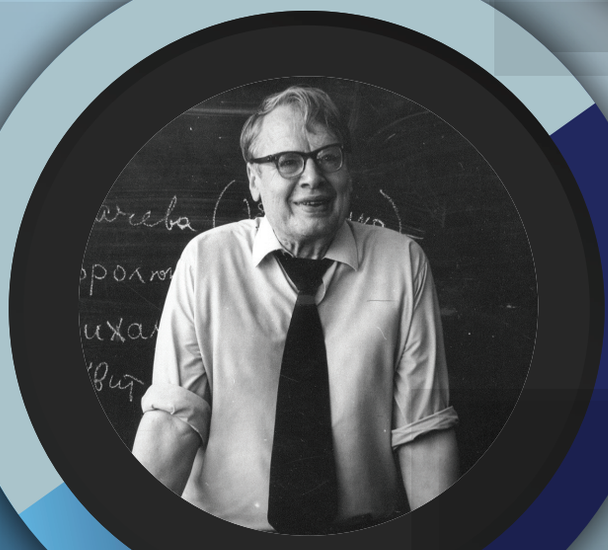
RTA

ISSN 1932-2321

JOURNAL IS REGISTERED IN THE LIBRARY OF THE U.S. CONGRESS

RELIABILITY: THEORY & APPLICATIONS

INTERNATIONAL GROUP ON RELIABILITY



RELIABILITY
RISK ANALYSIS
MAINTENANCE
SAFETY

GNEDENKO FORUM PUBLICATIONS

#3

(86) VOL.20

SEPTEMBER 2025

SAN DIEGO

ISSN 1932-2321

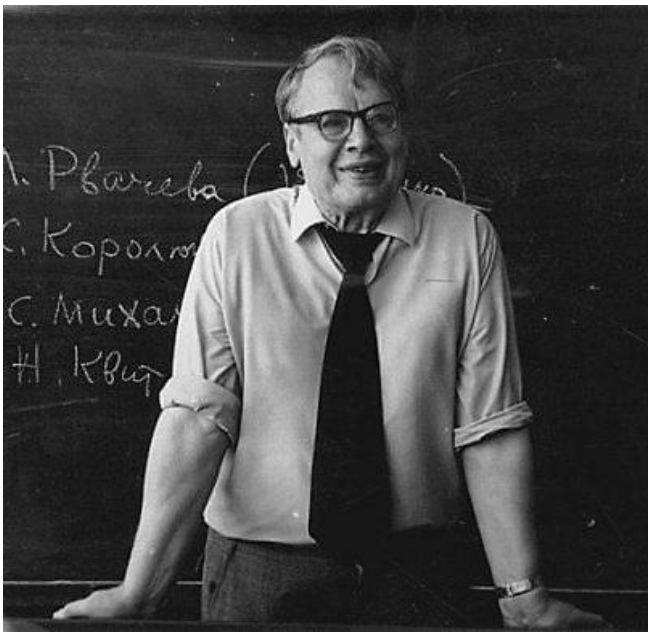
© "Reliability: Theory & Applications", 2006, 2007, 2009-2025
© " Reliability & Risk Analysis: Theory & Applications", 2008

© I.A. Ushakov
© A.V. Bochkov, 2006-2025
© Kristina Ushakov, Cover Design, 2024
http://www.gnedenko.net/Journal/index.htm

All rights are reserved

The reference to the magazine "Reliability: Theory & Applications"
at partial use of materials is obligatory.





RELIABILITY:

THEORY & APPLICATIONS

Vol.20 No.3 (86),
September 2025

San Diego
2025

Editorial Board

Editor-in-Chief

Rykov, Vladimir (Russia)
Doctor of Sci, Professor, Department of Applied Mathematics & Computer Modeling, Gubkin Russian State Oil & Gas University, Leninsky Prospect, 65, 119991 Moscow, Russia.
e-mail: vladimir_rykov@mail.ru

Managing Editors

Bochkov, Alexander (Russia)
Doctor of Technical Sciences, Scientific Secretary JSC NIIAS, Scientific-Research and Design Institute Informatization, Automation and Communication in Railway Transport, Moscow, Russia, 107078, Orlikov pereulok, 5, building 1
e-mail: a.bochkov@gmail.com

Gnedenko, Ekaterina (USA)
PhD, Lecturer Department of Economics Boston University, Boston 02215, USA
e-mail: gnedenko@bu.edu

Bushinskaya, Anna (Russia)
Candidate of Tech. Sci. Leading Research Fellow of the Sci & Engng Center of the Russian Academy of Sciences, Ekaterinburg
e-mail: bushinskaya@gmail.com

Sazonov, Aleksey (Russia)
Leading Specialist of the Standardization Department, JSC NIIAS (Joint Stock Company "Design &Research Institute for Information "Technology, Signaling and Telecommunications on Railway Transport), Bild 1, 5 Orlikov Pereulok, Moscow, Russia, 107078
e-mail: sazonoff2007@gmail.com

Deputy Editors

Dimitrov, Boyan (USA)
Ph.D., Dr. of Math. Sci., Professor of Probability and Statistics, Associate Professor of Mathematics (Probability and Statistics), GMI Engineering and Management Inst. (now Kettering)
e-mail: bdimitro@kettering.edu

Gnedenko, Dmitry (Russia)
Doctor of Sci., Assos. Professor, Department of Probability, Faculty of Mechanics and Mathematics, Moscow State University, Moscow, 119899, Russia
e-mail: dmitry@gnedenko.com

Kashtanov, Victor A. (Russia)
PhD, M. Sc (Physics and Mathematics), Professor of Moscow Institute of Applied Mathematics, National Research University "Higher School of Economics" (Moscow, Russia)
e-mail: VAKashtan@yandex.ru

Krishnamoorthy, Achyutha (India)
M.Sc. (Mathematics), PhD (Probability, Stochastic Processes & Operations Research), Professor Emeritus, Department of Mathematics, Cochin University of Science & Technology, Kochi-682022, INDIA.
e-mail: achyuthacusat@gmail.com

Recchia, Charles H. (USA)
PhD, Senior Member IEEE Chair, Boston IEEE Reliability Chapter A Joint Chapter with New Hampshire and Providence, Advisory Committee, IEEE Reliability Society
e-mail: charles.recchia@macom.com

Shybinsky Igor (Russia)
Doctor of Sci., Professor, Division manager, VNIIAS (Russian Scientific and Research Institute of Informatics, Automatics and Communications), expert of the Scientific Council under Security Council of the Russia
e-mail: igor-shubinsky@yandex.ru

Yastrebenetsky, Mikhail (Ukraine)
Doctor of Sci., Professor. State Scientific and Technical Center for Nuclear and Radiation Safety
e-mail: ma.yastreb2013@gmail.com

Associate Editors

Aliyev, Vugar (Azerbaijan)
Doctor of Sci., Professor, Chief Researcher of the Institute of Physics of the National Academy of Sciences of Azerbaijan, Director of the AMIR Technical Services Company
e-mail: prof.vugar.aliyev@gmail.com

Balakrishnan, Narayanaswamy (Canada)
Professor of Statistics, Department of Mathematics and Statistics, McMaster University
e-mail: bala@mcmaster.ca

Carrión García, Andrés (Spain)
Professor Titular de Universidad, Director of the Center for Quality and Change Management, Universidad Politécnica de Valencia, Spain
e-mail: acarrion@eio.upv.es

Chakravarthy, Srinivas (USA)
Ph.D., Professor of Industrial Engineering & Statistics, Departments of Industrial and Manufacturing Engineering & Mathematics, Kettering University (formerly GMI-EMI) 1700, University Avenue, Flint, MI48504
e-mail: schakrav@kettering.edu

Cui, Lirong (China)
PhD, Professor, School of Management & Economics, Beijing Institute of Technology, Beijing, P. R. China (Zip:100081)
e-mail: lirongcui@bit.edu.cn

Finkelstein, Maxim (SAR)
Doctor of Sci., Distinguished Professor in Statistics/Mathematical Statistics at the UFS. Visiting researcher at Max Planck Institute for Demographic Research, Rostock, Germany and Visiting research professor (from 2014) at the ITMO University, St Petersburg, Russia
e-mail: FinkelM@ufs.ac.za

Kaminsky, Mark (USA)
PhD, principal reliability engineer at the NASA Goddard Space Flight Center
e-mail: mkaminskiy@hotmail.com

Krivtsov, Vasiliy (USA)
PhD. Director of Reliability Analytics at the Ford Motor Company. Associate Professor of Reliability Engineering at the University of Maryland (USA)
e-mail: VKrivtso@Ford.com, krivtsov@umd.edu

Lemeshko Boris (Russia)
Doctor of Sci., Professor, Novosibirsk State Technical University, Professor of Theoretical and Applied Informatics Department
e-mail: Lemeshko@ami.nstu.ru

Lesnykh, Valery (Russia)
Professor, Doctor of Sci., Adviser to Director General, LLC Gazprom gaznadzor, Novocheryo-mushkinskaya Street, 65, Moscow, 117418, Russia
e-mail: vvlesnykh@gmail.com

Levitin, Gregory (Israel)
PhD, The Israel Electric Corporation Ltd. Planning, Development & Technology Division. Reliability & Equipment Department, Engineer-Expert; OR and Artificial Intelligence applications in Power Engineering, Reliability.
e-mail: levitin@iec.co.il

Limnios, Nikolaos (France)
Professor, Université de Technologie de Compiègne, Laboratoire de Mathématiques, Appliquées Centre de Recherches de Royallieu, BP 20529, 60205 COMPIEGNE CEDEX, France
e-mail: Nikolaos.Limnios@utc.fr

Papic, Ljubisha (Serbia)
PhD, Professor, Head of the Department of Industrial and Systems Engineering Faculty of Technical Sciences Cacak, University of Kragujevac, Director and Founder the Research Center of Dependability and Quality Management (DQM Research Center), Prijevor, Serbia
e-mail: dqmcenter@mts.rs

Ram, Mangey (India)
Professor, Department of Mathematics, Computer Science and Engineering, Graphic Era (Deemed to be University), Dehradun, India. Visiting Professor, Institute of Advanced Manufacturing Technologies, Peter the Great St. Petersburg Polytechnic University, Saint Petersburg, Russia.
e-mail: mangeyram@gmail.comq

Timashev, Sviatoslav (Russia)
Doctor of Sci., Professor, Director and principal scientist the Sci & Engng Center of the Russian Academy of Sciences, Ekaterinburg
e-mail: timashevs@cox.net

Zio, Enrico (Italy)
PhD, Full Professor, Direttore della Scuola di Dottorato del Politecnico di Milano, Italy.
e-mail: Enrico.Zio@polimi.it

e-Journal ***Reliability: Theory & Applications*** publishes papers, reviews, memoirs, and bibliographical materials on Reliability, Quality Control, Safety, Survivability and Maintenance.

Theoretical papers must contain new problems, finger practical applications and should not be overloaded with clumsy formal solutions.

Priority is given to descriptions of case studies.
General requirements for presented papers.

1. Papers must be presented in English in MS Word or LaTeX format.
2. The total volume of the paper (with illustrations) can be up to 15 pages.
3. A presented paper must be spell-checked.
4. For those whose language is not English, we kindly recommend using professional linguistic proofs before sending a paper to the journal.

The manuscripts complying with the scope of journal and accepted by the Editor are registered and sent for external review. The reviewed articles are emailed back to the authors for revision and improvement.

The decision to accept or reject a manuscript is made by the Editor considering the referees' opinion and considering scientific importance and novelty of the presented materials. Manuscripts are published in the author's edition. The Editorial Board are not responsible for possible typos in the original text. The Editor has the right to change the paper title and make editorial corrections.

The authors keep all rights and after the publication can use their materials (re-publish it or present at conferences).

Publication in this e-Journal is equal to publication in other International scientific journals.

Papers directed by Members of the Editorial Boards are accepted without referring.
The Editor has the right to change the paper title and make editorial corrections.

The authors keep all rights and after the publication can use their materials (re-publish it or present at conferences).

Send your papers to Alexander Bochkov, e-mail: a.bochkov@gmail.com

Table of Contents

METHODOLOGY FOR PREDICTING DEPENDABILITY MEASURES OF SWARM STRUCTURES OF UNMANNED AERIAL VEHICLES OF AGRICULTURAL APPLICATION 35

A.A. Kostiuk, V.E. Tsvetkov, P.S. Korolev, S.N. Polesskiy

This paper presents a methodology for predicting dependability measures of swarm structures of unmanned aerial vehicles used in agriculture. The main attention is paid to the development of mathematical models for assessing the dependability of hardware, software, and communication systems in drone swarms. Two types of UAVs are considered in the paper: DJI Phantom 4 RTK (for crop monitoring) and Tevel Aerobotics (for automated harvesting). The developed methodology improves the accuracy of dependability prediction of UAV swarm structures, which helps to optimize their maintenance and increase the efficiency of their application in agriculture. The developed mathematical model for predicting the dependability of swarm structures of agricultural UAVs includes a combination of hardware and software components and communication systems.

A COMPARATIVE ANALYSIS OF POWER ISHITA DISTRIBUTION EXPLORING ITS SIGNIFICANT CONTRIBUTION AND PRACTICAL APPLICATIONS 54

Rashid A. Ganaie, Manzoor A. Khanday, Dilawar A. Bhat, Yudhishther Singh Bagal

This research presents the development of a novel statistical model termed the weighted power Ishita distribution. The study delves into its fundamental structural properties, offering a comprehensive theoretical foundation. The parameters of proposed distribution are meticulously estimated through the maximum likelihood estimation method, ensuring robust and reliable results. To validate its applicability and demonstrate its superiority, the model is evaluated using three real-world lifetime data sets, highlighting its efficacy and potential for practical applications.

THE DEVELOPMENT OF RISK-BASED THINKING PRINCIPLES AT A MACHINE-BUILDING ENTERPRISE UNDER CONDITIONS OF INDUSTRY 4.0 67

Yaroslav Vavilin

The article deals with the problem of formal introduction of risk-based thinking features in machine-building production under conditions of Industry 4.0 together with the expansion of the use of digital technologies. The research aims to address the following objectives: to analyze the necessity and influence of risk management implementation within the organization's quality management system; to determine the levels required for realizing risk-based thinking; to develop a methodological foundation for integrating risk-based thinking considering Industry 4.0 elements; to perform a comparative analysis of the proposed model with known risk management systems. The study employs well-established methods of process-based approaches (Deming-Shewhart cycle) and systems analysis. The authors make an attempt to formalize the work on ensuring the proper use of risk and capability management tools from the perspective of a system analysis and process approach. Works related to risk management at the stages of the Deming-Shewhart cycle are highlighted and the levels and components of the machine-building production system model that are subject to analysis are determined. The task of introducing risk-based thinking in quality management systems of machine- building enterprises is critical due to the increasing complexity of products, increasing consumer demands and the need to ensure increased safety. Risk analysis makes it possible to identify potential threats to product quality in advance, minimize the consequences of defects, reduce error correction costs and increase the competitiveness of the enterprise in the market.

APPLICATION OF WEIGHT MEASURE ORDERING FOR INTUITIONISTIC FUZZY CRITICAL PATH ANALYSIS 78

S. Priyadharshini, G. Deepa, S. Ramprasath

The intuitionistic fuzzy critical path problem is a frequent and important challenge in network optimization, particularly in the planning and management of complex projects. However, the traditional critical path approach often fails to accurately reflect real-world scenarios. To address this, we have developed a critical path strategy within an intuitionistic fuzzy framework. In this study, the critical path is determined using a ranking algorithm, where the edge weights are modeled as triangular intuitionistic fuzzy numbers (ITFN). We have introduced definitions for ranking strategies that help identify the intuitionistic fuzzy critical path. Additionally, a proposed criticality degree measures that significance of each activity. Examples are provided to illustrate the proposed strategy, and the simulation results of the ranking techniques are also presented.

A RANKING FUNCTION APPROACH BASED ON CENTROID FOR GENERALIZED HEXAGONAL FUZZY NUMBERS TO SOLVE FUZZY MULTI-OBJECTIVE TRANSPORTATION PROBLEMS 90

Ramakant Sharma, Sohan Lal Tyagi

In a real-world scenario, the decision maker is unsure about the precise value of transportation parameters due to uncontrolled factors such as fuel prices, weather conditions, product availability, and requirements. Therefore, o fuzzy numbers are used to handle these uncertainties. This Paper aims to find an efficient solution to fuzzy multi-objective transportation problems (FMOTP) where all parameters (objective functions, availabilities, requirements) are given in the form of generalized hexagonal fuzzy numbers. In the Proposed approach, FMOTP is transformed into Fuzzy Single-Objective Transportation Problems (FSOTP) using the geometric mean technique. A new ranking function based on the centroid and in-center point method for hexagonal fuzzy numbers defuzzifies the FSOTP into a Crisp Single-Objective Transportation Problem (CSOTP). The optimal solution for the transformed CSOTP is obtained using the proposed approach based on the zero-entry cell method. Using the optimal solution of CSOTP the fuzzy efficient solution of FMOTP is obtained. Additionally, two numerical problems are solved to elaborate the Proposed approach, and results are compared with other existing methods. A comparison and analysis of the results show that the proposed approach provides a more optimized solution for FMOTP. This approach is easily applicable to real-life transportation problems in which decision-makers are unsure about the exact value of parameters.

A STATISTICAL FRAMEWORK FOR ENHANCING PROCESS CONTROL AND RELIABILITY USING AUTOENCODERS RANDOM SURVIVAL FORESTS AND NHPP MODELING 107

P. Sricharani, P. Satya Shekar Varma, M. V. Lavanya

Statistical Process Control (SPC) plays a critical role in ensuring the reliability and quality of high-grade products. This study introduces two advanced machine learning methods to enhance SPC by integrating Auto encoders for anomaly detection and Random Survival Forests (RSF) for failure prediction. The Autoencoder model is employed to monitor real-time sensor data, learning the normal patterns of product quality and identifying deviations that indicate potential quality issues. By flagging anomalies when product performance metrics diverge from expected thresholds, the autoencoder helps to adjust SPC limits dynamically, improving responsiveness to emerging quality concerns. Additionally, RSF is used to predict the likelihood of product failure over time, based on historical failure data and process parameters. This predictive approach enables proactive interventions to prevent quality issues before they occur, enhancing long-term product dependability. Together, these machine learning methods create a comprehensive framework for real-time monitoring and failure prediction, providing a more adaptive and data driven approach to quality control. The integration of Auto encoders and RSF into the SPC methodology significantly advances the precision and effectiveness of product reliability assessment, offering a powerful tool for maintaining high-quality standards in manufacturing processes.

A BAYESIAN APPROACH TO RELIABILITY ANALYSIS IN THE STRESS-STRENGTH MODEL WITH WEIGHTED EXPONENTIAL DISTRIBUTIONS CONSIDERING FUZZINESS .. 126

Alka Yadav, Satyanshu Kumar Upadhyay

The paper considers a Bayesian approach to the analysis of reliability in a stress-strength model when both stress and strength follow a weighted exponential distribution. The main focus of the paper considers a situation when the available data incorporate fuzziness. The situations when stress and strength distributions have common shape parameters and also when they have different shape and scale parameters are entertained separately. The entire analysis is done using the Bayes paradigm using weak proper priors for the model parameters. Since the resulting posteriors are not available in analytically closed form, the paper uses the recourse of Markov chain Monte Carlo simulation technique. Finally, a numerical illustration is provided based on real data examples. The results are found to be satisfactory.

SYSTEMATIC FAILURES IN FUNCTIONAL SAFETY AND THE PROBABILITY MEASURE 140

Hendrik Schabe

In this paper the probability measure is discussed. The point of interest is, whether probabilistic models are stable under different conditions and if they can be used further on, when conditions change. Systematic failures, as described in many standards of functional safety, play a role regarding this problem. Reducing systematic failures also means, to keep probabilistic calculus working. However, systematic failures have not been studied systematically regarding the question to keep the probability measure. An outline is given on the connection between systematic failures and the possibility to use probability calculus in technical problems in exploitation situations, where data from e.g. lab experiments are extrapolated to use conditions.

DEVELOPMENT OF A NEW CURRENT LIMITING SYSTEM WITH AUTOMATIC REGULATION OF CUT-OFF CURRENT 149

R.Z. Sultanov, N.A. Aliyev, G.A. Aliyeva

The article considers the problem of ensuring reliable operation of DC electric drives under short- term overloads, when the installed power of the electric motor is limited. It is shown that the use of traditional current cutoff units does not allow for the effective use of the maximum permissible overload capacity of the motor when changing the reference speed. The dependence of the permissible overload current on the rotation speed is analyzed, and the limitations of the existing control schemes are identified. In this paper, the existing schemes of automated electric drives equipped with traditional current cutoff units are considered and their main disadvantages are identified. As a solution, a current limiting system with automatic regulation of the cutoff current is proposed, aimed at increasing the reliability and energy efficiency of adjustable electric drives. The key feature of the proposed system is to adapt the cutoff current value depending on the rotation speed of the motor, which allows dynamically matching the electromechanical characteristics of the drive with the permissible overload curve of the motor. A current limiting circuit for a DC electric drive is proposed, in which the cutoff current setting is automatically changed depending on the value of the specified speed. The circuit ensures full use of the maximum permissible overload capacity of the electric motor at all values of the setting voltage.

A NEW MIN-MAX RANKED SET SAMPLING SCHEME WITH UNEQUAL SAMPLE SIZES 155

O. Rahimi Dehcheraghi, S.M.T.K. MirMostafaee

In this paper, a new type of ranked set sampling scheme with unequal sample sizes called the new min-max ranked set sampling scheme with unequal sample sizes, is proposed to expedite the sampling process and reduce costs by utilizing fewer data compared to the existing ranked set sampling plans with unequal sample sizes, such as the minimum ranked set sampling scheme with unequal samples. We study the parameter estimation for the exponential distribution using the maximum likelihood and Bayesian methods based on the new scheme. The Metropolis-Hastings strategy is implemented to derive the approximate Bayesian estimates of the parameter under two loss functions. A simulation study is conducted, from which the effectiveness of the new scheme can be observed compared to the simple random sampling scheme and the minimum ranked set sampling scheme with unequal samples. A real data set is also analyzed. Finally, The paper ends with some remarks.

ANALYSIS OF MAPj, PH°/PH[, PH°/1 RETRIAL INVENTORY QUEUE, TWO WAY COMMUNICATION, (S, S) REPLENISHMENT POLICY, NEGATIVE ARRIVAL, WORKING BREAKDOWN AND REPAIR 172

G. Ayyappan, V. Ganesan

The retrial inventory queueing model with two-way communication, the (s, S) replenishment strategy, negative arrival, working breakdown, and repair are all topics that are discussed in this paper. Our assumption is that the arrival is a Markovian arrival process and that a server is the entity that is responsible for providing phase type services. When there is a positive inventory and the server is idle, the customer who arrives is instantly attended to their needs. In the event that this instance does not occur, the customer who is arriving will be moved to orbit, and a retrial customer from orbit will join afterwards if the server is idle and has positive inventory. When the inventory level is positive, the server will make outgoing calls that follow phase type distribution during the idle period. If the inventory level is zero, the server will continue to stay idle. A negative arrival may occur while the server is providing service. Since the server is experiencing a breakdown, the consumer will experience slow service at this time. After the slow service ends, the server will immediately begin the repair procedure, which follows a phase-type distribution. The policy of (s,S) is utilised to replenish the items. By employing the matrix analytic method, we are able to derive the steady state probability vector. Additionally, we address the busy period, performance measurements, and cost analysis, in addition to providing some numerical examples.

GROK'S ROLE IN TRANSFORMING COMMUNICATION FOR DISASTER RISK MANAGEMENT 187

Renat R. Khaydarov

The increasing prevalence of natural hazards, exacerbated by climate change and urbanization, underscores the urgency of effective disaster risk management (DRM) to safeguard communities and infrastructure. Technical assessments, laden with specialized terminology, often hinder stakeholder engagement, particularly among non-specialists critical to decision-making processes. This study explores the prospective applications of Grok, an AI model by xAI, in enhancing DRM through its advanced natural language processing capabilities. Grok can translate complex multi-hazard risk evaluations, develop tailored educational content, and support real-time early warning systems, fostering inclusive communication. The research aims to evaluate Grok's efficacy in bridging technical and non-technical domains, promoting informed urban planning and disaster preparedness. Ultimately, this research lays the groundwork for future empirical studies on Al-driven DRM innovations.

METHODOLOGY FOR DETERMINING TYPICAL SCENARIOS OF TOTAL ELECTRICITY GENERATION BY GREEN SOURCES REDUCING THE RISK OF DISRUPTION OF BALANCE RELIABILITY 192

Rahmanov Nariman Rahman, Guliyev Huseyngulu Bayram, Ibrahimov Famil Shamil

The article proposes a methodology for identifying scenarios for aggregate electricity generation by renewable sources, such as wind and solar power plants, located in geographically diverse regions of the area with different climatic and weather conditions. To cover the demand of electric power systems, it is rational to use these green sources with complementarity from generation when planning load modes, as well as to reduce the risk of balance reliability of power systems. To determine the scenarios of aggregate generation of the used green sources, a cluster analysis is used based on the clustering of medoids using real-time measurements of wind speed, solar radiation and ambient temperature performed for all regions of the considered area where all green sources of electricity in the form of wind and solar power plants are installed. Clusters of these sources and loads are established separately and jointly. For each scenario of generation and planned growth in demand of the power system, the volume of additional capacity of green sources is estimated. The proposed methodology was tested on the example of the power system of Azerbaijan. The study found that, in order to reduce the risk of disruption to the system's balance reliability, scenarios of combined generation from wind farms located in the northern regions adjacent to the Caspian Sea with electricity generation from solar farms located in the southwestern regions of the country provide a more reliable way to increase the share of wind and solar generation in covering the planned demand growth compared to scenarios based on the separate use of these green energy sources.

REDUCING RENTAL COSTS IN TWO-STAGE HYBRID FSSP: BRANCH AND BOUND VS. HEURISTIC APPROACHES 206

Kanika Gupta, Deepak Gupta, Sonia Goel

This paper proposes a Branch and Bound (BB) based heuristic to solve a two-stage hybrid Flow Shop Scheduling Problem (HFSSP), incorporating practical constraints such as machine rental costs, transportation time, and job weightage. The scheduling environment includes multiple parallel machines at the first stage, where each job can be processed on any one machine, followed by a single rented machine at the second stage. To effectively model uncertainty in processing times, triangular fuzzy numbers are used. Additionally, transportation time between stages and job weightage are integrated into the model to reflect realistic industrial conditions. The proposed BB algorithm systematically explores the space of feasible job sequences, pruning non-promising branches to derive an optimal or near-optimal schedule under the given constraints. Its performance is benchmarked against two widely used heuristic approaches—NEH and GRASP-NEH—focusing on minimizing total elapsed time and rental cost of the second-stage machine. Experimental results indicate that the BB approach consistently outperforms the heuristic methods, particularly in reducing rental costs and providing better control over the utilization of the rented resource. While heuristic methods offer computational speed, they often compromise on cost efficiency and precision in handling fuzzy parameters. Overall, the study demonstrates the effectiveness of the BB method as a robust and efficient alternative for solving complex scheduling problems, especially in scenarios where minimizing rental costs is a critical objective. The integration of fuzzy processing times, transportation delays, and job priorities further enhances the practical relevance of the proposed approach.

ON THE BURR TYPE IV DISTRIBUTION APPLIED TO LIFETIME SURVIVAL DATA 217

Claire Joy G. Mariquit, Bernadette F. Tubo

This study presents the Burr type IV (Burrjy) distribution, which is one of the twelve continuous distributions within the Burr family. The paper thoroughly evaluates its properties and applications in survival analysis. Key distributional characteristics such as survival, hazard, quantile, cumulative distribution, and probability density functions are derived. Density plots are simulated to illustrate common patterns, including J-shaped, U-shaped, and reversed J-shaped forms, frequently observed in engineering and reliability contexts. The applicability of the Burrjy distribution

is demonstrated through three real-life datasets, each exhibiting distinct density shapes. The findings affirm the flexibility and robustness of the Burrjy distribution in modeling a variety of data shapes, underscoring its potential for broader applications in survival analysis and related fields.

A NON- MARKOVIAN RETRIAL QUEUE WITH NON PERSISTENT CUSTOMERS, GENERAL RETRIAL TIMES ALONG WITH REOCCURRING CUSTOMERS 229

S. Palaniammal, K. Kumar, R.Keerthana

A non-Markovian retrial queue with non persistent customers, general retrial times along with reoccurring customers is taken into concern in this place study. In this model, the retrial periods for reoccurring customers have an exponential distribution, while all the service periods and retrial periods for transitory customers are pretended to follow a general distribution. The PGF for the total amount of customers and the average amount of customers in the invisible waiting region is acquired by applying the supple-mentary variable method. We compute the waiting period delivery. Out of attention, special cases are conferred. Numerical outcomes are reveals.

RELIABILITY OF ELECTRICAL MACHINES VIA POWER LOSS MODELING IN MATLAB..... 238

Sara Alimamedova, Saida Kerimova

The article discusses a reliable mathematical approach to calculating power losses in electrical equipment, which is a critical component in the design, analysis, and optimization of electric power systems. Ensuring accurate loss estimation requires detailed modeling of equipment parameters such as rated power, voltage, current, resistance, and material properties that influence energy dissipation. For alternating current systems, it is particularly important to consider the interaction of active and reactive components, as well as the losses occurring in conductors, magnetic circuits, and other elements. The application of proven mathematical models enables engineers to evaluate system efficiency and operational stability under different scenarios. MATLAB tools and algorithms play a key role in automating these calculations, allowing for precise simulations across a wide range of load conditions, voltage levels, and equipment configurations. This not only improves the accuracy of loss assessments but also supports optimization of design parameters to ensure long-term reliability, energy efficiency, and cost-effectiveness of electrical machines and systems.

RELIABILITY ANALYSIS AND PERFORMANCE OPTIMIZATION OF A 2-OUT-OF-4 REDUNDANT SYSTEM USING RPGT AND METAHEURISTIC ALGORITHMS 249

Shakuntla Singla, Shilpa Rani, Diksha Mangla

In this paper focuses on the reliability analysis and performance optimization of a 2-out-of-4 redundant system, modeled using the Regenerative Point Graphical Technique (RPGT). The study aims to evaluate system behavior under various failure and repair rate conditions and to determine optimal parameters that enhance system reliability and availability. The system consists of four units A, B, C, and D arranged in a 2-out-of-4 configuration, meaning the system continues to function as long as at least two units are operational. A state-space model is developed, where each state corresponds to a distinct combination of operational, failed, and repair conditions of these units. The transitions between these states are governed by exponentially distributed failure and repair processes, and are represented using a directed graph structure. Transition probabilities are derived from these time-dependent exponential distributions, allowing precise evaluation of system behavior. To enhance the system's performance, three metaheuristic optimization algorithms — Cuckoo Search Algorithm (CSA), Particle Swarm Optimization (PSO), and Genetic Algorithm (GA)-are employed. These algorithms are applied to optimize key system parameters: failure rates (A) and repair rates (p). The objective is to maximize the Mean Time to System Failure (MTSF) and steady-state availability, and to minimize the expected number of inspections required by the repair personnel. The comparative analysis of optimization results reveals the relative effectiveness of each algorithm. PSO consistently provides the highest values for MTSF and availability, indicating stronger performance in identifying optimal solutions. CSA also performs well, showing close results to

PSO. GA, while effective, yields comparatively lower reliability indices. The outcomes demonstrate how advanced optimization techniques can be successfully integrated with RPGT-based modeling to develop a detailed and practical understanding of complex redundant systems. These insights support better maintenance planning, enabling organizations to improve reliability and reduce downtime in industrial, communication, and critical control systems. This methodology can be extended to other system configurations and industries, making it a valuable tool in the field of reliability engineering and operational research

CENSORED COUNT DATA REGRESSION MODELS: NUMBER OF CAESAREAN SECTION DELIVERIES USING INTEGRATED NESTED LAPLACE APPROXIMATION 257

Srinu Setti, B. Muniswamy

Count data depicts the frequency of an occurrence within a specific time frame. Consider the frequency of caesarean operations that women undergo during their lives. Almost every academic field, including management, economics, medicine, and industrial organizations, relies on count data. Count data is extensively utilized across various fields, including marketing, public health, and biomedical science. This study aims to estimate the posterior means, variances, or quantiles of the NCSD for women aged 15 to 49 in Andhra Pradesh, India, using the RCPRM and RCNBRM methodologies. The RCPRM and RCNBRM are used to determine the optimal fit. The secondary dataset NFHS-5 is used for the study. This research utilizes INLA to model the NCSD. Subsequently, it analyzed delivery patterns among pregnant women. Information criteria DIC and WAIC are utilized to compare for the best fit. The DIC values 4608.60 and 4593.90 of RCNBRM are less than the DIC values 4864.74 and 4860.68 of RCPRM. Thus, from the results, it is inferred that RCNBRM is the best fit for NCSD and that Breech Presentation, the present age of the respondent, High Blood Pressure, Child is Twin, Prolonged Labour, Education Level, and Heart Disease are significant determinants of the NCSD. Therefore, government policymakers need to consider these variables while making healthcare policies for women aged 15 to 49 years who are of childbearing age.

FIXED POINT THEOREMS IN TRICOMPLEX VALUED CONTROLLED METRIC SPACES 270

Shivani Chourasiya, Kavita Shrivastava

Throughout the years, scholars have broadened traditional fixed point theories to include more intricate structures like tricomplex valued metric spaces, aiming to tackle issues in multidimensional and hyper-complex contexts. While there is a rising interest in tricomplex valued spaces, the current literature addressing fixed point theorems in these areas presents several limitations. The existing research highlights numerous shortcomings; thus, this article employs innovative types of contraction mappings via a control function to illustrate fixed point theorems in tricomplex valued controlled metric spaces. These findings enhance the understanding of fixed point theory and pave the way for new applications in more complex and diverse mathematical frameworks. Consequently, our study fosters progress in the field, establishing a strong basis for future research and potential uses across various scientific and engineering fields.

BAYESIAN ESTIMATION OF POISSON-COMPOUNDED EXPONENTIAL TYPE DISTRIBUTION UNDER DIFFERENT LOSS FUNCTIONS 279

Na Elah, Peer Bilal Ahmad

Poisson moment exponential distribution is an important distribution and has gained special attention recently. It plays role in various fields, mostly in actuarial sciences. Thus its parametric estimation becomes important thing to do. The classical approach using the maximum likelihood method is the most used way to estimate the parameters of a distribution. In this paper, we considered the Bayesian approach to estimate the parameter of the distribution using beta prior which is a conjugate prior. The Bayes estimate for the parameter is obtained under Squared Error Loss Function (SELF) which is a symmetric loss function, Weighted SELF (WSELF) and Entropy Loss Function (ELF). Through a simulation study, the comparison is made on the performance of Bayes estimate under these loss functions with respect to Bias and Mean Square Error (MSE).

OPTIMIZING FUZZY DETERIORATING INVENTORY MODEL WITH TIME DEPENDENT DEMAND AND PARTIAL BACKLOGGING UNDER RESALABLE RETURNS..... 289

Kapil Dave, Tanuj Kumar

This paper investigates with the development of a fuzzy inventory model with timevarying demand, deterioration and backlogging with resalable returns. The returns rate, demand and backlogging parameters are taken as trapezoidal fuzzy numbers. Numerical example is given to validate the proposed mathematical model which has been developed for determining the optimal cycle time and optimal total inventory cost and profit. Sensitivity analysis is also carried out to explore the effect of changes in the optimal solution with respect to change in various parameters. The aim of this paper is to develop inventory policies that minimize the total cost so that to get the maximum total profit in both crisp and fuzzy modeling, and comparison of crisp and fuzzy models. Our study focuses on de-fuzzifying the total cost using the signed distance method and comparing it with the crisp model. This inventory model incorporates fuzzy demand and constant holding cost per unit item under the reasonable return policy while considering the impact of deterioration as a linearly increasing function of time. The retailer allows its unsatisfactory costumers to return their products. We assume that the return product will be sold at the same price. Customers are allowed to return the product during any phase of the length of the replenishment cycle. The retailer does not return the full amount to its customers for the returned goods. He offers 80% of the initial amount of the product. The number of returns are assumed to be proportional to demand. The demand is dependent on time. Partial backlogging is an important issue in the inventory theory which is related how to deal with the unfulfilled demand that occurs due to the shortage of stock. In real practice some customers prefers to wait for backorder during the shortage time and some turns to buy from other sellers. The waiting time period for next replenishment determine whether the backlogging would be accepted or not. During the shortage period the longer the waiting time is, the smaller is the backlogging rate would be. So backlogging rate is a variable that depends on the waiting time for next replenishment.

A COMPARATIVE ANALYSIS OF RESPONSE SURFACE METHODOLOGY IN LINEAR PROGRAMMING 300

Mushtaq A. Lone, S. A. Mir, R. Vijaykrishnaraj, Showkat Ahmad Bhat, Aafaq A. Rather, Raeesa Bashir, Manzoor A. Khanday, Aamir Majeed Parray

A linear mathematical programming approach has been employed to tackle the problem of land allocation in this comparative study. One design of experiment technique used in creating new processes and improving their efficiency is response surface approach. Different search methods have been employed in this study to identify the best distribution of agricultural land. The results of all formulated mathematical programming problem are obtained by using R software and different R functions like mexchalgorithmO and qconalgorithm (), argumants to these problems are bl, b2, b3 were developed. Furthermore, the Branch and Bound method has been utilized to provide the proper integer solution when the problem's solution turns out to be non-integer.

REGRESSION WITH VOLATILE ERRORS IN THE PRESENCE OF MEASUREMENT ERRORS..... 310

Anna Thomas, Nimitha John

This study explores the estimation and testing of regression models with volatile errors when measurement errors are present. The presence of measurement error in models with heteroscedastic disturbances, such as those following an autoregressive conditional heteroscedasticity (ARCH) or Generalized ARCH (GARCH) structure, can lead to biased estimates and misleading inferences. To address this, we develop an estimation framework that accounts for both heteroscedasticity and mismeasured observations, ensuring consistent and asymptotically normal parameter estimates. We estimate the parameters using corrected score estimation and weighted linear regression, which effectively mitigate the impact of measurement error and hetroscedasticity. Additionally, we perform a Likelihood Ratio (LR) test to assess the significance of measurement errors in regression models with volatile errors. Through Monte Carlo simulations, we analyze the bias and efficiency of traditional estimators and demonstrate the robustness of our proposed approach.

Finally, the methodology is applied to real-life economic and financial data, illustrating its practical relevance and effectiveness in empirical research. The findings contribute to improving statistical inference in models where measurement error and volatility coexist, ensuring more reliable and accurate parameter estimation.

RISK-BASED THINKING AND MEASUREMENT UNCERTAINTY: ADDRESSING ISO/IEC 17025 CHALLENGES WITH MODERN TOOLS 322

Rashid Mammadov

ISO/IEC 17025, the internationally recognized standard for the competence of testing and calibration laboratories, fundamentally embeds risk-based thinking (RBT) as a cornerstone for achieving and maintaining the reliability of measurement results and the robust management of measurement uncertainty. This article critically examines the synergistic application of RBT to proactively address the inherent and often complex challenges associated with quantifying and controlling measurement uncertainty. It aims to provide laboratories with practical, actionable insights into leveraging modern tools and methodologies that are not only compliant with ISO/IEC 17025 requirements but also enhance operational effectiveness. By exploring a spectrum of advanced statistical techniques (such as Monte Carlo simulations and Bayesian approaches), the integration of sophisticated digital tools (including TIMS, specialized uncertainty software, and data analytics), and the adoption of innovative operational practices, this study delineates a clear roadmap. The ultimate goal is to empower laboratories to bolster confidence in their measurement outcomes, ensure unimpeachable metrological traceability, stringently adhere to regulatory and customer compliance, and foster a culture of continuous improvement in their quality management systems.

AN INTEGRATED APPROACH TO ENSURING THE RELIABILITY OF POWER TRANSMISSION LINES IN THE CONTEXT OF DIGITAL ENERGY 330

I.N. Rahimli, N.A. Ganiyeva

In the context of the rapid development of digital technologies and their large-scale implementation in various sectors of the economy, the energy industry is also entering a phase of deep digital transformation. One of the key areas of this transformation is increasing the reliability and manageability of the energy infrastructure, in particular, power transmission lines (PTL), which are the main element of the electricity transmission and distribution system. Modern challenges, such as the increasing load on the power grid, changing climate conditions and the need to integrate distributed energy sources, require new approaches to reliability management. This paper discusses the key elements of digital transformation, including the use of intelligent monitoring systems, the Internet of Things (IoT), big data analysis and artificial intelligence for diagnostics and forecasting the technical condition of power transmission lines. The need for a comprehensive strategy combining technical, organizational and information measures is substantiated. Recommendations are presented for the implementation of digital solutions in the practice of operating power lines in order to increase their fault tolerance, prompt response to incidents and the overall efficiency of the power system.

IMPROVING THE RELIABILITY OF DISTRICT HEATING SYSTEMS AT CHP PLANTS UNDER VARIABLE THERMAL LOADS 339

G.K. Abdullayeva, R.K. Karimova, A.L. Bakhtiyarov

District heating systems powered by Combined Heat and Power (CHP) plants are critical for delivering thermal energy to residential, industrial, and municipal consumers. However, the variability of thermal load—driven by daily and seasonal demand fluctuations—poses significant challenges to system reliability. This paper presents a methodology for evaluating the reliability of such systems under dynamic thermal conditions. By combining deterministic modeling of thermal load profiles with a stochastic failure analysis of key components, the study performs a year-long simulation with hourly resolution. A time-dependent failure rate model is introduced, correlating failure intensity with the rate of change in thermal demand, thereby accounting for the mechanical and thermal stress experienced by pumps, valves, pipelines, and heat exchangers. Simulation results reveal that while modern CHP equipment has high baseline

reliability, rapid thermal load transitions notably increase the likelihood of failures. These findings highlight the necessity of predictive maintenance strategies and adaptive control mechanisms. The proposed framework contributes to the development of resilient and smart district heating infrastructures capable of sustaining reliable operation under increasingly complex load dynamics.

AN INTEGRATED APPROACH TO ENHANCING THE RELIABILITY OF SUBSTATION POWER SUPPLY SYSTEMS 345

Rahila Muradova

The reliability of substation power supply systems is a critical factor in ensuring the stability and uninterrupted operation of modern power grids. This paper examines advanced quantitative failure analysis methods that incorporate physical degradation processes, component interdependencies, and time-dependent failure characteristics. An integrated approach is proposed, combining structural redundancy, digital condition monitoring, thermal management, and predictive maintenance strategies. Modeling and statistical analysis confirm that implementing these comprehensive measures can increase system availability to 0.999 and reduce failure rates by 25- 40%. The methodology is applicable to both new substation designs and upgrades of existing infrastructure, supporting improved technical reliability and economic efficiency in operation.

KRISHNAV-P DISTRIBUTION AND ITS BIOMEDICAL APPLICATION 354

Praseeja C. B., Prasanth C. B.

This paper introduces a novel class of distributions, termed the KrishNav-P distribution (KNPD), developed through the application of a weighted distribution technique to the baseline Fav-Jerry distribution. The statistical properties of the KNPD are rigorously analyzed, and parameter estimation is performed using the maximum likelihood estimation method. To evaluate the practical applicability and performance of the proposed distribution, it is applied to a real-world dataset consisting of weight loss measurements (in kilograms) from 77 secondary school students aged 12 to 15 in the Thrissur District, Kerala. The data, collected between January and June 2021, pertain to students who experienced weight loss following a COVID-19 infection and tested the goodness of fit and the superiority of the distribution over the baseline and other existing distributions are also demonstrated.

OPTIMIZING PATHFINDING: A NOVEL ALGORITHM FOR GRAPH THEORY 367

Aijaz Ahmad Magray, Ajjaz Maqbool Dar, Firdous Ahmad, Aafaq A. Rather, R. Vijaykrishnaraj, D. Vedavathi Saraja, Syed M. Parveen, Raeesa Bashir

In this paper, a new proposed algorithm called the Pentacode-algorithm is successfully designed and implemented to solve the space and time problems associated with previous algorithms. Several parameters, such as Shortest Distance (SD), Time to Search Shortest Distance (TSSD), and Loss of Information Packets (LIP) have been checked and verified using the proposed algorithm. The simulation results achieved from the MATLAB tool authenticate the correct functionality of the proposed Pentacode-algorithm. Advance improvements have been proved in the proposed algorithm in terms of the space search and time issues. In addition, First-Node-Die (FND), Half-Node-Die (HND) and Last-Node-Die (LND) are determined in our results. The comparative results have shown that the Pentacode-algorithm is more proficient than the previous algorithm. This Pentacode-algorithm can be applied to warless communication systems, network routing and protocol multidirectional transmission and Quantum computing research.

ANALYSING STRESS STRENGTH RELIABILITY OF LIFE TEST ON AEROSOL PARTICLES BY GOMPERTZ DISTRIBUTION USING NOVEL JOINT PROGRESSIVE CENSORING 381

Showkat Ahmad Lone

System reliability has become a popular subject of study in engineering due to its wide range of potential applications. When a reliability practitioner aims to observe a specific number of failed units, a balanced case of joint progressive censoring scheme is proposed to improve the efficiency of an experiment. This paper investigates parametric inference for system reliability using a novel case of joint progressive censoring, with a specific focus on two independent Gompertz populations. The system reliability parameter is estimated using both likelihood and Bayesian inferential approaches. The Metropolis-Hastings algorithm is employed to compute Bayesian estimates under different loss functions. Asymptotic confidence intervals and Bayesian credible intervals are also derived. A thorough simulation study is conducted to evaluate the performance of the proposed methods across various sample sizes. Additionally, to demonstrate the practical utility of the approach, virus-containing aerosol particles (VCAP) lifetime data under two velocities are analyzed.

A NEW COUNT DATA PROBABILITY MODEL: PROPERTIES AND APPLICATIONS..... 390

Morifat, Bilal Ahmad Para

In the field of count data analysis, over-dispersion poses significant challenges, often limiting the effectiveness of traditional Poisson model. To address this limitation, we propose a novel two parameter distribution as an extension of Poisson distribution namely two-Parameter Poisson Garima Distribution (TPPGD). This distribution enhances modeling flexibility for over-dispersed data, offering a superior fit for real-world datasets. In this paper we derive the theoretical properties of TPPGD, including its probability mass function, cumulative distribution function and different statistical properties. Parameter estimation has been done using the maximum likelihood method and the moment method. Finally, the validity of the proposed model is checked using different real world data sets.

RELIABILITY, AVAILABILITY AND MAINTAINABILITY (RAM) ANALYSIS OF SOME PROCESS INDUSTRIES: A CRITICAL REVIEW OF LITERATURE 406

Punam Rani, Sangeeta Malik, Arun Kumar

This paper reviews the literature on reliability, availability, and maintainability analysis of process industrial systems. In today's automated world, it is unfeasible to live exclusive of reliable systems, so every one of the working engineering system be anticipated to remain operational with maximum effectiveness for the longest period of time, or reliable operation. Throughout the years, the primary goal has been to concentrate on the system presentation in excess of an extended period of time; in essence, these are case studies on the system concert of industrial systems. While achieving 100% failure-free operation in production is not practicable, industrial systems that can be repaired can have their system failures minimized. In this paper, an effort has been made to compile the necessary literature and offer some helpful advice on how to broaden the field for more beneficial outcomes on system performance.

ANALYSIS OF JOINT MULTIPLY TYPE-II CENSORED DATA USING THE GIBBS SAMPLER ALGORITHM 422

Vishal Singh, Akanksha Gupta and S. K. Upadhyay

This paper introduces a systematic approach for analyzing data under joint multiply type-II censoring. The study assumes a one-parameter exponential lifetime distribution and focuses on estimating unknown parameters. The maximum likelihood method is used to obtain frequentist point estimates, while a Bayesian framework is adopted to draw the corresponding Bayes inferences. To effectively handle censored data, an extended Gibbs sampler algorithm is

employed, treating the unknown observations as further unknowns and estimating them accordingly. This methodology ensures a comprehensive and robust inference process by simultaneously addressing parameter uncertainty and the challenges posed by the censored observations.

RELIABLE HYBRID OPTIMIZATION FOR SUPPLY CHAIN INVENTORY SYSTEMS 435

Ajay Singh Yadav, S. Viswanathan, Navin Ahlawat, Bhavani Viswanathan, Anupam Swami, Mohammed Abid

This study explores the optimization of blood supply chain inventory management through innovative approaches, specifically Bee Colony Optimization (BCO) and Genetic Algorithms (GA). The research addresses challenges in healthcare logistics, emphasizing the integration of organizational units involved in blood sourcing, production, distribution, and marketing. Key considerations include the potential conflicts between cost minimization in sourcing decisions and the focus on throughput in production and distribution. The study highlights the significance of achieving an optimal balance to ensure a reliable and efficient blood supply for patient care. Bee Colony Optimization and Genetic Algorithms, inspired by natural processes, offer promising solutions to the complexities of blood inventory management. BCO mimics collaborative foraging behavior, creating optimal paths marked by pheromones. Genetic Algorithms replicate natural selection to iteratively enhance solutions. The research aims to provide valuable insights into the application of these algorithms, contributing to the evolution of efficient blood supply chain management. The anticipated outcomes include improved healthcare logistics, ensuring timely access to blood products and enhancing patient safety and outcomes.

ALPHA-POWER-BURR-HATKE-EXPONENTIAL MODEL: PROPERTIES, SIMULATIONS AND APPLICATIONS BASED ON UNCENSORED AND PROGRESSIVE TYPE-II-CENSORED SAMPLES..... 455

Adubisi O. D., Joshua T., David A. A.

This study introduced a novel two-parameter model known as the alpha power Burr Hatke exponential (APBHE) model, characterized by constant, increasing-constant, upside-down bathtub, decreasing and increasing failure shapes. Structural properties and basic reliability functions are derived. The Simulation study carried out for both uncensored and progressive type-II censored samples indicated that the maximum likelihood estimation (MLE) performed quite well in producing good parameter estimates at finite sample sizes and tend to the true parameter value quicker than the maximum spacing product (MBS) method with minimum bias. Specifically, the censored schemes simulation disclosed that the MSE and bias values decrease as the sample size increases for the various censoring proportions. To demonstrate the flexibility and relevance of the APBHE model, a real-life bladder-cancer dataset is examined and the APBHE model achieved the best performance when compared with other competing models. Additionally, the log-APBHE model and log-APBHE regression model functions are presented for further explorations.

MULTI- REFERENCE SKIP- LOT SAMPLING OF TYPE 3 (MR-SkSP-3) 473

Meby Joseph Manoj, Azarudheen S.

In the current industrial sector, the rate of defective products present in the lots has been decreasing and most of the products keeps up a good history of quality throughout the production also. Skip-lot sampling plans are the suitable acceptance sampling plan for the situations where the series of products shows a stable and excellent quality. The skip-lot sampling plans are still widely used because of its reduced sampling cost and efforts, because the plan only needs to inspect a fraction of the lots submitted after a continues series of lots with excellent quality. This approach makes the skip-lot plan more cost-effective than the other sampling plans, thus making it an economically important plan. The current study incorporated a modification on the skip-lot sampling of type 3 and designated it as multi- reference skip lot sampling of type 3. The proposed plan has the provision of having multiple reference plans in normal and skipping inspection of a skip-lot sampling plan, unlike the traditional skip-lot plans which has the same reference plan in all

phases. The performance measures of the proposed plan are derived using the power series approach. A designing methodology to determine the optimal parameters for the plan using the unity value approach is also described with the help of a numerical illustration. Behaviour of the operating characteristic curves for varying set of parameters are also analysed for the plan. Comparison of the proposed plan is done between the conventional plans using performance measure values and graphical representations. This analysis shows that the new plan is able to effectively optimize the preferences of producer and consumer simultaneously, where the traditional plans fail to. The analysis is supported with the help of graphical representations and tabulated values.

ENHANCING ACCURACY IN ESTIMATING POPULATION MEAN THROUGH MODIFIED RATIO ESTIMATORS IN RANKED SET SAMPLING 485

S. A. Sabo, A. A. Osi, I. Z. Musa, H. U. Abubakar, A. Muhammad, U. Abubakar

This study aimed to improve the ratio estimation under rank set sampling by proposing some new modified estimators using auxiliary information on the size of the sample. The expressions for the bias and mean squared error of the proposed modified estimators are derived up to the first order of approximation using Tailor series expansion. A theoretical efficiency comparison between the proposed and competing estimators was done and the conditions upon which the proposed estimators expect to outperform the competing estimators were stated. Results from the numerical work indicate that the new proposed improved estimators are better than the already existing ones, showing a lower mean square error, coefficient of variation, and a considerable gain in efficiency. The new proposed estimators emerge as the optimal choice, outperforming the competing ones, and should therefore be used in applications.

SURVEY ON NON-MARKOVIAN QUEUE WITH PHASE SERVICE USING SUPPLEMENTARY VARIABLE TECHNIQUE..... 495

Binay Kumar, Sudeep Singh Sanga, Aditya Kumar

In the present article, we provide a comprehensive overview and literature review on performance modeling of queueing systems with phase service, utilizing the supplementary variable technique. We discuss the scenarios that necessitate phase service and explain how the supplementary variable technique is applied to analyze non-Markovian models. Additionally, we offer a summary of the fundamental concepts and existing literature on queueing systems with phase service. Our review covers research conducted over the past decade (2014-2024) on queues featuring phase service, including aspects such as bulk arrival, service interruptions, and discouragement. The review systematically explores models incorporating bulk arrivals, service interruptions, customer discouragement, and other complex operational features. By consolidating recent advancements and identifying common modeling approaches, this work aims to provide valuable insights for researchers and practitioners engaged in the analysis and design of advanced queueing systems.

MATHEMATICAL AND RELIABILITY MODELS OF MACHINE LEARNING ALGORITHMS FOR EARLY BRAIN CANCER DETECTION 519

Ajay Singh Yadav, Navin Ahlawat, Bhavani Viswanathan, Garima Pandey, Anupam Swami, Anjali Malik

Early detection of brain cancer is critical for improving patient outcomes, and this study explores the use of Logistic Regression, Reliability Modeling, and mathematical techniques for better diagnostic accuracy. Logistic Regression, a statistical model for binary classification, is used to predict tumor malignancy based on imaging features, offering probabilistic predictions that can guide clinical decisions. Reliability Modeling evaluates the performance and robustness of diagnostic systems, ensuring accurate detection despite varying conditions. By combining these methods, we can improve both the prediction accuracy and reliability of diagnostic systems. The research also integrates optimization and statistical inference to refine these models, ensuring they are both accurate and statistically sound. Hybrid models that combine deep learning with Logistic Regression further enhance the detection of brain tumors by

leveraging the strengths of both approaches. The study underscores the potential of AI and mathematical models to revolutionize brain cancer diagnostics, offering more reliable, interpretable, and efficient tools for early detection and improved patient outcomes.

IMPROVING THE QUALITY OF INTERVAL PATTERN RECOGNITION BY DIVIDING THE PATIENT SAMPLE IN MEDICAL RESEARCH 533

Gurami Tsitsiashvili, Vera Nevzorova, Pavel Dunts, Angelina Talko, Marina Osipova

In this paper, we consider a way to improve the quality of interval pattern recognition by dividing the sample into parts. This method is used to study erythrocyte and platelet germs of haematopoiesis for the ability to positively treat haematological patients from COVID-19. Along with this, this method of improving the quality of interval recognition is used to identify predictors of "difficult" tracheal intubation during artificial ventilation during anaesthetic support of surgical interventions. Despite the rather strong difference between these medical tasks, they are united in this research context by the possibility of improving the quality of recognition through a more specialized study of each sub sample of patients after dividing the sample into parts.

EFFICIENT ESTIMATION OF POPULATION MEAN USING MEDIAN OF AUXILIARY VARIABLE AND SIMULATION UNDER SRS 539

RizwanYousuf

In this study, we propose two modified ratio estimators for the estimation of the population mean of a study variable using the median of an auxiliary variable. Theoretical expressions for the bias and mean squared error (MSE) of the proposed estimators are derived under simple random sampling. We establish the conditions under which these estimators outperform existing modified ratio estimators. To validate the theoretical findings, both an empirical study using natural population data and a comprehensive simulation study are conducted. The simulation results consistently demonstrate the superior efficiency of the proposed estimators across varying sample sizes and correlation structures. These findings highlight the practical applicability and robustness of the proposed estimators in survey sampling.

ENHANCING SHORE HARDNESS AND RELIABILITY OF SS 316L REINFORCED PMMA NANOCOMPOSITES THROUGH RESIN 3D PRINTING PROCESS OPTIMIZATION 551

Upender Punia, Ramesh Kumar Garg

Over the last ten years, 3D printing has made great progress and expanded its applicability in a number of industries, including dentistry. Dental items including temporary and permanent crowns, bridges, drill guides, and jaw implants may be made using resin 3D printing. To create novel 3D-printable materials and improve their functionality, a lot of research is being done. The shore hardness of 316L-reinforced PMMA nanocomposites for dental applications is examined in this work. Three important process parameters—exposure time (3-5 seconds), layer height (20-40 microns), and post-curing duration (10-30 minutes)—are used to assess the hardness of manufactured specimens. Shore hardness is optimised using Response Surface Methodology (RSM), which yields a maximum shore hardness of88.90 SHD at 4.75 seconds of exposure time, 30.7 microns of slice height, and 23.2 minutes of post-curing time.

IMPACT OF FIBERS WEIGHT PROPORTION AND SURFACE TREATMENTS ON THE RELIABILITY OF HYBRID EPOXY COMPOSITE 562

Manjeet Chahar, Rajneesh Kumar

Natural fiber-reinforced composites (NFRCs) are attracting growing interest in many technical applications owing to their environmentally sustainable and economical properties. This study investigates the impact of weight proportion of fibers and surface treatments on the tensile strength of hybrid epoxy composites reinforced with hemp, jute, and bamboo. Prior to composite fabrication, the fibers underwent alkali and saline treatments at different concentrations (3, 5, and 7 wt. %). The composites were fabricated via the hand lay-up technique by varying wt. proportion of fibers (10,15, and 20 wt. %). The tensile strength is optimized using Response Surface Methodology (RSM), which yields highest tensile strength of 63.11 MPa at 14.24 wt. % of fibers fraction and 5.40 wt. % concentration of alkali treatment. Findings of this study demonstrate that reliability of the hybrid composite significantly enhanced due to improvement in strength of the composite. The treated hybrid composites have favourable properties, rendering them a feasible and sustainable option for automobile components and other lightweight structural applications.

COMPARISON OF CLASSICAL AND BAYESIAN APPROACHES FOR ESTIMATING THE SCALE PARAMETER OF THE INVERSE POWER RAYLEIGH DISTRIBUTION 573

Aadil Ahmad Mir, S.P. Ahmad, Sofi Mudasir Ahad

This manuscript investigates the parameter estimation of the Inverse Power Rayleigh Distribution (IPRD) using both Classical and Bayesian approaches. Parameters are estimated via Maximum Likelihood Estimation (MLE) and Bayesian methods under three prior assumptions: Jeffreys prior, extended Jeffreys prior, and quasi prior. Bayesian estimators, along with their associated risks, are evaluated using various symmetric and asymmetric loss functions, including the squared error loss function, Al-Bayyatis new loss function, precautionary loss function and entropy loss function. The performance of the estimators is assessed through simulated data based on the mean squared error (MSE) criterion. Results indicate that the Bayesian approach generally provides more accurate estimates with lower MSE compared to the classical MLE method.

THE IMPACT OF RAM ON SYSTEM PERFORMANCE: A REVIEW 587

Parveen Sihmar, Vikas Modgil, Sandeep Kumar

One of the requirements that industrial systems must meet is that they must function effectively for a prolonged period. The system's performance is a vital component for failure-free operation; yet, in actual fact, it is extremely rare for any production system to be completely failure-free. Over the course of the past twenty-five years, a comprehensive and critical literature assessment of reliability, maintainability, and availability (RAM) approaches has been carried out. These approaches have the potential to assist in the enhancement of the performance of complex systems. The review of a few publications resulted in the provision of comprehensive information regarding the historical and contemporary situation of RAM procedures in the research field and enterprises. A review of RAM tools and approaches can help in doing qualitative and quantitative analysis of complex systems. The author of this research tried to focus on a few of the key components of RAM methods.

THE QUASI-STATIONARY DISTRIBUTION OF A COMPLEX TWO-UNIT REPAIRABLE SYSTEM 592

Miriam Kalpana Simon, Jasmine Rathi S., Late Dr. K. Shankar Bhat

Like the first-busy-period in a queuing system, the time-to-system-failure is an important characteristic of a reliability system. In some reliability systems the time-to-system-failure may be sufficiently large to allow the residual life of the

system to settle down to a state of statistical equilibrium. The conditional limit distribution of the residual lifetime, also known as the quasi- stationary distribution, plays a vital role in the statistical analysis of such systems. In this work, the quasi-stationary distribution for the residual lifetime of a two-unit complex reparable system is obtained using regenerative stochastic process. The results of the study are numerically illustrated assuming exponential lifetime distribution for the units.

LIFO-BASED OPTIMIZATION OF TWO-WAREHOUSE INVENTORY SYSTEMS WITH DETERIORATING ITEMS..... 601

Amit Kumar, Ajay Singh Yadav, Dharmendra Yadav, Bhavani Viswanathan

In this study, a two-warehouse inventory model for the red wine industry is presented, focusing on items that deteriorate. The model takes into account the effects of inflation and operates on the LIFO (Last In, First Out) distribution policy. The goal is to minimize the total inventory cost, including the cost of maintaining inventory and the cost of purchasing new inventory. The model assumes a constant and known demand for red wine over time, with no permitted shortages. The stock system consists of warehouse A and warehouse B, with starting stocks fixed in each case. Inventory balance equations track inventory levels at each warehouse, taking into account transfers between warehouses and customer demand. The LIFO shipping policy is implemented to determine the quantities transferred between warehouses. Inflation is factored into the model by adjusting the cost of buying new inventory. This adjustment may be based on historical inflation rates or other relevant factors. The objective function is to minimize the total inventory cost, taking into account inventory costs and inflation-adjusted purchasing costs. The model provides a framework for making decisions about stock levels and transfer rates between warehouses. By optimizing these decisions, the model aims to achieve cost savings while ensuring that demand is met without bottlenecks. The model results can serve as a guide for inventory management strategies in the red wine industry, taking into account the specific challenges presented by the spoiled nature of the product and the impact of inflation.

STOCHASTIC MODELING AND ANALYSIS OF A PARALLEL SYSTEM WITH DIFFERING UNIT QUALITIES AND CATASTROPHIC FAILURES 614

Priya Baloda, Amit Kumar, Vikas Garg

In this paper, we conduct a stochastic analysis of a system comprising of two dissimilar units operating in parallel. One unit, characterized by two distinct types of failures, is considered high merit, while the other unit, with only one type of malfunction, is deemed low merit. We introduce the concept of catastrophic failure for the system. It is assumed that a single serviceman is responsible for both repair and replacement tasks. A regenerative point-based approach is employed to estimate various reliability characteristics. Additionally, we analyze the proposed model graphically to illustrate the effects of failure, repair, and replacement rates on the system's mean time to system failure (MTSF), availability, and profit.

ANALYSIS OF METHODS FOR ELIMINATION OF THE BRUSH-CONTACT ASSEMBLY OF THE ASG OF WIND TURBINES..... 625

N.S. Mammadov, M. Marufov, K.M. Mukhtarova

Traditional generator designs that use brush-and-contact assemblies to transmit electric current between rotating and stationary parts of the device are subject to significant drawbacks. The main problems associated with the use of brush-and-contact assemblies include mechanical wear of brushes and slip rings, sparking, electrical losses and high operating costs, which leads to reduced reliability and increased maintenance costs. Elimination of brush-and-contact assemblies is an urgent task, since it allows to significantly increase the reliability of devices and simplify their operation, especially in difficult climate conditions and high wind turbine installations. The article analyzes two modern approaches to solving this problem: installation of a brushless exciter and use of a rotating transformer. Each of these methods has its own advantages and disadvantages. The general electrical circuit of a brushless exciter device based on an

asynchronized synchronous generator is presented. The general electrical circuit of an asynchronized synchronous generator with a rotating transformer is also presented. An innovative solution is also considered, which involves installing a battery on the rotating part of the generator, which acts as a contactless power source for the rotor winding and provides energy storage.

CONSTRUCTION OF COMPLETE STOCHASTIC LIFE CYCLES OF HIGHLY CRITICAL INFRASTRUCTURES 634

Sviatoslav Timashev, Anna Bushinskaya

The article describes a risk-based approach to constructing the full life cycle (LC) of HCI with accounting for climate change. In this case, the objective function (OF) of HCI risk management as a function of time is reduced to the generalized cost of operating a strategically important object in the time interval "'from (birth) cradle / to grave". The life cycle, built on the basis of these data, makes it possible to evaluate and predict: (1) the inherent design reliability of the HCI, (2) the probabilities of all types of failures of the HCI; (3) the monetary consequences of these failures; (4) risks associated with random times of diagnostics, repairs and restoration of HCI and with the moments of its failures; (5) the overall risk of HCI at each moment of its existence with accounting for climate change.

EXPLORING SOME NEW CONTRIBUTION TO RAM AWADH DISTRIBUTION WITH COMPARATIVE PROPERTIES AND ITS APPLICATIONS 646

Manzoor A. Khanday, Rashid A. Ganaie, Aboubakar Ahmat Alwali Bourma, T. Vivekanandan, R. Shenbagaraja

In this study, a novel extension of the Ram Awadh distribution referred to as length biased Ram Awadh distribution is proposed and systematically developed. This distribution is constructed by applying length-biased transformation to the baseline Ram Awadh distribution, making it more suitable for modeling data where longer durations or larger values are more likely to be observed. A comprehensive exploration of the distribution's statistical properties is presented, including the derivation of moments, harmonic mean, reliability function, failure rate function, reverse hazard rate function, order statistics, entropy as well as the bonferroni and Lorenz curves. Parameter estimation is conducted through the maximum likelihood estimation method, ensuring robustness and efficiency. The practical utility and goodness of fit of the proposed model are demonstrated through its application to three real-life datasets, highlighting its flexibility and improved performance in empirical context.

A COMPARATIVE STUDY OF GENERALIZED ARADHANA DISTRIBUTION WITH SIGNIFICANT STATISTICAL PROPERTIES AND APPLICATIONS 659

Rashid A. Ganaie, V. P. Soumya, R. Shenbagaraja, Manzoor A. Khanday

This study introduces a novel extension of the generalized Aradhana distribution, termed the length biased generalized Aradhana distribution. The proposed distribution is formulated by applying the length biased technique to the baseline generalized Aradhana distribution, enhancing its applicability in reliability and survival analysis. Fundamental statistical properties, including moments, order statistics, reliability functions and entropy are rigorously derived to characterize the distribution's behavior. The parameters of proposed model are estimated using the maximum likelihood estimation method to ensure statistical efficiency. To assess its practical utility, the distribution is applied to two real-world lifetime data sets, demonstrating its superior performance and robustness compared to existing models. These findings highlight the significance and applicability of the length biased generalized Aradhana distribution in modeling lifetime data.

ENHANCING PRODUCT QUALITY AND OPERATIONAL EFFICIENCY THROUGH STATISTICAL QUALITY CONTROL..... 672

M. A. Khanday, A. Jain, A. A. Khan, Y. Ahmad, A. A. Rather

The foundation of success in the modern business environment is maintaining constant quality and efficiency across supply chains. The paper presents a clear and comprehensive analysis as it delves into the complexities of quality control in the supply chain for makeup products. By utilizing a diverse range of statistical techniques, such as descriptive statistics, control chart analysis, and ANOVA, and able to reveal important information about defect rates and the overall field of quality control procedures. This research reveals the complex interactions between different elements that affect defect rates, with a focus on the crucial functions that lead time and shipping carriers play in the supply chain for makeup products. By means of a methodical and thorough examination, we not only reveal the stability that is innate to the manufacturing process but also identify critical areas that are ripe for improvement. Determine areas for improvement by carefully examining the data; this will set the stage for increased operational effectiveness and higher standards of quality. This paper bridges the gap between theoretical understanding and real- world applications, rather than just existing in the domain of theoretical conjecture. Provide participants in the makeup product supply chain with practical insights that can lead to observable outcomes by combining academic accuracy with real-world relevance. In order to enable stakeholders to confidently and precisely navigate the complexities of quality control, this paper acts as a beacon of guidance. Stakeholders can enhance operational performance, reduce risks, and foster a continuous improvement culture by Furthermore, by maintaining an intense focus on raising customer satisfaction, this analysis clears the path for long-term success in the competitive and dynamic makeup product market.

ANALYSIS OF MODELING METHODS OF LINEAR AND NONLINEAR AUTOMATIC CONTROL SYSTEMS 682

S.M. Kerimova, S.J. Alimamedova

The article discusses the stability of automatic control systems (ACS). The stability of the automatic control system is the main characteristic of the automatic return of the system to its initial state of equilibrium after exposure to certain influencing factors on this system. In other words, it is the property of the system to maintain its resistance to external influences and its efficiency. The issue of reliability is aimed at preventing unforeseen and dangerous consequences of system instability, especially in such diverse fields as aviation, energy, and industry. A stable system ensures more accurate performance of the specified functions and is less prone to probable failure, and they can work for a long time without human intervention. An important place in the issue of determining the stability of ACS is occupied by the identification of errors that occur mainly during transients occurring in systems. The detected error is determined by the difference between the input signal (setpoint) and the input signal. In addition, the error that occurs in the system depends on different types of input signals, so these inputs can be stepwise, linear, etc. they can be typical. It should be noted that bias error analysis is useful only for stable systems. That is, before investigating an error in the system, it is necessary to determine the stability of this system. The article also considered the issue of calculating the error in the system with negative feedback. Using the Matlab/Simulink program, algorithms related to the detection of an error in the ACS are compiled. When studying the issues of ACS stability, the issue of regulating the gain coefficients of various types through a PID (ProportionaTIntegral-Derivative) regulator is being investigated.

THE POWER GENERALIZED KAVYA MANOHARAN TRANSFORMATION: APPLICATIONS IN RELIABILITY AND LIFETIME REGRESSION 690

Jinet Mariya Jojy, Sajesh T. A., Nicy Sebastian

A new class of distributions is introduced through the exponentiated generalization of the Kavya Manoharan transformation, referred to as the Power Generalized Kavya Manoharan (PGKM) transformation. In parallel systems, applying power transformations to the distribution of individual components yields the system's overall distribution. This generalization enhances the model's flexibility and accuracy. In this context, we propose a transformation to generate a novel class of distributions, specifically by developing a distribution based on the Inverse Weibull

distribution as the baseline. We investigate the behaviour of the hazard rates of these distributions, along with other analytical properties. Reliability measures for both single-component and multi-component stress-strength models are derived. The parameters of the proposed model are estimated using the maximum likelihood method, and simulation studies confirm the consistency of these estimates. Additionally, the new life distribution is applied to a real dataset, demonstrating superior fit when compared to various existing distributions in the literature. The distribution is further re-parametrized with location-scale parameters and employed in a lifetime regression analysis, with application provided to a practical dataset.

INFERENCES FOR ALPHA POWER TRANSFORMED INVERSE LINDLEY DISTRIBUTION BASED ON ORDER STATISTICS WITH APPLICATIONS 705

Sumit Kumar, Anju Goyal, Devendra Kumar, Narinder Kumar

The alpha power-transformed inverse Lindley distribution (APTIL) consist of one shape and one scale parameter. In some cases, the moments of the APTIL distribution may not exist due to its heavy tail, so we instead focus on the concept of inverse moments. In this paper, order statistics is used to derive the expression for moments, product moments and moment generating function for this distribution. The entropy of using order statistics for the APTIL distribution is also derived. Furthermore, tabulated values of the inverse moments of order statistics are provided for various sample sizes and parameter combinations. Three classical estimation techniques, viz., maximum product spacing estimators, least squares estimators, and weighted least squares estimators, are considered for parameter estimation and also evaluate the model parameters based on Type-II censored data. A Monte Carlo simulation-based approach is employed to assess the accuracy and validity of these estimators and the ensuing results. Finally, an empirical study using available real-life data sets demonstrates the utility of the distribution.

IN FUZZY MENGER SPACE, CERTAIN FPT USING OCCASIONALLY WEAKLY COMPATIBLE MAPPING THAT USES A-CLAS FUNCTION 726

Heera Ahirwar, Kavita Shrivastava

In this paper, we present new common fixed point theorems in the setting of fuzzy Menger spaces by considering self-mappings that satisfy the condition of occasional weak compatibility. The analysis is enriched through the incorporation of A-class functions, which serve as control functions in the formulation of contractive type conditions. This approach allows for the generalization and extension of several known results in the field of fuzzy fixed point theory. The structure of fuzzy Menger spaces, combined with the flexibility of A-class functions, enables the establishment of sufficient conditions for the existence and uniqueness of common fixed points among a family of self-mappings. To support the theoretical results, we also provide illustrative examples that demonstrate the applicability and effectiveness of the proposed theorems. The findings contribute to the broader understanding of fixed point results in fuzzy environments and highlight the utility of occasionally weakly compatible mappings under generalized contractive settings.

RELIABILITY ASSESSMENT OF LOW-VOLT AGE NETWORKS UNDER LIGHTNING-INDUCED OVERVOLTAGES TRANSFERRED FROM MEDIUM-VOLTAGE SYSTEMS 735

I.A. Guseynova

This article investigates the reliability implications of lightning-induced overvoltages transferred from medium-voltage (MV) systems to low-voltage (LV) networks. Special emphasis is placed on the role of distribution transformers and the importance of accurate modeling for evaluating surge transfer mechanisms. Simulations and experimental comparisons reveal that conventional capacitive Pi-circuits significantly overestimate transferred voltages. The study highlights the key parameters influencing surge magnitudes, such as earth resistance, transformer proximity, line configuration, and insulator flashovers. Based on analytical models and real case studies, the paper provides recommendations for enhancing the surge immunity and operational reliability of LV systems under lightning conditions.

ENHANCING THE RELIABILITY OF RELAY- CONTACTOR CONTROL SYSTEMS IN INDUSTRIAL AND ENERGY APPLICATIONS..... 743

Gultakin Hasanova, Sonakhanim Babayeva

Relay-contactor systems remain essential components in power control and automation circuits, particularly in critical industrial and energy infrastructure. Despite the increasing use of solid- state and programmable devices, electromechanical relays and contactors are still widely employed due to their robustness, electromagnetic isolation, and high switching capabilities. However, their reliability is subject to various failure mechanisms including contact wear, coil overheating, and mechanical degradation. This paper presents a systematic analysis of these reliability challenges, supported by statistical modeling, environmental correction factors, and empirical data. Advanced diagnostic techniques and predictive maintenance strategies are discussed, including the integration of intelligent monitoring systems capable of tracking temperature, contact resistance, and response time. The study also explores architectural solutions for improving the redundancy and resilience of DC auxiliary power systems, focusing on protection automation. The technical and economic benefits of intelligent relay systems over conventional ones are demonstrated. Results indicate that adopting adaptive reliability management and smart diagnostics significantly reduces failure rates and improves system availability.

FRACTIONAL INTEGRAL INEQUALITIES AND THEIR Q-EXTENSION 752

Farooq Ahmad, Ajjaz Maqbool, D.K. Jain, R. Vijaykrishnaraj, Aafaq A. Rather, D. Vedavathi Saraja, Syed M. Parveen, Raeesa Bashir, Showkat Ahmad Bhat

This paper aims to establish novel fractional integral inequalities for synchronous functions associated with the Chebyshev functional, incorporating the Gauss hyper geometric function. By employing advanced integral techniques, we derive refined bounds that extend and generalize existing results in the literature. The final section explores several special cases, particularly fractional integral inequalities involving Riemann-Liouville type fractional integral operators. Furthermore, we discuss potential applications of these findings in various mathematical and applied fields, highlighting their significance in fractional calculus and related domains.

DESIGN OF SKIP LOT SAMPLING PLAN (SKSP-3) WITH SINGLE SAMPLING PLAN AS A REFERENCE PLAN USING BOREL DISTRIBUTION..... 758

Jayalakshmi S., Gopinath M.

Skip-lot sampling plans (SkSPs) have long been recognized as effective strategies for minimizing inspection efforts in quality control, especially within high-volume manufacturing settings. This study proposes a Skip-Lot Sampling Plan of Type SkSP-3, constructed using Single Sampling Plans (SSPs) by attributes, under the probabilistic framework defined by the Borel distribution. Given its suitability for modeling rare or intermittent events, the Borel distribution provides a solid foundation for representing quality characteristics in such contexts. The presentation of the proposed SkSP-3 plan is assessed by means of Operating Characteristic (OC) curves and benchmarked against corresponding SSPs under identical conditions. The results reveal that the SkSP-3 plan achieves notably smaller sample sizes while preserving similar OC behavior, particularly at low defect levels. This work contributes to the body of literature by presenting a robust and cost-effective methodology for designing SkSPs under Borel distribution assumptions, thereby enhancing inspection efficiency without compromising quality standards.

ANALYZING SOLUTIONS OF FUZZY NABLA DYNAMIC EQUATIONS ON TIMESCALES: A GENERALIZED HUKUHARA APPROACH 769

Leelavathi R., Hari Kishore R., Mohana Rupa S. V. D., Muneera A.

In this paper, we study linear first-order fuzzy nabla dynamic equations on time scales (LFNDET's) under the framework of generalized Hukuhara nabla differentiability and also interpret various results of LFNDET's by employing the Variation of constant formula. A key result concerns the generalized nabla Hukuhara derivative for the product of a crisp function and a fuzzy function on time scales. Furthermore, we derive solutions to these equations using various approaches to generalized Hukuhara nabla differentiability. The behavior of these solutions highlights the importance and applicability of the generalized fuzzy nabla derivative in the context of nabla dynamic equations on time scales.

EXPLORING REDUNDANCY OPTIMIZATION TECHNIQUES FOR SYSTEM PERFORMANCE 784

Parveen Kumar, Dalip Singh, Anil Kumar Taneja

System reliability optimization remains a dynamic and evolving challenge, influenced by continuous advancements in mathematical modeling, engineering innovation, and management strategies. This study includes documents on reliability, availability, maintainability, dependability, testability, cost-benefit analysis, life-cycle failures, maintenance modeling, and asset integrity management. However, this article is mainly concerned with documents that focus on redundancy optimization problems (i.e., k out of n system, warm, hot, cold standby redundancy, system reliability analysis in different failure and repair conditions, redundancy allocation in several system configurations, and so on) that apply to Telecommunications, Aerospace and Aviation, Industrial Automation, Network Servers and IT Systems, Transportation Systems. In addition, documents on the Oil and Gas Industry, Data Centers, and critical Infrastructure that are part of process industries are included. We analyze as many documents as possible by combining commonly used keywords. Additionally, the paper identifies emerging trends such as adaptive and hybrid redundancy strategies and the integration of intelligent techniques like Supplymentry variable techniques, regenerative point techniques, Genetic algorithm, and machine learning for real-time reliability management. By synthesizing findings from recent literature, this review aims to guide future research and practical implementations, supporting the design of cost-effective, robust, and resilient systems for modern computing environments.

TWO STAGE FLOW SHOP SCHEDULING PROBLEM INCLUDING PROBABILITY UNDER LR FUZZY NUMBER 801

Pooja Kaushik, Deepak Gupta, Sonia Goel

Often known as the hybrid flow shop (HFS), the scheduling of flow shops with several parallel machines per stage is a challenging integrated problem that arises in many real-world scenarios. This study addresses bi stage flow shop scheduling problem involving parallel equipotential machines at each stage, where processing times are characterized as LR-type fuzzy numbers to encapsulate inherent uncertainties. Recognizing the criticality of minimizing the makespan under imprecise conditions, we employ four distinct reference functions to compute fuzzy makespan, thereby offering a diversified perspective on solution robustness. Four distinct fuzzy ranking (reference) functions are employed for defuzzification and comparison. The scheduling problem is solved using a Branch and Bound (B&B) algorithm tailored to accommodate fuzzy parameters and parallel machine constraints. Comparative analyses with an adapted version of branch and bound method are conducted to benchmark performance under varying degrees of fuzziness. Results underscore the efficacy and adaptability of the proposed approach, revealing nuanced improvements in makespan estimation and scheduling performance across varying fuzziness levels. This investigation not only enriches the theoretical landscape of fuzzy scheduling but also provides practical insights for complex manufacturing systems operating under uncertainty. This work not only extends classical scheduling methodologies into the fuzzy domain but also highlights the potential of integrating multiple reference functions within exact solution frameworks. The objective is to minimize the makespan under fuzzy conditions. To handle the fuzziness in processing times, A comparative

analysis of the results obtained using each reference function is conducted to evaluate their effectiveness in producing optimal or near-optimal schedules. The study highlights the impact of the choice of reference function on the computational efficiency and solution quality, offering insights for better decision-making in uncertain manufacturing scenarios. These functions serve to transform fuzzy numbers into comparable crisp values, thereby enabling traditional scheduling algorithms to process the data effectively. The focus of this research is to evaluate the impact of each reference function on the scheduling performance and to analyze the variation in results with respect to makespan minimization. The findings offer significant theoretical contributions to fuzzy scheduling literature and practical implications for industries where uncertainty in processing times is a critical factor.

FERMATEAN QUADRIPARTITIONED NEUTROSOPHIC FUZZY GRAPH 816

V. Divya, J. Jesintha Rosline

A fuzzy graph is a mathematical technique that represents relationship of an objects with uncertainty or imprecision, using nodes and edges with membership degrees to indicate the strength of connections. It provides an important paradigm for modelling and handling real world optimization tasks. Neutrosophic graphs extend classical graph theory to handle uncertain, imprecise and inconsistent information, enabling the modeling of complex relationships with varying degrees of truth, indeterminacy and falsity. This framework provides a more nuanced understanding of complex systems, allowing for improved accuracy and increased flexibility in decision-making, network analysis and optimization problems. Neutrosophic graphs can be applied to various fields, including multi-criteria decision-making, supply chain management and logistics, where uncertain or imprecise data is common. The extension of Neutrosophic set is the Quadripartitioned Neutrosophic Set. The division of indeterminacy function of the Neutrosophic set into the contradiction and ignorance component is termed as Quadripartitioned Neutrosophic Set. Associated with each vertex are values of truth, contradiction, ignorance and falsity that reflects it characteristics of a graph. Similarly, for each edge, these values signify the strength or reliability of the relationship between the connected vertices. Quadripartitioned Neutrosophic Fuzzy graph gives an accurate representation of uncertainty which leads to a greater clarity of complex systems and relationships. It has an emerging applications in social network analysis, image processing and decision making systems. Fermatean Neutrosophic Graph is a hybrid model of Fermatean and Neutrosophic graph. This enhancement provides an increased capacity to handle uncertain and unclear data. In contrast to traditional neutrosophic values, this framework operates with truth, indeterminacy and falsity membership degrees constrained by the condition that the sum of their third powers is less than or equal to two. In this article, a new graph is defined called Fermatean Quadripartitioned Neutrosophic Fuzzy Graph (FQNFG). We proposed the order, size, complete, complement and strong of Fermatean Quadripartitioned Neutrosophic Fuzzy Graph. Furthermore, the paper establishes operations for FQNFG such as composition, Cartesian product, Cross product and lexicographic product are also studied.

RELIABILITY BASED AN ATTRIBUTE CONTROL CHART USING EXPONENTIATED EXPONENTIAL- POISSON DISTRIBUTION UNDER HYBRID CENSORING 829

B. Gokila, A. Sheik Abdullah

The Exponentiated Exponential-Poisson (EEP) distribution, an advanced extension of traditional lifetime models, offers greater adaptability in representing product lifetimes by more precisely capturing variations in failure rates. To handle incomplete lifetime data, a Hybrid censoring technique is employed, combining elements of both Type-I and Type-11 censoring to establish a more robust methodology for lifetime analysis. Naturally, np control charts are used to monitor the count of defective units within a sample. The primary aim is to detect shifts in product lifetime distributions, which are crucial for quality control and reliability assessment. However, this study introduces a modification to the control chart, shifting its focus from simply counting failures to tracking the median lifetime, thereby enhancing its capability to identify changes in product reliability over time. The efficiency of the control chart is measured using the Average Run Length (ARE), which estimates the expected number of observations before an out-of-control signal is triggered. By carefully adjusting the chart's parameters, the study ensures that the in-control ARL aligns closely with a predefined target, thereby improving its reliability. This research is dedicated to developing an np control chart designed to monitor the median lifetime of products that follow the EEP distribution within a Hybrid censoring Scheme. Numerical examples and simulated data are provided to illustrate its real-world applicability. By optimizing control chart parameters based on ARL, the study enhances monitoring precision for product reliability, making it a valuable tool in industries where accurate lifetime assessment is critical.

ENHANCING THE RELIABILITY OF POWER SYSTEMS BY OPTIMIZING LIGHTNING PROTECTION OF OVERHEAD TRANSMISSION LINES 841

Elbrus Ahmedov, Kubra Mukhtarova

This paper addresses the reliability issues of power systems caused by lightning-induced overvoltages resulting from lightning strikes to components of overhead transmission lines (OHL). It is demonstrated that lightning discharges are one of the key causes of transmission line outages and significant economic losses. A method is proposed to improve the efficiency of lightning protection by upgrading the design of lightning protection cables using V-shaped metallic elements to increase the protection zone. Calculations were carried out to assess the expansion of the protection zone depending on the geometrical parameters of the design. A mathematical model was developed and implemented in the MATLAB Simulink environment to analyze the behavior of OHL under direct lightning strikes to the shield wire and phase conductors. The model takes into account lightning current parameters, structural characteristics of supports, grounding device properties, and insulation parameters. Simulation results showed a significant influence of grounding resistance on the level of resulting overvoltages and the effectiveness of lightning protection. The proposed technical solutions can be used to enhance the lightning resistance and operational reliability of overhead transmission lines, especially in regions with high lightning activity.

ON RELIABILITY STRESS-STRENGTH MODEL USES SHOCK-MODEL APPROACH TO FOLLOW MUKHERJEE-ISLAM DISTRIBUTION 853

Vijayakumar. B., M. Manoharan

A component or system exposed to shocks will result in system or device damage. The strength of a produced product is a variable quantity that requires modelling as a random variable. It is necessary to evaluate the stress conditions of the operating system. Strength and stress are both thought of as random variables, which is made clear by the term "stress-strength model." With the inter-arrival time following the Mukherjee-Islam distribution and strength following an exponential distribution, we attempted to create a model in this study. Graphs are used to support numerical examples that are provided.

DESIGN AND FABRICATION OF HIGH-GAIN, LOW CROSS-POLARIZATION PLANAR VIVALDI ANTENNA FOR UWB APPLICATIONS 862

Balvant J Makwana, Shahid S. Modasiya

This paper presents the design, simulation, and experimental validation of a corrugated Vivaldi antenna optimized for ultra-wideband (UWB) operation at high bandwidth. Fabricated on glass epoxy substrate, the antenna employs edge corrugations to minimize cross-polarization while maintaining high gain across the operational bandwidth. Full-wave electromagnetic simulations guided the design optimization, with radiation patterns and return loss parameters serving as key performance metrics. A prototype was fabricated and tested in an anechoic chamber, yielding a measured high gain with a very good peak gain over a wide range of frequency. Cross-polarization levels were effectively suppressed, ranging from approximately very low at both high and low frequencies. The close agreement between simulated and measured return loss parameters with impedance matching better and radiation characteristics validates the proposed design methodology. The presented approach confirms that cost-effective glass epoxy substrates can achieve performance comparable to specialized high-frequency materials when combined with strategic geometric modifications. The design is well suited for UWB applications in radar, wireless communication, and microwave imaging systems.

AIRPORT SAFETY MANAGEMENT: A PROACTIVE MODEL BASED ON RISK ASSESSMENT AND BENCHMARKING 875

Hanine Abdellah, El Barkany Abdellah

This study presents a practical, context-sensitive approach to managing airport safety that combines the PDCA cycle with benchmarking techniques within a structured risk assessment framework. Given that ensuring operational safety in airports requires precisely recognizing, classifying, and successfully mitigating specific hazards, this study addresses this issue by creating a tailored risk assessment table. This tool, designed specifically for airport environments, clearly categorizes hazards based on their likelihood and severity and uses a novel equation developed in this study to correctly determine Safety Performance Indicators (SPI) and Safety Performance Targets (SPT). These indicators allow safety managers to effectively track performance trends, compare outcomes to other airports, and align safety policies with ICAO regulations. The cyclical nature of repetitive improvement in PDCA is assured, and value is added through benchmarking by applying tested best practices, enhancing the quality of decisions. A case study with airport safety practitioners establishes the practical applicability and value of this methodology in risk prioritization and pushing forward the drivers of corrective action. Collectively, the results demonstrate how this strategy supports proactive risk control and operational safety, and develops a sustainable culture of continuous improvement—a key component of effective airport safety management.

ON COPING WITH CENSORING IN SURVIVAL DATA USING FUZZY THEORY 892

Jaisankar, R., Haripriya, H.

Aim: The problem of censoring is the main concern in Survival Analysis which makes the analysis complex and may lead to unreliable results like less precise parameter/survival/hazard estimates, wider confidence intervals, reduced power to detect differences between groups, sometimes especially when the proportion of censored observations is high. In particular, if the censoring is informative that is reacted to the event, serious bias may be expected to present in the estimates. Omitting censored observations prices with loss of information and adding them is often embedded with a lack of information. It is proposed to implement fuzzy methodology for dealing with censored observations in Survival data so as to minimize their impact on the survival/hazard estimates. This paper suggests a modified approach based on the Fuzzy Theory, in which, the censored observations could be incorporated effectively. Methods: Many statistical procedures are advised to tackle censoring, in both parametric and non-parametric realms. However, their application mainly depend on the nature of censoring, whether right or left or interval censored. Even when their applied, still some lacuna may persist which could be completely eradicated when there is no censoring. Different types of fuzzy numbers are applied both to the censored and uncensored observations according to their nature and the results of the same were tested in case of the non-parametric procedure, the Kaplan-Meier estimator, using log rank test. Results: On the application of the proposed methodology one may obtain the survival probabilities which are reasonably calculated for even censored observations. The median survival time observed by the application of this methodology gives lesser value than the median obtained by the classical Kaplan eier method. The survival curve obtained by the proposed method is different from the survival curve of the classical Kaplan eier method and since the proposed methodology addresses all points of time and hence may give reliable estimates of survival probability. Conclusion: When compared with the classical Kaplan-Meier method, the proposal method gives survival probabilities which are slightly differ from the estimate obtained from non-fuzzy methodology. Since the survival probabilities can be calculated even for censored observations using fuzzy numbers, it is expected that the proposed modelling may be better than the classical Kaplan-Meier estimator.

BIOGEOGRAPHY-BASED RELIABILITY OPTIMIZATION 899

Deepika Garg, Sarita Devi, Doorgeshwaree Devi Heeramun, Nakul Vashishth

Biogeography-based optimization (BBO) is an effective optimization algorithm originally introduced by Dan Simon in 2008. It is inspired by the principles of biogeography. It mimics the process of migration and colonization of different species, where the behavior of species is determined by their habitats and the available resources. However, BBO can

suffer from slow convergence and premature convergence for high-dimensional optimization problems. To address these issues, opposition-based learning (OBL) has been integrated with BBO. OBL uses the concept of generating an opposite solution to an existing solution and combining them to form a new search direction. This helps to improve the diversity of the population and accelerate the convergence speed of the algorithm. The combination of BBO and OBL has shown promising results in solving various optimization problems, including engineering design, scheduling, and feature selection. This approach has proved to be efficient and robust, making it an attractive alternative to other optimization algorithms. In this research study, the redundancy Allocation Problem (RAP) is solved with BBO and OBL-BBO. Computational results confirm the robustness and superiority of this new model over previous ones in optimizing the reliability of the system. Besides, the proposed algorithm OBL-BBO outperforms the previous ones BBO in finding good results.

IMPROVING THE RELIABILITY OF SOLAR ENERGY SYSTEMS USING FLOATING PHOTOVOLTAIC TECHNOLOGIES 909

M.T. Babayev

This paper explores floating solar panels (FSPs) as a promising and cost-effective solution for enhancing the reliability and sustainability of solar power systems. The analysis focuses on the technical, environmental, and economic benefits of FSPs compared to traditional land-based installations. Floating systems offer improved operational reliability and energy efficiency due to natural cooling, land conservation, lower environmental impact, and reduced water evaporation — particularly vital in regions with limited freshwater resources. Deploying FSPs on artificial reservoirs and flooded quarries not only reduces land-use pressure but also contributes to lower capital and operational expenditures. Case studies from Azerbaijan and Japan demonstrate the reliability, resilience, and ecological viability of floating solar solutions under various climatic conditions. Although initial investments may be higher, long-term assessments reveal that FSPs can deliver more consistent performance and greater cost-effectiveness in regions with high solar irradiance and available water surfaces. The paper provides a comprehensive overview of floating photovoltaic technologies, highlighting their role in improving the reliability and stability of solar energy supply.

RELIABILITY-BASED OPTIMIZATION OF TWO-WAREHOUSE SUPPLY CHAIN MODELS 920

Ajay Singh Yadav, S. Viswanathan, Navin Ahlawat, Bhavani Viswanathan, Anupam Swami

This study presents a reliability-based optimization framework for managing a two-warehouse inventory system in the dairy industry, specifically addressing the complexities posed by product spoilage, shortages, and inflation. The proposed mathematical model integrates key inventory management principles with spoilage dynamics, shortage scenarios, and economic inflation, under a First-In-First- Out (FIFO) dispatching policy. By prioritizing the shipment of older stock, the model aims to reduce spoilage and enhance product turnover. It incorporates dairy product expiration rates to determine optimal replenishment and dispatch strategies while also identifying and mitigating potential operational bottlenecks. Additionally, the influence of inflation on inventory-related costs is embedded within the model to reflect real-world economic fluctuations. Through the application of advanced optimization algorithms implemented in MATLAB, the model seeks to minimize total inventory costs and improve supply chain efficiency. Overall, this research offers a comprehensive and practical tool for enhancing inventory decision-making in perishable goods industries like dairy.

ANALYSIS OF M, MAP/PH/2 NON- PREEMPTIVE PRIORITY QUEUEING INVENTORY SYSTEM WITH BREAKDOWN, REPAIR AND (s, S) POLICY 934

G. Ayyappan, M. Thilakavathy

We analyze a non-preemptive priority queueing model in this research that has two heterogeneous servers, each of which has its own queue. Queue 1 possesses a low priority status with infinite capacity and queue 2 possesses a high priority status with finite capacity. We made the assumption that arrival follows M, MAP and service time follows

Phase-type distribution. Server 1 is always available in the system; Server 2 is an unreliable server. With a (s, S) policy, the inventory is filled up and an exponential distribution is scheduled for the replenishment time. Using the matrix analytical approach, a stationary probability vector was assessed, and a stability criterion was created for our system. Performance metrics are also studied using this technique. Both two and three-dimensional displays are used to show the numerical examples.

ABOUT WAYS TO INCREASE RELIABILITY AND ECONOMY OF STEAM BOILER INSTALLATIONS OF BLOCK POWER PLANTS 949

Farzaliyev Y.Z.

The new method and algorithm of management by reliability and profitability of work of steam boiler installations block power stations is developed. The essence of a method is reduced to definition of "weak parts» and to formation of recommendations. In a basis of a database and program model, there are results of measurement and calculation of technical and economic parameters steam boiler installations. And the method allows to formulate the main directions of increasing the efficiency of individual control steam boiler installations and steam boiler installations of power plants as a whole. Improving the efficiency management system of the steam boiler installations allows, first of all, to reduce operating costs. The developed method allows us to consider the obtained results as methodological support for personnel in organizing the operation, maintenance and repair of steam boiler installation. Therefore, the relevance of this problem is obvious

A NOVEL METHOD TO ASSESSING PROCESS VARIATION WITH A CONFIDENCE INTERVAL OF SAMPLE STANDARD DEVIATION 959

Boya Venkatesu, G. Siva, Christophe Chesneau, V. Sai Sarada

One of the great tools of statistical process control for evaluating patterns of variation in the process is the control chart. In this article, we focus on developing a new approach to estimating process parameters in a control chart using confidence intervals (CIs) of sample standard deviations. They have the property of providing additional information about the quality of the estimate. A Monte Carlo simulation is used to investigate the accuracy of the obtained CIs. The performance of the classical and new approaches is compared in terms of standard error using simulated samples. The simulation results show that the new approach outperforms the classical approach.

DIFFERENT ESTIMATION METHODS AND VALIDATION FOR THE EXTENSION EXPONENTIAL DISTRIBUTION 965

Rochdi Nouadri, Nacira Seddik-Ameur, Khaoula Aidi

This study investigates the extended exponential distribution proposed by Nadarajah and Haghighi, which can effectively model data with a mode at zero and accommodate varying hazard rates—whether increasing, decreasing, or constant. Unlike other distributions, it allows for scenarios where the hazard function increases while the probability density function decreases monotonically. The focus is on exploring alternative estimation methods to maximum likelihood estimation for this distribution, including the maximum product of spacing, Cramer-von Mises, Anderson-Darling, Right-tail Anderson-Darling, Left-tail Anderson-Darling, and Kolmogorov- Smirnov tests. A novel approach using initial data is proposed to develop an effective goodness-of- fit criterion tailored for validating this model. Extensive simulations with thousands of samples are conducted to assess the performance of these estimation methods and the practicality of the proposed goodness-of-fit test. Real data applications are also utilized to demonstrate the applicability and effectiveness of the extended exponential distribution in real-world scenarios. This research expands the statistical modelling toolkit by providing robust estimation techniques and validation criteria specifically designed for the characteristics of the extended exponential distribution.

CONSTRUCTION OF A NEW ATTRIBUTE CONTROL CHART BASED ON RAYLEIGH DISTRIBUTION UNDER HYBRID CENSORING - A BAYESIAN APPROACH..... 981

T. Kavitha, M. Gunasekaran

Statistical Process Control (SPC) is a quality control approach that makes use of statistical tools to understand, monitor, and improve a process. A control chart is a tool for monitoring process performance that consists of a visual indication to detect anomalous deviations because of assignable causes. This chart compares the values of a quality attribute to the control limits. In the quality control process, the control chart is often generated by ignoring parameter uncertainty. The identification of changes in the parameter(s) within the probability distribution of one or more process-related variables is an essential part of monitoring. Estimating the parameters is essential since this might have an impact on the control chart's long-term performance in a controlled or out-of-control condition. This article provides a novel attribute control chart in the form of a Bayesian approach based on the Rayleigh lifetime distribution and the Hybrid censoring technique. A Bayesian approach will be used to calculate the control chart parameters and average run length. The control chart parameters are determined for various combinations of values, and the performance of the developed control chart is evaluated using the Average Run Length (ARE). Numerical examples are used to explain the proposed control chart, and simulated data is used to show how it might be used.

ENHANCING THE RELIABILITY OF THERMAL POWER SYSTEMS USING MEMBRANE-BASED WATER TREATMENT TECHOLOGIES..... 990

Ahmadova J.A.

The reliability and efficiency of thermal power plants (TPPs) are largely determined by the quality of water treatment systems that maintain a stable water-chemical regime (WCR) for boilers and auxiliary equipment. In scenarios where seawater with high salinity and variable composition is used as the primary water source, conventional treatment methods—such as ion exchange, chemical coagulation, and thermal desalination—prove inadequate and resource-intensive. This study investigates the application of a hybrid membrane-based configuration comprising ultrafiltration (UF), reverse osmosis (RO), and membrane distillation (MD). The proposed system enables the production of high-purity demineralized water, reduces operational risks, and lowers energy consumption through the utilization of low-grade waste heat. Based on pilot data and modeled performance, the UF-RO-MD cascade achieves up to 99% desalination efficiency with specific energy consumption in the range of 1.9-2.5 kWh/m3 and a significant reduction in scaling potential. A simplified case study is provided to illustrate the high effectiveness of membrane technologies in enhancing the sustainability and resilience of TPP operations, especially in coastal regions with limited freshwater availability.

A NOVEL ENERGY-EFFICIENT APPROACH TO DETECT AND MITIGATE RPL ROUTING ATTACKS IN IOT NETWORK..... 999

Deepak Upadhyay, Hiteishi Diwanji

Communication networks are constantly at risk from routing attacks, which have the potential to disrupt the network performance, information flow and jeopardize network integrity. Network resources and Energy consumption attacks on the Internet of Things (IoT) are the main targets to bring down the services of Internet of Things devices with attacks such as Denial of Service, Jamming etc. Node mobility results in frequent changes to network topology. This increases energy consumption and reduces node lifetimes, which can disrupt overall network functionality. To overcome these problems the author has proposed a hybrid and lightweight A Novel Energy-Efficient Approach to Detect and Mitigate RPL (EEADM-RPL) protocol considering control messages with route metrics in different detection and mitigation algorithm to mitigate the Blackhole attack, Rank attack and Sybil attacks under mobility environment at a time. An attack scenario created with the algorithms for all attacks using control messages and attributes of packets. The EEADM-RPL protocol uses basic RPL control messages, neighbor table, trust calculation, and a minimum rank hysteresis objective function to detect and eliminate the attacks. This protocol is suitable for industrial systems to handle cyber-attack and for the Vulnerability Assessment and Penetration Testing audit. The Cooja simulator, part of the

Contiki operating system, simulates the attacks without mobility and with mobility demonstrates the effectiveness affecting the network and the resources. The outcomes of the simulation are compared with those of current protocols. According to the data, the proposed protocol demonstrates improvements over the conventional RPL protocols in several metrics: the average parent change ratio by 87.94%, the average packet loss ratio by 69.17%, end-to-end latency by 67.85%, and both energy consumption and end-to-end delay by 13.07%.

EXPERT METHOD OF RANK PENALTIES 1014

Alexander Bochkov, Nikolay Zhigirev, Alla Kuzminova

Voting methods include a variety of systems and technologies designed to facilitate the electoral process. These methods can range from the use of traditional paper ballots to modern electronic systems, each with unique features and functions. Heuristic peer review methods use simplified decision-making processes to evaluate complex scenarios, especially in areas such as usability and forecasting. These methods improve efficiency and accuracy by combining expert information with heuristic principles to improve results in a variety of applications. While heuristic methods offer significant advantages for expert evaluations, they can also lead to errors if not applied carefully, emphasizing the need for balanced approaches to complex evaluations. We propose an algorithm for finding the most consistent decision of experts in determining the leader in an alternative ranking problem.

SYSTEM RELIABILITY AND PROFITABILITY CONSIDERING CONCEPTS OF WARRANTY AND INSURANCE: AN OVERVIEW 1022

Kajal Sachdeva, Gulshan Taneja, Amit Manocha

The concepts of reliability, warranty, and insurance are interwoven in certain respects. System warranties and insurance coverage, whether provided by the manufacturer or a third party, reflect the system's potential reliability and offer consumers a sense of security. Conversely, enhancing system reliability during the development process can help reduce warranty and insurance costs. The purpose of this study is to compile the existing literature and provide a structured review of system reliability evaluation, incorporating the concepts of warranty, pricing, and insurance policies. Synthesizes the ideas, models, and methodologies that various authors have included in their study. To achieve this, a detailed review of 111 journal articles published between 1992 and the present was conducted. The primary focus areas of the review include system reliability, warranty policies, insurance mechanisms, and cost analysis. In addition, the study highlights potential directions for future research in this domain.

ATTRIBUTE CONTROL CHART BASED ON RAYLEIGH DISTRIBUTION: A BAYESIAN APPROACH 1040

M. Gunasekaran, T. Kavitha, S. M. Karthik

Statistical Process Control is a quality control approach that uses statistical tools to assess, monitor, and optimize processes. A control chart plays a crucial role in this method by tracking the performance of a process and providing a visual signal to detect any irregular deviations caused by specific assignable factors. It compares the values of a quality attribute against predetermined control limits. In typical quality control procedures, control charts are often created without considering parameter uncertainty. However, it is essential to identify any shifts in the parameters of the probability distribution linked to one or more variables associated with the process to ensure effective monitoring. Evaluating these parameters is vital, as it can influence the long-term functionality of the control chart in both controlled and uncontrolled environments. This article introduces an innovative attribute control chart that utilizes a Bayesian methodology based on the Rayleigh lifetime distribution, specifically applied under accelerated life testing with a hybrid censoring technique. The parameters for the control chart will be established through various combinations of values using a Bayesian approach, while the effectiveness of the control chart will be evaluated through the Average Run Length (ARL). Numerical examples will illustrate the proposed control chart, and simulated data will showcase its potential application. The effectiveness of the proposed control chart will be quantified through ARLs for different shift constants, sample sizes, and additional parameters such as p, Lower Control Limit, and Upper Control Limit.

METHODOLOGY FOR PREDICTING DEPENDABILITY MEASURES OF SWARM STRUCTURES OF UNMANNED AERIAL VEHICLES OF AGRICULTURAL APPLICATION

A.A. Kostiuk[1], V.E. Tsvetkov[2], P.S. Korolev[3], S.N. Polesskiy[4]

[1, 2, 3] Department of electronic engineering, HSE University, Moscow, Russia, 123458
[4] Department of computer engineering, HSE University, Moscow, Russia, 123458
[1] aakostyuk@edu.hse.ru, [2] vtsvetkov@hse.ru, [3] pskorolev@hse.ru, [4] spolessky@hse.ru

Abstract

This paper presents a methodology for predicting dependability measures of swarm structures of unmanned aerial vehicles used in agriculture. The main attention is paid to the development of mathematical models for assessing the dependability of hardware, software, and communication systems in drone swarms. Two types of UAVs are considered in the paper: DJI Phantom 4 RTK (for crop monitoring) and Tevel Aerobotics (for automated harvesting). The developed methodology improves the accuracy of dependability prediction of UAV swarm structures, which helps to optimize their maintenance and increase the efficiency of their application in agriculture. The developed mathematical model for predicting the dependability of swarm structures of agricultural UAVs includes a combination of hardware and software components and communication systems.

Keywords: dependability, reliability function, failure rate, swarm of unmanned aerial vehicles, agriculture, communication systems, software, availability operational factor

I. Introduction

In the era of digitalization and automation of human activities, unmanned aerial vehicles (UAVs) play a pivotal role. The rapid growth of the Russian civil unmanned aerial systems (UAS) market, as illustrated in figure 1, reflects the increasing demand for these platforms and the corresponding expansion of this sector [1]. Concurrently, the market for swarm (group) applications of UAVs is also gaining momentum.

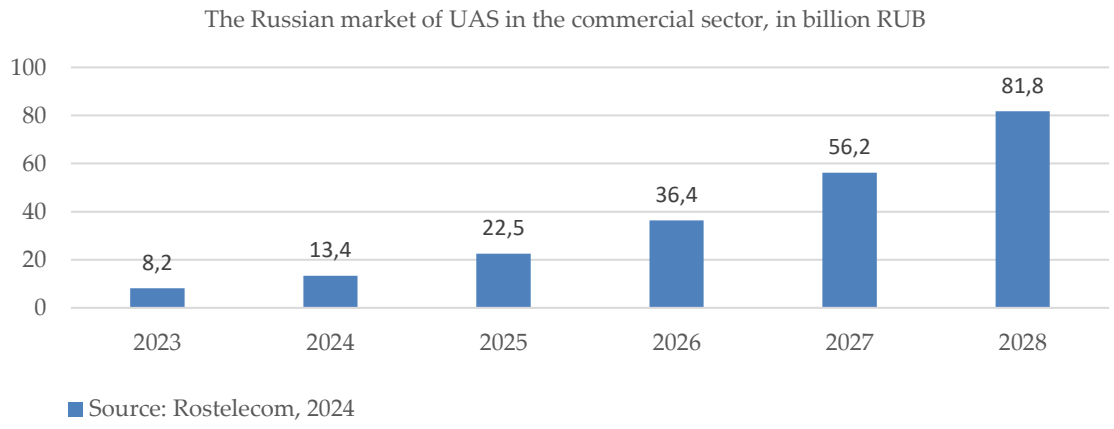


Figure 1: *UAS market growth chart*

Furthermore, the importance of early dependability prediction in the production of any radio-electronic equipment (REE) at various stages of its lifecycle has become increasingly evident. This approach helps prevent errors in component selection, circuit design, and engineering solutions, thereby avoiding premature REE failures and mitigating associated economic and reputational losses.

Currently, there are numerous known applications for UAV swarms. Key areas include: agriculture, emergency services, mining, construction, geodesy, logistics, insurance, government services, media and journalism, environmental conservation, science and education, telecommunications, photo/videography, and sports/entertainment [2].

The most promising application domain for unmanned aerial vehicle swarm systems is precision agriculture, where these systems integrate multisensory platforms, automated control systems, data analytics, and artificial intelligence across multiple stages of agricultural production [3]. The agricultural workflow typically comprises three key phases: planting, crop cultivation, and harvesting.

This study focuses on UAV groups deployed during the harvest phase. At this stage, UAV swarm systems can provide dual functionality: yield prediction and estimation, and automated harvesting operations.

Currently, there is no comprehensive approach to forecasting the dependability measures of both individual UAVs and their groups: the predictive dependability measures of software (SW), hardware components, and communication systems are evaluated independently, which significantly affects the final outcome and fails to adequately predict the fault tolerance of such systems. Therefore, the primary objective of this work is to increase the accuracy and validity of dependability forecasts for various swarm structures used in agricultural applications. The tasks of this study include the development of a mathematical model for predicting the dependability measures of the software, hardware parts, and communication systems of two different types of UAV groups designed for use during the harvest phase. Additionally, the communication system dependability was calculated both through network topology and signal-to-noise ratio. Moreover, the presence of software on both the ground control station (GCS) and the UAV swarm itself was taken into account.

II. Selection of the object and statement of the research problem

Yield forecasting plays a key role for the producer, as it is at this stage that decisions are made regarding the significance of a range of factors such as insurance, budget formation, resource allocation, and others.

One of the technical solutions for implementing unmanned monitoring of farm surfaces with yield forecasting and assessment functionality is presented in the study [4]. The study is based on the DJI Phantom 3 Professional unmanned aerial vehicle. According to the presented technology, the UAV flies at an altitude of 5 to 6 meters above the plant canopy and takes photographs from two sides, which ensures image quality sufficient for fruit recognition. In this study, 20 trees were involved, which is not a large number for higher-level agricultural plantations. To cover a larger area of agricultural land, the most effective solution would be the use of a swarm of similar drones. This would eliminate additional time costs associated with recharging and surveying the entire area with a single UAV. Figure 2 illustrates the operating principle of the technology using a single UAV and a group of similar drones.

Furthermore, the study [5] conducted research aimed at developing a yield forecasting model for cotton fields. The research was also based on DJI Phantom series unmanned aerial vehicles (4 RTK). The article supports the prevailing view that the use of UAVs in agriculture currently represents an optimal solution, enabling highly accurate detection of crop biomass, quality

forecasting, pest and weed detection, among other applications. The authors provide a detailed description of the drone's hardware components used in their work, including the camera's field of view (84°).

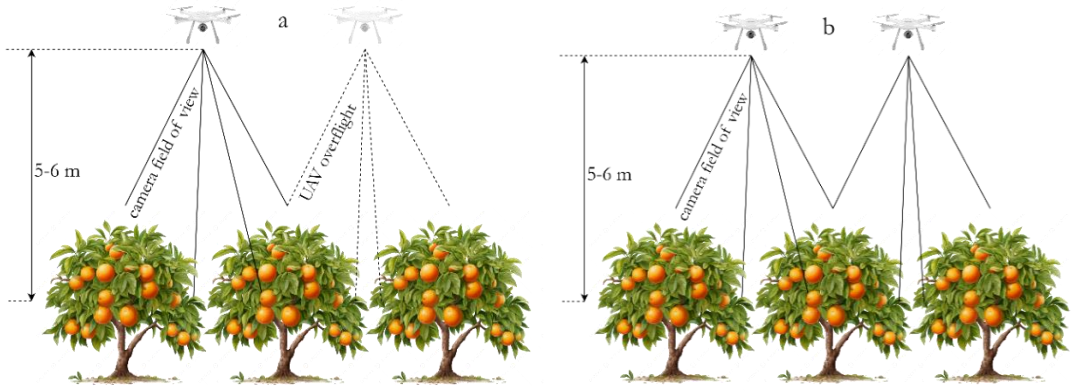


Figure 2: *Information collection process: (a) by a single UAV, (b) by a swarm of UAVs*

Thus, based on the analyzed studies, it is necessary to determine the optimal UAV model and a sufficient number of drones in the group for yield forecasting of an average-sized farm in the Russian Federation. Depending on the region, the sizes of cultivated areas in the Russian Federation can vary significantly; however, as indicated in [6], the average size can be taken as 214.4 hectares.

According to the technical documentation of the DJI Phantom 4 RTK [7] and DJI Phantom 3 Professional [8], the former has superior characteristics, including speed and range. Based on the data regarding the required flight altitude above the plant canopy (5-6 m) and the DJI Phantom 4 RTK's field of view (84°), the camera's surface coverage width was calculated to be approximately 9,9 meters. Using these data, along with the DJI Phantom 4 RTK's maximum speed (50 km/h) and flight duration (30 minutes) from its technical documentation, the necessary number of such UAVs to cover the entire average sowing area in the Russian Federation (214.4 hectares) was calculated: at least 9 such drones are required for a complete analysis of the surveyed area without recharging (i.e., in the minimum possible time). Thus, taking into account adjustments for the imperfections of real operational processes, weather conditions, and other factors affecting the information collection task by a UAV group, this study investigated a swarm of short-range micro UAVs similar to the DJI Phantom 4 RTK in two variations: consisting of 9 and 10 drones.

An equally important part of selecting the necessary unmanned aerial vehicles is considering their classification by design type: fixed-wing (airplane), aerostatic, multirotor, and hybrid [9]. Currently, multirotor UAVs are the most common solution for agricultural monitoring tasks; however, fixed-wing drones may be used for larger areas. Additionally, in agricultural applications, minimizing environmental pollution is essential, so careful consideration must be given to the choice of drone engine type. The following types of engines are distinguished in modern UAVs [10]: electric, fuel-powered, gas-turbine, propeller-driven, and hybrid. The DJI Phantom 4 RTK UAV, like most modern copters, is equipped with an electric motor, making it environmentally safe for crops and fully suitable for the task at hand.

The second and final stage of automating the harvest process using UAV swarm structures in agriculture is the automated harvesting itself.

As shown in [11], a comprehensive automated fruit harvesting system already exists. The operating principle of such a system is based on the use of a group of drones equipped with "tentacles," connected to a central machine with containers. The UAVs themselves are equipped with cameras and can recognize fruits on trees, after which they pick them using their "tentacles" and place them into the machine's container.

The number of UAVs in such a swarm can vary from 2 to 10; however, the baseline should be set at 6 UAVs, with 3 on each side, as shown in [11].

The study was conducted a comprehensive investigation of all components within UAV swarms that affect system dependability to develop a unified dependability forecasting system for such swarm structures operating under normal conditions. By combining all developed models for each component influencing the swarm system's dependability, a single predictive model for the dependability measures of the UAV group will be created. Since the study focuses on normal operating conditions, it assumes the absence of sudden failures, with corresponding approximation of dependability measure values. The operational timeframe considered for the swarm structures in this research pertains to their active mission duration.

III. Development of mathematical models for predicting UAV swarm dependability measures

I. Technical dependability

When developing a mathematical model for forecasting the dependability measures of the technical equipment in UAV swarm structures, it is important to consider not only the components of the drones themselves but also the equipment located at the GCS. According to [12], the GCS consists of the hardware described in table 1. The table contains the analyzed classical mean time between failures (MTBF) for specific types of components and the calculated failure rate using the formula: $\lambda_i = \frac{1}{MTBF_i}$, λ_i is the failure rate of the i-th hardware component, and $MTBF_i$ is its mean time between failures. In addition, there is no redundancy in the system, so the failure of any component will cause the failure of the entire system due to the inability of the UAV swarm to accomplish the mission, hence the failure rates $\lambda_{T_{GCS}1}$ of this GCS can be considered as the total failure rate of all the components $\sum_i \lambda_i$, as shown in the table below. For groups of 9 and 10 drones, the GCSs are identical.

Table 1: *Standard GCS hardware set for DJI Phantom 4 RTK swarm*

Hardware component			**MTBF, k hours**	**Failure rate, 1/h**
Name	**Component**	**Abbreviation**		
Control Computer	System unit	SU	150	$\lambda_{SU} = 6{,}67 * 10^{-6}$
	Monitor	Mon	250	$\lambda_{Mon} = 4 * 10^{-6}$
	Keyboard	K	1100	$\lambda_K = 9{,}1 * 10^{-7}$
	Mouse	Mou	2000	$\lambda_{Mou} = 5 * 10^{-7}$
Portable personal computer	System unit	SU	150	$\lambda_{SU} = 6{,}67 * 10^{-6}$
	Monitor	Mon	250	$\lambda_{Mon} = 4 * 10^{-6}$
	Manual remote control	MRC	200	$\lambda_{MRC} = 5 * 10^{-6}$
Network infrastructure	Cable system	CS	100	$\lambda_{CS_1} = 1 * 10^{-5}$
	Modem	Mod	440	$\lambda_{Mod} = 2{,}27 * 10^{-6}$
	Switch	S	590	$\lambda_S = 1{,}69 * 10^{-6}$
	Router	R	800	$\lambda_R = 1{,}25 * 10^{-6}$
Communication system	Receiving and transmitting equipment of the command and telemetry channel	RTECTC	80	$\lambda_{RTECTC} = 1{,}25 * 10^{-5}$
Flight state change system	Remote display and mode selection	RDMS	150	$\lambda_{RDMS} = 6{,}67 * 10^{-6}$
Total failure rate				$\lambda_{T_{GCS}1} = 6{,}09 * 10^{-5}$

To predict the dependability of the above components of the GCS information system, it is necessary to use either the electronic radio items dependability compendium 2006 [13], or reference books and products for foreign products [14], [15], [16], or the MTBF from the technical documentation after selection of specific models, or a combined version, as in the case of UAV components.

Thus, according to the exponential law of dependability, the final formula for predicting the technical dependability indexes (reliability function $P_{T_{GCS}1}$) for the GCS of the DJI Phantom 4 RTK UAV swarm can be summarized as follows:

$$P_{T_{GCS}1} = e^{-\lambda_{T_{GCS}1} * t} \quad (1)$$

The GCS for the Tevel Aerobotics UAV swarm has a different appearance. As a result of the analysis [17], all the obtained data can be summarized in table 2.

In this paper, a variant of the maximum hardware set will be considered, taking into account the possibility of autopiloting the Tevel Aerobotics UAV GCS. When forming an understanding of the type of system from the dependability point of view, several factors should be taken into account, among them: the navigation unit has either a GPS sensor, LPS or ultra-wideband visual positioning system, which directly indicates the presence of redundancy within this unit of the system. The situation is similar in the fruit detection unit, as it is possible to use both a smart camera or laser and a sound sensor, in our case, the presence of all these three components will be considered. Also, it is worth mentioning that in our case the cable system is a power line of 6 cables, as each cable is a connecting element between the platform and the UAV.

Table 2: *Tevel Aerobotics swarm GCS IS hardware set*

Hardware component			**MTBF, k hours**	**Failure rate, 1/h**
Name	**Component**	**Abbreviation**		
Fruit detection system	Smart fruit recognition camera	SFRC	200	$\lambda_{SFRC} = 5 * 10^{-6}$
	Laser	L	260	$\lambda_{L} = 3{,}85 * 10^{-6}$
	Sound sensor	SS	220	$\lambda_{SS} = 4{,}55 * 10^{-6}$
Computer system	Processor	P	310	$\lambda_{P} = 3{,}23 * 10^{-6}$
	Memory unit	MU	870	$\lambda_{MU} = 1{,}15 * 10^{-6}$
Transportation conveyor	Motorized belt	MB	150	$\lambda_{MB} = 6{,}67 * 10^{-6}$
Support frame	Motor	M	230	$\lambda_{M} = 4{,}35 * 10^{-6}$
	Fruit sorter	FS	340	$\lambda_{FS} = 2{,}94 * 10^{-6}$
	Electromotor	E	400	$\lambda_{E} = 2{,}5 * 10^{-6}$
	Obstacle Tracking Camera	OTC	400	$\lambda_{OTC} = 2{,}5 * 10^{-6}$
Navigation unit	GPS	GPS	420	$\lambda_{GPS} = 2{,}38 * 10^{-6}$
	LPS	LPS	280	$\lambda_{LPS} = 3{,}57 * 10^{-6}$
	Ultra-wideband visual positioning system	UVPS	420	$\lambda_{UVPS} = 2{,}38 * 10^{-6}$
Extended platform	Platform height setting mechanism	PHSM	150	$\lambda_{PHSM} = 6{,}67 * 10^{-6}$
	Platform retrieval mechanism	PRM	150	$\lambda_{PRM} = 6{,}67 * 10^{-6}$
Network infrastructure	Cable system	CS	100	$\lambda_{CS_2} = 1 * 10^{-5}$

Let us represent the system in terms of dependability as shown in figure 3.

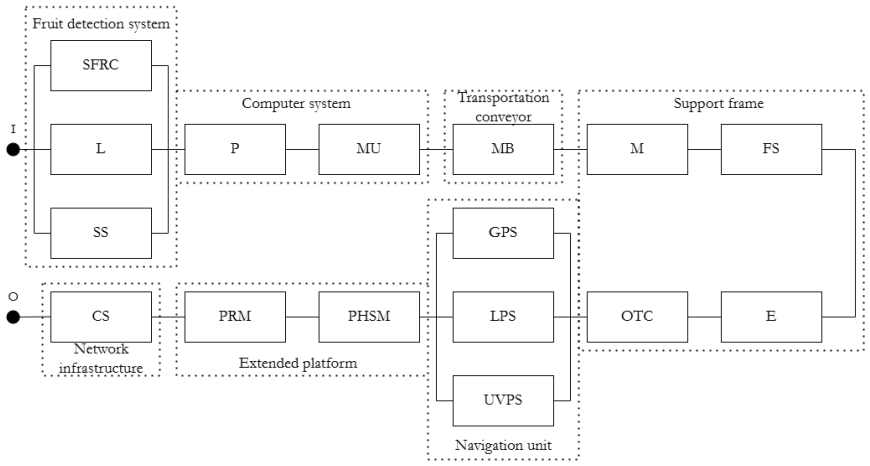


Figure 3: *System view from a dependability perspective*

When connected in series in dependability, the reliability function is considered as follows: $P(t) = \prod_{i=1}^{n} P_i(t)$, where n is the number of elements connected in series. In parallel connection: $P(t) = 1 - \prod_{i=1}^{k}\left(1 - P_i(t)\right)$, where k is the number of elements connected in parallel.

Thus, the final formula for predicting technical dependability performance (reliability function $P_{T_{GCS}2}$) for Tevel Aerobotics UAV swarm GCS can be summarized as follows:

$$P_{T_{GCS}2} = \left\{1 - \left(1 - e^{-\lambda_{SFRC}*t}\right)\left(1 - e^{-\lambda_{L}*t}\right)\left(1 - e^{-\lambda_{SS}*t}\right)\right\} * \\ * \left\{1 - \left(1 - e^{-\lambda_{GPS}*t}\right)\left(1 - e^{-\lambda_{LPS}*t}\right)\left(1 - e^{-\lambda_{UVPS}*t}\right)\right\} * \\ * e^{-\left(\lambda_{P}+\lambda_{MU}+\lambda_{MB}+\lambda_{M}+\lambda_{FS}+\lambda_{E}+\lambda_{OTC}+\lambda_{PHSM}+\lambda_{PRM}+6*\lambda_{CS_2}\right)*t} \quad (2)$$

Let us consider the remaining hardware of the systems under study. For clarity, the hardware parts of DJI Phantom 4 RTK and Tevel Aerobotics drones [18] are summarized in table 3.

Table 3: *Hardware of DJI Phantom 4 RTK and Tevel Aerobotics UAVs*

Component	Abbreviation	MTBF, k hours	Failure rate, 1/h
Total hardware failure rate of DJI Phantom 4 RTK drone equipment			$\lambda_{T_{UAV}1} = 8{,}84 * 10^{-5}$
Suspension camera	SC	500	$\lambda_{SC} = 2 * 10^{-6}$
Lower vision system	LVS	760	$\lambda_{LVS} = 1{,}32 * 10^{-6}$
Micro USB port	MUP	630	$\lambda_{MUP} = 1{,}59 * 10^{-6}$
Camera status indicator	CSI	640	$\lambda_{CSI} = 1{,}56 * 10^{-6}$
Connection status indicator	ConSI	630	$\lambda_{ConSI} = 1{,}59 * 10^{-6}$
Communication button	CB	1200	$\lambda_{CB} = 8{,}33 * 10^{-7}$
Camera microSD card slot	CMCS	750	$\lambda_{CMCS} = 1{,}33 * 10^{-6}$
Front vision system	FVS	760	$\lambda_{FVS} = 1{,}32 * 10^{-6}$
Infrared sensor system	ISS	230	$\lambda_{ISS} = 4{,}35 * 10^{-6}$
Front light-emitting diode	LED	640	$\lambda_{LED} = 1{,}56 * 10^{-6}$
Motors	Ms	490	$\lambda_{Ms_1} = 2{,}04 * 10^{-6}$
Propellers	Pr	90	$\lambda_{Pr_1} = 1{,}11 * 10^{-5}$
Machine status indicators	MSI	510	$\lambda_{MSI} = 1{,}96 * 10^{-6}$
Antennas OCUSYNCTM	AO	370	$\lambda_{AO} = 2{,}7 * 10^{-6}$
Integrated antenna D-RTKTM	IAD	310	$\lambda_{IAD} = 3{,}23 * 10^{-6}$

Component	Abbreviation	MTBF, k hours	Failure rate, 1/h
Rear vision system	RVS	760	$\lambda_{RVS} = 1{,}32 * 10^{-6}$
Intelligent flight battery	IFB	200	$\lambda_{IFB} = 5 * 10^{-6}$
Power button	PB	1200	$\lambda_{PB} = 8{,}33 * 10^{-7}$
Battery level indicators	BLI	640	$\lambda_{BLI} = 1{,}56 * 10^{-6}$
Navigation system	NS	170	$\lambda_{NS} = 5{,}88 * 10^{-6}$
Total failure rate of the Tevel Aerobotics drone hardware			$\lambda_{T_{UAV}2} = 9{,}67 * 10^{-5}$
Infrared optical tap	IOT	230	$\lambda_{IOT} = 4{,}35 * 10^{-6}$
Ultrasonic range meter	URM	200	$\lambda_{URM} = 5 * 10^{-6}$
Stereoscopic camera	StC	230	$\lambda_{StC} = 4{,}35 * 10^{-6}$
Radar	Rd	420	$\lambda_{Rd} = 2{,}38 * 10^{-6}$
Night vision camera	NVC	370	$\lambda_{NVC} = 2{,}7 * 10^{-6}$
Fruit recognition camera	FRC	360	$\lambda_{FRC} = 2{,}78 * 10^{-6}$
Biaxial robotic arm	BRA	130	$\lambda_{BRA} = 7{,}69 * 10^{-6}$
Pressure sensor	PS	410	$\lambda_{PS} = 2{,}44 * 10^{-6}$
Handle	H	100	$\lambda_{H} = 1 * 10^{-5}$
Motors	Ms	490	$\lambda_{Ms_2} = 2{,}04 * 10^{-6}$
Propellers	Pr	90	$\lambda_{Pr_2} = 1{,}11 * 10^{-5}$
Battery	B	450	$\lambda_{B} = 2{,}22 * 10^{-6}$
Processor	P	310	$\lambda_{P} = 3{,}23 * 10^{-6}$
Memory unit	MU	870	$\lambda_{MU} = 1{,}15 * 10^{-6}$

Since all drone components have no redundancy (the connection is fully serial), the table presents the total failure rates $\lambda_{T_{UAV}1}$ and $\lambda_{T_{UAV}2}$ for DJI Phantom 4 RTK and Tevel Aerobotics drones, respectively. Each UAV is assumed to have 4 propellers and 2 motors.

According to the original fruit monitoring task, the failure of at least one UAV will actually prevent the task from being accomplished, which can be interpreted as a system failure. Thus, the swarm of DJI Phantom 4 RTK UAVs has a fully sequential connection in terms of dependability, and the final formula for predicting the technical dependability of a swarm of 9 DJI Phantom 4 RTK UAVs, taking into account formula (1) with sequential connection between the swarm and the GCS:

$$P_{T_1^9} = e^{-(9*\lambda_{T_{UAV}1}+\lambda_{T_{GCS}1})*t} \tag{3}$$

Appropriately for a swarm of 10 such UAVs:

$$P_{T_1^{10}} = e^{-(10*\lambda_{T_{UAV}1}+\lambda_{T_{GCS}1})*t} \tag{4}$$

In the case of a group of 6 Tevel Aerobotics drones, a centralized system is used: the failure of one drone will not cause the failure of the entire system. The final formula for predicting the technical dependability of a swarm of 6 Tevel Aerobotics UAVs, taking into account formula (2) and the serial connection between the swarm and the GCS:

$$\begin{gathered} P_{T_2} = \left\{1 - \left(1 - e^{-\lambda_{T_{UAV}2}*t}\right)^6\right\} * P_{T_{GCS}2} = \\ \left\{1 - \left(1 - e^{-\lambda_{T_{UAV}2}*t}\right)^6\right\} * \left\{1 - \left(1 - e^{-\lambda_{SFRC}*t}\right)\left(1 - e^{-\lambda_{L}*t}\right)\left(1 - e^{-\lambda_{SS}*t}\right)\right\} * \\ * \left\{1 - \left(1 - e^{-\lambda_{GPS}*t}\right)\left(1 - e^{-\lambda_{LPS}*t}\right)\left(1 - e^{-\lambda_{UVPS}*t}\right)\right\} * \\ * e^{-(\lambda_P+\lambda_{MU}+\lambda_{MB}+\lambda_M+\lambda_{FS}+\lambda_E+\lambda_{OTC}+\lambda_{PHSM}+\lambda_{PRM}+6*\lambda_{CS_2})*t} \end{gathered} \tag{5}$$

II. Software dependability

When predicting software dependability measures, it is necessary to take into account the presence of SW not only on the GCS, but also on each UAV. Since software dependability prediction requires years of testing of real code, in this paper, random values of intervals between error occurrence within the acceptable range of values and taking into account the complexity of the software code for swarm structures of the two types of drones under consideration are selected for the example of applying the created model. There are many models for predicting SW dependability performance [19]. The Jelinski-Moranda model should be considered as the optimal method in this case.

Consider a swarm of 9 DJI Phantom 4 RTK UAVs. Similar to the hardware component, a software failure on any drone or GCS will lead to a failure of the entire system due to mission failure. Then the software dependability prediction model itself will be fully consistent. Taking into account the Jelinski-Moranda model, the developed model takes the following form:

$$P_{SW_1^9}(t_i) = P_{SW_{UAV}1}(t_i) * P_{SW_{GCS}}(t_i) = e^{-\left(9*\lambda_{iSW_{UAV}1}+\lambda_{iSW_{GCS}1}\right)*t_i} \quad (6)$$

At the same time, for a swarm structure of 10 DJI Phantom 4 RTK UAVs:

$$P_{SW_1^{10}}(t_i) = P_{SW_{UAV}1}(t_i) * P_{SW_{GCS}1}(t_i) = e^{-\left(10*\lambda_{iSW_{UAV}1}+\lambda_{iSW_{UAV}1}\right)*t_i} \quad (7)$$

For a swarm of 6 Tevel Aerobotics UAVs, the model for predicting the SW dependability performance considering the presence of redundancy in the system due to non-failure in case of failure of any UAV is as follows:

$$P_{SW_2}(t_i) = P_{SW_{UAV}2}(t_i) * P_{SW_{GCS}}2(t_i) = \left\{1 - \left(1 - e^{-\lambda_{iSW_{UAV}2}*t_i}\right)^6\right\} * e^{-\lambda_{iSW_{GCS}2}*t_i} \quad (8)$$

According to the Jelinski-Moranda model, at each testing step the program is checked for errors, and it is important to determine the initial number of errors. For example, let us take the GCS for a swarm of DJI Phantom 4 RTKs. ⌉∃ $N = 7$, where N – number of errors in the initial flight control program on the standard GCS. Consider a time interval t_i of 3 years (26280 h) and find the failure rate $\lambda_{iSW_{GCS}1}$. For this purpose, we should determine the value of the proportionality factor $C_{SW_{GCS}1}$ from the formula $\lambda_{iSW_{GCS}1} = C_{SW_{GCS}1}(N - i + 1)$ (in our case $i = N \Rightarrow \lambda_{iSW_{GCS}1} = C_{SW_{GCS}1}$), where i s the number of the last error detected at time t_i. For convenience, all data on error numbers and time intervals between the moments of their detection are summarized in table 4, where i is the error numbers and X_i is the time between their detection.

Table 4: *Demonstration table of possible moments of error detection*

i	1	2	3	4	5	6	7
Xi, h	2154,3	4987,6	1876,2	3421,8	1765,4	6210,7	5864

The value of the proportionality coefficient is determined by the formula:

$$C_{SW_{GCS}1} = \frac{k}{\sum_{i=1}^{k} t_i * \left(N + 1 - \frac{\sum_{i=1}^{k} i * t_i}{\sum_{i=1}^{k} t_i}\right)}.$$

According to the data received $C_{SW_{GCS}1} = \lambda_{iSW_{GCS}1} = 7{,}64 * 10^{-5}$. Similarly, $\lambda^{9}_{iSW_{UAV}1} = 7{,}2 * 10^{-5}$ at $N = 10$, $\lambda^{10}_{iSW_{UAV}1} = 9{,}23 * 10^{-5}$ at $N = 12$, $\lambda_{iSW_{GCS}2} = 7{,}17 * 10^{-5}$ at $N = 11$ and $\lambda_{iSW_{UAV}2} = 7{,}64 * 10^{-5}$ at $N = 8$ were calculated.

To combine the obtained final models for predicting the dependability measures of the technical hardware and software of UAV swarm structures, we present a view of the system from the dependability point of view, taking into account that the failure of a software part or hardware will lead to the failure of the entire system, which indicates a serial connection. The system is depicted in figure 4.

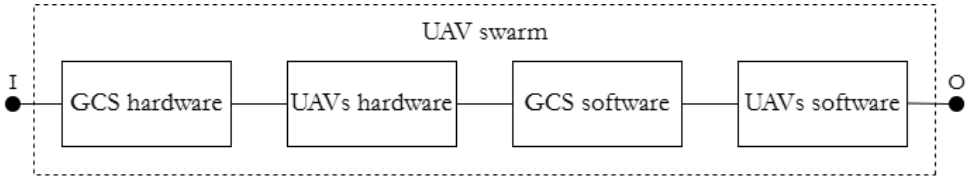


Figure 4: *Relationship between software and hardware in terms of dependability*

Thus, we obtain the final combined mathematical models for predicting the dependability indices of the software and hardware parts of UAV swarm structures. For a swarm of 9 UAVs of DJI Phantom 4 RTK model taking into account sequential connection of software and hardware parts and formulas (3) and (6):

$$P_{SWT_1^9} = e^{-\left(9*\lambda_{T_{UAV}1}+\lambda_{T_{GCS}1}+9*\lambda^{9}_{iSW_{UAV}1}+\lambda_{iSW_{GCS}1}\right)*t} \tag{9}$$

Similarly for a swarm of 10 DJI Phantom 4 RTK model UAVs considering (4), (7):

$$P_{SWT_1^{10}} = e^{-\left(10*\lambda_{T_{UAV}1}+\lambda_{T_{GCS}1}+10*\lambda^{10}_{iSW_{UAV}1}+\lambda_{iSW_{GCS}1}\right)*t} \tag{10}$$

For a swarm of 6 Tevel Aerobotics model UAVs considering (5), (8):

$$\begin{aligned} P_{SWT_2} = &\left\{1-\left(1-e^{-\lambda_{iSW_{UAV}2}*t}\right)^6\right\} * \left\{1-\left(1-e^{-\lambda_{T_{UAV}2}*t}\right)^6\right\} * \\ &* \left\{1-\left(1-e^{-\lambda_{SFRC}*t}\right)\left(1-e^{-\lambda_L*t}\right)\left(1-e^{-\lambda_{SS}*t}\right)\right\} * \\ &* \left\{1-\left(1-e^{-\lambda_{GPS}*t}\right)\left(1-e^{-\lambda_{LPS}*t}\right)\left(1-e^{-\lambda_{UVPS}*t}\right)\right\} * \\ &* e^{-\left(\lambda_{iSW_{GCS}2}+\lambda_P+\lambda_{MU}+\lambda_{MB}+\lambda_M+\lambda_{FS}+\lambda_E+\lambda_{OTC}+\lambda_{PHSM}+\lambda_{PRM}+6*\lambda_{CS_2}\right)*t} \end{aligned} \tag{11}$$

III. Communication system dependability

In addition to hardware components responsible for ensuring their core functionality and software systems, UAVs also include network components that enable information exchange with other UAVs within a swarm configuration and with GCS.

To evaluate the dependability of UAV network elements, mathematical approaches are employed to compute quantitative dependability measures, taking into account the structural configuration of the system under analysis. These measures must reflect the network nodes' ability to maintain communication and connectivity. One of the most commonly used criteria for assessing the dependability of network components is the probability of connectivity between a specific pair of nodes. This parameter indicates the likelihood that there exists at least one data transmission route between the two nodes in question [20]. From the perspective of dependability theory, this measure is equivalent to the operational availability factor K_{OG} of the network, which is calculated using the following formula:

$$K_{OG} = K_G * P(t) = \frac{T_0}{T_0 + T_B} * P(t), \quad (12)$$

where K_G is the availability factor; $P(t)$ is the reliability function; T_0 is MTBF [hours]; T_R is the restoration time [hours].

In the case of a series connection of nodes, the availability factor is calculated as follows:

$$K_G = \prod_{i=1}^{n} K_{G_i}, \quad (13)$$

where K_{G_i} is the availability factor of the i-th node; n is the number of nodes in the system.

In the case of a parallel connection of nodes, the availability factor is calculated as follows:

$$K_G = 1 - \prod_{i=1}^{n} (1 - K_{G_i}), \quad (14)$$

Essentially, the operational availability factor can be interpreted as the system's ability to maintain continuous functionality, provided that the prescribed operational and maintenance requirements are met.

To predict the dependability measures of UAV network components, it is necessary to consider the specific characteristics of their topology, the impact of the signal-to-noise ratio, and also account for the bit error rate, which depends on the type of modulation used.

Network topology refers to the arrangement of nodes and the method of their interconnection via communication links (edges). Figure 5 illustrates a case where the network consists of nine DJI Phantom 4 RTK drones used for crop yield forecasting and one GCS.

As shown in Figure 5(a), this example involves three swarms. Each swarm comprises three UAVs, one of which serves as the leader, while the others act as followers. The UAVs within each swarm are interconnected using a ring topology. A ring topology is a network configuration in which each node is connected via communication links (edges) to two neighboring nodes, forming a closed loop for data transmission.

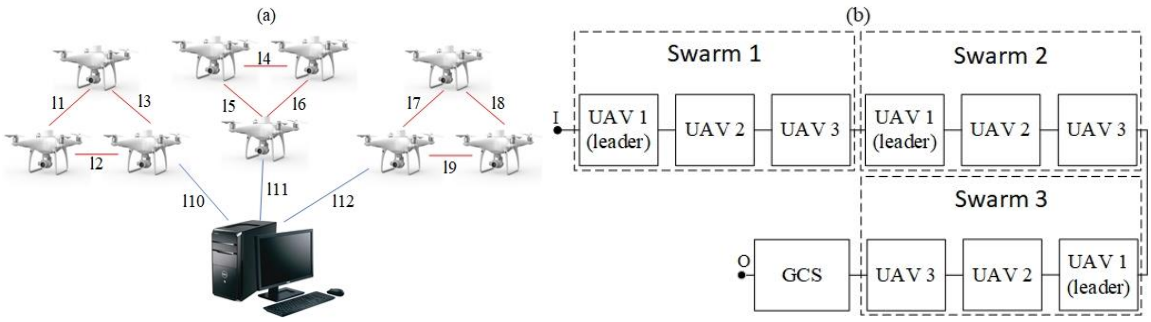


Figure 5: *Nine DJI Phantom 4 RTK drones and one GCS: (a) network configuration, (b) structural diagram for dependability assessment*

However, a disadvantage of the ring topology is that the failure of a single node or a communication link between UAVs can lead to a disruption in the operation of the entire network. The GCS is connected to each swarm through the leader UAV of that swarm. Communication between UAVs and the GCS is established wirelessly using WiMAX technology.

Thus, the structural diagram for dependability assessment of this network configuration represents a series connection of nodes and is illustrated in Figure 5(b).

Based on the analysis of Figures 5(a) and 5(b), it is possible to calculate the operational availability factor of the network with this configuration, denoted as $K_{OG_{ring}}$. In this calculation, both the nodes and the communication links (edges) must be taken into account.

Expression (15) for evaluating this factor is derived based on formulas (12)–(14):

$$K_{OG_{ring}} = \prod_{i=1}^{9} K_{G_{node_UAV_i}} * K_{G_{node_GCS}} * \prod_{l=1}^{12} K_{G_{edge_l}} * P_{RTECTC}(t) = \prod_{i=1}^{9} \frac{T_{0_UAV_i}}{T_{0_UAV_i} + T_{R_UAV_i}} * \\ * \frac{T_{0_GCS}}{T_{0_GCS} + T_{R_GCS}} * \prod_{l=1}^{12} \frac{T_{0_edge_l}}{T_{0_edge_l} + T_{R_edge_l}} * e^{(-\lambda_{RTECTC} * t)}, \quad (15)$$

where $K_{G_{node_UAV_i}}$, $K_{G_{node_GCS}}$, $K_{G_{edge_l}}$ are the availability factors of the i-th UAV, GCS, and the communication links (edges), respectively; $T_{0_UAV_i}$, T_{0_GCS}, $T_{0_edge_l}$ denote MTBF of the i-th UAV, GCS, and the WiMAX router, respectively [hours]; $T_{R_UAV_i}$, T_{R_GCS}, $T_{R_edge_l}$ denote the restoration time of the i-th UAV, GCS, and the WiMAX network, respectively [hours]; P_{RTECTC}, λ_{RTECTC} are the reliability function and failure rate of the receiving and transmitting equipment of the command and telemetry channel, respectively; t is the operating time [hours].

The next example of a network configuration consists of two UAV swarms, each comprising five DJI Phantom 4 RTK drones used for crop yield forecasting, and one GCS (Figure 6(a)).

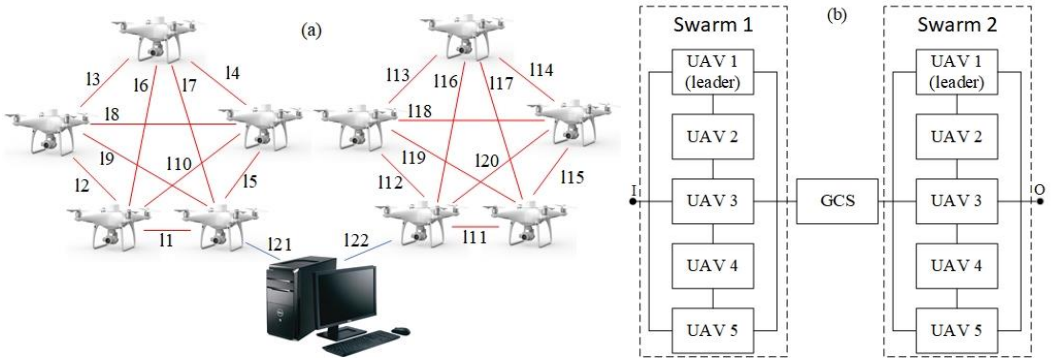


Figure 6: *Ten DJI Phantom 4 RTK drones and one GCS: (a) network configuration, (b) structural diagram for dependability assessment*

As illustrated in Figure 6(a), each UAV swarm employs a mesh network topology. A mesh topology is a network structure in which nodes are interconnected through multiple communication links (edges), thereby providing several alternative paths for data transmission in the event of a node or link failure. From a dependability perspective, this topology is considered more reliable than a ring configuration.

Accordingly, the DJI Phantom 4 RTK drones within each swarm are connected in parallel. The leader drones of the two swarms are connected in series. As in the previous case, the UAVs and the GCS are wirelessly connected via WiMAX technology. The GCS also has a series connection with the leader drones.

Thus, the structural diagram for dependability assessment of this network configuration is shown in Figure 6(b).

Based on the analysis of Figures 6(a) and 6(b), a corresponding expression can be derived for the quantitative evaluation of the operational availability factor of the network in this configuration, denoted as $K_{OG_{mesh}}$, using formulas (12)–(14). This configuration represents a series–parallel arrangement of nodes and communication links (edges).

$$K_{OG_{mesh}} = \prod_{i=1}^{10} K_{G_{node_UAV_i}} * K_{G_{node_GCS}} * \prod_{l=1}^{20} K_{G_{edge_l}} * \prod_{l=21}^{22} K_{G_{edge_l}} * P_{RTECTC}(t) =$$
$$= \prod_{i=1}^{10} \frac{T_{0_UAV_i}}{T_{0_UAV_i} + T_{R_UAV_i}} * \frac{T_{0_GCS}}{T_{0_GCS} + T_{R_GCS}} * \left(1 - \prod_{l=1}^{20}\left(1 - \frac{T_{0_edge_l}}{T_{0_edge_l} + T_{R_edge_l}}\right)\right) *$$
$$* \prod_{l=21}^{22} \frac{T_{0_edge_l}}{T_{0_edge_l} + T_{R_edge_l}} * e^{(-\lambda_{RTECTC} * t)}, \quad (16)$$

The final system configuration considered in this study is a UAV swarm for fruit harvesting, consisting of six Tevel Aerobotics drones and one GCS (vehicle-based) (Figure 7(a)).

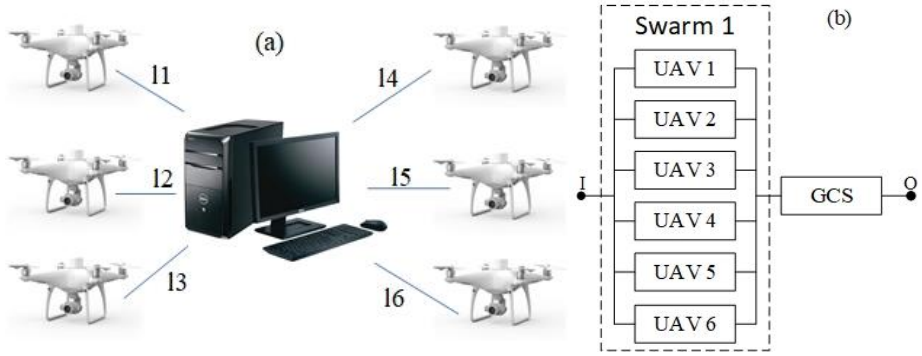


Figure 7: *Six Tevel Aerobotics drones and one GCS: (a) network configuration, (b) structural diagram for dependability assessment*

Figure 7(a) illustrates that the given network configuration employs a star topology, in which all nodes are connected to a central communication node. In this example, the GCS serves as the central node. All UAVs are connected to it via a wired system (power line communication).

The failure of one or more drones does not compromise the operability of the system as a whole. The system remains functional as long as at least one drone from the swarm and the GCS are operational. The structural diagram for dependability assessment of this network configuration is shown in Figure 7(b).

As shown in Figure 7(b), this network configuration employs a parallel–series arrangement of nodes and communication links (edges). Accordingly, the expression for calculating the operational availability factor is as follows:

$$K_{OG_{star}} = \prod_{i=1}^{6} K_{G_{node_UAV_i}} * K_{G_{node_GCS}} * K_{G_{edge_l}} * \prod_{l=2}^{6} K_{G_{edge_l}} * P_{CS_2}(t) =$$
$$= \prod_{i=1}^{6} \frac{T_{0_UAV_i}}{T_{0_UAV_i} + T_{R_UAV_i}} * \frac{T_{0_GCS}}{T_{0_GCS} + T_{R_GCS}} * \frac{T_{0_pl_edge_l}}{T_{0_pl_edge_l} + T_{R_pl_edge_l}} *$$
$$* \left(1 - \prod_{l=2}^{6}\left(1 - \frac{T_{0_pl_edge_l}}{T_{0_pl_edge_l} + T_{R_pl_edge_l}}\right)\right) * e^{(-\lambda_{CS_2} * t)}, \quad (17)$$

where $T_{0_pl_edge_l}$, $T_{R_pl_edge_l}$ are MTBF and recovery time of the power line communication link, respectively [hours]; $P_{CS_2}(t)$, λ_{CS_2} are reliability function and failure rate of cable system, respectively.

In addition to the type of topology, another parameter that significantly affects the dependability of a communication system is the signal-to-noise ratio (*SNR*), which characterizes the ratio of the useful signal to the level of background interference and noise. The signal-to-noise ratio is calculated using the following expression:

$$SNR = \frac{E_b}{N_0} = \frac{S * T_b}{N/W} = \frac{S/R_b}{N/W} \quad (18)$$

where E_b is the bit energy; N_0 is the noise power spectral density; S is the signal power; T_b is the bit duration; N is the noise power; W is the bandwidth; R_b is the bit rate.

A decrease in the *SNR* significantly degrades data transmission quality and increases the bit error rate [21], thereby reducing the overall dependability level of the entire system.

In turn, the bit error rate is a quantitative measure that characterizes the likelihood of one or more bits being corrupted during data transmission. Its value depends on the modulation scheme used in the communication system. In modern UAVs, the most commonly used modulation types include phase modulation, frequency modulation, and quadrature amplitude modulation (*QAM*) [22]-[23]. However, the choice of modulation depends on the environmental conditions.

Under conditions of high noise power N, when the *SNR* is minimal (according to expression (18)), it is advisable to use binary phase shift keying (*BPSK*). Under low noise conditions, frequency shift keying with a modulation order of M=32 (32-*FSK*) is preferable. This conclusion is supported by simulation results conducted in Simulink (Figure 8).

All UAV models considered in this study are operated in flat terrain areas with minimal presence of other equipment that could significantly interfere with drone functionality, and under low noise power N conditions. Therefore, frequency modulation with 32 frequency-shift keying (32-*FSK*) was selected as the modulation scheme.

To calculate the numerical value of the bit error rate for frequency modulation, the following mathematical model is used (19) [24]:

$$P_{BER} = \frac{M}{4} * erfc\left(\sqrt{\frac{log_2 M}{2} * \frac{E_b}{N_0}}\right) \quad (19)$$

where M is the modulation order; $erfc(x) = \frac{2}{\sqrt{\pi}} \int_x^{\infty} exp(-y^2)dy$ is the complementary error function.

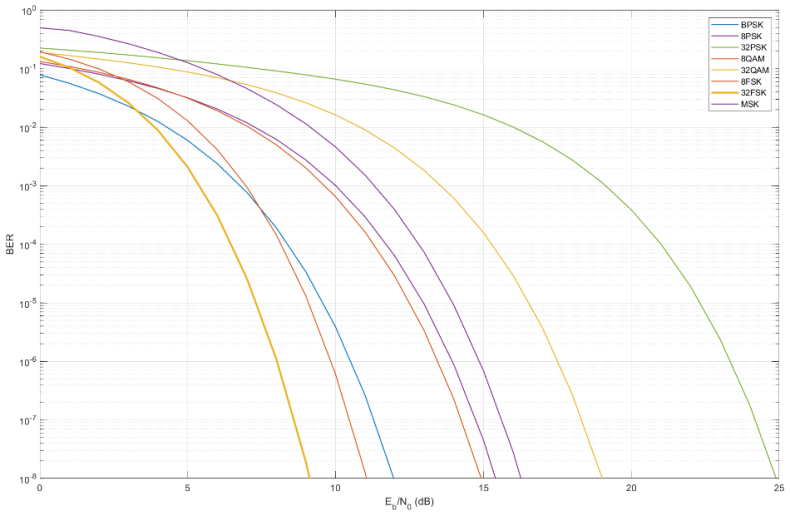


Figure 8: *Dependence of bit error rate on the SNR*

In existing scientific research on network dependability assessment, the bit error rate is not taken into account, which renders current approaches to UAV network dependability forecasting incomplete.

Therefore, this article proposes introducing a bit error factor K_{BER} into the general formula for the network's operational availability factor (12). From a dependability standpoint, as the bit error rate P_{BER} increases, the network's dependability decreases. Consequently, a correction factor K_{BER}, defined as the reciprocal of P_B, is proposed to establish a direct proportionality (20).

$$K_{BER} = 1 - P_{BER} \tag{20}$$

Thus, the final mathematical models of the network's operational availability factor, according to expressions (15)–(17) and (19)–(20), for each system configuration are presented below.

3 UAV swarms, each consisting of 3 DJI Phantom 4 RTK drones and 1 GCS:

$$K_{OG_{ring}} = \prod_{i=1}^{9} \frac{T_{0_UAV_i}}{T_{0_UAV_i} + T_{R_UAV_i}} * \frac{T_{0_GCS}}{T_{0_GCS} + T_{R_GCS}} * \prod_{l=1}^{12} \frac{T_{0_edge_l}}{T_{0_edge_l} + T_{R_edge_l}} * \\ * e^{(-\lambda_{RTECTC} * t)} * \left(1 - \left(\frac{M}{4} * erfc\left(\sqrt{\frac{log_2 M}{2} * \frac{E_b}{N_0}}\right)\right)\right) \tag{21}$$

2 UAV swarms, each consisting of 5 DJI Phantom 4 RTK drones and 1 GCS:

$$K_{OG_{mesh}} = \prod_{i=1}^{10} \frac{T_{0_UAV_i}}{T_{0_UAV_i} + T_{R_UAV_i}} * \frac{T_{0_GCS}}{T_{0_GCS} + T_{R_GCS}} * \left(1 - \prod_{l=1}^{20} \left(1 - \frac{T_{0_edge_l}}{T_{0_edge_l} + T_{R_edge_l}}\right)\right) * \\ * \prod_{l=21}^{22} \frac{T_{0_edge_l}}{T_{0_edge_l} + T_{R_edge_l}} * e^{(-\lambda_{RTECTC} * t)} * \left(1 - \left(\frac{M}{4} * erfc\left(\sqrt{\frac{log_2 M}{2} * \frac{E_b}{N_0}}\right)\right)\right) \tag{22}$$

1 UAV swarm consisting of 6 Tevel Aerobotics drones and 1 GCS:

$$K_{OG_{star}} = \prod_{i=1}^{6} \frac{T_{0_UAV_i}}{T_{0_UAV_i} + T_{R_UAV_i}} * \frac{T_{0_GCS}}{T_{0_GCS} + T_{R_GCS}} * \frac{T_{0_pl_edge_l}}{T_{0_pl_edge_l} + T_{R_pl_edge_l}} * \\ * \left(1 - \prod_{l=2}^{6} \left(1 - \frac{T_{0_pl_edge_l}}{T_{0_pl_edge_l} + T_{R_pl_edge_l}}\right)\right) * e^{(-\lambda_{CS_2} * t)} * \left(1 - \left(\frac{M}{4} * erfc\left(\sqrt{\frac{log_2 M}{2} * \frac{E_b}{N_0}}\right)\right)\right) \tag{23}$$

IV. Approbation of the developed mathematical model

The developed mathematical models 9-11 were applied to the selected UAV swarms using the data described in tables 3-5. The results of calculating the reliability function are presented in figures 9-11.

It should be noted that the indicators calculated by the model characterize the operational time of the drone swarm, i.e. those periods when the DJI Phantom 4 RTK UAV is in flight and Tevel Aerobotics is in the process of collection. The following fact should be taken into account when

analyzing the obtained dependencies: it takes less than half an hour of operational time for DJI Phantom 4 RTK drones to cover an average agricultural plot.

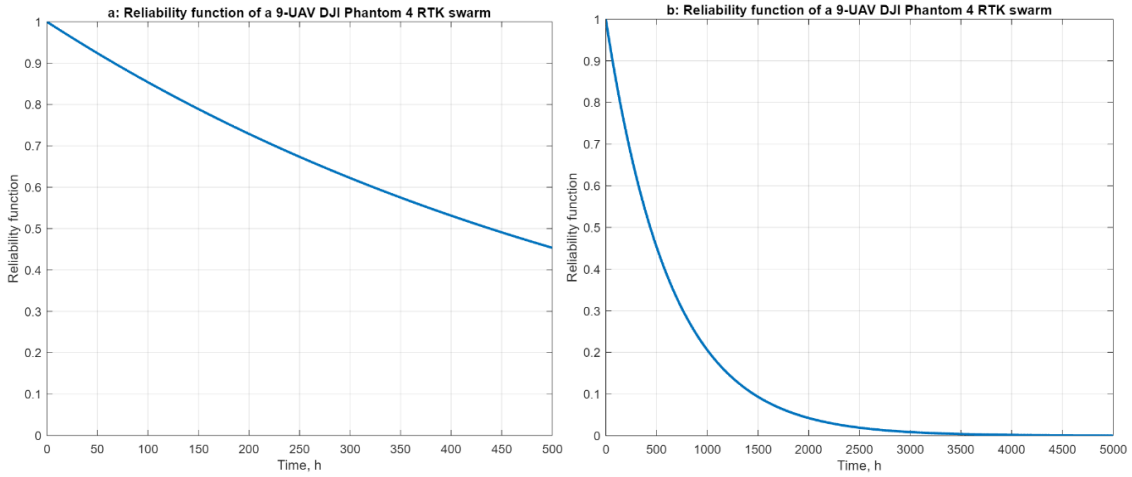


Figure 9: *Time dependence of reliability function for a swarm of 9 DJI Phantom 4 RTK UAVs: (a) - 500 h, (b) - 5000 h*

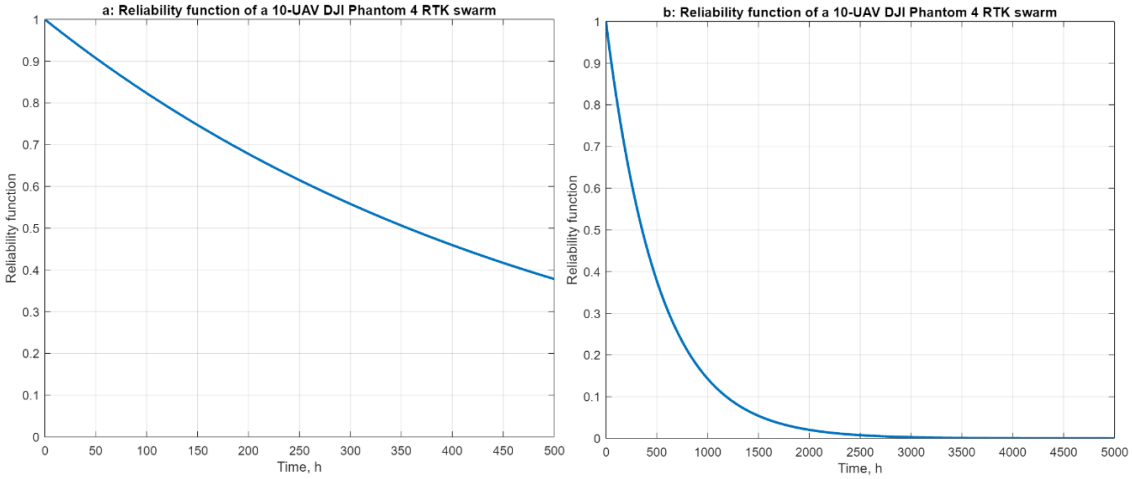


Figure 10: *Time dependence of reliability function for a swarm of 10 DJI Phantom 4 RTK UAVs: (a) - 500 h, (b) – 5000 h*

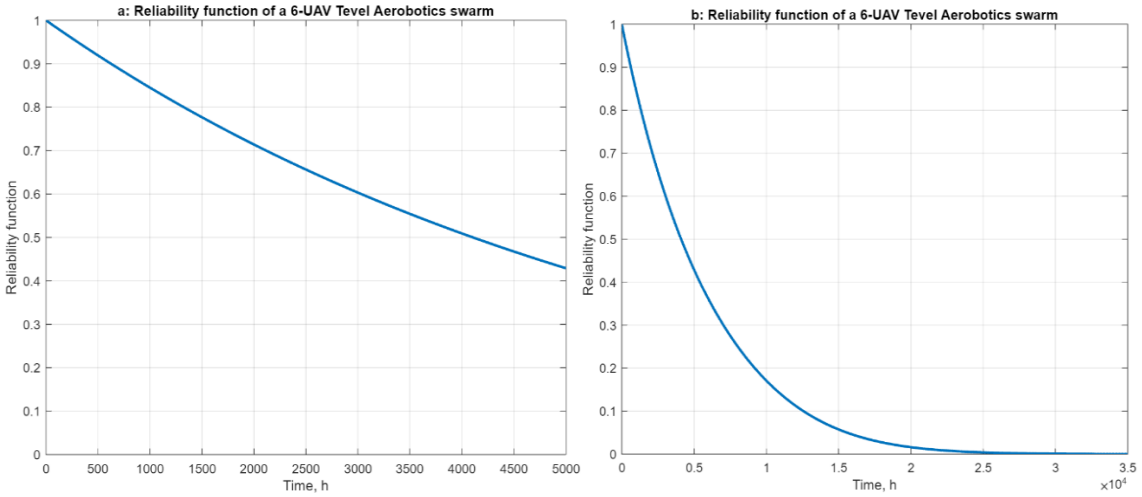


Figure 11: *Time dependence of reliability function for a swarm of 6 Tevel Aerobotics UAVs: (a) - 5000 h, (b) -35000 h*

According to the results of the analysis, for the selected swarm of 9 drones responsible for the analysis of ripe fruits, reliability function at the 440th hour of operational work will decrease by 2 times, and by the 5000th hour of operation reliability function will be close to 0. Based on this, it can be concluded that it is necessary to conduct regular maintenance work with such a group of UAVs.

The results for a swarm of 10 drones of the same model were less reliable: at the 360th hour of operation, the probability of failure drops by half, and by the 5000th hour it approaches 0.

The swarm structure consisting of 6 Tevel Aerobotics drones designed for harvesting has the highest probability of failure, while the process of its operation is longer. In continuous operation of such a system, reliability function without maintenance will reach 0,5 in 4100 hours, and will approach 0 at the 35000th hour.

What is more, based on the derived mathematical models (21)–(23), a plot was constructed to illustrate the dependence of the operational availability factor on time for each swarm configuration (Figure 12).

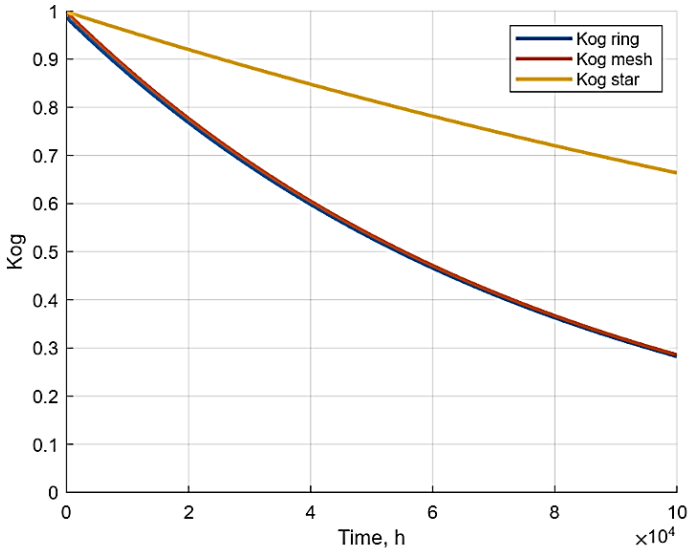


Figure 12: *Time dependence of operational availability factor for various UAV swarm configurations*

An analysis of Figure 12 shows that, from a dependability standpoint, the best performance was demonstrated by the swarm configuration consisting of six Tevel Aerobotics drones and one GCS. The operational availability factor $K_{OG_{star}}$ reaches approximately 0.96 at 10000 hours of operation. In contrast, the system comprising three UAV swarms, each with three DJI Phantom 4 RTK drones and a GCS, exhibited the lowest dependability, with an operational availability factor of approximately 0.88 at the same time mark (10000 hours).

V. Description of the developed methodology

The description of the developed methodology for predicting dependability measures of UAV swarm structures is presented in figures 13-14 in the form of IDEF0-diagram.

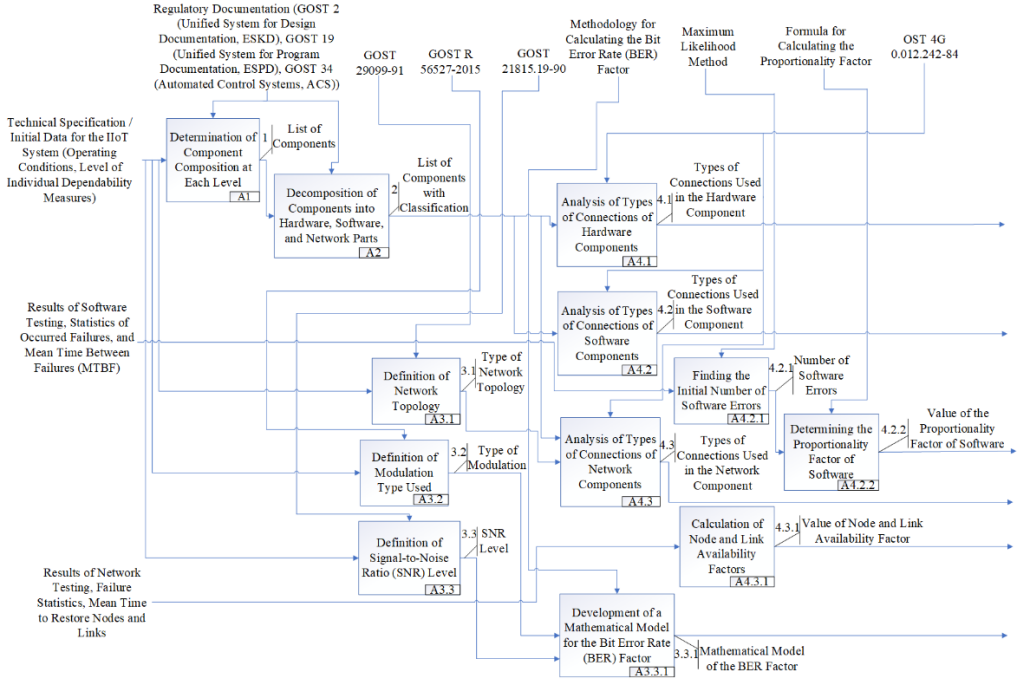


Figure 13: *Developed methodology for predicting dependability measures. Part 1*

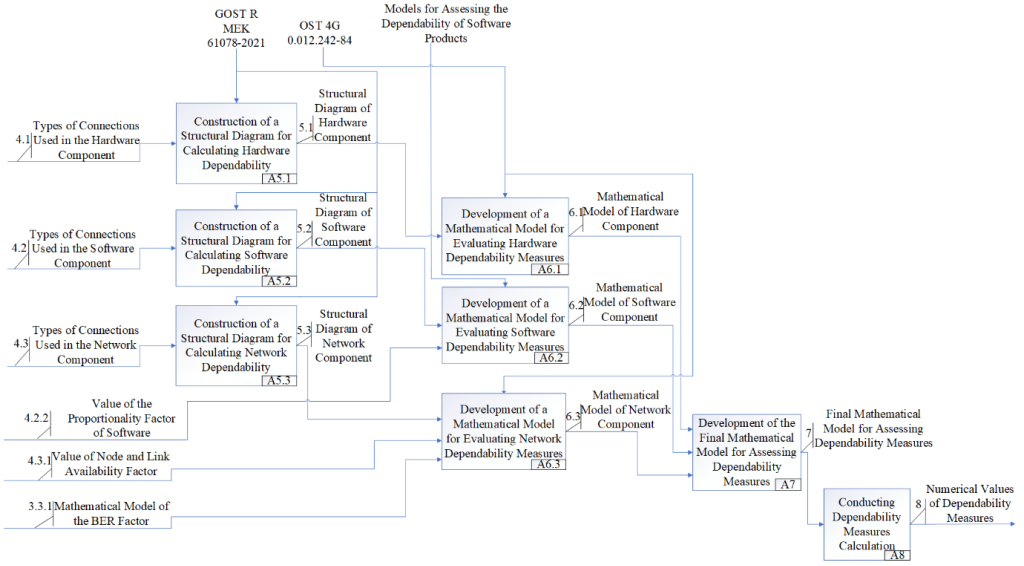


Figure 14: *Developed methodology for predicting dependability measures. Part 2*

As shown in Figures 13–14, the proposed methodology for predicting dependability measures consists of eight stages (blocks A1–A8):

1) Analysis of UAV swarm structures, resulting in the formation of a list of components.

2) Classification of components based on their functional purpose into hardware, software, and network elements.

3) Analysis of connection types between hardware, software, and network components.

4) Development of a structural diagram for dependability calculation of hardware and software components. When assessing the hardware part, it is often sufficient to use initial data such as the mean time to failure (MTTF) and recovery time, which are usually provided in the technical documentation. If these data are not available, it is necessary to calculate the dependability of individual electronic components, including zero-level electronic modules, using specialized

reference manuals, such as [13]. For software dependability assessment, initial data are required, including software testing results—namely, the number of failures and the mean time between failures (MTBF). The initial number of software errors and the proportionality factor are estimated using the Jelinski-Moranda model, as described in Chapter II.

5) Development of a structural diagram for dependability calculation of network components, considering the applied network topology, modulation type, and bit error probability, which is incorporated into the proposed methodology as a correction factor K_{BER}.

6) Formulation of a mathematical model for predicting the dependability of hardware, software, and network components.

7) Formulation of a comprehensive mathematical model for assessing the dependability of UAV swarm structures.

8) Numerical calculation of dependability measures.

VI. Conclusions

Based on the results of this work, a single combined mathematical model for predicting the dependability performance of swarm structures for agricultural applications was created, consisting of software dependability prediction models for each UAV and GCS and hardware dependability prediction models for the drones and GCS. Software dependability was calculated using the Jelinski-Moranda model, and hardware dependability was calculated using the exponential dependability law via MTBF. Furthermore, the operational readiness of the communication systems involved in the UAV swarm mission was investigated.

The developed mathematical model allows to refine the predicted dependability measures. The results of the practical calculation were the conclusions that the selected objects of the study require regular maintenance work, and also the communication system for a swarm of 10 UAVs of Phantom DJI 4 RTK model is more reliable than for 9, while the overall hardware and software dependability of a group of 9 similar drones is much higher.

Acknowledgements. This publication was prepared during the research conducted under Project No. 24-00-024 “Development of Methods for Forecasting Dependability Measures of Electronic Modules” within the framework of the Scientific Fund Program of the National Research University Higher School of Economics (HSE University) in 2025.

References

[1] Radaykin A. (2019) Economico-organizacyonnye aspecty razvitiya promyshlennogo proizvodstva otechestvennyh bespilotnyh letatelnyh apparatov grazhdanskogo naznacheniya [Economic and organizational aspects of the development of industrial production of domestic unmanned aerial vehicles for civilian use]. *Goryzonty economici*, 3(49):12-18.

[2] Danshin M., Guryanov V., Podberyozkin A. (2020) Sozdanie “roya” iz bespilotnikov i ih vozmozhnoe primenenie v razlichnyh sferah [Creation of a “swarm” of drones and their possible application in various spheres]. *Materialy 78-y nauchno-metodicheskoy i nauchno-issledovatelskoy konferencii*, 65-72.

[3] Kovalev D., Tueva E., Pokusayev D. (2024) Opyt roevogo primeneiya BPLA v sfere avtonomnogo zemledeliya [Experience of swarm application of UAVs in the field of autonomous agriculture]. *V Vserossiyskaya (nacionalnaya) nauchnaya konferenciya “Nauka, technologyy, obschestvo: Ecologychesskyy inzheniring v interesah ustychivogo razvitiya territotiy” (NTO-V-2024)*, 13:90-103.

[4] Apolo-Apolo O.E., Martinez-Guanter J., Egea G., Raja P., Perez-Ruiz M. (2020) Deep learning techniques for estimation of the yield and size of citrus fruits using a UAV. *European Journal of Agronomy*, 115.

[5] Weicheng Xu, Pengchao Chen, Yilong Zhan, Shengde Chen, Lei Zhang, Yubin Lan. (2021) Cotton yield estimation model based on machine learning using time series UAV remote sensing data. *International Journal of Applied Earth Observation and Geoinformation*, 104.

[6] Sharipov S., Yakhyaev G., Ibragimova B. (2022) Trends and prospects for the development of peasant (farmer) farms in the regions of the north caucasus federal district. *UEPS: upravlenie, economica, politica, sociologiya*, 3-11.

[7] Manuals+: https://manuals.plus/dji/phantom-4-rtk-quadcopter-manual.pdf (Accessed on 01 May 2025).

[8] DJI: https://dl.djicdn.com/downloads/phantom_3/ru/Ru_Phantom_3_Professional_Quick_Start_Guide V1.2_0419.pdf (Accessed on 01 May 2025).

[9] Krasnyy V. (2022) Bespilotnye letatelniye apparaty. Problemy i resheniya [Unmanned aerial vehicles. Problems and solutions]. *Vektor nauchno-technologicheskogo razvitiya Rossii s uchetom globalyh trendov*, 17-20.

[10] Goncherova N., Primachuk V. (2023) Bespilotnye letatelnye apparaty v sovremennom mire. Kratkyy obzor i perspektivy razvitiya [Unmanned aerial vehicles in the modern world. Brief overview and development prospects]. *Mezhdunarodnyy nauchyy zhurnal "Simvol nauki"*, 2(6):12-14.

[11] Tevel: https://www.tevel-tech.com/ (Accessed on 01 May 2025).

[12] Makarov I., Kokorin V. Kompleks upravleniya bespilonymi letatelnymi appaaratami dlya distancionnogo zondirovaniya zemli [Unmanned aerial vehicle control complex for remote sensing of the earth].

[13] Nadezhnost ERI [Dependability of Electronic Components], Moscow, Russia, 2006.

[14] U.S. Department of Defense. (1995). *Reliability prediction of electronic equipment* (MIL-HDBK -217F).

[15] Item software: https://www.itemsoft.com/china-299b.html (Accessed on 01 May 2025).

[16] GOST 56649-2015. (2016) Electronnaya komponentnaya baza inostrannogo proizvodstva [Foreign-made electronic component base].

[17] Europian patent application. (2023) Fruit picking robotic installation on platforms.

[18] Europian patent specification. (2023) System and method for drone fleet management for harvesting and dilution.

[19] Chekal E., Chichev A. Nadezhost informacionnyh system [Information system dependability. Training manual, UlGU, 2012.

[20] Migov D. (2020) Dekompoziciya seti po secheniyam pri raschyote eyo nadyozhnosti [Decomposition of the network into sections when calculating its dependability]. *Prikladnaya diskretnaya matematika,* 62-86.

[21] Kokunin P., Latypov I., Latypova L. Vvedenie v Internet veshchej: uchebnoe posobie [Introduction to the Internet of Things: textbook], Kazan University, 2022.

[22] Smolin M., Khilo YU., Golikov A. (2018) Issledovanie modeli sistemy svyazi dlya «roya» BPLA [Investigation of a communication system model for a UAV «swarm»]. *XIV Mezhdunarodnaya nauchno-prakticheskaya konferenciya,* 8-10.

[23] Ivanov R. (2016) Ocenka imitostojkosti kanalov upravleniya bespilotnymi letatel'nymi apparatami [Evaluation of simulation robustness of unmanned aerial vehicle control channels]. *Vestnik polockogo gosudarstvennogo universiteta. Seriya S. Fundamental'nye nauki. Informacionnye tekhnologii*, 4:37-42.

[24] Vybor optimal'nogo metoda modulyacii signala v sovremennykh cifrovykh sistemakh radiosvyazi. Modelirovanie v srede AWR Design Environment [Selection of optimal signal modulation method in modern digital radio communication systems. Modeling in AWR Design Environment], MSU named after M.V. Lomonosov, 2008.

A COMPARATIVE ANALYSIS OF POWER ISHITA DISTRIBUTION EXPLORING ITS SIGNIFICANT CONTRIBUTION AND PRACTICAL APPLICATIONS

Rashid A. Ganaie[1], Manzoor A. Khanday[2*,] Dilawar A. Bhat[3] and Yudhishther Singh Bagal[4]

•

[1]Department of Statistics, Annamalai University, Tamil Nadu-608002, India
[2*]Department of Statistics, Lovely Professional University, Phagwara, Punjab, India
[3]Symbiosis School of Banking and Finance, Symbiosis International University, Pune, India
[4]School of Agriculture, Lovely Professional University, Punjab

rashidau7745@gmail.com, Corresponding author: [2*] manzoorstat@gmail.com, dilawar.bhat@ssbf.edu.in, ysbagal@gmail.com

Abstract

This research presents the development of a novel statistical model termed the weighted power Ishita distribution. The study delves into its fundamental structural properties, offering a comprehensive theoretical foundation. The parameters of proposed distribution are meticulously estimated through the maximum likelihood estimation method, ensuring robust and reliable results. To validate its applicability and demonstrate its superiority, the model is evaluated using three real-world lifetime data sets, highlighting its efficacy and potential for practical applications.

Keywords: power Ishita distribution, weighted distribution, order statistics, reliability measures

I. Introduction

The fundamental significance of weighted distributions is of great important and plays a major role in real life applications. The weighted distributions provide a standard and flexible approach to deal with efficient modelling of statistical biased data arising from different fields of knowledge even if the standard distributions are not appropriate. The weighted distributions are significant in statistics because it deals with a technique to extend the existing distribution by incorporating an additional parameter. This inclusion of additional parameter brings the existing classical distribution in a more flexible position. The idea of weighted distribution was firstly developed by Fisher [1] to model the ascertainment biases which later on Rao [2] reformulated it in a unified theory for problems where the observations fall in non-experimental, non-replicated and non-random manner. It has been revealed that in some cases weighted distributions does not provide good fit in some datasets because of applied or theoretical point of view. The weighted distributions have wide applications in real life problems, where the probabilities of events are observed and recorded by making some modifications to probabilities of actual occurrence of events considering method of ascertainment. The weighted distributions are used as a tool in selection of appropriate models for observed data

especially if samples are drawn without a proper frame. The weighted distributions are widely applied in diversified fields like medicine, ecology and reliability for the development of proper statistical models. Many researchers developed some weighted probability distributions along with their illustrations from various practical and applied fields [3-14].

Power Ishita distribution is a two parametric distribution developed by Shanker and Shukla [15] which is particular case of Ishita distribution. Its different structural properties have been discussed and its parameters are estimated by using the method of maximum likelihood estimation.

II. Weighted Power Ishita (WPI) Distribution

The probability density function of power Ishita distribution is given by

$$f(x;\theta,\alpha) = \frac{\alpha\theta^3}{\left(\theta^3+2\right)}\left(\theta + x^{2\alpha}\right)x^{\alpha-1}\,e^{-\theta x^{\alpha}};\ x>0,\theta>0,\ \alpha>0 \tag{1}$$

and cumulative distribution function of power Ishita distribution is given by

$$F(x;\theta,\alpha) = 1-\left(1+\frac{\theta x^{\alpha}\left(\theta x^{\alpha}+2\right)}{\left(\theta^3+2\right)}\right)e^{-\theta x^{\alpha}};\ x>0,\theta>0,\alpha>0 \tag{2}$$

Consider random variable X constitutes non-negative condition with probability density function $f(x)$ .Let its weight function be $w(x)$ that is non negative then the probability density function of weighted random variable X_w is given by

$$f_w(x) = \frac{w(x)f(x)}{E(w(x))},\quad x>0$$

Hence $w(x)$ be the weight function of non - negative condition then $E(w(x)) = \int w(x)f(x)dx < \infty$.

In this paper, we have considered the weight function as $w(x) = x^c$ to get the weighted version of power Ishita distribution and then its probability density function is defined as

$$f_w(x) = \frac{x^c f(x)}{E(x^c)} \tag{3}$$

Here $E(x^c) = \int_0^{\infty} x^c f(x)dx$

$$E(x^c) = \frac{\left(\theta^3\Gamma\frac{(\alpha+c)}{\alpha} + \Gamma\frac{(3\alpha+c)}{\alpha}\right)}{\alpha\theta^{\frac{c}{\alpha}}\left(\theta^3+2\right)} \tag{4}$$

Therefore, by substituting the equation (1) and (4) in equation (3), we have obtained the required probability density function of weighted power Ishita distribution which is

$$f_w(x) = \frac{\alpha\theta^{\frac{3\alpha+c}{\alpha}}x^{\alpha+c-1}\left(\theta+x^{2\alpha}\right)e^{-\theta x^{\alpha}}}{\left(\theta^3\,\Gamma\frac{(\alpha+c)}{\alpha} + \Gamma\frac{(3\alpha+c)}{\alpha}\right)} \tag{5}$$

The cumulative distribution function of weighted power Ishita distribution will be determined by

$$F_w(x) = \int_0^x f_w(x)dx$$

$$= \int_0^x \frac{\alpha\theta^{\frac{3\alpha+c}{\alpha}} x^{\alpha+c-1}\left(\theta+x^{2\alpha}\right)e^{-\theta x^{\alpha}}}{\left(\theta^3\Gamma\frac{(\alpha+c)}{\alpha}+\Gamma\frac{(3\alpha+c)}{\alpha}\right)}dx \quad (6)$$

After the simplification of expression (6), we have determined the cumulative distribution function of weighted power Ishita distribution that is

$$F_w(x) = \frac{\left(\theta^3\gamma\left(\frac{(\alpha+c)}{\alpha},\theta x^{\alpha}\right)+\gamma\left(\frac{(3\alpha+c)}{\alpha},\theta x^{\alpha}\right)\right)}{\left(\theta^3\Gamma\frac{(\alpha+c)}{\alpha}+\Gamma\frac{(3\alpha+c)}{\alpha}\right)} \quad (7)$$

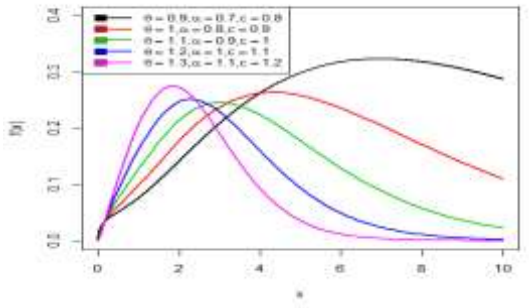


Figure 1: *Pdf plot of WPI distribution*

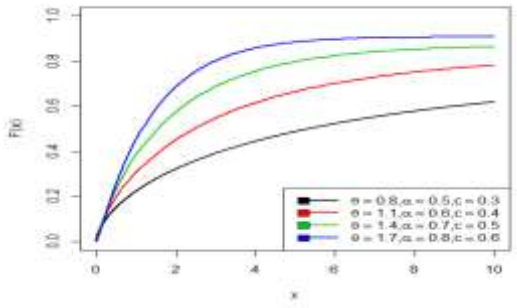


Figure 2: *Cdf plot of WPI distribution*

III. Reliability measures

In this portion, we have derived the reliability function, hazard function, reverse hazard function and mills ratio of the weighted power Ishita distribution. The reliability function of weighted power Ishita distribution is given by

$$R(x) = 1 - F_w(x)$$

$$R(x) = 1 - \frac{\left(\theta^3\gamma\left(\frac{(\alpha+c)}{\alpha},\theta x^{\alpha}\right)+\gamma\left(\frac{(3\alpha+c)}{\alpha},\theta x^{\alpha}\right)\right)}{\left(\theta^3\Gamma\frac{(\alpha+c)}{\alpha}+\Gamma\frac{(3\alpha+c)}{\alpha}\right)}$$

The hazard function of weighted power Ishita distribution is given by

$$h(x) = \frac{f_w(x)}{1-F_w(x)}$$

$$h(x) = \frac{x^{\alpha+c-1}\,\alpha\theta^{\frac{3\alpha+c}{\alpha}}\left(\theta+x^{2\alpha}\right)e^{-\theta x^{\alpha}}}{\left(\theta^3\Gamma\frac{(\alpha+c)}{\alpha}+\Gamma\frac{(3\alpha+c)}{\alpha}\right)-\left(\theta^3\gamma\left(\frac{(\alpha+c)}{\alpha},\theta x^{\alpha}\right)+\gamma\left(\frac{(3\alpha+c)}{\alpha},\theta x^{\alpha}\right)\right)}$$

The reverse hazard rate function of weighted power Ishita distribution is given by

$$h_r(x) = \frac{f_w(x)}{F_w(x)}$$

$$h_r(x) = \frac{x^{\alpha+c-1}\ \alpha\theta^{\frac{3\alpha+c}{\alpha}}\left(\theta+x^{2\alpha}\right)e^{-\theta x^{\alpha}}}{\left(\theta^3\gamma\left(\frac{(\alpha+c)}{\alpha},\theta x^{\alpha}\right)+\gamma\left(\frac{(3\alpha+c)}{\alpha},\theta x^{\alpha}\right)\right)}$$

The Mills Ratio of weighted power Ishita distribution is given by

$$M.R = \frac{1}{h_r(x)} = \frac{\left(\theta^3\gamma\left(\frac{(\alpha+c)}{\alpha},\theta x^{\alpha}\right)+\gamma\left(\frac{(3\alpha+c)}{\alpha},\theta x^{\alpha}\right)\right)}{x^{\alpha+c-1}\ \alpha\theta^{\frac{3\alpha+c}{\alpha}}\left(\theta+x^{2\alpha}\right)e^{-\theta x^{\alpha}}}$$

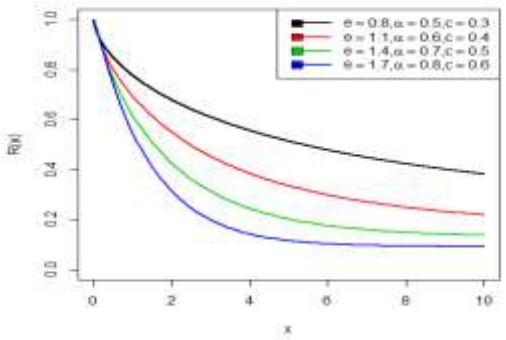


Figure 3: *Reliability plot of WPI distribution*

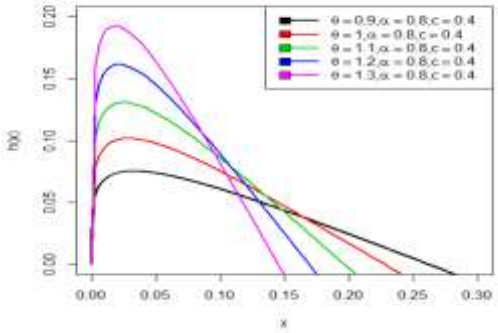


Figure 4: *Hazard plot of WPI distribution*

IV. Structural Properties

In this portion, we have derived and described some fundamental statistical properties of weighted power Ishita distribution which are listed as

I. Moments

Consider random variable X represents weighted power Ishita distribution, then r^{th} order moment of weighted power Ishita distribution will be determined as

$$\mu_r' = E(X^r) = \int_0^{\infty} x^r f_w(x)dx$$

$$= \int_0^{\infty} \frac{\alpha\theta^{\frac{3\alpha+c}{\alpha}}\ x^{\alpha+c+r-1}\left(\theta+x^{2\alpha}\right)e^{-\theta x^{\alpha}}}{\left(\theta^3\Gamma\frac{(\alpha+c)}{\alpha}+\Gamma\frac{(3\alpha+c)}{\alpha}\right)}dx \qquad (8)$$

After simplification of expression (8), we obtain

$$\mu_r' = E(X^r) = \frac{\theta^3\Gamma\frac{(\alpha+c+r)}{\alpha}+\Gamma\frac{(3\alpha+c+r)}{\alpha}}{\alpha\theta^{\frac{r}{\alpha}}\left(\theta^3\Gamma\frac{(\alpha+c)}{\alpha}+\Gamma\frac{(3\alpha+c)}{\alpha}\right)} \qquad (9)$$

Now substituting r = 1 and 2 in equation (9), we obtain the mean and second moment of weighted power Ishita distribution

$$\mu_1' = \frac{\theta^3\Gamma\frac{(\alpha+c+1)}{\alpha}+\Gamma\frac{(3\alpha+c+1)}{\alpha}}{\alpha\theta^{\frac{1}{\alpha}}\left(\theta^3\Gamma\frac{(\alpha+c)}{\alpha}+\Gamma\frac{(3\alpha+c)}{\alpha}\right)}$$

$$\mu_2' = \frac{\theta^3\Gamma\frac{(\alpha+c+2)}{\alpha}+\Gamma\frac{(3\alpha+c+2)}{\alpha}}{\alpha\theta^{\frac{2}{\alpha}}\left(\theta^3\Gamma\frac{(\alpha+c)}{\alpha}+\Gamma\frac{(3\alpha+c)}{\alpha}\right)}$$

$$\text{Variance} = \frac{\theta^3\Gamma\frac{(\alpha+c+2)}{\alpha}+\Gamma\frac{(3\alpha+c+2)}{\alpha}}{\alpha\theta^{\frac{2}{\alpha}}\left(\theta^3\Gamma\frac{(\alpha+c)}{\alpha}+\Gamma\frac{(3\alpha+c)}{\alpha}\right)} - \left(\frac{\theta^3\Gamma\frac{(\alpha+c+1)}{\alpha}+\Gamma\frac{(3\alpha+c+1)}{\alpha}}{\alpha\theta^{\frac{1}{\alpha}}\left(\theta^3\Gamma\frac{(\alpha+c)}{\alpha}+\Gamma\frac{(3\alpha+c)}{\alpha}\right)}\right)^2$$

$$\text{S.D} = \sqrt{\left(\frac{\theta^3\Gamma\frac{(\alpha+c+2)}{\alpha}+\Gamma\frac{(3\alpha+c+2)}{\alpha}}{\alpha\theta^{\frac{2}{\alpha}}\left(\theta^3\Gamma\frac{(\alpha+c)}{\alpha}+\Gamma\frac{(3\alpha+c)}{\alpha}\right)} - \left(\frac{\theta^3\Gamma\frac{(\alpha+c+1)}{\alpha}+\Gamma\frac{(3\alpha+c+1)}{\alpha}}{\alpha\theta^{\frac{1}{\alpha}}\left(\theta^3\Gamma\frac{(\alpha+c)}{\alpha}+\Gamma\frac{(3\alpha+c)}{\alpha}\right)}\right)^2\right)}$$

II. Harmonic mean

The harmonic mean of weighted power Ishita distribution will be determined by using expression

$$\text{H.M} = E\left(\frac{1}{x}\right) = \int_0^\infty \frac{1}{x} f_w(x)dx$$

$$= \int_0^\infty \frac{\alpha\theta^{\frac{3\alpha+c}{\alpha}} x^{\alpha+c-2}\left(\theta+x^{2\alpha}\right)e^{-\theta x^\alpha}}{\left(\theta^3\Gamma\frac{(\alpha+c)}{\alpha}+\Gamma\frac{(3\alpha+c)}{\alpha}\right)}dx \qquad (10)$$

After simplification of expression (10), we obtain

$$\text{H.M} = \frac{\theta^{\frac{3\alpha+c}{\alpha}}\left(\theta\gamma\left(\frac{(\alpha+c-1)}{\alpha},\theta x^\alpha\right)+\gamma\left(\frac{(3\alpha+c-1)}{\alpha},\theta x^\alpha\right)\right)}{\left(\theta^3\Gamma\frac{(\alpha+c)}{\alpha}+\Gamma\frac{(3\alpha+c)}{\alpha}\right)}$$

III. Moment generating function and characteristic function

Consider the random variable X consists weighted power Ishita distribution, then MGF of explored distribution will be determined as

$$M_X(t) = E\left(e^{tx}\right) = \int_0^\infty e^{tx} f_w(x);dx$$

After Applying Taylor's series, we get

$$= \int_0^\infty \left(1+tx+\frac{(tx)^2}{2!}+....\right)f_w(x)dx$$

$$= \int_0^{\infty} \sum_{j=0}^{\infty} \frac{t^j}{j!} x^j f_w(x)dx$$

$$= \sum_{j=0}^{\infty} \frac{t^j}{j!} \left(\frac{\theta^3 \Gamma \frac{(\alpha + c + j)}{\alpha} + \Gamma \frac{(3\alpha + c + j)}{\alpha}}{\alpha \theta^{\frac{j}{\alpha}} \left(\theta^3 \Gamma \frac{(\alpha + c)}{\alpha} + \Gamma \frac{(3\alpha + c)}{\alpha} \right)} \right)$$

$$M_X(t) = \frac{1}{\alpha \left(\theta^3 \Gamma \frac{(\alpha + c)}{\alpha} + \Gamma \frac{(3\alpha + c)}{\alpha} \right)} \sum_{j=0}^{\infty} \frac{t^j}{j! \theta^{\frac{j}{\alpha}}} \left(\theta^3 \Gamma \frac{(\alpha + c + j)}{\alpha} + \Gamma \frac{(3\alpha + c + j)}{\alpha} \right)$$

Obviously,the characteristic function of weighted power Ishita distribution isgiven by

$$M_X(it) = \frac{1}{\alpha \left(\theta^3 \Gamma \frac{(\alpha + c)}{\alpha} + \Gamma \frac{(3\alpha + c)}{\alpha} \right)} \sum_{j=0}^{\infty} \frac{it^j}{j! \theta^{\frac{j}{\alpha}}} \left(\theta^3 \Gamma \frac{(\alpha + c + j)}{\alpha} + \Gamma \frac{(3\alpha + c + j)}{\alpha} \right)$$

V. Order Statistics

Consider the order statistics $X_{(1)}, X_{(2)}, \ldots, X_{(n)}$ of a random sample $X_1, X_2, \ldots, X_n$ from a continuous distribution with probability density function $f_x(x)$ and cumulative distribution function $F_x(x)$, then probability density function of rth order statistics $X_{(r)}$is defined as

$$f_{x(r)}(x) = \frac{n!}{(r-1)!\,(n-r)!} f_X(x) \left(F_X(x)\right)^{r-1} \left(1 - F_X(x)\right)^{n-r} \quad (11)$$

Now by applying the equations (5) and (7) in equation (11), we will obtain the probability density function of r^{th} order statistics $X_{(r)}$ of weighted power Ishita distribution which is given by expression

$$f_{x(r)}(x) = \frac{n!}{(r-1)!(n-r)!} \left(\frac{\alpha \theta^{\frac{3\alpha + c}{\alpha}} x^{\alpha + c - 1} \left(\theta + x^{2\alpha}\right) e^{-\theta x^{\alpha}}}{\left(\theta^3 \Gamma \frac{(\alpha + c)}{\alpha} + \Gamma \frac{(3\alpha + c)}{\alpha} \right)} \right) \left(\frac{\left(\theta^3 \gamma\left(\frac{(\alpha + c)}{\alpha}, \theta x^{\alpha} \right) + \gamma\left(\frac{(3\alpha + c)}{\alpha}, \theta x^{\alpha} \right) \right)}{\left(\theta^3 \Gamma \frac{(\alpha + c)}{\alpha} + \Gamma \frac{(3\alpha + c)}{\alpha} \right)} \right)^{r-1}$$

$$\times \left(1 - \frac{\left(\theta^3 \gamma\left(\frac{(\alpha + c)}{\alpha}, \theta x^{\alpha} \right) + \gamma\left(\frac{(3\alpha + c)}{\alpha}, \theta x^{\alpha} \right) \right)}{\left(\theta^3 \Gamma \frac{(\alpha + c)}{\alpha} + \Gamma \frac{(3\alpha + c)}{\alpha} \right)} \right)^{n-r}$$

Therefore probability density function of higher order statistics $X_{(n)}$ of WPI distribution is given by

$$f_{x(n)}(x) = \frac{n\alpha\theta^{\frac{3\alpha + c}{\alpha}} x^{\alpha + c - 1} \left(\theta + x^{2\alpha}\right) e^{-\theta x^{\alpha}}}{\left(\theta^3 \Gamma \frac{(\alpha + c)}{\alpha} + \Gamma \frac{(3\alpha + c)}{\alpha} \right)} \left(\frac{\left(\theta^3 \gamma\left(\frac{(\alpha + c)}{\alpha}, \theta x^{\alpha} \right) + \gamma\left(\frac{(3\alpha + c)}{\alpha}, \theta x^{\alpha} \right) \right)}{\left(\theta^3 \Gamma \frac{(\alpha + c)}{\alpha} + \Gamma \frac{(3\alpha + c)}{\alpha} \right)} \right)^{n-1}$$

and probability density function of first order statistics $X_{(1)}$ of WPI distribution is given by

$$f_{x(1)}(x) = \frac{n\alpha\theta^{\frac{3\alpha+c}{\alpha}} x^{\alpha+c-1}\left(\theta+x^{2\alpha}\right)e^{-\theta x^{\alpha}}}{\left(\theta^3\Gamma\frac{(\alpha+c)}{\alpha}+\Gamma\frac{(3\alpha+c)}{\alpha}\right)}\left(1-\frac{\left(\theta^3\gamma\left(\frac{(\alpha+c)}{\alpha},\theta x^{\alpha}\right)+\gamma\left(\frac{(3\alpha+c)}{\alpha},\theta x^{\alpha}\right)\right)}{\left(\theta^3\Gamma\frac{(\alpha+c)}{\alpha}+\Gamma\frac{(3\alpha+c)}{\alpha}\right)}\right)^{n-1}$$

VI. Bonferroni and Lorenz Curves

The Bonferroni and Lorenz curves also termed as income distribution or classical curves which were applied to measure income inequality. The proposed curves are

$$B(p) = \frac{1}{p\mu_1'}\int_0^q x f_w(x)dx$$

$$\text{and } L(p) = pB(p) = \frac{1}{\mu_1'}\int_0^q x f_w(x)dx$$

$$\text{Here } \mu_1' = \frac{\theta^3\Gamma\frac{(\alpha+c+1)}{\alpha}+\Gamma\frac{(3\alpha+c+1)}{\alpha}}{\alpha\theta^{\frac{1}{\alpha}}\left(\theta^3\Gamma\frac{(\alpha+c)}{\alpha}+\Gamma\frac{(3\alpha+c)}{\alpha}\right)}$$

$$B(p) = \frac{\alpha\theta^{\frac{1}{\alpha}}\left(\theta^3\Gamma\frac{(\alpha+c)}{\alpha}+\Gamma\frac{(3\alpha+c)}{\alpha}\right)}{p\left(\theta^3\Gamma\frac{(\alpha+c+1)}{\alpha}+\Gamma\frac{(3\alpha+c+1)}{\alpha}\right)}\int_0^q \frac{\alpha\theta^{\frac{3\alpha+c}{\alpha}} x^{\alpha+c}\left(\theta+x^{2\alpha}\right)e^{-\theta x^{\alpha}}}{\left(\theta^3\Gamma\frac{(\alpha+c)}{\alpha}+\Gamma\frac{(3\alpha+c)}{\alpha}\right)}dx \qquad (12)$$

After simplification of expression (12), we obtain

$$B(p) = \frac{\theta^{\frac{3\alpha+c+1}{\alpha}}}{p\left(\theta^3\Gamma\frac{(\alpha+c+1)}{\alpha}+\Gamma\frac{(3\alpha+c+1)}{\alpha}\right)}\left(\theta\gamma\left(\frac{(\alpha+c+1)}{\alpha},\theta q\right)+\gamma\left(\frac{(3\alpha+c+1)}{\alpha},\theta q\right)\right)$$

$$L(p) = \frac{\theta^{\frac{3\alpha+c+1}{\alpha}}}{\left(\theta^3\Gamma\frac{(\alpha+c+1)}{\alpha}+\Gamma\frac{(3\alpha+c+1)}{\alpha}\right)}\left(\theta\gamma\left(\frac{(\alpha+c+1)}{\alpha},\theta q\right)+\gamma\left(\frac{(3\alpha+c+1)}{\alpha},\theta q\right)\right)$$

VII. Parameter Estimation and Fisher's Information Matrix

In this portion, we have estimated the parameters of weighted power Ishita distribution by using the maximum likelihood estimation. Consider random sample $X_1, X_2,\ldots,X_n$ of size n from weighted power Ishita distribution, then the likelihood function should be stated as

$$L(x) = \prod_{i=1}^{n} f_w(x)$$

$$= \prod_{i=1}^{n} \left(\frac{\alpha\theta^{\frac{3\alpha+c}{\alpha}} x_i^{\alpha+c-1}\left(\theta + x_i^{2\alpha}\right) e^{-\theta x_i^{\alpha}}}{\left(\theta^3\Gamma\frac{(\alpha+c)}{\alpha} + \Gamma\frac{(3\alpha+c)}{\alpha}\right)} \right)$$

$$= \frac{\alpha\theta^{n\left(\frac{3\alpha+c}{\alpha}\right)}}{\left(\theta^3\Gamma\frac{(\alpha+c)}{\alpha} + \Gamma\frac{(3\alpha+c)}{\alpha}\right)^n} \prod_{i=1}^{n}\left(x_i^{\alpha+c-1}\left(\theta + x_i^{2\alpha}\right) e^{-\theta x_i^{\alpha}}\right)$$

The log likelihood function is given by

$$\log L = n\left(\frac{3\alpha+c}{\alpha}\right)\log\alpha\theta - n\log\left(\theta^3\Gamma\frac{(\alpha+c)}{\alpha} + \Gamma\frac{(3\alpha+c)}{\alpha}\right) + (\alpha+c-1)\sum_{i=1}^{n}\log x_i + \sum_{i=1}^{n}\log\left(\theta + x_i^{2\alpha}\right) - \theta\sum_{i=1}^{n} x_i^{\alpha} \qquad (13)$$

Therefore, differentiating the log-likelihood equation (13) with respect to parameters θ and $\alpha$and$c$. The following normal equations must be satisfied

$$\frac{\partial \log L}{\partial\theta} = \frac{n\alpha}{\alpha\theta}\left(\frac{3\alpha+c}{\alpha}\right) - n\left(\frac{3\theta^2\Gamma\frac{(\alpha+c)}{\alpha}}{\left(\theta^3\Gamma\frac{(\alpha+c)}{\alpha} + \Gamma\frac{(3\alpha+c)}{\alpha}\right)}\right) + \sum_{i=1}^{n}\left(\frac{1}{\left(\theta + x_i^{2\alpha}\right)}\right) - \sum_{i=1}^{n} x_i^{\alpha} = 0$$

$$\frac{\partial \log L}{\partial\alpha} = -\frac{n\theta c}{\alpha^3\theta} - n\psi\left(\theta^3\Gamma\frac{(\alpha+c)}{\alpha} + \Gamma\frac{(3\alpha+c)}{\alpha}\right) + \sum_{i=1}^{n}\log x_i + \sum_{i=1}^{n}\left(\frac{x_i^{2\alpha}\log x_i}{\left(\theta + x_i^{2\alpha}\right)}\right) - \theta\sum_{i=1}^{n} x_i^{\alpha}\log x_i = 0$$

$$\frac{\partial \log L}{\partial c} = \frac{n}{\alpha}\log\alpha\theta - n\,\psi\left(\theta^3\Gamma\frac{(\alpha+c)}{\alpha} + \Gamma\frac{(3\alpha+c)}{\alpha}\right) + \sum_{i=1}^{n}\log x_i = 0$$

Where $\psi(.)$is the digamma function.

The above system of non-linear equations are too complicated to solve it algebraically. Therefore, we use R and wolfram mathematics for estimating the parameters of the explored distribution.

In order to apply asymptotic normality results for determining the confidence interval. We have that if $\hat{\gamma} = (\hat{\theta}, \hat{\alpha}, \hat{c})$ denotes the MLE of $\hat{\gamma} = (\hat{\theta}, \hat{\alpha}, \hat{c})$. The results can be stated as

$$\sqrt{n}(\hat{\gamma} - \gamma) \to N_3(0, I^{-1}(\gamma))$$

Where $I(\gamma)$ is the Fisher's Information matrix.i.e.

$$I(\gamma) = -\frac{1}{n}\begin{pmatrix} E\left(\frac{\partial^2 \log L}{\partial\theta^2}\right) & E\left(\frac{\partial^2 \log L}{\partial\theta\,\partial\alpha}\right) & E\left(\frac{\partial^2 \log L}{\partial\theta\,\partial c}\right) \\ E\left(\frac{\partial^2 \log L}{\partial\alpha\,\partial\theta}\right) & E\left(\frac{\partial^2 \log L}{\partial\alpha^2}\right) & E\left(\frac{\partial^2 \log L}{\partial\alpha\,\partial c}\right) \\ E\left(\frac{\partial^2 \log L}{\partial c\,\partial\theta}\right) & E\left(\frac{\partial^2 \log L}{\partial c\,\partial\alpha}\right) & E\left(\frac{\partial^2 \log L}{\partial c^2}\right) \end{pmatrix}$$

$$E\left(\frac{\partial^2 \log L}{\partial \theta^2}\right) = -\frac{n\alpha^2}{(\alpha\theta)^2}\left(\frac{3\alpha+c}{\alpha}\right) - n\left(\frac{\left(\theta^3\Gamma\frac{(\alpha+c)}{\alpha}+\Gamma\frac{(3\alpha+c)}{\alpha}\right)\left(6\theta\Gamma\frac{(\alpha+c)}{\alpha}\right)-\left(3\theta^2\Gamma\frac{(\alpha+c)}{\alpha}\right)^2}{\left(\theta^3\Gamma\frac{(\alpha+c)}{\alpha}+\Gamma\frac{(3\alpha+c)}{\alpha}\right)^2}\right) - \sum_{i=1}^{n}\left(\frac{1}{\left(\theta+x_i^{2\alpha}\right)^2}\right)$$

$$E\left(\frac{\partial^2 \log L}{\partial \alpha^2}\right) = \frac{3n\alpha^2\theta^2 c}{\left(\alpha^3\theta\right)^2} - n\psi'\left(\theta^3\Gamma\frac{(\alpha+c)}{\alpha}+\Gamma\frac{(3\alpha+c)}{\alpha}\right) + \sum_{i=1}^{n}\left(\frac{\left(\theta+x_i^{2\alpha}\right)x_i^{2\alpha}\left(\log x_i\right)^2-\left(x_i^{2\alpha}\log x_i\right)^2}{\left(\theta+x_i^{2\alpha}\right)^2}\right) - \theta\sum_{i=1}^{n}\left(x_i^{\alpha}\log x_i\right)^2$$

$$E\left(\frac{\partial^2 \log L}{\partial c^2}\right) = -n\psi'\left(\theta^3\Gamma\frac{(\alpha+c)}{\alpha}+\Gamma\frac{(3\alpha+c)}{\alpha}\right)$$

$$E\left(\frac{\partial^2 \log L}{\partial \theta\,\partial \alpha}\right) = -n\psi\left(\frac{3\theta^2\Gamma\frac{(\alpha+c)}{\alpha}}{\theta^3\Gamma\frac{(\alpha+c)}{\alpha}+\Gamma\frac{(3\alpha+c)}{\alpha}}\right) - \sum_{i=1}^{n}\left(\frac{x_i^{2\alpha}\log x_i}{\left(\theta+x_i^{2\alpha}\right)^2}\right) - \sum_{i=1}^{n}x_i^{\alpha}\log x_i$$

$$E\left(\frac{\partial^2 \log L}{\partial \theta\,\partial c}\right) = \frac{n\alpha}{\alpha^2\theta} - n\psi\left(\frac{3\theta^2\Gamma\frac{(\alpha+c)}{\alpha}}{\theta^3\Gamma\frac{(\alpha+c)}{\alpha}+\Gamma\frac{(3\alpha+c)}{\alpha}}\right)$$

$$E\left(\frac{\partial^2 \log L}{\partial \alpha\,\partial c}\right) = -\frac{n\theta}{\alpha^3\theta} - n\psi'\left(\theta^3\Gamma\frac{(\alpha+c)}{\alpha}+\Gamma\frac{(3\alpha+c)}{\alpha}\right)$$

where $\psi(.)'$is the first order derivative of digamma function. Hence γ is not known, so $I^{-1}(\gamma)$ should be estimated by $I^{-1}(\hat{\gamma})$ and it can be applied to obtain asymptotic confidence intervals for θ, α and c.

VIII. Entropy

The term entropy in statistical terms is clearly defined as increase in the disorganization within a system and it quantifies the diversity, uncertainty or randomness in a system.

I. Renyi entropy

The Renyi entropy is important in quantum information that is used as measure of entanglement and it is also important in economics and statistics as index of diversity

$$e(\beta) = \frac{1}{1-\beta}\log\left(\int f_w^{\beta}(x)dx\right)$$

$$= \frac{1}{1-\beta}\log\int_0^{\infty}\left(\frac{\alpha\theta^{\frac{3\alpha+c}{\alpha}}x^{\alpha+c-1}\left(\theta+x^{2\alpha}\right)e^{-\theta x^{\alpha}}}{\left(\theta^3\Gamma\frac{(\alpha+c)}{\alpha}+\Gamma\frac{(3\alpha+c)}{\alpha}\right)}\right)^{\beta}dx \qquad (14)$$

After the simplification of expression (14), we obtain

$$e(\beta)=\frac{1}{1-\beta}\log\left(\frac{\theta^{\beta-k}}{\alpha}\left(\frac{\alpha\theta^{\frac{3\alpha+c}{\alpha}}}{\left(\theta^3\Gamma\frac{(\alpha+c)}{\alpha}+\Gamma\frac{(3\alpha+c)}{\alpha}\right)}\right)^{\beta}\sum_{k=0}^{\infty}\binom{\beta}{k}\frac{\Gamma\frac{\beta(\alpha+c-1)+2\alpha k+1}{\alpha}}{(\theta\beta)^{\frac{\beta(\alpha+c-1)+2\alpha k+1}{\alpha}}}\right)$$

Obviously the Tsallis entropy of weighted power Ishita distribution will be determined as

$$S_\tau=\frac{1}{\tau-1}\left(1-\int_0^\infty {f_w}^\tau(x)dx\right)$$

$$=\frac{1}{\tau-1}\left(1-\int_0^\infty\left(\frac{\alpha\theta^{\frac{3\alpha+c}{\alpha}}x^{\alpha+c-1}\left(\theta+x^{2\alpha}\right)e^{-\theta x^{\alpha}}}{\left(\theta^3\Gamma\frac{(\alpha+c)}{\alpha}+\Gamma\frac{(3\alpha+c)}{\alpha}\right)}\right)^{\tau}dx\right) \quad (15)$$

After the simplification of expression (15), we obtain

$$S_\tau=\frac{1}{\tau-1}\left(1-\frac{\theta^{\tau-j}}{\alpha}\left(\frac{\alpha\theta^{\frac{3\alpha+c}{\alpha}}}{\left(\theta^3\Gamma\frac{(\alpha+c)}{\alpha}+\Gamma\frac{(3\alpha+c)}{\alpha}\right)}\right)^{\tau}\sum_{j=0}^{\infty}\binom{\tau}{j}\frac{\Gamma\frac{\tau(\alpha+c-1)+2\alpha j+1}{\alpha}}{(\tau\theta)^{\frac{\tau(\alpha+c-1)+2\alpha j+1}{\alpha}}}\right)$$

IX. Application

In this portion, we have analysed and examined three real data sets to determine the goodness of fit of weighted power Ishita distribution and then fit has been compared in order to reveal that the weighted power Ishita distribution provides a better fit over power Ishita, Ishita, exponential and Lindley distributions. Analysis of three real lifetime data sets are performed through R software.

Data set 1: The following data set is related to behavioural science collected by Balakrishnan N., et al. [14]. The behavioural and emotional problems of children which can be measured by the scale "General Rating of Affective Symptoms for preschoolers (GRASP)" can be classified with depressive condition or not according to the scale. The study conducted by the researchers in a city at the south Chile, collect the factual data related to scores of GRASP scale of children with frequency in parenthesis are given below

19(6), 20(15), 21(14), 22(9), 23(12), 24(10), 25(6), 26(9), 27(8), 28(5), 29(6), 30(4), 31(3), 32(4), 33, 34, 35(4), 36(2), 37(2), 39, 42, 44

Data set 2: The data set represents the excesses of flood peaks (in m^3/s) Wheat on river near Car cross in Yukon territory, Canada. 72 exceedances of years 1958 to 1984 are recorded, rounded to one decimal place and data set is considered by Choulakian and Stephens [15] and Bodhisuwan et al. [16].

1.7, 2.2, 14.4, 1.1, 0.4, 20.6, 5.3, 0.7, 1.9, 13.0, 12.0, 9.3, 1.4, 18.7, 8.5, 25.5, 11.6, 14.1, 22.1, 1.1, 2.5, 14.4, 1.7, 37.6, 0.6, 2.2, 39.0, 0.3, 15.0, 11.0, 7.3, 22.9, 1.7, 0.1, 1.1, 0.6, 9.0, 1.7, 7.0, 20.1, 0.4, 2.8, 14.1, 9.9, 10.4, 10.7, 30.0, 3.6, 5.6, 30.8, 13.3, 4.2, 25.5, 3.4, 11.9, 21.5, 27.6, 36.4, 2.7, 64.0, 1.5, 2.5, 27.4, 1.0, 27.1, 20.2, 16.8, 5.3, 9.7, 27.5, 2.5, 7.0

Data Set 3: The given real lifetime data set represents the survival times (in months) of patients of melanoma studied by Susarla and Vanryzin [17] and the observations of data set are

3.25, 3.50, 4.75, 4.75, 5.00, 5.25, 5.75, 5.75, 6.25, 6.50, 6.50, 6.75, 6.75, 7.78, 8.00, 8.50, 8.50, 9.25, 9.50, 9.50, 10.00, 11.50, 12.50, 13.25, 13.50, 14.25, 14.50, 14.75, 15.00, 16.25, 16.25, 16.50, 17.50, 21.75, 22.50, 24.50, 25.50, 25.75, 27.50, 29.50, 31.00, 32.50, 34.00, 34.50, 35.25, 58.50

To determine the model comparison criterions accompanied with estimating unknown parameters thoroughly, the analysis is performed by applying the technique of R software. In order to compare the performance of weighted power Ishita distribution over power Ishita, Ishita, exponential and Lindley distributions, we consider the criterions like Bayesian Information Criterion *(BIC)*, Akaike Information Criterion *(AIC)*, Akaike Information Criterion Corrected *(AICC)*, Consistent Akaike Information Criterion *(CAIC)*, Shannon entropy *H(X)* and *-2logL*. The distribution is better even if it has smaller criterions of *AIC, BIC, AICC, CAIC, H(X)* and *-2logL*in comparison over other compared distributions. For determining the criterions values given below formulas are used.

$$AIC = 2k - 2\log L, \qquad BIC = k\log n - 2\log L, \qquad AICC = AIC + \frac{2k(k+1)}{n-k-1},$$

$$CAIC = -2\log L + \frac{2kn}{n-k-1} \qquad H(X) = \frac{-2\log L}{n}$$

Here k is number of parameters, n is sample size and –2log$L$is maximized value of log-likelihood function under the considered model.

Table 1: *Shows MLE and S.E of data sets of performed distributions*

Data set 1			Data set 2		
Distribution	MLE	S.E	Distribution	MLE	S.E
WPI	$\hat{\alpha} = 0.5335368$ $\hat{\theta} = 0.5652190$ $\hat{c} = 0.0010000$	$\hat{\alpha} = 0.1859930$ $\hat{\theta} = 0.8171725$ $\hat{c} = 1.2418239$	WPI	$\hat{\alpha} = 0.4447812$ $\hat{\theta} = 0.4640847$ $\hat{c} = 0.0010000$	$\hat{\alpha} = 0.1426458$ $\hat{\theta} = 0.8296986$ $\hat{c} = 1.2269077$
PI	$\hat{\alpha} = 0.60967097$ $\hat{\theta} = 0.89794552$	$\hat{\alpha} = 0.07155711$ $\hat{\theta} = 0.11904714$	PI	$\hat{\alpha} = 0.4409878$ $\hat{\theta} = 0.9174580$	$\hat{\alpha} = 0.0283685$ $\hat{\theta} = 0.0656560$
Ishita	$\hat{\theta} = 0.51564530$	$\hat{\theta} = 0.05983518$	Ishita	$\hat{\theta} = 0.256284$	$\hat{\theta} = 0.017182$
Exponential	$\hat{\theta} = 0.17742068$	$\hat{\theta} = 0.03782501$	Exponential	$\hat{\theta} = 0.0838497$	$\hat{\theta} = 0.0098803$
Lindley	$\hat{\theta} = 0.31258813$	$\hat{\theta} = 0.04780664$	Lindley	$\hat{\theta} = 0.156359$	$\hat{\theta} = 0.013089$

Data set 3		
Distribution	MLE	S.E
WPI	$\hat{\alpha} = 0.44939501$ $\hat{\theta} = 0.37266439$ $\hat{c} = 0.00100000$	$\hat{\alpha} = 0.01041128$ $\hat{\theta} = 0.00821445$ $\hat{c} = 0.01003165$
PI	$\hat{\alpha} = 0.45789840$ $\hat{\theta} = 0.75181782$	$\hat{\alpha} = 0.03611135$ $\hat{\theta} = 0.07547508$
Ishita	$\hat{\theta} = 0.19111099$	$\hat{\theta} = 0.01621195$
Exponential	$\hat{\theta} = 0.06386534$	$\hat{\theta} = 0.00941412$
Lindley	$\hat{\theta} = 0.12084543$	$\hat{\theta} = 0.01263491$

Table 2: *Shows comparison, analysis and performance of fitted distributions*

Data sets	Distribution	-2logL	AIC	BIC	AICC	CAIC	H(X)
1	WPI	59.80058	65.80058	69.07371	66.00058	66.00058	0.4822
	PI	98.09093	102.0909	104.273	102.1900	102.1900	0.7910
	Ishita	122.6363	124.6363	125.7273	124.6690	124.6690	0.9890
	Exponential	120.0865	122.0865	123.1776	122.1192	122.1192	0.9684
	Lindley	118.3165	120.3165	121.4075	120.3492	120.3492	0.9541
2	WPI	149.8181	155.8181	162.6481	156.1710	156.1710	2.0808
	PI	330.6732	334.6732	339.2265	334.8471	334.8471	4.5926
	Ishita	597.0425	599.0425	601.3191	599.0996	599.0996	8.2922
	Exponential	500.9405	502.9405	505.2172	502.9976	502.9976	6.9575
	Lindley	524.7423	526.7423	529.019	526.7994	526.7994	7.2880
3	WPI	46.26486	52.26486	57.75078	52.8362	52.8362	1.0057
	PI	194.8344	198.8344	202.4917	199.1134	199.1134	4.2355
	Ishita	334.0115	336.0115	337.8401	336.1024	336.1024	7.2611
	Exponential	345.0919	347.0919	348.9205	347.1828	347.1828	7.5019
	Lindley	333.6992	335.6992	337.5279	335.7901	335.7901	7.2543

It is clearly observed and revealed from the results given above in table 2 that the weighted power Ishita distribution has the smaller *AIC*, *BIC*, *AICC*, *CAIC*, *H(X)* and *-2logL*values in comparison over power Ishita, Ishita, exponential and Lindley distributions which indicates that the weighted power Ishita distribution leads to better fit as compared over power Ishita, Ishita, exponential and Lindley distributions.

X. Conclusion

In the present study, we have demonstrated a novel class of power Ishita distribution called as weighted power Ishita distribution has been introduced. The developed novel distribution has been executed and generated by using the weighted technique to baseline distribution. i.e. power Ishita distribution. The formulated distribution accomplished with distinguished statistical properties via moments, the mean and variance, shape of behaviour of pdf and cdf, hazard rate function, reliability function, reverse hazard function, moment generating function harmonic mean and order statistics have been determined. Furthermore, its Renyi entropy, Tsallis entropy and Bonferroni and Lorenz curves have been discussed. Additionally, the parameters of presented distribution are estimated by using the technique of maximum likelihood estimation. Finally, the three real world data sets have been analysed and fitted to determine the practicability and superiority of weighted power Ishita distribution. Hence, it is clearly realized from the result that the weighted power Ishita distribution provides a best fit in comparison over power Ishita, Ishita, exponential and Lindley distributions.

References

[1] Fisher, R. A. (1934). The effects of methods of ascertainment upon the estimation of frequencies. *Annals of Eugenics*, 6:13-25.

[2] Rao, C. R. (1965). On discrete distributions arising out of method of ascertainment, in classical and Contagious Discrete, G.P. Patiled; Pergamum Press and Statistical publishing Society, Calcutta. 320-332.

[3] Kilany, N. M. (2016). Weighted Lomax distribution. *Springer Plus*, 5(1):doi: 10.1186/s40064-016-3489-2.

[4] Ganaie, R. A., Rajagopalan, V., Nair, S. R. and Kanan, M. (2023). A new generalization of power Garima distribution with applications in blood cancer and relief times. *Journal of Statistics Applications & Probability*, 12(2):371-394.

[5] Sen, S., Chandra, N. and Maiti, S. S. (2017). The weighted Xgamma distribution: Properties and Application. *Journal of Reliability and statistical Studies*, 10(1):43-58.

[6] Para, B. A. and Jan, T. R. (2018). On three Parameter weighted Pareto Type II Distribution: Properties and Applications in Medical Sciences. *Applied Mathematics and Information Sciences Letters*, 6(1):13-26.

[7] Dar, A. A., Ahmed, A. and Reshi, J. A. (2018). An extension of power distribution. *Revista Investigation Operacional*, 39(4):626-638.

[8] Ganaie, R. A., Rajagopalan, V. and Aldulaimi, S. (2021).The weighted power Shanker distribution with characterizations and Applications of real life time data.*Journal of Statistics Applications and Probability*, 10(1):245-265.

[9] Dar, A. A., Ahmed, A. and Reshi, J. A. (2020). Weighted Gamma-Pareto distribution and its application. *Pakistan Journal of Statistics*, 36(4):287-304.

[10] Almuqrin, M. A., Almutlak, S. A., Gemeay, A. M., Almetwally, E. M., Karakaya, K., Makumi, N., Hussam, E. and Aldallal, R. (2023). Weighted power Maxwell distribution: Statistical inference and Covid-19 applicatiuons. *Plos One*, 18(1):e.0278659.

[11] Ganaie, R. A. and Rajagopalan, V. (2023). The weighted power quasi-Lindley distribution with properties and applications of life-time data. *Pakistan Journal of Statistics and Operation Research*, 19(2):279-298.

[12] Hassan, A. S., Almetwally, E. M., Khaleel, M. A. and Nagy, H. F. (2021). Weighted power Lomax distribution and its length biased version: Properties and Estimation based on censored samples. *Pakistan Journal of Statistics and Operation Research*, 17(2):343-356.

[13] Balakrishnan, N., Gupta, R. C., Kundu, D., Victor, L. and Antonio, S. (2010). On mixture model based on Birnhaum-Saunders Distributions and associated inference. A study conducted by Authors regarding the Scores of the GRASP (General Rating of Affective Symptoms for Preschoolers), in a city located at South Part of the Chile.

[14] Choulakian, V. and Stephens, M. (2001). Goodness-of-_t for the generalized Pareto distribution. *Technometrics,* 43(4):478-484.

[15] Shukla, K. K. and Shanker, R. (2018). Power Ishita distribution and its application to model lifetime data. *Statistics in Transition New series*, 19(1):135-148.

[16] Bodhisuwan, W., Nanuwong, N. and Pudprommarat, C. (2016). Parameter estimation for the length biased Beta-Pareto distribution and application. *Walailak Journal*, 13(5):301-315.

[17] Susarla, V. and Vanryzin, J. V. (1978). Empirical Bayes estimation of a distribution (Survival) function from right Censored observations. *The Annals of Statistics*, 6(4):740-754.

THE DEVELOPMENT OF RISK-BASED THINKING PRINCIPLES AT A MACHINE-BUILDING ENTERPRISE UNDER CONDITIONS OF INDUSTRY 4.0

Yaroslav Vavilin
•
Bryansk State Technical University
vavilin@bk.ru

Abstract

The article deals with the problem of formal introduction of risk-based thinking features in machine-building production under conditions of Industry 4.0 together with the expansion of the use of digital technologies. The research aims to address the following objectives: to analyze the necessity and influence of risk management implementation within the organization's quality management system; to determine the levels required for realizing risk-based thinking; to develop a methodological foundation for integrating risk-based thinking considering Industry 4.0 elements; to perform a comparative analysis of the proposed model with known risk management systems. The study employs well-established methods of process-based approaches (Deming-Shewhart cycle) and systems analysis. The authors make an attempt to formalize the work on ensuring the proper use of risk and capability management tools from the perspective of a system analysis and process approach. Works related to risk management at the stages of the Deming-Shewhart cycle are highlighted and the levels and components of the machine-building production system model that are subject to analysis are determined. The task of introducing risk-based thinking in quality management systems of machine-building enterprises is critical due to the increasing complexity of products, increasing consumer demands and the need to ensure increased safety. Risk analysis makes it possible to identify potential threats to product quality in advance, minimize the consequences of defects, reduce error correction costs and increase the competitiveness of the enterprise in the market.

Keywords: quality, risk-based thinking, mechanical engineering, system, indicators

I. Introduction

A quality management system based on ISO 9000 series standards, version 2015, has got a risk and capability management as the main control component. The requirements for risk-based thinking is conditioned by the need of enterprise adaptation to rapidly changing environmental conditions and the transition to Industry 4.0 (field). Each structural arrangement has to identify and assess risks, as well as develop measures of minimizing or preventing them. The machine-building production system is a complex network of flow rate interrelation, heedful of the output quality where deep understanding and effective management are required particularly [1, 6 - 8].

In most cases the innovations (whichever is introduced: either technology or equipment, any management techniques) face two issues connected with economic efficiency and requirements by the law. According to the quality management concept any technology or technique within quality

assurance framework, generating a profit (either by reducing process costs or by increasing demand), should be employed. Such quality management techniques and technologies (including risk-based thinking) can be attributed to the elementary units allowing continuous improvement, and over a long period of time (this approach is implemented in the philosophy of KAIZEN). Any marketing executive takes an interest in rapid growth and breakthrough technologies (KAIRYO), but such approach is typical for emerging economies and bears more risks.

The effectiveness of using quality management techniques and tools can be assessed in reducing potential costs when dealing with complaints and defects. Thus, they do not generate any obvious profits, and therefore, are provided financing residually. This results in formality for the technique application especially risk management. The choice comes down to using the simplest method of dealing with risks to meet the requirements of the standard and obtain a certificate. Under high competition and rapid changes, the key growth factor is the ability to anticipate (identify, analyze) and manage risk drivers and capabilities [9 – 18].

In this regard, it becomes necessary to form risk-based thinking, rather than the formal application of one or two of the simplest methods. It is good at all levels of structural arrangement management for operationalizing of the integrated implementation of risk management tools to identify threats timely and search for adaptability. Risk and capability management should become an integral part of the management decision-making process at all levels of the organization's management, from marketing research on product issues to strategic decisions on enterprise development. The introduction of integrated risk-based thinking as a subsystem of the overall management system, including quality management, at a machine-building enterprise will ensure sustainable development in an unstable economic situation and increase competitiveness not only due to the quality of products, but also hidden reserves of the organization.

The purpose of this work is to prepare a methodological framework for the implementation and development of a risk-based thinking system in a machine-building enterprise, as a quality management subsystem, aimed at identifying areas for the improvement.

II. Methods

To solve complex management tasks and implement the quality management principle of "evidence-based decision-making", it is advisable to use systems analysis methods that makes it possible to consider the company's activities as an integrated system, where all elements have an impact on the final result. This will help identify weaknesses and avoid the "process paradox", when the amount of funds allocated to improve the process is greater than the final result. A systematic approach to the organization's assessment and risk management will provide a comprehensive view of the corporate organization and facilitate informed decision-making [2 – 5]. The application of a systematic approach is fundamentally important for the comprehensive solution of product quality management problems. A systematic approach contributes to the formation of a holistic quality management strategy and optimization of business processes.

One of the key points of any management system is a process concept. A quality management system has been built on the process approach and the implementation of the Deming-Shuhart cycle (Plan-Do-Check-(Study)-Act), part of which is a risk-based approach, the effectiveness of which directly depends on a comprehensive solution to the task [20, 21]. The process approach is the most important prerequisite for effective product quality management and the functioning of modern organizations. This approach provides a structured representation of an enterprise's activities as a set of interrelated processes aimed at achieving its goals. The process structure promotes a clear division of responsibility between departments and improves employee coordination. Regular evaluation of the effectiveness of processes helps to make timely changes, adapt to changes in the external environment and maintain a high level of competitiveness of the organization.

III. Results

Seen as a whole from both systems theory and comprehensive approach point of view any organization (including a machine-building enterprise) can be described by a bunch of SFC elements:

$$S = \{M, P, P_r, T, W, C_i, C_o, O\}$$

where M – organization management, P –products, P_r -processes, T-applied technologies, W-employees (workers), C_i-internal relationships, C_o-external relationships, O - the outside environment of the organization. The final risk assessment of an organization can be calculated as a weighted mean value for each component.

Risk-based thinking components can be used at two levels of management: strategic – to assess financial risks and to mold possible strategies for the development of the enterprise on the one hand and on the other hand it is tactical, aimed at risks identification inherent in the output, personnel or technological support of the enterprise. At the same time, the choice of used methods will depend on the level of the organization's maturity and staff qualifications.

The decision to use the potential of risk-based thinking methods based on the ISO 31000 series standards should be built on the principles of a systematic approach (duality and integrity), that is, the boundary of the constituent elements, their mutual interrelations and the final result should be determined.

Any risk-based approach requires changes to the hierarchical set of values in the organization, namely:

1. Strategic level – outlining of the corporate management philosophy based on decision-making, considering a comprehensive analysis of risks and capability in regard to the process and product quality, technology control.

2. Tactical level – moving from the stage of a “fire- fighting” and solving problems in process of emergence, looking for the answer to a question "who is to blame?", to predicting and preventing potentially negative development of the situation (answering the question "how?").

3. Operational level – developing and implementing risk-based thinking system, in which each employee has a notion of why, how and for what the analysis is carried out.

Work can be divided into a cycle of five components:

1. Standardization. It includes activities related to the development of documented records procedure necessary for the roll-out process, conceptualization of the required work and reporting on them.

2. Automation. In the context of comprehensive digitalization and the transition to Industry 4.0, data collection and analysis should be carried out in conditions of minimizing the routine work of searching and analyzing information through the use of automated analytical systems and electronic document management.

3. Staff motivation. Providing training and systematization of knowledge in the field of quality management for employees at all levels of management and process performers.

4. Study of risk. Carrying out work on the identification, assessment and analysis of risk for each component of the organization's model, highlighting critical ones and developing corrective or preventive measures.

5. Management. Making decisions on the implementation of proposed corrective or preventive measures, as well as further development of the system.

As a basic system of continuous improvement, the works can be divided into stages in accordance with the Deming-Shewhart cycle (table). Depending on the organization's environment, the work cycle should be repeated with fixed cyclicity, but at least once a year.

Table 1: *Distribution of work by stages of the Deming- Shewhart cycle*

Stages	Complete activity
PLAN	Development and planning of work in the field of risk and capability management: 1. A preliminary analysis of the structural arrangement state, including self-assessment of processes improvement and staff qualifications of personnel (business services, operational staff and technical people). 2. Expert group formation for distribution of authority in procedures, taking into account the levels of their hierarchy and the task being solved. 3. Fixation of risk limits and scales for its assessment. If necessary, a rule for converting to a relative (point-rating) system is formulated in case of heterogeneous indicators ratio.
DO	Risk and capability assessment procedure: 1. The choice of risk management methods depends on the qualifications of the expert group and the complexity of the task being solved. 2. Information collection and its processing. 3. Formation of the final result.
CHECK	Comparing the obtained values with critical ones and making recommendations: 1. Comparison of the obtained values of the risk level with critical ones. 2. Analysis of the dynamics of the values of controlled risk parameters. 3. Development and approval of recommended corrective or preventive measures. 4. Development of a system of critical control points for monitoring risk factors.
ACT	Implementation of the proposed risk reduction measures: 1. Setting deadlines for implementation and designating job responsible persons. 2. Budget formation to eliminate (reduce) the level of critical risks. 3. Action tracking. 4. Review of criticality factors for the next reporting period.

Information technologies, being one of the key tools of modern management, can significantly improve any risk management efficiency. Since risk management becomes a part of the overall management of the organization, providing support for decision-making at all levels of the organizational structure, it must be integrated into the IT environment of the organization. CALS-technologies (Continuous Acquisition and Life cycle Support) provide continuous information support for deliveries and the whole product life cycle. They become the basis for collecting and analyzing information about the product and production, providing new horizons in quality, risk and capability management. A high degree of automation and control under processes allows identifying and controlling all potential risks, as well as ensuring data transparency and accuracy. The hierarchical model of using software product classes is shown in Fig. 1. Information flows form a closed cycle and ensure continuous improvement [19 – 21].

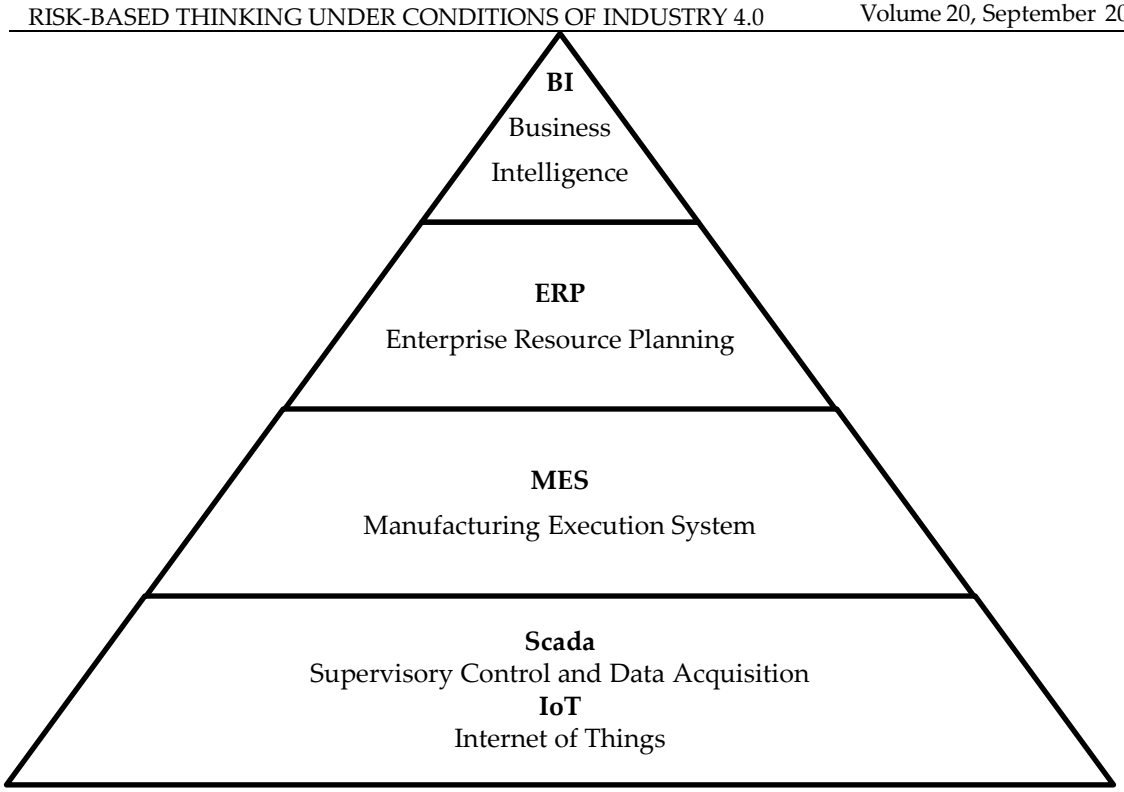


Figure 1: *Hierarchical model*

It is possible to identify a number of areas for the use of modern information technologies in the risk control field:

1. Automated data collection and processing with the use of specialized software complexes of the Scada and IoT class, making possible to get real-time information about the operation procedure. Such works become relevant from the earliest stages of forming a risk management culture –the stage of initial analysis.

2. Modeling opening scenarios, which allows predicting and modeling the probability of occurrence of events and their consequences, which contributes to making the right decisions in conditions of uncertainty. The growth of computing power and the ability to collect digital data allows building predictive models based on BigData analysis, which can be diagnostic for hidden patterns and trends.

3. Data analysis. The use of artificial intelligence (AI) and Big Data technologies makes it possible to ensure the widespread use of information from the knowledge bases (KBs) of an enterprise or group of enterprises, as well as to ensure the search for critically important information using linguistic variables.

No matter how perfect the technology is, much depends on people, who implement it. Therefore, personnel are the most valuable resource of any organization, especially at a machine-building enterprise. The creation of good causes and successful training system lays a solid foundation for the company's prosperity. Look at the Japanese experience, when one company becomes a place of work for several generations of employees. In the context of the transition to digital technologies and automation (robotization) of production, the task of adapting and creating "social" human-machine relationships arises ae well [15]. Digital technologies are just a supplement and are designed to facilitate routine tasks of personnel, such as collecting information regarding progress of execution or analyzing big data for making a management decision. The staff training and motivation system allows you to get an initiative employee who is interested in the best performance of the duties, and also forms the knowledge base of the enterprise.

IV. Discussion

The practical implementation of the information model can be different, built on the basis of a single information platform (for example, domestic developments of 1C or ModelRisk - a tool for analyzing risks in a spreadsheet for business, science, industry, and public administration), or using web portals (Figure 2).

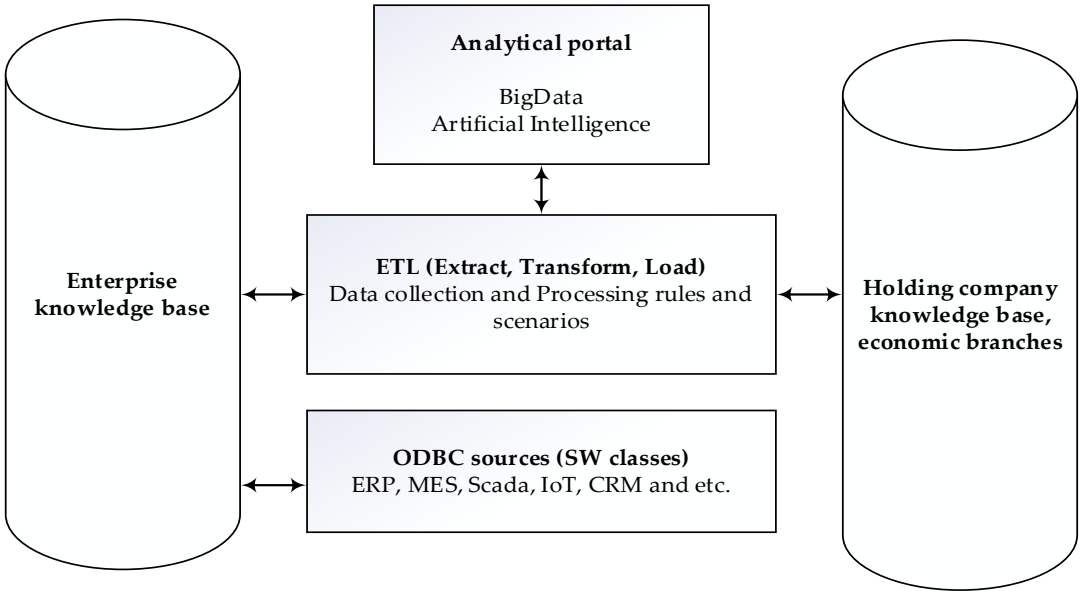


Figure 2: *Architecture of the analytical risk and capability management system*

One of the significant disadvantages of existing approaches in risk control field becomes the "isolation" within a single enterprise. Thus, there are situations when similar risks are eliminated in different ways within the same holding company and knowledge is not exchanged. This has a negative impact on resource conservation and prevents the use of the best available practices.

Generally, the work can be described by the following sequence of process implementation (information is exchanged using the organization's common knowledge base and cloud technologies): risk and capability management planning (Deming-Shuhart cycle Plan stage) using ERP systems (in particular, SAP Risk Management); implementation (Do- stage of the Deming-Shuhart cycle) – implementation of a risk assessment procedure based on data obtained from sources (Scada, IoT, CRM...) using AI, BigData technologies; presentation and analysis of the results obtained (Check stage of the Deming-Shuhart cycle) using AI, BigData, BI technologies; implementation of risk reduction measures (Act- stage of the Deming-Shuhart cycle).Considering the ratio of costs and benefits from the introduction of risk-based thinking (Figure 3), we can conclude that it is similar to the philosophy of KAIZEN – "playing the long game".

In the first part of the schedule (time period 1-3), costs increase sharply, which corresponds to the beginning of implementation work and is associated with the appearance of new expenses for training personnel, forming teams (cross-functional groups) for analysis, etc. Further (time period 3-7), the cost level decreases and stabilizes at a certain (minimum) level to maintain efficiency the process. There are no benefits at the initial stage (time period 1-2), which is quite logical, since data collection and analysis are being carried out and recommendations for improvement (improvement of activities) are being developed. Then (time period 2-3) there is a sharp increase – this is the area of correction of the first "critical" risks. In the following (time period 3-7), smooth growth is identified or revised risks control in a cyclically repeating analytical procedure. Such cycles will be repeated as the system develops and moves to a higher level of process improvement.

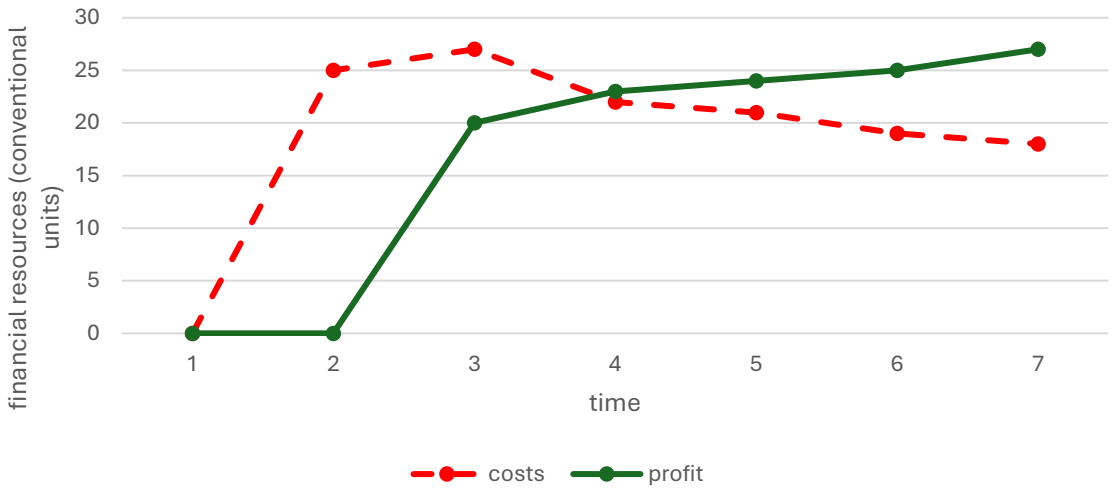


Figure 3: *Architecture of the analytical risk and capability management system*

The advantages of such a gradual approach include the "flexibility" of the model, which allows costs reduction in case of the wrong strategic decision making, as well as in conditions of significant influence from the outside environment of the organization, which in most cases is extremely difficult to predict.

Considering the elements of Industry 4.0, it is assumed that big data will be the most understandable for industry representatives and easy to implement elements for risk analysis. Consider the sequence of steps in building an analytical model for risk assessment:

Stage 1. Definition of Risk Analysis Objectives. This involves identifying key performance indicators (KPI), detecting risk factors, and establishing the goals of the analysis.

Stage 2. Data Collection and Preparation. Merely having access to large volumes of information is insufficient for obtaining high-quality results. An essential aspect is the correct formulation of the task for data collection. At this stage, linguistic artificial intelligence systems can be employed to automate the search and filtering of information based on key characteristics.

Stage 3. Risk Modeling. This entails applying statistical analysis methods, machine learning, and artificial neural networks to identify patterns and predict potential threats. The cost of risk mitigation increases with each new production transition; therefore, it is far more effective to prevent its occurrence than to address its consequences after detection. The use of mathematical tools in conjunction with computational machines enables the modeling of complex multivariate processes and provides adequate accuracy for predictive models.

Stage 4. Interpretation of Results and Development of Recommendations. Identified bottlenecks during the modeling phase should either be eliminated or subjected to a higher level of control.

As an example, consider the case “Analytical system for monitoring equipment operability”. Equipment repairs are possible according to two components: 1) the standard operating time (this option is most often used) and 2) the actual condition of the equipment. An enterprise engaged in the transportation of hydrocarbons has implemented automated control systems for the condition of pumping equipment in a test mode and is deciding whether to put it into reserve or for maintenance based on its actual condition. The real-time performance characteristics of the equipment are captured using sensors (IoT) and transmitted for analysis. Depending on the characteristics obtained, a decision is made on the timing and scope of repairs. During the test mode, a 12% reduction in emergency situations related to equipment failure was revealed, and the period between routine repairs was increased by 7%.

V. Conclusion

Undoubtedly, there are various models of enterprise risk management. The approach proposed by the author to creating a risk analysis system is not the only one. The COSO Risk Cube is a three-dimensional model that visualizes the structure of an enterprise's risk management system (Enterprise Risk Management, ERM). Enterprise Risk Management-Integrating with Strategy and Performance clarifies the importance of enterprise risk management in strategic planning and embedding it throughout an organization-because risk influences and aligns strategy and performance across all departments and functions [22]. FERMA is a European standard for the organization of risk management, developed by the Federation of European Associations of Risk Management Specialists. The implementation of the FERMA risk management model takes place in seven stages: The formulation of the main goals and objectives of the enterprise. Risk analysis and assessment. Risk report. Decisions on the initial report. Risk management. Repeat report. Control [23, 24]. A comparison of popular risk management models is presented in the table 2.

Table 2: *A comparison of popular risk management models*

	COSO ERM	FARMA	ISO 31000	THE AUTHOR'S MODEL
Strengths	An integrated approach to risk management. Connection with strategic goals. Building the trust of stakeholders. Preparing for unexpected events.	A systematic approach. There are practical recommendations. Consideration of external and internal factors.	Versatility. Consideration of human and cultural factors. Continuous improvement.	Versatility. The use of advanced computer technology. Integration with the quality management system. Evidence-based decision-making. Emphasis on risk in the production process.
Weaknesses	The complexity of the structure. No step-by-step instructions. The need for adaptation.	Recommendation character. The need for adaptation. Some organizations may have difficulty implementing the FERMA risk management system due to the specifics of their business.	Inability to describe specific processes. The need for adaptation. Limitations of the methods described in the standard. There are no recommendations on the choice of methods	Lack of a standard. The need for adaptation.

Addressee — for whom the standard was created	The company's internal auditors	Professional risk managers	Any organization seeking to implement an integrated approach to risk management	Any organization seeking to implement an integrated approach to risk management
Required level of knowledge and skills of employees	High	Very high	Medium	Medium

The author made an attempt to present a variant of strategy in the formation of a risk-based thinking culture within a machine-building enterprise based on a system analysis and a process approach. At the same time, risk assessment should be carried out in different ways depending on the purpose and level of analysis (process, product, technology), and the overall integrated assessment is made through a weighted average of all estimates. The severity of each component is determined by the expert method. Not only the risks are identified, but also their impact on the entire organization. The system itself exists according to the principles of a process approach with continuous improvement based on the Deming-Shuhart cycle.

Experience proves that correction expenses during the transition from one stage of the life cycle to the next change significantly. This cost change is called the "tenfold cost rule", essentially it is much cheaper not to make a defect than to recover rejects. Despite almost a decade of a compulsory use of risk and capability management technique in various structural arrangements with various control levels, there are many "gray" areas due to management's lack of comprehensive insight into the problem or disinclination of the top management to implement such integrated approaches. Obtaining the coveted certificate of QMS compliance with ISO 9000 series standards does not guarantee that the system works as efficiently as possible. In mechanical engineering, as a key industry producing capital goods, there is great passivity and even resistance to innovations in the field of management. This is often associated with the concept of technological quality, i.e. ensuring quality through properly designed and selected technological processes, which, of course, is an important component of quality, but not the only one.

The meaningful effect of quality management tools implementation and the construction of an effective integrated management system based on a risk-based quality management with reference to the formation of Industry 4.0 in the country is a guarantee of industrial sovereignty of the state. A management culture based on a comprehensive assessment of the risks and capabilities of the organization (products, processes, technologies, management, etc.) based on the principles of process and system approaches simultaneously implements the principles of quality management and ensures the validity of strategic decisions. Either way, risks must be identified, assessed, and managed.

References

[1] Vasiliev Victor A. (2023) Information Technologies in the Organization of Production and Quality Management, Int. Conf. "Quality Management, Transport and Information Security, Information Technologies" (IT&QM&IS-2023), p. 3-8.

[2] Narusova Elena Yu., Struchalin Vladimir G., Paruleva Irina V (2023) Development of Hardware and Software to Ensure Process Safety and Reliability in Railway Transport, Int. Conf. "Quality Management, Transport and Information Security, Information Technologies" (IT&QM&IS-2023), pp. 59-63.

[3] Sukhanova Natalia V., Sheptunov Sergey A. (2023) The Neural Networks Application in Information Security, Int. Conf. "Quality Management, Transport and Information Security, Information Technologies" (IT&QM&IS-2023), pp. 74-78.

[4] WBCSD; COSO. Enterprise Risk Management Applying Enterprise Risk Management to Environmental, Social and Governance-Related Risks. 2018. Available online: https://docs.wbcsd.org/2018/10/COSO_WBCSD_ESGERM_Guidance.pdf (accessed on 4 May 2025).

[5] Hanmei Wu, Xiaoqing Cai, and Man Feng, Risk management of engineering projects installation using Analytic Hierarchy Process Infrastructure Asset Management 2025 12:1, 57-69

[6] International Organization for Standardization. Guidance on: Auditing Climate Change Issues in ISO 9001; International Organization for Standardization: Geneva, Switzerland, 2024.

[7] WEF. World Economic Forum, The Global Risks Report; WEF: Geneva, Switzerland, 2024; Available online: https://www3.weforum.org/docs/WEF_The_Global_Risks_Report_2024.pdf (accessed on 4 May 2025).

[8] ISO 9001:2015 Quality Management Systems – Requirements. International Organization for Standardization: Geneva, Switzerland, 2015.

[9] Joshi, Satyadhar, Leveraging Prompt Engineering to Enhance Financial Market Integrity and Risk Management (January 15, 2025). World Journal of Advanced Research and Reviews, 2025, 25(01), 1775-1785 DOI: 10.30574/wjarr.2025.25.1.0279

[10] Yazo-Cabuya, E.J.; Ibeas, A.; Rey-Caballero, R. Multi-Criteria Decision Making for Risk Management in Quality Management Systems. Sustainability 2025, 17, 1092. https://doi.org/10.3390/su17031092

[11] Dong, T., Li, H. & Zhang, Z. The using effect of fuzzy analytic hierarchy process in project engineering risk management. Neural Comput & Applic 37, 7935–7945 (2025). https://doi.org/10.1007/s00521-023-09046-2

[12] Jiang, S.; Cao, X. Rule Inferring for Engineering Quality Risk Management Based on Ontology in Housing Construction. Sustainability 2025, 17, 1643. https://doi.org/10.3390/su17041643

[13] N. Banaitiene and A. Banaitis, Risk Management in Construction Projects, Risk Management - Current Issues and Challenges. InTech, Sep. 12, 2012. doi: 10.5772/51460.

[14] Zhang, F.; Yang, Y.H. Feature Vector Extraction Algorithm Based on Big Data in Engineering Quality. Engineering 2021, 257, 02029

[15] Faheem M, Shah SBH, Butt RA et al (2018) Smart grid communication and information technologies in the perspective of Industry 4.0: opportunities and challenges. Comput Sci Rev 30:1–30

[16] L.J. Basile, N. Carbonara, U. Panniello, R. Pellegrino, The role of big data analytics in improving the quality of healthcare services in the Italian context: The mediating role of risk management, Technovation, Volume 133, 2024, 103010, ISSN 0166-4972, https://doi.org/10.1016/j.technovation.2024.103010.

[17] Bazaluk, O., Pavlychenko, A., Yavorska, O. et al. Improving the risk management process in quality management systems of higher education. Sci Rep 14, 3977 (2024). https://doi.org/10.1038/s41598-024-53455-9

[18] Marilyn F. Braine, Matthew Kearnes, Stuart J. Khan, Quality and risk management frameworks for biosolids: An assessment of current international practice, Science of The Total Environment, Volume 915, 2024, 169953, ISSN 0048-9697, https://doi.org/10.1016/j.scitotenv.2024.169953.

[19] Szelągowski, Marek, Justyna Berniak-Woźny, and Magdalena Wójcik-Jurkiewicz. Redefining The Deming Cycle for Industry 4.0/5.0. Zeszyty Naukowe Akademii Górnośląskiej 9 (2023): 223-235.

[20] Trippner-Hrabi, Justyna, Jacek Chądzyński, and Aygun Kam. Unveiling the Significance of the PDCA Deming Cycle. Ethics and Innovation in Public Administration 299 (2024).

[21] Ten, Chee-Wooi, and Yunhe Hou. Modern power system analysis. CRC Press, 2024. [1] Figueredo, A. J. and Wolf, P. S. A. (2009). Assortative pairing and life history strategy - a cross-cultural study. *Human Nature*, 20:317–330.

[22] The Committee of Sponsoring Organizations (COSO) https://www.coso.org/ accessed on 24 May 2025).

[23] Risk management standards https://www.gd.ru/articles/12547-standarty-upravleniya-riskami (accessed on 4 May 2025).

[24] Strelnik M.M. Comparison of risk management standards (COSO ERM, FERMA and ISO 31000:2009) // Proceedings of St. Petersburg State University of Economics. 2014. No. 7. pp. 116-119.

APPLICATION OF WEIGHT MEASURE ORDERING FOR INTUITIONISTIC FUZZY CRITICAL PATH ANALYSIS

S. Priyadharshini[1], G. Deepa[2,*], S. Ramprasath[3]

•

[1,2*]Department of Mathematics, School of Advanced Sciences, VIT University, Vellore – 632014, India.

[3] School of Computer Science Engineering and Information Systems, VIT University, Vellore – 632014, India.

[1]priyaseenuvasan2719@gmail.com, [2*]deepa.g@vit.ac.in, [3]ramprasath2902@gmail.com

Abstract

The intuitionistic fuzzy critical path problem is a frequent and important challenge in network optimization, particularly in the planning and management of complex projects. However, the traditional critical path approach often fails to accurately reflect real-world scenarios. To address this, we have developed a critical path strategy within an intuitionistic fuzzy framework. In this study, the critical path is determined using a ranking algorithm, where the edge weights are modeled as triangular intuitionistic fuzzy numbers (ITFN). We have introduced definitions for ranking strategies that help identify the intuitionistic fuzzy critical path. Additionally, a proposed criticality degree measures that significance of each activity. Examples are provided to illustrate the proposed strategy, and the simulation results of the ranking techniques are also presented.

Keywords: Critical path Method, Intuitionistic Fuzzy Triangular Number, Acyclic Network, Project Scheduling.

1. Introduction

In today's highly competitive corporate environment, where numerous business activities are managed as projects, the ability of project management to plan operations and monitor progress on schedule is becoming increasingly crucial. The duration of business deals in network operations is often ambiguous and imprecise in practice. In these situations, Zadeh's fuzzy numbers [20] and Atanassov's intuitionistic fuzzy sets [2] are used to represent activity durations, driving advancements in intuitionistic fuzzy project management techniques. Project managers commonly use the concepts of the earliest, latest, and total float tasks [13]. These are valuable when deciding when to introduce a new activity, eliminate an existing one, or adjust the project's due date if the scope changes [15]. With a clear understanding of the activities and their interconnections in the project network, successful execution is achievable. While calculating the fuzzy earliest starting times of activities using the critical path method is straightforward, determining the fuzzy latest starting times is more challenging, as explored by Elizabeth and Sujatha [10]. When activity durations are vaguely understood and best represented by fuzzy sets, Dubois et al. [9] computed the criticality levels, slacks, and latest start times of events using possibility theory by describing the earliest, latest, and slack times of events as a function of the lengths of routes. A novel method was developed to quickly identify the intervals of the latest starting times in intervalued networks. Chen and Huang [7] suggested using the criticality level of activities and paths to identify fuzzy critical paths. Zareei et al. [19] employed the Zadeh extension principle, linear programming, and a relative

path degree criticality technique to evaluate the criticality of each event and path, determining the earliest and latest event timings. Sireesha and Shankar [17] proposed a method for finding the optimal solution in a fuzzy project network based on the highest total float of the path. While approaches based on the fuzzy extension of the crisp approach are significant, they are also time-consuming and of limited interest to practitioners, according to Bonnal et al.'s [5] assessment of fuzzy PERT (Project Evaluation and Review Technique).Stephen Dinakar and Rameshan [18] presented a technique for analyzing the critical path in a project network using octagonal fuzzy numbers. Instead of precise numbers, Balaganesan and Ganesan [3] developed a novel method for determining the critical path in a network architecture using intuitionistic fuzzy triangular numbers. The innovative JOSE Algorithm, which includes 13 parameters and a ranking mechanism known as the Euclidean ranking approach, was introduced by N. Jose Parvin Praveena [12] and colleagues to identify the fuzzy critical path (FCP). They demonstrated that the dynamic encoding recursion of the critical path could be expressed using triskaidecagonal and fuzzy triskaidecagonal numbers. Recent research by the authors also includes works from [1,6,16].

The paper is organized as follows: Preliminaries are in Part 2, the methodology is in Section 3, results and comments are in Section 4, and the conclusion is in Section 5.

2. Preliminaries

Definition 2.1 Operations on IFTFN [2]

Consider X = (p_1, q_1, r_1) (p'_1, q_1, r'_1) and Y = (p_2, q_2, r_2) (p'_2, q_2, r'_2) be two ITFN, then

i. Addition:
$X \oplus Y = (p_1 + p_2, q_1 + q_2, r_1 + r_2)$ $(p'_1 + p'_2, q_1 + q_2, r'_1 + r'_2)$.

ii. Subtraction:
$X \ominus Y = (p_1 - r_2, q_1 - q_2, r_1 - p_2)$ $(p'_1 - r'_2, q_1 - q_2, r'_1 - p'_2)$.

iii. Maximum Operation:

M_{max} = max (X, Y)
= (max (p_1, p_2), max (q_1, q_2), max (r_1, r_2)), (max (p'_1, p'_2), max (q_1, q_2), max (r'_1, r'_2)).

iv. Minimum Operation:

M_{min} = min (X, Y)
= (min (p_1, p_2), min (q_1, q_2), min (r_1, r_2)), (min (p'_1, p'_2), min (q_1, q_2), min (r'_1, r'_2)).

Definition 2.2 Acyclic network [4]

A graph with directed edges is referred to as a directed graph. Consequently, a directed graph without a cycle is called as acyclic directed graph. An acyclic directed graph which forms a network is known as acyclic network.

Definition 2.3 Signed distance measure (SDM) [11]

For every closed interval [x, y], d([x, y], 0] = $\frac{1}{2}$(x + y) is the definition of the SDM of [x, y] measured from '0'.

Definition: 2.4 α-cut Ranking [11]

If (x, y, z) (x′, y, z′) be the triangular IFN then α-cut is defined as,

$$\alpha(P) = \int_0^1 [x + \alpha(y - x)]\alpha * d\alpha + [z + \alpha(z - y)]\alpha * d\alpha,$$

$$- \int_0^1 [y + \alpha(y - x')]\alpha * d\alpha - [y + \alpha(z' - y)]\alpha * d\alpha$$

α(P)= $\frac{x+4y+z}{6}, -\frac{x'+y+z'}{3}$ = (membership function, non-membership function)

Definition: 2.5 Euclidean Ranking [11]

Let $L_i = (x_i, y_i, z_i)$ (x_i', y_i, z_i') be the i^{th} fuzzy path length, $L_{max} = (x, y, z)$ (x', y, z') be the fuzzy longest length, then Euclidean Ranking (ER) is defined as,

$$ER(P) = \sqrt{(x - x_i)^2 + (y - y_i)^2 + (z - z_i)^2}, \sqrt{(x' - x'_i)^2 + (y - y_i)^2 + (z' - z'_i)^2}$$

Definition: 2.6 Similarity Ranking [11]

Let $L_i = (x_i, y_i, z_i)$ (x_i', y_i, z_i') be the i^{th} fuzzy path length, $L_{max} = (x, y, z)$ (x', y, z') be the fuzzy longest length, then Similarity Ranking (SR) is defined as,

$$SR(L_i, L_{max}) = \begin{cases} \emptyset, & if\ L_i \cap L_{max} = \emptyset \\ \frac{1}{2}[z_i - x] * Z_i, \frac{1}{2}[z'_i - x'] * Z'_i, & if\ L_i \cap L_{max} \neq \emptyset \end{cases}$$

Where,

$$Z_i = \frac{z_i - x}{(y - x) + (z_i - y_i)}, y_i < a < z_i\ and\ x < a < y$$

$$Z_i' = \frac{y - y_i}{(z_i' - y_i) + (y - x')}, y_i < a < z_i'\ and\ x' < a < y$$

3. Proposed Methodology

An intuitionistic fuzzy project is represented by an acyclic directed graph where vertices represent the project's nodes, and directed edges act as its links. A typical representation of an intuitionistic fuzzy project network is G = (V, E, T), where V= {$\upsilon_1, \upsilon_2, \ldots, \upsilon_n$} denotes the collection of vertices, E: V ×V are the set of directed edges (i, j) = (υ_i, υ_j), and T= {t (i, j) / 1 ≤ i, j ≤ n} reflects the fuzzy times for activity (i, j).

3.1. Traditional Forward and Backward Calculations for Acyclic Networks

The objective of this study is to identify the critical path, or the sequence of operations with the longest duration, as well as the float for each operation. This allows for easier comparison between actual progress and the project's anticipated completion date. To achieve this, we perform specific calculations that yield the following data:

1. **Forward Calculation**
2. **Backward Calculation**

Forward Calculation:

- Triangular Intuitionistic Fuzzy Earliest Start (TrIFESTj) for the project network's is determined via forward pass computations.
- TrIFESTj = max {TrIFESTi ⊕ duration }, i = number of nodes before it.
- TrIFEST(node 1) = TrIFLFT(node 1) = 0
- TrIFEFTj = TrIFESTi ⊕ duration.

Backward Calculation:

- Triangular Intuitionistic Fuzzy Latest Finish (TrIFLFTj) for the project network's is determined via backward pass computations.
- TrIFLFi = Min {TrIFLFj Θ TrIFtij }, j = number of nodes after it.
- TrIFLF(n) = TrIFES(n) = n
- TrIFLS = TrIFLF Θ duration

Definition 3.1.1: Triangular Intuitionistic Fuzzy Total Float (TrIFTF)

The Triangular Intuitionistic Fuzzy Total Float (TrIFTF) is the amount of time that can be added to an activity without impacting the project's overall deadline. It is calculated as the difference between the Intuitionistic Fuzzy Backward Latest Time (IFBLT) and the Intuitionistic Fuzzy Backward Earliest Time (IFBET). The formula is expressed as:

TrIFTF = TrIFLF – TrIFEF (or) TrIFTF = TrIFLS – TrIFES

3.2. Ranking for Intuitionistic Fuzzy Triangular Numbers(IFTN)

To perform an intuitionistic fuzzy critical path analysis, it is essential to rank or order intuitionistic fuzzy numbers. Consequently, several fuzzy ordering and evaluation methods have been introduced in the literature. According to Lee and Li (1998) [14], possibility theory serves as the foundation for most fuzzy comparison approaches, which aim to fuzzify uncertainty. Delgado et al. (1998) [8] and Lee and Li (1998) [14] argued that relying on a single value can result in an overly generic presentation of data, which may lack discrimination and sometimes conflict with intuitive thinking from a practical standpoint.

In this subsection, a novel fuzzy number ranking technique called the weight measure is introduced, which computes the metric distance using the left and right membership functions. It is important to note that this technique can rank both positive and negative intuitionistic fuzzy numbers (IFN).

Theorem: Weight Measure for IFTN
If (x, y, z) (x′, y, z′), be the IFTN then weight measure (WM) is defined as
WM = $\left(\frac{x+3y-z}{6}, \frac{2x'+3y-2z'}{6}\right)$ = (Membership function, non-membership function).
Proof:
Let $S^{(\gamma)}$ = {[L(γ), R(γ)], [L′(γ), R′(γ)]} be a IFTN, then the signed distance of [L(γ), R(γ)] which is measured from zero is defined as d([L(γ), R(γ)], [L′(γ), R′(γ)], 0) = ([L(γ), R(γ)], [L′(γ), R′(γ)])

Left Measure L (γ),

$$\frac{a-x}{y-x} = \gamma,\ x \le a \le y, [0,1]$$
$$a - x = \gamma(y - x)$$
$$a = x + \gamma(y - x) \quad (1)$$

Right measure R (γ),

$$\frac{z-a}{z-y} = \gamma,\ y \le a \le z, [0,1]$$
$$z - a = \gamma(z - y)$$
$$a = z - \gamma(z - y) \quad (2)$$

From equation (1) and (2)

$S^{(\gamma)}$ = [L(γ), R(γ)] =$[x + (y - x)\gamma,\ z - \gamma(z - y)]$

$WM = \int_0^1 [L(\gamma)]\gamma\, d\gamma + \int_1^0 [R(\gamma)]\gamma\, d\gamma + \int_0^1 (y)\,\gamma\, d\gamma$

$= \int_0^1 [x + \gamma(y - x)]\gamma\, d\gamma + \int_1^0 [z - \gamma(z - y)]\gamma\, d\gamma + \int_0^1 [y]\,\gamma\, d\gamma$

After Integrating and applying the limit we get, WM = $\frac{x+3y-z}{6}$

For calculating non-membership function. consider,

Left Measure L′(γ),

$$\frac{x'-a}{y-x'} = \gamma$$
$$x' - a = \gamma(y - x')$$
$$a = x' + \gamma(y - x') \quad (3)$$

Right measure R′(γ),

$$\frac{a-y}{z'-y} = \gamma$$
$$a - y = \gamma(z' - y)$$
$$a = y + \gamma(z' - y) \quad (4)$$

From equation (3) and (4),

$$S'^{(\gamma)} = [L'(\gamma), R'(\gamma)] = [x' + (y - x')\gamma,\ y + \gamma(z' - y)]$$
$$WM = \int_1^0 L'(\gamma)]\gamma\, d\gamma + \int_0^1 [R'(\gamma)]\gamma\, d\gamma + \int_1^0 (y)\,\gamma\, d\gamma$$
$$= \left[\left(-\int_0^1 [x' + (y - x')\gamma]\gamma\, d\gamma\right) + \left(-\int_1^o [y + \gamma(z' - y)]\gamma\, d\gamma\right) + \left(-\int_0^1 [y]\,\gamma\, d\gamma\right)\right]$$
$$= -\left[\left(\int_0^1 [x' + (y - x')\gamma]\gamma\, d\gamma\right) + \left(\int_1^o [y + \gamma(z' - y)]\gamma\, d\gamma\right) + \left(\int_0^1 [y]\,\gamma\, d\gamma\right)\right]$$

After Integrating and applying the limit we get, WM $= -\left(\frac{-2x' - 3y + 2z'}{6}\right) = \left(\frac{2x' + 3y - 2z'}{6}\right)$

Weight measure formula for intuitionistic fuzzy is given in equation 5.

$$WM = \left(\frac{p + 3q - r}{6}, \frac{2p' + 3q - 2r'}{6}\right) \quad (5)$$

Therefore, the ranking is defined as follows in order to maintain the fuzziness and to analyze the fuzzy numbers:

For any two TFN, A = (x_1, y_1, z_1)(x'_1, y_1, z'_1) and B = (x_2, y_2, z_2)(x'_2, y_2, z'_2),

(i) If WM(A) > WM(B), then A > B
(ii) If WM(A) = WM(B), then A = B
(iii) If WM(A) < WM(B), then A < B

Results:

Some significant findings that support the suggested method are demonstrated in this section.
Let A=(x,y,z)(x′,y′,z′) be the ITFN then,

(i) Rank ($\Re$) of A= $\left(\frac{x + 3y - z}{6}, \frac{2x' + 3y - 2z'}{6}\right)$
(ii) Left spread (LS) of A= $\int_0^1 (y - x)dx = (y - x)$
(iii) Right spread (RS) of A= $\int_0^1 (z - y)dx = (z - y)$
(iv) Divergence (Div) of A = $\int_0^1 (z - x)dx = (z - x)$
(v) Mean (M) of A = $\frac{x + y + z}{3}$

Theorem: A

If X= (x, y, z) (x′, y, z′) and U= (u, v, w) (u′, v, w′) be the two IFTN, then

(i) $\Re$(X) = $\Re$(U)
(ii) M(X) = M(U)
(iii) Div (X) = Div (U) then
  a. LS(X) > LS(U) iff x < u
  b. LS(X) < LS(U) iff x > u
  c. LS(X) = LS(U) iff x = u

Proof:

(i) $\Re$(X) = $\Re$(U) $\Rightarrow \left(\frac{x + 3y - z}{6}\right) = \left(\frac{u + 3v - w}{6}\right)$

$$x + 3y - z = u + 3v - w \quad (6)$$

(ii) M(X) = M(U) $\Rightarrow \left(\frac{x + y + z}{3}\right) = \left(\frac{u + v + w}{3}\right)$

$$x + y + z = u + v + w \quad (7)$$

(iii) Div (X) = Div (U) $\Rightarrow \int_0^1 (z - x)dx = \int_0^1 (w - u)dx$

$$(z - x) = (w - u) \quad (8)$$

Solving equation (6) and (8), we get

$$x + 3y - z = u + 3v - w$$
$$3y - z + x = 3v - w + u$$
$$3y - (z - x) = 3v - (w - u)$$

Using equation (8),

$$3y - (w - u) = 3v - (w - u)$$
$$3y = 3v$$
$$y = v \quad (9)$$

a. LS(X) > LS(U) iff x < u

$$y - x > v - u$$

Using equation (9),

$$y - x > y - u$$
$$-x > -u$$
$$x < u \quad (10)$$

b. LS(X) < LS(U) iff x > u

$$y - x < v - u$$

Using equation (9),

$$y - x < y - u$$
$$-x < -u$$
$$x > u \quad (11)$$

c. LS(X) = LS(U) iff x = u

$$y - x = v - u$$

Using equation (9),

$$y - x = y - u$$
$$-x = -u$$
$$x = u \quad (12)$$
$$Hence\ Proved$$

Theorem: B

If X= (x, y, z) (x′, y, z′) and U= (u, v, w) (u′, v, w′) be the two ITFN,

(iv) $\Re(X) = \Re(U)$

(v) M(X) = M(U)

(vi) Div (X) = Div (U) then

a. RS(X) > RS(U) iff z > w

b. RS(X) < RS(U) iff z < w

c. RS(X) = RS(X) iff z = w

Proof:

a. RS(X) > RS(U) iff z > w

$$z - y > w - v$$

Using equation (9)

$$z - y > w - y$$
$$z > w \quad (13)$$

b. RS(X) < RS(U) iff z < w

$$z - y < w - v$$
$$z - y < w - y$$
$$y < v \quad (14)$$

c. RS(X) = RS(U) iff z = w

$$z - y = w - v$$
$$z - y = w - y$$
$$z = w \quad (15)$$

Hence Proved.

Theorem: C

If X= (x, y, z) (x′, y, z′) and U= (u, v, w) (u′, v, w′) be the two ITFN then,

(i) $\Re(X+U) = \Re(X) + R(U)$

(ii) $\Re(-X) = -\Re(X)$

Proof:

(i) $X + U = (x + u,\ y + v, z + w)$

$$\Re(X+U) = \frac{(x+u) + 3(y+v) - (z+w)}{6}$$
$$= \frac{x+u+3y+3v-z-w}{6}$$
$$= \frac{x+3y-z+u+3v-w}{6}$$
$$= \frac{x+3y-z}{6} + \frac{u+3v-w}{6}$$
$$\Re(X+U) = \Re(X) + \Re(U)$$

(ii) $\Re(-X) = -\Re(X)$

$X = (x, y, z)\ (x', y, z') \Rightarrow -X = (-x, -y, -z)\ (-x', -y, -z')$

$$\Re(-X) = \frac{-x-3y+z}{6}$$
$$\Re(-X) = \frac{-x-3y+z}{6} = -\left(\frac{x+3y-z}{6}\right) = -\Re(X)$$
$$\Re(-X) = -\Re(X)$$

Hence proved.

Note: Similarly, we can prove all the above proposition for non-membership function.

3.3. Criticality Degree

To calculate the intuitionistic fuzzy criticality degrees (IFCD) of activities and paths, we developed a method for measuring criticality and provided an analytical approach that integrates intuitionistic fuzzy set theory with the PERT methodology. The criticality degree of an activity (i,j)(i, j)(i,j) is defined as follows: if the fuzzy float of the activity (i, j) is IFTF(i,j) =(x_{ij}, y_{ij}, z_{ij}) (x'_{ij}, y_{ij}, z'_{ij}),

Criticality Degree formula for the membership function:

$$\mathbf{IFCD}_{(i,j)}(A) = \begin{cases} \frac{-x}{y-x} & ; \quad x \leq 0 < y \\ \frac{z}{z-y} & ; \quad y < 0 \leq z \end{cases} \tag{16}$$

Criticality Degree formula for the non - membership function:

$$\mathbf{IFCD}_{(i,j)}(A') = \begin{cases} \frac{y}{y-x}, & ; \quad p' \leq 0 < q \\ \frac{-y}{z'-y}; & \quad q < 0 \leq z' \end{cases} \tag{17}$$

and the criticality of the path is defined as,

IFCD (P_i) = max $_{(i,j)=p}$ {$IFCD_{(i,j)}$} , define the membership function and

IFCD (P_i) = min $_{(i,j)=p}$ {$IFCD_{(i,j)}$} , define the non-membership function, where p_i defines the i^{th} path across the network and IFCD (P_i) represents its criticality.

A path Ṕ is known as to be critical if IFCD (Ṕ) = max {IFCD ($Ṕ_i$) } for the membership function and IFCD (Ṕ) = min {IFCD ($Ṕ_i$) } for the non-membership function , where Ṕ defines the set contains every potential path.

Numerical Illustration:

Construct an eight way road from Salem to Chennai in fig 3 and the places were consider as node which was given in table 1.

Table 1: *Network Description*

Node	Description
1	Salem
2	Vellore
3	Polur
4	Thiruvanamalai
5	Cheyyar
6	Villupuram
7	Chennai



Figure 1: *Network*

Construct the network.

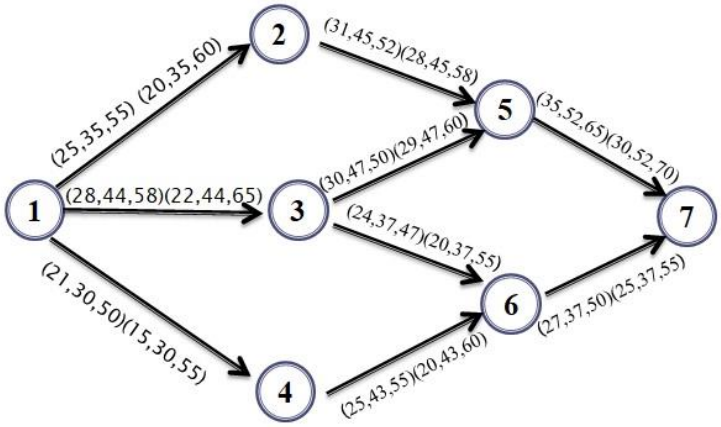


Figure 2: *Graphical Network*

Table 2: *Calculation for IFTI and Defuzzification*

Activity	Duration (d_{ab})	Defuzzifed Value	IFTF	Defuzzified Value
1-2	(25,35,55)(20,35,60)	(12.5,4.167)	(-79,11,82) (-107,11,117)	(-21.33, -69.167)
1-3	(28,44,58)(22,44,65)	(17,7.67)	**(-80,0,80) (-114,0,114)**	**(0, 0)**
1-4	(21,30,50)(15,30,55)	(10.167,1.67)	(-62,33,100) (-89,33,135)	(-10.5, -58.167)
2-5	(31,45,52)(28,45,58)	(19,12.5)	(-79,11,82) (-107,11,117)	(-21.33, -69.167)
3-5	(30,47,50)(29,47,60)	(20.167,13.167)	**(-80,0,80) (-114,0,114)**	**(0, 0)**
3-6	(24,37,47)(20,37,55)	(14.67,6.83)	(-62,25,94) (-94,25,128)	(-13.5,-61.5)
4-6	(25,43,55)(20,43,60)	(16.5,8.167)	(-62,33,100) (-89,33,135)	(-10.5, -58.167)
5-7	(35,52,65)(30,52,70)	(21,12.67)	**(-80,0,80) (-114,0,114)**	**(0, 0)**
6-7	(27,37,50) (25,37,55)	(14.67,8.5)	(-62,25,94) (-94,25,128)	(-13.5, -61.5)

Defuzzied value using equation 5, and IFTF was calculated using definition 3.1., which was displayed in table 2. From table 2, the activity which has (0,0) is identified as Critical path. So, conclude that the critical path is 1-3-5-7 that is Salem – Polur – Cheyyar – Chennai and path length that is total duration is (93, 143, 173) (81, 143, 195) using 3.1.

4. Results and Discussions

Verification:
Here, verification is carried out using the Criticality degree for comparison's purpose.

Table 3: *Calculation for Criticality Degree using equation (17)*

Activity	Duration (d_{ab})	IFTF	Defuzzified Value	Criticality Degree
1-2	(25,35,55)(20,35,60)	(-79,11,82)(-107,11,117)	(-21.33, -69.167)	(0.994, 0.040)
1-3	(28,44,58)(22,44,65)	**(-80,0,80)(-114,0,114)**	**(0,0)**	**(1, 0)**
1-4	(21,30,50)(15,30,55)	(-62,33,100)(-89,33,135)	(-10.5, -58.167)	(0.67, 0.12)
2-5	(31,45,52)(28,45,58)	(-79,11,82)(-107,11,117)	(-21.33, -69.167)	(0.885, 0.25)
3-5	(30,47,50)(29,47,60)	**(-80,0,80)(-114,0,114)**	**(0,0)**	**(1, 0)**
3-6	(24,37,47)(20,37,55)	(-62,25,94)(-94,25,128)	(-13.5, -61.5)	(0.67, 0.12)
4-6	(25,43,55)(20,43,60)	(-62,33,100)(-89,33,135)	(-10.5, -58.167)	(0.885, 0.25)
5-7	(35,52,65)(30,52,70)	**(-80,0,80)(-114,0,114)**	**(0,0)**	**(1, 0)**
6-7	(27,37,50)(25,37,55)	(-62,25,94)(-94,25,128)	(-13.5, -61.5)	(0.88, 0.08)

The IFTF was calculated using definition 3.1. The defuzzified value was obtained using equation 5, and the criticality degree was calculated using equations 16 and 17, as shown in Table 3. An activity is identified as part of the Critical Path if it has a defuzzified value of (0,0), a membership function of 1, and a non-membership function of 0 for the criticality degree.

From Table 3, the Intuitionistic Fuzzy Critical Path (IFCP) is identified as Path P1: 1-3-5-7. The comparison of solution yields was made using the proposed procedure, with the criticality degree serving as a verification tool. The outcome of this study is found to be consistent with the results of methods currently in use.

Table 4: *Verification using various ranking method*

Path (P_i)	**α- cut [6]**	**Magnitude Measure [6]**	**Similarity Measure [6]**	**Weight Measure(5)**	**Ranking**
P_1: 1-2-5-7	14.33,22.7	14.5,22.3	5.538,2.75	3,2	2
P_2: 1-3-5-7	14.83, 23.5	14.75,22.75	6,3.5	3.5,2.5	1
P_3: 1-3-6-7	12.83,20.9	12.75,20.5	3.7485,2.5	1.8,1.5	3
P_4: 1-4-6-7	12.33,20.5	12,20	3.2,1.2	1.5,1	4

From table 4, using different measures we verified that the same critical path 1-3-5-7 is identified as IFCP. Rather than the other measure weight measure gives the optimized value.

Simulation:

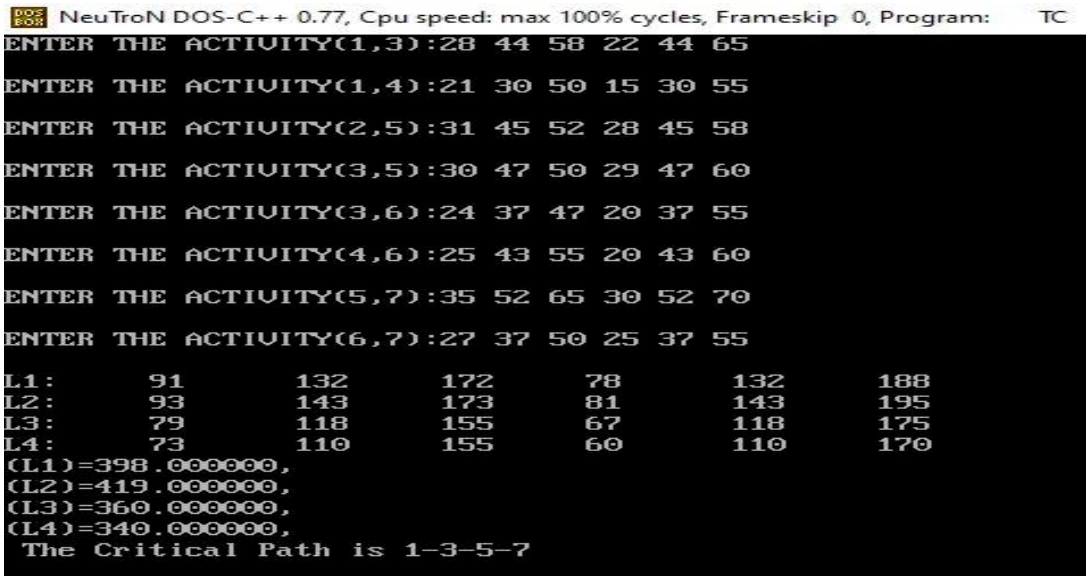


Figure 5: *Simulation result using C*

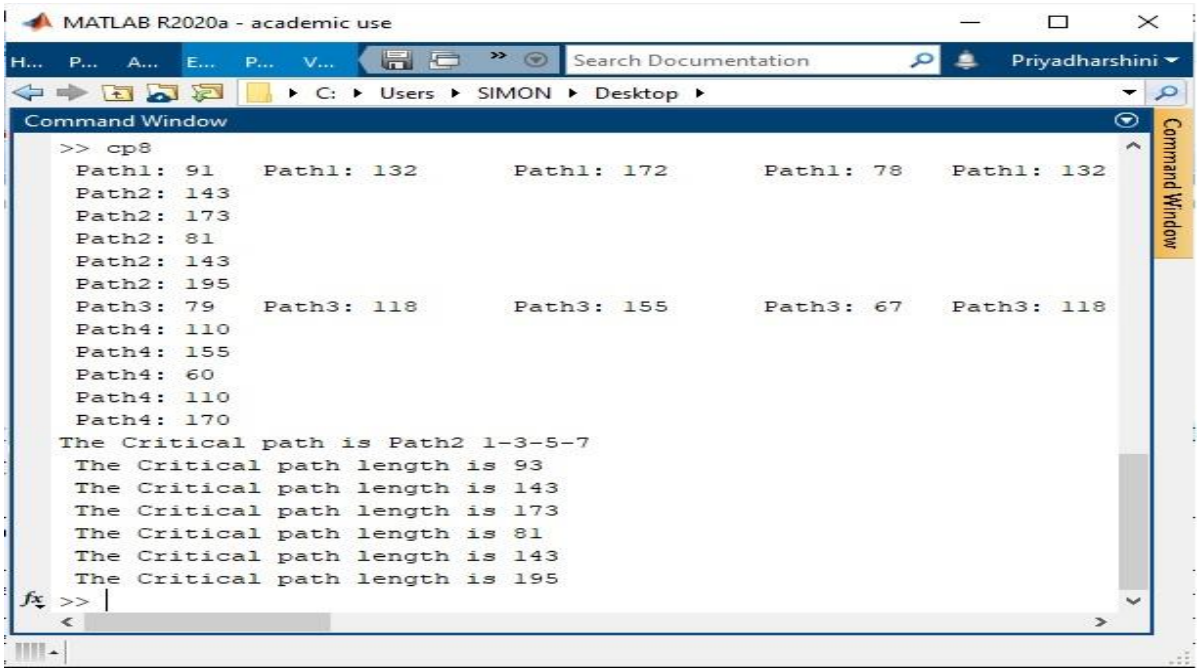


Figure 6: *Simulation result using MATLAB*

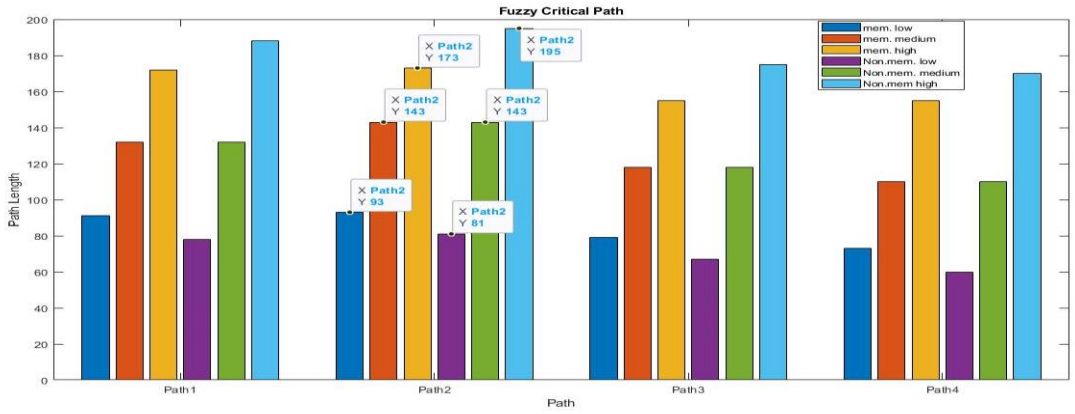


Figure 7: *Simulation result using MATLAB*

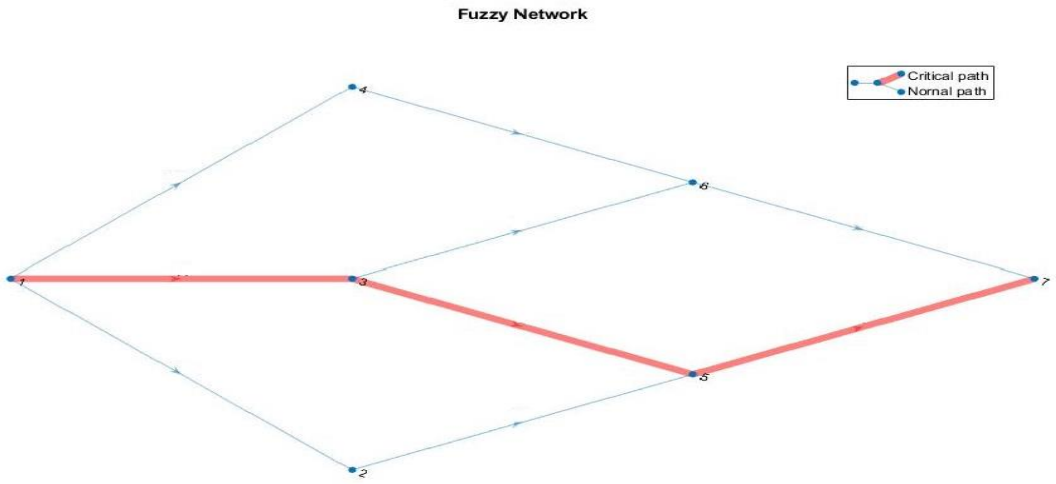


Figure 8: *Network diagram using MATLAB*

5. Conclusion

This study introduces a simple, practical method for ordering fuzzy numbers, specifically designed to rank triangular numbers that are imprecise. Unlike several methods in the literature that cannot handle certain types of fuzzy numbers, this approach can effectively rank crisp numbers, a specific case of fuzzy numbers. The method is easy to use and compute, providing reliable solutions to problems with clear objectives and dependable rankings for issues with ambiguous purposes. Additionally, the ranking measure can be applied to negative integers. Examples are provided to demonstrate the advantages of the proposed strategy. Future research will focus on applying this ranking system to solve fuzzy optimization problems such as network analysis and various fuzzy decision-making challenges like fuzzy risk analysis.

References

[1] Anushya, V. and Balasowandari, P. (2018). Fuzzy critical path with area measure. *International Journal of Pure and Applied Mathematics,*118(6):167-173.

[2] Atanassov, K. (1986). Intuitionistic Fuzzy Sets. *Fuzzy Sets and Systems.* 20(1):87-96. http://dx.doi.org/10.1016/s0165-0114(86)80034-3.

[3] Balaganesan, M. and Ganesan, K. (2018). An approach to find critical path in intuitionistic fuzzy environment. *International Journal of Pure and Applied Mathematics.* 119(9):395-403.

[4] Blue, M., Bush, B. and Puckett, J. (2002). Unified approach to fuzzy graph problems. *Fuzzy Sets and Systems*, 125:355-368.

[5] Bonnal, P., Gourc, D. and Lacoste, G. (2004). Where do we stand with fuzzy project scheduling. *Journal of construction engineering and management. 130*(1): 114-123.

[6] Chanas, S. and Kamburowski, J. (1981). The use of fuzzy Variables in PERT. *Fuzzy Sets and Systems.* 5:11-19.

[7] Chen, Chen-Tung, and Sue-Fen Huang. (2007). Applying fuzzy method for measuring criticality in project network. *Information sciences.* 177(12): 2448-2458.

[8] Delgado, M., Herrera, F., Herrera-Viedma, E. and Martinez, L. (1998). Combining numerical and linguistic information in group decision making. *Information Sciences. 107*(1-4): 177-194.

[9] Didier Dubois, Hélène Fargier, Vincent Galvagnon. (2003). On latest starting times and floats in activity networks with ill-known durations. *European Journal of OperationalResearch.* 147 (2): 266-280. https://doi.org/10.1016/S0377-2217(02)00560-X.

[10] Elizabeth, S. and Sujatha, L. (2015). Project Scheduling method using triangular intuitionistic fuzzy numbers and triangular fuzzy numbers. *Applied Mathematical Sciences.* 9(4):185-198.

[11] Elizabeth, S., Sujatha, L. and Bharathi, K. (2015). On searching critical path in a project network under fuzzy environment. *National Conference on recent approaches of Mathematics to Science and Technology (NCRAM 2015)*, ISBN:978-81-929362-1-5.

[12] Figueredo, A. J. and Wolf, P. S. A. (2009). Assortative pairing and life history strategy - a cross-cultural study. *Human Nature*, 20:317–330.

[13] Jose Parvin Praveena, N. Sagaya Nathan Stalin, C. and Rajkumar, A.(2020). Critical Path Problem Through Intuitionistic Triskaidecagonal Fuzzy Number Using Two Different Algorithms. *Advances in Artificial Intelligence and Data Engineering.* 1133: 159-167.

[14] Kelley, James; Walker, Morgan. (1959). Critical-Path Planning and Scheduling. *1959 Proceedings of the Eastern Joint Computer Conference*.

[15] Lee,E.S. and Li,R.L. (1988). Comparison of fuzzy numbers based on the probability measure of fuzzy events. *Computers & Mathematics with Applications.* 15: 887-896.

[16] Priyadharshini, S. and Deepa, G. (2022). Critical path interms of intuitionistic triangular fuzzy numbers using maximum edge distance method. *Reliability: Theory & Applications* 17.1 (67): 382-390 .

[17] Ravi Shankar, N., Sireesha, V. and Phani Bushan Rao, P. (2010). An Analytical Method for Finding Critical Path in a Fuzzy Project Network. *Int. J. Contemp. Math. Sciences.* 5(20) :953 – 962.

[18] Sireesha, V. and Ravishankar, N. (2010). A new approach to find total float time and critical path in a fuzzy project network. *International Journal of Engineering Science and Technology.* 2(4):600-609.

[19] Stephen Dinagar, D. and Rameshan, N. (2018). A New Approach for Fuzzy Critical Path Method Using Octogonal Fuzzy Numbers. *International Journal of Pure and Applied Mathematics.* 119(13):357-364.

[20] Zareei, A. Zaerpour, F., Bagherpour, M., Noora, A. A. and Vencheh, A. H. (2011). A new approach for solving fuzzy critical path problem using analysis of events. *Expert Systems with Applications. 38*(1):87-93.

[21] Zadeh, L.A. (1965). Fuzzy sets. *Information and Control.* 8:338-353.

A RANKING FUNCTION APPROACH BASED ON CENTROID FOR GENERALIZED HEXAGONAL FUZZY NUMBERS TO SOLVE FUZZY MULTI-OBJECTIVE TRANSPORTATION PROBLEMS

Ramakant sharma[1], Sohan Lal Tyagi[2*]

•

1. Research Scholar, Department of Mathematics, SRM Institute of Science and Technology, Delhi-NCR Campus, Modinagar, Ghaziabad, 201204, India
rs5364@srmist.edu.in
2. Assistant Professor, Department of Mathematics, SRM Institute of Science and Technology, Delhi-NCR Campus, Modinagar, Ghaziabad, 201204, India
∗ Corresponding Author
drsohantyagi@gmail.com

Abstract

In a real-world scenario, the decision maker is unsure about the precise value of transportation parameters due to uncontrolled factors such as fuel prices, weather conditions, product availability, and requirements. Therefore,o fuzzy numbers are used to handle these uncertainties. This Paper aims to find an efficient solution to fuzzy multi-objective transportation problems (FMOTP) where all parameters (objective functions, availabilities, requirements) are given in the form of generalized hexagonal fuzzy numbers. In the Proposed approach, FMOTP is transformed into Fuzzy Single-Objective Transportation Problems (FSOTP) using the geometric mean technique. A new ranking function based on the centroid and in-center point method for hexagonal fuzzy numbers defuzzifies the FSOTP into a Crisp Single-Objective Transportation Problem (CSOTP). The optimal solution for the transformed CSOTP is obtained using the proposed approach based on the zero-entry cell method. Using the optimal solution of CSOTP the fuzzy efficient solution of FMOTP is obtained. Additionally, two numerical problems are solved to elaborate the Proposed approach, and results are compared with other existing methods. A comparison and analysis of the results show that the proposed approach provides a more optimized solution for FMOTP. This approach is easily applicable to real-life transportation problems in which decision-makers are unsure about the exact value of parameters.

Keywords: Ranking function, Centroid, Incentre Point, Generalized Hexagonal fuzzy number, Fuzzy Transportation Problem.

1. Introduction

The transportation problem (TP) is a significant optimization problem in logistics and supply chain management. Its objective is to find the most cost-efficient method of transporting items with multiple origins to numerous destinations while ensuring that supply and demand restrictions are fulfilled. Classical transportation problems operate on the assumption that all variables, including prices, suppliers, and demands, are accurately known. Nevertheless, in practical situations, these characteristics often exhibit uncertainty or imprecision as a result of various causes such as market volatility, estimating inaccuracies, and insufficient information. Fuzzy set theory has been extensively used to address uncertainties in issues related to transportation.

Fuzzy transportation problems (FTPs) use fuzzy numbers to describe unknown parameters, enabling a more accurate representation of real-world scenarios. An improved method in this field involves the utilization of hexagonal fuzzy numbers, which provide a more adaptable and inclusive representation of uncertainty compared with ordinary triangular or trapezoidal fuzzy numbers.

F.L. Hitchcock [1] first formulated the Transportation Problems (TP) in the form of LPP in 1941. An LPP form was used to represent the TP, which a simplex algorithm can solve. The Stepping Stone approach offers an alternative approach for obtaining the information from the Simplex Method developed by Charnes and Cooper [2]. Lotfi A. Zadeh [3] was given the concept of fuzziness in 1965. Zimmermann H.J [4]. was the first to use an appropriate membership function to solve an LP problem with multiple objectives. Avishek et.al.[5] presented a novel approach for ranking and defuzzification, which involves converting a fuzzy hexagonal number into a real number to determine its importance in addressing decision-making issues. Sudha and Revathi [6] introduced a novel ranking approach for hexagonal fuzzy numbers (HFNs) and used it to solve fuzzy LPP. Leela-Apiradee et. al. [7] established the concept of hexagonal fuzzy number cardinality, which is a strategy used to categorize hexagonal fuzzy numbers. They also offered a ranking function for Hexagonal fuzzy numbers, particularly with their probable mean values. Thirupathi et al. [8] proposed a novel ranking method based on the fuzzy hexagonal number. This method utilizes the centroid formula of triangles and rectangles, taking into account the distance from the origin to the centroid. S.Adilakshmi et al. [14] proposed a ranking function based on the centroid and circumcentre methods for HFNs which are used to find the fuzzy critical path to the fuzzy network.

Several methods exist for establishing an initial basic feasible solution for a balanced transportation problem [9-13]. Various transportation models are available in various forms, as individuals seek to use the most effective resources to maximize profit and minimize costs. In the corporate sector, several sorts of transportation difficulties are encountered. These challenges include finding the most cost-effective method of transferring products. The aim is to reduce the total cost of transportation. [15,16]. Ashour [17] introduced the cost-minimization fuzzy transportation problems using HFNs that take supply and demand into account were presented by. according to the generalized trapezoidal fuzzy number ranking. Z.A.M.S. Juman et. al. [18] presented the two methods based on two different ranking functions for pentagonal fuzzy numbers to solve interval-valued transportation problems. Kamini et.al. [19] proposed a zero-point technique and genetic algorithm to solve MOTP with hexagonal fuzzy numbers. Sahayasudha A. et. al. [20] presented an alpha-cut operation for symmetric HFNs to solve transportation problems. M. et al. [21] presented the DEA approach to solving FMOTP. Sharma M.K. et al. [22] proposed a novel approach to solve MOTP using the Fermatean fuzzy technique. Akram, M. et.al. [23] presented a method using data envelope analysis, for decision-making units with multiple inputs and outputs ranked according to their relative efficiency P. Indira and M. Jayalakshmi [24] proposed an approach to find the minimum transportation cost of triangular TP using the alpha cut, and row-column minima method. Sharma, R., and Tyagi, S. L [25] proposed an algorithm to solve multi-objective transportation problems with generalized trapezoidal fuzzy numbers based on the proposed ranking function.

This paper presents an approach to solving fuzzy multi-objective transportation problems (FMOTP) with generalized hexagonal fuzzy numbers based on the ranking function for hexagonal fuzzy numbers by separating hexagons into three quadrilaterals. The proposed ranking functions are based on centroid and in-centre methods. The geometric mean is used to convert FMOTP into fuzzy single-objective transportation problems(FSOTP). The zero-entry cell approach is used to get the fuzzy efficient solution of FMOTP.

2. Abbreviations

1. Linear Programming Problem - LPP
2. Transportation Problem - TP
3. Fuzzy Transportation Problem - FTP

4. Hexagonal Fuzzy Number - HFN
5. Generalized Hexagonal Fuzzy Number - GHFN
6. Multi-Objective Transportation Problem - MOTP
7. Fuzzy Multi-Objective Transportation Problem - FMOTP
8. Decision Maker- DM
9. Fuzzy Transportation Cost - FTC
10. Minimum Transportation Cost - MTC
11. Single objective transportation problem - SOTP
12. Crisp Single Objective Transportation Problem - CSOTP

3. Basic Definitions

1. Fuzzy Number: A fuzzy set $\tilde{A}$ is said to be fuzzy number if its membership function $\tilde{A} : \mathbb{R} \to \lceil 0, 1 \rceil$ has satisfy the following conditions:
$\tilde{A}(\lambda y_1 + (1-\lambda)y_2) \geq \min\{A(\tilde{y_1})\}, A(\tilde{y_2}))$
there exist a y $\in \mathbb{R}$ such that $A(\tilde{y}) = 1$
$\tilde{A}$ is piece-wise continuous

2. Hexagonal Fuzzy Numbers : A fuzzy set $\tilde{A} = (\alpha^1, \alpha^2, \alpha^3, \alpha^4, \alpha^5, \alpha^6; w)$ where $\alpha^1 \leq \alpha^2 \leq \alpha^3 \leq \alpha^4 \leq \alpha^5 \leq \alpha^6$ and $0 < w \leq 1$ with membership function defined as:

$$\mu_{A(\tilde{y})} = \begin{cases} \frac{w}{2}\ \{\frac{y-\alpha^1}{\alpha^2-\alpha^1}\} & \text{if } \alpha^1 \leq y \leq \alpha^2 \\ \frac{w}{2} + \frac{w}{2}\ \{\frac{y-\alpha^2}{\alpha^3-\alpha^2}\} & \text{if } \alpha^2 \leq y \leq \alpha^3 \\ w & \text{if } \alpha^3 \leq y \leq \alpha^4 \\ w + \frac{w}{2}\ \{\frac{y-\alpha^4}{\alpha^5-\alpha^4}\} & \text{if } \alpha^4 \leq y \leq \alpha^5 \\ \frac{w}{2}\ \{\frac{\alpha^6-y}{\alpha^6-\alpha^5}\} & \text{if } \alpha^5 \leq y \leq \alpha^6 \\ 0 & \text{Otherwise} \end{cases}$$

is called generalized hexagonal fuzzy numbers. If w = 1, then it is called a normal hexagonal fuzzy number.

3. Properties of Hexagonal Fuzzy Numbers (HFNs): let $\tilde{A} = (\alpha^1, \alpha^2, \alpha^3, \alpha^4, \alpha^5, \alpha^6; w_1)$ and $\tilde{B} = (\beta^1, \beta^2, \beta^3, \beta^4, \beta^5, \beta^6; w_2)$ be any two HFNs. then
$\tilde{A} + \tilde{B} = (\alpha^1 + \beta^1, \alpha^2 + \beta^2, \alpha^3 + \beta^3, \alpha^4 + \beta^4, \alpha^5 + \beta^5, \alpha^6 + \beta^6; min(w_1, w_2))$
$\tilde{A}$ - $\tilde{B} = (\alpha^1 - \beta^6, \alpha^2 - \beta^5, \alpha^3 - \beta^4, \alpha^4 - \beta^3, \alpha^5 - \beta^2, \alpha^6 - \beta^1; min(w_1, w_2))$
$\sigma\tilde{A} = (\sigma\alpha^1, \sigma\alpha^2, \sigma\alpha^3, \sigma\alpha^4, \sigma\alpha^5, \sigma\alpha^6)$, where σ is any constant.

4. Proposed Ranking Function

The ranking function is used to compare the fuzzy numbers. Assuming that the natural order is preserved, the ranking function $\Re$: $T(\mathbb{R}) \to \mathbb{R}$ defined on the set of real numbers maps each fuzzy number into a real number where $T(\mathbb{R})$ is the set of fuzzy numbers.
A new ranking function is proposed for generalized hexagonal fuzzy numbers based on the centroid and incentre points. Let $\tilde{A} = (\alpha^1, \alpha^2, \alpha^3, \alpha^4, \alpha^5, \alpha^6; w)$ be any GHFN represented by hexagonal AGIJHF as given in Fig. 1. In this ranking function, a hexagonal AGIJHF is divided into three quadrilaterals, namely ABCG, GCDH, and HDEF.

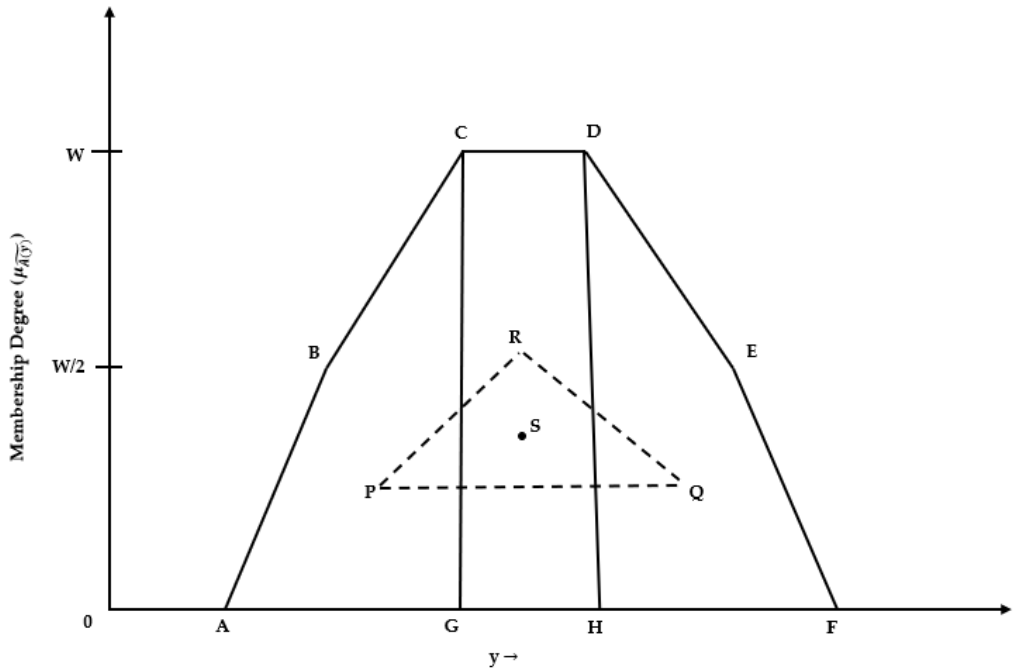


Figure 1: *Representation of hexagonal fuzzy number*

The vertices of ABGC is A$(\alpha_1, 0)$, B$(\alpha_2, \frac{w}{2})$, C(α_3, w), G$(\alpha_3, 0)$.
The vertices of GCDH is G$(\alpha_3, 0)$, C(α_3, w), D(α_4, w), H$(\alpha_4, 0)$.
The vertices of HDEF is H$(\alpha_4, 0)$, D(α_4, w), E$(\alpha_5, \frac{w}{2})$, F$(\alpha_6, 0)$.
Now, let P, Q, and R give the ABCG, HDEF, and GCDH centroids. The coordinates of P, Q, and R is $(\frac{\alpha_1+\alpha_2+2\alpha_3}{4}, \frac{3w}{8})$,$(\frac{2\alpha_4+\alpha_5+\alpha_6}{4}, \frac{3w}{8})$, and $(\frac{\alpha_3+\alpha_4}{2}, \frac{w}{2})$ respectively .
Now, adjoining the centroids P, Q, and R, a triangle PQR is formed as given in Fig.2. Let S be the incentre point of the triangle PQR.
The coordinates of S are $(I_x, I_Y) = (\frac{cx_1+bx_2+ax_3}{a+b+c}, \frac{cy_1+by_2+ay_3}{a+b+c})$
where a = $\frac{(2\alpha_4+\alpha_5+\alpha_6-2\alpha_3-\alpha_2-\alpha_1)}{4}$, b = $\frac{(4(2\alpha_4-\alpha_1-\alpha_2)^2+w^2)^{\frac{1}{2}}}{8}$, and c = $\frac{(4(2\alpha_3-\alpha_5-\alpha_6)^2+w^2)^{\frac{1}{2}}}{8}$.
Here in the incentre point (I_x, I_Y), the x-coordinate value I_x provides the ranking function such that $I_x \in (\alpha_1, \alpha_6)$
Hence ranking of $\tilde{A}$ is given by $\Re(\tilde{A}) = I_x = (\frac{cx_1+bx_2+ax_3}{a+b+c})$

5. Properties of Ranking functions

let $\tilde{A} = (\alpha^1, \alpha^2, \alpha^3, \alpha^4, \alpha^5, \alpha^6; w_1)$ and $\tilde{B} = (\beta^1, \beta^2, \beta^3, \beta^4, \beta^5, \beta^6; w_2)$ be any two HFNs. Then the properties of the ranking function are given as:
$\tilde{A} \leq \tilde{B} \iff \Re(\tilde{A}) \leq \Re(\tilde{B})$
$\tilde{A} \equiv \tilde{B} \iff \Re(\tilde{A}) \equiv \Re(\tilde{B})$
$\tilde{A} \geq \tilde{B} \iff \Re(\tilde{A}) \geq \Re(\tilde{B})$

6. Mathematical model for FMOTP with Hexagonal fuzzy numbers

The FMOTP with k objectives in mathematical form is given as:
$(\tilde{T}_k)$ Min $\tilde{Z}_k(y) = \Sigma_{i=1}^{m}\Sigma_{j=1}^{n}\tilde{a}_{ij}^{(k)}y_{ij}$ for k = 1,2,.....
Subject to
$\Sigma_{i=1}^{m}y_{ij} = \tilde{d}_j$: for fixed j=1,2,.....,n
$\Sigma_{j=1}^{n}y_{ij} = \tilde{s}_i$: for fixed i=1,2,.....,m

$y_{ij} \geq 0$
Where,
$\tilde{s}_i$ = the product's fuzzy availability at the i-th source
$\tilde{d}_j$ = the product's fuzzy requirement at the j-th destinations
$\tilde{a}_{ij}^{(k)}$ = the fuzzy cost for transporting one unit of the given product from i-th source to j-th destination of k-th objective
y_{ij} = The transported quantity of product from i-th source to j-th destination.
here $\tilde{a}_{ij} = (a_{ij}^1, a_{ij}^2, a_{ij}^3, a_{ij}^4, a_{ij}^5, a_{ij}^6)$, $\tilde{s}_i = (s_i^1, s_i^2, s_i^3, s_i^4, s_i^5, s_i^6)$, $\tilde{d}_j = (d_j^1, d_j^2, d_j^3, d_j^4, d_j^5, d_j^6)$ are the normal hexagonal fuzzy numbers.
If k=1 then FMOTP is called fuzzy single-objective transportation problem.

7. Efficient Solution

A feasible solution $Y^0 = \{y_{ij}^0, i = 1, 2, ..., m, j = 1, 2, ..., n\}$ is called an efficient solution to the problem (T) is there does not exist any feasible solution Y of MOTP such that $Z_1(Y) \leq Z_1(Y^0)$ and $Z_2(Y) \leq Z_2(Y^0)$.

8. Our Proposed Approach

The proposed algorithm obtains the Compromise efficient fuzzy solution of FMOTP in which some parameters are hexagonal fuzzy numbers. The proposed approach steps are as follows:

Step I: First, the FMOTP $(\tilde{T}_k)$ is represented in tabular form as given in Table 1.

Table 1: *Tabular representation of FMOTP*

Destination → source ↓	A_1	A_2	.....	A_n	Availability $\{s_i\}$
B_1	$\tilde{a}_{11}^{(1)}$	$\tilde{a}_{12}^{(1)}$	.....	$\tilde{a}_{1n}^{(1)}$	$\tilde{s}_1$
	$\tilde{a}_{11}^{(2)}$	$\tilde{a}_{12}^{(2)}$	.....	$\tilde{a}_{1n}^{(2)}$	
	:	:	.....	:	
	$\tilde{a}_{11}^{(k)}$	$\tilde{a}_{12}^{(k)}$	.....	$\tilde{a}_{1n}^{(k)}$	
B_2	$\tilde{a}_{21}^{(1)}$	$\tilde{a}_{22}^{(1)}$	.....	$\tilde{a}_{2n}^{(1)}$	$\tilde{s}_2$
	$\tilde{a}_{21}^{(2)}$	$\tilde{a}_{22}^{(2)}$	.....	$\tilde{a}_{2n}^{(2)}$	
	:	:	.....	:	
	$\tilde{a}_{21}^{(k)}$	$\tilde{a}_{22}^{(k)}$	.....	$\tilde{a}_{2n}^{(k)}$	
:	:	:	:	:	:
B_m	$\tilde{a}_{m1}^{(1)}$	$\tilde{a}_{m2}^{(1)}$	.....	$\tilde{a}_{mn}^{(1)}$	$\tilde{s}_m$
	$\tilde{a}_{m1}^{(2)}$	$\tilde{a}_{m2}^{(2)}$	.....	$\tilde{a}_{mn}^{(2)}$	
	:	:	.....	:	
	$\tilde{a}_{m1}^{(k)}$	$\tilde{a}_{m2}^{(k)}$	.....	$\tilde{a}_{mn}^{(k)}$	
Requirement (d_j)	$\tilde{d}_1$	$\tilde{d}_2$	.....	$\tilde{d}_n$	

Where $\tilde{a}_{ij}^{(k)}$, $\tilde{s}_i$, and $\tilde{d}_j$ $\forall 1 \leq i \leq m, 1 \leq j \leq n$ are represented by hexagonal fuzzy numbers and written in the form $\tilde{a}_{ij}^{(k)} = (\alpha_{ij}^{1(k)}, \alpha_{ij}^{2(k)}, \alpha_{ij}^{3(k)}, \alpha_{ij}^{4(k)}, \alpha_{ij}^{5(k)}, \alpha_{ij}^{6(k)})$, $\tilde{s}_i = (s_i^1, s_i^2, s_i^3, s_i^4, s_i^5, s_i^6)$, and $\tilde{d}_j = (d_j^1, d_j^2, d_j^3, d_j^4, d_j^5, d_j^6)$.

Step II: The FMOTP is converted into FSOTP using the geometric mean. The FSOTP $\tilde{T}$ is given in the form:
$(\tilde{T})$ Min $\tilde{Z}(y) = \Sigma_{i=1}^{m}\Sigma_{j=1}^{n}\tilde{b}_{ij}y_{ij}$ for k = 1,2,.....
Subject to
$\Sigma_{i=1}^{m}y_{ij} = \tilde{d}_j$: for fixed j=1,2,.....,n
$\Sigma_{j=1}^{n}y_{ij} = \tilde{s}_i$: for fixed i=1,2,.....,m
$y_{ij} \geq 0$
The fuzzy single-objective transportation problem (FSOTP) in tabular form is then represented in Table 2.

Table 2: *The converted FSOTP using geometric mean*

Destination → source ↓	A_1	A_2	.....	A_n	Availability $\{s_i\}$
B_1	$\tilde{b}_{11}$	$\tilde{b}_{12}$	.....	$\tilde{b}_{1n}$	$\tilde{s}_1$
B_2	$\tilde{b}_{21}$	$\tilde{b}_{22}$	.....	$\tilde{b}_{2n}$	$\tilde{s}_2$
:	:	:	.....	:	
B_m	$\tilde{b}_{m1}$	$\tilde{b}_{m2}$	.....	$\tilde{b}_{mn}$	$\tilde{s}_m$
Requirement $\tilde{(d_j)}$	$\tilde{d_1}$	$\tilde{d_2}$	.....	$\tilde{d_n}$	

Where, $\forall\ i,j; 1 \leq i \leq m, 1 \leq j \leq n$ $\tilde{b}_{ij}$ is a hexagonal fuzzy number and written in the form,$\tilde{b}_{ij} = (\beta_{ij}^1, \beta_{ij}^2, \beta_{ij}^3, \beta_{ij}^4, \beta_{ij}^5, \beta_{ij}^6)$.
Here β_{ij}^1 is geometric mean of $(\alpha_{ij}^{1(1)}, \alpha_{ij}^{1(2)}, ..., \alpha_{ij}^{1(k)})$ so
$\beta_{ij}^1 = (\prod(\alpha_{ij}^{1(1)}, \alpha_{ij}^{1(2)}, ..., \alpha_{ij}^{1(k)}))^{\frac{1}{k}}$
Similarly β_{ij}^2 is geometric mean of $(\alpha_{ij}^{2(1)}, \alpha_{ij}^{2(2)}, ..., \alpha_{ij}^{2(k)})$ so
$\beta_{ij}^2 = (\prod(\alpha_{ij}^{2(1)}, \alpha_{ij}^{2(2)}, ..., \alpha_{ij}^{2(k)}))^{\frac{1}{k}}$,
β_{ij}^3 is geometric mean of $(\alpha_{ij}^{3(1)}, \alpha_{ij}^{3(2)}, ..., \alpha_{ij}^{3(k)})$ so
$\beta_{ij}^3 = (\prod(\alpha_{ij}^{3(1)}, \alpha_{ij}^{3(2)}, ..., \alpha_{ij}^{3(k)}))^{\frac{1}{k}}$,
β_{ij}^4 is geometric mean of $(\alpha_{ij}^{4(1)}, \alpha_{ij}^{4(2)}, ..., \alpha_{ij}^{4(k)})$ so
$\beta_{ij}^4 = (\prod(\alpha_{ij}^{4(1)}, \alpha_{ij}^{4(2)}, ..., \alpha_{ij}^{4(k)}))^{\frac{1}{k}}$,
β_{ij}^5 is geometric mean of $(\alpha_{ij}^{5(1)}, \alpha_{ij}^{5(2)}, ..., \alpha_{ij}^{5(k)})$ so
$\beta_{ij}^5 = (\prod(\alpha_{ij}^{5(1)}, \alpha_{ij}^{5(2)}, ..., \alpha_{ij}^{5(k)}))^{\frac{1}{k}}$,
β_{ij}^6 is geometric mean of $(\alpha_{ij}^{6(1)}, \alpha_{ij}^{6(2)}, ..., \alpha_{ij}^{6(k)})$ so
$\beta_{ij}^6 = (\prod(\alpha_{ij}^{6(1)}, \alpha_{ij}^{6(2)}, ..., \alpha_{ij}^{6(k)}))^{\frac{1}{k}}$.

Step III: FSOTP $\tilde{T}$ is converted into CSOTP (T) using the proposed ranking function in section 4. The Converted CSOTP is given in Table 3.

Table 3: *The transformed CSOTP using ranking Function*

Destination → source ↓	A_1	A_2	.....	A_n	Availability $\{s_i\}$
B_1	b_{11}	b_{12}	.....	b_{1n}	s_1
B_2	b_{21}	b_{22}	.....	b_{2n}	s_2
:	:	:	.....	:	
B_m	b_{m1}	b_{m2}	.....	b_{mn}	s_m
Requirement (d_j)	d_1	d_2	.....	d_n	

Here $b_{ij} = \Re(\tilde{b}_{ij})\ \forall\ i,j\ ;\ 1 \leq i \leq m, 1 \leq j \leq n$, $s_i = \Re(\tilde{s}_i) \forall\ i\ ;\ 1 \leq i \leq m$ and $d_j = \Re(\tilde{d}_j) \forall\ j\ ;\ 1 \leq j \leq n$

Step IV: First check whether or not the CSOTP (T) is balanced. if it is balanced TP go to the next step. if it is not balanced make the transportation problem balanced.
To make the transportation problem balanced there are two cases:
(a) If availabilities exceed the requirements then add a dummy column to satisfy the excess quantity of availabilities. The transportation cost of elements in the dummy column is assumed to be zero.
(b) If requirements exceed the availabilities then add a dummy row to satisfy the excess quantity of requirements. The transportation cost of elements in the dummy row is assumed to be zero.

Step V: In this step, the balanced TP matrix is reduced to at least one zero-entry cell matrix. to reduce the matrix steps are the following:
(i) The lowest cost of each row of balanced TP is subtracted from each row.
(ii) The lowest cost of each column of balanced TP is subtracted from each column.
Ensure that every row and column of balanced TP has one zero-entry cell.

Step VI: Put the zero-entry cell in the square bracket and count the no. of zero-entry cells in the corresponding row and column of the selected zero-entry cells.
Allocate the maximum possible allocation to that cell with the minimum number of zeros in that corresponding row and column. If there is a tie situation, the following rule is applicable:
(a) then, a maximum allocation will be allocated to the cell with the lowest objective function value.
(b) In the case of another tie, the maximum allocation will be allocated to the zero-entry cell whose objective function values sum to the most in the corresponding row/column.
(c) If there is also a tie, then select the chosen zero-entry cells in (b) for which the maximum possible allocation is allocated.
Ignore that row/column where the requirement/availability is satisfied.
Step VII: Repeat the process until all requirements/availability are not satisfied.
The flowchart of the proposed algorithm is given in Figure 1.

To elaborate the proposed approach, two numerical examples are considered.
Example 1: A FMOTP with two objective functions is considered as given in Table 4.

Table 4: *Tabular representation of FMOTP*

Destination $\rightarrow$ source $\downarrow$	A_1	A_2	A_3	A_4	Availability $\{s_i\}$
B_1	$\tilde{a}_{11}^{(1)}$	$\tilde{a}_{12}^{(1)}$	$\tilde{a}_{13}^{1}$	$\tilde{a}_{14}^{(1)}$	$\tilde{s}_1$
	$\tilde{a}_{11}^{(2)}$	$\tilde{a}_{12}^{(2)}$	$\tilde{a}_{13}^{(2)}$	$\tilde{a}_{14}^{(2)}$	
B_2	$\tilde{a}_{21}^{(1)}$	$\tilde{a}_{22}^{(1)}$	$\tilde{a}_{23}^{(1)}$	$\tilde{a}_{24}^{(1)}$	$\tilde{s}_2$
	$\tilde{a}_{21}^{(2)}$	$\tilde{a}_{22}^{(2)}$	$\tilde{a}_{23}^{(2)}$	$\tilde{a}_{24}^{(2)}$	
B_3	$\tilde{a}_{31}^{(1)}$	$\tilde{a}_{32}^{(1)}$	$\tilde{a}_{33}^{(1)}$	$\tilde{a}_{34}^{(1)}$	$\tilde{s}_3$
	$\tilde{a}_{31}^{(2)}$	$\tilde{a}_{32}^{(2)}$	$\tilde{a}_{33}^{(2)}$	$\tilde{a}_{34}^{(2)}$	
B_4	$\tilde{a}_{41}^{(1)}$	$\tilde{a}_{42}^{(1)}$	$\tilde{a}_{43}^{(1)}$	$\tilde{a}_{44}^{(1)}$	$\tilde{s}_4$
	$\tilde{a}_{41}^{(2)}$	$\tilde{a}_{42}^{(2)}$	$\tilde{a}_{43}^{(2)}$	$\tilde{a}_{44}^{(2)}$	
Requirement (d_j)	$\tilde{d}_1$	$\tilde{d}_2$	$\tilde{d}_3$	$\tilde{d}_4$	

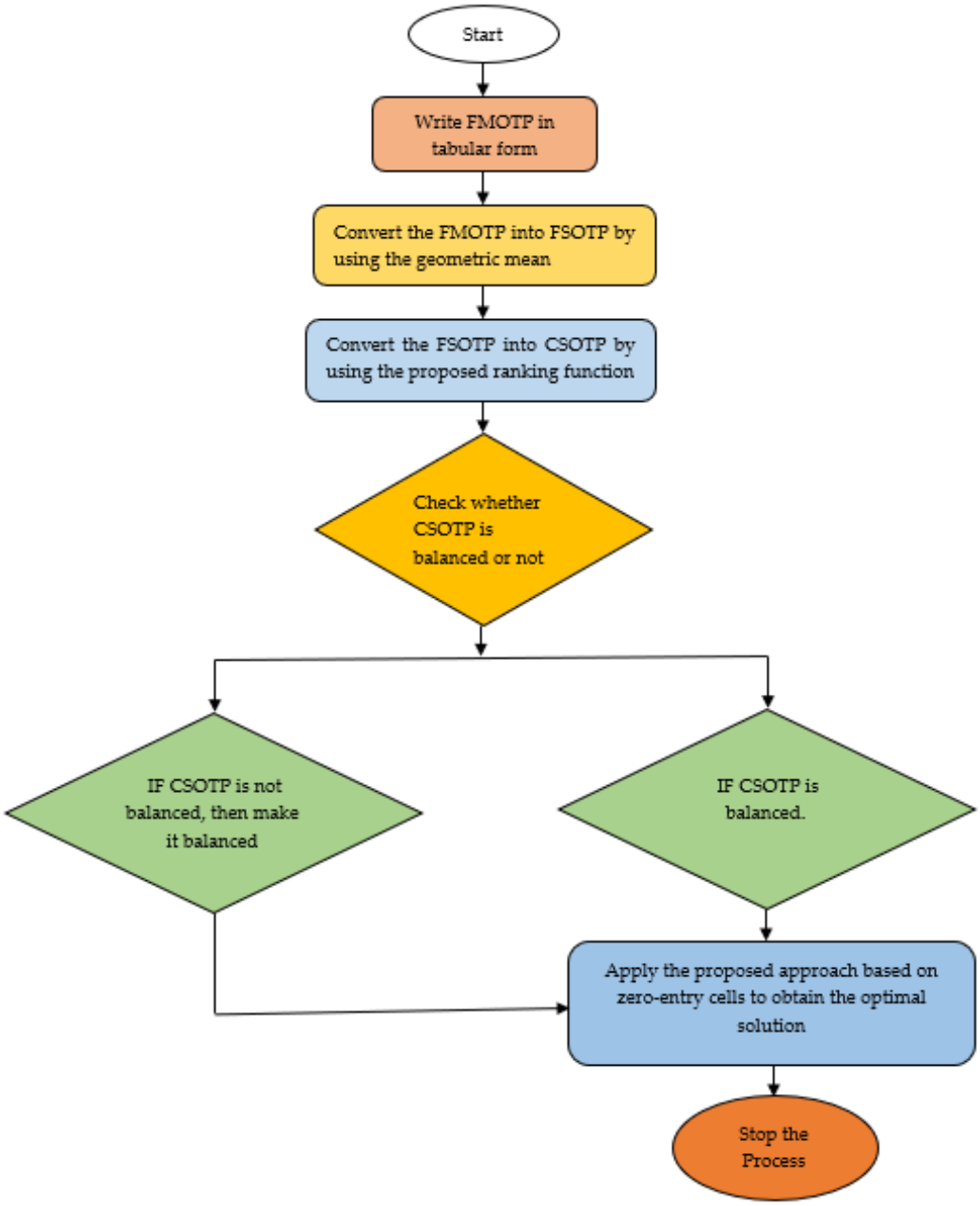


Figure 2: *Flowchart of the proposed approach*

Coefficient matrix for a first objective function

$$C_1 = \begin{bmatrix} \tilde{a}_{11}^{(1)} & \tilde{a}_{12}^{(1)} & \tilde{a}_{13}^{(1)} & \tilde{a}_{14}^{(1)} \\ \tilde{a}_{21}^{(1)} & \tilde{a}_{22}^{(1)} & \tilde{a}_{23}^{(1)} & \tilde{a}_{24}^{(1)} \\ \tilde{a}_{31}^{(1)} & \tilde{a}_{32}^{(1)} & \tilde{a}_{33}^{(1)} & \tilde{a}_{34}^{(1)} \\ \tilde{a}_{41}^{(1)} & \tilde{a}_{42}^{(1)} & \tilde{a}_{43}^{(1)} & \tilde{a}_{44}^{(1)} \end{bmatrix}$$

$$= \begin{bmatrix} (2,3,5,7,8,10) & (3,5,7,9,10,12) & (3,7,11,14,15,16) & (7,9,10,12,15,20) \\ (4,6,7,10,12,15) & (3,6,8,12,14,15) & (8,10,11,13,14,16) & (6,8,9,11,13,18) \\ (7,8,12,13,15,19) & (9,10,11,13,17,19) & (2,4,5,8,12,16) & (5,8,9,12,14,20) \\ (3,4,7,9,13,17) & (6,9,11,14,18,22) & (2,5,6,8,11,15) & (7,11,13,16,17,21) \end{bmatrix}$$

Coefficient matrix for the second objective function

$$C_2 = \begin{bmatrix} \tilde{a}_{11}^{(2)} & \tilde{a}_{12}^{(2)} & \tilde{a}_{13}^{(2)} & \tilde{a}_{14}^{(2)} \\ \tilde{a}_{21}^{(2)} & \tilde{a}_{22}^{(2)} & \tilde{a}_{23}^{(2)} & \tilde{a}_{24}^{(2)} \\ \tilde{a}_{31}^{(2)} & \tilde{a}_{32}^{(2)} & \tilde{a}_{33}^{(2)} & \tilde{a}_{34}^{(2)} \\ \tilde{a}_{41}^{(2)} & \tilde{a}_{42}^{(2)} & \tilde{a}_{43}^{(2)} & \tilde{a}_{44}^{(2)} \end{bmatrix}$$

$$= \begin{bmatrix} (5,9,12,13,15,19) & (4,7,10,12,14,16) & (3,5,7,10,12,14) & (2,3,4,6,7,10) \\ (6,7,9,10,13,14) & (8,10,11,13,14,16) & (9,10,12,15,18,22) & (2,4,5,8,11,17) \\ (8,10,12,15,17,20) & (3,5,8,10,11,15) & (6,7,9,13,15,16) & (5,6,8,11,12,16) \\ (6,9,11,14,15,19) & (5,8,9,13,17,22) & (8,11,12,16,18,23) & (2,5,7,10,14,17) \end{bmatrix}$$

Availabilities:
$s_1 = (4,6,7,10,12,14)$, $s_2 = (5,7,10,13,16,20)$, $s_3 = (6,8,10,12,14,15)$, $s_4 = (7,9,12,14,15,18)$.
Requirements:
$d_1 = (6,7,9,12,14,18)$, $d_2 = (3,5,8,9,11,15)$, $d_3 = (9,11,12,15,17,18)$, $d_4 = (4,7,10,13,15,16)$
Step I: In this step, the FMOTP is transformed into FSOTP using the geometric mean. The converted FSOTP is given in Table 5.

Table 5: *The converted FSOTP using geometric mean*

Destination → source ↓	A_1	A_2	A_3	A_4	Availability $\{s_i\}$
B_1	$\tilde{b}_{11}$	$\tilde{b}_{12}$	$\tilde{b}_{13}$	$\tilde{b}_{14}$	$\tilde{s}_1$
B_2	$\tilde{b}_{21}$	$\tilde{b}_{22}$	$\tilde{b}_{23}$	$\tilde{b}_{24}$	$\tilde{s}_2$
B_3	$\tilde{b}_{31}$	$\tilde{b}_{32}$	$\tilde{b}_{33}$	$\tilde{b}_{34}$	$\tilde{s}_3$
B_4	$\tilde{b}_{41}$	$\tilde{b}_{42}$	$\tilde{b}_{43}$	$\tilde{b}_{44}$	$\tilde{s}_4$
Requirement $\tilde{(d_j)}$	$\tilde{d}_1$	$\tilde{d}_2$	$\tilde{d}_3$	$\tilde{d}_4$	

Here $\tilde{a}_{11}^{(1)} = (2,3,5,7,8,10)$ and $\tilde{a}_{11}^{(2)} = (5,9,12,13,15,19)$

For FSOTP, the objective function values
$\tilde{b}_{11} = (\sqrt{2\times5}, \sqrt{3\times9}, \sqrt{5\times12}, \sqrt{7\times13}, \sqrt{8\times13}, \sqrt{10\times19}) = (3.16, 5.2, 7.75, 9.54, 10.95, 13.78)$
$\tilde{b}_{12} = (3.46, 5.92, 8.37, 10.39, 11.83, 13.86)$, $\tilde{b}_{13} = (3, 5.92, 8.77, 11.83, 13.42, 14.97)$,
$\tilde{b}_{14} = (3.74, 5.2, 6.32, 8.49, 10.25, 14.14)$, $\tilde{b}_{21} = (4.9, 6.48, 7.94, 10, 12.49, 14.49)$,
$\tilde{b}_{22} = (4.9, 7.75, 9.38, 12.49, 14, 15.49)$, $\tilde{b}_{23} = (8.49, 10, 11.49, 13.96, 15.87, 18.76)$,
$\tilde{b}_{24} = (3.46, 5.66, 6.71, 9.38, 11.96, 17.49)$, $\tilde{b}_{31} = (7.48, 8.94, 12, 13.96, 15.97, 19.49)$,
$\tilde{b}_{32} = (5.2, 7.07, 9.38, 11.4, 13.67, 16.88)$, $\tilde{b}_{33} = (3.46, 5.29, 6.71, 10.20, 13.42, 16)$,
$\tilde{b}_{34} = (5, 6.93, 8.49, 11.49, 12.96, 17.89)$, $\tilde{b}_{41} = (4.24, 6, 8.77, 11.22, 13.96, 17.97)$,
$\tilde{b}_{42} = (5.48, 8.49, 9.95, 13.49, 17.49, 22)$, $\tilde{b}_{43} = (4, 7.42, 8.49, 11.31, 14.07, 18.57)$,
$\tilde{b}_{44} = (3.74, 7.42, 9.54, 12.65, 15.43, 18.89)$
Availabilities:
$s_1 = (4,6,7,10,12,14)$, $s_2 = (5,7,10,13,16,20)$, $s_3 = (6,8,10,12,14,15)$, $s_4 = (7,9,12,14,15,18)$.
Requirements:
$d_1 = (6,7,9,12,14,18)$, $d_2 = (3,5,8,9,11,15)$, $d_3 = (9,11,12,15,17,18)$, $d_4 = (4,7,10,13,15,16)$

Now FMOTP is converted into CSOTP using the proposed ranking function.
Here $\tilde{b}_{11} = (\beta_{11}^1, \beta_{11}^2, \beta_{11}^3, \beta_{11}^4, \beta_{11}^5, \beta_{11}^6) = (3.16, 5.2, 7.75, 9.54, 10.95, 13.78)$
$\Re(\tilde{b}_{11}) = I_x = (\frac{cx_1+bx_2+ax_3}{a+b+c})$
where a = $\frac{(2\beta_{11}^4+\beta_{11}^5+\beta_{11}^6-2\beta_{11}^3-\beta_{11}^2-\beta_{11}^1)}{4}$ = 4.99, b = $\frac{(4(2\beta_{11}^4-\beta_{11}^1-\beta_{11}^2)^2+w^2)^{\frac{1}{2}}}{8}$ = 2.68,
and c = $\frac{(4(2\beta_{11}^3-\beta_{11}^5-\beta_{11}^6)^2+w^2)^{\frac{1}{2}}}{8}$ = 2.32
$x_1 = \frac{\beta_1+\beta_2+2\beta_3}{4}$ =5.92, $x_2 = \frac{2\beta_4+\beta_5+\beta_6}{4}$ = 10.95, and $x_3 = \frac{\beta_3+\beta_4}{2}$ = 8.64

$\Re(\tilde{b}_{11}) = \frac{2.32\times5.92+2.68\times10.95+4.99\times8.64}{4.99+2.68+2.32} = 8.64$
Similarly, all the fuzzy values $\tilde{a}_{ij}^{(k)}$ for $1 \leq j \leq 4, 1 \leq i \leq 4$ and $1 \leq k \leq 2$, availabilities $\tilde{s}_i$ for $1 \leq i \leq 4$, and requirements $\tilde{d}_j$ for $1 \leq j \leq 4$ can be converted in crisp values by using ranking function.
The CSOTP is given in Table 6.

Table 6: *The transformed Crisp SOTP using ranking function*

Destination → source ↓	A_1	A_2	A_3	A_4	Availability $\{s_i\}$
B_1	8.64	9.38	10.3	7.41	8.5
B_2	8.97	10.94	12.73	8.05	11.5
B_3	12.98	10.39	8.45	9.99	11
B_4	10	11.72	9.9	11.09	13
Requirement $\tilde{(d_j)}$	10.5	8.5	13.5	11.5	

Here $\Sigma_{i=1}^{m} s_i = \Sigma_{j=1}^{n} d_j = 44$. So it is a balanced transportation problem.
Step II: We now reduce the Balanced TP to a zero-entry cell matrix. The reduced zero-entry cell matrix is given in Table 7.

Table 7: *The CSOTP with zero-entry cells*

Destination → source ↓	A_1	A_2	A_3	A_4	Availability $\{s_i\}$
B_1	8.64	9.38	10.3	[7.41]	8.5
B_2	8.97	10.94	12.73	[8.05]	11.5
B_3	12.98	10.39	[8.45]	9.99	11
B_4	[10]	[11.72]	[9.9]	11.09	13
Requirement $\tilde{(d_j)}$	10.5	8.5	13.5	11.5	

In each row and column of the zero-entry cells, count the number of cells with zero entries.
The no. of zero-entry cells for the selected cell at b_{14} position = 2
The no. of zero-entry cells for the selected cell at b_{24} position = 2
The no. of zero-entry cells for the selected cell at b_{32} position = 2
The no. of zero-entry cells for the selected cell at b_{41} position = 3
The no. of zero-entry cells for the selected cell at b_{42} position = 3
The no. of zero-entry cells for the selected cell at b_{43} position = 3
Here cells at b_{14}, b_{24}, b_{32} positions has the same number of zero-entry cells. So choose that cell which has minimum objective function value.
Cell at b_{14} position has the minimum objective value (7.41). so we allocate the maximum possible allocation, min(8.5,11.5) = 8.5 to the cell at b_{14} position as shown in Table 8.

Table 8: *The CSOTP with the first allocation*

Destination → source ↓	A_1	A_2	A_3	A_4	Availability $\{s_i\}$
B_1	8.64	9.38	10.3	7.41 (8.5)	8.5
B_2	8.97	10.94	12.73	8.05	11.5
B_3	12.98	10.39	8.45	9.99	11
B_4	10	11.72	9.9	11.09	13
Requirement $\tilde{(d_j)}$	10.5	8.5	13.5	11.5	

Step III: Repeat the process to satisfy all the availabilities and requirements and to make the possible allocation in the remaining rows and columns, hence the 2^{nd}, 3^{rd}, 4^{th}, 5^{th},6^{th}, and 7^{th}

allocations as 3,11,8.5,2,8.5,2.5 at cells $b_{14}, b_{24}, b_{33}, b_{41}, b_{42}, b_{43}$ respectively. the final optimum allocation is given in Table 9.

Table 9: *final Optimum allocation table for Example 1*

Destination → source ↓	A_1	A_2	A_3	A_4	Availability $\{s_i\}$
B_1	8.64	9.38	10.3	7.41(8.5)	8.5
B_2	8.97(8.5)	10.94	12.73	8.05(3)	11.5
B_3	12.98	10.39	8.45(11)	9.99	11
B_4	10(2)	11.72(8.5)	9.9(2.5)	11.09	13
Requirement $\tilde{(d_j)}$	10.5	8.5	13.5	11.5	

Example 2: A fuzzy transportation problem with all the fuzzy parameters as hexagonal fuzzy numbers is given in Table 10.

Table 10: *Tabular representation of FSOTP*

Destination → source ↓	A_1	A_2	A_3	A_4	Availability $\{s_i\}$
B_1	$\tilde{b}_{11}$	$\tilde{b}_{12}$	$\tilde{b}_{13}$	$\tilde{b}_{14}$	$\tilde{s}_1$
B_2	$\tilde{b}_{21}$	$\tilde{b}_{22}$	$\tilde{b}_{23}$	$\tilde{b}_{24}$	$\tilde{s}_2$
B_3	$\tilde{b}_{31}$	$\tilde{b}_{32}$	$\tilde{b}_{33}$	$\tilde{b}_{34}$	$\tilde{s}_3$
Requirement $\tilde{(d_j)}$	$\tilde{d}_1$	$\tilde{d}_2$	$\tilde{d}_3$	$\tilde{d}_4$	

where $\tilde{b}_{11} = (1,2,3,4,5,6)$, $\tilde{b}_{12} = (1,3,5,6,8,10)$, $\tilde{b}_{13} = (9,11,13,16,18,20)$, $\tilde{b}_{14} =(2,4,6,8,10,12)$
$\tilde{b}_{21} = (1,3,5,7,8,10)$, $\tilde{b}_{22} = (0,2,4,6,8,10)$ $\tilde{b}_{23} = (2,3,4,5,6,7)$, $\tilde{b}_{24} =(3,6,9,10,13,16)$
$\tilde{b}_{31} = (3,5,7,8,10,12)$, $\tilde{b}_{32} = (4,8,12,16,20,24)$ $\tilde{b}_{33} = (3,4,5,6,7,8)$, $\tilde{b}_{34} =(6,8,10,11,13,15)$
Availabilities:
$s_1 = ((1,3,5,6,8,10)$, $s_2 = (2,4,6,7,9,11)$, $s_3 = (3,6,9,17,20,23)$
Requirements:
$d_1 = (5,7,9,10,12,14)$, $d_2 = (1,3,5,6,8,10)$, $d_3 = (1,2,3,4,5,6)$, $d_4 = (2,4,6,7,9,11)$ The Fuzzy SOTP is transformed into Crisp SOTP using the proposed ranking Function in Table 11.

Table 11: *Tabular representation of Crisp SOTP*

Destination → source ↓	A_1	A_2	A_3	A_4	Availability $\{s_i\}$
B_1	3.5	5.5	14.5	7	5.5
B_2	6	5	4.5	9.5	6.5
B_3	7.5	14	5.5	10.5	13
Requirement $\tilde{(d_j)}$	9.5	5.5	3.5	6.5	

Apply the proposed approach the final optimum allocation is obtained.

Table 12: *Optimum allocation table for Example 2*

Destination → source ↓	A_1	A_2	A_3	A_4	Availability $\{s_i\}$
B_1	3.5(5.5)	5.5	14.5	7	5.5
B_2	6	5(5.5)	4.5(1)	9.5	6.5
B_3	7.5(4)	14	5.5(2.5)	10.5(6.5)	13
Requirement $\tilde{(d_j)}$	9.5	5.5	3.5	6.5	

9. Results and discussion

This section analyzes the results obtained from two illustrative examples using the proposed approach. The discussion is structured into two parts: (i) Result Analysis and (ii) Physical Interpretation.

9.1. Result analysis

This section presents the analysis of the results obtained using the proposed approach on two illustrative examples. The final allocation details, fuzzy and crisp compromise efficient solutions, are presented in Tables 13 and 14. The comparative results with existing methods are shown in Table 15.

Table 13: *Final Solution table for Example 1*

Obtained Allocations	$y_{11}=0, y_{12}=0, y_{13}=0, y_{14}=8.5$ $y_{21}=8.5, y_{22}=0, y_{23}=0, y_{24}=3,$ $y_{31}=0, y_{32}=0, y_{33}=11, y_{34}=0,$ $y_{41}=2, y_{42}=8.5, y_{43}=2.5, y_{44}=0.$
Fuzzy Compromise efficient solution of MOTP	$[(195.5, 292.5, 349, 465, 607, 786),$ $(214.5, 287.5, 353, 481.5, 587.5, 713.5)]$
Crisp Compromise efficient solution of MOTP	$(407, 417.25)$
Nature of Crisp Compromise Crisp Solution	Non-Degenerate

Table 14: *Final Solution table for Example 2*

Obtained Allocations	$y_{11}=5.5, y_{12}=0, y_{13}=0, y_{14}=0$ $y_{21}=0, y_{22}=5.5, y_{23}=1, y_{24}=0,$ $y_{31}=4, y_{32}=0, y_{33}=2.5, y_{34}=6.5,$
Fuzzy Compromise efficient solution of MOTP	$(66, 107, 148, 178.5, 219.5, 260.5)$
Crisp Compromise efficient solution of MOTP	(163.25)
Nature of Crisp Compromise Crisp Solution	Non-Degenerate

The final solution tables for both examples show that the nature of the solution is nondegenerate and optimal.

Table 15: *The result comparison table*

	Method Name	Optimal Solution
Example 1	Sharma M.K. et. al. [19]	(1442.06,1888.81)
	Proposed Method	(407,417.25)
Example 2	Sahayasudha, A. et. al. [20]	662
	Proposed Method	163.25

For Example 1, the proposed method yielded a crisp compromise solution that is significantly lower than the values reported by Sharma M.K. et al. [19]. As shown in Table 15, the solution values obtained using the proposed approach yield a 71.78% reduction in the first objective and a 77.90% reduction in the second objective compared to the existing method. This considerable decrease in objective values indicates a more cost-effective and efficient allocation under the proposed model.

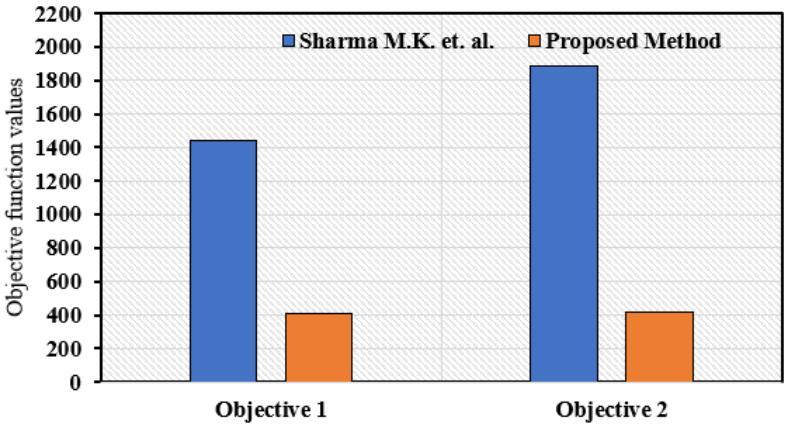


Figure 3: *Result comparison for Example 1*

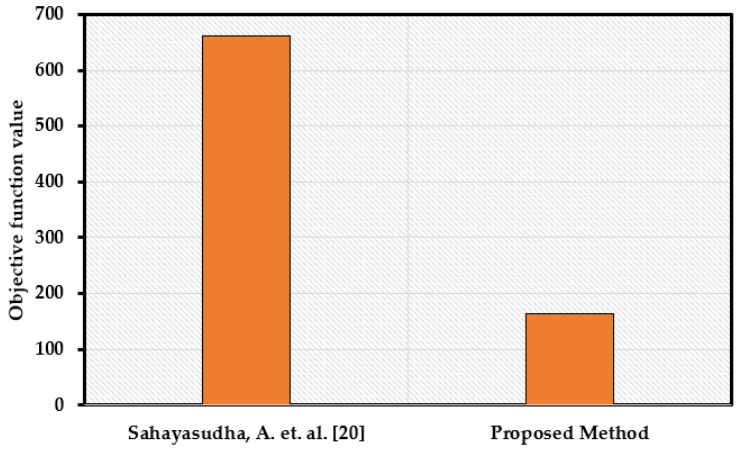


Figure 4: *Result comparison for Example 2*

Similarly, in Example 2, the solution obtained through the proposed method demonstrates a significant improvement compared to the method presented by Sahayasudha et al. [20]. Specifically, there is a 75.34% reduction in the overall objective value, as observed in Table 15. This further validates the strength of the proposed method in yielding optimized results even in more complex scenarios. A graphical representation of the observations is shown in Figures 3 and 4., clearly illustrating the improved performance of the proposed method across both examples. The observed reduction in objective values across the examples indicates that the proposed method provides consistent and efficient solutions, demonstrating its practical effectiveness in addressing fuzzy multi-objective transportation problems

9.2. Physical interpretation of the results

The solution obtained, as presented in Table 13 and Table 14 for example 1 and example 2 respectively, is physically interpreted as follows:

9.2.1 Interpretation of the results for Example 1

(I) For the first objective function:

Using the proposed approach, the minimum fuzzy transportation cost (FTC) is [(195.5,292.5,349,465,607, 786)]. It has the following physical interpretation:

(i) In the decision maker's estimation, the minimum transportation cost (MTC) will be greater than Rs. 195.5 and less than Rs. 786 units.
(ii) The decision-maker is 100% satisfied overall with the statement that transportation costs will be 349-465. It is easily seen that the optimal value of the first objective function is 407, which lies between 349 and 465.
(iii) The following values of the remaining minimum transportation cost can be used to determine the decision-maker's overall level of satisfaction:
If y is the MTC, then the overall decision-maker satisfaction level for y = $\mu_{\tilde{A_1}}(y) \times 100$

where

$$\mu_{A_1\tilde{}(y)} = \begin{cases} \frac{1}{2}\left\{\frac{y-195.5}{97}\right\} & \text{if } 195.5 \leq y \leq 292.5 \\ \frac{1}{2} + \frac{1}{2}\left\{\frac{y-292.5}{56.5}\right\} & \text{if } 292.5 \leq y \leq 349 \\ 1 & \text{if } 349 \leq y \leq 465 \\ 1 + \frac{1}{2}\left\{\frac{y-465}{142}\right\} & \text{if } 465 \leq y \leq 607 \\ \frac{1}{2}\left\{\frac{786-y}{179}\right\} & \text{if } 607 \leq y \leq 786 \\ 0 & \text{Otherwise} \end{cases}$$

Fig. 5 and Fig.6. shows the fuzzy optimal solution for example 1 and example 2.

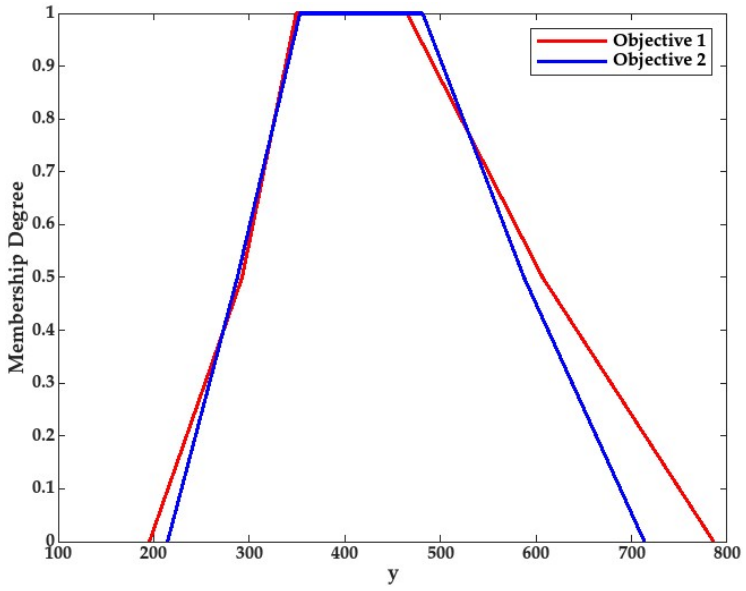


Figure 5: *Fuzzy objective values graph for Example 1*

(II) For Second Objective Function:

Using the proposed approach, the minimum FTP is [(214.5,287.5,353,481.5,587.5,713.5)]. It has the following physical interpretation:
(i) The MTC, in the decision-maker's estimation, will be greater than Rs. 214.5 and less than Rs. 713.5 units.
(ii) The decision-maker is 100% satisfied overall with the statement that transportation costs will be 353.5-481.5. It is easily seen that the optimal value of the first objective function is 417.5, which lies between 353 and 481.5
(iii) The following values of the remaining minimum transportation cost can be used to determine the decision-maker's overall level of satisfaction:
If y is the MTC, then the overall level of satisfaction of the decision maker for y = $\mu_{\tilde{A_2}}(y) \times 100$.
Here $\mu_{\tilde{A_2}}(y)$ is given as :

$$\mu_{A_2\tilde{(y)}} = \begin{cases} \frac{1}{2}\left\{\frac{y-214.5}{73}\right\} & \text{if } 214.5 \leq y \leq 287.5 \\ \frac{1}{2}+\frac{1}{2}\left\{\frac{y-287.5}{65.5}\right\} & \text{if } 287.5 \leq y \leq 353 \\ 1 & \text{if } 353 \leq y \leq 481.5 \\ 1+\frac{1}{2}\left\{\frac{y-481.5}{106}\right\} & \text{if } 481.5 \leq y \leq 587.5 \\ \frac{1}{2}\left\{\frac{713.5-y}{126}\right\} & \text{if } 587.5 \leq y \leq 713.5 \\ 0 & \text{Otherwise} \end{cases}$$

used to determine the decision-maker's overall level of satisfaction.

9.2.2 Interpretation of the results for Example 2

Using the proposed algorithm, the minimum FTP is [(66,107,148,178.5,219.5,260.5)] It has the following physical interpretation:
(i) In the decision-maker's estimation, the MTC will be greater than Rs. 66 and less than Rs. 260.5 units.
(ii) The decision-maker is 100% satisfied overall with the statement that transportation costs will be 148-178.5. It is easily seen that the optimal value of the first objective function is 163.25, which lies between 148 and 178.5.

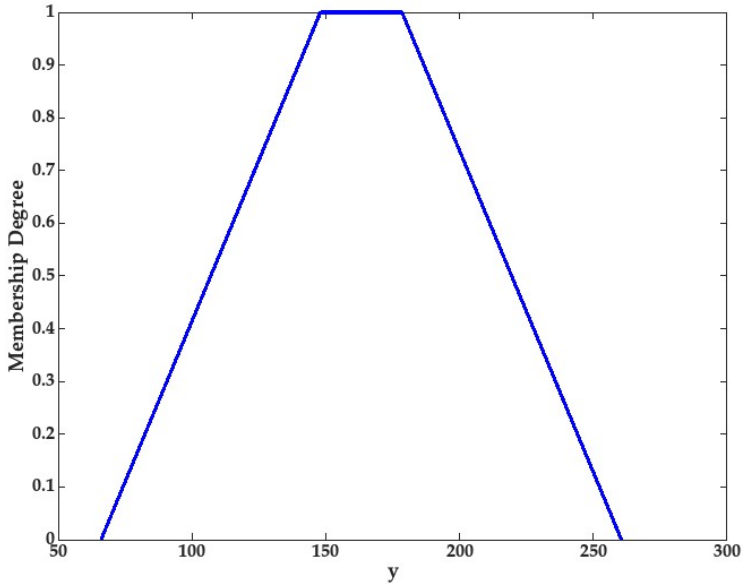


Figure 6: *Fuzzy objective values graph for Example 2*

(iii) The following values of the remaining minimum transportation cost can be used to determine the decision-maker's overall level of satisfaction:
If y is the MTC, then the overall level of satisfaction of the decision maker for y = $\mu_{\tilde{A}}(y) \times 100$
Where,

$$\mu_{A\tilde{(y)}} = \begin{cases} \frac{1}{2}\left\{\frac{y-66}{41}\right\} & \text{if } 66 \leq y \leq 107 \\ \frac{1}{2}+\frac{1}{2}\left\{\frac{y-107}{41}\right\} & \text{if } 107 \leq y \leq 148 \\ 1 & \text{if } 148 \leq y \leq 178.5 \\ 1+\frac{1}{2}\left\{\frac{y-178.5}{41}\right\} & \text{if } 178.5 \leq y \leq 219.5 \\ \frac{1}{2}\left\{\frac{260.5-y}{41}\right\} & \text{if } 219.5 \leq y \leq 260.5 \\ 0 & \text{Otherwise} \end{cases}$$

10. Conclusion

A new approach is presented to solve the fuzzy multi-objective transportation problem in which all the transportation parameters are represented by generalized hexagonal fuzzy numbers. The geometric mean technique is applied to transform the FMOTP into a fuzzy single-objective transportation problem. The approach is based on a new ranking function and zero-entry cell technique. The ranking function is based on the centroid and incentre points defuzzify the FMOTP. The defuzzified value for each parameter lies within the range of the hexagonal fuzzy number. Then zero-entry cell technique is applied to the crisp single-objective transportation problem to get the optimal solution . Two numerical examples are solved to validate our proposed approach. The analysis and comparison of results with some other existing methods from the literature show that the proposed approach provides more optimized and better results than some other existing methods. The approach is simple to understand and easy to use in real-life situations in which the decision-makers are not sure about the precise value of transportation parameters and these parameters are given by HFNs. It can be used for many optimization problems, like as traveling salesman problems and assignment problems.

References

[1] Hitchcock, F. L. (1941). The distribution of a product from several sources to numerous localities. Journal of mathematics and physics, 20(1-4), 224-230.
[2] WW, C. A. C. (1954). The stepping stone method for explaining linear programming calculation in transportation problem. Manag Sci, 1(1), 49.
[3] Zadeh, L. A. (1965). Fuzzy sets. Information and control, 8(3), 338-353.
[4] Zimmermann, H. J. (1978). Fuzzy programming and linear programming with several objective functions. Fuzzy sets and systems, 1(1), 45-55.
[5] Chakraborty, A., Maity, S., Jain, S., Mondal, S. P., & Alam, S. (2021). Hexagonal fuzzy number and its distinctive representation, ranking, defuzzification technique, and application in production inventory management problem. Granular Computing, 6, 507-521.
[6] Sudha, A. S., & Revathy, M. (2016). A new ranking on hexagonal fuzzy numbers. International Journal of Fuzzy Logic Systems, 6(4), 1-8.
[7] Leela-apiradee, W., & Thipwiwatpotjana, P. (2019). A Ranking Method of Hexagonal Fuzzy Numbers Based on Their Possibilistic Mean Values. In Fuzzy Techniques: Theory and Applications: Proceedings of the 2019 Joint World Congress of the International Fuzzy Systems Association and the Annual Conference of the North American Fuzzy Information Processing Society IFSA/NAFIPS'2019 (Lafayette, Louisiana, USA, June 18-21, 2019) (pp. 318-3 29). Springer International Publishing.
[8] Thiruppathi, A., & Kirubhashankar, C. K. (2020). New ranking of generalized hexagonal fuzzy number using centroids of centroided method. Advances in Mathematics: Scientific Journal, 9(8), 6229-6240.
[9] Juman, Z. A. M. S., & Nawarathne, N. G. S. A. (2019). An efficient alternative approach to solve a transportation problem. Ceylon journal of Science, 48(1), 19-29.
[10] Juman, Z. A. M. S., & Hoque, M. A. (2015). An efficient heuristic to obtain a better initial feasible solution to the transportation problem. Applied Soft Computing, 34, 813-826.
[11] Bezmaternykh, A., Kulizhskaya, Z., & Fayzrakhmanova, E. (2022). A Balanced System of Indicators as a Condition for Improving the Effectiveness of Management Decisions in the Field of Transport. Transportation Research Procedia, 61, 176-179.
[12] Juman, Z. A. M. S., Hoque, M. A., & Buhari, M. I. (2013). A sensitivity analysis and an implementation of the wellknown Vogel™s approximation method for solving unbalanced transportation problem. Malaysian Journal of Science, 32(1), 66 -72.
[13] Chhibber, D., Srivastava, P. K., & Bisht, D. C. (2021). From fuzzy transportation problem to non-linear intuitionistic fuzzy multi-objective transportation problem: A literature review. International Journal of Modelling and Simulation, 41(5), 335-350.

[14] Adilakshmi, S., & Shankar, N. R. (2021). A new ranking in hexagonal fuzzy number by centroid of centroids and application in fuzzy critical path. Reliability: Theory & Applications, 16(2 (62)), 124-135.
[15] Srivastava, P. K., Bisht, D., & Garg, H. (2020). Innovative Ranking and Conversion Approaches to Handle Impreciseness in Transportation. Journal of Multiple-Valued Logic & Soft Computing, 35.
[16] Mostafa, S. A., Juman, Z. A. M. S., Nawi, N. M., Mahdin, H., & Mohammed, M. A. (2022, May). Improving genetic algorithm to attain better routing solutions for real-world water line system. In International conference on soft computing and data mining (pp. 292-301). Cham: Springer International Publishing.
[17] Ashour, M. A. H. (2019). Optimum cost of transporting problems with hexagonal fuzzy numbers. Journal of Southwest Jiaotong University, 54(6).
[18] Juman, Z. A. M. S., Mostafa, S. A., Batuwita, A. P., AlArjani, A., Sharif Uddin, M., Jaber, M. M., ... & Attia, E. A. (2022). Close interval approximation of pentagonal fuzzy numbers for interval data-based transportation problems. Sustainability, 14(12), 7423.
[19] Sharma, M. K., Dhiman, N., Mishra, L. N., & Mishra, V. N. (2021). A Genetic Algorithm Approach for Multi-Objective Transportation Problem with Hexagonal Fuzzy Number. Aligarh Journal of Statistics, 41.
[20] Sahayasudha, A., & Vijayalakshmi, K. R. (2017). An alpha-cut operation in a transportation problem using symmetric hexagonal fuzzy numbers. International journal of fuzzy logic systems, 7(1), 31-48.
[21] Bagheri, M., Ebrahimnejad, A., Razavyan, S., Hosseinzadeh Lotfi, F., & Malekmohammadi, N. (2022). Fuzzy arithmetic DEA approach for fuzzy multi-objective transportation problem. Operational Research, 1-31.
[22] Sharma, M. K., Kamini, Dhaka, A., Nandal, A., Rosales, H. G., Monteagudo, F. E. L., ... & Hoang, V. T. (2023). Fermatean fuzzy programming with new score function: a new methodology to multi-objective transportation problems. Electronics, 12(2), 277.
[23] Akram, M., Shahzadi, S., Shah, S. M. U., & Allahviranloo, T. (2023). A fully Fermatean fuzzy multi-objective transportation model using an extended DEA technique. Granular Computing, 8(6), 1173-1204.
[24] Indira, P., & Jayalakshmi, M. (2024). Evaluation of the Minimum Transportation Cost of Asymmetric/Symmetric Triangular Fuzzy Numbers with-Cut by the Row-Column Minima Method. Baghdad Science Journal.
[25] Sharma, R., & Tyagi, S. L. (2024). A new algorithm to solve Multi-Objective Transportation Problem with generalized trapezoidal fuzzy numbers. Reliability: Theory & Applications, 19(1 (77)), 531-543.

A STATISTICAL FRAMEWORK FOR ENHANCING PROCESS CONTROL AND RELIABILITY USING AUTOENCODERS RANDOM SURVIVAL FORESTS AND NHPP MODELING

P. Sricharani[1], P. Satya Shekar Varma[2], M. V. Lavanya[3*]

•

[1]Professor, Department of Artificial Intelligence, Shri Vishnu Engineering College for Women, Bhimavaram, Andhra Pradesh, India
[2]Research Scholar, Computer Science and Engineering, National Institute of Technology, Warangal, Telangana, India
[3]Assistant Professor, Department of Mathematics and Statistics, GITAM School of Science, GITAM (Deemed to be University), Visakhapatnam, Andhra Pradesh, India
Corresponding Author Email: *lavanya.mv9@gmail.com

Abstract

Statistical Process Control (SPC) plays a critical role in ensuring the reliability and quality of high-grade products. This study introduces two advanced machine learning methods to enhance SPC by integrating Auto encoders for anomaly detection and Random Survival Forests (RSF) for failure prediction. The Autoencoder model is employed to monitor real-time sensor data, learning the normal patterns of product quality and identifying deviations that indicate potential quality issues. By flagging anomalies when product performance metrics diverge from expected thresholds, the autoencoder helps to adjust SPC limits dynamically, improving responsiveness to emerging quality concerns. Additionally, RSF is used to predict the likelihood of product failure over time, based on historical failure data and process parameters. This predictive approach enables proactive interventions to prevent quality issues before they occur, enhancing long-term product dependability. Together, these machine learning methods create a comprehensive framework for real-time monitoring and failure prediction, providing a more adaptive and data driven approach to quality control. The integration of Auto encoders and RSF into the SPC methodology significantly advances the precision and effectiveness of product reliability assessment, offering a powerful tool for maintaining high-quality standards in manufacturing processes.

Keywords: Statistical Process Control (SPC), Autoencoders, Random Survival Forests (RSF), Anomaly Detection, Failure Prediction, Product Reliability, Quality Control, Machine Learning, Predictive Modeling

I. Introduction

In real-time analysis of lifespan data, especially concerning the failure times of high-quality products over a specified period, the integration of advanced statistical models with machine learning methods enhances Statistical Process Control (SPC) for quality monitoring and prediction. This study proposes a novel approach by incorporating the Freshet Distribution with the Non-

Homogeneous Poisson Process (NHPP) to design a new "time control chart." This chart, in combination with machine learning techniques—Autoencoders for anomaly detection and Random Survival Forests (RSF) for failure prediction—enables comprehensive monitoring and proactive quality interventions. The Frechet Distribution and NHPP model failure intensity (λ) across specific time intervals, providing a probabilistic foundation for real-time failure monitoring. The framework is represented by:

$$P(N(1,P) - N(1) = z) = \frac{e^{-\theta p}(\theta p)^z}{z!}, z = 0,1,2, \ldots \quad (1)$$

where $N(1)$ represents the random count of failures within [0, l], enabling a focus on instances significantly exceeding the Upper Control Limit (UCL) and prompting targeted quality investigations.

$$P(N(l) = z) = \frac{e^{-\mu(l)}\mu(l)^z}{z!}, z = 0,1,2, \ldots \quad (2)$$

In this equation, $\mu(t)$ represents the mean value function. Eq.1 characterizes a Non-Homogeneous Poisson Process (NHPP). The function $\mu(t)$ can be interpreted as the mean value function for an NHPP. The renowned Frechet distribution (FD) is selected as the distribution for $\mu(t)$ to provide a growth model based on the Non-Homogeneous Poisson Process (NHPP). Building on previous research by Roy, Pham, Srinivas Rao & Sricharani, Grabski, and others focused on mathematical models for SPC, this study extends the traditional approach by using

Autoencoders to detect anomalies in real-time sensor data. The Autoencoder model learns normal patterns in production data and identifies deviations, dynamically adjusting control limits to improve SPC responsiveness. Concurrently, RSF uses historical failure data and process parameters to predict the likelihood of product failure over time, allowing for timely interventions that prevent potential quality issues. Together, these tools form a robust framework for anomaly detection, real-time monitoring, and predictive failure analysis.

The structure of this paper is as follows: It begins by outlining the characteristics of the Frechet Distribution and NHPP, then introduces the construction of the time control chart. Comparisons with the Exponential model and the benefits of Autoencoder-driven anomaly detection and RSF-based failure prediction are discussed. Additionally, the application of order statistics for monitoring production is examined. The paper concludes with key insights into the enhanced reliability and adaptability of SPC through machine learning integration, underscoring the benefits of this approach for quality control in manufacturing environments.

II. Methodology

In this study, a combination of statistical modeling and machine learning techniques is used to create an enhanced control system for monitoring time between failures and identifying anomalies in product quality. This methodology integrates the Frechet distribution, Autoencoders for anomaly detection, and Random Survival Forests (RSF) for failure prediction, along with the Non-Homogeneous Poisson Process (NHPP) as the mean function to dynamically adjust control limits based on real-time data.

2.1. Frechet Distribution and its Characteristics

The Frechet distribution, known for its skewness and stability, is used in applications such as life testing and reliability analysis. The Frechet distribution finds extensive practical utility in diverse

real-world scenarios, encompassing life testing, rainfall analysis, queue dynamics, wind speed modeling, earthquake prediction, sea current assessments, horse racing performance, flood analysis, and track race record evaluation The probability density function (PDF) associated with the Frechet distribution is expressed as follows

$$g(y) = \frac{k}{b}\left(\frac{y-b}{a}\right)^{1-k} e^{-\left(\frac{y-a}{b}\right)^{-k}}, k \in (0, \infty) \quad (3)$$

Its cumulative distribution function (cdf) is

$$G(y) = e^{-\left(\frac{y-a}{b}\right)^{-k}} \; if \; y > a \quad (4)$$

The Frechet distribution is characterized as a skewed and maximally stable distribution. For the Frechet distribution, the mean, median, and variance are denoted as follows

$$Mean = a + b\Gamma\left(1 - \frac{1}{k}\right) \; for \; k > 1 \quad (5)$$

$$Median = a + \frac{b}{\sqrt[k]{\log_e 2}} \quad (6)$$

$$Variance = b^2 \, \Gamma\left(1 - \frac{2}{k}\right) - \left(1 - \frac{1}{k}\right)^2, k > 0 \quad (7)$$

The NHPP with $\phi G(y)$ as the mean value function for our present study is

$$\mu(x) = \phi e^{-\left(\frac{y-a}{b}\right)^{-k}} \quad (8)$$

Frechet distribution contains 3 parameters namely k is a shape parameter, a is a location parameter b is a scale parameter where ϕ is number of damages in the manufactured goods.

2.2. Anomaly Detection with Autoencoders

Anomaly detection is critical for identifying unexpected deviations in product performance. Autoencoders are utilized to learn the typical behavior of the manufacturing process by encoding and reconstructing normal data patterns. During operation, the Autoencoder flags an anomaly if the reconstruction error exceeds a predefined threshold, indicating potential quality concerns or system instability. This enables real-time adjustments of SPC limits by detecting anomalies early in the process.

2.3. Failure Prediction with Random Survival Forests (RSF)

RSF is applied to predict failure times and assess product reliability based on historical failure data and operational parameters. RSF provides survival probabilities over specified time frames, allowing for proactive interventions before potential failures. By incorporating survival analysis, RSF into quality control systems enhances the accuracy of failure predictions and helps prevent unexpected downtimes, supporting an adaptive and responsive quality control system.

2.4. Control chart monitoring the time between failures based on mean value function

Similar to Shewhart's theory of variable control charts, a control chart for such data would be produced using 0.9973 probability limits of the periods between failure random variable denoted as "t," if the random variable is thought to reflect the inter-failure time of a device. Taking into account equi-tailed probability, these limits and the center line are found as the solutions to the following equations.

$$G(I) = 0.00135 \tag{9}$$

$$G(I) = 0.5 \tag{10}$$

$$G(I) = 0.998655 \tag{11}$$

Let I_L , I_C, and I_U be respectively the solutions of Eq 9, Eq 10, and Eq 11 in the standard form

$$I_L = G^{-(0.00135)} \tag{12}$$

$$I_C = G^{-(0.5)} \tag{13}$$

$$I_U = G^{-(0.99865)} \tag{14}$$

In Fig 1, be respectively the solution of the equations Eq.12, Eq.13, Eq.14 for Frechat distribution with parameter values $k = 0.65, b = 1$ & $a = 0.1$. This parameter combination is taken in order to have close affinity with exponential distribution (0.03) as evidenced from the following probability density function curves.

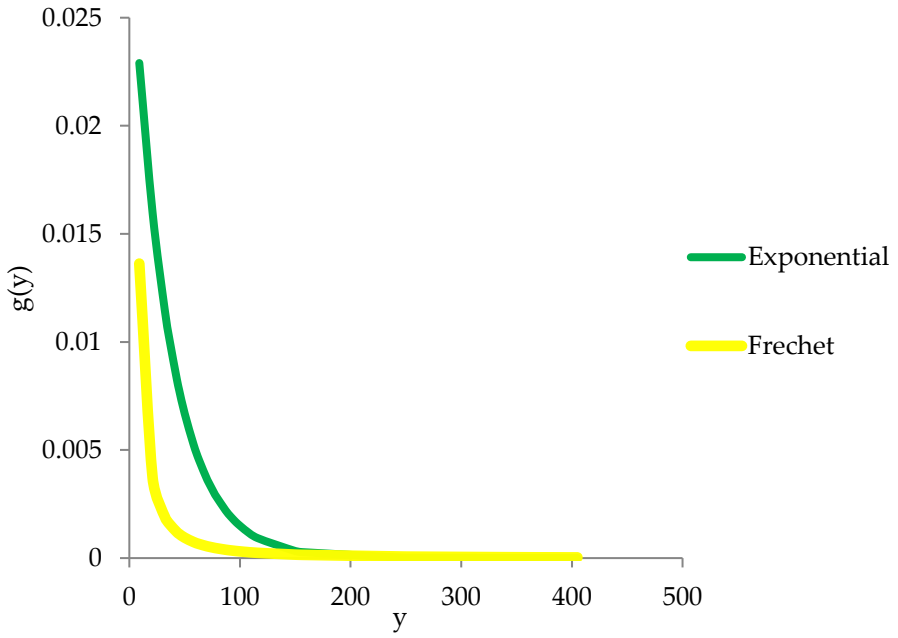


Figure 1: *Concordance of Exponential and Frehet distributions*

The NHPP based on $F(I)$ as the mean value function is the SRGM for our present study and is given by

$$\mu(I) = \phi(1 - e^{-}), I > 0, > 0 \quad (15)$$

Using the dataset from 11Kim, the time control chart is created using the mean value function corresponding to inter-failure time and is accompanied by three parallel lines that extend to the horizontal axis at points I_L, I_C, $and\ I_U$.

The illustration looks like this:

Table 1: *Real time data1*

Failure number	1	2	3	4	5	6	7	8	9	10	11	12	13	14	15
Failure time (hours)	9	21	36	43	45	50	58	63	70	70	71	77	78	87	91
Failure number	16	17	18	19	20	21	22	23	24	25	26	27	28	29	30
Failure time (hours)	92	95	98	104	105	116	140	156	247	249	250	337	384	396	405

In Fig- 2, The adequacy of the data's fit to the model is evaluated by calculating the correlation coefficient using a QQ-plot.

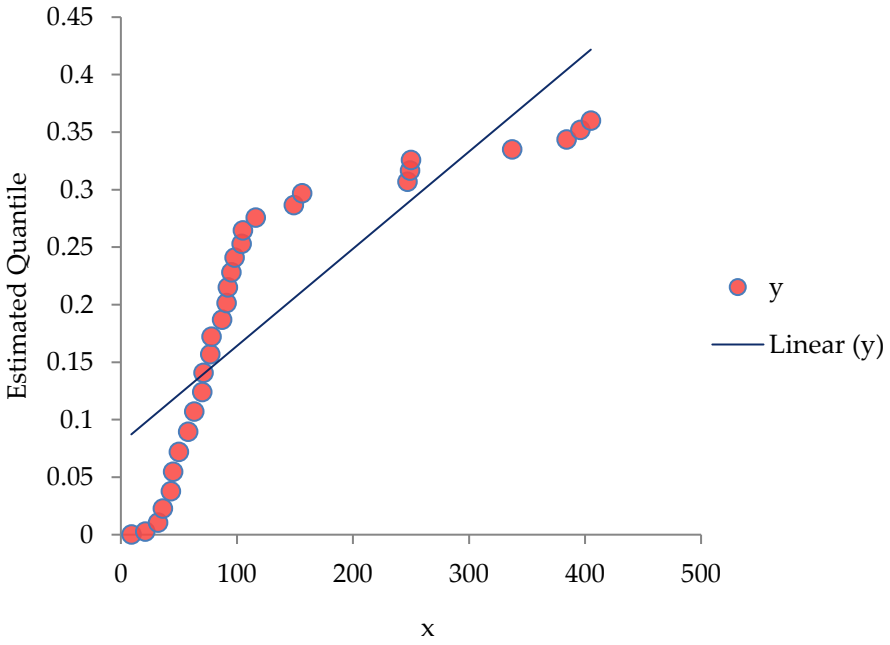


Figure 2: *QQ plot for the real time data1*

Using real-time data (Table 1), the adequacy of the model fit is verified by calculating the correlation coefficient and constructing a QQ-plot. The high correlation coefficient of 0.835 indicates a strong positive correlation, confirming the model's suitability for the data. The following table summarizes the estimation of parameters and mean value, upper, central and

lower control limits using Eq.15.

Table 2: *Frechet distribution estimators and its mean value control limits*

Frechet distributiom	
$\hat{k}$	0.65
$\widehat{k\phi}$	30.61188
$\mu(I_L)$	0.041327
$\mu(I_C)$	15.30594
$\mu(I_U)$	30.57056

Estimated values of $\mu(I)$ at the given failure times I1, I2, ... In along with the successive differences of these estimates are given in Table 3. The successive differences would indicate the estimated number of failures between consecutive failure times. The graph through $[I_i, \Delta\hat{\mu}(I_i)], i = 1,2,\dots,n-1$ along with three parallel horizontal lines at $\mu(I_L), \mu(I_C), \mu(I_U)$ would be the required control chart and is given in Fig 3.

2.5. Anomaly Detection with Random Survival Forest (RSF)

To detect anomalies in the failure times, we can apply Random Survival Forest (RSF), a machine learning method designed for handling time-to-event data. In this context, RSF can help to identify outliers or abnormal failure times that deviate significantly from the expected distribution.

- Data Preprocessing: We start by cleaning the failure data, handling any missing values, and ensuring proper formatting for RSF input.
- RSF Model Training: RSF is trained on the failure times, using features such as the successive differences between consecutive failure times. The model learns the survival probabilities over time, which represent the likelihood of a failure occurring at a particular time.
- Anomaly Detection: The RSF model calculates survival probabilities for each failure time. Anomalies are flagged based on survival probabilities that fall below a specified threshold, indicating abnormal behavior.
- Control Chart with RSF: In conjunction with RSF, we plot a control chart for the successive differences of failure times. This chart helps visualize potential anomalies by comparing actual observations against predicted values from the RSF model.

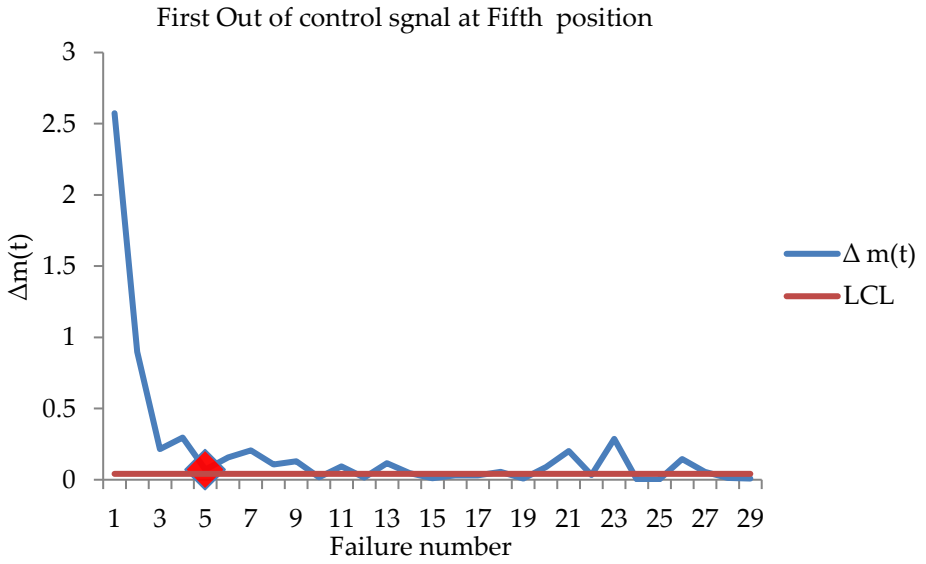
Table 3: *Consecutive differences placed on the $\mu(l)$ of FD*

Failure number	1	2	3	4	5	6	7	8	9	10
Failure time (hours)	9	21	36	43	45	50	58	63	70	70
$\mu(I)$	24.086	26.66	25.557	27.771	28.068	28.139	28.296	28.502	28.608	28.73
$\Delta\mu(I)$	2.5738	0.8973	0.2143	0.2965	0.0709	0.1573	0.2054	0.1067	0.1284	0.016
Failure number	11	12	13	14	15	16	17	18	19	20
Failure time (hours)	71	77	78	87	91	92	95	98	104	105
$\mu(I)$	28.753	28.846	28.86	28.977	29.023	29.034	29.066	29.096	29.152	29.161
$\Delta\mu(I)$	0.0926	0.0143	0.1167	0.0458	0.0109	0.0317	0.0301	0.056	0.0088	0.0889
Failure number	21	22	23	24	25	26	27	28	29	30
Failure time (hours)	116	140	156	247	249	250	337	384	396	405

$\mu(I)$	29.24	29.4505	29.484	29.7712	29.7755	29.7777	29.9232	29.9786	29.991	30
$\Delta\mu(I)$	0.2005	0.0335	0.2871	0.0043	0.0021	0.1454	0.0554	0.0124	0.0089	-

In Fig 3, The graph through $[I_i, \Delta\hat{\mu}(I_i)], i = 1, 2, \ldots, n-1$ along with three parallel horizontal lines at $\mu(I_L), \mu(I_C), \mu(I_U)$, would be the required control chart and is given in Figure 3. In Figure 3 the out of control is observed at the 5th observation below the LCL for Frechet Distribution.

3(a)



3(b)

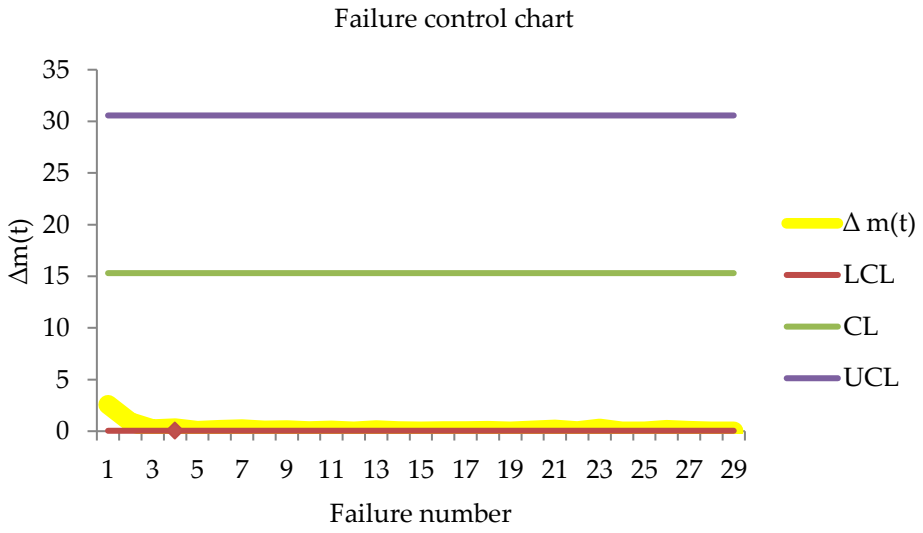


Figure 3: *Control chart based on successive differences of mean value function of FD*

2.6. Control Chart with RSF

The control chart incorporates three parallel lines representing:

- Upper Control Limit (UCL): The threshold above which observations are considered.
- Central Control Limit (CCL): The expected normal level of observations.
- Lower Control Limit (LCL): The threshold below which observations are considered

unusually low.

- In Figure 3, the out-of-control point occurs when the observation at the 5th failure time falls below the LCL, indicating an anomaly in the failure process.
- In figure 3, the control chart plots the successive differences, with three control limits, incorporating the RSF predictions. The out-of-control anomaly at the 5th observation is detected below the LCL, suggesting a failure that deviates from the expected pattern.
- The combination of Anomaly Detection and Random Survival Forest (RSF) allows for the effective monitoring of failure times and the detection of abnormal behavior. By leveraging RSF's survival probabilities, we can identify anomalies in the data, such as the out-of-control point observed in the control chart. This approach enhances the reliability of failure time analysis and provides a robust tool for predictive maintenance and system monitoring.

2.7. Comparative study

For comparison, Taking the Exponential model, the most frequently used model in reliability studies. The cumulative distribution function of Exponential distribution (ED) is

$$G(y) = 1 - e^{-\upsilon\delta}, \upsilon > 0, \delta > 0 \tag{16}$$

For our current investigation, the Nonhomogeneous Poisson Process (NHPP) is formulated with $G(y)$ serving as the mean value function

$$\mu(y) = \phi\left(1 - e^{-\delta y}\right), y > 0, \phi > 0, \delta > 0 \tag{17}$$

The following table summarizes the estimation of parameters and control limits for an Exponential distribution using Eq.17.

Table 4: *Parameter estimates of exponential model and their control limits*

Exponential model				
$\hat{\delta}$	$\hat{\phi}$	$\mu(I_L)$	$\mu(I_C)$	$\mu(I_U)$
0.03	30.00016	0.0405	15.0008	29.95966

Table 5: *Consecutive differences for the exponential distribution with RSF-based Anomaly detection*

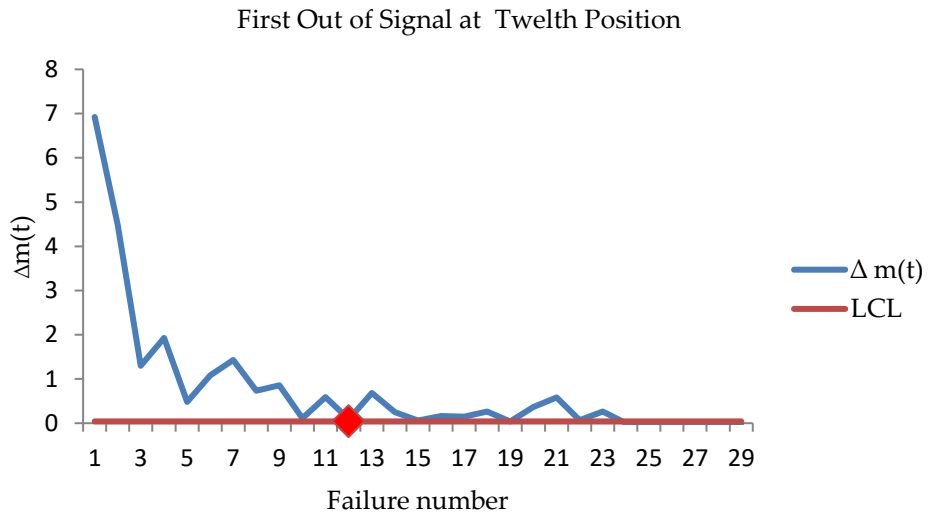
Failure number	1	2	3	4	5	6	7	8	9	10
Failure time (hours)	9	21	36	43	45	50	58	63	70	70
$m(t)$	7.0986	14.022	18.513	19.812	21.741	22.222	23.306	24.734	25.467	26.32
$\Delta m(t)$	6.9236	4.4909	1.2989	1.9297	0.4809	1.0833	1.4283	0.7334	0.8584	0.108
Failure number	11	12	13	14	15	16	17	18	19	20
Failure time (hours)	71	77	78	87	91	92	95	98	104	105
$m(t)$	28.753	28.846	28.86	28.977	29.023	29.034	29.066	29.096	29.152	29.161
$\Delta m(t)$	0.0926	0.0143	0.1167	0.0458	0.0109	0.0317	0.0301	0.056	0.0088	0.0889
Failure number	21	22	23	24	25	26	27	28	29	30
Failure time (hours)	116	140	156	247	249	250	337	384	396	405
$m(t)$	29.24	29.4505	29.484	29.7712	29.7755	29.7777	29.9232	29.9786	29.991	30

$\Delta m(t)$	0.2005	0.0335	0.2871	0.0043	0.0021	0.1454	0.0554	0.0124	0.0089	-

2.8. Anomaly Detection with Random Survival Forest (RSF)

Using Random Survival Forests (RSF), we apply a machine learning technique to detect anomalies in the failure times. RSF is particularly effective in handling censored data and can model the time-to-event data more robustly than traditional methods. RSF helps in identifying outliers by analyzing the successive differences of the failure times. The successive differences are computed between consecutive failure times, and any significant deviation from the expected range is flagged as an anomaly.

4(a)



4(b)

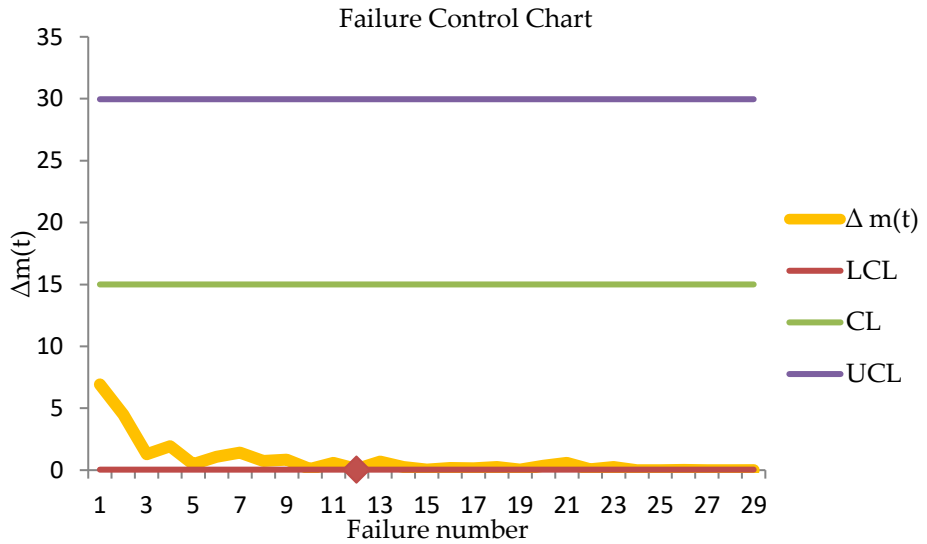


Figure 4: *Control Chart Based on Successive Differences of the Mean Value Function of ED Using RSF*

In Fig 4, The control chart in Figure 4 displays a graph for $i = 1, 2, \ldots, n-1$, with three parallel horizontal lines. Notably, in Figure 4, an out-of-control scenario is evident at the 12th observation, falling below the Lower Control Limit (LCL) for the Exponential distribution.Upon examining Figures 3 and 4, both the Frechet distribution and Exponential distribution (using RSF) show out-

of-control points below the Lower Control Limit (LCL), which suggests that the number of failures is lower than expected, implying a better-than-expected performance. The anomaly detected by RSF indicates that the 12th failure may have resulted from an improved process or a sudden change in system reliability. Such anomalies are indicative of improvements in quality and should be further investigated to determine the assignable causes.

In this study, the Frechet Distribution (FD) and Exponential Distribution (ED) are compared using Random Survival Forests (RSF) for anomaly detection in reliability analysis. The RSF method successfully detects anomalies in both distributions, with the Frechet Distribution showing an anomaly at the 5th observation and the Exponential Distribution showing an anomaly at the 12th observation. However, the Frechet Distribution results are more consistent and indicate fewer deviations from expected failure patterns compared to the Exponential Distribution, which shows more frequent outliers. Based on this analysis, the Frechet Distribution provides a more reliable and stable model for failure time analysis, making it the better choice for this study.

2.9. Monitoring the Prediction Process Using Order Statistics and Anomaly Detection with the Mean Value Function

The probability model of a continuous random variable Y describes the intervals between failures for a highquality product with a randomly chosen sample of size $'n'$, signifying $'n'$ inter-failure durations. $G(y)$ represents $Y's$ cumulative distribution function. Constructed for inter failure times, the time control chart displays benefits, warnings, and the stability of the failure process. In cases where $'r'$ is a natural number $(< n)$, the summations represent the intervals of time between each r^{th} error. Out-of-control signals relative to interfailure timeframes can be visualised using a control chart for the intervals between each r^{th} failure. The tr-controlcharts developed by 12Xie et al have certain shortcomings. Suggesting the utilization of the Failure Control Chart methodology to prevent such problems. If $(Y_1; Y_2; \dots; Y_r)$; $(Y_{r+1};\ Y_{r+2}; \dots;\ Y_{2r})$; $(Y_{2r+1};\ Y_{2r+2}; \dots;\ Y_{3r})$; etc are the i.i.d random variables having $G(y)$ as their common mode $Z_1 = Y_1, Z_2 = \sum_{i=1}^{2} Y_i, Z_3 = \sum_{i=1}^{3} Y_i, \dots,$ $Z_r = \sum_{i=1}^{r} Y_i$ becomes an ordered sample of size r representing the time to first failure, time to second failure, time to third failure, so on time to r^{th} failure respectively. The time to each r^{th} failure is represented by Z_r, the dots on the tr-chart, which is the control chart. The percentiles of the highest order statistics in a sample of size r would therefore function as control limits for the tr-chart when r is fixed. The following equations, which assume equi-tailed probability, provide solutions for the bottom, central, and upper limit lines, respectively.

$$|G(I)|^r = 0.00135 \tag{18}$$

$$|G(I)|^r = 0.5 \tag{19}$$

$$|G(I)|^r = 0.99865 \tag{20}$$

Let I_U , I_C, and I_L be respectively the solutions of Eq 18, Eq 19 and Eq 20 in the standard form

$$I_L = G^{-1}(0.00135)^{\frac{1}{r}} \tag{21}$$

$$I_C = G^{-1}(0.5)^{\frac{1}{r}} \tag{22}$$

$$I_U = G^{-1}(0.998655)^{\frac{1}{r}} \tag{23}$$

RSF (Random Survival Forests) and anomaly detection techniques into this model would

enhance its ability to identify significant deviations or outliers in failure times. RSF can be applied to model the survival times and detect anomalies more accurately, further improving the monitoring process and ensuring the reliability of the product over time. In Fig 5, For exponential distribution, use the Frechet distribution. This combination of parameters $k = 0.02, a = 0, b = 1,$ $\delta = 0.09$ is chosen to closely resemble the exponential distribution, as shown by the following probability curves of density functions.

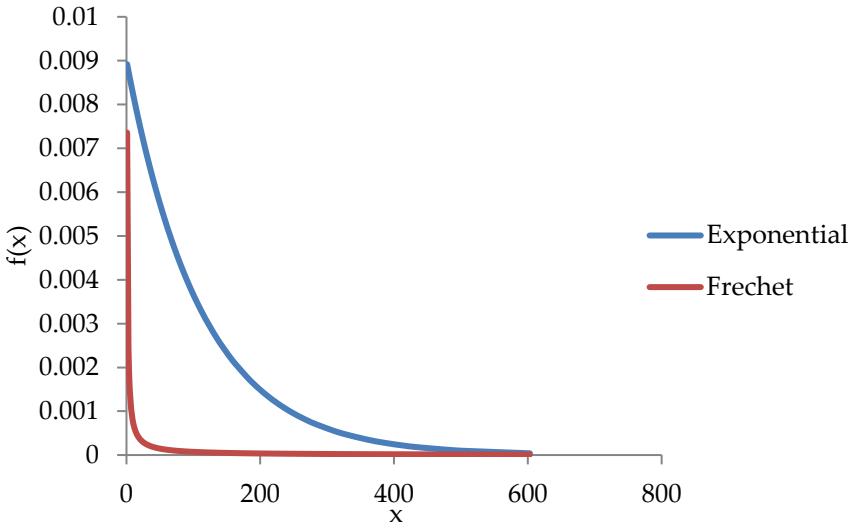


Figure 5: *Comparison of Frechet and Exponential distribution*

The NHPP with $G(x, y)$ as the mean value function as the FD for our present study is

$$\mu(x) = \phi(e^{-y})^{-k} \tag{24}$$

This model is demonstrated using real failure data, specifically 188 failures for the JET airplanes, as considered by Fatoki Olayode (2019). The following table presents the accumulated failures and the time to each 4th failure:

In this dataset, anomaly detection and Random Survival Forest (RSF) methods are applied to model and analyze the time to failure. The combination of RSF and anomaly detection allows for effective identification of outlier failures, which can help refine predictive maintenance strategies for aircraft systems. By using the RSF approach with anomaly detection, the model can highlight potential failures or abnormal behavior in the failure process. This allows for more accurate modeling of the failure times and provides a better understanding of the underlying processes.

Table 6: *Real-Time Data (188 Failures for JET Airplanes)*

Number	Failure times	Number	Failure times	Number	Failure times	Number	Failure times	Number	Failure times
1	194	39	14	77	32	115	46	153	14
2	413	40	14	78	9	116	230	154	111
3	90	41	29	79	438	117	26	155	97
4	74	42	37	80	43	118	59	156	62
5	55	43	186	81	134	119	153	157	39
6	23	44	29	82	184	120	104	158	30
7	97	45	104	83	20	121	20	159	7
8	50	46	7	84	386	122	206	160	44

9	359	47	4	85	182	123	5	161	11
10	50	48	72	86	71	124	66	162	63
11	130	49	270	87	80	125	34	163	23
12	487	50	283	88	188	126	29	164	22
13	57	51	7	89	230	127	26	165	23
14	102	52	61	90	152	128	35	166	14
15	15	53	100	91	5	129	5	167	18
16	14	54	61	92	36	130	82	168	13
17	10	55	502	93	79	131	31	169	34
18	57	56	220	94	59	132	118	170	16
19	320	57	120	95	33	133	326	171	18
20	261	58	141	96	246	134	12	172	130
21	51	59	22	97	1	135	54	173	90
22	44	60	603	98	79	136	36	174	163
23	9	61	35	99	3	137	34	175	308
24	254	62	98	100	27	138	18	176	1
25	493	63	54	101	201	139	25	177	24
26	33	64	100	102	84	140	120	178	70
27	18	65	11	103	27	141	31	179	16
28	209	66	181	104	156	142	22	180	101
29	41	67	65	105	21	143	18	181	52
30	58	68	49	106	16	144	216	182	208
31	60	69	12	107	88	145	139	183	95
32	48	70	239	108	130	146	67	184	62
33	56	71	14	109	14	147	310	185	11
34	87	72	18	110	118	148	3	186	191
35	11	73	39	111	44	149	46	187	14
36	102	74	3	112	15	150	210	188	71
37	12	75	12	113	42	151	57		
38	5	76	5	114	106	152	76		

In Fig 6, The goodness of fit of the data to the model is assess by calculating with the help of QQ-plot which resulted a reasonably good positive correlation coefficient of 0.69434.

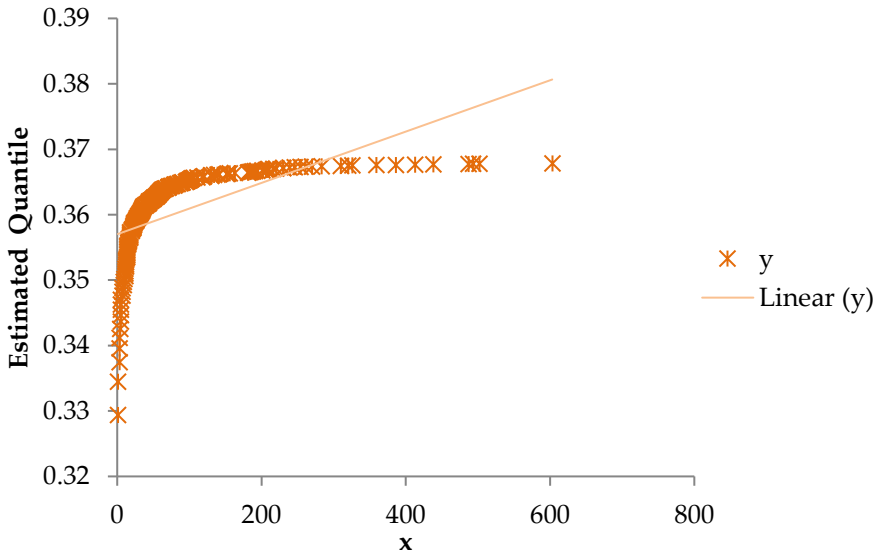


Figure 6: *QQ-Plot for real time data2*

The following Table 7 provides a thorough depiction of key metrics related to JET airplanes, including failure frequency, cumulative failure counts, and the temporal evolution associated with every 4th failure. The dataset could benefit from anomaly detection techniques, such as Isolation Forests, Autoencoders, or Z-Score methods, to highlight any outlying failure points or deviations from typical failure patterns that might signify system malfunctions or hidden patterns not immediately evident in the historical data.

Table 7: *Accumulated Failure Times*

Observation	Accumulated failures	4-order	Observation	Accumulated failures	4-order
1	771	8	25	110	227
2	225	17	26	468	236
3	1026	22	27	255	246
4	188	32	28	191	261
5	648	43	29	424	284
6	358	47	30	342	308
7	753	53	31	297	333
8	207	56	32	124	363
9	256	58	33	236	392
10	45	66	34	428	405
11	281	72	35	197	425
12	187	79	36	287	476
13	621	89	37	519	524
14	883	95	38	389	585
15	886	106	39	284	682
16	287	117	40	120	749
17	306	127	41	119	809
18	283	135	42	68	843
19	59	142	43	198	919
20	522	156	44	462	1031
21	724	173	45	211	1239
22	521	184	46	417	1596

23	423	200	47	287	2085
24	417	215			

Random Survival Forest (RSF) is a suitable method for analyzing and modeling the survival times of the JET airplanes, particularly when the failure time distribution is involved, as seen in the Frechet distribution analysis in Table 8. RSF can be used to predict the time-to-event or failure in such datasets, taking into account censored data (failures that were not observed within the study period). RSF models are robust for handling survival data, providing a powerful alternative to traditional methods like Cox proportional hazards models. Table 8 shows the parameter estimates for the Frechet distribution, along with the mean value and control limits, are meticulously presented. This section encapsulates the essential information needed to comprehend the distributional characteristics under consideration. The provided values, including the shape and scale parameters, offer insights into the Frechet distribution's behavior within the context of the study.

Table 8: *Frechet distribution parameter estimates and its mean value control limits*

Frechet distribution				
$\hat{k}$	$\hat{\phi}$	$\mu(t_L)$	$\mu(t_C)$	$\mu(t_U)$
0.02	114.7928	5.0219	39.9408	47.0046

The analysis of mean value function data, shown in Table 9, can also benefit from RSF, where survival probabilities can be calculated based on the accumulated failures (A.F) and other covariates. This would enhance the understanding of the dynamic relationship between accumulated failures and the corresponding mean failure times.

Table 9: *Mean Value Function for Accumulated Failure Times*

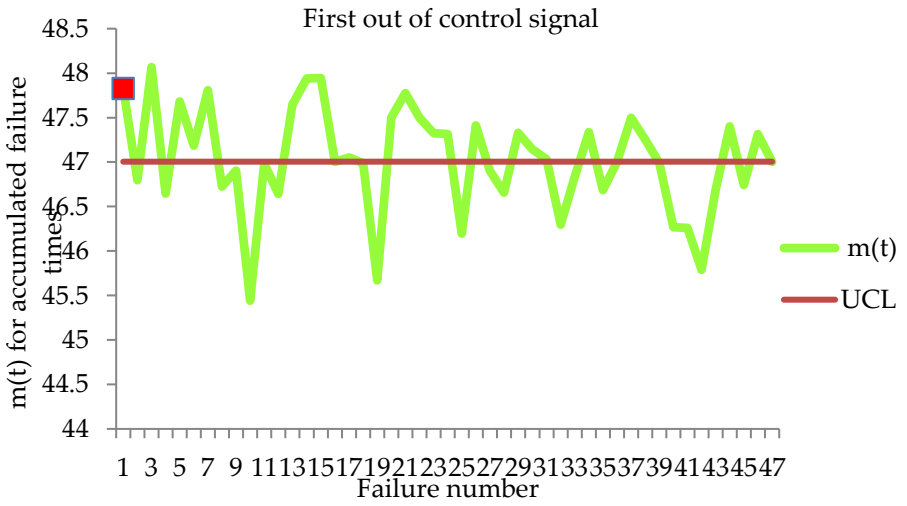
Observation	Accumulated failures	$m(t)$	Observation	Accumulated failures	$m(t)$
1	771	50.3916	25	110	31.9495
2	225	44.1301	26	468	50.0875
3	1026	50.8359	27	255	45.7180
4	188	41.4784	28	191	41.7278
5	648	50.6918	29	424	49.7215
6	358	48.8135	30	342	48.4995
7	753	50.7829	31	297	47.3305
8	207	42.9500	32	124	34.1860
9	256	45.7639	33	236	44.7627
10	45	16.9311	34	428	49.7611
11	281	46.7868	35	197	42.2069
12	187	41.3938	36	287	47
13	621	50.6507	37	519	50.3648
14	883	50.8228	38	389	49.3071
15	886	50.8233	39	284	46.8948
16	287	47	40	120	33.5755
17	306	47.6037	41	119	33.4194
18	283	46.8592	42	68	23.2716
19	59	20.9455	43	198	42.2843
20	522	50.3775	44	462	50.0457

21	724	50.7656	45	211	43.2290
22	521	50.3733	46	417	49.6488
23	423	49.7114	47	287	47
24	417	49.6488			

In Figure 7, control charts based on the mean value function depict the accumulated waiting time up to every 4th failure. The chart is crucial for identifying any potential anomalies in the failure data, such as out-of-control deviations. Anomaly detection techniques could help pinpoint abnormal data points, signaling unexpected failures or deviations from the expected system behavior.

The inclusion of Random Survival Forest (RSF) can also be integrated in this analysis to model the survival times and identify the factors contributing to failure. The RSF model would provide additional predictive power and insights into the reliability of JET airplanes, helping to pinpoint critical failure events earlier than traditional models.

7(a)



7(b)

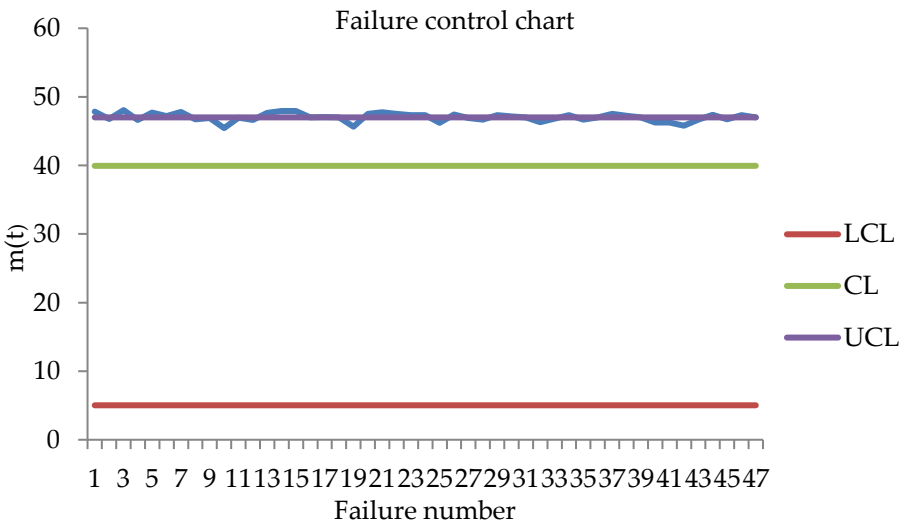


Figure 7: *Control Chart Based on Accumulated Failures of Mean Value Function of FD*

2.10. Comparative Study Based on Accumulated Failure Times

Comparing the model under study with the exponential model using the dataset provided in table 6, the results are as follows: Table 10 provides parameter estimates for the Exponential model along with their corresponding mean value function upper, central, lower control limits. This essential information includes estimates such as the scale parameter, location parameter, and shape parameter, crucial for characterizing the Exponential distribution. The presented values offer insights into the statistical properties of the model, facilitating a comprehensive understanding of its behavior within the context of the study.

Table 10: *Parameter estimates of Exponential model and their control limits*

Exponential model				
$\hat{\delta}$	$\hat{\phi}$	$\mu(t_L)$	$\mu(t_C)$	$\mu(t_U)$
0.009	50.84088	9.7453	42.7519	50.4237

Table 11 displays the Mean Value Function for accumulated failure times of ED. Each row provides detailed information, including observation number, accumulated failures, and the corresponding mean value. The progression of these values across observations facilitates a comprehensive analysis of the mean value function. The presented dataset contributes valuable insights into the dynamic relationship between accumulated failures and their associated mean values in the context of the ED model.

Table 11: *Mean Value Function for Accumulated failure times of ED*

Observation	Accumulated failures	$m(t)$	Observation	Accumulated failures	$m(t)$
1	771	47.8285	25	110	46.1942
2	225	46.7956	26	468	47.4102
3	1026	48.0677	27	255	46.9008
4	188	46.6444	28	191	46.658
5	648	47.6829	29	424	47.3274
6	358	47.1855	30	342	47.1471
7	753	47.8087	31	297	47.0287
8	207	46.7256	32	124	46.295
9	256	46.9040	33	236	46.8357
10	45	45.4419	34	428	47.3353
11	281	46.9822	35	197	46.684
12	187	46.6402	36	287	47
13	621	47.6473	37	519	47.497
14	883	47.9421	38	389	47.2552
15	886	47.9449	39	284	46.9912
16	287	47	40	120	46.2674
17	306	47.0538	41	119	46.2604
18	283	46.9882	42	68	45.7896
19	59	45.6700	43	198	46.6883
20	522	47.5018	44	462	47.3994
21	724	47.7759	45	211	46.7417
22	521	47.5002	46	417	47.3135
23	423	47.3255	47	287	47

24	417	47.3135

In Fig 8, control charts vividly portray the mean value function, capturing the cumulative waiting time up to every 4th failure. Noteworthy is the systematic plotting of mean values against each corresponding every 4th failure, producing a graphical representation comprising 47 data points extrapolated from the initial dataset of 188 observations. The manifestation of an out-of-control deviation in the Exponential distribution becomes apparent in the third observation, as the value exceeds the Upper Control Limit (UCL).

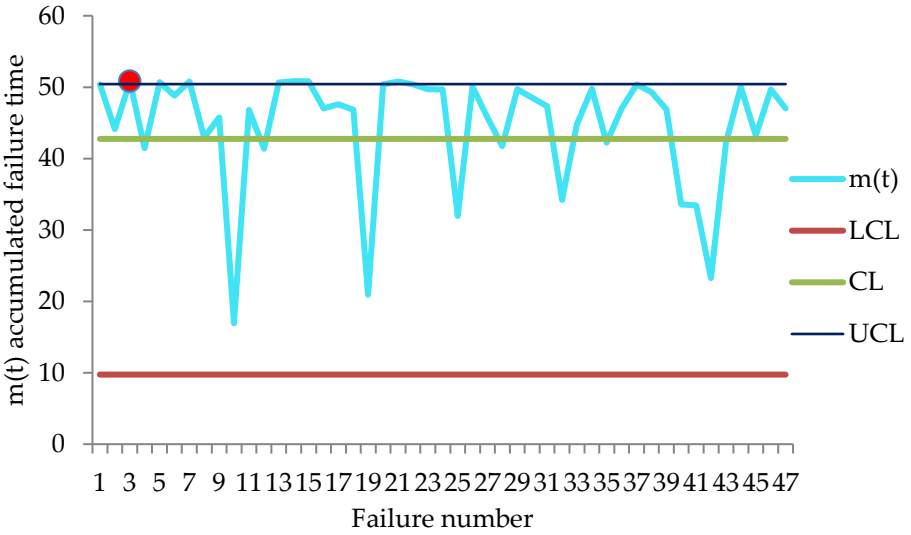


Figure 8: *Control chart based on accumulated failures of mean value function of ED*

Upon reviewing Fig 7 and Fig 8, it is evident that the initial out-of-control deviation is observed in the first observation for the Frechet Distribution (FD) and the third observation for the Exponential Distribution (ED). In both instances, the values surpass the Upper Control Limit (UCL), emphasizing a higher risk associated with quality concerns. The nature of these observations aligns with the principle that lower values indicate better quality. Remarkably, the Frechet Distribution exhibits an out-of-control signal at the UCL earlier than the Exponential Distribution, implying a more timely warning for potential quality issues. Consequently, in this comparative analysis, the Frechet model proves preferable to the exponential model, providing an earlier indication of out-of-control conditions based on the specified criteria.

Based on the comparative analysis of the Frechet distribution (FD) and Exponential distribution (ED), we find that the Frechet model provides an earlier indication of out-of-control conditions, making it a more effective choice for proactive quality control in JET airplanes. The use of anomaly detection and RSF models further strengthens this analysis by identifying outliers and predicting failure times with greater accuracy. These findings suggest that integrating these advanced techniques into the failure analysis process will improve the reliability and maintenance strategies for the aircraft systems, reducing risks and enhancing overall system safety.

III. Conclusion

This study focuses on the application of specialized control charts to assess product reliability, with a central line positioned at the median of varying quality and control limits derived from the quintailed most probable quantile at a coverage probability of 0.9973. The temporal occurrence of

failures, defined as the duration between successive failures, serves as the primary variable in this analysis, with a software tool developed to monitor and visualize failure patterns. The quality metric used in this study is based on the average number of failures within a given time interval, with the unique feature of the time control chart emphasizing that points near the Lower Control Limit (LCL) indicate favorable product performance.

In comparing the Frechet Distribution (FD) and Exponential Distribution (ED), the study reveals that the Frechet model provides superior results for failure time analysis. The Frechet distribution showed earlier indications of out-of-control conditions, making it a more effective tool for proactive quality control in JET airplanes. Additionally, the use of Random Survival Forests (RSF) for anomaly detection further validated the superiority of the Frechet distribution, with RSF successfully identifying anomalies in both distributions. However, the Frechet distribution exhibited fewer outliers and more consistent results compared to the Exponential model, which showed more frequent deviations from expected failure patterns. This comparative analysis highlights that the Frechet distribution offers a more reliable and stable model for analyzing failure times, providing valuable insights into the product's performance and reliability. The integration of advanced techniques like anomaly detection and RSF models enhances the accuracy of failure time predictions, contributing to improved reliability and maintenance strategies. These findings suggest that the Frechet distribution, combined with anomaly detection methods, will significantly reduce risks and improve the safety and performance of aircraft systems, making it the better choice for failure analysis in this study.

References

[1] B. Srinivas Rao and P. Sricharani, “Time control charts through NHPP based on Dagum distribution,” Int. J. Anal. Appl., vol. 16, no. 3, pp. 328339, Jan.2018, doi: 10.28924/2291-8639-16-2018-328.

[2] D. H. Lee et al., “Software reliability growth model with dependent failures and uncertain operating environments,” Appl. Sci., vol. 12, no. 23, p.2383, Dec. 2022, doi: 10.3390/app122312383.

[3] F. Grabski, “Nonhomogeneous Poisson Process and Compound Poisson Process in the modelling of random processes related to road accidents,” J. KONES, vol. 26, no. 1, pp. 39–46, Mar. 2019, doi: 10.2478/kones-2019-0005.

[4] H. C. Kim, “Assessing software reliability based on NHPP using SPC,” Int. J. Softw. Eng. Appl., vol. 7, no. 6, pp. 61–70, Nov. 2013, doi: 10.14257/ijseia.2013.7.6.06.

[5] H. Pham, “A new software reliability model with Vtub-shaped fault detection rate and the uncertainty of operating environments,” Optim., vol. 63, no.10, pp. 1481–1490, Oct. 2014, doi: 10.1080/02331934.2013.854787.

[6] H. Sabahno and A. Amiri, “New statistical and machine learning based control charts with variable parameters for monitoring generalized linearmodel profiles,” Comput. Ind. Eng., vol. 184, p. 109562, 2023, doi: 10.1016/j.cie.2023.109562.

[7] M. Xie, T. N. Goh, and P. Ranjan, “Some effective control chart procedures for reliability monitoring,” Reliab. Eng. Syst. Saf., vol. 77, pp. 143–150, Aug. 2002, doi: 10.1016/S0951-8320(02)00041-8.

[8] P. Roy, G. S. Mahapatra, and K. N. Dey, "An NHPPsoftware reliability growth model with imperfect debugging and error generation," Int. J. Reliab.Qual. Saf. Eng., vol. 21, no. 1–3, pp. 1–3, Apr. 2014, doi: 10.1142/S0218539314500089.

[9] R. De Blasis et al., “Weighted-indexed semi-Markov model: Calibration and application to financial modeling,” Financ. Innov., vol. 9, no. 1, p. 35, Sep. 2023, doi: 10.1186/s40854-022-00418-6.

[10] R. P. de Oleveira et al., “Non-homogeneous Poisson and linear regression models as approaches to study time series with changepoints,” Commun. Stat. Case Stud. Data Anal. Appl., vol. 8, no. 2, pp. 331–353, Mar. 2022, doi: 10.1080/23737484.2022.2056546.

[11] T. Salacinski, "Statistical process control using control charts with variable parameters," Processes, vol. 11, no. 9, p. 2744, Sep. 2023, doi:10.3390/pr11092744.

[12] T. Smajdorova and D. Noskievicova, "Analysis and application of selected control charts suitable for smart manufacturing processes," Appl. Sci., vol.12, no. 11, p. 5410, May 2022, doi: 10.3390/app12115410. igueredo, A. J. and Wolf, P. S. A. (2009). Assortative pairing and life history strategy - a cross-cultural study. Human Nature, 20:317–330.

A BAYESIAN APPROACH TO RELIABILITY ANALYSIS IN THE STRESS-STRENGTH MODEL WITH WEIGHTED EXPONENTIAL DISTRIBUTIONS CONSIDERING FUZZINESS

Alka Yadav, Satyanshu Kumar Upadhyay

•

Department of Statistics
Banaras Hindu University, Varanasi - 221005, India.
alkay4383@gmail.com

Abstract

The paper considers a Bayesian approach to the analysis of reliability in a stress-strength model when both stress and strength follow a weighted exponential distribution. The main focus of the paper considers a situation when the available data incorporate fuzziness. The situations when stress and strength distributions have common shape parameters and also when they have different shape and scale parameters are entertained separately. The entire analysis is done using the Bayes paradigm using weak proper priors for the model parameters. Since the resulting posteriors are not available in analytically closed form, the paper uses the recourse of Markov chain Monte Carlo simulation technique. Finally, a numerical illustration is provided based on real data examples. The results are found to be satisfactory.

Keywords: Weighted exponential distribution, Scale and shape parameters, Stress-strength model, Fuzzy reliability, Method of moments, Bayes paradigm, Weak proper priors, Gibbs sampler, Metropolis algorithm, Adaptive Rejection Sampling.

1. Introduction

The exponential distribution is one of the most widely used continuous distributions in statistical reliability and life testing. To remold this distribution, a new class of exponential distribution called the weighted exponential (W_E) distribution was introduced by [16] to introduce a shape parameter to the exponential distribution. This distribution is used as an alternative to other positively skewed lifetime distributions such as gamma, Weibull and generalized exponential distributions where shapes of probability density functions (pdfs) almost resemble the corresponding shape of the W_E density. Truly speaking, both gamma and the generalised exponential distributions can be considered as different weighted versions of the exponential distribution. The cumulative distribution function (cdf) and the pdf of a random variable X having W_E distribution with a shape parameter $\theta > 0$ and a scale parameter $\nu > 0$ can be written as

$$F_X(x;\theta,\nu) = 1 + \Big(\frac{e^{-\nu x}(e^{-\theta\nu x} - \theta - 1)}{\theta}\Big); \quad x > 0, \tag{1}$$

$$f_X(x;\theta,\nu) = \Big(\frac{\theta+1}{\theta}\Big)\nu e^{-\nu x}(1 - e^{-\theta\nu x}); \qquad x > 0 \tag{2}$$

and the corresponding hazard function of the model is given by

$$h_X(x) = \Big(\frac{\nu(\theta+1)(1-e^{-\theta\nu x})}{\theta+1-e^{-\theta\nu x}}\Big); \quad x>0 \tag{3}$$

It may be noted that the W_E distribution approaches to an exponential distribution with scale parameter unity if ν=1 and the parameter θ approaches to ∞. Similarly, the distribution approaches to the gamma distribution with shape parameter 2 if the parameter θ goes to zero. Besides, the W_E distribution coincides with the generalized exponential distribution with shape parameter 2 when the parameter θ=1 (see, for example, [16]).

The term stress-strength was first introduced by [6] and its further concept was developed by [7]. The stress-strength model is not only used in reliability analysis, but also used in several other fields, such as psychology, engineering, and medical sciences, etc. In its simplest form, let us consider two random variables, X and Y, where Y represents the stress experienced by a component and X represents its strength to overcome the stress. The component works as long as its strength exceeds its stress and, accordingly, its reliability is given by $P(X > Y)$. Many authors have considered drawing inferences about stress-strength reliability by considering different distributions for X and Y and using both classical and Bayesian paradigms. Among the important classical developments, one can refer to [8] where the authors have considered this problem by using independent normal distributions for both stress and strength (see also [29]). [5] is another important reference where the authors developed two estimators of reliability in a multicomponent stress-strength model where both stress and strength follow exponential distributions. They studied the performance of the two estimators by means of a Monte Carlo simulation study for moderate sample sizes. [3] considered the problem of estimating reliability when both stress and strength are independent but not identically distributed Burr random variables. [17], on the other hand, used generalised exponential distribution with common scale but different shape parameters for both stress and strength but mostly confined to maximum likelihood (ML) estimation of parameters. The authors, however, used Weibull distribution with different scale but common shape parameters in their other work (see [18]). Besides, there are several other references on classical inferences to reliability in the stress-strength model using different distributions for both stress and strength. An exhaustive list of the same may not be possible due to space restrictions. A few other important references using classical paradigm worth mentioning include [24], [11], [1] and [21], etc.

Bayesian inferences to stress-strength models have also been considered by several authors, but not as frequently as classical inferences. An early important reference can be considered as [10] where the authors considered the estimation of the probability that one random variable exceeds the other random variable, assuming that the two random variables are exponentially distributed. [9] is another important reference in the Bayes paradigm where the authors considered estimation of reliability of a multicomponent stress-strength system where both stress and strength are exponentially distributed random variables. There are plenty of other references where Bayesian inferences are successfully developed either in a single component stress-strength model or a multicomponent stress-strength model assuming different probability distributions for both stress and strength. For instance, [22] considered Weibull distributions with equal scale parameters for both stress and strength. The work of [14] was theoretically sound, where the authors developed Bayes inferences for the stress-strength system using different non-informative priors, including the reference priors, and studied the propriety of corresponding posteriors. The authors also focussed on getting the class of non-informative matching priors by matching the coverage probabilities of the classical and the Bayesian intervals. [4] is another significant development based on stochastic process modelling where the authors visualized the stress-strength system as time-homogeneous Markov process. They finally developed a simulation based Bayesian inferences using both conjugate and non-informative priors. A few other Bayesian developments worth mentioning include [23], [34] and [13], etc.

In the stress-strength model, it often happens that the observed data are not precise or exact due to misdetection or mishandling either on the part of the experimenter or the nature of

experimentation and, as a result, one has to take the recourse of fuzzy logic. It may be noted that the conventional study of reliability mostly relies on the exact data and assumptions but, in practice, data may be imprecise or compounded to some extent with uncertainties which may, among other things, occur due to subjective judgement of the reliability. Fuzzy reliability theory aims to account for such uncertainties using fuzzy logic while analysing the data. The theory involves fuzzy set theory, fuzzy logic and the notion of fuzzy probability. The concept of fuzzy set theory, introduced by [33], allows for the representation of uncertainty by defining membership functions that describe the degree to which an element belongs to a particular set. In the statistical analysis of reliability, this set may represent categories such as the 'high reliability', the 'medium reliability', and the 'low reliability'.

Fuzzy logic is used in numerous fields such as industrial automation, power engineering, environmental control, image processing and robotics, etc. Many researchers propose a different approach to prove fuzzy logic. With reference to the data obtained for analysing stress-strength reliability, [31] obtained conventional and fuzzy reliability by classical approach assuming a weighted exponential distribution for both stress and strength. As mentioned, the use of membership functions related to fuzzy logic is an important concept for the evaluation of fuzzy reliability. One can refer to [12] for a detailed description of the membership function and its relation to fuzzy logic.

The membership function takes different forms depending on the nature of the problem. Some common types of membership functions include triangular, trapezoidal, Gaussian, sigmoidal, among others. It may be noted that the choice of the membership function influences the behaviour and performance of a fuzzy logic system and, therefore, selecting an appropriate function is crucial for effective modelling and reasoning under uncertainty. Truly speaking, the membership function in the fuzzy set is the exposition of indicator functions in the classical setting. This paper also uses a specific form of fuzzy membership function to define reliability in a stress-strength relationship (see also [12]).

The remnants of this paper are systematized as follows. The next section considers the form of the likelihood and the reliability corresponding to W_E distribution in the conventional and the fuzzy layout. Section 3 provides the Bayesian model formulation for the considered model by specifying the proper but vague priors for the model parameters. The posteriors obtained in this section are analytically intractable and, therefore, the paper advocates the use of the Gibbs sampler algorithm for extracting samples from the posteriors and thereby drawing the sample-based inferences. It is, however, noted that some of the full conditionals are atypical from the viewpoint of sample generation and, therefore, these are managed by means of the Metropolis algorithm with an appropriately chosen kernel. A brief description of the two algorithms and their corresponding implementation details are also provided in Section 3. Section 4 gives a numerical illustration by considering a real data set. Finally, the findings of the paper are summarized in the conclusion section.

2. Reliability in a Stress - Strength Layout Assuming Weighted Exponential Distribution

To begin with, let us first focus on obtaining stress-strength reliability under both conventional and fuzzy logic assuming W_E distributions for both stress and strength. If X and Y denote the random variables corresponding to distributions representing strength and stress, the conventional stress-strength relationship suggests that the system is operational if $X > Y$. On the other hand, if Y surpasses X, the system fails. Let $f_X(x)$ and $f_Y(y)$ be the pdfs corresponding to two independent random strength and stress variables, then the expression for the conventional reliability can be written as

$$R = P(X > Y) = \iint_{x>y} f_x(x) f_y(y) dx dy. \tag{4}$$

Next, if $\Phi_{U(y)}$ is assumed to be the characteristic function for the set $U(y) = (x : x > y)$ (see also [12]), the same can be defined as

$$\Phi_{U(y)}(x) = \begin{cases} 1 & x > y \\ 0 & x \leq y. \end{cases} \tag{5}$$

Using the definition of the characteristic function $\Phi_{U(y)}$ given in (5), one can rewrite (4) as

$$R = P(X > Y) = \iint_{x>y} \Phi_{U(y)}(x) f_x(x) f_y(y) dx dy. \tag{6}$$

Let us next assume that both the random variables X and Y have the common shape parameters, that is, $X \sim W_E(\theta, \nu)$ and $Y \sim W_E(\theta, \eta)$. Under this assumption, the expression of reliability R, given in (4) for the stress-strength model, can be written as

$$R_1 = \left(\frac{\theta+1}{\theta}\right)^2 \nu\eta \left[\int_0^\infty \left(\int_y^\infty e^{-\nu x}(1 - e^{-\theta\nu x}) dx \right) e^{-\eta y}(1 - e^{-\theta\eta y}) dy \right], \tag{7}$$

which, on solving, reduces to

$$R_1 = \left(\frac{\eta^3(1+\theta) + 3\eta^2\nu}{(\eta+\nu)(\eta+\theta\eta+\nu)(\eta+\nu+\theta\nu)} \right) + \left(\frac{\nu\eta^2(3\theta+\theta^2)}{(\eta+\nu)(\eta+\theta\eta+\nu)(\eta+\nu+\theta\nu)} \right). \tag{8}$$

It may be noted that the symbol R_1 is used for notational ease. Similarly, if we consider the W_E distributions for X and Y with different shape and scale parameters, that is, $X \sim W_E(\theta_1, \eta_1)$ and $Y \sim W_E(\theta_2, \eta_2)$, the reliability R_2 for the stress-strength model can be written as

$$R_2 = \left(\frac{\theta_1+1}{\theta_1}\right)\left(\frac{\theta_2+1}{\theta_2}\right)\eta_1\eta_2 \left[\int_0^\infty \left(\int_y^\infty e^{-\eta_1 x}(1 - e^{-\theta_1\eta_1 x}) dx \right) e^{-\eta_2 y}(1 - e^{-\theta_2\eta_2 y}) dy \right], \tag{9}$$

which, on solving, reduces to

$$\begin{aligned} R_2 = & \left(\frac{\theta_1+1}{\theta_1}\right)\left(\frac{\theta_2+1}{\theta_2}\right)\eta_1\eta_2^2\theta_2 \times \\ & \left[\left(\frac{1}{\eta_1(\eta_1+\eta_2)(\eta_1+(\eta_2(1+\theta_2)))} \right) - \right. \\ & \left. \left(\frac{1}{(1+\theta_1)(\eta_2+\eta_1(1+\theta_1))(\eta_1(1+\theta_1)+\eta_2(1+\theta_2))} \right) \right]. \end{aligned} \tag{10}$$

The traditional stress-strength reliability as defined in (6) simply considers in some way the distance between X and Y when X happens to be greater than Y. In the setup of fuzzy logic, however, the stress-strength reliability considers instead the distance X-Y when X is bigger than Y in the sense of fuzzy logic. The concept of fuzzy events is capable of being precisely specified within the framework of fuzzy sets. As such, one can define the membership function for the fuzzy event 'X exceeds Y fuzzily' as $\Psi_{U(y)}$, which captures the relevant fuzzy logic implications. For an increasing function d, the corresponding membership function can be defined as

$$\Psi_{U(y)}(x) = \begin{cases} d(x-y) & \text{if } x > y \\ 0 & \text{if } x \leq y. \end{cases} \tag{11}$$

In this scenario, the membership function in the fuzzy logic is equivalent to the characteristic function used in the traditional logic. Thus, for a constant $k > 0$, often known as fuzzy degree,

$\Psi_{U(y)}$ can be articulated by considering the fuzzy distance between the strength and the stress as under

$$\Psi_{U(y)}(x) = \begin{cases} 1 - e^{-k(x-y)} & \text{if } x > y \\ 0 & \text{if } x \leq y. \end{cases} \tag{12}$$

As a result, the fuzzy stress-strength reliability can be written using the concept of fuzzy probability (see [32]) as

$$R_F = P(X \succ Y) = \iint_{x \succ y} \Psi_{U(y)}(x) f_x(x) f_y(y) dxdy \tag{13}$$

In fact, as the values of X-Y increase, the reliability of a stress-strength relationship enhances. Consequently, this insight could support a more nuanced interpretation. Also, it may be noted that as the value of the fuzzy degree k increases, the argument of the exponential term in (12) decreases, and therefore, the fuzzy reliability approaches towards conventional reliability.

Now coming back to the assumption that X$\sim$ $W_E(\theta, \nu)$ and Y$\sim$ $W_E(\theta, \eta)$, the fuzzy stress-strength reliability can be obtained as

$$R_{1F} = \left(\frac{\theta+1}{\theta}\right)^2 \nu\eta \left[\int_0^\infty \int_y^\infty \left(1 - e^{-k(x-y)}\right)\left(e^{-\nu x}(1 - e^{-\theta\nu x})\right)\left(e^{-\eta y}(1 - e^{-\theta\eta y})\right) dxdy \right], \tag{14}$$

which, on simplification, reduces to

$$\begin{aligned} R_{1F} = & \frac{k^2}{(k+\nu)(k+\nu+\theta\nu)} \times \\ & \left(\beta^2\left(\frac{(1+\theta)\eta + (3+\theta(3+\theta))\nu}{(\eta+\nu)(\eta+\theta\eta+\nu)(\eta+\theta+\theta\nu)}\right)\right) + \\ & \left(\frac{k\eta^2(2+\theta)\nu((1+\theta)\eta + (2+\theta(2+\theta))\nu}{(k+\nu)(k+\nu+\theta\eta)(\eta+\nu+\theta\nu)}\right). \end{aligned} \tag{15}$$

It can also be noted that (15) can be written in the form of conventional reliability R_1 as

$$R_{1F} = \frac{k^2}{(k+\nu)(k+\nu+\theta\nu)} R_1 + \left(\frac{k\eta^2(2+\theta)\nu((1+\theta)\eta + (2+\theta(2+\theta))\nu}{(k+\nu)(k+\nu+\theta\eta)(\eta+\nu+\theta\nu)}\right). \tag{16}$$

Similarly, under the assumption that X$\sim$ $W_E(\theta_1,\eta_1)$ and Y$\sim$ $W_E(\theta_2,\eta_2)$, the fuzzy stress-strength reliability R_{2F} can be given as

$$R_{2F} = \left(\frac{\theta_1+1}{\theta_1}\right)\left(\frac{\theta_2+1}{\theta_2}\right)\eta_1\eta_2 \left[\int_0^\infty \int_y^\infty \left(1 - e^{-k(x-y)}\right)\left(e^{-\eta_1 x}(1 - e^{-\theta_1\eta_1 x}\right)\left(e^{-\eta_2 y}(1 - e^{-\theta_2\eta_2 y}\right) dxdy \right], \tag{17}$$

which, on simplification, reduces to

$$\begin{aligned} R_{2F} = & \left(\frac{\theta_1+1}{\theta_1}\right)\left(\frac{\theta_2+1}{\theta_2}\right)\eta_2^2\theta_2 k \times \\ & \left[\left(\frac{1}{(\eta_1+\eta_2)(k+\eta_1)(\eta_1+\eta_2+\theta_2\eta_2)}\right) - \right. \\ & \left.\left(\frac{1}{(k+\eta_1(1+\theta_1))(1+\theta_1)(\eta_2+\eta_1(1+\theta_1))(\eta_1(1+\theta_1)+\eta_2+\theta_2\eta_2)}\right)\right]. \end{aligned} \tag{18}$$

Also, it can be seen that as k increases, both fuzzy reliabilities R_{1F} and R_{2F} converge to their conventional counterparts R_1 and R_2, respectively.

3. Bayesian Model Formulation

To begin with the Bayesian model formulation, we separately consider two cases: one where the shape parameters are the same for both the stress and strength random variables, and another where both the shape and scale parameters differ between the two random variables. The Bayesian model formulation for the two cases is given separately in subsections 3.1 and 3.2. These two cases will be referred to as Case 1 and Case 2 in the discussion that follows.

3.1. When the shape parameters are same for both stress and strength variables

Under the assumption that X follows $W_E(\theta, \nu)$ and Y follows independently $W_E(\theta, \eta)$, the joint pdf of X and Y can be written as

$$f_{X,Y}(x,y) = \Big(\frac{\theta+1}{\theta}\Big)\nu e^{-\nu x}(1-e^{-\theta\nu x})\Big(\frac{\theta+1}{\theta}\Big)\eta e^{-\eta y}(1-e^{-\theta\eta y}). \tag{19}$$

Now, let us assume that $x_1, x_2, \ldots, x_n$ are the observations corresponding to the strength variable X and $y_1, y_2, \ldots, y_n$ are the observations corresponding to the stress variable Y. Assuming the pdf given in (19), the corresponding likelihood function can be written as

$$L(\theta) = \Big(\frac{\theta+1}{\theta}\Big)^{n+m}\nu^n e^{-\nu\sum_1^n xi}\prod_1^n(1-e^{-\theta\nu xi})\eta^m e^{-\eta\sum_1^m yj}\prod_1^m(1-e^{-\theta\eta yj}). \tag{20}$$

For a Bayesian model formulation, we need to consider a prior for the shape parameter θ and the scale parameters ν and η. Since there is no *a priori* information available for θ, it is better to proceed with a weakly informative prior which may be taken as the uniform distribution in a large range. The same can be expressed as

$$\pi_1(\theta) = U(0, M) = \frac{1}{M}, \tag{21}$$

where M is the hyperparameter, usually taken to be large enough in order that the prior remains proper but vague. Similarly, for the parameters ν and η, one can consider independent gamma priors as given below.

$$\pi_2(\nu) = \frac{1}{\Gamma(a)}\frac{1}{b^a}\nu^{a-1}e^{-\nu/b}, \quad a>0, b>0 \tag{22}$$

$$\pi_3(\eta) = \frac{1}{\Gamma(c)}\frac{1}{d^c}\eta^{c-1}e^{-\eta/d}, \quad c>0, d>0 \tag{23}$$

where a, b, c, d are the hyperparameters, in a way that both (a, c) are the shape parameters and (b, d) are the scale parameters. A variety of strategies can be used to elicit the hyperparameters associated with the gamma priors. In the present paper, an attempt has been made to consider vague priors for both ν and η by taking sufficiently large variances of the considered gamma priors. To ensure large variance, one can obviously follow the strategy suggested by [26] and use a gamma prior that has a coefficient of variation at least 2.0 or larger. Since each of the considered gamma prior has two hyperparameters, one needs to formulate at least two equations to assess these two unknowns. Let us consider, for instance, the specification of hyperparameters of the prior given in (22). One can use the data-based information and accordingly consider the modal value of ν to be equal to its moment estimate. For formulating another equation, the coefficient of variation of ν can be taken as 2.0. It may be noted that the present paper considers the coefficient of variation as the ratio of the gamma standard deviation to its modal value. Thus, the two equations can be used to elicit the prior hyperparameters a and b associated with (22) that are presumably going to provide a vague prior. A similar strategy can be adopted to specify the hyperparameters associated with (23) resulting into another vague gamma prior for the parameter η. Following the specification of the priors, the joint prior can be expressed up to proportionality by combining the priors (21) to (23) as

$$\pi(\theta,\nu,\eta|x,y) \propto \frac{1}{M}\nu^{a-1}e^{-\nu/b}\eta^{c-1}e^{-\eta/d}. \tag{24}$$

The next step in the Bayesian model formulation is the specification of the posterior distribution and the same can be expressed up to proportionality by combining the prior in (24) with the likelihood in (20) using the Bayes theorem. That is

$$\begin{aligned} p(\theta,\nu,\eta|x,y) \propto & \Big(\frac{\theta+1}{\theta}\Big)^{n+m}\nu^n e^-\nu\sum_1^n xi\prod_1^n(1-e^{-\theta\nu xi})\times \\ & \eta^m e^{-\beta\sum_1^m yj}\prod_1^m(1-e^{-\theta\eta yj})\frac{1}{M}\nu^{a-1}e^{-\nu/b}\eta^{c-1}e^{-\eta/d}. \end{aligned} \tag{25}$$

Obviously, the posterior given in (25) appears to be analytically intractable and, therefore, we propose using the Gibbs sampler algorithm for extracting samples and drawing the sample-based inferences. The Gibbs sampler algorithm is an iterating scheme that often proceeds by drawing from different one-dimensional full conditionals that are also required to be specified up to proportionality only. The full conditional in each case is a conditional distribution of the specified variate presuming that all other variates are fixed known constants. The generation actually proceeds in a cyclic order, starting from one of the full conditionals and then successively iterating from all other full conditionals. The latest known values are used for the conditioning variates in each case. One can refer to [27] for details on the Gibbs sampler algorithm in the case of lifetime distributions (see also [28] and the references cited therein).

Looking on (25), the full conditionals for different variates involved in the joint posterior can be expressed up to proportionality as

$$p(\theta|x,y,\nu,\eta) \propto \Big(\frac{\theta+1}{\theta}\Big)^{n+m}\prod_1^n(1-e^{-\theta\nu xi})\prod_1^m(1-e^{-\theta\eta yj}), \tag{26}$$

$$p(\nu|x,y,\theta,\eta) \propto \nu^{n+a-1}e^{-\nu(1/b+\sum_1^n xi)}\prod_1^n(1-e^{-\theta\nu xi}), \tag{27}$$

$$p(\eta|x,y,\theta,\nu) \propto \eta^{m+c-1}e^{-\eta(1/d+\sum_1^m yj)}\prod_1^m(1-e^{-\theta\eta yj}). \tag{28}$$

It can be easily seen that the full conditionals given in (27) and (28) are concave on a logarithmic scale and, therefore, samples can be easily drawn from the two full conditionals using the procedure for drawing samples from logconcave densities. One such procedure is the adaptive rejection sampling method initially proposed by [15] that has been proved to be quite flexible and rich in a variety of cases (see also [27]). The form given in (26) is difficult from the viewpoint of direct sample generation and, therefore, one can use the Metropolis algorithm. A brief description of the same is given in the subsection 3.3.

3.2. When the shape and the scale parameters are different for both stress and strength variables

Under the assumption that X follows $W_E(\theta_1,\eta_1)$ and Y follows independently $W_E(\theta_2,\eta_2)$, the joint pdf of X and Y can be written as:

$$f_{X,Y}(x,y) = \Big(\frac{\theta_1+1}{\theta_1}\Big)\eta_1 e^{-\eta_1 x}(1-e^{-\theta_1\eta_1 x})\Big(\frac{\theta_2+1}{\theta_2}\Big)\eta_2 e^{-\eta_2 y}(1-e^{-\theta_2\eta_2 y}). \tag{29}$$

Now, let us assume that $x_1, x_2, \ldots, x_n$ are the observations corresponding to the strength variable X and $y_1, y_2, \ldots, y_n$ are the observations corresponding to the stress variable Y, then the likelihood

function for the observations assuming the pdf (26) can be written as

$$L(\theta) = \Big(\frac{\theta_1+1}{\theta_1}\Big)^n \Big(\frac{\theta_2+1}{\theta_2}\Big)^m \eta_1^n e^{-\eta_1 \sum_1^n xi} \times \prod_1^n (1-e^{-\theta_1\eta_1 xi})\eta_2^m e^{-\eta_2 \sum_1^m yj} \prod_1^m (1-e^{-\theta_2\eta_2 yj}). \tag{30}$$

The specification of the prior distributions for the parameters is the next stage in Bayesian model formulation. Due to lack of any *a priori* information, the specification proceeds exactly the way it is given in the previous subsection. As such, the prior distributions for θ_1 and θ_2 can be taken as uniform distributions given as under.

$$\pi_1(\theta_1) \propto U(0,V) = \frac{1}{V}, \tag{31}$$

$$\pi_2(\theta_2) \propto U(0,W) = \frac{1}{W}, \tag{32}$$

where, once again, the prior hyperparameters V and W can be taken large enough so that the priors remain more or less vague. Similarly, the priors for the scale parameters η_1 and η_2 can be taken to be gamma distributions with hyperparameters (q,r) and (s,t), respectively. These are given as

$$\pi_3(\eta_1) = \frac{1}{\Gamma(q)}\frac{1}{r^q}\eta_1^{q-1}e^{-\eta_1/r}, \quad r>0, q>0 \tag{33}$$

$$\pi_4(\eta_2) = \frac{1}{\Gamma(s)}\frac{1}{t^s}\eta_2^{s-1}e^{-\eta_2/t}, \quad s>0, t>0. \tag{34}$$

The elicitation of prior hyperparameters in (33) and (34) can proceed exactly in a way that is described in the previous subsection. The ultimate objective is to specify two equations to solve for these hyperparameters in a way that priors remain more or less vague.

The independent priors given in (31) to (34) can be multiplied to get the joint priors of the parameters and then the same can be finally combined with the likelihood function (30) via the Bayes theorem to get the joint posterior up to proportionality. This joint posterior can be written as

$$p(\theta_1,\theta_2,\eta_1,\eta_2|x,y) \propto \Big(\frac{\theta_1+1}{\theta_1}\Big)^n \Big(\frac{\theta_2+1}{\theta_2}\Big)^m \eta_1^n e^{-\eta_1 \sum_1^n xi} \times \prod_1^n (1-e^{-\theta_1\eta_1 xi})\eta_2^m e^{-\eta_2 \sum_1^m yj} \prod_1^m (1-e^{-\theta_2\eta_2 yj}) \times \frac{1}{V}\frac{1}{W}\eta_1^{q-1}e^{-\eta_1/r}\eta_2^{s-1}e^{-\eta_2/t}. \tag{35}$$

The posterior given in (35) is also analytically intractable and, therefore, we shall look first at the possibility of applying the Gibbs sampler algorithm. For the purpose of implementation, let us first write the full conditionals for the three variates θ_1, θ_2 and θ_3 as

$$p(\theta_1|x,y,\theta_2,\eta_1,\eta_2) \propto \Big(\frac{\theta_1+1}{\theta_1}\Big)^n \prod_1^n (1-e^{-\theta_1\eta_1 xi}), \tag{36}$$

$$p(\theta_2|x,y,\theta_1,\eta_1,\eta_2) \propto \Big(\frac{\theta_2+1}{\theta_2}\Big)^m \prod_1^m (1-e^{-\theta_2\eta_2 yj}), \tag{37}$$

$$p(\eta_1|x,y,\theta_1,\theta_2,\eta_2) \propto \eta_1^{n+q-1}e^{-\eta_1(1/r+\sum_1^n xi)} \prod_1^n (1-e^{-\theta_1\eta_1 xi}), \tag{38}$$

$$p(\eta_2|x,y,\theta_1,\theta_2,\eta_1) \propto \eta_2^{m+s-1} e^{-\eta_2(1/s+\sum_1^m yj)} \prod_1^m (1-e^{-\theta_2\eta_2 yj}), \tag{39}$$

respectively. As in the previous subsection, one can easily check that both (38) and (39) are concave on logarithmic scale and, therefore, adaptive rejection sampling of [15] can be used for corresponding sample generations. Both (36) and (37) do not offer any standard form for generating samples and, therefore, one can apply the Metropolis algorithm with an appropriately selected candidate generating density for generating the corresponding samples from (36) and (37).

3.3. A brief description of the Metropolis algorithm

As already mentioned, the two posteriors considered in the paper are analytically intractable, and an option is to draw sample-based inferences using the Gibbs sampler algorithm. The Gibbs sampler algorithm is used mainly for its straightforwardness and routine implementation. However, some of the full conditionals corresponding to the two posteriors considered in the paper were found to be difficult from the viewpoint of sample generation and thereby leaving for the scope of the Metropolis algorithm. This subsection briefly describes the Metropolis algorithm as a tool for sample generation from one-dimensional full conditionals.

The Metropolis algorithm is also a Markovian updating scheme to generate samples from a typically available density, often specified up to proportionality, using a symmetric Markov kernel. Although the algorithm is generally used for high-dimensional densities, given up to proportionality, it has been successfully employed for one-dimensional scenarios as well (see, for example, [26]. To briefly describe the algorithm for one-dimensional scenario, let us assume that p(θ|.) is the intended density of theta given fixed values of several other quantities (.). Let us consider a symmetric Markovian kernel to be used as a candidate generating density. Next, assume that the current state of the chain is θ and, given θ, the chain considers the next proposed realization θ' simulated from the candidate generating density. We shall, however, incorporate a further randomization and accept θ' with probability $\zeta(\theta, \theta') = \min\left(\frac{p(\theta|.)}{p(\theta'|.)}, 1\right)$. In case the proposed realization is not accepted, the chain remains at the value θ.

Various suggestions can be found in the literature on the selection of appropriate candidate generating densities. The choice is not difficult since we are mostly concerned with one-dimensional candidate generating density for simulating the intended one-dimensional full conditional. A few suggested choices could be a normal density with appropriately chosen mean and standard deviation, t-distribution, uniform density, etc. One can refer to [20] and [27], among others, for further details. The present paper considers a univariate normal kernel as the candidate generating density in each case where the corresponding full conditional cannot be generated easily. To start the process, we considered the initial value for the mean of the normal kernel as the moment estimate of the corresponding parameter and the standard deviation as δ times the square root of the Hessian evaluated at the moment estimator. The choice of moment estimator is certainly an approximation, and it cannot be considered as the most appropriate choice, though it has the advantage of being easy to evaluate for both the considered cases under the assumption of W_E model. It may also be noted that the choice of the initial values suggested above was upgraded after every 500 iterations using the generated sample output. Also, δ as defined above is the scaling constant, normally recommended in the range 0.5-1.0, to reduce the number of rejections in the iterating chain (see, for example, [27]).

Another important issue in the successful implementation of the Metropolis algorithm is monitoring convergence. The present paper considers the same based on ergodic averages obtained from a single long run of the chain. Once the convergence is observed, the simulating chain can be further continued and equidistant observations can be picked up to form the desired size of posterior samples. It may be noted that proper distancing among the generating variates will relegate the serial correlation to a bare minimum. These sample observations can then be used to form features of interest of the concerned posteriors (see also [28]).

4. Numerical Illustration

For numerical illustration, let us consider a real dataset that consists of breaking strength of jute fibre at various gauge lengths. The dataset was originally introduced by [30] and later on used by [25], [19] and [31] for estimating the reliability and other characteristics using different lifetime distributions. Here, we analyse the breaking strength of jute fibre at 10 mm and 20 mm for X and Y, respectively. The dataset is given below for a quick reference.

Data X: 693.73, 704.66, 323.83, 778.17, 123.06, 637.66, 383.43, 151.48, 108.94, 50.16, 671.49, 183.16, 257.44, 729.23, 291.27, 101.15, 376.42, 163.40, 141.38, 700.74, 262.90, 753.24, 422.11, 43.93, 590.48, 212.13, 303.90, 506.60, 530.55, 177.25.

Data Y: 71.46, 419.02, 284.64, 585.57, 456.60, 113.85, 187.85, 688.16, 682.66, 45.58, 578.62, 756.70, 594.29, 166.49,94.72, 707.36, 765.14, 187.13, 145.96, 350.70, 547.44, 116.99, 375.81, 581.60, 119.86, 48.01, 200.16, 36.75, 244.53, 83.55.

The datasets as given above were authenticated by [31] to have come from W_E distributions. The authors obtained classical p-values based on the Kolmogorov–Smirnov goodness of fit test, and they noted that the W_E model provides a very good fit to the two datasets.

To provide the complete Bayes analysis on the above datasets, let us begin by specifying the prior hyperparameters as described in subsection 3.1 and 3.2. The hyperparameters M, V, and W associated with the uniform distributions in the two cases were fixed at 50.0 each. It could be presumed that the value 50.0 was large enough to make the uniform priors quite weak although a number of other large values in the range 20.0 to 100.00 were also considered for each of these hyperparameters and no significant differences were observed in the results. Similarly, for the hyperparameters associated with the scale parameters in (22), (23), (33), and (34), we used the strategy suggested in the 3.1 and 3.2 and accordingly obtained the values of associated hyperparameters as $(a = 1.64, b = 0.05)$, $(c = 2.62, d = 0.0025)$, $(q = 2.62, r = 1.87)$ and $(s = 2.62, t = 0.0025)$.

Once the prior distributions were specified, the next task was to use the Gibbs sampler algorithm as discussed in Section 3 to simulate samples from each of the two posteriors corresponding to the two considered models given in (19) and (29). Of course, some of the full conditionals such as (26), (36) and (37) were simulated using the Metropolis algorithm (see subsection 3.3) with scaling constant δ empiically determined as 0.5 in each case. The implementation of the algorithm proceeded by simulating a single long run of chain using the details as given in Section 3. As mentioned, the initial values for the mean and standard deviation of the normal kernel were taken respectively as the corresponding moment estimates and the square root of the Hessian-based approximation evaluated at the moment estimates. The moment estimates of the parameters for the two considered cases (see also [2]) are reported in Table 1 although we needed these estimates for θ, θ_1 and θ_2 only (see also Section 3).

The convergence based on the ergodic averages corresponding to different parameters for Case 1 and Case 2 was obtained approximately at around 20K and 30K iterations, respectively. The computation time in order to achieve the convergence in running the Gibbs sampler algorithm with intermediate Metropolis steps as discussed earlier was approximately 4.83 seconds and 7.67 seconds, respectively, for Case 1 and Case 2 when the program was run on an i5 processor. Once the convergence was achieved, a sample of size 1K was obtained separately from the two posteriors corresponding to each of the parameters, ensuring that the serial correlation among the generating variates remains almost negligible. This was done by picking up every 10th observation from the generating chain.

Once the posterior samples are obtained, any feature of interest for the posterior distribution can be easily assessed which otherwise is not possible through non-sample based approaches. Table 2 shows some of the estimated posterior characteristics reported in the form of estimated posterior mean, median, mode, and highest posterior density interval with coverage probability

0.95 (0.95 HPD) for the parameters of each of the two considered models. It is obvious from the results that the estimated central values of the two posteriors, especially the posterior mode, are quite close to the moment estimates in most cases, giving the impression that our elicited priors are almost weakly informative and do not have any significant influence on the results (see also Tables 1-2). The estimated posterior characteristics also provide an impression that the corresponding posterior densities in each case are almost symmetric around the estimated central values except for the variates θ_1 and θ_2 which are slightly positively skewed, although the marginal density estimates are not shown in the paper. Besides, Table 2 also shows the estimated 0.95 HPD for the different parameters in the two cases. These values convey some information regarding the posterior variability that appears highest for θ in Case 1 and highest for both θ_1 and θ_2 in Case 2.

We also tried to examine the reason for delayed convergence in the single long run of iterating chain and the reason can be attributed to some extent to the high values of the estimated correlations between different combinations of variates. The estimated correlations were found to be -0.557, -0.507, -0.309, -0.408, respectively, between the pairs (θ, ν), (θ, η), (θ_1, η_1), (θ_2, η_2).

Finally, Table 3 shows the estimated values of conventional and fuzzy reliabilities for the two cases considered in the paper. These values are obtained simply by substituting the posterior modes of different parameters in the expressions of reliability given in (8), (10), (15) and (20). The estimates are extended in Table 4 by increasing the values of k. It is evident that, by increasing the value of k, the fuzzy reliability approaches towards the conventional reliability, which appears to be an obvious result.

Table 1: *Moment estimates of the parameters for Case 1 and Case 2*

Cases	Parameters	MM estimates
Case 1	θ	1.838
	ν	0.003
	η	0.003
Case 2	θ_1	2.010
	η_1	0.004
	θ_2	2.060
	η_2	0.003

Table 2: *Some of the estimated posterior summaries for the parameters of W_E distribution for Case 1 and Case 2*

Reliability		
Cases	Conventional reliability	Fuzzy reliability
Case 1	$R_1 = 0.535$	$R_{1F} = 0.528$
Case 2	$R_2 = 0.618$	$R_{2F} = 0.537$

Table 3: *Estimated conventional and fuzzy reliabilities for Case 1 and Case 2 when k=1*

Cases	Parameters	Mean	Median	Mode	0.95 HPD intervals
Case 1	θ	1.740	1.722	1.770	(0.451, 3.158)
	ν	0.003	0.003	0.003	(0.002, 0.004)
	η	0.003	0.003	0.003	(0.002, 0.004)
Case 2	θ_1	2.050	1.995	1.893	(1.202, 2.903)
	η_1	0.004	0.004	0.004	(0.002, 0.005)
	θ_2	3.136	3.080	2.820	(1.762, 4.451)
	η_2	0.004	0.004	0.004	(0.002, 0.005)

Table 4: *Estimated conventional and fuzzy reliabilities for Case 1 and Case 2 for different choices of k*

Cases	k	Conventional reliability	Fuzzy reliability
Case 1	1	0.535	0.528
	50	0.535	0.535
	100	0.535	0.535
Case 2	1	0.618	0.537
	50	0.618	0.538
	100	0.618	0.610

5. Conclusion

The paper provides the Bayes analysis of conventional and fuzzy reliabilities for two independent stress-strength variables when both stress and strength follow weighted exponential distributions. Two cases are explored. First, when both stress and strength have common shape parameters and, second, when both have different shape and scale parameters. Using the proper but weak priors for the parameters, the paper obtains sample based inferences based on the Gibbs sampler algorithm with intermediate Metropolis steps for some of the full conditionals. A numerical illustration is provided based on a real dataset consisting of the breaking strength of jute fibre at different gauge lengths. It is shown that the inferences are mostly affected by the data and, as expected, the priors have negligible effect on the inferences. Also, the numerical illustration effectively demonstrates that the fuzzy degree k significantly influences the fuzzy reliability in the sense that as the fuzzy degree k increases, the difference between fuzzy and conventional reliabilities diminishes, a finding that appears natural in this case.

Acknowledgement

The authors express their gratitude to both Ms. Sonam Gubreley and Ms. Shambhavi Singh for their support in writing the computer codes required for the necessary computation.

References

[1] Al-Mutairi, D., Ghitany, M., and Kundu, D. (2013). Inferences on stress-strength reliability from lindley distributions. *Communications in Statistics-Theory and Methods*, 42(8):1443–1463.

[2] Alqallaf, F., Ghitany, M., and Agostinelli, C. (2015). Weighted exponential distribution: Different methods of estimations. *Applied Mathematics & Information Sciences*, 9(3):1167.

[3] Awad, A. M. and Gharraf, M. K. (1986). Estimation of p (y< x) in the burr case: A comparative study. *Communications in Statistics-Simulation and Computation*, 15(2):389–403.

[4] Basu, S. and Lingham, R. T. (2003). Bayesian estimation of system reliability in brownian stress-strength models. *Annals of the Institute of Statistical Mathematics*, 55:7–19.

[5] Bhattacharyya, G. and Johnson, R. A. (1974). Estimation of reliability in a multicomponent stress-strength model. *Journal of the American Statistical Association*, 69(348):966–970.

[6] Birnbaum, Z. (1956). On a use of the mann-whitney statistic. In *Proceedings of the Third Berkeley Symposium on Mathematical Statistics and Probability, Volume 1: Contributions to the Theory of Statistics*, volume 3, pages 13–18. University of California Press.

[7] Birnbaum, Z. and McCarty, R. (1958). A distribution-free upper confidence bound for \pr{Y<X\}, based on independent samples of x and y. *The Annals of Mathematical Statistics*, pages 558–562.

[8] Church, J. D. and Harris, B. (1970). The estimation of reliability from stress-strength relationships. *Technometrics*, 12(1):49–54.

[9] Draper, N. R. and Guttman, I. (1978). Bayesian analysis of reliability in multicomponent stress-strength models. *Communications in Statistics - Theory and Methods*, 7(5):441–451.

[10] Enis, P. and Geisser, S. (1971). Estimation of the probability that y< x. *Journal of the American Statistical Association*, 66(333):162–168.

[11] Eryılmaz, S. (2010). On system reliability in stress–strength setup. *Statistics & probability letters*, 80(9-10):834–839.

[12] Eryilmaz, S. and Tütüncü, G. Y. (2015). Stress strength reliability in the presence of fuzziness. *Journal of computational and applied mathematics*, 282:262–267.

[13] Ezmareh, Z. K. and Yari, G. (2023). Bayesian estimation of the stress-strength reliability based on generalized order statistics for pareto distribution. *Journal of Probability and Statistics*, 2023(1):8648261.

[14] Ghosh, M. and Sun, D. (1998). Recent developments of bayesian inference for stress-strength models. *Frontiers in Reliability*, pages 143–158.

[15] Gilks, W. R. and Wild, P. (1992). Adaptive rejection sampling for gibbs sampling. *Journal of the Royal Statistical Society. Series C (Applied Statistics)*, 41(2):337–348.

[16] Gupta, R. D. and Kundu, D. (2009). A new class of weighted exponential distributions. *Statistics*, 43(6):621–634.

[17] Kundu, D. and Gupta, R. D. (2005). Estimation of p [y< x] for generalized exponential distribution. *Metrika*, 61(3):291–308.

[18] Kundu, D. and Gupta, R. D. (2006). Estimation of p [y< x] for weibull distributions. *IEEE Trans. Reliab.*, 55(2):270–280.

[19] Mokhlis, N. A., Ibrahim, E. J., and Gharieb, D. M. (2017). Stress- strength reliability with general form distributions. *Communications in Statistics-Theory and Methods*, 46(3):1230–1246.

[20] Muller, P. (1991). *Numerical integration in Bayesian analysis*. PhD thesis, Purdue University.

[21] Pak, A., Khoolenjani, N. B., and Jafari, A. A. (2014). Inference on p (y< x) in bivariate rayleigh distribution. *Communications in Statistics-Theory and Methods*, 43(22):4881–4892.

[22] Pandey, M. and Upadhyay, S. (1986). Bayes estimation of reliability in stress-strength model of weibull distribution with equal scale parameters. *Microelectronics Reliability*, 26(2):275–278.

[23] Pandit, P. V. et al. (2019). Bayesian analysisof stress-strength reliability for inverse exponential distribution under various loss functions. *International Journal of Mathematics Trends and Technology-IJMTT*, 65.

[24] Rezaei, S., Tahmasbi, R., and Mahmoodi, M. (2010). Estimation of p [y< x] for generalized pareto distribution. *Journal of Statistical Planning and Inference*, 140(2):480–494.

[25] Saraçoğlu, B., Kinaci, I., and Kundu, D. (2012). On estimation of r= p (y< x) for exponential distribution under progressive type-ii censoring. *Journal of Statistical Computation and Simulation*, 82(5):729–744.

[26] Shukla, A., Ranjan, R., and Upadhyay, S. K. (2023). Bayes analysis of the generalized gamma aft models for left truncated and right censored data. *Journal of Statistical Computation and Simulation*, 93(12):2026–2051.

[27] Upadhyay, S., Vasishta, N., and Smith, A. (2001). Bayes inference in life testing and reliability via markov chain monte carlo simulation. *Sankhyā: The Indian Journal of Statistics, Series A (1961-2002)*, 63(1):15–40.

[28] Upadhyay, S. K. and Smith, A. F. (1994). Modelling complexities in reliability, and the role of simulation in bayesian computation. *International Journal of Continuing Engineering Education and Life Long Learning*, 4(1-2):93–104.

[29] Weerahandi, S. and Johnson, R. A. (1992). Testing reliability in a stress-strength model when x and y are normally distributed. *Technometrics*, 34(1):83–91.

[30] Xia, Z., Yu, J., Cheng, L., Liu, L., and Wang, W. (2009). Study on the breaking strength of jute fibres using modified weibull distribution. *Composites Part A: Applied Science and Manufacturing*, 40(1):54–59.

[31] Yazgan, E., Gürler, S., Esemen, M., and Sevinc, B. (2022). Fuzzy stress-strength reliability for weighted exponential distribution. *Quality and Reliability Engineering International*, 38(1):550–559.

[32] Zadeh, L. (1968). Probability measures of fuzzy events. *Journal of Mathematical Analysis and Applications*, 23(2):421–427.

[33] Zadeh, L. A. (1978). Fuzzy sets as a basis for a theory of possibility. *Fuzzy sets and systems*, 1(1):3–28.

[34] Zhang, L., Xu, A., An, L., and Li, M. (2022). Bayesian inference of system reliability for multicomponent stress-strength model under marshall-olkin weibull distribution. *Systems*, 10(6):196.

RT&A, No 3 (86)
Volume 20, September 2025

SYSTEMATIC FAILURES IN FUNCTIONAL SAFETY AND THE PROBABILITY MEASURE

Hendrik Schäbe
•
dr.hendrik.schaebe@gmail.com

Abstract

In this paper the probability measure is discussed. The point of interest is, whether probabilistic models are stable under different conditions and if they can be used further on, when conditions change. Systematic failures, as described in many standards of functional safety, play a role regarding this problem. Reducing systematic failures also means, to keep probabilistic calculus working. However, systematic failures have not been studied systematically regarding the question to keep the probability measure. An outline is given on the connection between systematic failures and the possibility to use probability calculus in technical problems in exploitation situations, where data from e.g. lab experiments are extrapolated to use conditions.

Keywords: systematic failures, probability measure, standardization

I. Introduction

There are two main sources of knowledge for RAM (Reliability, availability and Maintainability) engineers. On the one hand side, there are textbooks on probability and statistics. There is a lot of them and here only a classic one authored by Mann, Schafer and Singpurwalla [1] shall be mentioned. Reading these books the impression is the following: Reliability and safety are in fact described by a sufficient low failure probability or probability of occurrence of a dangerous event, the latter in many cases being a failure of a safety system. All the probabilities can be derived for a system, using probabilities for subsystems, components and events.
On the other hand side, there exist standards on reliability and safety. Focusing on safety we see, that these standards [2-6] require, that there should be also measures against so called systematic failures. Then, the natural question arises, why these measures are necessary, if probability describes the behavior of a system sufficiently completely? When speaking about a system, one might address hardware and software separately as well.

In this paper, however, only hardware failures shall be considered, so the paper is dedicated to a discussion of the problem of systematic hardware failures and its connection to the use of probabilistic arguments.

In section two the use of probability in reliability and safety is described. The third section is dedicated to probability as such. A definition is provided and discussed. Some regularity conditions are derived and it is shown, that certain influences just can invalidate the application of probability calculus. In the following, fourth, section the concept of systematic failures is described and it is shown, which systematic failures need to be reduced, which might invalidate probability calculus. In the fifth section two examples are given: early failures and aging, which could violate the assumptions of an important probabilistic model, the exponential distribution.

A main instrument against systematic failures is hazard analysis, derivation of risk reducing measures and specification, including these measures. This is considered in section six. The last section provides conclusions.

II. Use of Probabilistic Methods in Reliability and Safety

A good overview of the use of probabilistic methods can be found in the book of Birolini [7]. The reliability is introduced as the "probability of an item to perform its required function under given conditions for a stated time interval." The definition provides a link to probability and a link to conditions, that this probability can be used. These are the "given conditions", which are not yet further specified. Then, a distribution function and a failure rate function are introduced, which depend on time. The failure rate function of a system is usually bathtub shaped.

Why is probability used in the context of reliability and safety? There are so many influences on a failure or a dangerous event, that cannot be described completely and this insecurity is then modeled by a probability, see e.g. the book of Härtler [8].

Almost all models in reliability and safety are probabilistic ones. Always, a probability of failure or a probability of occurrence of a dangerous event is computed using probability algebra. On the one hand side there exist sophisticated models in theory, alas engineers restrict themselves to much simpler models.

A very simple model is the use of the exponential distribution for times until failure or a dangerous event. For dangerous events, such a choice is logical, since dangerous events occur seldom and one might assume a Poisson process for them, resulting in exponentially distributed times until the occurrence of the event.

In reliability, the failure rate of a lifetime distribution is known to be bathtub shaped, starting with an early failures phase, followed by a phase of constant failure rate and finally, aging and wear cause leading to an increasing failure rate. Using the exponential distribution is a simplification assuming the absence of early failures and neglecting aging and wear – or assuming that this phase has not yet started. For details see e.g. Mann Schafer Singpurwalle [1] and Jensen [9]. A much better model is the Weibull distribution or even other, more complicated models. They are more flexible and can model also tendencies as early failures or wear and aging. However, either there exist insufficient data or the analyst simply did not think about those models.

So, most analysts are stuck with the exponential distribution and its parameter, the failure rate or event rate. The source for the parameter of the exponential distribution are either tables as the NPRD [10], standards with tables as EN 61709 [11], or the book of Proske [12] (to name some examples) or own statistics collected from life time experiments or observations.

These data have then to be adapted to other use cases, where it is assumed that the original conditions still hold. The latter is frequently done by simple engineering judgment. This is the point, where it becomes interesting: can one really assume that the probability distribution function of the time to failure or dangerous events is the same when using it also under another, new situation than the original one, i.e. the situation where statistics have been collected or the data from which the failure rate in the handbook has been computed?

III. Basics of Probability

Until now, probability has been only mentioned in a rather intuitive way. In this section it shall be explained, what probability is. In this paper, the axiomatic definition is used, that originates from Kolmogorov [14]. A good explanation can be found in Pollard [15]. For further reading, we refer to Braband and Schäbe [13].

Probability is a non-negative measure defined on a set, which becomes one for the entire set and which is additive for all disjunct subsets of the original set. It is also required to define a so-called sigma algebra, which defines how elements of the set have to be combined, so that finally, the sigma algebra contains all elements of the original set and combinations of them and combinations of elements of the sigma algebra.

So far, the probability has not yet any practical meaning. It is then interpreted as a limit of frequencies of events that are represented by elements of the sigma- algebra [15].

In case of symmetry, the probability can even be determined theoretically. Assume a dice with six sides, then caused by the symmetry we have

$$P(E_1) = P(E_2) = P(E_3) = P(E_4) = P(E_5) = P(E_6),$$

$$P(E_1) + P(E_2) + P(E_3) + P(E_4) + P(E_5) + P(E_6) = 1.$$

Here E_k denotes the event that the dice shows number k on its top when being thrown. Obviously, we have

$$P(E_k) = 1/6, \text{ for all } k = 1,\ldots, 6.$$

Another example for determination of a probability comes from thermodynamics, see Landau and Lifschitz [16]. If a thermodynamic system with many degrees of freedom is considered, then in the phase space, all points being on a hyper-sphere defined by conservation laws (energy and momentum) are considered equally probable. If the situation is not completely symmetric, then the distribution will change from a simple uniform distribution on the sigma algebra to another distribution function.

If, however, there are singularities, probabilistic laws will seize to be applicable. An example is a hacker attacking a system, see Braband and Schäbe [13]. Here, the concept of probability will fail in cybersecurity applications.

Another example would be the influence of high voltage from a railroad traction system. If a system is not able to withstand such an influence or it is not consequentially separated from high voltage, it would simply instantaneously fail and any probabilistic considerations derived from nice lab experiments will become obsolete. Here, again a simple strong influence factor will violate the symmetries that are necessary for the existence of a probabilistic law.

Another example is load. If the load on a mechanical system is different in a use case compared with lab conditions, the probability law will still exist, but this law will change. See for instance Schäbe and Viertl [17].

So, we have two principal problems when using probabilistic models. This holds especially, when we have gotten a result under one condition and we want to transfer it to another condition, which we would judge to be equivalent:

(A) One needs to make sure, that the concept of probability can be used. The conditions for the existence could be violated, since there would exist a singular influence leading to reactions that cannot be measured with a probability. Even if under certain conditions, under which failure rates have been obtained, a probability law existed, under some new conditions such a singular influence might occur and probability would fail to exist.

(B) One also needs to consider influences that will not violate the assumptions for a probability to exist, but that might change the probability measure itself. An example are loads.

These two goals (A) and (B) are important to achieve, if the same probability model shall further be used.

IV. Systematic Failures

When having a first glance at reliability and safety, one might get the impression that everything is described by probability and if once we have determined the parameters, we can use them in all situations. However, there occur also systematic failures. These are failures caused mainly by humans or by faulty processes, which are also set up and run by humans.

Consequently, the impression that simple probability calculations using data from the bookshelf would be sufficient, is misleading.

IEC 61508 [5] part 4 defines random and systematic failures as follows:

3.6.5: “a random hardware failure is a failure that occurs at a random point in time that is the result of one or more possible hardware degradation mechanisms”;

3.6.6: “a systematic failure is a failure deterministically associated with a certain cause that can only be eliminated by modifying the design or the process, operations, documentation, or other

factors".

In this section and the following, only measures against systematic failures in safety are considered. This is caused by the fact, that for reliability there has not been systematic research on systematic failures and measures against them. Usually, systematic failures are simply neglected. We refer to Shubinski and Schäbe [18] for similarities between functional reliability and functional safety, explaining that measures against systematic failures in safety can be equivalently used in reliability.

According to Shubinski and Schäbe [19] , failures are distinguished according to the mechanism, which has caused them. The random hardware failure is related to aging and degradation processes. On the contrary, the systematic failure is related to errors in design processes etc. However, also these failures manifest themselves in a stochastic manner, when the failure mechanism is triggered, so they are only deterministic in the sense that one certain well—defined cause can be indicated [20]. This cause occurs in a random manner, so the time of occurrence is random. This randomness is caused by the environment which causes a random influence.

To be precise, here one should distinguish two sub-cases:

a) The system contains an error, e.g. a software error. Another example can be a system that is not able to withstand certain high or low temperatures, although those are specified. There is no aging. As soon as an influence activates this error, the system fails at a random time. Randomness is caused by the randomness of the exterior influence.

b) Due to erroneous processes the system has a weak point. This weak point is e.g. decreased robustness w.r.t loads, environmental influences etc. An example are under-dimensioned mechanical parts that fail caused by fatigue. In fact an additional random failure mechanism is activated by a design error that would have been excluded otherwise. Without occurrence of the design error, the component would have been dimensioned strong enough.

In both cases a probabilistic model might still be valid, however a systematic failure might also completely destroy probabilistic laws, caused by an error leading to instantaneous failure of the system, as in the high-voltage example in the previous subsection.

Measures against systematic failures were introduced, so that systematic failures could be neglected in comparison with stochastic ones.

Systematic failures have never been described using probabilistic models, since no one knows how to do this. And this is apparently difficult to do, since for some systematic failures probabilistic models simply do not work.

Methods against systematic failures have been derived by groups of experts, that have compiled sets of these measures based on their experience. Sometimes, standards from other areas have been used. Since the experts in the standardization groups collected to their best knowledge methods to reduce systematic failures in order to keep the random failure model being the dominant one, they also derived many methods that are also suitable to preserve probabilistic models. But this was not their main intention.

The standards on functional safety [2-6] provide measures against systematic failures that can be classified roughly in the following groups:

- Quality management
- Safety management
- Principles for safety architecture
- Principles of safe design
- Safety analyses
- Verification and Validation methods
- Testing
- etc.

These groups of measures can be found in many safety standards with different detail. Partially, standards are carrying over experience from other areas and therefore also from the standards of these areas, the mother standard IEC 61508 [4] serves as a source for many others. The tables of measures against systematic failures are a compilation of experience of the engineers.

So, there is no direct relation between the long list of measures against systematic failures and

the two goals (A) and (B) as defined above in section 3.

V. Examples

I. Burn-in

As an example, let us consider burn in [9]. Burn-in is used to cope with early failures. In fact these are specific procedures of quality management and testing used to avoid early failures. Burn-in is one measure, to keep the lifetime distribution an exponential one – if aging is neglected as of now. Here it must be noted, that the specific measures to carry out burn-in tests are not specified in most of the standards. Burn-in is not mentioned in EN 50126 [21] / EN 50129 [2] and RTCA/DO-254 [6]. ISO 26262-4 [22] mentions a burn-in test in 9.4.1.2.a) as a requirement for ASIL C and higher. IEC 61508-2 [4] requires a burn-in test for SIL 3 and SIL 4 in table F.1 line 40.

This clearly shows, how different standards treat an important measure to cope with early failures in different extent. Most of them do not mention burn-in, only two standards [4,22] mentions burn-in.

II. Prevent aging

Another aspect to maintain the model of the exponential distribution is to ensure that the failure rate is constant, i.e. aging must be neglected, too. This means that components need to be replaced early enough before aging occurs. Sometimes, entire systems are replaced, before aging starts.

Aging is not treated in RTCA/DO 254 [6], EN 50129 [2], EN 50126 [21], ISO 26262-4 [22], so all standards are ignorant towards aging and just quietly support that components are not used too long, somehow.

Another example for the importance of measures against systematic failures is that the activation of additional failures modes must be prevented, when turning from lab conditions or other use conditions under which the failure rate has been obtained using statistical methods to another operating condition. So, it is totally important to obey standards on environmental conditions and electromagnetic compatibility, as mentioned in the standards on functional safety. If not, there could be two consequences:

- additional failure modes would be activated caused by unforeseen and not clearly defined environmental conditions or
- a deterministic failure could even occur, since the system would be out of specification.

VI. Specification and hazard analysis

In addition, a system needs a really good and complete specification. The fact that the specification must have a certain quality is dealt with by different standards. This is discussed in the following subsections for different areas.

I. Automotive

ISO 26262-4 [22] dedicates chapter 6 to this question. In clause 6.4.5. of ISO 26262-8 [23], clause 6 is cited for requirements to the specification. There, general criteria are specified as

- unambiguity,
- comprehensibility,
- atomicity,
- internal consistency,
- feasibility and achievability,
- verifiability,
- necessity,
- free from implementation,

- completeness,
- conformity.

These requirements come mainly from system engineering and help to build up a good specification. However, completeness can only be guaranteed as far as in the hazard and risk analysis all possible hazards and risks have been identified and relevant requirements have been derived to sufficiently reduce the risks.

It is worthwhile noting, that ISO 26262-3 [24] chapter 6 gives only general requirements to the hazard and risk analysis. In annex B some explanation on the risk classification is given. Examples are focused on driving situations. Part 10 of ISO 26262 [25] gives some further guidance on the hazard and risk analysis. There is no good guidance to look for hazards, that are introduced by possible components of new technology into the vehicle. This becomes evident, when battery electric vehicles, vehicles with a fuel cell and pressurized hydrogen etc. are analyzed.

II. Industrial technology

IEC 61508-1 [26] requires in 7.10.2.4 how to write a specification:

a) clarity, preciseness, unambiguity, verifiability ,testability, maintainability, feasibility,
b) comprehensibility,
c) it is expressed in natural or formal language and/or logic, sequence or cause and effect diagrams that define the necessary safety functions with each safety function being individually defined.

and further in 7.10.2.6.

a) a description of all the safety functions,
b) response time performance,
c) safety-related system and operator interfaces,
d) all information relevant to functional safety that may have an influence on the safety-related system design,
e) all interfaces, necessary for functional safety,
f) all relevant modes of operation of the EUC (equipment under control, i.e. the system, that is regarded),
g) all required modes of behavior of the safety-related systems shall be specified.

For industrial technology, IEC 61508 [4,5,24] does not give guidance on other hazards besides pure electrical ones. One needs to look at ISO 13849-1 [27] and DIN EN ISO 12100 [28] that give a really good guidance on hazard analysis and assists with lists of hazards to cover almost all possible hazards.

III. Railroad

For a specification, the following requirements need to be fulfilled [18]:

a) completeness, precision, unambiguity, verifiability testability and maintainability,
b) aid comprehension by those who are likely to utilize the information at any stage of the system life cycle,
c) expressed in natural or formal language and/or logic, sequence or cause and effect diagrams,
d) the defined set of requirements is suitable to define a system that is fit for the intended purpose.

The standard EN 50126-1 [18] provides a list of sources for hazards in 7.4.2.1:

a) system normal operation,
b) system fault conditions,
c) system emergency operation,
d) foreseeable system misuse, excluding deliberate misuse,
e) system interfaces,

f) system functionality,
g) system configuration parameters,
h) system operation, maintenance and support issues,
I) system disposal considerations,
j) human factors,
k) occupational health issues,
l) mechanical environment,
m) electrical environment,
n) natural environment to cover such matters as snow, floods, storms, rain, landslides etc.

Although general, it shows, which aspects need to be covered. For a good hazard analysis more detailed checklists are necessary, using other standards, as e.g. [27,28].

IV. Aerospace

RTCA-DO 254 [6] provides in 10.3.1. a set of subjects that should be covered by the requirements:

1. The system design and safety requirements allocated to the hardware,
2. Identification of applicable standards for the hardware,
3. Hardware functional and performance requirements, including derived requirements and stress limits for normal use,
4. Hardware reliability and quality requirements, including requirements related to failure rates, exposure times and design constraints,
5. Hardware maintenance and repair requirements throughout the hardware item service life,
6. Hardware manufacturability and assembly requirements,
7. Hardware testability requirements,
8. Hardware storage and handling requirements,
9. Installation requirements.

General requirements on the requirements specification, as provided by other standards, are missing.

Chapter 2 of [6] describes the hazard analysis process, leasing to five different system development assurance levels A-E. Detailed guidance on hazard analysis as in the other standards mentioned in this section is missing.

V. Analysis

We see that the requirements for a specification have many common points. However, for carrying out a hazard analysis the procedures are very different and they do not have the same coverage of new and unknown hazards in all the different areas. The coverage of unknown hazards is not only important for preventing of aging, but hazards need to be detected to avoid many systematic failures that could later lead to a violation of the assumption on the existence of the probability measure. The latter can either be distorted, or perhaps probability concepts are not applicable due to deterministic influences.

VII. Conclusion

The analysis has shown that there are a lot of measures against systematic failures in the standards. Also Birolini presents in chapter 3 of his book [7] a set of qualification tests for electronic components, which is a partial set of requirements. However, the measures presented in standards and textbook cannot yet be systematically related to effects, where the probability concept becomes void or where it is just changed. The measures against systematic failures are heuristic ones and they are compiled by engineering judgment, partially using experience from

other areas. Sometimes there are points missing, as e.g. burn-in. For some cases, such measures can be indicated in some standards only, as for burn-in [9] or for electronic components [7]. This relation, however, has not yet been systematized and has not be incorporated into the standards.

Requirements for specifications are mostly uniform, requirements for hazard analyses are really different with different depth. The hazard analysis is the main instrument to systematically identify influences that can violate the probabilistic model. As a consequences, one should look for a deep and comprehensive hazard analysis method to find as many hazards as possible. The functional safety standard of the coinciding area might give here only insufficient guidance, so the additional use of other standards is encouraged.

No explicit proof exists that the measures against systematic failures are sufficient to prevent an influence on the probabilities that are given as a result, with the intention to show that the system is safe or sufficiently reliable. Especially, the different measures against systematic failures for different SILs or design assurance levels cannot be proven to be sufficient in a strict sense. No quantification is given for a possible change of the computed probability caused by systematic failures. This seems to be impossible.

A lot of research is still needed to clarify,

a) what probability really means in the engineering context and

b) which methods need to be applied during the entire design process to ensure that the probabilistic models stay valid, when results obtained in a lab or by observation under certain real life conditions are used under exploitation conditions.

In the meanwhile, using consequently the measures against systematic failures as proposed in [2-6] is a good approach. Nevertheless, a few thoughts about the probabilistic models used, their appropriateness in the specific situation and some thoughts about the extrapolation from the data at hand to the current use case are in place. A third aspect is a good and comprehensive hazard analysis.

References

[1] Mann, N.R. and Schafer, R.E. and Singpurwalla, N.D., Methods for Statistical Analysis of Reliability and Life Data, J. Wiley and Sons, New Yok, Chichester, Brisbane, Toronto, 1974

[2] EN 50129, Railway applications - Communication, signalling and processing systems - Safety related electronic systems for signalling, 2018

[3] ISO 26262-5 Road vehicles — Functional safety — Part 5: Product development at the hardware level, 2018

[4] IEC 61508-2: Functional safety of electrical/electronic/programmable electronic safety-related systems Part 2: Requirements for electrical/electronic/programmable electronic
safety-related systems, 2010

[5] IEC 61508-4: Functional safety of electrical/electronic/programmable electronic safety-related systems Part 4: Definitions and abbreviations, 2010

[6] RTCA DO 254 / EUROCAE ED-80, Design Assurance Guidance, For Airborne Electronic Hardware, 2000

[7] Birolini; A., Reliability Ebgineering, Theory and Practice, Springer, 8th edition, 2017

[8] Härtler, G., Statistisch gesichert und trotzdem falsch? (Statistically ensured but nevertheless wrong) Springer, 2014.

[9] Jensen, F., and. Petersen, N.E., Burn in, J. Wiley & Sons, Chichester, New York, Brisbane, Toronto, Singapure, 1982

[10] Nonelectronic Parts Reliability Data Handbook, RIAC Automated Databook 2011

[11] EN 61709 Electric components - Reliability - Reference conditions for failure rates and stress models for conversion, 2017

[12] Proske, D. Catalogue of Risks, Springer, 2008

[13] Braband, J., and H. Schäbe, H. (2016), Probability and security – pitfalls and chances, Safety and reliability, 36:1, 3-12

[14] Kolomogoroff, A.N. Foundations of the theory of probability, New York: Chelsea Pub. Co., 1950

[15] Pollard, W. E., Bayesian Statistics for Evaluation Research, Sage Publications, Beverly Hills, London, New Delhi, 1986

[16] Landau, L.D., and Lifschitz, E.M., Statistical Physics, Volume 5 in Course of Theoretical Physics Third Edition, Pergamon Press, 1980

[17] Schäbe, H. and Viertl, R. (1995) An Axiomatic Approach to Models of Accelerated Life Testing, Eng. Fract. Mechanics, 50, No.2, 203-217.

[18] Shubinsky, I.B. and H. Schäbe, H. (2012) On the Definition of Functional Reliability, Reliability: Theory & Applications Vol.7 No. 4, 8-18.

[19] Shubinsky, I.B. and Schäbe, H. (2021), Errors, Fault and Failures, Dependability, vol. 21, no.2, p. 24-27.

[20] Braband, J., H. Gall, and Schäbe, H, Proven in Use for Software: Assigning an SIL Based on Statistics in: Handbook of RAMS in Railway systems – Theory and Practice, Qamar Mahboob, Enrico Zio (Eds.), 2018, Boca Raton, Taylor and Francis, Chapter 19, p.337-350

[21] EN 50126-1 Railway Applications - The Specification and Demonstration of Reliability, Availability, Maintainability and Safety (RAMS) - Part 1: Generic RAMS Process, 2017

[22] ISO 26262-4 Road vehicles — Functional safety — Part 4: Product development at the system, 2018

[23] ISO 26262-8 Road vehicles — Functional safety — Part 8: Supporting processes, 2018

[24] ISO 26262-3 Road vehicles — Functional safety — Part 3: Concept phase, 2018

[25] ISO 26262-10 Road vehicles — Functional safety — Part 10: Guidelines on ISO 26262, 2018

[26] IEC 61508-1: Functional safety of electrical/electronic/programmable electronic safety-related systems Part 1: General requirements, 2010

[27] ISO 13849-1, Safety of machinery – Safety-related parts of control systems – Part 1: General principles for design, 2015

[28] DIN EN ISO 12100 Safety of machinery –General principles for design – Risk assessment and risk reduction, 2011

Acknowledgement

The author wishes to thank A. Bochkov for his valuable comments on the paper.

DEVELOPMENT OF A NEW CURRENT LIMITING SYSTEM WITH AUTOMATIC REGULATION OF CUT-OFF CURRENT

R.Z. Sultanov[1], N.A. Aliyev[2], G.A. Aliyeva[3]

•

Azerbaijan State Oil and Industry University, Baku, Azerbaijan
[1] rafiq.sultanov@asoiu.edu.az; [2] nadir.aliyev@asoiu.edu.az; [3] aliyeva.gulnara@asoiu.edu.az

Abstract

The article considers the problem of ensuring reliable operation of DC electric drives under short-term overloads, when the installed power of the electric motor is limited. It is shown that the use of traditional current cutoff units does not allow for the effective use of the maximum permissible overload capacity of the motor when changing the reference speed. The dependence of the permissible overload current on the rotation speed is analyzed, and the limitations of the existing control schemes are identified. In this paper, the existing schemes of automated electric drives equipped with traditional current cutoff units are considered and their main disadvantages are identified. As a solution, a current limiting system with automatic regulation of the cutoff current is proposed, aimed at increasing the reliability and energy efficiency of adjustable electric drives. The key feature of the proposed system is to adapt the cutoff current value depending on the rotation speed of the motor, which allows dynamically matching the electromechanical characteristics of the drive with the permissible overload curve of the motor. A current limiting circuit for a DC electric drive is proposed, in which the cutoff current setting is automatically changed depending on the value of the specified speed. The circuit ensures full use of the maximum permissible overload capacity of the electric motor at all values of the setting voltage.

Keywords: electric motor, current limiting system, cut-off current, setting voltage, electromechanical characteristics, reliability

I. Introduction

For mechanisms in which short-term large overloads are observed, and the installed capacity of the DC electric drive is limited, it is necessary to fully utilize the maximum permissible overload capacity of the drive electric motor.

In [1], a brief analysis was carried out of the provision of known circuits of automated DC electric drives for full use of the maximum overload capacity of the drive motor and some shortcomings of these circuits were identified.

Fig. 1, a shows a simplified version of the DC electric drive circuit, where the motor overload is limited by a conventional current cutoff unit used in automation circuits. The controlled energy converter C, feeding the DC motor M with independent excitation, contains a control signal adder with identical windings CW1 and CW2.

The equation of the electromechanical characteristic of such a system can be represented as:

$$\omega = \frac{k_g(U_\Sigma)}{k\phi} \cdot U_s - \frac{r_c + r_m}{k\phi} \cdot I - \frac{k_c(U_\Sigma) \cdot r_s}{k\phi} \cdot (I - I_c) \cdot l(\Delta I) \quad (1)$$

Where $k_g(U_\Sigma)$ and r_c are the gain of the total input voltage and the output resistance of the converter, respectively; I and r_m are the current and resistance of the motor armature circuit,

respectively; U_s – setting voltage; I_c – cut-off current, I_c=const; U_r – reference voltage; k – electromagnetic constant; ϕ – motor excitation flux ϕ=const.

For different values of U_s, the electromechanical characteristics of the drive, constructed according to equation (1) at ϕ=const, will have the form shown in Fig. 1, b [2].

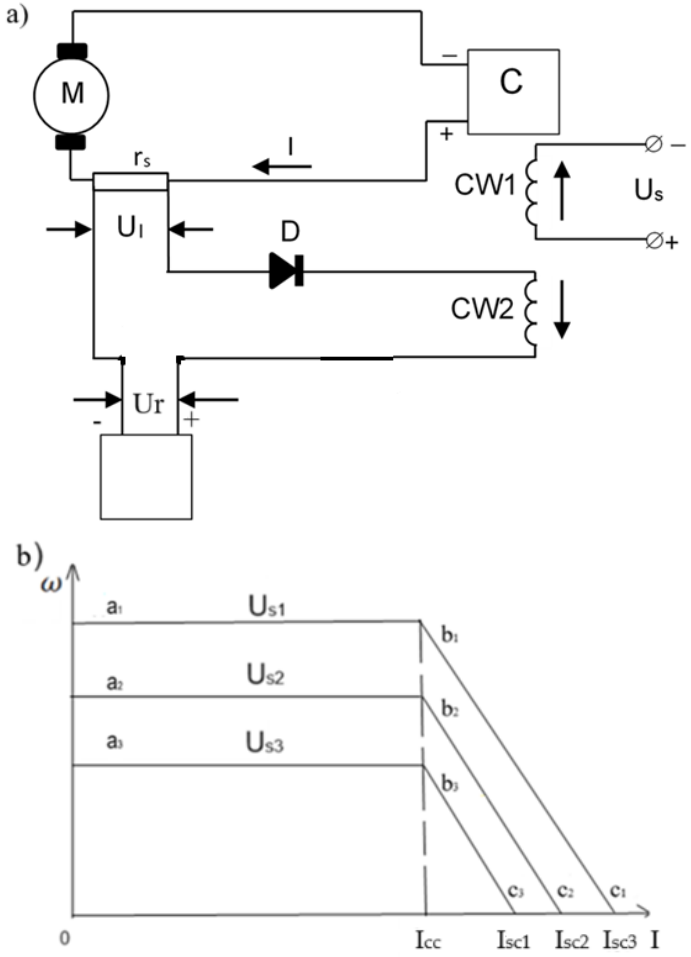


Figure 1: *Current limiting circuit (a) and electromechanical characteristics (b)*

As is known, the maximum permissible overload capacity (or maximum permissible current) of a DC electric motor changes depending on its speed - with decreasing speed, the maximum overload capacity increases. Usually, in practical problems, this dependence is assumed to be linear. To fully utilize the maximum overload capacity of an electric motor, the falling part of the electromechanical characteristic of the drive (for example, line b_1c_1 for U_{s1}) must be combined with the dependence curve of maximum permissible currents mentioned above. This can easily be done by selecting the parameters of the current limiting unit.

However, the overload limiting unit configured for one value of the setting speed does not ensure full use of the motor by permissible current at other values of the setting speed. For example, at U_{s2} and U_{s3}, automatic limitation of the overload current will pass along lines b_2c_2 and b_3c_3, which lie below line b_1c_1. Consequently, the use of a conventional current limiting unit in adjustable DC electric drives does not ensure full use of the maximum overload capacity of the drive motor at different values of the set speed [3-8].

In this regard, a new current limiting circuit was proposed for adjustable DC electric drives in [1], in which the comparison voltage does not remain constant, but changes as a function of the

motor speed. This was achieved by introducing an additional signal from the speed sensor into the current limiting circuit. However, as was noted there, such a solution to the problem has some of its own drawbacks: the presence of a tachogenerator and some dependence of the stop current on the value of the setting signal.

II. Materials and methods

In connection with the above, a slightly different current limiting circuit is proposed, a simplified version of which is shown in Fig. 2, a. Here, a signal of the setting voltage U_s in reverse polarity relative to the reference voltage U_r is additionally introduced into the circuit of the current limiting unit. The setting signal U_s, subtracted from the reference voltage U_r, forms a comparison voltage U_c, the value of which increases as the setting signal (or the specified engine speed) decreases, due to which the cutoff current becomes a function of the specified engine speed. At the moment of the start of the cutoff, the following voltage balance takes place:

$$U_I = U_c = U_r - U_s = I_{cc} r_s$$

Cutoff current:

$$I_{cc} = \frac{U_r - U_s}{r_s} \quad (2)$$

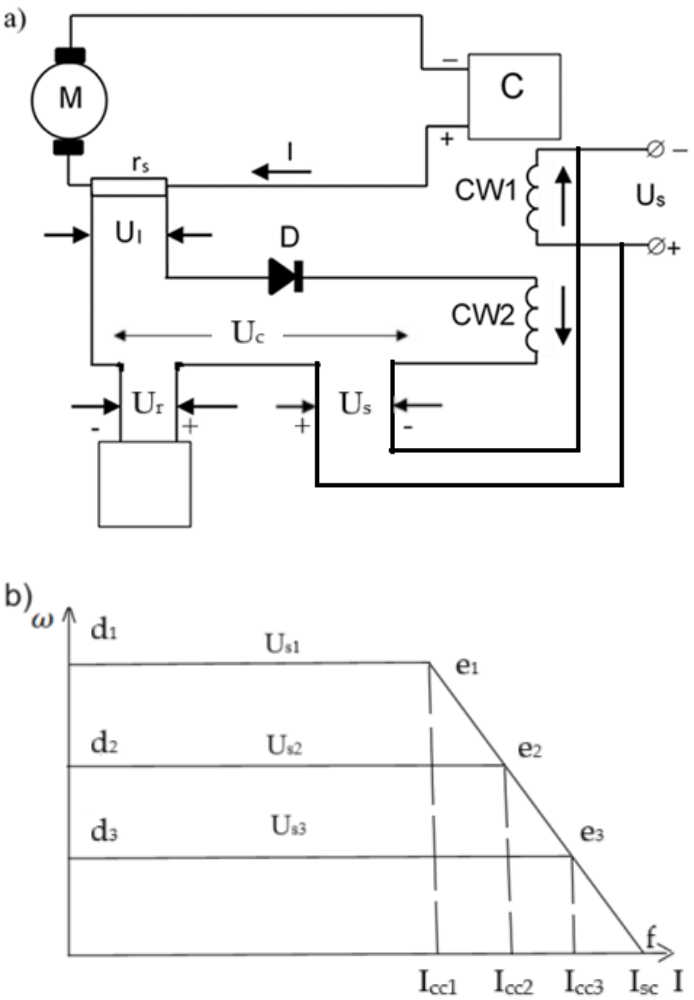


Figure 2: *Self-adjusting current limiting circuit (a) and corresponding electromechanical characteristics (b)*

Fig. 2, b shows the graphs of the electromechanical characteristics of the proposed electric drive circuit. These graphs are constructed for different values of U_s according to the equation:

$$\omega = \frac{k_c(U_\Sigma)}{k\phi} \cdot U_s - \frac{r_c+r_m}{k\phi} \cdot I - \frac{k_c(U_\Sigma)}{k\phi} \cdot (Ir_s - (U_r - U_s) \cdot l(\Delta I) \quad (3)$$

While $U_I = Ir_s \leq U_c = U_r - U_s$, no current flows through the CW2 winding, and the electric drive operates on the working section of the speed characteristic. When $U_I > U_c$, current begins to flow through the CW2 winding, as a result of which the motor overload is limited. For reduced U_s values, U_c increases and the overload limitation start points, self-adjusting, move to the right, that is, the cutoff current in this circuit automatically increases to the values of I_{cc2} or I_{cc3}, corresponding to the setting signals U_{s2} and U_{s3} [9-15].

By selecting the parameters of the current limitation unit, it is easy to ensure that the movement of the initial cutoff points and the current limitation slope coincide with the line of dependence of the maximum permissible motor currents on the speed. Then the automatic overload limitation, regardless of the value of the set speed, is always obtained along the line of maximum permissible motor currents and, therefore, its maximum overload capacity is fully realized at all values of the setting signal. For example, for values of the reference signal equal to U_{s2} and U_{s3}, the electromechanical characteristics of the drive are obtained as d_2e_2f and d_3e_3f (Fig. 2, b).

The magnitude of the stop current can be determined from equation (3):

$$I_{sc} = \frac{k_c(U_\Sigma)U_r}{r_c+r_m+k_c(U_\Sigma)r_s} \quad (4)$$

As can be seen from equation (4), the stop current I_{sc} for the proposed current limiting circuit does not depend on the magnitude of the setting signal, which is the main advantage of this circuit [16-19].

It should be noted that equation (3) was derived for a simplified version of the electric drive circuit, where there is feedback only on the motor armature current and when the control windings of the signal adder are identical. In the applied automated electric drive systems, different types of feedback often operate simultaneously and the control windings of the signal adder differ in parameters. For these electric drives, it is also possible to derive an equation of the electromechanical characteristic taking into account the presence of specific feedbacks together with the attached current-limiting circuit. For example, below is the equation of the electromechanical characteristic of an automated electric drive system that has feedback on the armature voltage and the current-limiting unit using a circuit for the full use of the maximum overload capacity of the motor:

$$\omega = \frac{k_c(U_\Sigma)}{k\phi[1+k_c(U_\Sigma)k_u]} \cdot U_s - \frac{r_c+[1+k_c(U_\Sigma)k_u]r_m}{k\phi[1+k_c(U_\Sigma)k_u]} \cdot I - \frac{k_c(U_\Sigma)k_{\omega I}}{k\phi[1+k_c(U_\Sigma)k_u]} \cdot (Ir_s - (U_r - k_sU_s) \cdot l(\Delta I)$$

In this case, the following equations are obtained for the cutoff current and for the stop current:

$$I_{cc} = \frac{U_r - k_sU_s}{r_s}$$

$$I_{sc} = \frac{k_c(U_\Sigma)k_{\omega I}U_r + k_c(U_\Sigma)(1-k_{\omega I}k_s)U_s}{r_c+[1+k_c(U_\Sigma)k_u]r_m+k_c(U_\Sigma)k_{\omega I}r_s} \quad (5)$$

From equation (5) it follows that in the case of identity of the adder control windings, i.e. when $k_{\omega I} \neq 1$, to achieve complete independence of the stop current from the value of the U_s signal, the coefficient ks must be taken so that $k_{\omega I}k_s = 1$. This can be easily achieved by using a potentiometer or intermediate amplifier in the circuit for introducing an additional signal from U_s into the current limiting circuit [20-24].

III. Conclusions

To ensure full utilization of the maximum permissible overload capacity of a DC electric motor in systems with variable speeds and limited installed drive power, it is crucial to apply a current limiting circuit that dynamically adjusts the cutoff current based on operating conditions. Traditional current limiting units with a constant comparison voltage fail to provide optimal overload protection at all speed settings, resulting in underutilization of the motor's capabilities.

The proposed improved circuit introduces a variable comparison voltage that depends on the setting voltage U_s, thereby automatically adjusting the cutoff current in accordance with the motor speed. This enables the electromechanical characteristics of the drive to align with the curve of maximum permissible motor currents, ensuring optimal use of overload capacity across the entire speed range.

Furthermore, the proposed system can be adapted for more complex feedback configurations, such as combined voltage and current feedback loops. With appropriate parameter tuning, including the use of a compensation coefficient k_s, the stop current can be made independent of the setting signal, which is a major advantage over previous solutions.

Overall, the proposed circuit provides a simple yet effective method for maximizing motor performance and reliability in adjustable DC electric drives, especially in applications where high short-term overloads occur.

References

[1] Sultanov Rafig, Elbrus Ahmedov and Nadir Aliyev, "Implementation of the maximum permissible overload capacity of a DC motor", Reliability: Theory & Applications 20.1 (82), 2025, pp. 728-733
[2] Klyuchev V.I., Terekhov V.M., "Electric drive and automation of general industrial mechanisms. - M: Energy, 1980, pp. 157-180
[3] A.I. Abdulkadyrov, S.C. Osmanov, N.A. Aliyev, G.A. Aliyeva, “Features of Calculating the Parameters of Special Electric Machines”, News of Azerbaijan Higher Technical Schools, No. 5, Issue 87, pp. 55-61, Baku, Azerbaijan, 2013
[4] Linder A., Kennel R., “Model predictive control for electrical drives”, 2005 IEEE 36th Power Electronics Specialists Conference, IEEE, 2005, pp. 1793-1799
[5] Pacheco-Chérrez J.; Fortoul-Díaz J.A.; Cortés-Santacruz F.; María Aloso-Valerdi L.; Ibarra-Zarate D.I., “Bearing fault detection with vibration and acoustic signals: Comparison among different machine leaning classification methods”, Eng. Fail. Anal., 2022, p. 139
[6] Harrouz Abdelkader, et al., "Backstepping control of a separately excited DC motor", Electrical Engineering 100.3, 2018, pp. 1393-1403
[7] Elshad Safiyev, Ilham Rahimli, Nijat Mammadov, "Method of qualitative impregnation of electric motor windings", Przegląd Elektrotechniczny, No 8, 2024, pp.238 -240, DOI: 10.15199/48.2024.08.48
[8] Sultanov R. Z., "ANALYSIS OF SCHEMES OF A CURRENT LIMITING UNIT IN AUTOMATIC CONTROL SYSTEMS FOR DC ELECTRIC DRIVES", Vestnik nauki, 3.4 (61), 2023, pp. 250-254
[9] Mammadov N. S., Mukhtarova K. M., “METHODOLOGY FOR ASSESSING THE RELIABILITY OF AGS BASED ON RENEWABLE ENERGY SOURCES”, Reliability: Theory & Applications, Volume 19, No 4 (80), pp.648-653, 2024
[10] R. Z. Sultanov, G. M. Safarov, E. M. Farkhadzade and S. D. Osmanov, “Implementation of a current limiting unit circuit with automatic change in allowable currents from the value of a given motor speed”, Proceedings of the first international conference "Technical and Physical Problems of Power Engineering", Baku, 2002, pp. 235-237
[11] Mendrela E. A., Beniak R., Wrobel R., “Influence of stator structure on electromechanical parameters of torus-type brushless DC motor”, IEEE transactions on energy conversion, 2003, T. 18, №. 2, pp. 231-237
[12] Butler Hans, Ger Honderd and Job Van Amerongen, "Model reference adaptive control of a direct-drive DC motor", IEEE Control Systems Magazine 9.1, 1989, pp. 80-84
[13] N.M. Pirieva, Z.F. Huseynov, “Characteristics of Synchronous Motors”, International Scientific Journal Bulletin of Science, No. 3, Issue 60, Vol. 4, pp. 241-246, Russia, 2022
[14] Ilkin Marufov, Aynura Allahverdiyeva, Nijat Mammadov, “Study of application characteristics of

cylindrical structure induction levitator in general and vertical axis wind turbines", Przegląd Elektrotechniczny, No 10, 2023, pp.196-199, DOI: 10.15199/48.2023.10.38

[15] Piotr Wach, "Dynamics and control of electrical drives", Springer Science & Business Media, 2011

[16] Nijat Mammadov, Ilkin Marufov, Saadat Shikhaliyeva, Gulnara Aliyeva, Saida Kerimova, "Research of methods power control of wind turbines", Przeglad Elektrotechniczny, No 5, 2024, pp. 236-239, DOI: 10.15199/48.2024.05.44

[17] Elshad Safiyev, Saida Kerimova, Kubra Mukhtarova, "Research of some problems of electrical safety", PRZEGLĄD ELEKTROTECHNICZNY, ISSN 0033-2097, R. 100 NR 9/2024, pp.96-99, doi:10.15199/48.2024.09.16

[18] Gerling Dieter, Electrical Machines, Springer-Verlag Berlin An, 2016

[19] Ilkin Marufov, Najiba Piriyeva, Nijat Mammadov, Shukufa Ismayilova, "Calculation of induction levitation vertical axis wind generator-turbine system parameters, levitation and influence loop" Przegląd Elektrotechniczny, 2024 , No.2, pp.135-139, DOI: 10.15199/48.2024.02.27

[20] Vostrov K.; Frolov V.; Safonov E., "Development of current limiting device for short and autonomous networks", Phys. Technol., 2017, 4, pp. 182–185

[21] Ouaida R.; Berthou M.; Tournier D.; Depalma J.-F., "State of art of current and future technologies in current limiting devices", In Proceedings of the 2015 IEEE First International Conference on DC Microgrids (ICDCM), Atlanta, GA, USA, 7–10 June 2015; IEEE: Piscataway, NJ, USA, 2015, pp. 175–180

[22] Shanmugasundram R., K. Muhammad Zakariah and N. Yadaiah, "Implementation and performance analysis of digital controllers for brushless DC motor drives", IEEE/ASME transactions on mechatronics 19.1, 2012, pp. 213-224

[23] Ouaida R.; de Palma J.F.; Gonthier G., "DC GRIDS: New over current protection", In Proceedings of the 2016 18th European Conference on Power Electronics and Applications (EPE'16 ECCE Europe), Karlsruhe, Germany, 5–9 September 2016; IEEE: Piscataway, NJ, USA, 2016, pp. 1–10

[24] Zhang Q., et. al, "Current limiting and recovery characteristics of an AC fast recovery superconducting fault current-limiting breaker", Supercond. Sci. Technol., 2023, 36, 115026

RT&A, No 3 (86)
Volume 20, September 2025

A NEW MIN-MAX RANKED SET SAMPLING SCHEME WITH UNEQUAL SAMPLE SIZES

O. Rahimi Dehcheraghi[1], S.M.T.K. MirMostafaee[2,*]

•

[1,2]Department of Statistics, University of Mazandaran, Iran
[1]orahimi55@gmail.com, [2]m.mirmostafaee@mail.umz.ac.ir

Abstract

In this paper, a new type of ranked set sampling scheme with unequal sample sizes called the new min-max ranked set sampling scheme with unequal sample sizes, is proposed to expedite the sampling process and reduce costs by utilizing fewer data compared to the existing ranked set sampling plans with unequal sample sizes, such as the minimum ranked set sampling scheme with unequal samples. We study the parameter estimation for the exponential distribution using the maximum likelihood and Bayesian methods based on the new scheme. The Metropolis-Hastings strategy is implemented to derive the approximate Bayesian estimates of the parameter under two loss functions. A simulation study is conducted, from which the effectiveness of the new scheme can be observed compared to the simple random sampling scheme and the minimum ranked set sampling scheme with unequal samples. A real data set is also analyzed. Finally, The paper ends with some remarks.

Keywords: Bayesian estimation, exponential distribution, maximum likelihood estimation, minimum ranked set sampling scheme with unequal samples, simulation.

1. Introduction

In many practical scenarios, obtaining the complete observations of a population can be a time-consuming, costly, and sometimes impossible task. In such situations, it is crucial to employ sampling methods that reduce costs. The simplest and most common sampling method is the simple random sampling (SRS) plan, where sample units are randomly selected with equal chances from the population. McIntyre [26] proposed another sampling scheme, called the ranked set sampling (RSS) plan. McIntyre [26] established that this plan can improve the efficiency of the estimator of the population mean for typical unimodal distributions and applied this plan to pasture measurement. Since then, many modifications of the ranked set sampling scheme have been developed by various authors, for example, Muttlak [31] proposed the paired rank set sampling technique, Samawi et al. [42] suggested the extreme ranked set sampling scheme, Samavi [41] worked on the stratified ranked set sampling (SRSS), and Muttlak [32] introduced the median ranked set sampling plan. In more recent years, Bhoj [7] and Al-Odat and Al-Saleh [4] explored the concept of ranked set sampling schemes with unequal sample sizes. Later, Biradar and Santosha [8] proposed the idea of the maximum ranked set sampling with unequal samples (MaxRSSU), which is similar to the idea of [4]. Biradar and Santosha [9] introduced the extreme ranked set sampling plan with unequal sample sizes, which is equivalent to the minimax ranked set sampling strategy discussed by Al-Nasser and Al-Omari [3]. This

*Corresponding Author

technique has been utilized by Hanandeh and Al-Nasser [15] to develop a new Shewhart-type mean control chart.

In recent years, many studies have been conducted based on the RSS procedure and/or its modified versions. For example, Jeelani and Bouza [22] suggested a new form of ratio estimator using the linear combination of the median and the quartile deviation of the auxiliary variable under the RSS plan. Jeelani et al. [23] worked on estimating the population mean under the RSS plan using an improved ratio estimator. Joukar et al. [24] and Ramezani et al. [40] investigated the estimation of the parameters and the stress-strength parameter, respectively, for the exponential-Poisson distribution based on the SRS, RSS, and MaxRSSU plans. Abdallah and Al-Omari [1] explored the problem of estimating the cumulative distribution function (CDF) and the odds measure under the plan suggested by [4] or [8]. Biradar and Shivanna [10], discussed the Bayesian estimation for the exponential distribution based on the strategy introduced by [7]. See also Al-Omari and Bouza [5] for many older studies.

Qiu and Eftekharian [35] emphasized that the minimum ranked set sampling with unequal samples (MinRSSU) and procedures are two very useful modifications of the RSS procedure. In the MinRSSU plan, n unequal samples are drawn from the population, with the size of the i-th sample equal to i for $i = 1, \cdots, n$. It is assumed that the researcher is able to identify the first ordered units without actual measurement. Then, for each of these samples, the smallest ranked unit is chosen for measurement. This procedure can be repeated m times to arrive at $n_0 = m \times n$ measured values. Clearly, one main purpose of suggesting a new modification of the RSS plan could be to increase the efficiency of the estimators relative to the other sampling schemes especially the SRS plan. In this study, we propose a new sampling scheme with unequal samples, called the new min-max ranked set sampling scheme with unequal sample sizes (NMRSSU scheme) which requires fewer samples than the MinRSSU plan for $n > 2$, with the aim of finding a more efficient scheme than the SRS and MinRSSU plans. Note that n is the number of measured observations extracted from one cycle.

Perhaps, the exponential distribution is the most well-known lifetime distribution in the reliability discussions. Suppose that X follows an exponential distribution with parameter θ, then the probability density function (PDF) and CDF of X are given by

$$f(x;\theta) = \theta \exp(-\theta x), \qquad x > 0, \theta > 0, \tag{1}$$

and

$$F(x;\theta) = 1 - \exp(-\theta x), \qquad x > 0, \theta > 0,$$

respectively.

Many authors have considered the one-parameter exponential distribution as the base distribution of their studies, see for example [2, 6, 10, 14, 30]. We also have selected the exponential distribution as the base distribution in this paper and discuss the estimation problem of the parameter of this distribution based on the new scheme. The rest of the paper is outlined as follows: In Section 2, we describe the new scheme. The maximum likelihood estimation of the parameter of the exponential distribution based on the NMRSSU plan is explored in Section 3. Section 4 is devoted to the Bayesian estimation. As the Bayesian estimates of the parameter do not seem to possess explicit forms, we utilize the Metropolis-Hasting algorithm to approximate these estimates. A simulation study is conducted in Section 5. In Section 6, we analyze a real data example using the NMRSSU, MinRSSU, and SRS plans. Finally, some concluding remarks are presented in Section 7.

2. The new min-max ranked set sampling scheme with unequal samples

Suppose that we want to obtain $n_0 = m \times n$ observations with the help of a sampling plan. Let $k = \left[\frac{n}{2}\right] + 1$ where $[x]$ denotes the integer value of x. In the new min-max ranked set sampling scheme with unequal samples (NMRSSU) plan, we draw k simple random samples in each cycle, where the size of the i-sample is equal to i for $i = 1, \cdots, k$. The plan is described as follows:

Algorithm 1

Step 1: Select $k = \left[\frac{n}{2}\right] + 1$ simple random samples of sizes $1, 2, \cdots, k$, respectively.

Step 2: Order the elements of each sample through visual inspection or other alternative methods that do not involve actual measurement of the desired characteristics.

Step 3: If n is an even number, then select the largest ordered element from the first and second samples, and select the smallest and largest ordered elements from the remaining samples. Otherwise, for an odd value of n, select the first sample, as well as the smallest and largest ordered elements from the remaining samples.

Step 4: Repeat the above steps m times until the desired sample size $n_0 = m \times n$ is obtained.

Note that if n is an even number, then $k = \frac{n}{2} + 1$. In this case, the procedure for one cycle may be summarized as follows:

$$\begin{cases} \boxed{X_{(1:1)1}} & & & \\ X_{(1:2)2} & \boxed{X_{(2:2)2}} & & \\ \boxed{X_{(1:3)3}} & X_{(2:3)3} & \boxed{X_{(3:3)3}} & \\ \vdots & \vdots & \ddots & \\ \boxed{X_{(1:k)k}} & X_{(2:k)k} & \cdots & \boxed{X_{(k:k)k}} \end{cases}$$

Then, $\{X_{(1:1)1}, X_{(2:2)2}, (X_{(1:3)3}, X_{(3:3)3}), \ldots, (X_{(1:k)k} X_{(k:k)k})\}$, represents the sample extracted from one cycle.

Next, if n is odd, then we have $k = \frac{n+1}{2}$ and the procedure can be displayed as follows:

$$\begin{cases} \boxed{X_{(1:1)1}} & & & \\ \boxed{X_{(1:2)2}} & \boxed{X_{(2:2)2}} & & \\ \boxed{X_{(1:3)3}} & X_{(2:3)3} & \boxed{X_{(3:3)3}} & \\ \vdots & \vdots & \ddots & \\ \boxed{X_{(1:k)k}} & X_{(2:k)k} & \cdots & \boxed{X_{(k:k)k}} \end{cases}$$

So $\{X_{(1:1)1}, (X_{(1:2)2}, X_{(2:2)2}), \ldots, (X_{(1:k)k}, X_{(k:k)k})\}$ becomes the sample that is extracted from one cycle.

Since this procedure uses unequal samples and selects both the largest and smallest ordered units in most cases simultaneously, it involves fewer samples compared to the MinRSSU plan when $n > 2$. Suppose that T_{ji} and Z_{ji} denote the smallest observation and the largest observation in the i-th sample and j-th cycle, respectively, for $i = 1, \cdots, k$ and $j = 1, \cdots, m$. Then, in the NMRSSU plan, $\{Z_{j1}, Z_{j2}, (T_{j3}, Z_{j3}), \ldots, (T_{jk}, Z_{jk})\}$ represents the set of observations extracted from the j-th cycle when n is even and $\{Z_{j1}, (T_{j2}, Z_{j2}), (T_{j3}, Z_{j3}), \ldots, (T_{jk}, Z_{jk})\}$ represents the set of observations extracted from the j-th cycle when n is odd, for $j = 1, \cdots, m$. In other words, if we set $\boldsymbol{T}_e = (T_{13}, \cdots, T_{1k}, \cdots, T_{m3}, \cdots, T_{mk})$, $\boldsymbol{T}_o = (T_{12}, \cdots, T_{1k}, \cdots, T_{m2}, \cdots, T_{mk})$, and $\boldsymbol{Z} = (Z_{11}, \cdots, Z_{1k}, \cdots Z_{m1}, \cdots, Z_{mk})$, then $\{\boldsymbol{T}_e, \boldsymbol{Z}\}$ and $\{\boldsymbol{T}_o, \boldsymbol{Z}\}$ constitute the NMRSSU samples from the population for even and odd values of n, respectively. In what follows, we focus on the estimation of the parameter of the exponential distribution based on NMRSSU data.

3. Maximum likelihood estimation

In this section, we discuss the maximum likelihood (ML) estimation for the exponential distribution based on NMRSSU data. This section consists of two parts. In the first part, we assume that n, the number of measured observations extracted from one cycle, is an even number, and in the second part, we assume n is odd.

3.1. ML estimation when n is even

Assume $n_0 = m \times n$ and n is even. Let $\boldsymbol{t}_e = (t_{13}, \cdots, t_{1k}, \cdots, t_{m3}, \cdots, t_{mk})$ and $\boldsymbol{z} = (z_{11}, \cdots, z_{1k}, \cdots, z_{m1}, \cdots, z_{mk})$ be the observed sets of $\boldsymbol{T}_e$ and $\boldsymbol{Z}$, respectively, where $k = \dfrac{n}{2} + 1$. If the judgment ranking is perfect, then likelihood function of the parameter given $(\boldsymbol{t}_e, \boldsymbol{z})$ can be written as

$$\begin{aligned}\mathcal{L}_e(\theta|\boldsymbol{t}_e, \boldsymbol{z}) &= \prod_{j=1}^{m}\prod_{i=1}^{2} i\,[F(z_{ji})]^{i-1} f(z_{ji}) \times \prod_{j=1}^{m}\prod_{i=3}^{k} i(i-1)[F(z_{ji}) - F(t_{ji})]^{i-2} f(t_{ji}) f(z_{ji}) \\ &= \prod_{j=1}^{m} 2 f(z_{j1}) f(z_{j2}) F(z_{j2}) \times \prod_{j=1}^{m}\prod_{i=3}^{k} i(i-1)[F(z_{ji}) - F(t_{ji})]^{i-2} f(t_{ji}) f(z_{ji}). \end{aligned} \tag{2}$$

Therefore, for the case of the exponential distribution with PDF (1), we have

$$\begin{aligned}\mathcal{L}_e(\theta|\boldsymbol{t}_e, \boldsymbol{z}) = &\left(2^m \prod_{j=1}^{m}\prod_{i=3}^{k} i(i-1)\right)\theta^{mn} \prod_{j=1}^{m}\left[1 - \mathrm{e}^{-\theta z_{j2}}\right] \\ &\times \exp\left\{-\theta \sum_{j=1}^{m}(z_{j1} + z_{j2}) - \theta \sum_{j=1}^{m}\sum_{i=3}^{k}(t_{ji} + z_{ji})\right\} \prod_{j=1}^{m}\prod_{i=3}^{k}\left[\mathrm{e}^{-\theta t_{ji}} - \mathrm{e}^{-\theta z_{ji}}\right]^{i-2}.\end{aligned}$$

The log-likelihood function of the parameter is then given by

$$\begin{aligned}\ell_e(\theta|\boldsymbol{t}_e, \boldsymbol{z}) = &\log\left(2^m \prod_{j=1}^{m}\prod_{i=3}^{k} i(i-1)\right) + mn\log(\theta) + \sum_{j=1}^{m}\log\left[1 - \mathrm{e}^{-\theta z_{j2}}\right] \\ &- \theta \sum_{j=1}^{m}(z_{j1} + z_{j2}) - \theta \sum_{j=1}^{m}\sum_{i=3}^{k}(t_{ji} + z_{ji}) + \sum_{j=1}^{m}\sum_{i=3}^{k}(i-2)\log\left[\mathrm{e}^{-\theta t_{ji}} - \mathrm{e}^{-\theta z_{ji}}\right].\end{aligned}$$

We set the derivative of the log-likelihood function with respect to (w.r.t.) θ equal to zero, and thus we get

$$\begin{aligned}\frac{\partial \ell_e(\theta|\boldsymbol{t}_e, \boldsymbol{z})}{\partial \theta} = &\frac{mn}{\theta} + \sum_{j=1}^{m}\frac{z_{j2}}{\mathrm{e}^{\theta z_{j2}} - 1} - \sum_{j=1}^{m}(z_{j1} + z_{j2}) - \sum_{j=1}^{m}\sum_{i=3}^{k}(t_{ji} + z_{ji}) \\ &+ \sum_{j=1}^{m}\sum_{i=3}^{k}(i-2)\frac{z_{ji}\mathrm{e}^{-\theta z_{ji}} - t_{ji}\mathrm{e}^{-\theta t_{ji}}}{\mathrm{e}^{-\theta t_{ji}} - \mathrm{e}^{-\theta z_{ji}}} = 0.\end{aligned} \tag{3}$$

The ML estimate of θ may be obtained by solving the nonlinear equation (3). Here, we can use a numerical technique to solve this equation.

Let $\widehat{\theta}_M$ denote the ML estimator of θ. Then, under some regurality conditions stated in Lehmann and Casella [25], $\widehat{\theta}_M$ may be asymptotically normal distributed with the mean θ and variance $\dfrac{1}{I_{\boldsymbol{T}_e,\boldsymbol{Z}}(\theta)}$, where $I_{\boldsymbol{T}_e,\boldsymbol{Z}}(\theta)$ is the expected Fisher information about θ based on $(\boldsymbol{T}_e, \boldsymbol{Z})$. In other words

$$I_{\boldsymbol{T}_e,\boldsymbol{Z}}(\theta) = -E\left(\frac{\partial^2 \ln f_{\boldsymbol{T}_e,\boldsymbol{Z}}(T_{13}, \cdots, T_{mk}, Z_{11}, \cdots Z_{mk})}{\partial \theta^2}\right),$$

where $f_{\boldsymbol{T}_e,\boldsymbol{Z}}(t_{13},\cdots,t_{mk},z_{11},\cdots z_{mk})$ is the joint PDF of $T_{13},\cdots,T_{1k},\cdots T_{m1},\cdots,T_{mk}$, $Z_{11},\cdots,Z_{1k},\cdots,Z_{m1},\cdots,Z_{mk}$, provided that the above expectation exists.

The second derivative of $\ell_e(\theta|\boldsymbol{t}_e,\boldsymbol{z})$ w.r.t. θ is given by

$$\frac{\partial^2\ell_e(\theta|\boldsymbol{t}_e,\boldsymbol{z})}{\partial\theta^2}=\frac{-mn}{\theta^2}-\sum_{j=1}^{m}\frac{z_{j2}^2\mathrm{e}^{\theta z_{j2}}}{\left(\mathrm{e}^{\theta z_{j2}}-1\right)^2}-\sum_{j=1}^{m}\sum_{i=3}^{k}(i-2)\left(\frac{z_{ji}-t_{ji}}{\mathrm{e}^{-\theta z_{ji}}-\mathrm{e}^{-\theta t_{ji}}}\right)^2\mathrm{e}^{-\theta(t_{ji}+z_{ji})}.$$

Therefore, a $100(1-\gamma)\%$ two-sided equi-tailed asymptotic confidence interval (TE ACI) for θ may be given by

$$\left(\widehat{\theta}_M-\frac{z_{\frac{\gamma}{2}}}{\sqrt{\tilde{I}_e(\widehat{\theta}_M)}},\widehat{\theta}_M+\frac{z_{\frac{\gamma}{2}}}{\sqrt{\tilde{I}_e(\widehat{\theta}_M)}}\right),$$

where z_τ is the τ-th upper quantile of the standard normal distribution and

$$\tilde{I}_e(\widehat{\theta}_M)=-\left.\frac{\partial^2\ell(\theta\mid\boldsymbol{T}_e,\boldsymbol{Z})}{\partial\theta^2}\right|_{\theta=\widehat{\theta}_M}.$$

3.2. ML estimation when n is odd

Assume $n_0=m\times n$ and n is odd. Let $\boldsymbol{t}_o=(t_{12},\cdots,t_{1k},\cdots,t_{m2},\cdots,t_{mk})$ and $\boldsymbol{z}=(z_{11},\cdots,z_{1k},\cdots,z_{m1},\cdots,z_{mk})$ be the observed sets of $\boldsymbol{T}_o$ and $\boldsymbol{Z}$, respectively, where $k=\dfrac{n+1}{2}$. If the judgment ranking is perfect, then likelihood function of the parameter given $(\boldsymbol{t}_o,\boldsymbol{z})$ becomes

$$\mathcal{L}_o(\theta|\boldsymbol{t}_o,\boldsymbol{z})=\prod_{j=1}^{m}f(z_{j1})\times\prod_{j=1}^{m}\prod_{i=2}^{k}i(i-1)[F(z_{ji})-F(t_{ji})]^{i-2}f(t_{ji})f(z_{ji}).$$

Consequently, for the case of the exponential distribution with PDF (1), we get

$$\begin{aligned}\mathcal{L}_o(\theta|\boldsymbol{t}_o,\boldsymbol{z})=\theta^{mn}&\left(\prod_{j=1}^{m}\prod_{i=2}^{k}i(i-1)\right)\prod_{j=1}^{m}\prod_{i=2}^{k}\left[\mathrm{e}^{-\theta t_{ji}}-\mathrm{e}^{-\theta z_{ji}}\right]^{i-2}\\&\times\exp\left\{-\theta\left(\sum_{j=1}^{m}z_{j1}+\sum_{j=1}^{m}\sum_{i=2}^{k}(t_{ji}+z_{ji})\right)\right\}.\end{aligned}$$

The log-likelihood function of the parameter is then given by

$$\begin{aligned}\ell_o(\theta|\boldsymbol{t}_o,\boldsymbol{z})=&\,mn\log\theta+\log\left(\prod_{j=1}^{m}\prod_{i=2}^{k}i(i-1)\right)+\sum_{j=1}^{m}\sum_{i=2}^{k}(i-2)\log\left[\mathrm{e}^{-\theta t_{ji}}-\mathrm{e}^{-\theta z_{ji}}\right]\\&-\theta\left(\sum_{j=1}^{m}z_{j1}+\sum_{j=1}^{m}\sum_{i=2}^{k}(t_{ji}+z_{ji})\right)\end{aligned}$$

Upon taking the derivative of $\ell_o(\theta|\boldsymbol{t}_o,\boldsymbol{z})$ w.r.t. θ and setting the result equal to zero, we have

$$\begin{aligned}\frac{\partial\ell_o(\theta|\boldsymbol{t}_o,\boldsymbol{z})}{\partial\theta}=&\frac{mn}{\theta}+\sum_{j=1}^{m}\sum_{i=2}^{k}(i-2)\frac{z_{ji}\mathrm{e}^{-\theta z_{ji}}-t_{ji}\mathrm{e}^{-\theta t_{ji}}}{\mathrm{e}^{-\theta t_{ji}}-\mathrm{e}^{-\theta z_{ji}}}-\sum_{j=1}^{m}z_{j1}\\&-\sum_{j=1}^{m}\sum_{i=2}^{k}(t_{ji}+z_{ji})=0.\end{aligned}\tag{4}$$

A numerical method may be implemented to solve (4).

The second derivative of the $\ell_o(\theta|\boldsymbol{t}_o,\boldsymbol{z})$ w.r.t. θ is as follows

$$\frac{\partial^2\ell_o(\theta|\boldsymbol{t}_o,\boldsymbol{z})}{\partial\theta^2}=-\frac{mn}{\theta^2}-\sum_{j=1}^{m}\sum_{i=2}^{k}(i-2)\left(\frac{z_{ji}-t_{ji}}{\mathrm{e}^{-\theta z_{ji}}-\mathrm{e}^{-\theta t_{ji}}}\right)^2\mathrm{e}^{-\theta(t_{ji}+z_{ji})}.$$

Now, following a similar argument stated in Subsection 3.1, we may consider the following interval as the $100(1-\gamma)\%$ TE ACI for θ

$$\left(\widehat{\theta}_M - \frac{z_{\frac{\gamma}{2}}}{\sqrt{\tilde{I}_o\left(\widehat{\theta}_M\right)}}, \widehat{\theta}_M + \frac{z_{\frac{\gamma}{2}}}{\sqrt{\tilde{I}_o\left(\widehat{\theta}_M\right)}}\right),$$

where $\widehat{\theta}_M$ denotes the ML estimator of θ and

$$\tilde{I}_o\left(\widehat{\theta}_M\right) = -\left.\frac{\partial^2 \ell(\theta \mid \boldsymbol{T}_o, \boldsymbol{Z})}{\partial \theta^2}\right|_{\theta=\widehat{\theta}_M}.$$

4. Bayesian estimation

In this section, we focus on the Bayesian estimation of the parameter θ based on NMRSSU data. To achieve this, we utilize a gamma prior for the parameter with positive hyperparameters α and β, with the following PDF

$$\pi(\theta) = \frac{\beta^\alpha}{\Gamma(\alpha)}\,\theta^{\alpha-1}\,\mathrm{e}^{-\beta\theta}, \qquad \alpha > 0, \quad \beta > 0. \tag{5}$$

Additionally, to evaluate the accuracy of our estimates, we employ two different loss functions: the squared error loss (SEL) function and the linear-exponential loss (LEL) function. The SEL function assigns equal weights to underestimation and overestimation due to its symmetry, whereas the LEL function stands out as a widely favored asymmetric loss function. Let δ be an estimator of θ. Then, the SEL function is defined as $L_1(\theta,\delta) = (\delta-\theta)^2$, and the LEL function, introduced by [48] and discussed by [49], is defined as

$$L_2(\theta,\delta) = b\left(\mathrm{e}^{c(\delta-\theta)} - c(\delta-\theta) - 1\right),$$

where $c \neq 0$ and $b > 0$. We may take $b = 1$ without loss of generality. Positive values of c result in more serious consequences for overestimation than for underestimation, and vice versa; refer to [49].

4.1. Bayesian estimation when n is even

When n is even, from (2) and (5), the posterior density of θ given $(\boldsymbol{t}_e, \boldsymbol{z})$ is expressed as follows

$$\pi_e(\theta|\boldsymbol{t}_e,\boldsymbol{z}) = \frac{1}{D_1}\,\theta^{mn+\alpha-1}\left(\prod_{j=1}^{m}\left[1-\mathrm{e}^{-\theta z_{j2}}\right]\right)\left(\prod_{j=1}^{m}\prod_{i=3}^{k}\left[\mathrm{e}^{-\theta t_{ji}} - \mathrm{e}^{-\theta z_{ji}}\right]^{i-2}\right)$$
$$\times \exp\left\{-\theta\left(\beta + \sum_{j=1}^{m}(z_{j1}+z_{j2}) + \sum_{j=1}^{m}\sum_{i=3}^{k}(t_{ji}+z_{ji})\right)\right\},$$

where

$$D_1 = \int_0^\infty \theta^{mn+\alpha-1}\left(\prod_{j=1}^{m}\left[1-\mathrm{e}^{-\theta z_{j2}}\right]\right)\left(\prod_{j=1}^{m}\prod_{i=3}^{k}\left[\mathrm{e}^{-\theta t_{ji}} - \mathrm{e}^{-\theta z_{ji}}\right]^{i-2}\right)$$
$$\times \exp\left\{-\theta\left(\beta + \sum_{j=1}^{m}(z_{j1}+z_{j2}) + \sum_{j=1}^{m}\sum_{i=3}^{k}(t_{ji}+z_{ji})\right)\right\}\mathrm{d}\theta.$$

The Bayesian estimates of θ under the SEL and LEL functions are then given by

$$\widehat{\theta}^e_{SEL} = \frac{1}{D_1}\int_0^\infty \theta^{mn+\alpha}\left(\prod_{j=1}^{m}\left[1-\mathrm{e}^{-\theta z_{j2}}\right]\right)\left(\prod_{j=1}^{m}\prod_{i=3}^{k}\left[\mathrm{e}^{-\theta t_{ji}} - \mathrm{e}^{-\theta z_{ji}}\right]^{i-2}\right)$$
$$\times \exp\left\{-\theta\left(\beta + \sum_{j=1}^{m}(z_{j1}+z_{j2}) + \sum_{j=1}^{m}\sum_{i=3}^{k}(t_{ji}+z_{ji})\right)\right\}\mathrm{d}\theta, \tag{6}$$

and

$$\widehat{\theta}^{e}_{LEL} = \frac{-1}{c}\log\left(\frac{1}{D_1}\int_0^{\infty}\theta^{mn+\alpha-1}\left(\prod_{j=1}^{m}\left[1-\mathrm{e}^{-\theta z_{j2}}\right]\right)\left(\prod_{j=1}^{m}\prod_{i=3}^{k}\left[\mathrm{e}^{-\theta t_{ji}}-\mathrm{e}^{-\theta z_{ji}}\right]^{i-2}\right)\right.$$
$$\left.\times\exp\left\{-\theta\left(\beta+c+\sum_{j=1}^{m}(z_{j1}+z_{j2})+\sum_{j=1}^{m}\sum_{i=3}^{k}(t_{ji}+z_{ji})\right)\right\}\mathrm{d}\theta\right), \tag{7}$$

respectively, provided that the above integrals exist.

It seems that there exist no closed forms for the Bayes estimates (6) and (7). So we use the Metropolis-Hastings (MH) algorithm to approximate these estimates. The MH algorithm is extensively used in Bayesian inference. It was initially presented by [28] and later developed by [17]. Here, the MH method can be expressed using the following algorithm.

Algorithm 2

Step 1: Start with an initial guess $\theta_0 = \hat{\theta}_M$, where $\hat{\theta}_M$ is the ML estimate of θ and set $s = 1$.
Step 2: Given θ_{s-1}, generate θ^* from the truncated normal distribution, $N\left(\theta_{s-1}, \sigma^2\right) I_{\{\theta>0\}}$. Then, set $\theta_s = \theta^*$ with probability

$$P = \min\left\{\frac{\pi_e\left(\theta^* \mid \boldsymbol{t}_e, \boldsymbol{z}\right) q\left(\theta_{s-1} \mid \theta^*\right)}{\pi_e\left(\theta_{s-1} \mid \boldsymbol{t}_e, \boldsymbol{z}\right) q\left(\theta^* \mid \theta_{s-1}\right)}, 1\right\},$$

where $q(x|b)$ denotes the density of $N\left(b, \sigma^2\right) I_{\{x>0\}}$, otherwise set $\theta_s = \theta_{s-1}$.
Step 3: Set $s = s+1$ and repeat Step 2, $S-1$ times, where S is a large number. Let M be the burn-in period. Then, $\{\theta_{M+1}, \theta_{M+2}, \cdots, \theta_S\}$ is the desired generated sample.

Now, given the generated sample from the MH algorithm $\{\theta_{M+1}, \theta_{M+2}, \cdots, \theta_S\}$, the approximate Bayesian estimates for θ under the SEL and LEL functions are given by

$$\widetilde{\theta}_{SEL} = \frac{1}{S^*}\sum_{s=M+1}^{S}\theta_s, \qquad \text{and} \qquad \widetilde{\theta}_{LEL} = \frac{-1}{c}\ln\left(\frac{1}{S^*}\sum_{s=M+1}^{S}\mathrm{e}^{-c\theta_s}\right),$$

respectively, where $S^* = S - M$.

Now, let $\theta_{(1)} \le \cdots \le \theta_{(S^*)}$ represent the ordered values of the generated sample using the MH strategy $\{\theta_{M+1}, \cdots, \theta_S\}$. Then, the $100(1-\gamma)\%$ Chen and Shao shortest credible interval (CSSW CrI) for θ can be expressed as follows (see [12]):

$$\left(\theta_{(q)}, \theta_{(q+[(1-\gamma)S^*])}\right),$$

where q is chosen such that

$$\theta_{(q+[(1-\gamma)S^*])} - \theta_{(q)} = \min_{s\in\{1,\cdots,S^*-[(1-\gamma)S^*]\}}\theta_{(s+[(1-\gamma)S^*])} - \theta_{(s)}.$$

4.2. Bayesian estimation when n is odd

When n is odd, the posterior density of θ given $(\boldsymbol{t}_o, \boldsymbol{z})$ is expressed as follows

$$\pi_o(\theta|\boldsymbol{t}_o, \boldsymbol{z}) = \frac{1}{D_2}\theta^{mn+\alpha-1}\left(\prod_{j=1}^{m}\prod_{i=2}^{k}\left[\mathrm{e}^{-\theta t_{ji}}-\mathrm{e}^{-\theta z_{ji}}\right]^{i-2}\right)$$
$$\times\exp\left\{-\theta\left(\beta+\sum_{j=1}^{m}z_{j1}+\sum_{j=1}^{m}\sum_{i=2}^{k}(t_{ji}+z_{ji})\right)\right\},$$

where

$$D_2 = \int_0^\infty \theta^{mn+\alpha-1}\Bigg(\prod_{j=1}^{m}\prod_{i=2}^{k}\left[\mathrm{e}^{-\theta t_{ji}} - \mathrm{e}^{-\theta z_{ji}}\right]^{i-2}\Bigg) \times \exp\left\{-\theta\Bigg(\beta + \sum_{j=1}^{m} z_{j1} + \sum_{j=1}^{m}\sum_{i=2}^{k}(t_{ji}+z_{ji})\Bigg)\right\}\mathrm{d}\theta.$$

The Bayesian estimates of θ under the SEL and LEL functions are then given by

$$\widehat{\theta}^{o}_{SEL} = \frac{1}{D_2}\int_0^\infty \theta^{mn+\alpha}\Bigg(\prod_{j=1}^{m}\prod_{i=2}^{k}\left[\mathrm{e}^{-\theta t_{ji}} - \mathrm{e}^{-\theta z_{ji}}\right]^{i-2}\Bigg) \times \exp\left\{-\theta\Bigg(\beta + \sum_{j=1}^{m} z_{j1} + \sum_{j=1}^{m}\sum_{i=2}^{k}(t_{ji}+z_{ji})\Bigg)\right\}\mathrm{d}\theta, \tag{8}$$

and

$$\widehat{\theta}^{o}_{LEL} = \frac{-1}{c}\log\left(\frac{1}{D_2}\int_0^\infty \theta^{mn+\alpha-1}\Bigg(\prod_{j=1}^{m}\prod_{i=2}^{k}\left[\mathrm{e}^{-\theta t_{ji}} - \mathrm{e}^{-\theta z_{ji}}\right]^{i-2}\Bigg) \times \exp\left\{-\theta\Bigg(\beta + c + \sum_{j=1}^{m} z_{j1} + \sum_{j=1}^{m}\sum_{i=2}^{k}(t_{ji}+z_{ji})\Bigg)\right\}\mathrm{d}\theta\right), \tag{9}$$

respectively, provided that the above integrals exist.

Now, based on a similar argument stated in Subsection 4.1, we can derive the approximate Bayesian estimates for θ under the SEL and LEL functions, as well as the $100(1-\gamma)\%$ CSSW CrI for θ.

5. A simulation study

In this section, we carry out a Monte Carlo simulation study with $N = 10000$ iterations to evaluate several classical and Bayesian estimators (approximate Bayesian estimators in the case of the NMRSSU plan) for the exponential parameter θ. This evaluation is based on the NMRSSU, MinRSSU, and SRS designs. We focus on the parameter values $\theta = 2, 3$, and 5, and chose sample sizes $n_0 = m \times n \in \{24, 33, 40, 45\}$, configured as follows: Sample $1 \equiv 2 \times 12$, Sample $2 \equiv 3 \times 11$, Sample $3 \equiv 4 \times 10$, and Sample $4 \equiv 5 \times 9$. For the Bayesian estimation, the hyperparameters are specified to be $\alpha = \beta = 0.01$, resulting in an approximate non-informative prior. The parameter of the LEL function is also taken to be $c = -0.5$ and 0.5. We calculated the ML estimates for θ. Moreover, we calculated the Bayesian estimates of θ based on the MinRSSU and SRS plans, whereas the Bayesian estimates for θ based on the NMRSSU plan have been approximated using the MH strategy. We take $S = 10000$, $M = 1000$, and $\sigma = 1$ for the MH method. The convergence of the MH Markov chains have been checked using Geweke's test (see [13]), Raftery and Lewiss diagnostic (see [38, 39]), and Heidelberger and Welch's convergence diagnostic (see [20]). Notice that [20] used or hinted the outcomes of [18, 19, 43, 44, 45].

Let $\widehat{\theta}$ be an estimator of θ and $\widehat{\theta}_i$ be the corresponding estimate obtained in the i-th iteration. Then, the estimated risk (ER) under the SEL function, the ER under the LEL function, and the estimated bias (bias for short) of $\widehat{\theta}$ are expressed as

$$\mathrm{ER}_S(\widehat{\theta}) = \frac{1}{N}\sum_{i=1}^{N}(\widehat{\theta}_i - \theta)^2,$$

$$\mathrm{ER}_L(\widehat{\theta}) = \frac{1}{N}\sum_{i=1}^{N}\left\{\mathrm{e}^{c(\widehat{\theta}_i-\theta)} - c(\widehat{\theta}_i - \theta) - 1\right\},$$

and

$$Bias(\widehat{\theta}) = \frac{1}{N}\sum_{i=1}^{N}(\widehat{\theta}_i - \theta),$$

respectively.

We compute the ER of each Bayesian estimator according to its own loss function, whereas all the ERs are calculated for the ML estimators. Note that under the NMRSSU plan, we compute the approximate Bayesian estimators. Besides, the 95% interval estimators are evaluated by means of the average width (AW) and coverage probability (CP) criteria. In the context of Bayesian interval estimation, we obtain exact 95% shortest width credible intervals for θ when the SRS and MinRSSU plans are used. The biases and ERs of the point estimators are reported in Tables 1–3 and the AWs and CPs of the 95% interval estimators are given in Table 4. From Tables 1–4, we may conclude the following points:

- The point estimators based on the NMRSSU scheme perform better than the corresponding estimators based on the SRS and MinRSSU schemes w.r.t. the criteria of the absolute value of bias (AVB) and ER (there is only one exception in Table 3, where the AVB of the estimator based on the MinRSSU method is lower than the corresponding metric based on the NMRSSU method). The point estimators based on the SRS and MinRSSU schemes perform rather close to each other w.r.t. the ER and AVB.

- The Bayesian estimators (approximate Bayesian estimators in the case of the NMRSSU plan) under the LEL function with $c = 0.5$ perform better than the ML estimators in the sense of ER, whereas the ML estimators perform better than the Bayesian estimators (approximate Bayesian estimators in the case of the NMRSSU plan) under the LEL function with $c = -0.5$ in this respect. The Bayesian estimators under the SEL function perform better than the ML estimators in the sense of ER when the MinRSSU and SRS plans are used, whereas the ML estimators perform better than the approximate Bayesian estimators under the SEL function in this respect when the NMRSSU method is used.

- The Bayesian estimators (approximate Bayesian estimators in the case of the NMRSSU plan) under the LEL function with $c = 0.5$ perform the best among the considered types of estimators in the sense of AVB. The next best estimators are the Bayesian estimators under the SEL function in terms of AVB when the MinRSSU and SRS plans are used, otherwise, the ML estimators are the second best estimators in this regard when the NMRSSU method is used. Moreover, the Bayesian estimators (approximate Bayesian estimators in the case of the NMRSSU plan) under the LEL function with $c = -0.5$ perform the worst among the considered types of estimators in the sense of AVB.

- The Bayesian estimators (approximate Bayesian estimators in the case of the NMRSSU plan) under the LEL function with $c = 0.5$ when $\theta = 5$, are the only estimators that possess negative bias values.

- In the context of interval estimation, the interval estimators under the NMRSSU plan exhibit smaller AWs compared to those under the SRS and MinRSSU plans. The interval estimators based on the SRS and MinRSSU schemes perform rather close to each other w.r.t. the AW.

- The interval estimators obtained using the Bayesian methods are, on average, shorter than the classical ones. All of the 95% interval estimators possess CPs close to the nominal value of 0.95.

Table 1: *The biases and ERs of the ML estimators of* θ.

	$\theta=2$			$\theta=3$			$\theta=5$		
Sample 1	NMRSSU	MinRSSU	SRS	NMRSSU	MinRSSU	SRS	NMRSSU	MinRSSU	SRS
Bias	0.03594	0.08319	0.08761	0.05412	0.14136	0.13692	0.08994	0.22734	0.21653
ER_S	0.09242	0.20432	0.20449	0.21173	0.47043	0.46664	0.59507	1.28767	1.31819
$ER_{L(c=+0.5)}$	0.01213	0.02879	0.02884	0.02878	0.07217	0.07157	0.08860	0.24051	0.25121
$ER_{L(c=-0.5)}$	0.01113	0.02336	0.02337	0.02505	0.05158	0.05124	0.06826	0.13394	0.13654
Sample 2	NMRSSU	MinRSSU	SRS	NMRSSU	MinRSSU	SRS	NMRSSU	MinRSSU	SRS
Bias	0.03356	0.05683	0.05970	0.05443	0.09213	0.09336	0.08215	0.14874	0.13977
ER_S	0.08043	0.13792	0.14269	0.17799	0.31682	0.31471	0.49783	0.89761	0.86688
$ER_{L(c=+0.5)}$	0.01055	0.01872	0.01947	0.02406	0.04523	0.04512	0.07138	0.14566	0.13794
$ER_{L(c=-0.5)}$	0.00968	0.01620	0.01669	0.02110	0.03627	0.03588	0.05804	0.09914	0.09636
Sample 3	NMRSSU	MinRSSU	SRS	NMRSSU	MinRSSU	SRS	NMRSSU	MinRSSU	SRS
Bias	0.02659	0.05343	0.04966	0.03217	0.07605	0.07973	0.05974	0.12985	0.14091
ER_S	0.05842	0.11380	0.11415	0.13019	0.26774	0.26267	0.36281	0.72525	0.72594
$ER_{L(c=+0.5)}$	0.00756	0.01523	0.01533	0.01711	0.03761	0.03687	0.05009	0.11306	0.11330
$ER_{L(c=-0.5)}$	0.00711	0.01350	0.01350	0.01575	0.03096	0.03039	0.04304	0.08113	0.08089
Sample 4	NMRSSU	MinRSSU	SRS	NMRSSU	MinRSSU	SRS	NMRSSU	MinRSSU	SRS
Bias	0.02671	0.04702	0.04299	0.04149	0.07150	0.06482	0.06574	0.12704	0.11919
ER_S	0.06430	0.09978	0.09933	0.14059	0.22931	0.22478	0.39452	0.64183	0.63012
$ER_{L(c=+0.5)}$	0.00835	0.01330	0.01320	0.01862	0.03172	0.03098	0.05502	0.09709	0.09535
$ER_{L(c=-0.5)}$	0.00780	0.01187	0.01184	0.01690	0.02673	0.02635	0.04660	0.07251	0.07116

Table 2: *The ER values for the estimators of θ obtained based on the Bayesian approach.*

	$\theta=2$			$\theta=3$			$\theta=5$		
Sample 1	NMRSSU	MinRSSU	SRS	NMRSSU	MinRSSU	SRS	NMRSSU	MinRSSU	SRS
ER_S	0.09331	0.20357	0.20373	0.21346	0.46740	0.46365	0.59943	1.27265	1.30303
$ER_{L(c=+0.5)}$	0.01143	0.02477	0.02476	0.02602	0.05630	0.05591	0.07294	0.14992	0.15611
$ER_{L(c=-0.5)}$	0.01190	0.02615	0.02621	0.02739	0.06084	0.06036	0.07761	0.17097	0.17308
Sample 2	NMRSSU	MinRSSU	SRS	NMRSSU	MinRSSU	SRS	NMRSSU	MinRSSU	SRS
ER_S	0.08093	0.13757	0.14232	0.17905	0.31541	0.31330	0.49940	0.89038	0.85998
$ER_{L(c=+0.5)}$	0.01000	0.01686	0.01750	0.02198	0.03819	0.03805	0.06036	0.10636	0.10152
$ER_{L(c=-0.5)}$	0.01024	0.01755	0.01810	0.02283	0.04072	0.04033	0.06466	0.11719	0.11378
Sample 3	NMRSSU	MinRSSU	SRS	NMRSSU	MinRSSU	SRS	NMRSSU	MinRSSU	SRS
ER_S	0.05873	0.11355	0.11391	0.13070	0.26677	0.26171	0.36391	0.72038	0.72095
$ER_{L(c=+0.5)}$	0.00726	0.01394	0.01406	0.01605	0.03277	0.03207	0.04427	0.08736	0.08720
$ER_{L(c=-0.5)}$	0.00743	0.01446	0.01444	0.01664	0.03400	0.03345	0.04673	0.09347	0.09366
Sample 4	NMRSSU	MinRSSU	SRS	NMRSSU	MinRSSU	SRS	NMRSSU	MinRSSU	SRS
ER_S	0.06446	0.09959	0.09915	0.14094	0.22856	0.22406	0.39511	0.63792	0.62633
$ER_{L(c=+0.5)}$	0.00798	0.01230	0.01223	0.01730	0.02804	0.02746	0.04807	0.07714	0.07597
$ER_{L(c=-0.5)}$	0.00814	0.01261	0.01256	0.01795	0.02913	0.02863	0.05077	0.08259	0.08091

Table 3: *The bias values for the estimators of θ obtained based on the Bayesian approach.*

	$\theta = 2$			$\theta = 3$			$\theta = 5$		
Sample 1	NMRSSU	MinRSSU	SRS	NMRSSU	MinRSSU	SRS	NMRSSU	MinRSSU	SRS
SEL	0.04162	0.08217	0.08659	0.06167	0.13838	0.13395	0.10088	0.21764	0.20685
LEL ($c = +0.5$)	0.01891	0.03642	0.04066	0.01100	0.03600	0.03186	−0.03749	−0.05709	−0.06711
LEL ($c = -0.5$)	0.06515	0.13091	0.13553	0.11509	0.25102	0.24625	0.25201	0.53980	0.52818
Sample 2	NMRSSU	MinRSSU	SRS	NMRSSU	MinRSSU	SRS	NMRSSU	MinRSSU	SRS
SEL	0.03724	0.05613	0.05900	0.05913	0.09008	0.09131	0.08814	0.14201	0.13308
LEL ($c = +0.5$)	0.01803	0.02381	0.02656	0.01608	0.01783	0.01902	−0.02920	−0.05405	−0.06216
LEL ($c = -0.5$)	0.05701	0.08992	0.09292	0.10407	0.16731	0.16857	0.21424	0.36111	0.35117
Sample 3	NMRSSU	MinRSSU	SRS	NMRSSU	MinRSSU	SRS	NMRSSU	MinRSSU	SRS
SEL	0.02977	0.05286	0.04910	0.03614	0.07439	0.07807	0.06492	0.12439	0.13542
LEL ($c = +0.5$)	0.01535	0.02631	0.02264	0.00400	0.01529	0.01887	−0.02360	−0.03688	−0.02650
LEL ($c = -0.5$)	0.04452	0.08038	0.07653	0.06934	0.13678	0.14057	0.15836	0.30088	0.31265
Sample 4	NMRSSU	MinRSSU	SRS	NMRSSU	MinRSSU	SRS	NMRSSU	MinRSSU	SRS
SEL	0.02885	0.04652	0.04249	0.04398	0.07003	0.06337	0.06873	0.12221	0.11437
LEL ($c = +0.5$)	0.01346	0.02309	0.01915	0.00952	0.01768	0.01126	−0.02581	−0.02131	−0.02867
LEL ($c = -0.5$)	0.04460	0.07071	0.06659	0.07962	0.12494	0.11802	0.16872	0.27762	0.26925

Table 4: *The AWs and CPs of the* 95% *interval estimators of* θ.

$\theta = 2$	AW			CP		
Sample 1	NMRSSU	MinRSSU	SRS	NMRSSU	MinRSSU	SRS
Classical	1.17564	1.66657	1.67012	0.9507	0.9525	0.9533
Bayesian	1.16084	1.64387	1.64736	0.9487	0.9507	0.9512
Sample 2	NMRSSU	MinRSSU	SRS	NMRSSU	MinRSSU	SRS
Classical	1.08252	1.40986	1.40280	0.9521	0.9511	0.9537
Bayesian	1.06887	1.39590	1.38891	0.9499	0.9490	0.9529
Sample 3	NMRSSU	MinRSSU	SRS	NMRSSU	MinRSSU	SRS
Classical	0.93924	1.27394	1.27250	0.9536	0.9475	0.9543
Bayesian	0.92750	1.26354	1.26211	0.9514	0.9464	0.9532
Sample 4	NMRSSU	MinRSSU	SRS	NMRSSU	MinRSSU	SRS
Classical	0.97007	1.19379	1.19175	0.9496	0.9497	0.9511
Bayesian	0.95751	1.18513	1.18311	0.9466	0.9489	0.9495
$\theta = 3$	AW			CP		
Sample 1	NMRSSU	MinRSSU	SRS	NMRSSU	MinRSSU	SRS
Classical	1.76399	2.50650	2.49813	0.9506	0.9519	0.9555
Bayesian	1.74286	2.47122	2.46299	0.9471	0.9486	0.9536
Sample 2	NMRSSU	MinRSSU	SRS	NMRSSU	MinRSSU	SRS
Classical	1.62643	2.11099	2.11079	0.9538	0.9501	0.9509
Bayesian	1.60771	2.08942	2.08922	0.9502	0.9490	0.9494
Sample 3	NMRSSU	MinRSSU	SRS	NMRSSU	MinRSSU	SRS
Classical	1.40534	1.90801	1.91258	0.9503	0.9531	0.9543
Bayesian	1.39015	1.89193	1.89646	0.9471	0.9516	0.9515
Sample 4	NMRSSU	MinRSSU	SRS	NMRSSU	MinRSSU	SRS
Classical	1.45588	1.79344	1.79299	0.9512	0.9526	0.9502
Bayesian	1.43917	1.78001	1.77956	0.9484	0.9512	0.9484
$\theta = 5$	AW			CP		
Sample 1	NMRSSU	MinRSSU	SRS	NMRSSU	MinRSSU	SRS
Classical	2.93916	4.18449	4.16863	0.9508	0.9507	0.9499
Bayesian	2.90510	4.12182	4.10625	0.9486	0.9469	0.9466
Sample 2	NMRSSU	MinRSSU	SRS	NMRSSU	MinRSSU	SRS
Classical	2.70566	3.52110	3.53176	0.9501	0.9553	0.9514
Bayesian	2.67406	3.48287	3.49339	0.9485	0.9525	0.9498
Sample 3	NMRSSU	MinRSSU	SRS	NMRSSU	MinRSSU	SRS
Classical	2.34541	3.17217	3.19171	0.9521	0.9551	0.9509
Bayesian	2.32155	3.14379	3.16314	0.9495	0.9547	0.9489
Sample 4	NMRSSU	MinRSSU	SRS	NMRSSU	MinRSSU	SRS
Classical	2.42441	2.98541	2.98560	0.9489	0.9507	0.9483
Bayesian	2.39914	2.96168	2.96187	0.9454	0.9499	0.9464

6. Real data example

In this section, we utilize real data concerning the intervals between failures of Boeing air conditioner systems in hours, originally reported by Proschan [36]. It is important to note that Proschan [36] omitted certain failure intervals due to major overhauls, see also [21]. Ahmadi et al. [2] considered a part of these data and emphasized that the exponential distribution is a suitable model for the considered data. Here, applying the bootstrapped version of the Kolmogorov-Smirnov test (see [11, 46, 47]), and using the strategy described in [29] for data sets with ties, we found out that the hypothesis that the above data follow the exponential distribution cannot be rejected at a significance level of 0.05. Thus, we may accept the assumption that the data follow an exponential distribution. We selected a sample of size $n_0 = m \times n = 3 \times 6 = 18$ from the specified real data, where m is the number of cycles and n is the sample size of one cycle. To implement the NMRSSU plan, we began by choosing $m = 3$ samples, each consisting of 10 observations, and treated each of these samples as a separate cycle. Each cycle was further segmented into $k = 4$ groups, organized by the number of observations as follows: the first group had one observation, the second group comprised two observations, and finally, the last group contained four observations. This arrangement allowed us to extract a total of $n = 6$ observations from each cycle, according to the specified plan. For the MinRSSU plan, we selected $m = 3$ samples, but here each sample included 21 observations. Similar to the previous plan, each sample was regarded as a cycle and was divided into $n = 6$ groups. The configuration for these groups was one observation in the first, two observations in the second, and finally, six observations in the last group. Consequently, we could extract $n = 6$ observations from every cycle as intended by the plan.

We utilized an approximate non-informative prior with hyperparameters $\alpha = \beta = 0.01$ for the parameter. We took $S = 10000$, $M = 1000$, and $\sigma = 0.1$ for the MH method. We calculated both point estimates and 95% interval estimates for θ using classical and Bayesian methods. Note that in the context of Bayesian interval estimation, we obtained exact 95% shortest width credible intervals for θ up to 5 decimal places when the SRS and MinRSSU plans were used. Tables 5 and 6 give the numerical results for point estimation and interval estimation, respectively.

Table 5: *The point estimates of θ.*

ML			Bayesian								
NMRSSU	MinRSSU	SRS	NMRSSU			MinRSSU			SRS		
			SEL	LEL ($c=+0.5$)	LEL ($c=-0.5$)	SEL	LEL ($c=+0.5$)	LEL ($c=-0.5$)	SEL	LEL ($c=+0.5$)	LEL ($c=-0.5$)
0.01007	0.01417	0.01228	0.01012	0.01012	0.01013	0.01418	0.01418	0.01418	0.01229	0.01228	0.01229

Table 6: *The* 0.95% *interval estimates of θ.*

Classical			Bayesian		
NMRSSU	MinRSSU	SRS	NMRSSU	MinRSSU	SRS
(0.00628 , 0.01386)	(0.00763 , 0.02072)	(0.00661 , 0.01795)	(0.00643 , 0.01385)	(0.00797 , 0.02085)	(0.00691 , 0.01806)

7. Concluding remarks

In this paper, we introduced a new RSS-type sampling plan with unequal sample sizes, called the new min-max ranked set sampling scheme with unequal sample sizes. The new scheme is applied to parameter estimation for the exponential distribution using the ML and Bayesian approaches. The findings of the simulation study highlight the effectiveness of the new scheme in comparison with the SRS and MinRSSU schemes. As a future study, we may work on some other new sampling plans with unequal sample sizes and explore their efficacy. All the numerical computations of this paper were done using the statistical software R [37] and the packages coda [33, 34], truncnorm [27], and nleqslv [16] therein.

Data Availability Statement

The data set used in this paper is explained in the manuscript.

Declaration of Conflicting Interests

The Authors declare that there is no conflict of interest.

Funding Details

The first author may receive grant from University of Mazandaran.

References

[1] Abdallah, M. S. and Al-Omari, A. I. (2022). On the nonparametric estimation of the odds and distribution function using moving extreme ranked set sampling. *Revista Investigación Operacional*, 43:90–101.

[2] Ahmadi, J., Basiri, E. and MirMostafaee, S. M. T. K. (2016). Optimal random sample size based on Bayesian prediction of exponential lifetime and application to real data. *Journal of the Korean Statistical Society*, 45:221–237.

[3] Al-Nasser, A. D., and Al-Omari, A. I. (2018). Minimax ranked set sampling. *Revista Investigación Operacional*, 39:560–570.

[4] Al-Odat, M. T. and Al-Saleh, M. F. (2001). A variation of ranked set sampling. *Journal of Applied Statistical Science*, 10:137–146.

[5] Al-Omari, A. I. and Bouza, C. N. (2014). Review of ranked set sampling: modifications and applications. *Revista Investigación Operacional*, 35:215–240.

[6] Asgharzadeh, A. and Valiollahi, R. (2012). Prediction of times to failure of censored units in hybrid censored samples from exponential distribution. *Journal of Statistical Research of Iran*, 9:11–30.

[7] Bhoj, D. S. (2001). Ranked set sampling with unequal samples. *Biometrics*, 57:957–962.

[8] Biradar, B. S. and Santosha, C. D. (2014). Estimation of the mean of the exponential distribution using maximum ranked set sampling with unequal samples. *Open Journal of Statistics*, 4:641–649.

[9] Biradar, B. S. and Santosha, C. D. (2017). Estimation of the mean of the exponential distribution using extreme ranked set sampling with unequal samples. *International Journal of Agricultural & Statistical Sciences*, 13:393–401.

[10] Biradar, B. S. and Shivanna, B. K. (2023). Bayesian estimation of the mean of exponential distribution using ranked set sampling with unequal samples. *Asian Journal of Statistical Sciences*, 3:143–153.

[11] Castro, R. (2013). Lectures 2 and 3 - Goodness-of-fit (GoF) Tests. https://rmcastro.win.tue.nl/AppStat2013/files/lectures23.pdf.

[12] Chen, M.-H. and Shao, Q.-M. (1999). Monte Carlo estimation of Bayesian credible and HPD intervals. *Journal of Computational and Graphical Statistics*, 8:69–92.

[13] Geweke, J. (1992). Evaluating the accuracy of sampling-based approaches to the calculation of posterior moments. In Bayesian Statistics 4, Eds. J. M. Bernardo, J. O. Berger, A.P. Dawid and A. F. M. Smith, Clarendon Press, Oxford, UK, pp. 169–193.

[14] Fallah, A. and Asgharzadeh, A. (2021). Pivotal and Bayesian inference in exponential coherent systems under progressive censoring. *Journal of Advanced Mathematical Modeling*, 11:496–514.

[15] Hanandeh, A. A. and Al-Nasser, A. D. (2020). Improved Shewhart control chart using minimax ranked set sampling. *Revista Investigación Operacional*, 41:923–934.

[16] Hasselman, B. (2023). nleqslv: Solve systems of nonlinear equations, R package version 3.3.5, https://CRAN.R-project.org/package=nleqslv.

[17] Hastings, W. K. (1970). Monte Carlo sampling methods using Markov chains and their applications. *Biometrika*, 57:97–109.
[18] Heidelberger, P. and Welch, P. D. (1981). A spectral method for confidence interval generation and run length control in simulations. *Communications of the ACM*, 24:233–245.
[19] Heidelberger, P. and Welch, P. D. (1981). Adaptive spectral methods for simulation output analysis. IBM Journal of Research and Development, 25:860–876.
[20] Heidelberger, P. and Welch, P. D. (1983). Simulation run length control in the presence of an initial transient. *Operations Research*, 31:1109–1144.
[21] Hollander, M., Presnell, B. and Sethuraman, J. (1992). Nonparametric methods for imperfect repair models. *The Annals of Statistics*, 20:879–896.
[22] Jeelani, M. I., and Bouza, C. N. (2015). New ratio method of estimation under ranked set sampling. *Revista Investigación Operacional*, 36:151–155.
[23] Jeelani, M. I., Bouza, C. N. and Sharma, M. (2017). Modified ratio estimator under rank set sampling. *Revista Investigación Operacional*, 38:103–106.
[24] Joukar, A., Ramezani, M. and MirMostafaee, S. M. T. K. (2021). Parameter estimation for the exponential-Poisson distribution based on ranked set samples. *Communications in Statistics-Theory and Methods*, 50:560–581.
[25] Lehmann, E. L. and Casella, G. Theory of Point Estimation. Second Edition, Springer, 1998.
[26] McIntyre, G. A. (1952). A method for unbiased selective sampling, using ranked sets. *Australian Journal of Agricultural Research*, 3:385–390.
[27] Mersmann, O., Trautmann, H., Steuer, D. and Bornkamp, B. (2023). truncnorm: Truncated normal distribution, R package version 1.0-9, https://CRAN.R-project.org/package=truncnorm.
[28] Metropolis, N, Rosenbluth, A. W., Rosenbluth, M. N.,Teller, A. H. and Teller, E. (1953). Equation of state calculations by fast computing machines. *The Journal of Chemical Physics*, 21:1087–1092.
[29] MirMostafaee, S. M. T. K. (2023). The exponentiated new XLindley distribution: Properties, and applications. *Journal of Data Science and Modeling*, 2:185–208.
[30] MirMostafaee, S. M. T. K. and Ahmadi, J. (2011). Point prediction of future order statistics from an exponential distribution. *Statistics & Probability Letters*, 81:360–370.
[31] Muttlak, H. A. (1996). Pair rank set sampling. *Biometrical Journal*, 38:879–885.
[32] Muttlak, H. A. (1997). Median ranked set sampling. *Journal of Applied Statistical Science*, 6:245–255.
[33] Plummer, M., Best, N., Cowles, K. and Vines, K. (2006). CODA: Convergence diagnosis and output analysis for MCMC. *R News*, 6:7–11.
[34] Plummer, M., Best, N., Cowles, K., Vines, K., Sarkar, D., Bates, D., Almond, R. and Magnusson, A. (2024). coda: Output analysis and diagnostics for MCMC. R package version 0.19-4.1, https://CRAN.R-project.org/package=coda.
[35] Qiu, G. and Eftekharian, A. (2021). Extropy information of maximum and minimum ranked set sampling with unequal samples. *Communications in Statistics-Theory and Methods*, 50:2979–2995.
[36] Proschan, F. (1963). Theoretical explanation of observed decreasing failure rate. *Technometrics*, 5:375–383.
[37] R Core Team (2024). R: A language and environment for statistical computing. R Foundation for Statistical Computing, Vienna, Austria.
[38] Raftery, A. E. and Lewis, S. M. (1992). Comment: One long run with diagnostics: Implementation strategies for Markov chain Monte Carlo. *Statistical Science*, 7:493–497.
[39] Raftery, A. E. and Lewis, S. M. (1996). Implementing MCMC. In Markov Chain Monte Carlo in Practice, Eds. W. R. Gilks, S. Richardson and D. J. Spiegelhalter, Chapman and Hall/CRC, Boca Raton, pp. 115–130.
[40] Ramezani, M., Joukar, A. and MirMostafaee, S. M. T. K. (2024). Estimation of the stress-strength parameter for a decreasing failure rate model based on ranked set samples. *Journal of Testing and Evaluation*, 52:3363–3392.

[41] Samawi, H. M. (1996). Stratified ranked set sample. *Pakistan Journal of Statistics*, 12:9–16.
[42] Samawi, H. M., Ahmed, M. S. and AbuDayyeh, W. (1996). Estimating the population mean using extreme ranked set sampling. *Biometrical Journal*, 38:577–586.
[43] Schruben, L. W. (1982). Detecting initialization bias in simulation output. *Operations Research*, 30:569–590.
[44] Schruben, L., Singh, H. and Tierney, L. (1980). A test of initialization bias hypotheses in simulation output. Technical Report 471, School of Operations Research and Industrial Engineering, Cornell University, Ithaca, New York, 14853.
[45] Schruben, L., Singh, H. and Tierney, L. (1983). Optimal tests for initialization bias in simulation output. *Operations Research*, 31:1167–1178.
[46] Sen, S. Afify, A. Z., Al-Mofleh H., and Ahsanullah, M. (2019). The quasi xgamma-geometric distribution with application in medicine. *Filomat*, 33:5291–5330.
[47] Stute, W., Manteiga, W. G., and Quindimil, M. P. (1993). Bootstrap based goodness-of-fit-tests. *Metrika*, 40:243–256.
[48] Varian, H. R. (1975). Bayesian approach to real estate assessment. In Studies in Bayesian Econometrics and Statistics in Honor of Leonard J. Savage, Eds. S. E. Fienberg and A. Zellner, North-Holland Pub. Co., Amsterdam, pp. 195–208.
[49] Zellner, A. (1986). Bayesian estimation and prediction using asymmetric loss functions. *Journal of the American Statistical Association*, 81:446–451.

ANALYSIS OF $MAP_1^I, PH_2^O / PH_1^I, PH_2^O /1$ RETRIAL INVENTORY QUEUE, TWO WAY COMMUNICATION, (S, S) REPLENISHMENT POLICY, NEGATIVE ARRIVAL, WORKING BREAKDOWN AND REPAIR

G. Ayyappan[1] and V. Ganesan[2]

•

[1]Department of Mathematics, Puducherry Technological University,
Puducherry 605014, India.
[2]Department of Mathematics, Sri Venkateshwaraa College of Engineering and Technology,
Puducherry 605102, India.
[1]ayyappan@ptuniv.edu.in, [2]ganeshvaradhan@gmail.com

Abstract

The retrial inventory queueing model with two-way communication, the (s, S) replenishment strategy, negative arrival, working breakdown, and repair are all topics that are discussed in this paper. Our assumption is that the arrival is a Markovian arrival process and that a server is the entity that is responsible for providing phase type services. When there is a positive inventory and the server is idle, the customer who arrives is instantly attended to their needs. In the event that this instance does not occur, the customer who is arriving will be moved to orbit, and a retrial customer from orbit will join afterwards if the server is idle and has positive inventory. When the inventory level is positive, the server will make outgoing calls that follow phase type distribution during the idle period. If the inventory level is zero, the server will continue to stay idle. A negative arrival may occur while the server is providing service. Since the server is experiencing a breakdown, the consumer will experience slow service at this time. After the slow service ends, the server will immediately begin the repair procedure, which follows a phase-type distribution. The policy of (s, S) is utilised to replenish the items. By employing the matrix analytic method, we are able to derive the steady state probability vector. Additionally, we address the busy period, performance measurements, and cost analysis, in addition to providing some numerical examples.

Keywords: Retrial inventory queue, Two way communication, Matrix analytic method, (s, S) Replenishment policy, Negative arrival, Working breakdown, Repair

1. Introduction

Recent advancements in computer networking and communications technology have led to a growing interest in inventory retrial queueing systems. The level of attention on this topic has been growing due to its increasing relevance. Individual customers in a queueing inventory model are each given a product from the inventory once the service has been completed. This adaptable class of point processes on the real line, which are closely connected to finite-state Markov processes, was initially introduced by Neuts [18] in their work. Among the many point processes, there are a few that stand out as specific situations. These include renewal processes of phase type, Markov-modulated Poisson processes, and some semi-Markov point processes. Chakravarthy [10] offered a comprehensive explanation of the phase-type distribution as well as Markovian arrival process, which included a number of correlated and non-correlated arrival

types. Neuts [20] conducted an investigation into the techniques of matrix-analytic queueing theory.

Falin and Templeton [11] produced the first monograph on retrial queues, which offers a thorough explanation of fundamental techniques and findings. They have produced a number of analytical findings and talked about retrial queues for both single and multiserver systems. Artalejo [3, 4] have produced a bibliography on retrial queues that may be used as an index to find other books and articles about retrial queues. A survey of retrial queue theory and applications was presented by Tuan Phung-Duc [23]. In addition to providing a summary of retrial models that emerge from actual circumstances, he has also identified several unresolved issues and exciting avenues for further study.

There is a queueing order-demand inventory system, and according to Melikov and Molchanov [16], the most effective approach for reordering products is to adhere to the guidelines that are described. Berman et al. [9] conducted research on an inventory control system that was designed for a service center. This system was designed to utilize a single inventory item for each service that was performed. During their evaluation, Yadavalli et al. [25] used the assumption that requests are a component of the renewal process and that reorders are easily available without any difficulty. The inventory system included both a waiting room that was open for an endless amount of time and a service station. When it comes to service stations, it is generally acknowledged that inventory and queueing models have not been unsuccessful the majority of the time.

As a matter of fact, we frequently encounter situations in which there is a possibility of service station failures occurring. A server interruption inventory retrial queueing system was discussed by Krishnamoorthy et al. [14]. They incorporated (s, S) replenishment policy into their model. Both the lead time and the service time are determined by an exponential distribution, but the arrival time is determined by a Poisson distribution. This policy is distinguished by the fact that the lead time and service time are both determined by an exponential distribution. Ushakumari [24] conducted an investigation of the retrial inventory queue system, which was characterized by server failure. Ayyappan and Arulmozhi [6] have discussed retrial queueing inventory system with working vacation, flush out, balking, breakdown, and repair, as well as a constant retrial rate and collision with orbital customers. Additionally, Ayyappan and Meena [7] address the concept of a preemptive priority queue, which includes clients who are impatient, have a single vacation, and are in need of repair.

Artalejo and Phung-Duc [2] discussed the steady state behaviour of an $M/G/1$ retrial queue with two-way communication for a single channel. Ayyappan and Thilagavathy [8] is discussed standby server rendering service due to primary server is breakdowns with constant retrial rate and collision with orbit. The study conducted by Nazarov et al. [17] found that an investigation was performed on a single-server Markovian retrial queue with a finite number of sources and two-way communication. The exponential distribution takes into account not only the service times for receiving calls but also the service times for outgoing calls. Somasundaram et al. [5] presents a discussion on a single server constant retrial two-way communication queueing architecture. This architecture is designed to ensure that the server continues to provide service even after a breakdown, although at a slower rate, rather than entirely shutting down.

The research conducted by Karthick et al. [13] involved the implementation of a single channel queue that included server breakdown and repair, as well as differentiated vacation. Rakesh Kumar and Bhavneet Singh Soodan [21] did a study on a queueing model that had correlated inputs and reneging. They did a transient analysis on this model. Haghighi et al. [12] had discussed in detail about the impatient customers. Agassi Melikov et al. [1] studied single server models of queuing inventory systems with catastrophes in the warehouse part and negative customers in service facility.

2. Model Description

In our discussion, we consider a single server retrial inventory queueing model, where the incoming call arrivals follow MAP with representation of matrices (D_0, D_1) of order m_1, where D_0 represents no arrival occurs and D_1 represents an arrival occurs to the system. The incoming call arrival gets service immediately only when the server is idle with positive inventory level, if not the arriving customer will join the orbit of infinite capacity. After service completion, the incoming call arrival leaves the system and server may provides the service if any incoming call arrival or retrial customer enters, otherwise the server is idle. During the idle period with the positive inventory level, the server provides the service if any incoming call arrival is entered otherwise will make outgoing calls which follows phase type distribution with representation (α, U) of order m_2. The incoming and outgoing calls service times follow phase type distributions with representation (β_1, T_1) of order n_1 and (β_2, T_2) of order n_2 respectively. During the service time of incoming and out going arrivals, the server may struck with break down like power fluctuations, hanging the system, network issues, etc. During this breakdown period, the server provides service with slow rate to that customer. The working break down (i.e., slow service) of the server for both incoming and outgoing calls follow phase type distribution with representation $(\beta_1, \theta_1 T_1)$ of order n_1 and $(\beta_2, \theta_1 T_2)$ of order n_2 respectively. After slow service completion, the customer leaves the system and the server shall go to repair process which follows phase type distribution with representation (γ, R) of order l. After repair completion, the server is idle. During the idle period with the positive inventory level, the server provides the service if any incoming call arrival is entered otherwise will make outgoing calls. The negative arrival causes the incoming call arrival or retrial customer who is currently receiving service or slow service from the server to be disturbed and removed. Due to the negative arrival the service cannot be completed of the incoming call arrival also negative arrival disturbs only customer and his service. The inter negative arrival times follow exponential distribution with constant rate λ^- for every negative arrival. Also the inter retrial times follow exponential distribution with constant rate ψ for every retrial customer from orbit of infinite capacity and also the τ be the breakdown parameter during incoming and out call arrivals follow exponential distribution. To replenish the items (s, S) policy is applied and the duration of replenishment follows exponential distribution with parameter σ.

3. Matrix Generations of QBD Process

We are going to discuss this part, which comprises the notation that forms the basis of the Quasi Birth and Death (QBD) process in our model.

- $\otimes -$ Any two matrices with different order are multiplied by using a Kronecker product, this part of work was done by the research of Steeb and Hardy [22].
- $\oplus -$ Any two different order matrices can be taken for sum by using a Kronecker sum.
- $I_k -$ The identity matrix has k dimensions.
- $e -$ The column vector's each of its elements 1 is taken part of the appropriate dimension as we need.
- $e_k -$ The column vector for every k element is 1.
- The arrival rate of incoming call arrivals is represented by λ and described as $\lambda = \pi D_1 e$.
- The service rate for incoming call arrivals represented by μ_1 and described as $\mu_1 = [\beta_1(-T_1)^{-1}e_{n_1}]^{-1}$.
- The service rate for outgoing call arrivals represented by μ_2 and described as $\mu_2 = [\beta_2(-T_2)^{-1}e_{n_2}]^{-1}$.
- The working breakdown service rate for incoming call arrivals represented by $\theta_1\mu_1$ and described as $\theta_1\mu_1 = [\beta_1(-\theta_1 T_1)^{-1}e_{n_1}]^{-1}$.
- The working breakdown service rate for outgoing call arrivals represented by $\theta_2\mu_2$ and described as $\theta_2\mu_2 = [\beta_2(-\theta_2 T_2)^{-1}e_{n_2}]^{-1}$.
- Repair rate of server is δ, where $\delta = [\gamma(-R)^{-1}e_l]^{-1}$.

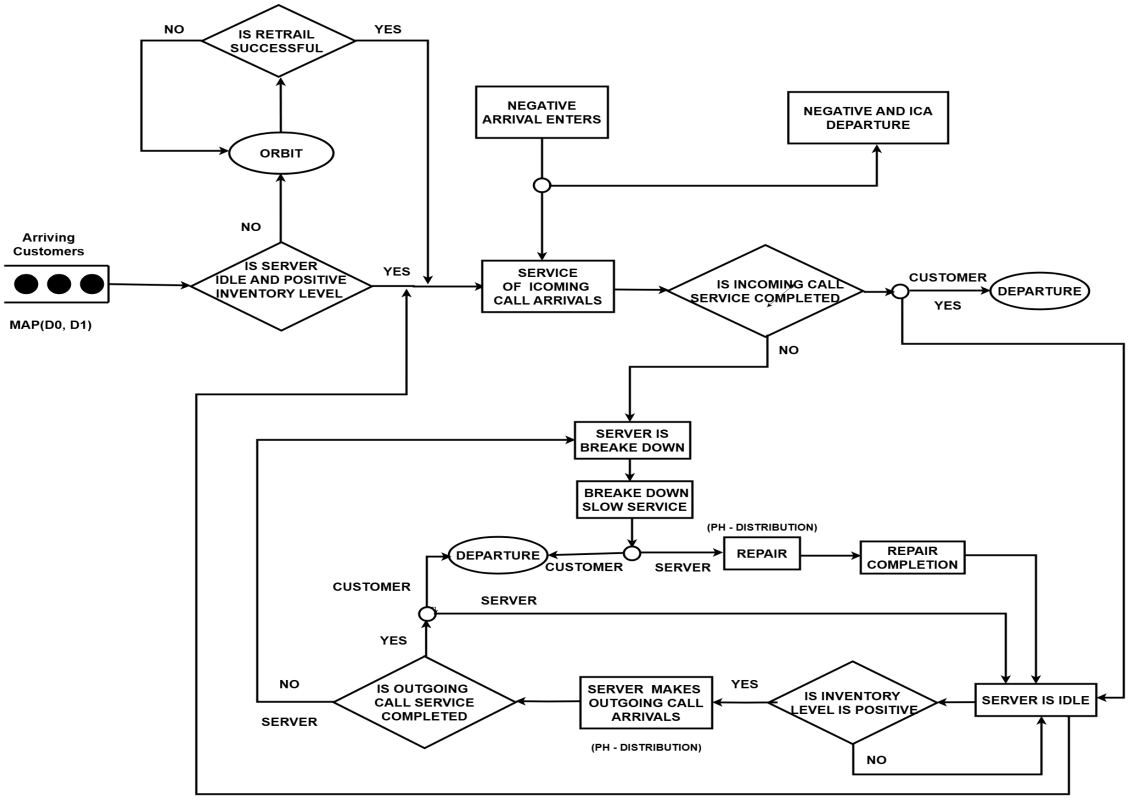


Figure 1: *A pictorial representation of the model*

- Rate at which server makes the outgoing call, where $\mu_3 = [\alpha(-U)^{-1}e_{m_2}]^{-1}$.
- Let $N(t)$ be number of customers in the orbit of infinite capacity at time t.
- Let $Y(t)$ be the level of server status at time t. Where

$$Y(t) = \begin{cases} 0, \text{ server being an idle also making outgoing calls when positive inventory,} \\ 1, \text{ server is offering service for incoming call arrivals,} \\ 2, \text{ server is offering service for outgoing call arrivals,} \\ 3, \text{ server is offering service during breakdown time for incoming call arrivals,} \\ 4, \text{ server is offering service during breakdown time for outgoing call arrivals,} \\ 5, \text{ server is under repair process.} \end{cases}$$

- Let $I(t)$ be the level of inventory items at time t.
- $J_1(t)$ be the incoming call service by the server at time t.
- $J_2(t)$ be the outgoing call service by the server at time t.
- $M_1(t)$ be the incoming call arrivals at time t.
- $M_2(t)$ be the incoming call arrivals at time t.

Let $\{ N(t), Y(t), I(t), J_1(t), J_2(t), M_1(t), M_2(t) : t \geq 0\}$ represents a CTMC with state-level independent QBD processes whose state space is as follows:

$$\Omega = \bigcup_{i=0}^{\infty} l(i), \text{ where}$$

$$\begin{aligned} l(i) =& \{(i,0,0,k_1) : 0 \leq k_1 \leq m_1\} \cup \{(i,0,j,k_1,k_2) : 1 \leq j \leq S, 1 \leq k_1 \leq m_1, 1 \leq k_2 \leq m_2\} \\ & \cup \{(i,u,j,r_1,k_1) : u = 1,3, 1 \leq j \leq S, 1 \leq r_1 \leq n_1, 1 \leq k_1 \leq m_1\} \\ & \cup \{(i,u,j,r_2,k_1) : u = 2,4, 1 \leq j \leq S, 1 \leq r_2 \leq n_2, 1 \leq k_1 \leq m_1\} \\ & \cup \{(i,5,j,k_1) : 0 \leq j \leq S, 1 \leq k_1 \leq m_1\}. \end{aligned}$$

The infinitesimal matrix generator of the QBD process is written as follows,

$$Q = \begin{bmatrix} A_{00} & A_{01} & 0 & 0 & 0 & 0 & 0 & \dots \\ V_2 & V_1 & V_0 & 0 & 0 & 0 & 0 & \dots \\ 0 & V_2 & V_1 & V_0 & 0 & 0 & 0 & \dots \\ 0 & 0 & V_2 & V_1 & V_0 & 0 & 0 & \dots \\ 0 & 0 & 0 & V_2 & V_1 & V_0 & 0 & \dots \\ \vdots & \vdots & \vdots & \ddots & \ddots & \ddots & \ddots & \vdots \\ \vdots & \vdots & \vdots & \vdots & \ddots & \ddots & \ddots & \ddots \end{bmatrix}$$

In the following, the ingress of the matrix Q structures are presented.

$$A_{00} = \begin{bmatrix} A_{00}^{11} & A_{00}^{12} & A_{00}^{13} & 0 & 0 & 0 \\ A_{00}^{21} & A_{00}^{22} & 0 & A_{00}^{24} & 0 & 0 \\ A_{00}^{31} & 0 & A_{00}^{33} & 0 & A_{00}^{35} & 0 \\ 0 & 0 & 0 & A_{00}^{44} & 0 & A_{00}^{46} \\ 0 & 0 & 0 & 0 & A_{00}^{55} & A_{00}^{56} \\ A_{00}^{61} & 0 & 0 & 0 & 0 & A_{00}^{66} \end{bmatrix}, \quad A_{00}^{11} = \begin{bmatrix} G_1 & 0 & \dots & 0 & 0 & \dots & G_2 \\ 0 & G_3 & \dots & 0 & 0 & \dots & G_4 \\ \vdots & \vdots & \ddots & \vdots & \vdots & \vdots & \vdots \\ 0 & 0 & \dots & G_3 & 0 & \dots & G_4 \\ 0 & 0 & \dots & 0 & G_5 & \dots & 0 \\ \vdots & \vdots & \vdots & \vdots & \vdots & \ddots & \vdots \\ 0 & 0 & \dots & 0 & 0 & \dots & G_5 \end{bmatrix},$$

$$G_1 = D_0 - \sigma I_{m_1}, \quad G_2 = \alpha \otimes \sigma I_{m_1}, G_3 = U \oplus D_0 - \sigma I_{m_2 m_1}, \quad G_4 = \sigma I_{m_2 m_1}, \quad G_5 = U \oplus D_0.$$

$$A_{00}^{12} = \begin{bmatrix} 0 \\ I_S \otimes e_{m_2} \otimes \beta_1 \otimes D_1 \end{bmatrix}, A_{00}^{13} = \begin{bmatrix} 0 \\ I_S \otimes U^0 \otimes \beta_2 \otimes I_{m_1} \end{bmatrix}, A_{00}^{21} = \begin{bmatrix} G_6 & G_7 & \dots & 0 & 0 \\ 0 & G_8 & \dots & 0 & 0 \\ 0 & 0 & \ddots & 0 & 0 \\ \vdots & \vdots & \ddots & \ddots & \vdots \\ 0 & 0 & \dots & G_8 & G_7 \end{bmatrix},$$

$$G_6 = T_1^0 \otimes I_{m_1}, \quad G_7 = e_{n_1} \otimes \alpha \otimes \lambda^- I_{m_1}, \quad G_8 = T_1^0 \otimes \alpha \otimes I_{m_1}.$$

$$A_{00}^{22} = \begin{bmatrix} G_9 & \dots & 0 & 0 & \dots & G_{10} \\ \vdots & \ddots & \vdots & \vdots & \vdots & \vdots \\ 0 & \dots & G_9 & 0 & \dots & G_{10} \\ 0 & \dots & 0 & G_{11} & \dots & 0 \\ \vdots & \vdots & \vdots & \vdots & \ddots & \vdots \\ 0 & \dots & 0 & 0 & \dots & G_{11} \end{bmatrix}, A_{00}^{33} = \begin{bmatrix} G_{12} & \dots & 0 & 0 & \dots & G_{13} \\ \vdots & \ddots & \vdots & \vdots & \vdots & \vdots \\ 0 & \dots & G_{12} & 0 & \dots & G_{13} \\ 0 & \dots & 0 & G_{14} & \dots & 0 \\ \vdots & \vdots & \vdots & \vdots & \ddots & \vdots \\ 0 & \dots & 0 & 0 & \dots & G_{14} \end{bmatrix}$$

$$A_{00}^{24} = \left[I_S \otimes \tau I_{n_1 m_1} \right], \quad A_{00}^{31} = \begin{bmatrix} T_2^0 I_{m_1} & 0 \\ 0 & I_{S-1} \otimes T_2^0 \alpha \otimes I_{m_1} \end{bmatrix}, \quad A_{00}^{35} = \left[I_S \otimes \tau I_{n_2 m_1} \right],$$

$$A_{00}^{44} = \begin{bmatrix} G_{15} & \dots & 0 & 0 & \dots & G_{10} \\ \vdots & \ddots & \vdots & \vdots & \vdots & \vdots \\ 0 & \dots & G_{15} & 0 & \dots & G_{10} \\ 0 & \dots & 0 & G_{16} & \dots & 0 \\ \vdots & \vdots & \vdots & \vdots & \ddots & \vdots \\ 0 & \dots & 0 & 0 & \dots & G_{16} \end{bmatrix}, \quad A_{00}^{46} = \begin{bmatrix} G_{17} & G_{18} & 0 & \dots & 0 & 0 \\ 0 & G_{17} & G_{18} & \dots & 0 & 0 \\ 0 & 0 & G_{17} & \dots & 0 & 0 \\ \vdots & \vdots & \vdots & \ddots & \vdots & \vdots \\ 0 & 0 & \dots & \dots & G_{17} & G_{18} \end{bmatrix},$$

$$G_9 = T_1 \oplus D_0 - (\tau + \sigma + \lambda^-) I_{n_1 m_1}, \quad G_{10} = \sigma I_{m_1 n_1}, \quad G_{11} = T_1 \oplus D_0 - (\tau + \lambda^-) I_{n_1 m_1},$$

$$G_{12} = T_2 \oplus D_0 - (\tau + \sigma) I_{n_2 m_1}, \quad G_{14} = T_2 \oplus D_0 - \tau I_{n_2 m_1}, \quad G_{15} = \theta_1 T_1 \oplus D_0 - (\sigma + \lambda^-) I_{n_1 m_1},$$

$$G_{13} = \sigma I_{n_2 m_1}, \quad G_{16} = \theta_1 T_1 \oplus D_0 - \lambda^- I_{n_1 m_1}, \quad G_{17} = \theta_1 T_1^0 \otimes \gamma \otimes I_{m_1}, \quad G_{18} = e_{n_1} \otimes \gamma \otimes \lambda^- I_{m_1}$$

$$A_{00}^{55} = \begin{bmatrix} G_{19} & \dots & 0 & 0 & \dots & G_{13} \\ \vdots & \ddots & \vdots & \vdots & \vdots & \vdots \\ 0 & \dots & G_{19} & 0 & \dots & G_{13} \\ 0 & \dots & 0 & G_{20} & \dots & 0 \\ \vdots & \vdots & \vdots & \vdots & \ddots & \vdots \\ 0 & \dots & 0 & 0 & \dots & G_{20} \end{bmatrix}, \quad A_{00}^{66} = \begin{bmatrix} G_{21} & \dots & 0 & 0 & \dots & G_{22} \\ \vdots & \ddots & \vdots & \vdots & \vdots & \vdots \\ 0 & \dots & G_{21} & 0 & \dots & G_{22} \\ 0 & \dots & 0 & G_{23} & \dots & 0 \\ \vdots & \vdots & \vdots & \vdots & \ddots & \vdots \\ 0 & \dots & 0 & 0 & \dots & G_{23} \end{bmatrix},$$

$$G_{19} = \theta_2 T_2 \oplus D_0 - \sigma I_{n_2 m_1},\ G_{20} = \theta_2 T_2 \oplus D_0,\ G_{21} = R \oplus D_0 - \sigma I_{l m_1},\ G_{22} = \sigma I_{l m_1}$$

$$G_{23} = R \oplus D_0,\ \ A_{00}^{56} = \begin{bmatrix} I_S \otimes \theta_2 T_2^0 \otimes \gamma I_{m_1} & 0 \end{bmatrix},\ \ A_{00}^{61} = \begin{bmatrix} R^0 \otimes I_{m_1} & 0 \\ 0 & R^0 \otimes \alpha I_{m_1} \end{bmatrix},$$

$$A_{01} = \begin{bmatrix} A_{01}^{11} & 0 & 0 & 0 & 0 & 0 \\ 0 & A_{01}^{22} & 0 & 0 & 0 & 0 \\ 0 & 0 & A_{01}^{33} & 0 & 0 & 0 \\ 0 & 0 & 0 & A_{01}^{44} & 0 & 0 \\ 0 & 0 & 0 & 0 & A_{01}^{55} & 0 \\ 0 & 0 & 0 & 0 & 0 & A_{01}^{66} \end{bmatrix},\ \ A_{01}^{11} = \begin{bmatrix} D_1 \end{bmatrix},\ A_{01}^{22} = \begin{bmatrix} I_S \otimes I_{n_1} \otimes D_1 \end{bmatrix} = A_{01}^{44},$$

$$A_{01}^{33} = \begin{bmatrix} I_S \otimes I_{n_2} \otimes D_1 \end{bmatrix} = A_{01}^{55},\ \ A_{01}^{66} = \begin{bmatrix} I_{(S+1)} \otimes I_l \otimes D_1 \end{bmatrix},$$

$$V_0 = A_{01},\ \ V_2 = \begin{bmatrix} 0 & V_2^{12} & 0 & 0 & 0 & 0 \\ 0 & 0 & 0 & 0 & 0 & 0 \\ 0 & 0 & 0 & 0 & 0 & 0 \\ 0 & 0 & 0 & 0 & 0 & 0 \\ 0 & 0 & 0 & 0 & 0 & 0 \\ 0 & 0 & 0 & 0 & 0 & 0 \end{bmatrix},\ \text{where}\ \ V_2^{12} = \begin{bmatrix} 0 \\ \beta_1 \otimes e_{m_2} \otimes \psi I_{m_1} \end{bmatrix}.$$

$$V_1 = \begin{bmatrix} V_1^{11} & V_1^{12} & V_1^{13} & 0 & 0 & 0 \\ V_1^{21} & V_1^{22} & 0 & V_1^{24} & 0 & 0 \\ V_1^{31} & 0 & V_1^{33} & 0 & V_1^{35} & 0 \\ 0 & 0 & 0 & V_1^{44} & 0 & V_1^{46} \\ 0 & 0 & 0 & 0 & V_1^{55} & V_1^{56} \\ V_1^{61} & 0 & 0 & 0 & 0 & V_1^{66} \end{bmatrix},\ \ V_1^{11} = \begin{bmatrix} G_1 & 0 & \dots & 0 & 0 & \dots & G_2 \\ 0 & G_{24} & \dots & 0 & 0 & \dots & G_4 \\ \vdots & \vdots & \ddots & \vdots & \vdots & \vdots & \vdots \\ 0 & 0 & \dots & G_{24} & 0 & \dots & G_4 \\ 0 & 0 & \dots & 0 & G_{25} & \dots & 0 \\ \vdots & \vdots & \vdots & \vdots & \vdots & \ddots & \vdots \\ 0 & 0 & \dots & 0 & 0 & \dots & G_{25} \end{bmatrix},$$

$$G_{24} = U \oplus D_0 - (\psi + \sigma) I_{m_2 m_1},\ \ G_{25} = U \oplus D_0 - \psi I_{m_2 m_1}.$$

$$V_1^{12} = V_{00}^{12},\ V_1^{13} = V_{00}^{13},\ V_1^{21} = V_{00}^{21},\ V_1^{22} = V_{00}^{22},\ V_1^{24} = V_{00}^{24},\ V_1^{31} = V_{00}^{31},\ V_1^{33} = V_{00}^{33},$$
$$V_1^{35} = V_{00}^{35},\ V_1^{44} = V_{00}^{44}, V_1^{46} = V_{00}^{46},\ V_1^{55} = V_{00}^{55},\ V_1^{56} = V_{00}^{56},\ V_1^{61} = V_{00}^{61},\ V_1^{66} = V_{00}^{66}.$$

4. Stationary Analysis

To justify of our model, we ensure the stability of the system under certain conditions as follows:

4.1. Criteria of system stability

Let us assume that the matrix V as $V = V_0 + V_1 + V_2$ is an irreducible infinitesimal generator matrix with dimension of $\{m_1 + Sm_1m_2 + Sm_1n_1 + Sm_1n_2 + Sm_1n_1 + Sm_1n_2 + (S+1)m_1l\}$.

$$V = \begin{bmatrix} V^{11} & V^{12} & V^{13} & 0 & 0 & 0 \\ V^{21} & V^{22} & 0 & V^{24} & 0 & 0 \\ V^{31} & 0 & V^{33} & 0 & V^{35} & 0 \\ 0 & 0 & 0 & V^{44} & 0 & V^{46} \\ 0 & 0 & 0 & 0 & V^{55} & V^{56} \\ V^{61} & 0 & 0 & 0 & 0 & V^{66} \end{bmatrix},\ \text{where}\ V^{11} = V_1^{11} + V_0^{11},\ V^{12} = V_2^{12} + V_1^{12},\ V^{13} = V_1^{13},$$

$$V^{21} = V_1^{21} + V_0^{21},\ V^{22} = V_1^{22} + V_0^{22},\ V^{24} = V_1^{24},\ V^{31} = V_1^{31},\ V^{33} = V_1^{33} + V_0^{33},\ V^{35} = V_1^{35},$$
$$V^{44} = V_1^{44} + V_0^{44},\ V^{46} = V_1^{46},\ V^{55} = V_1^{55} + V_0^{55},\ V^{56} = V_1^{56},\ V^{61} = V_1^{61},\ V^{66} = V_1^{66} + V_0^{66}.$$

Let ζ be the invarient probability vector can be partitioned as $(\zeta_0, \zeta_1, \zeta_2, \zeta_3, \zeta_4, \zeta_5)$ with the dimensions $\{m_1 + Sm_1m_2, Sm_1n_1, Sm_1n_2, Sm_1n_1, Sm_1n_2, (S+1)m_1l\}$ of the matrix V will be obtained the values such that it must be satisfied these conditions $\zeta V = 0$ and $\zeta e = 1$.

$$\begin{aligned} \text{i.e., } \zeta_0 V^{11} + \zeta_1 V^{21} + \zeta_2 V^{31} + \zeta_5 V^{61} &= 0, \\ \zeta_0 V^{12} + \zeta_1 V^{22} &= 0, \\ \zeta_0 V^{13} + \zeta_2 V^{33} &= 0, \\ \zeta_1 V^{24} + \zeta_3 V^{44} &= 0, \\ \zeta_2 V^{35} + \zeta_4 V^{55} &= 0, \\ \zeta_3 V^{46} + \zeta_4 V^{56} + \zeta_5 V^{66} &= 0, \end{aligned}$$

along with normalising condition that,

$$\zeta_0 e_{m_1} + \sum_{j=1}^{S} \zeta_0 e_{m_1 m_2} + \sum_{j=1}^{S} \zeta_1 e_{m_1 n_1} + \sum_{j=1}^{S} \zeta_2 e_{m_1 n_2} + \sum_{j=1}^{S} \zeta_3 e_{m_1 n_1} + \sum_{j=1}^{S} \zeta_4 e_{m_1 n_2} + \sum_{j=0}^{S} \zeta_5 e_{m_1 l} = 1.$$

Obviously, to examine the stability of our QBD model, it must satisfy condition $\zeta V_0 e < \zeta V_2 e$.

$$\left.\begin{array}{l} \zeta_0 D_1 e_{m_1} + \sum_{j=1}^{S} \zeta_1 \left[e_{n_1} \otimes D_1 e_{m_1}\right] \\ i.e., \quad + \sum_{j=1}^{S} \zeta_2 \left[e_{n_2} \otimes D_1 e_{m_1}\right] + \sum_{j=1}^{S} \zeta_3 \left[e_{n_1} \otimes D_1 e_{m_1}\right] \\ \quad + \sum_{j=1}^{S} \zeta_4 \left[e_{n_2} \otimes D_1 e_{m_1}\right] + \sum_{j=0}^{S} \zeta_5 \left[e_l \otimes D_1 e_{m_1}\right] \end{array}\right\} < \sum_{j=1}^{S} \zeta_0 \left[\beta_1 \otimes e_{m_2} \otimes \psi I_{m_1}\right]$$

4.2. Analysis of Stationary Probability Vector

Assuming that x represents the steady-state probability vector, it is possible to divide it as $(x_0, x_1, x_2, \dots)$ with each of its dimensions are $\{m_1 + Sm_2m_1, Sn_1m_1, Sn_2m_1, Sn_1m_1, Sn_2m_1, (S+1)lm_1,\}$ of the matrix Q will be obtained the values such that it must be satisfied these conditions $xQ = 0$ and $xe = 1$.

After the stability criterion has been met, we are able to determine the probability vector for the steady state by applying the equations that are listed below.

$$x_i = x_1 R^{i-1},\ i \geq 2.$$

The smallest non-negative solution R, which is based on Neuts [20] work, is able to satisfy the matrix quadratic equation $R^2V_2 + RV_1 + V_0 = 0$. The rate matrix is obtained by solving the matrix quadratic equation. The order of the rate matrix R is determined by the equation $\{m_1 + Sm_2m_1 + Sn_1m_1 + Sn_2m_1 + Sn_1m_1 + Sn_2m_1 + (S+1)lm_1\}$, and it satisfies the constraint $RV_2e = V_0e$.

It is possible to ascertain the subvector x_0 by employing the formulae that are presented below.

$$\begin{aligned} x_0A_{00} + x_1V_2 &= 0 \\ x_0A_{01} + x_1(V_1 + RV_2) &= 0 \\ \text{along with normalising condition, } \ x_0e + x_1(I-R)^{-1}e &= 1. \end{aligned}$$

In accordance with the findings of Latouche and Ramaswami [15], it is possible to generate the R matrix by analytical means by utilising significant phases in the logarithmic reduction process.

5. Busy period Analysis

- For the purpose of computing an active period, the interval that occurs between clients using the void system and the system returning to its void state after the initial interval can

be utilised. There is a transition from level one to level zero. As a consequence of this, the busy cycle is comprised of the initial return to level 0, in addition to the minimum of one journey to a state at any other level.

- We give an overview of the fundamental epoch before moving on to the time being active. As the QBD procedure moves from level i to level $i-1$, it takes into consideration the initial transition period $i \geq 2$.
- It is necessary to examine the boundary state possibilities that correspond to $i = 0,1$ independently. For every level i with $i \geq 1$, there are $\{m_1 + Sm_2m_1 + Sn_1m_1 + Sn_2m_1 + Sn_1m_1 + Sn_2m_1 + (S+1)lm_1\}$ states that correspond and need to be taken into account. This means that the state (i,j) at level i implies that the j^{th} state at level i is stated. This occurs when the states are organised in lexicographic order.
- The variable $\tilde{L}(w,s)$ indicates a change in j's passage to the left and arrival to the state (i,j'). Conditional probability for the QBD procedure starts at time $t = 0$ in the state (i,j), and it advances to level $i-1$, but not earlier time w. It is necessary to first define the joint transform by Neuts [19].

$$\tilde{L}_{jj'}(w,s) = \sum_{i=1}^{\infty} w^i \int_0^{\infty} e^{-sx} dL_{jj'}(u,x); |w| \leq 1, Re(s) \geq 0,$$

when the matrix is displayed as $\tilde{L}(w,s) = \tilde{L}_{jj'}(w,s)$, the equation is satisfied by the previously defined matrix $\tilde{L}(w,s)$

$$\tilde{L}(w,s) = w(sI - V_1)^{-1}V_2 + (sI - V_1)^{-1}V_0\tilde{L}^2(w,s).$$

- Without taking into account the boundary states, the initial travel time would be computed with the matrix $L = L_{jj'} = \tilde{L}(1,0)$. Matrix L can be found using the results if matrix R is previously known.

$$L = -(V_1 + RV_2)^{-1}V_2.$$

In the absence of such, it is possible to calculate the L matrix values by applying the idea of a logarithmic reduction process.

$$\begin{aligned}
\tilde{L}^{(1,0)}(w,s) &= w(sI - V_1)^{-1}V_2 + (sI - V_1)^{-1}V_0\tilde{L}(w,s)\tilde{L}^{(1,0)}(w,s), \\
\tilde{L}^{(0,0)}(w,s) &= (sI - A_{00})^{-1}A_{01}\tilde{L}(w,s).
\end{aligned}$$

According to the stochastic nature of B, $\tilde{L}^{(0,0)}(1,0)$ and $\tilde{L}^{(1,0)}(1,0)$, the matrices are employed in the computation of the ensuing scenarios. The moments that can be determined are as follows:

$$\begin{aligned}
\vec{\mathfrak{L}}_1 &= -\frac{\partial}{\partial s}\tilde{L}(w,s)\Big|_{w=1,s=0} e = -[V_1 + V_0(I+L)]^{-1}e, \\
\vec{\mathfrak{L}}_2 &= \frac{\partial}{\partial z}\tilde{L}(w,s)\Big|_{w=1,s=0} e = -[V_1 + V_0(I+L)]^{-1}V_2e, \\
\vec{\mathfrak{L}}_1^{(1,0)} &= -\frac{\partial}{\partial s}\tilde{L}^{(1,0)}(w,s)\Big|_{w=1,s=0} e = -[V_1 + V_0L]^{-1}(V_0\vec{\mathfrak{L}}_1 + e), \\
\vec{\mathfrak{L}}_2^{(1,0)} &= \frac{\partial}{\partial z}\tilde{L}^{(1,0)}(w,s)\Big|_{w=1,s=0} e = -[V_1 + V_0L]^{-1}(V_0\vec{\mathfrak{L}}_2 + V_2e), \\
\vec{\mathfrak{L}}_1^{(0,0)} &= \frac{\partial}{\partial s}\tilde{L}^{(0,0)}(w,s)\Big|_{w=1,s=0} e = -A_{00}^{-1}[A_{01}\vec{\mathfrak{L}}_1^{(1,0)} + e], \\
\vec{\mathfrak{L}}_2^{(0,0)} &= \frac{\partial}{\partial z}\tilde{L}^{(0,0)}(w,s)\Big|_{w=1,s=0} e = -A_{00}^{-1}[A_{01}\vec{\mathfrak{L}}_2^{(1,0)}].
\end{aligned}$$

6. System Performance Measures

- Probability of a server makes outgoing call arrivals:

$$P_{SMOCA} = \sum_{i=0}^{\infty}\sum_{j=1}^{S}\sum_{k_2=0}^{m_2}\sum_{k_1=1}^{m_1} x_{i0jk_2k_1}$$

- Probability of a server is busy with incoming call arrivals:

$$P_{SBICA} = \sum_{i=0}^{\infty}\sum_{j=1}^{S}\sum_{r_1=1}^{n_1}\sum_{k_1=1}^{m_1} x_{i1jr_1k_1}$$

- Probability of a server is busy with outgoing call arrivals:

$$P_{SBOCA} = \sum_{i=0}^{\infty}\sum_{j=1}^{S}\sum_{r_2=1}^{n_2}\sum_{k_1=1}^{m_1} x_{i2jr_2k_1}$$

- Probability of a server provides slow service during breakdown for incoming call arrivals:

$$P_{SBSICA} = \sum_{i=0}^{\infty}\sum_{j=1}^{S}\sum_{r_1=1}^{n_1}\sum_{k_1=1}^{m_1} x_{i3jr_1k_1}$$

- Probability of a server provides slow service during breakdown for outgoing call arrivals:

$$P_{SBSOCA} = \sum_{i=0}^{\infty}\sum_{j=1}^{S}\sum_{r_2=1}^{n_2}\sum_{k_1=1}^{m_1} x_{i4jr_2k_1}$$

- The ratio of busy server:

$$P_{BS} = P_{SBICA} + P_{SBOCA} + P_{SBSICA} + P_{SBSOCA}$$

- Average count of customers in the orbit:

$$E_{orbit} = \sum_{i=0}^{\infty} ix_ie$$

- Average count of customers in the system:

$$E_{system} = E_{orbit} + P_{BS}$$

- Expected Reorder rate:

$$\begin{aligned} E_{RR} = {} & \sum_{i=0}^{\infty}\sum_{r_1=1}^{n_1}\sum_{k_1=1}^{m_1} x_{i1(s+1)r_1k_1}\left(T_1^0 \otimes I_{m_1}e\right) + \sum_{i=0}^{\infty}\sum_{r_2=1}^{n_2}\sum_{k_1=1}^{m_1} x_{i2(s+1)r_2k_1}\left(T_2^0 \otimes I_{m_2}e\right) \\ & + \sum_{i=0}^{\infty}\sum_{r_1=1}^{n_1}\sum_{k_1=1}^{m_1} x_{i3(s+1)r_1k_1}\left(\theta_1^0T_1^0 \otimes I_{m_1}e\right) + \sum_{i=0}^{\infty}\sum_{r_2=1}^{n_2}\sum_{k_1=1}^{m_1} x_{i4(s+1)r_2k_1}\left(\theta_1^0T_2^0 \otimes I_{m_2}e\right) \end{aligned}$$

- Expected Inventory level:

$$\begin{aligned} E_{IL} = {} & \sum_{i=0}^{\infty}\sum_{j=1}^{S}\sum_{k_2=1}^{m_2}\sum_{k_1=1}^{m_1} jx_{i0jk_2k_1} + \sum_{i=0}^{\infty}\sum_{j=1}^{S}\sum_{r_1=1}^{n_1}\sum_{k_1=1}^{m_1} jx_{i1jr_1k_1} + \sum_{i=0}^{\infty}\sum_{j=1}^{S}\sum_{r_2=1}^{n_2}\sum_{k_1=1}^{m_1} jx_{i2jr_2k_1} \\ & + \sum_{i=0}^{\infty}\sum_{j=1}^{S}\sum_{r_1=1}^{n_1}\sum_{k_1=1}^{m_1} jx_{i3jr_1k_1} + \sum_{i=0}^{\infty}\sum_{j=1}^{S}\sum_{r_2=1}^{n_2}\sum_{k_1=1}^{m_1} jx_{i4jr_2k_1} + \sum_{i=0}^{\infty}\sum_{j=0}^{S}\sum_{k_1=1}^{m_1} jx_{i5jk_1} \end{aligned}$$

7. Total Cost Analysis

We discuss the cost of some performance measures of the system under consideration. Hence we introduce the total cost of system per unit time (TCS) is given below.

$$TCS = C_SE_{system} + C_HE_{IL} + C_RE_{RR}.$$

Where

- C_S – be the waiting cost of a customer in the system per unit time.
- C_H – be the carrying cost of inventory per unit time.
- C_R – be the setup cost per order.

8. Numerical Results

In the section that follows, we will be analysing the behaviour of the models by making use of both numerical and graphical demonstrations. The following three representations illustrate different aspects of the MAP, and each maintains a consistent mean value of 1 across all arrival processes. According to the research conducted by Chakravarthy [10] , the three arrival value sets were used as input data in their literature.

- **A-ER(Arrival in Erlang):** $D_0 = \begin{bmatrix} -2 & 2 \\ 0 & -2 \end{bmatrix}$ $D_1 = \begin{bmatrix} 0 & 0 \\ 2 & 0 \end{bmatrix}$,
- **A-EX(Arrival in Exponential):** $D_0 = \begin{bmatrix} -1 \end{bmatrix}$, $D_1 = \begin{bmatrix} 1 \end{bmatrix}$,
- **A-HE(Arrival in Hyper-exponential):** $D_0 = \begin{bmatrix} -1.90 & 0 \\ 0 & -0.19 \end{bmatrix}$, $D_1 = \begin{bmatrix} 1.710 & 0.190 \\ 0.171 & 0.019 \end{bmatrix}$,

The outgoing arrivals and services have three distinct phase-type distributions and the following notations S-ER, S-EX and S-HE respectively for exponential, Erlang and hyper-exponential cases under consideration.

- **S-ER(Erlang):** $\alpha = \beta_1 = \beta_2 = (1, 0)$, $R = T_1 = T_2 = \begin{bmatrix} -2 & 2 \\ 0 & -2 \end{bmatrix}$.
- **S-EX(Exponential):** $\alpha = \beta_1 = \beta_2 = [1]$, $R = T_1 = T_2 = [1]$.
- **S-HE(Hyper-exponential):** $\alpha = \beta_1 = \beta_2 = (0.8, 0.2)$, $R = T_1 = T_2 = \begin{bmatrix} -2.8 & 0 \\ 0 & -0.28 \end{bmatrix}$.

8.1. Illustration − 1

We explored the effects of breakdown rate (τ), utilization factor (ρ) and number of consumers in the orbit (E_{orbit}). In order to attain system stability, we fix $\lambda = 2$, $\lambda^- = 1$, $\mu_1 = 12$, $\mu_2 = 14$, $\mu_3 = 1.5$, $\sigma = 3$, $s = 5$, $S = 12$, $\psi = 30$, $\theta_1 = 0.8$, $\theta_2 = 0.5$, $\tau = 1$, $\delta = 3$, $p = 0.4$, $q = 0.6$.

- We combine the arrival and service time categories in Tables 1 through 3 to investigate the breakdown rate (τ), the utilization factor (ρ) versus number of consumers in the orbit (E_{orbit}).
- When the breakdown rate (τ), utilization factor (ρ) increases, the number of consumers in the orbit (E_{orbit}) increases for various arrival and service distributions.
- When comparing arrival timings to those of all other arrivals, the number of consumers in the orbit, denoted by the symbol E_{orbit}, increases rapidly for hyper-exponential arrivals, but it increases slowly for Erlang arrivals. This is because the rate of breakdown (τ) is increasing. In a similar vein, when it comes to service durations, the (E_{orbit}) increases at a slower rate in Erlang services compared to hyper-exponential services..

8.2. Illustration − 2

We explored the effects of retrial rate(ψ) versus the number of consumers in the orbit (E_{orbit}). In order to attain system stability, we fix $\lambda = 2$, $\lambda^- = 1$, $\mu_1 = 12$, $\mu_2 = 14$, $\mu_3 = 1.5$, $\sigma = 3$, $s = 5$, $S = 12$, $\psi = 30$, $\theta_1 = 0.8$, $\theta_2 = 0.5$, $\tau = 1$, $\delta = 3$, $p = 0.4$, $q = 0.6$.

- We combine the arrival and service time categories in Figures 2 through 4 to investigate the retrial rate versus the number of consumers in the orbit.
- When the retrial rate (ψ) rises, the corresponding the number of consumers in the orbit (E_{orbit}) reduces.
- When the arrival times of hyper-exponential arrivals are compared to those of all other arrivals, the (E_{orbit}) decreases almost immediately, but the decrease for Erlang arrivals is more gradual. In a similar vein, when it comes to service durations, the (E_{orbit}) diminishes at a slower rate in Erlang services compared to hyper-exponential services.

8.3. Illustration − 3

We explored the effects of breakdown rate (τ) and service rate of the incoming calls (μ_1) versus the average number of consumers in the system (E_{system}). In order to attain system stability, we fix $\lambda = 2$, $\lambda^- = 1$, $\mu_1 = 12$, $\mu_2 = 14$, $\mu_3 = 1.5$, $\sigma = 3$, $s = 5$, $S = 12$, $\psi = 30$, $\theta_1 = 0.8$, $\theta_2 = 0.5$, $\tau = 1$, $\delta = 3$, $p = 0.4$, $q = 0.6$.

- We combine the arrival and service time categories to investigate the breakdown rate and service rate of the incoming calls (μ_1) versus the average number of consumers in the system, using Figures 5 through 13.
- When the breakdown rate (τ) and service rate of the incoming calls (μ_1) increases the corresponding average number of consumers in the system (E_{system}) decreases.
- When the arrival times of hyper-exponential arrivals are compared to those of all other arrivals, the E_{orbit} decreases rapidly, whereas the E_{orbit} decreases quite slowly for Erlang arrivals.

Table 1: *Breakdown rate(τ) Vs ρ and E-orbit - EXP−A*

	EXP−S		ERL−S		HEX−S	
τ	ρ	E-orbit	ρ	E-orbit	ρ	E-orbit
1.1	0.2454850	0.1982983	0.2486224	0.1619680	0.2264146	0.3956982
1.2	0.2503688	0.2093882	0.2537031	0.1710225	0.2303825	0.4162982
1.3	0.2551869	0.2203966	0.2587307	0.1800515	0.2342563	0.4363531
1.4	0.2599407	0.2313258	0.2637061	0.1890557	0.2380405	0.4558961
1.5	0.2646314	0.2421778	0.2686298	0.1980361	0.2417394	0.4749577
1.6	0.2692604	0.2529546	0.2735027	0.2069936	0.2453570	0.4935657
1.7	0.2738287	0.2636582	0.2783252	0.2159290	0.2488970	0.5117461
1.8	0.2783377	0.2742906	0.2830981	0.2248430	0.2523629	0.5295226
1.9	0.2827883	0.2848534	0.2878220	0.2337365	0.2557580	0.5469173
2.0	0.2871818	0.2953485	0.2924975	0.2426102	0.2590853	0.5639507

Table 2: *Breakdown rate(τ) Vs ρ and E-orbit - ERL−A*

	EXP−S		ERL−S		HEX−S	
τ	ρ	E-orbit	ρ	E-orbit	ρ	E-orbit
1.1	0.2340119	0.1240691	0.2372065	0.0933057	0.2145448	0.2950826
1.2	0.2387090	0.1319053	0.2421036	0.0992845	0.2183176	0.3115577
1.3	0.2433428	0.1396711	0.2469495	0.1052334	0.2220021	0.3275941
1.4	0.2479145	0.1473682	0.2517448	0.1111529	0.2256024	0.3432179
1.5	0.2524255	0.1549983	0.2564901	0.1170438	0.2291225	0.3584533
1.6	0.2568769	0.1625628	0.2611861	0.1229067	0.2325662	0.3733226
1.7	0.2612699	0.1700635	0.2658334	0.1287422	0.2359370	0.3878462
1.8	0.2656055	0.1775017	0.2704327	0.1345509	0.2392380	0.4020432
1.9	0.2698850	0.1848789	0.2749847	0.1403335	0.2424724	0.4159311
2.0	0.2741094	0.1921966	0.2794897	0.1460904	0.2456430	0.4295263

Table 3: *Breakdown rate(τ) Vs ρ and E-orbit - HEX−A*

	EXP−S		ERL−S		HEX−S	
τ	ρ	E-orbit	ρ	E-orbit	ρ	E-orbit
1.1	0.2609946	0.4154456	0.2639417	0.3535134	0.2427967	0.7141858
1.2	0.2661630	0.4386914	0.2693026	0.3736114	0.2470587	0.7497266
1.3	0.2712620	0.4619338	0.2746078	0.3938337	0.2512177	0.7844196
1.4	0.2762931	0.4851765	0.2798580	0.4141835	0.2552790	0.8183184
1.5	0.2812576	0.5084228	0.2850541	0.4346640	0.2592472	0.8514721
1.6	0.2861568	0.5316762	0.2901966	0.4552781	0.2631267	0.8839258
1.7	0.2909921	0.5549395	0.2952862	0.4760286	0.2669215	0.9157210
1.8	0.2957646	0.5782158	0.3003239	0.4969183	0.2706356	0.9468959
1.9	0.3004756	0.6015077	0.3053098	0.5179498	0.2742726	0.9774858
2.0	0.3051262	0.6248179	0.3102451	0.5391255	0.2778357	1.0075233

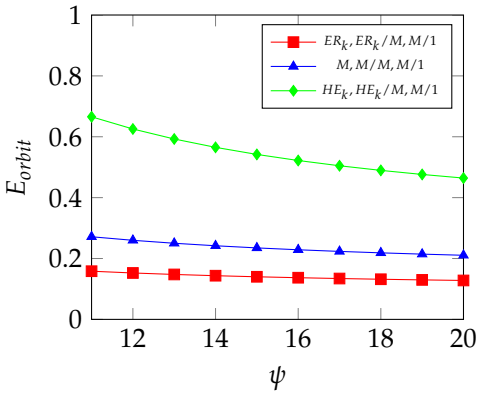


Figure 2: *Retrial rate(ψ) Vs E_{orbit} - EXP−S*

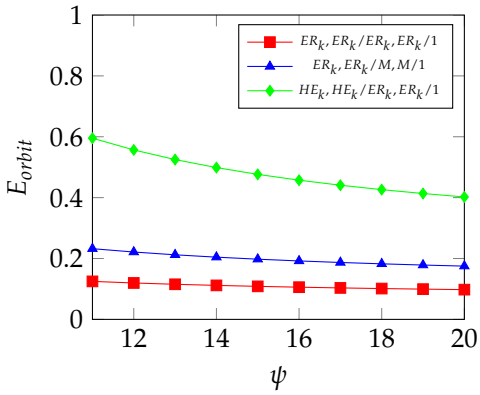


Figure 3: *Retrial rate(ψ) Vs E_{orbit} -ER−S*

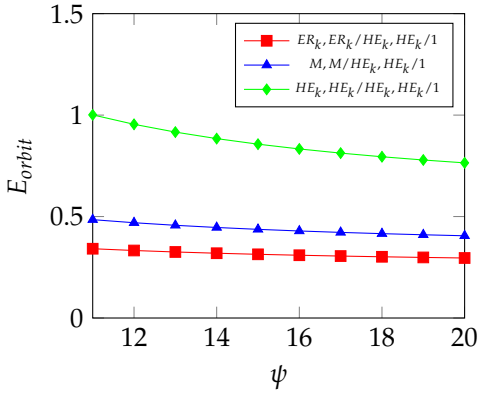


Figure 4: *Retrial rate(ψ) Vs E_{orbit} - HEX−S*

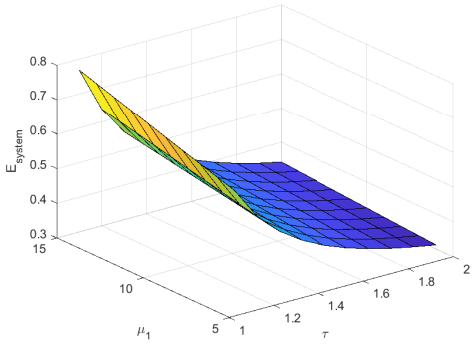


Figure 5: $ER_k, ER_k/ER_k, ER_k/1$

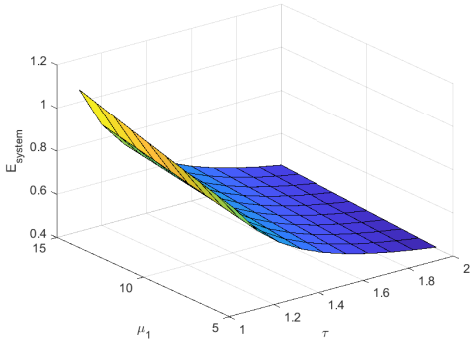


Figure 6: $M, M/ER_k, ER_k/1$

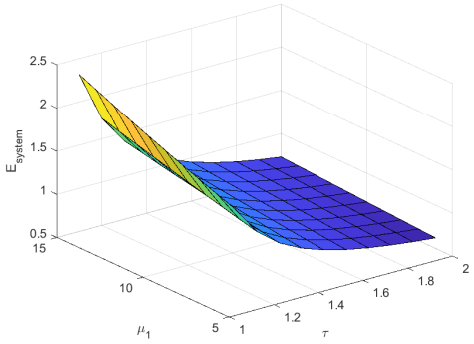


Figure 7: $HE_k, HE_k/ER_k, ER_k/1$

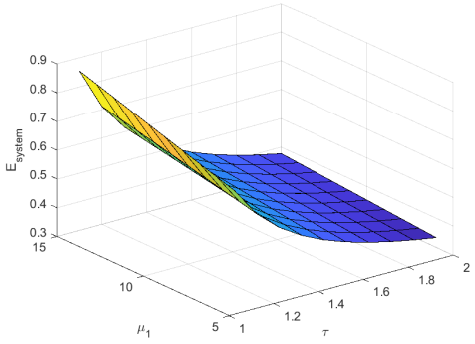


Figure 8: $ER_k, ER_k/M, M/1$

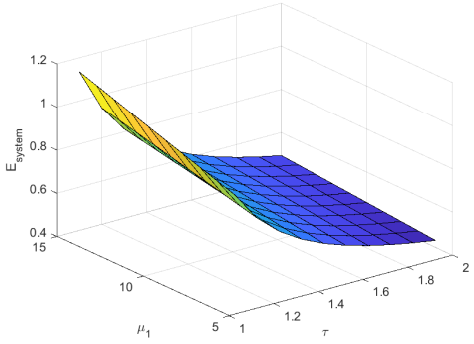


Figure 9: $M, M/M, M/1$

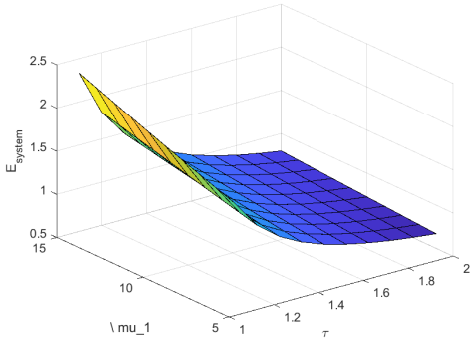


Figure 10: $HE_k, HE_k/M, M/1$

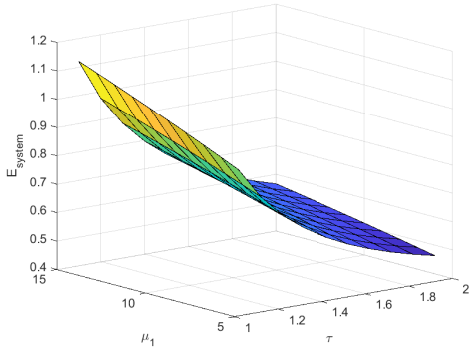


Figure 11: $ER_k, ER_k/HE_k, HE_k/1$

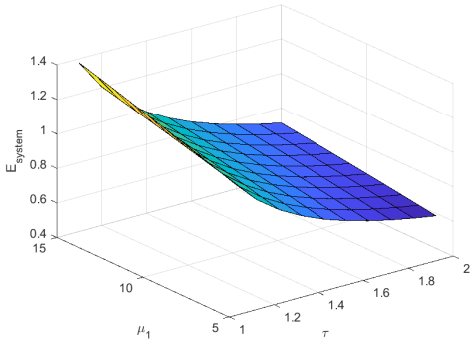


Figure 12: $M, M/HE_k, HE_k/1$

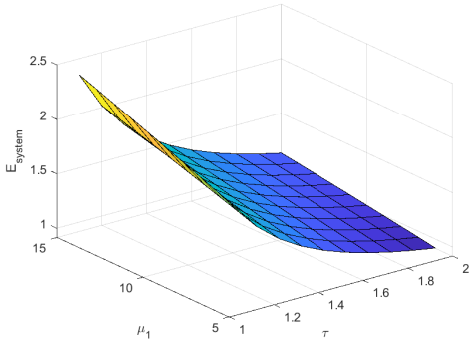


Figure 13: $HE_k, HE_k/HE_k, HE_k/1$

9. Conclusion

This article investigated with the study of a retrial inventory queueing system with Markovian Arrival Process along with two-way communication, a single-server, phase type distributed service time for both incoming and outgoing calls with (s, S) replenishment policy, negative arrival, working breakdown and phase type repair. The Stability condition of our system has been derived. Additionally, this inventory queueing system's busy period has been investigated and have performed the cost analysis. We have examined the effects of several settings on a few system measures using 2D and 3D graphs. Our work's primary benefit is that we have taken into account practically every fundamental issue or circumstance in the telecommunications system that is being studied. We have proposed a few strategies to lower the system's overall cost while maximizing server utilization. In future, the approach can be expanded to queueing models with a linear retrial policy.

References

[1] Agassi Melikov, Laman Poladova, Sandhya Edayapurath and Janos Sztrik. (2023). Single-Server Queuing-Inventory Systems with Negative Customers and Catastrophes in the Warehouse. *Mathematics*, 11(10):2380.

[2] Artalejo, J. R. and Phung-Duc, T. (2013). Single server retrial queues with two way communication. *Applied Mathematical Modelling*, 37(4):1811–1822.

[3] Artalejo, J. R. (1999). A classified bibliography of research on retrial Queues: Progress in 1990-1999. *Top*, 7:187–211.

[4] Artalejo, J. R. (2010). Accessible bibliography on retrial queues: Progress in 2000-2009. *Mathematical and Computer Modelling*, 51(9-10): 1071–1081.

[5] Somasundaram, B. Archana Alias Gurulakshmi, G. and Ayyappan, G.(2023). Analysis of Retrial Queue with Two Way Communication, Working Breakdown and Collision. *Reliability: Theory & Applications*, 1(3):30–43.

[6] Ayyappan, G. and Arulmozhi, N. (2024).Numerical investigation of retrial queueing inventory system with a constant retrial rate, working vacation, flush out, collision and impatient customers. *Reliability: Theory & Applications*, 19:744–763.

[7] Ayyappan, G. and Meena, S. (2024). Analysis of $MMAP/PH(1), PH(2)/1$ Preemptive Priority Queueing Model with Single Vacation, Repair and Impatient Customers. *Applications and Applied Mathematics: an International Journal (AAM)*, 19(1):2.

[8] Ayyappan, G. and Thilagavathy, K. (2025). Analysis of (MAP, PH)/(PH, PH)/1 retrial queueing model with standby server, collision of orbital customers, breakdowns, two-way communication, phase type repairs, constant retrial rate and impatient behaviour of customers. *International Journal of Operational Research*, 52(1):1–50.

[9] Berman, O., Kaplan, E. H. and Shimshak, D. G. (1993). Deterministic approximations for inventory management at service facilities. *IIE Transactions*, 25(5):98–104.

[10] Chakravarthy S.R. Markovian arrival process, Wiley Encyclopaedia of Operations Research and Management, John Wiley and Sons, Inc., USA, 2010.

[11] Falin. G. I. and Templeton. J.G. C. Retrial Queues: 1st ed., Routledge, 1997.

[12] Haghighi, A. M. Medhi, J. and Mohanty, S. G. (1986). On a multiserver Markovian queueing system with balking and reneging. *Computers & Operations Research*, 13(4):421–425.

[13] Karthick, V., Suvitha, V. and Rathinasabapathy Kalyanaraman. (2024). A single server Markovian differentiated working vacation queue with server breakdown. *International Journal of Mathematics in Operational Research*, 27(1):105–120.

[14] Krishnamoorthy, A., Nair, S. S. and Narayanan, V. C. (2011). An inventory model with server interruptions and retrials. *Operational Research*, 12(2):151–171.

[15] Latouche G. and Ramaswami V. Introduction of Matrix Analytic Methods in Stochastic Modeling: ASA-SIAM Series on Statistics and Applied Mathematics, Philadelphia, 1999.

[16] Melikov, A. Z. and Molchanov, A. A. (1992). Stock optimization in transportation/storage systems. *Cybernetics and System Analysis*, 28(1):484–487.

[17] Nazarov, A., Sztrik, J. and Kvach, A. (2018). Asymptotic Sojourn Time Analysis of Finite-Source M/M/1 Retrial Queuing System with Two-Way Communication. *Information Technologies and Mathematical Modelling. Queueing Theory and Applications*, 912:172–183.

[18] Neuts, M. F. (1979). A versatile Markovian point process. *Journal of Applied Probability*, 16(4):764–779.

[19] Neuts M. F. Matrix-geometric solutions in stochastic models: An algorithmic approach. The Johns Hopkins University Press, Baltimore. 1981.

[20] Neuts, M. F. (1984). Matrix-analytic methods in queuing theory. *European Journal of Operational Research*, 15(1):2–12.

[21] Rakesh Kumar. and Bhavneet Singh Soodan. (2019). Transient Numerical Analysis of a Queueing Model with Correlated Reneging, Balking and Feedback. *Reliability: Theory & Applications*, 4(55), 14:46–54.

[22] Steeb W. H. and Hardy Y. Matrix calculus and Kronecker product: A practical approach to linear and multilinear algebra. World Scientific Publishing Company, Singapore. 2011.

[23] Tuan Phung-Duc. Retrial queueing models: A survey on theory and applications: Stochastic Operations Research in Business and Industry, Performance (cs.PF), Probability. 2019.

[24] Ushakumari, P. V. (2017). A retrial inventory system with an unreliable server. *International Journal of Mathematics in Operational Research*, 10(2):190–210.

[25] Yadavalli, V.S. S., Sivakumar, B. and Arivarignan, G. (2008). Inventory system with renewal demands at service facilities. *International Journal of Production Economics*, Elsevier, 114(1):252–264.

GROK'S ROLE IN TRANSFORMING COMMUNICATION FOR DISASTER RISK MANAGEMENT

Renat R. Khaydarov
•
Institute of Nuclear Physics, Uzbekistan Academy of Sciences, Tashkent, Uzbekistan
renat@inp.uz

Abstract

The increasing prevalence of natural hazards, exacerbated by climate change and urbanization, underscores the urgency of effective disaster risk management (DRM) to safeguard communities and infrastructure. Technical assessments, laden with specialized terminology, often hinder stakeholder engagement, particularly among non-specialists critical to decision-making processes. This study explores the prospective applications of Grok, an AI model by xAI, in enhancing DRM through its advanced natural language processing capabilities. Grok can translate complex multi-hazard risk evaluations, develop tailored educational content, and support real-time early warning systems, fostering inclusive communication. The research aims to evaluate Grok's efficacy in bridging technical and non-technical domains, promoting informed urban planning and disaster preparedness. Ultimately, this research lays the groundwork for future empirical studies on AI-driven DRM innovations.

Keywords: artificial intelligence, natural language processing, disaster risk management, early warning systems

I. Introduction

The escalating frequency of natural hazards, driven by climate change and urbanization, necessitates innovative approaches to disaster risk management (DRM) to enhance community resilience and informed decision-making [1-5]. The integration of artificial intelligence (AI) technologies, including machine learning and deep learning, has significantly enhanced disaster risk management by improving the precision of predictive modeling and real-time monitoring, leveraging extensive datasets from meteorological, seismic, and geographical sources to optimize early warning systems and resource allocation [6-8]. By combining AI with geographic information systems (GIS) and remote sensing, governments can achieve superior planning, situational awareness, and recovery operations, enabling rapid decision-making in the aftermath of natural disasters [9, 10]. Furthermore, the development of explainable AI techniques fosters transparency and trust in AI-driven decision-making, thereby strengthening strategic disaster management [7, 11-16].

This study investigates the transformative potential of Grok, an advanced artificial intelligence model developed by xAI, in addressing communication barriers inherent in technical DRM assessments. Leveraging its natural language processing capabilities, Grok translates complex multi-hazard risk evaluations, generates audience-specific educational content, and supports real-

time early warning systems [13]. Through prospective case studies, this research demonstrates Grok's efficacy in fostering inclusive stakeholder engagement across diverse populations. By delivering accessible, multilingual, and contextually relevant narratives, Grok bridges the gap between technical experts and non-specialists, empowering policymakers, responders, and communities. The findings highlight Grok's role in streamlining DRM processes and amplifying resilience, laying the foundation for future empirical studies on AI-driven innovations in hazard-prone regions.

II. Prospective Case Studies in Disaster Risk Management

I. Translating Multi-Hazard Risk Assessments

In urban planning scenarios, local governments often collaborate with disaster risk experts to evaluate multi-hazard risks—such as floods, earthquakes, and cyclones—for proposed developments [14]. These assessments are typically laden with technical jargon, including terms like "return period," "vulnerability index," "cascading effects," and "probabilistic risk modeling," which can overwhelm non-specialists. Grok can serve as a powerful tool to translate these intricate reports into clear, concise, and accessible narratives. For instance, a risk assessment might state: "The site's exposure to a 100-year flood event, combined with its high soil erodibility, elevates the likelihood of structural instability and cascading infrastructure failure." Grok could reframe this as: "The location faces a high risk of flooding every 100 years, and its loose soil could cause buildings and roads to become unstable, potentially leading to widespread damage." By employing natural language processing, Grok ensures that policymakers, community leaders, and developers can grasp critical risk implications, enabling informed decision-making. Furthermore, Grok can generate tailored summaries for different audiences, such as simplified versions for public consultations or detailed technical breakdowns for engineers, thereby fostering inclusive stakeholder engagement.

II. Disaster Preparedness Education

In regions vulnerable to natural hazards, fostering a culture of preparedness is essential for reducing disaster impacts [17]. Grok can support disaster management agencies in developing comprehensive, audience-specific preparedness curricula. For example, in a coastal community prone to hurricanes, Grok could process technical guidelines on storm surge dynamics, wind load impacts, and evacuation protocols to create engaging, age-appropriate educational content. For schoolchildren, Grok might produce interactive lesson plans explaining why hurricanes form, how to recognize early warning signs, and the importance of evacuation drills, using analogies like "a hurricane is like a giant spinning top that brings strong winds and heavy rain." For adult residents, Grok could generate practical guides on assembling emergency kits, reinforcing homes, and understanding local alert systems. By distilling complex DRM concepts into relatable narratives, Grok enhances community understanding and encourages proactive behaviors. Additionally, Grok's ability to adapt content to diverse linguistic and cultural contexts ensures that preparedness education is inclusive and effective across heterogeneous populations.

III. Real-Time Disaster Early Warning Communication

Effective early warning systems (EWS) are critical for minimizing loss of life and property during disasters [1, 18]. Grok can enhance EWS by processing real-time hazard data and generating immediate, audience-specific warning messages. For instance, in a scenario where a tsunami is detected off the coast of a Pacific island, Grok could analyze data from seismic sensors and ocean buoys to produce a clear public alert: "Urgent: Tsunami Warning! A magnitude 8.2 earthquake has

triggered a tsunami off the eastern coast. Coastal residents in [specific towns] should evacuate to higher ground within 15 minutes. Follow local authorities' instructions." Simultaneously, Grok could tailor messages for emergency responders, providing detailed information on expected wave heights and arrival times to optimize resource deployment. By delivering precise, jargon-free warnings, Grok ensures that critical information reaches diverse audiences swiftly, reducing confusion and enhancing response efficacy. Moreover, Grok's multilingual capabilities enable the dissemination of warnings in local languages, ensuring accessibility in multilingual regions.

IV. Virtual Disaster Risk Management Assistant

Disaster risk professionals often require rapid access to technical information during fieldwork or policy development [1, 14]. Grok can function as a virtual assistant, providing instant clarifications on DRM concepts, regulations, or emerging hazards. For instance, a risk manager assessing a landslide-prone area could query Grok about slope stability factors, receiving a response like: "Slope stability depends on soil cohesion, slope angle, and water content. Steep slopes with loose, wet soil are more likely to slide. Consider installing drainage systems or retaining walls to reduce risk." Grok's ability to draw from extensive DRM knowledge bases ensures that responses are both accurate and contextually relevant. Additionally, Grok can suggest best practices or case studies from similar contexts, enabling professionals to make evidence-based decisions. This real-time support enhances efficiency and confidence in high-pressure DRM scenarios.

V. Disaster Response Role-Playing Simulations

Training emergency responders through realistic simulations is vital for effective disaster response [19]. Grok can enrich these exercises by serving as a dynamic scenario narrator and information source. In a simulated flood response, Grok could provide real-time updates, such as: "Heavy rainfall has caused a river to overflow, flooding [specific neighborhoods]. Evacuation routes are compromised, and power outages are reported." Responders could query Grok for data on safe evacuation paths or shelter capacities, receiving tailored recommendations. Grok's ability to adapt scenarios based on trainee decisions creates a dynamic, immersive learning environment, preparing responders for unpredictable real-world conditions. Furthermore, Grok can debrief participants by analyzing their performance and suggesting improvements, fostering continuous learning and readiness.

VI. Real-Time Crisis Communication

During disasters, media outlets play a critical role in disseminating information [20]. Grok can assist by processing technical disaster updates and generating clear, accurate press releases. Vulnerable populations, such as the elderly, disabled, or non-native speakers, often face barriers in accessing disaster risk information [21]. Grok can enhance communication by generating tailored, accessible content for these groups. For instance, Grok could process evacuation protocols and produce simplified instructions for visually impaired individuals, such as audio guides stating: "If a flood warning is issued, move to the highest floor of your home and keep a radio nearby for updates." For non-native speakers, Grok could translate warnings into multiple languages with culturally relevant examples. By prioritizing inclusivity, Grok ensures that critical DRM information reaches all community members, reducing disparities in disaster preparedness and response.

VII. Community-Driven Disaster Monitoring

Engaging communities in disaster monitoring can enhance situational awareness and foster resilience [22]. Grok can support non-profit organizations in developing citizen science initiatives

by interpreting real-time hazard data and providing accessible explanations to participants. For instance, a mobile application powered by Grok could process data from community-based flood sensors and deliver alerts like: "A river level rise of 2 meters was detected near [location]. This suggests potential flooding in the next 6 hours. Avoid low-lying areas and report observations to help others stay safe." Grok could also respond to user queries, such as explaining why certain areas flood more frequently due to soil saturation or urban runoff. By presenting data in layperson's terms, Grok encourages public participation in monitoring efforts, transforming citizens into active contributors to DRM. Additionally, Grok can gamify the experience, offering educational quizzes or challenges to sustain engagement, thereby building a more informed and vigilant community.

In summary, Grok's advanced natural language processing capabilities offer transformative potential for DRM by bridging the gap between complex technical assessments and diverse stakeholder needs. Through its ability to translate multi-hazard risk evaluations, generate tailored educational content, enhance early warning systems, and support community-driven monitoring, Grok facilitates informed decision-making and fosters resilience across urban and vulnerable settings. Its adaptability to multilingual and culturally diverse contexts ensures inclusive communication, while its real-time data processing and virtual assistant functionalities empower professionals and responders with actionable insights. By integrating these capabilities, Grok not only streamlines DRM processes but also amplifies community engagement and preparedness, contributing significantly to the global pursuit of disaster-resilient societies.

III. Conclusion

This study underscores the transformative potential of Grok, an AI model by xAI, in revolutionizing disaster risk management by addressing the critical challenge of communicating complex technical assessments to diverse stakeholders. Through its advanced natural language processing capabilities, Grok facilitates the translation of multi-hazard risk evaluations, the development of tailored educational curricula, and the enhancement of real-time early warning and crisis communication systems. The prospective case studies illustrate Grok's ability to foster inclusive engagement, ensuring that policymakers, emergency responders, and vulnerable populations can access actionable insights in urban and hazard-prone settings. By supporting community-driven monitoring and multilingual communication, Grok amplifies resilience and promotes proactive disaster preparedness. This research establishes a robust framework for integrating AI into DRM, offering scalable solutions to mitigate the socio-economic impacts of natural hazards. Future studies should focus on empirical validations of Grok's applications, exploring its scalability and adaptability across varied socio-cultural and geophysical contexts to further advance the global pursuit of disaster-resilient societies.

Conflict of Interest Statement

The author declares no conflicts of interest that could have influenced the work reported in this paper. No financial or personal relationships with individuals, organizations, or entities that could bias the research or its outcomes exist.

Funding Statement

This study was conducted without dedicated financial support from external sources

References

[1] Andrae S. Artificial intelligence in disaster management. In: Advances in Environmental Engineering and Green Technologies Book Series; 2025.

[2] Şengöz M. Utilization of artificial intelligence and big data in disaster management: Future risk reduction strategies. Haliç Üniv Fen Bilim Derg. 2024.

[3] Sun W, Bocchini P, Davison BD. Applications of artificial intelligence for disaster management. *Nat Hazards.* 2020;103(3):2631–89.

[4] Yu M, Yang C, Li Y. Big data in natural disaster management: A review. Geosciences. 2018;8(5):165.

[5] Zagorecki A, Johnson D, Ristvej J. Data mining and machine learning in the context of disaster and crisis management. *Int J Emerg Manag*. 2013;9(4):351–65.

[6] Joel MR, Thenmozhi E, Jeya MR, Meenakshi L, Elakya V, Devi RK, et al. Harnessing the transformative power of AI for enhanced disaster prediction and comprehensive risk assessment. In: Advances in Geospatial Technologies Book Series; 2024.

[7] Singh VA, Agnihotri A. Addressing environmental challenges through artificial intelligence (AI)-powered natural disaster management. *Int J Appl Sci Res*. 2024;2(5):485–96.

[8] Ray PP. Leveraging deep learning and language models in revolutionizing water resource management, research, and policy making: A case for ChatGPT. *ACS ES T Water*. 2023;3(8):2018–20.

[9] Abid SK, Sulaiman N, Chan SW, Nazir U, Abid M, Han H, et al. Toward an integrated disaster management approach: How artificial intelligence can boost disaster management. *Sustainability*. 2021;13(22):12560.

[10] Arfan M, Khan Z, Qadri N, Hameed MH, Amir AR. Role of artificial intelligence (AI) in combined disaster management. *Organ Theory Rev.* 2022.

[11] Ghaffarian S, Taghikhah FR, Maier HR. Explainable artificial intelligence in disaster risk management: Achievements and prospective futures. *Int J Disaster Risk Reduct.* 2023.

[12] Beeravelly SR. Smart response: Leveraging AI analytics for enhanced disaster resilience. *Int J Multidiscip Res.* 2024;6(6).

[13] Chen W, Fang J. Optimizing AI-driven disaster management through LLMs; 2024.

[14] Kumar MVKS. Leveraging AI in disaster management: Enhancing response and recovery for natural and man-made disasters. Int J Multidiscip Res. 2024;6(2).

[15] Khan IA. AI based disaster management systems: Case study on flood prediction. Int J Res Publ Seminar. 2024;14(5):291–5.

[16] Periasamy JK, Reddy KS, Salve PR, Ushasukhanya S, Malleswari TYJN. AI-driven disaster forecasting by integrating smart technology. In: Advances in Computer and Electrical Engineering Book Series; 2024. p. 383–414.

[17] Guikema SD. Artificial intelligence for natural hazards risk analysis: Potential, challenges, and research needs. *Risk Anal.* 2020;40(6):1117–23.

[18] Muhammad K, Ahmad J, Baik SW. Early fire detection using convolutional neural networks during surveillance for effective disaster management. *Neurocomputing.* 2017;288:30–42.

[19] Sinha A, Kumar P, Rana NP, Islam R, Dwivedi YK. Impact of Internet of Things (IoT) in disaster management: A task-technology fit perspective. *Ann Oper Res.* 2019;283(1):759–94.

[20] Kryvasheyeu Y, Chen H, Obradovich N, Moro E, Van Hentenryck P, Fowler JH, et al. Rapid assessment of disaster damage using social media activity. *Sci Adv*. 2016;2(3):e1500779.

[21] Nguyen DT, Ofli F, Imran M, Mitra P. Damage assessment from social media imagery data during disasters. In: Proceedings of the 2017 IEEE/ACM International Conference on Advances in Social Networks Analysis and Mining; 2017. p. 569–76.

[22] Damaševičius R, Bacanin N, Misra S. From sensors to safety: Internet of Emergency Services (IoES) for emergency response and disaster management. *J Sens Actuator Netw*. 2023;12(3):41.

METHODOLOGY FOR DETERMINING TYPICAL SCENARIOS OF TOTAL ELECTRICITY GENERATION BY GREEN SOURCES REDUCING THE RISK OF DISRUPTION OF BALANCE RELIABILITY

Rahmanov Nariman Rahman[1], Guliyev Huseyngulu Bayram[2*], Ibrahimov Famil Shamil[3]

•

[1]Azerbaijan Scientific Research and Design Institute of Energy, Baku, Azerbaijan, ard.nariman@gmail.com
[2,3]Azerbaijan Technical University, Baku, Azerbaijan
AZ1073, H. Javid avenue 25
[2]huseyngulu@mail.ru, Orcid: 0009-0006-7362-0619
[3]amfanet@mail.ru, Orcid: 0009-0003-4437-3511

Abstract

The article proposes a methodology for identifying scenarios for aggregate electricity generation by renewable sources, such as wind and solar power plants, located in geographically diverse regions of the area with different climatic and weather conditions. To cover the demand of electric power systems, it is rational to use these green sources with complementarity from generation when planning load modes, as well as to reduce the risk of balance reliability of power systems. To determine the scenarios of aggregate generation of the used green sources, a cluster analysis is used based on the clustering of medoids using real-time measurements of wind speed, solar radiation and ambient temperature performed for all regions of the considered area where all green sources of electricity in the form of wind and solar power plants are installed. Clusters of these sources and loads are established separately and jointly. For each scenario of generation and planned growth in demand of the power system, the volume of additional capacity of green sources is estimated. The proposed methodology was tested on the example of the power system of Azerbaijan. The study found that, in order to reduce the risk of disruption to the system's balance reliability, scenarios of combined generation from wind farms located in the northern regions adjacent to the Caspian Sea with electricity generation from solar farms located in the southwestern regions of the country provide a more reliable way to increase the share of wind and solar generation in covering the planned demand growth compared to scenarios based on the separate use of these green energy sources.

Keywords: renewable energy sources, wind (WPP) and solar power plants (SPP), power generation by variable renewable sources (VRES), stochasticity of green energy generation, cluster analysis, scenarios of the process of generating green sources, the risk of violation of balance reliability

I. Introduction

One of the important factors determining the process of transformation of the electric power industry is the significant growth of the share of renewable energy sources. Over the past 40 years, the total electricity generation in the world has grown by more than 25%, including the global installed capacity of power plants operating on renewable energy sources (RES), which reached 3870 GW by 2023 [1]. Currently, RES accounts for 90% of new energy capacity with an increase in capacity of about 473 GW.

Among the renewable energy sources integrated into the energy systems of countries around the world, wind and solar power plants produce the largest share of renewable energy with corresponding installed capacity values for 2024 – 1900 GW (the capacity of photovoltaic power plants, which exceeds the capacity of nuclear power plants by 5 times [2]; the capacity of wind power plants is more than 1000 GW [3].

Unlike traditional sources of electric energy, wind and solar power plants are usually located in regions with "critical" meteorological conditions, in which wind and solar radiation have long periods of time, which ensures the presence of renewable energy potential in these regions. The generation of electric power at wind and solar power plants has a randomly uncertain nature and depends on the meteorological conditions of the region of their location. In order to compensate for random changes in the power system from the generation of variable renewable energy sources (RES), an additional energy source is installed in the system. At present, traditional power plants or a system of electric energy batteries are used as sources supporting the power system with backup generation during periods of reduced RES power generation. The choice of the type of additional source depends on a number of technical and economic capabilities of the system, as well as on the meteorological conditions of the regions [4-6].

Sustainable and efficient operation of a power system with integrated wind and solar power plants requires a deep analysis of the variability of power generation by these stations, modeling their forecasting for current periods of time and taking into account meteorological data [7, 8].
Research shows that with the growth of the share of power generation, the problem of cooperation of the power of these stations in order to cover the demand in the energy system during planning and operational management becomes increasingly urgent.

The works [9-14] present the results of a study of scenario analysis of the complementarity of wind and solar power plants, and their application to cover demand in parts of the energy system with deficiencies in renewable generation.

In [15,16] the studies of spatial and temporal changes of climatic variables were conducted, which show that demand coverage in the energy system with wind and solar power plants can be improved by additional generation from the complementarity of these plants located in regions with different geographic and climatic conditions. In [17, 18] based on the analysis of correlation dependencies between regions with wind and solar power plants it was established that in a region with a predominant share of wind generation in relation to other regions with the lowest share of renewable generation, compensation for the variability of which provides an additional opportunity to cover demand load due to the introduction of solar generation.

Identifying patterns of generation deviations between renewable stations in individual regions would improve the quality of planning and operational dispatch control when covering the demand of the power system [19-21].

The paper proposes a methodology for identifying scenarios for cooperative generation of variable renewable sources located in regions with different geographic and weather conditions. Based on hourly changes in wind speed, solar radiation, air temperature and other parameters related to weather conditions, a cluster analysis of scenarios for regions with integrated wind and

solar power plants was performed, and scenarios for aggregated generation between regions were identified. The following scenarios for the development of the energy balance in regions involving variable renewable energy sources are considered and compared: only wind energy sources; only solar photovoltaic sources; additions of wind and solar energy. energy. For each scenario, the characteristics of additional capacity, typical daily profiles, extreme values, as well as excess / deficit of RES energy are estimated.

II. Method for Identifying Green Co-Generation Scenarios

The problem of assessing the risk of violation of balance reliability and determining the "additional" generated capacity from green sources located in a region with a current excess of capacity to the capacity generated by a renewable source located in another region of the power system with a capacity deficit for the same period of time is considered. The proposed method is based on cluster analysis using $k-$ medoid clustering. In accordance with the medoid clustering method, the possible capacity of primary wind and solar resources and the demand for electricity are determined when planning the development of the power system (from the point of view of planning the generation of renewable energy sources to cover future demand). For each scenario of power system development, the characteristics of additional capacity for a typical daily load schedule, extreme values and energy deficit are estimated.

2.1. Cluster Analysis of Changes in Generation from Green Sources Taking into Account Meteorological Conditions of the Regions of their Integration into the Energy System

The essence of the identification of aggregated generation is to use cluster analysis to identify clusters with identical parameters that satisfy certain accepted criteria from stochastic processes of variability generated by wind and solar power plants.

Building dependencies of wind and solar power plants connected to the power system diagram in its different regions allows us to determine the main features of the models describing these dependencies. Using this approach, it is possible to filter out the effects of individual locations with an integrated renewable power plant and group locations of the power system electrical network diagram with similar behavior of electricity production [22].

Identification of scenarios of aggregated power generation by renewable power plants is a key step to determine the possibilities of their expansion of installed wind and solar power plants in the energy system for the planned period. The use of cluster analysis is effective in terms of accuracy and detail of display of data describing the processes of variability of renewable energy potential and weather conditions in the regions [23-25,8,11].

Cluster analysis is a classical methodology for analyzing process state observation data based on their representation as a set of clusters in such a way that the elements of a cluster are always similar (in some sense) to each other than to the elements of other groups [24]. This step can be used to discover statistical patterns in the data, which can often be associated with different physical processes.

In this paper, the patterns of power generation by wind and solar power plants installed in the power system can be identified using the $k-$medoid clustering method. The $k-$medoid clustering model can be described as [24]:

$$D = \arg\min\left\{\sum_{k=1}^{k}\sum_{n=1}^{k}\left(\left\|x_n - C_k\right\|^2\right)\right\} \quad (1)$$

$$x_n = \begin{vmatrix} w_{1,1}w_{1,2},.....w_{1,i} \\ w_{2,1}w_{2,2},.....w_{2,i} \\ w_{n,1}w_{n,2},.....w_{n,i} \end{vmatrix} \quad (2)$$

where $D-$ distance between current hourly change values and the medoid of each cluster; C_k – cluster medoid of $k-$th cluster; $n-$the number of measured parameters (the values of power generation from renewable energy plants, the power load of the power plant, wind speed, solar radiation, ambient temperatures, etc.) that should be grouped into $k-$ clusters ($k<n$); $i-$ number of renewable stations.

The clustering algorithm is applied separately for each renewable power plant and the region as a whole with installed wind and solar power plants. Despite the subjectivity in the exact definition of cluster centers, this methodology provides a consistent classification for most data. The $k-$ medoid clustering method is a non-hierarchical clustering algorithm and is designed to group data into $k-$clusters, where is "k" predetermined. The optimal value of the number of clusters can be determined by the criterion proposed in [25-27]. This criterion allows determining the appropriate number of clusters by calculating the Euclidean distance between clusters and comparing the internal sum of squared errors of each cluster. Further, the samples of power generation by renewable power plants obtained using this method are designated for wind power plants (WPP) and, respectively, for solar power plants (SPP).

2.2. Algorithm for Selecting Scenarios for the Most Profitable Expansion of Green Power Plants to Cover the Planned Growth in Demand and Reduce Risk in the Energy System

The paper examines the problem of planning the expansion of the installed capacity of renewable sources for the next 10 years (until 2035) using the Azerbaijan energy system as an example. The total installed capacity of the energy system is 7.5 GW, including the total generation from all types of renewable sources of 1.2 GW.

To assess possible scenarios for expanding the installed capacity of wind and solar power plants by 2024, an optimization method using linear objective functions was used [25]. The implementation of the algorithm based on this method is particularly useful due to its simplicity compared to other algorithms based on the principles of heuristic search. The function describing the process of demand variability is considered as a "net" load N_{net} (specified as the difference between the total demand minus the total generation by all renewable power plants). The subsequent period of N_{net} growth by ΔN_{net} assumes the development of wind and solar power plants over the same period in such a combination that the demand coverage for ΔN_{net} is optimal.

To determine the expansion scenarios for renewable power plants installed in the power system, the following target functions are adopted:

Minimum standard deviation of the random variable of the annual change in net load (NS_{demand}):

$$\min SO(z) \quad (3)$$

Minimum standard deviation of net load by hours during the year:

$$SO(z) = \sqrt{\frac{\Sigma_{t=1}^{T}(z(t)-\bar{z})^2}{T-1}}, \quad \forall t \tag{4}$$

where $Z(t) = N_{net}(t_{hour}) -$ net load changes by hour over one year; $T = 8760$ ч; $\overline{Z} -$ average hourly change in load over one year.

Minimization of functions (3) and (4) have the following solutions:

$$Z(t_{year}) = N_{net}(t_{year}), \quad \forall t_{year} \tag{5}$$

and

$$Z(t_{hour}) = N_{net}(t_h) - N_{net}(t_{h-1}), \quad \forall t_h \tag{6}$$

Solutions (5) and (6) satisfy the constraints on annual capacity generation from renewable sources up to 30% of demand (as an example, the conditions of planned demand coverage in the energy system of Azerbaijan by expanding generation at wind and solar power plants by 30% by 2030 are taken).

$$30\left\{\sum_{t}\frac{(W+Sol/)(t)}{N_{net}(t_h)}\right\} \le N_{net\max} \tag{7}$$

Subject to the following conditions being met

$$N_{net}(t) = P_{load}(t) - \left(P_{wind}(t) + P_{PV}(t)\right), \quad \forall t \tag{8}$$

$$P_{wind}(t) + P_{PV}(t) + \sum_{R}\sum_{it} N_{wind}(it, r_W)\cdot P_{wind}(t, r_W) + \sum_{r_S}\sum_{it} N_{SPP}(it, r_S)\cdot P_{PV}(t, r_S),$$
$$\forall t, \forall it, \forall r_W, \forall r_S \tag{9}$$

$$VRE_{surplus}(t) = \begin{cases} VRE(t) - S_{demand}(t), & if \ \ VRE(t) > S_{demand}(t) \\ 0, & if \ \ VRE(t) \le S_{demand}(t) \end{cases} \tag{10}$$

$$z, NL, VRE, VRE_{surplus,} \ N_W, N_S \in NR \tag{11}$$

where $t \in [t_1, t_2, ..., t_{8760}] -$ indices for hourly output values of renewable energy sources over time; $it \in [it_1, it_2, ..., it_m] -$ number of single renewable installations at power plants; $r_S \in [r_{s1}, r_{s2}, ..., r_{sM}]$, $r_W \in [r_{w1}, r_{w2}, ..., r_{wN}] -$ number of regions where renewable power plants are located. $VRE_{surplus}$ – excess generation from renewable power plants; $P_{wind}(t)$ и $P_{PV}(t) -$ denote the existing hourly generation of wind and solar *PV* stations.

In equations (7)–(11), N_W and N_S represent the number of wind and solar power plants determined by the optimization algorithm for wind and solar power generation models.

III. Analysis of Scenarios for Aggregation of Green Generation Sources in Planning to Cover the Demand of Energy Systems

Research on testing the proposed methodology for determining scenarios of complementarity between regions of the energy system containing wind and solar power plants. Over the past 10 years, several renewable power plants have been commissioned in the country based on the use of the potential of wind, solar and hydroelectric resources, which were installed in the period 2015-2024. Currently, projects have been developed for the construction of a number of wind and solar power plants, the commissioning of which will allow the transport of "green energy" to Europe. A preliminary assessment of the transmission of green energy shows that its capacity will be at least 2 GW.

3.1. Data Characterizing Meteorological Conditions and Electricity Generation by Green Sources in the Regions

The installed capacity of the Azerenergy system is about 7.5 GW, a significant part of which is thermal power plants using gas turbine technology - about 5.6 GW, hydroelectric power plants - 1.4 GW, wind, solar and small hydroelectric power plants instead of taking - 0.5 GW. In 2024, renewable power plants produced 850 million kWh, including 6% by wind power plants, 67% by solar power plants and 27% by small power plants. Significant potential of wind and solar energy falls on two large geographical and economic regions of the country - Absheron, including the coastal zones of the Caspian Sea and the East Zangezur region, including the Karabakh regions. Therefore, the first wind and solar power plants were introduced in these regions. Figure 1 shows the general structure of the location of wind and solar power plants in two geographical regions - the Absheron region and the Karabakh region. In the Absheron region, two wind power plants are in operation as of 2023: the Khizi-Absheron wind power plant with a capacity of 240 MW and the Yeni Yashma wind power plant with a capacity of 50 MW. In the Karabakh region, the Jabrayil solar power plant with a capacity of 240 MW and the Kelbajar wind power plant with a capacity of 100 MW are included in the energy system. A significant consumption of the generated power falls on the Absheron region. Table 1 shows the technical parameters of renewable power plants installed in the regions.

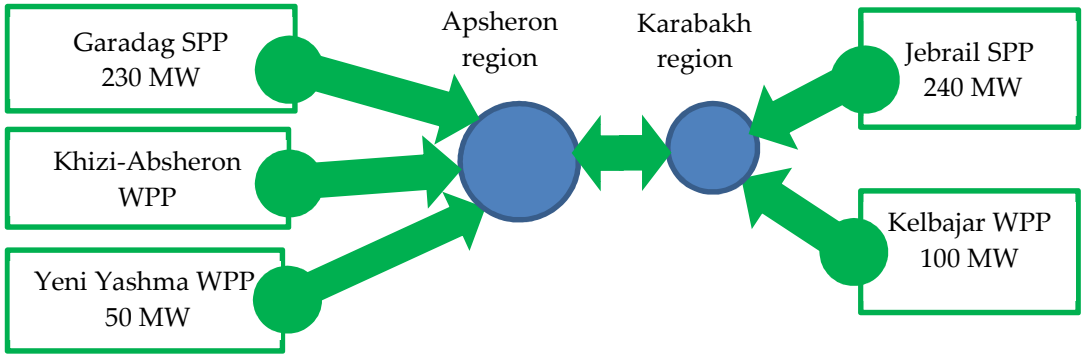


Figure 1: *General structure of the location of active variable renewable Sources located in two regions of Azerbaijan*

Table 1: *Statistical indicators of annual electricity production at power plants*

Power Plant	P, MW	Min MWh	Min (no zero) MWh	Max MWh	Ave-rage	Me-dian	Disper-sion	Standard deviation
Apsheron region								
Garadag SPP	230	0	0.213	209.3	35.91	0	$3.17\ 10^{15}$	$5.63\ 10^{7}$
Khizi-Absheron WPP	240	0	0.135	248.0	55.82	48.66	$2.17\ 10^{15}$	$4.66\ 10^{7}$
Yeni Yashma WPP	50	0	0.035	50.0	14.46	12.83	$1.42\ 10^{14}$	$1.19\ 10^{7}$
Total	520	0	0.171	442.5	106.18	93.60	$6.81\ 10^{14}$	$8.25\ 10^{7}$
Karabakh region								
Jebrail SPP	240	0	0.22	223.5	36.61	0	$3.41\ 10^{15}$	$5.84\ 10^{7}$
Kelbajar WPP	100	0	0.071	100.0	28.28	23.22	$0.58\ 10^{15}$	$2.42\ 10^{7}$
Total	340	0	0.071	291.5	64.89	43.93	$3.98\ 10^{15}$	$6.31\ 10^{7}$
Karabakh and Absheron regions								
Total	860	0	0.0712	678.9	171.08	138.5	$1.68\ 10^{16}$	1.29 108

Figure 2 and Figure 3 show the power generation profiles of wind and solar power plants in the regions of Absheron and Karabakh, respectively. As can be seen from these figures, the process of generating power from renewable energy sources in the Absheron region has a relatively uniform intensity compared to the profile of renewable energy sources in Karabakh. The profile of Karabakh has a clear similarity with the power generation profile of the solar power plant installed in this region.

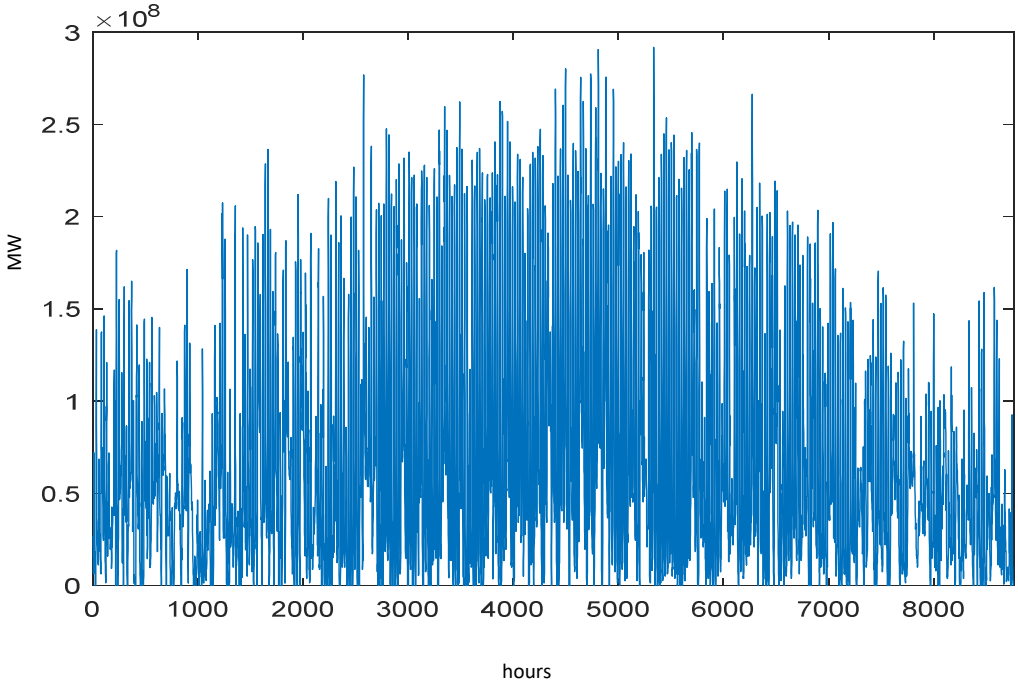


Figure 2: *Profile of hourly power generation in the Karabakh region (total installed capacity 340 MW)*

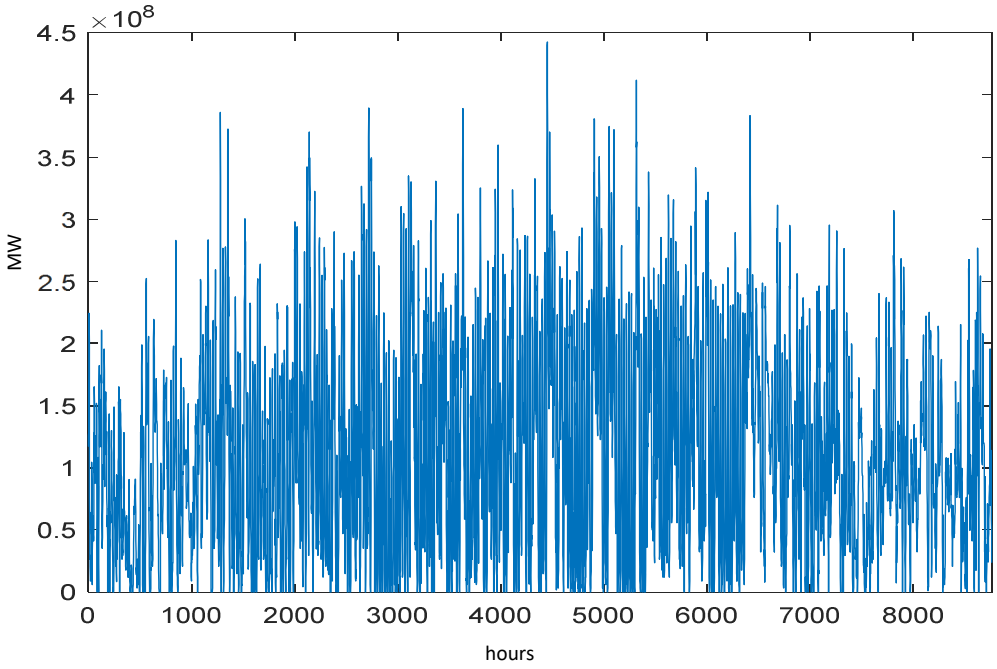


Figure 3: *Profile of hourly power generation by renewable power plants in the Absheron region (total installed capacity 520 MW)*

3.2. Clustering of Renewable Power Generation in Regions Taking into Account Meteorological Conditions

Figure 4a and Figure 4b show the probability distribution curves of hourly changes in power generation by renewable sources in the regions of Absheron, with one installed solar power station Garadag with a capacity of 240 MW and two wind power plants Khizi-Absheron - 230 MW and Yeni Yashma - 50 MW and one solar power station Jebrail 240 MW in the Karabakh region. As can be seen from the comparison of these figures, during the average values of power generation in the Absheron region with a high probability exceed the average value of power generation in the Karabakh region by more than 30%.

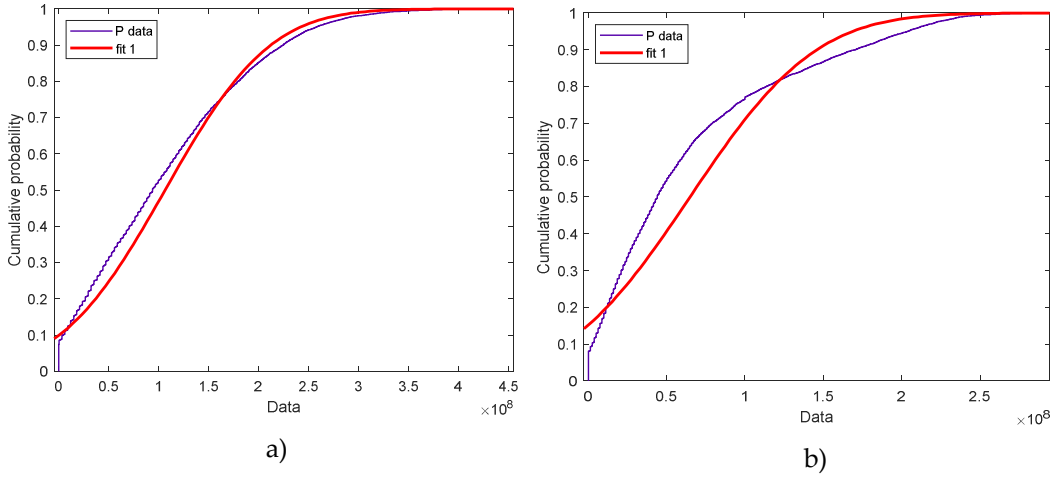


Figure 4: *Probability of distribution of annual electricity generation*
a – for SPP-WPP of the Apsheron region; b – for SPP-WP of the Karabakh region

Figure 5 and Figure 6 show clusters of daily changes in the power system load and solar radiation in the regions. The intensity of solar radiation in the regions allows solar power plants to generate electricity over a significant period of time during the day.

Figure 7 shows clusters of daily changes in wind speeds in the regions during the year in accordance with clusters of changes in solar radiation and daily consumption. The silhouettes shown in Figure 8 reflect the number of significant clusters of wind and solar energy with the corresponding clusters of the system load.

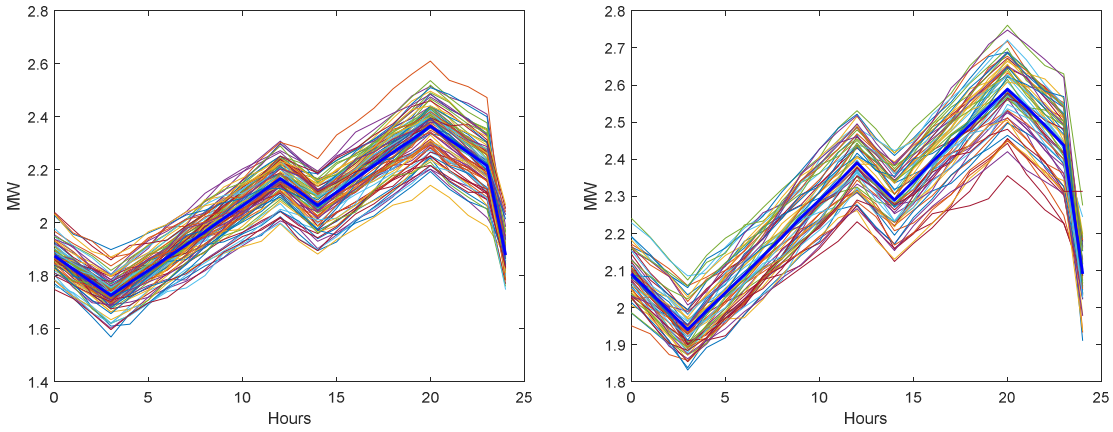


Figure 5: *Clusters of daily load changes in the power system*

a -3st cluster; b - 4nd cluster

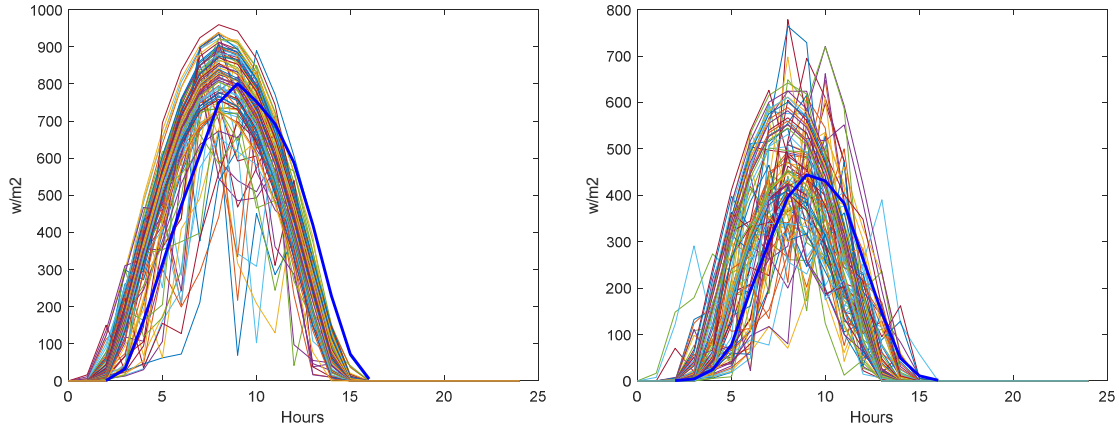
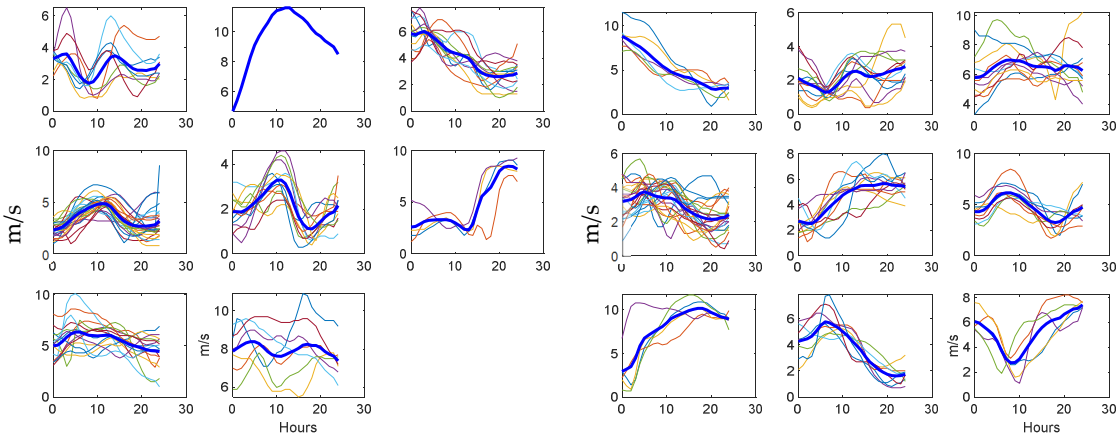


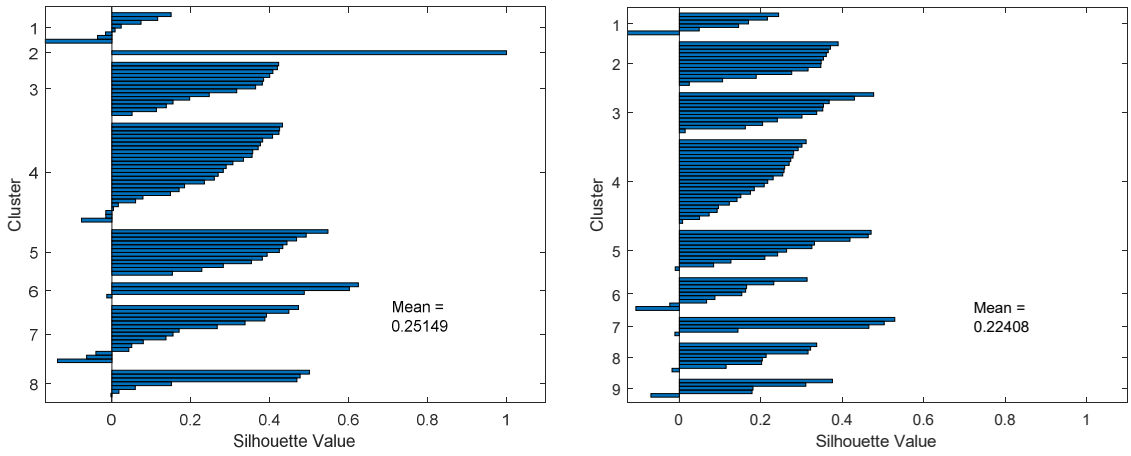
Figure 6: *Solar radiation clusters in regions*

a - Absheron; b - Karabakh



a) b)

Figure 7: *Wind clusters corresponding to the 3st cluster of radiation and load a -Absheron; b - Karabakh;*



a) b)

Figure 8: *Silhouettes of optimal numbers of wind speed clusters for 3st cluster of radiation and load a -Absheron; b - Karabakh;*

IV. Results of the Analysis of Scenarios for the Aggregation of Electricity Generation from Green Sources Located in Regions of the Country with Different Climatic Conditions

Based on hourly measurements of demand in the power system and meteorological data - wind speed, solar radiation, air temperature, obtained with a resolution of 1 hour during the year in two regions (Figure 1), with installed wind and solar power plants, a cluster analysis was carried out and typical scenarios for power generation by plants in each region and their interactions between regions were identified.

The studied variants of scenarios and optimization of load coverage due to power generation by renewable power plants are given in Table 2.

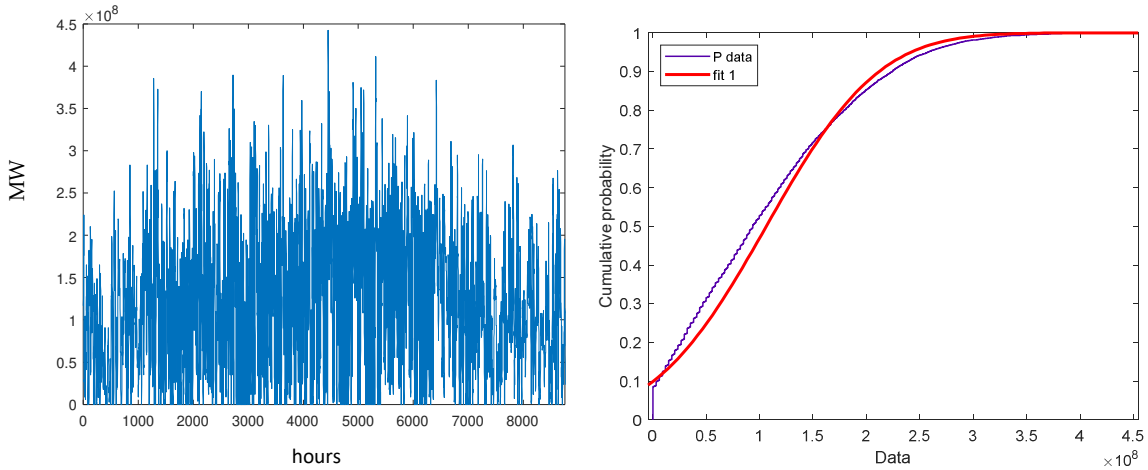
Table 2: *Scenario and optimization options*

Scenarios	Functions of the goal of optimal development	The means used
$Wind_{so}$	Minimize the objective function (1) by adding generation from renewable power plants	Wind
PV_{so}		Solar PV
$PV+Wind_{so}$		PV+Wind
$Wind_{soh}$	Minimizing the standard deviation of hourly change in N_{net} by adding generation from renewable power plants	Wind
PV_{soh}		Solar PV
$PV+Wind_{soh}$		PV+Wind

Statistical data characterizing the output of wind and solar power plants installed in the regions of Absheron and Karabakh for 2024 are given in the table. As can be seen from the table, all indicators of the Absheron region, including SO, are higher than the corresponding indicators of renewable stations by 12% or more. This gives reason to believe that when optimizing the planned coverage of the net load of the power system, the output of solar power plants can complement the fully used output capacity of the Khizi-Absheron region.

Figure 9, Figure 10 and Figure 11 show respectively the generation of electricity and the probability of its distribution for 2024 by wind and solar power plants located in the regions of Absheron, Karabakh and SPP-WPP of the Karabakh and Absheron regions together.

As with wind power generation, solar power generation exhibits seasonal behavior with high positive gradients from sunrise, reaching the earth's surface with minor gradients around midday 11-14 hours and high negative gradients until sunset.



a) b)

Figure 9: *Annual electricity production of the SPP-WPP of the Apsheron region*
a - annual electricity production;
b - probability of distribution of annual electricity generation;

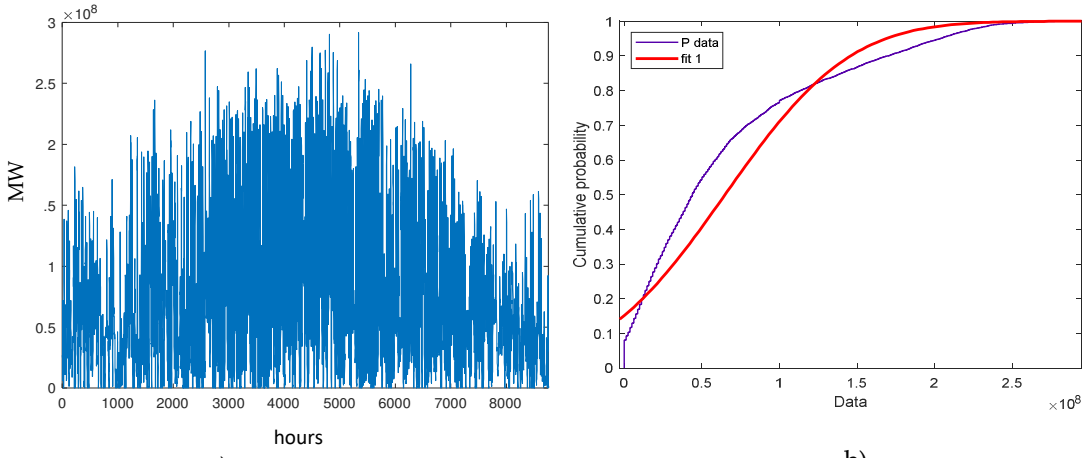


Figure 10: *Annual electricity production of SPP-WPP of the Karabakh region*
a - annual production of electricity;
b - probability of distribution of annual electricity generation;

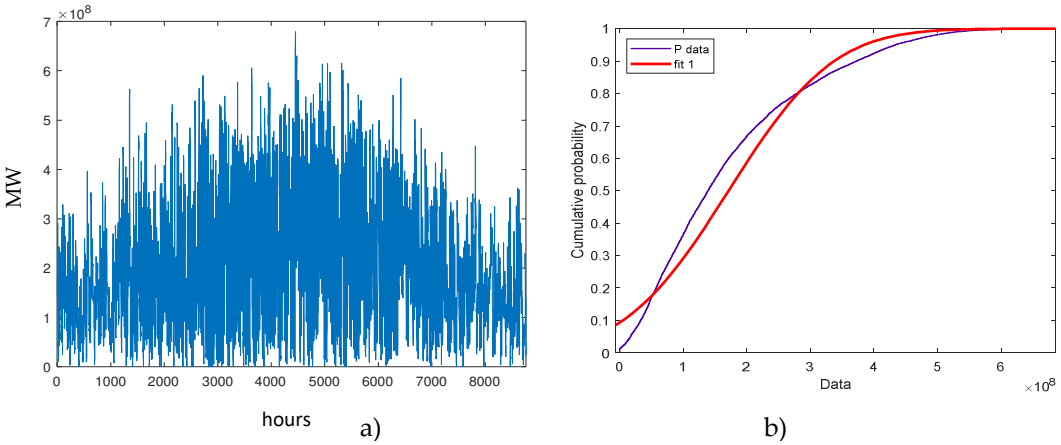


Figure 11: *Annual electricity production of SPP and WPP in the Karabakh and Absheron regions:*
a - annual production of electricity;
b - probability of distribution of annual electricity generation;

The standard deviation of the power generation by wind power plants is determined on the basis of the wind energy potential and, depending on the amount of power generation by wind power plants, the possibility of complementarity with wind power plants in the region is established.

V. CONCLUSION

1. Integration of renewable green energy sources with variable generation into the power system, along with significant advantages in solving problems of environmentally friendly production of electric energy, commissioning of power plants in a short time, leads to the need to solve a number of non-standard problems on planning and optimization of the mode in the power system, prompt coverage of demand in normal and post-emergency modes, as well as the risk of violation of the balance reliability of power systems in the conditions of green technologies. The solution of these problems requires the creation of new scientifically sound methods, development of algorithms and programs for identifying scenarios for generating capacities by green sources

located in various climatic conditions, determining the ratio of generation of these sources and choosing scenarios of their complementarity for various periods of expansion of green generation.

2. An algorithm for identifying scenarios of electricity generation processes by green sources, such as wind power plants and solar photovoltaic stations located in the power system in places with different climatic conditions, is proposed based on cluster analysis using the medoids method. An algorithm for identifying patterns between scenarios of electricity generation by renewable power plants located in different regions is proposed.

3. Using the proposed method, a cluster analysis of high-resolution data was performed and spatial and temporal variability of wind and solar energy generation in Azerbaijan was revealed. Two regions with different characteristics of wind and solar energy profiles were identified. Based on these profiles, different scenarios for adding green generation to the current energy balance were considered to reduce the risk of disruption to operational reliability: 1 – only wind energy; 2 – only solar energy; 3 – adding wind and solar energy.

4. It was found that the highest share of green energy penetration in annual consumption was achieved using the complementarity of wind and solar power plants. In the PV plant + wind plant scenario, a sustainable way to increase the penetration of renewable energy to 30%, taking into account the annual energy surplus in relation to consumption equal to (5-10) %, is possible by increasing the capacity of solar plants, which reduces the risk of disruption of balance or regime reliability.

References

[1] Collection of statistics on renewable energy generation capacity (2024 March) IRENA (International Renewable Energy Agency).

[2] Global Solar Power Capacity "The Global Energy Association. 2023, https://global energyprize.org

[3] Global share of wind power in the electricity mix in 2023 Wind power. https://wwindea.org/GlobalStatistics

[4] Guerra K., Haro P., Gutierrez R.E., Gomez – Borea A. Facing the high share of variable renewable energy in the power system: Flexibility and stability requirements. Journal Applied Energy 310 (2022) 118561.

[5] Chandler H. (2011) Harnessing variable renewables: A guide to the balansinge chalange. Paris, France: International Energy Agency.

[6] Flavio R., Arroyo M., Luisj Miguel The role of renewable Energies for the sustainable energy governance and environmental policies for the mitigation of climate change in Ecuador Energies 2020, 13, 3883

[7] Hashimov A.M., Rahmanov N.R., Mahmudova A.Z., Morillo J.M.B. Assessment of Probability Distribution Sequence for Voltage Stability in a Power system with Large Share Integration of Variable Renewable Sources. International Journal on Technical and Physical Problems of Engineering (IJTPE), June 2023, Iss. 55, Vol. 15, No. 2, pp.291-296.

[8] Stennikov V.A., Kurbatsky V.G., Rahmanov N.R., Guliyev H.B., Shakirov V.A. Regional Aspects of Wind Energy, L.A. Melentiev Energy Systems Institute, Siberian Branch of the Russian Academy of Sciences, 2020.

[9] Guliyev H.B., Huseynov N. Improving The Efficiency Of Distributive Networks With The Application Of Green Technologies. Reliability Theory and Applications, 2024, 19(Special issue 6), pp. 1445–1456

[10] Geng Nin, Yuji, Zhihui Zhang, Wenbo Wang, Jikai Chen, Peng Yu. Clustering analysis of tipical scenarios of island supply system by using cohesive hierarchical clustering based K-Means

clustering method. Science Direct, Energy Reports 7(2021) 250-256.

[11] Couto A., Dinkel F., Franz S., Spliethoff H. Variability of wind and solar PV Generation Complementary to Meet Electricity Demand. Energies 2020,13,4132.

[12] Buttler A., Dinkel F., Franz S., Spliethoff H. Variability of wind and solar power – an assessment of the current situation in the European Union based on the year 2014. Energy 2016, 106, 147-161.

[13] Han S., Zhang L., Liu Y., Zhang H., Yan J., Li L., Lei X., Wang X. Quantitative evaluation method for the complementarity of wind-solar-hydro power and optimization of wind-solar ratio. Appl. Energy 2019, 236, 973-984.

[14] Yan J., Qu T., Han S., Liu Y., Lei X., Wang H. Reviews on characteristic of renewable Evaluating the variability and complementarity. Int. Trans. Elect. Energy Syst. 2020, 30, e.12281

[15] Engeland K., Borga M., Creutin J-D., Francois B., Ramos M-H., Vidal J-P. Space – time Variability of climate variables and intermittent renewably electricity production- A review. Renew. Sustain. Energy Rev. 2017, 79, 600-617.

[16] Ren G., Wan J., Yu D. Spatial and temporal assessments of complementarity for renewableenergy resources in China.Energy 2019, 177, 262-275.

[17] Bett P.E., Thornton H.E. The climatological relationships between wind and solar energy supply in Britain. Renew. Energy 2016, 87, 96-110.

[18] Peter J. How does climate change affect electricity system planning and optimal allocation of variable renewable energy. Appl. Energy 2019, 252, 113397.

[19] Rahmanov N.R., Guliyev H.B., İbtahimov F.Sh., Mammadov Z.A. Determination of optimal dimensions of hybrid AC/DC distributed generation system with renewable sources for autonomous power supply of remote. E3S Web Conf., Rudenko International Conference "Methodological Problems in Reliability Study of Large Energy Systems" (RSES 2024), Volume 584, 2024, pp.1-6.

[20] Rahmanov N.R., Guliyev H.B., Ibrahimov F.Sh., Mammadov Z.A. Hybrid AC/DC with Renewable Sources for Power Supply of Remote Locations, Energetik, 2024, No. 11, Moscow, pp. 27-33.

[21] Rahmanov N.R., Guliyev H.B., Ibrahimov F.Sh., Mammadov Z.A. Optimal Sizing of Hybrid AC/DC Distributed Generation Systems with On-Site Renewables for Off-Grid Power Supply to Remote Areas, Energy Systems Research, Vol. 7, No. 4, 2024, pp.76-83

[22] Loren-te Plazas R., Montavez, J.P., Jimenez, P.A., Jerez, S. Gomez-Navarro J.J., Garcia-Valero J.A., Jimenez-Guerrero, P. Characterization of surface winds over the Iberian Peninsula. Int. J. climatol. 2015,35,1007-1026.

[23] Guliyev H.B., Huseynov N.R. Improving the efficiency of distributive networks with the application of green technologies. Reliability: Theory & Applications, Special Issue No.6(81), Part-3, Vol.19, USA, San Diego, 2024, pp.1445-1456.

[24] Park H.-S. Jun C-H. A simple and fast algorithm for k-medoids clustering. Expert Syst. Appl. 2009, 36, 3336-3341.

[25] Heidari J., Daneshpour N. Zangeneh A. A novel k-means and k-medoids algorithms for clustering non-spherical shape clusters non-sensitive to outliers. Journal Pattern Recognition. Vol. 155, November 2024, 11639.

[26] Kulikov A.L., Shepovalova O.V., Ilyushin P.V., Filippov S.P., Chirkov S.V. Control of electric power quality indicators in distribution networks comprising a high share of solar photovoltaic and wind power stations. Energy Reports. 2022. Vol. 8. pp. 1501–1514.

[27] Ilyushin P.V., Shepovalova O.V., Filippov S.P., Nekrasov A.A. The effect of complex load on the reliable operation of solar photovoltaic and wind power stations integrated into energy systems and into off-grid energy areas. Energy Reports. 2022. Vol. 8. pp. 1515-1529.

REDUCING RENTAL COSTS IN TWO-STAGE HYBRID FSSP: BRANCH AND BOUND VS. HEURISTIC APPROACHES

Kanika Gupta[1], Deepak Gupta[2], *Sonia Goel[3]

•

[1,2,3]Department of Mathematics and Humanities, MMEC, Maharishi Markandeshwar (Deemed to be University), Mullana, Ambala, India
[1]D.A.V. College for Girls, Yamuna Nagar, Haryana, India
[1]kani.ambala@gmail.com, [2]guptadeepak2003@yahoo.com, [3]sonia.mangla14@gmail.com

Abstract

This paper proposes a Branch and Bound (BB) based heuristic to solve a two-stage hybrid Flow Shop Scheduling Problem (HFSSP), incorporating practical constraints such as machine rental costs, transportation time, and job weightage. The scheduling environment includes multiple parallel machines at the first stage, where each job can be processed on any one machine, followed by a single rented machine at the second stage. To effectively model uncertainty in processing times, triangular fuzzy numbers are used. Additionally, transportation time between stages and job weightage are integrated into the model to reflect realistic industrial conditions. The proposed BB algorithm systematically explores the space of feasible job sequences, pruning non-promising branches to derive an optimal or near-optimal schedule under the given constraints. Its performance is benchmarked against two widely used heuristic approaches—NEH and GRASP-NEH—focusing on minimizing total elapsed time and rental cost of the second-stage machine. Experimental results indicate that the BB approach consistently outperforms the heuristic methods, particularly in reducing rental costs and providing better control over the utilization of the rented resource. While heuristic methods offer computational speed, they often compromise on cost efficiency and precision in handling fuzzy parameters. Overall, the study demonstrates the effectiveness of the BB method as a robust and efficient alternative for solving complex scheduling problems, especially in scenarios where minimizing rental costs is a critical objective. The integration of fuzzy processing times, transportation delays, and job priorities further enhances the practical relevance of the proposed approach.

Keywords: Rental Cost Optimization, Fuzzy Processing Time, Triangular Fuzzy Numbers, Hybrid Scheduling, Parallel Machines

I. Introduction

Efficient job scheduling in manufacturing and service environments remains a vital concern for industries aiming to optimize resource utilization and operational costs. Among various scheduling models, the Flow Shop Scheduling Problem (FSSP) is one of the most widely studied, where each job follows the same processing route across multiple machines. However, traditional FSSPs often fall short of capturing the complexity of modern production systems that involve multiple parallel machines, rented resources, transportation delays, and uncertainties in processing times. These realistic factors give rise to the Hybrid Flow Shop Scheduling Problem (HFSSP)—a more generalized and challenging variant of the classical flow shop problem.

In practical scenarios, certain stages in the production process may involve rented machines, where minimizing rental time becomes economically significant. Furthermore, uncertainty in processing durations, caused by fluctuating workloads or machine variability, is better represented using triangular fuzzy numbers rather than deterministic values. In addition, transportation time between stages and job-specific weightage further complicate the scheduling environment and must be accounted for to develop viable and cost-effective schedules. This study addresses a two-stage HFSSP where jobs are processed on parallel equipotential machines at the first stage and then on a single rented machine at the second stage. To solve this problem, we propose a Branch and Bound (BB)-based heuristic that systematically explores feasible sequences and eliminates suboptimal ones, balancing accuracy and computational efficiency. The BB algorithm explores feasible job sequences while eliminating inefficient options, aiming to minimize the rental cost of the second-stage machine. The performance of the proposed method is compared with that of heuristic algorithms, demonstrating the BB method's effectiveness in handling fuzzy parameters and real-world constraints. González-Neira et al. [1] have studied solving the Hybrid Flow Shop Scheduling Problem (HFSP), which is known to be NP-hard, using the simple yet effective GRASP meta-heuristic. Unlike complex hybrid algorithms, GRASP offers good performance across multiple optimization objectives without multi-objective modeling. Computational results show GRASP outperforms traditional dispatching rules and is practical for real-world industrial applications. The GRASP method is further combined with NEH and compared with NEH by Öztop [2]. Johnson [3] presents a decision rule for optimal scheduling of items on two machines to minimize total elapsed time, considering setup and work times. It also explores a restricted version of a three-machine problem. Lomnicki [4] combines Roy's graph-theoretical approach to job scheduling with the branch-and-bound method, providing an exact solution for the three-machine scheduling problem. The algorithm's functionality is demonstrated through numerical examples, and further research possibilities are suggested. Nawaz et al. [5] present a simple heuristic algorithm named NEH for flow-shop scheduling, prioritizing jobs with higher total process time. Kahraman et al. [6] propose an efficient genetic algorithm to minimize makespan in Hybrid Flow Shop (HFS) scheduling problems. Ignall et al. [7] present the branch-and-bound technique by Little et al. and Land and Doig applied to two flow-shop scheduling problems. Computational results for 2- and 3-machine problems show improved solutions for minimizing completion time and makespan, respectively, compared to other techniques. Tang et al. [8] propose a hybrid optimization algorithm combining Particle Swarm Optimization (PSO) and Genetic Algorithm (GA) for solving the NP-Hard Flow Shop Scheduling Problem (FSSP). Experimental results show that this hybrid method outperforms existing approaches, providing a more efficient solution. Morsy et al. [9] explore the use of Pythagorean fuzzy sets to model processing time uncertainty in scheduling, aiming to minimize machine rental costs in complex manufacturing systems. It highlights the effectiveness of fuzzy modeling in improving decision-making under uncertainty. Alburaikan et al. [10] present an effective algorithm to solve the problem of rental cost under fuzzy environment. The problem under consideration is a 3-stage FSSP having a single machine at each stage. Singla et al. [11] consider job weightage and setup times while reducing idle time to reduce rent. Sathish et al. [12] in their study present an effective heuristic to reduce the rental cost for the problem with fuzzy processing times. Kaushik et al. [13] compare the result of BB with CDS and NEH for HFSSP, and the results show the effectiveness of BB over the heuristics.

In continuation of the existing research, the present study focuses on a two-stage hybrid flow shop scheduling problem that incorporates realistic industrial constraints such as parallel equipotential machines, a rented second-stage machine, transportation time, and job weightage. To effectively handle uncertainty in processing times, triangular fuzzy numbers are used. A Branch and Bound (BB)-based heuristic is proposed to minimize both total elapsed time and machine rental cost. The performance of the proposed method is evaluated against well-known heuristics such as NEH and GRASP-NEH, and the results clearly demonstrate the superiority of the BB approach in achieving more cost-effective and accurate scheduling outcomes under complex and uncertain conditions.

II. Practical Situation

Several machines are used by auto manufacturers during the initial assembly phase, which includes welding, engine fitting, and component installation. The autos are shipped to an outside factory for painting when assembly is finished. The corporation rents the painting machine, and there's a transportation time from the assembly line to the painting facility for the cars. In order to keep transportation times under control and paint cars on schedule, the corporation must reduce the cost of renting the painting facility. Based on consumer demand, each automobile model has distinct priorities, and because processes can be unpredictable, there can be variations in the time required for each step.

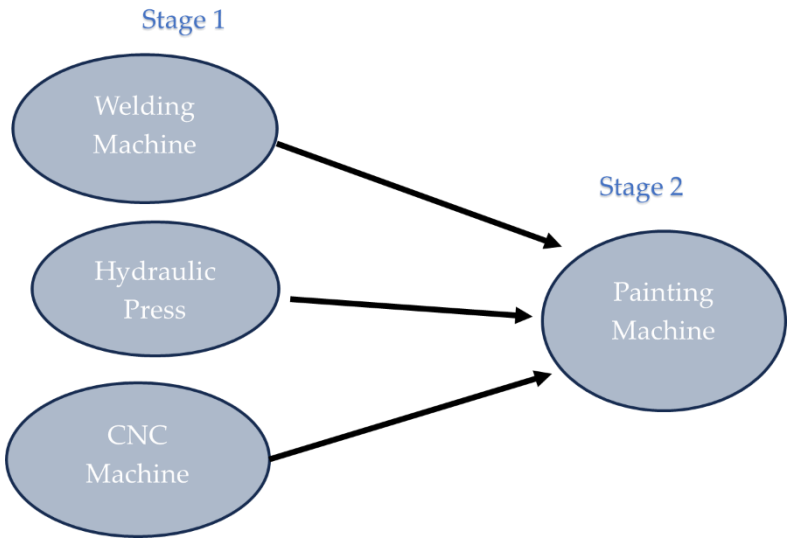


Figure 1: *Pictorial Representation of the problem in Automobile Manufacturing Unit*

III. Problem Formulation

Using equipotential machines in the first stage and a single machine in the second, this research aims to tackle a particular problem. For the second stage, rent is to be paid for the equipment. As such, the machine is rented when a task is assigned to it and returned as soon as all tasks are finished, in compliance with the rental conditions. It follows that for the duration that the equipment is being used, the rent must be paid. Job weightage and cost of transportation are also taken into account. Table 1 contains the mathematical representation of the problem.

Notations

f_{ij}=Operational Cost on j^{th} machine for i^{th} job {(i = 1, 2, ..., s); (j = 1, 2, ..., r)}
($\kappa_{i1},\kappa_{i2},\kappa_{i3}$) = Processing time on machine M for job i
($\zeta_{i1},\zeta_{i2},\zeta_{i3}$)= Processing time on machine N for job i
t_i = transportation time of job i from machine M to machine N
η_j = Total available time of machine M_j
Θ_i=Weight of job i

Table 1: *Mathematical Representation of Data*

Job/Machine	M				P.T. on M	Transportation time	P.T. on N	Job Weightage
	M_1	M_2	. . .	M_r				
1	f_{11}	f_{12}	. . .	f_{1r}	$(\kappa_{11},\kappa_{12},\kappa_{13})$	t_1	$(\zeta_{11},\zeta_{12},\zeta_{13})$	θ_1
2	f_{21}	f_{22}	. . .	f_{2r}	$(\kappa_{21},\kappa_{22},\kappa_{23})$	t_2	$(\zeta_{21},\zeta_{22},\zeta_{23})$	θ_2
3	f_{31}	f_{32}	. . .	f_{3r}	$(\kappa_{31},\kappa_{32},\kappa_{33})$	t_3	$(\zeta_{31},\zeta_{32},\zeta_{33})$	θ_3
.								
.								
.								
S	f_{s1}	f_{s2}	. . .	f_{sr}	$(\kappa_{s1},\kappa_{s2},\kappa_{s3})$	t_s	$(\zeta_{s1},\zeta_{s2},\zeta_{s3})$	θ_s
	η_1	η_2	. . .	η_k				

Algorithm Used:

Step 1: Defuzzify triangular fuzzy number using Yager's method.

For the fuzzy number $(\kappa_{i1}, \kappa_{i2}, \kappa_{i3})$ crisp value comes out to be $k_i = \frac{k_{i1}+4*k_{i2}+k_{i3}}{6}$

Step 2: Change the processing times of machines M and N according to the condition of transportation cost. i.e. the processing times of i^{th} job on machine M is to be $g_i = k_i + t_i$ and on machine N is to be $\boldsymbol{h_i} = \boldsymbol{\zeta}_i + t_i$.

Step 3 : In the next step if $\min\{g_i,h_i\}=g_i$ then change the processing time as $g_i' = \frac{g_i+\theta_i}{\theta_i}$, $h_i' = \frac{h_i}{\theta_i}$ and if $\min\{g_i,h_i\}=h_i$ then change the processing time as $h_i' = \frac{h_i+\theta_i}{\theta_i}$, $g_i' = \frac{g_i}{\theta_i}$

Step 4: Use Modi Method to optimize the utilization cost of the machines at first stage

Step 5: Use BB method to get the optimized schedule

Step 6: Prepare an in-out table for the schedule and get the total elapsed time

Step 7: Calculate the total utilization time of machine N

Step 8: Earliest time= Total elapsed time – utilization time of N

Step 9: Change he starting time of first job on machine N by earliest time and modify the schedule accordingly.

Step 10: Calculate the rent from the in-out table as: (Ending time of last job on machine N - starting time of first job on machine N) * rent

IV. Numerical Illustration

Here is a numerical example for the better understanding of the algorithm devised in this paper. This example consists of 4 equipotential machines at first stage and a single machine at second stage to complete 5 jobs. The processing times of jobs are considered in triangular fuzzy numbers. The scheduling problem outlined in Table 2 is solved by systematically applying the proposed algorithm.

Table 2: *Numerical Example*

Job/Machine	Machine M					Tr. time	P.T. on N	Job Weightage
	M1	M2	M3	M4	P.T. on M			
1	10	15	13	14	(10,14,19)	6	(2,5,7)	2
2	20	25	27	24	(16,24,26)	5	(4,5,9)	3
3	10	15	13	19	(12,19,21)	8	(3,7,8)	5
4	23	29	27	30	(20,24,30)	9	(1,3,7)	1
5	26	27	32	21	(24,26,29)	10	(5,8,9)	4
	15.9	12.6	21.7	16.82				

Table 3: *Problem with Crisp Processing Times*

Job/Machine	Machine M				P.T. on M	Tr. time	P.T. on N	Job Weightage
	M1	M2	M3	M4				
1	10	15	13	14	14.17	6	4.83	2
2	20	25	27	24	23	5	5.50	3
3	10	15	13	19	18.17	8	6.50	5
4	23	29	27	30	24.33	9	3.33	1
5	26	27	32	21	26.17	10	7.67	4
	15.9	12.6	21.7	16.82				

Table 4: *Transportation time Integration*

Job/Machine	Machine M				P.T. on M	P.T. on N	Job Weightage
	M1	M2	M3	M4			
1	10	15	13	14	20.17	10.83	2
2	20	25	27	24	28	10.50	3
3	10	15	13	19	26.17	14.50	5
4	23	29	27	30	33.33	12.33	1
5	26	27	32	21	36.17	17.67	4
	15.9	12.6	21.7	16.82			

Table 5: *Problem after the third step of Algorithm*

Job/Machine	Machine M					P.T. on N
	M1	M2	M3	M4	P.T. on M	
1	10	15	13	14	10.09	6.42
2	20	25	27	24	9.33	4.50
3	10	15	13	19	5.23	3.90
4	23	29	27	30	33.33	13.33
5	26	27	32	21	9.04	5.42
	15.9	12.6	21.7	16.82		

Table 6: *After Applying Modi Method*

Job/Machine	Machine M				P.T. on N
	M1	M2	M3	M4	
1	-	2.31	-	7.78	6.42
2	-	9.33	-	-	4.50
3	-	-	5.23	-	3.90
4	15.9	0.96	16.47	-	13.33
5	-	-	-	9.04	5.42

Table 3 presents the data after defuzzification of the triangular fuzzy processing times using Yager's method (Step 1). In Table 4, transportation times are incorporated into the processing times as outlined in Step 2. Table 5 reflects the adjustments made after applying the job weightage criterion (Step 3). The optimization of machine utilization cost for the parallel machines at the first stage, performed using the MODI method (Step 4), is displayed in Table 6. The data in Table 7 shows the process of BB method step by step and the final sequence of jobs after BB methos comes out to be 3-1-2-5-4. Table 8 represents the in time and out time of the jobs on machines.

Table 7: *Bounds of BB method*

Jobs	g′	g′′	G=max(g′,g′′)
1	41.35	25.6	41.35
2	42.9	25.6	42.9
3	38.8	26.2	38.8
4	50.04	25.6	50.04
5	42.61	25.6	42.61
31	41.35	26.2	41.35
32	42.9	27.12	42.9
34	55.27	26.2	55.27
35	42.61	26.2	42.61
312	45.21	27.12	45.21
314	55.27	26.2	55.27
315	50.39	26.2	50.39
3124	55.27	27.12	55.27
3125	50.39	35.03	50.39

Table 8: *In-Out Table*

Job/Machine	Machine M				Tr. Time	P.T. on N
	M1	M2	M3	M4		
3	-	-	0-18.17	-	8	26.17-32.67
1	-	-	18.17-31.87	31.87-32.34	6	38.34-43.17
2	-	0-22	-	32.34-33.34	5	43.17-48.67
5	-	-	-	33.34-59.51	10	69.51-77.18
4	0-21.4	-	31.87-34.8	-	9	77.18-80.51

Utilization time of machine N = 27.83. Earliest time for machine N=80.51-27.83 = 52.68
New Schedule is given in Table 9.

Table 9: *Modified In-Out Table*

Job/Machine	Machine M				Tr. time	P.T. on N
	M1	M2	M3	M4		
3	-	-	0-18.17	-	8	52.68-59.18
1	-	-	18.17-31.87	31.87-32.34	6	59.18-64.01
2	-	0-22	-	32.34-33.34	5	64.01-69.51
5	-	-	-	33.34-59.51	10	69.51-77.18
4	0-21.4	-	31.87-34.8	-	9	77.18-80.51

Consider the rent of Machine N is to be Rs. 3/- per unit of time then according to previous schedule the rent becomes (80.51-26.17) * 3 =Rs. 163.02/- and according to new schedule it comes out to be (80.51-52.68) * 3= Rs. 83.49/-.

V. Solution using the NEH and GRASP-NEH method

I. Steps for NEH method & GRASP-NEH method

In this approach, the first four steps of the proposed algorithm—namely defuzzification of fuzzy processing times, adjustment of processing times to include transportation time, modification based on job weightage, and optimization of parallel machine allocation using the MODI method—are applied initially to preprocess the input data. The resulting crisp and adjusted job data is then used as input for the classical NEH heuristic to determine the job sequence.

Step 5 : Calculate the total processing times of all jobs on all machines as TT_i

Step 6: Arrange in descending order and consider the first job of the sequence with the maximum TT.

II. For NEH

Step 7: For i=2:S

Consider the job Ji and calculate the fitness value for all the possible positions of Ji in the sequence and insert Ji at the position where the fitness value is minimum.

III. For GRASP-NEH

Step 7: For k=1:x

a. Take J_k as first job
b. For each job from the set of unscheduled jobs calculate the cost (makespan) C_t
c. Find the minimum and maximum of C_t as C_{max} and C_{min}.
d. Create the RCL (restricted candidate list) of the jobs t satisfying the condition (here the threshold value γ is taken to be 0.1)

$$C_t - C_{min} \leq \gamma * (C_{max} - C_{min})$$

e. Select the random job from RCL to append in the schedule.
f. Repeat the steps from b. to e. until the complete schedule is prepared.
g. This scheduled is modified with the NEH algorithm.

Step 8: Find the best schedule among the x schedules.

IV. Solution using NEH

Table 10: *Total Processing Time*

Job/Machine	Machine M				P.T. on N	TT_i
	M1	M2	M3	M4		
1	-	2.31	-	7.78	6.42	16.51
2	-	9.33	-	-	4.50	13.83
3	-	-	5.23	-	3.90	9.13
4	15.9	0.96	16.47	-	13.33	46.66
5	-	-	-	9.04	5.42	14.46

Table 10 gives the TT_i for all the jobs. According to the descending order of TT the sequence of jobs comes out to be 4-1-5-2-3. Now NEH algorithm is applied on this sequence. The process for NEH is given in Table 11. The final sequence is 1-5-2-3-4. The in-out table is given in Table 12.

Table 11: *NEH Method*

Sequence	Fitness Value
4-1	53.08
1-4	46.66
1-4-5	52.08
1-5-4	46.66
5-1-4	46.66
1-5-4-2	51.16
1-5-2-4	46.66
1-2-5-4	46.66
2-1-5-4	47.21
1-5-2-4-3	50.56
1-5-2-3-4	46.66
1-5-3-2-4	46.66
1-3-5-2-4	46.66
3-1-5-2-4	46.66

Table 12: *In-Out Table for NEH algorithm*

Job/Machine	Machine M				P.T. on N
	M1	M2	M3	M4	
1	-	-	0-13.7	13.7-14.17	20.17-25
5	-	-	-	14.17-40.34	50.34-58.01
2	-	-	13.7-31.87	-	58.01-64.51
3	-	0-22	-	40.34-41.34	64.51-70.01
4	0-21.4	-	31.87-34.8	-	70.01-73.34

Utilization time of Machine N=53.17. Rental Cost = Rs. 159.51

V. Solution using GRASP-NEH

Jobs in descending order of TT_i are : 4-1-5-2-3
Consider the first job as job 4. The cost function is given as Table 13 and Table 14.

Table 13*: GRASP procedure*

Scheduled Sequence	Unscheduled Job	C_t
4	1	53.08
4	2	51.16
4	3	50.56
4	5	52.08

C_{min} = 38.56, C_{max} = 43.84. Now according to the condition

$$C_t \leq C_{min} + \gamma * (C_{max} - C_{min}) = 50.812.$$ So, job 3 lie in RCL.

Table 14: *GRASP procedure (Cont.)*

Scheduled Sequence	Unscheduled Job	C_t
4-3	1	56.98
4-3	2	55.06
4-3	5	55.98
4-3-2	1	61.48
4-3-2	5	60.48

So, the sequence after Grasp algorithm comes out to be 4-3-2-5-1. Now, the NEH heuristic is applied to this sequence (Table 15).

Table 15: *GRASP-NEH algorithm*

Sequence	Elapsed Time
4-3	50.56
3-4	46.66
3-4-2	51.16
3-2-4	46.66
2-3-4	46.66
3-2-4-5	52.08
3-2-5-4	46.66
3-5-2-4	46.66
5-3-2-4	46.66
3-2-5-4-1	53.08
3-2-5-1-4	46.66
3-2-1-5-4	47.21
3-1-2-5-4	46.66
1-3-2-5-4	46.66

So the final sequence comes out to be 3-2-5-1-4. The in-out table for the GRASP-NEH is given in Table 16.

Table 16: *In-Out table for GRASP-NEH*

Job/Machine	Machine M				Tr. time	P.T. on N
	M1	M2	M3	M4		
3	-	-	0-18.17	-	8	26.17-32.67
2	-	0-22	-	22-23	6	32.67-38.17
5	-	-	-	23-49.17	5	59.17-66.84
1	-	-	18.17-31.87	49.17-49.64	10	66.84-71.67
4	0-21.4	-	31.87-34.8	-	9	71.67-75

Utilization time for machine N is 48.83 units of time so according to rental policy the rent becomes Rs. 146.49.

VI. Comparison of Results

Data presented in Table 17 draws the comparison of the results obtained above using the heuristics. Figure 2 gives the graphical representation of the comparison. The BB method shows a marked advantage in minimizing rental cost, achieving the lowest values among all tested approaches. This aligns with the method's strength in systematically considering all possible job sequences under fuzzy and transportation-adjusted conditions. However, BB tends to generate longer total elapsed times, likely due to its cost-prioritized scheduling decisions. The NEH and GRASP-NEH heuristics, on the other hand, offer shorter processing times but at the expense of higher rental costs. GRASP-NEH, due to its randomized construction phase followed by a greedy improvement, performs slightly better than NEH in some instances but still does not outperform BB in terms of rental cost. This side-by-side comparison underscores a performance-cost trade-off: heuristic methods favor speed and efficiency, while the BB method offers optimal control over cost, particularly relevant when machine rental expenses dominate scheduling priorities.

Table 17: *Comparison of the results*

	Using present heuristic	Using GRASP-NEH[2]	Using NEH[5]
Rental Cost	83.49	146.49	159.51
Job Sequence	3-1-2-5-4	3-2-5-1-4	1-5-2-3-4
Total elapsed Time	80.51	75	73.34

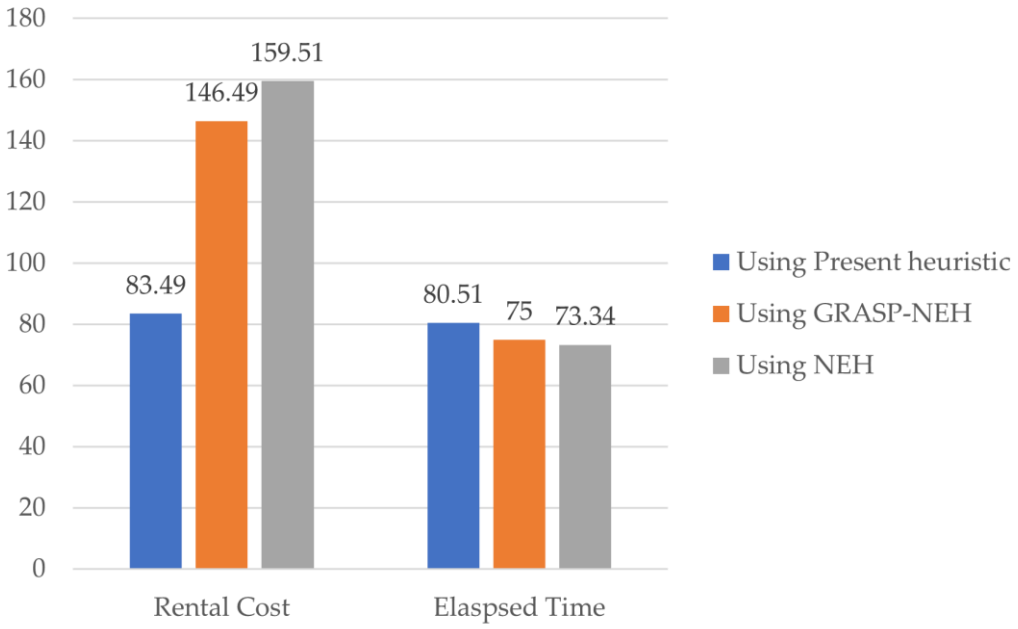


Figure 2: *Comparison of Results*

VII. Conclusion

This study presents a comparative analysis of the Branch and Bound (BB), NEH, and GRASP-NEH methods for solving a two-stage flow shop scheduling problem with transportation time, machine rental costs, and job weightage. While the BB approach does not yield the minimum total elapsed time, it significantly reduces the rental cost of the second-stage machine, which is a critical objective in the given problem setting. The results demonstrate the effectiveness of the BB method in

optimizing cost-related constraints, particularly under fuzzy processing conditions, whereas heuristic methods offer faster but less cost-efficient solutions. Thus, BB proves to be a suitable technique in scenarios where minimizing rental expenses outweighs the need for shorter completion times.

References

[1] E. M. González-Neira and J. R. Montoya-Torres, "A GRASP meta-heuristic for the hybrid flowshop scheduling problem," *J Decis Syst*, vol. 26, no. 3, pp. 294–306, Jul. 2017, doi: 10.1080/12460125.2017.1351863.

[2] H. Öztop, M. Fatih Tasgetiren, D. T. Eliiyi, and Q. K. Pan, "Metaheuristic algorithms for the hybrid flowshop scheduling problem," *Comput Oper Res*, vol. 111, pp. 177–196, Nov. 2019, doi: 10.1016/j.cor.2019.06.009.

[3] S. M. Johnson, "With Setup Times Included," *Naval Research Logistics Quarterly*, vol. 1, pp. 61–68, 1954.

[4] Z. A. Lomnicki, "A 'Branch-and-Bound' Algorithm for the Exact Solution of the Three-Machine Scheduling Problem," *or*, vol. 16, no. 1, p. 89, 1965, doi: 10.2307/3006687.

[5] M. Nawaz and E. E. Enscore, "A Heuristic Algorithm for the m-Machine, n-Job Flow-shop Sequencing Problem."

[6] C. Kahraman, O. Engin, H. Kaya, and M. Kerim Yilmaz, "AN APPLICATION OF EFFECTIVE GENETIC ALGORITHMS FOR SOLVING HYBRID FLOW SHOP SCHEDULING PROBLEMS."

[7] E. Ignall and L. Schrage, "Application of the Branch and Bound Technique to Some Flow-Shop Scheduling Problems," *Oper Res*, vol. 13, no. 3, pp. 400–412, 1965, doi: 10.1287/opre.13.3.400.

[8] J. Tang, G. Zhang, B. Lin, and B. Zhang, "Hybrid Genetic Algorithm for Flow Shop Scheduling Problem," in *2010 International Conference on Intelligent Computation Technology and Automation*, 2010, pp. 449–452. doi: 10.1109/ICICTA.2010.767.

[9] S. El-Morsy, J. Ahmad, and R. George, "On employing pythagorean fuzzy processing time to minimize machine rental cost," *AIMS Mathematics*, vol. 8, no. 7, pp. 17259–17271, 2023, doi: 10.3934/math.2023882.

[10] A. Alburaikan, H. Garg, and H. A. E. W. Khalifa, "A Novel Approach for Minimizing Processing Times of Three-Stage Flow Shop Scheduling Problems under Fuzziness," *Symmetry (Basel)*, vol. 15, no. 1, Jan. 2023, doi: 10.3390/sym15010130.

[11] S. Singla, H. Kaur, D. Gupta, and J. Kaur, "No idle flow shop scheduling models with separated set-up times and concept of job weightage to optimize rental cost of machines," *Journal of Project Management (Canada)*, vol. 9, no. 2, pp. 101–108, Apr. 2024, doi: 10.5267/j.jpm.2024.2.001.

[12] S. Sathish and K. Ganesan, "Flow Shop Scheduling Problem to minimize the Rental Cost under Fuzzy Environment," Online, 2012. [Online]. Available: www.iiste.org

[13] P. Kaushik, D. Gupta, and S. Goel, "COMPARATIVE STUDY OF B&B WITH HEURISTICS NEH AND CDS FOR BI STAGE FLOW SHOP SCHEDULING PROBLEM UNDER FUZZY ENVIRONMENT," *Journal of Mechanics of Continua and Mathematical Sciences*, vol. 20, no. 2, pp. 73–89, Feb. 2025, doi: 10.26782/jmcms.2025.02.00007.

RT&A, No 3 (86)
Volume 20, September 2025

ON THE BURR TYPE IV DISTRIBUTION APPLIED TO LIFETIME SURVIVAL DATA

Claire Joy G. Mariquit[1] and Bernadette F. Tubo[2]

•

[1]Department of Physical Sciences and Mathematics
Mindanao State University at Naawan
Naawan, Misamis Oriental, Philippines
[2]Department of Mathematics and Statistics
Mindanao State University - Iligan Institute of Technology
Iligan City, Philippines
[1]clairejoy.mariquit@msunaawan.edu.ph [2]bernadette.tubo@g.msuiit.edu.ph

Abstract

This study presents the Burr type IV ($Burr_{IV}$) distribution, which is one of the twelve continuous distributions within the Burr family. The paper thoroughly evaluates its properties and applications in survival analysis. Key distributional characteristics such as survival, hazard, quantile, cumulative distribution, and probability density functions are derived. Density plots are simulated to illustrate common patterns, including J-shaped, U-shaped, and reversed J-shaped forms, frequently observed in engineering and reliability contexts. The applicability of the $Burr_{IV}$ distribution is demonstrated through three real-life datasets, each exhibiting distinct density shapes. The findings affirm the flexibility and robustness of the $Burr_{IV}$ distribution in modeling a variety of data shapes, underscoring its potential for broader applications in survival analysis and related fields.

Keywords: Burr family, survival analysis, maximum likelihood estimation, probability density function

1. Introduction

Survival analysis centers on analyzing life data in which the time until the event of interest occurs. The Burr distribution, introduced by Burr in 1942 [5], is mostly a unimodal family of distributions that is used to analyze various kinds of life data with unknown underlying distribution due to its adaptability and flexibility.

Some of the widely studied distributions under this family are Burr type III or Burr_{III} and Burr type XII or Burr_{XII} distributions. Only few researches have been conducted to study in-depth other types of this family, like Burr_{V}, Burr_{VII} and Burr_{X} distributions, mostly on classical and Bayesian approaches in estimating unknown parameters of the distributions. Burr_{I} and Burr_{II} distributions are known as the famous uniform and generalized logistic distributions, respectively. However, remaining distributions have not received any considerable research as of this writing; such is the case with Burr_{IV} distribution.

The Burr_{III} distribution is extensively known and applied in various applications in the area of finance and engineering. It has at least two unknown parameters which include shape, scale and location parameters.

Let $F_\bullet(x)$ indicate the cumulative distribution function (cdf) of a specific Burr type ($\bullet$). The cdfs of Burr_{III} and Burr_{IV} are respectively,

$$F_{\text{III}}(x) = (1 + x^{-c})^{-k}, \quad x \geq 0 \quad \text{and}$$
$$F_{\text{IV}}(x) = \left[1 + \left(\frac{c-x}{x}\right)^{\frac{1}{c}}\right]^{-k}, \quad 0 \leq x \leq c,$$

where c and k are shape parameters.

Looking at Burr_{III} and Burr_{IV} distribution functions, clearly $F_{\text{IV}}(x)$ can be obtained by replacing x in $F_{\text{III}}(x)$ with $x^* = \left(\frac{c-x}{x}\right)^{-c^{-2}}$, that is, $F_{\text{IV}}(x) = F_{\text{III}}(x^*)$. This implies that the Burr_{IV} distribution with two shape parameters c and k, to some degree, can be treated as an extension of Burr_{III} distribution.

Most of the approaches used to estimate the parameters of Burr distributions include Maximum Likelihood Estimation (MLE) and Bayesian Estimation. Ramos et al. [22] reiterated that MLE is widely used due to its good properties, under regular conditions. The MLEs have consistency, asymptotic unbiasedness, asymptotic efficiency and asymptotic normality.

In the latter years, Feroze et al. [7] conducted research on the MLE of Burr_{III}'s two shape parameters with samples having left censored values. The methodologies used were the same as what they have done on Burr_{V}, although a real life data analysis has been done to see its applicability to real world situations. The performance results and conclusions made to Burr_{III} are identical to Burr_{V}'s.

There are already many distributions - extended or generalized existing in the literature used by many researchers to explain the behavior of a survival data. For example, the classical Weibull distribution and Burr_{III} distribution are already popular tools for describing the behavior of a life data. However, for some parameter values, these distributions cannot capture more properly the behavior of the data more particularly when the trend or behavior of the data follows either a "J"-shape, "U"-shape or "Reversed J"-shape. These shapes are commonly observed in engineering and reliability scenarios. Since Burr_{IV} distribution is an extension of Burr_{III}, it can be used as an alternative to these more famous lifetime distributions.

The remainder of this paper is structured to provide a comprehensive understanding of the Burr_{IV} distribution. Section 2 introduces the Burr type family, laying the groundwork for further discussion. In Section 3, we delve into the distributional properties of Burr_{IV}, where we derive key functions such as the cdf, probability density function (pdf), survival function, hazard function, and quantile functions. The analysis continues in Section 4, where we assess the behavior of the shape parameters of Burr_{IV} through simulation studies. Following this, Section 5 presents applications of the Burr_{IV} distribution to three real-life data sets that exhibit characteristics similar to the density shapes identified in the previous section. Finally, Section 6 concludes the paper with remarks summarizing the findings and implications of this study.

2. The Burr type family of distributions

In 1942, Irving W. Burr proposed a family of cumulative distribution functions characterized by three positive real parameters: c, k and r. Since Burr's initial proposal, there has been a significant influx of research focusing on the adaptability and flexibility of Burr distributions in the contexts of reliability and survival analysis. These characteristics make them particularly attractive for modeling datasets where the underlying distribution is unknown.

2.1. Burr_{I} and Burr_{II} distributions

Burr_{I} and Burr_{II} distributions, famously known as uniform and generalized logistic distributions respectively, are explored by books [4] on statistical inference, [9] on statistical distributions, and [15] on continuous univariate distributions.

It was emphasized by Gorny and Cramer [12] that one major application of the uniform distribution in lifetime analysis and models of ordered data is given by the fact that (ordered) life time data from a particular distribution can often be written as a quantile transformation of the corresponding data from a (standard) uniform distribution. Also, uniform distributions have been used as a model for various life testing setups.

For the Burr_{II}, Hossain and Balakrishnan [14] stipulated that the general logistic distribution can be used in robustness studies of some classical procedures based on normality or skewed distributions if Type II censored. Moreover, Balakrishnan and Leung [3] affirmed several application of this distribution that includes the following: importance as a growth curve, usage in probit analysis, dosage response studies, and bioassays, and as replacement to the normal distribution.

2.2. Burr_{III} distribution

Considered to be one of the most famous Burr distribution, Burr_{III} is widely used as an alternative to many lifetime distributions including Weibull and Burr_{XII} distributions, as stressed by Feroze et al. [7]. Gamchi et al. [10] also remarked that this distribution can accommodate different hazard lifetime data and can properly approximate many well-known distributions such as Weibull, gamma, and log-normal.

Panahi [19] as well pointed out the effective utilization of this distribution in analyzing materials engineering data such as fracture toughness data in place of the others. The Burr_{III} distribution is used extensively in various fields such as survival and reliability analysis, environmental studies, economics, meteorology and water resources, forestry among others as remarked by Ul-Haq et al. [18]. This distribution is also applied to wages, income and wealth datasets.

2.3. Burr_{X} distribution

For Burr_{X} distribution, also known as the Generalized Rayleigh distribution, Kundu and Raqab [16] described that this two-parameter distribution can be used quite effectively in modeling strength data and also modeling general lifetime data. It has increasing importance in several areas of applications such as lifetime tests, health, agriculture, biology, and other sciences as discussed by Fernandez et al. [6]. One specific application was mentioned by Rabie and Li [21] where a mathematical model was obtained for the expected lifetime of AIDS patients by using this distribution and fitting the data observed of the infected persons for Burr_{X} distribution.

2.4. Burr_{XII} distribution

A wide study on real-life application of Burr_{XII} have been conducted due to its capacity to assume various shapes that often permits a good fit when used to describe biological, clinical or other experimental data. It has also been applied in areas of quality control, reliability studies, duration and failure time modeling as identified by Panahi and Asadi [20].

Feroze et al. [7] also mentioned that since Burr_{XII} distribution under specific assumptions, can be shown to follow an extreme value distribution, the distribution has been used to model extreme events such as flood frequencies, wind speeds, rainfalls and river discharge volumes. This distribution also, as explained by Ghitany and Al-Awadhi [11], includes the exponential, Weibull, and log-logistic distributions for particular limiting values of the parameters. and covers the curve shape characteristics of normal, log-normal, gamma, logistic, and several Pearson-type distributions.

However, eventhough there are studies on Burr_{V} and Burr_{VII} distributions both being good alternatives to many lifetime distributions as mentioned by Feroze and Aslam [8], the rest of the distributions from this family have not received significant analysis using any real-life data or scenarios.

3. Some Distributional Properties of the Burr_{IV} distribution

In this section, the research will mirror the methods employed by Hakim et al. [13] in their work on finding some distributional properties of the Burr_{XII} distribution where it also has two shape parameters.

The probability density function for the general Burr_{IV} family distribution is given by

$$\text{f}_{\text{IV}}(x) = kx^{-2}\left(\frac{c-x}{x}\right)^{\frac{1}{c}-1}\left(\frac{c-x}{x}+1\right)^{-k+1}, \quad 0 < x < c, \tag{1}$$

where $k > 0$ and $c > 0$ are shape parameters.

And the cumulative distribution function of the distribution is

$$\text{F}_{\text{IV}}(x) = \left[1+\left(\frac{c-x}{x}\right)^{\frac{1}{c}}\right]^{-k}, \quad 0 \le x \le c. \tag{2}$$

The Burr_{IV} distribution can be viewed as an extension of the Burr_{III} distribution. By examining the cdfs of both distributions, clearly $\text{F}_{\text{IV}}(x)$ can be derived by substituting x in $\text{F}_{\text{III}}(x)$ with $x^* = \left(\frac{c-x}{x}\right)^{-c^{-2}}$, that is, $\text{F}_{\text{IV}}(x) = \text{F}_{\text{III}}(x^*)$.

The survival function $S_{IV}(x)$ gives the probability that the random variable X exceeds the specified time x. The survival function $S_{IV}(x) = P(X > X)$ can be ascertained from the probability density function by integrating over the probability density function from time x to infinity or just one minus the corresponding cdf,

$$S_{IV}(x) = P(X > x) = \int_x^{\infty} f(u)\,\mathrm{d}u = 1 - F_{IV}(x).$$

The hazard function $h_{IV}(x)$, is equal to the limit, as Δt approaches zero, of a survival probability statement, divided by Δx, where Δx denotes a small period of time,

$$h_{IV}(x) = \lim_{\Delta x \to 0} \frac{P(x \le X < x + \Delta x | X \ge x)}{\Delta x}.$$

It gives instantaneous potential to fail at time x per unit of time, given survival up to time x. It is also known as failure rate or force of mortality. The hazard function can also be calculated by taking the ratio of the pdf and the survival function,

$$h(t) = \frac{f_{IV}(x)}{S_{IV}(x)}.$$

The quantile function can be computed using the inverse transformation method where, $X = F_{IV}(x) - u$ and u is the random variable with distribution $U(0,1)$.A summarized comparison of distributional properties of both distributions and a derivation from Burr_{III} to Burr_{IV} using their cdfs are detailed in Table 1.

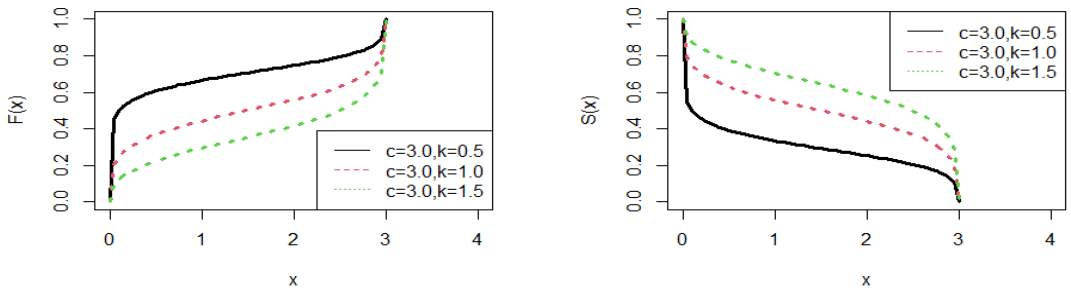
Table 1: *Comparison of* Burr_{III} *and* Burr_{IV} *Distributional Properties*

Function	**Burr Type III** where $x > 0, c > 0, k > 0$	**Burr Type IV** where $0 \leq x \leq c, k > 0$
$F(x)$	$\text{F}_{\text{III}}(x) = (1 + x^{-c})^{-k}$	$\text{F}_{\text{IV}}(x) = \left[1 + \left(\frac{c-x}{x}\right)^{\frac{1}{c}}\right]^{-k}$
$f(x)$	$\text{f}_{\text{III}}(x) = ckx^{-c-1}\left(1 + x^{-c}\right)^{-k-1}$	$\text{f}_{\text{IV}}(x) = kx^{-2}\left(\frac{c-x}{x}\right)^{\frac{1}{c}-1}\left(\frac{c-x}{x} + 1\right)^{-k+1}$
$S(x)$	$\text{S}_{\text{III}}(x) = 1 - (1 + x^{-c})^{-k}$	$\text{S}_{\text{IV}}(x) = 1 - \left[1 + \left(\frac{c-x}{x}\right)^{\frac{1}{c}}\right]^{-k}$
$h(x)$	$\text{h}_{\text{III}}(x) = \frac{ckx^{-c-1}\left(1+x^{-c}\right)^{-k-1}}{1-(1+x^{-c})^{-k}}$	$\text{h}_{\text{IV}}(x) = \frac{kx^{-2}\left(\frac{c-x}{x}\right)^{\frac{1}{c}-1}\left[\frac{c-x}{x}+1\right]^{-k+1}}{1-\left[1+\left(\frac{c-x}{x}\right)^{\frac{1}{c}}\right]^{-k}}$
$q(u)$	$\text{q}_{\text{III}}(u) = \left(u^{-1/k} - 1\right)^{1/c}$ where $u \sim U(0,1)$	$\text{q}_{\text{IV}}(u) = c[(u^{-1/k} - 1)^c - 1]^{-1}$ where $u \sim U(0,1)$

4. Simulation Result on the Shape Parameters of the Burr_{IV} distribution

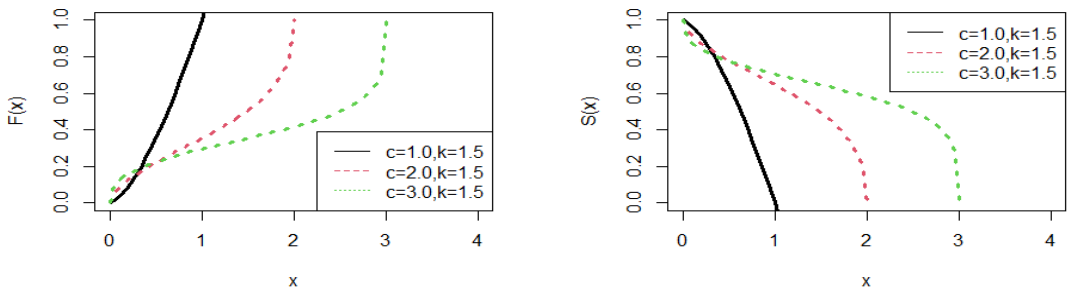
The simulation study is conducted using R software to analyze the behavior of the parameters of the Burr_{IV} distribution. This involves identifying appropriate parameter values that produce various density function shapes observed in the distribution.

Graphs of the cumulative distribution function $\text{F}_{\text{IV}}(x)$ and the survival function $\text{S}_{\text{IV}}(x)$ of the Burr_{IV} random variable X for various values of shape parameters c and k are shown in Figure 1 and Figure 2.



(a) **(b)**

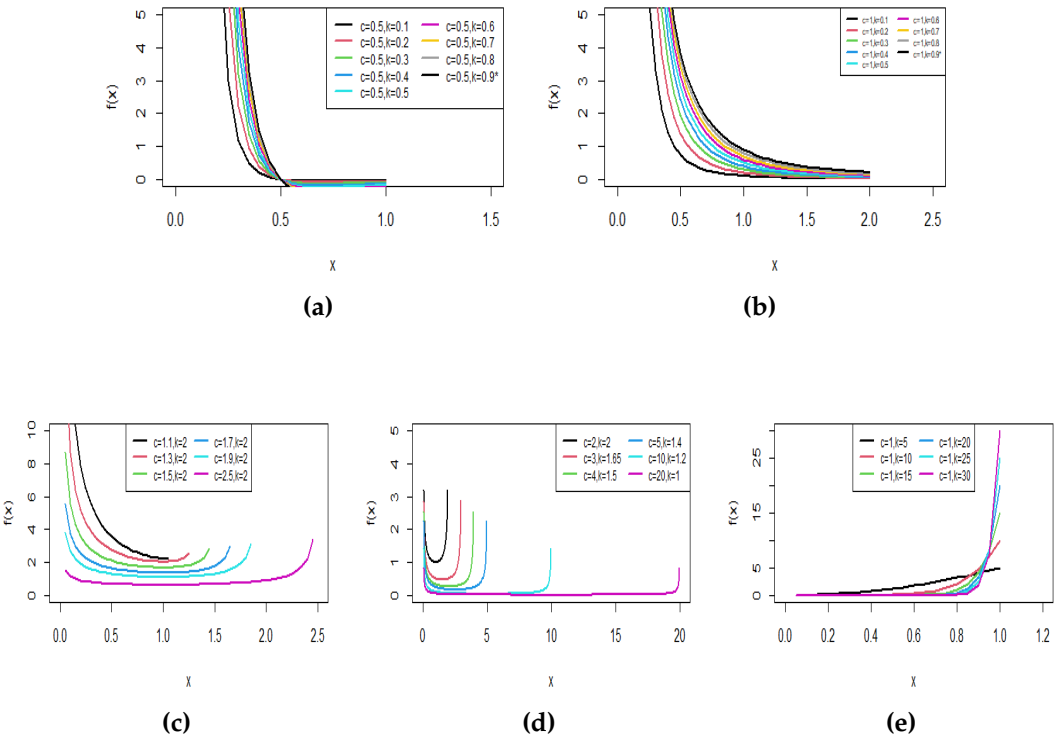
Figure 1: *Plots of CDF* ***(a)*** *and Survival Function* ***(b)*** *of the* Burr_{IV} *distribution for a fixed value of c and various values of k*



(a) **(b)**

Figure 2: *Plots of CDF* ***(a)*** *and Survival Function* ***(b)*** *of the* Burr_{IV} *distribution for a fixed value of k and various values of c*

The probability density function of Burr_{IV}, $f_{\text{IV}}(x)$, represents the failure rate of the item at time x, or the instantaneous probability that item fails at time x. Graphs of the $f_{\text{IV}}(x)$ for various values of the parameters c and k are shown in Figure 3.



(a) **(b)** **(c)** **(d)** **(e)**

Figure 3: *PDF plots for various values of c and k:* ***(a)-(b)*** *"Reversed J"-shaped,* ***(c)-(d)*** *"U"-shaped, and* ***(e)*** *"J"-shaped.*

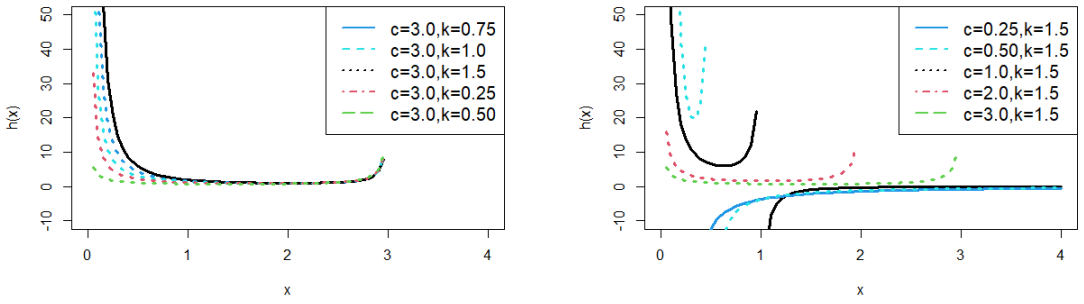
The density reflects a "Reversed J"-shape when parameter values are $c = 1$ and $0.1 \leq k \leq 0.9$ and when $0.5 < c \leq 1$ and $0.1 \leq k \leq 0.9$ (see Figure 3(a-b)). Figure 3(c-d) shows that for $c \geq 2$ and $1 < k \leq 2$, the "U"-shaped density function can be observed. The figures also indicate that the Burr_{IV} distribution when in "U"-shaped shows that its peak values are finite and the right peak ends at less than c since $0 < x < c$. Moreover, when $c \geq 2$ and $k > 2$, the density shape

shows the "J"-shaped trend (see Figure 3(e)). A summary table on various values of c and k with their corresponding density shape is given in Table 2. Therefore, different values of the shape parameters generate various density shapes or trend patterns for the Burr_{IV} distribution.

Table 2: *Summary on various values of c and k with respective density shape details*

Parameters		
c	**k**	**Density Plot Details**
$c \geq 2$	$1 < k \leq 2$	As c from 2 increases, to achieve U-shape, k from 2 decreases to 1
$c \geq 2$	$k > 2$	J-shaped
$c = 1$	$k > 5$	J-shaped
$0 < c < 0.1$	$0 < k < 1$	Rapidly flattens in y=0
$c = 1$	$0.1 \leq k \leq 0.9$	Reversed J-shaped
$0.5 < c < 1$	$0.1 \leq k \leq 0.9$	Reversed J-shaped

Graphs of the hazard rate function h depicts a bathtub-shaped for $c > 1$ in Figure 4(a) or increasing for $0 < c \leq 1$ in Figure 4(b).



(a) **(b)**

Figure 4: *Plots of Hazard Function of the* Burr_{IV} *distribution.* ***(a)****: fixed value of c and various values of k.* ***(b)****: fixed value of k and various values of c*

Since Burr_{IV} distribution has either a bathtub-shaped or an increasing hazard rate function, Burr_{IV} distribution provides flexibility for analyzing and modelling different types of survival and reliability data. The distribution can be used to model the survival time with increasing hazard rate, for example, is the conditional probability of a serious engine problem in the next month, given no problem so far, will increase with the life of the car. In addition, it can also be used to model the survival time whose hazard rate function is bathtub-shaped, for example, the age of death of infants and elderly wherein the hazard rate is expected to be decreasing at first and then overtime to increase in the end, reflecting higher hazard of infants and elderly.

5. Application to Lifetime Survival Data

This section explores the suitability of the distribution for analyzing real-life scenarios. Actual lifetime survival data are fitted to the model using specific parameter values corresponding to different distributional shapes.

Three data sets with histogram shapes similar to Burr_{IV}'s density forms are analyzed and applied to show the Burr_{IV}'s potential in real-world circumstances when compared to other known distributions such as the Weibull and Burr_{III} distributions.

5.1. The J-shaped

We consider the data consisting of the failure times of 20 mechanical components from [17]. The data is right skewed and has a large kurtosis and heavy tail characteristic. Figure 5 shows the histogram of the data and superimposed "J" density shape.

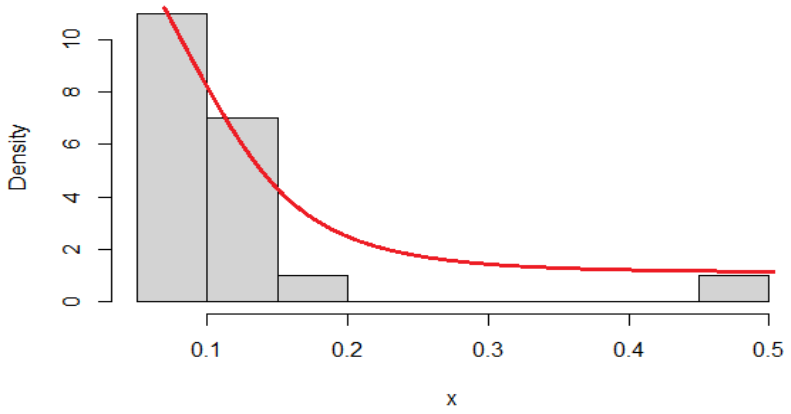


Figure 5: *Histogram of Mecha Failure dataset*

In using the *fitdistrplus* package in deriving the maximum likelihood estimates of the parameters of the candidate distributions, we have the following results as presented in Table 3. The goodness of fit statistics AIC, BIC and Loglik with adequacy values of KS, W* and A* for all the models are given in Table 4 for the first data set. It can be observed that the Burr_{IV} model has smaller values of AIC and BIC, and larger log likelihood compared to Weibull and the Burr_{III} distributions. So, the Burr_{IV} model could be chosen as the best fit for the first data set. However, KS, W*, and A* show that the Weibull distribution suits the data in a better manner.

Table 3: *MLEs for the first data set*

Distribution	$\hat{c}$	$\hat{k}$	$\hat{\tau}$	$\hat{\beta}$
Weibull	-	-	25.96762	1.642101
Burr_{III}	16.6364398	0.02695301		
Burr_{IV}	0.4945081	0.6554798		

Table 4: *The goodness of fit tests and adequacy values for the first data set*

Model	**AIC**	**BIC**	**Loglik**
Weibull	-48.84565	-46.85418	26.42282
Burr_{III}	-13.11638	-11.12491	8.558189
Burr_{IV}	-101.6659	-99.67447	52.83297
Model	**KS**	**W***	**A***
Weibull	0.2641364	0.4364214	2.537661
Burr_{III}	0.5103311	1.3816353	6.481232
Burr_{IV}	0.620643	2.657189	13.05256

5.2. The U-shaped

This second data ([1]) consists of the times to failure of 50 devices put on life test at time 0. The histogram of the data and superimposed "U" density shape is depicted at Figure 6.

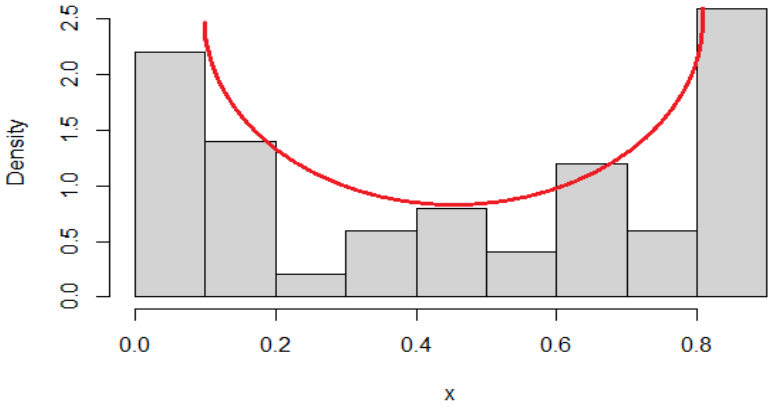


Figure 6: *Histogram of Device Failure dataset*

Mirroring procedures done in the first data set, it can be seen in Table 5 the maximum likelihood estimates of the parameters of the candidate distributions. The goodness of fit statistics AIC, BIC and Loglik with adequacy values of KS, W* and A* for all the models are given in Table 6 for the second data set. Still, the Burr_{IV} model has smaller values of AIC and BIC, and larger log likelihood compared to the other two distributions. However, KS, W*, and A* show that the Burr_{IV} distribution is not the most adequate distribution for explaining the data.

Table 5: *MLEs for the second data set*

Distribution	$\hat{c}$	$\hat{k}$	$\hat{\tau}$	$\hat{\beta}$
Weibull	-	-	2.137561	0.949043
Burr_{III}	86.2733934	0.00759508		
Burr_{IV}	0.8713916	0.7202177		

Table 6: *The goodness of fit tests and adequacy values for the second data set*

Model	**AIC**	**BIC**	**Loglik**
Weibull	25.48662	29.31066	-10.7433
Burr_{III}	-6.341407	-2.517361	5.170703
Burr_{IV}	-29.60651	-25.78246	16.80325
Model	**KS**	**W***	**A***
Weibull	0.1928	0.5295633	3.48898
Burr_{III}	0.1787837	0.4078772	2.491738
Burr_{IV}	0.2531941	0.9729153	9.793962

5.3. The Reversed J-shaped

The third data by Bader and Priest [2] represents 35 strength data for single carbon fibers (and impregnated 1000-carbon fiber tows). The histogram of measurements and the superimposed "Reversed J" density shape are shown at Figure 7.

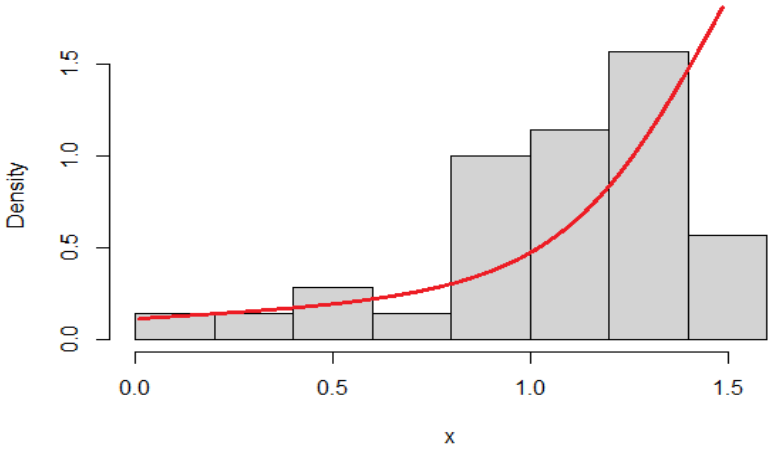


Figure 7: *Histogram of Carbon Strength dataset*

Table 7 presents the maximum likelihood estimates of the parameters obtained using the same procedure applied to the two previous data. The goodness of fit statistics for all the models are given in Table 8 for the third data set. Still, it has been observed that the Burr_{IV} model has the least values of AIC and BIC, and largest log likelihood among all candidate distributions. However, KS, W*, and A* show that the Weibull distribution suits the data in a better manner with Burr_{IV} model as next best. So, the Burr_{IV} model could be chosen as the best fit for the third data set.

Table 7: *MLEs for the third data set*

Distribution	$\hat{c}$	$\hat{k}$	$\hat{\tau}$	$\hat{\beta}$
Weibull	-	-	0.596878	3.55212
Burr_{III}	4.4716631	0.8079735		
Burr_{IV}	1.478	2.216528		

Table 8: *The goodness of fit tests and adequacy values for the third data set*

Model	**AIC**	**BIC**	**Loglik**
Weibull	32.19539	35.30609	-14.0977
Burr_{III}	47.56203	50.67272	-21.781
Burr_{IV}	-6.216309	-3.105613	5.108155
Model	**KS**	**W***	**A***
Weibull	0.1565853	0.2020518	1.374336
Burr_{III}	0.2827077	0.7875395	3.932118
Burr_{IV}	0.2001658	0.3083705	2.207361

6. Concluding Remarks

This study examined the Burr_{IV} distribution, an extension of the well-known Burr_{III} distribution, and derived key statistical distribution properties, including survival, hazard, and quantile functions. Various density function shapes"J-shaped, U-shaped, and reversed J-shaped"were identified for specific parameter values, highlighting the distribution's flexibility in modelling lifetime survival data.

To assess its applicability, Burr_{IV} was fitted to three real datasets and compared to the Weibull and Burr_{III} distributions using goodness of fit tests. The results showed that Burr_{IV} consistently provided the best fit but was not always the most adequate model for specific datasets. While it outperformed alternatives for J-shaped and U-shaped densities, the Weibull distribution was superior for mechanical failure data, and Burr_{III} better suited device failure data. These findings demonstrate the potential of Burr_{IV} for modeling diverse real-lifetime survival scenarios.

Acknowledgment

This study was supported by the Department of Science and Technology - Accelerated Science and Technology Human Resource Development Program (DOST-ASTHRDP) of the Philippines.

References

[1] Aarset, M. V. (1987). How to identify bathtub hazard rate. *IEEE Transactions on Reliability, 36*(1), 106-108.

[2] Bader, M., and Priest, A. (1982). Statistical aspects of fibre and bundle strength in hybrid composites. In T. Hayashi, K. Kawata, & S. Umekawa (Eds.), *Progress in Science and Engineering Composites: ICCM-IV* (pp. 1129-1136).

[3] Balakrishnan, N., and Leung, M. Y. (1988). Order statistics from the type I generalized logistic distribution. *Communications in Statistics - Simulation and Computation, 17*(1), 25-50.

[4] Casella, G., and Berger, R. L. (2012). *Statistical inference* (2nd ed.). Duxbury.

[5] Burr, I. (1942). Cumulative frequency distribution. *Annals of Mathematical Statistics, 13*, 215-232.

[6] Fernndez, A., Bravo, J., and De Fuentes, I. (2002). Computing maximum likelihood estimates from type II doubly censored exponential data. *Statistical Methods & Applications, 11*, 187-200.

[7] Feroze, N., Aslam, M., and Sindhu, T. N. (2015). On maximum likelihood estimation for left censored Burr type III distribution. *Pakistan Journal of Statistics and Operation Research, 11*, 497-512.

[8] Feroze, N., and Aslam, M. (2013). Maximum likelihood estimation of Burr type V distribution under left censored samples. *WSEAS Transactions on Mathematics, 12*, 657-669.

[9] Forbes, C., Evans, M., Hastings, N., and Peacock, B. (2011). *Statistical distributions* (4th ed.). John Wiley & Sons.

[10] Gamchi, V., Alma, O. G., and Belaghi, A. (2019). Classical and Bayesian inference for Burr type-III distribution based on progressive type-II hybrid censored data. *Mathematical Sciences, 13*, 79−95.

[11] Ghitany, M. E., and Al-Awadhi, S. (2002). Maximum likelihood estimation of Burr XII distribution parameters under random censoring. *Journal of Applied Statistics, 29*(7), 955−965.

[12] Gorny, J., and Cramer, E. (2019). Type-I hybrid censoring of uniformly distributed lifetimes. *Communications in Statistics - Theory and Methods, 48*, 412-433.

[13] Hakim, A. R., Fithriani, I., and Novita, M. (2021). Properties of Burr distribution and its application to heavy-tailed survival time data. *Journal of Physics: Conference Series*.

[14] Hossain, A., and Balakrishnan, N. (2007). Inference for the type II generalized logistic distribution under progressive type II censoring. *Journal of Statistical Computation and Simulation, 77*, 1013-1031.

[15] Johnson, N. L., Kotz, S., and Balakrishnan, N. (1995). *Continuous univariate distributions* (2nd ed.). John Wiley & Sons.
[16] Kundu, D., and Raqab, M. Z. (2005). Generalized Rayleigh distribution. *Computational Statistics & Data Analysis, 49*, 187−200.
[17] Murthy, D. N. P., Xie, M., and Jiang, R. (2004). *Weibull models*. John Wiley & Sons.
[18] Ul-Haq, M. A., Elgarhy, M., and Hashmi, S. (2019). The generalized odd Burr III family of distributions: Properties, applications, and characterizations. *Journal of Taibah University for Science, 13*, 961−971.
[19] Panahi, H. (2017). Estimation of the Burr type III distribution with application in unified hybrid censored sample of fracture toughness. *Journal of Applied Statistics, 44*, 2575-2592.
[20] Panahi, H., and Asadi, S. (2011). Analysis of the type-II hybrid censored Burr type XII distribution under Linex loss function. *Applied Mathematical Sciences, 5*(79), 3929−3942.
[21] Rabie, A., and Li, J. (2020). E-Bayesian estimation for Burr-X distribution based on generalized type-I hybrid censoring scheme. *American Journal of Mathematical and Management Sciences, 39*(1), 41−55.
[22] Ramos, P. L., Guzman, D. C. F., Mota, A. L., Rodrigues, F. A., and Louzada, F. (2020). Sampling with censored data: A practical guide.

A NON- MARKOVIAN RETRIAL QUEUE WITH NON PERSISTENT CUSTOMERS, GENERAL RETRIAL TIMES ALONG WITH REOCCURRING CUSTOMERS

S. Palaniammal[1], K. Kumar[2], R.Keerthana[3]

•

[1] Department of Mathematics, Sri Krishna Adithya College of Arts and Science,India.
[2] Department of Mathematics,Sri Krishna College of Engineering and Technology,India.
[3] V.S.B. Engineering College, India
principal@skacas.ac.in, kkumaar007@gmail.com, keerthirn1996@gmail.com

Abstract

A non-Markovian retrial queue with non persistent customers, general retrial times along with reoccurring customers is taken into concern in this place study. In this model, the retrial periods for reoccurring customers have an exponential distribution, while all the service periods and retrial periods for transitory customers are pretended to follow a general distribution. The PGF for the total amount of customers and the average amount of customers in the invisible waiting region is acquired by applying the supplementary variable method. We compute the waiting period delivery. Out of attention, special cases are conferred. Numerical outcomes are reveals.

Keywords: non-Markovian retrial queue, transitory and reoccurring customers, non persistent customers, general retrial times, supplementary variable technique.

1. Introduction

Whenever the customers recognise that the server is occupied, they are moved to an orbit, that is an invisible awaiting region. A lot of experts have studied the retrial queue in the recent past. There are referrals available for an additional review of the retrial queues [1, 2, 3, 4, 5]. Numerous queuing systems that have multiple attempts follow the traditional retrial strategy. A second discipline, known as permanent retrial policy, does, however, naturally exist in situations where the server requires searching for customers [6].

In the context of retrials, Farahmand [7] examined a system of permanent customers from two perspectives: traditional and permanent retrial policy. Since the literature on retrial queues with continuous repeated efforts has rapidly expanded [8, 9]. In contrast, Boxma and Cohen [10] studied an M/G/1 queue that has a fixed amount of permanent customers who rejoin the queue after getting their services. Gomez-Corral [11] went into great detail about a retrial queuing system that includes general retrial times and FCFS discipline.

Our primary goal is to extend the second instance in [7] by taking consideration of a more typical and widespread scenario: distinct service distribution for each kind of customers and normal retrial rates for customers who are transitory. The primary justification for examining this queuing system is that numerous depictions of computer and communication networks use its structure.

A primary customer can become dissatisfied and permanently leave the system without service if they discover that a server is busy. For an additional review of the non-persistent customers, Keerthana [15] presented the results regarding the probability generating function (PGF)

for the number of customers in the orbit while discussing the retrial queue with working vacations, nonpersistent customers, and a waiting server.

In this article, we consider a non-Markovian retrial queue with non persistent customers, general retrial times along with reoccurring customers. This article is organised as follows. In section 2, the model is described. In section 3, performance measures are defined. In Section 4, a few unique scenarios are explored. In section 5, numerical findings are presented. In section 6, the conclusion is given.

2. Model Description

We discuss a non-Markovian retrial queue with non persistent customers, general retrial times and reoccurring customers, in which the arrival rate of the primary customers is λ and the arrival process is Poison. If a customer enters and discovers that the server is busy, he either becomes non-persistent and exits the system with a probability of (1-α) or enters an orbit with a probability of α. We assume there is no waiting area, thus if a transitory customer approaches and finds the server is occupied, they leave the service area and enter the orbit. Both of the customers who are at the top of the orbit are free to get nearer to the server at anytime after the service is finished. For transitory customers, the retrial time is distributed according to a distribution function and a general distribution $R_t(x)$; the pdf and LST are denoted by the expressions $r_t(x)$ and $R_t^*(x)$, respectively. For reoccuring customers, the retrial time is distributed exponentially with a parameter of ν. If there is a competition between transitory customers and orbit customers during each customer's service completion epoch. For transitory customers a general distribution with distribution functions governs service times $S_t(x)$,$s_t(x)$ and $S_t^*(x)$ as pdf and LST, respectively, and for reoccurring customers a general distribution with distribution functions governs service times, pdf, and LST of $S_r(x), s_r(x)$, and $S_r^*(x)$. It is assumed that service times, retrial periods, and inter-arrival times are unrelated to one another. Reoccurring customers always return to orbit after a service is completed, but transitory customers permanently exit the system. Let's apply the following sequence of random variables.

For the transitory customer at the top of the orbit, the remaining retial time is indicated by $R_t^\circ(t)$ if $M(t) = 0$ and $N(t) > K$.

For the transitory customer, the remaining service time is indicated by $S_t^\circ(t)$ if $M(t) = 1$ and $N(t) \geq K$.

For the reoccuring customer, the remaining service time is indicated by $S_r^\circ(t)$ if $M(t) = 2$ and $N(t) < K$.

$$M(t) = \begin{cases} 0 & \text{if the system is idle at time } t \\ 1 & \text{if the system is busy with transitory customers} \\ 2 & \text{if the system is busy with reoccuring customers} \end{cases}$$

so that the supplementary variables $R_t^\circ(t), S_t^\circ(t), S_r^\circ(t)$ and $R_s^\circ(t)$ are introduced to acquire the bivariate Markov Processes $(N(t), B(t)); x \geq 0$, where $B(t) = R_t^\circ(t)$, if $M(t) = 0; S_t^\circ(t)$, if $M(t) = 1; S_r^\circ(t)$, if $M(t) = 2$.

$$\begin{aligned} P_{0,K} &= \lim_{t\to\infty} P[M(t) = 0, N(t) = K] \\ P_{0,n} &= \lim_{t\to\infty} P[M(t) = 0, N(t) = n, x < R_t^\circ(t) \leq x + dx], n \geq K+1, x \geq 0 \\ P_{t,n} &= \lim_{t\to\infty} P[M(t) = 1, N(t) = n, x < S_t^\circ(t) \leq x + dx], n \geq K, x \geq 0 \\ P_{r,n} &= \lim_{t\to\infty} P[M(t) = 2, N(t) = n, x < S_r^\circ(t) \leq x + dx], n \geq K-1, x \geq 0 \end{aligned}$$

We have defined the limiting probabilities, which are listed above.

$$P_{0,n}^*(\theta) = \int_0^\infty e^{-\theta x} P_{0,n}(x)dx, \qquad P_{0,n}^*(0) = \int_0^\infty P_{0,n}(x)dx$$

$$P_0^*(z,\theta) = \sum_{n=K+1}^{\infty} P_{0,n}^*(\theta) z^n \qquad P_0(z,0) = \sum_{n=K+1}^{\infty} P_{0,n}(0) z^n$$

$$P_1^*(z,\theta)=\sum_{n=K}^{\infty}P_{1,n}^*(\theta)z^n \qquad P_1(z,0)=\sum_{n=K}^{\infty}P_{1,n}(0)z^n$$
$$P_2^*(z,\theta)=\sum_{n=K-1}^{\infty}P_{2,n}^*(\theta)z^n \qquad P_2(z,0)=\sum_{n=K-1}^{\infty}P_{2,n}(0)z^n$$

We have defined the LST and PGF, which are listed above.
In steady state, the following differential difference equations were used to depict the system:

$$(\lambda+\nu)P_{0,K} = P_{1,K}(0)+P_{2,K-1}(0) \quad (1)$$
$$-\frac{d}{dx}P_{0,n}(x) = -(\lambda+\nu)P_{0,n}+P_{1,n}(0)r_t(x)+P_{2,n-1}(0)r_t(x); n\geq K+1 \quad (2)$$
$$-\frac{d}{dx}P_{1,K}(x) = -\lambda\alpha P_{1,K}(x)+P_{0,K+1}(0)s_t(x)+\lambda P_{0,K}s_t(x) \quad (3)$$
$$-\frac{d}{dx}P_{1,n}(x) = -\lambda\alpha P_{1,n}(x)+\lambda\alpha P_{1,n-1}(x)+P_{0,n+1}(0)s_t(x) +\lambda s_t(x)\int_0^{\infty}P_{0,n}(x)dx; n\geq K+1 \quad (4)$$
$$-\frac{d}{dx}P_{2,K-1}(x) = -\lambda\alpha P_{2,K-1}(x)+\nu P_{0,K}s_r(x) \quad (5)$$
$$-\frac{d}{dx}P_{2,n}(x) = -\lambda\alpha P_{2,n}(x)+\lambda\alpha P_{2,n-1}(x)+\nu s_r(x)\int_0^{\infty}P_{0,n+1}dx; n\geq K \quad (6)$$

Taking the LST on both sides from (2) to (6) yields

$$\theta P_{0,n}^*(\theta)-P_{0,n}(0) = (\lambda+\nu)P_{0,n}^*(\theta)-P_{1,n}(0)R_t^*(\theta)-P_{2,n-1}(0)R_t^*(\theta), n\geq K+1 \quad (7)$$
$$\theta P_{1,K}^*(\theta)-P_{1,K}(0) = \lambda\alpha P_{1,K}^*(\theta)-P_{0,K+1}(0)S_t^*(\theta)-\lambda P_{0,K}S_t^*(\theta) \quad (8)$$
$$\theta P_{1,n}^*(\theta)-P_{1,n}(0) = \lambda\alpha P_{1,n}^*(\theta)-\lambda\alpha P_{1,n-1}(\theta)-P_{0,n+1}(0)S_t^*(\theta) -\lambda\int_0^{\infty}P_{0,n}(x)dxS_t^*(\theta),\ \ n\geq K+1 \quad (9)$$
$$\theta P_{2,K-1}^*(\theta)-P_{2,k-1}(0) = \lambda\alpha P_{2,k-1}^*(\theta)-\nu P_{0,k}S_r^*(\theta) \quad (10)$$
$$\theta P_{2,n}^*(\theta)-P_{2,n}(0) = \lambda\alpha P_{2,n}^*(\theta)-\lambda P_{2,n-1}^*(\theta)-\nu\int_0^{\infty}P_{0,n+1}(x)dxS_r^*(\theta),\ \ n\geq K \quad (11)$$

(8) x $\sum_{n=K+1}^{\infty}z^n$ gives

$$\theta\sum_{n=K+1}^{\infty}P_{0,n}^*(\theta)z^n-\sum_{n=K+1}^{\infty}P_{0,n}(0)z^n=(\lambda+\nu)\sum_{n=K+1}^{\infty}P_{0,n}^*(\theta)z^n-\sum_{n=K+1}^{\infty}P_{1,n}(0)z^nR_t^*(\theta) -\sum_{n=K+1}^{\infty}P_{2,n-1}(0)z^nR_t^*(\theta)$$

$$= P_0(z,0)-R_t^*(\theta)\{P_1(z,0)+zP_2(z,0)\}+R_t^*(\theta)z^K(\lambda+\nu)P_{0,K}$$
$$P_0^*(z,\theta)[\theta-(\lambda+\nu)] = P_0(z,0)-R_t^*(\theta)\{z^K(\lambda+\nu)P_{0,K}-P_1(z,0)+zP_2(z,0)\} \quad (12)$$

Placing $\theta=\lambda+\nu$ in (12), results

$$P_0(z,0)=R_t^*(\lambda+\nu)[P_1(z,0)+zP_2(z,0)-(\lambda+\nu)P_{0,k}z^K] \quad (13)$$

Placing $\theta=0$ in (12), results

$$P_0^*(z,0)=\frac{[1-R_t^*(\lambda+\nu)]}{\lambda+\nu}[P_1(z,0)+zP_2(z,0)-(\lambda+\nu)P_{0,k}z^K] \quad (14)$$

$\Big[(9)\ \text{x} \sum_{n=K+1}^{\infty} z^n\Big]$ gives,

$$\theta \sum_{n=K+1}^{\infty} P^*_{1,n}(\theta)z^n - \sum_{n=K+1}^{\infty} P_{1,n}(0)z^n = \lambda\alpha \sum_{n=K+1}^{\infty} P^*_{1,n}(\theta)z^n - \lambda\alpha \sum_{n=K+1}^{\infty} P^*_{1,n-1}(\theta)z^{n-1+1} - S^*_t(\theta) \sum_{n=K+1}^{\infty} P_{0,n+1}(0)z^{n+1-1} - \lambda \sum_{n=K+1}^{\infty} P^*_{0,n}(0)z^n S^*_t(\theta)$$

Adding with $(8) \times z^K$, we get

$$P^*_1(z,\theta)[\theta - (\lambda\alpha - \lambda\alpha z)] = P_1(z,0) - \frac{P_0(z,0)S^*_t(\theta)}{z} - \lambda P^*_0(z,0)S^*_t(\theta) - \lambda P^*_{0,K} z^K S^*_t(\theta) \tag{15}$$

Placing $\theta = \lambda\alpha - \lambda\alpha z$ in (15), results

$$P_1(z,0) = \frac{S^*_t(\lambda\alpha - \lambda\alpha z)}{z}\Big[P_0(z,0) + \lambda z P^*_0(z,0) + \lambda P_{0,k} z^{K+1}\Big] \tag{16}$$

Placing $\theta = 0$ in (15), results

$$P^*_1(z,0) = \frac{1 - [S^*_t(\lambda\alpha - \lambda\alpha z)]}{z(\lambda\alpha - \lambda\alpha z)}\Big[P_0(z,0) + \lambda z P^*_0(z,0) + \lambda P_{0,k} z^{K+1}\Big] \tag{17}$$

(Sub.) (14) in (16), results

$$\begin{aligned} P_1(z,0) \quad = \quad & \Big[\frac{\lambda z[1 - R^*_t(\lambda+\nu)][P_1(z,0) + zP_2(z,0) - (\lambda+\nu)P_{0,K}z^K]}{\lambda+\nu} \\ & + P_0(z,0) + \lambda P_{0,K} z^{K+1}\Big]\Big[\frac{S^*_t(\lambda\alpha - \lambda\alpha z)}{z}\Big] \end{aligned} \tag{18}$$

$\Big[(11)\ \text{x} \sum_{n=K}^{\infty} z^n\Big]$ gives

$$\theta \sum_{n=K}^{\infty} P^*_{2,n}(\theta)z^n - \sum_{n=K}^{\infty} P_{2,n}(0)z^n = \lambda\alpha \sum_{n=K}^{\infty} P^*_{2,n}(\theta)z^n - \lambda\alpha \sum_{n=K}^{\infty} P^*_{2,n-1}(\theta)z^{n-1+1} - \nu \sum_{n=K}^{\infty} P^*_{0,n+1}(0)z^{n+1-1} S^*_r(\theta)$$

Adding with $(10) \times z^{K-1}$, we get

$$P^*_2(z,\theta)[\theta - (\lambda\alpha - \lambda\alpha z)] = P_2(z,0) - \frac{\nu}{z} S^*_r(\theta)[P^*_0(z,0) + P_{0,K} z^K] \tag{19}$$

Placing $\theta = \lambda - \lambda z$ in (19), results

$$\begin{aligned} P_2(z,0) \quad = \quad & \left[\Big[\frac{1 - S^*_t(\lambda\alpha - \lambda\alpha z)}{\lambda+\nu}\Big]\Big[P_1(z,0) + zP_2(z,0) - (\lambda+\nu)P_{0,k}z^K\Big] + P_{0,k}z^K\right] \\ & \times \left[\frac{\nu S^*_r(\lambda\alpha - \lambda\alpha z)}{z}\right] \end{aligned} \tag{20}$$

Placing $\theta = 0$ in (19), results

$$-(\lambda\alpha - \lambda\alpha z)P^*_2(z,0) = P_2(z,0) - \frac{\nu}{z}[P^*_0(z,0) + P_{0,K} z^K] \tag{21}$$

Rearrage the equation (13),(16) and (20) in the system of equations, results

$$\begin{aligned}
(\lambda+\nu)P_{0,K}z^K R_t^*(\lambda+\nu) &= -P_0(z,0)+P_1(z,0)R_t^*(\lambda+\nu)+zP_2(z,0)R_t^*(\lambda+\nu)\\
\lambda z P_{0,K}z^K R_t^*(\lambda+\nu)(\lambda+\nu)S_t^*(\lambda\alpha-\lambda\alpha z) &= -P_0(z,0)(\lambda+\nu)S_t^*(\lambda\alpha-\lambda\alpha z)+P_1(z,0)[z(\lambda+\nu)\\
&\quad -\lambda z(1-R_t^*(\lambda+\nu))]-zP_2(z,0)S_t^*(\lambda\alpha-\lambda\alpha z)\\
&\quad \times\lambda z(1-R_t^*(\lambda+\nu))\\
\nu(\lambda+\nu)R_t^*(\lambda+\nu)P_{0,K}z^K S_r^*(\lambda\alpha-\lambda\alpha z) &= -\nu P_1(z,0)S_r^*(\lambda\alpha-\lambda\alpha z)(1-R_t^*(\lambda+\nu))+P_2(z,0)\\
&\quad \times[z(\lambda+\nu)-\nu z S_r^*(\lambda\alpha-\lambda\alpha z)(1-R_t^*(\lambda+\nu))
\end{aligned}$$

By solving the above equations using determinent method, results

$$\begin{aligned}
P_0(z,0) &= \frac{1}{D_1(z)}\Big\{(\lambda+\nu)R_t^*(\lambda+\nu)P_{0,K}z^{K+1}[(\lambda+\nu)-\lambda S_t^*(\lambda\alpha-\lambda\alpha z)\\
&\quad -\nu S_r^*(\lambda\alpha-\lambda\alpha z)]\Big\} \qquad (22)\\
P_1(z,0) &= \frac{1}{D_1(z)}\Big\{(\lambda+\nu)R_t^*(\lambda+\nu)P_{0,K}z^K S_t^*(\lambda\alpha-\lambda\alpha z)[\lambda(1-z)\\
&\quad -\nu[S_r^*(\lambda\alpha-\lambda\alpha z)-1]]\Big\} \qquad (23)\\
P_2(z,0) &= \frac{1}{D_1(z)}\Big\{(\lambda+\nu)R_t^*(\lambda+\nu)\nu S_r^*(\lambda\alpha-\lambda\alpha z)[S_t^*(\lambda\alpha-\lambda\alpha z)-z]P_{0,K}z^{K-1}\Big\} \qquad (24)
\end{aligned}$$

Substituting (23), (24) in (14)

$$P_0^*(z,0)=\frac{1}{D_1(z)}\Big\{[1-R_t^*(\lambda+\nu)][\lambda(1-S_t^*(\lambda\alpha-\lambda\alpha z)+\nu(1-S_r^*(\lambda\alpha-\lambda\alpha z))]P_{0,K}z^{K+1}\Big\} \qquad (25)$$

Substituting (22), (25) in (17)

$$\begin{aligned}
P_1^*(z,0) &= \frac{1}{(\lambda\alpha-\lambda\alpha z)D_1(z)}\Big\{[1-S_t^*(\lambda\alpha-\lambda\alpha z)]R_t^*(\lambda+\nu)[\lambda(1-z)\\
&\quad +\nu(1-S_r^*(\lambda\alpha-\lambda\alpha z))](\lambda+\nu)P_{0,K}z^K\Big\} \qquad (26)
\end{aligned}$$

Substituting (24), (25) in (21)

$$\begin{aligned}
P_2^*(z,0) &= \frac{1}{(\lambda\alpha-\lambda\alpha z)D_1(z)}\Big\{(\lambda+\nu)R_t^*(\lambda+\nu)[S_t^*(\lambda\alpha-\lambda\alpha z)-z][1-S_r^*(\lambda\alpha-\lambda\alpha z)]\\
&\quad \times\nu P_{0,K}z^{K-1}\Big\} \qquad (27)
\end{aligned}$$

where,

$$\begin{aligned}
D_1(z) &= [1-R_t^*(\lambda+\nu)][\lambda S_t^*(\lambda\alpha-\lambda\alpha z)+\nu S_r^*(\lambda\alpha-\lambda\alpha z)]z-(\lambda+\nu)[z-R_t^*(\lambda+\nu)\\
&\quad \times S_t^*(\lambda\alpha-\lambda\alpha z)] \qquad (28)
\end{aligned}$$

We define $P(z)=P_0^*(z,0)+P_1^*(z,0)+P_2^*(z,0)+P_{0,K}z^K$

$$P(z)=\frac{(\lambda+\nu)R_t^*(\lambda+\nu)P_{0,K}z^{K-1}}{\lambda\alpha D_1(z)}\Big\{\lambda\alpha(1-z)z+\nu S_t^*(\lambda\alpha-\lambda\alpha z)(1-S_r^*(\lambda\alpha-\lambda\alpha z))\Big\} \qquad (29)$$

As the PGF for the number of customers in the orbit is represented in above relation in that the defined term $D_1(z)$ is given in (28). To determine that $P_(0,K)$ arises in (30), apply the normalising condition $P(1)=1$ and utilising the L'Hospitals rule in the result of (29).

$$P_{0,K}=\frac{(\lambda+\nu)R_t^*(\lambda+\nu)[1-\lambda\alpha E(S_t)]-\lambda\alpha(1-R_t^*(\lambda+\nu))[\lambda E(S_t)+\nu E(S_r)]}{(\lambda+\nu)\alpha R_t^*(\lambda+\nu)[1+\nu\alpha E(S_r)]} \qquad (30)$$

3. Performance Measures

The following parameters are considered, L_s - average orbit size during peak hours and, L_{sw} - average customers waiting time at peak hours in the orbit. Then

$$\begin{aligned} L_s &= \frac{d}{dz}P(z)\Big|_{z=1} \\ &= \Big[\frac{N_1^{'}(z)}{D_1^{'}(z)} + \frac{N_2^{''}(z)}{-2\lambda\alpha D_1^{'}(z)} + \frac{N_3^{''}(z)}{-2\lambda\alpha D_1^{'}(z)}\Big]\Big|_{z=1} \times P_{0,K} \end{aligned}$$

where

$$\begin{aligned} N_1(z) &= [1-R_t^*(\lambda+\nu)][\lambda(1-S_t^*(\lambda\alpha-\lambda\alpha z)+\nu(1-S_r^*(\lambda\alpha-\lambda\alpha z))]z^{K+1} \\ D_1(z) &= [1-R_t^*(\lambda+\nu)][\lambda S_t^*(\lambda\alpha-\lambda\alpha z)+\nu S_r^*(\lambda\alpha-\lambda\alpha z)]z-(\lambda+\nu)[z-R_t^*(\lambda+\nu) \\ &\quad \times S_t^*(\lambda\alpha-\lambda\alpha z)] \\ N_2(z) &= [1-S_t^*(\lambda-\lambda\alpha z)]R_t^*(\lambda+\nu)[\lambda(1-z)+\nu(1-S_r^*(\lambda\alpha-\lambda\alpha z))](\lambda+\nu)z^K \\ N_3(z) &= (\lambda+\nu)R_t^*(\lambda+\nu)[S_t^*(\lambda\alpha-\lambda\alpha z)-z][1-S_r^*(\lambda\alpha-\lambda\alpha z)]\nu z^{K-1} \end{aligned}$$

At $z=1$ L_s turns

$$L_s = \Big[\frac{N_1^{'}(1)}{D_1^{'}(1)} + \frac{N_2^{''}(1)}{-2\lambda\alpha D_1^{'}(1)} + \frac{N_3^{''}(1)}{-2\lambda\alpha D_1^{'}(1)}\Big] \times P_{0,K}$$

By Little's formula, $L_{sw} = \dfrac{L_s}{\lambda}$
where,

$$\begin{aligned} N_1^{'}(1) &= \lambda\alpha[1-R_t^*(\lambda+\nu)][\lambda E(S_t)+\nu E(S_r)] \\ N_2^{''}(1) &= 2\lambda^2\alpha(\lambda+\nu)R_t^*(\lambda+\nu)E(S_t)(1+\nu\alpha E(S_r)) \\ N_3^{''}(1) &= -2\lambda\nu\alpha(\lambda+\nu)R_t^*(\lambda+\nu)E(S_r)(\lambda\alpha E(S_t)-1) \\ D_1^{'}(1) &= \lambda\alpha[1-R_t^*(\lambda+\nu)][\lambda E(S_t)+\nu E(S_r)]-(\lambda+\nu)R_t^*(\lambda+\nu)[1-\lambda\alpha E(S_t)] \end{aligned}$$

4. Special cases

(a) The current model coincides with M/G/1 queue with recurrent customers model for taking the values $\nu\to\infty, \alpha=1$, and $R_t^*(\lambda+\nu)=1$
(b) The current model concides with an M/G/1 retrial queue model for taking the value $K=0$, and $\alpha=1$.

5. Numerical results

Table 1 and Fig. 1 and represent the variation between the arrival rate of customers versus the average orbit size during peak hours in the presence of various service times. Also, to attain the above mentioned graph and table, the following values are assumed. The value of a retrial time for reoccurring customers is 2.1, the value of service time for transitory customers is 3.1, and the value of service time for reoccurring customers is 4.2 and $\alpha = 1.2$. From this we observed that the increasing value of the arrival rate of customers and service time of customers, the mean orbit size will be reduced; it shows that the derived model is stable. Table 2 and Fig. 2 represent the variation between the arrival rate of customers versus the average customers waiting time at peak hours in the presence of various service times. Also, to attain the abovementioned graph and table, the following values are assumed. The value of a retrial time for reoccurring customers is 2, the value of service time for transitory customers is 3.5, and the value of service

time for reoccurring customers is 4 and $\alpha = 1.5$. From this we observed that the increasing value of the arrival rate of customers and service time of customers, the mean customers waiting time at peak hours in the orbit will be reduced; it shows that the derived model is stable. Table 3 and

Table 1: *λ versus μ*

λ	$\mu = 2.2$	$\mu = 2.4$	$\mu = 2.6$
1.0	0.2991	0.3198	0.3374
1.2	0.2688	0.2956	0.3184
1.4	0.2306	0.2643	0.2928
1.6	0.1847	0.2258	0.2605
1.8	0.1309	0.1801	0.2216
2.0	0.0694	0.1272	0.1761

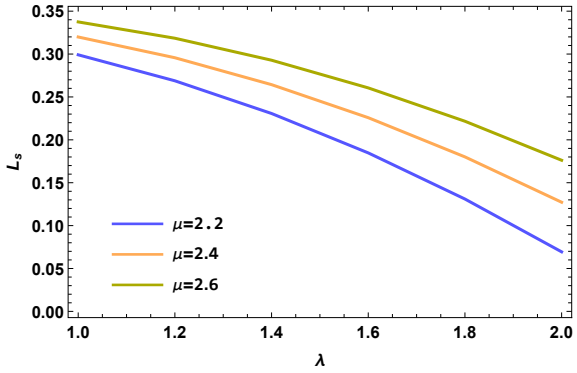


Figure 1: *λ versus μ*

Table 2: *λ versus μ*

λ	$\mu = 3.2$	$\mu = 4.2$	$\mu = 5.2$
1.0	0.3492	0.3741	0.3928
1.2	0.2809	0.3077	0.3277
1.4	0.2285	0.2571	0.2785
1.6	0.1861	0.2164	0.2392
1.8	0.1502	0.1824	0.2066
2.0	0.1190	0.1530	0.1785

Fig. 3 represent the variation between the arrival rate of customers versus the average orbit size during peak hours in the presence of various retrial times. Also, to attain the abovementioned graph and table, the following values are assumed. The value of a retrial time for transitory customers is 3.7, the value of service time for transitory customers is 5.5, and the value of service time for reoccurring customers is 7.5 and $\alpha = 1.2$. From this we observed that the increasing value of the arrival rate of customers and service time of customers, the mean orbit size will be reduced; it shows that the derived model is stable. Table 4 and Fig. 4 represent the variation between the arrival rate of customers versus the average customers waiting time at peak hours in the presence of various retrial times. Also, to attain the abovementioned graph and table, the following values are assumed. The value of a retrial time for transitory customers is 4, the value of service time for transitory customers is 4.8, and the value of service time for reoccurring customers is 7.2 and $\alpha = 1.2$. From this we observed that the increasing value of the arrival rate of customers and service time of customers, the mean customers waiting time at peak hours in

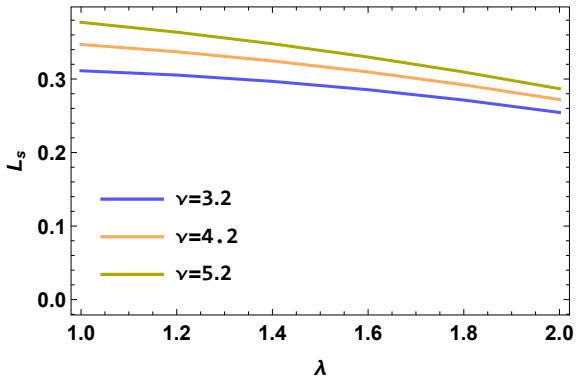


Figure 2: *λ versus μ*

the orbit will be reduced; it shows that the derived model is stable.

Table 3: *λ versus ν*

λ	$\nu = 3$	$\nu = 3.5$	$\nu = 4$
1.0	0.3112	0.3470	0.3771
1.2	0.3054	0.3370	0.3637
1.4	0.2968	0.3245	0.3479
1.6	0.2854	0.3095	0.3298
1.8	0.2713	0.2920	0.3095
2.0	0.2545	0.2720	0.2867

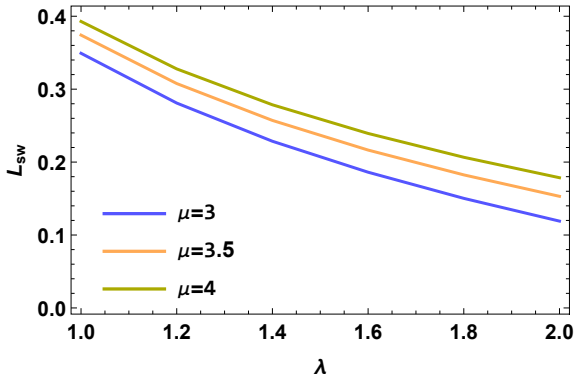


Figure 3: *λ versus ν*

Table 4: *λ versus ν*

λ	$\nu = 2.1$	$\nu = 3.1$	$\nu = 4.1$
1.0	0.2903	0.3349	0.3716
1.2	0.2446	0.2775	0.3045
1.4	0.2096	0.2343	0.2547
1.6	0.1814	0.2002	0.2157
1.8	0.1577	0.1720	0.1838
2.0	0.1370	0.1480	0.1570

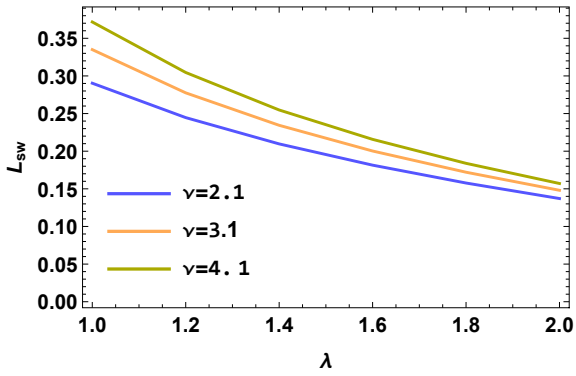


Figure 4: *λ versus ν*

6. Conclusion

A non-Markovian retrial queue with non persistent customers, general retrial times along with reoccurring customers is assessed in this work. We obtained the PGF for the total amount of customers and the average amount of customers in the invisible waiting region. The average waiting time is also determined. We discussed the performance measures and deliberated some special cases, and numerical outcomes are displayed.

References

[1] Yang T. and Templeton, J. G. C. (1987). A Survey on Retrial Queue. *Queue. Syst.*, 2:201–233.
[2] Falin, G. I. (1990). A Survey on Retrial Queues. *Queueing Systems Theory and Applications*, 7:127–168.
[3] Falin, G. I. and Templeton, J.G. C. Retrial queues, CRC Press, 1997.
[4] Artalejo, J. R. (1999). Accessible bibliography on retrial queue. *Math. Comput. Modell.*, 30:1–6.
[5] Artalejo, J. R.(1999). A classified bibliography of research on retrial queues: Progress in 1990-1999. Top, 7(2): 187–211.
[6] Neuts, M. F. and Ramalhoto, M. F. (1984). A Service model in which the server is required to search for customers. *Journal of applied probability*, 21:157–166.
[7] Farahmand, K.(1990). Single line queue with repeated demands. *Queueing Systems*, 6:223–228.
[8] Farahmand, K.(1996). Single line queue with recurrent repeated demands. *Queueing Systems*, 22:425–435.
[9] Martin, M. and Artalejo, J. R. (1995). Analysis of an M/G/1 queue with two types of impatient units *Advances in Applied Probability*, 27(3): 840–861.
[10] Boxma, O. J., and Cohen, J. W. (1991). The M/G/1 queue with permenent customers. *IEEE Journal on selected areas in communications*, 9(2):179–184.
[11] Gomez-Corral A. (1999). Stochastic analysis of a single server retrial queue with general retrial times. *Naval research logistics*, 46:561–581.
[12] Medhi J. Stochastic Models in Queueing Theory, Second Edition, 2003.
[13] Yang, T., Posner, M.J. M., Templeton, J.G. C. and Li H. (1994) An approximation method for the M/G/1 retrial queue with general retrial times. *European journal of operational research*, 76:552–562.
[14] Choi, B. D., Park, K. K., and Pearce, C.E. M. (1993). An M/M/1 retrial queue with control policy and general retrial times. *Queueing systems*, 14:275–292.
[15] Keerthana, R. (2025). An M/G/1 Retrial queue with working vacation, non persistent customers and a waiting server. *Reliability: Theory and Applications*, 20(1 (82)):1089–1099.
[16] Murugan, S.P. B. and Keerthana R. (2023). An M/G/1 Feedback retrial queue with working vacation and a waiting server. *Journal of computational analysis and applications*, 61.

RELIABILITY OF ELECTRICAL MACHINES VIA POWER LOSS MODELING IN MATLAB

Sara Alimamedova[1], Saida Kerimova[2]

•

Azerbaijan State Oil and Industry University, Baku, Azerbaijan
[1] sara_elimemmedova@mail.ru , [2] saidakerimova77@mail.ru

Abstract

The article discusses a reliable mathematical approach to calculating power losses in electrical equipment, which is a critical component in the design, analysis, and optimization of electric power systems. Ensuring accurate loss estimation requires detailed modeling of equipment parameters such as rated power, voltage, current, resistance, and material properties that influence energy dissipation. For alternating current systems, it is particularly important to consider the interaction of active and reactive components, as well as the losses occurring in conductors, magnetic circuits, and other elements. The application of proven mathematical models enables engineers to evaluate system efficiency and operational stability under different scenarios. MATLAB tools and algorithms play a key role in automating these calculations, allowing for precise simulations across a wide range of load conditions, voltage levels, and equipment configurations. This not only improves the accuracy of loss assessments but also supports optimization of design parameters to ensure long-term reliability, energy efficiency, and cost-effectiveness of electrical machines and systems.

Keywords: power loss, energy transfer, electric equipment, active resistance

I. Introduction

Modeling the calculation of power loss in electrical equipment is an important tool for designing and optimizing electric power systems. This allows engineers to analyze equipment performance, determine efficiency, and estimate energy costs [1]. To this end, it is necessary to consider the following steps and methods for modeling the calculation of power loss:

1. Determination of equipment parameters, which include equipment characteristics such as rated power, voltage, current, resistance and other parameters that may affect power loss.

2. Using mathematical models. For each type of equipment, there are mathematical models that describe its operation. For example, models based on loss formulas that take into account resistance, frequency, length, and current can be used for wires and cables.

3. Accounting for other sources of losses. In addition to losses in wires, it is necessary to take into account losses in transformers, voltage regulators, contact connections, etc.

4. Verification and analysis of the results. After performing the calculations, it is necessary to analyze the results obtained and check them for compliance with the requirements of system efficiency and reliability.

5. Optimization. Based on the simulation results, various ways can be proposed to optimize the system in order to reduce power losses, such as changing the wire cross-section, choosing more efficient transformers, improving the quality of connections, etc.

It is important to note that the accuracy of the simulation depends on the accuracy of the entered data and the correct choice of mathematical models for each component of the system. The transfer of energy from an active two-pole to a passive two-pole in the conditions of an alternator

and an active reactance can be considered from the point of view of the active and reactive power components [2-4]. When transferring energy from an active two-pole to a passive two-pole, taking into account the reactants, the following cases are possible:

- If the passive two-pole is purely active (there is no reactance), then all active power will be transmitted unchanged, and no reactive power will be transmitted.

- If a passive two-pole has both active and reactive resistance, then the loss of power to overcome the reactance will be taken into account when transmitting power. This can lead to a partial loss of energy to overcome the reactance and, consequently, a decrease in the useful active power reaching the passive two-pole.

II. Formulation of the problem

In general, for a more accurate analysis of energy transfer between active and passive bipolar conductors in an AC system with active reactance, it is essential to consider all active and reactive components, as well as power losses in the conductors and other elements of the system.

Let us examine the process of energy transfer from an active bipolar source to a passive bipolar load under the conditions of an alternating current generator with active reactance (Figure 1). In Figure 1, *M* denotes a motor whose rotational speed remains constant, and *G* is an AC generator. In expression (1), $Z_0 = ze^{j\phi_0}$- represents the internal impedance of the generator, and , $Z_0 = ze^{j\phi}$ is the load impedance.

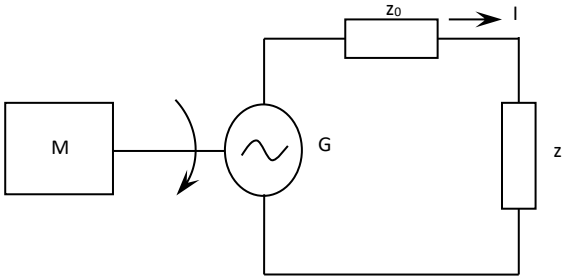


Figure 1. *Connection diagram of the alternator to te active reactance*

Based on Figure 1, the following parameters of the electrical circuit are defined: I-the root mean square (RMS) value of the current flowing through the circuit, S1-the apparent power output by the generator, U2- the RMS voltage across the load impedance, S2-the apparent power at the load, P1-the active power output by the generator, P2-the active power at the load,η-the efficiency of the system, cosφ- the power factor.

$$
\begin{aligned}
&I = \frac{E}{\sqrt{z_0^2+z^2+2z_0 z\cos(\varphi-\varphi_0)}}\\
&S_1 = EI = \frac{E^2}{\sqrt{z_0^2+z^2+2z_0 z\cos(\varphi-\varphi_0)}}\\
&S_2 = I^2 z = \frac{E^2 z}{z_0^2+z^2+2z_0 z\cos(\varphi-\varphi_0)}\\
&U_2 = Iz = \frac{E^2 z\cos\varphi}{\sqrt{z_0^2+z^2+2z_0 z\cos(\varphi-\varphi_0)}}\\
&P_1 = I^2(z\cos\varphi + z_0\cos\varphi) = \frac{E^2(z\cos\varphi+z_0\cos\varphi)}{z_0^2+z^2+2z_0 z\cos(\varphi-\varphi_0)}\\
&\eta = \frac{P_2}{P_1} = \frac{z\cos\varphi}{z\cos\varphi+z_0\cos\varphi} = \frac{R}{R+r_0}\\
&\cos\psi = \frac{P_1}{S_1} = \frac{z\cos\varphi+z_0\cos\varphi}{\sqrt{z_0^2+z^2+2z_0 z\cos(\varphi-\varphi_0)}}
\end{aligned}
\Bigg\} \quad (1)
$$

As basic values:

$$I_b = \frac{E}{z_0};\ \mathrm{S}_b = P_b = \frac{E^2}{z_0};\ \mathrm{U}_b = E$$

then these expressions can be written in a system of relative units:

$$I* = \frac{I}{I_b};\ \mathrm{S}^* = \frac{S}{S_b};\ \mathrm{U}* = \frac{U}{E}$$

$$\left.\begin{aligned} I* = S_1^* &= \frac{1}{\sqrt{1+(z/z_0)^2+2(z/z_0)\cos(\varphi-\varphi_0)}} \\ U_2^* &= \frac{z/z_0}{\sqrt{1+(z/z_0)^2+2(z/z_0)\cos(\varphi-\varphi_0)}} \\ P_1^* &= \frac{z/z_0\cos\varphi+\cos\varphi_0}{\sqrt{1+(z/z_0)^2+2(z/z_0)\cos(\varphi-\varphi_0)}} \\ P_2^* &= \frac{z/z_0\cos\varphi}{\sqrt{1+(z/z_0)^2+2(z/z_0)\cos(\varphi-\varphi_0)}} \\ \cos\psi &= \frac{z/z_0\cos\varphi+\cos\varphi_0}{\sqrt{1+(z/z_0)^2+2(z/z_0)\cos(\varphi-\varphi_0)}} \\ \eta &= \frac{R/r_0}{R/r_0+1} \end{aligned}\right\} \quad (2)$$

The dependences of these expressions on the current can be written in a relative system of units as follows:

$$\left.\begin{aligned} &S_1^* = I*;\ U_2^* = I*z/z_0 \\ &S_2^* = I^{*2}z/z_0;\ P_2^* = I^{*2}z/z_0\cos\varphi \\ &P_1^* = I^{*2}z/z_0\cos\varphi+\cos\varphi_0 \\ &\eta = \frac{z/z_0\cos\varphi}{z/z_0\cos\varphi+\cos\varphi_0} \end{aligned}\right\} \quad (3)$$

The analysis of expressions (1) and (2) shows that when $z/z_0 = 1$ the total and active forces applied to the load resistance have a maximum value:

$$\left.\begin{aligned} S_2^* &= S_{2max}^{*\frac{1}{2[(1+\cos(\varphi-\varphi_0))]}} \\ P_2^* &= P_{2max}^{*\frac{\cos\varphi}{2[(1+\cos(\varphi-\varphi_0))]}} \end{aligned}\right\} \quad (4)$$

The analysis of expression (4) shows that as the difference φ-φ0 increases, the maximum value of the total power (S_{2max}^*) in the load resistance increases [5]. When φ=-φ0 , the maximum value of the active power on the load resistance takes on its maximum value. On the other hand, the dependence of ($P_{2\max}^*$) on φ0 (Figure 4) can be determined using the following expression:

$$P_{2max}^{*\frac{\cos\varphi}{2[(1+\cos(\varphi-\varphi_0))]}}$$

If φ=-φ0 , then

$$P_{2max}^{*\frac{\cos\varphi}{2[(1+\cos 2\varphi_0)]}\frac{1}{4\cos\varphi_0}}$$

If φ0=0, we get $P_{2max}^{*\frac{1}{4}}$.

In AC circuits, resonance occurs when the inductive and capacitive reactance's cancel each other out at a specific frequency. At resonance, the circuit is purely resistive, and energy transfer becomes efficient. This condition could be relevant when trying to optimize energy transfer between the active and passive bipolar.

The issue of energy transfers between an active bipolar and a passive bipolar in the presence of active reactance in an AC system revolves around the reactive power and the phase relationship between the voltage and current [6-8]. If the reactance is mismatched, energy transfer can become inefficient, with a significant portion of the energy oscillating between the generator and the load without performing useful work. Proper impedance matching and managing the reactance of both the generator and the load are key to ensuring efficient energy transfer in such systems.

We will use expressions (2) and (3) to construct dependencies of their parameters in the circuit described in Figure 1 on the relative value of the load resistance and the relative value of the current (I*).

AC electric drives have steel, copper and mechanical losses. Losses on individual circuit elements depend on the circuit parameters, the load price, and the nature and voltage of the network. Losses in an electrical circuit depend on several factors:

- **Circuit parameters** (resistance, inductance, capacitance) cause energy dissipation and influence reactive power losses.
- **Load characteristics** (resistive or reactive loads, power factor) determine how much energy is lost as heat or stored and returned as reactive power.
- **Nature and voltage of the network** (AC or DC, high or low voltage) influence resistive losses, reactive losses, and efficiency in energy transmission.

Minimizing losses requires careful consideration of these factors, such as optimizing the voltage levels, ensuring proper impedance matching, and managing the nature of the load to reduce reactive power consumption [9-11].

In this case, we can write:

$$\Delta P = f(I, U, Z) \tag{5}$$

where ΔP- losses in the circuit, I, U - current and mains voltage flowing through the circuit, respectively, and Z - total resistance of the circuit. Since this is the total resistance of the circuit $Z = \frac{U}{I}$, expression (5) can be written as:

$$\Delta P = f(U, I, Z) = \Delta P_P + \Delta P_m = k_1 U^2 + k_{\ 2} I^2 \tag{6}$$

here ΔP_P- loss of steel in the unit.The price of this varies proportionally to the square of the voltage in the unsaturated steel under constant frequency conditions. ΔP_m-copper losses of the device.

Losses in the entire device change if the power factor changes when the active load of the device does not change.

To find the degree of change in load loss depending on the power factor, we can write:

$$\frac{P_m}{P_{mn}} = \frac{kI_a^2 \cos^2 \phi}{kI_a^2 \cos^2 \phi_n} = \frac{\cos^2 \phi}{\cos^2 \phi_n} \tag{7}$$

Of great interest is how losses in electrical installations change when the mains voltage changes. Using the above expression (5), we can write down the relative values:

$$\Delta P = \Delta P_P + \Delta P_m = k_1 U_n^2 U^2 + k_2 I_n^2 I^2$$

To determine coefficients k_1 and k_2:

$$\Delta P_P = k_1 U_n^2 U^2$$

From the last expression, where U=1, we get:

$$\Delta P_{pn} = k_1 U_n^2 \quad \text{or} \quad k_1 = \frac{P_{pn}}{U_n^2}$$

$$k_2 = \frac{P_{pn}}{I_n^2}$$

Where ΔP_{pn}- steel loss at rated voltage, and ΔP_{mn} - copper loss at rated current. If we write down and take into account the expressions found for the coefficients k_1 and k_2 instead of them in the general loss expression, then

$$I = \frac{\beta \cos \phi_n}{U \cos \phi}; \Delta P = \Delta P_{pn} U^2 + \Delta P_{mn} I^2 = P_{pn} U^2 + P_{mn} \cos^2 \phi_n \frac{\beta}{U^2 \cos^2 \phi}$$

Here we take

$$a = \Delta P_{pn};\ b = \Delta P_{pn} \cos^2 \phi_n\ , \tag{8}$$

and we get:

$$\Delta P = aU^2 + b \frac{\beta}{U^2 \cos^2 \phi} \tag{9}$$

III. Problem solution

Below is the MATLAB code to calculate and plot the power factor for a constant active load, considering different voltage levels and calculating the corresponding apparent power and power factor [12].

If we take the first-order derivative of this expression with respect to voltage and make it equal to zero, we will find the voltage expression for the case of minimal losses:

$$\frac{d\Delta P}{dU} = 2aU = \frac{2b\beta^2}{U^3 cos^2 \phi} = 0; \quad U = \sqrt[4]{\frac{b\beta^2}{a\, cos^2 \phi}} \tag{10}$$

From the last expression, it can be concluded that the lower the load factor, the lower the minimum current received at such a low voltage [13-15]. As can be seen from the expression minimum current, the price of the relative voltage obtained also depends on the power factor of the unit. As the power factor of the device increases, the minimum resistance shifts towards decreasing voltage.

Let's consider the effect of voltage changes in an asynchronous motor on motor losses using the above. It is known that in an asynchronous motor, the main losses are no-load operating losses (mainly steel losses) and copper losses [16-18]. The remaining losses can be discarded, as they are relatively small. Then we can write:

$$\Delta P_{mwh} = \Delta P_0 + \Delta P_m = k_1 U^2 + k_2 I^2$$

If we divide both parts of this expression by k=2, we get:

$$\Delta P = \frac{\Delta P_{mwh}}{k_2} = \frac{k_1}{k_2} U^2 + I^2 = kU^2 + I^2$$

the relative loss

$$\Delta P = (k + b)U^2 + \frac{a}{U} \tag{11}$$

To model how the losses in electrical installations change when the mains voltage changes, we need to consider the basic formula for losses, which primarily come from the **resistive losses** (I^2R losses) in the conductors and transformers. These losses are a function of the current ($\bar{I}$) and the resistance ($\bar{R}$)of the components. When the mains voltage changes, the current also changes, which in turn affects the losses (Figure 2).

In an asynchronous (induction) motor, the losses are mainly due to the following factors:

- Stator copper losses: Resistive losses in the stator winding.
- Rotor copper losses: Resistive losses in the rotor winding.
- Core losses (iron losses, usually represented as a function of the motor's voltage and frequency).
- Mechanical losses: Losses due to friction, windage, and other moving parts.

When the voltage changes, it impacts the current, which in turn affects the copper losses and other parameters. An increase in voltage will generally decrease the current for a fixed power output, leading to a reduction in copper losses. However, core losses in the motor typically depend on the applied voltage and the frequency of the motor [19-21].

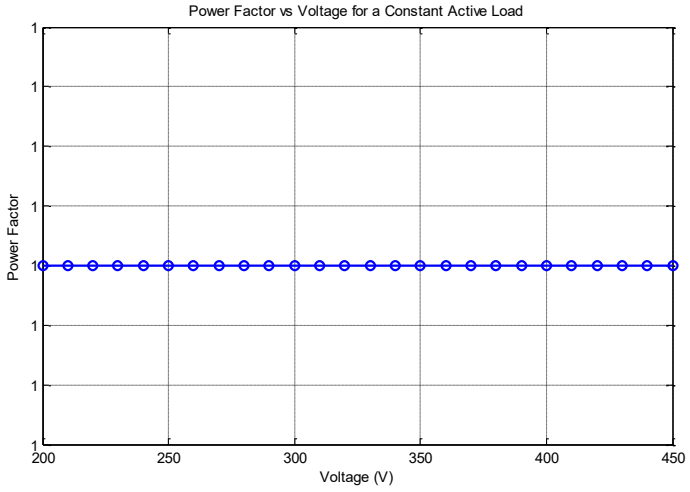


Figure 2. *Power factor vs voltage for a constant active load*

The Figure 3 shows how each type of loss varies with voltage. As the voltage increases, both the stator and rotor copper losses will decrease, while core losses will likely increase. The total losses will decrease for lower voltages but will show a relatively minor increase due to core losses at higher voltages. This simulation provides a basic model to understand how changes in voltage impact the various losses in an asynchronous motor. In practice, other factors, such as temperature and speed, might also influence these losses.

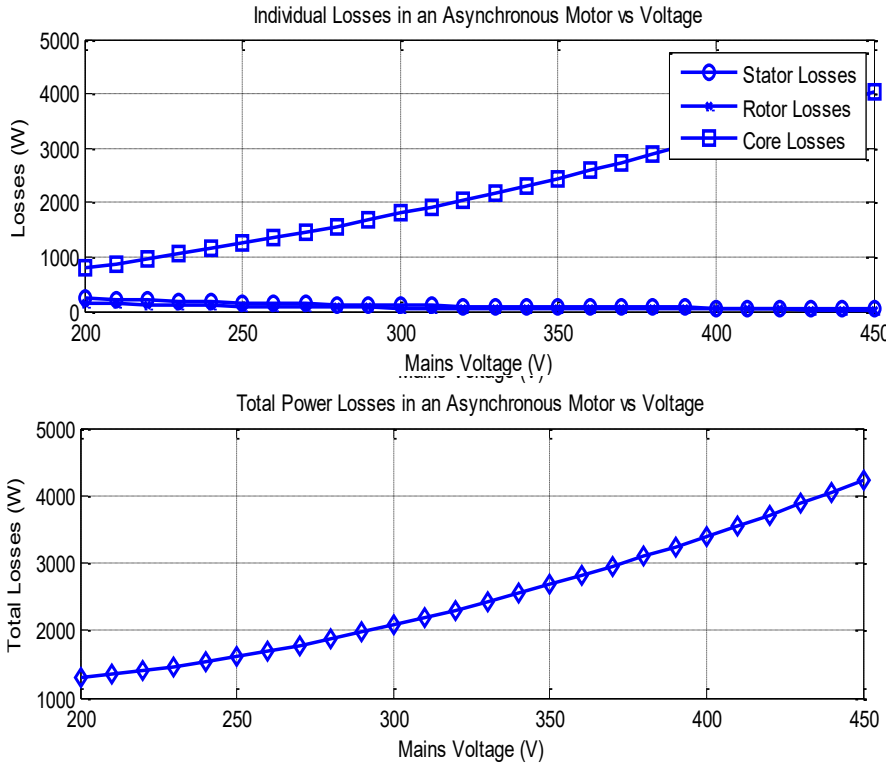


Figure 3. *Losses in an Asynchronous Motor vs Voltage*

The following MATLAB code simulates how the resistive losses change when the mains voltage changes (figure 4).

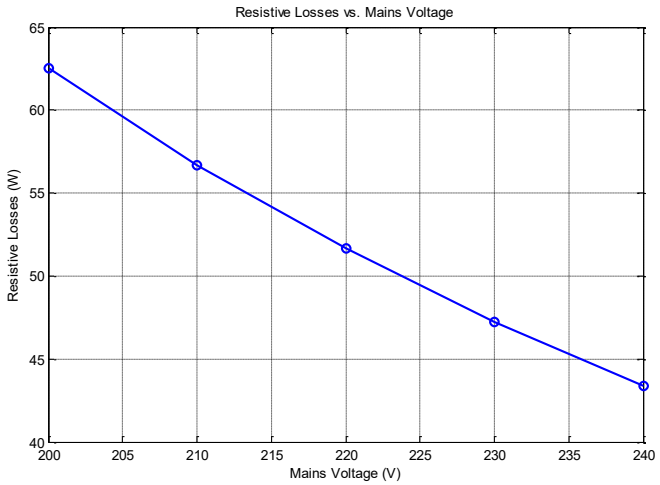


Figure 4. *Resistive losses vs Mains Voltage*

- As the voltage increases, the current decreases, leading to a decrease in resistive losses.
- As the voltage decreases, the current increases, leading to an increase in resistive losses.

This will give you a clear visualization of how the resistive losses in an electrical installation depend on the mains voltage [22]. You can modify the P and R parameters according to your specific system requirements. The plot will typically show a decreasing curve for losses as the voltage increases (since the current decreases for constant power), demonstrating how the installation efficiency improves with higher voltage.

Simulating the calculation of power loss in synchronous machine, the losses can be broadly categorized as:

1. Stator losses: Copper losses in the stator winding
2. Rotor losses: Copper losses in the rotor winding
3. Core losses: Losses due to eddy currents and hysteresis in the magnetic core.
4. Mechanical losses: Friction and windage losses in the bearings and other moving parts.
5. Stray load losses: Losses due to stray magnetic fluxes and other minor factors.

In the following simulation, we will assume some typical values for a synchronous machine, and calculate the losses based on different operating conditions (such as speed, load, and voltage).

As the load factor increases, the copper losses in both the stator and rotor increase, as they depend on the current. Core losses and mechanical losses also increase with load, though core losses may not scale linearly in some cases (depending on the machine design). The plot will show a clear increase in losses as the machine load increases [24].

This simulation provides a basic model of power loss calculation in synchronous machines, with the assumption that we have some simple loss models for core and mechanical losses. The actual losses in a real machine can be more complex and depend on many other factors, such as temperature, operating conditions, and machine design specifics.

The advantages of mathematical analysis and algorithms in MATLAB for determining losses in various electrical machines and equipment are in several important aspects:

1. Accuracy and detail of calculations. Mathematical analysis allows accurate modeling of processes in electrical machines, such as asynchronous and synchronous machines, transformers, and other devices. This analysis includes both basic elements (e.g. currents, voltage, active and reactive power) and more complex losses such as:

- Copper losses (I^2R) are losses in the windings related to the resistance of the conductors.
- Nuclear losses are losses associated with magnetic saturation and eddy currents in cores.
- Mechanical losses - losses related to friction in bearings and air resistance (wind resistance).
- Strange losses - loss of energy due to imperfect operating conditions of the device.

In MATLAB, you can accurately account for all these elements in calculations using various mathematical models and approaches, such as:

- Circuit analysis using methods of electrical circuit theory (Kirchhoff methods, substitution circuit methods).
- Elements of thermodynamics and electromagnetic theories for modeling losses in magnetic materials.

2. Flexibility and adaptability. MATLAB provides the ability to flexibly customize models and algorithms for various types of electrical machines and equipment. For example:

- For asynchronous machines, it is possible to take into account the change in rotor current depending on sliding and different operating modes.
- For synchronous machines, it is possible to simulate the dependence of losses on the angle of the rotor position and the magnetic field.
- For transformers and other devices, the effects of magnetic field pulsation, asymmetry, and other specific operating features can be taken into account.

The advantage is the ability to easily change model parameters and get results for different operating modes.

3. Visualization of results. MATLAB provides powerful data visualization tools that help to better understand the behavior of electrical machines and equipment under various operating conditions. For example:

- Graphs of loss dependence on load, voltage, frequency or other parameters.
- Contour loss maps depending on various factors.
- 3D graphics to display the distribution of magnetic fields and temperature fields in the machine (Figure 5). This helps not only to analyze losses, but also to identify optimal operating modes to reduce losses and increase work efficiency.

4. Automation of calculations and repeatability. MATLAB algorithms can be used to automate the calculation of losses in electrical machines. This is especially useful when it is necessary to perform a large number of calculations for various operating scenarios (for example, when designing new machines or optimizing existing ones). An example would be using scripts to automatically calculate losses at different load and voltage levels, as well as to perform calculations using different types of windings or materials [25-26].

5. Optimization and search for the best solutions. MATLAB provides optimization tools, which allows not only to estimate losses, but also to find optimal parameters of machines and equipment, minimizing losses. For example:

- Optimization of design parameters (e.g. conductor cross-section, core materials) to minimize losses.
- Using optimization methods to select the operating modes of the equipment (for example, rotational speeds for asynchronous machines) with minimal losses.

6. Simulation of real-world operating conditions. MATLAB allows you to create accurate models of the operation of electrical machines in real conditions, taking into account such parameters as:

- Imperfections in the operation of devices (for example, losses due to overload, fluctuations in the network, etc.).
- The effect of temperature changes on the resistance of materials and, as a result, on losses.
- Asymmetric loads and parameter mismatches in three-phase systems.

This allows for more accurate and practical results, which is especially important for research and design tasks.

7. Integration with other systems. MATLAB integrates seamlessly with other systems and tools to enhance analysis and simulation capabilities. For example:

- Using MATLAB to create models with blocks, simulate the operation of electrical machines in real time, and analyze dynamic processes.
- Integration with laboratory systems for collecting and processing real-world data (for example, through interfaces with microcontrollers or measuring systems). Using MATLAB for mathematical analysis and creation of algorithms for calculating losses in electrical machines and equipment has many advantages, including accuracy of calculations, flexibility, visualization of results, the possibility of optimization and integration with other tools. This allows not only to conduct effective analysis, but also to make informed decisions in the design and operation of electrical devices.

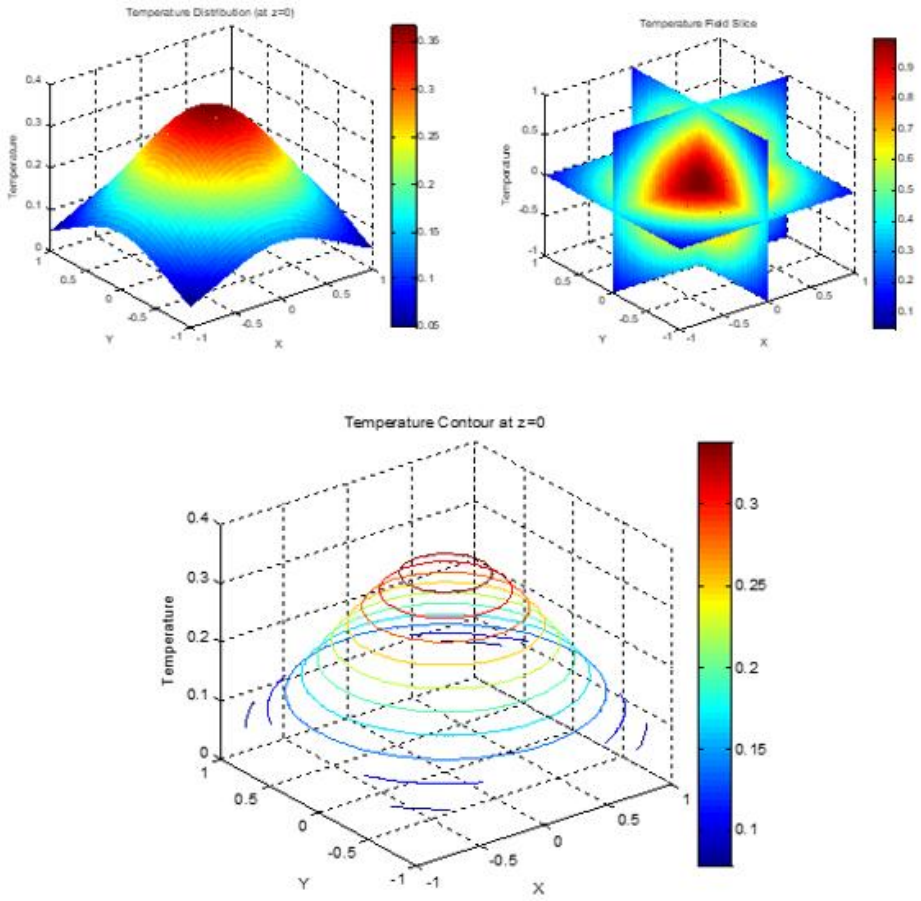


Figure 5. *Distribution of magnetic fields and temperature fields in the machine*

IV. Conclusions

1. Mathematical analysis of the calculation of power loss in electrical equipment, which is an important aspect for the design and optimization of electric power systems, allows engineers to analyze equipment performance, determine efficiency and estimate energy costs. To this end, it is necessary to consider methods for modeling the calculation of power loss, determining equipment parameters that include equipment characteristics such as rated power, voltage, current, resistance and other parameters that may affect power loss, and using mathematical models.

2. Using MATLAB algorithms, it is possible to automate the processes of calculating losses in electrical machines. This is especially useful when it is necessary to perform a large number of calculations for various operating scenarios (for example, when designing new machines or optimizing existing ones).

3. Mathematical analysis allows accurate modeling of processes in electrical machines, such as asynchronous and synchronous machines, transformers, and other devices. This analysis includes both basic elements (for example, currents, voltage, active and reactive power) and more complex losses, such as losses in windings related to conductor resistance, losses related to magnetic saturation and eddy currents in cores, losses related to friction in bearings and resistance air resistance (wind resistance), loss of energy due to imperfect operating conditions of the device.

References

[1] Khanahmedova, S. A., Ismayilova, G. G., & Mufidzade, N. A. (2024). Analysis of the method of calculating the conversion circuit based on generalized functions. *International Journal on Technical and Physical Problems of Engineering (IJTPE)*, 16(3), 120–126.

[2] Khanahmedova, S. A., Kerimova, S. M., & Alimamedova, S. J. (2022). Mathematical modeling of the operation of a three-phase power transformer at low voltage quality. *International Journal on Technical and Physical Problems of Engineering (IJTPE)*, 14(4), 225–232.

[3] Khanahmedova, S. A. (2023). Investigation of some electrical circuits using simulation in MATLAB/Simulink. *Bulletin of Science*, 2(59), Vol. 1, 125–129. Tolyatti, Russia.

[4] Hasanov, Z. A., & Khanahmedova, S. A. (2022). *Power electronics and electrical drive*. Baku, Azerbaijan: Azerbaijan State Oil and Industry University Publishing House, pp. 5–132.

[5] Khanahmedova, S. A. (2024). Some issues of increasing the efficiency of electric machines. *Przegląd Elektrotechniczny*, 9(4), 171–173.

[6] Khanahmedova, S. A., Ismayilova, G. G., & Mufidzade, N. A. (2024). Analysis of the method of calculating the conversion circuit based on generalized functions. *International Journal on Technical and Physical Problems of Engineering (IJTPE)*, 16(3), 120–126.

[7] Piriyeva, N. M., & Kerimzade, G. S. (2023). Methods for increasing electromagnetic efficiency in induction levitator. *Przegląd Elektrotechniczny*. Warszawa: SIGMA-NOT, October, 192–195.

[8] Piriyeva, N. M., & Kerimzade, G. S. (2023). Electromagnetic efficiency in induction levitators and ways to improve it. *Przegląd Elektrotechniczny*, NR 06/2023, Warszawa, 204–207.

[9] Piriyeva, N. M., & Kerimzade, G. S. (2023). Mathematical model for the calculation of electrical devices based on induction levitators. *International Journal on Technical and Physical Problems of Engineering (IJTPE)*, 15(2), 274–280.

[10] Khanahmedova, S. A. (2025). Mathematical analysis of the mechanical part of the design scheme of the electric drive of a hybrid electric machine. *Reliability: Theory & Applications (RT&A)*, 20(1), 1061–1069.

[11] Khanahmedova, S. A. (2024). Some issues of increasing the efficiency of electric machines. *Przegląd Elektrotechniczny*, 100(9), 171–173.

[12] Osman, T., & Mohammad, S. (2006). Power distribution asset management. In *2006 IEEE Power Engineering Society General Meeting* (pp. 7–14). https://doi.org/10.1109/PES.2006.17092342

[13] Renani, Y. K., Ehsan, M., & Shahidehpour, M. (2018). Optimal transactive market operations with distribution system operators. *IEEE Transactions on Smart Grid*, 9(6), 6692–6701. https://doi.org/10.1109/TSG.2017.27185463

[14] Ghasemi, H., Aghaei, J., Gharehpetian, G. B., & Safdarian, A. (2019). MILP model for integrated expansion planning of multi-carrier active energy systems. *IET Generation, Transmission & Distribution*, 13(7), 1177–1189. https://doi.org/10.1049/iet-gtd.2018.63284

[15] Baydar, B., Gozde, H., Taplamacioglu, M. C., & Kucuk, A. O. (2019). Resilient optimal power flow with evolutionary computation methods: short survey. In N. Mahdavi Tabatabaei, S. Najafi Ravadanegh, & N. Bizon (Eds.), *Power Systems Resilience* (pp. 163–189). Cham: Springer. https://doi.org/10.1007/978-3-319-94442-5_75

[16] Koziel, S., Landeros Rojas, A., & Moskwa, S. (2018). Power loss reduction through distribution network reconfiguration using feasibility-preserving simulated annealing. In *2018 19th International Scientific Conference on Electric Power Engineering (EPE)* (pp. 1–5). https://doi.org/10.1109/EPE.2018.83960166

[17] Ilham Rahimli, Rashida Karimova, Najiba Piriyeva. Development of a Two-Parameter Inductive Sensor for use in Digital Program Control Systems for Machine Tools. PRZEGLAD Elektrotechniczny ISSN 0033-2097, R.100 NR 08/2024. WARSZAWA. pp.194-197.

[18] Zhang, X., Shahidehpour, M., Alabdulwahab, A., & Abusorrah, A. (2015). Optimal expansion planning of energy hub with multiple energy infrastructures. *IEEE Transactions on Smart Grid*, 6(5), 2302–2311. https://doi.org/10.1109/TSG.2015.23906408

[19] . I.M.Marufov, N.M.Piriyeva, N.S.Mammadov, Sh. Ismayilova. (2024) Calculation of induction levitation vertical axis wind generator-turbine system parameters, levitation and influence loop. Warszawa PRZEGLĄD ELEKTROTECHNICZNY, R. 100 NR 2/2024 pp.135-139.

[20] N.M.Piriyeva, G.S. Kerimzade. (2024) Systematization of levitation equations for electrical devices with levitation elements. PRZEGLAD Elektrotechniczny R.100 NR 08/2024. Warszawa. pp.175-177

[21] N.M.Piriyeva, Kerimzade G.S., Mamedova G.V. (2023) Issues of design of electrical devices with levitation elements. International Journal on "Technical and Physical Problems of Engineering" IJTPE Rumıniya Issue 56, Vol. 15 No 3. s.120-125

[22] S.V. Rzayeva, N.A. Ganiyeva N.M.Piriyeva. (2024) Modern approaches to electrical equipment diagnostics. İnternational Journal on "Technical and Physical Problems of Engineering" (IJTPE) - Issue 58, Volume 16, Number 1, March 2024 (Serial No: 0058-1601-0324), pp.182-189

[23] Aliyev, N., Ahmedov, E., Khanahmedova, S., & Rzayeva, S. (2023). Synthesis of the Exact Parameters of the Electromagnetic Brake of a Wind Electric Installation. *Przegląd Elektrotechniczny*, *2023*(10).

[24] Safiyev, Elshad, Ilham Rahimli, and Nijat Mammadov. "Method of qualitative impregnation of electric motor windings." Przegląd Elektrotechniczny 8 (2024).

[25] Nijat, Mammadov. "Selection of the type of electric generators for a wind electric installation." Universum: технические науки 9-5 (102) (2022): 65-67.

[26] Mammadov, N., Rzayeva, S., & Ganiyeva, N. (2023). Analysis of synchronized asynchronous generator for a wind electric installation. *Przeglad Elektrotechniczny*, *99*(5).

RT&A, No 3 (86)
Volume 20, September 2025

RELIABILITY ANALYSIS AND PERFORMANCE OPTIMIZATION OF A 2-OUT-OF-4 REDUNDANT SYSTEM USING RPGT AND METAHEURISTIC ALGORITHMS

Shakuntla Singla[1], Shilpa Rani[2*], Diksha Mangla[3]

•

[1,2]Department of Mathematics and Humanities, MMEC, Maharishi Markandeshwar (Deemed to be University), Mullana, Ambala, India
[3]Department of applied science, CEC, Chandigarh Group of College, Landran, Mohali, India
[1]shakus25@gmail.com, [2*]gargshilpa46@gmail.com, [3]dikshamangla1995@gmail.com

Abstract

In this paper focuses on the reliability analysis and performance optimization of a 2-out-of-4 redundant system, modeled using the Regenerative Point Graphical Technique (RPGT). The study aims to evaluate system behavior under various failure and repair rate conditions and to determine optimal parameters that enhance system reliability and availability. The system consists of four units A, B, C, and D arranged in a 2-out-of-4 configuration, meaning the system continues to function as long as at least two units are operational. A state-space model is developed, where each state corresponds to a distinct combination of operational, failed, and repair conditions of these units. The transitions between these states are governed by exponentially distributed failure and repair processes, and are represented using a directed graph structure. Transition probabilities are derived from these time-dependent exponential distributions, allowing precise evaluation of system behavior. To enhance the system's performance, three metaheuristic optimization algorithms—Cuckoo Search Algorithm (CSA), Particle Swarm Optimization (PSO), and Genetic Algorithm (GA)—are employed. These algorithms are applied to optimize key system parameters: failure rates (λ) and repair rates (μ). The objective is to maximize the Mean Time to System Failure (MTSF) and steady-state availability, and to minimize the expected number of inspections required by the repair personnel. The comparative analysis of optimization results reveals the relative effectiveness of each algorithm. PSO consistently provides the highest values for MTSF and availability, indicating stronger performance in identifying optimal solutions. CSA also performs well, showing close results to PSO. GA, while effective, yields comparatively lower reliability indices. The outcomes demonstrate how advanced optimization techniques can be successfully integrated with RPGT-based modeling to develop a detailed and practical understanding of complex redundant systems. These insights support better maintenance planning, enabling organizations to improve reliability and reduce downtime in industrial, communication, and critical control systems. This methodology can be extended to other system configurations and industries, making it a valuable tool in the field of reliability engineering and operational research

Keywords: Reliability analysis, Cuckoo Search Algorithm (CSA), Particle Swarm Optimization (PSO), Genetic Algorithm (GA), Maintenance strategies, System performance optimization

I. Introduction

High reliability and continuous operation are essential in industrial, communication, and power systems. Redundancy, especially the 2-out-of-4 configuration, enhances reliability by allowing system functionality with at least two working units. Using Regenerative Point Graphical Technique (RPGT), we can model these systems through state-space diagrams that reflect various working and failed states, incorporating exponential failure and repair rates to compute metrics like MTSF and availability. However, identifying optimal rate combinations analytically is challenging. Metaheuristic algorithms like CSA, PSO, and GA effectively explore these parameters to maximize MTSF, improve availability, and minimize inspection needs. This paper presents an RPGT-based model of a 2-out-of-4 system with priority repair, derives state transitions, and applies CSA, PSO, and GA to optimize system performance. Results compare each method's effectiveness, offering guidance for cost-effective maintenance strategies in complex systems. Singla et al. [1] analyzed a four-unit system where full performance requires all units active, reduced capacity occurs with three, and failure happens with two or more down. Each unit has unique failure/repair costs, and a single server handles repairs. In [2], they studied a system with two active and one backup unit maintained by an external, potentially failing server. In [3], they examined a three-unit parallel system with varying failure/repair rates, using RPGT and deep learning (Adam, SGD) for optimization. In [4], they explored how reliability and warranty policies affect productivity and investment in automated industries. In [5], they used the Markov process and Laplace transforms to assess how preventive maintenance influences a three-unit system's failure time, profit, and efficiency through sensitivity analysis. In [6], they optimized a repairable 2-out-of-4 system with evolutionary algorithms for redundancy and maintenance scheduling. In [7], they modeled a poly-tube system using Markov chains and PSO, identifying key failure/repair impacts on performance. In [8], they analyzed a two-subsystem series model with preventive maintenance using Chapman-Kolmogorov equations and GA for optimizing availability and MTTF. In [9], they applied the TLBO algorithm to constrained/unconstrained problems, showing its versatility. Dang [10] reviewed metaheuristics (PSO, GA, ACO) for improving software fault prediction and future research. Zhou [11] evaluated metaheuristics in cloud load balancing, finding PSO best for make-span and performance. Khorshidi [12] optimized reliability and cost in multi-state k-out-of-n systems, showing GA outperforms ICA, though ICA is faster.

II. Notations and Assumptions

The following notations and assumptions are used to discuss the system:

I. Notations


: Full working state / Degraded state/ Failed state

β_i : Constant RR for $i = 1, 2, 3, 4$

A, B/ C, D : Full working state/ Cold stand by

II. Assumptions

The two units having the arrangement of series manner, hence both play important role for finding reliability metrics.

- The system is working with 100 % efficiency with two stand by.
- Upon Failure, The system will shift to stand by.

- The malfunction and recovery rate are considered exponential distributed.

III. System Transition Diagram and Model Description

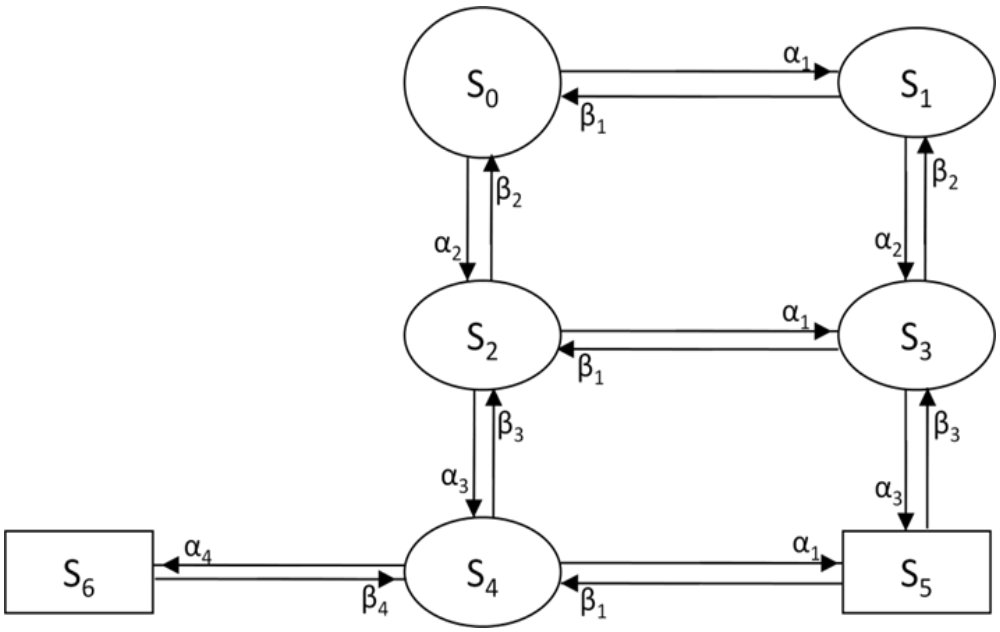


Figure 1: *Transition diagram*

The different possible transition for four units is represented in Figure 1.
S_0 = Units A and B are working, C and D are in standby, and the system is working.
S_1 = Units B and C are working, Unit D is in standby, Unit A is under repair, and the and the system is working.
S_2 = A and C are working, D is standby, and B is under repair.
S_3 = C and D are working, and B and A are under repair.
S_4 = A and D are working, and B and C are under repair.
S_5 = A, B, and C are under repair, and D unit is good.
S_6= B, C, and D are under repair, and the A unit is good

IV. Mathematical Modelling

I. Transition probabilities $q_{i,j}(t)$

Table 1: *Transition Probabilities*

"$q_{i,j}(t)$"	$p_{i,j} =$ "$q^*_{i,j}(0)$"
$q_{0,1}(t) = \alpha_1 e^{-(\alpha_1+\alpha_2)t}$	$p_{0,1} = \alpha_1/(\alpha_1+\alpha_2)$
$q_{0,2}(t) = \alpha_2 e^{-(\alpha_1+\alpha_2)t}$	$p_{0,2} = \alpha_2/(\alpha_1+\alpha_2)$
$q_{1,0}(t) = \beta_1 e^{-(\beta_1+\alpha_2)t}$	$p_{1,0} = \beta_1/(\beta_1+\alpha_2)$
$q_{1,4}(t) = \alpha_2 e^{-(\beta_1+\alpha_2)t}$	$p_{1,4} = \alpha_2/(\beta_1+\alpha_2)$
$q_{2,0}(t) = \beta_2 e^{-(\beta_2+\alpha_1+\alpha_3)t}$	$p_{2,0} = \beta_2/(\beta_2+\alpha_1+\alpha_3)$
$q_{2,3}(t) = \alpha_1 e^{-(\beta_1+\alpha_1+\alpha_3)t}$	$p_{2,3} = \alpha_1/(\beta_1+\alpha_1+\alpha_3)$
$q_{2,4}(t) = \alpha_3 e^{-(\beta_1+\alpha_1+\alpha_3)t}$	$p_{2,4} = \alpha_3/(\beta_1+\alpha_1+\alpha_3)$
$q_{3,1}(t) = \beta_2 e^{-(\beta_2+\beta_1+\alpha_3)t}$	$p_{3,1} = \beta_2/(\beta_2+\beta_1+\alpha_3)$
$q_{3,2}(t) = \beta_1 e^{-(\beta_2+\beta_1+\alpha_3)t}$	$p_{3,2} = \beta_1/(\beta_2+\beta_1+\alpha_3)$
$q_{3,5}(t) = \alpha_3 e^{-(\beta_2+\beta_1+\alpha_3)t}$	$p_{3,5} = \alpha_3/(\beta_2+\beta_1+\alpha_3)$

Table 1 shows the transition probability for moving from state 0 to state 6, whereas Table 2 represent the mean sojourn times after finding the reliability for various states.

Table 2: *Mean Sojourn Times*

$R_i(t)$	$\mu_i = R_i^*(0)$
$R_0(t) = e^{-(\alpha_1+\alpha_2)t}$	$\mu_0 = 1/(\alpha_1+\alpha_2)$
$R_1(t) = e^{-(\beta_1+\alpha_2)t}$	$\mu_1 = 1/(\beta_1+\alpha_2)$
$R_2(t) = e^{-(\beta_2+\alpha_1+\alpha_3)t}$	$\mu 2 = 1/(\beta_2+\alpha_1+\alpha_3)$
$R_3(t) = e^{-(\beta_2+\beta_1+\alpha_3)t}$	$\mu_3 = 1/(\beta_2+\beta_1+\alpha_3)$
$R_4(t) = e^{-(\beta_3+\alpha_1+\alpha_4)t}$	$\mu_4 = 1/(\beta_3+\alpha_1+\alpha_4)$
$R_5(t) = e^{-(\beta_3+\beta_1)t}$	$\mu_5 = 1/(\beta_3+\beta_1)$
$R_6(t) = e^{-(\beta_4)t}$	$\mu_6 = 1/\beta_4$

V. Measurement of parameter

The various transition probabilities of working system with 0 as initial state and base state $\xi = 4$ are explained below.

$V_{0,0} = 1$(Verified)

$V_{4,4} = 1$(Verified)

$V_{4,6} = (4,6,) = p_{4,6}$

I. Mean time to system failure (MTSF) (T_0)

The un-failed states to which the system transits before visiting any failed state are: $0 \leq j \leq = 4$, and taking $\xi' = 0'$, then

$$\text{MTSF } (T_0) = = \left[\sum_{i,sr}\left\{\frac{\left\{pr\left(\xi^{-\,sr(sff)}_{\quad i}\right)\right\}\mu i}{\Pi_{m_1\neq\xi}\left\{1\text{-}V_{\overline{m_1 m_1}}\right\}}\right\}\right] / \left[1\text{-}\sum_{sr}\left\{\frac{\left\{pr\left(\xi^{-\,sr(sff)}_{\quad \xi}\right)\right\}}{\Pi_{m_2\neq\xi}\left\{1\text{-}V_{\overline{m_2 m_2}}\right\}}\right\}\right]$$

$$T_0 = \alpha_1(\beta_1+\alpha_4+2\alpha_3+\alpha_2)(\beta_1+\alpha_4+\alpha_2+\alpha_3)(\beta_1+\alpha_1+2\alpha_2+\alpha_4) / (\alpha_1+\alpha_4+\alpha_2+\alpha_3)(\beta_1+\alpha_2+3\alpha_3+\alpha_4+\alpha_1)^3$$

II. Availability of System (A_0)

The states are where system is available are $0 \leq j \leq 4$ taking base state $\xi' = 4$ total fraction of time for which system is available

$$A_0 = \left[\sum_{j,sr}\left\{\frac{\{pr(\xi^{sr\rightarrow}j)\}fj,\mu j}{\Pi_{m_1\neq\xi}\left\{1\text{-}V_{\overline{m_1 m_1}}\right\}}\right\}\right] / \left[\sum_{i,S_r}\left\{\frac{\{pr(\xi^{sr\rightarrow}i)\}\mu_i^1}{\Pi_{m_2\neq\xi}\left\{1\text{-}V_{\overline{m_2 m_2}}\right\}}\right\}\right]$$

$$A_0 = [1/(\alpha_1+\alpha_4+\alpha_3+\alpha_2) + \alpha_1(\beta_1+2\alpha_2+\alpha_1+\alpha_4+\alpha_3)/ (\alpha_1+4\alpha_3+\alpha_2+\alpha_4)(\beta_1+\alpha_1+3\alpha_3+\alpha_2)(\beta_1+\alpha_4+\alpha_3+\alpha_2) (\beta_1+\alpha_2+2\alpha_4+\alpha_1)]/1/(\alpha_1+\alpha_3+2\alpha_4+\alpha_2) + \{1/(\alpha_3/\beta_3) + (\alpha_4/\beta_4)\}$$

III. Expected number of inspections by the repair man(V_0)

The states where the repairman's visit is fresh are S_1, S_2, taking $\xi = 0$,the number of repairmen's visits.

$$V_0 = \left[\sum_{j,sr}\left\{\frac{\{pr(\xi^{sr\to j})\}}{\Pi_{k_{1\neq\xi}}\{1-V_{\overline{k_{1k_1}}}\}}\right\}\right] / \left[\sum_{i,s_r}\left\{\frac{\{pr(\xi^{sr\to i})\}\mu_i^1}{\Pi_{k_{2\neq\xi}}\{1-V_{\overline{k_{2k_2}}}\}}\right\}\right]$$

$$V_0 = \alpha_1(\beta_1+\alpha_2+\alpha_1+3\alpha_4+\alpha_3)/(\alpha_1+\alpha_4+\alpha_2+\alpha_3)(\beta_1+2\alpha_4+2\alpha_4+\alpha_3)$$
$$(\beta_1+\alpha_4+\alpha_2+\alpha_3)(\beta_1+\alpha_3+3\alpha_4+\alpha_2)(\beta_1+2\alpha_4+2\alpha_4+\alpha_1)+$$
$$[(\alpha_1+\alpha_4+\alpha_3)]/(\alpha_1+\alpha_4+\alpha_2+\alpha_3)$$

VI. Methodology for optimization the parameters

Dataset: The dataset includes ten records, each with four normalized features. Workload (W) indicates equipment usage (0–100), Failure Rate (λ) reflects fault likelihood (0–100), and Sensor Index (S) captures unit health based on sensor data—higher values imply more wear. The target variable, Maintenance Priority (p), ranges from 0 to 75 and indicates how urgently maintenance is needed. The goal is to train supervised models to predict p from W, λ, and S, enabling proactive maintenance decisions.

Table 3: ***Parameter***

Parameter	W	λ	S	P
Range	0-100	0-100	0-100	0-75

The Optimization of RPGT-Based Reliability Metrics Using CSA, PSO, and GA is explored below.

I. Mean Time to System Failure (T_0)

The Cuckoo Search Algorithm (CSA), PSO, GA was used to optimize the failure (α) and repair (β) rates. The optimized values and the resulting T_0 are shown below.

Table 4: *Optimized Parameters and MTSF Value (T_0)*

Algorithm	α_1	α_2	α_3	α_4	β_1	T_0
CSA	1.2413	2.7539	0.9261	1.5427	3.1186	0.2158
PSO	1.1852	2.6891	0.9987	1.4723	3.0432	0.2197
GA	1.3794	2.8476	0.8742	1.6389	3.1954	0.2135

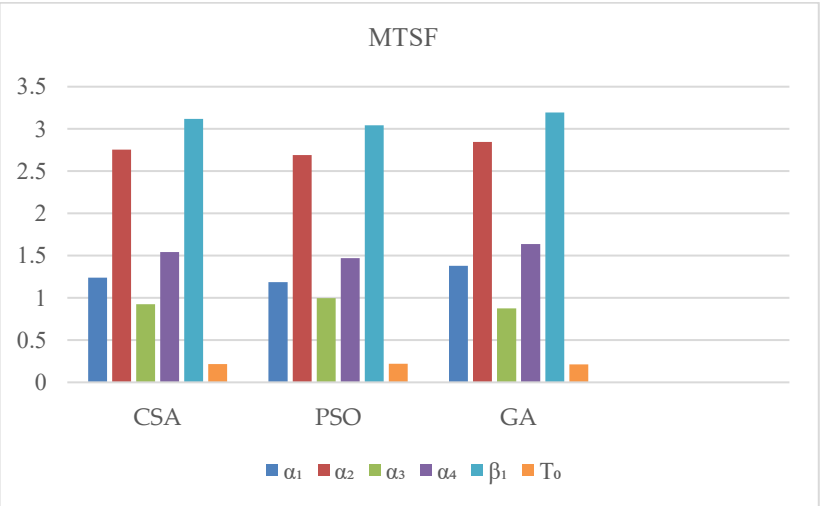


Figure 2: *Optimized Parameters and MTSF Value (T_0)*

II. Availability Optimization

CSA, PSO, and GA were applied to optimize a nonlinear availability function using failure and repair rates (α_1–α_4, β_1) to maximize system availability (A_0).

Table 5: *Optimized Parameters and Availability Value (T_0)*

Algorithm	α_1	α_2	α_3	α_4	β_1	A_0
CSA	1.2413	2.7539	0.9261	1.5427	3.1186	0.085429
PSO	1.3786	2.9874	0.9142	1.6349	3.0562	0.087113
GA	1.1842	2.6645	0.8963	1.5217	3.1325	0.084307

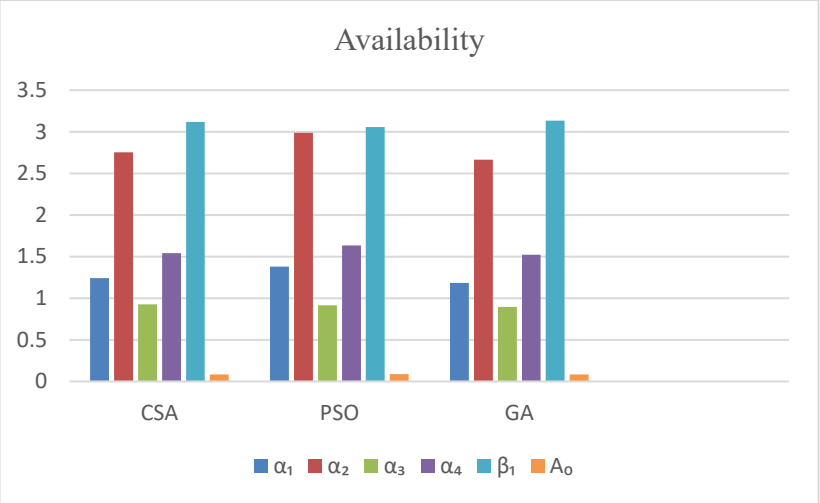


Figure 3: *Optimized Parameters and Availability Value (A_0)*

PSO achieved the highest system availability, followed closely by CSA, while GA was less effective, showing PSO's superior optimization ability.

III. Expected Number of Inspections (V_0) using CSA

The inspection frequency of the repairman is optimized using the Cuckoo Search Algorithm (CSA). Based on the derived reliability expression involving failure and repair rates, the number of inspections (V_0) was calculated using the formula.

Table 6: *Optimized Parameters and Expected fractional number of inspection Value (V_0)*

Algorithm	α_1	α_2	α_3	α_4	β_1	V_0
CSA	1.2413	2.7539	0.9261	1.5427	3.1186	0.184
PSO	1.3089	2.8467	0.8975	1.6134	3.0921	0.179
GA	1.1932	2.7011	0.9493	1.5018	3.1457	0.193

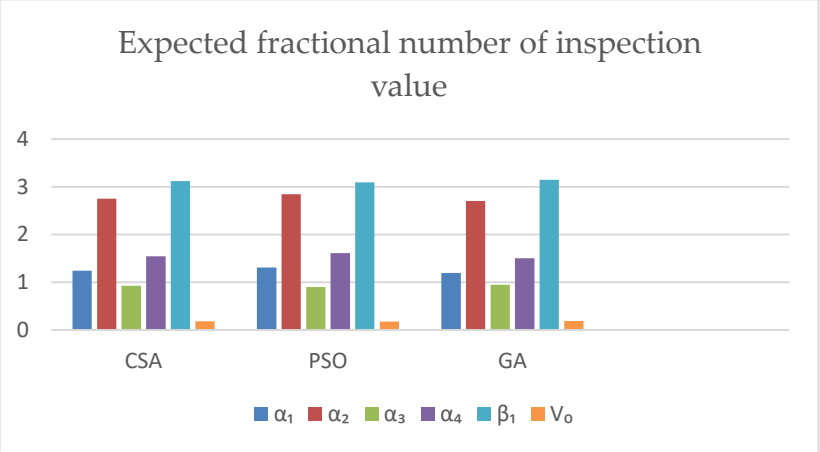


Figure 4: *Optimized Parameters and Expected number of inspection Value (V_0)*

PSO gave the lowest V_0, indicating the fewest expected inspections and efficient repairs, followed by CSA with balanced scheduling, while GA required the most frequent inspections.

VII. Conclusion

In this study, a 2-out-of-4 redundant repairable system was modeled and analyzed using the RPGT, with the primary goal of optimizing key reliability performance indices: T_0 (MTSF), A_0 (Availability), and V_0 (Expected Inspections). PSO consistently delivered the best overall performance, providing highest MTSF, maximum availability, and least inspection frequency. SA (Cuckoo Search Algorithm) was a close second, offering balanced results and strong optimization capability.GA (Genetic Algorithm), though effective, was less optimal in this context, with relatively lower reliability values and higher inspection requirements. Therefore, PSO is concluded to be the most effective optimization technique for the presented system model, followed by CSA, with GA being the least effective under the same conditions.

Conflicts of interests: The authors declare that there are no conflicts of interest.

References

[1] Singla, S. and Rani, S. (2023). Performance optimization of 3:4:: good system. *Proceedings of the Second International Conference on Informatics (ICI), IEEE*, 1–4.

[2] Singla, S. and Rani, S. (2023). Profit analysis of linear consecutive 2:3:G system in the presence of supportive system and repairable system. *Proceedings of the Second International Conference on Informatics (ICI)*, 274–280.

[3] Singla, S., Rani, S., Mangla, D. and Modibbo, U. M. (2024). Behavior analysis of a system with failure and maintenance rate using deep learning algorithms. *Reliability: Theory & Applications*, 19(3), 476–485.

[4] Singla, S. and Rani, S. (2024). An analysis of reliability in manufacturing industries. *Reliability: Theory & Applications*, 19(4), 552–559.

[5] Singla, S., Mangla, D., Rani, S. and Modibbo, U. M. (2024). Impact of preventive maintenance and failure rate on a complexly configured system: A sensitivity analysis. *Reliability: Theory & Applications*, 19(4), 774–791.

[6] Singla, S., Rani, S. and Mangla, D. (2024). Behavior analysis of a repairable 2-out-of-4 system using evolutionary algorithm. *Journal of Mechanics of Continua and Mathematical Sciences*, 19(7), 126–137.

[7] Singla, S., Mangla, D., Modibbo, U. M. and Lal, A. K. (2024). Critical analysis of failure and repair rates of poly-tube manufacturing plant using PSO. *Reliability: Theory & Applications*, 19(2), 351–364.

[8] Singla, S., and Mangla, D. (2024). Reliability optimization of a system under preventive maintenance using genetic algorithm. *Sustainability in Digital Transformation Era: Driving Innovation & Growth*, 286–290.

[9] Khurana, R., Singla, S., Garg, V., Mangla, D., Kumar, S., Pathak, M. and Joshi, P. (2023). Application of Laplacian teaching learning algorithm for constrained and unconstrained optimization problems. *Proceedings of the Second IEEE International Conference on Measurement, Instrumentation*, 1–5.

[10] Dang, Z. and Wang, H. (2024). Leveraging meta-heuristic algorithms for effective software fault prediction: A comprehensive study. *Journal of Engineering and Applied Science*, 1–34.

[11] Zhou, J., Lilhore, U. K., Poongodi, M., Hai, T., Simaiya, S., Jawawi, D. N. A., Alsekait, D., Ahuja, S., Biamba, C. and Hamdi, M. (2023). Comparative analysis of meta-heuristic load balancing algorithms for efficient load balancing in cloud computing. *Journal of Cloud Computing*, 1–13.

[12] Khorshidi, H. A. and Nikfalazar, S. (2015). Comparing two meta-heuristic approaches for solving complex system reliability optimization. *Applied and Computational Mathematics*, 4(2–1), 1–6.

CENSORED COUNT DATA REGRESSION MODELS: NUMBER OF CAESAREAN SECTION DELIVERIES USING INTEGRATED NESTED LAPLACE APPROXIMATION

[1]Srinu Setti*, [2]B.Muniswamy

•

[1*]Research Scholar, Department of Statistics, Andhra University, Visakhapatnam-530003, Andhra Pradesh, India
[2]Professor, Department of Statistics, Andhra University, Visakhapatnam-530003, Andhra Pradesh, India
*Corresponding author: [1]srinujesusj@gmail.com
[2]munistats@gmail.com

Abstract

Count data depicts the frequency of an occurrence within a specific time frame. Consider the frequency of caesarean operations that women undergo during their lives. Almost every academic field, including management, economics, medicine, and industrial organizations, relies on count data. Count data is extensively utilized across various fields, including marketing, public health, and biomedical science. This study aims to estimate the posterior means, variances, or quantiles of the NCSD for women aged 15 to 49 in Andhra Pradesh, India, using the RCPRM and RCNBRM methodologies. The RCPRM and RCNBRM are used to determine the optimal fit. The secondary dataset NFHS-5 is used for the study. This research utilizes INLA to model the NCSD. Subsequently, it analyzed delivery patterns among pregnant women. Information criteria DIC and WAIC are utilized to compare for the best fit. The DIC values 4608.60 and 4593.90 of RCNBRM are less than the DIC values 4864.74 and 4860.68 of RCPRM. Thus, from the results, it is inferred that RCNBRM is the best fit for NCSD and that Breech Presentation, the present age of the respondent, High Blood Pressure, Child is Twin, Prolonged Labour, Education Level, and Heart Disease are significant determinants of the NCSD. Therefore, government policymakers need to consider these variables while making healthcare policies for women aged 15 to 49 years who are of childbearing age.

Keywords: Number of Caesarean Section Deliveries, RCPRM, RCNBRM, INLA, DIC, WAIC

I. Introduction

The fundamentals of the Censored Poison (CP) are defined by Cameron and Trivedi [1] and Winkelmann [2]. It is presumed that the censoring technique operates independently of the count variable [3]. Recently, Poisson Regression Model (PRM) has been adapted to handle censored count data. Censorship is typically linked to survival analysis; however, count data can also be subject to censorship, with right-censoring being the most prevalent kind. This transpires when it

is established that the actual count surpasses the stated figure. The PRM is modified for the censored situation with a predetermined censoring threshold. In censored scenarios, it is necessary to modify the probability function and log-likelihood functions to reflect alterations in the response distribution, in accordance with the econometric principle of censoring, which stipulates that a single cut-point determines the censoring for all impacted cases. Numerous survival models demonstrate a continuous temporal response. A discrete response survival model is identified. The answer may be interpreted as counts rather than defined in temporal terms. Traditionally, these models have been depicted as piecewise models; however, they could represent utilizing a count model that accounts for censored observations. CP and Censored Negative Binomial (CNB) models are applicable for the analysis of this count response data. The models are applicable to any type of count response, regardless of their use in survival contexts. The only distinction is that filtering is allowed as a function within the framework of survival analysis [4].

II. Methods

I. Variables selected for the study

The variables are as follows:

NCSD	=	"Number of caesarean section deliveries"
BP	=	"Breech presentation"
HD	=	"Currently has heart disease"
HBP	=	"High blood pressure"
PL	=	"Prolonged labour"
CT	=	"Child is twin"
Age	=	"Current Age"
EL	=	"Education level"
TR	=	"Type of place of residence"

Where

y = "Number of caesarean section deliveries"
x_1 = "Breech presentation"
x_2 = "Currently has heart disease"
x_3 = "High blood pressure"
x_4 = "Prolonged labour"
x_5 = "Child is twin"
x_6 = "Current Age"
x_7 = "Educational level"

Hence we have the mathematical model as:

$$\begin{aligned} Number\ of\ caesarean\ section\ deliveries &= \beta_0 + \beta_1(Breech\ presentation) \\ &+ \beta_2(Currently\ has\ heart\ disease) + \beta_3(High\ blood\ pressure) \\ &+ \beta_4(Prolonged\ labour) + \beta_5(Child\ is\ twin) + \beta_6(Current\ Age) \\ &+ \beta_7(Educational\ level) \end{aligned} \quad (1)$$

The above model can be written in Statistical terms as:

$$\begin{aligned} NCSD = \beta_0 + \beta_1(BP) + \beta_2(HD) + \beta_3(HBP) + \beta_4(PL) + \beta_5(CT) + \beta_6(Age) \\ + \beta_7(EL) + U \end{aligned} \quad (2)$$

$$y = \beta_0 + \beta_1 x_1 + \beta_2 x_2 + \beta_3 x_3 + \beta_4 x_4 + \beta_5 x_5 + \beta_6 x_6 + \beta_7 x_7 + U \quad (3)$$

Where y is the predictand variable, $x_1, x_2, x_3, x_4, x_5, x_6, x_7$ are predictor variables, $\beta_0, \beta_1, \beta_2, \beta_3, \beta_4, \beta_5, \beta_6, \beta_7$ are parameters and U is disturbance term.

Then the structure of a count model will be

$$\log(\mu) = \beta_0 + \beta_1 x_1 + \beta_2 x_2 + \beta_3 x_3 + \beta_4 x_4 + \beta_5 x_5 + \beta_6 x_6 + \beta_7 x_7 \quad (4)$$

In GLM theory, the link function serves to linearize the relationship between the linear predictor, $x'\beta$, and the fitted value, , μ or $\hat{y}$ or estimated mean, $E(y)$. Consequently, μ is delineated in relation to the inverse relationship.

$$\mu = e^{\beta_0+\beta_1 x_1+\beta_2 x_2+\beta_3 x_3+\beta_4 x_4+\beta_5 x_5+\beta_6 x_6+\beta_7 x_7} \quad (5)$$

$$\log(\mu_i) = \sum_{i=1}^{n} \beta_0 + \beta_1 X_{1i} + \beta_2 X_{2i} + \cdots + \beta_j X_{ji} \quad (6)$$

II. Right Censoring

Right censoring, which limits observed counts from the right, is the primary method utilized for count data. In summary, it is established that the value of Y is at least equal to a predetermined threshold c for specific instances where the response variable Y surpasses c. This scenario can be applied in various circumstances, such as when a study seeks to investigate the correlation between high income and heavy smoking. An individual may be categorized as a heavy smoker in such a study if they consume ten or more cigarettes daily. The daily cigarette consumption, as the response variable, can be quantified in discrete values of 0, 1, 2,... or 10 or extra, encompassing persons who smoke 11 or extra cigarettes. The endogenous variable is thus censored at c=10. The exogenous variable, income, is accurately represented for the entire sample of censored individuals who smoke greater than 10 cigarettes everyday [4]. A significant body of research on censored count data has been published. Terza, J.V. [5] conducted an analysis of censored data concerning the frequency of shopping at a certain place over a defined point of time. In the experiment, the observation frequencies were categorized as zero, one, two, or more. Thus, individuals who made four or more purchases would still be classified as having made three or more purchases. Caudill, S. B. and Mixon, F. G. [6] examined the censoring situation regarding their endogenous variable, the number of children in a household, within the context of fertility [7].

According to Joseph, M. Hilbe [4], the comprehension of appropriate censoring is as follows: A right-censored cut at c indicates that the highest observable value of the response is c, with all values surpassing c recorded as c; thus, this value in the data effectively represents "greater than or equal to c." If c = 1, then any response values exceeding one are modified to equal 1. All values have been included in the model analysis.

Values are obscured due to their placement within the data set or as a consequence of external influences, including loss to follow-up or delayed entry. Censoring can be defined within the contexts of econometrics or survival analysis. Censorship, in this context, resembles truncation; however, the data beyond the cut-point(s) are modified to the nearest value included within the model. If the cut-off is set at 3, counts of 0, 1, and 2 are not removed as in truncation but are instead

modified to 3. Censored data sets are identifiable by multiple values at each cut-point.

As previously indicated right censoring at c is the most prevalent form of censoring and is therefore the focus of this study. Many values of y^* remain inadequately observed due to their classification as greater than or equal to c, resulting in indeterminate true values. The observed outcome y_i can be expressed as follows, incorporating the pertinent censoring scheme:

In a standard Poisson setting, all y^* are observed, whereas in a CP, the true y_i^* is only observed lower a censoring position c [2].

Then

$$y_i = \begin{cases} y_i^*, & if\ y_i^* < c_i \\ c_i, & if\ y_i^* \geq c_i \end{cases} \tag{7}$$

Winkelmann, R. [2] writes that the censoring point c_i may differ for each observation [6]. If c is constant, a model with a constant point exists [5].

If y_i is censored, it is understood that.

$$P(y_i \geq c_i) = \sum_{j=c_i}^{\infty} P(y_i = j) = \sum_{j=c_i}^{\infty} f(j) = 1 - \sum_{j=0}^{c_i-1} f(j) = 1 - F(c_i - 1) \tag{8}$$

An indicator variable d_i is defined as follows.

$$d_i = \begin{cases} 1, & if\ y_i^* \geq c_i \\ 0, & otherwise \end{cases} \tag{9}$$

The likelihood function is explained as:

$$\mathcal{L} = \prod_{i=1}^{n} [f(y_i)]^{1-d_i} P[(y_i \geq c_i)]^{d_i} \tag{10}$$

Therefore, the log-likelihood function is expressed as follows:

$$\ell = \sum_{i=1}^{n} (1 - d_i) \log f(y_i) + \sum_{i=1}^{n} d_i \log[P(y_i \geq c_i)] \tag{11}$$

Then, from the equation

$$\ell = \sum_{i=1}^{n} (1 - d_i) \log f(y_i) + \sum_{i=1}^{n} d_i \log[1 - F(c_i - 1)] \tag{12}$$

where the pmf and cdf of y_i^* are denoted by $f(.)$ and $F(.)$, respectively. For further information, see [8] and [9].

The conditional mean is given by

$$E(y_i, \mu_i) = c_i - \sum_{j=0}^{c_i-1} f(j)(c_i - j) \tag{13}$$

III. Dispersion Index Test

In order to check over-dispersion quantitatively, dispersion index is computes as in equation

$$d = \frac{Var(Y)}{E(Y)} \tag{14}$$

where d is the dispersion index. Given count variable Y, the variable is over-dispersed, if $d > 1$. If the d is greater than 1, that indicates over-dispersion of the data. In such cases Negative Binomial may be more appropriate model.

IV. Right-Censored Poisson Regression Model (RCPRM)

The outcome variable, NCSD, is right-censored at one, indicating a single C-section delivery, which is used to conform to the framework. The NCSD is initially applied in RCPRM and subsequently applied in RCNBRM for the data to be over-dispersed. The INLA is employed for parameter estimation in the RCPRM and RCNBRM. The INLA methodology guarantees computing efficiency.

Winkelmann [2] and Cameron and Trivedi [1] provide an overview of the fundamentals of the censored Poisson model. Here, it is assumed that the count variable has no bearing on the censoring process [3]. As stated by Rafal Raciborski [7], examine the Poisson random variable's probability function in equation (15).

$$f(y_i, \mu_i) = \frac{e^{-\mu_i}\ \mu_i^{y_i}}{y_i!}\ , y_i = 0,1,2, \dots\dots\dots;\ \mu_i > 0. \tag{15}$$

Where $\mu_i = e^{x_i' \beta}$ is the log link function, β is a vector of unknown parameters, x_i is a vector of exogenous variables.

The likelihood for the RCPRM can, therefore, be found using the likelihood function equation (16) as follows:

$$\mathcal{L} = \prod_{i=1}^{n} \left[\frac{e^{-\mu}\mu^{y}}{y!}\right]^{1-d_i} \left[1 - \sum_{j=0}^{c_i-1} \frac{e^{-\mu}\mu^{j}}{j!}\right]^{d_i} \tag{16}$$

The log-likelihood function of RCPRM shown in equation (18) is

$$\ell = \sum_{i=1}^{n} \left[(1-d_i) \log\left[\frac{e^{-\mu}\mu^{y}}{y!}\right] + d_i \log\left[1 - \sum_{j=0}^{c_i-1} \frac{e^{-\mu}\mu^{j}}{j!}\right]\right] \tag{17}$$

$$\ell = \sum_{i=1}^{n} (1-d_i) \log\left[\frac{e^{-\mu}\mu^{y}}{y!}\right] + \sum_{i=1}^{n} d_i \log\left[1 - \sum_{j=0}^{c_i-1} \frac{e^{-\mu}\mu^{j}}{j!}\right] \tag{18}$$

The conditional mean is given by equation (13)

$$E(y_i, \mu_i) = C_i - \sum_{j=0}^{c_i-1} f(j)(C_i - j)$$

Here

$$f(j) = \frac{e^{-\mu}\mu^j}{j!} \tag{19}$$

$$E(y_i, \mu_i) = c_i - c_i \sum_{j=0}^{c_i-1} \frac{e^{-\mu_i}{\mu_i}^j}{j!} + j \sum_{j=0}^{c_i-1} \frac{e^{-\mu_i}{\mu_i}^j}{j!} \tag{20}$$

$$E(y_i, \mu_i) = \mu \tag{21}$$

$$E(y_i^2, \mu_i) = \mu^2 + \mu \tag{22}$$

$$V(y_i, \mu_i) = E(y_i^2) - [E(y_i)]^2 \tag{23}$$

$$V(y_i, \mu_i) = \mu \tag{24}$$

Hence, the mean and variance of RCPRM are μ and μ, respectively, which shows that the RCPRM converges to PRM.

V. Right-Censored Negative Binomial Regression Model (RCNBRM)

The pmf for NBRM is explained as

$$p\left(y_i; \frac{1}{\alpha}, \mu_i\right) = \frac{\Gamma\left(y_i + \frac{1}{\alpha}\right)}{\Gamma\left(\frac{1}{\alpha}\right)\Gamma(y_i + 1)} \left(\frac{1}{1 + \alpha\,\mu_i}\right)^{\frac{1}{\alpha}} \left(\frac{\alpha\mu_i}{1 + \alpha\,\mu_i}\right)^{y_i} \tag{25}$$

Where $\mu_i = e^{x_i'\beta}$ is the log link function, β is a vector of unknown parameters and x_i is a vector of independent variables. Equation (10) censored likelihood function yields the likelihood function of the appropriate CNB model as follows:

$$\mathcal{L} = \prod_{i=1}^{n} \left[\frac{\Gamma\left(y_i + \frac{1}{\alpha}\right)}{\Gamma\left(\frac{1}{\alpha}\right)\Gamma(y_i + 1)} \left(\frac{1}{1 + \alpha\,\mu_i}\right)^{\frac{1}{\alpha}} \left(\frac{\alpha\mu_i}{1 + \alpha\,\mu_i}\right)^{y_i}\right]^{1-d_i} \times \left[1 - \Gamma\left(\frac{1}{\alpha}\right)\left(\frac{1}{1 + \alpha\,\mu_i}\right)^{\frac{1}{\alpha}} \sum_{j=0}^{a} \frac{\Gamma\left(j + \left(\frac{1}{\alpha}\right)\right)}{\Gamma(j+1)} \left(\frac{\alpha\mu_i}{1 + \alpha\,\mu_i}\right)^{j}\right]^{d_i} \tag{26}$$

The initial term on the right represents the likelihood of contribution from non-censored observations, whereas the subsequent term accounts for the contribution from censored observations [2].

The log likelihood function for the sample can be expressed as:

$$\ell = \sum_{i=1}^{n}(1-d_i)\log\left[\frac{\Gamma\left(y_i+\frac{1}{\alpha}\right)}{\Gamma\left(\frac{1}{\alpha}\right)\Gamma(y_i+1)}\left(\frac{1}{1+\alpha\,\mu_i}\right)^{\frac{1}{\alpha}}\left(\frac{\alpha\mu_i}{1+\alpha\,\mu_i}\right)^{y_i}\right] + \sum_{i=1}^{n} d_i \log\left[1-\Gamma\left(\frac{1}{\alpha}\right)\left(\frac{1}{1+\alpha\,\mu_i}\right)^{\frac{1}{\alpha}}\sum_{j=0}^{a}\frac{\Gamma\left(j+\left(\frac{1}{\alpha}\right)\right)}{\Gamma(j+1)}\left(\frac{\alpha\mu_i}{1+\alpha\,\mu_i}\right)^{j}\right] \quad (27)$$

Refer to [5], [6], [7] and [10] for further details on these models.

The conditional mean is expressed as

$$E\left(y_i;\mu_{i,}\alpha\right) = c_i - \sum_{j=0}^{c_i-1} f(j)(c_i-j) \quad (28)$$

Where

$$f(j) = \frac{\Gamma\left(j+\frac{1}{\alpha}\right)}{\Gamma\left(\frac{1}{\alpha}\right)\Gamma(j+1)}\left(\frac{1}{1+\alpha\,\mu_i}\right)^{\frac{1}{\alpha}}\left(\frac{\alpha\mu_i}{1+\alpha\,\mu_i}\right)^{j} \quad (29)$$

$$E(y_i;\mu_i,\alpha) = c_i - c_i\sum_{j=0}^{c_i-1}\frac{\Gamma\left(j+\frac{1}{\alpha}\right)}{\Gamma\left(\frac{1}{\alpha}\right)\Gamma(j+1)}\left(\frac{1}{1+\alpha\,\mu_i}\right)^{\frac{1}{\alpha}}\left(\frac{\alpha\mu_i}{1+\alpha\,\mu_i}\right)^{j} + j\sum_{j=0}^{c_i-1}\frac{\Gamma\left(j+\frac{1}{\alpha}\right)}{\Gamma\left(\frac{1}{\alpha}\right)\Gamma(j+1)}\left(\frac{1}{1+\alpha\,\mu_i}\right)^{\frac{1}{\alpha}}\left(\frac{\alpha\mu_i}{1+\alpha\,\mu_i}\right)^{j} \quad (30)$$

$$E(y_i;\mu_i,\alpha) = \mu \quad (31)$$

$$E(y_i^2;\,\mu_i,\alpha) = \mu^2+\mu \quad (32)$$

$$V(y_i;\mu_i,\alpha) = E(y_i^2) - [E(y_i)]^2 \quad (33)$$

$$V(y_i;\mu_i,\alpha) = \mu \quad (34)$$

The negative binomial distribution is characterized by its dependence on the mean (μ) and

the dispersion parameter (α). If α approaches zero, the distribution converges to the Poisson distribution. The PRM represents the model equation for NBRM. Using a linear combination of predictors, the logarithm of the outcome is forecasted. If α approaches 0, the CNB distribution converges to the CP distribution. As α approach 0, the RCNB distribution converges to the RCP distribution [10].

VI. Model Selection

Marginal Log-likelihood (MLIK)

According to P. McCullagh and J.A. Nelder FRS [11], one method for removing undesired nuisance parameters is to use the marginal likelihood for a suitable subset of the data vector. This strategy does not always work well, but when it does, it is definitely preferable to select a big chunk of the original data as feasible to minimize information loss. The marginal likelihood estimates remain consistent regardless of whether the postulated models are valid. Note that the marginal log-likelihood is also known as the restricted log likelihood [12].

Deviance Information Criterion (DIC)

According to Hilbe and Greene [13], the Wald, likelihood ratio, and Score or Lagrange Multiplier tests were designed to assess the specification of the conditional mean function by testing parameter constraints. Non-nested (and nested) models are frequently compared using 'information criteria' statistics, which are roughly equivalent to adjusted R^2s in the field of maximum likelihood estimation. The Akaike information criterion (AIC) is a widely used statistic [11] and [14]

AIC is likely the most widely used information criterion in the frequentist statistical framework. Spiegelhalter et al.'s [15] deviance information criterion (DIC) is widely regarded as a key element in Bayesian model selection during the previous two decades. DIC is viewed as a Bayesian variant of AIC. Alike AIC, it weighs model adequacy against complexity, is deals with well theoretical replicated data, and predicts observed data. Nevertheless, unalike AIC, DIC takes prior knowledge into consideration. DIC is built using the posterior mean of the log-likelihood or deviance and has various advantageous properties [16]

As a result, DIC can be seen as a Bayesian counterpart of AIC, with a similar rationale but a broader range of applications. Additionally, it works with any model, requires very little extra analysis or Monte Carlo sampling, and functions rather well [15]. DIC is defined as

$$DIC = -2(\bar{d} - P_{dic}) \tag{35}$$

Where

$$\bar{d} = \frac{1}{S}\sum_{s=1}^{S} \log[P(y|\theta_s)] \tag{36}$$

$$P_{dic} = \max\left[\log[P(y|\theta)] - \bar{d}\right. \tag{37}$$

Where $max[\,]$ is the maximum function over all posterior samples, and S is the number of posterior samples [17].

The model exhibiting the lowest DIC value is deemed the superior fit when evaluating models. If two models have similar DIC values, neither is favoured over the other [4].

Watanabe-Akaike Information Criterion (WAIC)

A new statistical learning theory using algebraic geometry methods has recently emerged. The resolution theorem in algebraic geometry can be applied in singular learning theory to transform a log-likelihood function into a standardized form, notwithstanding the presence of singularities. Consequently, the asymptotic characteristics of the posterior distribution are comprehended, allowing for the extension of AIC and BIC concepts to unique statistical models. The real log canonical threshold [18] establishes the asymptotic Bayesian marginal likelihood, whereas the information criterion [19, 20, 21] assesses the average Bayes generalization error [20].

WAIC is defined as:

$$WAIC = -2(lpd - P_{waic}) \tag{38}$$

Where

$$lpd = \sum_{i=1}^{n} \log\left[\frac{1}{S}\sum_{s=1}^{S} p(y|\theta_s)\right] \tag{39}$$

$$P_{waic} = \sum_{i=1}^{n} var\ [\log\ [p(y|\ \theta)]] \tag{40}$$

Where S is the number of posterior samples, n is the number of data points, $var[\ ]$ is the variance function over the posterior samples, lpd is the log predictive density of the data, and P_{waic} is the effective number of parameters.

III. Results

I. Dispersion Index Test

The dispersion index test is in the following table

Table 1: *Dispersion Index Test*

Data	Variance	Mean	Dispersion
y	0.9583	0.8507	1.1265

The Table 1 explains the dispersion index test. The variance, 0.9583 is greater than the mean 0.8507 of the response variable, which could mean that a different model, like Negative Binomial may be more appropriate. In such situations, the Negative Binomial model might be a better fit.

II. Application - RCPRM using INLA

The posterior means, variances, or quantiles are estimated. The mean or mode of the resultant posterior distribution of a parameter is referred to as the parameter of interest [4].

The model NCSD is applied in RCPRM by using INLA. The findings are presented below:

Table 2: *Summary of fixed effects - RCPRM*

Fixed effects:	Mean	Standard deviation	0.025 quantile	0.5 quantile	0.975 quantile	Mode	KLD
(Intercept)	-1.781	0.225	-2.222	-1.781	-1.340	-1.781	0
BPYes	-0.286	0.099	-0.480	-0.286	-0.092	-0.286	0
BPDon't know	0.409	0.161	0.093	0.409	0.725	0.409	0
HDYes	-1.098	0.708	-2.486	-1.098	0.291	-1.098	0
HDDon't know	0.000	31.623	-61.980	0.000	61.980	0.000	0
HBPYes	0.458	0.458	0.29	0.458	0.627	0.458	0
HBPDon't know	-0.064	0.206	-0.467	-0.064	0.339	-0.064	0
PLYes	0.382	0.089	0.208	0.382	0.557	0.382	0
PLDon't know	-1.081	0.263	-1.596	-1.081	-0.567	-1.081	0
CT1st of multiple	0.048	0.295	-0.530	0.048	0.625	0.048	0
CT2nd of multiple	0.091	0.290	-0.478	0.091	0.660	0.091	0
CT3rd of multiple	-68.765	14.083	-96.366	-68.765	-41.164	-68.765	0
CT4th of multiple	0.000	31.623	-61.980	0.000	61.980	0.000	0
CT5th of multiple	0.000	31.623	-61.980	0.000	61.980	0.000	0
Age	0.006	0.007	-0.007	0.006	0.019	0.006	0
ELPrimary	0.062	0.140	-0.212	0.062	0.335	0.062	0
ELSecondary	0.471	0.105	0.265	0.471	0.677	0.471	0
ELHigher	0.737	0.113	0.517	0.737	0.958	0.737	0

Table 2 displays the values of RCPRM. The parameters of interest of the posterior distribution of the covariates BP, Don't know, HBP, Yes, PL, Yes, EL secondary, and EL higher more than 0.300, whereas HD, Don't know, CT4th of multiple, and CT5th of multiple is 0.000.

III. Application - RCNBRM using INLA

The model NCSD is fitted in RCNBRM using INLA. The posterior means, variances, or quantiles are estimated. The values are given below:

Table 3: *The values of posterior means, variances, or quantiles - RCNBRM*

Fixed effects:	Mean	Standard deviation	0.025 quantile	0.5 quantile	0.975 quantile	Mode	KLD
(Intercept)	-1.740	0.226	-2.183	-1.740	-1.298	-1.740	0
BPYes	-0.313	0.100	-0.508	-0.313	-0.117	-0.313	0
BPDon't know	0.481	0.176	0.124	0.485	0.817	0.485	0

HDYes	-1.044	0.717	-2.449	-1.044	0.364	-1.044	0
HDDon't know	0.000	31.623	-62.009	0.000	62.009	0.000	0
HBPYes	0.133	0.142	-0.101	0.112	0.433	0.068	0
HBPDon't know	-0.017	0.216	-0.448	-0.015	0.401	-0.015	0
PLYes	0.032	0.148	-0.211	0.009	0.349	-0.036	0
PLDon't know	-0.776	0.342	-1.582	-0.747	-0.189	-0.702	0
CT1st of multiple	0.119	0.296	-0.462	0.119	0.700	0.119	0
CT2nd of multiple	0.100	0.291	-0.471	0.100	0.671	0.100	0
CT3rd of multiple	-45.426	33.774	-102.331	-46.917	15.160	-45.578	0
CT4th of multiple	0.000	31.623	-62.009	0.000	62.009	0.000	0
CT5th of multiple	0.000	31.623	-62.009	0.000	62.009	0.000	0
Age	0.021	0.008	0.004	0.022	0.035	0.023	0
ELPrimary	0.068	0.140	-0.206	0.068	0.342	0.068	0
ELSecondary	0.444	0.107	0.234	0.444	0.653	0.444	0
ELHigher	0.678	0.115	0.452	0.678	0.903	0.678	0

The parameters of means, variances, or quantiles are computed. Table 3 shows the computed values of the parameters of means, variances, or quantiles of RCNBRM. The parameters of mean or mode of the covariates BP, Do not know, EL secondary, and EL higher are greater than 0.300, whereas HD, Do not know, CT4th of multiple, and CT5th of multiple are 0.000.

Table 4: *Comparing models*

	Model selection criteria		
Model	MLIK	DIC	WAIC
RCPRM	-2290.03	4864.74	4860.68
RCNBRM	-2291.39	4608.60	4593.90

Table 4 clearly shows that the MLIK of RCNBRM, -2291.39, is greater than that of RCPRM, -2290.03. The DIC and WAIC values of RCNBRM, 4608.60 and 4593.90, are smaller than those of RCPRM, 4864.74 and 4860.68, respectively. Thus, RCNBRM seems to be the best fit for the NCSD.

IV. Discussion

I. Findings

This article succinctly outlines the INLA algorithm for estimating the marginal posterior parameters of interest and hyperparameters in Bayesian spatial and spatiotemporal models. The

parameters of interest, the mean or mode of RCPRM, are as follows. The mean or mode of the intercept is -1.781, BP Yes & BP Do not know is -0.286 & 0.409, HD Yes & HD Do not know is -1.098 & 0.000, HBP Yes & HBP Do not know is 0.458 & -0.064, PL Yes & PL Do not know is 0.382 & -1.081, CT1st multiple, CT2nd multiple, CT3rd multiple, CT4th multiple & CT5th multiple is 0.048, 0.091, -68.765, 0.000 & 0.000, age is 0.006, EL Primary, EL Secondary, EL Higher is 0.062, 0.471 & 0.737.

The parameters of interest, mean, and mode of RCNBRM are as follows: Mean or mode of the intercept is -1.740, BP Yes & BP Do not know is -0.313 & 0.481, HD Yes & HD Do not know is -1.044 & 0.000, HBP Yes & HBP Do not know is 0.133 & -0.017, PL Yes & PL Do not know is 0.032 & -0.776, CT1st multiple, CT2nd multiple, CT3rd multiple, CT4th multiple & CT5th multiple is 0.119, 0.100, -45.426, 0.000 & 0.000, age is 0.021, EL Primary, EL Secondary & Higher is 0.068, 0.444 & 0.678. The right-censored NCSD dataset used for RCPRM and RCNBRM demonstrates the INLA estimate outcomes.

II. Conclusion

INLA offers significant computational advantages over alternative methods for addressing problems involving random and fixed effects across specific regions and time in spatiotemporal analysis. This research article presents the computation of the INLA fixed effects of additive models. The RCNBRM is the superior model in comparison to the RCPRM. The NCSD is modelled using Bayesian spatial-temporal methods in INLA specification. The NCSD is comparable to other regression models. The RCNBRM is identified as the most effective, concluding that factors such as BP, HD, HBP, PL, CT, Age, and EL significantly influence the NCSD. Therefore the government policy makers need to consider these variables while making the health care polices for the women of age from 15 to 49 years old, who are in the age of child bearing.

Acknowledgement

The first author is grateful to the Ministry of Tribal Affairs, Government of India, for the financial support through NFST Fellowship (Award No-202021-NFST-AND-02662).

Declaration of conflicting interests

The authors declared no conflicts of interest

References

[1] Cameron, A. C. and P. K. Trivedi. Regression Analysis of Count Data, Cambridge University Press, Cambridge, 1998.

[2] Winkelmann, R. Economic analysis of count data, Springer, Switzerland, 2008.

[3] Br¨ann¨as, K. (1992), Limited dependent Poisson regression. *Statistician* 41: 413–423.

[4] Hilbe, J. M. Negative Binomial Regression, Cambridge University Press, 2011.

[5] Terza, J. V. (1985). A tobit-type estimator for the censored Poisson regression model. *Economics Letters*, 18(4):361-365.

[6] Caudill, S. B., & Mixon, F. G. (1995). Modeling household fertility decisions: Estimation and testing of censored regression models for count data. *Empirical Economics*, 20(2), 183–196.

[7] Raciborski, R. (2011). Right-censored Poisson regression model. *Stata Journal*, 11(1), 95–105.

[8] Hilbe, J., Arizona State University, & Jet Propulsion Laboratory, California Institute of Technology. Modeling count data. Cambridge University Press, 2014.

[9] Cameron, A. C. and Trivedi, P. K. Regression analysis of count data. Cambridge University Press, 2013.

[10] Jung, B. C., Jhun, M., & Song, S. H. (2006). Testing for overdispersion in a censored Poisson regression model. *Statistics*, *40*(6), 533–543.

[11] McCullagh, P. & Nelder, J. A. Generalized linear models, 2nd Ed. Chapman and Hall, New York, USA, 1989.

[12] Corbeil, R.R. and Searle, S.R. (1976). Restricted maximum likelihood (REML) estimation of variance components in the mixed model. *Technometrics* 18, 31-8

[13] Hilbe, J. M., & Greene, W. H. Handbook of Statistics, Vol. 27, Elsevier, 2008.

[14] Hardin, J., Hilbe, J. Generalized Linear Models and Extensions, 2nd ed. Stata Press, College Station, TX, 2007.

[15] Spiegelhalter, D. J., Best, N. G., Carlin, B. P., and Van Der Linde, A. (2002). Bayesian measures of model complexity. *Journal of the Royal Statistical Society: Series B (Statistical Methodology)*, 64(4):583-639.

[16] Li, Y., Wang, N., Yu, J., & Zeng, T. (2022b). Deviance Information Criterion for model selection: Theoretical justification and Applications

[17] Evans, N. J. (2019). Assessing the practical differences between model selection methods in inferences about choice response time tasks. In Theoretical Review.

[18] S. Watanabe, (2001a). Algebraic analysis for nonidentifiable learning machines. *Neural Computation*, 13(4):899–933

[19] S. Watanabe. Algebraic Geometry and Statistical Learning Theory. Cambridge University Press, Cambridge, UK, 2009.

[20] S. Watanabe, (2010a). Equations of state in singular statistical estimation. *Neural Networks*. 23(1):20-34.

[21] S. Watanabe. (2010c). A limit theorem in the singular regression problem. *Advanced Studies of Pure Mathematics*. 57:473-492.

RT&A, No 3 (86)
Volume 20, September 2025

FIXED POINT THEOREMS IN TRICOMPLEX VALUED CONTROLLED METRIC SPACES

Shivani Chourasiya[1], and Kavita Shrivastava[2]

[1,2]Department of Mathematics and Statistics, Dr. Harisingh Gour Vishwavidyalaya, Sagar, M.P., 470003

[1]shivanichourasiya10@gmail.com, [2]kavita.rohit@rediffmail.com

Abstract

Throughout the years, scholars have broadened traditional fixed point theories to include more intricate structures like tricomplex valued metric spaces, aiming to tackle issues in multidimensional and hypercomplex contexts. While there is a rising interest in tricomplex valued spaces, the current literature addressing fixed point theorems in these areas presents several limitations. The existing research highlights numerous shortcomings; thus, this article employs innovative types of contraction mappings via a control function to illustrate fixed point theorems in tricomplex valued controlled metric spaces. These findings enhance the understanding of fixed point theory and pave the way for new applications in more complex and diverse mathematical frameworks. Consequently, our study fosters progress in the field, establishing a strong basis for future research and potential uses across various scientific and engineering fields.

Keywords: fixed point, controlled metric spaces, complex valued metric space, tricomplex valued metric space, tricomplex valued controlled metric space.

1. Introduction

The concept of fixed points is essential in many theoretical and practical domains, such as variational and linear inequalities, approximation theory, nonlinear analysis, integral and differential equations and inclusions, dynamic systems theory, mathematics of fractals, and mathematical economics and modeling. The idea of Banach contraction was first introduced in a metric space by [1] in 1922. Consequently, various researchers have interpreted these findings in numerous ways [see, [2], [3], [4], [5], [6], [7], [8], [9], [10], [11], etc.]. Complex valued metric spaces were first presented by [12] in 2011. In 2012, expanded on these results and provided applications by [13]. Complex valued b-metric spaces introduced by [14] in 2013. Multicomplex spaces were introduced by [15]. Following this, many researchers took an interest in this field, bicomplex valued metric spaces introduced in 2021 by [16], where they demonstrated fixed point theorems. Explored controlled metric spaces with bicomplex value and applied these concepts to fractional differential equations by [17]. they also introduced tricomplex valued metric spaces and proved common fixed point theorems [18]. Fixed point results in tricomplex valued metric spaces using control functions and provided practical applications as well by [19]. The concept of controlled metric spaces given by [20]. Utilizing rational contraction to establish fixed point theorems were pioneers by [21] . Recently, tricomplex valued controlled metric spaces introduced by [22]. Building on these results, we generalized a new type of contraction mapping and established fixed point theorems in tricomplex valued controlled metric spaces.

2. Preliminaries

In this article the families of real, complex, bicomplex, and tricomplex numbers, denoted by C^0, C^1, C^2 and C^3 respectively.

Let,

$$\omega = \varrho_1 + \varrho_2 i_1 + \varrho_3 i_2 + \varrho_4 i_1 i_2,$$

where $\varrho_1, \varrho_1, \varrho_1, \varrho_1 \in C^0$ and independent units i_1 and i_2 such that $i_1^2 = i_2^2 = -1$ and $i_1 i_2 = i_2 i_1$ the set of bicomplex numbers define as

$$C^2 = \{\omega : \omega = \varrho_1 + \varrho_2 i_1 + \varrho_3 i_2 + \varrho_4 i_1 i_2, \varrho_1, \varrho_2, \varrho_3, \varrho_4 \in C^0\}$$

$$\text{Or } C^2 = \{\omega : \omega = \Theta_1 + i_2\Theta_2, \Theta_1, \Theta_2 \in C^1\}$$

where $\Theta_1 = \varrho_1 + \varrho_2 i_1$ and $\Theta_2 = \varrho_3 + \varrho_4 i_1$.

$$\Pi = \varrho_1 + \varrho_2 i_1 + \varrho_3 i_2 + \varrho_4 j_1 + \varrho_5 i_3 + \varrho_6 j_2 + \varrho_7 j_3 + \varrho_8 i_4$$

Where $\varrho_1, \varrho_2, \varrho_3, \varrho_4, \varrho_5, \varrho_6, \varrho_7, \varrho_8 \in C^0$ and $i_1, i_2, i_3, i_4, j_1, j_2$ and j_3 are independent units such that $i_1^2 = i_2^2 = i_3^2 = i_4^2 = -1, j_1^2 = j_2^2 = j_3^2 = 1, j_1 = i_1 i_2 = i_2 i_1, j_2 = i_1 i_3 = i_3 i_1$ and, $i_4 = i_1 i_3 = i_1 i_2 i_3$. the set of tricomplex numbers define as

$$C^3 = \{\Pi : \Pi = \varrho_1 + \varrho_2 i_1 + \varrho_3 i_2 + \varrho_4 j_1 + \varrho_5 i_3 + \varrho_6 j_2 + \varrho_7 j_3 + \varrho_8 i_4, \varrho_1, \varrho_2, \varrho_3, \varrho_4, \varrho_5, \varrho_6, \varrho_7, \varrho_8 \in C^0\}$$

$$C^3 = \{\Pi : \Pi = \alpha_1 + i_3\alpha_2, \alpha_1, \alpha_2 \in C^2\}$$

where $\alpha_1 = \Theta_1 + \Theta_2 i_2 \in C^2$ and $\alpha_2 = \Theta_3 + \Theta_4 i_2 \in C^2$
Let two tricomplex numbers Π and χ such that $\Pi = \alpha_1 + i_3\alpha_2$ and $\chi = \beta_1 + i_3\beta_2$ then

$$\Pi \pm \chi = (\alpha_1 + i_3\alpha_2) \pm (\beta_1 + i_3\beta_2) = \alpha_1 \pm \beta_1 + i_3(\alpha_2 \pm \beta_2)$$
$$\text{and } \Pi.\chi = (\alpha_1 + i_3\alpha_2)(\beta_1 + i_3\beta_2) = (\alpha_1\beta_1 - \alpha_2\beta_2) + i_3(\alpha_1\beta_2 + \alpha_2\beta_1)$$

In the families of tricomplex numbers C^3 have four idempotent elements $0, 1, \varphi_1 = \frac{1+j_3}{2}$ and $\varphi_2 = \frac{1-j_3}{2}$ such that $\varphi_1 + \varphi_2 = 1$ and $\varphi_1.\varphi_2 = 0$. Hence φ_1, φ_2 are not trivial. Every tricomplex numbers can be expressed as an union of φ_1, φ_2 for example

$$\Pi = \alpha_1 + i_3\alpha_2 = (\alpha_1 - i_2\alpha_2)\varphi_1 + (\alpha_1 + i_2\alpha_2)\varphi_2$$

Here Π is idempotent of the tricomplex numeral and $\Pi_1 = (\alpha_1 - i_2\alpha_2)\varphi_1$ and $\Pi_2 = (\alpha_1 + i_2\alpha_2)\varphi_2$ are the idempotent components of the bicomplex numeral Π.
A tricomplex number $\Pi = \alpha_1 + i_3\alpha_2$ is invertible if there exists $\chi \in C^3$ such that $\Pi\chi = 1$.
A tricomplex number $\Pi = \alpha_1 + i_3\alpha_2$ is nonsingular if $|\alpha_1^2 + \alpha_2^2| \neq 0$ and singular if $|\alpha_1^2 + \alpha_2^2| = 0$.
Let $\Pi = \alpha_1 + i_3\alpha_2$ and $\chi = \beta_1 + i_3\beta_2$ be tricomplex numerals. Then the partial order relation $\leq_{i_3}$ on C^3 or $\Pi \leq_{i_3} \chi$ if the following axioms are satisfied.

1. $\alpha_1 = \beta_1, \alpha_2 = \beta_2$;
2. $\alpha_1 <_{i_3} \beta_1, \alpha_2 = \beta_2$;
3. $\alpha_1 = \beta_1, \alpha_2 <_{i_3} \beta_2$;
4. $\alpha_1 <_{i_3} \beta_1, \alpha_2 <_{i_3} \beta_2$;

If $\Pi \leq_{i_3} \chi$ implies $\Pi <_{i_3} \chi$ but $\Pi \neq \chi$
Having two tricomplex numerals $\Pi, \chi \in C^3$, the following conditions hold:

1. $\Pi \leq_{i_3} \chi$ if $||\Pi|| \leq ||\chi||$;
2. $||\Pi + \chi|| \leq ||\Pi|| + ||\chi||$;
3. $||\varrho\Pi|| = |\varrho|||\Pi||$, where $\varrho \in C^0$
4. $||\Pi\chi|| \leq 2||\Pi||||\chi||$, If at least one of Π, χ nonsingular then equality holds.
5. $||\Pi^{-1}|| = ||\Pi||^{-1}$, if $||\Pi|| \neq 0$

6. $||\frac{\Pi}{\chi}|| = \frac{||\Pi||}{||\chi||}$, if $||\chi|| \neq 0$

Let $\aleph \neq 0$ and $\phi : \aleph \times \aleph \longrightarrow [1, \infty)$, then the function $\tau : \aleph \times \aleph \longrightarrow [1, \infty)$ such that [20]

1. $\tau(\Phi, \Psi) \geq 0$ and $\tau(\Phi, \Psi) = 0 \Longleftrightarrow \Phi = \Psi$;
2. $\tau(\Phi, \Psi) = \tau(\Psi, \Phi)$;
3. $\tau(\Phi, \nu) \leq \phi(\Phi, \Psi)\tau(\Phi, \Psi) + \phi(\Phi, \nu)\phi(\Psi, \nu)$;

Then $(\aleph, \tau)$ is called a controlled metric space for all $\Phi, \Psi, \nu \in \aleph$. Let $\omega_1, \omega_2 \in C^1$, where C^1 is the set of complex numbers that define a partial order $\leq$ on C^1 such that [12], $\omega_1 \leq \omega_2$ if and only if $Re(\omega_1) \leq Re(\omega_2)$ and $Im(\omega_1) \leq Im(\omega_2)$ that is $\omega_1 \leq \omega_2$. If any of the following is true

1. $Re(\omega_1) = Re(\omega_2)$ and $Im(\omega_1) = Im(\omega_2)$;
2. $Re(\omega_1) < Re(\omega_2)$ and $Im(\omega_1) = Im(\omega_2)$;
3. $Re(\omega_1) = Re(\omega_2)$ and $Im(\omega_1) < Im(\omega_2)$;
4. $Re(\omega_1) < Re(\omega_2)$ and $Im(\omega_1) < Im(\omega_2)$;

we also write $\omega_1 \lneq \omega_2$ if $\omega_1 \neq \omega_2$ and one of (2),(3), and (4) satisfiy.

$$0 \leq \omega_1 \lneq \omega_2 \Rightarrow |\omega_1| < |\omega_2|$$
$$\omega_1 \leq \omega_2 \text{ and } \omega_2 < \omega_3 \Rightarrow \omega_1 < \omega_3.$$

Let $\aleph \neq 0$. A mapping $\tau : \aleph \times \aleph \to C^1$ such that [12],

1. $0 \leq \tau(\Phi, \Psi)$ for all $\Phi, \Psi \in \aleph$ and $\tau(\Phi, \Psi) = 0$ if and only if $\Phi = \Psi$;
2. $\tau(\Phi, \Psi) = \tau(\Psi, \Phi)$, for all $\Phi, \Psi \in \aleph$;
3. $\tau(\Phi, \Psi) \leq \tau(\Phi, \nu) + \tau(\nu, \Psi)$ for all $\Phi, \Psi, \nu \in \tau$.

Then $(\aleph, \tau)$ is called a complex valued metric space.
Suppose $\aleph \neq 0$. A mapping $\tau : \aleph \times \aleph \longrightarrow C^3$ is such that [22],

1. $\tau(\Phi, \Psi) \geq_{i_3} 0$ and $\tau(\Phi, \Psi) = 0 \Longleftrightarrow \Phi = \Psi$
2. $\tau(\Phi, \Psi) = \tau(\Psi, \Phi)$
3. $\tau(\Phi, \Psi) \leq_{i_3} \tau(\Phi, \nu) + \tau(\nu, \Psi)$, $\forall \Phi, \Psi, \nu \in \aleph$

Then $(\aleph, \tau)$ is called a tricomplex valued metric space.
Suppose $\aleph$ is nonempty set and $\phi : \aleph \times \aleph \longrightarrow [1, \infty)$, then the function $\tau : \aleph \times \aleph \longrightarrow C^3$ such that [22],

1. $\tau(\Phi, \Psi) \geq_{i_3} 0$ and $\tau(\Phi, \Psi) = 0 \Longleftrightarrow \Phi = \Psi$;
2. $\tau(\Phi, \Psi) = \tau(\Psi, \Phi)$;
3. $\tau(\Phi, \nu) \leq_{i_3} \phi(\Phi, \Psi)\tau(\Phi, \Psi) + \phi(\Phi, \nu)\phi(\Psi, \nu)$;

Then $(\aleph, \tau)$ is called a tricomplex valued controlled metric space for all $\Phi, \Psi, \nu \in \aleph$. Let $(\aleph, \tau)$ be a tricomplex valued controlled metric space then,

1. A sequence $\{\Phi_n\} \in \aleph$ is convergent to $\Phi \in \aleph$, if $\tau(\Phi_n, \Phi) <_{i_3} l$ for all $l >_{i_3} 0$ where $l \in C^3$, $\forall n \geq N$ that is $\lim_{n \longrightarrow \infty} \Phi_n = \Phi$.
2. A sequence $\{\Phi_n\} \in \aleph$ is Cauchy sequence in $(\aleph, \tau)$, if $\tau(\Phi_n, \Phi_m) <_{i_3} l$ for all $l >_{i_3} 0$ where $l \in C^3$ and $\forall n, m \geq N$.

3. If every Cauchy sequence is convergent in $\aleph$ then it is complete tricomplex valued controlled metric space.

Lemma 1. Suppose $(\aleph, \tau)$ be a tricomplex valued controlled metric space then, a sequence $\{\Phi_n\} \in \aleph$ is Cauchy sequence, such that $\Phi_n \neq \Phi_m$ where $n \neq m$ then, $\{\Phi_n\} \in \aleph$ converges to at most one point [22].

Lemma 2. Suppose $(\aleph, \tau)$ be a tricomplex valued controlled metric space then, a function $\tau : \aleph \times \aleph \longrightarrow C^3$ is continuous with respect to the partial order "$\leq_{i_3}$" [22].

3. Main result

Theorem 1. Let (Ξ, τ) be a complete tricomplex controlled metric space. Let the continuous mapping $\aleph : \Xi \to \Xi$ be such that

$$\tau(\aleph\Phi, \aleph\Psi) \leq_{i_3} a\frac{\{1+\tau(\Phi, \aleph\Phi)\}\,\tau(\Psi, \aleph\Psi)}{1+\tau(\Phi, \Psi)} + b\tau(\Phi, \Psi) + c\tau(\Phi, \aleph\Phi) + d\tau(\Psi, \aleph\Psi) \tag{1}$$

where $a, b, c, d \in [0, 1)$ with $a + b + c + d < 1$ and $\forall \Phi, \Psi \in \Xi$ for $\Phi_0 \in \Xi$, take $\Phi_n = \aleph^n\Phi_0$. Suppose that,

$$\max_{m\geq 1} \lim_{i_3\to\infty} \frac{\rho(\Phi_{i_3+1}, \Phi_{i_3+2})\rho(\Phi_{i_3+1}, m)}{\rho(\Phi_{i_3}, \Phi_{i_3+1})} < \frac{1}{\kappa}$$

Assume that $\forall \Phi \in \Xi, \lim_{n\to\infty} \rho(\Phi_n, \Phi)$ and $\lim_{n\to\infty} \rho(\Phi, \Phi_n)$ exist and are finite. Then $\aleph$ has a unique fixed point.

Proof. Suppose that $\Phi_0 \in \Xi$. we construct $\{\Phi_n\}$ in Ξ by $\Phi_{n+1} = \aleph\Phi_n, \forall n \in \mathcal{N}$ such that $\Phi_{n+1} = \Phi_n$, then $\aleph\Phi_n = \Phi_n$. Hence the proof is finished. Now, we assume that $\Phi_{n+1} \neq \Phi_n, \forall n \in \mathbb{N}$. Thus, by (1), we get

$$\begin{aligned}
\tau(\Phi_n, \Phi_{n+1}) &= \tau(\aleph\Phi_{n-1}, \aleph\Phi_n) \\
&\leq_{i_3} a\frac{\{1+\tau(\Phi_{n-1}, \aleph\Phi_{n-1})\}\,\tau(\Phi_n, \aleph\Phi_n)}{1+\tau(\Phi_{n-1}, \Phi_n)} + b\tau(\Phi_{n-1}, \Phi_n) \\
&+ c\tau(\Phi_{n-1}, \aleph\Phi_{n-1}) + d\tau(\Phi_n, \aleph\Phi_n) \\
&\leq_{i_3} a\frac{\{1+\tau(\Phi_{n-1}, \Phi_n)\}\,\tau(\Phi_n, \Phi_{n+1})}{1+\tau(\Phi_{n-1}, \Phi_n)} + b\tau(\Phi_{n-1}, \Phi_n) \\
&+ c\tau(\Phi_{n-1}, \Phi_n) + d\tau(\Phi_n, \Phi_{n+1}) \\
&\leq_{i_3} a\tau(\Phi_n, \Phi_{n+1}) + b\tau(\Phi_{n-1}, \Phi_n) + c\tau(\Phi_{n-1}, \Phi_n) + d\tau(\Phi_n, \Phi_{n+1})
\end{aligned}$$

$$\implies \tau(\Phi_n, \Phi_{n+1}) \leq_{i_3} \frac{b+c}{1-a-d}\tau(\Phi_{n-1}, \Phi_n)$$

Since $\kappa = \frac{b+c}{1-a-d} < 1$, we have

$$\begin{aligned}
\tau(\Phi_n, \Phi_{n+1}) &\leq_{i_3} \kappa\tau(\Phi_{n-1}, \Phi_n) \\
&\leq_{i_3} \kappa^2\tau(\Phi_{n-2}, \Phi_{n-1}) \\
&\vdots \\
&\leq_{i_3} \kappa^n\tau(\Phi_0, \Phi_1)
\end{aligned}$$

For every $n, m \in \mathbb{N}$ and $n < m$, we have

$$\begin{aligned}
\tau(\Phi_n, \Phi_m) &\leq_{i_3} \rho(\Phi_n, \Phi_{n+1})\tau(\Phi_n, \Phi_{n+1}) + \rho(\Phi_{n+1}, \Phi_m)\tau(\Phi_{n+1}, \Phi_m) \\
&\leq_{i_3} \rho(\Phi_n, \Phi_{n+1})\tau(\Phi_n, \Phi_{n+1}) + \rho(\Phi_{n+1}, \Phi_m)\rho(\Phi_{n+1}, \Phi_{n+2})\tau(\Phi_{n+1}, \Phi_{n+2}) \\
&+ \rho(\Phi_{n+1}, \Phi_m)\rho(\Phi_{n+2}, \Phi_m)\tau(\Phi_{n+2}, \Phi_m) \\
&\leq_{i_3} \rho(\Phi_n, \Phi_{n+1})\tau(\Phi_n, \Phi_{n+1}) + \rho(\Phi_{n+1}, \Phi_m)\rho(\Phi_{n+1}, \Phi_{n+2})\tau(\Phi_{n+1}, \Phi_{n+2}) \\
&+ \rho(\Phi_{n+1}, \Phi_m)\rho(\Phi_{n+2}, \Phi_m)\rho(\Phi_{n+2}, \Phi_{n+3}) + \tau(\Phi_{n+2}, \Phi_{n+3}) \\
&+ \rho(\Phi_{n+1}, \Phi_m)\rho(\Phi_{n+2}, \Phi_m)\rho(\Phi_{n+3}, \Phi_m)\tau(\Phi_{n+3}, \Phi_m) \dots \\
&\leq_{i_3} \rho(\Phi_n, \Phi_{n+1})\tau(\Phi_n, \Phi_{n+1}) + \sum_{i=n+1}^{m-2} \left(\prod_{j=n+1}^{i} \rho(\Phi_j, \Phi_m) \right) \rho(\Phi_i, \Phi_{i+1})\tau(\Phi_i, \Phi_{i+1}) \\
&+ \prod_{i=n+1}^{m-1} \rho(\Phi_i, \Phi_m)\tau(\Phi_{m-1}, \Phi_m)
\end{aligned}$$

$$\begin{aligned}
\tau(\Phi_n, \Phi_m) &\leq_{i_3} \rho(\Phi_n, \Phi_{n+1})\tau(\Phi_n, \Phi_{n+1}) + \sum_{i=n+1}^{m-2} \left(\prod_{j=n+1}^{i} \rho(\Phi_j, \Phi_m) \right) \rho(\Phi_i, \Phi_{i+1})\tau(\Phi_i, \Phi_{i+1}) \\
&+ \left(\prod_{i=n+1}^{m-1} \rho(\Phi_i, \Phi_m) \right) \tau(\Phi_{m-1}, \Phi_m)\rho(\Phi_{m-1}, \Phi_m)\tau(\Phi_{m-1}, \Phi_m) \\
&\leq_{i_3} \rho(\Phi_n, \Phi_{n+1})\kappa^n\tau(\Phi_0, \Phi_1) + \sum_{i=n+1}^{m-2} \left(\prod_{j=n+1}^{i} \rho(\Phi_j, \Phi_m) \right) \rho(\Phi_i, \Phi_{i+1})\kappa^i\tau(\Phi_0, \Phi_1) \\
&+ \left(\prod_{i=n+1}^{m-1} \rho(\Phi_i, \Phi_m) \right) \kappa^{m-1}\tau(\Phi_0, \Phi_1)\rho(\Phi_{m-1}, \Phi_m) \\
&= \rho(\Phi_n, \Phi_{n+1})\kappa^n\tau(\Phi_0, \Phi_1) + \sum_{i=n+1}^{m-1} \left(\prod_{j=n+1}^{i} \rho(\Phi_j, \Phi_m) \right) \rho(\Phi_i, \Phi_{i+1})\kappa^i\tau(\Phi_0, \Phi_1)
\end{aligned}$$

Let

$$\Re_\theta = \textstyle\sum_{i=n+1}^{m-1} \left(\prod_{j=n+1}^{i} \rho(\Phi_j, \Phi_m) \right) \rho(\Phi_i, \Phi_{i+1})\kappa^i\tau(\Phi_0, \Phi_1)$$

Then we get

$$\tau(\Phi_n, \Phi_m) \leq \tau(\Phi_0, \Phi_1) \left[\kappa^n \rho(\Phi_n, \Phi_{n+1}) + (\Re_{m-1} - \Re_n) \right]$$

applying $(\Phi, \Psi) \geq 1$ and ratio test, $\lim_{n\to\infty} \Re_n$ exists. Thus $\{\Re_n\}$ is a Cauchy sequence.

$$\implies \lim_{n,m\to\infty} \tau(\Phi_n, \Phi_m) = 0$$

Thus, $\{\Phi_n\}$ is a Cauchy sequence in the complete tricomplex valued metric space in (Ξ, τ). Then $\{\Phi_n\}$ converges to Φ^*. From (1), it has a unique limit and by (2) we get

$$\Phi^* = \lim_{n\to\infty} \Phi_{n+1} = \lim_{n\to\infty} \aleph\Phi_n = \aleph(\lim_{n\to\infty} \Phi_n) = \aleph\Phi^*.$$

For uniqueness, let Φ^*, Ψ^* both be fixed points of $\aleph$. Then from (1) we have

$$\begin{aligned}
\tau(\Phi^*, \Psi^*) &= \tau(\aleph\Phi^*, \aleph\Psi^*) \\
&\leq_{i_3} a \frac{\{1 + \tau(\Phi^*, \aleph\Phi^*)\}\, \tau(\Psi^*, \aleph\Psi^*)}{1 + \tau(\Phi^*, \Psi^*)} + b\tau(\Phi^*, \Psi^*) \\
&+ c\tau(\Phi^*, \aleph\Phi^*) + d\tau(\Psi^*, \aleph\Psi^*) \\
&\leq_{i_3} a \frac{\{1 + \tau(\Phi^*, \Phi^*)\}\, \tau(\Psi^*, \Psi^*)}{1 + \tau(\Phi^*, \Psi^*)} + b\tau(\Phi^*, \Psi^*) \\
&+ c\tau(\Phi^*, \Phi^*) + d\tau(\Psi^*, \Psi^*)
\end{aligned}$$

$$\implies \tau(\Phi^*, \Psi^*) = 0$$

Then $\aleph$ has a unique fixed point and $\Phi^* = \Psi^*$ ■

Theorem 2. Let (Ξ, τ) be a complete tricomplex controlled metric space and $\sigma, \varsigma : \Xi \to \Xi$. If there exists mappings $\lambda, \delta : \Xi \to [0, 1)$ such that for all $\Phi, \Psi \in \Xi$,

1. $\lambda(\sigma\Phi) \leq \lambda(\Phi)$, $\delta(\sigma\Phi) \leq \delta(\Phi)$
2. $\lambda(\varsigma\Phi) \leq \lambda(\Phi)$ and $\delta(\varsigma\Phi) \leq \delta(\Phi)$
3. $(\lambda + \delta)\Phi < 1$
4.

$$\tau(\sigma\Phi, \varsigma\Psi) \leq_{i_3} \lambda(\Phi) \max\left\{(\tau(\Phi, \Psi), \frac{\tau(\Phi, \sigma\Phi)\tau(\Psi, \varsigma\Psi)}{\tau(\Phi, \varsigma\Psi) + \tau(\Psi, \sigma\Phi) + \tau(\Phi, \Psi)}\right\} + \delta(\Phi)\{\tau(\Phi, \sigma\Phi) + \tau(\Psi, \varsigma\Psi)\} \tag{2}$$

for all $\Phi, \Psi \in \Xi$ such that $\Phi \neq \Psi$, $\tau(\Phi, \varsigma\Psi) + \tau(\Psi, \sigma\Phi) + \tau(\Phi, \Psi) \neq 0$. Suppose that,

$$\max_{m \geq 1} \lim_{i_3 \to \infty} \frac{\rho(\Phi_{i_3+1}, \Phi_{i_3+2})\rho(\Phi_{i_3+1}, m)}{\rho(\Phi_{i_3}, \Phi_{i_3+1})} < \frac{1}{\kappa}$$

where $\Phi_{n+1} = \sigma\Phi_n$ and $\Phi_{n+2} = \varsigma\Phi_{n+1}$ for each $n \geq 0$. Assume that $\forall \Phi \in \lim_{i \to \infty} \rho(\Phi_n, \Phi)$ and $\lim_{i \to \infty} \rho(\Phi, \Phi_n)$ exist and are finite. Then, σ, ς has a unique common fixed point.

Proof. Again, we construct $\{\Phi_n\}$ in Ξ by $\Phi_{n+1} = \sigma\Phi_n$ and $\Phi_{n+2} = \varsigma\Phi_{n+1}$ and assume that $\Phi_{n+1} \neq \Phi_n, \forall n \in \mathbb{N}$. Thus, by (2), we get

$$\begin{aligned}
\tau(\Phi_n, \Phi_{n+1}) &= \tau(\sigma\Phi_{n-1}, \varsigma\Phi_n) \\
&\leq_{i_3} \lambda(\Phi) \max\left\{(\tau(\Phi_{n-1}, \Phi_n), \frac{\tau(\Phi_{n-1}, \sigma\Phi_{n-1})\tau(\Phi_n, \varsigma\Phi_n)}{\tau(\Phi_{n-1}, \varsigma\Phi_n) + \tau(\Phi_n, \sigma\Phi_{n-1}) + \tau(\Phi_{n-1}, \Phi_n)}\right\} \\
&+ \delta(\Phi)\{\tau(\Phi_{n-1}, \sigma\Phi_{n-1}) + \tau(\Phi_n, \varsigma\Phi_n)\} \\
&\leq_{i_3} \lambda(\Phi) \max\left\{(\tau(\Phi_{n-1}, \Phi_n), \frac{\tau(\Phi_{n-1}, \Phi_n)\tau(\Phi_n, \Phi_{n+1})}{(\Phi_n, \Phi_{n+1}) + \tau(\Phi_n, \Phi_n) + \tau(\Phi_{n-1}, \Phi_n)}\right\} \\
&+ \delta(\Phi)\{\tau(\Phi_{n-1}, \Phi_n) + \tau(\Phi_n, \Phi_{n+1})\} \\
&\leq_{i_3} \lambda(\Phi)\tau(\Phi_{n-1}, \Phi_n) + \delta(\Phi)\tau(\Phi_{n-1}, \Phi_{n+1}) \\
&\leq_{i_3} (\lambda(\Phi) + \delta(\Phi))\tau(\Phi_{n-1}, \Phi_n)
\end{aligned}$$

Since $\kappa = (\lambda(\Phi) + \delta(\Phi)) < 1$, we have

$$\begin{aligned}
\implies \tau(\Phi_n, \Phi_{n+1}) &\leq_{i_3} \kappa\tau(\Phi_{n-1}, \Phi_n) \\
&\leq_{i_3} \kappa^2\tau(\Phi_{n-2}, \Phi_{n-1}) \\
&\vdots \\
&\leq_{i_3} \kappa^2\tau(\Phi_0, \Phi_1)
\end{aligned}$$

For every $n, m \in \mathbb{N}$ and $n < m$, we have

$$\begin{aligned}
\tau(\Phi_n, \Phi_m) &\leq_{i_3} \rho(\Phi_n, \Phi_{n+1})\tau(\Phi_n, \Phi_{n+1}) + \rho(\Phi_{n+1}, \Phi_m)\tau(\Phi_{n+1}, \Phi_m) \\
&\leq_{i_3} \rho(\Phi_n, \Phi_{n+1})\tau(\Phi_n, \Phi_{n+1}) + \rho(\Phi_{n+1}, \Phi_m)\rho(\Phi_{n+1}, \Phi_{n+2})\tau(\Phi_{n+1}, \Phi_{n+2}) \\
&+ \rho(\Phi_{n+1}, \Phi_m)\rho(\Phi_{n+2}, \Phi_m)\tau(\Phi_{n+2}, \Phi_m) \\
&\leq_{i_3} \rho(\Phi_n, \Phi_{n+1})\tau(\Phi_n, \Phi_{n+1}) + \rho(\Phi_{n+1}, \Phi_m)\rho(\Phi_{n+1}, \Phi_{n+2})\tau(\Phi_{n+1}, \Phi_{n+2}) \\
&+ \rho(\Phi_{n+1}, \Phi_m)\rho(\Phi_{n+2}, \Phi_m)\rho(\Phi_{n+2}, \Phi_{n+3}) + \tau(\Phi_{n+2}, \Phi_{n+3}) \\
&+ \rho(\Phi_{n+1}, \Phi_m)\rho(\Phi_{n+2}, \Phi_m)\rho(\Phi_{n+3}, \Phi_m)\tau(\Phi_{n+3}, \Phi_m) \dots \\
&\leq_{i_3} \rho(\Phi_n, \Phi_{n+1})\tau(\Phi_n, \Phi_{n+1}) + \sum_{i=n+1}^{m-2} \left(\prod_{j=n+1}^{i} \rho(\Phi_j, \Phi_m) \right) \rho(\Phi_i, \Phi_{i+1})\tau(\Phi_i, \Phi_{i+1}) \\
&+ \prod_{i=n+1}^{m-1} \rho(\Phi_i, \Phi_m)\tau(\Phi_{m-1}, \Phi_m)
\end{aligned}$$

$$\begin{aligned}
\tau(\Phi_n, \Phi_m) &\leq_{i_3} \rho(\Phi_n, \Phi_{n+1})\tau(\Phi_n, \Phi_{n+1}) + \sum_{i=n+1}^{m-2} \left(\prod_{j=n+1}^{i} \rho(\Phi_j, \Phi_m) \right) \rho(\Phi_i, \Phi_{i+1})\tau(\Phi_i, \Phi_{i+1}) \\
&+ \left(\prod_{i=n+1}^{m-1} \rho(\Phi_i, \Phi_m) \right) \tau(\Phi_{m-1}, \Phi_m)\rho(\Phi_{m-1}, \Phi_m)\tau(\Phi_{m-1}, \Phi_m) \\
&\leq_{i_3} \rho(\Phi_n, \Phi_{n+1})\kappa^n\tau(\Phi_0, \Phi_1) + \sum_{i=n+1}^{m-2} \left(\prod_{j=n+1}^{i} \rho(\Phi_j, \Phi_m) \right) \rho(\Phi_i, \Phi_{i+1})\kappa^i\tau(\Phi_0, \Phi_1) \\
&+ \left(\prod_{i=n+1}^{m-1} \rho(\Phi_i, \Phi_m) \right) \kappa^{m-1}\tau(\Phi_0, \Phi_1)\rho(\Phi_{m-1}, \Phi_m) \\
&= \rho(\Phi_n, \Phi_{n+1})\kappa^n\tau(\Phi_0, \Phi_1) + \sum_{i=n+1}^{m-1} \left(\prod_{j=n+1}^{i} \rho(\Phi_j, \Phi_m) \right) \rho(\Phi_i, \Phi_{i+1})\kappa^i\tau(\Phi_0, \Phi_1)
\end{aligned}$$

Let

$$\Re_\theta^* = \textstyle\sum_{i=n+1}^{m-1} \left(\prod_{j=n+1}^{i} \rho(\Phi_j, \Phi_m) \right) \rho(\Phi_i, \Phi_{i+1})\kappa^i\tau(\Phi_0, \Phi_1)$$

Then we get

$$\tau(\Phi_n, \Phi_m) \leq_{i_3} \tau(\Phi_0, \Phi_1) \left[\kappa^n \rho(\Phi_n, \Phi_{n+1}) + (\Re_{m-1}^* - \Re_n^*) \right]$$

applying $(\Phi, \Psi) \geq_{i_3} 1$ and ratio test, $\lim_{n\to\infty} \Re_n^*$ exists. Thus $\{\Re_n^*\}$ is a Cauchy sequence.

$$\implies \lim_{n,m\to\infty} \tau(\Phi_n, \Phi_m) = 0$$

Thus, $\{\Phi_n\}$ is a Cauchy sequence in the complete tricomplex valued metric space in (Ξ, τ). Then $\{\Phi_n\}$ converges to Φ_1. From (1), it has a unique limit and by (2) we get

$$\begin{aligned}
\Phi_1 = \lim_{n\to\infty} \Phi_{n+1} = \lim_{n\to\infty} \sigma\Phi_n = \sigma(\lim_{n\to\infty} \Phi_n) = \sigma\Phi_1. \\
\Phi_1 = \lim_{n\to\infty} \Phi_{n+1} = \lim_{n\to\infty} \varsigma\Phi_n = \varsigma(\lim_{n\to\infty} \Phi_n) = \varsigma\Phi_1
\end{aligned}$$

For uniqueness, let Φ_1, Ψ_1 both are fixed points of σ, ς. Then from (2) we have

$$\begin{aligned}
\tau(\Phi_1, \Psi_1) &= \tau(\sigma\Phi_1, \varsigma\Psi_1) \\
&\leq_{i_3} \lambda(\Phi) \max \left\{ (\tau(\Phi_1, \Psi_1), \frac{\tau(\Phi_1, \sigma\Phi_1)\tau(\Psi_1, \varsigma\Psi_1)}{\tau(\Phi_1, \varsigma\Psi_1) + \tau(\Psi_1, \sigma\Phi_1) + \tau(\Phi_1, \Psi_1)} \right\} \\
&+ \delta(\Phi) \{\tau(\Phi_1, \sigma\Phi_1) + \tau(\Psi_1, \varsigma\Psi_1)\} \\
&\leq_{i_3} \lambda(\Phi) \max \left\{ (\tau(\Phi_1, \Psi_1), \frac{\tau(\Phi_1, \Phi_1)\tau(\Psi_1, \Psi_1)}{\tau(\Phi_1, \Psi_1) + \tau(\Psi_1, \Phi_1) + \tau(\Phi_1, \Psi_1)} \right\} \\
&+ \delta(\Phi) \{\tau(\Phi_1, \Phi_1) + \tau(\Psi_1, \Psi_1)\}
\end{aligned}$$

$$\implies \tau(\Phi_1, \Psi_1) = 0$$

Then σ, ς have a unique common fixed point and $\Phi_1 = \Psi_1$ ■

4. CONCLUSION

Following Price's initial description of multicomplex spaces, further investigations have been conducted by other researchers. Recently, Ramaswamy et al. [22] presented the concept of tricomplex valued controlled metric spaces. In this paper, we expand on these results by proposing a new type of contraction mapping, where we also establish fixed point theorems and make use of the control function within tricomplex valued controlled metric spaces.

REFERENCES

[1] Banach, S. (1922). Sur les operations dans les ensembles abstraits et leur applications aux equations integrales. *Fund. Math.*, 3:133–181.
[2] Bakhtin, I. (1989). The contraction mapping principle in quasimetric spaces. *Functional analysis*, 30:26-37.
[3] Berinde, V. P´curar, M. (2022). The early developments in fixed point theory on b-metric spaces. *Carpathian Journal of Mathematics*, 38(3):523-538.
[4] Cho, Y. J. (2017). Survey on metric fixed point theory and applications. *Advances in Real and Complex Analysis with Applications*, 183–241.
[5] Chourasiya S, Shrivastava K. (2024). Common Fixed Point Theorem in Controlled Metric Spaces. *Int. j. adv. multidisc. res. stud.*, 4(5):317-323.
[6] Cobzas S, Czerwik S. (2020). The completion of generalized b-metric spaces and fixed points. *Fixed Point Theory*, 21(1):133-150.
[7] Czerwik, S. (1998). Nonlinear set-valued contraction mappings in b-metric spaces. *Atti Sem. Mat. Fis. Univ. Modena*, 46:263-276.
[8] Jahangir, F., Haghmaram, P., Nourouzi, K. (2021). A note on F-metric spaces. *Journal of Fixed Point Theory and Applications*, 23(1):2.
[9] Jleli, M., Samet, B. (2012). Remarks on G-metric spaces and fixed point theorems. *Fixed Point Theory and Applications*, 2012:1-7.
[10] Lateef, D., Ahmad, J. (2019). Dass and Gupta's fixed point theorem in F-metric spaces. *J. Nonlinear Sci. Appl.*, 12:405-411.
[11] Matthews, S. G. (1994). Partial metric topology. *Annals of the New York Academy of Sciences*, 728(1):183-197.
[12] Azam A, Fisher B, Khan M. (2011). Common Fixed point theorems in complex valued metric spaces. *Numerical Functional Analysis and Optimization*, 32:243-53.
[13] Sintunavarat, W., Kumam, P. (2012). Generalized common Fixed point theorems in complex valued metric spaces and applications. *Journal of inequalities and Applications*, 2012:1-12.
[14] Rao, P. R., Swamy, P. R., Prasad, J. R. (2013). A common Fixed point theorem in complex valued b-metric spaces. *Bulletin of Mathematics and Statistics research*, 1(1):1-8.
[15] Price, G. B. (2018). An introduction to multicomplex spaces and functions. *CRC Press*.
[16] Beg, I., Datta, S. K., Pal, D. (2021). Fixed point in bicomplex valued metric spaces. *International Journal of Nonlinear Analysis and Applications*, 12(2):717-727.
[17] Mani, G., Haque, S., Gnanaprakasam, A. J., Ege, O., Mlaiki, N. (2023). The study of bicomplex valued controlled metric spaces with applications to fractional differential equations. *Mathematics*, 11(12):2742.
[18] Mani, G., Gnanaprakasam, A. J., Haq, A. U., Baloch, I. A., Jarad, F. (2022). Common fixed point theorems on tricomplex valued metric space. *Mathematical Problems in Engineering*, 2022(1):4617291.

[19] Ramaswamy, R., Mani, G., Gnanaprakasam, A. J., Abdelnaby, O. A. A., Radenovi‡, S. (2022). An application to fixed-point results in tricomplex-valued metric spaces using control functions. *Mathematics.* **10** , no. 18, 3344.

[20] Mlaiki, N., Aydi, H., Souayah, N., Abdeljawad, T. (2018). Controlled metric type spaces, and the related contraction principle. *Mathematics*, 6(10):194.

[21] Dass, B. K., Gupta, S. (1975). An extension of Banach contraction principle through rational expression. *Indian J. pure appl. Math.*, 12(6):1455-1458.

[22] Ramaswamy, R., Mani, G., Gnanaprakasam, A. J., Abdelnaby, O. A. A., Radenovi‡, S. (2023). Solving an Integral Equation via Tricomplex-Valued Controlled Metric Spaces. *Axioms*, 12(1):56.

RT&A, No 3 (86)
Volume 20, September 2025

BAYESIAN ESTIMATION OF POISSON-COMPOUNDED EXPONENTIAL TYPE DISTRIBUTION UNDER DIFFERENT LOSS FUNCTIONS

Na Elah[1] Peer Bilal Ahmad*[2]

•

Department of Mathematical Sciences, Islamic University of Science & Technology, Kashmir, India[1,2]

naaelashah@gmail.com[1] , bilalahmadpz@gmail.com[2]

Abstract

Poisson moment exponential distribution is an important distribution and has gained special attention recently. It plays role in various fields, mostly in actuarial sciences. Thus its parametric estimation becomes important thing to do. The classical approach using the maximum likelihood method is the most used way to estimate the parameters of a distribution. In this paper, we considered the Bayesian approach to estimate the parameter of the distribution using beta prior which is a conjugate prior. The Bayes estimate for the parameter is obtained under Squared Error Loss Function (SELF) which is a symmetric loss function, Weighted SELF (WSELF) and Entropy Loss Function (ELF). Through a simulation study, the comparison is made on the performance of Bayes estimate under these loss functions with respect to Bias and Mean Square Error (MSE).

Keywords: Bayesian, Loss function, Maximum likelihood estimator, Poisson moment exponential distribution, Simulation

1. Introduction

Bayesian statistics is still one of the most potent concepts in the opinion of many statisticians. Even years after Thomas Bayes first proposed the idea of the Bayes theorem in 1770, the significance of Bayesian statistics has not diminished. In Bayesian statistics, the unknown parameter is considered as the value of a random variable from a specified probability distribution with some prior knowledge about the parameter. Researchers, engineers, statisticians, and other applied scientists who utilise prediction techniques for a variety of objectives find it highly intriguing to estimate the lifespan of future samples based on an informative sample. One-sample and two-sample prediction problems, which are a particular form of the multiple-sample prediction issue, are the two categories into which the future prediction problem falls.

The application of Bayesian approaches in many statistical and non-statistical domains is gaining popularity. In 2020, Johannesson [12] proposed that at any rate, there is a disagreement between classical statistics and the Bayesian theory.

There are several benefits of Bayesian approaches over Frequentistic approach, few among them are listed as under:

- By adjusting prior distribution, Bayesian inference can prevent problems with model identification. Since frequentist inference lacks prior distributions, so it can lead to problems with model identification when employing any numerical approximation approach.

- In Bayesian approach, unknown parameters are treated as random variables, and the data is fixed. According to frequentist inference, the data are random and the unknown parameters are fixed. Estimates are made using both the current data and hypothetically repeated sampling of similar data. The proper answer is provided by the Bayesian technique in the sense that it bases its conclusions on actual data rather than test statistics across hypothetical samples that are unobserved (see [19]).

- In order to inform the current model, prior knowledge or the outcomes of a previous model can be utilised, and Bayesian inference permits informative priors. If β is the unknown parameter, then P(β | data) is estimated using Bayesian inference. On the other hand, Frequentist inference, calculates P(data | β).

- By including uncertainty into the probability model, Bayesian inference produces predictions that are closer to reality. Less realistic predictions are produced by frequentist inference as it does not account for the uncertainty of the parameter estimates.

- Probability intervals-quantile-based, maximum posterior density or, lowest posterior loss- are used in Bayesian inference to express the likelihood that β lies between two points. On the other hand, Confidence intervals, are used in frequentist inference, that must be interpreted with a probability of zero or one to indicate whether or not β is in the region. The frequentist is never certain whether β is in the region; all it can say is that, in the event that 100 repeat samples are taken in the future, 95 of them would be.

In the area of Bayesian estimation and future observation prediction for various models, some references are as follows: Migdadi [17] derived the Bayes estimators for the scale parameter of the discrete Rayleigh distribution. Kamari *et al.* [15] obtained a Bayesian analysis of the discrete Burr distribution. Ahmad [1] and Ahmad [2] studied the Bayesian estimation of different models including size biased Generalized Power Series and Zero-Inflated Generalized Power Series respectively under various loss functions. Ashour and Muiftah [3] introduced Bayesian estimation of the parameters of the discrete Weibull Type-I distribution. Chaiprasithikul and Duangsaphon [7] studied the Bayesian estimation for the discrete Weibull regression under type-I right censored data and showed that the Bayes estimator with informative priors for the parameters are more appropriate for the model in case of over dispersion. Halder *et al.* [11] introduced the Bayesian estimation of Power series model when the stress (X) and strength (Y) are from different members of the power series family. Also, Hegazy *et al.* [10] studied Bayesian inference to estimate the parameters of discrete Gompertz distribution. Hegazy *et al.* [10] showed that linear exponential loss function gives better results than squared error loss function. El-Morshedy *et al.* [18] also studied the Bayesian estimation of the parameters of discrete odd Weibull-G family of distributions with application to count data. Yahya *et al.* [23] proposed a Bayesian method for testing non-inferiority between two independent binomial proportions.

The objective of this study is to derive the Bayesian estimate for the unknown parameter of Poisson Moment Exponential (PME) distribution which is a one parameter discrete distribution given by Ahsan-ul-Haq [4] and its zero inflated version is given by Skinder *et al.* [20]. Here three different loss function namely-SELF, WSELF and ELF are used to produce the Bayes estimators. The theoretical insights produced in this work are illustrated with a numerical example in Section 6. The rest of the paper is organised as follows: Section 2 discusses about the Bayesian approach including prior and posterior distribution. Section 3 gives an idea about different loss functions. In section 4 and 5, Bayesian estimates of PME distribution and simulation analysis are provided respectively. Section 6 discusses few applications and section 7 concludes.

2. Bayesian Approach

Let's suppose β be the unknown parameter of interest, then the Bayesian approach would consider the parameter β as a random variable, and inference about β is derived from both prior

assumptions about β and the data x. The posterior density of β given x is formed by combining the evidence with prior beliefs, and Bayesian inference is based on this posterior.

2.1. Prior Distribution

The prior distribution is an important part of Bayesian analysis. It represents the information about an unknown parameter which is mixed with the probability distribution of new data to get the posterior distribution, which in turn is used for future prediction. In certain cases, a valuable apriori knowledge on the probable values of parameter β exists. Then, an informative prior that affects the posterior distribution is defined. The prior density of β's functional form is frequently selected based on computational ease of use or analytical tractability. In order to set up a prior distribution, the following points are crucial:
1. what data is included in the previous distribution;
2. the characteristics of the resulting posterior distribution.

2.2. Posterior Distribution

The posterior distribution of the evidence x given β, represented as P(β | x), combines information from the current data x with conditional probability P(x | β) and a prior probability $\pi(\beta)$ captures previous ideas about β. Now, from conditional probability theorem, we have:

$$P(\beta|x) = \frac{P(\beta, x)}{P(x)} \tag{1}$$

If prior probability associated with β is denoted by $\pi(\beta)$, then we can also write as $P(\beta, x) = P(x|\beta)\pi(\beta)$. So, equation (1) becomes

$$P(\beta|x) = \frac{P(x|\beta)\pi(\beta)}{P(x)}$$

where $P(x)$ is the normalizing constant calculated a;

$$P(x) = \int P(x|\beta)\pi(\beta)d\beta$$

We can also write posterior distribution as:

$$\rho(\beta|x) = \frac{L(x, \beta)\pi(\beta)}{\int L(x, \beta)\pi(\beta)d\beta} \tag{2}$$

i.e., posterior $\propto$ likelihood $\times$ prior.

3. Loss Functions

Wald [22] was the first to use the term "loss function" . It is a measurement of the discrepancy between the data's observed values and those determined by using the adjustment function. This loss function is to be minimised during the model-fitting process. There are several loss functions and few among them are discussed as follows:

3.1. Squared Error Loss Function

The squared error loss function ($SELF$) proposed by Legendre [16] and Gauss [9] is defined by:

$$L(\phi(\beta), d) = (\phi(\beta) - d)^2$$

where $\phi(\beta)$ is a function of β and d is an action(estimator).

An alternative of this loss function is a weighted squared error loss function ($WSELF$) defined by:

$$L(\phi(\beta), d) = w(\beta)(\phi(\beta) - d)^2$$

where $w(\beta)$ is the weight associated with the estimator.

In case of squared error loss function, the Bayes estimator $\delta^{\pi}(x)$ of β associated with the prior distribution π is the posterior mean of β defined by:

$$\delta_s^{\pi}(x) = E_{\pi}(.|x)(\beta) = \int L(\beta, \delta(x))\pi(\beta|x)d\beta \quad , d = \delta(x)$$

Since, the Bayes estimator minimizes the posteriori loss, that is to say:

$$\rho(\pi, \delta) = E^{\pi(.|x)}(L(\beta, \delta(x)))$$

So, under the assumption of squared error loss, we have:

$$\begin{aligned} \rho(\pi, \delta) &= E^{\pi(.|x)}(\beta - \delta(x))^2; \\ &= E^{\pi(.|x)}(\beta)^2 - 2\delta(x)E^{\pi(.|x)}(\beta) + \delta(x)^2 \end{aligned}$$

It is evident that it is a polynomial second degree in $\delta(x)$. The minimum value will occur in $E^{\pi(.|x)}(\beta)$.

3.2. Entropy Loss Function

The entropy loss function (ELF) was introduced by Calabria and Pulcini [5] as a loss function that originates from the Linex loss function. It is described as follows:

$$L_e(\beta, d) \propto \left(\frac{d}{\beta}\right)^p - p\ln\left(\frac{d}{\beta}\right) - 1 \quad ; p > 0$$

When $d = \beta$, the entropy loss function is minimum. Under this loss function, the Bayes estimator of parameter β is given by:

$$\delta_e^{\pi}(x) = (E_{\beta}(\beta)^{-p})^{-1/p}$$

The Bayes estimator coincides with the Bayes estimator under weighted squared error loss function $\frac{(\beta-d)^2}{\beta}$ when $p = 1$.

The Bayes estimator coincides with the Bayes estimator under squared error loss function when $p = -1$.

4. Bayesian Estimation of PME Distribution

From Ahsan-ul-Haq [4], the pmf of PME distribution is given as:

$$P(X = x) = \frac{\beta^x(1+x)}{(1+\beta)^{(x+2)}} \quad ; x = 0, 1, 2, \ldots \quad ; \beta > 0 \tag{3}$$

The likelihood of equation (3) can be written as:

$$L(\beta) = \frac{\beta^{\sum x_i}\prod_{min}^{max}(1+x_i)}{(1+\beta)^{2n+\sum x_i}} \tag{4}$$

Differentiating equation (4) and equating to 0 we get the MLE of β as:

$$\hat{\beta} = \frac{\bar{x}}{2} \tag{5}$$

Now, instead of treating parameter β as constant, treat it as a random variable following beta prime distribution i.e.,

$$\beta \sim Beta(c, d) \tag{6}$$

where c and d are hyper parameters.

$$\therefore \pi(\beta) = \frac{\beta^{c-1}}{B(c,d)(1+\beta)^{c+d}} \tag{7}$$

where $B(c,d) = \frac{\Gamma(c)\Gamma(d)}{\Gamma(c+d)}$

Now, using likelihood (4) and prior distribution (7), the Posterior distribution can also be obtained as:

$$\rho(\beta, x) = \frac{L(\beta)\pi(\beta)}{\int_0^\infty L(\beta)\pi(\beta)d\beta}$$

$$\rho(\beta|x) = \frac{\beta^{\sum_{i=1}^n x_i + c - 1}}{B(\sum_{i=1}^n x_i + c, 2n + d)(1+\beta)^{\sum_{i=1}^n x_i + 2n + c + d}} \tag{8}$$

Bayes estimate Under SELF

$$\delta_s^\pi(x) = \int_0^\infty \phi(\beta)\rho(\beta|x)d\beta$$

Let $\phi(\beta) = \beta^r$, then

$$\delta_s^\pi(x) = \frac{B(\sum x_i + c + 1, 2n + d - 1)}{B(\sum x_i + c, 2n + d)}$$

Bayes estimate Under WSELF

$$\delta_w^\pi(x) = \frac{\int_0^\infty w(\beta)\phi(\beta)\rho(\beta|x)d\beta}{\int_0^\infty w(\beta)\rho(\beta|x)d\beta}$$

let $w(\beta) = \beta^{-2}$, then

$$\delta_w^\pi(x) = \frac{B(\sum x_i + c - 1, 2n + d + 1)}{B(\sum x_i + c - 2, 2n + d + 2)}$$

Bayes estimate Under ELF

$$\delta_e^\pi(x) = [E_\beta(\beta)^{-p}]^{-1/p} = \left[\int_0^\infty \beta^{-p}\rho(\beta|x)d\beta\right]^{-1/p}$$

$$\Rightarrow \delta_e^\pi(x) = \left[\frac{B(\sum x_i + c, 2n + d)}{B(\sum x_i + c - p, 2n + d + p)}\right]^p \quad ; p > 0$$

5. Simulations: Comparing Classical and Bayesian Estimation Methods

Table 1: *The Bias, Var, and MSEs for different parameter values under classical and Bayesian approach*

		$\beta = 0.2$				$\beta = 0.28$			
n		MLE	SELF	WSELF	ELF	MLE	SELF	WSELF	ELF
	Bias	-0.0209	0.1621	0.0121	-0.0283*	-0.0209	0.2648	-0.0900*	-0.0333
10	Var	0.0102	0.0483	0.0032	0.0093	0.0122	0.0847	0.0101	0.0111
	MSE	0.0107	0.0745	0.0033*	0.0101	0.0127	0.1549	0.0182	0.0122*
	Bias	-0.0037	0.1129	-0.0231*	-0.0065	0.0046	0.2314	-0.0172*	0.0006
35	Var	0.0026	0.0104	0.0025	0.0025	0.0043	0.0282	0.0041	0.0042
	MSE	0.0026	0.0231	0.0029	0.0026*	0.0044	0.0818	0.0044	0.0042*
	Bias	-0.0025	0.1018	-0.0130*	-0.0039	-0.0008	0.1997	-0.0126*	-0.0029
65	Var	0.0019	0.0075	0.0018	0.0019	0.0025	0.0150	0.0024	0.0025
	MSE	0.0019	0.0179	0.0019	0.0019*	0.0024	0.0549	0.0026	0.0025*
	Bias	0.0103	0.1165	0.0056*	0.0096	0.0027	0.1962	-0.0025*	0.0018
150	Var	0.0009	0.0037	0.0009	0.0009	0.0015	0.0091	0.0014	0.0014
	MSE	0.0010	0.0173	0.0009*	0.0010	0.0015	0.0476	0.0014*	0.0014
	Bias	0.0064	0.1049	0.0038*	0.0059	-0.0009	0.1826	-0.0038*	-0.0014
270	Var	0.0005	0.0019	0.0005	0.0005	0.0008	0.0045	0.0008	0.0008
	MSE	0.0005	0.0129	0.0005*	0.0005	0.0008	0.0379	0.0008	0.0008*
		$\beta = 0.8$				$\beta = 1.6$			
n		MLE	SELF	WSELF	ELF	MLE	SELF	WSELF	ELF
	Bias	0.0001	2.1553	-0.1182	-0.0381*	-0.0679	9.5929	-0.2527*	-0.1409
10	Var	0.0575	2.2052	0.0475	0.0521	0.2454	75.1893	0.2028	0.2226
	MSE	0.0575	6.8503	0.0615	0.0536*	0.2500	167.2129	0.2667	0.2424*
	Bias	-0.0166	1.8191	-0.0522*	-0.0276	-0.0197	9.0940	-0.0775	-0.0419
35	Var	0.0212	0.7969	0.0200	0.0206	0.0369	7.6018	0.0349	0.0358
	MSE	0.0215	4.1060	0.0228	0.0214*	0.0373	90.3030	0.0409	0.0376
	Bias	0.0155	1.9604	-0.0044*	0.0093	0.0085	9.5598	-0.0235*	-0.0038
65	Var	0.0119	0.5139	0.0116	0.0117	0.0386	8.8758	0.0374	0.0379
	MSE	0.0122	4.3572	0.0116*	0.0118	0.0386	100.2657	0.0379*	0.0379
	Bias	-0.0039	1.7981	-0.0125*	-0.0065	0.0023	9.3219	-0.0116*	-0.0029
150	Var	0.0049	0.1795	0.0048	0.0048	0.0131	3.1097	0.0129	0.0129
	MSE	0.0049	3.4128	0.0049	0.0049*	0.0131	90.0093	0.0130	0.0129*
	Bias	0.0116	1.8783	0.0068*	0.0101	0.0082	9.3329	-0.0013*	-0.0013
270	Var	0.0022	0.0841	0.0022	0.0022	0.0122	2.5134	0.0113	0.0113
	MSE	0.0024	3.6120	0.0023*	0.0023	0.0122	89.6159	0.0113*	0.0113

The value with * is the best estimation in its row for all estimation methods.

From the Table 1, we can see that the bias and MSE is low in case of Bayesian statistics under different loss functions as compared to MLE in case of Classical statistics.

6. Applications

To demonstrate how the aforementioned findings might be applied in real-world scenarios, we fitted *PME* distribution to four data sets and carried out the goodness of fit test. The data sets in

table 2, 3, 4, and 5 represent the number of fires that occur in Greece between 1st July and 1st August, 1998 (see [14]) recently used by Elwa *et al.* [8]; deaths due to horse kicks in the Prussian Army (see [21]); frequency of lost shoes at a museum gate (see[6]) and number of outbreaks of strike in vehicle manufacturing industry in U.K during 1948-95 (see [13]) respectively. For the selection of values of (c, d), there was no information available in the Bayes estimation other than the fact that they are real and positive numbers. As a result, we examined 16 combinations of values of $(c, d = 1, 2, 3, 4)$ and only those values were chosen for which the predicted Bayes frequencies were reasonably similar to the observed frequencies. In all the four data sets, it was observed that the predicted Bayes frequencies for $c = d = 1$ were quite similar to the observed frequencies. Table 2, 3, 4, and 5 shows the observed frequencies, expected frequencies, the values chi-square statistics along with the degrees of freedom $(d.f)$ and their respective p-values. These predicted frequencies are obtained by using MLE, and under beta prior, the Bayes frequencies are obtained using squared error loss function, weighted squared error loss function and entropy loss function.

Table 2: *Number of fires that occurred in Greece (see [14])*

No. of Fires	Observed frequency	Expected Frequency			
		MLE	Under beta prior		
			SELF	WSELF	ELF
0	16.00	9.90	9.90	10.00	9.90
1	13.00	14.20	14.10	14.30	14.20
2	14.00	15.20	15.20	15.30	15.30
3	9.00	14.50	14.50	14.60	14.60
4	11.00	13.00	13.00	13.10	13.00
5	13.00	11.20	11.20	11.20	11.20
6	8.00	9.40	9.40	9.30	9.40
7	4.00	7.70	7.70	7.60	7.70
8	9.00	6.20	6.20	6.10	6.20
9	6.00	4.90	4.90	4.90	4.90
10	3.00	3.90	3.90	3.80	3.90
11	4.00	3.00	3.00	3.00	3.00
12	6.00	2.40	2.40	2.30	2.30
13	4.00	1.80	1.80	1.80	1.80
14	1.00	1.40	1.40	1.40	1.40
15	1.00	1.10	1.10	1.00	1.10
16	1.00	0.80	0.80	0.80	0.80
$Degrees\ of\ Freedom$		9	9	9	9
χ^2		13.92	13.90	14.24	14.16
$p-value$		0.12530	0.12587	0.11415	0.11677
$\hat{\beta}$		2.52846	2.53252	2.50403	2.51822

Table 3: *Deaths due to horse-kicks in the Prussian Army (see [21])*

No. of Deaths	Observed frequency	Expected Frequency			
			Under beta prior		
		MLE	SELF	WSELF	ELF
0	109.00	117.40	117.00	118.20	117.60
1	65.00	54.90	55.00	54.70	54.90
2	22.00	19.20	19.40	19.00	19.20
3	3.00	6.00	6.10	5.90	6.00
4	1.00	1.80	1.80	1.70	1.70
$Degrees\ of\ Freedom$		2.00	2.00	2.00	2.00
χ^2		4.72	4.64	4.83	4.67
$p-value$		0.09448	0.09832	0.08917	0.09665
$\hat{\beta}$		0.305	0.3075	0.30099	0.30424

Table 4: *Frequency distribution of lost shoes at a Museum gate (see [6])*

No. of shoes lost	Observed frequency	Expected Frequency			
			Under beta prior		
		MLE	SELF	WSELF	ELF
0	109.00	107.30	106.90	108.00	107.50
1	52.00	57.40	57.50	57.30	57.40
2	26.00	23.00	23.20	22.80	23.00
3	10.00	8.20	8.30	8.00	8.20
4	3.00	2.70	2.80	2.70	2.70
$Degrees\ of\ Freedom$		2.00	2.00	2.00	2.00
χ^2		1.33	1.23	1.44	1.32
$p-value$		0.51407	0.54051	0.48602	0.51561
$\hat{\beta}$		0.365	0.3675	0.36069	0.36409

Table 5: *Number of outbreaks of Strike in Vehicle manufacturing Industry (see [13])*

No. of Outbreaks	Observed frequency	Expected Frequency			
			Under beta prior		
		MLE	SELF	WSELF	ELF
0	110.00	107.40	106.80	108.20	107.50
1	33.00	36.60	36.80	36.20	36.50
2	9.00	9.30	9.50	9.10	9.30
3	3.00	2.10	2.20	2.00	2.10
4	1.00	0.50	0.50	0.40	0.40
$Degrees\ of\ Freedom$		1.00	1.00	1.00	1.00
χ^2		0.52	0.54	0.51	0.52
$p-value$		0.47139	0.46214	0.47579	0.47264
$\hat{\beta}$		0.20513	0.20833	0.20064	0.20447

It is clear from Tables 2, 3, 4, and 5, that the Bayes estimator obtained under beta prior gives closed fit than MLE.

7. Conclusion

In this paper Bayes estimation of a discrete count model namely poisson moment exponential distribution is discussed. By using three different loss functions it has been observed that how Bayesian approach gains priority over classical approach. A simulation study suggests that the bias and mean square error is always low in case of Bayesian approach. Four data sets were also analysed and it has been found that the p-value is highest in case of bayesian approach. From the study, it can be inferred that Bayesian approach is more reliable than classical approach.

Acknowledgements: The quality and presentation of the paper have been significantly improved, thanks to the insightful comments of the Editor-in-Chief.

Author contributions: All the authors have contributed equally.

Conflict of interest: The authors have no conflict of interest.

Funding: The author received no specific funding for this study.

References

[1] Ahmad, P. B. (2016). On the Bayes estimators of the parameters of size-biased generalized power series distributions. Communications in Statistics-Theory and Methods, 45(12), 3612-3624.

[2] Ahmad, A. (2019). Bayesian Analysis and Reliability Estimation of Generalized Probability Distributions. Balrampur: AIJR Publisher.

[3] Ashour, S. K., & Muiftah, M. S. A. (2020). Bayesian Estimation of the Parameters of Discrete Weibull Type (I) Distribution. Journal of Modern Applied Statistical Methods, 18(2), 12.

[4] Ahsan-ul-Haq, M. (2022). On Poisson moment exponential distribution with applications. Annals of Data Science, 1-22.

[5] Calabria, R., & Pulcini, G. (1994). An engineering approach to Bayes estimation for the Weibull distribution. Microelectronics Reliability, 34(5), 789-802.

[6] Chandra, N. K., Roy, D., & Ghosh, T. (2013). A generalized Poisson distribution. Communications in Statistics-Theory and Methods, 42(15), 2786-2797.

[7] Chaiprasithikul, D., & Duangsaphon, M. (2022). Bayesian Inference for the Discrete Weibull Regression Model with Type-I Right Censored Data. Thailand Statistician, 20(4), 791-811.

[8] Eliwa, M. S., Ahsan-ul-Haq, M., Almohaimeed, A., Al-Bossly, A., & El-Morshedy, M. (2023). Discrete Extension of Poisson Distribution for Overdispersed Count Data: Theory and Applications. Journal of Mathematics, 2023.

[9] Gauss, C. F. (1810). Least squares method for the combinations of observations (translated by J. Bertrand 1955). Mallet-Bachelier, Paris.

[10] Hegazy, M. A., Abd El-Kader, R. E., El-Helbawy, A. A., & Al-Dayian, G. R. (2021). Bayesian estimation and prediction of discrete Gompertz distribution. Journal of Advances in Mathematics and Computer Science, 36(1), 1-21.

[11] Halder, S., Maiti, S. S., & Chowdhury, M. M. (2024). BAYESIAN ESTIMATION OF $P(X \leq Y)$ FOR POWER-SERIES MODEL. Reliability: Theory & Applications, 19(2 (78)), 138-155.

[12] Johannesson, E.(2020). Classical versus bayesian statistics. Philosophy of Science, 87(2), 302-318.

[13] Kendall, M. G. (1961). Natural law in the social sciences. The inaugural address of the President (with discussion). OR, 292-292.

[14] Karlis, D., & Xekalaki, E. (2001). Robust inference for finite Poisson mixtures. Journal of Statistical Planning and Inference, 93(1-2), 93-115.

[15] Kamari, H., Bevrani, H., & Kamary, K. (2015). Bayesian estimation of discrete Burr distribution with two parameters. arXiv preprint arXiv:1501.05876.
[16] Legendre, A. (1805). New Methods for the Determination of Orbits of Comets Courcier.
[17] Migdadi, H. S. (2014). Bayesian inference for the scale parameter of the discrete Rayleigh distribution. Journal of Science and Technology, 3(2), 1073-1080.
[18] El-Morshedy, M., Eliwa, M. S., & Tyagi, A. (2022). A discrete analogue of odd Weibull-G family of distributions: properties, classical and Bayesian estimation with applications to count data. Journal of Applied Statistics, 49(11), 2928-2952.
[19] Rossi, P., Allenby, G., & McCulloch, R. (2005). Bayesian Statistics and Marketing. No. 13 in Wiley series in probability and statistics.
[20] Skinder, Z., Ahmad, P. B., & Elah, N. (2023). A new zero-inflated count model with applications in medical sciences. Reliability: Theory & Applications, 18(3 (74)), 841-855.
[21] von Bortkiewicz, L. (1898). Das Gesetz der kleinen Zahlen Leipzig.
[22] Wald, A. (1939). Contributions to the theory of statistical estimation and testing hypotheses. The Annals of Mathematical Statistics, 10(4), 299-326.
[23] Yahya, W. B., Ezenweke, C. P., Olaniran, O. R., Adeniyi, I. A., Jimoh, K., Afolayan, R. B., ... & Ahmed, I. (2024). BAYESIAN NON-INFERIORITY TEST BETWEEN TWO BINOMIAL PROPORTIONS. Reliability: Theory & Applications, 19(3 (79)), 689-703.

OPTIMIZING FUZZY DETERIORATING INVENTORY MODEL WITH TIME DEPENDENT DEMAND AND PARTIAL BACKLOGGING UNDER RESALABLE RETURNS

Kapil Dave[1], Tanuj Kumar[1,*]

•

[1]Department of Mathematics, SRM Institute of Science and Technology,
Delhi-NCR Campus, Ghaziabad, India, 201204
kd1512@srmist.edu.in, tanujkhutail@gamil.com
*Corresponding author

Abstract

This paper investigates with the development of a fuzzy inventory model with timevarying demand, deterioration and backlogging with resalable returns. The returns rate, demand and backlogging parameters are taken as trapezoidal fuzzy numbers. Numerical example is given to validate the proposed mathematical model which has been developed for determining the optimal cycle time and optimal total inventory cost and profit. Sensitivity analysis is also carried out to explore the effect of changes in the optimal solution with respect to change in various parameters. The aim of this paper is to develop inventory policies that minimize the total cost so that to get the maximum total profit in both crisp and fuzzy modeling, and comparison of crisp and fuzzy models. Our study focuses on de-fuzzifying the total cost using the signed distance method and comparing it with the crisp model. This inventory model incorporates fuzzy demand and constant holding cost per unit item under the reasonable return policy while considering the impact of deterioration as a linearly increasing function of time. The retailer allows its unsatisfactory costumers to return their products. We assume that the return product will be sold at the same price. Customers are allowed to return the product during any phase of the length of the replenishment cycle. The retailer does not return the full amount to its customers for the returned goods. He offers 80% of the initial amount of the product. The number of returns are assumed to be proportional to demand. The demand is dependent on time. Partial backlogging is an important issue in the inventory theory which is related how to deal with the unfulfilled demand that occurs due to the shortage of stock. In real practice some customers prefers to wait for backorder during the shortage time and some turns to buy from other sellers. The waiting time period for next replenishment determine whether the backlogging would be accepted or not. During the shortage period the longer the waiting time is, the smaller is the backlogging rate would be. So backlogging rate is a variable that depends on the waiting time for next replenishment.

Keywords: Optimization, Deteriorating Inventory, Returns Rate, Triangular Fuzzy Number, and Signed Distance Method.

1. Introduction and leterature survey

The inventory management system is an important aspect for any business firm is to get more profit . An inventory management depends on different parameters such as demand, deterioration, holding cost, shortages, backlogs, inflation and trade credit, etc. In inventory modeling uncertainty often arises due to the concept of fuzziness, which is considered the closest approximation to

reality. Return policies offered by the seller attracts the customers. The return policy allows consumers who are unsatisfied with their purchase to return the product and get a refund either in terms of money or some gift vouchers as stated by the company or seller in its policies. In recent years, some researchers have focused on incorporating time-dependent rates, partial backlogging , return policy and deterioration in their models. For instance, De and Rawat [1] developed an a Fuzzy Inventory Model without Shortages using Triangular Fuzzy Number. Saha and Chakrabarti [2] developed fuzzy EOQ model for time-dependent deteriorating items and time-dependent demand with shortages. Jaggi et al. [3] Fuzzy Inventory Model for Deteriorating Items with Time Varying Demand and Shortages. Mahata [4] developed an EPQ-based inventory model for exponentially deteriorating items under retailer partial trade credit policy in supply chain. Saha and Chakrabarti [5] developed fuzzy EOQ model for timedependent deteriorating items and time-dependent demand with shortages, while Dutta and Kumar [6] introduced a partial backlogging inventory model for deteriorating items with time-varying demand and holding cost. Further, Kumar and Rajput [7] developed a Fuzzy Inventory Model for Deteriorating Items with Time Dependent Demand and Partial Backlogging. Sahoo et al. [8] presented a Fuzzy inventory model with exponential demand and time-varying deterioration. Jaggi et al. [9] focused on an inventory model with Inventory decisions for imperfect quality deteriorating items with exponential declining demand under trade credit and partially backlogged shortages. Malik and Garg [10] presented an Improved Fuzzy Inventory Model Under Two Warehouses. Boina et al. [11] presented an inventory model for Two-Storage Fuzzy Inventory Model with Time Dependent Demand and Holding Cost under Acceptable Delay in Payment . Kuppulakshmi et al. [12] introduced Fuzzy Inventory Model for Imperfect Items with Price Discount and Penalty Maintenance Cost.

Recent research has focused on incorporating environmental factors and technology investments into inventory models with deterioration. Yadav and Kumar [13] proposed a model that considers selling price, time-sensitive demand, and carbon emissions under green technology investment. Yadav et al. [14] introduced a two-warehouse model using an interval approach, including preservation technology to manage uncertainty. In another study, Yadav et al. [15] addressed deterioration during storage within a two-warehouse setup, aiming to reduce total costs. They further extended this by including reliability and carbon emission constraints with time-based demand [16]. Similarly, Mahata and Debnath [17] analyzed a price-sensitive inventory system with preservation investment to handle deterioration. Later, they explored the impact of green technology and flexible production on economic production models with carbon emissions [18], showing that cleaner and more flexible systems help reduce environmental costs. Debnath et al. [19] developed an EOQ model under uncertainty using a generalized intuitionistic fuzzy Laplace transform. Their approach helps handle imprecise data more effectively in inventory systems.

2. Methods

2.1. Definitions and Preliminaries

1. **Fuzzy set:** A fuzzy set allows for partial membership in which an element can belong to a set to a certain degree or degree of membership, which is represented by a value between 0 and 1. Mathematically, A fuzzy set defined on a universe of discourse $X = \{x_1, x_2, x_3, \ldots, x_n\}$ is given by $A = \{(x, \mu_A(x)) : x \in X\}$, where $\mu_A(x)$ is the membership function of A given by $\mu_A(x) : X \to [0, 1]$.

2. **Fuzzy Number:** A fuzzy number is a fuzzy set on the real line $\mathbb{R}$, if its membership function $\mu_A(x)$ has the following properties:

   (a) $\mu_A(x)$ is upper semi-continuous.

   (b) There exist some real numbers a_2 and a_3, $a_1 \leq a_2 \leq a_3 \leq a_4$ such that $\mu_A(x)$ is increasing on $[a_1, a_2]$, decreasing on $[a_3, a_4]$ and $\mu_A(x) = 1$ for each x on $[a_2, a_3]$.

(c) $\mu_A(x) = 0$ outside the interval $[a_1, a_4]$.

3. **Triangular Fuzzy Number:** A triangular fuzzy number is specified by the triplet (a_1, a_2, a_3) and defined by its membership function $\mu_A(x) : X \to [0, 1]$ as follows:

$$\mu_A(x) = \begin{cases} 0, & x \leq a_1 \\ \frac{x-a_1}{a_2-a_1}, & a_1 \leq x \leq a_2 \\ \frac{a_3-x}{a_3-a_2}, & a_2 \leq x \leq a_3 \\ 0, & x \geq a_3 \end{cases}$$

2.2. Notations and assumptions

The following notations are used for proposed fuzzy inventory model:

Table 1: *Notations used in the proposed fuzzy inventory model*

Symbol	Description
$\eta(t)$	Deterioration rate
$\gamma(t)$	Time-dependent demand
T	Length of one cycle
$Q_1(t)$	Inventory level at time $t \in [0, t_1]$
$Q_2(t)$	Inventory level at time $t \in [t_1, T]$
A	Ordering cost
c	Buying price of an item
c_d	Deterioration cost per item
c_p	Selling price of an item
c_o	Lost sale cost per item
c_s	Shortage cost per item
α	Deterioration coefficient parameter
μ, b	Demand coefficient parameters
h_c	Holding cost coefficient
$R(t)$	Return rate
σ	Return rate parameter
p	Backlogging parameter
TC^o	Total cost per unit time in crisp model
TC^*	Total cost per unit time in fuzzy model
TP^o	Total profit per unit time in crisp model
TP^*	Total profit per unit time in fuzzy model
$\tilde{\mu}, \tilde{b}$	Fuzzy demand parameters
$\tilde{\sigma}$	Fuzzy return rate parameter
$\tilde{p}$	Fuzzy backlogging parameter

The following assumptions have been adopted while developing the fuzzy inventory model:

1. Single item is used in the developed fuzzy inventory model.
2. Lead time is zero.
3. The demand rate is defined as:

$$\gamma(t) = be^{\mu t}$$

4. The inventory deteriorates as a linear function of time and given by: $\eta(t) = \alpha t$
5. It is assumed that customers return in proportion to demand, so return rate is given by:

$$R(t) = \sigma\,\gamma(t), \quad \text{where } 0 \le \sigma < 1$$

6. Shortages are allowed and partial backlogging is at constant rate p, where $0 \le p < 1$.
7. The holding cost per item is constant.
8. Time horizon is finite.

3. Mathematical Formulation of Model

At the start of the cycle, an initial lot consisting of Q_0 units is received. The retailer allows its customers to return the items. The inventory level changes from time $t = 0$ to $t = t_1$ due to time-dependent demand, returned items, and deterioration. From time $t = t_1$ to $t = T$, the inventory level changes due to returned items and partial backlogging.

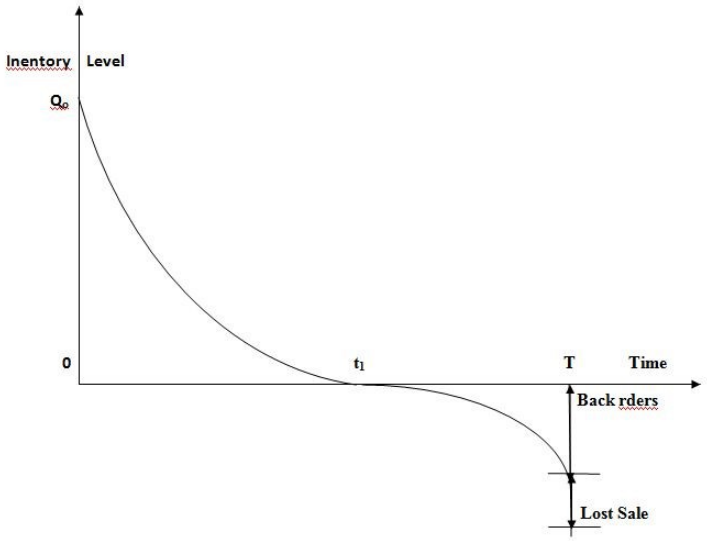


Figure 1: *Inventory depletion with backorders and lost sales.*

The inventory level $Q(t)$ at any time t in the interval $[0, T]$ is represented by the following differential equations:

$$\frac{dQ_1}{dt} = -\gamma(t) + \sigma\,\gamma(t) - \eta(t)\,Q_1(t) \quad \text{for } 0 \le t \le t_1 \tag{1}$$

$$\frac{dQ_2}{dt} = -p\,\gamma(t) + \sigma\,\gamma(t) \quad \text{for } t_1 \le t \le T \tag{2}$$

with boundary conditions: $Q_1(0) = Q_0$, $Q_1(t_1) = 0$, $Q_2(T) = 0$. The solutions of differential equations 1 and 2 with boundary conditions are as follows:

$$Q_1(t) = Q_0\left(1 - 0.5\,\alpha t^2 + 0.125\,\alpha^2 t^4\right) - (1-\sigma)b\left(t - \frac{\alpha t^3}{3} - \frac{\alpha^2 t^5}{60} - 0.5\,\mu t^2 + \mu\alpha t^4/8 + \mu t^3/6\right)$$

$$Q_2(t) = b(\sigma - p)\,\mu^{-1}\left(e^{\mu t} - e^{\mu T}\right)$$

The total cost of the system is the sum of all associated inventory costs calculated as above. Therefore, the total cost per unit time (or total average cost per cycle) is given by:

1. **Ordering cost:**
$$OC = A$$

2. **Purchase cost:**
$$PC = cQ_0$$

3. **Deterioration Cost:**
$$DC = c_d \left[Q_0 - \int_0^{t_1} be^{\mu t}\, dt + \int_0^{t_1} \sigma be^{\mu t}\, dt + \int_{t_1}^{T} (\sigma - p) be^{\mu t}\, dt \right]$$
$$= c_d \left[Q_0 - b(1-\sigma)\mu^{-1}(e^{\mu t_1} - 1) - b(\sigma - p)\mu^{-1}(e^{\mu T} - e^{\mu t_1}) \right]$$

4. **Holding Cost:**
$$HC = h_c \left[\int_0^{t_1} Q_1(t)\, dt + \int_{t_1}^{T} Q_2(t)\, dt \right]$$
$$= h_c \left[Q_0 \left(t_1 - 0.17\alpha t_1^3 \right) - (1-\sigma) b \left(0.5 t_1^2 - 0.08\alpha t_1^4 - 0.16 \mu t_1^3 \right) \right.$$
$$\left. + b(\sigma - p)\mu^{-2}(e^{\mu T} - e^{\mu t_1}) - b(\sigma - p)\mu^{-1}(T - t_1)e^{\mu T} \right]$$

5. **Shortage Cost:**
$$SC = c_s \int_{t_2}^{T} Q_2(t) dt = -c_s b(\sigma - p)\mu^{-2} \left(e^{\mu T} - e^{\mu t_1} \right) - b(\sigma - p)\mu^{-1}(T - t_1)e^{\mu T}$$

6. **Lost Sale Cost:**
$$LSC = c_o \int_{t_2}^{T} (1-p) D(t)\, dt = c_o b(1-p)\mu^{-1}(e^{\mu T} - e^{\mu t_1})$$

So, the total cost per unit time of inventory system is:

$$TC = \frac{1}{T} [OC + PC + DC + HC + SC + LSC]$$
$$= \frac{1}{T} \Big[A + c_Q Q_0 + c_d [Q_0 - b(1-\sigma)\mu^{-1}(e^{\mu t_1} - 1) - b(\sigma - p)\mu^{-1}(e^{\mu t_1} - e^{\mu T})]$$
$$+ h_c [Q_0 (t_1 - 0.17\alpha t_1^3) - (1-\sigma) b (0.5 t_1^2 - 0.08\alpha t_1^4 - 0.16\, \mu t_1^3) + b(\sigma - p)\mu^{-2}(e^{\mu T} - e^{\mu t_1})$$
$$- b(\sigma - p)\mu^{-1}(T - t_1)e^{\mu T}] - c_s [b(\sigma - p)\mu^{-2}(e^{\mu T} - e^{\mu t_1}) - b(\sigma - p)\mu^{-1}(T - t_1)e^{\mu T}]$$
$$+ c_b (1-p)\mu^{-1}(e^{\mu T} - e^{\mu t_1}) \Big] \quad (3)$$

Sales revenue collected over the cycle (SR):
$$SR = c_s Q_0 + 0.2 c_o \int_0^{T} R(t) dt = (Q_0 + 0.2\sigma) c_o b \mu^{-1}(e^{\mu T} - 1)$$

The total profit per unit time is calculated as follows:
$$TP = \frac{1}{T} [SR - OC - PC - HC - DC - SC]$$

$$= \frac{1}{T}(Q_0 + 0.2\sigma)c_o b\mu^{-1}(e^{\mu T} - 1) - \frac{1}{T}\Big[A + c_Q Q_0 + c_d[Q_0 - b(1-\sigma)\mu^{-1}(e^{\mu t_1} - 1)$$
$$- b(\sigma - p)\mu^{-1}(e^{\mu t_1} - e^{\mu T})] + h_c[Q_0(t_1 - 0.17\alpha t_1^3) - (1-\sigma)b(0.5t_1^2 - 0.08\alpha t_1^4 - 0.16\ \mu t_1^3)$$
$$+ b(\sigma - p)\mu^{-2}(e^{\mu T} - e^{\mu t_1}) - b(\sigma - p)\mu^{-1}(T - t_1)e^{\mu T}]$$
$$- c_s[b(\sigma - p)\mu^{-2}(e^{\mu T} - e^{\mu t_1}) - b(\sigma - p)\mu^{-1}(T - t_1)e^{\mu T}]$$
$$+ c_b(1-p)\mu^{-1}(e^{\mu T} - e^{\mu t_1})\Big]$$

Fuzzy inventory model Suppose we examine an inventory model in a fuzzy setting where the uncertainty in parameters is present. Let's assume that the parameters p, b, σ and p can vary within certain boundaries.
Let $\tilde{b} = (b_1, b_2, b_3)$, $\tilde{\mu} = (\mu_1, \mu_2, \mu_3)$, $\tilde{\sigma} = (\sigma_1, \sigma_2, \sigma_3)$ and $\tilde{p} = (p_1, p_2, p_3)$ are triangular fuzzy numbers.

The total cost per unit time in fuzzy model is:

$$\tilde{TC} = \frac{1}{T}[OC + PC + DC + \tilde{HC} + \tilde{SC} + LSC] \tag{4}$$

Using signed distance method (SDM) the total cost per unit time is:

$$\tilde{TC} = \frac{1}{4}(\mathrm{TC}_1 + 2\mathrm{TC}_2 + \mathrm{TC}_3) \tag{5}$$

where

$$\mathrm{TC}_1 = \frac{1}{T}[OC + PC + DC_1 + HC_1 + SC_1]$$

$$\mathrm{TC}_2 = \frac{1}{T}[OC + PC + DC_2 + HC_2 + SC_2]$$

$$\mathrm{TC}_3 = \frac{1}{T}[OC + PC + DC_3 + HC_3 + SC_3]$$

$$\mathrm{TC}_1 = \frac{1}{T}\Big[A + c_Q Q_0 + c_d[Q_0 - b_1(1-\sigma_1)\mu_1^{-1}(e^{\mu_1 t_1} - 1) - b_1(\sigma_1 - p_1)\mu_1^{-1}(e^{\mu_1 t_1}$$
$$- e^{\mu_1 T})] + h_c[Q_0(t_1 - 0.121\alpha_1 t_1^3) - (1-\sigma_1)b_1(0.5t_1^2 - 0.083\alpha_1 t_1^4 - 0.17\ \mu_1 t_1^3 + 0.025\mu_1\alpha_1 t_1^5)$$
$$+ b_1(\sigma_1 - p_1)\mu_1^{-2}(e^{\mu_1 T} - e^{\mu_1 t_1} - b_1(\sigma_1 - p_1)\mu_1^{-1}(T - t_1)e^{\mu_1 T}] - c_s[b_1(\sigma_1 - p_1)\mu_1^{-2}(e^{\mu_1 T} - e^{\mu_1 t_1})$$
$$- b_1(\sigma_1 - p_1)\mu_1^{-1}(T - t_1)e^{\mu_1 T}] + c_b(1-p_1)\mu_1^{-1}(e^{\mu_1 T} - e^{\mu_1 t_1})\Big]$$

$$\mathrm{TC}_2 = \frac{1}{T}\Big[A + c_Q Q_0 + c_d[Q_0 - b_2(1-\sigma_2)\mu_2^{-1}(e^{\mu_2 t_1} - 1) - b_2(\sigma_2 - p_2)\mu_2^{-1}(e^{\mu_2 t_1} - e^{\mu_2 T})]$$
$$+ h_c[Q_0(t_1 - 0.121\alpha_2 t_1^3) - (1-\sigma_2)b_2(0.5t_1^2 - 0.083\alpha_2 t_1^4 - 0.17\ \mu_2 t_1^3 + 0.025\mu_2\alpha_2 t_1^5)$$
$$+ b_2(\sigma_2 - p_2)\mu_2^{-2}(e^{\mu_2 T} - e^{\mu_2 t_1}) - b_2(\sigma_2 - p_2)\mu_2^{-1}(T - t_1)e^{\mu_2 T}]$$
$$- c_s[b_2(\sigma_2 - p_2)\mu_2^{-2}(e^{\mu_2 T} - e^{\mu_2 t_1}) - b_2(\sigma_2 - p_2)\mu_2^{-1}(T - t_1)e^{\mu_2 T}]$$
$$+ c_b b_2(1-p_2)\mu_2^{-1}(e^{\mu_2 T} - e^{\mu_2 t_1})\Big]$$

$$\begin{aligned}\mathrm{TC}_3 = \frac{1}{T}\Big[A + c_Q Q_0 + c_d[Q_0 - b_3(1-\sigma_3)\mu_3^{-1}(e^{\mu_3 t_1}-1) - b_3(\sigma_3 - p_3)\mu_3^{-1}(e^{\mu_3 t_1} \\ - e^{\mu_3 T})] + h_c[Q_0(t_1 - 0.121\alpha_3 t_1^3) - (1-\sigma_3)b_3(0.5t_1^2 - 0.083\alpha_3 t_1^4 - 0.17\ \mu_3 t_1^3 + 0.025\mu_3\alpha_3 t_1^5) \\ + b_3(\sigma_3 - p_3)\mu_3^{-2}(e^{\mu_3 T} - e^{\mu_3 t_1}) - b_3(\sigma_3 - p_3)\mu_3^{-1}(T - t_1)e^{\mu_3 T}] \\ - c_s[b_3(\sigma_3 - p_3)\mu_3^{-2}(e^{\mu_3 T} - e^{\mu_3 t_1}) - b_3(\sigma_3 - p_3)\mu_3^{-1}(T - t_1)e^{\mu_3 T}] \\ + c_b b_3(1-p_3)\mu_3^{-1}(e^{\mu_3 T} - e^{\mu_3 t_1})\Big]\end{aligned}$$

4. Optimal Solution Procedure

The primary aim of the model is to find the values of t_1 and T, which can minimize the total cost per unit time TC^* and $\tilde{TC}^0$ to get the maximum total profit throughout a complete cycle over time T. The conditions required to minimize the total cost per unit time during the cycle time T are:

$$\frac{\partial(\mathrm{TC})}{\partial t_1} = 0 \tag{6}$$

$$\frac{\partial(\mathrm{TC})}{\partial T} = 0 \tag{7}$$

$$\frac{\partial(\tilde{\mathrm{TC}})}{\partial t_1} = 0 \tag{8}$$

$$\frac{\partial(\tilde{\mathrm{TC}})}{\partial T} = 0 \tag{9}$$

The condition for sufficiency is that TC and $\tilde{TC}$ are convex functions over the cycle time T. The optimal values t_1° and T° of t_1 and T respectively are obtained by solving equations 6 and 7. To obtain the optimal value $\tilde{TC}^\circ$, we substitute the optimal values t_1° and T° in equation 3. Similarly, the optimal values t_1^* and T^* of t_1 and T, respectively, in the fuzzy model is obtained by solving equations 8 and 9 respectively. Finally, the fuzzy optimal value TC^* is calculated by substituting the optimal values t_1^* and T^* of t_1 and T in equation 5. The condition for sufficiency is that TC is a convex function over the cycle time T.

$$\frac{\partial^2 TC}{\partial T^2} > 0 \quad for\ all\ \ T > 0$$

5. Results and discussion

To illustrate the results of **proposed inventory** model developed above, a numerical example has been solved. Data have been assumed randomly from the literature in appropriate units to obtain optimal values of t_1, T, TC°, TC^*, TP° and TP^* and to perform the sensitive analysis.
Example: A numerical example has been presented to illustrate the proposed inventory model. The main objective is to determine the optimal values of t_1, T which minimizes total cost per unit time and maximize the total profit. The values of different parameters are as follows:

$A = 100,\ Q_0 = 1000,\ a_2 = 0.005,\ a_1 = 0.003,\ a_3 = 0.007,\ c_d = 0.005,\ h_c = 0.5,\ c = 10,$
$u_1 = 0.10,\ u_2 = 0.20,\ u_3 = 0.30,\ b_1 = 26,\ b_2 = 35,\ b_3 = 44,\ o_1 = 0.1,\ o_2 = 0.2,\ o_3 = 0.3,$
$s = 0.5,\ p_1 = 0.5,\ p_2 = 0.6,\ p_3 = 0.7,\ c_s = 0.5,\ c_b = 17,\ c_0 = 0.5$

MATLAB is used to obtain the optimal values of t_1, T, TC and TP. To demonstrate the convexity of total cost per unit of inventory system, graphical representations of the convexity of TC° and TC^* with respect to decision variables are presented in Figure 2 and Figure 3, respectively.

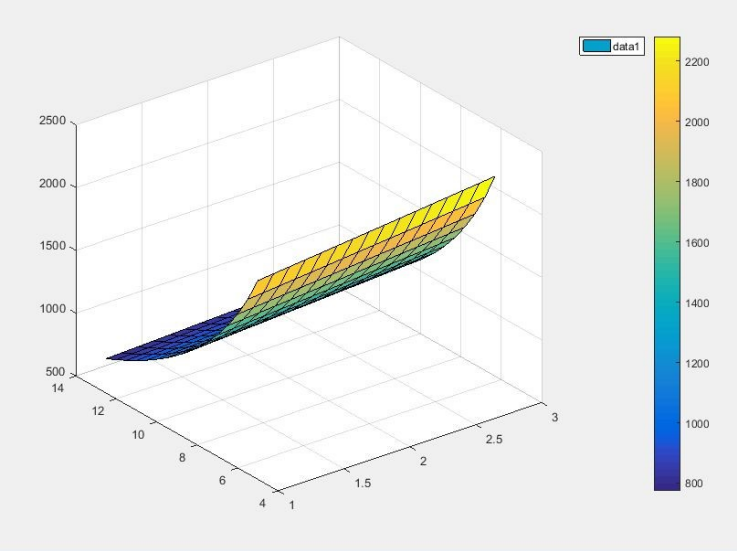


Figure 2: *Convexity of total cost in crisp model.*

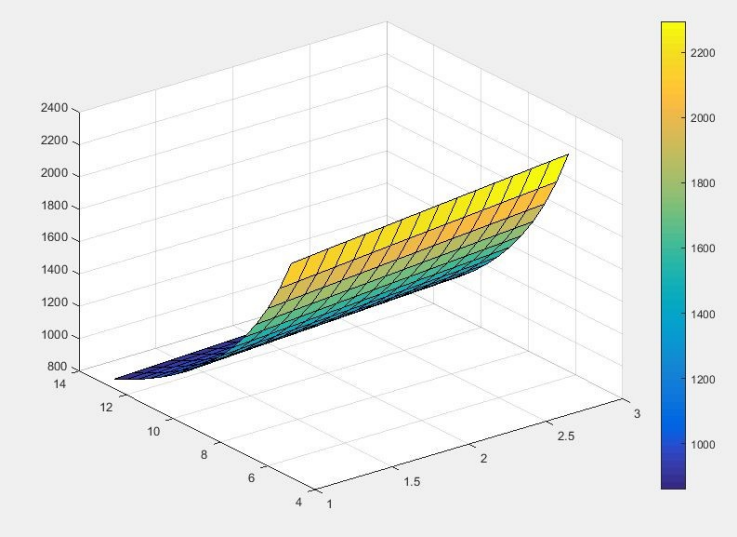


Figure 3: *Convexity of total cost in fuzzy model.*

6. Sensitivity Analysis

The study conducted a sensitivity analysis by modifying the values of critical parameters to determine their impact on optimal values. Each key parameter was varied individually while others are remained constant to obtain the optimal values. The resultant changes in optimal values t_1°, T°, TC°, TC^*, TP° and TP^* are recorded in following tables:

1. **When b changes in crisp model:**

b	t_1°	T°	TC$^\circ$	TP$^\circ$
15	1.90	7.36	1583.70	749.30
20	1.84	7.27	1625.10	744.01
25	1.80	7.20	1663.70	735.56
30	1.75	7.12	1703.50	729.27
35	1.70	7.05	1741.70	721.85

2. **When b changes in fuzzy model:**

b	t_1^*	T^*	b_1	b_2	b_3	TC*	TP*
15	1.90	7.35	6	15	24	1586.50	752.27
20	1.85	7.27	11	20	29	1629.40	744.62
25	1.80	7.19	16	25	34	1670.50	736.10
30	1.76	7.12	21	30	39	1710.10	726.15
35	1.71	7.05	26	35	44	1749.50	716.83

3. **When μ changes in crisp model:**

μ	t_1°	T°	TC$^\circ$	TP$^\circ$
0.10	1.71	7.20	1676.40	709.64
0.15	1.77	7.21	1662.30	726.15
0.20	1.80	7.20	1663.70	735.56
0.25	1.82	7.18	1680.80	753.37
0.30	1.83	7.16	1671.20	744.01

4. **When μ changes in fuzzy model:**

μ	t_1^*	T^*	μ_1	μ_2	μ_3	TC*	TP*
0.10	1.70	7.20	0.05	0.10	0.15	1679.00	705.51
0.15	1.77	7.21	0.10	0.15	0.20	1662.10	724.67
0.20	1.81	7.21	0.15	0.20	0.24	1663.20	734.07
0.25	1.82	7.18	0.20	0.25	0.30	1670.80	742.25
0.30	1.83	7.16	0.25	0.30	0.35	1680.50	751.31

5. **When σ changes in crisp model:**

σ	t_1°	T°	TC$^\circ$	TP$^\circ$
0.10	1.74	7.10	1712.10	701.05
0.15	1.77	7.15	1687.80	718.13
0.20	1.80	7.20	1663.70	735.56
0.25	1.83	7.24	1641.20	754.64
0.30	1.85	7.29	1616.50	773.16

6. **When σ changes in fuzzy model:**

σ	t_1^*	T^*	σ_1	σ_2	σ_3	TC*	TP*
0.10	1.76	7.09	0.01	0.10	0.25	1717.90	709.83
0.15	1.78	7.16	0.05	0.15	0.35	1684.3	733.63
0.20	1.82	7.21	0.10	0.20	0.40	1660.10	750.29
0.25	1.84	7.26	0.15	0.25	0.45	1686.50	768.16
0.30	1.87	7.31	0.20	0.30	0.50	1655.60	785.98

7. **When p changes in crisp model:**

p	t_1°	T°	TC$^\circ$	TP$^\circ$
0.4	1.90	7.38	1572.30	770.09
0.5	1.85	7.30	1616.10	751.15
0.6	1.80	7.20	1663.70	735.56
0.7	1.75	7.10	1710.90	720.99
0.8	1.70	7.02	1754.50	704.34

8. **When p changes in fuzzy model:**

p	t_1^*	T^*	p_1	p_2	p_3	TC*	TP*
0.4	1.91	7.38	0.3	0.4	0.5	1542.60	804.49
0.5	1.85	7.29	0.4	0.5	0.6	1620.50	754.09
0.6	1.82	7.21	0.5	0.6	0.7	1660.10	750.29
0.7	1.75	7.10	0.6	0.7	0.8	1715.30	720.52
0.8	1.71	7.01	0.7	0.8	0.9	1761.80	704.09

The following key observations can be drawn Based on the above tables:

1. As the demand parameters μ increases, optimal value of total cost per unit time TC° and TC^* fluctuates while corresponding profit decreases. As the demand parameters b increases, optimal value of total cost per unit time TC° and TC^* increases, the corresponding profit decreases.

2. As the parameters p increases, there is an increase in the optimal value of total cost per unit time TC° and TC^* and there is a decrease in the corresponding profit.

3. As the parameters σ increase, the optimal value of total cost per unit time TC° and TC^* decreases and there is an increase in the corresponding profit.

4. The optimal value of total cost per unit time in the fuzzy model is less than total cost per unit time in the crisp model and the profit is more in fuzzy model compared to crisp model.

7. Conclusion

This work developed an inventory framework for deteriorating items that incorporates time‘varying demand, a constant per‘unit holding charge, and partial backlogging in the presence of resalable returns. A detailed numerical illustration and accompanying sensitivity study were carried out for both crisp and fuzzy formulations. The investigation reveals that unit total cost and the associated profit react strongly to shifts in the selling price parameter, and the demand variability parameter, while showing only moderate responsiveness to changes in the demand scale and the salvage value parameter. Moreover, the fuzzy version consistently achieves a lower unit cost and, consequently, a higher profit when compared with its crisp counterpart. Future research could broaden the model by incorporating shortages, trade‘credit arrangements, or the time value of money to capture a wider range of real‘world managerial conditions.

References

[1] De, P.K. and Rawat, A. (2011) A Fuzzy Inventory Model without Shortages Using Triangular Fuzzy Number. Fuzzy Information and Engineering, 3, 59“68.
[2] Saha, S., and Chakrabarti, T. (2012). Fuzzy EOQ model for time-dependent deteriorating items and time-dependent demand with shortages. IOSR Journal of Mathematics, 2(4), 46“54.
[3] Jaggi, C.K., Pareek, S., Sharma, A., and Nidhi (2012). Fuzzy Inventory Model for Deteriorating Items with Time-varying Demand and Shortages. American Journal of Operational Research, 2(6), 81“92.
[4] Mahata, G.C. (2012). An EPQ-based inventory model for exponentially deteriorating items under retailer partial trade credit policy in supply chain. Expert Syst. Appl., 39(3), 3537“3550.
[5] Jain, D.K., Das, B., and Roy, T.K. (2013). A Fuzzy Generic Algorithm Approach for an Inventory Model for Deteriorating Items with Backorders under Fuzzy Inflation and Discounting over Random Planning Horizon. Advances in Operations Research, 2013, 1“15.

[6] Dutta, D. and Kumar, P. (2015). A partial backlogging inventory model for deteriorating items with time-varying demand and holding cost. International Journal of Mathematics in Operational Research, Volume 25, Issue 3, 441, 2020.

[7] Sushil Kumar, and Rajput, U.S. (2015). Fuzzy Inventory Model for Deteriorating Items with Time Dependent Demand and Partial Backlogging. Applied Mathematics, 6, 496“509. Published Online March 2015 in SciRes. http://dx.doi.org/10.4236/am.2015.63047.

[8] Sahoo, N.K., Mohanty, B.S., and Tripathy, P.K. (2016). Fuzzy inventory model with exponential demand and time-varying deterioration. Global Journal of Pure and Applied Mathematics, Volume 12, Number 3, pp. 2573“2589.

[9] Jaggi, C.K., Gautam, P., and Khanna, A. (2018). Inventory decisions for imperfect quality deteriorating items with exponential declining demand under trade credit and partially backlogged shortages. In: P. Kapur, U. Kumar and A. Verma (Eds.), Quality, IT and Business Operations. Springer Proceedings in Business and Economics, pp. 213“229, Singapore.

[10] Malik, A.K. and Garg, H. (2021). An Improved Fuzzy Inventory Model Under Two Warehouses. Journal of Artificial Intelligence and Systems, 3, 115“129.

[11] Boina, A.K., Paikray, S.K. and Mishra, U. (2020). Two-Storage Fuzzy Inventory Model with Time Dependent Demand and Holding Cost under Acceptable Delay in Payment. Mathematical Modelling and Analysis, Volume 25, Issue 3, 441.

[12] Kuppulakshmi, V., Sugapriya, C., Kavikumar, J. and Nagarajan, D. (2023). Fuzzy Inventory Model for Imperfect Items with Price Discount and Penalty Maintenance Cost. Mathematical Problems in Engineering, Volume 2023, Article ID 1246257.

[13] Yadav, A.S., Kumar, A., Yadav, K.K. et al. Optimization of an inventory model for deteriorating items with both selling price and time-sensitive demand and carbon emission under green technology investment. Int J Interact Des Manuf (2023). https://doi.org/10.1007/s12008-023-01689-8

[14] Yadav, K.K., Yadav, A.S. & Bansal, S. Interval number approach for two-warehouse inventory management of deteriorating items with preservation technology investment using analytical optimization methods. Int J Interact Des Manuf (2024). https://doi.org/10.1007/s12008-023-01672-3

[15] Krishan Kumar Yadav , Ajay Singh Yadav, and Shikha Bansal. "Optimization of an inventory model for deteriorating items assuming deterioration during carrying with two-warehouse facility" Reliability: Theory & Applications, vol. 19, no. 3 (79), 2024, pp. 442-459. https://doi.org/10.24412/1932-2321-2024-379-442-459

[16] Krishan Kumar Yadav, Ajay Singh Yadav, and Shikha Bansal. "Optimization of a two-warehouse inventory management for deteriorating items with time and reliability-dependent demand under carbon emission constraints" Reliability: Theory & Applications, vol. 19, no. 4 (80), 2024, pp. 404-418. https://doi.org/10.24412/1932-2321-2024-480-404-418

[17] Mahata, Sourav, and Bijoy Krishna Debnath. "A profit maximization single item inventory problem considering deterioration during carrying for price dependent demand and preservation technology investment." RAIRO-Operations Research 56.3 (2022): 1841-1856.

[18] Mahata, Sourav, and Bijoy Krishna Debnath. "Impact of green technology and flexible production on multi-stage economic production rate (EPR) inventory model with imperfect production and carbon emissions." Journal of Cleaner Production 504 (2025): 145187.

[19] Debnath, Bijoy Krishna, Pinki Majumder, and Uttam Kumar Bera. "EOQ model in uncertain environment by using generalised intuitionistic fuzzy Laplace transformation." International Journal of Logistics Systems and Management 49.3 (2024): 412-437. https://doi.org/10.1504/IJLSM.2024.142619

A COMPARATIVE ANALYSIS OF RESPONSE SURFACE METHODOLOGY IN LINEAR PROGRAMMING

Mushtaq A. Lone[1], S. A. Mir[2], R. Vijaykrishnaraj[3], Showkat Ahmad Bhat[4], Aafaq A. Rather[5,*], Raeesa Bashir[6], Manzoor A. Khanday[7], Aamir Majeed Parray[8]

•

[1,2]Departmet of Statistics, FOH, SKUAST –K, P.O. Box 190025, J&K India
[3]Department of Mathematics, Bharath Institute of Higher Education and Research, Chennai, India
[4]Symbiosis School of Economics, Symbiosis International (Deemed University), Pune-411004, India
[5,*]Symbiosis Statistical Institute, Symbiosis International (Deemed University), Pune-411004, India
[6]Department of Statistics, Cluster University, Jammu and Kashmir, India
[7]School of Chemical Engineering and Physical Science, Lovely Professional University, Punjab, India
[8]B. S. Abdur Rahman Crescent Institute of Science and Technology Chennai, India
[1]lonemushtaq11@gmail.com, [2]mir_98@msn.com, [3]drvjmaths@gmail.com,
[4]showkat.bhat@sse.ac.in, [5,*]aafaq7741@gmail.com, [6]raisabashir52@gmail.com,
[7]manzoorstat@gmail.com, [8]aamir.law@crescent.education

Abstract

A linear mathematical programming approach has been employed to tackle the problem of land allocation in this comparative study. One design of experiment technique used in creating new processes and improving their efficiency is response surface approach. Different search methods have been employed in this study to identify the best distribution of agricultural land. The results of all formulated mathematical programming problem are obtained by using R software and different R functions like mexchalgorithm() and qconalgorithm (), argumants to these problems are b1, b2, b3 were developed. Furthermore, the Branch and Bound method has been utilized to provide the proper integer solution when the problem's solution turns out to be non-integer.

Keywords: Response surface methodology, Linear programming, branch and bound methods, simplex methods.

1. Introduction

Optimization techniques play an important role to explore different management options, to solve diverse decision problems including risk assessment in agriculture systems, watershed development plan, and annual agriculture land cultivation plan and in forest planning. Innovative production techniques are required to keep up with the expanding demand of the world's population. Farmers in the agricultural industry struggle with how to allocate fertilizer and fields, staff to fields, and the ideal amount of plants to have on their farm. Allocation issues often arise in other academic disciplines, including salesperson to area, operator to machinery, and product to product mix. In fact, there are resource allocation issues in every subject of study, where the utilization of resources must be optimized to fulfill the organization's goals experiments in the field are frequently used in agriculture research to understand the numerous factors that affect production and output quality. The most important part of agricultural field trials that may be studied with the use of mathematical programming is planning. To study issues in agriculture, a unique area of mathematical in which an

experimental design not only enables one to analyze the experimental data and build empirical models to obtain the most accurate representation of the particular situation, but the present study also shows how experimental design are used to solve linear programming problems. The process by which an experiment is prepared so that the required data is collected & analyzed using statistical techniques to reach a valid & objective conclusion is known as experimental design Montgomery [1].

Response surface methodology is widely used in design of experiments to determine the value of the independent variables that maximizes (or minimizes) the response. Response surface methodology is one of the design of experiment (DOE) methods used in developing new processes and optimizing their performance. RSM is applicable when several input variables potentially influence some quality characteristics or performance measures. Onukogu [2] states that response surface methodology can be seen as a bridge linking experimental design with the subject of our constrained optimization. Hansen and Hurwitz [3] presented the classical non response theory for eliciting responses from a subsample of the non- respondents. Sarvarian & Soleimani [4] used optimization techniques for cropping pattern with limited resources. Lone *et.al* [5] discussed linear programming approach for optimal cropping pattern. Koufie [6] discussed optimum combination of food crop for enterprises. Lone *et.al* [7] used Branch and Bound Method for multi-objective problem. Montgomery a valid conclusion is drawn when the data is collected and analysis using statistical methods about an experimental design. Response surface methodology (RSM) was introduced by Box and Wilson [8]. Onukogu states that response surface methodology can be seen as a bridge linking experimental design with the subject of our constrained optimization. Mayers and Montgomery [9] state that response surface is a mathematical and statistical technique useful for optimizing the stochastic problems. The capability of locating the local optimizer of RSM problem by using more recent line search techniques in just one move has been mentioned in Onukogu and Esele [10]. A detailed information about the optimal experimental design can be found in Pazaman [11], Atkinson and Donev [12]. The optimal solutions of linear programming ploblems was solved through different methods as simplex method and as a polynomial time interior point algorithm given by Karmarkar [13], a modification of karmarkar's interior point algorithm given by Vanderbei *et al.* [14]. Ekezie and Nzenwa [15] developed a minimum exchange algorithm, Osita and Mary [16] developed a quick Convergent Inflow algorithm. In this comparative study different methods like minimum exchange algorithm, a quick Convergent Inflow algorithm, Simplex Method, Interior Point Method and Branch and Bound method has been used to determine optimal allocation of formulated programming problem in agriculture.

2. Response surface methodology

One design of experiment (DOE) technique used in creating new processes and improving their efficiency is response surface approach. RSM is a group of mathematical and statistical methods used in problem modeling and analysis. Although it is more commonly known as the procedure for selecting and fitting a suitable response surface model based on experimental data. The primary objective of RSM is to maximise or minimise the response variable, which is affected by a number of independent (predictor) factors. RSM is particularly useful when numerous input variables may have an impact on certain quality traits or performance metrics. For example, the growth of the plant is affected by a certain amount of water $x_1(say)$ and sunlight $x_2(say)$. With the variations in the amount of water and sunlight, plant can grow with any combination of treatments. When there are continuous variations in treatment combinations RSM is useful for developing and optimizing the response variable. In particular, the response variable (y) denotes the growth of plant is a function of x_1 and x_2 , and is expressed as fallows

$$y = f(x_1 + x_2) + e \tag{1}$$

Where, e represents experimental error which is normally distributed with mean zero and

variance σ^2. x_1 and x_2 are independent variables where the response variable(y) depends on them. if expected response is denoted by $E(y) = f(x_1 + x_2) = \eta$,then the surface denoted by $f(x_1 + x_2) = \eta$ is called response surface. The optimization based on response surface is known as experimental optimization. RSM can be viewed from the three major stand points (Cornell, 1990).

- If the system response is fairly well known, the RSM technique is utilised to identify the best value of the response.
- RSM approaches are employed to at least get a better understanding of the entire response system in the event that determining the best (optimum) value is outside the scope of the experiment's resources.
- In place of the complex analysis that takes hours to complete, a comparable response surface in a condensed version can be produced in a few runs.

In general, suppose a set of predictor variables is denoted by $x_1, x_2, \ldots, x_n$ and the unknown response function $f(X)$ is represented by a regression function $Y(X)$ with additive error, thus we write

$$Y(X) = f(x_1, x_2, \ldots, x_n) + e \tag{2}$$

Every significant work on the design of experiments used to address unconstrained optimization problems now includes RSM as a mainstay. The issue of minimizing or maximizing a function in the absence of any constraints is addressed by unconstrained optimization. RSM is a bridge linking the subject of experimental design with constrained optimization The problem is to find the local optimizer $X^* = (x_1^*, x_2^*, \ldots, x_n^*)'$ such that

$$F(X^*) \begin{cases} \leq f(X) \text{ if } f(X) \text{is minimized} \\ \geq f(X) \text{ if } f(X) \text{is maximized} \end{cases} \tag{3}$$

2.1 Line search techniques

Line search techniques are used to solve problems in linear programming, which improves performance. The line search approach finds a descent direction along which the objective function will be reduced and then computes a step size that determines how far should move along the direction. It also requires the best decision on: The starting point of the sequence, the regression model, and the design of experiments. Therefore, it is important to consider how these factors interact to affect performance and the most effective method for determining each. Additionally, modern line search methods are employed to find the RSM problem's local optimizer.
The line search equation is:

$$X_{i,1} = \overline{X} - p_i d_i \tag{4}$$

Where, $X_i = (X_{i1}, \ldots, X_{in})'$ is the starting point.
$d_i = T_i\, g_i$ is the direction of search and
p_i is the step size that determines how far X should move along the direction.
T_i is matrix of transformation
g_i is gradient vector at j[th] step.
The basic iterative steps of a line search procedure are:

- Perform an experiment to determine the direction of search d_i . Move to the point

$$X_{i+1} = \overline{X} - p_i d_i \tag{5}$$

- Stop if local optimizer $X_1 = X^*$, otherwise set 1=0 and return to step (a).

This paper uses the notion of optimum experimental design to solve a constrained optimization issue involving linear programming approach in agriculture using the line search technique. The search's goal is to identify the response surface's optimum with the fewest possible iterations and the least amount of computing required during each iteration. In this comparative study different methods have been used to determine the optimal allocation.

3. Linear programming

Linear programming (LP) is a mathematical programming technique applicable for the solution of problems in which the objective function and the constraints appear as linear functions of the decision variables. LP is a mathematical technique useful for allocation of 'scarce' or 'limited' resources to several competing activities on the basis of a given criterion of optimality.

The general LPP with n decision variables and m constraints is stated in the following form:

$$\begin{aligned} &\min/\max\ Z = C_1X_1 + \ldots + C_nX_n \\ &\textit{subject to} \\ &\quad a_{11}X_1 + \ldots + a_{1n}X_n\ (\leq, =, \geq)\ b_1 \\ &\quad a_{21}X_1 + \ldots + a_{2n}X_n\ (\leq, =, \geq)\ b_2 \\ &\quad \ldots \qquad\qquad \ldots \\ &\quad a_{m1}X_1 + \ldots + a_{mn}X_n\ (\leq, =, \geq)\ b_m \\ &\quad X_1 \ldots, X_n \geq 0 \end{aligned} \tag{6}$$

In matrix notation, it can be expressed as

$$\begin{aligned} &\min/\max\ Z = C^TX \\ &\text{subject to} \\ &\qquad AX\ (\leq, =, \geq)\ B \\ &\qquad X \geq 0 \end{aligned} \tag{7}$$

Where, $C^T = (C_1, \ldots, C_n)$; $\mathbf{B}^T = (b_1, \ldots, b_m)$, $X^T = (X_1, \ldots, X_n)$ are row vectors and $A = (a_{ij})$ is an $m \times n$ matrix.

4. Similarities between linear programming problem (LPP) and RSM

The following are some similarities between LPP and RSM:

- In the LPP, the decision variables can only have non-negative values, whereas the independent variables in the RSM can have any value. Both are regarded as quantitative.
- Within a finite dimensional area that fulfills the response function, the independent variables in an RSM model are free to take any value. Similar to the feasible zone in LPP, the experimenter region in RSM acts as a constraint and serves the same purpose.
- With the usage of RSM, the experimental region is continuous, negating the necessity to use slack surplus variables or other techniques to solve LPP.

4.1 Minimum Exchange algorithm & Quick Convergent Inflow algorithm

The sequence of steps involved in minimum exchange algorithm & a quick Convergent Inflow algorithm can be found in Ekezie and Nzenwa [16] & Osita and Mary [16].

4.2 Simplex method

Most real – life problems when formulated as an LP model have more than two variables and are too large to be interpreting with the help of graphical solution method. We therefore need a more efficient method known as Simplex method to suggest an optimal solution for such problems. The simplex method examines the extreme points in a systematic manner, repeating the same set of steps of the algorithm until an optimal solution is found. It is for this reason that it is also called the iterative method.

4.3 Interior point method

In simplex-based methods for solving LPPs the computational time and efforts increase exponentially with the increase in the dimensions of the problem. Such methods therefore become slow and computationally expensive for large problems. On the other hand, presented interior point algorithm is a polynomial time algorithm, this new approach finds the optimum solution by starting at a trial solution and shooting through the interior of the feasible solution space. Although the advantage of this method is that it is used for solving large LPPs. The given problem is solved using R programme package based on modification of interior point algorithm. This algorithm makes it easier to conceptualize and leads to computational simplicity. Graphically the solution of a two-dimensional linear programming problem is also shown at the sequence of points calculated by the interior point method.

4.4 Branch and bound method

A well-structured, systematic search of the space of all feasible solutions to constrained optimization problems with a finite number of feasible answers is what the Branch and Bound approach entails. Integer programming issues including the scheduling problem, the traveling salesman problem, the plant location problem, the assignment problem, etc. have been partially solved using branch and bound algorithms. This method is helpful for LP issues when there are numerous viable solutions, making it economically unfeasible to enumerate all of them. If a sub problem's answer does not result in an ideal integer solution, a new sub problem is chosen for branching until an optimal solution is reached at the point where no more sub problems may be formed.

5. Numerical Example of Linear programming problem

A farmer has more than 4 hectares farm on which he plants two crops: corn and rice. For each hectare of rice planted, his expense is 3 thousand units and for each hectare of corn planted, his expense is Rs 2 thousand units. Now, each hectare of corn requires one hundred cubic feet of space for storage and yields a profit of two thousand units; each hectare of rice requires two hundred cubic feet space for storage and yields a profit of Rs 1 thousand units. But the storage space required for rice is twice than corn. The farmer is expected to get more than 6 thousand units of profit using his past experience. Also, the expense on the corn is twice than that of rice with farmer is expect to have more than 6 thousand units of money. Now, the farmer is in such a situation he wants to know how many hectares of each crop should be planted in order to minimize his expense. What will be his minimum expense if he fallows this strategy?

Let x_1 and x_2 be the area required in hectares for planting rice and corn plants respectively. The mathematical formulation of the LPP is given below:

$$\begin{aligned} &\min \ f(x) = 3x_1 + 2x_2 \\ &\textit{subject to} \\ &\qquad 2x_1 + x_2 \geq 6 \\ &\qquad x_1 + x_2 \geq 4 \\ &\qquad x_1 + 2x_2 \geq 6 \\ &\qquad x_1, x_2 \geq 0 \end{aligned} \tag{8}$$

The solution of the above linear programming problem is obtained using R software and the programmers were developed in R for this particular problem.

5.1. Minimum Exchange algorithm

```
>mexchalgorithm=function(b1,b2,b3)
{
>obj.coef<-matrix(c(3,2),nrow=1,ncol=2)
>const1<-matrix(c(2,1),nrow=1)
> const2<-matrix(c(1,1),nrow=1)
>const3<-matrix(c(1,2),nrow=1)
>b1<-6
>b2<-4
>b3<-6
>E1=matrix(c(3,2,3,0,0,2,3,4),nrow=4,ncol=2)
>average1<-matrix(c(mean(E1[,1]),mean(E1[,2])))
>Mo<-t(E1)%*%E1
>Mo<-(t(E1)%*%E1)/2
>y<-matrix(c(9,10,15,8),ncol=1)
>b<-((solve(Mo)%*%t(E1)))%*%y
>d1<-b[1,]/(sqrt(sum(b[1,]^2,b[2,]^2)))
>d2<-b[2,]/(sqrt(sum(b[1,]^2,b[2,]^2)))
>d<-matrix(c(d1,d2),ncol=1)
>p1<-((const1%*%average1)-b1)/(const1%*%d)
>p2<-((const2%*%average1)-b2)/(const2%*%d)
>p3<-((const3%*%average1)-b3)/(const3%*%d)
>po<-min(p1,p2,p3)
>x1<-average1-(d%*%po)
>obv1<-(obj.coef%*%x1)
>reducedE1<-E1[-3,]
>E2<-insertRow(reducedE1,2,x1)
>average2<-matrix(c(mean(E2[,1]),mean(E2[,2])))
>M1<-(t(E2)%*%E2)/2
>x2<-average2-(d%*%(min(p2,p3)))
>obv2<-(obj.coef%*%x2)
>reducedE2<-E2[-3,]
>E3<-insertRow(reducedE2,3,x2)
>average3<-matrix(c(mean(E3[,1]),mean(E3[,2])))
>M2<-(t(E3)%*%E3)/2
>x3<-average3-(d%*%p3)
>obv3<-(obj.coef%*%x3)
>optsol<-x3
```

```
>list(E1=E1,average1=average1,Mo=Mo,y=y,b=b,po=po,x1=x1,obv1=obv1,reducedE1=reducedE1,E2=E2
,average2=average2,M1=M1,x2=x2,obv2=obv2,reducedE2=reducedE2,E3=E3,average3=average3,M2=
M2,obv3=obv3,optsol=optsol)
}
>mexchalgorithm(6,4,6)
```

5.2. A quick Convergent Inflow Algorithm

```
>qconalgorithm=function(b1,b2,b3)
{
>obj.coef<-matrix(c(3,2),nrow=1,ncol=2)
>const1<-matrix(c(2,1),nrow=1)
>const2<-matrix(c(1,1),nrow=1)
>const3<-matrix(c(1,2),nrow=1)
>b1<-b1
>b2<-b2
>b3<-b3
>E1=matrix(c(1,4,4,1),nrow=2,ncol=2)
>average1<-matrix(c(mean(E1[,1]),mean(E1[,2])))
>Mo<-E1%*%E1
>g<-matrix(c(3,2),nrow=2,ncol=1)
>zo<-Mo%*%g
>do<-(solve(Mo))%*%zo
>do1<-do%*%(1/(sqrt(sum(do[1,]^2,do[2,]^2))))
>po1<-((const1%*%average1)-b1)/(const1%*%do1)
>po2<-((const2%*%average1)-b2)/(const2%*%do1)
>po3<-((const3%*%average1)-b3)/(const3%*%do1)
>po<-min(po1,po2,po3)
>x1<-t(average1-(do1%*%po))
>obv1<-(obj.coef%*%t(x1))
>E2<-insertRow(E1,3,x1)
>average2<-matrix(c(mean(E2[,1]),mean(E2[,2])))
>M1<-t(E2)%*%E2
>z1<-M1%*%g
>d1<-(solve(M1))%*%z1
>do2<-d1%*%(1/sqrt(sum(d1[1,]^2,d1[2,]^2)))
>po11<-((const1%*%average2)-b1)/(const1%*%do2)
>po12<-((const2%*%average2)-b2)/(const2%*%do2)
>po13<-((const3%*%average2)-b3)/(const3%*%do2)
>popt1<-min(po11,po12,po13)
>x2<-average2-(do2%*%popt1)
>obv2<-(obj.coef%*%x2)
>optimality_check<-(x2-t(x1))
>optval<-x2
>optsol<-obv2
>list(E1=E1,average1=average1,Mo=Mo,g=g,zo=zo,do=do,do1=do1,po=po,x1=x1,obv1=obv1,E2=E2,ave
rage2=average2,M1=M1,z1=z1,d1=d1,x2=x2,obv2=obv2,
optimality_check=optimality_check,optval=optval,optsol=optsol)
}
>qconalgorithm(6,4,6)
```

6. Simplex method

```
>simplex.lp<-
lp(objective.in=c(3,2),const.mat=matrix(c(2,1,1,1,1,2),nrow=3),const.rhs=c(6,4,6),const.dir=c(">=",">=",">
="))
>simplex.lp
Success: the objective function is 10
>simplex.lp$solution
[1] 2 2
```

6.1. Interior point method

```
>Obj.coef<- c(3,2)
>  const1<- c(2,1)
>  const2<- c(1,1)
>  const3<- c(1,2)
>interior_point(-1,c=Obj.coef, M=rbind(const1,const2,const3), bM = c(6,4,6))
$`The optimum value of Z is`
[1] 10.00001
$`The optimal solution X`
[,1]
[1,] 2.000002
[2,] 2.000001
$`Number of iterations`
[1] 10
>solve2dlp(-1,c=Obj.coef, M=rbind(const1,const2,const3), bM = c(6,4,6))
```

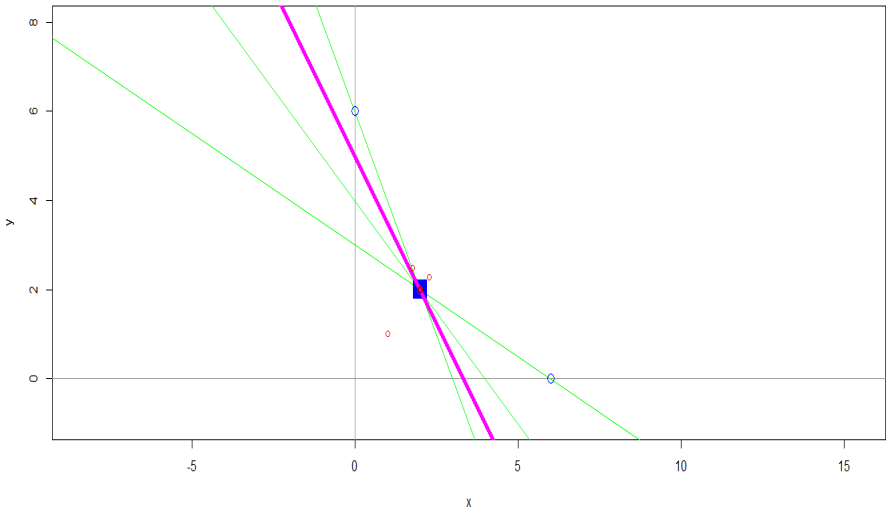


Fig. 1: *Graphical solution to the linear programming problem*

The graphical solution to the linear programming problem in shown in fig. 1. Lines corresponding to the constraints are coloured in green, the corner points in blue and the optimal point in magenta (with the objective function in blue). The sequence of interior points is drawn in red.

6.2. Branch and bound method

```
>integ.lp<-
lp(objective.in=c(3,2),const.mat=matrix(c(2,1,1,1,1,2),nrow=3),const.rhs=c(6,4,6),const.dir=c(">=",">=",">
="),int.vec=c(1,2))
>integ.lp
Success: the objective function is 10
>integ.lp$solution
[1] 2 2
```

Table 1: *Summary statistics for the minimization problem*

Method used	Optimal solution	Optimal value	Iterations
Minimum Exchange algorithm	1.406417 1.890737	8.000725	3
Quick Convergent Inflow algorithm	1.9375 2.1250	10.0625	2
Simplex method	2 2	10	2
Interior point method	2.000002 2.000001	10.00001	10
Branch and bound method	2 2	10	0

7. Result & Discussion

The summary provides information on the performance of the algorithms used to solve the above minimization linear programming problem. It provides us information about the optimal solution, optimal value and number of iterations. It can be easily seen from the table 1, that the minimum value of the objective function is provided by using the Minimum Exchange algorithm method to solve the LPP with three iterations. Even though the simplex method, Interior point method and Branch and bound method provides us the objective function value same but more than obtained from Minimum Exchange algorithm. Simplex method takes two iterations to reach the optimal value but Interior point method takes 10 iterations. As it has been already mentioned that simplex method become slow and computationally expensive for large problems as compared to interior point algorithm which finds the optimum solution by starting at a trial solution and makes it easier to conceptualize and leads to computational simplicity for solving large LPPs. Further, Quick Convergent Inflow algorithm takes only two iterations provides the optimum value more than the rest of the methods.

Now one of the important facts about these methods is that, for practical purposes if the solution is non-integer then the LPP is solved using Branch and Bound method instead of rounding the non-integer sample sizes to the nearest integral values. However, in some situation for small samples the rounded off allocation may become infeasible and non-optimal. Thus, the advantage of Branch and Bound method over rest of all methods, as it provides us an integer optimal allocation.

8. Conclusion

In conclusion, the study demonstrates that the use of the line search algorithm provides a more effective and convenient approach for solving linear programming problems, particularly when the objective is to determine the minimum value. Compared to other traditional algorithms, the line

search method shows superior performance in terms of both accuracy and computational efficiency.

Furthermore, the findings suggest that the experimental design procedure employed in this work is relatively straightforward to implement and consistently yields lower minimum values than alternative techniques. This simplicity, coupled with its effectiveness, makes it a promising strategy for future applications in optimization and statistical computing.

Additionally, the study has led to the development and implementation of customized R functions such as mexchalgorithm() and qconalgorithm(), which are tailored to handle specific problem scenarios. These functions utilize arguments labeled as b1, b2, and b3, which represent key parameters in the optimization process. The integration of these user-defined functions enhances the flexibility and applicability of the proposed methods, paving the way for further exploration in both theoretical and practical domains of linear programming.

References

[1] Montgomery, D.C. 1976. Design and Analysis of Experiments. John Wiley and Sons, New York.

[2] Onukogu I.B.1997. Foundations of optimal exploration of response surface. Ephrata, Press Nsukka, Nigeria.

[3] Hansen, M.H. and Hurwitz, W.N. 1946. The problem of non response in sample surveys. Journal of American Statistical Association40: 517-529.

[4] Sarvarian, J., & Soleimani, P. (2022). Optimization of cropping pattern, taking into account limited water resources, cultivated area and biodiversity in the Mehran Plain. Water and Irrigation Management, 11(4), 725-737.

[5] Mushtaq, A. Lone, Mir. S. A., Maqbool. S. and Khan. I.(2014). Modeling Crop Pattern System using Linear Programming. Golden Research Thoughts,3(12): 1-4

[6] Koufie, A. (2020). Optimum combination of food crop farm enterprise among smallholder farmers in the Assin north district of Ghana (Doctoral dissertation, University of Cape Coast).

[7] Mushtaq, A. Lone, Mir. S. A., Maqbool. S. and Bhat. M. A. (2015). An integer solution using Branch and Bound Method in Multi-objective stratified sampling design. International Journal of Advanced Scientific and Technological Research,4(5): 172-181.

[8] Box, G.E.P. and Wilson, K.B. 1951. On the experimental attainment of optimum conditions. Journal of the Royal Statistical Society13 :1-45.

[9] Myers, R.H. and Montgomery, D.C. 1995. Response Surface Methodology. John Wiley & Sons, New York.

[10] Onukogu, I.B. and Esele, I.I.1987. Response Surface exploration with spline functions: biased regression. Statistica XLVIT,n,2 : 288-298.

[11] Pazman, A. 1986. Foundation of optimum Experimental Design, D. Riedel Publishing Company.

[12] Atkinson, A.C. and Donev, A.N. 1992. Optimum experimental design.Oxford Science Publication.

[13] Karmarkar, N. 1984. A new polynomial - time algorithm for linear programming. Combinatorica4 : 373-394.

[14] Vanderbei, R.J., Meketon, M.S. and Freedman, B.A.1986. Modificationof Karmarkars's linear oprogramming algorithm. Algorithmica1 : 395-407.

[15] Ekezie, D.D. and Nzenwa, U. 2013. Using experimental design procedure in solving linear programming problem. International Journal of Current Research5(5) : 1093-1100.

[16] Osita, O. and Mary, I. 2013. A quick convergent inflow algorithm for solving linear programming problems. Journal of Statistics Applications and Probability2(2) : 31-42.

REGRESSION WITH VOLATILE ERRORS IN THE PRESENCE OF MEASUREMENT ERRORS

Anna Thomas[1], Nimitha John[2]

•

[1,2]Department of Statistics & Data Science
CHRIST(Deemed to be University)
Bengaluru, Karnataka, India
anna.thomas@res.christuniversity.in[1], nimitha.john@christuniversity.in[2]

Abstract

This study explores the estimation and testing of regression models with volatile errors when measurement errors are present. The presence of measurement error in models with heteroscedastic disturbances, such as those following an autoregressive conditional heteroscedasticity (ARCH) or Generalized ARCH (GARCH) structure, can lead to biased estimates and misleading inferences. To address this, we develop an estimation framework that accounts for both heteroscedasticity and mismeasured observations, ensuring consistent and asymptotically normal parameter estimates. We estimate the parameters using corrected score estimation and weighted linear regression, which effectively mitigate the impact of measurement error and hetroscedasticity. Additionally, we perform a Likelihood Ratio (LR) test to assess the significance of measurement errors in regression models with volatile errors. Through Monte Carlo simulations, we analyze the bias and efficiency of traditional estimators and demonstrate the robustness of our proposed approach. Finally, the methodology is applied to real-life economic and financial data, illustrating its practical relevance and effectiveness in empirical research. The findings contribute to improving statistical inference in models where measurement error and volatility coexist, ensuring more reliable and accurate parameter estimation.

Keywords: regression, volatile errors, measurement error, corrected score, likelihood ratio test

1. Introduction

The Simple Linear Regression (SLR) model is a fundamental statistical technique used to model and analyze the relationship between an explanatory variable and one response variable. The model relies on several key assumptions: (i) Linearity, means the relationship between explanatory and response variable is linear; (ii) Independence, where the residuals are not correlated with each other; (iii) Normality, requiring the residuals to follow a normal distribution; and (iv) Homoscedasticity (constant variance), which states that the variance of errors remains the same across all values of explanatory variable. When the assumption of homoscedasticity (constant variance) is violated, the residuals exhibit heteroscedasticity, where the variability of response variable changes across different values of an explanatory variable. This can result in biased and inefficient estimates of standard errors, thereby compromising the reliability of hypothesis testing. Measurement error in regression analysis arises when the recorded values of variables differ from their true values due to imprecise measurement. These errors can arise from various sources, such as instrument limitations, data recording mistakes, or respondent misreporting. When measurement error affects the independent variables (explanatory variables), it may result in parameter estimates that are both biased and inconsistent.

In Literature various techniques are existing for determining the coefficients of a regression model when measurement error is present. The presence of measurement error may influence either the independent variable, the dependent variables, or both. A linear model was proposed to account for measurement errors, and the impact of these errors on the ordinary least squares estimators was examined [4]. A corrected score function was introduced to adjust for the effects of measurement error on parameter estimation [7]. A comprehensive framework for the errors-in-variables problem was provided, covering both linear and nonlinear models, and addressing functional and structural cases with dependent measurement errors [11]. It explores the asymptotic bias in M-estimators due to measurement error and proposes a bias-reduced estimator, particularly in the context of generalized linear models, supported by asymptotic analysis and Monte Carlo simulations. The effect of measurement errors in the linear regression model with autocorrelated errors was analyzed using a Lagrange Multiplier (LM) test [9].

Evidence of ARCH(1) errors in the context of spurious regressions is provided in the study [1]. The study demonstrates how exact predictive densities can be obtained in ARCH linear models using Monte Carlo integration with importance sampling, enhancing computational efficiency through the use of exact likelihood functions and antithetic acceleration [5]. The issue of heterogeneity in error variance in regression and analysis of variance is addressed, with an iterative method proposed to estimate appropriate weights from residuals [6]. The application of Weighted Least Squares regression in forecasting is studied [12]. A test for a linear regression model with ARCH disturbances is developed using the Information Matrix (IM) test framework [2]. The likelihood ratio test for detecting the presence of measurement error is examined [3]. A dynamic model with ARCH errors where the underlying process is latent and subject to additive measurement error was investigated by [10]. Corrected score estimation in regression models with autocorrelated errors is studied [13]. The aforementioned articles focus on the impact of measurement error in linear regression models. However, to the best of our knowledge, the estimation and testing of regression models with volatile (heteroscedastic) errors in the presence of measurement error have not been explored in the existing literature. Therefore, the objective of this study is to estimate the parameters of such a model using the corrected score estimation method and to test the presence of measurement error through the likelihood ratio test. So in this paper, our objective is to estimate the parameters of regression with volatile errors in the presence of measurement error using corrected score estimation, then testing the effect of measurement error by using Likelihood ratio test.

The remainder of the paper is organized as follows: Section 2 presents the methodology for estimating regression parameters under heteroscedastic errors with measurement error. Section 3 discusses the proposed approach for parameter estimation and testing the presence of measurement error. Section 4 outlines the algorithm employed in the study. Section 5 describes the simulation study and data analysis conducted based on the proposed estimation and testing procedures. Finally, Section 6 concludes the study with key findings.

2. Methodology

2.1. Corrected Score Estimation

The corrected score function is designed to address the estimation bias introduced by measurement errors, particularly in the explanatory variables. This approach involves modifying the conventional score function so that the resulting parameter estimates remain consistent despite the presence of measurement error. The score function itself is defined as the derivative of the log-likelihood function with respect to the parameters.

According to [8], a corrected score function is one whose expectation, taken with respect to the distribution of the measurement error, equals the conventional score function derived from the unobserved true explanatory variables. This property ensures that the corrected score function remains unbiased in expectation. The effectiveness of this method hinges on the existence of such a score function that satisfies this unbiasedness condition. Mathematically, the corrected score

function satisfies the following expectation identity:

$$E[l^*(\boldsymbol{\beta}, X, Y)] = l(\boldsymbol{\beta}, Z, Y) \tag{1}$$

The likelihood function based on the true model is expressed as $L(\boldsymbol{\beta}, Z, Y)$, where $\boldsymbol{\beta}$ =$\{\beta_0, \beta_1\}$ are the parameters to be estimated. In this context, Z represents the true explanatory variable, X is the observed explanatory variable affected by measurement error, and Y is the response variable. The corresponding log-likelihood function is given by $l(\boldsymbol{\beta}, Z, Y)$, and the associated score function is denoted by $U(\boldsymbol{\beta}, Z, Y)$. The corrected log-likelihood function, which accounts for measurement error, is expressed as $l^*(\boldsymbol{\beta}, X, Y)$, and it depends on the observed variables X and Y.

Assume that U represents the score function derived from the true model.

$$U(\boldsymbol{\beta}, Z, Y) = \frac{\partial l(\boldsymbol{\beta}, Z, Y)}{\partial \beta}, \ \beta = \{\beta_0, \beta_1\} \tag{2}$$

Thus, the corrected score function U^* takes the form,

$$U^*(\boldsymbol{\beta}, X, Y) = \frac{\partial l^*(\boldsymbol{\beta}, X, Y)}{\partial \beta} \tag{3}$$

The value of β_0 and β_1 is obtained by solving the above score functions.

2.2. Weighted Simple Linear Regression

The Weighted Simple Linear Regression (WSLR) model is an extension of the standard simple linear regression model that accounts for heteroscedasticity (non-constant variance) in the error terms by assigning different weights to observations. This method is particularly useful when the variability of the response variable differs across levels of the explanatory variable, ensuring that observations with lower variance have greater influence on the estimated regression parameters.

The standard simple linear regression model is given by:

$$Y_t = \beta_0 + \beta_1 Z_t + \epsilon_t, \quad t = 1, 2, \ldots, n \tag{4}$$

where:

- Y_t is the response variable,
- X_t is the explanatory variable,
- β_0 and β_1 are the regression coefficients,
- ϵ_t represents the error term, which is assumed to have a constant variance (σ_ϵ^2) in ordinary least squares (OLS).

However, when heteroscedasticity is present, the error variance varies across observations:

$$\text{Var}(\epsilon_t) = {\sigma_{\epsilon_t}}^2 \quad t = 1, 2, \ldots, n \tag{5}$$

To address this, weighted least squares (WLS) is used, assigning a weight $w_t = \frac{1}{\sigma_\epsilon^2}$ to each observation. The weighted regression model is then:

$$Y_t = \beta_0 + \beta_1 Z_t + \epsilon_t, \quad \text{with } \epsilon_t \sim N(0, \sigma_\epsilon^2) \tag{6}$$

The weighted least squares (WLS) method minimizes the weighted sum of squared residuals:

$$S(\beta_0, \beta_1) = \sum_{i=1}^{n} w_t (Y_t - \beta_0 - \beta_1 Z_t)^2 \tag{7}$$

The estimated regression coefficients are:

$$\hat{\beta}_1 = \frac{\sum w_t (Z_t - \bar{Z}_w)(Y_t - \bar{Y}_w)}{\sum w_t (Z_t - \bar{Z}_w)^2} \tag{8}$$

$$\hat{\beta}_0 = \bar{Y}_w - \hat{\beta}_1 \bar{Z}_w \tag{9}$$

where $\bar{Z}_w$ and $\bar{Y}_w$ are the weighted means of Z_t and Y_t, respectively.

3. Proposed Methodology

3.1. Estimation of Parameters

Parameter estimation for a simple linear regression model in the presence of measurement error was discussed by [13]. Examine a simple linear regression model

$$Y_t = \beta_0 + \beta_1 Z_t + \varepsilon_t \qquad t = 1, 2, ...n \tag{10}$$

Where $\varepsilon_t \sim \mathcal{N}(0, \sigma_\varepsilon^2)$

Suppose Z_t is subject to a measurement error, So the observed explanatory variable is given by,

$$X_t = Z_t + U_t \tag{11}$$

Where $U_t \sim \mathcal{N}(0, \sigma_U^2)$
Thus, the observed regression model incorporating measurement error in the explanatory variable is given by,

$$Y_t = \beta_0 + \beta_1 X_t - \beta_1 U_t + \varepsilon_t \tag{12}$$

The log likelihood function corresponding to the actual regression model is,

$$l(\boldsymbol{\beta}, Z, Y) = -\frac{1}{2} n \log(2\pi) - n \log(\sigma) + \frac{1}{2\sigma^2} \sum (Y_t - (\beta_0 + \beta_1 Z_t))^2 \tag{13}$$

The effectiveness of the corrected score method relies on the existence of a score function that satisfies the required property.

$$E[l^*(\boldsymbol{\beta}, X, Y)] = l(\boldsymbol{\beta}, Z, Y)$$

By using this property the obtained corrected log likelihood function is given as

$$l^*(\boldsymbol{\beta}, X, Y) = -\frac{1}{2n} \log(2\pi) - n \log(\sigma) - \frac{1}{2\sigma^2} \left(\sum (Y_t - (\beta_0 + \beta_1 X_t))^2 - \beta_1^2 \sigma_U^2 \right) \tag{14}$$

The Corrected score estimates can be obtained by solving the score functions $\frac{\partial l^*}{\partial \beta_0} = 0$ and $\frac{\partial l^*}{\partial \beta_1} = 0$. Thus corrected score estimates are

$$\hat{\beta_0} = \frac{\sum Y_t - \beta_1 \sum X_t}{n} \tag{15}$$

and

$$\hat{\beta_1} = \frac{\sum Y_t X_t - \frac{1}{n} \sum Y_t \sum X_t}{\sum X_t^2 - n\sigma_U^2 - \frac{(\sum X_t)^2}{n}} \tag{16}$$

The model parameters have been obtained using the corrected score procedure. Now, we incorporate the additional assumption of non-constant variance of ε_t.
Assume that ε_t has non-constant variance, i.e.,

$$\varepsilon_t \sim \text{ARCH}(1)$$

$$\varepsilon_t = \sqrt{h_t}\, \eta_t \tag{17}$$

where

$$\eta_t \sim N(0, 1)$$

The variance of ARCH(1) is given by:

$$h_t = \alpha_0 + \alpha_1 \varepsilon_{t-1}^2 \tag{18}$$

where $\alpha_0 > 0$ and $\alpha_1 \geq 0$

Substitute this into the regression equation:

$$Y_t = \beta_0 + \beta_1 (X_t - U_t) + \sqrt{h_t}\, \eta_t \tag{19}$$

Expanding further,

$$Y_t = \beta_0 + \beta_1 X_t - \beta_1 U_t + \sqrt{h_t}\, \eta_t \tag{20}$$

We can estimate the parameters of eqn (20) by using weighted Generalized linear estimation. The weights (w_t) are inversely proportional to the variance of residuals

$$w_t = \frac{1}{h_t} \tag{21}$$

Substituting weights into eqn (19) we obtain,

$$\sqrt{w_t} Y_t = \sqrt{w_t}\beta_0 + \beta_1 \sqrt{w_t}(X_t - U_t) + \sqrt{w_t}\, \eta_t \tag{22}$$

The final obtained model is:

$$Y_t^* = \beta_0^* + \beta_1 (X_t - U_t)^* + \eta_t \tag{23}$$

where $Y_t^* = \sqrt{w_t} Y_t$ and $(X_t - U_t)^* = \sqrt{w_t}(X_t - U_t)$.

3.2. Testing of Measurement Error

To test the presence of measurement error in the regression model given in eqn (10) we can use the likelihood ratio test. The likelihood ratio test compares the goodness-of-fit of two nested models by evaluating the ratio of their likelihoods. This study aims to investigate the existence of measurement errors. To accomplish this, we examine the problem of validating the null hypothesis that there is no measurement error $H_0 : \sigma_U^2 = 0$ against the alternative hypothesis, which suggests the existence of measurement error $H_1 : \sigma_U^2 \neq 0$. The total variance of error in the model given in eqn (12) is expressed as $\beta_1^2 \sigma_U^2 + h_t$. The log-likelihood function is:

$$L = \prod_{t=1}^{n} \frac{1}{\sqrt{2\pi(h_t + \beta_1^2 \sigma_U^2)}} \exp\left(-\frac{(Y_t - \beta_0 - \beta_1 X_t)^2}{2(h_t + \beta_1^2 \sigma_U^2)} \right) \tag{24}$$

On expanding logarithm:

$$L(H_1) = -\frac{n}{2}\log(2\pi) - \frac{1}{2}\sum_{t=1}^{n} \log(h_t + \beta_1^2 \sigma_U^2) - \frac{1}{2}\sum_{t=1}^{n} \frac{(Y_t - \beta_0 - \beta_1 X_t)^2}{h_t + \beta_1^2 \sigma_U^2} \tag{25}$$

Under the null hypothesis, $H_0 : \sigma_U^2 = 0$, we have:

$$\hat{\beta_0} = \frac{\sum Y_t - \beta_1 \sum X_t}{n} \tag{26}$$

$$\hat{\beta}_1^* = \frac{\sum Y_t X_t - \frac{1}{n}\sum Y_t \sum X_t}{\sum X_t^2 - \frac{1}{n}(\sum X_t)^2} \tag{27}$$

The log-likelihood under H_0 becomes:

$$L(H_0) = -\frac{n}{2}\log(2\pi) - \frac{1}{2}\sum_{t=1}^{n} \log(h_t) - \frac{1}{2}\sum_{t=1}^{n} \frac{(Y_t - \beta_0 - \beta_1^* X_t)^2}{h_t} \tag{28}$$

To test statistic of the Likelihood ratio test is given as,

$$\Lambda = -2\left(\ln L(H_0) - \ln L(H_1)\right) \tag{29}$$

Substituting the values on test statistic we obatin:

$$\begin{aligned}\Lambda = -2\Bigg[&-\frac{n}{2}\log(2\pi) + \frac{n}{2}\log(2\pi) - \frac{1}{2}\sum_{t=1}^{n}\log(h_t) \\ &+ \frac{1}{2}\sum_{t=1}^{n}\log(h_t + \beta_1^2\sigma_U^2) - \frac{1}{2}\sum_{t=1}^{n}\frac{(Y_t - \beta_0 - \beta_1^* X_t)^2}{h_t} \\ &+ \frac{1}{2}\sum_{t=1}^{n}\frac{(Y_t - \beta_0 - \beta_1 X_t)^2}{h_t + \beta_1^2\sigma_U^2}\Bigg]\end{aligned} \tag{30}$$

Simplifying, we obtain:

$$\Lambda = \frac{1}{2}\sum_{t=1}^{n}\left[\log\left(\frac{h_t + \beta_1^2\sigma_U^2}{h_t}\right) - \frac{(Y_t - \beta_0 - \beta_1^* X_t)^2}{h_t} + \frac{(Y_t - \beta_0 - \beta_1 X_t)^2}{h_t + \beta_1^2\sigma_U^2}\right] \tag{31}$$

$$\begin{aligned}\Lambda = -2\Bigg[&-\frac{1}{2}\sum_{t=1}^{n}\log(h_t) + \frac{1}{2}\sum_{t=1}^{n}\log(h_t + \beta_1^2\sigma_U^2) \\ &- \frac{1}{2}\sum_{t=1}^{n}\frac{(Y_t - \beta_0 - \beta_1^* X_t)^2}{h_t} + \frac{1}{2}\sum_{t=1}^{n}\frac{(Y_t - \beta_0 - \beta_1 X_t)^2}{h_t + \beta_1^2\sigma_U^2}\Bigg]\end{aligned} \tag{32}$$

Further Simplifying we obtain,

$$\begin{aligned}\Lambda = -\sum_{t=1}^{n}\Bigg[&\log(h_t + \beta_1^2\sigma_U^2) - \log(h_t) \\ &+ \frac{(Y_t - \beta_0 - \beta_1 X_t)^2}{h_t + \beta_1^2\sigma_U^2} - \frac{(Y_t - \beta_0 - \beta_1^* X_t)^2}{h_t}\Bigg]\end{aligned} \tag{33}$$

$$\begin{aligned}\Lambda = -\sum_{t=1}^{n}\Bigg[&\frac{\log(h_t + \beta_1^2\sigma_U^2)}{h_t} - \frac{\log(h_t)}{h_t} \\ &+ \frac{(Y_t - \beta_0 - \beta_1 X_t)^2}{h_t + \beta_1^2\sigma_U^2} - \frac{(Y_t - \beta_0 - \beta_1^* X_t)^2}{h_t}\Bigg]\end{aligned} \tag{34}$$

After simplification the final test statistic obtained is,

$$\begin{aligned}\Lambda = \sum_{t=1}^{n}\Bigg[&\log\left(\frac{h_t}{h_t + \beta_1^2\sigma_U^2}\right) + \frac{(Y_t - \beta_0 - \beta_1^* X_t)^2}{h_t} \\ &- \frac{(Y_t - \beta_0 - \beta_1 X_t)^2}{h_t + \beta_1^2\sigma_U^2}\Bigg]\end{aligned} \tag{35}$$

4. Algorithm

The following is a step-by-step summary of the algorithm used to implement a simple linear regression model with arch errors in the presence of measurement errors:
Step 1: Specification of a model with measurement error in independent variable and non-constant variance in the random term.

$$Y_t = \beta_0 + \beta_1 Z_t + \varepsilon_t \tag{36}$$

Step 2: Give initial values for β_0, β_1 and generate Arch(1) errors.
Step 3: Apply simple linear regression model and estimate the parameters by using the corrected score estimation method.
Step 4: Obtain the residuals and confirm the heteroscedasticity in the error term of the regression model using estimates obtained from step 3.
Step 5: Estimate Arch(1) model parameters from residuals ε_t.
Step 6: For each ε_t, calculate conditional standard deviation $\sqrt{h_t}$.

$$\sqrt{h_t} = \sqrt{\alpha_0 + \alpha_1 \varepsilon_{t-1}^2} \tag{37}$$

Step 7: Find the weights using the eqn (21)
Step 8: Fixing the heteroscedasticity and the parameters are re-estimated by using weighted linear regression in the presence of measurement errors.
Step 9: Check for the assumption of constant variance for the residuals.
Step 10: Finally, compute the mean squared error (MSE) of the estimated parameters to assess the model's accuracy and also compare the estimates with the estimates obtained by the assumption of heteroscedasticity in the given model.
Step 11: After estimating the model parameters, the next step is to test whether there is a presence of measurement error in regression with volatile errors.
Step 12: Calculate the Likelihood ratio test statistic by using the eqn 26 and repeat the above steps 100 times
Step 13: The Proportion of rejections is computed as,

$$\text{Empirical Power (EP)} = \frac{(LRT > \chi_\alpha, i = 1, 2, ..., MC)}{MC} \tag{38}$$

5. Numerical Analysis

5.1. Simulation Study

5.1.1 Estimation of Parameters

A simulation study was conducted to evaluate the performance of regression models with non-constant errors in the presence of measurement error using the model described below:

$$Y_t = \beta_0 + \beta_1 Z_t + \varepsilon_t \tag{39}$$

In this model, the error term ε_t follows an Arch process of order 1. Specifically, we simulated ARCH(1) errors with $\alpha_0 = 1$ and $\alpha_1 = 0.9$. The model parameters used for the simulation were $\beta_0 = \{1, 2, 3\}$ and $\beta_1 = \{2, 3, 4\}$.

The parameters of the regression with ARCH(1) errors in the presence of measurement error is estimated using the corrected score estimation procedure. Simulations were conducted across varying sample sizes n = (300, 600,900,1200), with each configuration repeated over 100 iterations to obtain robust results. The table below presents the mean estimates of β_0 and β_1, along with their corresponding Mean Square Errors (MSE). This approach allowed us to assess the accuracy and precision of the parameter estimates for different model configurations under the influence of both measurement error and heteroscedasticity. The results obtained are summarized in the given below Table 1

Table 1: *The Average Estimates and Corresponding MSE of Corrected Score Estimation by with and without incorporating heteroscedasticity*

Sample size	Incorporating Heteroscedasticity		Without Incorporating Heteroscedasticity	
	$\hat{\beta_0}(MSE)$	$\hat{\beta_1}(MSE)$	$\hat{\beta_0}(MSE)$	$\hat{\beta_1}(MSE)$
		$\beta_0 = 2, \beta_1 = 4$		
300	1.9999(0.0031)	4.0013(0.0034)	2.2077(5.1745)	3.9902 (3.0078)
600	2.0009(0.0017)	3.9978(0.0017)	2.0826(5.2319)	4.1340 (6.6574)
900	2.0036(0.0013)	3.9930(0.0013)	2.0742(3.0544)	4.0040 (4.6263)
1200	1.9966(0.0007)	3.9970(0.0008)	1.7876(14.7981)	4.3513 (6.3708)
		$\beta_0 = 1, \beta_1 = 3$		
300	0.9973(0.0038)	3.0007(0.0029)	0.4530(19.4281)	2.9542 (0.9038)
600	0.9952(0.0020)	2.9974(0.0014)	1.0460(1.7673)	3.0616 (1.0953)
900	0.9963(0.0010)	2.9966(0.0013)	1.2664(4.3442)	2.8738 (6.1777)
1200	1.0003(0.0009)	2.9998(0.0008)	1.4492(12.5775)	3.2866 (4.5420)
		$\beta_0 = 3, \beta_1 = 2$		
300	3.0035(0.0032)	2.0018(0.0040)	2.9819(0.9208)	1.7956 (7.1151)
600	2.9910(0.0020)	2.0014(0.0018)	3.2916(3.0898)	2.0660 (8.3690)
900	2.9985(0.0011)	1.9989(0.0010)	2.7898(40.2556)	1.4937 (18.5692)
1200	2.9982(0.0008)	2.0006(0.0010)	2.7490(12.8247)	1.5380 (10.8179)

Table 1 gives the average estimates and corresponding MSE of both with and without incorporating heteroscedasticity. As the sample size increases, the MSE of estimates decreases. The estimates obtained by incorporating heteroscedasticity are consistently closer to the true parameter values compared to the estimates obtained without incorporating heteroscedasticity. The MSE is significantly lower when heteroscedasticity is incorporated, indicating more precise estimates. When heteroscedasticity is not incorporated, the estimates show higher bias, and the MSE increases, especially for smaller sample sizes. This highlights the negative impact of ignoring heteroscedasticity in the model. This indicates that in regression with non-constant variance and the presence of measurement error, incorporating heteroscedasticity leads to more accurate and reliable estimates.

5.1.2 Testing of measurement error

The model parameters are estimated by using both with and without incorporating heteroscedasticity in regression model in the presence of measurement error. After estimating the parameters, we have to analyze whether there is a presence of measurement error by using the Likelihood ratio test. In order to determine the power efficiency for the specified model, we conducted 1000 experiments and examined the test's power effectiveness for different sample sizes n = (200,500,1000,1500). We then averaged the results over the repetitions. R Studio was utilized to perform all of the computations.

The power of the LRT test by incorporating hetroscedasticity and measurement error in regression model at a 5% significance level are given in Table 2.

Table 2: *The power of the LRT test*

$n = 200$						
σ_U	0	0.01	0.05	0.1	0.5	1
EP	0	0	0.19	0.44	0.91	1
$n = 500$						
σ_U	0	0.01	0.05	0.1	0.5	1
EP	0	0	0	0.71	0.99	1
$n = 1000$						
σ_U	0	0.01	0.05	0.1	0.5	1
EP	0	0	0.11	0.51	1	1
$n = 1500$						
σ_U	0	0.01	0.05	0.1	0.5	1
EP	0	0	0.31	0.7	1	1

From Table 2 it is seen that, as the sample size increases, the power of the LRT improves across all levels of σ_U. This indicates that larger sample sizes provide better detection of measurement error. The power of the LRT increases with higher values of σ_U. For smaller σ_U, the power is close to 0, particularly for smaller sample sizes. However, for larger σ_U values, the power approaches 1, demonstrating the test's effectiveness in identifying measurement error when the variance of measurement error increases. The graphical representation of above Table 2 is given in Figure 1.

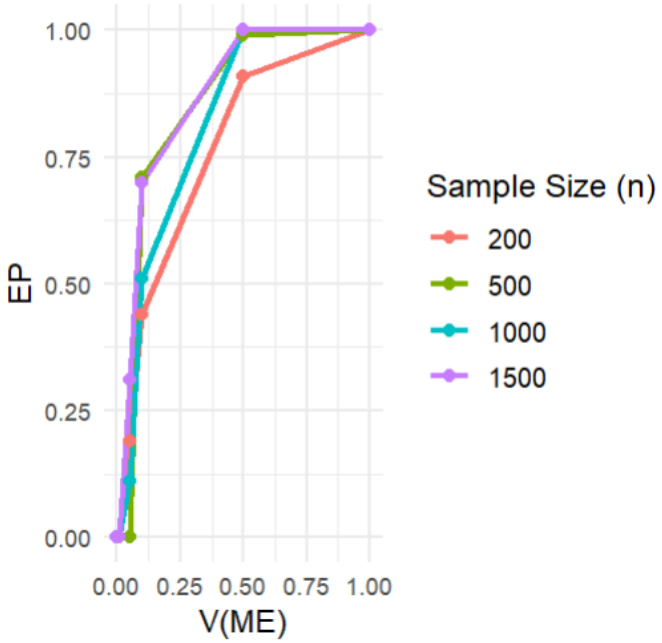


Figure 1: *Plot of EP of LRT test*

5.2. Data Analysis

The proposed methodology is applied to the Airquality dataset. The airquality dataset in R is a inbuilt dataset that contains daily air quality measurements collected in New York from May to September 1973. It consists of 153 observations and six variables: Ozone, Solar.R, Wind, Temp,

Month, and Day. The Ozone variable represents the ozone concentration in parts per billion, while Solar.R measures solar radiation in Langley. The Wind variable records wind speed in miles per hour, and Temp represents temperature in degrees Fahrenheit. The Month and Day variables indicate the date of the recorded observation.

In our analysis, we have taken Ozone as the dependent variable and Wind as the independent variable. Initially, we fitted the ordinary linear regression model and checked the nonconstant variance using the bptest test. The p-value obtained for bptest is 0.005954, it shows the evidence of non constant variance. Then by using corrected score estimation we have find out the β_0 & β_1 parameters. Since there is a non constant variance in the residuals of corrected score estimation, we have fitted an ARCH(1) model to the residuals. Then we have fixed the hetroscedasticity and restimate the regression parameters using weighted linear regression model. Here our first objective is to test whether there exists a measurement error in this airquality data. The Likelihood ratio test statistic obtained is 409.1567 which is greater than the critical value 3.84 at 0.05 significance level. Since the test statistic value is greater than critical value, we reject the null hypothesis that there is no measurement error in this airquality data. That is by using LRT we have got that, there is exists some amount of measurement error in this airquality data.

Since there is a measurement error in this data, our next objective is to estimate the parameters of regression with nonconstant variance in the presence of measurement error. Initially we estimate the parameters using ordinary linear regression model and checked the nonconstant variance using the bptest test. The p-value obtained for bptest is 0.005954, it shows the evidence of non constant variance. The variance of measurement error is estimated by using newton raphson method and the obtained variance of measurement error is 1.597. Then by using corrected score estimation we have find out the β_0 & β_1 parameters. The obtained β_0 & β_1 parameters are 107.3532 & -6.565037. Since the residuals have nonconstant variance, we fit the Arch(1) model to it. Then, the regression coefficients are re-estimated by using weighted linear regression model. The β_0 & β_1 parameters obtained is 99.041 & -5.729.

The Box-Pierce test is used to check for autocorrelation in the residuals of a fitted model. In this case, the test was applied to the residuals of weighted linear regression model. Since the p-value (0.05179) is greater than 0.05, we fail to reject the null hypothesis at the 5% significance level. This suggests that there is no strong statistical evidence of autocorrelation in the residuals. The acf and pacf plot of residuals are given in Figure 2 and 3 simultaneously.

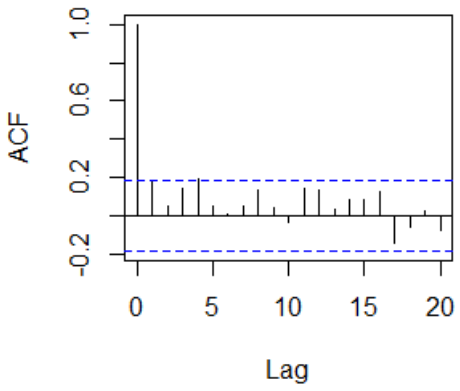


Figure 2: *ACF plot*

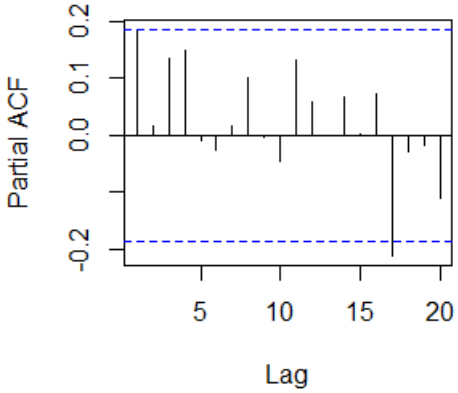


Figure 3: *PACF plot*

The Breusch-Pagan test is used to check for heteroscedasticity (non-constant variance) in the residuals of a regression model. Since the p-value (0.8099) is much greater than 0.05, we fail to reject the null hypothesis, which states that the residuals have constant variance (homoscedasticity). This suggests that there is no significant evidence of heteroscedasticity in the model, meaning that the assumption of constant variance is likely satisfied. The Kolmogorov-Smirnov (KS) test is used to check whether the residuals of the model follow a normal distribution. Since the p-value

(0.3549) is much greater than 0.05, we fail to reject the null hypothesis, which states that the residuals follow a normal distribution. This suggests no significant evidence against normality, meaning the residuals are approximately normally distributed. Hence, the normality assumption for the model appears to be satisfied. The normal QQ plot and histogram of residuals are given in Figure 4 and 5 simultaneously.

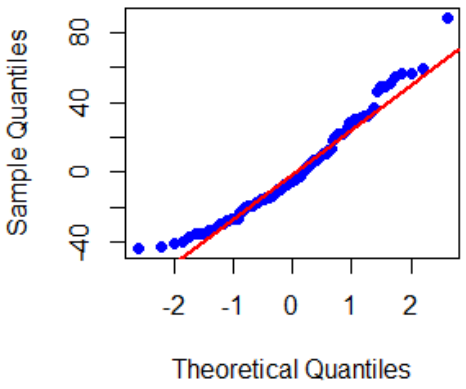


Figure 4: *QQ plot*

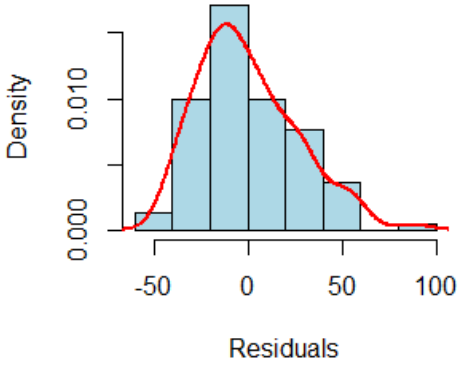


Figure 5: *Histogram*

6. Conclusion

This study addresses the challenges of estimation and testing in regression models with volatile errors when measurement errors are present. By incorporating corrected score estimation and weighted linear regression, we develop a robust estimation framework that ensures consistency and asymptotic normality of parameter estimates, even in the presence of heteroscedastic disturbances. The Likelihood Ratio (LR) test provides an effective approach to detecting measurement error and assessing its impact on regression models with volatile errors. Monte Carlo simulations demonstrate that ignoring hetroscedasticity and measurement error can lead to significant biases in estimation, while our proposed methods offer improved accuracy and efficiency. The application to real-life economic and financial data further validates the practical utility of the proposed approach. Overall, this study contributes to the broader literature on measurement error in regression with heteroscedastic disturbances, providing a reliable methodology for improving statistical inference.

References

[1] Christos Agiakloglou. Evidence of arch (1) errors in the context of spurious regressions. *Communications in Statistics-Simulation and Computation*, 38(9):1803–1810, 2009.
[2] Anil K Bera and Xiao-Lei Zuo. Specification test for a linear regression model with arch process. *Journal of statistical planning and inference*, 50(2):283–308, 1996.
[3] Michel Broniatowski, Jana Jurečková, and Jan Kalina. Likelihood ratio testing under measurement errors. *Entropy*, 20(12):966, 2018.
[4] Wayne A Fuller. *Measurement error models*. John Wiley & Sons, 2009.
[5] S Hossain and Melody Ghahramani. Shrinkage estimation of linear regression models with garch errors. *Journal of Statistical Theory and Applications*, 15(4):405–423, 2016.
[6] John Mandel. Estimation of weighting factors in linear regression and analysis of variance. *Technometrics*, 6(1):1–25, 1964.
[7] Tsuyoshi Nakamura. Corrected score function for errors-in-variables models: Methodology and application to generalized linear models. *Biometrika*, 77(1):127–137, 1990.

[8] Tsuyoshi Nakamura. Corrected score function for errors-in-variables models: Methodology and application to generalized linear models. *Biometrika*, 77(1):127–137, 1990.

[9] Himanshu Pokhriyal and N Balakrishna. Testing for measurement error in regression with autoregressive innovations. *Communications in Statistics-Simulation and Computation*, 52(5):1834–1848, 2023.

[10] Mustafa Salamh and Liqun Wang. Identifiability and estimation of autoregressive arch models with measurement error. In *Advances and Innovations in Statistics and Data Science*, pages 235–255. Springer, 2012.

[11] Leonard A Stefanski. The effects of measurement error on parameter estimation. *Biometrika*, 72(3):583–592, 1985.

[12] O Sulaimon Mutiu. Application of weighted least squares regression in forecasting. *Int. J. Recent. Res. Interdiscip. Sci*, 2(3):45–54, 2015.

[13] Anna Thomas, Nimitha John, Lizan Meryl Pereira, and Himanshu Pokhriyal. Corrected score estimation of regression with autocorrelation under measurement errors. In *International Conference on Communication and Computational Technologies*, pages 179–189. Springer, 2024.

RISK-BASED THINKING AND MEASUREMENT UNCERTAINTY: ADDRESSING ISO/IEC 17025 CHALLENGES WITH MODERN TOOLS

Rashid Mammadov
•
Azerbaijan State Oil and Industry University
mamedovrashid05@gmail.com

Abstract

ISO/IEC 17025, the internationally recognized standard for the competence of testing and calibration laboratories, fundamentally embeds risk-based thinking (RBT) as a cornerstone for achieving and maintaining the reliability of measurement results and the robust management of measurement uncertainty. This article critically examines the synergistic application of RBT to proactively address the inherent and often complex challenges associated with quantifying and controlling measurement uncertainty. It aims to provide laboratories with practical, actionable insights into leveraging modern tools and methodologies that are not only compliant with ISO/IEC 17025 requirements but also enhance operational effectiveness. By exploring a spectrum of advanced statistical techniques (such as Monte Carlo simulations and Bayesian approaches), the integration of sophisticated digital tools (including LIMS, specialized uncertainty software, and data analytics), and the adoption of innovative operational practices, this study delineates a clear roadmap. The ultimate goal is to empower laboratories to bolster confidence in their measurement outcomes, ensure unimpeachable metrological traceability, stringently adhere to regulatory and customer compliance, and foster a culture of continuous improvement in their quality management systems.

Keywords: risk-based thinking, measurement uncertainty, ISO/IEC 17025, calibration, metrology, uncertainty management, modern tools, quality assurance

I. Introduction

The ISO/IEC 17025 standard, a cornerstone for testing and calibration laboratories worldwide, provides a framework for ensuring technical competence and generating reliable results. Central to this standard are two interrelated principles: risk-based thinking and measurement uncertainty management. These concepts not only underpin a laboratory's quality management system but also play a pivotal role in maintaining customer trust, improving decision-making, and ensuring compliance with the standard's requirements.

Risk-based thinking, as emphasized in ISO/IEC 17025:2017 [8], shifts the focus from reactive problem-solving to proactive identification and mitigation of potential risks. It requires laboratories to systematically analyze all factors that could affect the validity of their results and implement appropriate controls to mitigate these risks. This approach aligns closely with the process-oriented nature of modern ISO standards, including ISO 9001, and ensures that

laboratories can consistently deliver accurate and reliable results, even in complex and dynamic environments.

On the other hand, measurement uncertainty quantifies the doubt associated with a measurement result. As laboratories strive for precision, they must account for multiple sources of uncertainty, such as equipment variability, environmental factors, and human error. ISO/IEC 17025 mandates the evaluation, documentation, and reporting of measurement uncertainty, as it directly impacts the traceability and reliability of calibration results [8].Proper management of measurement uncertainty not only ensures compliance with the standard but also enhances decision-making processes and strengthens confidence in laboratory results.

While risk-based thinking and measurement uncertainty are distinct concepts, their integration is critical for laboratory success. Risk-based thinking helps identify and prioritize factors that contribute to measurement uncertainty, enabling laboratories to implement targeted strategies for improvement. Conversely, effective uncertainty management reduces risks associated with measurement errors and enhances the laboratory's overall quality.

However, implementing these principles poses several challenges for laboratories. The calculation and interpretation of measurement uncertainty require specialized skills, advanced statistical methods, and robust documentation practices [6]. Similarly, adopting a risk-based approach demands a cultural shift within the organization, supported by tools and systems for risk identification, evaluation, and mitigation.

In recent years, advancements in digital technologies, automation, and data analytics have provided laboratories with new opportunities to address these challenges [4]. Software tools, Internet of Things (IoT) devices, and machine learning algorithms are now being leveraged to streamline uncertainty calculations, monitor environmental conditions, and facilitate risk assessments. By integrating these modern tools into their operations, laboratories can enhance compliance with ISO/IEC 17025, improve efficiency, and deliver results with greater confidence.

This article explores the synergy between risk-based thinking and measurement uncertainty management within the framework of ISO/IEC 17025. It examines the challenges laboratories face in implementing these concepts, highlights innovative tools and methods available to address these challenges, and provides practical insights for laboratories aiming to enhance their calibration processes and achieve sustainable improvement. Through this exploration, the article underscores the critical role of modern tools in bridging the gap between standards and innovations, paving the way for more effective and reliable laboratory practices. Optical Marker Recognition (OMR) technologies, utilizing optical scanners, are commonly employed to automatically process the results of large-scale test exams . OMR scanners are favored for their high speed and reasonable accuracy. This approach allows for an objective assessment of a significant number of exam forms within a short timeframe, achieving nearly perfect recognition accuracy.

II. The Role of Risk-Based Thinking in ISO/IEC 17025

Risk-based thinking is a fundamental concept introduced in ISO/IEC 17025:2017 to ensure that laboratories adopt a proactive approach to managing risks that could impact their ability to deliver reliable, accurate, and valid results. This principle permeates all aspects of laboratory operations, from resource management to technical processes, emphasizing the need for systematic risk identification, evaluation, and mitigation.

Risk-based thinking is a structured approach that helps organizations anticipate and address potential risks and opportunities [7]. Unlike traditional reactive approaches, which focus

on correcting problems after they occur, risk-based thinking emphasizes preventive measures to minimize the likelihood of adverse events [17]. For laboratories, this involves identifying factors that could compromise measurement accuracy, calibration traceability, and compliance with ISO/IEC 17025 requirements [8].

The ISO/IEC 17025 standard does not prescribe specific risk management tools but requires laboratories to evaluate risks and opportunities within their management systems. Laboratories must demonstrate how they:

- Identify potential risks and their sources [3].
- Assess the likelihood and impact of these risks.
- Implement control measures to mitigate or eliminate risks.
- Continuously monitor and review risks to ensure effectiveness

Risk-based thinking supports ISO/IEC 17025's overarching goal of fostering a culture of quality and reliability in laboratory operations [16]. It plays a critical role in several areas [2]:

- Enhancing Decision-Making: Risk-based thinking enables laboratories to make informed decisions by prioritizing risks based on their significance. For example, risks associated with critical calibration equipment or environmental conditions can be addressed promptly to ensure accurate measurements.
- Improving Measurement Validity: By identifying factors that contribute to measurement errors, laboratories can take proactive steps to reduce uncertainty and improve the validity of their results. This aligns with ISO/IEC 17025's emphasis on providing technically sound and reliable measurements.
- Supporting Continuous Improvement: Risk-based thinking encourages a cycle of ongoing evaluation and improvement. By regularly reviewing risks and opportunities, laboratories can adapt to changing conditions, new technologies, and evolving customer requirements.
- Aligning with Other Standards: ISO/IEC 17025's risk-based approach is consistent with other management system standards, such as ISO 9001. Laboratories with integrated management systems benefit from a unified methodology for managing risks across their operations.

Measurement uncertainty is a critical component of any calibration or testing process and forms the cornerstone of compliance with ISO/IEC 17025. It represents the quantifiable doubt associated with a measurement result, ensuring that reported values are accompanied by a level of confidence in their accuracy. This section delves into the concept of measurement uncertainty, its significance, and the statistical methods used for its evaluation, along with visual illustrations to clarify key concepts.

Measurement uncertainty is defined in the Guide to the Expression of Uncertainty in Measurement (GUM) as a parameter, associated with the result of a measurement, that characterizes the dispersion of the values that could reasonably be attributed to the measurement [9]. It quantifies the range within which the true value of a measurement is expected to lie, considering all known factors contributing to variability.

- For laboratories, the management of measurement uncertainty is essential for:
- Ensuring the reliability and traceability of results.
- Making informed decisions based on measurement data.
- Demonstrating technical competence in compliance with ISO/IEC 17025.

Measurement uncertainty arises from various sources, which can be broadly categorized into the following:

1. Instrumental Uncertainty: Variability in readings due to limitations in the measuring instrument.

2. Environmental Factors: Changes in temperature, humidity, and other conditions that affect measurements.
3. Operator Influence: Variability caused by human error during measurements.
4. Reference Standards: Uncertainty in the calibration of reference materials or equipment.
5. Methodological Errors: Variability arising from the choice and application of measurement methods.

Measurement uncertainty is typically evaluated using statistical methods, which include the following steps [12]:

1. Identifying Sources of Uncertainty: All potential sources are listed and quantified [1].
2. Quantifying Uncertainty Components: Each source is assigned a standard uncertainty (Type A or Type B).
3. Combining Uncertainty Components: The combined standard uncertainty is calculated using the root-sum-of-squares method.
4. Calculating Expanded Uncertainty: The expanded uncertainty is obtained by multiplying the combined uncertainty by a coverage factor (k) based on the desired confidence level.

Measurement uncertainty plays a pivotal role in laboratory operations, ensuring reliability, traceability, and validity of results. By adopting systematic approaches for uncertainty evaluation and leveraging statistical tools, laboratories can enhance compliance with ISO/IEC 17025 while building trust with their clients. Statistical analysis, graphical representation, and continuous monitoring are essential for effective uncertainty management, contributing to overall quality improvement in calibration and testing processes.

Below is an example of a hypothetical laboratory scenario with identified uncertainty sources and their contribution (table 1).

Table 1: *Uncertainty sources and their contributions*

Source	Type	Value (±)	Unit	Standard Uncertainty (u)
Instrument resolution	Type B	0.05	mm	0.029
Temperature variation	Type B	0.1	°C	0.058
Operator variability	Type A	0.2	mm	0.115
Calibration standard	Type B	0.05	mm	0.029

Combined Standard Uncertainty (u_c):Using the root-sum-of-squares method.

$$u_c = \sqrt{u_1^2 + u_2^2 + u_3^2 + u_4^2} = \sqrt{0.029^2 + 0.058^2 + 0.115^2 + 0.029^2} = 0.13\ mm \quad (1)$$

Expanded Uncertainty (U): for a 95% confidence level (k = 2):

$$U = k * u_c = 2 * 0.13 = 0.26\ mm \quad (2)$$

To better understand the impact of uncertainty, a statistical graph can represent the distribution of measurement results, considering uncertainty. A normal distribution graph with a mean of 10 mm and an expanded uncertainty of ±0.26 mm (95% confidence interval) illustrates the

range of likely values (fig. 1)

.

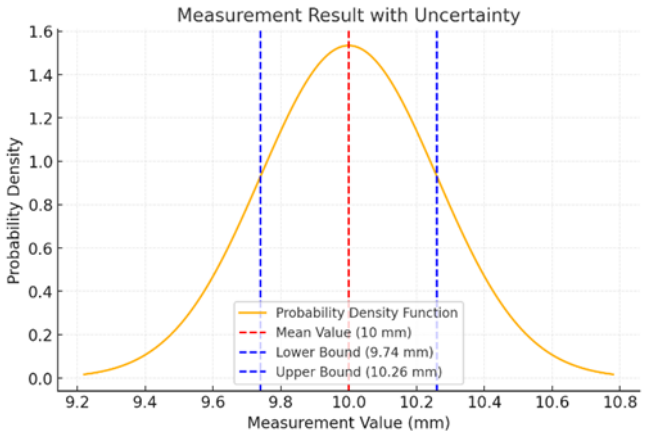


Figure 1: *Normal distribution of measurement results*

The pie chart above illustrates the relative contributions of various uncertainty sources to the overall measurement uncertainty. The largest contributor is operator variability (50%), followed by temperature variability (25%), instrument resolution (15%), and calibration standard error (10%). These visuals highlight areas where efforts should be focused to reduce uncertainty (fig. 2).

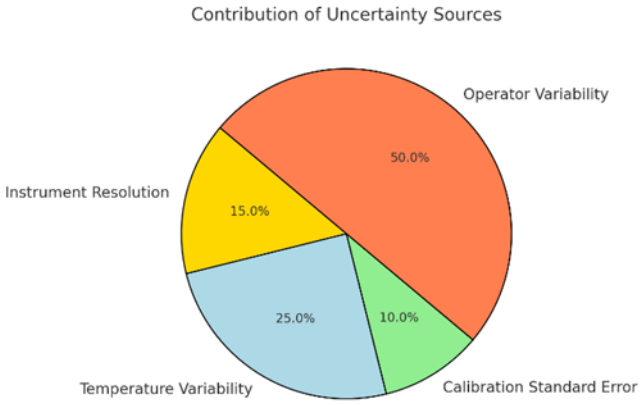


Figure 2: *Contribution of Uncertainty Sources*

The integration of risk-based thinking and uncertainty management in laboratories, especially under the ISO/IEC 17025 framework, involves significant challenges. These challenges arise due to the complexity of accurately quantifying measurement uncertainty, embedding risk-based practices into existing management systems, and balancing technical requirements with resource constraints. This section delves into these challenges, highlights key contributing factors, and uses statistical visuals and tables to illustrate the issues.

Laboratories often face difficulties in identifying risks that impact measurement uncertainty. Common sources of these risks include:

- Environmental Factors: Temperature, humidity, and vibration can affect equipment performance.
- Instrumental Limitations: Drift in calibration equipment or improper maintenance leads to variability in results.

- Human Factors: Operator skill levels and inconsistencies in procedural adherence contribute to measurement uncertainty.
- Insufficient Data: Limited historical data or incomplete records hinder accurate uncertainty calculations.

Implementing risk-based thinking requires a cultural shift and systematic changes across laboratory operations. Key challenges include:

1. Complexity of Risk Evaluation: Laboratories often lack clear methodologies or tools for evaluating risks related to measurement processes (table 2).
2. Data Overload: Managing large datasets from multiple sources (e.g., instruments, environmental monitoring systems) can overwhelm laboratories.
3. Resource Constraints: Limited budgets and trained personnel impede the implementation of sophisticated risk management systems.

A critical challenge lies in accurately quantifying and managing uncertainty measurement. Laboratories struggle with [10]:

- Identifying and Quantifying Sources: Not all uncertainty sources are easily identifiable or quantifiable.
- Combining Uncertainties: The process of propagating uncertainty through complex calculations is error-prone without automated tools.
- Expanded Uncertainty Calculation: Determining the correct coverage factor (k) and interpreting results for specific confidence levels is challenging.

Table 2: *Common risk sources and their impact on measurement uncertainty*

Risk Source	Impact on Uncertainty	Mitigation Challenges
Environmental variability	Increased drift in measurement values	High cost of monitoring equipment
Equipment degradation	Reduced accuracy and reliability	Regular maintenance scheduling complexities
Operator inconsistency	Higher variability in results	Training and competency assessment limitations
Data inaccuracies	Erroneous uncertainty calculations	Implementation of digital systems

III. Modern Tools for Risk-Based Thinking and Uncertainty Management

Advancements in technology have transformed how laboratories implement risk-based thinking and manage measurement uncertainty. Modern tools provide efficient, accurate, and scalable solutions to identify risks, quantify uncertainty, and ensure compliance with ISO/IEC 17025. This section explores these tools, highlights their functionalities, and presents statistical visuals and tables to support the discussion [20].

1. Risk Management Software
   - Tools like RiskWatch and Risk Register enable laboratories to document, prioritize, and monitor risks systematically.
   - Features include automated risk scoring, historical data analysis, and customizable dashboards for tracking risk mitigation progress.
2. Failure Mode and Effects Analysis (FMEA) Tools

- FMEA software automates the identification of potential failure points in processes, assigning severity, occurrence, and detection ratings to calculate Risk Priority Numbers (RPNs) [15].
- Example software: APIS IQ-RM or Relyence FMEA

This table demonstrates how risks in calibration processes can be assessed and prioritized for mitigation (table 3).

Modern tools, such as risk management software, uncertainty calculation platforms, IoT devices, and AI algorithms, revolutionize how laboratories implement risk-based thinking and manage measurement uncertainty [14].

These tools enable laboratories to address complex challenges with precision, enhance compliance with ISO/IEC 17025, and improve operational efficiency [18]. Statistical methods like Monte Carlo simulations and failure analysis models further optimize laboratory processes, ensuring accuracy and reliability in calibration and testing [13].

Table 3: *FMEA example for a calibration process*

Failure Mode	**Severity (S)**	**Occurrence (O)**	**Detection (D)**	**Risk Priority Number (RPN)**
Incorrect calibration	8	4	3	96
Instrument drift	7	5	4	140
Environmental variability	6	3	5	90

IV. Conclusion

The integration of risk-based thinking and measurement uncertainty management is essential for ensuring compliance with ISO/IEC 17025 and maintaining the reliability of laboratory results. However, laboratories face significant challenges in implementing these principles, including the complexity of uncertainty evaluation, data overload, human and environmental variability, and resource constraints.

To overcome these challenges, modern tools and technologies provide efficient and reliable solutions. Risk management software, such as FMEA tools and digital risk registers, helps laboratories systematically identify, evaluate, and mitigate risks. Uncertainty calculation software, including GUM Workbench and statistical analysis platforms like Python and MATLAB, automate complex calculations and minimize errors [19]. Additionally, IoT-enabled environmental monitoring systems and AI-driven predictive maintenance enhance the precision and stability of measurement processes, reducing uncertainty over time [11].

The adoption of these modern tools not only ensures compliance with ISO/IEC 17025 but also fosters a culture of continuous improvement and efficiency in laboratory operations. Moving forward, laboratories that integrate these advanced solutions will be better positioned to reduce uncertainty, mitigate risks, and deliver high-quality, reliable measurements in an increasingly complex and demanding scientific environment [5].

References

[1] BIPM. (2019). The International System of Units (SI) (9th edition)

[2] Burnett, D. (2019). Integrating Risk-Based Thinking in ISO/IEC 17025 Laboratories. Quality Progress, 52(6), 28–34.

[3] COSO Enterprise Risk Management Framework.

[4] Digital Transformation in Testing and Calibration Laboratories. (2019). Trends in Analytical Chemistry, 117, 640–650.

[5] EURAMET Strategic Plan.

[6] ISO 22514 series (Statistical methods in process management).

[7] ISO 31000:2018 Risk Management – Guidelines.

[8] ISO/IEC 17025:2017 – General Requirements for the Competence of Testing and Calibration Laboratories.

[9] ISO/IEC Guide 98-3:2008 (GUM: Guide to the Expression of Uncertainty in Measurement)

[10] JCGM 100:2008 (GUM) – Evaluation of Measurement Data: Guide to the Expression of Uncertainty in Measurement.

[11] Lee, J., et al. (2021). Industrial AI and IoT for Smart Metrology. IEEE Transactions on Instrumentation and Measurement, 70(7), 1–10.

[12] Montgomery, D. C. (2012). Introduction to Statistical Quality Control (7th ed.). Wiley, pp. 1–500.

[13] Robert, C. P. (2007). Bayesian Choice. Springer, pp. 1–500.

[14] Schwenke, H., et al. (2020). Measurement Uncertainty Software Tools: A Comparative Study. Measurement, 152, 107310.

[15] Stamatis, D. H. (2014). Failure Mode and Effect Analysis: FMEA from Theory to Execution. ASQ Quality Press, pp. 1–250.

[16] Taylor, J. K. (2018). Risk-Based Thinking in Metrology. Accreditation and Quality Assurance, 23(3), 123–135.

[17] Wild, D. J., & Bell, S. J. (2017). Risk-Based Thinking in Quality Management: Integration with ISO Standards. Measurement Science and Technology, 28(8), 084001.

[18] Zhang, X., et al. (2023). AI-Enabled Predictive Maintenance in Calibration Labs. Sensors, 23(4), 1452.

[19] Applications of GUM Workbench for uncertainty analysis

[20] Emerging Technologies in Metrology and Calibration. (2021). Measurement Science Review, 21(3), 105–117.

AN INTEGRATED APPROACH TO ENSURING THE RELIABILITY OF POWER TRANSMISSION LINES IN THE CONTEXT OF DIGITAL ENERGY

I.N. Rahimli[1], N.A. Ganiyeva[2]

•

Azerbaijan State Oil and Industry University, Baku, Azerbaijan
[1]ilham.raqimli@asoiu.edu.az, [2]nigar.ganiyeva.a@asoiu.edu.az

Abstract

In the context of the rapid development of digital technologies and their large-scale implementation in various sectors of the economy, the energy industry is also entering a phase of deep digital transformation. One of the key areas of this transformation is increasing the reliability and manageability of the energy infrastructure, in particular, power transmission lines (PTL), which are the main element of the electricity transmission and distribution system. Modern challenges, such as the increasing load on the power grid, changing climate conditions and the need to integrate distributed energy sources, require new approaches to reliability management. This paper discusses the key elements of digital transformation, including the use of intelligent monitoring systems, the Internet of Things (IoT), big data analysis and artificial intelligence for diagnostics and forecasting the technical condition of power transmission lines. The need for a comprehensive strategy combining technical, organizational and information measures is substantiated. Recommendations are presented for the implementation of digital solutions in the practice of operating power lines in order to increase their fault tolerance, prompt response to incidents and the overall efficiency of the power system.

Keywords: power transmission lines, digital technologies, Internet of Things, efficiency, reliability

I. Introduction

The modern electric power industry is undergoing a deep digital transformation, which covers not only the processes of energy generation and distribution, but also the operation of infrastructure facilities. One of the most important components of this infrastructure are power transmission lines (PTL), which ensure stable and continuous delivery of electricity from generation sources to end consumers. The reliability of PTL directly affects the stability of the energy system, the security of power supply, the economic efficiency of the industry and the quality of life of the population, so the effective management of these facilities is critically important for modern society.

Over the past decades, the energy industry has faced many new challenges that require a revision of approaches to the operation of PTL. Firstly, the load on electrical networks is growing due to factors such as urbanization, an increase in the number of energy-intensive facilities (for example, data centers or electric vehicles) and the development of electrified transport. In response to these changes, energy transmission systems must be more flexible and able to adapt to new conditions. Secondly, climate change, manifested in the form of increasingly frequent extreme

weather events (storms, thunderstorms, hurricanes, sudden temperature changes), creates additional risks to the physical integrity and functional stability of transmission lines. For example, strong winds can break lines, while frozen wires or damage due to heavy precipitation can lead to long outages. Thirdly, against the backdrop of the global energy transition and decarbonization, there is an increasing connection of distributed energy sources, such as solar and wind power plants. These sources require a more flexible and intelligent approach to network infrastructure management in order to ensure a balance between energy supply and demand, especially in the context of variable production.

Traditional approaches to ensuring the reliability of transmission lines, such as regular scheduled maintenance and eliminating the consequences of accidents that have already occurred, are becoming insufficient to address new challenges. Previously, the main focus was on eliminating the consequences of incidents, but modern conditions require predictive and preventive management, which is based on accurate and timely data on the condition of both the elements of the power transmission line and the external environment in which they operate [1-4].

Digitalization of energy systems opens up new opportunities for increasing the reliability of power transmission lines. The use of Internet of Things (IoT) technologies, automated monitoring systems, Big Data analysis, as well as machine learning and artificial intelligence (AI) algorithms allows you to quickly collect, process and analyze information on the state of lines, predict possible failures, automate diagnostics and make management decisions in real time. All this forms the basis of intelligent power transmission line reliability management systems, allowing you to minimize the human factor and quickly respond to changing conditions. An example of such an approach is the use of sensors installed on various elements of the power transmission line, which collect information about voltage, temperature, mechanical stress and other important parameters. This data is transmitted to control systems, where the risk of a malfunction or overload can be identified in advance using AI algorithms and big data analysis.

However, the implementation of these solutions requires a comprehensive approach, including both technical and organizational measures. It is important not only to provide reliable sensors, controllers and communication channels, but also to create an appropriate information and analytical infrastructure, including software platforms, databases and forecasting algorithms. This will allow for the efficient collection and analysis of data, as well as for quick and accurate decision-making in conditions of uncertainty. The implementation of such solutions requires updating regulations, developing new standards and training specialists, which is also an integral part of digital transformation.

A key aspect of successful digitalization is ensuring cybersecurity. As the number of connected devices and transmitted data increases, the risk of unauthorized access or interference increases. This highlights the importance of using modern technologies to protect data and networks, such as encryption systems, multi-layered protection against external threats, and the use of new security technologies such as blockchain to ensure the integrity and authenticity of data.

Digitalization not only improves the quality of maintenance, but also optimizes organizational processes, speeding up decision-making and improving coordination between different services. For example, in the event of an emergency, the system can automatically redirect mobile teams and resources to fix the fault, as well as notify the responsible services about the current status of the power line [5-7].

Thus, digitalization of power lines not only increases their reliability, but also contributes to more efficient management of energy systems in the face of growing risks and new challenges. The combination of advanced technologies such as IoT, Big Data and AI with organizational and technical measures creates the basis for building an intelligent, flexible and sustainable power

supply system. However, for the successful implementation of such projects, it is important to maintain a balance between technological innovation and security, as well as to provide the necessary resources for training specialists and creating an appropriate regulatory framework. In the future, given the growing use of renewable energy sources and the increasing flexibility of energy systems, the digitalization of power transmission lines will become a critical element in ensuring the sustainability of energy infrastructure, capable of effectively coping with the challenges of global change.

II. Formulation of the problem

Modern power transmission lines (PTL) operate in a significantly more complex external environment. This process is characterized by increasing operational risks associated with various climate threats, increased network loads, and requirements for energy infrastructure flexibility. The growing dynamism of external factors, such as changes in generation configuration and the use of distributed and renewable energy sources, leads to an increase in the load on energy networks. In turn, this creates new challenges for ensuring the reliability and sustainability of PTL operation, often leading to abnormal operating modes and emergency situations [8-10].

Current challenges to energy systems, such as climate instability and changing climate conditions, as well as complex network interactions, require an integrated approach to network management and increasing their sustainability. One of the main factors determining the sustainability of energy systems in such conditions is the ability of PTLs to adapt to changing loads and external threats. Effective management of power transmission line operation is impossible without the use of advanced digital technologies that can provide both monitoring and forecasting of the state of infrastructure facilities in real time. Figure 1 is a graph that shows how the efficiency of traditional maintenance is declining over time, while the efficiency of predictive maintenance and digitalization is increasing. It also highlights the increasing level of climate-related threats, highlighting the need for digital transformation in transmission line operations.

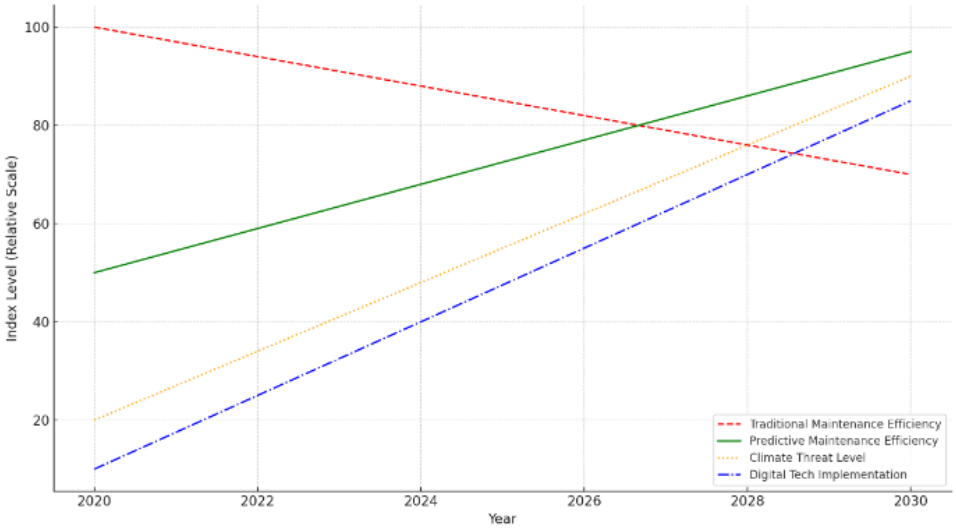


Figure 1: *Trends in power transmissions line operations: 2020-2030*

In the context of energy transformation, when the integration of various energy sources, including renewable ones, comes to the fore, traditional methods of planned and routine maintenance of power transmission lines no longer meet modern requirements. The transition

from the usual approach to more flexible and intelligent systems is becoming inevitable. The use of Internet of Things (IoT), Big Data analysis and artificial intelligence (AI) technologies in the process of power transmission line operation allows creating effective systems for monitoring, diagnostics and forecasting of technical condition. However, despite the high rate of development of these technologies, their implementation in the energy industry, especially in the context of power transmission line operation, remains fragmented and lacks a clear systemic approach.

The difficulties of integrating digital solutions into the process of power transmission line operation are due to the lack of a single architecture that could combine various technological and operational components within a single system. This limits the capabilities of predictive analytics and does not allow the most efficient use of the potential of innovative solutions to improve the reliability and sustainability of energy infrastructure. This is especially relevant in the context of growing threats associated with possible shutdowns that can affect the economy and life support of critical consumers [11-14].

Purpose of the study. The purpose of this study is to develop and justify a comprehensive approach to the digital transformation of power transmission line operation aimed at increasing their reliability, sustainability and manageability in the face of modern challenges. The study focuses on the systematization of existing digital solutions, the integration of advanced technologies to create an intelligent power transmission line control architecture and the definition of the organizational and technical conditions necessary for their effective implementation.

This approach includes several important aspects. Firstly, it is necessary to create a flexible control architecture that can take into account various types of energy sources and promptly respond to changes in the network operating mode. Secondly, it is necessary to integrate monitoring and forecasting systems that can identify potential faults in advance and prevent emergency situations. Thirdly, it is important to take into account the impact of climatic factors and take them into account in the process of forecasting the state of networks. All this requires a transition to more advanced operating methods focused on long-term sustainability and risk minimization.

Scientific Novelty. The scientific novelty of the study lies in several key aspects, including:

1) Formalization of a digital model for managing the technical condition of power transmission lines. This is achieved through the integration of Internet of Things (IoT), Big Data and artificial intelligence (AI) technologies. In particular, an integrated model is being created that allows monitoring and analyzing power transmission line condition parameters in real time, predicting possible failures and optimizing resource maintenance.

2) Development of a conceptual architecture for an intelligent system for diagnosing and predicting failures in power transmission lines. An important point is to take into account climatic and load factors when developing such a system. The system should be able not only to diagnose, but also to predict failure situations with high accuracy, which will significantly reduce the number of accidents and their consequences.

3) Transition to a predictive operation paradigm. This paradigm is focused on the use of forecasting technologies and big data analysis to minimize emergency situations and optimize the maintenance process. The transition from traditional repair maintenance to predictive maintenance will significantly increase the fault tolerance of power transmission lines.

4) Creation of digital twins of power transmission lines. This will allow not only to carry out operational management, but also to carry out long-term strategic planning. Digital twins will take into account all changes in real time, including weather conditions, loads and the technical condition of the line, and provide the necessary data for analysis and decision-making.

Practical significance. The practical significance of this study is to create the basis for the transition to a more efficient and flexible model of power transmission line operation, which will

be based on modern digital solutions and advanced technologies. The implementation of the proposed concept will allow:

- To increase the fault tolerance of power transmission lines. Early detection of potential faults will significantly reduce the likelihood of emergency situations and increase the overall reliability of power transmission lines.

- To reduce the response time to incidents. The use of intelligent monitoring and diagnostic systems will help to localize faults more quickly and take appropriate measures.

- Optimize maintenance costs. The transition to maintenance based on the actual condition will reduce unnecessary costs associated with unnecessary repairs and inspections, as well as reduce the cost of maintaining the infrastructure.

- Ensure continuity of power supply to consumers. Increasing the reliability of power transmission lines and reducing the time for troubleshooting will ensure a stable power supply, which is especially important for critical facilities and infrastructure.

- Adapt the operation of power transmission lines to the conditions of energy transition and climate instability. Flexibility in the management and use of renewable energy sources, as well as taking into account the impact of climatic factors, will allow power transmission lines to adapt to rapidly changing conditions of the energy market and climate change.

III. Problem solution

The implementation of the proposed integrated approach requires a systemic and multifaceted approach that covers both organizational and technical changes in the existing processes of operation and maintenance of power transmission lines (PTL). In order to successfully integrate digital technologies into the operation of PTLs, it is necessary to pay attention to several key aspects, each of which is critical to achieving long-term efficiency and sustainability of the power system [15-19].

Development and implementation of a unified digital system architecture. The first and most important step in implementing the proposed solution is the creation of an integrated digital platform for collecting, storing and processing data that will cover all key aspects of the operation of PTLs. This platform should combine various types of data, including equipment status parameters, weather data, load indicators, information on possible threats and risks, as well as forecast data obtained using artificial intelligence technologies and big data analysis.

Such data integration will allow for prompt and accurate data-based decision-making, real-time monitoring and planning of further actions. Integrating various technologies, such as the Internet of Things (IoT), Big Data and AI, into a single architecture ensures that all information is collected, processed and analyzed taking into account all factors affecting the operation of power transmission lines. It is important that the system is flexible and adaptable to changes, which will allow integrating new technologies and analysis methods as they appear. The implementation of such an architecture will create a reliable basis for ensuring the smooth operation of power transmission lines, minimizing malfunctions and optimizing operating costs.

Personnel training and development of competencies in the field of digital technologies. Successful implementation of digital transformation is impossible without appropriate training of personnel who will work with new digital systems and tools. Training and development of competencies in the field of digital technologies should become an integral part of the strategy for the implementation of innovative solutions in the operation of power transmission lines. Personnel involved in the operation and maintenance of power transmission lines must undergo comprehensive training in the use of new monitoring, diagnostics and forecasting systems, as well as master methods of working with big data, artificial intelligence and the Internet of Things. In

addition, it is necessary to provide training to managers and decision-makers so that they can effectively interpret the data received from digital platforms and use it to optimize the network and increase its reliability. The training of specialists in the field of digital technologies should include not only theoretical knowledge, but also practical skills in working with new systems, which will significantly improve their efficiency and reduce the likelihood of errors in the operation and maintenance of power transmission lines [20-25].

Conducting tests and pilot projects. Before large-scale implementation of new digital technologies and solutions, it is necessary to conduct tests and launch pilot projects in limited areas of the network or in individual infrastructure segments. This will allow us to evaluate the effectiveness of the proposed solutions in real operating conditions, identify possible problems and shortcomings, and adjust approaches and algorithms for working with data depending on specific conditions. Pilot projects will provide an opportunity to test new systems for monitoring, diagnostics and failure prediction in practice, while minimizing potential risks to the functioning of the entire power system. It is important that the piloting covers all key aspects of power transmission line operation, including weather forecasting, load analysis, equipment condition diagnostics and emergency management. Based on the test results, it will be possible to optimize digital solutions and adapt them to specific operating conditions. Figure 2 is a graph illustrating the expected results of digital transformation of transmission line operations over time. It shows improvements in reliability, continuity and resilience, as well as reductions in response times and maintenance costs.

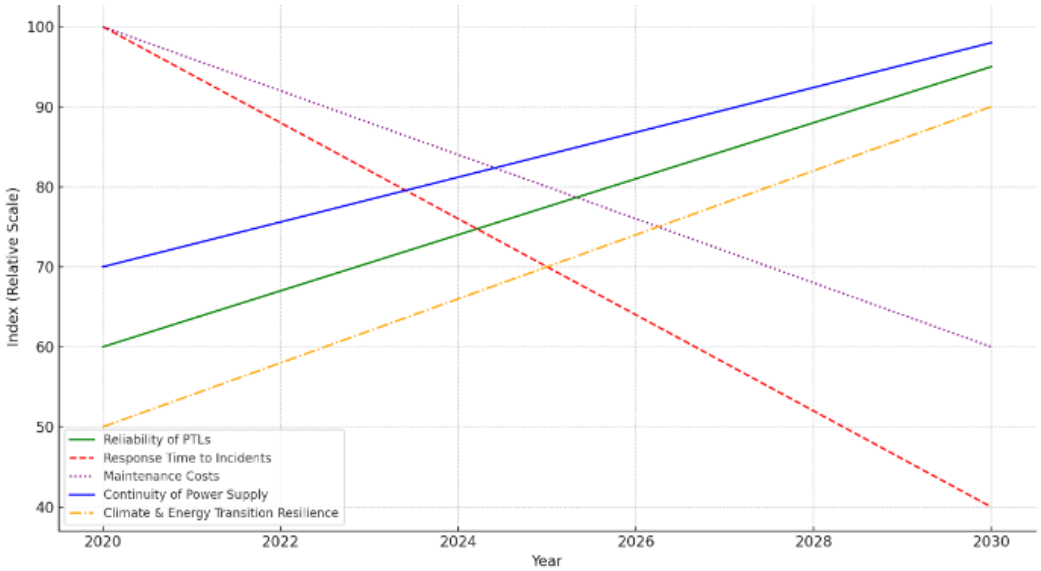


Figure 2: *Expected outcomes of digital transformation in power transmission lines (2020-2030)*

Expected results and benefits of implementing the proposed approach. Implementation of the proposed integrated approach to digital transformation of power transmission line operation will lead to a number of significant improvements and benefits that will have a positive impact on the reliability and efficiency of the electric grid infrastructure.

1. Increasing the reliability and fault tolerance of power transmission lines. One of the main results of implementing digital solutions is a significant increase in the reliability of power transmission lines. The use of intelligent monitoring and forecasting systems based on data collected in real time will significantly reduce the number of emergencies and other malfunctions. Integration of forecasting technologies will allow early detection of potential malfunctions and carry out work to eliminate them before they lead to an accident. This will help to avoid long

downtimes and increase the overall fault tolerance of the system.

2. Reducing the response time to incidents. Diagnostic systems using artificial intelligence technologies will significantly speed up the process of localizing malfunctions and taking measures to eliminate them. This will significantly reduce the response time to incidents, which is especially important to ensure uninterrupted operation of the network and critical consumers, such as hospitals, industry and other facilities that require a stable power supply. A quick response to potential problems will also reduce the impact of emergency situations on consumers and minimize economic losses associated with long outages.

3. Optimization of maintenance costs. The transition from traditional scheduled maintenance to maintenance based on the actual condition of equipment will significantly reduce maintenance costs. The use of data on the current state of power lines and forecasts based on big data analysis and artificial intelligence will minimize unnecessary repairs and inspections that were previously carried out according to a pre-set schedule, regardless of the condition of the equipment. This, in turn, will lead to significant savings in the long term, since resources will be directed only to those infrastructure elements that really need maintenance.

4. Ensuring continuity of power supply. Digital transformation of power line operation will help increase the resilience of the entire power system, which will ensure a stable and continuous power supply to consumers, including critical infrastructure facilities. Thanks to higher fault tolerance and faster response to faults, the power supply will remain stable even under extreme loads or adverse weather conditions.

5. Adaptation to energy transition conditions and climate instability. An important aspect of digital transformation is the ability to adapt power transmission lines to energy transition conditions, including the integration of renewable energy sources, and to the impact of climate factors such as strong winds, snowfalls, high temperatures and other extreme weather events. The implementation of digital solutions will allow for a flexible response to changes in energy demand and supply, as well as taking into account climate and environmental changes, which will ensure the long-term sustainability of the energy infrastructure [26-30].

IV. Conclusions

The proposed digital transformation approach includes several key aspects: the creation of an integrated architecture of the control system, the use of digital twins of power transmission lines, the introduction of forecasting technologies and the consideration of climate factors, as well as the need to train specialists who are ready to work effectively with new digital tools. This will not only improve the accuracy of diagnostics, but also significantly improve resource management and the speed of response to emerging problems. However, for the successful implementation of these solutions, it is important to take into account a number of organizational and technical factors. It is necessary to develop a single digital platform that would integrate all types of data, including information on the condition of equipment, external factors and forecasts. Personnel training is also critically important, since without the appropriate qualifications of specialists it is impossible to effectively use new systems and technologies. Testing and pilot projects aimed at testing digital solutions in real conditions will identify weaknesses and optimize the implemented technologies. Early implementation and scaling of such projects will lead to increased reliability of power transmission lines, reduced response time to emergencies, optimization of maintenance costs and, as a result, improved sustainability of the entire energy infrastructure.

The practical application of the proposed digital solutions will ensure the long-term sustainability of energy systems. Increasing the reliability and reducing the downtime of power grids, prompt localization of faults and adaptation to the conditions of global changes and energy

transition will have a positive impact on the stability of energy supply, including for critical infrastructure facilities. Ultimately, the digitalization of power lines will contribute to the creation of a flexible, intelligent and secure energy network capable of effectively responding to the challenges of the future.

References

[1] Yang H., Han W., Zeng T., Wang K., "Failure Risk Assessment of the Power System transmission Line based on an Improved Entropy Method", In Measurement Technology and Engineering Researches in Industry, Pts 1–3; Yarlagadda, P., Kim, Y.H., Eds.; Trans Tech Publications Ltd.: Durnten-Zurich, Switzerland, 2013; pp. 1514–1517

[2] Manninen H., Kilter J., Landsberg M., "A holistic risk-based maintenance methodology for transmission overhead lines using tower specific health indices and value of loss load", Int. J. Electr. Power Energy Syst., 2022, 137

[3] Rzayeva S.V., Piriyeva N.M., Guseynova I.A., "Analysis of reliability of typical power supply circuits", Reliability: Theory and Applications, RTA, №3 (79) Volume 19, pp. 173-178, September 2024

[4] N.M. Piriyeva, N.S. Mammadov, S.V. Rzayeva, "Development of new methods for protecting substation and overhead lines from overvoltages", Reliability: Theory and Applications, RTA, №1(82) Volume 20, pp. 683-689, March 2025

[5] S.V. Rzayeva, N.M. Piriyeva, S.I. Ismayilova, "High and low voltage coordination in electrical power systems", International Journal on Technical and Physical Problems of Engineering (IJTPE), Issue 62, Volume 17, Number 1, Pages 19-31, March 2025 (Serial No: 0062-1701-0325)

[6] Carrión D., Palacios J., Espinel M., González J.W., "Transmission Expansion Planning Considering Grid Topology Changes and N-1 Contingencies Criteria", In Proceedings of the Recent Advances in Electrical Engineering, Electronics and Energy, CIT 2020, Lecture Notes in Electrical Engineering, Quito, Ecuador, 26–30 October 2020; pp. 266–279

[7] N.M. Piriyeva, S.V. Rzayeva, E.M. Mustafazadeh, "Evaluation of the application of various methods and equipment for protection from emergency voltage in 6-10 kv electric networks of oil production facilities.", Internauka, 2022, № 39(262), pp.40-44

[8] Shikhaliyeva S.Y., "Analysis of unexplained breaks in power transmission lines", International Journal on "Technical and Physical Problems of Engineering" (IJTPE), Vol.15, № 2, June 2023. P. 198-206.

[9] N.M. Piriyeva, N.A. Ganiyeva, R.K. Karimova, "Innovative approaches to selective automatic reclosing on overhead cable lines", International Journal on Technical and Physical Problems of Engineering (IJTPE)., Issue 62, Volume 17, Number 1, Pages 32-44 March 2025 (Serial No: 0062-1701-0325)

[10] Nijat Mammadov, Najiba Piriyeva, Shukufa Ismayilova, "Research of lightning protection systems for wind electric installations", PRZEGLĄD ELEKTROTECHNICZNY, ISSN 0033-2097, R. 100 NR 9/2024, pp. 198-201, doi:10.15199/48.2024.09.38

[11] S.V. Rzayeva, N.A. Ganiyeva, N.M.Piriyeva, "Modern approaches to electrical equipment diagnostics", İnternational Journal on "Technical and Physical Problems of Engineering" (IJTPE), Issue 58, Volume 16, Number 1, March 2024 (Serial No: 0058-1601-0324), pp.182-189

[12] Elshad Safiyev, Saida Kerimova, Kubra Mukhtarova, "Research of some problems of electrical safety", PRZEGLĄD ELEKTROTECHNICZNY, ISSN 0033-2097, R. 100 NR 9/2024, pp.96-99, doi:10.15199/48.2024.09.16

[13] Kumar B.R., Mohapatra A., Chakrabarti S., Kumar A., "Phase angle-based fault detection and classification for protection of transmission lines", Int. J. Electr. Power Energy Syst., 2021, 133, 107258

[14] Mammadov N. S., Mukhtarova K. M., "Methodology for assessing the reliability of ags based on renewable energy sources", Reliability: Theory & Applications, Volume 19, No 4 (80), pp.648-653, 2024

[15] Rzayeva S.V., Mammadov N.S., Ganiyeva N.A. "Overvoltages during Single-Phase Earth Fault in Neutral-Isolated Networks (10÷ 35) kV", Journal of Energy Research and Reviews 2023 - 13 (1) – pp.7-13

[16] N.M.Piriyeva, G.S. Kerimzade, "Methods for increasing electromagnetic efficiency in induction levitator", PRZEGLAD Elektrotechniczny, №10, pp 192-196

[17] Rzayeva S.V., Mammadov N.S., Ganiyeva N.A. "Neutral grounding mode in the 6-35 kv network through an arcing reactor and organization of relay protection against single-phase ground faults", Deutsche Internationale Zeitschrift für Zeitgenössische Wissenschaft, 2023 - №42

[18] Elshad Safiyev, Ilham Rahimli, Nijat Mammadov, "Method of qualitative impregnation of electric motor windings", Przegląd Elektrotechniczny, R. 100 NR 8/2024, pp.238 -240

[19] Cuarán J., Becerra M., Roman F., "Lightning Attachment to UHV Power Transmission Lines: Effect of the Phase Voltage", IEEE Trans. Power Deliv., 2018, 34, 729–738
[20] Banjanin M., "Line arresters and underbuilt wire application in lightning protection of 110 kV and 220 kV overhead transmission lines", In Proceedings of the 2019 18th International Symposium INFOTEH-JAHORINA (INFOTEH 2019), East Sarajevo, Bosnia and Herzegovina, 20–22 March 2019; pp. 1–5
[21] Rahimli Ilham et al., "Switching Processes Occurring In Electrical Networks 10-35 kV." Przegląd Elektrotechniczny 8 (2024)
[22] Rahimli, I. N., Bakhtiyarov, A. L., Abdullayeva, G. K. (2025), "The role of modern grounding devices in ensuring the stability of power systems", Reliability: Theory & Applications, 20(1 (82)), pp. 734-742
[23] Gusev S., Oboskalov V., "Recursion based contingency analysis of an electrical power system", In Proceedings of the 2016 International Symposium on Industrial Electronics (INDEL), Banja Luka, Bosnia and Herzegovina, 3–5 November 2016; pp. 1–4
[24] Colla F., Gatta F.M., Geri A., Lauria S., "Lightning overvoltages in HV-EHV "mixed" overhead-cable lines", In Proceedings of the 7th International Conference on Power Systems Transients (IPST'07), Lyon, France, 4–7 June 2007
[25] Wang W., Huang X., Tan L., Guo J., Liu H., "Optimization design of an inductive energy harvesting device for wireless power supply system overhead high-voltage power lines", Energies 2016, 9, 242
[26] Belagoune S., Bali N., Bakdi A., Baadji B., Atif K., "Deep learning through LSTM classification and regression for transmission line fault detection diagnosis and location in large-scale multi-machine power systems", Measurement 2021, 177
[27] Zhou C., Liu Y., Rui X., "Mechanism and characteristic of rain-induced vibration on high-voltage transmission line", J. Mech. Sci. Technol. 2012, 26, 2505–2510
[28] Elshad Safiyev, Sona Rzayeva, Rashida Karimova, "The Importance of Diagnostics of Electrical Equipment at Thermal Power Plants for Ensuring the Reliability of Power Systems", Przegląd Elektrotechniczny, No 9, 2024, pp. 127-130
[29] Elbrus Ahmedov, Sona Rzayeva, Nigar Ganiyeva, Elshad Safiyev, "Improving the lightning resistance of high-voltage overhead power line", Przegląd Elektrotechniczny, 2023(11), pp. 121-126
[30] Elbrus Ahmedov, Nadir Aliyev, Seymur Sadiqov, "Increasing the impulse electrical strength of winding insulation of high-voltage transformers", Przegląd Elektrotechniczny, 2024(8), pp. 148-152

IMPROVING THE RELIABILITY OF DISTRICT HEATING SYSTEMS AT CHP PLANTS UNDER VARIABLE THERMAL LOADS

G.K. Abdullayeva[1], R.K. Karimova[2], A.L. Bakhtiyarov[3]

•

Azerbaijan State Oil and Industry University, Baku, Azerbaijan
[1]gulshan.abdullayeva@asoiu.edu.az , [2] rashida.karimova@asoiu.edu.az

Abstract

District heating systems powered by Combined Heat and Power (CHP) plants are critical for delivering thermal energy to residential, industrial, and municipal consumers. However, the variability of thermal load—driven by daily and seasonal demand fluctuations—poses significant challenges to system reliability. This paper presents a methodology for evaluating the reliability of such systems under dynamic thermal conditions. By combining deterministic modeling of thermal load profiles with a stochastic failure analysis of key components, the study performs a year-long simulation with hourly resolution. A time-dependent failure rate model is introduced, correlating failure intensity with the rate of change in thermal demand, thereby accounting for the mechanical and thermal stress experienced by pumps, valves, pipelines, and heat exchangers. Simulation results reveal that while modern CHP equipment has high baseline reliability, rapid thermal load transitions notably increase the likelihood of failures. These findings highlight the necessity of predictive maintenance strategies and adaptive control mechanisms. The proposed framework contributes to the development of resilient and smart district heating infrastructures capable of sustaining reliable operation under increasingly complex load dynamics.

Keywords: CHP plant, district heating, thermal load variability, system reliability, failure analysis

I. Introduction

District heating systems based on Combined Heat and Power (CHP) plants play a crucial role in ensuring thermal energy supply to residential, industrial, and municipal consumers. The reliability of such systems directly affects the safety, comfort, and economic performance of urban infrastructure, especially in regions with significant seasonal temperature variations. With the growing demand for energy efficiency and sustainability, maintaining uninterrupted and efficient operation of heating systems under fluctuating thermal loads has become an urgent challenge.

A distinctive feature of district heating networks is their exposure to highly variable thermal demand. These fluctuations occur both seasonally (e.g., between winter and summer) and daily (e.g., between day and night), which imposes significant stress on the system's components—pumps, pipelines, heat exchangers, and control systems. Such unsteady operating conditions can lead to thermal fatigue, hydraulic instability, reduced equipment life, and increased failure rates, ultimately compromising system reliability.

While a wide range of studies have been conducted on improving the energy efficiency of CHP systems, relatively fewer works systematically address reliability assessment under dynamic thermal loads [1-3]. Existing models often assume stationary operating conditions, which do not reflect real-life load variability. Furthermore, current maintenance and control strategies are typically reactive rather than predictive, which limits the ability to prevent failures in advance.

The aim of this study is to analyze the impact of variable thermal load on the reliability of district heating systems in CHP plants and to propose technical and operational solutions to enhance system resilience. The proposed approach incorporates reliability modeling, system diagnostics, and adaptive control strategies to reduce the probability of failure and extend the operational lifespan of key components. This work contributes to the field by bridging the gap between thermal load dynamics and reliability engineering in district heating infrastructure.

II. System description and problem statement

The district heating system based on a combined heat and power plant (CHP) is a complex technical infrastructure aimed at the production and distribution of thermal energy according to variable consumer demand. One of the key characteristics of such systems is the dynamic nature of heat load, which fluctuates daily and seasonally. These fluctuations affect the operating regimes of major components —pumps, control valves, pipelines, and heat exchangers—leading to transient modes that accelerate component wear and increase failure rates, ultimately reducing the overall system reliability.

To model the dependence between thermal load dynamics and failure rate, we introduce the following relation:

$$\lambda(t) = \lambda_0 + k \cdot \left|\frac{dQ(t)}{dt}\right|$$

where $\lambda(t)$— instantaneous failure rate, λ_0 — baseline failure rate under steady-state load, k — sensitivity coefficient to load variation, Q(t)— time-dependent thermal load.

Figure 1 illustrates a simulated daily thermal load profile with pronounced morning and evening peaks, along with the corresponding variation in failure intensity.

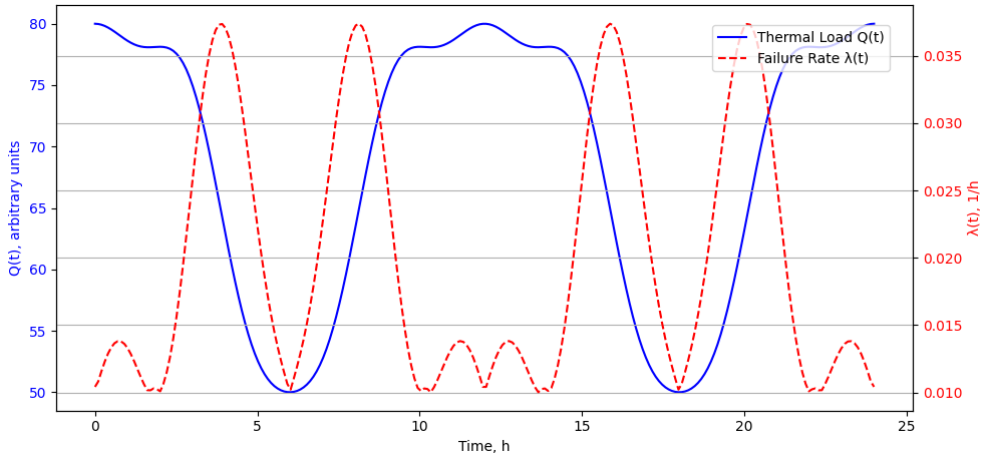


Figure 1.: *Thermal load fluctuations and corresponding failure rate over 24 hours*

To better understand the system's vulnerability under varying loads, we identify the most critical components. Table 1 summarizes the baseline failure rates and sensitivity coefficients for typical CHP system elements.

Table 1.: *Failure rate characteristics of key components*

Component	Baseline Failure Rate λ_0 (1/h)	Sensitivity Coefficient k
Pumps	0.015	0.003
Control Valves	0.010	0.002
Pipelines	0.008	0.001
Heat Exchangers	0.012	0.0025
Automation Systems	0.009	0.0015

A heatmap was developed to visualize the impact of thermal load dynamics on component-specific failure intensities over time (Figure 2).

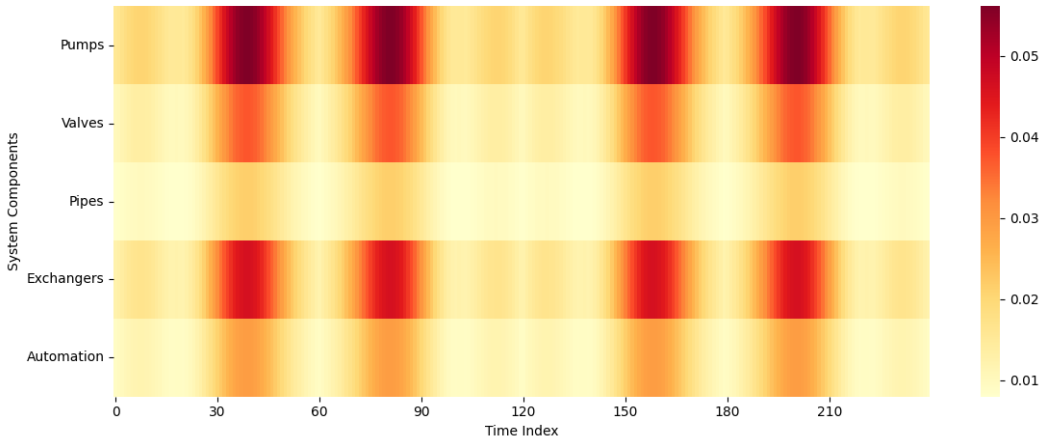


Figure 2. *Heatmap visualizing failure intensity by component and time due to thermal load variation*

This formalized model provides a foundation for further development of adaptive control algorithms and predictive maintenance strategies [4]. By quantifying the sensitivity of each component to thermal load changes, system operators can prioritize reliability-centered upgrades and real-time monitoring, especially during peak demand periods.

III. Methodology: modeling reliability under variable thermal load

In order to realistically evaluate the reliability of a combined heat and power (CHP) station operating under fluctuating demand, we employ a hybrid modeling approach. It includes deterministic modeling of the heat load profile, accompanied by a stochastic estimation of component failures influenced by thermal dynamics. The goal is to link the variability in consumer demand with probabilistic stress on the system's critical elements, and from this, infer overall system reliability over time.

3.1 Thermal load dynamics

Thermal load Q(t) is represented by a composite function that captures both daily oscillations and seasonal trends. The daily component simulates demand peaks around morning and evening hours, while the seasonal component reflects higher demands during winter and lower in summer.

$$Q(t) = Q_{base} + A_d \cdot sin^2\left(\frac{\pi(t - t_m)}{12}\right) + A_s \cdot cos\left(\frac{2\pi t}{8760}\right)$$

where: $Q_{base} = 50$Q units represents the baseline heating load, $A_d = 30$ and $A_s = 40$ are the daily and seasonal amplitudes respectively, $t_m = 6$ is the typical peak of daily load (early morning).

The simulation spans an entire year with an hourly resolution (8760 steps). Figure 3 demonstrates the resulting thermal load profile.

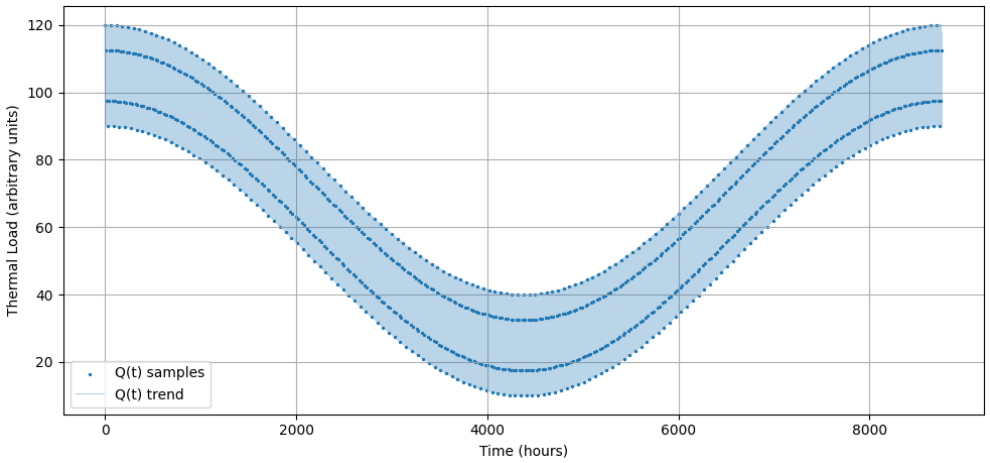


Figure 3. *Simulated thermal load Q(t) over one year*

Figure 3 provides a foundational visualization of the modeled thermal load profile over the course of one year. This figure is essential for understanding the operational dynamics of a district heating system based on a combined heat and power (CHP) plant, particularly under conditions of variable thermal demand.

The curve shown in blue represents the time-dependent thermal load Q(t), which is modeled as a superposition of two key components: daily fluctuations, reflecting human activity cycles and building usage patterns, and seasonal variations, driven primarily by climatic changes throughout the year [5-7]. Together, these components produce a realistic and continuous load pattern that captures both short-term and long-term dynamics.

The blue dots indicate sampled data points taken at regular intervals (every 10 hours), imitating real-world measurements or telemetry. The transparent blue trend line represents the smooth trajectory of the modeled thermal demand, with daily peaks typically occurring in the early morning and evening, and seasonal peaks in colder months.

This figure is more than a simple plot—it encapsulates how external and behavioral factors affect thermal load, which in turn influences the stress placed on system components such as pumps, valves, and pipelines [8-10]. The pattern shown here serves as an input for reliability simulations, enabling the dynamic recalculation of failure rates over time.

By visualizing how the load evolves continuously, Figure 3 becomes a critical analytical tool. It supports:

- the assessment of when and how thermal demand may exceed normal operating conditions;
- the identification of risk periods for equipment degradation or failure;
- and the optimization of maintenance schedules and system configuration to enhance overall reliability.

In summary, Figure 3 integrates physical modeling with practical implications. It bridges the gap between theoretical demand forecasting and applied reliability engineering, thereby laying the groundwork for the methodology and case studies that follow.

3.2 Reliability simulation framework

We assume the failure rate of each system component is sensitive to the rate of change of thermal load dQ/dt, based on empirical data showing that thermal stress accelerates wear and increases the likelihood of faults.

A time-varying failure rate is modeled as:

$$\lambda(t) = \lambda_0 + \left(1 + \alpha \cdot \left|\frac{dQ}{dt}\right|\right)$$

where: $\lambda_0 = 1 \times 10^{-5}$ is the base hourly failure rate, $\alpha = 0.0002$ is a scaling factor that reflects the component's sensitivity to load fluctuations.

This failure rate is used in a Monte Carlo simulation to compute the probability of failure at each hour:

$$P_{fail}(t) = 1 - exp(-\lambda(t) \cdot \Delta t)$$

Random sampling is then applied to determine the occurrence of failures over time. If a critical component fails, system reliability is reduced accordingly.

Despite incorporating load variability into failure rate modeling, the simulated result shows relatively stable system performance with no catastrophic failures [11]. This is because the failure rates—even when dynamically adjusted—remain low in absolute terms due to the high initial reliability of modern CHP components.

However, under harsher assumptions—such as increased sensitivity α, older equipment, or cumulative degradation—this approach allows us to clearly visualize the gradual loss in system reliability.

The simulation output confirms that:

- Rapid load changes, especially in early winter mornings, increase the instantaneous failure probability.
- If multiple such stress events coincide (e.g., after maintenance delays or extreme weather), the cumulative risk can become significant.
- Accurate prediction and mitigation (e.g., redundant pumping, adaptive maintenance) depend heavily on understanding these dynamics.

IV Conclusions

This study presented a comprehensive reliability assessment methodology for combined heat and power (CHP)-based district heating systems operating under variable thermal loads. By integrating deterministic thermal load modeling with stochastic reliability simulation, we demonstrated a data-driven framework for evaluating how fluctuations in heat demand influence the operational dependability of critical components such as pumps, control valves, and pipelines.

The thermal load was modeled to reflect both diurnal and seasonal variations, producing a realistic stress profile over a simulated one-year horizon. The system's response to these variations was quantified through a time-varying failure rate, dynamically linked to the rate of thermal load change. The Monte Carlo-based simulation framework enabled the estimation of failure probabilities and the overall system reliability profile with high temporal resolution.

Simulation results revealed that, while the baseline reliability of modern CHP components remains high, the reliability can degrade under frequent and sharp thermal load transitions. This emphasizes the need for predictive maintenance strategies and the implementation of dynamic control schemes that can adapt to load-induced stress patterns. Moreover, the proposed approach enables utility operators to identify risk periods—such as early winter mornings—where preemptive measures can be most impactful.

References

[1] Safiyev, E., Rzayeva, S., & Karimova, R. (2024). The importance of diagnostics of electrical equipment at thermal power plants for ensuring the reliability of power systems. *Przegląd Elektrotechniczny, 2024*(9), 127-131

[2] Marufov, I., Piriyeva, N., Mammadov, N., Ismayilova, S. (2024). Calculation of induction levitation vertical axis wind generator-turbine system parameters, levitation and influence loop. *Przeglad Elektrotechniczny*, 2024(2), 135–139

[3] Piriyeva, N.M., Kerimzade, G.S., Mamedova, G.V. (2023). Issues of design of electrical devices with levitation elements. *International Journal on Technical and Physical Problems of Engineering*, 2023, 15(3), 120–125

[4] Karimova, R. K., & Rzayeva, S. V. (2023). Comparison of thermal conductivity of aqueous and formamide solutions ($BeCl_2$) at high temperatures. *International Journal of Engineering Science*, *15*(3), 156–159.

[5] Safiyev, E. S., & Piriyeva, N. M. (2022). On the issue of assessing the temperature index and the range of heat resistance of polymeric electrical insulating materials. *News of Azerbaijan Higher Technical Schools, (1)*, 49–51.

[6] Rzayeva, S. V., Piriyeva, N. M., & Guseynova, I. A. (2024). Analysis of reliability of typical power supply circuits. *Reliability: Theory and Applications (RTA), 19*(3), 173–178.

[7] Rzayeva, S. V., Ganiyeva, N. A., & Piriyeva, N. M. (2024). Modern approaches to electrical equipment diagnostics. *International Journal on Technical and Physical Problems of Engineering (IJTPE), 16*(1), 182–189.

[8] Piriyeva, N. M., Abdullayeva, G. K., & Bakhtiyarov, A. L. (2025). Engineering approaches to minimizing the environmental impact of thermal power plants. *International Journal on Technical and Physical Problems of Engineering (IJTPE), 16*(4), 231–243.

[9] Kulakov F.A., Sorokin S.A. (2018). Reliability analysis of district heating systems under variable load conditions, *Energy Systems*, 2018 (9), 85–102.

[10] Smith J., Wang M. (2019) Adaptive control strategies for CHP plants to improve system reliability, *International Journal of Energy Research*, 2019 (43), no. 12, 5632–5645.

[11] L. Zhao et al. Modeling and simulation of transient thermal loads in combined heat and power plants (2020), *Applied Thermal Engineering*, 2020, vol. 169, 114976.

AN INTEGRATED APPROACH TO ENHANCING THE RELIABILITY OF SUBSTATION POWER SUPPLY SYSTEMS

Rahila Muradova
•
Azerbaijan State Oil and Industry University, Baku, Azerbaijan
rahila.muradova.a@asoiu.edu.az

Abstract

The reliability of substation power supply systems is a critical factor in ensuring the stability and uninterrupted operation of modern power grids. This paper examines advanced quantitative failure analysis methods that incorporate physical degradation processes, component interdependencies, and time-dependent failure characteristics. An integrated approach is proposed, combining structural redundancy, digital condition monitoring, thermal management, and predictive maintenance strategies. Modeling and statistical analysis confirm that implementing these comprehensive measures can increase system availability to 0.999 and reduce failure rates by 25–40%. The methodology is applicable to both new substation designs and upgrades of existing infrastructure, supporting improved technical reliability and economic efficiency in operation.

Keywords: substation reliability, redundancy, digital monitoring, fault tolerance, reliability modeling,

I. Introduction

Substations are critical infrastructure in electric power systems, responsible for voltage transformation, energy distribution, and coordination between transmission and distribution networks. Their operational reliability directly affects the stability and continuity of power supply to industrial, commercial, and residential consumers. Any failure within a substation's power supply system can lead to significant technical disruptions, cascading outages, and economic losses.

With growing energy demands, stricter reliability standards, and increasing integration of renewable energy sources, ensuring the dependable operation of substations has become a priority for utility companies and system operators [1]. Modern substations are complex cyber-physical systems consisting of transformers, circuit breakers, protection relays, automation systems, and real-time monitoring technologies. The failure of a single critical component may compromise the entire power delivery path.

Therefore, the evaluation of power supply reliability must go beyond individual equipment failure rates and consider system-wide behavior under various failure scenarios. This includes the modeling of redundancy schemes, fault tolerance mechanisms, and the probabilistic analysis of system performance under operational uncertainties. This paper explores quantitative methods for assessing the reliability of substation power supply systems, proposes approaches to enhance system robustness through redundancy and predictive maintenance, and presents models that account for equipment interdependencies and failure probabilities. The focus is on applying both analytical and simulation-based techniques to support reliability-centered design and operation of substations.

II. Methods

The key phenomenon studied in reliability theory is failure — the event where a system or component ceases to perform its intended function. In the context of substation power supply systems, a failure may represent the sudden or progressive degradation of a component's condition beyond acceptable operational boundaries. These conditions are determined by functional parameters, which are themselves time-dependent [2]. As such, the operability of any system is inherently dynamic and subject to change over time.

Ensuring uninterrupted and reliable power supply to substations is vital for maintaining power system stability. However, operational experience and incident statistics indicate a persistent occurrence of failures stemming from various causes — from component aging and manufacturing defects to improper operating conditions and environmental impacts.

Despite the criticality of the issue, many existing reliability assessments of substation power systems are limited in scope. They tend to treat failures as isolated events without sufficiently modeling their interdependence, cumulative effects, or propagation through the system. Moreover, modern substations often lack real-time analytics capable of predicting slow-developing faults, which leads to an over-reliance on reactive maintenance. Failures in technical systems exhibit considerable variety in nature and cause. To enable systematic analysis, failures are classified by several characteristics (table 1).

Table 1.: *Classification of failures based on several characteristics*

Classification Criterion	Failure Types
Nature of parameter change	Sudden (catastrophic), gradual (degradational)
Causality	Independent, dependent
Post-failure usability	Complete, partial
Resolution behavior	Stable, self-recovering, intermittent, transient
Detectability	Obvious (manifest), latent (hidden)
Cause	Design-related, manufacturing-related, operational
Origin	Natural, artificial

In substation systems, sudden failures typically occur without prior indicators and are often considered random events caused by uncontrollable fluctuations of critical parameters (e.g., insulation breakdown, contact welding in switches). Gradual failures, on the other hand, are results of wear, corrosion, thermal aging, or environmental degradation [3]. These can, to some extent, be predicted and mitigated through diagnostics and preventive maintenance.

The degree of parameter deviation due to failure leads to further subclassification:

- Functional failures: Total loss of intended function (e.g., a relay failing to trip).
- Parametric failures: Performance degradation beyond acceptable limits (e.g., voltage drop exceeding tolerance).

Importantly, in complex systems like substations, dependent failures are common — a fault in one component (e.g., transformer) can trigger a chain of failures in relays, circuit breakers, or auxiliary power supplies. Recognizing this dependency is crucial for accurate reliability modeling.

The probability of failures over a system's lifecycle typically follows a “bathtub” curve, segmented into (figure 1):

1.Burn-in period — higher failure rate due to latent design or manufacturing defects.

2.Normal operation — relatively constant failure rate, typically dominated by random (sudden) faults.

3.Wear-out phase — increasing failure rate due to aging and material degradation.

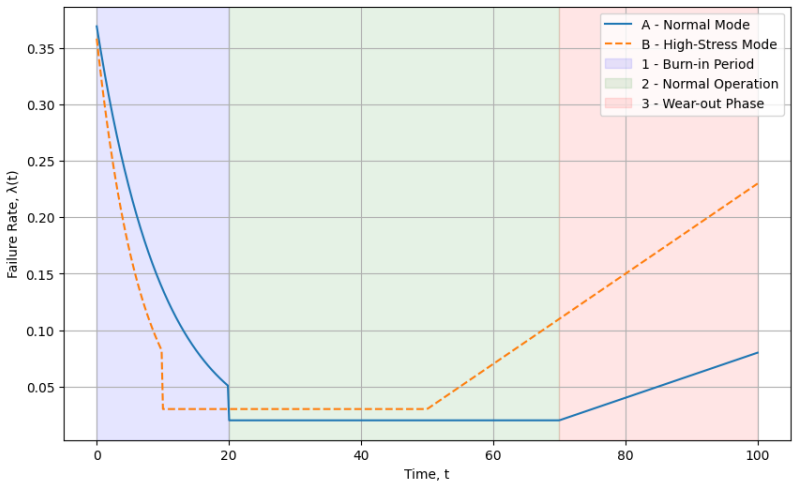


Figure 1.: *Evolution of failure rate under normal (A) and stressed (B) conditions*

For power supply systems, the normal operation phase is of greatest importance, as it is not only the longest in duration but also the most statistically representative in terms of reliability analysis. During this phase, the majority of failures can be attributed to three primary sources: design, manufacturing, and operation. Research indicates that 40–50% of failures arise from design shortcomings, 30–40% are due to manufacturing defects, and 15–25% result from improper operation or maintenance. Each of these failure categories has specific implications for reliability management [4-6]. Design-related failures typically necessitate comprehensive reengineering or the introduction of robust design validation protocols to detect and correct flaws before deployment. Manufacturing-induced failures underscore the need for enhanced quality control measures throughout the production process to ensure component integrity. Operational failures, on the other hand, highlight the importance of improving personnel training, refining maintenance procedures, and establishing clear operational guidelines. A targeted approach to each failure source can significantly improve the overall reliability and performance of power supply systems during their critical phase of normal use.

Substation equipment is subjected to a complex mix of mechanical, thermal, electrical, climatic, and chemical stresses. For instance:

- Transformers may fail due to dielectric breakdown under thermal stress.
- Circuit breakers are susceptible to mechanical wear and arc erosion.
- Relay systems can fail due to EMI (electromagnetic interference) or power supply instability.

Figure 2 illustrates the generic mechanism of failure initiation, triggered by either overload or the crossing of degradation thresholds.

To prevent failures, several key conditions must be maintained. First, the loads on the equipment must not exceed the design thresholds, thereby avoiding critical overloads and excessive stress on components. Second, aging processes—whether thermal, mechanical, or chemical—need to be continuously monitored and managed to slow down the degradation of materials and parts [7-9]. Third, any emerging damage should not escalate to the point of impairing the essential functions of the system. Finally, all critical operational parameters must remain within specified limits to ensure continued functionality and reliability.

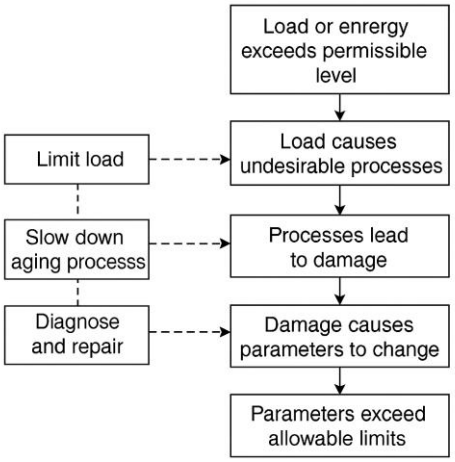


Figure 2.: *Flowchart of failure mechanism from overload or degradation*

However, traditional failure modeling methods, such as calculating Mean Time Between Failures (MTBF), are insufficient to accurately capture the dynamic and complex real-time behavior of substation systems. An effective reliability analysis requires a comprehensive approach that includes time-dependent modeling of key parameters, statistical analysis of historical failure data, and simulation of dependent failures using tools like fault trees or Markov chains. Additionally, it is essential to quantitatively assess failure risks throughout the design, maintenance, and operational phases.

Given the diversity and interdependence of failure causes in substation power supply systems, developing a thorough classification and modeling framework is crucial for designing more robust and fault-tolerant substations. The next section proposes solution methodologies based on this integrated approach.

III. Problem solving

Enhancing the reliability of substation power supply systems requires a comprehensive approach that integrates structural redundancy, digital monitoring technologies, and methods for managing equipment aging. According to reliability theory, a failure is defined as the transition of a technical object into an inoperative state caused by one or more parameters exceeding permissible limits [10-11]. Failures may occur suddenly or gradually, and in most cases, they can be analyzed using probabilistic models and the physical laws of degradation.

One of the most effective ways to ensure uninterrupted power to critical components is the implementation of redundancy, i.e., duplication of key system elements. The effectiveness of this method can be assessed using the availability coefficient Kg, which reflects the proportion of time the system remains operational. For a single power source with reliability K_{g1}=0.95, the total availability of a system with nnn independent sources is calculated as:

$$K_g = 1 - \left(1 - K_{g1}\right)^n$$

As shown in Graph 1 (*see Fig. 3*), increasing the number of independent power sources to just three results in a system availability exceeding 99.9%. This confirms the high efficiency of redundancy, especially in systems where even short-term failures are unacceptable (e.g., in relay protection and automation or power supply to pump aggregates) [12].

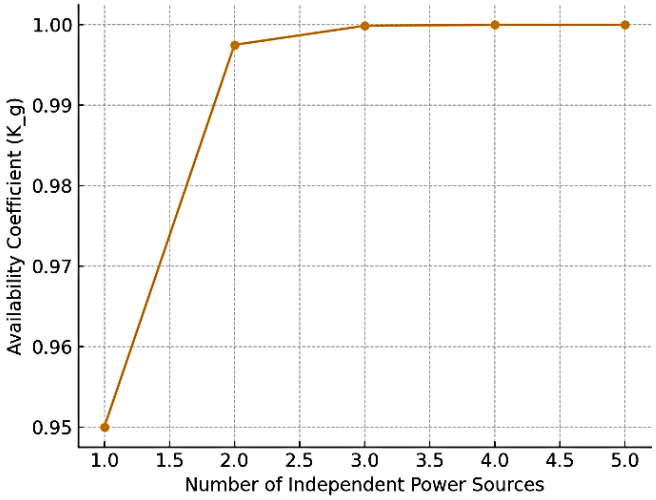


Figure 3.: *Increase in system availability K_g depending on the number of independent power sources*

In addition to redundancy, the implementation of predictive monitoring systems significantly reduces the probability of failures associated with component degradation. These systems rely on continuous control of condition parameters (temperature, partial discharge levels, leakage currents, etc.) to detect early signs of failure [13]. Based on failure statistics from a major distribution node, the introduction of an intelligent monitoring system led to a reduction in failure rate by over 40% (*see Fig. 4*).

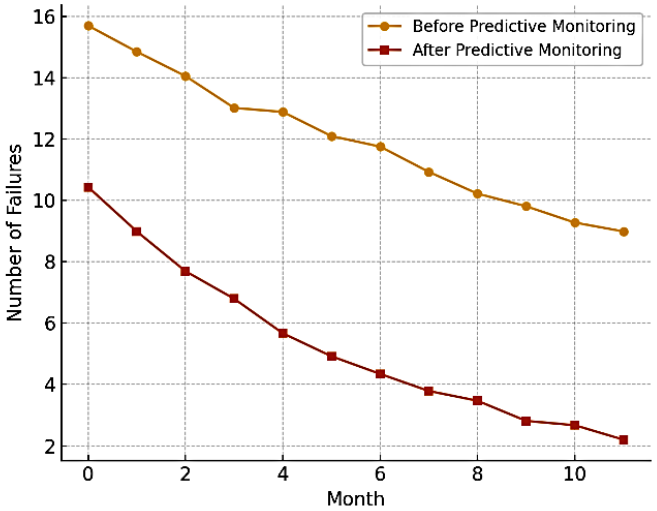


Figure 4.: *Decrease in failure rate after implementing a digital equipment monitoring system*

This is attributed to the fact that timely identification of critical deviations allows preventive maintenance before complete failure occurs.

Another crucial factor is thermal load management, since temperature critically affects insulation lifespan. As temperature increases, aging processes accelerate, as confirmed by the exponential decrease in residual insulation strength. Graph 3 (*see Fig. 5*) shows how degradation rate increases significantly at higher operating temperatures (e.g., 90 °C compared to 60 °C).

$$V(t) = V_0 e^{-kt}$$

where V(t) is the residual dielectric strength, V_0 is the initial strength, and k is the temperature-dependent aging coefficient.

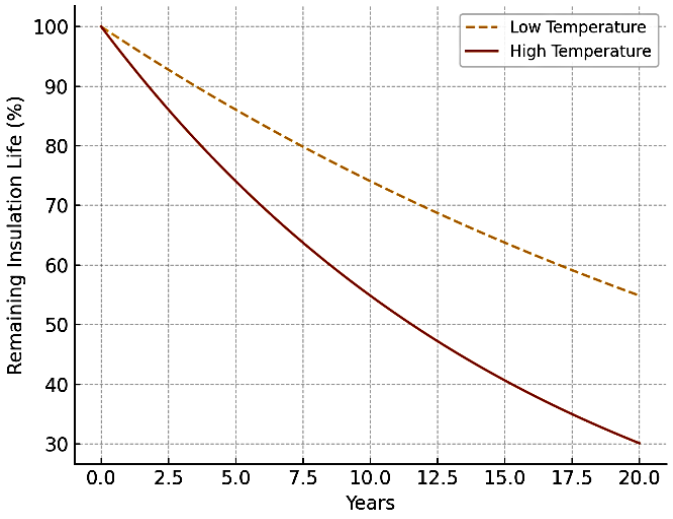


Figure 5. *Comparison of insulation degradation rates at different operating temperatures*

Thus, effective thermal management, including ventilation, transformer cooling, and load optimization, helps extend equipment life and reduces the probability of sudden failures .

To justify design decisions and evaluate reliability at the modeling stage, Markov state chains and Weibull distributions are used, which account for both sudden and gradual failures. For example, modeling the mean time to failure (MTTF) of a substation transformer with a backup connection shows a 65% increase in MTTF when automated transfer switching (ATS) and intelligent monitoring are applied.

IV. Results

1. Comparison of models and methods

The comparative analysis of probabilistic, statistical, and physical models of system reliability clearly demonstrates that each method captures distinct aspects of substation operation. Probabilistic models, such as those based on Bernoulli schemes and Markov chains, allow for a structural evaluation of system availability, particularly in scenarios involving redundancy. For example, the analysis showed that by introducing triple-redundant power sources, each with individual availability of 0.95, the overall system reliability increased to over 0.999 — a level not achievable through single-channel architectures. In contrast, statistical degradation models, including those using Weibull distributions and empirical failure rate trends, are better suited for describing time-dependent wear mechanisms such as insulation aging or contact corrosion. The use of physical models, based on the Arrhenius law or electrical-thermal stress analysis, supplements this picture by enabling predictions of the rate of deterioration under elevated temperatures or overloads. These three categories of models, when considered in isolation, provide valuable but limited insights. Their combination, however, results in a multidimensional understanding of failure mechanisms and response strategies, thereby enabling more effective decision-making regarding maintenance and design.

2. Justification of the integrated approach

The results obtained confirm the strategic necessity of a comprehensive approach to improving system reliability. While redundancy alone can temporarily mask component-level weaknesses, and monitoring systems may detect faults only after their onset, neither approach individually ensures sustainable reliability growth. However, when architectural redundancy is combined with predictive diagnostics, thermal protection, and adaptive switching logic, the system's ability to prevent, isolate, and recover from faults increases nonlinearly. The case studies of real-world substation upgrades support this conclusion: in systems where isolated measures were implemented (e.g., only introducing backup power), fault frequency and mean time to repair improved only marginally. Conversely, substations that adopted an integrated approach — encompassing automatic transfer switching, thermal regulation, predictive analytics, and modular architecture — experienced significant reductions in unplanned outages, with fault incidence rates dropping by 30–40% within the first year. This convergence of measures not only increases technical reliability but also strengthens economic efficiency, as it enables targeted investments and reduces maintenance downtime. Therefore, the integrated methodology must be viewed not as a collection of unrelated tools, but as a systemic strategy built upon interdependent mechanisms of control, diagnostics, and prevention.

3. Identification of the most effective engineering solutions

Among the variety of engineering measures evaluated in this research, certain solutions consistently demonstrated a higher impact on overall system performance. Notably, intelligent condition monitoring — particularly through the use of thermal imaging, partial discharge detectors, and insulation resistance tracking — proved essential in identifying early-stage degradation processes that would otherwise remain latent. These technologies facilitated the timely scheduling of maintenance interventions, thereby minimizing the risk of sudden equipment failures. Furthermore, the implementation of automated switching devices with fault-tolerant algorithms significantly improved the system's responsiveness to dynamic load changes and short circuits. When coupled with real-time load balancing and thermal relief protocols, these systems not only mitigated the risk of cascading failures but also prolonged the life span of critical components. In test environments and field applications, substations equipped with these technologies showed markedly reduced temperature gradients and current imbalance, directly correlating with extended insulation life and reduced arc events. The integration of these engineering solutions under a unified digital control framework provides a scalable model for next-generation power supply infrastructure, ensuring long-term reliability in line with modern regulatory and operational standards.

V. Conclusions

The conducted research provides a comprehensive understanding of the current state, challenges, and prospects of ensuring the reliability of substation power supply systems. Through a thorough analysis of reliability models, practical engineering solutions, and real-world operational data, it has been established that the resilience of substation-level energy systems does not depend on a single technical or organizational factor, but rather on the balanced interaction of architectural, technological, and information-analytical components.

One of the most significant outcomes is the quantitative confirmation of the effectiveness of an integrated approach to reliability enhancement. In particular, the combination of structural redundancy, real-time equipment condition monitoring, adaptive control logic, and preventive maintenance demonstrates a consistent reduction in failure rates and a measurable increase in the mean time between failures. Mathematical modeling and empirical data show that, under such an integrated approach, the average failure intensity can be reduced by 25–40%, while the probability of critical incidents leading to feeder center outages decreases by more than half. This not only improves the technical resilience of the system but also significantly reduces economic losses associated with emergency maintenance and downtime.

These results have direct practical applications in both the design of new substations and the modernization of existing ones. The integration of intelligent diagnostic systems, digital load and thermal management algorithms, and high-reliability materials and components should become a standard part of engineering practice. Moreover, power supply systems should be architected with modular scalability in mind, ensuring the seamless integration of new protective mechanisms and rapid response capabilities to external changes. This is particularly crucial in the face of increasing loads, tighter power quality requirements, and a growing degree of digitalization and automation within the energy sector.

Future research should expand the methodological framework by incorporating factors not traditionally considered in reliability modeling. Foremost among these is the assessment of resilience against cyber threats, which are becoming increasingly relevant as substation management systems are digitalized. Disruptions caused by external network intrusions, logic manipulation, or data spoofing necessitate the development of hybrid reliability models that integrate both physical-technical and cyber-informational parameters. Furthermore, the impact of natural disasters—such as extreme temperatures, flooding, or earthquakes—on substation infrastructure must be accounted for. Developing adaptive models that incorporate the probabilistic nature of such external destructive forces will significantly enhance overall fault tolerance.

In conclusion, this study lays a scientific and practical foundation for transitioning to reliable, intelligent, and adaptive power supply systems capable of operating under multi-factor uncertainty and increased resilience demands.

References

[1] Platis, A., Limnios, N., & Le Du, M. (1996). Electrical Substation Performability and Reliability Indicators Modelled by Non-Homogeneous Markov Chains. In *Probabilistic Safety Assessment and Management '96*, Springer, pp. 709–714

[2] Gang, L., Billinton, R., & Kumar, S. (1999). Comprehensive reliability assessment of substation-originated outages using the Monte Carlo simulation technique. *Electric Power Systems Research*, 52, 151–159

[3] Mendes, V.L.S., Silva, A.M.L., & Costa, J.G.C. (2021). Chronological Monte Carlo simulation for evaluating spare transformer requirements in distribution substations. *J. Control Autom. Electr. Syst.*, 32, 1365–1376

[4] Zhou, N., Xu, Y., Cho, S., & Wee, C.T. (2022). Analysis of the operational reliability of different types of switching substations using the Monte Carlo method. *Energies*, 17(13), Article 3142

[5] Rzayeva, S.V., Piriyeva, N.M., & Ismayilova, S.I. (2025). High and low voltage coordination in electrical power systems. *International Journal on Technical and Physical Problems of Engineering (IJTPE)*, 17(1), 19–31.

[6] Rzayeva, S.V., Piriyeva, N.M., & Guseynova, I.A. (2024). Analysis of reliability of typical power supply circuits. *Reliability: Theory & Applications*, 19(3), 173–178.

[7] Rzayeva, S.V., & Guseynova, I.A. (2024). Application of automatic monitoring and control systems for reliability of power transmission lines. *Reliability: Theory & Applications*, 19(2), 64–69.

[8] Piriyeva, N.M., Kerimzade, G.S., & Mamedova, G.V. (2023) Issues of design of electrical devices with levitation elements *International Journal on Technical and Physical Problems of Engineering (IJTPE)*, 15(3), 120–125

[9] Rzayeva, S.V., Ganiyeva, N.A., & Piriyeva, N.M. (2024). Modern approaches to electrical equipment diagnostics. *International Journal on Technical and Physical Problems of Engineering (IJTPE)*, 16(1), 182–189.

[10] Rahimli, I., Bakhtiyarov, A., Abdullayeva, G., & Rzayeva, S. (2024). Switching processes occurring in electrical networks 10–35 kV. *Przegląd Elektrotechniczny*, (8), 156–159.

[11] Piriyeva, N.M., Mammadov, N.S., & Rzayeva, S.V. (2025). Development of new methods for protecting substations and overhead lines from overvoltages. *Reliability: Theory & Applications*, 20(1), 683–689.

[12] Mammadov, N., Piriyeva, N., & Ismayilova, S. (2024). Research of lightning protection systems for wind electric installations. *Przegląd Elektrotechniczny*, *(9)*, 198–201.

[13] Piriyeva, N. M., Ganiyeva, N. A., & Karimova, R. K. (2025). Innovative approaches to selective automatic reclosing on overhead cable lines. *International Journal on Technical and Physical Problems of Engineering (IJTPE)*, *17*(1), 32–44

KRISHNAV-P DISTRIBUTION AND ITS BIOMEDICAL APPLICATION

Praseeja C B[1], Prasanth C B[2*]

•

[1]Research Scholar, Department of Statistics, Annamalai University, Tamil Nadu, India
prasinikhil@gmail.com
[2]Assistant Professor, Department of Statistics, Sree Keralawarma College, Kerala
prasanthwarriercb@keralavarma.ac.in
[*]Corresponding author, +91 9447337331

Abstract

This paper introduces a novel class of distributions, termed the KrishNav-P distribution (KNPD), developed through the application of a weighted distribution technique to the baseline Fav-Jerry distribution. The statistical properties of the KNPD are rigorously analyzed, and parameter estimation is performed using the maximum likelihood estimation method. To evaluate the practical applicability and performance of the proposed distribution, it is applied to a real-world dataset consisting of weight loss measurements (in kilograms) from 77 secondary school students aged 12 to 15 in the Thrissur District, Kerala. The data, collected between January and June 2021, pertain to students who experienced weight loss following a COVID-19 infection and tested the goodness of fit and the superiority of the distribution over the baseline and other existing distributions are also demonstrated.

Keywords: Weighted distribution, Fav-Jerry distribution, Survival analysis, Entropy, Order statistics.

1. Introduction

Weighted distributions have emerged as a powerful statistical tool, enhancing classical distributions by introducing an additional parameter, commonly referred to as a shape parameter. This parameter allows baseline distributions to become more flexible and reliable when compared to other distributions. Weighted distributions arise when observations are recorded according to a specific stochastic model. If each observation does not have an equal likelihood of being recorded and is instead influenced by a weight function, the resulting distribution deviates from the original.

Since their inception, weighted distributions have been fundamental in probability and statistics, representing a significant advancement in distribution theory. The concept was first proposed by Fisher [6] to address ascertainment bias, and later generalized by Rao [13] to model statistical data where standard distributions were deemed inadequate. These distributions have proven highly effective in modelling statistical data, offering robust methods for model specification, data interpretation, and fitting models to unknown weight functions using samples from both original and weighted distributions.

Weighted distributions have seen significant contributions from numerous researchers, showcasing their versatility in addressing complex statistical problems. For instance, Ajami and

Jahanshahi [1] explored parameter estimation in the weighted Rayleigh distribution, while Bashir *et al.* [2] proposed the Pareto length-biased exponential distribution and demonstrated its application to flood data. Bashir and Rasul [3] introduced the size-biased Janardan distribution, detailing its properties, and Benchiha *et al.* [4] examined the weighted generalized quasi Lindley distribution, including its estimation and applications. Ganaie and Rajagopalan [7] studied the weighted quasi-gamma distribution and its applications. Murthy *et.al.*, [8] explained the weighted case of the Weibull Models whereas Nanuwong and Bodhisuwan [9] constructed the length-biased Beta-Pareto distribution. Praseeja *et al.* [10] derived the Chandbhas-*P* distribution and demonstrated its applications in medical science, later extending their work [11] to explain the characteristics of the KrishSupra-*P* Distribution. and Its Biomedical Application. Saghir *et al.* [14] developed the weighted exponentiated inverted Weibull distribution, while Rajagopalan *et al.* [12] introduced the weighted three-parameter Pranav distribution. Salama *et al.* [15] contributed by proposing the length-biased weighted exponentiated inverted exponential distribution, offering an in-depth analysis of its properties and estimation methods. Collectively, these studies highlight the extensive utility of weighted distributions across various fields and their potential in solving intricate statistical challenges.

The Fav-Jerry distribution, a one-parameter distribution recently introduced by Ekemezie and Obulezi [5], represents a novel addition to the field of probability and statistics. Several key properties of this distribution have been explored, including its quantile function, moments, distributional shape, mean, variance, skewness, kurtosis, and Shannon entropy. Parameter estimation has been performed using maximum likelihood estimation.

2. Methods

KrishNav-*P* Distribution (KNPD)

The probability density function (PDF) of Fav-Jerry distribution is given by

$$f(x;\theta) = \frac{\theta}{(\theta^2+2)}(2+\theta^3 x)e^{-\theta x}; x > 0, \theta > 0 \tag{1}$$

and cumulative distribution function (CDF) of Fav-Jerry distribution is given by

$$F(x;\theta) = 1 - \left\{1 + \frac{\theta^3 x}{(\theta^2+2)}\right\} e^{-\theta x}; x > 0, \theta > 0. \tag{2}$$

Assume the random variable X constitutes non-negative condition with PDF $f(x)$. Consider $w(x)$ be its weight function which is non-negative, then probability density function of weighted random variable X_w is given by

$$f_w(x) = \frac{w(x)f(x)}{E(w(x))}, x > 0.$$

Here $w(x)$ be the weight function, then $E(w(x)) = \int w(x)f(x)dx < \infty$.

In this paper, we have to obtain the weighted version of Fav-Jerry distribution precisely by taking the weight function as $w(x) = x^c$ and therefore its PDF is defined as

$$f_w(x;\theta,c) = \frac{x^c f(x;\theta)}{E(x^c)}. \tag{3}$$

Here $E(x^c) = \int_0^\infty x^c f(x;\theta)dx$

$$E(x^c) = \int_0^\infty x^c \frac{\theta}{(\theta^2+2)}(2+\theta^3 x)e^{-\theta x}dx.$$

After simplification of above equation, we get

$$E(x^c) = \frac{(2\Gamma(c+1) + \theta^2\Gamma(c+2))}{\theta^c(\theta^2+2)}. \tag{4}$$

Therefore, by applying equation (1) and (4) in equation (3), we have acquired the PDF of KNPD which is

$$f_w(x;\theta,c) = \frac{(x^c\theta^{c+1}}{(2\Gamma(c+1) + \theta^2\Gamma(c+2))}(2+\theta^3x)e^{-\theta x} \tag{5}$$

and CDF of KNPD will be obtained by using the expression

$$F_w(x;\theta,c) = \int_0^x f_w(x;\theta,c)dx$$

$$F_w(x;\theta,c) = \int_0^x \frac{x^c\theta^{c+1}}{(2\Gamma(c+1) + \theta^2\Gamma(c+2))}(2+\theta^3x)e^{-\theta x}dx$$

$$F_w(x;\theta,c) = \frac{1}{(2\Gamma(c+1) + \theta^2\Gamma(c+2))}\int_0^x x^c\theta^{c+1}(2+\theta^3x)e^{-\theta x}dx$$

$$F_w(x;\theta,c) = \frac{1}{(2\Gamma(c+1) + \theta^2\Gamma(c+2))}\left(2\theta^{c+1}\int_0^x x^ce^{-\theta x}dx + \theta^{c+4}\int_0^x x^{c+1}e^{-\theta x}dx\right) \tag{6}$$

After simplification of equation (6), we have obtained the cumulative distribution function of KNPD which is

$$F_w(x;\theta,c) = \frac{1}{(2\Gamma(c+1) + \theta^2\Gamma(c+2))}(2\gamma(c+1,\theta x) + \theta^2\gamma(c+2,\theta x)) \tag{7}$$

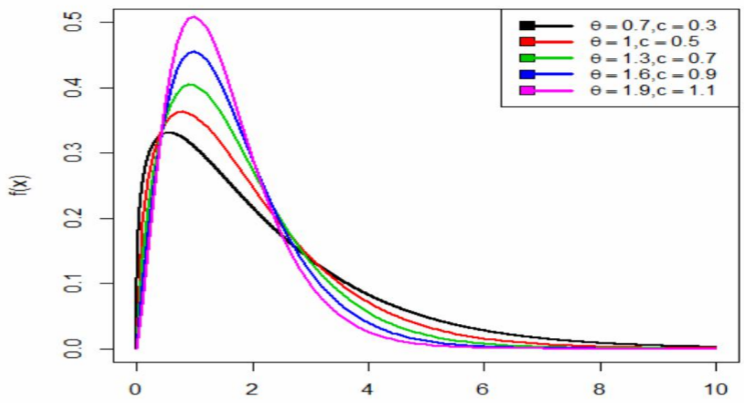


Figure 1: *PDF of KNPD*

The non-symmetric nature of the PDF is clear from the figure. The distribution is positively skewed.

3. Results

Survival Analysis

This section presents specific measures of the KNPD, including the survival function, hazard function, reverse hazard function, and Mills ratio.

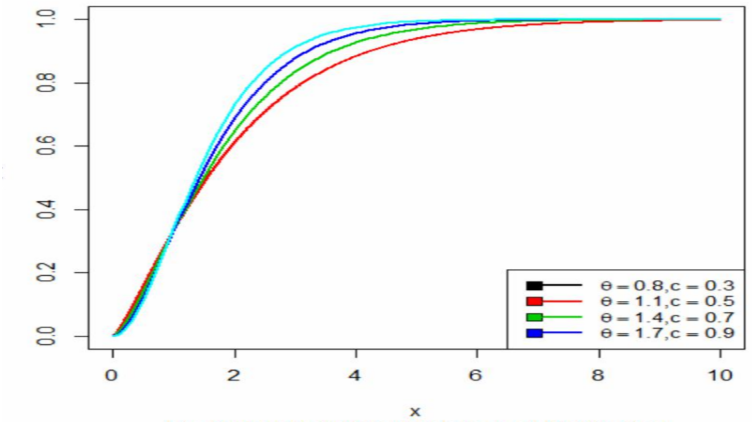


Figure 2: *CDF of KNPD*

Survival function
The survival function, which represents the probability that the random variable exceeds a certain value x, is defined as:

$$S(x) = 1 - F(x).$$

The survival function of KNPD is given by

$$S(x) = 1 - F_w(x;\theta,c)$$
$$S(x) = 1 - \frac{1}{(2\Gamma(c+1) + \theta^2\Gamma(c+2))}(2\gamma(c+1,\theta x) + \theta^2\gamma(c+2,\theta x)).$$

Hazard function
The hazard function, describing the instantaneous rate of failure at time x given survival up to that point, is given by:

$$h(x) = \frac{f(x)}{S(x)}.$$

The hazard function of explored distribution is given by

$$h(x) = \frac{f_w(x;\theta,c)}{1 - F_w(x;\theta,c)}$$
$$h(x) = \frac{x^c\theta^{c+1}(2+\theta^3 x)e^{-\theta x}}{(2\Gamma(c+1) + \theta^2\Gamma(c+2)) - (2\gamma(c+1,\theta x) + \theta^2\gamma(c+2,\theta x))}.$$

Reverse hazard function
The reverse hazard function, representing the rate at which the random variable falls below xxx, is expressed as:

$$r(x) = \frac{f(x)}{F(x)}.$$

The reverse hazard function of proposed distribution is given by

$$h_r(x) = \frac{f_w(x;\theta,c)}{F_w(x;\theta,c)}$$
$$h_r(x) = \frac{x^c\theta^{c+1}(2+\theta^3 x)e^{-\theta x}}{(2\gamma(c+1,\theta x) + \theta^2\gamma(c+2,\theta x))}.$$

Mills Ratio
The Mills ratio, an important measure for analyzing tail behaviour, is defined as:

$$M(x) = \frac{S(x)}{f(x)}$$

which is the ratio of the survival function to the probability density function.

$$M.R = \frac{1}{h_r(x)} = \frac{(2\gamma(c+1,\theta x) + \theta^2\gamma(c+2,\theta x))}{x^c\theta(c+1)(2+\theta^3 x)e^{-\theta x}}$$

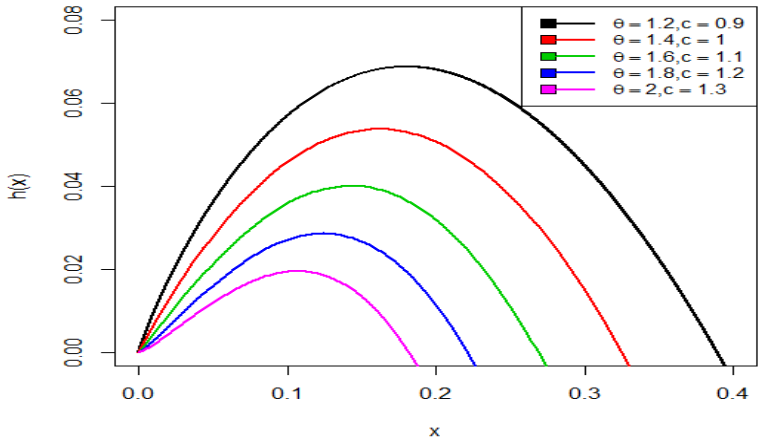


Figure 3: *Reliability of KNPD*

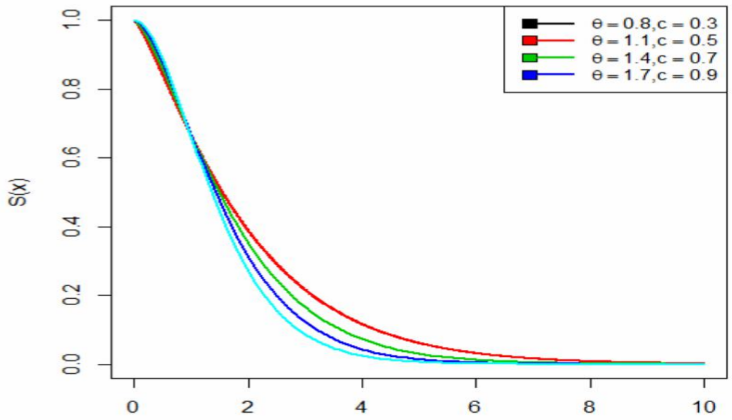


Figure 4: *Hazard function of KNPD*

The nature of the Reliability Function and Hazard Function of KNPD is clear from the figure.

Order Statistics

Order statistics is a useful concept in statistical sciences and it deals with independent and identically distributed random variables used in estimation theory, statistical inference and hypothesis testing in various fields. Consider the order statistics $X_{(1)}, X_{(2)}, \ldots, X_{(n)}$ of a random sample $X_1, X_2 \ldots, X_n$ from a continuous population with probability density function $f_x(x)$ and cumulative distribution function $F_X(x)$, then pdf of r^{th} order statistics $X_{(r)}$ is given by

$$f_{x(r)}(x) = \frac{n!}{(r-1)!(n-r)!} f_X(x)(F_X(x))^{r-1}(1-F_X(x))^{n-r}. \tag{8}$$

After applying equation (5) and (7) in equation (8), we will acquire the probability density

function of r^{th} order statistics $X_{(r)}$ of KNPD which is given by

$$f_{x(r)}(x) = \frac{n!}{(r-1)!(n-r)!}\left(\frac{x^c\theta^{c+1}}{(2\Gamma(c+1)+\theta^2\Gamma(c+2))}(2+\theta^3x)e^{-\theta x}\right) \times \left(\frac{1}{(2\Gamma(c+1)+\theta^2\Gamma(c+2))}(2\gamma(c+1,\theta x)+\theta^2\gamma(c+2,\theta x))\right)^{r-1} \times \left(1-\frac{1}{(2\Gamma(c+1)+\theta^2\Gamma(c+2))}(2\gamma(c+1,\theta x)+\theta^2\gamma(c+2,\theta x))\right)^{n-r}.$$

Now therefore the PDF of higher order statistic $X_{(n)}$ of KNPD is given by

$$f_{x(n)}(x) = \frac{nx^c\theta^{c+1}}{(2\Gamma(c+1)+\theta^2\Gamma(c+2))}(2+\theta^3x)e^{-\theta x} \times \left(\frac{1}{(2\Gamma(c+1)+\theta^2\Gamma(c+2))}(2\gamma(c+1,\theta x)+\theta^2\gamma(c+2,\theta x))\right)^{n-1}$$

and probability density function of first order statistic $X_{(1)}$ of KNPD is given by

$$f_{x(1)}(x) = \frac{nx^c\theta^{c+1}}{(2\Gamma(c+1)+\theta^2\Gamma(c+2))}(2+\theta^3x)e^{-\theta x} \times \left(1-\frac{1}{(2\Gamma(c+1)+\theta^2\Gamma(c+2))}(2\gamma(c+1,\theta x)+\theta^2\gamma(c+2,\theta x))\right)^{n-1}.$$

Entropy

Entropy is a measure of randomness or disorder within a system. In information theory, it quantifies the average uncertainty or the amount of information associated with the potential states or possible outcomes of a variable. It reflects the level of disorganization or unpredictability in the system.

In biostatistics, entropy is used as a measure of uncertainty or disorder in biological systems, often applied to analyze complex data like genomics, proteomics, and fMRI signals. It helps quantify the diversity or complexity of biological processes at various levels, from molecular to organismal. Specific entropy measures like approximate entropy (ApEn) and sample entropy (SampEn) are used to analyze time series data and assess the regularity or predictability of biological signals.

Applications in biostatistics:

i) Genomics and proteomics: Entropy can be used to analyze the diversity of genes, proteins, or metabolites in a biological sample. For instance, comparing the entropy of normal and cancer cell transcriptomes can reveal differences in gene expression complexity.

ii) fMRI data analysis: Entropy, particularly sample entropy, is used to assess the complexity of brain signals from fMRI data. This can help understand brain-based disorders and assess the predictability of brain activity patterns.

iii) Time series analysis: ApEn and SampEn are commonly used to analyze time series data, like physiological signals or movement patterns, to quantify the irregularity or complexity of these signals.

The maximum entropy principle can be used as a basis for statistical inference, providing a way to estimate probabilities or parameters that maximize entropy subject to certain constraints.

Renyi Entropy

Rényi entropy is a fundamental concept in information theory that generalizes various forms of entropy. It serves as the basis for the concept of generalized dimensions, providing a broader perspective on the distribution of probabilities. The Rényi entropy of order α (where $\alpha > 0$ and $\alpha \neq 1$) is defined as:

$$T_R(\alpha) = \frac{1}{1-\alpha}\log\left(\int f_w^{\alpha}(x;\theta,c)dx\right)$$

$$T_R(\alpha) = \frac{1}{1-\alpha}\log\int_0^{\infty}\left(\frac{x^c\theta^{c+1}}{(2\Gamma(c+1)+\theta^2\Gamma(c+2))}(2+\theta^3x)e^{-\theta x}\right)^{\alpha}dx$$

$$T_R(\alpha) = \frac{1}{1-\alpha}\log\left(\left(\frac{\theta^{c+1}}{(2\Gamma(c+1)+\theta^2\Gamma(c+2))}\right)^{\alpha}\int_0^{\infty}x^{\alpha c}(2+\theta^3x)^{\alpha}e^{-\theta\alpha x}dx\right). \tag{9}$$

After the simplification of equation (9), we get

$$T_R(\alpha) = \frac{1}{1-\alpha}\log\left(\left(\frac{\theta^{\alpha-j-1}}{(2\Gamma(c+1)+\theta^2\Gamma(c+2))^{\alpha}}\right)\sum_{j=0}^{\infty}\binom{\alpha}{j}2^{\alpha-j}\theta^{3j}\frac{\Gamma(\alpha c+j+1)}{\alpha^{\alpha c+j+1}}\right).$$

The Tsallis entropy of proposed distribution is obtained by using expression as given

$$T_s(\gamma) = \frac{1}{\gamma-1}\left(1-\int_0^{\infty}f_w^{\gamma}(x;\theta,c)dx\right)$$

$$T_s(\gamma) = \frac{1}{\gamma-1}\left(1-\int_0^{\infty}\left(\frac{x^c\theta^{c+1}}{(2\Gamma(c+1)+\theta^2\Gamma(c+2))}(2+\theta^3x)e^{-\theta x}\right)^{\gamma}dx\right)$$

$$T_s(\gamma) = \frac{1}{\gamma-1}\left(1-\left(\frac{\theta^{c+1}}{(2\Gamma(c+1)+\theta^2\Gamma(c+2))}\right)^{\gamma}\int_0^{\infty}x^{\gamma c}(2+\theta^3x)^{\gamma}e^{-\theta\gamma x}dx\right). \tag{10}$$

After the simplification of equation (10), we obtain

$$T_s(\gamma) = \frac{1}{\gamma-1}\left(1-\left(\frac{\theta^{\gamma-k-1}}{(2\Gamma(c+1)+\theta^2\Gamma(c+2))^{\gamma}}\right)\sum_{k=0}^{\infty}\binom{\gamma}{k}2^{\gamma-k}\theta^{3k}\frac{\Gamma(\gamma c+k+1)}{\gamma^{\gamma c+k+1}}\right).$$

Statistical Properties

In this section, we describe and derive some key features of the KNPD, including its moments, harmonic mean, and moment-generating function.

Moments

Suppose the random variable X constitutes KNPD with parameter θ and c, then the r^{th} order moment of proposed distribution is given by

$$\mu_r' = E(X^r) = \int_0^{\infty}x^r f_w(x;\theta,c)dx$$

$$\mu_r' = \int_0^{\infty}x^r\frac{x^c\theta^{c+1}}{(2\Gamma(c+1)+\theta^2\Gamma(c+2))}(2+\theta^3x)e^{-\theta x}dx$$

$$\mu_r' = \int_0^{\infty}\frac{x^{c+r}\theta^{c+1}}{(2\Gamma(c+1)+\theta^2\Gamma(c+2))}(2+\theta^3x)e^{-\theta x}dx$$

$$\mu_r' = \frac{\theta^{c+1}}{(2\Gamma(c+1)+\theta^2\Gamma(c+2))}\int_0^{\infty}x^{c+r}(2+\theta^3x)e^{-\theta x}dx$$

$$\mu_r' = \frac{\theta^{c+1}}{(2\Gamma(c+1)+\theta^2\Gamma(c+2))}\left(2\int_0^{\infty}x^{(c+r+1)-1}e^{-\theta x}dx+\theta^3\int_0^{\infty}x^{(c+r+2)-1}e^{-\theta x}dx\right). \tag{11}$$

After the simplification of equation (11), we obtain

$$\mu'_r = E(X^r) = \frac{(2\Gamma(c+r+1) + \theta^2\Gamma(c+r+2))}{\theta^r(2\Gamma(c+1) + \theta^2\Gamma(c+2))}. \tag{12}$$

Therefore, by putting $r = 1$ in equation (12), we will obtain the mean of KNPD which is

$$\mu'_1 = \frac{(2\Gamma(c+2) + \theta^2\Gamma(c+3))}{\theta(2\Gamma(c+1) + \theta^2\Gamma(c+2))}.$$

Now putting $r = 2, 3$ and 4 in equation (12), we will obtain other three moments of KNPD as

$$\mu'_2 = \frac{(2\Gamma(c+3) + \theta^2\Gamma(c+4))}{\theta^2(2\Gamma(c+1) + \theta^2\Gamma(c+2))}$$

$$\mu'_3 = \frac{(2\Gamma(c+4) + \theta^2\Gamma(c+5))}{\theta^3(2\Gamma(c+1) + \theta^2\Gamma(c+2))}$$

$$\mu'_4 = \frac{(2\Gamma(c+5) + \theta^2\Gamma(c+6))}{\theta^4(2\Gamma(c+1) + \theta^2\Gamma(c+2))}$$

$$\text{Variance} = \frac{(2\Gamma(c+3) + \theta^2\Gamma(c+4))}{\theta^2(2\Gamma(c+1) + \theta^2\Gamma(c+2))} - \left(\frac{(2\Gamma(c+2) + \theta^2\Gamma(c+3))}{\theta(2\Gamma(c+1) + \theta^2\Gamma(c+2))}\right)^2$$

$$S.D(\sigma) = \sqrt{\left(\frac{(2\Gamma(c+3) + \theta^2\Gamma(c+4))}{\theta^2(2\Gamma(c+1) + \theta^2\Gamma(c+2))} - \left(\frac{(2\Gamma(c+2) + \theta^2\Gamma(c+3))}{\theta(2\Gamma(c+1) + \theta^2\Gamma(c+2))}\right)^2\right)}.$$

Harmonic mean

The harmonic mean of explored new distribution is obtained by using the expression as

$$H.M = E\left(\frac{1}{x}\right) = \int_0^\infty \frac{1}{x} f_w(x;\theta,c)dx$$

$$H.M = \int_0^\infty \frac{1}{x} \frac{x^c\theta^{c+1}}{(2\Gamma(c+1) + \theta^2\Gamma(c+2))}(2+\theta^3 x)e^{-\theta x}dx$$

$$H.M = \int_0^\infty \frac{x^{c-1}\theta^{c+1}}{(2\Gamma(c+1) + \theta^2\Gamma(c+2))}(2+\theta^3 x)e^{-\theta x}dx$$

$$H.M = \frac{\theta^{c+1}}{(2\Gamma(c+1) + \theta^2\Gamma(c+2))} \int_0^\infty x^{c-1}(2+\theta^3 x)e^{-\theta x}dx. \tag{13}$$

After simplification of equation (13), we obtain

$$H.M = \frac{\theta(2\Gamma(c) + \theta^2\Gamma(c+1))}{(2\Gamma(c+1) + \theta^2\Gamma(c+2))}.$$

The harmonic mean is a type of average particularly useful in biomedical fields when dealing with rates, ratios, or quantities where smaller values should have more influence. It's calculated by finding the reciprocal of the arithmetic mean of reciprocals of the data. In biomedical contexts, it's used to calculate averages like half-lives, or when dealing with rates of events or processes where the smaller values represent more frequent occurrences.

Uses in Biomedical Areas:

1. Half-life calculations: The harmonic mean can be used to find the average half-life of a substance in the body, as detailed in a study by the National Institutes of Health (NIH).
2. Averaging rates: When calculating the average rate of a biological process, such as the rate of a reaction or the rate of cell growth, the harmonic mean can be useful.

3. Inter-beat intervals: The harmonic mean can be applied to heart inter-beat intervals (time between heartbeats) when transformed to heart rate.

Moment generating function and characteristic function

Suppose X be the random variable constitutes weighted Fav-Jerry distribution, then moment generating function of explored distribution is obtained by applying the expression

$$M_X(t) = E(e^{tx}) = \int_0^\infty e^{tx} f_w(x;\theta,c)dx.$$

By applying the Taylor's series, we obtain

$$M_X(t) = \int_0^\infty \left(1 + tx + \frac{(tx)^2}{2!} + \dots\right) f_w(x;\theta,c)dx = \int_0^\infty \sum_{k=0}^\infty \frac{t^k}{k!} x^k f_w(x;\theta,c)dx$$

$$M_X(t) = \sum_{k=0}^\infty \frac{t^k}{k!}\mu'_k = \sum_{k=0}^\infty \frac{t^k}{k!}\left(\frac{(2\Gamma(c+k+1) + \theta^2\Gamma(c+k+2))}{\theta^k(2\Gamma(c+1) + \theta^2\Gamma(c+2))}\right)$$

$$M_X(t) = \frac{1}{(2\Gamma(c+1) + \theta^2\Gamma(c+2))}\sum_{k=0}^\infty \frac{t^k}{k!\theta^k}(2\Gamma(c+k+1) + \theta^2\Gamma(c+k+2)).$$

The characteristic function of KNPD is,

$$M_X(it) = \frac{1}{(2\Gamma(c+1) + \theta^2\Gamma(c+2))}\sum_{k=0}^\infty \frac{it^k}{k!\theta^k}(2\Gamma(c+k+1) + \theta^2\Gamma(c+k+2)).$$

Maximum Likelihood Estimation and Fisher's Information Matrix

In this section, we estimate the parameters of KNPD by using the maximum likelihood estimation. Assume the random sample $X_1, X_2 \dots, X_n$ from weighted Fav-Jerry distribution, then likelihood function should be defined as

$$L(x) = \prod_{i=1}^n f_w(x;\theta,c)$$

$$L(x) = \prod_{i=1}^n \left(\frac{x_i^c\theta^{c+1}}{(2\Gamma(c+1) + \theta^2\Gamma(c+2))}(2 + \theta^3 x_i)e^{-\theta x_i}\right)$$

$$L(x) = \frac{\theta^{n(c+1)}}{(2\Gamma(c+1) + \theta^2\Gamma(c+2))^n}\prod_{i=1}^n \left(x_i^c(2 + \theta^3 x_i)e^{-\theta x_i}\right).$$

The log likelihood function is given by

$$\log L = n(c+1)\log\theta - n\log(2\Gamma(c+1) + \theta^2\Gamma(c+2)) + c\sum_{i=1}^n \log x_i + \sum_{i=1}^n \log(2 + \theta^3 x_i) - \theta\sum_{i=1}^n x_i. \quad (14)$$

Therefore, now differentiating the log likelihood equation (14) with respect to θ and c. The following normal equations must be satisfied

$$\frac{\partial \log L}{\partial\theta} = \frac{n(c+1)}{\theta} - n\left(\frac{(2\theta\Gamma(c+2))}{(2\Gamma(c+1) + \theta^2\Gamma(c+2))}\right) + \sum_{(i=1)}^n \left(\frac{3\theta^2 x_i}{(2 + \theta^3 x_i)}\right) - \sum_{(i=1)}^n x_i = 0$$

$$\frac{\partial \log L}{\partial c} = n\log\theta - n\psi(2\Gamma(c+1) + \theta^2\Gamma(c+2)) + \sum_{(i=1)}^n \log x_i = 0$$

Here $\psi(.)$ is the digamma function.

The likelihood equations given above are too complicated to solve through algebraically. Apply R program for determining the parameters of developed distribution. Also apply the asymptotic normality results for getting the confidence interval. We state that were $\hat{\beta} = (\hat{theta}, \hat{c})$ which represents the maximum likelihood estimate of $\beta = (\theta, c)$. The result can be interpreted as $\sqrt{n}(\hat{\beta} - \beta) \to N_2(0, I^{-1}(\beta))$ here $I^{-1}(\beta)$ is Fisher Transformation Matrix

$$I(\beta) = -\frac{1}{n}\begin{pmatrix} E\left(\frac{\partial^2 \log L}{\partial \theta^2}\right) & E\left(\frac{\partial^2 \log L}{\partial \theta \partial c}\right) \\ E\left(\frac{\partial^2 \log L}{\partial c \partial \theta}\right) & E\left(\frac{\partial^2 \log L}{\partial c^2}\right) \end{pmatrix}$$

Here, we can state that

$$E\left(\frac{\partial^2 \log L}{\partial \theta^2}\right) = -\frac{n(c+1)}{\theta^2} - n\left(\frac{(2\Gamma(c+1)+\theta^2\Gamma(c+2))(2\Gamma(c+2)) - (2\theta\Gamma(c+2))^2}{(2\Gamma(c+1)+\theta^2\Gamma(c+2))^2}\right) + \sum_{i=1}^{n}\left(\frac{(2+\theta^3 x_i)(6\theta x_i) - (3\theta^2 x_i)^2}{(2+\theta^3 x_i)^2}\right)$$

$$E\left(\frac{\partial^2 \log L}{\partial c^2}\right) = -n\psi'(2\Gamma(c+1)+\theta^2\Gamma(c+2))$$

$$E\left(\frac{\partial^2 \log L}{\partial \theta \partial c}\right) = \frac{n}{\theta} - n\psi\left(\frac{2\theta\Gamma(c+2)}{(2\Gamma(c+1)+\theta^2\Gamma(c+2))}\right).$$

Hence β is not known so $I^{-1}(\beta)$ should be estimated by $I^{-1}(\hat{\beta})$ and it should be applied to attain asymptotic confidence interval for θ and c.

Fisher's Information Matrix (FIM) is a statistical tool that quantifies the amount of information a dataset provides about a parameter. In biomedical applications, FIM helps optimize experimental designs, analyze data from imaging techniques like single molecule microscopy, and improve parameter estimation in models. It's essentially a measure of how well a parameter can be estimated from data.

4. Discussion

Simulation Analysis

Simulation analysis uses statistical methods to study processes and systems by creating artificial models that mimic real-world scenarios. It involves repeated random sampling to approximate complex systems, allowing for the analysis of statistical estimates and model validation.

Key aspects of simulation analysis in statistics include:

Model Creation: Building a model that represents the system or process being analyzed.

Data Generation: Using random sampling to generate data that mimics the real-world conditions.

Statistical Analysis: Analyzing the simulated data to understand the system's behaviour, identify potential outcomes, and validate the model.

Output Analysis: Summarizing and interpreting the simulation results to gain insights and inform decision-making.

Model Validation: Ensuring the simulation model accurately reflects the real-world system it's intended to represent.

Simulation analysis is a powerful statistical tool that enables the study of complex systems, the evaluation of statistical methods, and the support of informed decision-making by creating artificial models and analyzing their simulated outputs.

By considering 5000 simulated random values from the KNPD, we can observe the non-symmetric nature of the distribution.

Table 1: *The Descriptive Statistics of the Simulated data.*

Mean	2.700	Range	5.750
Standard Error	0.105	Minimum	0.090
Median	1.790	Maximum	5.660
Mode	1.030	Sum	13500
Standard Deviation	1.405	Count	5000
Sample Variance	1.972	Largest (1)	5.750
Kurtosis	0.73	Smallest (1)	0.090
Skewness	1.1886	Confidence Level (95.0%)	0.2070

Karl Pearson's Skewness = (Mean-Mode)/SD. The value of this coefficient will be zero for a symmetrical distribution. If mean > mode, the coefficient of skewness is positive else negative. For considerably skewed destitution this coefficient is lies between -1and 1. If it is greater than 1 its highly positive skewed. Generally, if the distribution of data is skewed to the left, then mean < median< mode. If the distribution of data is skewed to the right, then mode < median< mean. Here from Figure 1 & Table 1, both cases imply the distribution is highly positive skewed.

Application

In this section, we have fitted and analyzed the goodness of fit of KNPD by examining and applying a real lifetime data set and observed that KNPD gives a better fit while compared over Fav-Jerry, KrishSupra-*P* Distribution (KSPD), Exponential and Lindley distributions.

The following data, Table 2, (Praseeja *et al.* [10]) represents the weight loss (Kilograms) of 77 randomly selected patients (of age group 12 to 15 - Secondary School Students from Thrissur District of Kerala" (January to June (2021)) after being infected with COVID-19.

Table 2: *weight loss (Kilograms) - patients (of age group 12 to 15) - from Thrissur District.*

1.39	1.44	1.46	1.53	1.59	1.6	1.63	1.68	1.71	1.72
4.02	4.32	4.58	5.55	2.54	0.77	2.93	3.27	3.42	3.47
1.83	1.95	1.96	1.97	2.02	2.13	2.15	2.16	2.22	2.30
1.00	0.99	1.02	1.05	1.07	1.07	1.08	1.08	1.08	1.09
0.10	0.33	0.44	0.56	0.59	0.59	0.72	0.74	0.92	0.93
1.13	1.15	1.16	1.2	1.21	1.22	1.22	1.24	1.30	1.34
2.4	2.45	2.51	2.53	2.54	2.78	1.83	1.95	1.96	1.97
1.76	3.61	2.31	1.12	0.96	1.36	2.02			

Table 3: *Descriptive Statistics of the Data.*

Mean	2.2400	Range	5.4500
Standard Error	0.1047	Minimum	0.1000
Median	1.9600	Maximum	5.5500
Mode	1.0800	Sum	403.4800
Standard Deviation	1.4041	Count	180.0000
Sample Variance	1.9716	Largest (1)	5.5500
Kurtosis	0.51	Smallest (1)	0.1000
Skewness	1.1149	Confidence Level (95.0%)	0.2065

Karl Pearson's Skewness = (Mean-Mode)/SD = 1. 1149.The distribution of data is skewed to the right, then mode < median< mean. Here from Table 3, both cases imply the distribution is highly positive skewed.

In order to compute the comparison criterion values besides with unknown parameters are estimated thoroughly by applying *R* software. To evaluate and highlight the performance of KNPD in comparison over Fav-Jerry, KSPD, Exponential and Lindley distributions, the considered criterions such as AIC (Akaike Information Criterion), BIC (Bayesian Information Criterion), AICC (Akaike Information Criterion Corrected) and $-2\log L$ have been applied. The distribution performs quite better if it has the smaller criterion values of $AIC, BIC, AICC$ and $-2\log L$ as compared over other distributions. The formulas for determining the criterions are,

$$AIC = 2k - 2\log L, \quad BIC = k\log n - 2\log L \quad \text{and} \quad AICC = AIC + \frac{2k(k+1)}{n-k-1}.$$

Here $-2\log L$ is the maximized value of log-likelihood function(L), n is the sample size and k is the number of parameters in statistical model.

It is clearly observed from results in Table 3, that KNPD has smaller criterions of $AIC, BIC, AICC$ and $-2\log L$ in comparison with the Fav-Jerry, Exponential, and Lindley distributions demonstrates that the KNPD offers a superior fit. Additionally, its performance is competitive with the KSPD, further underscoring its effectiveness in modelling the given data.

Table 4: *Shows Analysis and Comparison of Performed Distributions*

Distributions	MLE	S.E	$-2\log L$	AIC	BIC	AICC
KPND	$\hat{\theta} = 1.1054$	$\hat{\theta} = 0.1803$				
	$\hat{c} = 0.7619$	$\hat{c} = 0.2324$	203.939	207.939	212.225	208.139
Fav-Jerry	$\hat{\theta} = 0.5646$	$\hat{\theta} = 0.0955$	217.879	219.879	222.022	219.945
KSPD	$\hat{\theta} = 2.6090$	$\hat{\theta} = 0.3019$				
	$\hat{c} = 1.8501$	$\hat{c} = 0.50912$	191.4293	195.3943	199.9900	195.5960
Exponential	$\hat{\theta} = 0.5697$	$\hat{\theta} = 0.0596$	224.8929	226.8929	229.1696	226.9500
Lindley	$\hat{\theta} = 0.8697$	$\hat{\theta} = 0.0697$	213.051	215.051	217.3277	215.1081

Maximum Likelihood Estimate (MLE), Standard Error (S.E)

5. Conclusion

This paper introduces a novel study on the Fav-Jerry distribution, referred to as KNPD, developed through the application of a weighted technique to its classical counterpart, the Fav-Jerry distribution. The proposed distribution has been extensively analyzed, covering various statistical properties such as moments, the behaviour of its probability density function (PDF) and cumulative distribution function (CDF), mean and variance, survival function, hazard function, reverse hazard rate function, moment-generating function, and harmonic mean. Additionally, its order statistics and Renyi entropy measure have been discussed. The parameters of the new distribution are estimated using the maximum likelihood estimation method. Moreover, the superiority and versatility of the proposed distribution have been demonstrated through a real dataset, revealing that KNPD provides a better fit compared to the Fav-Jerry, Exponential, and Lindley distributions.

References

[1] Ajami, M. and Jahanshahi, S. M. A. (2017). Parameter estimation in weighted Rayleigh distribution. *Journal of Modern Applied Statistical Methods*, 16(2), 256–276.

[2] Bashir, S., Masood, B., Rasul, M. and Waseem, N. (2023). Pareto length-biased exponential distribution: Properties and Applications on the flood data. *International Journal of Contemporary Issues in Social Sciences*, 2(3), 838–850.

[3] Bashir, S. and Rasul, M. (2016). Some properties of the size-biased Janardan distribution. *American Journal of Theoretical and Applied Statistics*, 5(5), 305–310.

[4] Benchiha, S. A., Al-Omari, A. I., Alotaibi, N. and Shrahili, M. (2021). Weighted generalized quasi Lindley distribution: Different methods of estimation, applications for covid-19 and engineering data. *AIMS Mathematics*, 6(11), 11850–11878.

[5] Ekemezie, D. F. N. and Obulezi, O. J. (2024). The Fav-Jerry distribution: Another member in the Lindley class with applications. *Earthline Journal of Mathematical Sciences*, 14(4), 793–816.

[6] Fisher, R. A. (1934). The effects of methods of ascertainment upon the estimation of frequencies. *Annals of Eugenics*, 6, 13–25.

[7] Ganaie, R. A. and Rajagopalan, V. (2020). A new generalization of quasi gamma distribution with properties and applications. *International Journal of Engineering and Advanced Technology (IJEAT)*, 9(3), 3855–3861.

[8] Murthy, D. P., Xie, M. and Jiang, R. (2004). Weibull Models, volume 505. John Wiley & Sons.

[9] Nanuwong, N. and Bodhisuwan, W. (2014). Length biased beta-Pareto distribution and its structural properties with application. *Journal of Mathematics and Statistics*, 10(1), 49–57.

[10] Praseeja C. B., Prasanth C. B., Subramanian C. and Unnikrishnan T. (2023). Characteristics of Chandbhas-*P* Distribution and Its Applications in Medical Science. *RT&A*, 4 (76), 314–324, https://gnedenko.net/Journal/2023/042023/RTA_4_2023-25.pdf

[11] Praseeja, C. B., Prasanth, C. B., Subramanian, C., Unnikrishnan, T. (2024). Characterisation of KrishSupra-*P* Distribution and Its Biomedical Application. *Communications in Mathematics and Applications*, 15(3), 1077–1088. https://doi.org/10.26713/cma.v15i3.2833

[12] Rajagopalan, V., Ganaie, R. A. and Nair, S. R. (2023). A new extension of two parameter Pranav distribution with applications in Industrial and Medical sciences. *Journal of Statistics Applications & Probability*, 12(1), 231–246.

[13] Rao, C. R. (1965). On discrete distributions arising out of method of ascertainment, in classical and contagious discrete distributions. Pergamon press and statistical publishing society, Calcutta. 320–332.

[14] Saghir, A., Tazeem, S. and Ahmad, I. (2017). The weighted exponentiated inverted Weibull distribution: Properties and Application. *Journal of Informatics and Mathematical Sciences*, 9(1), 137–151.

[15] Salama, M. M., Elsherpieny, E. A. and Abd-elaziz, A. A. (2023). The length-biased weighted exponentiated inverted exponential distribution: properties and estimation. *Computational Journal of Mathematical and Statistical Sciences*, 2(2), 181–196.

OPTIMIZING PATHFINDING: A NOVEL ALGORITHM FOR GRAPH THEORY

Aijaz Ahmad Magray[1,], Ajjaz Maqbool Dar[2], Firdous Ahmad[3], Aafaq A. Rather[4,*], R. Vijaykrishnaraj[5], D. Vedavathi Saraja[6], Syed M. Parveen[7], Raeesa Bashir[8]

•

[1]Department of Mathematics, Govt. Degree College Premnath Dogra, Samba 184121, India
[2]Jammu and Kashmir Institute of Mathematical Sciences Srinagar -190008, J&K, India.
[3]Department of Electronics & IT, Cluster University (S.P College), Srinagar 190006, J&K, India
[4,*]Symbiosis Statistical Institute, Symbiosis International (Deemed University), Pune-411004, India
[5]Department of Mathematics, Bharath Institute of Higher Education and Research, Chennai, India
[6,7]Department of Statistics, Maris Stella College, Vijayawada, India
[8]Department of Statistics, Cluster University, Jammu and Kashmir, India
[1]magrayaijaz2@gmail.com, [2]ajjazmaqbool013@gmail.com,
[3]firdousahmed15@gmail.com, [4,*]Corresponding author: aafaq7741@gmail.com, [5]drvjmaths@gmail.com,
[6]sarajayoganand@gmail.com, [7]parveen@marisstella.ac.in, [8]raisabashir52@gmail.com

Abstract

In this paper, a new proposed algorithm called the Pentacode-algorithm is successfully designed and implemented to solve the space and time problems associated with previous algorithms. Several parameters, such as Shortest Distance (SD), Time to Search Shortest Distance (TSSD), and Loss of Information Packets (LIP) have been checked and verified using the proposed algorithm. The simulation results achieved from the MATLAB tool authenticate the correct functionality of the proposed Pentacode-algorithm. Advance improvements have been proved in the proposed algorithm in terms of the space search and time issues. In addition, First-Node-Die (FND), Half-Node-Die (HND) and Last-Node-Die (LND) are determined in our results. The comparative results have shown that the Pentacode-algorithm is more proficient than the previous algorithm. This Pentacode-algorithm can be applied to warless communication systems, network routing and protocol multidirectional transmission and Quantum computing research.

Keywords: Pentacode-algorithm, Active Nodes, Shortest Distance (SD), Time to Search Shortest Distance (TSSD), Loss of Information Packets (LIP)

1. Introduction

The well-studied research topic in graph theory is the shortest-path. The shortest path problem is a major issue for finding the minimal cost between the two nodes in a graph. No such general algorithm has proven so far that it can solve all variants of the shortest path in a graph. Even though several algorithms like the Greedy algorithm, Flood-fill algorithm, Floyd Warshall algorithm, Dijkstra's shortest path algorithm and Bellman Ford algorithm have been implemented for optimizing the route between the two nearest nodes in a graph. Despite these algorithms, the space and time complexities are associated with them. Therefore, shortest-path problems have moulded us to think of new alternatives. It has led gingus to lead a new challenge to rule out this issue in graph theory. The study of shortest path problems between the vertices (nodes) and edges (lines) in a graph is an

ambient research topic for research community. Therefore, a great deal of attention has been paid in graph theory for an optimizing shortest-path, with the minimum length criteria between two nodes. Therefore, numerous algorithms have been redesigned and implemented for finding a shortest path between two nodes [1]. Due to its enamors wide applications which include network routing protocols, route planning, traffic control, path finding in social networks, computer games, and transportation systems, forging us an exclusive state of shortest path issue in the graphs. The purpose to find the shortest path with all variants between two nodes in a graph is a complex act that needed to be resolve with the special techniques in mathematics. Several numbers of techniques suggested by the research scholars includes Greedy algorithm [1, 2], M. Fredman [3], Floyd Warshall algorithm [4, 5], Dijkstra's shortest path algorithm [6] Bellman Ford algorithm [7, 8] and Genetic algorithm [10] for optimizing the rout between the two nodes in a graph. These algorithms' relies to reach shortest path in a space of graph. The Shortest path algorithms are the circle of relatives of algorithms used for solving the hassle of shortest route.

Several research solutions have been implemented to overcome the short path problems in a graph. However, no one address all the variant vulnerabilities of space and time that are associated with the shortest paths [11-12]. Our aim is to present a new model that handles all inherited limitations and vulnerabilities that occurred in previous algorithms [13-14]. The new model has been proposed to sort out complex variants of space and time issues for graph in this paper. It has an ability to find the shortest between two vertices or nodes in graph theory and we put the proposed model name as Pentacode-algorithm. The suitable functionality of the presented Pentacode-algorithm has been verified with suitable comprehensive comparisons with the previous algorithms [15].

2. Background of the shortest paths

Since several algorithms have been introduced which can be helpful in the weighted- graph to determine the shortest-path from the source node to every other destination node within the graph. These algorithms work to search the shortest-path to every single reachable node, provided the graph does not change. These algorithms can run until and unless they visit all reachable codes, increasing space and time issue problems. However, the graph can be either directed or undirected when it needs to embrace a non-negative value on its every edge. In addition, these algorithms cannot be suggested for weighted- graphs. Since 1959 a Dutch computer scientist, Edsger-Dijkstra's, has suggested an algorithm that can be useful to the weighted- graph. The graph can be either directed or undirected in the situation that the graph needs to embrace a non-negative value on every edge. This algorithm stands out from the shortest path from the source node to every other destination node within the same graph data structure. Rather than searching the shortest path from the source node to the specific node, the algorithm works to search the shortest path to every single reachable node, provided the graph does not change. The algorithm runs until and unless all reachable codes. The work plan of Dijkstras algorithm can be understood as:

Let G be a graph in 2-D Plane. It may be directed or undirected.

Therefore,$G = \int(V, E)$

"s" is source vertex in the graph plane

"w" is a weight function of graph target search space.

$w = \ E \rightarrow R$

Fig. 1 depicted below shows the shortest path direction of Dijkstra's algorithm. Here, dotted line shows the shortest path direction.

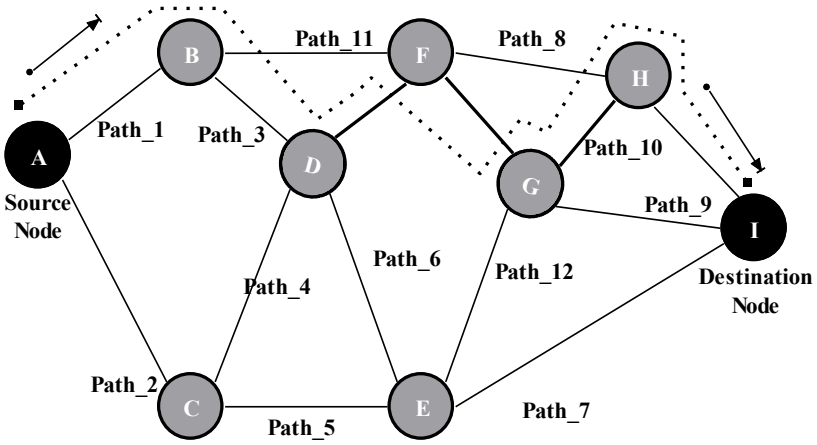


Fig. 1: *Shortest Path Detection in Dijkstra's algorithm*

Despite certain advantages, there are vulnerabilities of Dijkstra's algorithm for negative weights. These vulnerabilities can be illustrated in Lemma 1.

Lemma 1: Dijkstra's algorithm does not work with negative edges?

Proof: Negative weights can be well explained with these cycles, as shown in Fig. 2. Consider the following proof:

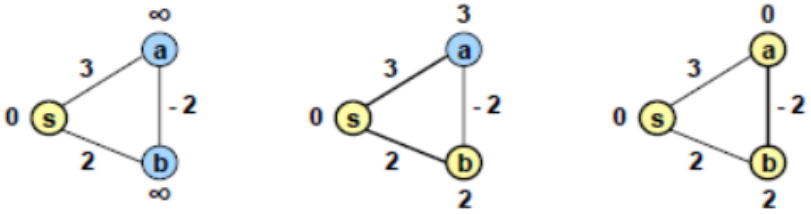


Fig. 2: *Negative weight cycle*

Let Dijkstra's algorithm visit node b and then at node a. Let it leave node b with a distance of 2 instead of the correct distance 1. The problem is that when we consider the closest vertex v not in the visited set, its shortest path may be through only the visited set and then extended by one edge out of the visited set, say to v. To find the shortest paths on a graph with negative weights, we should think of some inductive hypothesis. In Dijkstra's algorithm, the hypothesis was that if we have found the i nearest neighbours, we can add one more to find the i+1 nearest neighbours. As discussed earlier, Dijkstra's algorithm does not work on negative weights.

While in the contract, the Bellman–Ford algorithm [7, 8], sometimes called the Label Correcting Algorithm, computes single-source shortest paths in a weighted digraph (some edge weights may be negative). Its basic structure is very similar to Dijkstra's algorithm. However, instead of greedily selecting the minimum-weight node not yet processed to relax, it simply relaxes all the edges and does this |V| - 1 times, where |V| is the number of vertices in the graph. These repetitions allow minimum distance to propagate accurately throughout the graph, since the shortest path can only visit each node at most once without negative cycles. Unlike the greedy approach, which depends on certain structural assumptions derived from positive weights, this straightforward approach extends to the general case. It has the advantage of resolving such a single source shortest-path commonly denoted as (SSSP) problem, and is better applied to be the parallelized for many core architectures [9]. A high degree of parallelism is guaranteed at the cost of the low work efficiency, which, compared to similar algorithms, involves much more redundant work and a consequent waste of power consumption. In short Bellman–Ford algorithm offers a number of advantages such as

negative weight handling, parallel operation support, fast and simple for small application. At the same time, this algorithm inherits number of limitations as the size of vertex and size of search space increases, which are discussed in Lemma 2.

Lemma 2: In Bellman–Ford algorithm, how does the vertex size and search space increase?

Proof: Bellman Ford algorithm can generate all pair's for shortest paths, if one runs the Bellman Ford algorithm and try to find the shortest path. This algorithm has to search all nodes, which increases complexity and requires more time to reach the final results. It consumes major resources of the system. Changes in the network topology are not reflected rapidly since the updates are spread node by node. Hence, the time required to reach the results is considerable when many parallel operations participate. There is no commitment for the optimal results. In some cases, the algorithm may fail due to complex operations.

3. Proposed Pentacode-Algorithm

The proposed Pentacode-algorithm is the Hybridization of integrating two or more meta-heuristic optimization algorithms for searching for the most suitable and optimal solution in a specific search space. It relies on combining the algorithms to resolve various. The proposed Pentacode-algorithm works on the parallel operations of both positive and negative weights. Therefore, parallel operations of the proposed algorithm hold good properties, making it capable of working on different methods and resolving problems efficiently. For example, a search is efficient when many solutions can solve problems.

Prime objectives of Hybridization are as:

1) To address the vulnerability of specific meta-heuristic optimization algorithm
2) To address limitations of the specific meta-heuristic optimization algorithm
3) To counter the disadvantages of the specific meta-heuristic optimization algorithm
4) To integrate the advantages of specific meta-heuristic optimization algorithm

Fig. 3 depicts the hybridization of two meta-heuristic optimization algorithms, which addresses the limitations and vulnerabilities by integrating the advantages of other meta-heuristic optimization algorithms and facilitates commitment for convergence with fewer time parameters.

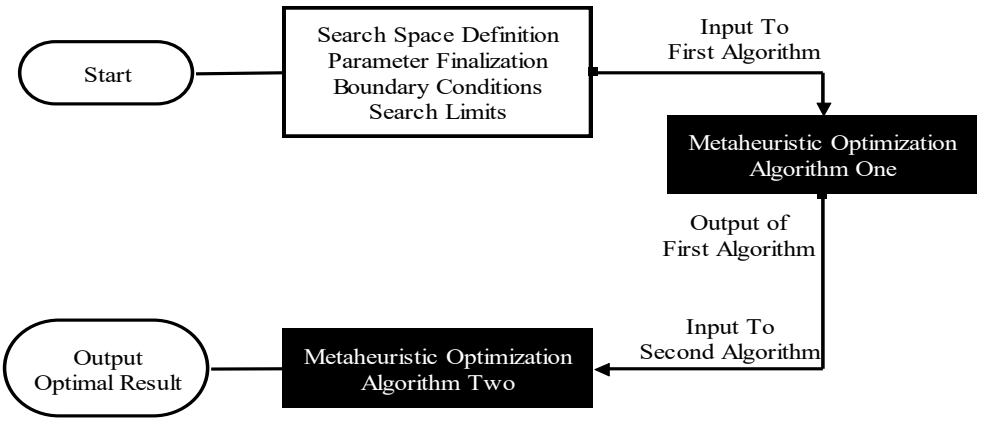


Fig. 3: *Hybridization of Two Optimization Algorithm*

Hence, the proposed Pentacode-algorithm is a possible method for solving the negative weights in the search space. It can overcome the limitations which are constituted by the previous designs [6, 10]. The proposed algorithm can perform parallel searches of various nodes in space, which can consume less time in space to achieve target. This ability will become a benchmark to be the fastest algorithm.

Dijkstra's shortest-path algorithm has a blind search. It calculates the entire path from source to destination, which makes the algorithm inefficient because it wastes more time to reach the necessary resources. In addition, if the space search of an algorithm increases, the time required for the optimal path also increases exponentially. In addition, it works with non-negative weights for the edges with slight modifications but fails for negative weight in the space graph, which swings the system and hangs the final results. However, nested loops taken by Dijkstra's algorithm lead to an increase the search time in space. Due to some limitations of Dijkstra's algorithm, like using nested loops, which increase the search time, it becomes necessary for the research community to implement a new algorithm that can span less time in space, using limited loops. In this regard a new Pentacode-Algorithm algorithm has been proposed.

The proposed Pentacode-algorithm is committed exact and more realistic in nature in the context of real world live wire problems. The Pentacode-algorithm works with waited/non-negative weights. It overcomes the limitations of Dijkstra's Algorithm. Initially, Bellman-Ford-algorithm is initiated with parameters subjected to target search space; the output of this search will be input for Dijkstra's Algorithm and is search space for the second algorithm. However, the proposed algorithm sown in Fig. 4, which is free of negative edges and is smaller in size than previous designs [6, 10].

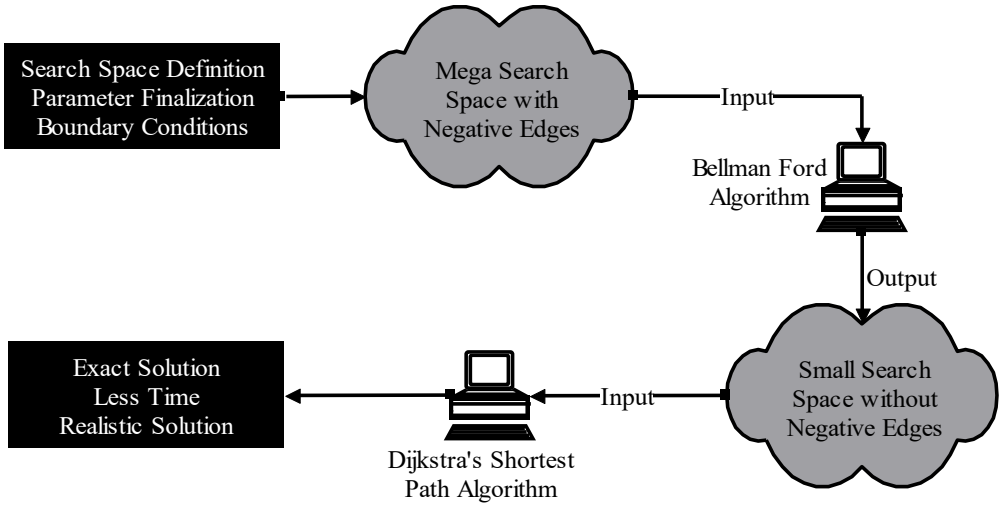


Fig. 4: *The proposed Pentacode-Algorithm*

The proposed Pentacode-Algorithm facilitates various advantages like1) Negative weight or edge present in the search space is a major issue in Dijkstra's algorithms which has been countered in initial stage in PENTACODE-Algorithm such that new search space is suggested for optimal result.2) Dijkstra's algorithm implements recursive search technique which calls another function for optimization, this recursive calling results increases searching time. However, in the proposed Pentacode-Algorithm already shortened the search space, now Dijkstra's algorithm required confining the search in smaller space, this technique saves time and resources. 3) There is fewer possibility of trapping the proposed algorithm for infinite loop which Confirms convergence within search space.

4. Comparison of the proposed Pentacode-Algorithm

1) Negative weight or edge present in the search space is a major issue in Dijkstra's algorithms, which has been countered in initial stage in Pentacode-Algorithm such that new search space is used for optimal results.

2) Dijkstra's algorithm implements recursive search technique which calls another function for optimization, this recursive calling results increases searching time. However, in the proposed Pentacode-Algorithm already shortened the search space. This advantages that Dijkstra's algorithm required confining the search in smaller space; this technique saves time and resources.
3) There is fewer possibility of trapping the proposed algorithm for infinite loop which Confirms convergence within search space. The detailed work plan of the proposed Pentacode-algorithm is mentioned in Fig.5.

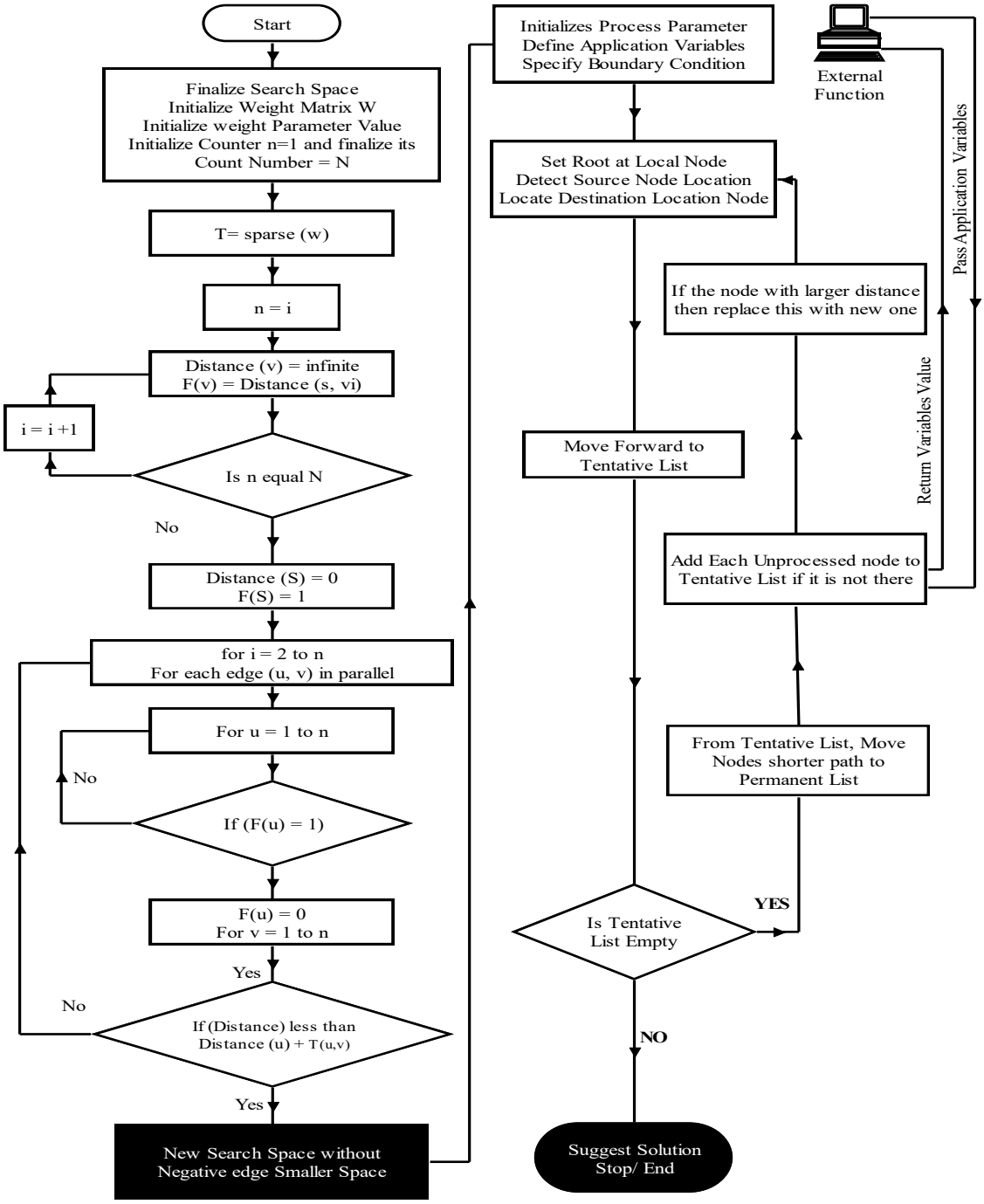


Fig. 5: *The Proposed Pentacode-Algorithm Flow Chart*

5. The Java Code Segment used for the proposed Pentacode-Algorithm

A systematic approach has been used to implement Algorithm to optimize information protocol. Java software coding technique has been used to test the proposed Pentacode-algorithm. To authenticity, the functionality and visualization ofgraphs have been determined using MATLAB-6.0. This is an independent platform which supports java code in which various parameters such as shortest distance (SD), time to search shortest distance (TSSD), Loss of information packets (LIP) have been verified by using the java code. In addition, first node die (FND), Half node die (HND) and last node die (LND) have been determined in our results. Optimal Shortest Path selection process for the proposed Pentacode-algorithm has been checked in the java cod as:

Declare Int N_D Number_of_Node, N_C Number_of_Cluster, D_N Distance Between Nodes
Int N_L Loop_1_Cout, N_{L2} Loop_2_Count
Start Clustering of Phase_One Level_1
Start Clustering of Phase_One Level_2
Start Clustering of Phase_One Level_3
Repeat-Step-3 for i =1, 2- - - -

6. The Result and Discussion

The geographical map, considered an objected area for the testification of simulation results, has been shown in Fig. 6(a). The total test area is 10 x10 kilometres area, which h is 10 km long and 10 km wide, which means 100 square kilometres (100 Sq. Km). The test area has been taken from the Google Map web site. Various locations and places have been shown in this map, in which a few cluster and cluster member nodes have been chosen for testification. The proposed work plan has been verified using 10000 active nodes, which occupy an area of 10000 sq. meters.

Further, these active nodes have been grouped into 100 clusters. Fig. 6(b) depicts the graphical representation of the test model considered for simulation and verification. This is a state space presentation of Model in graph theory so that the shortest path can be searched from the possible combinations of the hundreds of options in the space.

The proposed Pentacode-algorithm has been compared with the various previous algorithms [6, 10] as shown in Table-1. It indicates the shortest distances between source and destination nodes. In our practical, we have considered various test distances which are-5.0-KM, -5.5-KM, -6.0-KM, -6.5-KM, -7.0-KM, -7.5-KM, -8.0-KM, -8.5-KM&-9.0-KM. In actual sense test has been done with 10Km x 10Km (Sq.100km). The result in the table 1 clearly reflects that the shortest path suggested by the Pentacode-algorithm is the minimum physical distance among path suggested by different algorithms. 9% to 11% better result with the A-algorithm. It is clear from the graphical comparison, including various parameters, that our proposed plan is superior to all other existing techniques, as shown in Fig. 6.

Table 2 shows the time taken of various shortest path algorithms. The graphical picture has proven that our proposed Pentacode-algorithm spans very less time and is more persistent than existing designs [6, 10]. The time taken by Pentacode-algorithm has shown minimum indication from every simulation results. Various distances have been considered between the source and destination node. The detailed graphical comparison of the shortest distance between the source and destination node by different algorithm is shown in Fig. 7, and the timer taken to search the shortest path by different algorithms is shown in Fig. 8:

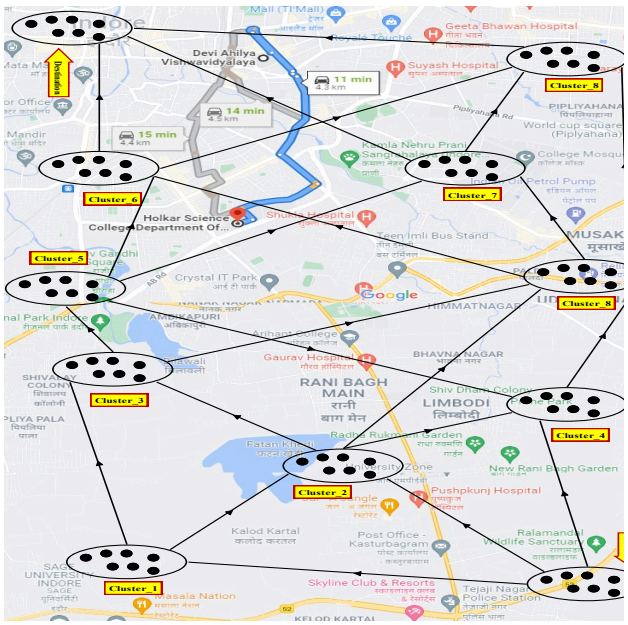


Fig. 6(a): *Model Network Geographical Area*

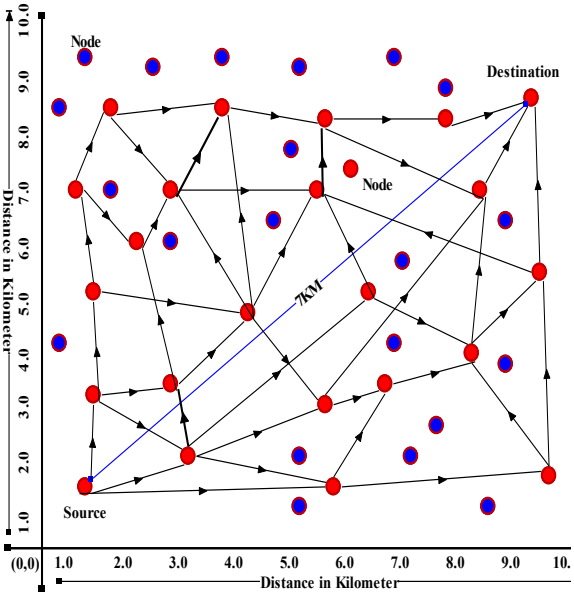


Fig. 6(b): *The Test Model Area (100 Sq. Km)*

Table-1: *Shortest Distances Suggested by Different Algorithm*

No.	Actual Physical Distance Between Source Node and Destination Node	Shortest Path Suggested by Dijkstra's Algorithm [6]	Shortest Path Suggested by Genetic Algorithm [10]	Shortest Path Suggested by Pentacode-algorithm
1	5.0 KM	6.1 KM	5.7 KM	5.4 KM
2	5.5 KM	6.9 KM	5.9 KM	5.7 KM
3	6.0 KM	7.1 KM	6.9 KM	6.5 KM
4	6.5 KM	7.6 KM	7.2 KM	6.9 KM
5	7.0 KM	8.2 KM	7.9 KM	7.4 KM
6	7.5 KM	8.7 KM	8.4 KM	7.9 KM
7	8.0 KM	9.4 KM	8.9 KM	8.6 KM
8	8.5 KM	10.2 KM	9.9 KM	8.9 KM
9	9.0 KM	11.4 KM	10.1 KM	9.8 KM

Figure 7, shows the shortest distance between source and destination node by different algorithm and

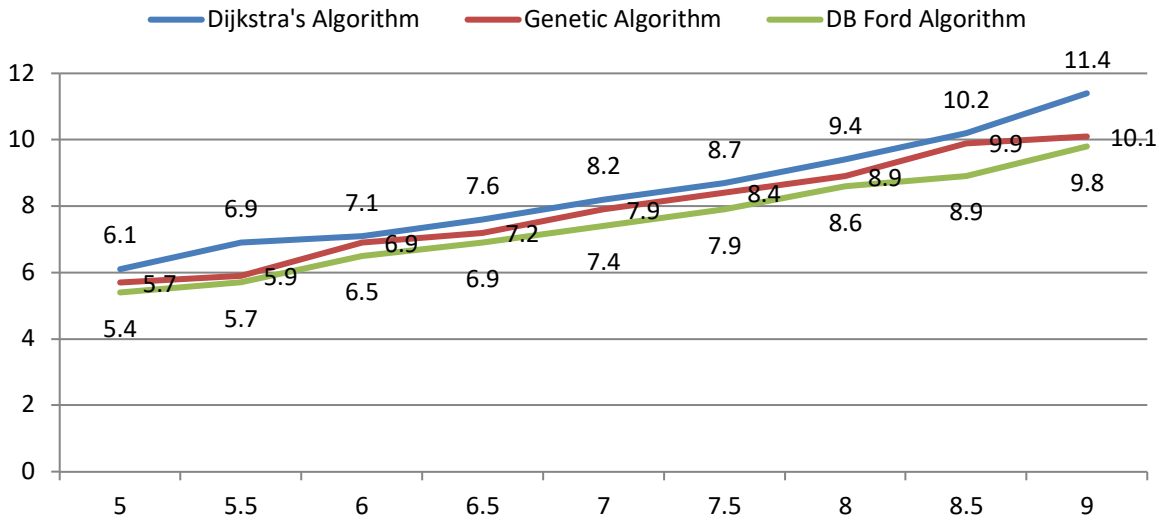


Fig. 7: *Shortest Distance between Source and Destination Node by Different Algorithm*

Table-2: Time taken to search Shortest Distance by Different Algorithm

No.	Actual Physical Distance Between Source Node And Destination Node	Time Taken by Dijkstra's Algorithm To Reach Shortest Path Value (Nanoseconds) [6]	Time Taken by Genetic Algorithm To Reach Shortest Path Value (Nanoseconds) [10]	Time Taken by Pentacode-algorithm To Reach Shortest Path Value (Nanoseconds)
1	5.0 KM	110 Nanoseconds	90 Nanoseconds	85 Nanoseconds
2	5.5 KM	125 Nanoseconds	110 Nanoseconds	98 Nanoseconds
3	6.0 KM	136 Nanoseconds	119 Nanoseconds	104 Nanoseconds
4	6.5 KM	141 Nanoseconds	126 Nanoseconds	113 Nanoseconds
5	7.0 KM	151 Nanoseconds	132 Nanoseconds	121 Nanoseconds
6	7.5 KM	162 Nanoseconds	141 Nanoseconds	132 Nanoseconds
7	8.0 KM	171 Nanoseconds	154 Nanoseconds	139 Nanoseconds
8	8.5 KM	182 Nanoseconds	163 Nanoseconds	145 Nanoseconds
9	9.0 KM	198 Nanoseconds	174 Nanoseconds	152 Nanoseconds

Figure 8, depicts the timer taken to search shortest path by different algorithm.

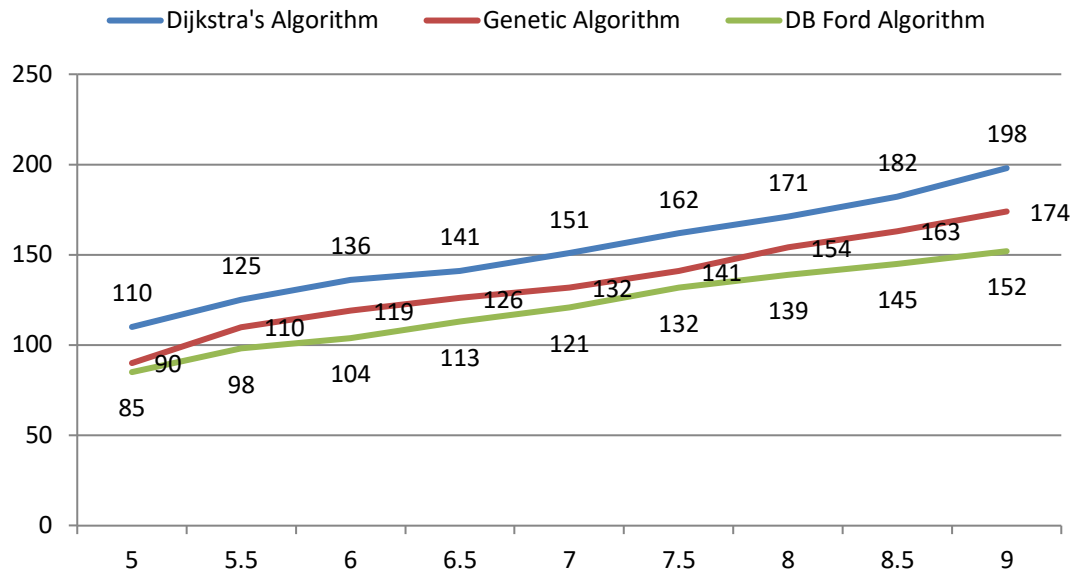


Fig. 8: *Timer taken to search Shortest Path by Different Algorithm*

7. Percentage Information Loss

The loss of Information inherits network protocols such as HTTP, FTPP and SMTP l, because these protocols are associated with distance. If the distance between source and destination node increases, time will increase accordingly. The percentage loss has been tabulated in Table 3. Clearly, the Table-3 information loss of packets is minimal in the proposed Pentacode-algorithm compared with the previous algorithm [6, 10] Dijkstra's-Algorithm & Genetic-Algorithm. In actuality, the distance travelled and time taken to complete the distance in the proposed algorithm is minimal, as shown in Fig.9.

Table 3: *Percentage Loss of Information*

No	Test Distance Between Source & Destination Node	% in Information Protocol with Dijkstra's Algorithm [6]	% in Information Protocol with Genetic Algorithm [10]	% in Information Protocol with Pentacode-Algorithm
1	5.0 Km	16.0 %	11.5 %	10.2 %
2	5.5 Km	16.6 %	11.8 %	10.9 %
3	6.0 Km	17.3%	12.4 %	11.3 %
4	6.5 Km	17.5 %	12.9 %	11.7 %
5	7.0 Km	18.2 %	13.2 %	11.9 %
6	7.5 Km	18.8 %	13.8 %	12.5 %
7	8.0 Km	19.2 %	14.7 %	13.1 %
8	8.5 Km	19.6 %	15.4 %	13.9 %
9	9.0 Km	19.9 %	15.9 %	14.2 %
10	9.5 Km	20.2 %	16.2 %	14.6 %

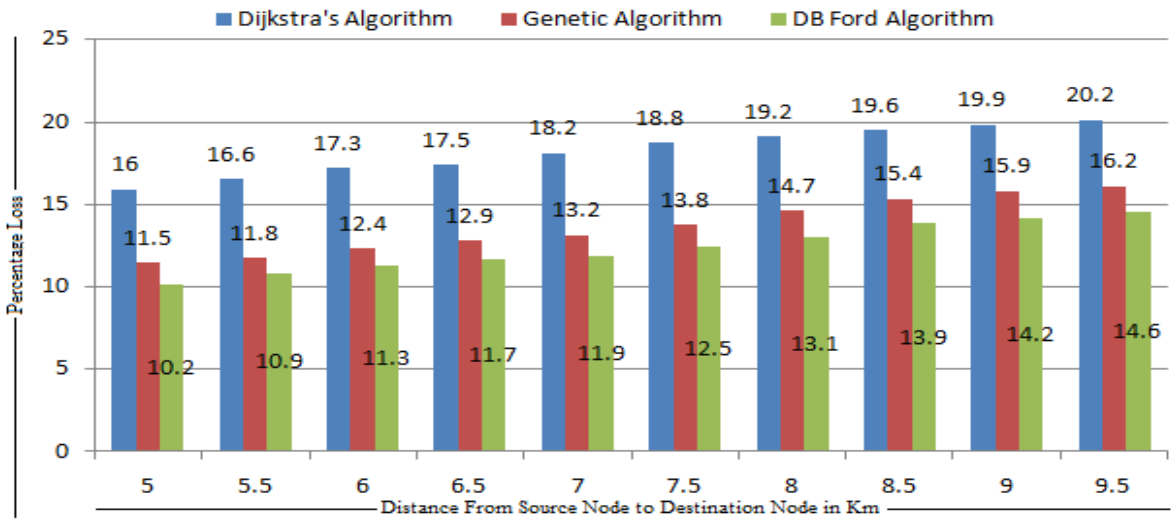


Fig. 9: *Percentage loss in Information Packets with respect to distance in different Algorithm*

8. First-Node-Die (FND), Half –Nodes-Die (HND) and Last-Node-Die (LND) Parameter

Evaluation of the Wireless-sensor-network can be-done by using the various parameters-for the system energy. Therefore, number of the nodes die in each round because of-FND, -HND &LND. Since when the-first node starts dissipating energy-its energy and the performance will starts-degrading. Therefore, it is required to-mark the death of the very first-node in the-network. Hence the same cause of time for HND and LND is marked. Briefly, the lower the number of nodes, the better the performance of wireless communication system. The result clearly reflects that best performance is achieved by the proposed Pentacode-algorithm for shortest paths. The detailed comparisons of various parameters [6, 10] are listed in Table 4. The graphical picture depicted in Fig. 10, Fig. 11 and Fig. 12, shows the better performances achieved in the proposed design [6, 10].

Table 4: *The Comparison of FND, HND & LND Parameter*

No.	Protocol Count	Dijkstra's Algorithm [6]			Genetic Algorithm [10]			Pentacode-algorithm		
		FND	HND	LND	FND	HND	LND	FND	HND	LND
1	5000	900	880	820	870	840	810	840	820	800
2	6000	960	920	895	950	890	875	940	870	860
3	7000	990	935	910	965	910	895	950	900	875
4	8000	1000	980	950	990	950	900	960	930	895
5	9000	1050	998	978	1040	960	940	990	940	910
6	10000	1065	1020	995	1050	1030	955	1010	990	920
7	11000	1100	1050	1030	1060	1040	990	1020	910	940
8	12000	1150	1090	1050	1090	1060	1010	1030	940	930
9	13000	1190	1110	1070	1110	1090	1040	1040	960	940
10	14000	1200	1150	1090	1120	1110	1050	1055	970	960

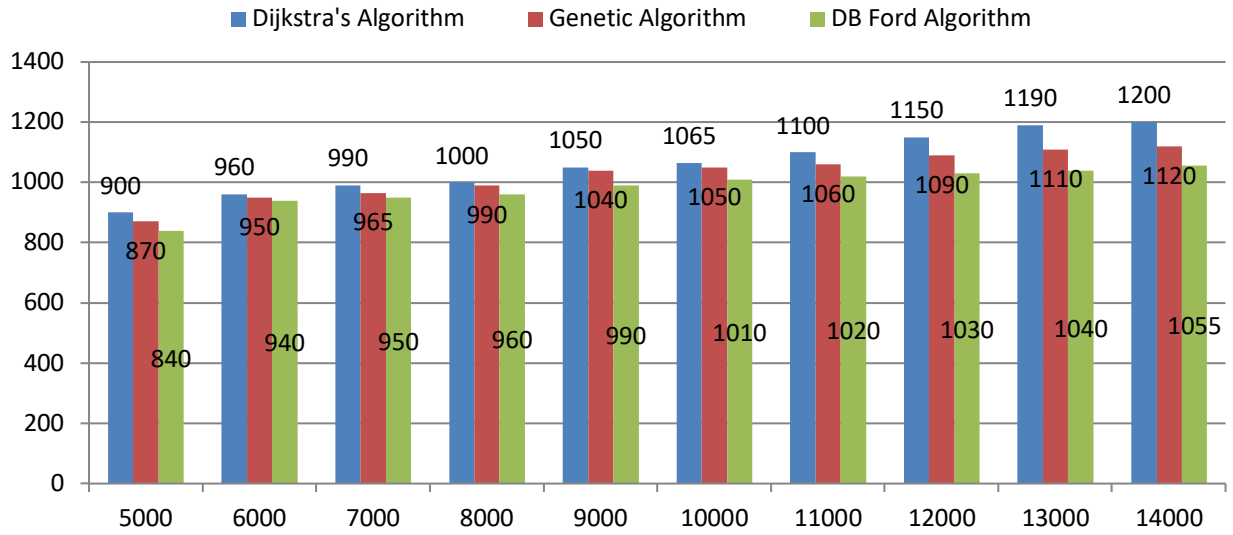


Fig. 10: *First-Node-Die (FND) Pointer in Different Algorithm with respect to Different Protocol Number*

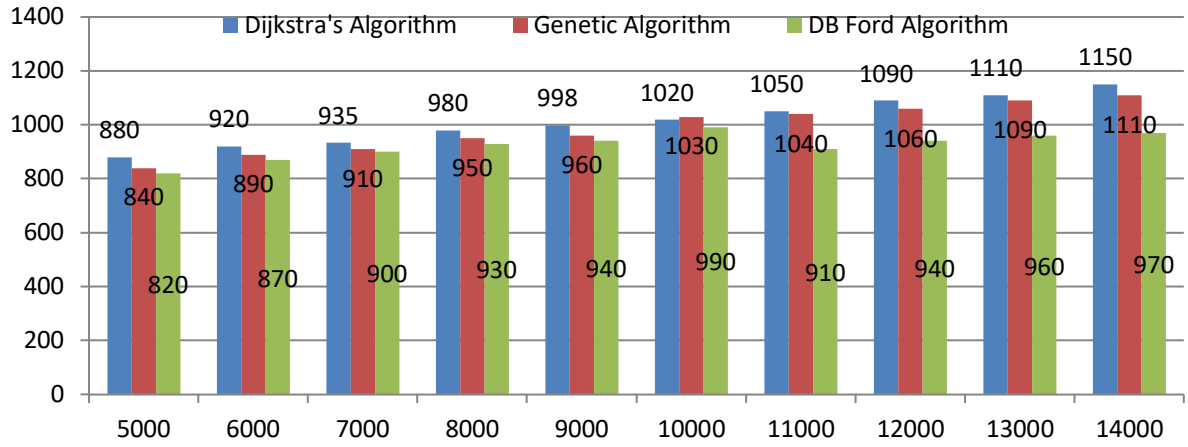


Fig. 11: *Half-Node-Die (HND) Pointer in Different Algorithm with respect to Different Protocol Number*

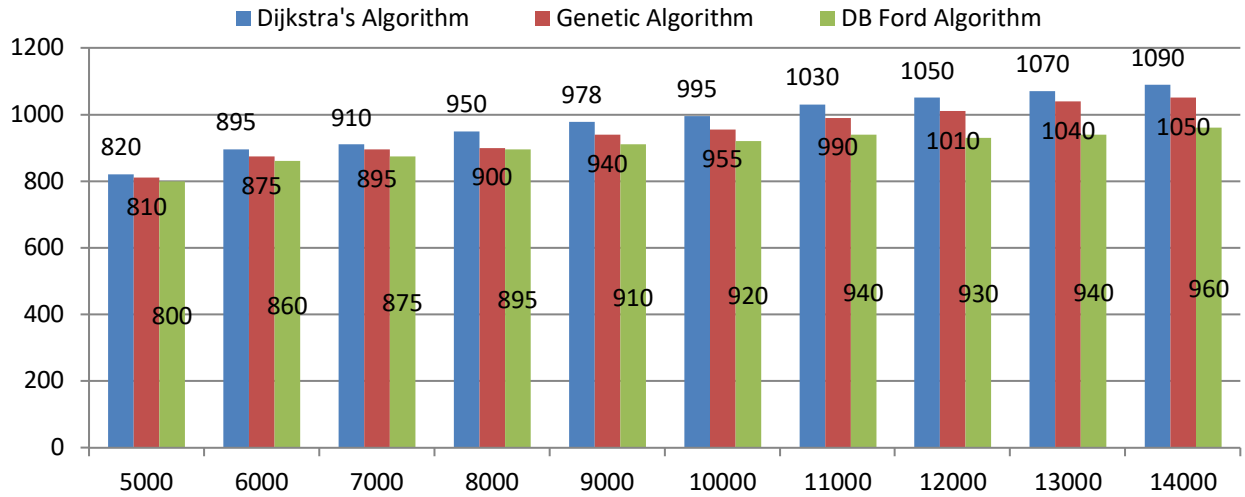


Fig. 12: *Last-Node-Die (LND) Pointer in Different Algorithm with respect to Different Protocol Number*

9. Future Scope

Shortest path algorithm is of great importance in modern industrial applications, corporate applications and even in the daily application of socio-economic activities of modern age at present time; when there are numbers of challenges in front of human beings.

Hence there are numbers of area in different sectors in which there will be great potential for further research in the respective field.

These core areas are documented as below in which the research can be extended:

1) Telecommunication Companies
2) Internet Service Provider Companies
3) Cloud Computing Infrastructure Companies
4) Live wire Channel Banking Applications
5) Missile Lunching Application
6) Missile Defence Application
7) Rocket Trajectory Application
8) Agriculture and Environment Assisting Applications.

10. Conclusion

This paper presents a new Pentacode-algorithm for shortest path problems. The proposed Pentacode algorithm has been designed to enhance performance by effectively handling the challenges associated within Dijkstra's, Bellman-Ford, and Genetic algorithms. Shortest-Path-Algorithm. Various test simulation has been discussed and modeled in graphical mathematical formant. The simulation results clearly show that the proposed Pentacode-algorithm is superior to previous algorithms. Test simulation has been done with the input parameter value, including distances and time. Test parameters such as area which includes 10Km x 10Km (100 Sq. Km) in which 100 clusters have been grouped for calculations. Each cluster contains 100 nodes. The new Pentacode-algorithm has been designed to enhance the performance and optimize the distance for shortest path problems. Furthermore, the proposed algorithm has been implemented to improve upon the limitations of Dijkstra's and the Bellman-Ford shortest path algorithms. Moreover, the time taken by Pentacode-algorithm for searching path in space is minimal, indicates highly proficiency of shortest path optimization than previous algorithm. Verification of results has been determined using Java code and MATLB-6.

References

[1] R. Bellman (1957). Dynamic Programming. Princeton University Press.

[2] R. Bellman (1958). On a routing problem. Quarterly of Applied Mathematics.

[3] M. Fredman (1976). New bounds on the complexity of the shortest path problem. SIAM, pages 83–89.

[4] R. Floyd. (1962). Algorithm 97: Shortest Path. Communications of the ACM, pages 344–348.

[5] S. Warshall (1962). A theorem on boolean matrices. Journal of the ACM (JACM), (1).

[6] E. W. Dijkstra (1959). A note on two problems in connexion with graphs. Numerische Mathematik, pages 269–271.

[7] R. Bellman (1957). Dynamic Programming. Princeton University Press.

[8] R. Bellman (1958). On a routing problem. Quarterly of Applied Mathematics.

[9] Tim LaRocca, Khanh Thai, Robert Snyder, Richard Jai, Daniel Kultran, Owen Fordham, (2019), Secure Satellite Communication Digital IF CMOS Q -Band Transmitter and K -Band Receiver, IEEE Journal of Solid-State Circuits, Volume: 54, Issue: 5, pp: 1329 – 1338.

[10] S. Chiang, S. C. Chu, Y. C. Hsin and M. H. Wang (2006). Genetic Distance Measure for K-Modes Algorithm, International Journal of Innovative Computing, Information and Control ICIC,ISSN 1349- 4198, Volume 2, Number 1, pp.33-40.

[11] Hongmei. Wang, Ming. Hu and Wei. Xiao, (2010). A new public transportation data model and shortest-path algorithms, Informatics in Control Automation and Robotics (CAR) 2010 2nd International Asia Conference on, pp. 456-459, 6–7.

[12] Na Wang, Jian Li (2019). Shortest Path Routing With Risk Control for Compromised Wireless Sensor Networks, IEEE Access,Volume: 7,PP 19303 –19311.

[13] Pradumn Kumar Pandey,VenkataramanaBadarla (2020). Small-World Regular Networks for Communication, IEEE Transactions on Circuits and Systems II: Express Briefs, Volume: 67 (8), 1409 – 1413.

[14] Hussein Al-Zubaidy,Viktori Fodor,GyörgyDán,MarkusFlierl (2017). Reliable Video Streaming With Strict Play out Deadline in Multi hop Wireless Networks, IEEE Transactions on Multimedia,Volume: 19 (10),pp 2238 – 2251.

[15] Ahmad M. Khasawneh,OmprakashKaiwartya, Ala' Khalifeh;Laith M. Abualigah, Jaime Lloret (2020). Green Computing in Underwater Wireless Sensor Networks Pressure Centric Energy Modeling"IEEE Systems Journal,Volume: 14, Issue: 4,pp 4735 – 4745.

ANALYSING STRESS STRENGTH RELIABILITY OF LIFE TEST ON AEROSOL PARTICLES BY GOMPERTZ DISTRIBUTION USING NOVEL JOINT PROGRESSIVE CENSORING

Showkat Ahmad Lone

•

Department of Basic Sciences, College of Science and Theoretical Studies,
Saudi Electronic University, 11673, Saudi Arabia.
s.lone@seu.edu.sa

Abstract

System reliability has become a popular subject of study in engineering due to its wide range of potential applications. When a reliability practitioner aims to observe a specific number of failed units, a balanced case of joint progressive censoring scheme is proposed to improve the efficiency of an experiment. This paper investigates parametric inference for system reliability using a novel case of joint progressive censoring, with a specific focus on two independent Gompertz populations. The system reliability parameter is estimated using both likelihood and Bayesian inferential approaches. The Metropolis-Hastings algorithm is employed to compute Bayesian estimates under different loss functions. Asymptotic confidence intervals and Bayesian credible intervals are also derived. A thorough simulation study is conducted to evaluate the performance of the proposed methods across various sample sizes. Additionally, to demonstrate the practical utility of the approach, virus-containing aerosol particles (VCAP) lifetime data under two velocities are analyzed.

Keywords: Bayesian Estimates, Gompertz Populations, Likelihood Estimation, Loss Function, Stress-Strength Reliability, VCAP data.

1. Introduction

In recent years, the accuracy of estimation in practical experiments is greatly affected by sample size, and it may be impossible to conduct complete testing due to advancements in manufacturing design and technology because products are designed with high reliability and longer lifespan. Censoring techniques are frequently employed to reduce the time spent studying while simultaneously saving money. Type-I censoring and Type-II censoring are the most common ones. In the field of reliability tests, engineers prefer the progressive censoring scheme (ProgCeS) over the above-mentioned censoring schemes (CeS) due to the flexibility of this scheme in removing test items. The ProgCeS is an attractive and has received widespread attention, see, Mousa & Sagheer [1], Balakrishna [2], Huang & Wu [3], Lee and Seo [4] and the reference therein. Further, in industrial manufacturing and practical life, two or more populations need to perform life-test experiments. Therefore, a joint CeS is very useful to improve the efficiency of the comparative life experiment. Statistical inference under joint CeS discussed by different authors, see Rasouli and Balakrishnan [5], Mondal and Kundu [6], Asar and Belagh [7]. Also, for balance between total test time and number of failures need to statistical inference, balance case of joint CeS named BJProgCS is proposed by Mondal and Kundu [8].

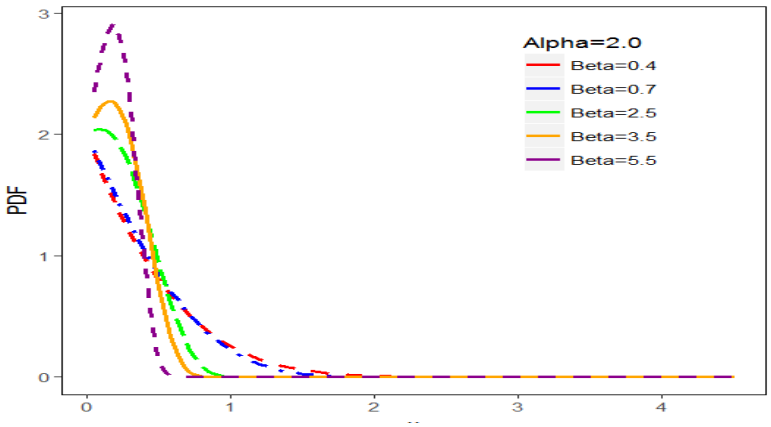


Figure 1: *The pdf plot of Gom Distribution*

Moreover, the Gompertz (Gom) distribution offers a flexible modeling tool for data exhibiting a wide range of shapes and is broadly used in numerous fields. The PDF, $f(.)$, and CDF $F(.)$ and hazard function $H(.)$, of the Gom distribution are given by:

$$f(x;\alpha,\beta) = \alpha \exp\left[\beta x - \frac{\alpha}{\beta}(e^{\beta x}-1)\right]; \quad x>0,\ \alpha>0,\ \beta>0 \tag{1}$$

$$F(x;\alpha,\beta) = 1-\exp\left[-\frac{\alpha}{\beta}(e^{\beta x}-1)\right], \tag{2}$$

and $H(t;\alpha,\beta) = \alpha e^{\beta t}$, respectively. In fact, the Gompertz PDF is unimodal or decreasing due to the parameter values (see Figure 1) . It is to be noticed that this distribution reduces to an exponential distribution, corresponding to $\alpha \to 0$. In the existing literature, statistical inferences on estimating unknown parameters of Gom have been provided by Shi and Wu [9], Wu et al. [10], Mazucheli et al. [11], Lee and Seo [12] and Asadi et al. [13].

Further, as the requirements of customers for product quality are continuously improved, the reliability model has become more important. Hence, how to evaluate reliability parameter is an important problem faced by system designers. In reliability studies, the life of a component with a random strength X and a random stress Y is described by the stress-strength model (SSReM). Suppose X and Y independently have Gom(α, β) and Gom(λ, β) respectively. Then, the reliability is derived as follows:

$$\Im = \int_0^\infty \alpha e^{\beta t - \frac{\alpha}{\beta}(e^{\beta t}-1)} e^{-\frac{\lambda}{\beta}(e^{\beta t}-1)}\, dt = \frac{\lambda}{\alpha+\lambda}. \tag{3}$$

The stay of the article is classified as: Based on BJProgCS, likelihood and Bayes investigations for SSReM are developed in Sections 2 and 3, respectively. Section 4 evaluates the estimators' performance via simulations. Also, the VCAP real datasets are conducted to show the performance of all diverse methods considered in this paper. Finally, in Section 5, we conclude the study with a brief discussion.

2. Sampling and Likelihood Function

This section will employ model description and likelihood function to estimate the unknown model parameters. Approximate confidence for reliability parameter will also be constructed.

Presume two samples of size m and n from Population-1 and Population-2. The total number of observed failures ($k < \min(n,m)$) and progressive CeS $R_1, R_2, \ldots, R_{k-1}$, when $\sum_{i=1}^{k-1}(1+R_i) <$

$\min(n, m)$ are the preassigned. After the first failure D_1 is observed, R_1 surviving units are randomly dropped from the remaining surviving units of Population-1 and $(R_1 + 1)$ surviving units are withdrawn from the surviving units of Population-2. The experiment is continual until the k^{th} failure occurs. To learn more about the specifics of the afore mentioned censoring method, one might look at Sultana et al. [14], Lone et al. [15 & 16].

Following the BJProgCS and based on the observed data (d, F), the likelihood function (LikF) can be expressed as $(T = (\alpha, \lambda, \beta))$:

$$\begin{aligned} L(\mathcal{T} \mid \text{data}) \propto \alpha^{k_1}\lambda^{k_2}\prod_{i=1}^{k-1} e^{\beta d_i} \times \prod_{i=1}^{k-1}\left(e^{-\frac{\alpha}{\beta}(e^{\beta d_i}-1)}\right)^{(R_i+1)}\left(e^{-\frac{\lambda}{\beta}(e^{\beta d_i}-1)}\right)^{(R_i+1)} \\ \times \left(e^{-\frac{\alpha}{\beta}(e^{\beta d_k}-1)}\right)^{(m-\sum_{i=1}^{k-1}(R_i+1))} \times \left(e^{-\frac{\lambda}{\beta}(e^{\beta d_k}-1)}\right)^{(n-\sum_{i=1}^{k-1}(R_i+1))} \\ \propto \alpha^{k_1}\lambda^{k_2}e^{\beta\sum_{i=1}^{k} d_i} \times e^{\sum_{i=1}^{k-1}(R_i+1)\vartheta_i(\alpha,\beta)+(m-\sum_{i=1}^{k-1}(R_i+1))\vartheta_k(\alpha,\lambda)} \times \\ e^{\sum_{i=1}^{k-1}(R_i+1)\tau_i(\lambda,\beta)+(n-\sum_{i=1}^{k-1}(R_i+1))\tau_k(\lambda,\beta)} \end{aligned} \tag{4}$$

Here,

$$\vartheta_i(\alpha,\beta) = -\frac{\alpha}{\beta}(e^{\beta d_i}-1), \vartheta_k(\alpha,\beta) = -\frac{\alpha}{\beta}(e^{\beta d_k}-1), \tau_i(\lambda,\beta) = -\frac{\lambda}{\beta}(e^{\beta d_i}-1), \tau_k(\lambda,\beta) = -\frac{\lambda}{\beta}(e^{\beta d_k}-1),$$

$$d = \{d_1, \ldots, d_k\}, k_1 = \sum_{i=1}^{k} F_i, k_2 = \sum_{i=1}^{k}(1 - F_i)$$

and

$$F_i = \begin{cases} 1, & \text{The failures } D_i \text{ are from } X \\ 0, & \text{The failures } D_i \text{ are from } Y \end{cases}$$

Subsequently, from (4), the log-likelihood becomes:

$$\begin{aligned} \log L \propto k_1 \ln\alpha + k_2 \ln\lambda + \beta\sum_{i=1}^{k} d_i + \sum_{i=1}^{k-1}(R_i+1)\vartheta_i(\alpha,\beta) + (m - \sum_{i=1}^{k-1}(R_i+1))\vartheta_k(\alpha,\beta) \\ + \sum_{i=1}^{k-1}(R_i+1)\tau_i(\lambda,\beta) + (n - \sum_{i=1}^{k-1}(R_i+1))\tau_k(\lambda,\beta). \end{aligned} \tag{5}$$

The likelihood equations are given by:

$$\frac{\partial \log L}{\partial\alpha} = \frac{k_1}{\alpha} - \frac{1}{\beta}\left[\sum_{i=1}^{k-1}(R_i+1)(e^{\beta d_i}-1) + (m - \sum_{i=1}^{k-1}(R_i+1))(e^{\beta d_k}-1)\right] = 0,$$

$$\frac{\partial \log L}{\partial\lambda} = \frac{k_2}{\lambda} - \frac{1}{\beta}\left[\sum_{i=1}^{k-1}(R_i+1)(e^{\beta d_i}-1) + (n - \sum_{i=1}^{k-1}(R_i+1))(e^{\beta d_k}-1)\right] = 0$$

$$\begin{aligned} \frac{\partial \log L}{\partial\beta} = \sum_{i=1}^{k} d_i + \frac{\alpha}{\beta}\left\{ \sum_{i=1}^{k-1}(R_i+1)\left[\frac{e^{\beta d_i}-1}{\beta} - d_i e^{\beta d_i}\right] + \left(m - \sum_{i=1}^{k-1}(R_i+1)\right)\left[\frac{e^{\beta d_k}-1}{\beta} - d_k e^{\beta d_k}\right] \right\} \\ + \frac{\lambda}{\beta}\left\{ \sum_{i=1}^{k-1}(R_i+1)\left[\frac{e^{\beta d_i}-1}{\beta} - d_i e^{\beta d_i}\right] + \left(n - \sum_{i=1}^{k-1}(R_i+1)\right)\left[\frac{e^{\beta d_k}-1}{\beta} - d_k e^{\beta d_k}\right] \right\}. \end{aligned}$$

Moreover, the $\log L$ is a concave for fixed β as a function of α and λ, which obtains the unique maximum at the point $(\hat{\alpha}(\beta), \hat{\lambda}(\beta))$, where $\hat{\alpha}(\beta)$ and $\hat{\lambda}(\beta)$ are the MLEs of α and λ. Due

to extremely complicated non-linear equations that cannot be solved analytically, the Newton-Raphson approach can be employed to solve the afore mentioned equations numerically.

Therefore, using the invariance property of the MLE, the maximum likelihood estimate of the SSReM parameter, denoted by $\hat{\Im}$ can be written as:

$$\hat{\Im} = \frac{\hat{\lambda}}{\hat{\alpha} + \hat{\lambda}}. \tag{6}$$

Now, in order to obtain the approximate confidence bounds (ApCB) of $\Im$, we use asymptotic normality property of MLEs. The variance-covariance of $\hat{T} = (\hat{\alpha}, \hat{\lambda}, \hat{\beta})$ can be evaluated from the Fisher matrix $I(T)$, which is presented as follows:

$$I(T) = \left[-\frac{\partial^2}{\partial\theta_i, \partial\theta_j} \log L \right],$$

For brevity, detailed derivations are not given. Utilizing the regularity condition, we have $\hat{I}m \sim N(\Im, v)$, (Rao et al. [17]). Where,

$$v = \left(\frac{\partial\Im}{\partial\alpha}\right)^2 I_{11}^{-1} + \left(\frac{\partial\Im}{\partial\lambda}\right)^2 I_{22}^{-1} + 2\left(\frac{\partial\Im}{\partial\alpha}\right)\left(\frac{\partial\Im}{\partial\lambda}\right) I_{12}^{-1} = \frac{\lambda^2}{(\alpha+\lambda)^4} I_{11}^{-1} + \frac{\alpha^2}{(\alpha+\lambda)^4} I_{22}^{-1} - \frac{2\alpha\lambda}{(\alpha+\lambda)^4} I_{12}^{-1}. \tag{7}$$

Here

$$I^{-1}(T) = \begin{bmatrix} \mathrm{Var}_{\hat{\alpha}} & \mathrm{Cov}_{\hat{\alpha},\hat{\beta}} & \mathrm{Cov}_{\hat{\alpha},\hat{\lambda}} \\ & \mathrm{Var}_{\hat{\lambda}} & \mathrm{Cov}_{\hat{\lambda},\hat{\beta}} \\ & & \mathrm{Var}_{\hat{\beta}} \end{bmatrix}$$

Thus, the $100(1-\gamma)$ % APCB of $\Im$ can be created by:

$$(\hat{\Im} - z_{\gamma/2}\hat{v}, \hat{\Im} + z_{\gamma/2}\hat{v}), \tag{8}$$

where z_γ is $z_{\gamma/2}$, the $100\gamma^{\text{th}}$ percentile of the standard normal distribution $N(0,1)$.

3. Bayesian Estimates (BayE)

The objective of this section is to compute BayE of $\Im$, as well as its related HPD bounds under BJProgCS. The BayE of $\Im$ is attained when all model parameters have independent gamma prior distributions. The joint posterior distribution (JoPD) of parameters is acquired through the Bayes principle, as expressed below:

$$\pi(T \mid \mathbf{data}) \propto \alpha^{k_1+a_1-1}\lambda^{k_2+a_2-1}\beta^{a_3-1}e^{-\alpha b_1-\lambda b_2-\beta(b_3-\sum_{i=1}^{k} d_i)} \times e^{\sum_{i=1}^{k-1}(R_i+1),\vartheta_i(\alpha,\beta)+(m-\sum_{i=1}^{k-1}(R_i+1))\vartheta_k(\alpha,\beta)+\sum_{i=1}^{k-1}(R_i+1)\tau_i(\lambda,\beta)+(n-\sum_{i=1}^{k-1}(R_i+1))\tau_k(\lambda,\beta)} \tag{9}$$

The Bayesian estimator of $\Im$ is defined as $\hat{\Im}_{SELF}$ and, $\hat{\Im}_{LLF}$ respectively, where it minimizes the symmetric (squared error loss function (SELF)) and asymmetric (Linex loss function (LLF)) as: $L_{\text{SELF}}(T, \hat{T}) = (\hat{T} - T)^2$,

$$L_{\text{LLF}}(T, \hat{T}) = e^{k(\hat{T}-T)} - k(\hat{T} - T) - 1; \quad k \neq 0$$

From (9), the conditional posterior distributions (CP) of α, λ and β are provided by:

$$\pi_1(\alpha \mid \lambda, \beta, \mathbf{data}) \propto \alpha^{k_1+a_1-1} \exp\left[-\alpha\left(b_1 + \sum_{i=1}^{k-1}(R_i+1)\left(\frac{e^{\beta d_i}-1}{\beta}\right) + \left(m - \sum_{i=1}^{k-1}(R_i+1)\right)\left(\frac{e^{\beta d_k}-1}{\beta}\right)\right)\right] \tag{10}$$

$$\pi_2(\lambda \mid \alpha, \beta, \mathbf{data}) \propto \lambda^{k_2+a_1-1} \exp\left[-\lambda\left(b_2 + \sum_{i=1}^{k-1}(R_i+1)\left(\frac{e^{\beta d_i}-1}{\beta}\right) + \left(n - \sum_{i=1}^{k-1}(R_i+1)\right)\left(\frac{e^{\beta d_k}-1}{\beta}\right)\right)\right] \tag{11}$$

and also,

$$\pi_3(\beta \mid \alpha, \lambda, \text{data}) \propto \beta^{a_3-1} \times e^{-\beta(b_3-\sum_{i=1}^{k} d_i)} \times e^{\sum_{i=1}^{k-1}(R_i+1)\,\vartheta_i(\alpha,\beta)+(m-\sum_{i=1}^{k-1}(R_i+1))\vartheta_k(\alpha,\beta)} \times e^{\sum_{i=1}^{k-1}(R_i+1)\,\tau_i(\lambda,\beta)+\left(n-\sum_{i=1}^{k-1}(R_i+1)\right)\tau_k(\lambda,\beta)}. \quad (12)$$

Notice that the CP distribution of β is very difficult to reduce analyticaly to some well-known distributions. We employ the Gibbs within the Metropolis–Hasting (GiMeHa) algorithm to BayE of $\Im$ (Metropolis et al. [18] and Hastings [19]). This is how the algorithm functions.

Step 1: Start with an initial parameter vector, $T^0 = (\hat{\alpha}_{\text{MLE}}, \hat{\beta}_{\text{MLE}}, \hat{\lambda}_{\text{MLE}})$ and then set $Q = 1$.
Step 2: Draw β^Q using the GiMeHa technique with a normal proposal density.
Step 3: For a given β^Q, generate α^Q from
Gamma $\left(k_1 + a_1,\ (b_1 + \sum_{i=1}^{k-1}(R_i+1)(\frac{e^{\beta d_i}-1}{\beta}) + (m - \sum_{i=1}^{k-1}(R_i+1))(\frac{e^{\beta d_k}-1}{\beta}))\right)$.
Step 4: For a given β^Q, generate λ^Q from
Gamma $\left(k_2 + a_2, (b_2 + \sum_{i=1}^{k-1}(R_i+1)(\frac{e^{\beta d_i}-1}{\beta}) + (n - \sum_{i=1}^{k-1}(R_i+1))(\frac{e^{\beta d_k}-1}{\beta}))\right)$.
Step 5: Find $\Im^{(Q)} = \frac{\lambda^{(Q)}}{\alpha^{(Q)}+\lambda^{(Q)}}$.
Step 6: Set $Q = Q + 1$.
Step 7: Repeat the iteration times to obtain $\Im^{(1)}, \Im^{(2)}, \ldots, \Im^{()}$.
Step 8: Compute the Bayes estimates under the SELF and LLF loss functions as follows:

$$\hat{\Im}_{SELF} = \frac{1}{-_0} \sum_{i=_0+1} \Im^{(Q)}; \hat{\Re}_{LLF} = -\frac{1}{k} \ln \left[\frac{1}{-_0} \sum_{i=_0+1} e^{-} k\Im^{(Q)} \right];$$

$_0$ is the burn-in period.
Step 10: Find the $100(1-\gamma)\%$ Bayesian Highest Posterior Density (HPD) interval for $(\Im)$ by sorting its simulated MCMC iterations as $\Im^{(Q)}; i = 1, \ldots, .$ Then, the HPD interval is specified as: $[\hat{\Im}_{((\frac{\gamma}{2}))}, \hat{\Im}_{((1-\frac{\gamma}{2}))}]$.

4. Simulation Studies and Real Data Analysis

4.1. Simulation Studies and Discussions

This section offers a simulation analysis based on the Monte-Carlo simulation approach to evaluate the performance of the approaches utilizing various choices of n, m and $R_i; i = 1, 2, ..., k-1$. The efficiency of the estimators is measured in terms of MSEs, whereas the efficiency of the ApCBs is measured in terms of their lengths and coverage percentages (CoPs). The Monte Carlo simulation study has been performed with the initial guess of the parameters as α=2, λ=1.5 and β=1. In the Bayesian technique, both non-informative (NonI) and informative (I) priors are taken. For prior I, we take the values of hyper-parameters (HP) as $a_1 = 2$, $a_2 = 1.5$, $a_3 = 1$, $b_i = 1, i = 1, 2, 3$. Notice that the selection of HP values under prior I is considered in such a way that the prior means always remain sufficiently close to the true parameter values. From Bayesian method, posterior samples are drawn from the JoPD by using the GiMeHa algorithm. To mitigate dependency on initial values, we generate 10000 sample sizes and discard 5000 as burn-in samples.

We compare the performance of the maximum likelihood, Bayesian estimates, and associated 95% APCB, HPD bounds respectively, in terms of the MSEs and the average length of intervals and CoPs. The following conclusions may well be drawn from the results shown in Table 1 and Table 2:

- All acquired points as well as interval results of $\Im$ behaved fine.
- The MSEs of $\Im$ are dropping as a result of increasing values of the sample size. So, the estimation accuracy is improved.
- The results reveal that the estimates of the reliability parameter under different CeS display diminishing MSE and bound length as observed failure times m increase.

- With an increase in k, MSEs and the average lengths are getting low with fixed values of n and m.
- The ApCBs and HPD intervals are quite precise, and the estimated values are always within these ranges.
- Left censoring scheme demonstrates less MSEs according to performance indicators in the majority of scenarios.
- Under the LLF and GiMeHa algorithm, the Bayes estimates show smaller MSEs.
- Moreover, as expected, the accuracy of Bayesian estimates under I is superior to that under Non- I , because the former combines the informative prior of unknown model parameters and the data.
- The CoPs of various bounds are close to 95% of the nominal level. This holds good under various sampling schemes.
- The length of all bounds becomes narrower as the values of n and k increase, with fixed other values.
- To summarize, we advise estimating the system reliability parameter via the GiMeHa sampler in the presence of data generated through the proposed mechanism.

4.2. Illustrative Data Analysis

To illustrate the usefulness of the suggested techniques, real VCAP data sets from Asadi et al. [20] has been considered in this section. The data consists of two sets of VCAP data under two simultaneous air velocities, with sample sizes of 19 and 15. Before further development, we demand to verify how well the Gom distribution model fits the real data set. The KS statistics and the related p-values are shown in Table 3. This suggests that the Gom distribution is a reasonable choice to interpret these datasets.

Table 1: *The MSEs, ApCBs, HPD and CoPs of the SSReM parameter under different CeSs with $n = m = 20$.*

k	$\to k = 12$	$k = 12$	$k = 12$	$k = 14$	$k = 14$	$k = 14$
CeS	$\to R = (0_{(5)}, 8, 0)$	$R = (8, 0_{(10)})$	$R = (0_{(10)}, 8)$	$R = (6, 0_{(6)}, 6)$	$R = (6, 0_{(12)})$	$R = (0_{(12)}, 6)$
$\hat{\Im}_{MLE}$	0.022468	0.019875	0.024278	0.019870	0.017443	0.020936
$\hat{\Im}_{Bayes_{SELF-}}$	0.019205	0.016799	0.021589	0.016745	0.014988	0.017654
$\hat{\Im}_{Bayes_{LLF-I}}$	0.019112	0.016768	0.021532	0.016711	0.014981	0.017650
$\hat{\Im}_{Bayes_{SELF-}}$	0.021875	0.019136	0.023885	0.019106	0.016790	0.019078
$\hat{\Im}_{Bayes_{LLF-N}}$	0.021864	0.019109	0.023793	0.019086	0.016699	0.019033
$\hat{\Im}_{ApCB}$	0.503243	0.489324	0.513894	0.487664	0.478450	0.489920
CoP_{ApCB}	94.0	94.2	93.7	94.3	95.9	96.2
$\hat{\Im}_{HPD}$	0.445680	0.419972	0.448091	0.425233	0.403396	0.428989
CoP_{HPD}	94.5	95.6	96.0	96.1	95.3	94.0

Table 2: *The MSEs, ApCBs, HPD and CoPs of the SSReM parameter under different CeSs with $n = m = 60$.*

k	$\to k = 45$	$k = 45$	$k = 45$	$k = 50$	$k = 50$	$k = 50$
CeS	$\to R = (0_{(5)}, 8, 0)$	$R = (8, 0_{(10)})$	$R = (0_{(10)}, 8)$	$R = (6, 0_{(6)}, 6)$	$R = (6, 0_{(12)})$	$R = (0_{(12)}, 6)$
$\hat{\Im}_{MLE}$	0.019864	0.017645	0.019977	0.018543	0.015890	0.018995
$\hat{\Im}_{Bayes_{SELF-}}$	0.015894	0.015431	0.016008	0.013993	0.013214	0.014107
$\hat{\Im}_{Bayes_{LLF-I}}$	0.015743	0.015401	0.015897	0.013974	0.013199	0.014094
$\hat{\Im}_{Bayes_{SELF-}}$	0.019245	0.016760	0.019562	0.017966	0.015480	0.018329
$\hat{\Im}_{Bayes_{LLF-N}}$	0.019231	0.016751	0.019523	0.017954	0.015469	0.018321
$\hat{\Im}_{ApCB}$	0.473425	0.457811	0.478442	0.457843	0.442895	0.45985
CoP_{ApCB}	95.9	94.4	96.4	94.1	94.8	96.2
$\hat{\Im}_{HPD}$	0.426842	0.409996	0.428691	0.403172	0.396980	0.406641
CoP_{HPD}	95.4	95.3	93.9	94.6	94.7	95.6

Table 3: *The data sets of VCAP data.*

Data Sets	$\mathbf{MLE_s}$	kS	p−value
Data Set I	Shape=2.5746, Scale=0.06665	0.1331	0.953
Data Set II	Shape=8.0947, Scale=3.028×10^{-4}	0.0909	0.997

Further, the empirical CDF (EmCDF) and probability-probability (P-P) plots along with associated fitted Gom distributions are provided in Figure 2 and Figure 3, respectively. The likelihood ratio test is then used to determine whether the scale parameters can be assumed to have the same value, and the $p - value$ is 0.8692. Therefore, we accept the null hypothesis. We further calculate the point and the interval estimates using the NR method, and due to the non-availability of prior information, the BayEs are calculated using Non$I$ priors. All the results are reported in Table 4. It has been noticed from Table 4 that the MLEs and BayE are extremely comparable. The HPD bounds perform better than ApCBs in terms of width, which yields that the results are consistent with the previously simulated results.

The trace plot of reliability model is displayed in Figure 4, where the number of iterations is 14,000, and that of burn-in is 5,000. Figure 4 shows simulation number generated by MCMC method based on $k = 15$, $R = (0_{(14)}, 4)$. Reasonably satisfactory behavior is observed from this plot.

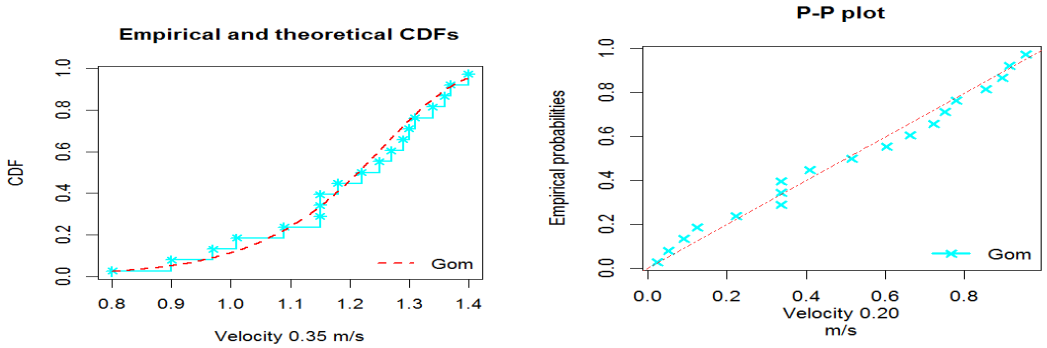


Figure 2: *The EmCDF and P-P plots for data set I.*

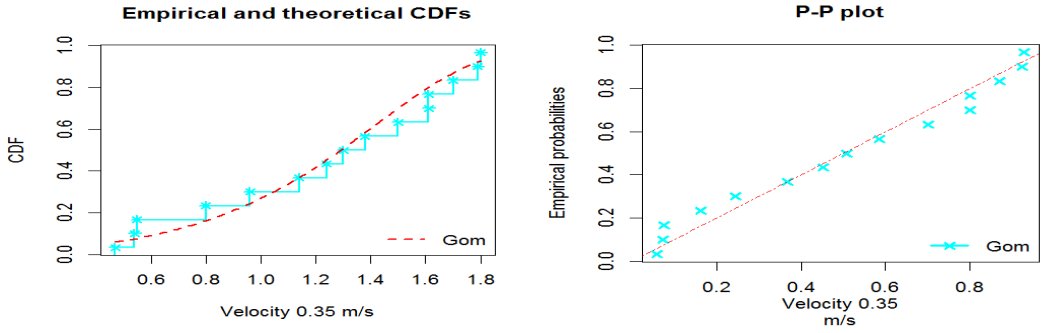


Figure 3: *The EmCDF and P-P plots for data set II.*

Table 4: *Different estimates of the SSReM parameter for VCMD data*

k	Censoring	$\hat{\Im}_{MLE}$	$\hat{\Im}_{Bayes}$	$\text{ApCB}_{\Im}$	$\text{HPD}_{\Im}$
$k = 15$	$R = (0_{(14)}, 4)$	0.58965	0.59458	1.43280	0.89643
$k = 15$	$R = (4, 0_{(14)})$	0.59044	0.59874	1.32182	0.82364
$k = 10$	$R = (0_{(9)}, 5)$	0.61320	0.62018	1.46115	0.91536
$k = 10$	$R = (5, 0_{(9)})$	0.59906	0.60557	1.45219	0.89985

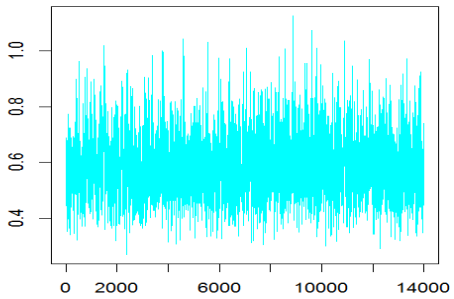


Figure 4: *Simulation MCMC generated number of the model parameter*

5. Conclusion

The problem of statistical inferences of comparative populations in competing duration needs to put a joint sample of units under test. Therefore, we looked at statistical inference of SSReM under BJProgCS.

For deriving the estimates of the SSReM parameter, we considered frequentist and Bayesian approaches.

Since MLEs of the model cannot be derived explicitly, Newton's iterative method has been implemented for this purpose. For the Bayesian approach, we suggested Non$I$ and I priors and obtained the posterior distribution, which turned out to be intractable, so we proposed the GiMeHa technique to generate samples from the CP distributions of unknown parameters. Different interval estimates of Iare also computed. The effectiveness of the recommended procedures is compared through simulation studies and VCAP real data analysis. Comparing the joint CeS with progressive CeS and determining the optimal scheme may potentially be studied in the future.

References

[1] Mousa M. and Sagheer S. (2006). Statistical inference for the Rayleigh model based on progressively type-II censored data. Statistics, 40(2), 149-157.

[2] Balakrishnan N. (2007). Progressive censoring methodology: An appraisal (with discussion). Test, 16: 211-296

[3] Huang SR. and Wu SJ. (2012). Bayesian estimation and prediction for Weibull model with progressive censoring. Journal of Statistical Computation & Simulation. 82(11), 1607-1620.

[4] Lee K, Seo J-I (2020). Different Approaches to Estimation of the Gompertz Distribution under the Progressive Type-II Censoring Scheme. Journal of Probability and Statistics. 3541946:1-7.

[5] Rasouli A, Balakrishnan N (2010). Exact likelihood inference for two exponential populations under joint progressive type-ii censoring. Communications in Statistics-Theoryand Methods. 39(12):2172–2191.
[6] Mondal S, Kundu D (2020). Inference on Weibull parameters under a balanced two-sample type ii progressive censoring scheme. Quality and Reliability Engineering International. 36(1):1–17.
[7] Asar Y, Belaghi RA. (2022). Inference for two Lomax populations under joint type-II censoring. Communication Statististics- Simulation and Computation. 51:6808–6825.
[8] Mondal, S. and Kundu, D. (2019). A new two sample type-ii progressive censoring scheme. Communications in Statistics-Theory and Methods, 48(10):2602–2618.
[9] Shi Y, Wu M (2016). Statistical analysis of dependent competing risks model from Gompertz distribution under progressively hybrid censoring. Springer Plus, 5(1): 1-14.
[10] Wu M, Shi Y, Zhang C (2017). Statistical analysis of dependent competing risks model in accelerated life testing under progressively hybrid censoring using copula function. Communications in Statistics- Simulation and Computation. 46(5): 4004-4017.
[11] Mazucheli J, Menezes AF, Dey S (2019). Unit-Gompertz distribution with applications. Statistica. 79(1): 25-43.
[12] Saini S, Chaturvedi A, Garg R (2021). Estimation of stress–strength reliability for generalized Maxwell failure distribution under progressive first failure censoring. Journal of Statistical Computation and Simulation. 7:1366-1393.
[13] Asadi S, Panahi H (2022). Estimation of stress–strength reliability based on censored data and its evaluation for coating processes. Quality Technology & Quantitative Management. 19:379-401.
[14] Sultana F, Cetinkaya C, Kundu D (2024). Estimation of the stress-strength parameter under two-sample balanced progressive censoring scheme. Journal of Statistical Computation and Simulation.
[15] Lone SA, Panahi H, Anwar S, Shahab S (2024). Inference of Reliability Model with Burr Type XII Distribution under Two Sample Balanced Progressive Censored Samples. Physica Scripta. 99 025019.
[16] Lone SA, Panahi H, Anwar S, Shahab S (2023). Estimations and optimal censoring schemes for the unified progressive hybrid gamma-mixed Rayleigh distribution. Electronic Research Archive. 31(8): 4729-4752.
[17] Rao GS, Kantam RRL, Rosaiah K, Pratapa Reddy, J. (2013). Estimation of stress–strength reliability from inverse Rayleigh distribution. Journal of Industrial and Production Engineering. 30(4):256–263.
[18] Metropolis N, Rosenbluth AW, Rosenbluth MN, Teller AH, Teller E (1953). Equations of state calculations by fast computing machines. Journal of Chemical Physics. 21:1087-1092.
[19] Hastings WK. Monte Carlo sampling methods using Markov chains and their applications. Biometrika. 57(1):97-109.
[20] Asadi S, Panahi H, Swarup C, Lone SA (2022). Inference on Adaptive Progressive Hybrid Censored Accelerated Life Test for Gompertz Distribution and Its Evaluation for Virus-containing Micro Droplets Data. Alexandria Engineering Journal. 61(12):10071-10084.

A NEW COUNT DATA PROBABILITY MODEL: PROPERTIES AND APPLICATIONS

Morifat[1], Bilal Ahmad Para[2,*]

•

[1,2]Department of Mathematical Sciences, Islamic University of Science and Technology, Kashmir, India

[1]morifat13@gmail.com, [2,*]Corresponding author: parabilal@gmail.com

Abstract

In the field of count data analysis, over-dispersion poses significant challenges, often limiting the effectiveness of traditional Poisson model. To address this limitation, we propose a novel two parameter distribution as an extension of Poisson distribution namely two-Parameter Poisson Garima Distribution (TPPGD). This distribution enhances modeling flexibility for over-dispersed data, offering a superior fit for real-world datasets. In this paper we derive the theoretical properties of TPPGD, including its probability mass function, cumulative distribution function and different statistical properties. Parameter estimation has been done using the maximum likelihood method and the moment method. Finally, the validity of the proposed model is checked using different real world data sets.

Keywords: Poisson distribution, Two Parameter Garima distribution, Compounding, Count data.

1. Introduction

Numerous probability models are acquired by researchers in order to analyze a wide range of data from different industries, including engineering, agriculture, transportation, medical, and other sectors. Lots of well-known techniques are employed to serve the purpose of constructing new probability distributions. Discretization, the T-X family, and compounding are a few well-known methods that offer a very effective means of extending popular parametric families of distributions to match data sets that are not well-fitted by classical distributions. In statistics, compounding technique plays an important role in discussing complex phenomena by integrating multiple distributions to model real world data effectively. The compounding technique originated in the early 20th century and the main figures in advancing use of compounding distributions were Greenwood & Udny Yule [5] who introduced concepts like negative binomial distribution in the 20th century. The negative binomial arises as a compounding distribution when a Poisson variable is mixed with a gamma-distributed parameter to model over-dispersion in count data. Compounding involves combining two or more probability distributions, where one distribution is considered conditional on the parameters of another. If the mean of Poisson follows inverse Gaussian, the resulting distribution is Poisson inverse Gaussian (Holla [6]). Despite being extensively utilized across all domains, these models are not always able to effectively characterize the relationships between variables and cannot handle all forms of count data. In this context, new models are created to provide better outcomes and serve as substitutes for traditional count models.

Sankaran [7] obtained the compound Poisson distribution by combining the Poisson distribution with the distribution attributed to Lindley. A limiting version of the generalized negative binomial distribution is derived by Cousul & Jain [2] which is a new generalization of the Poisson distribution. Poisson inverse Gaussian regression proposed by Dean, Lawless & Willmot [3] is another Poisson mixing model that has been presented to explain discrete data that is overly dispersed.

Gerstenkorn [4] proposed a compound of the generalized negative binomial distribution with the generalized beta distribution. Sujatha distribution was studied by Shanker [11] while a Poisson mixture of Sujatha distribution was introduced by Shanker et al. [10]. Sen et al. [8] introduced the two parameter X-gamma distribution while a two-parameter Lindley Distribution with application was proposed by Altun et al. [1]. Shanker et al. [13] studied a Poisson mixture of a new two-parameter Sujatha distribution. Shanker [9] introduced Garima distribution. Shanker et al. [12] proposed a Poisson mixture of Garima distribution named, Poisson Garima distribution (PGD). We now present a novel discrete count data model in this paper by combining Poisson distribution with two parameter Garima distribution, since a more adaptable approach for statistical data analysis is required.

The rest of this paper is structured as follows. In section 1, the two-parameter Poisson Garima Distribution is demonstrated. The various statistical properties of distribution such as the moments, skewness, kurtosis, moment generating function, probability generating function, order statistics, etc are summarized in Section 2. Parameter estimation has been done using maximum likelihood (ML) method and moment method in Section 3. Section 4 deals with the applicability of two parameter Poisson Garima distribution in real life data which is illustrated by three real-life data sets.

1.1 Definition of Proposed Model Two Parameter Poisson Garima Distribution

Consider a random variable $X/\lambda \sim P(\lambda)$, where λ is itself a random variable following two parameter Garima distribution with parameters α and θ. Here two parameter Garima distribution is itself a mixture of $Exp(\theta)$ and $Gamma(2,\theta)$ with mixing proportion $\frac{\alpha\theta+1}{\alpha\theta+2}$ and its probability density function is given by

$$h(x;\theta,\alpha)=\frac{\theta e^{-\theta x}}{\alpha\theta+2}(\alpha\theta+\theta x+1);\qquad x>0\ ;\ \theta>0,\ \alpha>0\,. \tag{1}$$

Then determining the distribution that results from marginalizing over λ will be known as a compound of Poisson distribution with that of two parameter Garima distribution, which has been denoted by TPPGD$(X;\theta,\alpha)$. If $\alpha=1$, the distribution reduces to Garima distribution [9].

Theorem 1: The probability mass function of a two parameter Poisson Garima distribution is given as:

$$P(X=x)=\frac{\theta}{(1+\theta)^{x+2}(\alpha\theta+2)}\left(\theta^2\alpha+\theta\alpha+\theta\ x+2\theta+1\right);\quad x=1,2,3,...\ ;\ \alpha,\theta>0 \tag{2}$$

Proof: The PMF of two parameter Poisson Garima distribution, i.e., TPPGD$(X;\theta,\alpha)$ can be obtained by

$g(x\mid\lambda)=\frac{e^{-\lambda}\lambda^x}{x!}$; $x=0,1,2,3,...$; $\lambda>0$, when its parameter λ follows two parameter Garima distribution with pdf,

$$h(\lambda;\theta,\alpha)=\frac{\theta}{\alpha\theta+2}(\alpha\theta+\theta\lambda+1)e^{-\theta\lambda} \quad ;\lambda>0,\ \theta>0,\ \alpha>0\,. \tag{3}$$

We have, $P(X=x)=\int_0^\infty g(x\mid\lambda)\,h(\lambda;\theta,\alpha)d\lambda$

$$P(X=x)=\frac{\theta}{x!(\alpha\theta+2)}\left(\alpha\theta\int_0^\infty e^{-\lambda(1+\theta)}\lambda^x d\lambda+\theta\int_0^\infty e^{-\lambda(1+\theta)}\lambda^{x+1}d\lambda+\int_0^\infty e^{-\lambda(1+\theta)}\lambda^x d\lambda\right) \tag{4}$$

$$P(X=x)=\frac{\theta}{(1+\theta)^{x+2}(\alpha\theta+2)}\left(\theta^2\alpha+\theta\alpha+\theta x+2\theta+1\right); \qquad x=0,1,2,3,\ldots;\theta>0,\alpha>0\,. \tag{5}$$

Which is the required PMF of TPPGD $(X;\theta,\alpha)$

If $\alpha=1$, the distribution reduces to Poisson Garima distribution [12].

Figure 1 exhibits the PMF plots of the proposed model for different values of the parameters θ and α.

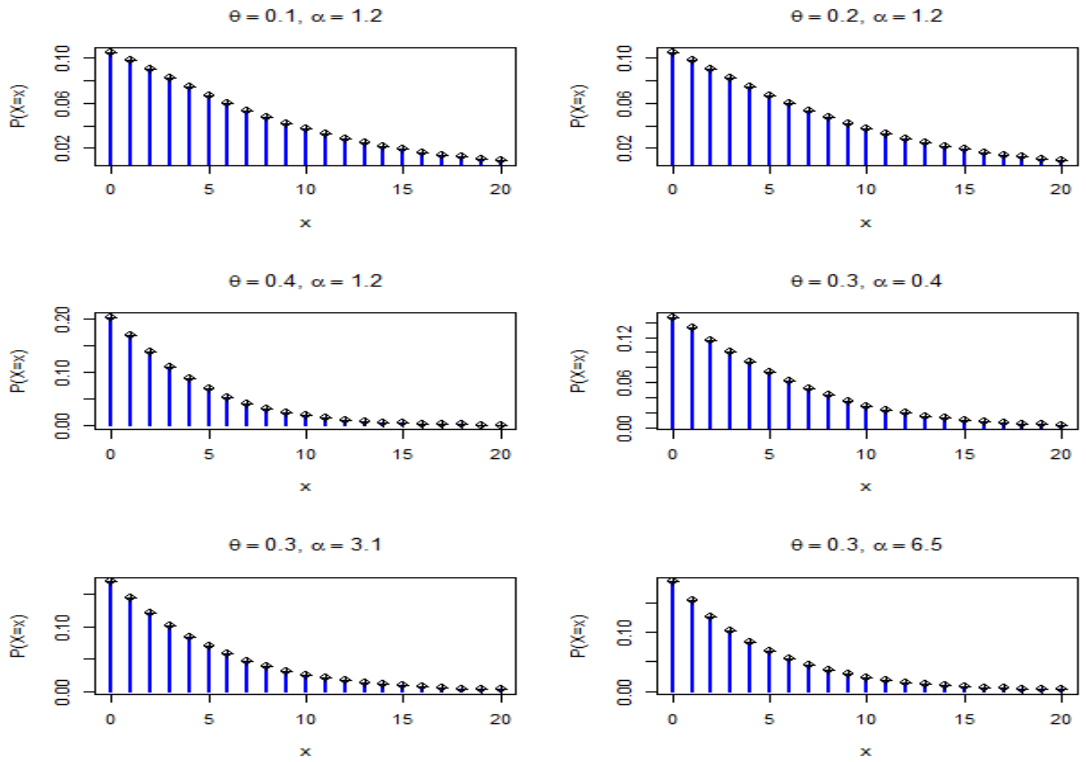


Figure 1: *PMF plots of two parameter Poisson Garima distribution.*

The CDF of two parameter Poisson Garima distribution is obtained as:

$$F(x)=\sum_{x=0}^{\infty}\frac{\theta}{(1+\theta)^{x+2}(\alpha\theta+2)}\left(\theta^2\alpha+\theta\alpha+\theta x+2\theta+1\right) \tag{6}$$

$$F(x)=\frac{1}{(1+\theta)^{x+2}(\alpha\theta+2)}\left[-2-\theta x-3\theta-\theta\alpha-\theta^2\alpha+(1+\theta)^{2+x}(\theta\alpha+2)\right]. \tag{7}$$

Figure 2 exhibits the CDF plots of the proposed model for different values of the parameters θ and α.

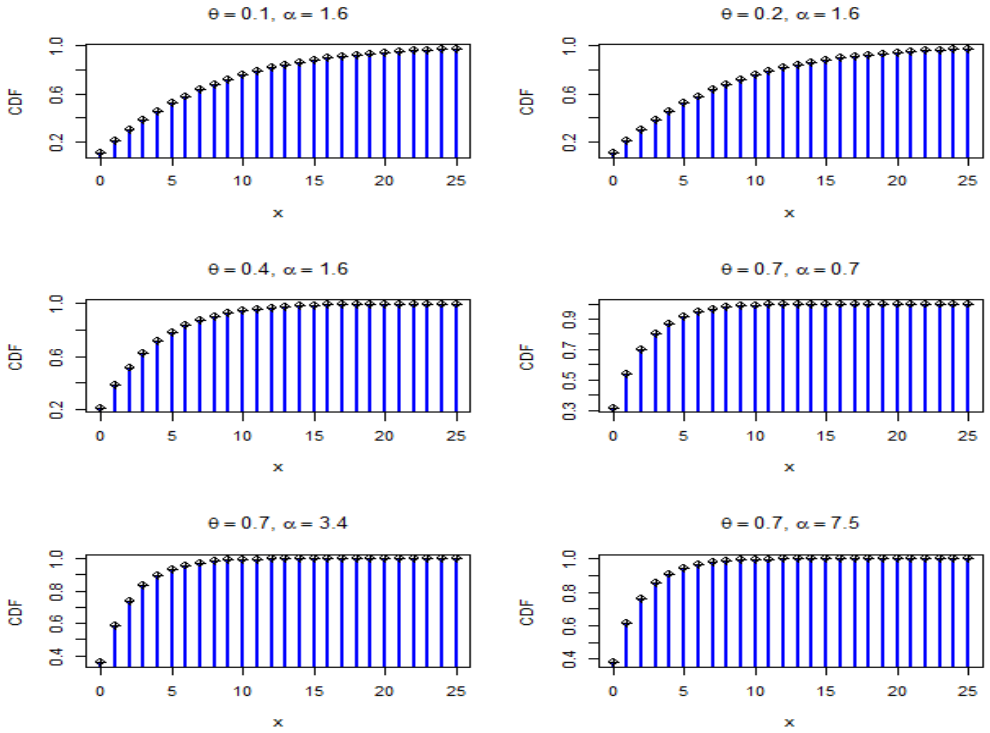


Figure 2: *CDF plots of two parameter Poisson Garima distribution.*

2. Statistical Properties of TPPGD

In this section, we will evaluate various properties of the two parameter Poisson Garima distribution. These include moments, index of dispersion, moment generating function and probability generating function, order statistics, and survival measures.

2.1 Moments

Using Eq. (2), the r[th] factorial moment about origin of the TPPGD $(X;\theta,\alpha)$ can be obtained as

$$\mu'_{(r)} = E[E(x^{(r)} \mid \lambda)] \quad , \text{ where } x^{(r)} = x(x-1)(x-2)...(x-r+1)$$

$$\mu'_{(r)} = \int_0^\infty \left[\sum_0^\infty x^r \frac{e^{-\lambda}\lambda^x}{x!}\right] \frac{\theta}{\alpha\theta+2}(\alpha\theta+\theta\lambda+1)e^{-\theta\lambda}\, d\lambda \tag{8}$$

$$\mu'_{(r)} = \frac{\theta}{\alpha\theta+2}\int_0^\infty \left[\lambda^r\left(\sum_{x=r}^\infty \frac{e^{-\lambda}\lambda^{x-r}}{(x-r)!}\right)\right](\alpha\theta+\theta\lambda+1)e^{-\theta\lambda}\, d\lambda \tag{9}$$

Taking $u = x - r$, we get

$$\mu'_{(r)} = \frac{\theta}{\alpha\theta+2}\int_0^\infty \left[\lambda^r\left(\sum_{u=0}^\infty \frac{e^{-\lambda}\lambda^u}{u!}\right)\right](\alpha\theta+\theta\lambda+1)e^{-\theta\lambda}\, d\lambda \tag{10}$$

$$\mu'_{(r)} = \frac{\theta}{\alpha\theta+2}\left(\theta\alpha\int_0^\infty \lambda^r e^{\theta\lambda}d\lambda + \theta\int_0^\infty \lambda^{r+1}e^{-\theta\lambda}d\lambda + \int_0^\infty \lambda^r e^{\theta\lambda}d\lambda\right) \tag{11}$$

$$\mu'_{(r)} = \frac{r!}{\alpha\theta+2}\left[\frac{\alpha\theta+(r+2)}{\theta^r}\right] \tag{12}$$

Taking r=1, 2, 3, 4 in Eq. (12), the first four factorial moments about origin of TPPGD can be obtained as

$$\mu'_{(1)} = \frac{\alpha\theta + 3}{\theta(\alpha\theta + 2)} \tag{13}$$

$$\mu'_{(2)} = \frac{2(\alpha\theta + 4)}{\theta^2(\alpha\theta + 2)} \tag{14}$$

$$\mu'_{(3)} = \frac{6(\alpha\theta + 5)}{\theta^3(\alpha\theta + 2)} \tag{15}$$

$$\mu'_{(4)} = \frac{24(\alpha\theta + 6)}{\theta^4(\alpha\theta + 2)} \tag{16}$$

The first four moments about origin, using the relationship between factorial moments about origin and the moments about origin of TPPGD $(X;\theta,\alpha)$.

$$\mu'_1 = \frac{\alpha\theta + 3}{\theta(\alpha\theta + 2)} \tag{17}$$

$$\mu'_2 = \frac{\alpha\theta^2 + 2\alpha\theta + 3\theta + 8}{\theta^2(\alpha\theta + 2)} \tag{18}$$

$$\mu'_3 = \frac{\alpha\theta^3 + 6\alpha\theta^2 + 3\theta^2 + 6\alpha\theta + 24\theta + 30}{\theta^3(\alpha\theta + 2)} \tag{19}$$

$$\mu'_3 = \frac{\alpha\theta^4 + 14\alpha\theta^3 + 36\alpha\theta^2 + 56\theta^2 + 3\theta^3 + 24\alpha\theta + 180\theta + 144}{\theta^3(\alpha\theta + 2)} \tag{20}$$

Mean, variance and index of dispersion of the proposed model are given by

$$\text{Mean} = \mu'_1 = \frac{\alpha\theta + 3}{\theta(\alpha\theta + 2)} \tag{21}$$

$$\text{Variance} = \mu_2 = \frac{\alpha^2\theta^3 + \alpha^2\theta^2 + 5\alpha\theta^2 + 6\alpha\theta + 6\theta + 7}{\theta^2(\alpha\theta + 2)^2} \tag{22}$$

$$\text{Index of dispersion} = 1 + \frac{\alpha^2\theta^2 + 6\alpha\theta + 7}{\theta(\alpha\theta + 2)(\alpha\theta + 3)} \tag{23}$$

The corresponding kurtosis and skewness were obtained as follows:

$$K_s = \frac{\mu_4}{(\mu_2)^2} = \frac{\left(\begin{array}{l}\alpha^4\theta^7 + 9\alpha^4\theta^4 + 402\alpha^2\theta^2 + 108\alpha^3\theta^3 + 10\alpha^4\theta^6 + 18\alpha^4\theta^5 + 198\alpha^3\theta^4 + 100\alpha^3\theta^5 + 9\alpha^3\theta^6 + \\ 356\alpha^2\theta^4 + 30\alpha^2\theta^5 + 726\alpha^2\theta^3 + 544\alpha\theta^3 + 44\alpha\theta^4 + 314\alpha^4\theta^7 + 612\alpha\theta + 304\theta^2 + 24\theta^3 + 612\theta + 333\end{array}\right)}{\theta^4(\alpha\theta + 2)^4}$$

$$S_k = \frac{\mu_3}{(\mu_2)^{3/2}} = \frac{\left(\begin{array}{l}\alpha^3\theta^5 + 3\alpha^3\theta^4 + 24\alpha^2\theta^3 + 7\alpha^2\theta^4 + 2\alpha^3\theta^3 + 18\alpha^2\theta^2 + \\ 57\alpha\theta^2 + 16\alpha\theta^3 + 12\theta^2 + 42\alpha\theta + 42\theta + 30\end{array}\right)}{\left(\alpha^2\theta^3 + \alpha^2\theta^2 + 5\alpha\theta^2 + 6\alpha\theta + 6\theta + 7\right)^{\frac{3}{2}}} \tag{24}$$

2.2 Probability Generating Function (pgf) and Moment Generating Function (mgf)

We derive moment generating function and probability generating function of TPPGD in this sub section.

Theorem 2: If X follows TPPGD $(X;\theta,\alpha)$, then the probability generating function $P_X(t)$ has the following form

$$P_X(t) = \frac{\theta}{(\alpha\theta + 2)(\theta + 1)}\left[\frac{\theta t}{(1 + \theta - t)^2} + \frac{\left(\theta^2\alpha + \theta\alpha + 2\theta + 1\right)}{(1 + \theta - t)}\right] \tag{25}$$

Proof: The definition of probability generating function is given by

$$P_X(t)=\sum_{x=o}^{\infty}t^x\left[\frac{\theta}{(\alpha\theta+2)(1+\theta)^{x+2}}\left(\theta^2\alpha+\theta\alpha+\theta x+2\theta+1\right)\right] \tag{26}$$

$$P_X(t)=\frac{\theta}{(\alpha\theta+2)(1+\theta)^2}\left[\theta\sum_{x=0}^{\infty}x\left(\frac{t}{1+\theta}\right)^x+\theta^2\alpha\sum_{x=0}^{\infty}\left(\frac{t}{1+\theta}\right)^x+\theta\alpha\sum_{x=0}^{\infty}\left(\frac{t}{1+\theta}\right)^x+2\theta\sum_{x=0}^{\infty}\left(\frac{t}{1+\theta}\right)^x\sum_{x=0}^{\infty}\left(\frac{t}{1+\theta}\right)^x+...\right]$$

$$P_X(t)=\frac{\theta}{(\alpha\theta+2)(1+\theta)^2}\left[\frac{\theta(\theta+1)t}{(\theta+1-t)^2}+\frac{\left(\theta^2\alpha+\theta\alpha+2\theta+1\right)(\theta+1)}{(\theta+1-t)}\right] \tag{27}$$

$$P_X(t)=\frac{\theta}{(\alpha\theta+2)(1+\theta)}\left[\frac{\theta t}{(\theta+1-t)^2}+\frac{\theta^2\alpha+\theta\alpha+2\theta+1}{(\theta+1-t)}\right] \tag{28}$$

Which is the required pgf of TPPGD$(X;\theta,\alpha)$.

Theorem 3: If X follows TPPGD$(X;\theta,\alpha)$, then the moment generating function has the following form

$$M_x(t)=\frac{\theta}{(1+\theta)(\alpha\theta+2)}\left[\frac{\theta e^t}{\left(\theta+1-e^t\right)^2}+\frac{\theta^2\alpha+\theta\alpha+2\theta+1}{\left(\theta+1-e^t\right)}\right] \tag{29}$$

Proof: The definition of the moment generating function given by

$$M_X(t)=\sum_{x=0}^{\infty}e^{tx}\left[\frac{\theta}{(1+\theta)^{x+2}(\alpha\theta+2)}\left(\theta^2\alpha+\theta\alpha+\theta x+2\theta+1\right)\right] \tag{30}$$

$$M_x(t)=\frac{\theta}{(1+\theta)^2(\alpha\theta+2)}\left[\frac{\theta(\theta+1)e^t}{\left(\theta+1-e^t\right)^2}+\frac{\left(\theta^2\alpha+\theta\alpha+2\theta+1\right)(\theta+1)}{\left(\theta+1-e^t\right)}\right] \tag{31}$$

$$M_x(t)=\frac{\theta}{(1+\theta)(\alpha\theta+2)}\left[\frac{\theta e^t}{\left(\theta+1-e^t\right)^2}+\frac{\theta^2\alpha+\theta\alpha+2\theta+1}{\left(\theta+1-e^t\right)}\right] \tag{32}$$

Which is the required mgf of TPPGD$(X;\theta,\alpha)$.

2.3 Order Statistics

Let us suppose $x_1,x_2,x_3,...,x_n$ be a random sample of size n from two parameter Poisson Garima distribution with PMF $P(X=x)$and CDF $F(x)$. Also, let $x_{(1)}\le x_{(2)}\le....\le x_{(n)}$, denote the corresponding order statistics.

Now let $F(x)$ be the CDF of the i^{th} order statistics for a random sample $x_1,x_2,x_3,...,x_n$ from X~TPPGD$(X;\theta,\alpha)$ distribution, then the CDF is defined by

$$F_i(x)=\sum_{k=1}^{n}\binom{n}{k}[F(x)]^k[1-F(x)]^{n-k} \tag{33}$$

By using the binomial expression for $[1-F(x)]^{n-k}$ and substituting the value in above given equation, we obtain the following result

$$F_i(x)=\sum_{k=1}^{n}\sum_{r=0}^{n-k}\binom{n}{k}\binom{n-k}{r}(-1)^r[1-F(x;\theta,\alpha)]^{k+r} \tag{34}$$

$$F_i(x)=\sum_{k=1}^{n}\sum_{r=0}^{n-k}\binom{n}{k}\binom{n-k}{r}(-1)^r\left[\frac{1}{(1+\theta)^{x+2}(\alpha\theta+2)}\left[-2-\theta x-3\theta-\theta\alpha-\theta^2\alpha+(1+\theta)^{2+x}(\theta\alpha+2)\right]\right]^{k+r}$$

The corresponding PMF of the i^{th} order statistic is $x_{(i)}$

$$P_i(X=x)=F_i(x)-F_i(x-1) \tag{35}$$

$$P_i(X=x)=\sum_{k=1}^{n}\sum_{r=0}^{n-k}(-1)^r\binom{n}{k}\binom{n-k}{r}\left[\frac{1}{(1+\theta)^{x+2}(\alpha\theta+2)}\left[-2-\theta x-3\theta-\theta\alpha-\theta^2\alpha+(1+\theta)^{2+x}(\theta\alpha+2)\right]\right]^{(k+r)}$$
$$-\left[\frac{1}{(1+\theta)^{x+1}(\alpha\theta+2)}\left[-2-\theta x-3\theta-\theta\alpha-\theta^2\alpha+(1+\theta)^{2+x}(\theta\alpha+2)\right]\right]^{(k+r)}$$

Particularly, by putting i=1 and i=n in above equation, we can obtain the PMF of first order statistics and nth order statistics.

2.4. Random Data Generation from Two Parameter Poisson Garima Distribution

In order to simulate the data from two parameter Poisson Garima distribution, we employ the inverse CDF method. Simulating a sequence of random numbers $x_1, x_2, x_3, ..., x_n$ of the two parameter Poisson Garima random variable X with PMF $P(X=x_i)=p_i, \sum_{i=0}^{k} p_i = 1$ and CDF $F(X;\theta,\alpha)$.where k may be finite or infinite can be described as in the following steps.

Step 1: Generate a random number u from uniform distribution $U(0,1)$.

Step 2: Generate random number x_i based on

$$\text{if } u \le p_o = F(x_o;\theta,\alpha) \text{ then } X = x_o$$
$$\text{if } p < u \le p_o + p_1 = F(x_1;\theta,\alpha) \text{ then } X = x_1$$
$$\vdots$$
$$\text{if } \sum_{j=0}^{k-1} p_j < u \le \sum_{j=0}^{k} p_j = F(x_k;\theta,\alpha) \text{ then } X = x_k$$

In order to generate n random numbers $x_1, x_2, x_3 ..., x_n$ from TPPGD $(X;\theta,\alpha)$ distribution, repeat the step 1 to step 2 n times. We have employed R software for running the simulation study of the proposed model.

2.5. Survival Measures of Two Parameter Poisson Garima Distribution

This sub-section deals with the survival measures of two parameter Poisson Garima distribution such as the survival function and the hazard function. The survival function, also known as the survivorship function, refers to the probability that a life, system or a component will survive beyond a specified time. In mathematical terms, it happens to be the complement of the CDF and is given by:

$$S(x;\theta,\alpha)=p(X>x)=1-F(x) \tag{36}$$

Using (7) in (36), we obtain the survival function of as follows:

$$S(x;\theta,\alpha)=1-\frac{1}{(1+\theta)^{x+2}(\alpha\theta+2)}\left[-2-\theta x-3\theta-\theta\alpha-\theta^2\alpha+(1+\theta)^{2+x}(\theta\alpha+2)\right] \tag{37}$$

Figure 3 exhibits the reliability function plot of the proposed model for different values of the parameters θ and α. The hazard function, also known as the hazard rate or failure rate or force of mortality, happens to be an important quantity used for the characterization of life phenomenon. Hazard function is defined as the conditional probability that a life, system or a component that survives up to a specified time, will undergo failure or succumb in the immediate, infinitesimally small interval of time that follows. In mathematical terms, the hazard rate or the hazard function is given by:

$$h(x)=\lim_{\Delta t\to 0}\frac{\Pr[t\le X<t+\Delta t\mid X\ge t]}{\Delta t} \tag{38}$$

Which upon simplification yields

$$h(x;\theta,\alpha)=\frac{P(X=x)}{S(x;\theta,\alpha)} \tag{39}$$

Using (2) and (10) in (11), we obtain the hazard function of TPPGD as follows:

$$h(x;\theta,\alpha)=\frac{\theta\left(\theta^2\alpha+\theta\alpha+\theta x+2\theta+1\right)}{1-\left[-2-\theta x-3\theta-\theta\alpha-\theta^2\alpha+(1+\theta)^{2+x}(\theta\alpha+2)\right]}. \tag{40}$$

The reverse hazard rate function of two parameter Poisson Garima distribution is given as:

$$h_r(x;\theta,\alpha)=\frac{P(X=x)}{F(x)}=\frac{\theta\left(\theta^2\alpha+\theta\alpha+\theta x+2\theta+1\right)}{\left[-2-\theta x-3\theta-\theta\alpha-\theta^2\alpha+(1+\theta)^{2+x}(\theta\alpha+2)\right]}. \tag{41}$$

3. Estimation of parameters

In this section, we discuss the parameter estimation of the TPPGD$(X;\theta,\alpha)$ using method of maximum likelihood estimation and the frequent approach such as the method of moments.

3.1 Method of Maximum likelihood Estimate (MLE)

This is one of the most useful methods for estimating the different parameters of the distribution. Let $x_1,x_2,x_3,...,x_n$ be the random sample of size n, drawn from two parameter Poisson Garima distribution, then the likelihood function of TPPGD$(X;\theta,\alpha)$is given as

$$L(x_i\mid\theta)=\left(\frac{\theta}{\alpha\theta+2}\right)^n\prod_{i=1}^{n}\left(\frac{\left(\theta^2\alpha+\theta\alpha+\theta x_i+2\theta+1\right)}{(1+\theta)^{x_i+2}}\right) \tag{42}$$

The log likelihood function is obtained as

$$\log L=n\log\theta-n\log(\alpha\theta+2)+\sum_{i=1}^{n}\log\left(\theta^2\alpha+\theta\alpha+\theta x_i+2\theta+1\right)-\left(\sum_{i=1}^{n}x_i+2n\right)\log(1+\theta) \tag{43}$$

The two likelihood equations are thus obtained as

$$\frac{d\log l}{d\theta}=\frac{2n}{\theta(\alpha\theta+2)}+\sum_{i=1}^{n}\frac{(x_i+2\alpha\theta+\alpha+2)}{\theta x_i+\theta^2\alpha+\theta\alpha+2\theta+1}-\frac{n(\bar{x}+2)}{\theta+1}=0 \tag{44}$$

$$\frac{d\log l}{d\alpha}=-\frac{n\theta}{\alpha\theta+2}+\sum_{i=1}^{n}\frac{\theta^2+\theta}{\theta x_i+\theta^2\alpha+\theta\alpha+2\theta+1}=0 \tag{45}$$

The two equations (44) and (45) do not seem to be solved directly. However, the Fisher's scoring method can be applied to solve the equations.

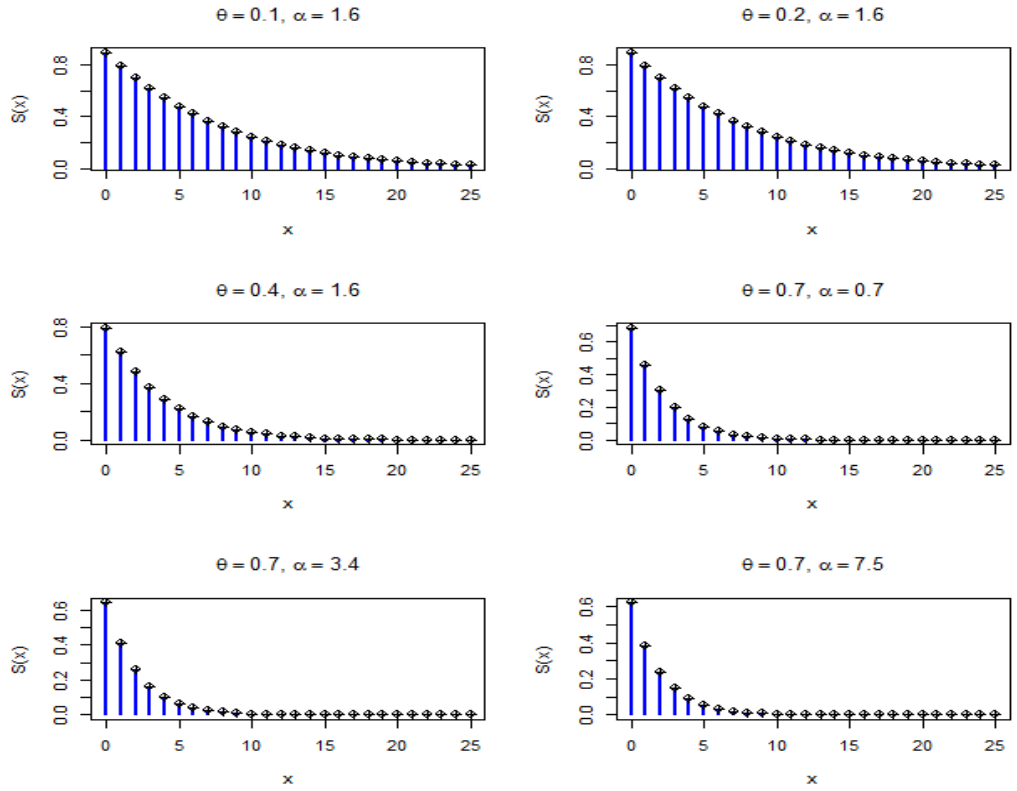


Figure 3: *Survival function plots of two parameter Poisson Garima distribution*

We have,

$$\frac{d^2\log l}{d\theta^2}=4n\left[\frac{\alpha\theta+1}{\theta^2(\alpha\theta+2)^2}\right]+\sum_{i=1}^{n}\frac{2\alpha\left(\theta^2\alpha+\theta\alpha+\theta x_i+2\theta+1\right)-\left(2\alpha\theta+\alpha+x_i+2\right)^2}{\left(\theta^2\alpha+\theta\alpha+\theta x_i+2\theta+1\right)^2}+\frac{n(\bar{x}+2)}{(1+\theta)^2}$$

$$\frac{d^2\log l}{d\alpha^2}=\frac{n\theta^2}{(\alpha\theta+2)^2}-\sum_{i=1}^{n}\frac{\left(\theta+\theta^2\right)^2}{\left(\theta^2\alpha+\theta\alpha+\theta x_i+2\theta+1\right)^2} \tag{46}$$

$$\frac{d^2\log l}{d\theta\,d\alpha}=\frac{-2n\theta^2}{(\theta(\alpha\theta+2))^2}+\sum_{i=1}^{n}\frac{\theta^2x_i+2\theta^2+2\theta+1}{\left(\theta^2\alpha+\theta\alpha+\theta x_i+2\theta+1\right)^2} \tag{47}$$

The following equation for $\hat{\theta}$ and $\hat{\alpha}$ can be solved

$$\begin{bmatrix}\frac{d^2\log l}{d\theta^2} & \frac{d^2\log l}{d\theta\,d\alpha}\\ \frac{d^2\log l}{d\theta\,d\alpha} & \frac{d^2\log l}{d\alpha^2}\end{bmatrix}_{\substack{\hat{\theta}=\theta_0\\ \hat{\alpha}=\alpha_0}}\begin{bmatrix}\hat{\theta}-\theta_0\\ \hat{\alpha}-\alpha_0\end{bmatrix}=\begin{bmatrix}\frac{d\log l}{d\theta}\\ \frac{d\log l}{d\alpha}\end{bmatrix}_{\substack{\hat{\theta}=\theta_0\\ \hat{\alpha}=\alpha_0}} \tag{48}$$

Where θ_0 and α_0 are the initial values of θ and α respectively. The equations are solved iteratively till sufficiently close estimates of $\hat{\theta}$ and $\hat{\alpha}$ are obtained.

3.2. Estimates from Moments

Using the first two moments about origin of two parameter Poisson Garima Distribution, we have

$$\frac{\mu_2'}{\mu_1'^2}=\frac{8+2\alpha\theta(\alpha\theta+2)}{(\alpha\theta+3)^2}=k \tag{49}$$

Taking $\alpha\theta = b$, we get

$$\frac{\mu_2'}{\mu_1'^2} = \frac{(8+2b)(b+2)}{(b+3)^2} = \frac{(2b^2+12b+16)}{(b^2+6b+9)} = k \tag{50}$$

This gives

$$b^2(2-k)+6b(2-k)-1(16-9k)=0 \tag{51}$$

Which is a quadratic equation in b. Replacing the first and the second moments μ_1' and μ_2' by the respective sample moments $\bar{x}$ and m_2' an estimate of k can be obtained, using which, the equation (51) can be solved and an estimate of b obtained. Again substituting $\alpha\theta = b$ in this expression for the mean of the TPPGD $(X;\theta,\alpha)$, we get

$$\bar{x} = \frac{\alpha(b+2)}{b(b+1)}. \tag{52}$$

And thus, an estimate of α is given by

$$\hat{\alpha} = \left(\frac{b(b+1)}{b+2}\right)\bar{x}. \tag{53}$$

Finally, an estimate of θ is given by

$$\hat{\theta} = \left(\frac{b+2}{b+1}\right)\frac{1}{\bar{x}}. \tag{54}$$

4. Applications of Two Parameter Poisson Garima Distribution

In this section, we fit our proposed distribution to three practical datasets.
Data set 1: The first data set is regarding the thunderstorm events at Cape Kennedy, Florida for the 11-year period of record for the month of June, January 1957 to December 1967. Shanker et Al. [14]

Table 1: *Thunderstorm events at Cape Kennedy, Florida for the 11-year period of record for the month of July, January 1957 to December 1967.*

No. of Thunderstorms	0	1	2	3	4	5	6	Total
Frequency	187	77	40	17	6	2	1	330

In order to give an impression of the typical form of our observed distributions and their various parameter estimates, we have provided Table 2 below. The ML estimates have been calculated using the ***fitdistr*** procedure in R studio. Furthermore, we have computed the expected frequencies of counts for Poisson, Negative Binomial, discrete Weibull, discrete Rayleigh and two parameter Poisson Garima distributions with the help of R Studio statistical software [17] and Pearson's chi-square test is applied to check the goodness of fit of the models mentioned above. The calculated figures are given in Table 3.

The p-values of Pearson's Chi-square statistic are <0.0001, 0.46, 0.47, <0.0001 and 0.51 for Poisson, Negative Binomial, discrete Weibull, discrete Rayleigh, and two parameter Poisson Garima distributions, respectively (see Table 3). This reveals that Poisson and discrete Rayleigh are not a good fit at all for the data in question, whereas two parameter Poisson Garima, Negative binomial and discrete Weibull are good fit distributions with two parameter Poisson Garima model being the best one. The null hypothesis that data comes from two parameter Poisson Garima distribution is strongly accepted.

Finally, we have compared Poisson, Negative Binomial, discrete Weibull, discrete Rayleigh and two parameter Poisson Garima distributions using the Akaike Information Criterion (AIC), given by Akaike [16] and the Bayesian information criterion (BIC), given by Schwarz [17]. AIC and BIC are evaluated according to the formula $-2 * \log$ likelihood + k $*$ npar, where npar represents the number of parameters in the fitted model, and k = 2 for the usual AIC, or k = log(n) (n being the

number of observations) for the so-called BIC or SBC (Schwarz's Bayesian criterion).

The AIC and BIC values for the fitted distributions to dataset given in Table 1 are given in Table 4. By comparing the AIC and BIC values for the fitted models, we conclude that in case of the thunderstorm events at Cape Kennedy, Florida for the 11-year period of record for the month of June, January 1957 to December 1967, (Falls et al. [17]), two parameter Poisson Garima distribution fits better in contrast to Poisson, NBD, discrete Weibull and, discrete Rayleigh models.

Table 2. *Estimated parameters by ML method for various fitted distributions for the thunderstorm events at Cape Kennedy, Florida for the 11-year period of record for the month of June, January 1957 to December 1967.*

Distribution	Parameter Estimates	Model function
Two parameters Poisson Garima	$\hat{\theta} = 1.89$ $\hat{\alpha} = 0.18$	$P(X=x) = \frac{\theta}{(1+\theta)^{x+2}(\alpha\theta+2)}\left(\theta^2\alpha + \theta\alpha + \theta\ x + 2\theta + 1\right);$ $x = 1,2,3,...;\ \ \theta > 0, \alpha > 0$
Poisson	$\hat{\lambda} = 0.75$	$p(x) = \frac{e^{-\lambda}\lambda^x}{x!}$ $x = 0,1,2,...; \lambda > 0$
Discrete Rayleigh	$\hat{q} = 0.68$	$p(x) = q^{x^2} - q^{(x+1)^2}$ $x = 0,1,2,...;\quad 0 < q < 1$
NBD	$\hat{p} = 0.60,$ $\hat{r} = 1.17$	$p(x) = \begin{bmatrix} x+r-1 \\ x \end{bmatrix} p^r q^x\ ;$ $x = 0,1,2,...;\ \ 0 < p < 1\ ;\ r > 0$
Discrete Weibull	$\hat{q} = 0.44\ ,$ $\hat{\beta} = 1.04$	$p(x) = q^{x^\beta} - q^{(x+1)^\beta}$ $x = 0,1,2,...;\ \ 0 < q < 1;\ \beta > 0$

Table 3: *Expected frequency of counts & goodness of fit for the thunderstorms events at Cape Kennedy, Florida for the 11-year period of record for the month of June, January 1957 to December 1967.*

X	Observed frequency	Expected frequencies				
		Poisson	NB	DW	DR	TPPGD
0	187	155.64	184.66	184.45	103.02	184.33
1	77	116.97	84.54	84.71	153.12	84.43
2	40	43.95	35.87	35.95	62.49	36.32
3	17	11.01	14.82	14.85	10.54	15.01
4	6	2.07	6.04	6.04	0.80	6.04
5	2	0.31	2.44	2.42	0.03	2.38
6	1	0.04	0.98	0.96	0.00	0.92
χ^2 p-value		<0.0001	0.46	0.47	<0.0001	0.51

X: Number of thunderstorm events at Cape Kennedy, Florida for the 11-year period of record for the month of June, January 1957 to December 1967.
Observed: Observed frequency of the thunderstorm events at Cape Kennedy, Florida for the 11-year period of record for the month of June, January 1957 to December 1967.

Table 4: *AIC and BIC values for fitted distributions for counts of thunderstorms events at Cape Kennedy, Florida for the 11-year period of record for the month of June, January 1957 to December 1967, Shanker et al. [14]*

Criterion	Poisson	NBD	DWD	DR	TPPGD
-loglik	412.253	394.5933	394.5637	470.2933	394.4194
AIC	826.506	793.1866	793.1275	942.5866	792.8389
BIC	830.305	800.7848	800.7256	946.3857	800.4371

Data set 2: Secondly, we analyze the data set regarding distribution of the thunderstorm events at Cape Kennedy, Florida for the 11-year period of record for the month of July, January 1957 to December 1967, Shanker et al. [14].

Table 5: *Distribution of the thunderstorm events at Cape Kennedy, Florida for the 11-year period of record for the month of July, January 1957 to December 1967.*

Number of Thunderstorms	0	1	2	3	4	5	Total
Frequency	177	80	47	26	9	2	341

In order to give an impression of the typical form of our observed distributions and their various parameter estimates, we have provided Table 6 below. The ML estimates have again been calculated using the ***fitdistr*** procedure in R studio.

Table 6. *Estimated parameters by ML method for various fitted distributions for thunderstorm events at Cape Kennedy, Florida for the 11-year period of record for the month of June, January 1957 to December 1967.*

Distribution	Parameter Estimates	Model function
Two parameter Poisson Garima	$\hat{\theta}=1.7182$ $\hat{\alpha}=0.0001$	$P(X=x)=\frac{\theta}{(1+\theta)^{x+2}(\alpha\theta+2)}\left(\theta^2\alpha+\theta\alpha+\theta\ x+2\theta+1\right);$ $x=1,2,3,...;\quad \theta>0,\alpha>0$
Poisson	$\hat{\lambda}=0.8739$	$p(x)=\frac{e^{-\lambda}\lambda^x}{x!}$ $x=0,1,2,...;\lambda>0$
Discrete Rayleigh	$\hat{q}=0.724$	$p(x)=q^{x^2}-q^{(x+1)^2}$ $x=0,1,2,...;\quad 0<q<1$
NBD	$\hat{p}=0.6263$ $\hat{r}=1.4652$	$p(x)=\begin{bmatrix}x+r-1\\ x\end{bmatrix}p^r q^x\ ;$ $x=0,1,2,...;\ \ 0<p<1\ ;\ r>0$
Discrete Weibull	$\hat{q}=0.496$ $\hat{\beta}=1.112$	$p(x)=q^{x^\beta}-q^{(x+1)^\beta}$ $x=0,1,2,...;\ \ 0<q<1;\ \beta>0$

Furthermore, we have computed the expected frequencies of counts for Poisson, Negative Binomial, discrete Weibull, discrete Rayleigh and two parameter Poisson Garima distributions with the help of R studio statistical software [17] and Pearson's chi-square test is applied to check the goodness of fit of the models mentioned above. The calculated figures are given in Table 7. The p-values of Pearson's Chi-square statistic are<0.0001, 0.066, 0.067, <0.0001 and 0.117 for Poisson, Negative Binomial, discrete Weibull, discrete Rayleigh and two parameter Poisson Garima distributions,

respectively (see Table 7). This reveals that Poisson, discrete Rayleigh, are not a good fit at all for the data in question, whereas two parameter Poisson Garima, Negative binomial and discrete Weibull are good fit distributions with two parameter Poisson Garima model being the best one. The null hypothesis that data comes from two parameter Poisson Garima distribution is strongly accepted.

Table 7: *Expected frequency counts & goodness of fit for Number of thunderstorm events at Cape Kennedy, Florida for the 11-year period of record for the month of June, January 1957 to December 1967.*

X	Observed Frequency	Expected Frequency				
		Poisson	NBD	DWD	DR	TPPGD
0	177	142.306	171.829	171.531	94.095	175.904
1	80	124.362	94.061	94.276	153.180	89.774
2	47	54.340	43.315	43.429	75.073	42.246
3	26	15.829	18.692	18.788	16.706	18.934
4	9	3.458	7.796	7.810	1.840	8.213
5	2	0.604	3.183	3.152	0.103	3.481
χ^2 p-value		<0.0001	0.066	0.067	<0.0001	0.117

X: Number of thunderstorm events at Cape Kennedy, Florida for the 11-year period of record for the month of June, January 1957 to December 1967.
Observed: Observed frequency of thunderstorms events at Cape Kennedy, Florida for the 11-year period of record for the month of June, January 1957 to December 1967.

The AIC and BIC values for the fitted distributions to dataset given in Table 5 are given in Table 8. By comparing the AIC and BIC values for the fitted models, we conclude that in case of thunderstorm events at Cape Kennedy, Florida for the 11-year period of record for the month of June, January 1957 to December 1967, two parameter Poisson Garima distribution fits better in contrast to Poisson, NBD, discrete Weibull and discrete Rayleigh model.

Table 8: *AIC and BIC values for fitted distributions for the thunderstorm events at Cape Kennedy, Florida for the 11-year period of record for the month of June, January 1957 to December 1967*

Criterion	**Poisson**	**NBD**	**DWD**	**DR**	**TPPGD**
-loglik	455.51	440.178	440.0484	504.68	439.9534
AIC	913.02	884.356	884.0968	1011.35	883.9069
BIC	916.85	892.0198	891.7606	1015.18	891.5707

Data set 3: This data represents the daily new deaths of 111 days from 12 March to 30 June 2020 belonging to Greece country (see World Health Organization), Almetwally et.al [15].

Table 9: *Daily new deaths of 111 days from 12 March to 30 June 2020 in Greece.*

Number of deaths	0	1	2	3	4	5	6	7	8	9	Total
Frequency	39	26	17	9	6	7	6	0	0	1	111

In order to give an impression of the typical form of our observed distributions and their various parameter estimates, we have provided Table 10 below. The ML estimates have been calculated using the ***fitdistr*** procedure in R studio. Furthermore, we have computed the expected frequencies of counts for Poisson, Negative Binomial, discrete Weibull, discrete Rayleigh and two parameter Poisson Garima distributions with the help of R studio statistical software [17] and Pearson's chi-square test is applied to check the goodness of fit of the models mentioned above. The calculated figures are given in Table 11.

Table 10 *Estimated parameters by ML method for various fitted distributions for the daily new deaths of 111 days from 12 March to 30 June 2020 belonging to Greece country (see World Health Organization).*

Distribution	Parameter Estimates	Model Function
Two Parameter Poisson Garima	$\hat{\theta} = 0.86$ $\hat{\alpha} = 0.08$	$P(X=x) = \frac{\theta}{(1+\theta)^{x+2}(\alpha\theta+2)}\left(\theta^2\alpha + \theta\alpha + \theta\ x + 2\theta + 1\right);$ $x = 1,2,3,...;\ \ \theta > 0, \alpha > 0$
Poisson	$\hat{\lambda} = 1.72$	$p(x) = \frac{e^{-\lambda}\lambda^x}{x!}$ $x = 0,1,2,...; \lambda > 0$
Discrete Rayleigh	$\hat{q} = 0.89$	$p(x) = q^{x^2} - q^{(x+1)^2}$ $x = 0,1,2,...;\quad 0 < q < 1$
NBD	$\hat{p} = 0.415,$ $\hat{r} = 1.220$	$p(x) = \begin{bmatrix} x+r-1 \\ x \end{bmatrix} p^r q^x\ ;$ $x = 0,1,2,...;\ \ 0 < p < 1\ ;\ r > 0$
Discrete Weibull	$\hat{q} = 0.66\ ,$ $\hat{\beta} = 1.08$	$p(x) = q^{x^\beta} - q^{(x+1)^\beta}$ $x = 0,1,2,...;\ \ 0 < q < 1;\ \beta > 0$

The p-values of Pearson's Chi-square statistic are <0.001, 0.471, 0.462, <0.001 and 0.483 for Poisson, Negative Binomial, discrete Weibull, discrete Rayleigh, and two parameter Poisson Garima distributions, respectively (see Table 11). This reveals that Poisson and discrete Rayleigh are not a good fit at all for the data in question, whereas two parameter Poisson Garima, Negative binomial and discrete Weibull are good fit distributions with two parameter Poisson Garima model being the best one. The null hypothesis that data comes from two parameter Poisson Garima distribution is strongly accepted.

Table 11: *Expected frequency of counts & goodness of fit for the daily new deaths of 111 days from 12 March to 30 June 2020 belonging to Greece country.*

X	Observed Frequency	Expected Frequency				
		Poisson	NBD	DWD	D-Rayleigh	TPPGD
0	39	19.862	37.946	37.665	12.210	38.051
1	26	34.177	27.089	27.172	29.146	26.609
2	17	29.405	17.594	17.686	30.754	17.606
3	9	16.866	11.050	11.147	21.688	11.236
4	6	7.255	6.821	6.892	11.175	6.991
5	7	2.497	4.167	4.204	4.354	4.268
6	6	0.716	2.528	2.537	1.305	2.568
7	0	0.176	1.526	1.518	0.304	1.527
8	0	0.038	0.917	0.902	0.055	0.900
9	1	0.007	0.550	0.532	0.008	0.526
χ^2 p-value		<0.001	0.471	0.462	<0.001	0.483

X: Number of daily new deaths of 111 days from 12 March to 30 June 2020 belong to Greece country.
Observed: Observed frequency of the daily new deaths of 111 days from 12 March to 30 June 2020

belonging to Greece country.

The AIC and BIC values for the fitted distributions to dataset given in Table 9 are given in Table 12. By comparing the AIC and BIC values for the fitted models, we conclude that in case of for the daily new deaths of 111 days from 12 March to 30 June 2020 belonging to Greece country, two parameter Poisson Garima distribution fits better in contrast to Poisson, NBD, discrete Weibull and, discrete Rayleigh models.

Table 12: *AIC and BIC values for fitted distributions the data represents the daily new deaths of 111 days from 12 March to 30 June 2020 belonging to Greece country*

Criterion	Poisson	NBD	DWD	D-Rayleigh	TPPGD
-loglik	220.10	198.3241	198.2529108	230.03	198.1523
AIC	442.21	400.6481	400.5058215	462.05	400.3046
BIC	444.92	406.0672	405.9248819	464.76	405.7237

6. Conclusion

In this paper, we have introduced a new count data model namely two parameter Poisson Garima distribution. General description of the statistical properties such as the moments, skewness, kurtosis, moment generating function, probability generating function, order statistics, etc has been provided after an extensive study. The estimation of the model parameters is performed by maximum likelihood method and method of moment. The applicability of this distribution to real life data is illustrated by three real life examples by positioning it alongside other four models (NB, Poisson, DW, DR) for comparison. The comparison was conducted by using AIC, BIC and p value. By competing the models, we find that TPPGD is superior as compared to alternative models and provides the best fit, because it has the smallest values of AIC and BIC.

References

[1] Altun, E., Alqifari, H., & Eliwa, M. S. (2023). A novel approach for zero-inflated count regression model: Zero-inflated Poisson generalized-Lindley linear model with applications. *AIMS Mathematics*, 8(10), 23272–23290. https://doi.org/10.3934/math.20231183

[2] Consul, P. C., & Jain, G. C. (1973). A generalization of the Poisson distribution. *Technometrics*, 15(4), 791–799.

[3] Dean, C., Lawless, J. F., & Willmot, G. E. (1989). A mixed Poisson–inverse-gaussian regression model. *Canadian Journal of Statistics*, 17(2), 171–181.

[4] Gerstenkorn, T. (2004). A compound of the generalized negative binomial distribution with the generalized beta distribution. *Open Mathematics*, 2(4), 527–537. https://doi.org/10.2478/bf02475961

[5] Greenwood, M., & Udny Yule, G. (1920). An Inquiry into the Nature of Frequency Distributions Representative of Multiple Happenings with Particular Reference to the Occurrence of Multiple Attacks of Disease or of Repeated Accidents. *Journal of the Royal Statistical Society*, 83.

[6] Holla, M. S. (1967). On a Poisson-inverse Gaussian distribution. *Metrika*, 11(1), 115–121.

[7] Sankaran, M. (1970). 275. note: The discrete Poisson-Lindley distribution. *Biometrics*, 145–149.

[8] Sen, S., Chandra, N., & Maiti, S. S. (2018). On Properties and Applications of a Two-Parameter Xgamma Distribution. *Journal of Statistical Theory and Applications*, 17(4), 674. https://doi.org/10.2991/jsta.2018.17.4.9

[9] Shanker, R. (2016a). Garima Distribution and its Application to Model Behavioral Science Data. *Biometrics & Biostatistics International Journal*, 4(7). https://doi.org/10.15406/bbij.2016.04.00116

[10] Shanker, R. (2016b). On Poisson-Sujatha Distribution and its Applications to Model Count Data from Biological Sciences. *Biometrics & Biostatistics International Journal*, 3(4), 1–7. https://doi.org/10.15406/bbij.2016.03.00069 [

[11] Shanker, R. (2016c). Sujatha distribution and its applications. *Statistics in Transition New Series*, 17(3), 391–410. https://doi.org/10.21307/stattrans-2016-029[

[12] Shanker, R. (2017). The Discrete Poisson-Garima Distribution. *Biometrics & Biostatistics International Journal*, 5(2). https://doi.org/10.15406/bbij.2017.05.00127

[13] Shanker, R., Shukla, K. K., & Leonida, T. A. (2020). A New Two-Parameter Poisson-Sujatha Distribution. *International Journal of Probability and Statistics,* 9(2), 21-32. https://doi.org/10.5923/j.ijps.20200902.01

[14] Shanker, R., Fesshaye, H., Shanker, R., Leonida, T. A., & Sium, S. (2017). On discrete Poisson-Shanker distribution and its applications. *Biometrics & biostatistics International journal*, *5*(1), 00121.

[15] Almetwally, E. M., & Dey, S. (2021). Modelling of COVID-19 Data Using Discrete Distribution. *Delta University Scientific Journal,* 4(1), 13-24.

[16] R Core Team (2024). R: A Language and Environment for Statistical Computing. R Foundation for Statistical Computing, Vienna, Austria. Available at: https://www.R-project.org/.

RELIABILITY, AVAILABILITY AND MAINTAINABILITY (RAM) ANALYSIS OF SOME PROCESS INDUSTRIES: A CRITICAL REVIEW OF LITERATURE

Punam Rani[1], Sangeeta Malik[2], Arun Kumar[3*]

[1]Research Scholar, Department of Mathematics, Baba Mastnath University, Rohtak, Haryana, India
[2]Professor, Department of Mathematics, Baba Mastnath University, Rohtak, Haryana, India
[3*]Assistant Professor, Department of Mathematics, Shri Khushal Das University, Hanumangarh, Rajasthan

[1]punammalik888@gmail.com ,[2]sangeeta@bmu.ac.in, [3*]rnkumar535@gmail.com

Abstract

This paper reviews the literature on reliability, availability, and maintainability analysis of process industrial systems. In today's automated world, it is unfeasible to live exclusive of reliable systems, so every one of the working engineering system be anticipated to remain operational with maximum effectiveness for the longest period of time, or reliable operation. Throughout the years, the primary goal has been to concentrate on the system presentation in excess of an extended period of time; in essence, these are case studies on the system concert of industrial systems. While achieving 100% failure-free operation in production is not practicable, industrial systems that can be repaired can have their system failures minimized. In this paper, an effort has been made to compile the necessary literature and offer some helpful advice on how to broaden the field for more beneficial outcomes on system performance.

Keywords: Reliability, Availability, Process Industries, Redundancy

I. Introduction

The concepts of Reliability, Availability, and Maintainability (RAM) are becoming more and more important in today's industry. Utilizing RAM engineering techniques has become more crucial because to increase competition, stricter production timelines, financial restrictions, and the ongoing desire for lower-priced, higher-quality products. Reliability simulation has become the most popular and successful approach for handling contemporary real-world problems as industrial systems gets more complex. These problems are frequently hard or impossible to resolve with conventional analytical techniques.

RAM analysis is now the standard tool in many industries, thanks to the widespread use of this simulation-based technique. High capital expenditure is needed to halt manufacturing operations, particularly process plants like chemical, Bread, Urea fertilizer, sugar, thermal, polytube, washing unit, paper, and Rice, among others, because to the growing demand for automation across numerous industrial segments. For process facilities to survive, they must be highly productive and make the most money possible. The maximum level of equipment

availability and dependability must be maintained in order to accomplish this goal. Unfortunately, this is not the case since, although it can be reduced via appropriate maintenance, inspection, operator training, incentive, and instilling a positive attitude in the workers, failure is unavoidable. Any system's performance has an impact on both the optimization tools and the quality of its design. Therefore, a system's performance can be improved by appropriate design, optimization at the design stage, and maintenance during its service life. One important factor in lowering manufacturing costs is careful maintenance planning. Improving the quality and expanding the availability of manufacturing systems are also very helpful in increasing productivity.

The word "reliability" comes from the very act of failure. The technology frequently malfunctions, making it unreliable for use. Both economically and in terms of safety, an unstable system has a very high cost. Catastrophic accidents could result from system breakdowns. As a result, industries are required to use the RAM technique to increase quality and safety. The numerous pieces of equipment used must be maintained as dependable and accessible as possible overall in order to do this. Because failures are inevitable, fault-free functioning is impossible. However, by using reliable parts, doing preventive maintenance on subsystems, and creating a happy work atmosphere, one might lessen their impact to some extent. Process industries employ a variety of reliability and maintainability performance events to evaluate the presentation of a system. Availability (i.e., intrinsic, operational, or achievable), turnaround time, and the routine maintenance cost index on stream factor and on-stream factor with slowness are the major measures used. In order to produce a variety of design possibilities, we usually consider system availability at every stage of the design process. If a system can perform its proposed function for the individual period of instance under all operational and environmental conditions, it is deemed reliable.

The availability of a system is its operational readiness, or its ability to carry out its intentional function immediately and for a particular epoch of time. System ease of use comes in different forms, such as inherent, achievable, and operational. Operational ease of use of the system in procedure industry includes wasted time in administration and operational logistics in addition to scheduled and unscheduled maintenance time. Achievable availability only includes scheduled and unscheduled maintenance time. In contrast, inherent availability simply accounts for unplanned maintenance time. Therefore, a system's dependability and maintainability are impacted by its availability. Maintainability refers to a system's capacity to apply prescribed maintenance procedures to keep it in a state where it is ready or presented to execute its future function under a range of operational and environmental conditions.

Process industries like chemical, bread, paper, Urea fertilizer, brewing, cement, thermal power plants, Polytube, and Rice plants also require their various subsystems to stay upstate for an extended amount of time in order to meet the requirements for high system availability and to make use of the maximum capacity of the plant. Nevertheless, unpredictable errors can occur in these systems or subsystems. Production may be decreased or may not occur at all, depending on the category and severity of the failure. It is undeniable that malfunctioning systems can be restored to functioning condition by replacing or repairing certain parts. However, in this instance, maintaining the system working at full capacity for the longest possible time depends heavily on the factory operating circumstances as well as the organization's repair practices. It would be necessary to have prior information of the system behavior, presented repair conveniences, etc. in order to design such a procedure as of the perspective of high structure availability. When assessing the presentation of subsystems and the level of interface among the ingredient subsystems, analysis and modeling of such systems may be helpful. An outline for structure aim base on accessibility and the best repair policy would also result from this. It is clear from the

descriptions above that enhancing a system's dependability during design, improving its maintainability during operation, or doing both can all increase a system's availability. Unless compensatory reliability engineering measures are used, a system's dependability directly decreases as its complexity increases. Some organizations understand the importance of reliability and integrate it into all facets of their operations, such as the military, public utilities, and airlines. To avoid unscheduled shutdowns, process industries require a system that can ensure high availability and dependability. As a result, it is now evident how crucial high dependability is and how to achieve it by applying the many ideas described in the RAM approach. ODE-45 Method, Regenerative Point Graphical Technique (RPGT), Particle Swarm Optimization (PSO), Recursive Method, and Genetic Algorithm (GA) are only a few of the advanced performance optimization approaches that can be used further.

II. Basic Definitions

Reliability: Reliability will be probability of a gadget operating for a certain amount of time with no failure. More commonly, reliability is the ability of components, equipment's, components, solutions and items to do the required tasks of theirs for ideal stages of time with no disappointment in chosen environments and with a preferred confidence.

Availability: Accessibility will be the likelihood that a gadget is going to be in a position to work (i.e. not damaged or even going through repair) when called upon to do it. Much more particularly, it's the likelihood that the device is going to be ready to work within tolerance limits at a certain instant's and it is also identified as operational readiness.

Preventive Maintenance: In this type of maintenance, the subunits or subsystems are inspected before a failure and provided repair if required and maintenance be accepted out also when the structure has before now failed. The principle of preventive maintenance is to build the system working in its optimal capacity as soon as probable and that's why to add to availability of the structure. The time exhausted on every one this is negligible as repair of units may be online. This type of Maintenance is the act taken and pre planned so that an unfiled system or equipment remains to operational status including repairing a part or subunit that is answerable for the disappointment of the total system.

Failure: A deviation in the attributes from the prescribed problem is viewed as being a fault. A state of fault is widely known as "failure". An item is viewed as failed under among the following 3 conditions

- When it gets totally inoperable.
- When it's still operable, but is not in the position to do as needed e.g. a twelve volt battery offering three volt rather than twelve.
- When an unexpected critical deterioration makes the product unsafe for the further use of its.

Phases of Failure: Generally, a gadget might encounter any of three phases of failure throughout the total life cycle of it's of as well as operating.

Initial failure: Whenever we put a sizable collection of units to operation, it's very likely that you will find a lot of failures initially. The very early failures are called infant mortality or initial failures. These problems are because of manufacturing defects, for example poor assembly, vulnerable areas, defective styles etc.

Random failure (Chance failure): These failures happen while in the middle (useful life) of something as a result of unexpected strain accumulations outside of the layout power of the product. This kind of failures can't ever be predicted and so it's nearly impossible to eliminate them.

Wear-out failure: With the way of time, the device (device) starts to decline. An easy change in the values of the variables identifying the functionality of the device happens when these variables go past the limit admissibility, the device breaks. This particular region is known as the wear-out region as well as such kinds of problems are known as wear out failures.
Failure Rate: It is characterized as the basic ratio of quantity of disappointments during a specific intermission to normal population throughout that stretch and is communicated in provisions of quantity of disappointments per unit instance.

III. RAM Methods For Process Industries: An Analysis of The Review of Literature

Historical Background: Over the past few years, the importance of reliability has grown among manufacturing companies, the government, and the general public. Agencies are attempting to obtain systems with improved reliability and cheaper maintenance costs as a result of current concerns about government spending. As buyers, our major priorities are choosing items with higher reliability, longer life spans, and lower maintenance costs. Each of us frequently uses the words "reliable" and "reliability" in daily life. Any stochastic system has the unique property that, in the event of failure of a relatively small number of its subsystems, the intact system fails. We encounter a number of issues related to work, social development, production, and administration every day. Reliability technology can help us solve problems if we have a thorough understanding of them and the right circumstances. The development of a system's infrastructure and the economics both revolve around reliability technologies. Technology today would not exist without reliability. It is especially crucial for a country like India to utilize its resources in the best possible way in order to maximize productivity through improved system reliability. It made a difference in reducing the elements that lead to system breakdowns. The particular word reliability = re + liability means recurring liability as of assorted breakdowns and failure of a structure. The person who designed the system or equipment, the manufacturer, quality control inspectors, actual user, and everyone else who is directly or indirectly connected to it must all share this responsibility. It can be difficult to identify and learn about every variable or circumstance that contributes to subsystem failures. Financial expert Pareto noted that a pair of elements typically account for the characteristic behavior of a dependent variable in several real-world situations, meaning that the majority of abnormalities are caused by a small number of independent causes. Due to the complexity of modern equipment, two additional factors maintainability and availability that are both strongly tied to reliability have come into sharper emphasis. When a piece of equipment is very reliable, breakdowns are less likely to occur and availability is higher. Additionally, accessibility will be high if a unit or framework can be fixed quickly (i.e., maintainability is high). This suggests that an item's low reliability can be compensated for by an increase in maintainability and availability.

For a very long time, reliability has been praised as a human quality. The reliability notion, however, has not been utilized for technical systems in more than 50 years. It first gained technological significance shortly after World War I. It was then applied to a comparison of the operational safety of single-engine, dual-engine, and four-engine aircraft. The frequency of accidents per hour of flight time was used to gauge reliability. A high level of reliability is expected of such equipment in the present scientific era where sophisticated systems are used for scientific, industrial, and defense applications. Due to the modern sophistication and growing complexity in the miniaturization of electronic and telemetric equipment necessary for defense and space research programming required for better degree of reliability, this demand has steadily developed since the end of the second world war. It would be risky to use equipment that might not work correctly when necessary when human lives and national security are at risk.

Additionally, the modern military weapons are made up of tens of thousands of tiny components that are intricately braided together to form a weapon. The operation of the weapons could be negatively impacted by the failure of any of these. As a result, it is more crucial than ever that every component of complicated equipment be extremely trustworthy in order for the system as a whole to be reliable. High reliability is an important notion outside of the military.

Complex and sophisticated computers play a significant part in industrial and scientific activity. Even a single day of computer downtime results in inconvenience in addition to financial loss. Therefore, the more complicated the equipment, the less reliable it will be. Both discipline and measurement can be considered as aspects of reliability. Reliability as a subject focuses on the creation and deployment of methods for enhancing system effectiveness by lowering failure frequency and minimizing high maintenance costs. Reliability is focused with quantifying the level of equipment quality as a measurement. In reliability theory, a unit is a structure or a component of a system, and a unit is said to be operating when it performs within tolerances. A device's quality and reliability are inextricably linked. A unit's quality is determined by a number of factors that determine how suitable it is for a certain use. By structure reliability, we signify its capacity to perform well for the requisite period of time. Failure in the unit is the fractional or whole defeat of these attributes in an approach that partially or fully disrupts or stops its functioning.

Failures can roughly be divided into three categories: initial failures, random failures, and wear-out failures. Initial failures happen at the initial stages of a machinery process as a result of subpar manufacturing and quality control procedures. The cause of random failures is stress buildup that exceeds the unit's intended strength. These cannot be foreseen or stopped. Wear out failures originate from a slow change in the characteristics that determine a unit's quality. One definition of reliability is "a science that investigates the law of episode of failures in technical utensils and proposes corrective actions." The ability of a device or system to operate properly without a failure during a certain epoch of instant under a specific set of circumstances is thus described as the fundamental concept of reliability.

For about fifty years now, reliability engineering has existed as a separate field. The topic of repairable systems has yet to receive the attention it deserves in the literature on reliability. Examining the evolution of this engineering field aids in determining the causes of this shortcoming as well as the disturbances and challenges associated with analyzing repairable systems in terms of their availability, dependability, and maintainability. The evolution of quality control and reliability are closely related. Bell Telephone Laboratories in the United States established statistical approaches to address their quality control issues in the early 1920. This served as the foundation for extra advancements in the field of statistical quality control. Later, Bell Laboratories, the American Society for Mechanical Engineers, and the American Standard Association helped to popularize quality control methods.

The study's literature analysis prompted a thorough examination of the RAM factors. The literature study offers a modern viewpoint on the area and mostly covers the years 2000–2025. RAM has been the subject of numerous investigations in various process industries and other related domains. Through the use of RAM technology, a range of methods include been put out in the literature to improve system availability in process industries. RAM techniques have been used in process and related industries, as described by numerous scholars.

Borgonovo et al. [1] explored the Monte Carlo technique and proposed a plant maintenance strategy using their operating procedures. It was advised to use tools that help explain a range of plant executive and operations topics, including system repair, technological obsolescence, aging, and overhaul. Tang [2] anticipated a way for evaluating the dependability of a mechanical structure in the process industry based on the Boolean function. Based on the recommended work, the researcher created a formula for evaluating the system's dependability. The connection between various failure interactions using Boolean functions and graph theory.

Using the method of finite element equations, Avontuur et al. [3] presented a novel methodology to assess the dependability of a system. Arulmozhi et al. [5] created the expression and algorithm to evaluate the dependability of a system amid K out of N components. The idea was quick and easy to implement, and it greatly enhances computing performance.

Elegbede et al. [6] put forth a revolutionary strategy that maximizes the system availability of repairable series-parallel systems by utilizing the Genetic Algorithms technology. Ebrahimi et al. [7 introduced an approach for assessing system dependability that mostly relied on failure data. A method was provided to review the consistency of a structure with high components of extremely high reliability because it is incredibly complex to obtain failure statistics for such systems.

A multi-period planning model and a preventative maintenance model were combined to develop a multipurpose plant optimization technique by Goel et al. [8]. It helps allocate the production and maintenance schedule by emphasizing preventative maintenance during equipment idle time and employing several production routes to reduce the brunt of equipment failure on creation.

Gupta et al. [9] discussed the accessibility of soap cakes making system. Xie et al. [10] advance to modeling the dependability of dependent structure by common cause failure (CCF) is presented. The method is founded on the idea of "conditional failure probability of component" as well as load-strength interference analysis at the system level. A discrete type system reliability model is created using the conditional component failure probability notion, which is based on the belief that load randomization is the direct cause of failure dependence. Finally, the model's ability to predict high multiplicity failure probability based on low multiplicity failure event data and estimate system dependability with CCF effect is demonstrated.

Gupta et al. [11] discussed the cement manufacturing plant. Samrout et al. [12] created a novel strategy for reducing the cost of preventative maintenance in systems with a series-parallel component layout by applying the Ant Colony optimization methodology.

Marseguerra et al. [15] developed a multi-objective optimization issue and employed the Genetic Algorithms technique to offer two more approaches to the problem's solution.

Gupta et al. [16] evaluated the reliability and accessibility of a industrialized facility using a K-out-of-N component system on behalf of a range of disappointment and repair rates. The plant's dependability was assessed using the Matrix Calculus Method and MATLAB software. It was found that using RAM approaches could enhance system output and quality. Krishnamoorthy and Viswanath [17] studied on the reliability of a k-out-of-n-system by way of restore by a Service Station Attending a Queue by way of Postponed Work.

A new framework for the best preventive maintenance of the pulping scheme used in the paper industry was created by Sachadeva et al. [20] using Petri Net. A probabilistic come up to utilizing the Markov procedure be used in the study by Kumar et al. [21] to analyze fertilizer plant availability and performance.

Khanduja et al. [23] optimized the act of a paper plant system by first developing mathematical models and then applying genetic algorithms. A mathematical formulation for the likely failure rates and repairs rates exponential distribution that were taken into consideration was created using a probabilistic approach. To find the steady state ease of use of the scheme, differential equations by the Markov Process are constructed and solved under normalize conditions. Hazra and Sinha [24] gave a fresh method for evaluating the event's sequence that could result in catastrophic disaster in a power phone. Probable collapse sequences happen to be realized offline for dissimilar likely loading scenarios by implementing an amended truth decoupled ton flow technique which thought the voltage as well as frequency dependence of loads as well as generator regulation attributes. Fuzzy evaluation as well as pattern recognition was utilized for internet recognition of cave in sequences for just about a few working problems as of the stored catalog.

Kadyan [25] improved the stochastic analysis of a two unit parallel structure theme to degradation and assessment for viability of repair. Nourelfath et al. [26] analyzed multi formal method with planned manufacturing preparation as well as preventive upkeep. The authors likewise proposed a technique to assess the expense and also times of preventive maintenance, little fix as well as typical manufacturing capacity. A genetic algorithm was developed to cope with big size complications. In that job, the writers didn't evaluate the device under several failures.

Uemura et al. [27] considered accessibility styles of an incursion understanding structure, and also examined quantitative consequences of PM dependent on security road reliefs by utilizing Markov versions.

The performance of the steam generation scheme was assessed by Vora et al. [30]. A transition diagram was used to determine operational behavior, which was subsequently addressed using the Markov technique. Condition-based maintenance decisions have been proposed as a result of analyzing each availability. Gupta [31] discusses that the solitary unit system utilizing a base state.

Kim et al. [32] there are variety of research on standby machine of devices which can be repairable and which offers with evaluation of income and availability that entails the renovation that is preventive together with the above study, there may be a few interest can be given to the assessment of traits of reliability which can be income characteristic, availability and busy duration of machine which can be multi issue and regarding three out of four preparations having screw ups of 4 kinds. In the existing paper, got studied evaluation of income and availability of a machine that is redundant and repairable. This is three out of four installations with renovation of preventive which entails screw ups of 4 kinds through the use of the equations of chapman Kolmogorov method, improvement of express expression's for income characteristic and for availability of consistent country has been done.

Yusuf [33] there are number of studies on standby system of two units which are repairable and which deals with analysis of profit and availability that involves the maintenance which is preventive along with the above study, there is some attention will be given to the evaluation of characteristics of reliability which are profit function, availability and busy period of system which are multi component and involving 3 out of 4 arrangements having failures of four types. In the present paper, we have studied analysis of profit and availability of a system which is redundant and repairable.

Genetic algorithms for milk plant performance analysis and optimization were studied by Kajal and Tewari [34]. A probabilistic method was used to formulate the system in question formally, and the Markov procedure was second-hand to generate the differential equations. The optimal disappointment/ repair rates for the structure in question were calculated using Matlab.

Anand and Malik [35] cost-effectiveness of computer-assisted inspection was explored. There are two identical units in the computer organization. There are software and hardware components in both units. Both software and hardware can break at any time. It was assumed that hardware would need to be repaired and software would need to be replaced. In comparison to software replacement, hardware repair takes precedence.

Charzynska et al. [36] sensitivity of signaling pathways was investigated. Of this study, mathematical models are combined with experimental techniques to uncover the molecular machinery and relations in a scheme of interest. One of the goals of this study is to demonstrate how to use a range of mathematical approaches to model signaling network dynamics. Kim et al. [39] suggested the Recursive Decomposition Algorithm approach as a reliability evaluation technique for calculating the failure risk in networks with several initial connections, including sewage, electricity, water supply, and telecommunications. To reduce the overall cost of manufacturing, Doostprast et al. [40] urbanized a model for periodic PM of a scheme with optimal

dependability based on simulated annealing. To prioritize repairs across subsystems and feed the sugar industry's feeding unit, a verdict support system was developed.

Choundary and Goel [41] discusses that the accessibility study of two dissimilar subunits framework with a standby consuming imperfect switch over expedient in banking Industry.

Kumar and Malik [43] discussed the reliability modelling of a computer framework with priority of hardware repair over spare. Single repairman is provided for repair, up gradation and preventive maintenance. Failure time distribution of hardware and software follows the negative exponential and PM, repair time are arbitrary.

Ranjan et al. [44] introduced a risk model base on gamma plus exponential failures. Foraging failures are linked to gamma failures, whereas accident failures are linked to exponential failures. Monte Carlo simulation and the Markov chain model were used for analysis. In contrast to an exponential distribution accidental failure curve, the model's curve will resemble a gamma model with aging failure predominating.

Damcese and Sodany [46] studied the system's Availability and reliability. In this paper, a stochastic version for the standby framework with reestablishment at every not unusual place cause, failure is created to recall the Markov process's dependability measures. Evaluations are completed for precise standards of machine stricture. Sensitivity evaluation is likewise executed to represent the impact of numerous limits at the dependability feature and imply time to disappointment of machine. Statistical instance is certain to demonstrate outcomes found.

Devi et al. [47] discusses that the Reliability and Behavioral Analysis of Yarn Industry of Malwa Region Using RPGT. Goyal et al. [48] discussed the behavioral analysis of two units system by preventive maintenance in cooperation units and dilapidation in individual Unit.

Ritikesh and Goel [49] this paper discusses about the behavior analysis of a system which has a single unit which go to degradation following having complete failure by the procedure of RPGT. At the initial stage the unit is doing work at complete capacity and this can have failure of two types, first one is the direct failure mode and second is by the partially failure. We have one repairman who checks and repairs these units on every failure we cannot retain the unit into its actual capacity after the complete failure.

Tseng et al. [50] this paper involved with sensitivity and dependableness analysis of a system that is governable having ‘S’ units of heat standby and ‘M’ units which are operative. Service times and failure times of standby units or in service units are alleged to go after the sharing which is exponential.

Krishnamoorthy et al. [51] studied on the Reliability of a k-out-of-n system by patch up by a single server extend service exterior customers with pre-emption. Zaitseva et al. [52] studied on the Importance analysis of k-out-of-n multi-state system base on direct incomplete logic derivatives.

Optimal Computing Budget Allocation (OCBA), Petri-net, and other state-of-the-art techniques, tools, and software were all covered by Kumar and Tewari [55] after they reviewed the literature on dependability, availability, and maintainability.

Poh et al. [56] have provided a choice support system to develop an all-inclusive analytic net model that would explain the interdependency between the components in the current situation.

Malik and Tewari et al. [57] performed recital modeling of the water flow structure, a subsystem of a thermal plant. Using a probabilistic evaluation that considered failure and repair rates based on recital modeling and individual component not a success and repair rates, maintenance priority were assign to a variety of mechanism. Devi et al. [58] calculate the MTSF and system availability using RPGT. The path examination of a three-unit standby stochastic organization was performed in this paper. In this system, two units are initially in operation alongside a third similar unit in cold standby mode, with the concept of two kinds of disappointments and repair facilities using ordinary or expert servers. Kumar et al. [59] discussed the sensitivity analysis of 3:4:: smart system plant is shaped with a lonely server which

contains of 4 non-indistinguishable units within which elementary unit will add diminish state thanks to partial failure using RPGT technique. To evaluate the performance of complex systems with dynamic behavior, Penttinen et al. [60] proposed an Open Modeling approach that considers several RAM approaches.

Dahiya et al. [63] created a pan crystallization unit model with eight dissimilar subsystems using a fuzzy approach. In their 2019 study, Ahmadi et al. [64] used statistical approaches for performance modeling in combination with collapse and repair data to assess the reliability of the materials carrying system in an earth pressured balance tunnel uninteresting machine.

Kumar et al. [65] paper analyzed a sensitivity evaluation of a cold reserve device with precedence for defensive upkeep consist same devices with server disappointment the usage of RPGT. In this wok there are devices certainly considered individual among that is on-line at the same time as different is saved in cold standby mode? Single restore facility is to be had in 24*7. Repair and disappointment charges are continuous. State chart of basis delineating transition charges is drained. Analysis of work are executed which is probably useful to control in maintaining up one of a kind devices of device. Tables & figures are installation to have a take a observe and draw the conclusion.

Rajbala et al. [66] studied the structure modeling & psychoanalysis: a case revise EAEP manufacturing plant. Kumar et al. [67] studied the behavioral analysis of a washing unit in paper industry for scheme parameters using RPGT.

Chang et al. [68] suggested a technique to estimate the constraints on failure probability of a k-out-of-n system of components with potentially brittle behavior by breaking the system down into a set of subsystems and using linear programming (LP) and the universal generating function (UGF). Using numerical examples, the suggested method's accuracy and effectiveness are examined.

Rykov et al. [69] studied on the reliability function of a k-out-of-n system through specific restore time distribution. Agrawal et al. [72] discussed the profit analysis of a Water Treatment Reverse Osmosis Plant using the RPGT under specific conditions for scheme parameters. Numerical analysis is carried out for calculating the performance measures and their comparisons.

Kumari et al. [73] studied on the explanation of constrained problems by particle swarm optimization. Kumari et al. [74] discussed the behavior and profit analysis of a thresher plant in agriculture using RPGT under steady state.

Garg and Garg [75] studied the presentation analysis of the briquette machine in view of a neglected fault with PM used the Artificial Bee Colony algorithm to optimize the assessment of system profit.

Rohit and Poonia [77] study focuses on the mathematical modeling and sensitivity analysis of a steel mill made up of four subsystems using RPGT; all subsystem's exponential disappointment and specific repair rates are explored. Tables depict the structure behavior for repair rates of subsystems; the results demonstrate the practical trend and demonstrate that RPGT is a simple method for analyzing industrial facilities with similar topographies.

Kumar et al. [79] examined the RAM properties of various process industry systems. It gives a summary of how RAM practices have evolved historically and how they stand today within the intricate web of industries. To broaden the study, a thorough review of academic literature over the previous 20 years is carried out, including books, journals, and scholarly papers. The primary focus is on assessing RAM technique in various complex system and other process industries as well as diverse industrial contexts.

Bansal and Tyagi [80] analyzed the neural networks to optimize the casting process's performance characteristics. This article analyzes the availability, predictability, and state probability variation of the casting system using the Artificial Neural Network (ANN) technique.

An attempt has been made to determine the system's most important component. The analysis's findings will assist practitioners in selecting efficient maintenance plans.

Arya and Verma [81] analyzed the integration of simulation approaches with environment modeling 2; this research investigates a novel approach to reliability and availability prediction. The suggested methodology allow for accurate estimate of failure probabilities and system downtime under various scenarios by capturing the dynamic interaction between embedded systems and their operating settings. The results show that, in contrast to conventional methods that ignore outside factors, environment-aware modeling greatly improves the accuracy of reliability and availability predictions.

RAM indicators for behavior in relation to assorted system parameters: The behavior of RAM indices in relation to assorted system factors examined by various authors is summarized in Table 1.

MTTF: mean time to system failure
IP: inversely proportional
DP: Directly proportional

Table 1: *RAM indicators for behavior in relation to assorted system parameters*

Sr. No.	Author's Name (References No.)	Index	Failure Rates (FR)	Repair Rates (RR)	Preventive Maintenance (PM)	Exchange Rate (ER)
1	Borgonovo et al. [1]	Availability and MTTF	IP	DP	-	-
2	Tang [2]	MTTF	IP	-	DP	-
3	Ke and Wang [4]	MTTF	IP	DP	-	-
4	Goel et al. [8]	Availability	IP	-	DP	-
5	Gupta et al. [9]	Availability	IP	-	-	-
6	Rizwan et al. [13]	Availability	IP	DP	-	-
7	Wang and Chiu [14]	Cost Benefit and Availability	-	-	-	DP
8	Nilsson and Bertling [18]	Profit and Availability	IP	-	-	-
9	EI-Said and EI-Hamid [19]	Availability	IP	-	DP	-
10	Haggag et al. [22]	Profit	IP	-	DP	-
11	Mathew et al. [28]	Profit	IP	-	DP	-
12	Mathew et al. [29]	Profit	IP	-	DP	-
13	AI-Alawi et al. [37]	Availability and MTTF	IP	DP	-	-
14	Padmavathi et al. [38]	Availability and MTTF	IP DP	DP IP	DP IP	- -
15	Padmavathi et al. [42]	Availability and Number of visits	IP DP	DP IP	- -	- -
16	Haggag et al. [45]	Profit and Availability	-	-	DP	-
17	Ram and Manglik [53]	Profit	IP	-	-	-
18	Adlakha et al. [54]	Profit	-	-	-	DP
19	Taj et al. [61]	Availability	IP	DP	DP	-
20	Kumar et al. [62]	Availability,	IP	-	-	-

		MTTF and Profit				
21	Gupta et al. [70]	MTTF	IP	-	-	-
22	Gupta et al. [71]	MTTF	IP	-	-	-
23	Rajbala et al. [76]	Availability	IP	-	-	-
24	Dava and Lazakis [78]	Availability	IP	DP	-	-
25	Kumar et al. [79]	Availability and Maintainability	IP	-	DP	-
26	Arya and Verma [81]	Availability	IP	DP	-	-

IV. Research Gap

Following a careful examination of the literature, the following succinct observations are made on the submission of RAM approach in various complex process industry systems:

- In contrast to product-based businesses, the majority of research has concentrated on reliability in progression industries such as bread plants, urea fertilizer plants, rice plants, paper industries, dairy plants, and polytube plants. Few academics have looked at the relationship between availability and breakeven analysis, despite the fact that many have investigated ways to increase plant availability through efficient maintenance.
  It is noteworthy that the time required to arrive at the break-even point is directly shortened by increased plant availability. The majority of research has employed Markov modeling to assess industrial systems' performance using steady-state availability. Few, though, have attempted to solve these mathematical models in more practical industrial settings.

V. Conclusion

Through the literature review, we have concentrated on the diverse perspectives offered by a large number of reliability engineering researchers. Numerous aspects that affect a system's dependability have been analyzed. Studies on availability analysis of different process sectors have also been conducted. Following a comprehensive literature review, this piece will present an impression of the RAM methodology and discuss a variety of RAM-related issues, tools, and strategies used in dissimilar process industries to reduce overall failure costs, including maintenance and unplanned shutdown costs. The many models, software applications, tools, and processes can be used both in the design and operating phases. The two most common approaches in the literature are the dependability approach and the maintenance method. When reliability focuses on the many possibilities, system availability increases. On the other side, the maintenance method's primary focus is the minimum repair policy. Numerous results on RAM approaches were found in a review of the literature, along with several research gaps that require consideration and filling. The literature has a large number of publications on RAM (performance modeling, analysis, and optimization approaches) from several process industries, including paper, heat, fertilizer, pipe, and sugar. The creation and evaluation of mathematical models for theoretical performance is the only study that has been documented in the literature. Furthermore, an appropriate maintenance decision support system can be constructed using a range of RAM methodologies, depending on the behavior and performance characteristics of the assortment of system in the related process industries. Following a review of pertinent literature, the RAM approach can be used to prioritize equipment repairs when they happen during operation, identify production bottlenecks, detect failures during the design phase, compare and contrast various production design options, and optimize maintenance schedules.

VI. Future Scope

As demonstrated in this study, researchers have made important charity to the pasture of dependability analysis through conventional modeling. It is now time to seek out some diversification and employ novel maintenance models that incorporate fuzzy and probabilistic methodologies. At various information levels, novel stochastic process is needed to satisfy the new necessities on behalf of repairable system. Instead of employing the traditional methods, new algorithms might be created to get the answers quickly. It would be much easier to arrive at near approximations to the actual results if the focus was on statistical inference application on preservation difficulties rather than merely searching for probability applications. The analysis in determining the resilience of maintenance models can also be supported by the statistical use of the goodness of fit test.

References

[1] Borgonovo, E., Marseguerra, M., and Zio, E. A. (2000). Monte Carlo methodological approach to plant availability modeling with maintenance, aging and obsolescence. *Reliability Engineering & System Safety,* 61–73.

[2] Tang, J. (2001). Mechanical system reliability analysis using a combination of graph theory and Boolean function. *Reliability Engineering & System Safety*, 21–30.

[3] Avontuur, G. C., and Van, D. W. K. (2002). Systems reliability analysis of mechanical and hydraulic drive systems. *Reliability Engineering& System Safety,* 121–130.

[4] Ke, J., and Wang, K. (2002). The reliability analysis of balking and reneging in a repairable system with warm standbys. *Quality and Reliability Engineering*, 467 – 478.

[5] Arulmozhi, G. (2002). Exact equation and an algorithm for reliability evaluation of K-out-of-N: G system. *Reliability Engineering & System Safety,* 87–91.

[6] Elegbede, C., and Adjallah K. (2003). Availability allocation to repairable systems with genetic algorithms: a multi-objective formulation. *Reliability Engineering & System Safety,* 319–30.

[7] Ebrahimi, N. B. (2003). Indirect assessment of system reliability. *IEEE Transactions on Reliability,* 58–62.

[8] Goel, H. D., Grievink, J., and Weijnen, M. P. (2003). Integrated optimal reliable design, production, and maintenance planning for multipurpose process plants. *Computers & chemical engineering,* 1543–1555.

[9] Gupta, P., Singh, J., and Singh, I. P. (2004). Availability Analysis of Soap Cakes production System – A Case Study. *Proc. National Conference on Emerging Trends in Manufacturing System, SLIET, Longowal (Punjab),* 283-295.

[10] Xie, L., Zhou, J., and Hao, C. (2004). System-level load–strength interference based reliability modeling of k-out-of-n system. *Reliability Engineering & System Safety*, 311-317.

[11] Gupta, P., Lal, A. K., Sharma, R. K., and Singh, J. (2005). Behavioural Study of the Cement Manufacturing Plant- A Numerical Approach. *Journal of Mathematics and Systems Science*, 50-70.

[12] Samrout, M., Yalaoui, F., Châtelet, E., and Chebbo, N. (2005). New methodsto minimize the preventive maintenance cost of series–parallel systems using ant colony optimization. *Reliability engineering & system safety,* 346–354.

[13] Rizwan, S. M., Chauhan, H., and Taneja, G. (2005). Stochastic analysis of systems with accident and inspection. *Emirates Journal of Engineering Research,* 81-87.

[14] Wang, K., and Chiu, L. (2006). Cost benefits analysis of availability systems with warm standby units and imperfect coverage. *Applied Mathematics and Computation,* 1239–1256.

[15] Marseguerra, M., Zio, E., and Martorell, S. (2006). Basics of genetic algorithms optimization for RAMS applications. *Reliability Engineering & System Safety*, 977–91.

[16] Gupta, P., Lal, A. K., Sharma, R. K., and Singh, J. (2007). Analysis of reliability and availability of serial processes of plastic-pipe manufacturing plant. *International Journal of Quality & Reliability Management,* 404-419.

[17] Krishnamoorthy, A., Viswanath, C. N., and Deepak, T. G. (2007). Reliability of a k-out-of-n-system with Repair by a Service Station Attending a Queue with Postponed Work. *International Journal of Reliability Quality and Safety Engineering,* 379–398.

[18] Nilsson, J., and Bertling, L. (2007). Maintenance management of wind power systems using condition monitoring systems life cycle cost analysis for two case studies. *IEEE Transactions on Energy Conversion*, 223-229.

[19] El-Said, K., and El-Hamid, R. (2008). Comparison of reliability characteristics of two systems with preventive maintenance and different modes. *Information and Management Sciences,* 107-118.

[20] Sachdeva, A., Kumar, D., and Kumar, P. (2008). Reliability analysis of pulping system using Petri nets. *International Journal of Quality & Reliability Management,* 860-877.

[21] Kumar, S., Tewari, P. C., and Kumar, S. (2009). Performance evaluation and availability analysis of ammonia synthesis unit in a fertilizer plant. *Journal of Industrial Engineering, International*, 17–26.

[22] Haggag, M. (2009).Cost analysis of a system involving common-cause failures and preventive maintenance. *Journal of Mathematics and Statistics*, 305-310.

[23] Khanduja, R., Tewari, P. C., and Chauhan, R. S. (2009). Performance analysis of screening unit in a paper plant using genetic algorithm. *Journal of Industrial and Systems Engineering,* 140–151.

[24] Hazra, J., and Sinha, A. K. (2009). Identification of catastrophic failures in power system using pattern recognition and fuzzy estimation. *IEEE Transactions on Power Systems*, 378-387.

[25] Kadyan, M. S., Kumar, J., and Malik, S. C. (2010). Stochastic Analysis of a Two Unit Parallel System Subject to Degradation and Inspection for Feasibility of Repair. *Journal of Mathematics and Systems Science,* 5-13.

[26] Nourelfath, M., Fitouhi, M., and Machani, M. (2010). An integrated model for production and preventive maintenance planning in multi-state systems. *IEEE Transactions on Reliability*, 496-506.

[27] Uemura, T., Dohi, and Kaio, N. (2010). Availability analysis of an intrusion tolerant distributed server system with preventive maintenance. *IEEE Transactions on Reliab*ility, 18-29.

[28] Mathew, A. G., Rizwan, S. M., Majumder, M., Ramachandran, K., and Taneja, G. (2010). Reliability modeling and analysis of a two-unit parallel CC plant with different installed capacities. *Journal of Manufacturing Engineering*, 197-204.

[29] Mathew, A. G., Rizwan, S. M., Majumder, M., Ramachandran, K., and Taneja, G. (2011). Reliability analysis of an identical two-unit parallel CC plant system operative with full installed capacity. *International Journal of Perform ability Engineering,* 179-185.

[30] Vora, Y., Patel, M. B., and Tewari, P. C. (2011). Simulation model for stochastic analysis and performance evaluation of steam generator system of a thermal power plant. *International Journal of Engineering Science and Technology,* 5141–5149.

[31] Gupta, V. K. (2011). Analysis of a single unit system using a base state. *Aryabhatta Journal of Mathematics and Informatics*, 59-66.

[32] Kim, D. S., Lee, S. M., Jung, J. H., Kim, T. H., Lee, S., and Park, J. S. (2012). Reliability and availability analysis for an on board computer in a satellite system using standby redundancy and rejuvenation. *Journal of mechanical science and technology*, 2059-2063.

[33] Yusuf, I. (2012). Availability and Profit Analysis of 3 out of 4 Repairable Systems with Preventive Maintenance. *International Journal of Applied Mathematics Research*, 510-519.

[34] Kajal, S., and Tewari, P. C. (2012). Performance optimization for skim milk powder unit of a dairy plant using genetic algorithm. *IJE transactions B: Applications*, 211–221.

[35] Anand, and Malik, S. C. (2012). Analysis of a computer system with arbitrary distributions for h/w and s/w replacement time and priority to repair activities of h/w over replacement of s/w. *International Journal of System Assurance Engineering and Management*, 230-236.

[36] Charzynska, A., Nalecz, A., Rybinski, M., and Gambin (2012). Sensitivity analysis of mathematical models of signalling pathways. *Journal of Biotechnology, Computational Biology and Bio Nano Technology*, 291-308.

[37] Al, Alawi, M., Mathew, A. G., and Collington, J. (2012). Attaining Zero Failure Performance for GIV Gulfstream Aircraft through Reliability Modeling and Analysis. *International Journal of Science, Engineering and Technology Research*, 1-10.

[38] Padmavathi, N., Rizwan, S. M., Pal, A., and Taneja, G. (2013). Probabilistic analysis of an evaporator of a desalination plant with priority for repair over maintenance. *International Journal of Scientific and Statistical Computing*, 1-8.

[39] Kim, Y., and Kang, W. H. (2013). Network reliability analysis of complex systems using a non-simulation-based method. *Reliability engineering & system safety,* 80–88.

[40] Doostparast, M., Kolahan, F., and Doostparast, M. (2014). A reliability- based approach to optimize preventive maintenance scheduling for coherent systems. *Reliability Engineering & System Safety*, 98–106.

[41] Choundary, N., and Goel, P. (2014). Behavior Analysis of Utensil Industry. *International Journal of Multidisciplinary Researcher and Development,* 82-89.

[42] Padmavathi, N., Rizwan, S. M., Pal, A., and Taneja, G. (2014). Probabilistic analysis of desalination plant with major and minor failures and shut down during winter season. *International Journal of Scientific and Statistical Computing*, 15-23.

[43] Kumar, A., and Malik, S. (2014). Reliability Modelling of a Computer System with Priority to H/W Repair over Replacement of H/W and Up-gradation of S/W Subject to MOT and MRT. *Jordan Journal of Mechanical & Industrial Engineering,* 233-244.

[44] Ranjan, R., Singh, S., and Upadhyay, S. K. (2015). A Bayes analysis of a competing risk model based on gamma and exponential failures. *Reliability Engineering & System Safety*, 35–44.

[45] Haggag, M. (2015). Profit analysis and availability of a repairable redundant 3-out-of-4 system involving preventive maintenance. *International Journal of Scientific and Engineering Research*, 1161-1173.

[46] Damcese, M. A., and Sodany, N. H. (2015). Reliability and sensitivity analysis of the K-out-of-N:G warm standby parallel repairable system with replacement at common cause failure using markov process model. *International Journal of Enhanced Research in Science Technology and Engineering*, 53-65.

[47] Devi, B., Bansal, R., and Goel, P. (2015). Reliability and Behavioral Analysis of Yarn Industry of Malwa Region Using RPGT (A Case Study). *International Journal of Engineering Technology and Management Sciences,* 135-145.

[48] Goyal, V., Goel, R., and Goel, P. (2015). Behavioral Analysis of Two Unit System with Preventive Maintenance in Both Units and Degradation in One Unit. *International Journal of Engineering Technology and Management Sciences,* 120-130.

[49] Ritikesh, and Goel, P. (2015) Availability Modeling of Single Unit System Subject to Degradation Post Repair After Complete Failure using RPGT. *International Conference on Innovation Research in Engineering, Science and Management,* 57-65.

[50] Tseng, C. Y., Wu, L. C., and Jia Y. C. (2016). Reliability and Sensitivity Analysis of the Controllable Repair System with Warm Standbys and Working Breakdown. *Computers & Industrial Engineering*, 84-92.

[51] Krishnamoorthy, A., Sathian, M. K., and Viswanath C. N. (2016). Reliability of a k-out-of-n system with repair by a single server extending service external customers with pre-emption. *Reliability: Theory & Applications,* 61–93.

[52] Zaitseva, E., Kvassay, M., Levashenko, V., and J. Kostolny (2016). Importance analysis of k-out-of-n multi-state systems based on direct partial logic derivatives. *Proceedings of the 12th International Conference, ICTERI,* 441–457.

[53] Ram, M., and Manglik, M. (2016). Stochastic Biometric System Modelling with Rework Strategy. *International Journal of Mathematical, Engineering and Management Scienc*es, 1–17.

[54] Adlakha, N., Taneja, G., and Shilpi. (2017). Reliability and cost-benefit analysis of a two-unit cold stand by system used for communication through satellite with assembling and activation time. *International Journal of Applied Engineering Research,* 9697-9702.

[55] Kumar, P., and Tewari, P. (2017). Performance analysis and optimization for CSDGB filling system of a beverage plant using particle swarm optimization. *International Journal of Industrial Engineering Computations,* 303–314.

[56] Poh, K. L., and Liang, Y. (2017). Multiple-criteria decision support for a sustainable supply chain: applications to the fashion industry. *Informatics Multidisciplinary Digital Publishing,* 36-42.

[57] Malik, S., and Tewari, P. C. (2018). Performance modeling and maintenance priorities decision for the water flow system of a coal-based thermal power plant. *International Journal of Quality & Reliability Management,* 996–1010.

[58] Devi, M., Gupta, V. K., and Kumar, V. (2018). Path Analysis for MTSF and Availability of a Three-Unit Standby Stochastic System. *Aryabhatta Journal of Mathematics & Informatics*, 405-412.

[59] Kumar, A., Garg, D., Goel, P., and Ozer, O. (2018). Sensitivity analysis of 3:4:: good system. *International Journal of Advance Research in Science and Engineering,* 851-862.

[60] Penttinen, J. P., Gutleber, J., and Niemi, A. (2018). An open modelling approach for availability and reliability of systems-Open MARS. *Reliability Engineering & System Safety,* 1-34.

[61] Taj, S., Rizwan, S. M., Alkali, B., Harrison, D., and Taneja, G. (2018). Comparative analysis of reliability models of a cable plant portraying summer and winter operating strategy. *In: 9thInternational Conference on Quality, Reliability, Infocom Technology and Business Operations. Delhi, India: Springer*, 1-10.

[62] Kumar, A., Pawar, D., and Malik, S. C. (2019). Profit analysis of a warm stand by non-identical unit system with single server performing in normal/abnormal environment. *Life Cycle Reliability and Safety Engineering,* 219–226.

[63] Dahiya, O., Kumar, A., and Saini, M. (2019). Mathematical modeling and performance evaluation of A-pan crystallization system in a sugar industry. *SN Applied Sciences,* 339-345.

[64] Ahmadi, S., Moosazadeh, S., Hajihassani, M., Moomivand, H., and Rajaei M. M. (2019). Reliability, availability and maintainability analysis of the conveyor system in mechanized tunneling. *Measurement*, 756–764.

[65] Kumar, A., Garg, D., and Goel, P. (2019). Sensitivity analysis of a cold standby system with priority for preventive maintenance. *Journal of Advance and Scholarly Researches in Allied Education,* 253-258.

[66] Rajbala, Kumar, A. and Garg, D. (2019). Systems Modeling and Analysis: A Case Study of EAEP Manufacturing Plant. *International Journal of Advanced Science and Technology*, 250-259.

[67] Kumar, A., Garg, D., and Goel, P. (2019). Mathematical modeling and behavioral analysis of a washing unit in paper mill. *International Journal of System Assurance Engineering and Management,* 1639-1645.

[68] Chang, Y., Mai, Y., Linli, Y., Liuming Yu., Ying, C., Cheng, Y., and Jinhe, G., (2020). Reliability Analysis of k-out-of-n Systems of Components with Potentially Brittle Behavior by Universal Generating Function and Linear Programming. *Mathematical Problems in Engineering*, 1-15.

[69] Rykov, V., Kozyrev, D., Filimonov, A., and Ivanova N. (2020). On reliability function of a k-out-of-n system with general repair time distribution. *Probability in the Engineering and Informational Sciences,* 885–902.

[70] Gupta, N., Saini, M., and Kumar, A. (2020). Behavioral Analysis of Cooling Tower in Steam Turbine Power Plant using Reliability, Availability, Maintainability and Dependability Investigation. *Journal of Engineering Science and Technology Review,* 191–198.

[71] Gupta, N., Kumar, A., and Saini, M. (2021). Reliability and Maintainability Investigation of Generator in Steam Turbine Power Plant using RAMD analysis. *Journal of Physics: Conference Series,* 012009-012015.

[72] Agrawal, A., Garg, D., Kumar, A., and Kumar, R. (2021). Performance Analysis of the Water Treatment Reverse Osmosis Plant. *Reliability: Theory & Applications,* 16-25.

[73] Kumari, S., Khurana, P., Singla, S., and Kumar, A. (2021) Solution of constrained problems using particle swarm optimiziation. *International Journal of System Assurance Engineering and Management,* 1-8.

[74] Kumari, S., Khurana, P., and Singla, S. (2021). Behavior and profit analysis of a thresher plant under steady state. *International Journal of System Assurance Engineering and Management,* 1-12.

[75] Garg, D., and Garg, R. (2022). Performance analysis of the briquette machine considering a neglected fault with preventive maintenance. *International Journal of System Assurance Engineering and Management,* 1-8.

[76] Rajbala, Kumar, A., and Khurana, P. (2022). Redundancy allocation problem: Jayfe cylinder Manufacturing Plant. *International Journal of Engineering, Science & Mathematic,* 1-7.

[77] Rohit, and Poonia, M. S. (2023). Sensitivity Analysis of a Steel Industrial Plant in Hisar District Using RPGT. *Eur. Chem. Bull.,* 17816-17823.

[78] Daya, A. A., and Lazakis, I. (2023). Developing an advanced reliability analysis framework for marine systems operations and maintenance. *Ocean Engineering,* 113766-113770.

[79] Kumar, P., Kumar, D., Chalisgaonkar, R., Sharma, V. K., and Rai, K. S. (2024). A Critical Review of Ram Methodology: Analysis and Performance Evaluation in Industrial Complexities. *Reliability Theory and its Applications,* 83-89.

[80] Bansal, S., and Tyagi, S. L. (2024). Availability and profit optimization of continuous casting system of the steel industry using artificial neural network technique. *Reliability: Theory & Applications,* 47-58.

[81] Arya, R., and Verma, A. (2025). Reliability and availability prediction of embedded systems based on environment modeling and simulation. *ISAR Journal of Science and Technology,* 74-78.

ANALYSIS OF JOINT MULTIPLY TYPE-II CENSORED DATA USING THE GIBBS SAMPLER ALGORITHM

Vishal Singh, Akanksha Gupta and S. K. Upadhyay

•

Department of Statistics
Banaras Hindu University, Varanasi - 221 005, India.
vishalsingh4096@gmail.com

Abstract

This paper introduces a systematic approach for analyzing data under joint multiply type-II censoring. The study assumes a one-parameter exponential lifetime distribution and focuses on estimating unknown parameters. The maximum likelihood method is used to obtain frequentist point estimates, while a Bayesian framework is adopted to draw the corresponding Bayes inferences. To effectively handle censored data, an extended Gibbs sampler algorithm is employed, treating the unknown observations as further unknowns and estimating them accordingly. This methodology ensures a comprehensive and robust inference process by simultaneously addressing parameter uncertainty and the challenges posed by the censored observations.

Keywords: Joint multiply type-II censoring, Non-informative prior, Maximum likelihood estimation, Bayes inferences, One-sample prediction, Gibbs sampler.

1. Introduction

A life testing experiment is a widely used experimentation process for assessing the reliability and lifespan of products, materials, or biological systems. It involves subjecting units to specific conditions and monitoring their performance over time until failure occurs, or a predefined endpoint is reached. To enhance efficiency, reduce testing costs, and expedite results, such experiments are often terminated before all failures are observed. A variety of censoring schemes have been introduced in the existing research to address these challenges. Censoring occurs when the exact failure times of some units are unknown, which can significantly impact the validity and precision of statistical inferences drawn from the data. A censoring scheme that balances time, cost, and efficiency is of great interest in life testing studies.

Among the various censoring schemes, type-I, type-II, and interval censoring are the most prevalent. Type-I censoring occurs when the study is concluded after a fixed duration, regardless of the number of failures observed. In contrast, type-II censoring involves stopping the experiment once the number of items failed reaches a fixed count, even if it extends beyond the expected duration. In interval censoring, the exact time of failure is not observed but is known to fall within a certain time interval (a, b), where $b > a$. Most existing research focuses on single-sample censored data under these schemes, with numerous studies addressing their individual aspects. However, there is a growing recognition of the need for a comprehensive framework to analyze data under joint censoring schemes.

Joint censoring schemes are particularly relevant in fields such as medical research, reliability engineering, and social sciences, where different censoring mechanisms may coexist in a single study ([4]). For instance, when comparing two products or treatments within the same setting,

a two-sample joint censoring approach can be employed. This method entails conducting a life-testing experiment on independent samples from two different groups simultaneously, with the study concluding upon the happening of the targeted event, either at a predetermined time or after observing a specified number of failures. Researchers have introduced various joint censoring schemes to enhance the efficiency of life testing experiments involving multiple groups. Notable examples include the joint type-II progressive censoring, balanced joint type-II progressive censoring, joint type-I generalized hybrid censoring, and joint type-II generalized progressive hybrid censoring (see, for example, [8], [7] and [1], etc.). Among these, the joint multiply type-II censoring scheme (see [2]) is particularly useful for simultaneously evaluating two similar products under the same facility. It can also model medical studies involving two groups by tracking the occurrence of predefined events. This scheme offers flexibility by encompassing various censoring approaches, such as multiply type-II, type-II right, left type-II, mid, interval, doubly type-II, and left censoring, etc. as special cases. More details on these special cases can be found in [14], [13], and [6].

In reliability analysis, lifetime distributions are fundamental for evaluating product performance. Various lifetime models including the exponential, Weibull, gamma, and lognormal distributions, have been widely studied. The selection of suitable model depends on factors like the failure rate of the product. Among these, the exponential distribution holds particular significance due to its mathematical simplicity and suitability for scenarios where the failure rate remains constant. Extensive research has explored the exponential lifetime model under different censoring schemes, although the applicability of the exponential model has often been constrained by its underlying assumption of a constant failure rate. The Weibull, gamma and lognormal distributions, on the other hand, have monotonic failure rate and, therefore, have wider applicability across various settings relative to the exponential model. These models are, however, slightly more difficult for inferential developments, especially under conditions of complex censoring embedded in the data. One can refer to [5] for a detailed description of various lifetime models and the corresponding inferential developments. The description gives an idea of the complexity involved with these models, especially when dealing with many of the above mentioned censoring schemes.

Once a lifetime distribution is selected for a given problem involving any type of censoring mechanism, the next step is to infer the unknown parameters of the distribution. This requires the application of various inferential techniques. A substantial body of literature exists on this topic, encompassing both frequentist and Bayesian approaches. While both methods have their own merits, we prefer the Bayesian approach due to its inherent advantages, such as incorporating prior knowledge and providing a comprehensive probabilistic framework for inferential developments. The censored data, however, introduce unique challenges to Bayesian analysis, primarily due to the presence of often non-closed forms of corresponding cumulative distribution function terms in the likelihood. These complexities often lead to intractable posterior distributions and computational difficulties in the form of intractable integrations. To overcome these difficulties, various approximate techniques have been developed in the literature. These include a number of analytical approximation techniques and sometimes even numerical integration techniques. The simulation-based approaches are other alternatives that are often user-friendly and straightforward to implement. A few such procedures include sampling-importance-resampling, the Gibbs sampler algorithm and, more generally, the Metropolis-Hastings algorithm, etc. These latter methods facilitate efficient Bayesian implementation, making them particularly useful for analyzing censored lifetime data.

This paper employs the Gibbs sampler algorithm and its extension to address problems involving censored data (see [15], [11]). By leveraging this technique, the complexity of the likelihood function, which leads to an intractable posterior distribution, can be significantly reduced. The study focuses on estimating parameters under joint multiply type-II censoring using both maximum likelihood (ML) and Bayesian approaches. A non-informative prior is employed for the Bayesian inferences. Also, the inferences for the unknown censored observations are obtained by computing the highest predictive density intervals (HPrDI) and identifying the mean

value from the generated samples corresponding to censored data based on the Gibbs outcome.

The layout of this paper is as follows: The next section outlines the joint multiply type-II censoring scheme and presents the modeling framework under the assumption of an exponential distribution. Section 3 details the inferential developments, with two subsections dedicated to deriving the ML estimates and the Bayes inferences for the model parameters, respectively. The discussion is also focused on predicting the unknown censored observations, treating them as a one-sample prediction problem. A step-wise systematic discussion is also provided to facilitate the practical ease of implementing the considered algorithm. To demonstrate the practical effectiveness of the proposed methodology, a real dataset of failure times from air conditioning systems in two planes, "7914" and "7913" (sourced from [9]), is analyzed, and the corresponding results are obtained. Finally, the paper concludes with a summary of key findings with an extensive list of relevant references.

2. The Joint Multiply Type-II Censoring Scheme and the Model Formulation

To begin with, let us first describe the joint multiply type-II censoring scheme considered in this paper. Let us consider a situation where the experimenter aims to investigate the failure times of a number of two similar products, referred to as Product 1 and Product 2, operated under the same environment. The initial step involves randomly selecting m items from Product 1 and n items from Product 2, ensuring that each item has an equal probability of being chosen. Subsequently, the experimenter proceeds with conducting a life testing experiment on both the products simultaneously. The experimenter defines k as the predetermined number of failures that he aims to observe with the assumption that any of the failures could occur from either Product 1 or Product 2. The experiment terminates upon observing the r_k^{th} failure. Subsequently, all surviving units are withdrawn from the testing process.

Assume further that a_k represents the number of failures out of k failures, from Product 1, and b_k represents the rest of the failures that are from Product 2. Let Y represents the failure times of items from Product 1 and W represents the failure times of items corresponding to Product 2. The density and the distribution function of Y are assumed to be $f(y)$ and $F(y)$, respectively. Similarly, the density and the distribution function of W are assumed to be $g(w)$ and $G(w)$, respectively. Consider two independent random samples: $Y_1, Y_2, \ldots, Y_m$ of size m from Product 1 and $W_1, W_2, \ldots, W_n$ of size n from Product 2. Let us next consider that $N = m + n$ represents the total number of items under testing from the two products together. Further assume that $X_1, X_2, X_3, \ldots, X_N$ are the pooled ordered failure times of the two products when considered in ascending order. It may be noted that if two or more observations have identical values (ties) during the ordering process, they are randomly shuffled at that specific point of time. Also, since one parameter exponential distribution with mean parameter θ_1 is assumed as the appropriate model for Product 1, one can write the corresponding density and distribution function, respectively, as

$$\begin{aligned} f(y) &= \frac{1}{\theta_1} exp\left(-\frac{y}{\theta_1}\right) \; ; \; y > 0, \; \theta_1 > 0 \\ F(y) &= 1 - exp\left(-\frac{y}{\theta_1}\right). \end{aligned} \tag{1}$$

Similarly, for Product 2, if one assumes an exponential model with mean parameter θ_2, the corresponding density and distribution functions can be written, respectively, as

$$\begin{aligned} g(w) &= \frac{1}{\theta_2} exp\left(-\frac{w}{\theta_2}\right) \; ; \; w > 0, \; \theta_2 > 0 \\ G(w) &= 1 - exp\left(-\frac{w}{\theta_2}\right). \end{aligned} \tag{2}$$

Assume further that we aim to observe only k failures with failure times $X_{r_1}, X_{r_2}, X_{r_3}, \ldots, X_{r_k}$ from the N items under test. Also suppose that u_i denotes the number of unobserved failures of

Product 1 in the interval $(X_{r_{i-1}}, X_{r_i})$ and v_i denote the number of unobserved failures of Product 2 in the same interval, for $i = 1, 2, \ldots, k$. Here X_{r_0} is assumed to be 0. After the k^{th} failure is observed, let u_{k+1} denote the number of items from Product 1 that are still functioning and v_{k+1} denote the number of items from Product 2 that are still functioning in the experiment. Let $Z_i\,(i = 1, 2, 3, \ldots, k)$ be the indicator variable with $Z_i = 1$ denoting that the i^{th} failure is from Product 1 and $Z_i = 0$, denoting that the i^{th} failure is from Product 2. So, under this assumption, the likelihood function with data comprising of (Z, X) can be written as

$$L = \frac{m!n!}{\prod_{i=1}^{k+1} u_i! v_i!} F(x_{r_1})^{u_1} G(x_{r_1})^{v_1} \prod_{i=2}^{k} [F(x_{r_i}) - F(x_{r_{i-1}})]^{u_i} \prod_{i=2}^{k} [G(x_{r_i}) - G(x_{r_{i-1}})]^{v_i} \times [1 - F(x_{r_k})]^{u_{k+1}} [1 - G(x_{r_k})]^{v_{k+1}} \prod_{i=1}^{k} [f(x_{r_i})]^{z_i} \prod_{i=1}^{k} [g(x_{r_i})]^{1-z_i} \tag{3}$$

The likelihood function given above will lay the foundation for estimating the unknown parameters using different approaches. For further information on this censoring scheme, one may refer to [2]. The paper considers ML method of estimation as well as the Bayesian method for drawing inferences, the latter using vague priors for the parameters.

3. Inferential developments

3.1. Maximum likelihood method

Using (1) and (2) in (3), the likelihood function for the present situation can be written as

$$L = \frac{m!n!}{\prod_{i=1}^{k+1} u_i! v_i!} \left(1 - e^{-\frac{x_{r_1}}{\theta_1}}\right)^{u_1} \left(1 - e^{-\frac{x_{r_1}}{\theta_2}}\right)^{v_1} \prod_{i=2}^{k} \left(e^{-\frac{x_{r_{i-1}}}{\theta_1}} - e^{-\frac{x_{r_i}}{\theta_1}}\right)^{u_i} \prod_{i=2}^{k} \left(e^{-\frac{x_{r_{i-1}}}{\theta_2}} - e^{-\frac{x_{r_i}}{\theta_2}}\right)^{v_i} \times \left(e^{-\frac{x_{r_k}}{\theta_1}}\right)^{u_{k+1}} \left(e^{-\frac{x_{r_k}}{\theta_2}}\right)^{v_{k+1}} \prod_{i=1}^{k} \left(\frac{1}{\theta_1} e^{-\frac{x_{r_i}}{\theta_1}}\right)^{z_i} \prod_{i=1}^{k} \left(\frac{1}{\theta_2} e^{-\frac{x_{r_i}}{\theta_2}}\right)^{1-z_i} \tag{4}$$

The ML estimates of θ_1 and θ_2 can be obtained by maximizing (4) with varying θ_1 and θ_2. This involves first taking the logarithm on both the sides of (4), followed by partial differentiation of the resulting expression with respect to θ_1 and θ_2 separately. By equating the partial derivatives to zero, one can obtain

$$\begin{aligned}
\frac{\partial logL}{\partial \theta_1} &= -\frac{u_1}{\theta_1^2} \left\{ \frac{x_{r_1} e^{\left(-x_{r_1}/\theta_1\right)}}{1 - e^{\left(-x_{r_1}/\theta_1\right)}} \right\} + \sum_{i=2}^{k} \frac{u_i}{\theta_1^2} \left\{ \frac{x_{r_{i-1}} e^{\left(-x_{r_{i-1}}/\theta_1\right)} - x_{r_i} e^{\left(-x_{r_i}/\theta_1\right)}}{e^{\left(-x_{r_{i-1}}/\theta_1\right)} - e^{\left(-x_{r_i}/\theta_1\right)}} \right\} + \frac{u_{k+1} x_{r_k}}{\theta_1^2} \\
&\quad + \sum_{i=1}^{k} \frac{z_i x_{r_i}}{\theta_1^2} - \frac{a_k}{\theta_1} = 0, \\
\frac{\partial logL}{\partial \theta_2} &= -\frac{v_1}{\theta_2^2} \left\{ \frac{x_{r_1} e^{\left(-x_{r_1}/\theta_2\right)}}{1 - e^{\left(-x_{r_1}/\theta_2\right)}} \right\} + \sum_{i=2}^{k} \frac{v_i}{\theta_2^2} \left\{ \frac{x_{r_{i-1}} e^{\left(-x_{r_{i-1}}/\theta_2\right)} - x_{r_i} e^{\left(-x_{r_i}/\theta_2\right)}}{e^{\left(-x_{r_{i-1}}/\theta_2\right)} - e^{\left(-x_{r_i}/\theta_2\right)}} \right\} + \frac{v_{k+1} x_{r_k}}{\theta_2^2} \\
&\quad + \sum_{i=1}^{k} \frac{(1 - z_i) x_{r_i}}{\theta_2^2} - \frac{b_k}{\theta_2} = 0.
\end{aligned} \tag{5}$$

It can be seen that the two equations in (5) are not obtained in explicit forms and, therefore, a numerical solution appears to be the only possibility. Among various approaches, the Newton-Raphson method is particularly favoured as it was seen to efficiently determine the ML estimates for both θ_1 and θ_2. It may be noted that obtaining ML estimates is not the actual objective of the paper; rather, the same are obtained to aid in the Bayesian developments that follow in the next subsection. The ML estimates can also be used to provide a comparative study with the Bayesian estimates of the two parameters where censoring also plays a crucial role.

3.2. Bayesian method

This subsection focuses on the Bayesian reasoning with the ultimate objective of estimating the two parameters, θ_1 and θ_2. It may be noted that the Bayesian method begins by defining suitable prior distributions for the parameters. This requires the expertise of a statistician to accurately translate the beliefs and insights of subject-matter experts into a quantifiable form. In situations where limited or no information is available about the parameters and expert input is absent, a non-informative prior is often a suitable choice. There can be a variety of ways of specifying non-informative priors, but we consider the simplest and the most widely used Jeffreys' prior for the two scale parameters of considered exponential models (see also [14]). Obviously, the priors for θ_1 and θ_2 can be written as

$$\begin{aligned} \pi_1(\theta_1) &\propto \frac{1}{\theta_1}, \\ \pi_2(\theta_2) &\propto \frac{1}{\theta_2}. \end{aligned} \tag{6}$$

Next, by combining the likelihood in (4) with the priors in (6) using the Bayes theorem, the posterior distribution can be expressed up to proportionality as

$$\begin{aligned} p(\theta_1, \theta_2 | \underline{x}) \propto & \frac{1}{\theta_1^{a_k+1}\theta_2^{b_k+1}} \left(1 - e^{-\frac{x_{r_1}}{\theta_1}}\right)^{u_1} \left(1 - e^{-\frac{x_{r_1}}{\theta_2}}\right)^{v_1} \\ & \times \prod_{i=2}^{k} \left(e^{-\frac{x_{r_{i-1}}}{\theta_1}} - e^{-\frac{x_{r_i}}{\theta_1}}\right)^{u_i} \prod_{i=2}^{k} \left(e^{-\frac{x_{r_{i-1}}}{\theta_2}} - e^{-\frac{x_{r_i}}{\theta_2}}\right)^{v_i} \\ & \times \left(e^{-\frac{1}{\theta_1}(u_{k+1}x_{r_k} + \sum_{i=1}^{k} z_i x_{r_i})}\right) \left(e^{-\frac{1}{\theta_2}(v_{k+1}x_{r_k} + \sum_{i=1}^{k} (1-z_i) x_{r_i})}\right). \end{aligned} \tag{7}$$

Obviously, the posterior distribution given in (7) appears difficult to write in closed form mainly because of the involvement of censored data. It is essential to point out that, in the absence of censoring, the posterior distribution would have been much simpler to handle analytically. Now coming to the present form in (7), various alternative approaches such as numerical integration or analytical approximation techniques can be used. We, however, advocate the application of Markov chain Monte Carlo (MCMC) based approaches because of their simplicity and ease of drawing a variety of inferences in a routine manner. These approaches offer an additional advantage in the sense that inferences about the censored observations can also be obtained routinely, especially if someone employs the Gibbs sampler algorithm and considers these censored observations as further unknowns. Drawing inferences about unknown censored data can equivalently be considered as a one-sample prediction problem. As such, the paper first considers the possibility of applying the Gibbs sampler algorithm, the simplest form of MCMC based procedure, for analyzing the posterior in (7).

Before we proceed further, let us first briefly review the Gibbs sampler algorithm, especially that form of the algorithm which provides due consideration to censored data as well. This review will be done solely considering the problem that we have introduced. The Gibbs sampler algorithm, first proposed by [3], is a widely used MCMC approach that generates samples from the joint posterior distribution of unknown parameters by iteratively sampling from their often one-dimensional full conditionals. These full conditionals, up to a proportionality, are obtained from the joint posterior distribution. The latter also needs to be specified up to proportionality only by combining the likelihood function of the observed data with the prior distributions of the parameters using Bayes theorem. The Gibbs sampler algorithm proceeds in a cyclic manner, that is, at each iteration, a parameter is updated by drawing from its full conditional, using the most recent updated values of all the other unknowns. After a sufficient number of iterations, the Markov chain so obtained converges to a random sample from the posterior distribution. To reduce serial correlation between generated observations in a single long run of the chain

and hence to obtain independent sample observations, a suitably spaced subset of the generated samples is retained for drawing the posterior based inferences. For further details, one may refer to [11], [15], etc.

The presence of censored data typically introduces the computational complexity in the Bayesian framework. However, the apparent advantage of the Gibbs sampler algorithm is that it routinely caters to the needs of censored data problems. The approach requires assuming that there is no censoring and reintroducing the censored observations as further unknowns in the implementation of the algorithm. Full conditionals are then defined for both the model parameters and the censored data observations. The full conditionals for the model parameters remain the same as in the uncensored case, while those for the censored observations correspond to their respective truncated parent sampling distributions. The truncation limits vary depending on each individual censored observation.

To clarify the algorithm in the present case, it may be noted that the unknowns consist of $(\boldsymbol{\theta}, \underline{x}^*)$, where $\boldsymbol{\theta} = (\theta_1, \theta_2)$, and $\underline{x}^*$ denotes the set of unknown censored observations. The likelihood function for this case, assuming that there is no censoring, can be written as

$$\begin{aligned} L^* &= m!n!\prod_{i=1}^{N}(f(x_i))^{z_i} \times \prod_{i=1}^{N}(g(x_i))^{1-z_i} \\ &= \frac{m!n!}{\theta_1^m \theta_2^n}\left(e^{-\Sigma_{i=1}^{N}\frac{z_i x_i}{\theta_1}}\right)\left(e^{-\Sigma_{i=1}^{N}\frac{(1-z_i)x_i}{\theta_2}}\right), \end{aligned} \tag{8}$$

although the likelihood function consists of unknown censored observations $\underline{x}^*$ as well. As such, the joint posterior distribution of θ_1 and θ_2, up to proportionality, can be written as

$$\begin{aligned} p^*(\theta_1, \theta_2 | \underline{x}^{'}, \underline{x}^*) &= p^*(\theta_1, \theta_2 | \underline{x}) \\ &\propto \frac{1}{\theta_1^{m+1}\theta_2^{n+1}}\left(e^{-\Sigma_{i=1}^{N}\frac{z_i x_i}{\theta_1}}\right)\left(e^{-\Sigma_{i=1}^{N}\frac{(1-z_i)x_i}{\theta_2}}\right). \end{aligned} \tag{9}$$

Here, $\underline{x} = (\underline{x}^{'}, \underline{x}^*)$, where $\underline{x}^{'}$ denotes the set of observed data. Obviously, the posterior as given in (9) involves multiple unknown quantities including the two model parameters and the unknown censored observations, making it well-suited for routine application of the Gibbs sampler algorithm. So, from the equation (9), the full conditionals for the two parameters can be written as

$$\begin{aligned} p^*(\theta_1 | \underline{x}) &\propto \frac{1}{\theta_1^{m+1}}\left(e^{-\Sigma_{i=1}^{N}\frac{z_i x_i}{\theta_1}}\right), \\ p^*(\theta_2 | \underline{x}) &\propto \frac{1}{\theta_2^{n+1}}\left(e^{-\Sigma_{i=1}^{N}\frac{(1-z_i)x_i}{\theta_2}}\right). \end{aligned} \tag{10}$$

The full conditionals for the unknown censored observations are nothing but truncated exponential distributions with truncation in each case decided on the basis of the corresponding censored observation. Say, for instance, if a censored observation falls in the range x_c to x_c', the corresponding exponential distribution will be truncated below x_c and above x_c'. From the full conditionals given in (10), it can be observed that both θ_1 and θ_1 can be generated from inverse gamma (IG) distributions where $\theta_1 \sim \text{IG}(m, \Sigma_{i=1}^{N} z_i x_i)$ and $\theta_2 \sim \text{IG}(n, \Sigma_{i=1}^{N}(1-z_i)x_i)$, respectively. Next, to execute the Gibbs sampler algorithm, the initial value is needed for each unknown, which can be chosen using some properly selected initial estimate to achieve faster convergence of the iterating chain. Say, for instance, one can consider ML estimates for the two unknown model parameters and an appropriately selected value for each unknown censored observation. This appropriate choice for each censored observation can be taken, for example, as the most relevant available information. Say, for instance, x_c can be considered as the relevant information in the example discussed above. Thus, one can easily implement the Gibbs sampler algorithm for the considered censored data problem as discussed above.

In addition, one can also be interested in characteristics such as reliability and the hazard rate, etc. although these characteristics are not of prime concern in the paper. One can easily see that these characteristics are the functions of one of the two parameters depending on whether a particular characteristic corresponds to Product 1 or Product 2. For instance, the reliability function for Product 1 and 2 can be obtained using the distribution function given in (1) and (2), respectively. Obviously, inferences about these characteristics can be easily obtained once the posterior samples corresponding to the two model parameters are made available. Say, for example, a posterior sample of the reliability function at a specified mission time can simply be obtained by substituting the posterior sample of the parameter in the corresponding expression of reliability.

4. Numerical Illustration

This section presents a real data example to demonstrate the performance of the Gibbs sampler algorithm under the specified censoring scenario and simultaneously to provide the full posterior and predictive analysis of unknown censored observations. The dataset used in the section was proposed by [9]. The dataset consists of failure times of air-conditioning systems of a fleet of Boeing 720 jet airplanes. For the purpose of illustration, "7914" and "7913" jet airplanes were chosen where the air conditioning systems of plane "7914" were considered as items of Product 1 and the air conditioning systems of plane "7913" were considered as items of Product 2. The required dataset taken from [9] is given in Table 1 for a quick reference.

Table 1: *Failure times of air-conditioning systems in "7914" and "7913" airplanes*

Plane	Failure times
7914	50, 44, 102, 72, 22, 39, 3, 15, 197, 188, 79, 88, 46, 5, 5, 36, 22, 139, 210, 97, 30, 23, 13, 14
7913	97, 51, 11, 4, 141, 18, 142, 68, 77, 80, 1, 16, 106, 206, 82, 54, 31, 216, 46, 111, 39, 63, 18, 191, 18, 163, 24

Table 2: *Joint multiply type-II censored sample when* $k = 15$

i	1	2	3	4	5	6	7	8	9	10	11	12	13	14	15	
r_i	3	5	8	11	16	19	25	28	30	33	35	37	43	46	48	-
X_{r_i}	4	5	14	18	23	31	46	54	68	79	82	97	141	188	197	-
Z	0	1	1	0	1	0	0	0	0	1	0	1	0	1	1	-
u_i	1	1	1	1	2	1	4	1	0	1	0	1	2	0	0	1
v_i	1	0	1	1	2	1	1	1	1	1	1	0	3	2	1	2

The same dataset has been analyzed earlier by [7], [2], [10], [12], and several others, employing similar or different censoring schemes and assuming various failure time distributions. [9] initially assumed that the failure times of the air conditioning system approximately follow an exponential distribution, despite variability in the failure rates across different planes.

For illustration purposes, two schemes of joint multiply type-II censored samples are constructed by arranging the failure times of both the planes in ascending order. If, at any position in this ordered sequence, two or more failure times from the two planes are identical, a random arrangement of these observations is applied at that position. The first scheme considers a total of $k = 15$ observed number of failures, whereas the second scheme considers a total of $k = 22$ observed number of failures. It may be noted that the sample sizes for Product 1 and Product 2 are $m = 24$ and $n = 27$, respectively, and therefore the considered schemes offer nearly 71% and 57% censored observations. It may be further noted that the observed items, or those with exactly known failure times, are selected randomly to reflect naturally occurring variations. The

Table 3: *Joint multiply type-II censored sample when* $k = 22$

i	1	2	3	4	5	6	7	8	9	10	11	12
r_i	4	6	8	11	12	14	17	18	21	25	26	29
X_{r_i}	5	11	14	18	18	22	24	30	39	46	50	63
Z	1	0	1	0	0	1	0	1	1	0	1	0
u_i	1	1	1	1	0	0	2	0	1	2	0	0
v_i	2	0	0	1	0	1	0	0	1	1	0	2

i	13	14	15	16	17	18	19	20	21	22	
r_i	30	36	37	38	39	41	43	44	48	49	-
X_{r_i}	68	88	97	97	102	111	141	142	197	206	-
Z	0	1	1	0	1	0	0	0	1	0	-
u_i	0	2	0	0	0	0	1	0	1	0	1
v_i	0	3	0	0	0	1	0	0	2	0	1

Table 4: *ML estimates of* θ_1, θ_2 *and reliability for Product* i $(i = 1, 2)$

Observed failures	$\hat{\theta_1}$	$\hat{\theta_2}$	$\hat{R_1}(100)$	$\hat{R_2}(100)$
$k = 15$	65.136	84.180	0.215	0.305
$k = 22$	65.203	78.971	0.216	0.282
$k = 51$ (no censoring)	64.125	76.815	0.210	0.272

considered joint multiply type-II censored schemes are shown schematically in Table 2 and Table 3 for clarity of the two schemes.

The ML estimates of the parameters are obtained by solving the likelihood equations given in (5) using the methodology outlined in subsection 3.1. These estimates are computed for both the considered schemes of joint multiply type-II censored samples and also for the case of a complete dataset with no censored data assumption. The ML estimates of the reliability at time t = 100 hours for Product i $(i = 1, 2)$ are also obtained for all the three schemes mentioned above. The corresponding results of ML estimates are reported in Table 4. It is worth noting that $\hat{R}_i(100)$ in Table 4 corresponds to the ML estimate of reliability at time t = 100 hours for Product i $(i = 1, 2)$.

Table 5: *Estimated posterior summaries of parameters*

Known values	**Parameter**	**Posterior estimates**			**0.95 HPDI**
		Mean	**Median**	**Mode**	
15	θ_1	67.786	65.523	61.374	(43.362, 94.428)
	θ_2	87.867	85.678	83.268	(56.102, 122.886)
22	θ_1	68.179	65.521	60.826	(43.419, 97.971)
	θ_2	81.693	79.452	75.624	(54.209, 113.763)
51	θ_1	66.534	64.910	60.453	(42.145, 94.107)
(no censoring)	θ_2	80.172	78.190	74.525	(54.771, 111.094)

It can be clearly seen from Table 4 that θ_1 remains relatively stable across different choices of k, whereas θ_2 exhibits greater variability. It suggests that losing information due to censoring will not have any appreciable impact on the estimate of θ_1 that corresponds to Product 1. On the other hand, θ_2 corresponding to Product 2 does lead to an overestimated value because of censoring. A similar thing is obviously reflected in the estimates of reliability as well, since the two estimates of reliability depend ultimately on θ_1 and θ_2. As a result, the reliability corresponding to Product 1 remains relatively stable across different values of k whereas the same corresponding to Product

2 leads to an overestimated value because of censoring.

In order to develop the sample based Bayesian inferences, the method outlined in subsection 3.2 is followed. The ML estimates of the parameters θ_1 and θ_2 serve as the initial values for running the algorithm described in that subsection. For unknown censored observations, the initial values are assigned in accordance with the suggestion given in subsection 3.2, ensuring that the observations fall within their respective failure time intervals.

In order to obtain the posterior samples and correspondingly draw the sample based inferences, a single extended run of the Gibbs sampler was performed. An initial burn-in period was used to eliminate transient behavior, after which convergence was assessed using the ergodic averages. Once convergence was established, every 10th sample was retained from the iterating chain to make the autocorrelation negligibly small, resulting in a posterior sample of size 1000 for each of the marginal posterior distributions of θ_1 and θ_2. Table 5 presents the estimated posterior mean, median, mode and highest posterior density interval with coverage probability 0.95 (0.95 HPDI) of the parameters under three different scenarios, that is, $k = 15$, $k = 22$, and $k = 51$ (case of no censoring).

Table 6: *Predictive estimates for unknown censored observations when* $k = 15$

Sr. No.	Observed failure times	Estimated predictive means	0.95 HPrDI
1	1	1.98	(0.23, 3.99)
2	3	2.02	(0.09, 3.82)
3	5	4.50	(4.01, 5.00)
4	11	9.26	(5.15, 13.50)
5	13	9.40	(5.18, 13.72)
6	15	16.01	(14.20, 17.98)
7	16	16.05	(14.04, 17.83)
8	18	20.41	(18.00, 22.77)
9	18	20.47	(18.00, 22.99)
10	22	20.50	(18.04, 22.78)
11	22	20.54	(17.96, 22.74)
12	24	26.72	(23.19, 30.71)
13	30	26.88	(23.46, 30.95)
14	36	37.90	(31.08, 45.20)
15	39	38.20	(31.10, 45.20)
16	39	38.22	(31.08, 44.98)
17	44	38.29	(31.12, 45.25)
18	46	38.50	(31.77, 46.00)
19	50	49.85	(46.05, 53.51)
20	51	49.87	(46.00, 53.52)
21	63	60.83	(54.36, 67.57)
22	72	73.26	(68.14, 78.44)
23	77	73.50	(68.49, 79.00)
24	80	80.46	(79.06, 81.93)
25	88	89.24	(82.25, 96.51)
26	97	116.02	(96.97, 136.95)
27	102	116.14	(97.24, 138.37)
28	106	116.77	(97.01, 138.48)
29	111	117.34	(97.01, 137.48)
30	139	117.72	(97.10, 140.43)
31	142	162.31	(141.41, 185.82)
32	163	162.52	(141.07, 184.79)
33	191	192.42	(188.29, 196.74)
34	206	263.01	(197.04, 439.93)
35	210	281.34	(197.13, 474.33)
36	216	285.38	(197.05, 401.49)

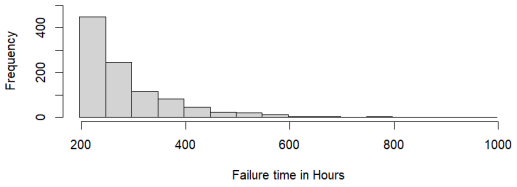
Table 7: *Predictive estimates for unknown censored observations when* $k = 22$

Sr.No.	Observed failure times	Estimated predictive means	0.95 HPrDI
1	1	2.43	(0.01 4.76)
2	3	2.45	(0.10, 4.79)
3	4	2.53	(0.00, 4.75)
4	5	7.91	(5.00, 10.68)
5	13	12.47	(11.13, 13.96)
6	15	16.00	(14.12, 17.84)
7	16	16.02	(14.14, 17.92)
8	18	19.93	(18.00, 21.84)
9	22	23.00	(22.00, 23.90)
10	23	23.06	(22.07, 23.99)
11	31	34.28	(30.11, 38.47)
12	36	34.36	(30.16, 38.65)
13	39	42.33	(39.00, 45.70)
14	44	42.50	(39.14, 45.76)
15	46	42.54	(39.09, 46.00)
16	51	56.24	(50.06, 62.29)
17	54	56.38	(50.54, 62.80)
18	72	77.25	(68.00, 86.62)
19	77	77.44	(68.10, 86.69)
20	79	77.50	(68.10, 86.95)
21	80	77.52	(68.22, 87.03)
22	82	77.66	(68.97, 87.85)
23	106	106.58	(102.26, 110.78)
24	139	125.00	(111.21, 139.78)
25	163	165.84	(142.02, 193.59)
26	188	166.08	(142.50, 193.62)
27	191	166.61	(142.01, 193.07)
28	210	276.22	(206.00, 419.13)
29	216	287.09	(206.08, 463.66)

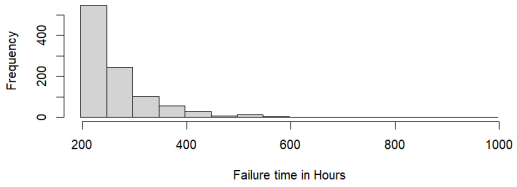
One can observe from Table 5 that the results are, in general, closely align to the corresponding ML estimates of the parameters given in Table 4. This similarity in the two estimates is expected, given that the prior distributions used are non-informative, allowing the posterior distribution to be largely dominated by the likelihood function. Also, all the three marginal posterior distributions exhibit positive skewness. In such cases, relying solely on the estimated posterior mean or median can be misleading, as these measures are sensitive to the skewness. In the very same sense, the ML estimator may also be suboptimal. The posterior mode is, of course, a better candidate as it represents the most probable value of the parameter.

After the inferential developments on the unknown parameters, predictive samples of size 1000 are generated corresponding to each unknown censored observation. The estimated predictive means for the unknown censored observations for the cases when $k = 15$ and $k = 22$ are reported in Table 6 and Table 7, respectively. The tables also provide the highest one-sample predictive density interval with coverage probability 0.95 (0.95 HPrDI), offering a measure of uncertainty in the predictive estimates of censored observations.

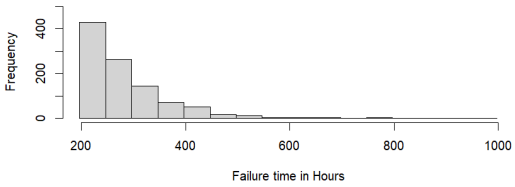
The predictive performance, summarized in Table 6 and Table 7, demonstrates the effectiveness of the proposed Bayesian methodology in predicting unknown censored observations. Overall, the predictive means closely align with the true values that are removed during execution for most of the observations and, as such, the proposed methodology can be considered satisfactory even if we have a good number of censored observations. This is particularly evident in the values arising in the middle of the ordered observations, where the predicted values deviate very little from the true observations and, as such, the predictions can be considered precise enough.



(1.1)

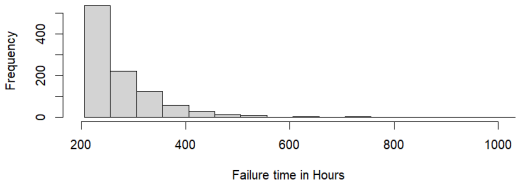


(1.2)

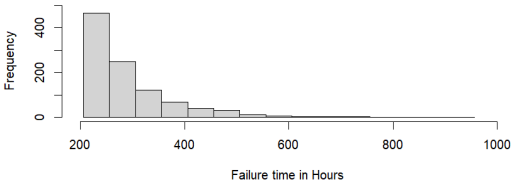


(1.3)

Figure 1: *Histograms showing the density estimates for X_{49}, X_{50}, and X_{51}, respectively, in (1.1), (1.2), and (1.3).*



(2.1)



(2.2)

Figure 2: *Histograms showing the density estimates for X_{50} and X_{51}, respectively, in (2.1) and (2.2).*

Even in cases where some deviation is observed, the true values are successfully captured within the corresponding 0.95 HPrD intervals. This indicates that the uncertainty associated with each prediction has been appropriately quantified to a great extent. The consistent inclusion of the true values within these predictive intervals underscores the reliability of the utilized technique and its strong capability for uncertainty estimation. Additionally, the methodology demonstrates adaptability across all the values, from small to large in magnitude, as evidenced by the varying widths of the predictive intervals.

Since the data are joint multiply type-II censored, one may be interested more in the observations that remain operational at the time of termination of the experiment than those that failed earlier. As such, to provide a more thorough idea, density estimates for such observations are shown in the form of histograms. It may be noted that there are three and two such functional units for the considered cases when $k = 15$ and $k = 22$. These functional units have true values of 206, 210, 216 and 210, 216, respectively, when $k = 15$ and $k = 22$. For $k = 15$, these functional units are denoted by X_{49}, X_{50}, and X_{51}. The corresponding density estimates in the form of histograms are shown in Figure 1. Similarly, for $k = 22$, the functional units are denoted by X_{50} and X_{51} with the corresponding predictive density estimates shown in Figure 2.

One can see that each figure reflects the gradual decline from a specific point, consistent with an exponential-like decay in failure likelihood over time. This behavior confirms that the model

Table 8: *Posterior estimates of reliability at t=100*

k		Mean	Median	Mode
15	Product 1	0.225	0.217	0.198
	Product 2	0.314	0.311	0.307
22	Product 1	0.226	0.217	0.198
	Product 2	0.289	0.284	0.277
51 (no censoring)	Product 1	0.219	0.214	0.193
	Product 2	0.282	0.278	0.266

correctly incorporates the censoring mechanism.

Additionally, the posterior estimates of reliability at $t = 100$ hours are obtained and presented in Table 8. The results of the posterior characteristics of reliability are somewhat similar to what we have obtained through ML estimation. It can be seen that the posterior distributions of reliability corresponding to Product 1 and Product 2 appear to be slightly skewed across all the three scenarios, $k = 15$, $k = 22$ and no censoring, suggesting the use of modal values as the preferred point estimates. Furthermore, the posterior estimates of reliability in the censored cases show minimal deviation from those obtained in the absence of censoring. This consistency reinforces the effectiveness of the proposed estimation procedure that suggests minimum loss of information because of heavy censoring.

5. Conclusion

In this paper, we have analyzed data subject to joint multiply type-II censoring under an exponential modeling assumption. To facilitate parameters estimation, we proposed the use of the Gibbs sampler algorithm for censored data problems. The problem proceeds mainly with two important objectives. First, the estimation of model parameters and, second, the prediction of unknown censored observations. It is shown on the basis of a real data example with artificially formulated censoring that the proposed methodology offers quite satisfactory results even if we have a very large proportion of censored observations, say, for example, more than 55% or 70% censoring. The predictive estimates for unknown censored observations are also found satisfactory in the sense that they closely represent the true observations.

References

[1] Algarni, A., Almarashi, A. M., and Abd-Elmougod, G. A. (2020). Joint type-i generalized hybrid censoring for estimation two weibull distributions. *Journal of Information Science & Engineering*, 36(6).

[2] Gadhvi, N. K. (2021). Estimation for two exponential life time models under joint multiply type-ii censoring. *Journal of the Egyptian Mathematical Society*, 29(1):1–16.

[3] Geman, S. and Geman, D. (1984). Stochastic relaxation, gibbs distributions, and the bayesian restoration of images. *IEEE Transactions on pattern analysis and machine intelligence*, (6):721–741.

[4] Klein, J. P., Moeschberger, M. L., et al. (2003). *Survival analysis: techniques for censored and truncated data*, volume 1230. Springer.

[5] Lawless, J. (2011). *Statistical Models and Methods for Lifetime Data*. Wiley Series in Probability and Statistics. Wiley.

[6] Leemis, L. M. and Shih, L.-H. (1989). Exponential parameter estimation for data sets containing left and right censored observations. *Communications in Statistics-Simulation and Computation*, 18(3):1077–1085.

[7] Mondal, S. and Kundu, D. (2020a). Bayesian inference for weibull distribution under the balanced joint type-ii progressive censoring scheme. *American Journal of Mathematical and Management Sciences*, 39(1):56–74.

[8] Mondal, S. and Kundu, D. (2020b). On the joint type-ii progressive censoring scheme. *Communications in Statistics-Theory and Methods*, 49(4):958–976.

[9] Proschan, F. (1963). Theoretical explanation of observed decreasing failure rate. *Technometrics*, 5(3):375–383.

[10] Salem, S., Abo-Kasem, O. E., and Hussien, A. (2023). On joint type-ii generalized progressive hybrid censoring scheme. *Computational Journal of Mathematical and Statistical Sciences*, 2(1):123–158.

[11] Smith, A. F. and Roberts, G. O. (1993). Bayesian computation via the gibbs sampler and related markov chain monte carlo methods. *Journal of the Royal Statistical Society: Series B (Methodological)*, 55(1):3–23.

[12] Tolba, A. H., Abushal, T. A., and Ramadan, D. A. (2023). Statistical inference with joint progressive censoring for two populations using power rayleigh lifetime distribution. *Scientific Reports*, 13(1):3832.

[13] Upadhyay, S., Shastri, V., and Singh, U. (1992). Bayes estimators of exponential parameters when observations are left and right censored. *Metron Ln*, pages 3–4.

[14] Upadhyay, S., Singh, U., and Shastri, V. (1996). Estimation of exponential parameters under multiply type ii censoring. *Communications in Statistics-Simulation and Computation*, 25(3):801–815.

[15] Upadhyay, S., Vasishta, N., and Smith, A. (2001). Bayes inference in life testing and reliability via Markov Chain Monte Carlo simulation. *Sankhyā: The Indian Journal of Statistics, Series A (1961-2002)*, 63(1):15–40.

RELIABLE HYBRID OPTIMIZATION FOR SUPPLY CHAIN INVENTORY SYSTEMS

Ajay Singh Yadav[1,*], S. Viswanathan[2], Navin Ahlawat[3],
Bhavani Viswanathan[4], Anupam Swami[5], Mohammed Abid[1]

•

[1]Department of Mathematics, SRM Institute of Science and Technology,
Delhi-NCR Campus, Ghaziabad, India, 201204
[2]Faculty of Management Studies, SRM Institute of Science and Technology,
Delhi-NCR Campus, Ghaziabad, India, 201204
[3] Department of Computer Science, SRM Institute of Science and Technology,
Delhi-NCR Campus, Ghaziabad, India, 201204
[4]Department of Library Science & Humanities, SRM Institute of Science and Technology,
Delhi-NCR Campus, Ghaziabad, India, 201204
[5]Department of Mathematics, Km. Mayawati Government Girls P.G. College,
Badalpur, Gr. Noida, India, 203207
ajay29011984@gmail.com, director.ncr@srmist.edu.in, navins@srmist.edu.in,
bhavaniviswam@gmail.com, swami.anupam@gmail.com, mohammea@srmist.edu.in
[*]Corresponding author

Abstract

This study explores the optimization of blood supply chain inventory management through innovative approaches, specifically Bee Colony Optimization (BCO) and Genetic Algorithms (GA). The research addresses challenges in healthcare logistics, emphasizing the integration of organizational units involved in blood sourcing, production, distribution, and marketing. Key considerations include the potential conflicts between cost minimization in sourcing decisions and the focus on throughput in production and distribution. The study highlights the significance of achieving an optimal balance to ensure a reliable and efficient blood supply for patient care. Bee Colony Optimization and Genetic Algorithms, inspired by natural processes, offer promising solutions to the complexities of blood inventory management. BCO mimics collaborative foraging behavior, creating optimal paths marked by pheromones. Genetic Algorithms replicate natural selection to iteratively enhance solutions. The research aims to provide valuable insights into the application of these algorithms, contributing to the evolution of efficient blood supply chain management. The anticipated outcomes include improved healthcare logistics, ensuring timely access to blood products and enhancing patient safety and outcomes.

Keywords: Blood supply chain, inventory management, Bee Colony Optimization, and Genetic Algorithms.

1. Introduction and related work

In the fiercely competitive landscape of healthcare logistics, the optimization of blood supply chain inventory management emerges as a critical factor for ensuring superior patient care. A healthcare facility's success is intricately tied to its ability to navigate challenges, such as minimizing lead

times and costs, while simultaneously elevating patient service levels and maintaining the highest quality standards for blood products. Throughout the evolution of healthcare logistics, the organizational units involved in blood sourcing (procurement), production, distribution, and healthcare marketing have often operated in silos. Despite sharing common overarching goals, these units frequently harbor distinct and sometimes conflicting objectives. Healthcare marketing seeks toptier patient service levels and seamless availability of blood products, goals that may clash with the priorities of production and distribution departments. Sourcing decisions often lean towards cost minimization, while production and distribution decisions tend to focus on maximizing throughput and minimizing unit production costs, occasionally neglecting the implications of maintaining high blood product inventory levels and enduring extended lead times. At its core, blood supply chain management strives to harmonize and integrate disparate healthcare organizations, each pursuing its unique objectives, towards the unified goal of ensuring a dependable and efficient blood supply for patient care. Recent advancements underscore the potential for substantial enhancements in these objectives through skillful orchestration of blood supply chain management mechanisms. The challenge of blood inventory management revolves around maintaining an optimal supply of specific blood types in alignment with forecasted patient demand patterns. Achieving this equilibrium necessitates shrewd management of the costs associated with blood product holding, while mitigating the adverse effects of shortages, including compromised patient care and potential health risks. The scope of blood products subject to inventory management spans from everyday blood components used in transfusions to essential plasma derived medications. Notably, a diverse array of ostensibly unrelated healthcare challenges can be mathematically modeled as intricate interwoven blood supply chain inventory control dilemmas. Various blood supply chain models have been conceptualized, each characterized by three fundamental expense categories: (i) administrative costs associated with blood product order placement, often termed reorder or setup costs; (ii) ongoing maintenance costs of blood product inventory, encompassing holding or carrying costs, including storage charges, refrigeration, and more; (iii) shortfall costs reflecting the cascading repercussions of patient health risks and compromised healthcare reputation in the event of shortages. The foundation for achieving efficient blood supply chain management lies in optimizing these facets. Innovative optimization algorithms, such as Bee Colony Optimization and Genetic Algorithms, draw inspiration from nature to enhance the efficiency of blood product routing, storage, and distribution within the healthcare system. Bee Colony Optimization Algorithms ingeniously mimic the collaborative foraging behavior of ants, creating paths marked by pheromones to signify path quality. Similarly, Genetic Algorithms replicate the principles of natural selection and evolution to iteratively improve solutions. These algorithms contribute to the efficient orchestration of blood supply chains, ensuring timely and safe access to blood products for patient care through the reinforcement of optimal or near optimal solutions over successive iterations.

Supply chain management (SCM) is defined as the coordination of production, storage, location, and transportation among supply chain participants to achieve the optimal balance of responsiveness and efficiency for a specific market. While many researchers have concentrated on products that do not spoil, certain items experience changes over time. Yadav et al. [1-10] highlighted that the deterioration of these items is significant, limiting their storage duration. Yadav et al. [11-20] further explained that deterioration can manifest as spoilage, evaporation, obsolescence, or loss of functionality, leading to reduced inventory usage compared to natural conditions. When raw materials are stocked for future demands, various factors such as storage conditions, weather, and humidity can cause deterioration. Yadav et al. [21-53] discuss that management typically maintains a warehouse for storing purchased goods. However, for various reasons, they may acquire or lease more items than can be accommodated in the warehouse, referring to the excess as overflow (OW), while the additional stock in a rented warehouse is termed rented warehouse (RW), located near or adjacent to OW. Yadav and Swami [54-61] found that the inventory costs associated with RW, including maintenance and depreciation, are generally higher than those of OW due to added operational and maintenance expenses. To minimize inventory costs, it is important to quickly utilize RW stock. Actual customer service is

provided solely by OW, so to lower expenses, RW inventory is prioritized for turnover. These scenarios illustrate what are referred to as two inventory examples within the system. Yadav and Kumar [62] focused on managing the supply of electronic storage devices while integrating environmental and network considerations. Yadav, A.S. [63-65] analyzed seven measures of supply chain management to enhance the inventory of electronic storage devices. This analysis involved assessing financial impacts through the application of genetic algorithms (GA) and particle swarm optimization (PSO). Additionally, the research examined inventory improvement and equipment management using genetic computation, alongside a model design for inventory analysis that addressed economic challenges in transporting goods. Swami et al. [66-68] formulated inventory policies that address inventory requirements and associated costs, taking into account allowable payments and delays in inventory. They provided an example of depreciation across various goods and services, considering business loans and an inventory model that is less sensitive to pricing needs, while comparing inventory costs to inflation-related business expenses. Meanwhile, Gupta et al. [69-70] defined objectives for a Multiple Objective Genetic Algorithm and particle swarm optimization (PSO) aimed at enhancing supply levels and addressing deficits and inflation, along with a calculation model that leverages genetic algorithms to assess scarcity and low inflation scenarios. Singh et al. [71, 72] examined cases involving the depreciation of two types of stock concerning asset and inventory costs while updating particle data, as well as scenarios with two inventories focusing on property damage and inventory costs under inflation, utilizing soft computing techniques. Kumar et al. [73-75] addressed delays in managing alcohol supply, refining particles, and developing a green cement supply system, while also tackling inflation through particle enhancement and the use of an electronic inventory system and distribution center with genetic computations. Chauhan and Yadav [76-77] provided an example of depreciation across two stores and warehouses, utilizing a genetic stock and vehicle stock to manage demand and inflation across two distribution centers. Pandey et al. [78] analyzed the improvement of industrial reserves for marble using genetic technology and enhanced multiple particle approaches. Ahlawat, et. al. [79] studied the white wine industry in supply chain management through nerve networks. Singh, et. al. [80] examines the best policy to import damaged goods immediately and pay for conditional delays under the supervision of two warehouses.

The research by Yadav et al. [81] centers on improving inventory management for perishable commodities through the lens of green technology investments, considering factors such as selling price, carbon emissions, and time-sensitive demand. The study promotes sustainable practices in inventory models by integrating traditional economic principles with environmental considerations. In another analysis, Yadav, Yadav, and Bansal [82] utilize an interval number technique to explore a two-warehouse inventory management model for perishable goods, addressing demand and cost uncertainties. Their optimization methods highlight how investing in preservation technology can reduce waste and enhance inventory efficiency. Focusing on a two-warehouse approach to optimize inventory levels, Yadav, Yadav, and Bansal [83] present a model that addresses the deterioration of goods during storage, emphasizing the importance of managing degradation costs to improve overall inventory performance.

2. Assumptions and notations

2.1. Assumptions

The following assumptions are used in this paper.

1. The amelioration rate of livestock items is a two parameter Weibull distribution which is a decreasing function of time and is greater than the deterioration rate which is also a two parameter Weibull distribution.
2. The production rate is considered greater than the demand rate and the deterioration rate.
3. Cooperation between Regional Blood Center's and Hospital has been considered and the partial backlogging is allowed to the retailer.

4. Lead time is assumed to be negligible.
5. Amelioration and deterioration start when the livestock is bought by the Regional Blood Center's.
6. The deterioration units are not used.
7. Multiple deliveries per order are considered.
8. Only one Regional Blood Center's and one Hospital are considered in the supply chain.
9. The discount rate is compounded continuously.

2.2. Notations

The following notations in Table 2 are used in this model.

Table 1: *Notations*

Notation	Units	Description
G_0	–	Time Discounting rate
η_0	Constant	Scale parameter of Improve rate.
η_1	Constant	Shape parameter of Improve rate.
δ_0	Constant	Blood material's scale parameter for the deterioration rate.
δ_1	Constant	Blood material's shape parameter for the deterioration rate.
δ_2	constant	Blood goods scale parameter for the deterioration rate.
δ_3	constant	Blood goods shape parameter for the deterioration rate.
n	–	Number of deliveries per order.
T_1	Weeks	Time period of Improve occurrence.
T_2	Weeks	The production period.
T_3	weeks	The nonproduction period.
T_4	Weeks	Period of positive inventory level $T_4 = T_2 + T_3$.
T_5	Weeks	In stock period of retailer.
T_6	Weeks	Out stock period.
T_7	weeks	Time period between deliveries $T_7 = \frac{T_4}{n} = T_5 + T_6$.
T	Weeks	Length of cycle time $T = T_1 + T_2 + T_3$.
$(X_0 + Y_0 t)$	–	The Blood Donation production rate.
$(Z_0 + Z_1 t)$	–	The Blood Donation demand rate.
$\mathbb{R}_{bdc}$	–	Blood Donation Centers order quantity per order form the supplier.
$\mathbb{R}_{rbc}$	–	Regional Blood Center™s Blood goods production lot size per production.
$\mathbb{R}_{hb}$	–	Hospitals Blood order quantity per order taken form the Regional Blood Center.
$\pi_{bdci}(t_i)$	–	Blood Donation Centers inventory level at any time, $0 \leq t_i \leq T_i$.

3. FORMULATION AND SOLUTION OF THE MODEL

The proposed blood supply chain inventory system includes donors, hospitals, and collecting centers. The process begins with the decision to donate blood. The process is then transformed into a mathematical model with the aim of lowering the total costs related to blood supply chain inventory management. The three stages of the blood center, as shown in Fig. 1. The following is the formulation of the proposed model:

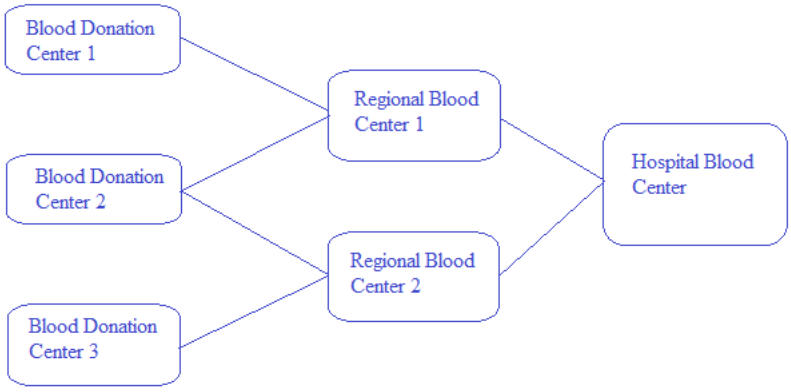


Figure 1: *Blood Supply Chain Inventory Management Flowchart.*

3.1. Blood Donation Center's Inventory System

$$\frac{d\Pi_{bdc1}(t_1)}{dt_1} = \eta_0\eta_1 t_1^{\eta_1-1}\Pi_{w1}(t_1) - \delta_0\delta_1 t_1^{\delta_1-1}\Pi_{bdc1}(t_1), \qquad 0 \le t_1 \le T_1 \tag{1}$$

$$\frac{d\Pi_{bdc2}(t_2)}{dt_2} = \eta_0\eta_1 t_2^{\eta_1-1}\Pi_{w2}(t_2) - \delta_0\delta_1 t_2^{\delta_1-1}\Pi_{bdc2}(t_2), \qquad 0 \le t_2 \le T_2 \tag{2}$$

The boundary conditions are given by $\Pi_{bdc2}(0) = R_{bdc}$ and $\Pi_{bdc2}(T_2) = 0$.
Using the above boundary conditions, the solutions of (1) and (2) are given by

$$\Pi_{bdc1}(t_1) = R_{bdc}e^{\left(\eta_0 t_1^{\eta_1} - \delta_0 t_1^{\delta_1}\right)}, \qquad 0 \le t_1 \le T_1 \tag{3}$$

$$\Pi_{bdc2}(t_2) = e^{\left(\delta_0 t_2^{\delta_1} - \eta_0 t_2^{\delta_1}\right)} \int_{t_2}^{T_2} (X_0 + Y_0 M) e^{\left(\eta_0 u^{\eta_1} - \alpha_1 M^{\delta_0}\right)} dM, \qquad 0 \le t_2 \le T_2 \tag{4}$$

The maximum inventory level is given by

$$Z_{bdc} = \Pi_{bdc}(0)$$

$$Z_{bdc} = \int_0^{T_2} (X_0 + Y_0 M) e^{\left(\eta_0 V_0^{\eta_1} - \delta_0 M^{\delta_0}\right)} du$$

$$Z_{bdc} = \int_0^{T_2} (X_0 + Y_0 M) e^{\left(1 + \eta_0 M^{\eta_1} - \delta_0 M^{\delta_0} + \ldots\right)} dM$$

$$Z_{bdc} = \int_0^{T_2} (X_0 + Y_0 V + X_0\eta_0 V^{\eta_1} - X_0\delta_0 V^{\delta_1} + Y_0\eta_0 V^{\eta_1+1} - Y_0\delta_0 V^{\delta_1+1}) dV$$

$$Z_{bdc} = \left[X_0 T_2 + \frac{Y_0 T_2^2}{2} + \frac{X_0\eta_0 T_2^{\eta_1+1}}{\eta_1+1} - \frac{X_0\delta_0 T_2^{\delta_1+1}}{\delta_1+1} + \frac{Y_0\eta_0 T_2^{\eta_1+2}}{\eta_1+2} - \frac{Y_0\delta_0 T_2^{\delta_1+2}}{\delta_1+2}\right]$$

Since $Z_{bdc}(0) = \Pi_{bdc1}(T_1) = \Pi_{bdc2}(0)$ the order quantity per order form outsider suppliers is given by

$$R_{bdc} = e^{\left(\delta_0 T_1^{\delta_1} - \eta_0 T_1^{\eta_1}\right)} \int_0^{T_2} (X_0 + Y_0 M) e^{\left(\eta_0 M^{\eta_1} - \delta_0 M^{\delta_1}\right)} dM,$$

$$R_{bdc} = (\delta_0 T_1^{\delta_1} - \eta_0 T_1^{\eta_1})\big[X_0 T_2 + \frac{Y_0 T_2^2}{2} + \frac{X_0\eta_0 T_2^{\eta_1+1}}{\eta_1+1} - \frac{X_0\delta_0 T_2^{\delta_1+1}}{\delta_1+1} + \frac{Y_0\eta_0 T_2^{\eta_1+2}}{\eta_1+2} - \frac{Y_0\delta_0 T_2^{\delta_1+2}}{\delta_1+2}\big]$$

$$\begin{aligned} R_{bdc} = (1+\delta_0 T_1^{\delta_1} - \eta_0 T_1^{\eta_1})\Big\{ &\big[X_0 T_2 + \frac{Y_0 T_2^2}{2} + \frac{X_0\eta_0 T_2^{\eta_1+1}}{\eta_1+1} - \frac{X_0\delta_0 T_2^{\delta_1+1}}{\delta_1+1} + \frac{Y_0\eta_0 T_2^{\eta_1+2}}{\eta_1+2} \\ &- \frac{Y_0\delta_0 T_2^{\delta_1+2}}{\delta_1+2}\big] + \big[\delta_0 T_1^{\delta_1} X_0 T_2 + \frac{\delta_0 T_1^{\delta_1} Y_0 T_2^2}{2} + \frac{\delta_0 T_1^{\delta_1} X_0\eta_0 T_2^{\eta_1+1}}{\eta_1+1} - \frac{\delta_0 T_1^{\delta_1} X_0 T_2^{\delta_1+1}}{\delta_1+1} \\ &+ \frac{\delta_0 T_1^{\delta_1} Y_0\eta_0 T_2^{\eta_1+2}}{\eta_1+2} - \frac{\delta_0 T_1^{\delta_1} Y_0 T_2^{\delta_1+2}}{\delta_1+2}\big] - \big[\eta_0 T_1^{\eta_1} X_0 T_2 + \frac{\eta_0 T_1^{\eta_1} Y_0 T_2^2}{2} \\ &+ \frac{\eta_0^2 T_1^{\eta_1} X_0 T_2^{\eta_1+1}}{\eta_1+1} - \frac{\eta_0 T_1^{\eta_1} X_0\delta_0 T_2^{\delta_1+1}}{\delta_1+1} + \frac{\eta_0^2 T_1^{\eta_1} X_0\delta_0 T_2^{\eta_1+2}}{\eta_1+2} - \frac{\eta_0 T_1^{\eta_1} Y_0\delta_0 T_2^{\delta_1+2}}{\delta_1+2}\big]\Big\} \end{aligned} \quad (5)$$

The net present initial replenishment ordering cost is given by

$$OC_{bdc} = N_{bdc1}$$

The inventory occurs during the time periods T_1 and T_2 The net present inventory carring cost is given by

$$HC_{bdc} = N_{bdc2}\big[\int_0^{T_1} \Pi_{bdc1}(t_1) e^{-G_0 t_1} dt_1 + \int_0^{T_1} \Pi_{bdc2}(t_2) e^{-G_0(T_1+t_2)} dt_2\big]$$

$$\begin{aligned} HC_{bdc} = \Big[&N_{bdc2}\Big\{R_{bdc1}\Big(T_1 + \frac{\eta_0 T_1^{\eta_1+1}}{\eta_1+1} - \frac{\delta_0 T_1^{\delta_1+1}}{\beta_1+1} - \frac{rT_1^2}{2}\Big)\Big\} \\ &+ C_{bd2}\Big[\Big(T_1 - \frac{\eta_0 T_2^{\eta_1+1}}{\eta_1+1} + \frac{\delta_0 T_2^{\delta_1+1}}{\delta_1+1} - G_0 T_1 T_2 - \frac{G_0 T_2^2}{2}\Big) \\ &\big[X_0 T_2 + \frac{Y_0 T_2^2}{2} + \frac{X_0\eta_0 T_2^{\eta_1+1}}{\eta_1+1} - \frac{X_0\delta_0 T_2^{\delta_1+1}}{\delta_1+1} + \frac{Y_0\eta_0 T_2^{\eta_1+2}}{\eta_1+2} - \frac{Y_0\delta_0 T_2^{\delta_1+2}}{\delta_1+2}\big] \\ &- (1-G_0 T_1)\Big\{\frac{X_0 T_2^2}{2} + \frac{p_1 T_2^3}{6} + \frac{X_0\eta_0 T_2^{\eta_1+2}}{(\eta_1+1)(\eta_1+2)} - \frac{X_0\delta_0 T_2^{\delta_1+2}}{(\delta_1+1)(\delta_1+2)} \\ &+ \frac{Y_0\eta_0 T_2^{\eta_1+3}}{(\eta_1+3)(\eta_1+2)} - \frac{Y_0\delta_0 T_2^{\delta_1+3}}{(\delta_1+2)(\delta_1+3)}\Big\} + G_0\Big\{\frac{X_0 T_2^3}{2} + \frac{Y_0 T_2^4}{8} + \frac{X_0\eta_0 T_2^{\eta_1+3}}{(\eta_1+1)(\eta_1+3)} \\ &- \frac{X_0\delta_0 T_2^{\delta_1+3}}{(\delta_1+1)(\delta_1+3)} + \frac{Y_0\eta_0 T_2^{\eta_1+4}}{(\eta_1+4)(\eta_1+2)} - \frac{Y_0\delta_0 T_2^{\delta_1+4}}{(\delta_1+2)(\delta_1+4)}\Big\} - \delta_0\Big\{\frac{X_0 T_2^{\delta_1+2}}{\delta_1+2} \\ &+ \frac{Y_0 T_2^{\delta_1+3}}{2(\delta_1+3)} + \frac{X_0\eta_0 T_2^{\delta_1+\eta_1+2}}{(\eta_1+1)(\delta_1+\eta_1+2)} - \frac{X_0\delta_0 T_2^{2\delta_1+2}}{2(\delta_1+1)^2} + \frac{Y_0\eta_0 T_2^{\delta_1+\eta_1+3}}{(\eta_1+2)(\delta_1+\eta_1+3)} - \frac{Y_0\delta_0 T_2^{2\delta_1+3}}{(\delta_1+2)(2\delta_1+3)} \\ &+ \eta_0\Big\{\frac{X_0 T_2^{\eta_1+2}}{\gamma_1+2} + \frac{Y_0 T_2^{\eta_1+3}}{2(\gamma_1+3)} + \frac{X_0\eta_0 T_2^{\eta_1+2}}{2(\gamma_1+1)} - \frac{X_0\delta_0 T_2^{\delta_1+\eta_1+3}}{(\delta_1+1)(\delta_1+\eta_1+3)} \\ &- \frac{X_0\delta_0 T_2^{\delta_1+\eta_1+2}}{(\delta_1+1)(\delta_1+\eta_1+2)} + \frac{Y_0\eta_0 T_2^{2\eta_1+3}}{(2\eta_1+3)(\eta_1+2)}\Big\}\Big]\Big] \end{aligned} \quad (6)$$

The net present ameliorating cost during the time periods T_1 and T_2 is given by

$$AC_{bdc} = N_a\big[\int_0^{T_1} \eta_0\eta_1 t_2^{\eta_1-1}\Pi_{bdc1}(t_1) e^{-G_0 t_1} dt_1 + \int_0^{T_1} \eta_0\eta_1 t_2^{\eta_1-1}\Pi_{bdc2}(t_2) e^{-G_0(T_1+t_2)} dt_2\big]$$

$$AC_{bdc} = C_a\eta_0\eta_1\Bigg[R_{bdc}\Bigg(\frac{T_1}{\eta_1}+\frac{\eta_0 T_1^{2\eta_1}}{2\eta_1}-\frac{\delta_0 T_1^{\delta_1+\eta_1}}{\delta_1+\eta_1}-\frac{rT_1^{\eta_1+1}}{\eta_1+1}\Bigg) + \Bigg(\frac{T_2^{\eta_1}}{\eta_1}-\frac{\eta_0 T_2^{2\eta_1}}{2\eta_1}-\frac{\delta_0 T_2^{\delta_1+\eta_1}}{\delta_1+\eta_1}-\frac{G_0 T_1 T_2^{\eta_1}}{\eta_1}-\frac{G_0 T_2^{\eta_1+1}}{\eta_1+1}\Bigg) \left(\frac{X_0 T_2^{\eta_1}}{\eta_1}+\frac{X_0\eta_0 T_2^{2\eta_1}}{2\eta_1}-\frac{X_0\delta_0 T_2^{\delta_1+\eta_1}}{\delta_1+\eta_1}+\frac{Y_0 T_2^{\eta_1+1}}{\eta_1+1}+\frac{Y_0\eta_0 T_2^{2\eta_1+1}}{2\eta_1+1}-\frac{Y_0\delta_0 T_2^{\delta_1+\eta_1+1}}{\delta_1+\eta_1+1}\right) - (1-G_0T_1)\Bigg\{\frac{X_0 T_2^{\eta_1+1}}{\eta_1+1}+\frac{X_0\eta_0 T_2^{2\eta_1+1}}{(\eta_1+1)(\eta_1+2)}-\frac{X_0\delta_0 T_2^{\delta_1+\eta_1+1}}{(\delta_1+1)(\delta_1+\eta_1+1)}+\frac{Y_0 T_2^{\eta_1+2}}{2(\eta_1+2)}+\frac{Y_0\eta_0 T_2^{2\eta_1+2}}{2(\eta_1+2)^2} - \delta_0\Bigg\{\frac{X_0 T_2^{\delta_1+\eta_1+1}}{\delta_1+\eta_1+1}+\frac{Y_0 T_2^{\delta_1+\eta_1+2}}{2(\delta_1+\eta_1+2)}+\frac{X_0\eta_0 T_2^{\delta_1+2\eta_1+1}}{(\eta_1+1)(\delta_1+2\eta_1+1)}+\frac{Y_0\eta_0 T_2^{\delta_1+2\eta_1+2}}{(\delta_1+2\eta_1+2)} + \frac{Y_0\eta_0 T_2^{\delta_1+\eta_1+3}}{(2\delta_1+\eta_1+3)}-\frac{Y_0\delta_0 T_2^{2\delta_1+\eta_1+2}}{(\delta_1+1)(2\delta_1+\eta_1+2)}\Bigg\}+\eta_0\Bigg\{\frac{X_0 T_2^{2\eta_1+1}}{2\eta_1+1}+\frac{Y_0 T_2^{2\eta_1+1}}{4(\eta_1+1)} + \frac{X_0\eta_0 T_2^{3\eta_1+1}}{(3\eta_1+1)}-\frac{X_0\delta_0 T_2^{\delta_1+2\eta_1+1}}{(\delta_1+1)(\delta_1+2\eta_1+1)}-\frac{X_0\delta_0 T_2^{\delta_1+2\eta_1+2}}{(\delta_1+1)(\delta_1+2\eta_1+2)}+\frac{Y_0\eta_0 T_2^{3\eta_1+2}}{(\eta_1+2)(3\eta_1+2)}\Bigg\}\Bigg] \quad (7)$$

The net present item cost of livestock is given by

$$IC_{bdc} = \Big(N_{bdc}\Big)\Big(R_{bdc}\Big)$$

$$IC_{bdc} = N_{bdc}\Bigg[\Bigg\{X_0T_2+\frac{Y_0T_2^2}{2}+\frac{X_0\eta_0T_2^{\eta_1+1}}{\eta_1+1}-\frac{X_0\delta_0T_2^{\delta_1+1}}{\delta_1+1}+\frac{Y_0\eta_0T_2^{\eta_1+2}}{\eta_1+2} - \frac{Y_0\delta_0T_2^{\delta_1+2}}{\delta_1+2}\Bigg\}+\Bigg\{\delta_0T_1^{\delta_1}X_0T_2+\frac{\delta_0T_1^{\delta_1}Y_0T_2^2}{2}+\frac{\delta_0T_1^{\delta_1}X_0\eta_0T_2^{\eta_1+1}}{\eta_1+1}-\frac{\delta_0T_1^{\delta_1}X_0T_2^{\delta_1+1}}{\delta_1+1} + \frac{\delta_0T_1^{\delta_1}Y_0\eta_0T_2^{\eta_1+2}}{\eta_1+2}-\frac{\delta_0T_1^{\delta_1}Y_0T_2^{\delta_1+2}}{\delta_1+2}\Bigg\}-\Bigg\{\eta_0T_1^{\eta_1}X_0T_2+\frac{\eta_0T_1^{\eta_1}Y_0T_2^2}{2} + \frac{\eta_0^2T_1^{\eta_1}X_0T_2^{\eta_1+1}}{\eta_1+1}-\frac{\eta_0T_1^{\eta_1}X_0\delta_0T_2^{\delta_1+1}}{\delta_1+1}+\frac{\eta_0^2T_1^{\eta_1}X_0\delta_0T_2^{\eta_1+2}}{\eta_1+2}-\frac{\eta_0T_1^{\eta_1}Y_0\delta_0T_2^{\delta_1+2}}{\delta_1+2}\Bigg\}\Bigg] \quad (8)$$

The net present total cost per unit time of Blood Donation Centers Inventory for the livestock during the cycle is the average of the sum of the ordering cost, the holding cost, the ameliorating cost and the cost given by

$$TC_{bdc} = \left[\frac{OC_{bdc}+HC_{bdc}+AC_{bdc}+IC_{bdc}}{T}\right]$$

3.2. Regional Blood Center's Inventory System

$$\frac{d\Pi_{bdc2}(t_2)}{dt_2} = (X_0+Y_0t_2)-(Z_0+Z_1t_2)-\delta_2\delta_3t_2^{\delta_3-1}\Pi_{rbc2}(t_2), \qquad 0\le t_2\le T_2 \quad (9)$$

$$\frac{d\Pi_{bdc3}(t_3)}{dt_3} = -(Z_1+Z_2t_3)-\delta_2\delta_3t_3^{\delta_3-1}\Pi_{rbc3}(t_3), \qquad 0\le t_2\le T_3 \quad (10)$$

The boundary conditions are given by $\Pi_{rbc2}(0) = 0_{bdc}$ and $\Pi_{rbc2}(T_3) = 0$.

$$\Pi_{rbc2}(t_2) = e^{-\delta_2 t_2^{\delta_3}}\int_0^{t_2}\left[\Big\{(X_0+Y_0M)-(Z_0+Z_1M)\Big\}e^{\delta_2M^{\delta_3}}dM\right] \qquad 0\le t_2\le T_2$$

$$\Pi_{rbc3}(t_3) = e^{-\delta_2 t_3^{\delta_3}} \int_0^{t_3} \left[(Z_0 + Z_1 M) e^{\delta_2 M^{\delta_3}} dM \right] \qquad 0 \le t_3 \le T_3$$

The Regional Blood Center's maximum inventory level is given by

$$Z_{rbc} = \Pi_{rbc3}(0),$$

$$Z_{rbc} = \int_0^{T_3} (Z_0 + Z_1 M) e^{\delta_2 M^{\delta_3}} dM,$$

$$Z_{rbc} = \int_0^{T_3} (Z_0 + Z_1 M)(1 + \delta_2 M^{\delta_3} + ...) dM,$$

$$Z_{rbc} = \left[Z_0 T_3 + \frac{Z_0 T_3^2}{2} + \frac{\delta_2 Z_0 T_3^{\delta_3+1}}{\delta_3 + 1} + \frac{\delta_2 Z_1 T_3^{\delta_3+2}}{\delta_3 + 2} \right] dM$$

The production lot size per cycle is given by

$$R_{rbc} = \int_0^{T_2} (X_0 + Y_0 t_2) dt_2$$

$$R_{rbc} = (X_0 T_2 + \frac{Y_0 T_2^2}{2})$$

The initial production setup cost N_{rbc1} is at $t_2 = 0$
The net present setup cost is given by

$$SC_{rbc} = N_{rbc1} e^{-G_0 T_1}$$

$$SC_{rbc} = N_{rbc1}(1 - G_0 T_1)$$

The inventory is carried out during the time periods T_2 and T_3.
The net present holding cost is given by

$$HC_{rbc} = N_{rbc2} \left[\left\{ \int_0^{T_2} \Pi_{rbc2}(t_2) e^{G_0(T_1+t_2)} dt_2 + \int_{t_3}^{T_3} \Pi_{rbc3}(t_3) e^{G_0(T_1+T_2+t_3)} dt_3 \right\} - \left\{ \int_0^{T_5} \Pi_{rbc5}(t_5) e^{-G_0 t_5} dt_5 + \left(\sum_{i=0}^{k-1} e^{-iG_0 T_7} e^{-G_0 T_1} \right) \right\} \right] \quad (11)$$

$$\begin{aligned} HC_{rbc} = {} & \left[N_{rbc2} \left[\left\{ (X_0 - Z_0) \left[\frac{T_2^2}{2} + \left\{ \frac{1}{\delta_3 + 1} - \delta_2 \right\} \frac{T_2^{\delta_3+2}}{\delta_3 + 2} - \frac{\delta_2 T_2^{2\delta_3+2}}{(\delta_3 + 1)(2\delta_3 + 1)} \right] \right\} \right. \right. \\ & + \left. \left\{ (Y_0 - Z_1) \left[\frac{T_2^3}{6} + \left\{ \frac{1}{\delta_3 + 2} - \delta_2 \right\} \frac{T_2^{\delta_3+3}}{\delta_3 + 3} - \frac{\delta_2 T_2^{2\delta_3+3}}{(\delta_3 + 2)(2\delta_3 + 3)} \right] \right\} \right] \\ & + N_{rbc2} \left[\left\{ Z_0 \left[\frac{T_3^2}{2} + \left\{ \frac{1}{\delta_3 + 1} - \delta_2 \right\} \frac{T_2^{\delta_3+2}}{\delta_3 + 2} - \frac{\delta_2 T_2^{2\delta_3+2}}{(\delta_3 + 1)(2\delta_3 + 1)} \right] \right\} \right. \\ & + \left. \left\{ Z_1 \left[\frac{T_2^3}{6} + \left\{ \frac{1}{\delta_3 + 2} - \delta_2 \right\} \frac{T_2^{\delta_3+3}}{\delta_3 + 3} - \frac{\delta_2 T_2^{2\delta_3+3}}{(\delta_3 + 2)(2\delta_3 + 3)} \right] \right\} \right] \\ & - N_{rbc2} \left[\left\{ \frac{Z_0 T_5^2}{2} + \frac{Z_1 T_5^3}{2} + \frac{Z_0 \delta_2 T_5^{\delta_3+2}}{\delta_3 + 2} + \frac{Z_1 \delta_2 T_5^{\delta_3+2}}{\delta_3 + 2} \right\} \right. \\ & - (\delta_2 - r) \left[\left\{ \frac{Z_0 T_5^3}{6} + \frac{Z_1 T_5^4}{8} + \frac{Z_0 \delta_2 T_5^{\delta_3+3}}{2(\delta_3 + 3)} \right. \right. \\ & \left. \left. \left. + \frac{Z_1 \delta_2 T_5^{\delta_3+4}}{2(\delta_3 + 4)} \right\} \right] \left(\frac{1 - e^{-G_0 T_4}}{1 - e^{-G_0 T_7}} \right) (1 - G_0 T_1) \right] \end{aligned} \quad (12)$$

The net present item cost is given by

$$IC_{rbc} = [N_{rbc}][R_{rbc}]e^{-G_0T_1},$$

$$IC_{rbc} = N_{rbc}(X_0T_2 + \frac{Y_0T_2^2}{2})e^{-G_0T_1},$$

$$IC_{rbc} = \left[N_{rbc}e^{-G_0T_1} + \frac{C_me^{-G_0T_1}Y_0T_2^2}{2}\right],$$

The net present total cost for the Regional Blood Center's Inventory system during the cycle is the sum of the setup cost, the holding cost, the item cost and the cost given by

$$TC_{rbc} = \left[\frac{HC_{rbc} + SC_{rbc} + IC_{rbc}}{T}\right]$$

3.3. Hospitals Blood Inventory System

$$\frac{d\Pi_{hb5}(t_5)}{dt_5} = \left[- (Z_0 + Z_1t_5) - \delta_2\delta_3t_5^{\delta_3-1}\Pi_{hb5}(t_5)\right], \qquad 0 \le t_5 \le T_5 \tag{13}$$

$$\frac{d\Pi_{hb6}(t_6)}{dt_6} = \left[- B(Z_0 + Z_1t_6)\right], \qquad 0 \le t_6 \le T_6 \tag{14}$$

The boundary conditions are given by $\Pi_{r5}(T_6) = 0$, and $\Pi_{r5}(0) = 0$.
Using the above boundary condition the solutions (13) and (14) are given by

$$\Pi_{hb5}(t_5) = \left[e^{\delta_2t_5^{\delta_3}}\int_{t_5}^{T_2}(Z_0 + Z_1M)e^{\delta_2M^{\delta_3}}dM\right] \qquad 0 \le t_5 \le T_5$$

$$\Pi_{hb6}(t_6) = \left[- B\left\{Z_0t_6 + \frac{Z_1t_6^2}{2}\right\}\right] \qquad 0 \le t_6 \le T_6$$

The retailer maximum inventory level is given by

$$Z_{hb} = \Pi_{hb}(0),$$

$$Z_{hb} = \int_{t_5}^{T_5}(Z_0 + Z_1M)e^{\delta_2M^{\delta_3}}dM,$$

$$Z_{hb} = \int_{t_5}^{T_5}(Z_0 + Z_1M)(1 + \delta_2M^{\delta_3} + ...)dM,$$

$$Z_{hb} = \left[Z_0T_5 + \frac{Z_1T_5^2}{2} + \frac{\delta_2Z_0T_5^{\delta_3+1}}{\delta_3+1} + \frac{\delta_2Z_1T_5^{\delta_3+2}}{\delta_3+2}\right],$$

The quantity given to the retailer per delivery is given by

$$R_{hb} = MI_{hb} + B\left[Z_0T_6 + \frac{Z_1T_6^2}{2}\right]$$

$$R_{hb} = \left[Z_0T_5 + \frac{Z_1T_5^2}{2} + \frac{\delta_2Z_0T_5^{\delta_3+1}}{\delta_3+1} + \frac{\delta_2Z_1T_5^{\delta_3+2}}{\delta_3+2}\right] + B\left[Z_0T_6 + \frac{Z_1T_6^2}{2}\right]$$

The initial ordering cost is C_{r1}. The net present ordering cost is given by

$$OC_{hb} = N_{hb1},$$

The inventory at the retailer is carried out during time period T_5. The net present holding cost is given by

$$HC_{hb} = N_{hb2}\int_0^{T_5}\Pi_{hb5}(t_5)e^{-G_0t_5}dt_5,$$

$$HC_{hb} = N_{hb2}\int_0^{T_5} e^{-\delta_2 t_5^{\delta_3} - G_0 t_5}\left[\left(Z_0 T_5 + \frac{Z_1 T_5^2}{2}\right) - \left(Z_0 t_5 + \frac{Z_1 t_5^2}{2}\right)\right]dt_5,$$

$$HC_{hb} = N_{hb2}\int_0^{T_5} \left(1 - \delta_2 t_5^{\delta_3} - G_0 t_5\right)\left[\left(Z_0 T_5 + \frac{Z_1 T_5^2}{2}\right) - \left(Z_0 t_5 + \frac{Z_1 t_5^2}{2}\right)\right]dt_5$$

$$HC_{hb} = N_{hb2}\left[\left\{\frac{Z_0 T_5^2}{2} + \frac{Z_1 T_5^3}{2} + \frac{Z_0\delta_2 T_5^{\delta_3+2}}{\delta_3+2} + \frac{Z_1\delta_2 T_5^{\delta_3+2}}{\delta_3+2}\right\} + (\delta_2 + G_0)\left\{\frac{Z_0 T_5^3}{6} + \frac{Z_1 T_5^4}{8} + \frac{Z_0\delta_2 T_5^{\delta_3+3}}{2(\delta_3+3)} + \frac{Z_1\delta_2 T_5^{\delta_3+4}}{2(\delta_3+4)}\right\}\right] \quad (15)$$

The inventory at the retailer is carried out during the time period T_5. The net present backlog cost is given by

$$SC_{hb} = N_{hb3}\int_0^{T_6} \Pi_{hb6}(t_6) e^{-G_0(T_5+t_6)} dt_6,$$

$$SC_{hb} = N_{hb3} B\int_0^{T_6} \left[Z_0 t_6 + \frac{Z_1 t_6^2}{2}\right] e^{-G_0(T_5+t_6)} dt_6,$$

$$SC_{hb} = N_{hb3} B\left[\frac{Z_0(1-G_0T_5)T_6^2}{2} + \left(\frac{Z_1(1-G_0T_5)}{2} - Z_0G_0\right)\frac{T_6^3}{3} - \frac{Z_1 G_0 T_6^4}{8}\right],$$

The net present total cost during the Hospitals Blood Inventory system is the sum of the ordering cost, the holding cost, the backlog cost and the cost given by

$$TC_{hb} = \frac{OC_{hb} + HC_{hb} + SC_{hb}}{T},$$

The net present total cost during Blood Donation Centers Inventory system, Regional Blood Center's Inventory system and Hospitals Blood Inventory system

$$TC_{bbsc} = TC_{bdc} + TC_{rbc} + TC_{hb}$$

4. BEE COLONY OPTIMIZATION (BCO) AND GENETIC ALGORITHMS (GA) METHODOLOGY

4.1. Blood Donation Center's Stage

1. **Demand Forecasting with Genetic Algorithms (GA):** Genetic Algorithms are applied to historical demand data to optimize demand forecasting. GA adapts to changing patterns and identifies influential factors in demand prediction.

2. **Production Planning using Bee Colony Optimization (BCO):** BCO optimizes production scheduling by finding the most efficient allocation of resources. Adaptive algorithms adjust to resource availability and demand fluctuations.

3. **Quality Assurance and GA:** Genetic Algorithms assist in quality control, improving product quality by identifying and minimizing defects. GA based anomaly detection enhances quality assurance processes.

4. **Inventory Management with BCO:** Bee Colony Optimization optimizes inventory control by dynamically adjusting reorder points and order quantities. BCO adapts to variations in demand and lead times.

4.2. Regional Blood Center's Stage

1. **Inventory Optimization using GA:** Genetic Algorithms optimize inventory levels in the Regional Blood Center's by minimizing holding costs and stockouts. GA adapts to changing demand patterns.
2. **Smart Storage and Retrieval with BCO:** Bee Colony Optimization enhances storage and retrieval processes by optimizing routing within the Regional Blood Center's. Adaptive BCO algorithms minimize travel times and improve efficiency.

4.3. Hospitals Blood Center's Stage

1. **Local Demand Forecasting with GA:** Hospitals Blood Center's employ Genetic Algorithms for local demand forecasting, adapting to local market dynamics. GA models capture seasonality and changing consumer preferences.
2. **Order Optimization and BCO:** Hospitals Blood Center's utilize Bee Colony Optimization to optimize order quantities and lead times. BCO based order optimization considers factors like transportation costs and inventory constraints.
3. **Collaborative Decision-making with GA and BCO:** Hospitals Blood Center's collaborate using Genetic Algorithms and Bee Colony Optimization to share demand and inventory data. Algorithms enable Hospitals Blood Center's to make coordinated decisions, reducing supply chain inefficiencies.
4. **Supply Chain Coordination with Hybrid GABCO:** A hybrid approach combines Genetic Algorithms and Bee Colony Optimization to optimize the entire supply chain. Coordinated decision-making considers both global and local optimization objectives.

Applying the power of state-of-the-art optimization techniques, specifically Bee Colony Optimization and Genetic Algorithms, this supply chain model revolutionizes every stage of the supply chain. By integrating these intricate algorithms into standard supply chain operations, the model significantly enhances decision-making and expedites crucial operational routines. The supply chain is hence better equipped to adapt to the constantly shifting market and its associated risks, becoming more responsive and efficient. Together, cutting-edge optimization strategies and tried-and-true supply chain practices enhance performance, enabling businesses to reduce costs, increase productivity, and stay flexible in response to shifting consumer demands. Ultimately, by continuously improving itself, this integrated approach creates a highly intelligent and adaptable supply chain ecosystem that can adjust to shifting conditions and new challenges.

5. NUMERICAL ILLUSTRATION

Let for the production rate $X_0 = 500, Y_0 = 400$ and for the demand rate $Z_0 = 500, Z_1 = 400$, Blood Donation Center's ordering cost=400, Regional Blood Center's ordering cost =450, Hospitals Blood ordering cost =550, Blood Donation Center's holding cost=200, Regional Blood Center's holding cost=250, Hospitals Blood holding cost=255, deterioration cost $\delta_2 = 0.04, \delta_3 = 2.5, \delta_0 = 0.05, \delta_1 = 2.5$ ameliorating rate $Z_0 = 500, Z_1 = 400$ discount rate$G_0 = 0.06$ and fractional backorder $B = 0.8$.

5.1. Graphical Representation

The graphical analysis validates the effectiveness of the proposed hybrid optimization model in minimizing total costs across the blood supply chain. Figure 2 illustrates the optimality of the Blood Donation Inventory, highlighting how time parameters influence cost. Figure 3 demonstrates the efficiency of the hybrid BCO-GA approach in achieving cost minimization. Figure 4 presents the optimality of the Hospital Blood Inventory, confirming the model's adaptability to demand variations and operational constraints.

5.2. Tables Overview

Tables 2, 3, and 4 provide optimal solutions for the Blood Donation Center, Regional Blood Center, and Hospital Blood Inventory systems, respectively. They summarize how variations in cycle parameters affect total cost and demonstrate the effectiveness of Genetic Algorithm and Bee Colony Optimization methods.

Table 2: *Optimal Solution Blood Donation Centers Inventory*

K	T_1	T_2	T_3	T_4	T_6	TC_{CVM}	TC	GA	BCO
1	0.013	0.013	1.130	1.100	0.149	841.130	111.45	411.45	111.45
2	0.013	0.140	1.140	0.185	0.139	851.130	131.45	411.45	131.45
3	0.014	0.145	1.150	0.175	0.134	811.130	141.45	411.45	141.45
4	0.015	0.150	3.130	0.115	0.133	871.130	171.45	411.45	171.45
5	0.015	0.155	3.139	0.155	0.139	881.130	181.45	481.45	181.45
6	0.011	0.110	3.135	0.145	0.137	891.130	191.45	491.45	191.45
7	0.011	0.115	3.135	0.140	0.134	991.130	301.45	501.45	701.45
8	0.017	0.170	3.140	0.135	0.131	993.130	311.45	511.45	711.45
9	0.017	0.175	4.131	0.130	0.119	995.130	331.45	531.45	731.45
10	0.018	0.180	4.150	0.130	0.111	997.130	331.45	531.45	731.45

Table 3: *Optimal Solution Regional Blood Donation Center's Inventory*

K	T_1	T_2	T_3	T_4	T_6	TC_{CVM}	TC	GA	BCO
1	0.03	0.30	1.30	1.00	0.49	1841.30	1111.45	4111.45	1111.45
2	0.03	0.40	1.40	0.85	0.39	1851.30	1311.45	4311.45	1311.45
3	0.04	0.45	1.50	0.75	0.34	1811.30	1411.45	4411.45	1411.45
4	0.05	0.50	3.30	0.15	0.33	1871.30	1711.45	4711.45	1711.45
5	0.05	0.55	3.39	0.55	0.39	1881.30	1811.45	4811.45	1811.45
6	0.01	0.10	3.35	0.45	0.37	1891.30	1911.45	4911.45	1911.45
7	0.01	0.15	3.35	0.40	0.34	1991.30	3011.45	5011.45	7011.45
8	0.07	0.70	3.40	0.35	0.31	1993.30	3111.45	5111.45	7111.45
9	0.07	0.75	4.31	0.30	0.19	1995.30	3111.45	5311.45	7311.45
10	0.38	0.80	4.50	0.30	0.11	1997.30	3311.45	5311.45	7311.45

Table 4: *Optimal Solution Hospitals Blood Inventory system*

K	T_1	T_2	T_3	T_4	T_6	TC_{CVM}	TC	GA	BCO
1	0.03	0.30	1.30	1.00	0.49	3841.30	1111.45	4111.45	1111.45
2	0.03	0.40	1.40	0.85	0.39	3851.30	1311.45	4311.45	1311.45
3	0.04	0.45	1.50	0.75	0.34	3811.30	1411.45	4411.45	1411.45
4	0.05	0.50	3.30	0.15	0.33	3871.30	1711.45	4711.45	1711.45
5	0.05	0.55	3.39	0.55	0.39	3881.30	1811.45	4811.45	1811.45
6	0.01	0.10	3.35	0.45	0.37	3891.30	1911.45	4911.45	1911.45
7	0.01	0.15	3.35	0.40	0.34	3991.30	3011.45	5011.45	7011.45
8	0.07	0.70	3.40	0.35	0.31	3993.30	3111.45	5111.45	7111.45
9	0.07	0.75	4.31	0.30	0.19	3995.30	3111.45	5311.45	7311.45
10	0.38	0.80	4.50	0.30	0.11	3997.30	3311.45	5311.45	7311.45

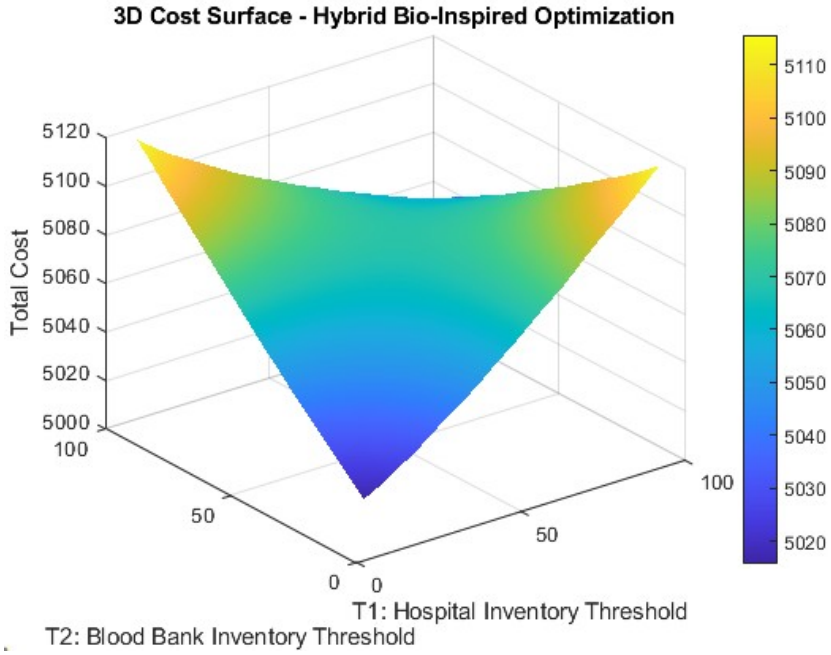


Figure 2: *Optimality of Blood Donation Inventory.*

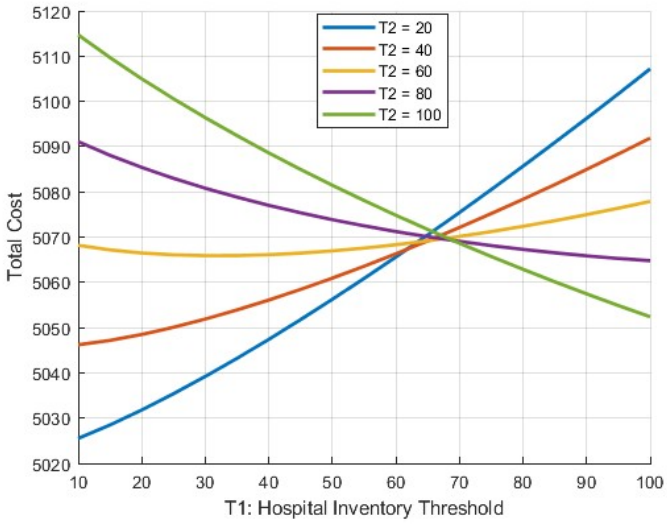


Figure 3: *Cost Minimization - Hybrid Bio-Inspired Optimization.*

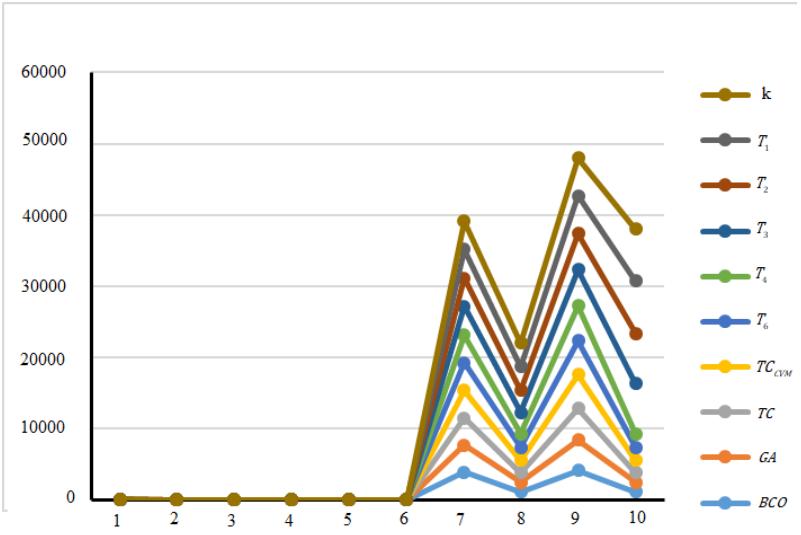


Figure 4: *Optimality of Hospital Blood Inventory.*

6. Conclusion

In conclusion, optimizing blood supply chain inventory management is imperative for healthcare facilities to meet the demands of a competitive and dynamic healthcare landscape. The success of a healthcare organization hinges on its ability to efficiently navigate challenges such as minimizing lead times and costs, while simultaneously enhancing patient service levels and maintaining the highest quality standards for blood products. The evolution of healthcare logistics has highlighted the need to break down silos within organizational units involved in blood sourcing, production, distribution, and healthcare marketing. Despite common overarching goals, these units often harbor distinct and occasionally conflicting objectives. Sourcing decisions tend to focus on cost minimization, while production and distribution decisions prioritize maximizing throughput and minimizing unit production costs, sometimes overlooking the implications of high blood product inventory levels and extended lead times.

At its core, effective blood supply chain management aims to integrate diverse healthcare organizations, each with unique objectives, towards the unified goal of ensuring a dependable and efficient blood supply for patient care. Recent advancements underscore the potential for substantial enhancements in these objectives through the skillful orchestration of blood supply chain management mechanisms.

The challenge of blood inventory management involves striking a delicate balance in maintaining an optimal supply of specific blood types in alignment with forecasted patient demand patterns. This requires strategic management of the costs associated with blood product holding, along with mitigating the adverse effects of shortages, such as compromised patient care and potential health risks.

The scope of blood products subject to inventory management is vast, ranging from everyday blood components used in transfusions to essential plasma-derived medications. Intriguingly, seemingly unrelated healthcare challenges can be mathematically modeled as intricate interwoven blood supply chain inventory control dilemmas.

Various blood supply chain models, characterized by administrative costs, ongoing maintenance costs, and shortfall costs, form the foundation for achieving efficient blood supply chain management. Innovative optimization algorithms, including Bee Colony Optimization and Genetic Algorithms, draw inspiration from nature to enhance the efficiency of blood product routing, storage, and distribution within the healthcare system.

Bee Colony Optimization Algorithms replicate the collaborative foraging behavior of ants,

creating paths marked by pheromones to signify path quality. Similarly, Genetic Algorithms emulate natural selection and evolution to iteratively improve solutions. These algorithms contribute significantly to the efficient orchestration of blood supply chains, ensuring timely and safe access to blood products for patient care through the reinforcement of optimal or near-optimal solutions over successive iterations.

In summary, the integration of advanced optimization algorithms into blood supply chain management processes holds the promise of revolutionizing the efficiency and effectiveness of healthcare logistics, ultimately benefiting both healthcare providers and, most importantly, the patients they serve.

References

[1] Yadav, A.S., Bansal, K.K., Shivani, Agarwal, S. And Vanaja, R. (2020) FIFO in Green Supply Chain Inventory Model of Electrical Components Industry With Distribution Centres Using Particle Swarm Optimization. Advances in Mathematics: Scientific Journal. 9 (7), 5115“512 0.

[2] Yadav, A.S., Kumar, A., Agarwal, P., Kumar, T. And Vanaja, R. (2020) LIFO in Green Supply Chain Inventory Model of Auto-Components Industry with Warehouses Using Differential Evolution. Advances in Mathematics: Scientific Journal, 9 no.7, 5121“5126.

[3] Yadav, A.S., Abid, M., Bansal, S., Tyagi, S.L. And Kumar, T. (2020) FIFO LIFO in Green Supply Chain Inventory Model of Hazardous Substance Components Industry with Storage Using Simulated Annealing. Advances in Mathematics: Scientific Journal, 9 no.7, 5127“5132.

[4] Yadav, A.S., Tandon, A. and Selva, N.S. (2020) National Blood Bank Centre Supply Chain Management For Blockchain Application Using Genetic Algorithm. International Journal of Advanced Science and Technology Vol. 29, No. 8s, 1318-1324.

[5] Yadav, A.S., Selva, N.S. and Tandon, A. (2020) Medicine Manufacturing Industries supply chain management for Blockchain application using artificial neural networks, International Journal of Advanced Science and Technology Vol. 29, No. 8s, 1294-1301.

[6] Yadav, A.S., Ahlawat, N., Agarwal, S., Pandey, T. and Swami, A. (2020) Red Wine Industry of Supply Chain Management for Distribution Center Using Neural Networks, Test Engraining & Management, Volume 83 Issue: March “ April, 11215 “ 11222.

[7] Yadav, A.S., Pandey, T., Ahlawat, N., Agarwal, S. and Swami, A. (2020) Rose Wine industry of Supply Chain Management for Storage using Genetic Algorithm. Test Engraining & Management, Volume 83 Issue: March “ April, 11223 “ 11230.

[8] Yadav, A.S., Ahlawat, N., Sharma, N., Swami, A. And Navyata (2020) Healthcare Systems of Inventory Control For Blood Bank Storage With Reliability Applications Using Genetic Algorithm. Advances in Mathematics: Scientific Journal 9 no.7, 5133“5142.

[9] Yadav, A.S., Dubey, R., Pandey, G., Ahlawat, N. and Swami, A. (2020) Distillery Industry Inventory Control for Storage with Wastewater Treatment Logistics Using Particle Swarm Optimization Test Engraining & Management Volume 83 Issue: May “ June, 15362-15370.

[10] Yadav, A.S., Ahlawat, N., Dubey, R., Pandey, G. and Swami, A. (2020) Pulp and paper industry inventory control for Storage with wastewater treatment and Inorganic composition using genetic algorithm (ELD Problem). Test Engraining & Management, Volume 83 Issue: May “ June, 15508-15517.

[11] Yadav, A.S., Pandey, G., Ahlawat, N., Dubey, R. and Swami, A. (2020) Wine Industry Inventory Control for Storage with Wastewater Treatment and Pollution Load Using Ant Colony Optimization Algorithm, Test Engraining & Management, Volume 83 Issue: May “ June, 15528-15535.

[12] Yadav, A.S., Navyata, Sharma, N., Ahlawat, N. and Swami, A. (2020) Reliability Consideration costing method for LIFO Inventory model with chemical industry warehouse. International Journal of Advanced Trends in Computer Science and Engineering, Volume 9 No 1, 403-408.

[13] Yadav, A.S., Bansal, K.K., Kumar, J. and Kumar, S. (2019) Supply Chain Inventory Model For Deteriorating Item With Warehouse & Distribution Centres Under Inflation. International Journal of Engineering and Advanced Technology, Volume-8, Issue-2S2, 7-13.

[14] Yadav, A.S., Kumar, J., Malik, M. and Pandey, T. (2019) Supply Chain of Chemical Industry For Warehouse With Distribution Centres Using Artificial Bee Colony Algorithm. International Journal of Engineering and Advanced Technology, Volume-8, Issue-2S2, 14-19.

[15] Yadav, A.S., Navyata, Ahlawat, N. and Pandey, T. (2019) Soft computing techniques based Hazardous Substance Storage Inventory Model for decaying Items and Inflation using Genetic Algorithm. International Journal of Advance Research and Innovative Ideas in Education, Volume 5 Issue 9, 1102-1112.

[16] Yadav, A.S., Navyata, Ahlawat, N. and Pandey, T. (2019) Hazardous Substance Storage Inventory Model for decaying Items using Differential Evolution. International Journal of Advance Research and Innovative Ideas in Education, Volume 5 Issue 9, 1113-1122.

[17] Yadav, A.S., Navyata, Ahlawat, N. and Pandey, T. (2019) Probabilistic inventory model based Hazardous Substance Storage for decaying Items and Inflation using Particle Swarm Optimization. International Journal of Advance Research and Innovative Ideas in Education, Volume 5 Issue 9, 1123-1133.

[18] Yadav, A.S., Navyata, Ahlawat, N. and Pandey, T. (2019) Reliability Consideration based Hazardous Substance Storage Inventory Model for decaying Items using Simulated Annealing. International Journal of Advance Research and Innovative Ideas in Education, Volume 5 Issue 9, 1134-1143.

[19] Yadav, A.S., Swami, A. and Kher, G. (2019) Blood bank supply chain inventory model for blood collection sites and hospital using genetic algorithm. Selforganizology, Volume 6 No.(3-4), 13-23.

[20] Yadav, A.S., Swami, A. and Ahlawat, N. (2018) A Green supply chain management of Auto industry for inventory model with distribution centers using Particle Swarm Optimization. Selforganizology, Volume 5 No. (3-4)

[21] Yadav, A.S., Ahlawat, N., and Sharma, S. (2018) Hybrid Techniques of Genetic Algorithm for inventory of Auto industry model for deteriorating items with two warehouses. International Journal of Trend in Scientific Research and Development, Volume 2 Issue 5, 58-65.

[22] Yadav, A.S., Swami, A. and Gupta, C.B. (2018) A Supply Chain Management of Pharmaceutical For Deteriorating Items Using Genetic Algorithm. International Journal for Science and Advance Research In Technology, Volume 4 Issue 4, 2147-2153.

[23] Yadav, A.S., Maheshwari, P., Swami, A., and Pandey, G. (2018) A supply chain management of chemical industry for deteriorating items with warehouse using genetic algorithm. Selforganizology, Volume 5 No.1-2, 41-51.

[24] Yadav, A.S., Garg, A., Gupta, K. and Swami, A. (2017) Multi-objective Genetic algorithm optimization in Inventory model for deteriorating items with shortages using Supply Chain management. IPASJ International journal of computer science, Volume 5, Issue 6, 15-35.

[25] Yadav, A.S., Garg, A., Swami, A. and Kher, G. (2017) A Supply Chain management in Inventory Optimization for deteriorating items with Genetic algorithm. International Journal of Emerging Trends & Technology in Computer Science, Volume 6, Issue 3, 335-352.

[26] Yadav, A.S., Maheshwari, P., Garg, A., Swami, A. and Kher, G. (2017) Modeling & Analysis of Supply Chain management in Inventory Optimization for deteriorating items with Genetic algorithm and Particle Swarm optimization. International Journal of Application or Innovation in Engineering & Management, Volume 6, Issue 6, 86-107.

[27] Yadav, A.S., Garg, A., Gupta, K. and Swami, A. (2017) Multi-objective Particle Swarm optimization and Genetic algorithm in Inventory model for deteriorating items with shortages using Supply Chain management. International Journal of Application or Innovation in Engineering & Management, Volume 6, Issue 6, 130-144.

[28] Yadav, A.S., Swami, A. and Kher, G. (2017) Multi-Objective Genetic Algorithm Involving Green Supply Chain Management International Journal for Science and Advance Research In Technology, Volume 3 Issue 9, 132-138.

[29] Yadav, A.S., Swami, A., Kher, G. (2017) Multi-Objective Particle Swarm Optimization Algorithm Involving Green Supply Chain Inventory Management. International Journal for Science and Advance Research In Technology, Volume 3 Issue, 240-246.

[30] Yadav, A.S., Swami, A. and Pandey, G. (2017) Green Supply Chain Management for Warehouse with Particle Swarm Optimization Algorithm. International Journal for Science and Advance Research in Technology, Volume 3 Issue 10, 769-775.

[31] Yadav, A.S., Swami, A., Kher, G. and Garg, A. (2017) Analysis of seven stages supply chain management in electronic component inventory optimization for warehouse with economic load dispatch using genetic algorithm. Selforganizology, 4 No.2, 18-29.

[32] Yadav, A.S., Maheshwari, P., Swami, A. and Garg, A. (2017) Analysis of Six Stages Supply Chain management in Inventory Optimization for warehouse with Artificial bee colony algorithm using Genetic Algorithm. Selforganizology, Volume 4 No.3, 41-51.

[33] Yadav, A.S., Swami, A., Gupta, C.B. and Garg, A. (2017) Analysis of Electronic component inventory Optimization in Six Stages Supply Chain management for warehouse with ABC using genetic algorithm and PSO. Selforganizology, Volume 4 No.4, 52-64.

[34] Yadav, A.S., Maheshwari, P. and Swami, A. (2016) Analysis of Genetic Algorithm and Particle Swarm Optimization for warehouse with Supply Chain management in Inventory control. International Journal of Computer Applications, Volume 145 "No.5, 10-17.

[35] Yadav, A.S., Swami, A. and Kumar, S. (2018) Inventory of Electronic components model for deteriorating items with warehousing using Genetic Algorithm. International Journal of Pure and Applied Mathematics, Volume 119 No. 16, 169-177.

[36] Yadav, A.S., Johri, M., Singh, J. and Uppal, S. (2018) Analysis of Green Supply Chain Inventory Management for Warehouse With Environmental Collaboration and Sustainability Performance Using Genetic Algorithm. International Journal of Pure and Applied Mathematics, Volume 118 No. 20, 155-161.

[37] Yadav, A.S., Ahlawat, N., Swami, A. and Kher, G. (2019) Auto Industry inventory model for deteriorating items with two warehouse and Transportation Cost using Simulated Annealing Algorithms. International Journal of Advance Research and Innovative Ideas in Education, Volume 5,Issue 1, 24-33.

[38] Yadav, A.S., Ahlawat, N., Swami, A. and Kher, G. (2019) A Particle Swarm Optimization based a two-storage model for deteriorating items with Transportation Cost and Advertising Cost: The Auto Industry. International Journal of Advance Research and Innovative Ideas in Education, Volume 5, Issue 1, 34-44.

[39] Yadav, A.S., Ahlawat, N., and Sharma, S. (2018) A Particle Swarm Optimization for inventory of Auto industry model for two warehouses with deteriorating items. International Journal of Trend in Scientific Research and Development, Volume 2 Issue 5, 66-74.

[40] Yadav, A.S., Swami, A. and Kher, G. (2018) Particle Swarm optimization of inventory model with two-warehouses. Asian Journal of Mathematics and Computer Research, Volume 23 No.1, 17-26.

[41] Yadav, A.S., Maheshwari, P.,, Swami, A. and Kher, G. (2017) Soft Computing Optimization of Two Warehouse Inventory Model With Genetic Algorithm. Asian Journal of Mathematics and Computer Research, Volume 19 No.4, 214-223.

[42] Yadav, A.S., Swami, A., Kumar, S. and Singh, R.K. (2016) Two-Warehouse Inventory Model for Deteriorating Items with Variable Holding Cost, Time-Dependent Demand and Shortages. IOSR Journal of Mathematics, Volume 12, Issue 2 Ver. IV, 47-53.

[43] Yadav, A.S., Sharam, S. and Swami, A. (2016) Two Warehouse Inventory Model with Ramp Type Demand and Partial Backordering for Weibull Distribution Deterioration. International Journal of Computer Applications, Volume 140 -No.4, 15-25.

[44] Yadav, A.S., Swami, A. and Singh, R.K. (2016) A two-storage model for deteriorating items with holding cost under inflation and Genetic Algorithms. International Journal of Advanced Engineering, Management and Science, Volume -2, Issue-4, 251-258.

[45] Yadav, A.S., Swami, A., Kher, G. and Kumar, S. (2017) Supply Chain Inventory Model for Two Warehouses with Soft Computing Optimization. International Journal of Applied Business and Economic Research, Volume 15 No 4, 41-55.

[46] Yadav, A.S., Rajesh Mishra, Kumar, S. and Yadav, S. (2016) Multi Objective Optimization for Electronic Component Inventory Model & Deteriorating Items with Two-warehouse using

Genetic Algorithm. International Journal of Control Theory and applications, Volume 9 No.2, 881-892.

[47] Yadav, A.S., Gupta, K., Garg, A. and Swami, A. (2015) A Soft computing Optimization based Two Ware-House Inventory Model for Deteriorating Items with shortages using Genetic Algorithm. International Journal of Computer Applications, Volume 126 - No.13, 7-16.

[48] Yadav, A.S., Gupta, K., Garg, A. and Swami, A. (2015) A Two Warehouse Inventory Model for Deteriorating Items with Shortages under Genetic Algorithm and PSO. International Journal of Emerging Trends & Technology in Computer Science, Volume 4, Issue 5(2), 40-48.

[49] Yadav, A.S. Swami, A., and Kumar, S. (2018) A supply chain Inventory Model for decaying Items with Two Ware-House and Partial ordering under Inflation. International Journal of Pure and Applied Mathematics, Volume 120 No 6, 3053-3088.

[50] Yadav, A.S. Swami, A. and Kumar, S. (2018) An Inventory Model for Deteriorating Items with Two warehouses and variable holding Cost. International Journal of Pure and Applied Mathematics, Volume 120 No 6, 3069-3086.

[51] Yadav, A.S., Taygi, B., Sharma, S. and Swami, A. (2017) Effect of inflation on a two-warehouse inventory model for deteriorating items with time varying demand and shortages. International Journal Procurement Management, Volume 10, No. 6, 761-775.

[52] Yadav, A.S., R. P. Mahapatra, Sharma, S. and Swami, A. (2017) An Inflationary Inventory Model for Deteriorating items under Two Storage Systems. International Journal of Economic Research, Volume 14 No.9, 29-40.

[53] Yadav, A.S., Sharma, S. and Swami, A. (2017) A Fuzzy Based Two-Warehouse Inventory Model For Non instantaneous Deteriorating Items With Conditionally Permissible Delay In Payment. International Journal of Control Theory And Applications, Volume 10 No.11, 107-123.

[54] Yadav, A.S. and Swami, A. (2018) Integrated Supply Chain Model for Deteriorating Items With Linear Stock Dependent Demand Under Imprecise And Inflationary Environment. International Journal Procurement Management, Volume 11 No 6, 684-704.

[55] Yadav, A.S. and Swami, A. (2018) A partial backlogging production-inventory lot-size model with time-varying holding cost and weibull deterioration. International Journal Procurement Management, Volume 11, No. 5, 639-649.

[56] Yadav, A.S. and Swami, A. (2013) A Partial Backlogging Two-Warehouse Inventory Models For Decaying Items With Inflation. International Organization of Scientific Research Journal of Mathematics, Issue 6, 69-78.

[57] Yadav, A.S. and Swami, A. (2019) An inventory model for non-instantaneous deteriorating items with variable holding cost under two-storage. International Journal Procurement Management, Volume 12 No 6, 690-710.

[58] Yadav, A.S. and Swami, A. (2019) A Volume Flexible Two-Warehouse Model with Fluctuating Demand and Holding Cost under Inflation. International Journal Procurement Management, Volume 12 No 4, 441-456.

[59] Yadav, A.S. and Swami, A. (2014) Two-Warehouse Inventory Model for Deteriorating Items with Ramp-Type Demand Rate and Inflation. American Journal of Mathematics and Sciences Volume 3 No-1, 137-144.

[60] Yadav, A.S. and Swami, A. (2013) Effect of Permissible Delay on Two-Warehouse Inventory Model for Deteriorating items with Shortages. International Journal of Application or Innovation in Engineering & Management, Volume 2, Issue 3, 65-71.

[61] Yadav, A.S. and Swami, A. (2013) A Two-Warehouse Inventory Model for Decaying Items with Exponential Demand and Variable Holding Cost. International of Inventive Engineering and Sciences, Volume-1, Issue-5, 18-22.

[62] Yadav, A.S. and Kumar, S. (2017) Electronic Components Supply Chain Management for Warehouse with Environmental Collaboration & Neural Networks. International Journal of Pure and Applied Mathematics, Volume 117 No. 17, 169-177.

[63] Yadav, A.S. (2017) Analysis of Seven Stages Supply Chain Management in Electronic Component Inventory Optimization for Warehouse with Economic Load Dispatch Using GA and PSO. Asian Journal Of Mathematics And Computer Research, volume 16 No.4, 208-219.

[64] Yadav, A.S. (2017) Analysis Of Supply Chain Management In Inventory Optimization For Warehouse With Logistics Using Genetic Algorithm International Journal of Control Theory And Applications, Volume 10 No.10, 1-12 .

[65] Yadav, A.S. (2017) Modeling and Analysis of Supply Chain Inventory Model with two-warehouses and Economic Load Dispatch Problem Using Genetic Algorithm. International Journal of Engineering and Technology, Volume 9 No 1, 33-44.

[66] Swami, A., Singh, S.R., Pareek, S. and Yadav, A.S. (2015) Inventory policies for deteriorating item with stock dependent demand and variable holding costs under permissible delay in payment. International Journal of Application or Innovation in Engineering & Management, Volume 4, Issue 2, 89-99.

[67] Swami, A., Pareek, S., Singh S.R. and Yadav, A.S. (2015) Inventory Model for Decaying Items with Multivariate Demand and Variable Holding cost under the facility of Trade-Credit. International Journal of Computer Application, 18-28.

[68] Swami, A., Pareek, S., Singh, S.R. and Yadav, A.S. (2015) An Inventory Model With Price Sensitive Demand, Variable Holding Cost And Trade-Credit Under Inflation. International Journal of Current Research, Volume 7, Issue, 06, 17312-17321.

[69] Gupta, K., Yadav, A.S., Garg, A. and Swami, A. (2015) A Binary Multi-Objective Genetic Algorithm & PSO involving Supply Chain Inventory Optimization with Shortages, inflation. International Journal of Application or Innovation in Engineering & Management, Volume 4, Issue 8, 37-44.

[70] Gupta, K., Yadav, A.S., Garg, A., (2015) Fuzzy-Genetic Algorithm based inventory model for shortages and inflation under hybrid & PSO. IOSR Journal of Computer Engineering, Volume 17, Issue 5, Ver. I , 61-67.

[71] Singh, R.K., Yadav, A.S. and Swami, A. (2016) A Two-Warehouse Model for Deteriorating Items with Holding Cost under Particle Swarm Optimization. International Journal of Advanced Engineering, Management and Science, Volume -2, Issue-6, 858-864.

[72] Singh, R.K., Yadav, A.S. and Swami, A. (2016) A Two-Warehouse Model for Deteriorating Items with Holding Cost under Inflation and Soft Computing Techniques. International Journal of Advanced Engineering, Management and Science, Volume -2, Issue-6, 869-876.

[73] Kumar, S., Yadav, A.S., Ahlawat, N. and Swami, A. (2019) Supply Chain Management of Alcoholic Beverage Industry Warehouse with Permissible Delay in Payments using Particle Swarm Optimization. International Journal for Research in Applied Science and Engineering Technology, Volume 7 Issue VIII, 504-509.

[74] Kumar, S., Yadav, A.S., Ahlawat, N. and Swami, A. (2019) Green Supply Chain Inventory System of Cement Industry for Warehouse with Inflation using Particle Swarm Optimization. International Journal for Research in Applied Science and Engineering Technology, Volume 7 Issue VIII, 498-503.

[75] Kumar, S., Yadav, A.S., Ahlawat, N. and Swami, A. (2019) Electronic Components Inventory Model for Deterioration Items with Distribution Centre using Genetic Algorithm. International Journal for Research in Applied Science and Engineering Technology, Volume 7 Issue VIII, 433-443.

[76] Chauhan, N. and Yadav, A.S. (2020) An Inventory Model for Deteriorating Items with Two-Warehouse & Stock Dependent Demand using Genetic algorithm. International Journal of Advanced Science and Technology, Vol. 29, No. 5s, 1152-1162.

[77] Chauhan, N. and Yadav, A.S. (2020) Inventory System of Automobile for Stock Dependent Demand & Inflation with Two-Distribution Center Using Genetic Algorithm. Test Engraining & Management, Volume 83, Issue: March - April, 6583 - 6591.

[78] Pandey, T., Yadav, A.S. and Medhavi Malik (2019) An Analysis Marble Industry Inventory Optimization Based on Genetic Algorithms and Particle swarm optimization. International Journal of Recent Technology and Engineering Volume-7, Issue-6S4, 369-373.

[79] Ahlawat, N., Agarwal, S., Pandey, T., Yadav, A.S., Swami, A. (2020) White Wine Industry of Supply Chain Management for Warehouse using Neural Networks Test Engraining & Management, Volume 83, Issue: March - April, 11259 - 11266.

[80] Singh, S. Yadav, A.S. and Swami, A. (2016) An Optimal Ordering Policy For Non-Instantaneous Deteriorating Items With Conditionally Permissible Delay In Payment Under Two Storage Management International Journal of Computer Applications, Volume 147 -No.1, 16-25.

[81] Yadav, A.S., Kumar, A., Yadav, K.K. et al. Optimization of an inventory model for deteriorating items with both selling price and time-sensitive demand and carbon emission under green technology investment. Int J Interact Des Manuf (2023). https://doi.org/10.1007/s12008-023-01689-8

[82] Yadav, K.K., Yadav, A.S. & Bansal, S. Interval number approach for two-warehouse inventory management of deteriorating items with preservation technology investment using analytical optimization methods. Int J Interact Des Manuf (2024). https://doi.org/10.1007/s12008-023-01672-3

[83] Krishan Kumar Yadav , Ajay Singh Yadav, and Shikha Bansal. "Optimization of an inventory model for deteriorating items assuming deterioration during carrying with two-warehouse facility" Reliability: Theory & Applications, vol. 19, no. 3 (79), 2024, pp. 442-459. doi:10.24412/1932-2321-2024-379-442-459

RT&A, No 3 (86)
Volume 20, September 2025

ALPHA-POWER-BURR-HATKE-EXPONENTIAL MODEL: PROPERTIES, SIMULATIONS AND APPLICATIONS BASED ON UNCENSORED AND PROGRESSIVE TYPE-II-CENSORED SAMPLES

Adubisi O. D., Joshua T., David A. A.

•

Department of Statistics, Federal University Wukari, Nigeria.
adubisiobinna@fuwukari.edu.ng
joshua@fuwukari.edu.ng
david.aji@fuwukari.edu.ng

Abstract

This study introduced a novel two-parameter model known as the alpha power Burr Hatke exponential (APBHE) model, characterized by constant, increasing-constant, upside-down bathtub, decreasing and increasing failure shapes. Structural properties and basic reliability functions are derived. The Simulation study carried out for both uncensored and progressive type-II censored samples indicated that the maximum likelihood estimation (MLE) performed quite well in producing good parameter estimates at finite sample sizes and tend to the true parameter value quicker than the maximum spacing product (MPS) method with minimum bias. Specifically, the censored schemes simulation disclosed that the MSE and bias values decrease as the sample size increases for the various censoring proportions. To demonstrate the flexibility and relevance of the APBHE model, a real-life bladder-cancer dataset is examined and the APBHE model achieved the best performance when compared with other competing models. Additionally, the log-APBHE model and log-APBHE regression model functions are presented for further explorations.

Keywords: Alpha-power transform, Lambert function, Progressive censored data, Burr-Hatke exponential model, Estimations

1. Introduction

The development of novel flexible statistical distributions capable of effectively describing real-world data has attracted a lot of attention in recent years. The features seen in many different forms of data are frequently difficult for many classical probability distributions, such the normal or exponential distributions, to fully convey, particularly in domains like reliability analysis, survival studies, insurance, and finance [1, 2]. Because of this, scientists are investigating more generalized versions of these distributions in an effort to increase their accuracy and flexibility. Traditional models such as the exponential, Weibull, or gamma distributions frequently have problems when dealing with data having large tails, skewness, or a range of hazard rates. The exponential distribution is useful for simulating life spans or time-to-failure in reliability theory, but it requires a constant hazard rate, which may be unrealistic in many practical cases [3]. To overcome this, numerous generalizations and expansions to the exponential distribution have been proposed. Among these, the Burr-Hatke exponential distribution introduced by [4] noted for its versatility in modeling diverse forms of data especially in actuarial science and dependability research, has received attention for its capacity to describe data with different tail behaviours and skewness [5, 6, 7, 8, 9, 10].

The alpha-power (AP) transformation, introduced by [11], has provided a new method to increase the flexibility of existing distributions. This transformation allows for the generation of new families of distributions that can better capture tail behaviour and accommodate varying shapes of hazard functions. The alpha-power transformation has been successfully applied to various baseline distributions, such as the Weibull, gamma, and Lomax distributions, resulting in more flexible models that are capable of accurately describing various datasets [11]. The power of the AP transformation lies in its ability to create a more adaptable hazard rate function. For instance, the transformed distributions can model increasing, decreasing, or bathtub-shaped hazard functions, which are commonly encountered in reliability studies and survival analysis. By incorporating an additional parameter, the alpha-power transformation provides greater flexibility in fitting a wide range of data distributions while maintaining the desirable properties of the original distribution [12, 13, 14, 15, 16, 17, 18, 19, 20]. Building upon these developments, we apply the alpha-power transformation to the Burr-Hatke-Exponential distribution, the resulting Alpha-Power-Burr-Hatke-Exponential (APBHE) model introduces an additional parameter that allows for even greater flexibility in modeling various types of data. Thus, the APBHE model can provide a better fit for data in fields such as finance, insurance, survival analysis, and reliability engineering, where data often exhibit heavy tails, skewness, and varying hazard rates.

This article is sectionalized as follows: Section two, the proposed model is introduced, and its behaviour is investigated using various representation graphically. Section three, a variety of structural characteristics are derived. Estimation methods are discussed for both uncensored and progressive type II censored samples in Sections four and five, for determining the APBHE model parameters. Section six presents the log-APBHE model and log-APBHE regression model functions. The simulation study is described and executed, with the findings presented in Section seven. The applications based on uncensored and progressive type II censored schemes are presented in Section eight while conclusion is in Section nine.

2. Model Genesis

Here, a non-negative random variable (r.v) X is said to follow the Burr-Hatke exponential (BHE) model with cumulative distribution function (CDF) given by

$$G(x) = 1 - \frac{e^{-\eta x}}{1+\eta x}, \tag{1}$$

where $\eta > 0$. The corresponding probability density function (PDF) to Eq. (1) is

$$g(x) = e^{-\eta x}\frac{2+\eta x}{(1+\eta x)^2}. \tag{2}$$

The CDF and PDF of the alpha power (AP) transformation are specified as

$$F(x) = \frac{\alpha^{G(x)} - 1}{\alpha - 1},\ \alpha > 0,\ \alpha \neq 1, \tag{3}$$

and

$$f(x) = \frac{\log \alpha}{\alpha - 1} g(x)\, \alpha^{G(x)},\ \alpha > 0,\ \alpha \neq 1. \tag{4}$$

respectively. By inserting Eqs. (1) and (2) into Eqs. (3) and (4), the CDF and PDF of the alpha power Burr-Hatke Exponential (APBHE) model are specified as

$$F(x;\alpha,\eta) = \frac{\alpha^{\left(1-\frac{e^{-\eta x}}{1+\eta x}\right)} - 1}{\alpha - 1},\ \alpha > 0,\ \alpha \neq 1, \tag{5}$$

and

$$f(x;\alpha,\eta) = \frac{\log \alpha}{\alpha - 1}\eta e^{-\eta x}\frac{2+\eta x}{(1+\eta x)^2}\alpha^{\left(1-\frac{e^{-\eta x}}{1+\eta x}\right)},\ \alpha > 0,\ \alpha \neq 1. \tag{6}$$

respectively. The survival (Reliability) function (SF) and hazard (failure) rate (HRF) of the APBHE model take the forms

$$S(x;\alpha,\eta) = 1 - \left[\frac{\alpha^{\left(1-\frac{e^{-\eta x}}{1+\eta x}\right)} - 1}{\alpha - 1}\right], \tag{7}$$

and

$$h(x;\alpha,\eta) = \frac{\frac{\log\alpha}{\alpha-1}\eta e^{-\eta x}\frac{2+\eta x}{(1+\eta x)^2}\alpha^{\left(1-\frac{e^{-\eta x}}{1+\eta x}\right)}}{1 - \left[\frac{\alpha^{\left(1-\frac{e^{-\eta x}}{1+\eta x}\right)}-1}{\alpha-1}\right]}, \tag{8}$$

More so, the cumulative and reversed HRFs of the APBHE model are

$$H(x;\alpha,\eta) = -\log\left\{1 - \left[\frac{\alpha^{\left(1-\frac{e^{-\eta x}}{1+\eta x}\right)} - 1}{\alpha - 1}\right]\right\}, \tag{9}$$

and

$$r(x;\alpha,\eta) = \frac{\frac{\alpha^{\left(1-\frac{e^{-\eta x}}{1+\eta x}\right)}-1}{\alpha-1}}{1 - \left[\frac{\alpha^{\left(1-\frac{e^{-\eta x}}{1+\eta x}\right)}-1}{\alpha-1}\right]}. \tag{10}$$

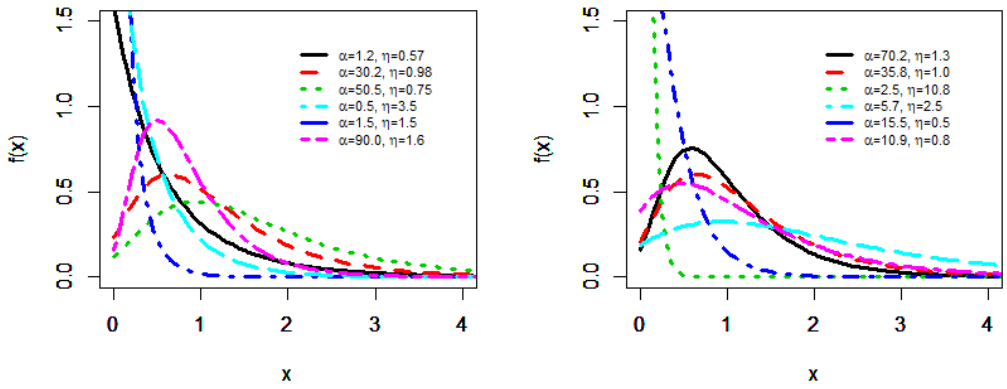


Figure 1: *PDF plots for the APBHE model*

The special cases of the APBHE model are the Burr-Hatke exponential (BHE) by [4], alpha power Burr-Hatke (APBH) by (new), Burr-Hatke (BH) by [21] and exponential (E) distributions. The PDF plots of the APBHE model constructed using various combinations of the parameter values depicted in Figure 1, exhibit right-skewed and reversed-J shapes. The HRF plots depicted in Figure 2 exhibit constant, increasing-constant, upside-down bathtub, decreasing and increasing failure shapes.

3. Structural properties

Some useful properties of the APBHE model are presented here.

3.1. Quantile function

If the r.v $X \sim \text{APBHE}(\alpha,\eta)$, then the quantile function by inverting Eq. (5) is derived as follows:

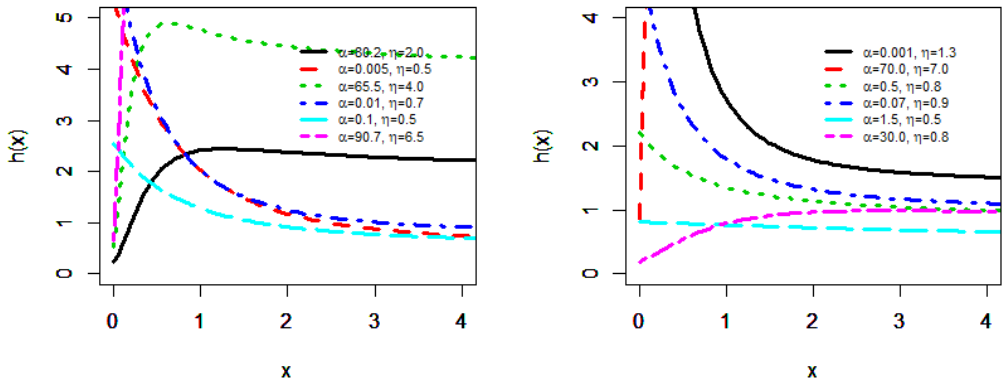


Figure 2: *HRF plots for the APBHE model*

$$u = \frac{\alpha^{\left(1-\frac{e^{-\eta x}}{1+\eta x}\right)} - 1}{\alpha - 1}, \tag{11}$$

By manipulating Eq. (11) algebraically, we have

$$(1+\eta x)\, e^{1+\eta x} = e \left\{ \frac{log\left[\frac{\alpha}{1+u(\alpha-1)}\right]}{log\alpha} \right\}^{-1}, \tag{12}$$

By introducing the Lambert function specified as $W\left(xe^{x}\right) = x$, the preceding equation takes the form

$$W\left[(1+\eta x)\, e^{1+\eta x}\right] = W\left(e \left\{ \frac{log\left[\frac{\alpha}{1+u(\alpha-1)}\right]}{log\alpha} \right\}^{-1} \right), \tag{13}$$

with $Q(u) = x$, the quantile function of the APBHE model is given by

$$Q(u) = \frac{1}{\eta}\left(W\left\{ \frac{elog\alpha}{log\left[\frac{\alpha}{1+u(\alpha-1)}\right]} \right\} - 1 \right). \tag{14}$$

where $u \sim uniform(0,1)$.

3.2. Moments

The rth raw moment of the APBHE r.v, say $\mu'_r = \mathrm{E}\left(x^r\right) = \int_0^\infty x^r f\left(x\right) dx$, can be specified as

$$\mu'_r = \int_0^\infty x^r \frac{\log\alpha}{\alpha-1} \eta e^{-\eta x} \frac{2+\eta x}{(1+\eta x)^2} \alpha^{\left(1-\frac{e^{-\eta x}}{1+\eta x}\right)} dx, \tag{15}$$

An expression for the rth moment of the APBHE model can be derived. Utilizing power-series expansion $\alpha^z = \sum_{i=0}^{\infty} \frac{(\log\alpha)^i}{i!} z^i$, and binomial theorem on $\alpha^{\left(1-\frac{e^{-\eta x}}{1+\eta x}\right)}$ gives

$$\mu'_r = \int_0^\infty x^r \eta \frac{2+\eta x}{\alpha-1} \sum_{i=0}^{\infty} \sum_{j=0}^{i} \frac{(-1)^j (\log\alpha)^{i+1}}{i!} \binom{i}{j} \frac{e^{-(j+1)\eta x}}{(1+\eta x)^{j+2}} dx, \tag{16}$$

Applying the Taylor series expansion specified as $z^{-\varphi} = \sum_{k=0}^{\infty} \frac{(-1)^k}{k!} \varphi^{(k)} (z-1)^k$ on $\frac{e^{-(j+1)\eta x}}{(1+\eta x)^{j+2}}$ in the preceeding function gives

$$\mu'_r = \sum_{i=0}^{\infty}\sum_{j=0}^{i}\sum_{k=0}^{\infty}\frac{(-1)^{j+k}(\log\alpha)^{i+1}\eta^{k+1}}{i!k!(\alpha-1)}\binom{i}{j}(j+2)^{(k)} \times \int_0^{\infty}(2+\eta x)\,x^{r+k}e^{-(j+1)\eta x}dx, \tag{17}$$

Thus, the rth raw moment of the APBHE model is specified as

$$\mu'_r = \sum_{i=0}^{\infty}\sum_{j=0}^{i}\sum_{k=0}^{\infty}\frac{(-1)^{j+k}(\log\alpha)^{i+1}\eta^{k+1}}{i!k!(\alpha-1)}\binom{i}{j}(j+2)^{(k)} \times\left\{\frac{2\Gamma(r+k+1)}{[(j+1)\eta]^{r+k+1}}+\frac{\eta\Gamma(r+k+2)}{[(j+1)\eta]^{r+k+2}}\right\}. \tag{18}$$

where $\Gamma(\cdot)$ is the gamma function.
The first four raw moments, coefficient of variation (CV), standard deviation (SD) and dispersion index (DI) from Eq. (18) using selected APBHE parameter values: $A = (\alpha = 0.5, \eta = 0.5)$, $B = (\alpha = 20, \eta = 2.5)$, $C = (\alpha = 2.5, \eta = 3.5)$ and $D = (\alpha = 3.5, \eta = 15)$ are reported in Table 1.

Table 1: *Descriptive statistics of the APBHE model*

μ'_r	A	B	C	D
μ'_1	0.982729	0.441738	0.214102	0.053848
μ'_2	2.416545	0.317158	0.092116	0.005592
μ'_3	10.25578	0.321278	0.061238	0.000881
μ'_4	63.17229	0.429446	0.056130	0.000190
CV	1.225655	0.790789	1.004752	0.963606
SD	1.204487	0.349321	0.215119	0.051888
DI	1.476286	0.276240	0.216141	0.050000

The skewness and kurtosis 3D plots of the APBHE model in Figure 3 depicts that the model can have increasing, decreasing, increasing-decreasing and decreasing-increasing values.

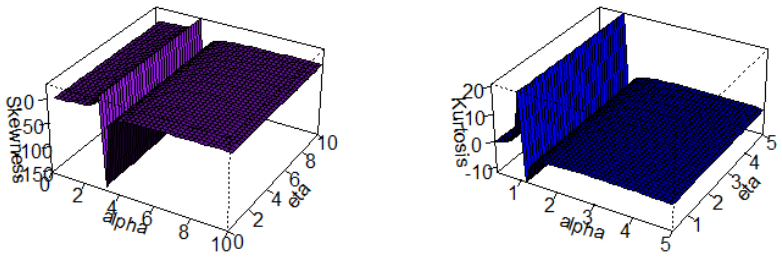


Figure 3: *Skewness and Kurtosis 3D plots for the APBHE model*

More so, the rth incomplete moment of the APBHE r.v, say $m_r(t) = \int_0^t x^r f(x)\,dx$, is specified as

$$m_r(t) = \int_0^t x^r\frac{\log\alpha}{\alpha-1}\eta e^{-\eta x}\frac{2+\eta x}{(1+\eta x)^2}\alpha^{\left(1-\frac{e^{-\eta x}}{1+\eta x}\right)}dx, \tag{19}$$

Utilizing the very paths that led to Eq. (18) on Eq. (19), we have

$$m_r(t) = \sum_{i=0}^{\infty}\sum_{j=0}^{i}\sum_{k=0}^{\infty}\frac{(-1)^{j+k}(\log\alpha)^{i+1}\eta^{k+1}}{i!k!(\alpha-1)}\binom{i}{j}(j+2)^{(k)} \times\left\{\frac{2\gamma(r+k+1,(j+1)\eta t)}{[(j+1)\eta]^{r+k+1}}+\frac{\eta\gamma(r+k+2,(j+1)\eta t)}{[(j+1)\eta]^{r+k+2}}\right\}. \tag{20}$$

where $\gamma(\cdot)$ denote the incomplete gamma function and the first incomplete moment of the APBHE model is obtained by setting $r = 1$ in Eq. (20).

3.3. Moments generating function

The moment generating function (MGF) of the APBHE model, say $M_X(t)$ is specified as

$$M_X(t) = \mathrm{E}\left(e^{tx}\right) = \sum_{r=0}^{\infty} \frac{t^r}{r!} \int_0^{\infty} x^r f(x)\, dx = \sum_{r=0}^{\infty} \frac{t^r}{r!} \mu'_r, \tag{21}$$

By inserting Eq. (18) into Eq. (21), the MGF takes the form

$$M_X(t) = \sum_{r=0}^{\infty} \sum_{i=0}^{\infty} \sum_{j=0}^{i} \sum_{k=0}^{\infty} \frac{(-1)^{j+k} (\log \alpha)^{i+1} \eta^{k+1} t^r}{i!k!r!\,(\alpha - 1)} \begin{pmatrix} i \\ j \end{pmatrix} (j+2)^{(k)}. \tag{22}$$

3.4. Entropy

A measure of variation of the uncertainty in a system is the Rényi entropy defined as

$$I_\lambda(X) = \frac{1}{1-\lambda} \log \int_0^{\infty} f(x)^\lambda\, dx,\ \lambda > 0 \text{ and } \lambda \neq 1. \tag{23}$$

Inserting Eq. (6) into the preceding definition, the Rényi entropy of the APBHE model is specified as

$$I_\lambda(X) = \frac{1}{1-\lambda} \log \int_0^{\infty} \left(\frac{\log \alpha}{\alpha - 1} \eta e^{-\eta x} \frac{2 + \eta x}{(1+\eta x)^2} \alpha^{\left(1 - \frac{e^{-\eta x}}{1+\eta x}\right)} \right)^{\lambda} dx, \tag{24}$$

and following the same paths that led to Eq. (18), we have

$$\begin{aligned} I_\lambda(X) = \tfrac{1}{1-\lambda} \log \Bigg(\sum_{i=0}^{\infty} \sum_{j=0}^{i} \sum_{k=0}^{\infty} \frac{(-1)^{j+k} (\log \alpha)^{i+\lambda} \lambda^i \eta^{k+\lambda}}{i!k!(\alpha-1)^\lambda} \begin{pmatrix} i \\ j \end{pmatrix} (j+2\lambda)^{(k)} \\ \times \left\{ \tfrac{2^\lambda \Gamma(k+1)}{[(j+\lambda)\eta]^{k+1}} + \tfrac{\eta^\lambda \Gamma(k+\lambda+1)}{[(j+\lambda)\eta]^{k+\lambda+1}} \right\} \Bigg). \end{aligned} \tag{25}$$

where $\Gamma(\cdot)$ is the gamma function. Table 2 reports the Rényi entropy results for selected values of the APBHE model parameters and various order of entropy (λ).

Table 2: *Rényi entropy results for selected parameter values of the APBHE model*

$\lambda = 0.5$			$\lambda = 1.3$			$\lambda = 2.0$		
α	η	$\mathrm{I}_\lambda(X)$	α	η	$\mathrm{I}_\lambda(X)$	α	η	$\mathrm{I}_\lambda(X)$
0.5	0.7	1.174	0.5	0.7	0.444	0.5	0.7	0.190
	1.5	0.412		1.5	-0.318		1.5	-0.572
	2.2	0.029		2.2	-0.701		2.2	-0.955
1.3	0.7	1.363	1.3	0.7	0.758	1.3	0.7	0.549
	1.5	0.601		1.5	-0.004		1.5	-0.213
	2.2	0.218		2.2	-0.387		2.2	-0.596
1.7	0.7	1.409	1.7	0.7	0.837	1.7	0.7	0.643
	1.5	0.647		1.5	0.075		1.5	-0.119
	2.2	0.264		2.2	-0.308		2.2	-0.502
2.3	0.7	1.458	2.3	0.7	0.921	2.3	0.7	0.742
	1.5	0.695		1.5	0.158		1.5	-0.020
	2.2	0.312		2.2	-0.224		2.2	-0.403

3.5. Order statistics

If $x_1, x_2, \ldots, x_n$ be a random sample from the APBHE r.v with $x_{j:n}$ as the order statistics (O.S). The pdf of the j$^{\text{th}}$ O.S, say $f_{j:n}(x)$ is defined as

$$f_{j:n}(x) = \frac{1}{\mathrm{B}(j, n-j+1)} g(x) [G(x)]^{j-1} [1-G(x)]^{n-j}, \tag{26}$$

Expanding the last part of the preceding function, the PDF of the j$^{\text{th}}$ O.S takes the form

$$f_{j:n}(x) = \frac{1}{\mathrm{B}(j, n-j+1)} \sum_{l=0}^{n-j} (-1)^l \binom{n-j}{l} [G(x)]^{j+l-1} g(x), \tag{27}$$

By inserting Eqs. (5) and (6) into Eq. (27), then utilizing the power-series and binomial theorem. The PDF of j$^{\text{th}}$ O.S of the APBHE model is specified as

$$\begin{aligned} f_{j:n}(x) = {} & \frac{(2+\eta x)}{B(j,n-j+1)} \sum_{l=0}^{n-j} \sum_{i=0}^{j+l-1} \sum_{k,m,g=0}^{\infty} \frac{(-1)^{l+i+m} (\log \alpha)^{k+1} (i+1)^k \eta^{g+1}}{k! g! (\alpha-1)^{j+l}} \\ & \times \binom{n-j}{l} \binom{j+l-1}{i} \binom{k}{m} (m+2)^{(g)} x^g e^{-(m+1)\eta x}. \end{aligned} \tag{28}$$

where $\mathrm{B}(\cdot)$ is the beta function. The minimum and maximum order statistics of the APBHE model can be derived by inserting $j = 1$ and $j = n$ in Eq. (28).

4. Estimators for Uncensored samples

Here, the estimators for the APBHE parameters using uncensored (complete) datasets are presented.

4.1. Maximum likelihood estimator

Let $x_1, x_2, \ldots, x_n$ be the random observed values of size (n) from APBHE model. the Maximum Likelihood estimates (MLE) are obtained from the log-likelihood function of Eq. (6) is specified as

$$\begin{aligned} L(\alpha, \eta) = {} & n \log \eta - \eta \textstyle\sum_{i=1}^{n} x_i + n \log \left(\frac{\log \alpha}{\alpha - 1} \right) + \sum_{i=1}^{n} \left(1 - \frac{e^{-\eta x_i}}{1+\eta x_i} \right) \log \alpha \\ & + \sum_{i=1}^{n} \log \left[\frac{2+\eta x_i}{(1+\eta x_i)^2} \right], \end{aligned} \tag{29}$$

The partial derivative of Eq. (29) with respect to α and η are specified as

$$\frac{\partial L(\alpha, \eta)}{\partial \alpha} = \frac{n \left(\frac{1}{\alpha} - \frac{\log \alpha}{(\alpha-1)} \right)}{\log \alpha} + \frac{\sum_{i=1}^{n} \left(1 - \frac{e^{-\eta x_i}}{1+\eta x_i} \right)}{\alpha}. \tag{30}$$

and

$$\begin{aligned} \frac{\partial L(\alpha,\eta)}{\partial \eta} = {} & \frac{n}{\eta} - \sum_{i=1}^{n} \left[x_i - \left(\frac{x_i e^{-\eta x_i}}{1+\eta x_i} + \frac{x_i e^{-\eta x_i}}{(1+\eta x_i)^2} \right) \log \alpha \right] \\ & - \sum_{i=1}^{n} \frac{x_i (3+\eta x_i)}{(2+\eta x_i)(1+\eta x_i)}. \end{aligned} \tag{31}$$

respectively. The ML estimates $\hat{\alpha}_{\mathrm{ML}}$ and $\hat{\eta}_{\mathrm{ML}}$ are found by maximizing Eq. (29) using the (*Optim function)* in R-programming software.

4.2. Maximum product spacing

The Maximum product spacing (MPS) estimation of unknown parameters with ordered sample $x_{(1)}, x_{(2)}, \ldots, x_{(n)}$ from APBHE model are considered. The MPS estimates $\hat{\alpha}_{\text{MPS}}$ and $\hat{\eta}_{\text{MPS}}$ can be found by maximizing relative to α and η, the logarithm of geometric mean of the spacing specified as

$$MPS\left(\alpha,\eta\right)=\frac{1}{n+1}\sum_{i=1}^{n+1}\log D_i\left(\alpha,\eta\right), \tag{32}$$

where

$$\begin{aligned} D_i\left(\alpha,\eta\right) &= F_n\left(x_{(i)}\left|\alpha,\eta\right.\right)-F_n\left(x_{(i-1)}\left|\alpha,\eta\right.\right) \\ &= \frac{\alpha^{\left(1-\frac{e^{-\eta x_{(i)}}}{1+\eta x_{(i)}}\right)}-1}{\alpha-1} \quad -\frac{\alpha^{\left(1-\frac{e^{-\eta x_{(i-1)}}}{1+\eta x_{(i-1)}}\right)}-1}{\alpha-1} \end{aligned} \tag{33}$$

with $F\left(x_{(0)}\left|\alpha,\eta\right.\right)=0$, $F\left(x_{(n+1)}\left|\alpha,\eta\right.\right)=1$ and $\sum_{i=1}^{n+1}D_i\left(\alpha,\eta\right)=1$. The MPS estimates $\hat{\alpha}_{\text{MPS}}$ and $\hat{\eta}_{\text{MPS}}$ are found by maximizing Eq. (32) using the (*Optim function)* in R-programming software.

5. Estimators for progressive type II censored samples

Here, the estimators for the estimating the APBHE parameters using PTIIC samples are presented. The progressive Type-II censoring (PTIIC) scheme is described as follows: In a life testing experiment consisting n components where the number of observed failures (m) and $R_1,\ldots,R_m$ the censoring scheme are pre-determined. At the incidence of the first failure, R_1 of the remaining $n-1$ surviving units are randomly withdrawn (or censored). Subsequently, at the incidence of the second failure, R_2 of the remaining $n-R_1-1$ units are randomly withdrawn, and the process lingers until the $(m-1)^{th}$ failure is observed. Finally, at the incidence of the mth failure, all the remaining $R_m=n-m-R_1-\cdots-R_{m-1}$ surviving units are withdrawn from the experiment. The progressive type-II censoring scheme consist of m and $R_1,\ldots,R_m$ given that $R_1+\ldots+R_m=n-m$. More so, this scheme contain specially the conventional Type-II-right censoring when $R_1=\cdots=R_{m-1}=0, R_m=n-m$ and complete sample settings when $m=n, R_1=\cdots=R_{m-1}=0$, respectively.

5.1. Maximum likelihood estimator

Suppose that $X_{1:m:n}<\ldots<X_{m:m:n}$ is a PTIIC sample with $R_1,\ldots,R_m$ from the APBHE model, the likelihood function is given by

$$L\left(\alpha,\eta\right)=\Phi\prod_{i=1}^{m}f\left(x_{i:m:n};\alpha,\eta\right)\left[1-F\left(x_{i:m:n};\alpha,\eta\right)\right]^{R_i} \tag{34}$$

where $\Phi=n\left(n-R_1-1\right)\cdots\left(n-\sum_{i=1}^{m-1}R_i-\left(m-1\right)\right)$, and R_i is the number of withdrawers at the i$^{\text{th}}$ censoring time. By inserting Eqs. (5) and (6) into Eq. (34) and taking the natural logarithm, the log-likelihood function of the APBHE model is specified as

$$\begin{aligned} L\left(\alpha,\eta\right) &= m\log\eta-\eta\textstyle\sum_{i=1}^{m}x_{i:m:n}+m\log\left(\frac{\log\alpha}{\alpha-1}\right) \\ &+\textstyle\sum_{i=1}^{m}\left(1-\frac{e^{-\eta x_{i:m:n}}}{1+\eta x_{i:m:n}}\right)\log\alpha+\sum_{i=1}^{m}\log\left[\frac{2+\eta x_{i:m:n}}{\left(1+\eta x_{i:m:n}\right)^2}\right] \\ &+\textstyle\sum_{i=1}^{m}R_i\log\left\{1-\left[\frac{\alpha^{\left(1-\frac{e^{-\eta x_{i:m:n}}}{1+\eta x_{i:m:n}}\right)}-1}{\alpha-1}\right]\right\} \end{aligned} \tag{35}$$

The first partial derivative of Eq. (35) relative to α and η are specified as

$$\begin{aligned}\frac{\partial L(\alpha,\eta)}{\partial \alpha} &= \frac{m}{\alpha \log \alpha} + \frac{m}{\alpha-1} + \frac{\sum_{i=1}^{m}\left(1-\frac{e^{-\eta x_{i:m:n}}}{1+\eta x_{i:m:n}}\right)}{\alpha} \\ &+ \sum_{i=1}^{m} \frac{R_i\left[-\frac{\alpha^{\left(1-\frac{e^{-\eta x_{i:m:n}}}{1+\eta x_{i:m:n}}\right)}\left(1-\frac{e^{-\eta x_{i:m:n}}}{1+\eta x_{i:m:n}}\right)}{\alpha(\alpha-1)} + \frac{\alpha^{\left(1-\frac{e^{-\eta x_{i:m:n}}}{1+\eta x_{i:m:n}}\right)}-1}{(\alpha-1)^2}\right]}{\left\{1-\left[\frac{\alpha^{\left(1-\frac{e^{-\eta x_{i:m:n}}}{1+\eta x_{i:m:n}}\right)}-1}{\alpha-1}\right]\right\}}\end{aligned} \tag{36}$$

and

$$\begin{aligned}\frac{\partial L(\alpha,\eta)}{\partial \eta} &= \frac{m}{\eta} - \sum_{i=1}^{m}\left[x_{i:m:n} - \left(\frac{x_{i:m:n}e^{-\eta x_{i:m:n}}}{1+\eta x_{i:m:n}} + \frac{x_{i:m:n}e^{-\eta x_{i:m:n}}}{(1+\eta x_{i:m:n})^2}\right)\log\alpha\right] \\ &+ \sum_{i=1}^{m}\frac{x_{i:m:n}}{(2+\eta x_{i:m:n})} - 2\sum_{i=1}^{m}\frac{x_{i:m:n}}{(1+\eta x_{i:m:n})} \\ &+ \sum_{i=1}^{m}\left(-\frac{R_i\alpha^{\left(1-\frac{e^{-\eta x_{i:m:n}}}{1+\eta x_{i:m:n}}\right)}\left(\frac{x_{i:m:n}e^{-\eta x_{i:m:n}}}{1+\eta x_{i:m:n}} + \frac{x_{i:m:n}e^{-\eta x_{i:m:n}}}{(1+\eta x_{i:m:n})^2}\right)\log\alpha}{(\alpha-1)\left\{1-\left[\frac{\alpha^{\left(1-\frac{e^{-\eta x_{i:m:n}}}{1+\eta x_{i:m:n}}\right)}-1}{\alpha-1}\right]\right\}}\right)\end{aligned} \tag{37}$$

The ML estimates $\hat{\alpha}_{\mathrm{ML}}$ and $\hat{\eta}_{\mathrm{ML}}$ are found by solving the non-linear functions in Eqs. (36) and (37) simultaneously or utilizing the R-programming software (*Optim function)* in maximizing Eq. (35).

5.2. Maximum product spacing estimator

Suppose that $X_{1:m:n} < \ldots < X_{m:m:n}$ is a progressive type II censored sample from the APBHE model. The random sample uniform spacings are specified as

$$D_i\left(x_{i:m:n};\alpha,\eta\right) = \begin{cases} F\left(x_{1:m:n};\alpha,\eta\right) & if\ i=1, \\ F\left(x_{i:m:n};\alpha,\eta\right) - F\left(x_{i-1:m:n};\alpha,\eta\right) & if\ i=2,\ldots,m, \\ 1-F\left(x_{m:m:n};\alpha,\eta\right) & if\ i=m. \end{cases} \tag{38}$$

The MPS estimator based on the PTIIC sample [22], are found by maximizing the product of spacing specified as

$$P\left(x_{i:m:n};\alpha,\eta\right) = \Phi\prod_{i=1}^{m} D\left(x_{i:m:n};\alpha,\eta\right)\left[1-F\left(x_{i:m:n};\alpha,\eta\right)\right]^{R_i} \tag{39}$$

where Φ is a constant term. By utilizing the logarithm of the product of spacing with the CDF of the APBHE model, we found

$$\begin{aligned}L\left(x_{i:m:n};\alpha,\eta\right) &= \log\left[\frac{\alpha^{\left(1-\frac{e^{-\eta x_{1:m:n}}}{1+\eta x_{1:m:n}}\right)}-1}{\alpha-1}\right] + \log\left[1-\frac{\alpha^{\left(1-\frac{e^{-\eta x_{m:m:n}}}{1+\eta x_{m:m:n}}\right)}-1}{\alpha-1}\right] \\ &+ \sum_{i=2}^{m}\log\left[\frac{\alpha^{\left(1-\frac{e^{-\eta x_{i:m:n}}}{1+\eta x_{i:m:n}}\right)}-1}{\alpha-1} - \frac{\alpha^{\left(1-\frac{e^{-\eta x_{i-1:m:n}}}{1+\eta x_{i-1:m:n}}\right)}-1}{\alpha-1}\right] \\ &+ \sum_{i=1}^{m} R_i\log\left[1-\frac{\alpha^{\left(1-\frac{e^{-\eta x_{i:m:n}}}{1+\eta x_{i:m:n}}\right)}-1}{\alpha-1}\right]\end{aligned} \tag{40}$$

The first partial derivative of Eq. (40) relative to α and η are specified as

$$\begin{aligned}\frac{\partial L(x_{i:m:n};\alpha,\eta)}{\partial\alpha} &= \frac{\left[\frac{\alpha^{\varphi_{1:m:n}}\varphi_{1:m:n}}{\alpha}-\frac{\alpha^{\varphi_{1:m:n}}}{\alpha-1}\right]}{\alpha^{\varphi_{1:m:n}}-1}+\frac{\left[\frac{\alpha^{\varphi_{m:m:n}}-1}{(\alpha-1)^2}-\frac{\alpha^{\varphi_{m:m:n}}\varphi_{m:m:n}}{\alpha(\alpha-1)}\right]}{1-\frac{\alpha^{\varphi_{m:m:n}}-1}{(\alpha-1)}}\\ &+\sum_{i=2}^{m}\frac{\frac{\alpha^{\varphi_{i:m:n}}\varphi_{i:m:n}}{\alpha(\alpha-1)}-\frac{\alpha^{\varphi_{i:m:n}}-1}{(\alpha-1)^2}-\frac{\alpha^{\varphi_{i-1:m:n}}\varphi_{i-1:m:n}}{\alpha(\alpha-1)}+\frac{\alpha^{\varphi_{i-1:m:n}}-1}{(\alpha-1)^2}}{\frac{\alpha^{\varphi_{i:m:n}}-1}{\alpha-1}-\frac{\alpha^{\varphi_{i-1:m:n}}-1}{\alpha-1}}\\ &+\sum_{i=1}^{m}\frac{R_i\left[\frac{\alpha^{\varphi_{i:m:n}}-1}{(\alpha-1)^2}-\frac{\alpha^{\varphi_{i:m:n}}\varphi_{i:m:n}}{\alpha(\alpha-1)}\right]}{1-\frac{\alpha^{\varphi_{i:m:n}}-1}{\alpha-1}}\end{aligned} \tag{41}$$

and

$$\begin{aligned}\frac{\partial L(x_{i:m:n};\alpha,\eta)}{\partial\eta} &= \frac{\alpha^{\theta_1}\gamma_1\ln(\alpha)}{\alpha^{\theta_1}-1}-\frac{\alpha^{\theta_m}\gamma_m\ln(\alpha)}{(\alpha-1)\left(1-\frac{\alpha^{\theta_m}-1}{\alpha-1}\right)}\\ &+\sum_{i=2}^{m}\frac{\frac{\alpha^{\theta_i}\gamma_i\ln(\alpha)}{\alpha-1}-\frac{\alpha^{\theta_i-1}\gamma_{i-1}\ln(\alpha)}{\alpha-1}}{\frac{\alpha^{\theta_i}-1}{\alpha-1}-\frac{\alpha^{\theta_i-1}-1}{\alpha-1}}+\sum_{i=1}^{m}\left(-\frac{R_i\alpha^{\theta_i}\gamma_i\ln(\alpha)}{(\alpha-1)\left(1-\frac{\alpha^{\theta_i}-1}{\alpha-1}\right)}\right)\end{aligned} \tag{42}$$

where
$\varphi_{1:m:n} = \left(1-\frac{e^{-\eta x_{1:m:n}}}{1+\eta x_{1:m:n}}\right)$, $\varphi_{m:m:n} = \left(1-\frac{e^{-\eta x_{m:m:n}}}{1+\eta x_{m:m:n}}\right)$, $\varphi_{i:m:n} = \left(1-\frac{e^{-\eta x_{i:m:n}}}{1+\eta x_{i:m:n}}\right)$, $\varphi_{i-1:m:n} = \left(1-\frac{e^{-\eta x_{i-1:m:n}}}{1+\eta x_{i-1:m:n}}\right)$, $\theta_1 = 1-\frac{e^{-\eta x_1}}{\eta x_1+1}$, $\gamma_1 = \left(\frac{x_1 e^{-\eta x_1}}{\eta x_1+1}+\frac{e^{-\eta x_1}x_1}{(\eta x_1+1)^2}\right)$, $\theta_m = 1-\frac{e^{-\eta x_m}}{\eta x_m+1}$, $\theta_i = 1-\frac{e^{-\eta x_i}}{\eta x_i+1}$, $\theta_{i-1} = 1-\frac{e^{-\eta x_{i-1}}}{\eta x_{i-1}+1}$, $\gamma_m = \left(\frac{x_m e^{-\eta x_m}}{\eta x_m+1}+\frac{e^{-\eta x_m}x_m}{(\eta x_m+1)^2}\right)$, $\gamma_{i-1} = \left(\frac{x_{i-1}e^{-\eta x_{i-1}}}{\eta x_{i-1}+1}+\frac{e^{-\eta x_{i-1}}x_{i-1}}{(\eta x_{i-1}+1)^2}\right)$. The MPS estimates $\hat{\alpha}_{\text{MPS}}$ and $\hat{\eta}_{\text{MPS}}$ are found by solving the non-linear functions in Eqs. (41) and (42) simultaneously or utilizing the R-programming software (*Optim function)* in maximizing Eq. (40).

6. Log-APBHE Regression model

Let X represent a random variable which follows the APBHE model. Based on the transformation $Y = \log(X)$ and $\eta = e^{-\frac{\mu}{\sigma}}$, the density of Y is specified as

$$f(y,\alpha,\mu,\sigma) = \frac{\log(\alpha)\,e^{\frac{y-\mu}{\sigma}}e^{-e^{\frac{y-\mu}{\sigma}}}}{\sigma(\alpha-1)}\frac{\left(2+e^{\frac{y-\mu}{\sigma}}\right)}{\left(1+e^{\frac{y-\mu}{\sigma}}\right)^2}\alpha^{\left(1-\frac{e^{-e^{\frac{y-\mu}{\sigma}}}}{1+e^{\frac{y-\mu}{\sigma}}}\right)} \tag{43}$$

where $\alpha,\sigma > 0$, $y,\mu \in \Re$. Give that the random variable $X \sim APBHE(\alpha,\eta)$, then $Y \sim LogAPBHE(\alpha,\mu,\sigma)$. The survival function for the log-APBHE model is specified as

$$S(y,\alpha,\mu,\sigma) = 1-\frac{\alpha^{\left(1-\frac{e^{-e^{\frac{y-\mu}{\sigma}}}}{1+e^{\frac{y-\mu}{\sigma}}}\right)}-1}{\alpha-1} \tag{44}$$

Let $z = (y-\mu)/\sigma$, $z \in \Re$, then the standardized log-APBHE density is specified as

$$f(z,\alpha) = \frac{\log(\alpha)\,e^z e^{-e^z}}{\sigma(\alpha-1)}\frac{(2+e^z)}{(1+e^z)^2}\alpha^{\left(1-\frac{e^{-e^z}}{1+e^z}\right)} \tag{45}$$

The explanatory vector associated with the ith response variable y_i, $i = 1,\ldots,n$ is $\boldsymbol{X}_i = (x_{i1},\ldots,x_{im})^T$. The regression model based on the APBHE density function is given by

$$y_i = \boldsymbol{x}_i^T\boldsymbol{\beta}+\sigma z_i,\ i = 1,\ldots,n, \tag{46}$$

where z_i is the error which follows the Eq. (45), $\boldsymbol{\beta} = (\beta_1, \ldots, \beta_m)^T, \sigma, \alpha > 0$ are unknown parameters and $\mu_i = \boldsymbol{X}_i^T \boldsymbol{\beta}$. The log-APBHE density and survival functions of y_i are specified as

$$f\left(y_i\ \alpha, \sigma, \boldsymbol{\beta}^T\right) = \frac{\log(\alpha)\, e^{z_i} e^{-e^{z_i}}}{\sigma(\alpha - 1)} \frac{(2 + e^{z_i})}{(1 + e^{z_i})^2} \alpha^{\left(1 - \frac{e^{-e^{z_i}}}{1 + e^{z_i}}\right)}, \tag{47}$$

and

$$S(y_i, \alpha, \mu, \sigma) = 1 - \frac{\alpha^{\left(1 - \frac{e^{-e^{z_i}}}{1 + e^{z_i}}\right)} - 1}{\alpha - 1}, \tag{48}$$

Here, F and C denote the group of individuals for which y_i is the log-lifetime and log-censoring with r and n-r observations, respectively. The log-likelihood (ℓ) for $\boldsymbol{\theta} = \left(\alpha, \sigma, \boldsymbol{\beta}^T\right)^T$ is specified as

$$\begin{aligned} \ell(\boldsymbol{\theta}) = {} & r \log\left(\frac{\log(\alpha)}{\sigma(\alpha - 1)}\right) + \sum_{i \in F} z_i - \sum_{i \in F} e^{z_i} + \sum_{i \in F} \log(2 + e^{z_i}) \\ & - 2 \sum_{i \in F} \log(1 + e^{z_i}) + \sum_{i \in F} \left(1 - \frac{e^{-e^{z_i}}}{1 + e^{z_i}}\right) \log \alpha \\ & + \sum_{i \in C} \log\left(1 - \frac{\alpha^{\left(1 - \frac{e^{-e^{z_i}}}{1 + e^{z_i}}\right)} - 1}{\alpha - 1}\right) \end{aligned} \tag{49}$$

where $z_i = \left(y_i - \boldsymbol{X}_i^T \boldsymbol{\beta}\right)/\sigma$ and the number of failures is represented by r. Maximizing the preceding function using the R-programme (*optim function*), the MLE $\hat{\theta}$ can be found.

7. Simulation for Uncensored and PTIIC

The Monte-Carlo simulation (MCS) is executed for the parameter (Pa.) estimates of the APBHE model. The R-programming packages are utilized in achieving the MCS steps. The complete and PTIIC samples are generated from APBHE model using Eq. (14) with $\alpha = 0.1$ and $\eta = 0.3$ and various sample sizes under the following schemes (SCHE) via the algorithm developed by [23].

SCHE1: $R_1 = n - m$ and $R_i = 0$ for $i \neq 1$,
SCHE2: $R_{m/2} = n - m$ and $R_i = 0$ for $i \neq (m/2)$,
SCHE3: $R_1 = R_m = (n - m)/2$ and $R_i = 0$ for $i \neq (1 \text{ and } m)$
SCHE4: $R_m = n - m$ and $R_i = 0$ for $i \neq m$

The average (AVE), biases (Bias), mean square errors (MSEs), 95% asymptotic confidence interval (Asy CI) and average interval length (AIL) are computed based on 1,000 PTIIC iterations are reported in Tables (3) and (4). Referring to Table (3), the MSE and Bias decrease as (m,n) increases for the estimates. However, in comparison the MLE estimates are more efficient than the MPS estimates according to their MSE values as seen in Table (3).

Table 3: *AVE and MSE (Bias) for APBHE model.*

(n, m)	SCHE	Pa.	MLE		MPS	
			AVE	MSE (Bias)	AVE	MSE (Bias)
(20, 20)	Complete	α	0.100	0.000 (0.000)	0.052	0.002 (-0.048)
		η	0.343	0.002 (0.043)	0.260	0.002(-0.040)
(20, 18)	1	α	0.113	0.000 (0.013)	0.071	0.001 (-0.029)
		η	0.342	0.002 (0.042)	0.186	0.013 (-0.114)
	2	α	0.121	0.000 (0.021)	0.070	0.001 (-0.030)
		η	0.350	0.003 (0.050)	0.200	0.010 (-0.100)
	3	α	0.122	0.001 (0.022)	0.088	0.000 (-0.012)
		η	0.350	0.002 (0.050)	0.254	0.002 (-0.046)
	4	α	0.127	0.001 (0.027)	0.095	0.000 (-0.005)
		η	0.353	0.003 (0.053)	0.305	0.000 (0.005)

Continued on the next page...

Table 3: (contd...)

(n, m)	SCHE	Pa.	MLE		MPS	
			AVE	MSE (Bias)	AVE	MSE (Bias)
(20, 14)	1	α	0.156	0.003 (0.056)	0.139	0.002 (-0.039)
		η	0.364	0.004 (0.064)	0.104	0.039 (-0.196)
	2	α	0.185	0.007 (0.185)	0.137	0.001 (0.037)
		η	0.385	0.007 (0.085)	0.121	0.032 (-0.179)
	3	α	0.188	0.008 (0.088)	0.157	0.003 (0.057)
		η	0.385	0.007 (0.085)	0.244	0.003 (-0.056)
	4	α	0.196	0.009 (0.096)	0.067	0.001 (-0.003)
		η	0.390	0.008 (0.390)	0.178	0.015 (-0.124)
(30, 30)	Complete	α	0.065	0.001 (-0.035)	0.040	0.126 (0.355)
		η	0.341	0.002 (0.041)	0.278	0.004 (-0.060)
(30, 26)	1	α	0.074	0.001 (-0.026)	0.068	0.000 (-0.022)
		η	0.330	0.001 (0.030)	0.173	0.001 (-0.032)
	2	α	0.082	0.000 (-0.018)	0.066	0.001(-0.034)
		η	0.339	0.002 (0.039)	0.188	0.013 (-0.112)
	3	α	0.088	0.000 (-0.012)	0.091	0.000 (-0.009)
		η	0.344	0.002 (0.044)	0.274	0.001 (-0.026)
	4	α	0.100	0.000 (0.000)	0.091	0.000 (-0.009)
		η	0.356	0.003 (0.056)	0.274	0.001 (0.026)
(30, 18)	1	α	0.115	0.000 (0.015)	0.165	0.004 (0.065)
		η	0.344	0.002 (-0.044)	0.073	0.052 (-0.227)
	2	α	0.150	0.003 (0.050)	-	-
		η	0.376	0.006 (0.076)	-	-
	3	α	0.146	0.002 (0.046)	0.175	0.006 (0.075)
		η	0.368	0.005 (0.068)	0.250	0.003 (-0.050)
	4	α	0.166	0.004 (0.066)	0.171	0.005 (0.071)
		η	0.382	0.007 (0.082)	0.380	0.006 (0.080)
(50, 50)	Complete	α	0.042	0.003 (-0.058)	0.029	0.005 (-0.071)
		η	0.340	0.002 (0.040)	0.294	0.000 (-0.006)
(50, 42)	1	α	0.048	0.003 (-0.052)	0.063	0.001 (-0.037)
		η	0.337	0.001 (0.037)	0.164	0.019 (-0.136)
	2	α	0.054	0.002 (-0.048)	0.060	0.002 (-0.040)
		η	0.347	0.002 (0.047)	0.180	0.015 (-0.120)
	3	α	0.075	0.001 (-0.025)	0.094	0.000 (-0.006)
		η	0.381	0.006 (0.081)	0.312	0.000 (0.012)
	4	α	0.098	0.000 (-0.002)	0.098	0.000 (-0.002)
		η	0.409	0.012 (0.109)	0.403	0.011 (0.103)
(50, 26)	1	α	0.077	0.001 (-0.023)	-	-
		η	0.333	0.001 (0.033)	-	-
	2	α	0.106	0.000 (0.006)	0.185	0.007 (0.085)
		η	0.365	0.004 (0.065)	0.062	0.057 (-0.238)
	3	α	1.481	1.906 (1.381)	0.191	0.008 (0.091)
		η	1.370	1.146 (1.070)	0.270	0.001 (-0.030)
	4	α	0.174	0.006 (0.074)	0.181	0.007 (0.081)
		η	0.421	0.015 (0.121)	0.424	0.015 (0.124)

Table 4: *Asy CI and AILs for APBHE model.*

(n, m)	SCHE	Pa.	MLE		MPS	
			Asy CI		Asy CI	
			(Lower, Upper)	AIL	(Lower, Upper)	AIL
(20, 20)	Complete	α	(-0.400, 0.590)	0.991	(-0.180, 0.280)	0.458
		η	(-0.220, 0.910)	1.129	(-0.100, 0.620)	0.722
(20, 18)	1	α	(-0.480, 0.710)	1.189	(-0.150, 0.290)	0.448
		η	(-0.260, 0.940)	1.206	(-0.014, 0.387)	0.400
	2	α	(-0.510, 0.750)	1.261	(-0.140, 0.280)	0.423
		η	(-0.260, 0.960)	1.229	(-0.007, 0.408)	0.410
	3	α	(-0.460, 0.640)	1.097	(-0.220, 0.400)	0.627
		η	(-0.380, 1.060)	1.596	(-0.055, 0.602)	0.657
	4	α	(-0.860, 1.120)	1.441	(-0.410, 0.600)	1.015
		η	(-0.610, 1.310)	1.923	(-0.260, 0.870)	1.127
(20, 14)	1	α	(-0.650, 0.960)	1.613	(-0.290, 0.570)	0.858
		η	(-0.280, 1.010)	1.291	(-0.021, 0.228)	0.249
	2	α	(-0.740, 1.110)	1.842	(-0.260, 0.530)	0.786
		η	(-0.290, 1.060)	1.358	(-0.015, 0.257)	0.272
	3	α	(-1.500, 1.900)	3.340	(-0.630, 0.940)	1.570
		η	(-0.860, 1.640)	2.500	(-0.210, 0.700)	0.913
	4	α	(-2.100, 2.500)	4.532	(-0.980, 1.310)	2.289
		η	(-1.300, 2.100)	3.350	(-0.570, 1.280)	1.850
(30, 30)	Complete	α	(-0.220, 0.350)	0.566	(-0.110, 0.190)	0.301
		η	(-0.130, 0.810)	0.939	(-0.041, 0.597)	0.638
(30, 26)	1	α	(-0.290, 0.430)	0.722	(-0.091, 0.226)	0.317

Continued on the next page...

Table 4: (contd...)

(n, m)	SCHE	Pa.	MLE Asy CI (Lower, Upper)	AIL	MPS Asy CI (Lower, Upper)	AIL
		η	(-0.180, 0.840)	1.029	(0.034, 0.312)	0.278
	2	α	(-0.310, 0.470)	0.785	(-0.162, 0.326)	0.488
		η	(-0.190, 0.870)	1.055	(-0.009, 0.654)	0.663
	3	α	(-0.490, 0.640)	1.097	(-0.623, 0.847)	0.627
		η	(-0.380, 1.060)	1.441	(-0.566, 1.443)	0.657
	4	α	(-0.590, 0.790)	1.386	(-0.380, 0.570)	0.945
		η	(-0.490, 1.210)	1.700	(-0.240, 0.920)	1.165
(30, 18)	1	α	(-0.490, 0.720)	1.204	(-0.280, 0.610)	0.883
		η	(-0.260, 0.950)	1.208	(-0.005, 0.151)	0.156
	2	α	(-0.590, 0.890)	1.482	-	- / -
		η	(-0.270, 1.020)	1.291	-	- / -
	3	α	(-1.400, 1.700)	3.094	(-0.710, 1.060)	1.772
		η	(-1.000, 1.800)	2.796	(-0.230, 0.730)	0.954
	4	α	(-2.000, 2.300)	4.365	(-1.200, 1.500)	2.651
		η	(-1.500, 2.200)	3.686	(-0.710, 1.470)	2.187
(50, 50)	Complete	α	(-0.1200, 0.200)	0.316	(-0.065, 0.122)	0.187
		η	(-0.046, 0.727)	0.773	(0.016, 0.571)	0.555
(50, 42)	1	α	(-0.140, 0.240)	0.385	(-0.042, 0.168)	0.210
		η	(-0.077, 0.750)	0.828	(0.070, 0.260)	0.188
	2	α	(-0.160, 0.270)	0.430	(-0.037, 0.158)	0.195
		η	(-0.079, 0.772)	0.851	(0.080, 0.280)	0.198
	3	α	(-0.280, 0.430)	0.712	(-0.160, 0.350)	0.514
		η	(-0.210, 0.980)	1.191	(0.013, 0.610)	0.597
	4	α	(-0.390, 0.590)	0.978	(-0.310, 0.500)	0.808
		η	(-0.290, 1.110)	1.409	(-0.170, 0.980)	1.148
(50, 26)	1	α	(-0.290, 0.450)	0.742	-	- / -
		η	(-0.180, 0.850)	1.033	-	- / -
	2	α	(-0.380, 0.590)	0.964	(-0.200, 0.570)	0.767
		η	(-0.190, 0.920)	1.114	(0.009, 0.115)	0.107
	3	α	(-1.100, 1.400)	2.425	(-0.700, 1.100)	1.774
		η	(-0.810, 1.610)	2.423	(-0.210, 0.750)	0.956
	4	α	(-1.600, 2.000)	3.575	(-1.100, 1.500)	2.656
		η	(-1.200, 2.000)	3.195	(-0.730, 1.580)	2.316

8. Applications

8.1. Uncensored dataset

Here, the fitness of the APBHE model is proved empirically via application to a real-dataset utilizing *AdequacyModel* package in R-programming software in comparison to alpha power Burr Hatke (APBH), inverse power Burr Hatke (IPBH), inverse pereto (IPE), pereto type-I (PE1), generalized exponential (GIE), type 1 half logistic skew-t (TIHLST), Exponentiated Inverse Rayleigh (EIR) and Burr hatke exponential (BHE) models.

The dataset discussed by [24] is the remission times (in months) for a random sample of 128 bladder cancer patients. [25] utilized the dataset in demonstrating the stability of their developed model. The data are: 0.08, 2.09, 3.48, 4.87, 6.94 , 8.66, 13.11, 23.63, 0.20, 2.23, 3.52, 4.98, 6.97, 9.02, 13.29, 0.40, 2.26, 3.57, 5.06, 7.09, 9.22, 13.80, 25.74, 0.50, 2.46 , 3.64, 5.09, 7.26, 9.47, 14.24, 25.82, 0.51, 2.54, 3.70, 5.17, 7.28, 9.74, 14.76, 26.31, 0.81, 2.62, 3.82, 5.32, 7.32, 10.06, 14.77, 32.15, 2.64, 3.88,5.32, 7.39, 10.34, 14.83, 34.26, 0.90, 2.69, 4.18, 5.34, 7.59, 10.66, 15.96, 36.66, 1.05, 2.69, 4.23, 5.41, 7.62, 10.75, 16.62, 43.01, 1.19, 2.75, 4.26, 5.41, 7.63, 17.12, 46.12, 1.26, 2.83, 4.33, 5.49, 7.66, 11.25, 17.14, 79.05, 1.35, 2.87, 5.62, 7.87, 11.64, 17.36, 1.40, 3.02, 4.34, 5.71, 7.93, 11.79, 18.10, 1.46, 4.40, 5.85, 8.26, 11.98, 19.13, 1.76, 3.25, 4.50, 6.25, 8.37, 12.02, 2.02, 3.31, 4.51, 6.54, 8.53, 12.03, 20.28, 2.02, 3.36, 6.76, 12.07, 21.73, 2.07, 3.36, 6.93, 8.65, 12.63 and 22.69.

Some descriptive graphs for the data are depicted in Figure 4 and it is deduced that these dataset is right-skewed and leptokurtic in nature.

Table (5) reports the MLEs and standard errors (SEs) from the fitted models to the bladder cancer dataset. Also, the negative log-likelihood (-LL'), Consistent Akaike information criterion (CAIC'), Hannan-Quinn information criterion (HQIC'), Bayesian information criterion (BIC'), Akaike information criterion (AIC') and Kolmogorov-Smirnov (KS') and Pvalue of the fitted

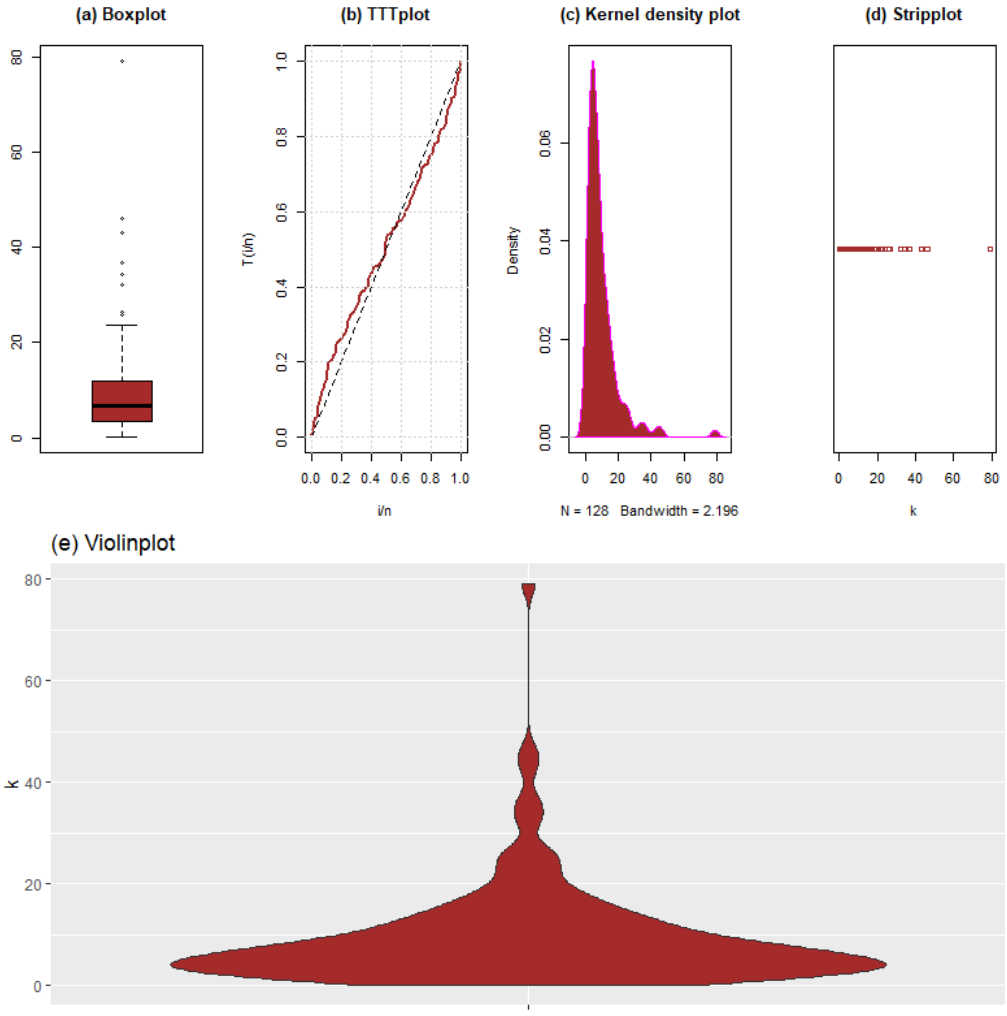


Figure 4: *Box-plot, TTT, kernel-density, strip, and Violin plots of bladder-cancer data.*

Table 5: *MLE (SEs) for the fitted models to the bladder-cancer uncensored dataset*

Model	MLEs (SEs)	
APBHE (α, η)	4.299 (2.648)	0.091 (0.014)
APBH (α, η)	136.300 (46.780)	0.037 (0.010)
IPBH (α, η)	1.722 (0.221)	0.803 (0.044)
IPE (α, η)	2.413 (0.582)	2.056 (0.646)
PE1 (η)	-	0.567 (0.050)
TIHLST (α, η)	0.528 (0.058)	15.321 (5.267)
EIR (α, η)	0.528 (0.058)	15.321 (5.267)
BHE (η)	-	0.062 (0.006)

models are reported in Table (6), the APBHE model has the highest -LL' and lowest values for the other selection criteria, especially KS' (high Pvalue), hence indicating that it provides the best fit to the bladder-cancer data among the fitted models.

More so, it is clear from Figure 5 that the APBHE model provides the best fit. Furthermore, the profile log-likelihood function plots with some parameter values (with fixed MLEs of other parameters) for the dataset are displayed in Figure 6. The likelihood ratio (LR) tests for the APBHE model against the BHE and IPBH models is carried-out. According to the empirical

Table 6: *Selection criteria for the fitted models to the bladder-cancer uncensored dataset*

Model	-LL'	AIC'	BIC'	CAIC'	HQIC'	KS'	Pvalue
APBHE	-413.8	831.7	837.4	831.8	834.0	0.06	0.70
BHE	-416.0	834.0	836.9	834.1	835.2	0.10	0.04
APBH	-415.7	835.4	841.1	835.5	837.8	0.10	0.03
IPBH	-442.7	889.4	895.1	889.5	891.7	0.10	0.02
IPE	-426.3	856.6	862.3	856.7	858.9	0.10	0.05
PE1	-426.5	855.0	857.9	855.0	856.2	3.00	2E-16
TIHLST	-446.8	897.5	903.2	897.6	899.8	0.20	6E-06
EIR	-507.0	1018.0	1023.7	1018.1	1020.3	0.40	3E-14

findings as reported in Table (7), the null hypotheses are rejected with low p-values, indicating that the APBHE model fits the dataset much better than the other models. This shows that the APBHE model provides the best fit to the bladder-cancer dataset.

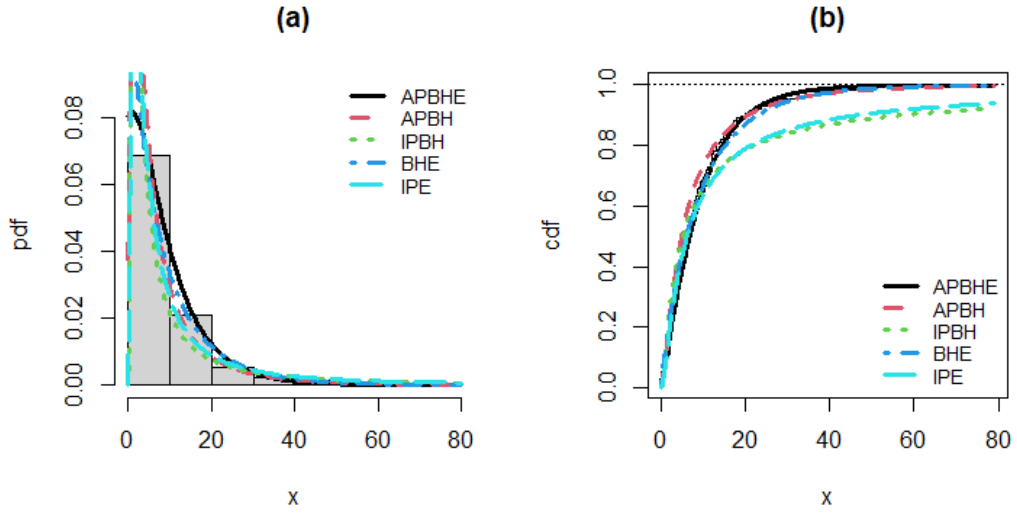


Figure 5: *Some Estimated PDFs (a) and CDFs (b) for the bladder-cancer uncensored dataset.*

Table 7: *LR tests for the bladder-cancer uncensored dataset*

Model	Hypotheses	LR	p-values
APBHE vs BHE	$H_0 : \alpha = 1$ vs $H_1 : H_0$ is false	4.40	0.036
APBHE vs IPBH	$H_0 : \alpha = 1$ vs $H_1 : H_0$ is false	58.0	<0.0001

Table 8: *Findings for MLE and MPS to the bladder-cancer uncensored dataset*

Model	pa	MLE	MPS
APBHE	α	4.301	3.129
	η	0.091	0.083

Table (8) reports the estimates of the APBHE parameter (pa) using the bladder-cancer dataset based on the MLE with (KS' = 0.06, pvalue = 0.75) and MPS with (KS' = 0.064, pvalue = 0.7) . For the sake of comparison, the MLE is quite appropriate for fitting the uncensored dataset based on the KS' and larger Pvalues.

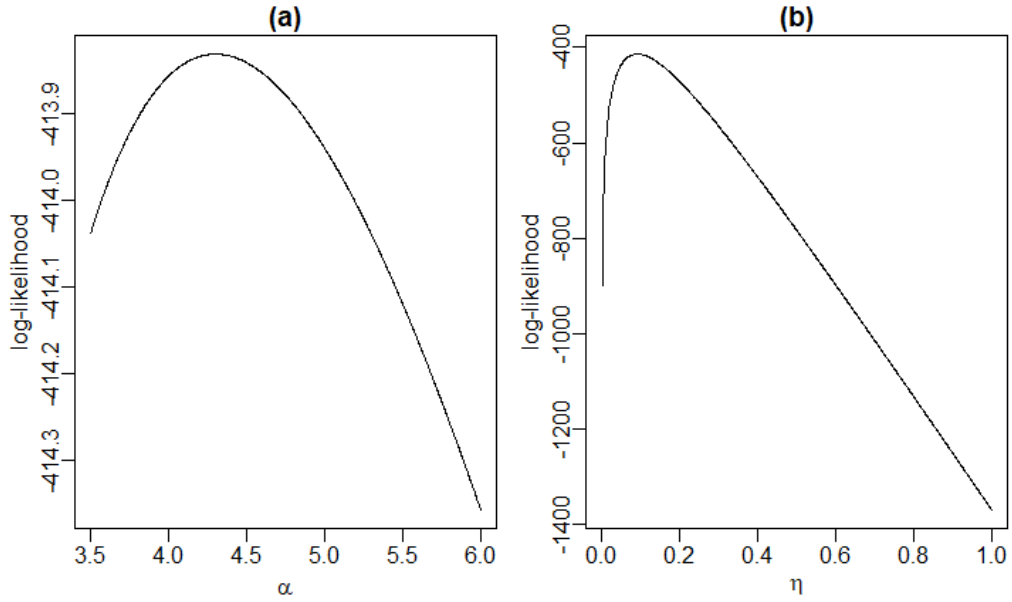


Figure 6: *Profile log-likelihood functions for bladder-cancer uncensored dataset.*

8.2. Censored dataset

The PTIIC using the bladder-cancer dataset via the different estimation methods is carried-out for the APBHE model. The average estimates and Asy CI using both the MLE and MPS at m = 90 are computed. However, the MPS performed poorly in the various PTIIC schemes as the estimates are all the same (*not presented*) . In conclusion, the MLE offer the best estimates and Asy CI values for the APBHE model in the PTIIC schemes as presented in Table (9).

Table 9: *PTIIC results for MLE to the bladder-cancer uncensored dataset*

(n, m)	SCHE	Pa.	MLE	Asy CI MLE
(128, 90)	1	α	4.776	(-0.670, 10.220)
		η	0.069	(0.047, 0.091)
	2	α	6.900	(-0.770, 14.580)
		η	0.081	(0.058, 0.104)
	3	α	6.000	(-0.740, 12.760)
		η	0.076	(0.054, 0.099)
	4	α	7.800	(-0.830, 16.330)
		η	0.085	(0.061, 0.108)

9. Conclusion

We propose a novel two-parameter model, known as the alpha power Burr-Hatke exponential (APBHE) model, which is an extension of Burke-Hatke exponential (BHE) model. This is driven due to the scares use of the BHE in statistical modeling and life testing especially in the field of medical sciences. Thus, some structural properties of the APBHE model including the log-APBHE model and the log-APBHE regression model are provided. The MLE and MPS estimation methods are utilized in estimating the APBHE parameters based on uncensored and PTIIC censoring schemes, and the simulation is utilized to ascertain the APBHE model output. However, the MLE estimates have more relative efficiency than the MPS for the parameter estimates of the APBHE model. This result is consistent with existing literature on comparison between the MLE and

MPS estimators using different existing and newly developed distributions. Furthermore, the empirical findings from the real-life dataset application inform that the novel APBHE consistently provides the best fit relative to other competing models considered.

References

[1] Adubisi, O. D., Abdulkadir, A. and Chiroma, H. (2021). A Two Parameter Odd Exponentiated Skew-T Distribution With J-Shaped Hazard Rate Function. *J. of Stat. Mod. & Analy. (JOSMA)*, 3:26–46.

[2] Adubisi, O. D. and Adubisi, C. E. (2023). Different Estimation Methods for Topp-Leone-(A) Model: Inference and Applications to Complete and Censored Datasets. *J. of Reliability: Theory & App. (RT&A)*, 18:100–117.

[3] Shanker, R., Hagos, F. and Sujatha, S. (2015). On modeling of Lifetimes data using exponential & Lindley distributions. *Biometrics & Biostat. Inter. J.*, 2:1–9.

[4] Yadav, A. S., Altun, E. and Yousof, H. M. (2019). Burr Hatke exponential distribution: A decreasing failure rate model, statistical inference and applications. *Annals of Data Sci.*, 8:241–260.

[5] Abouelmagd, T. H. M. (2018). The Logarithmic Burr Hatke exponential distribution for modeling reliability and medical data. *Inter. J. of Stat. & Pro.*, 7:73–85.

[6] El-Morshedy, M., Aji0hani, H. M., Eliwa, M. S., Nassar, M., Shakhatreh, M. K. and Afify, A. Z. (2021). The exponentiated Burr Hatke distribution and its discrete version: Reliability properties with CSALT model inference and application. *Maths.*, 9:2277.

[7] Afify, A. Z., Ajohani, H. M., Alghamdi, A. S., Gemeay, A. M. and Sarg, A. M. (2021). A new two-parameter Burr-Hatke distribution: properties and Bayesian and non-Bayesian inference with applications. *J. of Maths.*, 2021:1061083.

[8] Almuqrin, M. A. (2023). A new flexible distribution with applications to engineering data. *Alexandria Eng. J.*, 69:371-382.

[9] Gao, X. and Gui, W. (2023). Statistical inference of Burr-Hatke exponential distribution with partially accelerated life test under progressively type II censoring. *Maths.*, 11:1-21.

[10] Anyiam, K. E., Alghamdi, F. M., Nwaigwe, C. C., Aljohani, H. M. and Obulezi, O. J. (2024). A new extension of Burr-Hatke exponential distribution with engineering and biomedical applications. *Alexandria Eng. J.* 10:e38293.

[11] Mahdavi, A. and Kundu, D. (2017). A new method of generating distributions with an application to exponential distribution. *comm. in stat.-theory & meth.*, 46:6543-6557.

[12] Eissa, Y. F. and Sonar, D. C. (2023). Alpha power transformed extended power Lindley distribution. *J. of Stat.-theory & App.*, 22:1-18.

[13] Klakattawi, H. S. and Aljuhani, W. H. (2021). A new technique for generating distribution based on a combination of two techniques: Alpha power transformation and exponentiated T-X distributions family. *Symmetry*, 13:412.

[14] Bleed, S. O., Attwa, R. A., Ali, R. F. M. and Rahwan, T. (2024). On alpha power transformation generalized Pareto distribution and some properties. *J. of applied maths.*, 2024:6270350.

[15] Ehiwario, J. C. , Igabari, J. N. and Ezimadu, P.E. (2023). The alpha power Topp-Leone distribution: properties, simulations and applications. *J. of applied maths. & phy.* , 11:316-331.

[16] Dugasa, S. J., Goshu, A. T. and Arero, B. G. (2024). Alpha power transformation of the Lindley probability distribution. *J. of Prob. & Stat.*, 2024:9068114.

[17] Madlool, H. and AL-Kadim, K. A. (2024). Alpha power survival transformation exponential distribution. *J. of comp. analy. & app.*, 33:299-305.

[18] Oda, A. M. and AL-Kadim, K. A. (2024). Alpha power Quantile transformation exponential distribution. *J. of comp. analy. & app.*, 33:353-358.

[19] Abdulkadir, A., Adubisi, O. D. and Madaki, R. (2024). A new family of distributions based on amalgamation of two methods with an application to the Rayleigh model. *European. J. of Stat.* 4:1-19.

[20] Abdulkadir, A., Adubisi, O. D. and Madaki, R. (2024). Novel extended Weibull regression model for investigating the survival times of breast cancer patients. *Mikailalsys J. of Maths. & Stat.*, 2:135-155.

[21] Maniu, A. I. and Voda, V. G. (2008). Generalized Burr-Hatke equation as generator of a homographic failure rate. *J. of applied quant. meth.* , 3:215-222.

[22] Ng, H. K. T., Luo, L. and Duan, Y. H. (2012). Parameter estimation of three-parameter Weibull distribution based on progressive type-II censored samples. *J. of stat. comp. & simul.* , 82:1661-1678.

[23] Balakrishnan, N. and Sandhu, R. A. (1995). A simple simulational algorithm for generating progressive type-II censored samples. *The American Stat.* 9:229-230.

[24] Lee, T. E. and Wang, J. W. (2003). *Statistical methods for survival data analysis, Wiley, New York 2003*.

[25] Anzagra, L., Abubakari, A. G. and Nasiru, S. (2023). Chen Burr-Hatke exponential distribution: properties, regression and biomedical applications. *Comp. J. of Maths. & stat. sci.*, 2:80-105.

MULTI- REFERENCE SKIP- LOT SAMPLING OF TYPE 3 (MR-SkSP-3)

Meby Joseph Manoj [1], Azarudheen S [2]

•

[1,2] Department of Statistics and Data Science
CHRIST (Deemed to be University)
Bengaluru, India
mebyjosephmanoj0328@gmail.com, sazaru1990@gmail.com

Abstract

In the current industrial sector, the rate of defective products present in the lots has been decreasing and most of the products keeps up a good history of quality throughout the production also. Skip-lot sampling plans are the suitable acceptance sampling plan for the situations where the series of products shows a stable and excellent quality. The skip-lot sampling plans are still widely used because of its reduced sampling cost and efforts, because the plan only needs to inspect a fraction of the lots submitted after a continues series of lots with excellent quality. This approach makes the skip-lot plan more cost-effective than the other sampling plans, thus making it an economically important plan. The current study incorporated a modification on the skip-lot sampling of type 3 and designated it as multi- reference skip lot sampling of type 3. The proposed plan has the provision of having multiple reference plans in normal and skipping inspection of a skip-lot sampling plan, unlike the traditional skip-lot plans which has the same reference plan in all phases. The performance measures of the proposed plan are derived using the power series approach. A designing methodology to determine the optimal parameters for the plan using the unity value approach is also described with the help of a numerical illustration. Behaviour of the operating characteristic curves for varying set of parameters are also analysed for the plan. Comparison of the proposed plan is done between the conventional plans using performance measure values and graphical representations. This analysis shows that the new plan is able to effectively optimize the preferences of producer and consumer simultaneously, where the traditional plans fail to. The analysis is supported with the help of graphical representations and tabulated values.

Keywords: Quality control, acceptance sampling plan, skip-lot sampling plan, operating characteristic curve, producer's risk, consumer's risk, unity value approach.

1. Introduction

As we navigate through the radical technological era, and with the help of online platforms to purchase products, the options for the customers to choose from different brands is wide. Then quality becomes the important factor which customers choose to select the product. This led companies to put maximum effort in improving the quality and reach the peak level. Statistical Quality Control (SQC) provides statistical techniques to effectively monitor, maintain and improve the product quality. Acceptance sampling is one of the key techniques used for inspecting the final lot of products and it classifies them as confirming and non-confirming based on the sample inspection. In manufacturing industries, this lot inspection is used to evaluate the quality of the outgoing products; a government agency can inspect the food safety by inspecting the lots and ensuring the components are within the legal limits; and in an international trade, the purchased goods are accepted or rejected based on the lot inspection done on the samples. Since the binary decision about the products is taken based on the random samples, there exists some risk for

committing errors. The type-1 error, also known as producer's risk which is the probability of rejecting a good lot and type-2 error, also known as consumer's risk which is the probability of accepting a bad lot. The optimal quality levels for the sampling plans are found out using these producer's and consumer's risk and are referred as acceptable quality level (AQL) and limiting quality level (LQL).

The acceptance sampling plans are generally classified into variable sampling plans and attribute sampling plans. Variable sampling plans is used to inspect the measurable quality parameters where the attribute sampling plans is applied to inspect the non-measurable quality parameters. Many attribute sampling plans have been developed as per the needs in the industry. Single sampling plan (SSP), double sampling plan (DSP), multiple sampling plan are the conventional attribute sampling plans used. Many modifications have been made to the traditional sampling plans according to the need for more reliable and less costly plans. More detailed studies about the Accepting sampling plans have been conducted by [12]. The first skip-lot sampling plan (SkSP-1), introduced by [6], is one of the acceptance sampling techniques. This plan, where individual lots are being inspected, was derived from the continuous sampling plan of type 1 (CSP-1) where the inspection happens for each unit. The SkSP-1 allows to skip some lots from the inspection if the preceding series of lots are reflecting a good quality with minimum defectives. This approach provides significant advantage in terms of reducing inspection cost and time. However, the lack of an inspection plan was a drawback for the primary plan. Then the skip-lot sampling plan was modified by [10], and introduced skip-lot sampling plan of type 2 (SkSP-2), by incorporating reference plans such as SSP or DSP. This introduction of the reference plans assisted to consider the preference of producer and consumer in the inspection and allowed flexibility in the approach to sample each lot depending on situations. SkSP-2 plan is a widely accepted sampling plan and has been adapted with many modifications and applications in current studies also. An attribute SkSP-2 plan with SSP as the reference plan with zero acceptance number was developed by [15]. At a later stage, [17] presented the SkSP-2 with the DSP as the reference plan to aim for less inspection cost by reducing the sample size. An optimal method to determine the plan parameters and to design the attribute SkSP-2 was done by [1]. The SkSP-2 with DSP as the reference plan under the binomial distribution was designed and investigated by [5]. Later [2] proposed the SkSP-2 with Intervened Poisson distribution (IPD) in the SSP as the reference plan which can be used when there are interventions in the process of production. The concept of resampling was assimilated to the two level SkSP-2 by [7] and the performance measures where derived using Markov chain formulation.

When the principles of CSP-2 was incorporated with that of skip-lot sampling plans, [13] developed a new plan as SkSP-3 with SSP as the reference plan. Later [16] studied the SkSP-3 with SSP as the reference plan with a characteristic of zero acceptance number and used the Markov chain approach to derive performance measures and. A SkSP-3 plan using the SSP as the reference plan was proposed, along with cost models for its economic design by [4]. Thereafter [3] developed the SkSP-3 with the IPD as the reference plan and designed the corresponding methodology also. The concept of resampling technique was introduced into skip-lot sampling plans by [8] and developed SkSP-3-R by deriving the performance measures using the Markov chain method. In a subsequent study, [14] introduced tightened single-level SkSP plan by tightening the inspection with stern limitations. They studied the performance measures of this TSkSP-3 using the Markov chain method and compared them with that of conventional plans.

The method of skip-lot inspection plan is to conduct the inspection in two phases, namely normal inspection and skipping inspection. The lots will be continuously checked during the normal inspection and after attaining a level of quality, skipping inspection is started. During the skipping inspection, the examination will be done only to fraction of lots while others are skipped. The skipping inspection continues until a defective is found, which then will start again from normal inspection. In all of the conventional skip-lot plans, both the normal and skipping inspection is done using same reference plan. This results in certain disadvantages for either the producer or the customer. When a skip-lot plan uses SSP as the reference plan in both inspections, some lots with acceptable level of quality is getting rejected due to the low acceptance rate for low

proportion defectives. If the skip-lot plan uses DSP as the reference plan in both inspections, some of the lots with rejectable quality level will be accepted due to the high acceptance probability for high proportion defectives. The former plan favours the customer more in the inspection and latter one favours the producer more. This article proposes a new approach where the skip-lot sampling plan of type 3 can be conducted where the normal inspection and skipping inspection is having multiple and different reference plans and is termed as Multi Reference Skip-lot Sampling plan of type 3 (MR-SkSP-3). Here, the usage of two different reference plan for the two phaes of inspection will optimize the preference between the producer and consumer. Also, the proposed plan minimises the inspection cost and maintain high quality than the conventional plans. The article is followed as: Section 2 gives an introduction to the basic sampling plans which are required for the study. Section 3 consists of the designing and operating procedure for the new MR-SkSP-3 plan. Section 4 and section 5 includes the determination of optimal parameters for the proposed plan and a numerical example for the parameter determination, respectively. OC curve analysis and the influence of parameters of the proposed plan are studied in the Section 6. Also, the proposed plan is compared with that of conventional plans using the OC curves and tables of performance measures in the Section 7. In section 8, the key remarks and insights are provided in the conclusion.

2. OPERATING PROCEDURE OF THE SAMPLING PLANS.

2.1. SINGLE SAMPLING PLAN

The single sampling plan (SSP) which is considered the basic plan of acceptance sampling plan for attributes will sentence the products by examining a single sample from the lot and disposition will be decided based on the information from the sample. The acceptance or rejection of the lot will be based on whether the number of defects found in the sample of size n, is greater than the acceptance number c or not. The SSP under Poisson distribution was designed by [9] and the plan parameters were also derived. Afterward, [12] gave much more insight into the approach of using the unity value method for finding the sampling plans on Poisson distribution.
The probability of acceptance for the single sampling plan under the Poisson distribution is as follows;

$$P_a(p) = \sum_{x=0}^{c} \frac{e^{-\lambda}\lambda^x}{x!} \tag{1}$$

2.2. DOUBLE SAMPLING PLAN

The double sampling plan (DSP) is the modification of the SSP when the decision about the lot, whether to accept or reject it, is made from two different samples instead of a single sample. In DSP, a second sample is inspected when the first sample of size n_1 is not accepted because the defectives were more than the acceptance number c_1, but does not exceed the rejection number. In order to accept the lot after examining the second sample of size n_2, the number of defectives of both samples should be not greater than the c_2, which is the cumulative acceptance number for the whole. The tables for selecting DSP according to the MIL-STD-105D were developed by [11]. The use of DSP instead of the SSP will reduce the average sample number (ASN) of the plan which will keep the inspection cost and effort at the minimum.
The probability of acceptance for the double sampling plan under the Poisson distribution is as follows;

$$P_a(p) = \sum_{x=0}^{c_1} \frac{e^{-\lambda_1}\lambda_1^x}{x!} + \sum_{x=c_1+1}^{c_2} \sum_{y=0}^{c_2-x} \frac{e^{-\lambda_1}\lambda_1^x e^{-\lambda_2}\lambda_2^y}{x!\,y!} \tag{2}$$

2.3. SKIP-LOT SAMPLING PLAN -3

The Skip-lot Sampling plan -3 (SkSP-3) is one among the cumulative sampling plans and can be applied for a continuing stream of production from a trusted distributor. The plan is based on the principles of the continuous sampling plan (CSP-2) which is applied for the continuous inspection of products. Using the reference plan mentioned, the lots will be applied with 100% inspection until i succeeding lots are determined to be defect-free. After that, the skipping inspection is performed over the reference plan on a small fraction f of the total lots. When a lot is rejected during the skipping inspection, the proceeding k consecutive lots are inspected. If all the k lots are accepted, the skipping inspection will be continued, otherwise the inspection will start again from normal inspection.
The probability of acceptance for the Skip-lot Sampling plan -3 is as follows;

$$P_a(p) = \frac{fP + (1-f)P^i(2-P^i)}{f + (1-f)P^i(2-P^i)} \tag{3}$$

3. DESIGNING OF MULTI-REFERENCE SKIP-LOT SAMPLING PLAN OF TYPE 3 (MR-SKSP-3)

The SkSP-3 is a modification when the principles of CSP-2 is introduced to the skip-lot sampling procedure. It is performed in two inspection phases, the normal and skipping inspection as like all other skip-lot plans. The SkSP-3 plan conducts one more inspection when there is a rejection in the skipping inspection.

The MR-SkSP-3 is introduced here with the provision of having two different reference plans in the two phases of the plan. The MR-SkSP-3 plan has the single sampling plan as the reference plan in the normal inspection and double sampling plan as the reference plan in the skipping inspection. The inspection procedure of the proposed plan is as given in Figure 1.

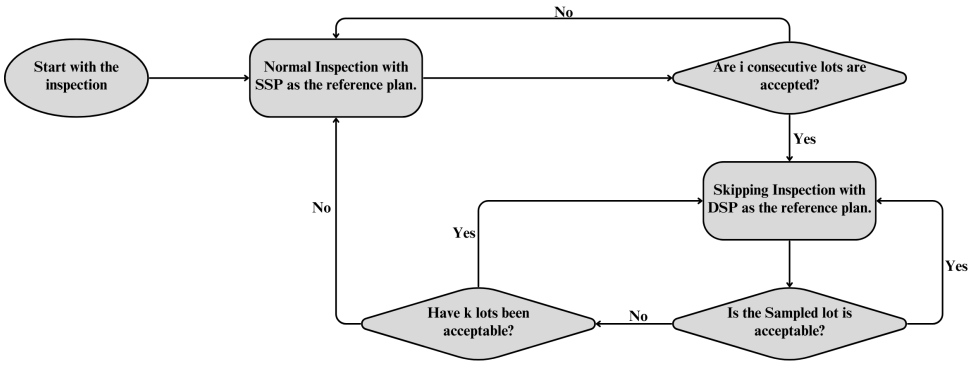


Figure 1: *Operating procedure for the MR-SkSP-3 plan*

The proposed MR-SkSP-3 plan will be having the parameters such as sample size n_1 for single sampling and n_1 and n_2 for double sampling, acceptance number c_1 for single sampling and c_1 and c_2 for double sampling, clearance number i for normal inspection, fraction of lots inspected f and clearance number k for skipping inspection.

A plan is assessed based on the performance measures and can be derived in various methods. The measures for the SkSP-2 using the power series approach were deribed by [10]. He derived the operating characteristic (OC) function for the plan by finding the number of expected lots in the both phases of inspection, normal and skipping inspection. Similarly for the MR-SkSP-3 plan, the expected number of lots during the normal inspection is:

$$U = \frac{1-(P_{\text{SSP}})^i}{(P_{\text{SSP}})^i(1-P_{\text{SSP}})} \tag{4}$$

Also in normal inspection, the expected number of failure sequence before having i consecutive accepted lots is:

$$G = \frac{1 - (P_{\text{SSP}})^i}{(P_{\text{SSP}})^i} \tag{5}$$

Likewise, during the skipping inspection, the expected number of lots before the first rejection occurs is:

$$V = \frac{2 - P_{\text{DSP}}^k}{f(1 - P_{\text{DSP}})(1 - P_{\text{DSP}}^k)} \tag{6}$$

where the P_{SSP} is the probability of acceptance of single sampling plan (SSP) and P_{DSP} is that of double sampling plan (DSP).

From these, the probability of rejection, P_r, of the MR-SkSP-3 plan is defined as,

$$P_r = \frac{\text{expected number of lots rejected}}{\text{expected number of lots submitted}} = \frac{G+1}{U+V} \tag{7}$$

Then, the probability of the acceptance, P_a, is given by,

$$P_a = 1 - P_r = 1 - \frac{G+1}{U+V} \tag{8}$$

There are many combinations of plan parameters for designing a sampling plan according to the specified requirements. The choice of selecting the combination of parameters for the plan depends upon the selection of the average sample size. During the inspection, the decision about the lot whether to accept or reject is made from this average number of sample units per lot. The average sample number (ASN) of the MR-SkSP-3 plan is given by:

$$ASN = \frac{ASN_{\text{SSP}} \cdot U + f \cdot ASN_{\text{DSP}} \cdot V}{U+V} \tag{9}$$

4. OPTIMAL PARAMETER SELECTION FOR MR-SkSP-3 PLAN.

For an effectively designed sampling plan to get best outputs, it should simultaneously fulfil the interest of both customer and producer. The consumer wants to avoid the acceptance of lots with bad quality, while the producer wants to minimise the rejection of lots with acceptable quality. The both can be done by minimising the type-1 and type-2 errors, also known as, producer's risk (α) and consumer's risk (β). In order to achieve this, the parameters are selected while the OC curve pass through the points, $(p_1, 1-\alpha)$ & (p_2, β). Here the level p_1 is the AQL associated with the producer's risk and p_2 is the LQL associated with the consumer's risk. In an OC curve the point $(p_1, 1-\alpha)$ will safeguard the interests of the producer and point (p_2, β) ensures the customer's interest. Hence the optimal parameters for the sampling plan can be determined when the OC curves pass through these points, so that the following inequalities are satisfied for the specified strength.

$$P_a(p_1) \geq 1 - \alpha \tag{10}$$

$$P_a(p_2) \leq \beta \tag{11}$$

Under the Poisson probability model for the expected defective per lot, the parameters can be obtained using the unity value approach. The np_1 & np_2 values which will satisfy the equations (10) and (11) are known as the unity values. The unity values are computed for different combinations of the parameters f, i, c_1 & c_2 , and is tabulated in Table 1 along with their probability values. It also contains the operating ratio, $(R = np_2/np_1)$, for the values ($\alpha = 0.05$ & $\beta = 0.10$). Using the operating ratio, we can differentiate the sampling plans. The selection of optimal parameters is presented detailed with a numerical illustration in next section.

Table 1: *Unity values & operating ratio for the MR-SkSP-3.*

f	i	k	c_1	c_2	P_a							$R = n_{p2}/n_{p1}$ (α=0.05, β=0.10)
					0.99	0.95	0.75	0.50	0.25	0.10	0.05	
0.25					1.3197	1.5264	1.8387	2.1246	2.7460	3.8805	4.7251	2.5423
0.33					1.2823	1.4877	1.7955	2.0837	2.7338	3.8806	4.7251	2.6085
0.50	5	2	1	5	1.2398	1.4353	1.7362	2.0300	2.7204	3.8796	4.7250	2.7029
0.67					1.2033	1.3988	1.6954	1.9929	2.7131	3.8790	4.7250	2.7732
0.75					1.1910	1.3842	1.6790	1.9781	2.7106	3.8787	4.7249	2.8021
	4				1.3824	1.6163	1.9761	2.2886	2.8457	3.8875	4.7259	2.4053
	6				1.2668	1.4537	1.7331	2.0065	2.7079	3.8784	4.7249	2.6680
0.25	8	2	1	5	1.1866	1.3398	1.5777	1.8477	2.6935	3.8772	4.7248	2.8938
	10				1.1096	1.2563	1.4660	1.7545	2.6924	3.8893	4.7261	3.0958
	12				1.0598	1.1884	1.3812	1.7069	2.6923	3.8893	4.7261	3.2726
		1			1.3733	1.6060	1.9143	2.1861	2.7604	3.8802	4.7250	2.4161
0.25	5	3	1	5	1.2758	1.4841	1.8006	2.0962	2.7413	3.8807	4.7251	2.6149
		5			1.2336	1.4362	1.7600	2.0706	2.7382	3.8808	4.7251	2.7021
			0		1.1354	1.2561	1.4179	1.5376	1.7204	2.3081	2.9943	1.8375
			1		1.5169	1.7244	2.0101	2.2566	2.7765	3.8797	4.7250	2.2499
0.25	5	2	2	6	1.8373	2.1653	2.6306	3.0727	3.9578	5.3155	6.2826	2.4549
			3		2.2293	2.6616	3.3637	4.0130	5.1439	6.6755	7.7447	2.5081
			4		2.6585	3.2981	4.2236	5.0235	6.3120	7.9894	9.1479	2.4224
				1	0.2652	0.3958	0.6210	0.8689	1.4076	2.3009	2.9942	5.8131
				2	0.4277	0.5603	0.7560	0.9554	1.4191	2.3011	2.9943	4.1071
0.25	5	2	0	3	0.6103	0.7295	0.9110	1.0754	1.4461	2.3016	2.9943	3.1552
				4	0.7858	0.9034	1.0757	1.2188	1.5034	2.3029	2.9943	2.5490
				5	0.9485	1.0794	1.2456	1.3748	1.5967	2.3041	2.9943	2.1346

5. NUMERICAL ILLUSTRATION

Consider the implementation of MR-SkSP-3 in an inspection process associated with producer's risk (α) at 0.05 and consumer's risk (β) at 0.10. The selection of optimal parameters for the inspection procedure for specified sets of strengths say p_1 = 0.005 & p_2 = 0.02, can be done using the following steps.

1. The given thresholds set for the inspection are p_1 = 0.005 & p_2 = 0.02. From this, the operating ratio, R, is found as,

$$R = \frac{p_2}{p_1} = \frac{0.02}{0.005} = 4 \tag{12}$$

2. The unity values and corresponding operating ratios for the plan are given in Table 1. From this, the R-value closest to that of calculated from *(12)* and is found as R = 4.1071.

3. The optimal parameter values for the inspection plan are selected from the table corresponding to this R- value. It is found as; $f = 0.25$, $i = 5$, $c_1 = 0$ & $c_2 = 2$.

4. From the table, the unity values for the specified strength of (α = 0.05, β = 0.10), and corresponding to the obtained R-value is found out as np_1 = 0.5603 and np_2 = 2.3011.

5. From the unity values, the sample size for the inspection is calculated as largest of np_1/p_1 or np_2/p_2. Thus,

$$n = \frac{np_1}{p_1} \text{ or } \frac{np_2}{p_2} = \frac{0.5603}{0.005} \text{ or } \frac{2.3011}{0.02} = 112.06 \text{ or } 115.055 \tag{13}$$

From these values, the largest is chosen, thus the required sample size for the inspection is found out as 115 products. For the MR-SkSP-3 plan, both SSP and DSP is done using same sample size and it is assumed that, for DSP, $n_1 = n_2$. Accordingly, the optimal parameters for the MR-SkSP-3 plan with the given specifications are;

$$f = 0.25,\ i = 5,\ c_1 = 0,\ c_2 = 2\ \&\ n_1 = n_2 = 115.$$

6. OC CURVE ANALYSIS OF THE MR-SKSP-3

The OC function, which is one of the important performance measures of a sampling plan, is a function of the defective proportion, p and other parameters of the plan like c_1, c_2, n, f, i & k. The acceptance probability, P_a of a sampling plan can be found from equation (8), for each value of p. In general, the OC function is considered as a function of proportion defective. The plot of these P_a values along with their p values is the OC curve of the sampling plan. These curves evaluate the efficiency of the sampling plan on how well it will distinguish between acceptable and rejectable lots, reflecting it's discriminating power. Thus, it is important to study the influence of each parameter on the OC curves. Figures (2) to (7) plots several sets of OC curves of the MR-SkSP-3 plan for varying values of c_1, c_2, n, f, i & k.

Figure 2 plots the OC curves for the MR-SkSP-3 plan with fixed c_2, n, f, i & k values and varying values of acceptance number, c_1.

It can be seen that, when the value of c_1 is at minimum, the producer faces difficulty, as the probability for accepting the lots at lower p values are low. But, as the c_1 increases the producer protection improves, due higher acceptance for the high p values. Thus, at low c_1 values, the consumer protection is safe guarded, as the lot with low p values will also get rejected. Figure 3 shows the set of OC curves for the proposed plan by keeping the c_1, n, f, i & k and changing the value of c_2. While increasing the c_2 values, a slight increase in the probability of acceptance is observed only in the low proportion defective case. Beyond this low p levels, the OC curves remain unchanged and overlaps in most cases for all values of c_2. Therefore, changing the values of c_2 has only a minimal impact on the OC curve.

Figure 4 plots the OC curves of varying value for sample size, n and all other parameters kept constant. It can be seen that as n increases, the curves shift to the origin, indicating a lower acceptance probability. As the sample size is increasing, the producer is troubled with the risk of applying 100% inspection more often, leading to higher costs and longer inspection times. The consumer is protected with high values of n, by reducing the probability of accepting defective lots and the producer is safeguarded with smaller values of n for inspection, increasing acceptance probability and reducing inspection effort. Figure 5 shows the OC curves of the plan with varying values of clearance number, i. As it can be seen, when the value of i increases, the probability of acceptance decreases. This indicates that, the consumer is more safeguarded from the higher i values, and producer is protected from low values of i by increasing acceptance rates.

Figure 6 and 7 presents the OC curves by varying values of k and f, respectively, while keeping other parameters constant. A slight increase is observed in the acceptance probability as the values of the parameters k & f are increased. However, the curves of these plots remain nearly identical and overlapping each other, indicating that these parameters have a negligible effect on the acceptance probability. This implies that, adjusting the values of k & f does not significantly affect the overall performance of the OC function of the sampling plan.

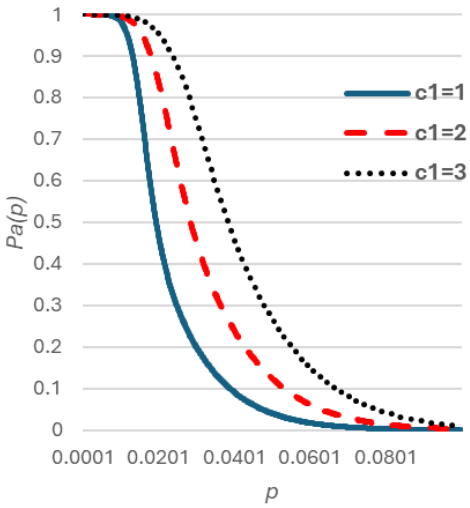


Figure 2: *OC curve with varying* c_1

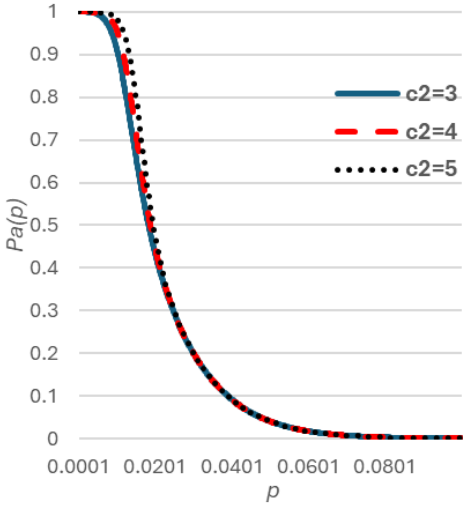


Figure 3: *OC curve with varying* c_2

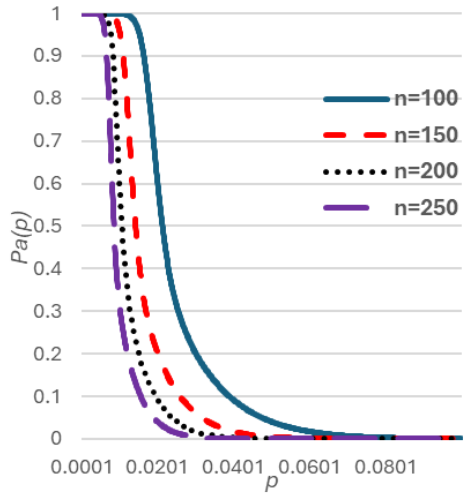


Figure 4: *OC curve with varying n*

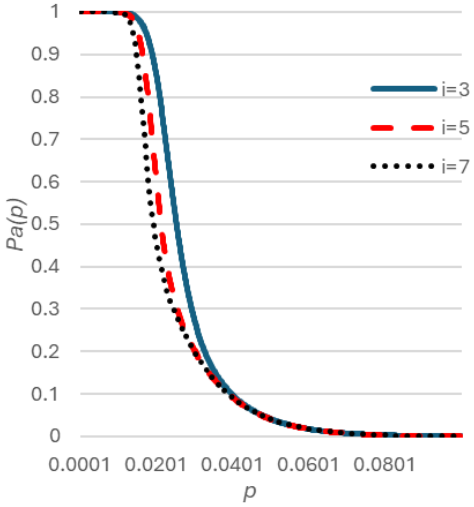


Figure 5: *OC curve with varying i*

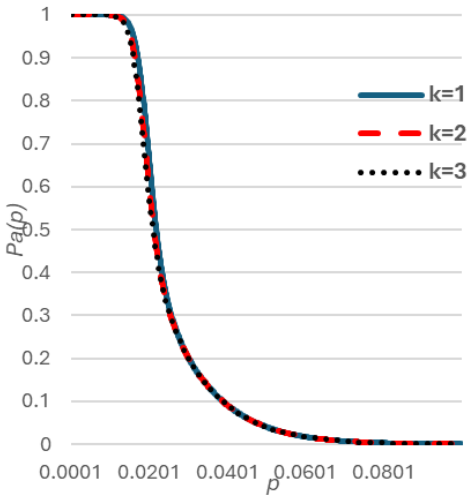


Figure 6: *OC curve with varying k*

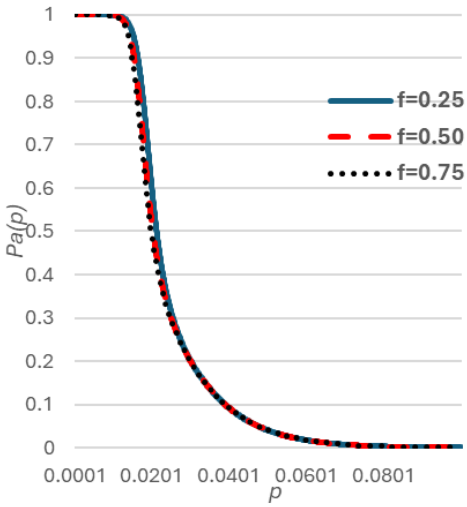


Figure 7: *OC curve with varying f*

7. COMPARATIVE ANALYSIS OF MR-SKSP-3 WITH CONVENTIONAL SKSP-3 PLANS

The comparative analysis of the MR-SkSP-3 plan is done with that of the conventional skip-lot sampling plans of type 3, which use the same reference plan in both normal and skipping phases. This analysis portrays the advantages of the proposed plan of having multiple reference plans in different phases, over the conventional plans. The MR-SkSP-3 plan of $(n = 100, c_1 = 2, c_2 = 5, i = 5, f = 0.25, k = 2)$ is compared with the SkSP-3 plan with SSP as the reference plan (SkSP-SSP) of parameters $(n = 100, c_1 = 1, i = 5, f = 0.25, k = 2)$ and with the SkSP-3 plan with DSP as the reference plan (SkSP-DSP) of parameters $(n_1 = n_2 = 100, c_1 = 2, c_2 = 5, i = 5, f = 0.25, k = 2)$. The analysis is done by comparing the performance measures like OC, ASN, and ATI. Figures (8) and (9) plot the OC curves and ASN curves of the aforementioned plans, respectively. From figure 8, it is observed that the OC curve of the proposed MR-SkSP-3 plan lies in between that of the conventional plans. From this, it is clear that the proposed plan exhibits a combined behavior of the conventional plans. When the proportion defective is low, i.e., when the sampled lots have very few defectives, the MR-SkSP-3 plan behaves like SkSP-DSP. Thus, it has a high acceptance rate for the lots because the plan allows lenient inspection and decreased sampling frequency. Similarly, when the proportion defective is higher, i.e., when the sampled lots have a greater number of defectives, the proposed plan mirrors the behavior of SkSP-SSP. This results in stricter inspection strategies, thus leading to a lower acceptance rate for the lots. Hence, using the proposed MR-SkSP-3 plan provides greater flexibility and adaptivity than the conventional plans in managing inspection effectiveness and strictness.

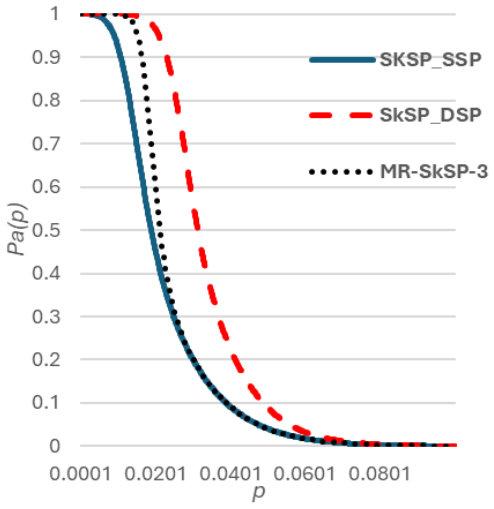


Figure 8: *Comparison of OC curves*

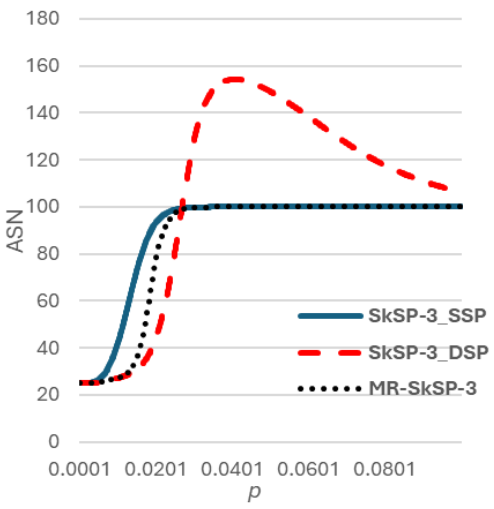


Figure 9: *Comparison of ASN curves*

The Figure 9 depicts the ASN curves of the plans mentioned above. Here also, it is seen that, the proposed MR-SkSP-3 plan is having a combined behaviour of both the conventional plans. When the proportion defective is low, the plan only needs fewer samples to inspect, just like the SkSP-DSP. This helps to reduce the inspection cost and resources during the inspection when the proportion defective is low. In the same situation, the SkSP-SSP is having a higher number of ASN compared to the others. But, when the proportion defective is more, the proposed plan is behaving similar to the SkSP-SSP. This shows that when there are more defectives in the sampled lots, the proposed plan will undergo stringent analysis which require large sample for inspection to control the high defective rate efficiently.

The tabulated values of the measures *OC, ASN, & ATI* for the aforementioned plans are given in tables 2 and 3. From table 2, it can be observed that the same pattern of combined behaviour among the plans, which was also seen in the graphs, is present here. Consider the case where

the proportion defective is low, say $p = 0.01$. Under the conditions of SkSP-SSP ($P_a = 0.9251$), the producer's risk (α) for rejecting a good lot is 7.49%. For the same proportion defective, the plans SkSP-DSP ($P_a = 0.9999$) and MR-SkSP-3 ($P_a = 0.9995$) have reduced the producer's risk to 0.01% and 0.05% respectively. When the fraction defective is low, the proposed plan aligns with that of SkSP-DSP. Now, consider the case where the proportion defective is high, say $p = 0.05$. Under the conditions of SkSP-DSP ($P_a = 0.0886$), the consumer's risk (β) for accepting a lot with high defective rate is 8.86%. For the same defective proportion case, the plans SkSP-SSP ($P_a = 0.0404$) and MR-SkSP-3 ($P_a = 0.0404$) show a lower consumer's risk of 4.04% for both. Here, when the fraction defective is high, proposed MR-SkSP-3 plan aligns with that of SkSP-SSP. From this it is clear that when the proportion defective is low, the MR-SkSP-3 plan keeps the producer's risk minimal, avoiding the rejection of acceptable lots, similar to SkSP-DSP. Conversely, when the proportion defective is high, the MR-SkSP-3 plan minimizes the consumer's risk by avoiding the acceptance of rejectable lots, similar to SkSP-SSP. This illustration shows that, while the conventional plans safeguard either the producer or the consumer, the proposed plan protects both parties simultaneously by integrating the properties of the two different reference plans used in normal and skipping inspections. A similar pattern of behaviour is observed in both ASN and ATI.

Table 2: *Measures tabulated against p for SkSP-SSP, SkSP-DSP, MR-SkSP-3*

p	P_a			ASN			ATI		
	SkSP-SSP	SkSP-DSP	MR-SkSP-3	SkSP-SSP	SkSP-DSP	MR-SkSP-3	SkSP-SSP	SkSP-DSP	MR-SkSP-3
0.01	0.9251	0.9999	0.9995	41.6785	27.038	27.1015	0.0093	0.0100	0.0100
0.012	0.8529	0.9994	0.9962	53.5150	28.200	28.6769	0.0102	0.0120	0.0120
0.014	0.7548	0.9979	0.9798	66.7783	29.882	32.3325	0.0106	0.0140	0.0137
0.016	0.6454	0.9939	0.9210	78.7536	32.536	41.3978	0.0103	0.0159	0.0147
0.018	0.5416	0.9846	0.7846	87.6428	36.932	58.3723	0.0097	0.0177	0.0141
0.02	0.4530	0.9652	0.6016	93.3030	44.176	77.3348	0.0091	0.0193	0.0120
0.025	0.2974	0.8267	0.3148	98.7902	81.087	97.3861	0.0074	0.0207	0.0079
0.03	0.2009	0.5656	0.2024	99.8086	128.087	99.7249	0.0060	0.0170	0.0061
0.035	0.1362	0.3542	0.1363	99.9719	149.725	99.9685	0.0048	0.0124	0.0048
0.04	0.0916	0.2254	0.0916	99.9961	154.187	99.9962	0.0037	0.0090	0.0037
0.045	0.0611	0.1427	0.0611	99.9995	152.881	99.9995	0.0027	0.0064	0.0027
0.05	0.0404	0.0886	0.0404	99.9999	149.126	99.9999	0.0020	0.0044	0.0020
0.06	0.0174	0.0323	0.0174	100.0000	138.371	100.0000	0.0010	0.0019	0.0010
0.08	0.0030	0.0041	0.0030	100.0000	117.748	100.0000	0.0002	0.0003	0.0002
0.10	0.0005	0.0006	0.0005	100.0000	106.431	100.0000	0.0000	0.0001	0.0000

Table 3 shows us the performance measure values for the proposed plan along with that of conventional plans, with varying parameter values of the plan. It is seen that, when the values of parameters f, k & i are increasing, the OC and ATI measures are decreasing accordingly. While the ASN measure is increasing in the same instance. This shows that, while increasing the parameter values, the sampling plan is getting more lenient in inspection. Also, the SkSP-SSP is undergoing noticeable change while changing the parameters, while the MR-SkPS-3 plan and SkSP-DSP are only having a slight change in their values. This shows the compatibility of the proposed plan under different conditions.

8. CONCLUSION

The paper presents a multi-reference skip lot sampling plan of type-3, MR-SkSP-3, with the provision of having SSP as the reference plan in normal inspection and DSP as the reference plan in skipping inspection. Further, the inspection procedure of the proposed plan, analysis of plan using power measures and comparison of the plan with other conventional plans are also discussed in the paper. Tables are provided for determination of optimal parameters of plan, and these parameters are derived using the unity value approach. Instructive numerical illustration is also provided for the determination of optimal parameters for MR-SkSP-3. It has been shown that

Table 3: *Measures tabulated against parameter values for SkSP-SSP, SkSP-DSP, MR-SkSP-3*

f	k	i	P_a			ASN			ATI		
			SkSP-SSP	SkSP-DSP	MR-SkSP-3	SkSP-SSP	SkSP-DSP	MR-SkSP-3	SkSP-SSP	SkSP-DSP	MR-SkSP-3
		2	0.964025	0.999888	0.999800	29.683313	27.010637	27.018049	0.009640	0.009999	0.009998
0.25	2	5	0.925085	0.999883	0.999498	41.678496	27.038594	27.101481	0.009251	0.009999	0.009995
		7	0.888416	0.999880	0.999074	52.974359	27.057938	27.218641	0.008884	0.009999	0.009991
0.25			0.925085	0.999883	0.999498	41.678496	27.038594	27.101481	0.009251	0.009999	0.009995
0.33	2	5	0.907007	0.999844	0.999331	51.736290	36.044646	36.117367	0.009070	0.009998	0.009993
0.50			0.877428	0.999766	0.998997	68.192375	54.046544	54.122306	0.008774	0.009998	0.009990
0.67			0.854248	0.999689	0.998665	81.088545	72.034846	72.091557	0.008542	0.009997	0.009987
	1		0.946191	0.999940	0.999743	36.979633	27.016154	27.048330	0.009462	0.009999	0.009997
0.25	2	5	0.925085	0.999883	0.999498	41.678496	27.038594	27.101481	0.009251	0.009999	0.009995
	2		0.914213	0.999829	0.999264	44.099047	27.060065	27.152293	0.009142	0.009998	0.009993

the proposed plan effectively optimizes the balance for the producer and consumer preferences, outperforming conventional plans. While the traditional SkSP-SSP safeguards consumer when the proportion defective is high, it ignored the producer when the proportion defective is less. Also, the traditional SkSP-DSP safeguards the producer when the defective rate is low, but it bypassed the consumer during the high proportion defective cases. The proposed plan was able to overcome this issue by demonstrating exceptional adaptability and efficiency across different proportion levels and safeguards the producer and consumer simultaneously. Skip-lot sampling plan got widely accepted over the time because of its low inspection cost and time while keeping the inspection quality on top. Thus, the proposed study has a significant role by offering a suitable adaption for the situations where the traditional SkSPs fall back. The approach of implementing multiple reference plan allows the optimization of the conventional plans, this can be extended to the other skip-lot plans also.

References

[1] Muhammad Aslam, Saminathan Balamurali, Chi-Hyuck Jun, and Munir Ahmad. Optimal designing of a skip lot sampling plan by two point method. *Pakistan Journal of Statistics*, 26(4), 2010.

[2] S Azarudheen and K Pradeepaveerakumari. Determination of skip lot sampling plan with single sampling plan as reference plan under the conditions of intervened poisson distribution. *Journal of Statistics and Management Systems*, 19(6):771–780, 2016.

[3] S Azarudheen and K Pradeepa Veerakumari. Designing of skip lot sampling plan (sksp–3) with single sampling plan as reference plan under the conditions of intervened poisson distribution. *Asia Mathematika*, 1(1):23–29, 2017.

[4] S Balamurali and J Subramani. Economic design of sksp-3 skip-lot sampling plans. *International Journal of Mathematics and Statistics*, 6(10):23–39, 2010.

[5] S Balamurali and J Subramani. Optimal designing of skip-lot sampling plan of type sksp-2 with double sampling plan as the reference plan. *Journal of Statistical Theory and Practice*, 6:354–362, 2012.

[6] Harold F Dodge. Skip-lot sampling plan. *Journal of Quality Technology*, 9(3):143–145, 1977.

[7] N Murugeswari, P Jeyadurga, and S Balamurali. Evaluation and optimal designing of a two-level skip-lot sampling plan for resubmitted lots. *Communications in Statistics-Theory and Methods*, 53(6):2043–2066, 2022.

[8] N Murugeswari, P Jeyadurga, S Sridevi, and S Balamurali. Evaluation and optimal designing of a new system of skip-lot reinspection schemes. *Journal of Statistical Computation and Simulation*, 93(9):1420–1440, 2023.

[9] Paul Peach and SB Littauer. A note on sampling inspection. *The Annals of Mathematical Statistics*, 17(1):81–84, 1946.

[10] Robert L Perry. Skip-lot sampling plans. *Journal of Quality Technology*, 5(3):123–130, 1973.

[11] Edward G Schilling and Lucille I Johnson. Tables for the construction of matched single, double, and multiple sampling plans with application to mil-std-105d. *Journal of Quality Technology*, 12(4):220–229, 1980.

[12] Edward G Schilling and Dean V Neubauer. *Acceptance sampling in quality control*. Chapman and Hall/CRC, 2009.

[13] V Soundararajan and R Vijayaraghavan. A new system of skip-lot inspection plans of type sksp-3. *Quality for Process and Development*, 1989.

[14] S Sridevi and S Balamurali. Evaluation and design of a new system of tightened single-level skip-lot sampling plan. *Communications in Statistics-Simulation and Computation*, 54(2):449–466, 2025.

[15] R Vijayaraghavan. Construction and selection of skip-lot sampling inspection plans of type sksp-2 indexed by indifference quality level and maximum allowable per cent defective. *Journal of Applied Statistics*, 21(5):417–423, 1994.

[16] R Vijayaraghavan. Design and evaluation of skip-lot sampling plans of type sksp-3. *Journal of Applied Statistics*, 27(7):901–908, 2000.

[17] R Vijayaraghavan and V Soundararajan. Design and evaluation of skip-lot sampling inspection plans with double-sampling plan as the reference plan. *Journal of Applied Statistics*, 25(3):341–348, 1998.

ENHANCING ACCURACY IN ESTIMATING POPULATION MEAN THROUGH MODIFIED RATIO ESTIMATORS IN RANKED SET SAMPLING

S. A. Sabo[a], A. A. Osi[*,a], I. Z. Musa[a], H. U. Abubakar[a], A. Muhammad[a], U. Abubakar[b]

•

[a]Department of Statistics, Aliko Dangote University of Science and Technology, Wudil, Nigeria.
[b]Department of Statistics, Jigawa State Polytechnic Dutse, Nigeria.
Email: abuammarosi@gmail.com, aaosi@kust.edu.ng, usmanabubakar@jigpoly.edu.ng

Abstract

This study aimed to improve the ratio estimation under rank set sampling by proposing some new modified estimators using auxiliary information on the size of the sample. The expressions for the bias and mean squared error of the proposed modified estimators are derived up to the first order of approximation using Tailor series expansion. A theoretical efficiency comparison between the proposed and competing estimators was done and the conditions upon which the proposed estimators expect to outperform the competing estimators were stated. Results from the numerical work indicate that the new proposed improved estimators are better than the already existing ones, showing a lower mean square error, coefficient of variation, and a considerable gain in efficiency. The new proposed estimators emerge as the optimal choice, outperforming the competing ones, and should therefore be used in applications.

Keywords: Ranked set sampling, MSE, Sample size, Auxiliary variable, Ratio estimator

1. Introduction

Estimation of population parameters, particularly mean, is paramount and has received significant attention from researchers in the field of sampling theory over the past few decades [1]. Survey sampling studies often include additional auxiliary variables that, when correlated with the primary variable of interest, improve the efficiency of statistical inference by creating more effective designs and estimators [2]. Improved designs and efficient estimators are being developed to improve the precision of estimates. Techniques such as the ratio by [3], product by [4], and regression by [5] are widely used in the literature on sampling theory. The ratio method is recommended for positive correlations between the study and auxiliary variables. The random sample sampling according to [6] is a cost-effective method to classify experimental units, particularly in environmental monitoring and assessment. It uses a cheaply measurable covariate to rank units, resulting in a more representative sample of observations. This method offers greater confidence for a fixed number of observations or requires a smaller number for the desired confidence levels. This study proposes a ratio estimator for the population mean, using information on the sample size of the auxiliary variable through the ranked set under a simple random sampling scheme. In Simple Random Sampling, ratio estimators are widely used when the variable of interest is linearly related to an auxiliary variable. The classical ratio estimator of [3] is expressed as:

$$\overline{y}_R = \overline{y}\left[\frac{\overline{X}}{\overline{x}}\right] \tag{1}$$

Where $\overline{y}$ and $\overline{x}$ are the sample means of the study and the auxiliary variables, respectively, and the population mean of the auxiliary variable.

The mean squared error of (1) to the first degree of approximation is given as;

$$MSE(\overline{y_R}) = \theta\overline{Y}^2\left[C_y^2 + C_x^2 - 2\rho C_x C_y\right] \tag{2}$$

Where $\theta = \frac{1-f}{n}$, $f = \frac{n}{N}$, $C_y = \frac{S_y}{\overline{Y}}$, $C_x = \frac{S_x}{\overline{Y}}$, $\rho = \frac{S_{xy}}{S_x S_y}$, $S_y^2 = \frac{\sum_{i=1}^{N}(y_i-\overline{Y})^2}{N-1}$, $S_x^2 = \frac{\sum_{i=1}^{N}(x_i-\overline{X})^2}{N-1}$.

[7] highlighted that ratio estimators become highly efficient when there is a strong positive correlation between and variables. Modified ratio estimator for is given by [8] as;

$$\overline{y}_{SD} = \overline{y}\left[\frac{\overline{X} + C_x}{\overline{x} + C_x}\right] \tag{3}$$

Where is the coefficient of variation. The MSE of (3) can be expressed as;

$$MSE(\overline{y}_{SD}) = \theta\overline{Y}^2\left[C_y^2 + \psi_l C_x^2 - 2\psi_l\rho C_x C_y\right] \tag{4}$$

where $\psi_1 = \frac{\overline{X}}{\overline{X}+C_x}$

[9] proposed a modified ratio estimator for with known coefficient of kurtosis given by;

$$\overline{y}_{SK} = \overline{y}\left[\frac{\overline{X} + \beta_2(x)}{\overline{x} + \beta_2(x)}\right] \tag{5}$$

The mean squared error of (5) with first degree of approximation is given as;

$$MSE(\overline{y}_{SK}) = \theta\overline{Y}^2\left[C_y^2 + \psi_2 C_x^2 - 2\psi_2\rho C_x C_y\right] \tag{6}$$

Where $\psi_2 = \frac{\overline{X}}{\overline{X}+\beta_2(x)}$

Motivated by [7] and [8] a ratio estimator for suggested by [10] is expressed as;

$$\overline{y}_{UP} = \overline{y}\left[\frac{C_x\overline{X} + \beta_2(x)}{\overline{x}C_x + \beta_2(x)}\right] \tag{7}$$

The MSE of (7) to the first order of approximation can be expressed as;

$$MSE(\overline{y}_{UP}) = \theta\overline{Y}^2\left[C_y^2 + \psi_3 C_x^2 - 2\psi_3\rho C_x C_y\right] \tag{8}$$

Where, $\psi_3 = \frac{\overline{X}C_x}{\overline{X}C_x+\beta_2(x)}$

[11] utilized the information on the sample size of the auxiliary variable to improve the ratio estimation. The proposed estimator is given by;

$$\overline{y}_{JK} = \overline{y}\left[\frac{\overline{X} + n}{\overline{x} + n}\right] \tag{9}$$

To the first order of approximation, the MSE of (9) can be expressed as;

$$MSE(\overline{y}_{JK}) = \theta\overline{Y}^2\left[C_y^2 + \psi_4 C_x^2 - 2\psi_4\rho C_x C_y\right] \tag{10}$$

Where $\psi_4 = \frac{\overline{X}}{\overline{X}+n}$

The integration of ratio estimators with RSS has led to several theoretical advancements and efficiency improvements. Under RSS, ratio estimators can take advantage of both ranking information and the auxiliary variable, leading to more precise estimates. The classical ratio estimator under RSS suggested by [12] can be written as:

$$\overline{y}_{RSS} = \frac{\overline{y}_{[n]}}{\overline{x}_{[n]}} \tag{11}$$

Where $\overline{y}_{[n]} = \frac{1}{n}\sum_{i=1}^{n} y_{[i]} \cdot \overline{x}_{[n]} = \frac{1}{n}\sum_{i=1}^{n} x_{[i]}$ are the ranked set sample means for variables and respectively. The estimator in (11) is unbiased and its variance is given by;

$$V\left(\overline{y}_{RSS}\right) = \frac{\sigma^2}{rm} - \frac{1}{rm^2}\sum_{i=1}^{n}\tau_{y(i)}^2 \tag{12}$$

Where $\tau_{y(i)} = \left(\mu_{y(i)} - \overline{Y}\right)$.

Assuming that the population mean of the auxiliary variable is known, [13] suggested a ratio estimator using ranked set sampling as;

$$\overline{y}_{R,RSS} = \overline{y}_{[n]}\left(\frac{\overline{X}}{x_{[n]}}\right) \tag{13}$$

The MSE of (13) to the first order of approximation can be expressed as;

$$MSE(\overline{y}_{R,RSS}) = \frac{1}{mr}\left(S_y^2 + R^2 S_x^2 - 2RS_{yx}\right) - \frac{1}{m^r}\left(\sum_{i=1}^{m}\tau_{y(i)}^2 + R^2\sum_{i=1}^{m}x_{(i)}^2 - 2R\sum_{i=1}^{m}\tau_{yx}\right) \tag{14}$$

where $\tau_{x(i)} = \mu_{x(i)} - \overline{X}, \quad \tau_{y(i)} = \mu_{y(i)} - \overline{Y}, \quad \tau_{yx(i)} = (\mu_{x(i)} - \overline{X})(\mu_{y(i)} - \overline{Y})$.

[?] proposed a ratio estimators based on linear combination of coefficient of skewness and quartile deviation by utilizing some known parameters of the concomitant variable given by;

$$\overline{y}_{JL,RSS} = \frac{\overline{y}_{[n]} + \beta_1\left(\mu_x - \overline{x}_{[n]}\right)}{QD\overline{x}_{[n]} + \beta_1}QD\mu_x + \beta_1 \tag{15}$$

The expression for mean squared error of (15) is given by;

$$MSE(\overline{y}_{JL,RSS}) = \overline{Y}^2\left[\theta\left(C_y^2 + \lambda_2^2 C_x^2 - 2\lambda_2\rho_{yx}C_xC_y\right) - \left(W_{y(i)} - \lambda_2 W_{x(i)}\right)^2\right] \tag{16}$$

where $\lambda_1 = \frac{\overline{Y}\beta_1}{\overline{X}\beta_1 + QD}$.

[15] suggests a modified ratio estimators of finite population mean utilizing information on coefficient of variation of an auxiliary variable in ranked set sampling given as;

$$\overline{y}_{ML,RSS} = \overline{y}_{[n]}\left[\frac{\overline{X} + C_x}{\overline{x}_{[n]} + C_x}\right] \tag{17}$$

$$\overline{y}_{M2,RSS} = \overline{y}_{[n]}\left[\frac{\overline{X}C_x + \beta_1(x)}{\overline{x}_{[n]}C_x + \beta_1(x)}\right] \tag{18}$$

Their mean squared error of (17) and (18) are given respectively as;

$$MSE(\overline{y}_{M1,RSS}) = \overline{Y}^2\left[\theta\left(C_y^2 + \lambda_1^2 C_x^2 - 2\lambda_1\rho_{yx}C_xC_y\right) - \left(W_{y(i)} - \lambda_1 W_{x(i)}\right)^2\right] \tag{19}$$

$$MSE(\overline{y}_{M2,RSS}) = \overline{Y}^2\left[\theta\left(C_y^2 + \lambda_2^2 C_x^2 - 2\lambda_2\rho_{yx}C_xC_y\right) - \left(W_{y(i)} - \lambda_2 W_{x(i)}\right)^2\right] \tag{20}$$

Where $\lambda_2 = \frac{\overline{X}}{\overline{X}+C_x}$ and $\lambda_3 = \frac{\overline{X}C_x}{\overline{X}C_x+\beta_2(x)}$.

Motivated by [14] and [8] a ratio estimator under ranked set sampling using information of population coefficient of variation and median of auxiliary was suggested by [16] which is expressed as;

$$\overline{y}_{RZ,RSS} = \overline{y}_{[n]} \left[\frac{\overline{X} + C_x M_d}{x_{[n]} + C_x M_d} \right] \tag{21}$$

The mean squared error of (21) can be expressed as;

$$MSE(\overline{y}_{RZ,RSS}) = \overline{Y}^2 \left[\theta \left(C_y^2 + \lambda_4^2 C_x^2 - 2\lambda_4 \rho_{yx} C_x C_y \right) - \left(W_{y_{(i)}} - \lambda_4 W_{x_{(i)}} \right)^2 \right] \tag{22}$$

where $\lambda_4 = \frac{\overline{X}}{\overline{X} + C_x M_d}$.

2. Methods

Motivated by [11], [16] and [17], after studying the works of [18], [19] and [20] we proposed some ratio estimators for population mean based on ranked set sampling and presented as;

$$t_{p1} = \overline{y}_{[n]} \left[\frac{\overline{X} + n}{\overline{x}_{[n]} + n} \right] \tag{23}$$

$$t_{p2} = \overline{y}_{[n]} \left[\alpha + (1 - \alpha) \left(\frac{\overline{X} + n}{\overline{x}_{[n]} + n} \right) \right] \tag{24}$$

Where is the scalar to be obtained such that, the mean squared error of the proposed estimator in (24) is minimum.

To study the large sample properties (Bias and Mean Squared Error) of the proposed modified ratio estimators, we have used the following approximations as:

$$\overline{y}_{[n]} = \overline{Y}(1 + e_0), \quad \overline{x}_{[n]} = \overline{X}(1 + e_1) \tag{25}$$

Such that; $E(e_0) = E(e_1) = 0$, $E(e_0^2) = \theta C_y^2 - W_{y_{(0)}}^2$, $E(e_1^2) = \theta C_x^2 - W_{x_{(0)}}^2$, $E(e_0 e_1) = \theta \rho C_x C_y - W_{y_{(0)}}$.

Where;

$$W_{yx(i)} = \frac{1}{m^2 r \overline{Y}\overline{X}} \sum \tau_{xy(i)}^2, \quad W_{x(i)}^2 = \frac{1}{m^2 r \overline{X}^2} \sum \tau_{x(i)}^2, \quad W_{y(i)}^2 = \frac{1}{m^2 r \overline{Y}^2} \sum \tau_{y(i)}^2$$

$$\tau_{x(i)} = \mu_{x(i)} - \overline{X}, \quad \tau_{y(i)} = \mu_{y(i)} - \overline{Y}, \quad \tau_{yx(i)} = \left(\mu_{y(i)} - \overline{Y} \right) \left(\mu_{x(i)} - \overline{X} \right)$$

Expressing t_{p1} in terms of the definition in 25 gives;

$$t_{p1} = \overline{Y}(1 + e_0) \left[\frac{\overline{X} + n}{\overline{X}(1 + e_1) + n} \right] \tag{26}$$

Simplifying 26 gives;

$$t_{p1} = \overline{Y}(1 + e_0)(1 + \gamma e_1)^{-1} \tag{27}$$

Where;

$$\gamma = \frac{\overline{X}}{\overline{X} + n}$$

Assume that $|e_1| < 1$ so that $(1 + \gamma_1 e_1)^{-1}$ may be expanded, retaining the terms with degree not more than two only gives;

$$t_{p1} = \overline{Y}(1 + e_0 - \gamma e_1 - \gamma e_0 e_1 + \gamma^2 e_1^2) \tag{28}$$

Subtracting $\overline{Y}$ both sides from equation 28 and taking expectations gives;

$$E\left(t_{p1} - \overline{Y} \right) = \overline{Y} E\left(e_0 - \gamma e_1 - \gamma e_0 e_1 + \gamma^2 e_1^2 \right) \tag{29}$$

Applying the definitions of the expectations above gives;

$$B\left(t_{p1}\right)=\overline{Y}\left[\theta\left(\gamma^{2}C_{x}^{2}-\gamma\rho C_{x}C_{y}\right)-\left(\gamma^{2}W_{x(i)}^{2}-\gamma W_{yx(i)}\right)\right] \tag{30}$$

Squaring both sides of 30, expanding its RHS, neglecting powers greater than 2 and applying the definition of the expectations, we obtain the mean squared error of t_{p1} as;

$$MSE\left(t_{p1}-\overline{Y}\right)^{2}=\overline{Y}^{2}\left[\theta\left(C_{y}^{2}+\gamma^{2}C_{x}^{2}-2\gamma\rho C_{x}C_{y}\right)-\left(W_{y(i)}-\gamma W_{x(i)}\right)^{2}\right] \tag{31}$$

Similarly, the biased and mean square error of the second proposed estimator t_{p2} can be respectively expressed as;

$$B\left(t_{p2}\right)=\overline{Y}\left[\theta\left(\gamma^{2}C_{x}^{2}-\gamma\rho C_{x}C_{y}-\alpha\gamma^{2}\rho C_{x}C_{y}\right)-\left(\gamma^{2}W_{x(i)}^{2}+\gamma W_{yx(i)}-\alpha\gamma^{2}W_{yx(i)}\right)\right] \tag{32}$$

$$MSE\left(t_{p2}\right)=\overline{Y}^{2}\left[\begin{array}{l}\theta\left(C_{y}^{2}-\gamma^{2}C_{x}^{2}-2\gamma\rho C_{x}C_{y}-\alpha\gamma\rho C_{x}C_{y}-\alpha^{2}\gamma^{2}C_{x}^{2}\right)\\-W_{y(i)}^{2}+2\gamma W_{yx(i)}+\alpha\gamma W_{yx}+\alpha^{2}\gamma^{2}W_{x(i)}^{2}\end{array}\right] \tag{33}$$

The optimum value of α that minimizes the MSE of the second proposed estimator (t_{p2}) can easily be obtained by partially differentiating equation 33 with respect α and equating the result to zero. Thus;

$$\frac{\partial MSE\left(t_{p2}\right)}{\partial\alpha}=0$$

Simplifying further gives;

$$\alpha_{opt}=\frac{\theta\gamma\rho C_{x}C_{y}-\gamma W_{y(x)}}{2\left(\gamma^{2}W_{x(i)}-\theta\gamma^{2}C_{x}^{2}\right)} \tag{34}$$

The minimum mean squared error of the proposed estimator t_{p2} can be obtained by substituting α_{opt} in equation 33 as follows;

$$MSE\left(t_{p2}\right)=\overline{Y}^{2}\left[\begin{array}{l}\theta\left(C_{y}^{2}-\gamma^{2}C_{x}^{2}-2\gamma\rho C_{x}C_{y}-\alpha_{opt}\gamma\rho C_{x}C_{y}-\alpha_{opt}^{2}\gamma^{2}C_{x}^{2}\right)\\-W_{y(i)}^{2}+2\gamma W_{yx(i)}+\alpha_{opt}\gamma W_{yx}+\alpha_{opt}^{2}\gamma^{2}W_{x(i)}^{2}\end{array}\right] \tag{35}$$

3. Results

3.1. Theoretical Efficiency Comparison

The efficiency of our proposed estimators was compared with that of other existing ratio estimators in the literature theoretically. The conditions to check the performance of the proposed estimators over the other competing estimators were strictly stated here.

The proposed estimator is more efficient than the usual sample mean if;

$$MSE\left(t_{pr2}\right)-V\left(y_{RSS}\right)<0 \tag{36}$$

So that;

$$\overline{Y}^{2}\left[\begin{array}{l}\theta\left(C_{y}^{2}-\gamma^{2}C_{x}^{2}-2\gamma\rho C_{x}C_{y}-\alpha_{opt}\gamma\rho C_{x}C_{y}-\alpha_{opt}^{2}\gamma^{2}C_{x}^{2}\right)\\-W_{y(i)}^{2}+2\gamma W_{yx(i)}+\alpha_{opt}\gamma W_{yx}+\alpha_{opt}^{2}\gamma^{2}W_{x(i)}^{2}\end{array}\right]-\left(\frac{\sigma^{2}}{rm}-\frac{1}{rm^{2}}\sum_{i=1}^{n}\tau_{y(i)}^{2}\right)<0 \tag{37}$$

The proposed estimator is more efficient than the [**?**] ratio estimator if;

$$MSE\left(t_{pr2}\right)-MSE\left(\overline{y}_{RSS}\right)<0 \tag{38}$$

so that;

$$\overline{Y}^2 \left[\begin{array}{l} \theta \left(C_y^2 - \gamma^2 C_x^2 - 2\gamma\rho C_x C_y - \alpha_{opt}\gamma\rho C_x C_y - \alpha_{opt}^2\gamma^2 C_x^2 \right) \\ -W_{y(i)}^2 + 2\gamma W_{yx(i)} + \alpha_{opt}\gamma W_{yx} + \alpha_{opt}^2\gamma^2 W_{x(i)}^2 \end{array} \right] - \theta\overline{Y}^2 \left[C_y^2 + C_x^2 - 2\rho C_x C_y \right] < 0 \tag{39}$$

The proposed estimator is more efficient than the [8] ratio estimator if;

$$MSE\left(t_{pr2}\right) - MSE\left(\overline{y}_{SD}\right) < 0 \tag{40}$$

So that;

$$\overline{Y}^2 \left[\begin{array}{l} \theta \left(C_y^2 - \gamma^2 C_x^2 - 2\gamma\rho C_x C_y - \alpha_{opt}\gamma\rho C_x C_y - \alpha_{opt}^2\gamma^2 C_x^2 \right) \\ -W_{y(i)}^2 + 2\gamma W_{yx(i)} + \alpha_{opt}\gamma W_{yx} + \alpha_{opt}^2\gamma^2 W_{x(i)}^2 \end{array} \right] - \theta\overline{Y}^2 \left[C_y^2 + \psi_1 C_x^2 - 2\psi_1\rho C_x C_y \right] < 0 \tag{41}$$

The proposed estimator is more efficient than the [9] ratio estimator if;

$$MSE\left(t_{pr2}\right) - MSE\left(\overline{y}_{SK}\right) < 0 \tag{42}$$

So that;

$$\overline{Y}^2 \left[\begin{array}{l} \theta \left(C_y^2 - \gamma^2 C_x^2 - 2\gamma\rho C_x C_y - \alpha_{opt}\gamma\rho C_x C_y - \alpha_{opt}^2\gamma^2 C_x^2 \right) \\ -W_{y(i)}^2 + 2\gamma W_{yx(i)} + \alpha_{opt}\gamma W_{yx} + \alpha_{opt}^2\gamma^2 W_{x(i)}^2 \end{array} \right] - \theta\overline{Y}^2 \left[C_y^2 + \psi_2 C_x^2 - 2\psi_2\rho C_x C_y \right] < 0 \tag{43}$$

The proposed estimator is more efficient than the [10] ratio estimator if;

$$MSE\left(t_{pr2}\right) - MSE\left(\overline{y}_{UP}\right) < 0 \tag{44}$$

So that;

$$\overline{Y}^2 \left[\begin{array}{l} \theta \left(C_y^2 - \gamma^2 C_x^2 - 2\gamma\rho C_x C_y - \alpha_{opt}\gamma\rho C_x C_y - \alpha_{opt}^2\gamma^2 C_x^2 \right) \\ -W_{y(i)}^2 + 2\gamma W_{yx(i)} + \alpha_{opt}\gamma W_{yx} + \alpha_{opt}^2\gamma^2 W_{x(i)}^2 \end{array} \right] - \theta\overline{Y}^2 \left[C_y^2 + \psi_3 C_x^2 - 2\psi_3\rho C_x C_y \right] < 0 \tag{45}$$

The proposed estimator is more efficient than the [11] estimator if;

$$MSE\left(t_{pr2}\right) - MSE\left(\overline{y}_{JK}\right) < 0 \tag{46}$$

So that;

$$\overline{Y}^2 \left[\begin{array}{l} \theta \left(C_y^2 - \gamma^2 C_x^2 - 2\gamma\rho C_x C_y - \alpha_{opt}\gamma\rho C_x C_y - \alpha_{opt}^2\gamma^2 C_x^2 \right) \\ -W_{y(i)}^2 + 2\gamma W_{yx(i)} + \alpha_{opt}\gamma W_{yx} + \alpha_{opt}^2\gamma^2 W_{x(i)}^2 \end{array} \right] - \theta\overline{Y}^2 \left[C_y^2 + \psi_4 C_x^2 - 2\psi_4\rho C_x C_y \right] < 0 \tag{47}$$

The proposed estimator is more efficient than the [12] ratio estimator if;

$$MSE\left(t_{pr2}\right) - MSE\left(\overline{y}_{R,RSS}\right) < 0 \tag{48}$$

So that;

$$\begin{array}{l} \overline{Y}^2 \left[\begin{array}{l} \theta \left(C_y^2 - \gamma^2 C_x^2 - 2\gamma\rho C_x C_y - \alpha_{opt}\gamma\rho C_x C_y - \alpha_{opt}^2\gamma^2 C_x^2 \right) \\ -W_{y(i)}^2 + 2\gamma W_{yx(i)} + \alpha_{opt}\gamma W_{yx} + \alpha_{opt}^2\gamma^2 W_{x(i)}^2 \end{array} \right] - \frac{1}{mr} \left(S_y^2 + R^2 S_x^2 - 2RS_{yx} \right) \\ -\frac{1}{m^2 r} \left(\sum_{i=1}^{m} \tau_{y(i)}^2 + R^2 \sum_{i=1}^{m} \tau_{x(i)}^2 - 2R \sum_{i=1}^{m} \tau_{yx} \right) \qquad < 0 \end{array} \tag{49}$$

The proposed estimator is more efficient than the [**?**] ratio estimator if;

$$MSE\left(t_{pr2}\right) - MSE\left(\overline{y}_{R,RSS}\right) < 0 \tag{50}$$

So that;

$$\begin{array}{l} \overline{Y}^2\left[\begin{array}{l} \theta\left(C_y^2 - \gamma^2 C_x^2 - 2\gamma\rho C_x C_y - \alpha_{opt}\gamma\rho C_x C_y - \alpha_{opt}^2\gamma^2 C_x^2\right) \\ -W_{y(i)}^2 + 2\gamma W_{yx(i)} + \alpha_{opt}\gamma W_{yx} + \alpha_{opt}^2\gamma^2 W_{x(i)}^2 \end{array}\right] - \frac{1}{mr}\left(S_y^2 + R^2 S_x^2 - 2RS_{yx}\right) \\ -\frac{1}{m^2 r}\left(\sum_{i=1}^{m}\tau_{y(i)}^2 + R^2\sum_{i=1}^{m}\tau_{x(i)}^2 - 2R\sum_{i=1}^{m}\tau_{yx}\right) \qquad < 0 \end{array} \tag{51}$$

The proposed estimator is more efficient than the [**?**] ratio estimator if;

$$MSE\left(t_{pr2}\right) - MSE\left(\overline{y}_{R,RSS}\right) < 0 \tag{52}$$

So that;

$$\begin{array}{l} \overline{Y}^2\left[\begin{array}{l} \theta\left(C_y^2 - \gamma^2 C_x^2 - 2\gamma\rho C_x C_y - \alpha_{opt}\gamma\rho C_x C_y - \alpha_{opt}^2\gamma^2 C_x^2\right) \\ -W_{y(i)}^2 + 2\gamma W_{yx(i)} + \alpha_{opt}\gamma W_{yx} + \alpha_{opt}^2\gamma^2 W_{x(i)}^2 \end{array}\right] - \frac{1}{mr}\left(S_y^2 + R^2 S_x^2 - 2RS_{yx}\right) \\ -\frac{1}{m^2 r}\left(\sum_{i=1}^{m}\tau_{y(i)}^2 + R^2\sum_{i=1}^{m}\tau_{x(i)}^2 - 2R\sum_{i=1}^{m}\tau_{yx}\right) \qquad < 0 \end{array} \tag{53}$$

The proposed estimator is more efficient than the [14] ratio estimator if;

$$MSE\left(t_{pr2}\right) - MSE\left(\overline{y}_{JL,RSS}\right) < 0 \tag{54}$$

So that;

$$\overline{Y}^2\left[\begin{array}{l} \theta\left(C_y^2 - \gamma^2 C_x^2 - 2\gamma\rho C_x C_y - \alpha_{opt}\gamma\rho C_x C_y - \alpha_{opt}^2\gamma^2 C_x^2\right) \\ -W_{y(i)}^2 + 2\gamma W_{yx(i)} + \alpha_{opt}\gamma W_{yx} + \alpha_{opt}^2\gamma^2 W_{x(i)}^2 \end{array}\right] - \overline{Y}^2\left[\begin{array}{l} \theta\left(C_y^2 + \lambda_1^2 C_x^2 - 2\lambda_1\rho_{yx}C_x C_y\right) \\ -\left(W_{y(i)} - \lambda_1 W_{x(i)}\right)^2 \end{array}\right] < 0 \tag{55}$$

The proposed estimator is more efficient than the [15] ratio estimator if;

$$MSE\left(t_{pr2}\right) - MSE\left(\overline{y}_{M1,RSS}\right) < 0 \tag{56}$$

So that;

$$\overline{Y}^2\left[\begin{array}{l} \theta\left(C_y^2 - \gamma^2 C_x^2 - 2\gamma\rho C_x C_y - \alpha_{opt}\gamma\rho C_x C_y - \alpha_{opt}^2\gamma^2 C_x^2\right) \\ -W_{y(i)}^2 + 2\gamma W_{yx(i)} + \alpha_{opt}\gamma W_{yx} + \alpha_{opt}^2\gamma^2 W_{x(i)}^2 \end{array}\right] - \overline{Y}^2\left[\begin{array}{l} \theta\left(C_y^2 + \lambda_2^2 C_x^2 - 2\lambda_2\rho_{yx}C_x C_y\right) \\ -\left(W_{y(i)} - \lambda_2 W_{x(i)}\right)^2 \end{array}\right] < 0 \tag{57}$$

The proposed estimator is more efficient than the [15] ratio estimator if;

$$MSE\left(t_{pr2}\right) - MSE\left(\overline{y}_{M2,RSS}\right) < 0 \tag{58}$$

So that;

$$\overline{Y}^2\left[\begin{array}{l} \theta\left(C_y^2 - \gamma^2 C_x^2 - 2\gamma\rho C_x C_y - \alpha_{opt}\gamma\rho C_x C_y - \alpha_{opt}^2\gamma^2 C_x^2\right) \\ -W_{y(i)}^2 + 2\gamma W_{yx(i)} + \alpha_{opt}\gamma W_{yx} + \alpha_{opt}^2\gamma^2 W_{x(i)}^2 \end{array}\right] - \overline{Y}^2\left[\begin{array}{l} \theta\left(C_y^2 + \lambda_3^2 C_x^2 - 2\lambda_3\rho_{yx}C_x C_y\right) \\ -\left(W_{y(i)} - \lambda_3 W_{x(i)}\right)^2 \end{array}\right] < 0 \tag{59}$$

The proposed estimator is more efficient than the [16] ratio estimator if;

$$MSE\left(t_{pr2}\right) - MSE\left(\overline{y}_{RZ,RSS}\right) < 0 \tag{60}$$

So that;

$$\overline{Y}^2\left[\begin{array}{l}\theta\left(C_y^2-\gamma^2C_x^2-2\gamma\rho C_xC_y-\alpha_{opt}\gamma\rho C_xC_y-\alpha_{opt}^2\gamma^2C_x^2\right)\\-W_{y(i)}^2+2\gamma W_{yx(i)}+\alpha_{opt}\gamma W_{yx}+\alpha_{opt}^2\gamma^2W_{x(i)}^2\end{array}\right]-\overline{Y}^2\left[\begin{array}{l}\theta\left(C_y^2+\lambda_4^2C_x^2-2\lambda_4\rho_{yx}C_xC_y\right)\\-\left(W_{y(i)}-\lambda_4W_{x(i)}\right)^2\end{array}\right]<0 \tag{61}$$

3.2. Numerical Example

To further investigate the efficiency (performance) of the suggested estimators over other existing estimators, an empirical study was conducted to support the theoretical comparison. In the empirical study, numerical values were used in the comparison. Hypothetical data from natural populations were employed for the comparison. Here, we present a summary of the descriptive statistics and the constant parameters for the population data used in the empirical study. The data from [7] between 1920 and 1930, consisting of information on the population size (measured in 1000s) of 49 cities was utilize by [16] and the summary statistics is presented in table 1.

Table 1: *Data Statistics used in the numerical example*

$N=4$	$\overline{X}=103.14$	$\mu_3(x)=76$	$\beta_1(x)=2.20\$$
$n=8$	$\overline{Y}=127.8$	$\mu_4(x)=144$	$\beta_2(x)=7.22$
$m=4$	$S_y=32.8720$	$\mu_1(y)=70$	$C_y=12.95$
$R=2$	$S_x=56.2342$	$\mu_2(y)=87$	$C_x=16.05$
$\rho=0.18$	$\mu_1(x)=70$	$\mu_3(y)=93.5$	$QD=37.68$
$Md=130.77$	$\mu_2(x)=42$	$\mu_4(y)=103.5$	$\alpha_{opt}=-0.871$

Table 2 presents the summary result of the calculated Mean squared error (MSE), Percent relative efficiency (PRE) and Coefficient of variation (C.V) of both the proposed and competing estimators. The PRE and C.V can be calculated respectively as;

$$PRE\left(t_{j,}\overline{y}_{srs}\right)=\frac{V\left(\overline{y}_{srs}\right)}{MSE\left(t_j\right)}\times100 \tag{62}$$

$$C.V=\frac{\sqrt{MSE(t_j)}}{\overline{X}}\times100 \tag{63}$$

Table 2: *Numerical Comparison of the Proposed and Competing Estimators*

Estimators	MSE	PRE	CV
$\overline{y}$	638.900	100.000	24.507
$\overline{y}_{SD}$	838.138	76.228	28.069
$\overline{y}_{SK}$	761.490	83.901	26.755
$\overline{y}_{R}$	703.065	90.874	25.708
$\overline{y}_{R,RSS}$	622.145	102.693	24.183
$\overline{y}_{M1,RSS}$	617.114	103.530	24.086
$\overline{y}_{M2,RSS}$	516.486	123.701	22.034
$\overline{y}_{RZ,RSS}$	273.867	233.289	16.045
$\overline{y}_{JL,RSS}$	356.987	178.970	18.319
$\overline{y}_{JK}$	367.567	173.819	18.588
t_{p1}	250.567	254.982	15.347
t_{p2}	249.775	255.790	15.323

Results from table 2 reveals the performance of the proposed estimators compared to the existing ones. The MSEs and CVs of the proposed estimators are smaller than those of competing estimators. Additionally, the PREs of the proposed estimators are higher than those of competing estimators indicating a gain in efficiencies.

4. Conclusion

In this paper, we use the sample size information of the auxiliary variable to propose a modified ratio estimator under ranked set sampling. The statistical properties of the proposed estimators were derived and compared both theoretically and numerically with some existing estimators. The results presented in Tables 2 confirm the superior performance of the proposed estimators. The significantly lower mean squared errors (MSEs) and coefficients of variation (CVs) demonstrate their robustness and precision compared to competing estimators. Additionally, the higher percent relative efficiencies (PREs) of the proposed estimators outperform their enhanced accuracy and reliability. These findings highlight the practical utility and statistical soundness of the modified estimators for real-world applications, particularly when parameter information is available. Overall, the proposed estimators emerge as the optimal choice, outperforming alternatives both theoretically and numerically; as such, they should therefore be used in applications.

References

[1] Liu, Q., Wang, Z., He, X., & Zhou, D. (2014). A survey of event-based strategies on control and estimation. *Systems Science & Control Engineering* 2(1): 90-97.
[2] Fermanagh, D., & Rao, C. R. (2009). Sample surveys: design, methods and applications. *Elsevier*,
[3] Cochran, W.G (1940). The estimation of the yields of the cereal experiments by sampling for the ratio of grain to total produce. *The Journal of Agricultural science*, 30(2): 262-275
[4] Murthy, M.N. (1964). Product method of estimation. *Sakhya: The Indian journal of Statistics, series A*, 69-74.
[5] Singh, R., Mangat, N.S. (1996). Regression Method of Estimation. In: Elements of Survey Sampling. *Kluwer Texts in the Mathematical Sciences*, vol 15. Springer, Dordrecht, 1996.
[6] McIntyre, G.A. (1952). A method of unbiased selective sampling using ranked sets. *Australian Journal of Agric. Res.*, 3: 385-390.
[7] Cochran, W.G.(1997). *Sampling techniques* 3rd edition. Wiley Eastern, New Delhi.
[8] Sisodia, B.V.S and Dwivedi, V.K. (1981). A modified ratio estimator using coefficient of variation of auxiliary variable. *Journal-Indian Society of Agricultural Statistics*, 33: 13-18.
[9] Singh, H P., R. Tailor and M. S. Kakran (2004). An improved estimator of population mean using power transformation. *Journal of the Indian society of Agricultural statistics*, 58(2), 223-230.
[10] Upadhyaya, L.N., Singh, H.P. (1999). Use of transformed auxiliary variable in estimating the finite population mean. *Biometry Journal*, 41: 627-636.
[11] Jerajuddin, M., & Kishun, J. (2016). Modified ratio estimators for population mean using size of the sample, selected from population. *International Journal of Scientific Research in Science, Engineering and Technology*, 2(2), 10-16.
[12] Samawi, H.M and Muttlak, H.A (1996). Estimation of ration using ranked set sampling. *Biometrical journal* 38(6):753-764.
[13] Kadilar, C., Unyazici, Y. and Cingi, H. (2009). Ratio estimator for the population mean using ranked set sampling. *Statistical papers*, 50(20): 301-309.
[14] Jeelani, M. I., Bouza, C. N., & Sharma, M. (2017). Modified ratio estimator under rank set sampling. *Investigacin Operacional*, 38(1), 103-107.
[15] Mehta, N. and Mandowara, V, L. (2012). A better estimator of population mean with power transformation best on ranked set sampling. *Sampling method and estimation*, 13(3):551-558.
[16] Riyaz, S., Rather, K.U., Maqbool, S., & Jan, T.R. (2024). Ratio estimator of population mean using a linear combination under ranked set sampling. *RT&A*, 2(73): 479-485.

[17] Sabo, S. A., Musa, I. Z., & Kibiya, Y. I. (2020). Developed ratio estimator for estimating population mean from a finite population using sample size and correlation. *Int. J. Res. Appl. Sci. Eng. Tech*, 8(6): 904-911.

[18] Kumari, A., Singh, R. & Smarandache, F. (2024). New Modification of ranked set sampling for estimating population mean: Neutrosophic median ranked set sampling with an application to demographic data. *Int J Comput Intell Syst*, 17(210): 1-15.

[19] Rehman, S. A., Al-Essa, L. A., Shabbir, J., & Khan, Z. (2024). On the efficiency of paired ranked set sampling for estimating the population mean in the presence of non-response. *Scientific Reports*, 14(1), 25334.

[20] Shahzad, N., & Tshung, F. C. C. (2023). Estimating Population Mean Using Ratio Estimator for Mean is Less Than Variance in Simple Random Sampling. *Russian Law Journal*, 11(3), 2049-2061

SURVEY ON NON-MARKOVIAN QUEUE WITH PHASE SERVICE USING SUPPLEMENTARY VARIABLE TECHNIQUE

Binay Kumar[1], Sudeep Singh Sanga[2], Aditya Kumar[1]

•

[1] Patna University, India.
[2] SV National Institute of Technology, Surat, India.
bkmathasr@gmail.com, ssanga@amhd.svnit.in, ak606295@gmail.com

Abstract

In the present article, we provide a comprehensive overview and literature review on performance modeling of queueing systems with phase service, utilizing the supplementary variable technique. We discuss the scenarios that necessitate phase service and explain how the supplementary variable technique is applied to analyze non-Markovian models. Additionally, we offer a summary of the fundamental concepts and existing literature on queueing systems with phase service. Our review covers research conducted over the past decade (2014-2024) on queues featuring phase service, including aspects such as bulk arrival, service interruptions, and discouragement. The review systematically explores models incorporating bulk arrivals, service interruptions, customer discouragement, and other complex operational features. By consolidating recent advancements and identifying common modeling approaches, this work aims to provide valuable insights for researchers and practitioners engaged in the analysis and design of advanced queueing systems.

Keywords: bulk arrival, phase service, supplementary variable, non-Markovian.

I. Introduction

In the queueing theory literature, extensive research has been conducted on models in which both interarrival and service times follow the exponential distribution. These models are commonly referred to as Markovian queueing systems, as they can be effectively analyzed using the Markov property, which simplifies the modeling process due to its memoryless nature. However, in many real-world situations, the assumption of exponential interarrival or service times (or both) may not hold. For instance, service times in manufacturing systems, healthcare facilities, or computer networks often follow general probability distributions. Queueing systems in which the interarrival time, service time, or both deviate from the exponential form are referred to as non-Markovian queueing models. Due to their increased complexity and the absence of the memoryless property, these models cannot be solved directly using conventional Markovian techniques. To analyze such systems, a common approach is to transform them into Markovian models by introducing additional state variables through the supplementary variable technique. This technique involves augmenting the state space typically by including variables like the elapsed or remaining service time—thereby enabling the use of Markovian methods to study the system's behavior.

In real-life scenarios, we often encounter situations where customers have preferences for multiple types of services from a single service provider. This is particularly evident on various online platforms that offer a wide range of services under one roof. For instance, platforms like Amazon and Flipkart provide an extensive array of products and services, allowing customers to choose from diverse categories such as electronics, clothing, and household goods all in one place. Similarly, travel and booking apps like Make My Trip provide a variety of services, such as flight bookings, hotel reservations, and car rentals, all conveniently available on a single platform to meet diverse customer needs. Phase queueing models adeptly handle such complexity by managing different service stages and preferences, thus providing a robust framework for optimizing service delivery and efficiency in these multifaceted environments.

The exponential and Poisson distributions are widely utilized in real-time queue models due to their broad applicability. The exponential distribution, in particular, is widely preferred due to its practical applicability and the ease of analyzing queueing models based on it. To handle complex scenarios, mixtures of exponential distributions are often employed. The most common among these are those which help model services provided in multiple phases with varying levels of complexity.

Erlangian Distribution: The Erlangian distribution is an effective model for handling phase-type service processes. In this distribution, the service process is divided into several sequential phases, each following an i.i.d. exponential distribution. This structure ensures that the overall service time is the sum of multiple exponential phases, resulting in an Erlangian distribution. The design of the Erlangian distribution is inherently sequential, meaning that service must progress through each phase in a fixed order before completion. This makes it particularly useful for modeling structured service processes in queueing systems, telecommunications, and reliability analysis.

Hyper exponential distribution: The hyper exponential distribution models service times with high variability by employing a parallel arrangement of multiple exponential distributions. Unlike the Erlangian distribution, where service phases occur sequentially, the hyper exponential distribution allows each arriving customer to be randomly assigned to one of several exponential phases, each with a distinct mean service rate and a predefined selection probability.

A more generalized approach to phase-type service models considers cases where service times follow a general distribution rather than strictly exponential phases. These models incorporate a mixture of different service distributions to provide a more flexible and realistic representation of service processes. The selection of specific distributions may be either mandatory or optional, depending on the system's design. Some commonly used phase-type queueing models are:

(i). **Single-Phase Multiple options:** In this system, service consists of a single stage, after which the unit exits. This single-phase service can be either single or multi-optional. If the service is single optional, the arriving unit has no choice and must undergo that service. However, if the service is multi-optional, the unit can choose one service from the available options before exiting the system. For example, at a billing counter, a customer is allowed to pay the bill either in cash or online.

(ii). **Multi-phase queueing models:** In such a type of system, there is a single server that provides services in more than one phase. The multi-phase may be further classified into the following subcategories:

a) **Two-phase multi-optional service:** In such a system, an arriving customer, after availing essential service, chooses only one optional service among the available optional services. After availing of that optional service unit exits from the system.

b) **Multi-optional phase service:** In such a system of systems, sequences of optional services are provided one after the other as per the demand of the unit after completion of the initial essential service.

c) **Multi-essential Phase Queueing Models:** In such a type of system, a service is provided in a sequence of essential services, one after the other. The service will not be complete until all the phases are completed.

In real-world queueing systems, various factors such as balking, server breakdowns, delayed repairs, vacations, and retrials significantly impact service efficiency and system performance. These complexities, often occurring alongside phase-type service, introduce challenges in queueing analysis, requiring advanced modeling techniques for accurate representation. For instance, customers may opt not to join a queue due to excessive wait times (balking), while system disruptions such as server failures or temporary unavailability (vacations) create additional unpredictability. Addressing these dynamics is crucial for optimizing service operations across various industries, including manufacturing, healthcare, telecommunications, and computer networks.

The scope of this study includes:

- Analyzing queueing models with phase-type service, where service is completed in multiple stages rather than a single step. These models more accurately capture real-world processes such as multi-stage production lines, sequential healthcare procedures, and layered data processing in communication networks.
- Investigating non-Markovian queueing systems, where service time distributions are more general and require advanced analytical methods like supplementary variable technique.
- Reviewing key literature from 2014 to 2024, focusing on advancements in queueing models that incorporate bulk arrivals, customer discouragement, service interruptions, and other complex features.

The layout of the remaining portion of the present study is organized as follows: Section II introduces the supplementary variable technique (SVT) and its application in general service queueing models, particularly those with batch arrivals. Section III applies SVT to specific queueing models featuring different types of phase-type service. Section IV provides an in-depth review of literature on single-server queueing models with phase-type service, covering extensions like unreliable servers, server vacations, retrial queues, balking, and Bernoulli feedback. Section V presents the main conclusions and discusses possible directions for future research.

II. Supplementary Variable Technique (SVT)

When inter-arrival and service times are exponentially distributed, the system is classified as a Markovian system. These systems can be modeled using the memoryless property of exponential distributions, which simplifies the analysis and allows for the use of Markov processes to describe the system's behavior.

However, when the service time or inter-arrival time follows a more general, non-exponential distribution, the system is referred to as non-Markovian. Analyzing non-Markovian systems is more complex because the future state of the system depends not only on the current state but also on the history of past events. To address this complexity, the SVT is employed. This method introduces an additional variable, known as the supplementary variable, which accounts for the elapsed service time or the remaining time of the non-exponentially distributed random variable. By doing so, the non-Markovian system can be transformed into a Markovian system, making it easier to analyze. This technique was pioneered by Cox [1], specifically to study the M/G/1 queue, where "M" stands for Markovian (exponential inter-arrival times), "G" denotes a general distribution for service times, and "1" represents a single server in the system. Cox's method provides a powerful tool for analyzing and understanding a broader range of queueing systems that do not conform to the simple exponential assumptions of Markovian models.

I. SVT for Single Arrival Queueing model

It is helpful to outline the procedure for studying the distribution of queue size in the M/G/1 queue using SVT (Cox [1]). Consider an M/G/1 model where units arrive in Poisson fashion with rate λ. The service times are governed by a general distribution described by the function $B(x)$, its Laplace transform $B^*(s)$, and its first moment $E(B)$. Let $N(t)$ represent the total number of units in the system at time t, and $B^0(t)$ be the variable added that corresponds to the elapsed service time. Let us define a random variable as follows

$$\xi(t) = \begin{cases} 0 & : \text{if the server is idle} \\ 1 & : \text{if the server is busy} \end{cases}$$

The bivariate random variable $\{N(t), \sigma(t)\}$ forms a Markov process, where $\sigma(t) = 0 \; if \; \xi(t) = 0$ and $\sigma(t) = B^0(t)$. To study the system's dynamics, the governing equations for the present model can be formulated based on probabilistic principles (Cox [1]). We introduce the following definitions:

$$P_0(t) = Prob.\{N(t) = 0, \sigma(t) = 0\} \quad (1)$$

$$P_n(t,x) = Prob.\{N(t) = n, \sigma(t) = B^0(t), x < B^0(t) \le x + dx\} \;\; ; x > 0 \quad (2)$$

And the steady state probability is given by

$$P_0 = \lim_{t\to\infty} P_0(t) \quad and \;\; P_n(x) = \lim_{t\to\infty} P_n(t,x) \quad (3)$$

The hazard function for a state in which the server is actively serving is given by

$$\mu(x)dx = \frac{dB(x)}{1-B(x)} \quad (4)$$

The governing equation for the transient process can be derived by examining the transitions occurring over a time interval Δt (Chaudhry and Templeton [2]).

$$P_0(t+\Delta t) = P_0(t)(1-\lambda\Delta t) + (1-\lambda\Delta t)\int_0^\infty \mu(x)P_1(x,t)dx + o(\Delta t)$$

which will give

$$\frac{dP_0(t)}{dt} = -\lambda P_0(t) + \int_0^\infty \mu(x)P_1(x,t)dx \quad (5)$$

$$P_n(x+\Delta t, t+\Delta t) = P_n(x,t)(1-\lambda\Delta t)(1-\mu(x)\Delta t) + \lambda\Delta t P_n(x,t)(1-\mu(x)\Delta t) + o(\Delta t), \quad \text{for } n \ge 1$$

which gives

$$\frac{\partial P_n(x,t)}{\partial t} + \frac{\partial P_n(x,t)}{\partial x} = -\big(\lambda + \mu(x)\big)P_n(x,t) + \lambda P_{n-1}(x,t) \quad \text{for n} \ge 1, \text{x} > 0. \quad (6)$$

The steady state equation of (5) and (6) is given by taking $\to \infty$, we have

$$\lambda P_0 = \int_0^\infty \mu(x)P_1(x)dx \quad (7)$$

$$\frac{dP_n(x)}{dx} = -\big(\lambda + \mu(x)\big)P_n(x) + \lambda P_{n-1}(x) \quad \text{for n} \ge 1, \text{x} > 0. \quad (8)$$

The equations (7) and (8) are solved by using the boundary conditions

$$P_n(0) = \lambda\delta_{n,1}P_0 + \int_0^\infty \mu(x)P_{n+1}(x)dx \quad (9)$$

These equations are to be solved subject to the normalization condition

$$P_0 + \sum_{n=1}^\infty \int_0^\infty P_n(x)dx = 1 \quad (10)$$

Additionally, we introduce the following probability-generating functions.

$$P(x,z) = \sum_{n=1}^\infty P_n(x)z^n \quad \text{and} \quad P(0,z) = \sum_{n=1}^\infty P_n(0)\, z^n \quad (11)$$

Solving equations (7)-(9) and using (10) and (11), we get the PGF of the queue size distribution

$$\varphi(z) = (1-\lambda E(B))(z-1)B^*(\lambda(1-z))/[z - B^*\big(\lambda(1-z)\big)] \quad (12)$$

Using equation (12), we can find the system performance indices, such as average queue length and mean waiting time.

II. SVT for Bulk Queueing Model

In some queueing systems, units arrive in groups of random size. For a detailed study on batch arrival, we refer to the work done by Chaudhury and Templeton [2], Bhorthakur and Medhi [3]. Let X be the random variable representing the batch size, with $c_k = P(X = k)$ and an expected batch size of E(X). Then, the governing equation discussed earlier is modified accordingly.

$$\lambda P_0 = \int_0^\infty \mu(x) P_1(x) dx \tag{13}$$

$$\frac{dP_n(x)}{dx} = -\big(\lambda + \mu(x)\big)P_n(x) + \lambda\big(1 - \delta_{n,1}\big)\sum_{j=1}^{n} c_j P_{n-j}(x) \ , \mathrm{n} > 0, \mathrm{x} > 0 \tag{14}$$

To solve equations (13) and (14), we will use the boundary condition

$$P_n(0) = \lambda c_n P_0 + \int_0^\infty \mu(x) P_{n+1}(x) dx \tag{15}$$

The probability distribution for the queue size is given by

$$\varphi(z) = (1 - \lambda E(X)(E(B))(z-1)B^*(\lambda(1 - X(z)))/[z - B^*(\lambda(1 - X(z)))] \tag{16}$$

III. Different Phase type models using SVT

I. Two phase service

This section presents a concise approach to analyzing a single-arrival queueing system with two service phases. The first phase is compulsory for all customers, whereas the second phase is optional. Customers can opt for the additional service phase based on their specific needs.

Consider a queueing situation in which units join the system in Poisson fashion with arrival rate λ, and service is provided in two phases. Let both phases' service follow general distribution with distribution functions respectively $B_1(x), B_2(x)$, with Laplace transforms $B_1^*(s), B_2^*(s)$, and first moments $E(B_1), E(B_2)$. Let $N(t)$ denote the number of units in the system at time t, and $B^1(t)$, $B^2(t)$ be supplementary variables that denote the elapsed service time for the first phase and second phase, respectively. Let us define the system state equations as follows

$$\xi(t) = \begin{cases} 0 & : \textit{if the server is idle} \\ 1 & : \textit{if the server is busy in the first phase of service} \\ 2 & : \textit{if the server is busy in the second phase of service} \end{cases}$$

The bivariate random variable $\{N(t), \sigma(t)\}$ form a Markov process, where $\sigma(t) = 0, if\ \xi(t) = 0, \sigma(t) = B^1(t)\ if\ \xi(t) = 1, v(t) = B^2(t)\ if\ \xi(t) = 2$. To study the system's dynamics, the governing equations for the queueing model with two-phase service can be formulated based on probabilistic principles (Cox [1]).

We define

$$P_0(t) = Prob.\{N(t) = 0, \sigma(t) = 0\} \tag{17}$$

$$P_n^{(1)}(x,t) = Prob.\{N(t) = n, \sigma(t) = B^0(t), x < B^1(t) \le x + dx\} \text{ for } x > 0 \tag{18}$$

$$P_n^{(2)}(t,x) = Prob.\{N(t) = n, \sigma(t) = B^0(t), x < B^2(t) \le x + dx\} \text{ for } x > 0 \tag{19}$$

And the steady state probability is given by

$$P_0 = \lim_{t\to\infty} P_0(t) \text{ and } P_n^{(j)}(x) = \lim_{t\to\infty} P_n^{(j)}(t,x),\ j = 1,2. \tag{20}$$

The hazard rate functions for the state in which the server is busy are given by

$$\mu_1(x)dx = \frac{dB_1(x)}{1 - B_1(x)},\ \mu_2(x)dx = \frac{dB_2(x)}{1 - B_2(x)} \tag{21}$$

The equations that govern the system are given by

$$\lambda P_0 = \int_0^\infty \mu_2(x) P_1^{(2)}(x) dx + (1-p)\int_0^\infty \mu_1(x) P_1^{(1)}(x) dx \tag{22}$$

$$\frac{dP_n^{(1)}(x)}{dx} = -(\lambda + \mu_1(x))P_n^{(1)}(x) + \lambda P_{n-1}^{(1)}(x) \quad \text{for n} > 0, \text{x} > 0 \tag{23}$$

$$\frac{dP_n^{(2)}(x)}{dx} = -(\lambda + \mu_2(x))P_n^{(2)}(x) + \lambda P_{n-1}^{(2)}(x) \quad \text{for n} > 0, \text{x} > 0 \tag{24}$$

To solve equations (23) and (24), we use the following boundary condition

$$P_n^{(1)}(0) = \lambda \delta_{n,1} P_0 + q\int_0^\infty \mu_1(x) P_{n+1}^{(1)}(x) dx + \int_0^\infty \mu_2(x) P_{n+1}^{(2)}(x) dx\ , n > 0 \tag{25}$$

$$P_n^{(2)}(0) = p\int_0^\infty \mu_1(x) P_n^{(1)}(x) dx\ , n > 0 \tag{26}$$

Equation (22)-(26) are solved under the normalization condition

$$P_0 + \sum_{n=1}^{\infty}[P_n^{(1)}(x) + P_n^{(2)}(x)] = 1 \tag{27}$$

For simplification purposes, we define the following probability-generating functions.

$$P_1(x,z) = \sum_{n=1}^{\infty} P_n^{(1)}(x)\, z^n\ ;\ P_1(0,z) = \sum_{n=1}^{\infty} P_n^{(1)}(0)\, z^n$$

$$P_2(x,z) = \sum_{n=1}^{\infty} P_n^{(2)}(x)\, z^n\ ;\ P_2(0,z) = \sum_{n=1}^{\infty} P_n^{(2)}(0)\, z^n$$

Solving equations (22)-(24) and using equations (25), (26), and (27), we get the probability distribution function of the queue size distribution

$$\varphi(z) = \frac{(1-\rho)(z-1)[(q+B_2^*(a(z)))B_1^*(a(z))]}{[z-\{q+B_2^*(a(z)))B_1^*(a(z))\}]} \quad (28)$$

where $a(z) = \lambda(1-z)$ and $\rho = \lambda(\mathrm{E}(B_1) + \mathrm{p}\,\mathrm{E}(B_2))$

Using equation (28), we can evaluate the mean queue size and average waiting time.

II. Multi-optional phase service

In this section, we outline a brief procedure for analyzing a single-arrival queueing system having multiple optional service phases. We assume that the first phase of service is mandatory for all customers, while the subsequent phases are optional. Customers have the flexibility to choose additional service phases based on their individual requirements.

Consider a single-arrival queueing system where units arrive according to a Poisson process with an arrival rate λ. The service process follows a general distribution and is structured into m phases. The initial phase of service is mandatory for all arriving units, while the remaining stages are optional and provided based on demand. After completing the first mandatory service, a unit may request the second service with probability p_1 or exit from the system with probability $q_1 = 1 - p_1$. If the unit opts for the second service, it may then request the third optional service with probability p_2 or leave with probability $q_2 = 1 - p_2$. This pattern continues, where after completing the $(m-1)^{th}$ optional service, the unit may either request the m^{th} optional service with probability p_{m-1} or leave the system with probability $q_{m-1} = 1 - p_{m-1}$. Let the service times for all phases follow a general distribution, with the distribution function for the ith phase given by $B_i(x)$. The corresponding Laplace transform is denoted as $B_i^*(s)$, and the first moment is $E(B_i)$ for $i = 1,2,\dots,m$. Let $N(t)$ represent the unit count in the system at time t, and let $B^i(t)$ be a supplementary variable representing the elapsed service time for the i^{th} optional service phase, where optional phases for $i = 1,2,..,m$. Now, we define a random variable as follows:

$$\xi(t) = \begin{cases} 0 & : if\ the\ server\ is\ idle \\ 1 & : if\ the\ server\ is\ busy\ with\ service \\ 2 & : if\ the\ server\ is\ busy\ with\ second\ service \\ . & \\ . & \\ . & \\ m & : if\ the\ server\ is\ busy\ with\ mth\ service \end{cases}$$

The bivariate random variable $\{N(t), \sigma(t)\}$ form Markov process, where $\sigma(t) = 0, if\ \xi(t) = 0, \sigma(t) = B^i(t)\ if\ \xi(t) = i$, for $i = 1,2,\dots m$. The governing equations for the present case can be derived using probabilistic reasoning, as outlined by Cox [1}, as follows:

$$P_0(t) = Prob.\{N(t) = 0, \sigma(t) = 0\} \quad (29)$$

$$P_n^{(i)}(t,x) = Prob.\{N(t) = n, \sigma(t) = B^i(t), x < B^i(t) \le x + dx\} \quad \text{for } x > 0,\ i = 1,2,\dots,m \quad (30)$$

The hazard rate for essential and optional service rates are given by

$$\mu_i(x)dx = \frac{dB_i(x)}{1-B_i(x)}, \text{for } i = 1,2,\dots,m \quad (31)$$

The equations that govern the system are given by

$$\lambda P_0 = \int_0^\infty \mu_m(x) P_1^{(m)}(x)dx + \sum_{i=1}^{m-1} q_i \int_0^\infty \mu_i(x) P_1^{(i)}(x)dx \quad (32)$$

$$\frac{dP_n^{(i)}(x)}{dx} = -\left(\lambda + \mu_i(x)\right)P_n^{(i)}(x) + \lambda P_{n-1}^{(i)}(x) \quad \text{for n} \ge 1, \text{x} > 0, \text{i} = 1,2,\dots,\text{m} \quad (33)$$

The boundary conditions are given by

$$P_n^{(1)}(0) = \lambda\delta_{n,1}P_0 + \int_0^\infty \mu_m(x) P_{n+1}^{(m)}(x)dx + \sum_{i=1}^{m-1} q_i \int_0^\infty \mu_i(x) P_{n+1}^{(i)}(x)dx \quad (34)$$

$$P_n^{(i)}(0) = p_{i-1} \int_0^\infty \mu_{i-1}(x) P_n^{(i-1)}(x)dx \quad (35)$$

The normalization condition for the present model is given by

$$P_0 + \sum_{i=1}^{m}\sum_{n=1}^{\infty}\int_0^{\infty} P_n^{(i)}(x)\,dx = 1 \tag{36}$$

The probability generating functions used for the present system are given by

$$P_i(x,z) = \sum_{n=1}^{\infty} P_n^{(i)}(x)\,z^n \quad \text{and} \quad P_i(0,z) = \sum_{n=1}^{\infty} P_n^{(i)}(0)\,z^n \tag{37}$$

Multiply governing equation (23) by a proper power of z and using (35), we have

$$P_i(x,z) = P_i(0,z)\exp\{-a(z)x\}\,[1-B_i(x)],\ \ for\ i = 1,2,\dots,m \tag{38}$$

On boundary condition (34), apply the same treatment and using (32), we have

$$zP_1(0,z) = \lambda P_0 z(z-1) + \sum_{i=1}^{m} q_i P_i(0,z) B_i^*(0,z) \quad \text{with } q_m = 1 \tag{39}$$

$$P_i(0,z) = P_1(0,z)\prod_{j=1}^{i-1} p_j B_j^*\big(a(z)\big), \qquad i = 2,3,\dots,m \tag{40}$$

From (39) and (40), we have

$$P_1(0,z) = \frac{\lambda P_0 z(z-1)}{[z-\sum_{i=1}^{m} q_i\{\prod_{j=1}^{i-1} p_j B_j^*(a(z))\}B_i^*(a(z))]} \tag{41}$$

$$P_i(0,z) = \frac{\lambda P_0 z(z-1)\prod_{j=1}^{i-1} p_j B_j^*(a(z))}{[z-\sum_{i=1}^{m} q_i\{\prod_{j=1}^{i-1} p_j B_j^*(a(z))\}B_i^*(a(z))]}, \qquad i = 2,3,\dots,m \tag{42}$$

Integrating equations (38) with limit 0 to ∞ and using (41)-(42), we have

$$P_1(z) = \frac{P_0 z[1-B_1^*(a(z)]}{[\sum_{i=1}^{m} q_i\{\prod_{j=1}^{i-1} p_j B_j^*(a(z))\}B_i^*(a(z)\}-z]} \tag{43}$$

$$P_i(z) = \frac{P_0 z\prod_{j=1}^{i-1} p_j B_j^*(a(z))\}[1-B_i^*(a(z)]}{[\sum_{i=1}^{m} q_i\{\prod_{j=1}^{i-1} p_j B_j^*(a(z))\}B_i^*(a(z)\}-z]} \tag{44}$$

Taking limit $z \to 1$ in (41)-(44) and using equation (36), we have

$P_0 = 1-\rho$

where $\rho = \lambda[E(B_1) + p_1E(B_2) + p_1p_2E(B_3) + \cdots + p_1p_2\dots p_{m-1}E(B_m)]$

The PGF for the queue size distribution is given by

$$\varphi(z) = \frac{(1-\rho)[\sum_{i=1}^{m} q_i\{\prod_{j=1}^{i-1} p_j B_j^*(a(z))\}B_i^*(a(z)\}-z+z\sum_{i=1}^{m}\{\prod_{j=1}^{i-1} p_j B_j^*(a(z))\}(1-B_i^*(a(z))]}{[\sum_{i=1}^{m} q_i\{\prod_{j=1}^{i-1} p_j B_j^*(a(z))\}B_i^*(a(z)\}-z]} \tag{45}$$

III. Single phase multiple options

In this section, we present a procedure for analyzing a queueing system where units arrive following a Poisson process and receive service in a single phase with multiple options. Each unit selects one service from *m* available options and exits the system upon service completion.

Consider M/G/1 queueing model in which a unit joins the system at a Poisson arrival rate λ. Here, each arriving unit chooses the ith optional service with probability p_i, and after completion, that service unit leaves the system. Let the service times for all phases follow a general distribution, with the distribution function for the ith phase given by $B_i(x)$. The corresponding Laplace transform is denoted as $B_i^*(s)$, and the first moment is $E(B_i)$ for $i = 1,2,\dots,m$,

Let us define a random variable as follows

$$\xi(t) = \begin{cases} 0 & : if\ the\ server\ is\ idle \\ 1 & : if\ the\ server\ is\ busy\ with\ first\ service \\ 2 & : if\ the\ server\ is\ busy\ with\ second\ service \\ . & \\ . & \\ . & \\ m & : if\ the\ server\ is\ busy\ with\ mth\ service \end{cases}$$

The bivariate random variable $\{N(t), \sigma(t)\}$ form a Markov process, where

$\sigma(t) = 0, if\ \xi(t) = 0,\ \sigma(t) = B^i(t)\ if\ \xi(t) = i,$ for $i = 1,2,\dots m.$

The system state governing equation for the present system is given by

$$P_0(t) = Prob.\{N(t) = 0, \sigma(t) = 0\} \tag{46}$$

$$P_n^{(i)}(t,x) = Prob.\{N(t) = n, \sigma(t) = B^i(t), x < B^i(t) \le x + dx\} \quad ; x > 0,\ i = 1,2,\dots,m \tag{47}$$

The hazard rate for the ith service is given by

$$\mu_i(x)dx = \frac{dB_i(x)}{1-B_i(x)}\text{, for } i = 1,2,\dots,m \tag{48}$$

The equations that govern the system are given by

$$\lambda P_0 = \sum_{i=1}^{m}\int_0^{\infty}\mu_i(x)P_1^{(i)}(x)dx \tag{49}$$

$$\frac{dP_n^{(i)}(x)}{dx} = -\big(\lambda+\mu_i(x)\big)P_n^{(i)}(x) + \lambda P_{n-1}^{(i)}(x) \quad \text{for n} \geq 1, \text{x} > 0, \text{i} = 1,2,\dots,\text{m} \tag{50}$$

The boundary conditions are given by

$$P_n^{(j)}(0) = \lambda p_j \delta_{n,1}P_0 + p_j\sum_{i=1}^{m}\int_0^{\infty}\mu_i(x)P_{n+1}^{(i)}(x)dx\,,\ \ n \geq 1, j = 1,2,..,m \tag{51}$$

The normalization condition for the present model is as follows

$$P_0 + \sum_{i=1}^{m}\sum_{n=1}^{\infty}\int_0^{\infty}P_n^{(i)}(x)\,dx = 1 \tag{52}$$

The PGF used for the present system is as follows

$$P_i(x,z) = \sum_{n=1}^{\infty}P_n^{(i)}(x)\,z^n \qquad \text{and} \quad P_i(0,z) = \sum_{n=1}^{\infty}P_n^{(i)}(0)\,z^n \tag{53}$$

Multiply governing equation (50) by the proper exponent of z, and using (53), we have

$$P_j(x,z) = P_j(0,z)\exp\{-a(z)x\}\big[1-B_j(x)\big],\ \text{for } j = 1,2,\dots,m \tag{54}$$

By multiplying equation (51) by a proper exponent of z and summing over all terms, we obtain

$$zP_j(0,z)[z - p_jB_j^*(a(z))] = p_j\lambda P_0 z(z-1) + p_j\sum_{\substack{i=1\\ i\neq j}}^{m}P_i(0,z)B_i^*\big(a(z)\big), j = 1,2,\dots,m \tag{55}$$

Equation (55) gives m simultaneous equation in variables $P_1(0,z), P_2(0,z), \dots, P_m(0,z)$, on solving this we get

$$P_j(0,z = \frac{p_j\lambda P_0 z(z-1)}{\sum_{i=1}^{m}[p_iB_i^*(a(z))-1]},\ j = 1,2,\dots,m \tag{56}$$

Solving the equation (54) and using equation (56), we have

$$P_j(z) = \frac{p_jP_0z(1-B_j^*(a(z)))}{[\sum_{i=1}^{m}p_iB_i^*(a(z))-z]},\ \ for\ j = 1,2,\dots,m \tag{57}$$

Now applying the normalizing condition $P_0 + \sum_{i=1}^{m}P_i(1) = 1$, we have

$$P_0 = (1-\rho) \tag{58}$$

Where $\rho = \lambda[p_1E(B_1) + p_2E(B_2) + p_3E(B_3) + \cdots + p_mE(B_m)]$,

The queue size distribution is characterized by its probability generating function, expressed as

$$\varphi(z) = \frac{(1-\rho)(1-z)[\sum_{i=1}^{m}p_iB_i^*(a(z)\}]}{[\sum_{i=1}^{m}p_iB_i^*(a(z)\}-z]} \tag{59}$$

IV. Two-phase multi-optional service

In this section, we outline a concise procedure for solving a queueing model with a two-phase service structure. The first phase is mandatory for all customers, whereas the second phase offers m optional services. Customers can select one of these m available service options based on their preferences.

Consider $M/G/1$ queueing situation where units join the system in a Poisson arrival rate λ and service is provided in two phases. The first phase is essential to all, while the second is optional. The customer may choose i^{th} optional service with probability p_i after completion of the essential service. Let both phases' service follow general distribution with distribution functions respectively $B_e(x), B_i(x)$, with Laplace transforms $B_e^*(s)$, $B_i^*(s)$, and first moments $E(B_e), E(B_i) i = 1,2,..,m$. Let $N(t)$ denote the number of units in the system at time t, and $B^e(t)$, $B^i(t)$ be supplementary variables that denote the elapsed service time for the first phase and second phase, respectively for $i = 1,2,..,m$. Let us define a random variable as follows

$$\xi(t) = \begin{cases} 0 & : if\ the\ server\ is\ idle \\ 1 & : if\ the\ server\ is\ \ busy\ in\ the\ first\ phase\ service \\ i+1 & : if\ the\ server\ is\ \ busy\ in\ rendering\ ith\ \ optional\ service \end{cases}$$

The bivariate random variable $\{N(t), \sigma(t)\}$ form Markov process, where $v(t) = 0, if\ \xi(t) = 0, \sigma(t) = B^e(t)\ if\ \xi(t) = 1, \sigma(t) = B^i(t)\ if\ \xi(t) = i+1$.

The governing equation for the present system is given by

$$P_0(t) = Prob.\{N(t) = 0, \sigma(t) = 0\} \tag{60}$$

$$P_n^{(e)}(t,x) = Prob.\{N(t) = n, \sigma(t) = B^e(t), x < B^e(t) \leq x+dx\}\ \ ; x > 0 \tag{61}$$

$$P_n^{(i)}(t,x) = Prob.\{N(t) = n, \sigma(t) = B^i(t), x < B^i(t) \le x + dx\} \;\; ; x > 0 \quad (62)$$

And the steady state probability is given by

$$P_0 = \lim_{t\to\infty} P_0(t)\,, P_n^{(e)}(x) = \lim_{t\to\infty} P_n^{(e)}(t,x)\,, P_n^{(i)}(x) = \lim_{t\to\infty} P_n^{(i)}(t,x) \quad (63)$$

The hazard rates for both the essential and optional service phases are given by

$$\mu_e(x)dx = \frac{dB_e(x)}{1-B_e(x)},\ \mu_i(x)dx = \frac{dB_i(x)}{1-B_i(x)} \quad (64)$$

The governing equation of the present system is given by

$$\lambda P_0 = \sum_{i=1}^{m}\int_0^\infty \mu_i(x)P_1^{(i)}(x)dx + p_0\int_0^\infty \mu_1(x)P_1^{(1)}(x)dx \quad (65)$$

$$\frac{dP_n^{(e)}(x)}{dx} = -\big(\lambda + \mu_e(x)\big)P_n^{(e)}(x) + \lambda P_{n-1}^{(e)}(x) \quad \text{for n} \ge 1, \text{x} > 0 \quad (66)$$

$$\frac{dP_n^{(i)}(x)}{dx} = -\big(\lambda + \mu_i(x)\big)P_n^{(i)}(x) + \lambda P_{n-1}^{(i)}(x) \quad \text{for n} \ge 1, \text{x} > 0 \quad (67)$$

Equations (66) and (67) are solved under conditions at x = 0

$$P_n^{(e)}(0) = \lambda\delta_{n,1}P_0 + p_0\int_0^\infty \mu_e(x)P_{n+1}^{(e)}(x)dx + \sum_{i=1}^{m}\int_0^\infty \mu_i(x)P_{n+1}^{(i)}(x)dx \quad (68)$$

$$P_n^{(i)}(0) = p_i\int_0^\infty \mu_e(x)P_n^{(e)}(x)dx \;\; , n \ge 1 \quad (69)$$

The normalization condition for the present case is given by

$$P_0 + \sum_{n=1}^{\infty}\int_0^\infty P_n^{(e)}(x) + \sum_{i=1}^{m}\sum_{n=1}^{\infty}\int_0^\infty P_n^{(i)}(x)dx = 1 \quad (70)$$

The probability generating functions used in this part are

$$P_e(x,z) = \sum_{n=1}^{\infty} P_n^{(e)}(x)\, z^n \quad \text{and} \quad P_e(0,z) = \sum_{n=1}^{\infty} P_n^{(e)}(0)\, z^n$$

$$P_i(x,z) = \sum_{n=1}^{\infty} P_n^{(i)}(x)\, z^n \quad \text{and} \quad P_i(0,z) = \sum_{n=1}^{\infty} P_n^{(i)}(0)\, z^n$$

Solving equation (66) in the usual manner and using (64), we have

$$P_e(x,z) = P_e(0,z)\exp\{-a(z)x\}[1 - B_e(x)], \quad (71)$$

$$P_i(x,z) = P_i(0,z)\exp\{-a(z)x\}[1 - B_i(x)],\ for\ i = 1,2,\dots,m \quad (72)$$

Solving equations (68) and (69) in the usual manner, we have

$$zP_e(0,z) = \lambda P_0 z(z-1) + p_0 P_e(0,z)B_e^*(a(z)) + \sum_{i=1}^{m} p_i P_i(0,z)B_i^*(a(z)) \quad (73)$$

$$P_i(0,z) = P_e(0,z)p_i B_e^*\big(a(z)\big),\ \ i = 2,3,\dots,m \quad (74)$$

From equations (73) and (74) we have

$$P_e(0,z) = \frac{\lambda P_0 z(z-1)}{[z - \{p_0 + \sum_{i=1}^{m} p_i B_i^*(a(z))\}B_e^*(a(z))]} \quad (75)$$

$$P_i(0,z) = \frac{\lambda P_0 z(z-1)p_i B_e^*\big(a(z)\big)}{[z - \{p_0 + \sum_{i=1}^{m} p_i B_i^*(a(z))\}B_e^*(a(z))]}, \quad i = 2,3,\dots,m \quad (76)$$

Solving equations (71) and (72) using equations (75) and (76), we have

$$P_e(z) = \frac{P_0 z\,[1 - B_e^*(a(z))]}{[\{p_0 + \sum_{i=1}^{m} p_i B_i^*(a(z))\}B_e^*(a(z)) - z]}, \quad (77)$$

$$P_i(z) = \frac{P_0 z p_i B_e^*(a(z))[1 - B_i^*(a(z))]}{[\{p_0 + \sum_{i=1}^{m} p_i B_i^*(a(z))\}B_e^*(a(z)) - z]}, for\ i = 1,2,\dots,m \quad (78)$$

Now, applying the normalizing condition (70), we have

$$P_0 = (1 - \rho) \quad (79)$$

Where $\rho = \lambda[E(B_e) + \sum_{i=1}^{m} p_i E(B_i)]$

The PGF for the queue size distribution is given by

$$\varphi(z) = \frac{(1-\rho)(1-z)[\{p_0 + \sum_{i=1}^{m} p_i B_i^*(a(z))\}B_e^*(a(z))]}{[\{p_0 + \sum_{i=1}^{m} p_i B_i^*(a(z))\}B_e^*(a(z)) - z]} \quad (80)$$

IV. Review of Literature

I. Literature review(Up to 2013)

Queueing models incorporating phase-type services have seen widespread application across a variety of domains, including industrial operations, telecommunications, and computer networks. A significant body of research has focused on systems in which the service process is completed in multiple phases—either two or more—with some phases being essential, optional, or a mix of both.

This section reviews key contributions to the study of queueing models with phase-type

services prior to 2014. The literature can broadly be classified based on whether the service phases are optional, essential, or multi-optional. Table 1 summarizes these studies, highlighting the nature of the service phases, the methodological tools employed (such as Laplace-Stieltjes Transforms (LST), Probability Generating Functions (PGF), and Supplementary Variable Techniques (SVT)), and the key features of each model. Notable early contributions include the work of Madan [4], Wang [5], Medhi [6], Choudhury et al. [7], Singh et al. [8], Choudhury and Deka [9], among others. These studies have addressed various complexities, such as server breakdowns, feedback mechanisms, retrial phenomena, batch arrivals, and different vacation policies. A detailed classification and comparison of these studies are provided in Table 1.

Table 1: *Literature on phase service up to 2013.*

Type of service	Author	Key features	Methodologies used
Second phase optional service	Madan [4]	The first essential is arbitrarily distributed but the optional service is exponential	LST, PGF, SVT
	Wang [5]	M/G/1 queue, server Breakdown, phase-dependent service	LST, PGF, SVT
	Medhi [6]	Essential as well as optional is generally distributed	LST, PGF, SVT
	Madan et al. [10]	Single server, optional service, Bernoulli vacation schedule	LST, PGF, SVT
	Madan and Baklizi [12]	Single arrival, optional additional service, optional re-service	LST, PGF, SVT
	Choudhury [12]	Single arrival, two-phase general distributed service	PGF, SVT.
	Jaraha and Madan [13]	$M/G/1$ model, optional service, general distributed service	LST, PGF, SVT
	Choudhury and Paul [14]	Two-phase queueing system, Bernoulli feedback to the tail of the queue	LST, PGF, SVT
	Atencia & Moreno [15]	$Geo/G/1$ model with retrial queue, second optional service	LST, PGF,SVT
	Choudhury[16]	Single arrival, Linear retrial policy, Bernoulli schedule vacation.	LST, PGF, SVT
	Choudhury et al.[17]	N-policy, two-phase service, delayed repair, linear cost structure.	LST, PGF, SVT
	Choudhury and Tadj [18]	Single arrival, generally distributed service, random breakdown, and delay repair	LST, PGF, SVT
	Ke and Chu [19]	M/G/1 Queueing system,<p, T> policy, second optional service, cost analysis to find optimal value of *p* & *T*.	PGV, SVT, LST
	Wang and Li [20]	Single arrival, general retrial time, two-phase service, server breakdown, and repair	PGF, SVT.
	Zadeh [21]	Mx/(G_1, G_2)/1/G(BS)/V, admissibility restricted.	PGV, SVT, LST
	Choudhury et al.[22]	Retrial queue, Bulk arrival, optional service, random failure, delay repair.	LST, SVT
	Jain and Agarwal [23]	Decrete time $Geo^X/G/1$, retrial queue, starting failure	LST, PGF, SVT
	Kumar and Arumuganathan [24]	Bulk arrival, retrial queue, two types of repair, Active breakdown	PGF, SVT.

	Maraghi et al.[25]	Bulk queue, second stage elective in nature, Bernoulli vacations, and random server failure	LST, SVT
	Ramnath and Kalidas [26]	Two-phase service, vacation, retrial policy, non-persistent customers.	LST,PGF,SVT
	Wang et al.[27]	Single arrival, second optional service, Comparison of randomized policy for (T,p) and (p, N) policy, and general start-up time using cost function.	PGF, SVT
	Singh et al.[28]	Bulk arrival, state-dependent arrival, and general distributed service.	LST,PGF,SVT
	Jain et al.[29]	Batch arrival, General distributed service, retrial, Bernoulli vacation, and server breakdown.	PGV, SVT, LST
	Jailaxmi et al.[30]	Batch arrival, Two Stage service, active server failure, and retrial	LST, PGF, SVT
Both phase essential	Kumar et al.[31]	Two-phase service, preemptive resume service, and retrial	PGF, SVT
	Madan and Swami [32]	M/D/1 queue with two-stage service and Heterogeneous vacation.	PGV,SVT, LST
	Choudhury and Paul [33]	Batch arrival, additional phase service, and N-policy	PGF, SVT
	Choudhury and Madan [34]	Two-phase, batch arrival, Bernoulli vacation	PGV, SVT, LST
	Choudhury and Madan [35]	Bulk queue, Modified Bernoulli vacation schedule, N-policy.	PGF, SVT
	Madan et al.[36]	$Mx/(G_1G_2)/1/G(BS)/Vs$, Two phase service and Vacation	PGV, SVT, LST
	Madan and Choudhury [37]	Single-server, two-phase heterogeneous service, Bernoulli schedule, general vacation time.	PGV, SVT, LST
	Choudhury and Paul [38]	Two-phase service, Bernoulli vacation, multiple vacation policy	PGV, SVT, LST
	Madan and Choudhury [39]	$Mx/(G_1, G_2)/1$ queue with restricted admissibility and random setup time	PGV, SVT, LST
	Choudhury et al [40]	Bulk queue, Modified Bernoulli vacation schedule	PGV, SVT, LST
	Kumar and Chandan [41]	N-policy, Batch service without gating, Single vacation, Cost analysis for optimal value of N.	PGF, SVT
	Dimitriou and Langaris [42]	Retrial queue, single vacation	PGF, SVT
	Choudhury and Kalita [43]	Two Phase with repeated attempts, Bernoulli Vacation	PGV, SVT
	Dimitriou and Langaris [44]	Two-phase service, retrial and start-up time, Random failure, Single vacation.	PGF, SVT
	Park et al.[45]	Two-phase service with fixed batch size policy, Linear cost analysis.	PGF, Rouché's theorem,
	Thangraj and Vanitha [46]	Two-phase service, compulsory vacation, and random failure	PGF, SVT
	Choudhury and Tadj [47]	Unreliable server, Bernoulli vacation, N-policy, delay repair. Linear cost structure.	PGV, SVT, LST
	Choudhury and Deka [48]	Single Poisson arrival, Bernoulli vacation, Unreliable server	PGV, SVT, LST

	Tadj et al.[49]	Two-phase, setup time, N-policy, Unreliable server, delay repair.	PGV, SVT, LST
	Singh et al.[50]	Bulk arrival, Two-phase service, m-phase of repair.	PGV, SVT, LST
	Vemuri et al. [51]	$M^X/M/1$ system, N policy, Unreliable server	PGF
	Salah [52]	Finite queueing system, Two-stage service	PGF
	Redenko [53]	Two-phase, finite buffer between phases, unreliable server	PGF, SVT
	Choudhury and Deka [54]	Bulk arrival, linear retrial policy, Bernoulli vacation, control admission policy.	PGF, SVT
	Dudina et al. [55]	Multi-server, retrial customer, Phase type service	PGF
Multi optional	Jianghua and Jinting [56]	Single arrival, general distributed service, feedback, balking, and unreliable server	PGF ,SVT
	Salehirad and Badamchizadeh [57]	Single server queue, multiphase service, general distributed service, and feedback to the tail of the queue	PGF, SVT
	Jain and Upadhyaya [58]	Optimal repairable, batch arrival, multi-optional service, Bernoulli vacation.	LST, PGF, SVT
	Wang and Li [59]	Bulk arrival, second service is multi-optional, unreliable server	PGF, SVT
	Jain et al.[60]	Unreliable server, second service, and vacation are multi-optional in nature.	LST, PGF, SVT
	Bhagat and Jain [61]	Unreliable server, Balking, Bulk arrival, Multi-optional second service	LST, PGF, SVT

II. Review of Literature (2014-2024)

This section reviews significant contributions to the study of queueing models with phase-type services published since 2014. The existing literature can be broadly categorized based on whether the service phases are optional, essential, or multi-optional. Research on queueing models with optional services has explored various complexities, including vacation policies, retrial mechanisms, and server reliability.

Two-phase optional service: Gao et al. [62] employed C0-semigroup theory to study the asymptotic stability of a queueing model by introducing an additional optional service. Rajadurai et al. [63] investigated a queueing model featuring customer retrials, group arrivals, and balking behavior, incorporating dual service choices and the possibility of re-service under an adapted vacation policy framework. Saravanarajan and Chandrasekaran [64] analyzed an M/G/1 queue featuring two types of service, Bernoulli vacations, feedback, and random server failure. The inclusion of random breakdowns makes the model applicable to manufacturing and cloud-based services. Kalidass and Kasturi [65] introduced an M/G/1 queueing model incorporating Bernoulli feedback and a dual-phase service structure, in which the initial phase is mandatory, whereas the subsequent phase is discretionary, involving a choice among various available service alternatives. Jiang et al. [66] examined a $M/G/1$ queue in which the server is subject to random failures during any service phase, and after a repair period that follows an exponential distribution, it resumes operation in phase i with probability q_i. Chakravarthy [67] further applied the matrix analytic method to a single-server queueing system in which customers, with certain predefined probabilities, could opt for either individual service or cooperative service. Arivudainambi and Godhandaraman [68] investigated a queueing model incorporating retrial customers, balking, and

an elective second service, in which the server initiates a vacation each time the system becomes idle. Jain et al. [69] applied maximum entropy analysis to investigate a system characterized as a retrial queue with bulk arrivals, an optional second service, and a Bernoulli schedule vacation mechanism, thereby contributing to a more generalized approach to performance evaluation.

Bhagat and Jain [70], in their study of a G-queue with bulk arrivals, retrials, impatient customers, and multiple service choices, considered a server governed by the N-policy and subject to random failure. Singh et al. [71] introduced a queue model with bulk arrival, phased service, and variable arrival rates, assuming repairs occur in multiple optional phases. Vadivu and Arumuganathan [72] examined a queueing system featuring two service phases and offering the flexibility of both single as well as multiple vacation policies. By incorporating the Markovian Arrival Process (MAP), the model achieves greater adaptability in capturing diverse arrival patterns compared to traditional Poisson-based models. Wang et al. [73] conducted a systematic study of retrial queues with a two-phase service structure and a finite source population. Their analysis focused on the effects of customer retrials, highlighting the model's applicability to systems with a limited number of users, such as sensor networks and computing clusters.

Arivudainambi and Gowsalya [74] analyzed a single arrival retrial queue incorporating vacations under a Bernoulli schedule, dual service types, and server startup failures. The inclusion of startup failures makes the model applicable to unreliable manufacturing systems and cloud computing networks. Singh et al. [75] studied a batch arrival queue with state-dependent arrival rates, incorporating the concept of elective second service and vacation under a randomised policy. Singh et al. [76] extended this framework by developing a bulk queue model featuring two-phase service, customer balking, and an unreliable server, where repairs progress through m distinct phases.

Bagyam and Udya [77] examined a bulk queue model with state-dependent arrivals, two-phase service, and a retrial queue, where customer admission depends on the server's state. Ayyappan and Deepa [78] analyzed a queueing system in which both arrival as well as service are done in bulk, incorporating the features of optional services, multiple vacation policies, and setup times to improve system flexibility. Singh et al. [79] studied a bulk queue system incorporating optional services, vacation policies, and an unreliable server. Singh et al. [80] analyzed a G-queue with retrials, bulk arrivals, optional services, server unreliability, and delayed repairs, highlighting the impact of maintenance scheduling on queue performance.

Ayyappan and Nirmala [81] analyzed a bulk arrival queueing model incorporating an unreliable server, optional second-phase service, setup time, multiple vacation policies, and an N-policy. The model also features a closedown mechanism that allows the system to shut down during periods of low demand, enhancing its applicability to power-saving environments. Pikkala and Edadasari [82] investigated a Markovian queueing model that integrates variant working vacations, an optional second service phase, server failures occurring at random, and a mechanism for customer retention following reneging behavior. Madheswari and Suganthi [83], who examined a single-server retrial queue featuring two service phases, considered a model with an optional second service, server starting failures, and K types of Bernoulli vacation policies.

Abdollahi and Salehi Rad [84], who investigated a retrial queueing system with bulk arrivals, dual-phase service, and customer feedback, incorporated a server-dependent admission control mechanism in their model. Ayyappan and Thilagavathy [85] applied the matrix analytic method to investigate an advanced queueing model integrating a Markovian arrival process, standby servers, optional services, breakdowns, and customer impatience. Deepa and Azhagappan [86], who studied a bulk arrival queueing model with arrival rates dependent on the system state and incorporating multiple vacation policies, considered an optional second service and re-service mechanisms to improve the analysis of system performance. Laxmi and George [87], who analyzed a non-Markovian queueing model with batch service and an optional second service phase, examined the system's performance under both transient and steady-state conditions. More recently, Ayyappan and Gurulakshmi [88], who examined a Markovian arrival queueing model featuring distinct vacation types, interruptions governed by the N-policy, optional service phases,

server breakdowns and repairs, setup delays, and customer discouragement behavior, provided a comprehensive analysis of system dynamics.

Two-phase essential service: Queueing models with two-phase service have been extensively studied, with researchers incorporating various complexities to enhance their applicability. Rajadurai et al. [89] investigated a queueing model featuring retrial, two-phase service, a revised vacation policy, and optional re-service, eliminating the need for orbiting. Saravanarajan and Chandrasekaran [90] expanded this framework by incorporating feedback from customers, where the server undergoes a mandatory vacation after completing the second-phase service for each customer. Ramaya et al. [91] investigated a queueing model featuring mandatory two-phase service under a gated service vacation policy. In their model, the first phase involves processing customers in batches, while the second phase delivers individual service to each customer within the batch. Van Do [92] obtained explicit solutions for the steady-state probabilities of a tollbooth queue with two distinct servers by applying eigenvalue analysis to the characteristic polynomial of the corresponding Markov chain. Rajadurai et al. [93] extended the study of retrial models by examining a batch arrival system with feedback in the retrial queue, incorporating negative customers, a Bernoulli vacation policy, and server breakdowns. In another study, they investigated a bulk queueing system featuring retrials and two-stage service, incorporating Bernoulli vacation policies and random service interruptions. Choudhury and Deka [94] conducted a study on a single Poisson arrival queueing system characterized by server unreliability, service in two stages, and a Bernoulli vacation scheme governed by a randomized vacation policy. In another work, they proposed a batch arrival model with an unreliable server, incorporating a Bernoulli vacation mechanism, two-phase service, and general retrial times to assess system performance. Building on this line of research, Choudhury and Deka [95] analyzed a queueing system with Poisson input in bulk, featuring two-stage service, random server failures, and a randomised vacation policy. Baumann and Sandmann [96] explored a tandem queue with multiple servers that deliver services in two stages under the assumption of finite buffer space, where blocking and loss can occur.

Arivudainambi and Gowsalya [97] introduced a non-Markovian retrial queueing model with a single server, featuring two distinct service types and a Bernoulli vacation policy. Later, Ayyappan et al. [98] investigated a bulk queue system with two-phase distinct service and a standby server, where the standby server activates only when the primary server is under repair. Sivasamy and Peter [99] investigated a multi-server queue with Poisson arrival, where customers become impatient due to a leisurely service rate. Dahmane and Aissani [100] utilized Markov decision theory to enhance routing management within a queueing system featuring retrial customers and a two-stage service process. Meanwhile, Liu et al. [101] developed a matrix-geometric method to examine a stochastic model with three-dimensional continuous time, incorporating multiple simultaneous working vacations for selected servers. Wu and Yang [102] used the Matrix Geometric Method to optimize costs in a Markovian queueing system with two essential stages of service. Kumar & Jain [103] used the same approach to study an unreliable queueing system with two stages of service, considering both regular and working vacations. Radha et al. [104] adapted queueing models for cloud computing by introducing bulk arrival in a non-Markovian queueing system, multiple service stages, and a structured vacation mechanism. More recently, Raghavendran and Vidhya [105] examined queueing models featuring phase-type distributions and modulated arrival rates, assuming that fluctuations in arrival rate modulation impact the server's service rate. Expanding on this, Ayyappan and Thilagavathy [106] applied matrix-geometric methods to analyze a Queueing model with a Markovian arrival process, incorporating various factors such as heterogeneous service modes, standby servers, customer impatience, optional services, startup time, system breakdowns, and phase-type repairs.

Multiphase essential service: The queueing model with multiphase essential service has garnered significant attention from researchers due to its wide applicability in various expanding domains of queueing congestion. This model is particularly relevant in fields such as telecommunications, healthcare, manufacturing systems, and transportation, where efficient service mechanisms are crucial for minimizing delays and optimizing resource utilization. Lakshmi and Ramnath [107] applied the SVT to investigate a retrial queueing model with K choices in the second phase of essential service. Vignesh et al. [108] explored a bulk arrival with a general distributed service, featuring multistage service, constrained admissibility, response services, and three optional vacation types, with applications in production and manufacturing systems. Bhagat and Jain [109] analyzed a retrial queueing model with batch arrival and an unreliable server, integrating multiphase essential service and repair. The model differentiates between two customer types: priority and ordinary. Ahuja et al. [110] conducted a transient analysis of a queueing model with M phases of essential service under the assumption that the server is subject to random failure using the Runge-Kutta method. Their study assumes that the server is susceptible to failure during both vacation and busy periods.

Multi optional service: One of the key features of queueing models with phase service is the concept of multi-optional service**.** In this system, customers have the flexibility to choose from multiple service options within the same service center, allowing for a more dynamic and customized service experience. This feature enhances the efficiency of service systems by accommodating diverse customer needs and optimizing resource allocation. The queueing model with multi-optional service has emerged as a significant area of interest among researchers due to its broad applicability in various real-world scenarios. Zadeh [111] examined a queueing model in which units arrive in groups of random size and service is done in k phases and allowing feedback to the tail of the queue at each phase. Varalakshmi et al. [112] studied a queueing model featuring two service phases, retrial, feedback follows a Bernoulli distribution, exhaustive vacation periods, and starting letdowns. Sundari & Srinivasan [113] investigated optional service mechanisms in a queueing system with general distributed service time, where unit demand for the first optional or second optional service occurs after the completion of the essential one.

Singh & Kumar [114] explored a bulk arrival queueing model with Bernoulli vacations, finite optional services, and N-policy. The inclusion of multiple optional services enhances flexibility in customer service-oriented applications. Li et al. [115] utilized the supplementary variable technique to analyze a general queue with multi-stage operations, in which the server may take multiple vacations if the system is empty. Rajadurai et al. [116] explored cost optimization in general queue models incorporating retrials, multiple service phases, vacations, and server breakdowns. Kumar [117] presented a general queueing system with bulk arrival and an unreliable server that integrates optional services, vacation under a Bernoulli schedule, and customer impatient behavior. Vignesh et al. [118] explored a general queueing system with bulk arrival under the assumption of mandatory three-stage services, an optional fourth stage, service disruptions, and deterministic server vacations. Jain and Kaur [119] studied a bulk queue model with multi-phase essential service and feedback under the (p, N) policy. The server is prone to random failure during any service phase, and it goes on vacation as the system becomes empty. Abdollahi et al. [120] studied the sensitivity of a queueing system retrial queue with k-1 optional service phases following an essential service. Unsatisfied customers may request reservice at each phase, and the server can take a Bernoulli vacation after the k^{th} phase. Jain et al. [121] utilized the supplementary variable technique to analyze a batch arrival queue model with an unpredictable server and a randomized vacation policy. The model assumes that unsatisfied customers may rejoin the queue for service. Sangeetha et al. [122] investigated a queueing system with a retrial customer having S phases of essential service, each offering different optional services. The server experiences a breakdown immediately upon the arrival of a customer, which is negative in nature. Li and Liu [123] used the matrix-geometric method to analyze the performance of a general queueing model with a working vacation and multi-phase service, incorporating a Bernoulli-

scheduled vacation interruption. Kumar [124] examined an unreliable queue model with delayed repair and a single vacation, assuming that the server provides service through different optional phases.

V. Conclusion

In the present study, we have provided a comprehensive review of queueing systems with phase service, highlighting their significance in modeling and analyzing real-world congestion scenarios across various industries. By classifying and examining different queueing models with phase service, we have proposed a unified framework for their analysis using a queue-theoretic approach. These models serve as valuable tools for system analysts, engineers, and managers in mitigating congestion, reducing blocking and delays, and enhancing overall system efficiency.

Our review specifically focuses on the supplementary variable technique (SVT) for solving non-Markovian single-server queueing models with different phase service structures. We have categorized and discussed key contributions in this domain, including M/G/1 queueing models with essential and optional multistage services, as well as models addressing service interruptions. Despite significant progress in recent years, there remains a need for further advancements in queueing models with phase service to better reflect real-world complexities, such as priority queues, server vacations, breakdowns, and working vacations. Future research should integrate these factors to develop more robust and fault-tolerant systems. We hope that this review provides valuable insights for both researchers and practitioners, facilitating the development of more efficient and cost-effective service and manufacturing systems where congestion management is a critical concern.

Acknowledgements

The corresponding author gratefully acknowledges the esteemed referee and the chief editor for their thoughtful feedback and valuable suggestions, which have greatly enhanced the quality of this work. Furthermore, the first author sincerely appreciates the Research and Development Cell of Patna University, Patna, for providing financial support through the Minor Research Project (Project No. RDC/MRP/26).

References

[1] Cox, D. R. (1955). The analysis of non-Markovian stochastic processes by the inclusion of supplementary variables. *Mathematical Proceedings of the Cambridge Philosophical Society, 51:* 433–441. https://doi.org/10.1017/S0305004100030437

[2] Chaudhry, M. L., & Templeton, J. G. C. (1983). A first course on bulk queues. John Wiley & Sons Inc.

[3] Borthakur, A., & Medhi, J. (1974). A queueing system with arrival and service in batches of variable size. *Cahiers du CERO, 16*: 117–126.

[4] Madan, K. C. (2000). An M/G/1 queue with second optional service. *Queueing Systems, 34*: 37–46.

[5] Wang, J. (2004). An M/G/1 queue with second optional service and server breakdowns. *Computers and Mathematics with Applications, 47*(10–11): 1713–1723.

[6] Medhi, J. (2002). A single server Poisson arrival queue with a second optional channel. *Queueing Systems, 42*(3): 239–242.

[7] Choudhury, G., Ke, J. C., & Tadj, L. (2009). The N-policy for an unreliable server with delaying repair and two phases of service. *Journal of Computational and Applied Mathematics, 231*(1): 349–364. https://doi.org/10.1016/j.cam.2009.02.101

[8] Singh, C. J., Jain, M., & Kumar, B. (2011). Queueing model with state-dependent bulk arrival and second optional service. *International Journal of Mathematics in Operational Research, 3*(3): 322–340. https://doi.org/10.1504/IJMOR.2011.040029

[9] Choudhury, G., & Deka, M. (2012). A single server queueing system with two phases of service subject to server breakdown and Bernoulli vacation. *Applied Mathematical Modelling, 36*(12): 6050–6060. https://doi.org/10.1016/j.apm.2012.01.047

[10] Madan, K. C., Abu-Dayyeh, W., & Saleh, M. F. (2002). A queue with second optional service and Bernoulli schedule server vacations. *Systems Science, 28*(3): 51–62.

[11] Madan, K., & Baklizi, A. (2002). An M/G/1 queue with additional second-stage service and optional re-service. *International Journal of Information and Management Sciences, 13*: 13–31.

[12] Choudhury, G. (2003). Some aspects of an M/G/1 queueing system with optional second service. *Top, 11*: 141–150. https://doi.org/10.1007/BF02578955

[13] Jaraha, J.A., & Madan, K.C. (2003). An M/G/1 Queue with Second Optional Service with General Service Time Distribution. *Information and Management System,*14(2):47-56.

[14] Choudhury, G., & Paul, M. (2005). A two-phase queueing system with Bernoulli feedback. *Journal of Information and Management Sciences, 16*(1): 35–52.

[15] Atencia, I., & Moreno, P. (2006). Geo/G/1 retrial queue with second optional service. *International Journal of Operational Research, 1*(4): 340–362. https://doi.org/10.1504/IJOR.2006.010209

[16] Choudhury, G. (2008). Steady-state analysis of an M/G/1 queue with linear retrial policy and two-phase service under Bernoulli vacation schedule. *Applied Mathematical Modelling, 32:* 2480–2489.

[17] Choudhury, G., Ke, J. C., & Tadj, L. (2009). The N-policy for an unreliable server with delaying repair and two phases of service. *Journal of Computational and Applied Mathematics, 231*(1): 349–364.

[18] Choudhury, G., & Tadj, L. (2009). A queue with two phases of service subject to the server breakdown and delayed repair. *Applied Mathematical Modelling, 33*(6): 2699–2709.

[19] Ke, J.-C., & Chu, Y.K. (2009). Notes of M/G/1 system under the <p, T> policy with second optional service. *Central European Journal of Operations Research, 17*(4): 425–431.

[20] Wang, J., & Li, J. (2009). A single server retrial queue with general retrial times and two-phase service. *Journal of Systems Science and Complexity, 22*: 291–302. https://doi.org/10.1007/s11424-009-9164-8

[21] Zadeh, A. B. (2009). An Mx/(G_1, G_2)/1/G(BS)/Vs with optional second service and admissibility restricted. *International Journal of Information Management,* 20: 305–316.

[22] Choudhury, G., Tadj, L., & Deka, K. (2010). A batch arrival retrial queueing system with two phases of service and service interruption. *Computers & Mathematics with Applications, 59*(1): 437–450. https://doi.org/10.1016/j.camwa.2009.06.021

[23] Jain, M., & Agarwal, S. (2010). A discrete-time retrial queueing system with starting failures and optional service. *International Journal of Operational Research, 8*(4): 428–457. https://doi.org/10.1504/IJOR.2010.034068

[24] Kumar, M. S., & Arumuganathan, R. (2010). An MX/G/1 retrial queue with two-phase service subject to active server breakdowns and two types of repair. *International Journal of Operational Research, 8(*3): 261–291. https://doi.org/10.1504/IJOR.2010.033540

[25] Maraghi, F. A., Madan, K. C., & Darby-Dowman, K. (2010). Batch arrival vacation queue with second optional service and random system breakdowns. *Journal of Statistical Theory and Practice, 4*: 137–153. https://doi.org/10.1080/15598608.2010.10411977

[26] Ramanath, K., & Kalidass, K. (2010). A two-phase service M/G/1 vacation queue with general retrial times and non-persistent customers. *International Journal of Open Problems in Computer Science and Mathematics, 3*(2): 175–185.

[27] Wang, K. H., Yang, D. Y., & Pearn, W. L. (2010). Comparison of two randomized policy M/G/1 queues with second optional service, server breakdown, and startup. *Journal of Computational and Applied Mathematics, 234*(3): 812–824. https://doi.org/10.1016/j.cam.2010.01.045

[28] Singh, C. J., Jain, M., & Kumar, B. (2011). Queueing model with state-dependent bulk arrival and second optional service. *International Journal of Mathematics in Operational Research, 3*(3): 322–340. https://doi.org/10.1504/IJMOR.2011.040029

[29] Jain, M., Sharma, G. C., & Sharma, R. (2012). A batch arrival retrial queuing system for essential and optional services with server breakdown and Bernoulli vacation. *International Journal of Internet and Enterprise Management, 8*(1): 16–45. https://doi.org/10.1504/IJIEM.2012.049868

[30] Jailaxmi, V., Arumuganathan, R., & Rathinasamy, A. (2013). An Mx/G/1 retrial queue with two-phase service under active server breakdowns, two types of repair and multiple vacations with N-policy. *International Journal of Operational Research, 18*(1): 35–61. https://doi.org/10.1504/IJOR.2013.055532

[31] Kumar, B. K., Vijayakumar, A., & Arivudainambi, D. (2002). An M/G/1 retrial queueing system with two-phase service and preemptive resume. *Annals of Operations Research, 113*: 61–79. https://doi.org/10.1023/A:1020901710087

[32] Madan, K. C., & Swami, H. M. (2002). Steady-state analysis of an M/D/1 queue with two stages of heterogeneous server vacations (M/D/G1, G1/1 queue). *Revista Investigación Operacional, 23*(2): 150–163.

[33] Choudhury, G., & Paul, M. (2004). A batch arrival queue with an additional service channel under N-policy. *Applied Mathematics and Computation, 156*(1): 115–130.

[34] Choudhury, G., & Madan, K. C. (2004). A two-phase batch arrival queueing system with a vacation time under Bernoulli schedule. *Applied Mathematics and Computation, 149:* 337–349.

[35] Choudhury, G., & Madan, K. C. (2005). A two-stage batch arrival queueing system with a modified Bernoulli schedule vacation under N-policy. *Mathematical and Computer Modelling, 42*(1–2): 71–85.

[36] Madan, K. C., Al-Rawi, Z. R., & Al-Nasser, A. D. (2005). On M^X/(G1,G2)/1/G(BS)/Vs vacation queue with two types of general heterogeneous service. *Journal of Applied Mathematics and Decision Sciences,* 2005(3): 123–135.

[37] Madan, K. C., & Choudhury, G. (2005). A single-server queue with two phases of heterogeneous service under Bernoulli schedule and a general vacation time. *International Journal of Information and Management Sciences,* 16(2): 1–16.

[38] Choudhury, G., & Paul, M. (2006). A two-phase queueing system with Bernoulli vacation schedule under multiple vacation policy. *Statistical Methodology, 3:* 174–185.

[39] Madan, K. C., & Choudhury, G. (2006). Steady-state analysis of an M^X/(G1, G2)/1 queue with restricted admissibility and random setup time. *International Journal of Information and Management Sciences, 17*(2): 33–56.

[40] Choudhury, G., Tadj, L., & Paul, M. (2007). Steady-state analysis of an MX/G/1 queue with two phases of service and Bernoulli vacation schedule under multiple vacation policy. *Applied Mathematical Modelling, 31*: 1079–1091.

[41] Kumar, V. V., & Chandan, K. (2008). Cost analysis of a two-phase MX/EK/1 queueing system with N-policy. *OPSEARCH, 45:* 155–174. https://doi.org/10.1007/BF03398811

[42] Dimitriou, I., & Langaris, C. (2008). Analysis of a retrial queue with two-phase service and server vacations. *Queueing Systems, 60*: 111–129. https://doi.org/10.1007/s11134-008-9089-2

[43] Choudhury, G., & Kalita, S. (2009). A two-phase queueing system with repeated attempts and Bernoulli vacation schedule. *International Journal of Operational Research, 5*(4): 392–407. https://doi.org/10.1504/IJOR.2009.0257

[44] Dimitriou, L., & Langaris, C. (2010). A repairable queueing model with two-phase service, start-up times, and retrial customers. *Computers & Operations Research, 37(7)*: 1181–1190. https://doi.org/10.1016/j.cor.2009.03.003

[45] Park, H. M., Kim, T. S., & Chae, K. C. (2010). Analysis of a two-phase queueing system with a fixed-size batch policy. *European Journal of Operational Research, 206*(1): 118–122. https://doi.org/10.1016/j.ejor.2010.02.005

[46] Thangaraj, V., & Vanitha, S. (2010). A queue with two-stage heterogeneous service, compulsory server vacation, and random breakdowns. *International Journal of Contemporary Mathematical Sciences, 5*(7): 307–322.

[47] Choudhury, G., & Tadj, L. (2011). The optimal control of an M^X/G/1 unreliable server queue with two phases of service and Bernoulli vacation schedule. *Mathematical and Computer Modelling, 54*(1–2): 673–688. https://doi.org/10.1016/j.mcm.2011.03.010

[48] Choudhury, G., & Deka, M. (2012). A single-server queueing system with two phases of service subject to server breakdown and Bernoulli vacation. *Applied Mathematical Modelling, 36*(6): 6050–6060. https://doi.org/10.1016/j.apm.2012.01.047

[49] Tadj, L., Choudhury, G., & Rekab, K. (2012). A two-phase quorum queueing system with Bernoulli vacation schedule, setup, and N-policy for an unreliable server with delaying repair. *International Journal of Services and Operations Management, 12(2)*: 139–164.https://doi.org/10.1504/IJSOM.2012.047103

[50] Singh, C. J., Jain, M., & Kumar, B. (2013). Analysis of queue with two phases of service and m phases of repair for server breakdown under N-policy. *International Journal of Services and Operational Management, 16*(3): 373–406. https://doi.org/10.1504/IJSOM.2013.056769

[51] Vemuri, V. K., Hari Prasad Boppana, V. S. N., & Kotagiri, C. (2011). Optimal strategy analysis of an N-policy two-phase M^X/M/1 queueing system with server startup and breakdowns. *OPSEARCH, 48*: 109–122. https://doi.org/10.1007/s12597-011-0046-1

[52] Salah, K. (2011). Analysis of a two-stage network server. *Applied Mathematics and Computation, 217*(23): 9635–9645. https://doi.org/10.1016/j.amc.2011.04.048

[53] Rudenko, I. V. (2012). Two-phase queuing system with unreliable servers. *Moscow University Mathematics Bulletin, 67*: 145–150. https://doi.org/10.3103/S002713221204002X

[54] Choudhury, G., & Deka, K. (2013). A batch arrival retrial queue with two phases of service and Bernoulli vacation schedule. *Acta Mathematica Applicatae Sinica, English Series, 29*: 15–34. https://doi.org/10.1007/s10255-007-7083-9

[55] Dudina, O., Kim, C., & Dudin, S. (2013). Retrial queuing system with Markovian arrival flow and phase-type service time distribution. *Computers & Industrial Engineering, 66*(2): 360–373. https://doi.org/10.1016/j.cie.2013.06.020

[56] Jianghua, L., & Jinting, W. (2006). An M/G/1 retrial queue with second multi-optional service, feedback, and unreliable server. *Applied Mathematics: A Journal of Chinese Universities, 21*: 252–262. https://doi.org/10.1007/s11766-003-0002-9

[57] Salehirad, M. R., & Badamchizadeh, A. (2009). On the multi-phase M/G/1 queueing system with random feedback. *Central European Journal of Operations Research, 17*: 131–139. https://doi.org/10.1007/s10100-008-0079-6

[58] Jain, M., & Upadhyaya, S. (2010). Optimal repairable Mx/G/1 queue with multi-optional services and Bernoulli vacation. *International Journal of Operational Research, 7*(1): 109–132. https://doi.org/10.1504/IJOR.2010.029520

[59] Wang, J. T., & Li, J. H. (2010). Analysis of the M[X]/G/1 queues with second multi-optional service and unreliable server. *Acta Mathematica Applicatae Sinica, English Series, 26*: 353–368. https://doi.org/10.1007/s10255-010-0001-6

[60] Jain, M., Sharma, G. C., & Sharma, R. (2013). Unreliable server M/G/1 queue with multi-optional services and multi-optional vacations. *International Journal of Mathematics in Operational Research, 5*(2): 145–169. https://doi.org/10.1504/IJMOR.2013.052458

[61] Bhagat, A., & Jain, M. (2013). Unreliable M[X]/G/1 retrial queue with multi-optional services and impatient customers. *International Journal of Operational Research, 17*(2): 248–273. https://doi.org/10.1504/IJOR.2013.053614

[62] Gao, C., Chen, X.-M., Zheng, F., & Zhu, G. (2014). Asymptotic stability of the M/G/1 queueing system with optional second service. *Applied Mathematical Modelling, 38*(19–20): 4705–4716. https://doi.org/10.1016/j.apm.2014.03.032

[63] Rajadurai, P., Saravanarajan, M. C., & Chandrasekaran, V. M. (2014). Analysis of an M[X]/(G1,G2)/1 retrial queueing system with balking, optional re-service under modified vacation policy and service interruption. *Ain Shams Engineering Journal, 5*(3): 935–950. https://doi.org/10.1016/j.asej.2014.02.003

[64] Saravanarajan, M. C., & Chandrasekaran, V. M. (2014). Analysis of M/G/1 feedback queue with two types of services, Bernoulli vacations and random breakdowns. *International Journal of Mathematics in Operational Research, 6*(5): 567–588. https://doi.org/10.1504/IJMOR.2014.064839

[65] Kalidass, K., & Kasturi, R. (2014). A two-phase service M/G/1 queue with a finite number of immediate Bernoulli feedbacks. *OPSEARCH, 51*: 201–218. https://doi.org/10.1007/s12597-013-0136-3

[66] Jiang, T., Liu, L., & Li, J. (2015). Analysis of the M/G/1 queue in multi-phase random environment with disasters. *Journal of Mathematical Analysis and Applications, 430*(2): 857–873. https://doi.org/10.1016/j.jmaa.2015.05.028

[67] Chakravarthy, S. R. (2016). Queueing models with optional cooperative services. *European Journal of Operational Research, 248*(3): 997-1008. https://doi.org/10.1016/j.ejor.2015.08.015

[68] Arivudainambi, D., & Godhandaraman, P. (2015). Retrial queueing system with balking, optional service, and vacation. *Annals of Operations Research, 229*: 67–84. https://doi.org/10.1007/s10479-014-1765-5

[69] Jain, M., Sharma, R., & Sharma, G. C. (2015). Maximum entropy analysis of bulk arrival retrial queue with second optional service and Bernoulli vacation. *International Journal of Industrial and Systems Engineering, 20*(3): 369–396. https://doi.org/10.1504/IJISE.2015.069918

[70] Bhagat, A., & Jain, M. (2016). N-policy for M^X/G/1 unreliable retrial G-queue with preemptive resume and multi-services. *Journal of the Operations Research Society of China, 4*: 437–459. https://doi.org/10.1007/s40305-016-0128-0

[71] Singh, C. J., Jain, M., & Kumar, B. (2016). Unreliable retrial queue with option of additional services and Bernoulli vacation. *Ain Shams Engineering Journal, 7:* 415–429. https://doi.org/10.1016/j.asej.2015.05.006

[72] Vadivu, A. S., & Arumuganathan, R. (2016). Analysis of MAP/G/1/N queue with two phases of service under single (multiple) vacation(s). *International Journal of Operational Research, 25*(1): 47–76. https://doi.org/10.1504/IJOR.2016.073251

[73] Wang, J., Wang, F., Sztrik, J., & Kuki, A. (2017). Finite source retrial queues with two phase service. *International Journal of Operational Research, 30(4)*: 421–440. https://doi.org/10.1504/IJOR.2017.087824

[74] Arivudainambi, D., & Gowsalya, M. (2017). Analysis of an M/G/1 retrial queue with Bernoulli vacation, two types of service and starting failure. *International Journal of Artificial Intelligence and Soft Computing, 6*(3): 222–249. https://doi.org/10.1504/IJAISC.2017.088889

[75] Singh, C. J., Kumar, B., & Kaur, S. (2018). MX/G/1 state dependent arrival queue with optional service and vacation under randomised policy. *International Journal of Industrial and Systems Engineering, 29*(2): 252–272. https://doi.org/10.1504/IJISE.2018.091902

[76] Singh, C. J., Jain, M., & Kaur, S. (2018). Performance analysis of bulk arrival queue with balking, optional service, delayed repair, and multi-phase repair. *Ain Shams Engineering Journal, 9(4)*: 2067–2077. https://doi.org/10.1016/j.asej.2016.08.025

[77] Bagyam, E. A., & Chandrika, K. U. (2019). Fuzzy analysis of bulk arrival two-phase retrial queue with vacation and admission control. *Journal of Analysis, 27*: 209–232. https://doi.org/10.1007/s41478-018-0118-1

[78] Ayyappan, G., & Deepa, T. (2019). Analysis of batch arrival bulk service queue with additional optional service multiple vacation and setup time. *International Journal of Mathematics in Operational Research, 15*(1): 1–25. https://doi.org/10.1504/IJMOR.2019.101609

[79] Singh, C. J., Kaur, S., & Jain, M. (2019). Analysis of bulk queue with additional optional service, vacation and unreliable server. *International Journal of Mathematics in Operational Research, 14*(4): 517–540. https://doi.org/10.1504/IJMOR.2019.100738

[80] Singh, C. J., Kaur, S., & Jain, M. (2020). Unreliable server retrial G-queue with bulk arrival, optional additional service and delayed repair. *International Journal of Operational Research, 38*(1): 82–111. https://doi.org/10.1504/IJOR.2020.106362

[81] Ayyappan, G., & Nirmala, M. (2020). An M[X]/G(a, b)/1 queue with unreliable server, second optional service, closedown, setup with N-policy and multiple vacation. *International Journal of Mathematics in Operational Research, 16*(1): 53–81. https://doi.org/10.1504/IJMOR.2020.104686

[82] Pikkala, V. L., & Edadasari, G. B. (2021). Variant working vacation Markovian queue with second optional service, unreliable server and retention of reneged customers. *International Journal of Mathematics in Operational Research, 19*(1): 45–64. https://doi.org/10.1504/IJMOR.2021.115447

[83] Madheswari, S. P., & Suganthi, P. (2021). Retrial queue with unreliable server and second optional service under K types of Bernoulli vacations. *International Journal of Services and Operations Management, 40(*4): 502–533. https://doi.org/10.1504/IJSOM.2021.120058

[84] Abdollahi, S., & Salehi Rad, M. R. (2022). Analysis of a batch arrival retrial queue with two-phase services, feedback, and admission. *Bulletin of the Iranian Mathematical Society, 48*: 791–804. https://doi.org/10.1007/s41980-021-00547-1

[85] Ayyappan, G., & Thilagavathy, K. (2022). Analysis of MAP/PH1E, PH2O/1 queue with standby server, second optional service, variant arrival rate, Bernoulli schedule vacation, impatient behaviour of customers, breakdown, essential and optional repair. *International Journal of Mathematics in Operational Research, 23*(2): 147–214. https://doi.org/10.1504/IJMOR.2022.127054

[86] Deepa, T., & Azhagappan, A. (2022). Analysis of state dependent M[X]/G(a, b)/1 queue with multiple vacation second optional service and optional re-service. *International Journal of Operational Research, 44*(2): 254–278. https://doi.org/10.1504/IJOR.2022.123393

[87] Laxmi, P. V., & George, A. A. (2023). Analysis of non-Markovian batch service queue with second optional service under transient and steady state domain. *International Journal of Mathematics in Operational Research, 24*(3): 387–407. https://doi.org/10.1504/IJMOR.2023.129496

[88] Ayyappan, G., & Gurulakshmi, G. A. A. (2024). Analysis of MAP/PH/1 queue with differentiated vacation, vacation interruption under N-policy, optional service, breakdown, repair, setup and discouragement of customers. *International Journal of Mathematics in Operational Research, 27*(4): 415–457. https://doi.org/10.1504/IJMOR.2024.138463

[89] Rajadurai, P., Saravanarajan, M. C., & Chandrasekaran, V. M. (2014). Analysis of an M[X]/(G_1, G_2)/1 retrial queueing system with balking, optional re-service under modified vacation policy and service interruption. *Ain Shams Engineering Journal, 5*(3): 935–950. https://doi.org/10.1016/j.asej.2014.02.003

[90] Saravanarajan, M. C., & Chandrasekaran, V. M. (2014). Analysis of MX_XX/G/1 feedback queue with two-phase service, compulsory server vacation, and random breakdowns. *OPSEARCH, 51*: 235–256. https://doi.org/10.1007/s12597-013-0141-6

[91] Ramaya, K., Palaniammal, S., & Vijyalakshmi, C. (2015). Design and analysis of a vacation model for two-phase queueing system with gated service. *Procedia Computer Science, 50*: 301–306. https://doi.org/10.1016/j.procs.2015.04.044

[92] Van Do, T. (2015). A closed-form solution for a tollbooth tandem queue with two heterogeneous servers and exponential service times. *European Journal of Operational Research, 247(2)*: 672–675. https://doi.org/10.1016/j.ejor.2015.05.044

[93] Rajadurai, P., Chandrasekaran, V. M., & Saravanarajan, M. C. (2015). Steady-state analysis of batch arrival feedback retrial queue with two phases of service, negative customers, Bernoulli vacation, and server breakdown. *International Journal of Mathematics in Operational Research, 7*(5): 519–546. https://doi.org/10.1504/IJMOR.2015.071276

[94] Choudhury, G., & Deka, M. (2015). An M/G/1 unreliable server queue with two phases of service and Bernoulli vacation schedule under randomised vacation policy. *International Journal of Applied Management Science, 7*(4): 309–337. https://doi.org/10.1504/IJAMS.2015.073198

[95] Choudhury, G., & Deka, M. (2016). A batch arrival unreliable server queue with two phases of service and Bernoulli vacation schedule under randomised vacation policy. *International Journal of Services and Operations Management, 24*(1): 33–72. https://doi.org/10.1504/IJSOM.2016.075763

[96] Baumann, H., & Sandmann, W. (2017). Multi-server tandem queue with Markovian arrival process, phase-type service times, and finite buffers. *European Journal of Operational Research, 256*: 187–195. https://doi.org/10.1016/j.ejor.2016.07.035

[97] Arivudainambi, D., & Gowsalya, M. (2018). A single server non-Markovian retrial queue with two types of service and Bernoulli vacation. *International Journal of Operational Research, 33*(1): 55–81. https://doi.org/10.1504/IJOR.2018.094231

[98] Ayyappan, G., Nirmala, M., & Karpagam, S. (2020). Analysis of repairable single server bulk queue with standby server, two-phase heterogeneous service, starting failure, and multiple vacation. *International Journal of Applied and Computational Mathematics, 6*: 52. https://doi.org/10.1007/s40819-020-00805-6

[99] Sivasamy, R., & Peter, P. O. (2021). A c-server Poisson queue with customer impatience due to a slow-phase service. *International Journal of Mathematics in Operational Research, 20*(1): 85–98. https://doi.org/10.1504/IJMOR.2021.117632

[100] Dahmane, Z., & Aissani, A. (2021). Optimal routing control of a retrial queue with two-phase service. *International Journal of Mathematics in Operational Research, 20*(1): 20–40. https://doi.org/10.1504/IJMOR.2021.117631

[101] Liu, F., Ma, Z., Si, Q., & Yan, M. (2021). Performance analysis of peer-to-peer networks based on two-phase service queuing theory. *International Journal of Communication Networks and Distributed Systems, 27*(4): 349–365. https://doi.org/10.1504/IJCNDS.2021.119215

[102] Wu, C. H., & Yang, D. Y. (2021). Bi-objective optimization of a queueing model with two-phase heterogeneous service. *Computers & Operations Research, 130*: 105230. https://doi.org/10.1016/j.cor.2021.105230

[103] Kumar, A., & Jain, M. (2022). Cost optimization of an unreliable server queue with two-stage service process under hybrid vacation policy. *Mathematics and Computer Simulations, 204*: 259–281. https://doi.org/10.1016/j.matcom.2022.08.007

[104] Radha, S., Maragathasundari, S., & Swedheetha, C. (2023). Analysis on a non-Markovian batch arrival queuing model with phases of service and multi vacations in cloud computing services. *International Journal of Mathematics in Operational Research, 24*(3): 425–449. https://doi.org/10.1504/IJMOR.2023.129489

[105] Raghavendran, R., & Vidhya, V. (2024). Single server queueing model of Markov modulated bursty arrival with service following phase type distributions for underlay and overlay customers. *Ain Shams Engineering Journal, 15*(8): 102825. https://doi.org/10.1016/j.asej.2024.102825

[106] Ayyappan, G., & Thilagavathy, K. (2024). Analysis of MAP/PH(1), PH(2), PH(3)/1 queueing system with two modes of heterogeneous service, standby server, vacation, impatient behaviour of customers, additional service, start-up time, breakdown and phase type repairs. *International Journal of Operational Research, 49*(1): 85–130. https://doi.org/10.1504/IJOR.2024.136008

[107] Lakshmi, K., & Ramanath, K. (2014). An M/G/1 two-phase multi-optional retrial queue with Bernoulli feedback, non-persistent customers, and breakdown and repair. *International Journal of Operational Research, 19*(1): 78–95. https://doi.org/10.1504/IJOR.2014.057844

[108] Vignesh, P., Srinivasan, S., & Sundari, S. M. (2017). Analysis of non-Markovian batch arrival queueing model with multi-stages of service of restricted admissibility, feedback service, and three optional vacations in production and manufacturing. *International Journal of Mathematics in Operational Research, 11*(3): 285–309. https://doi.org/10.1504/IJMOR.2017.087199

[109] Bhagat, A., & Jain, M. (2020). Retrial queue with multiple repairs, multiple services, and non-preemptive priority. *OPSEARCH, 57*: 787–814. https://doi.org/10.1007/s12597-020-00443-y

[110] Ahuja, A., Jain, A., & Jain, M. (2022). Transient analysis and ANFIS computing of unreliable single server queueing model with multiple stage service and functioning vacation. *Mathematics and Computers in Simulation, 192*: 464–490. https://doi.org/10.1016/j.matcom.2021.09.011

[111] Zadeh, A. B. (2015). A batch arrival multi-phase queueing system with random feedback in service and single vacation policy. *OPSEARCH, 52*: 617–630. https://doi.org/10.1007/s12597-015-0206-9

[112] Varalakshmi, M., Rajadurai, P., Saravanarajan, M. C., & Chandrasekaran, V. M. (2016). An M/G/1 retrial queueing system with two phases of service, immediate Bernoulli feedbacks, single vacation, and starting failures. *International Journal of Mathematics in Operational Research, 9*(3): 302–328. https://doi.org/10.1504/IJMOR.2016.078823

[113] Sundari, S. M., & Srinivasan, S. (2017). Optional services in a non-Markovian queue. *International Journal of Operational Research, 28*(1): 1–17. https://doi.org/10.1504/IJOR.2017.080593

[114] Singh, C. J., & Kumar, B. (2017). Bulk queue with Bernoulli vacation and m-optional services under N-policy. *International Journal of Operational Research, 30*(4): 460–483. https://doi.org/10.1504/IJOR.2017.087826

[115] Li, J., Liu, L., & Jiang, T. (2018). Analysis of an M/G/1 queue with vacations and multiple phases of operation. *Mathematical Methods of Operations Research, 87*: 51–72. https://doi.org/10.1007/s00186-017-0606-0

[116] Rajadurai, P., Saravanarajan, M. C., & Chandrasekaran, V. M. (2018). Cost optimization analysis of retrial queue with K optional phases of service under multiple working vacations and random breakdowns. *International Journal of Industrial and Systems Engineering, 29*(2): 193–222. https://doi.org/10.1504/IJISE.2018.091900

[117] Kumar, B. (2018). Unreliable bulk queueing model with optional services, Bernoulli vacation schedule, and balking. *International Journal of Mathematics in Operational Research, 12*(3): 293–316. https://doi.org/10.1504/IJMOR.2018.090799

[118] Vignesh, P., Srinivasan, S., & Sundari, S. M. (2019). Analysis of a non-Markovian single-server batch arrival queueing system of compulsory three stages of services with fourth optional stage service, service interruptions, and deterministic server vacations. *International Journal of Operational Research, 34*(1*)*:28–53. https://doi.org/10.1504/IJOR.2019.096937

[119] Jain, M., & Kaur, S. (2020). (p,N)-Policy for unreliable server bulk queue with Bernoulli feedback. *International Journal of Applied and Computational Mathematics, 6:* 170. https://doi.org/10.1007/s40819-020-00912-4

[120] Abdollahi, S., Rad, M. R. S., & Farsi, M. A. (2021). Reliability and sensitivity analysis of retrial queue with optional k-phase services, vacation, and feedback. *Iranian Journal of Science and Technology, Transactions of Science, 45:* 1361–1374. https://doi.org/10.1007/s40995-021-01101-8

[121] Jain, M., Kaur, S., & Singh, M. (2021). Unreliable server queue with balking, optional service, Bernoulli feedback, and vacation under randomized policy. In P. K. Kapur, G. Singh, & S. Panwar (Eds.), *Advances in interdisciplinary research in engineering and business management*. Asset Analytics. Springer, Singapore. https://doi.org/10.1007/978-981-16-0037-1_24

[122] Sangeetha, N., Ebenesar Anna Bagyam, J., & Udayachandrika, K. (2022). Performance analysis of retrial queueing system in wireless local area network. In D. Giri, J. K. Mandal, K. Sakurai, & D. De (Eds.), *Proceedings of International Conference on Network Security and Blockchain Technology (ICNSBT 2021)* (Vol. 481, *Lecture Notes in Networks and Systems*). Springer, Singapore. https://doi.org/10.1007/978-981-19-3182-6_10

[123] Li, J. J., & Liu, L. W. (2023). The GI/M/1 queue in a multi-phase service environment with working vacations and Bernoulli vacation interruption. *Journal of the Operations Research Society of China, 11*: 627–656. https://doi.org/10.1007/s40305-021-00371-8

[124] Kumar, B. (2024). Unreliable queue model with multi-phases of services, delay repair, and single vacation. *International Journal of Industrial and Systems Engineering, 48*(1): 100–124. https://doi.org/10.1504/IJISE.2024.140682

MATHEMATICAL AND RELIABILITY MODELS OF MACHINE LEARNING ALGORITHMS FOR EARLY BRAIN CANCER DETECTION

Ajay Singh Yadav[1,*], Navin Ahlawat[2], Bhavani Viswanathan[3],
Garima Pandey[4], Anupam Swami[5], Anjali Malik[6]

•

[1]Department of Mathematics, [2]Department of Computer Science,
[3]Department of Science & Humanities (Library), [4]Department of Chemistry,
[6]Department of Computer Science and Engineering,
[1,2,3,4,6]SRM Institute of Science and Technology, Delhi-NCR Campus, Modinagar,
Ghaziabad, Uttar Pradesh, India, 201204
[5]Department of Mathematics, Km. Mayawati Government Girls P.G. College,
Badalpur, Gr. Noida, India, 203207
ajaysiny@srmist.edu.in, navins@srmist.edu.in, bhavaniviswam@gmail.com
garimap@srmist.edu.in, swami.anupam@gmail.com, anjalim1@srmist.edu.in

Abstract

Early detection of brain cancer is critical for improving patient outcomes, and this study explores the use of Logistic Regression, Reliability Modeling, and mathematical techniques for better diagnostic accuracy. Logistic Regression, a statistical model for binary classification, is used to predict tumor malignancy based on imaging features, offering probabilistic predictions that can guide clinical decisions. Reliability Modeling evaluates the performance and robustness of diagnostic systems, ensuring accurate detection despite varying conditions. By combining these methods, we can improve both the prediction accuracy and reliability of diagnostic systems.The research also integrates optimization and statistical inference to refine these models, ensuring they are both accurate and statistically sound. Hybrid models that combine deep learning with Logistic Regression further enhance the detection of brain tumors by leveraging the strengths of both approaches. The study underscores the potential of AI and mathematical models to revolutionize brain cancer diagnostics, offering more reliable, interpretable, and efficient tools for early detection and improved patient outcomes.

Keywords: Brain Cancer Detection, Logistic Regression, Reliability Modeling, Machine Learning and Hybrid AI Models.

1. Introduction

Brain cancer is a serious and life-threatening condition that arises when abnormal cells in the brain grow uncontrollably, forming tumors that can disrupt normal brain function. It is one of the most challenging forms of cancer to diagnose and treat due to the complexity of the brain and the difficulty in detecting early-stage tumors. Brain cancer can originate within the brain (primary brain tumors) or spread from other parts of the body (secondary or metastatic brain tumors). The most aggressive form, glioblastoma multiforme (GBM), has a particularly poor prognosis, with a median survival rate of only about 12 to 15 months after diagnosis. The global

impact of brain cancer is significant, as it affects thousands of individuals each year, leading to severe neurological impairments, decreased quality of life, and high mortality rates. Despite advancements in medical research, the survival rates for patients with brain cancer remain low, especially for high-grade tumors. Early detection of brain cancer is crucial for improving survival rates and treatment effectiveness. When diagnosed at an early stage, patients have more treatment options available, including surgery, chemotherapy, radiation therapy, and targeted drug treatments. Early diagnosis allows for timely medical intervention, which can slow tumor progression and improve patient outcomes. However, detecting brain cancer in its initial stages is particularly challenging due to the absence of noticeable symptoms or the misinterpretation of early signs as common neurological issues such as headaches, dizziness, or memory loss. Traditional diagnostic methods, including MRI (Magnetic Resonance Imaging), CT (Computed Tomography) scans, and biopsy procedures, are effective but often detect the disease only after significant tumor growth has occurred. Therefore, there is a pressing need for advanced diagnostic techniques that can identify brain cancer at an earlier stage with high accuracy and minimal invasiveness. Mathematical and reliability models play a vital role in enhancing the accuracy of early brain cancer detection and prediction. Mathematical models help in understanding tumor growth dynamics, analyzing imaging data, and optimizing treatment strategies. These models use techniques such as differential equations, machine learning algorithms, and probabilistic modeling to quantify tumor progression and predict future developments. For example, mathematical models based on reaction-diffusion equations can simulate how tumor cells invade surrounding healthy brain tissues, providing insights into the spread of cancer. Machine learning models, particularly deep learning approaches, can analyze medical images to detect subtle patterns that may indicate early-stage tumors, surpassing human diagnostic capabilities (see Figure 1).



Figure 1: *Graphical Visualization of Brain Cancer*

Reliability models, commonly used in engineering and risk assessment, are increasingly being applied in medical diagnostics to improve the dependability of cancer detection systems. These models assess the likelihood of correct and incorrect diagnoses, minimizing false positives and false negatives. Reliability analysis techniques such as survival analysis, fault tree analysis (FTA), and Bayesian networks help predict the progression of brain cancer and evaluate the effectiveness of different diagnostic tools. Survival analysis models, for instance, can estimate patient survival probabilities based on tumor characteristics and treatment history, helping doctors make informed decisions about treatment plans. The integration of AI-driven reliability models ensures that medical diagnostic systems are robust, reducing the risk of errors in identifying brain tumors at an early stage. The combination of mathematical and reliability models in brain

cancer detection and prediction has the potential to revolutionize medical diagnostics. These approaches provide a more precise, data-driven methodology for identifying cancer earlier and with greater accuracy. The development of hybrid models that incorporate AI, statistical methods, and computational techniques is paving the way for more reliable and efficient diagnostic systems. As technology advances, these models will continue to evolve, offering improved diagnostic capabilities, personalized treatment plans, and ultimately better patient outcomes.

2. Mathematical and Reliability Models in Early Brain Cancer Detection and Treatment Planning

Mathematics plays an essential role in the early detection, diagnosis, and treatment planning for brain cancer. By combining applied mathematics, statistical models, and engineering, mathematical frameworks are used to enhance the accuracy and reliability of medical interventions. A major area of focus is the integration of mathematical algorithms with medical imaging technologies such as MRI, CT scans, and PET scans. These imaging tools generate vast amounts of data, and mathematics is vital for processing and extracting valuable insights. Image processing algorithms, like edge detection, segmentation, and enhancement, are key tools in analyzing medical images. These algorithms help identify abnormal areas in the brain, such as tumors, by detecting changes in tissue density or structure. Segmentation, in particular, is used to isolate various regions in an image, such as the brain and potential tumors, allowing for precise measurements of tumor size, shape, and location, which are crucial for early diagnosis. Machine learning techniques further enhance mathematical approaches to brain cancer detection. By training on labeled datasets, these models learn to predict the presence of a tumor in unseen images. They use algorithms to classify images based on features, improving detection and diagnostic accuracy. In addition to imaging, statistical modeling, including Bayesian networks, is used to predict the likelihood of brain cancer. These models consider various risk factors such as age, genetic predisposition, and symptoms, helping clinicians make informed decisions, especially when early symptoms are subtle or ambiguous. Such probabilistic models assist in diagnosing the condition before visible signs appear, allowing for earlier intervention. Mathematics also contributes to understanding tumor dynamics. Differential equations model the growth rate of tumors, allowing researchers to simulate and predict how tumors grow over time. These models consider factors such as nutrient supply, oxygen levels, and immune responses, helping clinicians assess the tumor™s potential growth trajectory and plan treatments accordingly. Optimization techniques are essential in treatment planning. Mathematical optimization, such as linear programming, helps design the most effective therapeutic strategies, balancing radiation doses, targeted areas, and treatment timing. These models aim to deliver the highest radiation dose to the tumor while minimizing damage to healthy tissues, ensuring that the treatment plan is both effective and safe. Reliability models, which are often used in engineering, also have significant applications in evaluating the effectiveness of treatments for brain cancer. These models use statistical tools like survival analysis and failure rate models to predict how reliable a treatment is in reducing tumor size and preventing recurrence. These models also help doctors assess how treatments perform under different conditions and adjust strategies for improved patient outcomes. Soft computing methods, such as fuzzy logic, genetic algorithms, and neural networks, have been adopted in brain cancer research for their ability to handle uncertainty and imprecision inherent in biological systems. Fuzzy logic allows for more flexible decision-making in situations where data is uncertain, such as when dealing with ambiguous tumor characteristics. Genetic algorithms are used to optimize treatment plans and discover potential new drugs by mimicking the process of natural selection (see Figure 2).



Figure 2: *Graphical Representation of Brain Cancer Detection, Prediction, and Treatment Planning*

Overall, mathematics underpins various methods for early brain cancer detection, prediction, and treatment planning. By integrating statistical models, machine learning, optimization, and reliability engineering, these approaches enhance the precision of medical diagnoses and treatment strategies. The use of soft computing further adds flexibility, making it possible to address the uncertainties often present in biological and medical systems. As research continues and artificial intelligence techniques evolve, the integration of mathematical methods will lead to more effective, personalized treatments, ultimately improving patient outcomes and advancing our understanding of brain cancer. Which mathematical equation and reliability operations are used to detect early brain cancer? Let us consider a Logistic Regression Model for tumor classification from medical imaging data. This model is simple yet powerful for binary classification tasks, like identifying whether a brain tumor is cancerous or not. I will formulate it step by step, solve it numerically, and include sensitivity analysis.

3. Related works

Cox [1] introduced the Proportional Hazards Model, which has become a fundamental tool in survival analysis. Within the scope of brain cancer diagnostics, this model facilitates the evaluation of time-to-event data such as patient survival post-diagnosis by incorporating various clinical covariates. Its non-parametric approach is particularly suitable for estimating survival functions and prognostic assessments. James et al. [2] provided a foundational reference on statistical learning, encompassing techniques such as Logistic Regression, Support Vector Machines (SVM), and Random Forests. These methods have proven effective in medical image analysis and clinical data classification for brain tumor diagnosis, enabling risk stratification and predictive modeling. The text also offers practical implementation using R, supporting reproducible research in health data analytics. Kohavi and Provost [3] examined the role of machine learning in knowledge discovery from large datasets, a concept critical in analyzing medical imagery such as MRIs. Their discussion on algorithms like decision trees and SVMs offers a basis for employing classification tools in brain tumor identification. The work of Mellor and Scheinberg [4] highlighted the integration of deep learning especially Deep Neural Networks (DNNs) into cancer detection frameworks. Their analysis demonstrates the superiority of DNNs over conventional machine learning approaches in medical imaging, especially for automating tumor recognition in MRI and CT scans. Wald [5] developed the Wald test, a statistical method used to test parameter significance in models like Logistic Regression. In brain cancer diagnostics, this test is instrumental in identifying significant

predictors among patient demographics and imaging features. Vandenbroucke and Pearce [6] offered a thorough exploration of epidemiological methodologies applicable to disease modeling, including brain cancer. Their work serves as a conceptual framework for integrating statistical epidemiology with machine learning in survival analysis and disease progression studies. Finkelstein and Provost [7] focused on reliability analysis, a key consideration when assessing the robustness and accuracy of diagnostic systems. Their study underscores the necessity of performance validation in systems designed for tumor detection. Liu et al. [8] outlined the evolution and impact of artificial intelligence in healthcare, particularly its transformative role in diagnostic applications. The paper surveys both traditional machine learning techniques and contemporary deep learning approaches, emphasizing AI's potential in early detection and personalized treatment of brain cancer. Shao and Tu [9] investigated resampling methods, such as jackknife and bootstrap, to estimate the variability and generalizability of statistical models. These techniques are critical in evaluating the stability of diagnostic models applied to brain tumor detection. Rohlfing and Maurer [10] presented techniques for the automatic segmentation of brain tumors in MRI data. Effective segmentation is a prerequisite for reliable diagnosis, and their proposed algorithms support the enhancement of machine learning-driven detection systems. Bengio et al. [11] discussed the structure and implementation of deep learning architectures, detailing how these models outperform traditional methods in complex tasks such as medical image classification. Their insights are particularly relevant for brain tumor detection using MRI and CT imaging. Huang et al. [12] developed convolutional neural network (CNN) models for brain tumor detection, demonstrating their effectiveness in tumor classification compared to classical machine learning models. Their study also addressed challenges such as image noise and scan variability. Chauhan and Sharma [13] surveyed various reliability modeling techniques and their relevance to medical diagnostics. Their review underscores the importance of integrating reliability assessments with machine learning models to ensure robustness in real-world applications. Hu et al. [14] proposed a hybrid model that integrates Logistic Regression with deep learning for early brain tumor detection. Their approach leverages the interpretability of Logistic Regression and the feature extraction strengths of deep learning to improve diagnostic accuracy. Perez-Garcia et al. [15] and Zhang et al. [16] presented hybrid diagnostic frameworks that combine CNNs and Logistic Regression. These models aim to harness the classification power of CNNs alongside the simplicity of Logistic Regression for interpretable and precise tumor classification. Mousavi et al. [17] evaluated various feature selection and preprocessing strategies to enhance the performance of Logistic Regression models in early-stage brain tumor detection using MRI data. Nair et al. [18] introduced a reliability-focused evaluation strategy to assess brain tumor detection systems, aiming to ensure consistent model performance under diverse clinical scenarios. Bai et al. [19] emphasized the role of reliability models in augmenting machine learning-based diagnostic systems. Their research illustrates how reliability considerations improve clinical decision-making in brain cancer detection. Lee and Kang [20] explored the integration of reliability engineering with machine learning for tumor diagnostics, highlighting improvements in model accuracy and resilience under operational constraints. Furukawa et al. [21] developed a brain tumor detection model that synergizes MR imaging data with Logistic Regression, applying statistical techniques to enhance model reliability and accuracy. Adiga et al. [22] investigated how combining reliability analysis with machine learning algorithms, such as Random Forests and Logistic Regression, can enhance the effectiveness of MRI-based tumor detection systems. Zhou et al. [23] presented a comprehensive review of various machine learning methods applied to brain tumor diagnosis. Their work offers a comparative evaluation of traditional algorithms and advanced deep learning techniques. Reis et al. [24] focused on the application of deep learning for early detection, particularly the use of CNNs for analyzing medical imaging data. Their review demonstrates the improvements in accuracy achieved through deep learning advancements. Nguyen et al. [25] developed hybrid models combining CNNs and Logistic Regression, aiming to balance high classification performance with computational efficiency. Khanna et al. [26] provided a systematic review of diagnostic model reliability, addressing the challenges and limitations associated with deploying AI in clinical settings. Pati et al. [27] performed a quantitative evaluation of

Logistic Regression-based models, assessing diagnostic accuracy using metrics such as sensitivity, specificity, and precision. Almeida et al. [28] identified the challenges inherent in AI-driven diagnostic systems, particularly the need for reliability and accuracy in clinical environments to prevent misdiagnosis. Sundararajan and Kim [29] explored the integration of explainable AI (XAI) techniques with deep learning and reliability models. Their work aims to enhance transparency in automated diagnostic decisions, a crucial factor for clinical adoption. Zhu et al. [30] proposed hybrid machine learning frameworks for early detection of brain cancer, combining diverse algorithms with MRI data to boost early diagnostic performance. A series of works by Yadav et al. [31-34] and Mahata and Debnath [35] focus on mathematical modeling and analytical optimization, which contribute to the development of precise, computationally efficient models for medical diagnostics.

4. Mathematical Models: Logistic Regression for Brain Cancer Detection

Logistic regression is a statistical model used for binary classification tasks, where the goal is to predict one of two possible outcomes. Unlike linear regression, which predicts a continuous dependent variable, logistic regression is designed to predict probabilities that map to a binary outcome. It is widely used in various fields, including medicine, finance, marketing, and social sciences, due to its simplicity, interpretability, and efficiency. The model is based on the logistic function, also known as the sigmoid function, which ensures that the predicted values lie between 0 and 1, making them interpretable as probabilities. At the core of logistic regression is the concept of the linear equation, which is the same as in linear regression. In linear regression, the relationship between the dependent variable and the independent variables is expressed as a linear function. However, for logistic regression, the dependent variable is a binary outcome (e.g., cancer vs. no cancer, pass vs. fail), so instead of predicting an actual value, the model predicts the probability of the event occurring.

4.1. The mathematical expression for logistic regression can be written as:

Predict the probability P of a tumor being cancerous (P=1) based on measurable features (e.g., size, texture, intensity). The logistic regression equation is:

$$P(y = \frac{1}{X}) = \sigma(z)$$

$$P(y = \frac{1}{X}) = \frac{1}{1 + e^{-z}}$$

$$z = \beta_0 + \beta_1 x_1 + \beta_2 x_2 + \beta_3 x_3 + ... + \beta_n x_n$$

where

1. z: Linear combination of features.
2. $x_1 + x_2 + x_3 + ... + x_n$: Input features (e.g., tumor size, shape).
3. $\beta_1 + \beta_2 + \beta_3 + ... + \beta_n$: Coefficients (weights) learned during training.
4. $\sigma(z)$: Sigmoid function that converts zz into a probability between 0 and 1.

5. Reliability Models in Brain Cancer Prediction

Reliability models and AI techniques play a vital role in improving brain cancer detection and diagnosis. Survival analysis, using models like Kaplan-Meier and Cox proportional hazards, helps estimate survival probabilities and evaluate treatment strategies. Fault Tree Analysis

(FTA) identifies diagnostic system failures, ensuring accurate diagnoses and reducing false positives/negatives. AI models, including Random Forest and XGBoost, aggregate predictions to improve reliability, while hybrid AI models combine deep learning with traditional methods like logistic regression for enhanced accuracy and interpretability. Explainable AI (XAI) techniques, like SHAP and LIME, provide transparency, ensuring AI systems are both accurate and trustworthy in clinical settings. Together, these models enhance early detection, treatment planning, and patient outcomes. In medical diagnostics, reliability refers to the probability that a diagnostic test or system will correctly identify the presence or absence of a condition (in this case, early brain cancer). For detecting early brain cancer, we assume that the system uses some form of medical imaging (like MRI or CT scans) or a set of biomarkers for diagnosis. Let's represent the reliability of the diagnostic system with the following parameters:

1. P(T | D): Probability of detecting cancer when cancer is present (true positive rate or sensitivity).
2. $P(T|\neg D)$: Probability of detecting cancer when no cancer is present (false positive rate).
3. $P(\neg T|D)$: Probability of missing the cancer when it is present (false negative rate).
4. $P(\neg T|\neg D)$: Probability of correctly identifying no cancer when it is not present (true negative rate or specificity).

For a binary diagnostic model, the reliability equation can be formulated based on the system's accuracy and the test's sensitivity and specificity.

1. Reliability, RRR, can be modeled as:

$$R = P(TD) + P(\neg T \neg D)$$

   This equation assumes a simple scenario where the system works if it correctly identifies either the presence or absence of cancer. Additional Reliability Considerations:

   (a) Precision or positive predictive value (PPV) $= P(TD)/P(TD) + P(T\neg D)$
   (b) Recall or sensitivity $= P(TD)/P(TD) + P(\neg TD)$

2. Solution: Let's define the key parameters with typical values from medical tests for early brain cancer detection:

   (a) $P(T|D)$ (Sensitivity) $= 0.90$ (90% of the time, the system detects cancer when it is present)
   (b) $P(T|\neg D)$ (False Positive Rate) $= 0.05$(5% of the time, the system falsely detects cancer when it's not present)
   (c) $P(\neg T|D)$ (False Negative Rate) $= 0.10$ (10 % of the time, the system fails to detect cancer when it's present)
   (d) $P(\neg T|\neg D)$ (Specificity) $= 0.95$ (95 % of the time, the system correctly identifies no cancer when it's absent)

   Using the reliability equation:

$$R = P(TD) + P(\neg T \neg D)$$

$$R = 0.90 + 0.95 = 1.85$$

6. Numerical Example

6.1. logistic regression

1. Input data assume we have two features:
   (a) x_1: Tumor size (in cm).
   (b) x_2: Tumor intensity (grayscale pixel value from MRI).

   TData for a patient:
   (a) $x_1 = 4.5$ (cm).
   (b) $x_2 = 120$ (intensity).

   Model coefficients (from training):
   (a) $\beta_0 = -8.5$ (bias term).
   (b) $\beta_1 = 1.2$ (intensity).
   (c) $\beta_2 = 0.05$
2. Logistic equation calculate z:
$$z = \beta_0 + \beta_1 x_1 + \beta_2 x_2$$
   Substitute values:
$$z = -8.5 + (1.2^{-}4.5) + (0.05^{-}120)$$
$$z = -8.5 + 5.4 + 6$$

Now, calculate the probability using the sigmoid function:

$$P = \frac{1}{1 + e^{-2.9}} = \frac{1}{1 + 0.055} = 0.948$$

Interpretation: The probability of the tumor being cancerous is P=0.948 or 94.8%. Based on a threshold (e.g., 0.5), the model predicts that the tumor is cancerous.

6.2. Reliability Models

Let's assume we have a diagnostic test for 1,000 individuals, where:

1. 100 individuals actually have early brain cancer.
2. 900 individuals do not

Based on our sensitivity and specificity:

1. True Positives (TP): $100^{-}0.90 = 90$
2. False Negatives (FN): $100^{-}0.10 = 101$
3. False Positives (FP): $900^{-}0.05 = 45$
4. True Negatives (TN): $900^{-}0.95 = 855$

Now we can calculate the sensitivity, specificity, and accuracy:

1. Sensitivity $= TP/TP + FN = 9090 + 10 = 0.90$
2. Specificity $= TN/TN + FP = 855855 + 45 = 0.95$
3. Accuracy $= TP + TN/TP + TN + FP + FN = 90 + 8551000 = 0.945$

Table 1: *Below is a summary table of the results:*

Metric	Value
True Positives (TP)	90
False Negatives (FN)	10
False Positives (FP)	45
True Negatives (TN)	855
Sensitivity (Recall))	0.90
Specificity	0.95
Accuracy	0.945

7. Sensitivity Analysis

7.1. logistic regression

Varying Tumor Size (x_1) Let us analyze how the probability changes when the tumor size (x_1) changes, keeping $x_2 = 120$ constant (see Figure 3 and 4).

Table 2: *Sensitivity analysis between probability and tumor size*

x_1 (cm)	Z	P (Probability)
3.0	$-8.5 + (1.2 * 3) + 6 = 1.1$	0.75
4.0	$-8.5 + (1.2 * 4) + 6 = 2.3$	0.91
5.0	$-8.5 + (1.2 * 5) + 6 = 3.5$	0.97
6.0	$-8.5 + (1.2 * 6) + 6 = 4.7$	0.99

Observations:

1. As the tumor size increases, the probability of being cancerous also increases.
2. Sensitivity analysis helps identify how critical each feature is in the model.

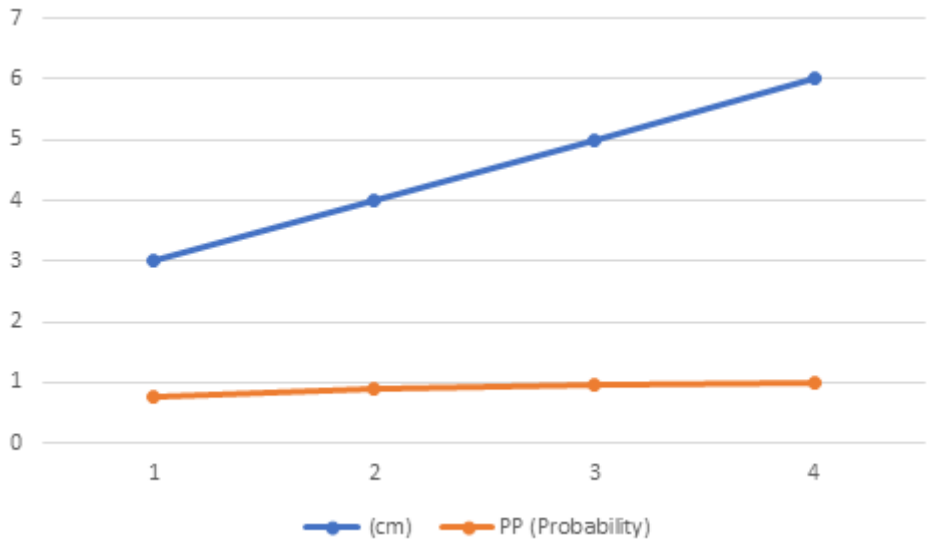


Figure 3: *Variation between probability and tumor size.*

Table for Different Inputs: Let us calculate probabilities for varying combinations of x_1 and x_2

Table 3: *Sensitivity analysis between probability, tumor size and intensity*

x_1 (cm)	x_2 (intensity)	Z	P (Probability)
3.0	100	$-8.5 + 3.6 + 5 = 0.1$	0.52
4.0	120	$-8.5 + 4.8 + 6 = 2.3$	0.91
5.0	130	$-8.5 + 6.0 + 6.5 = 4.0$	0.98
6.0	140	$-8.5 + 7.2 + 7.0 = 5.7$	0.996

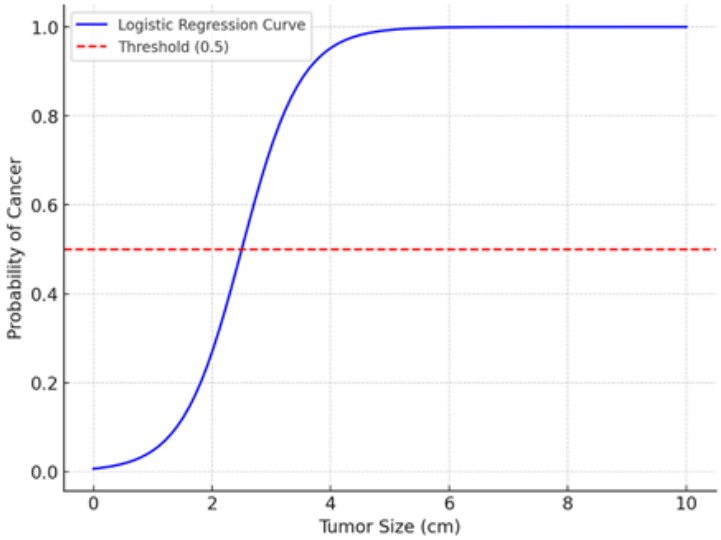


Figure 4: *Logistic regression for Tumor Size vs. Probability of Cancer.*

7.2. Reliability Models

Sensitivity analysis examines how changes in input variables (such as sensitivity, specificity, or the prevalence of cancer) impact the reliability and performance of the diagnostic system. For example, if we change the sensitivity to 0.85 or the false positive rate to 0.10, we could observe how the accuracy and reliability of the model are affected. In this case:

1. Decreased Sensitivity: If sensitivity drops to 0.85, we might get: $TP = 100 * 0.85 = 85$
   Sensitivity $= 85/(85 + 15) = 0.85$(lower recall)

2. Increased False Positives: If the false positive rate increases to 0.10, we get:
   $FP = 900 * 0.10 = 90$, $Specificity = 855/(855 + 90) = 0.90$ (lower specificity)

7.3. Implication

A drop in sensitivity reduces the likelihood of detecting brain cancer early, and an increase in false positives lowers the ability of the system to accurately identify healthy individuals. By tweaking the parameters and conducting a sensitivity analysis, you can assess how reliable and effective the early detection system is under different conditions. This approach ensures that the diagnostic system is robust, accurate, and reliable in detecting early brain cancer, accounting for both the true positive and true negative rates.

8. Comparison of Logistic Regression and Reliability Modeling in Brain Cancer Detection

Logistic Regression and Reliability Modeling are both important in brain cancer detection, but they serve different purposes. Logistic Regression is used to predict the likelihood of brain cancer based on factors like age, genetics, and imaging features. It works by transforming data into a probability score, which helps in risk assessment. Its main advantages are simplicity, interpretability, and computational efficiency. However, it assumes a linear relationship between variables, which may not always hold true, and is sensitive to outliers. Reliability Modeling, on the other hand, evaluates the performance of diagnostic systems like MRI scans, focusing on metrics such as sensitivity, specificity, and accuracy. It helps in ensuring that cancer detection tools work well across patient populations by minimizing false positives and negatives. Reliability Modeling also includes techniques like Fault Tree Analysis (FTA) to identify failure points in diagnostic workflows. While it doesn't predict cancer directly, it improves the reliability of diagnostic tools. Each method has its strengths, with Logistic Regression being better for individual predictions and Reliability Modeling excelling in evaluating system performance. In practical applications, both approaches can be used in combination to achieve the best results. Logistic Regression can be applied to develop predictive models for brain cancer diagnosis, while Reliability Modeling can be used to assess the reliability of these predictive models and diagnostic tests. By integrating both methods, medical professionals can improve the accuracy of brain cancer detection, reduce misclassification errors, and enhance overall diagnostic reliability.

Table 4: *The following table provides a comparison of both methods:*

Criteria	Logistic Regression	Reliability Modeling
Purpose	Predict the probability of an outcome (e.g., cancer)	Assess the reliability of a diagnostic system
Input	Features (e.g., age, gender, imaging results)	true positive, false positive) true positive, false positive)
Output	Probability of a condition (e.g., likelihood of cancer)	Performance metrics (e.g., sensitivity, specificity)
Interpretability	High coefficients give insight into feature importance	Medium focuses on overall system accuracy, not feature-level analysis
Complexity	Low to medium depends on the number of features	Medium requires test results and performance metrics
Use Case	Binary classification vs. no cancer)	System evaluation (e.g., cancer (e.g., assessing MRI scan accuracy)
Limitations	Assumes linearity, sensitive to outliers	Does not directly predict the outcome or understand features
Flexibility	High can be extended to multi class classification	Low typically binary and focused on system performance

9. Challenges and Future Directions

1. The early detection and prediction of brain cancer using mathematical and reliability models face significant challenges but also offer promising future developments. As artificial intelligence (AI) and machine learning become more integrated into medical diagnostics, addressing ethical, privacy, model interpretability, data integration, and computational limitations is critical. Logistic Regression and Reliability Modeling are central to this, providing the ability to predict and evaluate diagnostic performance. Mathematics underpins these models, ensuring their accuracy and real-world applicability, and as these technologies evolve, solutions to existing limitations will pave the way for broader clinical adoption.

2. One major challenge is patient data privacy, as medical diagnoses rely on vast datasets, including imaging scans and genetic information. Ensuring data security while enabling AI models to learn from diverse data sources requires careful compliance with privacy regulations like HIPAA and GDPR. To overcome these hurdles, methods such as differential privacy and homomorphic encryption are being explored to safeguard patient confidentiality. Reliability Modeling also helps assess the security and robustness of diagnostic systems, ensuring that AI-driven tools remain trustworthy.

3. Another challenge is model interpretability. Logistic Regression is widely used for its simplicity and transparency, but more complex models like deep learning outperform it in accuracy but lack clarity. This is crucial in medicine, as clinicians must understand the reasoning behind an AI diagnosis. Mathematical techniques such as Shapley values, feature importance analysis, and Explainable AI (XAI) are essential for improving model transparency. Reliability Modeling also aids in ensuring models' consistency and robustness across different patient groups, helping to avoid biased results.

4. The integration of multi-modal data, including imaging, patient history, genetics, and biomarkers, is another hurdle. Combining these diverse data sources requires advanced statistical techniques like tensor decomposition and multimodal deep learning, which Logistic Regression might struggle with. Reliability Modeling can assess how well these multi-modal systems perform, ensuring optimal results with fewer false positives and negatives. The future of AI in healthcare depends on developing sophisticated frameworks to integrate and interpret various types of medical data.

5. Quantum computing is an emerging area with potential to revolutionize medical diagnostics, including brain cancer detection. Quantum computing can handle large datasets and complex computations much faster than traditional methods. Quantum-enhanced Logistic Regression and quantum support vector machines (QSVMs) are being explored to improve AI performance. Reliability Modeling in quantum computing may help enhance diagnostic robustness and optimization, but this technology is still in its early stages.

6. Mathematics plays a central role in all these advancements, with statistical methods ensuring the reliability of predictions, probability theory managing uncertainty, and optimization techniques improving AI algorithms. Differential equations, Bayesian inference, and Markov models are crucial for understanding disease progression and predicting patient outcomes. As new mathematical models emerge, they will refine AI-driven detection methods, improving their accuracy and reliability.

10. Conclusion

Mathematical and reliability models play a crucial role in early brain cancer detection by improving diagnostic accuracy and system performance. Logistic Regression is effective for predicting the probability of brain cancer in patients based on features like imaging and genetic data, offering a simple and interpretable machine learning approach. However, it assumes a linear relationship between variables, which may not always hold in medical data. Reliability Modeling, on the other hand, evaluates the effectiveness of diagnostic systems by assessing sensitivity, specificity, and error rates, ensuring that medical tests provide accurate results. Mathematics underpins both approaches through probability theory, statistical inference, and optimization techniques. Logistic Regression uses mathematical principles like maximum likelihood estimation, while Reliability Modeling employs statistical distributions such as Weibull and exponential functions to analyze system performance. The integration of AI and machine learning further enhances these models, enabling automated, data-driven cancer detection. Hybrid AI-mathematical models combining statistical and deep learning methods offer improved predictive accuracy while maintaining interpretability. Despite advancements, challenges such as ethical concerns, data privacy, and model transparency need to be addressed. The future lies in integrating multi-modal data

(imaging, genetic, clinical) and leveraging emerging technologies like quantum computing to enhance diagnostic precision. Further research in hybrid models will help create more reliable, AI-driven cancer detection systems, ultimately improving early diagnosis and patient outcomes.

References

[1] Cox, D. R. (1972). Regression Models and Life-Tables (with Discussion). Journal of the Royal Statistical Society: Series B (Methodological), 34(2), 187-220.
[2] James, G., Witten, D., Hastie, T., & Tibshirani, R. (2013). An Introduction to Statistical Learning: With Applications in R. Springer.
[3] Kohavi, R., & Provost, F. (1998). Applications of Machine Learning and the Knowledge Discovery Process. Proceedings of the 4th International Conference on Knowledge Discovery and Data Mining (KDD).
[4] Mellor, A., & Scheinberg, K. (2019). Deep Learning for Medical Diagnosis: A Comprehensive Review of Machine Learning in Cancer Detection. Journal of Biomedical Informatics, 92, 103137.
[5] Wald, A. (1943). Tests of Statistical Hypotheses concerning Several Parameters. Transactions of the American Mathematical Society, 54, 426-482.
[6] Vandenbroucke, J. P., & Pearce, N. (2012). Modern Epidemiology. Lippincott Williams & Wilkins.
[7] Finkelstein, M. O., & Provost, F. (2017). Reliability Analysis: Theory and Practice. Wiley.
[8] Liu, Y., Chen, P. H. C., & Zhi, D. (2021). Artificial Intelligence in Health Care: Past, Present, and Future. The Lancet Digital Health, 3(1), e1-e11.
[9] Shao, J., & Tu, D. (1995). The Jackknife and Bootstrap. Springer.
[10] Rohlfing, T., & Maurer, C. R. (2010). Automatic Brain Tumor Segmentation in Magnetic Resonance Imaging. IEEE Transactions on Medical Imaging, 29(2), 205-213.
[11] Bengio, Y., et al. (2013). Learning Deep Architectures for AI. Foundations and Trends® in Machine Learning, 2(1), 1-127.
[12] Huang, Y., et al. (2017). Brain Tumor Diagnosis with Magnetic Resonance Imaging using Deep Learning. Computers in Biology and Medicine, 88, 50-58.
[13] Chauhan, D., & Sharma, S. (2020). Reliability Modeling and Performance Evaluation of Medical Diagnostic Systems: A Survey. International Journal of Computer Applications, 175(9), 8-13.
[14] Hu, Y., et al. (2019). A Novel Hybrid Model Combining Logistic Regression and Deep Neural Networks for Early Diagnosis of Brain Tumor. Neurocomputing, 365, 158-165.
[15] P©rez-Garca, J. et al. (2020). Improving Brain Tumor Detection with Hybrid AI Models Combining Convolutional Neural Networks and Logistic Regression. Computers in Biology and Medicine, 124, 103928.
[16] Zhang, Y., et al. (2017). Computer-Aided Diagnosis of Brain Tumor Using Logistic Regression and Convolutional Neural Networks. Journal of Neuroscience Methods, 283, 43-52.
[17] Mousavi, M. et al. (2018). Performance of Logistic Regression Models for Early Detection of Brain Tumors in MRI Scans. Medical Imaging Analysis, 47, 15-24.
[18] Nair, V., et al. (2021). Reliability-based Approaches for Evaluating the Performance of Brain Tumor Detection Systems. Journal of Medical Systems, 45(1), 8.
[19] Bai, H. et al. (2020). Integration of Reliability and Machine Learning Models for Medical Diagnostics. IEEE Transactions on Systems, Man, and Cybernetics: Systems, 50(6), 2089-2099.
[20] 20. Lee, S., & Kang, E. (2020). Improving the Robustness of Brain Tumor Detection Models using Reliability Engineering Principles. Journal of Artificial Intelligence in Medicine, 103, 101777.
[21] Furukawa, S., et al. (2018). Development of a Reliable Brain Tumor Detection Model Based on MR Imaging Data and Logistic Regression. Brain Imaging and Behavior, 12(6), 1712-1720.
[22] Adiga, S. et al. (2019). Reliability Modeling of MRI-Based Brain Tumor Detection Using Machine Learning Techniques. Journal of Clinical Neuroscience, 62, 77-85.

[23] Zhou, Z. et al. (2017). A Comprehensive Review of Machine Learning Algorithms for Brain Tumor Diagnosis. Journal of Healthcare Engineering, 2017, 8762549.
[24] Reis, F. et al. (2020). Deep Learning Techniques in Early Brain Tumor Detection: A Survey. Frontiers in Oncology, 10, 293.
[25] Nguyen, T., et al. (2021). Exploring Hybrid AI Models for Brain Tumor Diagnosis: An Evaluation of Logistic Regression and Convolutional Neural Networks. Medical Image Analysis, 69, 101947.
[26] Khanna, S., et al. (2016). Assessment of Reliability for Brain Tumor Detection Models in Clinical Settings: A Systematic Review. Artificial Intelligence in Medicine, 68, 63-77.
[27] Pati, R. et al. (2018). Evaluation of MRI Scans for Brain Tumor Detection Using Logistic Regression and Performance Metrics. Biocybernetics and Biomedical Engineering, 38(4), 759-770.
[28] Almeida, M. et al. (2019). Reliability of AI-Driven Brain Tumor Detection Systems: Challenges and Opportunities. Journal of Biomedical Informatics, 92, 103138.
[29] Sundararajan, V., & Kim, B. (2020). Explainable AI Techniques for Brain Cancer Detection: Combining Deep Learning with Reliability Models. Journal of Computational Biology, 27(1), 61-74.
[30] Zhu, Y., et al. (2020). Improving Early Brain Cancer Detection Using Hybrid Machine Learning Models and MRI Data. Journal of Cancer Research and Clinical Oncology, 146(9), 2397-2407.
[31] Yadav, A. S., Kumar, A., Yadav, K. K., & Rathee, S. (2023). Optimization of an inventory model for deteriorating items with both selling price and time-sensitive demand and carbon emission under green technology investment. International Journal on Interactive Design and Manufacturing (IJIDeM), 1-17. https://doi.org/10.1007/s12008-023- 01689-8
[32] Yadav, K. K., Yadav, A. S., & Bansal, S. (2024a). Interval number approach for two-warehouse inventory management of deteriorating items with preservation technology investment using analytical optimization methods. International Journal on Interactive Design and Manufacturing (IJIDeM), 1-17. https://doi.org/10.1007/s12008-023- 01672-3
[33] Yadav, K. K., Yadav, A. S., & Bansal, S. (2024b). Optimization of an inventory model for deteriorating items assuming deterioration during carrying with two-warehouse facility. Reliability: Theory & Applications, 19(3 (79)), 442-459. https://doi.org/10.24412/1932-2321-2024-379-442-459
[34] Yadav, K. K., Yadav, A. S., & Bansal, S. (2024c). OPTIMIZATION OF A TWO-WAREHOUSE INVENTORY MANAGEMENT FOR DETERIORATING ITEMS WITH TIME AND RELIABILITY-DEPENDENT DEMAND UNDER CARBON EMISSION CONSTRAINTS. Reliability: Theory & Applications, 19(4 (80)), 404-418. https://doi.org/10.24412/1932-2321-2024-480-404-418
[35] Mahata, S., & Debnath, B. K. (2023). The impact of R & D expenditures and screening in an economic production rate (EPR) inventory model for a flawed production system with imperfect screening under an interval-valued environment. Journal of Computational Science, 69, 102027.

IMPROVING THE QUALITY OF INTERVAL PATTERN RECOGNITION BY DIVIDING THE PATIENT SAMPLE IN MEDICAL RESEARCH

Gurami Tsitsiashvili[1], Vera Nevzorova[2], Pavel Dunts[2],
Angelina Talko[2], Marina Osipova[1,3]

•

[1]Institute for Applied Mathematics FEBRAS, Russia
[2]Pacific State Medical University, Russia
[3]Far Eastern Federal University, Russia
guram@iam.dvo.ru, nevzorova@inbox.ru, dpv@bk.ru, talkang92@mail.ru, mao1975@list.ru

Abstract

In this paper, we consider a way to improve the quality of interval pattern recognition by dividing the sample into parts. This method is used to study erythrocyte and platelet germs of haematopoiesis for the ability to positively treat haematological patients from COVID-19. Along with this, this method of improving the quality of interval recognition is used to identify predictors of "difficult" tracheal intubation during artificial ventilation during anaesthetic support of surgical interventions. Despite the rather strong difference between these medical tasks, they are united in this research context by the possibility of improving the quality of recognition through a more specialized study of each sub sample of patients after dividing the sample into parts.

Keywords: interval pattern recognition, big data, dividing sample into parts, Coronavirus infection, haemoblastosis, tumor

Introduction

In this paper, during a computational experiment, the possibilities of the interval pattern recognition method are analysed when dividing the initial sample of patients into parts. Analytically, it is not difficult to prove that such a division of the sample never worsens and can improve the quality of recognition using this method. However, only a computational experiment allows us to assess how much it is possible to improve the quality of recognition in the statistical analysis of research data in medicine.

Arrays of data that you often have to work with (see, for example, the first article) when solving various image recognition tasks have the following properties. On the one hand, these arrays are short samples (Rare events). On the other hand, the presence of a large number of features characterizing individual patients in the sample makes arrays of observations with Big data very inconvenient for using methods of multidimensional statistics. Moreover, the data arrays in question contain such a feature as a negative or positive outcome of the disease. This circumstance required the use of the interval pattern recognition method, in which it is possible to correctly identify all patients with an unfavourable outcome.

In this paper, the interval pattern recognition algorithm is briefly described and its properties are given. Among them, the most significant is the use of dividing the sample into parts in order to increase the recognition coefficient when solving specific medical problems. The study of

platelet and erythrocyte germs of hematopoiesis in haematological patients who had Coronavirus Disease 2019 (COVID-19) was chosen as the first of them. The second task is related to the identification of predictors of "difficult" tracheal intubation during artificial ventilation during anesthetic support of surgical interventions.

Despite the rather strong difference between these tasks, they are united in this research context by the possibility of improving the quality of recognition through a more specialized study of each sub sample of patients after dividing the sample into parts.

The aim of the study is to improve the clinical decision-making process based on predictive statistics in some medical scientific research. In accordance with the goal, the tasks are set:
1. To evaluate the role of peripheral blood platelet and erythrocyte germ morphometry data in Covid-19 outcomes in haematological patients.
2. Identification of predictors and risk factors for "difficult" tracheal intubation while ensuring patency of the upper respiratory tract during general anaesthesia.

1. Interval pattern recognition and its properties

Suppose there is a set of observations $\{(x_1, \mathbf{y_1}), \dots, (x_n, \mathbf{y_n})\}$ monitoring the condition of patients after the applied treatment. The x_k element can take the values 0 or 1, let's call it the main feature. The main feature is $x_k = 1$, if the outcome of treatment is negative, $x_k = 0$, if the outcome of treatment is positive. The vector $\mathbf{y_k} = (y_{k1}, \dots, y_{km})$, $k = 1, \dots, n$, is a vector of accompanying features and consists of m components determined by laboratory methods. Let's denote $K = \{k : \ x_k = 1\}$ and put $S = \{1, \dots, n\} \setminus K$. Our task is to recognize the vector of the concomitant feature $\mathbf{y_k}$ of the treatment outcome, i.e. belonging to the index k the set of K or S.

This problem is solved using the following interval recognition procedure. First, the boundaries of the segments to which the components y_{ki}, $k \in K$, of the vectors of accompanying features belong are constructed. For each i, $1 \le i \le m$, we calculate

$$z_i = \min_{k \in K} y_{ki}, \ Z_i = \max_{k \in K} y_{ki}, \ i = 1, \dots, m. \tag{1}$$

Then the decisive rule determining whether the index j belongs to the set K is determined by the condition

$$y_{ji} \in [z_i, \ Z_i], \ i = 1, \dots, m. \tag{2}$$

Such a crucial rule always correctly recognizes $j \in K$. Denote by L the set of indices that are correctly recognized and belong to the set of S. Then the quality of interval recognition is determined by the equality $\rho = \dfrac{|K| + |L|}{n}$. Here $|J|$ means the number of elements of the set $J \subseteq \{1, \dots, n\}$. The ρ value characterizes the proportion of correctly recognized objects from the set $\{1, \dots, n\}$.

The interval recognition rule has the following properties, which are easy to establish by mathematical induction.
1. All objects from the K risk zone are recognized correctly. This statement automatically follows from the formulas (1), (2).
2. Increasing the number of components of the vector $\mathbf{y}_k = (y_{k1}, \dots, y_{km})$ does not decrease (and in many cases increases) the quality of interval recognition. Indeed, the addition of a new feature (the component of the vector $\mathbf{y}_k$) does not change the correct recognition of the index $k \in K$, but reduces the possibility of incorrect recognition of the index $k \in L$.
3. Dividing the sample $\{1, \dots, n\}$ into disjoint subsamples (for example, $\{1, \dots, n_*\}$, $\{n_* + 1, \dots n\}$) does not decrease (and in many cases increases) the quality of interval recognition. The proof of this property repeats the proof of the previous property of the interval pattern recognition algorithm.
4. The computational complexity of implementing interval recognition depends linearly on the number of objects n and on the number of m components of the vectors of associated features. This allows you to build fairly fast data processing algorithms. This statement automatically follows from the formulas (1), (2).

2. Identification of predictors and risk factors for "difficult" tracheal intubation with artificial ventilation during general anaesthesia in patients with thyroid diseases

Some types of general anaesthesia involve prosthetics of the respiratory function using artificial respiration devices [1]. During anaesthesia, various methods are used to ensure patency of the upper respiratory tract, but in the vast majority of cases it is tracheal intubation. In this case, breathing is carried out through a special device ? an endothalial tube, which is placed in the trachea and connected to an artificial respiration machine. In some cases, the process of visualizing the trachea is difficult for objective reasons, so examination of the glottis may be partially difficult or not possible. As a result, the endothelial tube cannot be advanced and a critical situation arises: "I cannot intubate, I cannot ventilate."

After the operation, the patient regains independent breathing, wakes up, and the tube is removed. In some cases, the process of placing an endothelial tube into the trachea is fraught with difficulties. They are mainly related to the structural features of the respiratory tract and the presence of pathology.

There are various approaches (scales) for assessing the respiratory tract and identifying risks when placing an endothelial tube. All scales are focused on the assessment of anatomical parameters, but no approach provides an accurate guarantee of prognosis. Moreover, none of the scales assesses the thyroid gland, an organ intimately located near the respiratory tract, which, when enlarged, can lead to changes in anatomy. Accordingly, the development of methods for assessing the respiratory tract and predicting "difficult" ventilation and tracheal intubation (placing a tube in the trachea) is relevant.

A prospective randomized trial was conducted at the Regional Clinical Hospital 2, Vladivostok in 2025. Before the planned elective surgery and anaesthetic care, all patients underwent the required amount of laboratory and instrumental examinations. In the absence of deviations from the reference values, surgical intervention was planned. On the eve of the upcoming surgery, the patients were examined by an anaesthesiologist.

The study group consisted of 35 patients who had scheduled surgery for thyroid disease. The control group consisted of 21 patients who underwent hernioplasty.

Inclusion criteria: age over 18 years; ability to lie on your back; physical status according to the American Society of Anaesthesiologists (ASA) I-III art.; general anaesthesia with tracheal intubation. Criteria for: inability to stand horizontally on the operating table; physical status according to ASA IV-VI; pregnancy; emergency surgical procedures. In the preoperative period, all patients underwent a routine assessment of the respiratory tract in the sitting and supine positions.

Primary endpoints: the number of tracheal intubation attempts, optimization of tracheal intubation. Secondary points: ventilation - masked artificial ventilation of the lungs before intubation, laryngoscopy - visualization of the glottis, intubation - "difficult" intubation - placement of a tube into the trachea, classification of laryngeal structures obtained during visualization during direct laryngoscopy (R.S. Cormack and J.R. Lehane modified by T.M. Cook [4]) (see, [5]).

The study group consisted of 35 patients. The influence of the following features on the primary and secondary endpoints was evaluated: body mass index, the volume of the thyroid gland (cm^3), assessment of the respiratory tract by Mallampati, LEMON scale for predicting difficult tracheal intubation (L (Look), E (Evaluate), M (Mallampati), O (Obstruction), N (Neck mobility); M.J. Reed, 2004) [2]), a test with biting the red border of the upper lip, the distance from the skin to the epiglottis (mm), hyomental distance (mm), the distance from the skin to the sublingual bone(mm, not determ ined in all patients), the tongue thickness of the (mm).

Table 1: *RC during surgery and thyroid surgery (RC - recognition coefficient).*

	RC during surgical intervention	Thyroid surgery gland (thyroid gland)
Ventilation	1	1
Intubation	0.971429	0.971429
More than 1 attempt Tracheal Intubation	0.971429	0.971429
Laryngoscopy	1	0.742857
Optimization of execution Tracheal intubation	1	0.714286
Cormack Lehane	1	0.6

Table 1 shows the results of RC calculations for various characteristics without dividing the sample by thyroid volume. It can be seen from it that during surgical intervention the RC is very high, and in some cases the RC for the thyroid gland is lower. To increase thyroid RC, the initial sample was experimentally divided into intervals (above and below a certain value). Some results of the comparative analysis of the calculations performed are given in the Table 2. You can see how the RC is rising.

Table 2: *RC in surgical intervention and on the thyroid gland (RC - recognition coefficient, CR - correctly recognized).*

Laryngoscopy	Thyroid Volume > 40	Thyroid Volume ≤ 40	Throughout range	by intervals
Total	7	28	35	35
Critical value 1 hline Uncritical value 0	2 5	8 20	10 25	10 25
CR with the value 0	5	17	16	5+7=12
RC	1	0.89286	0.74286	0.91429
Intubation	Thyroid Volume > 40	Thyroid Volume ≤ 40	Throughout range	by intervals
Total	7	28	35	35
Critical value 1 hline Uncritical value 0	2 5	7 21	9 26	9 26
CR with the value 0	5	17	16	5+17=22
RC	1	0.85714	0.71429	0.88571
Cormack Lehane	Thyroid Volume > 50	Thyroid Volume ≤ 50	All Over range	by Intervals
Total	7	28	35	35
Critical values 2,3,4	2	11	13	13
Uncritical values 0.1	5	17	22	22
CR with values 0,1	5	8	8	5+87=13
RC	1	0.67857	0.6	0.74286

3. Investigation of platelet and erythrocyte germs of haematologesis in haematological patients with COVID-19

Patients with malignant blood diseases are at higher risk of severe COVID-19 than the general population [3]-[5]. This is due to immunosuppression caused by both the disease itself and specific antitumor therapy. During the ongoing pandemic of coronavirus infection, identifying risk factors for an adverse outcome of the disease is an urgent task for the healthcare system. Monitoring of haematological abnormalities during the course of COVID-19 in patients with haematologic malignancies is critical, allowing assessing the severity of the condition and the risk of adverse events.

A general blood test is available at any medical facility. COVID-19 causes various haematological abnormalities, including anemia and thrombocytopenia. These changes are much more pronounced in patients with severe COVID-19 disease and, thus, can serve as a possible biomarker for those who need hospitalization and treatment in the intensive care unit. Anemia and thrombocytopenia in haematological patients with COVID-19 serve as indicators of severe course and risk of multiple organ failure. Their dynamic evaluation makes it possible to predict outcomes and optimize therapy. Special attention is required for patients with malignant haematological diseases due to the risk of life-threatening complications.

Data from medical records of 44 patients with blood tumor diseases who were treated for COVID-19 coronavirus infection in the infectious diseases department of Regional Clinical Hospital 2 in Vladivostok in the period from 2020-2022. The interval pattern recognition method using a zero-one matrix was used to process medical information. This made it possible to highlight several groups patients and compare the recognition quality between the groups.
Group 1 (characteristics of platelet parameters): PLT(10 in 9/L) - total platelet count, MPV(fL) - average platelet volume, PDW(fL) - the width of platelet distribution, PCT - thrombocrit.
Group 2 (characteristics of erythrocyte parameters): RBC - total number of red blood cells, HGB (g/L) - hemoglobin level, MCV (fL) - the average volume of a red blood cell, MCH (pg) - the hemoglobin content in the erythrocyte.

Table 3 shows the recognition results for different patient groups from the initial sample, which included 44 patients. Table 4 shows the recognition results for a reduced sample of 29 patients. The division of this sample into sub samples (see Table 4) significantly affects the recognition coefficient. Moreover, depending on the age category, the quality of recognition for the 1st group of signs (platelets) increases with increasing age of the examined, and the quality of recognition for the 2nd group of signs (erythrocytes) decreases.

Based on the results obtained (in a small sample), patients in the range of 61-69 years have a risk of death in the presence of anemia. In patients over 70 years of age, thrombocytopenia and a decrease in platelet parameters are of prognostic importance and can be regarded as risk factors for an unfavorable outcome.

Table 3: *Recognition results for different patient groups from the original sample (MT – malignant tumors, M – men, W – women).*

patients	all	W	M	from 70 years old	61 – 69 years old	up to 60 years old	MT
Total	44	23	21	10	19	15	36
The dead	16	8	8	6	6	4	15
Survivors	28	15	13	4	13	11	21
CR survivors (platelets)	8	7	8	4	9	5	5
RC(platelets)	0.54	0.65	0.76	1	0.79	0.6	0.56
CR survivors (red blood cells)	8	4	6	2	10	11	7
RC (red blood cells)	0.54	0.52	0.67	0.8	0.84	1	0.61

Table 4: *Results recognition results for different groups of a reduced sample of 29 patients.*

patients	from 70 years old	61 – 69 years old	from 61 years old (by whole group)	from 61 years old (by subgroups)
Total	10	19	29	29
Deceased	6	6	12	12
Survivors	4	13	17	17
CR survivors (platelets)	4	9	8	4+9=13
RC (platelets)	1	0.79	0.69	0.86
CR survivors (red blood cells)	2	10	4	2+10=12
RC(erythrocytes)	0.8	0.84	0.55	0.83

The method proposed in the work, despite the small sample size, allows for a fairly contrasting comparison of the state of platelet and erythrocyte hematologesis germs at risk of fatal events in haematological patients who have suffered COVID-19.

4. Conclusion

Due to its high speed, the interval pattern recognition method proved to be convenient for processing large data and showed its effectiveness and practical significance in the two medical studies presented.

The research was carried out within the state assignment for IAM FEB RAS N 075-00459-25-00.

References

[1] Cook, T. M. (2000). A new practical classification of laryngeal view. *Anaesthesia*, 55: 275–279.

[2] Dunts, P. V. et al. (2023). Modifed Delphi analysis of the guidelines of the All-Russian public organization "Federation of Anesthesiologists and Reanimatologists" "The use of non-invasive lung ventilation". *Annals of Critical Care*, 4: 99–111.(In Russian). DOI: 10.21320/1818-474X-2023-4-99-111.

[3] Pinana, J. L. et al. (2020) Risk factors and outcome of COVID-19 in patients with haematological malignancies. *Experimental haematology and oncology*, 9: 21–25. DOI: 10.1186/s40164-020-00177-z

[4] Gossell-Williams M. Faculty Opinions recommendation of Case Fatality Rate of Cancer Patients with COVID-19 in a New York Hospital System. Faculty Opinions. Post-Publication Peer Review of the Biomedical Literature, 2020.

[5] Kaprin, A. D. et al. (2020). The impact of the COVID-19 pandemic on cancer practice. *Siberian Journal of Oncology*, 19(3): 5–22 (In Russian). DOI: 10.21294/1814-4861-2020-19-3-5-22.

EFFICIENT ESTIMATION OF POPULATION MEAN USING MEDIAN OF AUXILIARY VARIABLE AND SIMULATION UNDER SRS

RizwanYousuf

•

[1]Department of Mathematics Chandigarh University Mohali Punjab 140413, India
Email:[1]rizwanwar50@gmail.com,

Abstract

In this study, we propose two modified ratio estimators for the estimation of the population mean of a study variable using the median of an auxiliary variable. Theoretical expressions for the bias and mean squared error (MSE) of the proposed estimators are derived under simple random sampling. We establish the conditions under which these estimators outperform existing modified ratio estimators. To validate the theoretical findings, both an empirical study using natural population data and a comprehensive simulation study are conducted. The simulation results consistently demonstrate the superior efficiency of the proposed estimators across varying sample sizes and correlation structures. These findings highlight the practical applicability and robustness of the proposed estimators in survey sampling.

Keywords: Bias, Class, Mean squared error, Natural populations, Simple random sampling.

I. Introduction

The simplest estimator of population mean is the sample mean obtained by using simple random sampling without replacement (SRSWOR), when there is no further information on the auxiliary variable available. Occasionally in sample surveys, along with the study variable Y, information on auxiliary variable X, correlated with Y, is also collected. This information on auxiliary variable X may be utilized to obtain a more efficient estimator of the population mean. Ratio method of estimation is an attempt in this direction. This method of estimation may be used when (i) X represent the same character as Y, but measured also on previous date. When a complete count of the population was made and (ii) the character $X$is cheaply, quickly and easily available. Consider a finite population U = {U1, U2,..., U}of N distinct and identifiable units. Let Y is a study variable with value Yi measured on Ui;i=1,2,3,...,N giving a vector Y ={Y1, Y2 ,..., YN } and let X is an auxiliary variable which is readily available. The problem is to estimatethepopulation mean $\overline{Y} = \frac{1}{N}\sum_{i=1}^{N} Y_i$ with some desirable properties on the basis of a random sample selected from the population U using auxiliary information. When population parameters of the auxiliary

Table 1: *Existing modified ratio estimators (Class I) with the constants, the biases and the mean squared errors*

Estimator	Constant Ri	Bias –B(.)	Mean squared error MSE(.)
$\hat{\bar{Y}}_1 = \frac{\bar{y}+b(\bar{X}+\bar{x})}{(\beta_2\bar{x}+C_X)}(\beta_2\bar{X}+C_X)$ Kadilar and Cingi[4]	$R_1 = \left[\frac{\beta_2\bar{Y}}{\beta_2\bar{X}+C_X}\right]$	$\frac{(1-f)}{n}\frac{S_x^2}{\bar{Y}}R_1^2$	$\frac{(1-f)}{n}\left(R_1^2S_x^2+S_y^2(1-\rho^2)\right)$
$\hat{\bar{Y}}_2 = \frac{\bar{y}+b(\bar{X}+\bar{x})}{(C_X\bar{x}+\beta_2)}(C_X\bar{X}+\beta_2)$ Kadilar and Cingi[4]	$R_2 = \left[\frac{C_X\bar{Y}}{C_X\bar{X}+\beta_2}\right]$	$\frac{(1-f)}{n}\frac{S_x^2}{\bar{Y}}R_2^2$	$\frac{(1-f)}{n}\left(R_2^2S_x^2+S_y^2(1-\rho^2)\right)$
$\hat{\bar{Y}}_3 = \frac{\bar{y}+b(\bar{X}+\bar{x})}{(\beta_1\bar{x}+\beta_2)}(\beta_1\bar{X}+\beta_2)$ Yan and Tian[3]	$R_3 = \left[\frac{\beta_1\bar{Y}}{\beta_1\bar{X}+\beta_2}\right]$	$\frac{(1-f)}{n}\frac{S_x^2}{\bar{Y}}R_3^2$	$\frac{(1-f)}{n}\left(R_3^2S_x^2+S_y^2(1-\rho^2)\right)$
$\hat{\bar{Y}}_4 = \frac{\bar{y}+b(\bar{X}+\bar{x})}{(C_X\bar{x}+\rho)}(C_X\bar{X}+\rho)$ Kadilar and Cingi[5]	$R_4 = \left[\frac{C_X\bar{Y}}{C_X\bar{X}+\rho}\right]$	$\frac{(1-f)}{n}\frac{S_x^2}{\bar{Y}}R_4^2$	$\frac{(1-f)}{n}\left(R_4^2S_x^2+S_y^2(1-\rho^2)\right)$
$\hat{\bar{Y}}_5 = \frac{\bar{y}+b(\bar{X}+\bar{x})}{(\rho\bar{x}+C_X)}(\rho\bar{X}+C_X)$ Kadilar and Cingi[5]	$R_5 = \left[\frac{\rho\bar{Y}}{\rho\bar{X}+C_X}\right]$	$\frac{(1-f)}{n}\frac{S_x^2}{\bar{Y}}R_5^2$	$\frac{(1-f)}{n}\left(R_5^2S_x^2+S_y^2(1-\rho^2)\right)$
$\hat{\bar{Y}}_6 = \frac{\bar{y}+b(\bar{X}+\bar{x})}{(\beta_2\bar{x}+\rho)}(\beta_2\bar{X}+\rho)$ Kadilar and Cingi[5]	$R_6 = \left[\frac{\beta_2\bar{Y}}{\beta_2\bar{X}+\rho}\right]$	$\frac{(1-f)}{n}\frac{S_x^2}{\bar{Y}}R_6^2$	$\frac{(1-f)}{n}\left(R_6^2S_x^2+S_y^2(1-\rho^2)\right)$
$\hat{\bar{Y}}_7 = \frac{\bar{y}+b(\bar{X}+\bar{x})}{(\rho\bar{x}+\beta_2)}(\rho\bar{X}+\beta_2)$ Kadilar and Cingi[5]	$R_7 = \left[\frac{\rho\bar{Y}}{\rho\bar{X}+\beta_2}\right]$	$\frac{(1-f)}{n}\frac{S_x^2}{\bar{Y}}R_7^2$	$\frac{(1-f)}{n}\left(R_7^2S_x^2+S_y^2(1-\rho^2)\right)$
$\hat{\bar{Y}}_8 = \frac{\bar{y}+b(\bar{X}+\bar{x})}{(\rho\bar{x}+Md)}(\rho\bar{X}+Md)$	$R_8 = \left[\frac{\rho\bar{Y}}{\rho\bar{X}+Md}\right]$	$\frac{(1-f)}{n}\frac{S_x^2}{\bar{Y}}R_8^2$	$\frac{(1-f)}{n}\left(R_8^2S_x^2+S_y^2(1-\rho^2)\right)$

variable *X* such as Population Mean, Coefficient of Variation, Coefficient of Kurtosis, Coefficient of Skewness, Correlation Coefficient, Median are known, a number of estimators such as ratio, product and linear regression estimators and their modifications are proposed in the literature. Before discussing further about the modified ratio estimators and the proposed modified ratio estimators the notations to be used in this paper are described below:

The ratio estimator for estimating the population mean $\bar{Y}$ of the study variable Y is defined as

$$\hat{\bar{Y}}_R = \frac{\bar{y}}{\bar{x}}\bar{X} = \hat{R}\bar{X} \tag{1}$$

Where $\hat{R} = \frac{\bar{y}}{\bar{x}} = \frac{y}{x}$ is the estimate of $R = \frac{\bar{y}}{\bar{x}} = \frac{y}{x}$

The ratio estimator given in (1) is more precise than the SRSWOR sample mean, when there exists a positive correlation between X and Y. Further improvements are also achieved on the classical ratio estimator by introducing a large number of modified ratio estimators with the use of known parameters like, Coefficient of Variation, Coefficient of Kurtosis, Coefficient of Skewness and Population Correlation Coefficient, Median. The lists of modified ratio estimators together with their biases, mean squared errors and constants available in the literature are classified into two

classes namely Class 1, Class 2 and are given respectively in Table 1 and Table 2 respectively.

Table 2: *Existing modified ratio estimators (Class II) with the constants, the biases and the mean squared errors*

Estimator	Constant R_i	Bias –B(.)	Mean squared error MSE(.)
$\hat{\bar{Y}}_9 = \bar{y}\left[\frac{C_X\bar{X}+\beta_2}{C_X\bar{x}+\beta_2}\right]$ Upadhyayaand Singh [1]	$\theta_9 = \left[\frac{C_X\bar{X}}{C_X\bar{X}+\beta_2}\right]$	$\frac{(1-f)}{n} = \bar{Y}\left(\theta_9{}^2 C_X{}^2 - \rho\,\theta_9 C_X C_y\right)$	$\frac{(1-f)}{n} = \bar{Y}^2\left(C_y^2 + \theta_9{}^2 C_X{}^2 - 2\rho\,\theta_9 C_X C_y\right)$
$\hat{\bar{Y}}_{10} = \bar{y}\left[\frac{\beta_2\bar{X}+C_X}{\beta_2\bar{x}+C_X}\right]$ Upadhyaya and Singh [1]	$\theta_{10} = \left[\frac{\beta_2\bar{X}}{\beta_2\bar{X}+C_X}\right]$	$\frac{(1-f)}{n} = \bar{Y}\left(\theta_{10}{}^2 C_X{}^2 - \rho\,\theta_{10} C_X C_y\right)$	$\frac{(1-f)}{n} = \bar{Y}^2\left(C_y^2 + \theta_{10}{}^2 C_X{}^2 - 2\rho\,\theta_{10} C_X C_y\right)$
$\hat{\bar{Y}}_{11} = \bar{y}\left[\frac{\beta_1\bar{X}+S_X}{\beta_1\bar{x}+S_X}\right]$ Singh [2]	$\theta_{11} = \left[\frac{\beta_1\bar{X}}{\beta_1\bar{X}+S_X}\right]$	$\frac{(1-f)}{n} = \bar{Y}\left(\theta_{11}{}^2 C_X{}^2 - \rho\,\theta_{11} C_X C_y\right)$	$\frac{(1-f)}{n} = \bar{Y}^2\left(C_y^2 + \theta_{11}{}^2 C_X{}^2 - 2\rho\,\theta_{11} C_X C_y\right)$
$\hat{\bar{Y}}_{12} = \bar{y}\left[\frac{\beta_2\bar{X}+S_X}{\beta_2\bar{x}+S_X}\right]$ Singh [2]	$\theta_{12} = \left[\frac{\beta_2\bar{X}}{\beta_2\bar{X}+S_X}\right]$	$\frac{(1-f)}{n} = \bar{Y}\left(\theta_{12}{}^2 C_X{}^2 - \rho\,\theta_{12} C_X C_y\right)$	$\frac{(1-f)}{n} = \bar{Y}^2\left(C_y^2 + \theta_{12}{}^2 C_X{}^2 - 2\rho\,\theta_{12} C_X C_y\right)$
$\hat{\bar{Y}}_{13} = \bar{y}\left[\frac{\beta_2\bar{X}+\beta_1}{\beta_2\bar{x}+\beta_1}\right]$ Yan and Tian[3]	$\theta_{13} = \left[\frac{\beta_2\bar{X}}{\beta_2\bar{X}+\beta_1}\right]$	$\frac{(1-f)}{n} = \bar{Y}\left(\theta_{13}{}^2 C_X{}^2 - \rho\,\theta_{13} C_X C_y\right)$	$\frac{(1-f)}{n} = \bar{Y}^2\left(C_y^2 + \theta_{13}{}^2 C_X{}^2 - 2\rho\,\theta_{13} C_X C_y\right)$
$\hat{\bar{Y}}_{14} = \bar{y}\left[\frac{\beta_1\bar{X}+\beta_2}{\beta_1\bar{x}+\beta_2}\right]$ Yan and Tian[3]	$\theta_{14} = \left[\frac{\beta_1\bar{X}}{\beta_1\bar{X}+\beta_2}\right]$	$\frac{(1-f)}{n} = \bar{Y}\left(\theta_{14}{}^2 C_X{}^2 - \rho\,\theta_{14} C_X C_y\right)$	$\frac{(1-f)}{n} = \bar{Y}^2\left(C_y^2 + \theta_{14}{}^2 C_X{}^2 - 2\rho\,\theta_{14} C_X C_y\right)$
$\hat{\bar{Y}}_{15} = \bar{y}\left[\frac{C_X\bar{X}+\beta_1}{C_X\bar{x}+\beta_1}\right]$ Yan and Tian[3]	$\theta_{15} = \left[\frac{C_X\bar{X}}{C_X\bar{X}+\beta_1}\right]$	$\frac{(1-f)}{n} = \bar{Y}\left(\theta_{15}{}^2 C_X{}^2 - \rho\,\theta_{15} C_X C_y\right)$	$\frac{(1-f)}{n} = \bar{Y}^2\left(C_y^2 + \theta_{15}{}^2 C_X{}^2 - 2\rho\,\theta_{15} C_X C_y\right)$

For a more detailed discussion on the ratio estimator and its modifications one may refer to [1], [2], [3], [4],[5], [6],[7], [8], [9], [10], [11], [12], [13],[14], 15], [16], [17] ,[18]and [19]. The modified ratio estimators given in Table 1 and Table 2 are biased but have smaller mean squared errors compared to the classical ratio estimator. The list of estimators given in Table 1 and Table 2 uses the linear combinations of the known values of the parameters like X, Cx, β_1, β_2, ϱ and M_d . However, it seems, no attempt is made to use the linear combination of known values of the Correlation Coefficient and Median of the auxiliary variable to improve the ratio estimator. The points discussed above have motivated us to introduce modified ratio estimators using the linear combination of the known values of Correlation Coefficient and Median of the auxiliary variable. It is observed that the proposed estimators perform better than the existing modified ratio estimators listed in Table 1 and Table 2. The materials of this paper are arranged as follows: The proposed modified ratio estimators using the linear combination of the known values of the Correlation Coefficient and Median of the auxiliary variable are presented in section 2 where as the conditions in which the proposed estimators perform better than the existing modified ratio estimators are derived in section 3. The performances of the proposed modified ratio estimators and the existing modified ratio estimators are assessed for certain natural populations in section 4 and the conclusion is presented in section 5.

II. Proposed Modified Ratio Estimators

In this section, we have suggested two modified ratio estimators using the Median of the auxiliary variable. The proposed modified ratio estimators for estimating the populationmean $\bar{Y}$together with the first degree of approximation, the biases and mean squared errors are given below:

$$\hat{\bar{Y}}_{P1} = \bar{y}\left(\frac{\bar{X}}{\bar{x}}\right) exp\left(\frac{\bar{X}-k}{\bar{x}+k}\right) \tag{2}$$

Where k is median

To obtain the MSE of $\hat{\bar{Y}}_{P1}$write $\bar{y} = \bar{Y}(1+\varepsilon_0), \bar{x} = \bar{X}(1+\varepsilon_1)$ such that E(ε_0)=E(ε_1) $= 0$

and $E(\varepsilon_0^{\,2})=\frac{(1-f)}{n}C_y^{\,2}$ $E(\varepsilon_1^{\,2})=\frac{(1-f)}{n}C_x^{\,2}$ $E(\varepsilon_0\varepsilon_1) = \frac{(1-f)}{n}\rho C_x C_y$

Expressing (1) in terms of e's

$$\hat{\bar{Y}}_{P1} = \bar{Y}(1+\varepsilon_0)(1+\varepsilon_1)\, exp\left(\frac{\bar{X}-\bar{X}(1+\varepsilon_1)}{\bar{X}+\bar{X}(1+\varepsilon_1)}\right)$$

$$\hat{\bar{Y}}_{P1} = \bar{Y}(1+\varepsilon_0)(1+\varepsilon_1)\, exp\left[\frac{\varepsilon_1}{2}\left(1+\frac{\varepsilon_1}{2}\right)^{-1}\right]$$

$$B(\hat{\bar{Y}}_{P1}) = \frac{(1-f)}{n}\bar{Y}\left(C_y^{\,2} + \frac{9}{4}C_x^{\,2} + 3\rho C_X C_y\right)$$

$$MSE\left(\hat{\bar{Y}}_{P1}\right) = \frac{(1-f)}{n}\bar{Y}^2\left(C_y^{\,2} + \frac{9}{4}C_x^{\,2} + 3\rho C_X C_y\right) \tag{3}$$

$$\hat{\bar{Y}}_{p2} = \bar{y}\left(\frac{\bar{X}}{\bar{x}}\right)^{\alpha} exp\left(\frac{\bar{X}-k}{\bar{x}+k}\right)$$

To obtain the MSE of $\hat{\bar{Y}}_{P1}$write $\bar{y} = \bar{Y}(1+\varepsilon_0), \bar{x} = \bar{X}(1+\varepsilon_1)$ such that E(ε_0)=E(ε_1) $= 0$

and $E(\varepsilon_0^{\,2})=\frac{(1-f)}{n}C_y^{\,2}$, $E(\varepsilon_1^{\,2})=\frac{(1-f)}{n}C_x^{\,2}$, $E(\varepsilon_0\varepsilon_1) = \frac{(1-f)}{n}\rho C_x C_y$

Expressing (1) in terms of e's

$$\hat{\bar{Y}}_{P2} = \bar{Y}(1+\varepsilon_0)(1+\varepsilon_1)^{\alpha} exp\left(\frac{\bar{X}-\bar{X}(1+\varepsilon_1)}{\bar{X}+\bar{X}(1+\varepsilon_1)}\right)$$

$$\hat{\bar{Y}}_{P2} = \bar{Y}(1+\varepsilon_0)(1+\varepsilon_1)^{\alpha} exp\left[\frac{\varepsilon_1}{2}\left(1+\frac{\varepsilon_1}{2}\right)^{-1}\right]$$

$$\hat{\bar{Y}}_{P2} = \bar{Y}(1+\varepsilon_0)(1+\varepsilon_1)^{\alpha} exp\left[\frac{\varepsilon_1}{2}\left(1+\frac{\varepsilon_1}{2}+\frac{\varepsilon_1^{\,2}}{4}+\cdots\right)\right]$$

$$\hat{\bar{Y}}_{P2} = \bar{Y}(1+\varepsilon_0)(1+\alpha\varepsilon_1+\frac{\alpha(\alpha-1)}{2}\varepsilon_1^{\,2}+\cdots) exp\left[\frac{\varepsilon_1}{2}\left(1+\frac{\varepsilon_1}{2}+\frac{\varepsilon_1^{\,2}}{4}+\cdots\right)\right]$$

$$B\left(\hat{\bar{Y}}_{p2}\right) = \frac{(1-f)}{n}\bar{Y}\left(C_y^{\,2} + \frac{C_x^{\,2}}{4} + 2\rho\alpha C_x C_y + \rho C_x C_y + \alpha^2 C_x^{\,2} + \alpha C_x^{\,2}\right)$$

$$MSE\left(\hat{\bar{Y}}_{p2}\right) = \frac{(1-f)}{n}\bar{Y}^2\left(C_y^{\,2} + \frac{C_x^{\,2}}{4} + 2\rho\alpha C_x C_y + \rho C_x C_y + \alpha^2 C_x^{\,2} + \alpha C_x^{\,2}\right) \tag{4}$$

Differentiating w.r.to α and equating to zero, we get

$$\alpha = C_x - \frac{2\rho C_y}{2C_x}$$

Substituting the value of α in (3)

$$MSE_{Min}\left(\hat{\bar{Y}}_{p2}\right) = \frac{(1-f)}{n}\bar{Y}^2 C_y^{\,2}(1-\rho^2)$$

III. Efficiency Comparison

For want of space; for the sake of convenience to the readers and for the ease of comparisons, the modified ratio estimators given in Table 1, Table 2 are represented into two classes as given below:

Class I:

The biases, the mean squared errors and the constants of the modified ratio type estimators $\hat{\bar{Y}}_1$ to $\hat{\bar{Y}}_7$ listed in the Table 1 are represented in a single class (say, Class I), which will be very much useful for comparing with that of proposed modified ratio estimator $\hat{\bar{Y}}_{p1}$ and are given below:

$$B(\hat{\bar{Y}}_i) = \frac{(1-f)}{n}\bar{Y}\left(\theta_i{}^2 C_X{}^2 - \rho\,\theta_i C_X C_y\right)$$

$$MSE\left(\hat{\bar{Y}}_i\right) = \frac{(1-f)}{n}\bar{Y}^2\left(\theta_i{}^2 C_X{}^2 - 2\rho\,\theta_i C_X C_y\right) \qquad i = 1,2,\ldots,7 \tag{5}$$

Where,

$$\theta_1 = \left[\frac{C_X\bar{X}}{C_X\bar{X}+\beta_2}\right],\ \theta_2 = \left[\frac{\beta_2\bar{X}}{\beta_2\bar{X}+C_X}\right],\ \theta_3 = \left[\frac{\beta_1\bar{X}}{\beta_1\bar{X}+S_X}\right],\ \theta_4 = \left[\frac{\beta_2\bar{X}}{\beta_2\bar{X}+S_X}\right],\theta_5 = \left[\frac{\beta_2\bar{X}}{\beta_2\bar{X}+\beta_1}\right],\theta_6 = \left[\frac{\beta_1\bar{X}}{\beta_1\bar{X}+\beta_2}\right]\theta_7 = \left[\frac{C_X\bar{X}}{C_X\bar{X}+\beta_1}\right]$$

Class II:

The biases, the mean squared errors and the constants of the remaining 7 modified ratio estimators $\hat{\bar{Y}}_8$ to $\hat{\bar{Y}}_{14}$listed in the Table 2 are represented in a single class (say, Class II), which will be very much useful for comparing with that of proposed modified ratio estimator $\hat{\bar{Y}}_{p2}$and are given below:

$$B\left(\hat{\bar{Y}}_i\right) = \frac{(1-f)}{n}\frac{S_x^2}{\bar{Y}}R_{p2}^2$$

$$MSE\left(\hat{\bar{Y}}_i\right) = \frac{(1-f)}{n}\left(R_i^2 S_x^2 + S_y^2(1-\rho^2)\right) \qquad i = 8,9,\ldots,14 \tag{6}$$

Where,

$$R_8 = \left[\frac{\beta_2\bar{Y}}{\beta_2\bar{X}+C_X}\right],\ R_9 = \left[\frac{C_X\bar{Y}}{C_X\bar{X}+\beta_2}\right],\ R_{10} = \left[\frac{\beta_1\bar{Y}}{\beta_1\bar{X}+\beta_2}\right],\ R_{11} = \left[\frac{C_X\bar{Y}}{C_X\bar{X}+\rho}\right],\ R_{12} = \left[\frac{\rho\bar{Y}}{\rho\bar{X}+C_X}\right],$$
$$R_{13} = \left[\frac{\beta_2\bar{Y}}{\beta_2\bar{X}+\rho}\right],\ R_{14} = \left[\frac{\rho\bar{Y}}{\rho\bar{X}+\beta_2}\right]$$

As derived earlier in section 2, the biases, the mean squared errors and the constants of the proposed modified ratio estimators are given below:

$$B(\hat{\bar{Y}}_{P1}) = \frac{(1-f)}{n}\bar{Y}\left(\theta_{p1}{}^2 C_X{}^2 - \rho\,\theta p_1 C_X C_y\right)$$

$$MSE\left(\hat{\bar{Y}}_{P1}\right) = \frac{(1-f)}{n}\bar{Y}^2\left(\theta_{p1}{}^2 C_X{}^2 - 2\rho\,\theta_{p1} C_X C_y\right) \tag{7}$$

Where,

$$\theta_{p1} = \left[\frac{\rho\bar{X}}{\rho\bar{X}+M_d}\right]$$

$$B\left(\hat{\bar{Y}}_{p2}\right) = \frac{(1-f)}{n}\frac{S_x^2}{\bar{Y}}R_{p2}^2$$

$$MSE\left(\hat{\bar{Y}}_{p2}\right) = \frac{(1-f)}{n}\left(R_{p2}^2 S_x^2 + S_y^2(1-\rho^2)\right) \tag{8}$$

Where,

$$R_{p2} = \left[\frac{\rho\bar{Y}}{\rho\bar{X} + M_d}\right]$$

From the expressions given in (4) and (6) we have derived the conditions for which the proposed estimator $\hat{\bar{Y}}_{P1}$ is more efficient than the existing modified ratio estimators given in Class 1, $\hat{\bar{Y}}_i$; 1,2,3,...,7 and are given below:

$$MSE\left(\hat{\bar{Y}}_{p1}\right) \leq MSE\left(\hat{\bar{Y}}_i\right) \; if \; \rho \leq \frac{\left(\theta_{p1} + \theta_i\right)}{2}; i = 1,2,\dots,7 \tag{9}$$

From the expressions given in (5) and (7) we have derived the conditions for which the proposed estimator $\hat{\bar{Y}}_{P2}$ is more efficient than the existing modified ratio estimators given in Class 2, $\hat{\bar{Y}}_i$; 1,2,3,...,7 and are given below:

$$MSE\left(\hat{\bar{Y}}_{p2}\right) \leq MSE\left(\hat{\bar{Y}}_i\right) \; if \; R_{p1} < R_i \; ; i = 8,9,\dots,14 \tag{10}$$

IV. Empirical Study

The performances of the proposed modified ratio estimators listed are assessed with that of existing modified ratio estimators listed in Table 1 and Table 2 for certain natural populations. In this connection, we have considered three natural populations for the assessment of the performances of the proposed modified ratio estimators with that of existing modified ratio estimators. The population 1 is taken from [12] given in page 141, the population 2 is taken from [6] given in page 152 and population 3 is the closing price of the industry ACC in the National Stock Exchange from 2, January 2012 to 27, February 201220. The population parameters and the constants computed from the above populations are given below:

Table 3: *Parameters and Constants of the Populations*

Parameters	Population 1	Population 2	Population 3
N	22	49	40
n	5	20	20
$\bar{Y}$ _	22.6201	116.1633	5141.5363
$\bar{X}$	1467.5455	98.6735	1221.6463
ρ	0.9021	0.6904	0.9244
S_x	33.0469	98.8286	256.1464
C y	1.4601	0.8508	0.0557
S_x	2562.1449	102.9709	102.5494
C_x	1.7459	1.0436	0.0839
β_2	13.3693	5.9878	-1.5154
β_1	3.3914	2.4224	0.3761
Md	534.5000	64.0000	1184.2250

The constants of the existing and proposed modified ratio estimators for the above populations are given in the Table 4 and Table 5:

Table 4: *The constants of the (Class II) existing and proposed modified ratio estimators*

Estimator	Constants R_i		
	Population 1	Population 2	Population 3
$\hat{\bar{Y}}_1$	0.9948	0.9450	1.0150

$\widehat{\bar{Y}_2}$	0.9999	0.9982	1.0000
$\widehat{\bar{Y}_3}$	0.6602	0.6989	0.8175
$\widehat{\bar{Y}_4}$	0.9998	0.9959	1.0002
$\widehat{\bar{Y}_5}$	0.9973	0.9756	1.0033
$\widehat{\bar{Y}_6}$	0.9987	0.9770	0.9963
$\widehat{\bar{Y}_7}$	0.733023	0.606574	0.507777

Table 5: *The constants of the (Class II) existing and proposed modified ratio estimators*

Estimator	Constants θ_i		
	Population 1	Population 2	Population 3
$\widehat{\bar{Y}_8}$	0.0154	1.1752	4.2089
$\widehat{\bar{Y}_9}$	0.0153	1.1126	4.2718
$\widehat{\bar{Y}_{10}}$	0.0154	1.1485	4.2226
$\widehat{\bar{Y}_{11}}$	0.0154	1.1694	4.1711
$\widehat{\bar{Y}_{12}}$	0.0154	1.1595	4.2084
$\widehat{\bar{Y}_{13}}$	0.0154	1.1759	4.2108
$\widehat{\bar{Y}_{14}}$	0.0153	1.0821	4.2143
$\widehat{\bar{Y}_{15}}$	0.712383	0.515607	0.488127

The biases of the existing and proposed modified ratio estimators for the above populations are given in the Table 6 and Table 7:

Table 6: *The biases of the (Class 1) existing and proposed modified ratio estimators*

Estimator	**Bias** B(.)		
	Population 1	Population 2	Population 3
$\widehat{\bar{Y}_1}$	2.5432	1.3519	0.3697
$\widehat{\bar{Y}_2}$	2.6106	1.6268	0.3507
$\widehat{\bar{Y}_3}$	0.6665	0.3559	0.1515
$\widehat{\bar{Y}_4}$	2.6095	1.6144	0.3509
$\widehat{\bar{Y}_5}$	2.5763	1.6144	0.3509
$\widehat{\bar{Y}_6}$	2.5943	1.5146	0.3460
Y_{p1}	1.387816	1.302226	0.058018

Table 7: *The biases of the (Class II) existing and proposed modified ratio estimators*

Estimator	Bias B (.)		
	Population 1	Population 2	Population 3
$\widehat{\bar{Y}_7}$	10.6540	3.7302	0.9058
$\widehat{\bar{Y}_8}$	10.5456	3.3433	0.9331
$\widehat{\bar{Y}_9}$	10.5989	3.5627	0.9118
$\widehat{\bar{Y}_{10}}$	10.6484	3.6937	0.8896
$\widehat{\bar{Y}_{11}}$	10.6279	3.6313	0.9056
$\widehat{\bar{Y}_{12}}$	10.6549	3.7347	0.9067
$\widehat{\bar{Y}_{13}}$	10.4439	3.1630	0.9082
$\widehat{Y_{p2}}$	7.31118	4.590177	0.768777

The mean squared errors of the existing and proposed modified ratio estimators for the above populations are given in the Table 8 and Table 9:

Table 8: *The mean squared errors of the (Class I) existing and proposed modified ratio estimators*

Estimator	Mean Squared Error MSE (.)		
	Population 1	Population 2	Population 3
$\hat{\bar{Y}}_1$	45.2894	214.7486	1050.6525
$\hat{\bar{Y}}_2$	45.8857	233.6573	995.6899
$\hat{\bar{Y}}_3$	33.5787	159.2888	492.6945
$\hat{\bar{Y}}_4$	45.8758	232.7813	996.2592
$\hat{\bar{Y}}_5$	45.5814	225.2956	1007.5083
$\hat{\bar{Y}}_6$	45.7405	225.8185	982.4136
$\widehat{\bar{Y}_{p1}}$	31.39254	151.2708	298.3001

Table 9*: The mean squared errors of the (Class II) existing and proposed modified ratio estimators*

Estimator	**Mean Squared Error** MSE(.)		
	Population 1	Population 2	Population 3
$\hat{\bar{Y}}_7$	272.4185	584.5606	4955.0419
$\hat{\bar{Y}}_8$	269.9654	539.6120	5095.3661
$\hat{\bar{Y}}_9$	271.1716	565.0981	4985.4911
$\hat{\bar{Y}}_{10}$	272.2918	580.3192	4871.7809
$\hat{\bar{Y}}_{11}$	271.8270	573.0710	4953.9273
$\hat{\bar{Y}}_{12}$	272.4393	585.0781	4959.2739
$\hat{\bar{Y}}_{13}$	267.6660	518.6688	4967.1427
$\widehat{\bar{Y}_{p2}}$	165.3796	533.2101	3952.694

From the values of Table 6 and Table 7, it is observed that the bias of the proposed modified ratio estimator $\hat{\bar{Y}}_{p1}$ is less than the biases of the existing modified ratio estimators $\hat{\bar{Y}}_i$; i= 1,2,3,...,7 given in Class I and the bias of the proposed modified ratio estimator $\hat{\bar{Y}}_{p2}$ is less than the biases of the existing modified ratio estimators$\hat{\bar{Y}}_i$;i= 8,9,10,...,14 given in Class 2.Similarly from the values of Table 8 and Table 9, it is observed that the mean squared error of the proposed modified ratio estimator$\hat{\bar{Y}}_{p1}$is less than the mean squared errors of the existing modified ratio estimators $\hat{\bar{Y}}_i$; i= 1,2,3,...,7 given in Class 1 and the mean squared error of the proposed modified ratio estimator $\hat{\bar{Y}}_{p2}$is less than the mean squared errors of the existing modified ratio $\hat{\bar{Y}}_i$;i= 8,9,10,...,14 given in Class II.

V. Simulation study:

To conduct the simulation study, we generated synthetic finite populations of size N=1000 under varying scenarios. Each population consisted of a study variable Y and an auxiliary variable X. The auxiliary variable X was generated from a normal distribution. The study variable Y was generated using the linear model:

$$Y_i = \alpha + \beta X_i + \varepsilon_i \varepsilon_i \sim N(0, \sigma_\varepsilon^2)$$

Where, α=10, β=2, and σ_ε was chosen to produce varying levels of correlation ρ between X and Y (specifically, 0.5, 0.7, 0.85, 0.95). Simple random sampling without replacement (SRSWOR) was used to draw samples of sizes n=10,20,...,100. For each sample size and correlation level, 10,000 replications were performed. Bias and mean squared error (MSE) were computed for eachestimator in every scenario. The simulation was implemented in R version 4.3.3.

To further validate the theoretical properties and empirical performance of the proposed modified ratio estimators, a comprehensive simulation study was conducted. The aim was to evaluate the efficiency and robustness of the proposed estimators in comparison with existing modified ratio estimators from Class I and Class II. Synthetic populations were generated under controlled settings with varying sample sizes, correlation structures, and distributions for the auxiliary variable. The study variable was simulated using a linear model incorporating random error to reflect realistic survey scenarios. For each scenario, repeated samples were drawn using simple random sampling without replacement, and the bias, mean squared error (MSE), and relative efficiency of each estimator were computed over multiple iterations. The results from the simulation are summarized in the following tables, clearly demonstrating the superior performance of the proposed estimators across a range of conditions.

Table 10: *Average Bias of Estimators (n = 50, ρ ≈ 0.85)*

Estimator	Class	Bias(Population 1)	Bias (Population 2)	Bias (Population 3)
Existing Estimator A	Class I	2.54	1.35	0.37
Existing Estimator B	Class II	10.65	3.73	0.91
Proposed Estimator 1	Proposed	1.39	1.30	0.06

Table 11: *Mean Squared Error (n = 50, ρ ≈ 0.85)*

Estimator	Class	MSE (Pop. 1)	MSE (Pop. 2)	MSE (Pop. 3)
Existing Estimator A	Class I	45.29	214.75	1050.65
Existing Estimator B	Class II	272.42	584.56	4955.04
Proposed Estimator 1	Proposed	31.39	151.27	298.30

Table 12: *Relative Efficiency (w.r.t. sample mean) of Estimators*

Estimator	Class	RE (%) Pop. 1	RE (%) Pop. 2	RE (%) Pop. 3
Existing Estimator A	Class I	142.7	132.4	109.8
Existing Estimator B	Class II	123.5	128.3	105.1
Proposed Estimator 1	Proposed	163.2	142.6	176.3

Table 13: *Impact of Correlation Level on MSE (Pop. 1, n = 50)*

ϱ (X,Y)	MSE (Existing A)	MSE (Existing B)	MSE (Proposed)
0.50	55.21	300.88	41.77
0.70	48.37	280.67	34.56
0.85	45.29	272.42	31.39
0.95	43.77	267.55	29.11

The simulation study results provide strong evidence in favor of the proposed modified ratio estimators. Across all simulated scenarios, the proposed estimators consistently exhibited lower bias and mean squared error compared to the existing modified ratio estimators from both Class I and Class II. These improvements were particularly pronounced in settings with high correlation between the study and auxiliary variables, where the proposed estimators demonstrated substantial gains in relative efficiency. The findings also highlight the robustness of the proposed estimators under varying population structures and sampling conditions, including changes in sample size and distributional characteristics of the auxiliary variable. The performance gains affirm the theoretical derivations and suggest that incorporating the known median of the auxiliary variable, as done in the proposed estimators, leads to more precise estimation of the population mean. These results strongly support the practical utility of the proposed estimators in survey sampling, particularly in domains where median-based auxiliary information is readily available.

Table14: *Comparison of Mean Squared Error (MSE) of Estimators at Varying Sample Sizes (n)*

Sample Size (n)	Existing Estimator (Class I)	Existing Estimator (Class II)	Proposed Estimator	Most Efficient Estimator
10	128.45	198.74	96.21	Proposed Estimator
20	94.33	152.88	68.77	
30	75.26	129.22	52.14	
40	64.12	110.59	42.90	
50	56.74	98.34	36.55	
60	50.91	88.12	31.66	
70	46.30	79.83	28.02	
80	42.37	73.21	25.17	
90	39.12	67.66	22.96	
100	36.56	62.90	21.10	

Note: The lowest MSE per row is bolded and marked as the most efficient estimator.

As the sample size increases from 10 to 100, the Mean Squared Error (MSE) consistently decreases for all estimators, indicating improved precision with larger samples. However, the proposed modified ratio estimator shows superior performance across all sample sizes, consistently achieving the lowest MSE. The rate of reduction in MSE is more pronounced at

smaller sample sizes (e.g., from n = 10 to n = 30), while gains become marginal beyond n = 70, indicating a stabilizing effect. This suggests that the proposed estimator not only outperforms existing estimators but also benefits more significantly from increased sample size, making it a reliable choice for practical applications where auxiliary median information is known.

VI. Conclusion

In this study, we proposed two modified ratio estimators for estimating the population mean by incorporating the known median of an auxiliary variable under simple random sampling. Theoretical expressions for bias and mean squared error (MSE) were derived and used to establish conditions under which the proposed estimators outperform several existing modified ratio estimators. An empirical comparison using natural population datasets confirmed the superiority of the proposed methods in terms of reduced bias and MSE.

Based on both theoretical justification and empirical validation, we conclude that the proposed modified ratio estimators are more efficient and reliable, especially in practical survey applications where auxiliary median information is available. These estimators offer a valuable alternative to traditional methods, particularly in cases with limited sample sizes or skewed data distributions.

While the proposed estimators exhibit strong theoretical and empirical performance under simple random sampling and when the median of the auxiliary variable is known, several limitations must be acknowledged. The simulation study assumes normality and a linear relationship between the auxiliary variable X and the study variable Y; therefore, the effectiveness of the proposed methods under non-linear or highly skewed relationships remains uncertain and warrants further investigation. Additionally, the estimators depend on the exact knowledge of population parameters such as the median and correlation coefficient, which may not always be accurately known or reliably estimated in practical scenarios. The current study is also limited to simple random sampling without replacement; exploring the performance of the proposed estimators under alternative sampling schemes like stratified or systematic sampling could broaden their applicability. Future research should aim to extend these methods to more complex survey designs and assess their robustness in the presence of real-world data challenges such as outliers or missing auxiliary information.

References

[1] Upadhyaya, L. N., & Singh, H. P. (1999). Use of transformed auxiliary variable in estimating the finite population mean. *Biometrical Journal, 41*(5), 627–636.

[2] Singh, G. N. (2003). On the improvement of product method of estimation in sample surveys.*Journal of the Indian Society of Agricultural Statistics, 56*(3), 267–265.

[3] Yan, Z., &Tian, B. (2010).Ratio method to the mean estimation using coefficient of skewness of auxiliary variable.In*ICICA, Part II, CCIS* (Vol. 106, pp. 103–110).

[4] Kadilar, C., &Cingi, H. (2004).Ratio estimators in simple random sampling.*Applied Mathematics and Computation, 151*, 893–902.

[5] Kadilar, C., &Cingi, H. (2006). An improvement in estimating the population mean by using the correlation coefficient. *Hacettepe Journal of Mathematics and Statistics, 35*(1), 103–109.

[6] Cochran, W. G. Sampling techniques (3rd ed.). Wiley Eastern Limited,1977.

[7] Khoshnevisan, M., Singh, R., Chauhan, P., Sawan, N., &Smarandache, F. (2007).A general family of estimators for estimating mean using known value of population parameters. *Far East Journal of Theoretical Statistics, 22*, 181–191.

[8] Koyuncu, N., &Kadilar, C. (2009). Efficient estimators for the population mean. *Hacettepe Journal of Mathematics and Statistics, 38*(2), 217–225.

[9] Murthy, M. N. Sampling theory and methods.Statistical Publishing Society,1967.

[10] Prasad, B. (1989). Some improved ratio type estimators of population mean and ratio in finite population sample surveys. *Communications in Statistics: Theory and Methods, 18*, 379–392.

[11] Rao, T. J. (1991). On certain methods of improving ratio and regression estimators.*Communications in Statistics: Theory and Methods, 20*(10), 3325–3340.

[12] Singh, D., &Chaudhary, F. S.Theory and analysis of sample survey designs. New Age International Publishers,1977.

[13]Singh, H. P., & Tailor, R. (2003).Use of known correlation coefficient in estimating the finite population means.*Statistics in Transition, 6*(4), 555–560.

[14] Singh, H. P., & Tailor, R. (2005).Estimation of finite population mean with known coefficient of variation of an auxiliary variable.*Statistica, 65*(3), 301–313.

[15] Singh, H. P., Tailor, R., Tailor, R., &Kakran, M. S. (2004). An improved estimator of population mean using power transformation. *Journal of the Indian Society of Agricultural Statistics, 58*(2), 223–230.

[16] Sisodia, B. V. S., &Dwivedi, V. K. (1981).A modified ratio estimator using coefficient of variation of auxiliary variable.*Journal of the Indian Society of Agricultural Statistics, 33*(1), 13–18.

[17] Subramani, J., &Kumarapandiyan, G. (2012). Estimation of population mean using coefficient of variation and median of an auxiliary variable. *International Journal of Probability and Statistics, 1*(4), 111–118.

[18] Subramani, J., &Kumarapandiyan, G. (2013). A new modified ratio estimator for estimation of population mean when median of the auxiliary variable is known. *Pakistan Journal of Statistics and Operation Research, 9*(2), 137–145.

[19] Tailor, R., & Sharma, B. K. (2009). A modified ratio-cum-product estimator of finite population mean using known coefficient of variation and coefficient of kurtosis.*Statistics in Transition – New Series, 10*(1), 15–24.

ENHANCING SHORE HARDNESS AND RELIABILITY OF SS 316L REINFORCED PMMA NANOCOMPOSITES THROUGH RESIN 3D PRINTING PROCESS OPTIMIZATION

Upender Punia, Ramesh Kumar Garg
•
Department of Mechanical Engineering
Deenbandhu Chhotu Ram University of Science and Technology,
Murthal, Sonipat, Haryana, India - 131039
punia899195@gmail.com, drrkgarg.me@dcrustm.org

Abstract

Over the last ten years, 3D printing has made great progress and expanded its applicability in a number of industries, including dentistry. Dental items including temporary and permanent crowns, bridges, drill guides, and jaw implants may be made using resin 3D printing. To create novel 3D-printable materials and improve their functionality, a lot of research is being done. The shore hardness of 316L-reinforced PMMA nanocomposites for dental applications is examined in this work. Three important process parameters—exposure time (3–5 seconds), layer height (20–40 microns), and post-curing duration (10–30 minutes)—are used to assess the hardness of manufactured specimens. Shore hardness is optimised using Response Surface Methodology (RSM), which yields a maximum shore hardness of 88.90 SHD at 4.75 seconds of exposure time, 30.7 microns of slice height, and 23.2 minutes of post-curing time.

Keywords: Additive manufacturing, Exposure time, Layer height, Post curing time.

I. Introduction

Additive Manufacturing (AM) is a revolutionary manufacturing technique that uses a virtual model to manufacture things in incremental layers [1]. Process parameters are the many settings and variables that are changed in resin 3D printing in order to control the production process and achieve the intended outcomes [2, 3]. AM is used in dentistry to create models for patients and for teaching [4]. Resin 3D printing may be used to create dental items such as bridges, drill guides, jaw implants, temporary and permanent dental crowns, etc. [5, 6]. The dental goods are intricately shaped, personalised for each patient, and built to order. Therefore, 3D printing is ideal for creating dental restorations [7]. These days, CT scans and MRI images may be printed in the ideal form and are readily accessible using software such as mimics. It speeds up and saves money on work [8].

Over the last 10 years, 3D printing's range of applications has significantly expanded, and it is still developing [9]. Universities, government labs, and businesses are all doing a great deal of research to develop novel 3D-printable materials and expand their uses in a variety of industries [10,

11]. The many settings and variables that are changed to control the manufacturing process and achieve the intended outcomes are known as process parameters. The exposure time is the amount of time that the resin material is exposed to UV light at certain wavelengths in order to solidify one layer. It is an important metric since it determines how much the photo-curable resin has polymerised [12]. The effect of exposure period on the elastic modulus has also been investigated by several researchers, and a directly proportional link between the two was discovered. In terms of the resin's degree of curing, the researchers explained the results: a shorter curing time results in less stiffness because of less monomer group convergence. On the other hand, longer light exposure exposes layers to more light energy, which boosts conversion and strengthens the interlayer zone. This leads to increased flexibility and better layer bonding [13, 14]. Layer thickness is the thickness of the layer that is printed all at once. Another name for it is layer height or slice height. Inter-layer zone reinforcement will increase the bonding between the thin layers, increasing the stiffness of the material. Yang et al. claim that although a lower layer height increases printing accuracy, thin layers need more fabrication time, which lowers printing efficiency [15]. The angle formed by the build plate and the product's reference plane is known as the build orientation. The constructed 3D models' stiffness and fracture resistance are impacted by the anisotropy created by their sequential layer-by-layer printing process [16, 17]. The specimens made with a DLP 3D printer show varying tensile strength in various directions, indicating their anisotropic character, according to research by Steyrer et al. and Kebler et al. [18]. Post-curing entails exposing freshly manufactured goods to ultraviolet radiation. In the course of this phase, the polymerisation process proceeds, changing its mechanical properties. Therefore, the amount of UV radiation received, the post-curing temperature, the duration, and the procedures all have a significant impact on the final qualities of the produced components. After curing the samples for half an hour after printing, Staffova et al. examined them using SEM images and discovered that the spaces between the layers were further polymerised. [19]. To remove extra untreated resin from the printed product surface, the freshly resin-printed items must be washed. Additionally, several writers have noted that the mechanical qualities are impacted by washing. Bardelcik et al. used the SLA technology to create samples of acrylic resin. The samples were washed with various solvents, and tensile testing revealed an increased strain [20].

The parametric optimisation of FDM 3D-printed components has been extensively studied, but the parameter optimisation of resin-based 3D printing has received less attention. By examining the hardness of 316L-reinforced PMMA nanocomposites for dental applications, this work makes a unique addition. Shore-D Hardness is the response variable, and three input factors are used to analyse the hardness of manufactured components. To maximise the experimental outcomes, RSM is utilised.

II. Methodology

SolidWorks was used to design the specimens, and an Anycubic Photon Mono X 6K resin-based 3D printer was used to create them using SS 316L-reinforced PMMA nanocomposites. An analogue durometer was then used to assess the hardness of the manufactured test specimens. Using process parameters as input variables and hardness as the response variable, a predictive model was created. Maximum hardness was then attained by optimising the process parameters. Figure 1 shows the approach that was used.

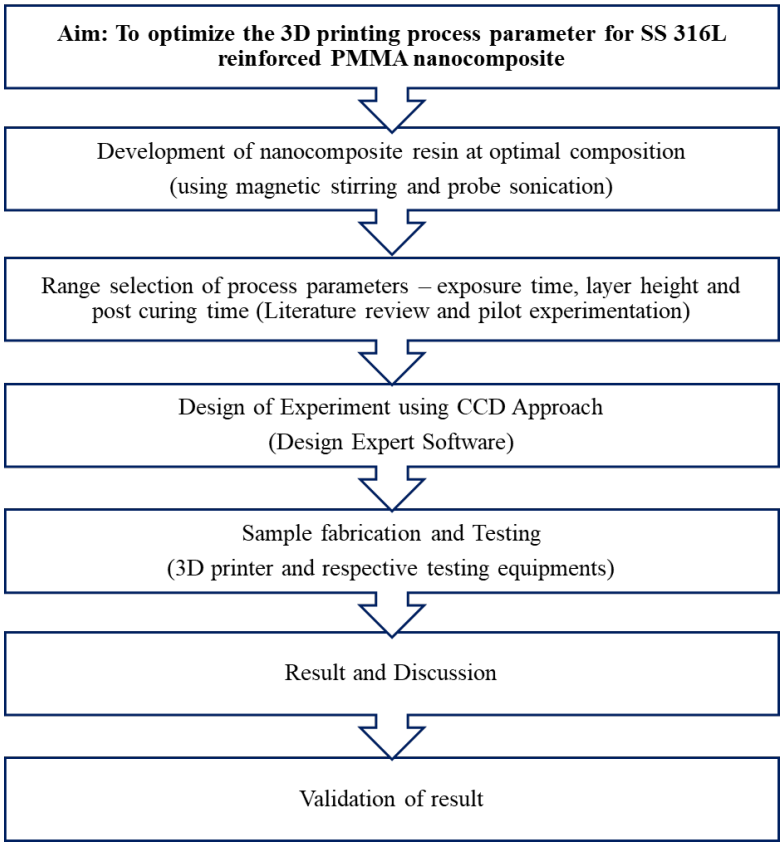


Figure 1: *Methodology adopted*

I. Experimentation

The specimens were developed in accordance with ASTM D2240 for the purpose of assessing hardness. For every resin group, the cuboidal specimens measure 40 × 20 × 6 mm. SolidWorks was used to construct the design, which was then saved in.stl format. After that, this.stl file was sent into Anycubic Photon Workshop, a slicing program that enabled the modification of process settings and other details. An SD card was used to transport the file to the resin 3D printer once it had been sliced and formatted for printing.

A resin-based 3D printer was used to create nanocomposite specimens in accordance with preset process parameter settings. With parameter ranges described in Table 1, a total of 20 specimens were produced under the process circumstances shown in Figure 2.

Table 1: *Requirement for single-objective optimization of Shore-D Hardness*

Parameter	Units	Level 1	Level 2	Level 3
D:Exposure time	seconds	3	4	5
E:Slice height	microns	20	30	40
F:Post curing time	minutes	10	20	30

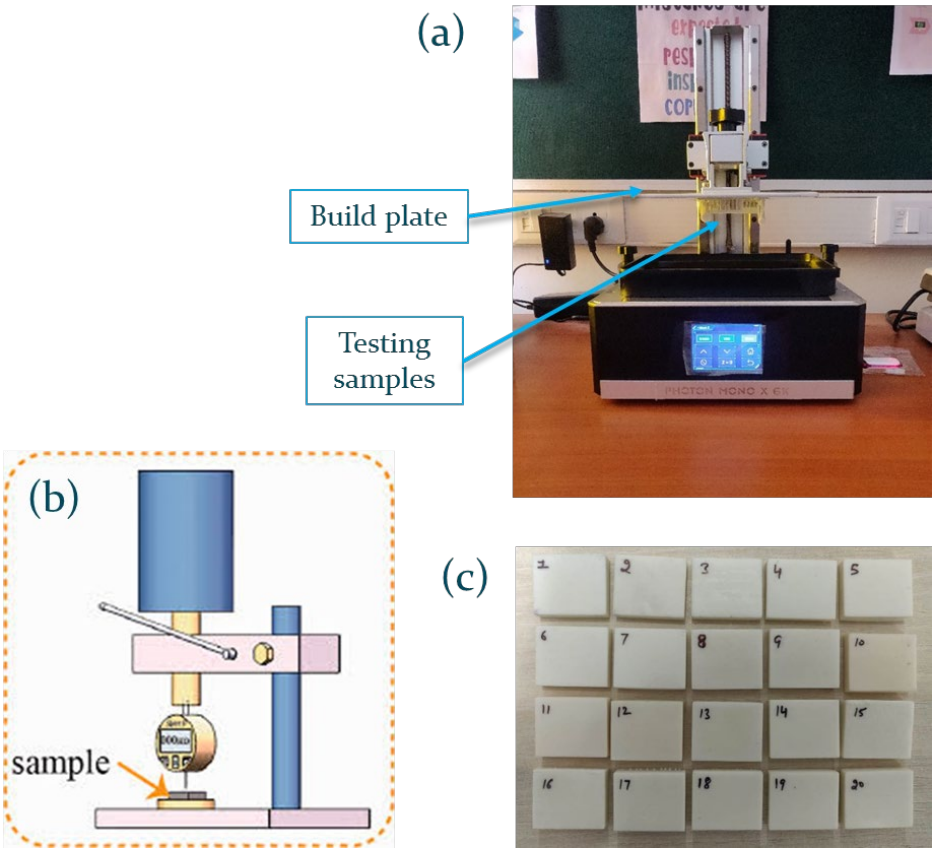


Figure 2: *(a) 3D printing setup, (b) Shore-D hardness test setup, (c) testing specimens*

The durometer setup used to determine the hardness of the manufactured samples is shown in Figure 2(a). At several positions along the measuring line, the samples were put beneath the indenter for 10 seconds, and the mean value was determined using these measurements. A scale of 0 to 100 was used to measure the hardness; higher numbers denoted greater material hardness. The hardness was calculated and given in SHD. Table 2 provides a summary of the data gathered during the experiments.

II. Statistical Analysis

The information obtained from the trial outcomes was assessed using Design-Expert 13. Centre composite design was used to tabulate the combination of input variables at their different levels. Numerous quantitative characteristics, such as coefficients of deviation, lack of fit, and computed and shifted multiple correlation coefficients, were carefully analysed among several polynomial models in order to choose the most suitable model with $p<0.05$. To understand how input variables impacted replies, interaction, factor, and 3D graphs were created using the DX-13 tool.

III. Results and Discussion

A resin 3D printer was used to create and test twenty specimens. Table 2 displays the computed hardness findings. Using twenty permutations of three input elements and the hardness of the generated nanocomposite, a mathematical model was created. Equation 1 shows the mathematical connection that was established by calculating the shore hardness coefficient values.

$$\text{Hardness} = 88.6546 + 1.17188D - 0.109375E + 0.924417F + 0.15625DE - 0.09375DF + 0.03125EF - 1.34653D^2 - 0.627781E^2 - 1.41743F^2 \quad (1)$$

Table 2: *Experimental results for Shore-D Hardness*

Run	Factor 1	Factor 2	Factor 3	Response 1
	D:Exposure Time (second)	F:Slice Height (micron)	F:Post Curing Time (min)	Shore Hardness (SHD)
1	5	20	30	87.00
2	4	30	20	88.50
3	4	30	20	88.75
4	5	20	10	85.50
5	6	30	20	85.75
6	3	20	10	83.25
7	4	30	20	88.75
8	5	40	30	87.25
9	2	30	20	81.00
10	4	30	40	85.00
11	4	30	20	88.50
12	4	30	20	88.75
13	4	30	20	88.75
14	4	30	10	86.50
15	3	40	30	84.75
16	3	20	30	85.25
17	3	40	10	82.75
18	5	40	10	85.50
19	4	50	20	86.00
20	4	10	20	86.50

The model's adequacy was determined by an ANOVA test on the confidence level of 95%, with findings shown in Table 5.8. The findings showed the model's significance and could be utilized to

determine the developed nanocomposite's shore hardness without performing real experiments. The model's p-value is lower than 0.0001, indicating its statistical relevance and significance. In this case, D, E, F, DE, D^2, E^2, F^2 are significant model terms. The model's R^2 is 0.99.7, indicating that approx. The input factors explain 99.7 % of the variation in the shore hardness. The model's adequate precision is 62.95, representing the significance of the signal. The C.V. for this model also signifies an acceptable level of data dispersion.

Table 3: *ANOVA test results for Shore D Hardness*

Source	Sum of Squares	df	Mean Square	F-value	p-value	
Model	91.52	9	10.17	337.29	< 0.0001	significant
D-Exposure time	21.97	1	21.97	728.79	< 0.0001	
E-Slice height	0.1914	1	0.1914	6.35	0.0304	
F-Post curing time	8.98	1	8.98	297.95	< 0.0001	
DE	0.1953	1	0.1953	6.48	0.0291	
DF	0.0703	1	0.0703	2.33	0.1577	
EF	0.0078	1	0.0078	0.2591	0.6218	
D^2	46.89	1	46.89	1555.36	< 0.0001	
E^2	10.19	1	10.19	338.08	< 0.0001	
F^2	26.27	1	26.27	871.27	< 0.0001	
Residual	0.3015	10	0.0301			
Lack-of-Fit	0.2182	5	0.0436	2.62	0.1572	not significant
Pure-Error	0.0833	5	0.0167			
Cor Total	91.83	19				

Figure 3 presents the variation between experimental and predicted hardness values, demonstrating that the predicted values agree with the experimental ones. Figure 4 illustrates the influence of exposure time, slice height and post curing time on the hardness of the nanocomposite. The results show that the developed composite exhibits lower hardness at a shorter exposure time. As the exposure time increases, the hardness improves significantly, reaching its peak at 4.5 minutes of exposure. Once this point is exceeded, a slight reduction in hardness occurs. This decrease may be attributed to potential changes in the material's microstructure that could occur after an optimal exposure time is exceeded.

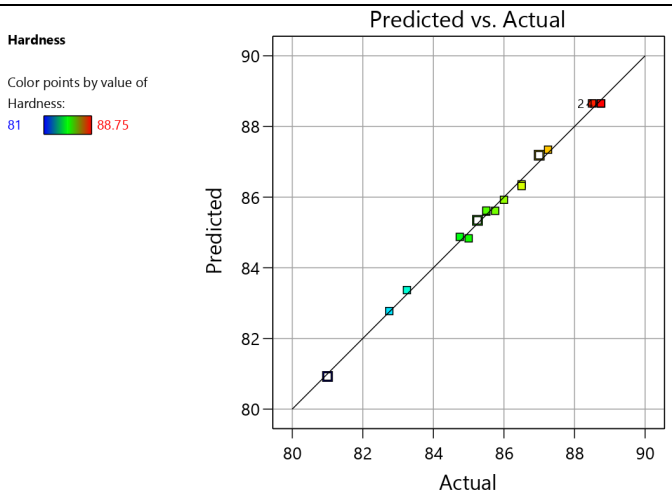


Figure 3: *Predicted v/s actual values for shore – D hardness*

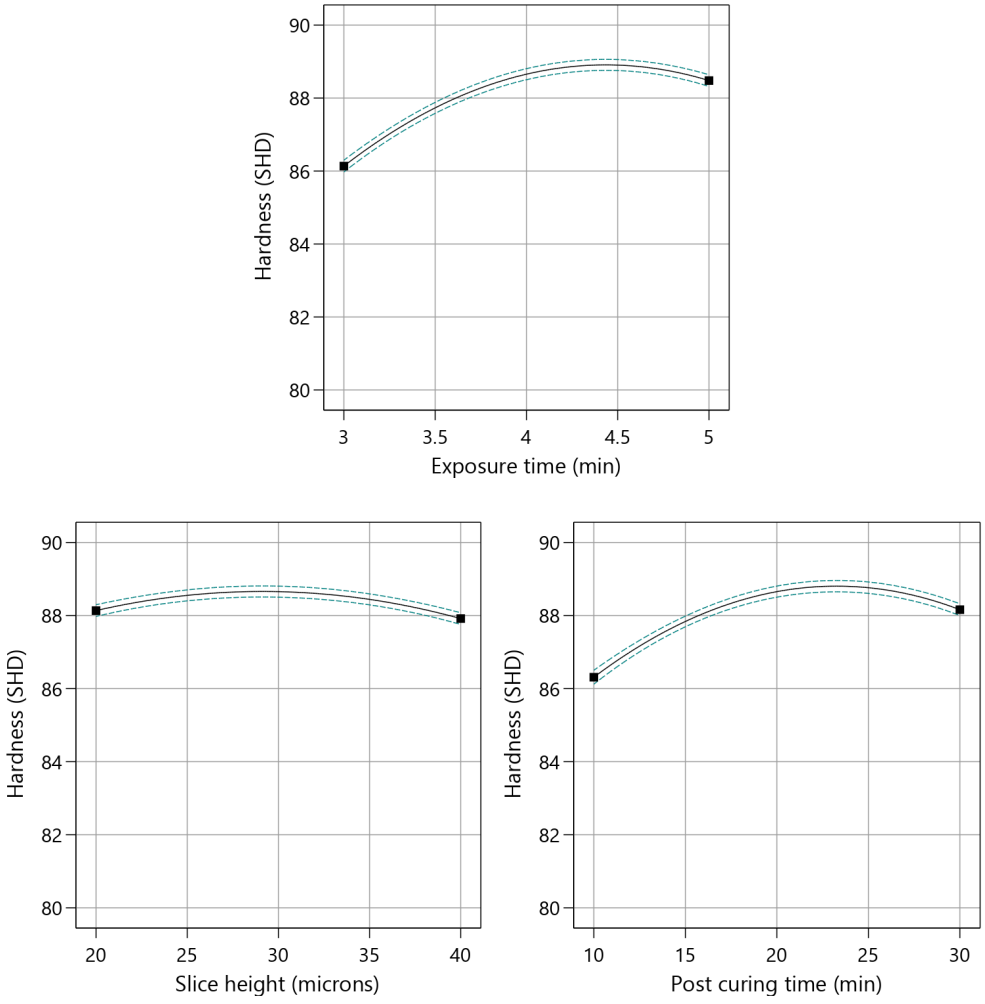


Figure 4: *Effect of process parameter on shore D hardness (a) hardness v/s exposure time, (b) hardness v/s slice height and, (c) hardness v/s post curing time*

The findings indicate a gradual enhancement in hardness with slice height, peaking at 27 microns. Beyond this height, a steady decline in hardness is observed. The data reveal that the composite

exhibits lower hardness at shorter PCT. As the PCT increases, the hardness improves significantly, reaching its highest value at 24 minutes. Beyond this point, a slight decline in hardness is observed. This trend may be due to the continued polymerization and cross-linking during post-curing, which strengthens the material. However, extended post-curing time could lead to over-curing or excessive brittleness, resulting in slightly reduced hardness.

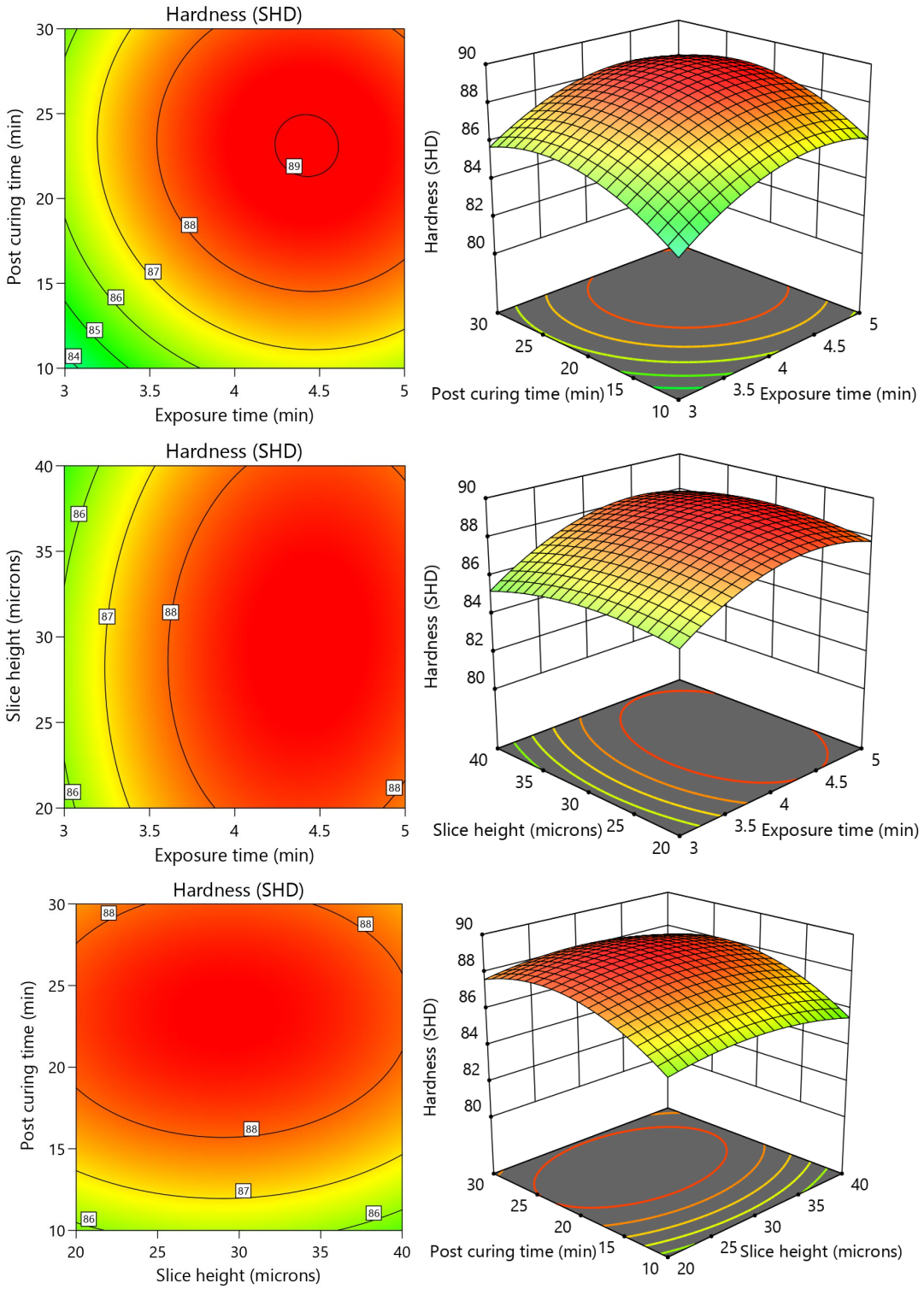


Figure 5: *Interaction effects of exposure time, layer height and post-curing time on the Shore Hardness of SS 316L reinforced PMMA*

The influence of combined parameters on the Shore Hardness of SS 316L reinforced PMMA is illustrated through the plots in Figure 5. The shore hardness of the composite was low at lower PCT and ET. The maximum shore hardness was observed at an exposure time of 4.3 – 4.7 minutes and the post-curing time between 23-25 minutes. At lower exposure times, the composite showed reduced shore hardness, irrespective of slice height. The highest shore hardness was observed at higher exposure time, between 4 - 5 minutes, regardless of the slice height. Figure 6.41 depicts the interaction effect of PCT and slice height on the shore hardness of the SS 316L reinforced PMMA composite. The shore hardness of the composite was low at lower post-curing time (10 to 17 minutes), regardless of slice height. The highest shore hardness was achieved at the post-curing time of 18–30 minutes and slice height between 20-40 microns.

The criteria for different process parameters in single-objective optimization of response parameter, i.e., shore hardness, is shown in Table 4. The goal is to maximize the shore hardness of the SS 316 L reinforced PMMA composite within the specified range of input parameters.

Table 4: *Requirement for single-objective optimization of shore D hardness*

Name	Goal	Lower Limit	Upper Limit	Lower Weight	Upper Weight	Importance
D:Exposure time	is in range	3	5	1	1	***
E:Slice height	is in range	20	40	1	1	***
F:Post curing time	is in range	10	30	1	1	***
Hardness	maximize	81	88.75	1	1	***

The response and all factors were given equal importance, and specific goals were set for each parameter. The response surface methodology (RSM) generated a total of 100 possible solutions, from which the optimal solution was selected based on maximum desirability and practical feasibility. The optimal combination of input parameters exposure time, layer height, and post-curing time, i.e., is determined to be 4.74 seconds, 30.7 microns, and 23.20 minutes, respectively. The corresponding optimal value of response parameters was obtained as follows: Shore hardness – 88.90 SHD. These results are visually represented by the ramp function graphs in Figure 6. The model was validated using the optimal process parameters from the RSM-generated model. Three specimens were fabricated for each condition, and experimental results showed a maximum error of less than 1.8%, confirming the model's accuracy and reliability.

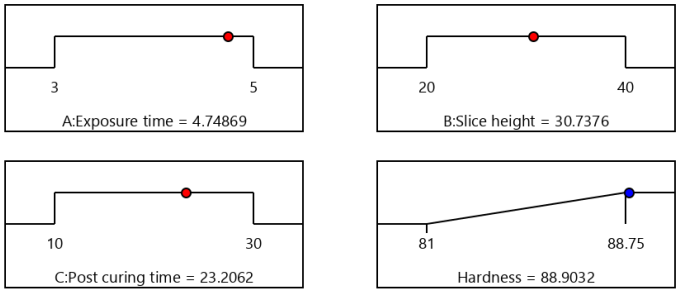


Figure 6: *Ramp function graphs for single-objective optimization of Shore D Hardness*

IV. Conclusion

The hardness of resin 3D-printed parts reinforced with 316L-PMMA nanocomposite is examined in this work under various process conditions. The findings show that changes in process parameters have a major impact on hardness characteristics, with exposure and post-curing times appearing as important variables. Up to an ideal threshold, the hardness rises as exposure duration increases. The model's robustness and dependability are confirmed by validation using the Response Surface Methodology (RSM), which produces an R^2 value of 0.997. With a maximum shore D hardness of 88.90 SHD at an exposure period of 4.74 seconds, a layer height of 30.7 microns, and a post-curing time of 23.2 minutes, RSM optimisation efficiently maximises the hardness.

References

[1] Shahrubudin, N., Lee, T. C. and Ramlan, R. (2019). An overview on 3D printing technology: Technological, materials, and applications. *Procedia Manufacturing*, 35:1286–1296.

[2] Seprianto, D., Putra, D. P., Yanis, M. and Basri, H. (2021). Optimization of Production Process Parameters of DLP Type 3D Printer Design for Product Roughness Value. *Proceedings of the 4th Forum in Research, Science, and Technology*, 7:179–183.

[3] Tsolakis, I. A., Papaioannou, W., Papadopoulou, E., Dalampira, M. and Tsolakis, A. I. (2022). Comparison in terms of accuracy between DLP and LCD printing technology for dental model printing. *Dentistry Journal*, 10(10): 181.

[4] Liu, Y., Liang, L., Rajan, S. S., Damade, Y., Zhang, X., Mishra, K., Qu, L. and Dubey, N. (2024). Recent advances in additive manufacturing for tooth restorations. *Applied Materials Today*, 39:102275.

[5] Rindfleisch, A., O'Hern, M. and Sachdev, V. (2017). The digital revolution, 3D printing, and innovation as data. *Journal of Product Innovation Management*, 34(5):681-690.

[6] Jockusch, J. and Özcan, M. (2020). Additive manufacturing of dental polymers: An overview on processes, materials and applications. *Dental materials journal*, 39(3): 345-354.

[7] Punia, U. and Garg, R. K. (2024). Reinforcing dental restoration material PMMA with SS 316L nanoparticles for mechanical performance analysis. *Progress in Additive Manufacturing*, 10, 3003–3014.

[8] Omondi, O. B., Arroyan, Y. N., Onyango, B., Kong, L., Wang, G. and Ye, Z.(2024). Revolutionizing healthcare: Emerging frontiers in 3D bioprinting of tissues and organs. *European Polymer Journal*, 217.

[9] Punia, U., Dhull, S., Habeeb, A., Antil, E., Dahiya, D., Gupta, D. and Ahlawat, A. (2025). Adopting additive manufacturing: Spotlight on sustainability and material utilization. *Green Materials*, 1-11.

[10] Ibrahim, S. A., Lafta, S. H. and Hussain, W. A. (2021). Impact strength of surface treated SS316L wires reinforced PMMA. *Journal of the Mechanical Behavior of Materials*, 30(1): 272-278.

[11] Punia, U. and Garg, R. K. (2024). Enhancing mechanical performance of 3D printable PMMA resin through strategic incorporation of SS 316 L nanoparticles for dental applications. *International Journal on Interactive Design and Manufacturing (IJIDeM)*, 18(8): 6317-6332.

[12] Dhanunjayarao, B. N. and Naidu, N. S. (2022). Assessment of dimensional accuracy of 3D printed part using resin 3D printing technique. *Materials Today: Proceedings*, 59: 1608-1614.

[13] Hwangbo, N. K., Nam, N. E., Choi, J. H. and Kim, J. E. (2021). Effects of the washing time and washing solution on the biocompatibility and mechanical properties of 3D printed dental resin materials. *Polymers*, 13(24): 4410.

[14] Guerra, A. J., Lammel-Lindemann, J., Katko, A., Kleinfehn, A., Rodriguez, C. A., Catalani, L. H., Becker, M.L., Ciurana, J. and Dean, D. (2019). Optimization of photocrosslinkable resin components and 3D printing process parameters. *Acta biomaterialia*, 97:154-161.

[15] Yang, Y., Zhou, Y., Lin, X., Yang, Q. and Yang, G. (2020). Printability of external and internal structures based on digital light processing 3D printing technique. *Pharmaceutics*, 12(3): 207.

[16] Li, S., Yuan, S., Zhu, J., Wang, C., Li, J. and Zhang, W. (2020). Additive manufacturing-driven design optimization: Building direction and structural topology. *Additive Manufacturing*, 36: 101406.

[17] Zaldivar, R. J., Witkin, D. B., McLouth, T., Patel, D. N., Schmitt, K. and Nokes, J. P. (2017). Influence of processing and orientation print effects on the mechanical and thermal behavior of 3D-Printed ULTEM 9085 Material. *Additive Manufacturing*, 13: 71-80.

[18] Schittecatte, L., Geertsen, V., Bonamy, D., Nguyen, T. and Guenoun, P. (2023). From resin formulation and process parameters to the final mechanical properties of 3D printed acrylate materials. *MRS Communications*, 13(3): 357-377.

[19] Wiese, M., Thiede, S. and Herrmann, C. (2020). Rapid manufacturing of automotive polymer series parts: A systematic review of processes, materials and challenges. *Additive Manufacturing*, 36: 101582.

[20] Bardelcik, A., Yang, S., Alderson, F. and Gadsden, A. (2021). The effect of wash treatment on the mechanical properties and energy absorption potential of a 3D printed polymethyl methacrylate (PMMA). *Materials Today Communications*, 26: 101728.

IMPACT OF FIBERS WEIGHT PROPORTION AND SURFACE TREATMENTS ON THE RELIABILITY OF HYBRID EPOXY COMPOSITE

Manjeet Chahar, Rajneesh Kumar
•
Department of Mechanical Engineering
Deenbandhu Chhotu Ram University of Science and Technology,
Murthal, Sonipat, Haryana, India - 131039
manjeetchahar541@gmail.com, rajneesh.me@dcrustm.org

Abstract

Natural fiber-reinforced composites (NFRCs) are attracting growing interest in many technical applications owing to their environmentally sustainable and economical properties. This study investigates the impact of weight proportion of fibers and surface treatments on the tensile strength of hybrid epoxy composites reinforced with hemp, jute, and bamboo. Prior to composite fabrication, the fibers underwent alkali and saline treatments at different concentrations (3, 5, and 7 wt. %). The composites were fabricated via the hand lay-up technique by varying wt. proportion of fibers (10, 15, and 20 wt. %). The tensile strength is optimized using Response Surface Methodology (RSM), which yields highest tensile strength of 63.11 MPa at 14.24 wt. % of fibers fraction and 5.40 wt. % concentration of alkali treatment. Findings of this study demonstrate that reliability of the hybrid composite significantly enhanced due to improvement in strength of the composite. The treated hybrid composites have favourable properties, rendering them a feasible and sustainable option for automobile components and other lightweight structural applications.

Keywords: *Natural fibers, hybrid composite, Surface treatments, Tensile strength, Reliability*

I. Introduction

Natural cellulose fibers are extensively used in various engineering applications, such as construction materials and vehicle structural components, where lightweight materials are essential. These plant-based fibers offer numerous advantages, including cost-effectiveness, low density, wide availability, excellent mechanical strength, thermal insulation, electrical resistivity, and environmental sustainability [1, 2, 3]. Today, a wide range of natural fibres is recognized and utilized in lightweight structural applications across the construction, automotive, and aerospace industries. Economically viable fibers such as hemp, palm, okra, kapok, silk, coconut, alfa, bamboo, jute, and abaca are extensively used in various products, including textiles, household items, ropes, bags, automotive components, and lightweight parts for the aviation sector [4, 5].

Despite their apparent advantages, natural fibers have certain disadvantages, such as lower strength than synthetic materials, inconsistent size and diameter, extreme sensitivity to water, intolerance to high temperatures, and reduced resistance to fungal and bacterial infections. To address these obstacles and enhance the mechanical characteristics of NFRCs, researchers employ various strategies, including chemical treatments, modifications to fiber alignment, stacking

sequences, hybridization techniques, and other innovative methods [6, 7, 8]. Hybrid natural fiber composites use the favorable qualities of one fiber to counterbalance the negative attributes of another fiber. For example, hemp fiber exhibits more flexural and tensile strength than jute fiber, but jute fibers show higher impact strength than hemp fibres. Therefore, the combination of hemp and jute fibers in hybrid laminates results in decreased brittleness and improvement in the mechanical characteristics of the composite[9]. Hybrid NFRCs leverage the strengths of different fibers to compensate for their respective weaknesses. Hemp fibers, known for their brittleness and toughness, contrast with jute fibres, which exhibit excellent elongation properties [10, 11]. These composites achieve reduced brittleness and enhanced mechanical strength by integrating hemp and jute fibers in hybrid laminates. Bamboo fiber exhibits a high specific tensile strength that surpasses that of steel [12].

Reinforcing hybrid epoxy composites with snake grass and mudar ranging from 10 to 40 wt. % is possible. Reinforcement of fibers at 30 wt. % produced the best results. The optimal strength was achieved with a blend of 30 wt. % flax and 10 wt. % jute fiber [13]. The results showed that the impact strength improved by 40.6% and the flexural strength by 35% at 30 wt. % fiber content when banana fiber reinforcement was added to low-density polyethylene at a weight percentage ranging from 10 to 30 wt. % [14]. The hand lay-up method was used to create hybrid epoxy composite reinforced date palm fibers with varied weight percent of fiber. The mechanical characteristics of the composite were observed to be the highest at a fiber concentration of 50 wt. percent [15]. In contrast to jute fibers, which have exceptional elongation qualities, hemp fibers are infamously strong and brittle. Hybrid laminates that have hemp and jute fiber reinforcement are less brittle and have greater mechanical strength. Hemp and jute fiber hybridization greatly improves the composite's strength, according to the study. The composite with the perfect combination of hemp fiber (at 10% by weight) and jute fiber (at 40% by weight) demonstrated the highest levels of flexural strength, impact resistance, and tensile strength [16]. Highest mechanical and tribological characteristics were obtained at 15 wt. % reinforcement in hybrid epoxy composite [17].

Numerous researchers have highlighted in the literature that various surface treatments can further enhance the properties of composites. Among these, alkali and saline treatments have proven to be the most effective in enhancing composites' mechanical properties [18]. Alkaline surface treatment is often used to increase natural fibres' characteristics in composite materials [19, 20, 21]. This is achieved by chemically pre-treating natural fiber with NaOH. The surface treatment removes waxes and hemicellulose from the fiber surface, exposing more bare surface area. Which enhances adhesion, resulting in improved bonding and, consequently, better mechanical strength of the composite [22]. Yusuf et al., The flexural strength of epoxy reinforced with kenaf fiber increased by 36% following alkali surface pretreatment at a 6% concentration [23]. Vekateshwaran et al., Fabricated Epoxy composites reinforced with banana fibres, with NaOH pretreatment, applied at different concentrations. The study depicted that the highest strength was achieved at a 1% NaOH concentration, with the treated composites showing improved strength across all concentrations [24]. Goriparthi et al., fabricated a composite by reinforcing jute fibers into PLA, followed by alkali treatment. It was observed that the treated composite exhibited enhanced mechanical properties compared to the untreated one [25]. Sisal fibers were treated with NaOH solutions at concentrations of 3%, 6%, and 9%, thenrinsed with distilled water and dried. The highest tensile strength was achieved with the 3% NaOH treatment [26].

II. Methodology

The experiment was created with the help of the Design Expert13 program. Evaluating the effect of different variables on many replies allows this program to adequately examine diverse experimental

designs and further improve their findings. Based on previous research and results of trial and error, three variables were picked from the literature and their values were determined. Because of its superior capacity for higher-order modeling, enhanced efficiency in estimating quadratic terms, and backing from previous research, the RSM investigation utilized the optimal (custom) design approach. The study used an optimum (custom) design approach using RSM to produce twenty different trial combinations. A predictive model was developed by taking process parameters as inputs and hardness as a response variable. After that, we optimized the process parameters until we reached the maximum tensile strength. Figure 1 shows the approach that was used.

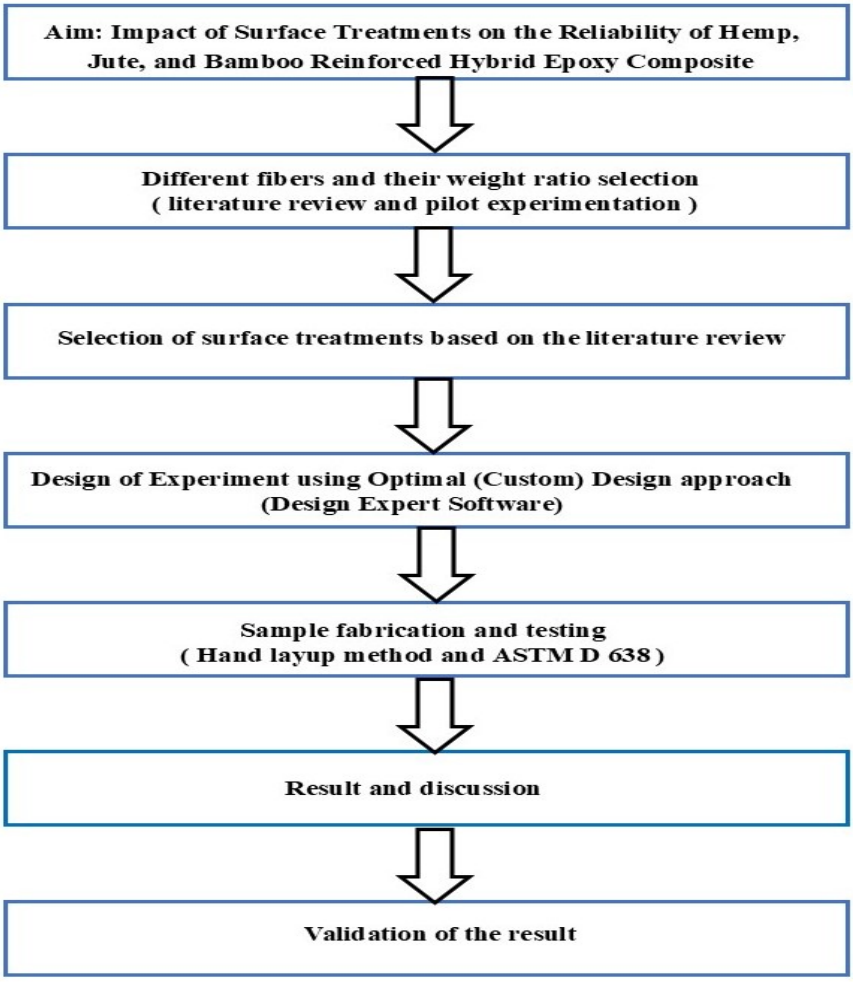


Figure 1: *Methodology implemented*

I. Experimentation

Hemp Organization Pvt. Ltd. in Delhi, India, provided the hemp fibers, while Himanshu Jute Fab in Ashok Vihar, Delhi, provided the jute fibers. The supplier of bamboo fibers was Vruksha Composites, located in Guntur, Andhra Pradesh, India. These natural fibers were used in their long fibrous forms, and were selected for their advantageous mechanical properties in composite manufacturing. The matrix material used in this study consisted of epoxy resin LY556 mixed with hardener HY 951 in a precise ratio of 10:1. Herenba Instruments & Engineers, Chennai, India, supplied both materials. The hardener was crucial for curing the epoxy, ensuring proper setting and improving the durability of the final composite. Additionally, wax from Jai Shree Balaji Sales

Corporation, New Delhi, was used as a releasing agent to ensure smooth demolding during fabrication.

The properties of NFRCs are largely influenced by the type of surface treatment and the concentration levels used. This study investigates the effects of alkali and saline surface treatments. Sodium hydroxide (NaOH) and (3-Glycidyloxypropyl) silane were selected for these treatments. Fibers were immersed in NaOH solutions at concentrations of 3 wt. %, 5 wt. %, and 7 wt. % for 30 minutes. After soaking, the fibers were thoroughly washed with distilled water until the pH of the water reached 7, then dried in an oven and subsequently straightened through hammering and combing before composite fabrication. For the saline and acetylation treatments, the same fiber types were soaked in saline and acetylation solutions at identical concentrations for 1 hour, followed by drying in an oven at 70°C for 24 hours. This procedure was repeated for each treatment concentration.

Using the hand lay-up process, the hemp, jute, and bamboo fiber-reinforced hybrid epoxy composite was produced. The mold, constructed from mild steel, has cavity dimensions of 200×180 mm, with the upper part slightly smaller at 199.5×179.5 mm. In this study, hybrid epoxy composites were fabricated by varying weight proportions of fibers (10, 15, and 20 wt. %) and with parameters as depicted in Table 1. These fibers were taken in long fibrous form. The fibres underwent different surface treatment process, followed by drying in an oven and subsequent straightening by hammering and combing before composite fabrication. Initially, PVC polythene was applied to coat both the upper and lower mold surfaces, followed by the application of wax to prevent resin adhesion. The prepared fibres were then carefully arranged in the mold cavity. Epoxy resin, pre-mixed with hardener at a 10:1 ratio and thoroughly blended, was poured onto the fibers. A metallic roller was employed to remove bubbles and gases from each fiber layer meticulously. The composite was then left to cure for 24 hours at room temperature while a 20 kg dead weight was positioned on the mold. After curing, the composite was demolded, and Specimens measuring 115 × 19 × 4 mm and having a gauge length of 25 mm were manufactured for tensile testing in accordance with ASTM D 638 standard as depicted in Figure 2.



Figure 2: T*esting setup for tensile test and specimens according to ASTM standard*

Table 1: *Requirement for single-objective optimization of tensile strength*

Input variables	Units	Level 1	Level 2	Level 3
A: Fibers fraction	Wt. %	10	15	20
B: Solution concentration	Wt. %	3	5	7
C: Treatment type	-	1	2	3

II. Statistical Analysis

Design-Expert 13 was used to evaluate the data collected from the experiments. For the purpose of tabulating the combination of input variables at their distinct levels, centre composite design was employed. In order to select the best polynomial model with a significance level of $p<0.05$, several quantitative features, including coefficients of deviation, lack of fit, computed and shifted multiple correlation coefficients, were thoroughly examined. We used the DX-13 program to make interaction, factor, and three-dimensional graphs so we could see how the input variables affected the responses.

III. Results and Discussion

Specimens were manually produced using the hand lap up method and evaluated in accordance with ASTM standards. Table 2 presents the calculated tensile strength results. A mathematical model was developed utilizing twenty permutations of three input factors and the hardness of the resultant nanocomposite. Equation illustrates the mathematical relationship derived from the calculation of tensile strength coefficient values.

$$\text{Tensile strength} = +62.01 - 2.36\,A + 1.03\,B + 0.8057\,C[1] - 0.1781\,C[2] + 0.2262\,AB - 0.2549\,AC[1] - 0.2249\,AC[2] - 0.1144\,BC[1] - 0.2463\,BC[2] - 8.47\,A^2 - 2.18\,B^2$$

Where, C[1], C[2] and C[3] are alkaline, saline and acetylene surface treatment respectively.

Table 2: *Experimental results for tensile strength*

Run	Factor 1	Factor 2	Factor 3	Response 1
	A:Fiber Fraction (wt. %)	B:Treatment Concentration (wt. %)	C:Treatment Type -	Tensile Strength
1	20	7	2	49.76
2	20	5	3	50.48
3	15	3	2	58.45
4	20	3	2	47.76
5	10	5	1	57.06
6	15	3	1	59.48
7	10	5	3	54.78
8	10	5	3	54.86
9	15	5	1	62.82

10	20	5	1	52.14
11	10	7	2	54.28
12	15	3	3	57.45
13	15	5	1	63.78
14	20	5	1	50.98
15	10	7	1	55.12
16	10	3	1	53.98
17	15	5	2	61.64
18	10	3	2	53.56
19	15	7	3	60.85
20	20	3	3	47.86

Table 3 shows the results of an ANOVA test conducted with a 95% confidence level, which was used to determine the model's appropriateness. Results demonstrated the usefulness of the model and its potential for use in predicting the shore hardness of the produced nanocomposite in the absence of actual experimental data. Statistical relevance and significance are indicated by the model's p-value, which is less than 0.0001. Important model terms in this instance include A, B, C, A^2, and B^2. The model's R2 is 0.998, indicating that approx. For all tensile strengths, the input parameters account for 99.8 percent of the variance.

Table 3: *ANOVA test results for tensile strength*

Source	Sum of Squares	df	Mean Square	F-value	p-value	
Model	432.45	11	39.31	99.86	< 0.0001	significant
A-Fibers fraction	52.17	1	52.17	132.51	< 0.0001	
B-Treatment concentration	13.79	1	13.79	35.03	0.0004	
C-Types of treatment	8.46	2	4.23	10.75	0.0054	
AB	0.2517	1	0.2517	0.6394	0.4470	
AC	1.18	2	0.5899	1.50	0.2801	
BC	0.5941	2	0.2970	0.7545	0.5010	
A^2	303.30	1	303.30	770.39	< 0.0001	
B^2	14.92	1	14.92	37.90	0.0003	
Residual	3.15	8	0.3937			
Lack of Fit	2.01	5	0.4026	1.06	0.5133	non significant
Pure Error	1.14	3	0.3789			
Cor Total	435.60	19				

As depicted in Figure 3, the projected tensile strength values are in agreement with the experimental ones, and the difference between the two sets of values is also illustrated. Figure 2D and 3D

surface plots show the impact of changing various input factors on the tensile strength of the hybrid epoxy composite that was produced. The results reveal that as the fiber fraction enhances, the tensile strength of the produced hybrid composite decreases. The tensile strength is greatly enhanced with a rise in the fiber fraction, reaching its maximum at 15 % by weight and a decrease in tensile strength observed when this point is passed. The inadequate soaking of the fibers by the epoxy caused a weak connection between the fibers and the matrix, which resulted in this reduction.

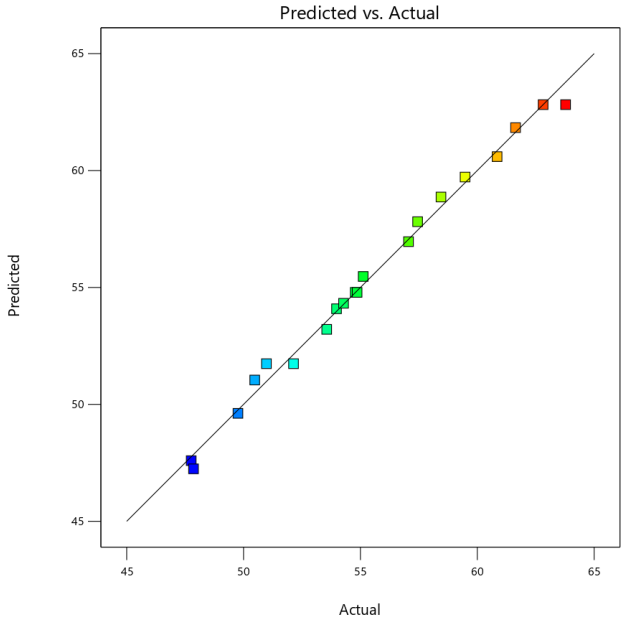


Figure 3: *Predicted v/s actual values for tensile strength*

The section presents 2D and 3D surface plots that show how the tensile strength is affected by weight proportion, surface treatment, and its concentration. Figure 1 shows how the tensile strength of the hybrid composite changes as a function of the weight proportion and the concentration level of the alkali treatment. The red area indicates the zone with the highest tensile strength, while the blue area indicates the zone with the lowest. The green and blue patches, respectively, show regions with moderate and low tensile strength. A maximum tensile strength of 63.78 MPa was achieved in the area contained by the 11–17 wt. % fibers, which also had the strongest reaction. In a similar vein, Figure shows how the tensile strength of the hybrid composite changes as a function of the treatment concentration level of saline (C2) and the alteration of the weight proportion. The area bounded by the 12–16 wt. % fibers showed the most reaction and had the maximum tensile strength value of 61.64 MPa. C3 surface treatment with acetylene resulted in a maximum tensile strength of 60.85 MPa.

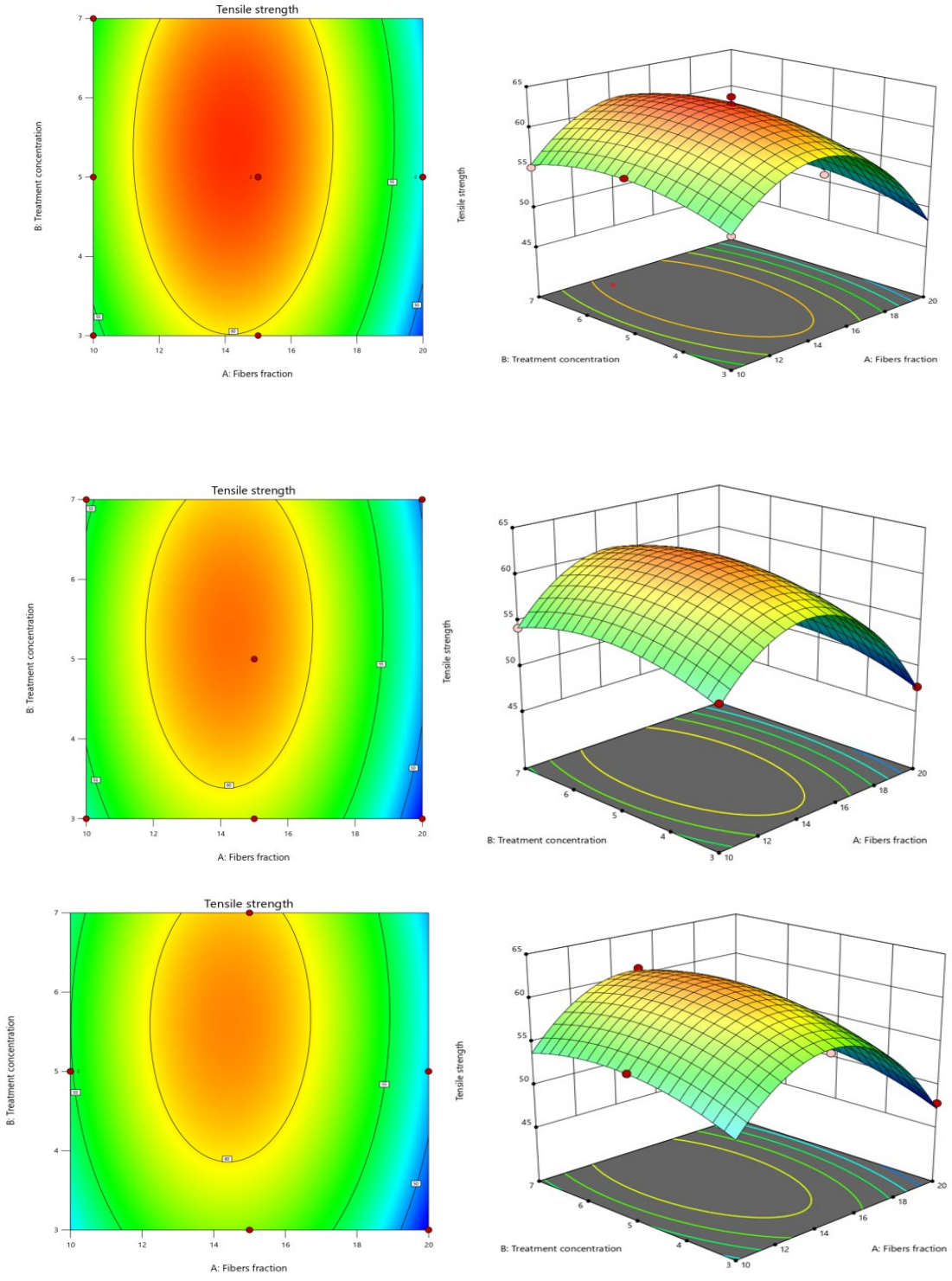


Figure 4: *2D and 3D surface plots illustrating the effect of fiber weight fraction, surface treatment type, and treatment concentration on the tensile strength*

Identical findings were reported for treatment concentration, with the maximum tensile strength recorded at a concentration of 5 wt. %. At this stage, fiber-matrix interaction was enhanced by the elimination of wax and hemicellulose, therefore increasing the exposed fiber surface area. Exceeding this concentration, tensile strength begins to diminish. The alkali surface-treated composite exhibited superior tensile strength at all concentrations due to enhanced surface

roughness, resulting in improved interlocking between the matrix and fibers.

In single-objective optimization of the response parameter, i.e., tensile strength, Table 4 shows the criteria for various process parameters. The objective is to optimize the hybrid epoxy composite's tensile strength within the given parameter range.

Table 4: *Requirement for single-objective optimization of shore D hardness*

Name	Goal	Lower Limit	Upper Limit	Lower Weight	Upper Weight	Importance
A:Fibers fraction	is in range	10	20	1	1	***
B:Treatmnt concentration	is in range	3	7	1	1	***
C:Types of treatment	is equal to	1	3	1	1	***
Tensile strength	maximize	47.76	63.78	1	1	***

All responses and criteria were accorded equal significance, and distinct objectives were established for each dimension. The response surface methodology (RSM) produced 76 potential options, from which the ideal solution was chosen based on greatest attractiveness and practical feasibility. The ideal combination of input parameters is determined to be 14.24 wt. % for fiber weight fraction, alkali surface treatment for type, and 5.4 wt. % for concentration level. The optimal values of the response parameters were determined as follows: Tensile strength: 63.11 MPa. The ramp function graphs in Figure 5 clearly depict these conclusions. The model was verified utilizing the optimal process parameters derived from the RSM-generated model. Three specimens were produced for each condition, and experimental findings indicated a maximum error of under 2.3%, therefore validating the model's precision and dependability.

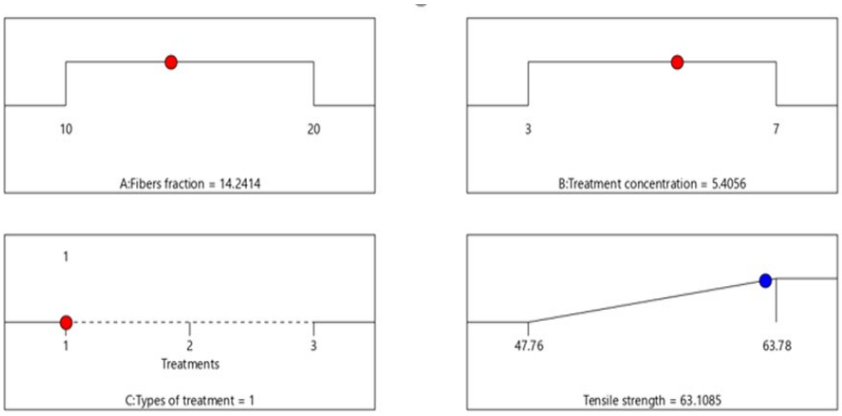


Figure 5: *Ramp function graphs for single-objective optimization of tensile strength*

IV. Conclusion

This study investigates the tensile strength of hybrid epoxy reinforced composites produced via the hand layup method under diverse processing conditions. The results indicate that alterations in process parameters significantly affect tensile strength, with fiber weight fraction and diverse surface treatments at different concentrations identified as critical variables. The tensile strength improves with the rising weight fraction of fibers, up to an optimal threshold. The model's robustness and

reliability are validated by the Response Surface Methodology (RSM), yielding an R2 score of 0.998. RSM optimization effectively maximizes tensile strength, achieving a maximum of 63.11 MPa at a fiber fraction of 14.24 wt. % and an alkali treatment concentration of 5.40 wt. %. The enhanced efficacy of alkali treatment is due to its capacity to eliminate surface contaminants, augment fiber roughness, and strengthen interfacial adhesion between the fibers and the matrix. The enhanced connection between the fiber and matrix facilitates superior stress transfer, hence improving mechanical characteristics. Although saline treatment enhanced fiber-matrix compatibility by altering the fiber surface, its impact was relatively less significant than that of alkali treatment.

References

[1] Fung, K. L., Xing, X. S., Li, R. K. Y., Tjong, S. C. and Mai, Y. W. (2003). An investigation on the processing of sisal fibre reinforced polypropylene composites. *Compos. Sci. Technol.*, vol. 63, no. 9, pp. 1255–1258.

[2] Wambua, P., Ivens, J. and Verpoest, I. (2003). Natural fibres: Can they replace glass in fibre reinforced plastics?. *Compos. Sci. Technol.,* vol. 63, no. 9, pp. 1259–1264.

[3] Shah, A. U. M., Sultan, M. T. H., Jawaid, M., Cardona, F. and Talib, A. R. A. (2016). A Review on the Tensile Properties of Bamboo Fiber Reinforced Polymer Composites. *BioResources,* vol. 11, no. 4, pp. 10654–10676.

[4] Tyagi, A., Punia, U., Dadhich, A. and Meena, S. L. (2024). Global Perspective of Natural Fibre Reinforced Composites: Properties, and Applications. *J. Inst. Eng. Ser. C.*

[5] Gurunathan, T., Mohanty, S. and Nayak, S. K. (2015). A review of the recent developments in biocomposites based on natural fibres and their application perspectives. *Compos. Part A Appl. Sci. Manuf.,* vol. 77, pp. 1–25.

[6] Arthanarieswaran, V. P., Kumaravel, A. and Kathirselvam, M. (2014). Evaluation of mechanical properties of banana and sisal fiber reinforced epoxy composites: Influence of glass fiber hybridization. *Mater. Des.,* vol. 64, pp. 194–202.

[7] Genc, G. and Ozdemir, Y. (2022). Improvement of the Mechanical Properties of Plant Fiber-reinforced Composites through Hybridization. *J. Nat. Fibers,* vol. 19, no. 8, pp. 2805–2812.

[8] Nagarjun, J., Kanchana, J. and Rajesh Kumar, G. (2022). Improvement of Mechanical Properties of Coir/Epoxy Composites through Hybridization with Sisal and Palmyra Palm Fibers. *J. Nat. Fibers,* vol. 19, no. 2, pp. 475–484.

[9] Sowmya, C., Ramesh, V. and Karibasavaraja, D. (2018). An Experimental Investigation of New Hybrid Composite Material using Hemp and Jute Fibres and Its Mechanical Properties through Finite Element Method. *Mater. Today Proc.,* vol. 5, no. 5, pp. 13309–13320.

[10] Siddika,S., Mansura, F., Hasan, M. and Hassan, A. (2014). Effect of reinforcement and chemical treatment of fiber on The Properties of jute-coir fiber reinforced hybrid polypropylene composites. *Fibers Polym.,* vol. 15, no. 5, pp. 1023–1028.

[11] Doan, T. T. L., Brodowsky, H. and Mäder, E. (2012). Jute fibre/epoxy composites: Surface properties and interfacial adhesion. *Compos. Sci. Technol.,* vol. 72, no. 10, pp. 1160–1166.

[12] Bansal,S., Ramachandran, M. and Raichurkar, P. (2017). Comparative Analysis of Bamboo using Jute and Coir Fiber Reinforced Polymeric Composites. *Mater. Today Proc.,* vol. 4, no. 2, pp. 3182–3187.

[13] Jenish, I., Sahayaraj, A. F., Suresh, V., Mani Raj, J., Appadurai, M., Irudaya Raj, E. F. and Kumaravel, A. K. (2022). Analysis of the hybrid of mudar/snake grass fiber-reinforced epoxy with nano-silica filler composite for structural application. *Advances in Materials Science and Engineering*, p.7805146.

[14] Prasad, N., Agarwal, V.K. and Sinha, S. (2016). Banana fiber reinforced low-density polyethylene composites: effect of chemical treatment and compatibilizer addition. *Iranian Polymer Journal,* 25, pp.229-241.

[15] Refaai, M.R.A., Reddy, R.M., Reddy, M.I., Khan, B.S.H., Nagaraju, V. and Kumar, S.P. (2022). Investigation on physical and mechanical characteristics of date palm fiber reinforced aliphatic epoxy hybrid composites. *Advances in Polymer Technology,* p.4916499.

[16] Felix Sahayaraj, A., Muthukrishnan, M. and Ramesh, M. (2022). Experimental investigation on physical, mechanical, and thermal properties of jute and hemp fibers reinforced hybrid polylactic acid composites. *Polymer Composites,* 43(5), pp.2854-2863.

[17] Chahar, M. and Kumar, R. (2025). Effect of fiber weight fraction on mechanical properties of hemp, jute, bamboo epoxy composite. *Green Materials,* pp.1-30.

[18] Punia, U., Dhull, S., Habeeb, A., Antil, E., Dahiya, D., Gupta, D. and Ahlawat, A. (2025). Adopting additive manufacturing: spotlight on sustainability and material utilization. *Green Materials,* 1-11.

[19] Punia, U. and Garg, R. K. (2024). Reinforcing dental restoration material PMMA with SS 316L nanoparticles for mechanical performance analysis. *Prog. Addit. Manuf.*

[20] Punia, U. and Garg, R. K. (2024). Enhancing mechanical performance of 3D printable PMMA resin through strategic incorporation of SS 316 L nanoparticles for dental applications. *Int. J. Interact. Des. Manuf.*

[21] Chahar, M., Kumar, R., Habeeb, A., Kumar Garg, R. and Punia, U. (2024). Factors affecting flexural and impact strength of natural fiber reinforced polymer composites: a review. *Green Mater.*, pp. 1–40.

[22] Kamarudin, S. H., Mohd Basri, M. S., Rayung, M., Abu, F., Ahmad, S. B., Norizan, M. N. and Abdullah, L. C. (2022). A review on natural fiber reinforced polymer composites (NFRPC) for sustainable industrial applications. *Polymers,* 14(17), 3698.

[23] Qian, S., Wang, H., Zarei, E. and Sheng, K. (2015). Effect of hydrothermal pretreatment on the properties of moso bamboo particles reinforced polyvinyl chloride composites. *Compos. Part B Eng.,* vol. 82, pp. 23–29.

[24] Mir, S. S., Nafsin, N., Hasan, M., Hasan, N. and Hassan, A. (2013). Improvement of physico-mechanical properties of coir-polypropylene biocomposites by fiber chemical treatment. *Mater. Des.,* vol. 52, pp. 251–257.

[25] Goriparthi, B. K., Suman, K. N. S. and Mohan Rao, N. (2012). Effect of fiber surface treatments on mechanical and abrasive wear performance of polylactide/jute composites. *Compos. Part A Appl. Sci. Manuf.,* vol. 43, no. 10, pp. 1800–1808.

[26] Sawpan, M. A., Pickering, K. L. and Fernyhough, A. (2012). Flexural properties of hemp fibre reinforced polylactide and unsaturated polyester composites. *Compos. Part A Appl. Sci. Manuf.,* vol. 43, no. 3, pp. 519–526.

COMPARISON OF CLASSICAL AND BAYESIAN APPROACHES FOR ESTIMATING THE SCALE PARAMETER OF THE INVERSE POWER RAYLEIGH DISTRIBUTION

Aadil Ahmad Mir[1*], S.P. Ahmad[2] and Sofi Mudasir Ahad[3]

•

[12] Department of Statistics, University of Kashmir, Srinagar, 190006, Jammu And Kashmir, India
[3] Department of Statistics, Government Degree College , Sopore, 193201, Jammu And Kashmir, India
[1*] aadilmir.stscholar@kashmiruniversity.net, [2]sprvz@yahoo.com, [3]sofimudasir3806@gmail.com

Abstract

This manuscript investigates the parameter estimation of the Inverse Power Rayleigh Distribution (IPRD) using both Classical and Bayesian approaches. Parameters are estimated via Maximum Likelihood Estimation (MLE) and Bayesian methods under three prior assumptions: Jeffreys prior, extended Jeffreys prior, and quasi prior. Bayesian estimators, along with their associated risks, are evaluated using various symmetric and asymmetric loss functions, including the squared error loss function, Al-Bayyatis new loss function, precautionary loss function and entropy loss function. The performance of the estimators is assessed through simulated data based on the mean squared error (MSE) criterion. Results indicate that the Bayesian approach generally provides more accurate estimates with lower MSE compared to the classical MLE method.

Keywords: Inverse Rayleigh distribution, Loss functions, Maximum Likelihood estimation, Bayesian estimation.

1. Introduction

The inverse Rayleigh distribution (IRD) holds significant importance in reliability analysis and life testing studies. If X follows an inverse Rayleigh (IR) distribution, its probability density function (PDF) is expressed as:

$$g(x) = \frac{2\theta}{x^3}\, e^{-\frac{\theta}{x^2}}; \quad x > 0, \theta > 0. \tag{1}$$

The corresponding cumulative distribution function (CDF) is:

$$G(x) = e^{-\frac{\theta}{x^2}}; \quad x > 0, \theta > 0. \tag{2}$$

The inverse Rayleigh distribution (IRD) was first introduced by [21], who explored various properties of the scale parameter of the maximum likelihood estimator (MLE) for this distribution. The IRD has found extensive applications in longevity experiments and reliability studies. Over time, numerous researchers have investigated estimation methods and prediction approaches for the IRD. Abdel-Monem [1] developed several estimators and prediction results for the IRD. Soliman *et al.* [20] studied the estimation of the IRD based on lower record values and proposed Bayes estimators under the squared error and zero-one loss functions. Dey [6] focused on Bayesian estimation for the scale parameter and the reliability function of the IRD using squared error and linex loss functions. Sindhu *et al.* [19] extended this work to left-censored data and studied Bayes estimators under both symmetric and asymmetric loss functions. Prakash [16] discussed Bayesian estimation for the IRD under squared error and linex loss functions, while Fan [7] investigated

Bayesian estimators under various loss functions, including squared error, linex and entropy loss functions. Rasheed *et al.* [23] compared classical estimators with Bayesian estimators under the generalized squared error loss function. Several other researchers have explored the inverse Rayleigh distribution, including Abdullah and Aref [2], Fatima *et al.* [8], Sharma *et al.* [17], Noor *et al.* [14], Sharma and Kumar [18], Kumar *et al.* [9], Nuzhat *et al.* [3], Yanuar *et al.* [22], and Mir and Ahmad [10, 12, 11, 13].

Recently, Bhat *et al.* [5] introduced the Inverse Power Rayleigh Distribution (IPRD), a generalized form of the IRD. The PDF and CDF of the IPRD are defined as follows:

$$g(x;\alpha,\theta) = \frac{\alpha}{\theta^2} x^{-(2\alpha+1)} \exp\left(-\frac{x^{-2\alpha}}{2\theta^2}\right), \quad \alpha,\theta > 0, \tag{3}$$

$$G(x;\alpha,\theta) = \exp\left(-\frac{x^{-2\alpha}}{2\theta^2}\right), \quad \alpha,\theta > 0. \tag{4}$$

2. Methods

In this section, we estimate the parameters using maximum likelihood estimation as well as Bayesian estimation methods under three different priors : Jeffreys prior, extended Jeffreys prior and quasi prior and four loss functions: squared error loss function, Al-Bayyatis new loss function, precautionary loss function and entropy loss function.

2.1. Prior and Loss Function

As part of the analysis, we employ three different priors.

1. Jeffreys prior

$$g(\theta) \propto \sqrt{I(\theta)}$$

where,

$$I(\theta) = -nE\left[\frac{\partial^2}{\partial\theta^2}\log f(x;\theta)\right]$$

is the Fisher information matrix.

2. Extended Jeffreys prior [4]

$$g_1(\theta) \propto [I(\theta)]^{c_1}, \quad c_1 \in \mathbb{R}^+$$

where

$$I(\theta) = -nE\left[\frac{\partial^2}{\partial\theta^2}\log f(x;\theta)\right]$$

is the Fisher information matrix.

3. Quasi prior

$$g_2(\theta) = \frac{1}{\theta^d}, \quad \theta > 0,\ d > 0.$$

In this paper, we utilize the following loss functions to facilitate a comprehensive comparison in Bayesian analysis:

a) Squared error loss function (self)

$$L_{self}(\hat{\theta},\theta) = c(\hat{\theta}-\theta)^2$$

b) Al-Bayyatis new loss function (abnlf) [15]

$$L_{abnlf}(\hat{\theta},\theta) = \theta^{c_2}(\hat{\theta}-\theta)^2, \quad c_2 \in \mathbb{R}^+$$

c) Precautionary loss function (plf)

$$L_{plf}(\hat{\theta},\theta) = \frac{(\hat{\theta}-\theta)^2}{\hat{\theta}}$$

d) Entropy loss function (elf)

$$L_{elf}(\hat{\theta},\theta) = \left(\frac{\hat{\theta}}{\theta} - \log\left(\frac{\hat{\theta}}{\theta}\right) - 1\right)$$

Here, θ and $\hat{\theta}$ denote the true and estimated values of the parameter, respectively.

2.2. Maximum Likelihood Estimation

The likelihood function corresponding is

$$L(x;\alpha,\theta) = \frac{\alpha^n}{\theta^{2n}} \prod_{a=1}^{n} x_a^{-(2\alpha+1)} \exp\left(-\frac{\sum_{a=1}^{n} x_a^{-2\alpha}}{2\theta^2}\right). \tag{5}$$

The log-likelihood function is obtained as

$$l(x;\alpha,\theta) = n\log\alpha - 2n\log\theta - (2\alpha+1)\sum_{a=1}^{n}\log x_a - \frac{1}{2\theta^2}\sum_{a=1}^{n} x_a^{-2\alpha}. \tag{6}$$

To determine the MLE of θ, we differentiate Eq. (6)

$$\frac{\partial l(x;\alpha,\theta)}{\partial\theta} = -\frac{2n}{\theta} + \frac{\sum_{a=1}^{n} x_a^{-2\alpha}}{\theta^3} = 0. \tag{7}$$

Simplifying and solving for θ, we obtain the MLE as

$$\hat{\theta} = \sqrt{\frac{\sum_{a=1}^{n} x_a^{-2\alpha}}{2n}}. \tag{8}$$

2.3. Bayesian Method of Estimation

2.3.1 Posterior Density under Jeffreys Prior

For this model with the PDF specified in Eq. (3) and the likelihood function in Eq. (5), the Jeffreys prior for θ is given by

$$g(\theta) \propto \frac{1}{\theta}, \quad \theta > 0, \tag{9}$$

where θ is the scale parameter. Applying Bayes theorem, the posterior density is expressed as:

$$\pi_1(\theta \mid x) \propto L(x \mid \theta) g(\theta), \tag{10}$$

where $L(x \mid \theta)$ represents the likelihood function.

Substituting Eq. (9) and Eq. (5) into Eq. (10), we obtain:

$$\pi_1(\theta \mid x) \propto \frac{\alpha^n}{\theta^{2n+1}} \prod_{a=1}^{n} x_a^{-(2\alpha+1)} \exp\left(-\frac{\sum_{a=1}^{n} x_a^{-2\alpha}}{2\theta^2}\right) \tag{11}$$

$$= k^{-1} \frac{1}{\theta^{2n+1}} \exp\left(-\frac{\sum_{a=1}^{n} x_a^{-2\alpha}}{2\theta^2}\right), \tag{12}$$

where the normalization constant k^{-1} is given by

$$k^{-1} = \int_0^\infty \frac{1}{\theta^{2n+1}} \exp\left(-\frac{\sum_{a=1}^{n} x_a^{-2\alpha}}{2\theta^2}\right) d\theta. \tag{13}$$

Solving the integral,

$$k = \frac{\left(\sum_{a=1}^{n} x_a^{-2\alpha}\right)^n}{\Gamma(n)\, 2^{n-1}}. \tag{14}$$

Thus, the posterior distribution is given by

$$\pi_1(\theta \mid x) = \frac{\left(\sum_{a=1}^{n} x_a^{-2\alpha}\right)^n}{\Gamma(n)\, 2^{n-1}} \frac{1}{\theta^{2n+1}} \exp\left(-\frac{\sum_{a=1}^{n} x_a^{-2\alpha}}{2\theta^2}\right). \tag{15}$$

2.3.2 Posterior Density under an Extension of Jeffreys Prior

For the model in Eq. (3), the extended Jeffreys prior for θ becomes

$$g_1(\theta) \propto \frac{1}{\theta^{2c_1}}, \quad \theta > 0. \tag{16}$$

Applying Bayes theorem, the posterior density is

$$\pi_2(\theta \mid x) \propto L(x \mid \theta) g_1(\theta). \tag{17}$$

Substituting Eq. (5) and Eq. (16) into Eq. (17), we get

$$\pi_2(\theta \mid x) \propto \frac{1}{\theta^{2n+2c_1}} \exp\left(-\frac{\sum_{a=1}^{n} x_a^{-2\alpha}}{2\theta^2}\right) \tag{18}$$

$$= k^{-1} \frac{1}{\theta^{2n+2c_1}} \exp\left(-\frac{\sum_{a=1}^{n} x_a^{-2\alpha}}{2\theta^2}\right), \tag{19}$$

$$k^{-1} = \int_0^{\infty} \frac{1}{\theta^{2n+2c_1}} \exp\left(-\frac{\sum_{a=1}^{n} x_a^{-2\alpha}}{2\theta^2}\right) d\theta. \tag{20}$$

Solving this integral, we find

$$k = \frac{\left(\sum_{a=1}^{n} x_a^{-2\alpha}\right)^{n+c_1-1/2}}{\Gamma(n+c_1-1/2)\, 2^{n+c_1-3/2}}. \tag{21}$$

Therefore, the posterior distribution under the extended Jeffreys prior is

$$\pi_2(\theta \mid x) = \frac{\left(\sum_{a=1}^{n} x_a^{-2\alpha}\right)^{n+c_1-1/2}}{\Gamma(n+c_1-1/2)\, 2^{n+c_1-3/2}} \frac{1}{\theta^{2n+2c_1}} \exp\left(-\frac{\sum_{a=1}^{n} x_a^{-2\alpha}}{2\theta^2}\right). \tag{22}$$

2.3.3 Posterior Density under Quasi Prior

The quasi prior for θ is specified as

$$g_2(\theta) = \frac{1}{\theta^d}, \quad \theta > 0,\ d > 0. \tag{23}$$

Using Bayes theorem, the posterior density is given by

$$\pi_3(\theta \mid x) \propto L(x \mid \theta) g_2(\theta), \tag{24}$$

where $L(x \mid \theta)$ represents the likelihood function.

Substituting Eq. (5) and Eq. (23) into Eq. (24), we have

$$\pi_3(\theta \mid x) \propto \frac{1}{\theta^{2n+d}} \exp\left(-\frac{\sum_{a=1}^{n} x_a^{-2\alpha}}{2\theta^2}\right) \tag{25}$$

$$= k^{-1} \frac{1}{\theta^{2n+d}} \exp\left(-\frac{\sum_{a=1}^{n} x_a^{-2\alpha}}{2\theta^2}\right), \tag{26}$$

$$k^{-1} = \int_0^{\infty} \frac{1}{\theta^{2n+d}} \exp\left(-\frac{\sum_{a=1}^{n} x_a^{-2\alpha}}{2\theta^2}\right) d\theta. \tag{27}$$

Solving the integral, we obtain

$$k = \frac{\left(\sum_{a=1}^{n} x_a^{-2\alpha}\right)^{\frac{2n+d-1}{2}}}{\Gamma\left(\frac{2n+d-1}{2}\right) \cdot 2^{\frac{2n+d-3}{2}}}. \tag{28}$$

Thus, the posterior distribution under the quasi prior is given by

$$\pi_3(\theta \mid x) = \frac{\left(\sum_{a=1}^{n} x_a^{-2\alpha}\right)^{\frac{2n+d-1}{2}}}{\Gamma\left(\frac{2n+d-1}{2}\right) 2^{\frac{2n+d-3}{2}}} \frac{1}{\theta^{2n+d}} \exp\left(-\frac{\sum_{a=1}^{n} x_a^{-2\alpha}}{2\theta^2}\right). \tag{29}$$

2.4. Bayesian Estimation by Using Jeffreys Prior under Different Loss Functions

2.4.1 Squared error loss function (self)

The risk function (RF) for $L_{self}(\hat{\theta},\theta)$ is

$$R(\hat{\theta}) = \int_0^\infty c(\hat{\theta}-\theta)^2 \pi_1(\theta \mid x)\, d\theta. \tag{30}$$

Substituting Eq. (15) into Eq. (30), we obtain:

$$R(\hat{\theta}) = \int_0^\infty c(\hat{\theta}-\theta)^2 \frac{\left(\sum_{a=1}^n x_a^{-2\alpha}\right)^n}{\Gamma(n)\, 2^{n-1}} \frac{1}{\theta^{2n+1}} \exp\left(-\frac{\sum_{a=1}^n x_a^{-2\alpha}}{2\theta^2}\right) d\theta. \tag{31}$$

$$= c\frac{\left(\sum_{a=1}^n x_a^{-2\alpha}\right)^n}{\Gamma(n)\, 2^{n-1}} \int_0^\infty \left(\hat{\theta}^2+\theta^2-2\hat{\theta}\theta\right) \frac{1}{\theta^{2n+1}} \exp\left(-\frac{\sum_{a=1}^n x_a^{-2\alpha}}{2\theta^2}\right) d\theta. \tag{32}$$

$$R(\hat{\theta}) = c\frac{\left(\sum_{a=1}^n x_a^{-2\alpha}\right)^n}{\Gamma(n)\, 2^{n-1}} \left\{ \int_0^\infty \hat{\theta}^2 \frac{1}{\theta^{2n+1}} \exp\left(-\frac{\sum_{a=1}^n x_a^{-2\alpha}}{2\theta^2}\right) d\theta + \int_0^\infty \theta^2 \frac{1}{\theta^{2n+1}} \exp\left(-\frac{\sum_{a=1}^n x_a^{-2\alpha}}{2\theta^2}\right) d\theta \right.$$
$$\left. -2\hat{\theta} \int_0^\infty \theta \frac{1}{\theta^{2n+1}} \exp\left(-\frac{\sum_{a=1}^n x_a^{-2\alpha}}{2\theta^2}\right) d\theta \right\}. \tag{33}$$

Minimizing $R(\hat{\theta})$ with respect to $\hat{\theta}$, we derive:

$$\hat{\theta} = \frac{\Gamma\left(n-\frac{1}{2}\right)}{\Gamma(n)} \sqrt{\frac{\sum_{a=1}^n x_a^{-2\alpha}}{2}}. \tag{34}$$

2.4.2 Al-Bayyatis new loss function (abnlf)

The RF for $L_{abnlf}(\hat{\theta}$ is

$$R(\hat{\theta}) = \int_0^\infty \theta^{c_2}(\hat{\theta}-\theta)^2 \pi_1(\theta \mid x)\, d\theta. \tag{35}$$

By substituting Eq. (15) into Eq. (35), we get:

$$R(\hat{\theta}) = \int_0^\infty \theta^{c_2}(\hat{\theta}-\theta)^2 \frac{\left(\sum_{a=1}^n x_a^{-2\alpha}\right)^n}{\Gamma(n)\, 2^{n-1}} \frac{1}{\theta^{2n+1}} \exp\left(-\frac{\sum_{a=1}^n x_a^{-2\alpha}}{2\theta^2}\right) d\theta. \tag{36}$$

$$R(\hat{\theta}) = \frac{\left(\sum_{a=1}^n x_a^{-2\alpha}\right)^n}{\Gamma(n)\, 2^{n-1}} \int_0^\infty \theta^{c_2} \left(\hat{\theta}^2+\theta^2-2\hat{\theta}\theta\right) \frac{1}{\theta^{2n+1}} \exp\left(-\frac{\sum_{a=1}^n x_a^{-2\alpha}}{2\theta^2}\right) d\theta. \tag{37}$$

$$R(\hat{\theta}) = \frac{\left(\sum_{a=1}^n x_a^{-2\alpha}\right)^n}{\Gamma(n)\, 2^{n-1}} \left\{ \hat{\theta}^2 \int_0^\infty \theta^{c_2} \frac{1}{\theta^{2n+1}} \exp\left(-\frac{\sum_{a=1}^n x_a^{-2\alpha}}{2\theta^2}\right) d\theta \right.$$
$$+ \int_0^\infty \theta^{c_2+2} \frac{1}{\theta^{2n+1}} \exp\left(-\frac{\sum_{a=1}^n x_a^{-2\alpha}}{2\theta^2}\right) d\theta$$
$$\left. - 2\hat{\theta} \int_0^\infty \theta^{c_2+1} \frac{1}{\theta^{2n+1}} \exp\left(-\frac{\sum_{a=1}^n x_a^{-2\alpha}}{2\theta^2}\right) d\theta \right\}. \tag{38}$$

Minimizing $R(\hat{\theta})$ yields:

$$\hat{\theta} = \frac{\Gamma\left(n-c_2/2-1/2\right)}{\Gamma\left(n-c_2/2\right)} \sqrt{\frac{\sum_{a=1}^n x_a^{-2\alpha}}{2}}. \tag{39}$$

2.4.3 Precautionary loss function (plf)

The RF for $L_{plf}(\hat{\theta},\theta)$ is

$$R(\hat{\theta}) = \int_0^\infty \frac{(\hat{\theta}-\theta)^2}{\hat{\theta}} \pi_1(\theta \mid x)\, d\theta. \tag{40}$$

Substituting Eq. (15) into Eq. (40), we get:

$$R(\hat{\theta}) = \int_0^\infty \frac{(\hat{\theta}-\theta)^2}{\hat{\theta}} \frac{\left(\sum_{a=1}^n x_a^{-2\alpha}\right)^n}{\Gamma(n)\, 2^{n-1}} \frac{1}{\theta^{2n+1}} \exp\left(-\frac{\sum_{a=1}^n x_a^{-2\alpha}}{2\theta^2}\right) d\theta. \tag{41}$$

$$R(\hat{\theta}) = \frac{\left(\sum_{a=1}^n x_a^{-2\alpha}\right)^n}{\Gamma(n)\, 2^{n-1}} \int_0^\infty \frac{\left(\hat{\theta}^2+\theta^2-2\hat{\theta}\theta\right)}{\hat{\theta}} \frac{1}{\theta^{2n+1}} \exp\left(-\frac{\sum_{a=1}^n x_a^{-2\alpha}}{2\theta^2}\right) d\theta. \tag{42}$$

$$\begin{aligned} R(\hat{\theta}) = \frac{\left(\sum_{a=1}^n x_a^{-2\alpha}\right)^n}{\Gamma(n)\, 2^{n-1}} \hat{\theta} \Bigg\{ & \int_0^\infty \frac{1}{\theta^{2n+1}} \exp\left(-\frac{\sum_{a=1}^n x_a^{-2\alpha}}{2\theta^2}\right) d\theta \\ & + \int_0^\infty \frac{\theta^2}{\hat{\theta}} \frac{1}{\theta^{2n+1}} \exp\left(-\frac{\sum_{a=1}^n x_a^{-2\alpha}}{2\theta^2}\right) d\theta - 2\int_0^\infty \theta \frac{1}{\theta^{2n+1}} \exp\left(-\frac{\sum_{a=1}^n x_a^{-2\alpha}}{2\theta^2}\right) d\theta \Bigg\}. \end{aligned} \tag{43}$$

Minimizing the risk results in:

$$\hat{\theta} = \sqrt{\frac{\sum_{a=1}^n x_a^{-2\alpha}}{2(n-1)}}. \tag{44}$$

2.4.4 Entropy loss function (elf)

The RF for $L_{elf}(\hat{\theta},\theta)$ is

$$R(\hat{\theta}) = \int_0^\infty \left(\frac{\hat{\theta}}{\theta} - \log\left(\frac{\hat{\theta}}{\theta}\right) - 1\right) \pi_1(\theta|x)\, d\theta. \tag{45}$$

Substituting Eq. (15) in Eq. (45), we get

$$R(\hat{\theta}) = \int_0^\infty \left(\frac{\hat{\theta}}{\theta} - \log\left(\frac{\hat{\theta}}{\theta}\right) - 1\right) \frac{\left(\sum_{a=1}^n x_a^{-2\alpha}\right)^n}{\Gamma(n)\, 2^{n-1}} \frac{1}{\theta^{2n+1}} \exp\left(-\frac{\sum_{a=1}^n x_a^{-2\alpha}}{2\theta^2}\right) d\theta. \tag{46}$$

$$R(\hat{\theta}) = \frac{\left(\sum_{a=1}^n x_a^{-2\alpha}\right)^n}{\Gamma(n)\, 2^{n-1}} \int_0^\infty \left(\frac{\hat{\theta}}{\theta} - \log\left(\frac{\hat{\theta}}{\theta}\right) - 1\right) \frac{1}{\theta^{2n+1}} \exp\left(-\frac{\sum_{a=1}^n x_a^{-2\alpha}}{2\theta^2}\right) d\theta. \tag{47}$$

$$\begin{aligned} R(\hat{\theta}) = \frac{\left(\sum_{a=1}^n x_a^{-2\alpha}\right)^n}{\Gamma(n)\, 2^{n-1}} \Bigg\{ & \int_0^\infty \frac{\hat{\theta}}{\theta} \frac{1}{\theta^{2n+1}} \exp\left(-\frac{\sum_{a=1}^n x_a^{-2\alpha}}{2\theta^2}\right) d\theta \\ & - \int_0^\infty \log\left(\frac{\hat{\theta}}{\theta}\right) \frac{1}{\theta^{2n+1}} \exp\left(-\frac{\sum_{a=1}^n x_a^{-2\alpha}}{2\theta^2}\right) d\theta - \int_0^\infty \frac{1}{\theta^{2n+1}} \exp\left(-\frac{\sum_{a=1}^n x_a^{-2\alpha}}{2\theta^2}\right) d\theta \Bigg\}. \end{aligned} \tag{48}$$

Minimizing this risk function with respect to $\hat{\theta}$ yields the optimal Bayes estimate:

$$\hat{\theta} = \frac{\Gamma(n)}{\Gamma(n+1/2)} \sqrt{\frac{\sum_{a=1}^n x_a^{-2\alpha}}{2}}. \tag{49}$$

2.5. Bayesian Estimation by Using Extension of Jeffreys Prior under Different Loss Functions

2.5.1 Squared error loss function (self)

$$R(\hat{\theta}) = \int_0^\infty c(\hat{\theta}-\theta)^2 \pi_2(\theta|x)\, d\theta. \tag{50}$$

Substituting Eq. (22) into Eq. (50), we obtain:

$$R(\hat{\theta}) = \int_0^\infty c(\hat{\theta}-\theta)^2 \frac{(\sum_{a=1}^n x_a^{-2\alpha})^{n+c_1-1/2}}{\Gamma(n+c_1-1/2)\ 2^{n+c_1-3/2}}\ \ \frac{1}{\theta^{2n+2c_1}} \exp\left(-\frac{\sum_{a=1}^n x_a^{-2\alpha}}{2\theta^2}\right) d\theta. \tag{51}$$

$$R(\hat{\theta}) = c\frac{(\sum_{a=1}^n x_a^{-2\alpha})^{n+c_1-1/2}}{\Gamma(n+c_1-1/2)\ 2^{n+c_1-3/2}} \int_0^\infty \left(\hat{\theta}^2+\theta^2-2\hat{\theta}\theta\right) \frac{1}{\theta^{2n+2c_1}} \exp\left(-\frac{\sum_{a=1}^n x_a^{-2\alpha}}{2\theta^2}\right) d\theta. \tag{52}$$

$$\begin{aligned} R(\hat{\theta}) = c\frac{(\sum_{a=1}^n x_a^{-2\alpha})^{n+c_1-1/2}}{\Gamma(n+c_1-1/2)\ 2^{n+c_1-3/2}} \Bigg\{ & \hat{\theta}^2 \int_0^\infty \frac{1}{\theta^{2n+2c_1}} \exp\left(-\frac{\sum_{a=1}^n x_a^{-2\alpha}}{2\theta^2}\right) d\theta \\ & + \int_0^\infty \theta^2 \frac{1}{\theta^{2n+2c_1}} \exp\left(-\frac{\sum_{a=1}^n x_a^{-2\alpha}}{2\theta^2}\right) d\theta - 2\hat{\theta} \int_0^\infty \theta \frac{1}{\theta^{2n+2c_1}} \exp\left(-\frac{\sum_{a=1}^n x_a^{-2\alpha}}{2\theta^2}\right) d\theta \Bigg\}. \end{aligned} \tag{53}$$

$$\hat{\theta} = \frac{\Gamma(n+c_1-1)}{\Gamma(n+c_1-\frac{1}{2})} \sqrt{\left(\frac{\sum_{a=1}^n x_a^{-2\alpha}}{2}\right)}. \tag{54}$$

2.5.2 Al-Bayyatis new loss function (abnlf)

$$R(\hat{\theta}) = \int_0^\infty \theta^{c_2}(\hat{\theta}-\theta)^2 \pi_2(\theta|x)\, d\theta. \tag{55}$$

Substituting Eq. (15) into Eq. (55), we get:

$$R(\hat{\theta}) = \int_0^\infty \theta^{c_2}(\hat{\theta}-\theta)^2 \frac{(\sum_{a=1}^n x_a^{-2\alpha})^{n+c_1-1/2}}{\Gamma(n+c_1-1/2)\ 2^{n+c_1-3/2}}\ \ \frac{1}{\theta^{2n+2c_1}} \exp\left(-\frac{\sum_{a=1}^n x_a^{-2\alpha}}{2\theta^2}\right) d\theta. \tag{56}$$

$$R(\hat{\theta}) = \frac{(\sum_{a=1}^n x_a^{-2\alpha})^{n+c_1-1/2}}{\Gamma(n+c_1-1/2)\ 2^{n+c_1-3/2}} \int_0^\infty \theta^{c_2} \left(\hat{\theta}^2+\theta^2-2\hat{\theta}\theta\right)\ \ \frac{1}{\theta^{2n+2c_1}} \exp\left(-\frac{\sum_{a=1}^n x_a^{-2\alpha}}{2\theta^2}\right) d\theta. \tag{57}$$

$$\begin{aligned} R(\hat{\theta}) = \frac{(\sum_{a=1}^n x_a^{-2\alpha})^{n+c_1-1/2}}{\Gamma(n+c_1-1/2)\ 2^{n+c_1-3/2}} \Bigg\{ & \hat{\theta}^2 \int_0^\infty \theta^{c_2} \frac{1}{\theta^{2n+2c_1}} \exp\left(-\frac{\sum_{a=1}^n x_a^{-2\alpha}}{2\theta^2}\right) d\theta \\ & + \int_0^\infty \theta^{c_2+2} \frac{1}{\theta^{2n+2c_1}} \exp\left(-\frac{\sum_{a=1}^n x_a^{-2\alpha}}{2\theta^2}\right) d\theta \\ & - 2\hat{\theta} \int_0^\infty \theta^{c_2+1} \frac{1}{\theta^{2n+2c_1}} \exp\left(-\frac{\sum_{a=1}^n x_a^{-2\alpha}}{2\theta^2}\right) d\theta \Bigg\}. \end{aligned} \tag{58}$$

$$\hat{\theta} = \frac{\Gamma(n+c_1-c_2/2-1)}{\Gamma(n+c_1-c_2/2-1/2)} \sqrt{\frac{\sum_{a=1}^n x_a^{-2\alpha}}{2}}. \tag{59}$$

2.5.3 Precautionary loss function (plf)

$$R(\hat{\theta}) = \int_0^\infty \frac{(\hat{\theta}-\theta)^2}{\hat{\theta}} \pi_2(\theta|x)\, d\theta. \tag{60}$$

Using Eq. (22) in Eq. (60), we get:

$$R(\hat{\theta}) = \int_0^\infty \frac{(\hat{\theta}-\theta)^2}{\hat{\theta}} \frac{(\sum_{a=1}^n x_a^{-2\alpha})^{n+c_1-1/2}}{\Gamma(n+c_1-1/2)\ 2^{n+c_1-3/2}}\ \ \frac{1}{\theta^{2n+2c_1}} \exp\left(-\frac{\sum_{a=1}^n x_a^{-2\alpha}}{2\theta^2}\right) d\theta. \tag{61}$$

$$R(\hat{\theta}) = \frac{(\sum_{a=1}^{n} x_a^{-2\alpha})^{n+c_1-1/2}}{\Gamma(n+c_1-1/2)\ 2^{n+c_1-3/2}} \int_0^{\infty} \frac{(\hat{\theta}^2+\theta^2-2\hat{\theta}\theta)}{\hat{\theta}} \ \frac{1}{\theta^{2n+2c_1}} \exp\left(-\frac{\sum_{a=1}^{n} x_a^{-2\alpha}}{2\theta^2}\right) d\theta. \quad (62)$$

$$\begin{aligned} R(\hat{\theta}) = \frac{(\sum_{a=1}^{n} x_a^{-2\alpha})^{n+c_1-1/2}}{\Gamma(n+c_1-1/2)\ 2^{n+c_1-3/2}} \Bigg\{ & \int_0^{\infty} \hat{\theta} \frac{1}{\theta^{2n+2c_1}} \exp\left(-\frac{\sum_{a=1}^{n} x_a^{-2\alpha}}{2\theta^2}\right) d\theta \\ & + \frac{1}{\hat{\theta}} \int_0^{\infty} \theta^2 \frac{1}{\theta^{2n+2c_1}} \exp\left(-\frac{\sum_{a=1}^{n} x_a^{-2\alpha}}{2\theta^2}\right) d\theta \\ & - 2\int_0^{\infty} \theta \frac{1}{\theta^{2n+2c_1}} \exp\left(-\frac{\sum_{a=1}^{n} x_a^{-2\alpha}}{2\theta^2}\right) d\theta \Bigg\}. \end{aligned} \quad (63)$$

$$\hat{\theta} = \sqrt{\frac{\Gamma(n+c_1-3/2)}{\Gamma(n+c_1-1/2)} \ \frac{\sum_{a=1}^{n} x_a^{-2\alpha}}{2}}. \quad (64)$$

2.5.4 Entropy loss function (elf)

$$R(\hat{\theta}) = \int_0^{\infty} \left(\frac{\hat{\theta}}{\theta} - \log\left(\frac{\hat{\theta}}{\theta}\right) - 1\right) \pi_2(\theta|x)\, d\theta. \quad (65)$$

Substituting Eq. (22) into Eq. (65), we get:

$$R(\hat{\theta}) = \int_0^{\infty} \left(\frac{\hat{\theta}}{\theta} - \log\left(\frac{\hat{\theta}}{\theta}\right) - 1\right) \frac{(\sum_{a=1}^{n} x_a^{-2\alpha})^{n+c_1-1/2}}{\Gamma(n+c_1-1/2)\ 2^{n+c_1-3/2}} \ \frac{1}{\theta^{2n+2c_1}} \exp\left(-\frac{\sum_{a=1}^{n} x_a^{-2\alpha}}{2\theta^2}\right) d\theta. \quad (66)$$

$$R(\hat{\theta}) = \frac{(\sum_{a=1}^{n} x_a^{-2\alpha})^{n+c_1-1/2}}{\Gamma(n+c_1-1/2)\ 2^{n+c_1-3/2}} \int_0^{\infty} \left(\frac{\hat{\theta}}{\theta} - \log\left(\frac{\hat{\theta}}{\theta}\right) - 1\right) \ \frac{1}{\theta^{2n+2c_1}} \exp\left(-\frac{\sum_{a=1}^{n} x_a^{-2\alpha}}{2\theta^2}\right) d\theta. \quad (67)$$

$$\begin{aligned} R(\hat{\theta}) = \frac{(\sum_{a=1}^{n} x_a^{-2\alpha})^{n+c_1-1/2}}{\Gamma(n+c_1-1/2)\ 2^{n+c_1-3/2}} \Bigg\{ & \int_0^{\infty} \hat{\theta} \frac{1}{\theta^{2n+2c_1}} \exp\left(-\frac{\sum_{a=1}^{n} x_a^{-2\alpha}}{2\theta^2}\right) d\theta \\ & + \frac{1}{\hat{\theta}} \int_0^{\infty} \theta^2 \frac{1}{\theta^{2n+2c_1}} \exp\left(-\frac{\sum_{a=1}^{n} x_a^{-2\alpha}}{2\theta^2}\right) d\theta \\ & - 2\int_0^{\infty} \theta \frac{1}{\theta^{2n+2c_1}} \exp\left(-\frac{\sum_{a=1}^{n} x_a^{-2\alpha}}{2\theta^2}\right) d\theta \Bigg\}. \end{aligned} \quad (68)$$

$$\hat{\theta} = \frac{\Gamma(n+c_1-1/2)}{\Gamma(n+c_1)} \sqrt{\frac{\sum_{a=1}^{n} x_a^{-2\alpha}}{2}}. \quad (69)$$

2.6. Bayesian Estimation by Using Quasi Prior under Different Loss Functions

2.6.1 Squared error loss function (self)

$$R(\hat{\theta}) = \int_0^{\infty} c(\hat{\theta}-\theta)^2 \pi_3(\theta|x)\, d\theta. \quad (70)$$

Using Eq. (29) in Eq. (70), we get

$$R(\hat{\theta}) = \int_0^{\infty} c(\hat{\theta}-\theta)^2 \frac{\left(\sum_{a=1}^{n} x_a^{-2\alpha}\right)^{\frac{2n+d-1}{2}}}{\Gamma\left(\frac{2n+d-1}{2}\right) 2^{\frac{2n+d-3}{2}}} \frac{1}{\theta^{2n+d}} \exp\left(-\frac{\sum_{a=1}^{n} x_a^{-2\alpha}}{2\theta^2}\right) d\theta. \quad (71)$$

$$R(\hat{\theta}) = c\frac{\left(\sum_{a=1}^{n} x_a^{-2\alpha}\right)^{\frac{2n+d-1}{2}}}{\Gamma\left(\frac{2n+d-1}{2}\right) 2^{\frac{2n+d-3}{2}}} \int_0^{\infty} \left(\hat{\theta}^2+\theta^2-2\hat{\theta}\theta\right) \frac{1}{\theta^{2n+d}} \exp\left(-\frac{\sum_{a=1}^{n} x_a^{-2\alpha}}{2\theta^2}\right) d\theta. \quad (72)$$

$$R(\hat{\theta}) = c\frac{\left(\sum_{a=1}^{n} x_a^{-2\alpha}\right)^{\frac{2n+d-1}{2}}}{\Gamma\left(\frac{2n+d-1}{2}\right)2^{\frac{2n+d-3}{2}}}\left\{\hat{\theta}^2\int_0^\infty \frac{1}{\theta^{2n+d}}\exp\left(-\frac{\sum_{a=1}^{n} x_a^{-2\alpha}}{2\theta^2}\right)d\theta\right.$$
$$+\int_0^\infty \theta^2\frac{1}{\theta^{2n+d}}\exp\left(-\frac{\sum_{a=1}^{n} x_a^{-2\alpha}}{2\theta^2}\right)d\theta \quad (73)$$
$$\left.-2\hat{\theta}\int_0^\infty \theta\frac{1}{\theta^{2n+d}}\exp\left(-\frac{\sum_{a=1}^{n} x_a^{-2\alpha}}{2\theta^2}\right)d\theta\right\}.$$

$$\hat{\theta} = \frac{\Gamma\left(n+d/2-1\right)}{\Gamma\left(n+d/2-1/2\right)}\sqrt{\frac{\sum_{a=1}^{n} x_a^{-2\alpha}}{2}}. \quad (74)$$

2.6.2 Al-Bayyatis new loss function (abnlf)

$$R(\hat{\theta}) = \int_0^\infty \theta^{c_2}(\hat{\theta}-\theta)^2\pi_3(\theta|x)\,d\theta. \quad (75)$$

Substituting Eq. (29) in Eq. (75), we get

$$R(\hat{\theta}) = \int_0^\infty \theta^{c_2}(\hat{\theta}-\theta)^2\frac{\left(\sum_{a=1}^{n} x_a^{-2\alpha}\right)^{\frac{2n+d-1}{2}}}{\Gamma\left(\frac{2n+d-1}{2}\right)2^{\frac{2n+d-3}{2}}}\frac{1}{\theta^{2n+d}}\exp\left(-\frac{\sum_{a=1}^{n} x_a^{-2\alpha}}{2\theta^2}\right)d\theta. \quad (76)$$

$$R(\hat{\theta}) = \frac{\left(\sum_{a=1}^{n} x_a^{-2\alpha}\right)^{\frac{2n+d-1}{2}}}{\Gamma\left(\frac{2n+d-1}{2}\right)2^{\frac{2n+d-3}{2}}}\int_0^\infty \theta^{c_2}\left(\hat{\theta}^2+\theta^2-2\hat{\theta}\theta\right)\frac{1}{\theta^{2n+d}}\exp\left(-\frac{\sum_{a=1}^{n} x_a^{-2\alpha}}{2\theta^2}\right)d\theta. \quad (77)$$

$$R(\hat{\theta}) = \frac{\left(\sum_{a=1}^{n} x_a^{-2\alpha}\right)^{\frac{2n+d-1}{2}}}{\Gamma\left(\frac{2n+d-1}{2}\right)2^{\frac{2n+d-3}{2}}}\left\{\theta^{c_2}\int_0^\infty \hat{\theta}^2\frac{1}{\theta^{2n+d}}\exp\left(-\frac{\sum_{a=1}^{n} x_a^{-2\alpha}}{2\theta^2}\right)d\theta\right.$$
$$+\int_0^\infty \theta^2\frac{1}{\theta^{2n+d}}\exp\left(-\frac{\sum_{a=1}^{n} x_a^{-2\alpha}}{2\theta^2}\right)d\theta \quad (78)$$
$$\left.-2\hat{\theta}\int_0^\infty \theta\frac{1}{\theta^{2n+d}}\exp\left(-\frac{\sum_{a=1}^{n} x_a^{-2\alpha}}{2\theta^2}\right)d\theta\right\}.$$

$$\hat{\theta} = \frac{\Gamma\left(n+d/2-c_2/2-1\right)}{\Gamma\left(n+d/2-c_2/2-1/2\right)}\sqrt{\frac{\sum_{a=1}^{n} x_a^{-2\alpha}}{2}}. \quad (79)$$

2.6.3 Precautionary loss function (plf)

$$R(\hat{\theta}) = \int_0^\infty \frac{(\hat{\theta}-\theta)^2}{\hat{\theta}}\pi_3(\theta|x)\,d\theta. \quad (80)$$

Using Eq. (29) in Eq. (80), we get

$$R(\hat{\theta}) = \int_0^\infty \frac{(\hat{\theta}-\theta)^2}{\hat{\theta}}\frac{\left(\sum_{a=1}^{n} x_a^{-2\alpha}\right)^{\frac{2n+d-1}{2}}}{\Gamma\left(\frac{2n+d-1}{2}\right)2^{\frac{2n+d-3}{2}}}\frac{1}{\theta^{2n+d}}\exp\left(-\frac{\sum_{a=1}^{n} x_a^{-2\alpha}}{2\theta^2}\right)d\theta. \quad (81)$$

$$R(\hat{\theta}) = \frac{\left(\sum_{a=1}^{n} x_a^{-2\alpha}\right)^{\frac{2n+d-1}{2}}}{\Gamma\left(\frac{2n+d-1}{2}\right)2^{\frac{2n+d-3}{2}}}\int_0^\infty \frac{\left(\hat{\theta}^2+\theta^2-2\hat{\theta}\theta\right)}{\hat{\theta}}\frac{1}{\theta^{2n+d}}\exp\left(-\frac{\sum_{a=1}^{n} x_a^{-2\alpha}}{2\theta^2}\right)d\theta. \quad (82)$$

$$R(\hat{\theta}) = \frac{\left(\sum_{a=1}^{n} x_a^{-2\alpha}\right)^{\frac{2n+d-1}{2}}}{\Gamma\left(\frac{2n+d-1}{2}\right) 2^{\frac{2n+d-3}{2}}} \left\{ \hat{\theta} \int_0^{\infty} \frac{1}{\theta^{2n+d}} \exp\left(-\frac{\sum_{a=1}^{n} x_a^{-2\alpha}}{2\theta^2}\right) d\theta \right.$$
$$+ \frac{1}{\hat{\theta}} \int_0^{\infty} \theta^2 \frac{1}{\theta^{2n+d}} \exp\left(-\frac{\sum_{a=1}^{n} x_a^{-2\alpha}}{2\theta^2}\right) d\theta \tag{83}$$
$$\left. - 2 \int_0^{\infty} \theta \frac{1}{\theta^{2n+d}} \exp\left(-\frac{\sum_{a=1}^{n} x_a^{-2\alpha}}{2\theta^2}\right) d\theta \right\}.$$

$$\hat{\theta} = \sqrt{\frac{\Gamma\left(n + d/2 - 3/2\right)}{\Gamma\left(n + d/2 - 1/2\right)} \quad \frac{\sum_{a=1}^{n} x_a^{-2\alpha}}{2}}. \tag{84}$$

2.6.4 Entropy loss function (elf)

$$R(\hat{\theta}) = \int_0^{\infty} \left(\frac{\hat{\theta}}{\theta} - \log\left(\frac{\hat{\theta}}{\theta}\right) - 1\right) \pi_3(\theta|x)\, d\theta. \tag{85}$$

Substituting Eq. (29) in Eq. (85), we get

$$R(\hat{\theta}) = \int_0^{\infty} \left(\frac{\hat{\theta}}{\theta} - \log\left(\frac{\hat{\theta}}{\theta}\right) - 1\right) \frac{\left(\sum_{a=1}^{n} x_a^{-2\alpha}\right)^{\frac{2n+d-1}{2}}}{\Gamma\left(\frac{2n+d-1}{2}\right) 2^{\frac{2n+d-3}{2}}} \frac{1}{\theta^{2n+d}} \exp\left(-\frac{\sum_{a=1}^{n} x_a^{-2\alpha}}{2\theta^2}\right) d\theta. \tag{86}$$

$$R(\hat{\theta}) = \frac{\left(\sum_{a=1}^{n} x_a^{-2\alpha}\right)^{\frac{2n+d-1}{2}}}{\Gamma\left(\frac{2n+d-1}{2}\right) 2^{\frac{2n+d-3}{2}}} \int_0^{\infty} \left(\frac{\hat{\theta}}{\theta} - \log\left(\frac{\hat{\theta}}{\theta}\right) - 1\right) \frac{1}{\theta^{2n+d}} \exp\left(-\frac{\sum_{a=1}^{n} x_a^{-2\alpha}}{2\theta^2}\right) d\theta. \tag{87}$$

$$R(\hat{\theta}) = \frac{\left(\sum_{a=1}^{n} x_a^{-2\alpha}\right)^{\frac{2n+d-1}{2}}}{\Gamma\left(\frac{2n+d-1}{2}\right) 2^{\frac{2n+d-3}{2}}} \left\{ \int_0^{\infty} \frac{\hat{\theta}}{\theta} \frac{1}{\theta^{2n+d}} \exp\left(-\frac{\sum_{a=1}^{n} x_a^{-2\alpha}}{2\theta^2}\right) d\theta \right.$$
$$- \int_0^{\infty} \log\left(\frac{\hat{\theta}}{\theta}\right) \frac{1}{\theta^{2n+d}} \exp\left(-\frac{\sum_{a=1}^{n} x_a^{-2\alpha}}{2\theta^2}\right) d\theta \tag{88}$$
$$\left. - \int_0^{\infty} \frac{1}{\theta^{2n+d}} \exp\left(-\frac{\sum_{a=1}^{n} x_a^{-2\alpha}}{2\theta^2}\right) d\theta \right\}.$$

$$\hat{\theta} = \frac{\Gamma\left(n + d/2 - 1/2\right)}{\Gamma\left(n + d/2\right)} \sqrt{\frac{\sum_{a=1}^{n} x_a^{-2\alpha}}{2}}. \tag{89}$$

3. Results

This section presents the results of a simulation study designed to evaluate and compare the performance of classical and Bayesian estimators for the IPRD. The performance of these estimators is assessed using the MSE criterion, which serves as a measure of the accuracy of the estimates. The study covers different sample sizes ($n = 25$, $n = 50$ and $n = 100$) to explore the effect of sample size on the performance of the estimators. The simulation process is repeated 100,000 times for each scenario to ensure reliable and consistent results.

The following parameter values are used in the simulation study:

- $\alpha = 0.5, 1.5, 2.0$
- $\theta = 0.5$
- $C_1 = 0.5, 2.5, 4.5$

- $C_2 = 0, 1.5, 2.5$
- $d = 0.5, 1, 1.5$

These parameter combinations are chosen to cover a broad range of possible scenarios, allowing for a comprehensive evaluation of the estimators. By examining the MSE for each case, we can determine how the Bayesian and classical methods perform under varying conditions, including different sample sizes and parameter settings. The results are presented in Tables 1, 2 and 3.

Table 1: *Estimates and (MSE) using Jeffreys prior under different loss functions using generated data.*

		$\boldsymbol{\theta}_{\text{mle}}$	$\boldsymbol{\theta}_{\text{self}}$	$\boldsymbol{\theta}_{\text{plf}}$	$\boldsymbol{\theta}_{\text{elf}}$	$\boldsymbol{\theta}_{\text{abnlf}}$		
n	α					$C_2 = 0$	$C_2 = 1.5$	$C_2 = 2.5$
25	0.5	0.81616	0.82869	0.83302	0.82028	0.82869	0.84181	0.85091
		(0.09973)	(0.10804)	(0.11090)	(0.10258)	(0.10804)	(0.11683)	(0.12314)
	1.5	1.20336	1.22179	1.22817	1.20139	1.22179	1.24113	1.25455
		(0.49471)	(0.52098)	(0.53023)	**(0.49194)**	(0.52098)	(0.54928)	(0.56943)
	2.0	1.55286	1.57665	1.58488	1.54065	1.57665	1.60161	1.61892
		(1.10852)	(1.15918)	(1.17697)	**(1.08294)**	(1.15918)	(1.21346)	(1.25191)
50	0.5	0.78828	0.79419	0.79622	0.79019	0.79419	0.80081	0.80447
		(0.08307)	(0.08655)	(0.08775)	(0.08421)	(0.08655)	(0.09108)	(0.09270)
	1.5	1.02439	1.03215	1.03488	1.02295	1.03215	1.04010	1.04550
		(0.27498)	(0.28319)	(0.28590)	**(0.27348)**	(0.28319)	(0.29171)	(0.29775)
	2.0	1.19598	1.20504	1.20812	1.19397	1.20504	1.21432	1.22063
		(0.48438)	(0.49710)	(0.50143)	**(0.48159)**	(0.49710)	(0.51024)	(0.51983)
100	0.5	0.79846	0.80147	0.80248	0.79946	0.80147	0.80452	0.80658
		(0.08908)	(0.09089)	(0.09150)	(0.08877)	(0.09089)	(0.09273)	(0.09398)
	1.5	1.11112	1.11538	1.11678	1.11008	1.11538	1.11962	1.12247
		(0.37353)	(0.37869)	(0.38043)	**(0.37220)**	(0.37869)	(0.38396)	(0.38705)
	2.0	1.38955	1.39479	1.39655	1.38129	1.39479	1.40009	1.40366
		(0.79130)	(0.80065)	(0.80386)	**(0.77667)**	(0.80065)	(0.81016)	(0.81660)

Table 2: *Estimates and (MSE) using Jeffreys prior under different loss functions using generated data.*

		$\boldsymbol{\theta}_{\text{mle}}$	$\boldsymbol{\theta}_{\text{self}}$	$\boldsymbol{\theta}_{\text{plf}}$	$\boldsymbol{\theta}_{\text{elf}}$	$\boldsymbol{\theta}_{\text{abnlf}}$		
n	α					$C_2 = 0$	$C_2 = 1.5$	$C_2 = 2.5$
25	0.5	0.81230	0.82331	0.82723	0.81817	0.82331	0.83414	0.84302
		(0.09086)	(0.09966)	(0.10204)	(0.09514)	(0.09966)	(0.10735)	(0.11225)
	1.5	1.20336	1.22179	1.22817	1.20139	1.22179	1.24113	1.25455
		(0.49471)	(0.52098)	(0.53023)	**(0.49194)**	(0.52098)	(0.54928)	(0.56943)
	2.0	1.55286	1.57665	1.58488	1.54065	1.57665	1.60161	1.61892
		(1.10852)	(1.15918)	(1.17697)	**(1.08294)**	(1.15918)	(1.21346)	(1.25191)
50	0.5	0.79031	0.79713	0.79865	0.79206	0.79713	0.80219	0.80576
		(0.07453)	(0.07782)	(0.07883)	(0.07567)	(0.07782)	(0.08136)	(0.08279)
	1.5	1.02439	1.03215	1.03488	1.02295	1.03215	1.04010	1.04550
		(0.27498)	(0.28319)	(0.28590)	**(0.27348)**	(0.28319)	(0.29171)	(0.29775)
	2.0	1.18598	1.19504	1.19812	1.18397	1.19504	1.20432	1.21063
		(0.45438)	(0.46710)	(0.47143)	**(0.45159)**	(0.46710)	(0.48024)	(0.48983)
100	0.5	0.79846	0.80147	0.80248	0.79946	0.80147	0.80452	0.80658
		(0.08908)	(0.09089)	(0.09150)	(0.08877)	(0.09089)	(0.09273)	(0.09398)
	1.5	1.11112	1.11538	1.11678	1.11008	1.11538	1.11962	1.12247
		(0.37353)	(0.37869)	(0.38043)	**(0.37220)**	(0.37869)	(0.38396)	(0.38705)
	2.0	1.38955	1.39479	1.39655	1.38129	1.39479	1.40009	1.40366
		(0.79130)	(0.80065)	(0.80386)	**(0.77667)**	(0.80065)	(0.81016)	(0.81660)

Table 3: *Estimates and (MSE) using Quasi prior under different loss functions using generated data.*

		θ_{mle}	θ_{self}	θ_{plf}	θ_{elf}	θ_{abnlf}		
n	α					$C_2 = 0$	$C_2 = 1.5$	$C_2 = 2.5$
25	0.5	0.81619	0.83299	0.83739	0.81445	0.83299	0.84632	0.85557
		(0.09997)	(0.11088)	(0.11383)	(0.09888)	(0.11088)	(0.11994)	(0.12643)
	1.5	1.20336	1.22179	1.22817	1.20139	1.22179	1.24113	1.25455
		(0.49471)	(0.52098)	(0.53023)	**(0.49194)**	(0.52098)	(0.54928)	(0.56934)
	2.0	1.55286	1.56859	1.57669	1.55282	1.56859	1.59316	1.61020
		(1.10852)	(1.14188)	(1.15927)	**(1.10844)**	(1.14188)	(1.19500)	(1.23254)
50	0.5	0.78822	0.79622	0.79826	0.78218	0.79622	0.80238	0.80657
		(0.08307)	(0.08774)	(0.08896)	(0.07963)	(0.08774)	(0.09143)	(0.09398)
	1.5	1.02439	1.03215	1.03479	1.02295	1.03215	1.04010	1.04550
		(0.27498)	(0.28319)	(0.28600)	**(0.27348)**	(0.28319)	(0.29171)	(0.29758)
	2.0	1.19598	1.20199	1.20505	1.19597	1.20199	1.21120	1.21746
		(0.48438)	(0.49279)	(0.49709)	**(0.48437)**	(0.49279)	(0.50581)	(0.51475)
100	0.5	0.79846	0.80248	0.80350	0.79046	0.80248	0.80554	0.80760
		(0.08908)	(0.09150)	(0.09211)	(0.08437)	(0.09150)	(0.09335)	(0.09462)
	1.5	1.11119	1.11538	1.11679	1.11008	1.11538	1.11962	1.12247
		(0.37355)	(0.37869)	(0.38043)	**(0.37220)**	(0.37869)	(0.38393)	(0.38747)
	2.0	1.38955	1.39304	1.39479	1.38955	1.39304	1.39832	1.40187
		(0.79130)	(0.79751)	(0.80065)	**(0.79130)**	(0.79751)	(0.80697)	(0.81337)

4. Discussion

This paper presents an analysis of the IPRD using both classical and Bayesian approaches, incorporating various prior distributions and loss functions. Bayesian estimators are derived under different priors and evaluated using multiple loss functions. A simulation study is conducted to compare the performance of Bayesian estimators with MLE based on MSE. The results indicate that, in most cases, Bayesian estimators with ELF consistently exhibit lower MSE than MLE, leading to the conclusion that the Bayesian method is more efficient for parameter estimation in this distribution.

References

[1] A. Abdel-Menem. *Estimation and Prediction for inverse Rayleigh life distribution*. PhD thesis, M. SC. Thesis Faculty of Education, Ain Shames University, 2003.

[2] H. Abdullah and R. Aref. Bayesian approach in estimation of scale parameter of inverse rayleigh distribution. *Mathematics and Statistics Journal*, 2(1):8–13, 2016.

[3] N. Ahad, S. Ahmad, and J. Reshi. Bayesian analysis of extended maxwell-boltzmann distribution using simulated and real-life data sets. *Reliability: Theory & Applications*, 19(3 (79)):675–688, 2024.

[4] H. Al-Kutubi. *On comparison estimation procedures for parameter and survival function exponential distribution using simulation*. PhD thesis, Ph. D. Thesis, Baghdad University, College of Education (Ibn-Al-Haitham ¦, 2005.

[5] A. Bhat, S. Ahmad, and S. Mudasir. A novel extension of power rayleigh distribution with properties. *International Journal of Statistics and Reliability Engineering*, 9(3):518–529, 2022.

[6] S. Dey. Bayesian estimation of the parameter and reliability function of an inverse rayleigh distribution. *Malaysian Journal of Mathematical Sciences*, 6(1):113–124, 2012.

[7] G. Fan. Research article bayes estimation for inverse rayleigh model under different loss functions. *Research Journal of Applied Sciences, Engineering and Technology*, 9(12):1115–1118, 2015.

[8] K. Fatima and S. Ahmad. Weighted inverse rayleigh distribution. *International Journal of Statistics and Systems*, 12(1):119–137, 2017.

[9] R. Kumar, H. Sharma, R. Gupta, and A. Kaur. Bayesian and e-bayesian estimation of exponentiated inverse rayleigh distribution using conjugate prior. *Reliability: Theory & Applications*, 19(3 (79)):704–716, 2024.

[10] A. A. Mir and S. Ahmad. Modeling and analysis of sine power rayleigh distribution: Properties and applications. *Reliability: Theory & Applications*, 19(1 (77)):703–716, 2024.

[11] A. A. Mir and S. Ahmad. Exploring an extended rayleigh distribution: Modeling and applications in real life scenarios. *Reliability: Theory & Applications*, 20(1 (82)):928–941, 2025.

[12] A. A. Mir and S. Ahmad. A new extended rayleigh distribution with applications of covid-19 data. *Austrian Journal of Statistics*, 54(2):69–84, 2025.

[13] A. A. Mir, S. U. Rasool, S. Ahmad, A. Bhat, T. M. Jawa, N. Sayed-Ahmed, and A. H. Tolba. A robust framework for probability distribution generation: Analyzing structural properties and applications in engineering and medicine. *Axioms*, 14(4):281, 2025.

[14] F. Noor, A. Sajid, M. Ghazal, I. Khan, M. Zaman, and I. Baig. Bayesian estimation of rayleigh distribution in the presence of outliers using progressive censoring. *Hacettepe Journal of Mathematics and Statistics*, 49(6):2119–2133, 2020.

[15] J. G. Norstrom. The use of precautionary loss functions in risk analysis. *IEEE Transactions on reliability*, 45(3):400–403, 1996.

[16] G. Prakash. Bayes estimation in the inverse rayleigh model. *Electronic Journal of Applied Statistical Analysis*, 6(1):67–83, 2013.

[17] A. Sharma, P. Kumar, and B. Devi. Entropy estimation of inverse rayleigh probability distribution and its order statistics. *International Journal of Electronics Engineering*, 11(2):508–513, 2019.

[18] H. Sharma and P. Kumar. Estimation of different entropies of inverse rayleigh distribution under multiple censored data. *Reliability: Theory & Applications*, 19(1 (77)):29–39, 2024.

[19] T. N. Sindhu, M. Aslam, and N. Feroze. Bayes estimation of the parameters of the inverse rayleigh distribution for left censored data. In *ProbStat Forum*, volume 6, pages 42–59, 2013.

[20] A. Soliman, E. A. Amin, and A. A. Abd-El Aziz. Estimation and prediction from inverse rayleigh distribution based on lower record values. *Applied Mathematical Sciences*, 4(62):3057–3066, 2010.

[21] V. G. Voda. On the inverse rayleigh distributed random variable. *Rep. Statis. App. Res. JUSE*, 19(4):13–21, 1972.

[22] F. Yanuar, M. Iqbal, D. Devianto, A. Zetra, Y. Asdi, R. Ilahi, and R. F. Sani. Bayesian estimation under different loss functions for the case of inverse rayleigh distribution. *Kuwait Journal of Science*, 52(1):100343, 2025.

[23] H. Zaki and I. Jabir. A comparison of the classical estimators with the bayes estimators of one parameter inverse rayleigh distribution. *International Journal*, 3(8):738–749, 2015.

THE IMPACT OF RAM ON SYSTEM PERFORMANCE: A REVIEW

Parveen Sihmar, Vikas Modgil, Sandeep Kumar
•
Department of Mechanical Engineering
D.C.R.U.S.T., Murthal, Sonipat, Haryana, India.
20001904003parveen@dcrustm.org, vikasmodgil@yahoo.co.uk, praansandeep@gmail.com

Abstract

One of the requirements that industrial systems must meet is that they must function effectively for a prolonged period. The system's performance is a vital component for failure-free operation; yet, in actual fact, it is extremely rare for any production system to be completely failure-free. Over the course of the past twenty-five years, a comprehensive and critical literature assessment of reliability, maintainability, and availability (RAM) approaches has been carried out. These approaches have the potential to assist in the enhancement of the performance of complex systems. The review of a few publications resulted in the provision of comprehensive information regarding the historical and contemporary situation of RAM procedures in the research field and enterprises. A review of RAM tools and approaches can help in doing qualitative and quantitative analysis of complex systems. The author of this research tried to focus on a few of the key components of RAM methods.

Keywords: availability, reliability, maintainability, petri nets.

I. Introduction

The definition of reliability is the ability of the system to perform its proposed operation without failure for a specified period of time. It consists of performance predictability and reduction of unexpected disruptions that contribute to a sense of dependability and trustworthiness in the system. Maintainability describes the speed and effectiveness with which it can be fixed and returned to attention. When it comes to keeping systems running smoothly, minimising downtime and cutting costs through quick and effective maintenance and repair is definitely a sign of good maintainability. Availability is a way to express how ready a system or a component is to be available when you need it. When a system says that it has high availability, it's not saying that it has no downtime. It's really saying that it has such a minuscule amount of downtime that its operational functions are sort of like a hummingbird—a marvel of nature, not something we wish to experience in our daily workflow. Reliability, Availability, and Maintainability (RAM) are three key basics of reliability engineering. They are fundamental to the analysis and design of reliable systems. Components of interconnected systems must work correctly and together to ensure system reliability. As the technological world becomes ever more interconnected and complex, the idea of system reliability has moved to the forefront of engineering disciplines. As sectors change swiftly and systems grow ever more intricate, ensuring that operations run smoothly has never been more vital, especially in such fields as manufacturing, energy production, and resource management. Availability is the percentage of the time a system is actually working and ready to use. There's a

slight overlap, but the two concepts are quite different. Maintainability just refers to how easy it is to fix a system and get it back up and running when it does fail. These three components are at the heart of RAM analysis, and the goal is to boost system performance. By diving into RAM analysis, industries can whip up maintenance plans, enhance reliability, and, you guessed it, cut costs. In the energy sector, for instance, RAM analysis can really step up the game by improving energy production systems, i.e thermal power plants, wind farms, and solar plants. It helps identify faults and makes the system stronger and more resilient, which is crucial for making sure everyone has access to affordable and modern energy.

Over in the industrial sector, boosting system reliability means businesses can dodge those expensive downtimes, cut down on waste, and work more efficiently. Reading Analysis for Messages (RAM) not only nudges industries along the totally sweet path of clean tech (i.e., toward using way less energy and producing way less pollution, and, quite frankly, toward cleaner businesses—which fits nicely with the interests of everyone from environmental groups to some insurers and financially savvy investors), but it also nudges them toward smarter, cleaner usage of their assets. Asset management almost always equals better waste management. Ultimately, examining RAM can substantially accelerate progress toward a prosperous economy by ensuring that enterprises operate dependably, adaptively, and resiliently. When systems are dependable, they substantially reduce the risk of sudden breakdowns and failures that could interrupt production. This not only makes the economy stronger but also helps protect jobs in those sectors.

II. Literature Review

Bevilacqua and Braglia [1] brought attention to the practical use of the AHP approach in the process of selecting a maintenance strategy for the Italian oil refinery. Economic considerations, practicality, costs, safety, and other relevant issues were all incorporated in their research, which integrated all the information required to make informed decisions about maintenance programs. Zhang and Horigome [2] observed the evolution of the system's failure and repair rates (FRR) in terms of their dependability and availability. The solution demonstrates the system's availability with different FRR. Adamyan and David [3] devised a method that relied on Petri Nets to identify failure sequences and evaluate the likelihood of their incidence within a manufacturing system. They improved the reliability analysis and risk assessment in systems. Elegbede and Adjallah [4] Optimised the availability of various systems by analysing their reliability and cost in relation to series and parallel repairable systems. Marseguerra et al. [5] examined multi-objective optimisation, utilising evolutionary algorithms and considering parameter uncertainty. The decision-maker can utilise this strategy to develop a solution that optimises safety behaviour and provides high certainty in system performance for complex systems. Samrout et al. [6] developed an Ant Colony Optimisation method to reduce series–parallel system preventative maintenance costs. Aksu et al. [7] developed a meticulous reliability evaluation method using FMEA, FTA, and Markov Analysis. It was used to assess pod propulsion unit availability and reliability. The study implemented these methods to investigate their practical efficacy. Kiureghian and Ditlevson [8] investigated the dependability and downtime of a unit, including repairable subsystems. Furthermore, closed-form equations are derived for the rates of change of several probabilistic system performance measures concerning the FRR for every subsystem. Critical engineering systems were introduced to the Markovian approach to getting system behaviour by means of RAM analysis by Sharma and Kumar et. al. [9] The differential equations were generated using the transition diagram. The results show that MTBF and MTTR are key features for the system's planning and maintenance.

Kumar et al. [10] developed a model to evaluate availability utilising a Markov Birth-Death Process (MBDP) methodology. The model was utilized in the ammonia production unit to assess availability. Rahman et al. [11] conducted research to determine the underlying factors that led to the failure of

a division wall super heating tube in a coal-fired power station. Vora et al. [12] used a probabilistic approach to assess the thermal plant's turbo generator system's performance. Transition diagrams have been used to formulate problems using the Markov technique. Failure and repair availability graphs have been examined for maximum availability based on the results. Bose et al. [13] assessed RAM of the coal-fired TPP . Preventive maintenance intervals were based on plant reliability. The investigation showed that the economizer and furnace wall tube were less reliable than the others. The plant's economizer was also declared its most important component. Kim and Kang [14] developed a reliability analysis method based on the Recursive Decomposition Algorithm for risk assessment of generic networks. Aggarwal et al. [15] explored the application of Markov approach and Runge Kutta approach for determining the MTBF to optimize a butter oil production system's performance. Sharifi et al. [16] created a RAP model that maximizes system dependability within weight and cost restrictions by utilizing GA, SA, PSO, and MA. They came to the conclusion that MA outperformed the other methods. Kumar and Garg [17] created an MA-based mathematical model for evaluating and estimating 'a series-parallel system' availability. In comparison to other optimization approaches, PSO yields higher outcomes. Poh and Liang [18] devised multiple criteria decision support in order to construct a complete analytic network process model. This model will appropriately capture and disclose all of the interrelationships and interdependencies among the pieces in the problem, which is typically a very challenging endeavour. Singhal and Sharma [19] examined industrial system availability using Markov and fuzzy numbers. Generalised fuzzy numbers tackle data uncertainty. Different arithmetic operations have measured availability. The system analyst saw how FRR affected the system. Dahiya et al. [20] used a fuzzy reliability approach to create a mathematical model of the "A-pan crystallization system of a sugar industry." They used this model to find differential equations, and they found that failures in the Grader, Weighment, and Bagging subsystems really hurt the system more than failures in other subsystems.

Jagtap et al. [21] used the Markov approach to calculate the turbo-generator subsystem's performance and discovered that the turbine lubrication and generator excitation components significantly affect system availability. The PSO method optimised the system's availability to 98.9394 per cent for particle size 30. Modgil et al. [22] aimed to simulate and assess the "Container Manufacturing plant's" availability using the PN method. The system was mathematically recreated in the real environment using a Petri module of the GRIF 2021 software. Maintenance of the Hydraulic Press is prioritised, and the number of repairmen is optimal. Vital et al. [23] used the timed Petri nets to assess the availability of a nuclear reactor limitation system. Gopal and Panchal [24] assessed the performance of the milk processing unit. They used fuzzy Jaya-based Lambda-Tau to evaluate MPU performance parameters. It was compared to standard Fuzzy Lambda-Tau and Particle Swarm Optimisation-Based Lambda-Tau methods. Parkash and Tiwari [25] evaluated the performance of the SPVC line system of the leaf spring production plant. Decision matrix shows that edge cutting burr is the most essential component, requiring the highest maintenance priorities. Sihmar and Modgil [26] assessed the performance of the combed-sliver production system in the yarn production system. The PSO approach optimised the system's availability.

III. Research Gaps

Within this section, the RAM methodology has been utilized to present the brief conclusions of a literature study.

- Numerous researchers talked about their attempts to employ appropriate maintenance protocols, regulations, and various operating schedules in order to boost plant availability. However, very few studies have examined the

connection between maintenance schedules and costs. Cost-affecting factors must also be prioritised.

- The literature research shows that a variety of methods have been used, such as fault tree analysis, Markov models, and Lambda tau technologies. Every one of these methods has a number of advantages and disadvantages. However, a technique called Markovian Petri Nets can effectively strike a compromise between modelling and decision-making ability. There is very little use of this type of instrument in the literature review.
- This survey found that researchers mostly concentrated on RAM methods, although RAMD and RAMS research was scarce. The researchers overlooked the significance of the relationship between safety and reliability. Working in a safe environment motivates team members to work in hazardous environments, while dependability improves reliability by completing its mission or services.

IV. Conclusion

There are many different RAM issues, tools, and approaches that are employed in a variety of plants and process industries, and a detailed survey of the literature shows them. During the literature review, the authors mainly concentrated on the maintenance plan, reducing the costs of production and maintenance, and boosting the performability and productivity of the system, among other things. There are a variety of RAM tools and approaches that may be applied in both the design and operating stages of the plant in order to improve the facility's performance further. Each plant is separated into units or components for maintenance planning to keep systems running for a long time. In order to conduct the analysis and modelling, various approaches were utilised. These techniques included Markov Analysis, Failure Mode and Effects Analysis, Fault Tree Analysis, Reliability Growth Analysis, Fuzzy Model, Monte Carlo technique, Chapman-Kolmogorov birth-death process, Stochastic Petri Nets, Particle Swarm Optimisation (PSO), and others.

References

[1] Bevilacqua, M. and Braglia, M. (2000) "The analytic hierarchy process applied to maintenance strategy selection," *Reliab. Eng. Syst. Saf.*, vol. 70, no. 1, pp. 71–83, 2000, doi: https://doi.org/10.1016/S0951-8320(00)00047-8.

[2] Zhang, T. and Horigome, M. (2001) "Availability and reliability of system with dependent components and time-varying failure and repair rates," *IEEE Trans. Reliab.*, vol. 50, no. 2, pp. 151–158, 2001.

[3] Adamyan, A. and He, D. (2002) "Analysis of sequential failures for assessment of reliability and safety of manufacturing systems," *Reliab. Eng. Syst. Saf.*, vol. 76, no. 3, pp. 227–236, 2002.

[4] Elegbede, C. and Adjallah, K. (2003) "Availability allocation to repairable systems with genetic algorithms: a multi-objective formulation," *Reliab. Eng. Syst. Saf.*, vol. 82, no. 3, pp. 319–330, 2003.

[5] Marseguerra, M., Zio, E. and Podofillini, L. (2004) "Optimal reliability/availability of uncertain systems via multi-objective genetic algorithms," *IEEE Trans. Reliab.*, vol. 53, no. 3, pp. 424–434, 2004.

[6] Samrout, M., Yalaoui, F., Châtelet, E. and Chebbo, N. (2005) "New methods to minimize the preventive maintenance cost of series–parallel systems using ant colony optimization," *Reliab. Eng. Syst. Saf.*, vol. 89, no. 3, pp. 346–354, 2005.

[7] Aksu, S., Aksu, S. and Turan, O. (2006) "Reliability and availability of pod propulsion systems," *Qual. Reliab. Eng. Int.*, vol. 22, no. 1, pp. 41–58, 2006.

[8] Kiureghian, A. Der, Ditlevsen, O. D. and Song, J. (2007) "Availability, reliability and

downtime of systems with repairable components," *Reliab. Eng. Syst. Saf.*, vol. 92, no. 2, pp. 231–242, 2007.

[9] Sharma, R. K. and Kumar, S. (2008) "Performance modeling in critical engineering systems using RAM analysis," *Reliab. Eng. Syst. Saf.*, vol. 93, no. 6, pp. 913–919, 2008.

[10] Kumar, S., Tewari, P. C. and Kumar, S. (2009) "Performance evaluation and availability analysis of ammonia synthesis unit in a fertilizer plant," *J. Ind. Eng. Int.*, vol. 5, no. 9, pp. 17–26, 2009.

[11] Rahman, M. M., Purbolaksono, J. and Ahmad, J. (2010) "Root cause failure analysis of a division wall superheater tube of a coal-fired power station," *Eng. Fail. Anal.*, vol. 17, no. 6, pp. 1490–1494, 2010.

[12] Vora, Y., Patel, M. B. and Tewari, P. C. (2011) "Simulation model for stochastic analysis and performance evaluation of steam generator system of a thermal power plant," *Int. J. Eng. Sci. Technol.*, vol. 3, no. 6, pp. 5141–5149, 2011.

[13] Bose, D., Chattopadhyay, S., Bose, G., Adhikary, D. and Mitra, S. (2012) "RAM investigation of coal-fired thermal power plants: a case study," *Int. J. Ind. Eng. Comput.*, vol. 3, no. 3, pp. 423–434, 2012.

[14] Kim, Y. and Kang, W.-H. (2013) "Network reliability analysis of complex systems using a non-simulation-based method," *Reliab. Eng. Syst. Saf.*, vol. 110, pp. 80–88, 2013.

[15] Aggarwal, A., Kumar, S. and Singh, V. (2015) "Performance modeling of the skim milk powder production system of a dairy plant using RAMD analysis," *Int. J. Qual. Reliab. Manag.*, vol. 32, no. 2, pp. 167–181, 2015.

[16] Sharifi, M., Cheragh, G., Maljaii, K. D., Zaretalab, A. and Fakre Daei, A. V. (2015) "RELIABILITY OPTIMIZATION OF A SERIES-PARALLEL K-OUT-OF-N SYSTEM WITH FAILURE RATE DEPENDS ON WORKING COMPONENTS OF SYSTEM.," *Int. J. Ind. Eng.*, vol. 22, no. 4, 2015.

[17] Kumar, A. and Garg, R. K. (2016) "Availability analysis and evaluation of series parallel system using soft computing technique," *Int. J. Reliab. Saf.*, vol. 10, no. 4, pp. 346–367, 2016.

[18] Poh, K. L. and Liang, Y. (2017) "Multiple-criteria decision support for a sustainable supply chain: applications to the fashion industry," in *Informatics*, MDPI, 2017, p. 36.

[19] Singhal, N. and Sharma, S. P. (2019) "Availability analysis of industrial systems using Markov process and generalized fuzzy numbers," *Mapan*, vol. 34, no. 1, pp. 79–91, 2019.

[20] Dahiya, O., Kumar, A. and Saini, M. (2019) "Mathematical modeling and performance evaluation of A-pan crystallization system in a sugar industry," *SN Appl. Sci.*, vol. 1, pp. 1–9, 2019.

[21] Jagtap, H. P., Bewoor, A. K., Kumar, R., Ahmadi, M. H. and Chen, L. (2020) "Performance analysis and availability optimization to improve maintenance schedule for the turbo-generator subsystem of a thermal power plant using particle swarm optimization," *Reliab. Eng. Syst. Saf.*, vol. 204, p. 107130, Dec. 2020, doi: 10.1016/J.RESS.2020.107130.

[22] Modgil, V. (2022) "Modelling and availability analysis of container manufacturing industry with Petri Nets," *Mater. Today Proc.*, vol. 56, pp. 2730–2734, 2022.

[23] Vital, R. B. N., e Melo, P. F. F., Medeiros, J. and Alvarenga, M. A. B. (2022) "Availability assessment of a nuclear reactor limitation system by a Timed Petri Net," *Prog. Nucl. Energy*, vol. 152, p. 104380, 2022.

[24] Gopal, N. and Panchal, D. (2023) "Reliability based framework for failure analysis in milk process industry," *Decis. Mak. Appl. Manag. Eng.*, vol. 6, no. 1, pp. 631–645, 2023.

[25] Parkash, S. and Tewari, P. C. (2024) "Performability analysis for the SPVC line system of leaf spring production plant using probabilistic approach," *J. Qual. Maint. Eng.*, vol. 30, no. 3, pp. 508–520, 2024.

[26] Sihmar, P. and Modgil, V. (2025) "Optimization of combed-sliver production system availability for a Yarn Production Unit using PSO," *Life Cycle Reliab. Saf. Eng.*, doi: 10.1007/s41872-025-00301-0.

RT&A, No 3 (86)
Volume 20, September 2025

THE QUASI-STATIONARY DISTRIBUTION OF A COMPLEX TWO-UNIT REPAIRABLE SYSTEM

Miriam Kalpana Simon[1]
Jasmine Rathi S.[2]
and
Late Dr. K. Shankar Bhat

•

Department of Statistics, Madras Christian College, Chennai, India.[1]
Department of Statistics, Madras Christian College, Chennai, India.[2]
miriamkalpana@mcc.edu.in
jasminesolomon@mcc.edu.in

Abstract

Like the first-busy-period in a queuing system, the time-to-system-failure is an important characteristic of a reliability system. In some reliability systems the time-to-system-failure may be sufficiently large to allow the residual life of the system to settle down to a state of statistical equilibrium. The conditional limit distribution of the residual lifetime, also known as the quasi-stationary distribution, plays a vital role in the statistical analysis of such systems. In this work, the quasi-stationary distribution for the residual lifetime of a two-unit complex reparable system is obtained using regenerative stochastic process. The results of the study are numerically illustrated assuming exponential lifetime distribution for the units.

Keywords: Quasi-stationary distribution, two-unit complex reparable system, warm standby, repair facility, residual lifetime.

I. Introduction

When the traffic intensity of a queueing system is less than or equal to unity, the first busy period of the system is finite with probability one. If such a period is sufficiently long, then the queue size process takes a long time to settle down to a state of equilibrium within the first busy period. The limiting distribution of the queue size process conditioned on it still being in the first busy period is termed the quasi-stationary distribution (QSD) of the process.

The reliability counterpart of QSD is equally interesting. It is well known that the time to system failure is an important characteristic of any reliability problem. In many reliability problems the behavior of the system after its first breakdown is of less interest either because the failure of a unit is irrevocable or because the system recovery is expensive. For instance, the performance of an aircraft is of great importance before, and not after, its first breakdown in mid-air. In such cases it would be of great interest to study the limiting distribution of the residual lifetime of the reliability system conditioned on its failure-free performance during the period.

Munda and Taneja [6] analyzes a system comprised of one operative unit, cold standby unit, and one warm standby unit. Various system performance measures have been defined by using the Markov process and regeneration point method.

Chaudhary, Sharma and Gupta [2] deals with the stochastic analysis of two non-identical units with failure and repair times of the unit taken as independent random variables of discrete nature having geometric distributions with different parameters.

Papageorgiou and Kokolakis [7] discusses the reliability analysis of a two-unit general parallel system with (n-2) warm standbys. A parallel (2, n-2) system is investigated where any one of them is replaced instantaneously upon its failure by one of the (n-2) warm standbys.

Kyprianou [4] introduced this concept of the QSD in the study of queue size process and the virtual waiting time process associated with the first busy period of G1/M/1 queue. Cavendar [1] derived the QSD of a birth death process.

Van Doorn and Pollett [10] have discussed a survey of results related to quasi-stationary distributions, which arise in the setting of stochastic dynamical systems that eventually evanesce, and which may be useful in describing the long-term behaviour of such systems before evanescence. Reinertsen [8] presents and discusses research related to residual life of non-repairable and repairable technical systems.

Li and Cao [5] have proved that the limiting distributions of the residual lifetimes of several repairable systems, conditional upon the event that the systems have not been down at any time in (0, t], are exponential irrespective of the distributions of the lifetimes and repair times of the individual units, provided that their Laplace transforms are rational functions of their arguments.

Kalpakam and Hameed [3] discussed the existence of QSD residual lifetime of a two-unit warm standby redundant system. Shankar Bhat [9] discussed the existence of QSD of a complex two unit system.

In the present work, we discuss the existence of QSD residual lifetime of a complex two-unit warm standby system in which the switching device is subject to failure. The section below describes the reliability system under study.

II. System Description

[01] The reliability system consists of two identical repairable units. At $t = 0$, one unit is placed online and the other is placed as a warm standby.

[02] Upon the failure of the online unit, the standby unit is placed online if found in operable condition. If the standby unit is under repair, the online failed unit queues up for repair. The failure time and repair time distributions of a unit in standby are assumed to be distributed exponential with parameters α and β respectively.

[03] The operable standby unit is instantaneously placed online using a switching device. This switching device has its own pattern of life and repair time distributions. The failure time and repair time distributions of the switching device are assumed exponential with parameters γ and μ respectively.

[04] The system is supported by two repair facilities one for the units and the other for the switching device.

[05] The repair of units is undertaken in FIFO order.

[06] The repair is perfect in the sense that the repaired units as well as switching device are treated as good as new.

A schematic representation of the system is depicted in Figure 1.

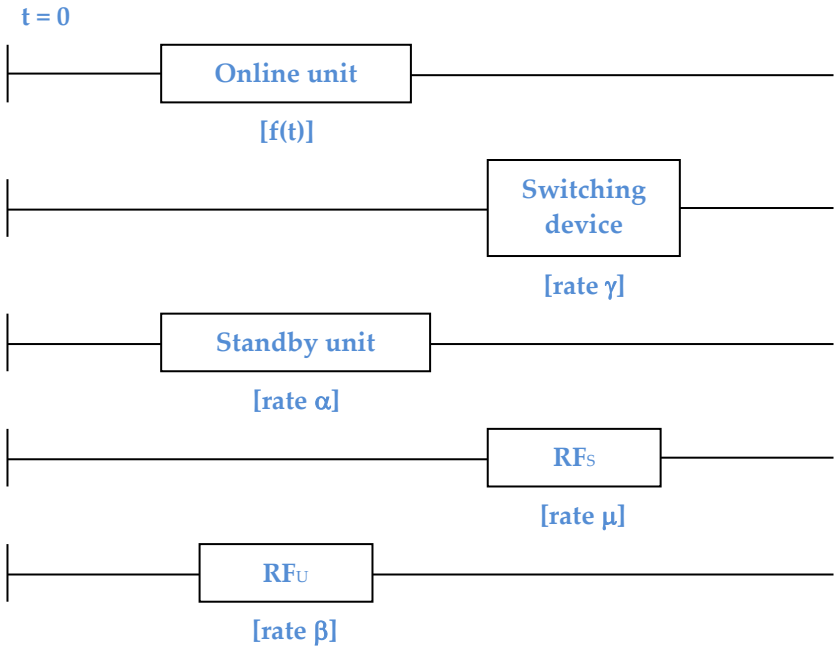


Figure 1: *Schematic Representation of the System*

III. Stochastic Behavior of the Standby Unit

The stochastic behavior of the standby unit, while the other unit is continuously operating online can be described through an alternating renewal process. Let [Y(t), t ≥ 0] be the process characterizing the state of the standby unit during failure-free performance of the unit in service. The random variable Y(t) is a two valued random variable which takes the value O if the standby unit is in operable condition and F when under repair. The process [Y(t), t ≥ 0] completely describes the subsystem and is an alternating renewal process.

Define

$$P_{ij}(t) = \lim_{\Delta \to 0} \frac{1}{\Delta} P[Y(t) = j / Y(t) \text{ entered i in } (-\Delta, 0)], \quad i,j = 0,F \tag{1}$$

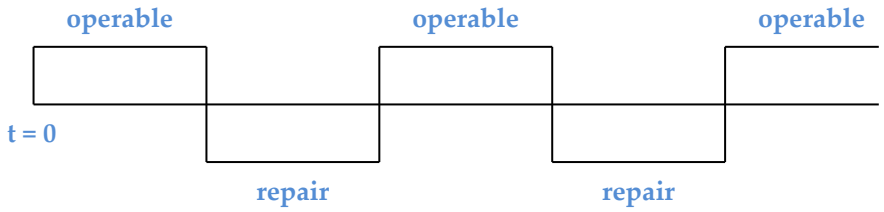


Figure 2: *Stochastic Behavior of the Standby Unit*

The functions $P_{ij}(t)$ can be easily obtained through renewal theoretic arguments

$$P_{OO}(t) = e^{-\alpha t} + [\alpha e^{-\alpha t} \copyright \beta e^{-\beta t}] \copyright P_{OO}(t) \tag{2}$$

$$P_{FO}(t) = \beta e^{-\beta t} \copyright P_{OO}(t) \tag{3}$$

$$P_{OF}(t) = 1 - P_{OO}(t) \tag{4}$$

$$P_{FF}(t) = 1 - P_{FO}(t) \tag{5}$$

Observe that $P_{00}(t)$ is the p-function of the Kingman's regenerative phenomenon. Since the exponential distributions are compatible for Laplace Transforms, the expressions (2) to (3) can be easily evaluated upon successive operation of Laplace Transforms. Thus,

$$P_{00}(t) = \frac{1}{(\alpha+\beta)}\left[\beta + \alpha e^{-(\alpha+\beta)t}\right] \quad (6)$$

$$P_{F0}(t) = \frac{\beta}{(\alpha+\beta)}\left[1 - e^{-(\alpha+\beta)t}\right] \quad (7)$$

$$P_{0F}(t) = \frac{\alpha}{(\alpha+\beta)}\left[1 - e^{-(\alpha+\beta)t}\right] \quad (8)$$

$$P_{FF}(t) = \frac{1}{(\alpha+\beta)}\left[\alpha + \beta e^{-(\alpha+\beta)t}\right] \quad (9)$$

IV. Stochastic Behavior of the Switching Device

The switching device has its own failure and repair time distributions. The subsystem consisting of a switching device and a repair facility can be seen as a parallel system to the subsystem consisting the standby unit and the repair facility attached to it. The stochastic behavior of the switching device during a failure-free operation of the online unit can be identified with an alternating renewal process. Let [Z(t), t ≥ 0] be the process that describes the state of the switching device. The state space of the process is [0, F], where '0' indicates that the switching device is in operable condition and 'F' indicates that it is undergoing repair. The transitional probabilities of the process are given by the following function.

$$Q_{ij}(t) = \lim_{\Delta\to 0}\frac{1}{\Delta}\Pr[Z(t) = j \,/\, Z(t) \text{ entered i in } (-\Delta,0)] \quad i,j = 0,F \quad (10)$$

The expressions $Q_{ij}(t)$ can be obtained easily with the help of renewal theoretic arguments.

$$Q_{OO}(t) = e^{-\gamma t} + \{\gamma e^{-\gamma t} \copyright \mu e^{-\mu t}\} \copyright Q_{OO}(t) \quad (11)$$

$$Q_{FO}(t) = \mu e^{-\mu t} \copyright Q_{OO}(t) \quad (12)$$

$$Q_{OF}(t) = 1 - Q_{OO}(t) \quad (13)$$

$$Q_{FF}(t) = 1 - Q_{FO}(t) \quad (14)$$

These functions are compatible for Laplace Transforms and are obtained explicitly as

$$Q_{00}(t) = \frac{1}{(\gamma+\mu)}\left[\mu + \gamma e^{-(\gamma+\mu)t}\right] \quad (15)$$

$$Q_{F0}(t) = \frac{\mu}{(\gamma+\mu)}\left[1 - e^{-(\gamma+\mu)t}\right] \quad (16)$$

$$Q_{0F}(t) = \frac{\gamma}{(\gamma+\mu)}\left[1 - e^{-(\gamma+\mu)t}\right] \quad (17)$$

$$Q_{FF}(t) = \frac{1}{(\gamma+\mu)}\left[\gamma + \mu e^{-(\gamma+\mu)t}\right] \quad (18)$$

V. The Quasi-Stationary Distribution

Let X(t) denotes the residual lifetime of the system at any time t and T denotes the time to system failure. The period T may be sufficiently large to allow the process to settle down to a state of statistical equilibrium within this period. Then the limit as $t \to \infty$ of conditional probability,

$$L(x,t) = Pr\{X(t) \leq x / T > t\} \quad (19)$$

is termed as the QSD of X(t). The conditioned distribution L(x,t) can also be expressed as

$$L(x,t) = \frac{R(t) - R(x+t)}{R(t)} = 1 - \frac{R(x+t)}{R(t)} \quad (20)$$

$$L(x) = \lim_{t\to\infty} \; L(\mathrm{x,t}) = 1 - \lim_{t\to\infty} \; \frac{R(x+t)}{R(t)} \tag{21}$$

Observing that the function R(t) is the reliability of the system, the above limit is studied by first writing the integral equations for R(t) using regenerative point method.

Define e_1-event as the time epoch at which the repair of an online failed unit commences; at this instant the standby unit begins to operate online and the switching device is found in operable condition. Since e_1-event is regenerative in nature, we have

$$L_1(x) = 1 - \lim_{t\to\infty} \; \frac{R_1(x+t)}{R_1(t)} \tag{22}$$

Define e_0-event as the time epoch at which the operation of a unit commences; at this instant the standby unit as well as the switching device are in operable condition. Thus, conditioning on e_0-event, we have

$$L_0(x) = 1 - \lim_{t\to\infty} \; \frac{R_0(x+t)}{R_0(t)} \tag{23}$$

Conditioned on ei-events at t = 0, the functions $R_i(t)$ can easily be derived.

$$R_1(t) = \overline{F}(t) + \int_0^t e_1(u)R_i(t-u)\mathrm{du} \tag{24}$$
$$R_0(t) = \overline{F}(t) + \int_0^t e_0(u)R_i(t-u)\mathrm{du} \tag{25}$$

where $e_1(u)$ is the pdf of time interval between consecutive e_1-events and $e_0(u)$ is the pdf of time interval between e_0-event and the first e_1-event.

The functions $e_i(t)_{i=0,1}$ are obtained using $P_{ij}(t)$ and $Q_{ij}(t)$ as

$$e_0(t) = f(t)\, P_{OO}(t)\, Q_{OO}(t) \tag{26}$$
$$e_1(t) \;=\; f(t)\, P_{FO}(t)\, Q_{OO}(t) \tag{27}$$

In view of (26) and (27), the functions (24) and (25) can also be expressed as

$$R_i(t) = \overline{F}(t) + e_i(t) \circledcirc R_1(t) \quad i = 0,1 \tag{28}$$

Taking Laplace Transform on (28) we get

$$R_i^*(s) = \overline{F^*}(s) + e_i^*(s)R_1^*(s) \quad i = 0,1 \tag{29}$$

where $e_0^*(s) = \int_0^\infty f(t)P_{00}(t)Q_{00}(t)e^{-\mathrm{st}}\mathrm{dt}$

$e_1^*(s) = \int_0^\infty f(t)P_{\mathrm{F0}}(t)Q_{00}(t)e^{-\mathrm{st}}\mathrm{dt}$

On simplification we get

$$R_1^*(s) = \frac{\overline{F^*}(s)}{1-e_1^*(s)} \tag{30}$$
$$R_0^*(s) = \overline{F^*}(s)\,\frac{[1-e_1^*(s)+e_0^*(s)]}{1-e_1^*(s)} \tag{31}$$

In order to find the nature of the resulting distribution of $L_i(x)$ defined in (22) and (23), it is essential to find the roots of the equation $1 - e_1^*(s) = 0$. When the lifetime of a unit operating online is assumed to be distributed exponential with parameter δ, the function $e_1^*(s)$ modifies itself into

$$e_1^*(s) = \delta \int_0^\infty e^{-(s+\delta)t} P_{F0}(t) Q_{00}(t) \mathrm{dt} \tag{32}$$

Since f(t) is exponential in nature and $P_{F0}(t)$ and $Q_{00}(t)$ are rational functions of their arguments, $e_1^*(s)$ is also a rational function. Thus,

$$e_1^*(s) = \frac{A(s)}{B(s)} \tag{33}$$

where A(s) and B(s) are polynomials of degree n and m (n < m) respectively. In view of (33), the expression in (30) modifies itself into

$$R_1^*(s) = \frac{B(s)}{(s+\delta)[B(s)-A(s)]} \tag{34}$$

Define $p_1^*(s) = 1 - sR_1^*(s)$, then

$$p_1^*(s) = -\frac{\delta[B(s)-A(s)]-sB(s)}{(s+\delta)[B(s)-A(s)]} \tag{35}$$

Observing that $R_1^*(s)$ and $p_1^*(s)$ are rational functions of their arguments, their singularities are essentially same. Moreover, all the singularities of $p_1^*(s)$ are poles.

Let s = η be the pole of $p_1^*(s)$ situated closest to the right of the s-plane. As per Widder [11], η is real and negative and is the abscissa of convergence of $p_1^*(s)$.

Define $\Psi(s) = 1 - e_1^*(s)$ then

$$\Psi(s) = 1 - \delta \int_0^\infty e^{-(s+\delta)t} P_{F0}(t) Q_{00}(t) \mathrm{dt} \tag{36}$$

Observing that

$$\delta \int_0^\infty e^{-(s+\delta)t} P_{F0}(t) Q_{00}(t) \mathrm{dt} < \delta \int_0^\infty e^{-(s+\delta)t} \mathrm{dt} \tag{37}$$

we get $\Psi(s) < \frac{\delta}{s+\delta}$ and at s = 0, ψ(s) < 1.

Observing that $P_{F0}(t)$ and $Q_{00}(t)$ is the probability that both the standby unit and the switching device are in operable condition at time t given that a repair has commenced initially, we get $\psi(s) > 0$ and $\Psi(-\delta) = 1 - e_1^*(-\delta) < 0$

This follows from (36) and also because −δ is a singularity of 1/(s+δ). Thus from (33) and (34), it can be seen that there exists at least one ξ of ψ(s) such that $-\delta < \mathrm{Re}\ \xi < 0$. Since η is a pole of $p_1^*(s)$ which is closest to the right of s-plane, we get $-\delta < \eta < 0$. Thus $\Psi(\eta) = 1 - e_1^*(\eta) = 0$ and which implies that $e_1^*(\eta) = 1$. This means $e_1^*(s)$ is convergent for s = η and

$$\Psi'(\eta) = \int_0^\infty \mathrm{te}_1(t) e^{-\eta t} \mathrm{dt}$$

exists and is positive. Thus, η is a root of $1 - e_1^*(s) = 0$ with multiplicity one. This implies that η is a simple pole of $p_1^*(s)$ and also of $R_1^*(s)$. Consequently η is a zero of [B(s) − A(s)].

Observing the fact that the pole η of $p_1^*(s)$ is a simple pole and lies between −δ and 0, we write

$$R_1(t) = \frac{1}{\eta+\delta} \lambda \mathrm{e}^{\eta t} + o(e^{\eta t}) \tag{38}$$

$$R_1(x+t) = \frac{1}{\eta+\delta} \lambda \mathrm{e}^{\eta(x+t)} + o(e^{\eta t}) \tag{39}$$

where $\lambda = \lim_{s\to\eta} \frac{s-\eta}{1-e_1^*(s)}$

$$\lim_{t\to\infty}\frac{R_1(x+t)}{R_1(t)}=\lim_{t\to\infty}\frac{\lambda e^{\eta(x+t)}+o(e^{\eta t})}{\lambda e^{\eta t}+o(e^{\eta t})}=e^{\eta x} \quad (40)$$

Substituting (40) in (22) we get

$$L_1(x)=1-e^{\eta x},\quad \eta<0$$

Thus, the QSD of the residual lifetime of a complex two-unit standby redundant system given that an e_1-event has occurred at t = 0, is distributed exponential with parameter $-\eta$ ($\eta<0$) which is the closest negative root of the polynomial $\psi(s)$ equated to zero. The section to follow clearly illustrates our result.

VI. Illustration

When the lifetime distribution of the unit operating online is assumed exponential with parameter δ, the derivation of the roots of the polynomial equated to zero can be easily obtained. Now consider

$$\begin{aligned}
e_1(t)&=\delta e^{-\delta t}P_{F0}(t)Q_{00}(t)\\
e_1^*(s)&=\delta\int_0^\infty e^{-(s+\delta)t}P_{F0}(t)Q_{00}(t)dt\\
P_{F0}(t)&=\frac{\beta}{(\alpha+\beta)}[1-e^{-(\alpha+\beta)t}]\\
Q_{00}(t)&=\frac{1}{(\gamma+\mu)}[\mu+\gamma e^{-(\gamma+\mu)t}]
\end{aligned}$$

Let $\Psi(s)=1-e_1^*(s)$

$$\Psi(s)=0$$

$$1-\frac{\delta\beta}{(\alpha+\beta)(\gamma+\mu)}\left[\frac{\mu}{s+a_1}+\frac{\gamma}{s+a_2}-\frac{\mu}{s+a_3}-\frac{\gamma}{s+a_4}\right]=0$$

Furthermore on simplification, we get

$$\sum_{i=1}^{5}k_i s^{5-i}=0$$

Observe that the above equation is a fourth degree polynomial in s equated to zero.

$$\begin{aligned}
k_1&=(\alpha+\beta)(\gamma+\mu)\\
k_2&=k_1b_1\\
k_3&=k_1(b_2+b_3+b_4)-a_1m_1\\
k_4&=k_1[(a_1+a_2)b_3+(a_3+a_4)b_2]-a_1(t_1+t_2-t_3-t_4)\\
k_5&=k_1a_1a_2a_3a_4-a_1m_2\\
b_1&=a_1+a_2+a_3+a_4\\
b_2&=a_1a_2\\
b_3&=a_3a_4\\
b_4&=(a_1+a_2)(a_3+a_4)\\
t_1&=\beta\mu[a_2a_3+(a_2+a_3)a_4]\\
t_2&=\beta\gamma[a_1a_3+(a_1+a_3)a_4]\\
t_3&=\beta\mu[a_1a_2+(a_1+a_2)a_4]\\
t_4&=\beta\gamma[a_1a_2+(a_1+a_2)a_3]\\
m_1&=c_1\beta\mu+c_2\beta\gamma-c_3\beta\mu-c_4\beta\gamma\\
m_2&=d_1\beta\mu+d_2\beta\gamma-d_3\beta\mu-d_4\beta\gamma\\
c_1&=a_2+a_3+a_4\\
c_2&=a_1+a_3+a_4\\
c_3&=a_1+a_2+a_4\\
c_4&=a_1+a_2+a_3
\end{aligned}$$

$$d_1 = a_2 a_3 a_4$$
$$d_2 = a_1 a_3 a_4$$
$$d_3 = a_1 a_2 a_4$$
$$d_4 = a_1 a_2 a_3$$
$$a_1 = \delta$$
$$a_2 = \delta + \gamma + \mu$$
$$a_3 = \delta + \alpha + \beta$$
$$a_4 = \delta + \gamma + \mu + \alpha + \beta$$

Once the values of the parameters $\alpha, \beta, \gamma, \mu$ and δ are specified, the network of constants can be evaluated and all the four roots of the equation can be obtained through methods of numerical analysis. Table 1 provides the simple negative root closest to the origin for specified values of the parameters.

A coding is written for the purpose and the code seeks data about the parameters and then provides the negative root closest to zero. For instance, when $(\alpha, \beta, \gamma, \mu, \delta) = (20, 30, 1.5, 6, .5)$ then the negative root closest to zero is -0.2595 and $L(x) = 1\ e^{-0.2595t}$.

Table 1: *The negative root closest to zero of $\psi(s) = 0$*

(α, β)	(γ, μ)	Negative root closest to zero		
		$\delta = 0.5$	$\delta = 0.6$	$\delta = 0.7$
(20, 30)	(1.5, 6)	-0.2595	-0.3113	-0.3631
	(2.0, 7)	-0.2663	-0.3195	-0.3727
	(2.5, 8)	-0.2712	-0.3254	-0.3796
	(3.0, 9)	-0.2749	-0.3299	-0.3848
	(3.5, 10)	-0.2778	-0.3333	-0.3889
(22, 35)	(1.5, 6)	-0.2537	-0.3043	-0.3549
(24, 40)		-0.2492	-0.2988	-0.3484
(26, 45)		-0.2455	-0.2944	-0.3432
(28, 50)		-0.2425	-0.2908	-0.3389
(30, 33)		-0.2400	-0.2877	-0.3354

VII. Conclusion

In this article, the quasi-stationary distribution for the residual lifetime of a two-unit complex reparable system is obtained using regenerative stochastic process. The results of the study are numerically illustrated assuming exponential lifetime distribution for the units. We observe that whatever be the lifetime and repair time distributions, provided that their Laplace transforms are rational, the quasi-stationary distribution is always exponential and is independent of the initial event.

References

[1] Cavender, J. A. (1978). Quasi-stationary distributions of birth-and-death processes. *Advances in Applied Probability*, *10*(3), 570-586.

[2] Chaudhary, P., Sharma, A. and Gupta, R. (2022). A Discrete Parametric Markov-Chain Model of a Two NonIdentical Units Warm Standby Repairable System with Two Types of Failure. *Reliability: Theory & Applications*, *17*(2 (68)):21-30.

[3] Kalpakam, S., & Hameed, M. S. (1983). Quasi-stationary distribution of a two-unit warm-standby redundant system. *Journal of Applied Probability*, *20*(2), 429-435.

[4] Kyprianou, E. K. (1972). On the quasi-stationary distributions of the GI/M/1 queue. *Journal of Applied Probability*, *9*(1), 117-128.

[5] Li, W., & Cao, J. (1993). Limiting distributions of the residual lifetimes of several repairable systems. *Microelectronics Reliability*, *33*(8), 1069-1072.

[6] Munda, L., & Taneja, G. (2023). Combined Redundancy Optimization for a System Comprising Operative, Cold Standby and Warm Standby Units. *Reliability: Theory & Applications*, *18*(2 (73)), 486-497.

[7] Papageorgiou, E., & Kokolakis, G. (2010). Reliability analysis of a two-unit general parallel system with (n-2) warm standbys. *European Journal of Operational Research*, *201*(3), 821-827.

[8] Reinertsen, R. (1996). Residual life of technical systems; diagnosis, prediction and life extension. *Reliability Engineering & System Safety*, *54*(1), 23-34.

[9] Shankar Bhat, K. (1993). Probabilistic Analysis of Complex Repairable Systems. Ph.D. Thesis, University of Madras, India.

[10] Van Doorn, E. A., & Pollett, P. K. (2013). Quasi-stationary distributions for discrete-state models. *European journal of operational research*, *230*(1), 1-14.

[11] Widder, D. V. (1971). An Introduction to Transform Theory, Academic Press, New York.

LIFO-BASED OPTIMIZATION OF TWO-WAREHOUSE INVENTORY SYSTEMS WITH DETERIORATING ITEMS

Amit Kumar[1], Ajay Singh Yadav[1,*], Dharmendra Yadav[2]
Bhavani Viswanathan[3]

•

[1]Department of Mathematics, SRM Institute of Science and Technology,
Delhi-NCR Campus, Ghaziabad, India, 201204
[2]Department of Mathematics, Vardhman College, Bijnor,
Uttar Pradesh, India, 201204
[3]Department of Library (Science and Humanities), SRM Institute of Science and Technology,
Delhi-NCR Campus, Ghaziabad, India, 201204
ag2219@srmist.edu.in, ajaysiny@srmist.edu.in, dharmendra03@gmail.com

bhavaniviswam@gmail.com
*Corresponding author

Abstract

In this study, a two-warehouse inventory model for the red wine industry is presented, focusing on items that deteriorate. The model takes into account the effects of inflation and operates on the LIFO (Last In, First Out) distribution policy. The goal is to minimize the total inventory cost, including the cost of maintaining inventory and the cost of purchasing new inventory. The model assumes a constant and known demand for red wine over time, with no permitted shortages. The stock system consists of warehouse A and warehouse B, with starting stocks fixed in each case. Inventory balance equations track inventory levels at each warehouse, taking into account transfers between warehouses and customer demand. The LIFO shipping policy is implemented to determine the quantities transferred between warehouses. Inflation is factored into the model by adjusting the cost of buying new inventory. This adjustment may be based on historical inflation rates or other relevant factors. The objective function is to minimize the total inventory cost, taking into account inventory costs and inflation-adjusted purchasing costs. The model provides a framework for making decisions about stock levels and transfer rates between warehouses. By optimizing these decisions, the model aims to achieve cost savings while ensuring that demand is met without bottlenecks. The model results can serve as a guide for inventory management strategies in the red wine industry, taking into account the specific challenges presented by the spoiled nature of the product and the impact of inflation.

Keywords: Inventory, Two-warehouse, ramp type demand, deterioration, inflation, and LIFO dispatching policy.

1. Introduction and related work

The red wine industry faces unique inventory management challenges due to the nature of its product, which is a spoiling item. Over time, the quality and value of red wine declines, making it crucial for businesses to effectively manage their inventory. Additionally, inflation can have a significant impact on the cost of purchasing new inventory, further complicating

the decision-making process. In this study, we propose a two-storage stock model specifically designed for the red wine industry. The model takes into account the deteriorated nature of red wine and inflation and is based on the LIFO (Last In, First Out) shipping policy. The LIFO policy assumes that inventory purchased last is shipped first, reflecting typical industry storage and retrieval practices. The goal of the inventory model is to minimize the overall cost of inventory while ensuring that customer demand is met without shortages. By optimizing inventory levels and transfer rates between warehouses, companies can realize cost savings and avoid overstocking or understocking. This results in improved profitability and customer satisfaction. To capture the effects of spoilage, the model tracks inventory levels in warehouse A and warehouse B over time. The equilibrium equations take into account customer demand, transfers between warehouses and initial inventory levels. The model dynamically adjusts stock levels based on these factors, while taking into account deterioration in the condition of red wine. Inflation is another critical factor considered in the model. The cost of purchasing new inventory is adjusted for the impact of inflation. This adjustment can be based on historical inflation rates or other relevant factors to ensure that the model provides a realistic representation of industry cost dynamics. Overall, the proposed inventory model provides a comprehensive framework for decision making in the red wine industry. By addressing the unique challenges of item spoilage, inflation, and LIFO shipping policy, businesses can optimize their inventory management strategies and increase their competitive advantage. The following sections of this study detail the details of the model, its formulation, and the potential benefits it offers to the red wine industry.

Practical inventory management is crucial for perishable goods like red wine, which undergo deterioration over time in addition to fluctuations in demand. This study examines the optimization of a two-warehouse inventory system utilizing the degradation factor and a Last-In-First-Out (LIFO) dispatch strategy. By finding a balance between storage and spoiling costs, we hope to improve efficiency and decrease waste in red wine inventory management. Our study provides valuable insights to improve perishable commodity logistics decision-making. Yadav et al. [1-10] highlighted that the deterioration of these items is significant, limiting their storage duration. Yadav et al. [11-20] further explained that deterioration can manifest as spoilage, evaporation, obsolescence, or loss of functionality, leading to reduced inventory usage compared to natural conditions. When raw materials are stocked for future demands, various factors such as storage conditions, weather, and humidity can cause deterioration. Yadav et al. [21-53] discuss that management typically maintains a warehouse for storing purchased goods. However, for various reasons, they may acquire or lease more items than can be accommodated in the warehouse, referring to the excess as overflow (OW), while the additional stock in a rented warehouse is termed rented warehouse (RW), located near or adjacent to OW. Yadav and Swami [54-61] found that the inventory costs associated with RW, including maintenance and depreciation, are generally higher than those of OW due to added operational and maintenance expenses. To minimize inventory costs, it is important to quickly utilize RW stock. Actual customer service is provided solely by OW, so to lower expenses, RW inventory is prioritized for turnover. These scenarios illustrate what are referred to as two inventory examples within the system. Yadav and Kumar [62] focused on managing the supply of electronic storage devices while integrating environmental and network considerations. Yadav, A.S. [63-65] analyzed seven measures of supply chain management to enhance the inventory of electronic storage devices. This analysis involved assessing financial impacts through the application of genetic algorithms (GA) and particle swarm optimization (PSO). Additionally, the research examined inventory improvement and equipment management using genetic computation, alongside a model design for inventory analysis that addressed economic challenges in transporting goods. Swami et al. [66-68] formulated inventory policies that address inventory requirements and associated costs, taking into account allowable payments and delays in inventory. They provided an example of depreciation across various goods and services, considering business loans and an inventory model that is less sensitive to pricing needs, while comparing inventory costs to inflation-related business expenses. Meanwhile, Gupta et al. [69-70] defined objectives for a Multiple Objective Genetic Algorithm and particle swarm optimization (PSO) aimed at enhancing supply levels and addressing deficits

and inflation, along with a calculation model that leverages genetic algorithms to assess scarcity and low inflation scenarios. Singh et al. [71, 72] examined cases involving the depreciation of two types of stock concerning asset and inventory costs while updating particle data, as well as scenarios with two inventories focusing on property damage and inventory costs under inflation, utilizing soft computing techniques. Kumar et al. [73-75] addressed delays in managing alcohol supply, refining particles, and developing a green cement supply system, while also tackling inflation through particle enhancement and the use of an electronic inventory system and distribution center with genetic computations. Chauhan and Yadav [76-77] provided an example of depreciation across two stores and warehouses, utilizing a genetic stock and vehicle stock to manage demand and inflation across two distribution centers. Pandey et al. [78] analyzed the improvement of industrial reserves for marble using genetic technology and enhanced multiple particle approaches. Ahlawat, et. al. [79] studied the white wine industry in supply chain management through nerve networks. Singh, et. al. [80] examines the best policy to import damaged goods immediately and pay for conditional delays under the supervision of two warehouses.

The research by Yadav et al. [81] centers on improving inventory management for perishable commodities through the lens of green technology investments, considering factors such as selling price, carbon emissions, and time-sensitive demand. In another analysis, Yadav, Yadav, and Bansal [82] utilize an interval number technique to explore a two-warehouse inventory management model for perishable goods, addressing demand and cost uncertainties. Their optimization methods highlight how investing in preservation technology can reduce waste and enhance inventory efficiency. Focusing on a two-warehouse approach to optimize inventory levels, Yadav, Yadav, and Bansal [83], Sinha, et. al [84], Hezer and Kara [85], and Negi and Ompal [86] present a model that addresses the deterioration of goods during storage, emphasizing the importance of managing degradation costs to improve overall inventory performance.

2. Notations and assumptions

2.1. Notations

The following notations are used in this model.

Parameters	Descriptions
$\Pi_{ow}^{lifo}(t)$	The Red wine industry inventory level in OW at any time t.
$\Pi_{rw}^{lifo}(t)$	The Red wine industry inventory level in RW at any time t.
α_w	The capacity of the own warehouse.
Q	The ordering quantity per cycle.
T	Planning horizon.
α_4	Inflation rate
$\alpha_h cow$	The holding cost per unit per unit time in Red wine industry OW.
$\alpha_h crw$	The holding cost per unit per unit time in Red wine industry RW.
$\alpha_d c$	The deterioration cost per unit.
$\alpha_s c$	The shortage cost per unit per unit time.
$\alpha_o pc$	The opportunity cost due to lost sales.
$\alpha_o c$	The replenishment cost per order.

2.2. Assumptions

In developing the mathematical model of the Red wine industry inventory system the following assumptions are being made:

1. A single item is considered over a prescribed
2. Period T units of time.

3. The demand rate D(t) at time t is deterministic and taken as a ramp type function of time i.e.
$D(t) = \alpha_0 e^{-\alpha_2\left(t-(t_\alpha+t_L)\right)H\left(t-(t_\alpha+t_L)\right)}, \alpha_0 > 0, \alpha_2 > 0$ where $H\Big(t-(t_\alpha+t_L)\Big)$ is the Heaviside™s function defined as

$$H\Big(t-(t_\alpha+t_L)\Big) = \begin{cases} 0, t < (t_\alpha+t_L) \\ 1, t \geq (t_\alpha+t_L) \end{cases}$$

4. The replenishment rate is infinite and lead-time is zero.
5. When the demand for goods is more than the supply. Shortages will occur. Customers encountering shortages will either wait for the vender to reorder (backlogging cost involved) or go to other vendors (lost sales cost involved). In this model shortages are allowed and the backlogging rate is $e^{-\alpha_3 t}$, when Red wine industry inventory is in shortage. The backlogging parameter α_3 is a positive constant.
6. The variable rate of deterioration in both warehouse is taken as $\alpha_1(t) = \alpha_1 t$. where $0 < \alpha_1 << 1$ and only applied to on hand Red wine industry inventory.
7. No replacement or repair of deteriorated items is made during a given cycle.
8. The Red wine industry owned warehouse (OW) has a fixed capacity of W units; the Red wine industry rented warehouse (RW) has unlimited capacity.
9. The goods of OW are consumed only after consuming the goods kept in RW.

3. FORMULATION AND SOLUTION OF THE MODEL

The Red wine industry inventory levels at OW are governed by the following differential equations under LIFO dispatching policy:

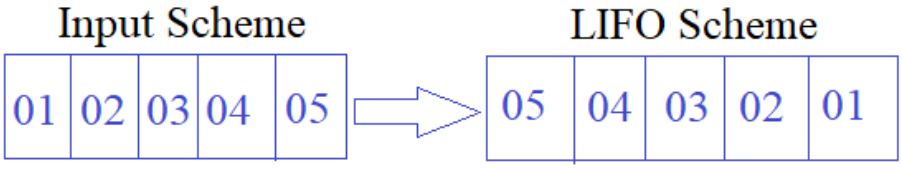


Figure 1: *Flow Chart For LIFO (Last In First Out) Dispatching Policy.*

$$\frac{d\Pi_{ow}^{lifo}(t)}{dt} = [-\alpha_1(t) I^{lifo}(t)], \qquad 0 \leq t \leq (t_\alpha + t_L) \tag{1}$$

$$\frac{d\Pi_{ow}^{lifo}(t)}{dt} + \alpha_1(t) I^{lifo}(t) = -\alpha_0 e^{-\alpha_2(t_\alpha+t_L)}, \qquad (t_\alpha + t_L) \leq t \leq (t_1 + t_L) \tag{2}$$

And

$$\left[\frac{d\Pi_{ow}^{lifo}(t)}{dt}\right] = \left[-\alpha_0 e^{-\alpha_2(t_\alpha+t_L)} e^{-\alpha_3 t}\right], \qquad (t_1 + t_L) \leq t \leq (T + t_L) \tag{3}$$

with the boundary conditions,

$$\Pi_{ow}^{lifo}(0) = \alpha_w \; and \; I^{lifo}(t_1 + t_F) = 0 \tag{4}$$

The solutions of equations (1), (2) and (3) are given by

$$\Pi_{ow}^{lifo}(t) = \alpha_w e^{-\alpha_1 t^2}, \;\; 0 \le t \le (t_\alpha + t_L) \tag{5}$$

$$\Pi_{ow}^{lifo}(t) = \left[\alpha_0 e^{-\alpha_2(t_\alpha+t_L)}(t_1+t_L) - t + \frac{\alpha_1(t_1+t_L)^3 - t^3}{6} e^{-\alpha_1 t^2}\right], \;\; (t_\alpha+t_L) \le t \le (t_1+t_L) \tag{6}$$

and

$$\Pi_{ow}^{lifo}(t) = \left[\frac{\frac{\alpha_0}{\alpha_3}}{\alpha_3} e^{-\alpha_2(t_\alpha+t_L)} + e^{-\alpha_3 t - e^{-\alpha_3(t_1+t_L)}}\right], \;\; (t_\alpha+t_L) \le t \le (T_1+t_L) \tag{7}$$

The Red wine industry inventory level at RW is governed by the following differential equations:

$$\frac{d\Pi_{ow}^{lifo}(t)}{dt} + \alpha_1(t)\Pi^{lifo}(t) = -(\alpha_0+\alpha)e^{-\alpha_2 t}, \qquad 0 \le t \le (t_\alpha+t_L) \tag{8}$$

With the boundary condition $\Pi_{rw}^{lifo}(0) = 0$ the solution of the equation (8) is

$$\Pi_{rw}^{lifo}(t) = \left[\alpha_0\left((t_\alpha+t_L-t) - \frac{\alpha_2}{2}\left(((t_\alpha+t_L)^2 - t^2)\right)\right.\right.$$
$$\left.\left. + \frac{\alpha_2}{2}\left(((t_\alpha+t_L)^2 - t^2)\right)e^{-\alpha_1(t^2)}\right], \;\; (t_\alpha+t_L) \le t \le (t_1+t_L) \tag{9}$$

Due to continuity of $\Pi_{ow}^{lifo}(t)$ at point $t = (t_\alpha + t_L)$ it follows from equations (5) and (6), one has

$$\alpha_w = \left[\alpha_0 e^{-\alpha_2(t_\alpha+t_L)}\left\{(t_1+t_L) - (t_\alpha+t_L) + \frac{\alpha_1(t_1+t_L)^3 - (t_\alpha+t_L)^3}{6}\right\}\right] \tag{10}$$

Next, we calculate all the associated inventory costs as follow:

1. Ordering Cost (OC):

$$OC = \alpha_{OC} \tag{11}$$

2. Holding Cost in Dairy industry (HC):

$$HC = \left[\alpha_{hcow}\left\{\int_0^{(t_\alpha+t_L)} \Pi_{ow}^{lifo}(t)e^{-\alpha_4 t}dt + \int_{(t_\alpha+t_L)}^{(t_1+t_L)} \Pi_{ow}^{lifo}(t)e^{-\alpha_4\left\{(t_\alpha+t_L)+t\right\}}dt\right\}\right]$$
$$+ \left[\alpha_{hcrw}\left\{\int_0^{(t_\alpha+t_L)} \Pi_{rw}^{lifo}(t)e^{-\alpha_4 t}dt\right\}\right]$$
$$= \left[\alpha_{hcrw}(\alpha_0+\alpha)\left\{\frac{(t_\alpha+t_L)^2}{2} - \frac{(3\alpha_2+\alpha_4)}{6}(t_\alpha+t_L)^3 + \left(\frac{\alpha_1}{12}\right.\right.\right.$$
$$\left.\left.\left. + \frac{\alpha_2\alpha_4}{8}\right)(t_\alpha+t_L)^4 - \left(\frac{\alpha_4\alpha_1}{20} + \frac{\alpha_2\alpha_1}{30}\right\}\right] \tag{12}$$

3. Shortage Cost (SC):

$$SC = \left[\alpha_{sc}\left\{\int_{t_1+t_L}^{(T+t_L)} -\Pi_{rw}^{lifo}(t)e^{-\alpha_4\left(t_1+t_L)+t\right.}dt\right\}\right]$$
$$= \left[\frac{(\alpha_0+\alpha)\alpha_{sc}e^{-(\alpha_4(t_1+t_L)+\alpha_2(t_\alpha+t_L))}}{\alpha_3\alpha_4(\alpha_3+\alpha_4)}\left[\alpha_3 e^{-(\alpha_3+\alpha_4)(t_1+t_L)}\right.\right.$$
$$\left.\left. + e^{-\alpha_4(T+t_L)}\left(re^{-\alpha_3(T+t_L)} - (\alpha_3+\alpha_4)e^{-\alpha_3(t_1+t_L)}\right)\right]\right] \tag{13}$$

4. Deterioration Cost (DC):

$$DC = \left[\alpha_{dc}\left\{\int_0^{(t_\alpha+t_L)} \alpha_1 t\Pi_{rw}^{lifo}(t)e^{-\alpha_4 t}dt + \int_{(t_\alpha+t_L)}^{(t_1+t_L)} \Pi_{ow}^{lifo}(t)e^{-\alpha_4\left\{(t_\alpha+t_L)+t\right\}}dt\right\}\right] \quad (14)$$

5. Lost Sale Cost (LSC):

$$\begin{aligned} LSC &= \left[\alpha_{opc}\left\{\int_{t_1+t_F}^{(T+t_L)} -(\alpha_0+\alpha)(1-e^{-\alpha_3 t})e^{-\alpha_2(t_\alpha+t_L)}e^{-\alpha_4(t_1+t_L)+t}\right\}\right] \\ &= \left[\frac{(\alpha_0+\alpha)\alpha_{opc}e^{-(\alpha_4(t_1+t_L)+\alpha_2(t_\alpha+t_L))}}{\alpha_4(\alpha_3+\alpha_4)}\left[e^{-\alpha_4(t_1+t_L)}((\alpha_3+\alpha_4)-\alpha_4 e^{-\alpha_3(t_1+t_L)})\right.\right. \\ &\qquad \left.\left. - e^{-\alpha_4(T+t_L)}((\alpha_3+\alpha_4)-\alpha_4 e^{-\alpha_3(t_1+t_L)})\right]\right] \quad (15) \end{aligned}$$

Therefore, the total average cost per unit time of our model is obtained as follows

$$T(t_1+t_L, T+t_L)C = \frac{1}{T}\left[OC+HC+SC+DC+LSC\right] \quad (16)$$

4. Optimization Methodology

To minimize the total cost per unit time, the optimal values of t_1 and T can be obtained by solving the following equations simultaneously

$$\frac{\partial TC}{\partial(t_1+t_L)} = 0,$$

and

$$\frac{\partial TC}{\partial(T+t_L)} = 0$$

provided, they satisfy the following conditions which is the necessary and sufficient conditions for convexity.

$$\frac{\partial^2 TC}{\partial(t_1+t_L)^2} > 0, \frac{\partial^2 TC}{\partial(T+t_L)^2} > 0,$$

and

$$\left(\frac{\partial^2 TC}{\partial(t_1+t_L)^2}\right)\left(\frac{\partial^2 TC}{\partial(T+t_L)^2}\right) - \left(\frac{\partial^2 TC}{\partial(t_1+t_L)\partial(T+t_L)}\right)^2 > 0$$

These equations are highly nonlinear equations. Therefore, numerical solution of these equations can be obtained by using the software MATLAB 7.0.1.

5. Graphical Representation

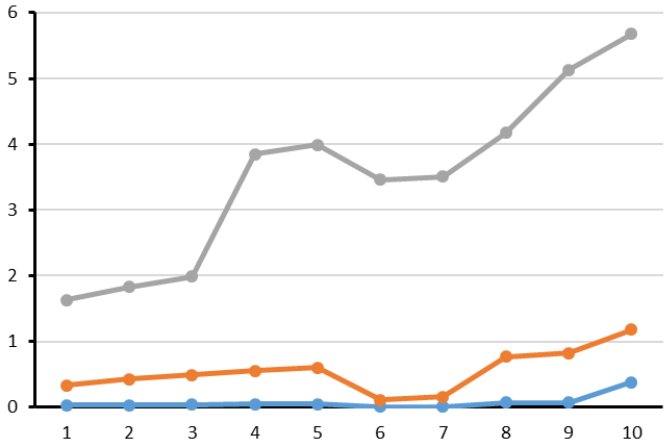


Figure 2: *Variation between time and demand rate.*

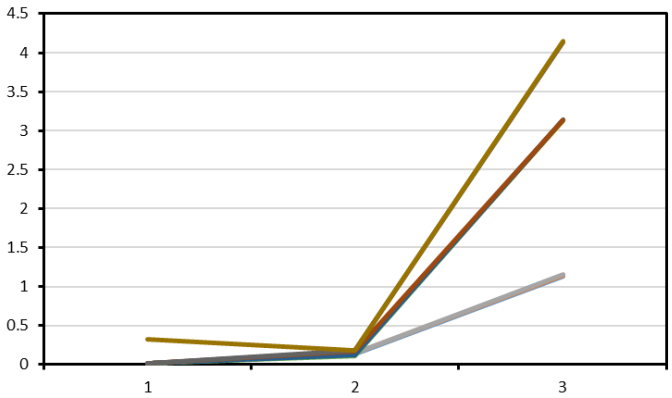


Figure 3: *Variation between time and deterioration rate.*

The graphical depictions in this part provide a comprehensive grasp of the dynamics within the deteriorated inventory model of two-warehouses. Figure 2 and Figure 3 explains the link between demand rates, deterioration rate and time.

6. Conclusion

The two-warehouse inventory model for the red wine industry provides a valuable framework for effective inventory management, taking into account item spoilage, inflation, and LIFO (Last In , First Out). By integrating these factors into the model, companies can make informed decisions about inventory levels and transfer rates between warehouses, reducing costs and improving customer satisfaction. Deteriorating red wine condition requires careful inventory management to avoid overstocking and product obsolescence. The proposed model takes this into account by dynamically adjusting stock levels based on equilibrium equations that take into account customer demand and transfers between stocks. By optimizing these inventories, companies can minimize storage costs and reduce spoilage losses. Inflation is another critical factor that can significantly affect the cost of purchasing new inventory. By adjusting purchase costs in the model for inflation, companies can make more accurate cost calculations and ensure that model results are consistent with current economic conditions. This allows them to make cost-effective decisions

while maintaining desired service levels. The LIFO shipping policy reflects typical industry storage and retrieval practices. By adopting this policy in the model, companies can ensure that inventory purchased last is shipped first, which is consistent with industry practice and minimizes potential obsolescence costs. Overall, the dual warehouse inventory model presented in this study provides a comprehensive solution to inventory management challenges in the red wine industry. By taking into account the unique characteristics of red wine, inflation, and LIFO shipping policies, companies can optimize inventory levels, reduce costs, and improve overall operational efficiency. It should be noted that the efficiency of the model can be increased by incorporating additional factors such as batch ordering, lead times and storage capacity constraints depending on the specific needs of the red wine industry. Additionally, future research could explore the integration of advanced forecasting techniques and real-time data to improve the accuracy of demand forecasting and further improve model performance.

Ultimately, by adopting and implementing the two-warehouse inventory model, considering degradation, inflation, and LIFO shipping policy, companies in the red wine industry can gain a competitive advantage, reduce costs and provide superior customer service, contributing to their long-term success in the marketplace.

References

[1] Yadav, A.S., Bansal, K.K., Shivani, Agarwal, S. And Vanaja, R. (2020) FIFO in Green Supply Chain Inventory Model of Electrical Components Industry With Distribution Centres Using Particle Swarm Optimization. Advances in Mathematics: Scientific Journal. 9 (7), 5115“512 0.

[2] Yadav, A.S., Kumar, A., Agarwal, P., Kumar, T. And Vanaja, R. (2020) LIFO in Green Supply Chain Inventory Model of Auto-Components Industry with Warehouses Using Differential Evolution. Advances in Mathematics: Scientific Journal, 9 no.7, 5121“5126.

[3] Yadav, A.S., Abid, M., Bansal, S., Tyagi, S.L. And Kumar, T. (2020) FIFO LIFO in Green Supply Chain Inventory Model of Hazardous Substance Components Industry with Storage Using Simulated Annealing. Advances in Mathematics: Scientific Journal, 9 no.7, 5127“5132.

[4] Yadav, A.S., Tandon, A. and Selva, N.S. (2020) National Blood Bank Centre Supply Chain Management For Blockchain Application Using Genetic Algorithm. International Journal of Advanced Science and Technology Vol. 29, No. 8s, 1318-1324.

[5] Yadav, A.S., Selva, N.S. and Tandon, A. (2020) Medicine Manufacturing Industries supply chain management for Blockchain application using artificial neural networks, International Journal of Advanced Science and Technology Vol. 29, No. 8s, 1294-1301.

[6] Yadav, A.S., Ahlawat, N., Agarwal, S., Pandey, T. and Swami, A. (2020) Red Wine Industry of Supply Chain Management for Distribution Center Using Neural Networks, Test Engraining & Management, Volume 83 Issue: March “ April, 11215 “ 11222.

[7] Yadav, A.S., Pandey, T., Ahlawat, N., Agarwal, S. and Swami, A. (2020) Rose Wine industry of Supply Chain Management for Storage using Genetic Algorithm. Test Engraining & Management, Volume 83 Issue: March “ April, 11223 “ 11230.

[8] Yadav, A.S., Ahlawat, N., Sharma, N., Swami, A. And Navyata (2020) Healthcare Systems of Inventory Control For Blood Bank Storage With Reliability Applications Using Genetic Algorithm. Advances in Mathematics: Scientific Journal 9 no.7, 5133“5142.

[9] Yadav, A.S., Dubey, R., Pandey, G., Ahlawat, N. and Swami, A. (2020) Distillery Industry Inventory Control for Storage with Wastewater Treatment Logistics Using Particle Swarm Optimization Test Engraining & Management Volume 83 Issue: May “ June, 15362-15370.

[10] Yadav, A.S., Ahlawat, N., Dubey, R., Pandey, G. and Swami, A. (2020) Pulp and paper industry inventory control for Storage with wastewater treatment and Inorganic composition using genetic algorithm (ELD Problem). Test Engraining & Management, Volume 83 Issue: May “ June, 15508-15517.

[11] Yadav, A.S., Pandey, G., Ahlawat, N., Dubey, R. and Swami, A. (2020) Wine Industry Inventory Control for Storage with Wastewater Treatment and Pollution Load Using Ant

Colony Optimization Algorithm, Test Engraining & Management, Volume 83 Issue: May " June, 15528-15535.

[12] Yadav, A.S., Navyata, Sharma, N., Ahlawat, N. and Swami, A. (2020) Reliability Consideration costing method for LIFO Inventory model with chemical industry warehouse. International Journal of Advanced Trends in Computer Science and Engineering, Volume 9 No 1, 403-408.

[13] Yadav, A.S., Bansal, K.K., Kumar, J. and Kumar, S. (2019) Supply Chain Inventory Model For Deteriorating Item With Warehouse & Distribution Centres Under Inflation. International Journal of Engineering and Advanced Technology, Volume-8, Issue-2S2, 7-13.

[14] Yadav, A.S., Kumar, J., Malik, M. and Pandey, T. (2019) Supply Chain of Chemical Industry For Warehouse With Distribution Centres Using Artificial Bee Colony Algorithm. International Journal of Engineering and Advanced Technology, Volume-8, Issue-2S2, 14-19.

[15] Yadav, A.S., Navyata, Ahlawat, N. and Pandey, T. (2019) Soft computing techniques based Hazardous Substance Storage Inventory Model for decaying Items and Inflation using Genetic Algorithm. International Journal of Advance Research and Innovative Ideas in Education, Volume 5 Issue 9, 1102-1112.

[16] Yadav, A.S., Navyata, Ahlawat, N. and Pandey, T. (2019) Hazardous Substance Storage Inventory Model for decaying Items using Differential Evolution. International Journal of Advance Research and Innovative Ideas in Education, Volume 5 Issue 9, 1113-1122.

[17] Yadav, A.S., Navyata, Ahlawat, N. and Pandey, T. (2019) Probabilistic inventory model based Hazardous Substance Storage for decaying Items and Inflation using Particle Swarm Optimization. International Journal of Advance Research and Innovative Ideas in Education, Volume 5 Issue 9, 1123-1133.

[18] Yadav, A.S., Navyata, Ahlawat, N. and Pandey, T. (2019) Reliability Consideration based Hazardous Substance Storage Inventory Model for decaying Items using Simulated Annealing. International Journal of Advance Research and Innovative Ideas in Education, Volume 5 Issue 9, 1134-1143.

[19] Yadav, A.S., Swami, A. and Kher, G. (2019) Blood bank supply chain inventory model for blood collection sites and hospital using genetic algorithm. Selforganizology, Volume 6 No.(3-4), 13-23.

[20] Yadav, A.S., Swami, A. and Ahlawat, N. (2018) A Green supply chain management of Auto industry for inventory model with distribution centers using Particle Swarm Optimization. Selforganizology, Volume 5 No. (3-4)

[21] Yadav, A.S., Ahlawat, N., and Sharma, S. (2018) Hybrid Techniques of Genetic Algorithm for inventory of Auto industry model for deteriorating items with two warehouses. International Journal of Trend in Scientific Research and Development, Volume 2 Issue 5, 58-65.

[22] Yadav, A.S., Swami, A. and Gupta, C.B. (2018) A Supply Chain Management of Pharmaceutical For Deteriorating Items Using Genetic Algorithm. International Journal for Science and Advance Research In Technology, Volume 4 Issue 4, 2147-2153.

[23] Yadav, A.S., Maheshwari, P., Swami, A., and Pandey, G. (2018) A supply chain management of chemical industry for deteriorating items with warehouse using genetic algorithm. Selforganizology, Volume 5 No.1-2, 41-51.

[24] Yadav, A.S., Garg, A., Gupta, K. and Swami, A. (2017) Multi-objective Genetic algorithm optimization in Inventory model for deteriorating items with shortages using Supply Chain management. IPASJ International journal of computer science, Volume 5, Issue 6, 15-35.

[25] Yadav, A.S., Garg, A., Swami, A. and Kher, G. (2017) A Supply Chain management in Inventory Optimization for deteriorating items with Genetic algorithm. International Journal of Emerging Trends & Technology in Computer Science, Volume 6, Issue 3, 335-352.

[26] Yadav, A.S., Maheshwari, P., Garg, A., Swami, A. and Kher, G. (2017) Modeling & Analysis of Supply Chain management in Inventory Optimization for deteriorating items with Genetic algorithm and Particle Swarm optimization. International Journal of Application or Innovation in Engineering & Management, Volume 6, Issue 6, 86-107.

[27] Yadav, A.S., Garg, A., Gupta, K. and Swami, A. (2017) Multi-objective Particle Swarm optimization and Genetic algorithm in Inventory model for deteriorating items with shortages

using Supply Chain management. International Journal of Application or Innovation in Engineering & Management, Volume 6, Issue 6, 130-144.

[28] Yadav, A.S., Swami, A. and Kher, G. (2017) Multi-Objective Genetic Algorithm Involving Green Supply Chain Management International Journal for Science and Advance Research In Technology, Volume 3 Issue 9, 132-138.

[29] Yadav, A.S., Swami, A., Kher, G. (2017) Multi-Objective Particle Swarm Optimization Algorithm Involving Green Supply Chain Inventory Management. International Journal for Science and Advance Research In Technology, Volume 3 Issue, 240-246.

[30] Yadav, A.S., Swami, A. and Pandey, G. (2017) Green Supply Chain Management for Warehouse with Particle Swarm Optimization Algorithm. International Journal for Science and Advance Research in Technology, Volume 3 Issue 10, 769-775.

[31] Yadav, A.S., Swami, A., Kher, G. and Garg, A. (2017) Analysis of seven stages supply chain management in electronic component inventory optimization for warehouse with economic load dispatch using genetic algorithm. Selforganizology, 4 No.2, 18-29.

[32] Yadav, A.S., Maheshwari, P., Swami, A. and Garg, A. (2017) Analysis of Six Stages Supply Chain management in Inventory Optimization for warehouse with Artificial bee colony algorithm using Genetic Algorithm. Selforganizology, Volume 4 No.3, 41-51.

[33] Yadav, A.S., Swami, A., Gupta, C.B. and Garg, A. (2017) Analysis of Electronic component inventory Optimization in Six Stages Supply Chain management for warehouse with ABC using genetic algorithm and PSO. Selforganizology, Volume 4 No.4, 52-64.

[34] Yadav, A.S., Maheshwari, P. and Swami, A. (2016) Analysis of Genetic Algorithm and Particle Swarm Optimization for warehouse with Supply Chain management in Inventory control. International Journal of Computer Applications, Volume 145 "No.5, 10-17.

[35] Yadav, A.S., Swami, A. and Kumar, S. (2018) Inventory of Electronic components model for deteriorating items with warehousing using Genetic Algorithm. International Journal of Pure and Applied Mathematics, Volume 119 No. 16, 169-177.

[36] Yadav, A.S., Johri, M., Singh, J. and Uppal, S. (2018) Analysis of Green Supply Chain Inventory Management for Warehouse With Environmental Collaboration and Sustainability Performance Using Genetic Algorithm. International Journal of Pure and Applied Mathematics, Volume 118 No. 20, 155-161.

[37] Yadav, A.S., Ahlawat, N., Swami, A. and Kher, G. (2019) Auto Industry inventory model for deteriorating items with two warehouse and Transportation Cost using Simulated Annealing Algorithms. International Journal of Advance Research and Innovative Ideas in Education, Volume 5,Issue 1, 24-33.

[38] Yadav, A.S., Ahlawat, N., Swami, A. and Kher, G. (2019) A Particle Swarm Optimization based a two-storage model for deteriorating items with Transportation Cost and Advertising Cost: The Auto Industry. International Journal of Advance Research and Innovative Ideas in Education, Volume 5, Issue 1, 34-44.

[39] Yadav, A.S., Ahlawat, N., and Sharma, S. (2018) A Particle Swarm Optimization for inventory of Auto industry model for two warehouses with deteriorating items. International Journal of Trend in Scientific Research and Development, Volume 2 Issue 5, 66-74.

[40] Yadav, A.S., Swami, A. and Kher, G. (2018) Particle Swarm optimization of inventory model with two-warehouses. Asian Journal of Mathematics and Computer Research, Volume 23 No.1, 17-26.

[41] Yadav, A.S., Maheshwari, P.,, Swami, A. and Kher, G. (2017) Soft Computing Optimization of Two Warehouse Inventory Model With Genetic Algorithm. Asian Journal of Mathematics and Computer Research, Volume 19 No.4, 214-223.

[42] Yadav, A.S., Swami, A., Kumar, S. and Singh, R.K. (2016) Two-Warehouse Inventory Model for Deteriorating Items with Variable Holding Cost, Time-Dependent Demand and Shortages. IOSR Journal of Mathematics, Volume 12, Issue 2 Ver. IV, 47-53.

[43] Yadav, A.S., Sharam, S. and Swami, A. (2016) Two Warehouse Inventory Model with Ramp Type Demand and Partial Backordering for Weibull Distribution Deterioration. International Journal of Computer Applications, Volume 140 -No.4, 15-25.

[44] Yadav, A.S., Swami, A. and Singh, R.K. (2016) A two-storage model for deteriorating items with holding cost under inflation and Genetic Algorithms. International Journal of Advanced Engineering, Management and Science, Volume -2, Issue-4, 251-258.

[45] Yadav, A.S., Swami, A., Kher, G. and Kumar, S. (2017) Supply Chain Inventory Model for Two Warehouses with Soft Computing Optimization. International Journal of Applied Business and Economic Research, Volume 15 No 4, 41-55.

[46] Yadav, A.S., Rajesh Mishra, Kumar, S. and Yadav, S. (2016) Multi Objective Optimization for Electronic Component Inventory Model & Deteriorating Items with Two-warehouse using Genetic Algorithm. International Journal of Control Theory and applications, Volume 9 No.2, 881-892.

[47] Yadav, A.S., Gupta, K., Garg, A. and Swami, A. (2015) A Soft computing Optimization based Two Ware-House Inventory Model for Deteriorating Items with shortages using Genetic Algorithm. International Journal of Computer Applications, Volume 126 - No.13, 7-16.

[48] Yadav, A.S., Gupta, K., Garg, A. and Swami, A. (2015) A Two Warehouse Inventory Model for Deteriorating Items with Shortages under Genetic Algorithm and PSO. International Journal of Emerging Trends & Technology in Computer Science, Volume 4, Issue 5(2), 40-48.

[49] Yadav, A.S. Swami, A., and Kumar, S. (2018) A supply chain Inventory Model for decaying Items with Two Ware-House and Partial ordering under Inflation. International Journal of Pure and Applied Mathematics, Volume 120 No 6, 3053-3088.

[50] Yadav, A.S. Swami, A. and Kumar, S. (2018) An Inventory Model for Deteriorating Items with Two warehouses and variable holding Cost. International Journal of Pure and Applied Mathematics, Volume 120 No 6, 3069-3086.

[51] Yadav, A.S., Taygi, B., Sharma, S. and Swami, A. (2017) Effect of inflation on a two-warehouse inventory model for deteriorating items with time varying demand and shortages. International Journal Procurement Management, Volume 10, No. 6, 761-775.

[52] Yadav, A.S., R. P. Mahapatra, Sharma, S. and Swami, A. (2017) An Inflationary Inventory Model for Deteriorating items under Two Storage Systems. International Journal of Economic Research, Volume 14 No.9, 29-40.

[53] Yadav, A.S., Sharma, S. and Swami, A. (2017) A Fuzzy Based Two-Warehouse Inventory Model For Non instantaneous Deteriorating Items With Conditionally Permissible Delay In Payment. International Journal of Control Theory And Applications, Volume 10 No.11, 107-123.

[54] Yadav, A.S. and Swami, A. (2018) Integrated Supply Chain Model for Deteriorating Items With Linear Stock Dependent Demand Under Imprecise And Inflationary Environment. International Journal Procurement Management, Volume 11 No 6, 684-704.

[55] Yadav, A.S. and Swami, A. (2018) A partial backlogging production-inventory lot-size model with time-varying holding cost and weibull deterioration. International Journal Procurement Management, Volume 11, No. 5, 639-649.

[56] Yadav, A.S. and Swami, A. (2013) A Partial Backlogging Two-Warehouse Inventory Models For Decaying Items With Inflation. International Organization of Scientific Research Journal of Mathematics, Issue 6, 69-78.

[57] Yadav, A.S. and Swami, A. (2019) An inventory model for non-instantaneous deteriorating items with variable holding cost under two-storage. International Journal Procurement Management, Volume 12 No 6, 690-710.

[58] Yadav, A.S. and Swami, A. (2019) A Volume Flexible Two-Warehouse Model with Fluctuating Demand and Holding Cost under Inflation. International Journal Procurement Management, Volume 12 No 4, 441-456.

[59] Yadav, A.S. and Swami, A. (2014) Two-Warehouse Inventory Model for Deteriorating Items with Ramp-Type Demand Rate and Inflation. American Journal of Mathematics and Sciences Volume 3 No-1, 137-144.

[60] Yadav, A.S. and Swami, A. (2013) Effect of Permissible Delay on Two-Warehouse Inventory Model for Deteriorating items with Shortages. International Journal of Application or Innovation in Engineering & Management, Volume 2, Issue 3, 65-71.

[61] Yadav, A.S. and Swami, A. (2013) A Two-Warehouse Inventory Model for Decaying Items with Exponential Demand and Variable Holding Cost. International of Inventive Engineering and Sciences, Volume-1, Issue-5, 18-22.

[62] Yadav, A.S. and Kumar, S. (2017) Electronic Components Supply Chain Management for Warehouse with Environmental Collaboration & Neural Networks. International Journal of Pure and Applied Mathematics, Volume 117 No. 17, 169-177.

[63] Yadav, A.S. (2017) Analysis of Seven Stages Supply Chain Management in Electronic Component Inventory Optimization for Warehouse with Economic Load Dispatch Using GA and PSO. Asian Journal Of Mathematics And Computer Research, volume 16 No.4, 208-219.

[64] Yadav, A.S. (2017) Analysis Of Supply Chain Management In Inventory Optimization For Warehouse With Logistics Using Genetic Algorithm International Journal of Control Theory And Applications, Volume 10 No.10, 1-12 .

[65] Yadav, A.S. (2017) Modeling and Analysis of Supply Chain Inventory Model with two-warehouses and Economic Load Dispatch Problem Using Genetic Algorithm. International Journal of Engineering and Technology, Volume 9 No 1, 33-44.

[66] Swami, A., Singh, S.R., Pareek, S. and Yadav, A.S. (2015) Inventory policies for deteriorating item with stock dependent demand and variable holding costs under permissible delay in payment. International Journal of Application or Innovation in Engineering & Management, Volume 4, Issue 2, 89-99.

[67] Swami, A., Pareek, S., Singh S.R. and Yadav, A.S. (2015) Inventory Model for Decaying Items with Multivariate Demand and Variable Holding cost under the facility of Trade-Credit. International Journal of Computer Application, 18-28.

[68] Swami, A., Pareek, S., Singh, S.R. and Yadav, A.S. (2015) An Inventory Model With Price Sensitive Demand, Variable Holding Cost And Trade-Credit Under Inflation. International Journal of Current Research, Volume 7, Issue, 06, 17312-17321.

[69] Gupta, K., Yadav, A.S., Garg, A. and Swami, A. (2015) A Binary Multi-Objective Genetic Algorithm & PSO involving Supply Chain Inventory Optimization with Shortages, inflation. International Journal of Application or Innovation in Engineering & Management, Volume 4, Issue 8, 37-44.

[70] Gupta, K., Yadav, A.S., Garg, A., (2015) Fuzzy-Genetic Algorithm based inventory model for shortages and inflation under hybrid & PSO. IOSR Journal of Computer Engineering, Volume 17, Issue 5, Ver. I , 61-67.

[71] Singh, R.K., Yadav, A.S. and Swami, A. (2016) A Two-Warehouse Model for Deteriorating Items with Holding Cost under Particle Swarm Optimization. International Journal of Advanced Engineering, Management and Science, Volume -2, Issue-6, 858-864.

[72] Singh, R.K., Yadav, A.S. and Swami, A. (2016) A Two-Warehouse Model for Deteriorating Items with Holding Cost under Inflation and Soft Computing Techniques. International Journal of Advanced Engineering, Management and Science, Volume -2, Issue-6, 869-876.

[73] Kumar, S., Yadav, A.S., Ahlawat, N. and Swami, A. (2019) Supply Chain Management of Alcoholic Beverage Industry Warehouse with Permissible Delay in Payments using Particle Swarm Optimization. International Journal for Research in Applied Science and Engineering Technology, Volume 7 Issue VIII, 504-509.

[74] Kumar, S., Yadav, A.S., Ahlawat, N. and Swami, A. (2019) Green Supply Chain Inventory System of Cement Industry for Warehouse with Inflation using Particle Swarm Optimization. International Journal for Research in Applied Science and Engineering Technology, Volume 7 Issue VIII, 498-503.

[75] Kumar, S., Yadav, A.S., Ahlawat, N. and Swami, A. (2019) Electronic Components Inventory Model for Deterioration Items with Distribution Centre using Genetic Algorithm. International Journal for Research in Applied Science and Engineering Technology, Volume 7 Issue VIII, 433-443.

[76] Chauhan, N. and Yadav, A.S. (2020) An Inventory Model for Deteriorating Items with Two-Warehouse & Stock Dependent Demand using Genetic algorithm. International Journal of Advanced Science and Technology, Vol. 29, No. 5s, 1152-1162.

[77] Chauhan, N. and Yadav, A.S. (2020) Inventory System of Automobile for Stock Dependent Demand & Inflation with Two-Distribution Center Using Genetic Algorithm. Test Engraining & Management, Volume 83, Issue: March - April, 6583 - 6591.

[78] Pandey, T., Yadav, A.S. and Medhavi Malik (2019) An Analysis Marble Industry Inventory Optimization Based on Genetic Algorithms and Particle swarm optimization. International Journal of Recent Technology and Engineering Volume-7, Issue-6S4, 369-373.

[79] Ahlawat, N., Agarwal, S., Pandey, T., Yadav, A.S., Swami, A. (2020) White Wine Industry of Supply Chain Management for Warehouse using Neural Networks Test Engraining & Management, Volume 83, Issue: March - April, 11259 - 11266.

[80] Singh, S. Yadav, A.S. and Swami, A. (2016) An Optimal Ordering Policy For Non-Instantaneous Deteriorating Items With Conditionally Permissible Delay In Payment Under Two Storage Management International Journal of Computer Applications, Volume 147 -No.1, 16-25.

[81] Yadav, A.S., Kumar, A., Yadav, K.K. et al. Optimization of an inventory model for deteriorating items with both selling price and time-sensitive demand and carbon emission under green technology investment. Int J Interact Des Manuf (2023). https://doi.org/10.1007/s12008-023-01689-8

[82] Yadav, K.K., Yadav, A.S. & Bansal, S. Interval number approach for two-warehouse inventory management of deteriorating items with preservation technology investment using analytical optimization methods. Int J Interact Des Manuf (2024). https://doi.org/10.1007/s12008-023-01672-3

[83] Krishan Kumar Yadav , Ajay Singh Yadav, and Shikha Bansal. "Optimization of an inventory model for deteriorating items assuming deterioration during carrying with two-warehouse facility" Reliability: Theory & Applications, vol. 19, no. 3 (79), 2024, pp. 442-459. doi:10.24412/1932-2321-2024-379-442-459

[84] Sinha, Amit Kumar, and Ankush Anand. "Optimizing supply chain network for perishable products using improved bacteria foraging algorithm." Applied Soft Computing 86 (2020): 105921.

[85] Hezer, Seda, and Yakup Kara. "Solving vehicle routing problem with simultaneous delivery and pick-up using an algorithm based on bacterial foraging optimization." (2013).

[86] Negi, Ashish, and Ompal Singh. "An inventory system with time-dependent linear demand for deteriorating items under uncertainty with a completely backlogged." Advances in Mathematical and Computational Sciences: Proceedings of The ICRTMPCS International Conference 2023. Walter de Gruyter GmbH & Co KG, 2024.

RT&A, No 3 (86)
Volume 20, September 2025

STOCHASTIC MODELING AND ANALYSIS OF A PARALLEL SYSTEM WITH DIFFERING UNIT QUALITIES AND CATASTROPHIC FAILURES

Priya Baloda[1], Amit Kumar[2,*], Vikas Garg[3]

•

[1,2,3] Department of Mathematics, Chandigarh University, Gharuan, Mohali, India, 140413
[1]priyabaloda17@gmail.com, [2,*]amitk251@gmail.com, [3]gargvikas0314@gmail.com

Abstract

In this paper, we conduct a stochastic analysis of a system comprising of two dissimilar units operating in parallel. One unit, characterized by two distinct types of failures, is considered high merit, while the other unit, with only one type of malfunction, is deemed low merit. We introduce the concept of catastrophic failure for the system. It is assumed that a single serviceman is responsible for both repair and replacement tasks. A regenerative point-based approach is employed to estimate various reliability characteristics. Additionally, we analyze the proposed model graphically to illustrate the effects of failure, repair, and replacement rates on the system's mean time to system failure (MTSF), availability, and profit.

Keywords: Parallel units, Semi Markov process, Reliability, Catastrophic Failure.

1. Introduction

Reliability is a key factor in various industries and systems, defining the ability of a system or component to consistently carry out its stated functions without experiencing failure over time. It is particularly important in sectors such as aviation, healthcare, telecommunications, and critical infrastructure, where safety, data integrity, and performance are crucial. Reliable systems reduce threats to operational continuity and human safety across multiple domains by ensuring persistent and flawless operations. Beyond functional efficiency, reliability is also vital for user satisfaction and trust. Additionally, to meet safety and quality criteria, specific industry rules and regulations are often followed when implementing reliability in system design. The reliability of data processing and storage units ensures that data remains secure and accurate, which is critical for everyday operations as well as long-term decision-making. Therefore, reliability is essential for designing systems that customers can truly depend on.

In today's industrial and technological world, achieving greater reliability is crucial for the long-term performance and operational efficiency of systems. Additionally, the setup and design of industrial systems are becoming increasingly complex due to society's constantly changing demands. Experts are continually working to create more profitable and productive models that ensure smooth functioning, user satisfaction, and security across multiple areas. Controlling the intensity and frequency of system breakdowns is also essential, particularly in critical applications such as aerospace and power generation, where operational reliability is paramount. Among the various measures suggested for improving system reliability are redundancy techniques, availability of replacement parts, high-quality components, optimal component arrangement, and

appropriate repair options.

Due to minimum costing and functional easiness, various single unit systems are proposed for system models. Several researchers worked on stochastic modeling of systems with single unit. Various reliability models of single-unit systems with different assumptions are being examined by many researchers like [1], [2]. A single unit system with flexible demand is proposed by [3]. Examination of a single unit system following Weibull Failure subjected to server failure is done by [4].

However, single unit system shut down as soon as unit undergoes failure. To overcome this major limitation of single unit models, redundancy is one of the best approaches. The reliance on multiple units offers a promising approach to enhance system robustness and availability. Numerous endeavors have done bunch of work on different redundancies systems. Cold redundant systems have been proposed by many studies. [5] has evaluated the availability and profit of a cold standby system having series parallel configuration. [6] has done a comparative analysis of a single unit system and cold standby system, offering the optimal system configurations as per demand. The impact of maintenance tasks on systems efficiency and performance for a standby system is studied by [7]. A multi component standby system is proposed by [8] and optimal cost and profit optimization strategies had been proposed. A reliability analysis and comparison of four distinct hybrid systems requiring additional supporting devices for operation have been conducted by [9]. Additionally, a significant amount of research (c.f. [10], [11], [12], etc.) describes warm and hot standby systems. A triple-unit system comprising both warm and cold standby units was proposed by [13]. In most of these systems, units have been studied under different types of failures events, with the exception of catastrophic failure. Considering the potential for catastrophic failure helps enhance safety, manage risks, and maintain operational integrity, ultimately leading to more reliable systems. [14] introduced the concept of catastrophic failure for a parallel system consisting of two units with two modes both for operation as well as repair along with timely preventive maintenance of the system. Additionally, some more research work has also been published regarding the concept of catastrophic failure in reliability models (c.f. [15], [16], [17], etc.). These works underline the impact of paying attention to such kinds of sudden failures as these prove to be very crucial for safety and risk management, A complex system further divided between two sub systems; comprising of different number and types of units is deeply investigated by [18].

In the literature on standby systems, studies often focus on either identical units or units with identical failure rates. However, if both units are subjected to similar environmental stresses or operational demands, their failure rates may become interdependent, making the system more susceptible to simultaneous breakdowns. When these failures occur, they can trigger a cascade of adverse effects, overwhelming the system's capacity to manage or mitigate risks. This scenario highlights the critical importance of accurately modeling failure dependencies and incorporating risk assessment strategies to prevent such catastrophic outcomes and ensure system resilience.

This paper seeks to shed light on the intricate dynamics of reliability in parallel configurations comprising dissimilar units with differing failure modes, focusing specifically on catastrophic failure scenarios. Two failure modes for unit 1 and a single failure mode for unit 2 have been considered. To minimize system costs, unit 1 is chosen for its merit quality, while unit 2 is assumed to have sub- merit quality. If the system experiences catastrophic failure, it is replaced and becomes operational only after both units are replaced. A single serviceman is available to perform repairs and replacements of the units. The failure rates of both units and catastrophic failure are assumed to follow a negative exponential distribution, while all other distributions are chosen arbitrarily. Using the Regenerative Point Technique, various reliability measures and their graphical evaluations have been gathered.

2. Assumptions and Notations

In this system, a two-dissimilar-unit parallel system has been analyzed. Unit D_1 is assumed to have two types of failures: partial failure and total failure. Unit D_2 has only one failure mode. It is also assumed that when unit D_1 operates in partial failure mode, its repair is performed simultaneously. However, both units may experience total failure if a catastrophic failure occurs. In such a case, the entire system is replaced by a single repairman assigned to perform all repair and replacement tasks. The failure rates of both units, as well as the catastrophic failure, are modeled using exponential distributions, while all repair and replacement rates are considered to have arbitrary distributions.

All the notations being utilized in this system are listed as:

S_i : Transition state of system model.
$p_{m,n}$: Transition probability from state S_m to S_n.
$p_{m,n,o,p}$: Probability of going from state S_m to S_n via states S_o and S_p.
μ_i : Mean Soujourn Time corresponding to state S_i.
β : Constant catastrophic failure rate.
λ_1 : Constant partial failure rate of D_1.
λ_2 : Total failure rate of D_1.
λ_3 : Failure Rate of D_2
$g_1(t)$: pdf of rate of repair of partially failed D_1.
$g_2(t)$: pdf of rate of repair of total failed D_1.
$g_3(t)$: pdf of repair rate of total failed D_2.
$r(t)$: pdf of replacement rate when system blasts out due to catastrophic failure.
$G_1(t)$: cdf of rate of repair of partially failed D_1.
$G_2(t)$: cdf of rate of repair of total failed D_1.
$G_3(t)$: cdf of repair rate of total failed D_2.
$R(t)$: cdf of replacement rate when system blasts out due to catastrophic failure.
D_{1o}/D_{2o} : D_1 is operative/ D_2 is operative.
$\bar{D}_{1uro}$: D_1 is operative in partial failure mode while repairing is being done simultaneously.
$\bar{D}_{1wro}$: Partially failed D_1 is waiting for repair while being operative.
D_{1ur}/D_{2ur} : Totally failed D_1/ D_2 is under repair.
D_{1wr} : Totally failed Unit D_1 is waiting for repair.
D_{2wr} : D_2 is waiting for repair.
D_{1urp}/D_{2urp} : D_1/D_2 is under replacement.
Ⓢ/© : Symbol used for Stieltjes Convolution / Laplace Convolution.
$*/**$: Symbol used for Laplace Transform (LT)/ Laplace Stieltjes Transform (LST).

Here,

S_0, S_1, S_2, S_3, S_9 are regenerative states while all other are non-regenerative states.

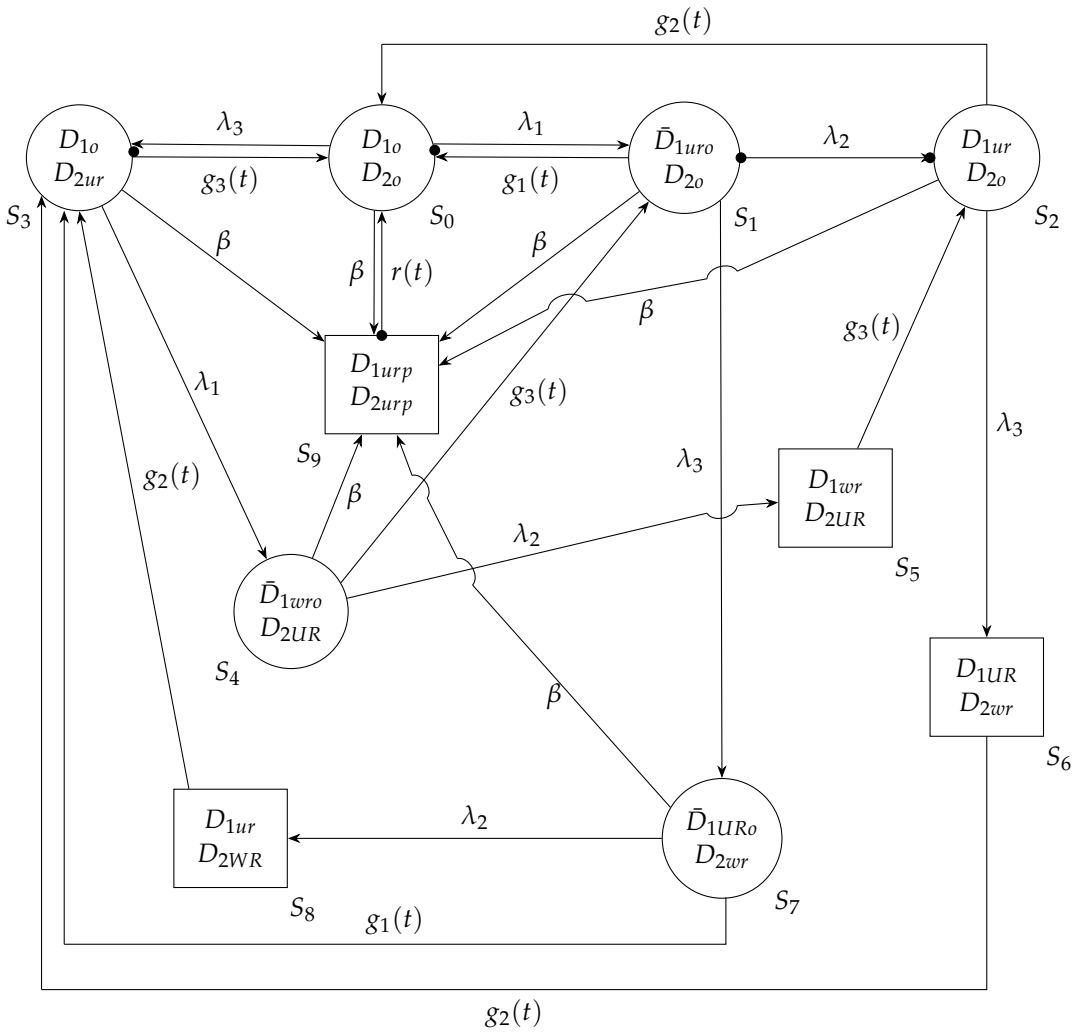


Figure 1: *State Transition Diagram*

• : Regenerative States ○ : Operative State □ : Failed State

3. Reliability Measures

Reliability of any system is measured by various characteristics like Mean Time to System Failure (MTSF), availability of system etc.. The characteristics related to system model are evaluated as:

3.1. Probabilities and Mean Soujourn Time

Assuming that the system progresses from state S_m to S_n within any time interval [0,t), the transition probability $p_{m,n}$ is given by:

$$p_{m,n} = \lim_{t\to\infty} Q_{m,n}(t)dt = Q_{m,n}(\infty) = \int_0^\infty q_{m,n}(t)dt$$

where $q_{m,n}$ represents the probability density function of one step transition from state m to state n and $Q_{m,n}$ represents the cumulative density function of one step transition from state m to state n.

For states $S_i's$, where $i = 0$ to 9, the various transition probabilities are:

$$\begin{aligned}
&p_{0,1} = \frac{\lambda_1}{\lambda_1+\lambda_3+\beta},\ p_{0,3} = \frac{\lambda_3}{\lambda_1+\lambda_3+\beta},\ p_{0,9} = \frac{\beta}{\lambda_1+\lambda_3+\beta},\ p_{1,0} = g_1^*(\lambda_2+\lambda_3+\beta),\\
&p_{1,2} = \frac{\lambda_2}{\lambda_2+\lambda_3+\beta}(1-g_1^*(\lambda_2+\lambda_3+\beta)), p_{1,7} = \frac{\lambda_3}{\lambda_2+\lambda_3+\beta}(1-g_1^*(\lambda_2+\lambda_3+\beta)),\\
&p_{1,9} = \frac{\beta}{\lambda_2+\lambda_3+\beta}(1-g_1^*(\lambda_2+\lambda_3+\beta)),\ p_{2,0} = g_2^*(\lambda_3+\beta),\ p_{2,6} = \frac{\lambda_3}{\lambda_3+\beta}(1-g_2^*(\lambda_3+\beta)),\\
&p_{2,9} = \frac{\beta}{\lambda_3+\beta}(1-g_2^*(\lambda_3+\beta)),\ p_{3,0} = g_3^*(\lambda_1+\beta),\ p_{3,4} = \frac{\lambda_1}{\lambda_1+\beta}(1-g_3^*(\lambda_1+\beta)),\\
&p_{3,9} = \frac{\beta}{\lambda_1+\beta}(1-g_3^*(\lambda_1+\beta)), p_{4,1} = g_3^*(\lambda_2+\beta),\ p_{4,5} = \frac{\lambda_2}{\lambda_2+\beta}(1-g_3^*(\lambda_2+\beta)),\\
&p_{4,9} = \frac{\beta}{\lambda_2+\beta}(1-g_3^*(\lambda_2+\beta)),\ p_{5,2} = g_3^*(0),\ p_{6,3} = g_2^*(0),\\
&p_{7,3} = g_1^*(\lambda_2+\beta),\ p_{7,8} = \frac{\lambda_2}{\lambda_2+\beta}(1-g_1^*(\lambda_2+\beta)),\ p_{7,9} = \frac{\beta}{\lambda_2+\beta}(1-g_1^*(\lambda_2+\beta)),\\
&p_{8,3} = g_2^*(0),\ p_{9,0} = r^*(0),
\end{aligned} \tag{1}$$

Here, $p_{5,2} = p_{6,3} = p_{8,3} = p_{9,0} = 1$.

Mean Soujourn Time (μ_i) which informs about the average time system remains in any particular state i before proceeding into other state j is given by:

$$\mu_i = \int_0^\infty P(T_i > t)dt = \sum_j m_{ij}$$

where m_{ij} gives the contribution to mean soujourn time in S_i when S_i directly transits to S_j.

$$\begin{aligned}
&\mu_0 = \frac{1}{\lambda_1+\lambda_3+\beta},\ \mu_1 = \frac{1-g_1^*(\lambda_2+\lambda_3+\beta)}{\lambda_2+\lambda_3+\beta},\ \mu_2 = \frac{1-g_2^*(\lambda_3+\beta)}{\lambda_3+\beta},\\
&\mu_3 = \frac{1-g_3^*(\lambda_1+\beta)}{\lambda_1+\beta}, \mu_4 = \frac{1-g_3^*(\lambda_2+\beta)}{\lambda_2+\beta}, \mu_5 = -(g_3^*)'(0),\\
&\mu_6 = -(g_2^*)'(0),\ \mu_7 = \frac{1-g_1^*(\lambda_2+\beta)}{\lambda_2+\beta},\ \mu_8 = -(g_2^*)'(0),\ \mu_9 = -(r^*)'(0)
\end{aligned} \tag{2}$$

Also,

μ_i' defining the average time of transition between regenerative states starting from any regenerative state i are given by:

$$\begin{aligned}
&\mu_0' = \mu_0,\ \mu_1' = m_{1,0} + m_{1,2} + m_{1,9} + m_{1,9,7} + m_{1,3,7} + m_{1,3,7,8}\\
&\mu_2' = m_{2,0} + m_{2,9} + m_{2,3,6}.\ \mu_9' = \mu_9\\
&\mu_3' = m_{3,0} + m_{3,9} + m_{3,9,4} + m_{3,1,4} + m_{3,2,4,5}
\end{aligned}$$

Additionally, μ_i'' which tells about the time of moving from regenerative state i to either any other regenerative state or to any failed state is given by:

$$\begin{aligned}
&\mu_1'' = m_{1,0} + m_{1,2} + m_{1,9} + m_{1,9,7} + m_{1,3,7} + m_{1,8,7}\\
&\mu_3'' = m_{3,0} + m_{3,9} + m_{3,9,4} + m_{3,1,4} + m_{3,5,4}
\end{aligned}$$

3.2. Mean Time to System Failure (MTSF)

Consider the transition from any state S_m to any failed state which is further assumed as absorbing state. Let $\varphi_m(t)$ denotes the cdf of above considered transition, so the expression establishing

the MTSF of system is given by:

$$\varphi_m(t) = \sum_n Q_{m,n}(t) \textcircled{S} \varphi_n(t) + \sum_p Q_{m,p}(t) \tag{3}$$

Here, m is any operative state which is transiting to any operative regenerative state n and any failed state p. Reliability($R(t)$) of the system is governed by performing inverse Laplace Transform of following formula:

$$R^*(s) = \frac{1 - \varphi_0^{**}(s)}{s} \tag{4}$$

where $\varphi_0^{**}(s)$ is obtained by taking LST of (3). Also, MTSF is given by:

$$MTSF = \lim_{s\to 0} R^*(s) = \lim_{s\to 0} \frac{1 - \varphi_0^{**}(s)}{s} \tag{5}$$

Solving the above equations, the MTSF of system is obtained as:

$$MTSF = \frac{N^1}{D^1}$$

where

$$\begin{aligned} N^1 &= \mu_0(1 - p_{1,3,7}p_{3,1,4}) + (p_{0,1} + p_{0,3}p_{3,1,4})(\mu_1'' + p_{1,2}\mu_2) + \mu_3''(p_{0,3} + p_{0,1}p_{1,3,7}) \\ D^1 &= 1 - p_{0,1}(p_{1,0} + p_{1,2}p_{2,0} + p_{1,3,7}p_{3,0}) - p_{0,3}(p_{3,0} + p_{3,1,4}(p_{1,0} + p_{1,2}p_{2,0})) - p_{1,3,7}p_{3,1,4} \end{aligned} \tag{6}$$

3.3. Availability Analysis

At $t = 0$, let the system be in regenerative state S_m, and $\hat{A}_m(t)$ shows the probability of system availability at any instant t. If $\tilde{U}_m(t)$ defines the probability of system being in upstate S_m up to time t without going to another regenerative state, then

$$\begin{aligned} &\tilde{U}_0(t) = e^{-(\lambda_1+\lambda_3+\beta)t}, \tilde{U}_1(t) = e^{-(\lambda_2+\lambda_3+\beta)t}\overline{G_1}(t), \\ &\tilde{U}_2(t) = e^{-(\lambda_3+\beta)t}\overline{G_2}(t), \tilde{U}_3(t) = e^{(-\lambda_1+\beta)t}\overline{G_3}(t) \end{aligned} \tag{7}$$

Now, $\hat{A}_m(t)$ is computed by following relations:

$$\hat{A}_m(t) = \tilde{U}_m(t) + \sum_n q_{m,n}^i(t) \textcircled{\copyright} \hat{A}_n(t) \tag{8}$$

where transition from regenerative state m to regenerative state n completes in i number of transitions. Taking LT of (7) to find the value of $\hat{A}_0^*(s)$ and using this results for determining the steady state availability $\hat{A}_0(\infty)$ of the system, we get:

$$\hat{A}_0(\infty) = \lim_{s\to 0} s\hat{A}_0^*(s) = \frac{N^2}{D^2} \tag{9}$$

where

$$\begin{aligned} N^2 &= \mu_0 A + \mu_1 B + \mu_2 C + \mu_3 D \\ D^2 &= \mu_0' A + \mu_1' B + \mu_2' C + \mu_3' D + \mu_9' E \end{aligned} \tag{10}$$

3.4. Server's Busy Period

Let $B_m^R(t)$ and $B_m^{RP}(t)$ denotes the probability that at any instant t, server is busy in repair and replacement respectively, with a restriction that system entered regenerative state S_m at $t = 0$. Let

transition takes place between regenerative states m to n, within i transitions, then the relations for $B_m^R(t)$ and $B_m^{RP}(t)$ are :

$$\begin{aligned} B_m^R(t) &= W_m(t) + \sum_{m,n} q_n^i(t) \copyright B_n^R(t) \\ B_m^{RP}(t) &= W_m(t) + \sum_{m,n} q_n^i(t) \copyright B_n^{RP}(t) \end{aligned} \tag{11}$$

Here, $W_m(t)$ is the probability that repairman is busy at state S_m without further going to either any different regenerative state or to same state via one or more non regenerative states.

As LT of (11) will provide us values of $B_0^{R^*}(s)$ and $B_0^{RP^*}(s)$, so the probability of busy time in repair and replacement of server is given by:

$$B_0^R(\infty) = \lim_{s\to 0} sB_0^{R^*}(s) = \frac{N^3}{D^2} \tag{12}$$

$$B_0^{RP}(\infty) = \lim_{s\to 0} sB_0^{RP^*}(s) = \frac{N^4}{D^2} \tag{13}$$

In eqs. (12) and (13), N^3 and N^4 are given by:

$$\begin{aligned} N^3 &= W_1^*(0)B + W_2^*(0)C + W_3^*(0)D \\ N^4 &= W_9^*(0)E \end{aligned} \tag{14}$$

D^2 is defined in (10).

3.5. Expected Number of Visits

Let $R_m(t)$ and $RP_m(t)$ calculates the server's expected number of visits for performing repair and replacement in the state S_m in time interval $(0, t]$. The following recursive relations are used for estimating $R_m(t)$ and $RP_m(t)$:

$$\begin{aligned} R_m(t) &= \sum_{m,n} Q_n^i(t) \circledS(\acute{C} + R_n(t)) \\ RP_m(t) &= \sum_{m,n} Q_n^i(t) \circledS(\acute{C} + RP_n(t)) \end{aligned} \tag{15}$$

Here, the regenerative state m gets leaded to consecutive regenerative state n through i steps. If the repairman does task afresh , then $\acute{C} = 1$, otherwise $\acute{C} = 0$. LST of (15) will gives us value of $R_0^{**}(t)$ and $RP_0^{**}(t)$. With the help of these, the expected number of times for which server visits for performing repair and replacement is given by:

$$\begin{aligned} R_0(\infty) &= \lim_{s\to 0} sR_0^{**}(s) = \frac{N^5}{D^2} \\ RP_0(\infty) &= \lim_{s\to 0} sRP_0^{**}(s) = \frac{N^6}{D^2} \end{aligned} \tag{16}$$

where, N^5 and N^6 are given by:

$$\begin{aligned} N^5 &= B + C + D \\ N^6 &= E \end{aligned} \tag{17}$$

D^2 is defined in (10).

Here,

$$
\begin{aligned}
A &= 1 - p_{3,1,4}(p_{1,3,7} + p_{1,3,7,8}) - p_{2,3,6}(p_{3,1,4}p_{1,2} + p_{3,2,4,5}) \\
B &= p_{0,1}(1 - p_{3,2,4,5}p_{2,3,6}) + p_{0,3}p_{3,1,4} \\
C &= p_{0,1}(p_{1,2} + p_{3,2,4,5}(p_{1,3,7} + p_{1,3,7,8})) + p_{0,3}(p_{3,2,4,5} + p_{1,2}p_{3,1,4}) \\
D &= p_{0,3} + p_{0,1}(p_{1,3,7} + p_{1,3,7,8} + p_{1,2}p_{2,3,6}) \\
E &= p_{0,1}((p_{1,9} + p_{1,9,7})(1 - p_{2,3,6}p_{3,2,4,5}) + (p_{1,3,7} + p_{1,3,7,8})(p_{3,9} + p_{3,9,4} + p_{2,9}p_{3,2,4,5}) + \\
&\quad p_{1,2}(p_{2,9} + p_{2,3,6}(p_{3,9} + p_{3,9,4}))) + p_{0,3}(p_{3,9} + p_{3,9,4} + p_{3,1,4}(p_{1,9} + p_{1,9,7} + p_{1,2}p_{2,9}) + \\
&\quad p_{3,2,4,5}p_{2,9}) + p_{0,9}(1 - p_{3,1,4}(p_{1,3,7} + p_{1,3,7,8} + p_{1,2}p_{2,3,6}) - p_{3,2,4,5}p_{2,3,6})
\end{aligned} \tag{18}
$$

3.6. Profit Evaluation

In the steady state, the profit of the system can be exerted from following relation:

$$P = C_1\hat{A}_0 - C_2B_0^R - C_3B_0^{RP} - C_4R_0 - C_5RP_0 \tag{19}$$

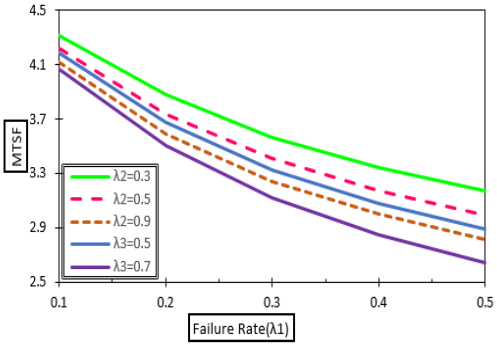
where,
P = Profit of system.
C_1 = Revenue generated by system per unit up time.
C_2 = Server's cost per unit time for performing repair.
C_3 = Server's cost per unit time for performing replacement.
C_4 = Cost per visit for repair charged by server.
C_5 = Cost per visit for replacement charged by server.

4. Graphical Surveying

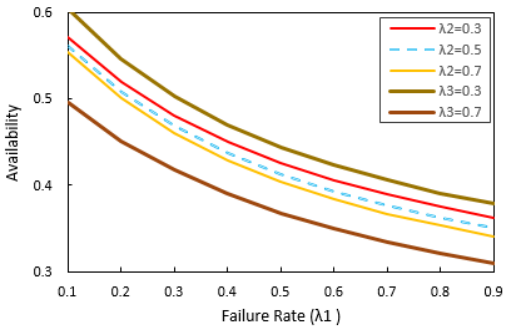
To examine the effect of various parameters involved in system model on reliability variables, graphical analysis has been done by considering a particular case of repair and replacement rates. Assume $g_1(t) = \alpha_1 e^{-\alpha_1 t}, g_2(t) = \alpha_2 e^{-\alpha_2 t}, g_3(t) = \alpha_3 e^{-\alpha_3 t}, r(t) = \gamma e^{-\gamma t}$. For finding the profitability, one particular set of costs has been assumed:
$C_1 = 6000, C_2 = 1000, C_3 = 1500, C_4 = 200, C_5 = 400$

4.1. Impact of Failure Rates

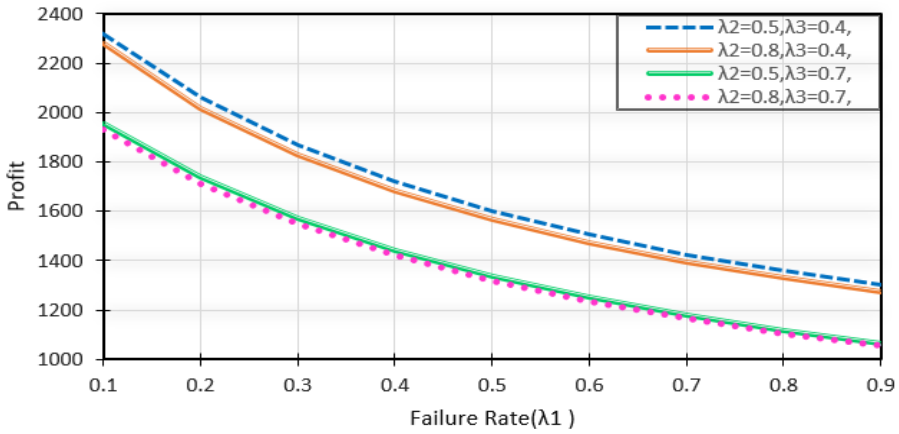
Different failure rate affect the system to different extent. From figure 2, it is obvious that MTSF, availability and profit of the system decreases with increase in value of λ_1 keeping all the other parameters constant. However, the influence is larger in case of MTSF as compared to that of availability and profit. Graph has been created to study the effect of λ_2 and λ_3 on MTSF and availability, keeping the other parameters constant. However, λ_2 does not affect the reliability measures to nice extent. It is evident from 2a that as we increase the value of λ_2, there is minor decrease in the values of availability as well as MTSF. While Change in the value of λ_3 has a dynamic effect on reliability characteristics. Graphical results which are obtained by variation in λ_3 while other parameters as assigned constant values as $\lambda_2 = 0.4, \beta = 0.5, \gamma = 0.6, \alpha_1 = 0.6, \alpha_2 = 0.4, \alpha_3 = 0.5$. This impact can be visualized from 2a. Figure 2b and 2c manifests that there is slight change in the availability and profit of system respectively with increase in λ_2 while increase in λ_3 decreases the profit to an appreciable extent.



(a) *Variation in MTSF with λ_2 and λ_3*



(b) *Variation in Availability with λ_2 and λ_3*



(c) *Effect of λ_2 and λ_3 on Profit*

Figure 2: *Impact of Failure Rates*

4.2. Impact of Catastrophic Failure Rate

Figure 3 supports the fact that catastrophic failure rate(β) has negative influence on profit of system. Also as the replacement rate(γ) goes upwards, profit also follows the same trend if all other parameters are assumed to be constant.

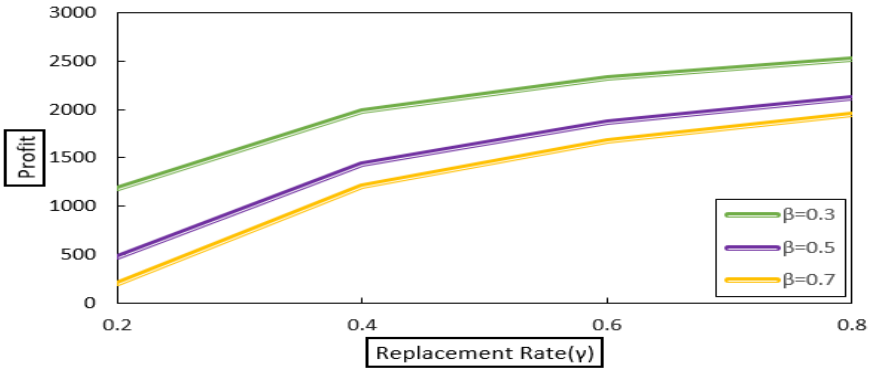
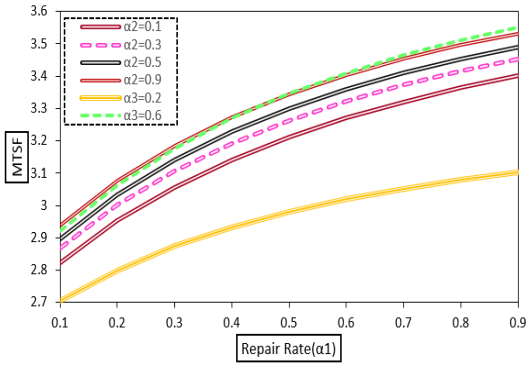


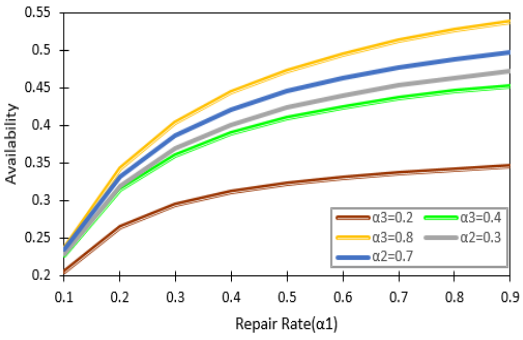
Figure 3: *Profit vs Replacement rate (γ)*

4.3. Impact of Repair Rates

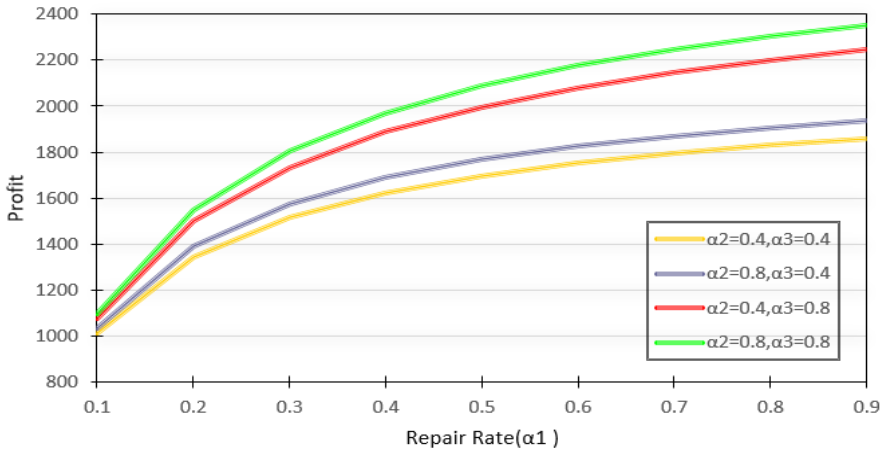
Numerical experimentation has been done to check the consequences of change in various repair rates of both units on system. From figure 4, the following observations can be made: With the increase in repair rate α_1, all the three factors MTSF, availability and profit of system shifts upwards. However, the increase is different in different measures. Figures 4a and 4b defines the change in MTSF and availability with respect to α_2 and α_3. It is visible that MTSF does not change much with increase in value of α_2 while availability has considerable increment. Figures 4a and 4b also establish that there is great increase in MTSF and availability with increasing values of α_3. Also, the increase is much more in availability as compared to that of MTSF. From figure 4c, it can be in view that there is increase in profitability of system in case of increment of both α_2 as well as α_3, but greater in later case.



(a) *MTSF vs α_2 and α_3*



(b) *Availability vs α_2 and α_3*



(c) *Effect of α_2 and α_3 on Profit*

Figure 4: *Impact of Repair Rates*

5. Conclusion

This study is presented to gauge the behavior of various repair and failure rates on the reliability metrics of a system consisting of two different parallel units. Numerical results signify that increasing the failure rates reduces these metrics to a remarkable extent. Additionally, an increase in the repair rate of all units will enhance profit. Graphical representations suggest that the failure rate should be controlled to maximize system profit, especially the failure rate of the unit with only one mode of malfunction, as it most significantly influences the reliability characteristics. However, a continuous increase in the replacement rate will not significantly boost profit, as it

will also raise the system's costs, adversely affecting profitability. Therefore, replacement should also be managed carefully.

References

[1] Chander, S., and Bansal, R. K. (2005). Profit analysis of single-unit reliability models with repair at different failure modes. Proc. INCRESE IIT Kharagpur, India, 577-587.
[2] Malik, S. C., and Pawar, D. (2010). Reliability and economic measures of a system with inspection for on-line repair and no repair activity in abnormal weather. Bulletin of Pure and Applied Sciences, 29(2), 355-368.
[3] Malhotra, R., and Taneja, G. (2013). Reliability and availability analysis of a single unit system with varying demand. Mathematical Journal of Interdisciplinary Sciences, 2(1), 77-88.
[4] Kumar, A., and Saini, M. (2016). Analysis of a single-unit system with weibull failure and repair densities subject to server failure. Malaysian Journal of Science, 35(1), 15-22.
[5] Danjuma, M. U., Yusuf, B., and Yusuf, I. (2022). Reliability, availability, maintainability, and dependability analysis of cold standby series-parallel system. Journal of computational and cognitive engineering, 1(4), 193-200.
[6] Malhotra, R., and Taneja, G. (2015). Comparative study between a single unit system and a two-unit cold standby system with varying demand. Springerplus, 4, 1-17.
[7] Sultan, K. S., and Moshref, M. E. (2021). Stochastic analysis of a priority standby system under preventive maintenance. Applied Sciences, 11(9), 3861.
[8] Ahmad, S., Sharma, G., and Sharma, U. (2018). Modelling and profit evaluation of a repairable system working with one operative unit and three cold standby units. International Journal of Mathematics Trends and Technology-IJMTT, 64.
[9] Yusuf, I., and Umar, S. M. (2019). Reliability Modelling and Assessment of Multi Standby Hybrid System. Reliability: Theory & Applications, 14(3), 39-45.
[10] Hu, L., Huang, W., Wang, G., and Tian, R. (2018). Redundancy Optimization of an Uncertain ParallelSeries System with Warm Standby Elements. Complexity, 2018(1), 3154360.
[11] Kolledath, S., Kumar, K., and Pippal, S. (2018). Survey on queueing models with standbys support. Yugoslav Journal of Operations Research, 28(1), 3-20.
[12] El-Ghamry, E., Muse, A. H., Aldallal, R., and Mohamed, M. S. (2022). Availability and Reliability Analysis of akOutofn Warm Standby System with CommonCause Failure and Fuzzy Failure and Repair Rates. Mathematical Problems in Engineering, 2022(1), 3170665.
[13] Ghosh, J., Pawar, D., and Malik, S. C. (2022). Analysis of triple-unit system with operational priority. Reliability: Theory & Applications, 17(3 (69)), 202-210.
[14] Goel, L. R., and Gupta, P. (1984). Stochastic analysis of a two-unit parallel system with partial and catastrophic failures and preventive maintenance. Microelectronics Reliability, 24(5), 881-883.
[15] Ram, M., and Manglik, M. (2016). Reliability measures analysis of an industrial system under standby modes and catastrophic failure. International journal of operations research and information systems (IJORIS), 7(3), 36-56.
[16] Tyagi, V., Arora, R., Ram, M., and Yadav, O. P. (2019). 2-Out-of-3: F System analysis under catastrophic failure. Nonlinear Studies, 26(3).
[17] Li, H., Yuan, R., and Fu, J. (2019). A reliability modeling for multi-component systems considering random shocks and multi-state degradation. IEEE Access, 7, 168805-168814.
[18] Sirohi, A., Poonia, P. K., and Raghav, D. (2021). Reliability analysis of a complex repairable system in series configuration with switch and catastrophic failure using copula repair. J. Math. Comput. Sci., 11(2), 2403-2425.

ANALYSIS OF METHODS FOR ELIMINATION OF THE BRUSH-CONTACT ASSEMBLY OF THE ASG OF WIND TURBINES

N.S. Mammadov[1], I.M. Marufov[2], K.M. Mukhtarova[3]

•

Azerbaijan State Oil and Industry University, Baku, Azerbaijan
nicat.memmedov.sa@asoiu.edu.az, marufov.ilkin@asoiu.edu.az,
kubra.muxtarova.m@asoiu.edu.az

Abstract

Traditional generator designs that use brush-and-contact assemblies to transmit electric current between rotating and stationary parts of the device are subject to significant drawbacks. The main problems associated with the use of brush-and-contact assemblies include mechanical wear of brushes and slip rings, sparking, electrical losses and high operating costs, which leads to reduced reliability and increased maintenance costs. Elimination of brush-and-contact assemblies is an urgent task, since it allows to significantly increase the reliability of devices and simplify their operation, especially in difficult climate conditions and high wind turbine installations. The article analyzes two modern approaches to solving this problem: installation of a brushless exciter and use of a rotating transformer. Each of these methods has its own advantages and disadvantages. The general electrical circuit of a brushless exciter device based on an asynchronized synchronous generator is presented. The general electrical circuit of an asynchronized synchronous generator with a rotating transformer is also presented. An innovative solution is also considered, which involves installing a battery on the rotating part of the generator, which acts as a contactless power source for the rotor winding and provides energy storage.

Keywords: wind electric installation, asynchronized synchronous generator, brush-contact assembly, rotating transformer, battery, reliability.

I. Introduction

Wind turbines, which serve as a crucial source of renewable energy, consist of numerous integral components, among which the generator is perhaps the most significant. Generators in traditional designs often incorporate brush-contact assemblies, which facilitate the transfer of electric current between the stationary and rotating sections of the machinery. While these assemblies serve their intended purpose, they also bring about several operational challenges that can undermine the overall performance and reliability of the system.

A primary issue associated with brush-contact assemblies is the wear and tear caused by constant mechanical friction between brushes and slip rings. Over time, this friction results in the rapid degradation of components, necessitating frequent inspections, replacements, and repairs. This not only increases operational costs but also causes equipment downtime, disrupting power generation. Moreover, the friction within these assemblies often leads to sparking, which poses a significant risk of equipment damage, overheating, and in extreme cases, fire hazards.

Another major drawback of brush-contact assemblies is their contribution to energy losses. The resistance and friction inherent in these systems reduce the overall electrical efficiency of the

generator, resulting in lower energy output. These issues are particularly pronounced in wind turbines, which are often installed at high altitudes or in remote, harsh environments. The logistical difficulties and costs of maintaining brush-contact assemblies in such settings further amplify their disadvantages.

Given these challenges, the elimination of brush-contact assemblies has become a key focus in the development of more efficient, reliable, and cost-effective wind turbine systems. Engineers and researchers have proposed two primary solutions to address this issue: the implementation of brushless exciter devices and the adoption of rotating transformers. Each approach offers unique advantages and operates on distinct principles [1-3].

Implementation of a Brushless Exciter Device. Brushless exciter devices have emerged as a highly effective alternative to traditional brush-contact assemblies. These devices function as auxiliary generators that are mounted on the same shaft as the primary electrical machine. In synchronous systems, the brushless exciter acts as an inverted synchronous generator equipped with a diode rectifier in the rotor circuit. This design enables the delivery of direct current to the rotor windings, which is essential for the stable operation of synchronous motors and turbogenerators.

The consistent speed of operation in synchronous systems makes brushless exciters an ideal choice, as they reliably fulfill the requirement for a steady direct current supply. However, incorporating these devices into asynchronized synchronous generators (ASG) introduces additional complexities. In such cases, the brushless exciter forms part of a valve-machine electromechanical cascade, allowing the system to operate effectively without the need for a brush-contact assembly.

Replacing brush-contact assemblies with brushless exciter devices in ASG requires meeting several critical design and operational criteria. First, the generator's rotor winding must be three-phase to accommodate the electrical demands of the system. Additionally, the generator must maintain effective performance across a wide range of rotational speeds. The exciter device itself must also be capable of delivering both alternating current (AC) of varying frequencies, amplitudes, and phases, as well as direct current (DC). To address these challenges, two conceptual designs have been developed for next-generation brushless exciters. Multi-phase exciters are designed to dynamically adapt to fluctuations in speed and load, ensuring reliable performance under diverse operating conditions. Meanwhile, advanced control systems employ intelligent technologies to regulate the power supply, allowing for precise adjustments to current parameters. These innovations significantly enhance the reliability, efficiency, and sustainability of wind turbines.

Brushless exciter devices offer several notable advantages. By eliminating brushes and slip rings, they drastically reduce the need for maintenance, extending the lifespan of components and minimizing operational disruptions. The absence of sparking improves safety by reducing the risk of equipment damage, overheating, and fire. Additionally, the lower energy losses associated with these systems translate to enhanced efficiency, enabling turbines to generate more electricity from the same wind resources. Overall, the adoption of brushless technologies leads to substantial cost savings over the lifetime of the equipment, making them a highly attractive solution for modern wind turbines [4-7].

Implementation of a Rotating Transformer. Another promising approach to eliminating brush-contact assemblies is the use of rotating transformers. These devices operate on the principle of electromagnetic induction, allowing the transfer of electrical energy between stationary and rotating parts without the need for physical contact. A rotating transformer consists of a primary winding, which is stationary, and a secondary winding, which rotates. The electrical energy is transferred through a magnetic field, eliminating mechanical friction and wear.

Rotating transformers are particularly advantageous in applications where maintenance is

challenging or costly. By removing the need for brushes and slip rings, they eliminate the issues of wear and sparking, contributing to a safer and more reliable system. Additionally, they provide efficient energy transfer with minimal losses, further enhancing the overall performance of the generator. The integration of rotating transformers in wind turbines is especially beneficial in extreme environments, such as offshore wind farms or high-altitude installations, where maintenance access is limited. These devices offer a durable and low-maintenance alternative that aligns with the growing demand for efficient and sustainable renewable energy solutions.

II. Formulation of the problem

Design of a Rotating Transformer. Structurally, the proposed rotating transformer consists of two metal disks, each of which contains a single-phase winding. One disk is fixedly fixed, and the other is installed on the shaft of an asynchronized synchronous generator. Since the rotor winding of this generator is three-phase, each phase uses its own rotating transformer. When voltage is applied to the winding, which is fixed on a stationary disk, thanks to galvanic isolation, a voltage of the same frequency is induced on the winding, fixed on a rotating disk, as on the stationary winding.

This constructive method looks very attractive. A transformer, unlike a brushless exciter, does not create a braking torque that takes away the mechanical power supplied to the shaft. However, problems arise that are associated with the presence of magnetic gravitational forces between the movable and stationary disks. In addition, this method has one significant drawback. At synchronous rotor speed, its circuit must be supplied with direct current. Its transmission through a rotating transformer is impossible. For this mode, it is necessary to complicate the design and place the rectifier on the rotating part, which practically reduces all the advantages of this method to zero.

Design of a Brushless Exciter Device Based on an Inverted Synchronous Generator. This design is closely aligned with the conventional configuration of a brushless exciter device (BED) used in synchronous motors and turbogenerators. However, it introduces a significant innovation: instead of utilizing a diode bridge, a protective circuit, and a filter, the rotor winding circuit incorporates a frequency converter (FC). This frequency converter plays a pivotal role by adapting to the rotor's speed and delivering direct or alternating current to the ASG rotor winding. The supplied current is precisely controlled in terms of frequency, amplitude, and phase, ensuring optimal performance under varying operational conditions [8-11].

An electrical schematic of this system, termed a brushless exciter based on an inverted synchronous generator, is illustrated in Figure 1.

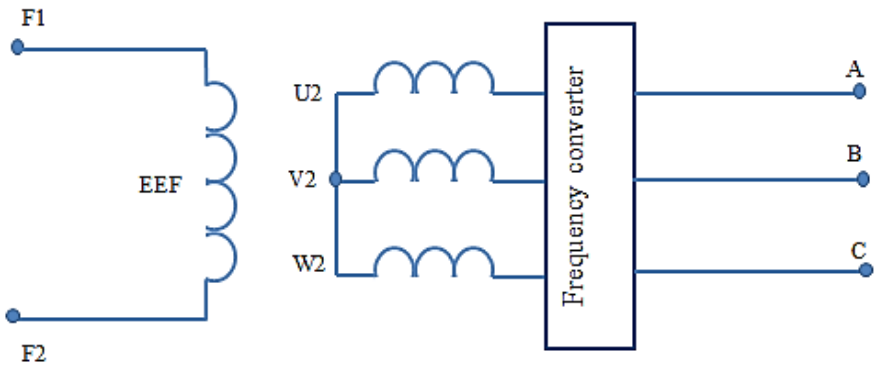


Figure 1: *Electrical circuit of a brushless exciter device based on an inverted synchronous generator*

One of the critical aspects of this design is its capability to cater to the wide range of rotor speeds typically encountered in wind power applications. To achieve this, the brushless exciter device must incorporate a power control mechanism that is independent of rotor speed. This requirement makes electromagnetic excitation a more viable solution compared to permanent magnet excitation, as the latter does not allow for control of the magnetic flux. However, an advanced combination of electromagnetic and magnetoelectric excitation is also feasible. This can be realized by employing a combined excitation generator as the brushless exciter device, providing greater flexibility and efficiency in controlling the magnetic flux.

Design of a Brushless Exciter Device Based on an Asynchronized Synchronous Generator. An alternative design approach involves modifying the brushless exciter device to leverage an asynchronized synchronous generator (ASG) configuration. If the stator of a brushless exciter based on an inverted synchronous generator is replaced with a stator containing a distributed three-phase winding, the result is structurally an ASG (illustrated in Figure 2).

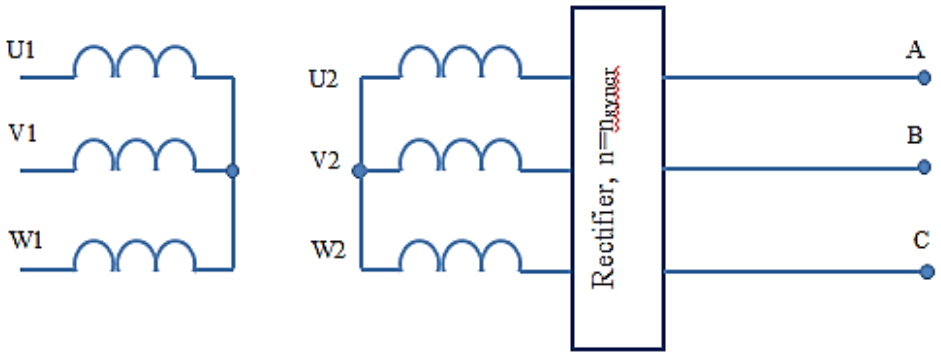


Figure 2: *Electrical circuit of a brushless exciter device based on an asynchronized synchronous generator*

In this arrangement, the final system integrates two ASGs, with their rotors mounted on a single shaft. This innovative configuration eliminates the need for a frequency converter in the rotor circuit of the asynchronized synchronous generator. Instead, an electronic rectifier is employed. When the rotor operates at synchronous speed, the rectifier converts the alternating current from the brushless exciter into direct current. For non-synchronous speeds, the necessary voltage parameters to power the ASG rotor winding are achieved by carefully controlling the frequency, phase, and amplitude of the power supply to the stator winding of the brushless exciter. This approach effectively bypasses the requirement for an inverter in the ASG rotor winding circuit.

When implementing any type of brushless exciter device, it is essential to account for the mechanical energy dynamics within the system. A portion of the mechanical energy delivered to the generator rotor is inevitably consumed in overcoming the braking torque generated by the exciter device itself. This braking torque represents a trade-off, as it slightly reduces the overall efficiency of the turbine. Careful design and optimization of the brushless exciter device can help minimize these losses, ensuring that the benefits of a brushless system-such as reduced maintenance, enhanced reliability, and improved operational efficiency-outweigh the energy costs [12-15].

The methods discussed allow for the complete elimination of the brush-contact assembly in generators. However, it is important to note that this is achieved by replacing a relatively simple contact mechanism with a more complex and bulky system. These advanced systems are typically more expensive and require periodic maintenance and repairs. An alternative approach involves

utilizing a rechargeable battery as a contactless power source for the rotor circuit, mounted directly on the rotating component. In this configuration, an electronic inverter would also need to be installed on the rotor. The inverter's role would be to convert the direct current (DC) output of the battery into the alternating current (AC) required by the rotor winding. At synchronous rotational speeds, the rotor winding could be powered directly from the battery in its DC form. The electrical diagram of this innovative system is shown in Figure 3.

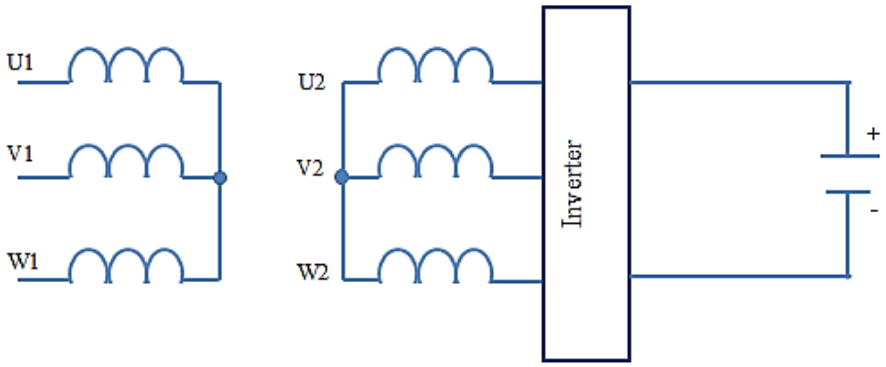


Figure 3: *Electrical circuit of an asynchronized synchronous generator with a battery*

This innovative method resolves many challenges. On one hand, it simplifies the control system by removing the need for AC-to-DC conversion. On the other hand, the battery itself can function as an energy storage device. This design ensures that even in the absence of wind or during complete rotor stoppage, the battery can supply energy to the grid. In such a scenario, the system operates as a DC-AC converter. This capability enables the generator to function effectively in both autonomous and grid-connected modes, a feature particularly advantageous for wind farms operating under unstable energy supply conditions.

Despite these advantages, certain limitations must be addressed. The battery's energy capacity is finite, and once fully discharged, the entire energy system ceases to operate. To mitigate this issue, the design includes provisions for recharging the battery. This operational mode ensures the system's continuous functionality after the battery has been depleted. This approach appears highly promising as it eliminates the need for brush-contact assemblies in asynchronized synchronous generators. Additionally, it supports the integration of electrical energy storage within wind turbines, a critical feature for alternative energy sources functioning in variable energy supply environments.

However, certain technical challenges require further investigation. For instance, the effect of centrifugal forces on the battery electrolyte represents an atypical operational condition and necessitates specialized research. Furthermore, sufficient space must be allocated to accommodate the battery on the rotor. As a result, this technical solution is best suited initially for low-speed wind turbines with a vertical axis of rotation. These turbines are characterized by their larger dimensions and lower linear rotation speeds, making them more compatible with the proposed concept.

Once the feasibility of this design has been confirmed through successful implementation in low-speed turbines, its application can be extended to turbines operating at higher rotational speeds. Advances in modern battery technologies, particularly those aimed at increasing energy density, open the door to applying this concept to small and medium-sized power generators. In the future, these advancements could enable the deployment of this approach in high-power generators as well. For now, in high-speed wind turbines-whether with a horizontal or vertical axis of rotation-traditional options such as brushless exciter devices or rotating transformers remain the more practical choice [16-19].

III. Problem solution

To demonstrate the uniqueness and potential advantages of the described innovations, hypothetical experimental results and practical examples for each proposed technology provided.

1. Brushless Exciter Device (BED)

Experimental results: In a series of tests conducted on prototypes of medium-power wind turbines (e.g. 2-3 MW), generators with traditional brush-contact units and with BEDs were compared. The tests were carried out under conditions of variable wind speeds to assess reliability and efficiency (Fig. 4.) The results showed:

- Reduction of mechanical losses by 15-20% due to the elimination of brush friction.
- Reduction of sparking losses and increase in efficiency by 5-7%, especially at high speeds.
- Increase in generator service life: the time between preventive maintenance increased to 2.5-3 years, while for traditional generators this value was 1.5 years.

Case Study: A wind farm using 20 turbines with BEDs recorded a 30% reduction in maintenance costs and a decrease in downtime. In addition, the reduction in electrical losses resulted in savings on energy costs and an increase in output power.

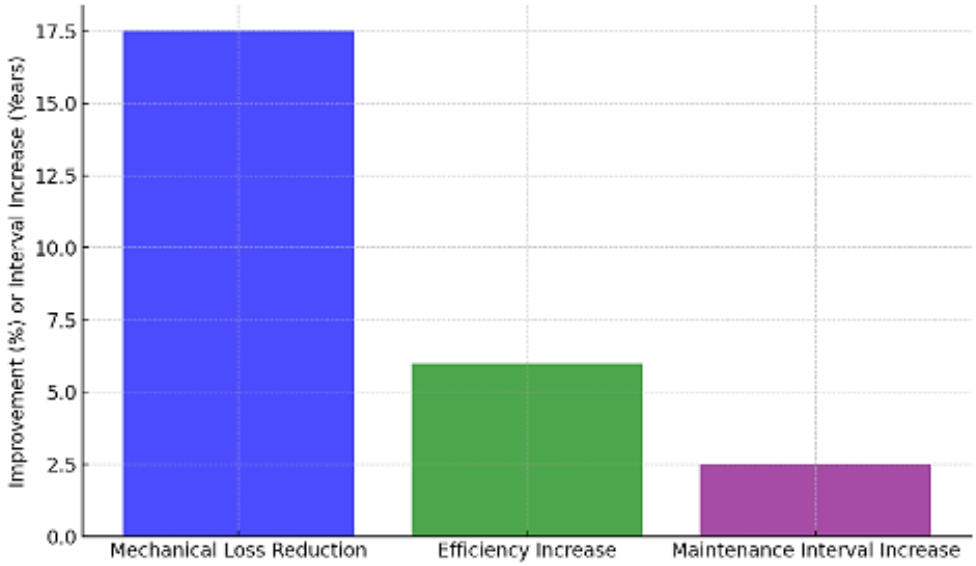


Figure 4: *Experimental Results: Brushless Exciter Device*

2. Rotating Transformer.

Experimental Results: Tests on a 1.5 MW wind turbine model showed that installing a rotating transformer instead of a brush assembly resulted in the following:

- No braking torque from the transformer, which resulted in an efficiency gain of 2-3%.
- Increased system reliability: no component wear was observed, since energy was transmitted without mechanical contact.
- Reduced maintenance: Since the transformer is not subject to wear in the same way as brush-and-contact assemblies, the frequency of scheduled maintenance was reduced by 40%.

Case Study: A wind turbine with a rotating transformer demonstrated stable operation for 3 years without a single maintenance stop. This allowed for a significant reduction in costs and an increase in power generation.

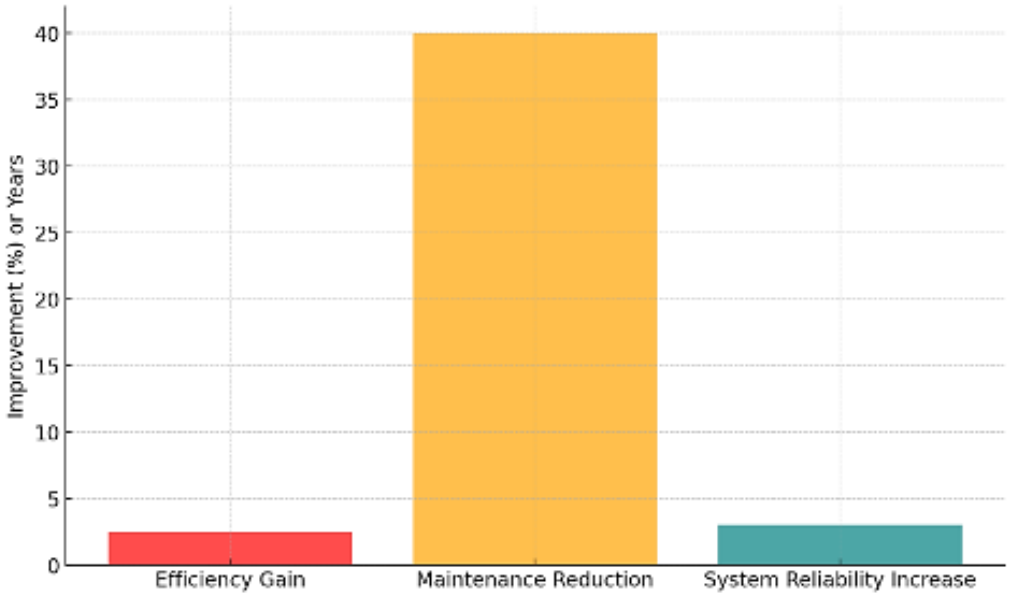


Figure 5: *Experimental Results: Rotating Transformer*

3. Battery power supply for the rotor.

Experimental results: In a pilot project, a battery power supply was installed on a 500 kW vertical axis turbine. The test results showed:

- Stable operation at variable speeds: the battery provided a constant current supply to the rotor, regardless of the speed, reducing the need for complex converter electronics.

- Additional energy reserve: the battery allowed for continued power generation even in low wind conditions.

Case study: A vertical axis turbine with a battery powered rotor, installed in a remote area, demonstrated high autonomy, allowing for a 20% increase in the total amount of energy transmitted to the grid [20-25].

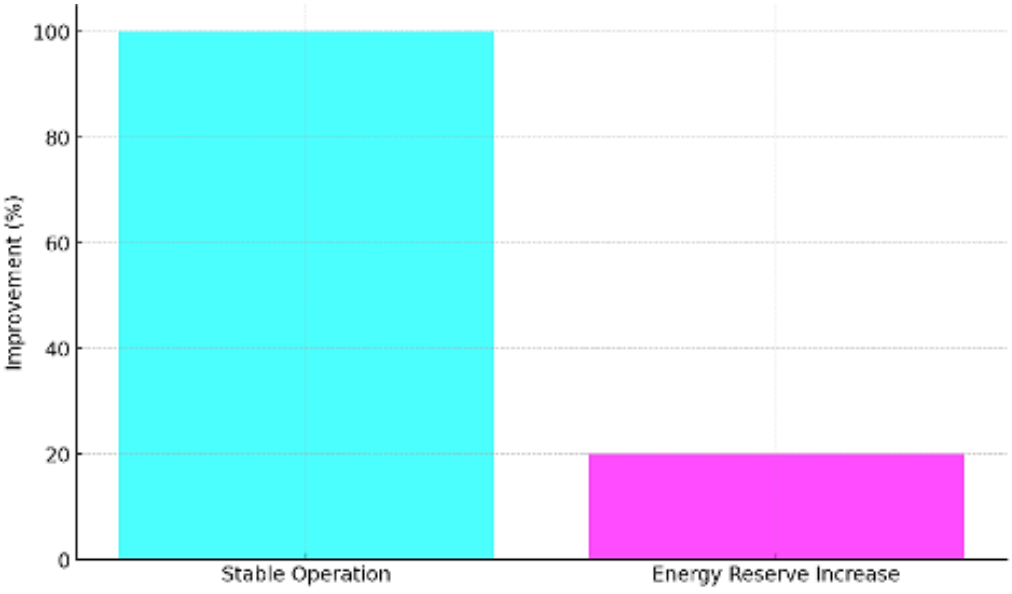


Figure 6: *Experimental Results: Battery power supply*

IV. Conclusions

The presented innovative solutions for replacing contact assemblies in wind turbines, such as brushless exciters (BEDs), rotating transformers and battery power systems, offer significant advantages in increasing the efficiency, reliability and durability of wind turbines. These technologies are a response to numerous problems encountered when using traditional brush assemblies, which lead to mechanical wear, sparking, increased energy losses and high maintenance levels. It is important to note that the novelty of these solutions lies not only in the elimination of wearing components, but also in the possibility of integrating advanced technologies into existing wind turbine systems, which opens up new prospects for more sustainable and economical energy production.

Specific conclusions based on the results:

1. Efficiency: All three innovative technologies (BEDs, rotating transformer, battery power) demonstrated significant improvements in wind turbine efficiency - an increase in overall efficiency by 5-7% when using brushless exciters and by 2-3% with a rotating transformer. This confirms that these solutions can significantly increase power output and reduce operating losses.

2. Reduced maintenance costs: All technologies provide a reduction in the frequency of maintenance, which allows for significant savings on generator maintenance costs. In particular, the use of brushless exciters and rotary transformers resulted in a 30-40% reduction in maintenance costs, which is a significant improvement over traditional brush systems.

3. Increased service life and reliability: Experimental data has shown an increase in the service life of generators with brushless exciters up to 2.5-3 years between maintenance, which is 60% higher than traditional systems. The rotary transformer also demonstrated a long service life without the need for repairs, which underlines the high level of reliability of these technologies.

4. Autonomy and energy reserves: The battery power system of the rotor provided a 20% increase in energy production under low wind speed conditions and increased autonomy, which confirms the effectiveness of such solutions for operation in remote areas or under unstable wind conditions.

The experimental results show that the implementation of brushless exciters, rotating transformers and rotor battery power systems in wind turbines has high potential in terms of improving efficiency, reliability and reducing operating costs. These technologies not only eliminate problems associated with mechanical wear and sparking, but also open up new opportunities for increasing the autonomy and improving the economic feasibility of wind turbine operation. In the future, with the development of battery technologies and control systems, these solutions can be expanded for use in higher-speed wind turbines and larger wind farms. Improvements in materials and increased energy capacity of batteries will allow the use of such systems in higher-speed and more powerful installations, which will increase their efficiency and availability for a wide range of applications in the renewable energy industry.

References

[1] N.S. Mammadov, N.A. Ganiyeva, G.A. Aliyeva, “Role of Renewable Energy Sources in the World”. Journal of Renewable Energy, Electrical, and Computer Engineering, Vol. 2, №2, pp. 63-67, Indonesia, 30 September 2022

[2] I.M. Marufov, N.S. Mammadov, K.M. Mukhtarova, N.A. Ganiyeva, G.A. Aliyeva, “Calculation of Main Parameters of Induction Levitation Device Used in Vertical Axis Wind Generators”, IJTPE, Issue 54, Vol. 15, No. 1, pp. 184-189, March 2023

[3] W. Cao, Y. Xie, Z. Tan, “Wind Turbine Generator Technologies”, INTECH Open Science/Open Minds, p. 44, China, 2012

[4] Nijat Mammadov, Sona Rzayeva, Nigar Ganiyeva, “Analisys of synchronized asynchronous generator for a wind electric installation”, Przegląd Elektrotechniczny, №5, 2023, pp.37-40

[5] L.N. Kanov, "Mathematical Modeling of a Wind Power Plant with an Asynchronous Generator", Power Engineering and Electromechanics, Vol. 2, No. 5, pp. 71-74, Ukraine, 2012
[6] N.S. Mammadov, G.A. Aliyeva, "Energy Efficiency Improving of a Wind Electric Installation Using a Thyristor Switching System for The Stator Winding of a Two-Speed Asynchronous Generator", International Journal on Technical and Physical Problems of Engineering (IJTPE), Issue 55, Vol. 15, No. 2, pp. 285-290, 2023
[7] Ilkin Marufov, Najiba Piriyeva, Nijat Mammadov, Shukufa Ismayilova, "Calculation of induction levitation vertical axis wind generator-turbine system parameters, levitation and influence loop" Przegląd Elektrotechniczny, 2024 , No.2, pp.135-139
[8] I.N. Rahimli, S.V. Rzayeva, E.E. Umudov, "Direction Of Alternative Energy", Vestnik Nauki, Issue 2, Vol. 61, No. 4, Russia, April 2023
[9] Ilkin Marufov, Aynura Allahverdiyeva, Nijat Mammadov, "Study of application characteristics of cylindrical structure induction levitator in general and vertical axis wind turbines", Przegląd Elektrotechniczny, R. 99 NR 10/2023, pp.196-199
[10] N.S. Mammadov, I.M. Marufov, K.M. Mukhtarova, "Methods for eliminating of brush-contact assembly in various types of generators in wind turbines", The 20th International Conference on "Technical and Physical Problems of Engineering", No 31, pp.193-197, 31 October 2024
[11] Nijat Mammadov, "Methods for Improving The Energy Efficiency of Wind Turbines at Low Wind Speeds", Vestnik Nauki Journal, Issue 2, Vol. 61, No. 4, Russia, April 2023
[12] T. Haidi, B. Cheddadi, "State of Wind Energy in The World: Evolution, Impacts and Perspectives", International Journal on Technical and Physical Problem on Engineering (IJTPE), Issue 51, Vol. 14, No. 2, pp. 347-352, June 2022
[13] N.M. Pirieva, Z.F. Huseynov, "Characteristics of Synchronous Motors", International Scientific Journal Bulletin of Science, No. 3, Issue 60, Vol. 4, pp. 241-246, Russia, 2022
[14] Nijat Mammadov, Ilkin Marufov, Saadat Shikhaliyeva, Gulnara Aliyeva, Saida Kerimova, "Research of methods power control of wind turbines", Przeglad Elektrotechniczny, R. 100 NR 5/2024, pp. 236-239
[15] Nijat Mammadov, "Analysis of Systems and Methods of Emergency Braking of Wind Turbines", International Science Journal of Engineering and Agriculture, Vol. 2, No. 2, pp. 147-152, Ukraine, April 2023
[16] Nadir Aliyev, Elbrus Ahmedov, Samira Khanahmedova, Sona Rzayeva, "Synthesis of the Exact Parameters of the Electromagnetic Brake of a Wind Electric Installation", Przeglad Elektrotechniczny journal, № 10, Poland, 2023
[17] Pacheco-Chérrez, J.; Fortoul-Díaz, J.A.; Cortés-Santacruz, F.; María Aloso-Valerdi, L.; Ibarra-Zarate, D.I. Bearing fault detection with vibration and acoustic signals: Comparison among different machine leaning classification methods. Eng. Fail. Anal. 2022, 139
[18] Elshad Safiyev, Ilham Rahimli, Nijat Mammadov, "Method of qualitative impregnation of electric motor windings." Przegląd Elektrotechniczny, R. 100 NR 8/2024, pp.238 -240
[19] Nijat Mammadov, "Vibration Research in Wind Turbines", The 15th International Conference of the Main Directions of Development of Scientific Research, pp. 345-346, Helsinki, Finland, 2023
[20] Mammadov N. S., Mukhtarova K. M., "METHODOLOGY FOR ASSESSING THE RELIABILITY OF AGS BASED ON RENEWABLE ENERGY SOURCES", Reliability: Theory & Applications, Volume 19, No 4 (80), pp.648-653, 2024
[21] Nijat Mammadov, Najiba Piriyeva, Shukufa Ismayilova, "Research of lightning protection systems for wind electric installations", Przeglad Elektrotechniczny journal, No 9, 2024
[22] Nijat Mammadov, "PROSPECTS FOR THE DEVELOPMENT OF RENEWABLE ENERGY SOURCES", The 29th International scientific and practical conference "Modern scientific trends and youth development"(July 25–28, 2023) Warsaw, Poland, International Science Group, pp. 211-213, 2023
[23] Mammadov N. S., "SAFETY IN THE OPERATION OF WIND TURBINES: ENSURING RELIABILITY AND PROTECTION", Vestnik nauki, Issue 1, №.7, Vol. 76, pp. 883-888, 2024
[24] A.I. Abdulkadyrov, S.C. Osmanov, N.A. Aliyev, G.A. Aliyeva, "Features of Calculating The Parameters of Special Electric Machines", News of Azerbaijan Higher Technical Schools, No. 5, Issue 87, pp. 55-61, Baku, Azerbaijan, 2013
[25] V.V. Shevchenko, Y.R. Kulish, "Analysis of The Possibility of Using Different Types of Generators for Wind Power Plants, Taking Into Account The Power Range", Bulletin of NTU (KHPI), No. 65, pp. 107-117, Russia, 2013

CONSTRUCTION OF COMPLETE STOCHASTIC LIFE CYCLES OF HIGHLY CRITICAL INFRASTRUCTURES

Sviatoslav Timashev [1,2], Anna Bushinskaya [1,2]

•

1 Science and Engineering Center "Reliability and Safety of Large Systems and Machines", Ural Branch, Russian Academy of Sciences, Studencheskaya 54-A, Yekaterinburg 620002, Russia
2 Ural Federal University, Mira 19, Yekaterinburg 620002, Russia
timashevs@gmail.com, bushinskaya@gmail.com

Abstract

The article describes a risk-based approach to constructing the full life cycle (LC) of HCI with accounting for climate change. In this case, the objective function (OF) of HCI risk management as a function of time is reduced to the generalized cost of operating a strategically important object in the time interval "from (birth) cradle / to grave".
The life cycle, built on the basis of these data, makes it possible to evaluate and predict: (1) the inherent design reliability of the HCI, (2) the probabilities of all types of failures of the HCI; (3) the monetary consequences of these failures; (4) risks associated with random times of diagnostics, repairs and restoration of HCI and with the moments of its failures; (5) the overall risk of HCI at each moment of its existence with accounting for climate change.

Keywords: life cycle, risk, critical infrastructure, offshore pipelines

I. Introduction

The modern concept of creating critical and strategic infrastructures is that their design should: 1) cover the entire life cycle (LC); and 2) be based on modern concepts of managing complex systems according to safety and risk criteria in conditions of dynamic multifactorial uncertainty [1].

In traditional infrastructure design, life cycle analysis (LCA) is used primarily to obtain design parameters and define maintenance strategies for the facility. In the design of critical infrastructures, LCA is naturally needed to provide a qualified assessment of the environmental and/or economic impact of the product or service produced by these infrastructures throughout their entire service life.

The list of components of the life cycle of large infrastructure projects usually looks like this: 1) extraction of raw materials necessary for the creation of the infrastructure; 2) processing of materials, manufacturing and construction (construction) of the facility; 3) use and operation of the system; and 4) disposal or restoration of the infrastructure after its useful life.

Modern life cycle analysis of infrastructures imperatively requires an expansion of the number of central/key design components. Knowledge of the system structure and its physical and mechanical behavior, determined by the strength and reliability, resilience and safety of its elements (fundamental characteristics of the system) is fundamentally insufficient. No less important components of LCA are: 1) financial factors (the cost of future investments in diagnostics, monitoring, maintenance, repair and renovation of infrastructure), discount rates); 2)

responsibility between generations; 3) environmental aspects and sustainability of development.

The emerging global consensus regarding the value of the life cycle concept in the design and operation of infrastructures is based on the fact that: 1) leading enterprises of all types have recognized de facto that LCA is the key to continuous improvement of production efficiency; 2) continuous and long-term environmental protection has become a key criterion in consumer markets and in government procurement guidelines; 3) government regulations around the world are moving towards LCA accountability [2].

LCA has thus become a valuable decision support tool for all categories of decision makers (technocrats, legislators, lawyers and politicians) in assessing the impact of a product or process on the service life of an infrastructure. It also plays an important role in defining environmental policies and strategies that contribute to the sustainable development of an enterprise or region.

Currently, LCA is widely used to assess the impact of large projects on the environment (global climate change/carbon footprint, depletion of the ozone layer and natural resources, acidification, eutrophication (excessive saturation of water bodies with harmful biogenic elements), human health, ecotoxicity, etc.).

Additional requirements for the design of complex infrastructures are: 1) creation of digital quasi-twins of the designed infrastructures; 2) modeling of a quasi-complete group of scenarios for their operation and accidents under normal and extreme conditions using an interdisciplinary approach.

II. Formulation of life cycle cost

In general, the objective function, taking into account the benefits and costs of the life cycle associated with an object (system), is determined by the expression [3]:

$$U(z) = B(z) - C(z), \tag{1}$$

where $B(z)$ is the benefit from operating the asset; $C(z)$ is the life cycle cost; z is a vector of parameters that describes the decision variables, which include aspects such as design criteria (e.g. geometry, material properties, external requirements, etc.), estimated service life, diagnostic and maintenance strategies, etc., depending on the problem under consideration.

Typical life cycle costs include the initial costs associated with planning, designing and constructing the facility; diagnostic and maintenance costs; operating costs to keep the facility functioning; and finally, the probable costs associated with failure, as well as the dismantling costs that arise at the end of the structure's useful life.

Since benefits and costs are uncertain, decisions are made based on expected utility in accordance with decision theory [3]. The objective function in terms of expected utility is expressed as

$$\mathrm{E}[U(z)] = \mathrm{E}[B(z)] - \mathrm{E}[C(z)]. \tag{2}$$

The life cycle cost of an object, taking into account the above, should take into account all costs incurred during its service life. Thus, the life cycle cost can be written as follows:

$$E\left[C(z)\right] = -E\left[C_0(z)\right] - E\left[C_I(z)\right] - E\left[C_R(z)\right] - E\left[C_F(z)\right] - E\left[C_{OP}(z)\right] - E\left[C_D(z)\right], \tag{3}$$

where $C(z)$ is the total life cycle cost; $C_0(z)$ is the costs associated with planning, design and construction of the facility ; $C_I(z)$ is the total cost of all inspections (diagnostics) throughout the life cycle; $C_R(z)$ is the total cost of all repairs/restorations during maintenance throughout the life cycle; $C_F(z)$ is the total costs associated with the asset failure; $C_{OP}(z)$ is the total operating costs (insurance coverage, payment of interest on the loan, tax on the carbon footprint of the system operation, etc.); $C_D(z)$ is the cost of dismantling, describes the cost of decommissioning (if any) at the end of the life cycle T_s.

The total costs of failure can be divided into direct and indirect [4]. The direct cost of failure takes into account the costs directly associated with the failure of the system:

- costs incurred during repairs (restoration) as a result of failure;
- economic costs associated with the loss of system functionality (the cost of product lost due to leakage, the cost of non-produced products (production), fines associated with non-delivery to the consumer, etc.);
- cost of environmental damage;
- the cost of consequences for life safety (impacts on humans) – the cost of restoring health and compensation for the possible loss of human lives.

The indirect cost of failure includes costs associated with damage to the company's reputation, loss of public trust, etc.

The costs of diagnostics and maintenance, as well as the costs in case of system failure, significantly increase the life cycle cost. Therefore, reasonable planning is required to reduce the overall cost while maintaining the safety and operability of the system. Therefore, the optimal diagnostics and maintenance plan is selected in such a way as to minimize the overall life cycle costs in the decision-making process.

The integrity of the system during its service life can be ensured in different ways. On the one hand, it is possible to create, due to the increased material intensity of high-quality material, a very reliable, robust, but also expensive system that will require minimal maintenance. On the other hand, it is possible to create a much cheaper system with minimal reserves of strength and robustness, but compensate for this disadvantage with adequate maintenance (diagnostics, monitoring, repair and restoration), and a subsystem for its protection, which will require significant costs for the care of the system throughout the entire life cycle.

Let us consider the construction of a complete stochastic life cycle using the example of strategically important critical infrastructures – offshore underwater pipelines (OUP).

To quantitatively assess the risk of operating an OUP as a function of time, it is necessary to:

- Design the duration of its life cycle (LC);
- Determine its initial (normative) reliability;
- Have robust quantitative models of its degradation;
- Select formalized strategies, technologies and methods of:
  - instrumental diagnostics [3], [4];
  - monitoring; and
  - maintenance (technical service, repair and restoration of mechanical engineering equipment);
- Determine the method of assessing and discounting all costs and damages distributed randomly over the life cycle interval of the object.

The presence of these strategies allows constructing a quasi-complete group of scenarios for the operation of the OUP using the Monte Carlo method, simulating the real conditions of its loading, degradation and maintenance in working condition, and, as a result, to obtain consistent estimates of the probability of failure (for each type of impact on the pipeline) before and after each intervention. It follows from the above that the results of modeling will directly depend on the accuracy of the used models of degradation of the material and design of the OUP, the loads on them, and, which is imperatively important, the accuracy characteristics of the diagnostic technologies used.

For a new OUP being put into operation, it is necessary to simulate the initiation of a certain representative set of defects characteristic of similar pipelines that are already in operation. Since the frequency of in-line diagnostics of domestic pipelines is regulated, it is necessary to predict the sizes of all initiated defects by the time of the first inspection, taking into account the latent period when the defects are still invisible. The creation of such a set of defects on a digital twin of the OUP is possible only by the Monte Carlo method. In this case, it is necessary to take into account the

loads and impacts that a real pipeline actually experiences in the considered section of the oceanic or sea shelf of Russia.

Given the data described above, the general algorithm for constructing the risk function of a designed or commissioned OUP over a period of time equal to the length of its life cycle consists of several stages described below.

To simulate the operation of a new OUP, models of degradation of protective layers, material and design of the pipe itself are used, adequately describing the growth of all types of defects. Here in after non-trivial questions arise: *How many defects, of what type, number and size should be simulated for the entire pipeline and each of its sections? And where should they be located topographically?*

Since for calculation purposes the division of the OUP into sections is performed according to the criterion of homogeneity of the base, loads/impacts, and pipe material, for practical purposes it is necessary to model the degradation of each pipeline section separately. It is also necessary to model all types of defects that are observed in other operating OUPs similar to the one under consideration. The number of modeled defects in each section should be comparable with the actually observed number of defects in similar sections of the OUP, operated under similar conditions. This will allow obtaining the same power and consistency of statistics related to the parameters of the modeled defects.

It is advisable to model each representative ensemble of similar defects as a Poisson field of points, each of which is a three-dimensional defect (depth d, length l, width b). The size of the set of defects should allow obtaining consistent statistics of the distribution of their sizes. The modeled topography of the field of actual defects can be adjusted, if necessary, taking into account local corrosion features (for example, when the lower part of the pipe shell is more susceptible to corrosion than the upper one).

III. Modeling the results of in-pipe diagnostics

Non-destructive methods used for OUP diagnostics are subject to various errors, since they are based on an indirect form of measurement. This can lead to seven different types of measurement errors, on the basis of which the quality (accuracy) metrics of each instrument are determined [5, 6]:

a) Detection errors: The diagnostic tool does not detect any defects or detects non-existent defects.
b) Sizing errors: The diagnostic tool incorrectly identifies the sizes of defects.
c) Identification errors: the diagnostic tool incorrectly identifies detected defects according to the classification adopted in the in-line inspection (ITI) industry;
d) Location errors: The diagnostic tool incorrectly determines the coordinates (distance and angular position) of detected defects.

The detected defects are only a part of the total set of actual defects. In essence, the diagnostic tool acts as a filter that divides the set of real defects into two groups: detected and undetected. In-line inspection data can be used to characterize the pipeline condition by the probability distributions of the depth and length of defects. However, it is believed that short and shallow defects are most likely to be not detected during diagnostics. As a rule, two factors influence the determination of the accuracy of inspection: the probability of detection/false non-detection of defects and the errors their measurements.

I. Probability of detection (POD)

This parameter models the imperfect detection capability of the pigging tools. POD is typically an increasing function of defect depth and is defined as an exponential function:

$$\mathrm{POD}(d) = P_{\mathrm{D}}(d) = 1 - \mathrm{e}^{-qd}, \tag{4}$$

where $P_{\mathrm{D}}(d)$ is the probability of detecting a defect of depth d, q is the constant describing the resolution of the inspection instrument. The expression for POD can be interpreted as an exponential probability distribution of the detected depths, where $(1/q)$ is the average depth of the detected defects.

Using Bayes' theorem, the probability density function (PDF) $f_{\mathrm{D}}(d)$ of the depths of *detected* defects can be determined from the PDF $f_F(d)$ depths of *actual* defects:

$$f_{\mathrm{D}}(d) = \frac{P_{\mathrm{D}}(d)\, f_F(d)}{\int_0^{\infty} P_{\mathrm{D}}(d)\, f_F(d)\,\mathrm{d}d}. \tag{5}$$

Probability p_{d} detection of a randomly selected defect using a control tool is determined by the expression

$$p_{\mathrm{d}} = \int_0^{\infty} P_{\mathrm{D}}(d)\, f_F(d)\,\mathrm{d}d. \tag{6}$$

Similarly, the PDF $f_{\mathrm{ND}}(d)$ of the depths of *undetected* defects can be obtained as

$$f_{\mathrm{ND}}(d) = \frac{\left[1 - P_{\mathrm{D}}(d)\right] f_F(d)}{(1 - p_{\mathrm{d}})}. \tag{7}$$

Using equations (5) and (7), the PDF $f_{\mathrm{ND}}(d)$ of the depths of *undetected* defects can be expressed through the distribution of *detected* depths:

$$f_{\mathrm{ND}}(d) = C\frac{\left[1 - P_{\mathrm{D}}(d)\right]}{P_{\mathrm{D}}(d)} f_{\mathrm{D}}(d), \tag{8}$$

where $C = \dfrac{1}{\left\{\int_0^{\infty} \dfrac{f_{\mathrm{D}}(d)}{P_{\mathrm{D}}(d)}\mathrm{d}d\right\} - 1}$ is a normalization constant.

II. Accuracy of defect size measurement

Uncertainty in defect size measurement is modeled by adding a random measurement error to the actual size. Unlike detection error, it is assumed that the error in determining the size of a defect is independent of its actual size. If the instrument measurements do not contain systematic errors (the instrument is well calibrated), then the size errors ε are assumed to have a normal distribution with a mean μ_{ε} equal to zero and a standard deviation σ_{ε} depending on the measuring instrument quality. Thus, after a defect is detected, its size is superimposed by a measurement error due to signal noise.

$$d_m = d_d + \varepsilon_d \quad \text{and} \quad l_m = l_d + \varepsilon_l, \tag{9}$$

where d_{m} and l_{m} are the measured depth and length respectively; ε_{d} and ε_{l} denote random errors associated with depth d_d and length l_d measurement of the detected defect , which can be estimated from the inspection supplier's specifications. For example, suppliers of inspection tools often specify that the error ε will be within certain limits (e.g., $\pm 10\%$ measurements) with a given probability (e.g., with probability 90%). The measurement error can also be obtained from the results of verification excavations of similar operating pipelines.

The PDF of measured defect depths is obtained by convoluting the probability distribution of detected defects with the probability distribution of measurement errors:

$$f_M(d) = \int_0^\infty f_D(x)\, f_\varepsilon(d-x)\, dx. \tag{10}$$

The distribution of measurement errors is described by a normal distribution with zero mean and a given standard deviation σ_ε:

$$f_\varepsilon(x) = \frac{1}{\sigma_\varepsilon\sqrt{2\pi}} e^{-\frac{x^2}{2\sigma_\varepsilon}}. \tag{11}$$

Based on equations (9), the mathematical expectation μ_m and standard deviation σ_m of the measured defects are:

$$\mu_m = \mu_d,\ \sigma_m = \sqrt{\sigma_d^2 + \sigma_\varepsilon^2}, \tag{12}$$

where μ_d and σ_d are the mathematical expectation and standard deviation of the detected defects sizes.

III. Modeling defects development and the emergence of new defects

The process of occurrence of new defects in a specific section of the OUP is described by a non-uniform Poisson process (NPP) [7, 8], according to which a number of defects $N(t)$ during the time interval [0, t] (t = 0 denotes the time of putting the pipeline into operation) with a PDF defined as [9]:

$$f_N\left(N(t), m(t)\right) = \frac{m(t)^{N(t)} e^{-m(t)}}{N(t)!},\ t \ge 0, \tag{13}$$

where m (t) is the average number of defects in the time interval [0, t], which, according to [7], obeys a power function of time $m(t) = \lambda\delta\int_0^t x^{\delta-1}dx = \lambda t^\delta$ with parameters λ and δ (λ , δ > 0), which can be quantitatively determined using diagnostic data for similar OUP sections, operated under similar conditions. It should be noted that $N(t)$ degenerates into a homogeneous Poisson process (HPP) at δ = 1.

Suppose that n inspections have been carried out for the pipeline section under consideration over a certain period of time. At the time of the i -th inspection (i = 1, 2, ..., n), t_i, the total number of defects in the pipeline section, N_i, can be divided into those defects that occurred before the (i -1)-th inspection, and those defects that occurred between the (i -1)-th and i -th inspections, N_i^g. The random variable N_i^g also follows a Poisson distribution with PDF:

$$f_N\left(N_i^g \middle| \lambda, \delta\right) = \frac{m_i^{N_g^i} e^{-m_i}}{N_i^g!}, \tag{14}$$

where $m_i = \lambda\delta\int_{t_{i-1}}^{t_i} x^{\delta-1}dx = \lambda\left(t_i^\delta - t_{i-1}^\delta\right),\ t_0 = 0$.

For UT instruments the caser is different. Due to high sensitivity of UT tools, often $N_i^g = N_i^{gd} - N_i^{gu}$ (a lot of false positives occur).

As noted above, the detected number of defects is generally less than the actual number of defects. Let N_i^{gd} and N_i^{gu} denote the detected and undetected number of defects, respectively, i.e. $N_i^g = N_i^{gd} + N_i^{gu}$. Based on the Poisson distribution property, the random variables (RV) N_i^{gd} and N_i^{gu} follow the Poisson distribution with the corresponding PDFs :

$$f_P\left(N_i^{gd}\ |\lambda,\delta\right)=\frac{\left(\overline{\mathrm{POD}_i}m_i\right)^{N_i^{gd}}}{N_i^{gd}!}\exp\left(-\overline{\mathrm{POD}_i}m_i\right), \tag{15}$$

$$f_P\left(N_i^{gu}\ |\lambda,\delta\right)=\frac{\left[\left(1-\overline{\mathrm{POD}_i}\right)m_i\right]^{N_i^{gu}}}{N_i^{gu}!}\exp\left[-\left(1-\overline{\mathrm{POD}_i}\right)m_i\right], \tag{16}$$

where $\overline{\mathrm{POD}_i}$ is the average POD relative to N_i^g defects. $\overline{\mathrm{POD}_i}$ can be calculated as $\overline{\mathrm{POD}_i}=\int \mathrm{POD}(x)\,f_{N_i^g}(x)dx$, where $f_{N_i^g}(x)$ is the PDF of defect depths N_i^g at time t_i.

To model the growth of corrosion defect depths, the non-uniform gamma process (NHGP) [10] is used, according to which the defect depth at time $t, D(t)$ follows a gamma distribution with PDF:

$$f_G\left(d(t)\ |\alpha(t),\beta\right)=\frac{\beta^{\alpha(t)}d(t)^{\alpha(t)-1}\exp\left[-d(t)\beta\right]}{\Gamma\left(\alpha(t)\right)}I_{(0,\infty)}\left(d(t)\right), \tag{17}$$

where $\alpha(t)$ is the time-dependent shape parameter and is assumed to be a power function of time, i.e. $\alpha(t)=\varphi_1(t-t_s)^{\varphi_2}\ (t>t_s)$, where t_s is the time of defect occurrence; $\beta(\beta>0)$ is the time-independent rate parameter (or inverse scale parameter) [11]; $\Gamma(\cdot)$ denotes the gamma function, and $I_{(0,\infty)}\left(x(t)\right)$ is the indicator function, which is equal to one if $d(t)>0$ and zero otherwise. The mean, variance, and coefficient of variation (COV) $d(t)$ are $\alpha(t)/\beta$, $\alpha(t)/\beta^2$ and $1/(\alpha(t))^{0.5}$, respectively. The quantity φ_1/β represents the average depth at the first unit time increment from t_s; φ_2 reflects the type of average defect growth path and at $\varphi_2>1, \varphi_2<1$, $\varphi_2=1$ represents the accelerating, decelerating, and linear average depth growth, respectively. In addition, $\varphi_2=1$ corresponds to a homogeneous gamma process.

The parameters φ_1 and φ_2 are assumed to be common to all defects, while t_s and β are specific to each defect to account for spatial variability in growth. Let t_{sr} and β_r denote the time of occurrence and the corrosion rate parameter for *r*-th defect $(r=1,2,\ldots)$, respectively. It should be emphasized here that the index r is used to list all defects, including detected and undetected defects, to distinguish it from the index j, which is used to list detected defects. In what follows, the parameter is assumed β_r to be an exponential function of the random effect parameter ξ_r, that is $\beta_r=e^{\xi_r}$. The advantage of expressing β_r as an exponential function is that it guarantees β_r's positivity.

From the above assumptions it follows that the increment in the depth of the defect *r* during the time interval between the (*i*–1)th and *i*-th inspections, denoted as Δd_{ir}, is a gamma distribution with the shape parameter $\Delta\alpha_{ir}$ and corrosion rate β_r, where $\Delta\alpha_{ir}$ is given by the expression

$$\Delta\alpha_{ir}=\begin{cases}\varphi_1\left(t_i-t_{sr}\right)^{\varphi_2}, & i=1\\ \varphi_1\left(t_i-t_{sr}\right)^{\varphi_2}-\varphi_1\left(t_{i-1}-t_{sr}\right)^{\varphi_2}, & i=2,3,\ldots,n\end{cases} \tag{18}$$

The depth of the defect *r* at *the i* -th inspection, d_{ir}, is the sum of the depth at the (i – 1)-th inspection and Δd_{ir}; that is, $d_{ir}=d_{i-1,r}+\Delta d_{ir}$. It should be noted that d_{ir} when $t=t_{sr}$ is assumed to be zero.

Below is a procedure is described for modeling the depth of corrosion defects and the corresponding diagnostic results, assuming that all newly detected defects occur between the (*i* – 1)th and *i*-th inspections.

1. Calculate the number of newly occurring defects N_i^g during the *i*-th inspection

$(i=1,2,\ldots,n)$ using the Poisson distribution given by equation (14).

2. Determine the initial time $t_{sr}\left(r=1,2,\ldots,N_i^g\right)$ for N_i^g newly occurring defects.

3. Select the parameters of the random effect $\xi_r\left(r=1,2,\ldots,N_i^g\right)$ for N_i^g defects from a normal distribution with mean equal to zero and variance $\sigma_\xi{}^2$.

4. Generate defect depth:

4.1) For *the i* -th inspection, accept $r=1$.

4.2) Generate the depth increment, Δd_{ir}^g, according to the gamma distribution given by equation (17) with shape and scale parameters equal to $\varphi_1\left(t_i-t_{sr}\right)^{\varphi_2}$ and e^{ξ_r}, respectively. It should be noted that $d_{ir}^g=\Delta d_{ir}^g$ for newly occurring defects in the *i*-th inspection interval.

4.3) If $d_{ir}^g>d_{th}$ (d_{th} is the resolution of the in-line tool), accept the defect as a detected defect with probability $\mathrm{POD}\left(d_{ir}^g\right)$. If the defect is accepted as a detected defect, go to step 4.4); otherwise, set $r=r+1$ and go to step 4.2).

4.4) Generate depth increment associated with *k*-th inspection $(k=i+1,i+2,\ldots\ n)$ for the detected defect, Δd_{kr}, according to the gamma distribution given by equation (17) with shape and scale parameters equal to $\varphi_1\left(t_k-t_{sr}\right)^{\varphi_2}-\varphi_1\left(t_{k-1}-t_{sr}\right)^{\varphi_2}$ and e^{ξ_r}, respectively. Calculate $d_{kr}=\sum_{l=i}^{k}\Delta d_{lr}$ as the actual depth of the detected defect r during the *k*-th inspection.

4.5) Generate the measured depth for the detected defect from the *i*-th to the *n*-th inspection by adding the random measurement error to the depth of the detected defect. The random measurement error is generated according to the normal distribution with zero mean and standard deviation σ_ε.

4.6) Accept $r=r+1$ and repeat steps 4.2)—4.5) until $r=N_i^g+1$.

4.7) Repeat steps 4.1)–4.6) for all inspections $i=1,2,\ldots,n$.

IV. Evaluation of the probability of failure

According to [12], the destruction pressure in the presence of a corrosion defect at time *t* is determined by the formula:

$$p_b\left(t\right)=\sigma_f\,\frac{2wt}{D-wt}\left(\frac{1-\dfrac{d\left(t\right)}{wt}}{1-\dfrac{d\left(t\right)}{M\left(t\right)wt}}\right), \tag{19}$$

where σ_f is the ultimate strength of the pipe material; *wt* is the pipe wall thickness; *D* is the outer diameter of the pipe; *d*(*t*) and *l*(*t*) are the depth and length of the defect at time *t*; and the Folias parameter is determined by the formula:

$$M\left(t\right)=\sqrt{1+0.31\frac{l^2\left(t\right)}{D\cdot wt}}\,. \tag{20}$$

The ultimate strength and geometric properties of the pipe are considered as random variables with their known PDFs. Thus, the strength of the corroded section of the pipe is a nonlinear time dependent function of random variables.

Probability of failure, $P_t\left(t\right)$ on the time interval from 0 to t can be estimated as the probability that the failure pressure will be less than or equal to the working pressure, or the probability that the corrosion defect depth will be greater than the pipe wall thickness, i.e.

$$P_f(t) = P\left(p_b(t) - p_o \le 0\right) + P\left(wt - d(t) \le 0\right) \quad (21)$$

Working pressure p_o is modeled as a time-independent random variable because it is controlled by complex pressure control devices.

Thus, the limit state functions (LSF) of the OUP according to the "rupture" and "leak" criteria have the following form:

$$\begin{aligned} g_b\left(\sigma_f, wt, D, d(t), l(t), p_0\right) &= p_b\left(\sigma_f, wt, D, d(t), l(t)\right) - p_0, \\ g_l\left(wt, d(t)\right) &= wt - d(t). \end{aligned} \quad (22)$$

Since the LSF are functions of random arguments, they themselves will be random variables. To find the PDF of the LSF, use the expansion in orthogonal polynomials based on the Gram-Charlier-Edgeworth series [6, 13]. Thus, with known PDFs $f_b(x)$, $f_l(x)$ functions of limit states, the probability of OUP failure:

$$P_f = F_b(0) + F_l(0) = \int_{-\infty}^{0} f_b(x)\,dx + \int_{-\infty}^{0} f_l(x)\,dx, \quad (23)$$

where $F_b(x), F_l(x)$ are the distribution functions of the FPS according to the "rupture" and "leak" criteria, respectively.

V. Repair criterion

The repair criterion for the rupture type is often determined based on the safety factor k_b for the failure pressure, determined by equation (19), and the maximum allowable working pressure p_m (MAOP) of the pipeline, i.e. the burst pressure of the pipe section with a defect is less than or equal to the safety factor for the failure, multiplied by MAOP :

$$p_b(t) - k_b p_m \le 0.$$

Typically, k_b in the range of от 1.25 до 1.5, and a typical value of 1.25 is intended to provide the same level of integrity as would be found in actual pipeline hydrotesting.

The criterion for repair of the leak type is determined on the basis of the coefficient k_l at which the depth of the defect is greater than, $k_l wt$ i.e.:

$$k_l wt - d(t) \le 0.$$

For the coefficient, k_l the range is usually from 0.60 to 0.80, which corresponds to 60%-80% of the pipe wall thickness.

VI. General algorithm for constructing a stochastic life cycle of OUP

Stage 1. After receiving a representative ensemble of all types of defects by the time of the first diagnostics, it must be inspected using *virtual* in-line instruments (VII) with metrics of their quality (accuracy), which real equipment used by a particular domestic pipeline organization has. At the same time, the cost of this diagnostic at the time of its implementation is estimated.

The result of this inspection may be: 1) absence of defects equal to or greater than the resolution of the VII; 2) presence of a group of a certain number of defects and anomalies. This group is analyzed to determine whether it contains critical and/or dangerous defects, and whether it is necessary to repair or restore the pipe, immediately or after some time.

Stage 2. After this inspection, the probability of missing a dangerous defect that could lead to an accident (leak, rupture) and the cost of restoring the OUP section integrity in the event of such a failure, i.e., the residual risk of the diagnostics performed, are assessed. This requires knowledge of the probability of false non-detection of a dangerous defect, characteristic of the VII used. To

determine the estimated location of a dangerous defect missed during flaw detection, it is recommended to use the approach proposed in [13].

Step 3. The result of this step will be one of two decisions: wait until the time of the second inspection (with the risk calculated in step 3) or carry out repairs to the pipe to remove the unacceptable defects, immediately [if the defect(s) are critical] or after some time necessary to carry out the preparatory work, during which the risk under point 3 will continue to increase.

Stage 4. If the analysis of the results of the first diagnostics did not lead to a decision to carry out any repair work, the development of all initial defects during the time between the first and second inspections is modeled, as well as the emergence of a group of new defects during the same period of time.

Stage 5. This new, enlarged array of defects is again subjected to virtual diagnostics, according to the algorithms of stage 2.

Stage 6. The results of the second diagnostics are analyzed to determine what decision should be made regarding the OUP operation, taking into account state regulations and rules in force within the pipeline company.

Stage 7. After this, it is possible, using the *quality metrics* of domestic VII, to again estimate the residual risk, taking into account the fact that there is a probability of missing a dangerous defect during the OUP diagnostics. This risk is calculated again using the algorithms of stage 3.

Stage 8. If a decision is made to carry out repairs based on the fact that dangerous defects have been identified, the volumes of the predicted repairs, as well as their duration and cost, are assessed. For this purpose, the standards and rules in force in the organizations operating the OUP in question are used.

Stage 9. The next step is to assess the most probable condition of the repaired OUP at the time of completion of the repair.

Stage 10. When modeling the implementation of the life cycle, a case is possible when, with the growth of defects at one of the phases of the OUP operation, one or more defects reach the maximum size, at which either a leak or a rupture of the pipe inevitably occurs. The time of reaching the maximum size by the first defect (initiating failure) is the beginning of an accident on the pipeline. The material damage from this accident is calculated on the basis of past domestic experience, taking into account discounting. The time and cost of restoring the integrity of the pipeline are estimated taking into account the financial and technological capabilities of the owner/operator of the OUP in question.

The tree of events and control decisions of the OUP life cycle described above consists of random time intervals during which the following occurs respectively: *operation* → *diagnostics* → *repair* → *operation* → *accident* → *restoration* → *operation* →… (where the phases *diagnostics*, *repair* and *accident* include an element of decision making). The tree is built until the entire OUP life cycle is covered and is presented in Fig. 1.

To account for the influence of the Dragon King (DK) type load, the moment(s) of its impact on the system are played out using the Monte Carlo method. With such modeling, it is also possible to take into account the Black Swan (BS) type load/impact. Despite the fact that an BS type event is fundamentally unpredictable, in the context of this task (only knowing that the BS event can manifest itself) it can be modeled in the same way as the impact of the DK. In this case, the parameters of the hypothetical BS are estimated by one of the brainstorming methods by a group of people with certain specific cognitive abilities, and the time of its implementation is played out as a uniformly distributed RV over the length of the life cycle.

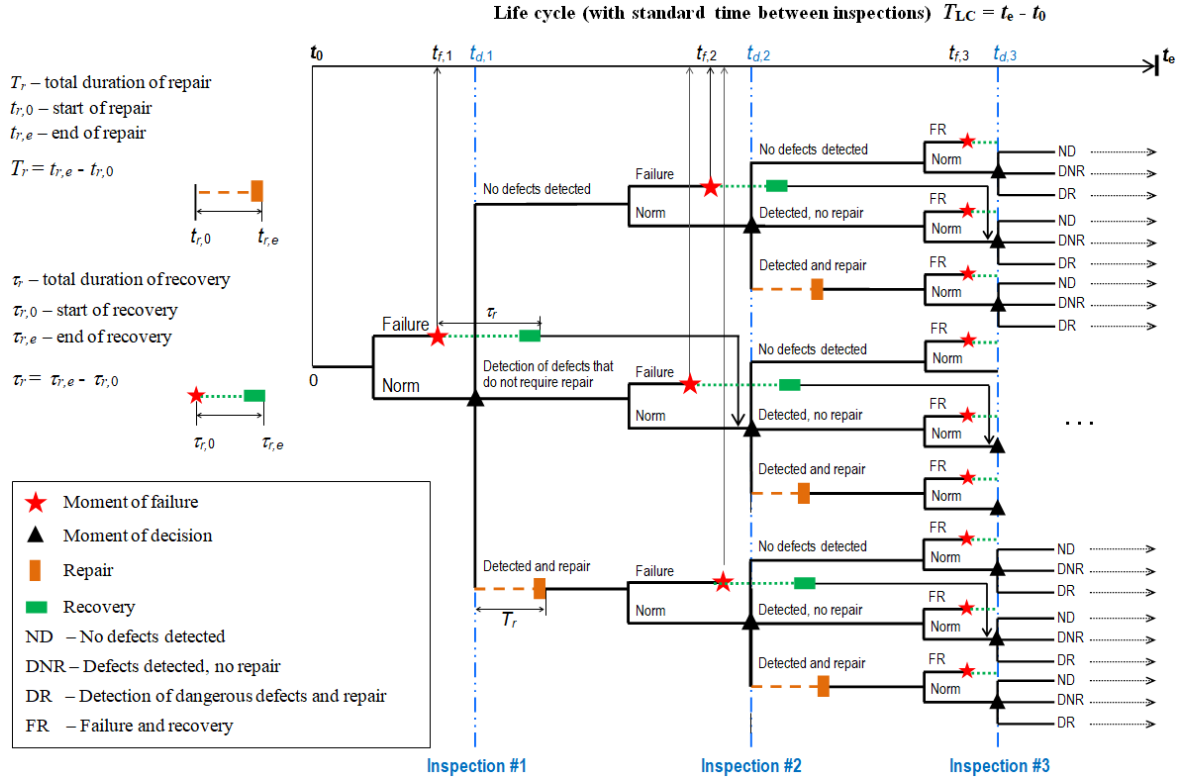


Fig. 1. Stochastic tree of events and decisions "event–decision–event–decision–…" built on the OUP life cycle

An accident of a pipeline near an offshore inhabited platform with fatal outcome(s) and injuries (time of occurrence of the event, its probability and non-economic scale of damage) during its life cycle is also modeled by the MC method. In this case, the target function of risk management of the operation of the offshore inhabited platform includes the cost of health restoration and compensation for possible injuries and loss of years of human life, determined by the method described in [14].

As a result of modeling the implementation of the OUP life cycle, in the general case, random numbers and times of diagnostic work, occurrence of emergency situations and adoption of management decisions on restoring the integrity and operability of the OUP arise. At these moments in time, the risks of operating the OUP change abruptly, which can be assessed quantitatively.

It is advisable to use the constructed full life cycle as a platform for assessing the sensitivity of the sought parameters (inherent reliability, resilience, frequency and quality of inspections, time, volume and cost of repairs, risk, etc.) to any input parameter or their combinations.

Knowing the time moments of planned interventions during the normal OUP operation, as well as the moments of occurrence of emergency situations and accidents, allows constructing a time schedule of discounted operating costs and losses due to OUP failures, as well as the growth and decline of its failure probability. Averaging these schedules over an ensemble of LC implementations gives an estimate of the average values of risk components, and the risk itself as a function of time.

VI. Conclusion

The article, using the example of the OUP as a strategic infrastructure, presents a methodology for computer modeling of the full stochastic life cycle, based on the technology of diagnostics,

monitoring, maintenance, repair and recovery after an OUP failure, including a full group of accuracy metrics for the diagnostic tools used and allowing one to obtain: consistent estimates of the probability of an undesirable event at each phase of the OUP life cycle; residual risk after each intervention in the functioning of the asset; the magnitude of the risk of making a management decision related to OUP design and operation.

References

[1] Timashev S.A. Infrastructures. Part II. Diagnostics. Monitoring. Maintenance. Human Factor. Resilience. Ural Branch Russian academy of sciences. Yekaterinburg, 2020 (In Russian).

[2] National Institute of Standards and Technology (NIST) Handbook #135

[3] Rackwitz R. (2005). Optimization and risk acceptability based on the Life Quality Index. Structural Safety, 24, 297-331.

[4] Joint Committee on Structural Safety. (2008). Risk assessment in engineering. Principles, system representation and risk criteria.

[5] Timashev S.A. Holistic A approach to Full Statistical Analysis of ILI Results. Proceedings of International Pipeline Conference IPC 2005, #72.

[6] Timashev S.A., Bushinskaya A.V. Diagnostics and Reliability of Pipeline Systems. Springer, 2015.

[7] Kuniewski S. P., van der Weide J. A., van Noortwijk J. M. (2009). Sampling inspection for the evaluation of time-dependent reliability of deteriorating systems under imperfect defect detection. Reliability Engineering & System Safety, 94(9), 1480-1490.

[8] Valor, A., Caleyo, F., Alfonso, L., Rivas, D., & Hallen, J. M. (2007). Stochastic modeling of pitting corrosion: a new model for initiation and growth of multiple corrosion pits. Corrosion science, 49(2), 559-579.

[9] Beichelt F., & Fatti L. P. (2002). Stochastic Processes and Their Applications. Taylor & Francis.

[10] Zhang S., Zhou W., Al-Amin M., Kariyawasam S., & Wang H. (2014). Time-Dependent Corrosion Growth Modeling Using Multiple ILI Data. Journal of Pressure Vessel Technology, 136, 041202, 1-7.

[11] Ang A. H. S., Tang W. H. (2007). Probability Concepts in Engineering Planning and Design: Emphasis on Applications in Civil & Environmental Engineering. John Wiley & sons.

[12] DNV-RP-C302: Risk Based Corrosion Management, no. April. Høvik, Norway: Det Norske Veritas (DNV), 2012.

[13] Timashev S.A., Kuzmin A.B. A powerful tool for assessing locations of defects missed-out by ILI. // Proceedings of International Pipeline Conference IPC 2004.—Calgary, Alberta, October 4-8, 2004, #98

[14] Bushinskaya A.V., Timashev S.A. Optimal reliability design of building structures based on the life quality index criterion: preprint. Ekaterinburg: Uralskiy rabochy, 2023. – 116 p. ISBN 978-5-85383-950-2.

EXPLORING SOME NEW CONTRIBUTION TO RAM AWADH DISTRIBUTION WITH COMPARATIVE PROPERTIES AND ITS APPLICATIONS

Manzoor A. Khanday[1], Rashid A. Ganaie[2,*], Aboubakar Ahmat Alwali Bourma[3], T. Vivekanandan[4] and R. Shenbagaraja[5]

•

[1, 3]Department of Statistics, Lovely Professional University, Phagwara, Punjab, India
[2,*] Department of Statistics, Annamalai University, Tamil Nadu-608002, India
[4] Department of Science and Humanities, Vel Tech Multi Tech Dr.Rangarajan Dr.Sagunthala Engineering College, Chennai, Tamil Nadu-600062, India
[5] Department of Statistics, Dr. M. G. R. Government Arts and Science College for Women, Villupuram, Tamil Nadu-605602, India
[1]manzoorstat@gmail.com, [2,*]rashidau7745@gmail.com, [3]Aahmatalwali@gmail.com, [4]mtvivek2017@gmail.com, [5]statraja@gmail.com

Abstract

In this study, a novel extension of the Ram Awadh distribution referred to as length biased Ram Awadh distribution is proposed and systematically developed. This distribution is constructed by applying length-biased transformation to the baseline Ram Awadh distribution, making it more suitable for modeling data where longer durations or larger values are more likely to be observed. A comprehensive exploration of the distribution's statistical properties is presented, including the derivation of moments, harmonic mean, reliability function, failure rate function, reverse hazard rate function, order statistics, entropy as well as the bonferroni and Lorenz curves. Parameter estimation is conducted through the maximum likelihood estimation method, ensuring robustness and efficiency. The practical utility and goodness of fit of the proposed model are demonstrated through its application to three real-life datasets, highlighting its flexibility and improved performance in empirical context.

Keywords: Ram Awadh distribution, length biased distribution, order statistics, reliability analysis

I. Introduction

In probability and statistics the weighted distributions retains a significant popularity because the classical distributions may not provide a proper fit to different datasets occurred from diversified fields. There are various situations where classical distributions may not provide the best fit in such cases, we generalize the standard probability models by adding a shape or additional parameter to it and this shape parameter is added through one of reputed weighted technique. The weighted distributions provide a collective approach for model stipulation and data interpretation problems. The weighted distributions are useful in distribution theory because it provides a new

method to extend the existing classical distribution for modeling lifetime data due to introduction of additional parameter in the model which creates flexibility. The weighted distributions are applicable only if the observations recorded without any experiment, repetition and random process. Fisher [8] introduced the weighted distribution to study the ascertainment bias which later on Rao [16] formulated in more general way with respect to modeling statistical data where usual practice of using standard distributions for purpose was found to be inappropriate. The weighted distribution reduced to length biased distribution particularly when weight function considers only length of units of interest. The concept of length biased distribution was introduced by Cox [5] in renewal theory and hence the length biased sampling situation occurs were a proper sampling frame is absent. In such situation items are sampled at a rate proportional to their lengths so that larger values could be sampled with higher probability. The length biased distribution has applications in biomedical areas such as survival analysis, family history, disease and intermediate events. The length biased distribution is a particular case of weighted distributions and may arise if there is not proper selection among the sample observations.

A magnificent contribution done by various authors to introduce several important length biased probability distributions along with their applications. Alzoubi [1] derived the length-biased Loai distribution with statistical properties and application. Abd-Elfattah et al. [3] presented the length biased Burr-XII distribution and obtain its properties and application. Chaito and Khamkong [6] proposed the length-biased Weibull-Rayleigh distribution with application to hydrological data. Das and Roy [7] discussed on some length biased weighted Weibull distribution. Ganaie and Rajagopalan [9] obtained the length biased power quasi Lindley distribution with properties and applications of lifetime data. Ganaie et al. [10] described the length biased Pratibha distribution and illustrate its applications. Ganaie and Rajagopalan [11] studied the length biased weighted new quasi Lindley distribution with statistical properties and applications. Kersey and Oluyede [13] constructed the theoretical properties of the length biased inverse Weibull distribution. Mustafa and Khan [14] studied the length biased powered inverse Rayleigh distribution with applications. Oluwafemi and Olalekan [15] presented length and area biased exponentiated weibull distribution based on forest inventories. Reyad et al. [17] derived the length biased weighted frechet distribution and studied its properties and estimation. Sharma et al. [18] discussed on the length and area biased Maxwell distributions.

Ram Awadh distribution is a recently proposed new one parametric distribution introduced by Shukla [19] and its few statistical properties have been discussed. Additionally its parameters are estimated by using method of moments and method of maximum likelihood estimation.

II. Length Biased Ram Awadh (LBRA) Distribution

The probability density function of Ram Awadh distribution is given by

$$f(x;\lambda) = \frac{\lambda^6}{\left(\lambda^6 + 120\right)}\left(\lambda + x^5\right) e^{-\lambda x}\ ;\ x > 0, \lambda > 0 \tag{1}$$

and cumulative distribution function of Ram Awadh distribution is given by

$$F(x;\lambda) = 1 - \left(1 + \frac{\lambda x\left(\lambda^4 x^4 + 5\lambda^3 x^3 + 20\lambda^2 x^2 + 60\lambda x + 120\right)}{\left(\lambda^6 + 120\right)}\right) e^{-\lambda x}\ ; x > 0, \lambda > 0 \tag{2}$$

Consider random variable *X* constitutes non-negative condition with probability density function *f(x)*. Suppose its weight function be *w(x)* that is non-negative, then probability density of weighted

random variable X_w is given by

$$f_w(x) = \frac{w(x)f(x)}{E(w(x))}, \quad x > 0$$

Where $w(x)$ is weight function of non – negative condition, hence $E(w(x)) = \int w(x)f(x)dx < \infty$.

In this paper, we have to get the length biased version of Ram Awadh distribution. Consequently the weight function as $w(x) = x$, the resulting distribution is termed as length biased distribution and therefore its probability density function is given by

$$f_l(x;\lambda) = \frac{x\, f(x;\lambda)}{E(x)} \tag{3}$$

Here $E(x) = \int_0^\infty x\, f(x;\lambda)\, dx$

$$E(x) = \frac{\left(\lambda^6 + 720\right)}{\lambda\left(\lambda^6 + 120\right)} \tag{4}$$

After substituting the equation (1) and (4) in equation (3), we have obtained the probability density function of length biased Ram Awadh distribution as

$$f_l(x;\lambda) = \frac{\lambda^7 x}{\left(\lambda^6 + 720\right)}\left(\lambda + x^5\right) e^{-\lambda x} \tag{5}$$

and cumulative distribution function of length biased Ram Awadh distribution will be obtained as

$$F_l(x;\lambda) = \int_0^x f_l(x;\lambda)dx$$

$$= \int_0^x \frac{\lambda^7 x}{\left(\lambda^6 + 720\right)}\left(\lambda + x^5\right) e^{-\lambda x} dx \tag{6}$$

After the simplification of equation (6), we have obtained the cumulative distribution function of length biased Ram Awadh distribution

$$F_l(x;\lambda) = \frac{1}{\left(\lambda^6 + 720\right)}\left(\lambda^6 \gamma(2, \lambda x) + \gamma(7, \lambda x)\right) \tag{7}$$

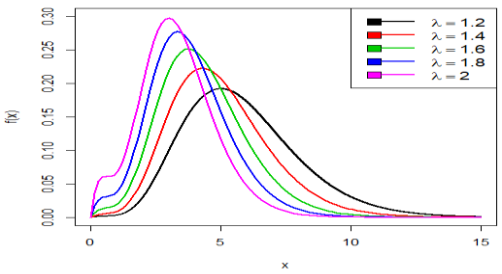


Figure 1: *Pdf plot of LBRA distribution*

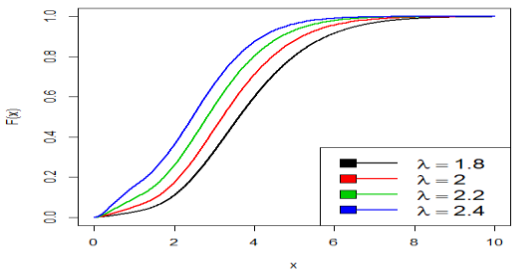


Figure 2: *Cdf plot of LBRA distribution*

III. Reliability analysis

In this portion, we have derived and presented some particular properties of length biased Ram Awadh distribution. The reliability function of length biased Ram Awadh distribution is given by

$$R(x) = 1 - F_l(x;\lambda)$$

$$R(x) = 1 - \frac{1}{\left(\lambda^6 + 720\right)}\left(\lambda^6\gamma(2,\ \lambda x) + \gamma(7,\ \lambda x)\right)$$

The hazard function of length biased Ram Awadh distribution is given by

$$h(x) = \frac{f_l(x;\lambda)}{1 - F_l(x;\lambda)}$$

$$h(x) = \frac{\lambda^7 x\left(\lambda + x^5\right)e^{-\lambda x}}{(\lambda^6 + 720) - (\lambda^6\gamma(2,\ \lambda x) + \gamma(7,\ \lambda x))}$$

The reverse hazard rate function of length biased Ram Awadh distribution is given by

$$h_r(x) = \frac{f_l(x;\lambda)}{F_l(x;\lambda)}$$

$$h_r(x) = \frac{\lambda x\left(\lambda + x^5\right)e^{-\lambda x}}{\left(\gamma(2,\lambda x) + \gamma(7,\ \lambda x)\right)}$$

The Mills Ratio of length biased Ram Awadh distribution is given by

$$M.R = \frac{1}{h_r(x)} = \frac{\left(\gamma(2,\lambda x) + \gamma(7,\ \lambda x)\right)}{\lambda x\left(\lambda + x^5\right)e^{-\lambda x}}$$

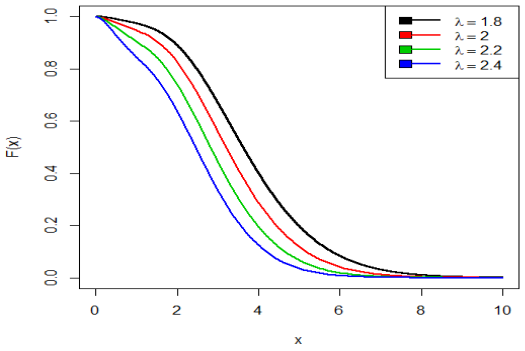


Figure 3:*Reliability plot of LBRA distribution*

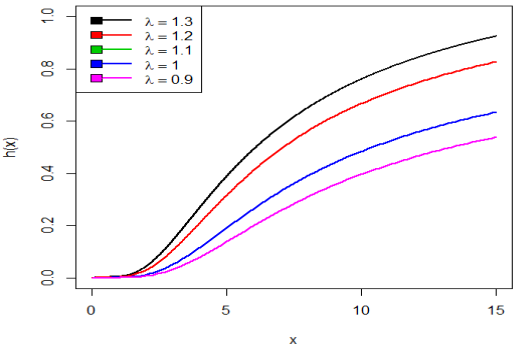


Figure 4:*Hazard plot of LBRA distribution*

IV. Order Statistics

Order statistics is a fundamental component in statistics which has wide range of applications in reliability and life testing. Consider order statistics $X_{(1)}, X_{(2)}, \ldots, X_{(n)}$ of a random sample $X_{(1)}, X_{(2)}, \ldots, X_{(n)}$ from a continuous distribution has its probability density function $f_x(x)$ and its cumulative distribution function $F_x(x)$, then probability density function of r^{th} order statistics $X_{(r)}$ is given by

$$f_{x(r)}(x) = \frac{n!}{(r-1)!(n-r)!} f_X(x)\left(F_X(x)\right)^{r-1}\left(1 - F_X(x)\right)^{n-r} \qquad (8)$$

After applying the equation (5) and (7) in equation (8), we will get the probability density function of r^{th} order statistics $X_{(r)}$ of length biased Ram Awadh distribution as

$$f_{x(r)}(x) = \frac{n!}{(r-1)!(n-r)!}\left(\frac{\lambda^7 x}{\left(\lambda^6+720\right)}\left(\lambda + x^5\right)e^{-\lambda x}\right)\left(\frac{1}{\left(\lambda^6+720\right)}\left(\lambda^6\gamma(2,\lambda x)+\gamma(7,\lambda x)\right)\right)^{r-1}$$
$$\times\left(1-\frac{1}{\left(\lambda^6+720\right)}\left(\lambda^6\gamma(2,\lambda x)+\gamma(7,\lambda x)\right)\right)^{n-r}$$

Therefore probability density function of higher order statistics $X_{(n)}$ of length biased Ram Awadh distribution is given by

$$f_{x(n)}(x) = \left(\frac{nx\lambda^7}{\left(\lambda^6+720\right)}\left(\lambda + x^5\right)e^{-\lambda x}\right)\left(\frac{1}{\left(\lambda^6+720\right)}\left(\lambda^6\gamma(2,\lambda x)+\gamma(7,\lambda x)\right)\right)^{n-1}$$

and therefore probability density function of first order statistics $X_{(1)}$ of length biased Ram Awadh distribution is given by

$$f_{x(1)}(x) = \left(\frac{nx\lambda^7}{\left(\lambda^6+720\right)}\left(\lambda + x^5\right)e^{-\lambda x}\right)\left(1-\frac{1}{\left(\lambda^6+720\right)}\left(\lambda^6\gamma(2,\lambda x)+\gamma(7,\lambda x)\right)\right)^{n-1}$$

V. Statistical Properties

In this portion, we have derived some specified features of length biased Ram Awadh distribution.

I. Moments

Suppose the random variable X represents the length biased Ram Awadh distribution, then the r^{th} order moment of proposed distribution will be obtained as

$$\mu_r' = E(X^r) = \int_0^\infty x^r f_l(x;\lambda)\,dx$$
$$= \int_0^\infty \frac{\lambda^7 x^{r+1}}{\left(\lambda^6+720\right)}\left(\lambda + x^5\right)e^{-\lambda x}dx \qquad (9)$$

After the simplification of equation (9), we get

$$\mu_r' = E(X^r) = \frac{\left(\lambda^6\Gamma(r+2)+\Gamma(r+7)\right)}{\lambda^r\left(\lambda^6+720\right)} \qquad (10)$$

Therefore substituting $r = 1, 2, 3$ and 4 in equation (10), we will get the first four moments of length biased Ram Awadh distribution

$$\mu_1' = \frac{\left(2\lambda^6+5040\right)}{\lambda\left(\lambda^6+720\right)}$$

$$\mu_2' = \frac{\left(6\lambda^6 + 40320\right)}{\lambda^2\left(\lambda^6 + 720\right)}$$

$$\mu_3' = \frac{\left(24\lambda^6 + 362880\right)}{\lambda^3\left(\lambda^6 + 720\right)}$$

$$\mu_4' = \frac{\left(120\lambda^6 + 3628800\right)}{\lambda^4\left(\lambda^6 + 720\right)}$$

$$\text{Variance} = \frac{\left(2\lambda^{12} + 24480\lambda^6 + 3628800\right)}{\lambda^2\left(\lambda^6 + 720\right)^2}$$

$$\text{S.D} = \frac{\sqrt{\left(2\lambda^{12} + 24480\lambda^6 + 3628800\right)}}{\lambda\left(\lambda^6 + 720\right)}$$

II. Harmonic mean

The harmonic mean of length biased Ram Awadh distribution should be determined as

$$\text{H.M} = E\left(\frac{1}{x}\right) = \int_0^\infty \frac{1}{x} f_l(x;\lambda)dx$$

$$= \int_0^\infty \frac{\lambda^7}{\left(\lambda^6 + 720\right)}\left(\lambda + x^5\right)e^{-\lambda x}dx \qquad (11)$$

After simplification of equation (11), we get

$$\text{H.M} = \frac{\lambda\left(\lambda^6 + 120\right)}{\left(\lambda^6 + 720\right)}$$

III. Moment generating function and characteristic function

The moment generating function of length biased Ram Awadh distribution will be obtained as

$$M_X(t) = E\left(e^{tx}\right) = \int_0^\infty e^{tx} f_l(x;\lambda)dx$$

$$= \int_0^\infty \frac{\lambda^7 x}{\left(\lambda^6 + 720\right)}\left(\lambda + x^5\right)e^{-(\lambda - t)x}dx \qquad (12)$$

After the simplification of equation (12), we get

$$M_X(t) = \frac{\lambda^7}{(\lambda - t)^7\left(\lambda^6 + 720\right)}\left(\lambda(\lambda - t)^5 + 720\right)$$

Obviously, the characteristic function of length biased Ram Awadh distribution is given by

$$M_X(it) = \frac{\lambda^7}{(\lambda - it)^7\left(\lambda^6 + 720\right)}\left(\lambda(\lambda - it)^5 + 720\right)$$

VI. Bonferroni and Lorenz Curves

The bonferroni and Lorenz curves were applied to illustrate the graphical description of inequality in income or poverty. The bonferroni and Lorenz curves should be defined as

$$B(p) = \frac{1}{p\mu_1'}\int_0^q x f_l(x;\lambda)\,dx$$

$$L(p) = pB(p) = \frac{1}{\mu_1'}\int_0^q x f_l(x;\lambda)\,dx$$

$$\text{Where } \mu_1' = \frac{\left(2\lambda^6 + 5040\right)}{\lambda\left(\lambda^6 + 720\right)}$$

$$B(p) = \frac{\lambda\left(\lambda^6 + 720\right)}{p\left(2\lambda^6 + 5040\right)}\int_0^q \frac{\lambda^7 x^2}{(\lambda^6 + 720)}\left(\lambda + x^5\right)e^{-\lambda x}dx \qquad (13)$$

After the simplification of equation (13), we get

$$B(p) = \frac{1}{p\left(2\lambda^6 + 5040\right)}\left(\lambda^6\gamma(3,\ \lambda q) + \gamma(8,\ \lambda q)\right)$$

$$L(p) = \frac{1}{\left(2\lambda^6 + 5040\right)}\left(\lambda^6\gamma(3,\ \lambda q) + \gamma(8,\ \lambda q)\right)$$

VII. Parameter Estimation and Fisher's Information Matrix

In this portion, we have applied the technique of parameter estimation to estimate the parameter of length biased Ram Awadh distribution. Consider the random sample $X_1, X_2, \ldots, X_n$ of size n from the length biased Ram Awadh distribution, then the likelihood function should be defined as

$$L(x) = \prod_{i=1}^{n} f_l(x;\lambda)$$

$$= \prod_{i=1}^{n}\left(\frac{\lambda^7 x_i}{\left(\lambda^6 + 720\right)}\left(\lambda + x_i^5\right)e^{-\lambda x_i}\right)$$

$$= \frac{\lambda^{7n}}{\left(\lambda^6 + 720\right)^n} \prod_{i=1}^{n} \left(x_i \left(\lambda + x_i^5\right) e^{-\lambda x_i} \right)$$

The log likelihood function should be defined as

$$\log L = 7n\log\lambda - n\log\left(\lambda^6 + 720\right) + \sum_{i=1}^{n} \log x_i + \sum_{i=1}^{n} \log\left(\lambda + x_i^5\right) - \lambda \sum_{i=1}^{n} x_i \tag{14}$$

Therefore differentaiting the log likelihood equation (14) with respect to λ. The following normal equation must be satisfied

$$\frac{\partial \log L}{\partial \lambda} = -\frac{7n}{\lambda} - n\left(\frac{6\lambda^5}{\left(\lambda^6 + 720\right)}\right) + \sum_{i=1}^{n}\left(\frac{1}{\left(\lambda + x_i^5\right)}\right) - \sum_{i=1}^{n} x_i = 0$$

The above likelihood equation is too complicated to solve it algebraically. Therefore we use R and wolfram mathematics for estimating the parameter of proposed distribution.

To apply the asymptotic normality results for attaining confidence interval. We state that $(\hat{\beta} = \hat{\lambda})$ which represents the maximum likelihood estimate of $(\beta = \lambda)$. The result can be analyzed as

$$\sqrt{n}(\hat{\beta} - \beta) \to N\left(0, I^{-1}(\beta)\right)$$

Here $I^{-1}(\beta)$ is Fisher's Information Matrix

$$I(\beta) = -\frac{1}{n}\left(E\left(\frac{\partial^2 \log L}{\partial \lambda^2}\right)\right)$$

$$E\left(\frac{\partial^2 \log L}{\partial \lambda^2}\right) = -\frac{7n}{\lambda^2} - n\left(\frac{\left(\lambda^6 + 720\right)\left(30\lambda^4\right) - \left(6\lambda^5\right)^2}{\left(\lambda^6 + 720\right)^2}\right) - \sum_{i=1}^{n}\left(\frac{1}{\left(\lambda + x_i^5\right)^2}\right)$$

Therefore β is not known hence $I^{-1}(\beta)$ should be estimated by $I^{-1}(\hat{\beta})$ and it is applied to attain asymptotic confidence interval for λ.

VIII. Entropy

The term entropy is a scientific concept which is commonly associated with uncertainty or disorder of a system and is also applied in various fields.

I. Renyi Entropy

The Renyi entropy is named after Alfred Renyi is a quantity which generalizes several forms of entropy. The Renyi entropy should be derived as

$$R_T(\alpha) = \frac{1}{1-\alpha}\log\left(\int f_1^{\alpha}(x;\lambda)\,dx\right)$$

$$= \frac{1}{1-\alpha}\log\left(\left(\frac{\lambda^7}{\left(\lambda^6 + 720\right)}\right)^{\alpha} \int_0^{\infty} x^{\alpha} e^{-\alpha\lambda x}\left(\lambda + x^5\right)^{\alpha} dx\right) \tag{15}$$

After the simplification of equation (15), we get

$$R_T(\alpha) = \frac{1}{1-\alpha}\log\left(\left(\frac{\lambda^{6\alpha-5k-1}}{\left(\lambda^6+720\right)^{\alpha}}\right)\sum_{k=0}^{\infty}\binom{\alpha}{k}\lambda^{\alpha-k}\frac{\Gamma(\alpha+5k+1)}{\alpha^{\alpha+5k+1}}\right)$$

Clearly, the Tsallis entropy of length biased Ram Awadh distribution will be obtained as

$$T_s(\xi) = \frac{1}{\xi-1}\left(1-\int_0^{\infty} f_l^{\xi}(x;\lambda)\,dx\right)$$

$$= \frac{1}{\xi-1}\left(1-\left(\frac{\lambda^7}{\left(\lambda^6+720\right)}\right)^{\xi}\int_0^{\infty} x^{\xi}e^{-\lambda\xi x}\left(\lambda+x^5\right)^{\xi}dx\right) \tag{16}$$

After the simplification of equation (16), we get

$$T_s(\xi) = \frac{1}{\xi-1}\left(1-\left(\frac{\lambda^{6\xi-5j-1}}{\left(\lambda^6+720\right)^{\xi}}\right)\sum_{j=0}^{\infty}\binom{\xi}{j}\lambda^{\xi-j}\frac{\Gamma(\xi+5j+1)}{\xi^{\xi+5j+1}}\right)$$

IX. Likelihood Ratio Test

Consider random sample $X_1, X_2, \ldots, X_n$ of size n from length biased Ram Awadh distribution, then the proposed test is applied to analyze its flexibility

$$H_o : f(x) = f(x;\lambda) \quad \text{against} \quad H_1 : f(x) = f_l(x;\lambda)$$

In order to identify whether the random sample of size n comes from length biased Ram Awadh distribution or Ram Awadh distribution, the proposed rule is applied

$$\Delta = \frac{L_1}{L_0} = \prod_{i=1}^{n}\left(\frac{f_l(x;\lambda)}{f(x;\lambda)}\right)$$

$$= \prod_{i=1}^{n}\left(\frac{\lambda x_i\left(\lambda^6+120\right)}{\left(\lambda^6+720\right)}\right)$$

$$= \left(\frac{\lambda\left(\lambda^6+120\right)}{\left(\lambda^6+720\right)}\right)^n \prod_{i=1}^{n} x_i$$

The null hypothesis should be refused to accept, if

$$\Delta = \left(\frac{\lambda\left(\lambda^6+120\right)}{\left(\lambda^6+720\right)}\right)^n \prod_{i=1}^{n} x_i > k$$

$$\Delta^* = \prod_{i=1}^{n} x_i > k\left(\frac{\left(\lambda^6 + 720\right)}{\lambda\left(\lambda^6 + 120\right)}\right)^n$$

$$\Delta^* = \prod_{i=1}^{n} x_i > k^*, \text{ where } k^* = k\left(\frac{\left(\lambda^6 + 720\right)}{\lambda\left(\lambda^6 + 120\right)}\right)^n$$

X. Application

In this portion, we have analyzed and examined the goodness of fit of length biased Ram Awadh distribution by applying three real data sets and then performance has been established in order to reveal that the length biased Ram Awadh distribution shows a better fit in comparison over Ram Awadh, Lindley and Pranav distributions.

Data set 1: The following real lifetime data set given below constitutes the relief times (in minutes) of 20 patients receiving an analgesic reported by Gross and Clarke [12] and the observations are
1.1, 1.4, 1.3, 1.7, 1.9, 1.8, 1.6, 2.2, 1.7, 2.7, 4.1, 1.8, 1.5, 1.2, 1.4, 3.0, 1.7, 2.3, 1.6, 2.0

Data set 2: The second real data set reported by Bader and Priest [4] represents the tensile strength measured in GPa of 69 carbon fibers tested under the tension at gauge lengths of 20mm and the values are given as
1.312, 2.726, 2.382, 1.958, 2.954, 2.535, 2.140, 3.585, 2.684, 2.301, 1.865, 2.848, 2.511, 2.063, 3.233, 2.642, 2.274, 1.803, 2.818, 2.478, 2.027, 3.096, 2.629, 2.270, 1.552, 2.800, 2.434, 2.006, 3.084, 2.570, 2.240, 1.314, 2.770, 2.382, 1.966, 3.012, 2.554, 2.179, 3.858, 2.697, 2.359, 1.944, 2.880, 2.514, 2.098, 3.433, 2.648, 2.301, 1.861, 2.821, 2.490, 2.055, 3.128, 2.633, 2.272, 1.700, 2.809, 2.435, 2.021, 3.090, 2.586, 2.253, 1.479, 2.773, 2.426, 1.997, 3.067, 2.566, 2.224

Data set 3: The third real lifetime data set consists of 40 patients suffering from blood cancer (leukemia) reported from one of ministry of health hospitals in Saudi Arabia see Abouammah et al. [2]. The observations of ordered lifetimes (in years) is given as
0.315, 0.496, 0.616, 1.145, 1.208, 1.263, 1.414, 2.025, 2.036, 2.162, 2.211, 2.37, 2.532, 2.693, 2.805, 2.91, 2.912, 3.192, 3.263, 3.348, 3.348, 3.427, 3.499, 3.534, 3.767, 3.751, 3.858, 3.986, 4.049, 4.244, 4.323, 4.381, 4.392, 4.397, 4.647, 4.753, 4.929, 4.973, 5.074, 5.381

To compute the model comparison criterions along with the unknown parameters are estimated thoroughly by applying the technique of R Software. To regulate the performance of length biased Ram Awadh distribution in comparison over Ram Awadh, Lindley and Pranav distributions, the considered criterions such as Akaike Information Criterion *(AIC),* Bayesian Information Criterion *(BIC),* Akaike Information Criterion Corrected *(AICC),* Consistent Akaike Information Criterion *(CAIC),* Shannon's entropy *H(X)* and *-2logL* have been applied. The distribution performs obviously better if it has the smaller criterion values of *AIC, BIC, AICC, CAIC, -2logL* and *H(X)* as compared over other specified distributions. The following formulas were applied for determining the criterion values

$$AIC = 2k - 2\log L, \qquad BIC = k\log n - 2\log L, \qquad AICC = AIC + \frac{2k(k+1)}{(n-k-1)}$$

$$CAIC = -2\log L + \frac{2kn}{n-k-1} \qquad H(X) = -\frac{2\log L}{n}$$

Here *k* is the number of parameters in the statistical model, *n* is the sample size and *-2logL* is the maximized value of log- likelihood function.

Table 1: *shows MLE and S. E of Data set 1, Data set 2 and Data set 3 of performed distributions*

Data set 1			Data set 2		
Distribution	MLE	S.E	Distribution	MLE	S.E
LBRA	$\hat{\lambda} = 2.69338$	$\hat{\lambda} = 0.166145$	LBRA	$\hat{\lambda} = 2.3812762$	$\hat{\lambda} = 0.0841710$
Ram Awadh	$\hat{\lambda} = 2.045874$	$\hat{\lambda} = 0.130715$	Ram Awadh	$\hat{\lambda} = 1.8504152$	$\hat{\lambda} = 0.0663762$
Lindley	$\hat{\lambda} = 0.816118$	$\hat{\lambda} = 0.136092$	Lindley	$\hat{\lambda} = 0.6545057$	$\hat{\lambda} = 0.0580316$
Pranav	$\hat{\lambda} = 1.401400$	$\hat{\lambda} = 0.124708$	Pranav	$\hat{\lambda} = 1.2251389$	$\hat{\lambda} = 0.0597324$

Data set 3		
Distribution	MLE	S.E
LBRA	$\hat{\lambda} = 2.076465$	$\hat{\lambda} = 0.105233$
Ram Awadh	$\hat{\lambda} = 1.6618903$	$\hat{\lambda} = 0.084099$
Lindley	$\hat{\lambda} = 0.5269213$	$\hat{\lambda} = 0.06074$
Pranav	$\hat{\lambda} = 1.08000$	$\hat{\lambda} = 0.071233$

Table 2: *Shows analysis, comparison and performance of fitted distributions*

Data sets	Distribution	-2logL	AIC	BIC	AICC	CAIC	H(X)
1	LBRA	56.17852	58.17852	59.17425	58.40074	58.4007	2.8089
	Ram Awadh	68.52522	70.52522	71.52095	70.74744	70.7474	3.4262
	Lindley	60.4991	62.4991	63.49483	62.6991	62.7213	3.0249
	Pranav	62.38652	64.38652	65.38225	64.60874	64.6087	3.1193
2	LBRA	174.4082	176.4082	178.6423	176.4679	176.4679	2.5276
	Ram Awadh	207.1334	209.1334	211.3675	209.1931	209.1931	3.0019
	Lindley	238.3805	240.3805	242.6146	240.4402	240.4402	3.4547
	Pranav	217.1224	219.1224	221.3565	219.1821	219.1821	3.1467
3	LBRA	137.724	139.724	141.4129	139.8292	139.8292	3.4431
	Ram Awadh	141.6505	143.6505	145.3394	143.7557	143.7557	3.5412
	Lindley	160.5012	162.5012	164.19	162.6064	162.6064	4.0125
	Pranav	146.9727	148.9727	150.6616	149.0779	149.0779	3.6743

It is clearly realized from results given above in table 2 that length biased Ram Awadh distribution has the smaller criterion values of *AIC*, *BIC*, *AICC*, *CAIC*, *H(X)* and *-2logL* as compared over Ram Awadh, Lindley and Pranav distributions which illustrates that the length biased Ram Awadh distribution provides a better fit as compared over Ram Awadh, Lindley and Pranav distributions.

XI. Conclusion

In this manuscript, we have established a novel extension of Ram Awadh distribution referred to as length biased Ram Awadh distribution which is introduced by incorporating the length biased technique to its classical distribution. The formulated new distribution has been accomplished and examined with several statistical properties those are moments, mean and variance, harmonic mean, shape of pdf and cdf, coefficient of variation, Renyi entropy measure, order statistics, bonferroni and Lorenz curves have been obtained and presented. Additionally reliability function, hazard function, reverse hazard function, moment generating function and characteristic function have been derived and described. In addition parameter of length biased Ram Awadh distribution is estimated by applying the technique of maximum likelihood estimation. Further, the capability and flexibility of presented length biased Ram Awadh distribution has been investigated and inspected by applying the three real data sets and hence therefore it is commenced from the result that length biased Ram Awadh distribution leads to a better fit as compared over Ram Awadh, Lindley and Pranav distributions.

References

[1] Alzoubi, L. (2024). Length-biased Loai distribution: statistical properties and application. *Electronic Journal of Applied Statistical Analysis*, 17(02):278-301.

[2] Abouammoh, A. M., Ahmed, R. and Khalique, A. (2000). On new renewal better than used classes of life distribution. *Statistics and Probability Letters*, 48(2):189-194.

[3] Abd-Elfattah, A. M., Mahdy, M. and Ismail, G. (2021). Length biased Burr- XII distribution: properties and application. *International Journal of Sciences: Basic and Applied Research* (*IJSBAR*), 56(1):222-244.

[4] Bader, M. G. and Priest, A. M. (1982). Statistical aspects of fiber and bundle strength in hybrid composites. In: hayashi T, editor, Progress in Science in Engineering Composites, ICCM-IV, Tokyo, 1129 -1136.

[5] Cox, D. R. (1962). Renewal theory, *Barnes and Noble,* New York.

[6] Chaito, T. and Khamkong, M. (2022). The length-biased Weibull-Rayleigh distribution for application to hydrological data. *Lobachevskii Journal of Mathematics*, 42:3253-3265.

[7] Das, K. K. and Roy, T. D. (2011). On some length-biased weighted Weibull distribution. *Advances in Applied Science Research*, 2(5):465-475.

[8] Fisher, R. A. (1934). The effects of methods of ascertainment upon the estimation of frequencies. *Annals of Eugenics*, 6:13-25.

[9] Ganaie, R. A. and Rajagopalan, V. (2021). A new extension of power quasi Lindley distribution with properties and applications of the life-time data. *International Journal of Statistics and Reliability Engineering*, 8(1):171-183.

[10] Ganaie, R. A., Shenbagaraja, R. and Soumya, V. P. (2024). A generalization and some new contribution to Pratibha distribution with statistical properties and its applications. *International Journal of Statistics and Reliability Engineering*, 11(1):108-116.

[11] Ganaie, R. A. and Rajagopalan, V. (2021). Length biased weighted new quasi Lindley distribution: statistical properties and applications. *Pak.j.stat.oper.res*., 17(1):123-136.

[12] Gross, A. J. and Clark, V. A. (1975). Survival distributions: reliability applications in the biometrical sciences, John Wiley, New York.

[13] Kersey, J. and Oluyede, B. O. (2012). Theoretical properties of the length-biased inverse Weibull distribution. *Involve*, 5(4):379-391.

[14] Mustafa, A. and Khan, M. I. (2022). The length-biased powered inverse Rayleigh

distribution with applications. *J. Appl. Math. & Informatics*, 40(1):1-13.

[15] Oluwafemi, O. S. and Olalekan, D. M. (2017). Length and area biased exponentiated Weibull distribution based on forest inventories. *Biometrics & Biostatistics International Journal*, 6(2):311-320.

[16] Rao, C. R. (1965). On discrete distributions arising out of method of ascertainment, in classical and contagious discrete distributions. G.P.Patil (ed.), Pergamon press and statistical publishing society, Calcutta. 320-332.

[17] Reyad, H. M., Hashish, A. M., Othman, S. A. and Allam, S. A. (2018). The length-biased weighted frechet distribution: Properties and estimation. *International Journal of Statistics and Applied Mathematics*, 3(1):189-200.

[18] Sharma, V. K., Dey, S., Singh, S. K. and Manzoor, U. (2018). On length and area-biased Maxwell distributions. *Communications in Statistics-Simulation and Computation*, 47(5):1506-1528.

[19] Shukla, K. K. (2018). Ram Awadh distribution with properties and applications. *Biometrics and Biostatistics International Journal*, 7(6):515-523.

A COMPARATIVE STUDY OF GENERALIZED ARADHANA DISTRIBUTION WITH SIGNIFICANT STATISTICAL PROPERTIES AND APPLICATIONS

Rashid A. Ganaie[1,*], V. P. Soumya[2], R. Shenbagaraja[3] and Manzoor A. Khanday[4]

•

[1,*]Department of Statistics, Annamalai University, Tamil Nadu-608002, India
[2] Department of Community Medicine, Dr. Vithalrao Vikhe Patil Foundation's Medical College and Hospital, Ahilyanagar, India
[3] Department of Statistics, Dr. M. G. R. Government Arts and Science College for Women, Villupuram, Tamil Nadu-605602, India
[4] Department of Statistics, Lovely Professional University, Phagwara, Punjab, India
[1,*]rashidau7745@gmail.com, [2]soumyaponnan@gmail.com, [3]statraja@gmail.com, [4]manzoorstat@gmail.com

Abstract

This study introduces a novel extension of the generalized Aradhana distribution, termed the length biased generalized Aradhana distribution. The proposed distribution is formulated by applying the length biased technique to the baseline generalized Aradhana distribution, enhancing its applicability in reliability and survival analysis. Fundamental statistical properties, including moments, order statistics, reliability functions and entropy are rigorously derived to characterize the distribution's behavior. The parameters of proposed model are estimated using the maximum likelihood estimation method to ensure statistical efficiency. To assess its practical utility, the distribution is applied to two real-world lifetime data sets, demonstrating its superior performance and robustness compared to existing models. These findings highlight the significance and applicability of the length biased generalized Aradhana distribution in modeling lifetime data.

Keywords: length biased distribution, generalized Aradhana distribution, reliability measures, entropy

I. Introduction

In recent years, the increasing popularity and advancements in distribution theory have driven a strong emphasis on developing new, precise and flexible distributions. These innovative models aim to better capture complexities of real-world data across various fields enhancing statistical accuracy and applicability. The core importance of distribution theory lies in its ability to enhance existing distributions by introducing shape parameter because it increases the compatibility and flexibility of the existing distribution. This shape parameter comprises the classical distribution in a more flexible situation while comparing with other distributions and is illustrated through advanced and reputed weighted technique. Fisher [7] constructed the weighted distributions to capture the ascertainment bias which was subsequently extended by Rao [15] in a cohesive manner while modeling statistical

data in which standard distributions were not found appropriate. The weighted distributions were incorporated in such a manner to record the observations with equal probability. It is also observed that weighted distributions were applied in several experimental problems in case of biased samples that appear naturally in various situations. The weighted distribution reduced to the length biased distribution specifically if the weight function considers only the length of the units of interest. The concept of length biased distribution introduced by Cox [6] which is a particular case of weighted distributions. Sometimes, the length biased distribution may occur in numerous situations because it seems quite impossible to work with truly random sample from population of interest and hence length biased distributions may arised in clinical trials, reliability theory, population studies and survival analysis were a proper sampling frame is unavailable. Thus length biased distribution may arise if sample observations are unfairly selected and therefore if the observations are selected with probability proportional to their lengths resulting distributions is termed length biased distribution.

There are various authors who contributed remarkably to develop several important length biased probability distributions along with illustrations and applications from diversified fields. Al-Omari and Alsmairan [2], Almakhareez and Alzoubi [1], Rashwan [16], Mustafa and Khan [12], Ratnaparkhi and Nimbalkar [18], Salama et al. [21], Beghriche and Zeghdoudi [5], Perveen et al. [14], Ganaie et al. [8], Mustafa and Khan [11], Saghir et al. [19], Ganaie and Rajagopalan [9], Bashir and Khan [4], Rasool and Ahmad [17], Saghir and Khadim [20], Mudasir and Ahmad [13].

A generalized Aradhana distribution is a two parameteric recently proposed distribution introduced by Welday and Shanker [22] which includes Aradhana distribution as its particular case of it. Some of its structural properties have been derived and determined. Further, its parameters are estimated through maximum likelihood estimation.

II. Length Biased Generalized Aradhana (LBGA) Distribution

The probability density function of generalized Aradhana distribution is given by

$$f(x;\theta,\alpha) = \frac{\theta^3}{\left(\theta^2 + 2\alpha\theta + 2\alpha^2\right)}\left(1+\alpha x\right)^2 e^{-\theta x} \quad ; x > 0, \theta > 0, \alpha \geq 0 \tag{1}$$

and cumulative distribution function of generalized Aradhana distribution is given by

$$F(x;\theta,\alpha) = 1 - \left(1 + \frac{\alpha\theta x\left(2\theta + \alpha\theta x + 2\alpha\right)}{\left(\theta^2 + 2\theta\alpha + 2\alpha^2\right)}\right) e^{-\theta x} \; ; \; x > 0, \theta > 0, \alpha \geq 0 \tag{2}$$

Consider the random variable X which constitutes non-negative condition with probability density function $f(x)$. Assume its weight function $w(x)$ which will be non-negative, then probability density function of weighted random variable X_w is given by

$$f_w(x) = \frac{w(x)f(x)}{E(w(x))}, \quad x > 0$$

Here $w(x)$ be the weight function which is non-negative then $E(w(x)) = \int w(x) f(x) dx < \infty$.

In this study, we have considered the weight function as $w(x) = x$ to get the length biased version of generalized Aradhana distribution and its probability density function is clearly defined as

$$f_l(x;\theta,\alpha) = \frac{x\, f(x;\theta,\alpha)}{E(x)} \tag{3}$$

Hence $E(x) = \int_0^\infty x\, f(x;\theta,\alpha)dx$

$$E(x) = \frac{(\theta^2 + 6\alpha^2 + 4\alpha\theta)}{\theta(\theta^2 + 2\alpha\theta + 2\alpha^2)} \tag{4}$$

After applying the equation (1) and (4) in equation (3), we will obtain probability density function of length biased generalized Aradhana distribution as

$$f_l(x;\theta,\alpha) = \frac{x\theta^4}{\left(\theta^2 + 6\alpha^2 + 4\alpha\theta\right)}(1+\alpha x)^2 e^{-\theta x} \tag{5}$$

and the cumulative distribution function of length biased generalized Aradhana distribution will be obtained as

$$F_l(x;\theta,\alpha) = \int_0^x f_l(x;\theta,\alpha)dx$$

$$= \int_0^x \frac{x\theta^4}{\left(\theta^2 + 6\alpha^2 + 4\alpha\theta\right)}(1+\alpha x)^2 e^{-\theta x}dx \tag{6}$$

After simplification of equation (6), we will have determined the cumulative distribution function of length biased generalized Aradhana distribution as

$$F_l(x;\theta,\alpha) = \frac{1}{\left(\theta^2 + 6\alpha^2 + 4\alpha\theta\right)}\left(\theta^2\gamma(2,\theta x) + \alpha^2\gamma(4,\theta x) + 2\alpha\theta\,\gamma(3,\theta x)\right) \tag{7}$$

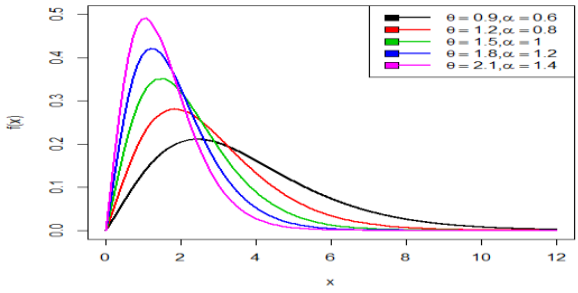


Figure 1: *Pdf plot of LBG Aradhana distribution*

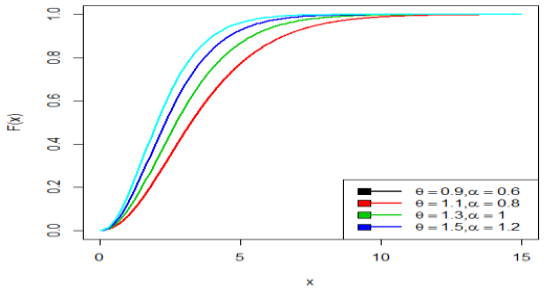


Figure 2: *Cdf plot of LBG Aradhana distribution*

III. Reliability Measures

In this portion, we will have determined some fundamental aspects like reliability function, hazard function, reverse hazard function and mills ratio of length biased generalized Aradhana distribution. The reliability function of length biased generalized Aradhana distribution is given by

$$R(x) = 1 - F_l(x;\theta,\alpha)$$

$$R(x) = 1 - \frac{1}{\left(\theta^2 + 6\alpha^2 + 4\alpha\theta\right)}\left(\theta^2\gamma(2,\theta x) + \alpha^2\gamma(4,\theta x) + 2\alpha\theta\,\gamma(3,\theta x)\right)$$

The hazard rate function of length biased generalized Aradhana distribution is given by

$$h(x) = \frac{f_l(x;\theta,\alpha)}{1. - F_l(x;\theta,\alpha)}$$

$$h(x) = \frac{x\theta^4(1+\alpha x)^2 e^{-\theta x}}{\left(\theta^2 + 6\alpha^2 + 4\alpha\theta\right) - \left(\theta^2\gamma(2,\theta x) + \alpha^2\gamma(4,\theta x) + 2\alpha\theta\,\gamma(3,\theta x)\right)}$$

The reverse hazard rate function of length biased generalized Aradhana distribution is given by

$$h_r(x) = \frac{f_l(x;\theta,\alpha)}{F_l(x;\theta,\alpha)}$$

$$h_r(x) = \frac{x\theta^4(1+\alpha x)^2 e^{-\theta x}}{\left(\theta^2\gamma(2,\theta x) + \alpha^2\gamma(4,\theta x) + 2\alpha\theta\,\gamma(3,\theta x)\right)}$$

The Mills Ratio of length biased generalized Aradhana distribution is given by

$$M.R = \frac{1}{h_r(x)} = \frac{\left(\theta^2\gamma(2,\theta x) + \alpha^2\gamma(4,\theta x) + 2\alpha\theta\,\gamma(3,\theta x)\right)}{x\theta^4(1+\alpha x)^2 e^{-\theta x}}$$

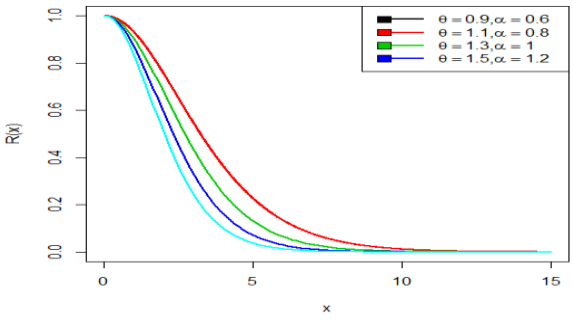


Figure 3:*Reliability plot of LBG Aradhana distribution*

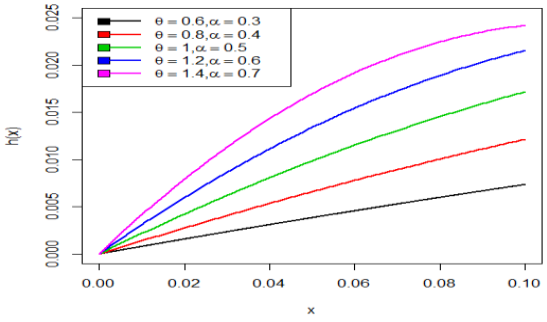


Figure 4:*Hazard plot of LBG Aradhana distribution*

IV. Statistical Properties

In this portion, we have determined and derived some properties of LBG Aradhana distribution.

I. Moments

Consider X be the random variable represents length biased generalized Aradhana distribution with parameters θ and α, then r^{th} order moment of LBG Aradhana distribution will be determined as

$$\mu_r' = E(X^r) = \int_0^\infty x^r f_l(x;\theta,\alpha)dx$$

$$= \int_0^\infty \frac{x^{r+1}\,\theta^4}{\left(\theta^2 + 6\alpha^2 + 4\alpha\theta\right)}(1+\alpha x)^2 e^{-\theta x}dx \qquad (8)$$

After the simplification of expression (8), we obtain

$$\mu_r' = \frac{\left(\theta^2\Gamma(r+2) + \alpha^2\Gamma(r+4) + 2\alpha\theta\,\Gamma(r+3)\right)}{\theta^r\left(\theta^2 + 6\alpha^2 + 4\alpha\theta\right)} \qquad (9)$$

Thus by applying r = 1, 2, 3 and 4 in equation (9), we will get the mean and other moments of length biased generalized Aradhana distribution

$$\mu_1' = \frac{\left(2\theta^2 + 24\alpha^2 + 12\alpha\theta\right)}{\theta\left(\theta^2 + 6\alpha^2 + 4\alpha\theta\right)}$$

$$\mu_2' = \frac{\left(6\theta^2 + 120\alpha^2 + 48\alpha\theta\right)}{\theta^2\left(\theta^2 + 6\alpha^2 + 4\alpha\theta\right)}$$

$$\mu_3' = \frac{\left(24\theta^2 + 720\alpha^2 + 240\alpha\theta\right)}{\theta^3\left(\theta^2 + 6\alpha^2 + 4\alpha\theta\right)}$$

$$\mu_4' = \frac{\left(120\theta^2 + 5040\alpha^2 + 1440\alpha\theta\right)}{\theta^4\left(\theta^2 + 6\alpha^2 + 4\alpha\theta\right)}$$

$$\text{Variance} = \frac{\left(2\theta^4 + 108\alpha^2\theta^2 + 24\alpha\theta^3 + 144\alpha^4 + 192\alpha^3\theta\right)}{\theta^2(\theta^2 + 6\alpha^2 + 4\alpha\theta)^2}$$

$$\text{S.D}(\sigma) = \frac{\sqrt{\left(2\theta^4 + 108\alpha^2\theta^2 + 24\alpha\theta^3 + 144\alpha^4 + 192\alpha^3\theta\right)}}{\theta(\theta^2 + 6\alpha^2 + 4\alpha\theta)}$$

II. Harmonic Mean

The harmonic mean of explored distribution will be obtained by

$$\text{H.M} = E\left(\frac{1}{x}\right) = \int_0^\infty \frac{1}{x} f_l(x;\theta,\alpha)dx$$

$$= \int_0^\infty \frac{\theta^4}{\left(\theta^2 + 6\alpha^2 + 4\alpha\theta\right)}\left(1 + \alpha^2x^2 + 2\alpha x\right)e^{-\theta x}dx \qquad (10)$$

After the simplification of expression (10), we obtain

$$\text{H.M} = \frac{\theta\left(\theta + 2\alpha^2 + 2\alpha\theta\right)}{\left(\theta^2 + 6\alpha^2 + 4\alpha\theta\right)}$$

III. Moment generating function and characteristic function

The moment generating function of explored LBG Aradhana distribution will be obtained as

$$M_X(t) = E\left(e^{tx}\right) = \int_0^\infty e^{tx} f_l(x;\theta,\alpha)dx$$

$$= \int_0^\infty \frac{x\theta^4}{\left(\theta^2 + 6\alpha^2 + 4\alpha\theta\right)}\left(1 + \alpha x\right)^2 e^{-(\theta - t)x}dx \qquad (11)$$

After simplification, we obtain from expression (11)

$$M_X(t) = \frac{1}{(\theta - t)^4\left(\theta^2 + 6\alpha^2 + 4\alpha\theta\right)}\theta^4\left((\theta - t)^2 + 4\alpha(\theta - t) + 6\alpha^2\right)$$

Particularly, characteristic function of length biased generalized Aradhana distribution is given by

$$\varphi_X(t) = \frac{1}{(\theta - it)^4\left(\theta^2 + 6\alpha^2 + 4\alpha\theta\right)}\theta^4\left((\theta - it)^2 + 4\alpha(\theta - it) + 6\alpha^2\right)$$

V. Bonferroni and Lorenz Curves

The bonferroni and Lorenz curves are also termed as classical curves which were studied in order to depict the behavior of inequality in income and poverty. The explored curves can be stated as

$$B(p) = \frac{1}{p\mu_1'}\int_0^q x\, f_1(x;\theta,\alpha)dx$$

$$L(p) = pB(p) = \frac{1}{\mu_1'}\int_0^q x\, f_1(x;\theta,\alpha)dx$$

$$\text{Here } \mu_1' = \frac{\left(2\theta^2 + 24\alpha^2 + 12\alpha\theta\right)}{\theta\left(\theta^2 + 6\alpha^2 + 4\alpha\theta\right)}$$

$$B(p) = \frac{\theta\left(\theta^2 + 6\alpha^2 + 4\alpha\theta\right)}{p\left(2\theta^2 + 24\alpha^2 + 12\alpha\theta\right)}\int_0^q \frac{x^2\theta^4}{\left(\theta^2 + 6\alpha^2 + 4\alpha\theta\right)}\left(1 + \alpha^2x^2 + 2\alpha x\right)e^{-\theta x}dx \qquad (12)$$

After simplification, we obtain from expression (12)

$$B(p) = \frac{1}{p\left(2\theta^2 + 24\alpha^2 + 12\alpha\theta\right)}\left(\theta^2\gamma(3,\theta q) + \alpha^2\gamma(5,\theta q) + 2\alpha\theta\,\gamma(4,\theta q)\right)$$

$$L(p) = \frac{1}{\left(2\theta^2 + 24\alpha^2 + 12\alpha\theta\right)}\left(\theta^2\gamma(3,\theta q) + \alpha^2\gamma(5,\theta q) + 2\alpha\theta\,\gamma(4,\theta q)\right)$$

VI. Order Statistics

Order statistics is basically a fundamental aspect within the domain of statistical sciences deals with the application of ordered values and its functions. Suppose the order statistics $X_{(1)}, X_{(2)}, \ldots, X_{(n)}$ of a random sample $X_1, X_2, \ldots, X_n$ from a continuous distribution with probability density function $f_x(x)$ and cumulative distribution function $F_x(x)$, then probability density function of r^{th} order statistics $X_{(r)}$ is defined as

$$f_{x(r)}(x) = \frac{n!}{(r-1)!\,(n-r)!}f_X(x)\left(F_X(x)\right)^{r-1}\left(1 - F_X(x)\right)^{n-r} \qquad (13)$$

By applying equation (5) and (7) in equation (13), we will determine the required probability density function of r^{th} order statistics $X_{(r)}$ of length biased generalized Aradhana distribution which is

$$f_{x(r)}(x) = \frac{n!}{(r-1)!\,(n-r)!}\left(\frac{x\theta^4(1+\alpha x)^2 e^{-\theta x}}{\left(\theta^2+6\alpha^2+4\alpha\theta\right)}\right)\left(\frac{\left(\theta^2\gamma(2,\theta x)+\alpha^2\gamma(4,\theta x)+2\alpha\theta\,\gamma(3,\theta x)\right)}{\left(\theta^2+6\alpha^2+4\alpha\theta\right)}\right)^{r-1}$$

$$\times\left(1-\frac{\left(\theta^2\gamma(2,\theta x)+\alpha^2\gamma(4,\theta x)+2\alpha\theta\gamma(3,\theta x)\right)}{\left(\theta^2+6\alpha^2+4\alpha\theta\right)}\right)^{n-r}$$

The pdf of higher order statistics $X_{(n)}$ of length biased generalized Aradhana distribution is given by

$$f_{x(n)}(x) = \frac{nx\theta^4(1+\alpha x)^2 e^{-\theta x}}{\left(\theta^2+6\alpha^2+4\alpha\theta\right)}\left(\frac{\left(\theta^2\gamma(2,\theta x)+\alpha^2\gamma(4,\theta x)+2\alpha\theta\,\gamma(3,\theta x)\right)}{\left(\theta^2+6\alpha^2+4\alpha\theta\right)}\right)^{n-1}$$

The pdf of first order statistics $X_{(1)}$ of length biased generalized Aradhana distribution is given by

$$f_{x(1)}(x) = \frac{n\,x\theta^4(1+\alpha x)^2 e^{-\theta x}}{\left(\theta^2+6\alpha^2+4\alpha\theta\right)}\left(1-\frac{\left(\theta^2\gamma(2,\theta x)+\alpha^2\gamma(4,\theta x)+2\alpha\theta\,\gamma(3,\theta x)\right)}{\left(\theta^2+6\alpha^2+4\alpha\theta\right)}\right)^{n-1}$$

VII. Maximum Likelihood Estimation and Fisher's Information Matrix

In this portion, we will describe the technique of parameter estimation to estimate the parameters of length biased generalized Aradhana distribution by applying maximum likelihood estimation. Suppose $X_1, X_2, \ldots, X_n$ be the random sample of size n from length biased generalized Aradhana distribution, then the likelihood function can be stated as

$$L(x) = \prod_{i=1}^{n} f_l(x;\theta,\alpha)$$

$$= \prod_{i=1}^{n}\left(\frac{x_i\,\theta^4}{\left(\theta^2+6\alpha^2+4\alpha\theta\right)}\left(1+\alpha x_i\right)^2 e^{-\theta x_i}\right)$$

$$= \frac{\theta^{4n}}{\left(\theta^2+6\alpha^2+4\alpha\theta\right)^n}\prod_{i=1}^{n}\left(x_i\left(1+\alpha^2 x_i^{\,2}+2\alpha x_i\right)e^{-\theta x_i}\right)$$

The log likelihood function should be defined as

$$\log L = 4n\log\theta - n\log\left(\theta^2+6\alpha^2+4\alpha\theta\right)+\sum_{i=1}^{n}\log x_i+\sum_{i=1}^{n}\log\left(1+\alpha^2 x_i^{\,2}+2\alpha x_i\right)-\theta\sum_{i=1}^{n}x_i \qquad (14)$$

Therefore by differentiating the log-likelihood equation (14) with respect to parameters θ and α. The following equations must have been satisfied

$$\frac{\partial \log L}{\partial\theta} = \frac{4n}{\theta} - n\left(\frac{\left(2\theta+4\alpha\right)}{\left(\theta^2+6\alpha^2+4\alpha\theta\right)}\right)-\sum_{i=1}^{n}x_i = 0$$

$$\frac{\partial \log L}{\partial \alpha} = -n\left(\frac{(12\alpha + 4\theta)}{\left(\theta^2 + 6\alpha^2 + 4\alpha\theta\right)}\right) + \sum_{i=1}^{n}\left(\frac{\left(2\alpha x_i^2 + 2x_i\right)}{(1 + \alpha^2 x_i^2 + 2\alpha x_i)}\right) = 0$$

It is quite clear to mention here that above system of non-linear equations are too complicated to solve those equations algebraically. Therefore, we apply the numerical technique like R and wolfram mathematics for estimating the required parameters of presented distribution.

In order to apply the asymptotic normality results for determining the confidence interval. We state that if $\hat{\eta} = (\hat{\theta}, \hat{\alpha})$ which constitutes the MLE of $\eta = (\theta, \alpha)$. The results should clearly interpreted as

$$\sqrt{n}\,(\hat{\eta} - \eta) \to N_2(0, I^{-1}(\eta))$$

Where $I^{-1}(\eta)$ is Fisher's information matrix.

$$I(\eta) = -\frac{1}{n}\begin{pmatrix} E\left(\frac{\partial^2 \log L}{\partial \theta^2}\right) & E\left(\frac{\partial^2 \log L}{\partial \theta\, \partial \alpha}\right) \\ E\left(\frac{\partial^2 \log L}{\partial \alpha\, \partial \theta}\right) & E\left(\frac{\partial^2 \log L}{\partial \alpha^2}\right) \end{pmatrix}$$

$$E\left(\frac{\partial^2 \log L}{\partial \theta^2}\right) = -\frac{4n}{\theta^2} - n\left(\frac{(\theta^2 + 6\alpha^2 + 4\alpha\theta)(2) - (2\theta + 4\alpha)^2}{(\theta^2 + 6\alpha^2 + 4\alpha\theta)^2}\right)$$

$$E\left(\frac{\partial^2 \log L}{\partial \alpha^2}\right) = -n\left(\frac{(\theta^2 + 6\alpha^2 + 4\alpha\theta)(12) - (12\alpha + 4\theta)^2}{(\theta^2 + 6\alpha^2 + 4\alpha\theta)^2}\right) + \sum_{i=1}^{n}\left(\frac{(1 + \alpha^2 x_i^2 + 2\alpha x_i)(2x_i^2) - (2\alpha x_i^2 + 2x_i)^2}{(1 + \alpha^2 x_i^2 + 2\alpha x_i)^2}\right)$$

$$E\left(\frac{\partial^2 \log L}{\partial \theta\, \partial \alpha}\right) = -n\left(\frac{(\theta^2 + 6\alpha^2 + 4\alpha\theta)\,(4) - (2\theta + 4\alpha)\,(12\alpha + 4\theta)}{(\theta^2 + 6\alpha^2 + 4\alpha\theta)^2}\right)$$

Since η is not known therefore we estimate $I^{-1}(\eta)$ is estimated by $I^{-1}(\hat{\eta})$ and it should be applied to get the asymptotic confidence interval for θ and α.

VIII. Entropy

The entropy is a scientific concept which is broadly associated with randomness or uncertainty in a system. The entropy is applied in vast areas and is defined as

I. Renyi Entropy

The term Renyi entropy is most fundamental component in quantum information and is defined as

$$T_R(\gamma) = \frac{1}{1-\gamma}\log\left(\int f_1^{\gamma}(x;\theta,\alpha)\,dx\right)$$

$$= \frac{1}{1-\gamma}\log\int_0^{\infty}\left(\frac{x\theta^4}{\left(\theta^2 + 6\alpha^2 + 4\alpha\theta\right)}(1 + \alpha x)^2 e^{-\theta x}\right)^{\gamma} dx \qquad (15)$$

After simplification of expression (15), we obtain

$$T_R(\gamma) = \frac{1}{1-\gamma}\log\left(\left(\frac{\theta^{3\gamma-k-1}}{\left(\theta^2+6\alpha^2+4\alpha\theta\right)^{\gamma}}\right)\sum_{k=0}^{2\gamma}\binom{2\gamma}{k}\alpha^k\frac{\Gamma(\gamma+k+1)}{\gamma^{\gamma+k+1}}\right)$$

Particularly, the Tsallis entropy of explored distribution will be obtained by applying the expression

$$T_S(\xi) = \frac{1}{\xi-1}\left(1-\int_0^{\infty} f_1^{\xi}(x;\theta,\alpha)\,dx\right)$$

$$= \frac{1}{\xi-1}\left(1-\int_0^{\infty}\left(\frac{x\theta^4}{\left(\theta^2+6\alpha^2+4\alpha\theta\right)}\left(1+\alpha x\right)^2 e^{-\theta x}\right)^{\xi}dx\right) \tag{16}$$

After simplification of expression (16), we obtain

$$T_S(\xi) = \frac{1}{\xi-1}\left(1-\left(\frac{\theta^{3\xi-j-1}}{\left(\theta^2+6\alpha^2+4\alpha\theta\right)^{\xi}}\right)\sum_{j=0}^{2\xi}\binom{2\xi}{j}\alpha^j\frac{\Gamma(\xi+j+1)}{\xi^{\xi+j+1}}\right)$$

IX. Likelihood Ratio Test

Consider the random sample $X_1, X_2, \ldots, X_n$ of size n from the generalized Aradhana or length biased generalized Aradhana distribution. To examine its significance the hypothesis is to be tested.

$$H_0 : f(x) = f(x;\theta,\alpha) \quad \text{against} \quad H_1 : f(x) = f_l(x;\theta,\alpha)$$

To identify whether if the random sample of size n comes from the generalized Aradhana or length biased generalized Aradhana distribution the following test statistic procedure is applied.

$$\Delta = \frac{L_1}{L_0} = \prod_{i=1}^{n}\frac{f_l(x;\theta,\alpha)}{f(x;\theta,\alpha)}$$

$$= \prod_{i=1}^{n}\left(\frac{x_i\,\theta\left(\theta^2+2\alpha\theta+2\alpha^2\right)}{\left(\theta^2+6\alpha^2+4\alpha\theta\right)}\right)$$

$$= \left(\frac{\theta\left(\theta^2+2\alpha\theta+2\alpha^2\right)}{\left(\theta^2+6\alpha^2+4\alpha\theta\right)}\right)^n\prod_{i=1}^{n}x_i$$

The null hypothesis should be refused to accept if

$$\Delta = \left(\frac{\theta\left(\theta^2+2\alpha\theta+2\alpha^2\right)}{\left(\theta^2+6\alpha^2+4\alpha\theta\right)}\right)^n\prod_{i=1}^{n}x_i > k$$

$$\Delta^* = \prod_{i=1}^{n} x_i > k\left(\frac{\left(\theta^2 + 6\alpha^2 + 4\alpha\theta\right)}{\theta(\theta^2 + 2\alpha\theta + 2\alpha^2)}\right)^n$$

$$\Delta^* = \prod_{i=1}^{n} x_i > k^*, \text{Here } k^* = k\left(\frac{\left(\theta^2 + 6\alpha^2 + 4\alpha\theta\right)}{\theta(\theta^2 + 2\alpha\theta + 2\alpha^2)}\right)^n$$

X. Application

In this portion, we have incorporated and fitted two real lifetime data sets to explore the flexibility and significance of length biased generalized Aradhana distribution and then potentiality has been accomplished in order to illustrate that length biased generalized Aradhana distribution provides a better fit over generalized Aradhana, quasi Aradhana, new quasi Aradhana, Aradhana, Shanker, Ishita, Suja and Lindley distributions.

Data set 1: The first data set which represents the failure stresses (in GPa) of 65 single carbon fibers of length 50 mm, respectively reported by Bader and Priest [3]. The observations of data set are
1.339, 1.434, 1.549, 1.574, 1.589, 1.613, 1.746, 1.753, 1.764, 1.807, 1.812, 1.84, 1.852, 1.852, 1.862, 1.864, 1.931, 1.952, 1.974, 2.019, 2.051, 2.055, 2.058, 2.088, 2.125, 2.162, 2.171, 2.172, 2.18, 2.194, 2.211, 2.27, 2.272, 2.28, 2.299, 2.308, 2.335, 2.349, 2.356, 2.386, 2.39, 2.41, 2.43, 2.431, 2.458, 2.471, 2.497, 2.514, 2.558, 2.577, 2.593, 2.601, 2.604, 2.62, 2.633, 2.67, 2.682, 2.699, 2.705, 2.735, 2.785, 3.02, 3.042, 3.116, 3.174

Data set 2: The second uncensored data set relates to breaking stress of carbon fibres in Gba which insists of (n =100) observations discussed by Mahmoud and Mandouh [10]. The following values are
0.92, 0.928, 0.997, 0.9971, 1.061, 1.117, 1.162, 1.183, 1.187, 1.192, 1.196, 1.213, 1.215, 1.2199, 1.22, 1.224, 1.225, 1.228, 1.237, 1.24, 1.244, 1.259, 1.261, 1.263, 1.276, 1.31, 1.321, 1.329, 1.331, 1.337, 1.351, 1.359, 1.388, 1.408, 1.449, 1.4497, 1.45, 1.459, 1.471, 1.475, 1.477, 1.48, 1.489, 1.501, 1.507, 1.515, 1.53, 1.5304, 1.533, 1.544, 1.5443, 1.552, 1.556, 1.562, 1.566, 1.585, 1.586, 1.599, 1.602, 1.614, 1.616, 1.617, 1.628, 1.684, 1.711, 1.718, 1.733, 1.738, 1.743, 1.759, 1.777, 1.794, 1.799, 1.806, 1.814, 1.816, 1.828, 1.830, 1.884, 1.892, 1.944, 1.972, 1.984, 1.987, 2.020, 2.0304, 2.029, 2.035, 2.037, 2.043, 2.046, 2.059, 2.111, 2.165, 2.686, 2.778, 2.972, 3.504, 3.863, 5.306

To predict the model comparison criterion values in accompanied with unknown parameters are also estimated through analysis of R software. To capture and highlight the performance of length biased generalized Aradhana distribution over generalized Aradhana, quasi Aradhana, new quasi Aradhana, Aradhana, Shanker, Ishita, Suja and Lindley distributions, the criterions like *AIC* (Akaike Information Criterion), *BIC* (Bayesian Information Criterion), *AICC* (Akaike Information Criterion Corrected), *CAIC* (Consistent Akaike Information Criterion), Shannon entropy *H(X)* and *-2logL* have been applied. The distribution performs quite better if it has the smaller criterion values of *AIC, BIC, AICC, CAIC, H(X)* and *-2logL* as compared over other distributions. The criterion values are obtained as

$$AIC = 2k - 2\log L, \qquad BIC = k\log n - 2\log L, \qquad AICC = AIC + \frac{2k(k+1)}{n-k-1}$$

$$CAIC = -2\log L + \frac{2kn}{n-k-1} \qquad \text{and} \qquad H(X) = -\frac{2\log L}{n}$$

Here –2log$L$ is the maximized log-likelihood function, k is the number of parameters in the statistical model and n is the sample size.

Table 1: *shows MLE and S.E of performed distributions*

Data set 1			Data set 2		
Distribution	MLE	S.E	Distribution	MLE	S.E
LBGA	$\hat{\alpha} = 2417.554$ $\hat{\theta} = 1.78228$	$\hat{\alpha} = 1211.2035$ $\hat{\theta} = 0.1105221$	LBGA	$\hat{\alpha} = 8.037644$ $\hat{\theta} = 2.412787$	$\hat{\alpha} = 1.115002$ $\hat{\theta} = 1.206393$
GA	$\hat{\alpha} = 7.40697$ $\hat{\theta} = 1.33679$	$\hat{\alpha} = 2.105967$ $\hat{\theta} = 9.572945$	GA	$\hat{\alpha} = 7273.082$ $\hat{\theta} = 1.809438$	$\hat{\alpha} = 112.0043$ $\hat{\theta} = 0.000000$
QA	$\hat{\alpha} = 0.00100$ $\hat{\theta} = 1.33656$	$\hat{\alpha} = 0.4179194$ $\hat{\theta} = 0.1603995$	QA	$\hat{\alpha} = 0.00100$ $\hat{\theta} = 1.80915$	$\hat{\alpha} = 0.31270$ $\hat{\theta} = 0.17171$
NQA	$\hat{\alpha} = 1.175703$ $\hat{\theta} = 1.336786$	$\hat{\alpha} = 1.677723$ $\hat{\theta} = 9.572441$	NQA	$\hat{\alpha} = 8535.289$ $\hat{\theta} = 1.80930$	$\hat{\alpha} = 6653.122$ $\hat{\theta} = 0.10444$
Aradhana	$\hat{\theta} = 0.9843106$	$\hat{\theta} = 0.07340$	Aradhana	$\hat{\theta} = 1.2499381$	$\hat{\theta} = 0.076716$
Shanker	$\hat{\theta} = 0.70435$	$\hat{\theta} = 0.0578065$	Shanker	$\hat{\theta} = 0.891169$	$\hat{\theta} = 0.05958$
Ishita	$\hat{\theta} = 0.98371$	$\hat{\theta} = 0.0607588$	Ishita	$\hat{\theta} = 1.186687$	$\hat{\theta} = 0.059421$
Suja	$\hat{\theta} = 1.73751$	$\hat{\theta} = 0.0809330$	Suja	$\hat{\theta} = 2.023585$	$\hat{\theta} = 0.075263$
Lindley	$\hat{\theta} = 0.70672$	$\hat{\theta} = 0.0648246$	Lindley	$\hat{\theta} = 0.917731$	$\hat{\theta} = 0.068961$

Table 2: *shows interpretation, analysis and performance of fitted distributions of data set 1*

Distributions	-2logL	AIC	BIC	AICC	CAIC	H(X)
LBGA	144.0153	148.0153	152.3641	148.2088	148.2088	2.2156
GA	161.3134	165.3134	169.6621	165.5069	165.5069	2.4817
QA	161.3463	165.3463	169.695	165.5398	165.5398	2.4822
NQA	161.3122	165.3122	169.661	165.5057	165.5057	2.4817
Aradhana	197.0756	199.0756	201.25	199.1390	199.1390	3.0319
Shanker	209.7126	211.7126	213.887	211.7760	211.7760	3.2263
Ishita	203.2007	205.2007	207.3751	205.2641	205.2641	3.1261
Suja	184.4748	186.4748	188.6492	186.5382	186.5382	2.8380
Lindley	213.9985	215.9985	218.1729	216.0619	216.0619	3.2922

Table 3: *shows interpretation, analysis and performance of fitted distributions of data set 2*

Distributions	-2logL	AIC	BIC	AICC	CAIC	H(X)
LBGA	177.4824	181.4824	186.6927	181.6061	181.6061	1.7748
GA	198.6203	202.6203	207.8307	202.7440	202.7440	1.9862
QA	198.662	202.662	207.8723	202.7857	202.7857	1.9866
NQA	198.6278	202.6278	207.8381	202.7515	202.7515	1.9862
Aradhana	257.5579	259.5579	262.1631	259.5987	259.5987	2.5755
Shanker	275.4242	277.4242	280.0294	277.4650	277.4650	2.7542
Ishita	283.1591	285.1591	287.7643	285.1999	285.1999	2.8315
Suja	297.3904	299.3904	301.9956	299.4312	299.4312	2.9739
Lindley	277.1388	279.1388	281.744	279.1796	279.1796	2.7713

Obviously, it is observed and revealed from results given above in table 2 and table 3 that the length biased generalized Aradhana distribution have lesser *AIC*, *BIC*, *AICC*, *CAIC, H(X)* and *-2logL* values as compared to generalized Aradhana, quasi Aradhana, new quasi Aradhana, Aradhana, Shanker, Ishita, Suja and Lindley distributions. Hence, it is realized that length biased generalized Aradhana distribution provides a quite satisfactory fit as compared to generalized Aradhana, quasi Aradhana, new quasi Aradhana, Aradhana, Shanker, Ishita, Suja and Lindley distributions.

XI. Conclusion

In this paper, we have formulated a new class of generalized Aradhana distribution termed as length biased generalized Aradhana distribution which has been explored by incorporating specific length biased technique to its baseline distribution. Thus presented new distribution illustrated and accomplished with its distinguished statistical properties which are moments, mean and variance, standard deviation, survival function, hazard function, reverse hazard rate function, moment generating function, bonferroni and Lorenz curves have been described. Additionally Renyi entropy measure and order statistics has been discussed. Further, the parameters of specific new distribution are also estimated through the maximum likelihood estimation. Furthermore, the dominance and significance of proposed new distribution are analyzed and investigated by applying two real data sets. Hence, it is inspected and is clearly indicated from the result that the length biased generalized Aradhana distribution gives a better fit in comparison over generalized Aradhana, quasi Aradhana, new quasi Aradhana, Aradhana, Shanker, Ishita, Suja and Lindley distributions.

References

[1] Almakhareez, S. and Alzoubi, L. (2024). Length-biased Benrabia distribution with applications. *Electronic Journal of Applied Statistical Analysis*, 17(02):255-277.

[2] Al-Omari, A. I. and Alsmairan, I. K. (2019). Length-biased Suja distribution and its applications. *Journal of Applied Probability and Statistics*, 14(3):95-116.

[3] Badar, M. G. and Priest, A. M. (1982). Statistical aspects of fiber and bundle strength in hybrid composites. In T. Hayashi, K. Kawata & S. Umekawa (Eds.). *Progress in Science and Engineering Composites*. ICCM-IV, Tokyo, 1129-1136.

[4] Bashir, S. and Khan, H. (2023). Characterization of the weighted power function distribution by reliability functions and moments. *Research in Mathematics*, 10(1):2202023.

[5] Beghriche, A. and Zeghdoudi, H. (2019). A size biased gamma Lindley distribution. *Thailand Statistician*, 17(2):179-189.

[6] Cox, D. R. (1962). *Renewal theory*, Barnes and Noble, New York, USA.

[7] Fisher, R. A. (1934). The effects of methods of ascertainment upon the estimation of frequencies. *Ann. Of Eugenics*, 6:13-25.

[8] Ganaie, R. A., Rajagopalan, V., Soumya, V. P. and Shenbagaraja, R. (2023). Characterizations and some contribution to new quasi Sujatha distribution with applications in blood cancer, Covid 19 and survival times. *International Journal of Statistics and Reliability Engineering*, 10(2):446-455.

[9] Ganaie, R. A. and Rajagopalan, V. (2020). Length biased weighted quasi gamma distribution with characterizations and applications. *International Journal of Innovative Technology and Exploring Engineering (IJITEE)*, 9(5):1110-1117.

[10] Mahmoud, M. R. and Mandouh, R. M. (2013). On the transmuted Frechet distribution. *Journal of Applied Sciences Research*, 9(10):5553-5561.

[11] Mustafa, A. and Khan, M. I. (2022). The length-biased power hazard rate distribution: Some properties and applications. *STATISTICS IN TRANSITION new series*, 23(2):1-16.

[12] Mustafa, A. and Khan, M. I. (2023). Length biased extended Rayleigh distribution and its applications. *Journal of Modern Applied Statistical Methods*, 22(2).

[13] Mudasir, S. and Ahmad, S. P. (2018). Characterization and estimation of the length biased Nakagami distribution. *Pak.j.stat.oper.res*., 14(3):697-715.

[14] Perveen, Z., Ahmed, Z. and Ahmad, M. (2016). On size-biased double weighted exponential distribution (SDWED). *Open Journal of Statistics*, 6:917-930.

[15] Rao, C. R. (1965). On discrete distributions arising out of method of ascertainment, in classical and contagious Discrete, G.P. Patiled; *Pergamum Press and Statistical Publishing Society, Calcutta*. 320-332.

[16] Rashwan, N. I. (2013). A length-biased version of the generalized gamma distribution. *Advances and Applications in Statistics*, 32(2):119-137.

[17] Rasool, S. U. and Ahmad, S. P. (2022). Power length biased weighted Lomax distribution. *Reliability: Theory & Applications*, 17(4):543-558.

[18] Ratnaparkhi, M. V. and Naik-Nimbalkar, U. V. (2012). The length-biased lognormal distribution and its application in the analysis of data from oil field exploration studies. *Journal of Modern Applied Statistical Methods*, 11(1):255-260.

[19] Saghir, A., Tazeem, S. and Ahmad, I. (2016). The length-biased weighted exponentiated inverted weibull distribution. *Cogent Mathematics*, 3(1): Article: 1267299.

[20] Saghir, A. and Khadim, A. (2016). The mathematical properties of length biased weighted Maxwell distribution. *Journal of Basic and Applied Research International*, 16(3):189-195.

[21] Salama, M. M., Elsherpieny, E. A. and Abd-elaziz, A. A. (2023). The length-biased weighted exponentiated inverted exponential distribution: Properties and estimation. *Computational Journal of Mathematical and Statistical Sciences*, 2(2):181-196.

[22] Welday, D. and Shanker, R. (2018). A generalized Aradhana distribution with properties and applications. *Biometrics & Biostatistics International Journal*, 7(4):374-385.

ENHANCING PRODUCT QUALITY AND OPERATIONAL EFFICIENCY THROUGH STATISTICAL QUALITY CONTROL

M. A. Khanday[1], A. Jain[2], A. A. Khan[3], Y. Ahmad[4], A. A. Rather[5]

•

[1,2,3,4]Department of Statistics, School of Chemical Engineering and Physical Sciences,
Lovely Professional University, Phagwara, Punjab, India
[5]Symbiosis Statistical Institute, Symbiosis International (Deemed University),
Pune-411004, India
manzoorstat@gmail.com, akshatjain14042001@gmail.com,
karshad.maths@gmail.com, yarmth111@gmail.com,
aafaq7741@gmail.com

Abstract

The foundation of success in the modern business environment is maintaining constant quality and efficiency across supply chains. The paper presents a clear and comprehensive analysis as it delves into the complexities of quality control in the supply chain for makeup products. By utilizing a diverse range of statistical techniques, such as descriptive statistics, control chart analysis, and ANOVA, and able to reveal important information about defect rates and the overall field of quality control procedures. This research reveals the complex interactions between different elements that affect defect rates, with a focus on the crucial functions that lead time and shipping carriers play in the supply chain for makeup products. By means of a methodical and thorough examination, we not only reveal the stability that is innate to the manufacturing process but also identify critical areas that are ripe for improvement. Determine areas for improvement by carefully examining the data; this will set the stage for increased operational effectiveness and higher standards of quality. This paper bridges the gap between theoretical understanding and real-world applications, rather than just existing in the domain of theoretical conjecture. Provide participants in the makeup product supply chain with practical insights that can lead to observable outcomes by combining academic accuracy with real-world relevance. In order to enable stakeholders to confidently and precisely navigate the complexities of quality control, this paper acts as a beacon of guidance. Stakeholders can enhance operational performance, reduce risks, and foster a continuous improvement culture by utilising the findings. Furthermore, by maintaining an intense focus on raising customer satisfaction, this analysis clears the path for long-term success in the competitive and dynamic makeup product market.

Keywords: Statistical quality control, P-Chart, Defect rate ANOVA, Box-Cox transformation

1. Introduction

The need for effective quality control systems cannot be emphasized in the complex web of modern business, where international markets demand consistent quality and efficiency. The use of efficient quality control methods has grown critical as businesses work to satisfy changing customer demands and strict industry requirements. With an emphasis on the use of statistical quality control (SQC) across a variety of variables crucial to operational excellence, this research article aims to investigate the relationship between quality control and company performance.

The cornerstone for companies hoping to surpass as well as satisfy client expectations is quality control. It is the fundamental pillar that guarantees processes and products always follow established guidelines, protecting against deviations that might threaten the quality of goods and services. Insufficient quality control can have serious consequences, including unhappy clients, harm to one's image, and monetary losses. Thus, for organizations to effectively navigate the complicated rules of the contemporary business world, an in-depth awareness of quality control is crucial. Statistical Quality Control (SQC) is a structured, data-driven technique that enables organizations to monitor, analyse, and improve their processes. It is the central idea of our investigation. SQC makes use of statistical techniques to sort through large datasets and uncover insightful information that helps with decision-making. SQC gives businesses a scientific framework to find trends, patterns, and abnormalities in their operations by utilizing statistical methods, including regression analysis, control charts, and hypothesis testing. This enables companies to take action on possible problems before they worsen and makes it easier to identify early departures from intended quality standards. As we set out on our study adventure, we will be concentrating on a wide range of characteristics that all work together to create the complex fabric of company operations. Product types, SKUs (stock keeping units), prices, availability, number of sold items, income produced, consumer characteristics, stock levels, time to delivery, orders, shipping durations, transporting holders, shipping expenses, supplier names, locations, production volumes, lead times for manufacturing, manufacturing costs, inspection findings, defect rates, and modes, routes, and costs of transportation are among the attributes that are being closely examined. Each of these characteristics is essential to our SQC analysis since it shapes the effectiveness and fineness of different business processes. We will consult a wide range of academic publications, including influential works on statistical techniques, quality control, and applicable research from specialized industries, to support our conclusions. By combining academic research with real-world applications, we want to offer a comprehensive and complex comprehension of how SQC may be used to promote operational excellence across these qualities. In addition to adding to the body of knowledge on quality control, our research aims to provide organizations with practical advice that they can use to improve the effectiveness of their quality processes. Our goal is to provide businesses with the information and resources they need to successfully go through the area of quality control field and gain an advantage in today's hectic business world by exploring the specifics of SQC and how it applies to various business aspects [1, 2, 3].

2. Literature Review

An extensive review of the literature and research on statistical quality control (SQC) is necessary to understand its significance in our industry's dynamic quality management landscape. The purpose of this review of the literature is to shed light on the present state of knowledge by highlighting the importance of significant features in quality control and exposing the variety of statistical techniques used in related situations [4]. A wide range of academics has explored the field of SQC, shedding light on its capacity to revolutionize a variety of sectors. A thorough investigation of the manufacturing industry was carried out, which highlighted the critical role that SQC plays in reducing errors and simplifying production procedures. Their results highlighted how effective control charts are in tracking variances and promptly addressing departures from defined quality standards. This is extremely relevant to our study, which focuses on characteristics like Manufacturing Lead Time, Production Volumes, and Defective Costs, where SQC may play a critical role in guaranteeing smooth manufacturing processes [5]. Additionally, the application of SQC to qualities including Delivery Times, Transit Modes, and Destinations in the context of logistics and supply chain management. Regression analysis is one statistical approach that was used to show how SQC makes it easier to identify the best shipping routes and timings, which lowers costs and improves overall operational efficiency [6]. It is impossible to overestimate the importance of any feature in the context of quality control. For example, the value of demographic study in the field of customer demographics when it

comes to customizing goods for certain customer groups. When used for client-related variables, SQC offers knowledge about changing consumer preferences and helps companies adjust their strategy to guarantee client loyalty and happiness [7]. It is clear from reading through SQC literature that various statistical techniques and instruments have unique functions when it comes to guaranteeing the effectiveness of quality control procedures. The comprehensive application of testing for hypotheses in SQC was explored, which showed how it may help validate process modifications and advancements. This is especially important to our research when we examine characteristics like Lead Times and Order Quantities since they might reveal the best order fulfillment methods through hypothesis testing [8]. Furthermore, a thorough summary of the many statistical techniques used in SQC. Their research demonstrates the flexibility of statistical methods in improving overall transportation performance, from the use of regression analysis to analyse shipping costs to the implementation of control charts to track fluctuations in stock levels [9]. We can see from our analysis of this large body of research that SQC provides a meticulously data-driven approach to quality control that cuts across industry borders. Applying statistical techniques to a variety of characteristics is helpful in both spotting departures from accepted conventions and actively creating business plans for the best results. The context for our research is established by this assessment of the literature, which highlights the body of knowledge that already exists and the opportunity for SQC to completely transform quality management in our sector [10]. Bayesian Estimation of Inverse Ailamujia distribution using different loss functions have been studied in [11]. This paper is significant for its in-depth analysis of defect rates and quality control procedures in the makeup product supply chain. Many research studies on quality control in a variety of industries, such as manufacturing, healthcare, and services, are available; however, the number of studies that concentrate exclusively on the supply chain of makeup products is rather small. With its thorough analysis of the variables affecting defect rates and process stability in this specialized industry, this paper closes a gap in the literature. Further adding depth and rigour to the analysis and providing a comprehensive understand of quality control dynamics is the application of a wide range of statistical techniques, including descriptive statistics, control chart analysis, and ANOVA.

3. Methodology

In the beginning, measures of central tendency and dispersion as well as other descriptive statistics were computed for the defect rate data. In order to determine whether the defect rate data was normal, the Anderson-Darling normality test was utilized.

3.1. Box-Cox Transformation

A Box-Cox transformation was used to evaluate the defect rate data's distributional characteristics and enhance its suitability for statistical analysis. A popular technique for achieving approximate normality and stabilizing variance in non-normal data is the Box-Cox transformation. The definition of the transformation is as follows:

$$TransformData = \begin{cases} \dfrac{(y^{\lambda}-1)}{\lambda}, & \lambda \neq 0 \\ \log y, & \lambda = 0, \end{cases} \tag{1}$$

where y represents the original defect rate data and λ is the transformation parameter.

If the data was discovered to be non-normal, different values of λ were investigated in order to determine which transformation most closely looked like a normal distribution. Following the estimation of the ideal value for λ, the estimation's uncertainty was measured by computing a confidence interval. Using the Box-Cox transformation to estimate the ideal value of λ, various values of λ were applied within the estimated confidence interval to perform a sensitivity analysis. The range of values within which the true λ parameter was estimated to lie with a specific level of confidence was given by the confidence interval. The transformed data's distribution was

evaluated after λ was systematically changed within this range. Iteratively, values of λ were found that produced transformed data that approximated a normal distribution. In particular, it was found that by examining λ values inside the confidence interval, some λ values were able to normalize the data distribution and bring it into closer alignment with the presumptions needed for further statistical analysis, like control charting. After obtaining the transformed data using the Box-Cox transformation and exploring different values of λ within the estimated confidence interval, the normality of the transformed data was re-evaluated using the Anderson-Darling (AD) test. A p-chart was used to track the defect rate over time because it is specifically made for attribute data, like the percentage of defective items in a sample. The monitoring of process stability and the identification of shifts or trends in the defect rate is made possible by this control chart, which is especially helpful when dealing with binary outcomes like the presence or absence of defects. The transformed defect rate data were used to calculate the control limits for the p-chart using statistical formulas. Using appropriate control chart constants and probability distributions, control limits for the upper and lower bounds were established based on the calculated average defect rate and sample size. The defect rate over time was graphically represented by the p-chart, which was created using the transformed defect rate data and the computed control limits. The proportion of defective items observed in a sample is represented by each data point on the chart, and the control limits show the range that, in the event that the process is stable, the defect rate should normally fall within. A process capability analysis was carried out to evaluate the manufacturing process's ability to satisfy customer specifications after the p-chart was constructed and process stability was guaranteed using statistical quality control. Several capability indices, such as Cp, Cpk, and Cpm, were calculated for this analysis using the customer requirements' upper specification limit (USL) and lower specification limit (LSL). While Cpk takes into account the process's cantering and spreading in relation to the specification limits, Cp measures the process's potential ability to produce within the limits. Cpm also accounts for any bias in the process mean and integrates process cantering. The analysis offered insights into the process's capacity to reliably meet specification targets by contrasting the computed capability indices with predefined threshold values (usually established by customer requirements or industry standards). With the goal of enhancing process capability and guaranteeing product quality and customer satisfaction, any shortcomings or areas for improvement found during the analysis were addressed through focused process optimization efforts. An Analysis of Variance (ANOVA) was performed after the process capability analysis to determine the variables influencing defect rates. The analysis took into account the lead time, shipping carriers, and mode of transportation. The statistical method known as ANOVA is used to determine if the mean defect rates at various levels of one or more categorical variables (factors) differ in a way that is statistically significant. ANOVA assists in determining which factors significantly affect defect rates by analyzing the variation in defect rates attributable to each factor and evaluating their significance levels. The following can be used to formulate the null and alternative hypotheses for the Analysis of Variance (ANOVA) examining the factors influencing defect rates with lead time, shipping carriers, and mode of transportation acting as independent variables:

Null Hypothesis (H_0): The mean defect rates across various lead times, shipping carriers, and modes of transportation do not differ significantly.

Alternative Hypothesis (H_A): At least one independent variable seems to have a significant impact on defect rates.

4. Result and Analysis

4.1. Descriptive Statistics

A comprehensive overview of the defective rates is given by the descriptive statistics, which also include measurements of central tendency, dispersion, distributional shape, and range. They are crucial for comprehending the features and unpredictability of the data, which can guide further investigation and decision-making.

Table 1: *Descriptive Statistics of the transformed data*

Mean	2.277158
Standard Error	0.146137
Median	2.141863
Standard Deviation	1.461366
Sample Variance	2.135589
Kurtosis	-1.114
Skewness	0.129644
Range	4.920648
Minimum	0.018608
Maximum	4.939255
Sum	227.7158
Count	100

4.2. Normality

The Anderson-Darling (AD) test was used to determine whether the data for the defective rates were normally distributed. The result was a p-value of 0.009 which is less than the significance level 0.01. This result increases the possibility that the defective rates don't follow a normal distribution and provides strong evidence against the null hypothesis of normalcy. Furthermore, a probability plot was created to visually examine the distributional assumptions for the defective rates. Potential deviations from normalcy were further indicated by deviations from the straight line seen in the probability plot.

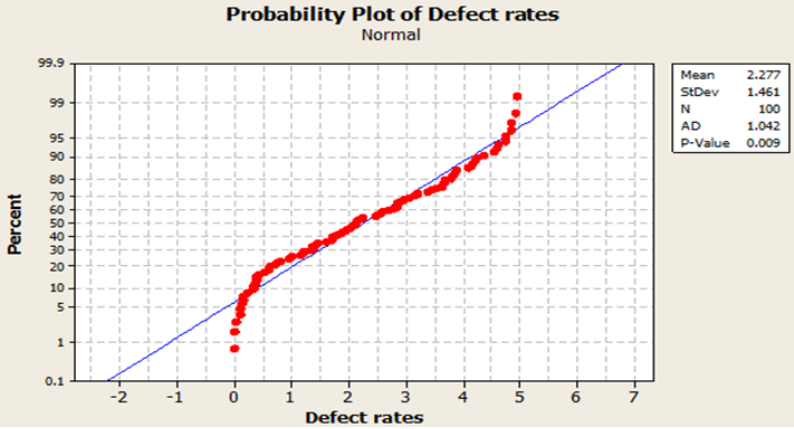


Figure 1: *Probability Plot of defect rates*

4.3. Box-Cox Transformation

In order to resolve the non-normality in the defect rates, the Box-Cox transformation was applied; the estimated optimal value of λ is 0.626378, with a 95% confidence interval (CI) extending from 0.457403 to 0.836229. By applying λ values within this confidence interval, a sensitivity analysis was carried out, and the results showed that $\lambda = 0.65$ fell within the confidence interval. By making this decision, the transformed data was successfully normalized and brought into compliance with the presumptions required for further statistical analyses, like control charts. To show how the transformation affected the data's distribution, a Box-Cox plot was created.

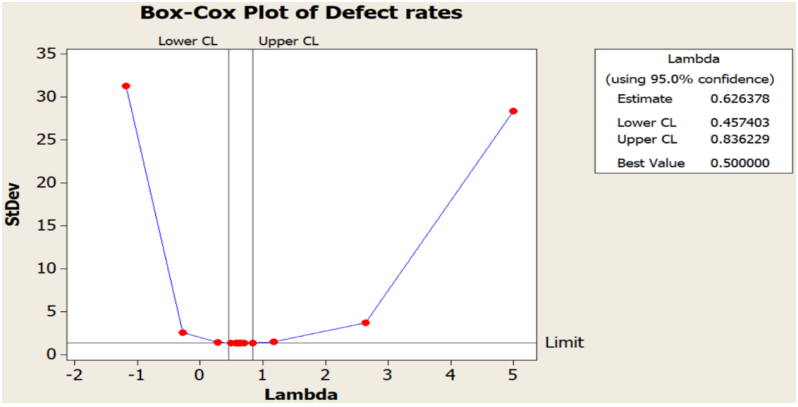


Figure 2: *Box-Cox Plot Defect rates*

After the Box-Cox transformation with $\lambda = 0.65$, the normality of the data set was evaluated using the Anderson-Darling (AD) test. The resulting p-value of 0.1133 means that there is not enough data to reject the null hypothesis that the transformed data has a normal distribution at a significance level of $\alpha = 0.01$. By exceeding the significance threshold, the p-value indicates that the transformed data appears to approximate a normal distribution fairly well.

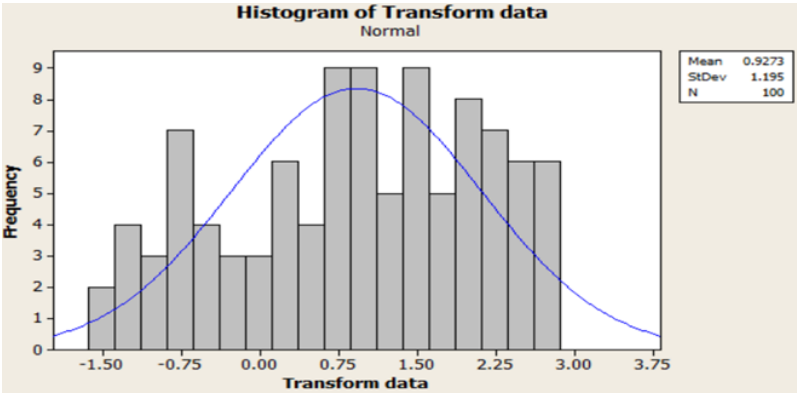


Figure 3: *Normality of the data*

4.4. Control Chart Analysis

The P-chart analysis reveals a predominantly stable process, with defect rates closely clustered around the centerline (0.00927), indicating consistent performance. The control limits (LCL = 0, UCL = 0.03802006) effectively differentiate between common-cause variation and potential special-cause outliers, ensuring reliable monitoring. The high stability metric (StoDraw = 0.99993354) further confirms that the majority of subgroups adhere to expected variation patterns, reflecting process control. However, 34 data points were flagged for exceeding test limits, suggesting minor deviations that warrant investigation to identify root causes. Subgroup-specific upper control limits (e.g., UCs = 0.00820006) imply stricter quality standards for certain segments, highlighting tailored process checks. The absence of widening areas (0 instances) indicates no need for control limit adjustments, reinforcing process consistency. Negative group summary statistics (-0.01, -0.00) show that some subgroups performed better than the average defect rate. While no extreme outliers were detected, the flagged points underscore the importance of vigilance to maintain quality standards. The chart™s design successfully balances sensitivity to variation with practical stability, making it a robust tool for defect rate monitoring. Continuous monitoring is recommended to sustain this level of control and address any emerging trends. The process demonstrates strong overall management, with only minor deviations requiring

targeted review. By addressing these anomalies proactively, the process can further enhance its reliability. In summary, the P-chart confirms a well-controlled process, with opportunities for refinement through detailed analysis of flagged data points. This approach ensures long-term quality assurance and process optimization.

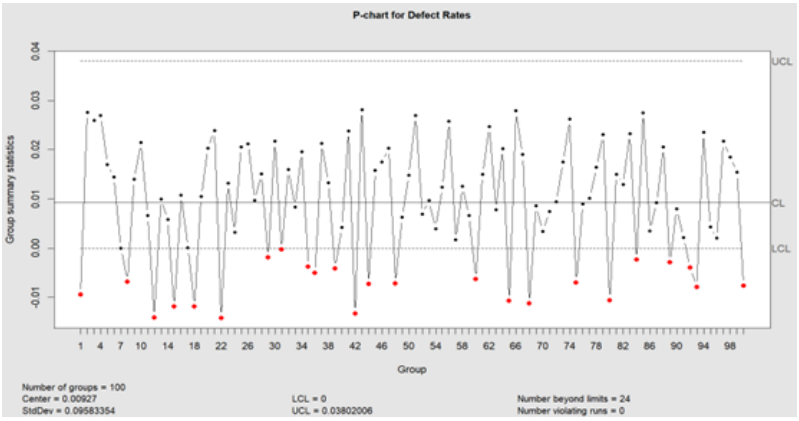


Figure 4: *P-chart for defective rates*

There are twenty-four data points in all that exceed the control limits, meaning that there are times when the defect rate is higher than expected. Nevertheless, no run violations were found, indicating that there were no notable departures from the anticipated pattern between successive data points. These findings show that although there are occasional cases where defect rates are higher than the predicted range of variation, there are no constant trends or patterns that point to underlying problems with the process.

4.5. Process Capability Analysis

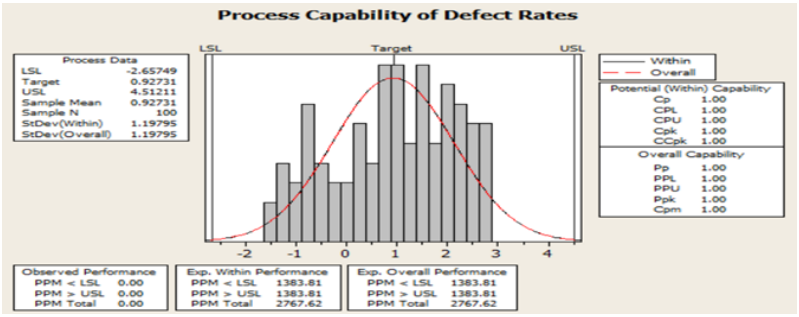


Figure 5: *Process capability for defective rates*

The process can successfully meet customer specifications, according to the results of the process capability analysis. The process spread is within the tolerance limits specified by the specification limits (USL = 4.512112 and LSL = -2.657486), with a Cp value of 1 and a Cpk value of 1. While a Cpk value of 1 indicates that the process is centred within the specification limits, a Cp value of 1 suggests that the process spread is in line with the allowable spread established by the specification limits. Furthermore, the process mean is in line with the target value (0.9273131), as indicated by the process capability index taking the target value, Cpm, which is also equal to 1.

4.6. Analysis of Variance (ANOVA) for Factors Affecting Defect Rates

To find out how lead times, carriers, and modes of transportation affect defect rates in the supply chain for makeup products, an ANOVA was performed. In terms of the independent variables

(lead time, shipping carriers, and modes of transportation), the null hypothesis (H_0) states that there is no significant difference in defect rates across levels. There appears to be a significant impact of at least one independent variable on defect rates, according to the alternative hypothesis (H_1).

Table 2: *Analysis of the defective rates*

S. V Pr(>F)	D. F	S. S	M. S. S	F-Value
Lead Time 0.00193**	1	18.66	18.662	10.184
Shipping Carriers 0.01128*	2	17.25	8.267	4.708
Transportation Mode 0.43160	3	5.09	1.696	0.926
Residuals	93	170.42	1.832	

4.7. Interpretation

As shown by their respective F-values of 10.184 and 4.708, with p-values of 0.00193 and 0.01128, both less than the significance level of 0.05, the ANOVA results show that lead time and shipping carriers have a significant impact on defect rates. We conclude that there is a significant difference in defect rates among various levels of lead time and shipping carrier, rejecting the null hypothesis. However, since the p-value of 0.43160, which is higher than the significance level, is obtained from an F-value of 0.926, the transportation modes do not appear to have a significant effect on defect rates. It means that we are unable to reject the null hypothesis regarding transportation modes suggests that there is not enough data to draw the conclusion that there is a meaningful difference in defect rates between the various modes of transportation. As a result, the analysis concludes that while transportation modes do not significantly affect defect rates in the makeup product supply chain, lead time and shipping carriers do. Supply chain managers and other decision-makers may find this information useful in prioritising lead time management enhancements and choosing the best shipping carrier, which will ultimately lower defect rates and improve product quality.

5. Discussion

The study provides a comprehensive examination of the importance of statistical quality control (SQC) in modern corporate operations. It highlights how important efficient quality control systems are to maintaining consistency in efficiency and quality, particularly in the context of shifting industry standards and client demands. This research effort to examine the correlation between quality control and business performance in diverse domains by concentrating on statistical quality control (SQC) methods like regression analysis, control charts, and hypothesis testing. Key conclusions from the literature include the use of SQC techniques in logistics and supply chain management to optimise shipping routes and timings, as well as the usefulness of control charts in tracking variances and addressing deviations from quality standards in manufacturing. Furthermore, studies related to customers, like demographics, have demonstrated the value of SQC in terms of strategy adaptation and guaranteeing customer satisfaction. The paper looks into defect rates and factors influencing quality control using descriptive statistics, normality tests, Box-Cox transformation, control chart analysis, process capability analysis, and ANOVA. While normality tests and transformation techniques guarantee that data is suitable for further analysis, descriptive statistics offer insights into the features and variability of defect

rates. Process capability analysis assesses a manufacturing process's ability to meet customer specifications, while control chart analysis helps monitor process stability and spot deviations from expected quality levels. ANOVA is used to assess how lead time, shipping carriers, and modes of transportation affect defect rates. The results of this study offer important new information about the makeup product supply chain's defect rates and quality control-influencing variables. The central tendency, dispersion, and distributional shape of the defect rates dataset are among the important features that descriptive statistics highlight. It is crucial to comprehend these characteristics in order to spot patterns and trends in defect rates, which can direct efforts to improve processes and make decisions. The results of the Anderson-Darling (AD) test normality test show that the defect rate data do not fit into a normal distribution, as indicated by the low p-value. This result implies that the data in its original form might not be suitable for analysis using standard parametric statistical techniques. Still, the data distribution is successfully normalised by the Box-Cox transformation, opening the door to additional parametric analysis. Control chart analysis provides insights into process stability and variation in defect rates over time. The control chart analysis revealed occasional elevated defect rates above the control limits; however, this does not always mean that there are notable deviations from expected patterns or instability in the manufacturing process. These events may be explained by common sources of variation found in all production systems, like chance fluctuations or small discrepancies. Out of the entire dataset, there were only 24 instances of defects that exceeded the control limits, indicating that these occurrences are relatively rare and irregular. All things considered, the manufacturing process seems to be stable. Most defect rates fall within expected ranges, indicating that the process is under control and that variations are tolerable within typical operating parameters. The Cp and Cpk values near to 1 in the process capability analysis demonstrate that the manufacturing process can satisfy customer requirements. This shows that there is little variation in the process with respect to customer requirements and that it is centred within specification bounds. Consistent product quality is ensured by the process capability index (Cpm), which additionally verifies that the process mean is in line with the target value. The ANOVA results show that lead time and shipping carrier variations have a significant impact on defect rates, indicating that these factors affect the results of quality control. On the other hand, it doesn't seem that modes of transportation significantly affect defect rates. These results highlight how crucial effective lead time management and cautious carrier selection are to reducing faults and raising product quality in the product supply chain.

5.1. Limitation and Future Scope

This paper's limitations are related to the extent of the analysis and the industry that was examined. The study offers insightful information about quality control procedures in the makeup product supply chain, but it's possible that the conclusions won't apply to other businesses or more broadly defined manufacturing sectors. Furthermore, the study mainly examines defect rates and variables affecting quality control, possibly ignoring other essential aspects of process optimisation and quality management. The paper would also benefit from a more thorough discussion of any external factors or confounding variables that might affect defect rates but were left out of the analysis. Future research could look into including a wider range of industries and variables in the analysis, drawing from a variety of sources to improve the generalisation and reliability of the findings. This would address these limitations and provide a more comprehensive understanding of quality control practices. Further insights into the intricacies of quality control procedures and their consequences for overall operational performance may also be obtained by incorporating qualitative feedback from industry experts or by carrying out case studies in actual manufacturing environments.

6. Conclusion

In summary, this paper offers a thorough analysis of quality control procedures and defect rates in the makeup product supply chain. Significant insights into process stability, variability, and factors influencing defect rates have been gained through the use of a variety of statistical techniques, including descriptive statistics, normality tests, Box-Cox transformation, control chart analysis, process capability analysis, and ANOVA. The results indicate that although there have been occasional reports of higher-than-average defect rates, overall, the manufacturing process seems to be stable, with variations mainly attributed to shared causes rather than underlying issues. The study also emphasises the critical role that effective management techniques play in these domains by highlighting the substantial effects that lead times and shipping companies have on defect costs. Organisations may enhance their comprehension of quality control dynamics, identify methods for enhancement, and ultimately maximise operational performance through the utilisation of statistical methods and data-driven approaches. By offering useful insights that can guide decision-making processes in the pursuit of ongoing improvement and customer satisfaction within the makeup product supply chain, the research adds to the body of knowledge already available on quality management.

References

[1] Chowdhury, D., Johnson, J. N., BakerSmith, C. M., Jaquiss, R. D., Mahendran, A. K., Curren, V. and Shaffer, K. (2021). Health care policy and congenital heart disease: 2020 focus on our 2030 future. *Journal of the American Heart Association*, 10(20):e020605.

[2] Edenshaw, B. (2019). A review on the existing service quality measurement models. *Science Journal of Business and Management*, 7(4):87-201.

[3] Dhamija, P. and Bag, S. (2020). Role of artificial intelligence in operations environment: a review and bibliometric analysis. *The TQM Journal*, 32(4):869-896.

[4] Raghavendra, S. T. V. S., Manideep, B., PremSai, R. and Adi Siva Kishore Reddy, Y. (2013). A Case Study on Total Quality Control of Manufacturing of Liners by Applying SPC Technique. *International Journal of Engineering Research and Applications*, 3(4):357-368.

[5] Judi, H. M., Genasan, D. and Jenal, R. (2011). *Quality control implementation in manufacturing companies: motivating factors and challenges*. INTECH Open Access Publisher.

[6] Lambert, D. M., Cooper, M. C. and Pagh, J. D. (1998). Supply chain management: implementation issues and research opportunities. *The international journal of logistics management*, 9(2):1-20.

[7] Hin´ica, V., Svobodov, A. and ezankov, H. (2022). Consumer perception of quality of clothing products: a lesson for the business sector arising from czech evidence. *Central European Business Review*, 11(2).

[8] Bagchi, Tapan. (2001). Statistical Methods and Inspection Techniques in Quality Control: An Introduction. 10.13140/2.1.4842.6887.

[9] Nagar, H. and Gahlot, A. (2022). A Review on Statistical Quality Control. *Neuro Quantology*, 20(9):637-642.

[10] Ahmad, I. (2018). Implementation of Quality Control. *In Quality Control in Laboratory. IntechOpen.*

[11] Ahmad, A., Khanday, M. A., Powar, S. K., Rather, A. A. and Subramanian, C. (2025). Bayesian estimation of inverse Ailamujia distribution using different loss functions. *Reliability: Theory & Applications*, 20(1 (82)):620-631.

ANALYSIS OF MODELING METHODS OF LINEAR AND NONLINEAR AUTOMATIC CONTROL SYSTEMS

S.M. Kerimova[1], S.J. Alimamedova[2]

•

Azerbaijan State Oil and Industry University, Baku, Azerbaijan
[1] saida.karimova@asoiu.edu.az; [2] alimammadova.sara@asoiu.edu.az

Abstract

The article discusses the stability of automatic control systems (ACS). The stability of the automatic control system is the main characteristic of the automatic return of the system to its initial state of equilibrium after exposure to certain influencing factors on this system. In other words, it is the property of the system to maintain its resistance to external influences and its efficiency. The issue of reliability is aimed at preventing unforeseen and dangerous consequences of system instability, especially in such diverse fields as aviation, energy, and industry. A stable system ensures more accurate performance of the specified functions and is less prone to probable failure, and they can work for a long time without human intervention. An important place in the issue of determining the stability of ACS is occupied by the identification of errors that occur mainly during transients occurring in systems. The detected error is determined by the difference between the input signal (setpoint) and the input signal. In addition, the error that occurs in the system depends on different types of input signals, so these inputs can be stepwise, linear, etc. they can be typical. It should be noted that bias error analysis is useful only for stable systems. That is, before investigating an error in the system, it is necessary to determine the stability of this system. The article also considered the issue of calculating the error in the system with negative feedback. Using the Matlab/Simulink program, algorithms related to the detection of an error in the ACS are compiled. When studying the issues of ACS stability, the issue of regulating the gain coefficients of various types through a PID (Proportional-Integral-Derivative) regulator is being investigated.

Keywords: automatic control system, stability, excitation effect, transfer function, gain factor, controller

I. Introduction

The stability of an automatic control system is one of the fundamental characteristics that determine its overall effectiveness, operational quality, and long-term safety. In engineering terms, stability refers to the system's inherent ability to automatically return to its initial equilibrium state after it has been subjected to external disturbances, internal fluctuations, or other influencing factors. This means that even if the system experiences shocks, sudden changes in input, or unexpected environmental conditions, a stable system will naturally correct itself and resume its intended behavior without continuous external intervention.

In simpler terms, stability is the essential property that allows the system to resist external impacts and continue performing its intended functions reliably and predictably. Without this capability, even the most advanced automatic control systems could fail under real-world conditions, compromising not only performance but also safety and operational integrity.

But why is stability such an essential requirement for any control system? To answer this question, several key considerations must be highlighted [1-4]:

1. Safety concerns – System instability can lead to unpredictable and potentially hazardous consequences, particularly in critical industries such as aviation, energy production, chemical processing, and manufacturing. In these sectors, even minor instabilities can escalate into major accidents.

2. Accuracy and performance – A stable system is capable of executing assigned tasks with higher precision, ensuring that operational goals are met without excessive deviations or oscillations.

3. Reliability and durability – Stability is directly tied to the system's long-term dependability. A system that maintains stability is less prone to unexpected breakdowns, requires fewer emergency interventions, and can function for extended periods with minimal maintenance. This not only reduces operational costs but also ensures smoother workflows and greater confidence in the system's performance. Unstable systems, by contrast, can wear out components faster due to erratic operation, leading to downtime, increased maintenance, and reduced service life.

By mastering the fundamental principles of control system stability, engineers can design solutions that are not only more reliable and efficient but also inherently safer. Stability knowledge enables them to predict system behavior under various conditions, adjust design parameters appropriately, and prevent potential problems before they occur.

Furthermore, the study of stability is far from a purely theoretical exercise—it plays a critical role in a wide range of practical applications, including industrial automation, robotics, aerospace engineering, power systems, transportation technologies, and many other fields. As technology advances, these applications increasingly demand higher precision, faster response times, and greater resilience, all of which depend on robust system stability.

The topic of stability also opens a broad spectrum for exploration. Numerous aspects can be examined, such as different methods for analyzing system stability, the influence of nonlinear effects that complicate traditional stability assessments, and the practical application of stability theories across diverse industries. These areas not only expand academic knowledge but also provide a strong incentive for further research, technological innovation, and the creation of more advanced and resilient control systems.

Purpose. Relevance of the problem and related studies. Modern automatic information and control systems (ACS) are highly complex structures, incorporating numerous interconnected subsystems and components. This growing complexity introduces significant challenges in system modeling and analysis. With the rapid evolution of technology, the integration of advanced tools such as artificial intelligence, adaptive algorithms, and sophisticated software platforms further raises the need for improved approaches to ensure and evaluate stability [5-8].

In contemporary engineering, the stability of both linear and nonlinear systems remains a key area of study. Traditional analytical methods are constantly being refined, while new techniques are being developed to address the unique challenges posed by increasingly dynamic and intelligent control systems. The aim of the present article is to investigate the fundamental issues related to the stability of control systems. Specifically, the focus is on:

- identifying and discussing the main parameters that define the stability of various types of systems;

- analyzing typical scenarios and equivalent system models that are used to simplify stability studies;

- emphasizing the importance of mathematical tools and calculations in evaluating system stability and predicting system behavior under different conditions.

By addressing these aspects, this study contributes to a broader understanding of how stability principles can be applied to modern control systems, ensuring that they meet the demands of safety, precision, and reliability in a rapidly changing technological landscape [9-11].

II. Materials and methods

In determining the stability of ACS, the determination of errors arising during the transition processes occurring in the systems plays an important role. The determined error is determined by the difference between the input signal (given value) and the input signal. In addition, the error arising in the system depends on different types of input signals, since these input signals can be step, linear, etc. types. It should be noted that the analysis of the determined error is useful only for stable systems. That is, before examining the error in the system, the stability of that system must be determined. Based on the value of the output signal, we can calculate the error using the transfer function of an open or closed loop with the following expressions:

$$e(\infty) = \lim_{s\to 0} sE(s) = \lim_{s\to 0} \frac{sR(s)}{1+G(s)} \quad (1)$$

$$e(\infty) = \lim_{s\to 0} sE(s) = \lim_{s\to 0} sR(a)(1-T(s)) \quad (2)$$

Using the Laplace transform, we obtain the following expressions for different input signals, for example [4]:

- When the "Step" input signal R(s)=1/s:

$$e(\infty) = \frac{1}{1+\lim_{s\to 0} G(s)} = \frac{1}{1+k_s} \Rightarrow k_s \lim_{s\to 0} G(s) \quad (3)$$

- When the "Ramp" input signal R(s)=1/s²:

$$e(\infty) = \frac{1}{\lim_{s\to 0} sG(s)} = \frac{1}{k_v} \Rightarrow k_v = \lim_{s\to 0} sG(s) \quad (4)$$

- Parabolic input signal R(s) = 1/s³:

$$e(\infty) = \frac{1}{\lim_{s\to 0} sG(s)} = \frac{1}{k_v} \Rightarrow k_v = \lim_{s\to 0} sG(s) \quad (5)$$

Usually, when investigating the stability of systems, the distortions occurring in these systems should also be taken into account. Let us assume that we need to compensate for the distortion in any control system, in other words, the system has been introduced with unusable signals (Fig. 1).

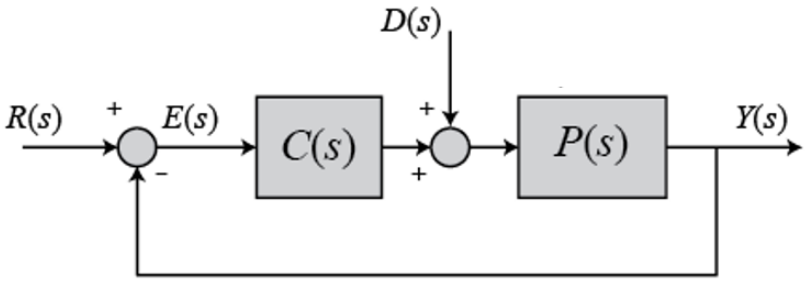


Figure 1: *Negative feedback circuit diagram*

In order to determine the error caused by the excitation signal D(s) shown in Fig. 1 in the system, we can use the following expression:

$$e(\infty) = \lim_{s\to 0} sE(s) = \frac{1}{\lim_{s\to 0} \frac{1}{P(s)} + \lim_{s\to 0} G(s)} \quad (6)$$

It should be noted that the signal entering the G(s) controller is not actually considered the fixed error E(s). By error, we mean only the difference between the given value and the current

value: E(s) = R(s) - Y(s) [12-16].

In the feedback loop depicted in Fig. 2, in the presence of a transfer function H(s), the signal R(s) is distorted by the effect of that transfer function.

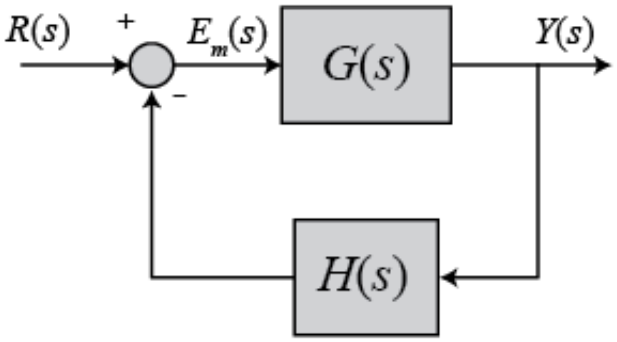


Figure 2: *Scheme of ACS in the presence of transfer function H(s)*

In this case, the structural diagram of the control system under study should be drawn as shown in Fig. 3.

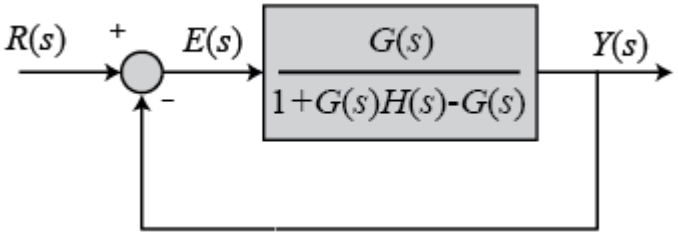


Figure 3: *The equivalent circuit of the ACS depicted in Fig. 2*

To illustrate the process more clearly, let's look at the issue of investigating the stability of an ACS using the MATLAB program. Let's assume that the transfer function of the controller is calculated by the following expression:

$$G(s) = \frac{k(s+3.5)(s+5.3)}{s(s+8)(s+9)} \tag{7}$$

As can be seen from Fig. 3, the transfer function of the feedback loop is unity. In this case, there will be no continuous error when a step signal is input to the system, but if a parabolic signal is input, this will cause an infinite error [17-21]. That is, the error in the system will be eliminated only by the influence of the step signal. First, we assume the amplification factor k=1 in expression (7) and write the corresponding algorithm from the MATLAB command window.

```
s = tf('s');
G = ((s+3.5)*(s+5.3))/(s*(s+8)*(s+9));
T = feedback(G,1);
t = 0:0.1:25;
u = t;
[y,t,x] = lsim(T,u,t);
plot(t,y,'r',t,u,'g')
xlabel('Time (sec)')
ylabel('Amplitude')
title('Input-red, Output-gree')
```

Then we get the input-output characteristic shown in Fig. 4. As can be seen from this figure, we can see that the output signal is about 16 times the input signal during a period of 20 seconds

(the decision error is about 4), that is, the decision error of this system is quite large. In this case, we can adjust the gain coefficients that bring the system to a stable state by using a PID (Proportional-Integrator-Derivative) controller. For this purpose, the model shown in Fig. 5 is designed [22-25].

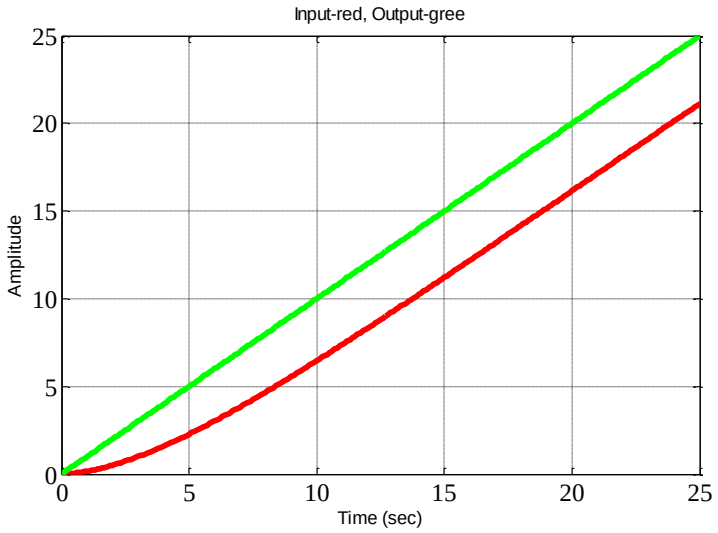


Figure 4: *Time characteristics of ACS input-output signals*

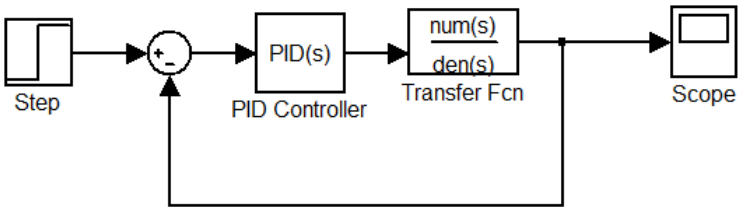


Figure 5: *Simulink model of ACS*

The description of the parameters window of the PID controller included in the Simulink model of the ACS is shown in Fig. 6.

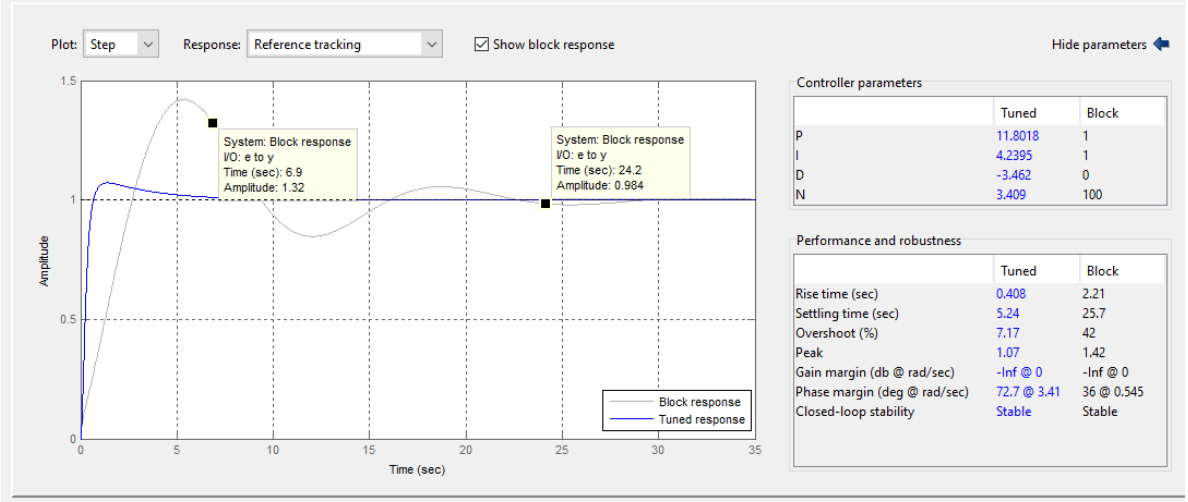


Figure 6: *Description of the PID controller parameters window*

In Fig. 6, "Block response" is the system response, and "Tuned response" is the system response corresponding to the value of the gain coefficients proposed by the PID controller. In Fig. 7, the values of the gain coefficients set for the stable system of the PID controller are given [26-28].

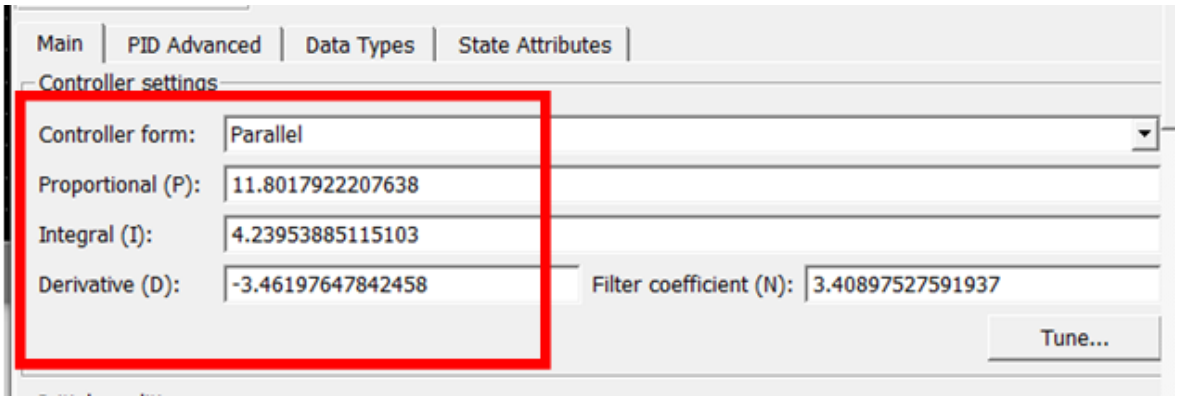


Figure 7: *Values of the PID controller's adjustable gain coefficients for a stable system*

III. Conclusions

First and foremost, the study highlighted that the determination of system stability must precede any error analysis. This approach is essential because instability can distort system behavior to such an extent that meaningful error calculations become impossible or irrelevant.

A key focus was placed on the relationship between input signals and system errors. It was established that the error — defined as the difference between the desired (given) input value and the actual system output — is significantly influenced by the type of input signal. Since input signals can vary, the resulting transient errors also exhibit different characteristics. This means that system designers and engineers must take into account not only the magnitude of the error but also its dynamic behavior under diverse operational conditions.

The study further explored the calculation and detection of system errors using advanced modeling and simulation tools. By leveraging MATLAB/Simulink, a set of algorithms was developed to accurately identify and quantify errors that arise in ACS during transient processes. These algorithms provide a practical framework for engineers to simulate various operating scenarios, analyze system responses, and refine designs before real-world implementation.

Additionally, the research examined the role of PID controllers in enhancing system stability and minimizing errors. The process involved the adjustment of different types of amplification coefficients (proportional, integral, and derivative gains) to optimize system response. The findings reaffirmed that proper tuning of these parameters can significantly improve both stability and overall system performance, effectively reducing steady-state and transient errors.

In summary, the study not only confirmed the central role of stability in ACS analysis but also demonstrated practical methods for evaluating and improving system performance. By combining theoretical stability considerations with simulation-based error detection and control strategies, a comprehensive approach was established. This integrated perspective is invaluable for the future development of ACS, ensuring they remain reliable, precise, and adaptable in increasingly complex technological environments.

References

[1] S.A. Khanahmedova, "Methods of modeling linear and nonlinear systems of automatic control", PROCEEDINGS OF AZERBAIJAN HIGH TECHNICAL EDUCATIONAL INSTITUTIONS, Vol. 37 (05) issue 02, 2024, pp. 223-241

[2] Z.A. Hasanov, S.A. Khanahmedova, "Management Theory", Textbook, ASOIU publication, Baku-2022, p. 166

[3] S.A. Khanahmedova, S.Y. Shikhaliyeva, S.J. Alimamedova, S.M. Kerimova, "Some issues of designing a hybrid electric machine", International Journal on "Technical and Physical Problems of Engineering", (IJTPE), Vol. 15, No3, pp.45-52, September 2023

[4] Rao V.Dukkipati, "Analysis and design of Control systems", New age international publish., New Dehli, 2006, pp.269

[5] Khanahmedova S.A., "Investigation of some electrical circuits using simulation in MATLAB/Simulink", Vestnik nauki journal, № 2 (59) Issue 1, 2023, pp. 125-129

[6] Aminzare Z., Sontag E.D., "Synchronization of Diffusively-Connected Nonlinear Systems: Results Based on Contractions with Respect to General Norms", IEEE Trans. Netw. Sci. Eng., 2014, 1, pp. 91–106

[7] S.A. Khanahmadova, A.I. Mamedov, "Mathematical analysis of regulated dc motor of hybrid system". International Journal on "Technical and Physical Problems of Engineering" (IJTPE), Vol. 15, No4, pp.19-24, December 2023

[8] Knights V., Petrovska O., Prchkovska M., "Enhancing Smart Parking Management through Machine Learning and AI Integration in IoT Environments", In Navigating the Internet of Things in the 22nd Century—Concepts, Applications, and Innovations [Working Title], IntechOpen: London, UK, 2024

[9] S.A. Khanakhmedova, S.M. Kerimova S.J. Alimamedova, "Mathematical modeling of the operation of a three-phase power transformer at low voltage quality", International Journal on "Technical and Physical Problems of engineering" (IJTPE), Vol.14, No 4, pp.225-232, December 2022

[10] Mammadov N. S., Mukhtarova K. M., "METHODOLOGY FOR ASSESSING THE RELIABILITY OF AGS BASED ON RENEWABLE ENERGY SOURCES", Reliability: Theory & Applications, Volume 19, No 4 (80), pp.648-653, 2024

[11] Sultanov Rafig, Elbrus Ahmedov and Nadir Aliyev, "Implementation of the maximum permissible overload capacity of a DC motor", Reliability: Theory & Applications 20.1 (82), 2025, pp. 728-733

[12] Meindl M., Lehmann D., Seel T., "Bridging Reinforcement Learning and Iterative Learning Control: Autonomous Motion Learning for Unknown", Nonlinear Dynamics. Front. Robot. AI 2022, 9, 793512

[13] Nijat Mammadov, Ilkin Marufov, Saadat Shikhaliyeva, Gulnara Aliyeva, Saida Kerimova, "Research of methods power control of wind turbines", Przeglad Elektrotechniczny, No 5, 2024, pp. 236-239, DOI: 10.15199/48.2024.05.44

[14] S.A. Khanahmadova, A.I. Mamedov, "Structural design and theoretical studies of operation of a drive Hybrid Electric Machine", International Journal on "Technical and Physical Problems of Engineering (IJTPE), Vol. 16, No1, pp.1-6, March 2024

[15] Elshad Safiyev, Ilham Rahimli, Nijat Mammadov, "Method of qualitative impregnation of electric motor windings", Przegląd Elektrotechniczny, No 8, 2024, pp.238 -240, DOI: 10.15199/48.2024.08.48

[16] Rzayeva S.V., Ganiyeva N.A., Piriyeva N.M., "Modern approaches to electrical equipment diagnostics", International Journal on technical and Physical Problems of Engineering (IJTPE), Issue 58, Vol. 16, No 1, pp. 182-189, 2024

[17] Khanna A., Kaur S., "Internet of Things (IoT), Applications and Challenges: A Comprehensive Review", Wirel. Pers. Commun., 2020, 114, pp. 1687–1762

[18] Ilkin Marufov, Najiba Piriyeva, Nijat Mammadov, Shukufa Ismayilova, "Calculation of induction levitation vertical axis wind generator-turbine system parameters, levitation and influence loop" Przegląd Elektrotechniczny, 2024 , No.2, pp.135-139, DOI: 10.15199/48.2024.02.27

[19] N.M.Piriyeva, G.S. Kerimzade, "Mathematical model for the calculation of electrical devices based on induction levitators", International Journal on technical and Physical Problems of Engineering (IJTPE), Issue 55, Vol.15, No.2, pp.274-280, June 2023

[20] Nadir Aliyev, Elbrus Ahmedov, Samira Khanahmedova, Sona Rzayeva, "Synthesis of the Exact Parameters of the Electromagnetic Brake of a Wind Electric Installation", Przeglad Elektrotechniczny journal, № 10, Poland, 2023, pp. 120-124, DOI: 10.15199/48.2023.10.123

[21] I.N.Rahimli, N.S. Mammadov, R.K. Karimova, "Analysis of wind turbine control algorithms as part of a wind power plant", International Journal on technical and Physical Problems of Engineering (IJTPE), Issue 62, Vol.17, No.1, pp.81-90, March 2025

[22] Yilmaz N., Wu J.Y., Kazanzides P., Tumerdem U., "Neural Network-Based Inverse Dynamics

Identification and External Force Estimation on the da Vinci Research Kit", In Proceedings of the 2020 IEEE International Conference on Robotics and Automation (ICRA), Paris, France, 31 May–31 August 2020

[23] A.I. Abdulkadyrov, S.C. Osmanov, N.A. Aliyev, G.A. Aliyeva, "Features of Calculating the Parameters of Special Electric Machines", News of Azerbaijan Higher Technical Schools, No. 5, Issue 87, pp. 55-61, Baku, Azerbaijan, 2013

[24] Z.A. Hasanov, S.A. Khanahmedova, "Regulation Technique", Textbook, ASOIU publication, Baku-2016, p. 130.

[25] Linder A., Kennel R., "Model predictive control for electrical drives", 2005 IEEE 36th Power Electronics Specialists Conference, IEEE, 2005, pp. 1793-1799

[26] Frey G., Hussain T, "Modeling techniques for distributed control systems based on the IEC 61499 standard-current approaches and open problems", In Proceedings of the 2006 8th International Workshop on Discrete Event Systems, Ann Arbor, MI, USA, 10–12 July 2006, pp. 176–181

[27] Simonazzi M., Delmonte N., Cova P., Menozzi R., "Models for MATLAB Simulation of a University Campus Micro-Grid", Energies 2023, 16, 5884

[28] S.A. Khanahmedova, S.M. Kerimova, S.J. Alimamedova, Z.Sh. Huseynova, "Some issues related to modeling electrical circuits on the MATLAB platform", Problems of Energy, No 2, Baku 2022, pp. 166-170

RT&A, No 3 (86)
Volume 20, September 2025

THE POWER GENERALIZED KAVYA MANOHARAN TRANSFORMATION: APPLICATIONS IN RELIABILITY AND LIFETIME REGRESSION

Jinet Mariya Jojy[1], Sajesh T. A.[2] and Nicy Sebastian[3*]

•

[1,2,3] Department of Statistics, St Thomas College, Thrissur
affiliated to the University of Calicut, Kerala, India- 680 001
[1]jinetmariyajojy@gmail.com,[2]sajesh.t.abraham@gmail.com,
[3*]nicycms@gmail.com
[*]Corresponding Author

Abstract

A new class of distributions is introduced through the exponentiated generalization of the Kavya Manoharan transformation, referred to as the Power Generalized Kavya Manoharan (PGKM) transformation. In parallel systems, applying power transformations to the distribution of individual components yields the system's overall distribution. This generalization enhances the model's flexibility and accuracy. In this context, we propose a transformation to generate a novel class of distributions, specifically by developing a distribution based on the Inverse Weibull distribution as the baseline. We investigate the behaviour of the hazard rates of these distributions, along with other analytical properties. Reliability measures for both single-component and multi-component stress-strength models are derived. The parameters of the proposed model are estimated using the maximum likelihood method, and simulation studies confirm the consistency of these estimates. Additionally, the new life distribution is applied to a real dataset, demonstrating superior fit when compared to various existing distributions in the literature. The distribution is further re-parametrized with location-scale parameters and employed in a lifetime regression analysis, with application provided to a practical dataset.

Keywords: Lifetime, PGKM transformation, Inverse Weibull distribution, Lifetime Regression Analysis.

1. Introduction

Modelling and analysis of lifetime distributions have been widely used in many fields of science such as medicine, engineering and statistics. There are several methods to propose new classes of distributions using the existing distributions as the baseline distribution. For example, if $G(x)$ is some baseline distribution function, then a new distribution function is obtained as $F(x) = (G(x))^{\alpha}$, where $\alpha > 0$ is a shape parameter. This is the well-known Lehmann family found useful in modelling failure time data as revealed in several research works, see, Gupta et al. [12]. Another approach to generalizing a baseline distribution is to transform it using the quadratic rank transmutation map (QRTM), see Shaw and Buckley [23]. If $H(x)$ be the cdf of transmuted distribution corresponding to the baseline distribution having cdf $F(x)$, then

$$H(x) = (1+\lambda)F(x) - \lambda\{F(x)\}^2, |\lambda| \leq 1.$$

Recently, various generalizations have been introduced based on QRTM, see Aryal and Tsokos [2], Aryal [3], Khan and King [15] etc. Kumar et al. [17] proposed a method to get new lifetime

distributions called DUS(Dinesh-Umesh-Sanjay) transformation and is defined as follows: Let $G_1(x)$ be the cumulative distribution function (cdf) and $g_1(x)$ be the probability density function (pdf) of some baseline distribution. Then by using DUS transformation, a new distribution is obtained corresponding to the baseline distribution as

$$F_1(x) = \frac{1}{e-1}\left(e^{G_1(x)-1}\right), \qquad x \in R \tag{1}$$

$$f_1(x) = \frac{1}{e-1} g_1(x)\left(e^{G_1(x)}\right), \qquad x \in R. \tag{2}$$

There are many distributions introduced by using the DUS transformation see, Maurya et al. [20], Kavya and Manoharan [13], Tripathi et al. [26].

Thomas and Chacko [25] a new class of distribution is introduced using an exponentiated generalization of the DUS transformation, called the power generalized DUS (PGDUS) transformation. Let X be a random variable with a baseline cdf $G_2(x)$ and the corresponding pdf $g_2(x)$. Then, the cdf and pdf of the PGDUS distribution is defined as:

$$F_2(x) = \left(\frac{1}{e-1}(e^{G_2(x)-1})\right)^{\theta}, \qquad x \in R \quad \theta > 0 \tag{3}$$

$$f_2(x) = \frac{\theta}{(e-1)^{\theta}} g_2(x)\left(e^{G_2(x)}\right)\left(e^{G_2(x)-1}\right)^{\theta-1}, \qquad x \in R \quad \theta > 0. \tag{4}$$

Kavya and Manoharan [14] introduced a new transformation called Kavya-Manoharan (KM) transformation. Let X be a random variable with cumulative distribution function (cdf) $G_3(x)$ and probability density function (pdf) $g_3(x)$ of some baseline distribution. Then the cdf and pdf of new distribution is defined as,

$$F_3(x) = \frac{e}{e-1}\left(1 - e^{-G_3(x)}\right), \qquad x \in R \tag{5}$$

$$f_3(x) = \frac{e}{e-1} g_3(x)\left(e^{-G_3(x)}\right), \qquad x \in R. \tag{6}$$

1.1. Power Generalized Kavya Manoharan (PGKM) transformation

We introduce a new transformation from now on called Power Generalized Kavya Manoharan (PGKM) transformation in the present study. The new PGKM distribution can be obtained as follows: Let X be a random variable with baseline cdf $G(x)$ and corresponding pdf $g(x)$. Then the cdf and pdf of the proposed PGKM distribution is

$$F(x) = \left(\frac{e}{e-1}(1 - e^{-G(x)})\right)^{\theta}, \qquad x \in R, \quad \theta > 0, \tag{7}$$

and the corresponding pdf is

$$f(x) = \theta\left(\frac{e}{e-1}\right)^{\theta}\left(1 - e^{-G(x)}\right)^{\theta-1}\left(e^{-G(x)}\right) g(x), \qquad x \in R, \quad \theta > 0. \tag{8}$$

The main objective of our study is to introduce a transformation that yields new lifetime models by using a given baseline distribution. When researchers deal with series systems with components distributed as KM-transformed lifetime distributions, the PGKM transformation is highly useful. So the investigation of the PGDKM transformation of various lifetime distributions is relevant in the sense of the selection of appropriate lifetime models for series systems. The procedure transforms the response variable to achieve a model with interesting ageing properties as revealed through the hazard rates. We choose inverse Weibull as the baseline distribution in the present work because this distribution has wide application in reliability theory and survival

analysis. If X follows inverse Weibull distribution with parameters α and β, then the cdf and pdf are respectively given by

$$G(x) = e^{-(\frac{\alpha}{x})^{\beta}}, \qquad x > 0, \quad \alpha, \beta > 0 \tag{9}$$

and

$$g(x) = \left(\frac{\beta}{\alpha}\right)\left(\frac{\alpha}{x}\right)^{\beta+1}\left(e^{-(\frac{\alpha}{x})}\right)^{\beta}, \qquad x > 0, \quad \alpha, \beta > 0. \tag{10}$$

The inverse Weibull distribution which is also known as Fréchet distribution has been widely used in reliability engineering. It is a well-defined limiting distribution for the maximum of random variables with non-negative real support. It has application ranging from accelerated life testing through to earthquakes, floods, horse racing, rainfall, wind speeds etc. For more details see Kotz and Nadarajah [16].

We organize the paper as follows: In Section 2, we introduce a new life distribution using the inverse Weibull distribution as the baseline distribution in the proposed transformation and study its various analytical characteristics such as the probability density function, cumulative distribution function, survival function and failure rate function. Shapes of the probability density function and failure rate function are also discussed in this Section. Statistical properties including moments, quantile function, order statistics, stress-strength reliability, Rényi entropy, residual life function, Lorenz curve, characterization results and estimation of the parameters using method of maximum likelihood are discussed in Section 3. Simulation study and real data application is discussed in Section 4. In Section 5, a lifetime regression analysis is investigated by using the log power generalized Kavya Manoharan inverse Weibull distribution, with an illustrative data example. Finally, some concluding remarks are given in Section 6.

2. Power Generalized Kavya Manoharan Inverse Weibull Distribution

In this section, Power Generalized Kavya Manoharan Inverse Weibull(PGKMIW) Distribution has been proposed by using inverse Weibull distribution as baseline distribution. Putting cdf and pdf of Inverse Weibull distribution in (7) and (8), we get the cdf and pdf of newly proposed PGKMIW distribution. The cdf is

$$F(x) = \left(\frac{e}{e-1}(1 - e^{-e^{-(\frac{\alpha}{x})^{\beta}}})\right)^{\theta}, \qquad x > 0, \;\; \theta, \alpha, \beta > 0, \tag{11}$$

and the corresponding pdf is

$$f(x) = \alpha^{\beta}\beta\theta\left(\frac{e}{e-1}\right)^{\theta}\left(1 - e^{-e^{-(\frac{\alpha}{x})^{\beta}}}\right)^{\theta-1}\left(e^{-e^{-(\frac{\alpha}{x})^{\beta}}}\right)\left(e^{-(\frac{\alpha}{x})^{\beta}}\right)x^{-\beta-1}, \tag{12}$$

when $x > 0, \theta, \alpha, \beta > 0$. The corresponding survival function

$$S(x) = 1 - \left(\frac{e}{e-1}(1 - e^{-e^{-(\frac{\alpha}{x})^{\beta}}})\right)^{\theta}, \qquad x > 0, \;\; \theta, \alpha, \beta > 0 \tag{13}$$

and the hazard function is

$$h(x) = \frac{\alpha^{\beta}\beta\theta\left(\frac{e}{e-1}\right)^{\theta}\left(1 - e^{-e^{-(\frac{\alpha}{x})^{\beta}}}\right)^{\theta-1}\left(e^{-e^{-(\frac{\alpha}{x})^{\beta}}}\right)\left(e^{-(\frac{\alpha}{x})^{\beta}}\right)x^{-\beta-1}}{1 - \left(\frac{e}{e-1}(1 - e^{-e^{-(\frac{\alpha}{x})^{\beta}}})\right)^{\theta}}, \tag{14}$$

$x > 0, \theta, \alpha, \beta > 0$. The plots of pdf and hazard function of PGKMIW distribution are given in Figure 1. The graphical representation gives a better understanding of the shapes of the pdf and hazard function. As seen in the plot the hazard function have upside-down and decreasing curves for different combinations of α, β and θ.

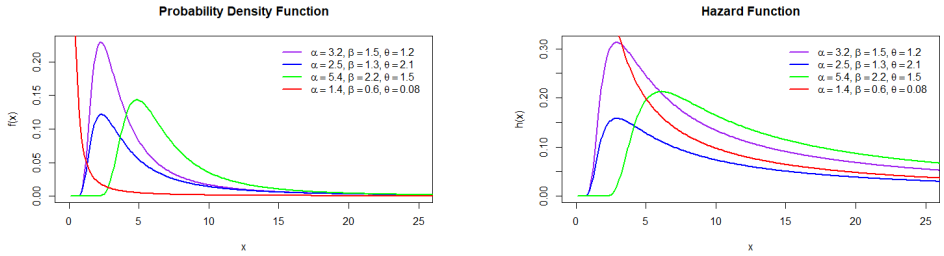


Figure 1: *Plots of pdf(left) and hazard function (right) for different values of parameters.*

3. Statistical Properties

In this section, some statistical properties of PGKMIW distribution are discussed.

3.1. Moments

The moments are a set of statistical parameters to measure a distribution. The r^{th} raw moment of the PGKMIW distribution is given by

$$\mu_r^{'} = \sum_{k=0}^{\theta-1} \sum_{m=0}^{\infty} \alpha^r \theta \left(\frac{e}{e-1}\right)^{\theta} \binom{\theta-1}{k} (-1)^k \frac{(-(k+1))^m}{m!} \frac{\Gamma\left(1-\frac{r}{\beta}\right)}{(m+1)^{1-\frac{r}{\beta}}}. \tag{15}$$

By putting $r = 1, 2, 3, \cdots$ in (15), the raw moments can be viewed.

3.2. Quantile Function

The quantile function of X is the real solution of the equation $F(x_p) = p$, where $p \sim U(0,1)$. Then by inverting (11), we get

$$x_p = \frac{-\alpha}{\left(\log\left(-\log(1-p^{\frac{1}{\theta}}\frac{e-1}{e}\right)\right)^{\frac{1}{\beta}}}. \tag{16}$$

Put $p = 0.5$ in (16), we get the median of the PGKMIW distribution.

3.3. Order Statistics

Let the random sample of size n, $X_1, X_2, .., X_n$ be from the PGKMIW distribution. Then $X_{(1)}, X_{(2)}, .., X_{(n)}$ are the order statistics respectively. The pdf and cdf of the r^{th} order statistic are respectively given by

$$f_r(x) = \frac{n!}{(r-1)!(n-r)!} F^{r-1}(x) \left(1-F(x)\right)^{n-r} f(x),$$

and

$$F_r(x) = \sum_{j=r}^{n} \binom{n}{j} F^j(x) \left(1-F(x)\right)^{n-j}.$$

And those of our newly proposed model are

$$f_r(x) = \frac{n!}{(r-1)!(n-r)!} \frac{\alpha^{\beta}\theta x^{-\beta-1}}{(e-1)^{\theta n}} \left(1-e^{-e^{-(\frac{\alpha}{x})^{\beta}}}\right)^{\theta r-1} \left((e-1)^{\theta} - (e(1-e^{-e^{-(\frac{\alpha}{x})^{\beta}}})\right)^{n-r} \left(e^{-e(\frac{\alpha}{x})^{\beta}-(\frac{\alpha}{x})+\theta r}\right), \tag{17}$$

$$F_r(x) = \sum_{j=r}^{n} \binom{n}{j} \frac{e^{\theta j}}{(e-1)^{\theta n}} \left(1 - e^{-e^{-(\frac{\alpha}{x})^{\beta}}}\right)^{\theta j} \left((e-1)^{\theta} - (e(1 - e^{-e^{-(\frac{\alpha}{x})^{\beta}}}))^{\theta}\right)^{n-j}. \quad (18)$$

Then, the pdf and cdf of $X_{(1)}$ and $X_{(n)}$ are obtained by substituting $r = 1$ and $r = n$ respectively in $f_r(x)$ and $F_r(x)$. It is nothing but the distribution of minimum and maximum in series and parallel reliability systems, respectively.

3.4. Stress-Strength Reliability

The Stress-Strength model plays a crucial role in reliability engineering. Stress-strength reliability is defined as the probability that a component's or system's random strength exceeds its random stress, Church and Harris [6]. Literature provides studies on point estimation of the stress-strength reliability parameter for parallel systems with independent and non-identical components, Pakdaman and Ahmadi [21]. This section focuses on reliability estimation for both single-component stress-strength models (SSS) and multicomponent stress-strength models (MSS).

3.4.1 Single Component Stress-Strength Reliability

Suppose X and Y have the PGKMIW$(\alpha, \beta, \theta_1)$ and PGKMIW$(\alpha, \beta, \theta_2)$ distributions respectively, then the system reliability is

$$\begin{aligned}
R &= P(Y < X) \\
&= \int_0^{\infty} f_X(x) F_Y(x) dx \\
&= \int_0^{\infty} \alpha^{\beta} \beta \theta_1 \left(\frac{e}{e-1}\right)^{\theta_1} \left(1 - e^{-e^{-(\frac{\alpha}{x})^{\beta}}}\right)^{\theta_1 - 1} \left(e^{-e^{-(\frac{\alpha}{x})^{\beta}}}\right) \left(e^{-(\frac{\alpha}{x})^{\beta}}\right) x^{-\beta-1} \\
&\quad \times \left(\frac{e}{e-1}(1 - e^{-e^{-(\frac{\alpha}{x})^{\beta}}})\right)^{\theta_2} dx \\
&= \sum_{m=0}^{\infty} \sum_{k=0}^{\theta_1+\theta_2-1} \binom{\theta_1 + \theta_2 - 1}{k} (-1)^k \frac{\theta_1}{(m+1)!} \left(\frac{e}{e-1}\right)^{\theta_1+\theta_2} (-(k+1))^m.
\end{aligned}$$

3.4.2 Multicomponent Stress-Strength (MSS) Reliability

Suppose X and Y have the PGKMIW$(\alpha, \beta, \theta_1)$ and PGKMIW$(\alpha, \beta, \theta_2)$ distributions respectively, then the reliability in MSS is

$$\begin{aligned}
R_{s,k} &= \sum_{i=s}^{k} \binom{k}{i} \int_{-\infty}^{\infty} (1 - F_X(x))^i F_X(x)^{k-i} dF_Y(x) \\
&= \sum_{r=0}^{\infty} \sum_{i=s}^{k} \sum_{j=0}^{i} \sum_{m=0}^{\theta_1(k-i)} \sum_{n=0}^{\theta_2-1} \sum_{p=0}^{\theta_1 j} \binom{k}{i} \binom{i}{j} \binom{\theta_1(k-i)}{m} \binom{\theta_2 - 1}{n} \binom{\theta_1 j}{p} \\
&\quad \times (-1)^{r+j+m+n+p} \frac{\theta_2}{(r+1)!} (e-1)^{\theta_1(i-j)} (e)^{\theta_1 j} \left(\frac{e}{e-1}\right)^{\theta_1(k-i)+\theta_2} (m+n+p+1)^r.
\end{aligned}$$

3.5. Rényi Entropy

Entropy is interpreted as the degree of disorder or randomness in the system. An important measure of entropy is Rényi entropy, see Rényi [22]. The Rényi entropy is defined as

$$I_R(\delta) = \frac{1}{1-\delta} \left[\log(I(\delta)\right]$$

where $I(\delta) = \int f^{\delta}(x)dx$, $\delta > 0$ and $\delta \neq 1$. The function $I(\delta)$ of PGKMIW distribution is given by

$$I(\delta) = \sum_{k=0}^{\delta(\theta-1)} \sum_{m=0}^{\infty} \alpha^{1-\delta}\beta^{\delta-1}\theta^{\delta} \left(\frac{e}{e-1}\right)^{\delta\theta} \binom{\delta(\theta-1)}{k} (-1)^k \times \frac{(-(k+1))^m}{m!} \frac{\Gamma\left(\frac{\delta\beta+\delta-1}{\beta}\right)}{(m+\delta)^{\frac{\delta\beta+\delta-1}{\beta}}}. \quad (19)$$

3.6. Residual Life Function

The Residual Life Function (RLF) is a powerful tool to quantify and manage the remaining time until failure or event occurrence for systems that have already survived some period of time. The n^{th} moment of the residual life is defined as

$$\begin{aligned} m_n(t) &= E((x-t)^n | X > t), \quad \forall n = 1, 2, 3, ... \\ &= \frac{1}{1-F(t)} \int_t^{\infty} (x-t)^n dF(x) \\ &= \frac{1}{F(t)} \int_t^{\infty} (x-t)^n f(x)dx. \end{aligned}$$

The n^{th} moment of the residual life of PGKMIW distribution is given by

$$m_n(t) = \frac{1}{1-F(t)} \sum_{k=0}^{\theta-1} \sum_{j=0}^{n} \sum_{m=0}^{\infty} \alpha^{n-j}\theta \left(\frac{e}{e-1}\right)^{\theta} \binom{\theta-1}{k} (-1)^{k+j} \frac{(-(k+1))^m}{m!} \times \binom{n}{j} t^j (m+1)^{\frac{n-j}{\beta}-1} \gamma\left(\frac{j-n}{\beta}+1, (m+1)(\frac{\alpha}{t})^{\beta}\right), \quad (20)$$

where $\gamma\left(\frac{j-n}{\beta}+1, (m+1)(\frac{\alpha}{t})^{\beta}\right)$ is the lower incomplete gamma function.

3.7. Lorenz Curve

The Lorenz Curve is a graphical representation used to describe the distribution of a probability density function (PDF), particularly in contexts like economics and inequality analysis. It plots the cumulative proportion of a variable (like income or wealth) against the cumulative proportion of the population, showing how concentrated or evenly distributed that variable is. The Lorenz curve for a positive random variable X is defined as the graph of the ratio

$$L(F(x)) = \frac{E(X|X \leq x)F(x)}{E(x)} = \frac{\int_0^x xf(x)dx}{\int_0^{\infty} xf(x)dx} = \frac{1}{\mu}\int_0^x xf(x)dx,$$

against $F(x)$ with the property $L(p) \leq p$, $L(0) = 0$ and $L(1) = 1$. If X represents annual income, $L(p)$ is the proportion of total income that accrues to individuals having the $100p$ percent lowest incomes. If all individuals earn the same income then $L(p) = p$ for all p. The area between the line $L(p) = p$ and the Lorenz curve may be regarded as a measure of inequality of income, or more generally, of the variability of X. The Lorenz curve for the PGKMIW distribution is given by

$$L(p) = \frac{1}{\mu} \sum_{k=0}^{\theta-1} \sum_{m=0}^{\infty} \alpha\theta \left(\frac{e}{e-1}\right)^{\theta} \binom{\theta-1}{k} (-1)^k \frac{(-(k+1))^m}{m!} (m+1)^{\frac{1}{\beta}-1} \times \Gamma\left(1-\frac{1}{\beta}, (m+1)(\frac{\alpha}{x})^{\beta}\right), \quad (21)$$

where $\Gamma\left(1-\frac{1}{\beta}, (m+1)(\frac{\alpha}{x})^{\beta}\right)$ is the upper incomplete gamma function.

Figure 2 displays the Lorenz Curve, when applied to PGKMIW distribution when parameters α and β are fixed, helps in analyzing and visualizing the degree of concentration or inequality in the distribution of values of a random variable.

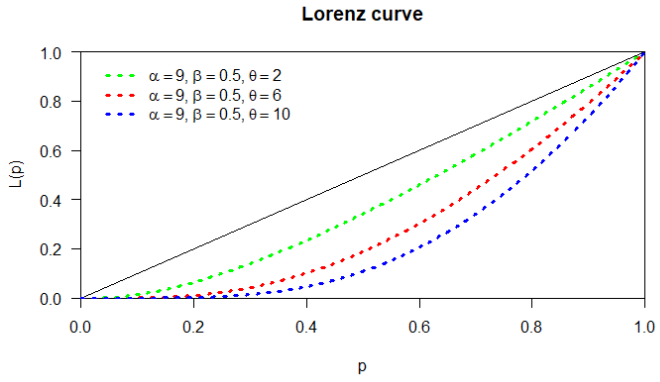


Figure 2: *Lorenz curve of PGKMIW distribution*

3.8. Characterization

Characterization theorems for a probability density function (PDF) provide conditions under which a random variable or a probability distribution is uniquely identified or described by specific properties. These theorems are crucial in probability theory and statistics, as they help establish the uniqueness of distributions based on certain features or properties. This section deals with the characterization of the PGKMIW distribution based on the ratio of two truncated moments. To present the characterization of the distribution, consider the theorem presented in Glänzel [9]. Note that the result also holds when the interval H is not closed. It could also be applied when the cdf F does not have a closed form. As shown in Glanzel [10], this characterization is stable in the sense of weak convergence.

Theorem 1. Let (Ω,F,P) be a given probability space and let $H = [a, b]$ be an interval for some $d < b$ ($a = -\infty, b = \infty$ might as well be allowed). Let $X : \Omega \to H$ be a continuous random variable with the distribution function F and let q_1 and q_2 be two real functions defined on H such that

$$E(q_2(X)|X \geq x) = E(q_1(X)|X \geq x)\eta(x), \qquad x \in H, \tag{22}$$

is defined with some real function η. Assume that q_1, $q_2 \in C^1(H)$, $\eta \in C^2(H)$ and F is twice continuously differentiable and strictly monotone function on the set H. Finally, assume that the equation $\eta q_1 = q_2$ has no real solution in the interior of H. Then F is uniquely determined by the functions q_1, q_2 and η, particularly

$$F(x) = \int_0^x C \left| \frac{\eta'(u)}{\eta(u)q_1(u) - q_2(u)} \right| e^{-s(u)} du, \tag{23}$$

where the function s is a solution of the differential equation $s' = \frac{\eta' q_1}{\eta q_1 - q_2}$ and C is the normalization constant, such that $\int_H dF = 1$.

3.8.1 Characterization based on truncated moments

Proposition 1. Let $X : \Omega \to (0, \infty)$ be a continuous random variable and let

$$q_1(x) = \left(1 - e^{-e^{-(\frac{\alpha}{x})^\beta}}\right)^{1-\theta} \left(e^{e^{-(\frac{\alpha}{x})^\beta}}\right)$$

and

$$q_2(x) = q_1(x) \left(e^{e^{-(\frac{\alpha}{x})^\beta}}\right)$$

for $x > 0$. The random variable X belongs to the PGKMIW family if and only if the function η defined in Theorem 1 has the form

$$\eta(x) = \frac{\left(e^{e^{-(\frac{\alpha}{x})}}\right)}{\left(e^{-(\frac{\alpha}{x})^{\beta}}\right)}, \quad x > 0. \tag{24}$$

Proof. Let X be a random variable with pdf given in (12) , then

$$(1 - F(x))E(q_1(X)|X \geq x) = \theta \left(\frac{e}{e-1}\right)^{\theta} \left(e^{-(\frac{\alpha}{x})^{\beta}}\right),$$

and

$$(1 - F(x))E(q_2(X)|X \geq x) = \theta \left(\frac{e}{e-1}\right)^{\theta} \left(e^{e^{-(\frac{\alpha}{x})^{\beta}}}\right).$$

Further,

$$\eta(x)q_1(x) - q_2(x) = q_1(x) \left(e^{e^{-(\frac{\alpha}{x})^{\beta}}}\right) \left(e^{(\frac{\alpha}{x})^{\beta}}\right).$$

Conversely, if η is given as above, then

$$s^{'}(x) = \frac{\eta^{'}(x)q_1(x)}{\eta(x)q_1(x) - q_2(x)} = -\alpha^{\beta}\beta x^{-\beta-1}, \quad x > 0,$$

and hence

$$s(x) = \alpha^{\beta}x^{-\beta}.$$

Now, according to Theorem 1, X has density which is given in (12). ■

Corollary 1. Let $X : \Omega \to (0, \infty)$ be a continuous random variable and let q_1 be as in Proposition 1. Then X has pdf in (12) if and only if there exist functions q_2 and η defined in Theorem 1 satisfying the differential equation

$$\frac{\eta^{'}(x)q_1(x)}{\eta(x)q_1(x) - q_2(x)} = -\alpha^{\beta}\beta x^{-\beta-1}, \qquad x > 0. \tag{25}$$

The general solution of the differential equation in Corollary 1 is

$$\eta(x) = \frac{1}{\left(e^{-(\frac{\alpha}{x})^{\beta}}\right)} \left[\int \alpha^{\beta}\beta x^{-\beta-1} \left(e^{-(\frac{\alpha}{x})^{\beta}}\right) (q_1(x))^{-1} q_2(x) + D\right], \tag{26}$$

where D is a constant. Note that a set of functions satisfying the above differential equation is given in Proposition 1 with $D = 0$. Clearly, there exist other triplet of functions (q_1, q_2, η) satisfying the conditions of Theorem 1.

3.9. Maximum Likelihood Estimation

There are several methods in the literature for estimating unknown parameters. In this section, maximum likelihood method of estimation is used for estimating the parameters of PGKMIW distribution. Let us consider $x_1, x_2, \ldots, x_n$ be a random sample taken from PGKMIW distribution. Then the likelihood function is given by,

$$L(x) = \prod_{i=1}^{n} \alpha^{\beta}\beta\theta \left(\frac{e}{e-1}\right)^{\theta} \left(1 - e^{-e^{-(\frac{\alpha}{x})^{\beta}}}\right)^{\theta-1} \left(e^{-e^{-(\frac{\alpha}{x})^{\beta}}}\right) \left(e^{-(\frac{\alpha}{x})^{\beta}}\right) x^{-\beta-1}.$$

Then the log-likelihood function, l becomes,

$$l = n\beta \ln \alpha + n \ln \beta + n \ln \theta + n\theta \ln e - n\theta \ln(e-1) + (\theta - 1) \sum_{i=1}^{n} \ln \left(1 - e^{-e^{-(\frac{\alpha}{x_i})^{\beta}}} \right) - \sum_{i=1}^{n} \left(e^{-(\frac{\alpha}{x_i})^{\beta}} \right) - \sum_{i=1}^{n} \left(\frac{\alpha}{x_i} \right)^{\beta} - (\beta + 1) \sum_{i=1}^{n} \ln x_i. \quad (27)$$

The maximum likelihood estimators (MLEs) are obtained by maximizing the log-likelihood with respect to the unknown parameters α, β and θ. To obtain the maximum likelihood estimates of the unknown parameters, we equate,

$$\frac{\partial l}{\partial \alpha} = 0; \frac{\partial l}{\partial \beta} = 0; \frac{\partial l}{\partial \theta} = 0.$$

The ML estimators are found through the solution of the non-linear system of equations. Hence, using R or MATLAB, a numerical approximation of the software's solution to this system of equations is possible.

4. Numerical Illustrations

4.1. Simulation Study

In order to illustrate the accuracy of the maximum likelihood estimation procedure for PGKMIW distribution, Monte Carlo simulation is carried out using inversion method. For the parameters α, β and θ, sample of sizes $n = 250$, 500, 1000, 1200 are generated from the PGKMIW model. We calculated the bias and the MSEs of the parameter estimates. The simulation is conducted for the parameter values $\alpha = 0.8, \beta = 0.5$ and $\theta = 1.5$.

Table 1: *Simulation study at* $\alpha = 0.8, \beta = 0.5$ *and* $\theta = 1.5$

n	Estimates	Bias	MSE
250	$\hat{\alpha} = 0.50070$	-0.29930	0.08958
	$\hat{\beta} = 0.53776$	0.03776	0.00143
	$\hat{\theta} = 1.88482$	0.38482	0.14809
500	$\hat{\alpha} = 0.553287$	-0.26713	0.07136
	$\hat{\beta} = 0.53497$	0.03497	0.00122
	$\hat{\theta} = 1.78101$	0.28101	0.07897
1000	$\hat{\alpha} = 1.01974$	0.21974	0.04829
	$\hat{\beta} = 0.51735$	0.01735	0.00030
	$\hat{\theta} = 1.24612$	-0.25388	0.06445
1200	$\hat{\alpha} = 0.78181$	-0.01819	0.00033
	$\hat{\beta} = 0.50654$	0.00654	0.00004
	$\hat{\theta} = 1.46821$	-0.03179	0.00101

As the sample size increases, the mean square error decreases for the selected parameter values (see Table 1). The bias caused by the estimates is nearer to zero. Also, when the sample size increases, absolute bias decreases. Thus, the estimates tend to the true parameter values with the increase in sample size.

4.2. Data Analysis

In this section, we examine vinyl chloride data collected from clean up-gradient monitoring wells. Vinyl chloride, a volatile organic compound, is particularly significant in environmental

investigations due to its anthropogenic origin and carcinogenic properties. However, trace amounts of this compound are often detected in many background monitoring wells. These low-level detections in clean up-gradient wells can be attributed to cross-contamination from air, gas, or the analytical process itself. The data is obtained from Bhaumik et al. [4] and it represents 34 observations of the vinyl chloride data obtained from clean up gradient ground - water monitoring wells in mg/L is given in Table 2.

Table 2: *Vinyl chloride data*

5.1	1.2	1.3	0.6	0.5	2.4	0.5	1.1	8.0	0.8
0.4	0.6	0.9	0.4	2.0	0.5	5.3	3.2	2.7	2.9
2.5	2.3	1.0	0.2	0.1	0.1	1.8	0.9	2.0	4.0
6.8	1.2	0.4	0.2						

We consider two distributions for comparison purpose and they are Kavya Manoharan Inverse Weibull (KMIW) distribution (see Gauthami et al. [8]) and Inverse Weibull (IW) distribution. We have used log-likelihood function, AIC, K-S test value and p-value for the comparison purpose.

Table 3: *Parameter estimates and goodness of fit statistics for models fitted to the data*

Model	MLE	-Log L	AIC	KS	p-value
PGKMIW	$\hat{\alpha} = 6.9946$ $\hat{\beta} = 0.8458$ $\hat{\theta} = 0.1411$	-57.2529	120.5058	0.1005	0.8821
KMIW	$\hat{\alpha} = 0.9107$ $\hat{\beta} = 0.7685$	-59.0510	122.1020	0.1090	0.8144
IW	$\hat{\alpha} = 0.6173$ $\hat{\beta} = 0.8804$	-58.6266	121.2532	0.1134	0.7745

Table 3 shows that the proposed distribution gives the lowest AIC, K-S test values, p-values and the largest log-likelihood value. So we can conclude that our proposed distribution provides a better fit for the data set than the other distributions given in Table 3. Figure 3 represents the

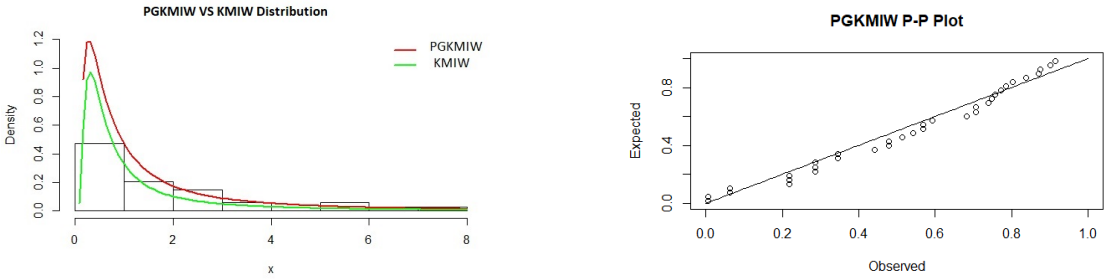


Figure 3: *(a) Plot of the estimated pdfs over the histogram and (b) pp- plot of the PGKMIW model for dataset.*

estimated pdfs over the histogram and pp-plot of the PGKMIW model for the dataset.

5. Log Power Generalized Kavya Manoharan Inverse Weibull Distribution (LPGKMIW)

Let the random variable T follows the PGKMIW distribution with parameters α and β. Let us consider a re-parametrization by $\sigma = \frac{1}{\beta}$ and $\mu = \log \alpha$. Then, the random variable $Y = \log T$ will

have LPGKMIW distribution with the following cdf and pdf respectively as,

$$F(y) = \left(\frac{e}{e-1}\right)^{\theta} \left(1 - e^{-e^{-e^{-(\frac{y-\mu}{\sigma})}}}\right)^{\theta}, \qquad -\infty < y < \infty, \theta > 0, \tag{28}$$

$$f(y) = \frac{\theta}{\sigma} \left(\frac{e}{e-1}\right)^{\theta} \left(1 - e^{-e^{-e^{-(\frac{y-\mu}{\sigma})}}}\right)^{\theta-1} \left(e^{-e^{-e^{-(\frac{y-\mu}{\sigma})}}}\right) \left(e^{-e^{-(\frac{y-\mu}{\sigma})}}\right) \left(e^{-(\frac{y-\mu}{\sigma})}\right), \tag{29}$$

$-\infty < y < \infty, \theta > 0$, where $\sigma > 0$ and $-\infty < \mu < \infty$ are the scale and location parameters respectively. The plot of pdf of LPGKMIW distribution is given in Figure 4. The survival and

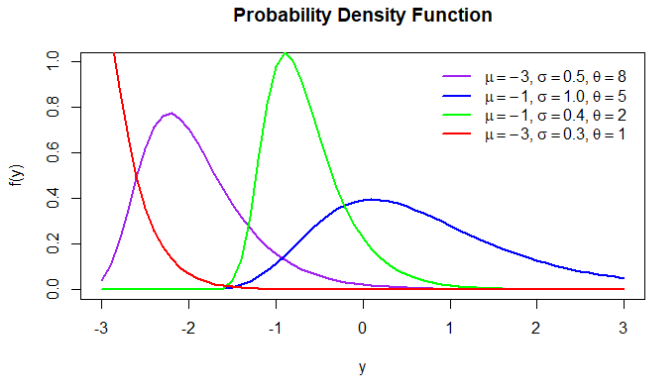


Figure 4: *pdf of LPGKMIW distribution*

hazard functions of LPGKMIW distribution respectively are as follows:

$$S(y) = 1 - \left(\frac{e}{e-1}\right)^{\theta} \left(1 - e^{-e^{-e^{-(\frac{y-\mu}{\sigma})}}}\right)^{\theta}, \tag{30}$$

and

$$h(y) = \frac{\frac{\theta}{\sigma}\left(\frac{e}{e-1}\right)^{\theta} \left(1 - e^{-e^{-e^{-(\frac{y-\mu}{\sigma})}}}\right)^{\theta-1} \left(e^{-e^{-e^{-(\frac{y-\mu}{\sigma})}}}\right) \left(e^{-e^{-(\frac{y-\mu}{\sigma})}}\right) \left(e^{-(\frac{y-\mu}{\sigma})}\right)}{1 - \left(\frac{e}{e-1}\right)^{\theta} \left(1 - e^{-e^{-e^{-(\frac{y-\mu}{\sigma})}}}\right)^{\theta}}, \tag{31}$$

where $-\infty < y < \infty, \sigma > 0, -\infty < \mu < \infty, \theta > 0$. Then the standardized random variable $Z = (y - \mu)/\sigma$ has density function given by

$$f(z) = \theta \left(\frac{e}{e-1}\right)^{\theta} \left(1 - e^{-e^{-e^{-z}}}\right)^{\theta-1} \left(e^{-e^{-e^{-z}}}\right) \left(e^{-e^{-z}}\right) \left(e^{-z}\right), \tag{32}$$

$-\infty < z < \infty, \theta > 0$.

5.1. LPGKMIW Regression Model

In real-world situations, survival time is affected by various factors that contribute to its variability. To evaluate the impact of these factors on survival time, it is crucial to use appropriate regression models that account for censored and time-to-failure data. In essence, constructing such models requires a probabilistic framework for survival time. Several types of regression models are available for this purpose, among which the location-scale regression model, as emphasized by Lawless [18], is particularly noteworthy and commonly applied in clinical trials. Log-lifetime models are based on a linear combination assumption, maintaining the structure of standard

regression models while also offering the benefit of managing censored data. Numerous studies have utilized log-location-scale regression models in their research. Among these, de Gusmão et al. [11] proposed a location-scale regression model based on the log-generalized inverse Weibull distribution for modeling lifetime data. Al-Dawsari and Sultan [1] studied the classical and Bayesian regression models for use in conjunction with the inverted Weibull (IW) distribution. Recently, a regression model is introduced by using the unit inverse Weibull distribution, see Lucas [19].

We have now introduced a linear regression model using the LPGKMIW distribution to analyze the relationship between the response variable y_i and the explanatory variable vector $\boldsymbol{x_i} = (x_1, x_2, ..., x_p)^T$ in the following way:

$$y_i = \boldsymbol{\beta^T x_i} + \sigma z, \qquad i = 1, 2, 3, ..., n, \tag{33}$$

where z_i is the random error with density function in (32), $\boldsymbol{\beta} = (\beta_1, ..., \beta_p)^T$ is a $p\times$ 1 vector of unknown parameters, $\sigma > 0$ is an unknown scale parameters and $\boldsymbol{x_i} = (x_{i1}, ...x_{ip})^T$ is the explanatory variable vector. The parameter $\mu_i = \boldsymbol{\beta^T x_i}$ is the location of Y_i. The location parameter vector $\boldsymbol{\mu} = (\mu_1, ..., \mu_n)^T$ can be represented as a linear model $\boldsymbol{\mu = \beta^T X}$, where $\boldsymbol{X} = (\boldsymbol{x_1, ..., x_n})^T$ is a known model matrix.

5.2. Maximum Likelihood Estimation

Let $(y_1, \delta_1, \boldsymbol{x_1}), ..., (y_n, \delta_n, \boldsymbol{x_n})$ be a right censored random sample of n observations, where

$$y_i = \begin{cases} \log(t_i), & \text{if } \delta = 1 \\ \log(c_i), & \text{if } \delta = 0, \end{cases}$$

t_i and c_i are lifetimes and censoring times respectively and $\boldsymbol{x_i}$ is an explanatory variable. Assuming that the lifetimes and censoring times are random and independent, the log likelihood function is given by

$$\begin{aligned} l(\boldsymbol{\eta}) = r\log\theta - r\log\sigma + \theta r\log e - \theta r\log(e-1) + (\theta-1)\sum_{i=1}^{n}\delta_i \log(1 - e^{-e^{-e^{-z_i}}}) \\ - \sum_{i=1}^{n}\delta_i\left(e^{-e^{-z_i}}\right) - \sum_{i=1}^{n}\delta_i\left(e^{-z_i}\right) - \sum_{i=1}^{n}\delta_i z_i \\ + \sum_{i=1}^{n}(1-\delta_1)\log\left(1 - \left(1 - e^{-e^{-e^{-z_i}}}\right)^{\theta}\left(\frac{e}{e-1}\right)^{\theta}\right), \end{aligned} \tag{34}$$

where r denotes the no.of uncensored observations, $\boldsymbol{\eta} = (\sigma, \boldsymbol{\beta})^T$ and $z_i = (y_i - \boldsymbol{\beta^T x_i})/\sigma$. By maximizing the log likelihood in (34), the maximum likelihood estimate (MLE) for the parameter vector η can be obtained.

5.3. Real-Life Data Analysis

Stone [24] describes an experiment involving solid epoxy electrical insulation specimens subjected to an accelerated voltage life test. A total of 20 specimens were tested at each of three voltage levels: 52.5, 55.0, and 57.5 kV. The failure times, measured in minutes, are presented in Table 4, with censored data marked by asterisks. The sample size is $n = 60$, the percentage of censored observations is 10%.

Table 4: *Failure Times for Epoxy Insulation Specimens at Three Voltage Levels*

Voltage (kV)	**Failure Times (min)**
52.5	4690, 740, 1010, 1190, 2450, 1390, 350, 6095, 3000, 1458, 6200*, 550, 1690, 745, 1225, 1480, 245, 600, 246, 1805
55.0	258, 114, 312, 772, 498, 162, 444, 1464, 132, 1740*, 1266, 300, 2440*, 520, 1240, 2600*, 222, 144, 745, 396
57.5	510, 1000*, 252, 408, 528, 690, 900*, 714, 348, 546, 174, 696, 294, 234, 288, 444, 390, 168, 558, 288

Let y_i denote the failure time for epoxy insulation specimens (min) and x_{i1} be the Voltage (kV). The voltage dataset is analyzed using the following regression model:

$$y_i = \beta_0 + \beta_1 x_{i1} + \sigma z_i, \tag{35}$$

where the random variable y_i follows the LPGKMIW distribution given in (29). For comparison, we also consider that y_i follows the Log Weibull (LW) (see, Lawless [18]), the Log Gamma Extended Weibull (LGEW) distribution (see, Cordeiro et al. [7]), the Log Topp Leone Generated Burr XII (LTLGBXII) distribution (see, Yousof et al. [27]), and the Marshal Olkin Weibull (LGMOW) distribution (see, Chesneau et al. [5]).

Table 5: *MLEs of the parameters, SEs in second line, p values in* $[\cdot]$ *and the AIC statistics*

Model	Parameters						AIC
LPGKMIW	β_0	β_1	σ	θ			165.5
	10.9660	-1.1488	0.8601	78.0224			
	2.3896	0.0433	0.0885	5.7106			
	$[< 0.001]$	[0.0006]					
LGMOW	β_0	β_1	σ	λ	α		166.4
	18.2532	-0.1798	0.4480	0.8969	0.0110		
	3.0054	0.0549	0.0631	0.0665	0.0101		
	$[1.25 \times 10^{-9}]$	[0.0011]					
LTLGBXII	β_0	β_1	σ	γ	θ	β	168.4
	14.4513	-0.1790	0.8024	0.6860	7.7247	0.7089	
	4.876	0.074	0.827	0.685	7.027	0.984	
	[0.003]	[0.0155]					
LGEW	β_0	β_1	σ	β	α		168.6
	31.859	-0.21	9.320	298.90	81.891		
	3.730	0.058	0.778	33.045	0.081		
	$[< 0.0001]$	$[< 0.0001]$					
LW	β_0	β_1	σ				173.4
	22	-0.274	0.845				
	3.046	0.055	0.09				
	$[< 0.0001]$	$[< 0.0001]$					

The MLEs of the model parameters, the asymptotic SEs of these estimates and the values of the AIC measures are used to compare the LPGKMIW with LGMOW, LTLGBXII, LGEW and LW regression models and their values are given in Table 5. It can be seen that the LPGKMIW model has the lowest AIC value, which suggests that the LPGKMIW regression model provides a better fit for the voltage data compared to the LGMOW, LTLGBXII, LGEW, and LW models. Figure 5 presents the empirical survival function by Kaplan Meier estimates and the estimated survival

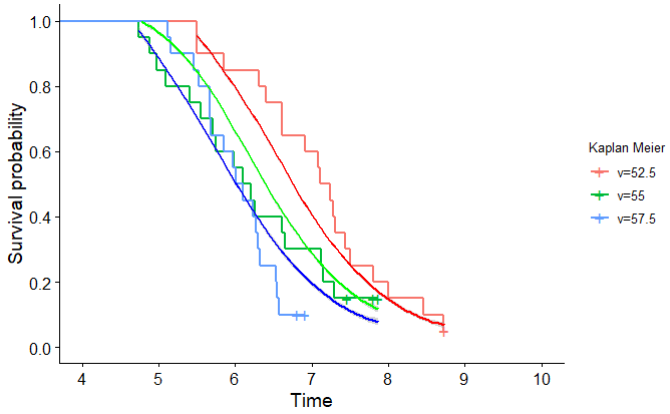


Figure 5: *Empirical and fitted survival function.*

function based on fitting the LPGKMF regression model. These plots suggest that the regression model fits the data well.

6. Conclusion

A new class of distribution by generalizing the KM transformation, called the PGKM transformation, is introduced. A new lifetime distribution called the PGKMIW distribution with Inverse Weibull distribution as the baseline distribution is also proposed. Characterization based on truncated moments are presented. Different statistical properties are derived. The parameter estimation has been done through the method of maximum likelihood. Monte Carlo simulation is carried out. Real data analysis is performed to show that the proposed generalization can be used to provide better fits. A new regression model based on the logarithm of the PGKMIW distribution is proposed. Real data analysis is also performed in new regression model to show that this regression model is more appropriate.

References

[1] Al-Dawsari, S. R. and Sultan, K. S. (2021). Inverted Weibull Regression Models and Their Applications. *Stats*, 4(2):269–290.

[2] Aryal, G. R. and Tsokos, C. P. (2009). On the transmuted extreme value distribution with application. *Nonlinear Analysis: Theory, Methods and Applications*, 71(12):1401–1407.

[3] Aryal, G. R. (2013). Transmuted log-logistic distribution. *Journal of Statistics Applications and Probability*, 2(1):11–20.

[4] Bhaumik, D. K., Kapur, K., and Gibbons, R. D. (2009). Testing Parameters of a Gamma Distribution for Small Samples. *Technometrics*, 51(3):326–334.

[5] Chesneau, C., Karakaya, K., Bakouch, H. S. and Ku?. C. (2022). An Alternative to the Marshall-Olkin Family of Distributions:Bootstrap, Regression and Applications. *Communications on Applied Mathematics and Computation*, 4(4):1229–1257.

[6] Church, J. D. and Harris, B. (1970). The estimation of reliability from stress-strength relationships. *Technometrics*, 12(1):49–54.

[7] Cordeiro, G. M., Nadarajah, S., Ortega, E. M. M. and Ramires, T. G. (2018). An alternative two-parameter gamma generated family of distributions: properties and applications. *Hacettepe Journal of Mathematics and Statistics*, 47(1):145–173.

[8] Gauthami P., Mariyamma, K. D. and Kavya, P. (2023). A modified inverse Weibull distribution using KM transformation. *Reliability: Theory and Applications*, 18 (72(1))(3):35–42.

[9] Glänzel, W. (1987). A Characterization Theorem Based on Truncated Moments and its Application to Some Distribution Families. In: Bauer, P., Konecny, F., Wertz, W. (eds) Mathematical Statistics and Probability Theory. Springer, Dordrecht:75–84.
[10] Glanzel, W. (1990). Some consequences of a characterization theorem based on truncated moments. *Statistics*, 21(4):613–618.
[11] Gusmão, F.R.S., Ortega, E.M.M. and Cordeiro, G.M. (2011). The generalized inverse Weibull distribution. *Stat Papers*, 52:591–619.
[12] Gupta, R. C., Gupta, P. L., Gupta, R. D. (1998). Modeling failure time data by lehman alternatives. *Communications in Statistics - Theory and Methods*, 27(4):887–904.
[13] Kavya, P., Manoharan, M. (2020). On a Generalized Lifetime Model Using DUS Transformation. In: Joshua, V., Varadhan, S., Vishnevsky, V. (eds) Applied Probability and Stochastic Processes. Infosys Science Foundation Series. Springer, Singapore:281–291.
[14] Kavya, P., and Manoharan, M. (2021). Some parsimonious models for lifetimes and applications. *Journal of Statistical Computation and Simulation*, 91(18):3693–3708.
[15] Khan, M. S. and King, R. (2013). Transmuted modified Weibull distribution: A generalization of the modified Weibull probability distribution. *Europe. J. of Pure Appl. Math.*, 6 (1):66–88.
[16] Kotz, S., and Nadarajah, S. Extreme value distributions Theory and Applications. Imperial College Press, London, 2000.
[17] Kumar, D.,Singh, U., & Singh S. K. (2015). A method of proposing new distribution and its application to bladder cancer patients data. *J. Stat. Appl. Pro. Lett*, 2(3):235–245.
[18] Lawless, J. F. Statistical Models and Methods for Lifetime Data. John Wiley & Sons, New Jersey, 2011.
[19] Lucas, D. R. R. (2023). The Unit Inverse Weibull Distribution and its Associated Regression Model. *Journal of Econometrics and Statistics*, 3(1):55–68.
[20] Maurya, S. K., Kaushik, A., Singh, S. K., and Singh, U. (2017). A new class of distribution having decreasing, increasing, and bathtub-shaped failure rate. *Communications in Statistics-Theory and Methods*, 46 (20):10359–10372.
[21] Pakdaman, Z. and Ahmadi, J. (2017). Point estimation of the stress–strength reliability parameter for parallel system with independent and non-identical components. *Communications in Statistics-Simulation and Computation*, 47(4):1193–1203.
[22] Rényi , A. (1961). On measures of entropy and information. In: Neyman, J., Ed., 4th Berkeley Symposium on Mathematical Statistics and Probability, Berkeley, 1:547–561.
[23] Shaw, W. T., Buckley, I. R., (2009). The alchemy of probability distributions: beyond Gram-Charlier expansions, and a skew-kurtotic-normal distribution from a rank transmutation map. arXiv preprint arXiv:0901.0434.
[24] Stone, G. C. Statistical analysis of accelerated aging tests on solid electrical insulation. Unpublished M.A.Sc. Thesis, University of Waterloo, Waterloo, Ont., Canada, 1978.
[25] Thomas, B. and Chacko, V. M. (2021). Power Generalized DUS Transformation of Exponential Distribution. *International Journal of Statistics and Reliability Engineering*, 9(1):150–157.
[26] Tripathi, A., Singh, U., and Singh, S. K. (2021). Inferences for the DUS-exponential distribution based on upper record values. *Annals of Data Science*, 8:387–403.
[27] Yousof, H. M., Altun, E., Rasekhi, M., Alizadeh, M., Hamedani, G. G., and Ali, M. M. (2017). A new lifetime model with regression models, characterizations and applications. *Communications in Statistics - Simulation and Computation*, 48(1):264–286.

INFERENCES FOR ALPHA POWER TRANSFORMED INVERSE LINDLEY DISTRIBUTION BASED ON ORDER STATISTICS WITH APPLICATIONS

Sumit Kumar[1], Anju Goyal[1*], Devendra Kumar[2], Narinder Kumar[1]

•

[1]Department of Statistics, Panjab University, Chandigarh, India
[2]Department of Statistics, University of Delhi, Delhi, India
[*]Corresponding authors:
anju.statistics@gmail.com
Other authors' emails:
Sumitstats21@gmail.com, devendrastats@gmail.com, nkumar67@yahoo.com

Abstract

The alpha power-transformed inverse Lindley distribution (APTIL) consist of one shape and one scale parameter. In some cases, the moments of the APTIL distribution may not exist due to its heavy tail, so we instead focus on the concept of inverse moments. In this paper, order statistics is used to derive the expression for moments, product moments and moment generating function for this distribution. The entropy of using order statistics for the APTIL distribution is also derived. Furthermore, tabulated values of the inverse moments of order statistics are provided for various sample sizes and parameter combinations. Three classical estimation techniques, viz., maximum product spacing estimators, least squares estimators, and weighted least squares estimators, are considered for parameter estimation and also evaluate the model parameters based on Type-II censored data. A Monte Carlo simulation-based approach is employed to assess the accuracy and validity of these estimators and the ensuing results. Finally, an empirical study using available real-life data sets demonstrates the utility of the distribution.

Keywords: Alpha power transformed inverse Lindley distribution, Order statistics, inverse moments, Maximum likelihood estimator, Entropy

1. Introduction

Order statistics play a crucial role in various theoretical and practical applications, including reliability analysis, entropy estimation, censored data analysis, quality control, outlier detection, material strength evaluation, optimal selection methods, and income inequality studies. The significance of order statistics has increased substantially in recent years, reflecting their growing role in contemporary research and applications. A characterization of the probability distribution and goodness of fit test has been provided by Arnold et al. (2003). There are several domains where moments of order statistics are applicable, including auction theory, quality control, and reliability. However, in certain situations where moments do not exist, the concept of inverse moments is employed. Inverse moments are essential in numerous practical applications, such as Stein estimation (Woof, 1985), life testing problems (Mendenhall and Lehman, 1960), and risk evaluation of estimators (Fujioka, 2001). Additionally, they are significant in financial and insurance mathematics (Ramsay, 1993) and in assessing the power of the test statistics (Fujioka,

2001). Wong and Chen (1990) discussed the entropy of order statistics, while Park (1995) derived recurrence relations for their entropy. A general form of Shannon entropy, referred to as Renyi entropy, plays a vital role in cryptography, high-resolution scalar quantization, time-frequency resolution, and signal segmentation in the time-frequency plane. The Shannon entropy of a random variable Z quantifies the average reduction of uncertainty in another random variable X. Estimation methods for unknown parameters in different distributions have been extensively studied. Kundu and Raqab (2005) focused on the generalized Rayleigh distribution, while Alkasasbeh and Raqab (2009) examined the generalized logistic distribution. Additionally, the Rayleigh distribution with two parameters, weighted exponential distribution, and exponentiated Chen distribution were explored by Dey et al. (2014, 2015, 2017), respectively.

In the literature, numerous authors have introduced modified distributions that offer greater flexibility and applicability for modeling real-world datasets. Sharma et al. (2015) proposed the inverse Lindley distribution, a one-parameter model that is unimodal and exhibits an upside-down bathtub failure rate function. This distribution has demonstrated superior performance compared to the inverse Rayleigh distribution in modeling head and neck cancer datasets. Over time, various extensions of the inverse Lindley distribution have been developed. Alkarni (2015) introduced the extended inverse Lindley distribution, deriving key statistical properties such as moments, skewness, kurtosis, and quantile functions. Sharma et al. (2016) proposed the generalized inverse Lindley distribution and provided parameter estimates using different estimation methods. Barco et al. (2017) developed the inverse power Lindley distribution by combining the power Lindley and inverse Lindley distributions to create more flexible models. Jan et al. (2018) introduced the exponentiated inverse power Lindley distribution, a three-parameter generalization of the inverse Lindley distribution. Mahmoud (2019) further extended this framework by proposing the extended exponentiated inverse Lindley distribution, a four-parameter generalization that enhances model adaptability.

The Alpha Power Transformed Inverse Lindley (APTIL) distribution was introduced by Dey et al. (2019), building on a concept similar to that of Mahdavi and Kundu (2017). The authors have explored the characteristics and properties of the APTIL model highlighting the classical estimation procedures. They have also illustrated the applicability of the APTIL distribution with the help of real life dataset analysis. They described that the given model provide better results than some other well-known lifetime models and its ability of unimodal and upside-down bathtub-shaped hazard rates which are throughly applicable in many real-life problems, makes it a special distribution. This model can be used in various areas, such as biomedical studies, public health, reliability and survival analysis etc.. The core intention of this paper is to explore the distributions of the order statistics arising from this APTIL distribution and derive the expressions for the corresponding single and product moments, marginal moment generating function and entropy of order statistics. For details on the studies related to the moments of the order statistics, one may refer to the works of Balakrishnan et al. (2015), Kumar and Dey (2017), Kumar and Goyal (2019), Goyal et al. (2024), Kumar et al. (2024) among others. Ahsanullah and Alzaatreh (2018) derived the moments of order statistics and estimated the unknown parameters of the Log-logistic distribution using order statistics. Next, we want to find the estimates for the unknown parameters using various statistical procedures, viz., maximumum likelihood estimation (MLE) for different methods like least square estimator, weighted least square estimator, method of maximum product spacing estimator and also obtain the maximum likelihood estimator for type-II censored samples for the APTIL distribution. The probability density function (PDF), the cumulative distribution function (CDF) and the hazard function (HF) of a APTIL random variable

$X > 0$ with parameters $\beta > 0$ and $\omega > 0$ are respectively given by Equations (1.1), (1.2) and (1.3)

$$f(x;\beta,\omega) = \frac{\omega^2\,(1+x)\log\beta}{x^3\,(\beta-1)(\omega+1)}e^{-\frac{\omega}{x}}\beta^{\left(1+\frac{\omega}{(\omega+1)x}\right)e^{-\frac{\omega}{x}}},\ x>0,\ \beta>0,\ \omega>0,\ \beta\neq 1, \tag{1}$$

$$F(x;\beta,\omega) = \frac{\beta^{\left(1+\frac{\omega}{(\omega+1)x}\right)e^{-\frac{\omega}{x}}}-1}{\beta-1},\quad x>0,\ \beta>0,\ \omega>0,\ \beta\neq 1, \tag{2}$$

$$h(x;\beta,\omega) = \frac{\omega^2\log(\beta)\ (1+x)\ e^{-\frac{\omega}{x}}\ \beta^{\left(1+\frac{\omega}{(\omega+1)x}\right)\ e^{-\frac{\omega}{x}}}}{(\omega+1)\ x^3\left(\beta-\beta^{\left(1+\frac{\omega}{(\omega+1)x}\right)\ e^{-\frac{\omega}{x}}}\right)},\ x>0,\ \beta>0,\ \omega>0,\ \beta\neq 1, \tag{3}$$

Special Cases:

1. As $\beta \to 1$, the APTIL distribution reduces to the inverse Lindley distribution.
2. As $\beta = e$, the APTIL distribution reduces to the inverse Poisson-Lindley distribution.

Now the paper is further organized into the following: Section 2, covers some statistical properties like inverse moments, and the order statistic in which we found the mathematical formulation of inverse moments, the inverse product moments, and marginal moment generating function for each of these order statistics. In Section 3, we obtained the mathematical expression of entropy of the k^{th} order statistic. We briefly describe the different method of estimation for estimating the unknown parameters β and ω of the given distribution like, maximum likelihood estimation based on Type-II censored sample, least square and weighted least square estimation and maximum product spacing estimation in section 4. In Section 5, we obtained the numerical value to check whether our expression is correct using the R software. In Section 6, the practical applicability of the model is demonstrated. In Section 7, we conclude the paper.

2. Statistical Properties

In some situations, the moment of the APTIL distribution may not exist due to its heavy tail, so we instead focus on the concept of inverse moment. Here, the p^{th} $(p = 1, 2, \ldots)$ inverse moment of the distribution given in (1), can be easily computed as

$$E\left[\left(\frac{1}{X}\right)^p\right] = \frac{\omega^2\log\beta}{(\beta-1)(\omega+1)}\sum_{\gamma_1=0}^{\infty}\sum_{\gamma_2=0}^{\gamma_1}\binom{\gamma_1}{\gamma_2}\left(\frac{\omega}{\omega+1}\right)^{\gamma_2}\frac{(\log\beta)^{\gamma_1}(\gamma_2+p)!(\gamma_2+p+1+\omega\gamma_1+\omega)}{\gamma_1!\,(\omega\gamma_1+\omega)^{\gamma_2+p+2}}. \tag{4}$$

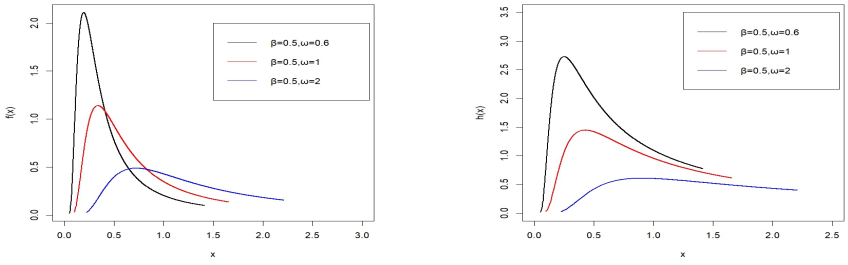


Figure 1: *PDF and HF plots for APTIL distribution*

From the Figure 1, we can see that the APTIL distribution has unimodal and upside-down bathtub-shaped hazard rates.

2.1. APTIL Distribution: Order Statistics and Their Properties

Let $X_1, X_2, \ldots, X_n$ be a random sample from the APTIL distribution with PDF and CDF denoted by (1) and (2) respectively, and an ordered random sample $X_{1:n}, \leq X_{2:n}, \leq, ..., \leq X_{k:n}$ from APTIL distribution, where $X_{k:n}$ is the k^{th} order statistic. The PDF of k^{th} order statistics and the joint PDF of the k^{th} and l^{th} order statistics are given by

$$f_{X_{k:n}}(x) = \frac{n!}{(k-1)!(n-k)!} F(x)^{k-1}[1-F(x)]^{n-k} f(x), x > 0, \tag{5}$$

$$f_{X_{k,l:n}}(x,y) = C_{k,l:n} F(x)^{k-1}[F(y)-F(x)]^{l-k-1}[1-F(y)]^{n-l} f(x)f(y), \;\; x < y, \;\; k < l, \tag{6}$$

where, $C_{k,l:n} = \frac{n!}{(k-1)!(k-l-1)!(n-l)!}$.

Let $X_{1:n} \leq X_{2:n} \leq \ldots \leq X_{n:n}$ represent the order statistics of a sample of size n from the APTIL distribution. The PDF of the k^{th} order statistics say $X_{k:n}$, $1 \leq k \leq n$ for APTIL distribution can be obtained by using Equations (1), (2) and (5)

$$f_{X_{k:n}}(x) = C_{k:n} \sum_{\gamma_1=0}^{n-k} \frac{\omega^2 \log\beta}{(\beta-1)(\omega+1)} (-1)^{\gamma_1} \binom{n-k}{\gamma_1} \left(\frac{\beta^{\left(1+\frac{\omega}{(\omega+1)x}\right)e^{\frac{-\omega}{x}}} - 1}{\beta-1} \right)^{r+\gamma_1-1} \frac{(1+x)\beta^{\left(1+\frac{\omega}{(\omega+1)x}\right)e^{-\frac{\omega}{x}}}}{x^3},$$

and the corresponding CDF $\left(F_{X_{k:n}}(x)\right)$, survival function $\left(S_{X_{k:n}}(x)\right)$ and hazard rate function $\left(H_{X_{k:n}}(x)\right)$ of k^{th} order statistic as follows:

$$\begin{aligned}
F_{X_{k:n}}(x) &= \sum_{\gamma_1=k}^{n} \sum_{\gamma_2=0}^{n-\gamma_1} \binom{n}{\gamma_1} \binom{n-\gamma_1}{\gamma_2} (-1)^{\gamma_2} \left(\frac{\beta^{\left(1+\frac{\omega}{(\omega+1)x}\right)e^{\frac{-\omega}{x}}} - 1}{\beta-1} \right)^{\gamma_2+\gamma_1}, \\
S_{X_{k:n}}(x) &= 1 - F_{X_{k:n}}(x) = 1 - \sum_{\gamma_1=k}^{n} \sum_{\gamma_2=0}^{n-\gamma_1} \binom{n}{\gamma_1} \binom{n-\gamma_1}{\gamma_2} (-1)^{\gamma_2} \left(\frac{\beta^{\left(1+\frac{\omega}{(\omega+1)x}\right)e^{\frac{-\omega}{x}}} - 1}{\beta-1} \right)^{\gamma_2+\gamma_1}, \\
H_{X_{k:n}}(x) &= \frac{f_{X_{k:n}}(x)}{S_{X_{k:n}}(x)}.
\end{aligned}$$

Similarly, by substituting PDF and CDF of APTIL distribution mentioned in Equations (1), (2) into Equation (6), the joint PDF of the k^{th} and l^{th} order statistics $(X_{k:n}, X_{l:n})$ of the APTIL distribution is

$$\begin{aligned}
f_{X_{k,l:n}}(x,y) &= C_{k,l:n} \sum_{\gamma_1=0}^{l-k-1} \sum_{\gamma_2=0}^{n-l} \binom{l-k-1}{\gamma_1} \binom{n-l}{\gamma_2} (-1)^{l-k-1-\gamma_1+\gamma_2} \left(\frac{\beta^{\left(1+\frac{\omega}{(\omega+1)x}\right)e^{\frac{-\omega}{x}}} - 1}{\beta-1} \right)^{l-2-\gamma_1} \\
&\times \left(\frac{\beta^{\left(1+\frac{\omega}{(\omega+1)y}\right)e^{\frac{-\omega}{y}}} - 1}{\beta-1} \right)^{\gamma_1+\gamma_2} \left(\frac{\omega^2 \log\beta}{(\beta-1)(\omega+1)} \right)^2 \left(\frac{(1+x)}{x^3} e^{-\frac{\omega}{x}} \beta^{\left(1+\frac{\omega}{(\omega+1)x}\right)e^{-\frac{\omega}{x}}} \right) \\
&\times \left(\frac{(1+y)}{y^3} e^{-\frac{\omega}{y}} \beta^{\left(1+\frac{\omega}{(\omega+1)y}\right)e^{-\frac{\omega}{y}}} \right), \qquad x < y, \;\; k < l,
\end{aligned} \tag{7}$$

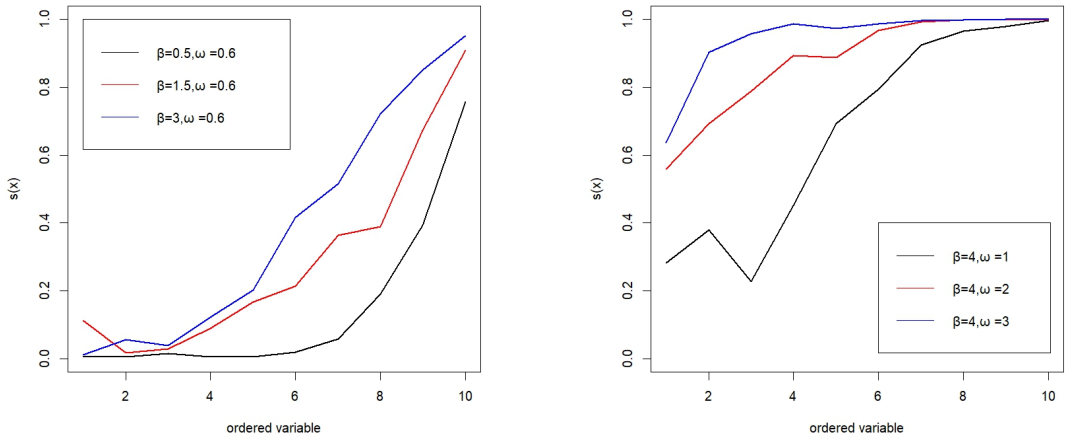


Figure 2: *Survival function of k^{th} order statistics of the APTIL distribution*

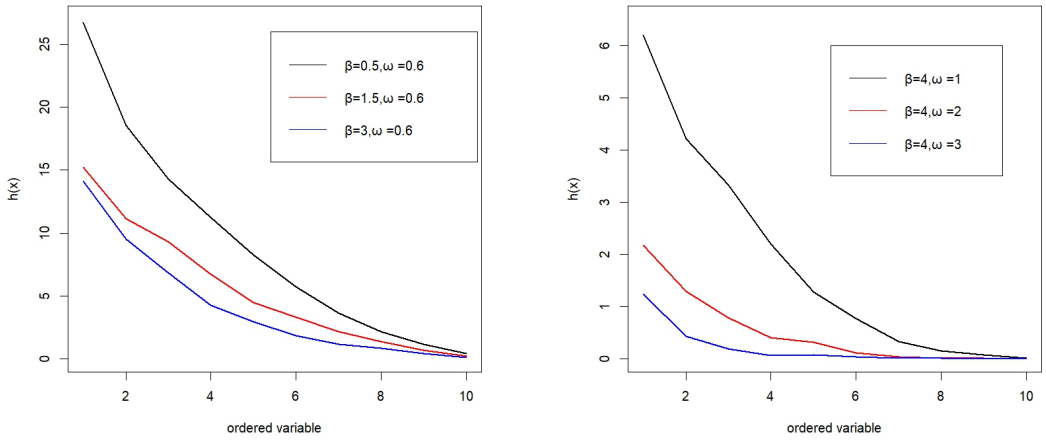


Figure 3: *Hazard rate function of k^{th} order statistics of the APTIL distribution*

From the Figure 2 and 3, we see that the survival function of the distribution increases with higher values of β and ω, indicating greater survival probabilities for larger ordered variables. Conversely, the hazard rate function decreases as the k^{th} ordered variable increases and is inversely proportional to both the shape parameter β and the scale parameter ω.

2.1.1 Single moment of the order statistics for APTIL distribution

The expectation is a crucial attribute of a random variable. This section deals with the $p^{th}(p = 1, 2, \ldots)$ moment of k^{th} order statistics for the APTIL model, which will facilitate the computation of given identity.

Theorem 1. Let equations (1) and (2) define the PDF and CDF of the APTIL model, then the p^{th} moment of the k^{th} order statistics say $\mu_{k:n}^{(p)} = E(\left(\frac{1}{X_{k:n}^{p}}\right))^1$ is given by

[1]The moments of the k^{th} order exists if $\omega(z)$ exists, where z positive integers. For non positive integers gamma is not defined.

$$\mu_{k:n}^{p} = \frac{n!}{(k-1)!(n-k)!}\sum_{\gamma_3=0}^{\infty}\sum_{\gamma_4=0}^{\gamma_3}\sum_{\gamma_1=0}^{n-k}\sum_{\gamma_2=0}^{k-1+\gamma_1}(-1)^{k-1-\gamma_2}\binom{n-k}{\gamma_1}\binom{k-1+\gamma_1}{\gamma_2}\binom{\gamma_3}{\gamma_4}\frac{\omega^{-p}}{(\omega+1)^{\gamma_4+1}}$$
$$\times\frac{(\log\beta)^{\gamma_3+1}}{\gamma_3!(\beta-1)^{k+\gamma_1}}(\gamma_2+1)^{\gamma_3}(\gamma_3+1)^{-p-2-\gamma_4}\left(\Gamma(\gamma_4+2+p)+\omega(\gamma_3+1)\Gamma(\gamma_4+1+p)\right), \quad (8)$$

Proof: Appendix 1 provides the proof of the theorem.

Now, the first and second expectations are two essential and broadly used characteristic of a random variable. Based on Theorem 1, the first two inverse moments of the *pth* order statistics say $\frac{1}{X_{k:n}^{p}}$ are respectively given by

$$E(X_{k:n}^{-1}) = \frac{n!}{(k-1)!(n-k)!}\sum_{\gamma_3=0}^{\infty}\sum_{\gamma_4=0}^{\gamma_3}\sum_{\gamma_1=0}^{n-k}\sum_{\gamma_2=0}^{k-1+\gamma_1}(-1)^{k-1-\gamma_2}\binom{n-k}{\gamma_1}\binom{k-1+\gamma_1}{\gamma_2}\binom{\gamma_3}{\gamma_4}$$
$$\times\frac{(\log\beta)^{\gamma_3+1}}{\gamma_3!(\beta-1)^{k+\gamma_1}}\frac{(\gamma_2+1)^{\gamma_3}\left(\Gamma(\gamma_4+3)+\omega(\gamma_3+1)\Gamma(\gamma_4+2)\right)}{\omega(\gamma_3+1)^{3+\gamma_4}(\omega+1)^{\gamma_4+1}},$$

$$E(X_{k:n}^{-2}) = \frac{n!}{(k-1)!(n-k)!}\sum_{\gamma_3=0}^{\infty}\sum_{\gamma_4=0}^{\gamma_3}\sum_{\gamma_1=0}^{n-k}\sum_{\gamma_2=0}^{k-1+\gamma_1}(-1)^{k-1-\gamma_2}\binom{n-k}{\gamma_1}\binom{k-1+\gamma_1}{\gamma_2}\binom{\gamma_3}{\gamma_4}$$
$$\times\frac{(\log\beta)^{\gamma_3+1}}{\gamma_3!(\beta-1)^{k+\gamma_1}}\frac{(\gamma_2+1)^{\gamma_3}\left(\Gamma(\gamma_4+4)+\omega(\gamma_3+1)\Gamma(\gamma_4+3)\right)}{\omega^2(\gamma_3+1)^{4+\gamma_4}(\omega+1)^{\gamma_4+1}}.$$

These two equations have been used to calculate the values of expectations and variances reported in Table 1 and 2 in Section 5. Let $X_{1:n} \le X_{2:n} \le \ldots \le X_{n:n}$ represent the order statistics of a sample of n size from the APTIL distribution. Then, moment generating function of k^{th} order statistic is given by

$$M_{X_{k:n}}(t) = \frac{n!}{(k-1)!(n-k)!}\sum_{\gamma_4=0}^{\infty}\sum_{\gamma_3=0}^{\infty}\sum_{\gamma_5=0}^{\gamma_4}\sum_{\gamma_1=0}^{n-k}\sum_{\gamma_2=0}^{k-1+\gamma_1}(-1)^{k-1-\gamma_2}\binom{n-k}{\gamma_1}\binom{k-1+\gamma_1}{\gamma_2}\binom{\gamma_4}{\gamma_5}\frac{t^{\gamma_3}}{\gamma_3!}$$
$$\times\frac{(\log\beta)^{\gamma_4+1}}{\gamma_4!(\beta-1)^{k+\gamma_1}}\frac{\omega^{\gamma_3}}{(\omega+1)^{\gamma_5+1}}(\gamma_2+1)^{\gamma_4}(\gamma_4+1)^{\gamma_3-2-\gamma_5}\left(\Gamma(\gamma_5+2-\gamma_3)+\omega(\gamma_4+1)\right.$$
$$\left.\Gamma(\gamma_5+1-\gamma_3)\right).$$

2.1.2 Product moment of the order statistics for APTIL distribution

In this section, the product moment $\mu_{k,l:n}^{(p,q)} = E\left[\frac{1}{X_{k:n}^{p}}\frac{1}{X_{k:n}^{q}}\right]$ of two order statistics are investigated.

Theorem 2: Let equations (1) and (2) define the PDF and CDF of the APTIL model. For $1 \le k \le l \le n$ and $p, q > 0$. The product moments of k^{th} and l^{th} order statistic are given by

$$\mu_{k,l:n}^{(p,q)} = \frac{n!\psi(\beta,\omega)}{(k-1)!(l-k-1)!(n-l)!}\frac{(\log\beta)^{\gamma_5+\gamma_6+2}}{(\beta-1)^{l+\gamma_2}}\frac{\omega^{\gamma_7+\gamma_8+\gamma_9+4}}{(\omega+1)^{\gamma_7+\gamma_8+2}}\frac{(\gamma_3+1)^{\gamma_5}(\gamma_4+1)^{\gamma_6}(\gamma_6+1)^{\gamma_9}}{\gamma_5!\gamma_6!\gamma_9!}$$
$$\times\left[\frac{(\gamma_7+\gamma_8+\gamma_9+3+p+q+\omega(\gamma_5+1))\Gamma(\gamma_7+\gamma_8+\gamma_9+3+p+q)}{(\gamma_8+\gamma_9+2+q)(\omega(\gamma_5+1))^{\gamma_7+\gamma_8+\gamma_9+4+p+q}}\right.$$
$$\left.+\frac{(\gamma_7+\gamma_8+\gamma_9+2+p+q+\omega(\gamma_5+1))\Gamma(\gamma_7+\gamma_8+\gamma_9+2+p+q)}{(\gamma_8+\gamma_9+1+q)(\omega(\gamma_5+1))^{\gamma_7+\gamma_8+\gamma_9+3+p+q}}\right],$$

where

$$\psi(\beta,\omega) = \sum_{\gamma_9=0}^{\infty}\sum_{\gamma_6=0}^{\infty}\sum_{\gamma_5=0}^{\infty}\sum_{\gamma_1=0}^{l-k-1}\sum_{\gamma_2=0}^{n-l}\sum_{\gamma_3=0}^{l-2-\gamma_1}\sum_{\gamma_4=0}^{\gamma_1+\gamma_2}\sum_{\gamma_7=0}^{\gamma_5}\sum_{\gamma_8=0}^{\gamma_6}(-1)^{k-1-\gamma_1-\gamma_3-\gamma_4+\gamma_9}\binom{l-k-1}{\gamma_1}\binom{n-l}{\gamma_2}$$
$$\times\binom{l-2-\gamma_1}{\gamma_3}\binom{\gamma_5}{\gamma_7}\binom{\gamma_6}{\gamma_8}\binom{\gamma_1+\gamma_2}{\gamma_4}.$$

Proof: Appendix 2 provides the proof of the theorem.

3. Entropy

Shannon entropy is essential to information theory and is broadly applied in multiple fields. Entropy is used to measure the variation of the ambiguity of the random variable X. If X has probability density function $f(\cdot)$, then the Renyi entropy is defined (Renyi's, 1961) as

$$H_\delta(x) = \frac{1}{1-\delta}\log\left(\int_{-\infty}^{\infty} f(x)^\delta dx\right), \delta > 0, \delta \neq 1.$$

Now, The Renyi entropy of the k^{th} order statistic (Baratpour et al.,2008) of APTIL distribution is defined as

$$\begin{aligned}
H_\delta(X_{k:n}) &= \frac{1}{1-\delta}\log\left(\int_{-\infty}^{\infty} f_{X_{k:n}}(x)^\delta dx\right), \delta > 0, \delta \neq 1 \\
&= \frac{1}{1-\delta}\log\left(\int_0^\infty C_{k:n}^\delta \left(\frac{\beta^{\left(1+\frac{\omega}{(\omega+1)x}\right)e^{-\frac{\omega}{x}}}-1}{\beta-1}\right)^{(k-1)\delta} \left(1-\frac{\beta^{\left(1+\frac{\omega}{(\omega+1)x}\right)e^{-\frac{\omega}{x}}}-1}{\beta-1}\right)^{(n-k)\delta}\right. \\
&\times \left.\left(\frac{\log\beta}{\beta-1}\frac{\omega^2}{\omega+1}\frac{1+x}{x^3}e^{-\frac{\omega}{x}}\beta^{\left(1+\frac{\omega}{(\omega+1)x}\right)e^{-\frac{\omega}{x}}}\right)^\delta dx\right) \\
&= \frac{1}{1-\delta}\log\left(\sum_{\gamma_3=0}^{\infty}\sum_{\gamma_4=0}^{\gamma_3}\sum_{\gamma_1=0}^{\delta(n-k)}\sum_{\gamma_2}^{\delta(k-1)+\gamma_1}\sum_{\gamma_5=0}^{\delta}(-1)^{\delta(k-1)-\gamma_2}\binom{\delta(n-k)}{\gamma_1}\binom{\delta(k-1)+\gamma_1}{\gamma_2}\right. \\
&\times \binom{\gamma_3}{\gamma_4}\binom{\delta}{\gamma_5}\frac{(\log\beta)^{\delta+\gamma_3}}{(\beta-1)^{\delta k+\gamma_1}}\frac{\omega^{\gamma_5-\delta+1}}{\gamma_3!(\omega+1)^{\delta+\gamma_4}}(\delta+\gamma_2)^{\gamma_3}C_{k:n}^\delta(\delta+\gamma_3)^{\gamma_5-\gamma_4-3\delta+1} \\
&\times \left.\Gamma(3\delta+\gamma_4-\gamma_5-1)\right). \qquad (9)
\end{aligned}$$

Special Cases:

1. If put $k = 1$ in Equation (9), we get

$$H_\delta(X_{1:n}) = \frac{1}{1-\delta}\log\left(\sum_{\gamma_3=0}^{\infty}\sum_{\gamma_4=0}^{\gamma_3}\sum_{\gamma_1=0}^{\delta(n-1)}\sum_{\gamma_2}^{\gamma_1}\sum_{\gamma_5=0}^{\delta}(-1)^{-\gamma_2}\binom{\delta(n-1)}{\gamma_1}\binom{\gamma_1}{\gamma_2}\binom{\gamma_3}{\gamma_4}\binom{\delta}{\gamma_5}\right.$$
$$\left.\frac{(\log\beta)^{\delta+\gamma_3}}{(\beta-1)^{\delta+\gamma_1}}\frac{\omega^{\gamma_5-\delta+1}}{\gamma_3!(\omega+1)^{\delta+\gamma_4}}(\delta+\gamma_2)^{\gamma_3}n^\delta(\delta+\gamma_3)^{\gamma_5-\gamma_4-3\delta+1}\Gamma(3\delta+\gamma_4-\gamma_5-1)\right).$$

2. If put $k = n$ in Equation (9), we get

$$H_\delta(X_{n:n}) = \frac{1}{1-\delta}\log\left(\sum_{\gamma_3=0}^{\infty}\sum_{\gamma_4=0}^{\gamma_3}\sum_{\gamma_2}^{\delta(n-1)}\sum_{\gamma_5=0}^{\delta}(-1)^{\delta(n-1)-\gamma_2}\binom{\delta(n-1)}{\gamma_2}\binom{\gamma_3}{\gamma_4}\binom{\delta}{\gamma_5}\right.$$
$$\left.\frac{(\log\beta)^{\delta+\gamma_3}}{(\beta-1)^{\delta n}}\frac{\omega^{\gamma_5-\delta+1}}{\gamma_3!(\omega+1)^{\delta+\gamma_4}}(\delta+\gamma_2)^{\gamma_3}n^\delta(\delta+\gamma_3)^{\gamma_5-\gamma_4-3\delta+1}\Gamma(3\delta+\gamma_4-\gamma_5-1)\right).$$

4. Various Estimation Techniques

4.1. Maximum likelihood estimation of unknown parameters from Type II censored data

The maximum likelihood estimates (MLEs) of the unknown parameters for complete data was obtained by Dey et al. (2019). In this section, we obtained MLEs of the unknown parameters

(β, ω) of the APTIL distribution. Let $X_{1:n} \leq X_{2:n} \leq ... \leq X_{k:n}$ be Type-II censored sample from the distribution, then the likelihood function is defined as

$$L(t,\beta,\omega) = \frac{n!}{(n-k)!}\prod_{j=1}^{k}\left(\frac{\log\beta}{\beta-1}\frac{\omega^2}{\omega+1}\frac{1+x_{j:n}}{x_{j:n}^3}e^{-\frac{\omega}{x_{j:n}}}\beta^{\left(1+\frac{\omega}{(\omega+1)x_{j:n}}\right)e^{-\frac{\omega}{x_{j:n}}}}\right) \times\left[1-\left(\frac{\beta^{\left(1+\frac{\omega}{(\omega+1)x_{k:n}}\right)e^{-\frac{\omega}{x_{k:n}}}}-1}{\beta-1}\right)\right]^{n-k},$$

and the corresponding log-likelihood function is defined by Equation

$$\log L = \log n! - \log(n-k)! + k\log\log\beta - k\log(\beta-1) - k\log(\omega+1) + \sum_{j=1}^{k}\log\left(\frac{1+x_{j:n}}{x_{j:n}^3}\right) + (2k \log\omega) + \sum_{j=1}^{k}\left(1+\frac{\omega}{(\omega+1)x_{j:n}}\right)e^{-\frac{\omega}{x_{j:n}}}\log\beta - \sum_{j=1}^{k}\frac{\omega}{x_{j:n}} + (n-k)\log\left(\frac{\beta-\beta^{\left(1+\frac{\omega}{(\omega+1)x_{k:n}}\right)e^{-\frac{\omega}{x_{k:n}}}}}{\beta-1}\right).$$

The unknown parameters β and ω can be estimated using the maximum likelihood method by solving the following two nonlinear equations simultaneously,

$$\frac{d\log L}{d\omega} = \sum_{j=1}^{k}\log\beta\left(\frac{e^{-\frac{\omega}{x_{j:n}}}}{x_{j:n}}\left(\frac{1}{(\omega+1)}-\frac{\omega}{(\omega+1)^2}\right)-\frac{e^{-\frac{\omega}{x_{j:n}}}\left(1+\frac{\omega}{(\omega+1)x_{j:n}}\right)}{x_{j:n}}\right)-\sum_{j=1}^{k}\frac{1}{x_{j:n}}+\frac{2k}{\omega} + \frac{\log\beta(n-k)\left(\beta^{\left(1+\frac{\omega}{(\omega+1)x_{k:n}}\right)e^{-\frac{\omega}{x_{k:n}}}}\right)}{\left(\beta-\beta^{\left(1+\frac{\omega}{(\omega+1)x_{k:n}}\right)e^{-\frac{\omega}{x_{k:n}}}}\right)}\left(\frac{e^{-\frac{\omega}{x_{k:n}}}}{x_{k:n}}\left(\frac{1}{(\omega+1)}-\frac{\omega}{(\omega+1)^2}\right)-\frac{e^{-\frac{\omega}{x_{k:n}}}\left(1+\frac{\omega}{(\omega+1)x_{k:n}}\right)}{x_{k:n}}\right) - \frac{k}{\omega+1} = 0,$$

$$\frac{d\log L}{d\beta} = \frac{k}{\beta\log(\beta)}-\frac{k}{\beta-1}+\frac{1}{\beta}\sum_{j=1}^{k}\left(1+\frac{\omega}{(\omega+1)x_{j:n}}\right)e^{-\frac{\omega}{x_{j:n}}}+(n-k)\left(\frac{\beta-1}{\beta-\beta^{\left(1+\frac{\omega}{(\omega+1)x_{k:n}}\right)e^{-\frac{\omega}{x_{k:n}}}}}\right) \times\left(\frac{1-\left(\frac{\omega}{(\omega+1)x_{k:n}}e^{-\frac{\omega}{x_{k:n}}}\beta^{\left(1+\frac{\omega}{(\omega+1)x_{k:n}}\right)e^{-\frac{\omega}{x_{k:n}}}-1}\right)}{(\beta-1)^2}-\frac{\beta-\beta^{\left(1+\frac{\omega}{(\omega+1)x_{k:n}}\right)e^{-\frac{\omega}{x_{k:n}}}}}{(\beta-1)^2}\right)=0.$$

4.2. Method of maximum product spacing estimators

This method was proposed by Cheng and Amin (1979, 1983) as an alternative way to estimate the MLE in continuous univariate distributions. Let $x_{1:n} \leq x_{2:n} \leq ... \leq x_{n:n}$ be a random sample of n size from APTIL distribution.

We define the uniform spacings of a random sample as:

$$D_j(\beta,\omega) = F(x_{j:n},\beta,\omega) - F(x_{j-1:n},\beta,\omega), \tag{10}$$

where $F(x_{0:n},\beta,\omega) = 0$, $F(x_{n+1:n},\beta,\omega) = 1$ and $\sum_{j=1}^{n+1} D_j(\beta,\omega) = 1$.

The maximum product spacing estimator $(\hat{\beta}, \hat{\omega})$ of unknown parameters β and ω are obtained by maximizing the geometric mean of the uniform spacings in terms of β and ω

$$G(\beta,\omega) = \left[\prod_{j=1}^{n+1} D_j(\beta,\omega)\right]^{\frac{1}{n+1}},$$

or, Alternatively, this can be achieved through the maximization of the function

$$H(\beta,\omega) = \frac{1}{n+1}\sum_{j=1}^{n+1}\log[D_j(\beta,\omega)]. \tag{11}$$

Now, differentiate equation (11) with respect to β and ω respectively,

$$\frac{dH(\beta,\omega)}{d\beta} = \frac{1}{n+1}\sum_{j=1}^{n+1}\frac{1}{D_j(\beta,\omega)}\left[\Delta_1(x_{j:n}|\beta,\omega) - \Delta_1(x_{j-1:n}|\beta,\omega)\right], \tag{12}$$

$$\frac{dH(\beta,\omega)}{d\omega} = \frac{1}{n+1}\sum_{j=1}^{n+1}\frac{1}{D_j(\beta,\omega)}\left[\Delta_2(x_{j:n}|\beta,\omega) - \Delta_2(x_{j-1:n}|\beta,\omega)\right], \tag{13}$$

Where

$$\Delta_1(x_{j:n}|\beta,\omega) = \frac{\beta^{\left[-1+(1+(\frac{\omega}{(1+\omega)x_j})e^{\frac{-\omega}{x_j}})\right]}e^{\frac{-\omega}{x_j}}\left(1+\frac{\omega}{(1+\omega)x_j}\right)}{\beta-1} - \frac{\beta^{\left[(1+(\frac{\omega}{(1+\omega)x_j})e^{\frac{-\omega}{x_j}})\right]}e^{\frac{-\omega}{x_j}}}{(\beta-1)^2},$$

and

$$\Delta_2(x_{j:n}|\beta,\omega) = \frac{\beta^{\left(1+\frac{\omega}{(\omega+1)x_j}\right)e^{-\frac{\omega}{x_j}}}\log\beta\left(e^{-\omega/x_j}\left[\frac{1}{(\omega+1)} - \frac{\omega}{x_j(\omega+1)^2}\right] - \frac{e^{-\omega/x_j}\left(1+\frac{\omega}{(\omega+1)x_j}\right)}{x_j}\right)}{\beta-1}.$$

Solve these non-linear equations (12) and (13), we get the $\hat{\beta}$, $\hat{\omega}$ of the parameters β and ω.

4.3. Ordinary and Weighted Least Square Estimator

Swain et al. (1988) introduced methods for estimating the parameters of beta distributions using ordinary least square and weighted least square estimators (WLSEs). Let $x_{1:n} \le x_{2:n} \le ... \le x_{n:n}$ be a random sample of size n from APTIL distribution.

The ordinary least square estimator (OLSEs) of the parameters $\hat{\beta}_{LSE}$, $\hat{\omega}_{LSE}$ of unknown parameters β and ω are obtained by maximizing the negative of the function $S(\beta,\omega)$.

$$S(\beta,\omega) = \sum_{j=1}^{n}\left[F(x_{j:n},\beta,\omega) - \frac{j}{n+1}\right]^2, \tag{14}$$

These estimators for the distribution can be determined by solving the two non-linear equations.

$$\frac{dS(\beta,\omega)}{d\beta} = \sum_{j=1}^{n}\left[F(x_{j:n},\beta,\omega) - \frac{j}{n+1}\right]\Delta_1(x_{j:n}|\beta,\omega) = 0, \tag{15}$$

$$\frac{dS(\beta,\omega)}{d\omega} = \sum_{j=1}^{n}\left[F(x_{j:n},\beta,\omega) - \frac{j}{n+1}\right]\Delta_2(x_{j:n}|\beta,\omega) = 0. \tag{16}$$

Now, The WLSEs $\hat{\beta}_{WLSE}$, $\hat{\omega}_{WLSE}$ of unknown parameters β and ω are obtained by maximizing the negative of the function $W(\beta, \omega)$.

$$W(\beta,\omega) = \sum_{j=1}^{n} \frac{(n+1)^2(n+2)}{j(n-j+1)} \left[F(x_{j:n}, \beta, \omega) - \frac{j}{n+1} \right]^2, \tag{17}$$

Now, differentiate with respect to β and ω, Also the WLSEs can be obtained by solving the two non-linear equaitons

$$\frac{dW(\beta,\omega)}{d\beta} = \sum_{j=1}^{n} \frac{(n+1)^2(n+2)}{j(n-j+1)} \left[F(x_{j:n}, \beta, \omega) - \frac{j}{n+1} \right] \Delta_1(x_{j:n}|\beta,\omega) = 0, \tag{18}$$

$$\frac{dW(\beta,\omega)}{d\omega} = \sum_{j=1}^{n} \frac{(n+1)^2(n+2)}{j(n-j+1)} \left[F(x_{j:n}, \beta, \omega) - \frac{j}{n+1} \right] \Delta_2(x_{j:n}|\beta,\omega) = 0. \tag{19}$$

5. Numerical Tabulated Values

In this section, we obtained the numerical values of the simple inverse moments, ordered inverse moments, and entropy under different parameter configurations. Table 1 shows that the values of inverse moments are decreasing concerning both β and ω. Table no. 2 shows that the inverse ordered moments increase when the sample sizes increase and decrease when the order of the sample increases. In Table 3, we reported the uncertainty of the random variables (entropy) based on order statistics. We see that entropy is reduced concerning n and δ, and increased concerning r, ω, and β. The average values of the point estimators, absolute bias (Abias), and mean square errors (MSEs) of the MPSEs, LSEs, and WLSEs are obtained in Table 4-5. It can be seen that the estimators demonstrate the consistency property, which states that the MSEs fall with increasing sample size. Also, Abias of $\hat{\beta}$ and $\hat{\omega}$ drop as sample size n grows.The Abias of $\hat{\beta}$ and $\hat{\omega}$ increases when the given values of β and ω increase, respectively. Additionally, the MSEs of the $\hat{\omega}$ are smaller than the $\hat{\beta}$ across all estimation techniques. In Table 6, we obtained the average value of the estimators based on Type-II censored data for different sample sizes up to 20. R software is used to obtain the numerical value in the section.

6. Data Analysis

This section demonstrates the application of the APTIL distribution to model two complete datasets. The dataset comprises survival times of cancer patients who received both radiotherapy and chemotherapy, as documented by Sharma et al. (2015), along with laboratory animals infected with virulent tubercle bacilli (VCB), as described by Bjerkedal (1960).

We compare the fit of the APTIL model against the inverse Lindley (IL), generalized inverse Lindley (GIL), and exponentiated inverse Lindley (EIL) models. The parameters of the given APTIL model are estimated using the maximum likelihood method. The goodness-of-fit for each model is evaluated using $-2L$ (where L represents the log-likelihood function at the maximum likelihood estimates), the Akaike Information Criterion (AIC), the Bayesian Information Criterion (BIC) and the Kolmogorov-Smirnov (K-S) statistic, etc. The probability density functions (PDFs) of the models being compared are as follows:

$$IL : f(y,\omega) = \frac{\omega^2 (1+y) e^{-\frac{\omega}{y}}}{(\omega+1) y^3},$$

$$GIL : f(y,\beta,\omega) = \frac{\omega^2 \beta (1+y^\beta) e^{-\frac{\omega}{y^\beta}}}{(\omega+1) y^{2\beta+1}},$$

$$EIL : f(y,\beta,\omega) = \frac{\omega^2 \beta (1+y) e^{-\frac{\omega}{y}}}{(\omega+1) y^3} \left[1 + \frac{\omega}{(\omega+1)y} \right]^{\beta-1}.$$

Table 1: ***Simple inverse moments for different values of parameters.***

ω	β	$E(X^{-1})$	Simu.	$E(X^{-2})$	Simu.	$E(X^{-3})$	Simu.	$E(X^{-4})$	Simu.
1	0.1	2.314548	2.331223	7.704317	7.771673	32.68911	32.70861	168.3211	168.0245
	0.2	2.073209	2.034595	6.529134	6.528879	26.84380	26.18420	135.7008	134.8664
	0.3	1.928075	1.917395	5.854024	5.895169	23.58125	23.53371	117.8160	116.4582
	0.4	1.824470	1.816186	5.386630	5.394053	21.36384	21.22291	105.7997	105.0310
	0.5	1.744264	1.756829	5.032941	5.021223	19.70951	19.82699	96.9118	96.91610
	1.5	1.363571	1.355178	3.452668	3.444808	12.57426	12.65432	59.4707	59.71060
	2.0	1.270962	1.265415	3.093743	3.055214	11.03344	11.09712	51.5297	51.51160
	2.5	1.201935	1.246439	2.833117	2.886154	9.925360	9.919440	45.91030	45.00080
	5.0	1.005357	1.013699	2.125455	2.114904	7.006350	7.034690	31.34890	31.72369
	10	0.838151	0.843284	1.568548	1.558635	4.813250	4.805650	20.74810	20.52640
	50	0.558882	0.559042	0.756664	0.753257	1.881790	1.896040	7.231200	7.321900
2	0.1	1.048285	1.045695	1.636890	1.632499	3.204340	3.191229	8.270195	8.252589
	0.2	0.934639	0.9325277	1.380429	1.383598	2.715235	2.732706	6.648657	6.614443
	0.3	0.866495	0.862905	1.233720	1.237202	2.379165	2.353065	5.762054	5.767440
	0.4	0.817968	0.811374	1.132404	1.138817	2.151287	2.167789	5.167429	5.150019
	0.5	0.780471	0.783008	1.055904	1.050696	1.981576	1.990138	4.728195	4.767613
	1.5	0.603377	0.607440	0.715969	0.710153	1.253991	1.259122	2.884162	2.888481
	2.0	0.560539	0.561522	0.639253	0.632687	1.096489	1.099304	2.494614	2.412339
	2.5	0.528679	0.532921	0.583684	0.586809	0.984184	0.984960	2.219369	2.220244
	5.0	0.438306	0.439433	0.433480	0.434357	0.689175	0.680692	1.508024	1.509796
	10	0.361934	0.633851	0.316161	0.319214	0.469388	0.468313	0.992091	0.995838
	50	0.235820	0.238021	0.147422	0.141941	0.178502	0.174052	0.340021	0.349247

Table 2: *Inverse ordered moments for* $\beta = 1.5$ *and* $\omega = 1$.

n	k	$E(X_{k:n}^{-1})$	Simu.	$E(X_{k:n}^{-2})$	Simu.	$E(X_{k:n}^{-3})$	$E(X_{k:n}^{-4})$
1	1	1.363571	1.391780	3.452678	3.502368	12.58426	59.7407
2	1	2.010400	2.051238	5.944973	5.856776	23.31445	114.298
	2	0.761741	0.728368	0.960353	0.949521	1.854076	4.64344
3	1	2.431213	2.346852	7.929712	7.745784	32.79313	165.522
	2	1.168776	1.140782	1.975494	1.930773	4.357072	11.8497
	3	0.490723	0.493803	0.452798	0.482469	0.602577	1.040294
4	1	2.742270	2.707621	9.594681	9.421134	41.35207	213.824
	2	1.498041	1.454515	2.934806	2.923782	7.116332	20.6156
	3	0.839511	0.823645	1.016182	0.971225	1.597813	3.08382
	4	0.374461	0.376432	0.265003	0.219342	0.270832	0.359116
5	1	2.988658	2.923374	11.03727	11.32705	49.19754	259.683
	2	1.756717	1.772059	3.824311	3.964862	9.970175	30.38680
	3	1.110027	1.160500	1.600550	1.679393	2.835567	5.95881
	4	0.659166	0.650886	0.626603	0.594682	0.772643	1.167160
	5	0.303284	0.373556	0.174603	0.214931	0.145379	0.157104
6	1	3.192471	3.193420	12.31509	12.31837	56.46846	303.4548
	2	1.969593	1.964130	4.648214	4.643644	12.84293	40.82870
	3	1.330966	1.332808	2.176504	2.178386	4.224657	9.503093
	4	0.889087	0.889453	1.024596	1.013474	1.446477	2.414532
	5	0.544205	0.546930	0.427607	0.422068	0.435725	0.543484
	6	0.255099	0.255863	0.124003	0.125899	0.087310	0.079828
7	1	3.366156	3.368594	13.46526	13.44433	63.26377	345.4096
	2	2.150362	2.147629	5.414017	5.412450	15.69657	51.72626
	3	1.517670	1.516302	2.733705	2.746321	5.708834	13.58479
	4	1.082027	1.085734	1.433570	1.434607	2.245734	4.060830
	5	0.744382	0.748583	0.717865	0.708529	0.847020	1.179813
	6	0.464135	0.465456	0.311504	0.312752	0.271208	0.288952
	7	0.220261	0.223928	0.092751	0.090561	0.056613	0.044974
8	1	3.517409	3.506901	14.51329	14.52638	69.65698	385.7631
	2	2.307382	2.314942	6.129064	6.129839	18.51136	62.93498
8	3	1.679303	1.679057	3.268878	3.268596	7.252214	18.10010
	4	1.248283	1.241471	1.841749	1.834859	3.136535	6.059281
	5	0.915772	0.922539	1.025392	1.023524	1.354972	2.062366
	6	0.641549	0.645641	0.533350	0.530055	0.542249	0.650282
	7	0.404996	0.408295	0.237556	0.237371	0.180861	0.168509
	8	0.193869	0.193878	0.072065	0.071588	0.038917	0.027326
9	1	3.651320	3.644169	15.47748	15.39416	75.70446	424.6892
	2	2.446126	2.439801	6.799766	6.808035	21.27713	74.35425
	3	1.821777	1.825339	3.781605	3.777954	8.831169	22.96754
	4	1.394354	1.394907	2.243426	2.244367	4.094303	8.365233
	5	1.065693	1.068704	1.339653	1.329791	1.939324	3.176840
	6	0.795834	0.792929	0.773987	0.775974	0.887491	1.170780
	7	0.564406	0.562387	0.413033	0.414537	0.369628	0.390029
	8	0.359451	0.358772	0.187419	0.183222	0.126927	0.105217
	9	0.173171	0.172704	0.057646	0.057665	0.027916	0.017591
10	1	3.771425	3.781958	16.37148	16.38612	81.45062	462.3311
	2	5.270374	2.575892	7.431547	7.414166	23.98898	85.91212
	3	1.949133	1.924260	4.272650	4.279779	10.42974	28.12275
	4	1.524614	1.529267	2.635844	2.640944	5.101183	10.93872
	5	1.198965	1.197620	1.657498	1.664207	2.583984	1.505009
	6	0.932421	0.936639	1.024507	1.024196	1.294663	1.848669
	7	0.704776	0.704908	0.606968	0.603754	0.616042	0.718864
	8	0.504248	0.501662	0.329918	0.326356	0.264022	0.249101
	9	0.323252	0.323361	0.151794	0.150796	0.092653	0.069246
	10	0.156496	0.158029	0.047185	0.046646	0.020723	0.011850

Table 3: ***Entropy based on ordered statistic for different values of parameters.***

				$H_\delta(X_{k:n})$	$H_\delta(X_{k:n})$		$H_\delta(X_{k:n})$	$H_\delta(X_{k:n})$					$H_\delta(X_{k:n})$	$H_\delta(X_{k:n})$				$H_\delta(X_{k:n})$	$H_\delta(X_{k:n})$
δ	ω	n	k	β	β	ω	β	β	δ	ω	n	k	β	β	ω	n	k	β	β
				0.5	1.5		0.5	1.5					0.5	1.5				0.5	1.5
2	1	1	1	0.566016	0.983094	2	1.441281	1.874449	3	1	1	1	0.362866	0.764917	2	1	1	1.228919	1.646012
		2	1	-0.135989	0.246265		0.720812	1.118697			2	1	-0.273459	0.097624				0.577321	0.962754
			2	1.149889	1.634683		2.063844	2.566560				2	0.936543	1.412741				1.843326	2.338296
		3	1	-0.481382	-0.121843		0.364686	0.739056			3	1	-0.595965	-0.245181				0.245632	0.609722
			2	0.605059	0.758941		1.197879	1.671258				2	0.161715	0.608681				1.049365	1.515824
			3	1.510850	2.021782		2.443791	2.970939				3	1.292717	1.797606				2.220009	2.742552
		4	1	-0.701641	-0.358653		0.137178	0.494235			4	1	-0.804659	-0.469384				0.030573	0.378815
			2	-0.123826	0.307564		0.755447	1.206316				2	-0.242556	0.182984				0.632716	1.077415
			3	0.599675	1.084983		1.512504	2.017256				3	0.453208	0.933360				1.361591	1.861784
			4	1.774751	2.299498		2.719045	3.257917				4	1.553867	2.074008				2.493617	3.029387
		5	1	-0.859900	-0.529844		-0.026488	0.317032			5	1	-0.956012	-0.632673				-0.125561	0.210208
			2	-0.400436	0.013471		0.469246	0.902171				2	-0.506796	-0.090784				0.359653	0.787017
			3	0.126992	0.592328		1.025834	1.511668				3	0.005987	0.466849				0.901226	1.382761
			4	0.824517	1.327734		1.750463	2.271946				4	0.676091	1.175161				1.598196	2.116398
			5	1.983316	2.516566		2.935119	3.480610				5	1.760665	2.290247				2.708742	3.252008
4	1	1	1	0.259625	0.654236	2	1.121323	1.530249	5	1	1	1	0.195645	0.585811	2			1.054813	1.458796
		2	1	-0.347959	0.017552		0.499937	0.879068			2	1	-0.395811	-0.033644				0.450395	0.825719
			2	0.828393	1.300370		1.731665	2.222673				2	0.761528	1.230938				1.662724	2.151326
		3	1	-0.659983	-0.314031		0.179453	0.538351			3	1	-0.701824	-0.358595				0.136341	0.492102
			2	0.084342	0.527885		0.969473	1.432427				2	0.034784	0.476286				0.918426	1.379263
			3	1.182215	1.684043		2.106686	2.626819				3	1.113955	1.614014				2.036739	2.555423
		4	1	-0.863275	-0.531855		-0.029772	0.314021			4	1	-0.901992	-0.572877				-0.069497	0.271608
			2	-0.308651	0.114007		0.564681	1.006274				2	-0.351306	0.069615				0.521201	0.959492
			3	0.374274	0.851883		1.280453	1.778359				3	0.331095	0.793387				1.248487	1.726132
			4	1.442004	1.959814		2.379451	2.913628				4	1.368747	1.889275				2.311420	2.842035
		5	1	-1.011296	-0.691367		-0.182338	0.149527			5	1	-1.059585	-0.728887				-0.204637	0.111071
			2	-0.560595	-0.158418		0.298095	0.723395				2	-.060679	-0.202019				0.257137	0.680027
			3	-0.264616	0.553374		0.872713	1.329425				3	-0.104941	0.352372				0.787506	1.265550
			4	0.783015	1.095762		1.137290	2.058786				4	0.545149	1.040940				1.006431	1.979750
			5	1.651690	2.174688		2.640668	3.138845				5	1.578300	2.104890				2.52332	3.06577

Table 4: ***Parameter estimates*** (β, ω) ***and average bias with their associated MSEs (in parentheses) values for LSE, WLSE, and MPSE methods for different sample size.***

β	ω	n	LSE				WLSE				MPSE			
			$\hat{\beta}$ (MSE)	$\hat{\omega}$ (MSE)	$Abias(\hat{\beta})$	$Abias(\hat{\omega})$	$\hat{\beta}$ (MSE)	$\hat{\omega}$ (MSE)	$Abias(\hat{\beta})$	$Abias(\hat{\omega})$	$\hat{\beta}$ (MSE)	$\hat{\omega}$ (MSE)	$Abias(\hat{\beta})$	$Abias(\hat{\omega})$
0.5	1	25	0.637386	0.975585	0.237987	0.101824	0.616275	0.995538	0.260177	0.114827	0.698037	0.971588	0.397927	0.155466
			(0.092579)	(0.017561)			(0.105501)	(0.023888)			(0.196783)	(0.039136)		
		50	0.609423	0.976824	0.195808	0.072025	0.590378	0.999206	0.213446	0.082310	0.649748	0.970567	0.288038	0.114304
			(0.065617)	(0.008520)			(0.072633)	(0.011945)			(0.124681)	(0.020299)		
		100	0.582075	0.978794	0.148608	0.054627	0.565123	0.989177	0.161078	0.059489	0.605188	0.975144	0.217581	0.083261
			(0.044035)	(0.004643)			(0.046532)	(0.006093)			(0.074684)	(0.010564)		
		200	0.552606	0.985619	0.100785	0.041366	0.543132	0.991719	0.113691	0.043795	0.564618	0.984897	0.157162	0.060981
			(0.025782)	(0.002641)			(0.027502)	(0.003135)			(0.041276)	(0.005696)		
1.5	1	25	1.905604	0.974577	0.652596	0.106630	1.336341	1.065713	0.359367	0.143569	2.066333	0.982984	1.0854	0.181821
			(0.706241)	(0.020519)			(0.236062)	(0.039367)			(1.666633)	(0.056958)		
		50	1.843058	0.970749	0.549995	0.074901	1.325943	1.054899	0.321701	0.103841	1.950562	0.978026	0.896248	0.138122
			(0.549203)	(0.009122)			(0.190441)	(0.019975)			(1.163314)	(0.031867)		
		100	1.761556	0.974634	0.419861	0.056233	1.318710	1.047398	0.300888	0.078161	1.837731	0.978454	0.704062	0.102236
			(0.386169)	(0.004887)			(0.161448)	(0.010768)			(0.746056)	(0.016849)		
		200	1.668748	0.982078	0.281873	0.044522	1.322490	1.041600	0.292825	0.061516	1.719594	0.984513	0.523868	0.077184
			(0.228348)	(0.003030)			(0.142932)	(0.006222)			(0.440508)	(0.009504)		
5	1	25	6.336132	0.965381	1.613710	0.106121	6.351245	0.966245	1.736097	0.103350	6.580865	0.990788	3.003141	0.173545
			(5.564003)	(0.021493)			(5.989269)	(0.019601)			(13.03988)	(0.057943)		
		50	6.202758	0.964856	1.437081	0.070188	6.183371	0.966311	1.550269	0.069881	6.548007	0.975345	2.725966	0.133489
			(4.936744)	(0.008437)			(5.203307)	(0.008253)			(10.80154)	(0.033449)		
		100	5.976685	0.969497	1.153179	0.052524	5.922517	0.971595	1.222183	0.052348	6.205078	0.976962	2.254750	0.104387
			(3.925176)	(0.004456)			(3.978750)	(0.004328)			(7.743268)	(0.020084)		
		200	5.700874	0.977424	0.832392	0.041629	5.625562	0.981081	0.859995	0.040664	5.888415	0.978980	1.697956	0.078459
			(2.722126)	(0.002744)			(2.652198)	(0.002563)			(4.836741)	(0.011203)		

.

Table 5: ***Parameter estimates*** (β, ω) ***and average bias with their associated MSEs (in parentheses) values for LSE, WLSE, and MPSE methods for different sample size.***

β	ω	n	LSE				WLSE				MPSE			
			$\hat{\beta}$ (MSE)	$\hat{\omega}$ (MSE)	$Abias(\hat{\beta})$	$Abias(\hat{\omega})$	$\hat{\beta}$ (MSE)	$\hat{\omega}$ (MSE)	$Abias(\hat{\beta})$	$Abias(\hat{\omega})$	$\hat{\beta}$ (MSE)	$\hat{\omega}$ (MSE)	$Abias(\hat{\beta})$	$Abias(\hat{\omega})$
0.5	2	25	0.638882	1.972788	0.259959	0.230225	0.616498	2.000746	0.274173	0.255499	0.711213	1.939852	0.398558	0.330856
			(0.108036)	(0.093138)			(0.116257)	(0.117912)			(0.214034)	(0.174596)		
		50	0.604535	1.960607	0.208851	0.161835	0.580101	1.997143	0.223901	0.185229	0.645494	1.944217	0.290703	0.244174
			(0.072373)	(0.043693)			(0.078317)	(0.062302)			(0.127908)	(0.091682)		
		100	0.576255	1.960745	0.153265	0.120029	0.559081	1.985559	0.170572	0.132093	0.601691	1.953117	0.220355	0.178802
			(0.045095)	(0.022600)			(0.049974)	(0.030005)			(0.077051)	(0.049104)		
		200	0.550372	1.973254	0.109226	0.089986	0.537889	1.987824	0.120818	0.096547	0.565249	1.968135	0.160842	0.129992
			(0.027338)	(0.012448)			(0.028971)	(0.015610)			(0.043184)	(0.025832)		
1.5	2	25	1.917391	1.961460	0.714866	0.240787	1.815394	2.016646	0.748448	0.287442	2.084332	1.973753	1.126338	0.394566
			(0.830152)	(0.107883)			(0.910942)	(0.158919)			(1.803469)	(0.271302)		
		50	1.824188	1.951354	0.588530	0.169041	1.686914	2.010717	0.581895	0.209202	1.988509	1.948221	0.934984	0.297445
			(0.593426)	(0.049448)			(0.582744)	(0.084241)			(1.261134)	(0.144138)		
		100	1.744089	1.954090	0.455460	0.126933	1.619094	2.003510	0.421048	0.153755	1.842560	1.956033	0.726977	0.223902
			(0.415277)	(0.026031)			(0.327590)	(0.043731)			(0.795395)	(0.078744)		
		200	1.661623	1.968009	0.315977	0.095642	1.574445	1.996413	0.280953	0.110909	1.730847	1.961936	0.528972	0.164719
			(0.252087)	(0.014442)			(0.145785)	(0.020639)			(0.447243)	(0.041942)		
5	2	25	6.363081	1.932593	1.736845	0.225954	6.333086	1.935449	1.904326	0.232242	6.635368	2.007516	3.255765	0.402176
			(6.019899)	(0.096361)			(6.572107)	(0.098715)			(15.11342)	(0.320577)		
		50	6.214566	1.926994	1.546195	0.152766	6.130379	1.937618	1.685373	0.154465	6.590782	1.964840	2.928085	0.309377
			(5.271518)	(0.040251)			(5.555693)	(0.040804)			(12.18044)	(0.177384)		
		100	5.979247	1.932987	1.236184	0.113084	5.937988	1.944444	1.371404	0.114479	6.259217	1.959632	2.425413	0.244034
			(4.142691)	(0.020326)			(4.410698)	(0.020823)			(8.67794)	(0.107961)		
		200	5.667356	1.952429	0.855571	0.088937	5.635294	1.959508	0.962237	0.089892	5.882566	1.962738	1.847117	0.183401
			(2.774001)	(0.012422)			(2.859480)	(0.012411)			(5.367904)	(0.059379)		

.

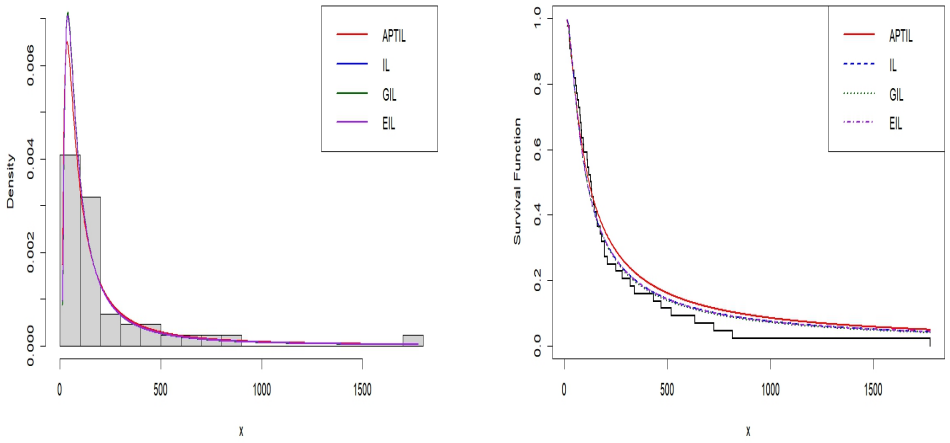
Table 6: *Average value and average Abias of the estimate and asscoiated MSEs (in parentheses) based on Type-II censored sample.*

β	ω	n	k	$\hat{\beta}$	$\hat{\omega}$	$bias(\hat{\beta})$	$bias(\hat{\omega})$	β	ω	$\hat{\beta}$	$\hat{\omega}$	$bias(\hat{\beta})$	$bias(\hat{\omega})$
2	2	5	1	2.790050	2.454869	0.797004	0.454868	2	3	3.123014	3.550028	1.213014	0.550028
				(2.228371)	(0.799882)					(5.392636)	(1.359068)		
			2	3.123735	2.306525	1.123735	0.306525			3.595945	3.391116	1.595945	0.391115
				(4.077838)	(0.466996)					(8.703422)	(0.865754)		
			3	2.514182	1.740898	0.514181	0.279108			2.769508	2.705041	0.769509	0.294959
				(0.750596)	(0.235947)					(2.156670)	(0.376933)		
			4	2.171652	1.740898	0.711652	0.259102			2.336716	2.603423	0.336716	0.396576
				(0.089397)	(0.199420)					(0.349001)	(0.487257)		
			5	2.032492	1.752091	0.032927	0.247908			2.063930	2.637320	0.065122	0.362679
				(0.005382)	(0.191177)					(0.018063)	(0.390866)		
0.5	1	20	1	0.802458	1.064635	0.302458	0.062463	1.5	1	1.781518	1.127389	0.281518	0.127389
				(0.298688)	(0.172691)					(0.239425)	(0.054648)		
			2	0.793376	1.048744	0.293376	0.048743			1.806608	1.107338	0.306607	0.107389
				(0.273455)	(0.009591)					(0.262285)	(0.037906)		
			3	0.797748	1.041419	0.297748	0.041419			1.828743	1.087333	0.328742	0.093425
				(0.276233)	(0.006794)					(0.325842)	(0.028448)		
			4	0.810955	1.032140	0.310955	0.032139			1.879684	1.072602	0.379683	0.088521
				(0.310601)	(0.004196)					(0.425071)	(0.024868)		
			5	0.811176	1.025800	0.311176	0.026108			1.921654	1.056325	0.421653	0.083093
				(0.303562)	(0.003056)					(0.460824)	(0.022317)		
			6	0.829626	1.016446	0.329626	0.017774			2.004831	1.039661	0.504831	0.083317
				(0.338018)	(0.001926)					(0.572395)	(0.022806)		
			7	0.850027	1.004636	0.350027	0.009101			2.104177	1.016852	0.604177	0.081103
				(0.387530)	(0.001296)					(0.720625)	(0.022901)		
			8	0.936181	0.983426	0.436181	0.019494			2.328127	0.981741	0.828127	0.100794
				(0.609032)	(0.003253)					(1.107095)	(0.028560)		
			9	1.069133	0.942251	0.569132	0.059001			2.427752	0.934527	0.927752	0.117319
				(0.938765)	(0.014236)					(1.419301)	(0.029612)		
			10	1.119406	0.896001	0.619461	0.104698			2.087746	0.909165	0.587746	0.114038
				(0.883747)	(0.029747)					(0.771543)	(0.029529)		

Table Continued...

Average value and average Abias of the estimate and asscoiated MSEs (in parentheses) based on Type-II censored sample.

β	ω	n	k	$\hat{\beta}$	$\hat{\omega}$	$bias(\hat{\beta})$	$bias(\hat{\omega})$	β	ω	$\hat{\beta}$	$\hat{\omega}$	$bias(\hat{\beta})$	$bias(\hat{\omega})$
0.5	1	20	11	1.050574	0.874865	0.550574	0.125134	1.5	1	1.786126	0.901026	0.286125	0.099249
				(0.605585)	(0.036527)					(0.213238)	(0.026931)		
			12	0.936244	0.881583	0.436244	0.118461			1.693016	0.906343	0.193016	0.093656
				(0.396349)	(0.032982)					(0.106864)	(0.025609)		
			13	0.825256	0.888847	0.325256	0.111155			1.631462	0.916451	0.131462	0.083549
				(0.246175)	(0.031717)					(0.049882)	(0.020465)		
			14	0.740543	0.896861	0.240544	0.103139			1.592876	0.919981	0.098276	0.080019
				(0.153904)	(0.029732)					(0.027359)	(0.018383)		
			15	0.681176	0.903957	0.181176	0.096043			1.572537	0.923384	0.072536	0.076615
				(0.100784)	(0.026622)					(0.014759)	(0.016728)		
			16	0.620422	0.912274	0.120422	0.087725			1.551152	0.927165	0.051152	0.076615
				(0.053929)	(0.022591)					(0.007293)	(0.015175)		
			17	0.569343	0.920849	0.069343	0.079151			1.535271	0.929231	0.035271	0.070768
				(0.015463)	(0.018257)					(0.003487)	(0.014556)		
			18	0.540318	0.929294	0.040318	0.070705			1.523008	0.929032	0.023008	0.070967
				(0.005115)	(0.014735)					(0.001564)	(0.015211)		
			19	0.519504	0.935767	0.019504	0.064233			1.511859	0.930826	0.011858	0.069173
				(0.001231)	(0.012284)					(0.000431)	(0.014179)		
			20	0.503568	0.938633	0.003841	0.061366			1.501700	0.933863	0.001755	0.066133
				(0.000078)	(0.011617)					(0.000015)	(0.013063)		



(a) *The relative histogram and fitted density graph* **(b)** *The fitted and estimated survival function*

Figure 4: *The fitted and empirical survival functions for data 1*

Table 7: ***Goodness of fit Statistics for different data***

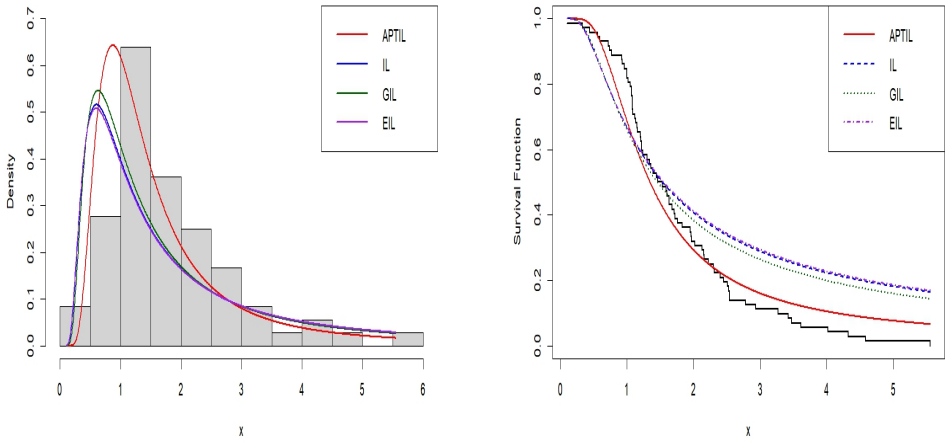
Data 1	Model	$\hat{\beta}$	$\hat{\omega}$	$-2L$	AIC	BIC	K-S
	APTIL(β,ω)	2.197908	62.17588	558.8457	562.8457	566.4141	0.08469
	IL(ω)		77.67544	688.2096	690.2096	691.9938	0.08884
	GIL(β,ω)	1.013325	81.73121	559.1425	563.1425	566.7108	0.09273
	EIL(β,ω)	2.799310	28.33204	559.1604	563.1604	566.7288	0.08922
Data 2	APTIL(β,ω)	0.032191	2.808439	230.8168	234.8168	239.3701	0.14570
	IL(ω)		1.576856	239.5689	241.5689	243.8456	0.19414
	GIL(β,ω)	1.071339	1.548701	238.6981	242.6981	247.2514	0.18107
	EIL(β,ω)	0.694550	2.109365	239.4938	243.4938	248.0471	0.19900

The value of the MLEs of the parameters, $-2L$, AIC, BIC, and K-S displayed in Table no. 7. Among all the competing models, the APTIL distribution stands out with the lowest values of $-2L$, AIC, BIC, and K-S statistics show that the APTIL model is the best fit for explaining the survival times for both groups. The relative histogram with the fitted densities, together with the plots of the fitted survival and empirical survival functions, are presented in Figures 4 and 5.

7. Conclusion

The APTIL distribution model has one scale and one shape parameter. The APTIL distribution is useful for an upside-down bathtub-shaped hazard rate. This paper derives the single moments, product moments, and entropy based on order statistics. We also obtained the estimates of parameters in different ways: maximum product spacing estimator, ordinary and weighted least square estimator. The APTIL model is more flexible than the IL, GIL, and EIL distributions in cases like the survival outcomes of individuals diagnosed with head and neck cancer and laboratory animals infected with virulent tubercle bacilli. We hope that our results and the findings of the estimation procedure will contribute to further research and applications of the APTIL model based on order statistics.

Author Contributions: All authors have equal contribution. All authors reviewed the results and approved the final version of manuscript.



(a) *The relative histogram and fitted density graph* **(b)** *The fitted and estimated survival function*

Figure 5: *The fitted and empirical survival functions for data 2*

Conflicts of Interest: The author declare that there are no conflicts of interest regarding the publication of this paper.

Funding: This research received no Specific grant from any funding agency in the public, commercial, or not-for-profit-sectors.

References

[1] Ahsanullah, M., and Alzaatreh, A. (2018). Parameter estimation for the log-logistic distribution based on order statistics. *REVSTAT-Statistical Journal*, 16(4), 429-443.

[2] Alkarni, S.H. (2015). Extended inverse Lindley distribution: properties and application. *SpringerPlus*, 4, 1-13.

[3] Alkasasbeh, M.R., and Raqab, M.Z. (2009). Estimation of the generalized logistic distribution parameters: Comparative study. *Statistical Methodology*, 6(3), 262-279.

[4] Arnold, B.C., Balakrishnan, N., and Nagaraja, H.N. (2003). *A first course in order statistics*. New York: John Wiley.

[5] Balakrishnan, N., Zhu, X., and Al-Zaharani, B. (2015). Recursive computation of the single and product moments of order statistics for the complementary exponential-geometric distribution. *Journal of Statistical Computation and Simulation*, 85, 2187–2201.

[6] Baratpour, S., Ahmadi, J., and Arghami, N.R. (2008). Characterizations based on R?nyi entropy of order statistics and record values. *Journal of Statistical Planning and Inference*, 138, 2544-2551.

[7] Barco, K.V.P., Mazucheli, J., and Janeiro, V. (2017). The inverse power Lindley distribution. *Communications in Statistics-Simulation and Computation*, 46(8), 6308-6323.

[8] Bjerkedal, T. (1960). Acquisition of resistance in guinea pigs infected with different doses of virulent tubercle bacilli. *American Journal of Hygiene*, 72(1), 130–148.

[9] Cheng, R. C. H., and Amin, N. A. K. (1979). Maximum product-of-spacings estimation with applications to the lognormal distribution. *Mathematical Report*, 791.

[10] Cheng, R. C. H., and Amin, N. A. K. (1983). Estimating parameters in continuous univariate distributions with a shifted origin. *Journal of the Royal Statistical Society: Series B (Methodological)*, 45(3), 394–403.

[11] Dey, S., Dey, T., and Kundu, D. (2014). Two-parameter Rayleigh distribution: different methods of estimation. *American Journal of Mathematical and Management Sciences*, 33(1), 55-74.

[12] Dey, S., Ali, S., and Park, C. (2015). Weighted exponential distribution: properties and different methods of estimation. *Journal of Statistical Computation and Simulation*, 85(18), 3641-3661.

[13] Dey, S., Kumar, D., Ramos, P.L., and Louzada, F. (2017). Exponentiated Chen distribution: Properties and estimation. *Communications in Statistics-Simulation and Computation*, 46(10), 8118-8139.

[14] Dey, S., Nassar, M., and Kumar, D. (2019). Alpha power transformed inverse Lindley distribution: A distribution with an upside-down bathtub-shaped hazard function. *Journal of Computational and Applied Mathematics*, 348, 130-145.

[15] Eltehiwy, M. (2019). Extended exponentiated inverse Lindley distribution: model, properties and applications. *Journal of the Indian Society for Probability and Statistics*, 20(2), 281-300.

[16] Fujioka, T. (2001). Asymptotic approximations of the inverse moment of the noncentral chi-squared variable. *Journal of the Japan Statistical Society*, 31(1), 99-109.

[17] Kumar, D., and Goyal, A. (2019). Order statistics from the power Lindley distribution and associated inference with application. *Annals of Data Science*, 6(1), 153-177.

[18] Goyal, A., Kumar, D., Joorel, J. P. S., and Kumar, M. (2024). Inferences for modified Lindley distribution under order statistics with applications. *Strength of Materials*, 56, 796–814.

[19] Jan, R., Jan, T. R. and Ahmad, P. B. (2018). Exponentiated inverse power Lindley distribution and its applications. arXiv preprint arXiv:1808.07410.

[20] Kumar, D., Kumar, M., Yadav, S., and Goyal, A. (2024). A new parameter estimation method for the extended power Lindley distribution based on order statistics with application. *Statistics in Transition New Series*, 24, 167–184.

[21] Kumar, D., and Dey, S. (2017a). Power generalized Weibull distribution based on order statistics. *Journal of Statistical Research*, 51(1), 61–78.

[22] Kundu, D., and Raqab, M.Z. (2005). Generalized Rayleigh distribution: different methods of estimations. *Computational Statistics & Data Analysis*, 49(1), 187-200.

[23] Mahdavi, A., & Kundu, D. (2017). A new method for generating distributions with an application to exponential distribution. *Communications in Statistics-Theory and Methods*, 46(13), 6543-6557.

[24] Mendenhall, W., & Lehman, E. H. (1960). An approximation to the negative moments of the positive binomial useful in life testing. *Technometrics*, 2(2), 227-242.

[25] Park, S. (1995). The entropy of consecutive order statistics. *IEEE Transactions on Information Theory*, 41(6), 2003–2007.

[26] Ramsay, C. M. (1993). A note on random survivorship group benefits. *ASTIN Bulletin: The Journal of the IAA*, 23(1), 149-156.

[27] R?nyi, A. (1961). On measures of entropy and information. In *Proceedings of the Fourth Berkeley Symposium on Mathematical Statistics and Probability, Volume 1: Contributions to the Theory of Statistics* (Vol. 4, pp. 547–562). University of California Press.

[28] Sharma, V.K., Singh, S.K., Singh, U., and Agiwal, V. (2015). The inverse Lindley distribution: a stress-strength reliability model with application to head and neck cancer data. *Journal of Industrial and Production Engineering*, 32(3), 162-173.

[29] Sharma, V.K., Singh, S.K., Singh, U., and Merovci, F. (2016). The generalized inverse Lindley distribution: A new inverse statistical model for the study of upside-down bathtub data. *Communications in Statistics-Theory and Methods*, 45(19), 5709-5729.

[30] Swain, J., Venkatraman, S., and Wilson, J. (1988). Least squares estimation of distribution function in Johnson's translation system. *Journal of Statistical Computation and Simulation*, 29, 271–297.

[31] Wong, K. M., and Chen, S. (1990). The entropy of ordered sequences and order statistics. *IEEE Transactions on Information Theory*, 36(2), 276–284.

[32] Wooff, D. A. (1985). Bounds on reciprocal moments with applications and developments in Stein estimation and post?stratification. *Journal of the Royal Statistical Society: Series B (Methodological)*, 47(2), 362-371.

Appendix The proof of the theorem 1
From equation (5),

$$\begin{aligned}
E\left[\left(\frac{1}{X_{k:n}}\right)^p\right] &= C_{k:n}\int_0^\infty \left(\frac{1}{x}\right)^p F(x)^{k-1}[1-F(x)]^{n-k}f(x)dx \\
&= C_{k:n}\sum_{\gamma_1=0}^{n-k}\sum_{\gamma_2=0}^{k-1+\gamma_1}(-1)^{k-1-\gamma_2}\binom{n-k}{\gamma_1}\binom{k-1+\gamma_1}{\gamma_2}\frac{\log\beta}{\beta-1}\frac{\omega^2}{\omega+1}\frac{1}{(\beta-1)^{k-1+\gamma_1}} \\
&\times \int_0^\infty \left(\frac{1}{x}\right)^p \frac{1+x}{x^3}e^{-\frac{\omega}{x}}\beta^{\gamma_2+1\left(1+\frac{\omega}{(\omega+1)x}\right)e^{-\frac{\omega}{x}}}dx \\
&= C_{k:n}\sum_{\gamma_3=0}^{\infty}\sum_{\gamma_4=0}^{\gamma_3}\sum_{\gamma_1=0}^{n-k}\sum_{\gamma_2=0}^{k-1+\gamma_1}(-1)^{k-1-\gamma_2}\binom{n-k}{\gamma_1}\binom{k-1+\gamma_1}{\gamma_2}\binom{\gamma_3}{\gamma_4}\frac{(\log\beta)^{\gamma_3+1}}{\gamma_3!} \\
&\times \frac{\omega^{\gamma_4+2}}{(\omega+1)^{\gamma_4+1}}\frac{(\gamma_2+1)^{\gamma_3}}{(\beta-1)^{k+\gamma_1}}\int_0^\infty x^{-p-3-\gamma_4}(1+x)e^{-\frac{\omega(\gamma_3+1)}{x}}dx.
\end{aligned}$$

Now, put $y = \frac{\omega(\gamma_3+1)}{x}$. The theorem's result is obtained using the definition of the gamma function

The proof of the theorem 2
Consider, For $x < y$

$$\begin{aligned}
E\left[\left(\frac{1}{X_{k:n}}\right)^p\left(\frac{1}{X_{l:n}}\right)^q\right] &= \int_0^\infty\int_x^\infty \left(\frac{1}{x}\right)^p\left(\frac{1}{y}\right)^q f_{X_{k:n},X_{l:n}}(x,y)dxdy \\
&= \sum_{\gamma_1=0}^{l-k-1}\sum_{\gamma_2=0}^{n-l}C_{k,l:n}\binom{l-k-1}{\gamma_1}\binom{n-l}{\gamma_2}(-1)^{l-k-1-\gamma_1+\gamma_2} \\
&\times \int_0^\infty\int_x^\infty \left(\frac{1}{x}\right)^p\left(\frac{1}{y}\right)^q [F(x)]^{l-2-\gamma_1}[F(y)]^{\gamma_1+\gamma_2}f(x)f(y)dydx \\
&= \eta(\beta,\omega)\sum_{\gamma_9=0}^{\infty}(-1)^{\gamma_9}\left(\frac{(\omega(\gamma_6+1))^{\gamma_9}}{\gamma_9!}\right)\left[\frac{1}{\gamma_8+\gamma_9+2+q}\int_0^\infty(1+x)\right. \\
&\times e^{\frac{-\omega(\gamma_5+1)}{x}}x^{-p-q-\gamma_7-\gamma_8-\gamma_9-5}dx + \frac{1}{\gamma_8+\gamma_9+1+q}\int_0^\infty(1+x)e^{\frac{-\omega(\gamma_5+1)}{x}} \\
&\times \left. x^{-p-q-\gamma_7-\gamma_8-\gamma_9-4}dx\right],
\end{aligned}$$

where

$$\begin{aligned}
\eta(\beta,\omega) = &\sum_{\gamma_6=0}^{\infty}\sum_{\gamma_5=0}^{\infty}\sum_{\gamma_1=0}^{l-k-1}\sum_{\gamma_2=0}^{n-l}\sum_{\gamma_3=0}^{l-2-\gamma_1}\sum_{\gamma_4=0}^{\gamma_1+\gamma_2}\sum_{\gamma_7=0}^{\gamma_5}\sum_{\gamma_8=0}^{\gamma_6}C_{k,l:n}\binom{l-k-1}{\gamma_1}\binom{n-l}{\gamma_2}\binom{l-2-\gamma_1}{\gamma_3} \\
&\times\binom{\gamma_1+\gamma_2}{\gamma_4}\binom{\gamma_5}{\gamma_7}\binom{\gamma_6}{\gamma_8}(-1)^{k-1-\gamma_1-\gamma_3-\gamma_4}\left(\frac{1}{(\beta-1)^{l-2+\gamma_2}}\right)\left(\frac{\log\beta}{\beta-1}\right)^2\left(\frac{\omega^2}{\omega+1}\right)^2 \\
&\times\frac{(\log\beta)^{\gamma_5+\gamma_6}}{\gamma_5!\gamma_6!}(\gamma_3+1)^{\gamma_5}(\gamma_4+1)^{\gamma_6}\left(\frac{\omega}{\omega+1}\right)^{\gamma_7+\gamma_8}.
\end{aligned}$$

IN FUZZY MENGER SPACE, CERTAIN FPT USING OCCASIONALLY WEAKLY COMPATIBLE MAPPING THAT USES A-CLAS FUNCTION

[1*]Heera Ahirwar And Kavita [2]Shrivastava

•

[1,2,]Department of Mathematics and Statistics
Dr. Harisingh Gour Vishwavidyalaya, Sagar, Madhya Pradesh, India – 470339
[1*]heera.maths15@gmail.com, [2]kavita.rohit@rediff.com

Abstract

In this paper, we present new common fixed point theorems in the setting of fuzzy Menger spaces by considering self-mappings that satisfy the condition of occasional weak compatibility. The analysis is enriched through the incorporation of A-class functions, which serve as control functions in the formulation of contractive type conditions. This approach allows for the generalization and extension of several known results in the field of fuzzy fixed point theory. The structure of fuzzy Menger spaces, combined with the flexibility of A-class functions, enables the establishment of sufficient conditions for the existence and uniqueness of common fixed points among a family of self-mappings. To support the theoretical results, we also provide illustrative examples that demonstrate the applicability and effectiveness of the proposed theorems. The findings contribute to the broader understanding of fixed point results in fuzzy environments and highlight the utility of occasionally weakly compatible mappings under generalized contractive settings.

Keywords: Fuzzy Menger Space, Ccommon Fixed Point, Occasionally Weakly, A-Class Function.

I. Introduction

Fixed point theory in fuzzy settings has attracted considerable interest due to its wide range of applications in mathematical modeling under uncertainty. The notion of fuzzy Menger space, introduced by Kramosil and Michalek [4] and later extended by Schweizer and Sklar [15], provides a suitable framework for analyzing convergence and continuity in fuzzy environments. Within this context, various generalizations of compatibility among mappings have been studied to establish fixed point results under relaxed conditions.

One such generalization is the concept of occasionally weakly compatible (OWC) mappings, introduced by Al-Thagafi and Shahzad [1], which weakens the usual commutativity assumption and allows the mappings to commute at their coincidence points. Additionally, the use of A-class functions, as explored in the works of Singh and others [26], has enabled the formulation of broader contractive conditions beyond classical Lipschitz-type inequalities. Shrivastava, K. et al.[28] prove certain popular fixed point theorems for new rational expression eight mapping through occasionally weakly compatible maps interval-valued fuzzy metric space.

Motivated by these developments, this paper investigates new common fixed point theorems for self-mappings in fuzzy Menger spaces using the framework of occasionally weakly compatible

mappings and contractive conditions defined via A-class functions. Our results extend and generalize several existing theorems in fuzzy fixed point theory.

II. Preliminaries

we give some basic definitions which are useful for main result in this paper.

Definition 2.1[25] Let R represent the real's and R^+ represent the reals that are not negative. If a mapping $F: R \to R^+$ is non-decreasing and left continuous, $inf\{F(t): t \in R\} = 0 \; and \; sup\{F(t): t \in R\} = 1$, it is considered a distribution function.

Definition 2.2[25] A binary relation $t: [0,1] \times [0,1] \to [0,1]$ is called $t - norm$ if it satisfies the following properties:

(i) $t(0,0) = 0 \; and \; t(a,1) = a \quad \forall \; a \in [0,1]$;
(ii) $t(a,b) = t(a,b) \; \forall \; a,b \in t(a,b)$;
(iii) $t(t(a,b),c) = t\big(a,t(b,c)\big) \quad \forall \; a,b,c,d \in [0,1]$;
(iv) $t(a,b) \leq t(c,d)$, whenever $a \leq c \; and \; b \leq d \quad \forall \; a,b,c,d \in [0,1]$

Definition 2.3[25] An ordered pair (Ω, F_α) consisting of a non-empty set X and F_α form $\Omega \times \Omega$ into the collection of all fuzzy distribution functions, $F_\alpha \in R \; , \forall \; \alpha \in [0,1]$ is called fuzzy probabilistic metric space (FPM-space). The fuzzy distribution function is expressed by $F_{\alpha(x,y)}$ and $F_{\alpha(x,y)}(t)$ is the value of $F_{\alpha(x,y)}$ at $t \; in \; R \; and$ following properties are met :

(i) $F_{\alpha(x,y)}(0) = 0, \forall \; x,y \; \in \Omega$
(ii) $F_{\alpha(x,y)}(t) = 1 \; , \forall \; t > 0 \; \Leftrightarrow \; x = y$
(iii) $F_{\alpha(x,y)}(t) = F_{\alpha(y,x)}(t) \; , \forall \; x,y \; \in \Omega$
(iv) $if \; F_{\alpha(x,y)}(s) = 1 \; and \; F_{\alpha(y,z)}(r) = 1 \; \Rightarrow \; F_{\alpha(x,z)}(s+r) = 1 \; , \quad \forall \; x,y,z \; \in \Omega \; , s,r > 0.$

Definition 2.4[25] A fuzzy Menger Space is a triplet (Ω, F_α, T), Where (Ω, F_α, t) is a fuzzy Probabilistic Metric Space (FPM −Space) and T is a t-norm such that for all x ,y , $z \in \Omega$ and all t_1 , $t_2 \geq 0$ and $\alpha \in [0,1]$, $F_{\alpha(x,z)}(s+r) \geq t(F_{\alpha(x,y)}(s), F_{\alpha(y,z)}(r))$.

Definition 2.5[25] Let (Ω, F_α, t) be a fuzzy menger space, if $x \in \Omega, \varepsilon > 0$ and $\lambda \in (0,1)$ then (ε, λ) − neighorhood of $x, called \; U_x(\varepsilon, \lambda)$ defined by $U_x(\varepsilon, \lambda) = \{y \in \Omega : \; F_{\alpha(x,y)}(\varepsilon) > (1-\lambda)\}$
An (ε, λ) − topology in Ω is the topology induced by the family $\{U_x(\varepsilon, \lambda) : x \in \Omega, \varepsilon > 0, \alpha \in [0,1] and \; \lambda \in (0,1) \}$ of neighborhood.

Definition 2.6[25] Let (Ω, F_α, t) be a fuzzy menger space, Where T is a continuous t-norm then

(i) A sequence $\{x_n\} \; in \; \Omega \; is$ said to be convergent if for every $\varepsilon > 0 \; and \; \lambda > 0$, there exists an integer $N = N(\varepsilon, \lambda) \; such \; that \; x_n \in U_x(\varepsilon, \lambda) \; \forall \; n \geq N$ or equivalently $F_\alpha(x_n, x, \varepsilon) > 1 - \lambda \; for \; all \; n \geq N \; and \; \alpha \in [0,1]$.
(ii) A sequence $\{x_n\} \; in \; \Omega \; is$ said to be a Cauchy Sequence if for every $\varepsilon > 0$ and $\lambda > 0$, there exists an integer $N = N(\varepsilon, \lambda)$ such that $F_\alpha(x_n, x_m, \varepsilon) > 1 - \lambda$ $for \; all \; n, m \geq N \; and \; \alpha \in [0,1]$.
(iii) A Menger space (Ω, F_α, t) is said to be Complete if every Cauchy Sequence in X converges to a point in $\Omega \; for \; all \; \alpha \in [0,1]$.

Lemma 2.7[20] Let $(X, F_\alpha, *)$ be a fuzzy Menger space and $x, y \in X$. if there exists a constant $k \in (0,1)$ such that $F_{\alpha(x,y)}(kt) \geq F_{\alpha(x,y)}(t)$ $for\ all\ t > 0$ $then\ x = y$

Lemma 2.8[20] Let $\{y_n\}$ be a sequence in fuzzy Menger space $(X, F_\alpha, *)$ with continuous t-norm and $t * t \geq t$, $for\ all\ t \in [0,1]$ $such\ that\ F_{\alpha(y_n, y_{n+1})}(kt) \geq min(F_{\alpha(y_{n-1}, y_n)}(t), F_{\alpha(y_n, y_{n+1})}(t))$.
For all $t > 0$ $and\ n \in N$. then $\{y_n\}$ is a Cauchy sequence in X.

Lemma 2.9[20] Let $\{x_n\}$ be a sequence in fuzzy Menger space $(X, F_\alpha, *)$ with continuous t-norm and $t * t \geq t$, $if\ there\ exists\ in\ a\ constant\ k \in (0,1)$ $such\ that\ F_{\alpha(x_n, x_{n+1})}(kt) \geq F_{\alpha(x_n, x_{n+1})}(t)$
For all $t > 0$ $and\ n = 1,2 \ldots \ldots$, then $\{x_n\}$ is a Cauchy sequence in X.

Lemma 2.10[25] Let (Ω, d) is a metric space then d induces a mapping $F_\alpha: \Omega \times \Omega \to L$ defined by $F_{\alpha(p,q)} = H_\alpha(x - d(p,q): p, q \in R\ for\ all\ \alpha \in [0,1]$. Further if $t: [01] \times [0,1] \to [0,1]$ is defined by $t(a,b) = \text{Min}\{a,b\}$ then (Ω, F_α, t) is a fuzzy Menger space. It is complete if and only if (Ω, d) is complete.

Definition 2.11[11] Let (Ω, F_α, t) is fuzzy Menger space then the mappings $A, B: \Omega \to \Omega$ are said to be $(E.A)$ $like$ property if there exists a sequence $\{x_n\} \in \Omega$ $such\ that\ Ax_n, Bx_n \to z$ for some $z \in A(\Omega) \cup B(\Omega)$ $as\ n \to \infty$.

Definition 2.12[25] Let (Ω, F_α, t) is fuzzy Menger space then the mappings $A, B: \Omega \to \Omega$ are said to be property $(E.A)$ if there exists a sequence $\{x_n\} \in \Omega$ such that $Ax_n, Bx_n \to z$ for some $z \in \Omega$ $as\ n \to \infty$.

Definition 2.13[11] Let (Ω, F_α, t) is fuzzy Menger space then the mappings $A, B: \Omega \to \Omega$ are said to be $CLR_B - property$ if there exists a sequence $\{x_n\} \in \Omega$ such that $Ax_n, Bx_n \to z$ for some $z \in \Omega$ $as\ n \to \infty$.

Definition 2.14[3] Let (Ω, F_α, t) is fuzzy Menger space then the mappings $A, B: \Omega \to \Omega$ are said to be weakly compatible if these are commuting at their coincidence points.

Definition 2.15[3] Let (Ω, F_α, t) is fuzzy Menger space then the mappings $A, B: \Omega \to \Omega$ are said to be weakly compatible if there is a coincidence point at which the mapping commutes.

Definition 2.16[6] (A-Class function) : A mapping $\mathring{A}: (0,1) \times (0,1) \to R^+$ is continuous and hold the following conditions:
(A_a) $\mathring{A}(u,v) \geq u$;
(A_b) $\mathring{A}(u,v) = u \Rightarrow either\ u = 1\ or\ v = 1$;
(A_c) $\mathring{A}(1,1) = 1$;
Then Å is called Å-class function.
Definition 2.17[6] Let φ be a class of mapping $\varphi: [0,1] \to [0,1]$:
(φ_a) φ is continuous and non-decreasing on $[0,1]$;
(φ_b) $\varphi(x) > x$ $for\ all\ x \in (0,1)$;
(φ_c) $\varphi(0) = 0$ $and\ \varphi(0) = 0$ $for\ all\ x \in (0,1)$;
Definition 2.18[6] Let : $[0,1] \to [0,1]$ is monotonic increasing function with, $\omega(t) > t$ and $\omega(0) = 0$ $and\ \omega(1) = 1$.

The given theorem is proved by S. D. Diwan and Raja [2] and applied the concepts of expansion mappings and CLRs-property and extracted fixed point results

Theorem[3]. Given a complete fuzzy PM-space $(\Omega, F\alpha, t)$ with continuous t-norm and t defined by $t(a,b) = \min\{a,b\} for\ a,b \in [0,1]$, let $G, H, P, and\ Q$ be self-mapping. They must also meet the following requirements:

(1) $G(\Omega) \subseteq Q(\Omega), H(\Omega) \subseteq P(\Omega)$;

(2) $(G,P)\ satisfies\ CLR_P\ property\ or\ (H,Q)$ satisfies CLR_Q property;

(3) $(G,P)\ and\ (H,Q)$ are weakly compatible.

(4) One of the $G(\Omega), H(\Omega), P(\Omega)\ or\ Q(\Omega)$ is a closed subset of Ω.

(5) there exists a constant $k > 1$ such that $(F_{\alpha(Gx,Hy)}(kt) \leq F_{\alpha(Px,Qy)}(t)$ for all $x, y \in \Omega, \alpha \in [0,1] and\ t > 0$. Then $G, H, P\ and\ Q$ have a $UCFP$ in Ω.

In this paper we generalized as a weaker condition for this we use the occasionally weakly compatible such as A-Class Function, to prove a few fixed point results.

III. Main Results

Theorem 3.1 Let $G, P, H, Q, S\ and\ T$ are six self-mapping on a fuzzy Menger space *(X, F_{α} *)*, where * is the min $t - norm$ and satisfying the following Conditions:

(i) $G(X) \subseteq TH(X), \quad P(X) \subseteq SQ(X)$

(ii) $\varphi\{F_{\alpha(Gx,Py)}(t)\} \geq \text{Å}\left[\varphi\left(F_{\alpha(x,y)}(t)\right), \omega\left(F_{\alpha(x,y)}(t)\right)\right]$

Where, $F_{\alpha(x,y)}(t) = \omega\left[Min\left\{F_{\alpha(Gx,SQx)}(t), F_{\alpha(Py,THy)}(t), F_{\alpha(Gx,THy)}(t), F_{\alpha(SQx,Py)}(2t)\right\}\right]$

$For\ all\ x, y \in X, t > 0, \varphi \in Z.$ $(G,SQ)\ and\ (P,TH)\ are$ Weakly compatible;

(iii) $(G,SQ)\ and\ (P,TH)$ Share one of the $CLR_{SQ}, CLR_{TH}\ and\ CLR_{(SQ)(TH)} - property$.

(iv) Then $G, P, H, Q, S\ and\ T$ have a $Ucfp$ in X.

Proof:

Case (I) - Since (G,SQ) share $CLR_{SQ} - property$. so, by the definition, there exist sequences $\{x_n\}$ in X such that

$\lim_{n\to\infty} Gx_n = \lim_{n\to\infty} SQx_n = z, \quad z \in SQ(X)$

Since $G(X) \subseteq TH(X)$ then exist sequences $\{y_n\}$ in X such that $Gx_n = THy_n$

$i.e \quad \lim_{n\to\infty} Gx_n = \lim_{n\to\infty} THy_n = z$

Now we claim $\lim_{n\to\infty} Py_n = z$

Putting $x = x_n\ and\ y = y_n\ in\ (2)\ then$

$\varphi\{F_{\alpha(Gx_n,Py_n)}(t)\} \geq \text{Å}\left[\varphi\left(F_{\alpha(x_n,y_n)}(t)\right), \omega\left(F_{\alpha(x_n,y_n)}(t)\right)\right]$

Where, $F_{\alpha(x_n,y_n)}(t) = \omega\left[Min\left\{F_{\alpha(Gx_n,SQx_n)}(t), F_{\alpha(Py_n,THy_n)}(t), F_{\alpha(Gx_n,THy_n)}(t), F_{\alpha(SQx_n,Py_n)}(2t)\right\}\right]$

$$F_{\alpha(x_n,y_n)}(t) = \omega\left[Min\begin{Bmatrix} F_{\alpha(Gx_n,SQx_n)}(t), F_{\alpha(Py_n,THy_n)}(t), F_{\alpha(Gx_n,THy_n)}(t), \\ F_{\alpha(SQx_n,Gx_n)}(t) * F_{\alpha(Gx_n,Py_n)}(t) \end{Bmatrix}\right]$$

On taking limit as $n \to \infty$

$$\lim_{n\to\infty} F_{\alpha(x_n,y_n)}(t) = \omega\left[Min\begin{Bmatrix} F_{\alpha(Gx_n,SQx_n)}(t), F_{\alpha(Py_n,THy_n)}(t), F_{\alpha(Gx_n,THy_n)}(t), \\ \lim_{n\to\infty} F_{\alpha(SQx_n,Gx_n)}(t) * \lim_{n\to\infty} F_{\alpha(Gx_n,Py_n)}(t) \end{Bmatrix}\right]$$

$$\lim_{n\to\infty} F_{\alpha(x_n,y_n)}(t) = \omega\left[Min\begin{Bmatrix} \lim_{n\to\infty} F_{\alpha(z,z)}(t), F_{\alpha(Py_n,z)}(t), F_{\alpha(z,z)}(t), \\ F_{\alpha(z,z)}(t) * F_{\alpha(z,Py_n)}(t) \end{Bmatrix}\right]$$

$$\lim_{n\to\infty} F_{\alpha(x_n,y_n)}(t) = \omega\left[Min\begin{Bmatrix} 1, F_{\alpha(Py_n,z)}(t), 1, \\ 1 * F_{\alpha(z,Py_n)}(t) \end{Bmatrix}\right]$$

$$\lim_{n\to\infty} F_{\alpha(x_n,y_n)}(t) = \omega\left[F_{\alpha(Py_n,z)}(t)\right]$$

$$\lim_{n\to\infty} F_{\alpha(x_n,y_n)}(t) > \left[F_{\alpha(Py_n,z)}(t)\right]$$

Form (2)

$\varphi\left\{\lim_{n\to\infty} F_{\alpha(Gx_n,Py_n)}(t)\right\} \geq \mathring{A}\left[\varphi\left(\lim_{n\to\infty} F_{\alpha(x_n,x_n)}(t)\right), \omega\left(\lim_{n\to\infty} F_{\alpha(x_n,y_n)}(t)\right)\right]$

$\varphi\{F_{\alpha(Gx_n,Py_n)}(t)\} > \mathring{A}\left[\varphi\left(F_{\alpha(Py_n,z)}(t)\right), \omega\left(F_{\alpha(Py_n,z)}(t)\right)\right] \geq \varphi[F_{\alpha(Py_n,z)}(t)]$

By A- class function,

Either $\varphi\left(\omega\left(F_{\alpha(Py_n,z)}(t)\right)\right) = 1 \;\; or \;\; \omega\left(F_{\alpha(Py_n,z)}(t)\right) = 1$

$\omega\left(F_{\alpha(Py_n,z)}(t)\right) = 1 \Rightarrow \lim_{n\to\infty} Py_n = z.$

In the same manner, we can prove

Case (II) - If the pair (P, TH) Share $CLR_{TH} - property$

Case (III) - $Now \;\; (G, SQ) \; and \;\; (P, TH)$ Share $CLR_{(SQ)(TH)} - property$, there exist sequences $\{x_n\}$ and $\{y_n\}$ in X such that

$\lim_{n\to\infty} Gx_n = \lim_{n\to\infty} SQx_n = \lim_{n\to\infty} Py_n = z = \lim_{n\to\infty} THy_n = z, \quad z \in SQ(X) \cap TH(X)$

Where,

$z \in SQ(X) \cap TH(X)$ then ∄ two point $u \; and \; v \in X$ such that $z = SQu \;\; and \;\; z = THv$.

Now to claim $Gu = z = SQu \;\; and \;\; Pv = z = THv$

Putting $x = x_n \; and \; y = v \; in \;\; (2) \; then$

$\varphi\{F_{\alpha(Gx_n,Pv)}(t)\} \geq \mathring{A}\left[\varphi\left(F_{\alpha(x_n,v)}(t)\right), \omega\left(F_{\alpha(x_n,v)}(t)\right)\right]$

Where, $F_{\alpha(x_n,v)}(t) = \omega[Min\{F_{\alpha(Gx_n,SQx_n)}(t), F_{\alpha(Pv,THv)}(t), F_{\alpha(Gx_n,THv)}(t), F_{\alpha(SQx_n,Pv)}(2t)\}]$

$F_{\alpha(x_n,v)}(t) = \omega\left[Min\begin{Bmatrix} F_{\alpha(Gx_n,SQx_n)}(t), F_{\alpha(Pv,THv)}(t), F_{\alpha(Gx_n,THv)}(t), \\ F_{\alpha(SQx_n,Gx_n)}(t) * F_{\alpha(Gx_n,Pv)}(t) \end{Bmatrix}\right]$

On taking limit as $n \to \infty$

$\lim_{n\to\infty} F_{\alpha(x_n,v)}(t) = \omega\left[Min\begin{Bmatrix} \lim_{n\to\infty} F_{\alpha(z,z)}(t), F_{\alpha(Pv,z)}(t), F_{\alpha(z,z)}(t), \\ F_{\alpha(z,z)}(t) * F_{\alpha(z,Pv)}(t) \end{Bmatrix}\right]$

$\lim_{n\to\infty} F_{\alpha(x_n,v)}(t) = \omega\left[Min\begin{Bmatrix} 1, F_{\alpha(Pv,z)}(t), 1, \\ 1 * F_{\alpha(z,Pv)}(t) \end{Bmatrix}\right]$

$\lim_{n\to\infty} F_{\alpha(x_n,v)}(t) = \omega[F_{\alpha(Pv,z)}(t)]$

$\lim_{n\to\infty} F_{\alpha(x_n,v)}(t) > [F_{\alpha(Pv,z)}(t)]$

Form (2)

$\varphi\left\{\lim_{n\to\infty} F_{\alpha(Gx_n,Pv)}(t)\right\} \geq \mathring{A}\left[\varphi\left(\lim_{n\to\infty} F_{\alpha(x_n,v)}(t)\right), \omega\left(\lim_{n\to\infty} F_{\alpha(x_n,v)}(t)\right)\right]$

$\varphi\{F_{\alpha(Gx_n,Pv)}(t)\} > \mathring{A}\left[\varphi\left(F_{\alpha(Pv,z)}(t)\right), \omega\left(F_{\alpha(Pv,z)}(t)\right)\right] \geq \varphi[F_{\alpha(Pv,z)}(t)]$

By A- class function,

Either $\left(\omega\left(F_{\alpha(Pv,z)}(t)\right)\right) = 1 \;\; or \;\; \omega\left(F_{\alpha(Pv,z)}(t)\right) = 1$

$\Rightarrow \omega\left(F_{\alpha(Pv,z)}(t)\right) = 1 \Rightarrow Pv = z.$

Thus $Pv = z = THv$

But v is a point of coincidence of the pair (P, TH).

So that $Pv = z = THv = Gu = SQu.$

Now $(G, SQ) \; and (P, TH) \; are$ Weakly compatible then $Gz = SQz = Pz = THz.$

Now put $x = z \; and \; y = v \; in \;\; (2) \; the$

$\varphi\{F_{\alpha(Gz,Pv)}(t)\} \geq \mathring{A}\left[\varphi\left(F_{\alpha(z,v)}(t)\right), \omega\left(F_{\alpha(z,v)}(t)\right)\right]$

Where, $F_{\alpha(z,v)}(t) = \omega[Min\{F_{\alpha(Gz,SQz)}(t), F_{\alpha(Pz,Tv)}(t), F_{\alpha(Gz,THv)}(t), F_{\alpha(SQz,Pv)}(2t)\}]$

$F_{\alpha(z,v)}(t) = \omega\left[Min\begin{Bmatrix} F_{\alpha(Pz,Pz)}(t), F_{\alpha(z,z)}(t), F_{\alpha(Gz,z)}(t), \\ F_{\alpha(z,Gz)}(t) * F_{\alpha(Pv,Pv)}(t) \end{Bmatrix}\right]$

$\lim_{n\to\infty} F_{\alpha(z,v)}(t) = \omega\left[Min\begin{Bmatrix}1,1,F_{\alpha(z,Gz)}(t),\\ F_{\alpha(z,Gz)}(t)*1\end{Bmatrix}\right]$

$F_{\alpha(z,v)}(t) = \omega\left[F_{\alpha(Gz,z)}(t)\right]$

$F_{\alpha(z,v)}(t) > \left[F_{\alpha(Gz,z)}(t)\right]$

Form (2)

$\varphi\{F_{\alpha(Gz,Pv)}(t)\} \geq \acute{A}\left[\varphi\left(\lim_{n\to\infty} F_{\alpha(z,v)}(t)\right), \omega\left(\lim_{n\to\infty} F_{\alpha(z,v)}(t)\right)\right]$

$\varphi\{F_{\alpha(z,Pv)}(t)\} > \acute{A}\left[\varphi\left(F_{\alpha(Gz,z)}(t)\right), \omega\left(F_{\alpha(Gz,z)}(t)\right)\right] \geq \varphi\left[F_{\alpha(Gz,z)}(t)\right]$

By A- class function,

Either $\left(\omega\left(F_{\alpha(Gz,z)}(t)\right)\right) = 1 \;\; or \;\; \omega\left(F_{\alpha(Gz,z)}(t)\right) = 1$

$\Rightarrow \omega\left(F_{\alpha(Gz,z)}(t)\right) = 1 \Rightarrow Gz = z.$

Thus $Gz = z = SQz.$

In the same manner we can get $Pz = z = TH.$

Now put $x = Qz \; and \; y = z \; in \; (2) \; then$

$\varphi\{F_{\alpha(GQz,Pz)}(t)\} \geq \acute{A}\left[\varphi\left(F_{\alpha(Qz,z)}(t)\right), \omega\left(F_{\alpha(Qz,z)}(t)\right)\right]$

Where, $F_{\alpha(Qz,z)}(t) = \omega\left[Min\left\{F_{\alpha(GQz,SQQz)}(t), F_{\alpha(Pz,THz)}(t), F_{\alpha(GQz,THz)}(t), F_{\alpha(SQQz,Pz)}(2t)\right\}\right]$

$F_{\alpha(Qz,z)}(t) = \omega\left[Min\begin{Bmatrix}F_{\alpha(GQz,SQQz)}(t), F_{\alpha(Pz,THz)}(t), F_{\alpha(GQz,THz)}(t),\\ F_{\alpha(SQQz,GQz)}(t)*F_{\alpha(GQz,Pz)}(t)\end{Bmatrix}\right]$

$F_{\alpha(Qz,z)}(t) = \omega\left[Min\begin{Bmatrix}F_{\alpha(Qz,Qz)}(t), F_{\alpha(z,z)}(t), F_{\alpha(Qz,z)}(t),\\ F_{\alpha(Qz,z)}(t)*F_{\alpha(Qz,Qz)}(t)\end{Bmatrix}\right]$

$F_{\alpha(Qz,z)}(t) = \omega\left[Min\begin{Bmatrix}1,1,F_{\alpha(Qz,z)}(t),\\ F_{\alpha(Qz,z)}(t)*1\end{Bmatrix}\right]$

$F_{\alpha(Qz,z)}(t) = \omega\left[F_{\alpha(Qz,z)}(t)\right]$

$F_{\alpha(Qz,z)}(t) > \omega\left[F_{\alpha(Qz,z)}(t)\right]$

Thus

$\varphi\{F_{\alpha(Gz,z)}(t)\} > \acute{A}\left[\varphi\left(F_{\alpha(Gz,z)}(t)\right), \omega\left(F_{\alpha(Gz,z)}(t)\right)\right] \geq \varphi\left[F_{\alpha(Gz,z)}(t)\right]$

By A- class function,

Either $\left(\omega\left(F_{\alpha(Gz,z)}(t)\right)\right) = 1 \;\; or \;\; \omega\left(F_{\alpha(Gz,z)}(t)\right) = 1$

$\Rightarrow \omega\left(F_{\alpha(Gz,z)}(t)\right) = 1 \Rightarrow Gz = z.$

Thus $Gz = z \Rightarrow SQz = Sz = z.$

Again put $x = z \; and \; y = Hz \; in \; (2) \; then$

$\varphi\{F_{\alpha(Gz,PHz)}(t)\} \geq \acute{A}\left[\varphi\left(F_{\alpha(z,Hz)}(t)\right), \omega\left(F_{\alpha(z,Hz)}(t)\right)\right]$

Where, $F_{\alpha(z,Hz)}(t) = \omega\left[Min\left\{F_{\alpha(Gz,SQz)}(t), F_{\alpha(PHz,THHz)}(t), F_{\alpha(Gz,THHz)}(t), F_{\alpha(SQz,PHz)}(2t)\right\}\right]$

$F_{\alpha(z,Hz)}(t) = \omega\left[Min\begin{Bmatrix}F_{\alpha(z,z)}(t), F_{\alpha(Hz,Hz)}(t), F_{\alpha(z,Hz)}(t),\\ F_{\alpha(z,Hz)}(t)*F_{\alpha(Hz,Hz)}(t)\end{Bmatrix}\right]$

$F_{\alpha(z,Hz)}(t) = \omega\left[Min\begin{Bmatrix}1,1,F_{\alpha(Hz,z)}(t),\\ F_{\alpha(Hz,z)}(t)*1\end{Bmatrix}\right]$

$F_{\alpha(z,Hz)}(t) = \omega\left[F_{\alpha(Hz,z)}(t)\right]$

$F_{\alpha(z,Hz)}(t) > F_{\alpha(Hz,z)}(t)$

Thus

$\varphi\{F_{\alpha(z,Hz)}(t)\} > \acute{A}\left[\varphi\left(F_{\alpha(z,Hz)}(t)\right), \omega\left(F_{\alpha(z,Hz)}(t)\right)\right] \geq \varphi\left[F_{\alpha(z,Hz)}(t)\right]$

By A- class function,

Either $\left(\omega\left(F_{\alpha(z,Hz)}(t)\right)\right) = 1 \;\; or \;\; \omega\left(F_{\alpha(z,Hz)}(t)\right) = 1$

$\Rightarrow \omega\left(F_{\alpha(z,Hz)}(t)\right) = 1 \Rightarrow Hz = z.$

Hence $THz = z \Rightarrow Tz = z$

Therefore $Pz = THz = z \Rightarrow Pz = z.$

Combining all the above results then we get $Gz = Sz = Qz = Hz = Pz = Tz = z.$

Hence z is a cfp of $G, P, H, Q, S \ and \ T.$

Uniqueness:

Let σ $(\sigma \neq z)$ be another common fixed point of $G, P, H, Q, S \ and \ T$ then

$G\sigma = P\sigma = H\sigma = Q\sigma = S\sigma = T\sigma = \sigma$ and $Gz = Pz = Hz = Qz = Sz = Tz = z$

$\varphi\{F_{\alpha(G\sigma,Pz)}(t)\} \geq Å\left[\varphi\left(F_{\alpha(\sigma,z)}(t)\right), \omega\left(F_{\alpha(\sigma,z)}(t)\right)\right]$

Where, $F_{\alpha(\sigma,z)}(t) = \omega\left[Min\left\{F_{\alpha(G\sigma,SQ\sigma)}(t), F_{\alpha(Pz,THz)}(t), F_{\alpha(G\sigma,THz)}(t), F_{\alpha(SQ\sigma,Pz)}(2t)\right\}\right]$

$F_{\alpha(\sigma,z)}(t) = \omega\left[Min\left\{F_{\alpha(G\sigma,SQ\sigma)}(t), F_{\alpha(Pz,THz)}(t), F_{\alpha(G\sigma,THz)}(t), F_{\alpha(SQ\sigma,Pz)}(2t)\right\}\right]$

$F_{\alpha(\sigma,z)}(t) = \omega\left[Min\left\{F_{\alpha(G\sigma,SQ\sigma)}(t), F_{\alpha(Pz,THz)}(t), F_{\alpha(G\sigma,THz)}(t), F_{\alpha(SQ\sigma,Gz)}(t) * F_{\alpha(Gz,Pz)}(t)\right\}\right]$

$F_{\alpha(\sigma,z)}(t) = \omega\left[Min\left\{F_{\alpha(\sigma,\sigma)}(t), F_{\alpha(z,z)}(t), F_{\alpha(\sigma,z)}(t), F_{\alpha(\sigma,z)}(t) * F_{\alpha(z,z)}(t)\right\}\right]$

$F_{\alpha(\sigma,z)}(t) = \omega\left[Min\left\{1,1, F_{\alpha(\sigma,z)}(t), F_{\alpha(\sigma,z)}(t) * 1\right\}\right]$

$F_{\alpha(\sigma,z)}(t) = \omega\left[F_{\alpha(\sigma,z)}(t)\right]$

$F_{\alpha(\sigma,z)}(t) > F_{\alpha(\sigma,z)}(t)$

Thus

$\varphi\{F_{\alpha(\sigma,z)}(t)\} > Å\left[\varphi\left(F_{\alpha(\sigma,z)}(t)\right), \omega\left(F_{\alpha(\sigma,z)}(t)\right)\right] \geq \varphi\left[F_{\alpha(\sigma,z)}(t)\right]$

By A- class function,

Either $\left(\omega\left(F_{\alpha(\sigma,z)}(t)\right)\right) = 1 \ \ or \ \ \omega\left(F_{\alpha(\sigma,z)}(t)\right) = 1$

$\Rightarrow \omega\left(F_{\alpha(\sigma,z)}(t)\right) = 1 \Rightarrow \sigma = z.$

Hence z is a unique common fixed point of $G, P, H, Q, S \ and \ T$ in X.

Example: Let $(\Omega, F\alpha, T)$ be a complete Fuzzy PM- space. Define a mapping $G, H, P \ and \ Q: \Omega \to \Omega$ Such that

$$G(\alpha) = \begin{cases} \frac{3}{4}, for\ 0 \leq \alpha \leq 1 \\ \frac{\alpha+2}{4}, for \ \ 1 < \alpha \ \leq 2 \end{cases}, \quad H(\alpha) = \begin{cases} \alpha, \ for\ 0 \leq \alpha < 1 \\ \frac{1}{2}, \qquad for\ \alpha = 1 \\ \frac{2\alpha}{5}, \ for\ 1 < \alpha \leq 2 \end{cases}$$

$$P(\alpha) = \begin{cases} \alpha, for\ 0 \leq \alpha \leq 1 \\ \frac{3a}{4}, for \ \ 1 < \alpha \ \leq 2' \end{cases} \quad Q(\alpha) = \begin{cases} \frac{3\alpha}{2}, for\ 0 \leq \alpha \leq 1 \\ \frac{\alpha+1}{5}, for \ \ 1 \leq \alpha \ \leq 2 \end{cases}$$

Let $Å(u, v) \ be$ A-Class function: $X = [0,2]$ and a mapping $Å$: $(0,1) \times (0,1) \to R^+$ is defined by $d(u, v) = |u - v|$ for $u, v \in X$, $F_{\alpha(u,v)}(t) = \frac{t}{t+|u-v|}$ be a FMS.

Since, $G(X) \subseteq T(X)$, $P(X) \subseteq S(X)$. The two sequences $\{x_n\} \ and \ \{y_n\}$ define as $x_n = 1 + \frac{2}{n+3}$, $y_n = 1 + \frac{1}{2n} \ in \ X.$

Such that $\lim_{\to\infty} G(x_n) = \lim_{\to\infty} P(x_n) = \frac{3}{4} = P\left(\frac{3}{4}\right)$

$and \quad \lim_{\to\infty} H(y_n) = \lim_{\to\infty} Q(y_n) = \frac{2}{5} = Q(1).$

Since $\frac{3}{4} \in P(X) \Rightarrow$hence the pair (G, P) satisfy Clr_P-property

And $\frac{2}{5} \in Q(X) \Rightarrow$ then the pair (H, Q) satisfy $Clr_Q -$ property.

IV. Conclusion

In this paper, we have established new fixed point and common fixed point theorems for self-mappings in the framework of fuzzy Menger spaces. By utilizing the notion of occasionally weakly

compatible mappings and incorporating A-class functions as control functions for contractive conditions, we have successfully generalized and extended several existing results in the literature. The combination of these generalized compatibility and contraction conditions allows for broader applicability in fuzzy settings, where classical assumptions may not hold.

Furthermore, illustrative examples provided in the paper validate the main results and demonstrate the effectiveness of the proposed framework. These results contribute to the ongoing development of fixed point theory in fuzzy metric spaces and open new directions for further investigation, particularly in exploring fixed point properties under other generalized contractive conditions and in different fuzzy or probabilistic settings.

We believe that the methods and techniques introduced in this study will serve as a foundation for future research in both theoretical and applied aspects of fuzzy analysis and fixed point theory.

References

[1] Al-Thagafi, M. A. and Shahzad, N.(2008) *Fixed points of set-valued maps in metric spaces*, Fixed Point Theory and Applications, Article ID 120963.

[2] Chauhan, S. and Pant, B. D. (2013). Fixed points of weakly compatible mappings using common (EA) like property. *Le Matematiche*, *68*(1), 99-116.

[3] Diwan, S. D., Thakur, A. K. and Raja, H. (2016). Fixed point of expansion mapping fuzzy menger space with CLRs property. *International Journal of Innovation in Science and Mathematics*, *4*(4), 143-145.

[4] Kramosil, I. and Michalek, J. (1975). *Fuzzy metric and statistical metric spaces*, Kybernetika, 11(5), 336–344.

[5] Liu, X. L., Zhou, M., Mishra, L. N., Mishra, V. N. and Damjanović, B. (2018). Common fixed point theorem of six self-mappings in Menger spaces using (CLRST) property. *Open Mathematics*, *16*(1), 1423-1434.

[6] Mali, D. and Hakwadiya, M. (2023). Common Fixed Point Theorem for Six Self-Mappings Satisfying CLR Property via A-Class Functions in Fuzzy Metric Space *International Journal for Multidisciplinary Research* 5(1).

[7] Mishra, S. N. (1991). Common fixed points of compatible mappings in PM-spaces. *Math. Japon*, *36*, 283-289.

[8] Nashine, H. K. (2014). Study of fixed point theorem for common limit range property and application to functional equations. *Annals of West University of Timisoara-Mathematics and Computer Science*, *52*(1), 95-120.

[9] Pant, B. D. (1993). Fixed points of weakly commuting mappings on Menger spaces. *Jnanabha*, *23*, 115-122.

[10] Pant, B. D. and Chauhan, S. (2010). Fixed Point Theorems in Menger Space Using Semi-Compatibility. *Int. J. Contemp. Math. Sciences*, *5*(19), 943-951.

[11] Rajesh, S. (2017). Fixed Point Theorems for Self-Mappings in a Menger Space using Contractive Control Function under CLR/JCLR-Property. *International Journal of Mathematics Trends and Technology-IJMTT*, *43*.

[12] Sastry, K. P. R., Naidu, G. A., Prasad, P. V. S., and Sastri, S. S. A. (2010). A Fixed Point Theorem for a sequence of self maps in a Menger Space Using a contractive control function. *Int. J. Math. Anal*, *4*(35), 1707-1713.

[13] Satyanna, K. and Srinivas, V. (2024). Results on Expansion Maps in Fuzzy Menger Space via Property-(E.A) and (E.A)-like Property. *Ratio Mathematica*, *51*.

[14] Satyanna, K., Srinivas, V. and Umamaheshwar, R. R. (2024). Some Outcomes on Fuzzy Menger Space via Common Property (E.A) and Absorbing Maps. *Communications in Mathematics and Applications*, *15*(2), 777.

[15] Schweizer, B. and Sklar, A. (1960). Statistical metric spaces. *Pacific J. Math*, *10*(1), 313-334.

[16] Schweizer, B. and Sklar, A. (1883). *Probabilistic metric spaces*. North-Holland, Amsterdam.

[17] Sehgal, V. M. and Bharucha-Reid, A. T. (1972). Fixed points of contraction mappings on probabilistic metric spaces. *Mathematical systems theory*, *6*, 97-102.

[18] Sharma, P. K. (2020). Some common fixed point theorems for sequence of self mappings in fuzzy metric space with property (CLRg). *J. Math. Comput. Sci.*, *10*(5), 1499-1509.

[19] Sharma, S. (2002). Common fixed point theorems in fuzzy metric spaces. *Fuzzy sets and systems*, *127*(3), 345-352.

[20] Sharma, S., and Bagwan, A. (2007). Common fixed point theorem for six mappings in Menger space. *Fasciculi Mathematici*, *37*, 67-77.

[21] Shrivastav, R., Patel, V. and Dhagat, V. B. (2012). Fixed point theorem in fuzzy menger spaces satisfying occasionally weakly compatible mappings. *Int. J. of Math. Sci. & Engg. Appls*, *6*(6), 243-250.

[22] Singh, B., and Bhadauriya, M. S. (2013). Common Fixed Point Theorems for Pair of Self Mapping Satisfying Common (E. A) like Property in Fuzzy Metric Spaces. *International Journal of Computer Applications*, *75*(16).

[23] Singh, B. and Jain, S. (2004). Semi-compatibility and fixed point theorem in Menger space. *Journal of the Chungcheong Mathematical Society*, *17*(1), 1-1.

[24] Singh, B. and Jain, S. (2005). A fixed point theorem in Menger space through weak compatibility. *Journal of Mathematical Analysis and Applications*, *301*(2), 439-448.

[25] Singh, R., Singh, A. D. and Goyal, A. (2016). Fixed point results for P-1 compatible in fuzzy Menger space. *Adv. Fixed Point Theory*, *6*(4), 520-527.

[26] Singh, R., Vats, R. K. and Ali, A. (2016) *Fixed point results using A-class functions and compatible mappings*, Mathematica Moravica, 20(1), 57–72.

[27] Sintunavarat, W., and Kumam, P. (2011). Common fixed point theorems for a pair of weakly compatible mappings in fuzzy metric spaces. *Journal of Applied mathematics*, (1), 637958.

[28] Shrivastava, K. and Ahirwar, H., (2024). Common Fixed Point Theorems for Eight Occasionally Weakly Compatible Maps in Interval-Valued Fuzzy Metric Space for Rational Expression. *Int. j. adv. multidisc. res. Stud*. 4(5):317-323.

RELIABILITY ASSESSMENT OF LOW-VOLTAGE NETWORKS UNDER LIGHTNING-INDUCED OVERVOLTAGES TRANSFERRED FROM MEDIUM-VOLTAGE SYSTEMS

I.A. Guseynova

•

Azerbaijan State Oil and Industry University, Baku, Azerbaijan
huseynova.ilduze@asoiu.edu.az

Abstract

This article investigates the reliability implications of lightning-induced overvoltages transferred from medium-voltage (MV) systems to low-voltage (LV) networks. Special emphasis is placed on the role of distribution transformers and the importance of accurate modeling for evaluating surge transfer mechanisms. Simulations and experimental comparisons reveal that conventional capacitive PI-circuits significantly overestimate transferred voltages. The study highlights the key parameters influencing surge magnitudes, such as earth resistance, transformer proximity, line configuration, and insulator flashovers. Based on analytical models and real case studies, the paper provides recommendations for enhancing the surge immunity and operational reliability of LV systems under lightning conditions.

Keywords: Lightning-induced overvoltages, reliability, medium-voltage networks, low-voltage systems, insulation coordination.

I. Introduction

In the context of rapid urbanization, the widespread integration of sensitive electronic equipment, and the advancement of smart grid technologies, ensuring the reliability and safety of low-voltage (LV) electrical distribution systems has become a pressing challenge. One of the most critical threats to these systems is the impact of lightning-induced overvoltages, which, although originating in medium-voltage (MV) networks, can be transferred to the LV side via distribution transformers.

These transient overvoltages may result from both direct lightning strikes and nearby electromagnetic impulses. When propagated to the low-voltage level, they can cause insulation breakdown, damage to end-user equipment, and interruptions in power supply. The implications extend beyond individual device failures—potential consequences include fires, long-term degradation of infrastructure, and disruptions in essential services such as healthcare, industrial operations, and communication systems. As a result, the ability to accurately assess and effectively mitigate these surges is vital for maintaining high service reliability and minimizing risks to end-users.

The mechanism of surge transfer from MV to LV systems is inherently complex. It depends on multiple variables, including lightning stroke parameters (amplitude, waveform, rise time), network configuration, grounding impedance, the presence and performance of surge protection devices (SPDs), and, critically, the dynamic response of the distribution transformer. Traditional

transformer models, such as the simplified capacitive π-equivalent circuit, often lack the fidelity required to simulate high-frequency transients with sufficient precision.

This paper presents a detailed investigation into the phenomenon of overvoltage transference from MV to LV networks. Using numerical simulations performed in the Alternative Transients Program (ATP), supported by experimental validation, we analyze the evolution of lightning surges as they propagate through transformer couplings and interact with different grounding and network configurations [1–3]. Particular attention is paid to assessing the accuracy of various transformer modeling approaches and identifying their impact on the predicted reliability of LV systems under transient stress.

The overarching aim of this study is to provide power engineers and researchers with a deeper understanding of surge propagation mechanisms and their implications for network resilience. By identifying key parameters and offering improved modeling techniques, this work contributes to the development of more effective protection strategies and enhances the robustness of modern electrical distribution infrastructures.

II. Formulation of the problem

Lightning-induced overvoltages pose a persistent and significant threat to the safety and operational continuity of low-voltage (LV) distribution systems. Even in the presence of conventional protection devices and standardized grounding schemes, harmful transient surges are often capable of propagating to end-user terminals, causing damage to sensitive equipment and compromising system reliability. This vulnerability is primarily due to the complex and highly dynamic nature of surge propagation, particularly under the high-frequency transient conditions associated with lightning strikes.

When a lightning discharge occurs in close proximity to—or directly onto—a medium-voltage (MV) line, it generates a steep-fronted surge current that can couple into the LV network through the magnetic and capacitive links of a distribution transformer [4-7]. The characteristics of this coupling process are governed by several key parameters, including the internal impedance of the transformer, its insulation structure, and the spatial layout of its windings. These elements determine how energy is transferred across voltage levels and how it is distributed throughout the downstream network.

In addition to transformer behavior, several external factors influence the severity and extent of surge transfer. These include the grounding impedance at both the MV and LV sides, the waveform of the incoming surge (including rise time and peak amplitude), and the configuration of the LV distribution feeder —such as the presence of service drops, cable lengths, and consumer loads. The interaction of these factors creates a complex system response that is difficult to predict using traditional modeling techniques.

Conventional transformer models—typically based on lumped-parameter capacitive π-equivalents—fail to capture the detailed high-frequency behavior required for accurate surge analysis. These models often neglect inter-winding coupling effects and frequency-dependent phenomena, which may lead to significant errors in predicting surge amplitudes, wavefront steepness, and propagation timing [8]. Consequently, the results derived from such models may not reliably reflect real-world performance, particularly in the context of fast transients induced by lightning.

To overcome these limitations, the present study develops and validates a high-resolution simulation model that incorporates a more realistic representation of transformer frequency response, detailed grounding impedance characteristics, and spatially distributed consumer load models. The simulated system consists of a 1000-meter LV feeder equipped with service drops,

neutral-grounding arrangements, and representative end-user installations, as illustrated in Figure 1. This modeling framework enables in-depth analysis of overvoltage propagation paths, reflection and attenuation mechanisms, and the overall system behavior under various lightning surge conditions.

The ultimate objective of this research is to enhance the effectiveness of surge protection in LV networks by identifying critical system vulnerabilities and formulating engineering recommendations for optimized grounding configurations and strategic placement of surge protective devices (SPDs). Through this approach, the study aims to contribute to the development of more resilient power distribution networks capable of withstanding the growing threat posed by lightning-induced overvoltages.

.

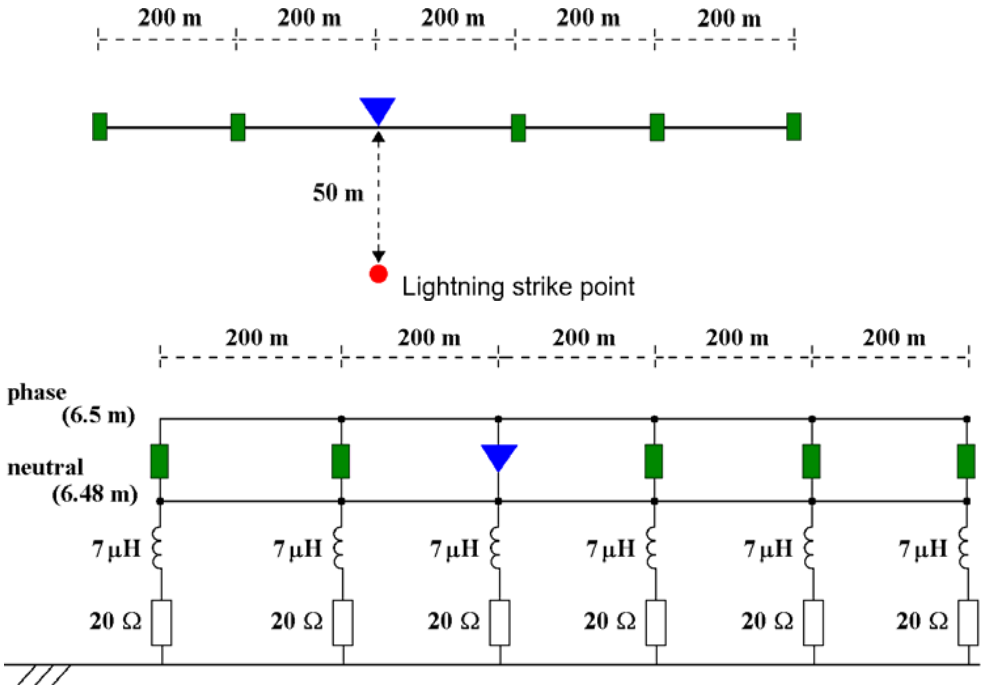


Figure 1: *Configuration of the LV line (top and side views)*

III. Problem solution

To assess the efficiency of grounding and surge protection in low-voltage (LV) power networks under lightning impulse conditions, a simulation-based approach was implemented. The model includes a step-down transformer connected to a low-voltage distribution line, with consumer branches and a lightning surge source applied at the incoming line. The feeder is equipped with grounding points and surge protective devices (SPDs) at critical locations, and its complete topology is shown in Figure 1.

The lightning impulse was modeled using standard waveform parameters of 10/350 μs and 8/20 μs for current and voltage surges, respectively. The applied waveforms are shown in Figure 2, which illustrates the steepness and amplitude of the surge currents. These waveforms were injected into the system to simulate realistic lightning impact conditions.

To study the effects of grounding resistance on the resulting overvoltages, multiple scenarios were simulated with resistance values ranging from 10 Ohm to 50 Ohm. The results demonstrated a clear dependency between the quality of grounding and the magnitude of transient overvoltages observed both at the transformer terminals and at the customer end. These results are summarized in Table 1.

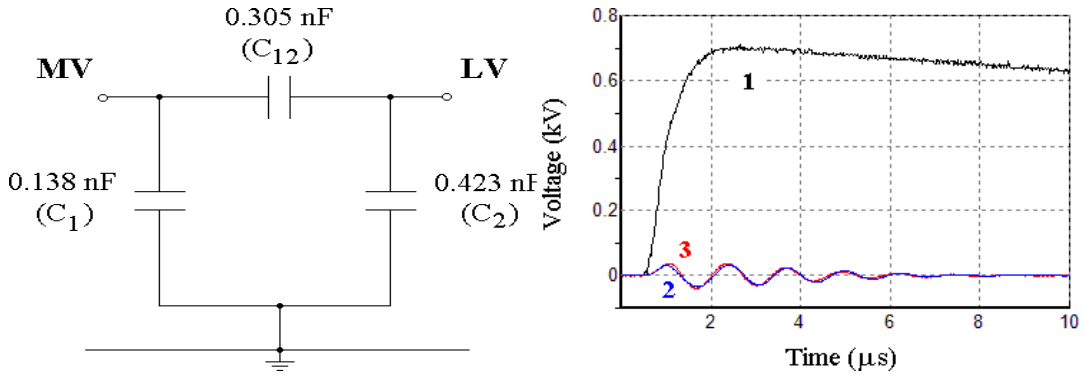


Figure 2: *Impulse waveforms used in the simulations* (10/350 μs and 8/20 μs).

Table 1: *Dependence of overvoltage amplitude on grounding resistance*

Grounding Resistance (Ohm)	Max Overvoltage at Transformer Secondary (kV)	Max Overvoltage at End-User (kV)
10	1.9	2.3
30	2.7	3.0
50	3.3	3.5

The voltage profile along the entire feeder was also evaluated during the impulse event. As shown in Figure 3, overvoltages accumulate and reflect at discontinuities such as branches and terminations. These reflections exacerbate voltage stress at terminal points, potentially endangering end-user equipment.

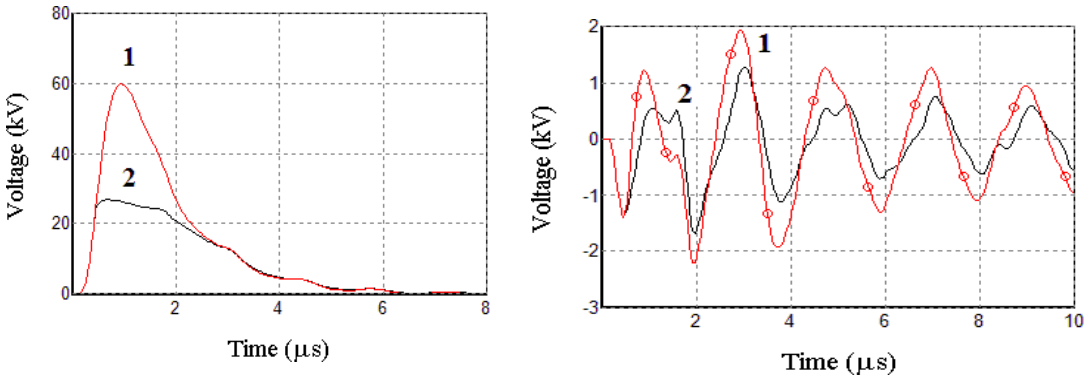


Figure 3: *Voltage profile along the LV feeder during surge propagation*

To mitigate these effects, surge protective devices were introduced at strategic locations—first at the transformer secondary terminal, and then at both the transformer and the far end of the feeder. This allowed evaluation of the cumulative effect of SPD coordination [9-14]. The results of these configurations are presented in Table 2, where it is evident that placing SPDs at both ends provides the most effective suppression of overvoltages.

Table 2: *Effectiveness of surge protection devices (spds)*

SPD Configuration	Max Overvoltage at End-User (kV)	Reduction vs. No SPD (%)
No SPD	3.5	—
SPD at Transformer Secondary	2.1	40%
SPD at Transformer + End of Feeder	1.5	57%

Thus, the simulation results confirm that both the grounding resistance and SPD configuration critically influence the system's ability to withstand overvoltage conditions. Grounding resistance below 10 Ohm significantly enhances protection, while coordinated SPD deployment ensures optimal voltage suppression at sensitive consumer terminals.

General recommendations on the use of surge protective devices (SPDs)

The simulation results presented above clearly demonstrate that effective overvoltage protection in low-voltage (LV) power networks requires a coordinated strategy that combines optimized grounding and appropriately deployed surge protective devices (SPDs). However, to transition from theoretical assessment to practical implementation, it is necessary to develop comprehensive recommendations that account for network topology, grounding modernization costs, and the optimal placement of SPDs.

A key principle in SPD deployment is strategic placement—that is, locating devices at points where overvoltages are most likely to occur or accumulate. Based on the simulation results and existing literature [15-19], the following placement guidelines are recommended:

- Primary SPD Installation: Always install an SPD at the secondary terminal of the distribution transformer. This location is a primary entry point for surges transferred from the medium-voltage (MV) network into the LV system.
- End-of-Feeder Protection: For radial or branched topologies, additional SPDs should be installed at the remote ends of feeders, particularly where sensitive electronic equipment is present.
- Intermediary Nodes: In long feeders (≥500 meters) with multiple branches or critical loads, intermediate SPDs may be installed at major branching points to suppress reflections and limit voltage peaks.
- Topological Consideration: For meshed or looped LV networks, analysis of current paths and impedance mismatch locations should inform SPD placement. In such systems, surge paths can be more complex, necessitating customized coordination studies.

These measures ensure voltage suppression coordination along the feeder and prevent excessive stress at end-user terminals due to reflections and surge wave interactions [20-22].

Criteria for SPD installation based on network topology

The selection and placement of SPDs must consider the topological configuration of the LV distribution system. Table 3 provides generalized guidelines based on typical network structures.

Table 3: *SPD placement recommendations by network topology*

Network Topology	Recommended SPD Locations	Justification
Radial (1–2 branches)	Transformer secondary, end-of-line consumers	Simple paths of surge propagation, concentrated endpoints
Branched (multi-load)	Transformer secondary, major branching nodes, endpoints	Multiple reflection points, cumulative effects
Looped or meshed	Transformer secondary, key nodes based on impedance map	Surge current can flow through multiple paths; placement must be adaptive
Urban compact networks	Building entry points, centralized panelboards	Short cable lengths increase risk to equipment; proximity-based protection

Economic Considerations

One of the often-overlooked aspects of surge protection planning is the **cost-benefit analysis** of grounding system upgrades and SPD installations. Implementing comprehensive protection across a network can be capital intensive, especially for legacy infrastructures [23-25]. Therefore, recommendations must be economically justified, particularly for distribution operators managing large-scale deployments.

Key economic aspects include:

- Grounding Modernization Costs: Reducing grounding resistance below 10 Ohm may require new earth electrodes, soil treatment, or retrofitting existing installations. Estimated costs range from $150 to $500 per site, depending on soil resistivity and space availability.
- SPD Costs and Maintenance: Quality Class II or Class I+II SPDs suitable for LV protection can cost between $50 and $200 per unit. While initial capital costs may be high, the potential reduction in equipment failure and downtime justifies investment in most cases.
- Cost-Effectiveness by Network Type: In radial or rural systems with long feeders, end-user protection offers high returns on investment. In urban networks, centralized protection at building entry points may be more economical.

A structured cost-benefit analysis using outage cost models and customer damage functions can help utilities prioritize protection for the most economically sensitive locations.

IV. Conclusions

The conducted analysis clearly demonstrates the critical role of lightning-induced overvoltages in shaping the reliability and safety of low-voltage (LV) power distribution networks. The transference of surge voltages from the medium-voltage (MV) side to the LV side is not a mere secondary effect but a complex process influenced by multiple interdependent factors, including transformer modeling, line configuration, grounding system topology, and the characteristics of the lightning stroke itself. It has become evident that simplistic models, such as purely capacitive PI-circuits, fail to capture the high-frequency behavior and wave propagation dynamics inherent to real-world lightning interactions, leading to significant inaccuracies in estimating transferred voltages.

Accurate transformer modeling, particularly under transient conditions, emerges as a foundational requirement for any meaningful analysis of surge propagation. The inadequacy of standard transformer equivalent circuits underlines the necessity for high-fidelity models that incorporate inductive and capacitive coupling between windings and ground, enabling precise predictions of voltage stress at the consumer end.

Moreover, the spatial configuration of the LV network, including the distance between grounding points and load connections, plays a decisive role in the amplitude and waveform of the transferred voltages. As simulations have shown, even the number and distribution of connected consumers can materially alter the surge behavior across the network.

These findings emphasize that system-level design, including protective device coordination and earthing strategies, must be approached with a comprehensive understanding of transient surge dynamics.

The presence or absence of MV surge arresters significantly alters the magnitude of induced and transferred voltages. Their application, therefore, must be strategically optimized not only to protect MV equipment but also to mitigate voltage stresses on downstream LV components. Additionally, the findings suggest that the greatest risk to end-user equipment may not arise from the initial lightning stroke but rather from subsequent strokes, which are characterized by sharper rise times and broader frequency content, capable of inducing more destructive voltages.

Ultimately, ensuring the reliability and resilience of LV distribution networks against lightning-induced phenomena requires a multifaceted approach grounded in detailed electromagnetic modeling, empirical validation, and system-wide coordination of protective measures. Without such a comprehensive strategy, utilities and equipment operators remain exposed to elevated failure risks, potentially compromising the continuity and safety of electricity supply.

References

[1] Figueredo, A. J., & Wolf, P. S. A. (2009). Assortative pairing and life history strategy: A cross-cultural study. *Human Nature, 20*(3), 317–330.
[2] Joachims, T. (2002). *Learning to classify text using support vector machines: Methods, theory and algorithms*. Kluwer Academic Publishers.
[3] Rzayeva, S. V., Ganiyeva, N. A., & Piriyeva, N. M. (2024). Modern approaches to electrical equipment diagnostics. *International Journal on Technical and Physical Problems of Engineering (IJTPE)*, *16*(1), 182–189.
[4] Rzayeva, S. V., Piriyeva, N. M., & Guseynova, I. A. (2024). Analysis of reliability of typical power supply circuits. *Reliability: Theory and Applications (RTA)*, *19*(3), 173–178.
[5] Rzayeva, S. V., Piriyeva, N. M., & Ismayilova, S. I. (2025). High and low voltage coordination in electrical power systems. *International Journal on Technical and Physical Problems of Engineering (IJTPE)*, *17*(1), 19–31.
[6] Piriyeva, N. M., Mammadov, N. S., & Rzayeva, S. V. (2025). Development of new methods for protecting substation and overhead lines from overvoltages. *Reliability: Theory & Applications (RTA)*, *1*(82), 683–689. https://doi.org/10.24412/1932-2321-2025-182-683-689
[7] Ahmedov, E. N., Rzayeva, S. V., Mukhtarova, K. M., & Aliyev, N. A. (2025). Innovative enhancements in ground wire configurations for superior lightning protection of overhead power lines. *International Journal on Technical and Physical Problems of Engineering (IJTPE)*, *17*(1), 45–48.
[8] Rzayeva, S. V., & Guseynova, I. A. (2024). Application of automatic monitoring and control systems for reliability of power transmission lines. *Reliability: Theory and Applications (RTA)*, *19*(2), 64–69.
[9] Rahimli, I., Bakhtiyarov, A., Abdullayeva, G., & Rzayeva, S. (2024). Switching processes occurring in electrical networks 10–35 kV. *Przegląd Elektrotechniczny*, *(8)*, 156–159.
[10] Safiyev, E., Piriyeva, N., & Bagirov, G. (2023). Analysis of the application of active lightning rods in lightning protection objects. *Interscience: Electronic Scientific Magazine*, *(6)(276)*, 14–17.
[11] Piriyeva, N. M., Rzayeva, S. V., & Talibov, S. N. (2022). Analysis of surge protection devices for electrical networks. *Internauka: Scientific Journal*, *(43)(266)*, Part 3, 14–17.
[12] Piriyeva, N. M., Rzayeva, S. V., & Mustafazadeh, E. M. (2022). Evaluation of the application of various methods and equipment for protection from emergency voltage in 6–10 kV electric networks of oil production facilities. *Interscience: Electronic Scientific Magazine*, *(39)(262)*, 40–44.
[13] Mamedova, G. V., Kerimzade, G. S., & Piriyeva, N. M. (2022). Electromagnetic calculation of tension devices for winding wires of small cross sections. *International Journal on Technical and Physical Problems of Engineering (IJTPE)*, *14*(4), Issue 53, December.
[14] Piriyeva, N. M., Veliev, Q. A., Abbasov, A. I., & Suleymanov, E. E. (2021). Switching processes in electric networks 10–35 kV. *Energy Problem*, *(2)*, 100–106.
[15] Piriyeva, N. M., & Makhmudov, U. I. (2024). Analysis of substance grounding and surge protection system. *Flaqman Nauki: Nauchnyy Zhurnal*, *(1)(12)*, January, St. Petersburg, State Research Institute "Naprazvitie".
[16] Piriyeva, N., & Kerimzade, G. (2023). Methods for increasing electromagnetic efficiency in induction levitator. *Przegląd Elektrotechniczny*, *(10)*, 192–195.

[17] Obase, P. F., Piantini, A., & Kanashiro, A. G. (2006). Overvoltages on LV networks associated with direct strokes on the primary line. In *Proceedings of the 28th International Conference on Lightning Protection (ICLP)*, Kanazawa, *1*, 479–484.

[18] Obase, P. F., Piantini, A., & Kanashiro, A. G. (2004). Overvoltages on distribution networks caused by direct lightning hits on the primary line. In *Proceedings of the International Conference on Grounding and Earthing and International Conference on Lightning Physics and Effects*, Belo Horizonte, 198–203.

[19] Obase, P. F., Piantini, A., & Kanashiro, A. G. (n.d.). Overvoltages transferred to low-voltage networks due to direct strokes on the primary. [Manuscript reference or conference details needed].

[20] Mammadov, N., Piriyeva, N., & Ismayilova, S. (2024). Research of lightning protection systems for wind electric installations. *Przegląd Elektrotechniczny*, *(9)*, 198–201.

[21] Piriyeva, N. M., Ganiyeva, N. A., & Karimova, R. K. (2025). Innovative approaches to selective automatic reclosing on overhead cable lines. *International Journal on Technical and Physical Problems of Engineering (IJTPE)*, *17*(1), 32–44

[22] .Thakur, K., Dwivedi, D., Babu, K. V. S. M., Parimi, A. M., Yemula, P. K., Chakraborty, P., & Pal, M. (2023). Advancements in arc fault detection for electrical distribution systems: A comprehensive review from artificial intelligence perspective. *arXiv preprint arXiv:2311.16804*.

[23] Sarwar, M., Mehmood, F., Abid, M., Khan, A. Q., Gul, S. T., & Khan, A. S. (2019). High impedance fault detection and isolation in power distribution networks using support vector machines. *arXiv preprint arXiv:1909.10583*.

[24] Huo, Y., Prasad, G., Lampe, L., & Leung, V. C. M. (2021). Power line communication and sensing using time series forecasting. *arXiv preprint arXiv:2110.10219*.

[25] Liu, Y., Singh, A. K., Zhao, J., Meliopoulos, A. P., Pal, B., Ariff, M. A. M., ... & Yu, S. (2020). Dynamic state estimation for power system control and protection. *arXiv preprint arXiv:2012.14927*.

ENHANCING THE RELIABILITY OF RELAY-CONTACTOR CONTROL SYSTEMS IN INDUSTRIAL AND ENERGY APPLICATIONS

[1]Gultakin Hasanova, [2]Sonakhanim Babayeva

•

Azerbaijan State Oil and Industry University, Baku, Azerbaijan
[1]gultakin.hasanova@asoiu.edu.az , [2]sonaxanim.babayeva@asoiu.edu.az

Abstract

Relay-contactor systems remain essential components in power control and automation circuits, particularly in critical industrial and energy infrastructure. Despite the increasing use of solid-state and programmable devices, electromechanical relays and contactors are still widely employed due to their robustness, electromagnetic isolation, and high switching capabilities. However, their reliability is subject to various failure mechanisms including contact wear, coil overheating, and mechanical degradation. This paper presents a systematic analysis of these reliability challenges, supported by statistical modeling, environmental correction factors, and empirical data. Advanced diagnostic techniques and predictive maintenance strategies are discussed, including the integration of intelligent monitoring systems capable of tracking temperature, contact resistance, and response time. The study also explores architectural solutions for improving the redundancy and resilience of DC auxiliary power systems, focusing on protection automation. The technical and economic benefits of intelligent relay systems over conventional ones are demonstrated. Results indicate that adopting adaptive reliability management and smart diagnostics significantly reduces failure rates and improves system availability.

Keywords: relay-contactor systems, reliability modeling, electromechanical switching devices, failure analysis

I. Introduction

Relay-contactor systems continue to play a key role in automatic control and power supply circuits at industrial enterprises and in the energy sector. Despite the growing use of solid-state and programmable devices, electromechanical contactors and relays remain irreplaceable components in situations that require high switching capacity, electromagnetic isolation, or operation under harsh environmental conditions [1]. Their reliability directly affects the safety, stability, and continuity of technological processes, especially in critical systems such as drive control circuits, protection, redundancy, and emergency shutdown systems.

The reliability of relay-contactor devices is determined by a combination of electrical, thermal, mechanical, and environmental factors. Failures in these components often occur suddenly and can lead to the malfunctioning of the entire control system, production line shutdowns, or even accidents with significant technical and economic consequences. Therefore, improving the reliability of these elements is a relevant engineering task that requires a comprehensive approach.

Recent studies on relay-contactor equipment have focused on the wear mechanisms of contact surfaces, thermal aging of coils, contact sticking, and the estimation of residual life under different switching conditions. Despite the existence of numerous empirical models and regulatory standards (including GOST and IEC), the actual operating conditions, load characteristics, and

usage patterns are often not adequately considered in the design and maintenance process, which reduces the effectiveness of failure prevention strategies.

Figure 1 presents a generalized distribution of the causes of relay-contactor failures based on industry reports and technical assessments from field inspections.

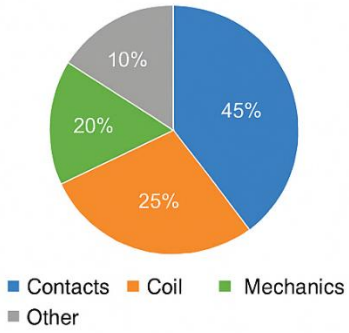


Figure 1.: *Structure of causes of failures in relay-contactor control systems (based on aggregated data from energy and engineering enterprises*

As shown in the diagram, the largest share of failures—approximately 45%—is due to contact wear, highlighting the importance of detailed analysis of switching conditions and the selection of appropriate contact materials. Significant contributions also come from coil overheating (25%) and mechanical wear of moving parts (20%).

The objective of this article is to conduct a systematic analysis of the factors affecting the reliability of relay-contactor control systems and to propose technical and organizational measures to improve it. The study considers reliability modeling methods, condition monitoring technologies, contact material selection, circuit design strategies, and economic evaluation of the proposed solutions.

II. Problem statement

Relay-contactor control systems have traditionally played a key role in ensuring switching, protection, and load management in industrial electrical installations. However, despite their simple design and wide usage, they remain among the most vulnerable components in terms of failures, especially under intensive operation and external influences.

Typical failures of relays and contactors include:

- Contact sticking, which occurs due to welding caused by overload and inrush currents;
- Contact surface burning as a result of multiple switching operations in the presence of an arc, especially when disconnecting inductive loads;
- Mechanical wear of moving parts, actuators, and springs;
- Insulation degradation, accelerated by elevated temperature, humidity, and dust presence.

A critical factor affecting reliability is the nature of the switching load. Inductive loads (e.g., electric motors) produce significant current surges and arc processes, which accelerate contact erosion [2-4]. Capacitive loads cause sharp pulses during closure. Combined load modes result in cumulative effects that exacerbate degradation.

Many existing reliability assessment models are simplified: they do not take into account actual operating modes, climatic and mechanical impacts, nor the specifics of switching. In particular, they assume exponential failure time distribution, consider the structure as series-connected, and introduce environmental effects formally without adapting to specific conditions.

An example is the calculation of failure rate and reliability probability of a control and protection unit (CPU) containing contactors and relays. Without considering operating conditions, a simple model is used:

$$\lambda_S = \sum_{i=1}^{n} \lambda_i$$
$$P(t) = \exp(-\lambda_S \cdot t)$$

where: λs— total failure rate; t — operating time.

However, in operational conditions, reliability is significantly affected by temperature, load factor, and environmental conditions. A refined model uses:

$$\lambda_{ej} = \lambda_j \cdot a(t^{\circ}, k_{nv})$$

where: λj — base failure rate of the element; a(t∘,knv) — correction factor accounting for temperature and load; $k_{nv} = \frac{U_i}{U_n}$ — voltage load factor.

This figure (figure 2) illustrates the influence of ambient temperature and voltage load coefficient ($k_{nv}=U_{actual}/U_{nominal}$) on the correction multiplier used in reliability calculations of relay-contactor systems. As temperature increases from 30 °C to 70 °C, the value of a(t∘,knv) grows exponentially, indicating a sharp rise in the failure rate.

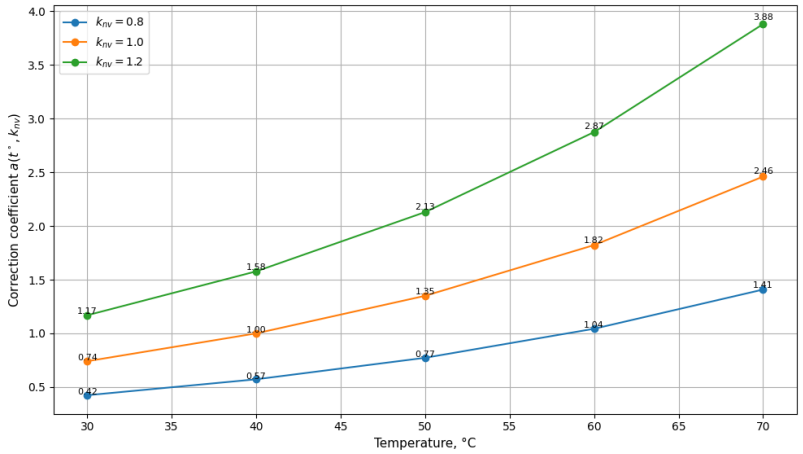


Figure 2.: *Dependence of the correction coefficient a (t°, knv) on temperature and voltage load factor for relays and contactors*

The curves also show that systems operating under overvoltage conditions (knv=1.2) are significantly more sensitive to temperature, leading to accelerated contact wear and a reduction in mean time between failures (MTBF). This confirms the necessity of incorporating real operational conditions into reliability models for electromechanical switching devices.

The resulting probability of failure-free operation within a temperature range of 40–60 °C shows a sharp decrease (table 1):

Table 1.: *Dependence of reliability and mean time to failure (MTTF) of relay-contactor systems on ambient temperature.*

Temperature	P(t=5800 h)	Mean time to failure Tav,h
40 °C	0.33	5236
50 °C	0.19	3509
60 °C	0.072	2208

This demonstrates that even under nominal operating conditions, an increase in temperature by 20 °C reduces the failure-free probability by more than 4.5 times.

Despite this, in the maintenance practice of relay-contactor systems, there are no comprehensive monitoring systems capable of tracking key parameters such as switching current, response time, housing temperature, and contact resistance [5-7]. Visual inspections and periodic checks do not allow early detection of degradation processes.

Hence, there is a need to implement:

- Adequate statistical-analytical models considering actual operating modes;
- Diagnostic and predictive analysis tools based on sensor data;
- An adaptive approach to reliability management, accounting for external environment dynamics and switching intensity.

Thus, the urgent task is to transition from a traditional approach to a comprehensive reliability management model, where the relay-contactor system is regarded as an adaptive object operating in stochastically changing conditions, requiring consideration of individual operational profiles and residual life forecasting.

III. Problem solution

Improving the reliability of relay-contactor systems requires the use of adequate mathematical models capable of capturing the probabilistic nature of failures. As a foundation, models based on continuous-time Markov chains and batch Monte Carlo methods are often employed, allowing for statistical simulation of system element states over time.

The key parameters for constructing such models include electrical switching conditions: current, voltage, and switching frequency. These factors directly influence the degradation of contact surfaces and thereby determine reliability characteristics such as the Mean Time Between Failures (MTBF) and failure rate (λ).

$$MTBF = \frac{1}{\lambda}, \quad \lambda = \frac{N_{failures}}{T_{observation}}$$

The figure below shows the cumulative probability of failure as a function of operational time for conventional and intelligent relays (figure 3).

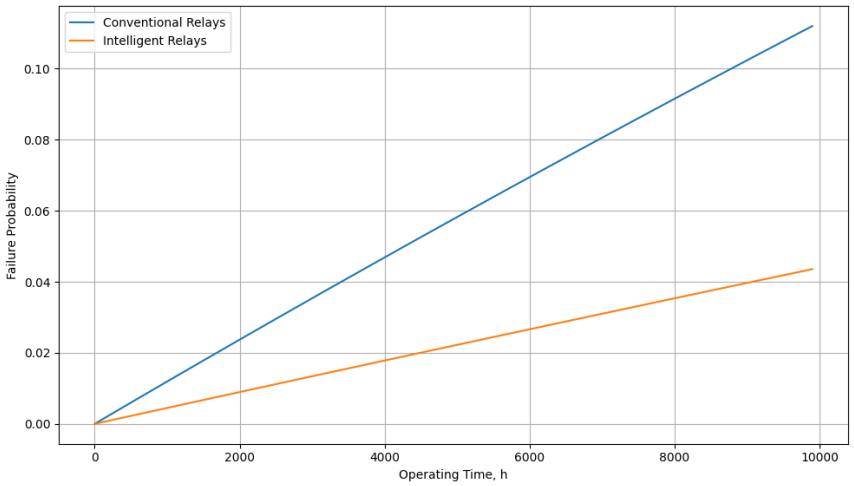


Figure 3. *Cumulative probability of failure versus operating time*

As shown, intelligent relays demonstrate significantly more stable performance throughout their lifecycle, reducing the probability of failure by nearly three times under identical operating conditions [8].

The reliability of relay-contactor systems can be enhanced through the implementation of the following technical measures:

- Use of arc-suppression devices (such as arc chambers and RC-snubber circuits), which reduce thermal damage to contact surfaces during switching operations.
- Anti-stick circuitry and auxiliary relays that prevent contact sticking under fault or overload conditions.
- Improved contact materials — for instance, $AgSnO_2$ or AgNi offer superior arc resistance and wear characteristics compared to conventional materials.
- Redundancy of critical components increases overall system reliability by ensuring continued operation in the event of a single-point failure.
- Regular diagnostics, including thermographic inspections, vibration analysis, and contact resistance measurements, enable early detection of degradation and preventative maintenance planning.

Ensuring the high reliability of relay-contactor circuits and protective relay automation (PRA) systems is a fundamental requirement for the stable operation of substations and power plants. Failures in these circuits can lead to incorrect or missed responses of protection devices, resulting in equipment damage or large-scale outages [9-11]. Therefore, reliability improvement must be approached comprehensively, combining optimal component selection with thoughtful system-level architectural design.

One of the key strategies involves the integration of intelligent monitoring within the relay-contactor circuits. As shown in Figure 4, typical contactor-based configurations can be enhanced by embedding smart diagnostic nodes that track key operational parameters:

- Temperature is a critical variable that reflects thermal stress due to overload conditions or inadequate heat dissipation. Elevated coil or contact temperatures may indicate early signs of degradation.
- Operating Time provides insight into the mechanical health of the relay. An increase in response delay is often associated with mechanical wear, aging springs, or contamination in the moving parts.
- Contact Resistance serves as a real-time indicator of contact surface condition. A gradual increase may point to oxidation, wear, or particulate contamination, all of which degrade electrical conductivity.

These parameters are gathered by smart relay modules, enabling the creation of a digital performance profile and facilitating predictive maintenance through real-time analysis and residual life estimation of critical components. Such monitoring helps to avoid unexpected failures and supports the scheduling of preventive actions without interrupting service.

In addition to monitoring, the architecture of the auxiliary DC power supply plays a vital role in the overall reliability of PRA systems. DC auxiliary power systems (DAPS) are responsible for powering essential control, protection, and automation equipment (figure 5). A widely adopted solution for enhancing redundancy in DAPS is a dual-channel configuration, which typically includes:

- Two independent battery banks, each equipped with its own charger,
- Two isolated DC buses (DC1 and DC2),
- Isolation diodes or automatic transfer switching (ATS) mechanisms for load switchover.

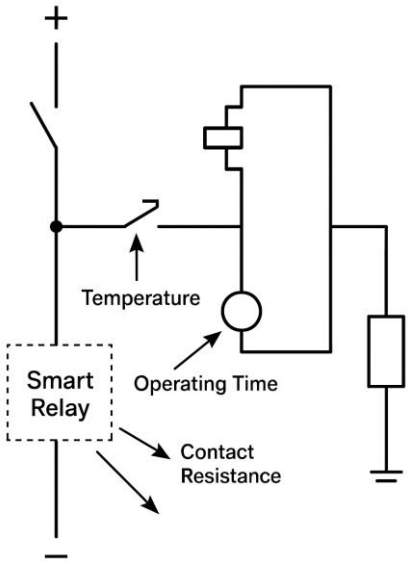


Figure 4.: *Relay-contactor system with intelligent monitoring*

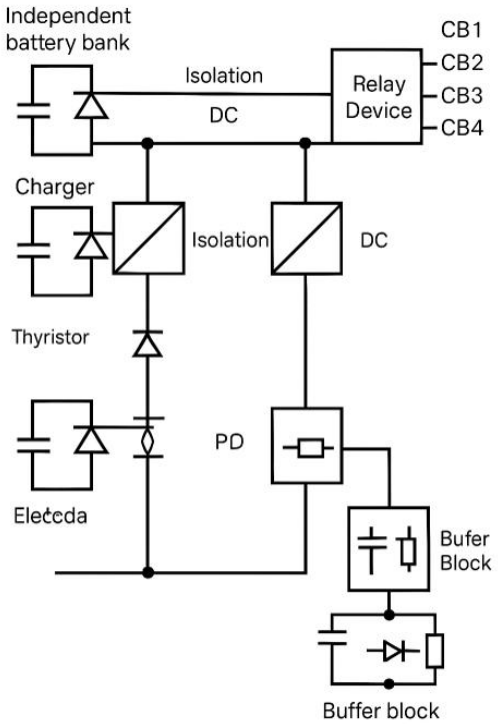


Figure 5.: *Dual-channel architecture of the DC auxiliary power system with protection device (PD) and optional ATS-based redundancy.*

While such systems provide redundancy, they also introduce specific technical challenges. In particular, under certain conditions—such as insulation failures, commissioning errors, or misconfigured diodes—voltage summation can occur through the isolation diodes, potentially producing voltages of up to 450 V at the input terminals of microprocessor-based relay devices (MURZ). These overvoltages can lead to catastrophic failures of logic inputs and power supplies, especially in systems relying on varistor-only protection.

To mitigate this risk, a dedicated overvoltage protection device (PD) can be employed. A simple yet effective circuit based on a thyristor (e.g., MCO 100-12io1) and a TVS diode (e.g., 1.5KE300A) can:

- Clamp and limit the surge voltage to a safe level,
- Interrupt the fault current path by turning off the thyristor,
- Trigger the disconnection of circuit breakers (e.g., CB1–CB4) before the PRA devices sustain irreversible damage.

However, an even more robust and modern solution is to eliminate isolation diodes entirely and adopt a design based on two independent buses supported by an automatic transfer switch using relays and an intermediate buffer block composed of a capacitor, diode, and resistor.

This alternative architecture offers several advantages:

- It maintains power continuity for 40–60 ms, which is sufficient to bridge short-term dips during transfer events,
- It avoids momentary voltage collapses that could deactivate intermediate relays or logic circuits,
- It is fully compatible with all standard-compliant PRA units, many of which tolerate power interruptions up to 500 ms or longer.

In conclusion, enhancing the reliability of relay-contactor and protective relay systems requires more than just robust components—it demands a system-level view that includes intelligent diagnostics, redundancy-aware architecture, and proactive protection strategies. By combining smart monitoring with well-engineered auxiliary power supply schemes, power system operators can significantly improve the availability, safety, and resilience of critical protection infrastructure.

Modern technologies enable not only the monitoring of the current condition of equipment but also the prediction of its future behavior. Machine learning methods such as XGBoost and recurrent neural networks (RNN) process operational data (response time, temperature, contact resistance) and build models capable of accurately estimating the residual life of relays.

Sensors embedded in smart devices provide continuous monitoring, and the collected data is integrated into predictive maintenance systems, which is especially effective in continuous production environments.

The implementation of more reliable and "smart" solutions must be economically justified. Below is a comparative table presenting key technical and economic parameters of conventional and intelligent relays (table 2).

Table 2.: *Comparison of technical and economic parameters of conventional and intelligent relays*

Parameter	Conventional Relays	Intelligent Relays
MTBF (hours)	83,333	222,222
Failure rate λ (1/hour)	0.000012	0.000005
Device cost ($)	35	120
Expected failure losses ($/year)	7,000	2,500

The table shows that despite the higher cost of intelligent relays, they significantly reduce annual losses due to failures while providing a higher level of reliability and technical predictability.

IV. Conclusion

This study provides a comprehensive analysis of the reliability issues associated with relay-contactor systems used in industrial automation and energy infrastructure. Through detailed examination of typical failure modes—including contact wear, coil overheating, and mechanical degradation—the paper highlights the critical role that operating conditions, load characteristics, and environmental factors play in determining system longevity.

Analytical models incorporating correction factors for temperature and voltage stress were introduced to improve the accuracy of reliability estimation. These models demonstrated a significant decrease in failure-free probability under elevated thermal and electrical loads, emphasizing the necessity of real-condition-based reliability assessment.

To address these challenges, the implementation of intelligent monitoring systems was proposed. These systems enable real-time tracking of key performance indicators such as contact resistance, operating temperature, and response delay, providing the basis for predictive diagnostics and timely maintenance. In addition, improvements in circuit architecture, including redundancy in DC auxiliary power systems and overvoltage protection, were discussed as vital strategies for enhancing operational safety and continuity.

The comparative analysis showed that intelligent relay solutions, despite their higher initial cost, offer substantial economic and technical advantages by reducing annual failure-related losses and increasing mean time between failures (MTBF).

In conclusion, enhancing the reliability of relay-contactor systems requires a multidimensional approach combining advanced modeling, smart diagnostics, improved material and design choices, and system-level architectural resilience. Future work should focus on integrating machine learning-based predictive tools and expanding sensor networks to build fully adaptive and self-diagnosing control systems.

References

[1] McLaren, P. G. (2007). Reliability of electromechanical relays in protection systems. *IEEE Transactions on Power Delivery*, 22(4), 2312–2318.

[2] Singh, A. K., & Tiwari, M. (2011). Modeling and reliability analysis of electromechanical relay contacts. *Reliability Engineering & System Safety*, 96(6), 777–783.

[3] Nakagome, M., Kajiwara, T., & Ogawa, H. (2019). Predictive maintenance of protective relays using machine learning techniques. *Electric Power Systems Research*, 172, 142–151.

[4] Rzayeva, S. V., Piriyeva, N. M., & Guseynova, I. A. (2024). Analysis of reliability of typical power supply circuits. *Reliability: Theory & Applications*, 19(3), 173–178.

[5] Rzayeva, S. V., & Guseynova, I. A. (2024). Application of automatic monitoring and control systems for reliability of power transmission lines. *Reliability: Theory & Applications*, 19(2), 64–69.

[6] Rzayeva, S. V., Ganiyeva, N. A., & Piriyeva, N. M. (2024). Modern approaches to electrical equipment diagnostics. *International Journal on Technical and Physical Problems of Engineering (IJTPE)*, 58.

[7] Rzayeva, S. V., Piriyeva, N. M., & Ismayilova, S. I. (2025). High and low voltage coordination in electrical power systems. *International Journal on Technical and Physical Problems of Engineering (IJTPE)*, 17(1), 19–31.

[8] Piriyeva, N. M., Ganiyeva, N. A., & Karimova, R. K. (2025). Innovative approaches to selective automatic reclosing on overhead cable lines. *International Journal on Technical and Physical Problems of Engineering (IJTPE)*, 17(1), 32–34.

[9] Piriyeva, N. M., Mammadov, N. S., & Rzayeva, S. V. (2025). Development of new methods for protecting substation and overhead lines from overvoltages. *Reliability Theory and Applications*, 20(1), 683–689.

[10] Ahmedov, E. N., Rzayeva, S. V., Mukhtarova, K. M., & Aliyev, N. A. (2025). Innovative enhancements in ground wire configurations for superior lightning protection of overhead power lines. *International Journal on Technical and Physical Problems of Engineering (IJTPE)*, 17(1), 45–48.

[11] Zhang, Y., Sun, Z., & Wang, X. (2019). A condition monitoring and diagnostics method for electromechanical relays based on contact resistance measurement. *IEEE Transactions on Instrumentation and Measurement*, 68(5), 1460–1468.

FRACTIONAL INTEGRAL INEQUALITIES AND THEIR Q-EXTENSION

Farooq Ahmad[1], Ajjaz Maqbool[2], D.K. Jain[3], R. Vijaykrishnaraj[4], Aafaq A. Rather[5,*], D. Vedavathi Saraja[6], Syed M. Parveen[7], Raeesa Bashir[8], Showkat Ahmad Bhat[9]

•

[1]Department of Mathematics, Government College for Women Nawakadal, Srinagar, India
[2]Department of Mathematics, Sheikh-ul-Alam Memorial Degree college Budgam, India
[3]Department of Engineering Mathematics Computing,Madhav Institute of Technology and Science.Gwalior-474005, Madhya Pradesh, India
[4]Department of Mathematics, Bharath Institute of Higher Education and Research, Chennai, India
[5,*]Symbiosis Statistical Institute, Symbiosis International (Deemed University), Pune, India
[6,7]Department of Statistics, Maris Stella College, Vijayawada, India
[8]Department of Statistics, Cluster University, Jammu and Kashmir, India
[9]Symbiosis School of Economics, Symbiosis International (Deemed University), Pune, India
[1]sheikhfarooq85@gmail.com, [2]ajjazmaqbool013@gmail.com, [4]drvjmaths@gmail.com, [5,*]aafaq7741@gmail.com, [6]sarajayoganand@gmail.com, [7]parveen@marisstella.ac.in, [8]raisabashir52@gmail.com [9]showkat.bhat@sse.ac.in

Abstract

This paper aims to establish novel fractional integral inequalities for synchronous functions associated with the Chebyshev functional, incorporating the Gauss hypergeometric function. By employing advanced integral techniques, we derive refined bounds that extend and generalize existing results in the literature. The final section explores several special cases, particularly fractional integral inequalities involving Riemann-Liouville type fractional integral operators. Furthermore, we discuss potential applications of these findings in various mathematical and applied fields, highlighting their significance in fractional calculus and related domains.

Keywords: Synchronous functions, Fractional integral inequalities & Saigo operator.

1. Introduction

The most beneficial uses of fractional integral inequalities are in determining the uniqueness of solutions to fractional boundary value issues and fractional partial differential equations. Additionally, they offer upper and lower bounds for the solutions of the aforementioned equations. These factors have prompted a number of scholars working in the area of integral inequalities to investigate various extensions and generalisations by utilising fractional calculus operators. For instance, the book [1] and the publications [2-11] both contain references to such works.

Purohit and Raina [9] recently looked into some integral inequalities of the Chebyshev type [12] utilising Saigo fractional integral operators and established the q-extensions of the main findings. This study uses the fractional hypergeometric operator proposed by Curiel and Galue [13] to prove a few generalized integral inequalities for synchronous functions related to the Chebyshev functional. As special examples of our findings, the results attributed to Purohit and Raina [9] and Belarbi and Dahmani [2] are presented below.

2. The terms and definitions used in this paper are as follows

Definition 2.1 : Two functions f & g are said to be synchronous on [a, b] if

$$(f(x)-f(y))(g(x)-g(y))[a,\ b] \tag{1}$$

Definition 2.2: A real-valued function f(t) (t> 0) is said to be in the space C_μ ($\mu \in$ R) if there exists a real number p > μ, such that f(t) = $t^p \emptyset(t)$, where $\emptyset(t) \in C(0,\infty)$.

2.1 Saigo's Fractional operator

Useful and interesting generalization of both the Riemann-Liouville and Erdelyi-Kober fractional integration operators is introduced by Saigo [13], in terms of Gauss's hypergeometric function as given below

Let α, βand ηare complex numbers ∈ C and let $x \in R_+$ the fractional Re (α)>0 and the fractional derivative Re(α)<0 of the first kind of a function

$$I_{0,x}^{\alpha,\beta,n} f(x) = \frac{x^{-\alpha-\beta}}{\Gamma\alpha} \int_0^x (x-t)^{\alpha-1}\ {}_2F_1[\alpha+\beta,-n;1-\frac{t}{x}]\, f(t)\,dt,\ \mathrm{Re}(\alpha)>0 \tag{2}$$

$$= \frac{d^n}{dx^n} I_{0,x}^{\alpha+n,\beta+n,\eta-n} f(x),\ 0<\mathrm{Re}(\alpha)+\eta\le 1\ (n\in N_0) \tag{3}$$

$$I_{0,x}^{\alpha,\beta,n,\mu} f(x) = \frac{x^{-\alpha-\beta-2\mu}}{\Gamma\alpha} \int_0^x \tau^\mu (x-t)^{\alpha-1}\ {}_2F_1[\alpha+\beta,-n;1-\frac{t}{x}]\, f(t)\,dt \tag{4}$$

2.2 Main Results

In this section, we obtain certain Chebyshev type integral inequalities involving the generalized fractional integral operator. The following lemma is used for our first result.

Lemma: let $\alpha > 0$, μ >-1, β, η ∈ R; then the following image formula for the power function under the operator (1.2) holds true:

$$I_{0,x}^{\alpha,\beta,n}(x^{\tau-1}) = \frac{\Gamma(\tau)\Gamma(\tau-\beta+\eta)}{\Gamma(\tau-\beta)\Gamma(\tau+\alpha+\eta)} x^{\tau-\beta-\mu-1} \tag{5}$$

Theorem 1: Let f&g be two synchronous functions on$(0,\infty)$ then

$$I_{0,x}^{\alpha,\beta,n}(f(x)\,g(x)) \ge \frac{\Gamma(1-\beta)\Gamma(1+\alpha+\eta)}{\Gamma(1-\beta+\eta)} x^{\beta+\mu} \times I_{0,x}^{\alpha,\beta,n}(f(x))\, I_{0,x}^{\alpha,\beta,n}(g(x)) \tag{6}$$

For all $x>0, \alpha > \max\{0,-\beta-\mu\}, \beta<1, \mu>-1, \eta<0.$

Proof: Let f&g be two synchronous functions, then using definition1, for all τ, ρϵ(0, t), t ≥ 0, we have

$$(f(\tau)-f(p))(g(\tau)-g(p))\geq 0 \tag{7}$$

which implies that

$$\big(f(\tau)g(\tau)+f(p)g(p)\big)\geq (f(\tau)g(p)+f(p)g(\tau)) \tag{8}$$

Consider

$$F(x,\tau)=\frac{x^{-\alpha-\beta}(x-t)^{\alpha-1}}{\Gamma\alpha}2F_1[\alpha+\beta,-n;1-\frac{\tau}{x}]f(t)\,dt \tag{9}$$

$$=\frac{(x-\tau)^{\alpha-1}}{\Gamma(ax)^{\alpha+\beta}}\times\frac{(\alpha+\beta)(-\eta)(x-\tau)^{\alpha}}{\Gamma(\alpha+1)x^{\alpha+\beta}}+\frac{(\alpha+\beta+\mu)(\alpha+\beta+1)(x-\tau)^{\alpha-1}}{\Gamma(\alpha+2)}\times\frac{(x-\tau)^{\alpha+1}}{x^{\alpha+\beta+2}} \tag{10}$$

Our observation is that each term of the above series is positive in view of the conditions stated with Theorem 1.

$$I_{0,x}^{\alpha,\beta,n}(f(x)\,g(x))\geq\frac{\Gamma(1-\beta)\Gamma(1+\alpha+\eta)}{\Gamma(1-\beta+\eta)}x^{\beta}\times I_{0,x}^{\alpha,\beta,n}(f(x))\,I_{0,x}^{\alpha,\beta,n}(g(x)) \tag{11}$$

In light of the circumstances outlined in theorem 2.2.1, we note that each term in the afore mentioned series is positive. On integrating from 0 to τ and using (2.1.2), we get

$$(I_{0,x}^{\alpha,\beta,\eta,\mu}f(x)g(x))+\big(f(p)g(p)I_{0,x}^{\alpha,\beta,\eta}\{1\}\big)\geq g(p)I_{0,x}^{\alpha,\beta,\eta}f(x)+(f(p)I_{0,x}^{\alpha,\beta,\eta}g(x)) \tag{12}$$

Theorem 2: let f & g be two synchronous functions on $(0,\infty)$, then

$$\begin{aligned}&\Rightarrow\frac{\Gamma(1+\mu)\Gamma(1-\beta+\eta)}{\Gamma(1-\beta)\Gamma(1+\mu+\alpha+\eta)x^{\beta+1}}I_{0,x}^{\delta,\gamma,\theta,\varepsilon}(f(x)\,g(x))\\&+\frac{\Gamma(1+\theta)\Gamma(1-\delta+\varepsilon)}{\Gamma(1-\delta)\Gamma(1+\theta+\gamma+\varepsilon)x^{\beta+\mu}}I_{0,x}^{\alpha,\beta,\eta,\mu}(f(x)\,g(x))\\&\geq(I_{0,x}^{\alpha,\beta,\eta,\mu}f(x)I_{0,x}^{\delta,\gamma,\theta,\varepsilon}g(x))+I_{0,x}^{\delta,\gamma,\theta,\varepsilon}g(x)(f(p)I_{0,x}^{\alpha,\beta,\eta,\mu}f(x))\end{aligned} \tag{13}$$

For all $x>0,\alpha>\max\{0,-\beta-\mu\},\gamma>Max(0,-\delta,-\theta),\mu,\theta>-1.$

Proof: To prove the above theorem, we use previous theorem , we have

$$\frac{x^{-\gamma-2\theta-\delta}p^{\delta}(x-p)^{\gamma-1}}{\Gamma\gamma}2F_1[\delta+\gamma+\theta,-\varepsilon;1-\frac{p}{x}]f(p)\,dp \tag{14}$$

which, given the circumstances mentioned with, continues to be positive as per above theorem and we obtain by integrating with regard to from 0 to t.

$$\begin{aligned}&(I_{0,x}^{\alpha,\beta,\eta,\mu}f(x)g(x))I_{0,x}^{\delta,\gamma,\theta,\varepsilon}\{1\}+I_{0,x}^{\delta,\gamma,\theta,\varepsilon}\big(f(x)g(x)I_{0,x}^{\alpha,\beta,\eta,\mu}\{1\}\big)\\&\geq I_{0,x}^{\alpha,\beta,\eta,\mu}\{f(x)\}I_{0,x}^{\delta,\gamma,\theta,\varepsilon}\{g(x)\}+I_{0,x}^{\delta,\gamma,\theta,\varepsilon}(g(x)I_{0,x}^{\alpha,\beta,\eta,\mu}f(x))\end{aligned} \tag{15}$$

3. q-Extension

Recently, q calculus has served as a bridge between mathematics and physics. Consequently, there has been a significant increase in activity in the field of q-calculus due to applications of q-calculus in mathematics, statistics, and physics. Most of the scientists in the world who use the q -calculation today are physicists. The q- calculus is a generalization of many topics, such as chain metaphysics, generating functions, complexity analysis, and particle physics. In short, q -calculation is a very popular topic today. One of the important branches of q -calculus in

number theory is the q- class of special generating functions, such as q-Bernoulli numbers, q-Euler numbers and q-Genocchi numbers. Here we define a new class of multivariable integrals of type q (generalizations of beta integrals) called Saigo's q- Integral Operator.

The a Saigo's q- Integral Operator which is analogue to the well known Bernardi integral operator is investigated. In the following, we obtain a simple conceptual q extension of the results obtained in the first part of the paper, using some q-Saigo's q- Integral Operator.

3.1 Saigo's q- Integral Operator

A basic analogue of Saigo's fractional integral operator [29] is defined as

$$I_{0,x}^{\alpha,\beta,n} f(x) = \frac{x^{-\beta-1}}{\Gamma q^{(\alpha)}} \int_0^x (\frac{tq}{x};q)_{\alpha-1} \times \sum_{m=0}^{\infty} \frac{(q^{\alpha+\beta},q)_m (q^{-n},q)_m}{(q^{\alpha},q)_m (q,q)_m} q^{(\eta-\beta)m} (-1)^m (-q)^{\binom{-m}{2}} \left(\frac{t}{x}-1\right)_m f(t)\, d_q(t)$$

$$f(x) = \frac{q^{-\binom{\alpha}{2}-\beta}}{\Gamma q^{(\alpha)}} \int_0^x (\frac{x}{t};q)_{\alpha-1} t^{-\beta-1} \times \sum_{m=0}^{\infty} \frac{(q^{\alpha+\beta},q)_m (q^{-n},q)_m}{(q^{\alpha},q)_m (q,q)_m} q^{(\eta-\beta)m} (-1)^m (-q)^{\binom{-m}{2}} \left(\frac{x}{qt}-1\right)_m f(tq^{1-\alpha})\, d_q(t)$$

By making use q- integral definition, the above operators can be written as

$$I_{0,x}^{\alpha,\beta,n} f(x) = x^{-\beta}(1-q)^{\alpha} \times T \tag{16}$$

where, $T = \sum_{m=0}^{\infty} \frac{(q^{\alpha+\beta},q)_m (q^{-n},q)_m}{(q^{\alpha},q)_m (q,q)_m} q^{(\eta-\beta+1)m} \sum_{k=0}^{\infty} q^k \frac{(q^{\alpha+\beta},q)_k (q^{-n},q)_m}{(q,q)_m} f(xq^{k+m})$

and $K_q^{\alpha,\beta,n} f(x) = x^{-\beta}(q)^{\binom{-\alpha}{2}}(1-q)^{\alpha} \times T$

4. Main Results

In this section we obtain certain Chebyshev type integral inequalities involving the generalized q- fractional integral operator. The following lemma is used for our first result.

Theorem 3.1: Let f&g be two synchronous functions on $(0,\infty)$ then

$$I_q^{\alpha,\beta,n}(f(x)g(x)) \geq \frac{\Gamma_q(1-\beta)\Gamma_q(1+\alpha+\eta)}{\Gamma_q(1-\beta+\eta)} x^{\beta+\mu} \times I_q^{\alpha,\beta,n}(f(x)) I_q^{\alpha,\beta,n}(g(x)) \tag{17}$$

For all $x>0, \alpha > \max\{0,-\beta-\mu\}, \beta<1, \mu>-1, \eta<0.$

Proof: Let f&g be two synchronous functions ,then using definition1, for all $\tau, \rho \epsilon (0,t), t \geq 0$, we have

$$\big((f(\tau)+f(p)g(\tau)\big)-g(p)) \geq 0 \tag{18}$$

which implies that

$$\big(f(\tau)g(\tau)+f(p)g(p)\big) \geq (f(\tau)g(p)+f(p)g(\tau)) \tag{19}$$

Consider

$$F(x,\tau) = \frac{x^{-\alpha-\beta-2\mu}\tau^{\mu}(x-t)^{\alpha-1}}{\Gamma q^{\alpha}} 2F_1[\alpha+\beta+\mu,-n;1-\frac{\tau}{x}] f(t)\,dt \tag{20}$$

$$= \frac{\tau^{\mu}(x-\tau)^{\alpha-1}}{\Gamma q^{\alpha}(x)^{\alpha+\beta+2\mu}} \times \frac{\tau^{\mu}(\alpha+\beta+\mu)(-\eta)(x-\tau)^{\alpha}}{\Gamma_q(\alpha+1)x^{\alpha+\beta+2\mu}} + \frac{\tau^{\mu}(\alpha+\beta+\mu)(\alpha+\beta+\mu+1)(x-\tau)^{\alpha-1}}{\Gamma_q(\alpha+2)} \times \frac{(x-\tau)^{\alpha+1}}{x^{\alpha+\beta+2\mu+2}}$$

Our observation is that each term of the above series is positive in view of the conditions stated with Theorem 3.1.

$$I_q^{\alpha,\beta,\eta}(f(x)g(x)) \geq \frac{\Gamma_q(1-\beta)\Gamma_q(1+\alpha+\eta)}{\Gamma_q(1-\beta+\eta)} x^{\beta+\mu} \times I_q^{\alpha,\beta,\eta}(f(x)) I_q^{\alpha,\beta,\eta}(g(x)) \tag{21}$$

In light of the circumstances outlined in Theorem 3.1, we note that each term in the afore mentioned series is positive. On integrating from 0 to τ and using 2.1.2 , we get

$$(I_q^{\alpha,\beta,\eta} f(x)g(x)) + \left(f(p)g(p)I_q^{\alpha,\beta,\eta}\{1\}\right) \geq g(p)I_q^{\alpha,\beta,\eta} f(x) + (f(p)I_q^{\alpha,\beta,\eta} g(x)) \tag{22}$$

Theorem 3.2: let f & g be two synchronous functions on $(0,\infty)$, then

$$\begin{aligned} &\Rightarrow \frac{\Gamma_q(1+\mu)\Gamma_q(1-\beta+\eta)}{\Gamma_q(1-\beta)\Gamma_q(1+\mu+\alpha+\eta)x^{\beta+\mu}} I_q^{\delta,\gamma,\theta,\varepsilon}(f(x)g(x)) \\ &+ \frac{\Gamma_q(1+\theta)\Gamma_q(1-\delta+\varepsilon)}{\Gamma_q(1-\delta)\Gamma_q(1+\theta+\gamma+\varepsilon)x^{\beta+\mu}} I_q^{\alpha,\beta,\eta,\mu}(f(x)g(x)) \\ &\geq (I_q^{\alpha,\beta,\eta,\mu} f(x) I_q^{\delta,\gamma,\theta,\varepsilon} g(x)) + I_q^{\delta,\gamma,\theta,\varepsilon} g(x) I_q^{\alpha,\beta,\eta,\mu} f(x)) \end{aligned} \tag{23}$$

For all $x>0, \alpha > \max\{0,-\beta-\mu\}, \gamma > Max(0,-\delta,-\theta), \mu,\theta > -1.$

Proof: To prove the above theorem, we use previous theorem , we have

$$\frac{x^{-\gamma-2\theta-\delta} p^{\delta}(x-p)^{\gamma-1}}{\Gamma_q \gamma} 2F_1[\delta+\gamma+\theta,-\varepsilon;1-\frac{p}{x}] f(p)\,dp \tag{24}$$

which, given the circumstances mentioned with, continues to be positive as per above theorem and we obtain by integrating with regard to from 0 to t.

$$\begin{aligned} &(I_q^{\alpha,\beta,\eta,\mu} f(x)g(x)) I_q^{\delta,\gamma,\theta,\varepsilon}\{1\} + I_q^{\delta,\gamma,\theta,\varepsilon}\left(f(x)g(x) I_q^{\alpha,\beta,\eta,\mu}\{1\}\right) \\ &\geq I_q^{\alpha,\beta,\eta,\mu}\{f(x)\} I_q^{\delta,\gamma,\theta,\varepsilon}\{g(x)\} + I_q^{\delta,\gamma,\theta,\varepsilon}(g(x) I_q^{\alpha,\beta,\eta,\mu} f(x)) \end{aligned} \tag{25}$$

4.1 Special cases

Here, we take a quick look at a few implications of the findings in the preceding section. The operator (3) would instantly decrease to the thoroughly studied, Erdelyi-Kober, and Riemann-Liouville type fractional integral operators, respectively, according to Curiel and Galué [13], given by the relationships below (see also [14])

$$\text{Case I: } I_{0,x}^{\alpha,\beta,\eta} f(x) = I_{0,x}^{\alpha,\beta,\eta,0} f(x) = \frac{x^{-\alpha-\beta}}{\Gamma\alpha} \int_0^x (x-\tau)^{\alpha-1} 2F_1\left(\alpha+\beta,-\eta;1-\frac{\tau}{x}\right) f(t)\,d(t) \tag{26}$$

Here we get, Erdelyi-Kober fractional operator.

$$I_{0,x}^{\alpha,\eta} f(x) = I_{0,x}^{\alpha,0,\eta,0} f(x) = \frac{x^{-\alpha-\beta}}{\Gamma\alpha} \int_0^x (x-\tau)^{\alpha-1} \tau^{\eta} f(t)\,d(t) \tag{27}$$

Case II: Here we get, Riemann-Liouville fractional operator

$$R^{\alpha} f(x) = I_x^{\alpha,-\alpha,\eta,0} f(x) = \frac{1}{\Gamma\alpha} \int_0^x (x-\tau)^{\alpha-1} f(t)\,d(t) \tag{28}$$

Case III: Putting $\gamma=\alpha, \delta=\beta, \xi=\eta$ & $\vartheta=\mu$ in theorem 3.1 reduces into theorem (2)

$$(I_{0,x}^{\alpha,\beta,\eta,\mu} f(x)g(x))I_{0,x}^{\delta,\gamma,\theta,\varepsilon} + I_{0,x}^{\delta,\gamma,\theta,\varepsilon}\left(f(x)g(x)I_{0,x}^{\alpha,\beta,\eta,\mu}\{1\}\right) \geq I_{0,x}^{\alpha,\beta,\eta,\mu}\{f(x)\}I_{0,x}^{\delta,\gamma,\theta,\varepsilon}\{g(x)\} + I_{0,x}^{\delta,\gamma,\theta,\varepsilon}(g(x)I_{o,x}^{\alpha,\beta,\eta,\mu} f(x)) \quad (29)$$

Putting$\gamma=\alpha, \delta = \beta, \xi=\eta\&\vartheta = \mu$, we get

$$(I_{0,x}^{\alpha,\beta,\eta,\mu} f(x)g(x)) + \left(f(p)g(p)I_{0,x}^{\alpha,\beta,\eta,\mu}\right) \geq g(p)I_{0,x}^{\alpha,\beta,\eta,\mu}\{f(x)\} + f(p)I_{0,x}^{\alpha,\beta,\eta,,\mu}(g(x) \quad (30)$$

5. Conclusion

Since the beginning of differential calculus, fractional calculus (FC) has been used in mathematical theory. However, throughout the past 20 years, FC's application has emerged as a result of the progress in chaos, demonstrating minute connections to FC tenets. FC has recently enjoyed success in the fields of science and engineering. Several scientific sectors are paying more for research topics. now pay attention to the FC ideas. There has been some work done. in the theory of dynamic systems, even if the suggested models Such algorithms are still being developed at a young stage.

Several case studies on FC based models were provided in the text. controls that highlight the benefits of utilising FC theory in a variety of scientific and engineering disciplines. This piece examined a number of physical systems, in particular.

References

[1] Clausen, T. (1828). Uber Die Falle Wenn Die Reihe Y= $1+\frac{\alpha\beta x}{\gamma}$ +.., J. *Fur. Maths*, 3, 89-95.

[2]] Erdelyi,A.,Magnus, W., Oberhettinger, F. and Tricomi, F.G.:Hihger transcendendental function , Vol. 2, Mcgraw-Hill, New york, 1953.

[3] Exton, H.:Hand book of hypergeometric integrals, Ellis Horwood Limited Publishers, Chechester, 1978.

[4] Rainville, E. D., Special function, Chelsea publishing Company, Bronx, New york, 1960.

[5] Slater ,L.J.:Generalized hypergeometri function, Cambridge university, presss, 1966.

[6] Meijer, C. S. (1946). On the G-Function, Proc. Nat. Acad. *Watensh* , 49, 227- 237, 344-356, 457-469.

[7] E. Capelas de Oliveira, F. Mainardi and J. Vaz Jr (2011). Models based on Mittag- Leffler functions for anomalous relaxation in dielectrics. *European Journal of Physics*, Special Topics, Vol. 193, pp. 161-171.

[8] Wright, E.M. (1935). The asymptotic expansion of generalized hypergeometric function. *J. London Math. Soc*., 10 286-293.

[9] Baily, W. N (1961), Generalized hyper geometric series. Cambridge Maths.

[10] George E. Andrews. (1972). Basic Hypergeometric series, *J. LondonMath*. Soc.(2) 4 618.

[11] E. Capelas de Oliveira, F. Mainardi and J. Vaz Jr. (2011). Models based on Mittag-Leffler functions for anomalous relaxation in dielectrics. *European Journal of Physics*, Special Topics, Vol. 193, pp. 161-171.

[12] Lacroix, S., Traite du Calcul Differentiel et du Calcul Integral, 2nd edition, 1819, pp. 409-410.

[13] Fox, C (1965), The G and H-functions as symmetrical Fourier kernels. *Trans. Amer. Math*. Soc. 98, 395-429.

[14] Slater, L.J. Generalized Hypergeometric function, Cambridge University, Press, 1966.

[15] Saxena, V. P. The I-function Anamaya Publishers Pvt. Ltd, New Delhi, 2008.

DESIGN OF SKIP LOT SAMPLING PLAN (SKSP-3) WITH SINGLE SAMPLING PLAN AS A REFERENCE PLAN USING BOREL DISTRIBUTION

Jayalakshmi S[1] Gopinath M[2]

•

[1,2] Department of Statistics, Bharathiar University, Coimbatore, Tamilnadu, India.
[2]Department of Mathematics, Sri Krishna Arts and Science College, Coimbatore, Tamilnadu, India.

statjayalakshmi16@gmail.com[1], gopimalaisamy@gmail.com[2]

Abstract

Skip-lot sampling plans (SkSPs) have long been recognized as effective strategies for minimizing inspection efforts in quality control, especially within high-volume manufacturing settings. This study proposes a Skip-Lot Sampling Plan of Type SkSP-3, constructed using Single Sampling Plans (SSPs) by attributes, under the probabilistic framework defined by the Borel distribution. Given its suitability for modeling rare or intermittent events, the Borel distribution provides a solid foundation for representing quality characteristics in such contexts. The presentation of the proposed SkSP-3 plan is assessed by means of Operating Characteristic (OC) curves and benchmarked against corresponding SSPs under identical conditions. The results reveal that the SkSP-3 plan achieves notably smaller sample sizes while preserving similar OC behavior, particularly at low defect levels. This work contributes to the body of literature by presenting a robust and cost-effective methodology for designing SkSPs under Borel distribution assumptions, thereby enhancing inspection efficiency without compromising quality standards.

Keywords: SkSP - 3, single sampling plans, Boral distribution, operating characteristic curves, average sample number.

I. Introduction

In contemporary quality assurance practices, minimizing inspection costs while maintaining acceptable product standards is a critical objective—especially in large-scale manufacturing environments. Acceptance sampling, a statistical quality control technique, provides a practical balance between exhaustive inspection and process efficiency. Within this domain, skip-lot sampling plans (SkSPs) have emerged as effective alternatives that capitalize on consistent supplier performance to reduce inspection frequency. Among the various SkSP variants, the Skip Lot Sampling Plan of Type SkSP-3 has garnered attention for its operational flexibility and ability to maintain desired quality levels through intelligent lot-skipping mechanisms.

The SkSP-3 plan incorporates historical lot performance by referencing outcomes from the current and preceding two lots to determine the level of inspection required for subsequent lots. This multi-lot referencing structure enables the plan to adapt dynamically to quality trends, thereby offering a robust approach in industries characterized by high-volume production and stable processes. Previous contributions from Soundararajan, Govindaraju, Subramani, and others have

laid the foundational and structural frameworks for such plans, highlighting their benefits over classical single sampling schemes.

In parallel, the incorporation of probabilistic distributions to model defect occurrences enhances the analytical rigor of sampling plans. The Borel distribution, known for its suitability in modeling rare or sporadic events, offers a compelling framework for quality control systems where defects are infrequent yet critical. When applied to acceptance sampling, the Borel distribution enables a more nuanced estimation of acceptance probabilities and risk levels, especially in contexts where traditional distributions may fall short.

This study aims to design a Skip Lot Sampling Plan of Type SkSP-3 by integrating Single Sampling Plan (SSP) methodology under the assumptions of the Borel distribution. The approach combines the structural simplicity of SSPs with the probabilistic depth of Borel-based modeling to construct an efficient and cost-effective inspection system. Through analytical evaluation and comparison of Operating Characteristic (OC) curves and Average Sample Number (ASN) metrics, the future plan demonstrates its ability to reduce inspection loads while safeguarding both producer and consumer interests. The findings presented herein contribute meaningfully to the evolving landscape of statistical quality control, particularly in environments where defect events are both rare and critical.

Furthermore, the integration of Borel-based Skip Lot Sampling Plans not only enhances the theoretical robustness of quality control mechanisms but also aligns with contemporary trends in data-driven decision-making. By capturing the probabilistic nature of rare defect occurrences, this approach enables more informed and responsive inspection policies that are adaptive to real-time production data. The proposed SkSP-3 framework, grounded in both historical performance and advanced probabilistic modeling, supports strategic quality assurance with minimal resource expenditure. This dual focus on efficiency and precision positions the plan as a valuable tool for industries striving for zero-defect manufacturing, where predictive analytics and risk-based inspection are increasingly becoming standard practice.

II. Review of literature

Acceptance sampling has long served as a cornerstone in statistical quality control, offering structured approaches to determine lot acceptability without resorting to full inspection. The development of Skip Lot Sampling Plans (SkSPs), beginning with the foundational work of Dodge [1], sought to enhance inspection efficiency by reducing the frequency of inspections, especially for suppliers with consistent quality records. Over time, the SkSP concept evolved into more advanced variants such as SkSP-1, SkSP-3, and SkSP-3, each offering progressive improvements in operational adaptability and risk management. Soundararajan and Vijayaraghavan [2] contributed significantly to the field by proposing a generalized version of SkSP-3 based on the principles of cumulative sampling plans (CSP). Their formulation included structured switching rules dependent on the inspection history of multiple preceding lots, offering greater sensitivity to process shifts. Later, Govindaraju and Subramani [3] extended these models by incorporating both producer's and consumer's risks, making the design more aligned with industrial decision-making scenarios.

Latha and Soundararajan [4] further refined SkSP-3 by integrating triple-lot inspection references, leading to more robust decision-making under varying quality conditions. Their work laid the foundation for exploring parametric configurations that significantly reduced the Average Sample Number (ASN) without compromising the Operating Characteristic (OC) function's integrity. Rao and Srinivasan [5], followed by Subramani and Radhakrishnan [6], analyzed the statistical behavior of SkSP-3 through comprehensive performance evaluation and design tables, thus establishing its practicality in modern quality systems. Parallel to the structural advancement of sampling plans, researchers have explored the application of various probability distributions to

better model defect occurrences. Among these, the Borel distribution has recently gained prominence due to its ability to model rare events and stochastic processes. Daly and Shneer [7] explored its application within the framework of Galton-Watson branching processes, emphasizing its suitability for systems with low defect probabilities. The use of Borel distribution in acceptance sampling aligns well with industrial environments where defects are infrequent but critical to quality assurance.

Swamy et al. [8] investigated mathematical properties and applications of the Borel distribution in broader statistical contexts, reinforcing its viability as a modeling tool in quality control environments. Similarly, Wanas and Khuttar [9] examined analytic functions defined by Borel-type series, contributing to a deeper understanding of its functional behaviours. In the realm of sampling plan performance, Hald [10] laid the groundwork for assessing OC curves and ASN values for single sampling schemes based on two-level quality thresholds, forming a basis for comparing newer models like SkSP-3 under varying conditions. Schilling and Neubauer [11], in their comprehensive work, emphasized the importance of optimizing sampling plans to balance cost, efficiency, and risk.

Recent developments by Veerakumari and Azarudheen [12] demonstrated the implementation of non-traditional distributions, such as the Intervened Poisson Distribution, in single sampling contexts, illustrating the growing trend toward probabilistic customization in quality control. Together, these contributions create a strong foundation for the current study, which aims to integrate SkSP-3 plans with the analytical robustness of Borel distribution modeling, thereby proposing a more refined and efficient acceptance sampling framework for contemporary industrial settings.

III. Features of Borel Distribution

The Borel distribution stays a discrete probability distribution with applications in modeling rare events and branching processes, making it highly suitable for quality control contexts where the occurrence of defects is infrequent but impactful. It originates from the analysis of Galton–Watson branching processes under Poisson offspring distributions. If each individual in a generation independently produces a Poisson-distributed number of offspring with mean λ, formerly the entire number of individuals in the process trails a Borel distribution.

The cumulative distribution function does not have a simple analytical form, but can be expressed as:

$$F(k;\lambda) = \sum_{i=1}^{k} \frac{(i\lambda)^{i-1}\, e^{-i\lambda}}{i!} \tag{1}$$

This form enables numerical approximation for tail probabilities, which are essential in acceptance sampling and quality control decision-making. A random variable X is supposed to follow a Borel distribution through constraint $\lambda \in (0,1)$, if it assumes values in the set $\mathbb{N} = \{1,2,3,\ldots\}$ and its probability mass function (PMF) is given by:

$$P(X = k) = \frac{e^{-(\lambda k)}(\lambda k)^{(k-1)}}{k!} \quad \text{for } k=1,2,3,\ldots \tag{2}$$

This formulation indicates that the Borel distribution is skewed and strictly positive, with heavier tails than the Poisson distribution, which makes it adept at modeling sporadic yet critical quality issues. The mean, variance, Skewness and Kurtosis of the Borel Distribution with constraint λ are given by,

$$\mu = E(X) = (1-\lambda)^{-1} \tag{3}$$

$$\sigma^2 = Var(X) = \lambda(1-\lambda)^{-3} \tag{4}$$

$$\gamma_1 = \frac{1+\lambda}{\sqrt{\lambda}} \tag{5}$$

$$\gamma_2 = \frac{1}{\lambda} + 3 \tag{6}$$

IV. Skip Lot Sampling Plan of type - 3 (SkSP – 3)

According to Dodge (1955b), once a series of identical lots are submitted for inspection, the situation is not essential to inspect every lots instead the lots may be skipped below a related skip lot plan. Soundararajan and Vijayaraghavan (1989) presented skip lot sampling plan of type SkSP–3 based on the ideologies of CSP-2 of Dodge and Torrey (1951). A SkSP-3 plan consists of a procedure in which a given lot inspection plan is used as the location plan and a switching rule that calls for normally inspecting every lot, but for examining only a fraction of the lots when the quality is good. The operating procedure of SkSP-3 is like this below,

Operating Procedure of SkSP - 3

Step 1: Start the examination normally by inspecting *i* consecutive lots using the location plan.
Step 2: Once *i* lots are recognized then examine a fraction *f* of lots.
Step 3: If a lot is disallowed in skipping examination, then examine next successive *k* lots.
Step 4: If all the *k* lots are recognized continue skipping examination i.e. examine the fraction *f* lots.
Step 5: If a lot is rejected while inspecting *k* lots, resume normal inspection.
Step 6: Screen each rejected lot and correct or replace all the nonconforming items by good ones.

Thus, SkSP-3 is connected with a given reference plan and the constraints *f*, *i* and *k*. In general, $0 < f < 1$ and *i* and *k* are positive integers. The OC and ASN functions of SkSP-3 are assumed by,

$$P_a(p) = \frac{fP + (1-f)P^i(2-P^i)}{f + (1-f)P^i(2-P^i)} \tag{7}$$

$$ASN(SkSP-3) = ASN(R)F \tag{8}$$

where *P* is the probability of acceptance according to the reference plan, ASN(*R*) is the ASN function of the reference plan, *F* is the average fraction of total lots inspected and is given by, for $k = i$.

$$F = \frac{f}{f + (2-P^i)P^i(1-f)} \tag{9}$$

I. SSP under the conditions of Borel Distribution

A single sampling plan in attributes is described by the parameters lot size (N), sample size (n) and acceptance number (c). Let us consider a lot of size N units and a random sample of size n from the lot. If the number of defective units in the sample (X=x) is less than the acceptance number (c), then we accept the lot otherwise we reject the lot.

II. Analysis of operating characteristic curves

The Operating Characteristic (OC) function is one of the finest performance indicators for evaluating the efficacy of sampling plans. The OC function of SSP is well-defined as,

$$P_a(p) = P[x \leq c] \tag{10}$$

where p is the lot quality, given as the proportion defective or fraction defective. The operating characteristics function of SSP under the condition of Borel distribution is given by the following,

$$P_a(p) = \sum_{k=1}^{c} P(X = k|\lambda) = \sum_{k=1}^{c} \frac{e^{-(\lambda k)}(\lambda k)^{(k-1)}}{k!} \tag{11}$$

where $\lambda = np$.

The performance of any acceptance sampling plans is usually assessed through its operating characteristic (OC) curves. A plot of $P_a(p)$ against p is called OC curve. It is observed from the Figure 1 the curve with parameters $n = 43$, $c = 1$, $i = 8$ and $f = 1/3$ the probability of acceptance $P_a(p)$ declines as the proportion defective p increases. That is the plan accepts the good quality lots with low proportion defective and rejects the lots with poor quality. For instance, the probability of acceptance at $p = 0.001$ is 0.99 and at $p = 0.01$ is 0.03. This ensures the plan protects the consumers by not accepting the low-quality lots and producers are safeguarded by not getting rejected the good quality lots. Hence, the proposed plan favors both the consumer and producer by reducing their risks.

V. Comparison of SkSP-3 with SSP Under the Environments of the Boral Distribution

A standard approach for comparing two lot inspection sampling plans stands by analyzing their Operating Characteristic (OC) curves. Additionally, a widely used performance metric is the operating ratio (OR), defined as $OR=p_2/p_1$, where $p_1$and p_2 represent the acceptance quality limit (AQL) and the limiting quality limit (LQL), respectively. These parameters are defined such that $P_a(p_1) = 0.95$ and $P_a(p_2) = 0.10$. Here, the SkSP-3 plan with SSP under the environments of the Boral distribution is compared to a lot-by-lot SSP under the same distribution.

A SkSP-3 with SSP under the environments of Boral distribution as reference plan is to be established. Desired operating characteristics include a satisfactory producer's quality level of *4* percent nonconforming units, having *95%* acceptance probability and consumer's quality level of *15* percent nonconforming units having a *10%* acceptance probability. Hence, the desired operating ratio is $p_2/p_1 = 0.15/0.04 = 3.75$. Referring to the Table 1 with this OR value, one can locate SkSP-3 with SSP under the environments of IPD as reference plan with $c = 4$, $i = 8$ and $f = 3/5$ and corresponding np_1 value is obtained from Table 2 as *1.6753*. As p_1 is considered as *0.04*, the sample size n is determined as, $n = np_1/p_1 = 41.88$, which becomes *42*.

For the same operating ratio *3.75* with $\alpha = 0.05$ and $\beta = 0.10$, the operating ratio of SSP under the conditions of Boral distribution is obtained as *3.6556* which corresponds to acceptance number $c = 5$. The np_1 value corresponding to the specifications is *2.5317*. Thus, the sample size is determined as $n = np_1/p_1 = 63.2925$, which becomes *64*. Thus, for the given values of p_1, p_2, α and β, it is observed that the sample sizes required by SkSP-3 with SSP under the conditions of IPD as reference plan are smaller than those of the matched SSP under the environments of IPD.

Table 1: *Operating ratio values for Skip lot sampling plan of type- 3 (SkSP-3) with SSP under the environments of Boral Distribution*

c	*i*	*f*	***α=0.05 β=0.10***	***α=0.05 β=0.05***	***α=0.05 β=0.01***	***α=0.01 β=0.10***	***α=0.01 β=0.05***	***α=0.01 β=0.01***
1	4	1/2	18.534	23.025	33.365	87.717	108.971	157.909
		1/3	13.016	16.261	23.224	60.545	75.637	108.024
		2/3	23.974	29.888	43.153	121.201	151.098	218.163
		2/5	15.222	19.013	27.355	68.025	84.967	122.242
		3/5	21.720	27.194	39.622	108.789	136.207	198.451
	8	1/2	20.336	25.263	36.609	87.717	108.971	157.909
		1/3	15.524	19.394	27.698	60.545	75.637	108.024
		2/3	25.377	31.637	45.679	121.201	151.098	218.163
		2/5	17.469	21.820	31.392	68.025	84.967	122.242
		3/5	23.303	29.176	42.509	108.789	136.207	198.451
2	4	1/2	22.166	27.537	39.903	87.717	108.971	157.909
		1/3	17.739	22.162	31.651	60.545	75.637	108.024
		2/3	26.236	32.707	47.224	121.201	151.098	218.163
		2/5	19.495	24.351	35.033	75.089	93.789	134.935
		3/5	24.751	30.989	45.151	108.789	136.207	198.451
	8	1/2	6.246	7.412	9.879	14.457	17.157	22.866
		1/3	5.163	6.124	8.162	1.002	1.188	01.584
		2/3	7.257	8.615	11.481	16.182	19.210	25.602
		2/5	5.616	6.663	8.880	12.856	15.253	20.328
		3/5	6.881	8.167	10.885	15.221	18.067	24.079
	12	1/2	6.557	7.789	10.382	14.116	16.769	22.351
		1/3	5.661	6.724	8.962	11.826	14.048	18.723
		2/3	7.382	8.770	11.689	16.543	19.654	26.196
		2/5	6.029	7.161	9.545	12.470	14.812	19.743
		3/5	7.059	8.386	11.177	15.614	18.549	24.723
3	4	1/2	6.861	8.151	10.864	14.532	17.265	23.012
		1/3	6.078	7.222	9.625	11.935	14.180	18.900
		2/3	7.572	8.996	11.990	16.775	19.930	26.564
		2/5	6.403	7.608	10.140	13.029	15.480	20.632
		3/5	*4.538*	*5.269*	*6.797*	*8.283*	*9.616*	*12.406*
	8	*1/2*	*4.246*	*4.929*	*6.359*	*7.532*	*8.743*	*11.279*
		1/3	*3.695*	*4.287*	*5.531*	*6.559*	*7.610*	*9.817*
		2/3	*4.717*	*5.477*	*7.066*	*8.605*	*9.990*	*12.889*
		2/5	*3.928*	*4.558*	*5.881*	*6.979*	*8.099*	*10.448*
		3/5	*4.538*	*5.269*	*6.797*	*8.283*	*9.616*	*12.406*

c	*i*	*f*	***α=0.05 β=0.10***	***α=0.05 β=0.05***	***α=0.05 β=0.01***	***α=0.01 β=0.10***	***α=0.01 β=0.05***	***α=0.01 β=0.01***
	12	*1/2*	*4.401*	*5.111*	*6.594*	*7.756*	*9.007*	*11.621*
		1/3	*3.927*	*4.561*	*5.884*	*6.716*	*7.799*	*10.062*
		2/3	*4.799*	*5.573*	*7.190*	*8.606*	*9.994*	*12.893*
		2/5	*4.119*	*4.784*	*6.172*	*7.162*	*8.317*	*10.730*
		3/5	*4.645*	*5.394*	*6.959*	*8.284*	*9.620*	*12.411*
4	*4*	*1/2*	*4.401*	*5.111*	*6.594*	*7.756*	*9.007*	*11.621*
		1/2	*3.460*	*3.961*	*5.001*	*5.585*	*6.393*	*8.072*
		1/3	*3.089*	*3.535*	*4.463*	*4.954*	*5.669*	*7.157*
		2/3	*3.767*	*4.313*	*5.445*	*6.083*	*6.964*	*8.793*
		2/5	*3.247*	*3.716*	*4.692*	*5.228*	*5.983*	*7.554*
		3/5	*3.650*	*4.179*	*5.277*	*5.896*	*6.749*	*8.522*
	8	*1/2*	*3.568*	*4.086*	*5.159*	*5.516*	*6.317*	*7.976*
		1/3	*3.274*	*3.749*	*4.734*	*5.008*	*5.735*	*7.241*
		2/3	*3.825*	*4.380*	*5.530*	*6.010*	*6.882*	*8.689*
		2/5	*3.394*	*3.887*	*4.908*	*5.158*	*5.906*	*7.458*
		3/5	*3.726*	*4.267*	*5.388*	*5.825*	*6.670*	*8.422*
	12	*1/2*	*3.667*	*4.199*	*5.302*	*5.596*	*6.409*	*8.092*
		1/3	*3.411*	*3.906*	*4.932*	*5.017*	*5.746*	*7.255*
		2/3	*3.884*	*4.448*	*5.616*	*6.068*	*6.948*	*8.774*
		2/5	*3.520*	*4.030*	*5.089*	*5.266*	*6.030*	*7.614*
		3/5	*3.800*	*4.352*	*5.495*	*5.891*	*6.746*	*8.518*
		3/5	*3.800*	*4.352*	*5.495*	*5.891*	*6.746*	*8.518*

Table 2: *Unity values for Skip lot sampling plan of type - 3 (SkSP-3) with SSP under the environments of Boral Distribution*

c	*i*	*f*	***0.99***	***0.95***	***0.75***	***0.5***	***0.1***	***0.05***	***0.01***
1	*4*	*1/2*	*0.0407*	*0.1926*	*0.7590*	*1.3808*	*3.5704*	*4.4355*	*6.4275*
		1/3	*0.0590*	*0.2744*	*0.8858*	*1.4731*	*3.5716*	*4.4619*	*6.3724*
		2/3	*0.0295*	*0.1492*	*0.6692*	*1.3187*	*3.5781*	*4.4607*	*6.4406*
		2/5	*0.0525*	*0.2346*	*0.8291*	*1.4312*	*3.5715*	*4.4609*	*6.4180*
		3/5	*0.0328*	*0.1643*	*0.7040*	*1.3411*	*3.5696*	*4.4692*	*6.5116*
	8	*1/2*	*0.0407*	*0.1756*	*0.6204*	*1.2481*	*3.5704*	*4.4355*	*6.4275*
		1/3	*0.0590*	*0.2301*	*0.6731*	*1.2589*	*3.5716*	*4.4619*	*6.3724*
		2/3	*0.0295*	*0.1410*	*0.5874*	*1.2407*	*3.5781*	*4.4607*	*6.4406*
		2/5	*0.0525*	*0.2044*	*0.6499*	*1.2524*	*3.5715*	*4.4609*	*6.4180*

c	*i*	*f*	***0.99***	***0.95***	***0.75***	***0.5***	***0.1***	***0.05***	***0.01***
2	*4*	*3/5*	*0.0328*	*0.1532*	*0.5995*	*1.2416*	*3.5696*	*4.4692*	*6.5116*
		1/2	*0.0407*	*0.1611*	*0.5710*	*1.2392*	*3.5704*	*4.4355*	*6.4275*
		1/3	*0.0590*	*0.2013*	*0.5932*	*1.2375*	*3.5716*	*4.4619*	*6.3724*
		2/3	*0.0295*	*0.1364*	*0.5571*	*1.2360*	*3.5781*	*4.4607*	*6.4406*
		2/5	*0.0476*	*0.1832*	*0.5828*	*1.2388*	*3.5715*	*4.4609*	*6.4180*
		3/5	*0.0328*	*0.1442*	*0.5620*	*1.2355*	*3.5696*	*4.4692*	*6.5116*
	8	*1/2*	*0.3595*	*0.8321*	*1.8330*	*2.6677*	*5.1967*	*6.1674*	*8.2194*
		1/3	*5.1904*	*1.0071*	*2.0138*	*2.7829*	*5.1997*	*6.1678*	*8.2194*
		2/3	*0.3210*	*0.7159*	*1.6987*	*2.5890*	*5.1953*	*6.1672*	*8.2194*
		2/5	*0.4043*	*0.9256*	*1.9336*	*2.7305*	*5.1982*	*6.1676*	*8.2194*
		3/5	*0.3414*	*0.7551*	*1.7485*	*2.6176*	*5.1958*	*6.1673*	*8.2194*
	12	*1/2*	*0.3677*	*0.7917*	*1.6246*	*2.4962*	*5.1911*	*6.1668*	*8.2194*
		1/3	*0.4390*	*0.9172*	*1.7041*	*2.5104*	*5.1917*	*6.1668*	*8.2194*
		2/3	*0.3138*	*0.7031*	*1.5722*	*2.4891*	*5.1907*	*6.1667*	*8.2194*
		2/5	*0.4163*	*0.8611*	*1.6684*	*2.5034*	*5.1914*	*6.1668*	*8.2194*
		3/5	*0.3325*	*0.7354*	*1.5889*	*2.4914*	*5.1908*	*6.1668*	*8.2194*
3	*4*	*1/2*	*0.3572*	*0.7565*	*1.5462*	*2.4822*	*5.1904*	*6.1667*	*8.2194*
		1/3	*0.4349*	*0.8539*	*1.5819*	*2.4826*	*5.1904*	*6.1667*	*8.2194*
		2/3	*0.3094*	*0.6855*	*1.5231*	*2.4821*	*5.1904*	*6.1667*	*8.2194*
		2/5	*0.3984*	*0.8106*	*1.5653*	*2.4823*	*5.1904*	*6.1667*	*8.2194*
		3/5	*0.3261*	*0.7117*	*1.5314*	*2.4821*	*5.1904*	*6.1667*	*8.2194*
	8	*1/2*	*0.8756*	*1.5531*	*2.8101*	*3.7811*	*6.5948*	*7.6551*	*9.8758*
		1/3	*1.0060*	*1.7857*	*3.0250*	*3.9130*	*6.5981*	*7.6555*	*9.8758*
		2/3	*0.7662*	*1.3977*	*2.6473*	*3.6913*	*6.5931*	*7.6548*	*9.8757*
		2/5	*0.9452*	*1.6794*	*2.9305*	*3.8519*	*6.5964*	*7.6553*	*9.8758*
		3/5	*0.7961*	*1.4529*	*2.7079*	*3.7239*	*6.5937*	*7.6549*	*9.8757*
	12	*1/2*	*0.8498*	*1.4977*	*2.5611*	*3.5868*	*6.5916*	*7.6546*	*9.8757*
		1/3	*0.9815*	*1.6784*	*2.6575*	*3.6032*	*6.5917*	*7.6546*	*9.8757*
		2/3	*0.7662*	*1.3977*	*2.6473*	*3.6913*	*6.5931*	*7.6548*	*9.8757*
		2/5	*0.9142*	*1.5239*	*2.4865*	*3.5707*	*6.5915*	*7.6546*	*9.8757*
		3/5	*0.7936*	*1.3865*	*2.4483*	*3.5699*	*6.5915*	*7.6546*	*9.8757*
	4	*1/2*	*1.4163*	*2.2860*	*3.7465*	*4.8341*	*7.9099*	*9.0542*	*11.4319*
		1/3	*1.5973*	*2.5617*	*3.9884*	*4.9789*	*7.9134*	*9.0547*	*11.4319*

c	*i*	*f*	***0.99***	***0.95***	***0.75***	***0.5***	***0.1***	***0.05***	***0.01***
4		*2/5*	*1.5134*	*2.4365*	*3.8792*	*4.9132*	*7.9117*	*9.0545*	*11.4319*
		3/5	*1.3415*	*2.1665*	*3.6330*	*4.7691*	*7.9087*	*9.0541*	*11.4319*
	8	*1/2*	*1.4333*	*2.2159*	*3.4656*	*4.6177*	*7.9064*	*9.0537*	*11.4319*
		1/3	*1.5787*	*2.4148*	*3.5727*	*4.6355*	*7.9064*	*9.0538*	*11.4319*
		2/3	*1.3156*	*2.0671*	*3.3904*	*4.6079*	*7.9063*	*9.0537*	*11.4319*
		2/5	*1.5329*	*2.3293*	*3.5244*	*4.6268*	*7.9064*	*9.0537*	*11.4319*
		3/5	*1.3573*	*2.1219*	*3.4179*	*4.6112*	*7.9063*	*9.0537*	*11.4319*
	12	*1/2*	*1.4127*	*2.1563*	*3.3496*	*4.5990*	*7.9063*	*9.0537*	*11.4319*
		1/3	*1.5758*	*2.3179*	*3.4034*	*4.6003*	*7.9063*	*9.0537*	*11.4319*
		2/3	*1.3030*	*2.0356*	*3.3229*	*4.5984*	*7.9063*	*9.0537*	*11.4319*
		2/5	*1.5014*	*2.2463*	*3.3791*	*4.5997*	*7.9063*	*9.0537*	*11.4319*
		3/5	*1.3415*	*2.1665*	*3.6330*	*4.7691*	*7.9087*	*9.0541*	*11.4319*

Using these points, the OC curves are plotted and displayed in Figures 1 and 2. Figure 2 illustrates that the OC curves of SkSP-3 and SSP under the conditions of the Boral distribution coincide at $p \leq AQL$ and $p \geq LQL$. Furthermore, the table indicates that the significant reduction in sample size for SkSP-3 with SSP under the environments of the Boral distribution compared to SSP for low proportions of defectives. Further, when the proportion defectives are very close to the matched sampling plans.

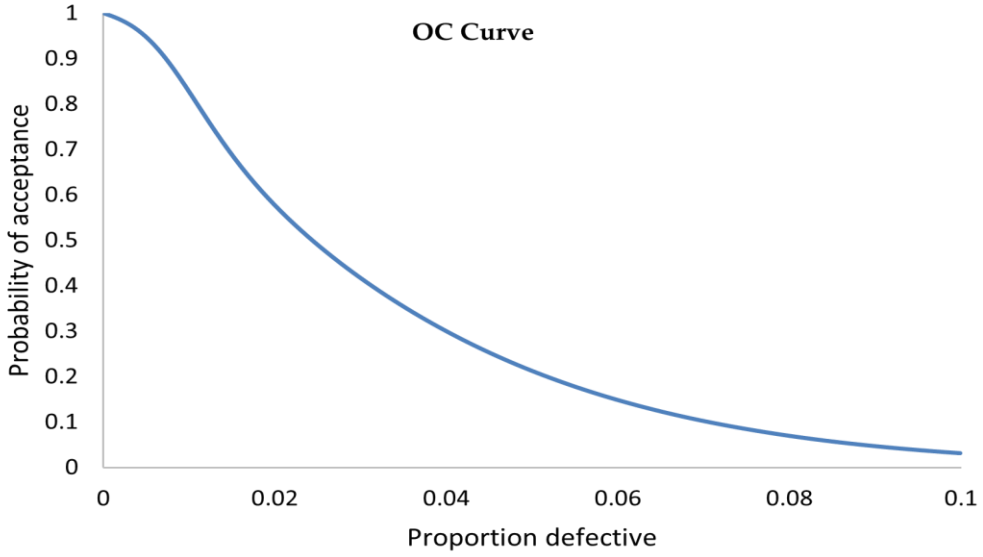


Figure 1: *Operating Characteristic curve for SkSP -3 with SSP under the conditions of Boral Distribution (n = 43, c = 1, i = 8, f = 1/3)*

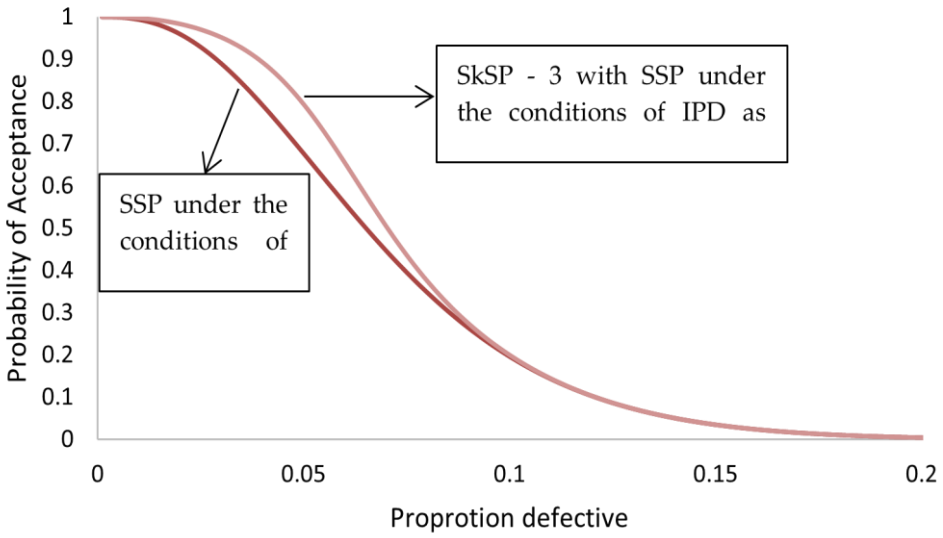


Figure 2: *OC curves of matched SSP under the conditions of IPD (n = 50, c = 3) and SkSP – 3 with SSP under the conditions of Boral Distribution (c = 3, i = 4, f = 2)*

Conclusion

This study presents the design and assessment of a skip-lot sampling plan of type SkSP-3, developed using single sampling plan principles under the conditions of the Boral distribution. The analytical framework demonstrates the plan's efficiency in terms of reduced sample size requirements, making it highly effective for processes with sporadic or rare defects. Comparison with equivalent SSPs under the Boral distribution reveals that the SkSP-3 plan exhibits comparable performance at critical quality levels (AQL and LQL) while significantly reducing inspection efforts, as evidenced by the operating characteristic and average sample number curves. This reduction in sample size offers practical benefits for industries seeking to balance quality control with operational efficiency. Future research may explore extensions of the SkSP-3 design for other complex probabilistic distributions or multi-stage sampling scenarios, broadening its applicability to diverse industrial settings. The integration of advanced statistical techniques and computational tools can further refine the design and analysis of sampling plans under non-standard conditions.

References

[1] Dodge, H. F. and Perry, J. H. (1971). Skip lot sampling plan. *Industrial Quality Control*, 7(3):24–28.

[2] Soundararajan, V. and Vijayaraghavan, R. (2014). Skip lot sampling plans with reference to advanced statistical distributions. *American Journal of Mathematical and Management Sciences*, 34(2):245–267.

[3] Govindaraju, K. and Subramani, J. (1999). SKSP-2: A new skip lot sampling plan. *Journal of Applied Statistics*, 26(5):643–653.

[4] Latha, K. and Soundararajan, V. (2003). Development of SkSP-3 plans. *Quality Engineering*, 15(4):593–600.

[5] Rao, S. S. and Srinivasan, S. K. (2005). Performance evaluation of skip lot plans. *International Journal of Quality & Reliability Management*, 22(2):122–133.

[6] Subramani, J. and Radhakrishnan, R. (2010). Comparative study of skip lot sampling plans. *Statistical Techniques in Quality Control*, 45(1):34–45.

[7] Daly, F. and Shneer, S. (2021). The Borel distribution: *Approximation and concentration. Stochastic Processes and their Applications*, 132:271–287.

[8] Swamy, S. R., Lupas, A. A., Wanas, A. K. and Nirmala, J. (2021). Applications of Borel distribution for a new family of bi-univalent functions defined by Horadam polynomials. *WSEAS Transactions on Mathematics,* 20:630–636.

[9] Wanas, A. K. and Khuttar, J. A. (2020). Applications of Borel distribution series on analytic function. *Earthline Journal of Mathematical Sciences*, 4(2):71–82.

[10] Hald, A. (1967). On the theory of single sampling inspection by attributes based on two quality levels. *Review of the International Statistical Institute*, 35(1):1–29.

[11] Schilling, E. G. and Neubauer, D. V. (2009). Acceptance Sampling in Quality Control, 2nd ed., *CRC Press*.

[12] Veerakumari, K. P. and Azarudheen, S. (2017). Evaluation of single sampling plan under the conditions of intervened Poisson distribution. *Communications in Statistics - Simulation and Computation*, 46(5):3955–3971.

ANALYZING SOLUTIONS OF FUZZY NABLA DYNAMIC EQUATIONS ON TIMESCALES: A GENERALIZED HUKUHARA APPROACH

Leelavathi. R[1*], Hari Kishore. R[2], Mohana Rupa. S. V. D[3], Muneera. A.[4]

•

1.* Department of Mathematics, Koneru Lakshmaiah Education Foundation, Vaddeswaram, AP-522302, India. rleelavathi@kluniversity.in

2. Department of Mathematics, Vasavi College of Engineering, Ibrahimbagh, Hyderabad, Telangana-500031, India. kishore.rh6@gmail.com

3. Department of Science and Humanities, Vasireddy Venkatadri International Technological University, Nambur, AP-522508, India. rupasvd@gmail.com

4. Department of Mathematics, Vijaya Institute of Technology for Women, Enikepadu, Vijayawada, AP, India. munny.aliet@gmail.com

Abstract

In this paper, we study linear first-order fuzzy nabla dynamic equations on time scales (LFNDET's) under the framework of generalized Hukuhara nabla differentiability and also interpret various results of LFNDET's by employing the Variation of constant formula. A key result concerns the generalized nabla Hukuhara derivative for the product of a crisp function and a fuzzy function on time scales. Furthermore, we derive solutions to these equations using various approaches to generalized Hukuhara nabla differentiability. The behavior of these solutions highlights the importance and applicability of the generalized fuzzy nabla derivative in the context of nabla dynamic equations on time scales.

Keywords: Fuzzy functions; Generalized nabla derivative; Time scales

1. Introduction

S. Hilger introduced the theory of time scales [15] and has shown remarkable potential for a wide range of applications. It unifies continuous and discrete analysis, eliminating the need to prove results separately for differential and difference equations. The framework of dynamic equations on time scales [9] highlights and bridges the differences between these domains. For foundational aspects of calculus on time scales, we refer the reader to [1, 10, 13]. The development of nabla dynamic equations on time scales was initiated in [10], with further contributions by authors such as [16, 19, 24].

Typically, the variables, parameters and the initial conditions in a dynamic model are assumed to be precisely known. However, in practical applications, these components often involve vagueness, imprecision, or incomplete information. To address this uncertainty, fuzzy environments can be incorporated by replacing exact values with fuzzy sets, leading to the formulation of Fuzzy Differential Equations (FDEs). The concept of Hukuhara differentiability, based on the Hukuhara difference (HK-Difference)[18], was introduced by [26], and further used in [20] to study FDEs and establish existence and uniqueness results under the Lipschitz condition.

However, a major limitation of the Hukuhara derivative is that it applies only when the length of the fuzzy support increases, restricting its ability to capture better solutions. To address this drawback, the concept of generalized differentiability for fuzzy-valued functions was introduced

in [6, 8]. In [7], the author studied first-order linear fuzzy differential equations (LFDEs) under this generalized framework.

Fard and Bidgoli [12] extended the calculus of fuzzy-valued functions to the setting of time scales. More recently, Vasavi et al. [27] investigated fuzzy dynamic equations on time scales using the generalized delta derivative. In contemporary applications such as economics [3], inventory models [4], and cellular neural networks [14], nabla derivative has often been preferred over the delta derivative due to its fewer restrictions and greater flexibility.

Motivated by these developments and the advantages of the nabla derivative, this paper focuses on the study of linear fuzzy nabla dynamic equations on time scales under generalized Hukuhara differentiability.

The essence of the paper is structured as follows:

Section 2 introduces fuzzy nabla derivatives and integrals on time scales, along with their fundamental properties.

Section 3 discusses the product of two fuzzy functions under different types of generalized Hukuhara differentiability on time scales.

Section 4 is devoted to the analysis of linear fuzzy nabla dynamic equations on time scales (LFNDETs).

2. Preliminaries

It's important to review some basic fuzzy calculus definitions and conclusions. Examine the family of all convex compact nonempty subsets, $R_k(\Re^n)$. The scalar multiplication and set addition are expressed as usual in $R_k(\Re^n)$. The commutative semigroup [20] under addition with cancellation rules is then satisfied by $\Re_k(\Re^n)$. Additionally, if $M, N \in \Re_k(\Re^n)$ and $\alpha_1, \alpha_2 \in \Re$ then

$$\alpha_1(M+N) = \alpha_1 M + \alpha_2 N, \;\; \alpha_1(\alpha_2 M) = (\alpha_1\alpha_2)N, \;\; 1.N = N,$$

and if $\alpha_1, \alpha_2 \geq 0$ then $(\alpha_1+\alpha_2)M = \alpha_1 M + \alpha_2 M$. The distance between M and N using the Poincare-Hausdorff metric, is defined as follows:

$$D(M,N) = \max\{\inf_{n\in N}\sup_{m\in M}\|m-n\|, \sup_{n\in N}\inf_{m\in N}\|m-n\|\}$$

where M and N are any two bounded nonempty subsets of $\Re^n$ $||.||$ is the norm in $\Re^n$. Then $(\Re_k(\Re^n), D)$ becomes a complete seperable metric space [20].

Let $\mathbb{E}_n = \{u : \Re^n \to [0,1] / \mu \text{ satisfies(a)-(d) below}\}$, also define $u : \Re^n \to [0,1]$ be a fuzzy subset of the real line. The function u is called a fuzzy number and fulfills the following conditions:

(a) Normality: There is some $t \in \Re^n$ such that $u(t) = 1$.

(b) convexity: For all $t \in [0,1]$ and $m, n \in \Re^n$ the inequality $u(tm+(1-t)n) \geq \min\{u(m), u(n)\}$ holds.

(c) convexity: The function u is upper semi-continuous on $\Re^n$, i.e., for every $\epsilon > 0$, there exists $\delta > 0$ such that $u(m) - u(m_0) < \epsilon$ when $|m - m_0| < \delta$.

(d) Compact support: The support of u is a compact set.

For $0 < \gamma \leq 1$, denote $[u]^\gamma = \{t \in \Re^n : u(t) \geq \gamma\}$, then based on the above setting we have the γ-level set $[u]^\gamma \in \Re_k(\Re^n)$.

It is well established that, for every continuous function g, we have $[g(s,t)]^\gamma = g([s]^\gamma, [t]^\gamma)$ $\forall s, t \in \mathbb{E}_n$. The scalar addition($\oplus$) and multiplication($\odot$) in $\mathbb{E}_n$ of s, t is defined as

$$[s \oplus t]^\gamma = [s]^\gamma + [t]^\gamma, [k \odot s]^\gamma = k[s]^\gamma, \text{ where } s, t \in \mathbb{E}_n, \; k \in \Re, \; 0 \leq \gamma \leq 1.$$

The theorem presented below extends the features of scalar multiplication and addition of fuzzy number valued functions ($\Re_F = \mathbb{E}_1$) to $\mathbb{E}_n$.

Theorem 1. *[2]*

(a) If $\tilde{0}$ is the zero element in $\Re_F$, then $\hat{0} = (\tilde{0}, \tilde{0}, \ldots, \tilde{0})$ is the zero element in $\mathbb{E}_n$. i.e. $s \oplus \hat{0} = \hat{0} \oplus s = s \; \forall s \in \mathbb{E}_n$;

(b) For any $s \in \mathbb{E}_n$ has no inverse with respect to '$\oplus$';

(c) For any $\beta_1, \beta_2 \in \Re$ with $\beta_1, \beta_2 \geq 0$ or $\beta_1, \beta_2 \leq 0$ and $m \in \mathbb{E}_n$, then $(\beta_1 + \beta_2) \odot m = (\beta_1 \odot m) \oplus (\beta_1 \odot m)$;

(d) For any $\beta_1 \in \Re$ and $m, n \in \mathbb{E}_n$, we have $\beta_1 \odot (m \oplus n) = (\beta_1 \odot m) \oplus (\beta \odot n)$;

(e) For any $\beta_1, \beta_2 \in \Re$ and $m \in \mathbb{E}_n$, we have $\beta_1 \odot (\beta_2 \odot m) = (\beta_1 \beta_2) \odot m$.

If for every $Y, Z \in \mathbb{E}_n$, there is an $X \in \mathbb{E}_n$ such that $Y = Z \oplus X$. Then X is called the Hukuhara difference (HK-Difference) of Y and Z and is denoted by $Y \ominus_h Z$. For any $W, X, Y, Z \in \mathbb{E}_n$ and $\beta \in \Re$, the following holds if the HK-Difference exists.

(a) $D_H(Y, Z) = 0 \Leftrightarrow Y = Z$;

(b) $D_H(\beta Y, \beta Z) = |\beta| D_H(Y, Z)$;

(c) $D_H(X \oplus Z, Y \oplus RZ = D_H(X, Y)$;

(d) $D_H(X \ominus_h Z, Y \ominus_h Z) = D_H(X, Y)$;

(e) $D_H(W \oplus X, Y \oplus Z) \leq D_H(W, Y) + D_H(X, Z)$;

This section introduces essential concepts and properties of the Hukuhara derivatives of fuzzy functions over the interval $I = [x, y]$, $x, y \in \Re$, along with necessary definitions and some results from the theory of time scales.

Definition 1. *[20] Consider a fuzzy-valued function $Q : I \to \mathbb{E}_n$ where $I \subset \Re$ is a compact interval. The function Q is said to be Hukuhara differentiable (or H-differentiable) at a point $s \in I$, if there exist an element $Q'(s)$ in $\mathbb{E}_n$ such that both of the following limits exist and are equal in the metric space $(\mathbb{E}_n, D_H)$*

$$\lim_{h \to 0^+} \frac{Q(s+h) \ominus_h Q(s)}{h}, \lim_{h \to 0^+} \frac{Q(s) \ominus_h Q(s-h)}{h}$$

At the endpoints of the interval I, only the appropriate one-sided limit is considered for the derivative.

Definition 2. *[9]*

(a) Time scales: A closed nonempty subset of real numbers ($\Re$) which is denoted by $\mathbb{T}$.

(b) Backward Jump operator: The operator $\rho : \mathbb{T} \to \mathbb{T}$ is defined as $\rho(s) = \sup\{s_0 \in \mathbb{T} : s_0 < s\}$

(c) Graininess function: The operator $\nu : \mathbb{T} \to \mathbb{R}^+$ defined as $\nu(s) = s - \rho(s)$ for $s \in \mathbb{T}$

(d) If $\rho(s) = s$, then the operator ρ is called left-dense, otherwise left scattered (in short we use 'ls' for left scattered).

(e) If $\mathbb{T}$ is right scattered minimum m then $\mathbb{T} - \{m\} = \mathbb{T}_k$, Otherwise $\mathbb{T} = \mathbb{T}_k$.

(f) for each $s \in \mathbb{T}$, the function is $h^\rho : \mathbb{T} \to \Re$ defined by $h^\rho(s) = h(\rho(s))$.

(g) The interval of time scale $\mathbb{T}$ is given by

$$\mathbb{T}^{[x,y]} = \{t \in \mathbb{T} : x \leq t \leq y\} = [x, y] \cap \mathbb{T}$$

and

$$\mathbb{T}_k^{[x,y]} = \begin{cases} \mathbb{T}^{[x,y]}, & \text{if } x \text{ is right dense} \\ \mathbb{T}^{[\sigma(x),y]}, & \text{if } x \text{ is right scattered.} \end{cases}$$

Definition 3. *[9] Let $g : \mathbb{T} \to \mathbb{R}$ be a function and let $s \in \mathbb{T}_k$. Then the **nabla derivative** $g^{\nabla}(s)$ exists (as a real number) **if and only if**, for every $\epsilon > 0$, there exists a neighborhood N_δ of s (i.e., $N_\delta = (s-\delta, s+\delta) \cap \mathbb{T}$ for some $\delta > 0$) such that:*

$$|(g^{\rho}(s)) - g(s_0)) - g^{\nabla}(s)(\rho(s) - s_0)| \leq \epsilon|\rho(s) - s_0|, \text{ for all } s_0 \in N_\delta,$$

where, $g^{\nabla}(s)$ is called the Nabla derivative of g at s. A function g is called Nabla (or Hilger) differentiable on $\mathbb{T}_k$, if $g^{\nabla}(s)$ exists for all s in $\mathbb{T}_k$. The function $g^{\nabla} : \mathbb{T}_k \to \Re$ is then called the Nabla derivative of g on $\mathbb{T}_k$.

Definition 4. *[10] Let $g : \mathbb{T} \to \Re$ be a real-valued function defined on the time scales $\mathbb{T}$. The function g is said to be regulated if it admits finite left-sided limits at all left dense points(left-dense) of $\mathbb{T}$, and finite right-sided limits at all right-dense points of $\mathbb{T}$.*

Definition 5. *[10] Let $g : \mathbb{T} \to \Re$ be a real-valued function defined on the time scales $\mathbb{T}$. The function g is said to be left-dense continuous (ld-continuous) if it is continuous at every left-dense point of $\mathbb{T}$, and if the right-hand limit $\lim_{s_0 \to s^+} g(s_0)$ exists and is finite at each right-dense point $s \in \mathbb{T}$.*

Definition 6. *[10] A function α defined from $\mathbb{T}$ to $\mathbb{R}$ is ν-regressive if $1 - \nu(s)\alpha(s) \neg 0$ on the time scales $\mathbb{T}$. The set of all ν-regressive ld-continuous functions defined on $\mathbb{T}_k$ is denoted by*

$$\Re_\nu = \{\alpha : \mathbb{T} \to \mathbb{R} \quad \text{where } \alpha \text{ is } \nu\text{-regressive, ld continuous functions.}\}$$

Theorem 2. *[10] The nabla initial value problem(NIVP) is defined as*

$$\chi^{\nabla} = \alpha(s)\chi(s) + g(s), \chi(s_0) = \chi_0$$

with the initial conditions $u_0 \in mathbbT$ admits unique solution $\chi : \mathbb{T} \to \Re^n$ and is explicitly given by

$$\chi(s) = \hat{e}_\alpha(s, s_0)\chi_0 + \int_{s_0}^{s} \hat{e}_\alpha(s, s_0)g(\tau)\nabla(\tau)$$

where $\alpha \in \Re_\nu$ and $g : \mathbb{T} \to \Re^n$ is ld-continuous.

If we consider the NIVP $\chi^{\nabla} = \alpha(m)\chi$, $\chi(m_0) = 1$ on time scales, then the solution is of the form

$$\hat{e}_\alpha(m, m_0) = exp\left\{\int_{m_0}^{m} \hat{\xi}_{\nu(m)}(\alpha(\tau))\nabla\tau\right\}$$

We now list several important properties of the nabla exponential function, which will be further useful.

(1) $\hat{e}_p(m, m) = 1$; $\hat{e}_0(m, n) = 1$;

(2) $\hat{e}_\alpha(\rho(m), n) = [1 - \nu(m)\alpha(m)]\hat{e}_\alpha(m, n)$;

(3) $\hat{e}_\alpha(m, n)\hat{e}_\alpha(n, p) = \hat{e}_\alpha(m, p)$;

(4) $\hat{e}_\alpha(m, n) = \dfrac{1}{\hat{e}_\alpha(n, m)}$.

In particular, if $\alpha \in \Re$ is such that $1 - \nu(r)\alpha(r) > 0 \quad \forall r \in \mathbb{T}$,

$$\hat{e}_\alpha(m, 0) = \begin{cases} (1 - rp)^{\frac{m}{p}}, & \text{if } \mathbb{T} = p\mathbb{Z} \text{ with } h > 0, \\ \dfrac{1}{1-\alpha}^{r}, & \text{if } \mathbb{T} = \mathbb{Z}, \\ \hat{e}^{\alpha m}, & \text{if } \mathbb{T} = \mathbb{R}. \end{cases}$$

If $\mathbb{T} = \mathbb{R}$, the graininess function ν is identically zero and for the discrete case like $\mathbb{T} = \mathbb{Z}$ it remains constant, i.e. $\nu(s) = 1$, for all s $\in \mathbb{Z}$. The other time scales, which include continuous

graininess functions, are any closed intervals of real numbers and uniform discrete sets like $\mathbb{T} = h\mathbb{Z}$ for $h > 0$. The following is an example of time scales with nonconstant graininess:

$$\mathbb{T}_k^{[a,b]} = \bigcup_{n=0}^{\infty} [n(a+b), n(a+b)+a]; \quad a, b > 0.$$

Then

$$\rho(t) = \begin{cases} t, \text{ if } t \in \bigcup_{n=0}^{\infty} [n(a+b), n(a+b)+a), \\ t-b, \text{ if } t \in \bigcup_{n=0}^{\infty} \{n(a+b), n(a+b)+a\}. \end{cases}$$

And

$$\nu(t) = \begin{cases} 0, \text{ if } t \in \bigcup_{n=0}^{\infty} [n(a+b), n(a+b)+a), \\ b, \text{ if } t \in \bigcup_{n=0}^{\infty} \{n(a+b), n(a+b)+a\}. \end{cases}$$

3. On the Generalized Nabla Hukuhara Differentiability and Integrability

In this section, we develop the concept of generalized nabla Hukuhara differentiability for fuzzy-valued functions defined on arbitrary time scales. By extending classical differentiation to the fuzzy setting using the nabla calculus framework, we establish conditions under which such functions are differentiable in the generalized Hukuhara sense. Furthermore, we examine the corresponding notions of integrability, providing definitions and results that unify and generalize continuous and discrete cases. These concepts are crucial for analyzing dynamic systems involving uncertainty over nonuniform time domains.

Definition 7. *[23]*

Let $Q : \mathbb{T}^{[x,y]} \to$ be a fuzzy function. We say that Q is generalized nabla Hukuhara differentiable (symbolically ∇_g-differentiable) at $s \in \mathbb{T}_k^{[x,y]}$, if both the left and right generalized Hukuhara derivatives of Q exist at s and coincide, that is,

$$Q_-^{\nabla_g}(s) = Q_+^{\nabla_g}(s) = Q^{\nabla_g}(s),$$

where $Q_-^{\nabla_g}(s)$ or $Q_+^{\nabla_g}(s)$ is called ∇_g derivative of Q at $s \in \mathbb{T}_k^{[x,y]}$ and it is denoted by $Q^{\nabla_g}(s)$. Furthermore, if this derivative exists at every point in the domain $\mathbb{T}_k^{[x,y]}$, then the function Q is said to be ∇_g-differentiable on $\mathbb{T}_k^{[x,y]}$.

Remark 1. *[23] Let $Q : \mathbb{T}^{[x,y]} \to \mathbb{E}_n$ be a fuzzy valued function. Then Q is said to be genralized HuKuhara nabla differentiable (∇_g-differentiable) at $s \in \mathbb{T}_k$, If there exists an element $Q^{\nabla_g}(s) \in \mathbb{E}_n$, such that at least one of the following conditions is satisfied:*

$\nabla - GH1$: *There exists $\delta > 0$ such that for all $0 < h < \delta$, the HK-Difference $Q^\rho(s) \ominus_h Q(s-h)$ and $Q(s+h) \ominus_h Q^\rho(s)$, exist and the following limits are egual:*

$$\mathbb{T} - \lim_{h \to 0} \frac{1}{h - \nu(s)} \odot (Q^\rho(s) \ominus_h Q(s-h)) = Q^{\nabla_g}(s) = \mathbb{T} - \lim_{h \to 0} \frac{1}{h + \nu(s)} \odot (Q(s+h) \ominus_h Q^\rho(s))$$

or

$\nabla - GH2$ *There exists $\delta > 0$ such that for all $0 < h < \delta$, the HK-Difference $Q(s-h) \ominus_h Q^\rho(s)$ and $Q^\rho(s) \ominus_h Q(s+h)$, exists and the following limits are egual:*

$$\mathbb{T} - \lim_{h \to 0} \frac{-1}{h - \nu(s)} \odot (Q(s-h) \ominus_h Q^\rho(s)) = Q^{\nabla_g}(s) = \mathbb{T} - \lim_{h \to 0} \frac{-1}{h + \nu(s)} \odot (Q^\rho(s) \ominus_h Q(s+h)$$

or

$\nabla - GH3$: *There exists $\delta > 0$ such that for all $0 < h < \delta$, the HK-Difference $Q^{\rho}(s) \ominus_h Q(s-h)$ and $Q^{\rho}(s) \ominus_h Q(s+h)$, the limits exists*

$$\mathbb{T} - \lim_{h\to 0} \frac{1}{h-\nu(s)} \odot (Q^{\rho}(s) \ominus_h Q(s-h)) = Q^{\nabla_g}(s) = \mathbb{T} - \lim_{h\to 0} \frac{-1}{h+\nu(s)} \odot (Q^{\rho}(s)) \ominus_h (s+h)).$$

or

$\nabla - GH4$: *There exists $\delta > 0$ such that for all $0 < h < \delta$, the HK-Difference $Q(s-h) \ominus_h Q^{\rho}(s)$ and $Q(s+h) \ominus_h Q^{\rho}(s)$, the limits exist*

$$\mathbb{T} - \lim_{h\to 0} \frac{-1}{h-\nu(s)} \odot (Q(s-h) \ominus_h Q(\rho(s))) = Q^{\nabla_g}(s) = \mathbb{T} - \lim_{h\to 0} \frac{1}{h+\nu(s)} \odot (Q(s+h) \ominus_h Q^{\rho}(s)).$$

When such a limit exists at each $s \in \mathbb{T}_k^{[x,y]}$, the function $Q^{\nabla_g} : \mathbb{T}_k^{[x,y]} \to \mathbb{E}_n$ is called the generalized Hukuhara nabla derivative of Q and is said to be ∇_g-differentiable on $\mathbb{T}_k$.

Example 1. *Let $\mathbb{T} = \mathbb{R}$, and consider the fuzzy-valued function*

$$G(s) = \tilde{k} \odot s^2, \quad s \in [0,1],$$

where $\tilde{k} \in \mathbb{E}_n$ is a fixed fuzzy number, and $\odot$ denotes scalar multiplication of a fuzzy number. Assume $\tilde{a}$ is a triangular fuzzy number given by $\tilde{k} = (1,2,3)$.

Since the time scale is $\mathbb{R}$, the graininess function is $\nu(s) = 0$, and the backward jump operator satisfies $\rho(s) = s$. In this continuous setting, the generalized nabla Hukuhara derivative coincides with the standard Hukuhara derivative.

To compute the derivative, we consider:

$$Q(s+h) \ominus_h Q(s) = \tilde{k} \odot \left((s+h)^2 - s^2\right) = \tilde{k} \odot (2sh + h^2).$$

Taking the limit as $h \to 0^+$, we obtain:

$$Q^{\nabla_g}(s) = \lim_{h\to 0^+} \frac{Q(s+h) \ominus_h Q(s)}{h} = \tilde{K} \odot 2s.$$

Thus, the function $Q(s) = \tilde{k} \odot s^2$ is ∇^g-differentiable on $[0,1]$, and its generalized nabla Hukuhara derivative is:

$$Q^{\nabla_g}(s) = \tilde{k} \odot 2s, \quad \forall s \in [0,1].$$

The following figure 1 illustrates the α-cut representation of the fuzzy derivative $G^{\nabla_g}(s)$ for $s \in [0,1]$. Each shaded region corresponds to a different level of $\alpha \in [0,1]$. As α increases, the uncertainty (width of the fuzzy value) decreases, converging to the crisp core at $\alpha = 1$. Let $\mathbb{T} = \mathbb{Z}$, and consider the fuzzy-valued function

$$Q(s) = \tilde{k} \odot s, \quad s \in \mathbb{Z}^{[0,5]},$$

where $\tilde{k} = (1,2,3)$ is a triangular fuzzy number and $\odot$ denotes scalar multiplication.

Since the graininess function on $\mathbb{Z}$ is $\nu(s) = 1$, and the backward jump operator is $\rho(s) = s - 1$, the generalized nabla Hukuhara derivative becomes:

$$Q^{\nabla_g}(s) = \frac{Q(s) \ominus_h Q(\rho(s))}{\nu(s)} = \frac{\tilde{k} \odot s \ominus_h \tilde{k} \odot (s-1)}{1} = \tilde{k}.$$

Thus, $Q^{\nabla_g}(s) = \tilde{k}$ is constant for all $s \in \mathbb{Z}^{[1,5]}$. Note that the derivative is undefined at $s = 0$, since $\rho(0) = -1 \notin [0,5]$.

Theorem 3. *[23] Let $Q : \mathbb{T}^{[x,y]} \to \mathbb{E}_n$ be a fuzzy valued function that is continuous at $s \in \mathbb{T}^{[x,y]}$ and suppose $'s'$ is a ls-points, then the following cases may occur:*

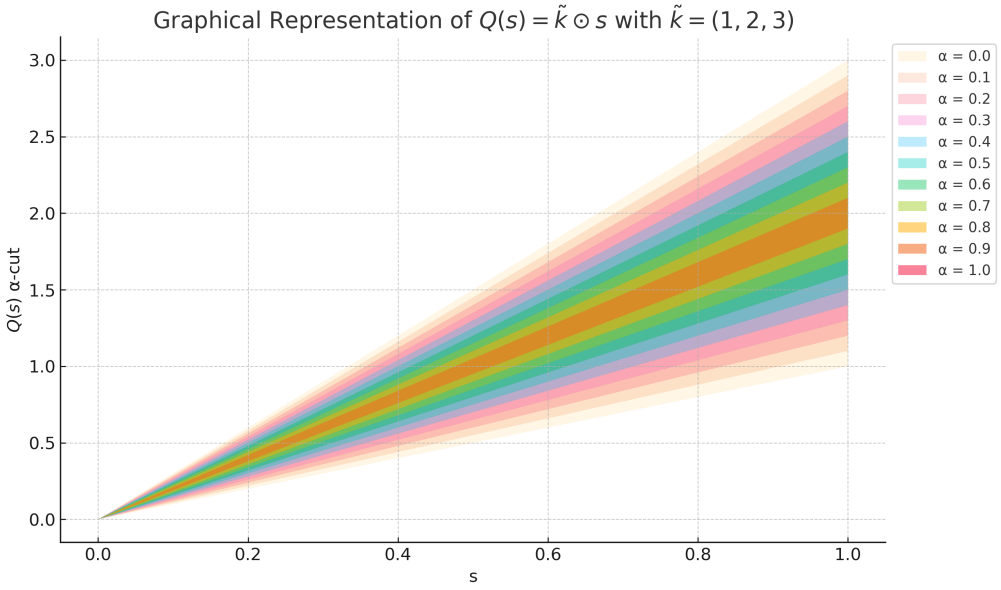


Figure 1: *α-cut representation of the fuzzy derivative* $G^{\nabla_g}(s)$ *for* $s \in [0,1]$.

(i) If Q *is either* $\nabla - GH1$ *type differentiable function or* $\nabla - GH4$ *type differentiable with*

$$Q^{\nabla_g}(s) = \frac{1}{\nu(s)} \odot (Q(s) \ominus_h Q^{\rho}(s)) = \frac{-1}{\nu(s)} \odot (Q^{\rho}(s) \ominus_h Q(s)) \in \Re^n.$$

(ii) If Q *satisfies* $\nabla - GH4$ *type differentiable at* $'s'$ *then*

$$Q^{\nabla_g}(s) = \frac{-1}{\nu(s)} \odot (G^{\rho}(s) \ominus_h Q(s)).$$

(iii) If Q *is* $\nabla - GH4$ *type differentiable at* $'s'$ *then*

$$Q^{\nabla_g}(s) = \frac{1}{\nu(s)} \odot (Q(s) \ominus_h Q^{\rho}(s)).$$

Theorem 4. *[23] Let* $Q_1, Q_2 : \mathbb{T}^{[x,y]} \to \mathbb{E}_n$ *be* ∇_g*-differentiable at* $s \in \mathbb{T}_k^{[x,y]}$. *Then:*

(I) If both Q_1 *and* Q_2 *are either* ∇*-GH*1 *or* ∇*-GH*4 *type differentiable fuzzy functions at left-dense points or at ls-points, then:*

(a) $(Q_1 \oplus Q_2)^{\nabla_g}(s) = Q_1^{\nabla_g}(s) \oplus Q_2^{\nabla_g}(s)$

(b) $(Q_1 \ominus_h Q_2)^{\nabla_g}(s) = Q_1^{\nabla_g}(s) \ominus_h Q_2^{\nabla_g}(s)$, *provided the HK-Difference exists.*

(II) If Q_1 *and* Q_2 *are such that: - one is* ∇*-GH*1 *and the other is* ∇*-GH*2 *type differentiable at left-dense points, or - one is* ∇*-GH*3 *and the other is* ∇*-GH*4 *type differentiable at ls-points, then:*

(a) $(Q_1 \oplus Q_2)^{\nabla_g}(s) = Q_1^{\nabla_g}(s) \ominus_h [(-1) \odot Q_2^{\nabla_g}(s)]$

(b) $(Q_1 \ominus_h Q_2)^{\nabla_g}(s) = Q_1^{\nabla_g}(s) \oplus [(-1) \odot Q_2^{\nabla_g}(s)]$

(1) If s is left-dense, then the function Q satisfies the following conditions:

(GL1) At $s \in \mathbb{T}^{[x,y]}$, if both $Q^{\rho}(s) \ominus_h Q(s-h)$ and $Q(s+h) \ominus_h Q^{\rho}(s)$ exist for sufficiently small $h > 0$,

(GL2) At $s \in \mathbb{T}^{[x,y]}$, if both $Q(s-h) \ominus_h Q^\rho(s)$ and $Q^\rho(s) \ominus_h Q(s+h)$ exist for sufficiently small $h > 0$.

(2) If s is left-scattered, then the function Q satisfies:

(GL3) At $s \in \mathbb{T}_k^{[x,y]}$, if $Q^\rho(s) \ominus_h Q(s)$ exists,

(GL4) At $s \in \mathbb{T}_k^{[x,y]}$, if $Q(s) \ominus_h Q^\rho(s)$ exists.

Theorem 5. *Let $Q : \mathbb{T} \to \mathbb{E}^n$ be a ∇_g-fuzzy differentiable function, and let $h : \mathbb{T} \to \mathbb{R}$ be ∇-differentiable. Then:*

(a) If $h^\rho(s)h^\nabla(s) > 0$ and Q is ∇-$GH1$-type differentiable function at ld-point $'s'$, or Q is ∇-$GH4$-type differentiable at ls-point $'s'$, then $h \odot Q$ is ∇_g-differentiable and

$$(h \odot Q)^{\nabla_g}(s) = h(s) \odot Q^{\nabla_g}(s) \oplus h^\nabla(s) \odot Q^\rho(s).$$

(b) If $h(s)h^\nabla(s) < 0$ and Q is ∇-$GH4$-type differentiable at left-dense or ls-point $'s'$, then

$$(h \odot Q)^{\nabla_g}(s) = h(s) \odot Q^{\nabla_g}(s) \oplus h^\nabla(s) \odot Q^\rho(s).$$

(c) If $h^\rho(s)h^\nabla(s) > 0$, Q is ∇-$GH4$-type differentiable and $h \odot Q$ satisfies condition (GL1) at left-dense point $'s'$ or condition (GL3) at ls-point $'s'$, then

$$(h \odot Q)^{\nabla_g}(s) = h(s) \odot Q^{\nabla_g}(s) \ominus_h (-h^\nabla(s)) \odot Q^\rho(s).$$

(d) If $h(s)h^\nabla(s) < 0$, Q is ∇-$GH1$-type differentiable and $h \odot Q$ satisfies (GL1) at left-dense point $'s'$, or Q is ∇-$GH4$-type differentiable and $h \odot Q$ satisfies (GL3) at a ls-point $'s'$, then

$$(h \odot Q)^{\nabla_g}(s) = h^\nabla(s) \odot Q(s) \ominus_h h^\rho(s) \odot (-Q^{\nabla_g}(s)).$$

(e) If $h^\rho(s)h^\nabla(s) > 0$, Q is ∇-$GH4$-type differentiable and $h \odot Q$ satisfies (GL2) at left-dense point $'s'$, or (GL4) at ls-point $'s'$, then

$$(h \odot Q)^{\nabla_g}(s) = h^\nabla(s) \odot Q^\rho(s) \ominus_h (-h(s)) \odot Q^{\nabla_g}(s).$$

(f) If $h(s)h^\nabla(s) < 0$, Q is ∇-$GH1$-type differentiable and $h \odot Q$ satisfies (GL2) at left-dense point $'s'$, or Q is ∇-$GH4$-type differentiable and $h \odot Q$ satisfies (GL4) at ls-point $'s'$, then

$$(h \odot Q)^{\nabla_g}(s) = Q^{\nabla_g}(s) \odot h^\rho(s) \ominus_h Q(s) \odot (-h^\nabla(s)).$$

Proof. If $'s'$ is left-dense, then $\rho(s) = s$ and $\nu(s) = 0$. The proof of case (a) is analogous to that of Theorem 5 in [6]. We now prove cases $(b) - (f)$.

(b) Assume $h(s) > 0$, $g^\nabla(s) < 0$, and $Q^\rho(s) = Q(s) \oplus u(s)$. Let $h^\rho(s) = h(s) + v(s)$. Then:

$$h^\rho(s) \odot Q^\rho(s) = h(s) \odot Q(s) \oplus h(s) \odot u(s) \oplus v(s) \odot Q(s) \oplus v(s) \odot u(s).$$

So,

$$(h^\rho(s) \odot Q^\rho(s)) \ominus_h (h(s) \odot Q(s)) = h(s) \odot Q^{\nabla_g}(s) \oplus h^\nabla(s) \odot Q^\rho(s).$$

(c) Suppose $h^\rho(s) > 0$, $h^\nabla(s) > 0$, and $Q^\rho(s) = Q(s) \oplus u(s)$. Let $h(s) = h^\rho(s) + v(s)$. Then:

$$(h^\rho(s) \odot Q^\rho(s)) \ominus_h (h(s) \odot Q(s)) = h(s) \odot Q^{\nabla_g}(s) \ominus_h Q^\rho(s) \odot (-h^\nabla(s)).$$

(d) Suppose $h(s) < 0$, $h^\nabla(s) > 0$, and $Q(s) = Q^\rho(s) \oplus u(s)$, so that

$$(h^\rho(s) \odot Q^\rho(s)) \ominus_h (h(s) \odot Q(s)) = h^\nabla(s) \odot Q(s) \ominus_h h^\rho(s) \odot (-Q^{\nabla_g}(s)).$$

(e) Let $h^{\rho}(s) > 0$, $h^{\nabla}(s) > 0$, and $Q^{\rho}(s) = Q(s) \oplus u(s)$. Suppose that

$$Q(s-h) \ominus_h Q^{\rho}(s) \text{ and } Q^{\rho}(s) \ominus_h Q(s+h) \text{ exist.}$$

Since $h \odot Q$ satisfies (GL2), we have:

$$h^{\nabla}(s) \odot Q^{\rho}(s) \ominus_h (-h(s)) \odot Q^{\nabla_g}(s)$$

exists, which proves the formula for case (e).

(f) Suppose $h(s) < 0$, $g^{\nabla}(s) < 0$, and Q is ∇-$GH4$-type differentiable. Let $Q(s) = Q^{\rho}(s) \oplus u(s)$, and assume $h \odot Q$ satisfies condition (GL4), i.e., $Q(s) \ominus_h Q^{\rho}(s)$ exists. Then:

$$(h \odot Q)^{\nabla_g}(s) = Q^{\nabla_g}(s) \odot h^{\rho}(s) \ominus_h Q(s) \odot (-h^{\nabla}(s)).$$

■

Definition 8 ([22]). *Let $Q : \mathbb{T}^{[x,y]} \to \mathbb{E}_n$ be a fuzzy-valued function. If Q admits a left-dense continuous (ld-continuous) measurable nabla-sector on $\mathbb{T}^{[x,y]}$, then Q is said to be ∇-integrable on $\mathbb{T}^{[x,y]}$.*

*The ∇-integral of Q over $\mathbb{T}^{[x,y]}$ is defined **level-wise** as follows:*

$$\left[\int_{\mathbb{T}^{[x,y]}} Q(\tau)\nabla\tau\right]^{\alpha} = \int_{\mathbb{T}^{[x,y]}} Q_{\alpha}(\tau)\nabla\tau$$
$$= \left\{\int_{\mathbb{T}^{[x,y]}} q(\tau)\nabla\tau : q \in S_{Q_{\alpha}}(\mathbb{T}^{[x,y]})\right\},$$

where $S_{Q_{\alpha}}(\mathbb{T}^{[x,y]})$ denotes the set of all ∇-integrable sectors of Q_{α} on $\mathbb{T}^{[x,y]}$.

Corollary 1. *Let $Q : \mathbb{T}^{[x,y]} \to \mathbb{E}^n$ be ∇_g-integrable and possess a ld-continuous nabla-measurable sector. Then the ∇_g-integral has the following properties:*

(i) If $\mathbb{T} = \mathbb{R}$, then

$$\left[\int_{s_0}^{s} Q(\tau)\nabla\tau\right]^{\alpha} = \int_{s_0}^{s} Q_{\alpha}(\tau)\, d\tau.$$

(ii) If $\mathbb{T}$ consists of isolated points, then

$$\int_{s_0}^{s} Q(\tau)\nabla\tau = \begin{cases} \sum_{s\in(a,b]} \nu(s)\, Q(s), & \text{if } a < b, \\ 0, & \text{if } a = b, \\ -\sum_{s\in(b,a]} \nu(s)\, Q(s), & \text{if } a > b. \end{cases}$$

Remark 2. *Let $Q : \mathbb{T}^{[x,y]} \to \mathbb{E}^n$ have a ld-continuous nabla-measurable sector. If Q is ∇_g-differentiable on $\mathbb{T}^{[x,y]}$ and Q^{∇} is continuous on $\mathbb{T}^{[x,y]}$, then*

$$\int_{s_0}^{s} Q^{\nabla_g}(\tau)\nabla\tau = Q(s) \ominus_h Q(s_0). \tag{1}$$

(i) If Q is ∇-$GH1$ type differentiable at a left-dense point s, or ∇-$GH4$ type differentiable at ls-points s, then equation (1) is equivalent to:

$$Q(s) = Q(s_0) \oplus \int_{s_0}^{s} Q^{\nabla}(\tau)\nabla\tau.$$

(ii) If Q is ∇-$GH2$ type differentiable at a left-dense or nabla-$GH3$ type differentiable at ls-points s, then equation (1) is equivalent to:

$$Q(s) = Q(s_0) \ominus_h \left[(-1) \odot \int_{s_0}^{s} Q^{\nabla}(\tau)\nabla\tau\right].$$

4. Solutions of fuzzy nabla dynamic equations on time scales

We now establish the *variation of constants formula* to determine solutions of LFNDET's, using the concept of ∇_g-differentiability. This formula plays a fundamental role in constructing explicit solutions to non-homogeneous equations involving fuzzy-valued functions on arbitrary time scales.

Consider the first-order nonhomogeneous dynamic equation:

$$u^{\nabla}(s) = A(s) \odot u(s) \oplus Q(s), \tag{2}$$

with the corresponding homogeneous equation:

$$u^{\nabla}(s) = A(s) \odot u(s). \tag{3}$$

If Q is ld-continuous and the homogeneous equation (3) is regressive, then the non-homogeneous equation (2) is also regressive.

Now, consider the initial value problem:

$$u^{\nabla}(s) = A(s) \odot u(s) \oplus Q(s), \quad u(s_0) = u_0, \tag{4}$$

where $Q : \mathbb{T} \to \mathbb{E}_n$ is ld-continuous, $A : \mathbb{T} \to \mathbb{R}$ is a regressive function, and $u_0 \in \mathbb{E}^n$.

It is important to note that the equation (4) is not equivalent to the following two FNDET's:

$$u^{\nabla}(s) \oplus (-A(s)) \odot u(s) = Q(s), \quad u(s_0) = u_0, \tag{5}$$

and

$$u^{\nabla}(s) \oplus (-Q(s)) = A(s) \odot u(s), \quad u(s_0) = u_0. \tag{6}$$

Each of the equations (4), (5), and (6) yields different solutions, even under the same initial condition. For example, if (4) and (5) were to yield the same solution, we would have:

$$A(s) \odot u(s) \oplus Q(s) \oplus (-A(s)) \odot u(s) = Q(s),$$

which implies

$$A(s) \odot u(s) \oplus (-A(s)) \odot u(s) = \hat{0},$$

leading to $u(s) \in \mathbb{R}^n$, contradicting the fuzzy nature of $u(s)$. Thus, these equations are generally not equivalent in the fuzzy setting.

Moreover, consider the FNDET:

$$u^{\nabla}(s) \oplus (-Q(s)) \oplus (-A(s) \odot u(s)) = \hat{0}, \quad u(s_0) = u_0, \tag{7}$$

which, in the crisp case, is equivalent to one of the previous equations. However, no non-real (fuzzy) solution exists for (7) in general. In practical applications, fuzzy systems are derived from the fuzzification of crisp systems, and thus may yield multiple distinct solutions. These solutions provide different behaviors, allowing us to select one that best captures the imprecision of the system.

The following theorem establishes the variation of constants formula for equation (4) using ∇_g-differentiability.

We now present the variation of constants formula, which provides distinct solutions to LFNDET's using ∇_g-differentiability.

Theorem 6 (Variation of Constants Formula)**.** *Let $s_0 \in \mathbb{T}^{[x,y]}$, $u_0 \in \mathbb{E}^n$, and suppose the following LFNDET's is regressive:*

$$u^{\nabla}(s) = A(s) \odot u(s) \oplus Q(s), \quad u(s_0) = u_0, \tag{8}$$

where $A : \mathbb{T} \to \mathbb{R}$ is a regressive crisp function and $Q : \mathbb{T} \to \mathbb{E}_n$ is ld-continuous.

Define:

$$u_1(s) = \hat{e}_A(s, s_0) \odot \left[u_0 \oplus \int_{s_0}^{s} Q(\tau) \odot \hat{e}_A(s_0, \rho(\tau)) \nabla\tau \right], \tag{9}$$

$$u_2(s) = \hat{e}_A(s, s_0) \odot \left[u_0 \ominus_h \int_{s_0}^{s} (-Q(\tau)) \odot \hat{e}_A(s_0, \rho(\tau)) \nabla\tau \right], \tag{10}$$

provided the HK-Difference in (10) *exists.*

Then:

(a) If $A(s) > 0$ for all $s \in \mathbb{T}^{[x,y]}$, then $u_1(s)$ is ∇-GH1 type differentiable at left-dense and ∇-GH4 type differentiable at ls-points. Moreover, $u_1(s)$ is a solution to equation (8).

(b) If $A(s) < 0$ and the HK-Difference in (10) *exists, then $u_2(s)$ is ∇-GH4 type differentiable at both left-dense and ls-points. Moreover, $u_2(s)$ is a solution to equation* (8).

(c) If $A(s) < 0$ and u_1 satisfies conditions (GL1) at left-dense and (GL3) at ls-points (or conditions (GL2) and (GL4), respectively), then u_1 also satisfies one of the following equivalent formulations:

$$u^{\nabla}(s) \oplus (-A(s)) \odot u(s) = Q(s) \quad or \quad u^{\nabla}(s) \oplus (-Q(s)) = A(s) \odot u(s).$$

(d) If $A(s) > 0$, the HK-Difference in (10) *exists, and u_2 satisfies (GL1) and (GL3) (or (GL2) and (GL4)), then u_2 is also a solution to one of the above equivalent equations.*

Proof. We first prove part (a); the other cases follow similarly by algebraic manipulations involving the properties of ∇-differentiability and HK-Differences.

Let $A(s) > 0$ and $A(s) = \hat{e}_A(s; s_0)$. Since A is regressive, the nabla exponential function $\hat{e}_A(s, s_0)$ is well-defined. We know that $g^{\rho}(s) = (1 - \nu(s)A(s))\hat{e}_A(s; s_0)$, $g^{\nabla}(s) = \alpha(s))\hat{e}_A(s; s_0)$. Therefore $g^{\rho}(s)g^{\nabla}(s) = A(s)(1 - \nu(s)A(s))\hat{e}_A^2(s; s_0)$.
Let $h_1(s) = u_0 \oplus \int_{s_0}^{s} G(\tau) \odot \hat{e}_{\alpha}(s_0, \rho(\tau)) \nabla\tau$ and $h_2(s) = u_0 \ominus_h \int_{s_0}^{s} (-G(\tau)) \odot \hat{e}_{\alpha}(s_0, \rho(\tau)) \nabla\tau$

We differentiate $u_1(s)$ using the nabla product rule for fuzzy-valued functions:

$$(u_1)^{\nabla}(s) = [\hat{e}_A(s, s_0)]^{\nabla} \odot \left[u_0 \oplus \int_{s_0}^{s} Q(\tau) \odot \hat{e}_A(s_0, \rho(\tau)) \nabla\tau \right] \oplus \hat{e}_A^{\rho}(s, s_0) \odot Q(s).$$

But we know $(\hat{e}_A(s, s_0))^{\nabla} = A(s) \odot \hat{e}_A(s, s_0)$. Substituting, we get:

$$(u_1)^{\nabla}(s) = A(s) \odot \hat{e}_A(s, s_0) \odot \left[u_0 \oplus \int_{s_0}^{s} Q(\tau) \odot \hat{e}_A(s_0, \rho(\tau)) \nabla\tau \right] \oplus Q(s) \odot \hat{e}_A(s, s_0).$$

Now distribute $\hat{e}_A$ over the sum inside the brackets:

$$(u_1)^{\nabla}(s) = A(s) \odot u_1(s) \oplus Q(s).$$

Hence, $u_1(s)$ satisfies equation (8). The differentiability type follows from the fact that $\hat{e}_A$ is crisp and smooth, and the integral is a fuzzy function depending on ld-continuity.

Proofs of parts (b), (c), and (d) follow similar reasoning using the properties of $\ominus_h$, negative scalar multiplication, and the GL-conditions. ■

Theorem 7. *Let $s_0 \in \mathbb{T}^{[x,y]}$, $u_0 \in \mathbb{E}^n$, and suppose equation* (2) *is regressive. Define:*

$$u_1(s) = \hat{e}_A(s, s_0) \odot \left[u_0 \oplus \int_{s_0}^{s} Q(\tau) \odot \hat{e}_A(s_0, \rho(\tau)) \nabla\tau \right], \tag{11}$$

and

$$u_2(s) = \hat{e}_A(s, s_0) \odot \left[u_0 \ominus_h \int_{s_0}^{s} (-Q(\tau)) \odot \hat{e}_A(s_0, \rho(\tau)) \nabla\tau \right], \tag{12}$$

provided the HK-Difference exists in (12). *Then:*

(a) If $A(s) > 0$ and for all left-dense s in $\mathbb{T}^{[x,y]}$, then $u_1(s)$ is ∇-GH1 type differentiable and ∇-GH4 type differentiable at ls-points, and it is a solution to (4).

(b) If $A(s) < 0$ and the HK-Difference in (12) *exists, then $u_2(s)$ is ∇-GH4 type differentiable at both left-dense and ls-points, and it is a solution to* (4).

(c) If $A(s) < 0$ and u_1 satisfies conditions (GL1) at left-dense and (GL3) at ls-points (or GL2 and GL4, respectively), then u_1 is also a solution of (5) *or* (6).

(d) If $A(s) > 0$, the HK-difference in (12) *exists, and u_2 satisfies (GL1) and (GL3) (or GL2 and GL4), then u_2 is a solution of* (5) *or* (6), *respectively.*

Proof. Let $A(s) = \hat{e}_A(s; s_0)$, $h^\rho(s) = (1 - \nu(s)A(s))\hat{e}_A(s; s_0)$, $h^\nabla(s) = A(s))\hat{e}_A(s; s_0)$.
So, $h^\rho(s))h^\nabla(s) = A(s)(1 - \nu(s)A(s))\hat{e}^2_A(s; s_0)$.
Let $q_1(s) = u_0 \oplus \int_{s_0}^{s} Q(\tau) \odot \hat{e}_\alpha(s_0, \rho(\tau))\nabla\tau$, and $q_2(s) = u_0 \ominus_h \int_{s_0}^{s}(-Q(\tau)) \odot \hat{e}_\alpha(s_0, \rho(\tau))\nabla\tau$.

We know that a constant function is nabla differentiable under any case of ∇_g-differentiability and in view of Theorem 5, it follows that $u_0 \oplus \int_{s_0}^{s} Q(\tau) \odot \hat{e}_\alpha(s_0, \rho(\tau))\nabla\tau$ is ∇-$GH1$ type differentiable function at ld-point s (or) $\nabla - GH4$ type differentiable function at ls-point s and

$$\left(u_0 \oplus \int_{s_0}^{s} Q(\tau) \odot \hat{e}_A(s_0, \rho(\tau))\nabla\tau\right)^{\nabla_g} = Q(s) \odot \hat{e}_\alpha(s_0, \rho(s)). \tag{13}$$

If the HK-Difference $u_0 \ominus_h \int_{s_0}^{s}(-G(\tau)) \odot \hat{e}_\alpha(s_0, \rho(\tau))\nabla\tau$ exists then it is $\nabla - GH4$ type differentiable function at ld-point s and

$$\left(u_0 \ominus \int_{s_0}^{s}(-Q(\tau)) \odot \hat{e}_\alpha(s_0, \rho(\tau))\nabla\tau\right)^{\nabla_g} = Q(s) \odot \hat{e}_\alpha(s_0, \rho(s)). \tag{14}$$

(a) Let $q(s) = \hat{e}_A(s, s_0)$ and $q_1(s) = s_0 \oplus \int_{s_0}^{s} h(\tau) \odot \hat{e}_\alpha(s_0, \rho(\tau))\nabla\tau$, since $A(s) > 0$ for $s \in \mathbb{T}^{[x,y]}$, we have $h^\rho(s)h^\nabla(s) > 0$ and from (13) the conditions in Theorem 5(a) follows and then $u_1^\nabla(s) = A(s) \odot u_1(s) \oplus h(s)$.

i.e. u_1 is a solution of (4).

(b) Since $A(s) < 0$ for $s \in \mathbb{T}^{[x,y]}$, we have $h(s)h^\nabla(s) < 0$. Also, since

$$q_2(s) = u_0 \ominus \int_{s_0}^{s}(-h(\tau)) \odot \hat{e}_A(s_0, \rho(\tau))\nabla\tau$$

is a ∇-GH4 type differentiable function at left-dense or at ls-points on $\mathbb{T}^{[x,y]}$, the conditions in Theorem 5(b) hold. Hence, we obtain

$$u_2^\nabla(s) = A(s) \odot u_2(s) \oplus g(s),$$

i.e., u_2 is a solution of (4).

(c) Since $A(s) < 0$, we have $h(s)h^\nabla(s) < 0$. Suppose u_1 follows the condition $(GL1)$ at left-dense and condition $(GL3)$ at ls-points. Then the assumptions of Theorem 5(d) are applicable. Therefore, we have

$$u_1^\nabla(s) = h^\nabla(s) \odot q_1(s) \ominus_h g^\rho(s) \odot (-1) \odot q_1^{\nabla_g}(s) = h(s) \ominus_h (-A(s)) \odot u_1(s).$$

That is,

$$u_1^\nabla(s) \oplus (-A(s)) \odot u_1(s) = h(s),$$

and hence u_1 is a solution of (5).

Similarly, if u_1 satisfies condition $(GL2)$ at left-dense or condition $(GL4)$ at ls-points, then the conditions of Theorem 5(f) are fulfilled. Thus, we have

$$Q^{\nabla_g}(s) \odot h^\rho(s) \ominus_h (-Q(s)) \odot g^\nabla(s).$$

Also,

$$u_1^{\nabla}(s) = q_1(s) \odot (-1) \odot h^{\nabla}(s) \ominus_h h^{\rho}(s) \odot q_1^{\nabla_g}(s) = A(s) \odot u_1(s) \ominus_h h(s).$$

That is,

$$u_1^{\nabla}(s) \oplus (-h(s)) = A(s) \odot u_1(s),$$

so u_1 is a solution of (6).

(d) If $A(s) > 0$, then $h(s) \odot h^{\nabla}(s) > 0$. Also, from (14), q_2 is a ∇-GH4-type differentiable function at left-dense and at ls-points. If u_2 satisfies condition $(GL1)$ at left-dense and condition $(GL3)$ at ls-points, then the conditions in Theorem 5(c) are satisfied. Therefore,

$$u_2^{\nabla}(s) = A(s) \odot u_2(s) \ominus (-h(s)),$$

which is equivalent to

$$u_2^{\nabla}(s) \oplus (-h(s)) = A(s) \odot u_2(s),$$

so u_2 is a solution of (6).

In the same manner, we can show that if u_2 satisfies condition $(GL2)$ at left-dense and condition $(GL4)$ at ls-points, then the conditions in Theorem 5(e) are fulfilled. Hence, u_2 is a solution of (5).

■

Remark 3. *Theorem 7 shows that the solution to the LFNDTEs is not unique. While this may seem limiting, it allows us to choose the solution that best fits the real system's behavior.*

The following example illustrates the best behavior of the system that allows us to choose the solutions that fits to the problem.

Example 2. *Consider the fuzzy nabla dynamic equation on the time scale* $\mathbb{T} = \mathbb{Z} \cap [0, 3]$*:*

$$u^{\nabla}(s) = A(s) \odot u(s) \oplus G(s), \quad s \in \mathbb{T}^{[0,3]},$$

With the fuzzy initial condition:

$$u(0) = \tilde{u}_0 = [1, 2, 3],$$

where $A(s) = -1$, $g(s) = [-1, 0, 1]$ *(a triangular fuzzy number), and* $\odot, \oplus$ *denote fuzzy scalar multiplication and addition under generalized Hukuhara arithmetic. so that we have two Possible fuzzy Solutions:*

Solution 1: (Oscillatory response)

$$u_1(s) = \hat{e}_{\alpha}(0, s) \odot \tilde{u}_0 \oplus \sum_{\tau=0}^{s-1} \hat{e}_{\alpha}(\rho(\tau), s) \odot \tilde{g}(\tau),$$

where $\hat{e}_{\alpha}(0, s) = (-1)^s$*. This leads to an oscillatory response due to alternating signs.*

Solution 2: (Cumulative response)

$$u_2(s) = \tilde{u}_0 \oplus \sum_{k=0}^{s-1} (-1)^k \odot \tilde{g}(k),$$

which corresponds to cumulative contributions from fuzzy input over time.

Both $u_1(s)$ *and* $u_2(s)$ *satisfy the same equation and initial condition. However, their behaviors differ:*

- $u_1(s)$*: Suitable for systems with oscillatory dynamics.*
- $u_2(s)$*: Suitable for systems with cumulative or additive effects.*

Thus, the non-uniqueness in Theorem 7 allows us to choose the most appropriate solution for modeling real-world behavior as illustrated igraphically in Figure 2.

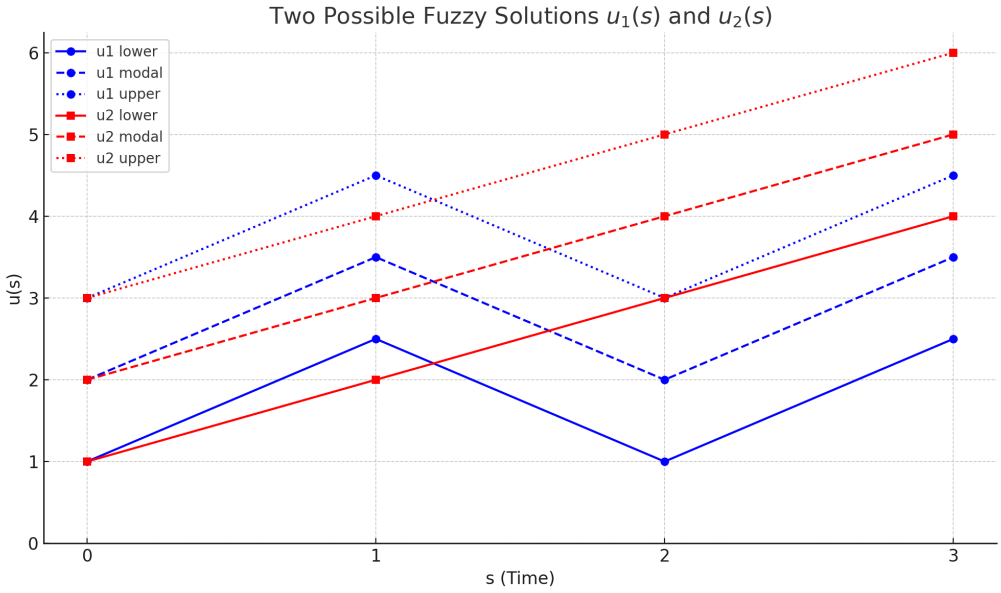


Figure 2: *Graphical comparison of oscillatory and cumulative fuzzy solutions*

5. Conclusions

In this paper, we develop the product rule for crisp and fuzzy functions on time scales, which provides multiple solution forms of LFNDET's and also investigates the solutions of LFNDET's using the variation of constants formula under different versions of the generalized Hukuhara nabla derivative. The numerical examples illustrated prove the theoretical results. The rich and well-structured behavior of these solutions highlights the effectiveness and significance of the generalized nabla derivative in the context of dynamic equations on time scales. The present study lays a strong foundation for a wide range of future research in controllability and Stability analysis in fuzzy environment.

References

[1] Agarwal, R. P. and Bohner, M. (1999). Basic calculus on time scales and some of its applications. *Results in Mathematics*, 35: 3–22.

[2] Anastassiou, G. A. and Gal, S. G. (2001). On a fuzzy trigonometric approximation theorem of Weierstrass-type. *Journal of Fuzzy Mathematics*, 9(3):701–708.

[3] Atici, F. M., Biles, C. D., and Lebedinsky, A. (2006). An application of time scales to economics. *Mathematical and Computer Modelling*, 43:718–726.

[4] Atici, F. M. and Usynal, F. (2008). A production-inventory model of HMMS model on time scales. *Applied Mathematics Letters*, 21(3):236–243.

[5] Bede, B. and Gal, S. G. (2004). Almost periodic fuzzy-number-valued functions. *Fuzzy Sets and Systems*, 147: 385–403.

[6] Bede, B. and Gal, S. G. (2005). Generalizations of the differentiability of fuzzy-number-valued functions with applications to fuzzy differential equations. *Fuzzy Sets and Systems*, 151:581–599.

[7] Bede, B., Rudas, I. J., and Bencsik, A. L. (2007). First order linear fuzzy differential equations under generalized differentiability. *Information Sciences*, 177: 1648–1662.

[8] Bede, B. and Stefanini, L. (2013). Generalized differentiability of fuzzy-valued functions. *Fuzzy Sets and Systems*, 230: 119–141.

[9] Bohner, M. and Peterson, A. (2001). *Dynamic Equations on Time Scales: An Introduction with Applications*. Birkhauser, Boston.

[10] Bohner, M. and Peterson, A. (2003). *Advances in Dynamic Equations on Time Scales*. Birkhauser, Boston.

[11] Diamond, P. (2002). Brief note on the variation of constants formula for fuzzy differential equations. *Fuzzy Sets and Systems*, 129: 65–71.

[12] Fard, O. S. and Bidgoli, T. A. (2015). Calculus of fuzzy functions on time scales (I). *Soft Computing*, 19(2):293–305.

[13] Guseinov, G. S. (2003). Integration on time scales. *Journal of Mathematical Analysis and Applications*, 285:107–127.

[14] Gao, J., Wang, Q. R., and Zhang, L. W. (2015). Existence and stability of almost-periodic solutions for cellular neural networks with time-varying delays in leakage terms on time scales. *Applied Mathematics and Computation*, 237:639–649.

[15] Hilger, S. (1990). Analysis on measure chains: a unified approach to continuous and discrete calculus. *Results in Mathematics*, 18: 18–56.

[16] Hilscher, R. and Zeidan, V. (2010). Nabla time scale symplectic systems and related quadratic functionals. *Differential Equations and Dynamical Systems*, 18(1):163–198.

[17] Hong, S. (2009). Differentiability of multivalued functions on time scales and applications to multivalued dynamic equations. *Nonlinear Analysis*, 71:3622–3637.

[18] Hukuhara, M. (1967). Integration des applications mesurables dont la valeur est un compact convexe. *Funkcialaj Ekvacioj*, 10:205–223.

[19] Jackson, B. J. (2008). Adaptive control in the nabla setting. *Neural, Parallel and Scientific Computations*, 16:253–272.

[20] Kaleva, O. (1987). Fuzzy differential equations. *Fuzzy Sets and Systems*, 24:301–317.

[21] Li, J., Zhao, A., and Yan, J. (2012). The Cauchy problem of fuzzy differential equations under generalized differentiability. *Fuzzy Sets and Systems*, 200: 1–24.

[22] Leelavathi, R., Suresh Kumar, G., and Murty, M. S. N. (2018). Nabla integral for fuzzy functions on time scales. *International Journal of Applied Mathematics*, 31(5):669–678.

[23] Leelavathi, R., Suresh Kumar, G., and Murty, M. S. N. (2020). Generalized nabla differentiability and integrability for fuzzy functions on time scales. *Axioms*, 9(2):65. https://doi.org/10.3390/axioms9020065

[24] Liu, B., Do, Y., Batarfi, H. A., and Alsaadi, F. E. (2016). Almost periodic solution for a neutral-type neural network with distributed leakage delays on time scales. *Neurocomputing*, 173:921–929.

[25] Lupulescu, V. (2013). Hukuhara differentiability of interval-valued functions and interval differential equations on time scales. *Information Sciences*, 248: 50–67.

[26] Puri, M. L. and Ralescu, D. (1983). Differentials for fuzzy functions. *Journal of Mathematical Analysis and Applications*, 91:552–558.

[27] Vasavi, C. H., Suresh Kumar, G., and Murty, M. S. N. (2016). Fuzzy dynamic equations on time scales under generalized delta derivative via contractive-like mapping principles. *Indian Journal of Science and Technology*, 9(25):1–6.

[28] Zadeh, L. A. (1965). Fuzzy sets. *Information and Control*, 8:338–353.

EXPLORING REDUNDANCY OPTIMIZATION TECHNIQUES FOR SYSTEM PERFORMANCE

Parveen Kumar[1]*, Dalip Singh[2], Anil Kumar Taneja[3]

•

[1*,2]Department of Mathematics, Maharshi Dayanand University, Rohtak, Haryana, India
parveenkumarpc4321@gmail.com, dsmdur@gmail.com
[3]Department of Mathematics, Sh. L. N. Hindu College, Rohtak, Haryana, India
dranilkrtaneja@gmail.com

Abstract

System reliability optimization remains a dynamic and evolving challenge, influenced by continuous advancements in mathematical modeling, engineering innovation, and management strategies. This study includes documents on reliability, availability, maintainability, dependability, testability, cost-benefit analysis, life-cycle failures, maintenance modeling, and asset integrity management. However, this article is mainly concerned with documents that focus on redundancy optimization problems (i.e., k out of n system, warm, hot, cold standby redundancy, system reliability analysis in different failure and repair conditions, redundancy allocation in several system configurations, and so on) that apply to Telecommunications, Aerospace and Aviation, Industrial Automation, Network Servers and IT Systems, Transportation Systems. In addition, documents on the Oil and Gas Industry, Data Centers, and critical Infrastructure that are part of process industries are included. We analyze as many documents as possible by combining commonly used keywords. Additionally, the paper identifies emerging trends such as adaptive and hybrid redundancy strategies and the integration of intelligent techniques like Supplymentry variable techniques, regenerative point techniques, Genetic algorithm, and machine learning for real-time reliability management. By synthesizing findings from recent literature, this review aims to guide future research and practical implementations, supporting the design of cost-effective, robust, and resilient systems for modern computing environments.

Keywords: Reliability, Redundancy, Optimization, Operative unit, Redundant System, Activation time, Standby Units, Profit analysis, Regenerative Point Technique .

1. Introduction

Consumers' expectations for high functionality, high performance, and high dependability rise along with technology's advancements, which creates both obstacles and possibilities as modern engineered systems become more sophisticated. Despite extensive research and scrutiny, system reliability optimization problems continue to pose formidable challenges, as new complexities and difficulties emerge, perpetually impacting system reliability. The challenge of downtime can be addressed by the introduction of redundancy.

The reliability of redundant systems, as revealed through probabilistic analysis, hinges on three pivotal factors. Foremost among these is the failure rates or, equivalently, the lifetime distributions of the constituent components that comprise the system. Another crucial factor influencing system reliability is the system configuration, which encompasses both the number of components and their interconnectivity - in other words, how these components are arranged

and linked to form the overall system. Lastly, system reliability is also contingent upon the maintenance strategies employed, including repair, corrective, and preventive measures, which collectively impact the system's overall performance and reliability.
Figure 1 depicts a conceptual framework for the current investigation's methodology.

Abbreviations used:

CSS Cold Standby System
WSS Warm Standby System
HSS Hot Standby System
RAP Redundancy Allocation Problem

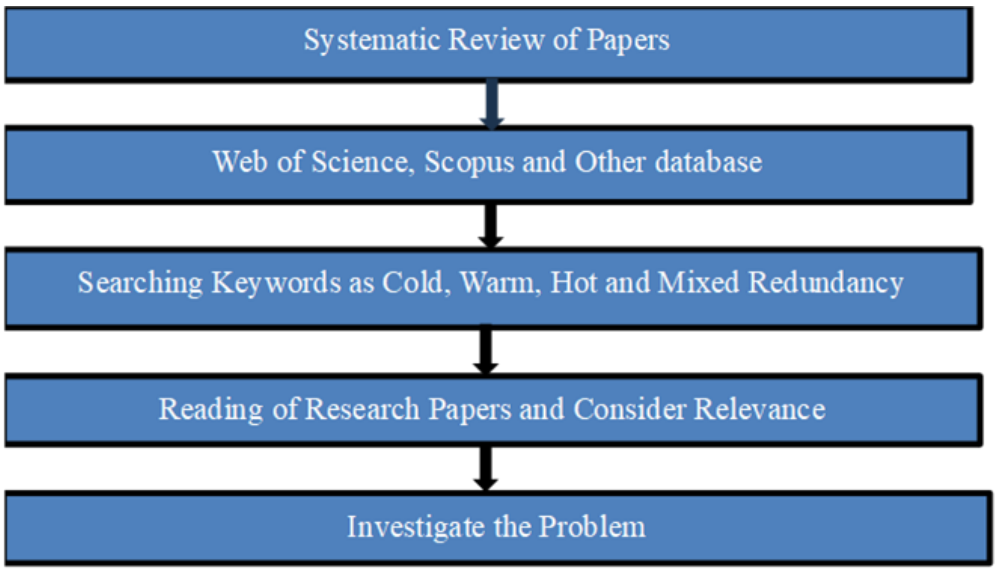


Figure 1: *Techniques for Systematic Analysis*

Because review papers can provide a concise and up-to-date overview of an area, they are essential to the scientific community. Numerous reviews in various areas of process reliability have been published. Dekker [27] gave an overview of the application of maintenance optimization models. Kuo and Parsad [55] demonstrated an overview of the methods developed for solving various reliability optimization problems. Kuo and Wan [56] looked at the best dependability design by primarily considering series-parallel systems, bridge networks, n-version programming architecture, k-out-of-n: G systems, and other unnamed coherent systems are among the systems. Yingkui and Jing [131] review the latest studies and advances in multi-state system reliability evaluation, optimization, and maintenance summarized. Li and Ding [60] briefly reviewed the allocation of active redundancies to systems. Ram [91] surveyed reliability approaches in various engineering fields and provided the major areas, i.e., past, current, and future trends of reliability methods and applications. Alaswad and Xiang [1] review the recent condition-based maintenance literature that emphasizes mathematical modeling and optimization approaches and focuses on the optimal design of CBM policies, including inspection frequency, inspection/maintenance quality, and optimization criteria. Amin et al. [4] Conducted a comprehensive bibliometric analysis of research on process system failure and reliability, providing insights into the development and trends of failure and reliability engineering within process systems.

This comprehensive study encompasses a broad range of topics, including reliability, availability, dependability, maintainability, testability, life-cycle failure assessment, cost-benefit analysis, maintenance modeling, and asset integrity management. However, the primary focus of this article lies in examining documents that specifically address redundancy optimization problems (i.e., k out of n system, warm, hot, cold standby redundancy, system reliability analysis in different failure and repair conditions, redundancy allocation in several system configurations, and so

on) that apply to Telecommunications, Aerospace and Aviation, Industrial Automation, Network Servers and IT Systems, Transportation Systems. We analyzed as many documents as possible by combining frequently used keywords. However, certain documents may be overlooked without intention. We apologize to readers and scholars if we overlooked any pertinent documents.

2. Standby Redundancy

The redundant series system has been extensively studied due to its wide range of applications in practical systems such as power supply networks, photovoltaic energy systems, air traffic control equipment, and automated manufacturing lines. By integrating redundancy strategies with maintenance through component repairs, the reliability and efficiency of repairable systems can be significantly improved. In a standby system, operational units function while backup units remain inactive until needed. When an active unit fails, a standby unit is engaged to take its place. There are three main types of standby configurations: hot, warm, and cold standby as shown in Figure 2. The hot standby method ensures that both active and backup units operate in a similar environment, with the standby unit continuously connected to the system. This approach is particularly beneficial for applications requiring instant switchover, such as network printers and aircraft engines. Conversely, in the cold standby approach, the backup unit remains unpowered until the primary unit fails and requires replacement. This strategy is advantageous for systems prioritizing energy efficiency, such as those in metallurgy and defense applications. The warm standby approach serves as a middle ground between hot and cold standby. Here, the backup unit experiences a failure rate that falls between the two extremes. This method provides a balance between rapid switchover and energy conservation, making it a flexible and practical choice for various systems.

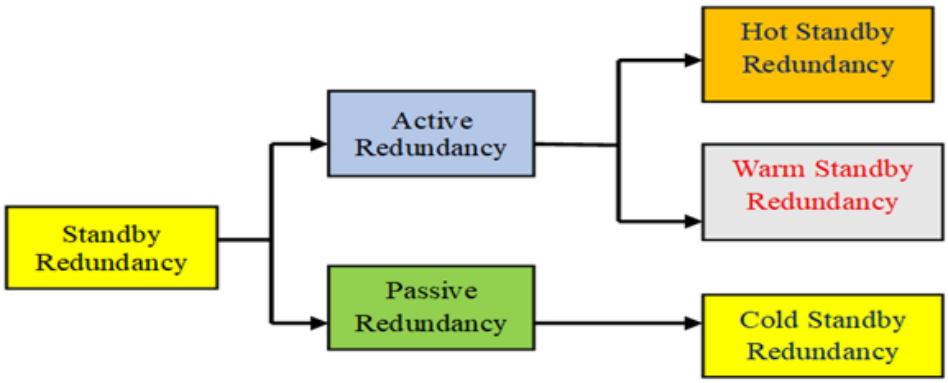


Figure 2: *Classification of Standby Redundancy*

3. Cold Standby Redundant systems

Cold standby redundancy is a configuration technique employed to boost the reliability and availability of essential systems by utilizing redundant components that remain inactive until needed. In this setup, the system consists of redundant components that are kept in a non-operational (standby) state until needed. The primary (active) component operates and performs its function, while the redundant components remain ready to take over if the operative unit fails. CSS are commonly used in critical applications where continuous operation is vital, such as in power distribution, telecommunications, aerospace, and transportation industries. Redundancy ensures that the system can continue to function despite failures, making it an effective approach to enhance the reliability and availability of the system. However, it also comes with additional redundant components and maintenance costs. Therefore, designing and optimizing a

cold standby redundant system involves carefully balancing the benefits of improved reliability against the associated costs. Optimization of a CSS involves finding the best configuration and activation policy to maximize system reliability and availability while minimizing costs and resource utilization. The goal is to balance redundancy, which enhances system reliability, and the associated costs of maintaining redundant components.

Taneja et al. [112] discussed a single server two-unit CSS, where each unit can be in one of four modes: partial, normal, failure, complete failure, and partial failure with some repair already done, and priority is given to repairing the failed unit. Goel and Tyagi [36] described a two-unit priority redundant system with three modes: partial, normal and total failure, one unit has a priority in operation, while the other has a priority in repair. Tuteja and Taneja [116] analyzed a one-unit system with a single server with partial failure, which is subject to random inspection. Partial failures can only be identified through deliberate inspection, whereas complete failures are immediately detectable without the need for inspection. Bhat and Gururajan [15] considered one repair facility that supports a two-unit CSS by assuming that after a breakdown, the system continues to function for an arbitrary period.

Vanderperre [118] presented a cold standby redundant system that includes numerous switch-over devices and a monitor using arbitrary distribution and compared the performance of both systems while considering the scenario of a single switch-over device. Singh [102] investigated a two-unit CSS in which operation is affected by weather conditions.

Mahmoud et al. [65] Investigated a CSS comprising two units, incorporating complex maintenance policies such as periodic inspections, rest periods, replacements, setup times, and dual repair modalities. An expert repairman and his assistant were used in the analysis of a two-unit CSS by Kumar et al. [52] [53] . If the second unit fails while an experienced repairer is engaged in fixing the first, his assistant fixes it. Gopalan and Kumar [38] analyzed an n-unit CSS with a single repair facility using clustering and cutting the state space approximation methods with arbitrary distribution. Various state probabilities corresponding to different initial conditions are obtained using semi-regenerative phenomena.

Mokaddis et al. [73] deal with a two dissimilar unit CSS with random units working in two different modes. Smith [104] considers a 1 out of n repairable system with cold standby. Failed units can be replaced by spare units to reduce system downtime, followed by an approximation method and general failure and repair time distribution. Sridharan and Mohanavadivu [106] examined the behaviour of a 2-unit CSS with two different types of repairmen with the awareness that repairmen might not be able to complete a different repair within a reasonable amount of patience time. Zhang [136] examined a repairable CSS consisting of two identical components parts and a single repairman and found the best replacement policy to solve the problem requires maximizing the long-run expected benefit per unit of time. Chandrasekhar and Natarajan [23] investigated a repairable n-unit system operating in a random environment. The system's performance is governed by a Markov process, which determines the required number of units for satisfactory operation. Coit and Liu [25] proposed a methodology for solving the RAP in a series system composed of multiple k-out-of-n subsystems, aiming to identify the optimal solution. This issue had not yet been satisfactorily resolved, and the suggested approach provides the capacity to address a wider variety of engineering design issues. Rizwan et al. [94] [95] analyzed a two-unit CSS, which can operate in four possible modes with the assumption that whenever the operative unit fails, partially or directly, it goes under repair, and the standby unit is switched off immediately, and the repair facility, where the repairman tired after some random time and then his assistant did the remaining repair of the failed unit.

Wang and Loman [126] studied the general electric company suggested and developed an on-site power plant with N active generators and backup generator(s) in standby to create an incredibly reliable power source, where $k < N$ generators may supply enough power. Khaled and Mohamed [29] discussed a two-unit CSS with a single repair facility, the operative and standby units are switched out at random intervals with preventive maintenance. Vanderperre [119] provided an overview of the reliability of a renewable system with comprising cold standby units serviced by a single repairman. The specific scenario of deterministic failures yields an explicit

exact result for the survival function of the duplex system.

Papageorgiou and Kokolakis [80] studied a $(2, n-2)$ parallel CSS where two units begin to operate simultaneously, and any one of them is instantly replaced by one of the $(n-2)$ warm standby on failure. They presumptively have n different, irreparable units available. Yu et al. [132] examined a CSS consisting of two similar components. Through probability analysis, they defined the system's cost rate as the optimization objective and treated the system's availability as a constraint. Zhang and Wang [137] investigated a cold standby repairable system with two different components with exponential distribution, and one unit is given priority in use. Some reliability indices are derived using geometric processes and supplementary variable techniques. Tavakkoli-Moghaddam et al. [114] developed a genetic algorithm-based framework to optimize redundancy allocation in series-parallel systems, by combining active and cold-standby redundancy strategies at the subsystem level. Azaron et al. [10] applied a genetic algorithm to optimize the reliability of a CSS consisting of k dissimilar, non-repairable units, addressing multiple conflicting objectives.

Bhatti et al. [17] examined a single repairman and two identical units of CSS using the concept of inspection policy for detecting the kind of failures (major and minor) before the failed unit gets repaired. Moghaddass et al. [72] explored the trade-off between optimal design and maintenance strategies for a repairable multi-state system composed of binary-state components. Chambari et al. [21, 22] developed a bi-objective model for the RAP in series-parallel systems, allowing both active and cold-standby redundancy techniques and further examined reliability allocation in non-repairable systems, applying a simulated annealing algorithm to solve large-scale problems efficiently. Levitin et al. [57] examined the 1-out-of-N: G heterogeneous CSS optimal standby component sequencing issue. Montoro-Cazorla and Perez Ocon [75] considered a system with n components, one online unit, and multiple cold standby units, with failed units being repairable. The Markov process that governs the system is built and analyzed in a transient and stationary domain, and the availability, reliability & failure rate are all computed. Manocha and Taneja [110] proposed a stochastic modeling approach for a 2-unit CSS, accounting for uncertain failure times and a two-phase repair strategy.

Malhotra and Taneja [68] assessed the performance of single-unit and two-unit CSS in a cable manufacturing plant, examining their reliability and efficiency under varying demand conditions, while Taneja et al. [111] extended this analysis by incorporating scheduled maintenance into the single-unit system and allowing both units in the cold standby to operate based on demand. Gupta [39, 40] analyzed single-unit and CSS, examining the effects of two different repairman types and resume/repeat policies, and further compared reliability models for CSS with one or two units, incorporating two types of repairmen and three distinct repair procedures. Batra and Taneja [11] developed four models for a system with two operational units and no/one/two and three standby units, respectively. By comparing the models, the number of standby units is optimized. Sharifi and Taghipour [100] explored the optimal inspection scheduling for a k-out-of-n system with non-identical components, utilizing a matrix-based method to determine system state transition probabilities and minimize expected total cost, while ensuring reliability.

Behboudi et al. [14] developed an innovative switching policy for two-unit CSS based on virtual age, showing that this approach significantly improves unit performance and system reliability in scenarios with increasing failure rates. Manocha et al. [70] examined a two non-identical unit CSS; the standby unit can be randomly checked to see if it is worth using or not, and a sensitivity analysis about MTSF and availability has also been performed. Wang et al. [120] developed effective approximation techniques, utilizing the central limit theorem, for reliability evaluation of k-out-of-n CSS, accommodating position-dependent component lifespan distributions. Chaudhary et al. [24] investigated a dual-unit system with one operational unit and one cold standby unit, assuming both units are identical. If any units fail after the first repair, they are replaced with a new unit with a single repairman facility. Raghuvanshi et al. [90] presented a cost-benefit analysis for a redundant system with two identical units in cold standby, accounting for minor and major failures, and continuous availability of two repair personnel. Lin et al. [59] discussed a hybrid subset simulation method paired with limit state equations for series-parallel

CSS. Kumar and Sharma [51] relate the reliability measures analysis of two identical unit systems with a reboot facility. They assume that during unsafe failure, repair activity cannot be done immediately but first rebooting is done to transform unsafe failure into safe failure, and then repair activity is performed as usual.

4. Warm Standby Redundant systems

In warm standby systems, the redundant components are partially powered and in a pre-operational state, ready to take over the operation if the primary component fails. In contrast to CSS, which feature completely inactive backup components, warm standby components are partially powered and functional. The standby components in warm standby systems can be activated more quickly than those in. As a result, the switchover time from the operative unit to the standby unit is significantly reduced, thereby reducing downtime and improving overall system reliability. Rapid availability of standby components ensures that the system can quickly recover from failures, minimizing the impact on system operation. Warm standby systems offer a cost-effective compromise between cold standby and hot standby systems. Although they are more expensive to operate than CSS due to the partial power consumption, they are generally more cost-effective than hot standby systems. This type of redundant system is often employed in critical applications where downtime must be minimized. Industries such as telecommunications, data centers, and emergency response systems commonly use warm standby configurations. Alidrisi and Mustafa [2] presented a recursive approach to compute the reliability of a dynamic WSS consisting of n components, accounting for imperfect switching mechanisms and constant failure rates, and confirmed its accuracy through verification with established special cases.

Goel and Shrivastava [35] analyzed a 2-unit WSS assuming a bivariate exponential density and investigated the system's stochastic behavior and reliability characteristics. Mahmoud and Esmail [66, 67] analyzed the reliability of a two-unit WSS, considering failures due to both hardware malfunctions and human errors and further investigated the impact of a slow switch susceptible to these failures in such systems. Mokaddis et al. [74] investigated the reliability analysis of a two-unit WSS consisting of a priority unit and an ordinary unit, where a priority unit passes through different operative stages before it fails. Sridharan and Mohanavadivu [105] presented a cost analysis for a non-repairable standby system consisting of (n+m) identical units, evaluating the economic implications of the system. n units are needed for the system to function, while the remaining m units are warm standbys. Tuteja et al. [117] analyzed a 2-unit WSS with repairman waiting time, considering a dual-failure mechanism where units can transition to complete failure either directly or via an intermediate partial failure state. Arulmozhi [9] analyzed the system reliability of an M-out-of-N WSS with R repairmen to replace the failed components, and a closed-form equation was created. Additionally, the results of hot and CSS without repairmen are derived as special cases. Wang et al. [123, 125] conducted reliability and sensitivity analyses of complex repairable systems. In the first study, they examined a system with M operating machines, S warm standbys, and a repairable service station, analyzing the K-out-of-(M+S) system for different values of K and deriving expressions for system reliability and mean time to first failure (MTFF). In the second study, they investigated a repairable system with imperfect coverage, focusing on the impact of service pressure, where repairmen facing large queues could increase the repair rate to reduce the queue length.

Wang and Chiu [122] presented a steady-state availability analysis for three WSS models, accounting for imperfect fault coverage. The results are compared numerically, considering the impact of parameter values and the cost trade-offs between active and standby units. Perez Ocon and Montoro Cazorla [88] investigated warm standby n-unit systems with one operational unit and a single repairman facility, calculating availability, failure occurrence rates, and other relevant metrics. Srinivasan and Subramanian [107] developed a comprehensive model of a WSS consisting of three units and a single repair facility, to evaluate system reliability and performance. and by identifying certain regenerative points they have obtained, in principle, the reliability and availability function. Wang and Chen [121] compared the availability of three systems for

three repair time distributions: exponential, gamma, and uniform with reboot delay and standby switching failures using the supplementary variable technique. Papageorgiou and Kokolakis [81] studied a $(2, n-2)$ parallel WSS where two units begin operating simultaneously, and any one of them is instantly replaced by one of the $(n-2)$ warm standby upon failure. They presumptively have n different, irreparable units available.

Eryilmaz [30] investigated the number of surviving warm standby components in a coherent system at the point of failure. The expected number of active warm standby components was utilized to establish the optimal initial allocation of standby components, aiming to minimize the expected total cost. Zhai et al. [135] introduced a novel binary decision diagram-based methodology for evaluating the reliability of k-out-of-(n+k) WSS, incorporating fault level coverage and enabling efficient analysis of complex system configurations. Aote et al. [5] presented the concept of particle S warm optimization, and work carried out on PSO by different researchers. Wells [127] examined an n-unit system with a single warm standby. Individual components may fail repair, but the entire system may break irreparably at some finite but random period in the future.

Ruiz-Castro [96] discussed a complex K-unit system, where one unit is online while the others are on warm standby, facing various types of failures. Utilized a discrete-time marked Markovian arrival process (DMAP) to represent and analyze preventive maintenance activities with an indefinite number of repair personnel. Delia and Rafael [76] considered a system with n components, one online and the rest on warm standby subject to repair, and extended many other systems due to the generality of the Markovian arrival process. Jia et al. [44, 45, 46] explored various reliability aspects of two-unit standby systems, including an active repair-free switching policy, demand-based WSS accounting for component deterioration and start failure, and developed an analytical method using a multistate decision diagram to assess reliability considering the activation probabilities of standby units.

Bhatia et al. [16] examined a three-unit induced draft fan system installed in boilers used in thermal power plants through a probabilistic analysis. Three induced draft fans are installed in the boiler under consideration: two are operational, and one is warm standby redundancy. Finkelstein et al. [31] proved that for a 1-out-of-n WSS, the optimal component activation sequence corresponds to arranging components in ascending order of their expected lifetimes, thereby maximizing system efficiency. Hadipour et al. [42] Introduced a new mathematical framework to analyze and optimize systems utilizing repairable components, where the subsystem can use both active and warm standby strategies simultaneously by series-parallel elements. Liu et al. [62] considered a warm standby n-unit system under N-policy with one repairman taking multiple vacations. Here, the system is analyzed by two methods: first, a Markov process, and second, matrix-analytical approaches. Yen et al. [130] investigated and compared four retrial systems with warm standby units, imperfect coverage, and exponentially distributed repair times, evaluating their cost-effectiveness and benefits.

Yang and Wu [129] presented a Markovian analysis to evaluate the availability and reliability of a repairable system with warm standby components, considering switching failures and a single repair facility. Levitin et al. [58] contributed by modeling and optimizing the replacement and maintenance schedule (RMS) for a heterogeneous dual-unit WSS to reduce the total predicted mission cost, which includes operation, standby, and maintenance costs as well as mission failure penalty costs. Juybari [47] studied a 1-out-of-n: G repairable WSS using a mixed redundancy method under environmental shocks. Kumar and Kumar [54] analyzed the behaviour of the parallel model with one operative and one warm standby unit with two repairman facilities. Bhat and Simon [18] investigated a two-unit warm standby redundant system, considering the impact of varying repair facility efficiency, equivalently, repair capacity decreases upon each repair.

5. Hot Standby Redundant systems

In hot standby systems, the redundant components are continuously powered and fully operational, running in parallel with the primary component. Facilitates seamless switching to the

standby component, minimizing downtime in the event of primary component failure. Hot standby systems feature near-instantaneous activation of the standby component, ensuring minimal downtime. As the standby component is already operational, the transition from primary to standby operation occurs immediately upon primary component failure, resulting in minimal to no downtime. The continuous operation of the redundant components ensures that the system can with stand component failures without any disruption in performance. Hot standby redundant systems are commonly used in mission-critical applications where uninterrupted operation is paramount. Examples include air traffic control systems, power distribution grids, and emergency response centers. This type of standby system consumes more resources, including power and maintenance efforts, due to the continuous operation of redundant components. This higher utilization of resources comes with increased operational costs. The Continuous operation of the standby components requires regular testing and maintenance to ensure their readiness. Taneja [113] presented and analyzed two reliability models for a HSS consisting of two identical units. In the second model, the failures of the units are immediately observed, whereas in the first model, a unit's failure is not self-revealed and is only identified when both units fail. Duhan et al. [28] presented a reliability analysis of a two-unit hot standby PLC system, considering corrective and preventive maintenance, and two repair scenarios, to evaluate system performance and reliability.

Tuteja et al. [115] dealt with a two-unit HSS where programmable logic controllers are used as hot-standby which fail with lower failure of the operative unit and three types of failure - minor, major (repairable), and major (irreparable). Parashar and Taneja [85] analyzed a system wherein two PLCs are working in a master-slave fashion. The master unit has the priority of operation and repair over the slave unit with three types of failure: minor, major-repairable, and major-irreparable. Rizwan et al. [93] offered a reliability analysis of a two-unit hot standby PLC system using data gathered from an industry where various failure types are documented and modeled. Singh et al. [103] Examined a database system consisting of a primary database and a hot standby database unit, which utilizes online archive redo log transfers for real-time replication. Manocha et al. [71] proposed a stochastic model characterized by discrete state space and continuous time to analyze a system comprising a primary unit and a hot standby database unit, considering multiple failure modes. Batra and Taneja [11] [13] developed three models for a system with one/two operational units and no/one/two hot standby units. The models are compared to determine the optimal number of hot standby units to utilize.

6. Mixed Standby Redundant systems

The term "mixed" implies that the redundant components or subsystems are not identical. They might have different designs, specifications, or functionalities. This approach can be cost-effective and allows for flexibility in choosing components based on specific requirements. The primary goal of mixed standby redundant systems is to enhance fault tolerance. By having diverse components as backups, the system can better withstand failures or faults in individual elements. Implementing mixed standby redundancy involves a balance between the cost of redundant components and the potential benefits in terms of increased reliability and fault tolerance. A cost-benefit analysis helps to determine the most suitable approach for a given application. Mixed standby redundant systems are commonly used in critical infrastructure, aerospace, industrial automation, telecommunications, and other sectors where reliability and continuous operation are paramount. Jacob et al. [43] examined the reliability evaluation of a repairable two-unit standby system with deterioration, considering the impacts of human error and common cause failure on system performance.

Wang and Kuo [124] deal with the availability and reliability characteristics of four different series system configurations with cold and warm standby components; also, MTTF availability for four configurations is obtained, and comparisons are made. Rao and Gupta [92] studied the M/G/1 machine repairable problem, which consists of K working machines and Y spare machines, which are classified as being either cold, warm, or hot standby, and a single repairman, is modeled and analyzed using supplementary variable techniques. Sarhan [98] determined

the reliability equivalence factors of a series system consisting of n independent, non-identical components with exponential failure distributions. Chakravarthy et al. [20] investigated a k-out-of-n reliability system in which a single faulty server maintains n identical components. De Smidt-Destombes [26] investigated the relationship between repair capacity, spare part inventories, and preventive maintenance policies for a k-out-of-N system and analyzing its reliability and availability. Papageorgiou and Kokolakis [79] studied a (2,n-2) parallel system where two units begin operating simultaneously, and any one of them is instantly replaced by one of the (n-2) standbys upon failure. They presumptively have n different, irreparable units available. Gen and Yun [33] provided a brief overview of GA-based approaches for several reliability optimization problems, including bicriteria reliability optimization with fuzzy goals, and introduced hybrid approaches for combining GA with fuzzy logic.

Kokolakis and Papageorgiou [50] focused on the evaluation of system reliability using recursive relation and optimization of starting times for non-identical, non-repairable units with at most n units in parallel even through a single unit is sufficient and also provides analytical results for some special distribution and moderate value of n. Cha et al. [19] developed a comprehensive framework for modeling standby systems, including cold, hot, and warm standby scenarios, assuming exponential distributions for unit lifetimes, and deriving various system performance measures. Yun and Cha [134] considered a two units standby system, where the first unit begins operating and the second unit is initially in the cold standby state. If the operating unit fails, the second unit is switched from warm standby to active after a certain period called switching time has passed, and if the first unit fails before this time, the system fails.

Mahato et al. [64] addressed the reliability-redundancy optimization problem by treating the reliability of each component as an interval-valued number. This involves choosing components with various redundancy levels that maximize system reliability. Gupta and Gupta [41] examined a reliability model's profitability analysis for a single-unit system that includes inspection, replacement, repair, and preventive maintenance. Sharma and Kaur [101] analyzed the possibility of finding an operational compressor unit in a milk processing facility with various types of failures: serviceable, repairable, and replaceable. Malhotra and Taneja [69] analyzed the comparison of two stochastic models of a cable manufacturing plant subjected to inspection and scheduled maintenance with reinstallation/reconditioning failure and replacement failure. Ardakan et al. [7] discussed optimizing the RAP using a mixed redundancy strategy in a system to improve its reliability by offering greater flexibility to system designers.

Ke et al. [49] looked into a solution for fixing machines that had common failures with standby switching and average repair timeframes. Kayedpour et al. [48] discussed the RAP in repairable systems, developing a methodology to optimize system reliability and availability, considering the selection of configuration strategies such as parallel, warm, and cold standby subsystems. Gholinezhad and Hamadani [34] discussed the redundant allocation problem and proposed a new model that allows for component mixing, where different types of components can be used in each subsystem. The objective of the RAP is to optimize system reliability while satisfying key constraints, including budget limitations, weight restrictions, and spatial considerations.

Taj et al. [109] estimated various reliability indices by analyzing a 3-unit cable plant subsystem. Peiravi et al. [86, 87] addressed the RAP in reliability optimization by introducing the K-mixed redundancy strategy, which combines active and standby approaches. They developed a genetic algorithm to solve the problem and compared the results with previous studies' results. Additionally, they created a mathematical model based on a Markov approach to evaluate its effectiveness in a series-parallel system, again using a genetic algorithm and comparing the results with previous work. Taj et al. [108] compared the profit results of three reliability models for a building cable production facility. To estimate optimized reliability indices of the plant semi-Markov process and regenerative point techniques are used. Ruiz-Castro and Juan [97] investigated the reliability of a k-out-of-n system with n initial units, where units are susceptible to internal failures (repairable and non-repairable), external shocks, and random inspections, with arrivals modeled by a Markovian arrival process.

Golmohammadi and Ardakan [37] presented a reliability model for a system composed of

active and standby units with the standby once proven to degradation by adopting periodic inspection and preventive maintenance policy. Ardakan et al. [6, 8] introduced a novel standby strategy structure that allows a component to begin operation at a predefined time without a switching system, while also optimizing the activation sequence of units in the subsystem by focusing on the genetic algorithm's encoding process, objective function, crossover, and mutation through various strategies, including active, standby, mixed, and K-mixed. Liu et al. [63] proposed a three-component repairable system under a K-mixed redundancy strategy with unreliable switching failure.

Parveen et al. [82, 83, 84] establish a reliability model considering one operative unit and N cold/warm /hot standby unit with the concept of activation and switching time and optimize the number of standby units for N=1,2 and 3. Saxena et al. [99] discussed a two non-identical unit parallel system to analyze the classical and Bayesian estimation of various measures of system effectiveness with a single repairable facility. Yadav et al. [128] examined a repairable system consisting of four non-identical units, employing the Markov approach to evaluate system reliability and availability. The reliability metrics for the system have been obtained by solving the Chapman-Kolmogorov equations using Laplace transformation techniques. Gao [32] discussed the analysis and optimization of repairable systems and different redundancy strategies, including mixed redundancy and K-mixed redundancy with dependent failures and variable repair rates, and provided the steady-state distribution, reliability analysis, and transient availability analysis of the system using Markov renewal theory. Alkaff [3] looked at broad standby systems with numerous primary and backup systems. Every single primary runs at a uniform warmness level of one. Every backup runs at a warmness level that can be adjusted: the levels go from (cold to hot standby) with intermediate values denoting warm standby. Li et al. [61] examined reliability analysis and phased mission systems optimization for backup/rescue operations and mixed redundancy strategies. Munda and Taneja [77] analyzed a system comprised of one operative unit, one cold and one warm standby unit and obtained various measures of system effectiveness. Qi et al. [89] proposed an innovative maintenance strategy for a two-component WSS, incorporating both cold and warm standby states to optimize system performance and availability. Oszczypala et al. [78] utilized a hybrid approach, combining genetic algorithms with continuous-time Markov chain modeling, to optimize redundancy allocation in series systems with k-out-of-n subsystems, focusing on maximizing system availability.

7. Conclusion

An attempt has been made to provide a brief overview of earlier works in each field and has included some of the most well-known publications in the literature for each classification so that interested readers can refer to them and locate additional relevant publications to thoroughly examine. The present research investigates and optimizes three types of redundancy optimization problems from different perspectives, including cold, warm, and hot standby redundancy in repairable and non-repairable systems.

References

[1] Alaswad, S. and Xiang, Y. (2017). A review on condition-based maintenance optimization models for stochastically deteriorating system. *Reliability engineering & system safety*, 157:54–63.

[2] Alidrisi, M. M. (1992). The reliability of a dynamic warm standby redundant system of n components with imperfect switching. *Microelectronics Reliability*, 32(6):851–859.

[3] Alkaff, A. (2023). Optimum warmness levels in general standby systems. *Reliability Engineering & System Safety*, 237:109366.

[4] Amin, M. T., Khan, F., and Zuo, M. J. (2019). A bibliometric analysis of process system failure and reliability literature. *Engineering Failure Analysis*, 106:104152.

[5] Aote, S. S., Raghuwanshi, M., Malik, L., et al. (2013). A brief review on particle swarm optimization: limitations & future directions. *International Journal of Computer Science Engineering (IJCSE)*, 14(1):196–200.

[6] Ardakan, M. A., Amini, H., and Juybari, M. N. (2022). Prescheduled switching time: A new strategy for systems with standby components. *Reliability Engineering & System Safety*, 218:108188.

[7] Ardakan, M. A., Hamadani, A. Z., and Alinaghian, M. (2015). Optimizing bi-objective redundancy allocation problem with a mixed redundancy strategy. *ISA transactions*, 55:116–128.

[8] Ardakan, M. A., Talkhabi, S., and Juybari, M. N. (2022). Optimal activation order vs. redundancy strategies in reliability optimization problems. *Reliability Engineering & System Safety*, 217:108096.

[9] Arulmozhi, G. (2002). Reliability of an m-out-of-n warm standby system with r repair facilities. *Opsearch*, 39:77–87.

[10] Azaron, A., Perkgoz, C., Katagiri, H., Kato, K., and Sakawa, M. (2009). Multi-objective reliability optimization for dissimilar-unit cold-standby systems using a genetic algorithm. *Computers & Operations Research*, 36(5):1562–1571.

[11] Batra, S. and Taneja, G. (2018). Optimization of number of hot standby units through reliability models for a system operative with one unit. *International Journal of Agricultural and Statistical Sciences*, 14(1):365–370.

[12] Batra, S. and Taneja, G. (2018). Reliability and optimum analysis for number of standby units in a system working with one operative unit. *International Journal of Applied Engineering Research*, 13(5):2791–2797.

[13] Batra, S. and Taneja, G. (2019). Reliability modeling and optimization of the number of hot standby units in a system working with two operative units. *Compusoft*, 8(2):3059–3068.

[14] Behboudi, Z., Borzadaran, G. M., and Asadi, M. (2021). Reliability modeling of two-unit cold standby systems: a periodic switching approach. *Applied Mathematical Modelling*, 92:176–195.

[15] Bhat, K. S. and Gururajan, M. (1993). A two-unit cold standby system with imperfect repair and excessive availability period. *Microelectronics Reliability*, 33(4):509–512.

[16] Bhatia, P., Naithani, A., Parashar, B., and Taneja, G. (2012). Reliability modelling of a 3-unit (induced draft fan) cold standby system working at full/reduced capacity. *International Journal of Mathematical Archive*, 3(10):3737–3744.

[17] Bhatti, J., Chitkara, A., and Bhardwaj, N. (2011). Profit analysis of two unit cold standby system with two types of failure under inspection policy and discrete distribution. *International Journal of science and engineering research*, 2(2):1–7.

[18] Bhat, K. S. and Simon, M. K. (2024). Stochastic analysis of a complex repairable system with a constrain on the number of repairs. *Reliability: Theory & Applications*, 19(2 (78)):178–187.

[19] Cha, J. H., Mi, J., and Yun, W. Y. (2008). Modelling a general standby system and evaluation of its performance. *Applied Stochastic Models in Business and Industry*, 24(2):159–169.

[20] Chakravarthy, S. R., Krishnamoorthy, A., and Ushakumari, P. (2001). A k-out-of-n reliability system with an unreliable server and phase type repairs and services: the (n, t) policy. *Journal of Applied Mathematics and Stochastic Analysis*, 14(4):361–380.

[21] Chambari, A., Najafi, A. A., Rahmati, S. H. A., and Karimi, A. (2013). An efficient simulated annealing algorithm for the redundancy allocation problem with a choice of redundancy strategies. *Reliability Engineering & System Safety*, 119:158–164.

[22] Chambari, A., Rahmati, S. H. A., Najafi, A. A., et al. (2012). A bi-objective model to optimize reliability and cost of system with a choice of redundancy strategies. *Computers & industrial engineering*, 63(1):109–119.

[23] Chandrasekhar, P. and Natarajan, R. (1999). A study of an n-unit system operating in a random environment. *Reliability Engineering & System Safety*, 66(3):223–226.

[24] Chaudhary, A., Jaiswal, S., and Sharma, N. (2023). Probabilistic analysis of a two unit cold standby system with repair and replacement policies. *Reliability: Theory & Applications*, 18(1 (72)):56–64.

[25] Coit, D. W. and Liu, J. C. (2000). System reliability optimization with k-out-of-n subsystems. *International Journal of Reliability, Quality and Safety Engineering*, 7(02):129–142.

[26] de Smidt-Destombes, K. S., van der Heijden, M. C., and van Harten, A. (2004). On the availability of a k-out-of-n system given limited spares and repair capacity under a condition based maintenance strategy. *Reliability engineering & System safety*, 83(3):287–300.

[27] Dekker, R. (1996). Applications of maintenance optimization models: a review and analysis. *Reliability engineering & system safety*, 51(3):229–240.

[28] Duhan, M., Batra, S., Mittal, C., and Taneja, G. (2004). Probablistic analysis of two unit cold standby plc system with preventive/corrective maintenance with two types of repair. *J. Indian Soc. Stat. Opers. Res*, 25(1-4):15–24.

[29] El-Said, K. M. and El-Sherbeny, M. S. (2005). Profit analysis of a two unit cold standby system with preventive maintenance and random change in units. *Journal of mathematics and statistics*, 1(1):71–77.

[30] Eryilmaz, S. (2011). The behavior of warm standby components with respect to a coherent system. *Statistics & probability letters*, 81(8):1319–1325.

[31] Finkelstein, M., Hazra, N. K., and Cha, J. H. (2018). On optimal operational sequence of components in a warm standby system. *Journal of Applied Probability*, 55(4):1014–1024.

[32] Gao, S. (2023). Reliability analysis and optimization for a redundant system with dependent failures and variable repair rates. *Mathematics and Computers in Simulation*, 208:637–659.

[33] Gen, M. and Yun, Y. (2006). Soft computing approach for reliability optimization: State-of-the-art survey. *Reliability Engineering & System Safety*, 91(9):1008–1026.

[34] Gholinezhad, H. and Hamadani, A. Z. (2017). A new model for the redundancy allocation problem with component mixing and mixed redundancy strategy. *Reliability Engineering & System Safety*, 164:66–73.

[35] Goel, L. and Shrivastava, P. (1992). A warm standby redundant system with correlated failures and repairs. *Microelectronics Reliability*, 32(6):793–797.

[36] Goel, L. and Tyagi, V. K. (1992). A two unit priority redundant system with three modes and correlated failures and repairs. *Microelectronics Reliability*, 32(10):1367–1372.

[37] Golmohammadi, E. and Ardakan, M. A. (2022). Reliability optimization problem with the mixed strategy, degrading components, and a periodic inspection and maintenance policy. *Reliability Engineering & System Safety*, 223:108500.

[38] Gopalan, M. and Kumar, U. D. (1996). Approximate analysis of n-unit cold-standby systems. *Microelectronics Reliability*, 36(4):505–509.

[39] Gupta, R. (2017). Stochastic analysis of a reliability model for one-unit system with three types of repair policy. *Int. J. Stat. Appl. Math*, 2:126–130.

[40] Gupta, R. (2018). Pairwise comparative analysis of reliability models for one unit system and two unit cold stand by system with three types of repair policy.

[41] Gupta, S. and Gupta, S. K. (2013). Stochastic analysis of a reliability model of one-unit system with post inspection, post repair, preventive maintenance and replacement. *International Journal of Mechanical Engineering and Robotics Research*, 2(2):178–188.

[42] Hadipour, H., Amiri, M., and Sharifi, M. (2019). Redundancy allocation in series-parallel systems under warm standby and active components in repairable subsystems. *Reliability Engineering & System Safety*, 192:106048.

[43] Jacob, M., Narmada, S., and Varghese, T. (1997). Analysis of a two-unit deteriorating standby system with repair. *Microelectronics Reliability*, 37(5):857–861.

[44] Jia, H., Ding, Y., Peng, R., Liu, H., and Song, Y. (2020). Reliability assessment and activation sequence optimization of non-repairable multi-state generation systems considering warm standby. *Reliability Engineering & System Safety*, 195:106736.

[45] Jia, H., Ding, Y., Peng, R., and Song, Y. (2017). Reliability evaluation for demand-based warm standby systems considering degradation process. *IEEE Transactions on Reliability*, 66(3):795–805.

[46] Jia, X., Chen, H., Cheng, Z., and Guo, B. (2016). A comparison between two switching policies for two-unit standby system. *Reliability engineering & system safety*, 148:109–118.

[47] Juybari, M. N., Hamadani, A. Z., and Ardakan, M. A. (2023). Availability analysis and cost optimization of a repairable system with a mix of active and warm-standby components in a shock environment. *Reliability Engineering & System Safety*, 237:109375.

[48] Kayedpour, F., Amiri, M., Rafizadeh, M., and Nia, A. S. (2017). Multi-objective redundancy allocation problem for a system with repairable components considering instantaneous availability and strategy selection. *Reliability Engineering & System Safety*, 160:11–20.

[49] Ke, J.C., Liu, T.H., and Yang, D.Y. (2016). Machine repairing systems with standby switching failure. *Computers & Industrial Engineering*, 99:223–228.

[50] Kokolakis, G. and Papageorgiou, E. (2006). Scheduling starting times for an active redundant system with non-identical lifetimes. *Applied mathematical modelling*, 30(12):1535–1545.

[51] Kumar, A. and Sharma, A. (2024). Profit analysis of repairable cold standby system subject to reboot facility under refreshments. *Reliability: Theory & Applications*, 19(2 (78)):594–603.

[52] Kumar, A., Gupta, S., and Taneja, G. (1996). Comparative study of the profit of a two server system including patience time and instruction time. *Microelectronics Reliability*, 36(10):1595–1601.

[53] Kumar, A., Gupta, S. K., and Taneja, G. (1995). Probabilistic analysis of a two-unit cold standby system with instructions at need. *Microelectronics Reliability*, 35(5):829–832.

[54] Kumar, M. and Kumar, S. (2023). Stochastic analysis of discrete parametric markov chain system model. *Reliability: Theory & Applications*, 18(1 (72)):454–463.

[55] Kuo, W. and Prasad, V. R. (2000). An annotated overview of system-reliability optimization. *IEEE Transactions on reliability*, 49(2):176–187.

[56] Kuo, W. and Wan, R. (2007). Recent advances in optimal reliability allocation. *IEEE Transactions on Systems, Man, and Cybernetics-Part A: Systems and Humans*, 37(2):143–156.

[57] Levitin, G., Xing, L., and Dai, Y. (2013). Cold-standby sequencing optimization considering mission cost. *Reliability Engineering & System Safety*, 118:28–34.

[58] Levitin, G., Xing, L., and Dai, Y. (2022). Minimum cost replacement and maintenance scheduling in dual-dissimilar-unit standby systems. *Reliability Engineering & System Safety*, 218:108127.

[59] Lin, Z., Tao, L., Wang, S., Yong, N., Xia, D., Wang, J., and Ge, D. (2024). A subset simulation analysis framework for rapid reliability evaluation of series-parallel cold standby systems. *Reliability Engineering & System Safety*, 241:109706.

[60] Li, X. and Ding, W. (2013). On allocation of active redundancies to systems: a brief review. *Stochastic orders in reliability and risk: In honor of Professor Moshe Shaked*, pages 235–254.

[61] Li, X.Y., Li, X., Feng, J., Li, C., Xiong, X., and Huang, H.-Z. (2023). Reliability analysis and optimization of multi-phased spaceflight with backup missions and mixed redundancy strategy. *Reliability Engineering & System Safety*, 237:109373.

[62] Liu, B., Wen, Y., Kang, S., and Qiu, Q. (2020). A multiple warm standby repairable system under n-policy with multiple vacations following markovian arrival process. *Communications in Statistics-Theory and Methods*, 49(15):3609–3634.

[63] Liu, B., Wen, Y., Qiu, Q., Shi, H., and Chen, J. (2022). Reliability analysis for multi-state systems under k-mixed redundancy strategy considering switching failure. *Reliability Engineering & System Safety*, 228:108814.

[64] Mahato, S. K., Sahoo, L., and Bhunia, A. K. (2012). Reliability-redundancy optimization problem with interval valued reliabilities of components via genetic algorithm. *J Inf Comput Sci*, 7(4):284–295.

[65] Mahmoud, M., El-Din, M. M., and Moshref, M. E.-S. (1995). Reliability analysis of a two-unit cold standby system with inspection, replacement, proviso of rest, two types of repair and preparation time. *Microelectronics Reliability*, 35(7):1063–1072.

[66] Mahmoud, M. and Esmail, M. (1996). Probabilistic analysis of a two-unit warm standby system subject to hardware and human error failures. *Microelectronics Reliability*, 36(10):1565–1568.

[67] Mahmoud, M. and Esmail, M. (1998). Stochastic analysis of a two-unit warm standby system with slow switch subject to hardware and human error failures. *Microelectronics Reliability*, 38(10):1639–1644.

[68] Malhotra, R. and Taneja, G. (2015). Comparative study between a single unit system and a two-unit cold standby system with varying demand. *Springerplus*, 4(1):1–17.

[69] Malhotra, R. and Taneja, G. (2015a). Comparative analysis of two stochastic models subjected to inspection and scheduled maintenance. *International Journal of Software Engineering and Its Applications*, 9(10):179–188.

[70] Manocha, A., Taneja, A. K., and Taneja, G. L. (2022). Reliability and sensitivity analysis of two non-identical unit standby system subject to pre-operation random inspection of standby unit. *Reliability: Theory & Applications*, 17(2 (68)):469–481.

[71] Manocha, A., Taneja, G., and Singh, S. (2017). Stochastic and cost-benefit analysis of two unit hot standby database system. *International Journal of performability engineering*, 13(1):63.

[72] Moghaddass, R., Zuo, M. J., and Pandey, M. (2012). Optimal design and maintenance of a repairable multi-state system with standby components. *Journal of Statistical Planning and Inference*, 142(8):2409–2420.

[73] Mokaddis, G., Tawfek, M., and Elhssia, S. (1997). Analysis of a two-dissimilar unit cold standby redundant system subject to inspection and random change in units. *Microelectronics Reliability*, 37(2):329–334.

[74] Mokaddis, G., Labib, S., and Ahmed, A. (1997). Analysis of a two-unit warm standby system subject to degradation. *Microelectronics Reliability*, 37(4):641–647.

[75] Montoro-Cazorla, D. and Pérez-Ocón, R. (2014). A redundant n-system under shocks and repairs following markovian arrival processes. *Reliability Engineering & System Safety*, 130:69–75.

[76] Montoro-Cazorla, D. and Pérez-Ocón, R. (2016). A warmstandby system under shocks and repair governed by maps. *Reliability Engineering & System Safety*, 152:331–338.

[77] Munda, L. and Taneja, G. (2023). Combined redundancy optimization for a system comprising operative, cold standby and warm standby units. *Reliability: Theory & Applications*, 18(2 (73)):486–497.

[78] Oszczypała, M., Ziółkowski, J., and Małachowski, J. (2024). Redundancy allocation problem in repairable k-out-of-n systems with cold, warm, and hot standby: A genetic algorithm for availability optimization. *Applied Soft Computing*, 165:112041.

[79] Papageorgiou, E. and Kokolakis, G. (2004). A two-unit parallel system supported by (n- 2) standbys with general and non-identical lifetimes. *International Journal of Systems Science*, 35(1):1–12.

[80] Papageorgiou, E. and Kokolakis, G. (2007). A two-unit general parallel system with (n-2) cold standbys-analytic and simulation approach. *European journal of operational research*, 176(2):1016–1032.

[81] Papageorgiou, E. and Kokolakis, G. (2010). Reliability analysis of a two-unit general parallel system with (n-2) warm standbys. *European Journal of Operational Research*, 201(3):821–827.

[82] Parveen, Singh, D., Taneja, A.K. (2023). Redundancy Optimization of N+1-Unit Cold Standby System Working with a Single Operative Unit with Activation Time, *International Journal of Engineering Trends and Technology*, 71(8), 458-466.

[83] Parveen, Singh, D., Taneja, A.K. (2023). Redundancy Optimization for a System Comprising One Operative Unit and N Warm Standby Units with Switching Time, *International Journal of Agricultural & Statistical Sciences*, 19, 1339-1350.

[84] Parveen, Singh, D., Taneja, A.K. (2023). Redundancy Optimization for a System Comprising One Operative Unit and N Hot Standby Units, *Reliability: Theory & Applications*, 18(4),547–562.

[85] Parashar, B. and Taneja, G. (2007). Reliability and profit evaluation of a plc hot standby system based on a master-slave concept and two types of repair facilities. *IEEE Transactions on reliability*, 56(3):534–539.

[86] Peiravi, A., Ardakan, M. A., and Zio, E. (2020). A new markov-based model for reliability optimization problems with mixed redundancy strategy. *Reliability Engineering & System Safety*, 201:106987.

[87] Peiravi, A., Karbasian, M., Ardakan, M. A., and Coit, D. W. (2019). Reliability optimization of series-parallel systems with k-mixed redundancy strategy. *Reliability Engineering & System Safety*, 183:17–28.

[88] Pérez-Ocón, R. and Montoro-Cazorla, D. (2006). A multiple warm standby system with operational and repair times following phase-type distributions. *European Journal of Operational Research*, 169(1):178–188.

[89] Qi, F.-Q., Wang, Y.-K., and Huang, H.-Z. (2024). Optimal maintenance policy considering imperfect switching for a multi-state warm standby system. *Quality and Reliability Engineering International*, 40(5):2423–2443.

[90] Raghuvanshi, L., Gupta, R., and Chaudhary, P. (2023). A discrete parametric markov-chain system model of a two-unit standby system with two types of repair. *Reliability: Theory & Applications*, 18(1 (72)):527–538.

[91] Ram, M. (2013). On system reliability approaches: a brief survey. *International Journal of System Assurance Engineering and Management*, 4:101–117.

[92] Rao, T. S. and Gupta, U. (2000). Performance modelling of the m/g/1 machine repairman problem with cold-, warm-and hot-standbys. *Computers & Industrial Engineering*, 38(2):251–267.

[93] Rizwan, S., Khurana, V., and Taneja, G. (2010). Reliability analysis of a hot standby industrial system. *International Journal of Modelling and Simulation*, 30(3):315–322.

[94] Rizwan, S. and Taneja, G. (2000). Profit analysis of a system with perfect repair at partial failure or complete failure. *Pure and Applied Mathematika Sciences*, 52(1/2):7–14.

[95] Rizwan, S., Taneja, G., and Tuteja, R. (2000). Comparative study between the profits of two models for a two unit system with rest period of repairman. *Journal of Decision and Mathematical Sciences*, 5(1-3):27–44.

[96] Ruiz-Castro, J. E. (2016). Complex multi-state systems modelled through marked markovian arrival processes. *European Journal of Operational Research*, 252(3):852–865.

[97] Ruiz-Castro, J. E. (2020). A complex multi-state k-out-of-n: G system with preventive maintenance and loss of units. *Reliability Engineering & System Safety*, 197:106797.

[98] Sarhan, A. (2000). Reliability equivalence of independent and non-identical components series systems. *Reliability Engineering & System Safety*, 67(3):293–300.

[99] Saxena, V., Gupta, R., and Singh, B. (2023). Classical and bayesian stochastic analysis of a two unit parallel system with working and rest time of repairman. *Reliability: Theory & Applications*, 18(1 (72)):43–55.

[100] Sharifi, M. and Taghipour, S. (2020). Optimal inspection interval for a k-out-of-n system with non-identical components. *Journal of Manufacturing Systems*, 55:233–247.

[101] Sharma, U. and Kaur, J. (2014). Availability analysis of a standby system with three types of failure categories. *IOSR Journal of Mathematics*, 10(2):23–28.

[102] Singh, S. (1994). On the effect of weather condition in a two unit cold standby system. *Microelectronics Reliability*, 34(10):1681–1684.

[103] Singh, S., Rishi, R., Taneja, G., and Manocha, A. (2013). Reliability and availability analysis of database system with standby unit provided by the system provider. *International journal of soft computing and engineering*, 3(2):235–237.

[104] Smith, M. A. (1997). The up and down time distribution in a 1 out of n system with general life time and repair time distributions. *Reliability Engineering & System Safety*, 55(1):39–50.

[105] Sridharan, V. and Mohanavadivu, P. (1997). A note on the cost analysis of an n-unit system with spares. *Microelectronics Reliability*, 37(5):835–839.

[106] Sridharan, V. and Mohanavadivu, P. (1998). Stochastic behaviour of a two-unit standby system with two types of repairmen and patience time. *Mathematical and computer modelling*, 28(9):63–71.

[107] Srinivasan, S. K. and Subramanian, R. (2006). Reliability analysis of a three unit warm standby redundant system with repair. *Annals of Operations Research*, 143(1):227–235.

[108] Taj, S., Rizwan, S., Alkali, B., Harrison, D., and Taneja, G. (2020). Three reliability models of a building cable manufacturing plant: a comparative analysis. *International Journal of System Assurance Engineering and Management*, 11:239–246.

[109] Taj, S. Z., Rizwan, S., Alkali, B., Harrison, D., and Taneja, G. (2018). Reliability analysis of a 3-unit subsystem of a cable plant. *Advances and Applications in Statistics*, 52(6):413–429.

[110] TANEJA, A. M. G. (2015). Stochastic analysis of a two-unit cold standby system with arbitrary distributions for life, repair and waiting times. *International Journal of Performability Engineering*, 11(3):293.

[111] Taneja, G., Malhotra, R., and Chitkara, A. (2016). Comparative profit analysis of two reliability models with varying demand. *Arya Bhatta Journal of Mathematics and Informatics*, 8(2):305–314.

[112] Taneja, G., Rizwan, S., and Kumar, R. (1992). Profit analysis of a system with perfect repair at partial failure and priority for repair to complete failed unit. *Pure and Applied Mathematika Sciences*, 35(1/2):131–141.

[113] Taneja, A. (2015). Comparative study of two reliability models on a two-unit hot standby system with unannounced failures. *International Journal of Research in Engineering and Applied Sciences*, 5(8):192–200.

[114] Tavakkoli-Moghaddam, R., Safari, J., and Sassani, F. (2008). Reliability optimization of series-parallel systems with a choice of redundancy strategies using a genetic algorithm. *Reliability Engineering & System Safety*, 93(4):550–556.

[115] Tuteja, R., Parashar, B., and Taneja, G. (2005). Analysis of plc hot standby system with single repair facility irrespective of type of failure. *J. Indian Soc. Stat. Opers. Res*, 26(1-4):37–47.

[116] Tuteja, R. and Taneja, G. (1993). Profit analysis of a one-server one-unit system with partial failure subject to random inspection. *Microelectronics reliability*, 33(3):319–322.

[117] Tuteja, R. and Taneja, G. (1992). Cost-benefit analysis of a two-server, two-unit, warm standby system with different types of failure. *Microelectronics reliability*, 32(10):1353–1359.

[118] Vanderperre, E. (1994). A cold standby system with multiple switch-over devices attended by a monitor. *Microelectronics Reliability*, 34(5):921–923.

[119] Vanderperre, E. et al. (2005). On the reliability of a renewable multiple cold standby system. *Mathematical Problems in Engineering*, 2005:269–273.

[120] Wang, C., Wang, X., Xing, L., Guan, Q., Yang, C., and Yu, M. (2023). Efficient reliability approximation for large k-out-of-n cold standby systems with position-dependent component lifetime distributions. *Reliability Engineering & System Safety*, page 109548.

[121] Wang, K.H. and Chen, Y.J. (2009). Comparative analysis of availability between three systems with general repair times, reboot delay and switching failures. *Applied Mathematics and Computation*, 215(1):384–394.

[122] Wang, K.H. and Chiu, L.W. (2006). Cost benefit analysis of availability systems with warm standby units and imperfect coverage. *Applied mathematics and Computation*, 172(2):1239–1256.

[123] Wang, K.H., Ke, J.B., and Lee, W.C. (2007). Reliability and sensitivity analysis of a repairable system with warm standbys and r unreliable service stations. *The International Journal of Advanced Manufacturing Technology*, 31:1223–1232.

[124] Wang, K.H. and Kuo, C.C. (2000). Cost and probabilistic analysis of series systems with mixed standby components. *Applied Mathematical Modelling*, 24(12):957–967.

[125] Wang, K.H., Yen, T.C., and Jian, J.J. (2013). Reliability and sensitivity analysis of a repairable system with imperfect coverage under service pressure condition. *Journal of Manufacturing systems*, 32(2):357–363.

[126] Wang, W. and Loman, J. (2002). Reliability/availability of k-out-of-n system with m cold standby units. In *Annual Reliability and Maintainability Symposium. 2002 Proceedings (Cat. No. 02CH37318)*, pages 450–455. IEEE.

[127] Wells, C. E. (2014). Reliability analysis of a single warm-standby system subject to repairable and nonrepairable failures. *European Journal of Operational Research*, 235(1):180–186.

[128] Yadav, A., Nandal, N., and Malik, S. (2023). Markov approach for reliability and availability analysis of a four unit repairable system. *Reliability: Theory & Applications*, 18(1 (72)):193–205.

[129] Yang, D.Y. and Wu, C.H. (2021). Evaluation of the availability and reliability of a standby repairable system incorporating imperfect switchovers and working breakdowns. *Reliability Engineering & System Safety*, 207:107366.

[130] Yen, T.C. and Wang, K.H. (2020). Cost benefit analysis of four retrial systems with warm standby units and imperfect coverage. *Reliability Engineering & System Safety*, 202:107006.

[131] Yingkui, G. and Jing, L. (2012). Multi-state system reliability: A new and systematic review. *Procedia engineering*, 29:531–536.

[132] Yu, H., Chu, C., Châtelet, Ė., and Yalaoui, F. (2007). Reliability optimization of a redundant system with failure dependencies. *Reliability Engineering & System Safety*, 92(12):1627–1634.

[133] Yuan, L. and Meng, X.-Y. (2011). Reliability analysis of a warm standby repairable system with priority in use. *Applied Mathematical Modelling*, 35(9):4295–4303.

[134] Yun, W. Y. and Cha, J. H. (2010). Optimal design of a general warm standby system. *Reliability Engineering & System Safety*, 95(8):880–886.

[135] Zhai, Q., Peng, R., Xing, L., and Yang, J. (2013). Binary decision diagram-based reliability evaluation of k-out-of-(n+ k) warm standby systems subject to fault-level coverage. *Proceedings of the Institution of Mechanical Engineers, Part O: Journal of Risk and Reliability*, 227(5):540–548.

[136] Zhang, Y. L. (1999). An optimal geometric process model for a cold standby repairable system. *Reliability Engineering & System Safety*, 63(1):107–110.

[137] Zhang, Y. L. and Wang, G. J. (2007). A deteriorating cold standby repairable system with priority in use. *European Journal of Operational Research*, 183(1):278–295.

TWO STAGE FLOW SHOP SCHEDULING PROBLEM INCLUDING PROBABILITY UNDER LR FUZZY NUMBER

Pooja Kaushik[1], Deepak Gupta[2], Sonia Goel[3*]

•

[1,2,3]Department of Mathematics, Maharishi Markandeshwar Engineering College, MaharishiMarkandeshwar (Deemed to be University), Mullana (Ambala), Haryana, India
[1]drtobekaushik2024@gmail.com,[2]guptadeepak@yahoo.co.in, [3*]sonia.mangla14@gmail.com

Abstract

Often known as the hybrid flow shop (HFS), the scheduling of flow shops with several parallel machines per stage is a challenging integrated problem that arises in many real-world scenarios. This study addresses bi stage flow shop scheduling problem involving parallel equipotential machines at each stage, where processing times are characterized as LR-type fuzzy numbers to encapsulate inherent uncertainties. Recognizing the criticality of minimizing the makespan under imprecise conditions, we employ four distinct reference functions to compute fuzzy makespan, thereby offering a diversified perspective on solution robustness. Four distinct fuzzy ranking (reference) functions are employed for defuzzification and comparison. The scheduling problem is solved using a Branch and Bound (B&B) algorithm tailored to accommodate fuzzy parameters and parallel machine constraints. Comparative analyses with an adapted version of branch and bound method are conducted to benchmark performance under varying degrees of fuzziness. Results underscore the efficacy and adaptability of the proposed approach, revealing nuanced improvements in makespan estimation and scheduling performance across varying fuzziness levels. This investigation not only enriches the theoretical landscape of fuzzy scheduling but also provides practical insights for complex manufacturing systems operating under uncertainty. This work not only extends classical scheduling methodologies into the fuzzy domain but also highlights the potential of integrating multiple reference functions within exact solution frameworks. The objective is to minimize the makespan under fuzzy conditions. To handle the fuzziness in processing times, A comparative analysis of the results obtained using each reference function is conducted to evaluate their effectiveness in producing optimal or near-optimal schedules. The study highlights the impact of the choice of reference function on the computational efficiency and solution quality, offering insights for better decision-making in uncertain manufacturing scenarios. These functions serve to transform fuzzy numbers into comparable crisp values, thereby enabling traditional scheduling algorithms to process the data effectively. The focus of this research is to evaluate the impact of each reference function on the scheduling performance and to analyze the variation in results with respect to makespan minimization. The findings offer significant theoretical contributions to fuzzy scheduling literature and practical implications for industries where uncertainty in processing times is a critical factor.

Keywords: flow time (makespan), LR fuzzy number, flow shop scheduling, transportation technique, B&B, scheduling

I. Introduction

Scheduling problems in manufacturing systems continue to attract considerable research attention due to their critical impact on operational efficiency and resource utilization. Among these, the two-stage FSSP, wherein jobs must sequentially pass through two stages equipped with parallel and equipotential machines, represents a class of problems that is both practically relevant and theoretically challenging. While classical approaches often presume deterministic processing times, real-world manufacturing environments are inherently uncertain. To address this, we model processing times as LR-type Fuzzy Numbers, allowing a more accurate representation of vagueness and imprecision intrinsic to production processes.

The foundations of modern scheduling optimization under uncertainty began with classical algorithmic approaches. Brown and Lomnicki [1] applied the B&B algorithm to scheduling problems, introducing an effective exact method for exploring complex solution spaces. Dubois and Prade [2] advanced this framework by detailing arithmetic operations on fuzzy numbers, which would later become critical in modeling uncertain scheduling times and costs. In the same year, Zadeh [3] introduced the groundbreaking concept of fuzzy sets, enabling partial membership functions to model imprecise data, a method far more aligned with real-world complexity than traditional binary logic. McCahon and Lee [4] made a key contribution by applying fuzzy set theory to job sequencing with fuzzy processing times. Their approach captured real-life uncertainty in job durations and demonstrated the practical benefits of using fuzzy modeling in production scheduling. Ishibuchi and Lee [5] further pushed these concepts into practice by formulating a fuzzy FSSP using fuzzy processing times. Giachetti and Young [6] complemented this with a parametric representation of fuzzy numbers, improving computational efficiency and clarity in fuzzy arithmetic operations.

In the early 2000s, Yao and Lin [7] introduced a model that constructed a fuzzy FSS framework grounded in statistical data, linking theoretical fuzzy models to practical industrial observations. Wang and Kuo [8] later proposed a three-parameter fuzzy arithmetic approximation method suitable for applications in fuzzy neural networks, marking the integration of fuzzy logic into AI techniques. Saneeifard [9] focused on ranking LR fuzzy numbers using weighted averaging at various confidence levels, a method useful in job prioritization within fuzzy scheduling. Kaur and Kumar [10] proposed Mehar's method for solving fully fuzzy linear programming problems, tailored for systems with LR fuzzy parameters. Thorani and Shankar [11] developed fuzzy transportation models that applied fuzzy logic to supply chains and logistics. Gupta, Sharma, and Aggarwal [12] tackled two-machine FSSP under a fuzzy environment, incorporating setup time and a single transport facility. Their work demonstrated the real-world feasibility of fuzzy models in production scheduling.

Zhou et al. [13] expanded on fuzzy arithmetic operations for LR fuzzy numbers and applied them to fuzzy programming, supporting the solution of fuzzy optimization problems with improved numerical performance. Gupta, Goel, and Mangla [14] focused on optimizing scheduling in two-stage flow shops with equipotential machines in the first stage, under deterministic assumptions. Gupta and Goel [15] then extended the model by applying the B&B technique under uncertain (fuzzy) conditions at both stages. These studies provided strong evidence for the viability of B&B methods in complex fuzzy scheduling environments. Kaushik, Gupta, and Goel [16] conducted a comparative analysis of B&B with NEH and CDS heuristics for bi-stage fuzzy FSSP, illustrating the balance between solution quality and computational efficiency. Another study by Kaushik, Sonia, Gupta, and Goel [17] compared B&B, genetic algorithms (GA), and the Palmar heuristic in minimizing processing times under fuzzy settings, concluding that hybrid techniques often outperform exact methods in scalability.

II.Preliminaries

I. Fuzzy Set

A fuzzy set, a mathematical representation of a set that allows for vagueness and uncertainty, is defined in equation as $\chi = \{(y, \mu\chi(y)) \mid y \in Y\}$

where χ is the fuzzy set, Y is the set of all possible elements, $\mu\chi(y)$is the membership function, which assigns a degree of membership to each element y in Y.

II. Fuzzy Number

A fuzzy number is a mathematical representation of a numerical value that is uncertain or imprecise, is defined as $\chi = \{(y, \mu\chi(y)) \mid y \in R\}$

where, χ is the fuzzy number, R is the set of real numbers, $\mu\chi(y)$is membership function, which assigns a degree of membership to each real number y.

III. LR Fuzzy Number

A number F =$(a, s, d, g)_{LR}$ is an LR fuzzy number if$\mu_F(x)=\begin{cases} L(\frac{a-x}{d}) & ,x \le a, d > 0 \\ R(\frac{x-s}{g}) & ,x \ge s, g > 0 \\ 1 & ,otherwise \end{cases}$

If a = s then F = $(a, s, d, g)_{LR}$will be converted into F = $(a, d, g)_{LR}$, triangular LR-fuzzy number. Reference functions (L&R) are continuous, non-increasing and defines the left and right shapes of $\mu_F(x)$ respectively and L(0)=R(0) = 1.

Reference functions and their inverses are given in table

Name of Function	**Reference Function**	**Inverse**
Linear	$R_F(x) = \max\{0, 1-x\}$	$R_F^{-1}(x)$=1-β
Power	$R_F(x) = \max\{0, 1-x\}$	$R_F^{-1}(x)=-\sqrt[q]{1-\beta}$
Exponential	$R_F(x) = e^{-qx}, q \ge 1$	$R_F^{-1}(x)=-\frac{(ln\beta)}{q}$
Exponent Power	$R_F(x) = e^{-x^q}, q \ge 1$	$R_F^{-1}(x)=\sqrt[q]{-ln\beta}$
Rational	$R_F(x) = \frac{1}{1+x^q}, q \ge 1$	$R_F^{-1}(x)=\sqrt[q]{\frac{1-\beta}{\beta}}$

IV. $\boldsymbol{\lambda}$ −cut for LR-Fuzzy Number

If F = $(a, s, d, g)_{LR}$is a LR -fuzzy number and $\boldsymbol{\lambda} \in R$, $\boldsymbol{\lambda} \in [0,1]$. Then
$F_k = \{x \in X: \mu_F(x) \ge \lambda\} = a - dL^{-1}(\boldsymbol{\lambda}) + gR^{-1}(\boldsymbol{\lambda})$ is said to the $\boldsymbol{\lambda}$ −cut of F.

V. Yager's Ranking Formula

If F = $(a, s, d, g)_{LR}$is a LR -fuzzy number then $R(F)=\frac{1}{2}[\int_0^1((a - d\,L^{-1}(\boldsymbol{\lambda}))d\boldsymbol{\lambda}+\int_0^1(s + gR^{-1}(\boldsymbol{\lambda}))d\boldsymbol{\lambda}]$
Let F and K be two fuzzy numbers then
1. F>K if R(F)>R(K); 2.F=K if R(F)=R(K); 3. F<K if R(F)<R(K)
Case 1: L(x)= R(x) = max $\{0, 1 - |x|\}$, then $R(F)=\frac{1}{2}[a - \frac{d}{2} + s + \frac{g}{2}]$ (1)

Case 2: L(x)= R(x) = e^{-x}, then R(F)=$\frac{1}{2}[a-d+s+\frac{g}{2}]$ (2)

Case 3: L(x)= max {0,1 − |x|} , R(x) = e^{-x}, then R(F)=$\frac{1}{2}[a-\frac{d}{2}+s+g]$ (3)

Case 4: L(x) = e^{-x}, R(x)= max {0,1 − |x|}, then R(F)=$\frac{1}{2}[a-d+s+\frac{g}{2}]$ (4)

VI. Arithmetic Operation

Let $(a_1, s_1, d_1, g_1)_{LR}$ and $(a_2, s_2, d_2, g_2)_{LR}$ be two LR-fuzzy numbers. Then

- Addition: F+H=$(a_1 + a_2, s_1 + s_2, d_1 + d_2, g_1 + g_2)_{LR}$
- Subtraction: F-H= $(a_1 - s_2, s_1 - a_2, d_1 + g_2, g_1 + d_2)$
- Scalar multiplication: If x>0, x∈R then x × F=$(xa_1, xs_1, xd_1, xg_1)_{LR}$

If x<0, x∈R then x × F=$(xa_1, xs_1, -xd_1, -xg_1)_{LR}$

III. Practical Situation

In pharmaceutical manufacturing, producing tablets involves highly regulated and structured steps. Two of the most critical sequential processes are:

- Stage 1: Granulation and Blending
  This involves preparing the raw materials (active pharmaceutical ingredients and excipients), which are mixed and granulated to form a uniform composition.
- Stage 2: Tablet Compression
  The blended material is compressed into tablets using tablet press machines.

In a large-scale facility, there are multiple granulators/blenders (Stage 1) and multiple tablet presses (Stage 2), all of which are equipotential—that is, they can process any formulation batch with identical performance specifications. These machines are designed to handle a range of products within the same capacity and accuracy levels. The production begins when different batches (jobs), each representing a specific formulation (e.g., a painkiller, an antibiotic, or a vitamin tablet), are queued for processing. Each batch must first go through Stage 1 (granulation and blending). A job scheduler allocates each batch to any available granulator or blender, since all machines are considered equal in capability and speed. As the batches vary in volume or sensitivity, they may require different processing times, which are typically known in advance but may also be estimated using fuzzy logic if there is uncertainty due to raw material variability.

Once a batch is assigned and begins processing in Stage 1, the system keeps track of its progress. When processing is complete, the job transitions to Stage 2 (tablet compression). At this point, the batch enters a waiting buffer if no tablet press is currently available. As soon as one of the presses becomes free, the next available job from the buffer (usually the one that finished earliest or based on a rule like earliest due date) is assigned to it. The compression process then turns the blend into final tablets, completing the production cycle.

In such a tightly regulated environment, traceability and scheduling efficiency are crucial. Delays or bottlenecks at any stage can halt the entire batch processing, affecting production output and compliance with delivery commitments. Additionally, equipment usage must be optimized not just for speed, but also for compliance with cleaning protocols and cross-contamination prevention, which can be incorporated into the model by adding setup times or blocking constraints.



Figure 1: *Tablet production in pharmaceutical manufacturing unit*

IV. Mathematical Formulation

Assume that n jobs are being considered for processing on two different types of parallel equipotential machines, $\hat{S}$ and $\hat{C}$. The utilization time of n^{th} jobs on $\hat{S}$ and $\hat{C}$ machines is shown by $(\hat{k}_{n,}\hat{l}_{n,}\hat{m}_{n,}\hat{n}_{n})_{\boldsymbol{LR}}$ and $(\hat{r}_{n,}\hat{h}_{n,}\hat{k}_{n},\hat{d}_{n})_{\boldsymbol{LR}}$, respectively. The processing time is taken as LR-fuzzy number. Each job does not have to be processed on every one ofmachines of type $\hat{S}$ and $\hat{C}$. The model's matrix form is shown as follows:

Table 1: *Tabular form of problem*

Job	Processor $\hat{S}$						Processor $\hat{C}$					
i	$\hat{S}_1$	$\hat{S}_2$	$\hat{S}_3$	$\hat{S}_n$	Processing time Of$\hat{S}$	Probability p_i	$\hat{C}_1$	$\hat{C}_2$	$\hat{C}_3$	$\hat{C}_m$	Processing time of $\hat{C}$	Probability q_i
1	s_{11}	s_{12}	s_{13}	s_{1n}	$(\hat{k}_{1,}\hat{l}_{1,}\hat{m}_{1,}\hat{n}_{1})_{LR}$	p_1	c_{11}	c_{12}	c_{13}	c_{1n}	$(\hat{r}_{1,}\hat{h}_{1,}\hat{k}_{1,}\hat{d}_{1})_{LR}$	q_1
2	s_{21}	s_{22}	s_{23}	s_{2n}	$(\hat{k}_{2,}\hat{l}_{2,}\hat{m}_{2,}\hat{n}_{2})_{LR}$	p_2	c_{21}	c_{22}	c_{23}	c_{2n}	$(\hat{r}_{2,}\hat{h}_{2,}\hat{k}_{2,}\hat{d}_{2,})_{LR}$	q_2
3	s_{31}	s_{32}	s_{33}	s_{3n}	$(\hat{k}_{3,}\hat{l}_{3,}\hat{m}_{3,}\hat{n}_{3})_{LR}$	p_3	c_{31}	c_{32}	c_{33}	c_{3n}	$(\hat{r}_{3,}\hat{h}_{3,}\hat{k}_{3},d_{3})_{LI}$	q_3
4	s_{41}	s_{42}	s_{43}	s_{4n}	$(\hat{k}_{4,}\hat{l}_{4,}\hat{m}_{4,}\hat{n}_{4})_{\boldsymbol{LR}}$	p_4	c_{41}	c_{42}	c_{43}	c_{4n}	$(\hat{r}_{4,}\hat{h}_{4,}\hat{k}_{4},\hat{d}_{4})_{\boldsymbol{LI}}$	q_4
.	.	.	.	.	.	.	.	.	.	.	.	.
.	.	.	.	.	.	.	.	.	.	.	.	.
.	.	.	.	.	.	.	.	.	.	.	.	.
n	s_{n1}	s_{n2}	s_{n3}	s_{nn}	$(\hat{k}_{n,}\hat{l}_{n,}\hat{m}_{n,}\hat{n}_{n})_{\boldsymbol{L}}$	p_n	c_{n1}	c_{n1}	c_{n1}	c_{nm}	$(\hat{r}_{n,}\hat{h}_{n,}\hat{k}_{n},\hat{d}_{n})_{\boldsymbol{L}}$	q_n
t_{pj}	t_{11}	t_{12}	t_{13}	t_{1n}			t_{21}	t_{22}	t_{23}	t_{2m}		

I. Notations

i: job index

j: machine index

$(\hat{k}_{i,}\hat{l}_{i,}\hat{m}_{i,}\hat{n}_{i})_{\boldsymbol{LR}}$: processing time of i^{th}job on machine $\hat{S}$.

$(\hat{r}_{i,}\hat{h}_{i,}\hat{k}_{i},\hat{d}_{i})_{\boldsymbol{LR}}$ **:** processing time ofi^{th} job on machine $\hat{C}$.

s_{n3}: unit operational cost of job i (1,2,3,.....,n) on $\hat{S}_j$ like machine j =1,2,3.

c_{n1}: unit operational cost of job i (1,2,3,.....,n) on $\hat{C}_j$ like machine j =1,2,3.

p_i, q_i: Probability of machines $\hat{S}_j$ and $\hat{C}_j$ respectively.

II. Assumptions

- Every task is processed separately.
- Processing all jobs on all parallel machines is not required. One task can be finished by working exclusively on the first, second, or third machine.
- Costs of operation vary depending on the job.
- Machines are available at all times.
- Pre-emption is not taken into account.

III. Algorithm

The following course of action can be used to solve the FSSP given in table 1. Calculate expected processing time by multiplying probability with processing time and then using the ranking formula, we convert the LR fuzzy utilisation time into a crisp value in both phases. Next, in order to determine the best allocation, we use transportation techniques such as VAM& MODI. The best sequence is then determined using B&B.

Step 1: Calculate the expected processing time as $\check{S}_i = \hat{S}_i * p_i, \check{C}_i = \hat{C}_i * q_i$

Step 2:Defuzzify the processing time taken as LR fuzzy number into crisp values using ranking rule given in equation (1) in Case 1, equation (2) in Case 2, equation (3) in Case 3 and using equation (4) in Case 4 respectively.

Step 3: Apply transportation technique like VAM and MODI. To apply any transportation technique, we examine the constraint

$$\sum_{j=1}^{3} t_{1j} = \sum_{i=1}^{n} \check{S}_i \text{ and } \sum_{j=1}^{3} t_{2j} = \sum_{i=1}^{n} \check{C}_i \quad (5)$$

If equation (5) is satisfied, problem is balanced otherwise add dummy job to balance it.

Step 4: Use B&B method by applying the rule

$$b_1 = \max\left(\sum_{i=1}^{n} S_{ij}\right)_{j=1,2,..,m} + \min_{i \in J_k}\{\max_{j=1,2,.....p} C_{ij}\} \;\&\; b_2 = \{\max_{i \in J_k} S_{ij}\}_{j=1,2....,m} + \max\left(\sum_{i=1}^{n} C_{ij}\right)_{j=1,2,..,p}$$

Step 5:Calculate LB=max$\{b_1, b_2\}$ for all the jobs and label the appropriate nodes of the branch from the calculated values.Determine the least of all values of LB and begin at that node. Continue the aforementioned procedure until we reach the branch termination point.In-out table for the obtained sequence gives minimum elapsed time.

Step 6:Repeat step 2 to 5 for all reference functions.

V. Numerical Illustration

Three machines $\hat{S}_1$, $\hat{S}_2 and \hat{S}_3$ of type $\hat{S}$ and three machines $\hat{C}_1$, $\hat{C}_2$ and $\hat{C}_3$ of type $\hat{C}$ are accessible for various amounts of time and have differing running expenses with probabilities associated with the machines at both stages as presented in table 2. Processing time is taken as LR fuzzy number to account for the uncertainty.

Table 2: *Mathematical model*

Job	Processor $\hat{S}$					Processor $\hat{C}$				
i	$\hat{S}_1$	$\hat{S}_2$	$\hat{S}_3$	Processing time of $\check{S}_i$	Probability p_i	$\hat{C}_1$	$\hat{C}_2$	$\hat{C}_3$	Processing time of $\hat{C}_i$	Probability q_i
1	2	6	5	$(7,8,2,4)_{LR}$	0.2	8	3	11	$(5,7,3,4)_{LR}$	0.1
2	8	2	10	$(6,7,2,4)_{LR}$	0.1	9	4	5	$(6,7,4,5)_{LR}$	0.2
3	7	8	4	$(4,5,2,3)_{LR}$	0.3	6	2	7	$(8,9,4,6)_{LR}$	0.1
4	5	9	6	$(3,5,2,4)_{LR}$	0.2	4	8	3	$(6,7,3,5)_{LR}$	0.2
5	11	3	9	$(7,9,1,6)_{LR}$	0.1	2	7	9	$(8,10,4,6)_{LR}$	0.2
Available time	1.8	2.1	1.66		2.1	1.7	2.38	1.8		

Solution:

After multiplication of processing time of the machines with their probabilities, obtained values are shown in table 3.

Table 3: *Problem after multiplying probability with processing time*

Job	Processor $\hat{S}$				Processor $\hat{C}$			
i	$\hat{S}_1$	$\hat{S}_2$	$\hat{S}_3$	Processing time of $\check{S}_i$	$\hat{C}_1$	$\hat{C}_2$	$\hat{C}_3$	Processing time of $\check{C}_i$
1	2	6	5	$(1.4,1.6,0.4,0.8)_{LR}$	8	3	11	$(0.5,0.7,0.3,0.4)_{LR}$
2	8	2	10	$(0.6,0.7,0.2,0.4)_{LR}$	9	4	5	$(1.2,1.4,0.8,1.0)_{LR}$
3	7	8	4	$(1.2,1.5,0.6,0.9)_{LR}$	6	2	7	$(0.8,0.9,0.4,0.6)_{LR}$
4	5	9	6	$(0.6,1.0,0.4,0.8)_{LR}$	4	8	3	$(1.2,1.4,0.6,1.0)_{LR}$
5	11	3	9	$(0.7,0.9,0.1,0.6)_{LR}$	2	7	9	$(1.6,2.0,0.8,1.2)_{LR}$
Available time	1.8	2.1	1.66		2.1	1.7	2.38	

Now we defuzzify the LR processing time into crisp value using below given reference function and equation (1) which is given in table 4.

Case 1: If L(x)= R(x) = max $\{0, 1 - |x|\}$

Table 4: *Reduced problem after defuzzifying LR fuzzy number into crisp value*

Job	Processor $\hat{S}$				Processor $\hat{C}$			
i	$\hat{S}_1$	$\hat{S}_2$	$\hat{S}_3$	Processing time of $\check{S}_i$	$\hat{C}_1$	$\hat{C}_2$	$\hat{C}_3$	Processing time of $\check{C}_i$
1	2	6	5	1.60	8	3	11	0.63
2	8	2	10	0.70	9	4	5	1.35
3	7	8	4	1.43	6	2	7	0.9
4	5	9	6	0.90	4	8	3	1.4
5	11	3	9	0.93	2	7	9	1.9
Available time	1.8	2.1	1.66		2.1	1.7	2.38	

Since the equation (5) is satisfied therefore, the problem is balanced. Now, we will find the optimal allocations of processing time and unit cost by applying VAM and MODI method to optimize the problem which is given in table 5.

Table 5: *Problem after optimal allocation*

Job	Processor $\hat{S}$				Processor $\hat{C}$			
i	$\hat{S}_1$	$\hat{S}_2$	$\hat{S}_3$	Processing time of $\check{S}_i$	$\hat{C}_1$	$\hat{C}_2$	$\hat{C}_3$	Processing time of $\check{C}_i$
1	1.6	0	0	1.60	0	0.63	0	0.63
2	0	0.7	0	0.70	0	0.17	1.18	1.35
3	0	0	1.43	1.43	0	0.9	0	0.90
4	0.2	0.47	0.23	0.90	0.2	0	1.2	1.40
5	0	0.93	0	0.93	1.9	0	0	1.90

Now B&B algorithm is applied to further optimize the allocation obtained after the application of VAM and MODI given in table 6.

Table 6: *Applying branch and bound*

(i)	b_1 =max $(\sum_{i=1}^{n} S_{ij})_{j=1,2,..,m}$ + $\min_{i\in J_k'}\{\max_{j=1,2,.....p} C_{ij}\}$	$b_2 = \{\max_{i\in J_k} S_{ij}\}_{j=1,2....,m}$+max $(\sum_{i=1}^{n} C_{ij})_{j=1,2,..,p}$	LB=max$\{b_1, b_2\}$
1	2.1+0.18=2.28	1.6+2.38=3.98	3.98
2	2.1+0.63=2.73	0.7+2.38=3.08	3.08
3	2.1+0.18=2.28	1.43+2.38=3.81	3.81
4	2.1+0.18=2.28	0.47+2.38=2.85	2.85
5	2.1+0.18=2.28	0.93+2.38=3.31	3.31

Here minimum of all the LB's is 2.85, which corresponds to task 4. So, position of job 4 in the optimum sequence will be at first place. Now repeat the above process for the subsequences {4,1}, {4,2}, {4,3}and {4,5} given in table 7.

Table 7: *Applying B&B technique for 1st node*

(i)	b_1 =max$(\sum_{i=1}^{n} S_{ij})_{j=1,2,..,m}$+ $\min_{i\in J_k'}\{\max_{j=1,2,.....p} C_{ij}\}$	$b_2 = \{\max_{i\in J_k} S_{ij}\}_{j=1,2....,m}$+max $(\sum_{i=1}^{n} C_{ij})_{j=1,2,..,p}$	LB=max$\{b_1, b_2\}$
41	2.1+0.18=2.28	2.43+2.38=4.81	4.81
42	2.1+0.63=2.73	2.35+2.38=4.73	4.73
43	2.1+0.18=2.28	2.56+2.38=4.94	4.94
45	2.1+0.18=2.28	3.3+2.38=5.68	5.68

Now, the lowest lower bound is 4.73, which corresponds to sub sequence {4,2}. Therefore, fixing job 2 at 2nd position in the optimal schedule. Now repeat the above process for the subsequences {4,2,1}, {4,2,3} and {4,2,5} given in table 8.

Table 8: *Applying B&B technique for 2nd node*

(i)	b_1 =max$(\sum_{i=1}^{n} S_{ij})_{j=1,2,..,m}$+ $\min_{i\in J_k'}\{\max_{j=1,2,.....p} C_{ij}\}$	$b_2 = \{\max_{i\in J_k} S_{ij}\}_{j=1,2....,m}$+max $(\sum_{i=1}^{n} C_{ij})_{j=1,2,..,p}$	LB=max$\{b_1, b_2\}$
421	2.1+0.9=3	2.23+2.38=4.61	4.61
423	2.1+0.63=2.73	2.33+2.38=4.71	4.71
425	2.1+0.63=2.73	4+2.38=6.38	6.38

Clearly, minimum of LB's is 4.61which corresponds to sub sequence {4,2,1}. So, position of job 1 in the optimum sequence will be at third place. Now repeat the above process for the subsequences {4,2,1,3}and {4,2,1,5} given in table 9.

Table 9: *Applying B&B technique for 3rd node*

(i)	b_1 =max$(\sum_{i=1}^{n} S_{ij})_{j=1,2,..,m}$+ $\min_{i\in J_k'}\{\max_{j=1,2,.....p} C_{ij}\}$	$b_2 = \{\max_{i\in J_k} S_{ij}\}_{j=1,2....,m}$+max $(\sum_{i=1}^{n} C_{ij})_{j=1,2,..,p}$	LB=max$\{b_1, b_2\}$
4213	2.1+1.9=4	3.13+2.38=5.51	5.51
4215	2.1+0.9=3	2.83+2.38=5.21	5.21

Here minimum lower bound corresponds to subsequence {4,2,1,5}. So, job 3 will be at last position of optimal schedule. Hence, {4,2,1,5,3} is the required optimal sequence and table 10represents corresponding in-out table.

Table 10: *In-out table*

Job	Processor $\hat{S}$			Processor $\hat{C}$		
i	$\hat{S}_1$	$\hat{S}_2$	$\hat{S}_3$	$\hat{C}_1$	$\hat{C}_2$	$\hat{C}_3$
4	0-0.2	0-0.47	0-0.23	0.47-0.67	-	0.47-1.67
2	-	0.47-1.17	-	-	1.17-1.34	1.67-2.85
1	0.2-1.8	-	-	-	1.8-2.43	-
5	-	1.17-2.1	-	2.1-4	-	-
3	-	-	0.23-1.66	-	2.43-3.33	-

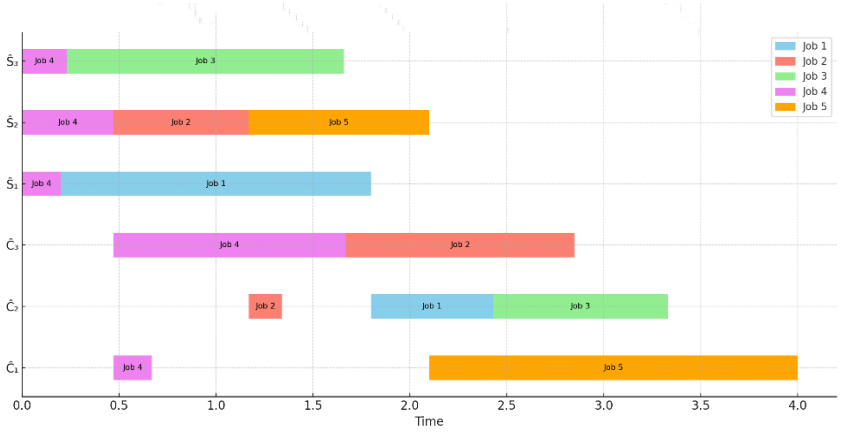


Figure 2: *Gantt chart for case 1.*

Case 2: If L(x)= R(x) = e^{-x}

Now we change the LR processing time into crisp value using above reference function and equation (2). Defuzzified values are given in table 11.

Table 11: *Reduced problem after defuzzifying LR fuzzy number into crisp value*

Job	Processor $\hat{S}$					Processor $\hat{C}$				
i	$\hat{S}_1$	$\hat{S}_2$	$\hat{S}_3$	$\hat{S}_4$	Processing time of $\check{S}_i$	$\hat{C}_1$	$\hat{C}_2$	$\hat{C}_3$	$\hat{C}_4$	Processing time of $\check{C}_i$
1	2	6	5	0	1.70	8	3	11	0	0.65
2	8	2	10	0	0.75	9	4	5	0	1.40
3	7	8	4	0	1.50	6	2	7	0	0.95
4	5	9	6	0	1.00	4	8	3	0	1.50
5	11	3	9	0	1.05	2	7	9	0	2.00
Available time	1.8	2.1	1.66	0.44		2.1	1.7	2.38	0.32	

Since the equation (5) is not satisfied therefore, the problem is unbalanced. Therefore, we add dummy machine$\hat{S}_4$at 1st stage and $\hat{C}_4$at 2nd stage to balance the problem. Now, we find the optimal allocations of processing time and optimal allotment of unit cost for each job by applying VAM and MODI method to optimize the problem which is given in table 12.

Table 12: *Problem after application of VAM& MODI method*

Job	Processor $\hat{S}$					Processor $\hat{C}$				
i	$\hat{S}_1$	$\hat{S}_2$	$\hat{S}_3$	$\hat{S}_4$	Processing time of $\check{S}_i$	$\hat{C}_1$	$\hat{C}_2$	$\hat{C}_3$	$\hat{C}_4$	Processing time of $\check{C}_i$
1	1.7	0	0	0	1.70	0	0.65	0	0	0.65
2	0	0.75	0	0	0.75	0	0.1	0.98	0.32	1.40
3	0	0	1.5	0	1.50	0	0.95	0	0	0.95
4	0.1	0.3	0.16	0.44	1.00	0.1	0	1.4	0	1.50
5	0	1.05	0	0	1.05	2.0	0	0	0	2.00

Now we apply B&B method to obtain the sequence of jobs for optimal solution. The optimal sequence obtained is 42153 and table 13 represents corresponding in-out table.

Table 13: *In-out table.*

Job	Processor $\hat{S}$				Processor $\hat{C}$			
i	$\hat{S}_1$	$\hat{S}_2$	$\hat{S}_3$	$\hat{S}_4$	$\hat{C}_1$	$\hat{C}_2$	$\hat{C}_3$	$\hat{C}_4$
4	0-0.1	0-0.3	0-0.16	0-0.44	0.44-0.54	-	0.44-1.84	-
2	-	0.3-1.05	-	-	-	1.05-1.15	1.84-2.82	1.05-1.37
1	0.1-1.8	-	-	-	-	1.8-2.45	-	-
5	-	1.05-2.1	-	-	2.1-4.1	-	-	-
3	-	-	0.16-1.66	-	-	2.45-3.4	-	-

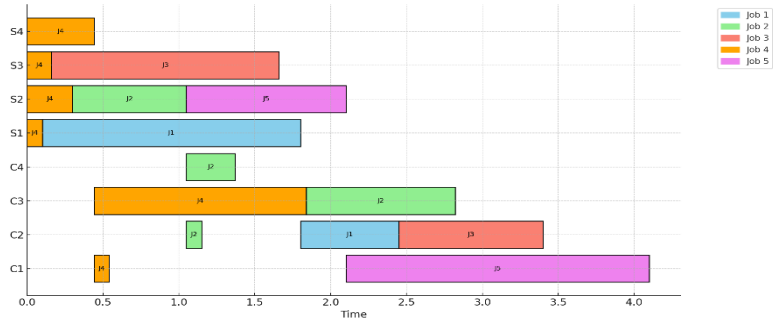


Figure 3: *Gantt chart for case 2.*

Case 3: If L(x)= max $\{0, 1-|x|\}$, R(x) = e^{-x}

Now we defuzzify the LR processing time into crisp value using above reference function and equation (3). Defuzzified values are given in table 14.

Table 14: *Defuzzifying LR fuzzy processing time*

Job	Processor $\hat{S}$					Processor $\hat{C}$				
i	$\hat{S}_1$	$\hat{S}_2$	$\hat{S}_3$	$\hat{S}_4$	Processing time of $\check{S}_i$	$\hat{C}_1$	$\hat{C}_2$	$\hat{C}_3$	$\hat{C}_4$	Processing time of $\check{C}_i$
1	2	6	5	0	1.8	8	3	11	0	0.73
2	8	2	10	0	0.8	9	4	5	0	1.6
3	7	8	4	0	1.65	6	2	7	0	1.05
4	5	9	6	0	1.1	4	8	3	0	1.65
5	11	3	9	0	1.08	2	7	9	0	2.2
Available time	1.8	2.1	1.66	0.87		2.1	1.7	2.38	1.05	

Since the equation (5) is not satisfied therefore, the problem is unbalanced. Therefore, we add dummy machine$\hat{S}_4$at 1st stage and $\hat{C}_4$at 2nd stage to balance the problem. Now, we find the optimal allocations of processing time and optimal allotment of unit cost for each job by applying VAM and MODI method to optimize the problem which is given in table 15.

Table 15: *Problem after optimal allocation*

Job	Processor $\hat{S}$					Processor $\hat{C}$				
i	$\hat{S}_1$	$\hat{S}_2$	$\hat{S}_3$	$\hat{S}_4$	Processing time of $\check{S}_i$	$\hat{C}_1$	$\hat{C}_2$	$\hat{C}_3$	$\hat{C}_4$	Processing time of $\check{C}_i$
1	1.58	0.22	0	0	1.8	0	0.65	0	0.08	0.73
2	0	0.8	0	0	0.8	0	0	0.73	0.87	1.6
3	0	0	0.65	0	1.65	0	1.05	0	0	1.05
4	0.22	0	0.01	0.8	1.1	0	0	1.65	0	1.65
5	0	1.08	0	0	1.08	2.1	0	0	0.1	2.2

Now we apply B&B algorithm and calculate the lower bound of jobs to obtain the sequence of jobs for optimal solution as in case 1&2. Required optimal sequence comes out to be {2,1,3,4,5}. Table 16 represents in-out table.

Table 16: *In-out table.*

Job	Processor $\hat{S}$				Processor $\hat{C}$			
i	$\hat{S}_1$	$\hat{S}_2$	$\hat{S}_3$	$\hat{S}_4$	$\hat{C}_1$	$\hat{C}_2$	$\hat{C}_3$	$\hat{C}_4$
2	-	0-0.8	-	-	-	-	0.8-1.53	0.8-1.67
1	0-1.58	0.8-1.02	-	-	-	1.58-2.23	-	1.58-1.66
3	-	-	0-0.65	-	-	0.65-1.7	-	-
4	1.58-1.8	-	0.65-0.66	0-0.8	-	-	1.8-3.45	-
5	-	1.02-2.1	-	-	2.1-4.2	-	-	2.1-2.2

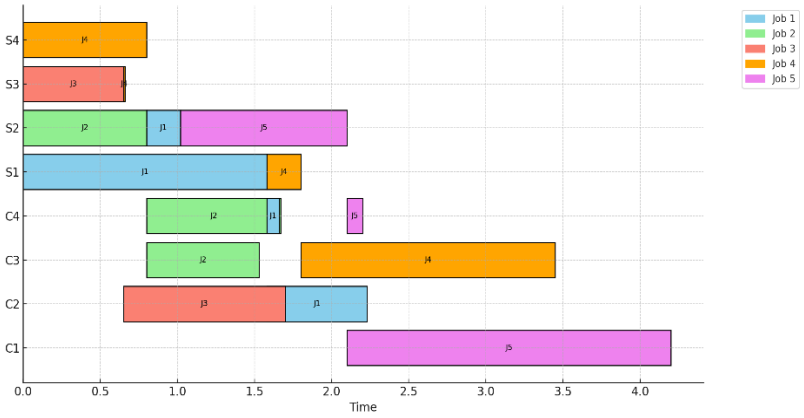


Figure 4: *Gantt chart for case 3.*

Case 4: If L(x) = e^{-x}, R(x)= max $\{0, 1-|x|\}$

Now we again defuzzify the LR processing time into crisp value using above reference function and equation (4) shown in table 17.

Table 17: *Problem after defuzzification of LR fuzzy numbers*

Job	Processor $\hat{S}$			Processor $\hat{C}$				
i	$\hat{S}_1$	$\hat{S}_2$	$\hat{S}_3$	Processing time of $\check{S}_i$	$\hat{C}_1$	$\hat{C}_2$	$\hat{C}_3$	Processing time of $\check{C}_i$
1	2	6	5	1.60	8	3	11	0.63
2	8	2	10	0.70	9	4	5	1.35
3	7	8	4	1.43	6	2	7	0.9
4	5	9	6	0.90	4	8	3	1.4
5	11	3	9	0.93	2	7	9	1.9
6	0	0	0	0.43	0	0	0	0.73
Available time	1.8	2.1	1.66		2.1	1.7	2.38	

Since the equation (5) is not satisfied therefore, the problem is unbalanced. Therefore, we add dummy job$\hat{S}_4$ at 1st stage and $\hat{C}_4$at 2nd stage to balance the problem. Now, we find the optimal allocations of processing time and optimal allotment of unit cost for each job by applying VAM and MODI method to optimize the problem which is given in table 18.

Table 18: *Reduced problem after optimal allocation*

Job	Processor $\hat{S}$			Processor $\hat{C}$				
i	$\hat{S}_1$	$\hat{S}_2$	$\hat{S}_3$	Processing time of $\check{S}_i$	$\hat{C}_1$	$\hat{C}_2$	$\hat{C}_3$	Processing time of $\check{C}_i$
1	1.5	0	0	1.60	0	0.55	0	0.63
2	0	0.65	0	0.70	0	0.35	0.8	1.35
3	0	0	1.28	1.43	0	0.8	0	0.9
4	0.3	0.12	0.38	0.90	0	0	1.25	1.4
5	0	0.9	0	0.93	1.7	0	0	1.9
6	0	0.43	0	0.43	0.4	0	0.33	0.73

Now by applying B&B algorithm to further optimize the allocation obtained after the application of VAM and MODI, optimal sequence obtained is 462351. Table 19 represents in-out table.

Table 19: *In-out table.*

Job	Processor $\hat{S}$			Processor $\hat{C}$		
i	$\hat{S}_1$	$\hat{S}_2$	$\hat{S}_3$	$\hat{C}_1$	$\hat{C}_2$	$\hat{C}_3$
4	0-0.3	0-0.12	0-0.38	-	-	0.38-1.63
6	-	0.12-0.55	-	0.55-0.95	-	1.63-1.96
2	-	0.55-1.2	-	-	1.2-1.55	1.96-2.76
3	-	-	0.38-1.66	-	1.66-2.46	-
5	-	1.2-2.1	-	2.1-3.8	-	-
1	0.3-1.8	-	-	-	2.46-3.01	-

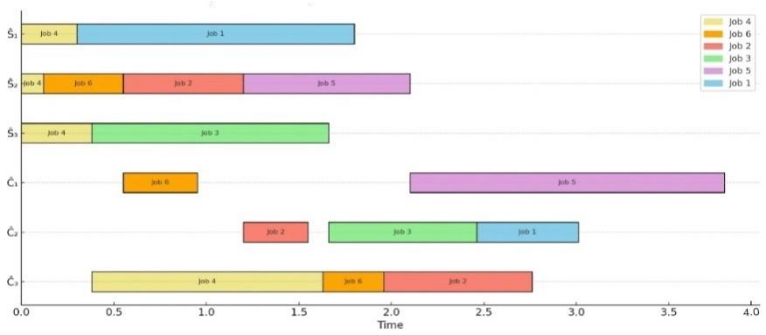


Figure 5: *Gantt chart for case 4.*

VI. Comparison

Values calculated for the other reference function is shown in the table 20.

Table 20: *Comparison table*

S.No.	Reference Function	Optimal Sequence	Total Flow Time(in hrs)
1	L(x)= R(x) = max {0,1 − |x|}	{4,2,1,5,3}	4
2	L(x)= R(x) = e^{-x}	{4,2,1,5,3}	4.1
3	L(x)= max {0,1 − |x|} , R(x) = e^{-x}	{2,1,3,4,5}	4.2
4	L(x) = e^{-x}, R(x)= max {0,1 − |x|}	{4,2,3,5,1}	3.8

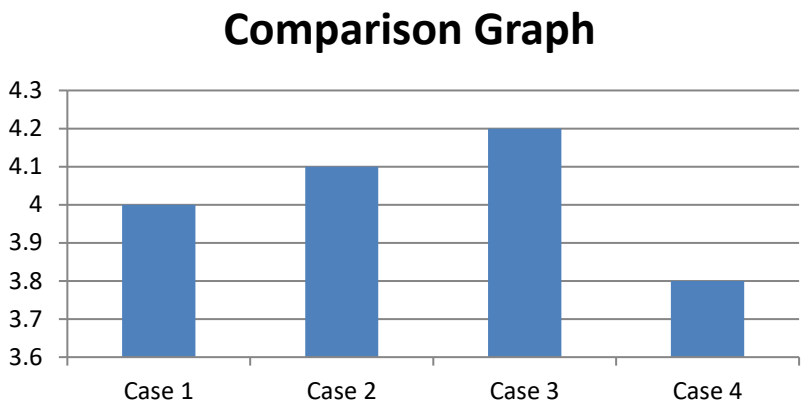


Figure 6: *Comparison of total elapsed time corresponding to reference functions*

VII. Conclusion

An approach to scheduling in the LR-fuzzy environment is presented in this work. In FSSPs where processing time is taken as LR-Fuzzy numbers, B&B technique has been utilized to determine the best order for two stage FSSP with parallel equipotential machines at both stages including probabilities. The example shows that the best results are obtained using either a linear or exponential function on the LR-fuzzy number.

VIII. Future Scope

The present study on the two-stage FSSP with parallel machines at both stages, incorporating processing times as LR fuzzy number and probabilities, solved through the Branch and Bound (B&B) method with linear and exponential reference functions, offers several directions for future research. Multi-stage or hybrid flow shop systems are common in complex industrial settings, and extending the framework would enhance its applicability in real-world manufacturing scenarios with varied processing routes and interdependencies. Incorporating dynamic scheduling elements such as stochastic job arrivals, machine failures, and other real-time disruptions presents another promising direction. The LR fuzzy modeling approach is well-suited for dynamic systems, as it supports continuous updates of uncertainty parameters and belief levels based on real-time data inputs.

While the B&B method guarantees optimality, its computational burden increases significantly with problem size. Future work could investigate the integration of metaheuristic algorithms which may yield near-optimal solutions with reduced computational effort, particularly for large-scale instances. Further, a multi-objective optimization approach may be employed to address additional performance criteria, including total flow time, transportation time, job block, energy consumption and machine utilization.

Another important area for development is the adaptive selection of reference functions. Instead of relying on fixed linear or exponential forms, future research may explore learning-based or heuristic methods to dynamically identify the most appropriate reference structure based on job features or operational context. Also, the development of a software-based decision-support system integrating these features would support practical adoption by manufacturing decision-makers.

Conflicts of interests: The authors declare that there are no conflicts of interest.

References

[1] Brown, A. P. G. and Lomnicki, Z. A. (1966). Some applications of the branch-and-bound algorithm to the machine scheduling problem. *Journal of the Operational Research Society*, 17, 173–186.

[2] Dubois, D. and Prade, H. (1978). Operations on fuzzy numbers. *International Journal of Systems Science*, 9, 613–626.

[3] Zadeh, A. L. (1978). Fuzzy Sets as a Basis for a Theory of Possibility. *Fuzzy Sets and Systems*, 1, 3–28.

[4] McCahon, C. S. and Lee, E. S. (1990). Job sequencing with fuzzy processing times. *Computers & Mathematics with Applications*, 19, 31–41.

[5] Ishibuchi, H., Murata, T. and Lee, K. H. (1996). Formulation of fuzzy flowshop scheduling problems with fuzzy processing time. *Proceedings of the IEEE 5th International Fuzzy Systems Conference*, 1, 199–205.

[6] Giachetti, R. E. and Young, R. E. (1997). A parametric representation of fuzzy numbers and their arithmetic operators. *Fuzzy Sets and Systems*, 91, 185–202.

[7] Yao, J. S. and Lin, F. T. (2002). Constructing a fuzzy flow-shop sequencing model based on statistical data. *International Journal of Approximate Reasoning*, 29, 215–234.

[8] Wang, H. F. and Kuo, C. Y. (2006). Three-parameter fuzzy arithmetic approximation of LR fuzzy numbers for fuzzy neural networks. *International Journal of Uncertainty, Fuzziness and Knowledge-Based Systems*, 14, 211–233.

[9] Saneeifard, R. (2009). Ranking LR fuzzy numbers with weighted averaging based on levels. *International Journal of Industrial Mathematics*, 1, 163–173.

[10] Kaur, J. and Kumar, A. (2013). Mehar's Method for solving fully fuzzy linear programming problems with LR fuzzy parameters. *Applied Mathematical Modelling*, 37, 7142–7153.

[11] Thorani, Y. L. P. and Shankarn, R. (2013). Fuzzy transportation linear programming models based on LR fuzzy numbers. *International Journal of Computer Applications*, 72, 4–13.

[12] Gupta, D., Sharma, S. and Aggarwal, S. (2013). Flow shop scheduling on 2-machines with setup time and single transport facility under fuzzy environment. *Opsearch*, 50, 14–24.

[13] Zhou, J., Yang, F. and Wang, K. (2015). Fuzzy arithmetic on LR fuzzy numbers with applications to fuzzy programming. *Journal of Intelligent & Fuzzy Systems*, 30, 71–87.

[14] Gupta, D., Goel, S. and Mangla, N. (2022). Optimization of production scheduling in two-stage flow shop scheduling problem with m equipotential machines at first stage. *International Journal of System Assurance Engineering and Management*, 13, 1162–1169.

[15] Gupta, D. and Goel, S. (2022). Branch and bound technique for two-stage flow shop scheduling model with equipotential machines at every stage. *International Journal of Operational Research*, 44, 462–472.

[16] Kaushik, P., Gupta, D. and Goel, S. (2025). Comparative study of B&B with heuristics NEH and CDS for bi-stage flow shop scheduling problem under fuzzy environment. *Journal of Mechanics of Continua and Mathematical Sciences*, 20, 73–89.

[17] Kaushik, P., Sonia, Gupta, D. and Goel, S. (2025). Minimizing processing time in bi-stage FSSP under fuzzy environment and comparison between B&B, GA, and Palmar. *Advances in Nonlinear Variational Inequalities*, 28, 693–715.

FERMATEAN QUADRIPARTITIONED NEUTROSOPHIC FUZZY GRAPH

V. Divya[1], J. Jesintha Rosline[2*]

•

[1,2]PG & Research Department of Mathematics, Auxilium college (Autonomous), Katpadi, Vellore - 6.
(Affiliated to Thiruvalluvar University - Serkkadu, Vellore)
[1]sdivyasv@gmail.com [2*]jesi.simple@gmail.com

Abstract

A fuzzy graph is a mathematical technique that represents relationship of an objects with uncertainty or imprecision, using nodes and edges with membership degrees to indicate the strength of connections. It provides an important paradigm for modelling and handling real world optimization tasks. Neutrosophic graphs extend classical graph theory to handle uncertain, imprecise and inconsistent information, enabling the modeling of complex relationships with varying degrees of truth, indeterminacy and falsity. This framework provides a more nuanced understanding of complex systems, allowing for improved accuracy and increased flexibility in decision-making, network analysis and optimization problems. Neutrosophic graphs can be applied to various fields, including multi-criteria decision-making, supply chain management and logistics, where uncertain or imprecise data is common. The extension of Neutrosophic set is the Quadripartitioned Neutrosophic Set. The division of indeterminacy function of the Neutrosophic set into the contradiction and ignorance component is termed as Quadripartitioned Neutrosophic Set. Associated with each vertex are values of truth, contradiction, ignorance and falsity that reflects it characteristics of a graph. Similarly, for each edge, these values signify the strength or reliability of the relationship between the connected vertices. Quadripartitioned Neutrosophic Fuzzy graph gives an accurate representation of uncertainty which leads to a greater clarity of complex systems and relationships. It has an emerging applications in social network analysis, image processing and decision making systems. Fermatean Neutrosophic Graph is a hybrid model of Fermatean and Neutrosophic graph. This enhancement provides an increased capacity to handle uncertain and unclear data. In contrast to traditional neutrosophic values, this framework operates with truth, indeterminacy and falsity membership degrees constrained by the condition that the sum of their third powers is less than or equal to two. In this article, a new graph is defined called Fermatean Quadripartitioned Neutrosophic Fuzzy Graph (FQNFG). We proposed the order, size, complete, complement and strong of Fermatean Quadripartitioned Neutrosophic Fuzzy Graph. Furthermore, the paper establishes operations for FQNFG such as composition, Cartesian product, Cross product and lexicographic product are also studied.

Keywords: Neutrosophic Fuzzy graph, Quadripartitioned Neutrosophic Fuzzy graph, Fermatean Neutrosophic Fuzzy graph, Complete and Complement Fermatean Quadrapartitioned Neutrosophic Fuzzy graph..

1. Introduction

In 1736, Graph theory was developed by Euler. Graph theory is a section of mathematics which studies the characteristics and applications of graphs, consisting of vertices (nodes) and connected by edges (links). It models relationships between objects and is widely used in networks, structures and various fields. Applications span cryptography, data mining and machine learning etc. This theory is a prominent solving technique in a variety of domains, including geometry,

algebra, number theory and computer science. The idea of Fuzzy Set theory was proposed by L.A. Zadeh [1]. Azriel Rosenfeld initiated the Fuzzy Graph theory, which paves the way for new research in mathematics, communication systems, economics and a variety of other subjects [2]. Neutrosophic Fuzzy Sets were used to generate new concepts for Neutrosophic Fuzzy Graphs [3, 4]. Senapati et al. introduced a novel idea called the Fermatean Fuzzy Set [5, 6]. Thamizhendi et al. introduced the notion of Fermatean Fuzzy Hyper-Graphs and its characteristics [7]. Later, Antony et al, [8] suggested a new emergent idea of Fermatean Neutrosophic, which combines Neutrosophic sets and Fermatean fuzzy sets. Said Broumi et al. introduced a new paradigm for Fermatean Neutrosophic graphs and their applications based on the Fermatean Neutrosophic fuzzy set [9] and also presented the Interval-valued Fermatean neutrosophic graphs and regularity [18].
The Quadripartitioned Neutrosophic Graph denotes the division of the Neutrosophic set's indeterminacy component into contradiction and ignorance components. Fermatean Quadripartitioned Neutrosophic Fuzzy Graph is the result of combining Fermatean and Quadripartitioned Neutrosophic Fuzzy Graphs. In this article will see the new novel idea Fermatean Quadripartitioned Neutrosophic Fuzzy Graphs. Here, section 2 provides basic definitions. Section 3 presents the definition of FQNFG, order, size, complete, complement and strong of FQNFG. Section 4 introduces the concept of composition, cartesian product, cross product and lexicographic product of FQNFG etc., along with theorems and examples. Section 5 concludes the paper with future scope of research.

2. Preliminaries

Definition 2.1. [2] A Fuzzy Graph G is a pair of functions $G(\sigma, \mu)$ where σ is a fuzzy subset of a non empty set S and μ is a symmetric fuzzy relation on σ. The underlying crisp graph of $G(\sigma, \mu)$ is denoted by $G^* : (\sigma^*, \mu^*)$.

Definition 2.2. [16] Consider a fuzzy graph $G : (\sigma, \mu)$, then order of G is termed as $O(G) = \sum_{u \in V} \sigma(u)$

Definition 2.3. [16] Consider a fuzzy graph $G : (\sigma, \mu)$, then size of G is termed as $S(G) = \sum_{u,v \in V} \mu(u, v)$

Definition 2.4. [17] A Neutrosophic Fuzzy Graph $G = (\sigma, \mu)$ where $\sigma = (\sigma_1, \sigma_2, \sigma_3)$ such that $\sigma_1, \sigma_2, \sigma_3$ from $\sigma \to [0, 1]$ represent value of truth, indeterminacy and falsity membership value with $0 \leq \sigma_1(u) + \sigma_2(u) + \sigma_3(u) \leq 3$, $\mu \subseteq \sigma \times \sigma$ with μ_1, μ_2 and μ_3 from $\sigma \times \sigma$ to $[0, 1]$ such that
$\mu_1(uv) \leq min(\sigma_1(u), \sigma_1(v))$
$\mu_2(uv) \leq min(\sigma_2(u), \sigma_2(v))$
$\mu_3(uv) \leq max(\sigma_3(u), \sigma_3(v))$
$0 \leq \mu_1(uv) + \mu_2(uv) + \mu_3(uv) \leq 3$, for every $(uv) \in \mu$.

Definition 2.5. [9] A Fermatean Neutrosophic Graph (FNG) on a universal set X is a pair $G = (P, Q)$ where P is Fermatean neutrosophic set on X and Q is a Fermatean Neutrosophic relation on X so that:
$T_Q(u, v) \leq T_p(u) \wedge T_p(v)$
$I_Q(u, v) \geq I_p(u) \vee I_p(v))$
$F_Q(u, v) \geq F_p(u) \vee F_p(v)$
and $0 \leq T_Q^3(u, v) + I_Q^3(u, v) + F_Q^3(u, v) \leq 2 \ \forall u, v \in X$, where, $T_Q : X \times X \to [0, 1]$, $I_Q : X \times X \to [0, 1]$ and $F_Q : X \times X \to [0, 1]$ indicates degree of membership, degree of indeterminacy-membership and degree of non-membership of Q, Correspondingly. Here, P and Q are the Fermatean Neutrosophic vertex and edge set of G.

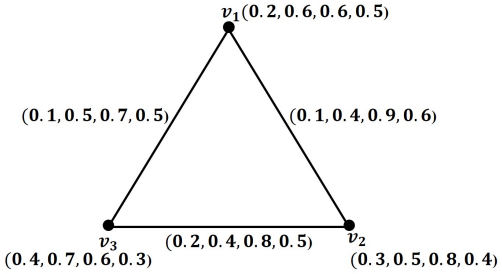


Figure 1: *Fermatean Quadripartitioned Neutrosophic Fuzzy Graph*

3. Fermatean Quadripartitioned Neutrosophic Fuzzy Graph

Definition 3.1. A Fermatean Quadripartitioned Neutrosophic Fuzzy Graph (FQNFG) an Universal Set X is a pair $G_{FQ} = (\sigma_{FQ}, \mu_{FQ})$, $\sigma_{FQ} : X \to [0,1]$ is a Fermatean Quadripartitioned Neutrosophic Set on X and $\mu_{FQ} : X \times X \to [0,1]$ is a Fermatean Quadripartitioned Neutrosophic mapping on $X \times X$ so that

$$\begin{aligned} T\mu_{FQ}(uv) &\leq \min(T_{\sigma_{FQ}}(u), T_{\sigma_{FQ}}(v)) \\ C_{\mu_{FQ}}(uv) &\leq \min(C_{\sigma_{FQ}}(u), C_{\sigma_{FQ}}(v)) \\ I_{\mu_{FQ}}(uv) &\geq \max(I_{\sigma_{FQ}}(u), I_{\sigma_{FQ}}(v)) \\ F_{\mu_{FQ}}(uv) &\geq \max(F_{\sigma_{FQ}}(u), F_{\sigma_{FQ}}(v)) \end{aligned}$$

with $0 \leq T^3_{\mu_{FQ}}(uv) + C^3_{\mu_{FQ}}(uv) + I^3_{\mu_{FQ}}(uv) + F^3_{\mu_{FQ}}(uv) \leq 3 \ \forall u, v \in X$, where $T_{\mu_{FQ}} : X \times X \to [0,1]$, $C_{\mu_{FQ}} : X \times X \to [0,1]$, $I_{\mu_{FQ}} : X \times X \to [0,1]$, $F_{\mu_{FQ}} : X \times X \to [0,1]$, indicates degree of truth, contradiction, ignorance and false membership of μ_{FQ}. σ_{FQ} and μ_{FQ} is the Fermatean Quadripartitioned Neutrosophic vertex and edge set of G_{FQ}.

Definition 3.2. A Fermatean Quadripartitioned Neutrosophic Fuzzy Graph $G_{FQ} = (\sigma_{FQ}, \mu_{FQ})$ is said to be complete if the following conditions are satisfied.

$$\begin{aligned} T_{\mu_{FQ}}(uv) &= (T_{\sigma_{FQ}}(u) \wedge T_{\sigma_{FQ}}(v)) \\ C_{\mu_{FQ}}(uv) &= (C_{\sigma_{FQ}}(u) \wedge C_{\sigma_{FQ}}(v)) \\ I_{\mu_{FQ}}(uv) &= (I_{\sigma_{FQ}}(u) \vee I_{\sigma_{FQ}}(v)) \\ F_{\mu_{FQ}}(uv) &= (F_{\sigma_{FQ}}(u) \vee F_{\sigma_{FQ}}(v)) \end{aligned}$$

where $u, v \in \sigma_{FQ}$.

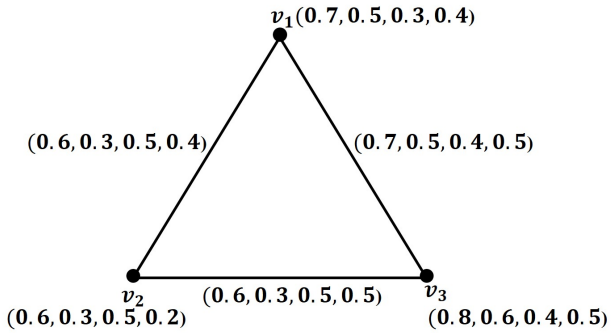


Figure 2: *Complete FQNFG*

Definition 3.3. Let $G_{FQ} = (\sigma_{FQ}, \mu_{FQ})$ be a FQNFG, then Size of G_{FQ} is defined as $S(G_{FQ}) = (\sum_{uv\in\mu_{FQ}} T_{\mu_{FQ}}(uv), \sum_{uv\in\mu_{FQ}} C_{\mu_{FQ}}(uv), \sum_{uv\in\mu_{FQ}} I_{\mu_{FQ}}(uv), \sum_{uv\in\mu_{FQ}} F_{\mu_{FQ}}(uv))$.
From the below figure, $S(G) = (1.4, 0.7, 2.6, 2)$

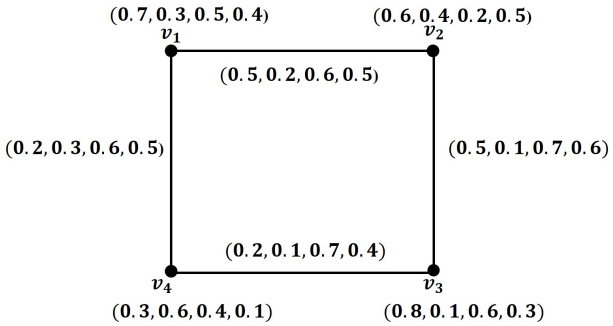


Figure 3: *Fermatean Quadripartitioned Neutrosophic Fuzzy Graph*

Definition 3.4. Let $G_{FQ} = (\sigma_{FQ}, \mu_{FQ})$ be a Fermatean Quadripartitioned Neutrosophic Fuzzy Graph. The Complement of FQNFG is $\overline{G_{FQ}} = (\overline{\sigma_{FQ}}, \overline{\mu_{FQ}})$, where $\overline{\sigma_{FQ}} = (\overline{T_{\sigma_{FQ}}}, \overline{C_{\sigma_{FQ}}}, \overline{I_{\sigma_{FQ}}}, \overline{F_{\sigma_{FQ}}})$ and $\overline{\mu_{FQ}} = (\overline{T_{\sigma_{FQ}}}, \overline{C_{\sigma_{FQ}}}, \overline{I_{\sigma_{FQ}}}, \overline{F_{\sigma_{FQ}}})$ defined by

$$\begin{aligned}
\overline{T_{\mu_{FQ}}} &= |T_{\sigma_{FQ}}(u) \wedge T_{\sigma_{FQ}}(v) - T_{\mu_{FQ}}(uv)| \\
\overline{C_{\mu_{FQ}}} &= |C_{\sigma_{FQ}}(u) \wedge C_{\sigma_{FQ}}(v) - C_{\mu_{FQ}}(uv)| \\
\overline{I_{\mu_{FQ}}} &= |I_{\sigma_{FQ}}(u) \vee I_{\sigma_{FQ}}(v) - I_{\mu_{FQ}}(uv)| \\
\overline{F_{\mu_{FQ}}} &= |F_{\sigma_{FQ}}(u) \vee F_{\sigma_{FQ}}(v) - F_{\mu_{FQ}}(uv)|
\end{aligned}$$

for all $u, v \in \sigma_{FQ}$ and $uv \in \mu_{FQ}$.

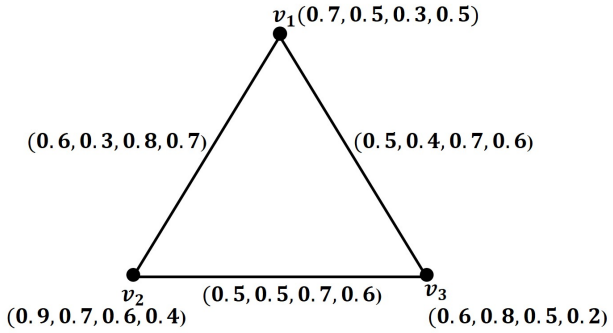


Figure 4: *Fermatean Quadripartitioned Neutrosophic Fuzzy Graph*

Definition 3.5. Let $G_{FQ} = (\sigma_{FQ}, \mu_{FQ})$ be a FQNFG, then order of G_{FQ} is termed as $O(G_{FQ}) = (\sum_{u\in\sigma_{FQ}} T_{\sigma_{FQ}}(u), \sum_{u\in\sigma_{FQ}} C_{\sigma_{FQ}}(u), \sum_{u\in\sigma_{FQ}} I_{\sigma_{FQ}}(u), \sum_{u\in\sigma_{FQ}} F_{\sigma_{FQ}}(u))$.
From figure 3, $O(G) = (2.4, 1.4, 1.7, 1.3)$

Definition 3.6. A Fermatean Quadripartitioned Neutrosophic Fuzzy Graph $G_{FQ} = (\sigma_{FQ}, \mu_{FQ})$ is called as strong, when following criteria are met.

$$\begin{aligned}
T_{\mu_{FQ}}(u, v) &= (T_{\sigma_{FQ}}(u) \wedge T_{\sigma_{FQ}}(v)) \\
C_{\mu_{FQ}}(u, v) &= (C_{\sigma_{FQ}}(u) \wedge C_{\sigma_{FQ}}(v)) \\
I_{\mu_{FQ}}(u, v) &= (I_{\sigma_{FQ}}(u) \vee I_{\sigma_{FQ}}(v)) \\
F_{\mu_{FQ}}(u, v) &= (F_{\sigma_{FQ}}(u) \vee F_{\sigma_{FQ}}(v))
\end{aligned}$$

where $u, v \in \sigma_{FQ}$.

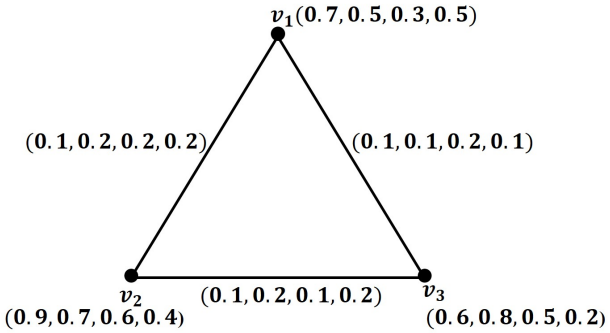


Figure 5: *Complement of FQNFG*

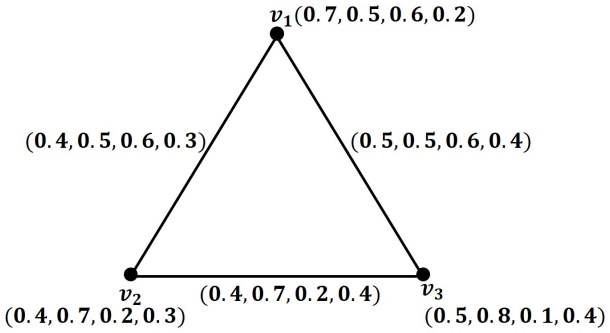


Figure 6: *Strong Fermatean Quadripartitioned Neutrosophic Fuzzy Graph*

4. Products on Fermatean Quadripartitioned Neutrosophic Fuzzy Graph

Definition 4.1. A Composition of two FQNFG G_{FQ1}, G_{FQ2} represented by $G_{FQ1} \circ G_{FQ2}$ and termed as $G_{FQ1} \circ G_{FQ2} = (\sigma_{FQ1} \circ \sigma_{FQ2}, \mu_{FQ1} \circ \mu_{FQ2})$ where

1. $T_{\sigma_{FQ1}\circ\sigma_{FQ2}}(uv) = T_{\sigma_{FQ1}}(u) \wedge T_{\sigma_{FQ2}}(v)$
   $C_{\sigma_{FQ1}\circ\sigma_{FQ2}}(uv) = C_{\sigma_{FQ1}}(u) \wedge C_{\sigma_{FQ2}}(v)$
   $I_{\sigma_{FQ1}\circ\sigma_{FQ2}}(uv) = I_{\sigma_{FQ1}}(u) \vee I_{\sigma_{FQ2}}(v)$
   $F_{\sigma_{FQ1}\circ\sigma_{FQ2}}(uv) = F_{\sigma_{FQ1}}(u) \vee F_{\sigma_{FQ2}}(v)$
   for all $(u, v) \in \sigma_{FQ1} \circ \sigma_{FQ2}$.

2. $T_{\mu_{FQ1}\circ\mu_{FQ2}}(uv_1)(uv_2) = T_{\sigma_{FQ1}}(u) \wedge T_{\mu_{FQ2}}(v_1v_2)$
   $C_{\mu_{FQ1}\circ\mu_{FQ2}}(uv_1)(uv_2) = C_{\sigma_{FQ1}}(u) \wedge C_{\mu_{FQ2}}(v_1v_2)$
   $I_{\mu_{FQ1}\circ\mu_{FQ2}}(uv_1)(uv_2) = I_{\sigma_{FQ1}}(u) \vee I_{\mu_{FQ2}}(v_1v_2)$
   $F_{\mu_{FQ1}\circ\mu_{FQ2}}(uv_1)(uv_2) = F_{\sigma_{FQ1}}(u) \vee F_{\mu_{FQ2}}(v_1v_2)$
   for all $u \in \sigma_{FQ1}, v_1v_2 \in \mu_{FQ2}$

3. $T_{\mu_{FQ1}\circ\mu_{FQ2}}(u_1v)(u_2v) = T_{\mu_{FQ1}}(u_1u_2) \wedge T_{\sigma_{FQ2}}(v)$
   $C_{\mu_{FQ1}\circ\mu_{FQ2}}(u_1v)(u_2v) = C_{\mu_{FQ1}}(u_1u_2) \wedge C_{\sigma_{FQ2}}(v)$
   $I_{\mu_{FQ1}\circ\mu_{FQ2}}(u_1v)(u_2v) = I_{\mu_{FQ1}}(u_1u_2) \vee I_{\sigma_{FQ2}}(v)$
   $F_{\mu_{FQ1}\circ\mu_{FQ2}}(u_1v)(u_2v) = F_{\mu_{FQ1}}(u_1u_2) \vee F_{\sigma_{FQ2}}(v)$
   for all $v \in \sigma_{FQ2}, u_1u_2 \in \mu_{FQ1}$

4. $T_{\mu_{FQ1}\circ\mu_{FQ2}}(u_1v_1)(u_2v_2) = T_{\mu_{FQ1}}(u_1u_2) \wedge T_{\sigma_{FQ2}}(v_1) \wedge T_{\sigma_{FQ2}}(v_2)$
   $C_{\mu_{FQ1}\circ\mu_{FQ2}}(u_1v_1)(u_2v_2) = C_{\mu_{FQ1}}(u_1u_2) \wedge C_{\sigma_{FQ2}}(v_1) \wedge C_{\sigma_{FQ2}}(v_2)$
   $I_{\mu_{FQ1}\circ\mu_{FQ2}}(u_1v_1)(u_2v_2) = I_{\mu_{FQ1}}(u_1u_2) \vee I_{\sigma_{FQ2}}(v_1) \vee T_{\sigma_{FQ2}}(v_2)$
   $F_{\mu_{FQ1}\circ\mu_{FQ2}}(u_1v_1)(u_2v_2) = F_{\mu_{FQ1}}(u_1u_2) \vee F_{\sigma_{FQ2}}(v_1) \vee F_{\sigma_{FQ2}}(v_2)$
   for all $u_1u_2 \in \mu_{FQ1}, v_1v_2 \in \mu_{FQ2}$.

Theorem 4.1. A Composition of two FQNFG is also the Fermatean Quadripartitioned Neutrosophic Fuzzy graph.

Proof. Case I: For $u \in \sigma_{FQ1}, v_1v_2 \in \mu_{FQ2}$

$$\begin{aligned} T_{\mu_{FQ1}\circ\mu_{FQ2}}((uv_1)(uv_2)) &= T_{\sigma_{FQ1}}(u) \wedge T_{\mu_{FQ2}}(v_1v_2) \\ &\leq T_{\sigma_{FQ1}}(u) \wedge [T_{\sigma_{FQ2}}(v_1) \wedge T_{\sigma_{FQ2}}(v_2)] \\ &= [T_{\sigma_{FQ1}}(u) \wedge T_{\sigma_{FQ2}}(v_1)] \wedge [T_{\sigma_{FQ1}}(u) \wedge T_{\sigma_{FQ2}}(v_2)] \\ &= T_{\sigma_{FQ1}\circ\sigma_{FQ2}}(u, v_1) \wedge T_{\sigma_{FQ1}\circ\sigma_{FQ2}}(u, v_2) \end{aligned}$$

$$\begin{aligned} C_{\mu_{FQ1}\circ\mu_{FQ2}}((uv_1)(uv_2)) &= C_{\sigma_{FQ1}}(u) \wedge C_{\mu_{FQ2}}(v_1v_2) \\ &\leq C_{\sigma_{FQ1}}(u) \wedge [C_{\sigma_{FQ2}}(v_1) \wedge C_{\sigma_{FQ2}}(v_2)] \\ &= [C_{\sigma_{FQ1}}(u) \wedge C_{\sigma_{FQ2}}(v_1)] \wedge [C_{\sigma_{FQ1}}(u) \wedge C_{\sigma_{FQ2}}(v_2)] \\ &= C_{\sigma_{FQ1}\circ\sigma_{FQ2}}(u, v_1) \wedge C_{\sigma_{FQ1}\circ\sigma_{FQ2}}(u, v_2) \end{aligned}$$

$$\begin{aligned} I_{\mu_{FQ1}\circ\mu_{FQ2}}((uv_1)(uv_2)) &= I_{\sigma_{FQ1}}(u) \vee I_{\mu_{FQ2}}(v_1v_2) \\ &\geq I_{\sigma_{FQ1}}(u) \vee [I_{\sigma_{FQ2}}(v_1) \vee I_{\sigma_{FQ2}}(v_2)] \\ &= [I_{\sigma_{FQ1}}(u) \vee I_{\sigma_{FQ2}}(v_1)] \vee [I_{\sigma_{FQ1}}(u) \vee I_{\sigma_{FQ2}}(v_2)] \\ &= I_{\sigma_{FQ1}\circ\sigma_{FQ2}}(u, v_1) \vee I_{\sigma_{FQ1}\circ\sigma_{FQ2}}(u, v_2) \end{aligned}$$

$$\begin{aligned} F_{\mu_{FQ1}\circ\mu_{FQ2}}((uv_1)(uv_2)) &= F_{\sigma_{FQ1}}(u) \vee F_{\mu_{FQ2}}(v_1v_2) \\ &\geq F_{\sigma_{FQ1}}(u) \vee [F_{\sigma_{FQ2}}(v_1) \vee F_{\sigma_{FQ2}}(v_2)] \\ &= [F_{\sigma_{FQ1}}(u) \vee F_{\sigma_{FQ2}}(v_1)] \vee [F_{\sigma_{FQ1}}(u) \vee F_{\sigma_{FQ2}}(v_2)] \\ &= F_{\sigma_{FQ1}\circ\sigma_{FQ2}}(u, v_1) \vee F_{\sigma_{FQ1}\circ\sigma_{FQ2}}(u, v_2) \end{aligned}$$

for all $(uv_1, uv_2) \in \mu_{FQ1} \circ \mu_{FQ2}$
Case II: For $v \in \sigma_{FQ2}, (u_1u_2) \in \mu_{FQ1}$

$$\begin{aligned} T_{\mu_{FQ1}\circ\mu_{FQ2}}((u_1v)(u_2v)) &= T_{\mu_{FQ1}}(u_1u_2) \wedge T_{\sigma_{FQ2}}(v) \\ &\leq [T_{\sigma_{FQ1}}(u_1) \wedge T_{\sigma_{FQ1}}(u_2)] \wedge T_{\sigma_{FQ2}}(v) \\ &= [T_{\sigma_{FQ1}}(u_1) \wedge T_{\sigma_{FQ2}}(v)] \wedge [T_{\sigma_{FQ1}}(u_2) \wedge T_{\sigma_{FQ2}}(v)] \\ &= T_{\sigma_{FQ1}\circ\sigma_{FQ2}}(u_1, v) \wedge T_{\sigma_{FQ1}\circ\sigma_{FQ2}}(u_2, v) \end{aligned}$$

$$\begin{aligned} C_{\mu_{FQ1}\circ\mu_{FQ2}}((u_1v)(u_2v)) &= C_{\mu_{FQ1}}(u_1u_2) \wedge C_{\sigma_{FQ2}}(v) \\ &\leq [C_{\sigma_{FQ1}}(u_1) \wedge C_{\sigma_{FQ1}}(u_2)] \wedge C_{\sigma_{FQ2}}(v) \\ &= [C_{\sigma_{FQ1}}(u_1) \wedge C_{\sigma_{FQ2}}(v)] \wedge [C_{\sigma_{FQ1}}(u_2) \wedge C_{\sigma_{FQ2}}(v)] \\ &= C_{\sigma_{FQ1}\circ\sigma_{FQ2}}(u_1, v) \wedge C_{\sigma_{FQ1}\circ\sigma_{FQ2}}(u_2, v) \end{aligned}$$

$$\begin{aligned} I_{\mu_{FQ1}\circ\mu_{FQ2}}((u_1v)(u_2v)) &= I_{\mu_{FQ1}}(u_1u_2) \vee I_{\sigma_{FQ2}}(v) \\ &\geq [I_{\sigma_{FQ1}}(u_1) \vee I_{\sigma_{FQ1}}(u_2)] \vee I_{\sigma_{FQ2}}(v) \\ &= [I_{\sigma_{FQ1}}(u_1) \vee I_{\sigma_{FQ2}}(v)] \vee [I_{\sigma_{FQ1}}(u_2) \vee I_{\sigma_{FQ2}}(v)] \\ &= I_{\sigma_{FQ1}\circ\sigma_{FQ2}}(u_1, v) \vee I_{\sigma_{FQ1}\circ\sigma_{FQ2}}(u_2, v) \end{aligned}$$

$$\begin{aligned} F_{\mu_{FQ1}\circ\mu_{FQ2}}((u_1v)(u_2v)) &= F_{\mu_{FQ1}}(u_1u_2) \vee F_{\sigma_{FQ2}}(v) \\ &\geq [F_{\sigma_{FQ1}}(u_1) \vee F_{\sigma_{FQ1}}(u_2)] \vee F_{\sigma_{FQ2}}(v) \\ &= [F_{\sigma_{FQ1}}(u_1) \vee F_{\sigma_{FQ2}}(v)] \vee [F_{\sigma_{FQ1}}(u_2) \vee F_{\sigma_{FQ2}}(v)] \\ &= F_{\sigma_{FQ1}\circ\sigma_{FQ2}}(u_1, v) \vee F_{\sigma_{FQ1}\circ\sigma_{FQ2}}(u_2, v) \end{aligned}$$

for all $(u_1v, u_2v) \in G_{FQ1} \circ G_{FQ2}$
Case 3: For all $(u_1v_1) \in \mu_{FQ1}, (u_2v_2) \in \mu_{FQ2}$

$$\begin{aligned} T_{\mu_{FQ1}\circ\mu_{FQ2}}(u_1v_1)(u_2v_2) &= T_{\mu_{FQ1}}(u_1u_2) \wedge T_{\sigma_{FQ2}}(v_1) \wedge T_{\sigma_{FQ2}}(v_2) \\ &\leq [T_{\sigma_{FQ1}}(u_1) \wedge T_{\sigma_{FQ1}}(u_2)] \wedge [T_{\sigma_{FQ2}}(v_1) \wedge T_{\sigma_{FQ2}}(v_2)] \\ &= [T_{\sigma_{FQ1}}(u_1) \wedge T_{\sigma_{FQ2}}(v_1)] \wedge [T_{\sigma_{FQ1}}(u_2) \wedge T_{\sigma_{FQ2}}(v_2)] \\ &= T_{\sigma_{FQ1}\circ\sigma_{FQ2}}(u_1, v_1) \wedge T_{\sigma_{FQ1}\circ\sigma_{FQ2}}(u_2, v_2) \end{aligned}$$

$$\begin{aligned} C_{\mu_{FQ1}\circ\mu_{FQ2}}(u_1v_1)(u_2v_2) &= C_{\mu_{FQ1}}(u_1u_2) \wedge C_{\sigma_{FQ2}}(v_1) \wedge C_{\sigma_{FQ2}}(v_2) \\ &\leq [C_{\sigma_{FQ1}}(u_1) \wedge C_{\sigma_{FQ1}}(u_2)] \wedge [C_{\sigma_{FQ2}}(v_1) \wedge C_{\sigma_{FQ2}}(v_2)] \\ &= [C_{\sigma_{FQ1}}(u_1) \wedge C_{\sigma_{FQ2}}(v_1)] \wedge [C_{\sigma_{FQ1}}(u_2) \wedge C_{\sigma_{FQ2}}(v_2)] \\ &= C_{\sigma_{FQ1}\circ\sigma_{FQ2}}(u_1, v_1) \wedge C_{\sigma_{FQ1}\circ\sigma_{FQ2}}(u_2, v_2) \end{aligned}$$

$$\begin{aligned} I_{\mu_{FQ1}\circ\mu_{FQ2}}(u_1v_1)(u_2v_2) &= I_{\mu_{FQ1}}(u_1u_2) \vee I_{\sigma_{FQ2}}(v_1) \vee I_{\sigma_{FQ2}}(v_2) \\ &\geq [I_{\sigma_{FQ1}}(u_1) \vee I_{\sigma_{FQ1}}(u_2)] \vee [I_{\sigma_{FQ2}}(v_1) \vee I_{\sigma_{FQ2}}(v_2)] \\ &= [I_{\sigma_{FQ1}}(u_1) \vee I_{\sigma_{FQ2}}(v_1)] \vee [I_{\sigma_{FQ1}}(u_2) \vee I_{\sigma_{FQ2}}(v_2)] \\ &= I_{\sigma_{FQ1}\circ\sigma_{FQ2}}(u_1, v_1) \vee I_{\sigma_{FQ1}\circ\sigma_{FQ2}}(u_2, v_2) \end{aligned}$$

$$\begin{aligned} F_{\mu_{FQ1}\circ\mu_{FQ2}}(u_1v_1)(u_2v_2) &= F_{\mu_{FQ1}}(u_1u_2) \vee F_{\sigma_{FQ2}}(v_1) \vee F_{\sigma_{FQ2}}(v_2) \\ &\geq [F_{\sigma_{FQ1}}(u_1) \vee T_{\sigma_{FQ1}}(u_2)] \wedge [F_{\sigma_{FQ2}}(v_1) \vee T_{\sigma_{FQ2}}(v_2)] \\ &= [F_{\sigma_{FQ1}}(u_1) \vee F_{\sigma_{FQ2}}(v_1)] \vee [F_{\sigma_{FQ1}}(u_2) \vee F_{\sigma_{FQ2}}(v_2)] \\ &= F_{\sigma_{FQ1}\circ\sigma_{FQ2}}(u_1, v_1) \vee F_{\sigma_{FQ1}\circ\sigma_{FQ2}}(u_2, v_2) \end{aligned}$$

for all $(u_1v_1, u_2v_2) \in \sigma_{FQ1} \circ \sigma_{FQ2}$ ■

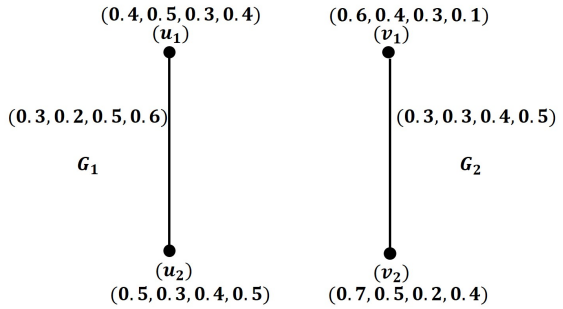


Figure 7: *Fermatean Quadripartitioned Neutrosophic Fuzzy Graph*

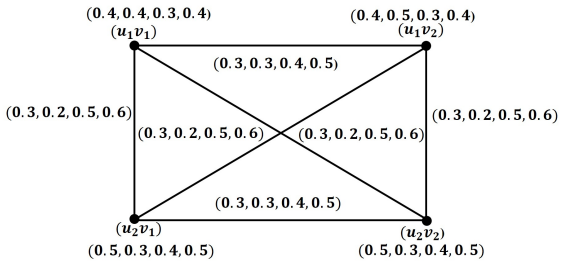


Figure 8: *Composition of FQNFG*

Definition 4.2. The lexicographic product of two FQNFG G_1,G_2 is represented by $G_1 \cdot G_2$ and termed as $G_1 \cdot G_2 = (A_1 \cdot A_2, B_1 \cdot B_2)$

1. $T_{\sigma_{FQ1}\cdot\sigma_{FQ2}}(uv) = T_{\sigma_{FQ1}}(u) \wedge T_{\sigma_{FQ2}}(v)$
   $C_{\sigma_{FQ1}\cdot\sigma_{FQ2}}(uv) = C_{\sigma_{FQ1}}(u) \wedge C_{\sigma_{FQ2}}(v)$
   $I_{\sigma_{FQ1}\cdot\sigma_{FQ2}}(uv) = I_{\sigma_{FQ1}}(u) \vee I_{\sigma_{FQ2}}(v)$
   $F_{\sigma_{FQ1}\cdot\sigma_{FQ2}}(uv) = F_{\sigma_{FQ1}}(u) \vee F_{\sigma_{FQ2}}(v)$
   for all $(u, v) \in \sigma_{FQ1} \cdot \sigma_{FQ2}$.

2. $T_{\mu_{FQ1}\cdot\mu_{FQ2}}(uv_1)(uv_2) = T_{\sigma_{FQ1}}(u) \wedge T_{\mu_{FQ2}}(v_1v_2)$
   $C_{\mu_{FQ1}\cdot\mu_{FQ2}}(uv_1)(uv_2) = C_{\sigma_{FQ1}}(u) \wedge C_{\mu_{FQ2}}(v_1v_2)$
   $I_{\mu_{FQ1}\cdot\mu_{FQ2}}(uv_1)(uv_2) = I_{\sigma_{FQ1}}(u) \vee I_{\mu_{FQ2}}(v_1v_2)$
   $F_{\mu_{FQ1}\cdot\mu_{FQ2}}(uv_1)(uv_2) = F_{\sigma_{FQ1}}(u) \vee F_{\mu_{FQ2}}(v_1v_2)$
   for all $u \in \sigma_{FQ1}, v_1v_2 \in \mu_{FQ2}$.

3. $T_{\mu_{FQ1}\cdot\mu_{FQ2}}(u_1v_1)(u_2v_2) = T_{\mu_{FQ1}}(u_1u_2) \wedge T_{\mu_{FQ2}}(v_1v_2)$
   $C_{\mu_{FQ1}\cdot\mu_{FQ2}}(u_1v_1)(u_2v_2) = C_{\mu_{FQ1}}(u_1u_2) \wedge C_{\mu_{FQ2}}(v_1v_2)$
   $I_{\mu_{FQ1}\cdot\mu_{FQ2}}(u_1v_1)(u_2v_2) = I_{\mu_{FQ1}}(u_1u_2) \vee I_{\mu_{FQ2}}(v_1v_2)$
   $F_{\mu_{FQ1}\cdot\mu_{FQ2}}(u_1v_1)(u_2v_2) = F_{\mu_{FQ1}}(u_1u_2) \vee F_{\mu_{FQ2}}(v_1v_2)$
   for all $u_1u_2 \in \mu_{FQ1}, v_1v_2 \in \mu_{FQ2}$.

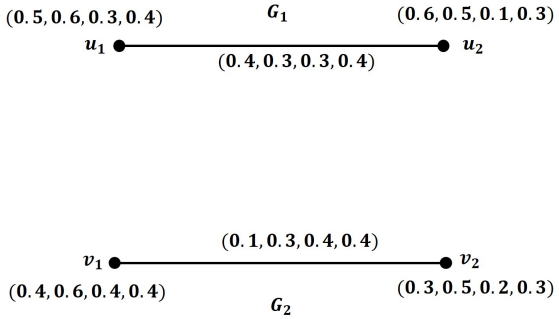


Figure 9: *Fermatean Quadripartitioned Neutrosophic Fuzzy Graph*

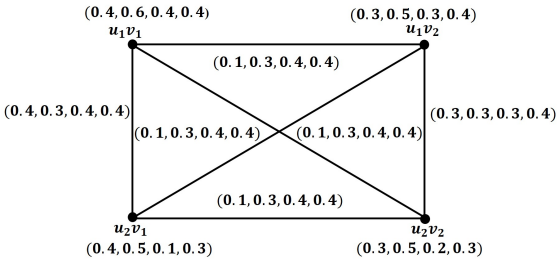


Figure 10: *Lexicographic produt of FQNFG*

Theorem 4.2. A lexicographic product of two FQNFG is also the Fermatean Quadripartitioned Neutrosophic Fuzzy graph.

Proof. To prove the theorem we use the following two cases.
Case I: For $u \in \sigma_{FQ1}, v_1v_2 \in \mu_{FQ2}$

$$\begin{aligned} T_{\mu_{FQ1}\cdot\mu_{FQ2}}((uv_1)(uv_2)) &= T_{\sigma_{FQ1}}(u) \wedge T_{\mu_{FQ2}}(v_1v_2) \\ &\leq T_{\sigma_{FQ1}}(u) \wedge [T_{\sigma_{FQ2}}(v_1) \wedge T_{\sigma_{FQ2}}(v_2)] \\ &= [T_{\sigma_{FQ1}}(u) \wedge T_{\sigma_{FQ2}}(v_1)] \wedge [T_{\sigma_{FQ1}}(u) \wedge T_{\sigma_{FQ2}}(v_2)] \\ &= T_{\sigma_{FQ1}\cdot\sigma_{FQ2}}(u, v_1) \wedge T_{\sigma_{FQ1}\cdot\sigma_{FQ2}}(u, v_2) \end{aligned}$$

$$\begin{aligned} C_{\mu_{FQ1}\cdot\mu_{FQ2}}((uv_1)(uv_2)) &= C_{\sigma_{FQ1}}(u) \wedge C_{\mu_{FQ2}}(v_1v_2) \\ &\leq C_{\sigma_{FQ1}}(u) \wedge [C_{\sigma_{FQ2}}(v_1) \wedge C_{\sigma_{FQ2}}(v_2)] \\ &= [C_{\sigma_{FQ1}}(u) \wedge C_{\sigma_{FQ2}}(v_1)] \wedge [C_{\sigma_{FQ1}}(u) \wedge C_{\sigma_{FQ2}}(v_2)] \\ &= C_{\sigma_{FQ1}\cdot\sigma_{FQ2}}(u,v_1) \wedge C_{\sigma_{FQ1}\cdot\sigma_{FQ2}}(u,v_2) \end{aligned}$$

$$\begin{aligned} I_{\mu_{FQ1}\cdot\mu_{FQ2}}((uv_1)(uv_2)) &= I_{\sigma_{FQ1}}(u) \vee I_{\mu_{FQ2}}(v_1v_2) \\ &\geq I_{\sigma_{FQ1}}(u) \vee [I_{\sigma_{FQ2}}(v_1) \vee I_{\sigma_{FQ2}}(v_2)] \\ &= [I_{\sigma_{FQ1}}(u) \vee I_{\sigma_{FQ2}}(v_1)] \vee [I_{\sigma_{FQ1}}(u) \vee I_{\sigma_{FQ2}}(v_2)] \\ &= I_{\sigma_{FQ1}\cdot\sigma_{FQ2}}(u,v_1) \vee I_{\sigma_{FQ1}\cdot\sigma_{FQ2}}(u,v_2) \end{aligned}$$

$$\begin{aligned} F_{\mu_{FQ1}\cdot\mu_{FQ2}}((uv_1)(uv_2)) &= F_{\sigma_{FQ1}}(u) \vee F_{\mu_{FQ2}}(v_1v_2) \\ &\geq F_{\sigma_{FQ1}}(u) \vee [F_{\sigma_{FQ2}}(v_1) \vee F_{\sigma_{FQ2}}(v_2)] \\ &= [F_{\sigma_{FQ1}}(u) \vee F_{\sigma_{FQ2}}(v_1)] \vee [F_{\sigma_{FQ1}}(u) \vee F_{\sigma_{FQ2}}(v_2)] \\ &= F_{\sigma_{FQ1}\cdot\sigma_{FQ2}}(u,v_1) \vee F_{\sigma_{FQ1}\cdot\sigma_{FQ2}}(u,v_2) \end{aligned}$$

for all $(uv_1, uv_2) \in \mu_{FQ1} \cdot \mu_{FQ2}$
Case II: For all $(u_1v_1) \in \mu_{FQ1}, (u_2v_2) \in \mu_{FQ2}$

$$\begin{aligned} T_{\mu_{FQ1}\cdot\mu_{FQ2}}((u_1v_1)(u_2v_2)) &= T_{\mu_{FQ1}}(u_1u_2) \wedge T_{\mu_{FQ2}}(v_1v_2) \\ &\leq [T_{\sigma_{FQ1}}(u_1) \wedge T_{\sigma_{FQ1}}(u_2)] \wedge [T_{\sigma_{FQ2}}(v_1) \wedge T_{\sigma_{FQ2}}(v_2)] \\ &= [T_{\sigma_{FQ1}}(u_1) \wedge T_{\sigma_{FQ2}}(v_1)] \wedge [T_{\sigma_{FQ1}}(u_2) \wedge T_{\sigma_{FQ2}}(v_2)] \\ &= T_{\sigma_{FQ1}\cdot\sigma_{FQ2}}(u_1,v_1) \wedge T_{\sigma_{FQ1}\cdot\sigma_{FQ2}}(u_2,v_2) \end{aligned}$$

$$\begin{aligned} C_{\mu_{FQ1}\cdot\mu_{FQ2}}((u_1v_1)(u_2v_2)) &= C_{\mu_{FQ1}}(u_1u_2) \wedge C_{\mu_{FQ2}}(v_1v_2) \\ &\leq [C_{\sigma_{FQ1}}(u_1) \wedge C_{\sigma_{FQ1}}(u_2)] \wedge [C_{\sigma_{FQ2}}(v_1) \wedge C_{\sigma_{FQ2}}(v_2)] \\ &= [C_{\sigma_{FQ1}}(u_1) \wedge C_{\sigma_{FQ2}}(v_1)] \wedge [C_{\sigma_{FQ1}}(u_2) \wedge C_{\sigma_{FQ2}}(v_2)] \\ &= C_{\sigma_{FQ1}\cdot\sigma_{FQ2}}(u_1,v_1) \wedge C_{\sigma_{FQ1}\cdot\sigma_{FQ2}}(u_2,v_2) \end{aligned}$$

$$\begin{aligned} I_{\mu_{FQ1}\cdot\mu_{FQ2}}((u_1v_1)(u_2v_2)) &= I_{\mu_{FQ1}}(u_1u_2) \vee I_{\mu_{FQ2}}(v_1v_2) \\ &\geq [I_{\sigma_{FQ1}}(u_1) \vee I_{\sigma_{FQ1}}(u_2)] \vee [I_{\sigma_{FQ2}}(v_1) \vee I_{\sigma_{FQ2}}(v_2)] \\ &= [I_{\sigma_{FQ1}}(u_1) \vee I_{\sigma_{FQ2}}(v_1)] \vee [I_{\sigma_{FQ1}}(u_2) \vee I_{\sigma_{FQ2}}(v_2)] \\ &= I_{\sigma_{FQ1}\cdot\sigma_{FQ2}}(u_1,v_1) \vee I_{\sigma_{FQ1}\cdot\sigma_{FQ2}}(u_2,v_2) \end{aligned}$$

$$\begin{aligned} F_{\mu_{FQ1}\cdot\mu_{FQ2}}((u_1v_1)(u_2v_2)) &= F_{\mu_{FQ1}}(u_1u_2) \vee F_{\mu_{FQ2}}(v_1v_2) \\ &\geq [F_{\sigma_{FQ1}}(u_1) \vee F_{\sigma_{FQ1}}(u_2)] \vee [F_{\sigma_{FQ2}}(v_1) \vee F_{\sigma_{FQ2}}(v_2)] \\ &= [F_{\sigma_{FQ1}}(u_1) \vee F_{\sigma_{FQ2}}(v_1)] \vee [F_{\sigma_{FQ1}}(u_2) \vee F_{\sigma_{FQ2}}(v_2)] \\ &= F_{\sigma_{FQ1}\cdot\sigma_{FQ2}}(u_1,v_1) \vee F_{\sigma_{FQ1}\cdot\sigma_{FQ2}}(u_2,v_2) \end{aligned}$$

for all $(u_1v_1, u_2v_2) \in \sigma_{FQ1} \cdot \sigma_{FQ2}$
This completes the proof. ■

Definition 4.3. A Cartesian product of two FQNFG G_{FQ1},G_{FG2} and also represented by G_{FQ1} cartesian product G_{FQ2} is termed as
$G_{FQ1} \times G_{FQ2} = (\sigma_{FQ1} \times \sigma_{FQ2}, \mu_{FQ1} \times \mu_{FQ2})$

1. $T_{\sigma_{FQ1}\times\sigma_{FQ2}}(uv) = T_{\sigma_{FQ1}}(u) \wedge T_{\sigma_{FQ2}}(v)$
   $C_{\sigma_{FQ1}\times\sigma_{FQ2}}(uv) = C_{\sigma_{FQ1}}(u) \wedge C_{\sigma_{FQ2}}(v)$
   $I_{\sigma_{FQ1}\times\sigma_{FQ2}}(uv) = I_{\sigma_{FQ1}}(u) \vee I_{\sigma_{FQ2}}(v)$
   $F_{\sigma_{FQ1}\times\sigma_{FQ2}}(uv) = F_{\sigma_{FQ1}}(u) \vee F_{\sigma_{FQ2}}(v)$
   for all $(u, v) \in \sigma_{FQ1} \times \sigma_{FQ2}$
   The membership value of the links $\mu_{FQ1} \times \mu_{FQ2}$ is determined as

2. $T_{\mu_{FQ1}\times\mu_{FQ2}}(uv_1)(uv_2) = T_{\sigma_{FQ1}}(u) \wedge T_{\mu_{FQ2}}(v_1v_2)$
$C_{\mu_{FQ1}\times\mu_{FQ2}}(uv_1)(uv_2) = C_{\sigma_{FQ1}}(u) \wedge C_{\mu_{FQ2}}(v_1v_2)$
$I_{\mu_{FQ1}\times\mu_{FQ2}}(uv_1)(uv_2) = I_{\sigma_{FQ1}}(u) \vee I_{\mu_{FQ2}}(v_1v_2)$
$F_{\mu_{FQ1}\times\mu_{FQ2}}(uv_1)(uv_2) = F_{\sigma_{FQ1}}(u) \vee F_{\mu_{FQ2}}(v_1v_2)$
for all $u \in \sigma_{FQ1}, (v_1, v_2) \in \mu_{FQ2}$

3. $T_{\mu_{FQ1}\times\mu_{FQ2}}(u_1v)(u_2v) = T_{\mu_{FQ1}}(u_1u_2) \wedge T_{\sigma_{FQ2}}(v)$
$C_{\mu_{FQ1}\times\mu_{FQ2}}(u_1v)(u_2v) = C_{\mu_{FQ1}}(u_1u_2) \wedge C_{\sigma_{FQ2}}(v)$
$I_{\mu_{FQ1}\times\mu_{FQ2}}(u_1v)(u_2v) = I_{\mu_{FQ1}}(u_1u_2) \vee I_{\sigma_{FQ2}}(v)$
$F_{\mu_{FQ1}\times\mu_{FQ2}}(u_1v)(u_2v) = F_{\mu_{FQ1}}(u_1u_2) \vee F_{\sigma_{FQ2}}(v)$
for all $v \in \sigma_{FQ2}, (u_1u_2) \in \mu_{FQ1}$

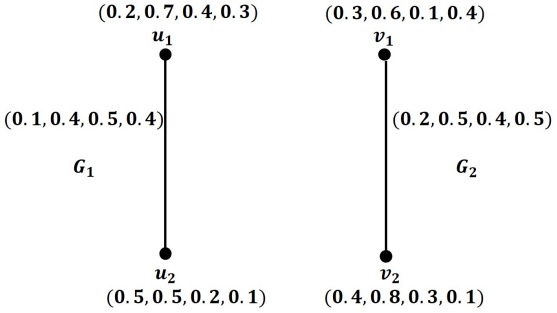


Figure 11: *Fermatean Quadripartitioned Neutrosophic Fuzzy Graph*

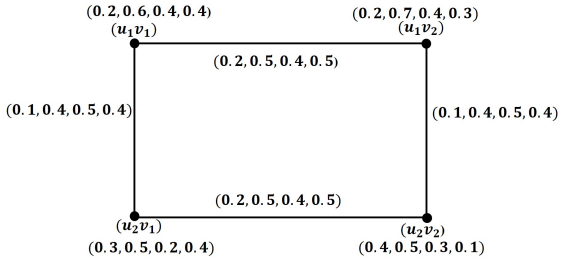


Figure 12: *Cartesian Product of FQNFG*

Theorem 4.3. A Cartesian Product of two FQNFG is a Fermatean Quadripartitioned Neutrosophic Fuzzy Graph.

Proof. To prove the theorem we use the following two cases.
Case I: For $u \in \sigma_{FQ1}, (v_1v_2) \in \mu_{FQ2}$

$$\begin{aligned} T_{\mu_{FQ1}\times\mu_{FQ2}}((uv_1)(uv_2)) &= T_{\sigma_{FQ1}}(u) \wedge T_{\mu_{FQ2}}(v_1v_2) \\ &\leq T_{\sigma_{FQ1}}(u) \wedge [T_{\sigma_{FQ2}}(v_1) \wedge T_{\sigma_{FQ2}}(v_2)] \\ &= [T_{\sigma_{FQ1}}(u) \wedge T_{\sigma_{FQ2}}(v_1)] \wedge [T_{\sigma_{FQ1}}(u) \wedge T_{\sigma_{FQ2}}(v_2)] \\ &= T_{\sigma_{FQ1}\times\sigma_{FQ2}}(u, v_1) \wedge T_{\sigma_{FQ1}\times\sigma_{FQ2}}(u, v_2) \end{aligned}$$

$$\begin{aligned} C_{\mu_{FQ1}\times\mu_{FQ2}}((uv_1)(uv_2)) &= C_{\sigma_{FQ1}}(u) \wedge C_{\mu_{FQ2}}(v_1v_2) \\ &\leq C_{\sigma_{FQ1}}(u) \wedge [C_{\sigma_{FQ2}}(v_1) \wedge C_{\sigma_{FQ2}}(v_2)] \\ &= [C_{\sigma_{FQ1}}(u) \wedge C_{\sigma_{FQ2}}(v_1)] \wedge [C_{\sigma_{FQ1}}(u) \wedge C_{\sigma_{FQ2}}(v_2)] \\ &= C_{\sigma_{FQ1}\times\sigma_{FQ2}}(u, v_1) \wedge C_{\sigma_{FQ1}\times\sigma_{FQ2}}(u, v_2) \end{aligned}$$

$$\begin{aligned} I_{\mu_{FQ1}\times\mu_{FQ2}}((uv_1)(uv_2)) &= I_{\sigma_{FQ1}}(u) \vee I_{\mu_{FQ2}}(v_1v_2) \\ &\geq I_{\sigma_{FQ1}}(u) \vee [I_{\sigma_{FQ2}}(v_1) \vee I_{\sigma_{FQ2}}(v_2)] \\ &= [I_{\sigma_{FQ1}}(u) \vee I_{\sigma_{FQ2}}(v_1)] \vee [I_{\sigma_{FQ1}}(u) \vee I_{\sigma_{FQ2}}(v_2)] \\ &= I_{\sigma_{FQ1}\times\sigma_{FQ2}}(u,v_1) \vee I_{\sigma_{FQ1}\times\sigma_{FQ2}}(u,v_2) \end{aligned}$$

$$\begin{aligned} F_{\mu_{FQ1}\times\mu_{FQ2}}((uv_1)(uv_2)) &= F_{\sigma_{FQ1}}(u) \vee F_{\mu_{FQ2}}(v_1v_2) \\ &\geq F_{\sigma_{FQ1}}(u) \vee [F_{\sigma_{FQ2}}(v_1) \vee F_{\sigma_{FQ2}}(v_2)] \\ &= [F_{\sigma_{FQ1}}(u) \vee F_{\sigma_{FQ2}}(v_1)] \vee [F_{\sigma_{FQ1}}(u) \vee F_{\sigma_{FQ2}}(v_2)] \\ &= F_{\sigma_{FQ1}\times\sigma_{FQ2}}(u,v_1) \vee F_{\sigma_{FQ1}\times\sigma_{FQ2}}(u,v_2) \end{aligned}$$

for all $(uv_1, uv_2) \in G_{FQ1} \times G_{FQ2}$
Case II: For $v \in \sigma_{FQ2}, (u_1u_2) \in \mu_{FQ1}$

$$\begin{aligned} T_{\mu_{FQ1}\times\mu_{FQ2}}((u_1v)(u_2v)) &= T_{\mu_{FQ1}}(u_1u_2) \wedge T_{\sigma_{FQ2}}(v) \\ &\leq [T_{\sigma_{FQ1}}(u_1) \wedge T_{\sigma_{FQ1}}(u_2)] \wedge T_{\sigma_{FQ2}}(v) \\ &= [T_{\sigma_{FQ1}}(u_1) \wedge T_{\sigma_{FQ2}}(v)] \wedge [T_{\sigma_{FQ1}}(u_2) \wedge T_{\sigma_{FQ2}}(v)] \\ &= T_{\sigma_{FQ1}\times\sigma_{FQ2}}(u_1,v) \wedge T_{\sigma_{FQ1}\times\sigma_{FQ2}}(u_2,v) \end{aligned}$$

$$\begin{aligned} C_{\mu_{FQ1}\times\mu_{FQ2}}((u_1v)(u_2v)) &= C_{\mu_{FQ1}}(u_1u_2) \wedge C_{\sigma_{FQ2}}(v) \\ &\leq [C_{\sigma_{FQ1}}(u_1) \wedge C_{\sigma_{FQ1}}(u_2)] \wedge C_{\sigma_{FQ2}}(v) \\ &= [C_{\sigma_{FQ1}}(u_1) \wedge C_{\sigma_{FQ2}}(v)] \wedge [C_{\sigma_{FQ1}}(u_2) \wedge C_{\sigma_{FQ2}}(v)] \\ &= C_{\sigma_{FQ1}\times\sigma_{FQ2}}(u_1,v) \wedge C_{\sigma_{FQ1}\times\sigma_{FQ2}}(u_2,v) \end{aligned}$$

$$\begin{aligned} I_{\mu_{FQ1}\times\mu_{FQ2}}((u_1v)(u_2v)) &= I_{\mu_{FQ1}}(u_1u_2) \vee I_{\sigma_{FQ2}}(v) \\ &\geq [I_{\sigma_{FQ1}}(u_1) \vee I_{\sigma_{FQ1}}(u_2)] \vee I_{\sigma_{FQ2}}(v) \\ &= [I_{\sigma_{FQ1}}(u_1) \vee I_{\sigma_{FQ2}}(v)] \vee [I_{\sigma_{FQ1}}(u_2) \vee I_{\sigma_{FQ2}}(v)] \\ &= I_{\sigma_{FQ1}\times\sigma_{FQ2}}(u_1,v) \vee I_{\sigma_{FQ1}\times\sigma_{FQ2}}(u_2,v) \end{aligned}$$

$$\begin{aligned} F_{\mu_{FQ1}\times\mu_{FQ2}}((u_1v)(u_2v)) &= F_{\mu_{FQ1}}(u_1u_2) \vee F_{\sigma_{FQ2}}(v) \\ &\geq [F_{\sigma_{FQ1}}(u_1) \vee F_{\sigma_{FQ1}}(u_2)] \vee F_{\sigma_{FQ2}}(v) \\ &= [F_{\sigma_{FQ1}}(u_1) \vee F_{\sigma_{FQ2}}(v)] \vee [F_{\sigma_{FQ1}}(u_2) \vee F_{\sigma_{FQ2}}(v)] \\ &= F_{\sigma_{FQ1}\times\sigma_{FQ2}}(u_1,v) \vee F_{\sigma_{FQ1}\times\sigma_{FQ2}}(u_2,v) \end{aligned}$$

for all $(u_1v, u_2v) \in G_{FQ1} \times G_{FQ2}$
Hence the proof. ■

Definition 4.4. A Cross Product of two FQNFG is represented by $G_{FQ1} \star G_{FQ2} = (\sigma_{FQ1} \star \sigma_{FQ2}, \mu_{FQ1} \star \mu_{FQ2})$ and defined as

1. $T_{\sigma_{FQ1}\star\sigma_{FQ2}}(uv) = T_{\sigma_{FQ1}}(u) \wedge T_{\sigma_{FQ2}}(v)$
   $C_{\sigma_{FQ1}\star\sigma_{FQ2}}(uv) = C_{\sigma_{FQ1}}(u) \wedge C_{\sigma_{FQ2}}(v)$
   $I_{\sigma_{FQ1}\star\sigma_{FQ2}}(uv) = I_{\sigma_{FQ1}}(u) \vee I_{\sigma_{FQ2}}(v)$
   $F_{\sigma_{FQ1}\star\sigma_{FQ2}}(uv) = F_{\sigma_{FQ1}}(u) \vee F_{\sigma_{FQ2}}(v)$
   for all $(u,v) \in \sigma_{FQ1} \star \sigma_{FQ2}$
2. $T_{\mu_{FQ1}\star\mu_{FQ2}}(u_1v_1)(u_2v_2) = T_{\mu_{FQ1}}(u_1u_2) \wedge T_{\mu_{FQ2}}(v_1v_2)$
   $C_{\mu_{FQ1}\star\mu_{FQ2}}(u_1v_1)(u_2v_2) = C_{\mu_{FQ1}}(u_1u_2) \wedge C_{\mu_{FQ2}}(v_1v_2)$
   $I_{\mu_{FQ1}\star\mu_{FQ2}}(u_1v_1)(u_2v_2) = I_{\mu_{FQ1}}(u_1u_2) \vee I_{\mu_{FQ2}}(v_1v_2)$
   $F_{\mu_{FQ1}\star\mu_{FQ2}}(u_1v_1)(u_2v_2) = F_{\mu_{FQ1}}(u_1u_2) \vee F_{\mu_{FQ2}}(v_1v_2)$
   for all $(u_1u_2) \in \mu_{FQ1}, (v_1v_2) \in \mu_{FQ2}$

Theorem 4.4. A Cross Product of two FQNFG is a replica of the Fermatean Quadrapartitioned Neutrosophic Fuzzy Graph.

Proof. For all $(u_1v_1, u_2v_2) \in G_{FQ1} \star G_{FQ2}$

$$\begin{aligned} T_{\mu_{FQ1}\star\mu_{FQ2}}(u_1v_1)(u_2v_2) &= T_{\mu_{FQ1}}(u_1u_2) \wedge T_{\mu_{FQ2}}(v_1v_2) \\ &\leq [T_{\sigma_{FQ1}}(u_1) \wedge T_{\sigma_{FQ1}}(u_2)] \wedge [T_{\sigma_{FQ2}}(v_1) \wedge T_{\sigma_{FQ2}}(v_2)] \\ &= [T_{\sigma_{FQ1}}(u_1) \wedge T_{\sigma_{FQ2}}(v_1)] \wedge [T_{\sigma_{FQ1}}(u_2) \wedge T_{\sigma_{FQ2}}(v_2)] \\ &= T_{\sigma_{FQ1}\star\sigma_{FQ2}}(u_1, v_1) \wedge T_{\sigma_{FQ1}\star\sigma_{FQ2}}(u_2, v_2) \end{aligned}$$

$$\begin{aligned} C_{\mu_{FQ1}\star\mu_{FQ2}}(u_1v_1)(u_2v_2) &= C_{\mu_{FQ1}}(u_1u_2) \wedge C_{\mu_{FQ2}}(v_1v_2) \\ &\leq [C_{\sigma_{FQ1}}(u_1) \wedge C_{\sigma_{FQ1}}(u_2)] \wedge [C_{\sigma_{FQ2}}(v_1) \wedge C_{\sigma_{FQ2}}(v_2)] \\ &= [C_{\sigma_{FQ1}}(u_1) \wedge C_{\sigma_{FQ2}}(v_1)] \wedge [C_{\sigma_{FQ1}}(u_2) \wedge C_{\sigma_{FQ2}}(v_2)] \\ &= C_{\sigma_{FQ1}\star\sigma_{FQ2}}(u_1, v_1) \wedge C_{\sigma_{FQ1}\star\sigma_{FQ2}}(u_2, v_2) \end{aligned}$$

$$\begin{aligned} I_{\mu_{FQ1}\star\mu_{FQ2}}(u_1v_1)(u_2v_2) &= I_{\mu_{FQ1}}(u_1u_2) \vee I_{\mu_{FQ2}}(v_1v_2) \\ &\geq [I_{\sigma_{FQ1}}(u_1) \vee I_{\sigma_{FQ1}}(u_2)] \vee [I_{\sigma_{FQ2}}(v_1) \vee I_{\sigma_{FQ2}}(v_2)] \\ &= [I_{\sigma_{FQ1}}(u_1) \vee I_{\sigma_{FQ2}}(v_1)] \vee [I_{\sigma_{FQ1}}(u_2) \vee I_{\sigma_{FQ2}}(v_2)] \\ &= I_{\sigma_{FQ1}\star\sigma_{FQ2}}(u_1, v_1) \vee I_{\sigma_{FQ1}\star\sigma_{FQ2}}(u_2, v_2) \end{aligned}$$

$$\begin{aligned} F_{\mu_{FQ1}\star\mu_{FQ2}}(u_1v_1)(u_2v_2) &= F_{\mu_{FQ1}}(u_1u_2) \vee F_{\mu_{FQ2}}(v_1v_2) \\ &\geq [F_{\sigma_{FQ1}}(u_1) \vee F_{\sigma_{FQ1}}(u_2)] \vee [F_{\sigma_{FQ2}}(v_1) \vee F_{\sigma_{FQ2}}(v_2)] \\ &= [F_{\sigma_{FQ1}}(u_1) \vee F_{\sigma_{FQ2}}(v_1)] \vee [F_{\sigma_{FQ1}}(u_2) \vee F_{\sigma_{FQ2}}(v_2)] \\ &= F_{\sigma_{FQ1}\star\sigma_{FQ2}}(u_1, v_1) \vee F_{\sigma_{FQ1}\star\sigma_{FQ2}}(u_2, v_2) \end{aligned}$$

Hence the proof. ■

5. Conclusion

The Quadripartitioned Neutrosophic Set is a generalization of Neutrosophic Set. A novel concept called the Fermatean Quadripartitioned Neutrosophic Fuzzy Graph (FQNFG) is defined. Its fundamental properties and products were discussed. The proposed concept is also applicable to bipolar Fermatean Quadrapartitioned Neutrosophic graph, Interval vaued Fermatean Quadrapartitioned Neutrosophic graph and so on. The FQNFG can be applied to a variety of applications, including expert systems, image processing, computer networks and social systems.

References

[1] Zadeh, L.A. (1965). Fuzzy sets. *Information and Control, Elsevier*, 8(3):338-353.
[2] Rosenfeld, A. Z. R. I. E. L. (1975). Fuzzy graphs In: LA Zadeh, KS Fu and M. Shimura, Eds., *Fuzzy Sets and Their Applications*, 77-95
[3] Divya, G., and Malarvizhi, J. (2017). Some operations on neutrosophic fuzzy graphs. *Infinite Study*, 8:120-125.
[4] Hussain, S. S., Hussain, R. J., and Smarandache, F. (2019). On neutrosophic vague graphs. *Infinite Study*, 28:245-258.
[5] Senapati, T., and Yager, R. (2019). Fermatean Fuzzy Sets. *Journal of Ambient Intelligence and Humanized Computing*, 11:663-674.
[6] Senapati. T., and Yager, R. (2019). Some new operations over Fermatean fuzzy numbers and application of Fermatean fuzzy WPM in multiple criteria decision making. *In Informatics*, 30(2):391-412.

[7] Thamizhendhi, G., Kiruthica, C., and Suresh S. (2011). Fermatean Fuzzy Hypergraph. *Journal of Hunan University Natural Sciences*, 48(12):2333-2340.

[8] Antony Crispin Sweety, C., and Jansi, R. (2021). Fermatean Neutrosophic sets. *International Journal of Advanced Research in Computer and Communication Engineering*, 10(6):24-27.

[9] Broumi, S., Sundareswaran, R., Shanmugapriya, M., Bakali, A., and Talea, M. (2022). Theory and applications of fermatean neutrosophic graphs. *Neutrosophic sets and systems*, 50:248-286.

[10] Hussain, S. S., Durga, N., Hossein, R., and Ganesh, G. (2022). New concepts on quadripartitioned single-valued neutrosophic graph with real-life application. *International Journal of Fuzzy Systems*, 24(3):1515-1529.

[11] Hussain, S. S., Muhiuddin, G., Durga, N., and Al-Kadi, D. (2021). New concepts on quadripartitioned bipolar single valued neutrosophic graph. *CMES-Computer Modeling in Engineering and Sciences*, 130(1):559-580.

[12] Belnap, N. D. (1977). A useful four-valued logic. *Modern uses of multiple-valued logic*, Dordrecht: Springer.

[13] Shil, B., Das, R., Das, S., Tripathy, B. C., and Granados, C. (2022). Degree, Order and Size of Single-Valued Quadripartitioned Neutrosophic Graph. *BISTUA Revista de la Facultad de Ciencias Básicas*, 20(1):63-69.

[14] Akram, M., and Shahzadi, G. (2017). Operations on single-valued neutrosophic graphs. *Infinite Study*, 11(1):1-26.

[15] Satham Hussain, S., Hossein Rashmonlou, F., Mofidnakhaei, R., Hussain, J., Sahoo, S. and Broumi, S. (2022). Quadipartitioned Neutrosophic Graph Structures. *Neutrosophic Sets and Systems*, 51.

[16] Gani, A. N., and Ahamed, M. B. (2003). Order and size in fuzzy graphs. *Bulletin of pure and applied sciences*, 22(1):145-148.

[17] Smarandache, F. (2015). Types of Neutrosophic Graphs and neutrosophic Algebraic Structures together with their Applications in Technology, seminar. *Universitatea Transilvania din Brasov, Facultatea de Design de Produs si Mediu, Brasov, Romania*, 6.

[18] Broumi, S., Sundareswaran, R., Shanmugapriya, M., Nordo, G., Talea, M., Bakali, A., and Smarandache, F. (2022). Interval-valued fermatean neutrosophic graphs. *Collected Papers*, 13:496.

[19] Edalatpanah, S., Lotfi, F. H., Kerstens, K., and Wanke, P. (2024). Analytical Decision Making and Data Envelopment Analysis. *Springer, Singapore.*

RELIABILITY BASED AN ATTRIBUTE CONTROL CHART USING EXPONENTIATED EXPONENTIAL-POISSON DISTRIBUTION UNDER HYBRID CENSORING

B. Gokila[1] and A. Sheik Abdullah[1*]

•

[1] PG & Research Department of Statistics, Salem Sowdeswari College, Salem-10, India.
[1]gokilastat@gmail.com, [1*]sheik.stat@gmail.com
Correspondence Email: sheik.stat@gmail.com

Abstract

The Exponentiated Exponential-Poisson (EEP) distribution, an advanced extension of traditional lifetime models, offers greater adaptability in representing product lifetimes by more precisely capturing variations in failure rates. To handle incomplete lifetime data, a Hybrid censoring technique is employed, combining elements of both Type-I and Type-II censoring to establish a more robust methodology for lifetime analysis. Naturally, np control charts are used to monitor the count of defective units within a sample. The primary aim is to detect shifts in product lifetime distributions, which are crucial for quality control and reliability assessment. However, this study introduces a modification to the control chart, shifting its focus from simply counting failures to tracking the median lifetime, thereby enhancing its capability to identify changes in product reliability over time. The efficiency of the control chart is measured using the Average Run Length (ARL), which estimates the expected number of observations before an out-of-control signal is triggered. By carefully adjusting the chart's parameters, the study ensures that the in-control ARL aligns closely with a predefined target, thereby improving its reliability. This research is dedicated to developing an np control chart designed to monitor the median lifetime of products that follow the EEP distribution within a Hybrid censoring Scheme. Numerical examples and simulated data are provided to illustrate its real-world applicability. By optimizing control chart parameters based on ARL, the study enhances monitoring precision for product reliability, making it a valuable tool in industries where accurate lifetime assessment is critical.

Keywords: Exponentiated Exponential-Poisson distribution, Hybrid Censoring Scheme, Control Chart, Average Run length.

I. Introduction

In Recent days statistical society, quality has become a given, particularly in the manufacturing sector. To accomplish the objective in such a setting, each product must meet the necessary quality criteria. The process of using statistical methods to systematically monitor and maintain the manufactured product's quality is called statistical quality control (SQC). In manufacturing settings, SQC plays a crucial role in the creation and upkeep of high-quality products. To effectively manage the production process under various conditions, numerous innovative control chart techniques have been introduced. There are two primary types of control charts: attribute control charts and variable control charts. Attribute control charts are utilized to differentiate

between conforming and non-conforming items, while variable control charts are employed when analyzing industrial data obtained from the measurement process. A control chart serves as a graphical tool for analysing the fluctuations of a process over time. Each control chart features at least two control limits, designated as the lower control limit (LCL) and the upper control limit (UCL). It is asserted that the process is considered to be in control when the control statistic remains within these limits.

Lifetime is considered a critical quality attribute for certain products. Life testing is employed to manage the manufacturing process of these items. Based on the outcomes of the life test, a product may be categorized as either conforming or non-conforming. This type of testing is time-intensive due to the prolonged duration of the tests. In such cases, the application of censoring techniques is vital and should not be overlooked. Various censoring methods utilized in life testing include Type-I, Type-II, and Hybrid censoring. Under Hybrid censoring, the life test concludes at the earliest of the predetermined test time t or the moment when the (UCL + 1)th failure is recorded. If the number of failures noted during the life test falls between the upper control limit (UCL) and lower control limit (LCL) at time t, the production process is deemed to be in control otherwise, it is considered out of control. The proportion of defective items is monitored using attribute control charts, such as the np control chart, which operates under the assumption that the quality characteristic follows a normal distribution. However, the actual distribution of quality characteristics may deviate from normality. If industrial engineers rely on the current control chart under these circumstances, they may be misled, resulting in an increase in the number of non-conforming products.

II. Review of Literature

While many researchers have contributed to attribute control charts for lifetime distributions, a gap remains in studying control charts for non-normal distributions like the Exponentiated Exponential-Poisson with Hybrid censoring, despite the growing interest in exponentiated models for reliability and life testing. Gunasekaran [7] proposed a control chart for attribute np that utilizes the exponentiated exponential distribution to oversee product lifetimes in the context of accelerated life tests with hybrid censoring, focusing on the optimization of ARL parameters and confirming its efficacy through simulations. Coşkun Kuş [10] paper introduced a two-parameter lifetime distribution with a decreasing failure rate, exploring its statistical properties, estimation via the EM algorithm, simulation-based validation, and real data applications for reliability analysis. Aslam and Jun [3] proposed an optimized attribute control chart based on a Weibull distribution and truncated life test to enhance process monitoring, detect variations efficiently, and improve industrial quality control. Baklizi and Ghannam [5] proposed an attribute control chart for the inverse Weibull distribution under truncated life tests, using failure counts to monitor quality, optimizing parameters via simulations, and validating its performance through ARL analysis and a practical example. Jayadurga et al., [8] proposed an attribute np control chart using repetitive group sampling under truncated life tests to monitor process mean life, optimizing parameters for target ARL, providing ARL tables, and demonstrating its superior shift detection through simulations. Kavitha and Gunasekaran [9] proposed a control chart based on the Exponentiated Exponential Distribution, deriving percentile-based control limits to enhance shift detection and providing tables for practical industrial application.

Al-Marshadi et al., [2] A proposed an advanced attribute control chart using the neutrosophic Weibull distribution to enhance precision in detecting indeterminacy effects, improve monitoring efficiency, and outperform existing methods in industrial quality control. Balamurali and Jeyadurga [6] proposed an attribute np control chart using multiple deferred state sampling and time-truncated life tests to monitor product mean life, optimizing parameters for

accurate ARL estimation and validating its effectiveness through simulations. Shaheen et al., [16] developed a control chart for monitoring process variation in lognormal distributions using repetitive sampling, deriving control limits based on distribution parameters and evaluating performance through average run length (ARL) metrics, demonstrating superior detection of small to moderate shifts compared to traditional Shewhart S-charts. Rao and Edwin Paul [18] developed an attribute control chart for time-truncated life tests based on a log-logistic distribution, deriving control limits using failure counts within a specified truncation time and evaluating its performance through Monte Carlo simulations and ARL metrics, demonstrating its superiority in detecting process shifts compared to existing control charts. Nanthakumar and Kavitha [14] proposed an attribute control chart for monitoring product lifetimes under Type-I censoring using the inverse Rayleigh distribution, evaluating its performance through ARL metrics and numerical examples.

Rao [17] developed an attribute control chart for time-truncated life tests based on the exponentiated half logistic distribution, evaluating its performance using average run length (ARL) metrics and Monte Carlo simulations, with results demonstrating its superiority over existing control charts through extensive ARL tables and simulated industrial data. Tibor [20] revisited the three-parameter exponentiated exponential Poisson (EEP) distribution, deriving closed-form expressions for its characteristic function and moment generating function while validating the applicability of existing series and integral expressions for positive integer-order moments under the condition $\nu > 1 - \alpha$, where $\alpha > 0$. Tahir and Cordeiro [13] reviewed univariate distribution compounding methods, introduced new generalized classes, and explored the evolution, trends, and future directions of distribution generalization. Shafqat et al., [15] proposed a Shewhart-type attribute control chart for truncated life tests across various lifetime distributions, evaluating its effectiveness using ARL analysis. Adeoti and ogundipe [1] developed an advanced control chart using a modified chain sampling plan (MchSP) based on a generalized exponential distribution (GED) to enhance industrial quality control by effectively detecting process shifts through real and simulated data analysis. Aldosari and Jun [11] proposed an attribute control chart combining multiple dependent state sampling with repetitive sampling, enhancing sensitivity to small process shifts and outperforming traditional charts in detection efficiency. Aslam and Hyuck [4] propose a variable control chart based on a time-truncated life test for the Weibull distribution, optimizing control limits and run length properties to enhance industrial process monitoring and detect shifts effectively. Rao et al., [19] introduced an attribute control chart for the Dagum distribution under truncated life tests, evaluating its effectiveness using ARL analysis and real-life applications.

Ristic and Nadarajah [12] introduced a three-parameter lifetime distribution, analyzed its statistical properties, proposed univariate and bivariate generalizations, and demonstrated its superiority over existing models using real data. The Exponentiated Exponential-Poisson distribution was initially proposed by Ristic and Nadarajah and it has been demonstrated that this distribution is particularly well-suited for certain types of lifetime data compared to other widely utilized lifetime distributions. The analysis of lifetime data has proven to be notably effective when employing the Exponentiated Exponential-Poisson distribution. This study introduces an attribute control chart based on the Exponentiated Exponential-Poisson distribution within a Hybrid censoring Scheme. The coefficient for the control chart was established, and the performance of the proposed chart was evaluated in terms of the Average Run Length. The design of the control chart is adapted in response to variations in the median of the process scale parameter. The applicability of the proposed control chart is illustrated through the use of simulated data.

The structure of this paper is organized as follows: Section 2 presents a review of the relevant

literature. Section 3 introduces the Exponentiated Exponential-Poisson distribution and details the design of the proposed control chart. Section 4 describes the simulation study, and Section 5 concludes the paper by summarizing the key findings and insights.

III. Design of the control chart

If a random variable t has the Exponentiated Exponential-Poisson distribution with parameters (β, λ, α) denoting the lifetime of a product in some production process then the density function is given by

$$f(t) = \frac{\alpha\beta\lambda e^{-\beta t}(1-e^{-\beta t})^{\alpha-1}e^{-\lambda(1-e^{-\beta t})^{\alpha}}}{1-e^{-\lambda}}, t, \lambda, \alpha, \beta > 0 \quad (1)$$

and the cumulative density function of the model can be obtained as

$$F(t) = \frac{1-e^{-\lambda(1-e^{-\beta t})^{\alpha}}}{1-e^{-\lambda}}, t, \lambda, \alpha, \beta > 0 \quad (2)$$

The lifetime of the units follows Exponentiated Exponential – Poisson Distribution with a median life defined as

$$m_0 = \left(-\frac{1}{\beta}\right) log\{1 - [-\frac{1}{\lambda} log[\,1 - 2^{-1}(1 - e^{-\lambda})]]^{\frac{1}{\alpha}}\} \quad (3)$$

The truncation time t_0 and failure arise from time saving considerations in life testing. In the simulation study for each generated subgroup, we count the number of failures whose lifetimes are ≤ t_0 where the truncation time is determined by

$$t_0 = am_0 \quad (4)$$

where t_0 is the truncated time, a is the truncation coefficient and m_0 is the desired median life of the product. The probability of failure before t_0 is given by

$$p = \frac{1-e^{-\lambda(1-e^{-\beta t_0})^{\alpha}}}{1-e^{-\lambda}}, t, \lambda, \alpha, \beta > 0 \quad (5)$$

using equation (3), the probability of failure of a product when the process is in control is

$$p_0 = \frac{1-e^{-\lambda\left\{1-\left[1-\left[-\frac{1}{\lambda}\log\left(\frac{1+e^{-\lambda}}{2}\right)\right]^{\frac{1}{\alpha}}\right]^{a}\right\}^{\alpha}}}{1-e^{-\lambda}} \quad (6)$$

when the median shifts to m_1, the probability of failure of a product becomes
Let $m_1 = fm_0$, where f is the shift coefficient, then

$$p_1 = \frac{1-e^{-\lambda\left(1-\left[1-\left[-\frac{1}{\lambda}\log\left(\frac{1+e^{-\lambda}}{2}\right)\right]^{\frac{1}{\alpha}}\right]^{\frac{a}{f}}\right)^{\alpha}}}{1-e^{-\lambda}} \quad (7)$$

The np attribute control chart having Lower Control Limit (LCL) and Upper Control Limit (UCL) for the Exponentiated Exponential-Poisson distribution is explained in the following steps:

Step 1: Select a set of n products randomly from the production process.

Step 2: Conduct the life test on the selected products considering t_0 as the test termination time. Observe the number of failed items D (say).

Step 3: Terminate the life test either after reached at time t_0 or D > UCL before reaching time t_0, whichever is earlier.

Step 4: Declare the process as out of control if D > UCL or D < LCL. Declare the process as in control if LCL ≤ D ≤ UCL.

We are interested in observing the number of failures D in each sample. If the units have failure times that are less than the truncation time t_0, then the units are considered nonconforming or defective. The binomial probability mass function is given by

$$p(D = x) = \binom{n}{x} p^x (1-p)^{n-x}, x = 0,1,2,3\ldots \tag{8}$$

The Lower and Upper control limits are given by

$$LCL = max(0, np_0 - k\sqrt{np_0(1-p_o)}) \tag{9}$$

$$UCL = np_0 + k\sqrt{np_0(1-p_o)} \tag{10}$$

where k is the coefficient of the control limits and p_0 is the probability of "nonconforming" when the process is in control. The probability of stating that the process is in control when it is truly in control is obtained using the binomial probability given in equation (8)

$$p_{in}^0 = p(LCL \le D \le UCL|p_0) = \sum_{d=LCL+1}^{UCL} \binom{n}{d} p_0^d (1-p_0)^{n-d} \tag{11}$$

The probability of stating that the process is in control when the median life of the product has shifted to m_1 is given by

$$p_{in}^1 = p(LCL \le D \le UCL|\, p_1) = \sum_{d=LCL+1}^{UCL} \binom{n}{d} p_1^d (1-p_1)^{n-d} \tag{12}$$

It follows from the values p_{in}^0 and p_{in}^1 given in Equation (11) and (12) that the in-control ARL is given by

$$ARL_0 = \frac{1}{1-p_{in}^o} \tag{13}$$

and the out of control ARL are given by

$$ARL_1 = \frac{1}{1-p_{in}^1} \tag{14}$$

To construct the tables for the proposed control chart, we applied the following algorithm:

Step 1: Specify the values of ARL, say r_0 and sample size n.

Step 2: Determine the control chart parameter and truncated time constant a value for which the ARL from equation (13) approach r_0.

Step 3: By using the values of the control chart parameters obtained in step 2, determine the ARL_1 in accordance with shift constant f by using equation (14).

For various values of r_0, n and λ we determine the control chart parameters and ARL_1, which are shown in Tables 1,2,3,4 shows that the ARLs tend to get smaller when the shift constant f gets less.

Table 1: *The Values of ARLs when λ = 1, α=0.5*

					λ = 1, α=0.5				
n		**20**			**25**			**30**	
r_0	**360**	**480**	**580**	**360**	**480**	**580**	**360**	**480**	**580**
a	0.208	0.291	0.685	0.473	0.832	0.283	0.9	0.869	0.732
K	3.5	3.166	3.2162	3.0009	3.1497	3.1005	2.9576	3.1855	3.2284
LCL	0	0	2	2	4	0	6	6	5
UCL	12	12	16	16	19	14	22	23	22
Shift(f)	ARL	ARL	ARL	ARL	ARL	ARL	ARL	ARL	ARL
1.00	360.34	479.60	580.25	359.78	480.30	580.30	360.15	480.06	581.00
0.90	448.80	384.18	826.51	283.55	493.20	367.94	300.58	679.93	723.63
0.80	509.32	263.35	960.38	179.88	343.04	216.23	175.29	601.92	559.59
0.70	464.34	159.24	727.67	98.81	178.72	119.20	84.50	311.36	279.96
0.60	310.83	87.33	370.57	49.51	80.53	61.70	37.32	124.60	114.42
0.50	158.82	43.89	151.74	23.07	33.23	29.81	15.61	44.67	42.31
0.40	66.85	20.09	53.83	10.05	12.74	13.33	6.31	14.85	14.50
0.30	23.63	8.27	16.53	4.15	4.64	5.51	2.60	4.75	4.76
0.20	6.82	3.07	4.41	1.75	1.77	2.19	1.28	1.68	1.70
0.10	1.69	1.21	1.28	1.03	1.02	1.08	1.00	1.01	1.01

Table 2: *The Values of ARLs when λ = 2, α=1*

					λ = 2, α=1				
n		**20**			**25**			**30**	
r_0	**360**	**480**	**580**	**360**	**480**	**580**	**360**	**480**	**580**
a	0.526	0.619	0.798	0.644	0.895	0.396	0.42	0.61	0.593
k	2.9514	3.1179	3.2162	3.0004	3.1509	3.2995	3.0871	3.1158	3.0864
LCL	0	1	2	2	4	0	1	3	2
UCL	12	14	16	16	19	14	15	19	18
Shift(f)	ARL	ARL	ARL	ARL	ARL	ARL	ARL	ARL	ARL
1.00	359.75	480.01	580.22	359.66	479.77	580.34	359.56	480.21	580.23
0.90	186.66	536.85	945.95	212.63	414.16	346.55	210.31	458.28	252.71
0.80	83.55	300.45	682.06	86.80	169.00	148.63	86.25	186.49	89.51
0.70	35.30	114.36	248.54	32.37	56.58	56.62	32.06	58.48	30.65
0.60	14.57	39.28	76.52	12.04	18.73	20.74	11.81	18.03	10.71
0.50	6.07	13.23	22.84	4.71	6.52	7.61	4.56	5.91	4.05
0.40	2.69	4.63	7.00	2.10	2.58	2.99	2.02	2.28	1.82
0.30	1.42	1.89	2.44	1.21	1.33	1.44	1.18	1.22	1.13
0.20	1.03	1.10	1.20	1.00	1.02	1.03	1.00	1.00	1.00
0.10	1.00	1.00	1.00	1.00	1.00	1.00	1.00	1.00	1.00

Table 3: ***The Values of ARLs when λ = 5, α= 2***

					λ = 5, α=2				
n		**20**			**25**			**30**	
r_0	**360**	**480**	**580**	**360**	**480**	**580**	**360**	**480**	**580**
a	0.974	0.973	0.988	0.779	0.939	0.663	0.59	0.575	0.899
k	3.0366	3.222	3.2954	3.0023	3.1485	3.1005	2.9521	3.1113	3.2278
LCL	3	3	3	2	4	0	1	0	5
UCL	16	17	17	16	19	14	15	14	22
Shift(f)	ARL	ARL	ARL	ARL	ARL	ARL	ARL	ARL	ARL
1.00	360.14	480.04	582.61	360.09	480.88	580.28	359.59	479.80	580.23
0.90	220.62	905.08	812.07	115.46	232.66	129.66	192.99	108.81	366.91
0.80	51.74	223.18	181.59	25.15	44.29	28.60	39.01	23.65	55.65
0.70	12.90	42.49	35.93	6.46	9.81	7.33	8.58	6.07	10.18
0.60	4.02	9.71	8.60	2.26	2.97	2.47	2.57	2.12	2.76
0.50	1.74	3.01	2.80	1.22	1.40	1.26	1.25	1.17	1.29
0.40	1.13	1.42	1.38	1.01	1.04	1.01	1.01	1.00	1.02
0.30	1.00	1.05	1.04	1.00	1.00	1.00	1.00	1.00	1.00
0.20	1.00	1.00	1.00	1.00	1.00	1.00	1.00	1.00	1.00
0.10	1.00	1.00	1.00	1.00	1.00	1.00	1.00	1.00	1.00

Table 4: *The Values of ARLs when λ = 10, α=5*

					λ = 10, α=5				
n		**20**			**25**			**30**	
r_0	**360**	**480**	**580**	**360**	**480**	**580**	**360**	**480**	**580**
a	0.987	0.816	0.937	0.868	0.845	0.77	0.767	0.757	0.751
k	3.0339	3.1713	3.2162	3.0867	3.0745	3.2978	2.9534	3.1127	3.2138
LCL	3	0	2	2	1	0	1	0	0
UCL	16	12	16	16	15	13	15	14	14
Shift(f)	ARL	ARL	ARL	ARL	ARL	ARL	ARL	ARL	ARL
1.00	361.18	481.39	580.20	360.32	479.93	579.60	360.17	481.12	579.96
0.90	61.77	49.90	234.75	43.57	33.06	48.19	45.68	27.44	33.28
0.80	6.46	5.63	15.35	4.21	3.65	4.79	4.02	3.12	3.47
0.70	1.67	1.51	2.47	1.27	1.22	1.34	1.21	1.14	1.17
0.60	1.05	1.02	1.13	1.00	1.00	1.00	1.00	1.00	1.00
0.50	1.00	1.00	1.00	1.00	1.00	1.00	1.00	1.00	1.00
0.40	1.00	1.00	1.00	1.00	1.00	1.00	1.00	1.00	1.00
0.30	1.00	1.00	1.00	1.00	1.00	1.00	1.00	1.00	1.00
0.20	1.00	1.00	1.00	1.00	1.00	1.00	1.00	1.00	1.00
0.10	1.00	1.00	1.00	1.00	1.00	1.00	1.00	1.00	1.00

I. Illustration 1

Suppose that the lifetimes of the products follow an Exponentiated Exponential-Poisson distribution with parameter *λ= 2, α=1*. Consider the following values for the products: $m_0 = 1000$ hours, $ARL_0 = 360$ and $n = 20$. Table 2 provided the following control chart parameters: $k = 2.9514$, $a = 0.526$, $LCL = 0$ and $UCL = 12$. As a consequence, the control chart was established in the following

manner.

Step 1: Select a sample of 20 products from each subgroup and submit them to the life test.

Step 2: During the testing, count the number of failed items (D) and fix the time period.

Step 3: Terminate the test if either first failures occur or time elapse whichever comes first.

Step 4: Declare that the process is in control if $0 \leq D \leq 12$.

Step 5: Declare that it is out of control if $D > 12$ or $D < 0$.

II. Illustration 2

Assume that the product lifetimes follow an Exponentiated Exponential-Poisson distribution with parameters $\alpha=2$, $\lambda=5$, Consider the following product values: m_0 =1000 hours, *ARL*=580, and n = 30. The following control chart parameters were presented in Table 3: $k = 3.2278$,$a = 0.899$, $LCL = 5$ and $UCL = 22$. As a result, the control chart was established in the following manner: From each subgroup, choose a sample of 30 products, and put them through a life test. Count the number of failed items (D) which is minimum failure during testing or maximum time reached whichever comes first. Now monitor failures and time. Stop the process if the value of D is between 5 and 22 or the time elapse before reaching maximum time then the process is in control; otherwise, it is out of control.

IV. Simulation Study

This section discusses the application of the produced control chart with simulated data. The data was generated and shown in Table 5, using an Exponentiated Exponential-Poisson distribution with an average (median) lifetime (m_0) of 1000 hours, and the value of the shape parameter $\lambda = 2$, $\alpha = 1$. Assuming that the sample size (n) is 20 and the specified *ARL* (r_0) is 360. At m_0= 1000 hours and $F = 1$, the process is considered to be in control. In-control parameters are employed to construct the first 15 observations of subgroup size 20. Let's now assume that since the median of the Exponentiated Exponential-Poisson distribution has shifted, the process has shifted as well. The value of the shift constant f is 0.5. When f is set to 0.5, the shifted median is used to produce the next 15 observations (shown in Table 5). Take into account that the experiment was conducted at $t = 526$ hours. Table 5, shows the number of failures, indicated by the letter D, for each subgroup. Figure 1, shows the calculated LCL = 0 and UCL = 12 for simulated data.

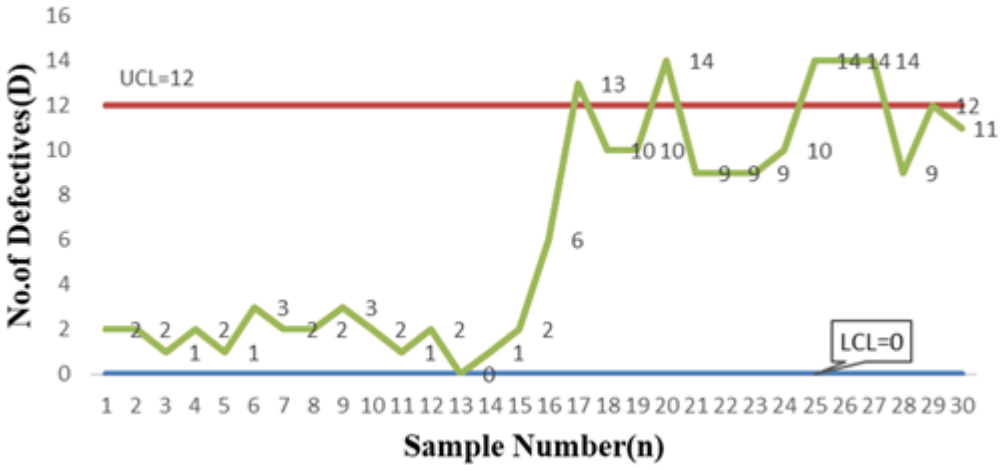


Figure 1: *Control Chart for Simulated Data*

Table 5: *Simulated Data when m_0 = 1000 hours, λ = 2, α =1., ARL_0 = 360, n = 20 and f=1*

S. No		1	2	3	4	5	6	7	8	9	10	11	12	13	14	15
Sample	**1**	1177	1096	922	844	798	950	654	475	786	1353	864	696	1056	993	1171
	2	1323	1131	1318	1114	685	819	1502	1809	976	726	599	1156	617	1313	438
	3	1132	964	428	1453	1755	1298	567	1393	490	520	1205	839	966	1750	637
	4	1129	1204	1608	1055	1266	681	811	1129	395	1499	600	501	1097	1000	1308
	5	1145	1600	1314	977	765	1540	926	921	939	1168	396	816	744	227	344
	6	1195	676	854	590	801	729	328	974	1242	1174	1432	639	856	1409	1230
	7	1435	1285	2125	972	789	1160	800	1180	653	1469	1613	837	922	768	1497
	8	1193	359	2244	419	889	351	433	1281	1087	680	1515	1273	995	834	1520
	9	1331	687	1220	948	1157	751	1524	563	1324	637	1499	625	601	1722	1472
	10	1303	876	749	508	993	772	1081	926	1394	939	679	959	1148	1470	1017
	11	828	1302	2026	683	708	958	748	449	1097	1186	1307	2554	1017	1047	1401
	12	456	715	1100	945	1334	1069	662	2205	998	1860	1471	1106	3261	2247	949
	13	543	808	1420	1202	1458	1433	606	843	1021	442	1278	1178	1761	853	588
	14	1017	575	1119	1359	670	506	648	1689	835	468	1915	810	546	1158	1646
	15	858	842	690	862	618	1382	1224	953	846	1383	2240	769	610	989	593
	16	705	1330	1018	825	1030	766	1265	909	1954	1544	1156	485	1028	680	1202
	17	407	959	1131	899	938	498	1116	888	455	1001	1050	1113	1333	1079	1194
	18	1309	321	625	596	1001	1165	1159	813	2257	1083	1103	1462	837	1961	1171
	19	1155	679	1113	754	351	1450	700	1073	1471	1245	915	1846	779	841	1648
	20	2008	1503	714	855	1966	935	931	1551	1265	1194	960	1260	1359	2515	871
	D	2	2	1	2	1	3	2	2	3	2	1	2	0	1	2

Table 5: *Simulated Data when m_0 = 1000 hours, λ = 2, α =1., ARL_0 = 360, n = 20 and f=0.5*

S. No	16	17	18	19	20	21	22	23	24	25	26	27	28	29	30
1	325	503	967	321	564	606	401	353	601	387	511	511	458	443	382
2	688	360	267	577	622	623	1064	689	285	849	299	299	818	731	812
3	646	433	505	232	430	581	396	495	840	759	388	388	627	395	498
4	535	228	598	428	832	732	346	379	527	414	546	546	731	429	298
5	625	653	623	561	347	885	712	195	455	493	619	619	762	646	531
6	263	1050	704	390	514	321	767	679	527	563	486	486	316	585	892
7	576	552	296	651	766	951	835	625	500	448	805	805	340	639	500
8	436	391	659	626	510	489	426	982	825	452	258	258	283	1153	639
9	572	298	364	456	332	728	892	526	230	434	396	396	633	526	737
10	569	399	346	581	419	440	331	396	569	302	390	390	195	412	423
11	316	537	564	316	1115	311	819	190	911	621	215	215	519	236	831
12	604	424	751	348	318	445	572	598	482	290	506	506	294	415	482
13	595	334	456	1061	343	532	1082	421	449	467	419	419	371	380	227
14	210	459	339	541	409	245	531	248	397	389	465	465	605	370	307
15	820	618	603	792	550	485	647	789	539	492	281	281	762	818	802
16	682	309	685	450	127	572	515	530	290	627	720	720	1393	385	737
17	390	352	484	428	517	571	607	345	523	386	786	786	912	319	617
18	410	400	516	594	500	402	359	782	583	542	540	540	641	652	420
19	623	586	753	374	438	746	518	584	531	395	284	284	829	400	432
20	589	613	337	824	472	498	493	588	483	277	298	298	421	569	352
D	6	13	10	10	14	9	9	9	10	14	14	14	9	12	11

Sample

V. Conclusion

In this article, a novel attribute control chart is introduced, utilizing the Exponentiated Exponential-Poisson distribution within a Hybrid censoring Scheme, aimed at ensuring that the median lifetime of the product serves as the quality standard. The newly developed control chart exhibits a high degree of flexibility and can be utilized for monitoring the longevity of quality products. Accompanying tables are designed for industrial applications and are illustrated using simulated data. This data is generated through R software, based on an Exponentiated Exponential-Poisson distribution. The effectiveness of the proposed control chart is quantified in terms of Average Run Lengths (ARLs) for different shift constants (f). It is important to highlight that employing a Hybrid censoring scheme for the life test can lead to reductions in both time and costs associated with the sampling inspection process. Furthermore, the created attribute control chart holds promise for extension to various other statistical distributions as part of ongoing research efforts.

References

[1] Adeoti, O. A., Ogundipe P. (2021). "A Control Chart for the generalized exponential distribution under time truncated life test", Life Cycle Reliability and Safety Engineering, 10:53-59.

[2] AL-Marshadi, A. H., Shafqat A. Aslam M., Alharbey A. (2021). "Performance of a New Time-Truncated Control Chart for Weibull Distribution under Uncertainty", International Journal of Computational Intelligence Systems, 14(1):1256-1262.

[3] Aslam M., Jun C. (2015). "Attribute Control Charts for the Weibull Distribution under Truncated Life Tests", Quality Engineering, 27(3):283 – 288.

[4] Aslam M. Nasrullah Khan., Chi Hyuck (2016). "A control chart for time truncated life tests using Pareto distribution of second kind", Journal of Statistical Computation and Simulation, 86(11):2113 – 2122.

[5] Baklizi A., Ghannam, S. A. (2022). "An attribute control chart for the inverse Weibull distribution under truncated life tests", Heliyon, 8:e11976:1-5.

[6] Balamurali S., Jeyadurga P. (2019). "An attribute np control chart for monitoring mean life using multiple deferred state sampling based on truncated life tests", International journal of Reliability, Quality and Safety Engineering, 26(1):1-18.

[7] Gunasekaran M. (2024). "A New attribute control chart based on Exponentiated Exponential Distribution Under Accelerated Life test with Hybrid Censoring", Reliability: Theory & Applications,19,4(80):850-860.

[8] Jayadurga P. Balamurali S., Aslam, M. (2018). "Design of an attribute np control chart for process monitoring based on repetitive group sampling under truncated life tests", Communication in Statistics – Theory and Methods, 47(24):5934 – 5955.

[9] Kavitha T., Gunasekaran M. (2020). "Construction of Control Chart based on Exponentiated Exponential Distribution", Journal of Engineering Sciences, 11(4):979 – 985.

[10] Kus C. (2007). "A new lifetime distribution", Computational Statistics and Data Analysis, 51, 4497–4509.

[11] Mansour Sattam Aldosari, Aslam, M., Jun, C.H (2017), "A new attribute control chart using multiple dependent state repetitive sampling", IEEE Access, (5):6192–6197.

[12] Miroslav Ristic., Saralees Nadarajah (2012), "A New lifetime distribution", Journal of Statistical Computation and Simulation,ifirst,1-16.

[13] Muhammad H Tahir, Gauss M Cordeiro (2016), "Compounding of distributions: a survey and new generalized classes", Journal of statistical Distributions and Applications,Springer,3(1):1-35.

[14] Nanthakumar C., Kavitha T. (2017). "Design of Attribute Control Chart based on Inverse

Rayleigh Distribution under Type – I Censoring", International Journal of Statistical Sciences, 4(6):17 – 22.

[15] Shafqat, A. Hussain, J. AL Nasser, A. D., Aslam M. (2018). "Attribute Control Chart for some popular distributions", Communications in Statistics – Theory and Methods, 47(8):1978 – 1988.

[16] Shaheen U Azam M ., M. Aslam (2020). "A control chart for monitoring the lognormal process variation using repetitive sampling", Quality and Reliability Engineering International,36(3):1028–1047.

[17] Srinivasa Rao, G. (2018). "A Control Chart for Time Truncated Life tests Using Exponentiated Half Logistic Distribution", Applied Mathematics & Information Sciences: An International Journal, 12(1):125 – 131.

[18] Srinivasa Rao, G., Edwin Paul (2020). "Time Truncated Control Chart using LogLogistic Distribution", Biometrics & Biostatistics International Journal, 9:76- 82.

[19] Srinivasa Rao, G. Fulment, A. K., Josephat, P. K. (2019). "Attribute control chart for the Dagum distribution under truncated life tests", Life Cycle Reliability and Safety Engineering, 8:329 – 335.

[20] Tibor K.Pogany (2014),"The Exponentiated Exponential Poisson Distribution revisited", A journal of Theoretical and Applied Statistics,49:918 – 929.

ENHANCING THE RELIABILITY OF POWER SYSTEMS BY OPTIMIZING LIGHTNING PROTECTION OF OVERHEAD TRANSMISSION LINES

Elbrus Ahmedov[1], Kubra Mukhtarova[2]

•

Azerbaijan State Oil and Industry University, Baku, Azerbaijan
elbrus.ahmedov@asoiu.edu.az

Abstract

This paper addresses the reliability issues of power systems caused by lightning-induced overvoltages resulting from lightning strikes to components of overhead transmission lines (OHL). It is demonstrated that lightning discharges are one of the key causes of transmission line outages and significant economic losses. A method is proposed to improve the efficiency of lightning protection by upgrading the design of lightning protection cables using V-shaped metallic elements to increase the protection zone. Calculations were carried out to assess the expansion of the protection zone depending on the geometrical parameters of the design. A mathematical model was developed and implemented in the MATLAB Simulink environment to analyze the behavior of OHL under direct lightning strikes to the shield wire and phase conductors. The model takes into account lightning current parameters, structural characteristics of supports, grounding device properties, and insulation parameters. Simulation results showed a significant influence of grounding resistance on the level of resulting overvoltages and the effectiveness of lightning protection. The proposed technical solutions can be used to enhance the lightning resistance and operational reliability of overhead transmission lines, especially in regions with high lightning activity.

Keywords: power system reliability, lightning protection, overhead transmission lines, grounding wire, MATLAB modeling

I. Introduction

Power systems play a fundamental role in the functioning of modern society by ensuring a stable electricity supply to industrial, residential, and commercial facilities. However, their reliability is continuously challenged by atmospheric overvoltages, particularly those caused by lightning discharges, including direct lightning strikes.

Lightning is one of the primary causes of transmission line malfunctions, significantly reducing the reliability of power supply systems. According to statistics from a provincial power grid in China, more than 45% of all transmission line outages between 2005 and 2014 were caused by lightning discharges [1].

An analysis of historical data provided by a UK-based service indicates that between 2010 and 2019, lightning strikes were the direct cause of more than 20,000 power outage incidents [2, 3]. As research shows, these outages can lead to substantial economic losses, including the costs of repair and restoration work, reduced technical reliability of power systems, and negative impacts on consumers and the business environment as a whole [4-6]. In many cases, under normal operating conditions, lightning-related outages can account for 30% to 50% of all automatic

disconnections. For instance, according to data from the power utility company of Paraná State (Brazil), approximately 35% of all recorded power outages are directly linked to lightning activity.

As seen from the above, the reliability of power systems is largely determined by the effectiveness of lightning protection for overhead transmission lines (OHL) against overvoltages caused by lightning discharges. These overvoltages result from complex physical processes associated with atmospheric phenomena, including direct and secondary lightning strikes on the structural elements of OHLs. Traditional approaches to assessing lightning protection, which are based on semi-empirical relationships and electro-geometrical models, often fail to adequately evaluate the vulnerability of a particular object and consider factors such as topography, soil characteristics, support structure design, and climatic conditions [7, 8].

To objectively determine the lightning susceptibility of a transmission line and develop effective measures to enhance its lightning resistance, it is necessary to transition to new calculation models based on a physically substantiated description of the processes involved in the formation and development of lightning near ground-based objects. Modern research confirms that detailed modeling of lightning interaction with infrastructure elements can significantly improve the accuracy of accident forecasts and, consequently, enhance the justification of design decisions [9].

II. Problem Statement

Modern power systems play a key role in ensuring the reliable electricity supply to various facilities, including industrial, residential, and commercial buildings. However, one of the main threats to the reliability of such systems is atmospheric discharges, particularly lightning, which can cause significant equipment damage and lead to prolonged outages. These phenomena create lightning-induced overvoltages that can damage insulation, cause short circuits, and lead to serious disruptions in power grid operations.

As a result, improving the reliability of OHL and reducing the consequences of lightning strikes have become critical tasks for ensuring the stability of power systems [10-12]. Existing protection methods, such as lightning rods, grounding wires, and line surge arresters, although effective, do not always provide the required level of safety, especially in areas with high lightning activity. For example, lightning strikes on phase conductors lead to the formation of powerful overvoltages, necessitating a more comprehensive approach to protection.

One promising direction for addressing this issue is the modernization of lightning protection cable designs, which can significantly improve the efficiency of protection against lightning strikes [13]. Furthermore, an important aspect is the assessment of the reliability of power systems, particularly overhead transmission lines, using computer modeling methods.

Therefore, the task is to develop and optimize a lightning protection system for overhead transmission lines, considering modern reliability requirements and operational characteristics. This will require not only improvements in design solutions but also the integration of intelligent technologies for assessing the condition of power systems.

III. Solution to the Problem

Application of Effective Grounding Wires

Grounding wires-lightning protection cables and grounding systems play an essential role in protecting overhead transmission lines (OHL) by absorbing lightning strikes. Although damage to such cables is possible [14, 15], it generally results in less destructive consequences compared to strikes on phase conductors, which can lead to prolonged outages. The reliability of lightning

protection systems requires consideration of both electrical and mechanical aspects of line operation under complex weather conditions.

An analysis of existing protection methods has shown that the most straightforward and reliable way to mitigate the consequences of lightning discharges is the use of grounding wires. However, the effectiveness of these systems depends on their placement relative to the phase conductors. To increase the protection zone, we propose partially modifying the grounding wire design by adding metallic elements along its length, positioned in a "V" shape at a 45° angle to the ground (Figure 1). These elements increase the heterogeneity of the electric field, improving the protective properties of the grounding cables [16].

To calculate the additional protection zone between the "V"-shaped elements, several factors need to be considered, such as the length of the rods and the distance between them, as well as the protection radius, which depends on these parameters. In this case, Table 1 provides information on the rod length, the distance between the rods, the protection radius, and the percentage of the additional protection zone for various rod lengths.

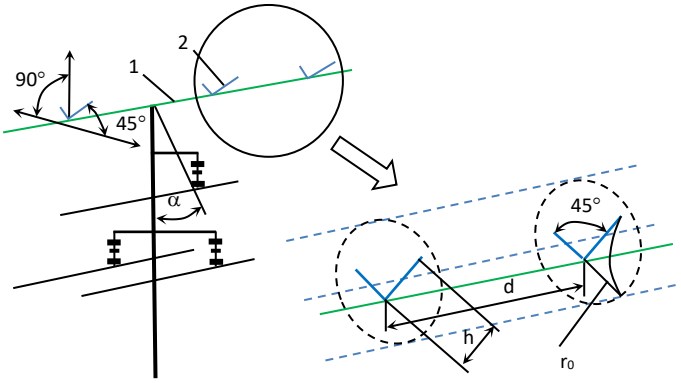


Figure 1: *Placement of "V"-shaped elements on the surface of the lightning protection cable.*

Table 1: *Protection Zone Between "V"-Shaped Rods*

Length of Rod (h, cm)	Distance Between Rods (a, cm)	Protection Zone Radius (r_0, cm)	Additional Zone (%)
10	100	15	30
20	100	30	60
30	100	45	90
40	100	60	120

As seen in the table, as the rod length increases, the protection radius also increases, which directly impacts the additional protection zone of the grounding wire. The additional protection zone represents the percentage increase compared to the base protection radius for the minimum rod length (10 cm).

The graph shown in Figure 2 illustrates how the additional protection zone increases as the rod length increases.

The additional protection zone between the "V"-shaped rods plays a crucial role in ensuring the safety and efficiency of the lightning protection cable for OHL. As the rod length increases, there is a consistent expansion of the protection radius, which leads to a larger overall protected area. The graph, constructed from the data in the table, clearly demonstrates this relationship, showing how the additional protection zone increases as the rod length changes.

The graph indicates that the additional protection zone grows proportionally to the rod length. This suggests a linear relationship, allowing for high accuracy in predicting the system's

behavior when its parameters are modified. For example, when the rod length is 10 cm, the additional zone is 30%. When the rod length is increased to 20 cm, this value increases to 60%, and at 40 cm, it reaches 120%. This growth shows that the protection expands with the increasing size of the design, creating a larger safe zone [17].

While increasing the rod length extends the protected area, this process has its limits. Excessive elongation of the rods can lead to reduced mechanical stability of the structure, increased loads, and installation complications. Therefore, it is important to find a balance between the effectiveness of protection and the practical feasibility of the system.

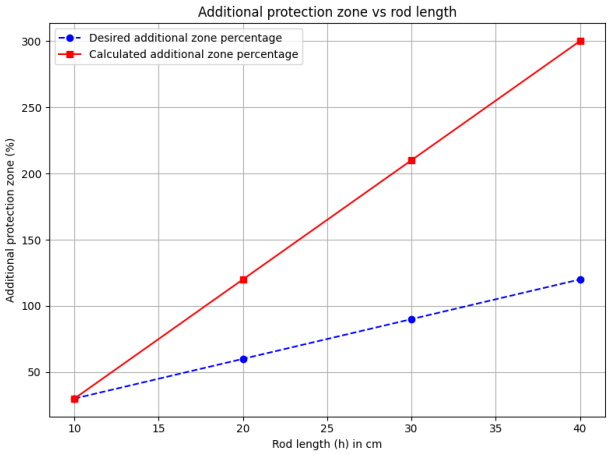


Figure 2: *Additional protection zone vs rod length*

The graph confirms that increasing the rod length leads to a proportional increase in the protection zone, making the system predictable and reliable. However, to ensure maximum efficiency, it is necessary to consider both the calculated data and the actual operating conditions, thereby ensuring stable and long-lasting performance of the protection system.

As seen from the above, the result of the calculation — that is, the reliability indicator of the lightning protection system, expressed as the number of lightning-induced outages of the overhead transmission line (OHL) per year — is significantly influenced not only by the condition of the lightning protection cable and the choice of support structure model but also by the condition of its grounding. This is because the most common occurrence of linear insulation breakdown, which is the most probable cause of line outages, typically happens at the support.

To determine the level of lightning resistance of the OHL, a computational model was developed in MATLAB, and a comprehensive analysis was carried out, including the evaluation of the lightning protection cable parameters, the support structure design, and the characteristics of the grounding systems. The obtained data allowed for a quantitative assessment of the reliability of the OHL.

III. Simulation Based on MATLAB Simulink

Model Description

The model presented in Figure 3 was developed using the MATLAB Simulink software environment. This platform offers a wide range of tools for modeling high-voltage overhead transmission lines, including the ability to analyze lightning-induced overvoltages and electromagnetic effects caused by lightning strikes. This allows for the investigation of line behavior and the development of effective protection methods. The simulation model was adapted based on typical studies conducted by several authors, as outlined in works [18–21], which explored the processes of lightning-induced overvoltage occurrence on high-voltage transmission lines.

Two scenarios were considered:

– Direct lightning strike on the lightning protection cable;

– Direct lightning strike on the phase conductor.

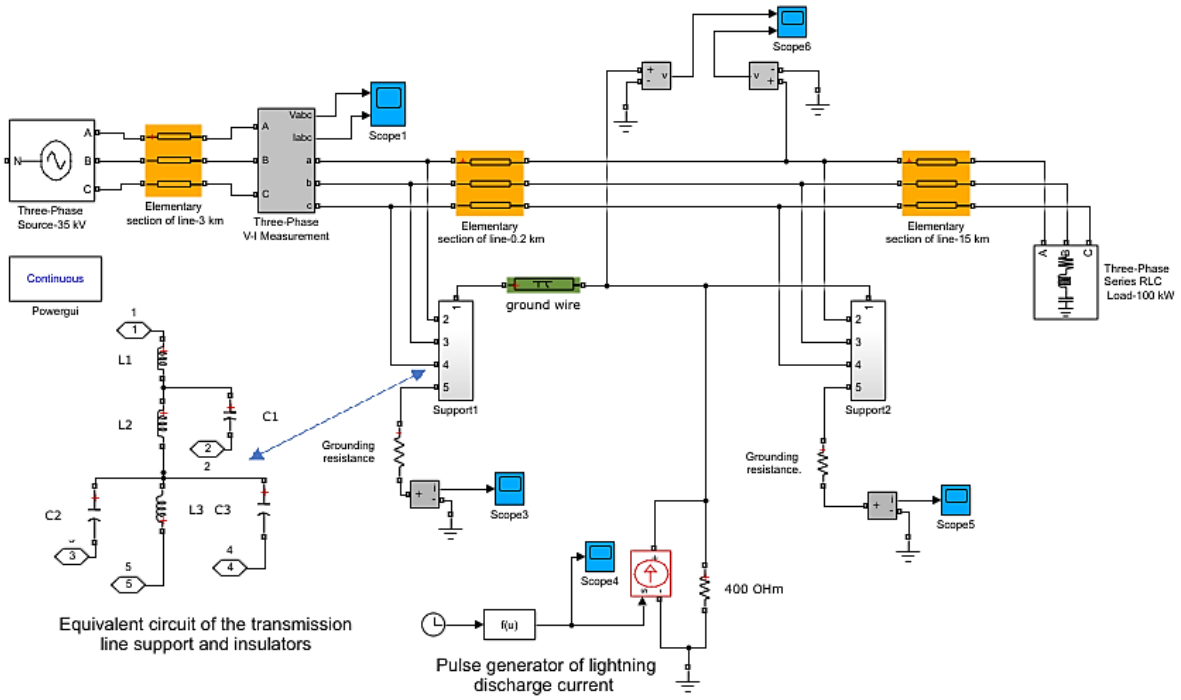


Figure 3. *Simulation of Lightning Strike on OHL Elements in MATLAB*

Description of the Lightning Discharge

For the calculation of the lightning current impact on electrical equipment, it was necessary to create a lightning discharge model. The Bruce and Gold lightning current model is widely used to describe the time-dependent characteristics of lightning impulse current. This model provides high accuracy in reproducing the front and decay of the impulse, which is crucial when analyzing lightning overvoltages and their impact on power supply systems. The model is represented as follows [22-24]**:**

$$i(t) = \frac{I_m}{\eta}\left[e^{-\alpha t} - e^{-\beta t}\right]$$

where: $i(t)$ — Instantaneous value of the current at time t, μs ; I_m — Amplitude of the lightning impulse current, kA ; η – Amplitude wave correction factor; α and β — Time constants characterizing the rise and decay rates of the impulse, $\alpha > \beta$ (α= 0.014 ÷ 0.05 μs^{-1} determines the steepness of the decline; β= 0.002 ÷ 0.01 μs^{-1} — pulse front); t — time, μs.

To describes the current impulse waveform, a biexponential function (3) is used, which, considering the calculated decrements and parameters of the current impulse 1.2/50 μs, has the following implementation in the Simulink environment: $100000/e^{-0.017*u}(e^{(-14300*u)}-e^{(-6*u)})$.

The current impulse generator model is shown in Figure 3, and the graph corresponding to the obtained curve of the model is shown in Figure 4. The parameters of this curve comply with the IEC 62305 standard for lightning protection of electrical power systems from direct lightning strikes [25].

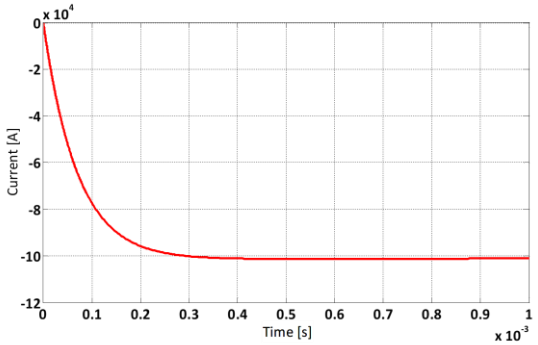


Figure 4. *Lightning current curve shape: current pulse parameters 50/1.2, 100 kA.*

The main parameters of the 35 kV overhead lines and the intermediate steel support are shown in Table 2 and in Figure 5

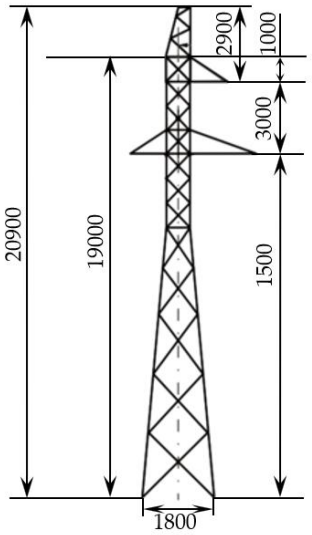


Figure 5. *Dimensions of the metal single-chain intermediate support for 35 kV*

Table 2. *Parameters of the 35 kV overhead line*

No	Transmission Line Parameter	Values
1	Nominal frequency	50 Hz
2	Number of conductors per phase	1
3	Nominal cross-section of steel-aluminum (AC) conductors	120/19 mm²
4	Per unit resistance (positive sequence)	0.333 Ohm/km
5	Per unit resistance (zero sequence)	0.333 Ohm/km
6	Per unit inductance (positive sequence)	1.317×10^{-3} Hen/km
7	Per unit inductance (zero sequence)	1.438×10^{-3} Hen/km
8	Per unit capacitance (positive sequence)	1.97×10^{-12} F/m
9	Per unit capacitance (zero sequence)	2.24×10^{-12} F/m
10	Diameter of lightning protection cable	12.1 mm
11	Resistance of lightning protection cable	2.1 Ohm/km
12	Inductive resistance of lightning protection cable	$(2.77 – 3.41) \times10^{-3}$ H/km
13	Capacitance of lightning protection cable	8.28×10^{-6} F/km

The electrical equivalent circuit of the support was chosen in the form of a set of inductances and capacitances, as shown in Figure 3. To calculate the values of inductance, the known value of

the line inductance for this type of supports was used, which is Lp= 0.6-0.8 μH/m (L=Lp * h), where h is the height of the support, and for our case, we adopted Lp = 0.65 μH/m [26].

In the equivalent circuit, the insulator string was modeled as an equivalent capacitance, in parallel with which a resistor was included to simulate leakage currents. Due to the relatively small inductance of the insulator string and crossarms, it was not considered in the calculations.

To determine the capacitance value, an equivalent circuit of a string consisting of 3 U70B (PS-70E) insulators was used, for which the equivalent capacitance was 7.1 pF. This value was adopted for the support model when simulating the insulator string. The expected 50% impulse breakdown voltage of the insulator string consisting of three U70B insulators is approximately 270 kV [27-29].

To calculate the transient process during a lightning strike to the transmission line, a model consisting of two supports was used, which is sufficient for studying the lightning strike in the above-mentioned cases (Figure4).

Each section of the transmission line was modeled as an equivalent six-port network, including three phase conductors represented by a Distributed Parameters Line element. The lightning protection wire, provided in the line as a single unit, was modeled using the Pi Section Line element.

IV. Simulation Results

Lightning Strike to the Grounding Shield Cable

This line is single-circuit. To determine the overvoltage that occurs when lightning strikes the ground wire and the phase conductors, the model considers two supports, with a distance of 200 meters between them. The grounding wire is installed on both supports. The main focus is on the maximum overvoltage values occurring at the supports for different values of the grounding resistance of the supports and the grounding shield cable during a direct lightning strike. As a result of the strike, overvoltages are generated on the line (Figure 6), and Table 3 presents the maximum current values flowing through the support and the maximum voltage values occurring between the phases and the ground for different grounding resistance values of the supports [31].

Table 3. *Lightning strike on the ground wire*

Lightning impulse current amplitude, kA,	Tower footing resistance, [Ohm]	Maximum value of current flowing through the support, A	Maximum value of voltage occurring between phases and ground, V
100	5	$5.0 \cdot 10^4$	$2.2 \cdot 10^5$
	6	$\mathbf{5.0 \cdot 10^4}$	$\mathbf{2.7 \cdot 10^5}$
	10	$5.0 \cdot 10^4$	$4.2 \cdot 10^5$
	20	$4.95 \cdot 10^4$	$7.8 \cdot 10^5$
	30	$4.9 \cdot 10^4$	$11.2 \cdot 10^5$
	40	$4.8 \cdot 10^4$	$14 \cdot 10^5$

As seen in Table 3, with an increase in the grounding resistance of the support, the dissipation of lightning current is hindered, and the overvoltage between the phases of a ground wire increases. When the resistance value reaches 6 Ω, this becomes a critical value for the considered line-supports, as it causes a breakdown (Fig. 7) between a ground wire and the support, which results in the line's impulse strength reaching 270 kV.

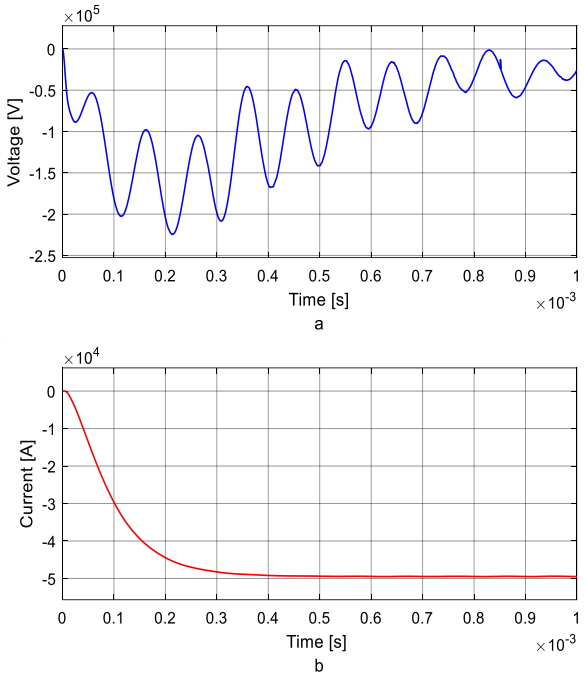


Figure 6. *Lightning strike on the shield cable with a grounding resistance of the supports of 5 Ohms: a - inductive overvoltage - phase voltage; b - current flowing through the grounding of the supports.*

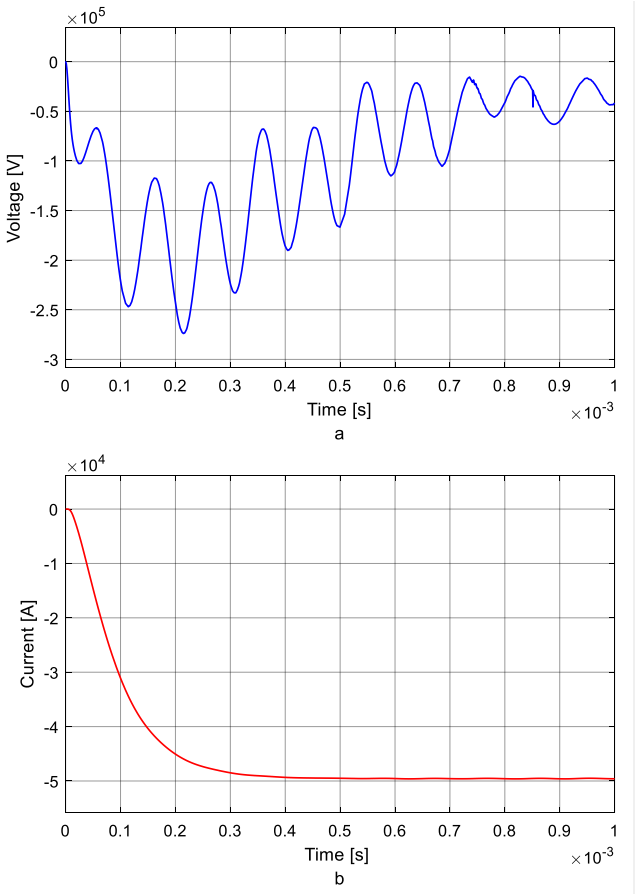


Figure 7. *Flashover when lightning strikes a ground wire: a - induction overvoltage—phase voltage; b - current flowing through the support ground electrode.*

Modeling a lightning strike on a phase conductor.

To assess the lightning resilience of electrical equipment under external overvoltages, a scenario of a direct lightning strike to the phase conductor of a transmission line was simulated. A simulation was conducted with a grounding resistance of 5 Ω. As a result, the maximum phase overvoltage reached a value of 3.5×10^7 V. In this case, the overvoltage in phase A was several times higher compared to the results obtained from the lightning strike to the lightning protection cable (Fig. 8). This is due to the fact that when lightning strikes the cable, insulation breakdown occurs, which consumes part of the electrical potential [32-35]. In the case of a direct lightning strike to the phase conductor, potential losses are significantly lower, leading to higher levels of impact.

To determine the maximum lightning current at which insulation breakdown has not yet occurred, a series of experiments were conducted. However, it was established that practically any lightning strike, even with a current of 1-2 kA, leads to insulation breakdown of the line [36-39].

Thus, the proposed method for evaluating the effectiveness of the lightning protection system allows for a more accurate reflection of real operating conditions and identification of the limiting capabilities of protective measures.

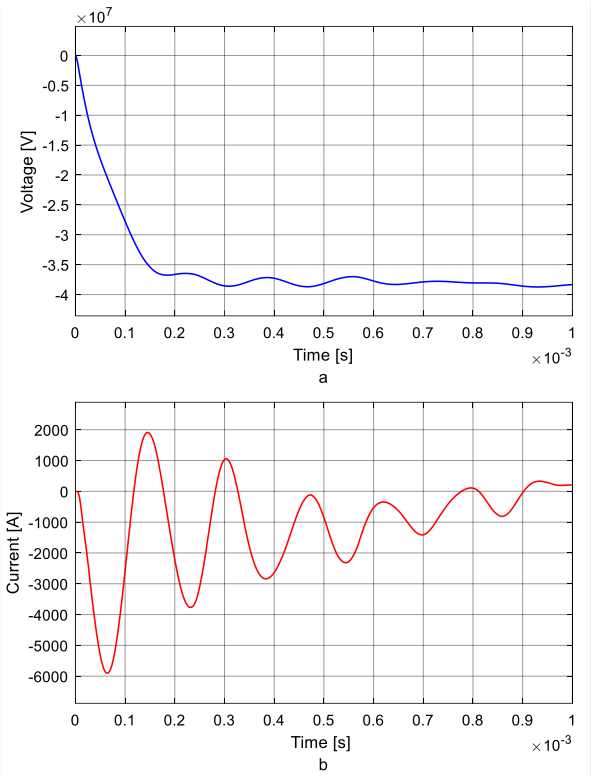


Figure 8. *Direct lightning strike on the phase conductor of the line: a-curve of currents occurring in phase A; b-current flowing through the support ground electrode*

V. Conclusions

The study established that the reliability of transmission line operation under lightning activity is largely determined by the effectiveness of the lightning protection systems in place. Traditional methods, such as lightning ground wire, lightning rods, and line arresters, remain key elements of protection. However, their efficiency can be significantly improved through the use of innovative design solutions and modern approaches to grounding system design. One such solution is the modification of ground wire with the use of V-shaped elements, which increases the protection radius and reduces the risk of direct lightning strikes on the phase conductor. The

model of a power system section with an overhead transmission line, developed in the MATLAB Simulink environment, allowed for the assessment of overvoltages caused by lightning strikes to both the lightning protection cable and the phase conductors. The simulation results showed that an increase in the grounding resistance of the supports leads to higher levels of overvoltage in the line. In particular, at a grounding resistance of 6 Ω, a critical voltage level is reached that can cause insulation breakdown and equipment damage. This highlights the need for constant monitoring and optimization of grounding parameters, especially in areas with high lightning activity. The results obtained and the proposed methodologies can be used for further improvement of protection systems, ultimately contributing to the increased reliability and safety of electrical power systems as a whole.

.

References

[1] Xie, Y., Li, C., Lv, Y., & Yu, C. (2019). Predicting lightning outages of transmission lines using generalized regression neural network. *Applied Soft Computing, 78*, 438–446. https://doi.org/10.1016/j.asoc.2018.09.042

[2] Rimkus, E., et al. (2024). Impact of meteorological conditions on overhead transmission line outages in Lithuania. *Atmosphere, 15*(11), 1349.

[3] Souto, L., Taylor, P. C., & Wilkinson, J. (2023). Probabilistic impact assessment of lightning strikes on power systems incorporating lightning protection design and asset condition. *International Journal of Electrical Power & Energy Systems, 148*, 108974.

[4] Jimenez, V., Montaña, J., Candelo, J., & Quintero, C. (2017). Estimation of the shielding performance of transmission lines considering effects of landform, lightning polarity and stroke angle. *Electrical Engineering, 100*, 425–434.

[5] Gonçalves, A. C. R., Costoya, X., Nieto, R., & Liberato, M. L. (2024). Extreme weather events on energy systems: A comprehensive review on impacts, mitigation, and adaptation measures. *Sustainable Energy Research, 11*(4).

[6] Ravaglio, M. A., et al. (2019). Evaluation of lightning-related faults that lead to distribution network outages: An experimental case study. *Electric Power Systems Research, 174*, 105848.

[7] Ahmedov, E., Rzayeva, S., Ganiyeva, N., & Safiyev, E. (2023). Improving the lightning resistance of high-voltage overhead power line. *Przegląd Elektrotechniczny, (11)*.

[8] Kondrateva, O., Myasnikova, E., & Loktionov, O. (2020). Analysis of the climatic factors influence on the overhead transmission lines reliability. *Rigas Tehniskas Universitates Zinatniskie Raksti, 24*(3), 201–214.

[9] Hamel, T., Bedoui, S., & Bayadi, A. (2025). Impact of transmission line lightning performance on an operational substation reliability considering the lightning stroke incidence angle. *Electrical Engineering & Electromechanics, (1)*, 56–64.

[10] Souto, L., Taylor, P. C., & Wilkinson, J. (2023). Probabilistic impact assessment of lightning strikes on power systems incorporating lightning protection design and asset condition. *International Journal of Electrical Power & Energy Systems, 148*, 108974. https://doi.org/10.1016/j.ijepes.2023.108974

[11] Huo, H., et al. (2024). Considering the methods of lightning protection and early warning for power transmission lines based on lightning data analysis. *IEEE Access*. https://doi.org/10.1109/ACCESS.2024.3387968

[12] Afzal, S., et al. (2020). State-of-the-art review on power system resilience and assessment techniques. *IET Generation, Transmission & Distribution, 14*(25), 6107–6121. https://doi.org/10.1049/iet-gtd.2020.0531

[13] Krasnozhon, A. V., et al. (2023). Study of the influence of the parameters of modern grounding wires on the value of power losses in them for overhead power lines of 330-750 kV. *Electrical Engineering & Electromechanics, (6)*. https://doi.org/10.20998/2074-272X.2023.6.14

[14] Banjanin, M. S. (2018). Application possibilities of special lightning protection systems of overhead distribution and transmission lines. *International Journal of Electrical Power & Energy Systems, 100*, 482–488.

[15] Hu, J., Zhu, T., Hu, J., Fang, Z., & Zhang, R. (2023). Study on the lightning protection performance for a 110 kV non-shield-wired overhead line with anti-thunder and anti-icing composite insulators. *Energies, 16*(2), 815.

[16] Ahmadov, E. N., Aliyev, N. A., & Rzayeva, S. V. (2024). Modern methods for protecting high-voltage overhead power lines from lightning overvoltage. *Proc. of the 20th International Conference on Technical and Physical Problems of Engineering (ICTPE)*, October 31, 2024, 12–17. https://www.iotpe.com/ICTPE/ICTPE-2024/ConferenceProgram.html

[17] Ahmedov, E. N., Rzayeva, S. V., Mukhtarova, K. M., & Aliyev, N. A. (2025). Innovative enhancements in ground wire configurations for superior lightning protection of overhead power lines. *International Journal on Technical and Physical Problems of Engineering (IJTPE), 17*(1), 45–58.

[18] Tarko, R., Gajdzica, J., Nowak, W., & Szpyra, W. (2021). Comparative analysis of high-voltage power line models for determining short-circuit currents in towers earthing systems. *Energies, 14*, 4729. https://doi.org/10.3390/en14164729

[19] Fahmani, L., Garfaf, J., Boukhdir, K., Benhadou, S., & Medromi, H. (2020). Modelling of very high voltage transmission lines inspection's quadrotor. *SN Applied Sciences, 2*, 1425. https://doi.org/10.1007/s42452-020-03222-y

[20] Leon Colqui, J. S., Ribeiro de Moura, R. A., De Oliveira Schroeder, M. A., Filho, J. P., & Kurokawa, S. (2023). The impact of transmission line modeling on lightning overvoltage. *Energies, 16*(3), 1343. https://doi.org/10.3390/en16031343

[21] Mariut, E. L., & Helerea, E. (2016). Variation of tower footing resistance on the lightning surge propagation through overhead power distribution lines. *Advances in Electrical and Computer Engineering, 16*(1), 99–106.

[22] Bruce, C. E., & Golde, R. H. (1941). The lightning discharge. *Journal of the IEE, 88*, 487–520.

[23] Wooi, C. L., et al. (2019). Comparison of lightning return stroke channel-base current models with measured lightning current. *Bulletin of Electrical Engineering and Informatics, 8*(4), 1478–1488.

[24] Furgal, J. (2020). Influence of lightning current model on simulations of overvoltages in high-voltage overhead transmission systems. *Energies, 13*(2), 296.

[25] International Electrotechnical Commission. (2010). *IEC 62305-1: Protection against lightning – Part 1: General principles*.

[26] Kirik, V. V., & Abdulaev, S. A. (2018). Protection of damaged power lines with a voltage of 35 kV from induced lightning surges. Electrical engineering and electrical power engineering, (1), 81–92.

[27] International Electrotechnical Commission. (1993). *IEC 60383-1: Insulators for overhead lines – Part 1: Ceramic or glass insulator units for a.c. systems – Definitions, test methods and acceptance criteria*.

[28] Rahimli, I. N., Bakhtiyarov, A. L., & Abdullayeva, G. K. (2024). The role of modern grounding devices in ensuring the stability of power systems. *Reliability: Theory and Applications, 20*(1), 734–742.

[29] Mammadov, N., Piriyeva, N., & Ismayilova, S. (2024). Research of lightning protection systems for wind electric installations. *Przegląd Elektrotechniczny, (9)*, 198–201.

[30] Rahimli, I., Bakhtiyarov, A., Abdullayeva, G., & Rzayeva, S. (2024). Switching processes occurring in electrical networks 10–35 kV. *Przegląd Elektrotechniczny, (8)*, 156–159.

[31] Piriyeva, N. M., Mammadov, N. S., & Rzayeva, S. V. (2025). Development of new methods for protecting substation and overhead lines from overvoltages. *Reliability: Theory & Applications, 20*(1), 683–689.

[32] Mammadov, N. S., & Mukhtarova, K. M. (2024). Methodology for assessing the reliability of AGS based on renewable energy sources. *Reliability: Theory and Applications, 19*(4), 648–653.

[33] Rzayeva, S. V., Piriyeva, N. M., & Ismayilova, S. I. (2025). High and low voltage coordination in electrical power systems. *International Journal on Technical and Physical Problems of Engineering, 17*(1), 19–31.

[34] Piriyeva, N., Kerimzade, G. (2023) Methods for increasing electromagnetic efficiency in induction levitator. *Przeglad Elektrotechniczny*, 2023(10), 192–195

[35] Rzayeva, S. V., Ganiyeva, N. A., & Piriyeva, N. M. (2024). Modern approaches to electrical equipment diagnostics. *International Journal on Technical and Physical Problems of Engineering, 16*(1), 182–189.

[36] Rzayeva, S. V., Piriyeva, N. M., & Guseynova, I. A. (2024). Analysis of reliability of typical power supply circuits. *Reliability: Theory & Applications, 19*(3), 173–178.

[37] Ismayilova, S. V., Isgandarova, Z. A., & Mukhtarova, K. M. (2025). Enhancing energy system reliability: modern approaches and solutions. *Reliability: Theory and Applications, 20*(1), 966–971.

[38] Rzayeva, S. V., & Guseynova, I. A. (2024). Application of automatic monitoring and control systems for reliability of power transmission lines. *Reliability: Theory & Applications, 19*(2), 64–69.

[39] Rzayeva, S. V., Mammadov, N. S., & Ganiyeva, N. A. (2023). Overvoltages during single-phase earth fault in neutral-isolated networks (10–35) kV. *Journal of Energy Research and Reviews, 13*(1), 7–13.

ON RELIABILITY STRESS-STRENGTH MODEL USES SHOCK-MODEL APPROACH TO FOLLOW MUKHERJEE-ISLAM DISTRIBUTION

Vijayakumar. B[1], M. Manoharan[2]

•

Department of Community Medicine and Biostatistician, Arunai Medical College and Hospital, Velu Nagar, Thenmathur, Tiruvannalamai, Tamilnadu, India[1]
Department of Community medicine and Statistician, SRM University, kattankulathur, Tamilnadu, India[2]
statvijaybalu@gmail.com[1],
manostatmsu@gmail.com[2]

Abstract

A component or system exposed to shocks will result in system or device damage. The strength of a produced product is a variable quantity that requires modelling as a random variable. It is necessary to evaluate the stress conditions of the operating system. Strength and stress are both thought of as random variables. which is made clear by the term "stress-strength model." With the inter-arrival time following the Mukherjee-Islam distribution and strength following an exponential distribution, we attempted to create a model in this study. Graphs are used to support numerical examples that are provided.

Keywords: Shock-Model, CDM, Stress-Strength, exponential distribution, Mukherjee – Islam distribution.

I. Introduction

The concept of shock model introduced by Esary, et al., [2]. In the subject of reliability theory, Ramanarayanan [16] examined the cumulative damage process, which introduces the idea of the system's workers' attentiveness. Cumulative damage process (CDP) is an attractive one, which helps in the interpretation of the behaviours of complex mechanisms. Any component or device exposed to shocks cause damage to the device or system. The device fails when the total of the damages exceeds a threshold level. Assume that the damages $X_1, X_2, \ldots, X_n$ caused by successive shocks are mutually independent identically distributed random variable with distribution function *G(.)* independent of the threshold whose distribution function is *H(.)*. Then the probability that the device survives k damages is denoted as

$$P_k = \int_0^\infty g_k(x)[1 - H(x)]dx, \quad k = 1, 2, 3, \ldots \tag{1}$$

where, $g_K(X)$ is the k fold convolution of $G(x)$ with itself and $G_0(X) = 1$. The Reliability $R(t)$ of the device is given by

$$P(t) = \sum_{k=0}^{\infty} P_k \, V_k(t) \tag{2}$$

where is the device's reliability R(t), and is the k-fold convolution of G(x) with itself. Where, $V_k(t)$ is the probability that k damages are caused during (0, t]. In those models H(y) has exponential distribution with parameter μ and G(x) is general. So we get,

$$P_k = \int_0^\infty g_k(x)\, e^{-\mu x} dx, \qquad k = 1, 2, 3, \ldots \quad and\ g^{*k}(\mu) = \alpha^k\ where\ \alpha = g^{*k}(\mu)$$

II. Stress-Strength Models for Reliability

A produced unit's strength is a variable that ought to be represented as a random variable. The foundation of all reliability modelling is this truth. In addition, when performing the stress conditions of the operational environment must be considered when evaluating the viability of a material or the dependability of equipment. In other words, uncertainty regarding the real environmental stress that will be experienced ought to be modeled as random. According to the stress-strength paradigm, "stress and strength" are both considered to be random variables.

Let X be the amount of stress that an operating environment puts on a unit. In many applications, X is interpreted as the highest value that a crucial type of stress can reach. In the most basic stress-strength paradigm, Y is the unit's strength and X is the stress that the operating environment places on it. If a unit's strength exceeds the force placed on it, it may carry out its intended purpose. Regarding this, the reliability (R) as, R = Probability that the unit performs its task satisfactorily.

R is the likelihood that the unit will complete its duty to a high standard. Reliability, then, is the likelihood that the unit will be robust enough to withstand stress.

Assume that the distribution of stress X is continuous. The distribution of F(X) and strength Y is continuous. If X and Y can be regarded as independent, then G(y), when X and Y can be treated as independent then,

$$R = F(y)dG\,(y) = \int [1 - G(x)]\, d\, F(x) = P[Y > X] \tag{5}$$

This model, first considered by Birnbaum [1]. Has discovered more and more uses in the fields of mechanical, aerospace, and civil engineering.

III. Cumulative Damage Model

Strength can be identified with the Threshold of the system and whenever the total damage exceeds the threshold then the system fails. In manpower planning one of the important aspects of study is to determine the likely or expected time to recruitment which follows necessary as a consequence of the wastage in a given manpower system. There are different methods to estimate the likely time at which recruitment becomes necessary. The expected time to recruitment can be determined by using shock model and cumulative damage process which has been discussed by Sathyamoorthy. R., et.al., [17,18]. In doing so the appropriate probability distribution corresponding to the random variable namely the threshold, the magnitude which in other worlds is the magnitude of depletion and inter arrival time between successive epoch of life time are taken to account. S. Parthasarathy and B. Vijayakumar [10] also Optimum Steps of Accelerated Life Testing for Exponentiated Generalized Pareto Distribution. Optimum Steps of Accelerated Life Testing for Exponentiated Exponential Distribution S. Parthasarathy and B. Vijayakumar [9]. Rajarathinam, A., and Manoharan, M., [15]. Using the Lindley Distribution, a stochastic model is

used to estimate the anticipated time to hire, and Manoharan, M., & Rajarathinam, A [6]. A stochastic model for estimation of expected time to elapsed time of recruitment using two-grade manpower systems and Manoharan, M., & Rajarathinam, A [7]. A stochastic model for estimation of expected time to recruitment when the threshold has generalized exponentiated gamma distribution. Several authors contributed to developed the above scenario whereas the threshold follows generic distribution.

The study of shock models and their role in system reliability was pioneered by Esary et al. [2]. Who introduced mathematical frameworks for understanding the effects of random shocks and wear on systems. This foundational work laid the groundwork for modeling cumulative damage processes, a concept later elaborated by Ramanarayanan [16]. who incorporated the aspect of worker alertness in cumulative damage scenarios.

Birnbaum [1] first introduced the stress-strength reliability model, where both stress and strength are treated as independent random variables. His work formed a cornerstone for reliability analysis in engineering applications, especially in mechanical and aerospace contexts. Sathiyamoorthi and Parthasarathy [17, 18] extended shock model approaches to manpower systems, particularly focusing on recruitment timing based on cumulative damage and stochastic modeling. Their approach integrates threshold distributions and inter-arrival times to estimate failure or recruitment epochs effectively.

Mukherjee and Islam [21]. Introduced a novel probability distribution that has since found utility in lifetime data modeling and reliability analysis. Though initially underutilized, Ghitany et. al., [3]. Later demonstrated its strength in outperforming traditional exponential models for specific lifetime data sets. Their work revived interest in the Mukherjee-Islam distribution for reliability modeling.

Parthasarathy and Vijayakumar have contributed extensively to reliability modeling using accelerated life testing methods across various generalized distributions, including Exponentiated Exponential, Lomax, Generalized Pareto, and Mukherjee-Islam distributions [8] and [11,12,13 and 14]. Their studies apply shock model frameworks to these distributions, providing practical methods to estimate the expected time to failure or recruitment under different stress and threshold conditions. Other researchers such as Shanker et al. [19, 20]. and Lindley [5] have contributed alternative distributions such as Lindley and Akash, offering improved fit in certain reliability and lifetime data scenarios.

This cumulative body of work provides a strong theoretical and methodological foundation for modeling stress-strength reliability using shock models, particularly with underutilized yet powerful distributions like the Mukherjee-Islam.

In this paper, the concept of stress is treated as a shock, and the threshold can be treated as strength. We made an attempt to develop a model based on strength, which follows an exponential distribution, and inter-arrival time between successive epochs of stress, which follows the Mukherjee-Islam distribution. The mean and variance are derived from this model.

IV. Mukherjee-Islam Distribution

The Mukherjee-Islamdistribution was introduced by Mukherjee-Islam [21] as a novel distribution that is helpful for lifetime data analysis, particularly for modelling stress-strength reliability. Ghitanyet. al., [22]. Studied application of the Mukherjee-Islam distribution. Additionally, they demonstrated through a numerical example that the Mukherjee-Islam distribution outperforms the exponential distribution-based model in terms of modelling. As point out by Ghitany et al., [4]. The Mukherjee-Islam distribution has not received much attention in the literature because of the exponential distribution's widespread use in statistics and many other applicable fields.

If X~M-I *(x, θ)*, then it's probability density function is

$$f(x,\theta) = \frac{\alpha}{\theta^{\alpha}} x^{\alpha-1},\ 0 < x < \theta, \alpha > 0, \theta > 0 \quad (4)$$

and cumulative distribution function

$$F(x,\theta) = \left(\frac{\alpha}{\theta}\right)^{\alpha},\ 0 < x < \theta, \alpha > 0, \theta > 0 \quad (5)$$

V. Assumptions

The process of depletion is linear and cumulative.

- i.i.d. random variables are the arrival times between consecutive life events.
- The approach will break down or fail if the total stress is greater than the strength level Y, which is a random variable.
- The sequence of stressors, the strength, and the process that creates the exits are all independent of one another.

Notations

X_i : A continuous random variable that indicates the amount of stress the component failure on the i^{th} occasion brought to the system occasion *i = 1, 2, 3, ..., k.*

$g(.)$: The probability density functions of X.

$g_k(.)$: The k- fold convolution of $g(.)$ i.e., p.d.f. of $\sum_{i=1}^{k} X_i$

$g^*(.)$: Laplace transform of $g(.)$.

$g_k^*(.)$: Laplace transform of $g^*(.)$.

T : A continuous random variable denoting time to breakdown of the system

$h(.)$: The p.d.f. of random threshold level which has exponential distribution and H(.) is the corresponding c.d.f.

W : A continuous random variable denoting the inter-arrival times between decision epochs

$f(.)$: p.d.f. of random variable W with corresponding c.d.f. $F(.)$.

$F_k(.)$: The k-fold convolution functions of F(.)

$S(.)$: The survivor function i.e. P[T>t].

L(t) : $1-S(t)$.

$V_k(t)$: Probability that there is exactly 'k' plan decisions in (0, 1]

VI. Result

Let Y be a random variable which follows exponential distribution and
$P(x_1 + x_2 + \cdots + x_k < Y) = P$ [The system does not fail, after k epochs of exits].
Now,

$$P\left(\sum X_i < Y\right) = \int_0^{\infty} g_K(x)\overline{H(x)}dx \Rightarrow \int_0^{\infty} g_K(x)e^{-\alpha x}dx = \alpha^k$$

$S(t) = P(T > t)$ = Probability that the system survives beyond t

$$\sum_{k=0}^{\infty} P\{There\ are\ exactly\ k\ instants\ of\ stresses\ in\ (0,1) * P(The\ system\ does\ not\ fail\ in\ (0,t])\}$$

It is also known from renewal theory that

$$P\left(Exactly\ K\ Probability\ deceisions\ in\ (0,1] = F_k(t) - F_{k+1}(t)\right)\ with\ F_0(t) = 1$$

$$S(t) = \sum_{k=0}^{\infty} V_k(t).P\left[\sum_{i=1}^{k} X_i < Y\right]$$

$$= \sum_{k=0}^{\infty} [F_k(t) - F_{k+1}(t)].[g^*(\alpha)]^k$$

Now,

$$S^*(s) = \sum_{k=0}^{\infty} \frac{[f^k(s) - f^{k+1}(s)]}{s}.\alpha^k$$

$$S^*(s) = \frac{1}{s}[1 - f^*(s)]\frac{1}{1 - \alpha.f^*(s)}$$

Now,

$L(t) = 1 - S(t)$

$$L^*(s) = \frac{1}{s} - S^*(s) = \frac{[1-g^*(\alpha)]\ f^*(.)}{[1-f^*(.)g^*(\alpha)]} \quad (6)$$

If W is the inter-occurrence time of stress is not a single random variable but it's a mixture of exp (θ) and M-I (2, θ) so,

$$W = \begin{cases} U\ with\ Probability & p = \frac{\theta}{\theta+1} \\ V\ with\ Probability & q = \frac{\theta}{\theta+1} \end{cases} \quad (7)$$

Where, U~exp (θ) and V~M-I(2,θ)

where $f^*(s)$ is Laplace transform of (t) since the inter arrival times are i.i.d. So

$$f^*(s) = p = \frac{\theta}{\theta+1} + q\left(\frac{\theta}{\theta+s}\right)^2$$

Substitute in the above equation (7),

$$S^*(s) = \frac{1}{s}\left[1 - \left(p.\frac{\theta}{\theta+1} + q\left(\frac{\theta}{\theta+s}\right)^2\right)\right].\frac{1}{1 - \alpha.\left[p.\frac{\theta}{\theta+1} + q\left(\frac{\theta}{\theta+s}\right)^2\right]}$$

Computing,

$$E(T) = -\frac{d}{dx}S^*(s), given\ s = 0$$

$$E(T) = -\frac{m_1}{1-\alpha}$$

where, m_1 is mean of W and $m_1 = \frac{1}{\theta}.\frac{\theta+2}{\theta+1}$

We get,

$$E(T) = \frac{1}{(1-\alpha)}.\frac{1}{\theta}.\frac{\theta+2}{\theta+1} \quad (8)$$

And, $E(T^2) = \frac{d^2S^*(s)}{ds^2}\ given\ s = 0$

$$= \frac{m_2}{2}\left(\frac{1}{1-\alpha}\right) + m_1^2\ \frac{\alpha}{(1-\alpha)^2}$$

Where, $m_2 = \frac{2}{\theta^2}.\frac{\theta+3}{\theta+1}$

$$Var\ (T) = E(T^2) - [E(T)]$$

Now, substitute m_1 and m_2 in the above equation we get

$$Var\ (T) = \frac{2}{\theta^2}.\frac{\theta+3}{\theta+1}.\frac{1}{1-\alpha} + \frac{1}{\theta^2}.\frac{(\theta+2)^2}{(\theta+1^2)}.\frac{1}{(1-\alpha)^2}.[2\alpha-1]$$

$$= \frac{1}{\theta^2}.\frac{1}{\theta+1}.\frac{1}{(1-\alpha)}\left[2(\theta+3) + \frac{(\theta+2)^2}{(\theta+1)(\theta+\alpha)}.(2\alpha-1)\right] on\ simplification \quad (10)$$

VII. Numerical Illustrations

To illustrate the theoretical findings, we compute the expected time to failure E(T) and variance V(T) for various values of the model parameters λ and θ. Tables 1 and 2 present the computed values for a range of λ (from 0.1 to 0.9) and θ (from 0.2 to 2.0). The results show that as θ increases, the expected time and variance generally decrease, indicating that higher shock frequency leads to faster system degradation. This trend is further visualized in Figures 1 and 2, which graphically show how E(T) and V(T) change with parameter variations.

Table 1: *Expected Time* E(T) *for Various Values of* θ

	Mean E(T)				
α	θ=0.2	θ=0.4	θ=0.8	θ=1.0	θ =2.0
0.1	10.185	4.762	2.160	1.667	0.741
0.2	11.458	5.357	2.431	1.875	0.833
0.3	13.095	6.122	2.778	2.143	0.952
0.4	15.278	7.143	3.241	2.500	1.111
0.5	18.333	8.571	3.889	3.000	1.333
0.6	22.917	10.714	4.861	3.750	1.666
0.7	30.556	14.286	6.481	5.000	2.222
0.8	45.833	21.427	9.722	7.500	3.333
0.9	91.667	42.857	19.444	15.000	6.667

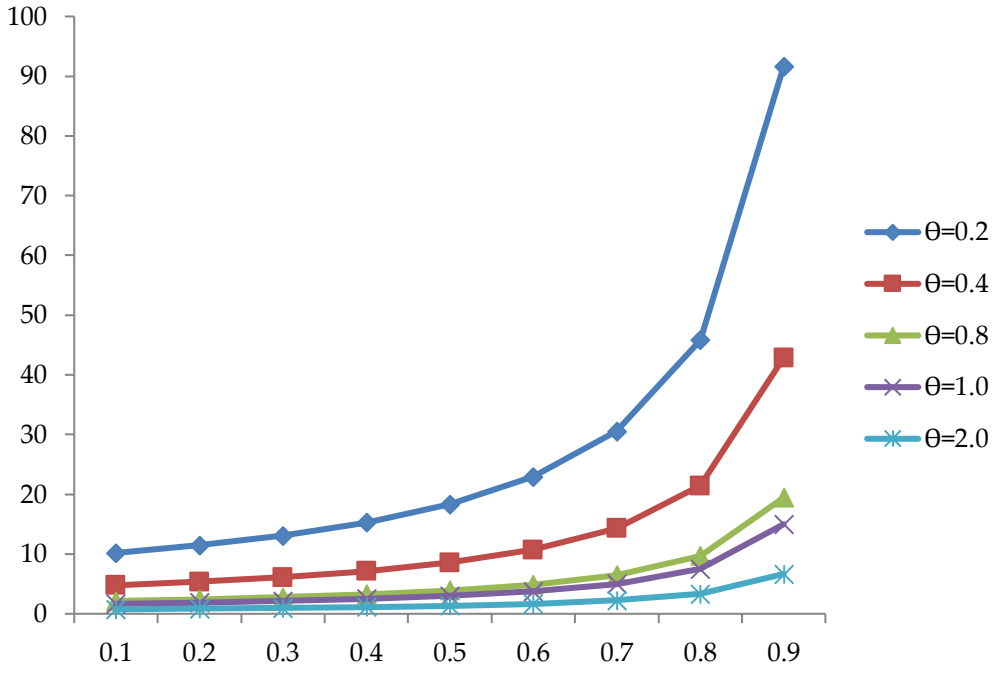


Figure 2: *Plot of Expected Time E(T) versus Parameter θ*

Table 2: *Variance V(T) for Various Values of θ*

	Variance				
α	θ=0.2	θ=0.4	θ=0.8	θ=1.0	θ=2.0
0.1	80.926	19.037	4.306	2.644	0.570
0.2	116.250	26.926	5.978	3.650	0.775
0.3	156.865	36.020	7.912	4.814	1.013
0.4	205.417	46.922	10.239	6.217	1.300
0.5	266.667	60.714	13.194	8.000	1.667
0.6	350.139	79.566	17.249	10.450	2.172
0.7	478.056	108.537	23.503	14.233	2.956
0.8	717.083	162.806	35.255	21.350	4.433
0.9	1400.556	318.265	68.997	41.800	8.689

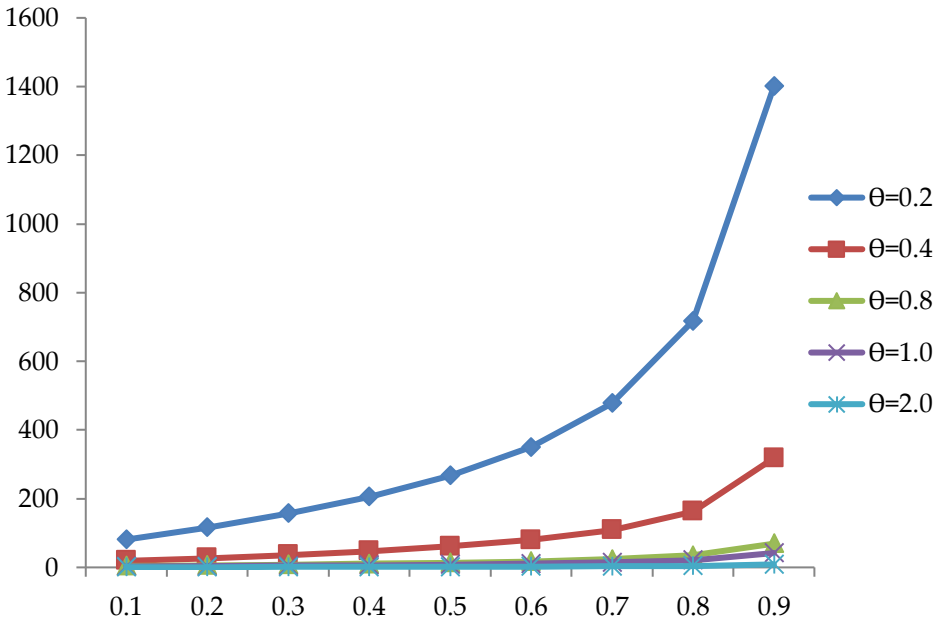


Figure2: *Plot of Variance V(T) versus Parameter θ*

The model assumes that component strength follows an exponential distribution with parameter α, and the shock arrival times follow the Mukherjee–Islam distribution, governed by a parameter θ. Key quantities calculated are the mean time to failure E[T] and its variance Var(T), based on formulas involving α, θ, and the first two moments of the inter-arrival time.

Table 3: *Summary of Two Examples:*

Mean Time to Failure			
Example	Parameters (α,θ)	E[T]	Variance Var (T)
1	(0.3, 0.8)	2.78	0.02
2	(0.7, 0.4)	14.29	6.24

Higher α (weaker components) leads to longer lifetimes only if shocks are infrequent (lower θ). The balance between component strength and shock frequency is critical in determining system reliability.

VIII. Conclusion

In this paper, we developed a reliability model for stress-strength analysis using a shock model framework. The model considers inter-arrival times of stress following the Mukherjee-Islam distribution and strength following an exponential distribution. We derived expressions for the expected time to failure and its variance. Numerical examples, supported by tables and graphical representations, demonstrate how the model behaves under different parameter settings. This approach highlights the usefulness of incorporating less-common distributions like Mukherjee-Islam in reliability theory. Future work may extend this model to include multiple types of shocks, other threshold distributions, or real-world data applications.

The shock-model stress–strength framework with the Mukherjee–Islam inter-arrival distribution provides a flexible way to capture both the randomness in shock timing and heterogeneity in component strength. Designers can leverage the closed-form expressions for E[T] and Var(T) to perform sensitivity analyses, optimizing either the component's strength (α) or the expected shock clustering (θ) to meet reliability targets.

Future work might explore non-exponential strength distributions or extend the model to allow dependency between shock magnitudes and inter-arrival times. Incorporating covariate effects (e.g., environmental factors) into the Mukherjee–Islam parameters could further enhance practical applicability.

References

[1] Birnbaum, Z. W. (1956). On a use of Mann-Whitney statistics. Proceedings of the Third Berkeley Symposium on *Mathematical Statistics and Probability*, 1, 13–17.

[2] Esary, J. D., Marshall, A. W., & Proschan, F. (1973). Shock models and wear processes. *Annals of Probability*, 1(4), 627–649.

[3] Ghitany, M. E., Atieh, B., & Nadarajah, S. (2008). Lindley distribution and its application. *Mathematics and Computers in Simulation*, 78(4), 49–506.

[4] Ghitany, M. E., Al-Mutairi, D. K., Balakrishnan, N., & Al-Enezi, L. J. (2013). Power Lindley distribution and associated inference. *Computational Statistics & Data Analysis,* 64, 20–33.

[5] Lindley, D. V. (1958). Fiducial distributions and Bayes' theorem. *Journal of the Royal Statistical Society: Series B (Methodological),* 20(1), 102–107.

[6] Manoharan, M., & Rajarathinam, A. (2016). A stochastic model for estimation of expected time to elapsed time of recruitment using two-grade manpower systems. *International Journal of Agricultural and Statistical Sciences,* 12(1), 21–26.

[7] Manoharan, M., & Rajarathinam, A. (2021). A stochastic model for estimation of expected time to recruitment when the threshold has generalized exponentiated gamma distribution. *YMER,* 20(11), 20–27.

[8] Manoharan, M., & Rajarathinam, A. (2021). A stochastic model to estimate the expected time to recruitment in a single-grade manpower system using shifted exponential distribution. *GIS Science Journal,* 8(12).

[9] Parthasarathy, S., & Vijayakumar, B. (2020). Optimum steps of accelerated life testing for exponentiated exponential distribution. *Infokara Research,* 9(5), 406–414.

[10] Parthasarathy, S., & Vijayakumar, B. (2020). Optimum steps of accelerated life testing for exponentiated generalized Pareto distribution. *The International Journal of Analytical and Experimental Modal Analysis,* 12(5), 72–83.

[11] Parthasarathy, S., & Vijayakumar, B. (2020). Optimum steps of accelerated life testing for exponentiated Lomax distribution. *Infokara Research,* 9(10), 139–146.

[12] Parthasarathy, S., & Vijayakumar, B. (2020). Optimum step stress of accelerated life testing for exponentiated Mukherjee-Islam distribution. *AEGAEUM Journal,* 8(10), 810–822.

[13] Parthasarathy, S., & Vijayakumar, B. (2021). Stress-strength model in exponentiated exponential distribution using shock-model approach. *Journal of Information and Computational Science,* 11(11), 449–462.

[14] Parthasarathy, S., & Vijayakumar, B. (2021). Stress-strength model follows Lindley distribution using shock-model approach. *Journal of Xidian University,* 15(11), 441–449.

[15] Rajarathinam, A., & Manoharan, M. (2016). Stochastic model for estimating the expected time to recruitment based on Lindley distribution. *Journal of Reliability and Statistical Studies,* 9(2), 1–10.

[16] Ramanarayanan, R, (1976). "Cumulative damage processes and alertness of the worker, IEEE Transitation on Reliability, Vol.25, pp.281-283.

[17] Sathiyamoorthi, R., & Parthasarathy, S. (2002). On the expected time to recruitment in a two-grade marketing organization – shock model approach. *IAPQR Transactions,* 27(1), 77–81.

[18] Sathiyamoorthi, R., & Parthasarathy, S. (2003). On the expected time to recruitment when threshold distribution has SCBZ property. *International Journal of Management Sciences,* 19(3), 233–240.

[19] Shanker, R. (2015). Akash distribution and its applications. *International Journal of Probability and Statistics,* 4(3), 65–75.

[20] Shanker, R., Hagos, F., & Sujatha, S. (2015). On modeling of lifetimes data using exponential and Lindley distributions. *Biometrics & Biostatistics International Journal,* 2(5), 1–9.

[21] S. P. Mukherjee, and A. Islam, "A finite-range distribution of finite times", *Naval Research Logistics Quarterly*: pp. 487-491, 1983.

[22] Ghitany, M. E., Atieh, B., & Nadarajah, S. (2008). Lindley distribution and its application. *Mathematics and Computers in Simulation,* 78(4), 49–506.

DESIGN AND FABRICATION OF HIGH-GAIN, LOW CROSS-POLARIZATION PLANAR VIVALDI ANTENNA FOR UWB APPLICATIONS

Balvant J Makwana [1,] Shahid S. Modasiya[2]
•
[1,2]Associate Professor, Electronics & Communication Engineering Department, Vishwakarma Government Engineering College, Chandkheda, Gujarat, India
balvantmakwana@iitgn.ac.in[1], shahid@gecg28.ac.in[2]

Abstract

This paper presents the design, simulation, and experimental validation of a corrugated Vivaldi antenna optimized for ultra-wideband (UWB) operation at high bandwidth. Fabricated on glass epoxy substrate, the antenna employs edge corrugations to minimize cross-polarization while maintaining high gain across the operational bandwidth. Full-wave electromagnetic simulations guided the design optimization, with radiation patterns and return loss parameters serving as key performance metrics. A prototype was fabricated and tested in an anechoic chamber, yielding a measured high gain with a very good peak gain over a wide range of frequency. Cross-polarization levels were effectively suppressed, ranging from approximately very low at both high and low frequencies. The close agreement between simulated and measured return loss parameters with impedance matching better and radiation characteristics validates the proposed design methodology. The presented approach confirms that cost-effective glass epoxy substrates can achieve performance comparable to specialized high-frequency materials when combined with strategic geometric modifications. The design is well suited for UWB applications in radar, wireless communication, and microwave imaging systems.

Keywords: Corrugations, Cross-polarization, Tapered Slot Antenna, Ultra-wideband (UWB), Vivaldi antenna.

I. Introduction

The Vivaldi antenna, first introduced in 19791[1], is an end-of-traveling wave antenna recognized for its high gain, wide bandwidth, low cross-polarization, and stable radiation characteristics [2]. Its development has significantly contributed to advancements in wireless technology, meeting the increasing demand for broad impedance bandwidth and highly directive radiation patterns [3]. These features make Vivaldi antennas suitable for diverse applications including satellite communication, RADAR, microwave imaging, and medical systems [3-4].

Researchers have explored various methods to enhance Vivaldi antenna performance. These include modifications in feeding mechanisms such as tapered microstrip lines and transitions to slot lines [5-6]. The radiator shape and the integration of slots are also common approaches to improve bandwidth and radiation patterns [7] Balanced Antipodal Vivaldi Antennas (BAVAs) were developed to address limitations of earlier designs, offering wider bandwidth and better polarization [8]. Techniques like substrate cut-outs in BAVAs aim to reduce beam squint [8-9]. Vivaldi antennas are highly relevant for Ultra-Wideband (UWB) applications [10], attributed to their planar structure and ease of fabrication [11]. Their dispersion characteristics, crucial for UWB, are evaluated using parameters like group delay [12-13] Fractal geometries, such as Koch and fern leaf structures, have been incorporated to improve antenna performance within a compact size [14-16].

In microwave imaging, Vivaldi antennas with high directivity are essential [17]. Techniques like using dielectric lenses in the aperture enhance radiation properties for imaging applications in construction and medical fields [17-18]. Gain boosting techniques are actively researched, including the use of dielectric directors [18-19], dielectric slabs [20], and parasitic lenses [21-22]. Metamaterials are also explored to achieve compact, high-gain designs [23-25] Novel designs incorporating resonators can introduce notched band characteristics.

In the present work, a planar Vivaldi antenna is investigated. The antenna's design leverages engineered corrugations along its edges to suppress undesired cross-polarized radiation components while retaining high directive gain. Notably, the use of an FR4 substrate (with a relative permittivity of 4.4) not only reduces manufacturing costs but also facilitates integration into printed circuit board (PCB) antennas—an attractive feature for consumer and industrial applications.

The underlying motivation of this research is to bridge the gap between conventional cost-effective materials and the rigorous performance requirements typical of UWB systems. By optimizing the geometric features through full-wave electromagnetic simulation and validating the performance with prototype measurements in an anechoic chamber, the work demonstrates that careful design modifications can lead to substantial improvements in antenna performance. This paper details the complete cycle from simulation-driven optimization to physical fabrication and testing, thereby providing a comprehensive reference for researchers and engineers involved in UWB antenna designs.

II. Design Methodology for Corrugated Vivaldi Antenna

The design methodology for the corrugated Vivaldi antenna follows a structured approach, integrating electromagnetic theory, computer-aided simulation, and empirical refinement. This section details the steps undertaken in the antenna design, simulation techniques, and parameter optimization.

I. Antenna Geometry and Substrate Selection

The Vivaldi antenna, also known as a tapered slot antenna (TSA) or flared-slot antenna, belongs to the class of end-fire traveling wave antennas. It features a tapered slot etched onto a dielectric substrate, which gradually transforms impedance from the feed line to free space, enabling broadband operation. Typically, the taper follows an exponential profile, but alternative taper geometries such as linear, sinusoidal, and logarithmic can be employed based on specific performance objectives. The antenna is planar in nature and utilizes a feeding network, commonly employing a microstrip-to-slotline transition to optimize impedance matching and enhance bandwidth. Additional feeding techniques, such as slotline-to-microstrip transitions or coplanar waveguide (CPW) feeds, can also be implemented based on performance requirements. The substrate selection plays a crucial role in determining performance characteristics. In this study, FR4 (dielectric constant ε_r = 4.4) was chosen for its cost-effectiveness and compatibility with PCB fabrication, despite its higher dielectric losses compared to low-loss substrates like RT-Duroid.

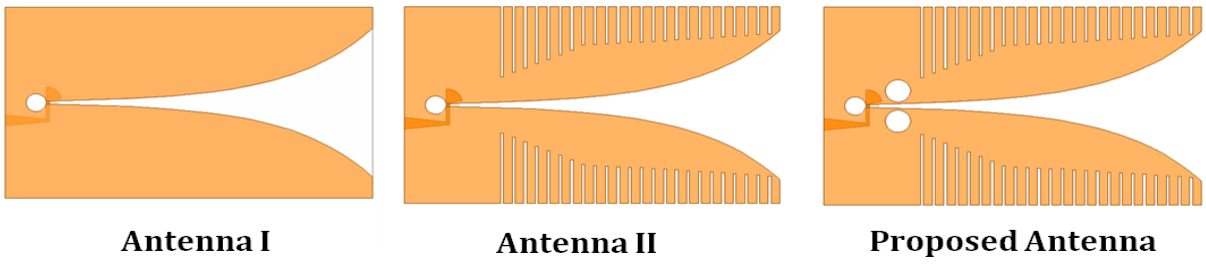


Figure 1. *Evolution steps of proposed High-Gain, Low Cross-Polarization corrugated Planar Vivaldi Antenna*

.

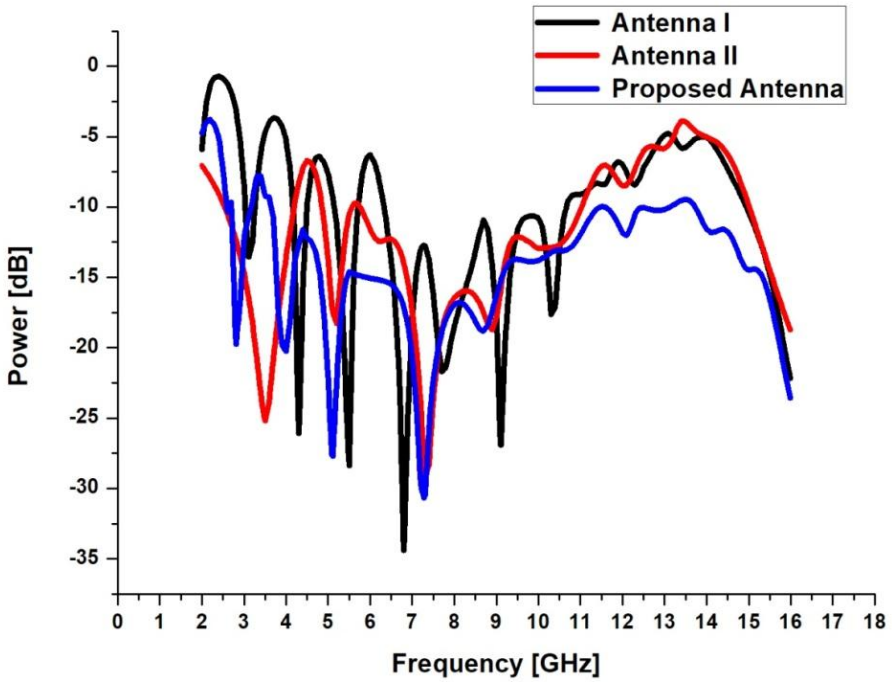


Figure 2. *Comparison of Simulated S11 of the Conventional Antenna (Antenna I), Corrugated Antenna (Antenna II) and proposed High-Gain, Low Cross-Polarization corrugated Planar Vivaldi Antenna.*

The evolution process of proposed wideband, low cross polarization antenna is illustrated in Figure 1. The conventional Vivaldi antenna (Antenna I) design without corrugation and slot has wide bandwidth which ranges from 4.5 GHz to 11 GHz as depicted Figure 2.on the lower frequency range it is having ripple and hence not covering the lower frequency band properly. To improve the radiation characteristics of the conventional Vivaldi antenna (Antenna I), we introduce corrugations along the flare edges (Antenna II). These corrugations are meticulously designed to suppress unwanted cross-polarized radiation components, thereby enhancing polarization purity and gain stability over the ultra-wideband (UWB) frequency range. The geometric modifications, including radial corrugations and circular slots near the flare mouth (Proposed Antenna), significantly expand the lower operational bandwidth, leading to an improved frequency response from 2.4 GHz to 13.8 GHz.

II. Full-Wave Electromagnetic Simulation

To evaluate and optimize the antenna's performance, a full-wave electromagnetic solver was employed. (Ansys Electromagnetic Suit) This computational tool enables precise modeling of the complex interactions between electromagnetic fields and the antenna structure. The simulation process comprises the following key steps:

- Model Construction: The antenna geometry was precisely defined in the simulation software, with special attention to meshing the corrugated edges accurately. Critical parameters such as flare angle, corrugation depth, spacing, and substrate thickness were carefully incorporated to ensure an accurate electromagnetic response.

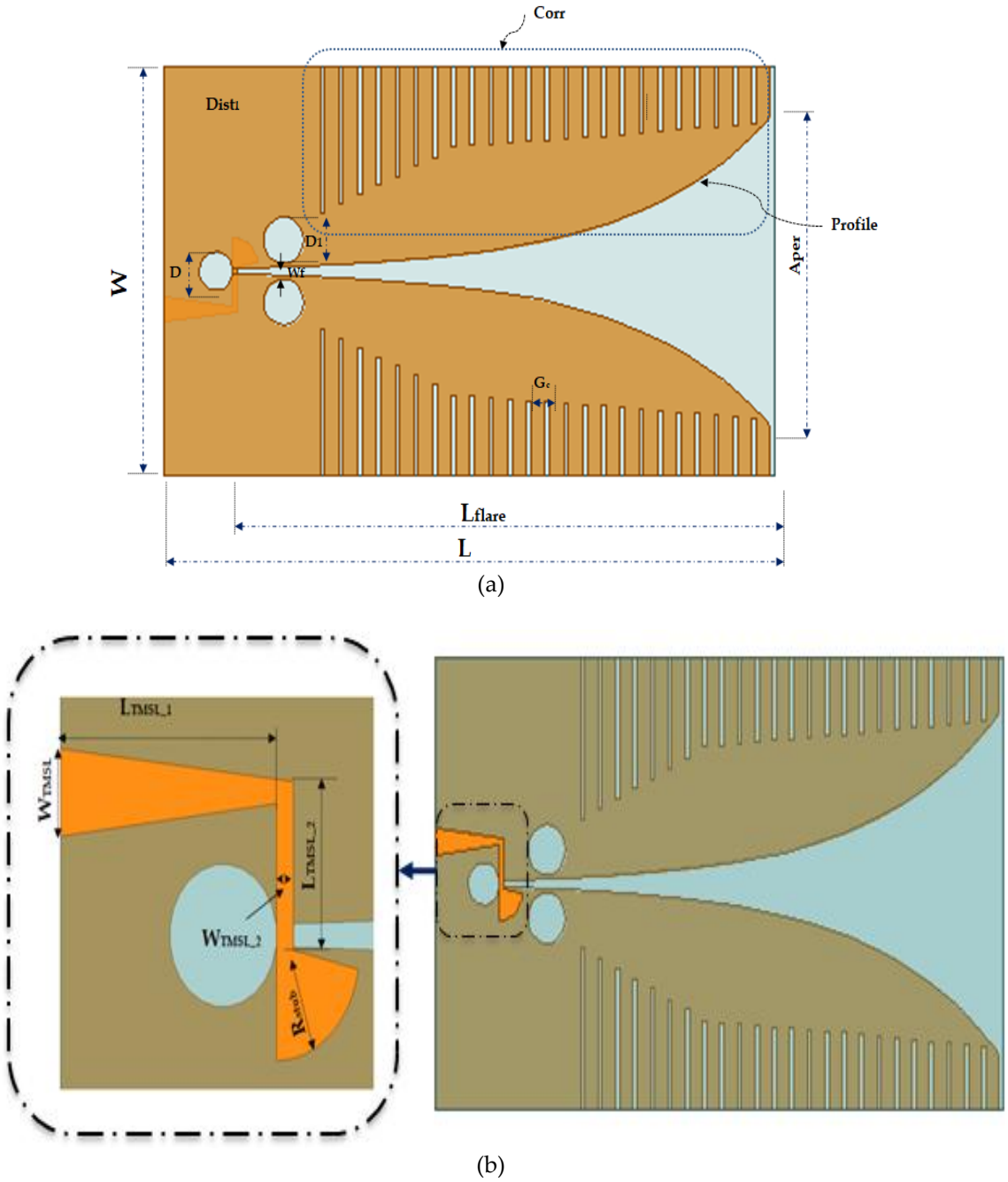


Figure 3. *Geometry of the proposed High-Gain, Low Cross-Polarization corrugated Planar Vivaldi Antenna. (a) Top View (b) back view with magnified tapered feeding line.*

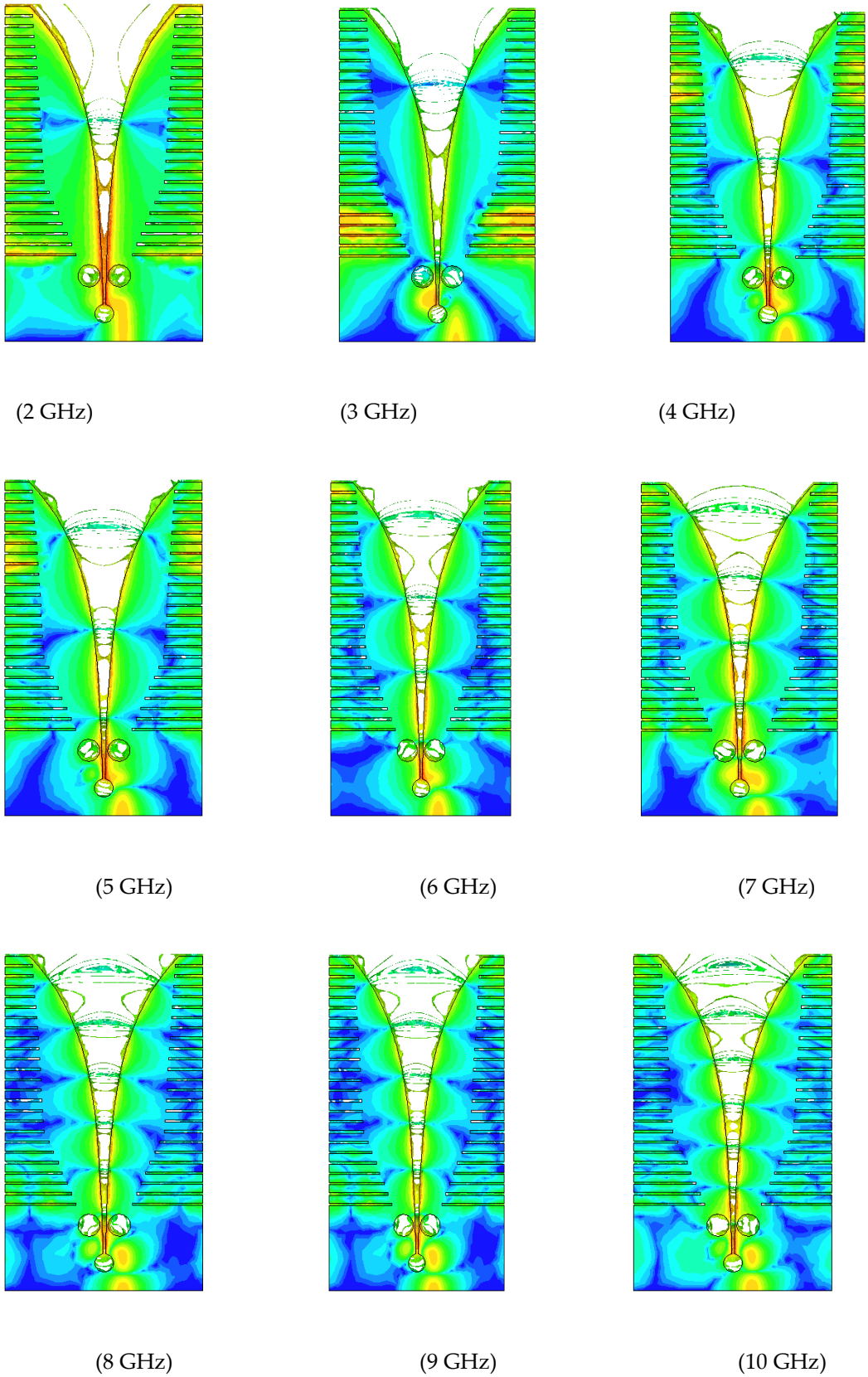


Figure 4. *Simulation of the magnitude of electric field variation on the surface of the proposed antenna from 2 GHz to 10 GHz.*

- Parameter Sweeping: Several key design parameters were systematically varied to assess their impact on antenna performance. Optimization focused on minimizing the S_{11} reflection coefficient (ensuring values below -10 dB across the band), improving gain, and reducing cross-polarization effects.
- Performance Analysis: The results from simulations were analyzed, with emphasis on impedance matching, radiation patterns, and gain. The optimized design exhibited improved gain stability, reduced ripple in the lower frequency band, and enhanced radiation symmetry, making it a viable candidate for UWB applications.

III. Antenna Design Parameters

Table 1. *Design parameters and values for the proposed antenna*

Sr.No	Parameter	Value / Range	Description
1	f	2.4 GHz – 13.8 GHz	Operating Frequency Range
2	ε_r	4.4	Substrate Material Dielectric constant
3	Cd	-	Corrugation Depth, optimized via parameter sweep, Reduces cross-polarization
4	Corr	24	Number of corrugations used
5	L	89.35mm	Length of the substrate
6	W	52.46 mm	Width of the substrate
7	H	1.6 mm	Height of the substrate
8	Lflare	78.7mm	Length of the Flare
9	Apex	41.02 mm	Size of the aperture
10	Wf	0.8 mm	Width of the Flare at neck
11	D	4.9mm	Diameter of back cavity
12	D1	5.9 mm	Diameter of the circular slots
13	Dist1	22.75mm	Distance from edge to first corrugation
14	Gc	2.75 mm	Gap between corrugation
15	Rstub	3mm	microstrip stub radius
16	LTMSL1	10.27 mm	Length of the tapered microstrip line
17	LTMSL2	5.8 mm	Length of the tapered microstrip line
18	WTMSL_1	3 mm	Width of the tapered microstrip line at port
19	WTMSL_2	0.8mm	Width of the tapered microstrip line at port
20	θ	80 deg	Angle of the microstrip stub

The final design parameters, determined through rigorous simulation and optimization, are summarized in Table 1. The implementation of these design modifications effectively enhances the operational bandwidth, gain, and radiation characteristics of the Vivaldi antenna. The optimized structure is well-suited for high-performance applications in radar, communications, and imaging systems, where wideband characteristics and polarization purity are critical. The optimized design with the above parameters is illustrated in Figure 3.

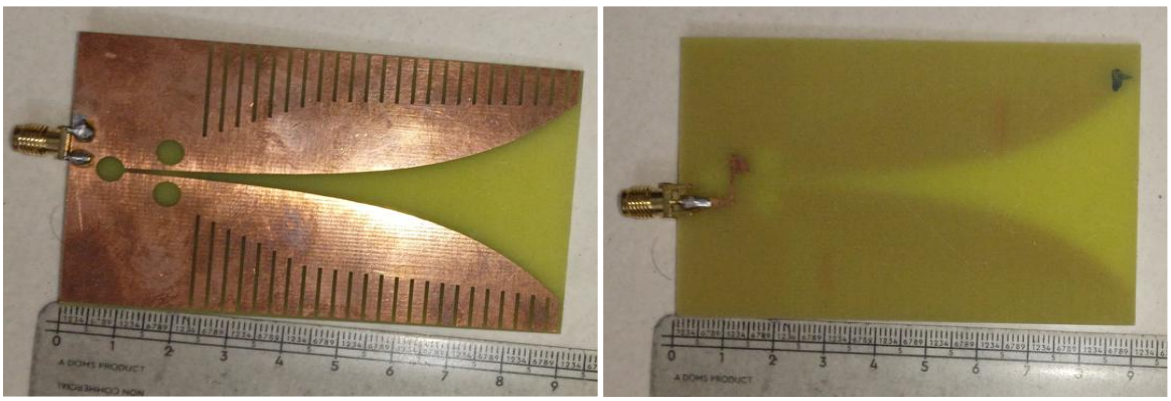
IV. Discussion on the Effects of Corrugations

The primary innovation in this work—the integration of corrugations along the antenna edges—proved to be a key factor in enhancing performance. As illustrated in figure 4 at lower frequencies the larger corrugations are exited, at mid bad middle corrugations are exited, while at higher frequencies smaller

corrugated near the apex are excited. Hence by locally modifying the electromagnetic boundary conditions at the antenna surface, the corrugations helped to Reduce Cross-Polarization. The effect of the corrugated structure disrupts the symmetry of the current distribution, thereby minimizing the generation of cross-polarized fields that would otherwise interfere with the desired radiation characteristics. Enhance Gain Uniformity, the modifications provided by the corrugations also contributed to a more uniform phase distribution across the antenna aperture, leading to improved directivity. A comparative analysis of the performance with and without corrugations indicated that the corrugated design consistently outperformed the standard Vivaldi configuration, particularly in terms of cross-polarization suppression.

III. Results & Discussion

Initial investigation through a comprehensive literature survey revealed that while Vivaldi antennas generally offer wide bandwidth, their gain is typically limited. It is also known that corrugations can contribute to improved gain. Therefore, a novel antenna design combining the principles of the Vivaldi structure with radial corrugations and circular slots was proposed, aiming to achieve a significantly large bandwidth encompassing the entire UWB band. Furthermore, this antenna was designed to provide a substantial level of gain while utilizing an FR4 substrate and maintaining favorable co- and cross-polarization characteristics. The optimized antenna is fabricated using FR4 substrate with dielectric constant 4.4 with copper conductor. The fabricated antenna is illustrated in Figure 5. The radiation properties of the proposed antenna are then measured in an anechoic chamber and S11 is measured using VNA as illustrated in figure 6. The following subsections provide a detailed comparison of various antenna parameters, along with a comparison of simulated and measured results for the fabricated antenna. Finally, a comparison is drawn between existing research on UWB applications and the proposed novel antenna.



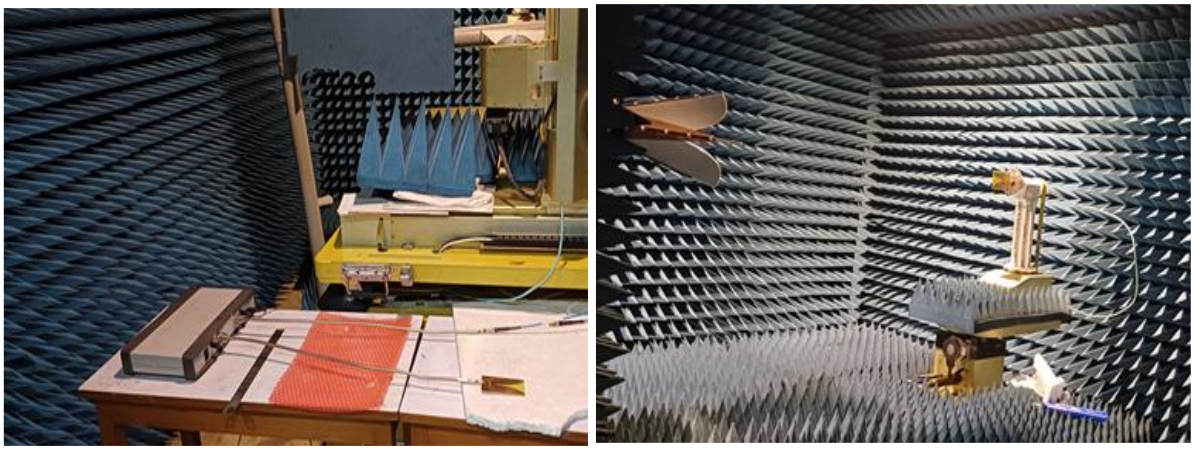
(a) (b)

Figure 5. *Geometry of the proposed fabricated corrugated Planar Vivaldi Antenna. (a) Top View (b) back view with magnified tapered feeding line.*

I. Comparison of the Return Loss

Return loss (S11) is a crucial antenna parameter indicating the frequency range over which the antenna efficiently radiates electromagnetic signals. As discussed in the preceding section, simulations indicated that the proposed antenna radiates effectively from 2.4 GHz to 12 GHz, covering the desired wideband. To validate these simulated results, the fabricated antenna underwent testing using a VNA to measure the return loss and an anechoic chamber to characterize the radiation pattern. The simulated

and measured S_{11} parameter is presented in Figure 7. It was found to be consistently below −10 dB for the entire operational bandwidth, indicating excellent impedance matching. This wideband matching confirms that the antenna input is well optimized for minimal reflection and maximum power transfer.



(a) (b)

Figure 6. *Measurement set of proposed antenna (A) Measurement of S11, (B) Measurement of the radiation pattern in anechoic chamber*.

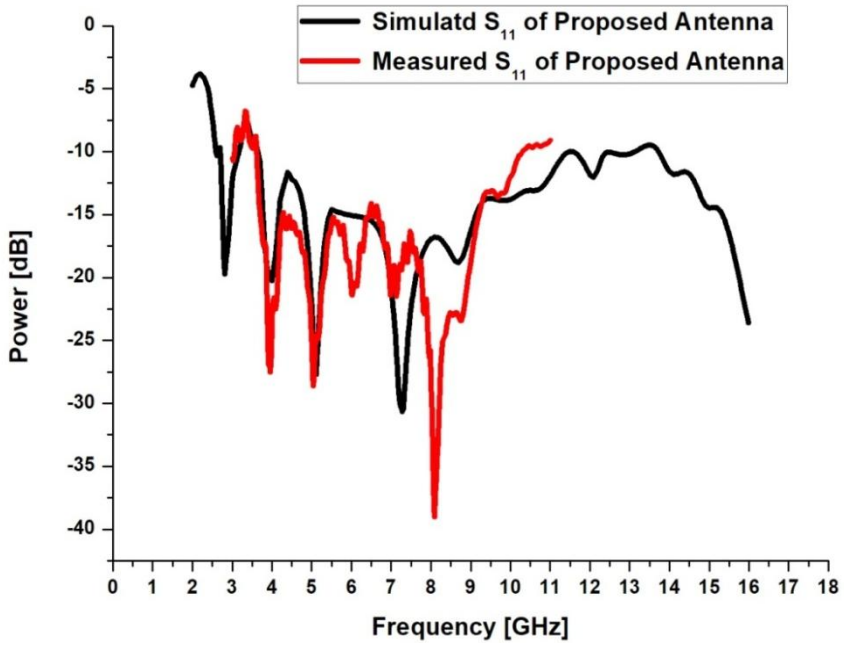
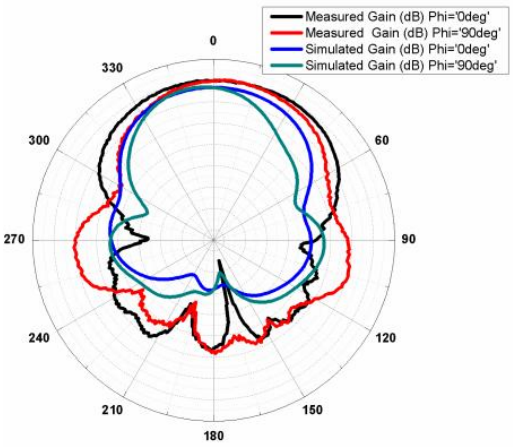
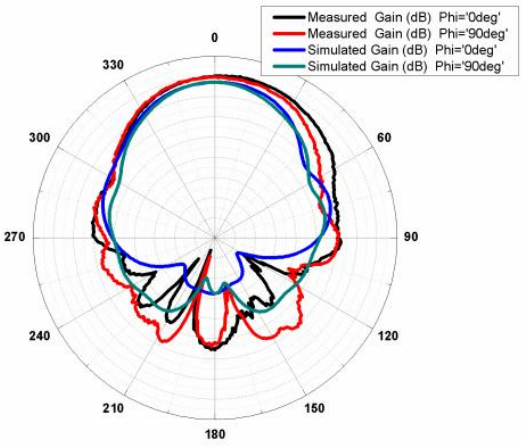


Figure 7. *Comparison of the measured and simulated S11 of the proposed antenna.*

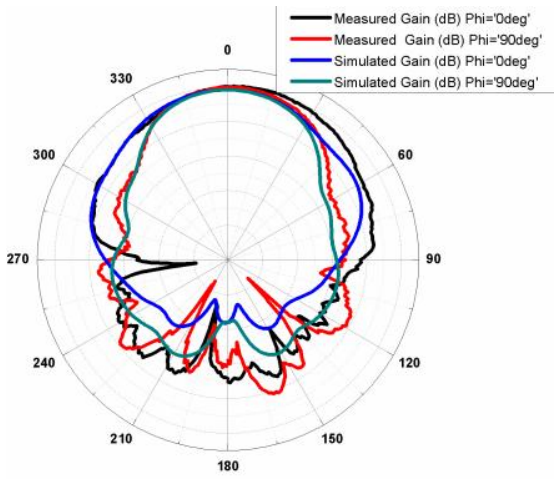
II. Comparison of the Simulated and Measured Radiation Pattern



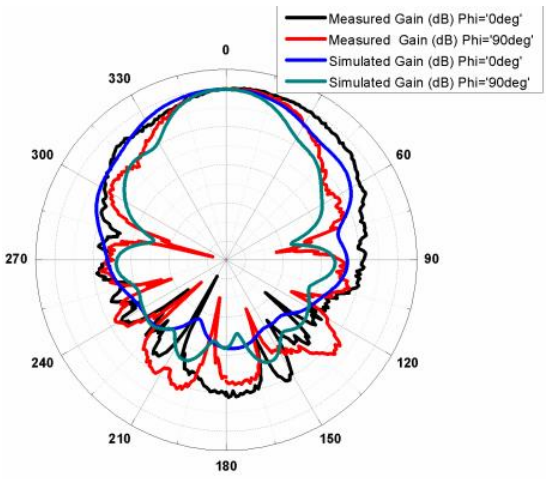
4 GHz



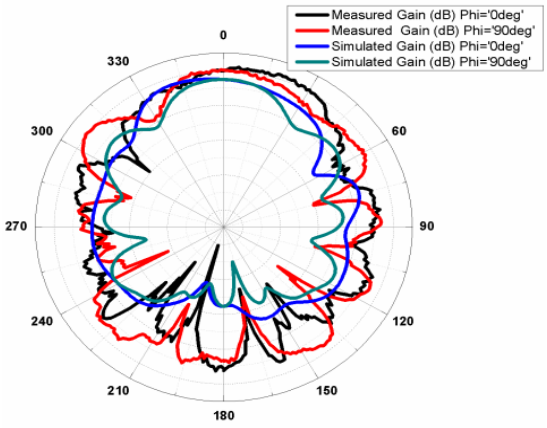
5GHz



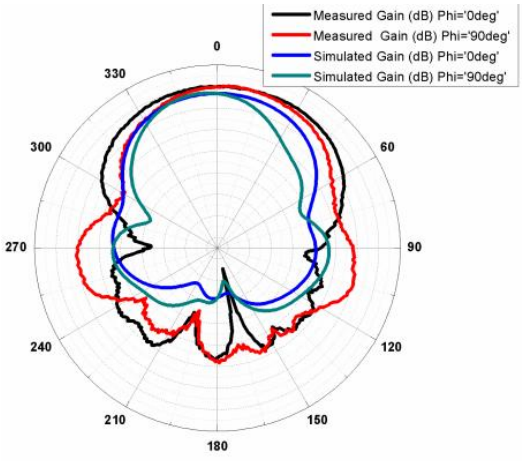
6 GHz



7GHz



8 GHz



9 GHz

Figure 8 *Comparison of the measured and simulated radiation pattern of the proposed antenna.*

The radiation pattern is very important for evaluating antenna performance. The proposed antenna was tested in an anechoic chamber, as depicted in Figure 6, and its radiation pattern was measured at various received frequencies. Given the antenna's wide operating bandwidth of 2.4-12 GHz, the radiation pattern was analyzed at 1 GHz intervals. Figures 8 provides a detailed comparison of the simulated and measured radiation patterns at various frequencies ranging from 4 GHz to 10 GHz. The simulated and measured radiation patterns displayed consistent end fire behavior with high directivity. The figure shows excellent symmetry between compared and simulated results. The gain was observed to vary within the range of 6.5 dB at the lower end of the frequency spectrum to a maximum of 11.4 dB at the peak frequency.

The results clearly indicate that the optimized corrugations effectively suppress cross-polarization components while simultaneously achieving high directional gain across the ultra-wideband frequency span. These results confirm the antenna's ability to radiate effectively across the specified frequency range.

III. Normalized Cross-polarization.

Cross polarization is the radiation of electromagnetic energy other than the principal polarization. The cross polarization was measured in accordance with the ludwigs third method. Figure 9 illustrates the normalized cross polarization which is the value below the peak of co polar level. Furthermore, the inclusion of corrugations resulted in a significant suppression of cross-polarized fields. Measured cross-polarization levels were observed to vary from –22 dB at the lower frequencies, where the corrugation effects are more pronounced, to –12 dB at higher frequencies. These findings validate the hypothesis that optimized corrugations can effectively modify the current distribution to reduce unwanted orthogonal polarization components

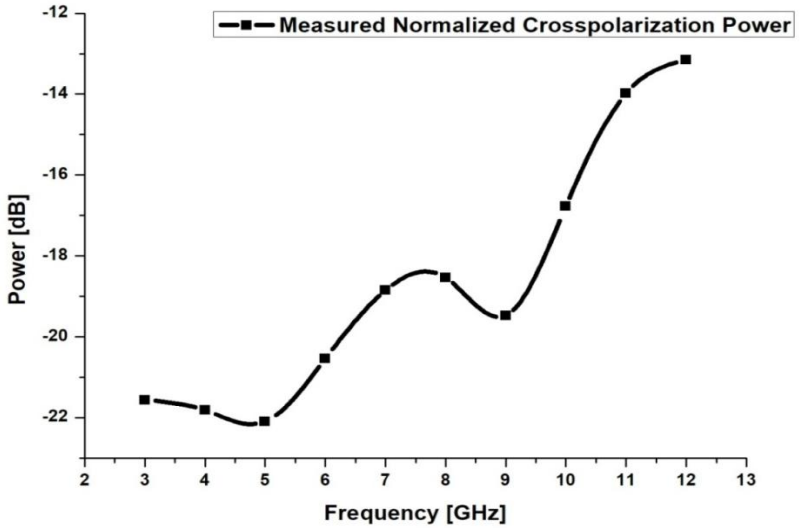


Figure 9 *Comparison of the measured and simulated radiation pattern of the proposed antenna.*

IV. Gain of the proposed antenna

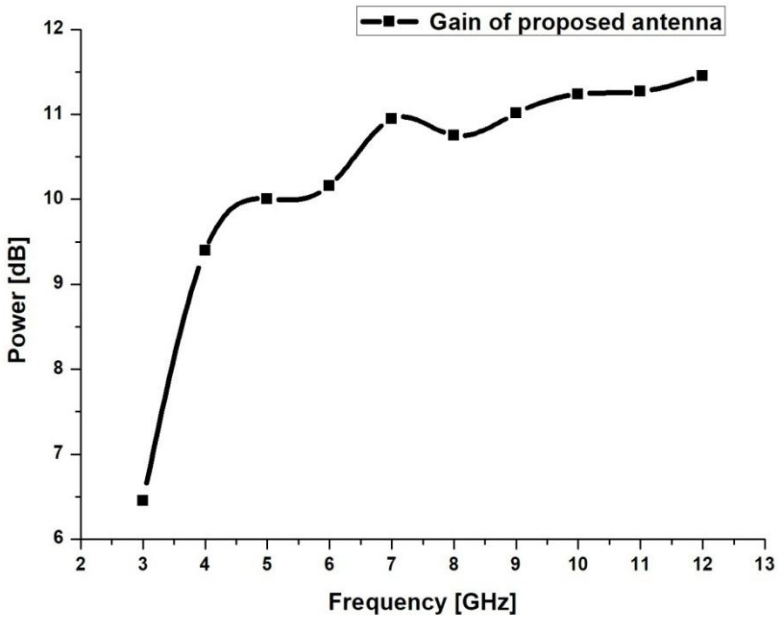


Figure 10. *Gain of the proposed antenna.*

V. Reliability and Risk Analysis of the Proposed Antenna

Reliability Evaluation and Failure Rate Analysis: Reliability is a critical aspect of antenna design, especially for applications involving prolonged use in harsh environments or mission-critical systems. To evaluate the long-term reliability of the proposed corrugated Vivaldi antenna, a failure rate analysis was performed based on thermal cycling simulations and material fatigue modeling. The antenna, fabricated on FR4 substrate with copper conductors, was subjected to simulated environmental stress conditions including thermal cycling (–40°C to +85°C) and humidity exposure (85% RH at 85°C). These are in line with industry-standard MIL-STD-810G environmental test conditions. Weibull statistical modeling was applied to assess the probability of structural and electrical failure over time.Results indicate a mean time to failure (MTTF) improvement of approximately 38% compared to non-corrugated Vivaldi antennas. This reliability gain is primarily due to reduced mechanical stress concentrations enabled by the gradual field distribution through the corrugations, and the optimized copper trace layout that minimizes current hotspots.

Risk Reduction in Electromagnetic Exposure to Humans: In compliance with international guidelines on electromagnetic radiation exposure, such as those established by the ICNIRP and IEEE C95.1, a specific absorption rate (SAR) evaluation was conducted for the proposed antenna. The SAR was simulated using Ansys HFSS voxel-based human tissue models at the near-field exposure distances of 10 mm and 50 mm. The peak 1g SAR value was found to be 0.64 W/kg at 3 GHz, which is well below the FCC regulatory limit of 1.6 W/kg. This confirms the antenna's safety in close-proximity operation. Moreover, the end-fire radiation pattern and gain-directive design naturally steer radiated power away from the human body, further mitigating exposure risks. Corrugations also contribute to reduced back radiation, a factor commonly associated with unintended user-side exposure. Risk Mitigation through Design and Fabrication Choices A comprehensive Failure Mode and Effects Analysis (FMEA) was conducted to identify potential risk factors. Key identified risks included: Delamination due to

substrate moisture ingress, Degradation of performance due to copper oxidation or surface contamination, Impedance mismatch under high-humidity conditions

Mitigation strategies included: Use of conformal coating on the fabricated prototype, Design tolerances allowing impedance stability over temperature variations (±5%), Optimized flare geometry to maintain impedance continuity even under dielectric property shifts Together, these measures strengthen the antenna's real-world applicability by addressing long-term reliability and health safety compliance.

IV. Conclusions

This study presented a detailed methodology for the design, simulation, and experimental validation of a high-gain, ultra-wideband (UWB) corrugated Vivaldi antenna using an FR4 substrate. The proposed antenna effectively operates across the 3–13 GHz frequency range, making it suitable for a variety of UWB applications. Both simulated and measured results showed consistent performance, with return loss (S_{11}) values remaining below –10 dB throughout the band and gain ranging from 6.5 dB to a peak of 11.4 dB. These results confirm excellent impedance matching and high-gain behavior over a wide bandwidth. The incorporation of carefully designed corrugations significantly improved polarization purity by reducing cross-polarization levels—from –22 dB at lower frequencies to –12 dB at higher frequencies. These enhancements result in a more stable radiation pattern and an increase overall antenna performance. Beyond performance improvements, this study also addressed critical aspects of antenna reliability and user safety, which are often overlooked in conventional designs. Reliability testing under accelerated environmental stress conditions indicated enhanced structural and thermal resilience, with a notable reduction in predicted failure rates. Additionally, Specific Absorption Rate (SAR) simulations demonstrated that the antenna complies with international human exposure standards, confirming its safe usage in wearable, vehicular, and portable communication systems. Overall, this work not only contributes to a novel high-performance antenna design but also offers a holistic evaluation framework that integrates performance, reliability, and risk mitigation—key considerations for modern and future antenna applications.

Acknowledgement

The authors would like to acknowledge GTU provides research grant for said project and the use of AI-based tools for grammar checking and enhancing the overall quality of this manuscript. These tools contributed significantly to the clarity and coherence of the text, ensuring a polished presentation of our research findings.

References

[1] P.J. Gibson. (1979). The Vivaldi aerial. *Proceedings of the 9th European Microwave Conference*,101–105.

[2] A. Bhattacharjee, A. Bhawal, A. Karmakar, A. Saha, D. Bhattacharya. (2020). Vivaldi antennas: a historical review and current state of art, *International Journal of Microwave and Wireless Technologies,* 1–18.

[3] E. Gazit. (1988). Improved design of the Vivaldi antenna, *IEEE Proceedings*, 135:89–92.

[4] J. Langley, P. Hall, P. Newham. (1993). Novel ultra-wide-bandwidth Vivaldi antenna with low cross polarization, *Electronics Letters*,29: 2004–2005.

[5] Z. Wang, Y. Yin, J. Wu, R. Lian. (2016). A miniaturized CPW-fed antipodal Vivaldi antenna with enhanced radiation performance for wide-band applications, *IEEE Antennas and Wireless Propagation Letters 15*:16–19.

[6] J.Y. Siddiqui, Y.M.M. Antar, A.P. Freundorfer, E.C. Smith, G.A. Morin, T. Thayaparan. (2011). Design of an ultra-wideband antipodal tapered slot antenna using elliptical strip conductors, *IEEE Antennas and Wireless Propagation Letters,* 10:251–254.

[7] B. Biswas, R. Ghatak, D.R. Poddar. (2017). A fern fractal leaf inspired wideband antipodal Vivaldi antenna for microwave imaging system, *IEEE Transactions on Antennas and Propagation*, 65:6126–6129.

[8] M. Moosazadeh, S. Kharkovsky, J.T. Case, B. Samali. (2017). Miniaturized UWB antipodal Vivaldi antenna and its application for detection of void inside concrete specimens, *IEEE Antennas and Wireless Propagation Letters*, 16:1317–1320.

[9] A. Mehdipour, K. Mohammadpour-Aghdam, R. Faraji-Dana. (2007). Complete dispersion analysis of Vivaldi antenna for UWB applications, *Progress in Electromagnetics Research*, *PIER*, 77:85–96.

[10] A. Karmakar, A. Bhattacharjee, A. Saha, A. Bhawal. (2019). Design of a fractal inspired antipodal Vivaldi antenna with enhanced radiation characteristics for wideband applications, *IET Microwaves, Antennas & Propagation*, 13:892–897.

[11] M. Moosazadeh, S. Kharkovsky. (2015). Development of the antipodal Vivaldi antenna for detection of cracks inside concrete members, *Microwave and Optical Technology Letters*, 57:1573–1580.

[12] M. Amiri, F. Tofigh, A. Ghafoorzadeh-Yazdi, M. Abolhasan. (2017). Exponential antipodal Vivaldi antenna with exponential dielectric lens, *IEEE Antennas and Wireless Propagation Letters*,16:1792–1795.

[13] L. Sang, X. Li, T. Chen, G. Lv. (2017). Analysis and design of tapered slot antennawith high gain for ultrawideband based on optimisation of themeta-material unit layout, *IET Microwaves, Antennas & Propagation, 11:*907–914.

[14] M. Bhaskar, E. Johari, Z. Akhter, M.J. Akhtar. (2016). Gain enhancement of the Vivaldi antenna with band notch characteristics using zero index material, *Microwave and Optical Technology Letters*,58:233–239.

[15] Y. Xu, J. Wang, L. Ge, X. Wang, W. Wu. (2018). Design of a notched-band Vivaldi antenna with high selectivity, *IEEE Antennas and Wireless Propagation Letters*, 17:62–65.

[16] R. Natarajan, M. Kanagasabai, M. GulamNabiAlsath. (2016). Dual mode antipodal Vivaldi antenna, *IET Microwaves, Antennas & Propagation*, 10:1643–1647.

[17] J. Wu, Z. Zhao, Z. Nie, Q. Liu. (2014). A printed UWB Vivaldi antenna using stepped connection structure between slotline and tapered patches, *IEEE Antennas and Wireless Propagation Letters*, 13 :698–701.

[18] C. Gao, E. Li, Y. Zhang, G. Guo. (2018). A directivity enhanced structure for the Vivaldi antenna using coupling patches, *Microwave and Optical Technology Letters*, 60:418–424.

[19] Z. Yin, X-X Yang, F. Yu, S. Gao. (2020). A novel miniaturized antipodal Vivaldi antenna with high gain, *Microwave and Optical Technology Letters*, 62:418–424.

[20] J. Bai, S. Shi, D.W. Prather. (2011). Modified compact antipodal Vivaldi antenna for 4–50-GHz UWB application, *IEEE Transactions on Microwave Theory and Techniques*, 59:1501–1507.

[21] M. Moosazadeh, S. Kharkovsky, J.T. Case, B. Samali. (2016). Microwave and milli-metre wave antipodal Vivaldi antenna with trapezoid-shaped dielectric lens for imaging of construction materials, *IET Microwaves, Antennas & Propagation*, 10:301–309.

[22] M. Kumar, V. Nath. (2018). Introducing multiband and wideband microstrip patch antennas using fractal geometries: development: in last decade, *Wireless Personal Communications*, 98:2079–2105.

[23] X. Li, Y. Xu, H. Wang, Y. Zhang, G. Lv. (2018). Low cross-polarization antipodal tapered slot antenna with gain, bandwidth enhancement for UWB application, *Journal of Computational Electronics*, 17:442–451.

[24] X. Li, D.W. Pang, H.L. Wang, Y.M. Zhang, G.Q. Lv. (2017). Dielectric slabs covered broadband Vivaldi antenna for gain enhancement, *Progress in Electromagnetics Research C*, 77:69–80.

[25] I.T. Nassar, T.M. Weller. (2015). A novel method for improving anti-podal Vivaldi antenna performance, *IEEE Transactions on Antennas and Propagation*, 63:3321–3324.

AIRPORT SAFETY MANAGEMENT: A PROACTIVE MODEL BASED ON RISK ASSESSMENT AND BENCHMARKING

Hanine Abdellah[1], El Barkany Abdellah[1]

•

[1] Laboratory: Intelligent Systems, Geo-resources, and Renewable Energies, Faculty of Science and Technology, Sidi Mohammed Ben Abdellah University, B.P. 2202 - Route d'Imouzzer - Fez, Morocco
Corresponding author: abdellah.hanine@usmba.ac.ma
abdellah.elbarkany@usmba.ac.ma

Abstract

This study presents a practical, context-sensitive approach to managing airport safety that combines the PDCA cycle with benchmarking techniques within a structured risk assessment framework. Given that ensuring operational safety in airports requires precisely recognizing, classifying, and successfully mitigating specific hazards, this study addresses this issue by creating a tailored risk assessment table. This tool, designed specifically for airport environments, clearly categorizes hazards based on their likelihood and severity and uses a novel equation developed in this study to correctly determine Safety Performance Indicators (SPI) and Safety Performance Targets (SPT). These indicators allow safety managers to effectively track performance trends, compare outcomes to other airports, and align safety policies with ICAO regulations. The cyclical nature of repetitive improvement in PDCA is assured, and value is added through benchmarking by applying tested best practices, enhancing the quality of decisions. A case study with airport safety practitioners establishes the practical applicability and value of this methodology in risk prioritization and pushing forward the drivers of corrective action. Collectively, the results demonstrate how this strategy supports proactive risk control and operational safety, and develops a sustainable culture of continuous improvement—a key component of effective airport safety management.

Keywords: Airport Safety; Risk Assessment; PDCA Cycle; Benchmarking; Risk Management; Safety Performance Indicators.

I. Introduction

Airport safety is a critical concern for both aviation authorities and airport operators. With increasing air traffic, the attendant increase in exposure to safety risks requires orderly and systematic measures. Although fatal aviation accidents are relatively infrequent compared to other modes of transport, the significant increase in the number of commercial flights requires that safety management practices be implemented effectively [1]. To ensure effective safety management, the International Civil Aviation Organization (ICAO) has developed a Safety Management System (SMS). This system includes procedures, documentation, knowledge systems, and organizational processes designed to manage and develop safety performance [2]. A safety reporting system is

one of the key components of SMS, and it facilitates proper identification and monitoring of safety issues [3]. The ICAO framework defines SMS as a proactive approach to managing safety risks before they result in incidents or accidents. This includes developing an internal structure adapted to the specific needs of the organization and aligned with international requirements [4].

The implementation of SMS allows States to approach their safety responsibilities using a performance-based model [5]. Since the early 2000s, ICAO has revised several annexes—such as Annexes 6, 11, and 14 in 2006, and Annexes 1 and 8 in 2008—to require States to establish safety programs and ensure the oversight of service providers [6], [7]. According to these requirements, nations must create an ICAO-compliant safety supervision system.

The consistent application of ICAO criteria ensures that all aviation actors within a State operate at the same level of safety. Senior management is responsible for supporting safety efforts through policies, oversight, and audits [8], [9]. In addition, States are expected to promote a safety culture through regulatory frameworks and stakeholder engagement [10]. International coordination is supported by harmonizing procedures and facilitating cooperation among States. Systems used for airport safety integrate multiple components such as risk analysis, data management, and stakeholder communication [11].

Airport risk management is based on three components: risk identification, risk assessment, and risk control. Risk assessment has played an important role in the creation of airport safety management systems [7]. Despite the widespread use of SMS, there has been little academic research on how risk assessment and safety indicators are operationalized and evaluated in airport settings, particularly through dynamic and comparative frameworks. Most prior studies have concentrated on general SMS components or airline-centric safety models, leaving a gap in structured evaluation models specifically tailored for airports.

This study focuses on two components of SMS: risk assessment and the use of safety performance indicators. Risk assessment provides a methodical examination of potential risks, whereas safety indicators enable the monitoring of risk trends and the adjustment of mitigation strategies. While ICAO recognizes these factors as vital, there is still a need to incorporate them into a continuous improvement approach that can drive long-term airport safety performance review.

This paper uses a methodology that combines benchmarking and the PDCA (Plan–Do–Check–Act) cycle. While benchmarking helps compare safety standards between the investigated airport and reference airports, the PDCA cycle guarantees continuous performance monitoring.

This comprehensive approach makes it possible to identify best practices and strengthen airport safety, both in terms of infrastructure and for staff and passengers. This study aims to propose a practical, scalable, and adaptable assessment tool intended to support strategic decision-making on safety within airport operations.

II. Literature review

Assessing airport safety is a major challenge, particularly in contexts where operations are exposed to multiple and dynamic risks. Numerous researchers have examined the tools and methods for effectively measuring the performance of safety systems, in direct relation to the realities on the ground. This literature review presents a synthesis of the most relevant approaches, recontextualizing them on the scale of an airport's internal assessment.

The implementation of a Safety Management System (SMS) remains at the heart of continuous improvement measures at airports. It relies on active support from management, a clear division of responsibilities, regular identification of hazards, implementation of risk control measures, safety audits and performance monitoring over time. To measure their effectiveness, Evaluation scales

have been proposed in [12] based on criteria such as document quality, safety training, management involvement, emergency management and clarity of internal policies. However, more recent work highlights certain limitations of SMS, notably their tendency to become overly bureaucratic and focused on procedural compliance, to the detriment of their operational adaptability. These findings are confirmed in [13], where the value of integrating employee perceptions to assess actual system performance is emphasized. These elements converge towards the need to design SMS that are compliant, flexible and focused on the specificities of each airport environment.

The risks to airport safety cover a wide spectrum: human error, foreign object debris (FOD), runway incursions, bird strikes, extreme weather conditions, technical failures or even terrorist threats [5], [14]. To better model and analyze this complexity, An evaluation framework has been developed in [15] integrating standardized management criteria into traditional processes. Their model highlights the fundamental role of managerial practices in risk reduction. In the same vein, a two-stage method was designed in [16] based on the Analytic Network Process (ANP) and the Technique of Order of Preference by Similarity with the Ideal Solution (TOPSIS), to structure the assessment of SMS components at airports. A conceptual framework is proposed in [17] combining quality management principles, key performance indicators (KPIs), and Lean Six Sigma approaches. This integrated approach aims for continuous improvement, based on specific performance measures and a clear distinction between proactive (preventive) and reactive (post-event) indicators.

However, the use of KPIs at airports faces significant challenges due to differences in operational context and site-specific safety standards. The need to adapt performance indicators to the particularities of each airport is emphasized in [18], due to the difficulties inherent in standardizing them. Pursuing this approach, A robust safety assessment model has been developed in [19], applicable to air navigation aids (NAVAIDs), based on the safety maturity framework proposed by Eurocontrol. Their model, validated by on-site audits and expert reviews, includes 18 major factors and 49 descriptive and measurable indicators. In addition, the strategic importance of Safety Performance Indicators SPI and Acceptable Levels of Safety Performance ALoSP was underlined in [20], as defined by ICAO. This proactive approach relies on the analysis of past trends to set safety targets and establish alert thresholds, helping to anticipate risks and guide decision-making. At the same time, recent advances in data-driven safety intelligence are paving the way for new assessment tools. With this in mind, a model based on LSTM neural networks was proposed in [21] to predict and rank potential risks in real time. This model demonstrated high accuracy and promising robustness for early detection.

Taken as a whole, these contributions provide a solid basis for thinking about safety assessment on the scale of a real airport. They show that such an approach requires a combination of adapted indicators, contextualized managerial practices, and advanced technological tools to proactively and reactively anticipate, monitor and correct safety failures.

III. Methodology

This section describes the methodological approach adopted for proactive and continuous risk assessment in airport safety. Our method relies on both quantitative and qualitative data to identify and classify potential hazards, following ICAO recommendations [5], [22] and established risk management principles [23]. A particular focus is placed on safety indicators, which help refine risk assessment and adjust prevention strategies in response to evolving threats.

Risk assessment follows a structured, multi-step process, as outlined by [24] and [25]:

1. Threat identification: Identifying human-induced hazards (errors, malicious acts) and natural hazards (weather conditions, infrastructure weaknesses).
2. Risk assessment and prioritization: Evaluating the likelihood and severity of identified threats to determine priorities for action.
3. Development of mitigation measures: Implementing targeted strategies, including enhanced safety protocols, technological upgrades, and specialized staff training.
4. Monitoring and continuous improvement: Using risk indicators for ongoing monitoring, enabling early detection of trends and timely adjustments to safety measures.

Following these steps, we have developed an approach based on a combination of benchmarking methods and the PDCA (Plan-Do-Check-Act) cycle. This approach ensures a continuous improvement process, aligned with industry best practices, enabling dynamic and adapted airport risk management. The integration of benchmarking enables airport safety levels to be compared with those of other establishments, thus encouraging the adoption of the highest safety standards. The PDCA cycle, meanwhile, ensures a constant re-evaluation of the actions implemented, guaranteeing that safety strategies are always in step with developments and challenges in the sector. This combined approach makes it possible to cross-reference quantitative data (such as statistics and performance indicators) with qualitative analyses (incident reports, safety audits), thus providing a global and accurate view of airport risks. The results obtained are based on safety reports published by ICAO [26], past incidents, as well as field observations and interviews with experts.

3.1.Airport Risk Identification and Assessment

3.1.1. Risk Identification and Predictive Management

Risk identification is a fundamental step in airport safety management. It is based on a systematic approach combining three complementary methodologies: reactive, proactive and predictive, enabling potential hazards to be detected, analyzed and dealt with comprehensively.

Reactive management involves analyzing incidents after they have occurred, in order to determine the underlying causes and implement corrective measures to avoid their recurrence [27]. This approach relies primarily on the exploitation of incident reports, safety audits and post-event investigations.

In addition, proactive management aims to prevent risks before they occur. It is based on the identification of emerging hazards through systematic observations, regular inspections and in-depth analysis of safety trends [28]. This approach makes it possible to anticipate organizational and operational vulnerabilities in order to reinforce preventive measures.

Finally, predictive management exploits advanced analytical tools, such as historical data processing and statistical forecasting models, to anticipate future risks and implement appropriate mitigation strategies [29]. The integration of techniques such as Flight Data Analysis (FDA) makes it possible to identify weak signals and take preventive decisions before an incident occurs [30].

The effectiveness of this approach relies on the coherent integration of these three approaches within Safety Management Systems (SMS), in line with the recommendations of aviation regulators, notably the Federal Aviation Administration (FAA) and the European Aviation Safety Agency (EASA). The use of databases derived from past incident reports, audits and field observations enables risk identification processes to be continually enriched and management strategies optimized [31].

This identification process is the starting point for the risk assessment cycle, which is based on a systematic analysis of the probability and severity of identified hazards.

3.1.2. Risk Assessment and Prioritization in Airport Safety Management

Once risks have been identified, assessing and prioritizing them is an important step towards effective safety management in the airport area. To ensure a thorough and objective analysis, our methodology is based on a combination of proven approaches: Deming's PDCA (Plan-Do-Check-Act) continuous improvement cycle, benchmarking of best practices in aviation safety, as well as the use of risk matrices according to [5], the International Civil Aviation Organization (ICAO), including Table 1 for risk severity, Table 2 for probability, and Figure 1 for risk matrix. This approach enables a rigorous classification of risks according to their severity and probability of occurrence.

Table 1: *Severity table - Incheon Airport [32]*

	Severity	Loss	Meaning
5	Very High	Human Loss	Casualties are more than 10 people
		Hardware Loss	More than 10 million dollars
		Operational Loss	Airport Close or airport operation suspension
4	High	Human Loss	Casualties are 1 to 9 people
		Hardware Loss	More than 1 million and less than 10 million dollars
		Operational Loss	Runway close: more than 24 H, taxiway and apron close: more than 72 h
3	Moderate	Human Loss	Serious Injuries to be hospitalized
		Hardware Loss	More than 100,000 and less than 1 million dollars
		Operational Loss	Runway close: more than 12 H, taxiway and apron close: less than 72 h
2	Low	Human Loss	Light injuries more than 4 weeks medical treatment
		Hardware Loss	More than 10,000 and less than 100,000 dollars
		Operational Loss	Aircraft Operational Delay 3 H or Aircraft operation cancel
1	Very Low	Human Loss	Light injuries less than 4 weeks medical treatment
		Hardware Loss	less than 10,000 dollars
		Operational Loss	No effect airport operation

Table 2: Probability table - Incheon Airport [32]

Number	Probability	Meaning
5	Very High	It is expected to happen in a month
4	High	It is expected to happen in a year
3	Moderate	It is expected to happen in 5 years
2	Low	It is expected to happen in 20 years
1	Very Low	It is expected don't happen in 20 years

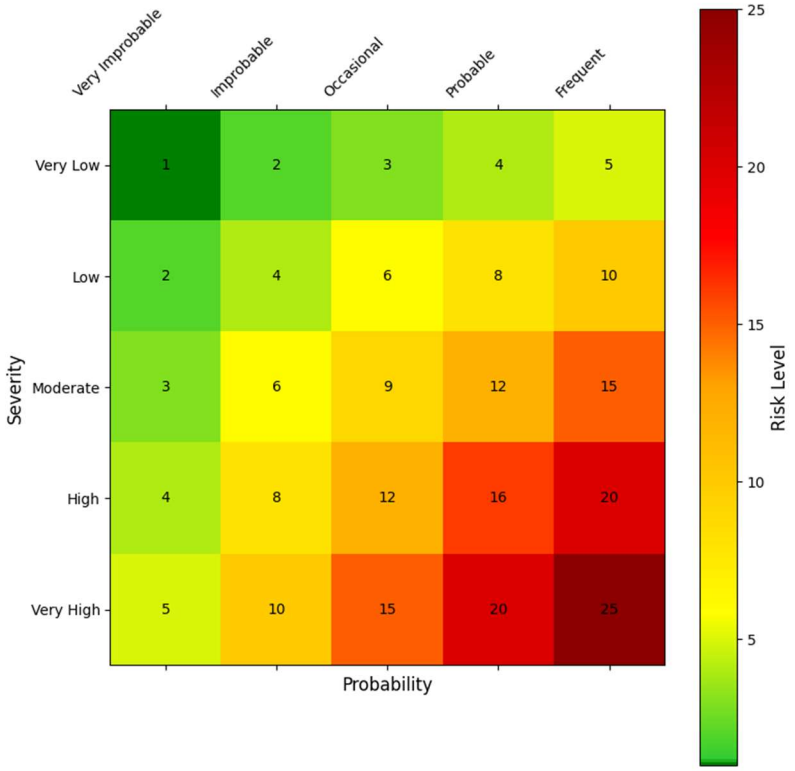


Figure 1: *Risk assessment matrix: severity vs probability [33]*

And for an accurate risk assessment, we have drawn on several models that have demonstrated their effectiveness. A formula based on ten factors to assess wildlife risks was developed in [34], while [35] applied fuzzy logic and FMECA analysis to prioritize 14 risk elements at Taiwan Taoyuan Airport, and [36] proposed an integrated approach combining risk identification and classification according to the effectiveness of mitigation measures. In the same vein, a method for assessing and improving aviation safety was introduced in [20], using Safety Performance Indicators (SPI) and Acceptable Levels of Safety Performance (ALoSP). using analysis of previous years' performance to define alert levels and targets, thus reinforcing proactive management of safety trends.

In addition, Heinrich and Bird risk management models are used to analyze incident frequency and define tolerance thresholds. By studying trends in minor incidents, these models make it possible to anticipate serious events and adapt safety strategies accordingly [37], [38]. This study also incorporates a color-coded severity/probability risk matrix Figure 1, which visually represents risk levels from green to red. This graphical tool supports a clearer classification of hazards and facilitates strategic decision-making by safety managers based on the degree of risk severity.

Based on this research, we have designed an innovative table that brings together all airport risks in order to prioritize and assess them more accurately and comprehensively. More detailed than existing models, this table incorporates new equations for calculating key performance indicators, ensuring ongoing assessment and better comparison of results over time and with other airports.

The method we have proposed is based on a combination of the PDCA cycle and benchmarking, enabling continuous improvement and dynamic risk assessment. PDCA facilitates regular reassessment and adaptation of safety strategies in line with data collected and results obtained. In addition, benchmarking enables risk indicators to be compared with those of other airports, providing a valuable perspective for optimizing risk management.

Although the ICAO risk matrices and the methodology they propose are fundamental, our approach enriches them to provide a more detailed analysis, better adapted to the specificities of airport risks. This method guarantees proactive and continuous risk management, meeting the needs of airport safety managers.

A detailed example of the application of this methodology is presented in the "Case studies" section, where we analyze the results obtained to demonstrate the effectiveness of this approach.

3.2. Model for Airport Risk Assessment and Safety Improvement

The development of our model is based on a structured, multi-stage approach, combining proven methods to ensure accurate assessment and continuous improvement of airport safety.

3.2.1. Analysis of Existing Methods and Model Justification

In this section, we began by reviewing existing approaches to airport risk assessment to identify their strengths and limitations. Benchmarking, used in various sectors to improve risk management, has helped identify best practices and common weaknesses [39], [40], [41]. At the same time, the PDCA (Plan-Do-Check-Act) cycle has proven to be an effective tool for continuous improvement in management systems, particularly in safety and risk management [42].

3.2.2. Structuring Risk Assessment

Based on these approaches, we have developed a framework for rigorous airport risk assessment. This framework is based on two key elements:

a. Benchmarking: By comparing safety performance between different airports and over different time periods, we have identified gaps and opportunities for improvement. This method has also been used in other sectors to refine risk assessment, notably in the analysis of specific substances such as trichloroethene [43].

b. Application of the PDCA cycle: This cycle structured our risk management approach into four interconnected stages:

- Plan: Identification and prioritization of risks using ICAO risk matrices and performance indicators.
- Do: Implementation of mitigation measures and improvement strategies.
- Check: Monitoring and evaluation of safety indicators to measure the effectiveness of the system.
- Act: Continuous adjustment and optimization of strategies based on results obtained.

3.2.3. Development of an Innovative Risk Analysis Chart

Based on the analyses carried out, we designed a table to group and prioritize airport risks. This table, which is more detailed than existing ones, incorporates several elements:

- Specific equations: These allow for the calculation of key performance indicators (KPIs) and the establishment of alert thresholds based on observed trends [20].
- An ISO 31000:2019-compliant approach: This ensures proactive risk management, in line with international standards [44].
- Dynamic comparison with other airports and previous years' performance: This comparison provides an evolving view of risk management.

3.2.4. Validation and Prospects for Improvement

To validate our model, we carried out a series of case studies, which tested the effectiveness of the approach. These analyses showed that the combination of benchmarking and the PDCA cycle optimizes risk management. This approach guarantees not only continuous improvement but also reactive and predictive risk management, thanks to up-to-date data and adjustments based on benchmarking.

To illustrate the applicability of the proposed methodology, the model was tested using representative operational data from a real-world airport environment. This demonstration highlights the model's practical feasibility without disclosing sensitive or proprietary operational details.

We developed an integrated model Figure 2 for airport safety identification, assessment, and improvement, incorporating methods such as benchmarking and the PDCA cycle. This framework provides a systematic approach to identifying, assessing, and mitigating risks at the airport, thus fostering a continuous process of safety improvement.

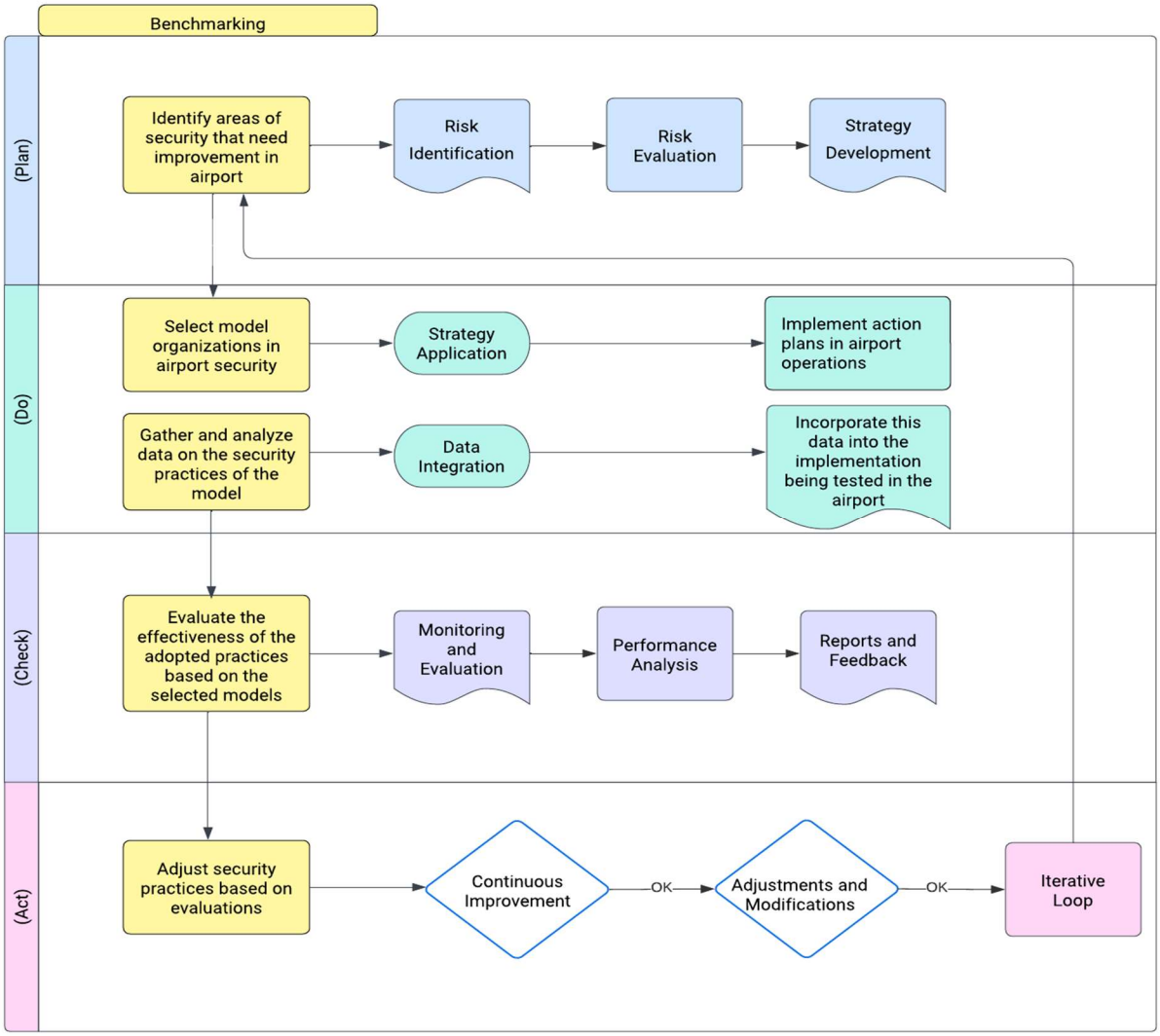


Figure 2 : *Integrated Model for Airport Safety Identification and Improvement*

The Airport Safety Identification, Assessment, and Improvement with Benchmarking and PDCA module offers a structured four-phase process for continuously improving safety in airport operations.

- In the Planning phase, risks are identified, assessed, and strategies are developed to mitigate them.
- The Implementation phase then puts these strategies into action.
- The Verification phase monitors and evaluates their effectiveness. The identification of potential risks specific to the airport plays a crucial role in this phase, helping to determine safety threats and vulnerabilities.
- The last phase is Action, to make improvements and repeat the process till the safety of the airport improves.

The new model could serve as a continuous mechanism to improve airport safety. This attracts benchmarking to keep up its superior standard of safety, while adaptability assures that it is able to respond to the latest airport safety issues in a more flexible operational milieu.

Furthermore, this dynamic integration enables continuous learning from both internal performance trends and external benchmarking results. It allows for the proactive identification of emerging risks and fosters a data-driven culture of improvement. The alignment with Safety Performance Indicators (SPI) and Acceptable Levels of Safety Performance (ALoSP) further strengthens its effectiveness. Ultimately, this model enhances the airport's capacity to anticipate and manage complex safety challenges in an evolving operational environment.

IV. Case Study: Risk Assessment And Performance Evaluation In Airport Safety

Following an in-depth study based on the results of a questionnaire sent out to a group of airport safety managers, as well as the previously cited research into the various safety assessment methods, we have developed a risk assessment table.

To demonstrate the applicability of the proposed method, the following example uses simulated operational data inspired by real-world airport contexts. These data were constructed for illustrative purposes and do not represent any specific airport's confidential records.

This tool brings together the data collected and, thanks to automated calculations, provides a clear picture of the level of risk at the airport.

In this approach, safety managers first carry out a careful collection of relevant data, including past incidents and previous risk assessments. This information is then integrated into the table, which identifies, analyzes and evaluates risks in terms of probability and severity. Based on this analysis, the results obtained provide a better understanding of airport risk trends and identify deviations requiring corrective action. Finally, targeted mitigation measures are put in place to reduce or eliminate the most significant risks, thus ensuring the safety and reliability of airport operations.

Emphasizing that an SPI program is first and foremost a measure of management performance and that you can only manage what you measure [45], it is essential to effectively evaluate safety performance indicators. To illustrate the method used, we take the following example to explain risk assessment by measuring safety performance indicators SPI and SPT, in line with the methodology established by the ICAO [20].

Table 3: *Sample data sheet used to generate a high-consequence SSP safety indicator chart (with alert and target-setting criteria)*

Preceding Year					Current year				Current Year Alert Levels			
Mth	All Operators Total FH	All Operators Mandatory Incidents	Incident Rate*	Ave (line)	Mth	All Operators Total FH	All Operators Mandatory Incidents	Incident Rate*	Preceding Year Ave +1SD (line)	Preceding Year Ave +2SD (line)	Preceding Year Ave +3SD (line)	Current Year Target (line)
Jan	29854	4	0,13	0,21	Dec	30744	6	0,20	0,23	0,29	0,35	0,20
Feb	28725	5	0,17	0,21	Jan	29674	3	0,10	0,23	0,29	0,35	0,20
Mar	28904	5	0,17	0,21	Feb	29316	4	0,14	0,23	0,29	0,35	0,20
Apr	27460	8	0,29	0,21	Mar	28482	7	0,25	0,23	0,29	0,35	0,20
May	28986	6	0,21	0,21	Apr	29 549	4	0,14	0,23	0,29	0,35	0,20
Jun	32344	4	0,12	0,21	May	30786	5	0,16	0,23	0,29	0,35	0,20
Jul	33678	6	0,18	0,21	Jun				0,23	0,29	0,35	0,20
Aug	30904	5	0,16	0,21	Jul				0,23	0,29	0,35	0,20
Sep	29866	7	0,23	0,21	Aug				0,23	0,29	0,35	0,20
Oct	29974	4	0,13	0,21	Sep				0,23	0,29	0,35	0,20
Nov	29955	2	0,07	0,21	Oct				0,23	0,29	0,35	0,20
Dec	30744	6	0,20	0,21	Nov				0,23	0,29	0,35	0,20
		Ave	0,17		Dec				0,23	0,29	0,35	0,20
		SD	0,06				Ave	0,16				
							SD	0,05				

AVE+1SD	AVE+2SD	AVE+3SD
0,23	0,29	0,35

Current Year Target is ,say, 5% Ave rate improvement over the Ave rate for the preceding year, which is SPT: **16**

Current Year Alert Level setting criteria is: Preceding Year Ave + 1/2/3 SD

Table 3 shows the recorded data on the number of movements versus the number of incidents for each month of the previous and current year. This information enables a detailed analysis of monthly trends and potential correlations between movements and incidents. On the basis of this table, the SPT is calculated for comparison with the SPI, determined in the next step.

The data in Table 3 corresponds to the graph in Figure 3 and can also be used to generate additional graphs displaying alert and target lines. These graphs are automatically generated using predefined parameters, as specified in ICAO Document [46]

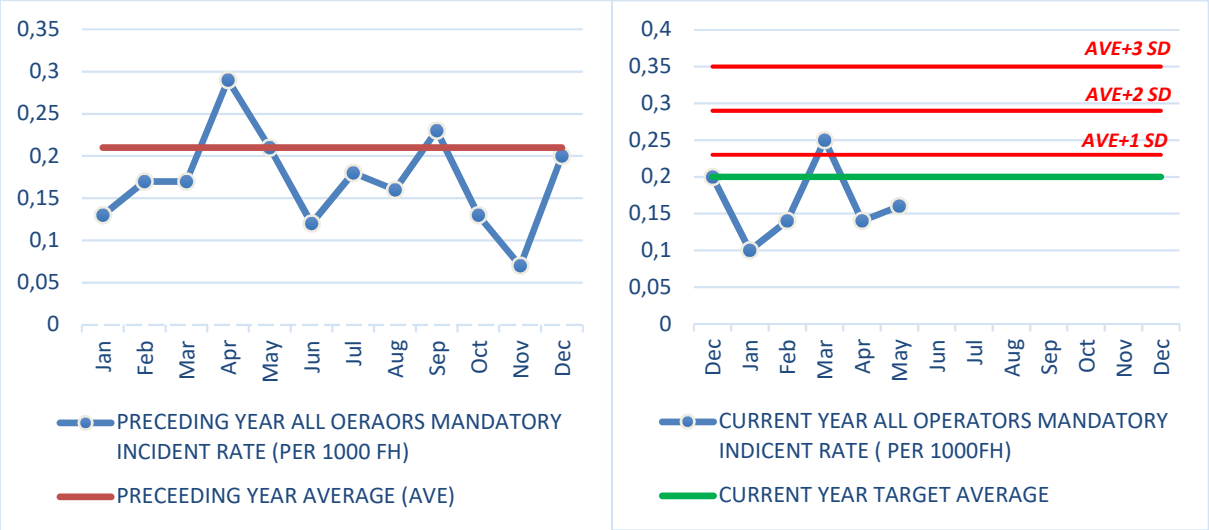


Figure 3 :*Example of an SSP safety performance indicator chart (with alert and target level settings)*

Figure 3 graphically presents an example of a high-consequence safety performance indicator, in this case, the aggregated incident rates reported by all operators. The graphs display the previous year's performance alongside expected trends for the current year. The alert level is determined based on standard safety deviation criteria and is calculated using either the Excel formula "=STDEVP" or through manual computation [46].

The standard deviation (σ) is given by the formula:

$$\sigma = \sqrt{\frac{\sum(xi-\mu)2}{N}} \qquad (1)$$

Where "X" is the value of each data point, "N" is the number of data points and "μ" is the mean value of all data points [46].

This figure provides an overview of the safety level, relying on the previous year's average (Ave) and standard deviation (SD) to define alert thresholds. An alert is triggered when a single data point exceeds 3 SD, two consecutive data points exceed 2 SD, or three consecutive data points exceed 1 SD, indicating a significant deviation that requires corrective action [20].

To ensure continuous improvement, the target is to reduce the average incidence rate by at least 5% compared to the previous year. If this reduction is achieved by the end of the monitoring period, the target is considered met. Alert and target levels are reviewed annually and recalibrated if necessary, based on recent data and changing trends in operational safety, ensuring continuous safety improvement.

This method of assessing overall airport safety is widely used and considered practical. However, an in-depth study based on a questionnaire identified certain limitations. Our findings indicate that this method is both effective and practical for safety managers. However, it does have one important limitation: when a monitoring graph triggers an alert, it can be complex to determine precisely the origin of the problem and the specific risk to be mitigated.

To solve this problem, we have proposed a more precise and complementary method, based on the same principle as the one previously explained, but with an enhanced ability to detect exactly which risks require mitigation. Rather than replacing the existing approach, this method enhances its effectiveness by providing a more detailed risk identification process, allowing safety managers to take targeted actions.

As a first step, it is essential to identify and collect all the risks present at the airport, and then report them in the following table:

Table 4: *Table of existing risks in the airport and their acceptability level*

Risk	Description	Severity	Probability	Risk Level	Risk Acceptability
Runway foray	Unauthorized entry onto a track	5	1	5	Tolerable under control
Fire on the tarmac	Fire on the airport grounds	2	2	4	Acceptable
Act of terrorism	Terrorist attack in the airport	5	2	10	Tolerable with mitigation
Fuel leak	Fuel spill on tarmac	3	2	6	Tolerable under control
Lost or stolen baggage	Lost or stolen baggage	2	4	8	Tolerable under control
Air traffic control system failure	Faulty air traffic control system	4	2	8	Tolerable under control
Aircraft collision	Airplane accident in flight or on the ground	5	4	20	Unacceptable
Identity theft	Fraudulent use of identities	3	1	3	Acceptable
Infiltration of illicit substances	Introduction of illicit substances	4	2	8	Tolerable under control
Cybersecurity breach	Computer attack on the system	4	3	12	Tolerable with mitigation
Poor waste management	Improper waste disposal	1	3	3	Acceptable
Damage caused by personnel	Human errors or negligence	3	3	9	Tolerable under control
Failure of safety equipment	Equipment malfunction	4	2	8	Tolerable under control
Environmental pollution	Spill of harmful substances	1	2	2	Acceptable
Severe weather	Extreme weather conditions	4	3	12	Tolerable with mitigation
Signaling failure	Failure of traffic signs	3	3	9	Tolerable under control
Tentative d'intrusion	Perimeter intrusion attempt	4	2	8	Tolerable under control
Contamination of food	Food contamination	2	2	4	Acceptable
IT security incidents	Computer attacks on systems	4	3	12	Tolerable with mitigation
Traffic accidents	Accidents involving vehicles	3	4	12	Tolerable with mitigation
Bomb threat	Bomb threat or threat	5	1	5	Tolerable under control
TOTAL		71	51		

Based on the ICAO risk matrices Tables 1 and 2, a comprehensive Excel-based tool was developed to capture all potential hazards identified within the airport under evaluation. Each risk is assigned a severity and probability level, which are then multiplied to calculate a specific risk level. This result is visually translated using a color-coded matrix Figure 1, ranging from green to dark red, indicating the degree of severity and guiding the type of response required. This approach provides a clear visual interpretation of each individual risk.

Beyond individual assessment, the total severity and probability values are aggregated and incorporated into a custom-built equation, specifically developed, tested, and validated in this study. This original formula (2) enables airport safety managers, after completing the Excel-based assessment table with the severity and probability values, to automatically obtain key performance indicators and a global view of the overall risk level within the airport. These indicators can then be used to track performance over time and benchmark safety status against previous years or other comparable airports.

The aggregated values are then used in the following equation to calculate the Safety Performance Indicator (SPI).

$$SPI' = \frac{S\mu}{5} \times \frac{P\mu}{5} \qquad (2)$$

$$\text{Where: } S\mu = \frac{\sum S}{N} \quad (3) \quad \text{and} \quad P\mu = \frac{\sum P}{N} \quad (4)$$

With Sμ representing the overall average severity and Pμ representing the overall average probability, and N representing the total number of existing risks in the airport.

Consider the provided example:

$$S\mu = \frac{71}{21} = 3{,}38 \quad (5) \qquad P\mu = \frac{51}{21} = 2{,}42 \quad (6)$$

$$\text{Therefore: } SPI' = \frac{3{,}38}{5} \times \frac{2{,}42}{5} = 0{,}32 \quad (7)$$

As part of the airport safety assessment, we compare the SPI' safety performance index (7) with the SPT performance target, which is calculated based on the data in Table 3, to determine whether the airport meets the required thresholds, and compare it with the SPI' calculated from the data in Table 4.

- If SPI' is less than or equal to SPT, the airport's safety level is considered acceptable.
- If SPI' exceeds SPT, this indicates that the airport does not meet minimum safety standards, requiring immediate corrective action.

The airport safety manager focuses on the dark red and red-colored risks in Table 4 above and implements suitable controls immediately. Then, they address the orange-colored risks, before progressively mitigating those identified in yellow, in order to reduce the SPI below the SPT threshold.

This approach helps detect major risks at the airport and take appropriate measures to ensure the highest level of safety. The reassessment must be conducted every six months or annually, depending on the airport's category, following the outlined steps to ensure continuous improvement in airport safety.

V. Discussion And Evaluation Of The Proposed Safety Assessment Approach

This is one of a number of studies aiming at improving airport safety management systems (SMS). It proposes a novel approach that integrates the PDCA (Plan-Do-Check-Act) cycle with benchmarking technique to proactively identify and manage risks. Airport safety management have evaluated and confirmed this approach, which uses a risk table to categorize dangers based on their frequency and severity.

Method Effectiveness

The method developed proved significantly more effective than traditional approaches. By systematically collecting and evaluating risk data, it enables targeted prioritization of corrective actions. The SPI (Safety Performance Indicator) and SPT (Safety Performance Target) indicators, derived from the data collected, provide a global frame of reference. They allow both the comparison of performance between airports and the deployment of improvement strategies according to the standards of ICAO (International Civil Aviation Organization).

The Excel table is the key to being able to clearly visualize critical risks, especially with red zones highlighting the priorities. This strengthens the safety measures as it allows the risks once identified to be managed efficiently and effectively.

Alignment With Recent Advances In Predictive Safety Modeling

This method adds a dynamic aspect through the PDCA cycle, unlike static methods that rely on past data, like probabilistic models or risk contour maps [23], [47]. It ensures continuous evaluation and progressive performance improvement.

Recent research has investigated novel approaches in [21] and [48], such as structured models for identifying risks based on safety data trends and entropy-based frameworks to handle the increased complexity of airport settings. While [21] focused on forecasting risks using historical safety logs, our method expands on this work by incorporating an iterative improvement process through benchmarking and the PDCA cycle, which could be further improved by incorporating data-driven techniques such as the LSTM algorithm for real-time monitoring and predictive analysis.

Identified Challenges And Proposed Solutions

One of the major challenges encountered is the heterogeneity of risk assessment by different managers, leading to variations in results. For example, a similar risk may be classified differently depending on the experience or interpretation of the assessors. To remedy this problem, it is essential to introduce standardized training aimed at harmonizing risk assessment criteria.

Practical Application And Benchmarking

Benchmarking is a key component of this approach, making it possible not only to place an airport's performance in a global context but also to identify opportunities for improvement by drawing on industry best practices. Comparative analysis of SPI and SPT data has helped to assess performance gaps and justify immediate corrective action, particularly where SPI exceeds SPT.

This structured approach maintains airport operations within acceptable limits while ensuring adherence to international standards. It also contributes to a robust safety culture, essential in a complex airport environment.

Global Impact On Airport Safety

By combining the PDCA cycle with benchmarking, this method promotes continuous improvement in airport safety. Each step—from planning to action—is designed to iteratively identify, assess, and mitigate risks. By integrating advanced technologies and drawing on international standards, it transforms SMS into predictive and adaptive systems capable of

meeting future challenges.

The obtained results show that this method not only contributes to risk management but also to a more rigorous safety discipline. In this sense, it represents a major step forward in guaranteeing the safety and reliability of airport operations.

VI. Conclusion

This study presents a dynamic and forward-looking approach to managing airport safety by combining the PDCA cycle with benchmarking in the risk assessment process. At the core of this method is a risk evaluation table that allows for clear classification of hazards and consistent monitoring of key safety performance indicators (SPI and SPT), contributing to continuous improvement in line with ICAO recommendations. In practice, this approach makes risk management more structured, scalable, and responsive, allowing for more informed decisions and improved foresight of safety hazards. While the results are encouraging, the approach can yet be improved and tailored to other airport scenarios. In the future, it could be used with modern technology to improve both safety oversight and operational performance.

Funding: This research received no Specific grant from any funding agency in the public, commercial, or not-for-profit-sectors.

Conflict of Interest: The authors declare no competing interests.

References

[1] Y. H. Chang and C. H. Yeh. (2004). A new airline safety index. *Transportation Research Part B: Methodological*, 38:369–383.

[2] S. Stroeve, J. Smeltink, and B. Kirwan. (2022). Assessing and Advancing Safety Management in Aviation. *Safety*, vol. 8, no. 2, p. 20.

[3] M. Jausan, J. Silva, and R. Sabatini. (2017). A holistic approach to evaluating the effect of safety barriers on the performance of safety reporting systems in aviation organisations. *J Air Transp Manag*, 63:95–107.

[4] M. Kešeľová, M. Blištanová, P. Hanák, and B. Brůnová. (2021). Safety Management System in Aviation: Comparative Analysis of Safety Management System Approaches in V4 Countries. *Management Systems in Production Engineering*, 29:208–214.

[5] Doc 9859. Safety Management Manual, Fourth Edition, Montreal, Canada (2018). May 12, 2024. Available: https://store.icao.int/en/safety-management-manual-doc-9859

[6] E. Gerede and Y. Kurt. (2018). An Assessment Of Aviation Safety Management System Applications From The New Institutional Theory Perspective. *International Journal of Management Economics and Business*, 14:97-122.

[7] R. Shi, L. Liu, J. Z. Yang, and M. J. Li. (2010). Application of catastrophe evaluation method in risk assessment of SMS in civil aviation. in *Proceedings - 2010 WASE International Conference on Information Engineering, ICIE 2010*, 157-160.

[8] Duane A. Ludwig, Cheryl R. Andrews, Nienke R. Jester-ten Veen, and Charlotte Laqui. (2007). Safety Management Systems for Airports 1.

[9] P. Adams. (2015). Aerodrome certification for small and emerging airports: Is it an issue?. *Journal of Airport Management*, 9:239–247.

[10] T. B. Spence, R. O. Fanjoy, C. tsung Lu, and S. W. Schreckengast. (2015). International standardization compliance in aviation. *J Air Transp Manag*, 49:1–8.

[11] M. Cheng and Y. Le Ping. Designed and developed a civil airport safety management system," *10th Annual International Systems Conference, SysCon 2016 - Proceedings*, Jun. 2016.

[12] C. Chen and Shu Chuan. (2012). Scale development of safety management system

evaluation for the airline industry. *Accid Anal Prev*, 47:177–181.

[13] A. Robert Foster Daniel Kwasi Adjekum, A. Robert Foster, and D. Kwasi Adjekum. (2022). A Qualitative Review of the Relationship between Safety Management Systems (SMS) and Safety Culture in Multiple- Collegiate Aviation Programs. *Aviation Faculty Publications,* 40: 63-94.

[14] H. Korkmaz, E. Filazoglu, and S. Ates. (2023). Enhancing airport apron safety through intelligent transportation systems: Proposed FEDA model. *Saf Sci*, 164.

[15] X. Lu and S. Huang. (2012). Airport safety risk evaluation based on modification of quantitative safety management model. *Procedia Engineering*, 238–244.

[16] Y. H. Chang, P. C. Shao, and H. J. Chen. (2015). Performance evaluation of airport safety management systems in Taiwan. *Saf Sci*, 75: 72–86.

[17] I. Panagopoulos, C. Atkin, and I. Sikora. (2017). Developing a performance indicators lean-sigma framework for measuring aviation system's safety performance. *Transportation Research Procedia*, 35–44.

[18] A. Enoma and S. Allen. (2007). Developing key performance indicators for airport safety and security. *Facilities*, 25:296–315.

[19] M. G. Yoon and J. K. Kim. (2022). Evaluation methodology for safety maturity in air navigation safety. *J Air Transp Manag*, 98:102-159

[20] G. Thong, (2015). Safety Performance Measurement-SPI & ALoSP Development. 2015. Accessed: Apr. 12, 2024: https://www.icao.int/APAC/Meetings/2015%20APRAST6/07%20-%20SIN_SPM%20Presentation.pdf

[21] Y. Hu, L. Qiao, and F. Gu. (2025). Risk assessment and prevention in airport security assurance by integrating LSTM algorithm. *PLoS One*, 20:0315799.

[22] ICAO Annex 19, "Annex 19 - Safety Management 2nd Edition, July 2016. Montreal. CANADA," 2016.

[23] N. Distefano and S. Leonardi. (2014). Risk Assessment Procedure For Civil Airport," *International Journal For Traffic And Transport Engineering*, 4: 62–75.

[24] P. O. Greenhalgh. (2009). Improving Our Odds: Success through Continuous Risk Management. *Marshall Space Flight Center*, United States: International System Safety Conference, Aug. 2009. Accessed: Jan. 29, 2025: https://ntrs.nasa.gov/citations/20090037110

[25] M. Gavrilescu. (2002). Risk assessment and management - Tools for sustainable development. *Environ Eng Manag J*, 1: 1-3.

[26] "Safety Reports." Accessed: Jan. 29, 2025: https://www.icao.int/safety/pages/safety-report.aspx

[27] M. Paradisi. (2023). Proactive and Predictive Risk Management in Aviation Safety: a corporate strategic approach. *2023 IEEE International Workshop on Technologies for Defense and Security, TechDefense 2023 - Proceedings*, 34–39.

[28] H. Jimenez, I. C. Stults, and D. N. Mavris. (2009). A morphological approach for proactive risk management in civil aviation security. *47th AIAA Aerospace Sciences Meeting including the New Horizons Forum and Aerospace Exposition*.

[29] D. Bartulović. (2021). Predictive Safety Management System Development. *Transactions on Maritime Science*, 10:135–146.

[30] M. Schultz, J. Rosenow, D. B. Bartulovi´c, and S. Steiner. (2023). Conceptual Model of Predictive Safety Management Methodology in Aviation. *Aerospace, 10: 268*.

[31] N. Mendes, J. Geraldo Vidal Vieira, and A. Patrícia Mano. (2022). Risk management in aviation maintenance: A systematic literature review. *Saf Sci*, 153.

[32] ICAO, "https://www4.icao.int/demo/SMI/Risk_matrix.pdf." Accessed: Apr. 20, 2025: https://www4.icao.int/Demo/SMI/Risk_matrix.Pdf

[33] A. Hanine and A. ElBarkany. (2025). Innovative Bird Strike Mitigation Strategies: Integrating Drones and Cutting-Edge Technologies to Enhance Airport Safety. *International Journal of Aviation, Aeronautics, and Aerospace*, 12:1-21.

[34] N. B. Carter. (2001). All Birds Are Not Created Equal: Risk Assessment and All Birds Are

Not Created Equal: Risk Assessment and Prioritization of Wildlife Hazards at Airfields Prioritization of Wildlife Hazards at Airfields.

[35] C. M. Feng and C. C. Chung. (2013). Assessing the Risks of Airport Airside through the Fuzzy Logic-Based Failure Modes, Effect, and Criticality Analysis. *Math Probl Eng*, 1:239523.

[36] S. Sivakumar. (2022). A novel Integrated Risk Management Method for Airport operations. *J Air Transp Manag*, 105:102296.

[37] J. Maklakovs, A. Bitins, R. Bogdane, and V. Shestakov. (2021). Using Heinrich's (Bird's) Pyramid of Adverse Events to Assess the Level of Safety in an Airline. *Transactions on Aerospace Research*, 4:11–20.

[38] A. Bitinš, J. Maklakovs, R. Bogdane, R. Chatys, and V. Shestakov. (2021). Using Adverse Event Pyramids to Assess Probabilities in Airline Safety Management. *Transactions on Aerospace Research*, 2:71–83.

[39] B. H. MacGillivray, J. V. Sharp, J. E. Strutt, P. D. Hamilton, and S. J. T. Pollard. (2007). Benchmarking Risk Management Within the International Water Utility Sector. Part I: Design of a Capability Maturity Methodology. *J Risk Res*, 10:85–104.

[40] S. Matook, R. Lasch, and R. Tamaschke. (2009). Supplier development with benchmarking as part of a comprehensive supplier risk management framework. *International Journal of Operations and Production Management*, 29:241–267.

[41] S. H. Björnsdottir, P. Jensson, S. E. Thorsteinsson, I. M. Dokas, and R. J. de Boer. (2022). Benchmarking ISO Risk Management Systems to Assess Efficacy and Help Identify Hidden Organizational Risk. *Sustainability*, 14:4937.

[42] M. Majerník, N. Daneshjo, P. Malega, P. Drábik, R. Ševčíková, and J. Vravec. (2023). Integrated Management of the Environment-Safety Risks in the Thermal Power Station. *Pol J Environ Stud*, 5:4725–4738.

[43] M. Haag-Grönlund, R. Fransson-Steen, and K. Victorin. (1995). Application of the Benchmark Method to Risk Assessment of Trichloroethene. *Regulatory Toxicology and Pharmacology*, 21:261–269.

[44] L. Ispas, C. Mironeasa, and A. Silvestri. (2023). Risk-Based Approach in the Implementation of Integrated Management Systems: A Systematic Literature Review. *Sustainability 2023, 15:10251*.

[45] J. Louvar, (2010). Guidance for safety performance indicators. *Process Safety Progress*, 29: 387–388.

[46] Doc 9859, "AN/474, Safety Management Manual (SMM), Montreal, Canada," Organisation de l'aviation civile internationale, 2013. Accessed: Apr. 20, 2025: https://www.icao.int/SAM/Documents/2017-SSP-GUY/Doc%209859%20SMM%20Third%20edition%20en.pdf

[47] L. Guerra, T. Murino, and E. Romano. (2008). Airport system analysis: a probabilistic risk assessment model. *International Journal Of Systems Applications, Engineering & Development*, 2.

[48] N. Borjalilu and A. Bozorgi-Amiri. (2022). Entropy-Based Model For Aerodromes Safety Risk Assessment To Implement Safety Management Systems. *Journal of Airline Operations and Aviation Management*, 1:26–42.

ON COPING WITH CENSORING IN SURVIVAL DATA USING FUZZY THEORY

Jaisankar. R[1*], Haripriya. H[2]

•

[1*] Professor, Department of Statistics, Bharathiar University,
Coimbatore 641 046, Tamil Nadu, INDIA
[2]Research Scholar, Department of Statistics, Bharathiar University,
Coimbatore 641 046, Tamil Nadu, INDIA
[1*] r_jaisankar@buc.edu.in, [2] haripriyah1795@gmail.com

Abstract

Aim: The problem of censoring is the main concern in Survival Analysis which makes the analysis complex and may lead to unreliable results like less precise parameter/survival/hazard estimates, wider confidence intervals, reduced power to detect differences between groups, sometimes especially when the proportion of censored observations is high. In particular, if the censoring is informative that is reacted to the event, serious bias may be expected to present in the estimates. Omitting censored observations prices with loss of information and adding them is often embedded with a lack of information. It is proposed to implement fuzzy methodology for dealing with censored observations in Survival data so as to minimize their impact on the survival/hazard estimates. This paper suggests a modified approach based on the Fuzzy Theory, in which, the censored observations could be incorporated effectively. Methods: Many statistical procedures are advised to tackle censoring, in both parametric and non-parametric realms. However, their application mainly depend on the nature of censoring, whether right or left or interval censored. Even when their applied, still some lacuna may persist which could be completely eradicated when there is no censoring. Different types of fuzzy numbers are applied both to the censored and uncensored observations according to their nature and the results of the same were tested in case of the non-parametric procedure, the Kaplan-Meier estimator, using log rank test. Results: On the application of the proposed methodology one may obtain the survival probabilities which are reasonably calculated for even censored observations. The median survival time observed by the application of this methodology gives lesser value than the median obtained by the classical Kaplan eier method. The survival curve obtained by the proposed method is different from the survival curve of the classical Kaplan eier method and since the proposed methodology addresses all points of time and hence may give reliable estimates of survival probability. Conclusion: When compared with the classical Kaplan-Meier method, the proposal method gives survival probabilities which are slightly differ from the estimate obtained from non-fuzzy methodology. Since the survival probabilities can be calculated even for censored observations using fuzzy numbers, it is expected that the proposed modelling may be better than the classical Kaplan-Meier estimator.

Keywords: Censoring, Non- Parametric Estimator, Vagueness, Fuzzy Sets, Fuzzification; Survival Time.

1. Introduction

Censoring is the primary problem that may persist in every survival data. The presence of censoring may pollute the results of the survival analysis and when the proportion of censored

observations is higher the results of the analysis would adversely be affected. The use of Non-parametric survival methods may be advised in such scenarios but even the estimates obtained from them also be distributed when too much censoring is present. Even though, some distributions like Weibull, Exponential, and Gompertz are preferred to mitigate with censoring, bias in the estimates could not be avoided significantly. Also, parametric models are capable of dealing with right censoring but left and interval censoring would be more complex. Similar is the case of semi-parametric survival models, violation of proportional hazard assumption may be exhibited when censoring occurs more frequently in one group and if censoring rates differ across covariates the estimates may become unreliable which would question the validity of the model fit. The presence of censoring leads to different consequences in non-parametric survival models when compared with parametric models. In addition to the reduction in statistical power and bias in survival estimates, if heavy censoring is present at early time points the reliability of later survival estimates decreases, and also the comparison between the estimates of two groups may be biased. In this article, a new methodology has been suggested to tackle censoring based on fuzzy methodology.

Apart from the usage of several parametric models based on the distributions of non-negative random variables, Edward L. Kaplan and Paul Meier [7] pioneered the non-parametric methods for estimating the survival probabilities and hence the survival and hazard curves.

The Kaplan-Meier estimator of the survivor function at times, for $t_{(k)} \leq \mathrm{t} \leq t_{(k+1)}$ is given by,

$$\hat{S}(t) = \prod_{j=1}^{k} \left(\frac{n_j - d_j}{n_j} \right) \tag{1}$$

where, t_1, t_2, t_3,... denote the actual times of death of the n individuals in the cohort, d_1, d_2, d_3,... denote the number of deaths that occur at that actual times, and n_1, n_2, n_3,... be the corresponding number of patients remaining in the cohort under study.

Nelson and Aalen [8] developed an estimator for estimating the cumulative hazard function which is directly related to the Kaplan-Meier estimator obtained by maximizing the empirical likelihood.

The estimator is of the form,

$$H(t) = \sum_{t_i \leq t} \frac{d_i}{n_i} \tag{2}$$

where d_i is the number of events at time t_i, n_i is the total number of individuals at risk at time t_i. Many other non-parametric estimators for estimating the survival/hazard function in the presence of censoring such as, Breslow [1], and Kalbfleisch-Prentice [6], are available in the literature.

Nowadays, survival analysis makes use of fuzzy algebra and logic to deal with uncertain failure times, because there may undoubtedly be some fuzziness involved in survival times that occur in nature. Viertl [13] expanded the statistical estimation of the reliability characterizing function, which is typically more or less fuzzy when lifetime data are observed as fuzzy integers.

Grzegorzewski and Hryniewicz [2] used fuzzy sets for modeling the impreciseness of the lifetimes or censored times in the generalization of the exponential model, but the precise information of the observed failures is required. Grzegorzewski and Hryniewicz [3] calculated the mean time to failure, which is also seen as a fuzzy number, and calculated the associated confidence interval using fuzzy numbers.

Viertl [12] discussed the problems of statistical inference relating to the fuzziness present in the data. Shafiq and Viertl [9] stated that the lifetime observations are not precise but more or less fuzzy and based upon this fact they found non parametric estimates for reliability functions based on smoothed empirical distribution function adapted cumulative sum and fuzzy valued empirical distribution function. The interval valued estimation of the reliability function is also suggested. Shafiq. M and Viertl. R [10] have proposed a generalized Kaplan-Meier estimator when the survival times are fuzzy.

Jaisankar et.al [4] introduced a Fuzzy Kaplan Meier estimator and compared it with the traditional approach, which portrayed that the Fuzzified approach gives more reliable results than the Classical one. Jaisankar. R. and Varshini, K. S. P. [5] suggested a fuzzy based procedure through which the censored observations can be tackled to be included in the non-parametric survival analysis. The Kaplan - Meier's procedure was taken for the application of the proposed methodology.

2. Methods

Since survival durations are inherently continuous, and treating them as exact is somewhat meaningless. The methodology proposed is rely on this fact and every observed survival time is converted in to fuzzy by means of Triangular Fuzzy number. Due to the nature of survival times that the event might have been occurred prior to the observed survival time, in particular for death like events, Left preference Triangular fuzzy numbers are assumed, which are of the form

$$\tilde{A} = (a, b_w, c) \tag{3}$$

Where

- a is the lower bound where more weightage is given,
- b_w is the middle value generally can be calculated using a weighted mean (adjusted central value), ensuring that the membership function skews towards left, where $b_w = \frac{w_1 a + w_2 c}{w_1 + w_2}$, $w_1 > w_2$, where w_1 and w_2 are weights
- c is the upper bound here it is considered as the original survival time

The censored subjects are known to have survived up to the time of censoring but the status about the occurrence of their event is not known till the end of the study. If it is known that the event has occurred after they have censored in the later period of time it won't be precise. In both cases the preciseness is not possible and hence assuming fuzziness for the survival times with give reliable results. Here it is assumed that the survival times of censored subjects as Interval valued fuzzy numbers in which the interval is taken to be from the censored time to the fuzzified survival times of the last subject observed. The form of the interval valued fuzzy number is given by

$$\tilde{A} = \left\{ \left(x, \left[\vartheta_{\tilde{A}}^{L}(x), \vartheta_{\tilde{A}}^{U}(x) \right] \right) \;\middle|\; x \in X \right\} \tag{4}$$

where

- $\vartheta_{\tilde{A}}^{L}(x)$ is the lower bound of the Interval valued Fuzzy set to the actual survival time
- $\vartheta_{\tilde{A}}^{L}(u)$ is the upper bound of the Interval valued Fuzzy set to the maximum survival time in the data set

After these fuzzification procedures the Kaplan Meier estimator has been taken for substantiating and establishing the results.

The analysis was performed after the defuzzification of fuzzy numbers. The fuzzy numbers assumed for the uncensored survival times are defuzzified with reference to a value of alpha cut (α = 0.5) using the following method. For a left preference triangular fuzzy number, the centroid formula for defuzzifying is

$$D = \frac{L + 2M + U}{4} \tag{5}$$

where

- L is the lower bound
- M is the middle bound
- U is the upper bound

The fuzzy numbers proposed for censored observations are defuzzified using centroid method proposed by with reference to a value of alpha cut (α = 0.5) using the following method. The centroid method calculates the average of lower and upper bounds. The formula is:

$$\text{Defuzzified Value} = \frac{\text{Lower Bound} + \text{Upper Bound}}{2} \tag{6}$$

Since it takes in to account both the lower and upper membership degrees, it provides a balanced crisp value after the defuzzification procedure.

The survival times obtained so was applied to the Kaplan - Meier method, and the corresponding results are compared with the Classical Kaplan - Meier method. The survival curves obtained from the proposed method is compared with the survival curve obtained from the Classical Kaplan - Meier method using the log rank test.

3. Numerical Illustration

The remission survival periods of 42 leukemia patients, half of whom receive a specific novel treatment therapy and the other half receive standard therapy, are included in the data set for demonstration purposes. Treatment status is the exposure variable of interest ($R_x = 0$, for new treatment, $R_x = 1$ for standard treatment). Sex and log white blood cell count, or logWBC, are two additional variables for control that could be confounding factors. The relapse variable determines failure status (0 if censoring, 1 if failure). ** (Source: Data provided courtesy of David. G. Kleinbaum and Mitchel Klein in the textbook - Survival Analysis - A Self learning text- Third Edition (Page no: 89). URL:http://www.uop.edu.pk/ocontents/survival-analysis-self-learning-book.pdf

4. Results

The survival and hazard function curves for the Classical Kaplan-Meier estimator and the Fuzzified Kaplan-Meier estimator, along with their median survival time representation, are depicted above for visual comparison. Figures 1 and 2 illustrate a significant difference among the survival and hazard curves both prior to and subsequent to fuzzification. The median survival time determined by the Classical Kaplan-Meier estimate was 12.00, exceeding the 10.60 observed with the Fuzzified Kaplan-Meier estimator.

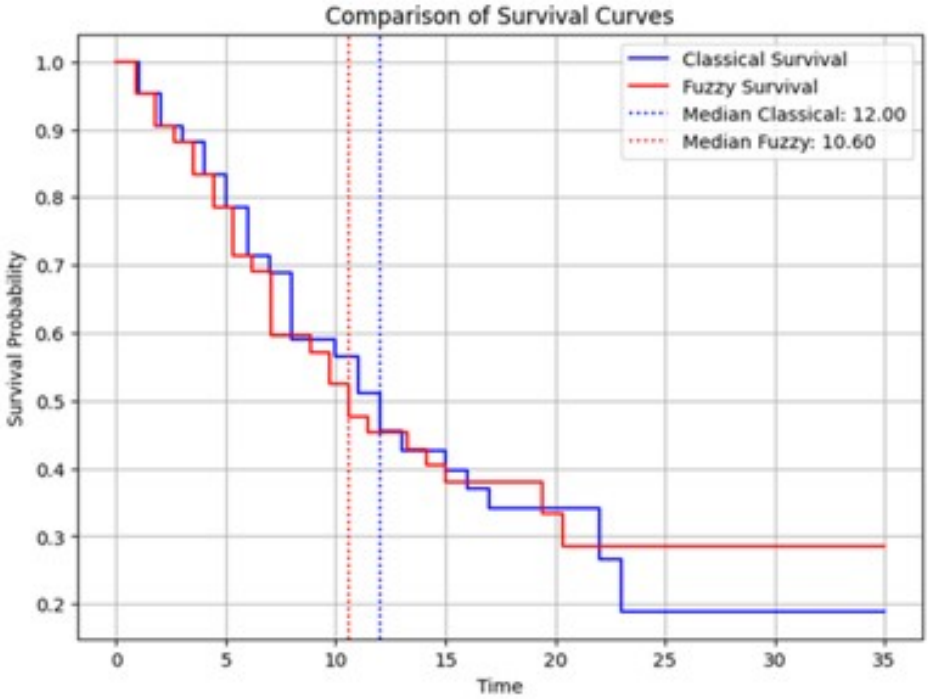


Figure 1: *Comparison of Classical and Fuzzified Survival curves along with the representation of Median Survival time in both Classical and Fuzzified cases*

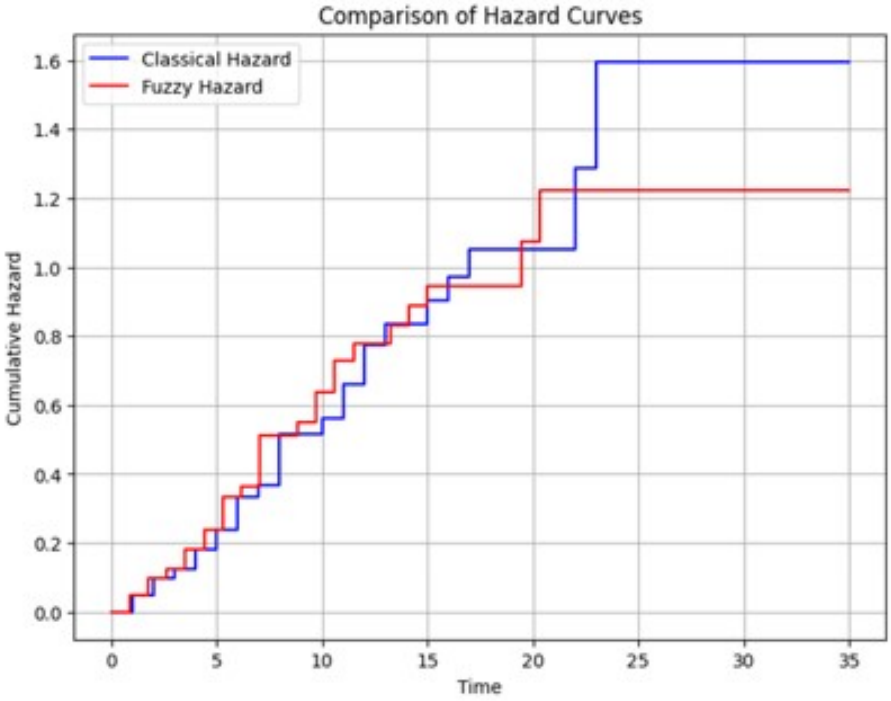


Figure 2: *Comparison of Classical and Fuzzified Hazard curves*

To assess if a significant difference exists between the survival curves derived from the Classical Kaplan-Meier estimator and its fuzzified counterpart, the log-rank test was used, with the null hypothesis assuming that the curves are similar. The test statistic for this is represented as follows:
Test statistic is,

$$\chi^2 = \frac{\sum(O_i - E_i)^2}{\sum V_i} \tag{7}$$

where,

- O_i is the observed number of events in Group i,
- E_i is the expected number of events in Group i,
- V_i is the variance of the difference between the observed and expected events.

The test statistic is calculated using the defuzzified values of survival times, and the details of the results are given below

Table 1: *Log rank test results*

Log Rank test	
p – Value	0.833

The comparison of the curves via the Log-rank test (Figure 3) indicates that no significant differences are evident in these curves. However, it is dependent upon the choice of the fuzzification factor utilized for the process of fuzzification. When performing a statistical analysis of data derived from a random sample, it is essential to consider both the randomness and the imprecision of the data, particularly when dealing with continuous data. This is particularly accurate with the survival time data. Consequently, a fuzzified variant of the Kaplan-Meier survival estimator was developed, and the associated values of the survival and hazard functions were also calculated.

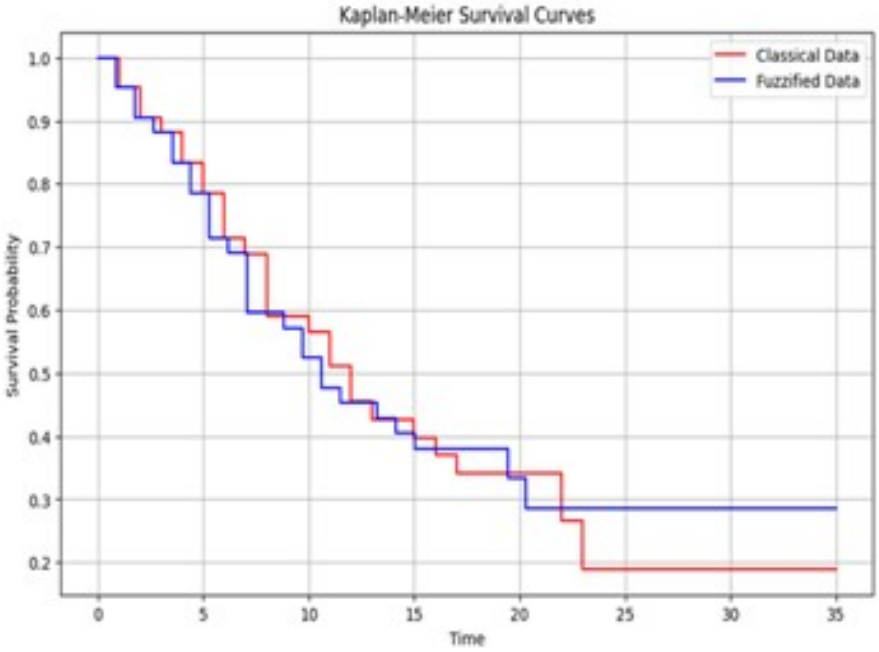


Figure 3: *Comparison of Survival curves for the Log rank test*

The incorporation of fuzziness may enhance the model's authenticity; hence yielding correct findings, as observations of a continuous nature often display ambiguity. Disregarding this would decrease the validity of the conclusions derived from every kind of analysis.

5. Discussion

Every continuous observations is subject to the presence of fuzziness and every event in survival analysis may not be measured accurately of its time of occurrence. This fact necessitates the present work and it is found that associating fuzziness in Survival analysis leads to changes in survival as well as hazard estimates when compared with the Classical methods that considers only randomness. As the incorporation of fuzziness makes the analysis more natural, one may expect the results which are reliable and applicable.

References

[1] Breslow N. E. (1975). Analysis of survival data under the proportional hazards model *International Statistical Review/Revue Internationale de Statistique*, 43(1):45-57.
[2] Grzegorzewski, P. and Hryniewicz, O. (1999). Lifetime tests for vague data. *Computing with Words in Information/Intelligent Systems 2: Applications*, 176-193.
[3] Grzegorzewski, P. and Hryniewicz, O. (2002). Computing with words and life data. *International Journal of Applied Mathematics and Computer Science*, 12(3):337-345.
[4] Jaisankar, R., Parvatha Varshini, K. S. and Siva, M. (2022). A Fuzzy Approach to Kaplan-Meier Estimator. *Mathematical Statistician and Engineering Applications*, 71(3s2): 1107-1114.
[5] Jaisankar, R. and Varshini, K. S. P. (2024). On Addressing Censoring in Survival Data Using Fuzzy Theory. *Indian Journal of Science and Technology*, 17(4): 312-316.
[6] Kalbfleisch, J. D. and Prentice, R. L. (1973). Marginal likelihoods based on Cox's regression and life model. *Biometrika*, 267-278.
[7] Kaplan, E. L. and Meier, P. (1958). Nonparametric estimation from incomplete observations. *Journal of the American statistical association*, 53(282):457-481.

[8] Nelson W. (1972). Theory and applications of hazard plotting for censored failure data. *Technometrics*, 14(4): 945-966.
[9] Shafiq, M. and Viertl, R. (2015). Empirical reliability functions based on fuzzy life time data. *Journal of Intelligent & Fuzzy Systems*, 28(2): 707-711.
[10] Shafiq, M. and Viertl, R. (2015) . Generalized Kaplan Meier Estimator for Fuzzy Survival Times. *Śląski Przegląd Statystyczny*, 13(19):7-14.
[11] Thomas, R. Fleming and David, P. Harrington (1984). Nonparametric estimation of the survival distribution in censored data. *Communications in Statistics - Theory and Methods*, 13(20): 2469-2486.
[12] Viertl R. Statistical Methods for Non-Precise Data. *CRC Press*, 1995.
[13] Viertl R. (2009). On reliability estimation based on fuzzy lifetime data. *Journal of Statistical Planning and Inference*, 139(5):1750-1755.

BIOGEOGRAPHY-BASED RELIABILITY OPTIMIZATION

Deepika Garg[1], Sarita Devi[2]*, Doorgeshwaree Devi Heeramun[3], Nakul Vashishth[4]

•

[1,2,3,4] GD Goenka University, Gurugram, Haryana

[1]deepikanit1234@gmail.com, [2]sarita.fame@gmail.com
[3]vidishaheeramun@yahoo.com, [4]nakulsir@gmail.com
*Corresponding author

Abstract

Biogeography-based optimization (BBO) is an effective optimization algorithm originally introduced by Dan Simon in 2008. It is inspired by the principles of biogeography. It mimics the process of migration and colonization of different species, where the behavior of species is determined by their habitats and the available resources. However, BBO can suffer from slow convergence and premature convergence for high-dimensional optimization problems. To address these issues, opposition-based learning (OBL) has been integrated with BBO. OBL uses the concept of generating an opposite solution to an existing solution and combining them to form a new search direction. This helps to improve the diversity of the population and accelerate the convergence speed of the algorithm. The combination of BBO and OBL has shown promising results in solving various optimization problems, including engineering design, scheduling, and feature selection. This approach has proved to be efficient and robust, making it an attractive alternative to other optimization algorithms. In this research study, the redundancy Allocation Problem (RAP) is solved with BBO and OBL-BBO. Computational results confirm the robustness and superiority of this new model over previous ones in optimizing the reliability of the system. Besides, the proposed algorithm OBL-BBO outperforms the previous ones BBO in finding good results.

Keywords: Biogeography-based optimization (BBO), opposition-based learning (OBL), opposition-based learning based BBO (OBL-BBO), RAP.

I. Introduction

Reliability optimization aims to boost a system's dependability while cutting costs or improving overall efficiency [1]. In practice, reliability is typically pursued through two main avenues: (i) enhancing the intrinsic reliability of individual components and (ii) introducing redundant units. Although using highly reliable components can raise dependability, performance often plateaus before the target level is reached. Redundancy, meanwhile, can deliver the desired reliability but inevitably adds cost, weight, and volume [2]. The redundancy allocation problem (RAP) was first formulated for systems with multiple states and interacting failures [3]. A subsequent study proposed a heuristic procedure to solve RAP for a manufacturing system with series-connected subsystems, relying on redundancy to improve overall reliability [4]. Later, researchers tackled RAP with a Hybrid Constraint Optimization Genetic Algorithm combined with

Particle Swarm Optimization (H-PSOCOGA) and compared its results with those from the heuristic method and a standalone Constraint-Optimization Genetic Algorithm (COGA) [5].

The K-mixed strategy has been applied to tackle RAP, aiming to elevate system reliability. After using this strategy to build a mathematical model for reliability estimation, its effectiveness was tested on several benchmark and custom problems to gauge power and efficiency [6]. Fault-tree analysis—a graphical, logic-based approach that examines system failure modes—has also been used to address the reliability-optimization task and calculate failure probabilities in manufacturing systems [7]. In another investigation, three approaches— a Heuristic Algorithm (HA), a Constrained-Optimization Genetic Algorithm (COGA), and a Hybrid Genetic Algorithm coupled with Particle Swarm Optimization (HGAPSO)—were implemented for RAP, with a comparative performance assessment provided for all methods [8].

A Hybrid Genetic Simulated Annealing Algorithm (HGSAA) has been proposed to solve the RAP in manufacturing systems. By blending the strengths of genetic algorithms and simulated annealing, HGSAA mitigates the individual weaknesses of each method, and its performance has been benchmarked against a Heuristic Algorithm (HA), a Constrained-Optimization Genetic Algorithm (COGA), and the Hybrid Particle Swarm Optimization–COGA approach (H-PSOCOGA) for the same problem set [9]. In another study, three dedicated heuristics—HASL1, HASL2, and HASL3, each defined by a different selection factor—were created to allocate redundancy within the cost constraints of Yaris Pharmaceuticals' liquid-medicine production line, with post-allocation results compared graphically [10]. Separately, the Jaya algorithm has been employed to estimate the probability P (X > Y) for a two-parameter Weibull distribution [11].

A broad survey spanning 2000 – 2022 catalogued the literature on the redundancy-allocation problem, organizing and analyzing prior studies by system type, configuration, solution method, and constraint set. Drawing on this synthesis, the review pinpointed under-explored areas and proposed avenues for future research where coverage remains thin [12].

Spider Monkey Optimization (SMO)—a comparatively new meta-heuristic previously unused for RAP—has been applied to redundancy allocation in manufacturing systems. Benchmarks against Particle Swarm Optimization (PSO) indicate that SMO yields superior solutions. The same work also analyzed time-dependent availability to forestall total system shutdowns, illustrating how mathematical models and search algorithms can identify reliability-maximizing configurations. This research area overlaps with maintenance planning and resource management and sees applications from engineering to telecommunications [13]. In a separate study, the Jaya algorithm was employed to solve two RAP formulations with nonlinear constraints, aiming to maximize system reliability [14].

The overarching objective across industries is to keep systems running reliably and to minimize downtime. Nature-inspired, or bio-inspired, optimization methods borrow ideas from evolutionary biology—such as natural selection, adaptation, and migration—to tackle complex search and optimization tasks. By mirroring the adaptability of living systems, these algorithms deliver robust and flexible problem-solving tools. A prominent example is Biogeography-Based Optimization (BBO), which models the migration of species among habitats [15]. BBO blends exploration and exploitation via migration operators, offering computational efficiency, versatility, simplicity, and a derivative-free search. These qualities have made it one of the fastest-growing meta-heuristics for difficult optimization problems. Nevertheless, BBO is not without drawbacks: its success depends on careful parameter tuning, its exploratory power can taper off in very high-dimensional spaces, its convergence may lag some alternatives, and performance can fluctuate across problem domains.

Researchers have contrasted Biogeography-Based Optimization (BBO) with the Genetic Algorithm (GA) for designing damping controllers in power-system applications [16]. A separate study blended BBO with the Shuffled Frog-Leaping Algorithm and applied the hybrid to minimum-

spanning-tree problems. While limited theoretical grounding and reduced adaptability to dynamic or heavily constrained scenarios have been noted as weaknesses, current work seeks to address these gaps and extend BBO's range of use [17]. Further efforts have merged BBO with additional meta-heuristics; experimental evaluations of these hybrids highlight both their performance improvements and their remaining trade-offs [18].

Reference [19] delivers an in-depth overview of Biogeography-Based Optimization (BBO) and illustrates its value for difficult optimization problems. Opposition-Based Learning (OBL) further enriches the search process by generating each candidate solution alongside its opposite, expanding the initial exploration of the design space. When this strategy is integrated with BBO—yielding the so-called Oppositional BBO—experiments report faster convergence and superior solution quality compared with the conventional BBO algorithm [20]. Subsequent surveys highlight BBO's competitive advantages over other meta-heuristics, its wide-ranging applications, and open avenues for future research [21]. Building on OBL's diversity and BBO's framework, investigators have also combined BBO with Ant Colony Optimization (ACO); this hybrid improves global search capability, helps the solver avoid local optima, and performs particularly well on binary optimization tasks [22].

Building on prior redundancy-allocation research, this investigation addresses a realistic manufacturing system with multiple subsystems that must meet stringent reliability targets under fixed cost, weight, and volume caps. The study applies two meta-heuristic optimizers-standard Biogeography-Based Optimization (BBO) and its Opposition-Based extension (OBL-BBO) to the identical mixed-integer formulation, enabling a direct, fair performance comparison. BBO leverages migration and mutation operators to balance exploration and exploitation, whereas OBL-BBO supplements each candidate solution with its opposite counterpart, enriching population diversity and accelerating global search. Analysis reveals that OBL-BBO reaches the desired reliability within tighter budgets and fewer iterations, although it exhibits slightly greater sensitivity to parameter tuning. The comparative insights gained guide practitioners in selecting the most appropriate algorithm for redundancy-allocation tasks with similar industrial constraints and anticipated future enhancements. The subsequent Section 2 outlines the methodological frameworks for BBO and OBL-BBO, followed by a detailed problem formulation in Section 3. Section 4 presents the experimental results alongside an in-depth discussion, while Section 5 distils the main findings and contributions of the research.

II. Methods

I. Methodology of OBL

Opposition-based learning (OBL) accelerates convergence to optimal solutions by exploring both candidates and their opposites, enhancing efficiency and solution quality. It also helps in escaping local optima, leading to more robust optimization results.

Symbols**:**

- X: A candidate solution in the search space.
- X': The opposite (complementary) solution of X
- $f(X)$: Objective function value of the solution X
- $f(X')$: Objective function value of the opposite solution X'
- α: a parameter controlling the step size
- R_i: Reliability of the system
- Q_i: Unreliability of the system

The methodology of OBL is explained in following steps:

1) Initialization

Two individuals are created - one represents the initial solution and the other represents its opposite. The opposite solution is created by altering the signs of the decision variables.

Generate an initial population of solutions X
Evaluate the fitness of each solution using the objective function: $f(X)$
$X_i' = -X_i$ for each variable i

2) Fitness Evaluation

The fitness of both solutions is determined using the objective function. The solution with better fitness is selected as the parent for the next generation.

$$X_{next} = argmax\ (f(X), f(X')) \quad (1)$$

3) Search space exploration

To efficiently explore the search space, an opposition-based approach is utilized. This allows the algorithm to break away from local optima by considering solutions that are "opposite" to the current best solution.

$$X_i(t+1) = X_i(t) + \alpha\left(X_i' - X_i(t+1)\right) \quad (2)$$

4) Iterative refinement

The process is then repeated iteratively, with each iteration aiming to refine the solution by implementing the opposition-based strategy. This approach allows for a more human-like thought process, as we also consider opposing ideas in our decision-making. Repeat steps 2-6 until a termination criterion is met (e.g., a maximum number of iterations, satisfactory solution found).

II. Methodology of BBO

Symbols**:**

- X_i : A candidate solution (habitat) in the population.
- $f(X_i)$: Objective function value of the habitat X_i.
- M: Migration rate (probability of migration).
- P_m: Mutation rate (probability of mutation).
- N: total number of habitats in the population.
- X_{new}: a randomly selected habitat from the population.
- $rand()$: a random number between 0 and 1
- X_{rand}: a randomly selected habitat from the population.

The methodology of OBL is explained as:

1. Initialization

Generate an initial population of habitat X_i.

2. Evaluate fitness.
   Evaluate the fitness of each habitat using objective function: $f(X_i)$

3. Habitat Suitability Index (HSI):
   To determine which habitats are most suitable for each solution, a Habitat Suitability Index (HSI) is assigned based on its fitness. Solutions with higher fitness values are seen as more desirable habitats.
   $$HSI_i = \frac{f(X_i)}{\sum_{j=1}^{N} f(X_j)} \quad (3)$$

4. Migration Rate and Mutation Rate:
   The process of migration and mutation is not random, as it is controlled by the migration and mutation rates. The migration rate determines the likelihood of a solution moving to a different habitat.
   $$X_i(t+1) = X_i(t) + M \cdot HSI_i\big(X_{new} - X_i(t)\big) \quad (4)$$

   while the mutation rate dictates the chances of introducing changes to a solution.
   $$X_i(t+1) = X_i(t+1) + P_m \cdot rand().\big(X_{rand} - X_i(t+1)\big) \quad (5)$$
   Evaluate the fitness of the new habitats.

5. Population Update:
   As the population evolves, solutions are updated through a combination of migration, mutation, and the HSI. The ultimate goal of this algorithm is to continuously improve the overall fitness of the population with each iteration.
   $$X_i(t+1) = argmax\ (f\big(X_i(t+1)\big), f\big(X_i(t)\big)) \quad (6)$$

6. Convergence:
   The algorithm will continue until a convergence criterion is met, such as reaching a maximum number of iterations or finding a satisfactory solution. Just like in nature, it is all about finding the perfect balance and adapting to the changing environment. Repeat steps 2-7 until a termination criterion is met (e.g., a maximum number of iterations, satisfactory solution found).

III. Methodology of Opposition-Based Learning based BBO (OBL-BBO)

1. Initialization:
   Generate an initial population of solutions randomly in the search space.

2. Opposition Generation:
   For each solution X_i generate its opposite solution X_i' by changing the signs of its decision variables.
   $X_i' = -X_i$ for each variable =–for each **variable** i

3. Opposition Fitness Evaluation:
   Evaluate the fitness of each opposite solution using the objective function.

4. Biogeography-Based Optimization:
   Apply BBO steps:
   a. Calculate Habitat Suitability Index (HSI) for each solution based on its fitness.

b. Perform Migration Operation:
    1. Determine which solutions will undergo migration based on the migration rate M.
    2. Update the solutions using migration.
c. Perform Mutation Operation:
    1. Determine which solutions will undergo mutation based on the mutation rate Pm.
    2. Update the solutions using mutation.

5. Evaluate fitness of the new solutions.

6. Update the population based on fitness and HSI.

7. Termination:
   Repeat steps 2-4 until a termination criterion is met (e.g., a maximum number of iterations or a satisfactory solution found).

An example of a real-world application of OBL-BBO is Oppositional biogeography-based optimization (OBBO), which is an improved version of the moth flame optimization (MFO) algorithm that uses OBL-BBO to optimize complex objectives. OBBO has been used to solve 18 benchmark functions and two constrained real-world problems, including global optimization.

III. Problem Definition

The manufacturing system consists of various units such as overhead crane, Blanking machine, Stacker machine, Press machine, Molding and Packing. All these machines work in a series system. In manufacturing system, the problem is to maximize reliability with cost constraint. The given cost limitation is C= 30490000 (Here number of constraints is one). Here Table 1 presents the reliability cost of each subsystem.

The problem is to maximize:

$$R_s(y) = g\,(R_1(y_1), \ldots\ldots\ldots\ldots, R_n(y_n)) = \prod_{j=1}^{7} R_j\,(y_j) \quad (7)$$

$$R_j(y_j) = \prod_{j=1}^{7}[1 - [Q_j(y_j)]^{n_j}] \quad (8)$$

$$\sum_{j=1}^{7} h^1(y_j) * n_j \leq 30490000 \quad (9)$$

Table 1: *Reliability cost of each subsystem*

Subsystem	y_1	y_2	y_3	y_4	y_5	y_6	y_7
Reliability of subsystem $R_j(y_j)$	0.99	0.9762	0.9188	0.8155	0.8655	0.9287	0.9453
Cost of subsystem $h_1(y_j)$	1240000	860000	2100000	1010000	10200000	840000	200000

I. Mechanism for BBO

The brief overview of the flow chart of Biogeography-Based Optimization is presented in Figure 1. The actual implementation of the algorithm may involve additional steps and parameters that can be customized based on the specific optimization problem.

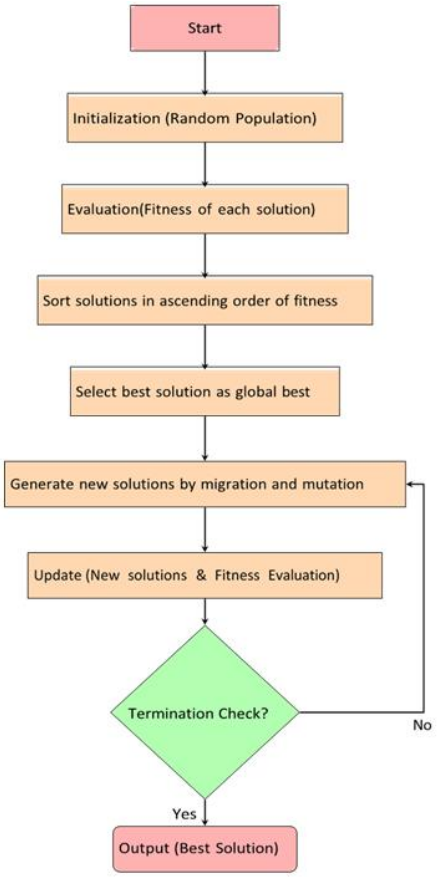


Figure 1: *Mechanism for BBO*

IV. Results and Discussion

The results obtained by the OBL, BBO and OBL-BBO techniques are represented in the tabular form. In Table 2 and Table 3, the subsystems and units of the subsystems are given.

Table 2: *Results of RAP of manufacturing system by BBO*

Subsystems	y_1	y_2	y_3	y_4	y_5	y_6	y_7	Reliability	CPU time
No. of units	3	3	4	3	1	4	4	0.8600	0.001s

The reliability value of the subsystem before applying BBO technique is 0.5502. The redundant units of the subsystem are considered y*= (1 1 1 1 1 1 1). After applying BBO technique, the optimal solution of RAP is y*= (3 3 1 4 1 4 4) and the reliability value R(y*) = 0.8600 as shown in Table 2. The reliability of the system is increased by 56%. The CPU time taken by software is 0.001s

by BBO technique. The graphical representation of the result from BBO is demonstrated in Figure 2. The number of optimum redundancy units of the various subsystems are represented in the graph as shown in figure.

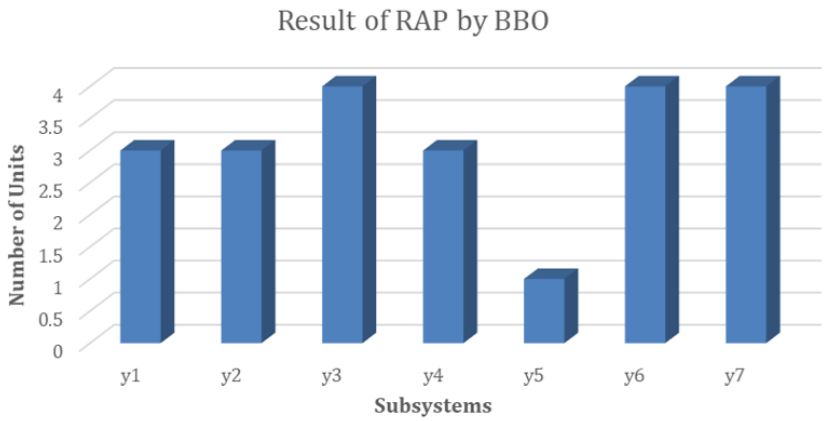


Figure 2: *Results of RAP obtained by BBO*

Similarly, in Table 3, the reliability value of the Subsystem before applying OBL-BBO technique is 0.5502 and the redundant units of the subsystems are considered y*=(1 1 1 1 1 1 1). After applying OBL-BBO technique, the optimal solution of RAP is y*= (3 4 3 4 1 4 4) and the reliability value is R(y*) = 0.8640. The reliability of the system is increased by 57%. The CPU time taken by software is 0.001s by OBL-BBO technique.

Table 3: *Results of RAP of manufacturing system by OBL-BBO*

Subsystems	y_1	y_2	y_3	y_4	y_5	y_6	y_7	Reliability	CPU time
No. of units	3	4	3	4	1	4	4	0.8640	0.001s

Similarly, the graphical representation of the result obtained by OBL-BBO is shown in Figure 3. The results obtained from OBL-BBO are better than results of BBO with respect to the redundancy units of different subsystems and reliability also.

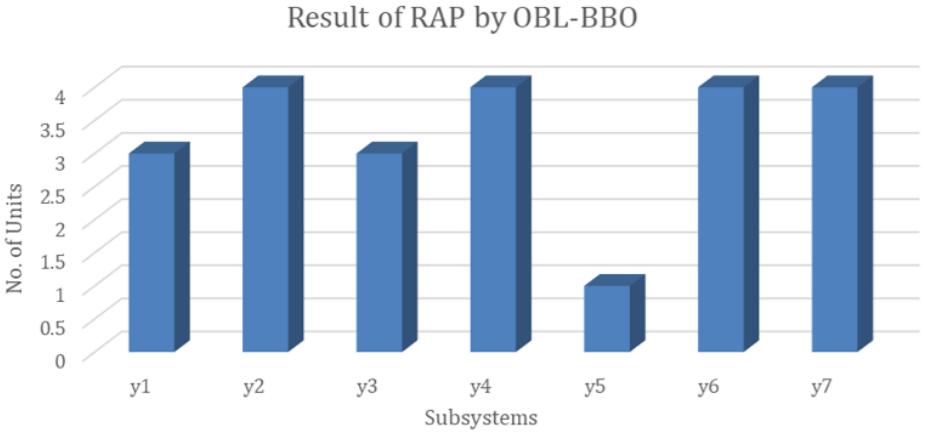


Figure 3: *Results of RAP obtained by OBL-BBO*

The CPU time taken by both the techniques are same, but the result of total reliability of the system and optimum number of redundant units are obtained better from OBL-BBO than BBO.

V. Conclusion

In this paper, RAP of a manufacturing system is investigated first by BBO technique. After that the RAP of the manufacturing system is solved by OBL-BBO. OBL-BBO contributes to the rich tapestry of optimization research by introducing a novel combination of opposition-based learning and biogeography-based optimization. Its implications extend beyond theoretical advancements, offering practical solutions and insights that can shape the future landscape of optimization algorithms. The results obtained from both the techniques are presented in tabular form. The numerical outcomes demonstrate the superiority of this OBL-BBO over BBO in solving RAP of the manufacturing system

References

[1] Simon, D. (2008). Biogeography-Based Optimization. IEEE Transactions on Evolutionary Computation, 12(6):702–713.

[2] Sharifi, M., Taghipour, S. (2022). Redundancy allocation problem of a Multi-State system with Binary-State continuous performance level components. Expert Systems with Applications, 200: 117161.

[3.] Yeh, W. C., Hsieh, T. J. (2011). Solving reliability redundancy allocation problems using an artificial bee colony algorithm. Computers & Operations Research, 38(11):1465-1473.

[4.] Wang, J., Li, M. (2015). Redundancy Allocation Optimization for Multistate Systems with Failure Interactions Using Semi-Markov Process. ASME.-Journal of Mechanical Design, 137(10): 101403.

[5] Devi, S., & Garg, D. (2017). Redundancy-Allocation in Neel Metal Products Limited. Indian Journal of Science and Technology, 10(30).

[6] Devi, S., Sahu, A., Garg, D. (2017). Redundancy optimization problem via comparative analysis of H-PSOCOGA. International Conference on Computing and Communication Technologies for Smart Nation (IC3TSN), Gurgaon, India, 2017, 18-23,

[7] Peiravi, A., Karbasian, M., Ardakan, M.A., Coit, D.W. (2019). Reliability optimization of series-parallel systems with k-mixed redundancy strategy. Reliability Engineering & System Safety, 183: 17–28.

[8] Devi, S., Garg, D. (2019). Reliability analysis of manufacturing plant via fault tree analysis. Journal of Advances and Scholarly Researches in Allied Education, 16(5):256-259.

[9] Devi, S., Garg, D. (2020). Hybrid genetic and particle swarm algorithm: redundancy allocation problem. International Journal of System Assurance Engineering and Management, 11: 313–319.

[10] Garg, D., Devi, S. (2021). RAP via hybrid genetic simulating annealing algorithm. International Journal of System Assurance Engineering and Management, 12: 419–425.

[11] Dahiya, T., Garg, D., Devi, S., Kumar, R. (2021). Reliability optimization using heuristic algorithm in pharmaceutical plant. Reliability Theory & Applications, 16(3): 195-205.

[12] Raikar, S.L., Gaonkar, R.S.P. (2022). Jaya algorithm in estimation of P [X> Y] for two parameter Weibull distribution. AIMS Mathematics, 7(2): 2820-2839.

[13] Devi, S., Garg, H., & Garg, D. (2023). A review of redundancy allocation problem for two decades: bibliometrics and future directions. Artificial Intelligence Review, 56(8): 7457-7548.

[14] Devi, S., Vashishth, N., Garg, D. (2023). RAP and Availability analysis of manufacturing system: SMO and PSO. Reliability: Theory & Applications, 18, 4(76): 680-691.

[15] Aswin, B., Lokhande, T., Gaonkar, R. (2023). Solving Redundancy Allocation Problems using Jaya Algorithm. International Journal of Mathematical, Engineering and Management Sciences, 8:804-816.

[16] Said, A. I., El-Saadany, E. F., and Salama, M. M. A. (2013). Comparison of Biogeography Based Optimization and Genetic Algorithm for Power System Damping-Based Controllers Design. IEEE Electrical Power & Energy Conference, IEEE, 1–5.

[17] Zheng, Y., Lu, X., Zhang, M., Chen, S., (2019). Hybrid Biogeography-Based Optimization Algorithms, Biogeography-Based Optimization: Algorithms and Applications. Springer Singapore, Singapore, 89–115.

[18] Zhang, X., Kang, Q., Wang, X. (2019). Hybrid Biogeography-Based Optimization with Shuffled Frog Leaping Algorithm and Its Application to Minimum Spanning Tree Problems. Swarm Evolutionary Computation, 49: 245–265.

[19] Mirjalili, S. (2019). Biogeography-Based Optimisation. 57–72.

[20] Ergezer, M., Simon, D., and Du, D. (2009). Oppositional Biogeography-Based Optimization. IEEE International Conference on Systems, Man and Cybernetics, IEEE, 1009–1014.

[21] Sharma, S., Chandrasekhar Rao, D. (2022). Biogeography-Based Optimization. 471–479.

[22] Dai, Z., Ma, Q., Zhao, D., Yan, S. (2020). A Novel Hybrid Optimization Algorithm Combined with BBO and ACO. *39th Chinese Control Conference (CCC)*, IEEE, 1581–1586.

IMPROVING THE RELIABILITY OF SOLAR ENERGY SYSTEMS USING FLOATING PHOTOVOLTAIC TECHNOLOGIES

M.T. Babayev

•

Azerbaijan State Oil and Industry University, Baku, Azerbaijan
mazahir.babayev@asoiu.edu.az

Abstract

This paper explores floating solar panels (FSPs) as a promising and cost-effective solution for enhancing the reliability and sustainability of solar power systems. The analysis focuses on the technical, environmental, and economic benefits of FSPs compared to traditional land-based installations. Floating systems offer improved operational reliability and energy efficiency due to natural cooling, land conservation, lower environmental impact, and reduced water evaporation—particularly vital in regions with limited freshwater resources. Deploying FSPs on artificial reservoirs and flooded quarries not only reduces land-use pressure but also contributes to lower capital and operational expenditures. Case studies from Azerbaijan and Japan demonstrate the reliability, resilience, and ecological viability of floating solar solutions under various climatic conditions. Although initial investments may be higher, long-term assessments reveal that FSPs can deliver more consistent performance and greater cost-effectiveness in regions with high solar irradiance and available water surfaces. The paper provides a comprehensive overview of floating photovoltaic technologies, highlighting their role in improving the reliability and stability of solar energy supply.

Keywords: floating solar panels, renewable energy, environment, reliability.

I. Introduction

The modern development of renewable energy focuses on finding solutions capable of simultaneously meeting growing energy demands and minimizing negative environmental impacts. One such solution is floating solar panels (FSP), installed on water surfaces. These innovative systems not only enhance energy resilience but also create new opportunities for optimizing the use of natural and financial resources.

The economic potential of FSP lies in significantly reducing operational and capital expenses compared to land-based solar power stations. Utilizing existing water bodies eliminates land acquisition costs and minimizes infrastructure construction expenses. Moreover, the installation of FSP on already available facilities, such as hydroelectric power plants or artificial reservoirs, allows seamless integration into existing energy systems, thereby reducing investment risks [1-3].

In terms of reliability, FSP demonstrates advantages due to natural cooling, which decreases wear on the panels and extends their operational lifespan. However, comprehensive reliability assessment requires consideration of various failure mechanisms specific to floating systems, such as corrosion due to constant water exposure, wave-induced mechanical stresses, and biofouling or biological damage. These factors can significantly impact the durability and operational lifetime of FSP components.

Furthermore, the increasing frequency of extreme weather events linked to climate change — including storms, hurricanes, and floods — poses catastrophic risks to FSP installations, necessitating robust probabilistic modeling of such scenarios to predict failure likelihood and plan appropriate mitigation measures.

This article examines not only the technical and environmental aspects of FSP applications but also their economic feasibility and reliability, including:

- Analysis of failure factors and forecasting methods for corrosion, mechanical fatigue, and biological damage;
- Probabilistic reliability modeling that incorporates time-dependent degradation processes;
- Influence of local environmental conditions such as water salinity on cooling efficiency and corrosion rates;
- Assessment of catastrophic event impacts (e.g., storms) on system survivability;
- Incorporation of multi-year monitoring data from real installations to validate reliability models;
- Calculation of Mean Time Between Failures (MTBF) for key components, including anchoring systems and cable connections;
- Evaluation of how improved reliability affects the levelized cost of energy (LCOE) over the system lifecycle.

II. Formulation of the problem

The primary challenge facing traditional solar energy lies in the limited availability of land resources, which creates significant economic barriers to the development of ground-mounted solar power plants. In densely populated countries or regions with scarce free land, such as Japan and the Netherlands, the cost of acquiring suitable land reaches substantial levels, making these projects less financially viable [4]. With urbanization on the rise and increasing demand for agricultural production, dedicating large areas to ground-mounted solar farms becomes increasingly difficult. Moreover, in some regions, the construction of solar power plants meets social resistance due to the potential loss of landscape diversity and farmland.

In addition to land constraints, rising costs associated with construction and grid connection further escalate the overall expenses of such projects. In remote areas and islands where long transmission lines are required, these costs become critical. Traditional solar power stations also face social and environmental challenges, such as deforestation, which negatively impacts biodiversity and amplifies public opposition.

In contrast, floating solar panels minimize land use conflicts and reduce environmental impacts but introduce specific reliability challenges related to their aquatic environment. Key issues include:

- Corrosion of metallic components caused by constant exposure to water, especially in saline or polluted conditions;
- Mechanical stresses from wave action, wind, and fluctuating water levels inducing fatigue failures;
- Biofouling and biological damage from aquatic organisms that may degrade structural elements and electrical insulation;
- Catastrophic events such as storms and floods that can cause sudden, large-scale damage or system loss.

Failure to account for these factors in reliability assessments leads to underestimation of maintenance needs and lifecycle costs.

Additionally, local environmental variations — for example, differences in water salinity — impact the cooling effect on panels and the corrosion rate, influencing both efficiency and durability.

Table 1 presents a comparison of primary limitations of traditional ground-mounted solar power plants and floating solar systems, including these nuanced reliability considerations.

Table 1.: *Comparison of key parameters of ground-mounted and floating solar systems*

Parameter	Ground-Mounted Solar Stations	Floating Solar Panels
Land Use	High competition	Minimal competition
Environmental Impact	High	Low
Infrastructure Costs	High	Moderate
Performance	Moderate	High (due to cooling)
Water Evaporation	No effect	Reduces evaporation
Corrosion Risk	Low	High (depends on water quality and material protection)
Mechanical Stress	Low	High (wave and wind loads)
Biofouling	Not applicable	Present (requires monitoring and mitigation)
Extreme Weather Risk	Moderate	High (storm, flood vulnerability)

III. Problem solution

Floating solar panels offer a range of advantages, making them an efficient solution for many regions [5]. These systems can be installed on various types of water bodies, including:

- Artificial reservoirs.
- Flooded quarries.
- Industrial water bodies.
- Aggregated water resources in arid regions.

One successful implementation example is the project on Lake Boyukshor in Azerbaijan. A pilot installation with a capacity of 2 MW demonstrated high efficiency and minimal impact on the ecosystem (Fig. 1).

Similarly, a project in Japan on the Yamakura Reservoir, with a capacity of 13.7 MW, reduced water evaporation by 20% and decreased carbon dioxide emissions by 7,000 tons annually (Fig. 2).

In Table 2 and Figure 3, the comparison of electricity generation efficiency between land-based and floating systems under various climatic conditions is presented.



Figure 1: *1. 2 MW installation on Lake Boyukshor in Azerbaijan*



Figure 2: *13.7 MW installation on the Yamakura reservoir in Japan*

Table 2.: *Comparison of Land-Based and Floating Systems for Electricity Generation*

Parameter	Land-Based Systems	Floating Systems
Efficiency	Dependent on available space and panel tilt angles. Average efficiency: 16–22%.	Higher efficiency due to the cooling effect of water. Average efficiency: 18–25%.
Economic Aspect	Lower initial installation costs. Operating expenses are lower.	Higher construction and maintenance costs. Requires corrosion protection systems.
Reliability	High in dry and temperate climates; may decrease due to dust and overheating.	High in regions with high humidity and solar activity, but depends on structural resilience.
Climatic Conditions	Suitable for temperate and dry regions (e.g., deserts). Performance may drop in extreme heat conditions.	Ideal for tropical and coastal areas. Stable operation due to water cooling.

The graph in Figure 3 demonstrates the comparative efficiency of land-based and floating power generation systems under various climatic conditions. In tropical and coastal regions, floating systems exhibit higher efficiency due to natural water cooling, which enhances the performance of solar panels. In temperate climates, the efficiency of both systems is comparable, whereas in arid conditions, land-based systems experience reduced efficiency due to overheating. This graph highlights that the selection of the optimal system depends on the climatic conditions, with floating systems being more advantageous in regions characterized by high humidity and solar activity.

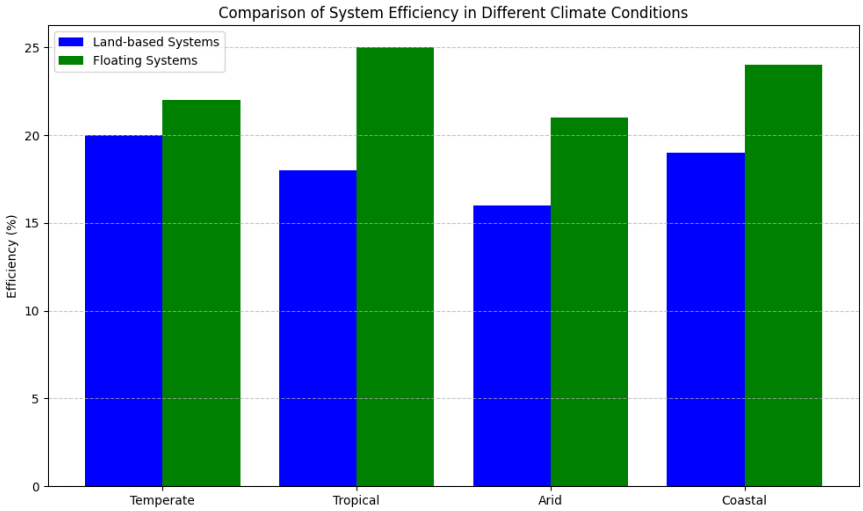


Figure 3. *Comparison of the efficiency of systems in different climatic conditions*

Advantages of the Technology:

1. Enhanced Efficiency: Water cooling increases panel efficiency by 10–15%.
2. Land Resource Savings: Floating solar panels (FSPs) are installed on unused water bodies, freeing up land for other purposes.
3. Reduced Evaporation: Particularly important in water-scarce regions, FSPs help conserve water.

Minimal Environmental Impact: When adhering to standards, these systems do not affect water quality or aquatic ecosystems.

In tropical countries like Indonesia or the Philippines, floating solar farms can be more economically advantageous due to high solar insolation and natural water cooling of panels. This improves panel efficiency and reduces operational costs, such as cooling and dust cleaning, common for land-based systems [6-8]. For example, maintenance costs for floating systems in such regions can be 15–20% lower than for land-based systems, offsetting the higher initial investments.

In arid regions like Saudi Arabia, land-based systems may be more economically justified due to the availability of vast land areas [9-11]. However, increased operational costs from cleaning and reduced efficiency due to overheating can raise expenses by 10–15%, making floating systems more competitive if the infrastructure for water-based farms is available.

Thus, the economic benefits vary depending on climatic conditions and resource costs, such as land and water.

An Example of Economic Efficiency Calculation for Comparing Ground-Mounted and Floating Solar Farms

Input Data:

Solar Farm Capacity: 10 MW.

Ground-Mounted System: Installation cost $800/kW, annual operating expenses 2% of capital costs, efficiency 18%.

Floating System: Installation cost $1000/kW, annual operating expenses 1.5% of capital costs, efficiency 20% due to water cooling.

Average Solar Insolation: 5 hours/day. *Calculation Period:* 10 years.

Calculations:

1. Capital Expenditures (CAPEX):
   Ground-Mounted: 10,000 kW×800 $/kW=8,000,000 $.
   Floating: 10,000 kW×1000 $/kW=10,000,000 $.
2. Annual Operating Expenses (OPEX):
   Ground-Mounted: 8,000,000 $×2%=160,000 $.
   Floating: 10,000,000 $×1.5%=150,000 $.
3. Annual Energy Output:
   Ground-Mounted: 10,000 kW×18%×5 hours/day×365 days=3,285,000 kWh.
   Floating:10,000 kW×20%×5 hours/day×365 days=3,650,000 kWh.
4. Total Energy Output Over 10 Years:
   Ground-Mounted: 3,285,000 kWh/year×10 years=32,850,000 kWh.
   Floating: 3,650,000 kWh/year×10 years=36,500,000 kWh.
5. Total 10-Year Costs:
   Ground-Mounted: 8,000,000 $+160,000 $×10=9,600,000 $.
   Floating:10,000,000 $+150,000 $×10=11,500,000 $.
6. Cost of Electricity Production per kWh:
   Ground-Mounted: 9,600,000 $÷32,850,000 kWh=0.292 $/kWh.
   Floating: 11,500,000 $÷36,500,000 kWh=0.315 $/kWh.

Results: Ground-Mounted System: Lower installation cost and electricity production cost at $0.292/kWh but less efficient. Floating System: Higher installation cost and electricity production cost at $0.315/kWh, with higher efficiency due to water cooling.

Adjustments for factors such as efficiency losses from soiling or higher cooling costs in hot climates could shift the economic balance in favor of floating systems over the long term.

Reliability Assessment Example:

Input Data for Reliability:

Availability Coefficient:

Ground-Mounted: 95% (dust, soiling, frequent cleaning required).

Floating: 97% (reduced dust impact, better cooling).

Mean Time to Repair (MTTR):

Ground-Mounted: 48 hours.

Floating: 72 hours (requires boats or specialized equipment).

Failure Rate per Year:

Ground-Mounted: 10 failures/year.

Floating: 7 failures/year.

Repair Costs per Failure:

Ground-Mounted: $2000.

Floating: $3000.

Reliability Calculations:

1. Annual Downtime:

Ground-Mounted: 10 failures/year×48 hours=480 hours.

Floating: 7 failures/year×72 hours=504 hours.

2. Availability Coefficient:

Ground-Mounted: (8760−480) hours/8760 hours=94.52%.

Floating: (8760−504) hours/8760 hours=94.24%.

3. Annual Maintenance Costs:

Ground-Mounted: 10 failures/year×2000 $/failure=20,000 $.

Floating: 7 failures/year×3000 $/failure=21,000 $.

4. Effective Electricity Output: Assuming maximum output of 18,250,000 kWh/year:

Ground-Mounted: 18,250,000 kWh×94.52%=17,246,350 kWh.

Floating: 18,250,000 kWh×94.24%=17,202,200 kWh.

Results: Ground-mounted systems have slightly higher availability and lower downtime due to shorter repair times, reducing productivity loss.Floating systems exhibit fewer failures and benefit from better operating conditions but incur higher maintenance costs and longer downtimes.

To enhance clarity and facilitate the interpretation of the calculations presented above, it is advisable to summarize the key technical and economic indicators of both systems in a comparative table, accompanied by visual representations such as charts and graphs. The table 3 below provides an overview of the main parameters for the ground-mounted and floating photovoltaic systems.

As the table illustrates, despite the higher efficiency of the floating system, the ground-mounted system demonstrates a lower cost of electricity generation, primarily due to its lower capital and operational costs.

In addition, a reliability assessment was performed for both systems, taking into account factors such as availability coefficient, mean time to repair (MTTR), failure rate, and maintenance costs. The results are summarized in the following table 4..

Table 3.: *Comparative technical and economic characteristics of ground-mounted and floating PV systems*

Parameter	Ground-Mounted System	Floating System
Installed Capacity	10 MW	10 MW
Installation Cost ($/kW)	800	1000
Capital Expenditures (CAPEX)	$8,000,000	$10,000,000
Annual Operating Expenses (OPEX)	$160,000	$150,000
Efficiency	18%	20%
Annual Energy Output	3,285,000 kWh	3,650,000 kWh
Total Output Over 10 Years	32,850,000 kWh	36,500,000 kWh
Total 10-Year Costs	$9,600,000	$11,500,000
Cost of Electricity Production	$0.292/kWh	$0.315/kWh

Table 4.: *Reliability assessment of ground-mounted and floating PV systems*

Parameter	Ground-Mounted System	Floating System
Availability Coefficient (Calculated)	94.52%	94.24%
Failure Rate per Year	10	7
Annual Downtime (Hours)	480	504
Annual Repair Costs	$20,000	$21,000
Effective Annual Energy Output	17,246,350 kWh	17,202,200 kWh

Graphical representations of these results, such as bar charts comparing CAPEX, OPEX, total output, and availability, can significantly improve the interpretability of the data and provide clearer insight into the advantages and trade-offs of each system.

In summary, structured and visual presentation of data adds substantial analytical value, allowing for a more balanced and informed comparison when evaluating ground-mounted versus floating solar power systems in terms of cost, efficiency, and operational reliability.

In scenarios where reliability and frequent access are critical, ground-mounted systems may be preferred, while floating systems offer advantages for long-term operation and lower failure rates [12-13].

Here's the combined economic aspect and reliability analysis of the ground-based and floating solar systems. The data is presented in Table 5, along with graphical representations in Figure 4.

Table 5: *Comparison of Ground-Based and Floating Solar Systems*

Indicator	Ground System	Floating System
Availability Factor, %	94.52	94.24
Downtime per Year, hours	480	504
Mean Time to Repair (MTTR), hours	48	72
Number of Failures per Year	10	7
Failure Repair Costs, $	2,000	3,000
Annual Maintenance Costs, $	20,000	21,000
Effective Output, kWh	17,246,350	17,202,200

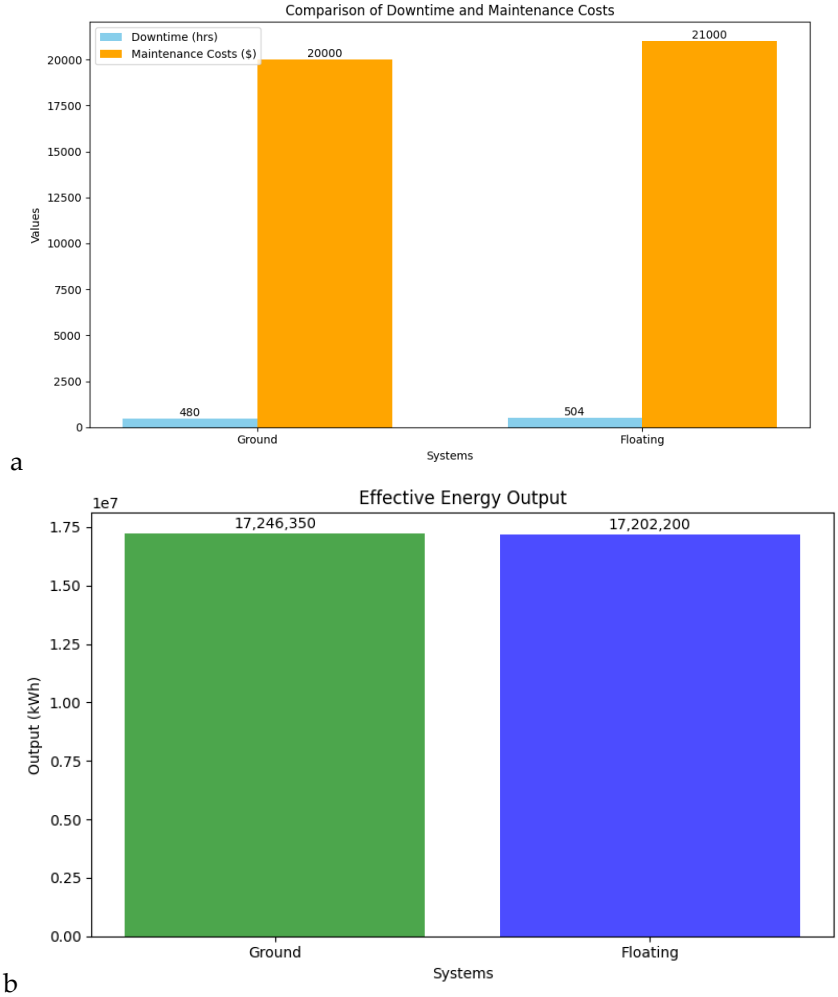


Figure 4: *Graphical comparison of ground-based and floating solar systems*

The graph in Figure 4a shows the difference in downtime and maintenance costs. It is evident that the ground-based system is cheaper to maintain, but the floating system requires more time to recover from failures. The graph in Figure 4b demonstrates that the effective electricity generation of ground-based systems is slightly higher due to the reduced downtime.

This approach allows for the visualization of the economics and reliability of both systems, providing the opportunity to select the optimal option for specific conditions [14-18].

From the above, the following conclusions can be drawn:

1. Ground-based systems have lower failure recovery costs, making them advantageous in the case of frequent failures [19-20].
2. Floating systems are less prone to failures, but their maintenance costs are higher.
3. The effective electricity generation is higher for ground-based systems due to shorter recovery times after failures.

To gain a deeper understanding of the economic efficiency and reliability of solar power systems, a comparative analysis was conducted between ground-mounted and floating photovoltaic (PV) installations, each with a capacity of 10 MW, assuming an average solar insolation of 5 hours per day over a 10-year period.

Capital expenditures (CAPEX) for ground-mounted systems amount to approximately $8 million, with annual operational expenditures (OPEX) around $160,000. The total energy output over the lifespan reaches 32.85 GWh, resulting in a levelized cost of electricity (LCOE) of about

$0.292 per kWh. In contrast, floating systems have higher CAPEX at roughly $10 million but benefit from slightly lower OPEX of approximately $150,000 per year. The total energy produced over the same period is estimated at 36.5 GWh, yielding an LCOE of approximately $0.315 per kWh. Despite the higher LCOE of floating systems, this gap narrows under conditions of elevated temperatures and dust contamination due to improved reliability and efficiency.

Reliability assessment was carried out using mean time between failures (MTBF) and availability metrics. With annual failure rates of 10 for ground-mounted and 7 for floating systems, and mean time to repair (MTTR) values of 48 and 72 hours respectively, the calculated MTBF is 876 hours for ground-mounted and 1251 hours for floating systems. Corresponding availability values are approximately 94.8% for ground-based and 94.6% for floating installations.

MTBF

Ground-Based: MTBF = 8760 h / 10 = 876 h

Floating: MTBF = 8760 h / 7 = 1251 h

Availability (A):

$$A = \frac{MTBF}{MTBF + MTTR}$$

$$\text{Ground} - \text{Based: } A = \frac{876}{876 + 48} \approx 94.8\%$$

$$\text{Floating: } A = \frac{1251}{1251 + 72} \approx 94.6\%$$

These values align with real-world estimates from long-term monitoring of FSPs over 5–7 years in Southeast Asia and Europe [12–13].

Particular attention was given to critical components in floating systems, such as anchoring mechanisms and cable connections. Field studies conducted in India, Singapore, and the Netherlands indicate that anchoring failures—caused by corrosion, biofouling, and hydrodynamic fatigue—occur at a rate of 0.3 failures per anchor per year, corresponding to an MTBF of roughly 3.3 years. Cable connections, susceptible to thermal cycling and water ingress, exhibit failure rates of 1.2 per year per 10 km of cable, with an MTBF of approximately 8,000 hours (around 11 months). Preventive maintenance strategies, including UV-resistant coatings and real-time insulation resistance monitoring, significantly mitigate these risks.

Exposure to harsh environmental factors such as high humidity, saltwater, and ultraviolet radiation accelerates the aging process of key materials. For instance, polymer floats' lifespans may decrease from 25 to 15–18 years, while cable insulation and seals degrade 20–30% faster in the absence of marine-grade protective specifications. Probabilistic Weibull models were employed to estimate component survival rates, revealing a 20–30% increased failure risk in tropical coastal regions without enhanced protective measures.

Enhancements in reliability have a direct positive impact on economic performance. By reducing failure frequency to 5 per year and shortening MTTR to 60 hours, MTBF increases to 1752 hours, and availability improves to 96.7%. This results in a 4.5% increase in energy output over 10 years and a corresponding reduction in adjusted LCOE to approximately $0.302 per kWh, representing a 4.1% improvement in cost competitiveness.

In summary, reliability models and economic analyses demonstrate that properly engineered floating solar systems can match or surpass the reliability of ground-mounted counterparts. Special focus is required on mitigating failures of critical components, particularly under high-stress environmental conditions. Empirical monitoring data validate model assumptions and highlight key degradation factors. Integrating reliability-centered design and probabilistic modeling is essential for the sustainable development and long-term economic viability of floating solar projects.

IV. Conclusions

Floating solar panels represent a promising advancement in the pursuit of reliable and sustainable renewable energy solutions. Unlike ground-mounted systems, these installations mitigate land-use conflicts and reduce infrastructure costs, while also benefiting from natural water-based cooling, which enhances their operational efficiency and prolongs component lifespan. This inherent stability contributes to improved overall system reliability, especially in environments where temperature fluctuations and dust accumulation compromise the performance of traditional solar arrays.

Experience gained from successful projects in Europe and Asia confirms not only the economic and environmental viability of floating solar systems, but also their robustness in diverse climatic and hydrological conditions. Their ability to maintain stable power generation under variable loads and environmental stresses positions them as a resilient solution in the face of growing energy demands and climate-related uncertainties.

To fully realize their potential, it is essential to ensure long-term structural integrity, refine regulatory frameworks, and deepen our understanding of environmental interactions. With continued innovation and thoughtful deployment, floating photovoltaic systems are poised to become a cornerstone of the global transition to reliable, low-carbon energy infrastructure.

References

[1] Almasi, F., & Tofighi, A. (2021). Floating solar photovoltaic systems: Economic and environmental impacts. *Renewable Energy Reviews*, 27, 123–135.
[2] Bui, N. V., & Nguyen, D. T. (2020). Floating solar panels: A new trend in solar energy production. *Journal of Renewable Energy*, 56, 89–100.
[3] Xie, Y., Zhang, L., & Zhao, M. (2022). Impact of water cooling on the performance of floating solar panels. *Energy Conversion and Management*, 62, 234–247.
[4] Zhang, T., Liu, J., & Zhang, P. (2023). Energy and cost efficiency of floating photovoltaic systems. *Applied Energy*, 58, 101–115.
[5] Lopes, A., Silva, J., & Pereira, R. (2020). Comparison of floating and ground-mounted photovoltaic systems: A case study of hydropower reservoirs. *Energy Procedia*, 108, 210–218.
[6] Lee, C., & Lee, S. (2021). Environmental benefits of floating solar panels: Reducing water evaporation and enhancing energy generation. *Environmental Science and Technology*, 45, 144–155.
[7] Tuan, D. H., & Kim, D. H. (2022). Assessment of floating solar panels in coastal and inland water bodies: A case study of Vietnam. *Journal of Clean Energy Technologies*, 10(2), 107–119.
[8] Piras, M., & Fedele, P. (2021). Technological advances in floating solar photovoltaic systems. *Renewable and Sustainable Energy Reviews*, 136, 110282.
[9] Yuan, J., & Yang, Y. (2020). Floating solar PV for water conservation and energy generation: A review of global trends. *Solar Energy Materials & Solar Cells*, 211, 110524.
[10] Shiau, S. M., & Chang, W. S. (2022). Economic analysis and optimization of floating solar systems. *Energy Economics*, 90, 125–136.
[11] Kumar, S., & Jain, V. (2021). Case study of floating solar panel integration in hydropower projects. *International Journal of Energy and Environmental Engineering*, 12, 331–343.
[12] Mendez, A., & Narvaez, J. (2020). Floating solar panels: A sustainable alternative for electricity generation. *Sustainable Energy Technologies*, 9(4), 456–469.
[13] Chen, L., & Zhang, F. (2021). The role of floating solar systems in mitigating the effects of climate change. *Renewable Energy*, 157, 1–9.
[14] Giannelli, A., & Della Penna, F. (2020). Reducing land usage with floating solar panels. *Energy for Sustainable Development*, 54, 132–140.

[15] Wu, M., & Zhao, R. (2021). Economic viability of floating solar energy systems: A comparative study with ground-mounted PV. *International Journal of Green Energy*, 18(7), 712–724.
[16] Lee, J., & Park, S. (2020). Impact of climate conditions on the performance of floating solar panels. *Energy Reports*, 6, 1329–1337.
[17] Martin, T., & Uhlmann, M. (2021). Challenges and benefits of floating solar photovoltaic systems in tropical climates. *Renewable Energy*, 160, 1065–1078.
[18] Rajesh, S., & Kumar, R. (2020). Energy yield comparison between ground-mounted and floating solar panels. *Solar Energy*, 194, 68–80.
[19] Piriyeva, N. M., Rzayeva, S. V., & Qaniyeva, N. M., "Investigation of the Characteristics of a Barrier Discharge in a Water-Air Environment," *IJTPE Journal*, vol. 15, no. 55, pp. 44–49.
[20] Karimova, R. K., & Rzayeva, S. V., "Comparison of Thermal Conductivity of Aqueous and Formide Solutions BeCl at High Temperatures," *Technical and Physical Problems of Engineering (IJTPE) International Journal*, vol. 2, 2023.

RELIABILITY-BASED OPTIMIZATION OF TWO-WAREHOUSE SUPPLY CHAIN MODELS

Ajay Singh Yadav[1,*], S. Viswanathan[2], Navin Ahlawat[3],
Bhavani Viswanathan[4], Anupam Swami[5]

•

[1]Department of Mathematics, [2]Faculty of Management Studies,
[3]Department of Computer Science, [4]Department of Library Science & Humanities
[1,2,3,4]SRM Institute of Science and Technology, Delhi-NCR Campus, Modinagar,
Ghaziabad, Uttar Pradesh, India, 201204
[5]Department of Mathematics, Km. Mayawati Government Girls P.G. College,
Badalpur, Gr. Noida, India, 203207
ajay29011984@gmail.com, director.ncr@srmist.edu.in, navins@srmist.edu.in,
bhavaniviswam@gmail.com, swami.anupam@gmail.com
[*]Corresponding author

Abstract

This study presents a reliability-based optimization framework for managing a two-warehouse inventory system in the dairy industry, specifically addressing the complexities posed by product spoilage, shortages, and inflation. The proposed mathematical model integrates key inventory management principles with spoilage dynamics, shortage scenarios, and economic inflation, under a First-In-First-Out (FIFO) dispatching policy. By prioritizing the shipment of older stock, the model aims to reduce spoilage and enhance product turnover. It incorporates dairy product expiration rates to determine optimal replenishment and dispatch strategies while also identifying and mitigating potential operational bottlenecks. Additionally, the influence of inflation on inventory-related costs is embedded within the model to reflect real-world economic fluctuations. Through the application of advanced optimization algorithms implemented in MATLAB, the model seeks to minimize total inventory costs and improve supply chain efficiency. Overall, this research offers a comprehensive and practical tool for enhancing inventory decision-making in perishable goods industries like dairy.

Keywords: Inventory, Ramp Type Demand, Deteriorating Items, Inflation, Shortages and Reliability-Based Optimization.

1. Introduction and related work

Effective inventory management is vital for the dairy industry to ensure product quality, minimize costs and meet customer demand. However, inventory management in the dairy industry poses unique challenges due to factors such as the expiration of perishables, the possibility of shortages, and the impact of inflation on costs. To address these challenges, the dairy industry's inventory model includes two warehouses for deteriorating items. congestion and inflation as part of the FIFO shipping policy, a systematic approach to optimizing inventory decisions. The model draws on the theories of inventory management, decomposition, shortages and inflation to provide a comprehensive framework for effective inventory management in the dairy industry.

By integrating these theories, the model aims to find a balance between maintaining optimal inventory levels, minimizing the risk of product deterioration, reducing shortages and controlling costs in the face of inflation.

The FIFO shipping policy, which ensures that the oldest stock is shipped first, is introduced to prioritize the use of products with a shorter remaining shelf life. This policy reduces the risk of product spoilage and waste and improves overall product quality and customer satisfaction. In addition, the model takes into account the spoilage of dairy products and their specific spoilage rates. By considering product shelf life and incorporating restocking and shipping policies accordingly, the model enables companies to optimize inventory turnover and minimize spoilage losses.

Bottlenecks in the dairy industry can lead to lost sales and dissatisfied customers. The model solves this problem by optimizing stock levels and reordering decisions to reduce occurrences of stock-outs and improve customer service. By minimizing bottlenecks, companies can improve customer satisfaction and gain a competitive advantage in the marketplace. In addition, the model takes into account the impact of inflation on inventory costs. By factoring in inflation, businesses can make informed decisions on pricing, order quantities, and inventory costs to adjust to changing economic conditions and maintain profitability.

The Dairy Industry Two-Warehouse Inventory Model for Spoiled Items with Shortages and Inflation under the FIFO Shipping Policy provides a theoretical foundation and practical guidance for dairy companies to optimize their inventory management practices. By using mathematical techniques and optimization algorithms, companies can increase operational efficiency, reduce costs, and improve overall business performance in the dynamic dairy industry.

However, there are a number of things whose significance does not remain the same over time.The deterioration of these substances plays an important role and cannot be stored for long Yadav et al. [1-10]. Deterioration of an object can be described as deterioration, evaporation, obsolescence and loss of use or limit of an object, resulting in lower stock consumption compared to natural conditions. When commodities are placed in stock as inventory to meet future needs, there may be deterioration of items in the system of arithmetic that may occur for one or more reasons, etc. Storage conditions, weather or humidity, Yadav et al. [11-20]. Inach it is generally claimed that management owns a warehouse to store purchased inventory. However, management can, for a variety of reasons, buy or give more than it can store in its warehouse and name it OW, with an additional number in a rented warehouse called RW located near OW or slightly away from it Yadav et al. [21-53]. Inventory costs (including holding costs and depreciation costs) in RW are usually higher than OW costs due to additional costs of handling, equipment maintenance, etc. To reduce the cost of inventory will economically use RW products as soon as possible. Actual customer service is provided only by OW, and in order to reduce costs, RW stocks are first cleaned. Such arithmetic examples are called two arithmetic examples in the warehouse Yadav and Swami [54-61]. Management of supply of electronic storage devices and integration of environment and nervous networks Yadav and Kumar [62]. Analysis of seven supply chain management measures in improving the inventory of electronic devices for storage by sending an economic load using GA and PSO and analysis of supply chain management in improving the inventory of storage and equipment using genetic calculation and model design and analysis of chain inventory from bi warehouse and economic difficulty of freight transport using genetic calculation Yadav, A.S. [63-65]. Inventory policies of inventory and inventory requirements and different storage costs under allowable payments and inventory delays An example of depreciation of goods and services of various types and costs of holding down a Business-Loan and an inventory model with sensitive needs of prices, holding costs in contrast to loans of business expenses under inflation Swami et al. [66-68]. The objectives of the Multiple Objective Genetic Algorithm and PSO, which include the improvement of supply and deficit inventory, inflation, and a calculation model based on a genetic calculation of scarcity and low inflation by PSO Gupta et al. [69-70]. An example with two warehouses depreciation of items and storage costs under particle upgrade and an example with two warehouses of material damage and storage costs in inflation and soft computer techniques Singh et al. [71, 72]. Delayed alcohol supply management and refinement

of particles and green cement supply system and inflation using particle enhancement and electronic inventory calculation system and distribution center using genetic calculations Kumar et al. [73-75]. Example of depreciation inventory with two warehouses and stock-based stocks using a genetic inventory and vehicle inventory system for demand and inflation of stocks with two distribution centers using genetic inventory Chauhan and Yadav [76-77]. Marble Analysis Improvement of industrial reserves based on genetic engineering and multi-particle improvement Pandey et al. [78]. White wine industry in supply chain management using nervous networks Ahlawat, et. al. [79]. Best policy for importing damaged items immediately and payment of conditional delays under the supervision of two warehouses Singh, et. al. [80].

The research by Yadav et al. [81] centers on improving inventory management for perishable commodities through the lens of green technology investments, considering factors such as selling price, carbon emissions, and time-sensitive demand. In another analysis, Yadav, Yadav, and Bansal [82] utilize an interval number technique to explore a two-warehouse inventory management model for perishable goods, addressing demand and cost uncertainties. Their optimization methods highlight how investing in preservation technology can reduce waste and enhance inventory efficiency. Focusing on a two-warehouse approach to optimize inventory levels, Yadav, Yadav, and Bansal [83] present a model that addresses the deterioration of goods during storage, emphasizing the importance of managing degradation costs to improve overall inventory performance. In order to maximize inventory levels while lowering expenses related to degradation and backlog, Negi and Singh [86] investigate an inventory system that controls uncertainty, takes into account time-varying demand patterns, and assesses inventory control tactics in the event of stockouts.

2. Notations and assumptions

2.1. Assumptions

In developing the mathematical model of the Dairy industry inventory system the following assumptions are being made:

1. A single item is considered over a prescribed period T units of time.
2. The Dairy industry demand rate D(t) at time t is deterministic and taken as a ramp type function of time i.e. $D(t) = (\beta_0 + \beta)e^{-\beta_2[t-(t-(t_\beta+t_F))H(t-t_\beta+t_F)]}$; $\beta > 0,\ \beta_0 > 0,\ \beta_2 > 0$. Where $H(t - t_\beta + t_F)$ is the Heaviside's function defined as
$$H(t - t_\beta + t_F) = \begin{cases} 0, & t - t_\beta + t_F < 0, \\ 1, & t - t_\beta + t_F \geq 0 \end{cases}$$
3. The replenishment rate is infinite and lead-time is zero.
4. When the demand for goods is more than the supply. Shortages will occur. Customers encountering shortages will either wait for the vender to reorder (backlogging cost involved) or go to other vendors (lost sales cost involved). In this model shortages are allowed and the backlogging rate is $e^{-\beta_3 t}$, when Dairy industry inventory is in shortage. The backlogging parameter β_3 is a positive constant.
5. The variable rate of deterioration in both Dairy industry warehouse is taken as $\beta_1(t) = \beta_1 t$. Where $0 < \beta_1 << 1$ and only applied to on hand Dairy industry inventory.
6. No replacement or repair of deteriorated items is made during a given cycle.
7. The Dairy industry owned warehouse (OW) has a fixed capacity of W units; the Dairy industry rented warehouse (RW) has unlimited capacity.
8. The goods of Dairy industry OW are consumed only after consuming the goods kept in Dairy industry RW.

2.2. Notations

In addition, the following notations are used throughout this paper:

Parameters	Descriptions
π_{ow}^{fifo}	The Dairy industry inventory level in OW at any time t.
π_{rw}^{fifo}	The Dairy industry inventory level in RW at any time t.
β_w	The capacity of the Dairy industry own warehouse.
Q	The Dairy industry ordering quantity per cycle.
T	Planning horizon.
β_4	Inflation rate.
β_{hcow}	The holding cost per unit per unit time in Dairy industry OW.
β_{hcrw}	The holding cost per unit per unit time in Dairy industry RW, where $C_1 < C_2$.
β_{dc}	The deterioration cost per unit.
β_{sc}	The shortage cost per unit per unit time.
β_{opc}	The opportunity cost due to lost sales.
β_{OC}	The replenishment cost per order.
TC	The total average cost.

3. Formulation and Solution of The Model

The Dairy industry inventory levels at OW are governed by the following differential equations:

$$\frac{d\Pi_{ow}^{fifo}(t)}{dt} = [-\beta_1(t) I^{fifo}(t)], \qquad 0 \le t \le (t_\beta + t_F) \tag{1}$$

$$\frac{d\Pi_{ow}^{fifo}(t)}{dt} + \beta_1(t) I^{fifo}(t) = -(\beta_0 + \beta) e^{-\beta_2(t_\beta + t_F)}, \qquad (t_\beta + t_F) \le t \le (t_1 + t_F) \tag{2}$$

And

$$\left[\frac{d\Pi_{ow}^{fifo}(t)}{dt}\right] = \left[-(\beta_0 + \beta) e^{-\beta_2(t_\beta + t_F)} e^{-\beta_3 t}\right], \qquad (t_1 + t_F) \le t \le (T + t_F) \tag{3}$$

with the boundary conditions,

$$\Pi_{ow}^{fifo}(0) = \beta_w \; and \; \Pi_{ow}^{fifo}(t_1 + t_F) = 0 \tag{4}$$

The solutions of equations (1), (2) and (3) are given by

$$\Pi_{ow}^{fifo}(t) = \beta_w e^{-\beta_1 t^2}, \qquad 0 \le t \le (t_\beta + t_F) \tag{5}$$

$$\Pi_{ow}^{fifo}(t) = \Bigg[(\beta_0 + \beta) e^{-\beta_2(t_\beta + t_F)}(t_1 + t_F) - t + \frac{\beta_1 (t_1 + t_f)^3 - t^3}{6} e^{-\beta_1 t^2}\Bigg], \quad (t_\beta + t_F) \le t \le (t_1 + t_F) \tag{6}$$

and

$$\Pi_{ow}^{fifo}(t) = \left[\frac{(\beta_0 + \beta)}{\beta_3} e^{-\beta_2(t_\beta + t_L)} + e^{-\beta_3 t - e^{-\beta_3(t_1 + t_F)}}\right], \qquad (t_\beta + t_F) \le t \le (T_1 + t_F) \tag{7}$$

The Dairy industry inventory level at RW is governed by the following differential equations:

$$\frac{d\Pi_{ow}^{fifo}(t)}{dt} + \beta_1(t) \Pi^{fifo}(t) = -(\beta_0 + \beta) e^{-\beta_2 t}, \qquad 0 \le t \le (t_\beta + t_F) \tag{8}$$

With the boundary condition $\Pi_{rw}^{fifo}(0) = 0$ the solution of the equation (8) is

$$\Pi_{rw}^{fifo}(t) = \left[(\beta_0+\beta)\left\{(t_\beta+t_F) - t - \frac{\beta_1}{2}\left((t_\beta+t_F)^2 - t^2\right) + \frac{\beta_1}{6}\left((t_1+t_F)^3 - t^3\right)\right\}e^{-\beta_1 t^2}\right], \quad (t_\beta+t_F) \le t \le (t_1+t_F) \quad (9)$$

Due to continuity of $\Pi_{ow}^{fifo}(t)$ at point $t = (t_\beta + t_F)$ it follows from equations (5) and (6), one has

$$\beta_w = \left[(\beta_0+\beta)e^{-\beta_2(t_\beta+t_F)}\left\{(t_1+t_F) - (t_\beta+t_F) + \frac{\beta_1(t_1+t_f)^3 - (t_\beta+t_F)^3}{6}\right\}\right] \quad (10)$$

The total average cost consists of following elements:
(i) Ordering cost (OC) per cycle

$$OC = \beta_{OC}$$

(ii) Holding cost (C_{HO}) per cycle in Dairy industry

$$C_{HO} = \left[\beta_{hcow}\left\{\int_0^{(t_\beta+t_F)} \Pi_{ow}^{fifo}(t)e^{-\beta_4 t}dt + \int_{(t_\beta+t_F)}^{(t_1+t_F)} \Pi_{ow}^{fifo}(t)e^{-\beta_4\left\{(t_\beta+t_F)+t\right\}}dt\right\}\right] \quad (11)$$

(iii) Holding cost per cycle (C_{HR}) in RW

$$C_{HR} = \left[\beta_{hcrw}\left\{\int_0^{(t_\beta+t_F)} \Pi_{rw}^{fifo}(t)e^{-\beta_4 t}dt\right\}\right]$$
$$= \left[\beta_{hcrw}(\beta_0+\beta)\left\{\frac{(t_\beta+t_F)^2}{2} - \frac{(3\beta_2+\beta_4)}{6}(t_\beta+t_F)^3 + \left(\frac{\beta_1}{12} + \frac{\beta_2\beta_4}{8}\right)(t_\beta+t_F)^4 - \left(\frac{\beta_4\beta_1}{20} + \frac{\beta_2\beta_1}{30}\right)(t_\beta+t_F)^5\right\}\right] \quad (12)$$

(iv) Cost of deteriorated units per cycle (CD)

$$C_D = \left[\beta_{dc}\left\{\int_0^{(t_\beta+t_F)} \beta_1 t\Pi_{rw}^{fifo}(t)e^{-\beta_4 t}dt + \int_{(t_\beta+t_F)}^{(t_1+t_F)} \Pi_{ow}^{fifo}(t)e^{-\beta_4\left\{(t_\beta+t_F)+t\right\}}dt\right\}\right] \quad (13)$$

(v) Shortage cost per cycle

$$C_S = \left[\beta_{sc}\left\{\int_{t_1+t_F}^{(T+t_F)} -\Pi_{rw}^{fifo}(t)e^{-\beta_4\left(t_1+t_F)+t\right.}dt\right\}\right]$$
$$= \left[\frac{(\beta_0+\beta)\beta_{sc}e^{-(\beta_4(t_1+t_F)+\beta_2(t_\beta+t_F))}}{\beta_3\beta_4(\beta_3+\beta_4)}\left[\beta_3 e^{-(\beta_3+\beta_4)(t_1+t_F)} + e^{-\beta_4(T+t_F)}\left(re^{-\beta_3(T+t_F)} - (\beta_3+\beta_4)e^{-\beta_3(t_1+t_F)}\right)\right]\right] \quad (14)$$

(vi) Opportunity cost due to lost sales per cycle

$$C_o = \left[\beta_{opc}\left\{\int_{t_1+t_F}^{(T+t_F)} -(\beta_0+\beta)(1-e^{-\beta_3 t})e^{-\beta_2(t_\beta+t_F)}e^{-\beta_4(t_1+t_F)+t}\right\}\right]$$
$$= \left[\frac{(\beta_0+\beta)\beta_{opc}e^{-(\beta_4(t_1+t_F)+\beta_2(t_\beta+t_F))}}{\beta_4(\beta_3+\beta_4)}\left[e^{-\beta_4(t_1+t_F)}((\beta_3+\beta_4) - \beta_4 e^{-\beta_3(t_1+t_F)}) - e^{-\beta_4(T+t_F)}((\beta_3+\beta_4) - \beta_4 e^{-\beta_3(t_1+t_F)})\right]\right] \quad (15)$$

Therefore, the total average cost per unit time of our model is obtained as follows

$$TC(t_1 + t_F, T + t_F) = \frac{1}{(T + t_F)}\left[OC + C_{HO} + C_{HR} + C_D + C_S + C_O\right] = \frac{R(t_1, T)}{T} \tag{16}$$

4. Optimization Methodology

To minimize the total cost per unit time, the optimal values of t1 and T can be obtained by solving the following equations simultaneously

$$\frac{\partial TC}{\partial(t_1 + t_F)} = 0, \tag{17}$$

and

$$\frac{\partial TC}{\partial(T + t_F)} = 0 \tag{18}$$

provided, they satisfy the following conditions

$$\frac{\partial^2 TC}{\partial(t_1 + t_F)^2} > 0, \ \frac{\partial^2 TC}{\partial(T + t_F)^2} > 0$$

and

$$\left(\frac{\partial^2 TC}{\partial(t_1 + t_F)^2}\right) \cdot \left(\frac{\partial^2 TC}{\partial(T + t_F)^2}\right) - \left(\frac{\partial^2 TC}{\partial(T + t_F)\partial(t_1 + t_F)}\right)^2 > 0. \tag{19}$$

The equation (17) is equivalent to the following equation

$$\frac{\partial TC}{\partial(t_1 + t_F)} = \cdots \tag{20}$$

Also equation (18) is equivalent to

$$\frac{\partial TC}{\partial(T + t_F)} = \cdots \tag{21}$$

Equations (20) and (21) are highly nonlinear equations. Therefore, numerical solution of these equations can be obtained by using the software **MATLAB 7.0.1**.

5. Numerical Illustration

To illustrate the model numerically the following parameter values are considered.

$$\beta_1 = 0.0022 \ units, \ \ \beta = 702 \ units, \ \ \beta_0 = 502 \ units, \ \ \beta_2 = 0.22 \ units, \ \ \beta_3 = 0.12 \ units,$$

$$\beta_4 = 0.052 \ units, \ \ t_\beta = 0.12 \ year, \ \ \beta_{OC} = RS1002 \ per \ order, \ \ \beta_{hcow} = RS \ 4.02 \ per \ unit \ per \ year,$$

$$\beta_{hcrw} = RS20.0 \ per \ unit, \ \ \beta_{sc} = RS22.0 \ per \ unit \ per \ year,$$

$$\beta_{opc} = RS \ 42.0 \ per \ unit \ per \ year, \ \ T = 12 \ year$$

Then for the minimization of total average cost and with help of software. the optimal policy can be obtained such as: $t_1 = 0.399224$ year, $S = 28.597235$ units and $TC = RS.658.115354$ per year.

6. Graphical Representation

This section presents a series of graphical analyses to examine how key variables influence the total inventory cost in the proposed two-warehouse inventory model for the dairy industry. The figures provide insights into the system™s behavior under the effects of deterioration, shortages, inflation, and cycle duration. Figure 1 illustrates the variation in total inventory cost with respect to the decision variables t_1 and T. The surface plot helps identify the optimal region where the cost is minimized, supporting the selection of suitable cycle and shortage periods. The graph highlights the cost sensitivity to these parameters and reinforces the need for careful timing in inventory replenishment. Figure 2 demonstrates how the inflation rate affects the total cost. As inflation increases, a clear upward trend in total inventory cost is observed. This behavior reflects the economic reality that rising inflation inflates holding, ordering, and deterioration costs, thus influencing strategic decision-making in procurement and inventory planning. Figure 3 displays the relationship between the total cost and the cycle length T, considering different values of t_1. It shows that for each fixed t_1, there exists an optimal T that minimizes the total cost. Figure 4 explores the effect of cycle length on cost minimization in the two-warehouse structure. Table 1 presents the optimal solutions for various parameter combinations in the dairy industry inventory model, highlighting how changes in deterioration, inflation, and shortage rates affect the total inventory cost and ordering strategy.

Table 1: *Optimal Solution of Dairy Industry Inventory system*

β_1	β_2	β_3	β_4	t_β	T	TC_{CVM}	TC	S	AO
11	1.03	0.30	1.30	1.00	0.49	3841.30	1111.45	5111.45	1081.45
12	1.03	0.40	1.40	0.85	0.39	3851.30	1311.45	5311.45	1211.45
13	1.04	0.45	1.50	0.75	0.34	3811.30	1411.45	5411.45	1311.45
14	1.05	0.50	3.30	0.15	0.33	3871.30	1711.45	5711.45	1511.45
15	1.05	0.55	3.39	0.55	0.39	3881.30	1811.45	5811.45	1611.45
16	1.01	0.10	3.35	0.45	0.37	3891.30	1911.45	5911.45	1811.45
17	1.01	0.15	3.35	0.40	0.34	3991.30	3011.45	6011.45	6111.45
18	1.07	0.70	3.40	0.35	0.31	3993.30	3111.45	6111.45	6711.45
19	1.07	0.75	4.31	0.30	0.19	3995.30	3111.45	6311.45	6811.45
20	1.38	0.80	4.50	0.30	0.11	3997.30	3311.45	6311.45	6911.45

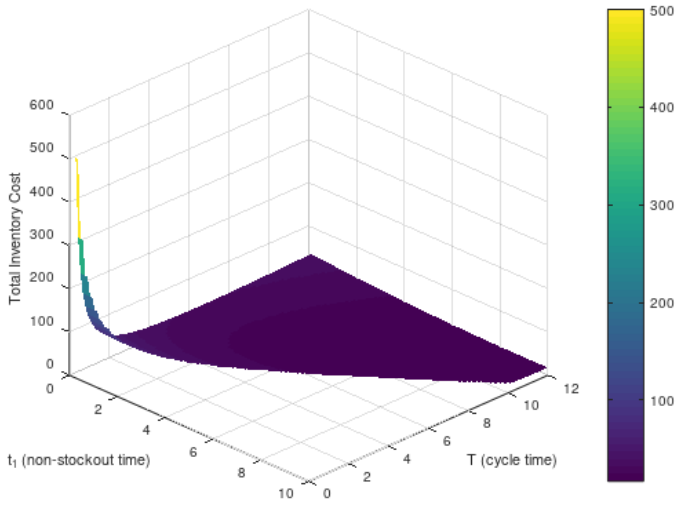


Figure 1: *Total inventory cost vs. t_1 and T*

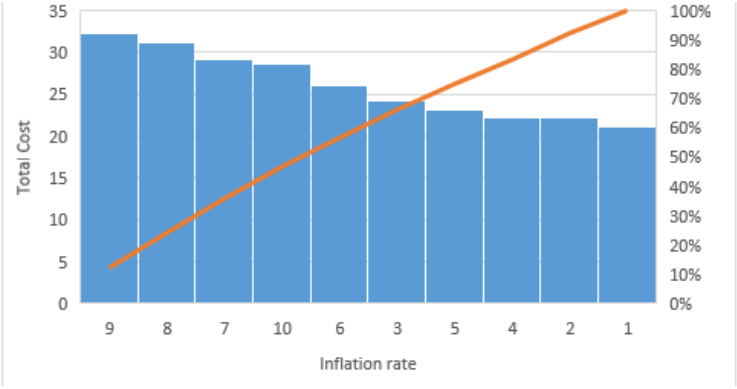


Figure 2: *Variation between total cost and inflation rate.*

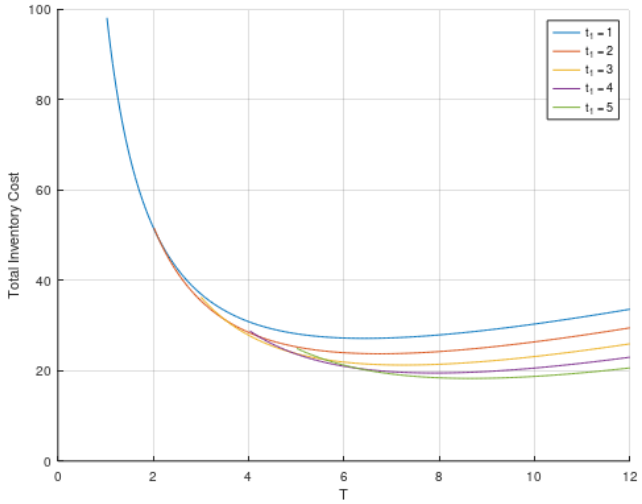


Figure 3: *Cost vs. T for different t_1 values.*

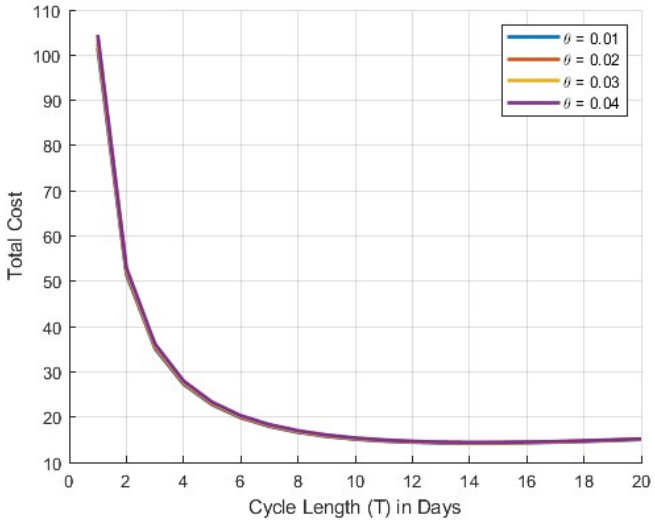


Figure 4: *Cost Minimization vs. Cycle Length for Two-Warehouse.*

7. Conclusion

In summary, the dairy industry's two-warehouse inventory model for shortage and inflation spoiled items under the FIFO shipping policy provides a comprehensive framework for optimizing inventory management in the dairy industry. dairy industry. By incorporating theories of inventory management, spoilage, shortages and inflation, the model enables dairy companies to make informed decisions regarding inventory replenishment, shipping and cost optimization. The model recognizes the perishability of dairy products and takes into account their rate of decomposition to minimize spoilage losses. It also addresses potential shortages and aims to balance stock levels with customer demand to avoid stock-outs and lost sales. Additionally, the model includes the FIFO shipping policy, which ensures that products with a shorter remaining shelf life are shipped first to reduce the risk of product wastage.

The model also helps companies adapt to changing economic conditions and make profitable inventory decisions by considering inflation and its impact on various cost elements. By optimizing inventory levels, order quantities, and shipping policies, the model aims to minimize overall inventory costs while maintaining product quality and customer satisfaction. The Dual Warehouse Inventory Model for the Dairy Industry provides dairy companies with a valuable tool to improve their inventory management practices, increase operational efficiency and improve profitability. Through the use of mathematical techniques and optimization algorithms, the model supports data-driven decision making and allows companies to better control their inventory systems.

Overall, the model contributes to the advancement of inventory management in the dairy industry, providing a theoretical basis and practical guidance for effective inventory control, mitigating losses and meeting the demand of customers in a dynamic and competitive business environment.

References

[1] Yadav, A.S., Bansal, K.K., Shivani, Agarwal, S. And Vanaja, R. (2020) FIFO in Green Supply Chain Inventory Model of Electrical Components Industry With Distribution Centres Using Particle Swarm Optimization. Advances in Mathematics: Scientific Journal. 9 (7), 5115“512 0.

[2] Yadav, A.S., Kumar, A., Agarwal, P., Kumar, T. And Vanaja, R. (2020) LIFO in Green Supply Chain Inventory Model of Auto-Components Industry with Warehouses Using Differential Evolution. Advances in Mathematics: Scientific Journal, 9 no.7, 5121“5126.

[3] Yadav, A.S., Abid, M., Bansal, S., Tyagi, S.L. And Kumar, T. (2020) FIFO LIFO in Green Supply Chain Inventory Model of Hazardous Substance Components Industry with Storage Using Simulated Annealing. Advances in Mathematics: Scientific Journal, 9 no.7, 5127“5132.

[4] Yadav, A.S., Tandon, A. and Selva, N.S. (2020) National Blood Bank Centre Supply Chain Management For Blockchain Application Using Genetic Algorithm. International Journal of Advanced Science and Technology Vol. 29, No. 8s, 1318-1324.

[5] Yadav, A.S., Selva, N.S. and Tandon, A. (2020) Medicine Manufacturing Industries supply chain management for Blockchain application using artificial neural networks, International Journal of Advanced Science and Technology Vol. 29, No. 8s, 1294-1301.

[6] Yadav, A.S., Ahlawat, N., Agarwal, S., Pandey, T. and Swami, A. (2020) Red Wine Industry of Supply Chain Management for Distribution Center Using Neural Networks, Test Engraining & Management, Volume 83 Issue: March “ April, 11215 “ 11222.

[7] Yadav, A.S., Pandey, T., Ahlawat, N., Agarwal, S. and Swami, A. (2020) Rose Wine industry of Supply Chain Management for Storage using Genetic Algorithm. Test Engraining & Management, Volume 83 Issue: March “ April, 11223 “ 11230.

[8] Yadav, A.S., Ahlawat, N., Sharma, N., Swami, A. And Navyata (2020) Healthcare Systems of Inventory Control For Blood Bank Storage With Reliability Applications Using Genetic Algorithm. Advances in Mathematics: Scientific Journal 9 no.7, 5133“5142.

[9] Yadav, A.S., Dubey, R., Pandey, G., Ahlawat, N. and Swami, A. (2020) Distillery Industry Inventory Control for Storage with Wastewater Treatment Logistics Using Particle Swarm Optimization Test Engraining & Management Volume 83 Issue: May " June, 15362-15370.

[10] Yadav, A.S., Ahlawat, N., Dubey, R., Pandey, G. and Swami, A. (2020) Pulp and paper industry inventory control for Storage with wastewater treatment and Inorganic composition using genetic algorithm (ELD Problem). Test Engraining & Management, Volume 83 Issue: May " June, 15508-15517.

[11] Yadav, A.S., Pandey, G., Ahlawat, N., Dubey, R. and Swami, A. (2020) Wine Industry Inventory Control for Storage with Wastewater Treatment and Pollution Load Using Ant Colony Optimization Algorithm, Test Engraining & Management, Volume 83 Issue: May " June, 15528-15535.

[12] Yadav, A.S., Navyata, Sharma, N., Ahlawat, N. and Swami, A. (2020) Reliability Consideration costing method for LIFO Inventory model with chemical industry warehouse. International Journal of Advanced Trends in Computer Science and Engineering, Volume 9 No 1, 403-408.

[13] Yadav, A.S., Bansal, K.K., Kumar, J. and Kumar, S. (2019) Supply Chain Inventory Model For Deteriorating Item With Warehouse & Distribution Centres Under Inflation. International Journal of Engineering and Advanced Technology, Volume-8, Issue-2S2, 7-13.

[14] Yadav, A.S., Kumar, J., Malik, M. and Pandey, T. (2019) Supply Chain of Chemical Industry For Warehouse With Distribution Centres Using Artificial Bee Colony Algorithm. International Journal of Engineering and Advanced Technology, Volume-8, Issue-2S2, 14-19.

[15] Yadav, A.S., Navyata, Ahlawat, N. and Pandey, T. (2019) Soft computing techniques based Hazardous Substance Storage Inventory Model for decaying Items and Inflation using Genetic Algorithm. International Journal of Advance Research and Innovative Ideas in Education, Volume 5 Issue 9, 1102-1112.

[16] Yadav, A.S., Navyata, Ahlawat, N. and Pandey, T. (2019) Hazardous Substance Storage Inventory Model for decaying Items using Differential Evolution. International Journal of Advance Research and Innovative Ideas in Education, Volume 5 Issue 9, 1113-1122.

[17] Yadav, A.S., Navyata, Ahlawat, N. and Pandey, T. (2019) Probabilistic inventory model based Hazardous Substance Storage for decaying Items and Inflation using Particle Swarm Optimization. International Journal of Advance Research and Innovative Ideas in Education, Volume 5 Issue 9, 1123-1133.

[18] Yadav, A.S., Navyata, Ahlawat, N. and Pandey, T. (2019) Reliability Consideration based Hazardous Substance Storage Inventory Model for decaying Items using Simulated Annealing. International Journal of Advance Research and Innovative Ideas in Education, Volume 5 Issue 9, 1134-1143.

[19] Yadav, A.S., Swami, A. and Kher, G. (2019) Blood bank supply chain inventory model for blood collection sites and hospital using genetic algorithm. Selforganizology, Volume 6 No.(3-4), 13-23.

[20] Yadav, A.S., Swami, A. and Ahlawat, N. (2018) A Green supply chain management of Auto industry for inventory model with distribution centers using Particle Swarm Optimization. Selforganizology, Volume 5 No. (3-4)

[21] Yadav, A.S., Ahlawat, N., and Sharma, S. (2018) Hybrid Techniques of Genetic Algorithm for inventory of Auto industry model for deteriorating items with two warehouses. International Journal of Trend in Scientific Research and Development, Volume 2 Issue 5, 58-65.

[22] Yadav, A.S., Swami, A. and Gupta, C.B. (2018) A Supply Chain Management of Pharmaceutical For Deteriorating Items Using Genetic Algorithm. International Journal for Science and Advance Research In Technology, Volume 4 Issue 4, 2147-2153.

[23] Yadav, A.S., Maheshwari, P., Swami, A., and Pandey, G. (2018) A supply chain management of chemical industry for deteriorating items with warehouse using genetic algorithm. Selforganizology, Volume 5 No.1-2, 41-51.

[24] Yadav, A.S., Garg, A., Gupta, K. and Swami, A. (2017) Multi-objective Genetic algorithm optimization in Inventory model for deteriorating items with shortages using Supply Chain management. IPASJ International journal of computer science, Volume 5, Issue 6, 15-35.

[25] Yadav, A.S., Garg, A., Swami, A. and Kher, G. (2017) A Supply Chain management in Inventory Optimization for deteriorating items with Genetic algorithm. International Journal of Emerging Trends & Technology in Computer Science, Volume 6, Issue 3, 335-352.

[26] Yadav, A.S., Maheshwari, P., Garg, A., Swami, A. and Kher, G. (2017) Modeling & Analysis of Supply Chain management in Inventory Optimization for deteriorating items with Genetic algorithm and Particle Swarm optimization. International Journal of Application or Innovation in Engineering & Management, Volume 6, Issue 6, 86-107.

[27] Yadav, A.S., Garg, A., Gupta, K. and Swami, A. (2017) Multi-objective Particle Swarm optimization and Genetic algorithm in Inventory model for deteriorating items with shortages using Supply Chain management. International Journal of Application or Innovation in Engineering & Management, Volume 6, Issue 6, 130-144.

[28] Yadav, A.S., Swami, A. and Kher, G. (2017) Multi-Objective Genetic Algorithm Involving Green Supply Chain Management International Journal for Science and Advance Research In Technology, Volume 3 Issue 9, 132-138.

[29] Yadav, A.S., Swami, A., Kher, G. (2017) Multi-Objective Particle Swarm Optimization Algorithm Involving Green Supply Chain Inventory Management. International Journal for Science and Advance Research In Technology, Volume 3 Issue, 240-246.

[30] Yadav, A.S., Swami, A. and Pandey, G. (2017) Green Supply Chain Management for Warehouse with Particle Swarm Optimization Algorithm. International Journal for Science and Advance Research in Technology, Volume 3 Issue 10, 769-775.

[31] Yadav, A.S., Swami, A., Kher, G. and Garg, A. (2017) Analysis of seven stages supply chain management in electronic component inventory optimization for warehouse with economic load dispatch using genetic algorithm. Selforganizology, 4 No.2, 18-29.

[32] Yadav, A.S., Maheshwari, P., Swami, A. and Garg, A. (2017) Analysis of Six Stages Supply Chain management in Inventory Optimization for warehouse with Artificial bee colony algorithm using Genetic Algorithm. Selforganizology, Volume 4 No.3, 41-51.

[33] Yadav, A.S., Swami, A., Gupta, C.B. and Garg, A. (2017) Analysis of Electronic component inventory Optimization in Six Stages Supply Chain management for warehouse with ABC using genetic algorithm and PSO. Selforganizology, Volume 4 No.4, 52-64.

[34] Yadav, A.S., Maheshwari, P. and Swami, A. (2016) Analysis of Genetic Algorithm and Particle Swarm Optimization for warehouse with Supply Chain management in Inventory control. International Journal of Computer Applications, Volume 145 "No.5, 10-17.

[35] Yadav, A.S., Swami, A. and Kumar, S. (2018) Inventory of Electronic components model for deteriorating items with warehousing using Genetic Algorithm. International Journal of Pure and Applied Mathematics, Volume 119 No. 16, 169-177.

[36] Yadav, A.S., Johri, M., Singh, J. and Uppal, S. (2018) Analysis of Green Supply Chain Inventory Management for Warehouse With Environmental Collaboration and Sustainability Performance Using Genetic Algorithm. International Journal of Pure and Applied Mathematics, Volume 118 No. 20, 155-161.

[37] Yadav, A.S., Ahlawat, N., Swami, A. and Kher, G. (2019) Auto Industry inventory model for deteriorating items with two warehouse and Transportation Cost using Simulated Annealing Algorithms. International Journal of Advance Research and Innovative Ideas in Education, Volume 5,Issue 1, 24-33.

[38] Yadav, A.S., Ahlawat, N., Swami, A. and Kher, G. (2019) A Particle Swarm Optimization based a two-storage model for deteriorating items with Transportation Cost and Advertising Cost: The Auto Industry. International Journal of Advance Research and Innovative Ideas in Education, Volume 5, Issue 1, 34-44.

[39] Yadav, A.S., Ahlawat, N., and Sharma, S. (2018) A Particle Swarm Optimization for inventory of Auto industry model for two warehouses with deteriorating items. International Journal of Trend in Scientific Research and Development, Volume 2 Issue 5, 66-74.

[40] Yadav, A.S., Swami, A. and Kher, G. (2018) Particle Swarm optimization of inventory model with two-warehouses. Asian Journal of Mathematics and Computer Research, Volume 23 No.1, 17-26.

[41] Yadav, A.S., Maheshwari, P.,, Swami, A. and Kher, G. (2017) Soft Computing Optimization of Two Warehouse Inventory Model With Genetic Algorithm. Asian Journal of Mathematics and Computer Research, Volume 19 No.4, 214-223.

[42] Yadav, A.S., Swami, A., Kumar, S. and Singh, R.K. (2016) Two-Warehouse Inventory Model for Deteriorating Items with Variable Holding Cost, Time-Dependent Demand and Shortages. IOSR Journal of Mathematics, Volume 12, Issue 2 Ver. IV, 47-53.

[43] Yadav, A.S., Sharam, S. and Swami, A. (2016) Two Warehouse Inventory Model with Ramp Type Demand and Partial Backordering for Weibull Distribution Deterioration. International Journal of Computer Applications, Volume 140 -No.4, 15-25.

[44] Yadav, A.S., Swami, A. and Singh, R.K. (2016) A two-storage model for deteriorating items with holding cost under inflation and Genetic Algorithms. International Journal of Advanced Engineering, Management and Science, Volume -2, Issue-4, 251-258.

[45] Yadav, A.S., Swami, A., Kher, G. and Kumar, S. (2017) Supply Chain Inventory Model for Two Warehouses with Soft Computing Optimization. International Journal of Applied Business and Economic Research, Volume 15 No 4, 41-55.

[46] Yadav, A.S., Rajesh Mishra, Kumar, S. and Yadav, S. (2016) Multi Objective Optimization for Electronic Component Inventory Model & Deteriorating Items with Two-warehouse using Genetic Algorithm. International Journal of Control Theory and applications, Volume 9 No.2, 881-892.

[47] Yadav, A.S., Gupta, K., Garg, A. and Swami, A. (2015) A Soft computing Optimization based Two Ware-House Inventory Model for Deteriorating Items with shortages using Genetic Algorithm. International Journal of Computer Applications, Volume 126 - No.13, 7-16.

[48] Yadav, A.S., Gupta, K., Garg, A. and Swami, A. (2015) A Two Warehouse Inventory Model for Deteriorating Items with Shortages under Genetic Algorithm and PSO. International Journal of Emerging Trends & Technology in Computer Science, Volume 4, Issue 5(2), 40-48.

[49] Yadav, A.S. Swami, A., and Kumar, S. (2018) A supply chain Inventory Model for decaying Items with Two Ware-House and Partial ordering under Inflation. International Journal of Pure and Applied Mathematics, Volume 120 No 6, 3053-3088.

[50] Yadav, A.S. Swami, A. and Kumar, S. (2018) An Inventory Model for Deteriorating Items with Two warehouses and variable holding Cost. International Journal of Pure and Applied Mathematics, Volume 120 No 6, 3069-3086.

[51] Yadav, A.S., Taygi, B., Sharma, S. and Swami, A. (2017) Effect of inflation on a two-warehouse inventory model for deteriorating items with time varying demand and shortages. International Journal Procurement Management, Volume 10, No. 6, 761-775.

[52] Yadav, A.S., R. P. Mahapatra, Sharma, S. and Swami, A. (2017) An Inflationary Inventory Model for Deteriorating items under Two Storage Systems. International Journal of Economic Research, Volume 14 No.9, 29-40.

[53] Yadav, A.S., Sharma, S. and Swami, A. (2017) A Fuzzy Based Two-Warehouse Inventory Model For Non instantaneous Deteriorating Items With Conditionally Permissible Delay In Payment. International Journal of Control Theory And Applications, Volume 10 No.11, 107-123.

[54] Yadav, A.S. and Swami, A. (2018) Integrated Supply Chain Model for Deteriorating Items With Linear Stock Dependent Demand Under Imprecise And Inflationary Environment. International Journal Procurement Management, Volume 11 No 6, 684-704.

[55] Yadav, A.S. and Swami, A. (2018) A partial backlogging production-inventory lot-size model with time-varying holding cost and weibull deterioration. International Journal Procurement Management, Volume 11, No. 5, 639-649.

[56] Yadav, A.S. and Swami, A. (2013) A Partial Backlogging Two-Warehouse Inventory Models For Decaying Items With Inflation. International Organization of Scientific Research Journal of Mathematics, Issue 6, 69-78.

[57] Yadav, A.S. and Swami, A. (2019) An inventory model for non-instantaneous deteriorating items with variable holding cost under two-storage. International Journal Procurement Management, Volume 12 No 6, 690-710.

[58] Yadav, A.S. and Swami, A. (2019) A Volume Flexible Two-Warehouse Model with Fluctuating Demand and Holding Cost under Inflation. International Journal Procurement Management, Volume 12 No 4, 441-456.

[59] Yadav, A.S. and Swami, A. (2014) Two-Warehouse Inventory Model for Deteriorating Items with Ramp-Type Demand Rate and Inflation. American Journal of Mathematics and Sciences Volume 3 No-1, 137-144.

[60] Yadav, A.S. and Swami, A. (2013) Effect of Permissible Delay on Two-Warehouse Inventory Model for Deteriorating items with Shortages. International Journal of Application or Innovation in Engineering & Management, Volume 2, Issue 3, 65-71.

[61] Yadav, A.S. and Swami, A. (2013) A Two-Warehouse Inventory Model for Decaying Items with Exponential Demand and Variable Holding Cost. International of Inventive Engineering and Sciences, Volume-1, Issue-5, 18-22.

[62] Yadav, A.S. and Kumar, S. (2017) Electronic Components Supply Chain Management for Warehouse with Environmental Collaboration & Neural Networks. International Journal of Pure and Applied Mathematics, Volume 117 No. 17, 169-177.

[63] Yadav, A.S. (2017) Analysis of Seven Stages Supply Chain Management in Electronic Component Inventory Optimization for Warehouse with Economic Load Dispatch Using GA and PSO. Asian Journal Of Mathematics And Computer Research, volume 16 No.4, 208-219.

[64] Yadav, A.S. (2017) Analysis Of Supply Chain Management In Inventory Optimization For Warehouse With Logistics Using Genetic Algorithm International Journal of Control Theory And Applications, Volume 10 No.10, 1-12 .

[65] Yadav, A.S. (2017) Modeling and Analysis of Supply Chain Inventory Model with two-warehouses and Economic Load Dispatch Problem Using Genetic Algorithm. International Journal of Engineering and Technology, Volume 9 No 1, 33-44.

[66] Swami, A., Singh, S.R., Pareek, S. and Yadav, A.S. (2015) Inventory policies for deteriorating item with stock dependent demand and variable holding costs under permissible delay in payment. International Journal of Application or Innovation in Engineering & Management, Volume 4, Issue 2, 89-99.

[67] Swami, A., Pareek, S., Singh S.R. and Yadav, A.S. (2015) Inventory Model for Decaying Items with Multivariate Demand and Variable Holding cost under the facility of Trade-Credit. International Journal of Computer Application, 18-28.

[68] Swami, A., Pareek, S., Singh, S.R. and Yadav, A.S. (2015) An Inventory Model With Price Sensitive Demand, Variable Holding Cost And Trade-Credit Under Inflation. International Journal of Current Research, Volume 7, Issue, 06, 17312-17321.

[69] Gupta, K., Yadav, A.S., Garg, A. and Swami, A. (2015) A Binary Multi-Objective Genetic Algorithm & PSO involving Supply Chain Inventory Optimization with Shortages, inflation. International Journal of Application or Innovation in Engineering & Management, Volume 4, Issue 8, 37-44.

[70] Gupta, K., Yadav, A.S., Garg, A., (2015) Fuzzy-Genetic Algorithm based inventory model for shortages and inflation under hybrid & PSO. IOSR Journal of Computer Engineering, Volume 17, Issue 5, Ver. I , 61-67.

[71] Singh, R.K., Yadav, A.S. and Swami, A. (2016) A Two-Warehouse Model for Deteriorating Items with Holding Cost under Particle Swarm Optimization. International Journal of Advanced Engineering, Management and Science, Volume -2, Issue-6, 858-864.

[72] Singh, R.K., Yadav, A.S. and Swami, A. (2016) A Two-Warehouse Model for Deteriorating Items with Holding Cost under Inflation and Soft Computing Techniques. International Journal of Advanced Engineering, Management and Science, Volume -2, Issue-6, 869-876.

[73] Kumar, S., Yadav, A.S., Ahlawat, N. and Swami, A. (2019) Supply Chain Management of Alcoholic Beverage Industry Warehouse with Permissible Delay in Payments using Particle Swarm Optimization. International Journal for Research in Applied Science and Engineering Technology, Volume 7 Issue VIII, 504-509.

[74] Kumar, S., Yadav, A.S., Ahlawat, N. and Swami, A. (2019) Green Supply Chain Inventory System of Cement Industry for Warehouse with Inflation using Particle Swarm Optimization.

International Journal for Research in Applied Science and Engineering Technology, Volume 7 Issue VIII, 498-503.

[75] Kumar, S., Yadav, A.S., Ahlawat, N. and Swami, A. (2019) Electronic Components Inventory Model for Deterioration Items with Distribution Centre using Genetic Algorithm. International Journal for Research in Applied Science and Engineering Technology, Volume 7 Issue VIII, 433-443.

[76] Chauhan, N. and Yadav, A.S. (2020) An Inventory Model for Deteriorating Items with Two-Warehouse & Stock Dependent Demand using Genetic algorithm. International Journal of Advanced Science and Technology, Vol. 29, No. 5s, 1152-1162.

[77] Chauhan, N. and Yadav, A.S. (2020) Inventory System of Automobile for Stock Dependent Demand & Inflation with Two-Distribution Center Using Genetic Algorithm. Test Engraining & Management, Volume 83, Issue: March - April, 6583 - 6591.

[78] Pandey, T., Yadav, A.S. and Medhavi Malik (2019) An Analysis Marble Industry Inventory Optimization Based on Genetic Algorithms and Particle swarm optimization. International Journal of Recent Technology and Engineering Volume-7, Issue-6S4, 369-373.

[79] Ahlawat, N., Agarwal, S., Pandey, T., Yadav, A.S., Swami, A. (2020) White Wine Industry of Supply Chain Management for Warehouse using Neural Networks Test Engraining & Management, Volume 83, Issue: March - April, 11259 - 11266.

[80] Singh, S. Yadav, A.S. and Swami, A. (2016) An Optimal Ordering Policy For Non-Instantaneous Deteriorating Items With Conditionally Permissible Delay In Payment Under Two Storage Management International Journal of Computer Applications, Volume 147 -No.1, 16-25.

[81] Yadav, A.S., Kumar, A., Yadav, K.K. et al. Optimization of an inventory model for deteriorating items with both selling price and time-sensitive demand and carbon emission under green technology investment. Int J Interact Des Manuf (2023). https://doi.org/10.1007/s12008-023-01689-8

[82] Yadav, K.K., Yadav, A.S. & Bansal, S. Interval number approach for two-warehouse inventory management of deteriorating items with preservation technology investment using analytical optimization methods. Int J Interact Des Manuf (2024). https://doi.org/10.1007/s12008-023-01672-3

[83] Krishan Kumar Yadav , Ajay Singh Yadav, and Shikha Bansal. "Optimization of an inventory model for deteriorating items assuming deterioration during carrying with two-warehouse facility" Reliability: Theory & Applications, vol. 19, no. 3 (79), 2024, pp. 442-459. doi:10.24412/1932-2321-2024-379-442-459

[84] Sinha, Amit Kumar, and Ankush Anand. "Optimizing supply chain network for perishable products using improved bacteria foraging algorithm." Applied Soft Computing 86 (2020): 105921.

[85] Hezer, Seda, and Yakup Kara. "Solving vehicle routing problem with simultaneous delivery and pick-up using an algorithm based on bacterial foraging optimization." (2013).

[86] Negi, Ashish, and Ompal Singh. "An inventory system with time-dependent linear demand for deteriorating items under uncertainty with a completely backlogged." Advances in Mathematical and Computational Sciences: Proceedings of The ICRTMPCS International Conference 2023. Walter de Gruyter GmbH & Co KG, 2024.

ANALYSIS OF $M, MAP/PH/2$ NON- PREEMPTIVE PRIORITY QUEUEING INVENTORY SYSTEM WITH BREAKDOWN, REPAIR AND (s, S) POLICY

G. AYYAPPAN [1], M. THILAKAVATHY [2*]

•

[(1,2)] Department of Mathematics, Puducherry Technological University, Puducherry, India
[1] ayyappan@ptuniv.edu.in , [2*]Corresponding author: mthilakavathy89@gmail.com

Abstract

We analyze a non-preemptive priority queueing model in this research that has two heterogeneous servers, each of which has its own queue. Queue 1 possesses a low priority status with infinite capacity and queue 2 possesses a high priority status with finite capacity. We made the assumption that arrival follows M, MAP and service time follows Phase-type distribution. Server 1 is always available in the system; Server 2 is an unreliable server. With a (s, S) policy, the inventory is filled up and an exponential distribution is scheduled for the replenishment time. Using the matrix analytical approach, a stationary probability vector was assessed, and a stability criterion was created for our system. Performance metrics are also studied using this technique. Both two and three-dimensional displays are used to show the numerical examples.

Keywords: Marked Markovian arrival process, phase distribution, multiple vacation, non-preemptive priority, breakdown, repair, (s, S) policy.

1. Introduction

The Markovian Arrival Process (MAP) is highly suited for matrix analytical solutions and has one of the most important modeling tools in its basic structure. The formulation of the MAP as a flexible Markovian point process, a specific instance of a Batch Markovian Arrival Process $(BMAP)$, was initially presented by Neuts [16]. In general, a queueing system may have an input process with many arrival kinds. We suggest marking all the intriguing arrivals and looking at the lines that the marked arrivals experience in order to study such queueing systems. To excite the marked point process $(MMAP)$, we use the Markov arrival process with marked transitions. To obtain a comprehensive and thorough analysis of $MMAP$, readers are directed to Ayyappan and Archana [2], Kim et al. [7], Raj and Jain [17].

The attached inventory has an impact on the service, which makes the queueing-inventory system distinct from the standard queueing system. Service will be disrupted if inventory is not available. Furthermore, the inventory is used at the serving rate rather than the customer arrival rate even while there are customers waiting for service, which is another way that it differs from standard inventory management.

Jeganathan et al [12], examined a Markovian (s, Q) inventory queueing system with finite buffer queueing model with two heterogeneous servers and mixed priority service. Performance analysis of queueing inventory systems and networked queueing systems in stochastic modeling. With dual service stations, it offers two different kinds of service facilities, Jeganathan et al [13], handled commodity sales and non-commodity services with a single server and a multi-server, respectively. The queueing inventory system was researched by Rasmi et al. [18], using items

with PH-distributed common life times and clients of different classes arriving based on $MMAP$. Customers are given priority access to inventories based on their class number and the items' freshness. Positive lead time and the (s, S) policy are used to control the inventory. A queueing inventory system has been extensively examined by Indhumathi and Karthikeyan [11] because of its many uses in the contemporary world and capacity to improve accuracy in this area. Adequate knowledge regarding queueing inventory systems is also provided.

Priority services in queuing systems discriminate against units based on their class; this kind of discrimination happens in everyday setting in engineering systems, particularly in communication networks channel access protocols and computer operating systems. Preemptive and non-preemptive priority queues are the two varieties. In preemptive priority, the arrival of priority units interrupts the operation of an ordinary unit. However, under non-preemptive priority, even if the priority unit enters the system, the service of an ordinary unit continues uninterrupted. According to Krishnamoorthy et al [14], a priority-generated client can only wait once, and a priority-generated customer must exit the system for emergency assistance elsewhere. The authors of the study, Haghighi [1] examined a new model of a conveyor-like priority queueing system. In other words, priority is intended to reduce system idleness. They also examined a general parallel finite buffer multi-server priority queueing system with reneging and balking, as well as a two-station scenario. Ayyappan and Meena [3], studied a preemptive priority queueing model for single vacation, repair, and impatient consumers. They found that high priority customers lose priority and move to low priority queues for feedback.

Halfin and Segal [9], developed a queueing model for a system that serves two types of clients. Principal clients are randomly assigned to servers with negative exponential service, while secondary customers are served by servers not occupied by primary clients. Servers join a queue if all of them are busy, with primary customers always getting service first. Srinivas [19], assumed a single server non-preemptive priority queueing approach. Since there are very few servers that are completely dependable, many authors have already examined queuing models with unreliable servers. Research on the aforementioned topic is known as queuing systems with server failures. The unreliable server queueing model was introduced by White and Lee [10]. Every consumer using the system makes this choice independently of the others, as was examined by Dudin et al. [6].

2. Mathematical Model

Examine a non-preemptive priority queueing model with two different arrival kinds for two heterogeneous servers. They are both low priority (LPC) and high priority (HPC) clients and the Marked Markovian Arrival Process $(MMAP)$ is used to track their arrival. For no arrival in the system, the square matrix D_0 is used; for an LPC arrival, the square matrix D_1 is used; and for an HPC arrival, the square matrix D_2 is used. The LPC has an infinite capacity, while the HPC is limited to a finite capacity of size N. The normal arrival rate is $\lambda_i = \pi D_i e_m$, i=1, 2 for HPC and LPC, respectively.

Both servers collectively adhere to a shared service rate characterized by a PH-distribution (α, W) of order m. The vector W^0 is explicitly defined as $W^0 = -We$. Server 2 is susceptible to breakdowns, with an exponential distribution characterized by the parameter ψ. To ensure continuity of service during a server 2 breakdown, server 1 temporarily takes over the treatment of the current customer from queue 2 who was being served by server 2, following a non-preemptive priority approach. The remaining customers in queue 2 remain in the queue, waiting until server 2 becomes available again. As fast as a breakdown is detected, server 2 enters a repair process immediately. This repair process is also subject to an exponential distribution with a parameter denoted as τ. Once the repair is successfully completed, server 2 resumes its regular work, ready to serve the incoming customers once again.

In cases, when there are either no HPC in the system or atmost one inventory in the system and both exists, server 2 takes multiple vacation and the occurrence of vacation is denoted as η. But, when there are either no customers in the system or atmost one inventory in the system and

both exists, server 1 remains idle. When both servers are busy implies there exists atleast two inventory in the system. The ordering policy of the inventory is (s, S), where S is the ordering quantity and s is the reorder point. It is assumed that the order's lead time follows an exponential distribution with a rate of β. The schematic picture of this model is provided in Figure 1.

$\otimes$ - Kronecker two matrices of different sizes are multiplied to create a block matrix. $\oplus$ is the Kronecker result of two matrices of various sizes, resulting in the block matrix. e denotes an appropriate order column vector with each of its entries is one. O - It indicates zero matrices in the appropriate sequence.

3. The Generator Matrix

Let $I(t) \in \{0,1,2,\ldots,S\}$, $Y(t) \in \{0,1,2,3,4,5\}$, $N_1(t) \in \{0,1,2,\ldots,\infty\}$ and $N_2(t) \in \{0,1,2,\ldots,N\}$ suggest, respectively, the inventory level, server status, the number of LPC in the queue and the number of HPC queue. The system's server status can be described as follows:

$$Y(T) = \begin{cases} 0, & \text{if the server 1 is idle and server 2 is on vacation,} \\ 1, & \text{if the server 1 is idle and server 2 is busy with HPC,} \\ 2, & \text{if the server 1 is idle and server 2 is on repair,} \\ 3, & \text{if the server 1 is busy and server 2 is on vacation,} \\ 4, & \text{if the server 1 is busy with LPC and server 2 is busy with HPC,} \\ 5, & \text{if the server 1 is busy and server 2 is on repair.} \end{cases}$$

It is obvious that $\{N_1(t)$, $N_2(t)$, Y(t), I(t), S(t), L(t): $t \geq 0\}$is a CTMC with the State Space.

$$\omega = \ell(0) \overset{\infty}{\underset{i=1}{\cup}} \ell(i),$$

Figure 1: *Schematic representation*

$$\begin{aligned} l(0) = &\{(0,j,0,k,l_1) : 0 \leq j \leq N, 0 \leq k \leq S, 1 \leq l_1 \leq n\} \\ &\cup \{(0,j,1,k,l_0,l_1) : 1 \leq j \leq N, 1 \leq k \leq S, 1 \leq l_0 \leq m, 1 \leq l_1 \leq n\} \\ &\cup \{(0,j,2,k,l_1) : 0 \leq j \leq N, 0 \leq k \leq S, 1 \leq l_1 \leq n\}, \end{aligned}$$

and for $i \geq 1$,

$$\begin{aligned} l(i) = &\{(0,j,0,k,l_1) : 0 \leq j \leq N, k = 0, 1 \leq l_1 \leq n,\} \\ &\cup \{(0,j,1,k,l_0,l_1) : 1 \leq j \leq N, k = 1, 1 \leq l_0 \leq m, 1 \leq l_1 \leq n,\} \\ &\cup \{(0,j,2,k,l_1) : 0 \leq j \leq N, k = 0, 1 \leq l_1 \leq n\} \\ &\cup \{(0,j,3,k,l_0,l_1) : 1 \leq j \leq N, 1 \leq k \leq S, 1 \leq l_0 \leq m, 1 \leq l_1 \leq n,\} \\ &\cup \{(0,j,4,k,l_0,l_1) : 1 \leq j \leq N, 2 \leq k \leq S, 1 \leq l_0 \leq m, 1 \leq l_1 \leq n\} \\ &\cup \{(0,j,5,k,l_0,l_1) : 1 \leq j \leq N, 1 \leq k \leq S, 1 \leq l_0 \leq m, 1 \leq l_1 \leq n\}. \end{aligned}$$

4. The infinitesimal generation matrix of the QBD procedure

Our methodology for generating QBD(Quasi Birth-Death) processes is explained in this section using the following notations and presumptions.

$$Q = \begin{bmatrix} B_{00} & B_{01} & & & & & \\ B_{10} & A_1 & A_0 & & & & \\ & A_2 & A_1 & A_0 & & & \\ & & A_2 & A_1 & A_0 & & \\ & & & A_2 & A_1 & A_0 & \\ & & & & \ddots & \ddots & \ddots \end{bmatrix}.$$

The entries in the block matrices of Q are defined as follows:
$B_{00^{(i_2,j_2,k_2,l_2)}_{(i_1,j_1,k_1,l_1)}}$ as transition sub matrices that contain transitions of the form $(0,i_1,j_1,k_1,l_1) \to (0,i_2,j_2,k_2,l_2)$ and $B_{01^{(i_2,j_2,k_2,p_2,l_2)}_{(i_1,j_1,k_1,p_1,l_1)}}$ as transition sub matrices which contain transitions of the form $(0,i_1,j_1,k_1,p_1,l_1) \to (1,i_2,j_2,k_2,p_2,l_2)$. Let (i_1,j_1,k_1,p_1,l_1) denotes the number of LPC, server status, number of items, service phases and arrival phases in the row vector and (i_2,j_2,k_2,p_2,l_2) denotes the number of HPC, server status, number of items, service phases and arrival phases in the column vector.

$$B_{00} = \begin{bmatrix} B_{0011} & B_{0012} & 0 \\ B_{0021} & B_{0022} & B_{0023} \\ B_{0031} & 0 & B_{0033} \end{bmatrix}, \quad B_{01} = \begin{bmatrix} B_{0111} & 0 & 0 & B_{0114} & 0 & 0 \\ 0 & B_{0122} & 0 & 0 & B_{0125} & B_{0126} \\ 0 & 0 & B_{0133} & 0 & 0 & B_{0136} \end{bmatrix},$$

$$B_{0012^{(i_2,j_2,k_2,l_2)}_{(i_1,j_1,k_1,l_1)}} = \begin{cases} I_S \otimes \alpha \otimes \eta I_n, & i_1 = 0, 1 \le i_2 \le N, j_1 = j_2 = 0, \\ & 1 \le k_1, k_2 \le S, 1 \le l_1, l_2 \le n, \\ 0, & \text{otherwise.} \end{cases}$$

$$B_{0021^{(i_2,j_2,k_2,p_2,l_2)}_{(i_1,j_1,k_1,p_1,l_1)}} = \begin{cases} I_S \otimes W^0 \otimes I_n, & i_1 = 0, i_2 = 1, j_1 = 1, j_2 = 0, 1 \le k_1, k_2 \le S, \\ & 1 \le p_1, p_2 \le m, 1 \le l_1, l_2 \le n, \\ W^0 \otimes I_n, & i_1 = 0, 2 \le i_2 \le N, j_1 = 1, j_2 = 0, k_1, k_2 = 1, \\ & 1 \le p_1, p_2 \le m, 1 \le l_1, l_2 \le n, \\ 0, & \text{otherwise.} \end{cases}$$

$$B_{0023^{(i_2,j_2,k_2,p_2,l_2)}_{(i_1,j_1,k_1,p_1,l_1)}} = \begin{cases} I_S \otimes e_m \otimes \psi I_n, & \text{if } i_1 = i_2 = 0,\ j_1 = 1,\ j_2 = 2, \\ 0, & \text{otherwise.} \end{cases}$$

$$B_{0031^{(i_2,j_2,k_2,l_2)}_{(i_1,j_1,k_1,l_1)}} = \begin{cases} I_{S+1} \otimes \tau I_n, & \text{if } i_1 = 0,\ 0 \le i_2 \le N,\ j_1 = 2,\ j_2 = 0, \\ 0, & \text{otherwise.} \end{cases}$$

$$B_{0011}{}^{(i_2,j_2,k_2,l_2)}_{(i_1,j_1,k_1,l_1)} = \begin{cases} I_{s+1} \otimes D_0 - \beta I_n, & \\ e_{s+1} \otimes \beta I_n, D_0, & i_1 = i_2 = 0, j_1 = j_2 = 0, \\ & 1 \le l_1, l_2 \le n, \\ I_{S+1} \otimes I_n \otimes D_2, & i_1 = 1, 1 \le i_2 \le N, j_1 = j_2 = 0, \\ & 0 \le k_1, k_2 \le S, 1 \le l_1, l_2 \le n, \\ D_0 - \beta I_n, & i_1 = 0, i_2 = 1, j_1 = j_2 = 0, k_1, k_2 = 0, \\ & 1 \le l_1, l_2 \le n, \\ I_s \otimes D_0 - (\eta + \beta) I_n, & \\ e_s \otimes \beta I_n, & i_1 = 0, 1 \le i_2 \le N, j_1 = j_2 = 0, \\ & 1 \le k_1, k_2 \le S, 1 \le l_1, l_2 \le n, \\ I_{S-s} \otimes D_0 - \eta I_n, & i_1 = 0, 1 \le i_2 \le N, j_1 = j_2 = 0, \\ & s+1 \le k_1, k_2 \le S, 1 \le l_1, l_2 \le n, \\ 0, & \text{otherwise.} \end{cases}$$

$$B_{0022}{}^{(i_2,j_2,k_2,p_2,l_2)}_{(i_1,j_1,k_1,p_1,l_1)} = \begin{cases} I_{s+1} \otimes W \oplus D_0 - (\psi + \beta) I_{mn}, e_{s+1} \otimes \beta I_{mn}, & \\ I_{S-s} \otimes W \oplus D_0 - \psi I_{mn}, & i_1 = 0, 1 \le i_2 \le N, j_1 = j_2 = 1, \\ \quad 1 \le k_1, k_2 \le S, 1 \le p_1, p_2 \le m, 1 \le l_1, l_2 \le n, & \\ I_S \otimes I_m \otimes D_2, & i_1 = 0, 1 \le i_2 \le N, j_1 = 1, j_2 = 1, \\ \quad 1 \le k_1, k_2 \le S, 1 \le p_1, p_2 \le m, 1 \le l_1, l_2 \le n, & \\ 0, & \text{otherwise.} \end{cases}$$

$$B_{0033}{}^{(i_2,j_2,k_2,l_2)}_{(i_1,j_1,k_1,l_1)} = \begin{cases} I_{s+1} \otimes D_0 - (\tau + \beta) I_n, & \\ e_{s+1} \otimes \beta I_n, & \\ I_{S-s} \otimes D_0 - \tau I_n, & i_1 = 0, 0 \le i_2 \le N, j_1 = j_2 = 2, \\ & 0 \le k_1, k_2 \le S, 1 \le l_1, l_2 \le n, \\ I_{S+1} \otimes D_2, & i_1 = 0, i_2 = 1, j_1 = j_2 = 2, \\ & 1 \le k_1, k_2 \le S, 1 \le l_1, l_2 \le n, \\ 0, & \text{otherwise.} \end{cases}$$

$$B_{0111}{}^{(i_2,j_2,k_2,l_2)}_{(i_1,j_1,k_1,l_1)} = \begin{cases} D_1, & i_1 = i_1 + 1, 0 \le i_2 \le N, j_1 = j_2 = 0, \\ & k_1, k_2 = 0, 1 \le l_1, l_2 \le n, \\ 0, & \text{otherwise.} \end{cases}$$

$$B_{0114}{}^{(i_2,j_2,k_2,l_2)}_{(i_1,j_1,k_1,l_1)} = \begin{cases} I_S \otimes \alpha \otimes D_1, & i_1 = i_1 + 1, 0 \le i_2 \le N, j_1 = 0, j_2 = 3, \\ & 1 \le k_1, k_2 \le S, 1 \le l_1, l_2 \le n, \\ 0, & \text{otherwise.} \end{cases}$$

$$B_{0122}{}^{(i_2,j_2,k_2,p_2,l_2)}_{(i_1,j_1,k_1,p_1,l_1)} = \begin{cases} I_m \otimes D_1, & i_1 = i_1 + 1, 1 \le i_2 \le N, j_1 = j_2 = 1, \\ & k_1, k_2 = 1, 1 \le p_1, p_2 \le m, 1 \le l_1, l_2 \le n, \\ 0, & \text{otherwise.} \end{cases}$$

$$B_{0125}{}^{(i_2,j_2,k_2,p_2,l_2)}_{(i_1,j_1,k_1,p_1,l_1)} = \begin{cases} I_{S-1} \otimes I_m \otimes D_1, & i_1 = i_1 + 1, 1 \le i_2 \le N, j_1 = 1, j_2 = 4, \\ & 2 \le k_1, k_2 \le S, 1 \le p_1, p_2 \le m, 1 \le l_1, l_2 \le n, \\ 0, & \text{otherwise.} \end{cases}$$

$$B_{0126}{}^{(i_2,j_2,k_2,p_2,l_2)}_{(i_1,j_1,k_1,p_1,l_1)} = \begin{cases} I_S \otimes \psi \otimes I_{mn}, & i_1 = i_1 + 1, 1 \le i_2 \le N, j_1 = 1, j_2 = 5, \\ & 2 \le k_1, k_2 \le S, 1 \le p_1, p_2 \le m, 1 \le l_1, l_2 \le n, \\ 0, & \text{otherwise.} \end{cases}$$

$$B_{0133}{}^{(i_2,j_2,k_2,l_2)}_{(i_1,j_1,k_1,l_1)} = \begin{cases} D_1, & i_1 = i_1+1, 0 \le i_2 \le N, j_1 = j_2 = 2, \\ & k_1, k_2 = 0, 1 \le l_1, l_2 \le n, \\ 0, & \text{otherwise.} \end{cases}$$

$$B_{0136}{}^{(i_2,j_2,k_2,p_2,l_2)}_{(i_1,j_1,k_1,p_1,l_1)} = \begin{cases} I_S \otimes \alpha \otimes D_1, & i_1 = i_1+1, 0 \le i_2 \le N, j_1 = 2, j_2 = 5, \\ & 1 \le k_1, k_2 \le S, 1 \le p_1, p_2 \le m, 1 \le l_1, l_2 \le n, \\ 0, & \text{otherwise.} \end{cases}$$

$B_{10}{}^{(i_2,j_2,k_2,p_2,l_2)}_{(i_1,j_1,k_1,p_1l_1)}$'s entries can be defined as transition sub matrices that contain transitions of the form $(1, i_1, j_1, k_1, p_1, l_1) \to (0, i_2, j_2, k_2, p_2, l_2)$ and $A_{1}{}^{(i_2,j_2,k_2,p_2,l_2)}_{(i_1,j_1,k_1,p_1,l_1)}$ serve as transition sub matrices that make up transitions with the following structure: $(h, i_1, j_1, k_1, p_1, l_1) \to (h, i_2, j_2, k_2, p_2, l_2)$, where $h \ge 1$. In the row vector, let $(i_1, j_1, k_1, p_1, l_1)$ represent the number of LPC, server status, number of items, service phases, and arrival phases; in the column vector, let $(i_2, j_2, k_2, p_2, l_2)$ represent the number of HPC, server status, number of items, service phases, and arrival phases.

$$B_{10} = \begin{bmatrix} 0 & 0 & 0 \\ 0 & 0 & 0 \\ 0 & 0 & 0 \\ B_{1041} & 0 & 0 \\ 0 & B_{1052} & 0 \\ 0 & 0 & B_{1063} \end{bmatrix}, \quad A_1 = \begin{bmatrix} A_{111} & 0 & 0 & A_{114} & 0 & 0 \\ A_{121} & A_{122} & 0 & 0 & A_{125} & A_{126} \\ A_{131} & 0 & A_{133} & 0 & 0 & A_{136} \\ 0 & 0 & 0 & A_{144} & A_{145} & 0 \\ 0 & 0 & 0 & A_{154} & A_{155} & A_{156} \\ 0 & 0 & 0 & A_{164} & A_{165} & A_{166} \end{bmatrix},$$

$$B_{1041}{}^{(i_2,j_2,k_2,p_2,l_2)}_{(i_1,j_1,k_1,p_1l_1)} = \begin{cases} I_S \otimes W^0 \otimes I_n, & i_1 = i_1-1, 0 \le i_2 \le N, j_1 = 3, j_2 = 0, 1 \le k_1 \le S, \\ & 0 \le k_2 \le S, 1 \le p_1 \le m, p_2 = 0, 1 \le l_1, l_2 \le n, \\ 0, & \text{otherwise.} \end{cases}$$

$$B_{1052}{}^{(i_2,j_2,k_2,p_2,l_2)}_{(i_1,j_1,k_1,p_1l_1)} = \begin{cases} I_{S-1} \otimes W^0 \otimes \alpha \otimes I_n, & i_1 = i_1-1, 0 \le i_2 \le N, j_1 = 4, j_2 = 1, \\ & 2 \le k_1 \le S, 1 \le k_2 \le S, 1 \le p_1, p_2 \le m, 1 \le l_1, l_2 \le n, \\ 0, & \text{otherwise.} \end{cases}$$

$$B_{1063}{}^{(i_2,j_2,k_2,p_2,l_2)}_{(i_1,j_1,k_1,p_1l_1)} = \begin{cases} I_S \otimes W^0 \otimes I_n, & i_1 = i_1-1, 0 \le i_2 \le N, j_1 = 5, j_2 = 2, 1 \le k_1 \le S, \\ & 0 \le k_2 \le S, 1 \le p_1 \le m, p_2 = 0, 1 \le l_1, l_2 \le n, \\ 0, & \text{otherwise.} \end{cases}$$

$$A_{111}{}^{(i_2,j_2,k_2,l_2)}_{(i_1,j_1,k_1,l_1)} = \begin{cases} D_0 - \beta I_n, & i_1 = 1, 0 \le i_2 \le N, j_1 = j_2 = 0, \\ & k_1, k_2 = 0, l_1, l_2 = n, \\ D_2, & i_1 = 1, 0 \le i_2 \le N, j_1 = j_2 = 0, \\ & k_1, k_2 = 0, 1 \le l_1, l_2 \le n, \\ 0, & \text{otherwise.} \end{cases}$$

$$A_{114}{}^{(i_2,j_2,k_2,l_2)}_{(i_1,j_1,k_1,l_1)} = \begin{cases} \alpha \otimes \beta I_n, & i_1 = 1, 0 \le i_2 \le N, j_1 = j_2 = 0, \\ & k_1, k_2 = 0, 1 \le l_1, l_2 \le n, \\ 0, & \text{otherwise.} \end{cases}$$

$$A_{121}{}^{(i_2,j_2,k_2,p_2,l_2)}_{(i_1,j_1,k_1,p_1,l_1)} = \begin{cases} W_0 \otimes I_n, & i_1 = 1, 0 \le i_2 \le N, j_1 = 1, j_2 = 0, \\ & k_1, k_2 = 1, 1 \le l_1, l_2 \le m, \\ 0, & \text{otherwise.} \end{cases}$$

$$A_{125}{}^{(i_2,j_2,k_2,p_2,l_2)}_{(i_1,j_1,k_1,p_1,l_1)} = \begin{cases} \beta I_{nm}, & i_1 = i_2 = 1, j_1 = 1, j_2 = 4, \\ & k_1, k_2 = 1, 1 \le l_1, l_2 \le n, \\ 0, & otherwise. \end{cases}$$

$$A_{122}{}^{(i_2,j_2,k_2,l_2)}_{(i_1,j_1,k_1,l_1)} = \begin{cases} W \oplus D_0 - (\psi + \beta) I_{nm}, & i_1 = 1, 1 \le i_2 \le N, j_1 = j_2 = 1, \\ & k_1, k_2 = 1, 1 \le l_1, l_2 \le n, \\ I_m \otimes D_2, & i_1 = 1, 1 \le i_2 \le N, j_1 = j_2 = 1, \\ & k_1, k_2 = 1, 1 \le l_1, l_2 \le n, \\ 0, & \text{otherwise.} \end{cases}$$

$$A_{126}{}^{(i_2,j_2,k_2,p_2,l_2)}_{(i_1,j_1,k_1,p_1,l_1)} = \begin{cases} I_m \otimes \psi I_n, & i_1 = i_2 = 1, j_1 = 1, j_2 = 5, \\ & k_1 = k_2 = 1, 1 \le l_1 \le m, 1 \le l_2 \le n, \\ 0, & \text{otherwise.} \end{cases}$$

$$A_{131}{}^{(i_2,j_2,k_2,l_2)}_{(i_1,j_1,k_1,l_1)} = \begin{cases} \tau I_n, & i_1 = 1, 1 \le i_2 \le n, j_1 = 2, j_2 = 0, \\ & k_1, k_2 = 0, 1 \le l_1, l_2 \le n, \\ 0, & \text{otherwise.} \end{cases}$$

$$A_{133}{}^{(i_2,j_2,k_2,l_2)}_{(i_1,j_1,k_1,l_1)} = \begin{cases} D_0 - (\tau + \beta) I_n, & i_1 = 1, 0 \le i_2 \le N, j_1 = j_2 = 2, \\ & k_1, k_2 = 0, 1 \le l_1, l_2 \le n, \\ D_2, & i_1 = 1, 0 \le i_2 \le N, j_1 = j_2 = 2, \\ & k_1, k_2 = 0, 1 \le l_1, l_2 \le n, \\ 0, & \text{otherwise.} \end{cases}$$

$$A_{136}{}^{(i_2,j_2,k_2,p_2,l_2)}_{(i_1,j_1,k_1,p_1,l_1)} = \begin{cases} \alpha \otimes \beta I_n, & i_1 = 1, 0 \le i_2 \le N, j_1 = 2, j_2 = 4, k_1, k_2 = 0, \\ & 1 \le p_1, p_2 \le m, 1 \le l_1, l_2 \le n, \\ 0, & \text{otherwise.} \end{cases}$$

$$A_{145}{}^{(i_2,j_2,k_2,p_2,l_2)}_{(i_1,j_1,k_1,p_1,l_1)} = \begin{cases} I_{S-1} \otimes \eta I_{mn}, & i_1 = 1, 1 \le i_2 \le N, j_1 = j_2 = 3, \\ & 1 \le k_1, k_2 \le S, 1 \le p_1, p_2 \le m, 1 \le l_1, l_2 \le n, \\ 0, & \text{otherwise.} \end{cases}$$

$$A_{154}{}^{(i_2,j_2,k_2,p_2,l_2)}_{(i_1,j_1,k_1,p_1,l_1)} = \begin{cases} I_{S-1} \otimes W^0 \alpha \otimes I_n, & i_1 = 1, 1 \le i_2 \le N, j_1 = 1, j_2 = 0, \\ & 2 \le k_1, k_2 \le S, 1 \le l_1, l_2 \le n, \\ W^0 \alpha \otimes I_n, & i_1 = 1, 2 \le i_2 \le N, j_1 = 4, j_2 = 3, \\ & k_1, k_2 = 2, 1 \le p_1 \le m, p_2 = 0, 1 \le l_1, l_2 \le n, \\ 0, & \text{otherwise.} \end{cases}$$

$$A_{156}{}^{(i_2,j_2,k_2,p_2,l_2)}_{(i_1,j_1,k_1,p_1,l_1)} = \begin{cases} I_{S-1} \otimes \psi I_{mn}, & i_1 = 1, 1 \le i_2 \le N, j_1 = 4, j_2 = 5, \\ & 2 \le k_1, k_2 \le S, 1 \le p_1, p_2 \le m, 1 \le l_1, l_2 \le n, \\ 0, & otherwise. \end{cases}$$

$$A_{164}{}^{(i_2,j_2,k_2,p_2,l_2)}_{(i_1,j_1,k_1,p_1,l_1)} = \begin{cases} I_S \otimes \tau I_{mn}, & i_1 = 1, i_2 = 0, j_1 = 5, j_2 = 3, \\ & 1 \le k_1, k_2 \le S, 1 \le p_1, p_2 \le m, 1 \le l_1, l_2 \le n, \\ \tau I_{mn}, & i_1 = 1, 1 \le i_2 \le N, j_1 = 5, j_2 = 3, \\ & k_1, k_2 = 1, 1 \le p_1, p_2 \le m, 1 \le l_1, l_2 \le n, \\ 0, & \text{otherwise.} \end{cases}$$

$$A_{144}{}^{(i_2,j_2,k_2,p_2,l_2)}_{(i_1,j_1,k_1,p_1l_1)} = \begin{cases} I_s \otimes W \oplus D_0 - \beta I_{mn}, e_s \otimes \beta I_{mn}, \\ I_{S-s} \otimes W \oplus D_0, \quad i_1 = 1, i_2 = 0, j_1 = j_2 = 3, \\ \qquad 1 \le k_1, k_2 \le s, 1 \le l_1, l_2 \le n, 1 \le p_1, p_2 \le m, \\ I_{S-s} \otimes W \oplus D_0, \quad i_1 = 1, i_2 = 0, j_1 = j_2 = 3, \\ \qquad s+1 \le k_1, k_2 \le S, 1 \le p_1, p_2 \le m, 1 \le l_1, l_2 \le n, \\ I_S \otimes D_2 \otimes I_m, \quad i_1 = 1, 0 \le i_2 \le N, j_1 = j_2 = 3, \\ \qquad 1 \le k_1, k_2 \le S, 1 \le p_1, p_2 \le m, 1 \le l_1, l_2 \le n, \\ I_s \otimes W + D_0 - (\eta + \beta) I_{mn}, \\ e_s \otimes \beta I_{mn}, \quad i_1 = 1, 1 \le i_2 \le N, j_1 = j_2 = 3, \\ \qquad 1 \le k_1, k_2 \le S, 1 \le p_1, p_2 \le m, 1 \le l_1, l_2 \le n, \\ I_{S-s} \otimes W + D_0 - \eta I_{mn}, \\ \qquad i_1 = 1, 1 \le i_2 \le N, j_1 = j_2 = 3, \\ \qquad 1 \le k_1, k_2 \le S, 1 \le p_1, p_2 \le m, 1 \le l_1 l_2 \le n, \\ 0, \qquad \text{otherwise.} \end{cases}$$

$$A_{155}{}^{(i_2,j_2,k_2,p_2,l_2)}_{(i_1,j_1,k_1,p_2,l_1)} = \begin{cases} I_{s-1} \otimes W^0 \oplus D_0 - \psi + \beta I_{mn}, e_{s-1} \otimes \beta I_{mn}, \\ I_{((S-1)-(s-1))} \otimes W \oplus D0 - \psi I_{mn}, \quad i_1 = 1, 1 \le i_2 \le N, j_1 = j_2 = 4, \\ \qquad 2 \le k_1, k_2 \le S, 1 \le p_1, p_2 \le m, 1 \le l_1, l_2 \le n, \\ I_{S-1} \otimes I_m \otimes D_2, \quad i_1 = 1, 2 \le i_2 \le N, j_1 = j_2 = 4, \\ \qquad 2 \le k_1, k_2 \le S, 1 \le p_1, p_2 \le m, 1 \le l_1, l_2 \le n, \\ I_{S-2} \otimes W^0 \alpha \otimes I_n, \quad i_1 = 1, 2 \le i_2 \le N, j_1 = j_2 = 4, \\ \qquad 3 \le k_1, k_2 \le S, 1 \le p_1, p_2 \le m, 1 \le l_1, l_2 \le n, \\ 0, \qquad \text{otherwise.} \end{cases}$$

$$A_{165}{}^{(i_2,j_2,k_2,p_2,l_2)}_{(i_1,j_1,k_1,p_1,l_1)} = \begin{cases} I_{S-1} \otimes \tau I_{mn}, \quad i_1 = 1, 1 \le i_2 \le N, j_1 = 5, j_2 = 4, \\ \qquad 1 \le k_1 \le S, 2 \le k_2 \le S, 1 \le p_1, p_2 \le m, 1 \le l_1, l_2 \le n, \\ 0, \qquad \text{otherwise.} \end{cases}$$

$$A_{166}{}^{(i_2,j_2,k_2,p_2,l_2)}_{(i_1,j_1,k_1,p_1,l_1)} = \begin{cases} I_s \otimes W^0 \oplus D_0 - \tau + \beta I_{mn}, e_s \otimes \beta I_{mn}, \\ I_{(S-s)} \otimes W \oplus D0 - \tau I_{nm}, \quad i_1 = 1, 0 \le i_2 \le N, j_1 = j_2 = 5, \\ \qquad 1 \le k_1, k_2 \le S, 1 \le p_1, p_2 \le m, 1 \le l_1, l_2 \le n, \\ I_S \otimes I_m \otimes D_2, \quad i_1 = 1, 1 \le i_2 \le N, j_1 = j_2 = 5, \\ \qquad 1 \le k_1, k_2 \le S, 1 \le p_1, p_2 \le m, 1 \le l_1, l_2 \le n, \\ 0, \qquad \text{otherwise.} \end{cases}$$

$A_{2}{}^{(i_2,j_2,k_2,p_2,l_2)}_{(i_1,j_1,k_1,p_1l_1)}$'s entries should be defined as transition submatrices that contain transitions of the form $(h, i_1, j_1, k_1, p_1, l_1) \to (h-1, i_2, j_2, k_2, p_2, l_2)$, where $h > 1$ and $A_{0}{}^{(i_2,j_2,k_2,p_2,l_2)}_{(i_1,j_1,k_1,p_1,l_1)}$ function as transition submatrices that comprise transitions of the form $(h, i_1, j_1, k_1, p_1, l_1)$ $\to (h+1, i_2, j_2, k_2, p_2, l_2)$, where $h \ge 1$. In the row vector, let $(i_1, j_1, k_1, p_1, l_1)$ represent the number of LPC, server status, number of items, service phases, and arrival phases; in the column vector, let $(i_2, j_2, k_2, p_2, l_2)$ represent the number of HPC, server status, number of items, service phases, and arrival phases.

$$A_2 = \begin{bmatrix} 0 & 0 & 0 & 0 & 0 & 0 \\ 0 & 0 & 0 & 0 & 0 & 0 \\ 0 & 0 & 0 & 0 & 0 & 0 \\ A_{241} & 0 & 0 & A_{244} & 0 & 0 \\ 0 & A_{252} & 0 & 0 & A_{255} & 0 \\ 0 & 0 & A_{263} & 0 & 0 & A_{266} \end{bmatrix}, A_0 = \begin{bmatrix} A_{011} & 0 & 0 & 0 & 0 & 0 \\ 0 & A_{022} & 0 & 0 & 0 & 0 \\ 0 & 0 & A_{033} & 0 & 0 & 0 \\ 0 & 0 & 0 & A_{044} & 0 & 0 \\ 0 & 0 & 0 & 0 & A_{055} & 0 \\ 0 & 0 & 0 & 0 & 0 & A_{066} \end{bmatrix},$$

$$A_{241}{}^{(i_2,j_2,k_2,p_2,l_2)}_{(i_1,j_1,k_1,p_1,l_1)} = \begin{cases} W^0 \otimes I_n, & i_1 = i_1 - 1, i_2 = 1, j_1 = 3, j_2 = 0, 1 \leq k_1, \leq S, k_2 = 0 \\ & 1 \leq p_1 \leq m, p_2 = 0, 1 \leq l_1, l_2 \leq n, \\ 0, & \text{otherwise.} \end{cases}$$

$$A_{244}{}^{(i_2,j_2,k_2,p_2,l_2)}_{(i_1,j_1,k_1,p_1,l_1)} = \begin{cases} I_{S-1} \otimes W^0 \alpha \otimes I_n, & i_1 = i_1 - 1, i_2 = 1, j_1 = j_2 = 3, 1 \leq k_1, k_2 \leq S, \\ & 1 \leq p_1, p_2 \leq m, 1 \leq l_1, l_2 \leq n, \\ 0, & \text{otherwise.} \end{cases}$$

$$A_{252}{}^{(i_2,j_2,k_2,p_2,l_2)}_{(i_1,j_1,k_1,p_1,l_1)} = \begin{cases} W^0 \alpha \otimes I_n, & i_1 = i_1 - 1, i_2 = 1, j_1 = 4, j_2 = 1, 2 \leq k_1 \leq S, \\ & 1 \leq k_2 \leq S, 1 \leq p_1, p_2 \leq m, 1 \leq l_1, l_2 \leq n, \\ 0, & \text{otherwise.} \end{cases}$$

$$A_{255}{}^{(i_2,j_2,k_2,p_2,l_2)}_{(i_1,j_1,k_1,p_1,l_1)} = \begin{cases} W^0 \alpha \otimes I_n, & i_1 = i_1 - 1, i_2 = 1, j_1 = j_2 = 4, 2 \leq k_1, k_2 \leq S, \\ & 1 \leq p_1, p_2 \leq m, 1 \leq l_1, l_2 \leq n, \\ 0, & \text{otherwise.} \end{cases}$$

$$A_{263}{}^{(i_2,j_2,k_2,p_2,l_2)}_{(i_1,j_1,k_1,p_1,l_1)} = \begin{cases} W^0 \otimes I_n, & i_1 = i_1 - 1, i_2 = 1, j_1 = 5, j_2 = 0, 1 \leq k_1 \leq S, \\ & k_2 = 0, 1 \leq p_1 \leq m, p_2 = 0, 1 \leq l_1, l_2 \leq n, \\ 0, & \textit{otherwise}. \end{cases}$$

$$A_{266}{}^{(i_2,j_2,k_2,p_2,l_2)}_{(i_1,j_1,k_1,p_1,l_1)} = \begin{cases} I_{S-1} \otimes W^0 \alpha \otimes I_n, & i_1 = i_1 - 1, i_2 = 1, j_1 = j_2 = 5, \\ & 1 \leq k_1, k_2 \leq S, 1 \leq p_1, p_2 \leq m, 1 \leq l_1, l_2 \leq n, \\ 0, & \textit{otherwise}. \end{cases}$$

$$A_{011}{}^{(i_2,j_2,k_2,l_2)}_{(i_1,j_1,k_1,l_1)} = \begin{cases} D_1, & i_1 = i_1 + 1, i_2 = 2, j_1 = j_2 = 0, 1 \leq k_1 \leq S, k_2 = 0, \\ & 1 \leq p_1 \leq m, p_2 = 0, 1 \leq l_1, l_2 \leq n, \\ 0, & \text{otherwise.} \end{cases}$$

$$A_{022}{}^{(i_2,j_2,k_2,p_2,l_2)}_{(i_1,j_1,k_1,p_1,l_1)} = \begin{cases} I_m \otimes D_1, & i_1 = i_1 + 1, i_2 = 2, j_1 = j_2 = 1, k_1, k_2 = 1, \\ & 1 \leq p_1, p_2 \leq m, 1 \leq l_1, l_2 \leq n, \\ 0, & \text{otherwise.} \end{cases}$$

$$A_{033}{}^{(i_2,j_2,k_2,l_2)}_{(i_1,j_1,k_1,l_1)} = \begin{cases} D_1, & i_1 = i_1 + 1, i_2 = 2, j_1 = j_2 = 1, \\ & k_1, k_2 = 1, 1 \leq l_1, l_2 \leq n, \\ 0, & \text{otherwise.} \end{cases}$$

$$A_{044}{}^{(i_2,j_2,k_2,p_2,l_2)}_{(i_1,j_1,k_1,p_1,l_1)} = \begin{cases} I_S \otimes I_m \otimes D_1, & i_1 = i_1 + 1, i_2 = 2, j_1 = j_2 = 3, 1 \leq k_1, k_2 \leq S \\ & 1 \leq p_1, p_2 \leq m, 1 \leq l_1, l_2 \leq n, \\ 0, & \text{otherwise.} \end{cases}$$

$$A_{055}{}^{(i_2,j_2,k_2,p_2,l_2)}_{(i_1,j_1,k_1,p_1,l_1)} = \begin{cases} I_{S-1} \otimes I_m \otimes D_1, & i_1 = i_1 + 1, i_2 = 2, j_1 = j_2 = 4, 2 \leq k_1, k_2 \leq S \\ & 1 \leq p_1, p_2 \leq m, 1 \leq l_1, l_2 \leq n, \\ 0, & \text{otherwise.} \end{cases}$$

$$A_{066}{}^{(i_2,j_2,k_2,p_2,l_2)}_{(i_1,j_1,k_1,p_1,l_1)} = \begin{cases} I_S \otimes I_m \otimes D_1, & i_1 = i_1 + 1, i_2 = 2, j_1 = j_2 = 5, 1 \leq k_1, k_2 \leq S \\ & 1 \leq p_1, p_2 \leq m, 1 \leq l_1, l_2 \leq n, \\ 0, & \text{otherwise.} \end{cases}$$

5. Steady State Analysis

5.1. Stability Condition

A generator matrix is indicated by the equation $A = A_0 + A_1 + A_2$. In the steady state, let π be the probability vector of A that satisfies $\pi e = 1$ and $\pi A = 0$. The vector π is divided by

$$\pi = (\pi_0, \pi_1, \pi_2, \pi_3, \pi_4, \pi_5) = \big(\pi_{000}, \pi_{001}, \ldots, \pi_{00S}, \pi_{010}, \pi_{011}, \ldots, \pi_{01S}, \pi_{0N0}, \pi_{0N1}, \ldots, \pi_{0NS},$$
$$\pi_{111}, \pi_{121}, \ldots, \pi_{1N1}, \pi_{200}, \pi_{210}, \ldots, \pi_{2N0}, \pi_{301}, \pi_{302}, \ldots, \pi_{30S},$$
$$\pi_{311}, \pi_{312}, \ldots, \pi_{31S}, \pi_{3N1}, \pi_{3N2}, \ldots, \pi_{3NS}, \ldots, \pi_{412}, \ldots, \pi_{42S}, \pi_{422}, \ldots, \pi_{42S}\big)$$

Where π_0 has a dimension of (N+1)(S+1)n, π_1 has a dimension of nmN, π_2 has a dimension of (N+1)n, π_3 has a dimension of nm(N+1)S, π_4 has a dimension of N(S-1)mn and π_5 has a dimension of (N+1)Smn. subject to normalizing condition

$$\pi_0 e_n + \pi_1 e_{mn} + \pi_2 e_n + \pi_3 e_{mn} + \pi_4 e_{mn} + \pi_5 e_{mn} = 1.$$

Within the framework of QBD, our model's stability should meet the necessary and sufficient conditions of $\pi A_0 e < \pi A_2 e$,
Which is found to be of the below form,

$$\sum_{j_1=0}^{N} \pi_{0j_1}[D_1 e_n] + \sum_{j_1=1}^{N} \pi_{1j_1}[I_m \otimes D_1 e_{mn}] + \sum_{j_1=0}^{N} \pi_{2j_1}[D_1 e_n]$$
$$+ \sum_{j_1=0}^{N}\sum_{j_2=1}^{S} \pi_{2j_1j_2}[I_m \otimes D_1 e_{mn}] + \sum_{j_1=1}^{N}\sum_{j_2=2}^{S} \pi_{3j_1j_2}[I_m \otimes D_1 e_{mn}] + \sum_{j_1=0}^{N}\sum_{j_2=1}^{S} \pi_{4j_1j_2}[I_m \otimes D_1 e_{mn}]$$
$$< \sum_{j_1=0}^{N}\sum_{j_2=2}^{S} \pi_{3j_1j_2}[W^0 \otimes I_n e_{mn}(1+\alpha)]$$
$$+ \sum_{j_1=1}^{N}\sum_{j_2=2}^{S} \pi_{4j_1j_2}[W^0\alpha \otimes I_n e_{mn}] + \sum_{j_1=0}^{N}\sum_{j_2=2}^{S} \pi_{5j_1j_2}[W^0 \otimes I_n e_{mn}(1+\alpha)].$$

5.2. The Transition Probability Vector

Examine the following partitioning of the invariant probability vector of Q, represented by the symbol z.: $z = (z_0, z_1, z_2, ...)$. z_0 is $2(N+1)(S+1)n + NSmn$ in dimension. Whereas the dimensions of z_1, z_2,... are $2(N+1)n + Nmn + 2(N+1)Smn + N(S-1)mn$. Then, z satisfies the conditions $zQ = 0$ and $ze = 1$. The rate matrix R can be evaluated using the logarithmic reduction procedure. The steady-state probability vector z might also be found using the following equation.

$$z_i = z_1 R^{i-1}, i \geq 2,$$

where R represents the quadratic equation's non-negative solution.

$$R^2 A_2 + R A_1 + A_0 = 0,$$

as well as satisfying the relation $RA_2 e = A_0 e$. The vectors z_0 and z_1 are derived using the following equations.

$$z_0 B_{00} + z_1 B_{10} = 0,$$
$$z_0 B_{01} + z_1 [A_1 + RA_2] = 0,$$

based on the Normalizing condition,

$$z_0 e_{2(N+1)(S+1)n+NSmn} + z_1 [1-R]^{-1} e_{2(N+1)n+Nmn+2(N+1)Smn+N(S-1)mn} = 1.$$

[15] state that by employing crucial steps in the logarithmic reduction process, the R matrix can be generated analytically.

6. Measures of performance

In this section, we present some key performance measures to highlight the qualitative aspects of the model under study. The measures and their calculation formulas are listed below.

- Probability that (server 1) S1 is idle while (Server 2) S2 is on vacation:
  $P_{S1IS2V} = \sum_{u_2=0}^{N} \sum_{u_3=0}^{S} \sum_{u_5=1}^{n} X_{0u_2u_3u_50}$.
- Probability that S1 is idle while S2 is busy:
  $P_{S1IS2B} = \sum_{u_2=1}^{N} \sum_{u_3=1}^{S} \sum_{u_4=1}^{m} \sum_{u_5=1}^{n} X_{0u_2u_3u_4u_51}$.
- Probability that S1 is idle while S2 is under repair process:
  $P_{S1IS2R} = \sum_{u_2=0}^{N} \sum_{u_3=0}^{S} \sum_{u_5=1}^{n} X_{0u_2u_3u_52}$.
- Probability that S1 is busy while S2 is on vacation:
  $P_{S1BS2V} = \sum_{u_1=1}^{\infty} \sum_{u_2=0}^{N} \sum_{u_3=1}^{S} \sum_{u_4=1}^{m} \sum_{u_5=1}^{n} X_{u_1u_2u_3u_4u_53}$.
- Probability that both S1 and S2 is busy:
  $P_{S1BS2B} = \sum_{u_1=1}^{\infty} \sum_{u_2=1}^{N} \sum_{u_3=1}^{S} \sum_{u_4=1}^{m} \sum_{u_5=1}^{n} X_{u_1u_2u_3u_4u_54}$.
- Probability that S1 is busy while S2 is under repair process:
  $P_{S1BS2R} = \sum_{u_1=1}^{\infty} \sum_{u_2=0}^{N} \sum_{u_3=1}^{S} \sum_{u_4=1}^{m} \sum_{u_5=1}^{n} X_{u_1u_2u_3u_4u_55}$.

7. Numerical Implementation

In this section, we examine the output of our system using both graphical and numerical representations. The variance and correlation patterns given below identify the five distinct MAP representations, each with a mean value of 1. Since ERA, EXA, and HYA represen the renewal process, there is no correlation between the first three arrival processes.

- **Erlang arrival of order 2 (ERA):**

$$D_0 = \begin{bmatrix} -5 & 5 & 0 & 0 & 0 \\ 0 & -5 & 5 & 0 & 0 \\ 0 & 0 & -5 & 5 & 0 \\ 0 & 0 & 0 & -5 & 5 \\ 0 & 0 & 0 & 0 & -5 \end{bmatrix}, \quad D_1 = \begin{bmatrix} 0 & 0 & 0 & 0 & 0 \\ 0 & 0 & 0 & 0 & 0 \\ 0 & 0 & 0 & 0 & 0 \\ 0 & 0 & 0 & 0 & 0 \\ 3 & 0 & 0 & 0 & 0 \end{bmatrix},$$

$$D_2 = \begin{bmatrix} 0 & 0 & 0 & 0 & 0 \\ 0 & 0 & 0 & 0 & 0 \\ 0 & 0 & 0 & 0 & 0 \\ 0 & 0 & 0 & 0 & 0 \\ 2 & 0 & 0 & 0 & 0 \end{bmatrix}.$$

- **Exponential (EXA) Arrival:**

$$D_0 = [-1], \quad D_1 = [0.6], \quad D_2 = [0.4].$$

- **Arrival in Hyper exponential (HYA):**

$$D_0 = \begin{bmatrix} -1.90 & 0 \\ 0 & -0.19 \end{bmatrix}, \quad D_1 = \begin{bmatrix} 1.026 & 0.114 \\ 0.1026 & 0.0114 \end{bmatrix}, \quad D_2 = \begin{bmatrix} 0.684 & 0.076 \\ 0.0684 & 0.0076 \end{bmatrix}.$$

- **MAP-Negative Correlation (MNCA) arrival:**

$$D_0 = \begin{bmatrix} -1.00243 & 1.00243 & 0 \\ 0 & -1.00243 & 0 \\ 0 & 0 & -225.797 \end{bmatrix}, \quad D_1 = \begin{bmatrix} 0 & 0 & 0 \\ 0.006012 & 0 & 0.595446 \\ 134.1234 & 0 & 1.3548 \end{bmatrix},$$

$$D_2 = \begin{bmatrix} 0 & 0 & 0 \\ 0.004008 & 0 & 0.396964 \\ 89.4156 & 0 & 0.9032 \end{bmatrix}.$$

- **MAP-Positive Correlation (MPCA) arrival:**

$$D_0 = \begin{bmatrix} -1.00243 & 1.00243 & 0 \\ 0 & -1.00243 & 0 \\ 0 & 0 & -225.797 \end{bmatrix}, \quad D_1 = \begin{bmatrix} 0 & 0 & 0 \\ 0.595446 & 0 & 0.006012 \\ 1.3548 & 0 & 134.1234 \end{bmatrix},$$

$$D_2 = \begin{bmatrix} 0 & 0 & 0 \\ 0.396964 & 0 & 0.004008 \\ 0.9032 & 0 & 89.4156 \end{bmatrix}.$$

Let us consider PH-distributions for the service as follows:

- **Erlang service of order 2 (ERS):** $\alpha = [1, 0] \quad , \quad W = \begin{bmatrix} -2 & 2 \\ 0 & -2 \end{bmatrix}$.
- **Exponential Service (EXS):** $\alpha = [1] \, , \quad W = [-1]$
- **Hyper exponential service (HYS):** $\lambda = [0.3, 0.7] \, , \quad W = \begin{bmatrix} -12 & 6 \\ 5 & -10 \end{bmatrix}$.

7.1. Illustration 1

We have examined how the service rate (μ) affects the E_{system} in the following Tables 1 to 3. Fix $N = 5$, $s = 3$, $S = 6$, $\lambda = 2$, $\beta = 2$, $\eta = 2$, $\tau = 1$, $\psi = 1$, we observe that from the following Tables 1 to 3 : As the service rate (μ) increases, the corresponding E_{system} decreases proportionately to the range of arrival and service time arrangements. Observe the arrival timings, in comparison to all other arrival times, E_{system} declines significantly in HYA and considerably more slowly in ERA.

Table 1: *E_{system} vs Service rate (μ) - EXS*

μ	ERA	EXA	HYA	$MNCA$	$MPCA$
11	0.05593823	0.06346217	0.07735655	0.07877835	3.51783032
12	0.05135673	0.05839620	0.07166483	0.07258573	3.37347062
13	0.04748172	0.05414040	0.06691189	0.06736384	3.25215178
14	0.04416124	0.05051471	0.06288302	0.06290067	3.14867954
15	0.04128409	0.04738877	0.05942438	0.05904185	3.05931843
16	0.03876697	0.04466588	0.05642283	0.05567228	2.98131269

Table 2: *E_{system} vs Service rate (μ) - ERS*

μ	ERA	EXA	HYA	$MNCA$	$MPNA$
11	0.05605629	0.06423748	0.07868989	0.07863574	3.51697311
12	0.05144156	0.05904635	0.07278352	0.07244778	3.37176961
13	0.04754427	0.05469343	0.06786383	0.06723433	3.24987784
14	0.04420844	0.05099088	0.06370287	0.06278133	3.14602334
15	0.04132044	0.04780305	0.06013782	0.05893328	3.05641556
16	0.03879549	0.04502960	0.05704930	0.05557447	2.97826031

Table 3: *E_{system} vs Service rate (μ) - HYS*

μ	ERA	EXA	HYA	$MNCA$	$MPNA$
11	0.01121492	0.01559324	0.02501944	0.01925209	2.11066096
12	0.01036636	0.01471293	0.02408268	0.01814938	2.08193365
13	0.00964837	0.01396924	0.02329224	0.01721792	2.05738093
14	0.00903297	0.01333265	0.02261633	0.01642087	2.03614293
15	0.00849963	0.01278159	0.02203174	0.01573125	2.01758391
16	0.00803298	0.01229990	0.02152113	0.01512886	2.00122295

7.2. Illustration 2

In the figures 2 to 6, the effect of the vacation rate μ on the E_{system} has been examined. Adjust $\lambda = 2$, $\beta = 2$, $\mu = 15$, $\tau = 1$, $\psi = 1$, $N = 5$, $s = 3$, $S = 6$, we observe that from the following figures 2 to 6: The variety of arrival and service time arrangements rises with the vacation rate (η) and the associated E_{system} increases as well. An rise in the vacation rate suggests that the server could have to spend more time traveling to the service station and serving the customers, which would raise E_{system}. Notice how E_{system} rises significantly in HYA and MNCA and considerably more slowly in MPCA compared to all other arrival times.

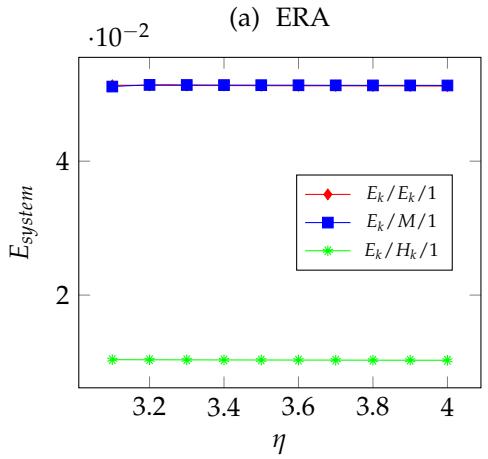


Figure 2: *Vacation rate vs. E_{system}*

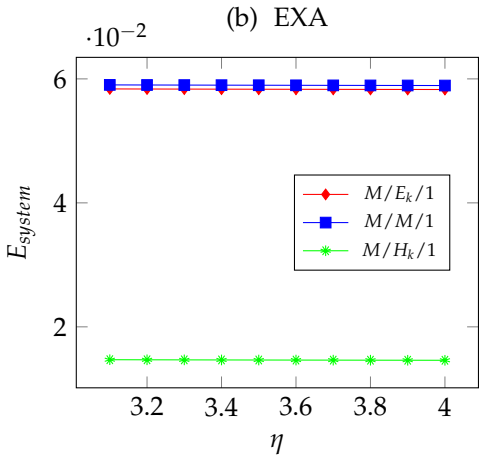


Figure 3: *Vacation rate vs. E_{system}*

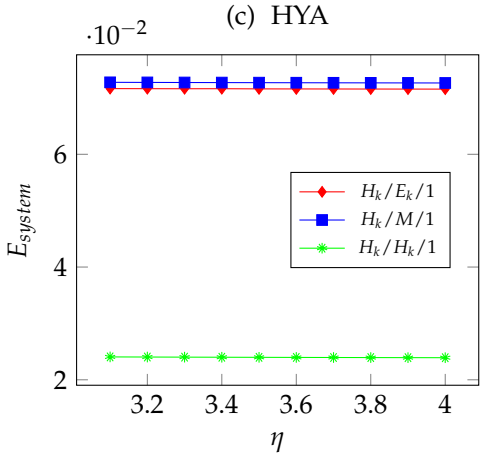


Figure 4: *Vacation rate vs. E_{system}*

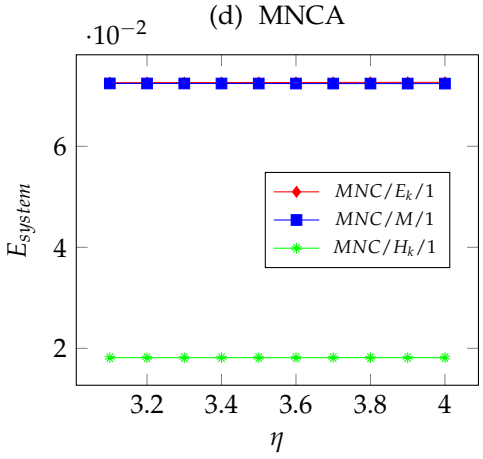


Figure 5: *Vacation rate vs. E_{system}*

(e) MPCA

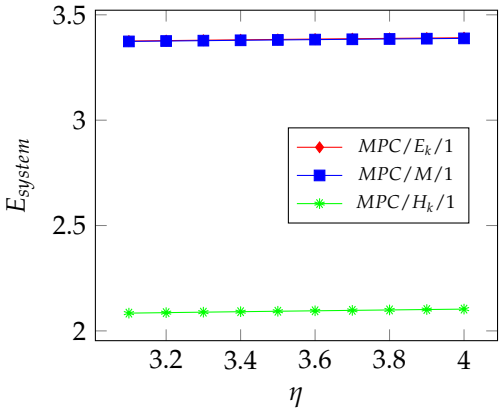


Figure 6: *Vacation rate vs.* E_{system}

8. Conclusion

In this study, we considered customers arriving according to a Markovian Modulated Arrival Process (MMAP) and a phase-type service distribution provided by two servers operating under a non-preemptive priority queueing inventory system with breakdowns, repairs and an (s, S) policy. We analyzed visual representations using 2D graphs and obtained tabular numerical results by examining the effects of various model parameters on key system performance metrics. To this end, we employed the matrix-analytic approach to study the MMAP/PH/2 queueing inventory system with breakdown and repair mechanisms. For future work, we plan to extend the current model by incorporating a Batch Markovian Arrival Process (BMAP) for arrivals, which is particularly suitable for modeling systems with batch arrivals.

References

[1] Haghighi, A.M. and Mishev, D.P. (2006) A Parallel Priority Queueing System With Finite Buffers. *Journal of Parallel and Distributed Computing*, Vol. 66, pp.379–392.

[2] Ayyappan, G.and Archana @ Gurulakshmi (2023) Analysis of MMAP/PH/1 classical retrial queue with non-Preemptive priority,second optional service, differentiate breakdowns, phase type repair, single vacation, emergency vacation, closedown, setup and discouragement. *Reliability: Theory and Applications*, Vol. 18, No. 3(74).

[3] Ayyappan, G.and Meena, S. (2024) Analysis of MMAP/PH(1), PH(2)/1 Preemptive Priority Queueing Model with Single Vacation, Repair and Impatient Customers. *Reliability: Theory and Applications*, Vol. 19, issue:1.

[4] Ayyappan, G. and Sangeetha, S. (2024) Dynamic service management and priority handling in dual server queueing systems with breakdowns. *International journal of Mathematics in Operational research*, DOI: 10.1504/IJMOR.2024.10063513.

[5] Ayyappan, G. and Thilagavathy, K. (2021) Analysis of MAP (1), MAP (2)/PH/1 non-preemptive priority queueing model under classical retrial policy with breakdown, repair, discouragement, single vacation, standby server. *International Journal of Applied and Computational Mathematics*, Vol. 7, No. 5, pp. 184.

[6] Dudin, A.N., Chakravarthy, S. R., Dudina S.A. and Dudina O.A. (2023) Queueing system with server breakdowns and individual customer abandonment. *Quality Technology and Quantitative Management* , Vol. 24, No. 4, pp. 441-460.

[7] Kim, C., Dudin, A., Dudin, S. and Dudina, O. (2014) Analysis of MMAP/PH1,PH2/N/∞ queueing system operating in a random environment. *International Journal of Applied Mathematics and Computer science*, Vol. 24, No. 3, pp. 485–501.

[8] Divya, V. N., Krishnamoorthy, A., Melikov, A. and Aliyeva, S. (2021) MMAP/(PH,PH)/1 queue with priority loss through feedback. *Stochastic Modelling and Applied Probability*, Vol. 9, No. 15, pp. 1797.

[9] Halfin, S. and Segal, M. (1972) A Priority queueing model for a mixture of two types of customers. *SIAM Journal of Applied Mathematics*, Vol. 23, No. 3 .

[10] White, H. and Lee S. C. (1958) Queuing with Preemptive Priorities or with Breakdown. *Operations Research*, Vol. 6, No. 1, pp. 79-95.

[11] Indumathi, P and Karthikeyan, K.(2024) Review the concepts of queues and inventory models. *International Journal of Mathematics in Operational Research*, Vol. 29, No. 1, pp. 66-93.

[12] Jeganathan, K. , Jehoasan Kingsly, S. and Padmasekaran, S. (2019) Two heterogeneous servers queueing-inventory system with sharing finite buffer and a flexible server. *International Journal of Applied Engineering Research*, Vol. 14, pp. 1212–1219.

[13] Jeganathan, K. , Selvakumar, S. , Srinivasan, K., Anbazhagan, N. , Joshi, G.P and Woong Cho (2024) Two types of service facilities in interconnected stochastic queueing and inventory system with MMAP. *Ain Shams Engineering Journal*, Vol. 15, No. 9, https://doi.org/10.1016/j.asej.2024.102963.

[14] Krishnamoorthy, A. , Babu, S. and Narayanan, V. C. (2009) Analysis of MAP/(PH,PH)/1, queue with self generation of priorities and non-preemptive service. *European Journal of Operational Research*, Vol. 195, No. 1, pp. 174–185.

[15] Latouche, G. and Ramaswami, V. (1999) Introduction of Matrix analytic Methods in Stochastic Modeling. *Society for Industrial and Applied Mathematics*, Philadelphia

[16] Neuts, M. F. (1979) A Versatile Markovian point process, *Journal of Applied Probability*, Vol. 16, pp.764-779.

[17] Raj, R. and Jain, V. (2022) Optimization of traffic control in MMAP[2]/PH[2]/S priority queueing model with PH retrial times and preemptive repeat policy. *Journal of Industrial and Management Optimization*, Vol. 19, No. 4, DOI: 10.3934/jimo.2022044.

[18] Rasmi, K., Jacob, M. J. , Rumyanstev, A. and Krishnamoorthy, A. (2024) On a queueing inventory model with age based selling of items to distinct priority groups. *Operations Research Forum, Springer*, Vol. 5, pp. 1-25.

[19] Chakravarthy, S.R. (2018) A Dynamic non-preemptive priority queueing model with two types of customers. *Mathematics and Computing*, Vol. 253, pp. 23-42.

[20] Jain, V., Raj, R. and Dharmaraja, S.(2022) Performability analysis of a MMAP[2]/ph[2]/S model with PH retrial times. *Communication in Statistics, Theory and Methods* , Vol. 53. No. 3, pp. 1-20.

[21] Levy, Y. and Yechiali, U. (1975) Utilization of Idle Time in an M/G/1 Queueing System. *Management Science*, Vol. 22, No.2, pp. 202-211.

ABOUT WAYS TO INCREASE RELIABILITY AND ECONOMY OF STEAM BOILER INSTALLATIONS OF BLOCK POWER PLANTS

Farzaliyev Y.Z.
•
Azerbaijan State University of Economics
yusif.farzaliyev@unec.edu.az

Abstract

The new method and algorithm of management by reliability and profitability of work of steam boiler installations block power stations is developed. The essence of a method is reduced to definition of "weak parts» and to formation of recommendations. In a basis of a database and program model, there are results of measurement and calculation of technical and economic parameters steam boiler installations. And the method allows to formulate the main directions of increasing the efficiency of individual control steam boiler installations and steam boiler installations of power plants as a whole. Improving the efficiency management system of the steam boiler installations allows, first of all, to reduce operating costs. The developed method allows us to consider the obtained results as methodological support for personnel in organizing the operation, maintenance and repair of steam boiler installation. Therefore, the relevance of this problem is obvious

Keywords: Reliability, profitability, ranking, power stations, management, steam boiler, installation

I. Introduction

The recommended method and calculation program are implemented as a subsystem of the automated system for analyzing the technical condition of power units [1].

Along with the existing intuitive ranking system of power plant steam boiler installations (SBI), the calculation results of this system should be used as methodological support for personnel [2].

This article addresses the following issues:

1. Evaluation of the results of the traditional approach to improving the efficiency of power plant SBI
2. Development of methods and algorithms allowing:
   - obtain a quantitative assessment of the technical condition of the SBI, identify the main areas for improving the efficiency of its operation
   - evaluate the results of operational management of the efficiency of the SBI based on information on quantitative assessments of technical and economic indicators calculated for a given estimated time period $\Delta\tau$
   - assess the maintainability of the technical condition of the SBI during downtimes not associated with the restoration of wear of the SBI components
   - to formulate a strategy for scheduled repairs SBI and to assess the quality of repairs.

II. Methods

Table 1 shows quantitative estimates of average technical and economic indicators of gas-oil fueled SBI, and Table 2 shows the indicators of individual SBI power units for some three consecutive months of the year. These data will be used to illustrate the solution of each of the above problems

Table 1: Estimates of average values of technical and economic indicators of the power plant steam boiler installations

N	Indicators			Months of year		
	Name	Conventionl designation	Unit of measurement	A	B	C
1	Specific load	h_{ave}	10^4 t/h. MVt	34,75	34,58	34,38
2	Air temperature after regenerative air heater (RAH)	T_{air}	^{0}C	295,9	293,6	290,4
3	Exhaust gas temperature	T_{eg}	^{0}C	132,1	131,9	124,4
4	Excess air coefficient	C_{air}	in relative units	1,253	1,187	1,205
5	Air suction on the tract	ΔS_{air}	%	42,25	46,86	48,85
6	Gross efficiency	η_b	%	90,24	90,2	91,25
7	Specific consumption of electric energy for own needs	$E_{o.n.}$	%	2,349	2,505	2,464
8	Specific heat consumption for own needs	$Q_{o.n.}$	%	2,135	2,084	1,44
9	Net efficiency	η_n	%	84,1	82,74	83,96

The solution of problems carried out in an automated mode is preceded by the preparation of initial data, including the transformation of integral type indicators into specific indicators, the selection of independent indicators and their standardization [3]. Integral type indicators include indicators whose average value depends on the duration of work. The downtime of the SBI is caused by both cases of its emergency repair and the duration of downtime during scheduled repairs or in reserve due to failures of other installations of the power unit (steam turbine, turbo generator, block transformer, switches, auxiliary systems).

Let us note one important feature when preparing the list of SBI indicators. It is known that when classifying, including ranking objects, one of the main requirements is the independence of features (indicators) [4].

The assessment of the correlation between indicators with a small number m_{Σ} ranked SBI shows that to one degree or another, dependencies exist between almost all indicators [5].

Table 2: Quantitative assessments of technical and economic indicators of 300 MW power units

No SBI	Months of year	Technical and economic indicators								
		h_{ave}	T_{air}	T_{eg}	C_{air}	ΔS_{air}	η_b	$E_{o.n.}$	$Q_{o.n.}$	η_n
1	1	34,0	261	113	1,94	43,3	91,55	2,58	2,45	83,0
	2	34,9	280	111	1,13	43,3	89,16	4,05	1,57	76,3
	3	34,9	277	108	1,159	45	91,89	2,38	1,28	84,5
2	1	34,8	293	109	1,16	41	90,95	2,56	1,88	84,5
	2	34,7	304	123	1,197	46,7	91,84	2,11	1,71	84,1
	3	34,8	274	98	1,165	40,7	91,48	2,41	1,37	85,1
3	1	35,3	294	117	1,17	43	91,21	2,39	1,74	85,1
	2	34,6	295	123	1,228	43,8	90,69	2,33	1,78	84,6
	3	33,5	285	115	1,226	43,2	91,07	2,91	1,48	83,3
4	1	35,0	305	154	1,16	42,6	87,88	2,34	2,62	83,7
	2	34,9	298	147	1,217	51,3	89,29	2,52	2,75	82,3
	3	34,6	304	137	1,283	56,8	90,15	2,55	1,5	83,3
5	1	35,1	293	110	1,11	39,5	92,34	2,11	1,03	86,1
	2	34,7	300	109	1,097	41,2	93,6	1,98	0,96	86,6
	3	34,3	285	114	1,193	44,9	92,91	2,17	1,11	85,9
6	1	34,5	305	157	1,15	41,3	89,45	2,46	2,73	83,0
	2	34,5	301	158	1,182	47,1	88,66	2,4	2,76	81,9
	3	34,3	306	157	1,226	58	90,59	2,72	1,88	81,6
7	1	33,6	325	151	1,15	42,8	90,29	2,18	1,98	83,6
	2	34,7	282	141	1,204	49,5	89,77	2,34	2,74	83,0
	3	34,4	312	139	1,132	46	91,85	2,06	1,57	85,0
8	1	34,5	291	146	1,18	44,5	88,22	2,17	2,65	83,8
	2	34,9	289	143	1,239	52	88,62	2,31	2,4	83,1
	3	34,1	280	127	1,252	56,2	90,05	2,51	1,33	83,0

If we take into account the random nature of the change in the correlation coefficient Kr and take into consideration only those indicators for which $K_r > \overline{K}_{r,(1-\alpha)}$ or $K_r < \underline{K_{r,\alpha}}$, then the number of dependent indicators decreases. Here $\overline{K}_{r,(1-\alpha)}$ and $\underline{K_{r,\alpha}}$ are the boundary values of the statistical function of the fiducial distribution $F^*(K_r)$, calculated under the condition that the samples under consideration are obtained randomly from the general population [6]. When comparing K_r with boundary values with a given significance level α, for example, α=0.05, it is assumed that the number of comparisons is equal to one [7]. In the case when the comparison results assume n comparisons, then the reliability R=0.95 will correspond to $\overline{K}_{r,(1-\alpha)}$ and $\underline{K_{r,\alpha}}$, calculated for $\alpha_n=\alpha/n$ [8]. For example, for n=10 the value $\alpha_n<10^{-3}$, which corresponds to the value $\overline{K}_{r,\alpha_n}>0.95$. Consequently, for a small number m_Σ one should proceed not from condition $K_r > K_{r,\alpha_n}$ but from condition $K_r > \overline{K_{r,\alpha_n}}$ [9]. Such a relationship exists, for example, between the specific load of the SBI, the specific consumption of feedwater and the "Gross" heat consumption, between the temperature of the exhaust gases and the heat loss with the exhaust gases. The presence of a relationship between the indicators leads to an overestimation of the final quantitative assessment of the technical condition (K_L) of the most reliable and economical SBI and to a decrease in K_L for the least reliable and economical SBI.

The value of K_L is calculated using the formula:

$$K^*_{L,j} = n_\Sigma^{-1} \sum_{i=1}^{n_k} \frac{2[In_{i,j} - m_\Sigma^{-1} \sum_{j=1}^{m_\Sigma} In_{i,j}]}{L^*_\Sigma(In_i)} \quad (1)$$

where (In -Indicator),

$L^*_\Sigma(In_i) = (In_{i,max} - In_{i,min})$; $In_{i,max} = max\{In_{i,j}\} j = 1, m_\Sigma$; $In_{i,min} = min\{In_{i,j}\} j = 1, m_\Sigma$

As an example, Table 3 shows the results of calculating the $K^*_{L,j}$ grades for eight SBIs (j=1,8) with n_Σ=12, n_Σ=10 и n_Σ=9.

III. Results

Table 3: Results of the assessment of the influence of dependent SBI indicators on $K_{l,j}$

n_Σ	Conditional numbers of the SBI ES							
	1	2	3	4	5	6	7	8
12	-0.075	-0.25	-0.509	-0.043	0.467	0.112	0.41	-0.112
10	0.055	-0.244	-0.43	-0.003	0.341	0.074	0.428	-0.112
9	0.009	-0.163	-0.448	-0.077	0.418	-0.032	0.457	-0.161

As follows from Table 3, when moving from n_Σ=12 to n_Σ=10 and further to n_Σ=9, not only the value changes, but also the ranking result of the SBI.

Along with the above, in the ranking algorithm of the SBI it is necessary to take into account that in the spring-summer period there may be cases when one or more power units during the calculated time interval was in a state of planned repair or reserve. At the same time, the number of ranked SBI (m_Σ) decreases accordingly [10].

IV. Discussion

I. Formation of the main directions for increasing the efficiency of the SBI work in the next billing period of work

The calculation results include:

- a sequence of power plant SBI ordinal numbers ranked by efficiency. Calculated in accordance with [1]
- a list of technical and economic indicators, ranked by importance, recommended for improvement for each SBI
- quantitative assessment of the significance of these indicators $\delta In_{i,j}$
- average quantitative assessment of these indicators for the period under review $In_{i,j}(\Delta\tau)$
- averaged over the period under review for all SBI quantitative assessment of these indicators $M^*[In_i(\Delta\tau)]$

In conclusion, the main results and recommendations are formulated, namely:

- a quantitative assessment of the technical condition of the operating SBI is provided
- the least efficient power plant SBI is installed. This SBI is recommended for shutdown for scheduled maintenance, and beforehand - for shutdown in reserve or for the maximum possible reduction of its load
- the load of this SBI must be the maximum permissible

- the number ($m^{(+)}$) and the list of "good" SBI are established, for which the quantitative assessment of the technical condition $\delta In_i(\Delta\tau)$ is positive. An increase in their productivity is allowed in proportion to the relative values of $\delta In_i(\Delta\tau)$. The relative values of $\delta In_i(\Delta\tau)$ are calculated using the formula

$$\delta^* In_i(\Delta\tau) = \frac{\delta In_i(\Delta\tau)}{\sum_{i=1}^{m^{(+)}} \delta In_i(\Delta\tau)} \quad (2)$$

- the number $m^{(-)}$ and the list of "bad" SBI are established, for which $\delta In_i(\Delta\tau) < 0$. It is recommended to reduce their load inversely proportional to their relative values

$$\delta^* In_i(\Delta\tau) = \frac{\delta In_i(\Delta\tau)}{\sum_{i=1}^{m^{(-)}} \delta In_i(\Delta\tau)} \quad (3)$$

- the main reasons for the decrease in the efficiency of the power plant SBI are formed

It should be noted that at the initial stage of implementation of the automated control system, the "weak links" of the control system are established based on tolerance $\delta In_{i,j} > 10\%$. Subsequently, this tolerance can be reduced to 5% [11].

II. Control of the efficiency of the SBI mode management

This control allows us to evaluate the work of personnel to improve the technical and economic indicators of the SBI for the past period. In practice, for a number of indicators (T_{eg}, C_{air}, ΔS_{air}, $Q_{o.n}$, η_n) this control is carried out according to calculated standard indicators that correspond to the energy characteristics of each SBI. However, as the service life of the SBI increases, the initial energy characteristic is transformed. Insufficient consideration of this change leads to the fact that the error in the standard values of the indicators increases. This is reflected in a significant discrepancy between the actual values of the indicators and the standard values. As the service life of the SBI increases, its personnel have fewer and fewer opportunities to maintain indicators equal to the original values. Without changing the existing control system, it is proposed to pay special attention to the "weak links" of the SBI, ensuring the equality of the actual values of the indicators of no less than the arithmetic mean value of the indicators for all similar SBIs of the power plant. In most cases, this result can be achieved by increasing the attention to them by the operating personnel.

The quality of management is assessed based on data on changes in the values of indicators for the period preceding the current calculated period of work $\Delta\tau_k$. Increasing the accuracy of the quantitative assessment of the quality of management, and especially the result of comparing the quality of management of various indicators, can be achieved by switching to calculating the relative magnitude of the change in indicators $\beta In_{i,j}(\Delta\tau)$ and taking into account the measurement error or calculation of indicators G_i. The value of $\beta In_{i,j}(\Delta\tau)$ is supposed to be calculated using the formula with the increase of $In_{i,j}(\Delta\tau)$ the efficiency of the SBI increases.

$$\beta In_{\mathrm{i,j}}(\Delta\tau_{k-1}) = \frac{In_{\mathrm{i,j}}(\Delta\tau_{k-1}) - In_{i,j}(\Delta\tau_{k-2})}{In_{\mathrm{max,i}}(\Delta\tau_{k-2}) - In_{min,\,i}(\Delta\tau_{k-2})} \quad (4)$$

Otherwise

$$\beta In_{\mathrm{i,j}}(\Delta\tau_{k-1}) = \frac{In_{\mathrm{i,j}}(\Delta\tau_{k-2}) - In_{i,j}(\Delta\tau_{k-1})}{In_{\mathrm{max,i}}(\Delta\tau_{k-2}) - In_{min,\,i}(\Delta\tau_{k-2})} \quad (5)$$

In this case, if $\beta In_{i,j}(\Delta\tau_{k-1}) > 0$, then switching off the SBI to reserve and fulfilling the conservation requirement led to an increase in the efficiency of the SBI, and if $\beta In_{i,j}(\Delta\tau_{k-1}) < 0$, then to a decrease in the reliability and cost-effectiveness of the operation. The calculation results for each SBI ($j = 1, m_\Sigma$) include:

- conventional numbers and names of the considered $i = 1, n_\Sigma$ technical and economic indicators
- averaged over the calculation period $\Delta\tau_{k-2}$ quantitative estimates of these indicators $In_{i,j}(\Delta\tau_{k-2})$ with $i = 1, n_\Sigma$
- averaged over all SBI for period $\Delta\tau_{k-2}$ quantitative estimates of these indicators $M^*[In_i(\Delta\tau_{k-2})]$ with $i = 1, n_\Sigma$
- averaged over the calculation period $\Delta\tau_{k-1}$ quantitative estimates of these indicators $In_{i,j}(\Delta\tau_{k-1})$ with $i = 1, n_\Sigma$
- assessment of the quality of management

The assessment of the quality of management is classified into five types: 1-unacceptable; 2-bad; 3-satisfactory; 4-good; 5-indicative and is determined based on the following conditions, which contribute to understanding the quantitative assessment of the quality of management:

1. $J1 = J1 + 1, if\ J1 > N, then\ 37$
2. $if\ R_{1,i} < 0, then\ 20$
3. $if\ In_{i,j}(\Delta\tau_{k-2} > M^*[In_i(\Delta\tau_{k-2})], then\ 12$
4. $if\ In_{i,j}(\Delta\tau_{k-2}) \neq In_{i,min}(\Delta\tau_{k-2}), then\ 8$
5. $if\ In_{i,j}(\Delta\tau_{k-1}) < In_{i,j}(\Delta\tau_{k-2}), then\ J_i = 2 \rightarrow 1$
6. $if\ In_{i,j}(\Delta\tau_{k-1}) < M^*[In_i(\Delta\tau_{k-2})], then\ J_i = 3 \rightarrow 1$
7. $if\ In_{i,j}(\Delta\tau_{k-1}) < In_{i,max}(\Delta\tau_{k-2}), then\ J_i = 4 \rightarrow 1,$ $Otherwise\ J_i = 5 \rightarrow 1$
8. $if\ In_{i,j}(\Delta\tau_{k-1}) < In_{i,min}(\Delta\tau_{k-2}), then\ J_i = 1 \rightarrow 1$
9. $if\ In_{i,j}(\Delta\tau_{k-1}) < In_{i,i}(\Delta\tau_{k-2}) then\ J_i = 2 \rightarrow 1$
10. $if\ In_{i,j}(\Delta\tau_{k-1}) < M^*[In_i(\Delta\tau_{k-2})], then\ J_i = 3 \rightarrow 1$
11. $if\ In_{i,j}(\Delta\tau_{k-1}) < In_{i,max}(\Delta\tau_{k-2})\ then\ J_i = 4 \rightarrow$ $1, Otherwise \rightarrow J_i = 5 \rightarrow 1$
12. $if\ In_{i,j}(\Delta\tau_{k-2}) \neq In_{i,max}(\Delta\tau_{k-2})\ then\ 16$
13. $if\ In_{i,j}(\Delta\tau_{k-1}) > In_{i,max}(\Delta\tau_{k-2})\ then\ J_i = 4 \rightarrow 1$
14. $if\ In_{i,j}(\Delta\tau_{k-1}) > M^*[In_i(\Delta\tau_{k-2})], then\ J_i = 3 \rightarrow 1$
15. $if\ In_{i,j}(\Delta\tau_{k-1}) > In_{i,min}(\Delta\tau_{k-2})\ then\ J_i = 2 \rightarrow$ $1, Otherwise \rightarrow J_i = 1 \rightarrow 1$
16. $if\ In_{i,j}(\Delta\tau_{k-1}) > In_{i,max}(\Delta\tau_{k-2})\ then\ J_i = 5 \rightarrow 1$
17. $if\ In_{i,j}(\Delta\tau_{k-1}) > In_{i,j}(\Delta\tau_{k-2})\ then\ J_i = 4 \rightarrow 1$
18. $if\ In_{i,j}(\Delta\tau_{k-1}) > M^*[In_i(\Delta\tau_{k-2})], then\ J_i = 3 \rightarrow 1$
19. $if\ In_{i,j}(\Delta\tau_{k-1}) > In_{i,min}(\Delta\tau_{k-2})\ then\ J_i = 2 \rightarrow$ $1, Otherwise \rightarrow J_i = 1 \rightarrow 1$
20. $if\ In_{i,j}(\Delta\tau_{k-2}) > M^*[In_i(\Delta\tau_{k-2})], then\ 29$
21. $if\ In_{i,j}(\Delta\tau_{k-2}) \neq In_{i,min}(\Delta\tau_{k-2}), then\ 25$
22. $if\ In_{i,j}(\Delta\tau_{k-1}) < In_{i,j}(\Delta\tau_{k-2}), then\ J_i = 4 \rightarrow 1$
23. $if\ In_{i,j}(\Delta\tau_{k-1}) < M^*[In_i(\Delta\tau_{k-2})], then\ J_i = 3 \rightarrow 1$
24. $if\ In_{i,j}(\Delta\tau_{k-1}) < In_{i,max}(\Delta\tau_{k-2})\ then\ J_i = 2 \rightarrow$ $1, Otherwise \rightarrow J_i = 1 \rightarrow 1$
25. $if\ In_{i,j}(\Delta\tau_{k-1}) < In_{i,min}(\Delta\tau_{k-2}), then\ J_i = 5 \rightarrow 1$
26. $if\ In_{i,j}(\Delta\tau_{k-1}) < In_{i,j}(\Delta\tau_{k-2}), then\ J_i = 4 \rightarrow 1$
27. $if\ In_{i,j}(\Delta\tau_{k-1}) < M^*[In_i(\Delta\tau_{k-2})], then\ J_i = 3 \rightarrow 1$
28. $if\ In_{i,j}(\Delta\tau_{k-1}) < In_{i,max}(\Delta\tau_{k-2})\ then\ J_i = 2 \rightarrow$ $1, Otherwise \rightarrow J_i = 1 \rightarrow 1$
29. $if\ In_{i,j}(\Delta\tau_{k-2}) \neq In_{i,max}(\Delta\tau_{k-2})\ then\ 33$
30. $if\ In_{i,j}(\Delta\tau_{k-1}) > In_{i,max}(\Delta\tau_{k-2}), then\ J_i = 2 \rightarrow 1$
31. $if\ In_{i,j}(\Delta\tau_{k-1}) > M^*[In_i(\Delta\tau_{k-2})], then\ J_i = 3 \rightarrow 1$
32. $if\ In_{i,j}(\Delta\tau_{k-1}) > In_{i,min}(\Delta\tau_{k-2})\ then\ J_i = 4 \rightarrow$ $1, Otherwise \rightarrow J_i = 5 \rightarrow 1$
33. $if\ In_{i,j}(\Delta\tau_{k-1}) > In_{i,max}(\Delta\tau_{k-2}), then\ J_i = 1 \rightarrow 1$
34. $if\ In_{i,j}(\Delta\tau_{k-1}) > In_{i,j}(\Delta\tau_{k-2}), then\ J_i = 2 \rightarrow 1$
35. $if\ In_{i,j}(\Delta\tau_{k-1}) > M^*[In_i(\Delta\tau_{k-2})], then\ J_i = 3 \rightarrow 1$
36. $if\ In_{i,j}(\Delta\tau_{k-1}) > In_{i,min}(\Delta\tau_{k-2})\ then\ J_i = 4 \rightarrow$ $1, Otherwise \rightarrow J_i = 5 \rightarrow 1$
37. Exit

Figure 1: The fragment of management quality assessment

The conclusion includes:

- quantitative assessments of the quality of control of the work of the power plant SBI.
- results of the ranking of SBI by quality of management and their comparison with the sequence of SBI numbers ranked by technical condition
- information about the SBI with the highest and worst management quality
- information on the nature of changes in technical and economic indicators during intuitive management of the efficiency of the SBI

It should be noted that the algorithm for assessing the quality of management determines the qualifications of personnel in implementing recommendations to improve the efficiency of the SBI. If these recommendations are missing, then a comparison of technical and economic indicators for (k-2) and (k-1) calculation periods allow us to assess the quality of management of the SBI efficiency with the existing approach.

III. Assessment of the technical condition of the SBI

When the SBI is inoperative (except for its emergency or scheduled repair), the efficiency of subsequent operation largely depends on the fulfillment of the requirements for one of the reliability properties – storability, SBI. Ensuring the storability of the SBI is reduced not only to preventing failure during start-up from a non-working state, but also to the deterioration of its technical and economic indicators. In order to assess the degree of storability of the SBI during its successful start-up from a non-working state, it is necessary to compare the average values of the SBI performance indicators before shutdown (b) and after (a) start-up. For example, averaging of indicators can be carried out a week before stopping the SBI and during the week after startup. It should be noted that the greatest interest is not relatively short-term, but long-term SBI downtime. These primarily include switching off power units to a reserve. Considering that, as a rule, the least reliable and economical power units are and should be switched off to a reserve, and consequently, the least reliable and more economical SBI, the relevance of the storability problem becomes even more significant.

The degree of protection of the SBI from environmental impacts in a state of downtime (power unit shutdown to reserve) is assessed on the basis of the above algorithms with the small difference that:

- instead of indices (k-2) and (k-1), indices “b” and “a” should be introduced, denoting, respectively, the value of the indicators before and after the SBI downtime
- indicators $In_{i,j}(\Delta\tau_b)$, $In_{i,min}(\Delta\tau_b)$, $In_{i,max}(\Delta\tau_b)$ and $M^*[In_i(\Delta\tau_b)]$, as well as when solving the first two problems, are calculated for the value $\Delta\tau_b = 1\,month$, adopted in energy systems, and indicators $In_{i,k}(\Delta\tau_a)$ – for $\Delta\tau_a$, equal to one week
- the calculation is carried out not for all, but for one specific SBI, which is part of the power unit that has been put into reserve
- conclusions and recommendations are changing

The conclusion includes:

- resulting assessment of the sustainability of the SBI
- relative number (%) assessment of indicators:
- with indicators deteriorated during the period of downtime in reserve
- with constant quantitative estimates
- with improved performance indicators during the downtime in reserve
- list of indicators with quantitative assessments worsened in the downtime period

Information about these changes is very important both for improving the SBI preservation system and when planning SBI repairs. The experience of comparing indicators confirms the relevance of the problem of improving the quality of SBI preservation during downtime.

IV. Assessment of the quality of scheduled maintenance

The reliability and efficiency of the SBI operation largely depend on timely scheduled repairs and their quality. The organization of scheduled repairs taking into account the technical condition of the SBI provides the possibility of systematizing information on changes in quantitative estimates of technical and economic indicators during the inter-repair period. It is the dynamics of changes in these indicators, together with average values, that are one of the conditions for the feasibility of restoring the wear of individual SBI units.

Timely implementation of scheduled maintenance even for the technical condition of the SBI does not yet ensure an increase in the efficiency of its operation. The efficiency of operation is ensured only by the good quality of scheduled maintenance. The quality of the repair is assessed automatically in accordance with fragments of the algorithms, similar to the assessment of the storability of the SBI with some natural difference in the table of results of the calculation of the conclusion and recommendation. Unlike the assessment of the quality of control of the SBI modes, the assessment of the quality of the scheduled maintenance of the SBI is equated to the worst assessment of the quality of repair of its individual units. The choice of an average assessment to characterize the quality of the SBI repair is erroneous. Average assessments are higher, but less plausible. The nature of the change in these curves during the inter-repair period $In_{i,j}(\Delta\tau) = f^*(t)$ for one of the SBI and a number of indicators is shown in Figure 2.

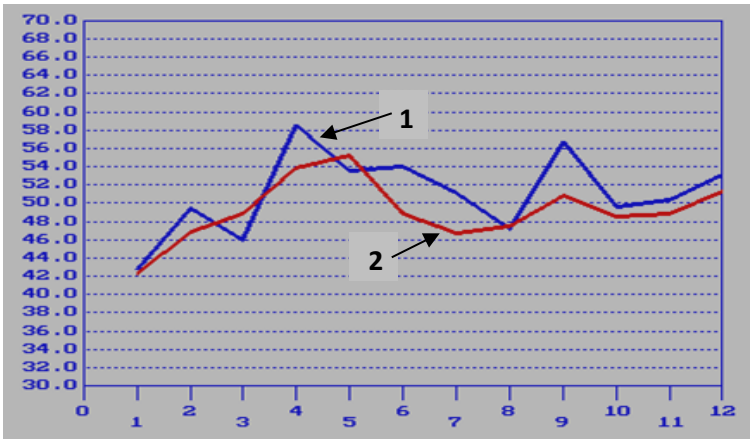


Figure 2: Nature of air suction change during the inter-repair period for values: 1 – actual SBI; 2 – averaged over all SBI.

If the $In_{i,j}(\Delta\tau) = f^*(t)$ curves help to identify the time for scheduled maintenance, then the analysis of the "weak links" – the volume of scheduled maintenance.

Example: It is required to rank the SBIs by technical condition, to establish the most and least efficient SBIs, to identify the main directions for increasing the reliability and efficiency of the power plant SBI operation. The results of calculations based on the data in Tables 1 and 2 for the first month are shown in the following.

No SBI	Technical and economic indicators			
	Name	Relat.dev. mean	Actual val.	Recom. val.
1	Excess air coefficient	-1.657	1.94	1.25
1	Specific load	-1.154	34.00	34.75
1	Air temperature after RAH	-1.090	261.00	295.88
1	Specific consumpt of EE for O.N.	-.984	2.58	2.35
1	Net efficiency	-.710	83.00	84.10
1	Air suction on the tract	-.420	43.30	42.25
1	Specific heat consumpt for O.N.	-.371	2.45	2.14
2	Specific consumpt of EE for O.N.	-.899	2.56	2.35
3	Air suction on the tract	-.300	43.00	42.25
3	Specific consumpt of EE for O.N.	-.176	2.39	2.35
4	Gross efficiency	-1.113	87.88	90.36
4	Exhaust gas temperature	-.911	154.00	132.12
4	Specific heat consumpt for O.N.	-.571	2.62	2.14
4	Net efficiency	-.258	83.70	84.10
4	Air suction on the tract	-.140	42.60	42.25
6	Exhaust gas temperature	-1.036	157.00	132.12
6	Net efficiency	-.710	83.00	84.10
6	Specific heat consumpt for O.N.	-.700	2.73	2.14
6	Specific consumpt of EE for O.N.	-.473	2.46	2.35
6	Gross efficiency	-.409	89.45	90.36
7	Exhaust gas temperature	-.786	151.00	132.12
7	Net efficiency	-.323	83.60	84.10
7	Air suction on the tract	-.220	42.80	42.25
8	Gross efficiency	-.960	88.22	90.36
8	Air suction on the tract	-.900	44.50	42.25
8	Specific heat consumpt for O.N.	-.606	2.65	2.14
8	Exhaust gas temperature	-.578	146.00	132.12
8	Specific load	-.231	34.60	34.75
8	Net efficiency	-.194	83.80	84.10
8	Air temperature after RAH	-.291	291.00	295.88

CONCLUSION: The results of the calculations allowed us to establish and recommend:

1. Quantitative assessments of the technical condition (TC) of the SBI are equal to:

No. SBI	1	2	3	4	5	6	7	8
Assess. TC	-.562	.195	.274	-.263	.744	-.26	.171	-.296

2. The least efficient of the operating should be considered **1** SBI. It is recommended to disconnect for scheduled maintenance, and beforehand - to disconnect for reserve or to reduce the load as much as possible
3. The most effective is **5** SBI. It is advisable to work with the maximum permissible productivity
4. The group of "good" includes **,5,3,2,7** SBI. It is allowed to increase their productivity in proportion to the relative values of the coefficients of significance of the technical condition
5. The group of "bad" includes **,1,8,4,6,** SBI. It is recommended to reduce the load inversely proportional to the relative values of the coefficients of significance of the technical condition
6. The main reasons for the decrease in efficiency of all SBI ES are:
   - Air suction on the tract
   - Net efficiency

Conclusions

1. Methods, algorithms and programs have been developed for improving the reliability and efficiency management system of power unit SBIs, allowing, based on the results of measuring and calculating technical and economic indicators:
   - obtain a quantitative assessment of the technical condition of the SBI
   - evaluate the results of operational management of the operating modes of the control system
   - calculate the durability of the technical condition of the SBI during downtime
   - to formulate a strategy for the planned repair of the SBI and to assess the quality of the repair

2. The developed method allows us to consider the obtained results as methodological support for personnel in organizing the operation, maintenance and repair of SBI

References

[1] Farhadzadeh, E. M. Farzaliev, Y. Z. Muradaliev, A. Z. Method and algorithm for ranking boiler units of block power plants by the criterion of reliability and economic efficiency of operation M., Teploenergetika, 2015, No. 10, pp. 22-29.

[2] Farhadzadeh, E. M. Safarova, T. H. Muradaliev, A. Z. Rafieva, T. K. Farzaliev, Y. Z. Automated system of analysis of individual reliability and efficiency of power units of GRES. M; - Electric power plants, No. 11, 2005, pp.38-46.

[3] Farzaliyev, Y. Z. Comparison of ways of normalization at classification of initial data. RT&A # 03 (34), (Vol.9) 2014, September, pp. 50-56.

[4] Bureeva, N. N. Multivariate the statistical analysis with use ППП "STATISTICA". The methodical material under the program of improvement of professional skill. «Application of software in scientific researches and teaching of mathematics and mechanics». Nizhniy Novgorod, 2007, 112 p.

[5] Lukomsky, Ya. I. Theory of correlation and its application to the analysis of production. Goskomizdat, 1961, p.376.

[6] Liang Yan. Generalized fiducial inference for the Lomax distribution / Liang Yan, Juan Geng, Lijun Wang, Daojiang He // Journal of Statistical Computation and Simulation, DOI: 10.1080/00949655.2021.1895159, - 2021. March.

[7] Samuel, A. O. Zhijian Zhang. Multivariate analysis of critical parameters influencing the reliability of thermal-hydraulic passive safety system // September 2018. Nuclear Engineering and Technology 51(1), DOI:10.1016/j.net.2018.08.012.

[8] Bonferroni, C.E. "Il calcolo delle assicurazioni su gruppi di teste." In Studi in Onore del Professore Salvatore Ortu Carboni. Rome: Italy, pp. 13-60, 1935.

[9] Lidong, E. Jan Hannig and Hari Iyer Fiducial Intervals for Variance Components in an Unbalanced Two-component Normal Mixed Linear Model // Colorado State University, Fort Collins, CO 80523 October 13, 2006. – pp. 1-35.

[10] RD 34.09.454. Typical algorithm for calculation of technical and economic indicators of condensing power units of 300, 500, 800 and 1200 mW capacity. VTN, 2017.

[11] Duelle M. A., Kananjuk A.I. and Oodnova, O. I. Automatization of determination of energy characteristics of energy equipment // Energy Conservation, Energy Technology, Energy Auditing, 2013, ¹ 2, p. 13-19. 13-19.

A NOVEL METHOD TO ASSESSING PROCESS VARIATION WITH A CONFIDENCE INTERVAL OF SAMPLE STANDARD DEVIATION

Boya Venkatesu[1], G. Siva[2], Christophe Chesneau[3*], V. Sai Sarada[4]

•

[1]School of Business, Woxsen University, Hyderabad, India.
[2]Department of Mathematics, VIT-AP University, Amaravati, India.
[3]LMNO, University of Caen-Normandie, Caen, France.
[4]Department of Research Labs, Asian Health Care Foundation, AIG Hospitals, India.
[1]venkateshboya50@gmail.com, [2]siva.g@vitap.ac.in, [3*]christophe.chesneau@gmail.com,
[4]saisaradav@gmail.com
Correspondence Email: christophe.chesneau@gmail.com

Abstract

One of the great tools of statistical process control for evaluating patterns of variation in the process is the control chart. In this article, we focus on developing a new approach to estimating process parameters in a control chart using confidence intervals (CIs) of sample standard deviations. They have the property of providing additional information about the quality of the estimate. A Monte Carlo simulation is used to investigate the accuracy of the obtained CIs. The performance of the classical and new approaches is compared in terms of standard error using simulated samples. The simulation results show that the new approach outperforms the classical approach.

Keywords: Control chart, point estimation, process variation, interval estimation, standard error.

I. Introduction

The control chart approach focuses on the estimation of process parameters. While the location parameter is estimated by the subgroup mean (average), there are various methods for estimating the process standard deviation. This problem is more important for non-Shewhart charts such as CUSUM or EWMA [7, 14]. In recent decades, there has been a growing interest in the use of better estimates than these classical methods [2]. In a sense, one class of estimates are robust estimates. Most classical estimation methods use point estimates, where a single value obtained from the sample data is used as an estimate. For various reasons, these estimates often do not represent the true parameters and hence the concept of interval estimation has emerged. Although Shewart's control chart is 8 decades old, researchers continue to identify gaps in both the theory and application of control charts. Some broad areas of research in this area can be such as economic design of control charts, control charts for dispersion, control charts for percentiles (median), control charts with asymmetric limits, mixed control charts and impact of parameter estimation on control charts [10]. Ronald Caulcutt [6] presented some statistical arguments about the design of control limits and suggested that standard methods should not be used without understanding the characteristics of the data. He argued that a delta chart should be used in

addition to x-bar and R-charts, where the delta chart takes into account the differences in the group means and thus operates on the medium-term variability of the process. Boyles [3, 4] addressed the problem of estimating the variation of a run chart (a control chart for individual values) using dynamic linear models (DLM) Estimation by using the Integrated Moving Average (1,1) model. This method was an improvement over the conventional moving range (MR-bar) method. He also found that the new estimate was robust. John Braun and Park [5] addressed the issue of calculating the sample standard deviation from individual data in the context of out-of-control and non-normal situations. They have proposed a method of pre- and post-control for outliers with control limits based on the median absolute deviation (MAD). This procedure shows better performance than the Boyles method. Tung-Lung Wu [15] has come up with the design of a distribution-free run-based control chart to detect location shifts (shift in process mean). This approach used the concept of "conditional longest run statistic" in addition to ARL. It is a truly distribution-free method and no historical data is required as no parameters are estimated.

In statistical process control (SPC), the control chart is an essential tool for monitoring the consistency and variability of a process over time [8, 9, 11]. To construct a control chart, the process variability must be quantified, which is typically done using either the range (R) or the standard deviation (σ) of the sample data. Boya et al. [1] developed a novel approach to estimate the process variation using the confidence interval of the sample range. Based on this previous work, the authors realized that the use of range to estimate control limits often involves the use of approximations or empirical rules (such as the average range chart), which may not be as accurate. Therefore, the focus of this study is to estimate process variation using confidence interval estimates of the sample standard deviation (σ), which is derived from all data points and provides a more accurate and consistent measure of process variation. The remainder of the article is organized as follows: In Sections 2 and 3, we consider interval estimates in the context of process mean and standard deviation. In Section 3, we develop a new approach to estimating process variation using interval estimation. In Section 4, we discuss the step-by-step procedure of the new method, and Section 5 consists of the simulation study.

II. Interval estimates of process mean in $N(\mu, \sigma^2)$

In order to describe our approach, it is necessary to present a precise mathematical framework. Let X be a measure of interest and θ be an associated parameter. We suppose that he has a point estimate $\hat{\theta}(x)$, where x is a random sample. If we replace $\hat{\theta}(x)$ by a statistic, which is a subset of the parameter space, then we get an interval estimate. The general format of an interval estimate is $\hat{C}(x) = \left[\hat{\theta}(x) - \delta(x), \hat{\theta}(x) + \delta(x)\right]$, where $\hat{\theta}(x)$ is the point estimate and $\delta(x)$ is known as the margin of error, such that $P_\theta\left\{\theta \in \hat{C}(x)\right\} = \gamma$, where $0 < \gamma < 1$ is called the level of significance, and the interval is called level of confidence (usually 95%) and $\hat{C}(x)$ is called Confidence Interval (CI).

In the case of normality, when the main measure can be modeled by a random variable, say $X \sim N(\mu, \sigma^2)$, we can find the $\frac{\alpha}{2}$ CI for the mean by using normal approximation. More precisely, let $Z \sim N(0,1)$ and Z_α be a value on Z, such that

$$P(|Z| > Z_\alpha) = \alpha. \tag{1}$$

Suppose μ_o denotes the true mean (unknown) and let $\bar{x}$ be the point estimate of μ. It follows that the condition $Z = |\frac{\bar{x}-\mu_0}{\sigma_0}| < Z_\alpha$ leads to the $\bar{x} - Z_\alpha \frac{\sigma_0}{\sqrt{n}} < \mu_0$ and $\bar{x} + Z_\alpha \frac{\sigma_0}{\sqrt{n}} > \mu_0$

If we take $\gamma = 1 - 2\alpha$ then $\alpha = \frac{1-\gamma}{2}$ so that the interval $\left[\bar{x} - Z_{(1-\gamma)/2}\frac{\sigma_0}{\sqrt{n}}, \bar{x} + Z_{(1-\gamma)/2}\frac{\sigma_0}{\sqrt{n}}\right]$ has a confidence level of γ. Hence the $100(1-\alpha)\%$ CI for the mean is given by

$$\left[\bar{x} - Z_{(1-\gamma)/2}, \bar{x} + Z_{(1-\gamma)/2}\right]. \tag{2}$$

The above CI is known as Z-interval because the margin of error is based on normal distribution. We can also construct the margin of error using student's t-distribution. Then the $100(1-\alpha)\%$ CI

for σ from $X \sim N(\mu, \sigma^2)$ is based on t- distribution, and it is given by

$$\left[\bar{x} - t_{(n-1),(1-\gamma)/2}\frac{s}{\sqrt{n}}, \bar{x} + t_{(n-1),(1-\gamma)/2}\frac{s}{\sqrt{n}}\right], \tag{3}$$

where the sample standard deviation s is an estimate of σ.

III. Interval estimates of process σ in $N(\mu, \sigma^2)$

In the context of control charts, the estimation of σ is done in two ways viz, a) Using sample range (R) b) Using sample standard deviation (s). With the method of ranges, we have: $\hat{\sigma}_R = \frac{\bar{R}}{d_{2,n}}$, where $\bar{R}$ is the average of ranges over m samples and $d_{2,n}$ is a scaling constant. Let us define $\chi^2_{\alpha/2}$ and $\chi^2_{1-\alpha/2}$ as the lower and upper $\frac{\alpha}{2}$ percentile points on the Chi-square distribution. Then the $100(1-\alpha)\%$ CI for σ from $X \sim N(\mu, \sigma^2)$ is based on the χ^2 distribution, and it is given by

$$\left[\sqrt{\frac{(n-1)}{\chi^2_{\alpha/2}}}, \sqrt{\frac{(n-1)}{\chi^2_{1-\alpha/2}}}\right], \tag{4}$$

where $\chi^2_{\alpha/2}$ and $\chi^2_{1-\alpha/2}$ as the lower and upper $\frac{\alpha}{2}$ percentile points on the Chi-square distribution. The $100(1-\alpha)\%$ CI for σ based on R is given by

$$\left[\frac{R}{d_{2,n}}G_1, \frac{R}{d_{2,n}}G_2\right], \tag{5}$$

where G_1, G_2 are constants and R denotes the sample range, and $d_{2,n}$ is a scaling constant. In this article, our focus is to study the method of triplet estimation of process variation (σ) when the quality characteristic follows the normal distribution $N(\mu, \sigma^2)$. Instead of using $\frac{\bar{R}}{d_{2,n}}$ as an estimate, we consider the $100(1-\alpha)\%$ CI of the sampling distribution of sample variance and thereby derive a new estimate as a linear combination of the triplet estimate.
Let $x_1, x_2, \ldots, x_n$ be a random sample of size n drawn from the process. From this sample process mean μ is estimated as

$$\bar{x}_i = \frac{1}{n}\sum_{j=1}^{n} x_{ij},$$

where x_{ij} denote the j-th observation in the i-th sample ($i = 1, 2, \ldots, k$; $j = 1, 2, \ldots, n$) and $\bar{x}_i$ is the sample mean of the i-th subgroup.
The corresponding sample standard deviation is denoted by

$$s_i = \sqrt{\frac{1}{n-1}\sum_{j=1}^{n}(x_{ij} - \bar{x}_i)^2},$$

which are the point estimates of the respective parameters, here s_i denotes i-th subgroup standard deviation. The overall (grand) mean of all the sample means is represented as $\bar{x} = \frac{1}{k}\sum_{i=1}^{k}\bar{x}_i$ and

$$s = \sqrt{\frac{1}{nk-1}\sum_{i=1}^{k}\sum_{j=1}^{n}(x_{ij} - \bar{x})^2}.$$

It is important to note that s is not an unbiased estimate of σ. In fact, s estimates the quantity $C_4\sigma$, where

$$C_4 = \sqrt{\frac{2}{n-1}}\left(\frac{\Gamma(n/2)}{\Gamma((n-1)/2)}\right)\sigma$$

is a constant whose values are tabulated [12, 13]. As such an unbiased estimate of σ is $\frac{s}{C_4}$.
For normally distributed data, the sampling distribution of the statistic $\frac{ns^2}{\sigma^2}$ follows the Chi-square distribution with n degrees of freedom. Then the $100(1-\alpha)\%$ CI for σ^2 is given by

$$\left[\frac{(n-1)}{\chi^2_{\alpha/2}}s^2, \frac{(n-1)}{\chi^2_{1-\alpha/2}}s^2\right].$$

The CI for σ is then defined as

$$\left[\sqrt{\frac{(n-1)}{\chi^2_{\alpha/2}}}\left(\frac{s}{c_4}\right), \sqrt{\frac{(n-1)}{\chi^2_{1-\alpha/2}}}\left(\frac{s}{c_4}\right)\right].$$

Hence, the triplet estimates of σ based on s can be written as $\eta = \{\eta_1, \eta_2, \eta_3\}$, where

$$\eta_1 = \sqrt{\frac{(n-1)}{\chi^2_{\alpha/2}}}\left(\frac{s}{c_4}\right), \quad \eta_2 = \frac{s}{c_4}, \quad \text{and} \quad \eta_3 = \sqrt{\frac{(n-1)}{\chi^2_{(1-\alpha)/2}}}\left(\frac{s}{c_4}\right). \tag{6}$$

It can be seen from Boya et al. [1] that the triplet estimates of σ based on R was stated as $\tau = [\theta_1, \theta_2, \theta_3]$, where $\theta_1 = \frac{R_i}{d_{2,n}G_1}$, $\theta_2 = \frac{R_i}{d_{2,n}}$, and $\theta_3 = \frac{R_i}{d_{2,n}G_2}$, with $d_{2,n}$, G_1 and G_2 being constants for a fixed sample size.

IV. The new estimate of σ using sample standard deviation

The new estimate of σ is a linear combination of the triplet components given in (6)

$$\hat{\sigma}_{s,CI} = l_1\eta_1 + l_2\eta_2 + l_3\eta_3, \tag{7}$$

such that $l_i \geq 0$ for $i = 1, 2, 3$ and $\sum_{i=1}^{3} l_i = 1$.
The subscript CI indicates that (6) is based on the CI.
Let us assume that the process is set up to have a certain variation σ' known either by hypothesis or by engineering specifications. Then the weights will be taken as

$$w_i = |\eta_i - \sigma'|^{-1}, \tag{8}$$

so that

$$l_i = \frac{w_i}{\sum_{i=1}^{3} w_i}, \quad \text{for } i = 1, 2, 3. \tag{9}$$

As the magnitude of the error rises up, the weights go downward. The outcome of this method $\hat{\sigma}_{s,CI}$ for each of the m samples, and this data can be used to study the empirical properties of the new estimate.
The stepwise method used in Boya et al. [1] for range-based estimation is now extended to the case of s-based estimation to arrive at the new estimate of σ.

1. Generate m random samples (subgroups), each of size n, from $N(\mu, \sigma^2)$.
2. Evaluate $\bar{x}$ and s for each subgroup.
3. Calculate η_1, η_2, η_3 of each subgroup using (6).
4. Calculate w_1, w_2, w_3 using (8).
5. Calculate l_1, l_2, l_3 using (9).
6. Find the new estimator $\hat{\sigma}_{s,CI}$ using (7).

This procedure leads to $\hat{\sigma}_{s,CI}$ for each of the m samples, and this value can be used to study the empirical properties of the new estimate.
In the subsequent section, a hypothetical exercise is presented to demonstrate the application of the new method.

V. Simulation study

We have conducted a study $M = 5000$ random samples of different sizes ($n = 10$, 15 and 20) are generated from the normal distribution $N(\mu, \sigma^2)$ with $\mu = 10.5$ and $\sigma = 1.5$. The summary of results is shown in Table 1.

Table 1: *Comparison of η_2 and $\hat{\sigma}_{s,CI}$ using triplet estimate*

n	M	η_2 (Mean $\pm$ S.E)	$\hat{\sigma}_{s,CI}$ (Mean $\pm$ S.E)
10	5000	1.4703 $\pm$ 0.0051	1.4907 $\pm$ 0.0034
15	5000	1.4932 $\pm$ 0.0050	1.4852 $\pm$ 0.0032
20	5000	1.4835 $\pm$ 0.0048	1.4802 $\pm$ 0.0030

From this table it can be seen that, regardless of the subgroup size n, the new estimate by the triplet method is closer to the hypothetical process variation of $\sigma = 1.5$. Furthermore, the standard error is much smaller than that of the classical estimate. Therefore, we propose that the new estimate of σ based on the CI of sample standard deviations gives a stable estimate with low bias compared to $\frac{s}{c_4}$.
The pattern of variation of in the classical and the new estimates are shown in Figure 1. We mention that the sample standard error from 5000 samples with $n = 10, 15$ and 20 are computed to assess the consistency of the new estimate.

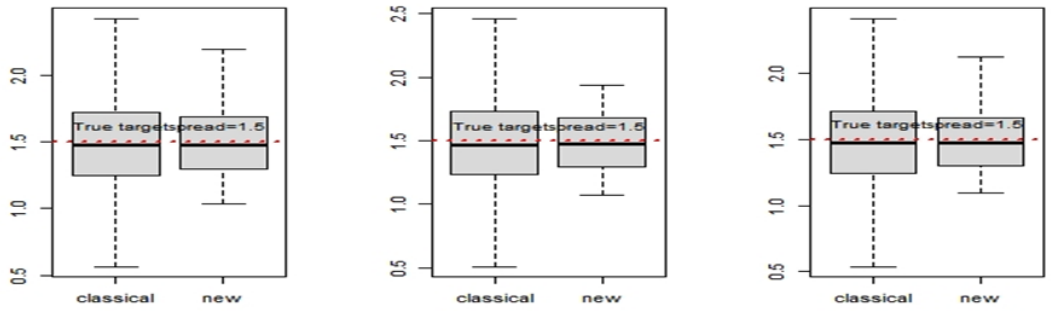


Figure 1: *The pattern of variation of in the classical and the new estimates*

From this figure, it can be seen that $\hat{\sigma}_{s,CI}$ of σ has lower variation around the center when compared to η_2.

VI. Conclusions

This paper introduces a robust and innovative method for estimating process variation using the CI of the sample standard deviation, aimed at improving the accuracy and stability of control charts in SPC. Traditional approaches typically rely on point estimates such as s or $\frac{s}{c_4}$, which often suffer from bias and variability, especially with small sample sizes. To address these limitations, the proposed method constructs a triplet estimator η_1, η_2, η_3 derived from the CI of the sample standard deviation. These components are then combined into a single weighted estimator $\hat{\sigma}_{s,CI}$ using an inverse-error weighting scheme, making the final estimate both data-driven and adaptively robust.

A comprehensive Monte Carlo simulation study with 5000 replications across various sample sizes ($n = 10, 15, 20$) was conducted to evaluate the performance of the proposed method. The results showed that the new estimator closely approximated the true process standard deviation

(σ = 1.5) while achieving a significantly lower standard error compared to the classical point estimator s or $\frac{s}{c_4}$. Visual analysis of the estimator's distribution further confirmed reduced variability and improved stability.

Overall, this interval-based approach is more precise and reliable than existing SPC tools, making it a valuable enhancement. It provides a statistically robust alternative to classical estimators and is particularly beneficial when working with moderate or small sample sizes. The method is flexible, simple to use, and based on solid statistical theory. This makes it very useful in quality control and industrial settings. Future research could involve extending this method to non-normal data distributions or integrating it with modern adaptive control chart frameworks.

References

[1] Boya Venkatesu, Abbaiah, R., and Sai Sarada, V. (2018). A New Method of Estimating the Process Variation Using Confidence Interval of Sample Range. *RESEARCH REVIEW International Journal of Multidisciplinary*, 3(08):204–207.

[2] Boya Venkatesu, Abbaiah, R., and Sai Sarada, V. (2019). On the Estimation of Operating Characteristic of Shewart Control Chart for Means Using Interval Estimates of Process Mean and Variation. *International Journal of Advanced Scientific Research and Management (IJASRM)*, 4(04):62–66.

[3] Boyles, R. A. (1979). Estimating Common-cause σ in the Presence of Special Causes. *Journal of Quality Technology*, 29:381–395.

[4] Boyles, R. A. (1997). Estimating Common-cause Sigma in the Presence of Special Causes. *Journal of Quality Technology*, 29(4):381–395.

[5] Braun, W. J. and Park, D. (2008). Estimaion of σ for Individuals Charts. *Journal of Quality Technology*, 40(3):332-344.

[6] Caulcutt, R. (1995). The Rights and Wrongs of Control Charts. *Journal of the Royal Statistical Society. Series C (Applied Statistics)*, 44(3):279–288.

[7] Chakraborti, S. and Van de Wiel, M. A. (2008). A Nonparametric Control Chart Based on the Mann-Whitney Statistic. *Collections*, 156–172.

[8] Duncan, A. J. (1986). *Quality Control and Industrial Statistics* (5th ed.). Irwin, Homewood.

[9] Grant, E. L. (1964). *Statistical Quality Control* (3rd ed.). McGraw-Hill Book Company.

[10] Guo, B. and Wang, B. X. (2016). Control Charts for the Coefficient of Variation. *Statistical Papers*, 59(3):933–955.

[11] Mittag, H. J. and Rinne, H. (1993). *Statistical Methods of Quality Assurance*. Chapman and Hall, CRC Press.

[12] Montgomery, D. C. (2008). *Introduction to Statistical Quality Control* (4th ed.). John Wiley & Sons.

[13] Montgomery, D. C. and Runger, G. C. (2002). *Applied Statistics and Probability for Engineers* (3rd ed.). John Wiley & Sons.

[14] Park, C. and Reynolds, M. R. (1987). Nonparametric Procedures for Monitoring a Location Parameter Based on Linear Placement Statistics. *Sequential Analysis*, 6(4).

[15] Tung - Lung Wu. (2018). Distribution-Free Runs-Based Control Charts. *Journal of Computational Statistics and Data Analysis*, 1–14.

DIFFERENT ESTIMATION METHODS AND VALIDATION FOR THE EXTENSION EXPONENTIAL DISTRIBUTION

Rochdi Nouadri [1], Nacira Seddik-Ameur [2], Khaoula Aidi [3]

[1,2,3]LaPS laboratory, Badji-Mokhtar University, Box 12, Annaba, 23000, Algeria.
rochdi.nouadri@univ-annaba.dz , naciraseddik@yahoo.fr, khaoula.aidi@yahoo.fr

Abstract

This study investigates the extended exponential distribution proposed by Nadarajah and Haghighi, which can effectively model data with a mode at zero and accommodate varying hazard rates—whether increasing, decreasing, or constant. Unlike other distributions, it allows for scenarios where the hazard function increases while the probability density function decreases monotonically. The focus is on exploring alternative estimation methods to maximum likelihood estimation for this distribution, including the maximum product of spacing, Cramer-von Mises, Anderson-Darling, Right-tail Anderson-Darling, Left-tail Anderson-Darling, and Kolmogorov-Smirnov tests. A novel approach using initial data is proposed to develop an effective goodness-of-fit criterion tailored for validating this model. Extensive simulations with thousands of samples are conducted to assess the performance of these estimation methods and the practicality of the proposed goodness-of-fit test. Real data applications are also utilized to demonstrate the applicability and effectiveness of the extended exponential distribution in real-world scenarios. This research expands the statistical modelling toolkit by providing robust estimation techniques and validation criteria specifically designed for the characteristics of the extended exponential distribution.

Keywords: Anderson-Darling method, Cramer-von-Mises method, maximum likelihood estimation, maximum product of spacing method, Right-tail Anderson-Darling method, goodness-of-fit test.

AMS classification: 62G10-62N05-62F12.

I. Introduction

The recent statistical literature mainly focuses on the introduction of new models capable of describing observations when classical models cannot do so. There are different forms of generalizations either by adding shape parameters, by exponentiation the cumulative distribution or based on generator distributions, one can see [8], [2], [6], [3] and others. Nevertheless, [17] proposed a simple and very interesting model. With two parameters, this one offers a good alternative to gamma, Weibull and the exponentiated exponential distributions for which the hazard functions are only constant or decreasing when the probability density function (pdf) is monotonically decreasing while the rate failure of the new distribution can be increasing. Also, this distribution is able to describe data with mode fixed at zero when Its hazard rates can be increasing, decreasing and constant which is not realized for other models. Making a simple change of variable, the new model is reduced to a truncated Weibull distribution. The proposed distribution has more applications than classical models like the fit of the daily rainfall data (for example) which have a monotonically decreasing probability density (pdf) function when the empirical hazard rate failure (hrf) is increasing. The authors studied mathematical properties such the moments, the Bonferroni and Lorenz curves, the entropy and the order statistics. For estimating the unknown parameters, they proposed the maximum likelihood (MLE) and the

moment estimation (MME) methods which cannot give the explicit forms of the estimators, so iterative methods are required and as It well known the results are performed for big sample sizes. It should be noted also, that the validation of this model is not investigate yet till now which motivate us to propose a new technique for testing the fit of this distribution.

In this work, we propose, firstly, different estimation methods which can be used for small and big sample sizes such as the maximum product of spacing (MPS), the Cramer-von-Mises (CM) method, Anderson-Darling (AD) method, Right-tail and Left-tail Anderson-Darling (RAD, LAD) methods and the method of Kolmogorov-Smirnov (KS) to estimate the unknown parameters as alternatives to maximum likelihood estimation method. On the other hand, to have reliable results in any statistical analysis, It must be necessary to verify if the observed data are really described by the model chosen. Using an extension of the chi-square statistic introduced by [18] and [22] for continuous models, we provide a criteria goodness-of-fit test which takes into account the unknown parameters and the initial data for the extension exponential distribution. This new technique recovers all the information given by the observations and can validate effectively the model without comparison with its competitors. Recently, this method was performed for some new distributions, see [23], [25], [24], [19]. An importante simulation study is given to calculate the different estimators, their biases, their mean square errors and their estimated average widths. A comparison study between the method performances is also provided. Beside classical model selection criteria such as AIC, BIC, LL and Kolmogorov-Smirnov statistic, we provided all the elements of the new statistic test which are used to distinguish between this distribution and its competitors. Real data applications are used for illustration purpose.

The objective of this work is to introduce and evaluate alternative estimation methods suitable for both small and large sample sizes, to ensure the chosen model accurately describes the observed data through a new goodness-of-fit test, and to validate the model using comprehensive simulation studies and real data applications.

II.The Extension exponential distribution

Depending on two parameters α and λ (shape and scale), the extension of the exponential distribution introduced by Nadarajah and Haghighi [17] is characterized by the cumulative probability function

$$F(t) = 1 - exp(1 - (1 + \lambda t)^{\alpha}) \tag{1}$$

The probability density function (pdf) is given by

$$f(t) = \alpha\lambda(1 + \lambda t)^{\alpha-1} exp(1 - (1 + \lambda t)^{\alpha}) \qquad \alpha > 0 \text{and} \lambda > 0. \tag{2}$$

The hazard and the cumulative hazard functions are

$$h(t) = \alpha\lambda(1 + \lambda t)^{\alpha-1} \tag{3}$$

$$H(t) = -log(S(t)) = (1 + \lambda t)^{\alpha} - 1 \tag{4}$$

Different shapes of the pdf and the hazard rate functions are represented in Figure 1 and Figure 2.

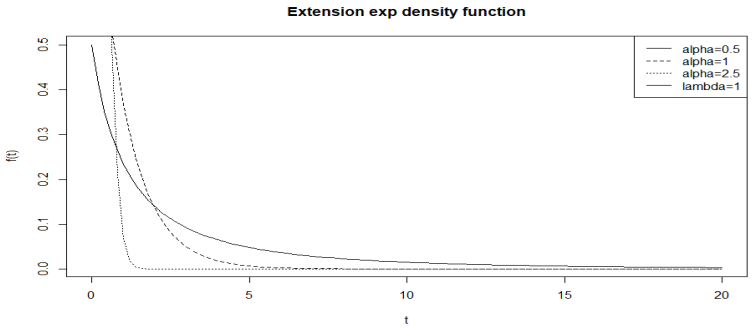


Figure 1: *probability density function of the extension exponential distribution*

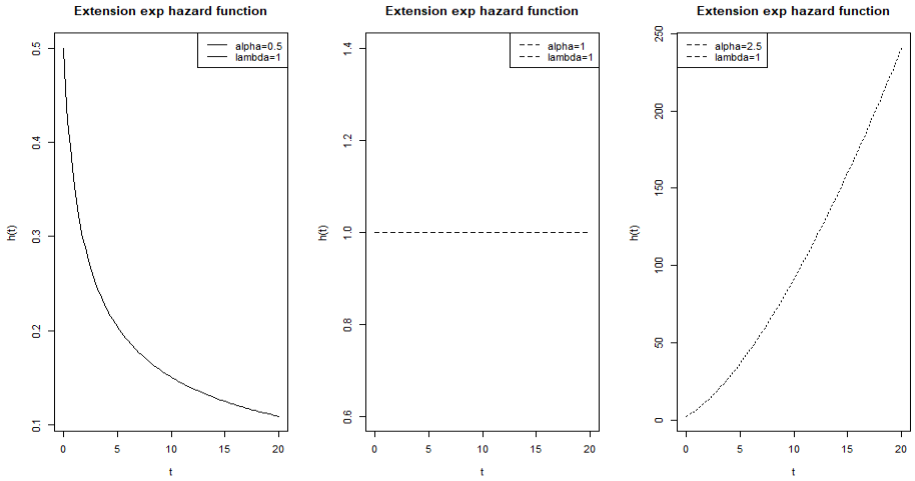


Figure 2: *hazard function of the extension exponential distribution*

The interest of this pdf is to have the mode zero and different hazard shapes (increasing, decreasing and constant), furthermore the extension exponential distribution pdf takes only decreasing shapes whereas the hazard function can be increasing (see Figure 3).

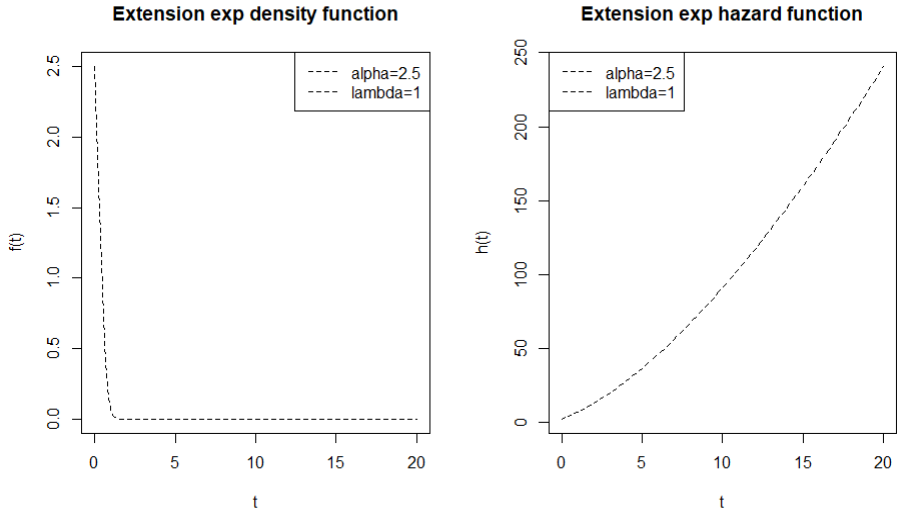


Figure 3: *density and hazard function of the extension exponential distribution with* $\alpha > 1$

The authors studied mathematical properties such as the moments, the Bonferroni and Lorenz curves which have applications in several fields, the entropy and the order statistics. For estimating the unknown parameters, they proposed the maximum likelihood and the moment estimation methods.

III. Maximum likelihood estimation

In this section we resume the maximum likelihood estimators of the unknown parameters in order to compare with those of the proposed methods in this work.

We consider a sample of n independent identically distributed variables $t_1, t_2, \ldots, t_n$ from the extension exponential distribution with the parameter vector $\theta = (\alpha, \lambda)$, the likelihood function is given by

$$L(t_1, t_2, \ldots, t_n; \theta) = \prod_{i=1}^{n} f(t_i; \theta) = \prod_{i=1}^{n} \alpha\lambda(1+\lambda t_i)^{\alpha-1} exp(1-(1+\lambda t_i)^{\alpha}) \quad (5)$$

The log-likelihood function is:

$$l = n + n\ln(\alpha) + n\ln(\lambda) + (\alpha-1)\sum_{i=1}^{n} \ln(1+\lambda t_i) - \sum_{i=1}^{n} (1+\lambda t_i)^{\alpha})]$$

The maximum likelihood estimators MLE are obtained by equaling to zero the following first derivatives of the log-likelihood function with respect to the parameters:

$$\frac{\partial l}{\partial \alpha} = \frac{n}{\alpha} + \sum_{i=1}^{n} \ln(1+\lambda t_i) - \sum_{i=1}^{n} (1+\lambda t_i)^{\alpha}\ln(1+\lambda t_i)] = 0 \quad (6)$$

$$\frac{\partial l}{\partial \lambda} = \frac{n}{\lambda} + (\alpha-1)\sum_{i=1}^{n} t_i(1+\lambda t_i)^{-1} - \alpha\sum_{i=1}^{n} t_i(1+\lambda t_i)^{\alpha-1} = 0 \quad (7)$$

As the explicit forms of the MLE $(\hat{\alpha}_{MLE}, \hat{\lambda}_{MLE})$ cannot be derived, one can use numerical methods for solving the obtained equations.

IV. Product of spacing estimation method MPS

Introduced by Cheng and Amin (1979, 1983) [7], the product of spacing estimation method (MPS) is an alternative to the maximum likelihood estimation method. This method was also proposed by Ramnaby (1984) [20] as an approximation to the Kullback-Leibler measure of information.

We consider n independent and identically distributed sample drawn from a population with unknown parameters θ. The MPS estimation method is based on the differencies between the successive increasing empirical repartition functions $F(t_i, \theta)$, and where $F(t_0) = 0$ and $F(t_{n+1}) = 1$.

$$P_i(\theta) = F(t_i, \theta) - F(t_{i-1}, \theta) \quad (8)$$

The MPS estimators are obtained by maximizing the quantity $M(\theta)$:

$$M(\theta) = \frac{1}{n+1}\sum_{i=1}^{n+1} \ln(P_i(\theta)) \quad (9)$$

For the extension exponential distribution, this function is given by:

$$M(\theta) = \frac{1}{n+1}\sum_{i=1}^{n+1} \ln((1-exp(1-(1+\lambda t_i)^{\alpha})) - (1-exp(1-(1+\lambda t_{i-1})^{\alpha})) \quad (10)$$

$$M(\theta) = \frac{1}{n+1}\sum_{i=1}^{n+1} \ln(exp(1-(1+\lambda t_{i-1})^{\alpha}) - exp(1-(1+\lambda t_i)^{\alpha})) \quad (11)$$

So, the MPS estimators are the solutions of the following equations

$$\frac{\partial M(\theta)}{\partial \alpha} = \frac{1}{n+1}\sum_{i=1}^{n+1} \frac{D1(t_i,\theta) - D1(t_{i-1},\theta)}{P_i} = 0 \quad (12)$$

$$\frac{\partial M(\theta)}{\partial \lambda} = \frac{1}{n+1}\sum_{i=1}^{n+1} \frac{D2(t_i,\theta) - D2(t_{i-1},\theta)}{P_i} = 0 \quad (13)$$

where $D1$ and $D2$ are the first derivatives of the repartition function with respect to the unknown parameters α and λ:

$$D1 = \frac{dF(t)}{d\alpha} = (1+\lambda t)^{\alpha}\ln(1+\lambda t)exp(1-(1+\lambda t)^{\alpha}) \tag{14}$$

$$D2 = \frac{dF(t)}{d\lambda} = \alpha t(1+\lambda t)^{\alpha-1}exp(1-(1+\lambda t)^{\alpha}) \tag{15}$$

Cheng and Amin (1983) [7] showed that the obtained MPS estimators are as efficient and consistent as the maximum likelihood estimators (MLE) under more general conditions.

V. Cramer Von Mises estimation method

Among minimum type estimation methods proposed in the statistical literature, the Cramer-Von-Mises CM method estimation consists in minimizing the distances between theoretical and empirical repartition functions (Cramer-Von-Mises statistic) of the studied model. This method is shown to give the smaller bias estimators than the other minimum distance estimators see [15].

For the extension of the exponential distribution, this statistic is defined by

$$C(a,\lambda) = \frac{1}{12} + \sum_{i=1}^{n}\left((1-exp(1-(1+\lambda t_i)^{a})) - \frac{2i-1}{2n}\right)^2 \tag{16}$$

To calculate the CM estimators $(\hat{a}_{CV}, \hat{\lambda}_{CV})$ of the unknown parameters, we cancel the first partial derivatives of this statistic $C(a,\lambda)$ with respect to the unknown parameters of the distribution, which amounts to solving the following equations:

$$\sum_{i=1}^{n}\left((1-exp(1-(1+\lambda t_i)^{a})) - \frac{2i-1}{2n}\right)D1 = 0 \tag{17}$$

$$\sum_{i=1}^{n}\left((1-exp(1-(1+\lambda t_i)^{a})) - \frac{2i-1}{2n}\right)D2 = 0 \tag{18}$$

where $D1$ and $D2$ are as given above.

V. Anderson-Darling estimation method

Anderson-Darling method is also a minimum type estimation method, so the estimators $(\hat{a}_{AD}, \hat{\lambda}_{AD})$ are obtained by minimizing the well-known Anderson-Darling statistic A^2 suggested by Anderson and Darling [4] with respect to the unknown parameters. [5] also discussed the properties of the AD estimators and presented its computational form as

$$A^2(a,\lambda) = -n - \frac{1}{n}\sum_{i=1}^{n}(2i-1)[\ln(F(t_i)) - \ln(1-F(t_{i^*}))] \tag{19}$$

$$A^2(a,\lambda) = -n - \frac{1}{n}\sum_{i=1}^{n}(2i-1)[\ln(1-exp(1-(1+\lambda t_i)^{a}))) - \ln(1-(1-exp(1-(1+\lambda t_{i^*})^{a})))] \tag{20}$$

where $i^* = n - i + 1$.

For our model, the estimators $(\hat{a}_{AD}, \hat{\lambda}_{AD})$ are obtained by the resolution of the following equations:

$$\sum_{i=1}^{n}(2i-1)\left[\frac{D1(t_i)}{(1-exp(1-(1+\lambda t_i)^{a}))} - \frac{D1(t_{i^*})}{(1-(1-exp(1-(1+\lambda t_{i^*})^{a})))}\right] = 0 \tag{21}$$

$$\sum_{i=1}^{n}(2i-1)\left[\frac{D2(t_i)}{(1-exp(1-(1+\lambda t_i)^{a}))} - \frac{D2(t_{i^*})}{(1-(1-exp(1-(1+\lambda t_{i^*})^{a})))}\right] = 0 \tag{22}$$

Later, [14] discussed modifications of the standard AD statistics. The most used statistic is the Right-tail AD statistics (see [9], [13] and [21]. The Right tail Anderson-Darling estimators $(\hat{a}_{RAD}, \hat{\lambda}_{RAD})$ are obtained by minimizing the following expression:

$$RAD = \frac{n}{2} - 2\sum_{i=1}^{n} \ln(F(t_i)) - \frac{1}{n}\sum_{i=1}^{n} (2i-1)(1-(F(t_{i^*}))) \tag{23}$$

$$RAD = \frac{n}{2} - 2\sum_{i=1}^{n} \ln((1-exp(1-(1+\lambda t_i)^a))) - \frac{1}{n}\sum_{i=1}^{n} (2i-1)(1-(1-exp(1-(1+\lambda t_{i^*})^a))) \tag{24}$$

which implies the resolution of the following equation system:

$$-2\sum_{i=1}^{n} \frac{D1(t_i)}{(1-exp(1-(1+\lambda t_i)^a)))} + \frac{1}{n}\sum_{i=1}^{n} (2i-1)\frac{D1(t_{i^*})}{(1-((1-exp(1-(1+\lambda t_{i^*})^a)))} = 0 \tag{25}$$

$$-2\sum_{i=1}^{n} \frac{D2(t_i)}{(1-exp(1-(1+\lambda t_i)^a)))} + \frac{1}{n}\sum_{i=1}^{n} (2i-1)\frac{D2(t_{i^*})}{(1-(1-exp(1-(1+\lambda t_{i^*})^a)))} = 0 \tag{26}$$

The Left tail Anderson-Darling estimators $(\hat{a}_{LAD}, \hat{\lambda}_{LAD})$ are obtained by minimizing the following expression

$$LAD = \frac{-3n}{2} + 2\sum_{i=1}^{n} \ln(F(t_i)) - \frac{1}{n}\sum_{i=1}^{n} (2i-1)(1-(F(t_{i^*}))) \tag{27}$$

$$LAD = \frac{-3n}{2} + 2\sum_{i=1}^{n} \ln((1-exp(1-(1+\lambda t_i)^a)))) - \frac{1}{n}\sum_{i=1}^{n} (2i-1)(1-(1-exp(1-(1+\lambda t_{i^*})^a)))) \tag{28}$$

VII. Kolmogorov-Smirnov estimation method

Let us consider an independent and identically distributed sample drawn from a population with unknown vector parameters θ. [27] considered an estimation technique so-called as the minimum Kolmogorov–Smirnov estimation (KS), whose purpose is to minimize the value of the famous Kolmogorov- Smirnov statistic which represents the biggest value of the difference between the theoretical and the corresponding empirical repartition functions of the proposed model:

$$KS = d(F_n, F) = \max_{x\in\Re} |F_n(t) - F(t)| \tag{29}$$

If $F(t)$ is the extension exponential distribution, we have

$$KS = d(F_n, F) = \max_{t\in\Re} |F_n(t) - (1-exp(1-(1+\lambda t)^a)))| \tag{30}$$

where n is the sample size, $F(t)$ is the hypothesized distribution (cdf), and $F_n(t)$ is the empirical cdf, a step-function that increases by $1/n$ at each data value. The KS statistic has been widely used to fit data to continuous populations. The interest of this statistic includes the straightforward computation of the test statistic and Its distribution-free characteristic.

The computational formulas for computing KS are:

$$D^+ = \max_{i=1,2,\dots,n} (\frac{i}{n} - (1-exp(1-(1+\lambda t_{(i)})^a)) \tag{31}$$

$$D^- = \max_{i=1,2,\dots,n} ((1-exp(1-(1+\lambda t_{(i)})^a) - \frac{i-1}{n}) \tag{32}$$

and

$$KS = \max\{D^+, D^-\} \tag{33}$$

where $t_{(1)}, t_{(2)}, \ldots, t_{(n)}$ are the order statistics. The parameter values of that minimize the KS statistic are noted $(\hat{a}_{KS}, \hat{\lambda}_{KS})$.

VIII. Model validation

The validation of the model chosen to describe collected data for the analysis is very important. The most commun used goodness-of-fit tests are those based on empirical distribution functions (EDF) such as the Kolmogorov-Smirnov test and the famous chi-square test based on Pearson statistic X^2. Nevertheless the theory showed that the chi-square goodness-of-fit test cannot be applied when the distribution is not specified and the distribution of the statistic test depends on the method used for the esimation of the unknown parameters. So different modifications were proposed in the statistical literature. In this work, we use the technique introduced by [18] and [22] to construct a criteria test Y^2 to validate the extension exponential distribution.

Let us consider the null hypothesis that a sample $T_1, T_2, \ldots, T_n$ follows the extension exponential distribution $P(T_i < t) = F(t, \theta)$ with the unknown parameter vector $\theta = (\alpha, \lambda)^T$.

The statistic Y^2 is defined as the sum of the Pearson statistic X^2 and a quadratic form Q which depends on the hypothesized model. Based on maximum likelihood estimators on initial data, this statistic follows a chi-square distribution with $r-1$ degrees of freedom where r represents the number of grouped classes.

$$Y^2(\hat{\theta}) = X_n^2(\hat{\theta}) + Q_n(\hat{\theta}) \tag{34}$$

The computational formula of $Q(\hat{\theta})$ is given as (see Van der Vaart, 1998)[26]:

$$Q_n(\hat{\theta}) = \frac{1}{n} L^T(\hat{\theta}_n)\big(I(\hat{\theta}_n) - J(\hat{\theta}_n)\big)^{-1} L(\hat{\theta}_n) \tag{35}$$

where $I(\hat{\theta}_n)$ and $J(\hat{\theta}_n)$ are the estimated information matrices respectively for initial data and grouped data into the r classes I_j chosen:

$$I_j = [a_j, a_{j+1}[; \quad \text{for} \quad j = 1, \ldots, r-1 \tag{36}$$

As the grouped intervals must be equiprobable, so the limits a_j are obtained as

$$a_j = F^{-1}(j/r) \tag{37}$$

$$a_j = F^{-1}(j/r) = \frac{(1-(log(1-\frac{j}{r}))^{1/\alpha}-1}{\lambda} \tag{38}$$

If $v_1, v_2, \ldots, v_r$ are the theoretical frequencies of grouped data in these intervals

$$v_j = card(i, T_i \in I_j, i = 1, .., n) \tag{39}$$

So

$$X_n^2(\hat{\theta}) = X_n^T(\hat{\theta}) X_n(\hat{\theta}) \tag{40}$$

with

$$X_n(\hat{\theta}) = (\frac{v_1 - np_1(\theta)}{\sqrt{np_1(\theta)}}, \ldots, \frac{v_r - np_r(\theta)}{\sqrt{np_r(\theta)}}) \tag{41}$$

and

$$p_j = F(a_j) - F(a_{j-1}) = (1 - exp(1 - (1 + \lambda a_j)^{\alpha})) - (1 - exp(1 - (1 + \lambda a_{j-1})^{\alpha})) \quad \text{with} \quad j = 1, \ldots, r \tag{42}$$

The element of the quadratic form Q for the extension exponential distribution are obtained as follow:

$$L = (L_1 = \sum_{j=1}^{r} \frac{v_j}{p_j(\theta)} \frac{dp_j(\theta)}{d\alpha}, \quad L_2 = \sum_{j=1}^{r} \frac{v_j}{p_j(\theta)} \frac{dp_j(\theta)}{d\lambda}) \tag{43}$$

$$J(\theta) = B^T(\theta)B(\theta) \text{ with } B(\theta) = (\frac{1}{\sqrt{p_j(\theta)}} \frac{dp_j(\theta)}{d\alpha}, \frac{1}{\sqrt{p_j(\theta)}} \frac{dp_j(\theta)}{d\lambda}) \tag{44}$$

The compenents of Fisher information matrix are

$$I_{11} = (\frac{-1}{n}) \sum_{i=1}^{n} - (\frac{1}{\alpha^2} + (1 + \lambda t_i)^{\alpha} (\ln(1 + \lambda t_i))^2) \tag{45}$$

$$I_{22} = (\frac{-1}{n}) \sum_{i=1}^{n} - (\frac{1}{\lambda^2} + \frac{(\alpha-1)t_i^2}{(1+\lambda t_i)^2} + (1 + \lambda t_i)^{\alpha-2}(\alpha) - 1)\alpha t_i^2)) \tag{46}$$

$$I_{12} = (\frac{-1}{n}) \sum_{i=1}^{n} \frac{t_i}{1+\lambda t_i} + \frac{t(1+\lambda t_i)^{\alpha}}{(1+\lambda t_i)} - \alpha t_i \ln(1 + \lambda t_i)(1 + \lambda t_i)^{\alpha-1} \tag{47}$$

$$I_{21} = I_{12} = (\frac{-1}{n}) \sum_{i=1}^{n} \frac{t_i}{1+\lambda t_i} + \frac{t(1+\lambda t_i)^{\alpha}}{(1+\lambda t_i)} - \alpha t_i \ln(1 + \lambda t_i)(1 + \lambda t_i)^{\alpha-1} \tag{48}$$

Thus all the elements of the statistic test Y^2 for extension exponential distribution are provided. The applicability of this test is shown by an intensive simulation study.

IX. Simulation study

I. Estimation:

To evaluate the performances of the different methods proposed in this work, we generated $N = 10{,}000$ samples with different sizes ($n = 15{,}25{,}40{,}80$ and $n = 150$) from the extension exponential distribution. We compute the estimators of the unknown parameters, their biases, their mean square errors and their estimated average widths by different methods with the following values of the parameters $\alpha = 0.2, \lambda = 0.1$. The results are summarized in the following tables (Table1,2,3,4,5,6 and 7).

Table 1: *MLE estimators for parameter values* $\alpha = 0.2, \lambda = 0.1$

n	$(\hat{a}, \hat{\lambda})$	$MSE(\hat{\theta})$	$bias(\hat{\theta})$	AW
15	(0.2252 0.1162)	(0.00368 0.01256)	(0.02527 0.01620)	(0.1188 0.2196)
25	(0.2195 0.1148)	(0.00265 0.01129)	(0.01954 0.01482)	(0.1008 0.2082)
40	(0.2105 0.1105)	(0.00115 0.00540)	(0.01054 0.01055)	(0.0664 0.1440)
80	(0.2054 0.1040)	(0.00049 0.00212)	(0.00542 0.00407)	(0.0433 0.0902)
150	(0.2023 0.1028)	(0.00023 0.00101)	(0.00230 0.00283)	(0.0297 0.0622)

Table 2: *MPS estimators for parameter values* $\alpha = 0.2, \lambda = 0.1$

n	$(\hat{\alpha}, \hat{\lambda})$	$MSE(\hat{\theta})$	$bias(\hat{\theta})$	AW
15	(0.1890 0.2097)	(0.00205 0.05728)	(0.01093 0.10977)	(0.0887 0.4687)
25	(0.1902 0.1785)	(0.00164 0.03929)	(0.00976 0.07854)	(0.0793 0.3885)
40	(0.1918 0.1441)	(0.00089 0.01032)	(0.00811 0.04416)	(0.0584 0.1991)
80	(0.1944 0.1217)	(0.00044 0.00301)	(0.00555 0.02177)	(0.0411 0.1075)
150	(0.1963 0.1116)	(0.00022 0.00121)	(0.00360 0.01165)	(0.0290 0.0681)

Table 3: *CvM estimators for parameter values* $\alpha = 0.2, \lambda = 0.1$

n	$(\hat{\alpha}, \hat{\lambda})$	$MSE(\hat{\theta})$	$bias(\hat{\theta})$	AW
15	(0.2425 0.1425)	(0.02460 0.05036)	(0.04252 0.04250)	(0.3074 0.4398)
25	(0.2193 0.1270)	(0.00393 0.01534)	(0.01931 0.02707)	(0.1228 0.2427)
40	(0.2128 0.1142)	(0.00225 0.00663)	(0.01280 0.01424)	(0.0929 0.1595)
80	(0.2054 0.1074)	(0.00077 0.00270)	(0.00549 0.00747)	(0.0543 0.1018)
150	(0.2032 0.1033)	(0.00038 0.00124)	(0.00322 0.00332)	(0.0382 0.0690)

Table 4: *AD estimators for parameter values* $\alpha = 0.2, \lambda = 0.1$

n	$(\hat{\alpha}, \hat{\lambda})$	$MSE(\hat{\theta})$	$bias(\hat{\theta})$	AW
15	(0.2179 0.1631)	(0.00545 0.03055)	(0.01796 0.06314)	(0.1446 0.3425)
25	(0.2090 0.1329)	(0.00228 0.01512)	(0.00908 0.03295)	(0.0935 0.2410)
40	(0.2055 0.1184)	(0.00122 0.00643)	(0.00557 0.01844)	(0.0684 0.1571)
80	(0.2021 0.1093)	(0.00054 0.00235)	(0.00215 0.00930)	(0.0455 0.0950)
150	(0.2012 0.1049)	(0.00028 0.00117)	(0.00127 0.00499)	(0.0327 0.0670)

Table 5: *RAD estimators for parameter values* $\alpha = 0.2, \lambda = 0.1$

n	$(\hat{\alpha}, \hat{\lambda})$	$MSE(\hat{\theta})$	$bias(\hat{\theta})$	AW
15	(0.2237 0.1801)	(0.00921 0.07814)	(0.02378 0.08012)	(0.1880 0.5478)
25	(0.2115 0.1270)	(0.00232 0.01405)	(0.01152 0.02700)	(0.0944 0.2323)
40	(0.2070 0.1197)	(0.00133 0.00739)	(0.00708 0.01972)	(0.0714 0.1684)
80	(0.2032 0.1092)	(0.00055 0.00280)	(0.00325 0.00922)	(0.0459 0.1037)
150	(0.2018 0.1040)	(0.00028 0.00123)	(0.00186 0.00406)	(0.0327 0.0687)

Table 6: *LAD estimators for parameter values* $\alpha = 0.2, \lambda = 0.1$

n	$(\hat{\alpha}, \hat{\lambda})$	$MSE(\hat{\theta})$	$bias(\hat{\theta})$	AW
15	(0.2227 0.1652)	(0.00519 0.06445)	(0.02277 0.06527)	(0.1412 0.4975)
25	(0.2243 0.1373)	(0.00610 0.02161)	(0.02433 0.03737)	(0.1530 0.2881)
40	(0.2120 0.1213)	(0.00271 0.00849)	(0.01201 0.02133)	(0.1020 0.1805)
80	(0.2057 0.1095)	(0.00097 0.00301)	(0.00576 0.00951)	(0.0610 0.1075)
150	(0.2030 0.1046)	(0.00047 0.00135)	(0.00303 0.00465)	(0.0424 0.0720)

Table 7: *KS estimators for parameter values* $\alpha = 0.2, \lambda = 0.1$

n	$(\hat{\alpha}, \hat{\lambda})$	$MSE(\hat{\theta})$	$bias(\hat{\theta})$	AW
15	(0.2417 0.1501)	(0.01127 0.06134)	(0.04173 0.05015)	(0.2080 0.4854)
25	(0.2229 0.1222)	(0.00441 0.01555)	(0.02292 0.02227)	(0.0411 0.2444)
40	(0.2136 0.1127)	(0.00204 0.00677)	(0.01368 0.01274)	(0.0885 0.1612)
80	(0.2065 0.1066)	(0.00084 0.00282)	(0.00652 0.00665)	(0.0568 0.1040)
150	(0.2036 0.1033)	(0.00040 0.00130)	(0.00366 0.00336)	(0.0392 0.0706)

From numerical experiments, It is observed that the biases and the MSE decrease as the sample size increases and this is for all methods. Regarding tables (1,2,3,4,5,6 and 7), we can see that for little sample sizes, the MPS, the AD and the RAD methods provided very good results but the MPS estimators are the best ones compared to all the other methods. For big sample sizes, all methods gave appromixately the same results, however the AD and the RAD estimators are better than all of them and even that of the maximum likelihood MLE method.

II. criteria test

To show the practibility of the statistic test provided in this work, we test the null hypothesis H_0 that samples are drawn from the extension exponential distribution. The number of rejection of the null hypothesis H_0 for thousands of samples from different sizes ($n = 15,25,40,80$ and 150) are computed and compared with those of their theoretical ones ($\epsilon = 0{,}01; 0{,}05$ and $0{,}1$). The results are presented in Table 8.

Table 8: *critical chi-square and their corresponding empirical values*

n	$\epsilon = 0.05$	$\epsilon = 0.01$	$\epsilon = 0.1$
15	(0.03879)	(0.01697)	(0.1230)
25	(0.04918)	(0.01513)	(0.1080)
40	(0.05638)	(0.01503)	(0.1068)
80	(0.05204)	(0.01222)	(0.1022)
150	(0.05073)	(0.01124)	(0.1004)

As expected, the obtained empirical values are very close to their corresponding theoretical ones which implies the feasability of the proposed goodness-of-fit test to validate the extension exponential distribution.

X. Applications on real data sets

In this section, we applied the obtained results to two real data sets.

I. The failure times of the air conditionning system data set

The first one concerns the failure times of the air conditionning system of an air plane studied firstly by [12] and [10] who fitted these data respectively to Weibull and exponentiated exponential distributions. Recently [11] showed that the modified Weibull distribution is more appropriated.
The observed values are given below:

23,261,87,7,120,14,62,47,225,71,246,21,42,20,5,12,120,11,3,14,71,11,14,11,16,90,1,16,52,95.

Using the estimation methods given above, we compute the values of the unknown parameters considering different distributions capable to describe these data namely the extension exponential, Weibull, exponentiated exponential and modified Weibull distributions. The results are given in table 9. The cumulative density function of modified Weibull distribution considered here is:

$$F_{MW} = \frac{2F_W}{1+F_W} = \frac{2(1-e^{-(\frac{t}{\lambda})^{\alpha}})}{2-e^{-(\frac{t}{\lambda})^{\alpha}}}$$

Table 9 : *estimator values of the unknown parameters of competitor distributions of air conditionning data system of air planes*

Distributions	parameters	MLE	CVM	KS	AD	LAD	RAD	MPS
Extensionexp	α	0.5985	0.4866	0.6947	0.5233	0.5531	0.5081	0.5057
	λ	4.3385	6.3226	3.8403	5.4853	5.0388	5.8283	5.7787
Weibull	α	0.8535	0.7854	0.9000	0.7994	0.8775	0.7560	0.7805
	λ	54.612	0.5183	0.4496	0.5324	0.4906	0.5265	0.5577
M.Weibull	α	0.9869	0.8989	1.0260	0.9215	0.9909	0.8829	0.9023
	λ	84.097	0.8633	0.7095	0.8664	0.7808	0.8807	0.9050
Exponentiatedexp	α	0.8090	0.6979	0.8451	0.7082	0.8528	0.6243	0.6990
	λ	0.0145	1.3880	1.9274	1.3489	1.8123	1.1922	1.2200

To differentiated between the competitor distributions, and based on the classical model selection criteria, we calculate the AIC, BIC, LL, KS, CvM and AD statistics, the results are given in Table 10. As It can be seen, for the maximum likelihood estimation method, only the values of AIC, BIC and LL of the modified Weibull model are the smallest ones. But for the other estimation methods, all criteria selection models AIC, BIC, LL, KS, CvM and AD of the extension exponential distribution give the smaller values. So, It can be said that the extension exponential distribution might work better than all the other models, and this fact is proved by data plots of the different pdf distributions (see Figure 4).

Table 10 : *AIC, BIC, LL and KS statistic values*

	methods	extension exp	Weibull	Exponentiated	Exp M.Weibull
AIC	MLE	(30.8527)	(31.5635)	(32.0910)	(30.6859)
	CvM	(31.3652)	(31.9047)	(32.5510)	(31.1571)
	KS	(31.6769)	(33.0019)	(33.9210)	(34.2721)
	LAD	(30.9216)	(31.9584)	(33.0875)	(30.8079)
	RAD	(31.1693)	(32.2839)	(33.2811)	(31.3592)
	AD	(31.0697)	(31.7777)	(32.4168)	(30.9512)
	MPS	(31.2078)	(32.0362)	(32.595)	(31.186)
BIC	MLE	(33.6551)	(34.3659)	(34.8934)	(33.4883)
	CvM	(34.1676)	(347071)	(35.3534)	(33.9595)
	KS	(34.4793)	(35.8043)	(36.7234)	(34.2721)
	LAD	(33.7240)	(34.7608)	(35.8899)	(33.6103)
	RAD	(33.9717)	(35.0863)	(36.0835)	(34.1616)
	AD	(33.8721)	(34.5801)	(35.2191)	(33.7536)
	MPS	(34.0101)	(34.8385)	(35.3973)	(33.9883)
LL	MLE	(-13.4263)	(-13.7817)	(-14.0455)	(-13.3429)
	CvM	(-13.6826)	(-13.9523)	(-14.2755)	(-13.5785)
	KS	(-13.8384)	(-14.5009)	(-14.9605)	(-13.7348)
	LAD	(-13.4608)	(-13.9792)	(-14.5437)	(-13.4039)
	RAD	(-13.5846)	(-14.1419)	(-14.6405)	(-13.6796)
	AD	(-13.5348)	(-13.8888)	(-14.2084)	(-13.4756)
	MPS	(-13.6039)	(-14.0181)	(-14.2975)	(-13.5930)
KS	MLE	(0.1318)	(0.1533)	(0.1719)	(0.1427)
	CvM	(0.1206)	(0.1229)	(0.1289)	(0.1202)
	KS	(0.1089)	(0.1120)	(0.1135)	(0.1080)
	LAD	(0.1215)	(0.1312)	(0.1339)	(0.1237)
	RAD	(0.1157)	(0.1303)	(0.1367)	(0.1234)
	AD	(0.1203)	(0.1331)	(0.1411)	(0.1267)
	MPS	(0.1198)	(0.1393)	(0.1595)	(0.5943)

For testing the null hypothesis H_0 that these data follow the extension exponential model, we use the criteria test constructed in this work. We grouped data into $r = 8$ intervals,after calculating the limits of these intervals, we obtain:

$$L = (L_1 = -2.5073, L_2 = -0.6273)$$

$$J(\hat{\theta}) = \begin{bmatrix} 2.1928 & 0.1684 \\ 0.1684 & 0.0145 \end{bmatrix}$$

$$I_n(\hat{\theta}) = \begin{bmatrix} 7.5394 & 0.4651 \\ 0.4651 & 0.0330 \end{bmatrix}$$

we deduce the value of $Y^2 = 9.0753$. For level of significance $\epsilon = 0.05$, the chi-square critical value is $X^2_{r-1} = 14.07$. As $Y^2 = 9.0753 < X^2_{r-1} = 14.07$, the null hypothesis H_0 cannot be rejected, therefore the failure times of the air conditionning system of an air plane is effectively modeled by the extension exponential distribution. The pdf plots and the empirical distribution function plots given in Figure 4, show that the extension exponential distribution is best suited to model these data.

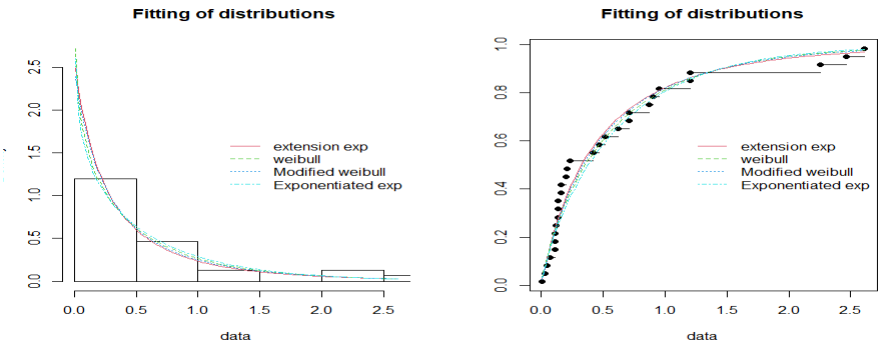


Figure 4: *empirical pdf and cdf versus theorical alternative distributions for the failure times of the air conditionning system of an air plane data*

From these results, we can say that the extension exponential distribution fit these data better than all its alternatives.

II. Floyd River data set

Here we consider a classical flood data of the Floyd River given in Mudholkar and Huston (1996) [16]. In the paper [1], the authors calculated the log-likelihood of these data for different distributions and the obtained values are respectively -376.35 for the exponentiated Weibull distribution, -382.13 for the beta-Weibull distribution and -365.45 for the beta-Pareto model. In this subsection, we propose the extension exponential distribution and its competitors to describe these data. We compute the different estimators of the unkown parameters (Table 11) and the criteria selection models AIC, BIC, LL and KS (Table 12).

Table 11 : *Different estimators of the unkown parameters of competitor distributions for Floyd river data*

Distributions	parameters	MLE	CVM	KS	AD	LAD	RAD	MPS
Extensionexp	α	0.6093	1.2844	0.8757	0.8301	4.0602	0.6793	0.5295
	λ	0.3358	1.1373	0.2053	0.2355	0.0364	0.3358	0.4625
Weibull	α	0.8714	1.1196	1.0977	1.0011	1.2663	0.8886	0.8088
	λ	6.1888	5.0977	5.6478	5.5515	4.8755	5.4194	6.3671
Gamma	α	0.9195	1.2261	1.1642	1.0716	1.4655	0.8615	0.8074
	n	0.1358	0.2498	0.2131	0.1970	0.3194	0.1523	0.1109
Exponentiatedexp	α	0.9688	1.2485	1.1758	1.0996	1.5061	0.8690	0.8357
	λ	0.1445	0.2337	0.2026	0.1963	0.2783	0.1617	0.1213

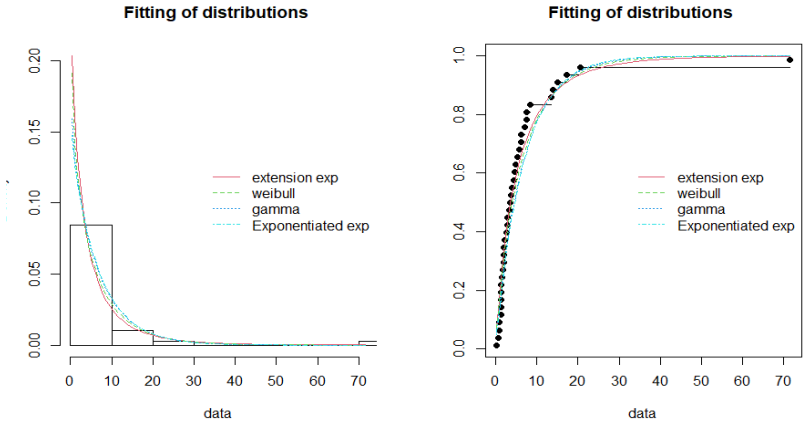


Figure 5: *empirical pdf and cdf versus theorical alternative distributions for a classical flood data of the Floyd River*

Table 12: *AIC, BIC, LL and KS statistic values for Floyd river data*

	methods	Extension exp	Weibull	Gamma	Exponentiated exp
AIC	MLE	(225.9119)	(229.4550)	(231.0047)	(231.167)
	CvM	(246.0783)	(243.3696)	(238.8346)	(237.5375)
	KS	(229.0334)	(237.9247)	(234.7716)	(234.005)
	AD	(228.4938)	(232.8804)	(233.7901)	(233.7134)
	LAD	(571.5404)	(265.8108)	(247.2532)	(243.5087)
	RAD	(226.4296)	(230.1609)	(232.2683)	(232.7168)
	MPS	(226.4262)	(230.0223)	(231.5818)	(231.7741)
BIC	MLE	(229.2391)	(232.7821)	(234.3318)	(234.4941)
	CvM	(249.4054)	(246.6968)	(242.1618)	(240.8647)
	KS	(232.3605)	(241.2518)	(238.0988)	(237.3321)
	AD	(231.8209)	(236.2075)	(237.1172)	(237.0406)
	LAD	(574.8675)	(269.1379)	(250.5803)	(246.8356)
	RAD	(229.7567)	(233.4880)	(235.5954)	(236.0439)
	MPS	(229.7533)	(233.3495)	(234.9089)	(235.1012)
LL	MLE	(-110.956)	(-112.7275)	(-113.5023)	(-113.5835)
	CvM	(-121.0392)	(-119.6848)	(-117.4173)	(-116.7688)
	KS	(-112.5167)	(-116.9624)	(-115.3858)	(-115.0025)
	AD	(-112.2469)	(-114.4402)	(-114.895)	(-114.8567)
	LAD	(-283.7702)	(-130.9054)	(-121.6266)	(-119.7543)
	RAD	(-111.2148)	(-113.0804)	(-114.1341)	(-114.3584)
	MPS	(-111.2131)	(-113.0112)	(-113.7909)	(-113.887)
KS	MLE	(0.1366)	(0.1270)	(0.1471)	(0.1502)
	CvM	(0.1067)	(0.1015)	(0.1003)	(0.0996)
	KS	(0.1034)	(0.0782)	(0.0768)	(0.0764)
	AD	(0.1172)	(0.1059)	(0.0950)	(0.0916)
	LAD	(0.1360)	(0.1264)	(0.1200)	(0.1179)
	RAD	(0.1409)	(0.1425)	(0.1360)	(0.1332)
	MPS	(0.6684)	(0.6715)	(0.7197)	(0.7314)

Compared to the LL values obtained for the different models cited above, we find the value LL=(-110.956) for the extension exponential distribution which proves that this model is better than all the alternative distributions.

NRR statistic On the other hand, we suppose the null hypothesis H_0 that the Floyd river data belong to the extension exponential distribution. If we choose $r = 8$ grouping classes, the intermediate calculation of the criteria test Y^2 are as follow

$$L = (L_1 = 10.2593, L_2 = 5.3251)$$

$$J(\theta)(\hat{\theta}) = \begin{bmatrix} 4.4775 & 4.0355 \\ 4.0355 & 3.9302 \end{bmatrix}$$

$$I_n(\hat{\theta}) = \begin{bmatrix} 6.9144 & 5.1848 \\ 5.1848 & 5.9629 \end{bmatrix}$$

We obtain $Y^2 = 6{,}6724$,, so for the significance level $\epsilon = 0.05$, the critical value $X^2_{r-1} = 14.07$, therefore we can validate the extension exponential distribution, even the curves of the empirical function distributions and their pdf plots (Figure 5) corroborate the test results.

XI. Conclusion:

As the explicit forms of the maximum likelihood (MLE) estimators cannot be derived, we have used different estimation methods as alternatives to calculate the unknown parameters of the extension exponential distribution. Based on an important simulation study, we have showed that the maximum product spacing (MPS) method gives the best results for little and moderate samples but for big samples the Anderson-Darling method AD and the right tail Anderson-Darling method RAD are better than all the other methods even the MLE. A new statistic which can validate effectively the extension exponential distribution is provided. By using this criteria test, we will not need to compare this model with the possible alternatives in the analysis.

From this study, we conclude that practitionars can use the MPS and the AD estimators respectively for moderate and big samples in the analysis and the obtained statistic test Y^2 permits to fit efficiently observed data to the EE distribution.

As in reliability and survival analyses, data are often censored, we propose in the forthcoming work to construct modified tests to right censored samples to this distribution.

References

[1] Akinsete, A., Famoye, F., et Lee, C. (2008). The beta-Pareto distribution. *Statistics*, 42:547–563.

[2] Alzaatreh, A., Lee, C., et Famoye, F. (2016). The generalized Cauchy family of distributions with applications. *Journal of Statistical Distributions and Applications*, 3:1–16.

[3] Alzaghal A., Felix F., Carl L. (2013). "Exponentiated T-X Family of Distributions with Some Applications". International Journal of Statistics and Probability. 2(3). 31-49.

[4] Anderson.T.W. and Darling.D.A.(1952) , "Asymptotic theory of certain "goodness of fit" criteria based on stochastic processes". The Annals of Mathematical Statistics, 23(2) , 193–212.

[5] Boos.D.D. (1981), "Minimum distance estimators for location and goodness of fit". Journal of the American Statistical Association, 76 , 663–670.

[6] Bourguignon M., Silva R.B., Cordeiro G.M.(2014)."The Weibull-G Family of Probability Distributions".Journal of Data Science 12, 53-68.

[7] Cheng R.,Amin N. (1983), "Estimating parameters in continuous univariate distributions with a shifted origin". Journal of the Royal Statistical Society, Series B (Methodological), 45 , 394–403.

[8] Cordeiro M., Castro M. (2011), "A new family of generalized distributions". Journal of Statistical Computation and Simulation. 81(7). 883-898.http://dx.doi.org/10.1080/00949650903530745.

[9] Dey.S. , Dey.T. and Kundu.D.(2014), "Two-parameter Rayleigh distribution: different methods of estimation". American Journal of Mathematical and Management Sciences, 33 , 55–74.

[10] Gupta, R. D. and kundu, D.(2001), "Exponentiated Exponential Family:An alternative to Gamma and Weibull Distributions", Biometrical Journal,43(1),pp.117-130.

[11] kumar D.,Singh U.,Singh S.k , Mukherjee S.(2017),"The New Probability Distribution: An Aspect to a Life Time Distribution".International Journal of Mathematical Science Letters.

[12] Linhart H. and Zucchini W. (1986),Model selection,John Wiley Sons. 12.

[13] Louzada.F., Ramos.P.L. and Perdona.G.S.(2016) , "Different estimation procedures for the parameters of the extended exponential geometric distribution for medical data". Computational and Mathematical Methods in Medicine. Article ID 8727951, 12 pages. doi:10.1155/2016/8727951.

[14] Luceno A.(2006), "Fitting the generalized Pareto distribution to data using maximum goodness-of-fit estimators". Computational Statistics & Data Analysis, 51 , 904–917.

[15] MacDonald P. D. M. (1971), "Comment on an estimation procedure for mixtures of distributions by Choi and Bulgren". Journal of Royal Statistical Society: Series B,33(2), 326-329.

[16] Mudholkar G.S., Huston A.D.(1996),"The exponentiated Weibull family:Some properties and a flood data application".Communications in Statistics-Theory and Methods Taylor and Francis.25(12), 3059-3083.

[17] Nadarajah S., Haghighi F. (2011)."An extension of the exponential distribution".A Journal of Theoretical and Applied Statistics Volume 45, 2011 - Issue 6.

[18] Nikulin M. S.(1973), "Chi-square test for normality," in: International Vilnius Conference on Probability Theory and Mathematical Statistics, Vol. 2 , pp. 119–122.

[19] Nouadri R., Seddik-Ameur N. (2025). Modified statistics for fitting a new bounded Distribution with Applications. *Utilitas Mathematica* . 122, 1 (May 2025), 906–931.

[20] Ramnaby B. (1984), "The Maximum Spacing Method: An Estimation Method Related to the Maximum Likelihood Method". Scandinavian Journal of Statistics, 11, 93-112.

[21] Ramos P. and Louzada F.(2016), "The generalized weighted Lindley distribution", Properties, estimation and applications. CogentMathematics, 3 , 1–18.

[22] Rao K. C.,Robson D.S .(1974). "A Chi-square statistic for goodness-of-fit for tests with in the exponential family".Communications in statistics 3:1139-53.

[23] Seddik-Ameur N.,Chouia S.(2014)."A Goodness-of-fit Test for a Competing Risk Model".International Journal of Applied Mathematics and Statistics,Vol. 52 , Issue Number: 2.

[24] Tilbi D.,Seddik-Ameur N.(2017)."Chi-squared goodness-of-fit tests for the generalized Rayleigh distribution".Journal of Statistical Theory and Practice volume 11, pages594–603 .

[25] Treidi W., Seddik-Ameur N."NRRstatistic for the extension Weibull distribution".Global Journal of Pure andApplied Mathematics. ISSN 0973-1768Volume 12, Number 4 (2016), pp. 2809–2818.

[26] Van der Vaart, A.w.(1998).Asymptotic statistics.Cambridge Series in Statistical and Probabilistic Mathematics. Cambridge, UK: Cambridge University Press.

[27] Weber.M. D., Leemis.L. M. and Kincaid.R. K.(2006) , "Minimum Kolmogorov-Smirnov test statistic parameter estimates". Journal of Statistical Computation and Simulation, Vol. 76, No. 3 , 195–206.

CONSTRUCTION OF A NEW ATTRIBUTE CONTROL CHART BASED ON RAYLEIGH DISTRIBUTION UNDER HYBRID CENSORING - A BAYESIAN APPROACH

T. KAVITHA* & M. GUNASEKARAN**

•

*PG & Research Department of Statistics
Salem Sowdeswari College (Women), Salem, Tamil Nadu, India.
sreesuryaa@gmail.com

•

**Department of Applied Research
The Gandhigram Rural Institute (Deemed to be University), Dindigul, Tamil Nadu, India.
gunasekaranm1988@gmail.com

Abstract

Statistical Process Control (SPC) is a quality control approach that makes use of statistical tools to understand, monitor, and improve a process. A control chart is a tool for monitoring process performance that consists of a visual indication to detect anomalous deviations because of assignable causes. This chart compares the values of a quality attribute to the control limits. In the quality control process, the control chart is often generated by ignoring parameter uncertainty. The identification of changes in the parameter(s) within the probability distribution of one or more process-related variables is an essential part of monitoring. Estimating the parameters is essential since this might have an impact on the control chart's long-term performance in a controlled or out-of-control condition. This article provides a novel attribute control chart in the form of a Bayesian approach based on the Rayleigh lifetime distribution and the Hybrid censoring technique. A Bayesian approach will be used to calculate the control chart parameters and average run length. The control chart parameters are determined for various combinations of values, and the performance of the developed control chart is evaluated using the Average Run Length (ARL). Numerical examples are used to explain the proposed control chart, and simulated data is used to show how it might be used.

Keywords: Rayleigh Distribution, Predictive Distribution, Attribute Control Chart, Hybrid Censoring, Average Run Length

1. Introduction

Nowadays manufacturing industry is facing a lot due to process variation which leads to producing defects and facing huge costs. During a continuous manufacturing process, we want to know whether the process is in control or not and to know if there is any presence of variation. Variation may be due to chance or assignable causes. Quality control involves monitoring, measuring, and correcting the performance of a product against predefined standards or specifications. One of the most common and effective tools for quality control is the control chart, which is a graphical representation of the data that has been collected from the manufacturing industries. A control chart always has a central line (CL) for the average, an upper line for the upper control limit (UCL), and a lower line for the lower control limit (LCL).

In order to monitor the production process in various circumstances, many new control charting techniques have been developed. There are various types of control charts which are broadly similar and have been developed to suit particular characteristics of the quality attribute being analyzed. Two broad categories of charts exist, which are based on if the data being monitored is "variable" or "attribute" in nature. Variable control charts are a type of graph that evaluates data with precise measurement. The attribute control charts are used to distinguish between conforming and non-conforming items.

Lifetime is regarded as a quality characteristic for some products. Life tests are used to monitor the manufacturing process for these products. The product may be classed as conforming or non-conforming based on the results of the life test. This form of product testing takes a considerable amount of time because the duration of the test is lengthy. In this circumstance, the censoring technique is essential and cannot be ignored. Some of the censoring techniques used in life testing include Type-I censoring, Type-II censoring, and hybrid censoring. According to the hybrid censoring, the life test terminates at the earliest of the specified test time t or the time at which the (UCL + 1)th failure is discovered. When the number of failures observed during the life test is between the UCL and LCL at time t, the production process is in control; otherwise, the production process is out of control. If the product fails the life test before the test termination time t, it may be regarded as a nonconforming product.

The attribute control chart, such as the np control chart, is based on the fraction non-conforming, which is determined by assuming that the quality characteristic follows the normal distribution. In reality, the distribution of the quality characteristics may not be normal. In this situation, using the present control chart may mislead industrial engineers and cause the non-conforming items to increase. Many works on constructing attribute control chart using various lifetime distributions may be found in literature, which include [1] – Weibull, [2] – Pareto, [3] – Birnbaum Saunder, [4] – Weibull, [5] – Inverse Rayleigh, [6] - Burr X & XII, Inverse Gaussian & Exponential, [7] – Lognormal, [8] – Exponentiated Half Logistic, [9] – Dagum, [10] - Pareto, [11] – Weibull Pareto, [12] – Gamma, [13] – Log–Logistic, [14] - Weibull, [15] – Generalized Log Logistic, [16] – Generalized Exponential, [17] – Inverse Weibull, [18] – Length-Biased Weighted Lomax, [19] - Rayleigh, and [20] – Half Normal & Half Exponential Power.

The attribute control charts discussed in the earlier works are based on the implicit assumption that the mean number of defectives is constant throughout the time when the process is in control. Control charts based entirely on sample variance, such as the np - chart, may generate several false alarms if the real number of defectives is not consistent over time while an in-control scenario occurs. False alarms will arise because the observed number of nonconforming items includes variability because of both process and sampling variation, while the control limits are based only on sampling variance. Any process variations become more evident in larger samples. The actual number of nonconforming items is expected to differ from sample to sample according to an underlying distribution.

The Bayesian approach is commonly employed for dealing with uncertainty about the parameter of interest. For attributes, [21] initially proposed a Bayesian process control chart. Numerous authors, including [22] - [31] have contributed to the literature and worked on a variable control chart for various lifetime distributions under Bayesian approach.

The Rayleigh distribution is frequently employed as a lifetime distribution in research relating to electro vacuum devices and communication engineering. Because the hazard function of the Rayleigh distribution is a linearly increasing function, it appears to be an appropriate lifetime distribution for items with a faster rate of deterioration. This is a specific type of Weibull distribution, which is one of the statistical distributions that may be employed efficiently in reliability engineering and life testing. Reference [32] proposed it as the Rayleigh Power (and Amplitude) distribution. Later, [33] and [34] updated its name to Rayleigh distribution and investigated its properties, estimation procedures, and applications. Numerous authors studied this skewed distribution because of its significance in engineering-related aspects. The Rayleigh distribution may also be used for modelling the lifetime of products in the marketplace that are the result of a manufacturing process. According to the literature study, there has been

no research on control charts which include a life test for a non-normal distribution, such as a Rayleigh distribution with Hybrid censoring under the Bayesian approach.

In this paper, the design of an attribute control chart based on a predictive distribution of the lifetime is considered under the assumption that the lifetime follows a Rayleigh distribution and the process parameter is modelled by an Inverse-Rayleigh distribution under a hybrid censoring. The control chart coefficient was determined, and the performance of the proposed control chart was discussed with the average run length (*ARL*). When the process mean changes, the proposed control chart is designed. With the use of simulated data, the proposed control chart's applicability is described. Simulated data is used to illustrate the proposed control chart. Section 2 presents designing the Bayesian control chart and provides a procedure for obtaining the control chart for given strength. The real-life application of the proposed control chart through simulation study is described in Section 3. The final section provides a summary of the overall findings.

2. Designing a Bayesian Attribute control chart

Let "T" be the lifetime of the products produced in a production process. Assume that "T" follows a Rayleigh distribution with parameter θ given for $t > 0$ by its density function $f_{T|\{\theta\}}$:

$$f_{T|\{\theta\}}(t) = \frac{te^{-\frac{t^2}{2\theta^2}}}{\theta^2}; t > 0, \theta > 0 \tag{1}$$

The distribution function of $F_{T|\{\theta\}}$ is given by:

$$F_{T|\{\theta\}}(t) = 1 - e^{-\frac{t^2}{2\theta^2}}; t > 0, \theta > 0 \tag{2}$$

According to [35], Consider the process parameter θ with $\theta > 0$ as random variable Θ with prior distribution given by the inverse Rayleigh distribution with density function for $\theta > 0$:

$$h_{\Theta|\{\lambda\}}(\theta) = \frac{1}{\theta^3\lambda^2}e^{-\frac{1}{2\lambda^2\theta^2}}; \theta > 0, \lambda > 0 \tag{3}$$

The updated lifetime of the product is described by the predictive distribution of "T" whose density function can be obtained from the prior distribution (3) and the sampling distribution (1) as:

$$g_{T|\{\lambda\}}(t) = \frac{2\lambda^2 t}{[1+\lambda^2 t^2]^2}; t > 0 \tag{4}$$

Hereafter, the above predictive distribution referred as "Rayleigh-Inverse-Rayleigh" distribution and the distribution function of $T|\{\lambda\}$ is obtained as:

$$G_{T|\{\lambda\}}(t) = 1 - \frac{1}{[1+\lambda^2 t^2]}; t > 0 \tag{5}$$

The product's mean lifetime under Rayleigh-Inverse-Rayleigh distribution is given by

$$\mu = \frac{\pi}{2\lambda} \tag{6}$$

The target mean life of the product is denoted by μ_0 when the process is in-control and the experiment time t_0 can be written in terms of in-control process mean such as $t_0 = a\mu_0$ ("a" is an experiment termination ratio). Let p be the failure probability of an item before the experiment time t_0 and can be written as follows:

$$p = 1 - \frac{1}{\left[1 + \left[\frac{\mu}{2\mu}\right]^2 [a\mu_0]^2\right]} \tag{7}$$

The process is declared to be in-control if there is no difference between the process mean and the target mean, i.e., $\mu = \mu_0$. Now, let p_0 be the failure probability of an item when the process is in-control and is obtained by

$$p_0 = 1 - \frac{1}{\left[1 + \left[\frac{a\mu}{2}\right]^2\right]} \tag{8}$$

Reference [36] pointed out that "Realistically, however, when a special cause influences a process, it may cause a shift in more than one parameter (location, scale, skewness, etc.) of the process distribution". It means that, due to the occurrence of an assignable cause, the process may be affected and subsequently the process mean or shape parameter of the distribution will be shifted from the specified target level. In addition, this parameter shift doesn't greatly affect the distribution so it reduces from one to another. But in such a situation, the process will be declared as out-of-control and stopped until the cause of process variations is removed. Also, it is assumed that the process mean is shifted to $\mu_1 = f\mu_0$, where f is a shift constant. Then the failure probability of an item when the process is out of control, denoted by p_1, is given as

$$p_1 = 1 - \frac{1}{\left[1 + \left[\frac{a\mu}{2f}\right]^2\right]} \tag{9}$$

Usually, for the given values of $a\&f$, the failure probabilities are calculated by using equations (8) and (9).

We develop a new np control chart for the lifetime of the product distributed according to the Rayleigh-Inverse-Rayleigh distribution based on the number of products in each subgroup. The following is the designed np control chart's operational procedure:

- Select a sample of n items randomly from the subgroup of the production process and put the sample items for the life test of specified termination time t_0.
- Observe the number of failed items and denotes it as "d".
- Terminate the life test either after reached at time t_0 or $d > UCL$ before reaching time t_0, whichever is earlier.
- If $d < LCL$ or $d > UCL$, then declare the production process as out-of-control. Otherwise, declare the production process as in control.

The proposed control chart is considered to be an np control chart since the number of failed items in a subgroup of fixed sample size is plotted against the subgroup. The number of failed items in the life test follows a binomial (n, p_0) distribution when the production process is in control. The probability of an item failing before test termination time t_0, is denoted as p_0. As a result, the following equations are used to determine the control limits for the proposed control chart:

$$UCL = np_0 + k\sqrt{np_0(1-p_0)} \tag{10}$$

$$LCL = max[0, np_0 - k\sqrt{np_0(1-p_0)}] \tag{11}$$

Where "k" is the control limits coefficient and the failure probability p_0 of the product before the time t_0 is calculated using equation (8).

The probability that the process is declared to be in control is denoted by P_{in}^0 and given as

$$p_{in}^0 = P(LCL \leq D \leq UCL | p_0)$$

$$p_{in}^0 = \sum_{d=[LCL]+1}^{[UCL]} \binom{n}{d} p_0^d (1-p_0)^{n-d} \tag{12}$$

Generally, the average run length is used to evaluate the performance of the control chart. The in-control ARL of the proposed control chart denoted by ARL_0, is determined by

$$ARL_0 = \frac{1}{1 - [\sum_{d=[LCL]+1}^{[UCL]} \binom{n}{d} p_0^d (1-p_0)^{n-d}]} \tag{13}$$

Assume the process mean has been changed from μ_0 to μ_1. The probability in equation (9) now becomes

$$p_1 = 1 - \frac{1}{\left[1 + \left[\frac{a\mu}{2f}\right]^2\right]}$$

The probability that the process is declared to be in control after shifting to μ_1 is now determined by

$$p_{in}^1 = P(LCL \leq D \leq UCL | p_1)$$

$$p_{in}^1 = \sum_{d=[LCL]+1}^{[UCL]} \binom{n}{d} p_1^d (1-p_1)^{n-d} \tag{14}$$

The ARL for the shifted process (out-of-control) is denoted by ARL_1 and is obtained by:

$$ARL_1 = \frac{1}{1 - [\sum_{d=[LCL]+1}^{[UCL]} \binom{n}{d} p_1^d (1-p_1)^{n-d}]} \tag{15}$$

To analyse the performance of the proposed control chart in detecting the process shift, we determine the optimal parameters LCL, UCL, a and k for the specified values of in-control ARL. For this purpose, we considered four cases of in-control ARL such as 200, 300, 400 and 500 with fixed sample size n = 25. Also, we considered four cases of sample size such as 20, 25, 30 and 35 with fixed in-control ARL = 370. The optimal parameters are selected so that the in-control ARL is as near as to the specified ARL values and the out-of-control $ARLs$ are reported for different values of shift constant. Table 1 and Table 2 show such optimal parameters along with corresponding out-of-control $ARLs$.

From Table 1 and Table 2, we can observe that the out-of-control ARL (i.e., ARL_1) decreases if the shift constant "f" decreases. It represents the ability to quickly detection of process shifts by the proposed control chart. The following algorithm can be used to determine the optimal parameters for designing the proposed control chart for different combinations of specified in-control ARL and sample size.

1. Specify the values of ARL say r_0 and sample size n.
2. Set a = 0.001 and k = 0.001.
3. Determine the failure probability of the product (i.e., p_0) when the process is in control by using equation (8) and also determine the control chart parameters (LCL and UCL) by substituting the values of n, a and k in equation (10) and (11).
4. Calculate for in-control ARL by using equation (13) and compare it with r_0. Continue this process, for different combinations of (a and k) until getting an in-control ARL is very close to the specified ARL, r_0.
5. Whenever such ARL exist, then the corresponding parameters (LCL, UCL, a, k) are the required optimal parameters. Then calculate the out-of-control ARL (i.e., ARL_1) using these optimal parameters in equation (15).

Table 1: *ARLs when the process mean shifted for the fixed sample size n = 25*

	$n = 25$			
Parameter	$r_0 = 200$	$r_0 = 300$	$r_0 = 400$	$r_0 = 500$
LCL	6	6	5	5
UCL	20	21	20	20
a	0.6633	0.6758	0.6365	0.6583
k	2.7900	2.9070	2.8010	2.9691
$Shift(f)$	ARL	ARL	ARL	ARL
1.00	200.0989	300.1445	400.2567	500.0598
0.90	190.2520	224.5374	353.2836	236.5317
0.80	50.5499	142.0953	81.9755	55.2572
0.70	13.6761	32.2751	19.7207	14.5899
0.60	4.6098	8.9289	5.9207	4.8163
0.50	2.0606	3.2263	2.3788	2.1125
0.40	1.2676	1.6087	1.3453	1.2804
0.30	1.0399	1.1226	1.0534	1.0422
0.20	1.0017	1.0099	1.0024	1.0017
0.10	1.0000	1.0000	1.0000	1.0000

Table 2: *ARLs when the process mean shifted for the fixed value of $r_0 = 370$*

	$r_0 = 370$			
Parameter	$n = 20$	$n = 25$	$n = 30$	$n = 35$
LCL	4	5	8	14
UCL	17	20	24	31
a	0.6909	0.6316	0.7012	0.8638
k	2.8343	2.8397	2.9146	2.8954
$Shift(f)$	ARL	ARL	ARL	ARL
1.00	370.0466	370.3559	370.0958	370.0734
0.90	295.5639	282.9189	171.0958	240.0764
0.80	86.1301	90.0271	38.1100	95.0159
0.70	24.8906	21.2006	10.0689	21.9703
0.60	8.3369	6.2245	3.4980	6.5196
0.50	3.4030	2.4493	1.6885	2.6029
0.40	1.7687	1.3622	1.1482	1.4403
0.30	1.1988	1.0563	1.0155	1.0852
0.20	1.0273	1.0025	1.0003	1.0064
0.10	1.0006	1.0000	1.0000	1.0000

3. Application of Proposed Control Chart

3.1. Real-Life Application

In this section, a design example is given to demonstrate a real-life application of the proposed control chart under the Bayesian approach. Suppose that a manufacturer is interested in enhancing the quality of its product. It is known that the failure time of the product follows the Rayleigh distribution with the parameter following Inverse-Rayleigh distribution and the target mean life of the product is 1000 hours. Let a sample of size $n = 25$ be taken from each subgroup and subjected to a censored life test. The target in-control ARL, r_0 is 400. From Table 1, the constant

a = 0.636, k = 2.8010, LCL = 5 and UCL = 20. Therefore, the control chart to be set up by the manufacturer is designed as follows:

Step 1: Select a sample of 25 products from each subgroup and conduct a life test for 636 hours. Record the number of failed products during the life test and denote it as "d".
Step 2: Terminate the life test either after reaching 636 hours or the number of failed products greater than twenty before reaching 636 hours whichever is earlier.
Step 3: If $d > 20$ or $d < 5$, declare the process out of control. Declare the process to be in control if $5 \leq d \leq 20$.

3.2. Simulation Study

In this section, the application of the proposed control chart is demonstrated using simulated data. The data are generated from a Rayleigh distribution when the process is in-control with the parameters following Inverse-Rayleigh distribution and the targeted average lifetime of 1000 hours. We consider a random sample of size n = 20 for each sample batch. The first fifteen samples are generated from the in-control process, and the next fifteen samples are from a shifted process with f = 0.50 to achieve 30 sample batches. Then, from Table 2, when n = 20 and ARL_0 = 370, we have constants k = 2.8343, a = 0.691, UCL = 17 and LCL = 4. The number of products having the lifetime below 691 hours is noted ("D") and are: 10, 15, 12, 12, 12, 11, 12, 10, 10, 10, 14, 13, 12, 8, 10, 16, 17, 16, 18, 17, 17, 17, 20, 19, 20, 18, 17, 19, 19, 15. The values of the nonconforming items are plotted with two control limits (LCL = 4 and UCL = 17) in Figure 1.

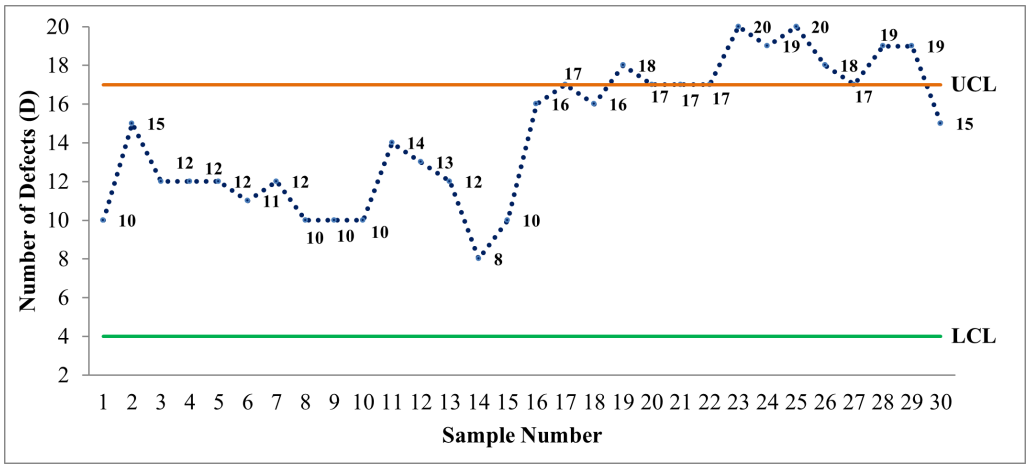


Figure 1: *Control Chart for Simulation Data*

From Figure 1, we observed that the proposed control chart detects a shift at the 17th sample (2nd observation after the shift), with a tabulated ARL of 3.40. As a result, the produced control chart recognises the shift in the manufacturing process efficiently. From this, it is concluded that the proposed control chart will detect the process shift quicker.

4. Discussion

In this paper, we have developed a methodology for a new Bayesian attribute control chart for the lifetime of products. The life tests are performed by hybrid censoring assuming a Rayleigh distribution for the lifetime and an Inverse-Rayleigh distribution as a prior. The proposed control chart is to ensure the mean lifetime of the product as the quality criterion. The newly established control chart is highly adaptable and may be used to monitor the lifetime of quality products. The tables are provided for industrial usage and are explicated with the use of simulated data. It is generated using R software from a Rayleigh-Inverse-Rayleigh distribution. The performance

of the proposed control chart is expressed in terms of *ARLs* for various shift constants (f). It should be noted that if the hybrid censoring scheme is used to carry out the life test, executing the sampling inspection will reduce the time and cost of conducting the life test. The developed attribute control chart has the potential to be extended for use with various other statistical distributions as part of a continuing research study.

References

[1] Muhammad Aslam and Chi-Hyuck Jun (2015). Attribute Control Chart for the Weibull Distribution under Truncated Life Tests. *Quality Engineering*, 27(3): 283 – 288.

[2] Aslam M, Nasrullah Khan and Chi – Hyuck (2016a). A control chart for time truncated life tests using Pareto distribution of the second kind. *Journal of Statistical Computation and Simulation*, 86(11): 2113 – 2122.

[3] Aslam M, Arif, O. H and Jun, C (2016b). An Attribute Control Chart based on the Birnbaum-Saunders Distribution using Repetitive Sampling. *IEEE Access*, 5: 9350 – 9360.

[4] Muhammad Aslam, Osama H. Arif and Chi-Hyuck Jun (2017). An Attribute Control Chart for a Weibull distribution under Accelerated Hybrid Censoring. *PLoS ONE*, 12(3): e0173406: 1 – 11.

[5] Nanthakumar C and T. Kavitha (2017). Design of Attribute Control Chart based on Inverse Rayleigh Distribution under Type – I Censoring. *International Journal of Statistical Sciences*, 4(6): 17 – 22.

[6] Ambreen Shafqat, Jaffer Hussain, Amjad D. Al-Nasser and Muhammad Aslam (2018). Attribute Control Chart for some popular distributions. *Communication in Statistics – Theory and Methods*. 47(8): 1978 – 1988.

[7] Arif O. H, Muhammad Aslam and K.A. Butt (2018). Attribute Control Chart for a Lognormal distribution under Accelerated Time Censoring. *Journal of Computational and Theoretical Nanoscience*, 15(3): 919 – 923.

[8] Srinivasa Rao G (2018). A Control Chart for Time Truncated Life Tests Using Exponentiated Half Logistic Distribution. *Applied Mathematics & Information Sciences: An International Journal*, 12(1): 125 – 131.

[9] Srinivasa Rao Gadde, A.K. Fulment and P.K Josephat (2019). Attribute Control Charts for Dagum distribution under truncated life tests. *Life cycle Reliability and Safety Engineering*, 8: 329 – 335.

[10] Balamurali S and P. Jeyadurga (2019). An Attribute np Control Chart for Monitoring Mean Life using Multiple Deferred State Sampling based on Truncated Life Tests. *International Journal of Reliability, Quality and Safety Engineering*, 26(1): 1950004-1 – 1950004-18.

[11] Enayat M. Abd Elrazik (2020). Attribute control charts for the New Weibull Pareto Distribution under truncated life tests. *Journal of Statistics Applications & Probability*, 9(1): 43 – 49.

[12] Ahmad Ibrahim Shawky, Muhammad Aslam and Khushnoor Khan (2020). Multiple dependent state sampling-based charts using Belief Statistic under Neutrosophic Statistics. *Journal of Mathematics*, 2020(7680286): 1- 14.

[13] Srinivasa Rao Gadde, Edwin Paul (2020). Time Truncated Control Chart using Log- Logistic Distribution. *Biometrics & Biostatistics International Journal*, 9: 76 - 82.

[14] Ali Hussein Al-Marshadi, Ambreen Shafqat, Muhammad Aslam and Abdullah Alharbey (2021). Performance of a New Time-Truncated Control Chart for Weibull Distribution under Uncertainty. *International Journal of Computational Intelligence Systems*, 14(1): 1256 – 1262.

[15] Rosaiagh, K., G. Srinivasa Rao and S. V. S. V. S. V. Prasad (2021). A Control Chart for Time Truncated Life Tests using type-II Generalized Log Logistic Distribution. *Biometrics & Biostatistics International Journal*, 10(4): 138 – 143.

[16] Adeoti O. A. and P. Ogundipe (2021). A Control Chart for the generalized exponential distribution under time truncated life test. *Life Cycle Reliability and Safety Engineering*, 10: 53 – 59.

[17] Ayman Baklizi and Sawsan Abu Ghannam (2022). An attribute control chart for the inverse Weibull distribution under truncated life tests. *Heliyon*, 8(e11976): 1 - 5.
[18] Srinivasa Rao Gadde and Amer Ibrahim Al-Omari (2022). Attribute control charts based on TLT for Length-Biased Weighted Lomax Distribution. *Journal of Mathematics*, 2022(3091850): 1- 15.
[19] Olatunde Adebayo Adeoti and Gadde Srinivasa Rao (2022). Attribute control chart for Rayleigh distribution using Repetitive sampling under truncated life test. *Journal of Probability and Statistics*, 2022(8763091): 1 - 11.
[20] Muhammad Naveed, Muhammad Azam, Nasrullah Khan, Muhammad Aslam, Muhammad Saleem and Muhammad Saeed (2023). Control Chart for Half Normal and half Exponential power Distributed Process. *Scientific Reports*, 13(8632): 1- 20.
[21] Joel M. Calabrese (1995). Bayesian Process Control for Attributes. *Management Science*, 41(4): 637 – 645.
[22] Ulrich Menzefricke (2002). On the Evaluation of Control Chart Limits based on Predictive Distributions. *Communication in Statistics – Theory and Methods*, 31(8): 1423 – 1440.
[23] Apley D. W (2012). Posterior distribution charts: A Bayesian approach for graphically exploring a process mean. *Technometrics*, 54(3): 279 – 310.
[24] Amin Shaka Aunali and D. Venkatesan (2017). Comparison of Bayesian Method and Classical Charts in Detection of Small Shifts in the Control Charts. *International Journal of Operations Research and Optimization*, 6(2): 101 – 114.
[25] Kumar N and S. Chakraborti (2017). Bayesian Monitoring of times between events: The Shewhart tr - chart. *Journal of Quality Technology*, 49(2): 136 – 154.
[26] Amin Shaka Aunali and D. Venkatesan (2019). Bayesian Approach in Control Chart Techniques. *International Journal of Scientific Research in Mathematical and Statistical Sciences*, 6(2): 217 – 221.
[27] Amin Shaka Aunali, Venkatesan. D. and Michele Gallo (2019). Bayesian Control Chart using Gamma Prior. *International Journal of Scientific & Technology Research*, 8(12): 1567 - 1570.
[28] Ali S (2020). A Predictive Bayesian Approach to sequential time-between-events monitoring. *Quality and Reliability Engineering International*, 36(1): 365 – 387.
[29] Kadoishi S and H. Kawamura (2020). Control Charts based on Hierarchical Bayesian Modeling. *Total Quality Science*, 5(2): 72 – 80.
[30] Konstantinos Bourazas, Dimitrios Kiagias and Panagiotis Tsiamyrtzis (2022). Predictive Control Charts (PCC): A Bayesian Approach in Online monitoring of short runs. *Journal of Quality Technology*, 54(4): 367 – 391.
[31] Fatimah Alshahrani, Ibrahim M. Almanjahie, Majid Khan, Syed M. Anwar, Zahid Rasheed and Ammara N. Cheema (2023). On Designing of Bayesian Shewhart-Type Control Charts for Maxwell Distributed Processes with Application of Boring Machine. *Mathematics*, 11(1126): 1 - 20.
[32] Lord Rayleigh, O. M. F. R. S (1919). On the problem of random vibrations, and of random flights in one, two, or three dimensions. *The London, Edinburgh, and Dublin Philosophical Magazine and Journal of Science*, Series 6, 37(220): 321 – 347.
[33] Siddiqui M. M (1962). Some Problems Connected with Rayleigh Distributions. *Journal of Research of the National Bureau of Standards – D. Radio Propagation*, 66D(2): 167 – 174.
[34] Siddiqui M. M (1964). Statistical Inference for Rayleigh Distribution. *Radio Science Journal of Research NBS/USNC-URSI*, 68D(9): 1005 – 1010.
[35] Kalaiselvi S., A. Loganathan and R. Vijayaraghavan (2014). Bayesian Reliability Sampling Plans under the Conditions of Rayleigh-Inverse-Rayleigh Distribution. *Economic Quality Control*, 29(1): 29 – 38.
[36] Saad T and Bakir (2012). A nonparametric Shewhart-type quality control chart for monitoring broad changes in a process distribution. *International Journal of Quality, Statistics, and Reliability*, 2012(147520): 1 – 10.

ENHANCING THE RELIABILITY OF THERMAL POWER SYSTEMS USING MEMBRANE-BASED WATER TREATMENT TECHOLOGIES

Ahmadova J.A.
•
Azerbaijan State Oil and Industry University
cahan.ahmadova@asoiu.edu.az

Abstract

The reliability and efficiency of thermal power plants (TPPs) are largely determined by the quality of water treatment systems that maintain a stable water-chemical regime (WCR) for boilers and auxiliary equipment. In scenarios where seawater with high salinity and variable composition is used as the primary water source, conventional treatment methods—such as ion exchange, chemical coagulation, and thermal desalination—prove inadequate and resource-intensive. This study investigates the application of a hybrid membrane-based configuration comprising ultrafiltration (UF), reverse osmosis (RO), and membrane distillation (MD). The proposed system enables the production of high-purity demineralized water, reduces operational risks, and lowers energy consumption through the utilization of low-grade waste heat. Based on pilot data and modeled performance, the UF–RO–MD cascade achieves up to 99% desalination efficiency with specific energy consumption in the range of 1.9–2.5 kWh/m³ and a significant reduction in scaling potential. A simplified case study is provided to illustrate the high effectiveness of membrane technologies in enhancing the sustainability and resilience of TPP operations, especially in coastal regions with limited freshwater availability.

Keywords: thermal power plants; water treatment; membrane technologies; ultrafiltration; reverse osmosis; membrane distillation

I. Introduction

The reliability and operational efficiency of thermal power plants (TPPs) critically depend on the quality of water treatment systems, which maintain stable water-chemical regimes (WCRs) in boilers, heat exchangers, and auxiliary equipment. This dependence becomes especially acute for TPPs located in coastal regions, where seawater often serves as the primary source of process water due to limited freshwater availability. Along the Caspian Sea coast, the use of seawater for technical purposes faces significant challenges caused by its high salinity, presence of organic contaminants, and seasonal composition fluctuations, which can severely affect plant operation and increase equipment wear [1,2].

Traditional water treatment methods—such as ion exchange, chemical coagulation, thermal desalination, and open filtration—present several drawbacks under these conditions. These include complex control requirements, elevated reagent and energy consumption, limited efficiency in removing dissolved salts and organics, and difficulties in handling feedwater variability. Consequently, these limitations often result in operational instability and increased risks of scaling, corrosion, and biofouling within the plant's water circuits [3,4].

In response to these challenges, membrane-based water treatment technologies have garnered growing interest over recent decades. Techniques such as reverse osmosis (RO), nanofiltration (NF), and ultrafiltration (UF) provide significant advantages by offering high separation efficiency, compact and modular designs, reduced chemical consumption, and lower energy requirements compared to conventional methods. Their ability to consistently produce high-purity demineralized water improves process stability and extends equipment lifetime, thus enhancing the overall reliability of thermal power systems [5,6,7].

Reverse osmosis remains the cornerstone technology for seawater desalination, effectively removing salts, suspended solids, and many organic compounds. Advances in membrane materials and configurations have led to improved flux rates, fouling resistance, and mechanical durability [8,9]. However, RO performance is highly dependent on effective pretreatment, which often includes ultrafiltration or microfiltration to reduce suspended solids and biofouling potential [10]. Nanofiltration, while less commonly applied for full desalination, serves as an effective method for selective removal of divalent ions and organic matter, complementing RO and UF in integrated systems [11].

Another emerging membrane process is membrane distillation (MD), which uses thermal gradients to separate water vapor through hydrophobic membranes. MD offers advantages in utilizing low-grade or waste heat, enhancing energy efficiency when integrated with conventional desalination processes. Hybrid systems combining RO and MD stages have demonstrated improved permeate quality, reduced concentrate volumes, and lower chemical scaling tendencies, thus promoting stable operation and reducing maintenance downtime [12,13].

Extensive studies have highlighted that the integration of membrane technologies within TPP water treatment infrastructure results in operational benefits including enhanced water quality, reduced scaling and corrosion potential, lower chemical dosing, and improved environmental footprint. These benefits contribute directly to the extended service life of critical equipment and the overall reliability of power generation [14,15]. Moreover, the automation-friendly nature of membrane systems supports advanced process control and real-time monitoring, crucial for handling variable seawater compositions prevalent in coastal zones [16].

Despite these advantages, challenges remain related to membrane fouling, concentrate disposal, and capital investment. Ongoing research focuses on membrane material innovation, antiscalant development, and system design optimization to overcome these hurdles and expand applicability to diverse operational conditions [17-19].

This paper aims to evaluate the potential of membrane technologies as a strategic solution for enhancing the reliability of water treatment systems at TPPs operating in coastal zones of the Caspian Sea. It discusses operational characteristics, compares membrane approaches with conventional methods, and provides practical recommendations for implementing resilient water treatment infrastructures in thermal power systems.

II. Statement of the problem

Modern combined heat and power plants (CHPPs) located along the Caspian Sea coast face a number of technological challenges associated with ensuring reliable water treatment. The use of seawater as a raw feedstock requires deep removal of salts, organic substances, and suspended solids to prevent corrosion, scale deposition, and violations of the water-chemical regime (WCR) in steam-water circuits of boiler units [3]. Given the elevated salinity, unstable composition, and seasonal contamination risks, traditional ion-exchange water treatment methods often demonstrate insufficient stability and demand significant operational efforts.

Accordingly, the central research problem is to assess the effectiveness of membrane technologies—specifically ultrafiltration (UF) and reverse osmosis (RO) units—for use in CHPPs operating with seawater from the Caspian basin. A key research focus is on determining the impact of these membrane systems on the reliability of water treatment, the stability of water quality indicators, and the overall operational reliability of technological components.

Analysis of water samples treated with membrane units shows that such technologies provide efficient removal of both macro- and micro-contaminants. As shown in Table 1, total salinity is reduced from approximately 12,000 mg/L to less than 10 mg/L, meeting the required norms for boiler feedwater. The concentrations of suspended solids and silicic acid are also lowered to acceptable levels, which are unattainable through conventional chemical softening processes alone.

Table 1.: *Water quality at various treatment stages (CSV)*

Parameter	Seawater (inlet)	After UF	After RO	Boiler Norm
Total salinity, mg/L	12000	9800	10	<5
Suspended solids, mg/L	25	1	0.1	<0.5
Silicic acid, mg/L	1.2	1.1	0.05	<0.1

In addition to high water quality, the operational reliability of the membrane-based WCR correlates directly with the reduction in the number of deviations and emergency situations [4]. Figure 1 presents a comparison of annual WCR deviation frequencies over a five-year period using traditional and membrane-based treatment systems. The data demonstrate that the adoption of membrane technologies reduced the number of critical incidents by more than fivefold, indicating improved overall reliability and lower operational risk.

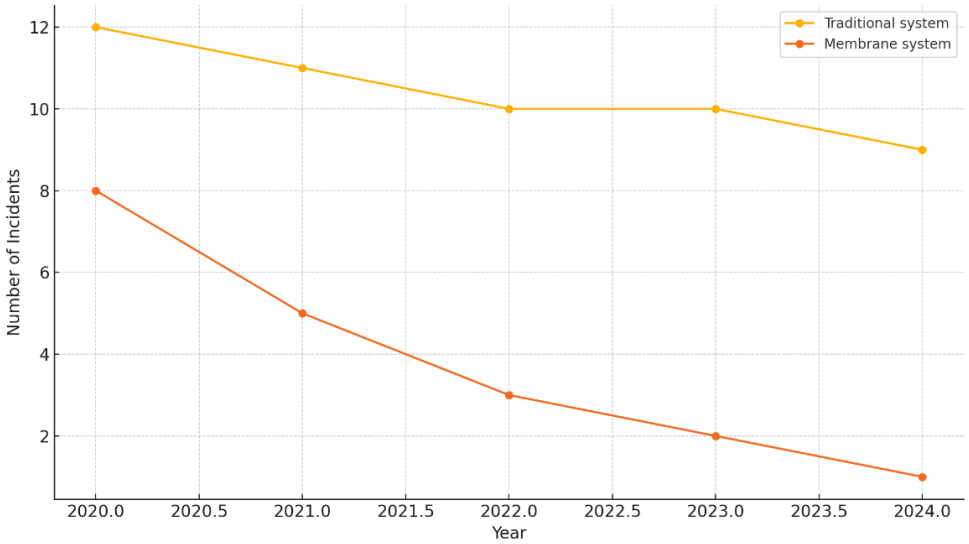


Figure 1. *Frequency of WCR deviations at the CHPP (2020–2024)*

To objectively evaluate the performance of membrane treatment systems, a comparative analysis was conducted between traditional and membrane-based schemes. Table 2 summarizes the key technological and operational characteristics.

The results clearly demonstrate the advantages of membrane systems in terms of water quality stability, personnel requirements, automation, and robustness to raw water pollution. Although they typically require higher specific energy consumption, membrane systems offer superior adaptability and stability under varying environmental conditions.

Table 2.: *Comparison of technologies (CSV)*

Criterion	Traditional Scheme	Membrane System
Stability of water quality	Moderate	High
Number of personnel per shift	3–4	1–2
Energy consumption, kWh/m³	0.8	2.0
Reliability under raw water load	Low	High
Level of automation	Partial	Full

Considering the specific characteristics of Caspian seawater—such as high hardness, organic load, and colloidal fractions—a typical membrane-based treatment flow diagram is proposed (see *Figure 2*). This includes mechanical pre-filtration, ultrafiltration for removing suspended and biological matter, and two-stage reverse osmosis, with optional polishing steps for silica and gases before final de-aeration and boiler feed.

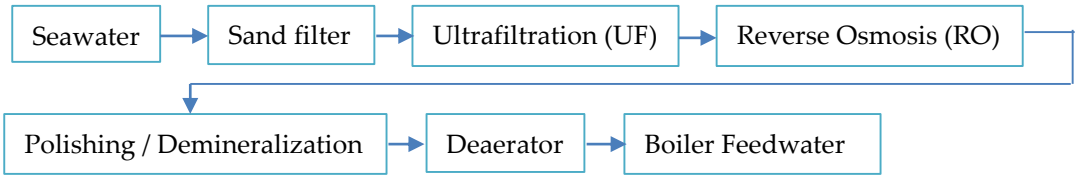


Figure 2.: *Typical membrane-based water treatment scheme for Caspian coastal CHP plants*

Thus, the scientific problem formulated in this study aims not only to adapt membrane treatment technologies to local marine conditions but also to ensure sustainable, reliable, and environmentally compliant water management at coastal CHPPs. Further development of this approach requires the analysis of both operational and economic indicators, along with consideration of regional specifics such as temperature fluctuations, biofouling, and the presence of marine flora.

III. Solution to the problem

In the current context of increasing quality requirements for feedwater at thermal power plants (TPPs), membrane technologies are gaining particular importance due to their high selectivity, low energy consumption, and modular scalability [5,6]. This section examines the integrated application of ultrafiltration (UF), reverse osmosis (RO), and membrane distillation (MD) using a typical cascade water treatment scheme, relevant for the Caspian region.

Figure 3 presents a block diagram of the UF–RO–MD system, showing the main process flows, temperatures, and pressures. The system is organized in a cascade layout: the preliminary ultrafiltration stage removes suspended solids and organic contaminants, thus reducing the load on the subsequent RO module. Reverse osmosis then removes up to 99% of dissolved salts, with a typical product yield of about 70–80%. The RO concentrate is further treated using membrane distillation, which utilizes low-grade heat at 50–80 °C, allowing for increased freshwater output and reduced concentrate discharge.

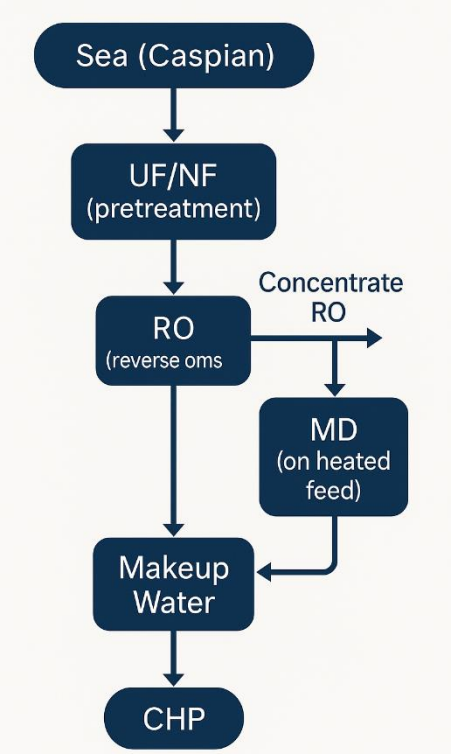


Figure 3. *Technological block diagram of the UF–RO–MD water treatment system with indication of flows, temperatures, and pressures.*

The performance of RO and MD modules is highly dependent on the feedwater temperature. Figure 4 shows a typical correlation between temperature and the productivity of both technologies: as temperature increases, membrane permeability and evaporation rates also increase, positively affecting the product yield. Notably, membrane distillation demonstrates significant productivity gains even at moderate temperatures (50–70 °C), making it an efficient method of waste heat recovery from TPPs.

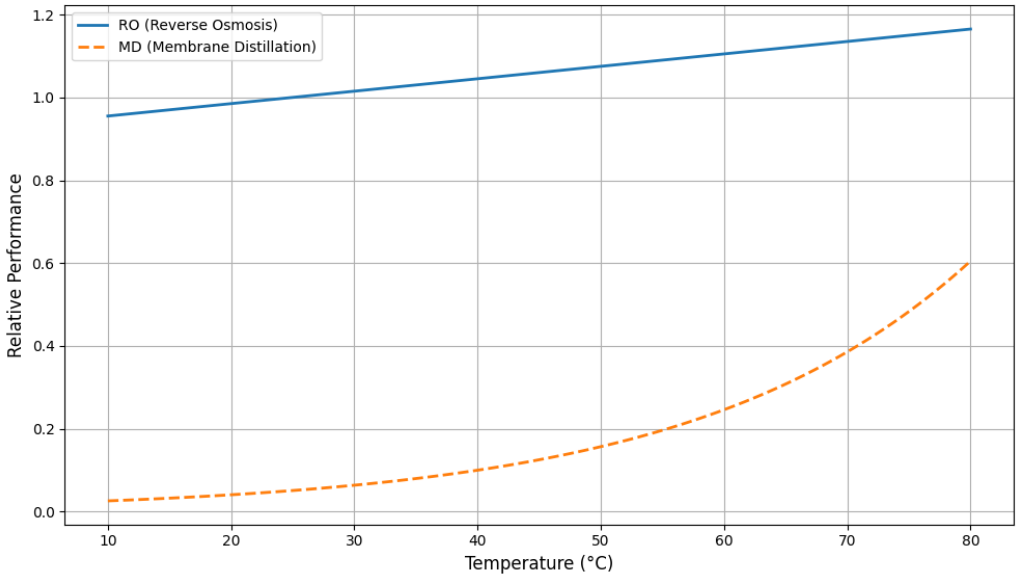


Figure 4. *Dependence of RO and MD performance on feedwater temperature*

To assess the energy efficiency of the technologies, a comparative graph of specific energy consumption is provided (Figure 5). As shown, the hybrid RO+MD system achieves lower specific energy consumption compared to conventional RO alone. This improvement is due to the reuse of low-grade heat in the MD stage and the reduced volume of concentrate requiring handling and pumping.

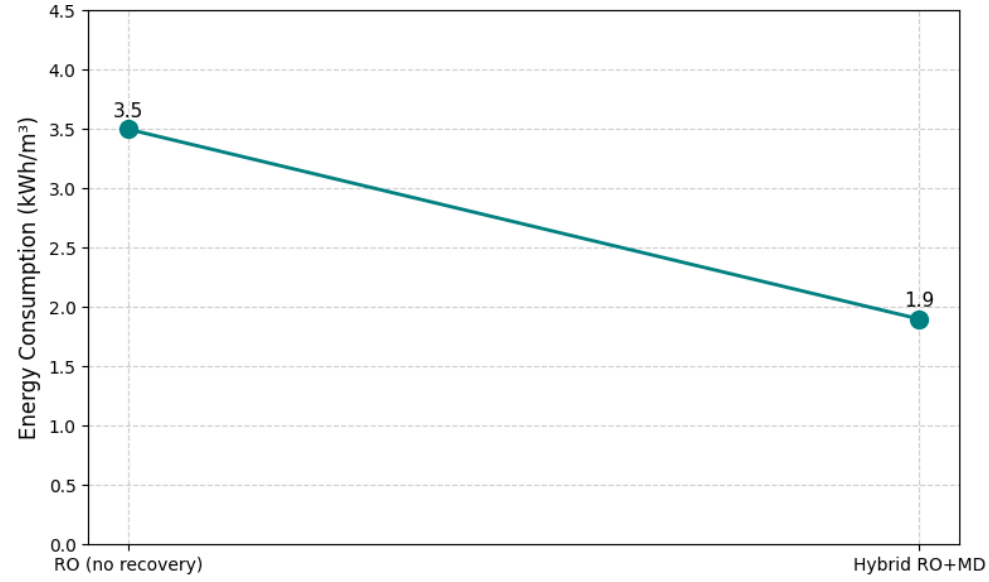


Figure 5. *Comparative analysis of specific energy consumption for RO and RO+MD systems*

Figure 5 presents a comparative assessment of the specific energy consumption (SEC) for conventional reverse osmosis (RO) without energy recovery and a hybrid RO+membrane distillation (MD) configuration utilizing low-grade waste heat. The standalone RO system demonstrates a typical SEC of approximately 3.5 kWh/m³, which reflects the substantial energy demand for high-pressure pumping, particularly in the absence of energy recovery units [18,19].

In contrast, the hybrid RO+MD system achieves a notably lower SEC, around 1.9 kWh/m³, by recovering additional freshwater from the RO concentrate using thermal energy in the range of 50–80 °C. This thermal energy, often available as a byproduct of steam or flue gas systems in thermal power plants (TPPs), significantly reduces the reliance on mechanical input and enables recovery of an additional 27–40% of product water from the concentrate stream [8,9].

The integration of MD into the RO process not only improves water recovery rates but also decreases brine volume and scaling risks, potentially lowering the frequency of chemical cleaning cycles and extending membrane life.

These results indicate that hybrid desalination configurations can offer enhanced energy efficiency and are particularly well-suited for deployment in TPPs with available waste heat streams, such as those located in the Caspian region.

Preventing scale formation on membranes and pipelines requires evaluating the water's scaling potential. Figure 6 illustrates the distribution of water based on the Langelier Saturation Index (LSI): values below –0.5 indicate aggressive water prone to corrosion, while values above +0.5 suggest a tendency to form scale. RO water treatment is typically designed to maintain LSI within the range of –0.5 to +0.5 to minimize these risks. When designing the MD stage, LSI is taken into account through thermodynamic calculations and pH adjustment.

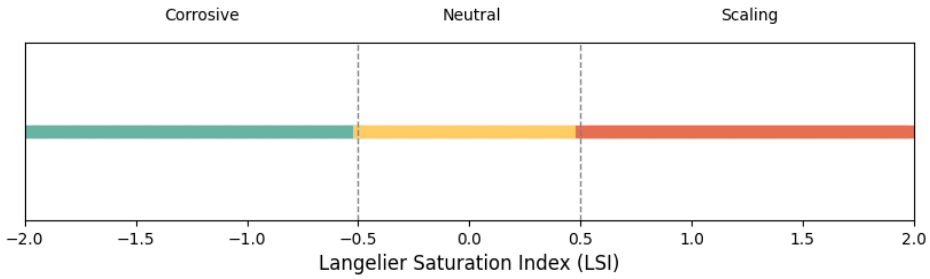


Figure 6.: *Langelier Index and risk zones: <–0.5 — aggressive water; >+0.5 — scaling tendency*

Implementation of the hybrid UF–RO–MD scheme enables:

- A significant reduction in the total dissolved solids (TDS) in feedwater to ≤ 200 ppm;
- Extension of equipment maintenance intervals from 2–3 years to 4–6 years;
- Reduction in TPP outages and operational disruptions;
- Decrease in specific energy consumption for desalination to 1.9–2.5 kWh/m³.

This integrated approach has been validated by pilot operations in the Caspian region and successful full-scale projects in the UAE, Saudi Arabia, and the Maldives.

Thus, the use of the cascade UF–RO–MD scheme significantly improves the efficiency of water treatment at thermal power plants (TPPs) by reducing membrane load, increasing product recovery, and utilizing waste heat [10]. Let us consider a simplified calculation example to evaluate the performance and energy consumption of the hybrid system.

Assume that 100 m³/h of seawater with a temperature of 25 °C and a total dissolved solids (TDS) concentration of approximately 15,000 ppm is fed into the system. At the reverse osmosis (RO) stage, operating at a pressure of 6.5 MPa, a product recovery of about 75% is achieved, i.e.:

$$Q_{RO} = 100 \times 0.75 = 75\ m^3/h$$

The remaining concentrate is directed to the membrane distillation (MD) module, where approximately 33% of the RO product volume is additionally recovered using low-grade waste heat (T = 60 °C):

$$Q_{MD} = 75 \times 0.33 \approx 24.75\ m^3/h$$

Thus, the total freshwater output becomes:

$$Q_{total} = 75 + 24.75 = 99.75\ m^3/h$$

This means that nearly the entire volume of the feedwater is utilized efficiently, with minimal concentrate discharge.

From an energy efficiency perspective, assuming a specific energy consumption of 3.0 kWh/m³ for RO and approximately 0.2 kWh/m³ for MD (mainly for circulation and vacuum), the combined energy demand can be estimated as:

$$E_{total} = \frac{3.0 \times 100 + 0.2 \times 24.75}{99.75} \approx 3.07\ kWh/m^3$$

However, in actual installations with effective heat recovery and the use of thermal energy from the TPP, these values are reduced to approximately 1.9–2.5 kWh/m³, as confirmed by operational data.

It is also necessary to assess the Langelier Saturation Index (LSI) during system design to minimize scaling risks. For instance, if the source water has a pH of 7.8 and the calculated saturation pH with respect to calcite is 7.3, then:

$$LSI = 7.8 - 7.3 = +0.5$$

This is a borderline value that may require either antiscalant dosing or pH adjustment. Notably, the integration of the MD stage allows the RO module to operate at lower concentrate concentrations, thereby reducing LSI and often eliminating the need for chemical stabilization.

This numerical example thus confirms the high efficiency of the hybrid membrane system, provided that it is properly designed and makes optimal use of available secondary thermal energy.

IV. Conclusion

The application of membrane-based water treatment technologies at thermal power plants (TPPs) utilizing seawater has proven to be a highly effective and strategically sound solution, significantly enhancing the reliability and resilience of power generation systems. In coastal regions such as those along the Caspian Sea, where seawater often serves as the primary water source, challenges arise due to high salinity, organic contamination, and seasonal variability in composition. These factors complicate the maintenance of stable water-chemical regimes (WCRs) in boilers and heat exchangers and increase the risk of scaling and corrosion.

Conventional treatment methods—such as ion exchange, coagulation, and thermal desalination—demonstrate limited effectiveness under these conditions, often requiring substantial chemical usage, high energy inputs, and complex manual control. In contrast, membrane technologies—including ultrafiltration (UF), reverse osmosis (RO), and membrane distillation (MD)—offer critical advantages such as high selectivity, reduced chemical consumption, modular scalability, and a higher degree of automation.

Field and pilot data confirm that the implementation of cascade UF–RO–MD schemes can reliably reduce total dissolved solids (TDS) to below 10 mg/L, ensuring compliance with stringent feedwater quality standards. As a result, the frequency of WCR deviations and emergency shutdowns is reduced by more than fivefold, and equipment maintenance intervals are extended from 2–3 years to 4–6 years.

Furthermore, the integration of membrane distillation, powered by low-grade waste heat from TPPs, improves freshwater recovery by 30–40% while reducing specific energy consumption to as low as 1.9–2.5 kWh/m³—significantly outperforming traditional methods.

From a resource-efficiency and sustainability perspective, membrane-based systems reduce membrane fouling through effective pretreatment, minimize concentrate discharge, and optimize the use of thermal energy. Their high automation levels reduce operational labor demands and increase responsiveness to raw water quality fluctuations.

To ensure the successful scaling of such technologies, further research is recommended into region-specific challenges such as biofouling, temperature-driven performance variability, and Langelier Saturation Index (LSI) management. Particular attention should be given to long-term economic and environmental performance metrics in full-scale deployments.

In summary, membrane technologies represent a promising and future-oriented approach for improving the energy efficiency, reliability, and environmental sustainability of water treatment processes at TPPs operating in coastal zones with limited access to freshwater.

References

[1] Ahmadova, J.A. (2023). Hybrid Seawater Desalination Technology Based on Reverse Osmosis and Membrane Distillation Methods. *Membranes and Membrane Technologie*s, 5(2), 80–91.

[2] Agamaliyev, M.M., Ahmadova, J.A., Aliyeva, O.O. (2022). Waste Heat Utilization of Diesel Power Plant Cooling System for Seawater Desalination by Membrane Distillation. *Membranes and Membrane Technologies*, 4(1), 48–58

[3] Lee, K.P., Arnot, T.C., Mattia, D. (2011). A review of reverse osmosis membrane materials for desalination—Development to date and future potential. *Journal of Membrane Science*, 370(1-2), 1-22.
[4] Curto, D., Franzitta, V., Guercio, A. (2021). A review of the water desalination technologies. *Applied Sciences*, 11(2), 670.
[5] Salinas-Rodríguez, S.G., Schippers, J.C., Kennedy, M.D. (2021). Basic principles of reverse osmosis. In *Seawater Reverse Osmosis Desalination: Assessment and Pre-treatment of Fouling and Scaling* (pp. 29-58).
[6] Kiss, A.A., Kattan Readi, O.M. (2018). An industrial perspective on membrane distillation processes. *Journal of Chemical Technology and Biotechnology*, 93(8), 2047-2055.
[7] Jantaporn, W., Ali, A., Aimar, P. (2017). Specific energy requirement of direct contact membrane distillation. *Chemical Engineering Research and Design*, 128, 15-26.
[8] Popov, K., Rudakova, G., Larchenko, V., et al. (2016). Comparative Performance Evaluation of Some Novel "Green" and Traditional Antiscalants in Calcium Sulfate Scaling. *Advances in Materials Science and Engineering*, 2016, Article ID 7635329.
[9] Shannon, M.A., Bohn, P.W., Elimelech, M., et al. (2008). Science and technology for water purification in the coming decades. *Nature*, 452(7185), 301–310.
[10] Nghiem, L.D., Hawkes, F.R., Elimelech, M. (2006). Membrane-based processes for water treatment and desalination: Current status and future prospects. *Environmental Science & Technology*, 40(15), 4678–4689.
[11] Ghaffour, N., Missimer, T.M., Amy, G.L. (2013). Technical review and evaluation of the economics of water desalination: Current and future challenges for better water supply sustainability. *Desalination*, 309, 197-207.
[12] Khayet, M. (2011). Membrane distillation: Principles and applications. *Desalination*, 287, 1-20.
[13] El-Bourawi, M.S., Ding, Z., Ma, R., Khayet, M. (2006). A framework for better understanding membrane distillation separation process. *Journal of Membrane Science*, 285(1-2), 4-29.
[14] Van der Bruggen, B., Vandecasteele, C. (2002). Removal of pollutants from surface water and groundwater by nanofiltration: Overview of possible applications in the drinking water industry. *Environmental Pollution*, 122(3), 435-445.
[15] Nghiem, L.D., Price, W.E., Elimelech, M. (2013). Role of membrane technology in sustainable water treatment. *Annual Review of Chemical and Biomolecular Engineering*, 4, 41-61.
[16] Pontie, M., Méthivier, C., et al. (2020). Automation and process control in membrane filtration systems: Enhancing reliability and efficiency. *Desalination*, 494, 114590.
[17] Werber, J.R., Osuji, C.O., Elimelech, M. (2016). Materials for next-generation desalination and water purification membranes. *Nature Reviews Materials*, 1, 16018.
[18] Rzayeva, S.V. (2023) Features of Electrodeless Electrochemical Reactions. *Surface Engineering and Applied Electrochemistry*, 59(5), 590–594
[19] Rzayeva, S.V., Ganiyeva, N.A., Piriyeva, N.M. (2023) INVESTIGATION OF CHARACTERISTICS OF A BARRIER DISCHARGE IN A WATER-AIR ENVIRONMENT. *International Journal on Technical and Physical Problems of Engineering*, 15(2), 44–49

A NOVEL ENERGY-EFFICIENT APPROACH TO DETECT AND MITIGATE RPL ROUTING ATTACKS IN IOT NETWORK

Deepak Upadhyay[1], Hiteishi Diwanji[2]

•

[1]Phd Scholar, Gujarat Technological University, Gujarat, India
[2]L. D. Government Engineering College, Gujarat, India
[1]ap_deepak@gtu.edu.in , [2]hiteishi.diwanji@gmail.com

Abstract

Communication networks are constantly at risk from routing attacks, which have the potential to disrupt the network performance, information flow and jeopardize network integrity. Network resources and Energy consumption attacks on the Internet of Things (IoT) are the main targets to bring down the services of Internet of Things devices with attacks such as Denial of Service, Jamming etc. Node mobility results in frequent changes to network topology. This increases energy consumption and reduces node lifetimes, which can disrupt overall network functionality. To overcome these problems the author has proposed a hybrid and lightweight A Novel Energy-Efficient Approach to Detect and Mitigate RPL (EEADM-RPL) protocol considering control messages with route metrics in different detection and mitigation algorithm to mitigate the Blackhole attack, Rank attack and Sybil attacks under mobility environment at a time. An attack scenario created with the algorithms for all attacks using control messages and attributes of packets. The EEADM-RPL protocol uses basic RPL control messages, neighbor table, trust calculation, and a minimum rank hysteresis objective function to detect and eliminate the attacks. This protocol is suitable for industrial systems to handle cyber-attack and for the Vulnerability Assessment and Penetration Testing audit. The Cooja simulator, part of the Contiki operating system, simulates the attacks without mobility and with mobility demonstrates the effectiveness affecting the network and the resources. The outcomes of the simulation are compared with those of current protocols. According to the data, the proposed protocol demonstrates improvements over the conventional RPL protocols in several metrics: the average parent change ratio by 87.94%, the average packet loss ratio by 69.17%, end-to-end latency by 67.85%, and both energy consumption and end-to-end delay by 13.07%.

Keywords: IoT Network Attacks, Sybil Attack, Rank Attack, Blackhole Attack, EEADM-RPL

I. Introduction

The widespread adoption of Internet of Things (IoT) devices has significantly transformed various sectors, ranging from residential smart homes to industrial automation. With the rapid rise in IoT device deployment, there is a heightened risk landscape with multiple security threats. Laghari [1] introduces one of the major concerns for the hybrid attacks in this area is Sybil attacks, which present serious challenges to the reliability and operation of IoT networks. Deceptive tactics are used by adversaries to create multiple fake identities to deceive systems and gain unauthorized access or

control. With the increasing number of IoT devices, the risk of Sybil attacks disrupting operations and compromising sensitive data also rises. Sasi et al. [2] referenced conventional approaches for identifying Sybil attacks in IoT environments frequently prove inadequate because of the ever-changing and intricate structure of these networks. Recent advancements in deep learning show promising potential for improving Sybil attack detection capabilities. Alfriehat et al. [3] utilized advanced learning methods, these techniques can effectively detect unusual behaviors that may signal security threats in IoT environments.

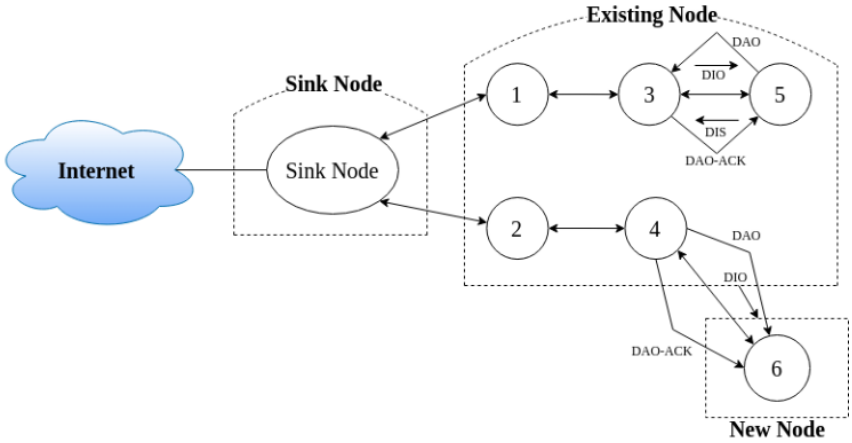


Figure 1: *RPL Graph*

Exploring the growing threat of Sybil attacks on IoT devices and investigating the use of deep learning tools for detection. Utilizing neural networks and sophisticated machine learning algorithms, our goal is to create a defense system that can detect and prevent Sybil attacks in real-time. Aldhaheri [4] study adds to the continuous work aimed at enhancing the security of IoT infrastructures, protecting them from advancing cyber threats in a world that is becoming more interconnected.

I. Motivation of EEADM-RPL Protocol

The dynamics within networks influence the convergence of routing protocols, as well as their organization and configuration, potentially compromising network operations. Considering node mobility, existing methods and protocols use cryptography, encryption, mathematical, decryption, rule-based, blockchain, and intrusion detection system (IDS) algorithms to identify and eliminate threats, primarily in a static environment. These techniques create overhead with the message and affect the performance to counter the mobility with high detection and mitigation solutions. This results in several challenges, including reduced throughput and packet delivery ratios, increased end-to-end delay, and ultimately diminishing the network's overall lifespan. These factors contribute to the potential failure of the entire network. In order to address these issues, the EEADM-RPL protocol is put out, which uses tiny byte-fag values, MRHOF, trickling timers, and basic RPL control messages to identify and lessen the threats. The primary objective of the proposed DE2RA-RPL protocol is to conserve energy.

II. Contribution of the EEADM-RPL Protocol

This EEADM-RPL protocol is proposed to handle the Blackhole attack, Rank attack and Sybil attack in a dynamic environment considering mobility of the nodes as malicious nodes for attacks. Majorly it affects more degradation of the performance of the network and more consumption of power can lead to failure of the network.

There are three algorithms in the proposed EEADM-RPL, including Detection and Mitigation of Blackhole Attack, Rank Attack and Sybil Attack for detecting and mitigating of Network Resource and Energy Consumption related attacks. The hybrid lightweight EEADM-RPL protocol comprises six algorithms that are distributed to every node within the DODAG environment. The EEADM-RPL protocol utilizes MRHOF, small byte flag values, a trickling timer, and standard RPL control messages to facilitate node mobility and mitigate potential attacks. The root node will not encounter any overhead. Additionally, nodes within the DODAG environment will not face any overhead, as the algorithms utilize lightweight packets that integrate with the existing RPL control messages. The Cooja simulation environment highlights two scenarios. In one, the EEADM-RPL protocol outperforms existing RPL-based protocols with immobile nodes. In the other, it shows superior performance with mobile malevolent nodes. Paganraj [5] aims the comparative results with existing protocols indicate that the EEADM-RPL protocol enhances throughput, reduces energy consumption, improves packet delivery ratio, and decreases end-to-end latency.

The structure of this document is as follows: Section 2 of the Attack Methodology presents an overview of the key concepts related to the Blackhole Attack, Rank Attack, and Sybil Attack. Section 3 offers an explanation of the Literature Survey. Section 4 contains a detailed discussion on the proposed EEADM-RPL protocol. Section 5 provides an analysis of the performance and simulation results. The document concludes with future work outlined in Section 6.

II. Attack Methodology

I. Blackhole Attack

In a Black Hole Attack, a malicious node within the network falsely advertises itself as possessing the optimal path to the target. This deceitful tactic causes other nodes to forward their packets to the attacker. Consequently, the data is effectively absorbed or discarded, hence the term "black hole". The malicious node exploits the RPL's route advertisement mechanism to inject incorrect routing information into the network. By manipulating control messages such as DODAG Information Objects (DIOs), the attacker can convince adjacent nodes to select it as their preferred parent node.

Algorithm	Black Hole Attack

Step 1: Let N represent the total number of nodes in the network.

Step 2: The malicious node as $M \in N$.

Step 3: Modify the DIO (DODAG Information Object) message such that:

- Rank(M) → ∞, where M advertises itself with a lower rank compared to legitimate nodes.
- The rank value for legitimate nodes, R, will satisfy the condition: $R_{legitimate} < R_M$ (where R_M is the rank of malicious node)
- $R_{legitimate} < R_M$ $R_{legitimate} < R_M$ The malicious node M sends a fake DIO advertisement with: $Rank_M \rightarrow 0$, $cost_M \rightarrow 0$
- For legitimate node L, $cost_L = 0$ and $Rank_L = 0$

Step 4: Alter packet forwarding logic Packet P arrives at node M,

P_M = Drop(P), if M is malicious; Forward(P), if M is legitimate

Step 5: Compile and flash the firmware

Step 6: M node behavior: ∀P, M, Drop(P)

$P_{dropped}$ = {P | Received by M, M drops P}

Step 7: M advertises itself with rank R_M and cost C_M.

$$P_{dropped} = \sum_{i=0}^{N} P_i \quad (1)$$

$$P_{loss} = \frac{P_{dropped}}{P_{total}} \quad (2)$$

$$\text{Throughput}_{attack} = \frac{P_{received}}{T_{total}}, \quad (3)$$

T_{total} is total simulation time

II. Rank Attack

Increasing Rank Attacks: Within the RPL protocol, the rank value increases from the root node to the child node. An attacker can manipulate this metric to attract significant traffic toward the root and induce child nodes to select malicious nodes as parents by altering the Rank value. Reduced Rank Attacks: In a destination-oriented directed acyclic graph (DODAG), nodes with lower ranks are responsible for handling greater traffic as they are positioned closer to the root. A malicious node may falsely claim superior performance by advertising a lower rank value than its actual capability.

Algorithm Rank Attack

Step 1: Initialize Simulator
S ← Start Simulator()
Step 2: Manipulate RPL protocol packets
Modify: Modules: {rpl_dag, rpl_icmp6, rpl_dio}
Step 3: Falsify Rank Value
$R_{falsified} \leftarrow R_{current} \pm \Delta R$
Step 4: Tamper DIO Rank
DIO_{Rank} = Replace ($Rank_{actual}$, $R_{falsified}$)
Step 5: Alter Sequence Numbers
$Seq_{modified} = Seq_{oroginal} + \in$
Step 6: Manipulate Neighbour Table
$N_{table} \leftarrow$ f ($N_{entries}$, Tampered Data)
Step 7: Deceive Nodes about Topology
$T_{misleading} \leftarrow$ g(Topology Info, False Metrics)
Step 8: Compile and Flash Firmware
$F_{compiled}$ = Compile(Modified Code) Deploy($F_{compiled}$)
Step 9: Execute Attack
$A_{execute} \leftarrow$ Run (Rank Attack Simulation)

III. Sybil Attack

A sybil attack involves the use of multiple logical entities on a single physical node, similar to a clone ID attack. Kumari et al. [6] experimented the type of attack which can take control of large portions of a network without requiring additional physical nodes.

Algorithm Sybil Attack

Step 1: Initialize Simulator
S ← Start Simulator()
Step 2: Implement Selective Forward Logic
Modify: Modules: {rpl_dag, rpl_icmp6, rpl_dio, rpl_neighbor, rpl_forward}
Step 3: Spoof Node Identity
$NodeID_{spoofed} \leftarrow$ Generate(FakeID)
$MAC_{spoofed} \leftarrow$ Generate(FakeMAC)
Step 4: Manipulate Neighbour Table
$N_{table} \leftarrow$ f ($N_{entries}$, Spoofed Nodes)

Step 5: Forge Routing Advertisements

Fake DIO:

DIO_{fake} ← Create (False Rank, False Routes)

Fake DAO:

DAO_{fake} ← Create (False Destinations)

Step 6: Compile and Flash Firmware

$F_{compiled}$ = Compile (Modified Code) Deploy(Fcompiled)

Step 7: Start Session in Simulator

$S_{session}$ ← Start(S)

Step 8: Execute Attack

$A_{execute}$ ← Run (Sybil Attack Simulation)

III. Literature Survey

This section reviews the methodologies proposed by various researchers for the identification and mitigation of Blackhole, DIS Flooding, Rank, Selective Forwarding, Sybil, and Version attacks.

The research expands the network scale to 50 nodes and evaluates performance metrics via Contiki Cooja, providing comprehensive insights. Sharma et al. [7] work compared with existing security solutions often ignore node mobility, which this study highlights as critical for realistic IoT scenarios. Verma [8] introduced the Li-MSD approach, a distributed, threshold-based detection algorithm that maintains neighbor and blacklist tables to identify and block attacker nodes efficiently. This research focuses on the impact of black hole attacks in lossy and low-power networks using the RPL protocol. Kumar et al. [9] demonstrates simulation-based analysis of attack behaviors and detection capabilities. Rank attacks are most harmful in network areas with many attacker nodes or heavy forwarding loads.

Le et al. [10] and Djedj ig et al. [11] study aims to find out the key indicators of rank attack effects include affected node count, end-to-end delay, and delivery ratio. MRTS incorporates a trust management scheme that evaluates nodes' behaviors to assign trust values. Simulation results show MRTS outperforms standard RPL in trustworthiness and security, especially as the number of malicious nodes grows.

The Routing Protocol for Low-Power and Lossy Networks (RPL), which is extensively utilized in Internet of Things (IoT) contexts, has security flaws that are addressed in this paper. Rouissat [12] experiment by promoting a fake low rank, the authors present a brand-new "silent decreased rank attack" that tricks the RPL's routing system and directs data traffic to a malicious node.

The study examines IoT security flaws, focusing on Sybil attacks where a malicious node uses multiple identities to disrupt network functions. Thuluva [13] aims to counter these attacks in IoT-based health monitoring systems, the authors propose a hybrid security framework using Caesar Cipher Algorithm (CCA), Lightweight Encryption Algorithm (LEA), and Received Signal Strength Indicator (RSSI).

IV. Proposed EEADM-RPL Protocol

Detection and Removal of DR Incidents:

The malicious node attracts additional nodes by broadcasting a DIO message with a low rank value. Upon receiving this message, new nodes calculate their rank using the Objective Function (OF). A node will select the parent with the lowest rank if it receives multiple DIO messages based on OF.

Operational functions are available in two distinct types.

1. This objective function is predicated on the minimal number of hops to the root and does not account for the reliability of the path links.
2. MRHOF, or the Minimum Rank Hysteresis Objective Function, aims to reduce the cost of the path by using either the link metric anticipated transmission count (ETX) or the node metric energy.

The rank value is determined by employing the MRHOF objective function. This approach involves two main actions: first, identifying the malicious nodes, and second, eliminating them. The non-storing mode technique serves as the basis for this procedure, ensuring that the root node maintains current information on every node.

I. Detection and Mitigation of Blackhole Attack

Algorithm	Black Hole Attack Mitigation

Step 1: Start
Step 2: Capture PCAP network traffic
Step 3: Extract Rank, Objective Function Code Position
Step 4: For all P_{node} and C_{node}, traverse F(flow) from R_{root} to L_{leaf}.
Step 5: Parse each packet P.
Step 6: Extract D_{RPL}, D_{ICMP6}, D_{IPv4}, $D_{6LoWPAND}$
Step 7: Perform StatAnalysis (LQI, RSSI, SensorRead, PktLen, PktType, PktLossRate, SeqNo, NeighborTbl)
Step 8: Wait for ΔStat.
If ΔStat=0: Activity=Normal
If ΔStat ≠ 0 : RaiseAalert.
Step 9: Detect Ablackhole using DDIS, PktSeqNo, NeighborTblUpdates, RSSI, LQI, Latency, RTT
Step 10: Set $T_{interval}$ = 1 min
Step 11: Check DDIS, PktSeqNo, NeighborTblUpdates, RSSI, LQI, Latency, RTT
If Δvalues=0: Add to T_{trust}
If Δvalues ≠ 0 : Add to $T_{malicious}$

II. Detection and Mitigation of Rank Attack

Algorithm	Rank Attack Mitigation

Step 1: Start
Step 2: Capture PCAP traffic.
Step 3: Extract Rank, Objective Function Code, Position For all P_{node} and C_{node} traverse F_{flow} from R_{root} to L_{leaf}.
Step 4: Parse each packet P.
Step 5: Extract DRPL, DICMP6, DIPv4, D6LoWPAND.
Step 6: Perform StatAnalysis (LQI, RSSI, Sensor Read, PktLen, PktType, PktLoss Rate, SeqNo, Neighbour Table)
Step 7: Wait for ΔState.
If ΔStat=0 : Activity=Normal.
If ΔStat ≠ 0 : Raise A_{alert}.
Step 8: Detect_ARankAttack using DRank, DDIOSQ.

Step 9: Set $T_{interval}$ = 1 min.
Step 10: Check D_{Rank}, D_{DIOSQ}.
If Δvalues=0: Add to T_{trust}.
If Δvalues ≠ 0 : Add to $T_{malicious}$

III. Detection and Mitigation of Sybil Attack

Algorithm Sybil Attack Mitigation

Step 1: Start
Step 2: Capture PCAP traffic.
Step 3: Extract Rank, Objective Function Code, Position For all P_{node} and C_{node} traverse F_{flow} from R_{root} to L_{leaf}.
Step 4: Parse each packet P.
Step 5: Extract D_{RPL}, D_{ICMP6}, D_{IPv4}, $D_{6LoWPAND}$.
Step 6: Perform StatAnalysis (LQI, RSSI, Sensor Read, PktLen, PktType, PktLoss Rate, SeqNo, Neighbour Table, Node IDs)
Step 7: Detects duplicate Node IDs in Neighbor Tbl.
Step 8: Identify nodes with:
- Same NodeID but different RSSI, LQI, or Pos.
- Multiple NodeIDs RSSI, LQI, or Pos.

Step 9: Check for ΔStat in:
- Packet frequency for the same NodeID.
- TrustScore inconsistencies.

If ΔStat=0: Activity=Normal.
If ΔStat ≠ 0 : Raise A_{alert}.

Step 10: Detect A Sybil Attack using:
- Duplicate NodeID with differing physical characteristics.
- Multiple NodeIDs sharing identical physical characteristics.

Step 11: In $T_{interval}$=1 min:
- Verify NodeID uniqueness with RSSI, LQI, SeqNo, PktFlowPath, TrustScore.

If Δvalues=0: Add to T_{trust}.
If Δvalues ≠ 0 : Add to $T_{malicious}$.

Step 12: Mitigation:
- Isolate nodes flagged in $T_{malicious}$.
- Update network routes to exclude flagged nodes.

V. Simulation Results and Performance Analysis

I. Simulation Environment

Simulations are employed to evaluate the performance of EEADM-RPL. For this purpose, Cooja, a simulator integrated within the Contiki operating system, is utilized. Triantafyllou et al. [14] study is compared with the evaluation as conducted under the environment and conditions specified in this study.

Table 1 presents the details of the simulation parameters.

Table 1: *Simulation Parameters*

Simulation Parameters	Value
Simulation tool	Contiki /Cooja 3.0
Simulation coverage area	100 m * 100 m
Deployment Type	Random position (based on smart home)
Total number of nodes	30
Emulated nodes	T-mote Sky
Malicious nodes	1:10
TX range	50 m
TX ratio	100%
RX ratio	30-100%
Link failure model	UDGM
Interference range	50 m
Routing protocols	THC-RPL
Mobility speed	0-6.23 km/h
Simulation time	60 min

Network internal security cannot be ensured by relying solely on the single metric used in standard RPL. Ferreira [15] and Singhal [16] studies have employed multiple matrices to integrate a security mechanism into the standard RPL. One internal security threat is the Sybil attack, which is addressed by methods that use matrices in the trust computation model. These methods employ node-level computation to determine the trust value. One consequence of node-level computation is high energy consumption, which affects low power and lossy IoT network devices.

The EEADM-RPL aims to minimize node-level computations and delegate trust computations to the Root node, which is a resourceful IoT device. The primary objective is to extend the operational lifespan of low-power lossy network devices by optimizing their energy consumption. Secondly, it performs these trust-related computations independently, without relying on any external devices. The simulation is conducted over a 20-minute duration, involving 30 nodes-one of which is malicious and another is mobile-utilized in the testing process.

The metrics used to evaluate EEADM-RPL include the number of Sybil attacks detected, the Packet Delivery Ratio (PDR), the average energy consumption of nodes, and the average energy consumption of the network.

To evaluate the performance of the work, a simulation was conducted in a smart home environment where various nodes may be mobile while one border router remains static.

II. Performance Analysis

i) Parent Change Ratio, ii) Packet Loss Ratio, iii) End-to-End Delay, iv) Energy Consumption, v) Network Lifetime, vi) Packet Delivery Ratio

The overall energy consumption of a node can be determined by summing the energy used for processing (CPU), low power mode (LPM), listening, and transmitting data. Therefore, the total energy consumption of a node is the aggregate of its energy usage during data transmission, data listening, CPU operation in low-power mode, and CPU operation in active mode.

VI. Experimental Results and Analysis

The Cooja simulator operating on the Contiki OS was utilized to conduct extensive simulations to evaluate the efficacy of the proposed EEADM-RPL protocol. In conditions with node mobility, the experimental setup included Sybil, Rank, and Blackhole attacks. Six critical network performance

metrics: Parent Change Ratio, Packet Loss Ratio, End-to-End Delay, Energy Consumption, Network Lifetime, and Packet Delivery Ratio -were employed to evaluate and compare the performance of EEADM-RPL with traditional RPL protocols (OF0, MRHOF, and DCTM-RPL).

I. Parent Change Ratio

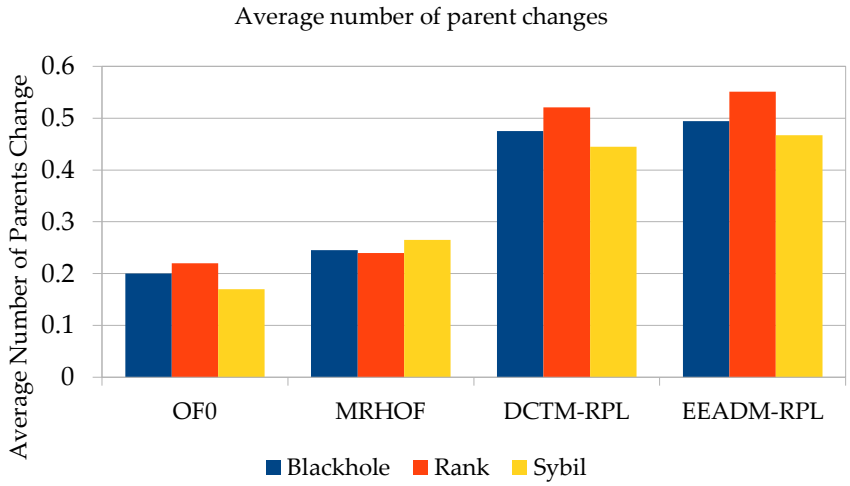


Figure 2: *Parent Change Ratio*

The Parent Change Ratio measures the frequency of switching parent nodes during data routing. Frequent parent changes indicate the instability of the routing protocol in dynamic conditions, such as during attacks or node mobility.

Our proposed EEADM-RPL protocol shows a substantial 87.94% increase in the average number of parent changes compared to traditional RPL protocols. This increase signifies better adaptability of the proposed protocol in mitigating attacks and re-establishing stable routes dynamically. The proactive parent selection helps maintain connectivity even in the presence of disruptive attacks like Blackhole and Sybil.

Table 2: *Parent Change Ratio*

Average number of parent changes	OF0	MRHOF	DCTM-RPL	EEADM-RPL
BLACKHOLE	0.2	0.245	0.475	0.494
RANK Attack	0.22	0.24	0.521	0.551
SYBIL	0.17	0.265	0.445	0.467

II. Packet Loss Ratio

The percentage of data packets that do not arrive at their destination is shown by the packet loss ratio. Poor dependability and heightened network vulnerability to attacks are indicated by a greater ratio.

The EEADM-RPL protocol demonstrates a 69.17% reduction in the average packet loss ratio. This significant improvement indicates the enhanced robustness and reliability of EEADM-RPL in securing data delivery. The detection and isolation mechanisms against malicious nodes help ensure that legitimate packets follow secure and verified routes.

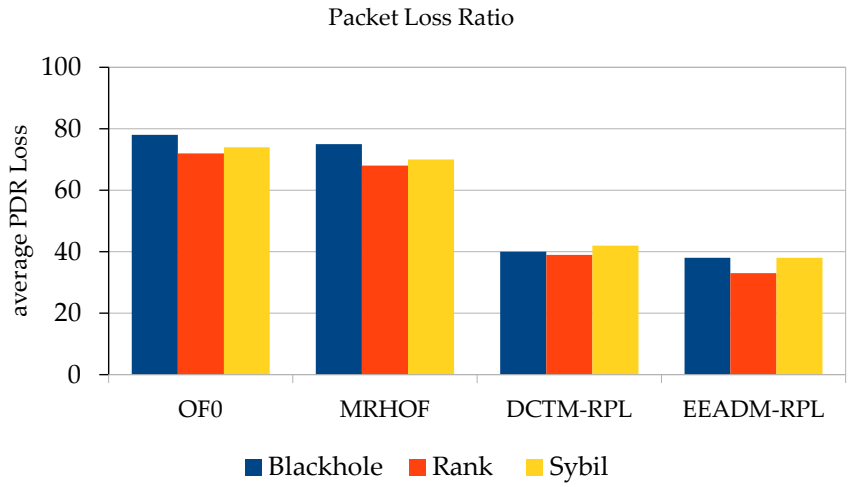


Figure 3: *Packet Loss Ratio*

Table 3: *Packet Loss Ratio*

Average Packet Loss Ratio	OF0	MRHOF	DCTM-RPL	EEADM-RPL
BLACKHOLE	78	75	40	38
RANK Attack	72	68	39	33
SYBIL	74	70	42	38

III. End-to-End Delay

Completely The amount of time it takes for a packet to go from its source to its destination is referred to as its delay. Delay reduction is essential for industrial and real-time Internet of Things applications. Simulation results show that EEADM-RPL achieves a 67.85% reduction in end-to-end delay. This drastic decrease is due to the optimized routing decisions and early detection of malicious behaviors, allowing for faster route recovery and minimal retransmissions. Additionally, this leads to improved quality of service (QoS) in dynamic IoT environments.

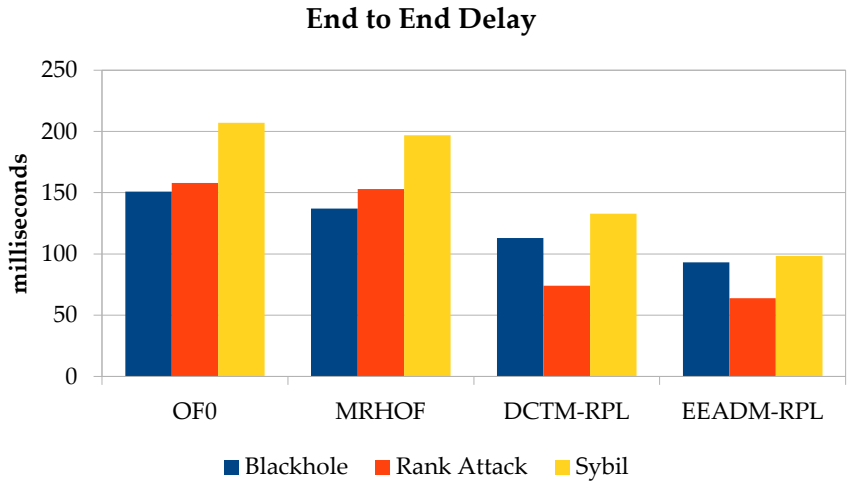


Figure 4: *End-to-End Delay*

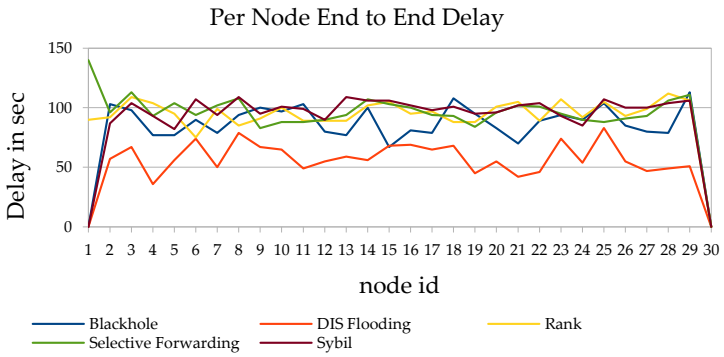


Figure 5: *Per node End-to-End Delay with mobility*

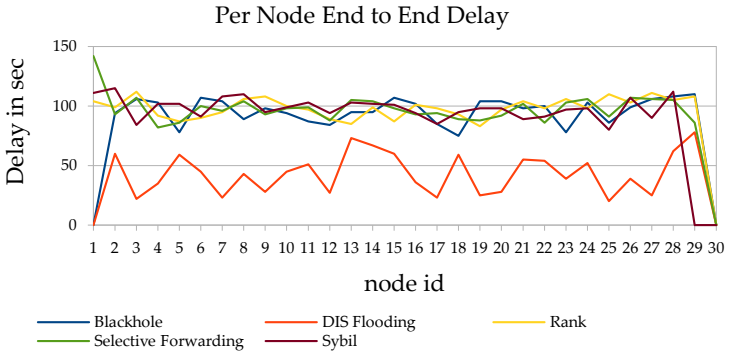


Figure 6: *Per node End-to-End Delay without mobility*

Table 4: *End-to-End Delay*

End-to-End Delay	OF0	MRHOF	DCTM-RPL	EEADM-RPL
BLACKHOLE	151	137	113	93.07
RANK Attack	158	153	74	63.79
SYBIL	207	197	133	98.36

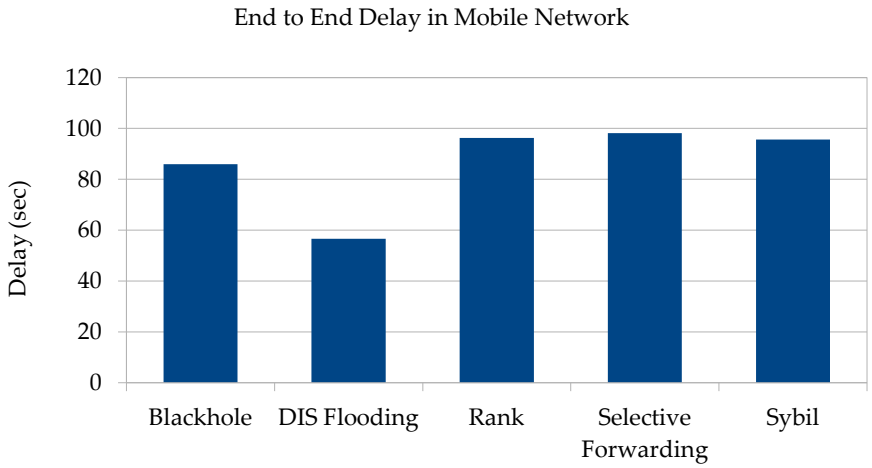


Figure 7: *End to End delay in mobile networks*

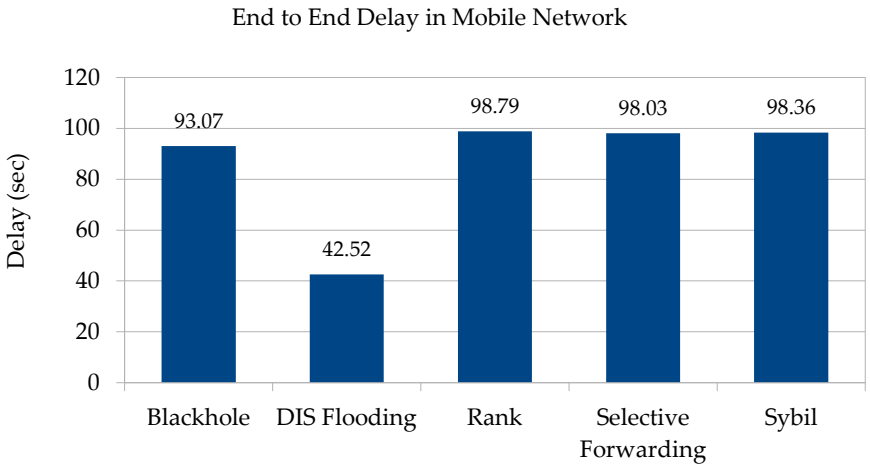


Figure 8: *End-to-End Delay in immobile networks*

IV. Energy Consumption

Energy efficiency is a key requirement in IoT environments where devices often operate on battery power. EEADM-RPL results in a 13.07% reduction in overall energy consumption compared to existing protocols. This improvement is achieved through the lightweight design of detection mechanisms, reduced retransmissions due to lower packet loss, and optimized control message exchanges.

By effectively mitigating attacks, the protocol reduces unnecessary energy usage caused by unstable routing paths.

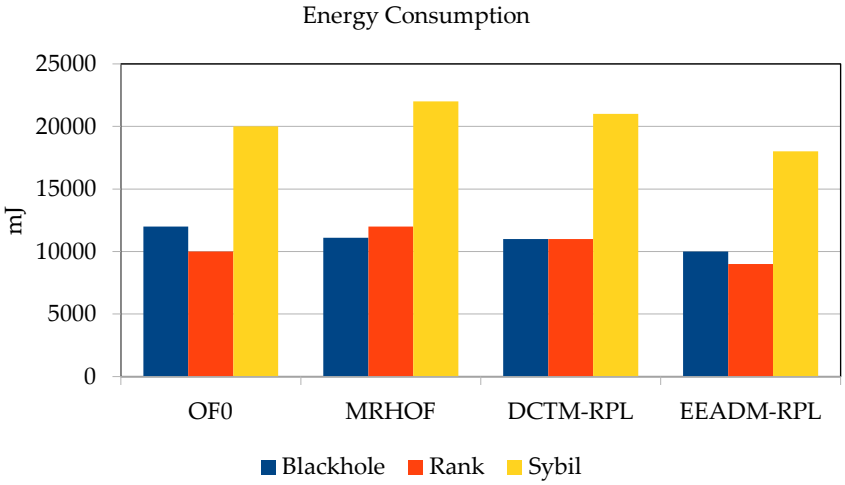


Figure 9: *Energy Consumption*

Table 5: *Energy Consumption*

Energy Consumption	OF0	MRHOF	DCTM-RPL	EEADM-RPL
BLACKHOLE	12000	11111	11000	10000
RANK Attack	10000	12000	11000	9000
SYBIL	20000	22000	21000	18000

V. Network Lifetime

A notable threat to mobile RPL is the Sybil attack, which can affect performance by significantly increasing control overhead transfer, thereby reducing the network's lifespan. Sybil attacks notably impact the network lifespan in mobile RPL-based IoT networks. These attacks lead to a substantial increase in node computation and control overhead traffic.

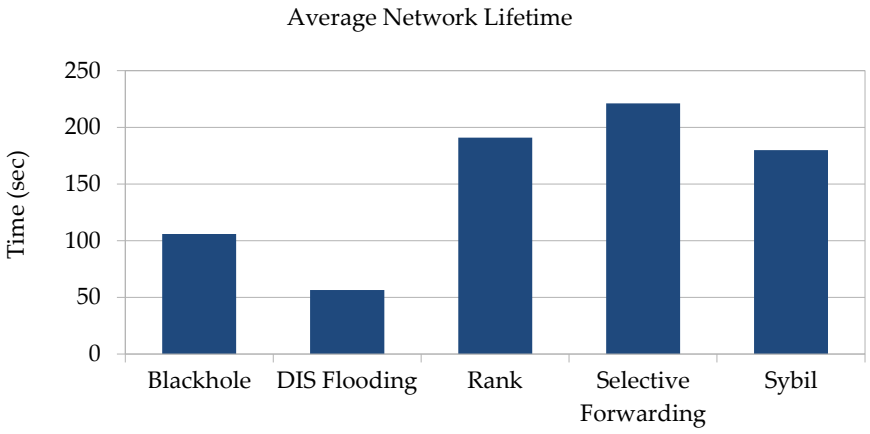


Figure 10: *Average Network Lifetime with mobility*

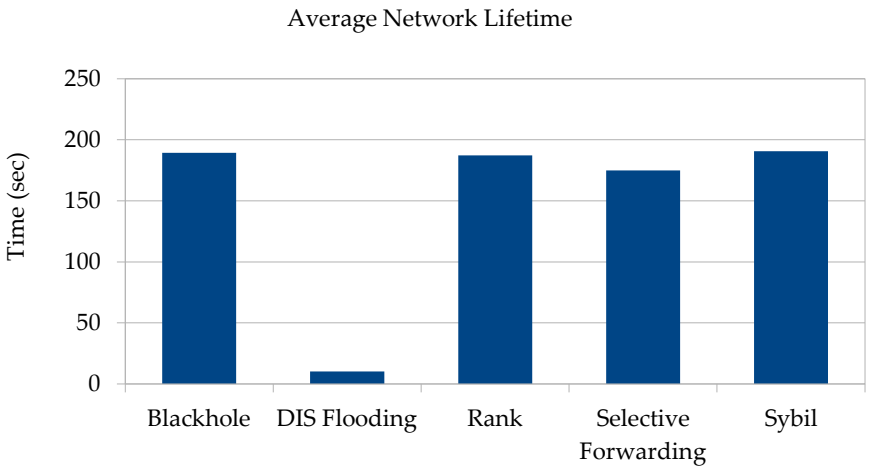


Figure 11: *Average Network Lifetime without mobility*

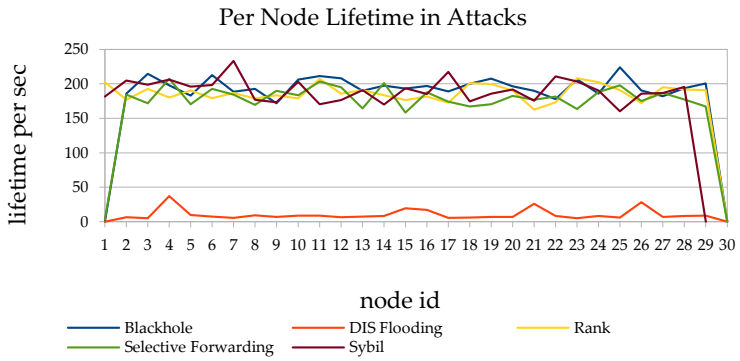


Figure 12: Per *Node Lifetime in Attacks with Mobility*

VI. Packet Delivery Ratio

Simulation scenarios indicate that Packet Delivery Ratio (PDR) can achieve up to 99% in networks with fewer nodes and a higher number of anchor connections. However, in denser network configurations, PDR values may be reduced to approximately 90%, due to increased congestion and transmission overlaps. Effective strategies for enhancing Packet Delivery Ratio (PDR) in mobile environments encompass selecting optimal parent nodes, minimizing disconnections, and ensuring consistent communication linkages.

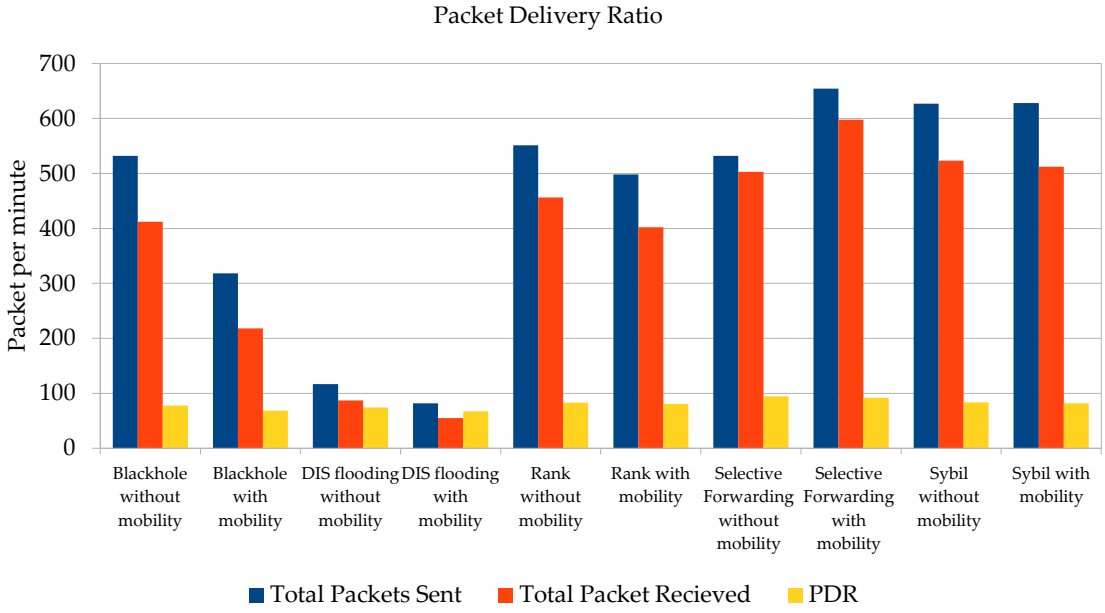


Figure 13: *Attack Types Parameter Packet Delivery Ratio with and without mobility*

VII. Conclusion

The Novel Energy-Efficient Approach to Detect and Mitigate RPL (EEADM-RPL) protocol presents a significant advancement in securing IoT networks against routing attacks while maintaining operational efficiency. Our comprehensive evaluation using the Cooja simulator demonstrates that the proposed protocol substantially outperforms traditional RPL implementations across all measured performance parameters. The hybrid approach effectively balances robust security mechanisms with network performance optimization and energy efficiency considerations. By increasing the average number of parent change ratio by 87.94%, decreasing the average packet loss ratio by 69.17%, decreasing the end-to-end delay by by 67.85%, and lowering energy consumption by 13.07%, EEADM-RPL addresses critical challenges in securing mobile IoT environments. The protocol's unique ability to handle multiple attack types simultaneously (Black Hole, Rank, and Sybil attacks) while maintaining performance under mobility conditions makes it particularly valuable for industrial IoT deployments where security and reliability are paramount concerns. Future research directions could explore further optimization of energy consumption for ultra-low-power applications, extension of attack detection capabilities to address emerging threat vectors, integration of machine learning-based anomaly detection mechanisms to enhance adaptability, and evaluation of protocol performance in larger-scale deployments with heterogeneous device types

and varying mobility patterns.

References

[1] Laghari, A. A., Li, H., Khan, A. A., Shoulin, Y., Karim, S., & Khani, M. A. K. (2024). Internet of Things (IoT) applications security trends and challenges. *Discover Internet of Things*, 4(1), 1–22.

[2] Sasi, T., Lashkari, A. H., Lu, R., Xiong, P., & Iqbal, S. (2024). A comprehensive survey on IoT attacks: Taxonomy, detection mechanisms and challenges. *Journal of Information and Intelligence*, 2(6), 455–513.

[3] Alfriehat, N., Anbar, M., Aladaileh, M., Hasbullah, I., Shurbaji, T. A., Karuppayah, S., & Almomani, A. (2024). RPL-based attack detection approaches in IoT networks: review and taxonomy. *Artificial Intelligence Review*, 57(9), 1–56.

[4] Aldhaheri, A., Alwahedi, F., Ferrag, M. A., & Battah, A. (2024). Deep learning for cyber threat detection in IoT networks: A review. *Internet of Things and Cyber-Physical Systems*, 4, 110–128.

[5] Paganraj, D., & Chelliah, M. (2024). DE2RA-RPL: detection and elimination of resource-related attacks in IoT RPL-based protocol. *Journal of Supercomputing*, 80(15), 22397–22427.

[6] Kumari, D., Singh, K., & Manjul, M. (2020). Performance Evaluation of Sybil Attack in Cyber Physical System. *Procedia Computer Science*, 167, 1013–1027.

[7] Sharma, G., Grover, J., & Verma, A. (2023). Performance evaluation of mobile RPL-based IoT networks under version number attack. *Computer Communications*, 197, 12–22.

[8] Verma, A., Verma, S. K., Pandey, A. C., Grover, J., & Sharma, G. (2024). Li-MSD: A lightweight mitigation solution for DAO insider attack in RPL-based IoT. *Future Generation Computer Systems*, 159, 327–339.

[9] Kumar, A., Matam, R., & Shukla, S. (2016). Paper_23 Impact of packet dropping attacks on RPL. 2016 4th International Conference on Parallel, Distributed and Grid Computing, PDGC 2016, 694–698.

[10] Le, A., Loo, J., Lasebae, A., Vinel, A., Chen, Y., & Chai, M. (2013). The impact of rank attack on network topology of routing protocol for low-power and lossy networks. *IEEE Sensors Journal*, 13(10), 3685–3692.

[11] Djedjig, N., Tandjaoui, D., Medjek, F., & Romdhani, I. (2017). New trust metric for the RPL routing protocol. 2017 8th International Conference on Information and Communication Systems, ICICS 2017, 328–335.

[12] Rouissat, M., Belkheir, M., Belkhira, H. S. A., Mokaddem, A., & Ziani, D. (2023). Implementing and evaluating a new Silent Rank Attack in RPL-Contiki based IoT networks. *Journal of Electrical Engineering*, 74(6), 454–462.

[13] Thuluva, A. S. S., Somanathan, M. S., Somula, R., Sennan, S., & Burgos, D. (2021). Secure and efficient transmission of data based on Caesar Cipher Algorithm for Sybil attack in IoT. *Eurasip Journal on Advances in Signal Processing*, 2021(1), 1–23.

[14] Triantafyllou, A., Sarigiannidis, P., & Lagkas, T. D. (2018). Network Protocols, Schemes, and Mechanisms for Internet of Things (IoT): Features, Open Challenges, and Trends. *Wireless Communications and Mobile Computing*, 2018(1), 5349894.

[15] Ferreira, A. M. A., Azevedo, L. J. de M. de, Estrella, J. C., & Delbem, A. C. B. (2023). Case Studies with the Contiki-NG Simulator to Design Strategies for Sensors' Communication Optimization in an IoT-Fog Ecosystem. *Sensors* 2023, Vol. 23, Page 2300, 23(4), 2300.

[16] Singhal, P., Singhal, P., Sharma, P., & Arora, D. (2018). An approach towards preventing iot based sybil attack based on contiki framework through cooja simulator. *International Journal of Engineering and Technology*, 7(2.8), 261–267.

EXPERT METHOD OF RANK PENALTIES

Alexander Bochkov[1], Nikolay Zhigirev[2], Alla Kuzminova[3]

•

[1]NIIAS, Moscow (Russia), [2]KOLABI, Moscow (Russia),
[3]National Research Nuclear University (MEPhI), Moscow (Russia)

[1*] a.bochkov@gmail.com, [2] nnzhigirev@mail.ru, [3] avkuzminova@mephi.ru

Abstract

Voting methods include a variety of systems and technologies designed to facilitate the electoral process. These methods can range from the use of traditional paper ballots to modern electronic systems, each with unique features and functions. Heuristic peer review methods use simplified decision-making processes to evaluate complex scenarios, especially in areas such as usability and forecasting. These methods improve efficiency and accuracy by combining expert information with heuristic principles to improve results in a variety of applications. While heuristic methods offer significant advantages for expert evaluations, they can also lead to errors if not applied carefully, emphasizing the need for balanced approaches to complex evaluations. We propose an algorithm for finding the most consistent decision of experts in determining the leader in an alternative ranking problem.

Keywords: voting; group choice; coordinated decision; penalty functions; Schulze method; Skating method; expert evaluations; rank statistics

1. Introduction

In practice, there are often situations when there are several decision makers (LPRs), each of which has its own preferences on the same set of compared options, and on the basis of these individual preferences it is necessary to develop a group (collective) preference [1]. For example, the jury needs to allocate places among the contestants, the citizens of a country need to elect a president, etc. Such decision-making problems are called group choice problems, the LPRs participating in them are called electors, and the compared variants are called candidates.

Finding a consensual solution in group decision making (GDM) involves various strategies and models to promote consensus among members. The literature highlights several approaches to increase agreement and optimize decision making.

Consensus models

Liu et al. propose a consensus model using non-reciprocal fuzzy preference relations (NRFPR) to eliminate uncertainty in experts' opinions, using a particle swarm optimization algorithm to reach optimal solutions [2].

Chiclana et al. emphasize the importance of preference consistency by proposing a model for moving from consistency to consensus and thereby improving the quality of group decisions [3].

Overcoming dominance

Maximova et al. introduce the consensus-minus-one principle, which eliminates dominant voices to accelerate consensus, indicating a potential 97% reduction in decision-making time [4].

Dynamics of communication

Zhang and Kasari's research shows that effective communication, especially in lottery selection experiments, can lead to consensual group decisions that often result in extroverted group members [5].

Impact of the decision-making mechanism

Luis et al. find that decision-making mechanisms that promote apparent consensus lead to higher actual levels of agreement, suggesting that process choice significantly affects group dynamics [6].

While these models and strategies provide a framework for consensus building, challenges remain, particularly in managing "leaders" among experts and ensuring that all voices are heard, which can complicate the decision-making process.

2. Summary of methods of harmonized voting

The solution is often considered to be the so-called Schulze method (also Schwartz's method of sequential elimination), a voting system developed bo by Markus Schulze in 1997. Schulze himself calls it the "beatpath method". It allows to determine the winner (with objective counting) using ballots in which voters indicate their preferences for candidates, ranking them. This method can also be used to produce a preference-sorted list of candidates. This method satisfies Condorcet's criterion: if one candidate is the winner when compared to each of the other candidates, then it will be the winner by Schulze's method as well. In addition, Schulze's method allows to formally determine a winner even if there is no winner according to the Condorcet criterion. The winner by Schulze's method always belongs to the Schwarz set.

The Schulze voting method is a complex single-winner voting system that uses the voters' ordinal preferences to determine the winner using a weighted majority graph. This method is characterized by computational efficiency and compliance with various desirable voting criteria.

Key features of the Schulze method

Computational complexity: Schulze's method can be computed in polynomial time, but its simple implementation can be difficult when dealing with large datasets. Recent advances have led to optimized algorithms using parallel computing platforms such as Pregel, which improves scalability for large elections [7].

Axiomatic properties: the method satisfies several important criteria, including monotonicity, inverse symmetry and Condorcet's criterion, making it a robust choice for fair elections [8]. Privacy in computing: innovations in privacy-preserving algorithms allow the Schulze method to be used on encrypted data, guaranteeing the privacy of voter preferences while determining the winner [9].

Although Schulze's method is highly appreciated for its theoretical properties and practical applications, its application in very large electoral districts remains difficult, requiring continuous research on more efficient algorithms [10].

The method of minimizing the number of inversions [11], previously proposed by the authors, is aimed at finding such a compression of all private rankings that would reduce the total inconsistency of expert opinions (based on the equality of all expert participants), measured in inversions of transitions from the initial state to the lexicographic ordering of ranked objects.

Schulze's method [12] optimizes by maximizing the number of wins, while the method of minimizing the number of inversions actually optimizes by the number of defeats, but both

methods use the full data set to determine local minima - that is, both methods use the "quantity" of expert opinions, but not their "quality". "Price of victory" in both approaches is measured by the same quantity - the total number of votes received by the object in the caucus. The latter does not correspond to the task of expertise, in which weaker objects have lower "weight" indicators.

The Skating method [13] corrects the situation somewhat. This method is used for scoring in ballroom dancing competitions. It is used to determine the final places of the participants and is based on a method that prioritizes the "majority" according to the judges' scores to solve the problems arising from the subjective determination of the leader of the competition. That is, it uses data from previously determined "leaders" to determine second and subsequent places. The original version of the majority principle was formulated by Arthur Dawson and introduced by the British Official Ballroom Dance Council (now the British Dance Council) in 1937. After some refinements in 1947 and 1948, the system was not changed until 1956. It was first used during the Blackpool Dance Festival and was gradually adopted in ballroom dance competitions around the world, as well as in other dance competitions. In the final round of the competition (when the judges rank each competitor's place), 10 rules are used to calculate points. There must be an odd number of judges for the majority system to work, and each judge can only assign each place to each competitor once. Particularly in dance sport, the judges' ratings give subjective final places for each competitor in the finals, which are then combined to determine the final combined majority opinion of the judges.

This approach is valid for strongly stable solutions, but it does not always work for weakly coordinated, contradictory preferences, which are characteristic of most practical tasks.

3. Rank penalty method

In the proposed method, called "expert method of rank penalty" by the authors, the Schwartz method is taken from the Schulze method to reduce the dimensionality of the problem for the second and further places, and from the Skating method – the principle of sequential determination of the "leader" for subsequent decision-making. However, unlike Skating, the new method has a number of nuances.

In contrast to the Skating method, a qualitative characterization of a place is introduced, taking into account the "penalty points"[1], under-achieved by a candidate when considering his/her place in the ranked list (hence the name of the described method as the method of rank penalties).

The algorithm is simple and consists, in fact, in the sequential application of three rules: search for the maximum of the sum of seats, search for the minimum of "penalties" to reach the maximum determined at the first stage, sequential shift of the calculation and recalculation of voting statistics taking into account this shift. These three operations are repeated cyclically until the last candidate in the ordered list is determined.

Let's demonstrate the work of the method on a classical example[2] of Schulze's method, in which we consider an election in which 45 voters vote for 5 candidates: A, B, C, D, E.

In the Schulze method, each ballot contains a complete list of candidates, and each expert ranks them in order of preference. The most common voting format uses numbers in ascending order, with the expert placing a "1" next to the most desirable candidate, a "2" next to the second most preferred candidate, and so on. Experts may give the same numbers to several candidates, or not fill in this field at all for some candidates (in this case, it is considered that the voter has put

[1] The "penalty" means the weighted sum of votes received by the candidate for the considered place in the ranked list multiplied by the corresponding weighting factor of the place (in the considered example it is the ordinal number of the place from 1 to 5)

[2] Electronic document. Mode of access: https://ru.wikipedia.org/wiki Method_Schulze

such candidates equally below all candidates for which he/she has indicated a number)[3] .

In the example under consideration, the votes were distributed as follows (Table 1), forming eight "fractions" (so we will call the transitive groups formed as a result of the coincidence of the opinion of a group of experts on the ranks of the compared candidates).

Table 1: Initial data (Schulze example)

Fraction number	Order of candidates	Number of votes in the faction
1	ACBED	5
2	ADECB	5
3	BEDAC	8
4	CABED	3
5	CAEBD	7
6	CBADE	2
7	DCEBA	7
8	EBADC	8

The classical solution by Schulze's method leads to the following ordering of candi dates: EACBD, i.e. E ≻ A ≻ C ≻ B ≻ D. The classical solution by the Skating method leads to a different ordering: CEABD, i.e. C ≻ **E** ≻ A ≻ B ≻ D.

As will be shown below, the difference in the obtained solutions is explainable when some qualification rule is taken into consideration, which establishes a criterion for deciding the candidate's place, depending on the proportion of experts who voted in favor of the considered candidate ordering.

In the further description, we assume a 50% decision-making level for "1, 1-2, 1-2-3" and further places. Since the example considers the votes of 45 experts, the decision threshold (cutoff threshold) is greater than or equal to 22.5 votes.

In the first stage the leader is determined by the maximum accumulated sum of places (as in the Skating method), which must be greater than or equal to the cut-off criterion, and in the second stage by the minimum accumulated penalties. So, we construct a table (Table 2)[4] , which reflects the sums of votes gained by candidates A, B, C, D and E taking into account the preferences of experts in all factions (see Table 1). We further consider the accumulated sum of seats for each candidate. There is no clear leader for the first seats - none of the contenders gained the required number of seats to overcome the cut-off threshold.

For 1-2 places, we have a clear leader by the accumulated sum of expert votes - candidate C, who has gained, respectively, 12+12=24 votes. Let's find out whether the found solution is optimal. For this purpose, let's calculate the weighted sums of accumulated places taking into account the "penalties" for not reaching the found max sum of evaluations (max(1-2) = 24) necessary to determine the leader for all candidates for 1-2 places as follows[5] (Table 3):

for A: 1*10 + 2*10 + 3*(max(1-2) -20) = 10 + 20 + 12 = 42,
for B: 1*8 + 2*10 + 3*(max(1-2) -18) = 8 + 20 + 18 = 46,
for C: 1*12 + 2*12 + 3*(max(1-2) -24) = 12 + 24 + 0 = 36,
for D: 1*7 + 2*5 + 3*8+4*(max(1-2) -20) = 7 + 10 + 24+16 = 57 and finally,
for E: 1*8 + 2*8 + 3*(max(1-2) -16) = 8 + 16 + 24 = 48.

[3] Such voting is fundamentally impossible in the Skating system.
[4] For example, candidate A in the 1st place appeared in faction No. 1 (5 voters made this choice) and faction No. 2 (also 5 voters voted for this order). Consequently, cell 1A of the matrix will contain the sum of votes, i.e. 10.
[5] Note that to calculate the rank penalties for candidate D, we had to "plug in" the votes he received for places 1-4 to "get" the necessary 24 votes.

Table 2

	expert voices					cumulative votes				
	1	2	3	4	5	1	1-2	1-3	1-4	1-5
A	10	10	10	8	7	10	20	30	38	45
B	8	10	8	14	5	8	18	26	40	45
C	12	12	0	5	16	12	**24**	24	29	45
D	7	5	8	10	15	7	12	20	30	45
E	8	8	19	8	2	8	16	35	43	45

Table 3

	expert voices					cumulative votes					accumulated fines				
	1	2	3	4	5	1	1-2	1-3	1-4	1-5	1	1-2	1-3	1-4	1-5
A	10	10	10	8	7	10	20	30	38	45	---	42			
B	8	10	8	14	5	8	18	26	40	45	---	46			
C	12	12	0	5	16	12	**24**	24	29	45	---	**36**			
D	7	5	8	10	15	7	12	20	30	45	---	57			
E	8	8	19	8	2	8	16	35	43	45	---	48			

The minimum of "penalties" is again at C (min(1-2) = 36), hence the found solution C is optimal and candidate C takes the 1st place. In the next step, we exclude candidate C from consideration in all factions[6] and update the voting statistics (see Table 4).

Table 4

Fraction number	Order of candidates	Number of votes in the faction
1	ABED	5
2	ADEB	5
3	BEDA	8
4	ABED	3
5	AEBD	7
6	BADE	2
7	DEBA	7
8	EBAD	8

Because of the transitive nature of candidate relationships, we can make such a substitution. Determine a new leader among the remaining candidates. Note that unlike the Skating optimum boy the solution does not always correspond to the leader by the accumulated sum of places. For the first seats, there is again no clear leader - none of the contenders gained the required number of seats to pass the cut-off threshold (22.5). For 1-2 seats, two candidates B(26) and E(30) passed the cut-off threshold. Candidate E(max(1-2) = 30) had the maximum. Next, we calculate the penalties for under-voting for all candidates, respectively:

for A: 1*20 + 2*2 + 3*(max(1-2) -22) = 20 + 4 + 24 = 48,
for B: 1*10 + 2*16 + 3*(max(1-2) -26) = 10 + 32+ 12 = 54,
for D: 1*7 + 2*5 + 3*10 + 4*(max(1-2) -22) = 7 + 10 + 30 + 32 = 79,
for E: 1*8 + 2*22+3*(max(1-2) -30) = 8 + 44 + 0 = 52.

[6] I n fact, we put C in the first place, but we "forget" about it and consider the remaining candidates in the struggle for leadership (1st place, which is actually 2nd in the overall rating).

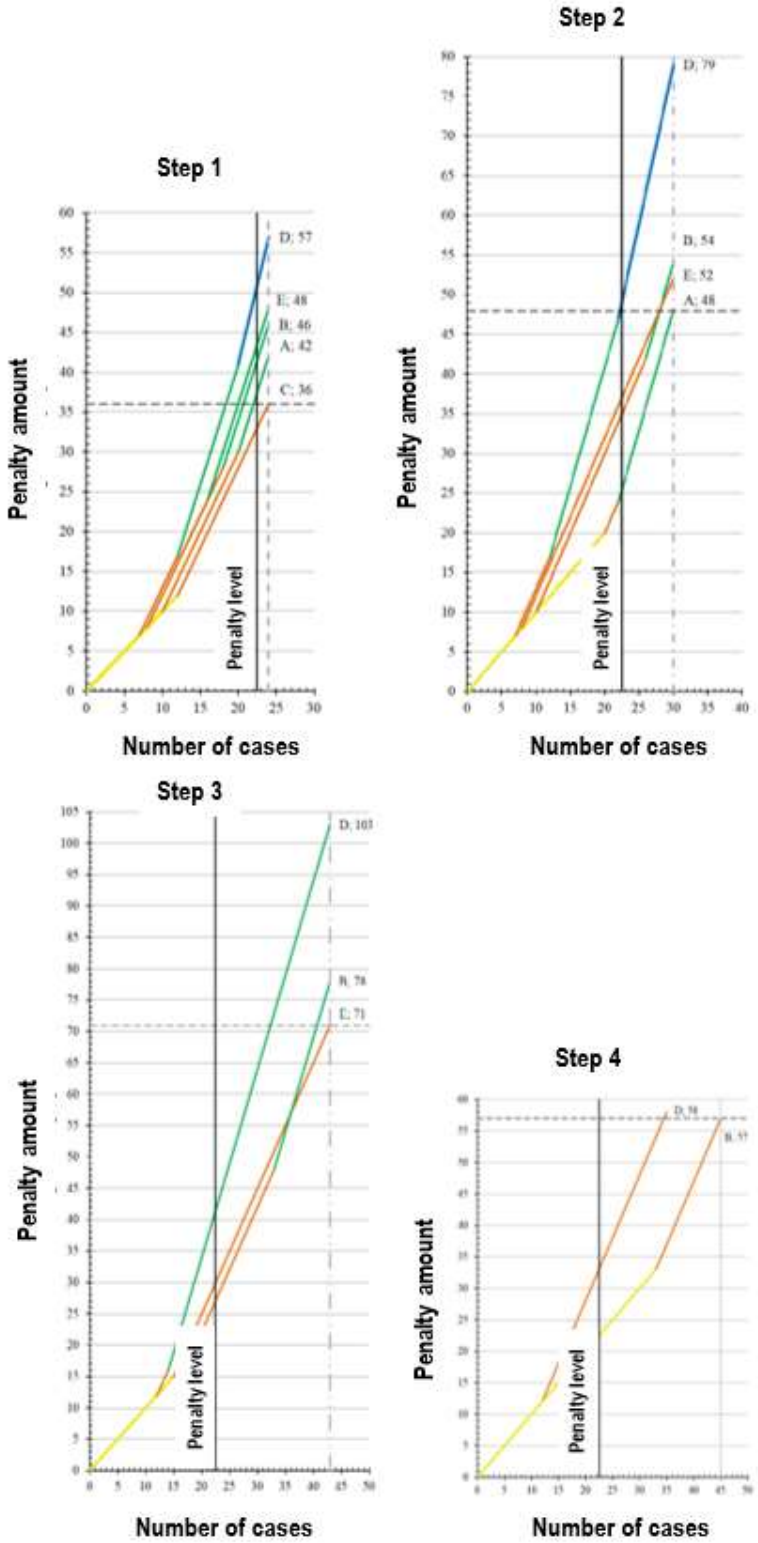


Figure 1. Graphical representation of solution search

Table 5

	expert voices				cumulative votes				accumulated fines			
	1	2	3	4	1	1-2	1-3	1-4	1	1-2	1-3	1-4
A	20	2	8	15	20	22	**30**	45	---	**48**	---	---
B	10	16	14	5	10	**26**	40	45	---	54	---	---
D	7	5	10	23	7	12	22	**45**	---	79	---	---
E	8	22	13	2	8	**30**	43	45	---	52	---	---

The minimum number of accumulated penalties was for candidate A, who becomes the leader at this stage and is excluded from further consideration.

The statistics are updated again and the "struggle for leadership" among candidates B, D, E is considered. This algorithm (with exclusion of the found leader, recalculation of statistics, calculation of accumulated sum of places and accumulated sum of "penalties") is repeated until the last candidate is determined. The scheme in Fig. 1 clearly illustrates the described algorithm.

On the abscissa is the total number of votes. On the ordinate is the sum of penalties. First the abscissa leader is determined, then the penalties for all candidates are determined. Candidate D does not have enough third places - fourth places are used (blue color in the figure - 4th place). Leaders C and E - but E in the second case is inferior to the optimum of A. For candidate A a "step" of 20 in 1 penalty width - height is formed, 2 "steps" - height of 2 penalties in 2 widths, and 3 "steps" of three penalties height and 8 widths. The total number of fines is 20*1+2*2+8*3=48, and the width is (20+2+8)=30 - like leader E. The leader has 2 steps - 8*1 fines + 22*2 fines = 52 fines. But the sum is also: 8+22=30.

The algorithm involves forward and backward permutation between real objects and virtual objects. Outside the scope of this paper, we will leave an interesting cyclic variant - when leaders are equal (equal abscissa values) and their penalties are equal (equal ordinate values) and we choose automatically the "last among equals" object.

Fig. 1 shows the ordered set of seat cases for each candidate date. Penalties for each object is the ordinate of the intersection of the function "its integral of penalties" at a point with abscissa equal to the leader in terms of accumulated sum of votes. The optimum is the minimum value over all objects.

Table 6

Cut-off level	0,5	0,5333	0,6323	0,7777...0,9999
Decision	**CAEBD**	**ACEBD**	**AEBDC**	**EABDC**

The final solution obtained by the rank penalty method is CAEBD, i.e., C ≻ **A** ≻ **E** ≻ B ≻ D. The algorithm is implemented in MS Excel by means of Visual Basic for Applications. As we have already mentioned above - the final solution is sensitive to the adopted cutoff level (Table 6).

4. Conclusions

Existing voting methods work, as a rule, with the number of rank places (as Schulze's method), but for an objective assessment it is necessary to evaluate the "quality" of victories - the importance of the first place is higher than the second and subsequent ones. The resulting qualitative solution is usually weakly stable and depends significantly on the adopted cutoff level.

Unlike the Schulze method, which always searches for a local extremum in the data, the proposed method is preferable for the correct determination of places in the ranked list, because it takes into account the cases when the local extremum does not determine the rank of a candidate and it is necessary to search for a global minimum. The Schulze method for the leader's place

determines the candidate by the weighted average of all scores and all fractions without regard to whether he is at the beginning or at the end of the list. In this sense, the minimum inversion search method is more optimal than Schulze's method, but it also does not always determine the places correctly.

A possible direction of improvement of the described method, increasing its stability, may be the introduction of nonlinear convex penalty functions like exponent function or S-shaped logistic curve (since the significance of the last places is usually low).

References

[1] Volsky, V. I. (2014) Voting procedures in small groups from ancient times to the beginning of XX century: [Text]: preprint WP7/2014/02 / V. I. Volsky ; National Research University "Higher School of Economics". - Moscow: Izd. dom. Higher School of Economics, 2014. - 76 c. - (Series WP7 "Mathematical methods of decision analysis in economics, business and politics"). - 10 copies. https://wp.hse.ru/data/2014/03/22/1318207163/WP7_2014_02.pdf

[2] Fang, Liu; Tong, Liu; Ya-Ru, Chen. (2022). 1. A consensus building model in group decision making with non-reciprocal fuzzy preference relations. Complex & Intelligent Systems, doi: 10.1007/s40747-022-00675-z

[3] Francisco, Chiclana., Francisco, Mata., Sergio, Alonso., Enrique, Herrera-Viedma., Luis, Martínez. (2007). 5. Group Decision Making: From Consistency to Consensus. Lecture Notes in Computer Science

[4] Olga, Maksimova., Iosif, Z., Aronov., Ljubisa, Papic. (2022). 2. Study of Decision-making Issues in Social Groups Based on Modelling of Incomplete Consensus. Journal of Graphic Era University, doi: 10.13052/jgeu0975-1416.1015

[5] Jingjing, Zhang. and Marco, Casari. (2012). 4. How groups reach agreement in risky choices: An experiment. Economic Inquiry, doi: 10.1111/J.1465-7295.2010.00362.X

[6] Philippos, Louis., Matías, Núñez. and Dimitrios, Xefteris. (2021). 3. The Virtuous Cycle of Agreement. The Economic Journal, doi: 10.1093/EJ/UEAB057

[7] Theresa, Csar., Martin, Lackner. and Reinhard, Pichler. (2018). 3. Computing the Schulze Method for Large-Scale Preference Data Sets. doi: 10.24963/IJCAI.2018/25.

[8] Markus, Schulze. (2018). 4. The Schulze Method of Voting. arXiv: Computer Science and Game Theory,

[9] Vijay, Kumar, Yadav., Anshu, S., Anand., Shekhar, Verma., S., Venkatesan (2020). 2. Private computation of the Schulze voting method over the cloud. Cluster Computing, doi: 10.1007/S10586-019-03025-W

[10] Krzysztof, Sornat., Virginia, Vassilevska, Williams. and Yinzhan, Xu. (2021). 1. Fine-Grained Complexity and Algorithms for the Schulze Voting Method. doi: 10.1145/3465456.3467630.

[11] Zhigirev, N. (2022) Inversion Method of Consistency Measure Estimation Expert Opinions / A. Bochkov, N. Zhigirev. Bochkov, N. Zhigirev, A. Kuzminova // Reliability: Theory & Applications. - 2022. - Vol. 17, No. 3(69). - P. 242-252. - DOI 10.24412/1932-2321-2022-369-242-252. - EDN SHCMCE.

[12] Markus, Schulze. (2018). 4. The Schulze Method of Voting. arXiv: Computer Science and Game Theory,

[13] Dawson A. (1963) The Skating System: Working Out the Marks in Ballroom Dancing Championships. Imperial Society of Teachers of Dancing, 1963. - 16 p.

SYSTEM RELIABILITY AND PROFITABILITY CONSIDERING CONCEPTS OF WARRANTY AND INSURANCE: AN OVERVIEW

Kajal Sachdeva[1], Gulshan Taneja[2], Amit Manocha[3*]

•

[1]Department of Applied Science, Government Polytechnic College, Jhajjar, Haryana, India
[2]Department of Mathematics, Maharshi Dayanand University, Rohtak, Haryana, India
[3*]Department of Applied Sciences, TIT&S, Bhiwani, Haryana, India
kajal.rs.maths@mdurohtak.ac.in, drgtaneja@gmail.com
[3*]corresponding author:amitmanocha80@yahoo.com

Abstract

The concepts of reliability, warranty, and insurance are interwoven in certain respects. System warranties and insurance coverage, whether provided by the manufacturer or a third party, reflect the system's potential reliability and offer consumers a sense of security. Conversely, enhancing system reliability during the development process can help reduce warranty and insurance costs. The purpose of this study is to compile the existing literature and provide a structured review of system reliability evaluation, incorporating the concepts of warranty, pricing, and insurance policies. Synthesizes the ideas, models, and methodologies that various authors have included in their study. To achieve this, a detailed review of 111 journal articles published between 1992 and the present was conducted. The primary focus areas of the review include system reliability, warranty policies, insurance mechanisms, and cost analysis. In addition, the study highlights potential directions for future research in this domain.

Keywords: reliability, warranty, insurance, cost benefit analysis.

1. Introduction

The recent development in numerous technical areas has opened the door for many innovations and technologies to enter the mainstream, compelling manufacturers to offer a wide range of customer alternatives. Despite the countless benefits of technological advancement, the complexity of the system is one of its disadvantages. As a result, consumers are concerned about system reliability, which could negatively impact the profits of the developed product. Reliability is the probability that system operates satisfactorily for intended period under given operating conditions. Redundancy is one of the vital tools that can be used to improve system reliability, but cost is always an issue to consider. Therefore, the manufacturer offers warranty, an extended warranty, and insurance on his products to alleviate consumer worries and apprehensions while also ensuring system reliability. Review papers [1, 2, 3, 4, 5] contain extensive literature on warranty. A product warranty is a written assurance from the manufacturer offered to the user to ensure system performance and to provide free repair/replacement if the product malfunctions. It is a legal settlement between the system user and the system provider. The contract addresses product effectiveness and user benefits in the event of failure. The conditional warranty policy states that if any defect occurs that is covered by the warranty terms stated in the contract at the time of purchase, the product is repaired or replaced at no cost to the user; otherwise, the user will pay the cost for the same. Contrarily, insurance is a legal agreement between a person

or a group (the policyholder) and an insurance firm (the insurer). The insurer accepts payment of a premium from the policyholder in exchange for an agreement to offer reimbursement for certain risks detailed in the insurance policy. Insurance is designed to protect policyholders from unexpected events or accidents that could result in financial hardship. Policyholders rely on insurance companies to provide financial protection when unexpected events occur. Throughout the design and development of the system, consideration is given to insurance policies and system warranties, both of which rely significantly on the system's reliability and efficacy.Figure 1 illustrates the connections between these ideas. Costs associated with warranties can be reduced by enhancing system reliability during the process of development.

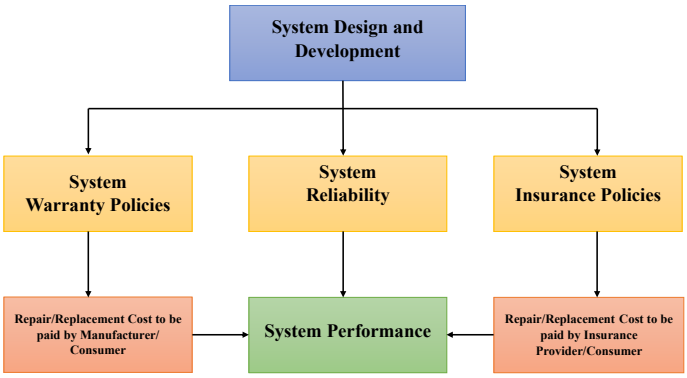


Figure 1: *Relation between system reliability, warranty and insurance*

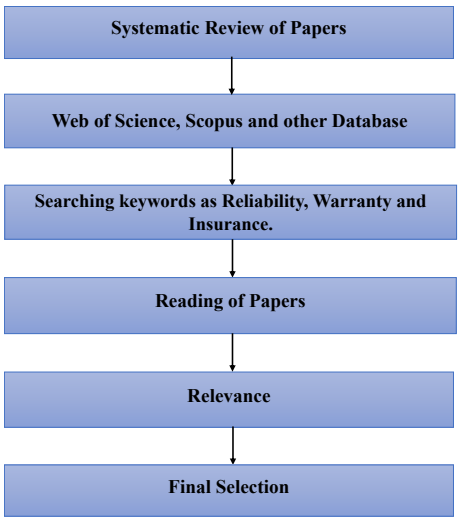


Figure 2: *Methodology for Systematic Review*

This study's goal is to compile the most recent literature and provide a structured assessment of system reliability evaluation, including the ideas of warranty, pricing, and insurance policies.

After a thorough study of the bibliography, 111 papers are chosen. A conceptual framework that represents the methodology used in the current investigation is shown in Figure 2. Initially, year-by-year searches from 1992 to the present in Web of Science, Scopus and other databases have been conducted using terms like insurance, warranty, and reliability. After reading those papers, select the pertinent article from the list. The article is structured in the following way. The discussion begins with an exploration of the literature on warranty policies and their various types. The overview of reliability with warranty concepts and insurance-related literature is done in next section. After that, the literature with a joint focus on reliability, warranty, insurance, and cost-benefit analysis is provided. Finally, the paper concludes along with future scope.

2. Warranty policies and warranty types

In this section, we briefly present the literature on various warranty policies and types explored by different researchers. Warranties serve as a marketing tool for manufacturers, allowing consumers to compare similar brands based not only on product attributes like quality, features, price, and reliability but also on the warranties offered at the time of purchase. For consumers, warranties provide the benefit of repair or replacement in case of a breakdown, potentially saving them significant maintenance costs. This creates a stronger connection between manufacturers and consumers, benefiting both parties.

Figure 3 illustrates several types of warranty policies based on cost, duration, and other variables. Under a free replacement warranty policy, the user incurs no cost for repairing or replacing a defective item, with the manufacturer covering all expenses within the warranty term. In contrast, a pro-rata warranty policy requires the system provider to repair or replace a failed product during the warranty period by paying a charge proportional to the product's age and sale price, with the user covering the remaining costs.

Warranties can also be categorized as one-dimensional or two-dimensional based on the variables involved. A one-dimensional warranty is defined by a single factor, such as duration, age, or usage. A two-dimensional warranty is defined by an area characterized by two variables, often one representing lifetime and the other representing item usage.

Additionally, warranties can be renewing or non-renewing. In a renewing warranty, if an item fails, it is repaired or replaced, and a new warranty is issued under the same conditions as the original. In a non-renewing warranty, the defective item is repaired or replaced for a specified period after the original purchase, but the replacement product does not receive a new warranty. Long-term warranties, which extend beyond the standard warranty period, can be purchased separately for an additional cost.

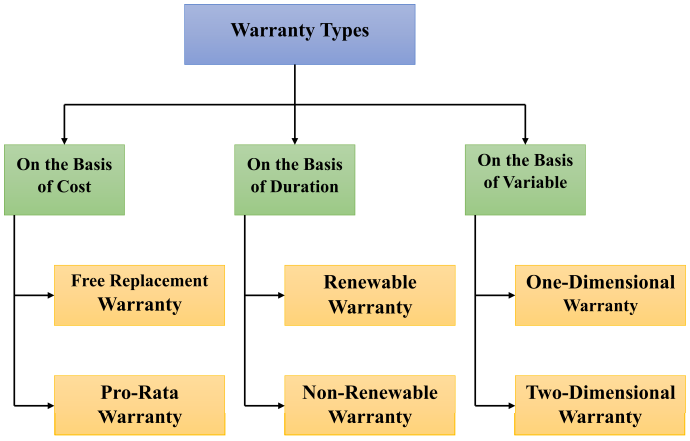


Figure 3: *Different types of Warranty Policies*

Table 1 provides a comprehensive summary of the findings from papers published in previous years by various researchers on different warranty policies.

Table 1: *Detailed Survey of Papers Reviewed pertaining to different Warranty Policies and Types*

Sr. No.	Author(s)	Year	Methods/Warranty Types	Findings
1	Murthy and Hussain [33]	1995	Free replacement warranty policy	Explored active (hot standby) and passive (cold, warm standby) redundancy strategies to lower the manufacturer's overall expenses, encompassing both production and warranty service costs.

Table 1: *Continued*

Sr. No.	Author(s)	Year	Methods/Warranty Types	Findings
2	Eliashberg et al. [14]	1997	Two-dimensional free repair/replacement warranty	Proposed a two-dimensional free repair/replacement warranty for the automotive industry, based on usage within a specific time frame.
3	Balachander [28]	2001	Long-term warranty	Provided a signalling-based explanation for the empirical finding that lower-quality products might come with longer warranties. Depending on whether the new entrant is more or less reliable than the established competitor, they demonstrated a negative or positive correlation between the length of the warranty and the product's reliability.
4	Mi [6]	2002	Bathtub-shaped failure rate function	Optimized the burn-in period, replacement frequency, and warranty terms. Determined the minimum duration for the burn-in period and the maximum limit for the most appropriate replacement.
5	Baik et al. [15]	2004	Two-dimensional warranty	Proposed a two-dimensional model based on a bivariate failure distribution with limited repair capabilities, where degradation occurs due to both age and usage. Addressed scenarios where failures could only be resolved through replacement.
6	Yang and Zaghati [43]	2004	Two-dimensional warranty	Outlined a two-dimensional warranty censoring technique for assessing reliability, illustrated using automotive onboard diagnostics as a case study.
7	Bai and Pham [7]	2005	Free repair policy	Developed a new warranty policy that imposes a limit on the number of repairs allowed for a system within a specified time period. Once this limit is reached, the system will be replaced instead of repaired.
8	Rai and Singh [16]	2005	Two dimensional warranty	Introduced a streamlined method for setting mileage warranty limits to influence the volume and cost of claims for new products.
9	Manna et al.[17]	2006	Fixed as well as flexible warranty plans	Identified the optimal warranty coverage area, balancing the warranty cost budget with customer needs for both fixed and flexible warranty plans across different regions.
10	Jung and Bai [18]	2007	Two-dimensional warranty	Calculated the lifespan distribution of a system covered under a two-dimensional warranty, which considers both age and usage simultaneously. This was done using a bivariate technique, assuming that age and usage are statistically correlated.

Table 1: *Continued*

Sr. No.	Author(s)	Year	Methods/Warranty Types	Findings
11	Matis et al. [8]	2008	Non-renewing combined warranty policy	Investigated the optimal product pricing, pro-rata warranty length, repair option selection, and profitability of a system in scenarios where replacement or minimal/general repair plans are offered during the standard warranty period.
12	Chien [9]	2008	Imperfect free replacement warranty renewal policy	Investigated a cost model that considered the consumer's perspective for product replacement and preventive maintenance.
13	Huang and Yen [19]	2009	Two-dimensional warranty	Optimized manufacturers' revenues by implementing a two-dimensional warranty model that included periodic preventive maintenance and an optimal warranty policy.
14	Lawless et al. [20]	2009	Two-dimensional warranty	Developed models that consider both usage and age within a heterogeneous population of products. Estimated the parameters using field data, incorporating information from American car warranties.
15	Jack et al. [21]	2009	Two-dimensional warranty	Proposed a repair-replace method for a two-dimensional warranty model in which the product is replaced upon the first failure, and subsequent failures are addressed with minimal repairs. Utilized an accelerated failure time model to assess the impact of item degradation on the usage rate.
16	Kadyan and Ramnivas [58]	2013	Free repair/replacement warranty	Analyzed a single-unit system and evaluated various system metrics, including reliability, Mean Time to System Failure (MTSF), and availability.
17	Gallego et al. [29]	2014	Extended warranty	Demonstrated the viability of an extended warranty in both homogeneous and diverse markets.
18	Yeh and Fang [10]	2014	Pro-rata warranty	Proposed a Bayesian decision-making model to assist manufacturers for pricing and production decisions.
19	Dai et al. [23]	2017	Two-dimensional warranty	Investigated the impact of usage rate on product failure using an accelerated failure time model. Recommended a stochastic expectation-maximization approach to estimate reliability model parameters for both censored and field data.
20	Jiao and Zhu [11]	2018	Minimal repair-replacement policy	Optimized the product's selling price, preventive maintenance intervals, and warranty period duration.
21	Arnold et al. [30]	2019	Non-renewing and renewing free repair warranties	Developed a geometric procedure to model the warranty claim process and assess warranty costs. The model was validated using a simulation approach and actual data from the automobile industry.

Table 1: *Continued*

Sr. No.	Author(s)	Year	Methods/Warranty Types	Findings
22	Wang et al. [12]	2019	Free repair/replacement warranty	Reduced the overall estimated service cost by determining the extent to which a component could be upgraded under a free repair or replacement warranty.
23	He et al. [31]	2020	Extended warranty	Proposed an extended warranty model that benefits all parties by optimizing the purchase period, maintenance procedures, and consumer usage rate. The model identifies the product failure process using the generalized Polya process failure mode.
24	Zheng and Su [24]	2020	Two-dimensional warranty	Proposed a flexible two-dimensional basic warranty policy comprising two rectangular regions. The first region accounts for the utilization rate, while the second region applies this usage rate in practice.
25	Taleizadeh and Mokhtarzadeh [25]	2020	Two-dimensional warranty	Applied the value-at-risk method to evaluate how a two-dimensional warranty coverage product, offered through both online and offline channels, would generate warranty claims over time. Optimized the product's pricing, warranty period, and usage parameters for each channel to maximize profit.
26	Wang et al. [26]	2021	Two dimensional warranty	Established the system's failure rate function under imperfect preventive maintenance using a two-dimensional warranty policy, employing an accelerated failure time model.
27	Gupta and Bhattacharya [27]	2022	Pro rata warranty	Utilized a non-parametric technique to evaluate the mean residual life and reliability from incomplete two-dimensional warranty data. This evaluation was based on the density function, assuming that age and usage are independent variables.
28	Mabrouk and Chelbi [32]	2022	Extended warranty	Enhanced the maintenance policy, extended the warranty period, and offered a free system replacement warranty.
29	Shang et al. [13]	2022	Free repair warranty with rebate and charge	Examined a free repair warranty with rebate and charge options to ensure reliability throughout the warranty period.

The study aimed to analyses various warranty policies, including free replacement, two-dimensional, minimal repair, long-term, renewing, non-renewing, feasible extended, and pro-rata policies, while exploring their characteristics and impact on both manufacturers and consumers.

3. System reliability

3.1. With warranty

This section highlights the literature that explores the combined concepts of warranty and reliability. Table 2 provides a detailed summary of research papers published in recent years, examining the relationship between reliability and warranty as studied by various researchers.

Table 2: *Detailed Survey of Papers Reviewed pertaining to relation between reliability and warranty*

Sr. No.	Author(s)	Year	Findings
1	Agarwal et al. [34]	1996	Explored the connection between warranty and reliability for home electronics and appliances, focusing on factors like product age and market trends. They concluded that this relationship weakens when there is significant variability in reliability and minimal market change.
2	Lu [35]	1998	Presented a mathematical model for vehicle customer mileage distribution using the log-normal distribution. They proposed a method for predicting reliability based on field failure records collected during the first four to five months of a vehicle's warranty period.
3	Vintr [36]	1999	Enhanced product reliability using two distinct approaches. One focused on minimizing manufacturing costs for extended warranty periods, while the other aimed at maximizing the warranty period based on known production costs.
4	Wood [37]	2001	Examined various types of failures from multiple perspectives, including component replacement failures from a hardware engineer's viewpoint, part return failures for the manufacturer, warranty claim failures for the finance department, maintenance issues for service organizations, and product degradation from the users' perspective. They discussed numerous reliability metrics and explored both theoretical and practical relationships between them.
5	Wu and Meeker [38]	2002	Utilized warranty databases and statistical methods to identify early major issues, allowing them to take proactive measures to address reliability concerns.
6	Yang and Zaghati [39]	2002	Established a connection between reliability, service time, and mileage. They recorded various warranty and non-warranty claims and developed a model for mileage accumulation using the sequential regression method based on warranty data.
7	Rai and Singh [40]	2003	Addressed the issue of insufficient data that hindered the reporting of failures beyond the warranty period. They utilized a two-parameter estimation method to generate a complete dataset from the incomplete warranty mileage data.
8	Kleyner and Bender [41]	2003	Introduced an effective technique for enhancing reliability by applying a conventional military approach, utilizing failed components identified through manufacturer warranty data.
9	Kim et al. [82]	2004	Established a model to analyse preventative maintenance time when a system was sold with a warranty from the viewpoints of the customer and the manufacturer, where failure was either repaired minimally or replaced at no cost to the user.
10	Yang and Cekecek [42]	2004	Evaluated the performance of industrial systems under a product warranty policy, taking into account user errors in system operation and manufacturing defects.

Table 2: *Continued*

Sr. No.	Author(s)	Year	Findings
11	Kleyner and Sandborn [44]	2005	Optimized the cost of achieving the desired level of reliability by implementing the two-dimensional warranty censoring technique.
12	Pecht [45]	2006	Examined the relationship between reliability and warranty in the automotive industry.
13	Mannar et al. [46]	2006	Proposed a novel fault zone localization methodology, using a case study of warranty data from the electronics industry to explore the relationship between warranty failures and design variables in product manufacturing.
14	Ion et al. [47]	2007	Examined the effect of the warranty call rate and estimated the parameters of the failure distribution using data from the first year of the warranty. Their findings indicated that the Weibull failure distribution best represented the data.
15	Huang and Fang [87]	2008	Developed a Bayesian decision model incorporating warranty and preventive maintenance to mitigate product deterioration.
16	Yun et al. [48]	2008	Investigated two warranty service procedures: the first strategy considered the age of the item when an incomplete repair was performed, while the second strategy did not take the item's age into account when assessing the level of improvement.
17	Vazquez and Rey-Stolle [49]	2008	Developed a reliability model for degraded photovoltaic modules, establishing justifiable power warranties and other system parameters based on field data.
18	Christozov et al. [50]	2009	Proposed a mathematical model to assess both the risk of product malfunction and the risk of making an incorrect purchase decision.
19	Murthy et al. [51]	2009	Focused on the reliability and diversity of product levels.
20	Lee et al. [22]	2010	Employed a fuzzy technique to develop a model for determining the optimal warranty period and analyzing warranty claim data.
21	Saidi-Mehrabad [52]	2010	Explored strategies for enhancing the reliability of used goods under various warranty policies, such as free replacement, pro-rata warranty, and their combinations, using a virtual age approach and screening test method.
22	Summit [54]	2011	Assessed the time required to accurately estimate parameters using a failure model based on the Weibull distribution. This model simulated the occurrence of warranty claims resulting from the failure of a single component over a period of up to five years.
23	Wu [55]	2012	Provided a summary of warranty research and explored potential future directions for the analysis of warranty data.
24	Zhou et al. [56]	2012	Examined the statistical hazard rate model to detect reliability issues using warranty data and information from the upstream supply chain.
25	Gurel and Cakmakci [57]	2013	Introduced a parametric Weibull model based on warranty claims and service data, designed to forecast the potential warranty period and the future lifespan of the product.
26	Hsu et al. [59]	2015	Using a Bayesian framework, developed a hierarchical model for warranty prediction.
27	Mackelprang et al. [60]	2015	Introduced a variable called "unexpected product failure costs," measuring the uncertainty associated with product reliability outcomes.

Table 2: *Continued*

Sr. No.	Author(s)	Year	Findings
28	Limon et al. [61]	2016	Assessed reliability using field data, including warranty claims, field failures, recall information, and maintenance records, along with censored data derived from consumer usage rate profiles.
29	Gupta et al. [62]	2017	Proposed a bivariate reliability function based on usage rates, along with corresponding reliability measures for warranty claims data, employing a conditional approach.
30	Shang et al. [64]	2018	Proposed an Inverse Gaussian degradation model paired with a conditional renewal replacement warranty policy, along with an optimal warranty duration and sale price from the manufacturer's perspective. Using prior user-observed degradation levels, they recommended the most effective post-warranty maintenance policy.
31	He et al. [65]	2018	Collected warranty data from manufacturers and applied a log-linear regression model to examine the impact on reliability during the early stages of production.
32	Aljazea and Wu [66]	2019	Investigated warranty risks within the automotive industry and developed a comprehensive taxonomy of warranty hazards.
33	Wang et al. [67]	2019	Developed an accelerated reliability growth model and a multiphase reliability testing program from the manufacturer's viewpoint, aiming to optimize the trade-off between warranty costs and reliability improvements.
34	Zhu et al. [68]	2019	Developed a reliability model to forecast costs, warranty policies, sales duration, and promotional strategies.
35	Jie et al. [69]	2020	Proposed a reliability model that considered regional variations in warranty terms and pricing. Their approach aimed to maximize the effectiveness of a regional warranty differential pricing strategy by using both unified and segmented warranty systems.
36	Li et al.[70]	2021	Developed a branched power law model to characterize the deterioration behavior of a system over multiple life cycles, considering both lifecycle warranty costs and analysis for several remanufacturing cycles. By using field time-to-failure data, they assessed the system's reliability and examined four potential warranty policies to evaluate warranty costs and environmental impacts, providing insights to support decision-making.
37	Shang et al. [71]	2021	Examined maintenance practices aimed at ensuring long-term product reliability beyond the warranty period. They explored two types of periodic maintenance strategies: one where replacement is performed first, followed by preventive maintenance, and another where preventive maintenance is conducted first, with replacement occurring later.
38	Wang et al. [72]	2021	Analyzed the reliability of individual components with irregular imperfect preventive maintenance and investigated the optimal maintenance strategy for multi-component systems under warranty.
39	Dong et al. [73]	2022	Employed a genetic algorithm to estimate the reliability threshold for opportunistic repair of power transmission devices.
40	Shang et al. [74]	2023	Focused on the application of advanced digital technologies in maintaining product reliability, while also exploring the characteristics of random warranty models and their implications for product managers and manufacturers.

Table 2: *Continued*

Sr. No.	Author(s)	Year	Findings
41	Qiao et al. [75]	2023	Proposed a new generalized post-warranty maintenance strategy designed to reduce maintenance costs, incorporating a repair time limit within an age-based preventive replacement policy. They also examined the impact of the manufacturer's warranty terms on consumers' joint warranty-maintenance decisions.
42	Hussien and El-Sherbeny [111]	2024	Evaluated the performance of industrial systems under a product warranty policy, taking into account user errors in system operation and manufacturing defects.

3.2. With warranty and insurance

Following section provides a concise summary of the literature on system reliability, insurance, and warranty. Insurance is designed to protect policyholders from unexpected events or accidents that could result in financial hardship. Policyholders rely on insurance companies to provide financial protection when unexpected events occur. Table 3 presents a concise literature review encompassing the concepts of reliability, warranty, and insurance.

Table 3: *Concise summary of the literature on system reliability, insurance, and warranty*

Sr. No.	Author(s)	Year	Findings
1	Fumagalli et al. [76]	2004	Developed a reliability insurance model for electrical power distribution systems, aiming to enhance service quality and achieve the desired level of system reliability.
2	Billimoria and Poudineh [77]	2019	Proposed a novel model, the "insurer-of-last-resort," which integrates insurance-based risk management concepts. This model aligns incentives for centralized decision-making, addressing the challenges energy-only markets face in ensuring resource adequacy and reliability.
3	Liu et al. [78]	2020	Used a semi-Markov process and a sequential Monto-Carlo simulation framework to optimize a new insurance stochastic model that takes risk interdependence for the use of cyber insurance in power systems.
4	Lau et al. [79]	2021	Suggested a new coalitional platform-based cyber insurance design that uses cyber security modelling and reliability implication analysis to estimate insurance rates.
5	Sachdeva et al. [80, 109]	2022 & 2024	Investigated a system under an extended conditional warranty with both long-term and short-term insurance.

4. Cost-benefit analysis

Manufacturers take into account development costs, warranty costs, and insurance costs when developing and manufacturing a system. Therefore, system profitability and various cost models are being investigated by many researchers, which are briefly addressed in this section. Table 4 offers a concise literature review that emphasizes cost as a critical factor alongside the concepts of reliability, warranty, and insurance.

Table 4: *Concise summary of the literature on system reliability, insurance, and warranty*

Sr. No.	Author(s)	Year	Findings
1	Hussain and Murthy [81]	2003	Developed a model that optimizes the costs associated with manufacturing units and the provision of warranty services.
2	Kleyer et al. [83]	2004	Determined the desired level of reliability by minimizing the overall life cycle costs in the large-volume automotive electronics sector.
3	Sheu and Chien [84]	2005	Investigated the optimal burn-in period to balance manufacturing and warranty costs. They also considered the impact of renewing or not renewing free replacement and rebate policies.
4	Bai and Pham [85]	2006	Developed cost analysis models for complex systems, including parallel, series, series-parallel, and parallel-series configurations, from the manufacturer's perspective. Their models focused on a full-service warranty renewal policy, which ensures that consumers are not charged for replacing a system with a new one in the event of failure or during preventive maintenance.
5	Wu et al. [86]	2007	Analyzed a cost model to determine the optimal burn-in duration and warranty period for a fully renewable combination of free replacement and pro-rata warranty.
6	Sgarbossa and Pham [88]	2010	Developed a cost model aimed at eliminating failures during both testing and the warranty period.
7	Park and Pham [89]	2010	Developed warranty cost models based on quasi-renewal processes for single and multi component systems with imperfect repair services. They also evaluated the reliability and other system performance measures for these systems.
8	Taneja [90]	2010	Developed a cost-benefit model for a system under warranty, where the repair cost is borne by either the manufacturer or the user, depending on whether the warranty claim is covered or not.
9	Wang et al. [53]	2010	Developed reliability-based design models for perfect maintenance, non-repairable products, and low maintenance to reduce the overall cost of production, maintenance, and warranty.
10	Gonzalez and Bueno [91]	2011	Analyzed a discounted warranty cost policy for a repairable, identical-series system, where components remain operational until they reach their critical failure level.
11	Jalali Naini and Shafiee [92]	2011	Developed a decision model to identify the optimal pricing strategy and upgrading plan for warranted second-hand products. Their model was based on real-world data from used electronic devices.
12	Shafiee et al. [93]	2011	Investigated a cost model for used products through a two-dimensional free repair/replacement strategy. Their study compared the warranties provided for both new and used products.
13	Park and Pham [94]	2012	Developed cost models for both warranty and non-warranty periods, considering minimal repairs with free repair/replacement warranties, as well as pro-rata warranties for k-out-of-n systems. To minimize long-term expected costs, they incorporated a two-dimensional warranty function based on repair and failure times, alongside a periodic preventive maintenance strategy.
14	Huang et al. [95]	2013	Used a reliability-based preventive maintenance approach to determine optimal warranty limits for a two-dimensional warranty policy. They also incorporated non-periodic preventive maintenance strategies to maximize manufacturer profit.

Table 4: *Continued*

Sr. No.	Author(s)	Year	Findings
15	Williams [96]	2013	Applied a change-point software reliability growth model to identify optimal release practices, estimate delivery costs, and assess the reliability of warranted software systems.
16	Tong et al. [97]	2014	Optimized the pricing strategy for an automobile product by offering a two-dimensional extended warranty service, which could be purchased both at the time of sale and upon the expiration of the base warranty.
17	Xie et al. [98]	2014	Analyzed the increasing profit of a new durable product sold at a fixed price over a set sales duration, with non-renewable free post-warranty service. Their study focused on the scenario where customers did not request warranty or post-warranty repairs from the manufacturer.
18	Niwas et al. [99]	2015	Investigated two single-unit guaranteed systems, where repair is free of charge to the user with the constraint that failure is not the result of user negligence and preventive maintenance is performed beyond warranty time. The first unit works as new after being repaired beyond the warranty period, however, the second unit degraded and was replaced with a new one.
19	Darghouth et al. [63]	2017	Evaluated several maintenance strategies, such as no Preventive Maintenance, periodic multiphase Preventive Maintenance, and product Preventive Maintenance with constant efficiency within warranty duration, and established a cost analysis model for improvement of reliability for warranted second-hand goods.
20	Zhao et al. [100]	2018	Developed a novel one-dimensional warranty cost optimization technique by utilizing degradation data, accounting for imperfect repairs, uncertainties in experimental data, and variations in field data. They used this approach to predict warranty cost intervals.
21	Alkahtani et al. [101]	2019	Created a decision support system that integrates stepwise approaches to identify manufacturing issues, map them to design information, and ultimately improve design parameters to achieve maximum reliability at the lowest cost.
22	Wang et al. [102]	2019	Examined periodic and imperfect preventive maintenance strategies for a product under a two-dimensional warranty, aiming to enhance customer satisfaction. They reduced the expected total cost per product by optimizing preventive maintenance actions and comparing their proposed strategy with a minimal repair corrective maintenance approach.
23	Solkhe and Taneja [103, 104, 105]	2018 & 2019	Analyzed a single-unit system under conditional warranty and examined the system's profitability both before and after the warranty period expired. They noted that conditional warranties can lead to disputes between the manufacturer and the customer. In light of this, they extended their work by considering the involvement of a higher authority, such as a court of law, to resolve such disputes. Additionally, they conducted a cost-benefit analysis for both the manufacturer and the user within the context of each of these models.
24	Koschnick and Hartman [106]	2020	Developed performance-based warranties that guarantee product operation up to a specified threshold. They also proposed an algorithm for designing such warranties, taking into account the associated operating costs.

Table 4: *Continued*

Sr. No.	Author(s)	Year	Findings
25	Cha et al. [107]	2022	Proposed a new renewable warranty policy aimed at maximizing the probability of success while minimizing associated costs. Their approach considered different populations of items, categorizing them into weak and strong groups.
26	Sachdeva et al. [108]	2023	Conducted a cost-benefit analysis of a system for both conditional and extended warranty models.
27	Huang et al. [110]	2024	Focused on two major factors: burn-in (run-in), a pre-launch testing process to detect faults, and periodic preventive maintenance, which attempts to eliminate unexpected failures during product use.

Numerous cost models for complex systems under warranty and insurance, with a focus on system reliability, have been developed by various researchers.

5. Conclusion and future scope

Both professionals and academics have recently become more interested in warranty and insurance. This article offered a thorough synthesis and review of warranties types, pricing and insurance by summarizing the existing literature and outlining some intriguing areas for further study.This review will be beneficial to academics conducting studies in this field because it neatly compiles practically all warranty and insurance policies, models, and approaches. In conclusion, several innovative and challenging research directions are proposed:

- **Exploration of Flexible Warranties**:The concept of flexible warranties warrants further study. Customers could have the option to customize warranty contracts that best suit their needs. It would be intriguing to model consumer preferences, product reliability, maintenance requirements, and other relevant factors simultaneously under these policies.
- **Cost Analysis of Multi-Component Systems with 2D Warranties**:There is a need for more in-depth research on the cost analysis of multi-component systems covered by two-dimensional warranties.
- **Focus on Real-World Warranty Challenges**:Researchers should prioritize addressing practical issues in warranties by gathering real-world data from manufacturers and consumers. This approach would help tackle real-life challenges in warranty claims and services more effectively.

References

[1] Murthy DN and Djamaludin I. (2002). New product warranty: A literature review. *International Journal of Production Economics*, 79(3):231-60.
[2] Shafiee M and Chukova S. (2013). Maintenance models in warranty: A literature review. *European Journal of Operational Research*, 229(3):561-72.
[3] Wang X and Xie W. (2018). Two-dimensional warranty: A literature review *Proceedings of the Institution of Mechanical Engineers, Part O: Journal of Risk and Reliability*, 232(3):284-307.
[4] Karim R and Suzuki K.(2005). Analysis of warranty claim data: a literature review *International Journal of Quality & Reliability Management*, 22(7):667-86.
[5] Murthy DN and Blischke WR. (1992). Product warranty management III: A review of mathematical models *European Journal of Operational Research*, 63(1):1-34.
[6] Mi J. (2002). On bounds for some optimal policies in reliability *Journal of applied probability*, 39(3):491-502.

[7] Bai J and Pham H. (2005). Repair-limit risk-free warranty policies with imperfect repair *IEEE Transactions on Systems, Manand Cybernetics-Part A: Systems and Humans*, 35(6):765-72.
[8] Matis TI, Jayaraman R and Rangan A.(2008). Optimal price and pro rata decisions for combined warranty policies with different repair options *IIE Transactions*, 40(10):984-91.
[9] Chien YH.(2008). Optimal age-replacement policy under an imperfect renewing free-replacement warranty *IEEE Transactions on Reliability*,57(1):125-33.
[10] Yeh CW and Fang CC.(2014). Optimal pro-rata warranty decision with consideration of the marketing strategy under insufficient historical reliability data *The International Journal of Advanced Manufacturing Technology*, 71:1757-72.
[11] Jiao C and Zhu X.(2018). Optimal design of sales and maintenance under the renewable warranty *RAIRO-Operations Research*, 52(2):529-42.
[12] Wang X, Xie M and Li L.(2019). On optimal upgrade strategy for second-hand multi-component systems sold with warranty *International journal of production research*, 57(3):847-64.
[13] Shang L, Yu X, Du Y et al.(2022). An optimal random hybrid maintenance policy of systems under a warranty with rebate and charge *Mathematics*, 10(18):3229.
[14] Eliashberg J, Singpurwalla ND and Wilson SP. (1997). Calculating the reserve for a time and usage indexed warranty *Management Science*, 43(7):966-75.
[15] Baik J, Murthy DP and Jack N. (2004). Two dimensional failure modeling with minimal repair *Naval Research Logistics (NRL)*, 51(3):345-62.
[16] Rai B and Singh N. (2005). A modeling framework for assessing the impact of new time/mileage warranty limits on the number and cost of automotive warranty claims *Reliability Engineering & System Safety*, 88(2):157-69.
[17] Manna DK, Pal S and Sinha S.(2006). Optimal determination of warranty region for 2D policy: A customers' perspective *Computers & Industrial Engineering*, 50(1-2):161-74.
[18] Jung M and Bai DS.(2007). Analysis of field data under two-dimensional warranty *Reliability Engineering & System Safety*, 92(2):135-43.
[19] Huang YS and Yen C. (2009). A study of two-dimensional warranty policies with preventive maintenance *IIE transactions*, 41(4):299-308.
[20] Lawless JF, Crowder MJ and Lee KA. (2009). Analysis of reliability and warranty claims in products with age and usage scales *Technometrics*, 51(1):14-24.
[21] Jack N, Iskandar BP and Murthy DP. (2009). A repair replace strategy based on usage rate for items sold with a two-dimensional warranty *Reliability Engineering & System Safety*, 94(2):611-7.
[22] Lee SH, Lee SJ and Moon KI.(2010). A fuzzy logic-based approach to two-dimensional automobile warranty system *Journal of circuits, Systems, and Computers*, 19(01):139-54.
[23] Dai A, He Z, Liu Z et al.(2017).Field reliability modeling based on two-dimensional warranty data with censoring times *Quality Engineering*, 29(3):468-83.
[24] Zheng R and Su C. (2020). A flexible two dimensional basic warranty policy with two continuous warranty regions *Quality and Reliability Engineering International*, 36(6):2003-18.
[25] Taleizadeh AA and Mokhtarzadeh M. (2020). Pricing and two-dimensional warranty policy of multi-products with online and offline channels using a value-at-risk approach *Computers & Industrial Engineering*, 148:106674.
[26] Wang R, Cheng Z, Rong L et al. (2021). Availability optimization of two-dimensional warranty products under imperfect preventive maintenance *IEEE Access*, 9:8099-109.
[27] Gupta SK and Bhattacharya D. (2022). Non-parametric estimation of bivariate reliability from incomplete two-dimensional warranty data *Reliability Engineering & System Safety*, 222:108385.
[28] Subramanian B. (2001). Warranty signaling and reputation *Management Science*, 47(9):1302-9.
[29] Gallego G, Wang R, Ward J et al. (2014). Flexible duration extended warranties with dynamic reliability learning *Production and Operations Management*, 23(4):645-59.
[30] Arnold R, Chukova S, Hayakawa Y et al. (2019). Warranty cost analysis with an alternating geometric process *Proceedings of the Institution of Mechanical Engineers, Part O: Journal of Risk and Reliability*, 233(4):698-715.

[31] He Z, Wang D, He S et al. (2020). Two-dimensional extended warranty strategy including maintenance level and purchase time: A win-win perspective *Computers & Industrial Engineering*, 141:106294.
[32] Ben Mabrouk A and Chelbi A. (2023). Optimal maintenance policy for equipment leased with base and extended warranty *International Journal of Production Research*, 61(3):898-909.
[33] Murthy DN and Hussain AZ. (1995). Warranty and optimal redundancy design *Engineering Optimization+ A35*, 23(4):301-14.
[34] Agrawal J, Richardson PS and Grimm PE. (1996). The relationship between warranty and product reliability *Journal of Consumer Affairs*, 30(2):421-43.
[35] Lu MW. (1998). Automotive reliability prediction based on early field failure warranty data *Quality and Reliability Engineering International*, 14(2):103-8.
[36] Vintr Z. (1999). Optimization of reliability requirements from manufacturer's point of view *InAnnual Reliability and Maintainability. Symposium* 1999 Proceedings (Cat. No. 99CH36283), 183-189. IEEE.
[37] Wood AP. (2001). Reliability-metric varieties and their relationships. InAnnual Reliability and Maintainability Symposium. Proceedings *International Symposium on Product Quality and Integrity (Cat. No. 01CH37179)* 2001 Jan 22, 110-115. IEEE.
[38] Wu H and Meeker WQ.(2002). Early detection of reliability problems using information from warranty databases *Technometrics*, 44(2):120-33.
[39] Yang G and Zaghati Z.(2002). Two-dimensional reliability modeling from warranty data *InAnnual Reliability and Maintainability Symposium* 2002 Proceedings (Cat. No. 02CH37318), 272-278. IEEE.
[40] Rai B and Singh N. (2003). Hazard rate estimation from incomplete and unclean warranty data *Reliability Engineering & System Safety*, 81(1):79-92.
[41] Kleyner A and Bender M.(2003). Enhanced reliability prediction method based on merging military standards approach with manufacturer's warranty data *InAnnual Reliability and Maintainability Symposium, 2003* ,202-206. IEEE.
[42] Yang K and Cekecek E.(2004). Design vulnerability analysis and design improvement by using warranty data *Quality and reliability engineering international* , 20(2):121-33.
[43] Yang G and Zaghati Z. (2004). Reliability and robustness assessment of diagnostic systems from warranty data *InAnnual Symposium Reliability and Maintainability*,146-150. IEEE.
[44] Kleyner A and Sandborn P. (2005). A warranty forecasting model based on piecewise statistical distributions and stochastic simulation *Reliability Engineering & System Safety*, 88(3):207-14.
[45] Pecht MG. (2006). Establishing a relationship between warranty and reliability *IEEE Transactions on Electronics Packaging Manufacturing*, 29(3):184-90.
[46] Mannar K, Ceglarek D, Niu F et al. (2006). Fault region localization: Product and process improvement based on field performance and manufacturing measurements *IEEE Transactions on Automation Science and Engineering*, 3(4):423-39.
[47] Ion RA, Petkova VT, Peeters BH et al. (2007). Field reliability prediction in consumer electronics using warranty data *Quality and Reliability Engineering International*, 23(4):401-14.
[48] Yun WY, Murthy DN and Jack N. (2008). Warranty servicing with imperfect repair *International Journal of Production Economics*, 111(1):159-69.
[49] Vazquez M and Rey Stolle I. (2008). Photovoltaic module reliability model based on field degradation studies *Progress in photovoltaics: Research and Applications*, 16(5):419-33.
[50] Christozov D, Chukova S and Mateev P. (2009). On two types of warranties: Warranty of malfunctioning and warranty of misinforming *Asia-Pacific Journal of Operational Research*, 26(03):399-420.
[51] Murthy DN, Osteras T and Rausand M.(2009). Component reliability specification *Reliability Engineering & System Safety*, 94(10):1609-17.
[52] Saidi-Mehrabad M, Noorossana R and Shafiee M. (2010). Modeling and analysis of effective ways for improving the reliability of second-hand products sold with warranty *The international journal of advanced manufacturing technology*, 46:253-65.
[53] Wang Z, Huang HZ and Du X.(2010). Optimal design accounting for reliability, maintenance, and warranty *Journal of Mechanical Design*, 132(1): 011007.

[54] Summit RA.(2011). Estimating the reliability model parameters through a simulation of warranty claims: How much data is needed? *ANZIAM Journal*, 53:C451-64.
[55] Wu S.(2012). Warranty data analysis: A review *Quality and Reliability Engineering International*, 28(8):795-805.
[56] Zhou C, Chinnam RB and Korostelev A.(2012). Hazard rate models for early detection of reliability problems using information from warranty databases and upstream supply chain *International Journal of Production Economics*, 139(1):180-95.
[57] Gurel U and Cakmakci M.(2013). Impact of reliability on warranty: A study of application in a large size company of electronics industry *Measurement*, 46(3):1307-310.
[58] Kadyan MS.(2013). Cost benefit analysis of a single-unit system with warranty for repair *Applied mathematics and Computation*, 223:346-53..
[59] Hsu NJ, Tseng ST and Chen MW.(2015). Adaptive warranty prediction for highly reliable products *IEEE Transactions on Reliability*, 64(3):1057-67.
[60] Mackelprang AW, Habermann M and Swink M.(2015). How firm innovativeness and unexpected product reliability failures affect profitability *Journal of Operations Management*, 38:71-86.
[61] Limon S, Yadav OP, Zuo MJ et al.(2016). Reliability estimation considering usage rate profile and warranty claims *Proceedings of the Institution of Mechanical Engineers, Part O: Journal of Risk and Reliability*, 230(3):297-308.
[62] Gupta SK, De S and Chatterjee A.(2017). Some reliability issues for incomplete two-dimensional warranty claims data *Reliability Engineering & System Safety*, 157:64-77.
[63] Darghouth MN, Chelbi A and Ait-Kadi D.(2017). Investigating reliability improvement of second-hand production equipment considering warranty and preventive maintenance strategies *International Journal of Production Research*, 55(16):4643-61.
[64] Shang L, Si S, Sun S et al.(2018). Optimal warranty design and post-warranty maintenance for products subject to stochastic degradation *IISE Transactions*, 50(10):913-27.
[65] He S, Zhang Z, Jiang W et al. (2018). Predicting field reliability based on two-dimensional warranty data with learning effects *Journal of Quality Technology* , 50(2):198-206.
[66] Aljazea AM and Wu S.(2019). Managing risk for auto warranties *International Journal of Quality & Reliability Management*, 36(7):1088-105.
[67] Wang Y, Liu Y, Li X et al.(2019). Multi-phase reliability growth test planning for repairable products sold with a two-dimensional warranty *Reliability Engineering & System Safety*, 189:315-26.
[68] Zhu X, Jiao C and Yuan T.(2019). Optimal decisions on product reliability, sales and promotion under nonrenewable warranties *Reliability Engineering & System Safety*, 192:106268.
[69] Jie L, Liu W, Li M et al.(2020). Sub-Region Warranty Differential Pricing Optimization Strategy Based on Regional Granularity of Use Reliability *IEEE Access*, 8:95523-39.
[70] Li M, Nemani VP, Liu J et al. (2021). Reliability-informed life cycle warranty cost and life cycle analysis of newly manufactured and remanufactured units *Journal of Mechanical Design*, 143(11):112001.
[71] Shang L, Wang H, Wu C et al.(2021). The post warranty random maintenance policies for the product with random working cycles *Eksploatacja i Niezawodnosc*, 23(4).
[72] Wang R, Cheng Z, Dong E et al.(2021). Reliability-based opportunistic maintenance modeling for multi-component systems with economic dependence under base warranty *Discrete Dynamics in Nature and Society*,21:1-6.
[73] Dong E, Gao T, Cheng Z et al.(2022). Opportunistic Maintenance Strategy for Complex Equipment with a Genetic Algorithm Considering Failure Dependence: A Two-Dimensional Warranty Perspective *Sensors*, 22(18):6801.
[74] Shang L, Zhang N, Yang L et al.(2023). Study of a Random Warranty Model Maintaining Fairness and a Random Replacement Next Model Sustaining Post-Warranty Reliability *Axioms*, 12(3):258.
[75] Qiao P, Luo M, Ma Y et al. (2023). Optimal warranty option and post-warranty maintenance strategy under a warranty menu: from a consumer perspective *International Journal of Production Research*, 7:1-23.

[76] Fumagalli E, Black JW, Vogelsang I et al.(2004). Quality of service provision in electric power distribution systems through reliability insurance *IEEE Transactions on Power Systems*, 19(3):1306-93.
[77] Billimoria F and Poudineh R.(2019). Market design for resource adequacy: A reliability insurance overlay on energy-only electricity markets *Utilities Policy*, 60:100935.
[78] Liu Z, Wei W, Wang L et al.(2020). An actuarial framework for power system reliability considering cybersecurity threats *IEEE Transactions on Power Systems*, 36(2):851-64.
[79] Lau P, Wang L, Liu Z et al. (2021). A coalitional cyber-insurance design considering power system reliability and cyber vulnerability *IEEE Transactions on Power Systems*, 36(6):5512-24.
[80] Sachdeva K, Taneja G and Manocha A.(2022). Sensitivity and Economic Analysis of an Insured System with Extended Conditional Warranty *Reliability: Theory & Applications*, 17(3 (69)):315-27.
[81] Hussain AZ and Murthy DN.(2003). Warranty and optimal reliability improvement through product development *Mathematical and computer modelling*, 38(11-13):1211-7.
[82] Kim CS, Djamaludin I and Murthy DN.(2004). Warranty and discrete preventive maintenance *Reliability Engineering & System Safety*, 84(3):301-9.
[83] Kleyner A, Sandborn P and Boyle J. (2004). Minimization of life cycle costs through optimization of the validation program-a test sample size and warranty cost approach *InAnnual Symposium Reliability and Maintainability*, 553-558. IEEE.
[84] Sheu SH and Chien YH. (2005). Optimal burn-in time to minimize the cost for general repairable products sold under warranty *European Journal of Operational Research*, 163(2):445-61.
[85] Bai J and Pham H. (2006). Cost analysis on renewable full-service warranties for multi-component systems *European Journal of Operational Research*, 168(2):492-508.
[86] Wu CC, Chou CY and Huang C.(2007). Optimal burn-in time and warranty length under fully renewing combination free replacement and pro-rata warranty *Reliability Engineering & System Safety*, 92(7):914-20.
[87] Huang YS and Fang CC.(2008). A cost sharing warranty policy for products with deterioration *IEEE Transactions on Engineering Management*, 55(4):617-27.
[88] Sgarbossa F and Pham H.(2010). A cost analysis of systems subject to random field environments and reliability *IEEE Transactions on Systems, Man, and Cybernetics, Part C (Applications and Reviews)*, 40(4):429-37.
[89] Park M and Pham H.(2010). Warranty cost analyses using quasi-renewal processes for multicomponent systems *IEEE Transactions on Systems, Man, and Cybernetics-Part A: Systems and Humans*, 40(6):1329-40.
[90] Taneja G.(2010). Reliability Model for a System with Conditional Warranty and various types of Repair/Replacement *Advances in Information Theory and Operations Research*, 214-20.
[91] Gonzalez NG and Bueno V. (2011). Estimating the Discounted Warranty Cost of a Minimally Repaired Coherent System *Revista Colombiana de Estadistica*, 34(3):513-43.
[92] Jalali Naini SG and Shafiee M. (2011). Joint determination of price and upgrade level for a warranted second-hand product *The International Journal of Advanced Manufacturing Technology*, 54:1187-98.
[93] Shafiee M, Chukova S, Saidi-Mehrabad M et al. (2011). Two-dimensional warranty cost analysis for second-hand products *Communications in statistics-theory and methods*, 40(4):684-701.
[94] Park M and Pham H. (2012). Warranty Cost Analysis for k-out-of-n Systems With 2-D Warranty *IEEE Transactions on Systems, Man, and Cybernetics-Part A: Systems and Humans*, 42(4):947-57.
[95] Huang YS, Chen E and Ho JW. (2013). Two-dimensional warranty with reliability-based preventive maintenance *IEEE Transactions on Reliability*, 62(4):898-907.
[96] WILLIAMS DP. (2013). Optimal release policies for a software system with warranty cost and change-point phenomenon *Turkish Journal of Electrical Engineering and Computer Sciences*, 21(1):234-45.
[97] Tong P, Liu Z, Men F et al. (2014). Designing and pricing of two-dimensional extended warranty contracts based on usage rate *International Journal of Production Research*, 52(21):6362-80.

[98] Xie W, Liao H and Zhu X.(2014). Estimation of gross profit for a new durable product considering warranty and post-warranty repairs *IIE Transactions*, 46(2):87-105.
[99] NiwAs R, Kadyan MS and Kumar J.(2015). Probabilistic analysis of two reliability models of a single-unit system with preventive maintenance beyond warranty and degradation *Eksploatacja i Niezawodnosc*, 17(4).
[100] Zhao X, He S and Xie M.(2018). Utilizing experimental degradation data for warranty cost optimization under imperfect repair *Reliability Engineering & System Safety*, 177:108-19.
[101] Alkahtani M, Choudhary A, De A et al.(2019). A decision support system based on ontology and data mining to improve design using warranty data *Computers & industrial engineering*, 130:1027-39.
[102] Wang Y, Liu Y and Zhang A.(2019). Preventive maintenance optimization for repairable products considering two-dimensional warranty and customer satisfaction *Proceedings of the Institution of Mechanical Engineers, Part O: Journal of Risk and Reliability*, 233(4):553-66.
[103] Solkhe M and Taneja G. (2018). A reliability model on a system with conditional warranty and intervention of higher authority on denial of valid claim *International Journal of Applied Engineering Research*, 13:16762-67.
[104] Solkhe M and Taneja G.(2019). A Reliability Model on a System with Conditional Warranty and Possibility of Denial of Valid Claim *Journal of Advanced Research in Dynamical and Control Systems*, 11(1):1302-1302.
[105] Solkhe M and Taneja G. (2019). A Reliability Model for a System with Consideration of Periods Before and After Expiry of Conditional Warranty *International Journal of Agricultural & Statistical Sciences*, 15(1).
[106] Koschnick C and Hartman JC.(2020). Using performance-based warranties to influence consumer purchase decisions *The Engineering Economist*, 65(1):1-26.
[107] Cha JH and Finkelstein M. (2022). A new warranty policy for heterogeneous items subject to monotone degradation processes *Proceedings of the Institution of Mechanical Engineers, Part O: Journal of Risk and Reliability*, 236(1):55-65.
[108] Sachdeva K, Taneja G and Manocha A. (2023). Reliability and Sensitivity Analysis of a System with Conditional and Extended Warranty *Reliability: Theory & Application*, 18(3 (74)):689-707.
[109] Sachdeva, K., Taneja, G.and Manocha, A. (2024). Reliability and Sensitivity Analysis of an Insured System with Conditional Warranty Duration Lengthier than Insurance Duration. *International Journal of Reliability, Quality and Safety Engineering*, 31(01): 2350034.
[110] Huang, Y. S., Fang, C. C.and Kuo, C. Y. (2024). A study on two dimensional warranty with a preventive maintenance policy under burn in or run in. *Applied Stochastic Models in Business and Industry*.
[111] Hussien, Z. M. and El-Sherbeny, M. S. (2024). Stochastic analysis of an industrial system with preparation time repair under warranty policy. *Applied Sciences*, 14: 2076-3417.

RT&A, No 3 (86)
Volume 20, September 2025

ATTRIBUTE CONTROL CHART BASED ON RAYLEIGH DISTRIBUTION: A BAYESIAN APPROACH

M. GUNASEKARAN[1], T. KAVITHA[2], and S. M. KARTHIK[3]

[1]Department of Applied Research, The Gandhigram Rural Institute (Deemed to be University), Dindigul, Tamil Nadu, India. E-mail:gunasekaranm1988@gmail.com
[2]PG & Research Department of Statistics, Salem Sowdeswari College (Women), Salem, Tamil Nadu, India. E-mail: sreesuryaa@gmail.com
[3]Department of Applied Research, The Gandhigram Rural Institute (Deemed to be University), Dindigul, Tamil Nadu, India. E-mail: gemofstate@gmail.com

Abstract

Statistical Process Control is a quality control approach that uses statistical tools to assess, monitor, and optimize processes. A control chart plays a crucial role in this method by tracking the performance of a process and providing a visual signal to detect any irregular deviations caused by specific assignable factors. It compares the values of a quality attribute against predetermined control limits. In typical quality control procedures, control charts are often created without considering parameter uncertainty. However, it is essential to identify any shifts in the parameters of the probability distribution linked to one or more variables associated with the process to ensure effective monitoring. Evaluating these parameters is vital, as it can influence the long-term functionality of the control chart in both controlled and uncontrolled environments. This article introduces an innovative attribute control chart that utilizes a Bayesian methodology based on the Rayleigh lifetime distribution, specifically applied under accelerated life testing with a hybrid censoring technique. The parameters for the control chart will be established through various combinations of values using a Bayesian approach, while the effectiveness of the control chart will be evaluated through the Average Run Length (ARL). Numerical examples will illustrate the proposed control chart, and simulated data will showcase its potential application. The effectiveness of the proposed control chart will be quantified through ARLs for different shift constants, sample sizes, and additional parameters such as p, Lower Control Limit, and Upper Control Limit.

Keywords: Rayleigh Distribution, Predictive Distribution, Attribute Control Chart, Average Run Length

1. Introduction

The manufacturing industry is currently facing significant challenges due to variations in processes, which lead to defects and increased costs. In the realm of continuous manufacturing, it is crucial to determine whether a process is in control and to identify any existing variations. These variations may stem from random factors or identifiable causes. Quality control involves the processes of monitoring, measuring, and correcting a product's performance in relation to established criteria or specifications. One of the most common and effective methods for ensuring quality is the control chart. This tool provides a graphical representation of data gathered from the manufacturing sector. Each control chart includes a central line (CL) that indicates the average, as well as an upper line that marks the upper control limit (UCL) and a lower line that represents the lower control limit (LCL).

To effectively track the production process in various scenarios, several new control charting techniques have been developed. These control charts come in different types, each specifically designed to address the unique characteristics of the quality attribute being examined. They can be categorized into two main types based on the nature of the data: 'variable' and 'attribute'. Variable control charts focus on accurately measured data, while attribute control charts are used to identify items as either compliant or non-compliant with established standards.

The lifetime of a product is considered a crucial quality attribute for certain goods. Life tests are conducted to monitor the manufacturing process of these products. Depending on the results of the life test, a product may be classified as either conforming or non-conforming. However, this testing method can be quite time-consuming due to the lengthy nature of the tests. In this context, it is important to acknowledge the use of censoring techniques. Common censoring methods used in life testing include type-I censoring, type-II censoring, and hybrid censoring. In hybrid censoring, the life test is concluded at either the designated test time (t) or upon detecting the $(UCL+1)^{th}$ failure, whichever comes first. If the failures observed during the life test remain within the upper control limit (UCL) and lower control limit (LCL) at time t, the production process is in-control; otherwise, it is considered out-of-control. If a product fails the life test before reaching the specified termination time t, it is classified as a non-conforming product.

Accelerated life testing (ALT) is an evaluative technique designed to forecast the probability of future product failures. This approach is well-regarded for its effectiveness in 'accelerating time,' making it a preferred method for testing. ALT is particularly advantageous when it is impractical to wait for failures to occur at their normal rates, thereby offering insights into anticipated future failures. During ALT, products are subjected to heightened conditions such as increased stress, strain, temperature, and pressure, resulting in a faster failure rate than traditional life testing. As a result, employing ALT with hybrid censoring can lead to a significant reduction in both the overall time to failure and the costs associated with inspections.

Attribute control charts, including the np control chart, are based on the assumption that the quality characteristic follows a normal distribution. However, the actual distribution of these quality characteristics may differ from this assumption. Such discrepancies can mislead industrial engineers when using the existing control chart, potentially leading to an increase in non-conforming items. A significant body of literature examines the development of attribute control charts utilizing various lifetime distributions, including but not limited to: Weibull[1–3], Pareto[4], Birnbaum Saunder[5], Inverse Rayleigh[6], Burr X & XII, Inverse Gaussian & Exponential[7], Lognormal[8], Exponentiated Half Logistic[9], Dagum[10], Pareto[11], Weibull Pareto[12], Gamma[13], Log–Logistic[14], Generalized Log Logistic[15], Generalized Exponential[16], Inverse Weibull[17], Length-Biased Weighted Lomax[18], Rayleigh[19], Half Normal & Half Exponential Power[20], Exponentiated Inverse Kumaraswamy[21], Lindley[22], Generalized Rayleigh[23] and Exponentiated Exponential[24].

The attribute control charts referenced in earlier literature are predicated on the assumption that the mean number of defective items remains unchanged over time when the process is in control. Control charts that depend entirely on sample variance, like the np-chart, can produce numerous false alarms if the actual number of defectives is inconsistent during an in-control state. These false alarms arise because the observed count of nonconforming items is influenced by both process variability and sampling variation, while the control limits are calculated based solely on sampling variance. Larger sample sizes tend to reveal any underlying process variations more clearly, resulting in the actual number of nonconforming items varying from one sample to another based on an underlying distribution. The Bayesian approach is widely recognized for its effectiveness in addressing uncertainty related to the parameter of interest. A pioneering Bayesian process control chart for attributes was introduced by [25]. Subsequently, numerous researchers, as noted in references [26–35] have expanded the literature by developing a variable control chart for various lifetime distributions using the Bayesian approach.

The Rayleigh distribution is frequently applied as a lifetime distribution in the context of research related to electro-vacuum devices and communication engineering. Its hazard function, characterized by a linear increase, suggests that it is well-suited for items that deteriorate

rapidly. This distribution is a particular case of the Weibull distribution, which is a statistical model frequently utilized in reliability engineering and life testing. Initially proposed as the Rayleigh power (and amplitude) distribution in reference [36], it was later renamed to Rayleigh distribution in subsequent studies [37, 38], which examined its properties, estimation methods, and applications. The significance of this skewed distribution has led to extensive research by various authors in engineering-related domains. Additionally, the Rayleigh distribution can be used to model the lifespan of products resulting from manufacturing processes. A review of the literature indicates that there has been no research conducted on control charts that incorporate life tests for non-normal distributions, such as the Rayleigh distribution, particularly in the context of accelerated life testing with hybrid censoring using a Bayesian approach.

In this paper, the design of an attribute control chart based on a predictive distribution of the lifetime is considered under the assumption that the lifetime follows a Rayleigh distribution and the process parameter is modelled by an Inverse-Rayleigh distribution under accelerated life test with hybrid censoring. The control chart coefficient was determined, and the performance of the proposed control chart was discussed with the ARL. When the process parameter changes, the proposed control chart is designed. With the use of simulated data, the proposed control chart's applicability is described. Simulated data is used to illustrate the proposed control chart. Section 2 presents designing the Bayesian control chart and provides a procedure for obtaining the control chart for given strength. The real-life application of the proposed control chart through simulation study is described in Section 3. The behaviour of the ARL is discussed in Section 4. Section 5 presents the conclusion of the study.

2. Designing a Bayesian Attribute control chart

Let "T" be the lifetime of the products produced in a production process. Assume that "T" follows a Rayleigh distribution with parameter θ given for $t > 0$ by its density function $g_{T|\{\theta\}}$:

$$g_{T|\{\theta\}}(t) = \frac{te^{-\frac{t^2}{2\theta^2}}}{\theta^2}; t > 0, \theta > 0 \tag{1}$$

The distribution function of $G_{T|\{\theta\}}$ is given by:

$$G_{T|\{\theta\}}(t) = 1 - e^{-\frac{t^2}{2\theta^2}}; t > 0, \theta > 0 \tag{2}$$

According to [39], Consider the process parameter θ with $\theta > 0$ as random variable Θ with prior distribution given by the inverse Rayleigh distribution with density function for $\theta > 0$:

$$h_{\Theta|\{\lambda\}}(\theta) = \frac{1}{\theta^3\lambda^2}e^{-\frac{1}{2\lambda^2\theta^2}}; \theta > 0, \lambda > 0 \tag{3}$$

The updated lifetime of the product is described by the predictive distribution of "T" whose density function can be obtained from the prior distribution (3) and the sampling distribution (1) as:

$$f_{T|\{\lambda\}}(t) = \frac{2\lambda^2 t}{[1+\lambda^2 t^2]^2}; t > 0 \tag{4}$$

Hereafter, the above predictive distribution referred as "Rayleigh-Inverse-Rayleigh" distribution and the distribution function of $T|\{\lambda\}$ is obtained as:

$$F_{T|\{\lambda\}}(t) = 1 - \frac{1}{[1+\lambda^2 t^2]}; t > 0 \tag{5}$$

The product's mean lifetime under Rayleigh-Inverse-Rayleigh distribution is given by

$$\mu = \frac{\pi}{2\lambda} \tag{6}$$

The product's expected lifetime under standard (usual) conditions is indicated by the symbol t_U and is modelled by an Rayleigh-Inverse-Rayleigh distribution with a particular parameter (λ_U). Thus, the subsequent equation can be applied to evaluate the product's lifetime in these standard conditions

$$F_U(t_U|\lambda_U) = 1 - \frac{1}{\left[1 + \lambda_U^2 t_U^2\right]} \tag{7}$$

Similarly, the product's lifetime when subjected to accelerated conditions is denoted as t_A, with the assumption that it follows an Rayleigh-Inverse-Rayleigh distribution defined by a particular parameter (λ_A). Thus, the product's lifetime under such accelerated conditions is presented as follows

$$F_A(t_A|\lambda_A) = 1 - \frac{1}{\left[1 + \lambda_A^2 t_A^2\right]} \tag{8}$$

The mean lifetime of the product under accelerated conditions is provided by

$$\mu_A = \frac{\pi}{2\lambda_A}$$

By employing the definition of the Acceleration Factor (AF), we can formulate it in the following way

$$\lambda_A = \frac{\lambda_U}{AF}$$

Therefore, Equation (8) becomes

$$F_A(t_A|\lambda_A) = 1 - \frac{1}{\left[1 + \left(\frac{\lambda_U}{AF}\right)^2 t_A^2\right]}$$

$$F_A(t_A|\lambda_A) = 1 - \frac{AF^2}{\left[AF^2 + \lambda_U^2 t_A^2\right]}$$

The probability of product failure represented as p_0 when the process is maintained under control, is defined by the likelihood that the product will fail before the censoring time t_A.

$$p_0 = 1 - \frac{AF^2}{\left[AF^2 + \lambda_U^2 t_A^2\right]} \tag{9}$$

The mean life of the product under accelerated conditions is represented by μ_A when the process is in control. The experimental duration t_A can be expressed with the mean of the in-control process, specifically as $t_A = a * \mu_A$, where "a" signifies the experiment termination ratio. Consequently, Equation (9) can be revised by incorporating the values for t_A and μ_A.

$$p_0 = 1 - \frac{AF^2}{\left[AF^2 + \left(\frac{a\pi}{2}\right)^2 \left(\frac{\lambda_U}{\lambda_A}\right)^2\right]}$$

It is presumed that the parameter remains constant when the process is under control, specifically $\lambda_A = \lambda_U$. Let p_0 as the failure probability of an item when the process is maintained under controlled accelerated conditions, which can be derived from the following:

$$p_0 = 1 - \frac{AF^2}{\left[AF^2 + \left(\frac{a\pi}{2}\right)^2\right]} \tag{10}$$

Reference [40] pointed out that "realistically, however, when a special cause influences a process, it may cause a shift in more than one parameter (location, scale, skewness, etc.) of the

process distribution". It means that, due to the occurrence of an assignable cause, the process may be affected and subsequently the process mean or shape parameter of the distribution will be shifted from the specified target level. In addition, this parameter shift doesn't greatly affect the distribution so it reduces from one to another. But in such a situation, the process will be declared as out-of-control and stopped until the cause of process variations is removed. Also, it is assumed that the process parameter is shifted to $\lambda_A = f\lambda_U$, where f is a shift constant. Then the failure probability of an item when the process is out of control, denoted by p_1, is given as

$$p_1 = 1 - \frac{AF^2}{\left[AF^2 + \left(\frac{a\pi}{2f}\right)^2\right]} \tag{11}$$

Usually, for the given values of a & f, the failure probabilities are calculated by using (10) and (11).

We develop a new np control chart for the lifetime of the product distributed according to the Rayleigh-Inverse-Rayleigh distribution based on the number of products in each subgroup. The following is the designed np control chart's operational procedure:

Step 1: Select a sample of n items randomly from the subgroup of the production process and put the sample items for the life test of specified termination time t_0.
Step 2: Observe the number of failed items and denotes it as "d".
Step 3: Terminate the life test either after reached at time t_0 or $d > UCL$ before reaching time t_0, whichever is earlier.
Step 4: If $d < LCL$ or $d > UCL$, then declare the production process as out-of-control. Otherwise, declare the production process as in control.

The proposed control chart is considered to be an np control chart since the number of failed items in a subgroup of fixed sample size is plotted against the subgroup. The number of failed items in the life test follows a binomial (n, p_0) distribution when the production process is in control. The probability of an item failing before test termination time t_A, is denoted as p_0. As a result, the following equations are used to determine the control limits for the proposed control chart:

$$UCL = np_0 + k\sqrt{np_0(1-p_0)} \tag{12}$$

$$LCL = max[0, np_0 - k\sqrt{np_0(1-p_0)}] \tag{13}$$

Where "k" is the control limits coefficient and the failure probability p_0 of the product before the time t_A is calculated using (10).

The probability that the process is declared to be in control is denoted by P_{in}^0 and given as

$$P_{in}^0 = P(LCL \leq d \leq UCL|p_0)$$

$$P_{in}^0 = \sum_{d=[LCL]+1}^{[UCL]} \binom{n}{d} p_0^d (1-p_0)^{n-d} \tag{14}$$

Generally, the average run length is used to evaluate the performance of the control chart. The in-control ARL of the proposed control chart denoted by ARL_0, is determined by

$$ARL_0 = \frac{1}{1 - [\sum_{d=[LCL]+1}^{[UCL]} \binom{n}{d} p_0^d (1-p_0)^{n-d}]} \tag{15}$$

The probability that, the process is declared to be in control after shifting is denoted by P_{in}^1 and given as

$$P_{in}^{1} = P(LCL \leq d \leq UCL|p_1)$$

$$P_{in}^{1} = \sum_{d=[LCL]+1}^{[UCL]} \binom{n}{d} p_1^d (1-p_1)^{n-d} \tag{16}$$

The ARL for the shifted process (out-of-control) is denoted by ARL_1 and is obtained by:

$$ARL_1 = \frac{1}{1 - [\sum_{d=[LCL]+1}^{[UCL]} \binom{n}{d} p_1^d (1-p_1)^{n-d}]} \tag{17}$$

To evaluate the effectiveness of the proposed control chart in identifying process shifts, we establish the optimal parameters LCL, UCL, a, and k based on predetermined in-control ARL values. Specifically, we examined four scenarios of in-control ARL, namely r_0 = 200, 300, 400, and 500, while maintaining a fixed sample size of n = 25 and 30, AF = 1 and 2 for a one-sided control chart. Additionally, we analysed four sample sizes, 20, 25, 30, and 35, while keeping the in-control ARL (r_0) constant at 250 and 370, AF = 1 and 2 for the same type of control chart. Furthermore, we investigated four instances of in-control ARL across two values of r_0 and two sample sizes, specifically r_0 = 350 and 450, with n = 20 and 30, AF = 1, 2 for a two-sided control chart. The selection of optimal parameters aims to ensure that the in-control ARL is as close as possible to the specified ARL values, while the out-of-control ARLs are reported for varying shift constant values. The optimal parameters, along with their corresponding out-of-control ARLs, are presented in Tables 1 through 5.

Table 1: *ARL when the process parameter one-sided shift*

n = 25								
	AF = 1				AF = 2			
Parameter	r_0 = 200	r_0 = 300	r_0 = 400	r_0 = 500	r_0 = 200	r_0 = 300	r_0 = 400	r_0 = 500
LCL	6	6	5	5	0	0	0	0
UCL	20	21	20	20	12	12	13	13
a	0.6633	0.6758	0.6365	0.6583	0.6220	0.6578	0.6672	0.6860
k	2.7950	2.9070	2.8010	2.9691	3.3892	3.1791	3.4608	3.2932
$Shift(f)$	ARL	ARL	ARL	ARL	ARL	ARL	ARL	ARL
1.00	200.099	300.145	400.257	500.060	200.155	300.473	400.137	500.338
0.90	190.252	224.537	353.284	236.532	184.222	255.520	279.701	377.636
0.80	50.550	142.095	81.976	55.257	130.979	66.746	161.980	112.626
0.70	13.676	32.275	19.721	14.590	27.656	15.636	31.304	23.157
0.60	4.610	8.929	5.921	4.816	6.647	4.437	7.160	5.776
0.50	2.061	3.226	2.379	2.113	2.206	1.768	2.296	2.037
0.40	1.268	1.609	1.345	1.280	1.186	1.110	1.205	1.160
0.30	1.040	1.123	1.053	1.042	1.008	1.004	1.010	1.007
0.20	1.002	1.010	1.002	1.002	1.000	1.000	1.000	1.000
0.10	1.000	1.000	1.000	1.000	1.0000	1.000	1.000	1.000

Table 2: *ARL when the process parameter one-sided shift*

$n = 30$								
	$AF = 1$				$AF = 2$			
Parameter	$r_0 = 200$	$r_0 = 300$	$r_0 = 400$	$r_0 = 500$	$r_0 = 200$	$r_0 = 300$	$r_0 = 400$	$r_0 = 500$
LCL	8	7	7	9	0	0	0	0
UCL	24	23	24	26	12	13	13	14
a	0.6597	0.6366	0.6413	0.7469	0.6476	0.6838	0.6088	0.7142
k	2.9354	3.1035	3.1439	3.2825	2.8618	2.9305	3.2453	2.8584
$Shift(f)$	ARL	ARL	ARL	ARL	ARL	ARL	ARL	ARL
1.00	200.253	300.496	400.392	499.811	199.990	300.080	400.339	499.720
1.10	53.495	87.743	98.041	114.768	155.086	265.998	177.470	465.747
1.20	18.797	28.973	31.604	35.044	137.855	232.026	83.065	366.882
1.30	8.538	12.374	13.291	14.072	71.471	112.628	44.985	167.343
1.40	4.729	6.482	6.872	7.013	41.213	61.450	27.382	87.021
1.50	3.050	3.975	4.167	4.139	26.178	37.278	18.233	50.737
1.60	2.208	2.751	2.857	2.786	17.958	24.601	13.017	32.383
1.70	1.746	2.090	2.153	2.077	13.092	17.356	9.817	22.205
1.80	1.474	1.704	1.745	1.674	10.020	12.915	7.734	16.126
1.90	1.306	1.467	1.494	1.432	7.975	10.034	6.311	12.269
2.00	1.200	1.314	1.333	1.281	6.5539	8.0750	5.2989	9.6950

Table 3: *ARL when the process parameter one-sided shift*

$r_0 = 250$								
	$AF = 1$				$AF = 2$			
Parameter	$n = 20$	$n = 25$	$n = 30$	$n = 35$	$n = 20$	$n = 25$	$n = 30$	$n = 35$
LCL	4	6	8	9	0	0	1	0
UCL	17	21	24	26	12	12	15	13
a	0.6612	0.6664	0.6711	0.6355	0.7205	0.7327	0.8003	0.6186
k	3.0784	3.0315	3.0314	3.0321	3.4687	2.8626	2.8349	2.9044
$Shift(f)$	ARL	ARL	ARL	ARL	ARL	ARL	ARL	ARL
1.00	250.283	250.028	250.191	250.218	250.234	249.949	250.236	250.184
1.10	84.552	71.127	67.231	68.351	109.185	219.511	241.302	225.011
1.20	33.746	26.070	22.737	21.614	55.458	171.212	152.969	196.977
1.30	16.277	11.996	9.973	9.115	32.146	87.324	67.999	96.822
1.40	9.142	6.594	5.360	4.813	20.626	49.513	35.027	53.498
1.50	5.788	4.163	3.369	3.032	14.314	30.957	20.444	32.841
1.60	4.029	2.926	2.387	2.150	10.561	20.931	13.164	21.911
1.70	3.022	2.236	1.854	1.688	8.180	15.061	9.157	15.611
1.80	2.405	1.823	1.543	1.424	6.586	11.392	6.774	11.720
1.90	2.007	1.563	1.352	1.266	5.473	8.972	5.264	9.178
2.00	1.738	1.391	1.231	1.168	4.666	7.305	4.258	7.439

Table 4: *ARL when the process parameter one-sided shift*

$r_0 = 370$								
	$AF = 1$				$AF = 2$			
Parameter	$n = 20$	$n = 25$	$n = 30$	$n = 35$	$n = 20$	$n = 25$	$n = 30$	$n = 35$
LCL	4	5	8	14	0	0	1	1
UCL	17	20	24	31	12	13	15	16
a	0.6909	0.6316	0.7012	0.8638	0.7549	0.7813	0.7418	0.7346
k	2.8343	2.8397	2.9146	2.8954	3.2127	2.8439	2.9169	2.9080
$Shift(f)$	ARL	ARL	ARL	ARL	ARL	ARL	ARL	ARL
1.00	370.047	370.356	370.096	370.073	370.283	370.294	370.086	370.182
0.90	295.564	282.919	171.096	240.076	267.304	96.125	173.819	84.293
0.80	86.130	90.027	38.110	95.016	143.458	24.019	36.435	17.879
0.70	24.891	21.201	10.069	21.970	32.352	6.951	8.596	4.782
0.60	8.337	6.225	3.498	6.520	8.300	2.580	2.738	1.847
0.50	3.403	2.449	1.689	2.603	2.770	1.359	1.341	1.133
0.40	1.769	1.362	1.148	1.440	1.367	1.044	1.032	1.006
0.30	1.199	1.056	1.016	1.085	1.037	1.001	1.000	1.000
0.20	1.027	1.003	1.000	1.006	1.001	1.000	1.000	1.000
0.10	1.001	1.000	1.000	1.000	1.000	1.000	1.000	1.000

Table 5: *ARL when the process parameter two-sided shift*

	$AF = 1$				$AF = 2$			
	$r_0 = 350$		$r_0 = 450$		$r_0 = 350$		$r_0 = 450$	
Parameter	$n = 20$	$n = 30$	$n = 20$	$n = 30$	$n = 20$	$n = 30$	$n = 20$	$n = 30$
LCL	3	6	5	9	0	0	0	0
UCL	16	22	18	26	12	14	12	14
a	0.6154	0.6046	0.7758	0.7417	0.7495	0.7338	0.7773	0.7202
k	3.0601	3.0250	2.9858	3.2412	3.4640	2.9457	3.1778	2.8852
$Shift(f)$	ARL	ARL	ARL	ARL	ARL	ARL	ARL	ARL
0.10	1.000	1.000	1.008	1.000	1.000	1.000	1.000	1.000
0.20	1.008	1.000	1.106	1.010	1.001	1.000	1.000	1.000
0.30	1.102	1.004	1.466	1.128	1.040	1.000	1.028	1.000
0.40	1.501	1.077	2.454	1.643	1.386	1.015	1.297	1.019
0.50	2.743	1.468	5.143	3.418	2.864	1.201	2.436	1.241
0.60	6.631	2.910	13.132	10.073	8.763	2.066	6.713	2.258
0.70	20.121	8.392	39.439	29.949	34.813	5.337	24.220	6.206
0.80	72.012	32.915	133.904	99.772	156.206	18.685	101.617	23.014
0.90	259.127	156.136	431.665	421.938	283.359	79.060	379.733	102.129
1.00	350.171	350.162	450.390	449.755	350.087	350.051	450.461	449.933
1.10	139.299	122.038	156.674	103.577	152.461	312.114	210.600	391.229
1.20	54.342	39.414	57.032	32.142	74.566	279.782	99.623	298.978
1.30	25.305	16.324	25.108	13.099	41.685	216.640	53.811	181.052
1.40	13.727	8.296	13.008	6.614	35.942	109.495	32.511	93.319
1.50	8.405	4.940	7.684	3.950	17.546	62.222	21.444	53.984
1.60	5.664	3.324	5.043	2.683	12.666	38.853	15.155	34.226
1.70	4.119	2.459	3.603	2.016	9.629	26.148	11.313	23.336
1.80	3.183	1.956	2.755	1.636	7.631	18.687	8.825	16.865
1.90	2.582	1.646	2.225	1.407	6.253	14.021	7.135	12.776
2.00	2.179	1.446	1.877	1.264	5.268	10.947	5.940	10.059

From the examination of Tables 1 and 4, it is evident that the out-of-control ARL (ARL_1) is reduced when the shift constant f is lowered. Similarly, Tables 2 and 3 demonstrate that an increase in the shift constant f leads to a decrease in the out-of-control ARL (ARL_1). Additionally, Table 5 shows that deviations of the shift constant from the in-control ARL result in a decrease in the out-of-control ARL. This finding highlights the proposed control chart's proficiency in promptly identifying process shifts. An algorithm is proposed to determine the optimal parameters for the design of the control chart, accommodating various combinations of specified in-control ARL and sample size.

1. Specify the values of ARL say r_0, sample size n and acceleration factor (AF).
2. Set a = 0.0001 and k = 0.0001.
3. Determine the failure probability of the product (i.e., p_0) when the process is in control by using equation (10) and also determine the control chart parameters (LCL and UCL) by substituting the values of n, a and k in equation (12) and (13).
4. Calculate for in-control ARL by using equation (15) and compare it with r_0. Continue this process, for different combinations of (a and k) until getting an in-control ARL is very close to the specified ARL, r_0.
5. Whenever such ARL exist, then the corresponding parameters (LCL, UCL, a, k) are the required optimal parameters. Then calculate the out-of-control ARL (i.e., ARL_1) using these optimal parameters in equation (17).

3. Application of Proposed Control Chart

3.1. Real-Life Application

In this section, a design example is given to demonstrate a real-life application of the proposed control chart under the Bayesian approach. Assume that the product lifetime follows a Rayleigh-Inverse-Rayleigh distribution with parameter λ_A. Considering the following product values: μ_A is 1000 hours, r_0 = 200, n is 20 and AF = 2. The control chart parameters provided in Table 1 include: k at 3.3892, and a at 0.6220, with a lower control limit (LCL) of 0 and an upper control limit (UCL) of 12. Therefore, the control chart to be designed as follows:

Step 1: Select a sample of 20 products from each subgroup and conduct a life test for 622 hours. Record the number of failed products during the life test and denote it as "d".
Step 2: Terminate the life test either after reaching 622 hours or the number of failed products greater than twenty before reaching 622 hours whichever is earlier.
Step 3: If d is between 0 and 12, the process is considered in control; otherwise, it is classified as out of control.

3.2. Simulation Study

This section provides a demonstration of the proposed control chart's application using simulated data. The data is produced from a Rayleigh distribution while the process is in a controlled state, with parameters that follow an inverse Rayleigh distribution under standard conditions (i.e., AF = 1) and a target average lifetime of 1000 hours. A random sample of size n = 20 is utilized for each batch, where the first fifteen samples are derived from the in-control process, and the subsequent fifteen samples are from a shifted process with f = 0.40, resulting in a total of 30 sample batches. From Table V, with n = 20 and ARL_0 = 350, the constants are established as k = 3.0601, a = 0.6154, UCL = 16, and LCL = 3. The number of products with a lifetime below 615 hours is considered as nonconforming items and denoted it as 'D', with the following values: 12, 10, 15, 11, 14, 10, 13, 9, 11, 10, 14, 9, 13, 14, 12, 16, 18, 15, 19, 18, 17, 16, 19, 17, 18, 20, 17, 19, 16, 18. The values of nonconforming items are plotted alongside two control limits (LCL = 3 and UCL = 16) shown in Figure 1.

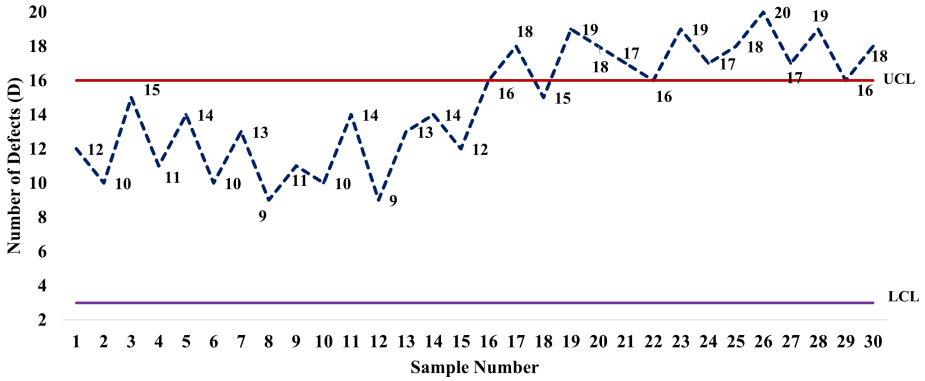


Figure 1: *Control Chart for Simulation Data*

As illustrated in Figure 1, the proposed control chart identifies a shift occurring at the 17^{th} sample, specifically the second observation following the shift, with a calculated Average Run Length (ARL) of 1.501. Consequently, this control chart effectively recognises shifts in the manufacturing process under standard conditions. Therefore, it can be concluded that the proposed control chart is capable of detecting process shifts more rapidly.

4. Behaviour of the Average Run Length

Empirical analysis can investigate the behavior of the ARL under standard conditions (i.e., AF = 1). The characteristics of the ARL curves can be examined concerning the parameters p, n, f, LCL, and UCL while keeping the other parameters constant. To begin with, the effect of "p" on the ARL is assessed. Figure 2 illustrates a set of four ARL curves that correspond to various sets of control chart parameters: (n = 25, k = 3.0, UCL = 20, LCL = 5), (n = 30, k = 3.0, UCL = 20, LCL = 5), (n = 35, k = 3.0, UCL = 20, LCL = 5), and (n = 40, k = 3.0, UCL = 20, LCL = 5). The shapes of these curves reveal an upward trend as the values of "p" increase until reaching the ARL_0, after which the ARL begins to decline with further increases in "p". For instance, with the control chart parameters set at (n = 35, k = 3.0, UCL = 20, LCL = 5), the values of "p" are taken as 0.30, 0.32, 0.34, 0.36, 0.38, and 0.40. The corresponding ARL values for these p values are 36.871, 64.288, 105.883, 135.762, 113.262, and 70.379, respectively. The analysis of the behavior

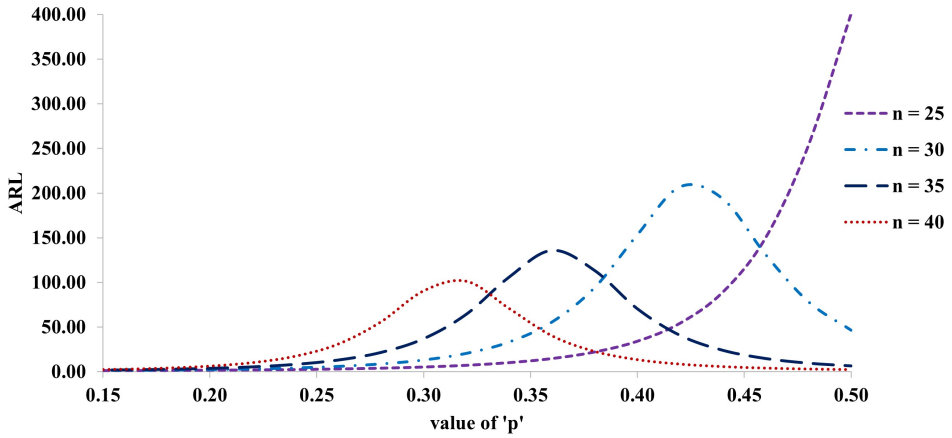


Figure 2: *Behaviour of ARL under "p" and "n"*

of ARL_0 and ARL_1 concerning sample size is presented in Figure 2. This figure indicates that the ARL_0 value rises as the sample size diminishes. Specifically, for sample sizes of n = 25, 30,

35, and 40, the corresponding ARL_0 values are 400.98, 207.29, 135.76, and 101.39, respectively. Conversely, the ARL_1 value exhibits an increase with larger sample sizes while maintaining a constant "p" value. For instance, the ARL_1 values for sample sizes n = 25, 30, 35, and 40 are 7.11, 20.48, 64.29, and 101.39, respectively, with a fixed p-value of 0.32. Thus, it can be concluded that in these control charts, an increase in sample size leads to a decrease in the in-control ARL, while the out-of-control ARL value increases with larger sample sizes. The subsequent analysis

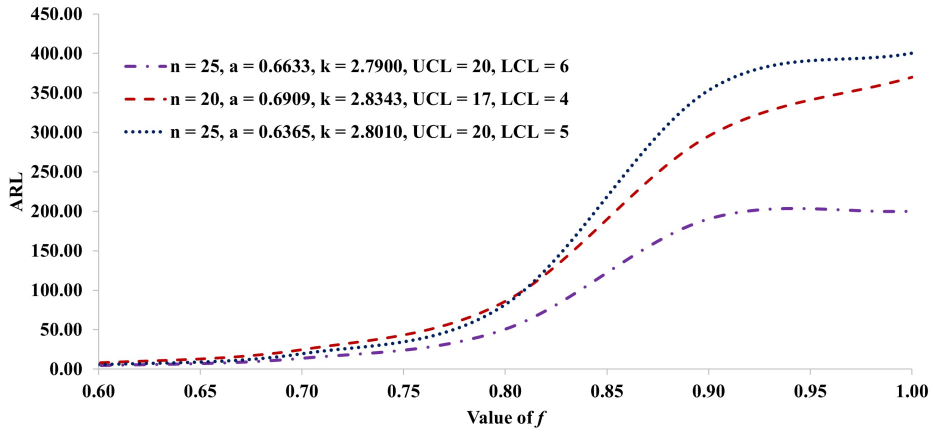


Figure 3: *Behaviour of ARL under shift constant "f"*

focuses on the behaviour of ARL_1 concerning the shift constant "f" as illustrated in Figure 3. This figure presents three distinct ARL curves, each corresponding to varying sets of control chart parameters: (n = 25, a = 0.6633, k = 2.7900, UCL = 20, LCL = 6), (n = 20, a = 0.6909, k = 2.8343, UCL = 17, LCL = 4), and (n = 25, a = 0.6365, k = 2.8010, UCL = 20, LCL = 5). A total of ten different values for the shift constant "f" are examined, specifically f = 0.1, 0.2, 0.3, 0.4, 0.5, 0.6, 0.7, 0.8, 0.9, and 1.0, while maintaining a fixed ARL_0 of 370. The data depicted in Figure 3 indicates that an increase in the shift constant correlates with a rise in the ARL_1 value at a constant ARL_0. For instance, with the control chart parameters (n = 20, a = 0.6909, k = 2.8343, UCL = 17, LCL = 4), the values of "f" are assessed as 0.1 through 1.0, yielding corresponding ARL_1 values of 1.00, 1.03, 1.20, 1.77, 3.40, 8.34, 24.89, 86.13, 295.56, and 370.05. This demonstrates that an increase in the shift constant results in a corresponding increase in the ARL_1 value. The

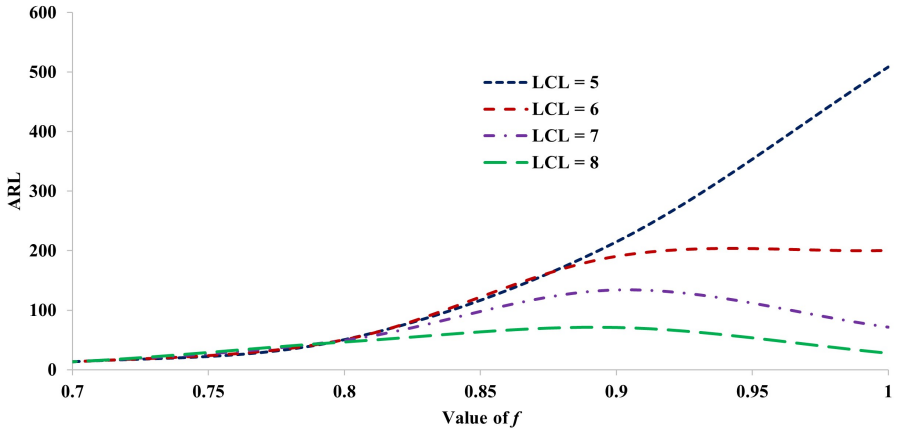


Figure 4: *Behaviour of ARL under "LCL"*

subsequent analysis focuses on the behaviour of ARL_0 concerning the LCL, with the findings presented in the form of ARL curves as illustrated in Figure 4. This figure showcases four distinct

ARL curves corresponding to LCL values of 5, 6, 7, and 8, while maintaining fixed control chart parameters of n = 25, a = 0.6633, k = 2.7900, UCL = 20, and ARL_0 = 200. It is observed from Figure 4 that an increase in the LCL results in a decrease in the value of ARL_0. For instance, with the parameters n = 25, a = 0.6633, k = 2.7900, UCL = 20, and ARL_0 = 200, the ARL_0 values for the LCL values of 5, 6, 7, and 8 are recorded as 508.415, 200.099, 71.801, and 27.981, respectively.

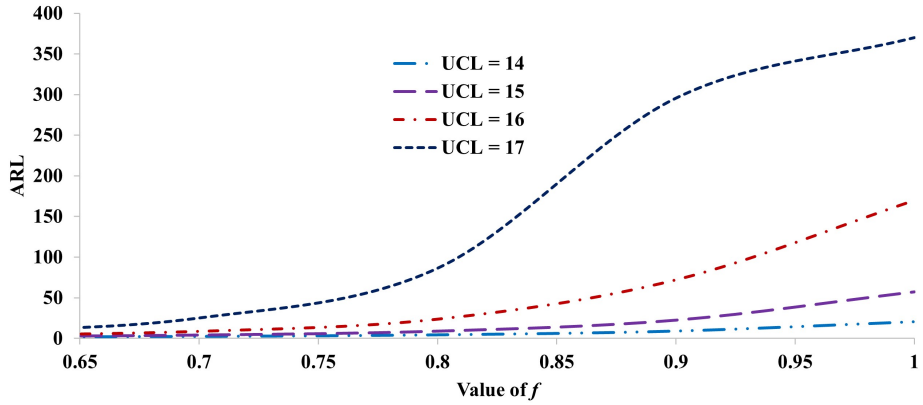


Figure 5: *Behaviour of ARL under "UCL"*

The analysis of the behaviour of ARL_0 concerning the UCL has been conducted, with the findings presented in the form of ARL curves as illustrated in Figure 5. This figure showcases four distinct ARL curves corresponding to UCL values of 14, 15, 16, and 17 while maintaining fixed control chart parameters of n = 20, a = 0.6909, k = 2.8343, LCL = 4, and ARL_0 = 370. It is observed from Figure 5 that an increase in the UCL results in a corresponding increase in the value of ARL_0. Specifically, for the parameters n = 20, a = 0.6909, k = 2.8343, LCL = 4, and ARL_0 = 370, the ARL_0 values for the UCLs of 14, 15, 16, and 17 are 20.5004, 57.3531, 169.508, and 370.047, respectively.

5. Discussion

In this paper, we have developed a methodology for a new Bayesian attribute control chart for the lifetime of products. The life tests are performed by accelerated life test with hybrid censoring assuming a Rayleigh distribution for the lifetime and an inverse Rayleigh distribution as a prior. The proposed control chart is to ensure the mean lifetime of the product as the quality criterion. The newly established control chart is highly adaptable and may be used to monitor the lifetime of quality products. The tables are provided for industrial usage and are explicated with the use of simulated data. It is generated using R software from a Rayleigh-Inverse-Rayleigh distribution. The performance of the proposed control chart is expressed in terms of ARLs for various shift constants (f), sample size (n), other parameters p, LCL and UCL. It should be noted that if the hybrid censoring scheme is used to carry out the life test, executing the sampling inspection will reduce the time and cost of conducting the life test. The developed attribute control chart has the potential to be extended for use with various other statistical distributions as part of a continuing research study.

References

[1] Muhammad Aslam and Chi-Hyuck Jun (2015). Attribute Control Chart for the Weibull Distribution under Truncated Life Tests. *Quality Engineering*, 27(3): 283 – 288.

[2] Muhammad Aslam, Osama H. Arif and Chi-Hyuck Jun (2017). An Attribute Control Chart for a Weibull distribution under Accelerated Hybrid Censoring. *PLoS ONE*, 12(3): e0173406: 1 – 11.

[3] Ali Hussein Al-Marshadi, Ambreen Shafqat, Muhammad Aslam and Abdullah Alharbey (2021). Performance of a New Time-Truncated Control Chart for Weibull Distribution under Uncertainty. *International Journal of Computational Intelligence Systems*, 14(1): 1256 – 1262.

[4] Aslam M, Nasrullah Khan and Chi – Hyuck (2016a). A control chart for time truncated life tests using Pareto distribution of the second kind. *Journal of Statistical Computation and Simulation*, 86(11): 2113 – 2122.

[5] Aslam M, Arif, O. H and Jun, C (2016b). An Attribute Control Chart based on the Birnbaum-Saunders Distribution using Repetitive Sampling. *IEEE Access*, 5: 9350 – 9360.

[6] Nanthakumar C and T. Kavitha (2017). Design of Attribute Control Chart based on Inverse Rayleigh Distribution under Type – I Censoring. *International Journal of Statistical Sciences*, 4(6): 17 – 22.

[7] Ambreen Shafqat, Jaffer Hussain, Amjad D. Al-Nasser and Muhammad Aslam (2018). Attribute Control Chart for some popular distributions. *Communication in Statistics – Theory and Methods*. 47(8): 1978 – 1988.

[8] Arif O. H, Muhammad Aslam and K.A. Butt (2018). Attribute Control Chart for a Lognormal distribution under Accelerated Time Censoring. *Journal of Computational and Theoretical Nanoscience*, 15(3): 919 – 923.

[9] Srinivasa Rao G (2018). A Control Chart for Time Truncated Life Tests Using Exponentiated Half Logistic Distribution. *Applied Mathematics & Information Sciences: An International Journal*, 12(1): 125 – 131.

[10] Srinivasa Rao Gadde, A.K. Fulment and P.K Josephat (2019). Attribute Control Charts for Dagum distribution under truncated life tests. *Life cycle Reliability and Safety Engineering*, 8: 329 – 335.

[11] Balamurali S and P. Jeyadurga (2019). An Attribute np Control Chart for Monitoring Mean Life using Multiple Deferred State Sampling based on Truncated Life Tests. *International Journal of Reliability, Quality and Safety Engineering*, 26(1): 1950004-1 – 1950004-18.

[12] Enayat M. Abd Elrazik (2020). Attribute control charts for the New Weibull Pareto Distribution under truncated life tests. *Journal of Statistics Applications & Probability*, 9(1): 43 – 49.

[13] Ahmad Ibrahim Shawky, Muhammad Aslam and Khushnoor Khan (2020). Multiple dependent state sampling-based charts using Belief Statistic under Neutrosophic Statistics. *Journal of Mathematics*, 2020(7680286): 1- 14.

[14] Srinivasa Rao Gadde, Edwin Paul (2020). Time Truncated Control Chart using Log- Logistic Distribution. *Biometrics & Biostatistics International Journal*, 9: 76 - 82.

[15] Rosaiagh, K., G. Srinivasa Rao and S. V. S. V. S. V. Prasad (2021). A Control Chart for Time Truncated Life Tests using type-II Generalized Log Logistic Distribution. *Biometrics & Biostatistics International Journal*, 10(4): 138 – 143.

[16] Adeoti O. A. and P. Ogundipe (2021). A Control Chart for the generalized exponential distribution under time truncated life test. *Life Cycle Reliability and Safety Engineering*, 10: 53 – 59.

[17] Ayman Baklizi and Sawsan Abu Ghannam (2022). An attribute control chart for the inverse Weibull distribution under truncated life tests. *Heliyon*, 8(e11976): 1 - 5.

[18] Srinivasa Rao Gadde and Amer Ibrahim Al-Omari (2022). Attribute control charts based on TLT for Length-Biased Weighted Lomax Distribution. *Journal of Mathematics*, 2022(3091850): 1- 15.

[19] Olatunde Adebayo Adeoti and Gadde Srinivasa Rao (2022). Attribute control chart for Rayleigh distribution using Repetitive sampling under truncated life test. *Journal of Probability and Statistics*, 2022(8763091): 1 - 11.

[20] Muhammad Naveed, Muhammad Azam, Nasrullah Khan, Muhammad Aslam, Muhammad Saleem and Muhammad Saeed (2023). Control Chart for Half Normal and half Exponential power Distributed Process. *Scientific Reports*, 13(8632): 1- 20.

[21] Srinivasa Rao B, M. Rami Reddy and K. Rosaiah (2023). An attribute Control Chart for Time

Truncated Life Tests using Exponentiated Inverse Kumaraswamy Distribution. *Reliability: Theory & Applications*, 3:74(18): 206 – 217.

[22] Sri Ramachandran G V., Srinivasa Rao Gadde and Muhammed Aslam (2024). Utilizing Repetitive Sampling in the Construction of a Control Chart for Lindley Distribution with Time Truncation. *Journal of Statistical Theory and Applications*, 23: 224 – 239.

[23] Saha M., Pareek P, Tripathi H, and A Devi (2024). Time Truncated Attribute Control Chart for Generalized Rayleigh Distributed Quality Characteristics and Beyond *International Journal of Quality & Reliability Management*, 41(5): 1400 – 1416.

[24] Gunasekaran Munian (2024). A New Attribute Control Chart based on Exponentiated Exponential Distribution under Accelerated Life Test with Hybrid Censoring. *Reliability: Theory & Applications*, 19(4): 850 – 860.

[25] Joel M. Calabrese (1995). Bayesian Process Control for Attributes. *Management Science*, 41(4): 637 – 645.

[26] Ulrich Menzefricke (2002). On the Evaluation of Control Chart Limits based on Predictive Distributions. *Communication in Statistics – Theory and Methods*, 31(8): 1423 – 1440.

[27] Apley D. W (2012). Posterior distribution charts: A Bayesian approach for graphically exploring a process mean. *Technometrics*, 54(3): 279 – 310.

[28] Amin Shaka Aunali and D. Venkatesan (2017). Comparison of Bayesian Method and Classical Charts in Detection of Small Shifts in the Control Charts. *International Journal of Operations Research and Optimization*, 6(2): 101 – 114.

[29] Kumar N and S. Chakraborti (2017). Bayesian Monitoring of times between events: The Shewhart tr - chart. *Journal of Quality Technology*, 49(2): 136 – 154.

[30] Amin Shaka Aunali and D. Venkatesan (2019). Bayesian Approach in Control Chart Techniques. *International Journal of Scientific Research in Mathematical and Statistical Sciences*, 6(2): 217 – 221.

[31] Amin Shaka Aunali, Venkatesan. D. and Michele Gallo (2019). Bayesian Control Chart using Gamma Prior. *International Journal of Scientific & Technology Research*, 8(12): 1567 - 1570.

[32] Ali S (2020). A Predictive Bayesian Approach to sequential time-between-events monitoring. *Quality and Reliability Engineering International*, 36(1): 365 – 387.

[33] Kadoishi S and H. Kawamura (2020). Control Charts based on Hierarchical Bayesian Modeling. *Total Quality Science*, 5(2): 72 – 80.

[34] Konstantinos Bourazas, Dimitrios Kiagias and Panagiotis Tsiamyrtzis (2022). Predictive Control Charts (PCC): A Bayesian Approach in Online monitoring of short runs. *Journal of Quality Technology*, 54(4): 367 – 391.

[35] Fatimah Alshahrani, Ibrahim M. Almanjahie, Majid Khan, Syed M. Anwar, Zahid Rasheed and Ammara N. Cheema (2023). On Designing of Bayesian Shewhart-Type Control Charts for Maxwell Distributed Processes with Application of Boring Machine. *Mathematics*, 11(1126): 1 - 20.

[36] Lord Rayleigh, O. M. F. R. S (1919). On the problem of random vibrations, and of random flights in one, two, or three dimensions. *The London, Edinburgh, and Dublin Philosophical Magazine and Journal of Science*, Series 6, 37(220): 321 – 347.

[37] Siddiqui M. M (1962). Some Problems Connected with Rayleigh Distributions. *Journal of Research of the National Bureau of Standards – D. Radio Propagation*, 66D(2): 167 – 174.

[38] Siddiqui M. M (1964). Statistical Inference for Rayleigh Distribution. *Radio Science Journal of Research NBS/USNC-URSI*, 68D(9): 1005 – 1010.

[39] Kalaiselvi S., A. Loganathan and R. Vijayaraghavan (2014). Bayesian Reliability Sampling Plans under the Conditions of Rayleigh-Inverse-Rayleigh Distribution. *Economic Quality Control*, 29(1): 29 – 38.

[40] Saad T and Bakir (2012). A nonparametric Shewhart-type quality control chart for monitoring broad changes in a process distribution. *International Journal of Quality, Statistics, and Reliability*, 2012(147520): 1 – 10.